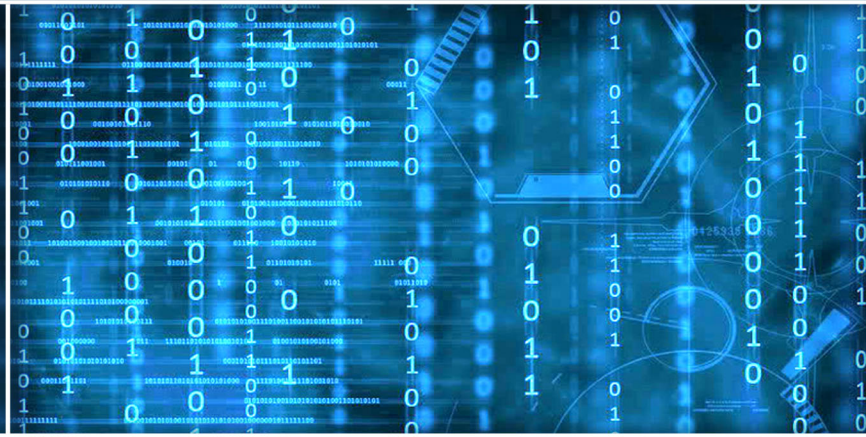


Volume 13 Issue 3

March 2022



ISSN 2156-5570(Online)

ISSN 2158-107X(Print)



Editorial Preface

From the Desk of Managing Editor...

It may be difficult to imagine that almost half a century ago we used computers far less sophisticated than current home desktop computers to put a man on the moon. In that 50 year span, the field of computer science has exploded.

Computer science has opened new avenues for thought and experimentation. What began as a way to simplify the calculation process has given birth to technology once only imagined by the human mind. The ability to communicate and share ideas even though collaborators are half a world away and exploration of not just the stars above but the internal workings of the human genome are some of the ways that this field has moved at an exponential pace.

At the International Journal of Advanced Computer Science and Applications it is our mission to provide an outlet for quality research. We want to promote universal access and opportunities for the international scientific community to share and disseminate scientific and technical information.

We believe in spreading knowledge of computer science and its applications to all classes of audiences. That is why we deliver up-to-date, authoritative coverage and offer open access of all our articles. Our archives have served as a place to provoke philosophical, theoretical, and empirical ideas from some of the finest minds in the field.

We utilize the talents and experience of editor and reviewers working at Universities and Institutions from around the world. We would like to express our gratitude to all authors, whose research results have been published in our journal, as well as our referees for their in-depth evaluations. Our high standards are maintained through a double blind review process.

We hope that this edition of IJACSA inspires and entices you to submit your own contributions in upcoming issues. Thank you for sharing wisdom.

Thank you for Sharing Wisdom!

Kohei Arai
Editor-in-Chief
IJACSA
Volume 13 Issue 3 March 2022
ISSN 2156-5570 (Online)
ISSN 2158-107X (Print)

Editorial Board

Editor-in-Chief

Dr. Kohei Arai - Saga University

Domains of Research: Technology Trends, Computer Vision, Decision Making, Information Retrieval, Networking, Simulation

Associate Editors

Alaa Sheta

Southern Connecticut State University

Domain of Research: Artificial Neural Networks, Computer Vision, Image Processing, Neural Networks, Neuro-Fuzzy Systems

Domenico Ciuonzo

University of Naples, Federico II, Italy

Domain of Research: Artificial Intelligence, Communication, Security, Big Data, Cloud Computing, Computer Networks, Internet of Things

Doroła Kaminska

Lodz University of Technology

Domain of Research: Artificial Intelligence, Virtual Reality

Elena Scutelnicu

"Dunarea de Jos" University of Galati

Domain of Research: e-Learning, e-Learning Tools, Simulation

In Soo Lee

Kyungpook National University

Domain of Research: Intelligent Systems, Artificial Neural Networks, Computational Intelligence, Neural Networks, Perception and Learning

Krassen Stefanov

Professor at Sofia University St. Kliment Ohridski

Domain of Research: e-Learning, Agents and Multi-agent Systems, Artificial Intelligence, e-Learning Tools, Educational Systems Design

Renato De Leone

Università di Camerino

Domain of Research: Mathematical Programming, Large-Scale Parallel Optimization, Transportation problems, Classification problems, Linear and Integer Programming

Xiao-Zhi Gao

University of Eastern Finland

Domain of Research: Artificial Intelligence, Genetic Algorithms

CONTENTS

Paper 1: Helping People with Social Anxiety Disorder to Recognize Facial Expressions in Video Meetings

Authors: Jieyu Wang, Abdullah Abuhussein, Hanwei Wang, Tian Qi, Xiaoyue Ma, Amani Alqarni, Lynn Collen

PAGE 1 – 6

Paper 2: Can the Futures Market be Predicted-Perspective based on AutoGluon

Authors: YangChun Xiong, ZiXuan Pan, BaiFu Chen

PAGE 7 – 12

Paper 3: Stochastic Rounding for Image Interpolation and Scan Conversion

Authors: Olivier Rukundo, Samuel Emil Schmidt

PAGE 13 – 22

Paper 4: Analysis of the Elderly's Internet Accessed Time using XGB Machine Learning Model for Solving the Level of the Information Gap of the Elderly

Authors: Hung Viet Nguyen, Haewon Byeon

PAGE 23 – 27

Paper 5: Accessibility of Bulgarian Regional Museums Websites

Authors: Todor Todorov, Galina Bogdanova, Mirena Todorova-Ekmekci

PAGE 28 – 34

Paper 6: Can Ready-to-Use RNNs Generate “Good” Text Training Data?

Authors: Jia Hui Feng

PAGE 35 – 38

Paper 7: Spectrum Pricing in Cognitive Radio Networks: An Analysis

Authors: Reshma C R, Arun kumar B. R

PAGE 39 – 44

Paper 8: Mobile-based Vaccine Registry to Improve Collection and Completeness of Maternal Immunization Data

Authors: Zubeda S. Kilua, Mussa A. Dida, Devotha N. Nyambo

PAGE 45 – 51

Paper 9: Personalized Desire2Learn Recommender System based on Collaborative Filtering and Ontology

Authors: Walid Qassim Qwaider

PAGE 52 – 56

Paper 10: Design Level Class Decomposition using the Threshold-based Hierarchical Agglomerative Clustering

Authors: Bayu Priyambadha, Tetsuro Katayama

PAGE 57 – 64

Paper 11: A Comparative Analysis of Multi-Criteria Decision Making Techniques for Ranking of Attributes for e-Governance in India

Authors: Bhaswati Sahoo, Rabindra Narayana Behera, Prasant Kumar Pattnaik

PAGE 65 – 70

Paper 12: Comparative Analysis of Lexicon and Machine Learning Approach for Sentiment Analysis

Authors: Roopam Srivastava, P. K. Bharti, Parul Verma

PAGE 71 – 77

Paper 13: COVID-19 Detection from X-Ray Images using Convolutional Neural Networks: A Literature Review

Authors: Othman A. Alrusaini

PAGE 78 – 88

Paper 14: Development of Mathematics Web-based Learning on Table Set-Up Activities

Authors: Gusti Ayu Dessy Sugiharni, I Made Ardana, I Gusti Putu Suharta, I Gusti Putu Sudiarta

PAGE 89 – 98

Paper 15: A Risk Management Framework for Large Scale Scrum using Metadata Outer Request Management Methodology

Authors: Rehab Adel, Hany Harb, Ayman Elshenawy

PAGE 99 – 109

Paper 16: Technique for Balanced Load Balancing in Cloud Computing Environment

Authors: Narayan A. Joshi

PAGE 110 – 118

Paper 17: A Heuristic Feature Selection in Logistic Regression Modeling with Newton Raphson and Gradient Descent Algorithm

Authors: Samingun Handoyo, Nandia Pradianti, Waego Hadi Nugroho, Yusnita Julyarni Akri

PAGE 119 – 126

Paper 18: HEMClust: An Improved Fraud Detection Model for Health Insurance using Heterogeneous Ensemble and K-prototype Clustering

Authors: Shamitha S Kotekani, V Ilango

PAGE 127 – 139

Paper 19: An Authorization Framework for Preserving Privacy of Big Medical Data via Blockchain in Cloud Server

Authors: Hemanth Kumar N P, Prabhudeva S

PAGE 140 – 150

Paper 20: Dynamic and Optimized Routing Approach (DORA) in Vehicular Ad hoc Networks (VANETs)

Authors: Satyanarayana Raju K, Selvakumar K

PAGE 151 – 156

Paper 21: Comparative Analysis of RSA and NTRU Algorithms and Implementation in the Cloud

Authors: Bambang Harjito, Henny Nurcahyaning Tyas, Esti Suryani, Dewi Wisnu Wardani

PAGE 157 – 164

Paper 22: A Conceptual Framework for using Big Data in Egyptian Agriculture

Authors: Sayed Ahmed, Amira S. Mahmoud, Eslam Farg, Amany M. Mohamed, Marwa S. Moustafa, Mohamed A. E. AbdelRahman, Hisham M. AbdelSalam, Sayed M. Arafat

PAGE 165 – 173

Paper 23: Design and Development for a Vehicle Tracking System

Authors: Tim Abe P. Andutan, Rosanna C. Ucat

PAGE 174 – 182

Paper 24: EMOGAME: Digital Games Therapy for Older Adults

Authors: Nita Rosa Damayanti, Nazlena Mohamad Ali

PAGE 183 – 191

Paper 25: A Paradigm for DoS Attack Disclosure using Machine Learning Techniques

Authors: Mosleh M. Abualhaj, Ahmad Adel Abu-Shareha, Mohammad O. Hiari, Yousef Alrabanah, Mahran Al-Zyoud, Mohammad A. Alsharaiah

PAGE 192 – 200

Paper 26: A Prediction Error Nonlinear Difference Expansion Reversible Watermarking for Integrity and Authenticity of DICOM Medical Images

Authors: David Muigai, Elijah Mwangi, Edwell T. Mharakurwa

PAGE 201 – 210

Paper 27: Deep Learning Framework for Physical Internet Hubs Inbound Containers Forecasting

Authors: El-Sayed Orabi Helmi, Osama Emam, Mohamed Abdel-Salam

PAGE 211 – 216

Paper 28: An Intelligent Anti-Jamming Mechanism against Rule-based Jammer in Cognitive Radio Network

Authors: Sudha Y, Sarasvathi V

PAGE 217 – 230

Paper 29: Rainfall Forecasting using Support Vector Regression Machines

Authors: Lemuel Clark Velasco, Johanne Miguel Aca-ac, Jeb Joseph Cajés, Nove Joshua Lactuan, Suwannit Chareen Chit

PAGE 231 – 237

Paper 30: Using Decision Tree Classification Model to Predict Payment Type in NYC Yellow Taxi

Authors: Hadeer Ismaeil, Sherif Kholeif, Manal A. Abdel-Fattah

PAGE 238 – 244

Paper 31: An Extended DBSCAN Clustering Algorithm

Authors: Ahmed Fahim

PAGE 245 – 258

Paper 32: Unsupervised Chest X-ray Opacity Classification using Minimal Deep Features

Authors: Mohd Zulfaezal Che Azemin, Mohd Izzuddin Mohd Tamrin, Mohd Adli Md Ali, Iqbal Jamaludin

PAGE 259 – 262

Paper 33: IoT based Speed Control for Semi-Autonomous Electric On-Road Cargo Vehicle

Authors: P. L. Arunkumar, M. Ramaswamy, T. S. Muruges

PAGE 263 – 272

Paper 34: A Novel Approach of Hyperspectral Imaging Classification using Hybrid ConvNet

Authors: Soumyashree M Panchal, Shivaputra

PAGE 273 – 281

Paper 35: Non-Repudiation-based Network Security System using Multiparty Computation

Authors: Divya K. S, Roopashree H. R, Yogeesh A C

PAGE 282 – 289

Paper 36: An Algorithm based on Convolutional Neural Networks to Manage Online Exams via Learning Management System Without using a Webcam

Authors: Lassaad K. SMIRANI, Jihane A. BOULAHIA

PAGE 290 – 299

Paper 37: A Cubic B-Splines Approximation Method Combined with DWT and IBP for Single Image Super-resolution

Authors: Victor Kipkoech Mutai, Elijah Mwangi, Ciira wa Maina

PAGE 300 – 310

Paper 38: Supervised Learning Techniques for Intrusion Detection System based on Multi-layer Classification Approach

Authors: Mansoor Farooq

PAGE 311 – 315

Paper 39: A Comprehensive Study of Different Types of Deduplication Technique in Various Dimensions

Authors: G. Sujatha, Jeberson Retna Raj

PAGE 316 – 323

Paper 40: PLA Mechanical Performance Before and After 3D Printing

Authors: Houcine SALEM, Hamid ABOUCHADI, Khalid ELBIKRI

PAGE 324 – 330

Paper 41: Detecting Hate Speech on Twitter Network using Ensemble Machine Learning

Authors: Raymond T Mutanga, Nalindren Naicker, Oludayo O Olugbara

PAGE 331 – 339

Paper 42: Methodology for Infrastructure Site Monitoring using Unmanned Aerial Vehicles (UAVs)

Authors: Cristian Benjamin Garcia Casierra, Carlos Gustavo Calle Sanchez, Javier Ferney Castillo Garcia, Felipe Munoz La Rivera

PAGE 340 – 348

Paper 43: Development of Pipe Inspection Robot using Soft Actuators, Microcontroller and LabVIEW

Authors: Mohd Aliff, Mohammad Imran, Sairul Izwan, Mohd Ismail, Nor Samsiah, Tetsuya Akagi, Shujiro Dohta, Weihang Tian, So Shimooka, Ahmad Athif

PAGE 349 – 354

Paper 44: Deep Learning-based Detection System for Heavy-Construction Vehicles and Urban Traffic Monitoring

Authors: Sreelatha R, Roopa Lakshmi R

PAGE 355 – 361

Paper 45: Classification of Autism Spectrum Disorder and Typically Developed Children for Eye Gaze Image Dataset using Convolutional Neural Network

Authors: Praveena K N, Mahalakshmi R

PAGE 362 – 370

Paper 46: Technological Affordances and Teaching in EFL Mixed-ability Classes during the COVID-19 Pandemic

Authors: Waheed M. A. Altohami, Mohamed Elarabawy Hashem, Abdulfattah Omar, Mohamed Saad Mahmoud Hussein

PAGE 371 – 380

Paper 47: Deep Learning Applications in Solid Waste Management: A Deep Literature Review

Authors: Sana Shahab, Mohd Anjum, M. Sarosh Umar

PAGE 381 – 395

Paper 48: Proposal of an Automated Tool for the Application of Sentiment Analysis Techniques in the Context of Marketing

Authors: Gabriel Elias Chanchi Golondrino, Manuel Alejandro Ospina Alarcon, Wilmar Yesid Campo Munoz

PAGE 396 – 402

Paper 49: Affinity Degree as Ranking Method

Authors: Rosyazwani Mohd Rosdan, Wan Suryani Wan Awang, Samhani Ismail

PAGE 403 – 410

Paper 50: Developing a Credit Card Fraud Detection Model using Machine Learning Approaches

Authors: Shahnawaz Khan, Abdullah Alourani, Bharavi Mishra, Ashraf Ali, Mustafa Kamal

PAGE 411 – 418

Paper 51: Bayesian Hyperparameter Optimization and Ensemble Learning for Machine Learning Models on Software Effort Estimation

Authors: Robert Marco, Sakinah Sharifah Syed Ahmad, Sabrina Ahmad

PAGE 419 – 429

Paper 52: A Robust Reversible Data Hiding Framework for Video Steganography Applications

Authors: Manjunath Kamath K, R. Sanjeev Kunte

PAGE 430 – 440

Paper 53: Automated Feature Extraction for Predicting Multiple Sclerosis Patient Disability using Brain MRI

Authors: Ali M. Muslim, Syamsiah Mashohor, Rozi Mahmud, Gheyath Al Gawwam, Marsyita binti Hanafi

PAGE 441 – 448

Paper 54: Random and Sequence Workload for Web-Scale Architecture for NFS, GlusterFS and MooseFS Performance Enhancement

Authors: Mardhani Riasegiawan, Nashihun Amien

PAGE 449 – 457

Paper 55: A Data Security Algorithm for the Cloud Computing based on Elliptic Curve Functions and Sha3 Signature

Authors: Sonia KOTEL, Fatma SBIAA

PAGE 458 – 465

Paper 56: Sentiment Analysis on Customer Satisfaction of Digital Banking in Indonesia

Authors: Bramanthyo Andrian, Tiarna Simanungkalit, Indra Budi, Alfian Farizki Wicaksono

PAGE 466 – 473

Paper 57: System Architecture for Brain-Computer Interface based on Machine Learning and Internet of Things

Authors: Shahanawaj Ahamad

PAGE 474 – 480

Paper 58: Wave Parameters Prediction for Wave Energy Converter Site using Long Short-Term Memory

Authors: Manzoor Ahmed Hashmani, Muhammad Umair, Horio Keiichi

PAGE 481 – 487

Paper 59: Dynamic User Activity Prediction using Contextual Service Matching Mechanism

Authors: M. Subramanyam, S. S. Parthasarathy

PAGE 488 – 498

Paper 60: Progressive 3-Layered Block Architecture for Image Classification

Authors: Munmi Gogoi, Shahin Ara Begum

PAGE 499 – 508

Paper 61: Face Recognition using Principal Component Analysis and Clustered Self-Organizing Map

Authors: Jasem Almotiri

PAGE 509 – 520

Paper 62: Performance Evaluation of Safe Avoidance Time and Safety Message Dissemination for Vehicle to Vehicle (V2V) Communication in LTE C-V2X

Authors: Hakimah Abdul Halim, Azizul Rahman Mohd Shariff, Suzi Iryanti Fadilah, Fatima Karim

PAGE 521 – 528

Paper 63: Design and Implementation of a Low-cost CO₂ Monitoring and Control System Prototype to Optimize Ventilation Levels in Closed Spaces

Authors: Ramces Cavallini-Rodriguez, Jesus Espinoza-Valera, Carlos Sotomayor-Beltran

PAGE 529 – 537

Paper 64: BCSM: A BlockChain-based Security Manager for Big Data

Authors: Hanan E. Alhazmi, Fathy E. Eassa

PAGE 538 – 545

Paper 65: A Review-based Context-Aware Recommender Systems: Using Custom NER and Factorization Machines

Authors: Rabie Madani, Abderrahmane Ez-zahout

PAGE 546 – 553

Paper 66: A Computer Vision-based System for Surgical Waste Detection

Authors: Md. Ferdous, Sk. Md. Masudul Ahsan

PAGE 554 – 565

Paper 67: Human-Computer Interaction in Mobile Learning: A Review

Authors: Nurul Amirah Mashudi, Mohd Azri Mohd Izhar, Siti Armiza Mohd Aris

PAGE 566 – 574

Paper 68: A Secure and Trusted Fog Computing Approach based on Blockchain and Identity Federation for a Granular Access Control in IoT Environments

Authors: Samia EL HADDOUTI, Mohamed Dafir ECH-CHERIF EL KETTANI

PAGE 575 – 584

Paper 69: Intraday Trading Strategy based on Gated Recurrent Unit and Convolutional Neural Network: Forecasting Daily Price Direction

Authors: Nabil MABROUK, Marouane CHIHAB, Zakaria HACHKAR, Younes CHIHAB

PAGE 585 – 592

Paper 70: Remote Healthcare Monitoring using Expert System

Authors: Prajoona Valsalan, Najam ul Hasan, Imran Baig, Manaf Zghaibeh

PAGE 593 – 599

Paper 71: An End-to-End Method to Extract Information from Vietnamese ID Card Images

Authors: Khanh Nguyen-Trong

PAGE 600 – 609

Paper 72: A New Text Summarization Approach based on Relative Entropy and Document Decomposition

Authors: Nawaf Alharbe, Mohamed Ali Rakrouki, Abeer Aljohani, Mashael Khayyat

PAGE 610 – 618

Paper 73: A Game Theory-based Virtual Machine Placement Algorithm in Hybrid Cloud Environment

Authors: Nawaf Alharbe, Mohamed Ali Rakrouki

PAGE 619 – 629

Paper 74: Ensuring Privacy Preservation Access Control Mechanism in Cloud based on Identity based Derived Key

Authors: Suresha D, K Karibasappa, Shivamurthy

PAGE 630 – 636

Paper 75: Multiple Hydrophone Arrays based Underwater Localization with Matching Field Processing

Authors: Shuo Jin, Xiukui Li

PAGE 637 – 645

Paper 76: High-quality Voxel Reconstruction from Stereoscopic Images

Authors: Arturo Navarro, Manuel Loiza

PAGE 646 – 653

Paper 77: Structural Information Retrieval in XML Documents: A Graph-based Approach

Authors: Imane Belahyane, Mouad Mammass, Hasna Abioui, Assmaa Moutaoukkil, Ali Idarrou

PAGE 654 – 659

Paper 78: Dynamic Support Range based Rare Pattern Mining over Data Streams

Authors: Sunitha Vanamala, L. Padma Sree, S. Durga Bhavani

PAGE 660 – 667

Paper 79: Energy Efficient Hop-by-Hop Retransmission and Congestion Mitigation of an Optimum Routing and Clustering Protocol for WSNs

Authors: Prakash K Sonwalkar, Vijay Kalmani

PAGE 668 – 676

Paper 80: A Novel Approach for Small Object Detection in Medical Images through Deep Ensemble Convolution Neural Network

Authors: J. Maria Arockia Dass, S. Magesh Kumar

PAGE 677 – 682

Paper 81: Software Reliability Prediction by using Deep Learning Technique

Authors: Shivani Yadav, Balkishan

PAGE 683 – 693

Paper 82: Performance Evaluation of Temporal and Frequential Analysis Approaches of Electromyographic Signals for Gestures Recognition using Neural Networks

Authors: Edwar Jacinto Gomez, Fredy H. Martinez Sarmiento, Fernando Martinez Santa

PAGE 694 – 701

Helping People with Social Anxiety Disorder to Recognize Facial Expressions in Video Meetings

Jieyu Wang^{1*}, Abdullah Abuhussein², Hanwei Wang³, Tian Qi⁴, Xiaoyue Ma⁵, Amani Alqarni⁶, Lynn Collen⁷

Department of Information Systems, St. Cloud State University, St. Cloud, USA^{1,2,7}

University College London, London, UK³

University of San Francisco, San Francisco, USA⁴

CNBD Applied Research Institute Co. Ltd, Beijing, China⁵

Information Technology and Security Department, Jazan University, Jazan, Saudi Arabia⁶

Abstract—According to previous research on social anxiety disorder (SAD) and facial expressions, those with SAD tend to view all faces as portraying negative emotions; thus, they are afraid of chatting with others when they cannot understand the real emotions being communicated. The advancement of facial recognition technology has given people opportunities to get a more precise emotional estimation of facial expressions. This study aims to investigate the practical effects of apps that detect facial expressions of emotion (e.g., AffdexMe) on people with SAD when communicating with other people through video chatting. We conducted empirical research to examine whether facial emotion recognition software can help people with SAD overcome the fear of chatting with others in video meetings and help them understand others' emotions to reduce communication conflicts. This paper presents the design of an experiment to measure participants' reactions when they video-chat with others using the AffdexMe application and to interview participants to get in-depth feedback. The results show that people with SAD could better recognize the emotions of others using AffdexMe. This results in more reasonable responses and better interaction during video chats. We also propose design suggestions to make the described approach better and more convenient to use. This research shed a light on the future design of emotion recognition in video chatting for people with disabilities or even ordinary users.

Keywords—Social phobia/social anxiety disorder; video meeting; facial expression recognition; emotion recognition; empirical research

I. INTRODUCTION

In modern times, mobile facial recognition applications have become more and more popular. Many mobile phone manufactures have developed facial recognition capabilities, including companies such as Samsung, Huawei, and Vivo. Facial recognition is technology which has the capability to identify or verify a person using a digital image or a video frame from a video source [1]. This process is often completed by comparing facial features with images stored in a database. Emotional recognition has been broadly studied by the computer vision community. It has been developed based on the application of facial recognition technology and aims to define individuals' emotions by analyzing their facial expressions. The currently available applications of facial recognition include area access control systems, checking attendance systems, facial recognition phone unlock, and even

logging onto banking apps and similar security applications. This widespread use of facial recognition has made many computing devices faster, safer, and easier to use in many ways. However, the application of emotion recognition using facial expressions is far less popular or widespread compared to other applications for facial recognition technology, in part because emotional recognition facial software faces challenges with recognizing moving objects, continuous detection of objects, unpredictable actions, and similar programming difficulties.

Emotion recognition is an interdisciplinary research field that is becoming very important for intelligent communication between humans and computers. It has been used in many areas such as gaming and entertainment, surveillance, robotics and many more. The potential for using video- and audio-aided emotion detection to identify and reduce the severity of psychological and mental disorders has recently gained attention from the research community. This is mainly attributable to advancements in artificial intelligence and video recording technologies.

According to the American Psychiatric Association [1], social phobia is a "persistent fear of one or more situations in which the person is exposed to possible scrutiny by others and fears that he or she may do something or act in a way that will be humiliating or embarrassing." It is estimated to be one of the most prevalent psychiatric disorders in the world [2], and is also known as social anxiety disorder (SAD). Generally, people with SAD feel embarrassed or fearful when interacting with others, especially strangers, and worry about being judged negatively [3]. They are more likely to misunderstand others' emotions in social situations.

Facial and emotional recognition tools and techniques can provide promising solutions for SAD patients. Many existing software tools can be used to analyze video content and recognize actions within them. These applications are being widely used in emotion recognition. AffdexMe [4] by Affectiva is one such app that analyzes and responds to facial expressions of emotion in real-time using the built-in camera on iOS or Android devices.

In this paper, we design and develop a solution that uses AffdexMe for emotion recognition to help people with SAD better communicate with others on video chatting platforms. Our proposed solution aims to enable SAD patients to

*Corresponding Author.

recognize the emotions of people with whom they communicate, and to help them to respond in appropriate ways. A usability testing experiment was conducted on participants with SAD for qualitative observation on approach effectiveness and usage behaviors.

The remainder of this paper is organized as follow. Section 2 presents the literature review and examines what others have done to tackle mental disorders using video-aided emotion recognition. Section 3 presents the study approach, experiment setup, and scenarios considered to demonstrate how AffdexMe is used to assist SAD patients. In Section 4, we present the evaluation method and results of the study. Discussions and study limitations are presented in Section 5. Finally, we conclude this work and lay out our future research plans in Section 6.

II. RELATED WORK

A. Technologies of Facial Recognition Systems

Facial expressions are able to communicate certain emotions such as anger, fear, or anxiety that people may have when they encounter certain situations [5]. Different facial features of experiment subjects were collected and successfully analyzed for the emotions of task subjects. Under certain conditions, the 2D facial recognition system used to recognize a flat face might not be useful for real-time, video-based facial emotion recognition. However, traditional still image-based facial recognition systems are not accurate enough when analyzing motions, even though motions can help to better analyze the emotions behind individuals' facial expressions in terms of psychology and physiology studies [6].

Yet, not all video-based facial emotion recognition applications are accurate and mature enough to be effective for widespread use. For example, Hirt et al. (2018) applied FaceReader to examine students' emotions of interest and boredom by video recording their facial expressions while reading, and later compared these emotional recognition results to student self-reports [7]. They found that the results from student self-reports were significantly different from those of the facial emotion recognition software. They concluded that until this discrepancy could be better analyzed and accounted for, the emotion recognition technology could not be formally applied to educational practice.

However, educational researchers have also argued the importance of facial emotion recognition to people with disabilities, such as, for example, preschool children with autism [8]. They emphasized the importance of intervention tools such as facial emotion recognition games to help children with autism understand facial expressions, which may lead them to exhibit more appropriate social behaviors. Researchers presented a facial emotion recognition game to children with autism as an early intervention. They also presented suggestions for the future design of a facial expression detection game.

B. Facial Expression and Social Anxiety Disorder (SAD)

Facial expression, as a type of nonverbal communication, plays a significant role in conveying speakers' messages and involves at least 65% of the total meaning of a conversation

[16], and yet people with social phobia have difficulties reading others' facial expressions and emotions. Researchers have found that such people have longer reaction times for almost all emotions and lower accuracy in emotion recognition [10,11]. Specifically, people with SAD tend to view various facial expressions as conveying negative feedback, whether they truly do or not.

Based on the research of Lange et al. [10], people with SAD tend to interpret negative feedback when they encounter the neutral faces of other people. They believe that a neutral face actually represents a negative emotion. With further questionnaires and experiments, researchers found that those with social anxiety disorder even viewed all facial symbols, including negative, positive, and neutral, as significantly threatening. Therefore, assistive technologies are required for this group of people so that they can communicate appropriately with others and actively join society instead of being gradually isolated from society.

C. Open-Source Facial Emotion Recognition Application: AffdexMe

Yu and Wang (2016) proposed an advanced, real-time, monocular, video-based facial expression recognition system that enabled more precise recognition of multiple variables [12]. An online statistical appearance model (OSAM) was used to track the facial movements of the participant, as shown in Fig. 1.

Based on different models created by the computer for analyzing the geometrically normalized facial mesh, the system was able to draw conclusions about participants' emotions when making different facial expressions. Examples are shown in Fig. 2 and 3.

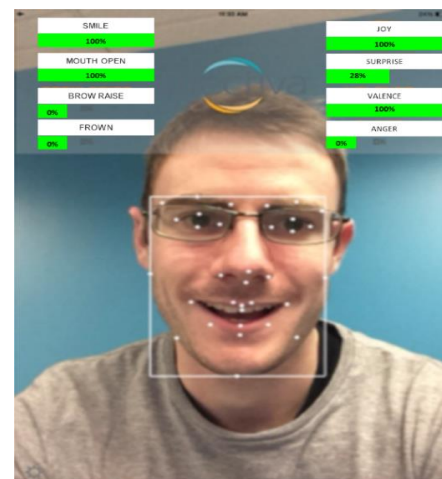


Fig. 1. A Sample Revised Interface of AffdexMe shows Six Emotions that can be Recognized by the Technology. Screenshots have been revised to Clarify the Font used in AffdexMe.

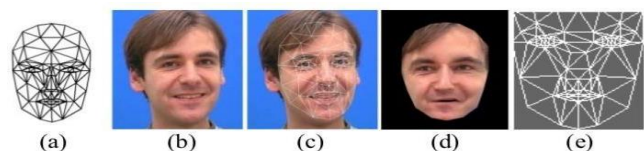


Fig. 2. The Process of Facial Recognition [5].



Fig. 3. Examples from the Facial Expression Recognition System [5].

McDuff et al. have also indicated that facial expressions can express certain emotions not only through still expressions but also through facial movement [13]. Their work provides the mechanism that enables facial expression recognition to work when analyzing users' emotions communicated by their facial movements. A Facial Action Coding System was used in their study to analyze facial expressions through analyzing the various actions according to the dataset from Affdex. This system automatically coded facial expressions when participants used the video chat platform Skype and analyzed the emotion of participants.

The traditional dataset for analyzing users' facial expressions has been manually collected; thus, it was difficult to classify diverse facial actions to indicate the emotions of users. However, the internet-based framework used by AffdexMe has enabled researchers to collect around 1.8 million online media videos of spontaneous facial responses [14]. Through active learning, the facial recognition system can learn 100 different scales of facial expression based on the movements of various facial features. This active learning method can help the computer system to recognize even more precise movements which are not similar to more common expressions such as smiles or closed eyes [14].

In sum, people with SAD tend to misunderstand facial emotions when they communicate with others, which makes it necessary to help them accurately classify the emotions behind different facial symbols such as positive or negative expressions. Therefore, a facial expression recognition system is needed for helping such people understand the true emotions behind facial features, and therefore reduce misunderstandings in communication. Our study aims to apply the AffdexMe facial emotion recognition technology to design a study to help people with SAD communicate with others appropriately. We also hope that our results can be generalized to the current global situation, in which people feel more isolated than ever before during the COVID-19 pandemic.

III. EXPERIMENTAL SETUP AND STUDY APPROACH

Our goal throughout this study is to help SAD patients to correctly interpret the emotions behind the facial expressions of others on video chat platforms. To achieve this goal, two groups of participants were asked to video chat with friends over Skype [15] for 10 minutes each. The first group included five ordinary participants (i.e., those not diagnosed with or symptomatic of SAD). The second group included five participants who self-reported themselves to have social anxiety disorder. Participants of both groups were undergraduate students at one university. Three of the participants with SAD were female and two were male

students; all of these participants had never previously heard about AffdexMe, had not used similar emotion recognition software before, and seldom video chatted with others prior to the study. The five ordinary participants with whom the SAD participants chatted agreed to participate in the experiment (Table I). Also, participants' informed consent was obtained according to research protocols. This involved a statement of consent to participate in the study and to use their photos for research purposes. We reduced study bias by requiring the SAD-free participants not to intentionally control their facial expressions.

During the 10-minute Skype call, an observer (Fig. 4) holding a smartphone sat with a SAD patient to capture the call with the SAD-free participant. Observer's smartphones had AffdexMe installed and running during the 10-minute video call. The AffdexMe app was used to detect six real-time emotions including joy, sadness, fear, anger, contempt, and disgust. AffdexMe also showed the percentage of certainty for every emotion detected. When the AffdexMe detected emotions, the observer verbally said a short sentence that described the emotion to the SAD patient. For example, when the application detected "sadness," the observer said: "He/she shows sadness."

The observer orally describing the emotions detected by AffdexMe was used to simulate the new function we are proposing here. In the future, we will develop this feature to automatically play recorded sentences that describe the detected emotions. Fig. 5 presents screenshots of AffdexMe output presenting a participant showing joy, disgust, and anger, respectively.

We interviewed each of the SAD patients after the video chatting session and asked them about their experiences when using this application in order to receive their feedback, determine if they encountered any problems, and see if they had any suggestions for improvement.

TABLE I. PARTICIPANTS

	Total Participants (10)	
	Ordinary Participants	Participants with SAD
Video chat	Five	Five



Fig. 4. Observer using AffdexMe to Detect Emotions in Skype Video-chat with Ordinary Participants.

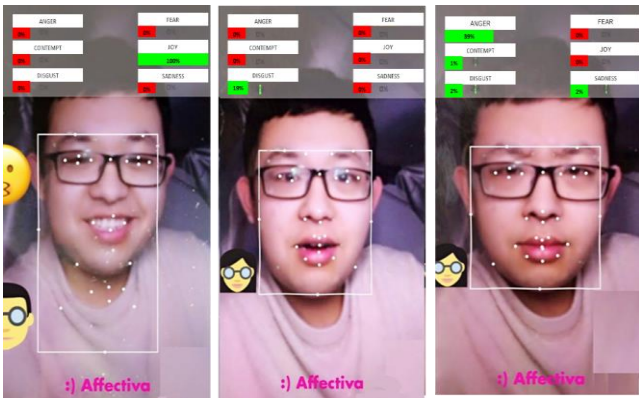


Fig. 5. AffdexMe Outputs on an Ordinary Participant to Help a Participant with SAD Understand Emotions. Screenshots have been Revised to Clarify the Font used in AffdexMe.

IV. RESULTS

During participants' chat sessions, AffdexMe successfully and continuously detected emotions with high success rates. After the 10-minute Skype call, we interviewed the SAD-participants and asked them about their experiences. The following questions were asked of participants:

- How did you like the application?
- What changes will you suggest making the application more effective?
- Do you think you would use an application like this regularly in your video calls? Why?

All participants reported that this application was helpful and supported them in reducing misinterpretation of emotions during video calls. Some participants reported that before using this application they could not accurately recognize others' emotions, as they often thought others felt unpleasant or otherwise negative emotions. One participant also reported that the application enabled them to comprehend others' emotions better and that they do not feel as nervous as they did before when video chatting with others. One of the participants expressed that she always found difficulties in interpreting emotions and often mistakenly regarded others' facial expressions as uncomfortable or angry; however, using the application, she was told that the person with whom she was video chatting showed no or neutral emotions, rather than negative ones.

When considering the application's functionality, a participant mentioned that the observer sound describing the detected emotion was too long (Table II). For example, when the participant-caller showed joy, the observer said, "She shows joy (Fig. 6)," but, before the sound ended, the participant-caller had already turned to another emotion. Therefore, the observer sometimes could not report the emotion promptly. The participant suggested that the sound could be simple and short, like "joy," or could read faster. Another participant thought the sound was helpful because in that case, he did not need to look at the application all the time. Nevertheless, the participant said that the sound was a little disruptive, as it distracted attention when listening to what the caller was talking about. Participants reported that they had to

pay attention to what the application said as well as what their conversation was about. All participants reported that it is more likely that they would download and regularly use a similar application if available for smartphones in the future.

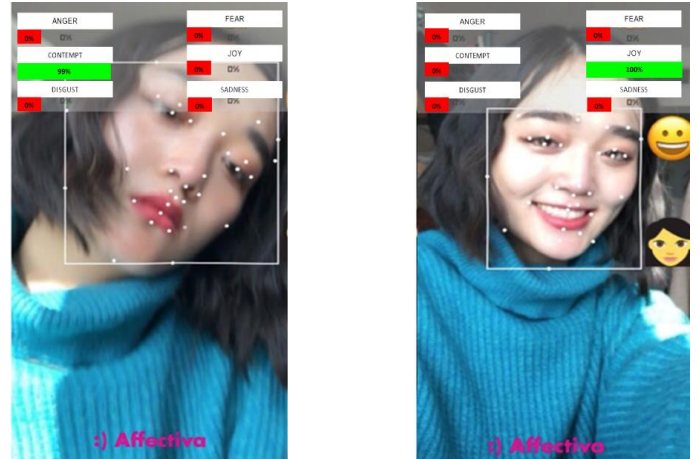


Fig. 6. AffdexMe Output showing One Emotion of a Person Called by One of the Participants. Screenshots have been Revised to Clarify the Font used in AffdexMe.

The designed solution to overcome the emotion recognition challenges encountered by SAD patients when communicating with others using video chatting apps was likable and beneficial according to our empirical study results. However, the study design may have subjected the results to bias. First, the number of participants interviewed in this work was relatively small and the findings may not be generalizable. However, we did try to overcome this limitation by providing more in-depth results about the subjects' perspectives on the research questions by interviewing participants rather than simply asking them to fill out a survey. This helped in being able to interpret the participants' facial gestures to get more reliable results. Additionally, the observer voice while describing the emotions detected by AffdexMe may have negatively impacted the cognitive performance of the SAD patients participating in this study. This issue can be resolved by recording different voices to describe the emotions and enable users to choose from a list of desired characters or possibly even languages.

TABLE II. EXPERIMENTAL FEEDBACK

Participants' Feedback	
Emotion	Functionality
<ul style="list-style-type: none"> • Comprehended others' emotions better • reduced misinterpretation of emotions • calmed nervousness 	<ul style="list-style-type: none"> • Should shorten the voice reminders' length • Voice reminders' distraction

V. DISCUSSION AND LIMITATIONS

Our study aims to help people with SAD to communicate effectively with others via facial emotion recognition technologies. Our observation and interview results suggested that this experimental design using facial emotion recognition helped the participants appropriately video chat with other participants. While only a limited amount of facial emotion

recognition research has been done to help people with SAD [7,8], the positive results of our study shed light on future related research design. As modern societies' environments are becoming more stressful due to factors including climate change disasters or pandemics such as COVID-19, this kind of individual assistive technology is needed to help people with SAD to adapt to the changing world. The results of our design can be generalized to other user groups, and even to ordinary people who need help when dealing with challenging communication methods.

Even though our design may help people with SAD to overcome their fears when interacting with others using video chat, there are some limitations in this study. For instance, we only recruited five participants with SAD to run the usability testing of this design. However, our sample size was based on the suggestion of Nelson (1993), who expressed that only five users can figure out 85% of the usability problems of a technology [9]. This study is only the first step to confirm that facial emotion recognition technologies can help people with SAD.

However, the practicability and conveniences of our design have many areas open to improvement. We suggest integrating the facial emotion recognition technology together with video social networks; in other words, inserting a facial emotion recognition function into video-chatting apps. Much existing social network software already has the function of video-chatting, such as Skype, WeChat, QQ, and Zoom. We plan to write codes to allow the emotion recognition function to operate during video-chatting, so that, when people are having video conversations, a small message box is placed at the corner on the screen. From the box, the user can read the computer's detection of emotion changes and the current emotion of the person being spoken to. We wish to design this function because video images can often be blurry, and a user may be able to see their communication partner but not be able to figure out the expressions on their faces, according to our experience of this study. With this new design, the user can better know the emotions of those with whom they chat and determine their own responses.

We also have specific suggestions for using facial emotion recognition to help people with visual disabilities. Such individuals cannot get any visual cues during communication, so they have more difficulty in interacting with others. We recommend adding a phonetic function to emotion recognition apps when people are video-communicating. When the talker shows strong emotion changes, the app will translate the emotion information into sounds. Therefore, visually-impaired people can get phonetic cues when communicating. This new function will allow them to better interact with others.

V. CONCLUSION

Our design demonstrated how a specific piece of facial emotion recognition technology helped people with SAD. Through experiments, observation, and interviews, we confirmed that facial emotion recognition as an assistive technology can help people with SAD to appropriately communicate with others via video chatting. This helps people with SAD better interact with others, allowing them to escape from isolation and be more involved in their societies. We also

proposed design suggestions for further development of this technology. We recommended adding a small text box to show the emotion of the talker instead of only using time-consuming phonetic reminders, in accordance with the feedback of our participants.

In future studies, we first plan to create a prototype to integrate the facial emotion recognition technology within a video-chat software. Then we will run usability tests to see if users evaluate it as useful and effective. If possible, we will further program this integration and publish it to serve people who need emotion recognition aid when communicating with others.

Moreover, we believe that the sound function is even more significant for visually-impaired people who may also need emotion recognition help when video-chatting with others. They cannot see the faces of other participants, and so they often cannot figure out their emotions. With our future studies, visually-impaired people can freely video-chat with others. The integrated app will tell them the emotion of the other person so that they can better deal with their social interactions. Of course, the sound function is mainly designed for visually-impaired people, so ordinary people may feel this function is useless and distracting. Therefore, we will add a sound switch button on the small box. If some users need or prefer to have the sound function, they can click on it to make the sound function active (those with visual disabilities may require others' help at the beginning). If some users feel the sound is annoying, they can simply turn it off.

In sum, our study has shed light on future facial emotion recognition designs, since there has been only very limited research discussing how this technology can be applied to serve people up to this point. We hope this study can encourage more researchers to work on this topic and invent more promising designs and apps.

ACKNOWLEDGMENT

We thank all our participants for their contributions.

REFERENCES

- [1] Edition, Fifth. "Diagnostic and statistical manual of mental disorders." Am Psychiatric Assoc 21, 2013, pp. 591-643.
- [2] Kessler, Ronald C., et al. "Lifetime prevalence and age-of-onset distributions of DSM-IV disorders in the National Comorbidity Survey Replication." Archives of general psychiatry 62, 6, 2005, pp. 593-602.
- [3] Lima, Laysa Karen Soares de, Erickson Duarte Bonifácio de Assis, and Nelson Torro. "Facial expressions and eye tracking in individuals with social anxiety disorder: a systematic review." Psicologia: Reflexão e Crítica 32, 2019.
- [4] Experience It. Available online: <https://www.affectiva.com/experience-it/> (accessed on 18 December 2020).
- [5] K. Chengeta, "Comparative Analysis of Emotion Detection from Facial Expressions and Voice Using Local Binary Patterns and Markov Models: Computer Vision and Facial Recognition." Proceedings of the 2nd International Conference on Vision, Image and Signal Processing, New York, NY, USA, 2018, pp. 1-6.
- [6] Yan, Yan, and Yu-Jin Zhang. "State-of-the-art on video-based face recognition." Encyclopedia of Artificial Intelligence. IGI Global, 2009, pp. 1455-1461.
- [7] Hirt, F.S.; Moser, I.; Werlen, E.; Imhof, C.; Bergamin, P., "A Comparison of Students' Emotional Self-Reports with Automated Facial Emotion Recognition in a Reading Situation," In Proceedings of the Sixth International Conference on Technological Ecosystems for

- Enhancing Multiculturality; Association for Computing Machinery: New York, NY, USA, October 24 2018, pp. 320–327.
- [8] Christinaki, E.; Vidakis, N.; Triantafyllidis, G., “Facial Expression Recognition Teaching to Preschoolers with Autism: A Natural User Interface Approach,” In Proceedings of the 6th Balkan Conference in Informatics; Association for Computing Machinery: New York, NY, USA, September 19 2013, pp. 141–148.
- [9] Nielsen, Jakob, and Thomas K. Landauer. "A mathematical model of the finding of usability problems." In Proceedings of the INTERACT'93 and CHI'93 conference on Human factors in computing systems, 1993, pp. 206-213.
- [10] Oh, K.S.; Lee, W.H.; Kim, S.; Shin, D.W.; Shin, Y.C.; Lim, S.W., “Impaired Facial Expression Recognition in Patients with Social Anxiety Disorder: A Case-Control Study,” *Cognitive Neuropsychiatry* 2018, 23, pp. 218–228.
- [11] Bell, C.; Bourke, C.; Colhoun, H.; Carter, F.A.; Frampton, C.; Porter, R.J., “The Misclassification of Facial Expressions in Generalised Social Phobia,” *Journal of Anxiety Disorders*, 25, 2010, pp. 278–283.
- [12] Yu, J. & Wang, Z. “A Monocular Video-Based Facial Expression Recognition System by Combining Static and Dynamic Knowledge”, In Proceedings of the 9th International Conference on Utility and Cloud Computing; Association for Computing Machinery: New York, NY, USA, December 6 2016, pp. 353–357.
- [13] McDuff, D.; Mahmoud, A.; Mavadati, M.; Amr, M.; Turcot, J.; Kaliouby, R. el AFFDEX SDK., “A Cross-Platform Real-Time Multi-Face Expression Recognition Toolkit”, In Proceedings of the 2016 CHI Conference Extended Abstracts on Human Factors in Computing Systems, Association for Computing Machinery, New York, NY, USA, May 7 2016, pp. 3723–3726.
- [14] Senechal, T., McDuff, D., & Kaliouby, R., “Facial action unit detection using active learning and an efficient non-linear kernel approximation,” In Proceedings of the IEEE International Conference on Computer Vision Workshops, 2015, pp. 10-18.
- [15] Skype. Communication Tool for Free Calls and Chat. Available online: <https://www.skype.com/en/> (accessed on 20 December 2020).
- [16] Wood, Julia T. “Interpersonal communication: Everyday encounters,” Cengage Learning, 2015.

Can the Futures Market be Predicted-Perspective based on AutoGluon

YangChun Xiong¹, ZiXuan Pan²

Department of Finance and Accounting
Guangzhou Huashang Vocational College, Guangzhou, China

BaiFu Chen³

School of Economics and Trade
Guangdong University of Finance, Guangzhou, China

Abstract—This paper discusses how to raise efficiency of predicting the Chinese futures market correlation coefficient. First, the predicted periods are divided by major events and the predictabilities between different periods are compared at the same time. Second, on this basis, an automatic machine learning framework, AutoGluon is applied to compare the predictive ability between different deep learning models such as LSTM and GRU. Results demonstrate that: (1) Compared by LSTM and GRU, AutoGluon can indeed raise efficiency of predicting. (2) The changes of prediction error between different periods can explain the influence of major events happened in futures market. (3) Although the predictive ability of many models decline over time, the performance of XGBoost is relatively stable, which can provide useful tools for market participants.

Keywords—AutoGluon; LSTM; GRU; Chinese futures market

I. INTRODUCTION

Financial time series forecasting methods include econometric method represented by ARIMA model and GARCH model, and deep learning methods represented by LSTM and GRU model. Futures market forecasting can also adopt the same method. The traditional econometric methods based on linear function hypothesis and model driven show good applicability in dealing with small amount of calculation and low-dimensional data. However, with the explosive growth of data volume in the era of big data, econometric method has gradually exposed its weaknesses.

The LSTM model was originally designed for natural language processing tasks. Now it has attracted more and more attentions in time series forecasting tasks. A large number of in-depth studies have been carried out on the use of LSTM model to predict future prices. The results showed that deep learning method has obvious advantages in forecasting accuracy compared with econometric methods. However, the deep learning models are too dependent on model structure and parameter adjustment, which makes it is difficult to deploy rapidly in different situations. In recent years, the automatic machine learning method represented by AutoGluon framework has performed excellently in various tasks relying on bagging and stacking strategy, and has attracted more and more attentions due to its ease of use.

Whether deep learning model or automatic machine learning method, the premise for predicting the future is that the data obeys the assumption of independent and identical distribution. A large number of studies have proved that it is difficult for financial market participants to get rid of

psychological effects such as greed and fear, resulting in the fact that historical data have a certain impact on future data, which leads to the fact that financial time series data are not completely independent before and after. At the same time, the impact of major events may change the expectations of market participants, making it difficult for financial time series data in different periods to maintain the same distribution assumption. These problems make many models highly fitting historical data in the training process have poor generalization ability in the testing process. Models that perfectly fit existing data cannot guarantee the same prediction accuracy in the future.

In short, the assumption that financial time series data obey the independent and identical distribution fundamentally challenges the basis of machine learning model to predict the future. The specific manifestation is the difference between training error and testing error, but the changes of difference may indicate the changes of market risk.

The innovation of this paper is that according to the time point of major public events (China's supply-side reform and the new corona epidemic), the futures index time series data are segmented and the correlation coefficients between varieties are calculated. By analyzing the difference between the training error and the testing error of the futures index correlation coefficient, new ideas are provided for the futures market prediction.

The structure of this paper is as follows: the second section is the literature review; the third section introduces the models used in this paper; the fourth section is the empirical analysis process; and the fifth section is the summary and enlightenment.

II. LITERATURE REVIEW

There are many studies on the use of econometric models to predict financial markets. Li Hongquan [1] used interval measurement method to study the crude oil price prediction. Zhang Y J, Yao T, He L Y [2] compared the abilities of different GARCH models to predict the crude oil market. Li Hongquan and Zhou Liang [3] used CoVaR, cross-sectional VaR, absorption ratio, Granger causality index and information spillover index to measure systemic financial risk, and examined the predictive ability of five indicators on macroeconomy in detail. Hong Yongmiao, Wang Shouyang [4] pointed out that the econometric methods focus on the relationships between the economic variables to reveal the inherent nature of economic operation, but due to the highly simplified and abstract mathematical model, many other

factors in reality may be not taken into account, which often results in model misdesign.

With the rapid development of artificial intelligence technology in the context of big data, machine learning, deep learning and text analysis have been widely used in the research of financial market prediction. Chen Y, He K, Tso G K F.[5] used deep learning model to predict the crude oil prices, R.A.de Oliveira, D.M.Q.Nelson, A.C.M.Pereira. The author in [6] studied the application of LSTM model in stock market forecasting. Mu Nianguo, Yao Honggang [7] proposed a prediction model of recurrent neural network based on attention mechanism, and found that the prediction effect of gated recurrent network was improved after adding attention mechanism. In addition, a large number of literatures focus on improving the prediction ability of deep learning model in stock and commodity markets [8]-[16]. The common point of the above research is using machine learning models to predict future prices directly, and the researches focused on improving the accuracy and speed of model prediction. Ensembles that combine predictions from multiple models have long been known to outperform individual models. Wang Y, Liu L, Wu C.[17] studied the effect of using time-varying parameter models to predict the crude oil prices. Sun Fuxiong et al. [18] took the Chinese listed companies as the research object, and put forward the combination model of stock suspension prediction. The empirical analysis results showed that the combination model prediction has achieved high accuracy. Zhou Hao et al. [19] proposed an improved crude oil price combination forecasting model, therefore proposed a dynamic particle swarm optimization algorithm. The experimental results showed that the predictions of combined model can greatly reduce the computational complexity and improve the prediction accuracy. Nick Erickson, Jonas Mueller et al. [20] proposed the AutoGluon framework based on automatic machine learning, which greatly simplifies the preliminary work such as feature engineering and parameter debugging of traditional machine learning models, and performs well in the prediction task of structured data. To our knowledge, there is no precedent to apply AutoGluon to the prediction of financial time series. In general, the research on the prediction of financial time series using single or combined models of econometrics and deep learning has been quite sufficient. But the research on the prediction performance of automatic machine learning is not sufficient enough, and the financial time series data do not obey the assumption of independent and identical distribution is always an unavoidable matter. In this paper, the AutoGluon framework is used for predicting the financial time series for the first time. By analyzing the difference between the training error and the testing error of the correlation coefficients of the futures index, the influence of major public events on the futures market is studied to explore the method of predicting the risk of China's futures market and provide reference for researchers.

III. MODELS DESCRIPTION

A. AutoGluon based on Automatic Machine Learning

In the past decades, many powerful machine learning models have emerged. But how to integrate these models is faced with many obstacles, such as model selection, model

integration, super-parameter adjustment, feature engineering, and data preprocessing. Automatic machine learning(AutoML) provides a possible solution through the combination of model selection algorithm and super-parameter optimization strategy. As a representative of AutoML, AutoGluon arranges and trains different models hierarchically, which saves training time and reduces overfitting by bagging and stacking strategy. It has long been found that the combination of multiple models can achieve better performance than single models. The popular AutoML uses bagging and stacking strategy to improve prediction ability and reduce variance. Specifically, several 'base' models are trained separately at each layer, then the outputs of each model are aggregated as features to be transmitted to the next layer for further training (stack) to achieve performance beyond the 'base' models. As a typical AutoML, AutoGluon embodies these ideas in Fig. 1.

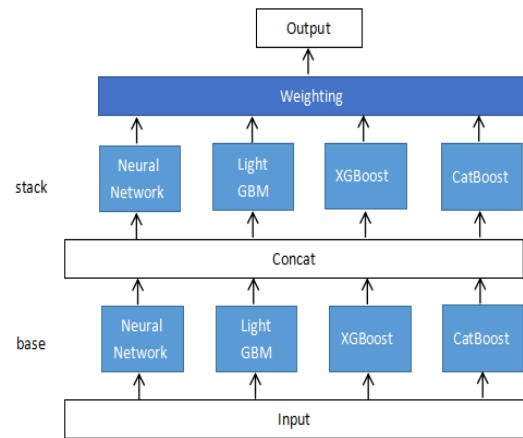


Fig. 1. AutoGluon's Multi-layer Stacking Strategy.

This paper select four representative machine learning algorithms to generate the basic model of AutoGluon, including artificial neural network, LightGBM algorithm, XGBoost algorithm and CatBoost algorithm. After the data were input into the model, different samples are formed by random repeated sampling, then the bagging strategy is applied to each layer to train the basic model on different samples by using four algorithms. At the same time, the stacking strategy is used to train the basic model on the same original data sample of each layer. Finally, all the scalars of each model output are connected to obtain a vector, and then a linear combination is made to obtain the final output of the model. The key codes are given in Fig. 2.

```
1.hyperparameters={'GBM':gbm_options,'NN':nn_options,'XGB':xgb_options,'CAT':cbm_options,}
2.time_limit = 1000 num_trials = 5
search_strategy = 'auto'
3.hyperparameter_tune_kwargs=
{'num_trials':num_trials,'scheduler':'local','searcher':search_strategy,}predictor=TabularPredictor(label=label).fit(train_data,time_limit=time_limit,num_stack_levels=1,num_bag_folds=3)
```

Fig. 2. Key Codes of AutoGluon.

B. LSTM and GRU

As branches of the recurrent neural network, LSTM and GRU models can solve the problem of gradient disappearance, and are often used for time series prediction. In order to compare with AutoGluon, Keras platform is applied to build LSTM and GRU models, and the key codes are given in Fig. 3.

```

1.Key codes of LSTM
model=Sequential()
model.add(LSTM(units=4,activation='tanh',recur
rent_activation='hard_sigmoid',input_shape =
(15 , 1)))model.add(Dense (units =1, activation
= 'linear'))

model.compile(loss='mean_absolute_error',opti
mizer = 'rmsprop')

history=model.fit(x_train,y_train,batch_size=1,
epochs=30, shuffle = True )

2.Key codes of GRU
model = Sequential()

model.add(GRU(units=4,return_sequences=Fals
e,activation='tanh',recurrent_activation='hard_si
gmoid', input_shape =(15 , 1)))

model.add(Dense(units=1,activation ='linear'))

model.compile(loss='mean_squared_error',optim
izer ='rmsprop')

history=model.fit(x_train,y_train, batch_size
=1,epochs =30)
    
```

Fig. 3. Key Codes of LSTM and GRU.

C. Model Assessment Index

There are many indexes to evaluate the fitting ability of machine learning model. This paper use mean square error (MSE) and mean absolute error (MAE) as model evaluation indexes. These can be calculated using the following formulas.

$$\begin{cases}
 MSE = \frac{1}{n} \sum_{i=1}^n (y_i - \hat{y})^2 \\
 MAE = \frac{1}{n} \sum_{i=1}^n |y_i - \hat{y}|
 \end{cases}
 \quad (1)$$

where n is the total number of samples, y_i is the actual value and \hat{y} is the predicted value.

Compared with MAE, MSE gives greater weight to outliers, so it is not as stable as MAE. For the fixed learning rate, the effective convergence of MSE is better than that of MAE, so MSE and MAE are used to evaluate the performance of the models.

IV. DATA DESCRIPTION AND EMPIRICAL ANALYSIS

A. Variables and Data

It is common to select extra-price indicators as explanatory variables to forecast future price. However, the available time of extra-price indicators often lags behind the price itself, which leads to the fact that the hindsight predictable

phenomenon cannot be realized in real time. Moreover, the reflexivity between some extra-price indicators and prices is hard to be falsified. For example, oil prices influence oil production and vice versa.

Therefore, this paper study the risk measurement of futures market by establishing the correlation coefficient time series between the futures index of rebar, iron ore and coke. The explained variable is the current value of the correlation coefficient of China's futures market price index, and the explanatory variable is the historical value of the correlation coefficient. The specific algorithm is to use the corr function of math module in python to calculate the correlation coefficient based on the daily closing price of futures index, and the number of cycles is 100.

This paper adopts the black industry index of South China Futures released by the tushare data community, which includes rebar, hot coil, iron ore, coke, coking coal, wire rod, manganese silicon and ferrosilicon. However, due to the different listing dates of each variety, the historical transactions of wire rod, manganese silicon, ferrosilicon, hot coil and coking coal are not active and the market influence is small. Considering the above factors, this paper only analyzes the futures price index of rebar, iron ore and coke for 2001 trading days from October 21, 2013 to December 31, 2021.

It can be seen from Table I that the original data (from 21 October 2013 to 31 December 2021) is divided into six intervals according to the approximate time points of China's supply-side reform and the new coronavirus epidemic. Then the correlation coefficients are calculated in each intervals. Finally, six training sets and six testing sets are generated, which are divided as follows.

TABLE I. DATASET PARTITION

Interval number	training sets date	testing sets date	reference
1	20131021-20141114	20141117-20151211	Before supply-side reform
2	20131021-20151211	20151214-20180205	In supply-side reform
3	20151214-20161108	20161109-20170927	After supply-side reform
4	20180223-20190212	20190213-20200123	Before new coronavirus
5	20180223-20200123	20200203-20211231	In new coronavirus
6	20200203-20210113	20210114-20211231	After new coronavirus

Then the training set and testing set are input into the model respectively. Finally, the results are compared and analyzed. The specific process is given in Fig. 4.

B. Empirical Analysis

For market participants, when a good fitting model of historical data (training set) can predict future data (testing set) within a certain error range, the risk is low. On the other hand the risk rises when the prediction error increases. Based on this, this paper proposes two hypotheses: 1) When the market is

influenced by external events, the risk will increase characterized by greater prediction error between the training set and the testing set. 2) When the market gradually adapts to the influence of external events, the risk will be reduced which is characterized by the decrease of prediction error between the training set and the testing set. If these two assumptions hold, it can be estimated that the market risk level by observing the change of the prediction error between the training set and the testing set, and then replace the model when the original model is obviously unable to adapt to market changes.

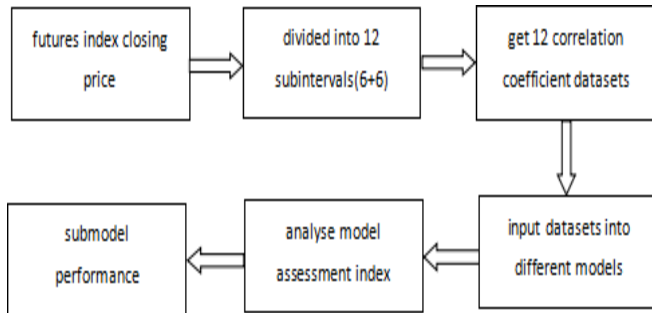


Fig. 4. Data Processing Procedure.

After inputting the dataset into different models, the output results are as follows.

where Ratio of error=Testing MSE / Training MSE, and the smaller the MSE index is, the better the fitting degree of the model to the dataset is.

It can be seen from Table II that AutoGluon framework has obvious advantages in fitting degree compared with LSTM model and GRU model in each training set, but it is completely backward in the testing set. Especially in interval 5, the error ratio of AutoGluon framework is as high as 24.22, which is far higher than that of other models. If the corresponding MSE index is carefully observed, it can be found that the MSE of the training set is only 0.01, and the MSE of the testing set is 0.35, which indicates that the AutoGluon framework has a certain overfitting phenomenon and leads to poor generalization ability of the model. Therefore, when measuring the prediction accuracy of the model, the MSE value of the model in a single interval cannot be used as the sole criterion, but the performance of the model on the training set and the testing set should be compared. However, even if the model performs well in both training set and testing set, it cannot guarantee that the model will have the same stable performance in the future.

Taking interval 2 (supply side reform) and interval 5 (new corona epidemic) as reference points, from interval 1 to interval 3 and from interval 4 to interval 6, it can be seen that the occurrence of two major events increases the error ratio of each model. This phenomenon confirms the first assumption mentioned above. One possible explanation is that the occurrence of major events leads to the increase of market risk, which is manifested as the decrease of model prediction ability. By comparing interval 3 and interval 4, the impact of old major events on the market gradually decreases as the error ratio decreases. This phenomenon confirms the second assumption mentioned above. But as major new events occur, the error ratio expands again. Although the error ratio has fluctuation,

but if the interval 1, 3, 4, 6 is divided into a group and the interval 2, 5 is divided into a group, the overall error ratio increases gradually. This shows that as time goes by and major events influence the market, the overall forecasting ability of the model is declining. The following Table III MAE index descriptive statistics also reflects the same characteristics.

TABLE II. DESCRIPTIVE STATISTICS OF MSE INDEX OF EACH MODEL

Interval number	1	2	3	4	5	6
LSTM						
Training MSE	0.1574 0	0.0878 0	0.0867 0	0.1244 0	0.1123 0	0.1093 0
Testing MSE	0.1041 0	0.1334 0	0.2061 0	0.1612 0	0.3829 0	0.4189 0
Ratio of error	0.6613 7	1.5193 6	2.3771 6	1.2958 2	3.4096 2	3.8325 7
GRU						
Training MSE	0.1606 2	0.0890 5	0.0887 9	0.1195 0	0.1079 8	0.1041 0
Testing MSE	0.1012 6	0.1375 5	0.2199 6	0.1559 6	0.3599 2	0.3812 0
Ratio of error	0.6304 3	1.5446 4	2.4773 1	1.3051 0	3.3332 1	3.6618 6
AutoGluon						
Training MSE	0.0337 0	0.0331 0	0.0240 0	0.0342 0	0.0148 0	0.0405 0
Testing MSE	0.2495 0	0.1717 0	0.1963 0	0.2022 0	0.3586 0	0.4049 0
Ratio of error	7.4035 6	5.1873 1	8.1791 7	5.9122 8	24.229 73	9.9975 3

TABLE III. DESCRIPTIVE STATISTICS OF MAE INDEX OF EACH MODEL

Interval number	1	2	3	4	5	6
LSTM						
Training MAE	0.3063 0	0.2195 0	0.184 80	0.27 670	0.2522 0	0.2410 0
Testing MAE	0.2446 0	0.2599 0	0.318 30	0.31 240	0.4284 0	0.4941 0
Ratio of error	0.7985 6	1.1840 5	1.722 40	1.12 902	1.6986 5	2.0502 1
GRU						
Training MAE	0.3036 7	0.2188 2	0.185 51	0.26 809	0.2408 3	0.2365 1
Testing MAE	0.2408 0	0.2610 3	0.326 63	0.30 724	0.4298 6	0.4733 5
Ratio of error	0.7929 7	1.1929 0	1.760 71	1.14 603	1.7849 1	2.0014 0
AutoGluon						
Training MAE	0.3036 7	0.2188 2	0.185 51	0.26 809	0.2408 3	0.2365 1
Testing MAE	0.2408 0	0.2610 3	0.326 63	0.30 724	0.4298 6	0.4733 5
Ratio of error	0.7929 7	1.1929 0	1.760 71	1.14 603	1.7849 1	2.0014 0

This paper use artificial neural network, LightGBM algorithm, XGBoost algorithm and CatBoost algorithm to generate AutoGluon framework sub-model for prediction. The dataset is divided into six intervals, and AutoGluon framework generates more than 30 sub-models in each interval. For simplification, this paper selects the interval before and after the outbreak of the new coronavirus (interval 5), and studies the top 10 performance sub-models in the training set and the testing set, respectively. The evaluation index is MAE as follows. It should be noted that the research conclusions of other intervals and MSE are basically consistent with this.

TABLE IV. COMPARISON OF AUTOGLUON SUBMODEL (INTERVAL 5)

Model ranking	Training set	MAE	Testing set	MAE
1	WeightedEnsemble_L3	0.08451	XGBoost_BAG_L1/T1	0.36506
2	LightGBM_BAG_L2/T4	0.08970	XGBoost_BAG_L1/T4	0.36529
3	LightGBM_BAG_L2/T1	0.09108	XGBoost_BAG_L1/T2	0.36655
4	LightGBM_BAG_L2/T3	0.09137	XGBoost_BAG_L1/T3	0.37448
5	LightGBM_BAG_L2/T2	0.09196	CatBoost_BAG_L1/T0	0.37494
6	CatBoost_BAG_L2/T2	0.09203	XGBoost_BAG_L1/T0	0.37667
7	CatBoost_BAG_L2/T0	0.09218	LightGBM_BAG_L1/T2	0.38039
8	CatBoost_BAG_L2/T1	0.09274	LightGBM_BAG_L1/T1	0.38174
9	WeightedEnsemble_L2	0.09306	LightGBM_BAG_L1/T0	0.38450
10	LightGBM_BAG_L2/T0	0.09474	LightGBM_BAG_L1/T4	0.38554

where ‘L’ represents the number of stacking layers, ‘T’ represents the parameter search times and ‘BAG’ represents the use of bagging strategy.

In the training set of six intervals, the prediction accuracy of the model is the highest, whether measured by MAE or MSE. However, in the testing set of each interval, Weighted Ensemble_L3 performs quite backward, which may be due to overfitting in the training process of weighted combination model, which also shows that the generalization ability of weighted combination model is weak. In the testing set, it is found that several models trained by XGBoost algorithm perform well. It is also worth noting that the same model performs poorly in the training set and does not enter the top ten.

Based on the characteristics of the AutoGluon framework, the more stacking layers and parameter search times, the more complex the sub-model trained will be. However, more complex models do not necessarily achieve better prediction results, which is quite obvious on several sub-models generated by XGBoost algorithm in Table IV testing set.

In general, from the perspective of model prediction accuracy, AutoGluon framework is generally better than

LSTM model and GRU model, especially in the training set. There is no significant difference between LSTM model and GRU model. It is particularly noteworthy that the testing/training error ratio of AutoGluon framework is much larger than that of LSTM model and GRU model, which indicates that AutoGluon framework has certain over-fitting phenomenon. But this does not affect the conclusion that AutoGluon framework has stronger overall prediction performance. At the same time, it is noteworthy that the testing/training error ratios of LSTM model and GRU model are smaller than those of AutoGluon framework, indicating that the prediction performance of LSTM model and GRU model is more stable.

V. CONCLUSION

In this paper, it is found that: (1) the impact of major events increases the difficulty of futures market prediction. At the same time, with the passage of time, it is more difficult to accurately predict the market through a single model, which is verified by comparing the change of interval error ratio before and after the event. (2) Although over-fitting phenomenon exist, the prediction accuracy of AutoGluon framework which consumes more resources is generally better than LSTM model and GRU model, but the overall performance difference between LSTM model and GRU model is trivial. (3) It may be meaningful to compare model performance only on specific datasets or tasks. By consuming more resources to train more complex weighted combination models, it is not certain to achieve better prediction results in specific tasks, while simple models are not necessarily inferior to complex models. The diversity of specific tasks and the ease of use of AutoGluon framework will make AutoGluon framework based on automatic machine learning have greater advantages over traditional machine learning methods in the future.

Based on these findings, such following suggestions are put forward: (1) In addition to MSE or MAE, ratio of error may be more suitable to measure the model prediction ability. (2) In order to improve the performance of time series prediction task model, XGBoost algorithm is worth being studied in the future.

REFERENCES

- [1] LI Hong-quan. Application of interval econometrics for crude oil price forecasting[J]. Computer Engineering and Applications, 2010, 46(6): 23-25.
- [2] Zhang Y J, Yao T, He L Y, et al. Volatility forecasting of crude oil market: Can the regime switching GARCH model beat the single-regime GARCH models[J]. International Review of Economics Finance, 2019, 59: 302-31.
- [3] LI Hongquan, Liang ZHOU. Systemic Financial Risk Measurement and Its Economic Forecasting Ability[J]. China Journal of Econometrics, 2021, 1(4): 892-903.
- [4] Hong Yongmiao, Wang Shouyang. How Is Big Data Changing Economic Research Paradigms?[J]. Management World, 2021, 37(10).
- [5] Chen Y, He K, Tso G K F. Forecasting crude oil prices: A deep learning based model[J]. Procedia Computer Science, 2017, 122: 300-307.
- [6] R.A.de Oliveira, D.M.Q.Nelson, A.C.M.Pereira. Stock markets price movement prediction with lstm neural networks[C]. //In 2017 International Joint Conference on Neural Networks (IJCNN), pages 1419-1426, 2017.
- [7] MU Nianguo, YAO Honggang. Application of attention mechanism based recurrent neural network in financial time series[J]. Modern Electronics Technique, 2021, 44 (14) : 1-5.

- [8] Zhang Xu,Xue Lei,Li Dun-Yu.Stock Analysis System Based on Financial TimeSeries and Public Opinion Analysis[J]. Industrial Control Computer,2018,31(04).
- [9] CHEN Jia, LIU Dongxue, WU Dashuo. Stock Index Forecasting Method Based on Feature Selection and LSTM Model[J]. Computer Engineering and Applications, 2019, 55(6): 108-112.
- [10] PENG Yan, LIU Yuhong, ZHANG Rongfen. Modeling and Analysis of Stock Price Forecast Based on LSTM[J]. Computer Engineering and Applications, 2019, 55(11): 209-212.
- [11] WANG Yan, GUO Yuankai. Application of Improved XGBoost Model in Stock Forecasting[J]. Computer Engineering and Applications, 2019, 55(20): 202-207.
- [12] SONG G, ZHANG Y F, BAO F X, et al. Stock prediction model based on particle swarm optimization LSTM [J] . Journal of Beijing University of Aeronautics and Astronautics , 2019, 45(12): 2533-2542.
- [13] GE Dao-Hui, LI Hong-Sheng, ZHANG Liang,LIU Ru-Yi,SHEN Pei-Yi, MIAO Qi-Guang. Survey of Lightweight Neural Network[J],Journal of Software, 2020, 31(9):2627-2653.
- [14] XU Haoran, XU Bo, XU Kewen. Analysis on Application of Machine Learning in Stock Forecasting[J]. Computer Engineering and Applications, 2020, 56(12): 19-24.
- [15] DANG Jianwu, CONG Xiaoqing. Research on Hybrid Stock Index Forecasting Model Based on CNN and GRU[J]. Computer Engineering and Applications, 2021, 57(16): 167-174.
- [16] ZHAO Hongrui, XUE Lei. Research on Stock Forecasting Based on LSTM-CNN-CBAM Model[J]. Computer Engineering and Applications, 2021, 57(3): 203-207.
- [17] Wang Y, Liu L, Wu C. Forecasting the real prices of crude oil using forecast combinations over time-varying parameter models[J]. Energy Economics, 2017, 66: 337–348.
- [18] SUN Fuxiong, LIU Guangming, ZENG Zixuan, PENG Mengqi. Research on Stock Suspension Prediction Based on Combination Model[J]. Computer Engineering and Applications, 2020, 56(18): 272-278.
- [19] ZHOUHao, ZHANGYifei,WANG Zhen,WANG Jue,WANG Shouyang. An improved research on optimization strategy of crude oil price forecast combination[J].System Engineering-Theory &Practice,2021,41(10): 2660-2668.
- [20] Nick Erickson, Jonas Mueller, Alexander Shirkov, Hang Zhang,PedroLarroy,MuLi,AlexanderSmola.AutoGluon-Tabular: Robust and Accurate AutoML for Structured Data[C]. //7th ICML Workshop on Automated Machine Learning (2020) Vienna.

Stochastic Rounding for Image Interpolation and Scan Conversion

Olivier Rukundo, Samuel Emil Schmidt
Department of Health Science and Technology
Faculty of Medicine, Aalborg University
Aalborg, Denmark

Abstract—The stochastic rounding (SR) function is proposed to evaluate and demonstrate the effects of stochastically rounding row and column subscripts in image interpolation and scan conversion. The proposed SR function is based on a pseudorandom number, enabling the pseudorandom rounding up or down any non-integer row and column subscripts. Also, the SR function exceptionally enables rounding up any possible cases of subscript inputs that are inferior to a pseudorandom number. The algorithm of interest is the nearest-neighbor interpolation (NNI) which is traditionally based on the deterministic rounding (DR) function. Experimental simulation results are provided to demonstrate the performance of NNI-SR and NNI-DR algorithms before and after applying smoothing and sharpening filters of interest. Additional results are also provided to demonstrate the performance of NNI-SR and NNI-DR interpolated scan conversion algorithms in cardiac ultrasound videos.

Keywords—Cardiac ultrasound; deterministic rounding; image quality; interpolation; pseudorandom number; scan conversion; stochastic rounding; video quality

I. INTRODUCTION

Image interpolation is an important type of estimation that pervades many engineering applications, where estimates of image pixel values at points other than the input or source grid are required and/or affect the desired results and/or the way to obtain them [1]. In digital image upscaling, the nearest neighbor interpolation (NNI) remains the fastest algorithm. NNI is used for estimating image pixel values at points of interest, and it is traditionally based on the deterministic rounding (DR) function. This type of function deterministically rounds off the subscripts of the grid coordinates of the output or destination image to enable the mapping of pixels from the source image into the destination image. However, in some NNI interpolated images cases, the image quality is often bad because of the presence of heavy jagged artefacts, especially at image objects' edges. Here, the DR function-based mapping remains main the inherent flaws that contribute to the presence of such heavy jagged artefacts. In this work, the stochastic rounding (SR) function is alternatively proposed to demonstrate and evaluate the effects or benefits of stochastically rounding row and column subscripts in NNI-based image interpolation and scan conversion. Note that, the scan conversion algorithm is used for translating input data (captured in different coordinates) into Cartesian coordinates (still more suitable for display) [9]. More information on the scan conversion system block diagram and the scan conversion

using bilinear interpolation examples are provided in [9], [10]. It is important to note that, when the fractional part of non-integer subscripts equals half a unity, this, key challenge in rounding functions, still raises the question of how or when to reasonably use the gain or loss of half a unity – and the SR function is the answer to this question. The rest of the paper is organized as follows: Section two introduces the literature review of interest. Section three presents the SR function. Section four presents numerical examples showing the comparison of results based on SR and DR functions. Section five presents experimental results. Relevant discussions are provided in Section six. The conclusion is given in Section seven.

II. LITERATURE REVIEW

There exist many image interpolation algorithms, in various categories, that were developed focusing on improving the accuracy or efficiency of the algorithm, depending on targeted applications including but not limited to rescaling, reslicing, rendering, zooming, coordinate transformations in two-dimensional data or scan conversion, tomographic reconstruction and image registration [1]. One of the most recent applications of interest is artificial intelligence (AI)-based image super-resolution [2], [3] - whose generalizable steps are shown in Fig. 1. Here, the authors' core idea was to enhance the quality of the bilinear interpolation images, by applying a set of pre-learned filters on the image patches, chosen by an efficient hashing mechanism [2]. In another example, presented in [3], the authors used the bicubic image interpolation algorithm to upscale the input or source image to meet the same size as the reference image before starting to recover from it, a resolution enhanced image comparable to the ground truth high-resolution image. Both bilinear and bicubic interpolation algorithms belong to the extra pixel category [4]. This category encompasses all image interpolation algorithms that create non-original pixels to achieve interpolation results [4]. The NNI algorithm belongs to the non-extra pixel category [4]. This category of image interpolation algorithms does not create non-original pixels to achieve interpolation results [5]. As mentioned earlier, the NNI algorithm remains the fastest among image interpolation algorithms [6], [7]. However, the NNI algorithm is based on the deterministic rounding for source image pixels selection. In [4], the author demonstrated that the best deterministic rounding (DR) function for nearest neighbor image interpolation purposes was the ceil function. In [8], authors proposed the stochastic rounding (SR) idea and, according to authors in [8], the SR idea was attracting renewed

interest in artificial intelligence/deep learning because it could improve the accuracy of the underlying computations.

Here, for $x \in \mathbb{R}$ with $x \notin \mathbb{F}$ (where $\mathbb{F} \subseteq \mathbb{R}$ denotes the floating-point number system), the authors considered two stochastic rounding modes shown in Eq. 1 and Eq. 2.

Mode-1:

$$fl(x) = \begin{cases} \lceil x \rceil & \text{with probability } 0.5 \\ \lfloor x \rfloor & \text{with probability } 0.5 \end{cases} \quad (1)$$

Mode-2:

$$fl(x) = \begin{cases} \lceil x \rceil & \text{with probability } p = (x - \lfloor x \rfloor) / (\lceil x \rceil - \lfloor x \rfloor) \\ \lfloor x \rfloor & \text{with probability } 1 - p \end{cases} \quad (2)$$

In the first mode (or Eq. 1) authors round $x \in \mathbb{R}$ with $x \notin \mathbb{F}$ up or down with equal probability to the respective nearest floating-point number. In the second mode (or Eq. 2), authors round with a probability that is 1 minus the relative distance of x to each of the nearest floating-point numbers. For $x \in \mathbb{R}$, $\lfloor x \rfloor = \max \{y \in \mathbb{F}: y \leq x\}$, $\lceil x \rceil = \min \{y \in \mathbb{F}: y \geq x\}$, so that $\lfloor x \rfloor \leq x \leq \lceil x \rceil$ with equality throughout if $x \in \mathbb{F}$. For $x \notin \mathbb{F}$, $\lfloor x \rfloor$ and $\lceil x \rceil$ are adjacent floating-point numbers. More details are provided in [8].

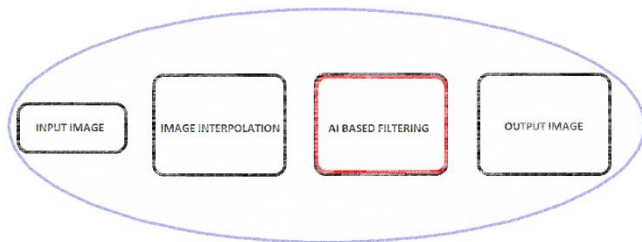


Fig. 1. An Example of Generalizable Steps for AI-based Image Super-Resolution Application Pervaded by Image Interpolation.

III. STOCHASTIC ROUNDING FUNCTION

Here, the stochastic rounding function is developed based on the equation that incorporates a rand function found in MATLAB. The MATLAB rand function is based on a new pseudorandom number generator named Mersenne Twister (MT). According to [11], the MT pseudorandom number generator seems to be the best among all generators ever implemented, with the period $2^{19937} - 1$ and 623-dimensional equidistributional property. Also, the success of this C-Code MT19937 has been achieved thanks to two new ideas added to the previous version, Generalized Feedback Shift Register (GFSR), namely, (1) the incomplete array, and (2) the inversive-decimation method [11]. In the experimental simulations, presented in this work, the pseudorandom number (r) was rounded to one digit. Also, the pseudorandom number was tuned to randomly vary between 0 and 0.5. In this way, it was possible to automate probabilities of stochastically rounding up or down thus achieving non-zero positive integers to be used as row and column subscripts of pixel coordinates. Note that, due to the intended application - of rounding non-integer row and column subscripts - Eq.3 incorporates conditions that allow it to only output non-zero positive integers.

$$sr(x) = \begin{cases} \lceil x - r \rceil, & \text{if } x > r \wedge (x \bmod 1) > 0 \\ \lfloor x \rfloor, & \text{otherwise} \end{cases} \quad (3)$$

In this way, the first condition ensures that any input index or subscript is greater than any pseudorandom number varying between 0 and 0.5. The second condition ensures that any input subscript is of non-integer type before proceeding to randomly rounding up or down. Note that, for $0 \leq r \leq 0.5$, it is an exception if $r > x$. Therefore, in such an exceptional case, the SR function rounds up (e.g., see Table I: See the first line in the 4X group).

Fig. 2 shows an example of destination pixel coordinates subscripts before round-off operations. In Fig. 2(a) and (b) results were obtained by doubling a 3-by-3 matrix and plotting the coordinates of the matrix elements. Note that, when the rounding operation is random - this results in stochastic pixel selection in NNI.

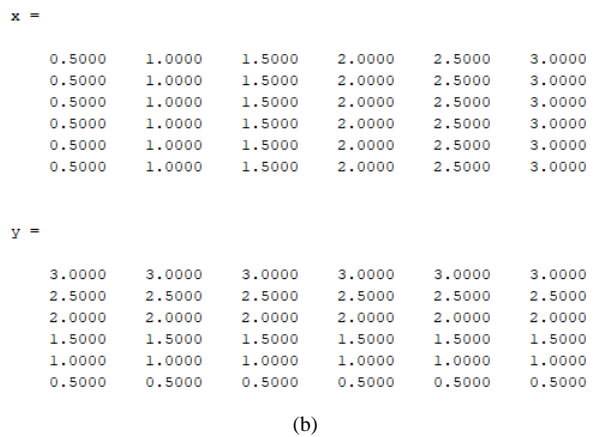
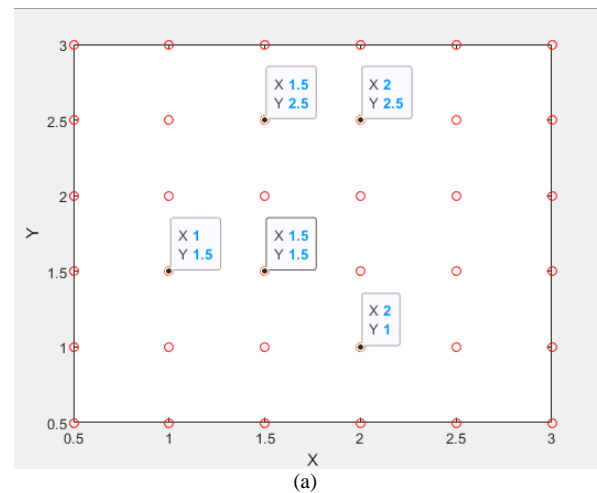


Fig. 2. (a) Shows Pixel Coordinate Subscripts before Round-off Operations. (b) Shows Row (y) and Column (x) Subscripts before Round-off Operations.

IV. NUMERICAL EXAMPLES

In Table I, the authors compare the output of SR and DR functions - after upscaling the original 3-by-3 matrix, two times, three times, and four times. As can be seen, Table I shows a column of subscripts, a column of random numbers, a column of DR results, and a column of SR results as well as columns of the elapsed time in both cases. Again, in Table I,

when the scaling ratio is equal to two, the SR results differ from the DR results, twice. The same happens when the scaling ratio is equal to three. When the scaling ratio is equal to four, the SR results differ from the DR results, three times, except that in this case, there is an exception, mentioned earlier - about when $x < r$.

TABLE I. X REPRESENTS SUBSCRIPTS AND R REPRESENTS A RANDOM NUMBER (ROUNDED TO ONE DIGIT). THE DR(x) IS EQUIVALENT TO THE CEIL(x) FUNCTION

ratio	x	r	DR(x)	SR(x)	DR (sec)	SR (sec)
2X	0.5000	0.4	1	1	$0.18 \times 1.0e-05$	$0.68 \times 1.0e-05$
	1.0000	0.5	1	1		
	1.5000	0.5	2	1		
	2.0000	0.1	2	2		
	2.5000	0.5	3	2		
	3.0000	0.3	3	3		
3X	0.3333	0.1	1	1	$0.15 \times 1.0e-05$	$0.60 \times 1.0e-05$
	0.6667	0.4	1	1		
	1.0000	0.3	1	1		
	1.3333	0.5	2	1		
	1.6667	0.3	2	2		
	2.0000	0.2	2	2		
	2.3333	0.4	3	2		
	2.6667	0.3	3	3		
	3.0000	0.1	3	3		
4X	0.2500	0.5	1	1	$0.04 \times 1.0e-05$	$0.17 \times 1.0e-05$
	0.5000	0.1	1	1		
	0.7500	0.4	1	1		
	1.0000	0	1	1		
	1.2500	0.4	2	1		
	1.5000	0.4	2	2		
	1.7500	0.4	2	2		
	2.0000	0.4	2	2		
	2.2500	0.5	3	2		
	2.5000	0.1	3	3		
	2.7500	0.3	3	3		
	3.0000	0.4	3	3		
	3.2500	0.4	4	3		
	3.5000	0.4	4	4		
	3.7500	0.5	4	4		
4.0000	0.1	4	4			

Note that, SR may also produce similar results to DR results, but that is not guaranteed because the SR's output relies on the pseudorandom value. Also, it is important to note that, the results presented in Table I are specific to a particular case of r value and input numbers. Still, in Table I, it can be seen, in the first case involving 2X (1.5 and 2.5), the SR behaved like the floor function, instead of the traditional

otherwise. In the second case involving 4X (1.5, 2.5, and 3.5), the SR behaved like the ceil function – in this way, the pseudo-randomness of the SR function has answered the question or removed the challenge of how to reasonably round a non-integer subscript in when the fractional part is equal to half a unity (i.e., 0.5). Note that, the most interesting point of DR and SR functions is that, when the fraction part of a non-integer equals 0.5, the DR function always rounds a non-integer in a predetermined or deterministic way, which is not the case with the SR function. Now, comparing the elapsed time or line reading time, it can be seen, in Table I, that the time taken by both the SR and DR functions (to round a given series of non-integers) is too small to make any significant difference.

V. EXPERIMENTS

A. Datasets, Smoothing / Sharpening Method, IQA Metrics

1) *Dataset*: Here, the used image dataset originated from the USC-SIPI Database of 210 Textures, Aerials, Miscellaneous, and Sequences images [12]. Here the author uses input images of 128 x 128 size and reference images of 512 x 512 size, all converted to 8bits using R2020a MATLAB. All experimental images are also available at the author's GitHub via [GitHub.com/orukundo](https://github.com/orukundo) [13].

2) *Smoothing / sharpening method*: The 2-D Gaussian smoothing kernel and sharpened using the unsharp masking methods - available in the MATLAB 2020a image processing toolbox - are used to extend experiments via evaluating smoothed and sharpened interpolation results.

3) *IQA metrics*: In the beginning, only full-reference (FR) IQA metrics are used. Those included the mean-squared error (MSE), structural similarity index (SSIM), and peak signal to noise ratio (PSNR). These FR-IQA metrics are selected to quantify or measure the closeness or similarity of modified or distorted images (i.e., in this case, interpolated images) against their corresponding pristine images (i.e., reference images), [14]. Note that for SSIM and PSNR, normally when the scores are higher (closer to 1 and 100) that means the better visual quality. For MSE when the scores are lower (closer to 0), that normally means better visual quality. Here, it is important to note that MATLAB's *tic* and *toc* command function is also used to check the elapsed time while reading code lines of the SR and DR functions (as shown in Table I). In the end, - given that there exist no reference images or videos for cardiac ultrasound images or videos - the video frames quality assessment is done using no-reference (NR) IQA metrics. The selected NR-IQA metric of interest is the Perception-based Image Quality Evaluator (PIQE) [15], [16]. Specifically, PIQE is used to calculate one frame's no-reference perceptual image quality after every 78-milliseconds for 10 000 milliseconds (i.e., entire video duration). This 78 milliseconds timestamp is estimated based on the number of frames of each video and the entire video duration as well as the suitability for graphical representation. To understand the PIQE scores, the quality scale, and score range are as follows: Excellent [0 ↔ 20]. Good [21 ↔ 35]. Fair [36 ↔ 50]. Poor [51 ↔ 80]. Bad [81 ↔ 100], [16]. For scan conversion operations, T5D data files are

used after being acquired from Duke University’s Experimental Ultrasound System, T5, [10], [17]. More information on Duke University’s Experimental Ultrasound System, T5 can be found via [18],[19],[20]. Note that, with T5D files, scan conversion operations are doable using a dedicated graphical user interface, developed in MATLAB, for post-processing of those ultrasound image sequences (from Duke University’s Experimental Ultrasound System, T5).

B. Automatic / Objective Evaluation Results (Natural Images)

In Table II and Table III, priority is given to NNI-DR and NNI-SR results over the bicubic and bilinear results – keeping in mind that traditional bicubic and bilinear algorithms generally perform much better than the traditional NNI algorithm.

TABLE II. SSIM, PSNR AND MSE METRICS SCORE ESTIMATES BEFORE APPLYING SMOOTHING AND SHARPENING FILTERS)

	SSIM		PSNR		MSE	
	NNI-DR	NNI-SR	NNI-DR	NNI-SR	NNI-DR	NNI-SR
IMAGE1	0.4809	0.5127	21.387	22.058	472.42	404.82
IMAGE2	0.5306	0.5688	21.443	22.391	466.41	374.34
IMAGE3	0.8713	0.8825	30.174	31.395	62.469	47.152
IMAGE4	0.8230	0.8388	23.667	24.903	279.46	210.24
IMAGE5	0.5555	0.5859	20.186	21.162	622.88	497.50
IMAGE6	0.5067	0.5480	20.606	21.586	565.45	451.30

TABLE III. SSIM, PSNR AND MSE METRICS SCORE ESTIMATES AFTER APPLYING SMOOTHING AND SHARPENING FILTERS

	SSIM		PSNR		MSE	
	NNI-DR	NNI-SR	NNI-DR	NNI-SR	NNI-DR	NNI-SR
IMAGE1	0.5112	0.5481	21.381	22.334	473.03	379.89
IMAGE2	0.5627	0.6081	21.338	22.658	477.77	352.58
IMAGE3	0.8857	0.9050	29.910	31.727	66.38	43.68
IMAGE4	0.8358	0.8637	23.221	25.070	309.67	202.32
IMAGE5	0.5876	0.6354	20.009	21.528	648.86	457.30
IMAGE6	0.5333	0.5895	20.516	21.977	577.32	412.45

C. Subjective / Human Evaluation Results (Natural Images)

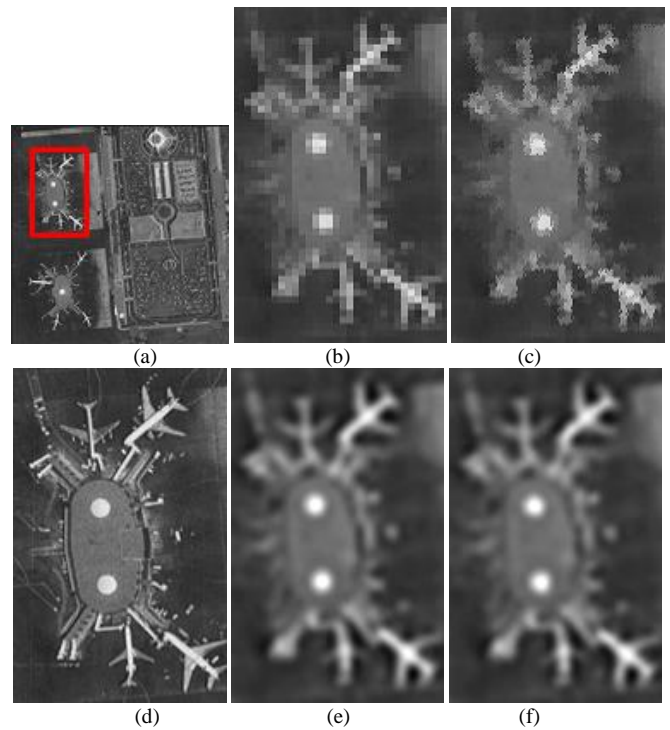


Fig. 3. (a) Input Image1. (b) NNI-DR Interpolated Image1. (c) NNI-SR Interpolated Image1. (d) RF Image1. (e) (b)-Filtered. (f) (c)-Filtered.

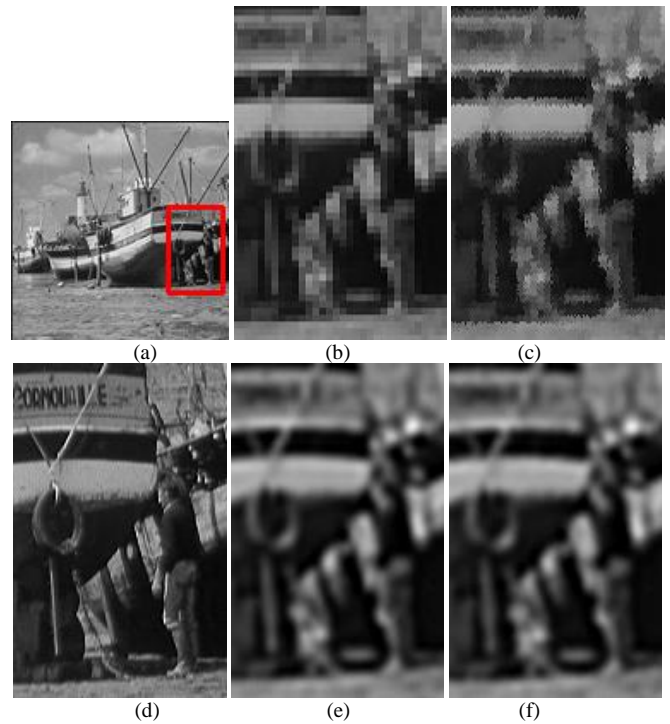


Fig. 4. (a) Input Image2. (b) NNI-DR Interpolated Image2. (c) NNI-SR Interpolated Image2. (d) RF Image2. (e) (b)-Filtered. (f) (c)-Filtered.

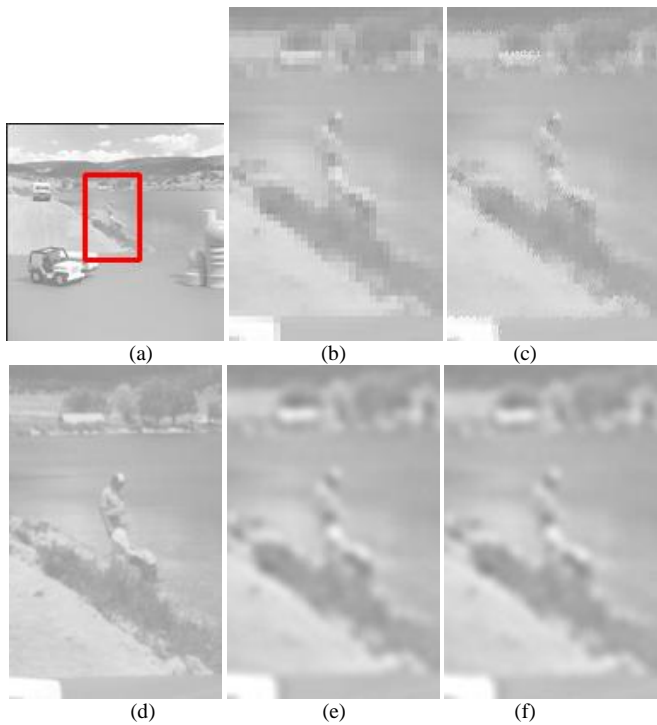


Fig. 5. (a) Input Image3. (b) NNI-DR Interpolated Image3. (c) NNI-SR Interpolated Image3. (d) RF Image3. (e) (b)-Filtered. (f) (c)-Filtered.

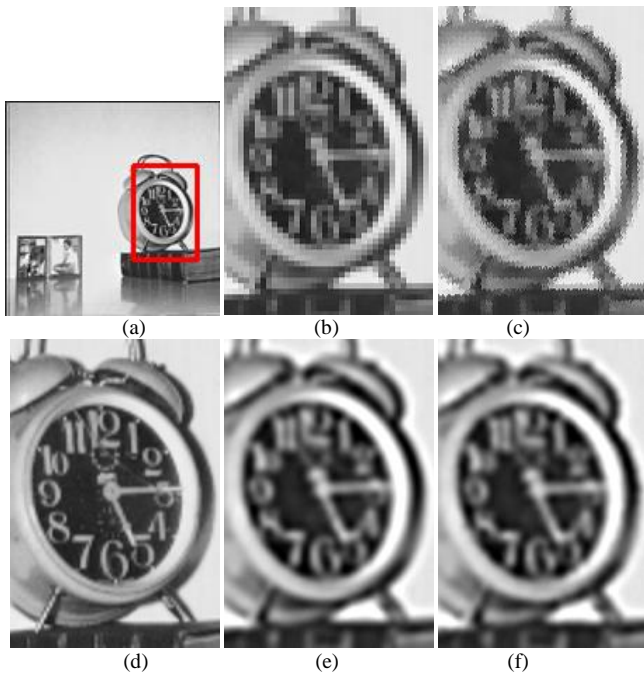


Fig. 6. (a) Input Image4. (b) NNI-DR Interpolated Image4. (c) NNI-SR Interpolated Image4. (d) RF Image4. (e) (b)-Filtered. (f) (c)-Filtered.

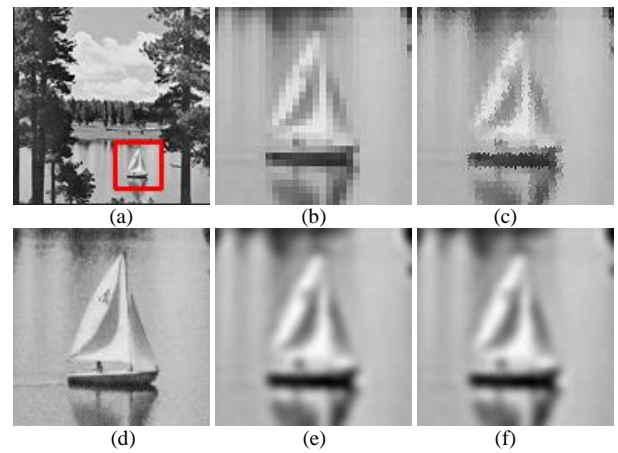


Fig. 7. (a) Input Image5. (b) NNI-DR Interpolated Image5. (c) NNI-SR Interpolated Image5. (d) RF Image5. (e) (b)-Filtered. (f) (c)-Filtered.



Fig. 8. (a) Input Image6. (b) NNI-DR Interpolated Image6. (c) NNI-SR Interpolated Image6. (d) RF Image6. (e) (b)-Filtered. (f) (c)-Filtered.

D. Subjective / Human Evaluation Results (Sectored Images)

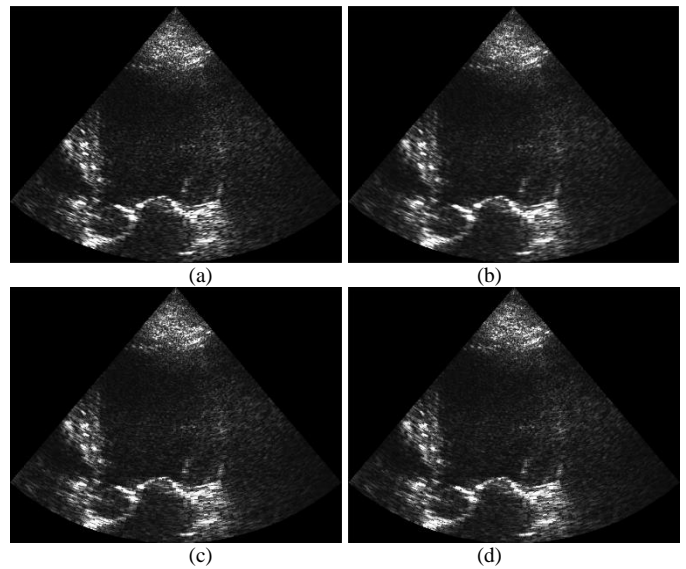


Fig. 9. (a) Bilinear, (b) Bilinear, (c) NNI-DR, (d) NNI-SR (Also see [36]: Interpolated Scan Conversion - 60).

VI. DISCUSSION

Table II shows columns of score estimates achieved by NNI-DR and NNI-SR algorithms (using the SSIM, PSNR, and MSE FR-IQA metrics). In all five image cases presented, the NNI-SR algorithm achieved score estimates slightly higher than the NNI-DR score estimates relevant to SSIM and PSNR. Also, in all five image cases, the NNI-SR algorithm achieved score estimates slightly lower than the NNI-DR score estimates relevant to MSE. The same situation is repeated in Table III, where, unlike in Table III, the results presented are achieved after applying the smoothing and sharpening filters. The Table II comparison concludes that the NNI-SR performed better than the NNI-DR, in this specific situation. However, from the author's observation, it is also possible that the slight betterment of the NNI-SR may have been caused by the fact that the content of NNI-SR images was better aligned with the content of the reference images than the content of the NNI-DR images.

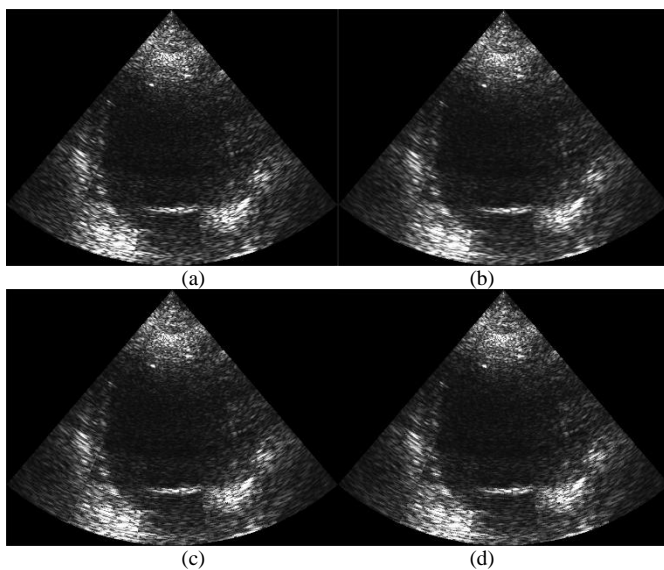


Fig. 10. (a) Bicubic, (b) Bilinear, (c) NNI-DR, (d) NNI-SR (Also see [36]: Interpolated Scan Conversion - 1000).

In Fig. 3, (b) and (c) images have both produced jagged edges on the outline of the planes as well as the rest of the building. Also, comparing the results achieved by NNI-SR and NNI-DR against the (d) RF image, it is clear that only the NNI-SR algorithm reconstructed the white dots in a way almost similar to the way such dots look in (d) image. Also, it is clear, the NNI-DR changed the three white dots or circles to squares. A similar situation did not repeat after smoothing and sharpening the results of NNI-DR and NNI-SR algorithms, shown in (e) and (f), respectively. Note that, here, getting a closer and clear view of the planes (and/or their locations) was not possible, even if the results could show plans and airport terminal (even without having previously seen the RF image in (d)). In Fig. 4, (b) and (c) images have shown jagged edges on the outline of the standing man as well as the rest of the ship edges. As can be seen, the NNI-DR algorithm produced so heavy jagged artefacts that the silhouette of the man disappeared completely, as shown in (b). Now, with the image produced by the NNI-SR algorithm, in (c), the man's silhouette

is only less hardly imaginable than in the NNI-DR case, shown in (b). After smoothing and sharpening, the results became too blurred that is impossible to imagine the man's silhouette, as shown in (e) and (f). If one sees the (e) and (f) images without having previously seen the RF image in (d), it is not possible to imagine the presence of a man's silhouette or ship edges. Here, it is also important to note that by cropping a small part of the image (a), the aim was to get a closer and clear view of the man. In Fig. 5(b) and (c) images have both produced heavy jagged edges on the outline of the two men as well as the rest of the beach. This demonstrates that getting a closer and clear view of the two men was not possible using both NNI-DR and NNI-SR. But, after smoothing and sharpening the (b) and (c) images, the results shown in (e) and (f) allow one to imagine the presence of two men, one standing and one sitting, without even having previously seen the RF image in (d). A similar situation is repeated in Fig. 6, Fig. 7, and Fig. 8.

Fig. 9 and Fig. 10 show two cardiac ultrasound imaging sectored images obtained using different interpolated scan conversion algorithms. Here, the bicubic interpolated scan conversion sectored image-(a) looks better than the rest of bilinear, NNI-DR, and NNI-SR interpolated scan conversion images in (b), (c), and (d), respectively. It is important to note that originally the frame rate was 60 and 1074 frames per second for images in Fig. 9 and Fig. 10, respectively. The value of frame rates could be seen on the Graphical User Interface developed for cardiac ultrasound video visualization. Note that relevant videos are available at <https://github.com/orukundo/Interpolated-Scan-Conversion-of-B-Mode-Cardiac-Ultrasound-Image-Sequences> (see the link entitled: Interpolated Scan Conversion-1000 and/or Interpolated Scan Conversion-60). Also, note that to easily perceive the video quality difference – relevant to the mentioned interpolated scan conversion algorithms - the monitor resolution must be high enough.

Further assessments were done via plotting and comparing graphs of pixel intensity distributions in NNI-DR and NNI-SR interpolated images against the pixel intensity distribution in reference images before and after filtering operations. Fig. 11(a) shows the number of pixels counts versus the corresponding number of bins in NNI-DR interpolated and unfiltered IMAGE1, NNI-SR interpolated and unfiltered IMAGE1, and RF IMAGE1. Fig. 11(b) shows the number of pixels counts versus the corresponding number of bins in NNI-DR interpolated and filtered IMAGE1, NNI-SR interpolated and filtered IMAGE1 and RF IMAGE1. As can be seen, in each case, none of the NNI-DR or NNI-SR results (represented by the blue and green line) matched perfectly with the RF results (represented by a red line). In other words, the number of pixels belonging to each bin of the FR IMAGE1 remained different from the number of pixels belonging to each bin of the NNI-DR and NNI-SR IMAGE1. This difference is also visible between NNI-DR and NNI-SR results, otherwise, it would not be possible to see the blue and green lines. Although not exactly at the same extent, a similar situation is generally repeated in Fig. 12, Fig. 13, Fig. 14, Fig. 15, and Fig. 16 based on IMAGE2, IMAGE3, IMAGE4, IMAGE5, and IMAGE6. Note that the number of empty bins in the source image remained equal to the number of empty bins in the images

interpolated by NNI-DR and NNI-SR (i.e., a condition in the non-extra pixel category).

In Fig. 17(a) and (b) cases, the video frames were repeatedly evaluated after 78 milliseconds (instead of evaluating every frame), in each of the 10-seconds videos. This option for evaluation of video frames was opted to better understand the performance of each interpolated scan conversion algorithm, or else understand why an image or frame quality was bad or good at a specific time, in ultrasound systems. Here, it is important to note that, in the past, many attempts were done to develop methods to assess the quality of ultrasound imaging systems automatically or objectively [21], [22], [23]. In the recent past, the author introduced an index for image interpolation quality assessment as a preliminary step to a suitable method for image quality assessment in ultrasound imaging – only focusing on undesirable artefacts, known as aliasing [24].

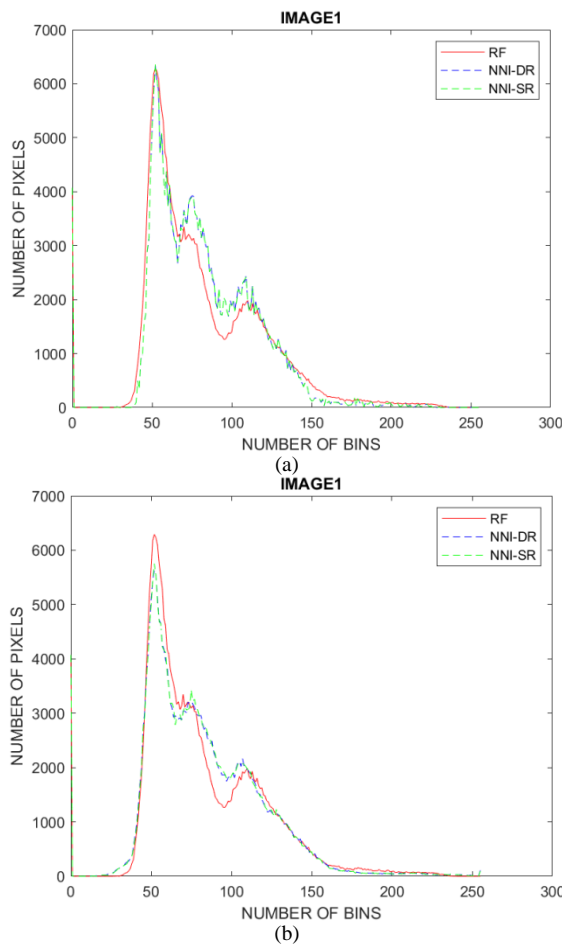


Fig. 11. (a) and (b) show the Number of Pixels Counts versus the Number of Bins in RF, NNI-DR and NNI-SR-based IMAGE1 before and after Filtering.

However, until now, the PIQE remains the only NR-IQA metric very sensitive to two interesting cases of undesirable artefacts in ultrasound imaging, namely: grain-like or speckle-like noise and blurriness. As can be seen, the bilinear interpolated scan conversion algorithm achieved the lowest mean score (i.e., blurriest video frames) in both (a) and (b) cases. Also, note that the current literature demonstrates that

the bilinear interpolation has always been associated with being the most blurriness productive among all non-adaptive interpolation algorithms [25], [26], [27], [28] even if it has proved to be useful in other image processing techniques [29], [30], [31]. The fact that bilinear performed poorer than others in both (a) and (b) cases, confirms its inherent flaw of being the most interpolation blurriness productive.

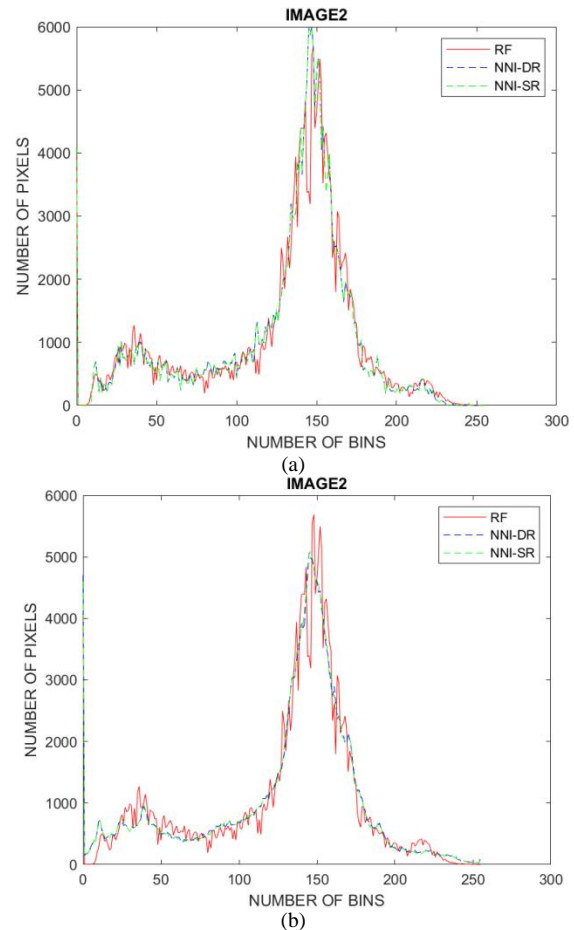


Fig. 12. (a) and (b) show the Number of Pixels Counts versus the Number of Bins in RF, NNI-DR and NNI-SR-based IMAGE2 before and after Filtering.

Now, considering (b), where the original video frame rate was 60, NNI-SR achieved higher PIQE scores than NNI-DR and in general, both NNI-DR and NNI-SR interpolated scan conversion algorithms achieved the best PIQE scores compared to the other two interpolation algorithms of the extra-pixel category. Considering (a), where the original video frame rate was 1074, the bicubic interpolated scan conversion algorithm demonstrated strength that would normally be expected, as it normally produces better image quality than most non-adaptive interpolation algorithms [32], [33], [34], [35]. The mean scores were provided, in the legend, to quickly assess the performance of each interpolated scan conversion algorithm. Note that, these mean scores are specific to these cases. Also, note that these mean score values may change. It is important to note that, the 78 milliseconds timestamp was adopted referring to the frame rate and video duration to enable the more informative and clearer plotting of graphs – otherwise with only 10 seconds videos, the graphs would have looked like

straight lines or similar. Note that the results in (a) and (b) also prove that the PIQE can be considered as the most suitable NR-IQA metric for ultrasound image quality assessment because, in (a) and (b) example, PIQE-based results match perfectly with the well-known performances of interpolation methods, mentioned.

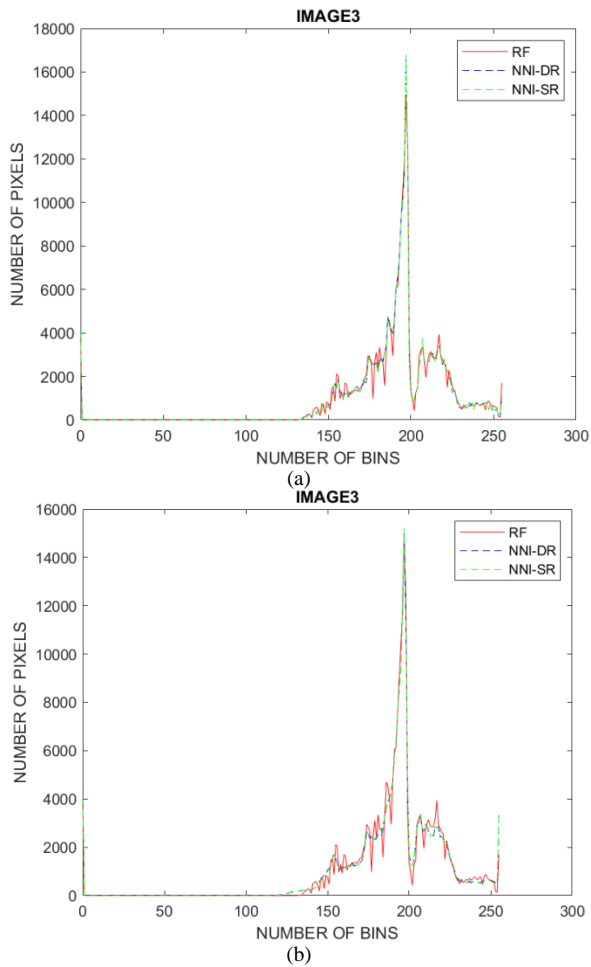


Fig. 13. (a) and (b) show the Number of Pixels Counts versus the Number of Bins in RF, NNI-DR and NNI-SR-based IMAGE3 before and after Filtering.

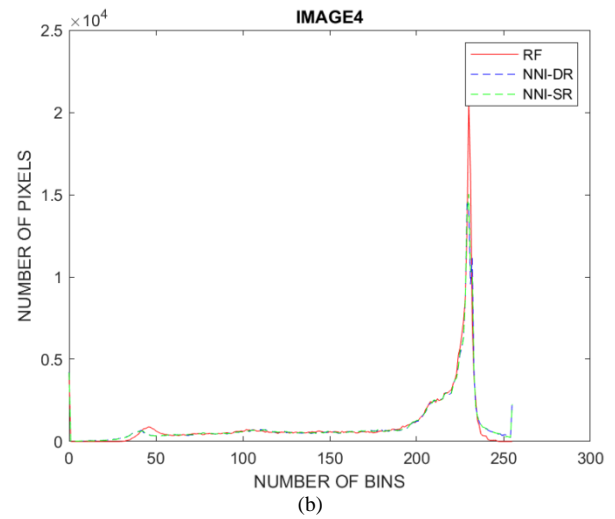
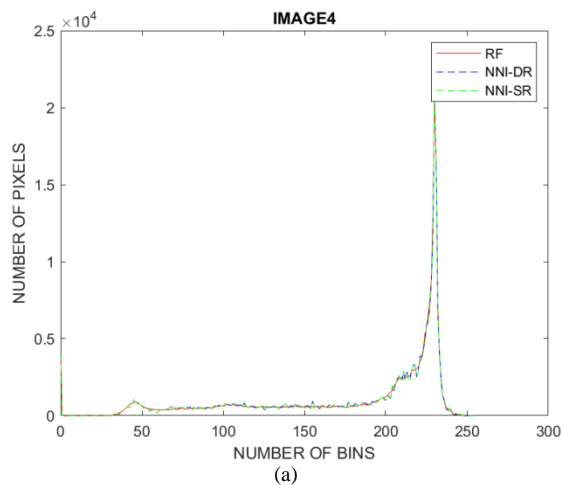


Fig. 14. (a) and (b) show the Number of Pixels Counts versus the Number of Bins in RF, NNI-DR and NNI-SR-based IMAGE4 before and after Filtering.

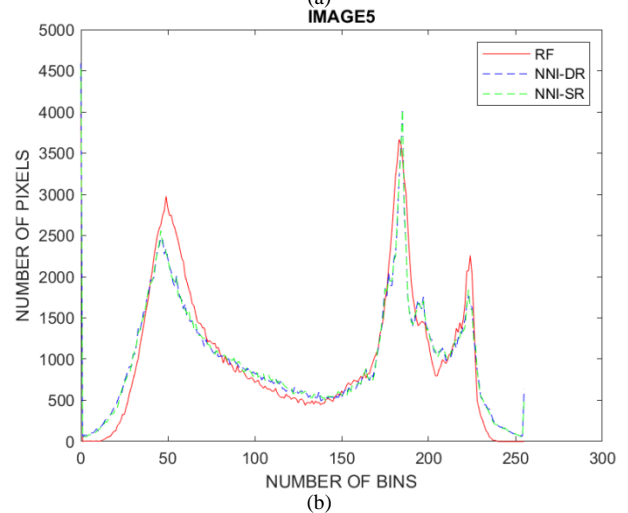
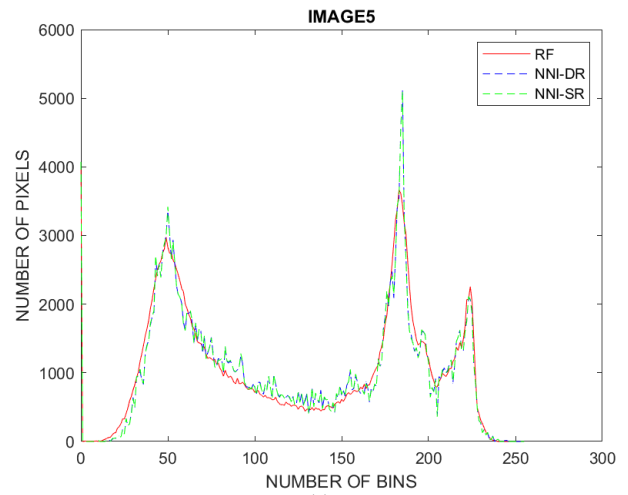


Fig. 15. (a) and (b) show the Number of Pixels Counts versus the Number of Bins in RF, NNI-DR and NNI-SR-based IMAGE5 before and after Filtering.

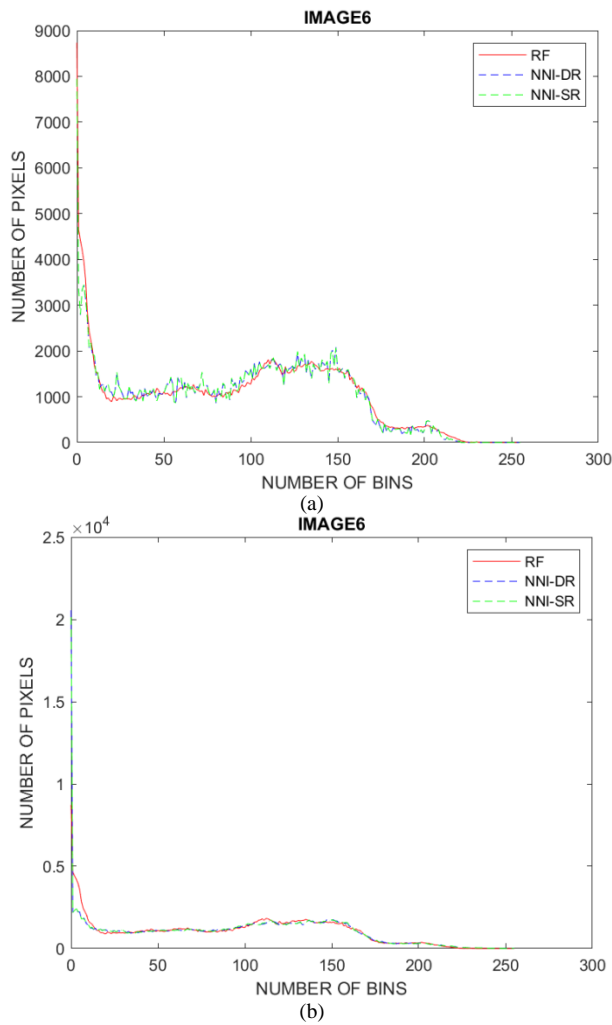


Fig. 16. (a) and (b) show the Number of Pixels Counts versus the Number of Bins in RF, NNI-DR and NNI-SR-based IMAGE6 before and after Filtering.

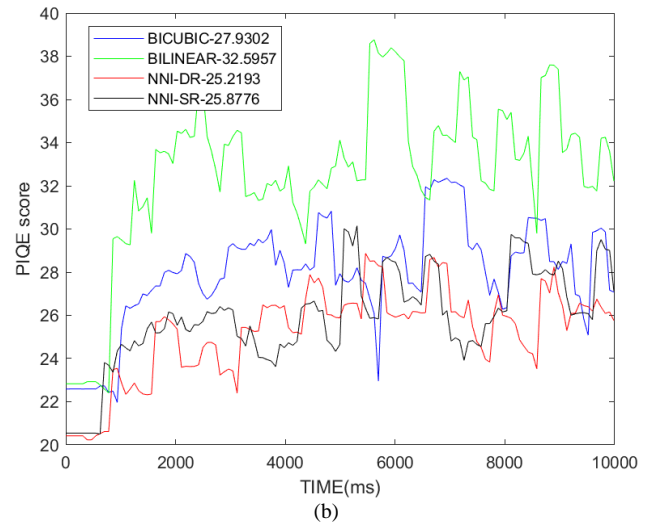
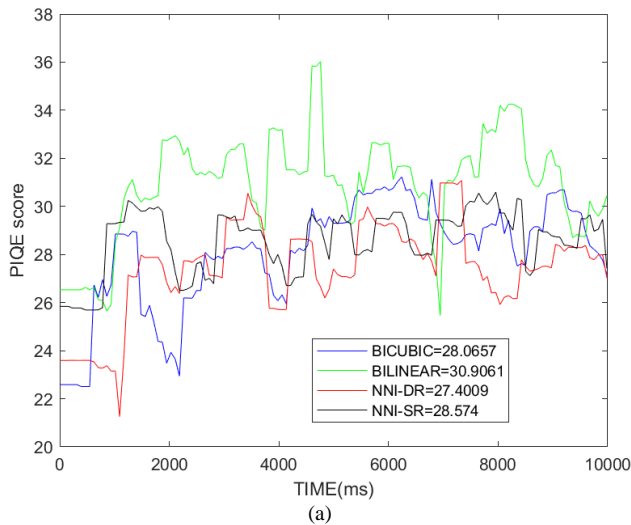


Fig. 17. (a): Video1 - Original Frame Rate Equals 1074. (b) Video2 - Original Frame Rate Equals 60.

VII. CONCLUSION

Evaluation and demonstration of effects of stochastically rounding row and column subscripts in NNI-based image interpolation and interpolated scan conversion were presented and discussed. Here, evaluation of effects of SR function was achieved using both human evaluation and automatic IQA metrics of interest while experimental demonstrations were conducted using natural and ultrasound images. With natural images, the automatic evaluation showed that the NNI-SR algorithm could achieve slightly better score estimates than the NNI-DR score estimates in terms of SSIM, PSNR and MSE - before and after applying the smoothing and sharpening filters. However, the human evaluation showed that both rounding functions could result in heavy jagged artefacts at the edges of image objects, with the exception after the smoothing and sharpening of interpolated images. With cardiac ultrasound images, the human evaluation suggested that the bicubic interpolated scan conversion algorithm could achieve the best results among the rest of the algorithms (in these specific cases involving sectorized images). With 60-fps and 1074 fps videos, the NNI-SR and NNI-DR almost tied in terms of PIQE scores thus raising the question of which algorithm could perform better than the other if longer videos were used. It is important to remind that relevant research challenges and extensive findings were presented and explained especially in the introduction and discussion parts. Future works could focus on applying the SR function in other engineering areas – for example, in a data augmentation to create more deep learning training samples, etc.

VIII. COMPETING INTEREST

The authors declare that they have no competing interests.

ACKNOWLEDGMENT

The authors would like to thank the reviewers and editors for their constructive comments. The author would like to thank Duke University, Biomedical Engineering Department for support.

REFERENCES

- [1] Kumar, A., Agarwal, N., et al., An efficient 2-D jacobian iteration modeling for image interpolation, 2012 19th IEEE International Conference on Electronics, Circuits, and Systems, pp. 977-980, (2012).
- [2] Romano, Y., et al., RAISR: Rapid and Accurate Image Super-Resolution, In: ArXiv:1606.01299v3, (2016).
- [3] Dong, C., Loy, C.C., He, K., Tang, X., Learning a Deep Convolutional Network for Image Super-Resolution, In: Fleet D., Pajdla T., Schiele B., Tuytelaars T. (eds) Computer Vision, ECCV, (2014).
- [4] Rukundo, O., Non-extra Pixel Interpolation, International Journal of Image and Graphics, 20(4), 2050031, (2020).
- [5] Rukundo, O., Evaluation of Rounding Functions in Nearest Neighbour Interpolation, International Journal of Computational Methods, 10 pages, (2021).
- [6] Rukundo, O., Cao, H.Q., Nearest Neighbour Value Interpolation, International Journal of Advanced Computer Science and Applications, 3(4), (2012).
- [7] Rukundo, O., Maharaj, B.T., Optimization of Image Interpolation based on Nearest Neighbour Algorithm, International Conference on Computer Vision Theory and Applications, Lisbon, 641-647, (2014).
- [8] Connolly, M., Higham, N., Mary, T., Stochastic Rounding and its Probabilistic Backward Error Analysis, SIAM Journal on Scientific Computing, Society for Industrial and Applied Mathematics, 43 (1), A566-A585, (2021).
- [9] Li, X.H., Ultrasound Scan Conversion on TI's C64x+ DSPs, TI Application Report, SPRAB32, (2009).
- [10] Rukundo, O., Schmidt, S.E., Von Ramm, O.T., Software Implementation of Optimized Bicubic Interpolated Scan Conversion in Echocardiography, In: ArXiv: 2005.11269, (2020).
- [11] Matsumoto, M. Nishimura, T., Mersenne Twister: A 623-dimensionally equidistributed uniform pseudorandom number generator, ACM Transactions on Modeling and Computer Simulation, 8(1), 3-30, (1998).
- [12] USC-SIPI Image Database: <<http://sipi.usc.edu/database/database.php>>, Accessed: 2021-10-12.
- [13] Modified-USC-SIPI-Image-Database: <<https://github.com/orukundo/Modified-USC-SIPI-Image-Database>>, Accessed: 2021-10-12.
- [14] Rukundo, O., Schmidt, S., Extrapolation for Image Interpolation, Proc. SPIE 10817, Optoelectronic Imaging and Multimedia Technology V, 108171F, (2018).
- [15] Venkatanath, N., Praneeth, D., et al., Blind Image Quality Evaluation Using Perception Based Features, In Proceedings of the 21st National Conference on Communications (NCC). Piscataway, NJ: IEEE, (2015).
- [16] Sheikh, H. R., Wang, Z., et al., LIVE Image Quality Assessment Database Release 2, <<https://live.ece.utexas.edu/research/quality>>, Accessed: 2021-10-12.
- [17] Moore, C., Castellucci, J., et al., Live High-Frame-Rate Echocardiography, IEEE Transactions on Ultrasonics, Ferroelectrics, and Frequency Control, 62(10), 1779-1787, (2015).
- [18] Andersen, M.V, Moore, C., et al., Quantitative Parameters of High-Frame-Rate Strain in Patients with Echocardiographically Normal Function, Ultrasound Med Biol., 45(5), 1197-1207, (2019).
- [19] Andersen, M.V, et al., Feature tracking algorithm for circumferential strain using high frame rate echocardiography, 2016 Computing in Cardiology Conference (CinC), pp. 885-888, (2016).
- [20] Andersen, M.V, Moore, C., et al., High-Frame-Rate Deformation Imaging in Two Dimensions Using Continuous Speckle-Feature Tracking, Ultrasound Med Biol., 42(11), 2606-2615, (2016).
- [21] Hemmsen, M.C., Petersen, M.M, et al., Ultrasound image quality assessment: a framework for evaluation of clinical image quality, Proc. SPIE 7629, Ultrasonic Imaging, Tomography, and Therapy, 76290C, (2010).
- [22] Zhang, S., Wang, Y., et al., CNN-Based Medical Ultrasound Image Quality Assessment, Complexity, vol. 2021, Article ID 9938367, 9 pages, (2021).
- [23] Sassaroli, E., Crane, C., et al., Image quality evaluation of ultrasound imaging systems: advanced B-modes, J Appl Clin Med Phys., 20(3), 115-124, (2019).
- [24] Rukundo, O., Schmidt, S., Aliasing Artefact Index for Image Interpolation Quality Assessment, Proc. SPIE 10817, Optoelectronic Imaging and Multimedia Technology V, 108171E, (2018).
- [25] Rukundo, O., Effects of Improved-Floor Function on the Accuracy of Bilinear Interpolation Algorithm, Computer and Information Science, 8(4), (2015).
- [26] Rukundo, O., Schmidt, S., Effects of Rescaling Bilinear Interpolant on Image Interpolation Quality, Proc. SPIE 10817, Optoelectronic Imaging and Multimedia Technology V, 1081715, (2018).
- [27] Rukundo, O., Wu, K.N., and Cao, H.Q., Image Interpolation based on the Pixel Value corresponding to the Smallest Absolute Difference, IEEE Int. Workshop on Advanced Computational Intelligence, 432-435, (2011).
- [28] Rukundo, O., Normalized Weighting Schemes for Image Interpolation Algorithms, In: ArXiv: 2011.08559, (2020).
- [29] Rukundo, O., Pedersen, M., Hovde, Ø., Advanced Image Enhancement Method for Distant Vessels and Structures in Capsule Endoscopy, Computational and Mathematical Methods in Medicine, (2017).
- [30] Rukundo, O., Half-Unit Weighted Bilinear Algorithm for Image Contrast Enhancement in Capsule Endoscopy, International Conference on Graphic and Image Processing, 106152Q-1 - 106152Q-9, SPIE, (2018).
- [31] Rukundo, O., Effects of Empty Bins on Image Upscaling in Capsule Endoscopy, International Conference on Digital Image Processing, 104202P-1 - 104202P-8, SPIE, (2017).
- [32] Ning, Y., Liu, Y., Zhang, Y. et al. Adaptive image rational upscaling with local structure as constraints. Multimed Tools Appl 78, 6889-6911 (2019).
- [33] Li, Y., Qi, F., Wan, Y., Improvements On Bicubic Image Interpolation, 4th Advanced Information Technology, Electronic and Automation Control Conference, 1316-1320, (2019).
- [34] Khan, S., Lee, D-H., et al., Image Interpolation via Gradient Correlation Based Edge Direction Estimation, Scientific Programming, Volume 2020, Article ID 5763837, 12 pages, (2020).
- [35] Sánchez-García, E, Balaguer-Beser, Á., et al., A New Adaptive Image Interpolation Method to Define the Shoreline at Sub-Pixel Level. Remote Sensing., 11(16):1880, (2019).
- [36] Interpolated Scan Conversion of B Mode Cardiac Ultrasound Sequences: <<https://github.com/orukundo/Interpolated-Scan-Conversion-of-B-Mode-Cardiac-Ultrasound-Image-Sequences>>, Accessed: 2021-10-12.

Analysis of the Elderly's Internet Accessed Time using XGB Machine Learning Model for Solving the Level of the Information Gap of the Elderly

Hung Viet Nguyen¹

Department of Artificial Intelligence
College of Computer Engineering, Inje University
Gimhae 50834, Republic of Korea

Haewon Byeon^{2*}

Department of Digital Anti-aging Healthcare
Graduate School (BK-21), Inje University
Gimhae 50834, Republic of Korea

Abstract—This study aims to construct machine learning models to predict the elderly's internet-accessed time. These models can resolve the information gaps in the present and future by analyzing information use factors such as internet access and mobile device usability. We analyzed 2,300 adults 55 years of age and older who participated in the national survey. This study followed a pipeline of five steps: primary data selection, data imputation to process missing data, feature ranking to identify most important features, machine learning algorithms to develop classifier models, and model evaluation. We applied the Extremely Randomized Trees classifier (Extra Tree) model, the Random Forest classifier (RF) model, and the Extreme Gradient Boosting classifier (XGB) model to look for feature ranking, then select feature importance. All classification models used the accuracy score to calculate the effect. In our study, the most accurate model for predicting the Internet access time of the elderly was the XGB model. The evaluation scores of the XGB machine learning model are very positive and bring high expectations. To solve the information gap of the elderly problem, we can use these effective models to predict the elderly object. Then, we can give some solutions to help them in a society with a strong information technology base.

Keywords—Information gap; machine learning; prediction model; elderly

I. INTRODUCTION

Articles related to the fourth industrial revolution, artificial intelligence (AI), robotics, autonomous vehicles, and unscrewed aerial vehicles appear in the media daily. As such, modern society is an information society. How does an information society affect the daily life of the elderly? Research began with these questions. Information Society is the development of information and communication technology.

It refers to a society in which valuable information can be created. It means that the center of existing economic activity is shifted from goods to information, services, and knowledge. Information becomes a vital resource as much as material or energy resources. In other words, through collecting, producing, processing, and storing information, the distribution of information is spread, and this is a society in which these actions are universal. With the rapid development of information and communication technology day by day, it is

rapidly entering into human life and making human life more convenient.

However, in a developing society, there are two people classes, one that does not have a computer or mobile device to access the internet, and one has those devices but cannot use it or has a low level of usage. They are the information-vulnerable class or the information-poor class [1, 2], and the representative targets are the disabled, the elderly, the low-income class, and farmers and fishers [3, 4]. An information gap is created between those who have access to new forms of information technology and those who do not. This information gap is expanding from the quantitative aspect of simply owning the internet or mobile device to the view of inequality among members of society arising from the qualitative aspect related to information literacy ability. Factors that cause this information gap include economic factors that can possess information devices, sociodemographic factors such as gender, age, race, and region, and cultural factors such as information literacy ability [5, 6, 7, 8, 9].

In this study, the level of the information gap of the elderly is predicted by the recent internet accessed time, and the factor recent internet accessed time is analyzed in terms of mobile usability factors. This study aims to construct machine learning models to predict the elderly's internet accessed time. These models can resolve the information gap in the present and future by analyzing information use factors such as internet access and mobile devices usability.

II. METHODS AND MATERIALS

A. Research Subjects

The data source for this study was the 2019 Digital Information Gap Survey. The number of respondents who participated in 2019 Digital Information Gap Survey is 15,000 people aged seven and over nationwide. A detailed description of the data source is presented in Choi (2020) [10]. We analyzed 2,300 adults aged 55 or older among the subjects who completed the survey.

B. Research Process

The programming language used in this research was Python version 3.7. This study followed a pipeline of five steps: primary data selection, data imputation to process

*Corresponding Author.

missing data, feature ranking to identify most important features, machine learning algorithms to develop classifier models, and model evaluation. The primary dataset had 2300 samples, with many missing values in 233 features. This study selected thirteen features involved in mobile devices usability of the elderly, which are encode by "code3 (whether or not you have a smartphone; 1=yes, 2=no), code7 (internet availability; 1=yes, 2=no), code15 (availability of mobile devices (e.g. display/sound/security/alarm); 1=not at all, 4=most are available), code16 (availability of mobile devices (e.g. wifi); 1=not at all, 4=most are available), code17 (whether you can move files from mobile device to computer; 1=not at all, 4=most are available), code18 (whether you can send files/photos from mobile device to others; 1=not at all, 4=most are available), code19 (whether necessary apps can be installed/deleted/updated on mobile devices; 1=not at all, 4=most are available), code20 (whether it can scan/repair the mobile device's malicious code (virus, spyware, etc.); 1=not at all, 4=most are available), code21 (whether you can write documents or materials (memo, word, etc.) on mobile device; 1=not at all, 4=most are available), code22 (whether you can connect and communicate with others over the Internet; 1=not at all, 4=most are available), code23 (whether you can actively exchange opinions on political and social issues or problems using the Internet; 1=not at all, 4=most are available), code24 (Whether you can protect yourself from personal information exposure; 1=not at all, 4=most are available), code25 (Whether you can be responsible for the use of the Internet; 1=not at all, 4=most are available)". The target variable was defined as recent internet use experience (1=within the last month, 2=over a month, 3=never used). The dataset table is presented in Fig. 1.

	code3	code7	code15	code16	code17	code18	code19	code20	code21	code22	code23	code24	code25	code26
0	1	1	3	3	3	3	3	3	3	3	3	3	3	1
1	1	1	3	2	2	3	3	2	2	3	2	2	3	1
2	1	1	2	2	3	3	2	2	2	3	2	2	2	1
3	1	1	2	2	2	3	2	2	3	1	1	1	1	1
4	1	1	4	4	4	4	4	3	3	3	3	3	3	1
...
2295	3	2	2	2	2	1	1	2	2	1	2	2	1	3
2296	3	2	1	2	1	1	1	2	2	2	1	2	2	3
2297	3	2	3	2	2	2	2	1	3	2	1	1	2	2
2298	3	2	3	3	3	3	4	3	3	2	1	2	2	2
2299	3	2	2	2	1	1	1	1	1	1	2	2	2	3

2300 rows x 14 columns

Fig. 1. Dataset Table.

code3 (whether or not you have a smartphone; 1=yes, 2=no), code7 (internet availability; 1=yes, 2=no), code15 (availability of mobile devices (e.g. display/sound/security/alarm); 1=not at all, 4=most are available), code16 (availability of mobile devices (e.g. wifi); 1=not at all, 4=most are available), code17 (whether you can move files from mobile device to computer; 1=not at all, 4=most are available), code18 (whether you can send files/photos from mobile device to others; 1=not at all, 4=most are available), code19 (whether necessary apps can be installed/deleted/updated on mobile devices; 1=not at all, 4=most are available), code20 (whether it can scan/repair the mobile device's malicious code (virus, spyware, etc.); 1=not at all, 4=most are available), code21 (whether you can write documents or materials (memo, word, etc.) on mobile device;

1=not at all, 4=most are available), code22 (whether you can connect and communicate with others over the Internet; 1=not at all, 4=most are available), code23 (whether you can actively exchange opinions on political and social issues or problems using the Internet; 1=not at all, 4=most are available), code24 (Whether you can protect yourself from personal information exposure; 1=not at all, 4=most are available), code25 (Whether you can be responsible for the use of the Internet; 1=not at all, 4=most are available), code26 (recent internet use experience; 1=within the last month, 2=over a month, 3=never used).

This study applied the Extremely Randomized Trees classifier (Extra Tree) model, Random Forest classifier (RF) model, and Extreme Gradient Boosting classifier (XGB) model to look for feature ranking then select feature importance [11, 12, 13]. Extreme gradient boosting (XGB) - a supervised Machine Learning (ML) algorithm was compared to Gradient Boosting classifier (GBM) model, K-Nearest Neighbors classifier (KNN) model, Random Forest (RF) model, and Extra Tree model then applied to make the most effective model with tuned hyperparameters. Three different feature ranking strategies were used for each model to determine the best combination of feature ranking techniques, number of features, and prediction model. A block diagram of the working process is shown in Fig. 2.

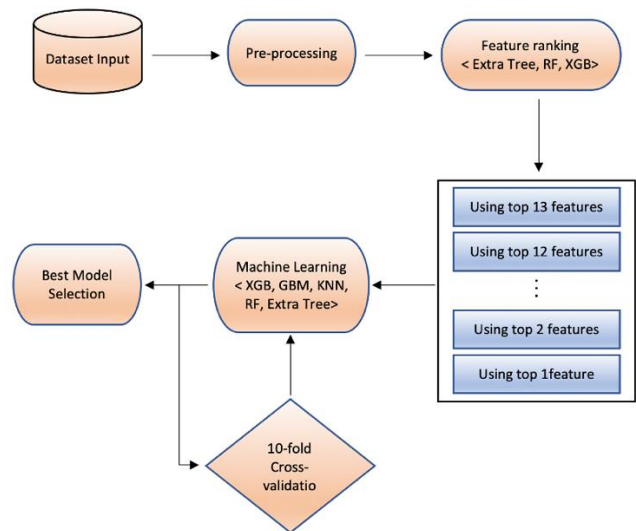


Fig. 2. Block Diagram of the Working Process.

C. Model Evaluation

All classification models used the accuracy score to calculate the effect. Models' accuracy can be defined as the relationship between true positives and true negatives.

Besides the accuracy score, this study also used Area Under the Curve (AUC) score to evaluate the model in case of which model's accuracy score is equal to the others' accuracy score. AUC measures the area beneath the ROC curve and is scale-invariant. It is also threshold invariant. AUC measures how good a model is at predicting True Positives and False Positives [14]. AUC ranges in value from 0 to 1. One model which mis-predicts 100% has an AUC of 0.0; one which predicts 100% correctly has an AUC of 1.0.

All machine learning models for prediction, augmentation, and feature ranking were developed using Python 3.7 codes that utilized the Scikit-Learn machine learning library. The best model's hyperparameters were tuned using the HyperOpt library and the stratified k-fold cross-validation, where the value of k was 10.

III. RESULTS AND DISCUSSION

A. Performance Evaluation of Machine Learning Models

Features' correlations were observed before finding feature ranking. Fig. 3 represents the correlation heatmap of the dataset. We can see that target data, code 26, has positive relations to code 3, code 7, and has negative relations to code 15, code 16, code 18, and code 19.

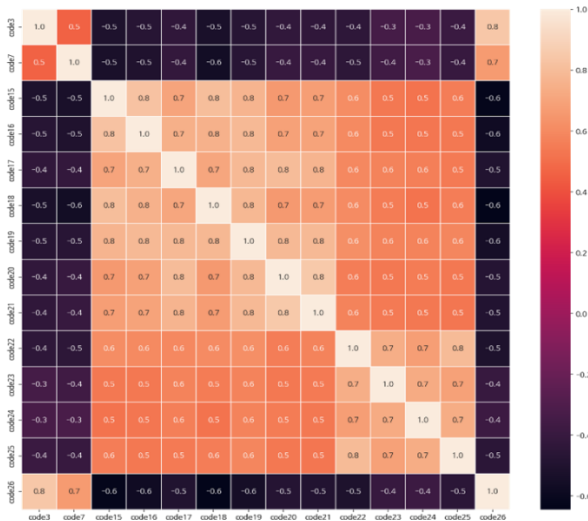


Fig. 3. Features Correlation Heatmap of the Dataset.

In this study, three different methods of feature ranking were applied (XGB, RF, and Extra Tree) [13]. As shown in Fig. 4, code3, code7, and code18 were the most important features in most cases. All three algorithms returned code3 as the most important feature. Code 3 represents the question about usable phone type at home, and code 7 represents the question about availability for using the internet at home. Code 18 was encoded to ask about users' ability to send files/photos from their mobile device to others.

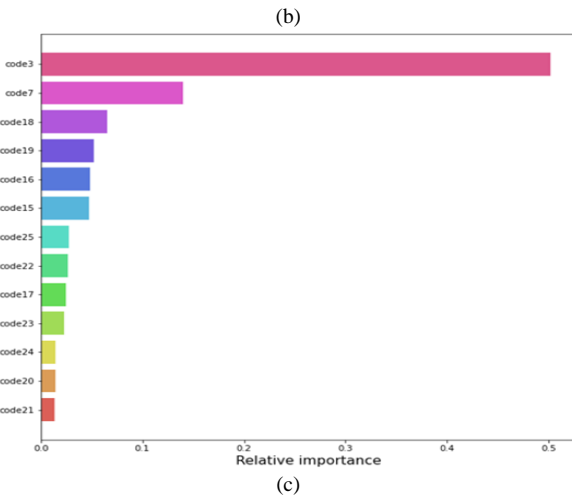
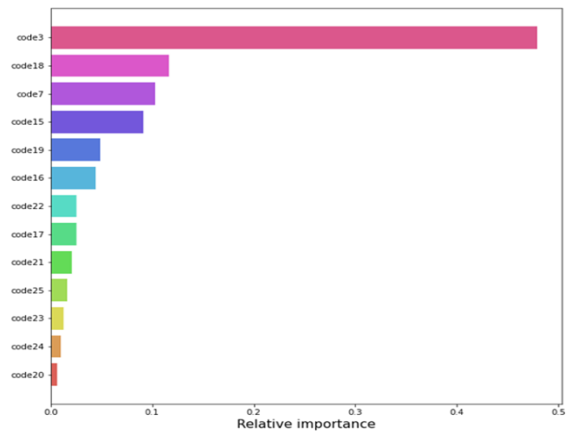
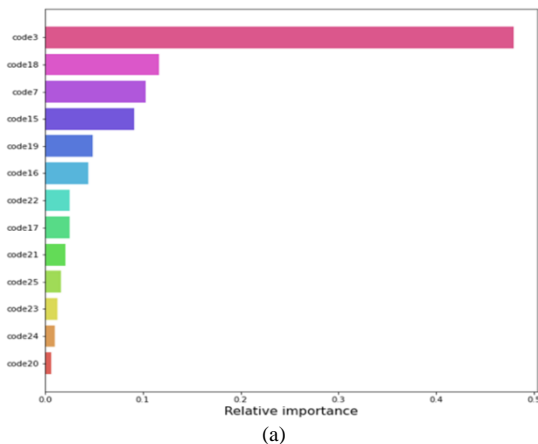


Fig. 4. Feature Ranking (a) Extra Tree Algorithm; (b) XGB Algorithm; (c) RF Algorithm.

code3 (whether or not you have a smartphone; 1=yes, 2=no), code7 (internet availability; 1=yes, 2=no), code15 (availability of mobile devices (e.g. display/sound/security/alarm); 1=not at all, 4=most are available), code16 (availability of mobile devices (e.g. wifi); 1=not at all, 4=most are available), code17 (whether you can move files from mobile device to computer; 1=not at all, 4=most are available), code18 (whether you can send files/photos from mobile device to others; 1=not at all, 4=most are available), code19 (whether necessary apps can be installed/deleted/updated on mobile devices; 1=not at all, 4=most are available), code20 (whether it can scan/repair the mobile device's malicious code (virus, spyware, etc.); 1=not at all, 4=most are available), code21 (whether you can write documents or materials (memo, word, etc.) on mobile device; 1=not at all, 4=most are available), code22 (whether you can connect and communicate with others over the Internet; 1=not at all, 4=most are available), code23 (whether you can actively exchange opinions on political and social issues or problems using the Internet; 1=not at all, 4=most are available), code24 (Whether you can protect yourself from personal information exposure; 1=not at all, 4=most are available), code25 (Whether you can be responsible for the use of the Internet; 1=not at all, 4=most are available), code26 (recent internet use experience; 1=within the last month, 2=over a month, 3=never used).

KNN and several Tree based ML models (RF algorithm, extra tree classifier, GBM, and XGBoost) were applied to analyze our dataset using the top feature, then the top two features, the top three features, etc., continuing for all 13 features [15]. This step identified the best combination of feature ranking model and a minimum number of features to achieve the best performance. As a fundamental machine learning algorithm, K Nearest Neighbor is a method of predicting output values based on a set of input values. It is one of the least complex machine learning algorithms. It classifies the data point on how its neighbor is classified. The KNN algorithm can compete with the most accurate models because it makes highly accurate predictions. The Random Forest is used in this study because it is stable and easy to implement and provides several interesting properties, including computing variables with excellent efficiency [16]. The extra tree classifier combines the results of multiple de-correlated decision trees collected into a "forest" to produce a classification result. It has been applied in this study because it is similar to RF; however, its construction method in the forest is optimal and faster than RF [13, 16, 17]. GBM and XGBoost are two popular techniques for ensemble ML, and their performance is good on structured and tabular data. These techniques are used to solve real-life data science problems and solve them with parallel tree boosting. While both XGB and GBM use gradient boosting as a principle, there are differences in the modeling details. Specifically, XGBoost uses a more formalized formalization to control overfitting, making it perform better [18]. These techniques were used because their impact has been widely recognized in many machine learning and data mining challenges [13].

Table I shows the performance of the top models for each of the five ML algorithms that employ three feature ranking approaches utilizing three feature ranking approaches. The XGB model using the XGB feature ranking method produced the best results. This model used 11 features, reaching 0.970 of accuracy score and 0.9894 of AUC score. For this model, selected variables included code3, code15, code18, code7, code25, code22, code23, code19, code21, code16, code20, code24, and code17. GBM came in second with an accuracy of 0.970, and its AUC score of 0.9884 is slightly lower than that of XGB. Therefore, the XGB model was chosen as the best model, and its hyper-parameters were tuned to get the most effective model.

B. Performance Evaluation of XGB Classifier Model

The best model obtained in this study is the XGB model with the XGB feature ranking method. The XGB Classifier model used 11 important selected features (code 3, code 7, code 15, code 18, code 19) as feature variables and code26 as the target variable. Feature and target variables were split to 70% for training and 30% for test. The XGB model's hyperparameters were tuned by the HyperOpt library. Developed by James Bergstra, Hyperopt is a powerful Python library for hyperparameter optimization. Hyperopt uses a form of Bayesian optimization to find the best parameters for a given model. It can optimize a model with hundreds of parameters [19]. After tuning the hyper-parameters, the best XGB Classifier's hyper-parameters are 'colsample_bytree': 0.66, 'gamma': 1.06, 'learning_rate': 0.43, 'max_depth': 6, 'min_child_weight': 1.0, 'n_estimators': 14, 'subsample': 0.83. The most effective XGB model had a 0.97 accuracy score and 0.9894 AUC score. The model can be evaluated to work extremely effectively.

TABLE I. ANALYZING THE PERFORMANCE OF DIFFERENT MACHINE LEARNING MODELS

Algorithm	Feature Selection Models	Number of features	Accuracy	Average Recall	Average Precision	Average F1 score	Average ROC_AUC
XGB	Extra Tree	12	0.968	0.968	0.968	0.967	0.989
	Random Forest	13	0.968	0.968	0.968	0.967	0.989
	XGB	11	0.970	0.970	0.970	0.969	0.989
GBM	Extra Tree	12	0.968	0.968	0.969	0.967	0.990
	Random Forest	10	0.968	0.968	0.968	0.967	0.988
	XGB	11	0.970	0.970	0.970	0.969	0.989
KNeighbors	Extra Tree	5	0.959	0.959	0.959	0.958	0.972
	Random Forest	2	0.962	0.962	0.962	0.962	0.949
	XGB	3	0.964	0.964	0.963	0.963	0.975
Random Forest	Extra Tree	11	0.964	0.964	0.963	0.963	0.986
	Random Forest	9	0.967	0.967	0.967	0.966	0.985
	XGB	4	0.965	0.965	0.965	0.964	0.989
ExtraTree	Extra Tree	3	0.962	0.962	0.962	0.961	0.982
	Random Forest	4	0.965	0.965	0.965	0.964	0.985
	XGB	4	0.965	0.965	0.965	0.964	0.985

IV. CONCLUSION

In this study, the level of the information gap of the elderly can be predicted as the recent internet accessed time, and the factor recent internet accessed time is analyzed in terms of mobile usability factors. This study constructed machine learning models to predict the elderly's internet accessed time through the elderly's mobile usability factors. XGB algorithm was used to design the machine learning model (XGB Classifier Model).

The evaluation scores of the XGB machine learning model are very positive and bring high expectations. To solve the information gap of the elderly problem, we can use these effective models to predict the elderly object. Then, we can give some solutions to help them in a society with a strong information technology base. For example, the authorities can give these people introductory training courses on information access skills to limit the information access gap of the elderly.

ACKNOWLEDGMENT

This research was supported by Basic Science Research Program through the National Research Foundation of Korea (NRF) funded by the Ministry of Education (NRF-2018R1D1A1B07041091, 2021S1A5A8062526) and 2022 Development of Open-Lab based on 4P in the Southeast Zone.

REFERENCES

- [1] R. Susło, M. Paplicki, K. Dopierała, and J. Drobnik., Fostering digital literacy in the elderly as a means to secure their health needs and human rights in the reality of the twenty-first century. *Family Medicine & Primary Care Review*, vol. 20, no. 3, pp. 271-275, 2018. doi: 10.5114/fmPCR.2018.78273.
- [2] G. M. Van Jaarsveld, The Effects of COVID-19 Among the Elderly Population: A Case for Closing the Digital Divide. *Frontiers in psychiatry* vol. 11 577427, 2020. doi: 10.3389/fpsy.2020.577427.
- [3] K. Hatamnezhad, P. Ghafari Ashtiyani, and F. Seyedi, Investigating the Relationship Between Electronic Literacy and Quality of Life of the Elderly in Arak, Iran. *Bulletin of Science, Technology & Society*, vol. 41, no. 1, Feb. 2021, pp. 3–9. doi: 10.1177/02704676211007360.
- [4] A. Powell, A. Bryne, and D. Dailey, The essential Internet: Digital exclusion in low - income American communities. *Policy & Internet*, vol. 2, no. 2, pp. 161-192, 2010. doi: 10.2202/1944-2866.1058.
- [5] B. Schäffer, The Digital Literacy of Seniors. *Research in Comparative and International Education*, vol. 2, no. 1, pp. 29–42, 2007. doi: 10.2304/rcie.2007.2.1.29.
- [6] D. Castilla, C. Botella, I. Miralles, J. Bretón-López, A. M. Dragomir-Davis, I. Zaragoza, and A. Garcia-Palacios, Teaching digital literacy skills to the elderly using a social network with linear navigation: A case study in a rural area. *International Journal of Human-Computer Studies*, vol. 118, pp. 24-37, 2018. doi: 10.1016/j.ijhcs.2018.05.009.
- [7] W. K. Shin, D. B. Lee, and M. Y. Park, Smartphone Adoption using Smartphone Use and Demographic Characteristics of Elderly. *Journal of the Ergonomics Society of Korea*, vol. 31, no. 5, pp. 695-704, 2012. doi: 10.5143/jesk.2012.31.5.695.
- [8] H. Lee, and S. H. Lee, A study on the relationship between level of digital informatization and satisfaction level of elderly people: Focusing on community, meeting, and community involvement activities. *Journal of Digital Convergence*, vol. 17, no. 2, pp. 1-7, 2019. doi: 10.14400/JDC.2019.17.2.001.
- [9] C. H. Wang, and C. L. Wu, Bridging the digital divide: the smart TV as a platform for digital literacy among the elderly. *Behaviour & Information Technology*, pp. 1-14, 2021. doi: 10.1080/0144929X.2021.1934732.
- [10] S. K. Choi, Current status of digital information gap for women with disabilities from a gender-conscious perspective and ways to support informatization education based on empowerment. *Journal of the Korea Institute of Information and Communication Engineering*, vol. 24, no. 5, pp. 655-661, 2020. doi:10.6109/JKIICE.2020.24.5.655.
- [11] Y. Liu, Y. Wang, and J. Zhang, New Machine Learning Algorithm: Random Forest. In *Information Computing and Applications*. Springer: Berlin/Heidelberg, Germany, 2012, pp. 246–252.
- [12] P. Geurts, D. Ernst, and L. Wehenkel, Extremely randomized trees. *Machine Learning*, vol. 63, pp. 3-42, 2006. doi: 10.1007/s10994-006-6226-1.
- [13] A. O. Alsayed, M. S. M. Rahim, I. AlBidewi, M. Hussain, S. H. Jabeen, N. Alromema, S. Hussain, and M. L. Jibril, Selection of the Right Undergraduate Major by Students Using Supervised Learning Techniques. *Applied Sciences*, vol. 11, no. 22, pp. 10639, 2021. doi: 10.3390/app112210639.
- [14] H. Byeon, Developing a nomogram for predicting the depression of senior citizens living alone while focusing on perceived social support. *World journal of psychiatry*, vol. 11, no. 12, pp. 1314, 2021. doi: 10.5498/wjpv.11.12.1314.
- [15] N. H. Chowdhury, M. B. I. Reaz, F. Haque, S. Ahmad, S. H. M. Ali, A. A. Bakar, and M. A. S. Bhuiyan, Performance Analysis of Conventional Machine Learning Algorithms for Identification of Chronic Kidney Disease in Type 1 Diabetes Mellitus Patients. *Diagnostics*, vol. 11, no. 12, pp. 2267, 2021. doi: 10.3390/diagnostics11122267.
- [16] C. Beaulac, and J. S. Rosenthal, Predicting University Students' Academic Success and Major Using Random Forests. *Research in Higher Education*, vol. 60, pp. 1048-1064, 2019. doi: 10.1007/s11162-019-09546-y.
- [17] R. Patil, and S. Tamane, A Comparative Analysis on the Evaluation of Classification Algorithms in the Prediction of Diabetes. *International Journal of Electrical and Computer Engineering*, vol. 8, no. 5, pp. 3966-3975, 2018. doi: 10.11591/ijece.v8i5.pp3966-3975.
- [18] A. Asselman, M. Khaldi, and S. Aammou, Enhancing the prediction of student performance based on the machine learning XGBoost algorithm. *Interactive Learning Environment*, pp. 1-20, 2021. doi: 10.1080/10494820.2021.1928235.
- [19] J. Bergstra, D. Yamins, and D. D. Cox, Making a Science of Model Search: Hyperparameter Optimization in Hundreds of Dimensions for Vision Architectures. *Proceedings of the 30th International Conference on Machine Learning*, vol. 28, no. 1, pp. 115-123, 2013.

Accessibility of Bulgarian Regional Museums Websites

Todor Todorov¹, Galina Bogdanova², Mirena Todorova–Ekmekci³

Faculty of Mathematics and Informatics, St. Cyril and St. Methodius University of Veliko Tarnovo, Veliko Tarnovo, Bulgaria¹
Institute of Mathematics and Informatics, Bulgarian Academy of Sciences, Sofia, Bulgaria¹
Institute of Mathematics and Informatics, Bulgarian Academy of Sciences, Sofia, Bulgaria²
Bulgarian Academy of Sciences, IEFSEM - Institute of Ethnology and³
Folklore Studies with Ethnographic Museum, Sofia, Bulgaria³

Abstract—Web accessibility is an inclusive practise that ensures everyone including people with disabilities can successfully work and interact with websites and use all their functionality. The research in the paper investigates the problem of web accessibility of Regional museums in Bulgaria and the compliance of their websites with the recommendations of Web Content Accessibility Guidelines 2.1 (WCAG 2.1), published by World Wide Web Consortium (W3C). The study presents the results of the user experience of people with disabilities regarding the accessibility of museums and exhibits in them. A methodology for automated testing of web accessibility with several software tools is described in the paper. Results from these tests are analysed and visualized with graphical tools. Some important conclusions about most common accessibility problems are given.

Keywords—Accessibility; museums; web accessibility; visual disability; disabled person; testing; automatic validation tools; WCAG criteria

I. INTRODUCTION

In present days Internet brings information to the user in a quick and easy way by just one mouse click. But this is not the case regarding people with different types of disabilities. According to the World Health Organization (WHO) a disabled person is anyone who has “a problem in body function or structure, an activity limitation, has a difficulty in executing a task or action; with a participation restriction”. In 2021 WHO reports [2] state that people identified as disabled are over 1 billion. The COVID pandemic dramatically increases the importance of the special needs of people and addressing the accessibility problem. One of the most important issues that all digital resources and site makers on the Internet should consider and work on is the accessibility for people with visual impairments. According to WHO 253 million people are affected by some form of blindness and visual impairment. This represents 3.2% of the world’s population, the second largest group of people with a certain type of disabilities. People with disabilities often have difficulty accessing the content of websites. Web accessibility includes good practices for removing these limitations through appropriate content design and organization. There is no clear correspondence between the good functionality of a website and its accessibility. In practice, designers and developers need to make additional efforts to understand the needs of people with disabilities and to adapt the developed web accessibility standards to their digital resources [3], [4].

World Wide Web Consortium (W3C) [8] presents Web Accessibility Initiative (WAI) [9] as guidelines and recommendations for web accessibility. WAI initiated the development of the Web Content Accessibility Guidelines (WCAG), which are now at version 2.1. The guidelines were built on four principles [8]:

- Perceivable - information and user interface components must be presentable to users in ways they can perceive;
- Operable - User interface components and navigation must be operable. The interface cannot require interaction that a user cannot perform;
- Understandable - users must be able to understand the information as well as the operation of the user interface;
- Robust - content must be robust enough that it can be interpreted reliably by a wide variety of user agents, including assistive technologies.

There are three compliance levels within WCAG 2.1 [5], [7]:

- Level A: Minimal compliance - prohibit elements that would make the website inaccessible;
- Level AA: Acceptable compliance - all the success criteria categorized as A and AA are satisfied. Used in most accessibility rules and regulations around the world;
- Level AAA: Optimal compliance - all the success criteria categorized as A, AA and AAA are satisfied.

The WAI Accessible Rich Internet Applications Suite (ARIA) [9] defines a way to make web content and web applications more accessible for dynamic content and advanced user interface controls developed with Ajax, HTML, JavaScript, and related technologies [6].

Aside from ethical and business justifications, there are legal reasons for applying Web Content Accessibility Guidelines in various nations and jurisdictions. In January 2017, the US Access Board approved a final rule to update Section 508 of the Rehabilitation Act of 1973. The new rule adopts seventeen WCAG 2.0 success criteria, but 22 of the 38

existing A-level and AA-level criteria were already covered by existing Section 508 guidelines. In EU Directive 2016/2102 requires websites and mobile applications of public sector bodies to conform with WCAG 2.1 Level AA. The European Parliament has approved the directive in October 2016, the European Commission updated the WCAG reference from 2.0 to 2.1 in December 2018 [22].

This paper presents results from an automated testing of accessibility of the websites of the Regional museums in Bulgaria. Some of the results are also discussed in relation to the user experience gathered by a group of volunteers with visual impairments. Section 2 shows an overview of other accessibility research articles related to museums. In Section 3 authors present the methodology of the conducted experiment. The results of the testing experiment are presented and discussed in Section 4.

II. ACCESSIBILITY AND BULGARIAN MUSEUMS

Digital museums are important part of today's digital world. The accessibility of their websites is even more important in last two years of world pandemic. There are a lot of research articles related to museum accessibility. In [12] is discussed how changes caused by the COVID-19 pandemic potentially pose a threat to the experience of disabled people, in particular blind and partially sighted visitors. Research [13] investigates the perspectives of 72 blind and partially sighted individuals on enhancing their visiting experience in museums. In [14] and [18] some case studies are presented, and the results and conclusions reveal that museums websites in Bulgaria and in other countries are still far from being considered accessible, and improvements in several areas are required.

The accessibility of museums includes not only visually impaired people being able to visit the museums, but also the content and objects in them being perceivable and understandable to them. Some of the possible and often used worldwide solutions to improve accessibility for the blind and visually impaired people in museums are to place Braille signs on all doors, secure stairs with handrail, tactile guide paths, audio information, Braille language plaques.

Unfortunately, this is not always enough for visually impaired people, who may not be able to find the appropriate Braille inscriptions. Even if they do find them, they often do not offer complete information about the objects like the full information that can be obtained by a person with normal vision in the museum or cultural site.

Increasing attention is being paid also to audio guides - cultural routes with audio sounds, voice guidance and digitally accessible content, libraries and archives.

Some common accessibility barriers for blind and visually impaired people and possible solutions include:

1) Getting main information about location, physical access points, work time, available cultural and historical exhibitions, collections, objects and information in the museum.

2) Finding, reading and understanding available information online and offline on sight.

3) Booking a visit for a person/ group with special needs, organizing companion or assistant help if needed.

4) Providing online directions with text or audio

5) An online map of site content with hyperlinks is greatly useful for those with disabilities.

6) Searching information or objects - a site needs to have an easy-to-find and operate search module/ tool on the first page. Usually, it is located in the top headline section, with an option to search with one or a few keywords in pages of the site or an available database and library with cultural and historical knowledge and object. In order to be found the data should be properly organized, categorized, described, meta tagged, etc. [20].

7) Digital accessibility of sites: Website need to be accessible for all types of users and devices from everywhere and it should not take too much time to load and open a page or find the most important information. More about site accessibility and criteria can be found in [11] and [19]. More about web accessibility of sites is also described in the next pages with research results.

Bulgaria has many natural wonders, historical and cultural relics and heritage. There are more than 180 museums in the country that preserve and expose unique samples of Bulgarian and world cultural heritage [10]. Most of them have sites with digital materials and information, virtual tours and exhibitions on the websites.

Bulgarian Ministry of Culture published a list with 50 cultural museums in 2020 that offer online services and tours, during the epidemic measures situation. Many of those sites and the ones reviewed by the authors in previous research papers [1] and [11] have short video tours, images and text digitized materials, but only a few of the sites show rich data repositories with large collections, annotated objects with captions, metatags and detailed categorized descriptions and search functionality. Some sites have simple education materials with basic games, images for printing and quizzes for kids; other museums use videos online in sites and social networks with people presenting exhibitions or objects, as more interactive digital storytelling [1].

Unfortunately, previous research of cultural sites shows that the accessibility of digital content and the websites of many of these museums in general is not at a high enough level. The survey conducted with volunteers with visual impairments found that over 80% of museums digital sites are not accessible to people with visual impairments, i.e., don't have an audio or text alternative. The results are similar in the negative aspect of the question "Is there access to museum-related materials in Braille, enlarged font and audio?" [11].

There are 30 Regional museums in Bulgaria with websites with information and digitized materials. In the next sections authors investigate the accessibility of these sites. Table I presents a list of Regional museums with their name, website URL and unique ID used for reference in the results section.

TABLE I. LIST OF MUSEUMS

ID	Name	URL
1	Regional Museum - Veliko Tarnovo	https://museumvt.com/bg/
2	Regional Museum - Gabrovo	https://h-museum-gabrovo.bg/
3	Regional Archaeological Museum - Plovdiv	https://www.archaeologicalmuseumplovdiv.org/
4	Regional Ethnographic Museum - Plovdiv	https://www.ethnograph.info/front/index.php
5	Regional Museum of Natural History – Plovdiv	https://rnhm.org/bg/home
6	Regional Museum - Plovdiv	https://historymuseumplovdiv.org/
7	Regional Museum - Burgas	https://www.burgasmuseums.bg/
8	Regional Museum - Ruse	https://www.museumruse.com/
9	Regional Museum - Varna	http://www.museumvarna.com/
10	Regional Museum - Pleven	https://rim-pleven.com/
11	Regional military museum - Pleven	http://panorama-pleven.com/
12	Regional Museum - Lovech	https://lovech-museum.bg/
13	History Museum - Sofia	https://www.sofiahistorymuseum.bg/index.php?lang=bg
14	Regional Museum - Yambol	http://yambolmuseum.eu/
15	Regional Museum - Vidin	http://museum-vidin.domino.bg/index2.htm
16	Regional Museum - Vratza	https://vratsamuseum.com/
17	Regional Museum - Silistra	https://www.museumsilistra.com/bg/
18	Regional Museum - Pernik	https://www.museumpernik.com/
19	Regional Museum - Smolyan	https://museumsmolyan.eu/
20	Regional Museum - Pazardzhik	https://museum-pz.com/wp/
21	Regional Museum - Sliven	http://museum.sliven.net/
22	Regional Museum - Razgrad	https://abritus.bg/
23	Regional Museum - Shumen	https://museum-shumen.eu/
24	Regional Museum - Montana	https://montana-museum.weebly.com/
25	Regional Museum - Kyustendil	http://www.kyustendilmuseum.primasoft.bg/bg/index.php
26	Regional Museum - Stara Zagora	https://www.rimstz.eu/
27	Regional Museum - Kardzhali	https://www.rim-kardzhali.bg/
28	Regional Museum - Haskovo	http://haskovomuseum.com/
29	Regional Museum - Dobrich	https://www.dobrichmuseum.bg/
30	Regional Museum - Blagoevgrad	https://museumbld.com/

III. METHODOLOGY

Automated evaluation software testing tools often called validators check the web site accessibility according to the guidelines defined by WCAG. They try to identify some errors and potential problems and give some recommendations about improvements of the web site accessibility. These automated tools are not panacea. They give an initial impression about the accessibility level of a web resource and can help developers about fixing general accessibility problems. For more detailed and complete accessibility test an additional manual testing should be conducted. Similar research and results on the topic can be found in [21]. During this manual testing all potential problems from automatic testing tools should be also addressed. It is not a rare case when automated testing tools give a false positive result indicating that the site is 100% accessible. Examples of such cases are presented in the next section. That is why additional manual testing is mandatory. However automated testing results can give a good overall impression about the web accessibility of a site. There are more than 150 automated testing tools in the Web Accessibility Evaluation Tools List from W3C. Three of them are selected to perform the tests of the website's accessibility of Bulgarian Regional museums.

1) *TAW* [15]: TAW is an automated tool for web site analysis based on WSAG recommendations. It is developed by the Spanish Foundation Centre for the Development of Information and Communication Technologies. It is available either as a browser extension or as a web service. It summarizes results in three categories “Problem” (should be fixed), “Warnings” (developer review is needed), “Not reviewed” (manual check is required). In the experiments performed are used options for Level AA accessibility checking with HTML, CSS, JS options enabled.

2) *WAVE* [16]: WAVE is another web accessibility test automation tool that also can be used either as a browser extension or as a web service. The report contains five categories that indicate and errors and features that should be addressed to improve accessibility.

3) *Lighthouse* [17]: It is an open source automated tool for quality improvement of the web site. It can be used as a web browser extension. The report gives scores and recommendations about different indicators. Only one of them is accessibility.

IV. RESULTS

Table II presents scores for all the museum sites with the three testing tools that were used in the research.

Result for each museum is shown on a separate row and assigned ID from first column corresponds to the ID from Table I. Same ID is used as a reference label on the other graphical results that follows next in this section.

TABLE II. ACCESSIBILITY TESTING SCORES OF MUSEUM SITES

	TAW															Lighthouse				WAVE					
	Problem					Warning					Not reviewed					P	A	B	S	E	C	A	F	St	A R
	P	O	U	R	T	P	O	U	R	T	P	O	U	R	T										
1	0	0	0	0	0	0	0	0	0	0	0	0	0	0	0	4	9	83	64	0	0	0	0	0	0
2	6	7	1	14	28	98	50	6	0	15 4	3	9	6	1	1 9	6	8	67	78	7	24	2 7	2 9	46	46
3	7	0	1	37	45	14	12	6	0	32	4	8	5	1	1 8	9	7	67	69	3	15	2 4	9	14	0
4	3	0	1	10	14	3	2	0	0	5	4	8	5	1	1 8	9	6	58	67	3	0	2 7	2	1	0
5	3 7	1 2	1 0	21	80	89	82	0	4	17 5	3	5	5	0	1 3	9	6	60	78	2 5	41	2 4	1 9	43	0
6	1 7	0	1	2	20	13	14	0	0	27	4	7	5	1	1 7	7	6	93	92	1 4	4	1 5	1	0	0
7	4	1 9	2	1	26	48	30	6	0	84	4	8	5	0	1 7	4	8	80	81	2 9	20	5	9	29	14
8	9	6	2	51	68	57	18	6	16	97	4	8	5	0	1 7	3	9	93	92	3	4	2 3	6	32	48
9	1 1	1	1	21	34	42	18	0	4	64	4	7	5	1	1 7	9	6	73	54	5	1	8	1 0	8	0
10	1 5	2 0	0	48	83	18	18	0	0	36	4	8	6	1	1 9	2	8	93	98	8	38	3 1	1 6	37	14
11	8	2	1	35	46	39	10	0	0	49	4	7	5	1	1 7	9	6	67	69	7	1	4 5	3	6	0
12	2 0	1 2	4	12	48	75	39	1 2	20	14 6	3	7	6	0	1 6	3	8	87	74	1 3	33	5 4	1 8	47	7
13	1 4	2 0	2	23	59	83	59	6	0	14 8	4	6	5	0	1 5	1	7	67	79	2 2	23	3 6	1 8	62	5
14	1 8	8 4	3	97	20 2	15 7	11 5	6	16 6	44 4	4	7	6	0	1 7	1	9	67	84	5 1	11 3	5 6	5 2	12 9	15
15	1	0	1	5	7	0	2	0	0	2	4	8	5	0	1 7	0	3 3	80	64	1	0	2	0	0	0
16	8 2	0	1	53	13 6	14 5	2	0	0	14 7	4	8	5	1	1 8	6	6	73	69	3 0	1	1 6	3	0	0
17	2 3	7	4	11	45	56 2	51	6	16	63 5	4	7	5	0	1 6	1	8	80	10 0	7	5	3 7	3 9	38	77
18	1 5	8	1	33	57	21	13	0	0	34	4	7	5	1	1 7	3	6	73	58	1 6	0	1 5	7	7	0
19	4	5	1	6	16	16	15	0	0	31	4	8	6	0	1 8	5	8	10 0	89	7	0	1	4	6	4
20	1 0	5	2	12	29	80	33	6	6	12 5	4	7	6	0	1 7	1	8	67	77	1 7	5	4 2	2 1	72	28
21	3 0	3	1	7	41	6	60	6	0	72	4	8	6	0	1 8	5	6	73	87	9	12	4 3	3	47	0
22	1 5	1 6	4	33	68	49	45	2 4	15	13 3	4	7	5	0	1 6	6	8	80	90	2 1	31	1 5	2 5	63	13
23	1 9	1 6	1	13	49	10 5	43	0	11	15 9	4	7	6	0	1 7	3	9	67	70	2 3	29	8 6	4 4	18	70
24	2 5	2 3	0	11 9	16 7	56	23	0	0	79	4	7	5	1	1 7	5	7	80	92	2 2	2	5	2	24	2
25	4 3	1 1	6	13 6	19 6	97	3	1 2	10	12 2	3	7	5	0	1 5	9	7	67	75	6	0	3 0	2 8	0	0
26	9	1 7	1	33	60	29	11	0	0	40	4	8	5	1	1 8	9	8	60	83	1 1	11	3 4	9	6	0
27	2	0	1	83	86	17	19	0	4	40	4	7	5	1	1 7	7	8	80	67	1	3	1 7	1 0	9	0
28	1 0	1 2	1	2	25	24	39	6	53	12 2	4	6	6	0	1 6	2	8	87	85	1 5	28	2 7	1 1	29	2
29	3 7	6 4	4	5	11 0	84	87	1 2	20	20 3	4	7	6	0	1 7	5	9	80	91	3 0	11 1	8 4	1 7	71	14
30	7	4	1	8	20	16	37	6	8	67	4	6	5	0	1 5	2	9	73	86	1 1	5	2 9	3	39	24

Lighthouse presents results for web site quality in five categories. In Table II, they are denoted as P (Performance), A (Accessibility), B (Best Practices), S (SEO). A special web application was created for automatic usage of Lighthouse API to test all the sites. The application performs three consecutive tests for each site and average the results.

Fig. 1 presents the results for the main criterion that considered – accessibility. Good results are those that are over 90. These are only 6 museums and only one of them is with score over 95. This is the Regional Museum of Dobrich (29). Regional Museum of Vidin (15) has the lowest score. Its site is with a very old-fashioned design even visually and also with bad technical implementation.

Considering data displayed on Fig. 2, the conclusion is that most of the museums (57%) are below the average Lighthouse score of 79 for all tested sites. Also, 80% of them are with a score below the acceptable value of 90. This means according to Lighthouse measurement Bulgarian regional museums websites are with low accessibility level.

Fig. 3 presents the other scores that Lighthouse uses to measure the quality of a web site. As a general conclusion it can be stated that websites with low accessibility level in most cases have low values on the other measurements too.

In the experiment is performed a manual testing for accessibility to the site of Regional Museum of Dobrich (29) which has the highest Lighthouse score. A group of volunteers with visual impairments found some additional problems that were not detected by the automation testing. For example, the main menu is totally inaccessible since it does not contain the necessary attributes for screen readers to find that there are dropdown options. Also, the dropdown list opens on mouse hover and not on Enter key click, which makes it totally inaccessible.

TAW testing tool displays potential problems and warnings according to the four accessibility principles: Perceivable (P), Operable (O), Understandable (U) and Robust (R). These results are presented on Table II for each site. The total number of potential accessibility errors are presented in the column marked with T on its header section. Results marked with red are from the sites where TAW was not able to perform the test because of some automation restrictions incorporated in the site.

On Fig. 4 are presented results for issues marked as “Problems” by TAW tests.



Fig. 1. Lighthouse Accessibility Scores of Tested Museum Sites.

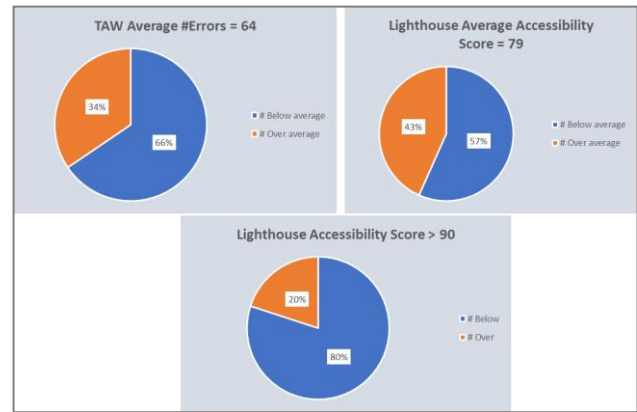


Fig. 2. Average Scores for Accessibility.

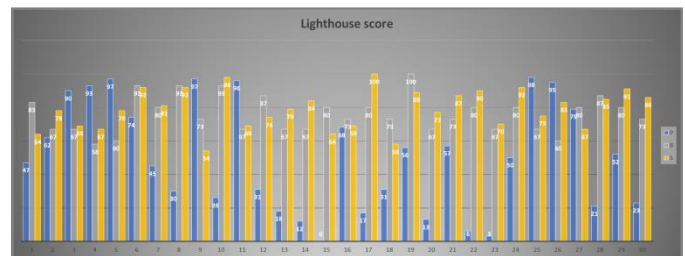


Fig. 3. Lighthouse other Scores.

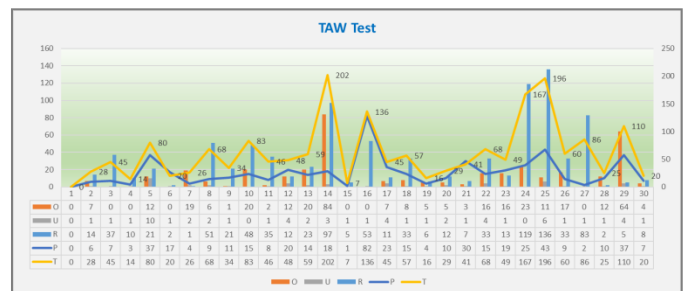


Fig. 4. TAW Scores.

A total number of potential problems detected on the site is indicated with yellow line.

The results of Regional Museum – Gabrovo (Number 2 in Table I), Regional Museum – Haskovo (28), Regional Museum – Blagoevgrad (30) and several other similar scores can be distinguished as museum sites with lowest scores number of accessibility problems. On the other side are Regional Museum – Yambol (14), Regional Museum – Montana (24) and Regional Museum – Kyustendil (25) with total number problems close to 200.

It's interesting to notice some controversial result for the same websites between the Lighthouse scores and those generated by TAW. For example, Regional Museum – Yambol (14) has accessibility score of 91 by Lighthouse but on the other hand TAW notices a total number of 202 problems. In fact, the TAW results are more adequate in this case, and this is confirmed by performed manual testing of the site by the group of volunteers. Most of the errors detected by TAW are related to bad menu navigation and not well-formed link tags. Also, there are a lot of problems connected to parsing – HTML not

well formed or not used according to specs. These problems are confirmed in manual testing but omitted in Lighthouse. Also, there are cases where Lighthouse evaluation is more precise than TAW. It has been already discussed the badly designed and totally inaccessible site of Regional Museum – Vidin (15) but TAW does not manage to find all the problems in this simple functionality and generates only 7 problems. On the other hand, Lighthouse correctly produces low score of only 33.

Reconsidering the results from Fig. 2 about the average number of TAW errors, it can be noticed that about 66% percent of the sites has below this average number of 64 errors. This could be considered as generally good result for overall accessibility.

WAVE produce a web accessibility report for a web site in five categories: Errors (E), Contrast Errors (C), Alerts (A), Features (F), Structural Elements (St), HTML5 and ARIA (AR).

The results for each category and for each of the tested sites are presented on Fig. 5.

Again, the site of the Regional Museum - Veliko Tarnovo (1) is not successfully tested due to access restrictions.

From other sites with the lowest levels of Errors and Contrast errors Regional Museum – Ruse (8) and Regional Museum – Kardzhali can be distinguished. Again, there are some false negative results like Regional Museum – Vidin (15). According to WAVE it has only 1 error and 2 alerts, but manual check proves that the accessibility problems in this case are much more.

An interesting and unique part of web site analysis with WAVE is that the developer receives a direct visual remark about the accessibility problematic elements on the page. Fig. 6 presents one such visual report about the problems related to the site of Regional Museum – Ruse (8).

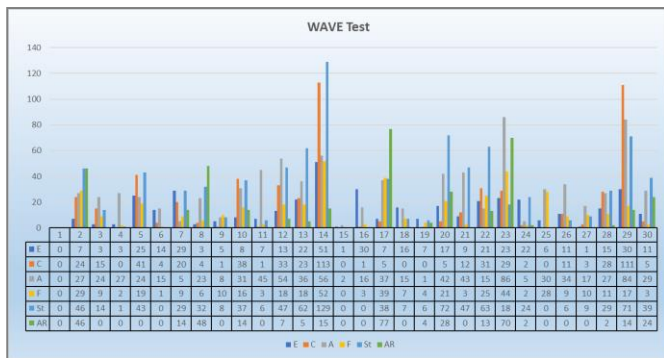


Fig. 5. WAVE Software Test Scores of the Experiment.

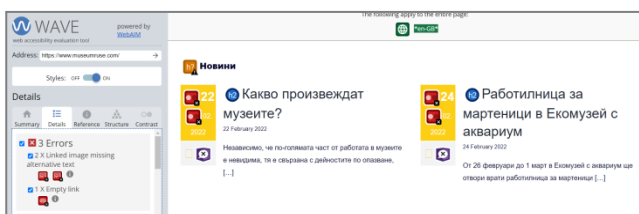


Fig. 6. WAVE Software Visual Report Screen from the Research.

V. CONCLUSION

The research in the paper investigated the important problem of web accessibility on museum sites. The research uses automatic web site testing tools and a group of volunteers – blind and with visual impairments for manual testing of 30 websites of Regional Museums in Bulgaria.

In general, the conclusion is that most of the web sites present below average and not a satisfactory level of digital accessibility. Most common accessibility problems found on the researched websites of museums are summarized as follows:

1) Heading elements are not in a sequentially descending order – tags from <h1> to <h6> are missing or are not used in proper way.

WCAG criteria:

- 1.3.1 Info and Relationships (Level A).
- 2.4.6 Headings and Labels (Level AA).

2) <html> element does not have a [lang] attribute - a screen reader assumes that the page is in the default language and might not announce the page's text correctly.

WCAG criteria:

- 3.1.1: Language of Page (Level A).

3) Links do not have a discernible name – if present they improve the navigation experience for screen reader users.

WCAG criteria:

- Success Criterion 2.4.4: Link Purpose (Level A).

4) Image elements do not have [alt] attributes - informative elements should aim for short, descriptive alternate text.

WCAG criteria:

- Success Criterion 1.1.1 (Non-text Content) (Level A).

5) Background and foreground colours do not have a sufficient contrast ratio - low-contrast text is difficult or impossible for many users to read.

WCAG criteria:

- Success Criterion 1.4.3: Contrast (Minimum) (Level AA).
- Understanding Success Criterion 1.4.6: Contrast (Enhanced) (Level AAA).

The volunteers with visual impairments in the experiment stated, during the research, that the automatic software results are useful for orientation and defining main points of sites they need to improve in order to comply with Web Content Accessibility Guidelines, but further real-time testing with visually impaired people is also needed, as the software cannot detect all important issues on sites concerning accessibility, functionality and usability of sites for visually impaired and blind people. This is a matter of further research and scientific papers.

Nevertheless, the existing web accessibility testing software for sites is very useful for web developers and site makers, as well as for institutions and museum representatives. They enable a vast number of sites and databases to be checked automatically in a very short time. Such automated software solutions are necessary in modern times with immense volumes of generated and uploaded online information and sites.

ACKNOWLEDGMENT

The research was funded by the National Science Fund of Bulgaria (scientific project "Digital Accessibility for People with Special Needs: Methodology, Conceptual Models and Innovative Ecosystems"), Grant Number KP-06-N42/4, 08.12.2020.

REFERENCES

- [1] M. Todorova-Ekmekci, T. Todorov, K. Sotirova-Valkova, "Usage of Innovative Technologies and Online Media Tools for Digital Presentation of Cultural Heritage in Bulgaria", In: Digital Presentation and Preservation of Cultural and Scientific Heritage, vol. 11, pp. 303-308, 2021, ISSN: 1314-4006.
- [2] World Health Organization, World Report on Vision. World Health Organization, Geneva, Switzerland, 2019. <https://www.who.int/publications/i/item/9789241516570>.
- [3] C. Ghidella, S. Murray, M. Smart, K. McKenna, L. Worrall, "Aphasia websites: An examination of their quality and communicative accessibility", Aphasiology, vol. 19 (12), pp. 1134–1146, 2005.
- [4] A. Obead, "An Accessibility Evaluation of the Websites of Top-ranked Hospitals in Saudi Arabia", International Journal of Advanced Computer Science and Applications (IJACSA), vol. 12(1), pp.692-698, 2021.
- [5] E. Pivetta, C. Flor, D. Satomi Saito, V. Ulbricht, "Analysis of an Automatic Accessibility Evaluator to Validate a Virtual and Authenticated Environment" International Journal of Advanced Computer Science and Applications (IJACSA), vol. 4(4), pp. 15-22, 2013.
- [6] E. Iseri, K. Uyar, U. Ilhan, "The accessibility of Cyprus Islands' Higher Education Institution Websites", Procedia Computer Science, vol. 120, pp. 967-974, 2017.
- [7] A. Basel, E. Bataineh, F. Kamoun, "E-Government Web Accessibility: WCAG 1.0 versus WCAG 2.0 Compliance", International Journal of Digital Information and Wireless Communications (IJDIWC) 3(4): pp.56-65, 2013.
- [8] W3C, World Wide Web Consortium, <https://www.w3.org>.
- [9] WAI, Web Accessibility Initiative, <https://www.w3.org/WAI/>.
- [10] Ministry of Tourism, "Statistical data," [Online]. Available: <http://www.tourism.government.bg/bg/kategorii/statisticheski-danni/>.
- [11] G. Bogdanova, N. Sabev, Z. Tomov and M. Ekmekci, "Physical and Digital Accessibility in Museums in the New Reality," 5th International Symposium on Multidisciplinary Studies and Innovative Technologies (ISMSIT), pp. 404-408, 2021.
- [12] R. Cecilia, "COVID-19 Pandemic: Threat or Opportunity for Blind and Partially Sighted Museum Visitors", Journal of Conservation and Museum Studies, vol. 19(1), pp. 1-8, 2021.
- [13] R. Vaz, D. Freitas, A. Coelho, "Perspectives of Visually Impaired Visitors on Museums: Towards an Integrative and Multisensory Framework to Enhance the Museum Experience", 9th International Conference on Software Development and Technologies for Enhancing Accessibility and Fighting Info-exclusion, pp.17-21, 2020.
- [14] A. Gassiot, R. Camprubí, "Accessibility of Museum Websites: The Case of Barcelona", Chapter in ICT Tools and Applications for Accessible Tourism, IGI Global, 2021.
- [15] TAW online web service. <http://tawdis.net/ingles.html?lang=en>.
- [16] WAVE Accessibility Tool website, <http://wave.webaim.org>.
- [17] Lighthouse, <https://developers.google.com/web/tools/lighthouse>.
- [18] N. Sabev, G. Bogdanova, "Digital and Physical Accessibility of Tourist Places in Bulgaria", Cultural and Historical Heritage: Preservation, Presentation, Digitalization (KIN Journal), vol. 4(2), ISSN 2367-8038, Institute of Mathematics and Informatics – Bulgarian Academy of Sciences, pp. 38–58, 2018.
- [19] N. Sabev, "A Journey in the Dark in the Virtual World", Cultural and Historical Heritage: Preservation, Presentation, Digitalization (KIN Journal), 3(1), ISSN 2367-8038, Institute of Mathematics and Informatics – Bulgarian Academy of Sciences, pp. 193–198, 2017.
- [20] K. Sotirova-Valkova, "FAIR Principles for Digital Repositories: Essence and Applications for Heritage Objects", Cultural and Historical Heritage: Preservation, Presentation, Digitalization (KIN Journal), vol. 6(2), pp. 64-76, 2020.
- [21] R. Lopes, L. Carriço, "On the Gap between Automated and In-Vivo Evaluations of Web Accessibility", Universal Access in Human-Computer Interaction. Applications and Services, 5th International Conference, UAHCI, pp. 735-744, 2009.
- [22] F. Paternò, F. Pulina1, C. Santoro1, H. Gappa, Y. Mohamad, "Requirements for Large Scale Web Accessibility Evaluation", International Conference on Computers Helping People with Special Needs. ICCHP 2020, Lucca, Italy, pp. 275–283, 2020.

Can Ready-to-Use RNNs Generate “Good” Text Training Data?

Jia Hui Feng

Engineering, Computer Mathematical Sciences
Auckland University of Technology
Auckland, New Zealand

Abstract—There is much research on the state-of-the-art techniques for generating training data through neural networks. However, many of these techniques are not easily implemented or available due to factors such as copyright of their research code. Meanwhile, there are other neural network codes currently available that are easily accessible for individuals to generate text data; this paper explores the quality of the text data generated by these ready-to-use neural networks for classification tasks. This paper’s experiment showed that using the text data generated by a default configured RNN to train a classification model can match closely with baseline accuracy.

Keywords—Neural networks; machine learning; text generation; classification; natural language processing; data augmentation; artificial intelligence

I. INTRODUCTION

Training data is crucial for machine learning tasks. In cases where there is little availability of training data due to limited time and resources, it becomes difficult for machines to be able to learn.

In the field of computer vision, there have been successes and benefits from using different methods to generate new training data; this is called data augmentation. This is done by creating new training data based on the original labeled training data. An example of data augmentation in image data is manipulating labeled training data of images through transformations such as rotation and cropping. This generates new training data images for the machine to learn from.

However, in the field of natural language processing (NLP), data augmentation has been a challenging problem as there have been difficulties in establishing universal rules for transformations in textual data while maintaining the quality of the label [1]. For example, the sentence “this is good” is a statement with positive intent, but with a small transformation such as swapping the words to make it “is this good,” it becomes a question with no positive intent; the meaning completely changes. There are also various studies on identifying effective ways to transform labeled textual training [1].

Another technique used to generate more training data is generative augmentation, where more new data is generated compared to switching or cropping images. There has been success in using GAN networks to generate more training data such as images of human faces [2].

Generative models have also been explored in the NLP field with existing language models [1]. There is ongoing research in generative models for both computer vision and NLP. However,

for an individual who is building a machine learning system with classification tasks, these state-of-the-art techniques for generating text data can be quite difficult to implement.

Thus, this paper’s intended purpose is to help individuals who want a “ready-to-use” method to generate more textual training data, by assessing the effectiveness of some of these available methods. The types of individuals that this is focused on are, for example, an entry-level data scientist who is hired in a small team for a machine learning and NLP project, a freelancer who is working on a personal project or a computer science student who is building a chatbot as part of their degree. A common task to implement is labeling data for training machine learning systems, thus classification is the task chosen for this experiment, allowing us to evaluate how “good” the generated training data is based on the accuracy results of the classification model.

There is currently much state-of-the-art research to help generate textual training data. However, much of this is not readily accessible due to copyright protection. Meanwhile, the state-of-the-art research that does have code available online is often complicated and difficult for entry level data scientists or coders to implement.

There are existing deep learning models available, such as TensorFlow [3] that are readily available for programmers to use; these are considered “ready-to-use” in this paper. There have been no studies though on the effectiveness of these neural network codes online. This research aims to perform an exploratory experiment on ready-to-use neural networks and the quality of the generated data.

II. RELATED WORKS

A. Generative Augmentation

Generative models are models that generate textual data; these models are often used in the research field in text generation. They have been explored in the use of data augmentation as they use the newly generated data as additional training data, this helps to increase the diversity of the text which can incorporate new information. Some generative models use pre-trained language models to improve their performance [1].

There are various state-of-the-art techniques, and research has been done on generative models for data augmentation. Although this is not the focus of this paper, most research on generative models in data augmentation shows minor improvements.

Rizos et al. [4] identified that one of the issues of online hate speech classification is not enough relevant training data that can be found online, and training on only a small amount of data will cause overfitting. Thus, they created an RNN that can generate data for online hate speech labeling to combat this issue. Their augmented data has improved 30% in hate speech class recall and 5.7% in macro-F1 score [4]. However, the authors state that further work can be done as the generative model was not the best performing augmentation method. In addition, it is only for short-text, and it is unknown whether the classification would be as effective for non-short text data.

Another technique, G-DAUG, was proposed by Yang et al. [5]. G-DAUG generates synthetic data using pretrained language models and then selects the most informative and diverse set of examples for augmentation. It has been shown to be effective on multiple common-sense reasoning QA setting benchmarks. However, the authors state that more improvements can be made to enhance the quality and diversity of the generated data [5].

Noise generation techniques are commonly used in generative methods as they help to solve the issue of class imbalance [1]; Qiu et al. [6] introduced a variation autoencoder (VAE) based method as a noise generation technique for text generation used in their paper. VAEs are autoencoders which transform input data into a latent representation. In their paper, however, it still only showed marginal improvements in classification tasks.

Generative Adversarial Network (GAN) is also another popular method used for data augmentation in computer vision [1]. There has been research in using GAN models for data augmentation in NLP, such as using the seqGAN architecture [7]. This is just like a GAN model, a generator, and discriminator, but used for textual data and the task of classification. There were, however, only minor improvements [1].

Many of the text generation techniques that have been explored in the research field are not readily available for the public to use. This is due to reasons such as copyright, or their research involves complex algorithms to be implemented in deep learning models, which may be time-consuming for individuals to implement. In addition, a lot of it is not for general use as their research findings are specific to a particular chosen field or topic.

Meanwhile, there has not been in-depth research on the quality of generated words from ready-to-use techniques.

III. EXPERIMENT DESIGN

The experiment was conducted by using benchmark text classification data, AG News [8], then using a CNN built from Python as a classification model to obtain the baseline accuracy rate, then using a ready-to-use RNN [5] to generate synthetic training data. The same CNN model is then used to train and test the original dataset in combination with the new generated training data to evaluate the accuracy of the textual training data.

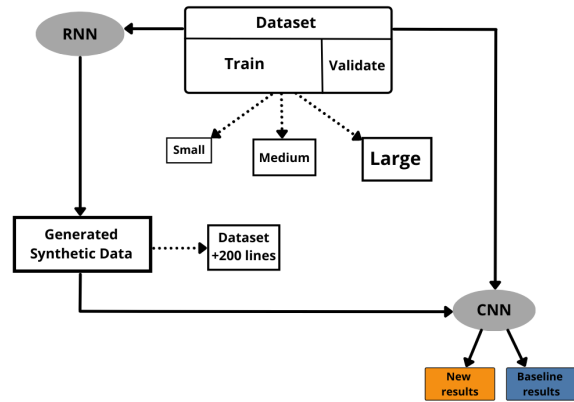


Fig. 1. Experiment Design Process.

As shown in the figure above (Fig. 1), there are three different sized datasets for this experiment. I first got the accuracy of small, medium and large baseline datasets, obtaining three baseline accuracy results. Then I used RNN to generate additional training data for each small, medium and large dataset. I then used the same CNN and tested the accuracy of the original dataset plus the newly generated synthetic training data.

A. Dataset

The dataset used was AG News which consists of four different classes, 1–4, where 1 is world, 2 is sports, 3 is business and 4 is science/technology [8].

- Dataset split ratio: 80% (training) and 20% (validating)
- Each label had an equal number of sentences
- Validating sets had a mixed number of labels

They were split into three different sized datasets:

- Size ratio: Sentences Total = Training/Validating
 - a. **Small:** 50/40/10
 - b. **Medium:** 500/400/100
 - c. **Large:** 1000/800/200

An equal number of labels were in the training sentences. For instance, in the “medium” training dataset of 400, there were 100 (400/4) sentences from each label.

In some real case scenarios, 1,000 sentences of a total dataset split for training and testing may not be considered a “large” dataset, it is though considered “large” respective to this experiment.

The sizes of the dataset were randomly chosen as there is no “common sized” dataset used in the real world. The figure below (Fig. 2) shows the original dataset with labels that were augmented.

1,"ATHENS, Greece - Greek sprinters Kostas Kenteris and Katerina Thanou pulled out of the Athens Games on Wednesday, nearly a week after they missed a drug test and were later hospitalized following a suspicious motorcycle crash. ""I'm withdrawing from the Olympics,"" Kenteris said after meeting with the International Olympic Committee's disciplinary commission..."

4, "The chief scientist at the National Aquarium in Baltimore has launched a review of the dolphin breeding program after the death of a 4-month-old dolphin."

3,"Hewlett-Packard shares fall after disappointing third-quarter profits, while the firm warns the final quarter will also fall short of expectations."

2,"With Scott Williamson bracing for a potentially grim diagnosis of his latest elbow injury, the Red Sox last night appeared poised to move on without him as Curtis Leskanic inched closer to rejoining the club. The Sox initially indicated they would make an announcement last night on Williamson's injury but changed their position during the first winning of the game ..."

Fig. 2. Original Dataset with Label [8].

Each dataset generated 200 lines of new training data. When the CNN is trained on the new training data, it also includes the original dataset. For instance, the small dataset was fed into the RNN model and generated 200 additional lines. This small dataset along with the 200 new additional sentences were fed into the classification model to test accuracy. This was to mimic a real case scenario where someone would use their existing training data in combination with the synthetically generated data. Similar to the choice of the sizes of dataset, generating 200 additional lines was also randomly chosen.

B. RNN

The RNN model chosen was textgenrnn created by Max Woolf [9], it is a Python 3 module that is built on top of Keras/TensorFlow. This model can be configured by the size, layers and whether to use a bidirectional option. This was chosen as it is free, quick to implement and can be easily customized for an individual level.

For this experiment, the RNN model had not been configured or changed, it simply used the default configuration and settings. This was so I could see how good just the default configuration was as some individuals who are in early entry to this field may not know how to do configurations in an RNN but still want to generate text training data.

The default model takes an input that converts each character to a 100-D character embedding vector and feeds into two LSTM layers [9]. The architecture of this RNN is shown in Fig. 3.

C. Text Classification Model

The CNN was built from Python's TensorFlow [3]. The architecture was as follows: input of up to 50 words, 1D convolutional layer of 128 filters of size 5 with ReLU activation function with a softmax output layer. The metrics used to evaluate accuracy were chosen through the TensorFlow CNN's configurations which returns binary accuracy [3].

In addition, GloVe [10] was used to train the 100-dimensional word embedding.

IV. RESULTS AND DISCUSSION

The results shown that for the small dataset the accuracy remains the same as shown in the table, at medium it becomes worse, but at the large dataset the accuracy catches up almost meeting the baseline. A visual comparison of the detailed results can be seen in Fig. 4.

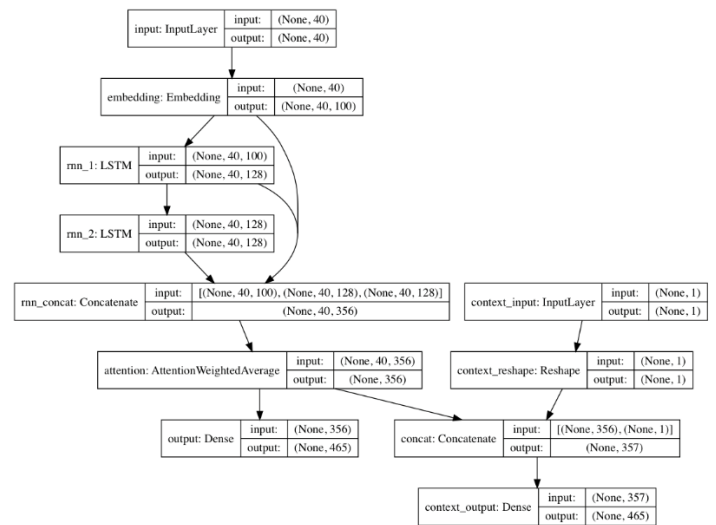


Fig. 3. Textgenrnn Architecture [9].

TABLE I. EXPERIMENT RESULTS

Dataset	Baseline accuracy	New dataset	New dataset accuracy
Small	40%	250/40/10	40%
Medium	70%	700/400/100	60%
Large	73%	1200/800/200	72%

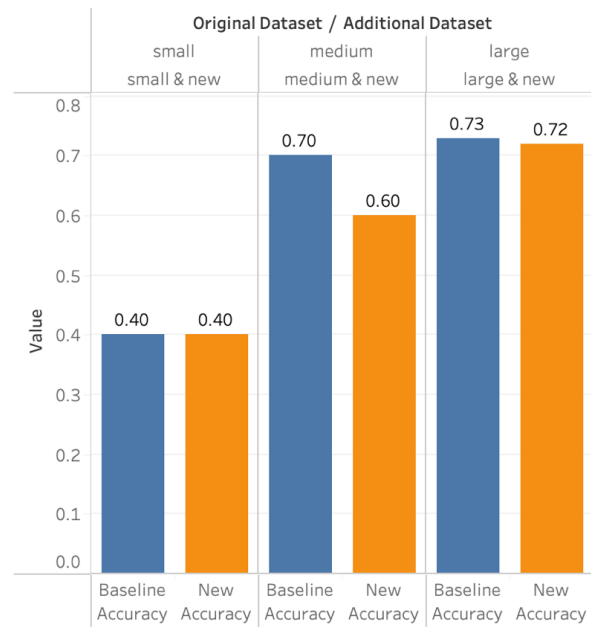


Fig. 4. Accuracy Visualization Comparison.

Southern Sunday hit the Brate Star victory and now skin.

Fig. 5. Label 2 Generated Example.

The results do not show a clear pattern, but it can be concluded (at least with this experiment) that this example

of a ready-to-use RNN of **default configurations** generates text training data that will likely closely match the baseline accuracy.

There was more investigation by looking at the generated text and a sample is given in Fig. 5. This is considered a label 2 which is "sports". At least with this example, it still seems that the generated data is still within the same topic.

In addition, the repository for textgenrnn [9] has made notes regarding the quality of the generated text data. The repository states that "results will vary greatly between datasets" [9] and that the best results are of datasets with at least 2,000–5,000 documents [9]. For smaller datasets, it is recommended to train it longer by setting *num_epochs* higher [5]. In this experiment, *num_epochs* was set at the default value of 1.

For the field of data augmentation in NLP in general, this experiment shows that more questions can be considered for generating text data, such as, "What are the characteristics of words that affect the CNN?" and "Are specific parameters of RNNs better for different types of text data?"

V. CONCLUSIONS AND FUTURE WORK

Although the experiment did not show obvious patterns for different factors in generating text data, it has answered the question the paper posed: Can ready-to-use RNNs generate "good" text data? Based on this experiment and this dataset, if an individual imports and runs this example of ready-to-use RNN with default settings, the classification results will likely match close to the baseline accuracy. With some more tweaks and adjustments, it is likely that the accuracy will improve, but more research can be conducted on the quality of ready-to-use RNNs with adjusted configurations.

Thus, in the future there can be more research conducted to further investigate the quality of the textual data and into not using default configurations – instead investigating through an RNN with adjusted parameters.

In addition, since this experiment only included three different sized datasets, more research can also be done with

more variety to discover more.

REFERENCES

- [1] M. Bayer, M.-A. Kaufhold, and C. Reuter, "A Survey on Data Augmentation for Text Classification," p. 35.
- [2] C. Shorten and T. M. Khoshgoftaar, "A survey on Image Data Augmentation for Deep Learning," *Journal of Big Data*, vol. 6, no. 1, p. 60, Dec. 2019. [Online]. Available: <https://journalofbigdata.springeropen.com/articles/10.1186/s40537-019-0197-0>
- [3] M. Abadi, A. Agarwal, P. Barham, E. Brevdo, Z. Chen, C. Citro, G. S. Corrado, A. Davis, J. Dean, M. Devin, S. Ghemawat, I. Goodfellow, A. Harp, G. Irving, M. Isard, Y. Jia, R. Jozefowicz, L. Kaiser, M. Kudlur, J. Levenberg, D. Mane, R. Monga, S. Moore, D. Murray, C. Olah, M. Schuster, J. Shlens, B. Steiner, I. Sutskever, K. Talwar, P. Tucker, V. Vanhoucke, V. Vasudevan, F. Viegas, O. Vinyals, P. Warden, M. Watteberg, M. Wicke, Y. Yu, and X. Zheng, "TensorFlow: Large-Scale Machine Learning on Heterogeneous Distributed Systems," p. 19.
- [4] G. Rizos, K. Hemker, and B. Schuller, "Augment to Prevent: Short-Text Data Augmentation in Deep Learning for Hate-Speech Classification," in *Proceedings of the 28th ACM International Conference on Information and Knowledge Management*. Beijing China: ACM, Nov. 2019, pp. 991–1000. [Online]. Available: <https://dl.acm.org/doi/10.1145/3357384.3358040>
- [5] Y. Yang, C. Malaviya, J. Fernandez, S. Swayamdipta, R. L. Bras, J.-P. Wang, C. Bhagavatula, Y. Choi, and D. Downey, "Generative Data Augmentation for Commonsense Reasoning," *arXiv:2004.11546 [cs]*, Nov. 2020, arXiv: 2004.11546. [Online]. Available: <http://arxiv.org/abs/2004.11546>
- [6] Y. L. Qiu, H. Zheng, and O. Gevaert, "Genomic data imputation with variational auto-encoders," *GigaScience*, vol. 9, no. 8, p. g1aa082, Aug. 2020. [Online]. Available: <https://academic.oup.com/gigascience/article/doi/10.1093/gigascience/g1aa082/5881619>
- [7] L. Yu, W. Zhang, J. Wang, and Y. Yu, "SeqGAN: Sequence Generative Adversarial Nets with Policy Gradient," *arXiv:1609.05473 [cs]*, Aug. 2017, arXiv: 1609.05473. [Online]. Available: <http://arxiv.org/abs/1609.05473>
- [8] X. Zhang, J. Zhao, and Y. LeCun, "Character-level Convolutional Networks for Text Classification," *arXiv:1509.01626 [cs]*, Apr. 2016, arXiv: 1509.01626. [Online]. Available: <http://arxiv.org/abs/1509.01626>
- [9] M. Woolf, "textgenrnn," 2017. [Online]. Available: <https://github.com/minimaxit/textgenrnn>
- [10] J. Pennington, R. Socher, and C. Manning, "Glove: Global Vectors for Word Representation," in *Proceedings of the 2014 Conference on Empirical Methods in Natural Language Processing (EMNLP)*. Doha, Qatar: Association for Computational Linguistics, 2014, pp. 1532–1543. [Online]. Available: <http://aclweb.org/anthology/D14-1162>

Spectrum Pricing in Cognitive Radio Networks: An Analysis

Reshma C R

Assistant Professor, Department of MCA
Research Scholar, VTU-RC, MCA Dept.
BMS Institute of Technology and Management
Yelahanka, Bengaluru, India

Arun Kumar B. R

Professor, Department of Computer Science & Engineering
Research Supervisor, VTU-RC, Dept. of MCA
BMS Institute of Technology and Management
Yelahanka, Bengaluru, India

Abstract—The wireless technology is applied in developing various applications in different trust areas. Due to this there is a huge demand for the spectrum band. The available spectrum can be shared among the primary users and the secondary users. The spectrum is utilized by the secondary user on rental basis. In this competitive world, the primary users provide a good quality for services to the end users for retaining the spectrum band. The pricing is one of the vital components in Cognitive Radio Networks (CRN) for owning/renting the spectrum. The spectrum is utilized by the secondary users when the spectrum is in idle state. This research work focuses on the spectrum pricing for the secondary users based on the price paid by the primary user. The primary users generate revenue, the same price is utilized for maintenance or annual fees which is to be paid to the governance of telecommunication department. The pricing and trading issues is one of the research areas for allocating the spectrum to the primary users. This research work focuses on providing spectrum to the secondary users with the minimal price for utilization during the specified time. The work highlights the open fact that there is a huge scarcity of the spectrum and the price are high, and not affordable to the individuals. Hence primary users lease/rent out the idle bandwidth for the secondary user. To utilize the spectrum for a dedicated period of time the secondary user has to pay the usage charges to the primary user. In this research work, various methods are presented for determining the price for the secondary users. The pricing components are analyzed by adapting the one-way Anova which compares the values among the groups. The results indicates that all the group means are not same and they are independent variables.

Keywords—Price; game theory; analysis of price; trading; usage

I. INTRODUCTION

The spectrum is one of the important resources for wireless communication. Due to the huge demand, there is a scarcity of spectrum band. These issues are resolved by cognitive radio networks. These radio networks are self-configurable hence these networks are called as intelligent radios. The spectrum hole is detected by using match-filtering method, cyclo-stationery and energy detection method. There are four different challenges in spectrum management:

- Spectrum Sensing: Detect the unused portion of the spectrum.

- Spectrum Decision: Based on internal/external policy allocating the available spectrum.
- Spectrum Sharing: sharing the available spectrum between Primary user (PU) and Secondary user (SU) without overlapping.
- Spectrum Mobility: Hand-off of the signal between the networks.

The spectrum allocation problem is solved by different perspectives such as criteria, approaches, techniques and challenges [1]. The spectrum pricing is one of the major criteria in spectrum utilization. Since individuals cannot purchase the spectrum band, the primary users are responsible of owing the spectrum. The underutilized spectrum or unused spectrum can be reused for various communication purpose by allocating the bandwidth to the secondary users. The primary user (PU) sends the signal status which indicates idle or busy state. If the channel state is idle. The allocation is based on the rental/leased method. The system works based on the sharing of the frequency band between the primary user and the secondary user. To improve the QoS for wireless communication, the economics plays a vital role for setting the charges based on the demand for the purpose of developing wireless technology. The available bandwidth is shared between the PUs and SUs on mutual agreement. The primary user decides to lease/rent some portion of the unused spectrum to the secondary user. This technique is called trading. In trading both users are involved. The spectrum allocation and pricing depend on the bandwidth that are available for bidding. Fig. 1 depicts the trading of spectrum between the PUs and SUs. The spectrum is shared among the primary user and secondary user.

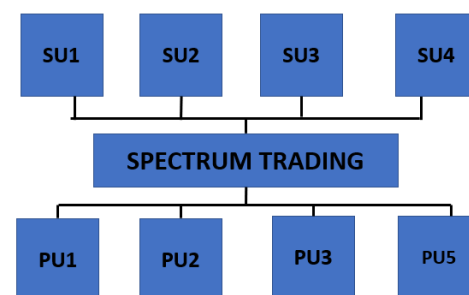


Fig. 1. Spectrum Trading.

The spectrum trading is a mutual agreement between the buyer and the seller. The licensed user needs to renew for the allocated spectrum bandwidth annually. The spectrum regulators or the managers fix the price depending on the services, usages and geographical locations.

II. LITERATURE REVIEW

There are certain parameters which are needed to be considered while utilizing the spectrum as a secondary user. One such parameter is price of the spectrum, owner of the spectrum etc. The researchers have proposed different spectrum allocation and pricing mechanisms. The process of allocation may be dynamic based on Vickery Auction method wherein the revenue is optimized [2]. Two models such as NLMF and NLMB are suggested which results in better pricing and maximum sharing of the spectrum. In NLMF mode the price is decided by the primary user and the values are set as 0 and 1. In NLMB the part of price is transferred to the SU and the primary user will never predominates. In this research, the work results in optimization of pricing when Nash equilibrium is combined with swarm particle [3]. The SU are imposed with the admission fee, the behavior is analyzed in two ways such as optimal and social behavior. The following assumptions are considered:

- The SU doesn't have any information.
- The SU packets are transmitted successfully.
- The cost for SU packet staying in the system is C per unit time.
- Net-benefit is and additional.
- The services are provided based on FCFS [4].

The secondary user can purchase the spectrum from primary user (PU) or through the broker by auction process where it does not include any interaction between PUs and SUs [5]. The two auction mechanisms are proposed first method is based on the received power, i.e., the users are charged based for the received SINR second method the receivers are co-located where the users can use total available bandwidth [6]. The spectrum trading is processed between multiple PU selling to the multiple SUs [7]. The pricing of spectrum was modeled as an evolutionary game and non-cooperative game. The power of the spectrum is one of the essential parameters which is recommended for fixing the price. Later the decision making is carried out for studying the behavioral models by using the utility Theory where rationality assumptions are made between the users [7-8]. There are two models one with monopoly PU market and the other with the multiple PU market. Spectrum trading is one of the efficient ways of using idle spectrum. The spectrum sharing models, spectrum trading form and related problems were discussed [9]. The multiple PUs has an opportunity to sell the spectrum to multiple SUs. The problem was modeled based on the evolutionary game and the competition among the SUs [10]. The quality of channel and maximum power that SU can transmit on the channel depends on the $P_{\min} \leq q \leq P_{\max}$.

The primary spectrum owner can fix the cost of the channel by the equation [11].

$$c(q) = C_0 + T(q) \quad (1)$$

The SU model prefers higher channel capacity, where the channel capacity for SU is given by Shannon-Hartley theorem [12]. Multiple bidders represent their bids for the available capacity of the bandwidth. There are issues in designing auctions i) attracting bidders ii) preventing bidders to control the auctions iii) maximizing the auctioneers revenue. The wireless service providers acquire the spectrum to provide service to the end users. The revenue generated by the end user indicates the true valuation price of the band. Later the true valuation price is used for the governance in forthcoming auctions. Spectrum allocation auctions can be synchronous and asynchronous. In asynchronous whenever the service is requested by the service providers the request can be serviced from coordinated access band (CAB) using pool of resources. In synchronous auction the spectrum bands are allocated/de-allocated in fixed time intervals. The service providers demand their request to the spectrum owner and what they are willing to pay for the allotted spectrum band [13].

III. SPECTRUM ALLOCATION PRICING OBJECTIVES AND PRINCIPLE

It is important to understand the pricing methodology to determine the spectrum price which certainly links with economical and market conditions along with the technological factors. The spectrum manager reviews the fee payment depending on type of use or type of user. This includes some of issues such as fiscal context, relevant principle and objective for certain types of spectrum fee, funding regulatory operations, demand and supply for spectrum and technology change.

A. Principles of Spectrum Pricing

The Spectrum management is important task which includes different activities such as spectrum planning, allocation, licensing, coordinating, sharing regional and global standards. The spectrum management principles reflect economical and behavioral aspects. The list of spectrum allocation pricing principles are as follows:

- 1) Spectrum should be allocated with the highest value.
- 2) Greater access to spectrum will be facilitated with least cost and least restrictive approach.
- 3) Promote regularity and flexibility in spectrum usage.
- 4) Fairness of price to all the licensed holders in the given frequency band.
- 5) The fee calculation should be clear and published as a document for maintain the transparency.
- 6) Administrative cost will be lower if the fee schedule is simpler.
- 7) Spectrum fee are set to take different parameters such as bandwidth, frequency band and coverage area.

B. Objectives

- 1) Spectrum price should promote efficient use of spectrum.
- 2) The cost of spectrum is associated with managing and regulating radio frequency should be covered from those who benefit from spectrum management.

3) Spectrum pricing should facilitate the achievement of government social and cultural activities [14].

IV. GAME THEORY FOR SPECTRUM UTILIZATION

Statement: The price P varies for the secondary users depending on the usage of the spectrum at any instant of time t .

Let su be the set of secondary users such that.

$$su = \{s_1, s_2, s_3, \dots, n\}$$

Let pu be the set of primary users such that.

$$pu = \{p_1, p_2, p_3, \dots, m\}$$

The primary user can offer any opportunistic spectrum to any secondary user when the spectrum is idle. There exists a relationship between the primary user and secondary user which can be represented by using the graph theory. According to Bipartite graph, any secondary user can utilize any primary users available or idle spectrum. Fig. 2 shows the mapping between the PU and SU.

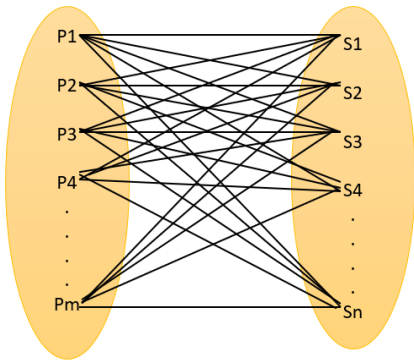


Fig. 2. Bipartite Graph showing the Relationship between PU and SU.

V. STRATEGY FOR PRICE COMPETENCY (SPC)

The available spectrum is identified based on the location Loc further the channel is allocated to the SUs. The status of the channel is obtained by the SUs and later the channel is allotted based on the usage with the time the price is evaluated. The procedure for evaluating the spectrum is calculated as follows:

Procedure for price competency

Step1: Let Loc be the location

P_k - Primary Spectrum

S_k - Secondary Spectrum

Step 2: $S_k \propto Loc$

Step 3: If ($Loc == 0$)

P_k is Available

else

Channel is busy

Step 4: $S_k = Ch$

Step5: Start $t=0$

Step 6: $P = P + \Delta$

Step 7: $Ut = \sum_{i=1}^n S \times L$

Step 8: $P = \frac{\lambda}{Ut}$

The SU searches the available bandwidth with the PU. If loc is found the PU assigns the location with the initial time t . once the process starts the price is evaluated dynamically based on the time where Δ is price variation with the usage time. The utility function (Ut) is evaluated depending on the number of users requesting for spectrum usage and the location. The initial price is set based on the usage of the spectrum.

VI. TWO-STAGE GAMES OF COMPLETE BUT IMPERFECT INFORMATION

The spectrum utilization by the secondary user can be assumed as a dynamic game. According to game theory. Consider p_1 and p_2 as players, A be the set of actions and S be the strategies.

The Gaming between the PU and SU involves the spectrum utilization effectively. The PU displays the channel information to the SU. Depending on the request price set by the PU. The analysis of the game is shown below:

- The player p_1 chooses an action A_1 from the feasible set $fs = \{I, O\}$.
- The player S observe the action A_1 and makes the decision A_2 from $fs_1 = \{I^c, O^c\}$.
- The payoff matrix is prepared by using the actions of each user $U_1\{A_1, A_2\}$ and $U_2\{A_1, A_2\}$.

The decision tree is represented below for the player S and P Fig. 3:

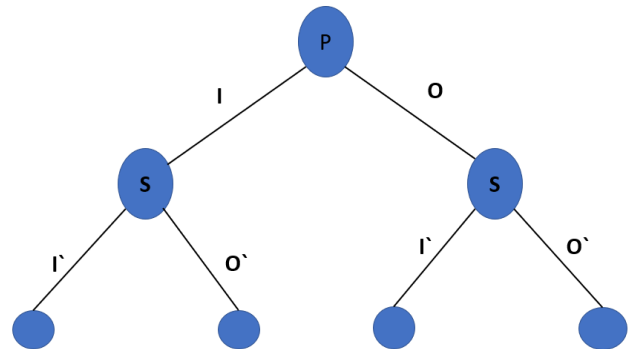


Fig. 3. Decision Tree for Channel Utilization.

The gaming strategy for the user is described below:

Strategy 1: If primary user P plays, I then Play I^c ; If player P plays O then it is denoted by (I^c, I^c)

Strategy 2: If Primary user P play, I then play O^c it is denoted by (I^c, O^c)

Strategy 3: If primary user P play, I then play O^c , if player P plays O , then denoted by (I^c, O^c)

Strategy 4: If player P plays, I then play O^c if player P plays O , then Play O^c denoted by (O^c, O^c)

The payoff matrix can be computed as below where the row represents the player 1 and column represents player 2. According to CR the player1 is PU and player2 is SU. The

strategy is designed between these two players based on the information of the channel state i.e., the channel state is dynamic which takes two different state Idle or Busy represented I and O respectively. The numeric value for the channel states is 1 and 0. The below table represents the payoff matrix for the game:

TABLE I. PAYOFF MATRIX

P2		I^c, I^c	I^c, O^c	O^c, I^c	O^c, O^c
P1					
I		(I, I)	(I, O)	(O, I)	(O, O)
O		(O, O)	(O, I)	(I, O)	(I, I)

Depending on the payoff matrix as shown in Table I, the secondary user makes a decision and then pays the rent to the primary user.

Assumptions:

- The spectral power is constant then the price is fixed which indicates QoS is good.
- The spectral power may vary due to uncertain, in that case the SU pays only for actual service provided.
- During the entire allotted time if the SU is unable to utilize the spectrum, then the price is considered as zero.

VII. EVALUATION OF SPECTRUM BY THE STANDARD ORGANIZATION

The TRAI uses the marginal cost of fund-based lending rate (MCLR) to index value based on the previous auctions. The spectrum evaluation methodologies were proposed by the international telecommunication union (ITU) they are listed below:

- price from previous auctions duly indexed.
- assessing producer surplus.
- production function approach.
- revenue surplus approach.

The other components are telecom index price or the consumer price index (CPI).

Methods for valuation of spectrum.

1) Base Rate: The interest rate can be used by banks or for computation. The base rate is used to calculate the present index value.

2) Weighted Average cost of Capital (WACC): The value of the firm is created based on the rate of returns of WACC. The cost is been invested in different types of shares such as investors of equity, debt, preference share, etc.

3) Cost Inflation Index (CII): The price of inflation rate is matched with the CII. An increase in the prices. The present value of the spectrum is calculated from the past.

4) Produce surplus method: the surplus is calculated when additional spectrum is allocated to an existing TSP. It is calculated as shown (The present value of the expenditure on the network during the next ‘y’ year without additional spectrum of ‘a’ MHz) – (Present value of the expenditure on the network during the next ‘y’ years with additional spectrum of ‘a’ MHz).

5) Production function approach: It is used for the technological relationship between quantities of physical inputs and quantities of output of goods. The production function is determined by the following equation: $X=Ay^\alpha z^\beta$.

x- Dependent variable can be minutes of use/ no. of subscribers.

y- Allocated spectrum.

z- No. of Base transceiver stations deployed by the service providers.

α and β – Percentage of change in minute of use for a percentage change in spectrum and BTS.

6) Revenue Surplus Approach: It is based on the concept of net present value. It estimates the TSP willingness to invest in spectrum based on their projection of potential revenue or surplus over the license period [15].

VIII. ANALYSIS OF SPECTRUM PRICING USING ANOVA

Spectrum pricing is a huge task that are carried out based on the regulations by the government. The pricing is categorized into reserved price, market price and revenue price. The bidder’s pays the reserved price for participating in the bidding auction. The participant will not receive the amount if he does not win the bid. Compared to the bidding price actually the reserve prices are higher. To identify the relationship between market price, reserved price and revenue price statistical method is applied. One-way Anova is applied to find out the relationship and independence among two or more groups. The Anova test is carried out using anaconda with python coding. The data is collected from the secondary source by the author [15]. The below Fig. 4 shows the actual values of the various prices.

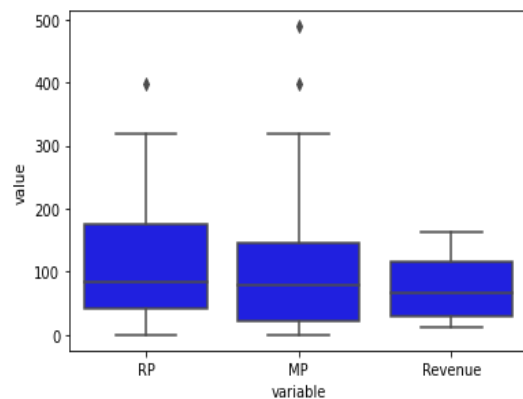


Fig. 4. Boxplot of Various Prices.

The F-value indicates the largest value associated with the independent variable which is real. The $Pr(>F)$ indicates the value which is calculated from the test would have occurred if null hypothesis of no difference among the groups are true. The below Table II shows the F-value and P-value.

Let the null hypothesis H_0 : All means of prices are same and H_1 : All the means of prices are different.

TABLE II. F-VALUE AND P-VALUE

F-value	P-value
1.3467	0.2674

The Table III describes the sum of squares among the groups and the degrees of freedom with the F-value and the P-value.

TABLE III. ANOVA TABLE SUMMARY

	Sum_sq	df	F	Pr(>F)
C(variables)	29995.8987	2	1.3467	0.26748
Residuals	701618.722095	63.0	NaN	NaN

According to the value of $Pr(>F)$ is 0.26748 evidence is small which indicates that all means are not same. The residuals represent the individual observation from the list it can take positive value if the individual observation is greater than the mean value. The residuals are negative if the individual observation is lesser than the mean value. The below Table IV describes the mean squares along with the sum of squares.

TABLE IV. MEAN SQUARE VALUES OF ANOVA TEST

	Mean_sq	Sum_sq	df	F	Pr(>F)
C (variables)	14997.949365	29995.8987	2	1.3467	0.26748
Residuals	11136.805113	701618.722095	63.0	NaN	NaN

Later post hoc test is conducted to verify the null hypothesis, this test is called Tukey's test which is tested for the group after the one-way Anova test. Anova specifies the significance of overall group but Tukey HSD performs on each group means where the means are different. Table V shows the Tukey HSD result.

The residuals are interpreted through the graphs which consists both the positive and negative values.

TABLE V. TUKEY HSD RESULT SUMMARY

	Group 1	Group 2	Diff	Upper	Lower	q-value	p-value
0	RP	MP	0.22	-76.147	76.602	0.010	0.90
1	RP	Revenue	45.3	-31.037	121.71	2.015	0.33
2	MP	Revenue	45.1	-31.265	121.48	2.004	0.33

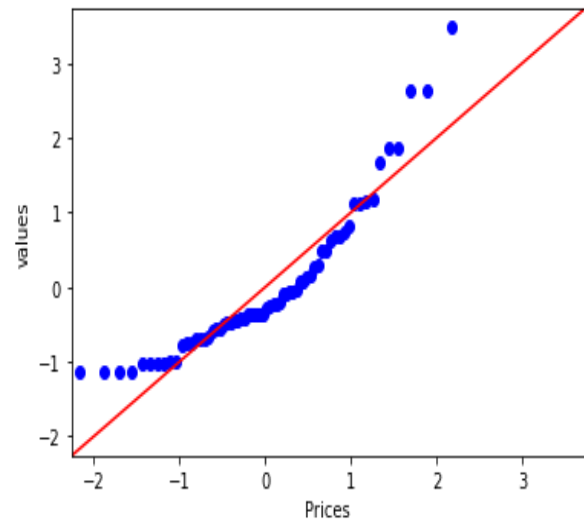


Fig. 5. Q-Q Plot of Residuals.

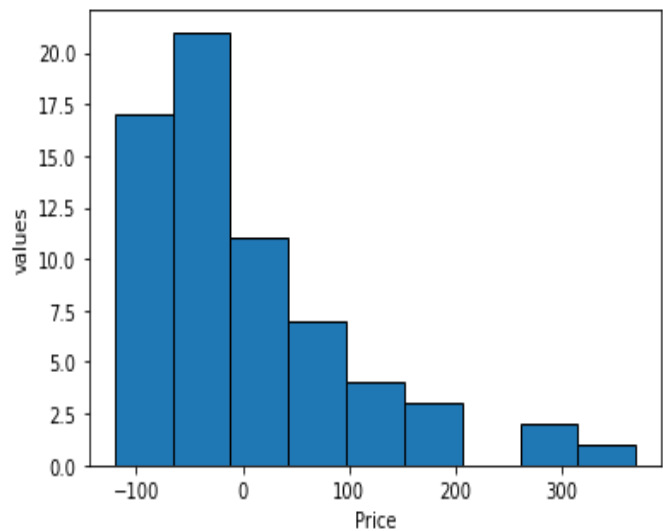


Fig. 6. Hist-Plot of Data.

IX. INFERENCE FROM THE EXPERIMENTAL TEST

The experiment result for analyzing various price components is discussed in this section. Fig. 4 is an actual data value plot which shows the variation of prices in Market Price Reserve Price and Revenue generated. In this the p-value is 0.2678 the null hypothesis is accepted indicating that all three group price values are considered. In post Tukey HSD test, it determines the significance difference between the groups. The results of p-value of Tukey HSD are 0.9, 0.3350 and 0.3386 which indicates there is no significance difference among the groups. Fig. 5 depicts the Q-Q plot of residuals of Anova Test which indicates that the price is non-normally distributed. Fig. 6 depicts the Histogram suggests that the values are normally distributed with extreme values greater than 300.

X. CONCLUSION

In this research work, the strategy for spectrum utilization among the users by applying game theory design mechanism is discussed which provides an incomplete information about spectrum status. The different price components were tested using Anova and later Post Hoc Tukey HSD was conducted to determine that there is no significance difference among the groups and in-between the groups. The residuals indicate that the price components are non-normally distributed and the histogram plot are normally distributed with errors. The future work will focus on minimizing the base rate for bidding the spectrum and maximizing the spectrum utilization with minimal price and time.

REFERENCES

- [1] Elias Z.Tragos , Sherali Zeadally, Alexandros G. Fragkiadakis and Vasilios A. Siris "Spectrum Assignment in Cognitive Radio Networks: A Comprehensive Survey, IEEE Communications Surveys & Tutorials, 2013.
- [2] V. Rodriguez, K Moessner, R. Tafazolli, "Auction Driven Dynamic Spectrum Allocation: Optimal bidding, Pricing and Service priorities for multi-rate, multi-class CDMA, IEEE PIRMC 3,2005.
- [3] Meng-Dung Weng, Bih-Hwang Lee and Jih-Ming Chen "Two-Novel Price-based algorithms for spectrum sharing in Cognitive Radio Networks, EURASIP Journal on Wireless Communications and Networks, 2013.
- [4] Shunfer Jin, Si Chen and Jin ling Zhang "Social Optimization and Pricing policy in cognitive Radio Networks with an Energy saving Strategy, Hindwai Publishing corporation, Mobile Information Systems, volume 2016.
- [5] Fan Wang, Marwan Krunz, shuguang Cui, "Price Based Spectrum Management in Cognitive Radio Networks", IEEE Journal of Selected Topics in Signal Processing Volume 2, Issue 1, 2008.
- [6] J. Huang, R Berry, ML Honig, "Auction Based Spectrum Sharing ACM/Springer Mobile Network Applications, volume 11 issue 3,405-418,2006.
- [7] D Niyato, E Hossain and Z Han, "Dynamic of Multiple-Seller and Multiple-Buyer Spectrum trading in Cognitive Radio Network: A Game theoretic model approach, IEEE transactions, Mobile computation, 2009.
- [8] J. Von Neumann, Q Morgenstern, Theory of Games and Economics Behavior, Princeton, NJ, USA, Princeton University Press 2007.
- [9] M. Osborne, A Rubinstein, "A Course in Game Theory Cambridge", MA MIT: Press 1994.
- [10] D. Niyato, E Hossain, "spectrum Trading in Cognitive Radio Network A Market Equilibrium-based approach", IEEE Wireless Communications, Volume 15, PP 71-80, December 2008.
- [11] D Niyato, E Hossain, Z. Han, "Dynamics of Network Selection in Heterogeneous Wireless Network: An Evolutionary Game Approach, IEEE Transactions on Vehicular Technology, Volume 58, Issue 4, May 2009.
- [12] Lin Gao, Xinbing Wang, Youyun Xu, Qian Zhang, "Spectrum Trading in Cognitive Radio Network Modeling Approach, IEEE Journal on Selected Areas in Communications, Volume 29, Issue 4, April 2011.
- [13] Shamik Sengupta, Mainak Chatterjee, "Designing Auction Mechanism for Dynamic Spectrum Access", Mobile Networks and Applications, Springer, 2008.
- [14] Guidelines for the review of spectrum pricing methodologies and preparations of spectrum fee schedules,ITU.
- [15] Rajat Kathuria, Mansi Kedia, Richa Sekhani, Kaushambi Bagchi, "Evaluating Spectrum Auctions, www.icrier.com, April 2019.

Mobile-based Vaccine Registry to Improve Collection and Completeness of Maternal Immunization Data

Zubeda S. Kilua, Mussa A. Dida, Devotha N. Nyambo
School of Computational and Communication Science and Engineering
The Nelson Mandela African Institution of Science and Technology
Tanzania

Abstract—Immunization during pregnancy and infancy significantly reduces morbidity and mortality of mothers, unborn fetuses, and young infants. Several studies show the merits of getting complete, quality, and accurate data on time to enhance policy and decision-making for society or country development. Despite the efforts by nations to ensure the success of maternal immunization through electronic immunization registries, limited resources such as poor internet access, shortage of electricity, and digital illiteracy in developing countries hinder the goal of full immunization of mothers and infants. Since 2015, immunization programs in Tanzania use internet-based information systems to collect immunization data from health facilities and submit them to the responsible authority for further decision-making such as the allocation of vaccines to health facilities. The internet-based media is not fully achieved in developing countries due to its cost and resource setting, thus, the responsible authority does not receive instant data to update its vaccine inventory and management activities which often results in partial immunization due to the unavailability of vaccines in some facilities. This challenge can be solved by having an affordable system that instantly incorporates and transmits vaccination details such as the utilization of vaccines and demands from each health facility to responsible authority with less resources. The present study proposes a USSD platform to enhance the receipt of real-time data by immunization authorities from both health facilities with poor and good internet connectivity at a lesser cost. A greater number of health facilities in Tanzania prefer to use both online and offline platforms for collecting and recording immunization data. As electronic immunization registry has been introduced in areas with limited resources, it is recommended the use online and offline platforms for data collection so that they can submit immunization data in real-time without the delays caused by poor resource setting.

Keywords—*Maternal immunization; electronic immunization registry; USSD; data collection; limited resource setting*

I. INTRODUCTION

Vaccination is among the most common measures in the world to improve maternal immunity and reduce the morbidity and mortality of babies and women. The reduction or elimination of maternal morbidity and mortality is critical for improving maternal health [1] to achieve the expansion of

health access in middle and low-income countries and attain the Sustainable Development Goals regarding maternal health [2], [3].

According to the World Health Organization (WHO) [4], current statistics indicate that more than 3 million people die worldwide annually from vaccine-preventable diseases such as measles, tetanus, poliomyelitis, and rubella, whereby approximately 50% of these deaths occur among children less than 5 years. Recent reports show that child mortality rates have reduced by 60% from 93 deaths per 1000 live births in 1990 to 38 deaths in 2019 worldwide [5]. However, measles and tetanus are still the leading cause of death to infants and mothers worldwide which can be preventable by vaccines (Fig. 1). The WHO, therefore, recommends that developing countries issue the tetanus vaccine during pregnancy to avoid maternal and neonatal deaths due to low levels of anti-tetanus antibodies [6].

Tanzania has made substantial progress in the area of health [7]. For instance, the life expectancy of its people has improved from 40 years in 1960 to 65 years in 2019 [8]. Similarly, the United States Agency for International Development (USAID) reports [9] show that child mortality has declined rapidly from 49.1 deaths per 1000 live births in 2009 up to 36 deaths per 1000 live births in 2019 [10] after achieving a 75% reduction of unvaccinated children in one year. In 2021, the immunization program in Tanzania ensured that every child got lifesaving vaccines through equal availability and distribution of vaccines in all regions. It further initiated the national immunization strategy to meet the immunization agenda 2030, by ensuring everyone is protected from vaccine-preventable diseases throughout their lives with high quality, effective, efficient, and equitable immunization services; and ensure an effective, efficient, and resilient immunization [11]. The present work is organized as follows: The background to the study is presented in Section II and a description of the developed system is provided in Section III. Sections IV and V provide the methodology and system requirements respectively. Sections VI, VII, and VIII present the results, discussions, and conclusions respectively.

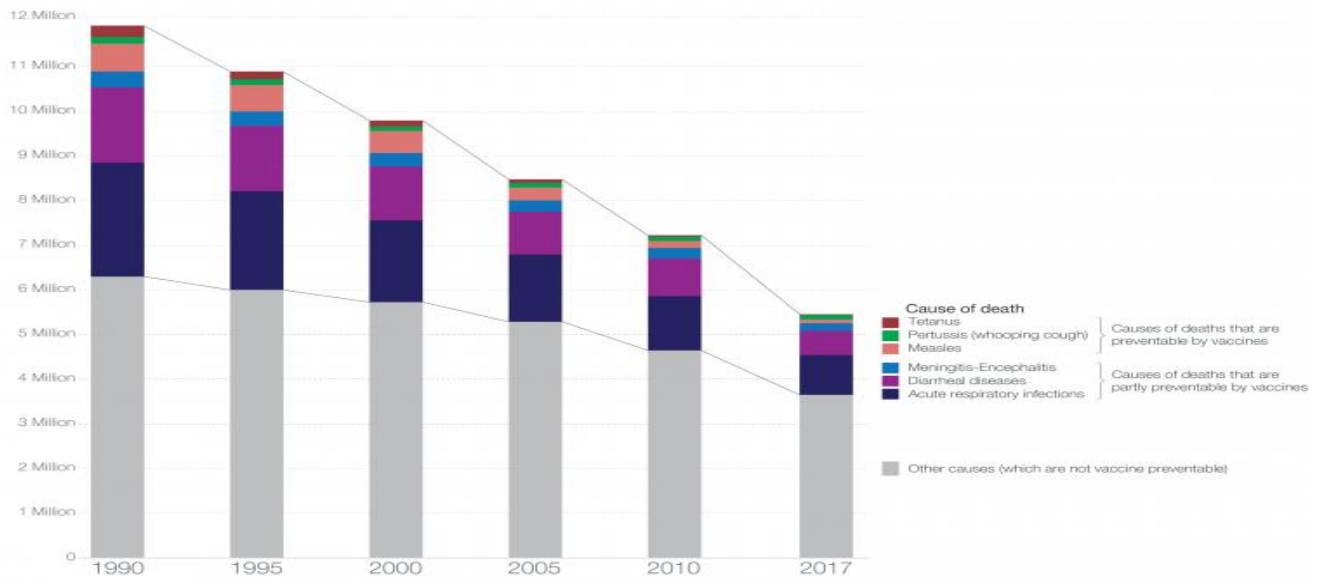


Fig. 1. Child Death due to Vaccine-preventable Disease [12].

II. BACKGROUND

According to Seymour et al. [13], the current immunization management system used for collecting and reporting immunization data in Tanzania is an internet-based platform. However, it is not yet fully achieved in Tanzania because the number of internet users is less compared to the total population. In January 2020, only 14.72 million people in Tanzania (25% of the population) had access to the internet out of a total population of 59,734,218 people [14]. Also reported by [15], another challenge is the rural-urban digital divide in developing countries which leads to poor performance of internet-based systems. Various techniques used to collect immunization data such as Electronic Immunization Register (EIR) and the vaccine immunization management system (VIMS) perform critical routine immunization service delivery by providing better collection, quality, and use of data [13]. The EIR, for instance, aims to improve immunization programs through better information management systems [16]. However, it is necessary to stimulate data collection, quality, and use [17].

The Tanzania immunization management registry (TiMR) which is integrated with a digital supply chain named the electronic immunization registry and logistics management information system (EIR-eLMIS) is used for stock notifications and supply of vaccines into various regions [18]. A model tested to check the impacts of EIR-eLMIS in 2017 provided an estimation of the declining stock-out rates in health facilities. Despite the adoption of eLMIS in health facilities, there still exist barriers such as poor internet connections, lack of electrical power, and digital illiteracy [18]. A second platform that is used to collect immunization data from the district level to the national level in Tanzania is VIMS which combines the existing platforms into single data collection [19]. However, there are various discussions about the poor internet access in

some areas which hinders the installation of VIMS in all health facilities [19]. The introduction of EIR in Zambia and Tanzania has enhanced regular reporting of vaccine stocks-out rates or declines in health facilities and shown that the EIR be built-in system for easy and routine monitoring [20].

The present work focuses on a real-time collection of immunization data using the Unstructured Supplementary Service Data (USSD) technology as an offline network access media because the use of the online-based systems in Tanzania is not yet fully achieved due to barriers like poor internet connections, shortage of electricity and digital illiteracy [18]. The USSD technology is a less-costly asset with better collection and aggregation of data [21], support resource-limited areas [22] as has been used for home-based health workers in South Africa [23], and health data reporting from lower levels to the national level in Uganda [22]. It can also be implemented with all kinds of users, including the illiterate and literate [24]. Other studies have used interactive voice response (IVR) and short message service (SMS) for data collection in information systems. However, the USSD shows more benefits such as providing a user interactive menu with its open-up design space compared to IVR and SMS [25] and is a more secured platform [26].

According to Vasuvedan et al. [27], there is slow-up immunization in sub-Saharan countries including Tanzania, where 72% of mothers reported delayed vaccination, especially in rural areas. Therefore, the USSD technology is proposed in the present study due to the following reasons: i) it works offline as well as online, ii) it works with less cost so can be implemented even in limited-resource setting areas, iii) it is a real-time data collection technique, iv) it can be used with digital illiteracy, and v) it has open up design space to receive more input from clients [21], [25].

III. DESCRIPTION OF THE DEVELOPED SYSTEM

The system which has been developed by this study has four components namely: login module, services menu, stock notifications, and vaccines ordering module. Users of the proposed system include health workers, heads of departments from reproductive and child health (RCH), regional immunization officers, and the regional database administrator. The health workers can access the system by dialing the given USSD code. The network operator submits the query to the USSD gateway which has been embedded with a mobile-based

vaccine registry. Health workers and heads of departments will receive the immunization register for data submission as well as stock details. The regional immunization officer will view data submitted from various health facilities in his/her region and generate a report on the utilization of vaccines and their demand in a particular region. The regional database administrator will be responsible for developing and maintaining the computerized database for his/her region. The conceptual framework of the proposed system is shown in Fig. 2.

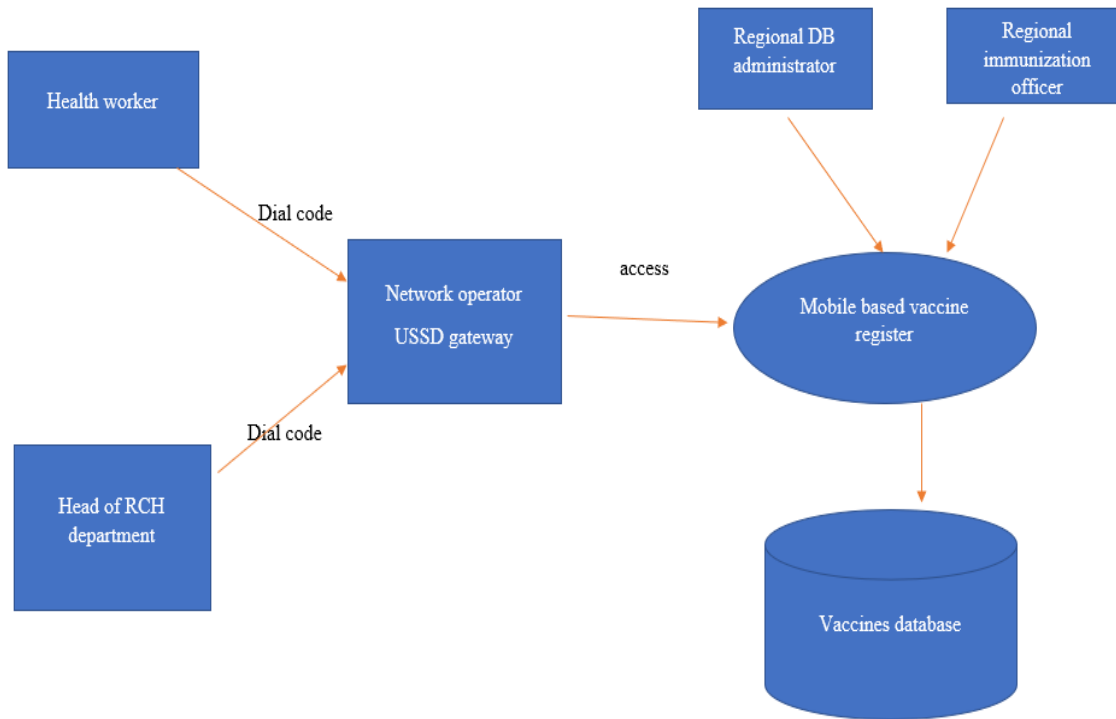


Fig. 2. The Conceptual Framework: Source: Authors.

IV. METHODOLOGY

A. Sampling

The study was conducted at 17 health facilities in Mpwapwa district Dodoma and 8 hospitals in Arusha town. A sample of 75 respondents was selected based on the sampling procedure given in sub-section B. The sample included 25 health officers (one per health facility) from the RCH department for the selected health facilities in Dodoma and Arusha region and 50 women (pregnant women and mothers) from various areas in Tanzania. The selection of the health facilities was based on accessibility to data, time to conduct research, and budget.

B. Sampling Procedure

Random sampling techniques were used to select the subset of health facilities while incorporating the time factor [28]. Snowballing sampling methods were used to select pregnant women and mothers because their total population is not easily accessible [29]. According to Parker et al. [30], snowballing is also a networking technique whereby one participant can help to identify another participant.

C. Data Collection

Based on the nature of the study, in-depth interviews and questionnaires were used as data collection tools. Individual in-depth interviews are used in most healthcare research because they provide a wide room to answer research questions [31]. Well-prepared questionnaires were also used to collect primary data from the health workers and pregnant women. The health workers were asked about the platform they used for collecting immunization data as well as stock management. However, the mothers were asked about their vaccination awareness and availability of vaccination services in the maternal clinic.

D. Data Analysis

The study used the R tool for the statistical computation of the collected data to get them cleaned, analyzed, and presented as shown in Tables III, IV, V, VI, and VII.

V. SYSTEM REQUIREMENTS

A. Functional and Non-Functional Requirements

The functional and non-functional system requirements are shown in Tables I and II, respectively.

TABLE I. FUNCTIONAL REQUIREMENTS

Requirements	Description
System should authenticate users	The system will allow only authorized users to log-in with their credential details such as password and facility number. Password categorize them into their roles whereby the health worker's password will be different from the head of department. After login they will interact with the system to view and submit vaccines details, they will not be able to edit any detail
System should record immunization details and submit to the regional immunization office	When the client attends the clinic, the health worker will issue the vaccines to him/her and after that should record it to the system
System should allow the health worker to view the card history	Every client will have a card number which he/she will get after registering in the clinic. Using the card number, the system should retrieve all vaccines she/he receive before. So that the health worker will be able to know the next required vaccine to issue to the patient
display the available stock	when the health worker issue the vaccines to the patient, the system should be able to deduct the number of vaccines in facility stock and when they require to view the available stock, they have to get exactly the remaining amount
Do ordering of vaccines	The system should allow only the head of RCH department to do ordering of vaccines based on his/her needs. This role will be available only to the head of department after log-ins, because he/she has the approval of ordering vaccines
To check nearby facility which has the available stock of vaccine	The system should be able to display the nearby facility which has the available stock so that can direct the patient to go and get the vaccines. Instead of asking them to come next time. This will help to reduce the number of partially-immunized patients

TABLE II. NON-FUNCTIONAL REQUIREMENTS

Requirements	Description
Availability	The system will be available both online and offline depending on the resources
Maintainability	The system shall be able to integrate with other external platforms such as VIMS, TiMR, EIR-eLMIS To support immunization program
Security	The system will ensure the authentication of users with their password as well as facility number also will ensure authorization, confidentiality, and integrity
Performance	The data submission with responses will be instant because the USSD working with session ID

B. Hardware and Software Requirements to Run System

There are three users of the system, namely, health workers, heads of RCH departments, and regional immunization officers. While the health workers and the heads of departments require any kind of mobile phone, the regional immunization officer requires a computer with the following minimum specification; operating system windows 8, RAM 4 GB, Processor intel icore 5 @ 2.20GHz, Hard disk 500 GB, and internet access.

VI. RESULTS

A. Data Collected for Requirements Gathering

The data were analyzed using the R tool. As shown in Table III, more health facilities have poor internet access and there is a lot of manual work in maternal clinics, such as the recording of data in registers (Table IV) and counting of remaining vaccines to get the stock detail (Table V).

Due to limited-resource settings in health facilities, most immunization data is recorded in paper-based registers.

TABLE III. INTERNET ACCESS IN HEALTH FACILITIES

	Region(s)		Chi-squared test
	Arusha (n, %)	Dodoma (n, %)	
If your answer is Yes there is a need for having a system that incorporates instant vaccination information, which method should be used?			$X^2 = 6.618$, $df = 1$, $p = 0.0101$
With internet	0 (0.0)	9 (100.0)	
Without internet	8 (50.0)	8 (50.0)	

TABLE IV. DATA RECORDING

	Region(s)		Chi-squared test
	Arusha (n, %)	Dodoma (n, %)	
After issuing vaccines to patients, what is done next for the recording information			$X^2 = 16.69$, $df = 2$, $p = 0.00024$
information is entered into the system instantly	7 (87.5)	1 (12.5)	
the information is copied to the paper and later entered into the system	0 (0.0)	2 (100.)	
the information is only recorded on paper	1 (6.7)	14 (939.3)	

TABLE V. COUNTING STOCK

	Region(s)		Chi-squared test
	Arusha (n, %)	Dodoma (n, %)	
As a health worker, how do you know the number of remaining vaccines in stock?			$X^2 = 3.4064$, $df = 1$, $p = 0.06494$
Counting	6 (27.3)	16 (72.7)	
Information systems	3 (75.0)	1 (25.0)	

B. User Requirements

Since health workers face limited resources such as poor internet, electricity, and digital literacy, they recommended a data collection platform that can work both online and offline (Table VI) and feature phones rather than smartphones for data collection (Table VII).

TABLE VI. SUGGESTED PLATFORMS

	Region(s)		Chi-squared test
	Arusha (n, %)	Dodoma (n, %)	
If your answer is Yes there is a need for having a system that incorporates instant vaccination information, which method should be used?			$X^2 = 6.618, df = 1, p = 0.0101$
With internet	0 (0.00)	9 (100.0)	
Without internet	8 (50.0)	8 (50.0)	

TABLE VII. TYPES OF MOBILE PHONES TO BE USED

	Region(s)		Chi-squared test
	Arusha (n, %)	Dodoma (n, %)	
If your answer is Yes for the health worker to use mobile phones, what type of mobile phones should be used?			$X^2 = 9.2437, df = 1, p = 0.0024$
Feature phones	8 (578.1)	6 (42.9)	
Smart phones	0 (0.0)	11 (100.0)	

C. Developed System

1) *User interface:* The system will give the user interface for health workers to access it by dialing a USSD code, but this will only be used by the RCH unit for the submission of immunization data. The health worker will be given a unique code for accessing the immunization registry (Fig. 3) and will log in using their facility number and password for the system to record the immunization details to a particular facility.

The health worker has to select the kind of service to be offered to a patient (Fig. 4A), for example, if the health worker is to issue a vaccine to a mother, she/he will select option 1 so the vaccines menu to be displayed (Fig. 4B). Similarly, if option 2 is selected, the period of children’s vaccines will be displayed as shown in Fig. 4C. After those services, the data has to be submitted to the regional immunization office as shown in Fig. 4D.

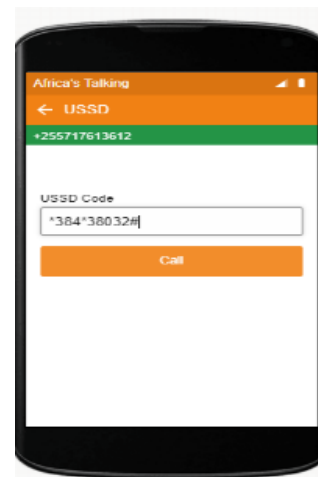


Fig. 3. Dialing USSD Code to Receive the Vaccine Registry.



Fig. 4. A Representation of the user Interface that will be used to Submit Immunization Data. (a): List of Services Available in the Registry, (b): List of Vaccines Issued to Mothers, (c): Periods of Vaccines to Children, (d): Data Submission.

2) *Backend interface:* The system dashboard will be used by the regional immunization officers to view real-time immunization data submitted by various health facilities. The data will be used to measure performance as well as vaccines utilization as shown in Fig. 5 to generate reports.



Fig. 5. System Dashboard.

VII. DISCUSSION

The EIR-eLMIS digital supply chain is used for stock notifications, the supply chain of vaccines into various regions [17]. Some researchers have tested various models to check the impact of EIR-eLMIS in Tanzania, and the findings show that the overall stock-out rate may be reduced from 7.1 to 2.1% monthly through the system compared to the excel-based system of recording health data [17]. Therefore, the use of an electronic immunization registry in the vaccine supply chain plays a major role in the availability of vaccines. However, the adoption of eLMIS in health facilities still faces some barriers such as poor internet connection, lack of electrical power, and digital literacy [17].

After system development and validation, the proposed system showed huge potential of having a platform that is suitable for the exchange of health information for both good and limited internet connectivity [32] by using a non-internet-based system to improve the routine reporting of health data [22]. However, Garner et al. [33] advance the need for affordable mobile phones for the achievements of mHealth in resource-limited areas since the use of smartphones remains limited. The USSD technology ejects the use of SMS in quick information exchanging service because USSD is almost seven times faster than SMS and cost-effective [34]. There is a need for real-time tracking of health data which is why we opted for the USSD [35].

VIII. CONCLUSION

In this study, a system was developed to enhance Tanzania's Ministry of Health and other immunization partners to receive real and accurate data instantly from health facilities from both rural and urban areas, showing the utilization of vaccines in maternal health so that the relevant authority can allocate vaccines based on demand. The use of the USSD platform will enable the remote health facilities which having poor internet access and electricity to submit immunization data instantly to the responsible authority and reduce the use of registers. The developed system may be used by the decision-makers of immunization programs.

ACKNOWLEDGMENT

The authors acknowledge the Ministry of Education, Science and Technology in Tanzania for funding this study as

well as the Nelson Mandela African Institution of Science and Technology for supporting the research.

REFERENCES

- [1] T. Firoz et al., "Measuring maternal health: focus on maternal morbidity," *Bull. World Health Organ*, vol. 91, pp. 794–796, 2013.
- [2] M. E. Kruk, M. Pate, and Z. Mullan, "Introducing the Lancet Global Health Commission on high-quality health systems in the SDG era," *Lancet Glob. Health*, vol. 5, no. 5, pp. e480–e481, 2017.
- [3] C. J. Murray, "Choosing indicators for the health-related SDG targets," *The Lancet*, vol. 386, no. 10001, pp. 1314–1317, 2015.
- [4] WHO, "Vaccines and immunization," 2020. <https://www.who.int/news-room/q-a-detail/vaccines-and-immunization-what-is-vaccination> (accessed Feb. 22, 2021).
- [5] WHO, "Child mortality and cause of death 2019," 2019. <https://www.who.int/data/gho/data/themes/topics/topic-details/GHO/child-mortality-and-causes-of-death>.
- [6] WHO, "Safety of immunization during pregnancy: a review of the evidence," World Health Organization: Global Advisory Committee on Vaccine Safety, Geneva, Switzerland, 2014. Accessed: Feb. 17, 2022. [Online]. Available: https://www.who.int/vaccine_safety/publications/safety_pregnancy_nov2014.pdf.
- [7] H. Afnan-Holmes et al., "Tanzania's countdown to 2015: an analysis of two decades of progress and gaps for reproductive, maternal, newborn, and child health, to inform priorities for post-2015," *Lancet Glob. Health*, vol. 3, no. 7, pp. e396–e409, 2015.
- [8] World Bank, "Life expectancy at birth, total (years) - Tanzania," 2022. <https://data.worldbank.org/indicator/SP.DYN.LE00.IN?end=2019&locations=TZ&start=1960>. (accessed Feb. 17, 2022).
- [9] USAID, "Maternal and Child Health Investments," Immunization in Tanzania, 2021. <https://www.usaid.gov/actingonthecall/stories/tanzania> (accessed Feb. 17, 2022).
- [10] A. O'Neill, "Tanzania: Infant Mortality Rate from 2009 to 2019," Statista, 2022. <https://www.statista.com/statistics/807807/infant-mortality-in-tanzania/> (accessed Feb. 17, 2022).
- [11] WHO, "Vaccines in the Western Pacific," 2021. [Online]. Available: <https://www.who.int/westernpacific/health-topics/vaccines-and-immunization>.
- [12] S. Vanderslott, "How is the world doing in its fight against vaccine preventable diseases? April 24, 2018 April 30, 2020," *Our World in Data*, 2018. <https://ourworldindata.org/vaccine-preventable-diseases> (accessed Feb. 17, 2022).
- [13] D. Seymour et al., "Electronic immunization registries in Tanzania and Zambia: shaping a minimum viable product for scaled solutions," *Front. Public Health*, p. 218, 2019.
- [14] S. Kemp, "Digital 2020: Tanzania," *DataReportal*, 2020. <https://datareportal.com/reports/digital-2020-tanzania> (accessed Feb. 17, 2022).
- [15] B. Furuho and S. Kristiansen, "A rural - urban digital divide? Regional aspects of Internet use in Tanzania," *Electron. J. Inf. Syst. Dev. Ctries.*, vol. 31, no. 1, pp. 1 – 15, 2007.
- [16] O. A. Ekhaguere, C. Kareiva, L. Werner, and B. E. Dixon, "Improving Immunization through Informatics: Perspectives from the BID Initiative Partnership with Tanzania and Zambia," in *Public Health Informatics and Information Systems*, J. Magnuson and B. E. Dixon, Eds. Cham: Springer, 2020, pp. 481–496.
- [17] L. Werner, D. Seymour, C. Puta, and S. Gilbert, "Three waves of data use among health workers: the experience of the Better Immunization Data Initiative in Tanzania and Zambia," *Glob. Health, Sci. Pract.*, vol. 7, no. 3, pp. 447–456, 2019.
- [18] S. S. Gilbert et al., "The impact of an integrated electronic immunization registry and logistics management information system (EIR-eLMIS) on vaccine availability in three regions in Tanzania: A pre-post and time-series analysis," *Vaccine*, vol. 38, no. 3, pp. 562–569, 2020.
- [19] R. Nshunju, M. Ezekiel, P. Njau, and I. Ulomi, "Assessing the Effectiveness of a Web-Based vaccine Information Management System on Immunization-Related Data Functions: An Implementation Research Study in Tanzania," USAID, Maternal and Child Survival Program,

2018. [Online]. Available: https://publications.jsi.com/JSIInternet/Inc/Common/_download_pub.cfm?id=21683&lid=3.
- [20] E. Carnahan et al., "Determinants of facility-level use of electronic immunization registries in Tanzania and Zambia: An observational analysis," *Global Health: Science and Practice*, vol. 8, no. 3, pp. 488–504, 2020.
- [21] M. Zhou, M. Herselman, and A. Coleman, "USSD technology a low cost asset in complementing public health workers' work processes," in *Bioinformatics and Biomedical Engineering*, vol. 9044, F. Ortuño and I. Rojas, Eds. Cham: Springer, 2015, pp. 57–64. [Online]. Available: https://doi.org/10.1007/978-3-319-16480-9_6.
- [22] J. Nakibuuka, A. R. Semwanga, and M. C. Were, "Implementation of USSD technology to improve quality of routinely reported health data in a resource-limited setting," in *Health Informatics Vision: From Data via Information to Knowledge*, vol. 262, J. Mantas, A. Hasman, and P. Gallos, Eds. IOS Press, 2019, pp. 162–165.
- [23] B. Wouters, J. Barjjs, G. Maponya, J. Maritz, and M. Mashiri, "Supporting home based health care in South African rural communities using USSD technology," San Francisco, California, United States of America, Aug. 2009, pp. 1–9. Accessed: Feb. 17, 2022. [Online]. Available: <http://hdl.handle.net/10204/3933>.
- [24] K. Otula Sigar and O. K. Jared, "A Critical Look of USSD Technology Adoption and Benefits," *Int. J. Adv. Res. Comput. Sci.*, vol. 5, no. 1, pp. 27–29, 2014.
- [25] T. Perrier, B. DeRenzi, and R. Anderson, "USSD: The third universal app," in *Proceedings of the 2015 Annual Symposium on Computing for Development*, New York, USA, 2015, pp. 13–21. [Online]. Available: <https://doi.org/10.1145/2830629.2830645>.
- [26] B. W. Nyamtiga, A. Sam, and L. S. Laizer, "Security Perspectives for USSD versus SMS in conducting mobile transactions: A case study of Tanzania," *Int. J. Technol. Enhanc. Emerg. Eng. Res.*, vol. 1, no. 3, pp. 38–43, 2013.
- [27] L. Vasudevan, J. N. Baumgartner, S. Moses, E. Ngadaya, S. G. Mfinanga, and J. Ostermann, "Parental concerns and uptake of childhood vaccines in rural Tanzania—a mixed methods study," *BMC Public Health*, vol. 20, no. 1, pp. 1–11, 2020.
- [28] F. W. Mugo, "Sampling in research," 2002. <http://www.socialresearchmethods.net/tutorial/Mugo/tutorial.htm> (accessed Feb. 18, 2022).
- [29] M. Naderifar, H. Goli, and F. Ghaljaie, "Snowball sampling: A purposeful method of sampling in qualitative research," *Stride. Dev. Med. Educ.*, vol. 14, no. 3, 2017.
- [30] C. Parker, S. Scott, and A. Geddes, *Snowball sampling*. New York, USA: SAGE Publications Limited, 2019. [Online]. Available: <http://dx.doi.org/10.4135/>.
- [31] B. DiCicco - Bloom and B. F. Crabtree, "The qualitative research interview," *Med. Educ.*, vol. 40, no. 4, pp. 314 – 321, 2006.
- [32] O. Yewande, Y. Adekunle, O. Alao, M. Agbaje, and E. Seun, "Development of a Health Information Exchange (HIE) system using the Unstructured Supplementary Service Data (USSD) Technology," *Am. J. Eng. Res.*, vol. 3, no. 26, pp. 1–10, 2020.
- [33] S. L. Garner, T. Sudia, and S. Rachaprolu, "Smart phone accessibility and mHealth use in a limited resource setting," *Int. J. Nurs. Pract.*, vol. 24, no. 1, p. e12609, 2018.
- [34] J. Sangnagouda, "USSD-A Potential Communication Technology that can Ouster SMS Dependency," *Int. J. Res. Rev. in Comput. Sci.*, vol. 2, no. 2, p. 295, 2011.
- [35] A. Dabas and C. Dabas, "Implementation of Real Time Tracking using Unstructured Supplementary Service Data," *World Acad. Sci. Eng. Technol.*, vol. 30, pp. 241–425, 2009.

Personalized Desire2Learn Recommender System based on Collaborative Filtering and Ontology

Walid Qassim Qwaider

Business Administration Dept., College of Administration and Humanities
Mustaqbal University, Qassim. Burydah 51411
Saudi Arabia

Abstract—In this century, attention has grown to recommendation systems (RS), especially in e-learning, to solve the problem of overloading information in e-learning systems. E-learning providers also play a major role in helping learners to find appropriate courses that fit their learning plan using Desire2Learn at Majmaah University. Although recommendation systems generally have a clear advantage in solving problems related to overloading information in various areas of e-business and making accurate recommendations, e-learning recommendation systems still have problems with overloading information about the characteristics of the learning recipient. Such as the appropriate education style, the level of skills provided and the student's level of education. In this paper, we suggest that a recommendation technique combining collaborative filtering and ontology be introduced to recommend courses for learning recipients through Desire2Learn. Ontology involves the integration of the characteristics of the learning recipient into the recommendation process as well as the classifications, while the liquidation process cooperates in the predictions and generates recommendations for e-learning. In addition, ontological knowledge is employed by the educational RS in the early stages if no assessments can be made to mitigate the cold start problem. The results of this study show that the proposed recommendation technique is distinguished and superior to the cooperative liquidation in terms of specialization and accuracy of the recommendation.

Keywords—Collaborative filtering; Desire2Learn; ontology; recommender system (RS); personalized Desire2Learn; PDRS

I. INTRODUCTION

Recommendation systems - enables users and experienced people to benefit from other experts with the same specialization and exchange notes, knowledge, and cooperation among them [9]. Recommendation systems were used to support users' decisions about their choice of information that they benefit from and who face multiple options and do not have the most appropriate option for them. The recommendation system was the solution in helping them to make the most appropriate decision from the available options [1].

In the late twentieth century, the technique of recommendation developed widely on the methods of book recommendation systems such as Amazon.Com and the Coursera recommendation system to address the issues faced by the company when overloading the information [2]. E-learning is also facing the same problems in downloading the

information within Desire2Learn provider systems to solve this problem through the automatic RS for appropriate courses for learners based on the learner's preference for the courses he/she enrolls in the semester and his or her academic record [10]. The RS is important to supporting learners through Desire2Learn providing customized recommendations for student courses and thus achieving the high potential for advanced customization [3].

The specialists in the field of RS are to make recommendations with multiple techniques, but provided that it is with the same area and related to the liquidation of information other than information about the subject matter [11]. Some researchers also said that special recommendation techniques such as collaborative filtration and duration on content could be more effective in some (traditional) cases because they rely on user entities and elements and do not take into account other user information to make additional recommendations [4].

In the Desire2Learn scenario, recipients of education have qualitative characteristics such as the nature of knowledge, the level of educational attainment, and the level of academic advising that affect the recipients of education [12]. Therefore, the traditional recommendation system that combines collaborative filtration and filtering on content cannot provide accurate recommendations to recipients of knowledge because it is not connected with the characteristics of recipients of further education. To provide excellence in specialization and accuracy in Desire2Learn proposals, the Recommendation system should contain the attributes of the recipient [5].

In this paper, we recommend the Desire2Learn recommendation technique to recommend Desire2Learn learning courses by combining collaborative filtering and methodology, with the primary objective being to improve the specialization and accuracy of recommendations. Anthropology is used to integrate the characteristics of the learner such as the nature of culture, the level of educational attainment, and the level of academic advising that affect the recipients of knowledge.

The rest of has been structured as follows: In Section II, we present the Literature survey, Related Work, RS techniques. Section III offers a framework of PDRS, Section IV discusses the Drsire2Learning RS method based on Ontology-CF. Section V Discussion and Result; and Section VI presents the conclusion and future work.

II. LITERATURE SURVEY

A. Previous Related Studies

Most recent studies have focused on recommendation systems by combining recommendation techniques as a way to develop effective, high-impact recommendations. This combination of techniques requires combining at least two techniques to develop performance more effectively. For instance, John et al. 2017, proposed the technique of recommendation, which proposes combining the cooperative liquidation and the ontology to recommend courses and various training courses through the Internet. To integrate the characteristics of learning recipients in the recommendation process with classifications with phytoogy, on the other hand, the filtering feature cooperates in classifying the exact assessment process and generating recommendations. The study showed that the accurate evaluation proposed recommendation progresses in the performance of the cooperative liquidation directly in terms of the allocation and process of evaluation accuracy of the recommendation [6]. Wei et al. describe an approach for technical recommendation containing CF and deep education to alleviate the cold startup problem of renewable elements. The study showed that the technique of the recommendation significantly improved performance and alleviate the problem of cold start [7]. Da Silva et al. used technology to develop that incorporates CF-based recommendation techniques and their integration with genetic algorithms. The results of the study indicate that performance has improved [15]. Saman et al. 2010, describes an approach for an electronic recommendation, whereby the system helps the recipient of the education the ability to research and choose the appropriate educational courses in their field of specialization. This web-based system includes presence language and Web (OWL), which is used to filter the language base as a recommendation method. The modules of the subsystem have an observer, a metafile, education, caches recommendations, and user interface [9]. Ting et al. propose a recommendation technique based on weblog exploration and a two-slide diagram, the conclusion of the study the combination of weblog and graph increases performance and improves recommendation results [14]. Yu 2008 presented Recommendations in Ontology to Promote CF's Social Building Recommendation, the results of the study showed that CF-based community-based recommendation techniques offer better performance than the conventional method [17]. Leyla 2010, presents a system based on a multi-model methodology to infer the educational content of the D2L base in universities. This multi-model acts as a model based on content and another model based on the recipient of knowledge. The oncology model is also used to represent courses through the hierarchy of definitions and sub conceptions. This combination of the learning recipient's epistemology and subgroup and the database used for mixed recommendations provides each of the rearrangements of files retrieved at different weights [13].

Qwaider 2017, The study presented an application on the D2L portal based on the database of the admission and registration system at Majmaah University, where EPERS can help students choose the courses in line with their educational level and the previous requirements for studying the course they wish to study, in this framework the developed D2L rules

related to Registering students with the courses they want to study that meet their needs [2]. This paper discusses the recommendation technique the necessity of Personalized Desire2Learn materials RS Based on CF algorithm and Ontology. Furthermore, there are many several problems for new items forecast with collaborative filtering algorithm and Ontology (CFO) recommendation technique based on issues. Compared with the filtering and ontology (Ontology-CF) and (algorithm-CF).

B. Recommendation Systems Techniques

Recommendation systems - enables users and experienced people to benefit from other experts with the same specialization and exchange notes [6], knowledge and cooperation among them, and it can be determined as any system that produces individual recommendations as a product that has an impact on directing the user in a way that is dedicated to the things of interest or useful purposes in the areas available options. Recommender systems were developed to support Internet users in the decision-making process by selecting information that would be useful to them when faced with situations where they did not have sufficient experience in the available alternatives. Collaborative filtering (F) does not rely on satisfaction analysis by the computer [15].

There are many algorithms used to measure the similarities of users' tastes in the proposed systems, including k-nearest neighbor k-NN and Pearson Correlation, It assumes that users will be similar in their choices as before and with the same amount of love for the same things. There are three major problems faced by the collaborative filtering system: cold start, expansion, scattering in the early stages [7].

In the content-based (CB) approach, Content-based filtering is the filtering method based on the content that describes the product and the user's preferences. Use keywords to describe this product and build a user account to identify the type of product they like [14]. In the knowledge-based (KB) technique, and recommends elements based on the comparison of the satisfaction of the features and the profile of the user's needs and preferences. In the Desire2Learn context. The satisfaction of each component is a set of learning materials constructed by analyzing the satisfaction of the elements that the user may see applied in the recommendation process [8].

Knowledge management is scientifically based because knowledge is categorized and based on predefined Ontology-based recommenders theory in structures or semi-data bases and KB recommender systems bases for use in so-called expert systems, knowledge-based systems, databases, case-building systems, etc. Where the computer uses the rules of reference to answer the questions of the investor, which reduces the problem of cold start, expansion, and scattering. In contrast, a hybrid recommender system approach combines collaborative filtration with content duration and can be more effective in some cases [9].

III. OUR RECOMMENDATION APPROACH FOR DESRS

Fig. 1 shows outlines of the general recommendation of e-learning (DESRS). The model contains the following main components: Student Profile, Learning Object Ontology, Student Database Preprocessing, Recommendation incentive,

(DKM), (LMT), Portal D2L. The following explain recommendation model works:

1) *Student profile*: The student's file contains all the information about the student. This information is obtained from the student, placed in his/her data, and stored. The student file includes the following information (student's name, gender, nationality, age, educational level, and cumulative average). The collaborative filtering recommendation engine has been done to take advantage of this information on student Ontology to make the expected recommendations [16].

2) *Learning object ontology*: Once the student has accepted the course, the next stage, learning resource ontology containing the name of the classes and the information about the educational material, has stored. The class that the student wishes to register for is the content format, such as text, image, etc.

3) *Student database preprocessing*: Database from both the student and learning object ontology and processed in a positive format for the recommendation incentive. The student's primary data processing component and the learning Ontology component.

4) *Recommendation incentive*: After data processing is completed, the drive calculates predictions of the target learner's assessment based on ontology. Finally, the Recommendation incentive creates customized recommendations for the target learner through D2L [14].

5) *Domain knowledge management (DKM)*: The teacher can provide the scientific material through the content icon and upload the classes online through the establishment of LMT.

6) *Learning Material Tree (LMT)*: In the curriculum tree, the name of the course or code where the tree of the curriculum is split into chapters and each chapter is split into study units and then sub-presented in different ways on the Internet such as PPT.

7) *Portal D2L*: The University uses the D2L program in the e-learning department where the teacher uploads the scientific material or training course on the D2L system and also contains the duties and tests, attendance system, absence, forums, meetings, virtual classes, and more.

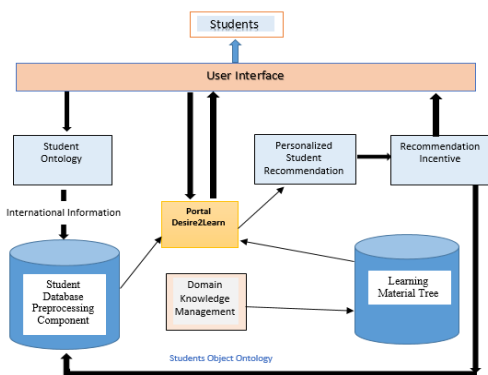


Fig. 1. Ontology-based Recommendation Desire2Learn Model.

The greater the similarity in the matrix the more similar the learning objects (the nearest neighbors). the learning objects are, Prediction based on mathematical models is computed using the k most similar LO (k nearest neighbors) who characterized by the most similar LO I, Using the most similar learning objects in the classification and evaluation process, the following mathematical formula was used:

$$sim(i, j) = \frac{\sum(r_{li} - \bar{r}_l)(r_{lj} - \bar{r}_l)}{\sqrt{\sum(r_{li} - \bar{r}_l)^2} \sqrt{\sum(r_{lj} - \bar{r}_l)^2}} \quad (1)$$

where r_{li} is the rating given to learning object i by learner l , \bar{r}_l is the mean rating of all the ratings provided by l based on ontology knowledge.

$$P_{l,i} = \frac{\sum_{t \in N} (Sim(i,t) \times r_{lt})}{\sum_{t \in N} (Sim(i,t))} \quad (2)$$

A. Recommendation Algorithm

For Fother conceptual recommendations (top r_{li}) for the determined learner based on the ontology and the forecast estimate (2), we use an algorithm (Algorithm 1).

Algorithm 1: Recommendations D2L (I, o, rit)

Input
learning objects of D2L
 $LO = \{i_1, i_2, i_3, \dots, i_n\}$
Ontology
 $O = \{student, LO\}$
Output
Foresee ratings and top N recommendations D2L
Procedure: Generate_Desire2Learn_Path
Method
1: for each, $I \in LO, o \in O$, do
2: Compute ontological likeness $Sim(iq, o, i)$ using (1)
end
3: Compute foresee ratings $P_{1,i}$ using (2)
4: Generate learning top N recommendation for target **Student** [t.

IV. APPLICATIONS AND EVALUATION

The study was conducted at the Majmaah University, MU-CSHSG. Table I presents a course entitled "Management Information Systems" (MIS), which is offered to non-specialized students who come from many other colleges. The number of students participating in the registration of the course 84 students using the electronic learning system D2L to reach them during the process of education for the second semester of the academic year 2018/2019. The D2L system allows students to register for the MIS course from various relevant scientific disciplines. Students have evaluated concerning whether the course is a mandatory requirement or a choice from other academic departments. The recommended system to identify students who study the course as the masters of the subject and students other than the students of specialization according to the MIS curriculum according to the appearance of the personal student obtained through the similarity in classification and ontological knowledge.

The algorithm based on ontology has been evaluated. The participating students were divided into the first group with the specialization and the second group that did not specialize in the course.

TABLE I. MU-CSHSG - MIS

No. of students pertinent	No. of students not pertinent	Total students	No. of ratings
32	52	84	33,124

A. Experimental Results

Two experiments have been used for the same students involved to extract algorithm performance evaluation. The first experiment is a set of CF and Ontology-CF. Experiment number two is algorithm-CF. Moreover, the results have been compared from the two operations.

1) *Accuracy experiments:* The MAE has been used to assess the accuracy of the algorithm in the application of this experiment. Mean absolute error (MAE) can predict accurately used rates, error assessment, and actual and predicted deviations of the proposed algorithms.

The results of the evaluation of the accuracy of the experiment showed that prediction in the Ontology-CF algorithm is more accurate than the conventional Algorithm-CF results. Ontology-CF and algorithm-CF results are more relevant to the number of neighbors (84). Outcomes Ontology-CF were generally superior to Algorithm-CF as illustrated in Fig. 2.

$$MAE = \frac{1}{n} \sum_{i=1}^n |p_i - r_i| \tag{3}$$

2) *Performance measure:* Fig. 3 shows the comparison of algorithms based on Ontology-CF and the Algorithm-CF algorithm. The F1 scale has been used to compare measurement (4).

$$F1 = \frac{2 \times precision \times recall}{precision + recall} \tag{4}$$

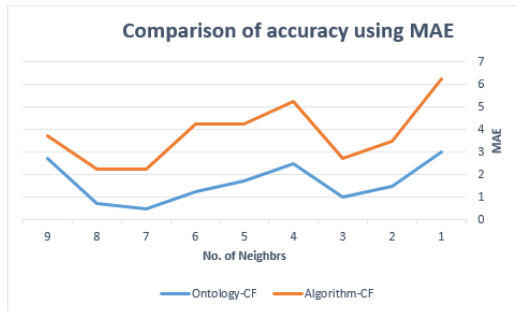


Fig. 2. Accuracy using MAE Measure.

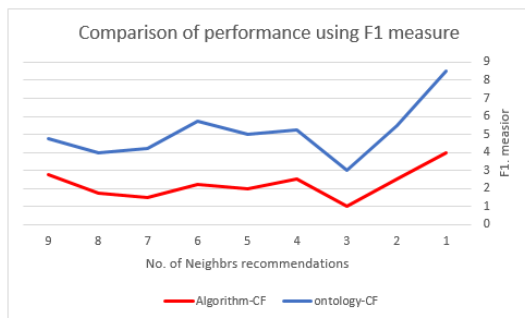


Fig. 3. Performance F1 Measure.

The F1 scale is accurate and recalls one value, which facilitates comparison and gives equal weight. As shown by the figure, Ontology-CF performance achieves the best performance in accuracy and recall from Algorithm-CF.

V. DISCUSSION AND RESULT

To evaluate the performance and accuracy of Ontology-CF compared to the same algorithm CF for the same students, the results of the experiment showed that the prediction of the Ontology-CF algorithm is more accurate than the traditional algorithm-CF results, Ontology-CF, and algorithm-CF are more accurate when the number of neighbors (84). Outcomes Ontology-CF are superior to algorithm-CF on their own. The reason for the superiority of Ontology-CF. One of the most critical advantages of Ontology-CF is generally the integration of student or learner characteristics, such as the nature of education, the level of educational attainment, and the level of academic advising that affect the recipients of training, the recommendation process using the knowledge of the field of ontology. Also, it helps to mitigate the problem of cold start through expansion, scattering the early stages of the Desire2Learn Recommender System in the deprivation of adequate valuation.

Fig. 3 shows the comparison of algorithms based on Ontology-CF and the algorithm-CF algorithm. The F1 scale was used to compare measurement (4). The F1 range is accurate and reminds one value, which facilitates comparison and gives equal weight. As shown by the figure, Ontology-CF performance achieves the best performance in accuracy and recall from Algorithm-CF on its own.

VI. CONCLUSION AND FUTURE WORK

The Desire2Learn recommender system has played an essential role in solving the problems of downloading information that increases educational resources through the Desire2Learn system. It is also possible for recipients of education to find the required educational courses within multiple and broad areas. However, conventional education techniques such as CF and CB continue to challenge by recipients of knowledge in different disciplines such as the nature of education, the level of educational attainment, and the level of academic advising that affect the recipients of education. In this study, the researcher presented a recommendation technique combining cystic fibrosis and ontology to recommend the use of courses in different disciplines for learners through Desire2Learn taking into account the features of the recipients of education. In this technique, no presence is used to integrate the characteristics of the learning recipient into the recommendation process. Results showed that the technology based on Ontology-CF outperformed the traditional performance of the CF algorithm on its own regarding performance and accuracy of prediction in the recommendations system. Also, it helps to mitigate the problem of cold start through expansion, scattering the early stages of the Desire2Learn Recommender System in the deprivation of adequate valuation. For future work, we will incorporate some courses and courses for the recipients of education. By establishing the science of existence using one of the programming languages such as the language Visual Basic (VB) and based on the database and ontology. Taking

into account the factor of time, location, and method of education.

ACKNOWLEDGMENT

The author would like to thank the Deanship of Scientific Research at Mustaqbal University for supporting this work.

REFERENCES

- [1] Anny, Leema.; Zameer, Gulzar. (2020). PCRS: Personalized Course Recommender System Based on Hybrid Approach. 6th International Conference on Smart Computing and Communications, 10.1016/j.procs.2017.12.067, KurukshehraIndia.
- [2] Qwaider, W. Q. (2017). A Personalized e-Learning Portal D2L Recommender System. Journal of Engineering and Applied Sciences, 12(8), 2084-2087.
- [3] Soo, Yeon Jeong; Young, Kuk Kim. (2022). Deep Learning-Based Context-Aware Recommender System Considering Contextual Features. Appl. Sci, 12, 45. <https://doi.org/10.3390/app12010045>.
- [4] Pandey. H.; Singh (2015). V. K, A Fuzzy Logic-based Recommender System for eLearning System with Multi-Agent Framework, International Journal of Computer Applications (0975 – 8887) Volume 122 – No.17.
- [5] Mohamed. K., Yassin, L., Abdelhak, T., Habeeb. S. (2022). A Survey of One Class E-Commerce Recommendation System Techniques, Electronics, 878. [HTTPS:// doi.org/10.3390/electronics11060878](https://doi.org/10.3390/electronics11060878).
- [6] John T., Zhendong N., Bakhti K., (2017). E-Learning RS Based on CF and Ontology, International Journal of Computer and Information Engineering Vol:11.
- [7] J. Wei.; J. He, K. Chen, Y. (2017). CF and deep learning-based RS for cold start items, Expert Syst. Appl., vol. 69.
- [8] Ain, Q. T., Ali, M., Riaz, A. (2017). Sentiment analysis using deep learning techniques: a review. Int J Adv Comput Sci Appl, 8(6), 424.
- [9] Chen, G.; Tan, X.; Guo, B.; Zhu, K.; Liao, P.; Wang, T.; Wang, Q.; Zhang X. SDFCNv2. (2021). SDFCNv2: An Improved FCN Framework for Remote Sensing Images Semantic Segmentation. 4902. <https://doi.org/10.3390/rs13234902>.
- [10] Sikka. R, Dhankhar. (2012). Survey Paper on E-Learning RS, International Journal of Computer Applications (0975 – 888) Volume 47– No.9.
- [11] Wei. S.; Penguin. S.; Peng. L. (2019). Hybrid Recommendation Algorithm Based on Weighted Bipartite Graph and Logistic, <https://www.researchgate.net/publication/335108492>.
- [12] Al-Bashiri, H., Abdulgabber, M. A. (2018). An improved memory-based collaborative filtering method based on the TOPSIS technique. PloS one, 13(10), e0204434.
- [13] Leyla Zhuhadar; Olfa Nasraou. (2009). Multi-model Ontology-based Hybrid RS in E-learning Domain. International Conference on Web Intelligence and Intelligent Agent Technology – Workshops. IEEE/WIC/ACM.
- [14] Ko, H.; Lee, S.; Park, Y. (2022). A Survey of Recommendation Systems: Recommendation Models, Techniques, and Application Fields, Electronics, 141. <https://doi.org/10.3390/electronics11010141>.
- [15] Mohamed, E.; Hassan, M.; Rodina, H.; Saeed., H.; Rehab. I. (2022). An evolutionary approach for combining results of RS techniques based on CF,” Information Sciences, <https://doi.org/10.1016/j.ins.2022.01.026>.
- [16] Nur. W.; Ridi. F; Sri S.Kusumawardani. (2022). A systematic review of ontology use in E-Learning recommender system, Computer and Education: Artificial Intelligence 3, 100047.
- [17] Baichuan Liu; Qingtao Zeng; Likun Lu; Yeli Li; Fucheng You. (2020). A survey of recommendation systems based on deep learning, Journal of Physics: Conference Series, doi:10.1088/1742-6596/1754/1/012148.

Design Level Class Decomposition using the Threshold-based Hierarchical Agglomerative Clustering

Bayu Priyambadha¹, Tetsuro Katayama²

Interdisciplinary Graduate School of Agriculture and Engineering, University of Miyazaki, Miyazaki, Japan^{1,2}
Faculty of Computer Science, Universitas Brawijaya, Malang, Jawa Timur, Indonesia¹

Abstract—Refactoring activity is essential to maintain the quality of a software's internal structure. It decays as the impact of software changes and evolution. Class decomposition is one of the refactoring processes in maintaining internal quality. Mostly, the refactoring process is done at the level of source code. Shifting from source code level to design level is necessary as a quick step to refactoring and close to the requirement. The design artifact has a higher abstraction level than the source code and has limited information. The challenge is to define new metrics needed in class decomposition using the design artifact's information. Syntactic and semantic information from the design artifact provides valuable data for the decomposition process. Class decomposition can be done at the level of design artifact (class diagram) using syntactic and semantic information. The dynamic threshold-based Hierarchical Agglomerative Clustering produces a more specific cluster that is considered to produce a single responsibility class.

Keywords—Refactoring; design level refactoring; software refactoring; hierarchical clustering; class decomposition

I. INTRODUCTION

Refactoring alters software's internal structure without changing the external behavior [1]. The primary purpose of the refactoring process is to preserve the quality of internal structure as the impact of change implementation in the evolution cycle of software. The quality of software's internal structure may decay during evolution. Many research and tools exist to expose the mostly get the structural decay as an impact of the software evolution [2]. The reduced quality of software's internal structure impacts the next changes. Decreasing the internal structure also decreases the maintainability of software and increases the effort of the next changes [3], [4]. Therefore, refactoring is recommended to solve the structural decay and to avoid the high cost that the developer must pay during the software changes process.

There are many options for refactoring the software artifact. Researchers already report and give guidance to refactoring based on the specific smells. One of the refactoring activities is the extract class. The class can be fat of functionality as an impact of the changes. The extract class decomposes the class due to class growth as changes happened during the evolution. According to the guidelines, the class must handle clear responsibility or function. Therefore, the extract class helps to maintain the class stay in clear functionality. Many research reports the methodology for class decomposition at the source

code level [5]–[14]. Mostly was done by using the clustering of the class elements based on various points of view and done at the source code level.

Hamdi et al. proposed the class decomposition methodology and named it Threshold-driven Class Decomposition based on the Agglomerative Hierarchical Clustering (AHC) algorithm [11]. The class decomposition uses several metrics that can only be easily calculated at the source code level. For example, direct and indirect call dependency, internal and external call dependency, and attribute sharing. The main result in the research of Hamdi is applying the threshold to HAC to determine the termination point in the process of decomposition. The result of Hamdi's algorithm sounds more promising in the case of termination state than the other approach.

Now-a-days, researchers have changed the refactoring object and shifted it to the design level. Shift to the design is considered necessary due to the easiness of model transformation. Model as an object of transformation is like a bridge between software artifacts (act integrally). It is bridging between the requirement and the implementation artifact. The model refinement is close to the requirement and implementation artifact. It will have an impact on both sides. It can also be used for software evolution and implementation in code. Vertical and horizontal model transformations are both possible. Vertical transformations are used when the source and target models have different levels of abstraction. On the other side, a horizontal transformation occurs when the source and target models have the same abstraction. The source model transformation does not impact the target model's behavior [15].

The class diagram is one of the design or model artifacts. The class diagram is more abstract than the source code. According to the limited information, working with the higher model level has a big challenge. The lower level of abstraction of the model has more detailed information than the higher level of the model. The similarity metric was used to do decomposition using Hamdi's approach. The metric is calculated based on the information in the source code. Using Hamdi's metric is difficult if the experiment's object is changed to the class diagram. The similarity value between elements is the mandatory requirement for clustering or decomposing using a hierarchical clustering algorithm. Shifting the experiment's object to the class diagram gives the

consequences to define the new similarity metric based on the information from the class diagram. One outcome of this research is determining the new similarity metrics calculated using all of the data or information from the class diagram. The metrics have a function to measure the distance between elements. In the case of class, it is not only the methods but also the attributes. The similarity metrics are considered the class's syntactic and semantic information in the class diagram. Besides shifting the experiment's object, the decomposition process only focused on the Blob class in the class diagram.

The rest of the paper is organized as follows. Section 2 summarizes the state of the arts of class decomposition approach. Section 3 describes the class usability and compactness of the class in the decomposition process. Sections 4 and 5 explain the proposed algorithm and the research scenarios. Section 6 describes the result and discussion. Then the last is the conclusion and future work in Section 7.

II. RELATED WORK

Several researchers are researching class decomposition as the refactoring activity. The class decomposition is used to maintain the class stay in the clear functionality. The development of research on class decomposition is as follows.

A Two-Step Technique for Extract Class Refactoring by Bavota et al. told about the extract class's approach based on the responsibility [5]. The object study is source code. This experiment considers the structural and semantic information inner the class. Specifically, this uses the metrics to measure the structural and semantic similarity. The metrics are Structural Similarity between Methods (SSM), Call-based Interaction between Methods (CIM), and Conceptual Similarity between Methods (CSM). The chains extraction (The Transitive Closure), as the proposed approach, is obtained by computing the transitive closure of the method-by-method matrix. The value of the matrix is calculated based on the combination of three metrics. Then, the approach is used to extract the class using the threshold minCohesion and minLength . minCohesion is the similarity value between methods, and minLength is the minimum chain length in the graph. By using both thresholds, the class is split into several classes.

The following paper from Bavota et al. discussed the identification of extract class refactoring opportunities using structural and semantic cohesion metrics [6]. In Bavota's refactoring process, the class partition process uses the MaxFlow-MinCut algorithm. Bavota implemented the algorithm as follows. In particular, let c be the class to be refactored and $M(c) = \{m_1, m_2, \dots, m_n\}$ be the set of its methods (including the constructor and static methods). The first main process in this approach is defining the graph showing the relationships between methods. The complete graph is defined as G_M . A set of weighted edges connects all the class's pairs of methods. The weight of each edge is represented by the value of the relatedness rate of a pair of methods. The weight of edges is computed by considering the Structural Similarity between Methods (SSM), Call-based Dependence between Methods (CDM), and Conceptual Similarity between Methods (CSM). Once the graph is

computed (weighted), a MaxFlow-MinCut algorithm is used to obtain a partition of the original class.

The next paper of Bavota et al. discussed the usefulness of using class structural and semantic information to extract class [7]. The structural and semantic are measured using SSM, CDM, and CSM. The final conclusion is that using a combination of structural and semantic information is worth doing extract class. This paper also said that the transitive closure approach is better than the MaxFlow-MinCut approach. Also, Bavota compares the transitive closure with the other approach, for example, Fokaefs et al., that uses a hierarchical clustering to extract class refactoring [10]. The transitive closure can split a Blob class into more than two classes, overcoming the MaxFlow-MinCut approach. And, it can automatically define the number of classes that should be extracted from a Blob class.

Isong Bassey et al. talk about the metric-based refactoring opportunities identification (ROI) for object-oriented software systems [14]. They carried out a comprehensive analysis on sixteen (16) primary studies to identify the state of the practice in ROI. This paper is summarized all refactoring opportunities that already existed before 2016. They separated analysis into three groups: the structural, the semantic, and the structural and semantic. This paper focuses on the source of information that can be used to identify the refactoring opportunities using the matrices. This paper summarized several research experiments, such as Al Dallal for the structural approach, Bavota and Al Dallal for the structural and semantic approach already published in several papers. All papers use a metric-based analysis approach. The same review is also already done by Al Dallal [16].

Wang Ying et al. talk about automatic software refactoring using weighted clustering [12]. This paper focuses on class-level refactoring. They consider the dependency relation between methods (as nodes) described as a network. Three matrices explain the relationships between methods, (i) attribute sharing (Sharing Attribute Weight/ SAW), (ii) method invocation (Method Invocation Weight/ MIW), and (iii) functional coupling (Functional Coupling Weight/ FCW). Not only the tree matrices but also Semantic Similarity Weight (SSW) is used to calculate the weight of the edge. The most beneficial cluster with the specific weight is chosen as the solution. The result is compared with the experiment conducted by Bavota and Fokaefs. Wang only compares the algorithm with Bavota and Fokaefs in terms of the effectiveness of clustering. Wang's approach can resolve cohesion and coupling problems without changing the code's external behavior. And, it can help to improve the understandability, flexibility, reusability, and maintainability of code.

Mohammed Hamdi talks about the class decomposition method using the Hierarchical Agglomerative Clustering (HAC) [11]. The decomposition is iterative until classes have a single responsibility. The main problem is considering the difficulty of terminating the decomposition process. This paper defines the notion of threshold to determine the termination point in the decomposition process. This paper explains that class responsibility is identified using method similarity based on internal and external class relationships. There are six

matrices, Internal Attribute Sharing (IAS), Internal Direct Call dependency (IDC), Internal Indirect Call dependency (IIC), Internal Method Sharing (IMS), External Indirect Call dependency (EIC), and External Call Dependency (ECD). By using the weighted AHC, the result is considered better. This approach looked like solving the problems of limitation of a number of resulting classes and the termination state of the decomposition process. The research conducted by Hamdi is the latest research that raises the problems in previous research.

III. SYNTACTIC AND SEMANTIC METRICS

Shifting to the design artifact, especially the class diagram, brings out the new challenge of defining new metrics. The metrics are used to calculate the similarity score between the class's elements (attribute and method) used in the decomposition process. The metrics are calculated based on the information in the class diagram. There are two approaches to define the similarity rate between class elements: syntactic and semantic analysis. It means that the two approaches measure the similarity score using the similarity of syntax and meaning.

The class diagram is one artifact that shows the relation of objects in the software system. It shows the inner structure of every class and the relation between them. When reading the class diagram, we got pure in the model level consisting of text and notation. It is not easy to collect information based on the image of the class diagram. However, by converting it into the XML file, all the information of the class diagram is easier to collect. [17], [18]. Extracting the information from the XML file uses the text-based extraction method. Therefore, syntactic and semantic analysis is appropriate to calculate the similarity metric from the XML class diagram.

A. The Type References Similarity (Syntactic)

Syntactic analysis means the analysis based on the actual syntax that lies on the class diagram. This approach is inspired by Al Dallal et al. [19] in their proposed cohesion metrics. In this approach, the class elements are considered a relationship if they have the same type. The type similarity is based on the type of attributes and methods (references variable or return value). The value will be 0 or 1. 0 means there is no relation, and one, there is a relation between method and attribute.

$$syn = \begin{cases} 1, & \text{similar type} > 0 \\ 0, & \text{similar type} \leq 0 \end{cases} \quad (1)$$

All the attribute and method data types are collected and then mapped into the relation matrix between them in every class.

B. The Meaning Similarity (Semantic) of the Label

Semantic analysis is the meaning analysis between attribute and method. This analysis considers the meaning of every label in the class (related to the class elements)—for example, the name of a method, attribute, and method's parameters. The label names are split into some words to make it easier to get the meaning. The semantic similarity is calculated based on the closest meaning between words with a value between 0 and 1. The higher value means the close of meaning. Semantic similarity can be calculated using the following formula.

$$sem = \frac{2.w_i.|w_1 \cap w_2| + w_s.(|s(w_1, w_2)| + |s(w_2, w_1)|)}{|w_1| + |w_2|} \quad (2)$$

Previously, the formula was used to calculate the semantic similarity between process names by Dijkman et al. [19]. From that formula, w_1 and w_2 are the word collections from every compared label. The words are extracted from the attributes or methods labels. The Dijkman's formula is considered appropriate to use in the case of class element's label. For an example of the splitting process, there is a label named "transcriptType." Then the "transcriptType" is split into "transcript" and "Type." Sometimes, the label of attributes or methods is written without using capital characters as a beginning of words. If not possible to split appropriately, then the splitting process is done by comparing the longest fragment of a word with the dictionary. If it exists in the dictionary, then it will be separated from the label. $s(w_1, w_2)$ or $s(w_2, w_1)$ is the number of words that have a synonym relationship between two labels. The synonymity of words is based on the calculation of relatedness by considering the depths of two words in the WordNet taxonomy (Wu-Palmer) [20]. A couple of words above 0.5 is considered a synonym. w_i and w_s are the weight that is defined for a similar word and the word that has semantic similarities (synonym). Dijkman defines the value of $w_i = 1$ and $w_s = 0.75$ [19].

C. Elements Similarity Metric

The element similarity metric is the combination of both syntactic and semantic metrics. The formula to calculate the similarity between method and attribute is described as follows. syn and sem are syntactic and semantic similarity scores respectively. Then, $e1$ and $e2$ are elements in the class. It can be the attributes or methods of the class. The whole formula for the element similarity metric is described as follows.

$$Sim(e1, e2) = \frac{syn + sem}{2} \quad (3)$$

This formula is used to define the similarity matrix that will be an input to the algorithm for decomposing the class.

IV. THRESHOLD-BASED AGGLOMERATIVE HIERARCHICAL CLUSTERING ALGORITHM

Threshold-based agglomerative hierarchical clustering is divided into static threshold and dynamic threshold hierarchical clustering. The difference between static and dynamic is the definition of the threshold. The static approach defines the threshold value at the beginning of the decomposition process. It is done only one time. The dynamic approach calculates the threshold in every cycle of the decomposition process. The threshold is adjusted based on the matrix changes in every step [11]. This research uses Hamdi's algorithm but is implemented at the design level. The similarity matrix considers syntactic and semantic aspects of the element's label. The decomposition is based on the similarity matrix composed using the formula (3) value. Later, the similarity matrix is used to compose the dissimilarity matrix to validate the decomposition result. Fig. 1. shows the dynamic threshold for threshold-based agglomerative hierarchical clustering. The static and dynamic threshold differences are located at the calculated threshold process. The calculation threshold is done once in the static approach and done in every process cycle in the dynamic approach. The process is run recursively and implemented in the prototype application.

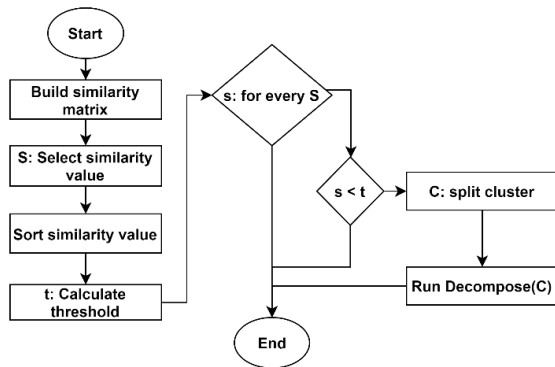


Fig. 1. Dynamic Threshold-based Agglomerative Hierarchical Clustering [11].

V. RESEARCH SCENARIOS

This chapter explains the scenarios of the experiment using new metrics from the class diagram and implements it using the threshold-based AHC by Hamdi. The scenario explains the dataset, tools, and validation process.

This experiment focuses on shifting from the source code to the design level. The proposed metric is implemented using two cases. First is the same case as Hamdi's paper (Transcript class), then called case 1. The Transcript class is regenerated as a class diagram using the Visual Paradigm and converted into XML files. It has been modified at the data type of the parameters variable using the types often used for those variables. The class Transcript is described as Fig. 2.

Second is the other case based on the smell dataset from the Landfill dataset [21]. Case 2 is the MDIApplication that is taken from the jHotDraw application. The MDIApplication is considered as Blob class based on the Landfill dataset. The MDIApplication is shown in the following Fig. 3.

The threshold-based agglomerative hierarchical clustering algorithm proposed by Hamdi et al. is implemented into the prototype application. This application is considered important due to the time of the calculation process. Also, the prototype application is built for the accuracy of the calculation. It also implements the tree-based keyword search algorithm useful for information collected over the XML class diagram [17]. The calculation of similarity meaning between words (semantic) is using the WordNet library for Java to support the semantic score between labels using formula (2).

The class diagram from the example cases (Fig. 2 and Fig. 3) is converted into an XML file then extracted using the prototype application. Then, the prototype application will automatically generate the similarity matrix based on the formula (3). Table I shows the value of similarity between elements (attributes and methods) of the Transcript class. Before that, the labels of every element are named using the prefix "a" for attribute, and "m" is for a method then followed by a number as elements index. Finally, the decomposition process is done using the threshold-based AHC (both static and dynamic). And the result of the experiment will be compared with the result of class decomposition at the source code level. Table II shows Hamdi's similarity matrix of the Transcript class.

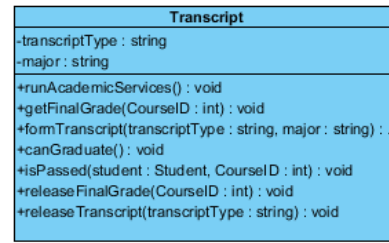


Fig. 2. Transcript Class.

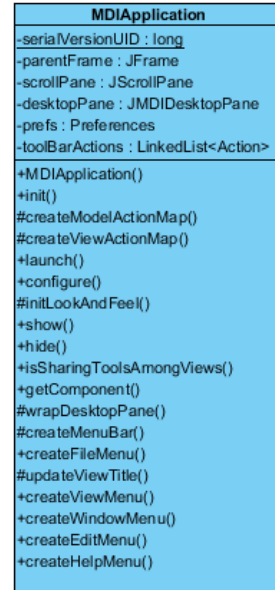


Fig. 3. MDIApplication Class from the jHotDraw.

TABLE I. THE SIMILARITY MATRIX OF TRANSCRIPT CLASS (DESIGN LEVEL)

	a1	a2	m1	m2	m3	m4	m5	m6	m7
a1		0.59	0.15	0.23	0.65	0.28	0.16	0.28	0.93
a2			0.15	0.09	0.58	0.19	0.05	0.14	0.65
m1				0.92	0.63	0.73	0.73	0.92	0.75
m2					0.71	0.78	1.00	1.00	0.88
m3						0.65	0.59	0.71	0.79
m4							0.71	0.83	0.80
m5								1.00	0.73
m6									0.94
m7									

TABLE II. THE SIMILARITY MATRIX OF TRANSCRIPT CLASS (PREVIOUS APPROACH) [11]

	m4	m5	m6	m7	m8	m9	m10
m4		0.25	0.33	0.25	0.25	0.32	0.25
m5			0.18	0.18	0.18	0.19	0.18
m6				0.08	0.08	0.26	0.2
m7					0.22	0.12	0.05
m8						0.05	0.05
m9							0.19
m10							

The validation uses two approaches. The first approach is by comparing the compactness rate using the Silhouettes index of cluster result. And the second approach is the conformance rate between the source code and the class diagram level's result. The compactness rate of every cluster resulting from the decomposition process will calculate using the Silhouettes index. Silhouettes index is the method that can be used to validate the consistency data in the cluster [22]. Then, the deep analysis of the result according to the applicability of the class is also considered important.

VI. RESULT AND DISCUSSION

A. Result of Experiment

The two metrics (*syn* and *sem*) are used to calculate the similarity between class elements then the similarity matrix is composed for every case. Finally, the similarity matrix from the two cases is used for the decomposition process using the prototype application. Case 1 is the decomposition process using class Transcript at the design level. The result of decomposition is differentiated based on the approach (static and dynamic threshold). First, the static threshold decomposition result is shown in Table III. Then, the result of the dynamic decomposition is shown in Table IV.

Table III shows the result of the decomposition process using the static threshold. It also shows the result of the Silhouettes index for every element inner the cluster. There are two clusters resulting from the static threshold decomposition process. The average of the Silhouettes index for all elements is 0.24.

Table IV shows the result of decomposition using the dynamic threshold. It is shown that the number of clusters resulting from the decomposition process is four clusters. Every element in the clusters has the Silhouettes index score that expresses the validity of the position of current elements in the specific cluster. If the score is close to 1, it is considered in the better cluster. Otherwise, it is considered the worse cluster. The average of Silhouettes from all elements is 0.35 using the dynamic threshold decomposition process.

Case 2 is taken from the jHotDraw application. The class MDIApplication will be decomposed due to the Blob indicators that are shown in the Landfill dataset. Same with the first case, the second case also threatened using the same experiment. The result of the static threshold decomposition is described in the following Table V.

There are two clusters resulting from the static threshold decomposition process. Every cluster represented the class after decomposition. Every element of the class has a Silhouettes index score representing the specific cluster's validity position. Many elements have negative of Silhouettes index. The average of Silhouettes for all elements is 0.08.

The dynamic decomposition result using case number two is described in Table VI. There are 12 clusters, and every element of each cluster is calculated. There are also many negative Silhouettes scores. The average Silhouettes of all elements is 0.15. This is because many clusters only have one element.

TABLE III. THE STATIC THRESHOLD DECOMPOSITION (CASE 1)

Cluster	Elements	Silhouettes Index
1	canGraduate	-0.52
	releaseTranscript	-0.31
	runAcademicServices	-0.72
	formTranscript	-0.03
	transcriptType	0.38
	major	0.37
2	isPassed	1.00
	releaseFinalGrade	1.00
	getFinalGrade	1.00
Average Silhouettes		0.24

TABLE IV. THE DYNAMIC DECOMPOSITION (CASE 1)

Cluster	Elements	Silhouettes Index
1	formTranscript	-0.34
	major	-0.11
2	canGraduate	-0.18
	runAcademicServices	-0.48
3	releaseTranscript	0.50
	transcriptType	0.80
4	isPassed	1.00
	releaseFinalGrade	1.00
	getFinalGrade	1.00
Average Silhouettes		0.35

TABLE V. THE STATIC DECOMPOSITION (CASE 2)

Cluster	Elements	Silhouettes Index
1	parentFrame	-0.12
	MDIApplication	-0.03
	desktopPane	0.01
	Show	-0.41
	isSharingToolsAmongViews	-0.01
	Hide	-0.39
	serialVersionUID	-0.03
	scrollPane	0.03
	Prefs	0.00
	2	createFileMenu
Init		0.01
getComponent		0.06
createViewActionMap		0.31
Configure		0.05
createModelActionMap		0.15
toolBarActions		-0.01
createViewMenu		0.30
updateViewTitle		0.32
createHelpMenu		0.34
createWindowMenu		0.30
initLookAndFeel		0.11
wrapDesktopPane		0.04
createMenuBar		0.21
createEditMenu		0.32
Launch	0.05	
Average Silhouettes		0.08

TABLE VI. THE DYNAMIC DECOMPOSITION (CASE 2)

Cluster	Elements	Silhouettes Index
1	isSharingToolsAmongViews	-0.12
	Prefs	-0.08
2	scrollPane	-0.27
3	parentFrame	0.00
	desktopPane	0.03
4	MDIApplication	0.27
	serialVersionUID	0.22
5	Show	-0.19
	Hide	-0.12
6	getComponent	-0.51
7	Launch	-0.62
8	createFileMenu	-0.84
	Init	-0.39
	initLookAndFeel	-0.49
	createMenuBar	-0.58
9	updateViewTitle	0.28
	Configure	0.08
10	createViewMenu	0.78
	createHelpMenu	0.89
	createWindowMenu	0.75
	createEditMenu	0.73
11	wrapDesktopPane	0.95
	toolBarActions	0.98
12	createViewActionMap	1.00
	createModelActionMap	1.00
Average Silhouettes		0.15

B. Compared with the Previous Approach

The result of the experiment using new metrics (*syn* and *sem*) at the design artifact shows different from the result of the previous approach. The previous approach uses six metrics at the source code level to calculate the similarity between class elements. The decomposition result using the previous approach will be assessed using the Silhouette index, then compared with the result of the current experiment. This comparison will focus on the Silhouette index value of decomposition using case 1.

The calculation of the Silhouette index of previous is based on the dissimilarity matrix calculated from the similarity matrix. The Silhouette index comparison of the previous and proposed approaches using case 1 is shown in Table VII. Based on the result shown in Table VII, the average of Silhouette using the previous approach is shown little different from the current approach. In the previous approach, using the static threshold, the average of the Silhouette index is 0.05. The dynamic threshold approach produces the average Silhouette as -0.02. The current approach for static and dynamic are 0.24 and 0.35, respectively. The experiment is used the prototype application to apply the decomposition using the previous approach's similarity matrix (Table II).

The previous experiment uses the six metrics to calculate the similarity between the class's elements at the source code level. The current experiment is done at the design level using

two metrics gathered from the class diagram. The comparison previous and proposed approach is to know how the conformance rate between each other.

Tables VIII and IX show the clustering result using each approach (previous and proposed). Using different metrics and objects of study, the previous and proposed approach results in the same number of clusters but different elements. The conformance is calculated by dividing the number of conformed elements at both results by the number of all elements. For example, for the static threshold AHC, four elements conform at both sides of the result. m4 and m6 are located at the same cluster (also m5 and m8). The rest element, m7, m9, and m10, are considered not to conform. It is similar to the dynamic threshold AHC. Four elements conform at both sides (m10, m7, m9, and m6). The conformance rate for both results is $\frac{4}{7} = 0.5714$. The proposed experiment uses two metrics from the class diagram to do the class decomposition results 0.5714 conformance rate.

C. Discussion

Tables III, IV, V, and VI show the result of the experiment, not only the number of the cluster but also the Silhouettes index score for every element. The Silhouettes index shows the validity of every element placed in a specific cluster. A higher score is better for Silhouettes.

TABLE VII. THE AVERAGE SILHOUETTE INDEX COMPARISON (CASE 1)

	Previous Approach		Current Approach	
	Static	Dynamic	Static	Dynamic
Case 1	0.05	-0.02	0.24	0.35

TABLE VIII. THE AVERAGE SILHOUETTE INDEX OF STATIC THRESHOLD (CASE 1)

Static Threshold			
Cluster	Previous	Cluster	Proposed
1	m5	1	m7
	m7		m10
	m8		m4
	m10		m6
2	m4	2	m8
	m6		m9
	m9		m5

TABLE IX. THE AVERAGE SILHOUETTE INDEX OF DYNAMIC THRESHOLD (CASE 1)

Dynamic Threshold			
Cluster	Previous	Cluster	Proposed
1	m5	1	m6
	m10	2	m7
2	m7	3	m4
	m8		m10
3	m9	4	m8
4	m4		m9
	m6		m5

The differences and the trend of the Silhouettes index between static and dynamic threshold AHC are interesting to discuss. Case 1 shows that the average of Silhouettes of static threshold is 0.25. And, the dynamic threshold has the average of Silhouettes is 0.35. In case 2 from jHotDraw, the static threshold shows that the average Silhouettes are 0.08 and 0.15 for the dynamic threshold. The dynamic threshold AHC produces the higher Silhouettes index score from the two cases. The dynamic threshold AHC is better than the static threshold AHC for those two cases in the design phase.

The comparison with the previous approach's average Silhouette shows a different trend. The previous approach shows that the static threshold AHC has a better value of the Silhouette index than a dynamic threshold. It is shown that the value of static and dynamic are 0.05 and -0.02, respectively. In this case, the value of the similarity matrix used in the experiment to decompose the class is taking an important position. The use of six metrics to calculate the similarity value and then decomposed using the static and dynamic threshold AHC is slightly lower than the use of two metrics (proposed experiment). The compactness of each cluster resulting from the decomposition process depends on the metrics used. Using two metrics, it shows the conformance rate of about 0.5714. It means that four elements conformed to each other (previous and proposed approach). With the 0.5714 conformance rate, the proposed approach's result has a better average of Silhouettes. But, this result cannot be used to justify which one is better. The decomposition result's correctness might be able to be found by deep analysis at the implementation level after the decomposition is finished.

The other angle of results shows that there are many elements with negative Silhouettes. It means that the elements are placed in the worse cluster. Silhouettes also show the density of every element in every cluster. The higher Silhouettes score shows the distance between elements inner the specific cluster is close to each other and far from the other cluster. High differentiation of distance between clusters is better for clustering results.

The decomposition of class using static and dynamic threshold AHC leaves the existence of many elements with a negative score of the Silhouettes index problem. To overcome this problem is needed to move the element with negative Silhouettes to the other cluster by comparing the Silhouettes score before and after movement. The better Silhouettes score will be chosen to increase the validity of the cluster.

The other point that is interesting to discuss is the result of clustering. The number of clusters between static and dynamic thresholds is always increased. The dynamic threshold produces more clusters than static. The static threshold produces less number of clusters, and the other side consists of a bigger element inner of every cluster and vice versa for the dynamic threshold AHC. Hamdi et al. said that the static threshold is suitable for fine-grained decomposition, and the dynamic is suitable for coarse-grained decomposition [11]. Based on the definition, the fine-grained will produce smaller objects.

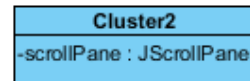


Fig. 4. Cluster Number Two.

Fine-grained produces more objects than coarse-grained decomposition. But it differs from Hamdi's result in the class diagram and uses the two metrics (*syn* and *sem*) for distance similarity calculation. In this experiment, using dynamic threshold AHC creates more clusters with smaller elements. And the static threshold produces a smaller number of clusters with a bigger number of elements in every cluster. It can happen because of the threshold. Different from the static, the dynamic threshold alters the threshold in every cycle of the decomposition process to find the separation limit. That is why the dynamic threshold has higher opportunities to create a new cluster in every decomposition cycle.

In the class decomposition process, the main purpose is to decompose the class by distinguishing the functionality of the class. The dynamic threshold AHC can find the single functionality inner the decomposed class. Using syntactic and semantic metrics in the class diagram, the dynamic threshold AHC is more distinctive than the static threshold to do decomposition. The dynamic threshold that is calculated on every cycle process makes the decomposition done in fine-grained size.

The dynamic threshold AHC results in more clusters than static, but the number of elements in every cluster is smaller than the static threshold. Some clusters only consist of one element, for example, cluster number two resulting from dynamic threshold decomposition of case 2 (see Table VI). The element in cluster number two is only scrollPane, and it is an attribute. From the detailed class in Fig. 3, the scrollPane has a private modifier. This will be the next interesting problem to discuss. Cluster number two will be one class with only one attribute and is private. Fig. 4 shows how cluster number two is realized into the class.

Class from cluster number two is doubtful to use. There is only one attribute, and it has a private modifier. The object from the class of cluster number two will be unable to access. The other word, the object will not collaborate with the other objects in the software system. The main purpose of object in the software system is to do sub-function to fulfill at least one of the software functionality. Ideally, the attribute is private to match the theory of information hiding. But, usually, at least there is one method that has a public modifier. The method has functioned as the object's boundary to access the data or process provided by the object. If there is no public method, then it will be an unuseful object. The movement process must solve this condition. For the class that only has private elements, the element must be moved to the other more valid cluster by comparing the validity or compactness rate of the element.

VII. CONCLUSION AND FUTURE WORK

The refactoring can be done by using the design artifact. This paper shows the new metrics from the class diagram to do the decomposition of class using the class diagram. The

metrics are *syn* and *sem* that measure using analysis of syntax and meaning. The metric uses the information gathered from the class diagram to calculate the similarity matrix. The decomposition process uses the algorithm from the previous approach but is implemented in the class diagram as a design-level artifact. The decomposition result shows a few points of conclusion.

The first conclusion is the differences between the previous and the current decomposition result. The current result of decomposition shows that the clusters resulting from the static and dynamic threshold AHC are more compact than the previous approach's result. It is validated using the Silhouette index to measure the compactness of the clusters.

Both approaches produce the same number of clusters, whether using the static or dynamic threshold AHC. But, some of the elements are different between previous and proposed approaches. The conformance rate of both (previous and proposed) approaches is 0,5714, with the proposed approach result showing higher compactness.

In the proposed experiment, there is a trend in the Silhouette index value of the proposed experiment's static and dynamic threshold result. The dynamic threshold is higher than static in the Silhouette value in both cases. Dynamic threshold AHC produces a more compact cluster than the static. The dynamic threshold AHC also produces more number of a cluster than the static threshold. On achieving single responsibility principles, the dynamic threshold AHC's result shows more specific than static because the result of the cluster consists of a lower number of elements but a higher Silhouette index as a measurement of compactness.

The result shows the advantages that can be obtained and shows that there are still shortcomings. The decomposition result still shows the elements that have the negative Silhouette value. The negative Silhouette value shows that the distances of the current element are far from the other elements in the same cluster. The other word, the negative Silhouette elements are considered the worse place. The enhancement for the moving mechanism of the negative element is considered important.

The result also shows that some clusters are considered unable to implement because the cluster may produce objects that cannot collaborate with others. The cluster that only has one element, specifically if the element has a private modifier, is considered a useless cluster. From this fact, it is considered important to include the modifier aspect to do the decomposition process. It is important to avoid the emergence of useless clusters.

REFERENCES

- [1] M. Fowler et al., *Refactoring Improving the Design of Existing Code Second Edition*, Second Ed. United State of America: Pearson Education - Wesley, 2019.
- [2] F. A. Fontana, P. Braione, and M. Zaroni, "Automatic detection of bad smells in code: An experimental assessment," *J. Object Technol.*, vol. 11, no. 2, 2012.
- [3] A. Yamashita and L. Moonen, "Exploring the impact of inter-smell relations on software maintainability: An empirical study," *Proc. International Conference on Software Engineering*, 2013.
- [4] F. Palomba, G. Bavota, M. Di Penta, F. Fasano, R. Oliveto, and A. De Lucia, "On the diffuseness and the impact on maintainability of code smells: a large scale empirical investigation," *Empir. Softw. Eng.*, vol. 23, no. 3, pp. 1188–1221, 2018.
- [5] G. Bavota, A. De Lucia, A. Marcus, and R. Oliveto, "A two-step technique for extract class refactoring," *ASE'10 - Proc. IEEE/ACM Int. Conf. Autom. Softw. Eng.*, pp. 151–154, 2010.
- [6] G. Bavota, A. De Lucia, and R. Oliveto, "Identifying Extract Class refactoring opportunities using structural and semantic cohesion measures," *J. Syst. Softw.*, vol. 84, no. 3, pp. 397–414, Mar. 2011.
- [7] G. Bavota, "Using structural and semantic information to support software refactoring," *Proc. - Int. Conf. Softw. Eng.*, pp. 1479–1482, 2012.
- [8] G. Bavota, A. De Lucia, A. Marcus, and R. Oliveto, "Automating extract class refactoring: an improved method and its evaluation," *Empir. Softw. Eng.*, vol. 19, no. 6, pp. 1617–1664, 2014.
- [9] M. Fokaefs, N. Tsantalis, E. Stroulia, and A. Chatzigeorgiou, "Identification and application of Extract Class refactorings in object-oriented systems," *J. Syst. Softw.*, vol. 85, no. 10, pp. 2241–2260, 2012.
- [10] M. Fokaefs, N. Tsantalis, A. Chatzigeorgiou, and J. Sander, "Decomposing object-oriented class modules using an agglomerative clustering technique," *IEEE Int. Conf. Softw. Maintenance, ICSM*, pp. 93–101, 2009.
- [11] M. Hamdi, R. Pethe, A. S. Chetty, and D. K. Kim, "Threshold-driven class decomposition," *Proc. - Int. Comput. Softw. Appl. Conf.*, vol. 1, pp. 884–887, 2019.
- [12] Y. Wang, H. Yu, Z. Zhu, W. Zhang, and Y. Zhao, "Automatic Software Refactoring via Weighted Clustering in Method-Level Networks," *IEEE Trans. Softw. Eng.*, vol. 44, no. 3, pp. 202–236, 2018.
- [13] N. Anquetil, A. Etien, G. Andreo, and S. Ducasse, "Decomposing God Classes at Siemens," *Proc. - 2019 IEEE Int. Conf. Softw. Maint. Evol. ICSME 2019*, pp. 169–180, 2019.
- [14] I. Bassey, N. Dladlu, and B. Ele, "Object-Oriented Code Metric-Based Refactoring Opportunities Identification Approaches: Analysis," *Proc. - 4th Int. Conf. Appl. Comput. Inf. Technol. 3rd Int. Conf. Comput. Sci. Appl. Informatics, 1st Int. Conf. Big Data, Cloud Comput. Data Sci.*, pp. 67–74, 2017.
- [15] M. Misbhauddin and M. Alshayeb, "UML model refactoring: a systematic literature review," *Empir. Softw. Eng.*, vol. 20, no. 1, pp. 206–251, 2013.
- [16] J. Al Dallal, "Identifying refactoring opportunities in object-oriented code: A systematic literature review," *Inf. Softw. Technol.*, vol. 58, pp. 231–249, 2015.
- [17] B. Priyambadha and T. Katayama, "Tree-based keyword search algorithm over the visual paradigm's class diagram XML to abstracting class information," *2020 IEEE 9th Glob. Conf. Consum. Electron. GCCE 2020*, pp. 280–284, 2020.
- [18] B. Priyambadha, T. Katayama, Y. Kita, H. Yamaba, K. Aburada, and N. Okazaki, "Utilizing the similarity meaning of label in class cohesion calculation," *J. Robot. Netw. Artif. Life*, vol. 7, no. 4, pp. 270–274, 2021.
- [19] R. Dijkman, M. Dumas, B. van Dongen, R. Käärrik, and J. Mendling, "Similarity of business process models: Metrics and evaluation," *Inf. Syst.*, vol. 36, no. 2, pp. 498–516, 2011.
- [20] J. B. Gao, B. W. Zhang, and X. H. Chen, "A WordNet-based semantic similarity measurement combining edge-counting and information content theory," *Eng. Appl. Artif. Intell.*, vol. 39, pp. 80–88, 2015.
- [21] F. Palomba et al., "Landfill: An open dataset of code smells with public evaluation," *IEEE Int. Work. Conf. Min. Softw. Repos.*, vol. 2015-Augus, pp. 482–485, 2015.
- [22] P. J. Rousseeuw, "Silhouettes: A graphical aid to the interpretation and validation of cluster analysis," *J. Comput. Appl. Math.*, vol. 20, pp. 53–65, 1987.

A Comparative Analysis of Multi-Criteria Decision Making Techniques for Ranking of Attributes for e-Governance in India

Bhaswati Sahoo¹, Rabindra Narayana Behera², Prasant Kumar Pattnaik³

School of Computer Engineering, Kalinga Institute of Industrial Technology, Deemed to be University, Bhubaneswar, India^{1,3}
National Informatics Center, Bhubaneswar, India²

Abstract—e-Governance is the system in which all the public services are made available in the online platform with the help of secured cyber architecture. Government along with the people have praised the ability of Information and communications technology (ICT) around the world in stimulating the various vital sectors of the economy. The advanced technologies have provided speed, inexpensive and convenient method of interaction and communication. In various developing and developed countries, these newly adopted technologies have shown direct positive impact on the country's productivity, efficiency and thus leads to rapid development. This work represents a comparative study of various Multi-Criteria Decision Making (MCDM) techniques like Technology, Multi-criteria Decision making, Ranking, Technique for Order of Preference by Similarity to Ideal Solution (TOPSIS), Weighted Sum Model (WSM) and Weighted Product Model (WPM) to find the ranking of various attributes responsible for better decision making for implementing successful e-Governance in developing country, India.

Keywords—e-Governance; information and communication technology; multi-criteria decision making; ranking; technique for order of preference by similarity to ideal solution (TOPSIS); usability; weighted sum model (WSM); weighted product model (WPM)

I. INTRODUCTION

The word e-Government refers to a broad set of applications defined and created in order to solve various administrative issues, i.e Government services or government sector-related issues. The development in utilize of Information Technologies and Communication Technology (ICT) has extended to new domains starting from entertainment and information sharing, to medicine, education and science [14]. Most of the e-Governance services are web-based applications. This helps the citizens for better access to the various e-Governance services [8]. e-Governance in India has advanced persistently beginning from digitization of government offices and departments to segregated sectors centered at adapting e-Governance usages in different areas of the government at various levels i.e. national, district, state or local levels. These segregated sectors were unified into a single vision and strategy given by the National e-Governance Plan (NeGP) in 2006 [3]. The NeGP takes a holistic scenario of e-Governance

plans, strategy and activities within the nation, merging them into a cumulative and collective view for a common shared cause. Revolving around this digitization concept, a huge nation-wide infrastructure is evolving and made accessible to the people of the remotest of villages, and expansive scale digitization of records is been undertaken to have easy, secured and reliable access over the Internet services. e-Governance plays a major component of the country's governance system and also is a vital part of the administrative reform agenda in developing country like India. The NeGP organization has the capability to accumulate large savings in costs by the method of sharing of core and support infrastructure, empowering interoperability through measures, and of presenting a seamless view of government to citizens. The ultimate objective is to allow transparent public services to citizens.

In the course of time various strategies are planned and are implemented for designing better e-Governance for the citizens. But despite of so many proposals, some fail because of the improper implementation attributes. In order to make a project successful, it is required to study all the critical factors starting from governance, management to implementation and getting feedback on services responsible for making a successful project.

Multi-criteria Decision making techniques (MCDM) are useful in cases where many factors stands validated for the success of one cause. The conflicting areas are analyzed effectively in this process of decision making. In a typical MCDM algorithm, weights are assigned to each criteria available for analysis, and basing on the weights, each criteria is analyzed with reference to some collected data or information. Basing on the algorithm, the criteria are ranked or weighted in order of their dependency for the success of a given solution. The method of structuring difficult problems properly and focusing on multiple attributes explicitly proceeds to more informed and good decisions. A number of approaches and techniques have been proposed and applied in different fields for better decision making considering various attributes of a problem [11, 12].

Therefore, in this paper various models of decision making are analysed in order to find the preference order of attribute ranking for making better decision for successful and proper implementation of e-Governance in India.

II. LITERATURE REVIEW

There are various authors who have used the methods such as TOPSIS, WPM and WSM for ranking various attributes in order provide efficiency in the system. Some of the noted works of the authors are cited below.

Mela et.al (2012) have selected various MCDM techniques like WSM, WPM, VIKOR, TOPSIS, PROMETHEE II for a comparative study for building design. They have tested against various criteria that are responsible for generating better designs [1].

Velasquez et.al (2013) have reviewed various MCDM techniques for better performance attributes. The authors have concluded that, MCDM techniques provides a whole new approach for better decision making for any problem which combines multi-criteria attributes for evaluation[2].

Mulliner et. al (2015) have compared the performance of methods like WPM, WSM, AHP, TOPSIS and COPRAS for assessment of sustainable housing affordability. The authors have evaluated 20 criteria and 10 alternatives taking Liverpool as a case study. The reason for using the MCDM techniques is to evaluate the robustness and contrasts in the result rankings [4].

Karande et.al (2016) compared the most popular six comprehensive MCDM methods such as WSM, WPM, MOORA, MULTIMOORA and WASPAS for industrial robot selection problems using two real time values. Local weights were under-taken and stability were maintained by designing proper interval ranges. MOORA have given robust and best values for the most critical criteria [5].

Kolios et.al (2016) have used the TOPSIS method from MCDM techniques in order to provide enrichment for accounting stochastic variable inputs. Along with TOPSIS, PROMETHEE is also used for predicting the optimum design alternative [6].

Ansar et.al (2018) have used various MCDM methods like WPM, WSM, AHP, TOPSIS, SMART on 10 alternatives and criteria in order to evaluate the success of information system selection. Among the MCDM techniques, TOPSIS resulted in better and sophisticated values for ranking the alternatives in their order for efficient information system selection [7].

Mondal et.al (2021) have implemented the MCDM techniques for evaluation of factors and attributes responsible for smart city governance. The author has used Agartala city for the case study. The work is focused the various applications under taken for Smart cities. Both qualitative and quantitative analysis has been implemented. After evaluation of the criteria and its attributes, the author concludes that it would take 5 years of time for completion of project for making Agartala a smart city [9].

Chakraborty et.al (2021) have applied Decision making trial and evaluation laboratory (DEMATEL) method for their work. They have taken the case studies of 98 Indian smart cities for evaluation against 11 criteria. The proposed work also include k-means clustering algorithm for reduction of datasets. Finally, after the application of MCDM techniques, they have found out the results along with strengths and weakness

relating to the progress of smart cities and measures for strengthening the lagging infrastructure for Smart cities [10].

III. METHODOLOGY

Multi-Criteria Decision Making techniques are used by decision makers for evaluating the conflicting criteria present as alternatives for taking proper and wise decision regarding a problem statement. Solving a particular problem has various options [12]. It may be finding the best alternative of the given set of alternatives, or ranking the alternatives to find the most critical factor for a given problem domain, or finding the deviation of the alternatives from a given set of most accurate alternatives or may be outranking the relations among the alternatives or may be deciding the criteria weights for each alternatives such that the best optimal solution are found from the given set of alternatives. A MCDM technique not only finds the best alternatives, it also provides a set of weak criteria or non-critical alternatives so that filtration can be made among the alternatives and would be helpful for the decision makers to take the best solution for the problem statement. Techniques like Aggregated Indices Randomization Method (AIRM), Analytical hierarchy Process (AHP), Analytical Network Process (ANP) are used for finding the weighted criteria for each alternative for finding the best solution to the given problem. Best Worst Method (BWM) is another technique used for finding the worst possibilities so that worst factors can be eliminated and best decision can be taken by the experts for decision-making. Some methods like ELECTRE and PEOMETHEE are used for outranking the alternatives and finding the most critical factors for decision-making in various fields. Techniques like Weighted Sum Model (WSM) and Weighted product Model (WPM) are used for finding the weights on each criterion for helping in decision making procedure. PAPRIKA is a technique to find the pairwise ranking among all possible alternatives available to find optimum solution. Ranking techniques such as Superiority and inferiority ranking method (SIR Method) , Technique for the Order of Prioritization by Similarity to Ideal Solution (TOPSIS) and Evaluation based on Distance from Average Solution (EDAS) are used for finding the differences among the similarity indices, or superiority and inferiority of alternatives for helping decision makers as most alternatives gets filtrated and best alternatives are outshined. Many MCDM techniques are available and each technique has some unique features for various problems. Techniques are applied looking into the problem statement defined and the results as desired by the researchers. In this research some MCDM Techniques like WSM, WPM and TOPSIS are used on the same set of criteria for evaluation of success of e-Governance Services in Indian Government. The techniques are compared and best fit technique is taken into account for the evaluation process.

A. Weighted Sum Model (WSM)

The importance of this technique is to simple add weights to each alternatives in the criteria for better assessment results [16]. The weights are evaluated using the following equation:

$$A_i^{\text{WSM-value}} = \sum w_j a_{ij} \text{ for } i= 1,2,3,\dots, n \text{ and } j= 1 \text{ to } n \quad (1)$$

This technique is helpful for ranking of alternatives for better decision making.

B. Weighted Product Model

The method is called dimensionless analysis as the mathematical components eliminate the units of measurement. It was first experimented by Bridgman and Miller and Starr in 1922 [15]. The equation is stated as follows:

$$P(A_K) = \prod (a_{Kj})^{w_j} \text{ for } K=1,2,3\dots m. \text{ and } j=1,2,3,\dots,n. \quad (2)$$

This method can also be used for comparison between two alternatives as per the following equation:

$$P(A_K/A_L) = \prod (a_{Kj}/a_{Lj})^{w_j} \text{ for } K, L=1,2,3\dots m. \text{ and } j=1,2,3,\dots,n \quad (3)$$

C. Technique for Order of Preference by Similarity to Ideal Solution (TOPSIS)

In the TOPSIS method, the objective is to choose the alternative by measuring the shortest geometric distance from the positive ideal solution (PIS) and the longest geometric distance from the negative ideal solution (NIS). The technique was developed by Ching-Lai Hwang and Yoon in 1981 [13]. In this technique of decision making, a set of alternatives are compared by identifying weights for each criterion, normalizing the scores for each criterion and finally calculating the distance from the most ideal alternative available.

Steps for TOPSIS Method:

1) Creating the evaluation matrix having n-criteria and m-alternatives, with the intersection of each alternative to the given criteria denoted as x_{ij} of size (n x m).

2) Next step is to normalize the matrix values to form a Normalized matrix (R).

$R = (r_{ij})_{n \times m}$ by the method.

$$r_{ij} = \frac{x_{ij}}{\sqrt{\sum_{k=1}^m x_{kj}^2}}, \quad i=1,2,3,\dots,m; j=1,2,3,\dots,n. \quad (4)$$

3) Next step is to calculate the weighted normalized decision matrix.

$$t_{ij} = r_{ij} \times w_j; \quad i=1,2,\dots,m \text{ and } j=1,2,\dots,n. \quad (5)$$

$$w_j = \frac{W_j}{\sum_{k=1}^n W_k}, \quad j=1,2,\dots,n \text{ so that } \sum_{i=1}^n w_i = 1, \text{ and } W_j \text{ is the original weight given to the indicator} \quad (6)$$

4) Finally, the worst alternative (A_w) and the best alternative (A_b) were determined.

$$A_w = \{ [\max(t_{ij} | i=1,2,3,\dots,m) | j \in J_-], [\min(t_{ij} | i=1,2,3,\dots,m) | j \in J_+] = \{t_{wj} | j=1,2,3,\dots,n\} \} \quad (7)$$

$$A_b = \{ [\min(t_{ij} | i=1,2,3,\dots,m) | j \in J_-], [\max(t_{ij} | i=1,2,3,\dots,m) | j \in J_+] = \{t_{bj} | j=1,2,3,\dots,n\} \} \quad (8)$$

$$J_+ = \{j=1,2,\dots,n | j\} \quad (9)$$

having positive impact value on the criteria and

$= \{j=1,2,\dots,n | j\}$ (10) having positive impact value on the criteria.

5) The distances between the chosen alternative i and the worst chosen alternative is calculated by

$$d_{iw} = \sqrt{\sum_{j=1}^n (t_{ij} - t_{wj})^2} \quad i=1,2,3,\dots,m. \quad (11)$$

the distance between the alternative i and best chosen condition is calculated by.

$$d_{ib} = \sqrt{\sum_{j=1}^n (t_{ij} - t_{bj})^2} \quad i=1,2,3,\dots,m. \quad (12)$$

Similarity to worst condition is calculated by:

$$s_{iw} = d_{iw} / (d_{iw} + d_{ib}), \quad 0 \leq s_{iw} \leq 1; \quad i=1,2,3,\dots,n \quad (13)$$

$s_{iw} = 1$ iff alternative is the best condition,

$s_{iw} = 0$ iff alternative is the worst condition.

The alternatives are ranked according to s_{iw} ($i=1,2,3,\dots,m$).

There are various criteria for evaluation of e-Governance projects at national, state, district and zonal level. The criteria are broadly classified as Governance, Management, Resources and Promotion.

Each broad criteria is again categorized into various sub-criteria such as follows:

Governance is sub categorized into ministerial and parliament. Management is divided into Administrative and opportunities. Resources are grouped into technical and non-technical and finally promotion is segregated as social media and advertisement.

Each sub-criteria is again divided into various alternatives as described below:

Ministerial covers policy maker, strategy planner, legal framework and stakeholders as its alternatives. Similarly, Parliament has political willingness, information sharing, scope and collaborations as its alternatives. Administrative encompasses administrative policies, administrative strategies, evaluation and financial budget as its alternatives for ranking of attributes. Opportunities has user friendly, design and navigation, leadership and economy as its alternative attributes. Technical criteria has ICT infrastructure, software development, security and privacy as its alternatives. Non-technical covers support staff, awareness, disaster recovery and helpdesk as the alternatives. Social media has Facebook, twitter, WhatsApp and Google share as its alternatives. Lastly, advertisement covers television, print media hoardings and airshows as its alternatives.

The division of criteria, sub-criteria and alternatives are designed in order to bring clarity in the valuation process and also it helps for better decision making as the attributes are collected take all- round aspects of e-Governance system in a developing country like India.

Questionnaire and feedback mechanism were taken into consideration to put the numeric values against each attribute and criteria for ranking of the attributes for good governance system in India.

Each criteria is evaluated in three different methods using TOPSIS, WPM and WSM. And ranking of attributes are made

depending on the importance of attributes for providing good governance system to the citizens through cyber space.

IV. RESULTS AND COMPARISON

Information and data were collected from various experts in the e-Governance sectors through questionnaire in various national, state and district level governance management systems. Along with this, feedback were also included that were collected from various existing e-Governance projects for making them successful at different levels of operation.

The methods like WSM, WPM and TOPSIS were used to analyse the responses obtained from the questionnaire and the feedback system. The responses were in both numeric grading and linguistic order. All the linguistic values were converted into numeric ranking in terms of percentage values and were mapped against each attributes. Finally the methods of WSM, WPM and TOPSIS were applied and the ranking of attributes from most preferable to least preferable are ranked in terms of 1, 2, 3 and 4.

The results are compared for each attribute in the following tables:

From Table I, it is noted that Strategy planner is given more priority as per TOPSIS method, WPM Method and WSM Method.

TABLE I. RANKING OF ALTERNATIVES FOR MINISTERIAL SUB-CRITERIA

SI No	Attributes	WSM	WPM	TOPSIS
1	Policy Maker	2	3	2
2	Legal Framework	3	2	3
3	Strategy Planner	1	1	1
4	Stakeholders	4	4	4

From Table II, scope has been given highest priority on analyzing in all the three methods.

TABLE II. RANKING OF ALTERNATIVES FOR PARLIAMENT SUB-CRITERIA

SI No	Attributes	WSM	WPM	TOPSIS
1	Political Willingness	4	2	4
2	Information sharing	3	3	2
3	Scope	1	1	1
4	Collaborations	2	4	3

The results in Table III, assigns highest priority to Evaluation in WPM and WSM method and Administrative policies in TOPSIS Method.

TABLE III. RANKING OF ALTERNATIVES FOR ADMINISTRATIVE SUB-CRITERIA

SI No	Attributes	WSM	WPM	TOPSIS
1	Administrative policies	4	2	2
2	Administrative policies	2	3	1
3	Evaluation	1	1	3
4	Financial Budget	3	4	4

TABLE IV. RANKING OF ALTERNATIVES FOR OPPORTUNITIES SUB-CRITERIA

SI No	Attributes	WSM	WPM	TOPSIS
1	User friendly	4	2	2
2	Leadership	2	3	1
3	Design and Navigation	1	1	3
4	Economy	3	4	4

From the Table IV, of Opportunities sub-criteria, TOPSIS ranks Leadership as most priority and WSM and WPM ranks Design and Navigation as the most preferred attribute.

As per Table V, ICT Infrastructure and software development are the most important attributes for governance system from the technical point of view.

TABLE V. RANKING OF ALTERNATIVES FOR TECHNICAL SUB-CRITERIA

SI No	Attributes	WSM	WPM	TOPSIS
1	ICT Infrastructure	1	2	1
2	Software Development	2	1	2
3	Security & Privacy	4	3	4
4	Accuracy	3	4	3

In Table VI, Awareness and Disaster recovery of the ICT systems are most important and hence are given highest priority.

TABLE VI. RANKING OF ALTERNATIVES FOR NON-TECHNICAL SUB-CRITERIA

SI No	Attributes	WSM	WPM	TOPSIS
1	Awareness	1	2	2
2	Disaster Recovery	2	1	1
3	Support staff	4	4	3
4	Help Desk	3	3	4

The importance of good governance system can be shared and spread through social media. Therefore, Facebook, Twitter are mostly used for sharing the information in promotion of e-Governance systems in Table VII.

TABLE VII. RANKING OF ALTERNATIVES FOR SOCIAL MEDIA SUB-CRITERIA

SI No	Attributes	WSM	WPM	TOPSIS
1	Face book	2	1	2
2	Twitter	1	4	1
3	WhatsApp	4	2	3
4	Google share	3	3	4

Television and print media are popularly used for advertising various e-Governance systems for its promotion as per the results shown in Table VIII.

Similarly the ranking order of all the criteria are done using WPM, WSM and TOPSIS Methodology.

TABLE VIII. RANKING OF ALTERNATIVES FOR ADVERTISEMENT SUB-CRITERIA

SI No	Attributes	WSM	WPM	TOPSIS
1	Television	2	1	2
2	Print Media	1	4	1
3	Hoardings	4	2	3
4	Air Shows	3	3	4

TABLE IX. RANKING OF SUB-CRITERIA

SI No	Attributes	WSM	WPM	TOPSIS
1	Ministerial	6	5	4
2	Parliament	5	6	5
3	Administrative	4	1	1
4	Opportunities	1	2	3
5	Technical	2	3	2
6	Non-Technical	3	4	6
7	Social Media	7	7	7
8	Advertisement	8	8	8

From the Table IX, the priority ranking of various sub-criteria are as follows:

Using WSM, the ranking order are Opportunities> Technical> Non-Technical> Administrative> Parliament> Ministerial> Social Media> Advertisement.

Using WPM, The ranking orders are Administrative> Opportunities> Technical> Non-Technical> Ministerial> Parliament> Social Media> Advertisement.

Using TOPSIS, the ranking order are Administrative>Technical>Opportunities> Ministerial>Parliament> Non-Technical>Social Media> Advertisement.

The final ranking of criteria that are responsible for success of e-Governance system is shown in Table X.

TABLE X. RANKING OF CRITERIA

SI No	Attributes	WSM	WPM	TOPSIS
1	Governance	2	1	1
2	Management	1	2	3
3	Resources	3	3	2
4	Promotion	4	4	4

The overall ranking of criteria are as follows:

In WSM method, Management> Governance> Resources> Promotion.

In WPM method, Governance> Management> Resources> Promotion.

In TOPSIS method, Governance> Resources> Management> Promotion.

The various criteria, sub-criteria and alternatives are compared and ranked according to their priority such that multi-criteria analysis can be done for better decision making for success of e-Governance in India.

V. CONCLUSION AND FUTURE WORK

The implementation of e-Governance in a developing country like India is very challenging in nature. The factors such as secured cyber space, advanced ICT infrastructure, disaster recovery strategies, proper planning, better scopes and collaborations are limited in India for which better facilities are not made available to the citizens. Moreover, Government plans and strategy also plays a vital role in the proper implementation and success of e-Governance Projects in India. The Government plans are not based on scientific weightage of various parameters for the success of e-Governance.

The above discussion in the results and comparison section gives the various ranking of alternatives and criteria. These priority ranking of criteria and alternatives are useful for better decision making approach in the Governance system as they are analysed by taking multiple criteria from all sectors of implementation starting from planning and governance to availability of resources and ICT support staff for helping citizens to become aware of the e-Governance Services. This paper mainly aims to provide the priority order ranking of the attributes that are possibly held responsible for healthy decision making process for real e-Governance in India so that it will reach enmass pan India to reach the unreachd.

REFERENCES

- [1] Mela, K., Tiainen, T., & Heinisuo, M. (2012). Comparative study of multiple criteria decision making methods for building design. *Advanced Engineering Informatics*, 26(4), 716-726.
- [2] Velasquez, M., & Hester, P. T. (2013). An analysis of multi-criteria decision making methods. *International Journal of Operations Research*, 10(2), 56-66.
- [3] Gupta, A., & Bansal, R. (2013, April). E-Governance: A Step Ahead. In 2013 Third International Conference on Advanced Computing and Communication Technologies (ACCT) (pp. 359-362). IEEE.
- [4] Mulliner, E., Malys, N., & Maliene, V. (2016). Comparative analysis of MCDM methods for the assessment of sustainable housing affordability. *Omega*, 59, 146-156.
- [5] Karande, P., Zavadskas, E., & Chakraborty, S. (2016). A study on the ranking performance of some MCDM methods for industrial robot selection problems. *International Journal of Industrial Engineering Computations*, 7(3), 399-422.
- [6] Kolios, A., Mytilinou, V., Lozano-Minguez, E., & Salonitis, K. (2016). A comparative study of multiple-criteria decision-making methods under stochastic inputs. *Energies*, 9(7), 566.
- [7] Daghouri, A., Mansouri, K., & Qbadou, M. (2018, December). Multi Criteria Decision Making methods for Information System Selection: A Comparative Study. In 2018 International Conference on Electronics, Control, Optimization and Computer Science (ICECOCS) (pp. 1-5). IEEE.
- [8] Sahoo, B., Behera, R. N., & Mohanty, S. (2018, July). International Cyber Attackers Eyeing Eastern India: Odisha-A Case Study. In *Science and Information Conference* (pp. 1328-1339). Springer, Cham.
- [9] Mondal, K., Pramanik, S., & Giri, B. C. (2021). NN-TOPSIS strategy for MADM in neutrosophic number setting. *Neutrosophic Sets and Systems*, 47, 66-92.
- [10] Chakraborty, S., Ghosh, S., Agarwal, S., & Chakraborty, S. (2021). An integrated performance evaluation approach for the Indian smart cities. *OPSEARCH*, 58(4), 906-941.

- [11] Mukherjee, P., Pattnaik, P. K., Al-Absi, A. A., & Kang, D. K. (2021). Recommended System for Cluster Head Selection in a Remote Sensor Cloud Environment Using the Fuzzy-Based Multi-Criteria Decision-Making Technique. *Sustainability*, 13(19), 10579.
- [12] https://en.wikipedia.org/wiki/Multiple-criteria_decision_analysis.
- [13] <https://en.wikipedia.org/wiki/TOPSIS>.
- [14] <https://en.wikipedia.org/wiki/E-governance>.
- [15] https://en.wikipedia.org/wiki/Weighted_product_model
https://en.wikipedia.org/wiki/Weighted_sum_model.

Comparative Analysis of Lexicon and Machine Learning Approach for Sentiment Analysis

Roopam Srivastava¹
Computer Science Dept.
Shri Venkateshwara University
Gajraula (U.P.), India

Prof. (Dr.) P.K. Bharti²
Computer Science Dept.
Shri Venkateshwara University
Gajraula (U.P.), India

Dr. Parul Verma³
Amity Institute of Information
Technology, Amity University
Lucknow, Lucknow (U.P.), India

Abstract—Opinion mining or analysis of text are other terms for sentiment analysis. The fundamental objective is to extract meaningful information and data from unstructured text using natural language processing, statistical, and linguistics methodologies. This further is used for deriving qualitative and quantitative results on the scale of ‘positive’, ‘neutral’, or ‘negative’ to get the overall sentiment analysis. In this research, we worked with both approaches, machine learning, and an unsupervised lexicon-based algorithm for sentiment calculation and model performance. Stochastic gradient descent (SGD) is utilized in this work for optimization for support vector machine (SVM) and logistic regression. AFINN and Vader lexicon are used for the lexicon model. Both the feature TF-IDF and bag of a word are used for classification. This dataset includes "Trip advisor hotel reviews". There are around 20k reviews in the dataset. Cleaned and preprocessed data were used in our work. We conducted some training and assessment. A classifier's accuracy is measured using evaluation metrics. In TF-IDF, the Support Vector Machine is the more accurate of the two classifiers used to assess machine learning accuracy. The classification rate in Bag of Words was 95.2 percent and the accuracy in TF-IDF was 96.3 percent on the support vector machine algorithm. VADER outperforms the Lexicon model with an accuracy of 88.7%, whereas AFINN Lexicon has an accuracy of 86.0%. When comparing the Supervised and unsupervised lexicon approaches, support vector machine model outperforms with a TFIDF accuracy of 96.3 percent and a VADER lexicon accuracy of 88.7%.

Keywords—NLP; sentiment analysis; SGD (stochastic gradient descent); machine learning; TFIDF; BoW; VADER; SVM; AFINN

I. INTRODUCTION

With the use of natural language processing, data from online reviews can be leveraged to extract business intelligence. It is an area of artificial intelligence and linguistics-focused on teaching computers to understand human language statements or words. It was designed to make users' life easier and also help them in communicating easily with the system using natural language [1]. The application of sentiment analysis is very broad and powerful, such as Expedia Canada; Canadians employ sentiment analysis when they see that people complain about their television station's music. Rather than dismissing a bad comment, Expedia capitalizes on it by airing all-new soulful music on their channel [2]. Supervised and unsupervised learning are two machine learning methodologies for sentiment classifiers. In a supervised technique, the classifier requires labeled training

data as well as the target. In the present study, sentiment classification is done using a supervised and unsupervised approach. Calculating the values of parameters of functions that minimize a cost function using ‘stochastic gradient descent is a simple yet effective optimization strategy that converges on a solution to a problem by selecting an arbitrary solution, examining the goodness of fit (under a loss function), and then stepping in the direction that minimizes loss. Support vector machine and logistic regression classifiers for this model’s accuracy are used in the first approach. Support vectors are the coordinates of each unique observation, to put it simply. The SVM classifier is a frontier that effectively separates the two classes (hyper-plane/line). The decision function only uses a subset of training points, making it memory efficient. Logistic regression is a supervised learning algorithm used most commonly to solve binary classification problems. The model might be developed using supervised learning to read the data and predict sentiment. More specifically, classification models would be used to solve the challenge. In another approach, using unsupervised lexicon-based models like ‘afinn lexicon’, Vader lexicon is used for sentiment analysis lexical model is a vocabulary of words that have been specifically matched for sentiment analysis, frequently including positive and negative phrases, as well as the magnitude of the polarity. We used the TF-IDF and BoW for feature engineering. Word embedding is a vector-based technique that represents text as a vector. To evaluate the classification system's accuracy, different evaluation measures, such as the F-Score and Accuracy score, have been employed. For text normalization, we employed various preprocessing steps like tokenization, stop words, lemmatization, n-gram, and punctuation removal to increase our system's performance. In this paper, Section II explains the related work and Section III tells the method, and workflow diagram in Section IV describes the result and discussion. Section V is the conclusion.

II. LITERATURE REVIEW

One can understand the analysis of sentiment as a type of data mining using computational linguistics, NLP, and text analysis for examining people's feelings. There are primarily two methods for extracting sentiment from reviews and categorizing the outcome as good or negative. Machine learning and lexicon-based approaches are examples. The lexicon-based strategy necessitates a predetermined lexicon, but the Machine Learning approach automatically classifies

the review and thus needs training data. Here, a task related to it is discussed. Utilizing an existing generated annotated corpus, using citation sentences, this study analyzes the sentiment expressed in scientific articles. There are 8736 citation sentences in this corpus. They used the classification method to create six different machine learning algorithms. The system's accuracy is then assessed using various evaluation indicators. Using n-gram features in SVM classifier, the author showed commendable accuracy with micro-F. In comparison to the baseline system, their solution enhanced performance by a maximum of nine percent [2]. This paper provides a framework for automatically classifying internet news articles and reviews several existing approaches for classifying online news articles. Various classifiers were tested to get high accuracy. Using a Bayesian classifier, the experimental technique obtained the best accuracy in terms of confusion measures [3]. It is an automated text classification that has long been seen as an essential tool for organizing and analyzing massive volumes of digital documents that are widely dispersed and expanding. It has been discovered that the classification performance of classifiers based on different training text corpus differs, even for the same classification strategy, and that these differences might be quite considerable in some cases [4]. In this study use of an imbalanced and multi-classed data set of large size was made to determine an effective approach for sentiment analysis. Both features, bag-of-words, and tf-idf together with multiple machine learning algorithms (SVM, LR, MultinomialNB, Forest Tree) were used. Using support vector machine and logistic regression with BoW techniques, their best approaches outperform well on SVM and LR [5]. To classify movie reviews, this article employs NLTK, Text Blob, and the VADER Sentiment Analysis Tool. The results of this study's experiments show that Vader outperforms in comparison to text blob [6]. They show how to extract sentiment from text using a lexicon-based technique. The Semantic Orientation CALculator (SO-CAL) integrates intensification and negation and uses dictionaries of words tagged with their semantic orientation (polarity and strength). SO-CAL is used in the polarity classification task, which entails labeling a text with a positive or negative label that reflects the text's attitude toward its major subject matter. It demonstrates that SO-performance CAL's is consistent across domains and in data that has never been seen before.[7] Researchers devised a multi-classification technique for studying tweets, and they used Vader to categorize tweets on the 2016 US election. According to the results, this Sentiment Analyzer was a good choice using Twitter data for sentiment analysis classification. A large amount of data could be classified rapidly by using VADER [8]. The use of a Rule-based classification system for improving sentiment analysis in online communities is also feasible. In addition to general-purpose sentiment analysis, researchers employ emoticons, modifiers, SWN-based sentiment classification, and domain-specific phrases to analyze evaluations within online communities. A disadvantage of this strategy in terms of classification efficacy for domain-specific words is the need for automatic classification and scoring of words [9]. In this study, the next word negation is used to classify the sentiment of text using frequency-inverse document frequency. For text classification,

the binary model of a "bag of words, tf-idf, and TF-IDF-NWN model" was also compared [10]. To automatically evaluate sentiment polarity and score, this method used an upgraded bag-of-words model that used word weight instead of term frequency to evaluate sentiment polarity and score. This technique may also classify reviews based on scientific topic area traits and keywords. This provided solutions to typical sentiment analysis issues that are suitable for use in a review system [11]. LeSSA was a new framework for textual sentiment classification that they had created. He made three key contributions: he established the K-means cluster from lexicon creation, offering a high-quality, broad-coverage sentiment lexicon, and he employed three strategies to build a high-quality training dataset for classification models. In terms of classification accuracy, their approach exceeds previous semi-supervised learning strategies [12]. In their research, they used four classifiers for sentiment analysis optimization: naive bayes, 'OneR', 'BFTree', and 'J48'. In terms of precision, F-measure, and correctly classified cases, OneR appears to be more promising than others. [13]. They used the word embedding technique is word2vec in their model for the word vector. Then applied the LDA model with weighted tf-idf. Their approach showed b [14].

III. METHODOLOGY

This section establishes the methodology's goal. Fig. 1 illustrates our process. We used the "trip advisor hotel review" dataset in my work. One can examine what constitutes a wonderful hotel with this dataset, which has 20k reviews scraped from Trip Advisor which was downloaded from kaggle.com. It has two columns 'Review' and 'Rating'. Five ratings appear in the rating column. Positive reviews receive a rating of (4,5), negative reviews (1,2), and neutral reviews (3) [15]. Our analysis only considers positive and negative reviews in our dataset. It is a comma-separated (.csv) file. We utilized the ScikitLearn python machine learning library, and for text processing, NLTK library from natural language processing for implementing the system. First, we do, data Pre-processing, calculating sentiment, features, and classification are all part of the classification process. In the unsupervised method, we used preprocessed data, then extract the data, model generation, calculating polarity score, and predicted sentiment.

Data Pre-Processing:

It is one of the initial steps in the feature engineering and modeling process. During the pre-process we clean the data, and normalize the corpus which has phrases and words into a standard form. This allows for document corpus standardization, which aids in the development of critical features and noise reduction caused by unwanted objects. We utilized the NLTK tool kit to perform data preprocessing. We go through the following procedures during test preparation, which is listed below:

- Cleaning Text-Unnecessary content, such as HTML tags, frequently appears in our text, adding little value to sentiment analysis. As a result, we must ensure that they are removed before extracting features.

- Lower Case-Because the computer sees lower case and upper case differently, if the text is in the same case, the machine can simply comprehend the words. To avoid problems like these, we should make all of the text in the same case, with a lower case being the best option.
- Remove special characters and digits-This is another text preprocessing strategy that can handle the words 'hurray' and 'hurray!' or game45. Because this type of word is difficult to digest, it is preferable to eliminate it or replace it with an empty string. For this, we employ regular expressions.
- Tokenization - Converting sentences into words.
- Stopword Removal - Stopwords are the most common words that provide no meaningful information in a text. It includes words like 'they', 'there', 'this', 'there', 'a', 'an', and 'the'. NLTK library is a commonly used library for stopwords removal. We can quickly add any new word to a list of terms by using the added technique. The function removes stopwords () helps eliminate stopwords from a corpus while keeping the most important and contextual words.
- Lemmatization - In the same way, as stemming removes affixes words to get to a word's fundamental form, lemmatization does the same. In actuality, it's a technique for reducing words to their lemma by comparing them to a linguistic dictionary. WordNetLemmatizer is a tool provided by nltk. The stem is commonly used for lemmatization. Now we get the clean review for further procedure.

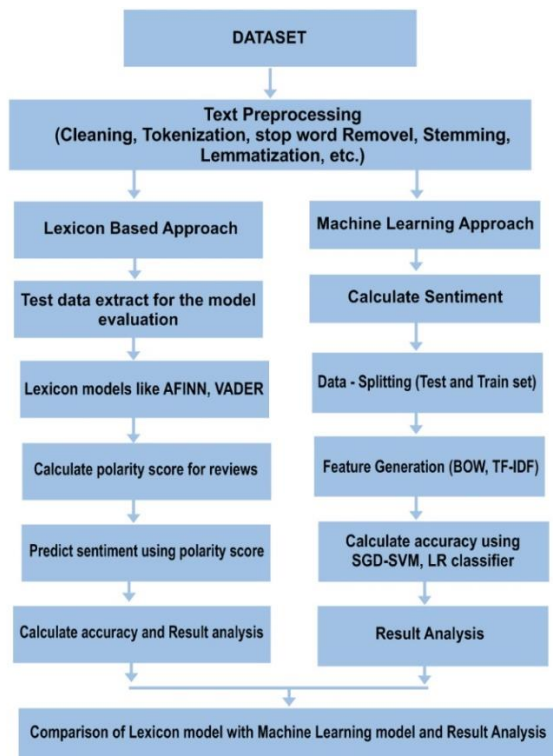


Fig. 1. The Flow of System Work.

A. Sentiment Calculation for ML Model

We calculate sentiment over 'Rating column in the dataset during supervised learning. Based on the rating column, we estimated sentiment. '1' denotes a positive sentiment, whereas '0' denotes a negative sentiment, the result of sentiment as depicted in Table I.

TABLE I. SENTIMENT EXAMPLE

Reviews	Sentiment
unique, great stay, wonderful time hotel monaco...	1(positive)
ok, nothing special charge diamond member hill...	0(negative)

B. Feature Engineering for Supervised Machine Learning Models with Bag of Word and TF-IDF

The process of transforming raw data into attributes helps aid predictive models in gaining a deeper understanding of the situation, resulting in enhancing the accuracy of previously unknown data. This is also known as feature engineering. The goal of feature-selection approaches is to reduce the dataset's dimensionality by deleting features that aren't essential to the classification [16]. A bag-of-words is converted text into vectors using the count vectorizer function. BOW extracts words from a text and creates a list of all the words and their frequency. To put it another way, a dictionary of all the words in the text is constructed. Because the structure of words and their meaning in context is gone, it is referred to as a bag of words. The combination of sequenced words in a text is referred to as an n-gram, with n denoting the number of words in the combination. When N equals 1, shows the text has a single word. If N equals 2, it refers to a pair of words that have been sequenced. In our classification, we used many types of N-grams, each of which yielded different results. Table II shows N-grams with various N values as an example based on the sentence "I like to eat pizza". The feature is employed as a bigram in our model.

TABLE II. N-GRAM

Value of N	Gram-Value	Example
N equals 1	Uni-gram	I, like, to, eat, pizza
N equals 2	Bi-gram	I like, like to, to eat, eat pizza
N equals 3	Tri-gram	I like to, like to eat, to eat pizza

1) Term Frequency-Inverse Document Frequency (TF-IDF) -The primary premise behind that words that occur more frequently in a document are given more weight than terms that appear less frequently. The frequency of each term is referred to as term frequency in this case. The tf-idf model performs effectively and prioritizes rare words over the binary bag of words approach, which treats all words equally [10]. Term frequency displays the significance of the word to a document, based on the assumption that the more terms in the document, the greater the importance.

$$tf = \text{frequency of a word} / \text{total word}$$

Inverse document frequency demonstrates how a term is genuinely useful. It is not required that a phrase that appears

frequently in some documents, such as stopwords, be relevant (the that, of, etc.). Stopwords obscure the context and should therefore be avoided. IDF operates in such a way that they are completely ignored calculated by:

$$IDF = \ln(\text{total no. of doc} / \text{no. of doc. that contain term})$$

2) Calculate TF-IDF for matrix generation- The tf-idf score (w) for a word in a corpus document is obtained by combining these two features. To create a composite weight for every phrase in each document by using the tf-idf model. Term 't' is given a weight in the document 'd' via the tf-idf weighting technique. When 't' appears repeatedly in a small number of documents, it has the maximum impact.

$$(tf - idf)_{t,d} = tf_{t,d} \times idf_t$$

When a term appears fewer or more times in a document, it is considered lower.

C. Classification Classifiers

The next stage is to use classification algorithms after preprocessing and feature selection. In the literature, several text classifiers have been proposed [17]. We employed machine learning algorithms such as SGD-Support Vector Machine (SVM) and Logistic Regression (LR).

- Support Vector Machine - Creates a decision boundary that is as robust as possible by using linearly separable classes. This indicates that the position of the boundary is determined by the points nearest to it. The decision boundary is a line or hyperplane that is as far away from either class's nearest training instance as possible. The SVM algorithm is a constraint-based optimization problem with inequality constraints. To address this problem, we employed support vector machine optimization with a hard margin (SGD).
- Stochastic Gradient Descent - Updates a set of coefficients by taking a "step" of a certain size in the opposite direction to the gradient, determining the gradient of the loss function at a specific point in the dataset, and updating the coefficients. The method modifies the coefficients iteratively, moving them away from the steepest ascent and toward the minimum, emulating a solution to the optimization issue.
- LR (Logistic Regression)- It is used when the dependent variable (target) is categorical. For binary and linear classification challenges, it is a simple and effective strategy. It's a straightforward classification model that produces outstanding results with linearly separable classes [18].

On a training review, build BOW and TF-IDF features, then transform test reviews into features and get the train and test shape. Using Logistic Regression and the SGD classifier for both features, before testing the model's performance, we fitted it to the train set and used predict to make predictions.

D. Sentiment Analysis using Unsupervised Lexicon-Based Models

This methodology stores specific information about words and phrases, such as sentiment polarity, objectivity, and subjectivity, with well knowledge bases, ontologies, lexicons, and databases. Many sentiment analysis methods rely heavily on an underlying opinion. "Lexicon features lists that are generally labeled according to their semantic orientation as either positive or negative is called sentiment lexicon" [21]. These lexicons frequently incorporate both positive and negative scores. There are a variety of popular lexical models for sentiment analysis. Some examples include the afinn and the Vader.

- AFINN Lexicon- It is one of the most basic and frequently used for sentiment analysis. It contains about 3300 words, each of which has a polarity score. The greatest features for conducting Twitter Sentiment Analysis are AFINN and Senti-strength. As a result, they're an excellent starting point for Twitter Sentiment Analysis [19].
- VADER Sentiment Lexicon- The sentiment dictionary with Valence The human-validated reasoning sentiment lexicon is of gold-standard quality [20]. It is open-source and included in the NLTK package, allowing it to be used directly on unlabeled text data. It is capable of detecting emotional polarity and intensity. It's a sentiment analysis model that can analyze a text by considering the text emotion's positive/negative polarity and its intensity. A decimal (float) value in the range [-1,1] indicates the text's polarity. It expresses the sentence's positive tone. When the polarity is less than zero it denotes negative polarity otherwise positive.

E. Sentiment Evaluation using Lexicon Model

Our unsupervised model, we used AFINN and VADER lexicon. We must first clean our data before proceeding with our analysis. It refers to the process of pre-processing and normalizing the text for analysis, which we have done earlier. Tokenized sentences are matched with words in the model to determine context and sentiment if any. We use a combining function such as sum or average to determine the final prediction about the overall text composition. In our work, using preprocessed data, we extract test reviews and test sentiments data for model evaluation. We then apply the above lexicon models to the reviews and calculate the polarity score as shown in Tables IIIA and IIIB.

TABLE III. (A). SENTIMENT AND POLARITY SCORE USING AFINN

Sample-Review	Sentiment	score
shame hotel wasn'tgood restaurant, arrived.....	negative	-0.5
great location, partial ocean view room larger.....	positive	19.0

(B).SENTIMENT AND POLARITY SCORE USING VADER

Sample-Review	Sentiment	score
shame hotel wasn't good restaurant, arrived.....	negative	-0.3
great location, partial ocean view room larger.....	positive	28.9

Using the polarity score, we predicted sentiment for review data, evaluated model performance, and predicted sentiment for positive and negative classes.

IV. RESULT AND DISCUSSION

We have done so to complete the experimental task. Due to any process, the maximum dataset which is to be generated is imbalanced. Using the above-mentioned data set, there are two columns in the dataset that is 'Review' and 'Rating'. Taking positive and negative reviews which have ratings (4,5) for positive and (1,2) for negative from the dataset. We used an imbalanced dataset with two classes ('positive' and 'negative') for work. Ten thousand sample reviews are taken from the dataset for a model. Review is preprocessed using the NLTK tool. The sentiment is calculated over the 'Rating label'. Training and testing sections of the dataset are separated, with test data making up 30% of the total for both machine learning and lexicon model, but only test data is used in the lexicon model. Various algorithms of machine learning are used for classification. The sentiment of the target dataset is utilized to generate features. In ML, feature generation was done by Bow and tf-idf, model is generated using classifiers such as SGD-SVM and logistic regression for accuracy calculation Stochastic Gradient Descent is used to solve hard margin support vector machine optimization. A fit function is used in the train set to fit the model and the prediction function applies to the test set, and objects were created for these functions. Can see in the Table IV(a) applied SVM and logistic regression as classifiers using a bag of word features for accuracy calculation. Table IV(b) shows that TFIDF features are used by both classifiers (SVM and LR) for accuracy. Stochastic Gradient Descent on Support Vector Machines was used. On comparing the result from the Table IV(a) and Table IV(b), we get that the SVM model performs well on both features. The SVM model using TF-IDF features performs the best, as can be observed, because of its high level of accuracy. 96.3 percent by displaying the graph

in Fig. 2. For both features, several classifiers such as MultinomialNB, Decision Tree, and Random Forest are used. On the bag of a word, these classifiers exhibit (82 percent, 74 percent, and 78 percent) accuracy, using tf-idf feature the classifiers give an accuracy of MultinomialNB, decision tree, and random forest (74 percent, 76 percent, and 78 percent). Hence we figure out that using tf-idf features our model shows the best result in supervised learning.

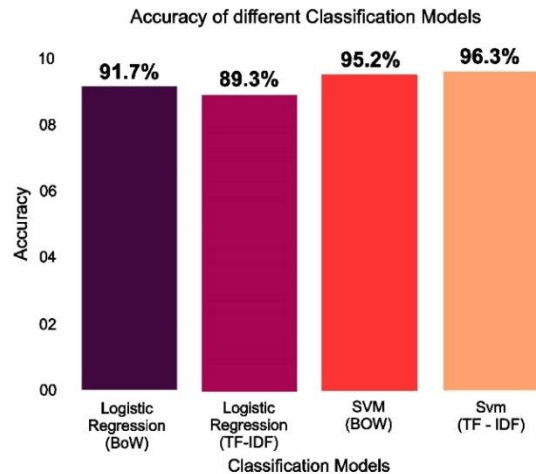


Fig. 2. Classification Model Accuracy.

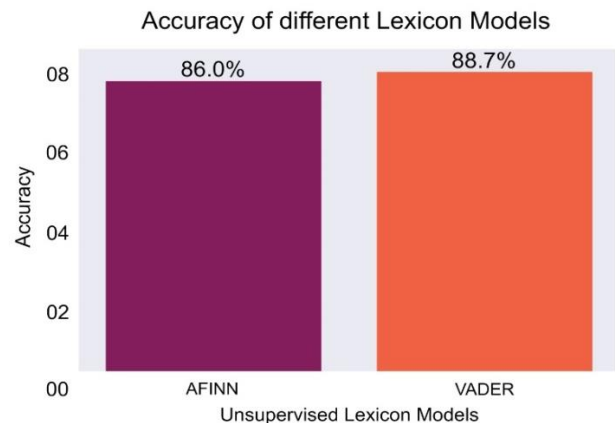


Fig. 3. Unsupervised Lexicon Model Accuracy

TABLE IV. (A). COMPARATIVE RESULT TABLE OF SUPERVISED LEARNING APPROACH USING BAG OF WORD

Class	LR-BOW				SVM-BOW			
	Precision	Recall	F1-Score	Accuracy	Precision	Recall	F-Score	Accuracy
0	0.86	0.59	0.70	0.917	0.87	0.84	0.85	0.952
1	0.92	0.98	0.95		0.97	0.97	0.97	

(B). COMPARATIVE RESULT TABLE OF SUPERVISED LEARNING APPROACH USING TFIDF

class	LR-TFIDF				SVM-TFIDF			
	Precision	Re-call	F1-score	Occur.	precision	Re-call	F1-Score	Occur.
0	0.97	0.36	0.53	0.893	0.95	0.82	0.88	0.963
1	0.89	1.00	0.94	-	0.97	0.93	0.98	

TABLE V. COMPARATIVE ANALYSIS OF PROPOSED APPROACH PERFORMANCE OF LEXICON-BASED APPROACHES

Class	AFINN Lexicon				VADER-Lexicon			
	Precision	Recall	F1-Score	Accuracy	Precision	Recall	F-Score	Accuracy
negative	0.59	0.78	0.67	0.86	0.91	0.43	0.58	0.887
positive	0.95	0.88	0.91		0.89	0.99	0.93	

During the unsupervised lexicon model, we extract 30% of test data. Proposed data are used in the model. For test review, the AFINN and VADER lexicon models were utilized to generate polarity scores and accuracy. We predicted sentiment using these polarity scores in the model. Positive and negative classes are used in it. The true label is used for the test sentiment whereas the predicted label is used for the predicted sentiment, for evaluating the model's performance. We used Afinn and Vader lexicon model for sentiment and accuracy. We calculate sentiment polarity using Afinn-score over the 'Review' column. For sentiment prediction, we used sentiment polarity. Now, the predicted label shows the predicted sentiment and the true label has test sentiment. We evaluate model performance and accuracy using these labels. Model performance using precision, recall, f-measure, accuracy for both classes. Performance results are shown in the Table V. The Vader ("Valence Aware Dictionary and sEntiment Reasoner") is a lexicon and rule-based tool for sentiment analysis. SentimentIntensityAnalyzer () function takes a string and produces a dictionary of scores in positive, negative, compound, etc. categories. A compounded score is a statistic that adds up all of the lexical ratings, normalized between -1 for the most severe negative and +1 for the most extreme positive. We apply this function over 'The 'Review' column of the dataset and predict sentiment using a compound score. We evaluated model performance using the predicted sentiment and test-sentiment label. On comparing the result for lexicon models, The Vader model exceeds the lexicon Afinn models with the highest 88.7% accuracy percent, which is depicted in the graph in Fig. 3.

Now, we compare both models, the supervised and unsupervised lexicon models. In the supervised model, on comparing Table IV(a) and (b) we get that SVM outperforms using feature *tf_idf* with the accuracy of 96.3% which is the VADER lexicon model performs well with 88.7% accuracy. As a result, the graph in Fig. 2 depicted a significant upgrade in the value of accuracy of classifier in the supervised model, and Fig. 3 shows the accuracy of lexicons in the unsupervised model, comparing the accuracy of both models from the graphs, we can see that the supervised model outperforms the lexicon approach.

V. CONCLUSION

In this paper, we analyze sentiment using both supervised and unsupervised models. For both features BoW and TFIDF, we employed SGD-SVM and logistic regression as classifiers, with bi-gram words in the classification model whereas AFINN and Vader lexicon was used in the unsupervised lexicon model. We discovered that the Vader lexical model is 88.7 percent more accurate than other lexical models. Other models' performance on the given data is found to be comparable to VADER. In terms of Supervised Learning

models, the SVM model on TF-IDF features is the best, with 96.3 percent accuracy. We may conclude that typical supervised models outperform lexicon models by equating the top models from both models. The limitation is that tone can be difficult to decipher vocally, and even more difficult to decipher in writing. Things become far more difficult when trying to analyze a huge volume of data having both subjective and objective responses.

REFERENCES

- [1] D.Khurana „A. Koli „K. Khatter., and S. Singh „, „Natural Language Processing: State of The Art”, Current Trends and Challenges”,<https://www.researchgate.net/publication/319164243>, August 2017.
- [2] H. Hassan Raza, M. Faizan, A. Hamza, A.Mushtaq „N. Akhtar.,” Scientific Text Sentiment Analysis using Machine Learning Techniques”, (IJACSA) International Journal of Advanced Computer Science and applications, Vol. 10, No. 12, 2019.
- [3] In European conference on machine learning (pp. 4-15). Springer, Berlin, Heidelberg, doi.org/10.1007/BFb0026666,1998.
- [4] M.lkonomakis., S.Kotsiantis., &V.Tampakas, ”Text classification using machine learning techniques” Issue 8, Volume 4, August 2005, pp. 966-974,WSEAS transactions on computers, 4(8), 966-974.
- [5] Md. Taufiqul Haque Khan Tusar, Md. Touhidul Islam, ” A Comparative Study of Sentiment AnalysisUsing NLP and Different Machine Learning Techniques on US Airline Twitter Data”, DOI:10.1109/ICECIT54077.2021.9641336,2021.
- [6] Venkateswarlu Bonta, Nandhini Kumaresh, and N. Janardhan, ” A Comprehensive Study on Lexicon Based Approaches for Sentiment Analysis”, Asian Journal of Computer Science and Technology ISSN: 2249-0701 Vol.8 No.S2, 2019, pp. 1-6.
- [7] Maite Taboada, Julian Brooke, Milan Tofiloski, Kimberly Voll, Manfred Stede, ” Lexicon-Based Methods for Sentiment Analysis”, https://doi.org/10.1162/COLI_a_00049, June 2011.
- [8] S.Elbagir and J.Yang., ” Twitter Sentiment Analysis Using Natural Language Toolkit and VADER Sentiment”, ISBN: 978-988-14048-5-5 ISSN: 2078-0958 (Print); ISSN: 2078-0966 (Online), Proceedings of the International MultiConference of Engineers and Computer Scientists 2019 IMECS 2019, March 13-15, 2019, Hong Kong.
- [9] Asghar MZ, Khan A, Ahmad S, Qasim M, Khan IA (2017) Lexicon-enhanced sentiment analysis framework using a rule-based classification scheme. PLoS ONE 12(2): e0171649. doi:10.1371.
- [10] B. Das, S. Chakraborty, ” An Improved Text Sentiment Classification Model Using TF-IDF and Next Word Negation”, 2018.pdf.
- [11] D.M.El-Din ” Enhancement Bag-of-Words Model for Solving the Challenges of Sentiment Analysis”, (IJACSA) International Journal of Advanced Computer Science and Applications, Vol. 7, No. 1, 2016.
- [12] Jawad Khan and Young-Koo Lee, ”LeSSA: A Unified Framework based on Lexicons and Semi-Supervised Learning Approaches for Textual Sentiment Classification”, Received: 21 November 2019; Accepted: 13 December 2019; Published: 17 December 2019.
- [13] J.Singh, G.Singh, and R.Singh, ” Optimization of sentiment analysis using machine learning classifiers”, Singh et al. Hum. Cent. Comput. Inf. Sci. (2017) 7:32 DOI 10.1186/s13673-017-0116-3.
- [14] W.Zhou, W. Hanbin, S. Hongguang, and S.Tieli, ” A Method of Short Text Representation Based on the Feature Probability Embedded Vector”, * Received: 4 July 2019; Accepted: 26 August 2019; Published: 28 August 2019.

- [15] Trip Advisor Hotel Review Dataset [https://doi.org/10.5281.zenodo.1219899](https://doi.org/10.5281/zenodo.1219899).
- [16] G. Forman, "An Experimental Study of Feature Selection Metrics for Text Categorization". *Journal of Machine Learning Research*, 3 2003, pp. 1289-1305.
- [17] Breiman, L. (2017). *Classification and regression trees*. Routledge.
- [18] Abdulhamit Subasi, "in *Practical Machine Learning for Data Analysis Using Python*", 2020.
- [19] M. S. Usha, Dr. M. Indra Devi, "Analysis of Sentiments using Unsupervised Learning Techniques", DOI: 10.1109/ICICES.2013.650820329, April 2013.
- [20] C.J. Hutto, Eric Gilbert, "VADER: A Parsimonious Rule-based Model for Sentiment Analysis of Social Media Text", 2014.
- [21] Liu, B. (2010), *Sentiment Analysis and Subjectivity*. In N. Indurkha & F. Damerou (Eds.), *Handbook of Natural Language Processing* (2nd ed.). Boca Raton, FL: Chapman & Hall.

COVID-19 Detection from X-Ray Images using Convoluted Neural Networks: A Literature Review

Othman A. Alrusaini

Department of Engineering and Applied Sciences
Applied College, Umm Al-Qura University
Makkah, Saudi Arabia

Abstract—This paper reviews a host of other peer-reviewed articles related to the detection of COVID-19 infection from X-ray images using Convoluted Neural Network (CNN) approaches. It stems from a background of a pandemic that has hit the world and negatively affected all spheres of life. The currently available testing mechanisms are invasive, expensive, time-consuming, and not everywhere. The paper considered 33 main articles supported by several other articles. The measurement metrics considered in this review are accuracy, precision, recall, F1-score, and specificity. The inclusion criteria for studies was that the article should have been written after the pandemic began, deliberates on CNN, and attempts to detect the disease from X-ray images. Findings suggest that transfer learning, support vector machines, long short-term memory, and other CNN approaches are highly effective in predicting the likelihood of the disease from X-rays. However, multi-class predictions seemed to score lowly on the accuracy score relative to their binary counterparts. Also, data augmentation significantly improved the performance of the models. Hence, the paper concluded that all reviewed approaches are effective. Recommendations are that analysts should integrate transfer learning procedures in the model formulation process, engage in data augmentation practices, and focus on classifying data based on binary classes.

Keywords—*Convoluted neural networks; COVID-19; chest x-ray; transfer learning; support vector machines; long short-term memory*

I. INTRODUCTION

COVID-19 is a respiratory disease caused by a relatively new virus belonging to the coronavirus family. It was discovered in late 2019, and it has since wreaked havoc globally [1] and compromised the global health system by clogging it with patients [2]. It has had a catastrophic effect on the economy, social lives, education, and other sectors of life. While the proportion of deaths resulting from this disease is low on average, the absolute number of deaths stands at 5.41 million [3]. One of the major issues aggravating the spread of COVID-19 is the fact that testing is not universally available to everyone [4, 5]. Governments prioritize persons with flu signs to take these tests. If one is detected positive, they are advised to quarantine and or hospitalized. This approach has helped arrest cases that would have spread undetected. The limitation with the testing approach is that there are limited testing equipment because of the novelty of the virus. Additionally, these testing systems are not available everywhere because some locations are remote. The tests are also invasive and time-consuming [6]. Artificial intelligence in

the form of convoluted neural networks comes in as a more convenient substitute [7]. It works by consolidating X-ray data from previously tested individuals and checking new ones against this database. The X-ray technology is available almost everywhere, which makes it a good candidate for a more inclusive testing system. With the right level of accuracy, it is possible for this new testing approach to become just as reliable.

The study investigates the effectiveness of different deep learning approaches in the detection of COVID-19 using X-ray images. The study is significant to stakeholders in the medical sector because the problem of testing individuals for the virus is clear [8, 9]. By presenting and discussing the effectiveness of different approaches, these practitioners will be able to objectively decide which approaches to adopt in enhancing the accuracy and reliability of their test results. The study is also significant to future researchers who may wish to read the comparisons between the selected approaches in detecting COVID-19 from examining X-ray images. The field of deep learning allows researchers to use several models in modeling problems and solutions. Not all models fit to all problem scenarios. Hence, this study will examine the approaches featuring prominently in the previous studies examining that have examined COVID-19 scenarios, which are CNN with transfer learning, CNN with support vector machines, CNN with Long Short-Term Memory, and other CNN approaches.

The first three approaches seem to be the basis of the majority of studies within the selected studies. The approaches have also been in use for quite some time, hence explaining the number of studies willing to integrate them into their models. Approaches that the researcher did not find to be thematically feature in many studies were consolidate in the fourth group of ‘other CNN approaches.’ A myriad of studies comprised this group. However, there was no central theme in the approaches considered within them. Finally, the study will investigate sundry approaches used in the detection of the virus from X-ray images. Ultimately, the study will compare the usefulness of these approaches with respect to their performance in precision, recall, F1-score, support, accuracy, sensitivity, specificity scores.

II. BACKGROUND

The COVID-19 pandemic is the worst pandemic that has plagued the world in recent times. It has succeeded in bringing the world to a halt in almost of spheres of life and has had a

devastating effect on the global population [10]. The economy has taken the biggest hit as estimates indicate that the global economy will have declined by about 5.7% in 2021 measured in GDP [11]. Social lives have also not been the same with stringent measures imposed on the public on how to interact with each other on top of travel restrictions. Places of worship have also experienced several restrictions from governing authorities [12]. But the most important statistics related to the number of people that have contracted the disease and those that have succumbed as a result. The World Health Organization estimates that there have been 274 million cases, while the number of deaths stands at 5.41 million [3]. Evidently, all people wish that this virus disappears because of the disastrous impact it has had on their lives and livelihoods.

To the time of writing, scientists have been successful in discovering an array of vaccines, which continue to be distributed across the world. The effectiveness of these vaccines to end the pandemic has been questioned because of several factors such as limited supply, vaccine hesitancy, and the rise of new variants like the most recent Omicron variant [13]. It seems that scientists have to strongly rely on testing and quarantining infected persons as a formidable way of arresting the virus. The challenges bedeviling this approach are many and significant. Firstly, the cost of testing is way beyond what ordinary people would afford, especially periodically [14]. Secondly, testing equipment is costly and limited in number. Thirdly, the tests take long before they are verified. The reading time taken by radiologists also needs to be reduced for efficiency purposes [15]. For these reasons (and many more), deep learning enthusiasts have been challenging themselves to map X-ray images from persons tested using the conventional approaches and mapping them to their results [16]. As a result, they have come up with models attempting to classify and predict one's COVID-19 status based on their chest X-ray scans.

The use of neural networks in classifying X-ray images of possible COVID-19 patients has been an ongoing research endeavor that has attracted the scholarly attention of several scholars, thereby creating a body of scholarly research that is growing by the day. These researchers have engaged with different methods, approaches, and techniques to improve the accuracy score of their models [5]. An examination of these approaches, techniques, and methods should inform the progress that has been made in this regard. It also gives other researchers the motivation to join the race for the attainment of 100% accuracy scores across the precision, recall, F1-score, support, accuracy, sensitivity, specificity scores [17]. This study reviews some of the most significant research papers that have engaged in this field, and therefore, compares the approaches used by the researchers.

III. METHODOLOGY

A. Study Design

The study adopts the design of a systematic literature review of peer-reviewed papers submitted and published in prominent journals. The review compares and contrasts findings reported in these studies and therefore gives an objective analysis on the same. The performance scores of the tests and procedures carried out in these analyses inform the

reliability of the approaches taken this study examines the accuracy, precision, recall/sensitivity, F1-score, specificity scores obtained in running the tests and suggests whether the approaches taken are reliable. These comparisons are the basis of the study recommending specific approaches while casting aspersions on the testing reliability of others.

B. Measurement Metrics

1) *Accuracy*: Accuracy refers to the level of correctness with which a model identifies the positives and negatives during classification. In a confusion matrix, True Positives and True Negatives are added and their ratio to the total number of subjects computed to give the accuracy score [18]. Many studies rely on this measure to determine the validity of their results.

2) *Precision*: Precision refers to the level of correctness with which a model identifies the positive cases out of all the positive cases detected. This computation involves taking the ratio of True Positives and False Positives from the confusion matrix [19]. It is a measurement metric that also features prominently in several studies.

3) *Recall (Sensitivity)*: Recall (otherwise known as sensitivity) refers to the proportion of correctly labelled positive cases against the total number of actual positive cases. It determines how accurately a model correctly detects positive cases [17]. The numerator is the number of positively labelled cases, while the denominator is the number of all positive cases regardless of whether they were detected as positive or not.

4) *F1-Score*: The F1-Score refers to a compromise between the precision and recall values. It is the harmonic mean between the two metrics [20]. The metric is reliable only if there is some balance between the two. Otherwise, if there is a tradeoff between them, the F1-Score is not likely to be high.

5) *Specificity*: Specificity refers to the proportion of actual negative cases that were predicted as negative by the model. It is the same as recall or sensitivity only that this time the group in focus contains negative cases.

C. Inclusion and Exclusion Criteria

The number of studies considered in this approach is 33, with additional studies backing up these papers by providing context. The researcher procedurally filtered out articles to remain with the ultimate 33 papers based on several criteria. On the criterion of relevance, several parameters were considered. Firstly, a study was considered only if it was about detecting COVID-19. Secondly, a study should be using CNN approaches for it to qualify. Thirdly, the CNN approaches should take chest X-ray images. On the time criterion, a study should have been conducted between 2019 and 2021. Since the disease was discovered in 2019, this filter did little to reduce the number of studies. Finally, the study considered the credibility criterion where a study was only considered if it was peer-reviewed. This filter was also responsible for eliminating web-based studies, those that did not have clear sources of data, and papers whose methodological approaches seemed flawed. Fig. 1 shows the paper search procedure, while Fig. 2 illustrates how the studies were filtered out.

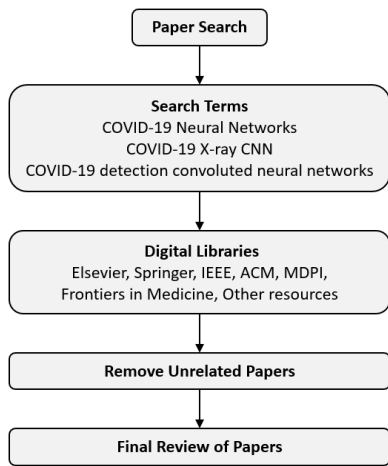


Fig. 1. Paper Search Procedure.

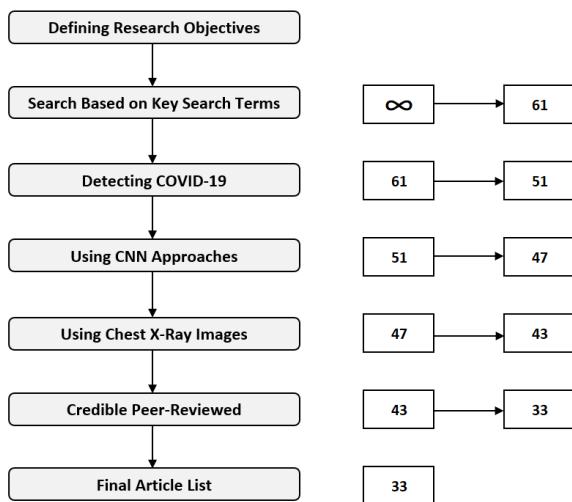


Fig. 2. Filtering Out Studies.

D. Definition of Key Terms and Abbreviations

ACGAN Auxiliary Classifier Generative Adversarial Network

ARIMA AutoRegressive Integrated Moving Average

AUC Area Under the Curve

Bayesnet Classifier A Bayesian network that is applied to CNN classification

CapsNet Capsule Neural Network

CFS Correlation-Based Feature Selection

CNN Convoluted Neural Networks

CNN-RF A hybrid of Convoluted Neural Network and Random Forest classifier

CNN-Softmax Convoluted Neural Network mostly applicable in a multi-class setting

Coro-Net One of the many models designed to detect coronavirus from xray images using CNN

DarkNet An open source high performance framework used to implement neural networks

DenseNet-121 It is a deep learning architecture that enable deep learning networks to to have a deeper reach but still maintain efficiency in its training

DTL Deep transfer learning

GDP Gross Domestic Product

Inception-ResNetV2 It builds on the inception family while also incorporating residual connections

InceptionV3 It is a CNN that assists in the detection of images and analysis of images

LSTM Long short-term memory

MobileNetV2 It is an architecture that assumes an inverted residual structure in which the input-output are thick bottleneck layers, and are not the expanded representation of the input

PA The Prophet Algorithm

ResNet It is an artificial neural network that works by stacking residual blocks to eventually form a network

ResNet101 A ResNet that is 101 layers deep

ResNet152 A ResNet that is 152 layers deep

ResNet18 A ResNet that is 18 layers deep

ResNet50 A ResNet that is 50 layers deep

ResNet50V2 A better performing version of ResNet50

RT-PCR Reverse transcription polymerase chain reaction

SqueezeNet It is a CNN that actively uses fire modules to reduce the number of parameters

SVM Support vector machines

VGG16 16 layers deep CNN

VGG19 19 layers deep CNN

Xception A CNN whose depth traverses 71 layers

IV. RESULTS

This section analyzes the application of three main CNN approaches in predicting COVID-19 positivity using X-ray images. The methods analyzed herein are transfer learning, support vector machines, and long-term short-term memory. Other minor CNN approaches are also analyzed in the fourth subsection. The goal is to establish their performance and with respect to the performance metrics discussed in the previous sections of this paper.

A. CNN with Transfer Learning

Several studies combined the convoluted neural networks with transfer learning to examine the model's outcome. In [21], the study applied a dense convoluted network with transfer learning and considered three labels, namely patients with COVID-19, with Pneumonia, and Normal. The study

worked with 112,120 chest X-ray images, which were obtained from 30,805 patients. The specific transfer learning approach adopted was known as twice-transfer learning whereby the study used the NIH ChestX-ray14 dataset as the intermediate step. The study reported an improvement in the model's effectiveness and the performance of the deep neural network, which is consistent with the findings established in [22]. Results indicated that the researchers were able to attain an accuracy of 100% on the dataset, which affirms the role played by transfer learning. These findings are similar to [23], whereby, the study employed the transfer learning approach with VGG19, MobileNetV2, Inception, Xception, and Inception-ResNetV2. The researchers assembled 1427 X-ray images. Accordingly, the study found that the application of the approach yielded remarkable positive results. The outcome yielded an accuracy of 96.78%, 98.66% sensitivity, and 96.46% specificity.

Some studies were prudent enough to mitigate the issue of small sample sizes by applying the transfer learning approach. The investigation by [24] is one such study, and it examined X-ray images to determine the effectiveness of deep learning and convoluted networks in detecting COVID-19. The dataset used consisted of 112 X-rays from each of the three classes – with COVID-19, with Pneumonia, and normal. Using transfer learning, the researchers successfully extracted knowledge from pre-trained models and used it on the model to be trained. Ultimately, the two best models by the study scored an accuracy of 95%. Sensitivity scores for the two best models VGG16 and VGG19 were 96% and 92%. Fig. 3 shows training loss, validation loss, training accuracy, and validation accuracy of the two top-performing epochs.

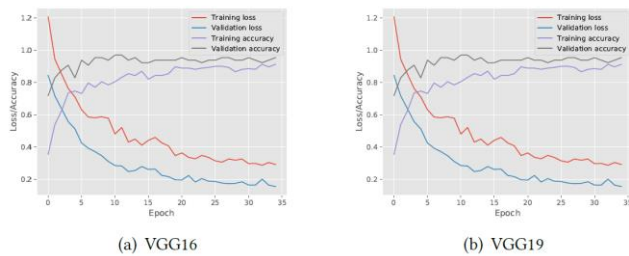


Fig. 3. Comparing VGG16 and VGG19 [24].

The investigation further constructed the confusion matrices for the models it ran, and the matrices for the two-top models VGG16 and VGG19 are shown in Fig. 4.

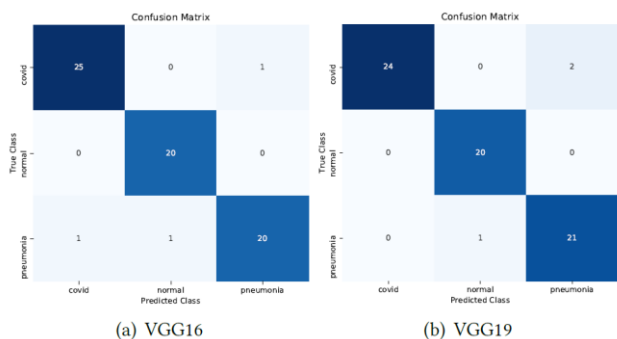


Fig. 4. Comparing Confusion Matrices between VGG16 and VGG19 [24].

Similar studies were conducted that reported findings resonating with those established in the above study. The research by [25] finds that transfer learning is an impeccable approach to boost the effectiveness of neural network models that predict COVID-19 from X-ray, ultrasound, and CT scan images. Using the VGG19 model, the study found that ultrasound images had the highest precision, which was 100%, followed by X-ray (86%), and CT scans (84%). Transfer learning algorithms are critical to the improvement of model results in neural networks [26]. Using publicly available datasets, the researchers report an accuracy of 96.3%, which they consider to be very high and reliable. The sample size employed was quite minimal as it comprised images from 65 male and 45 female sources, which totals 110. The confusion matrix suggests that out of the 34 sick patients, the model managed to correctly predict 33. On the other hand, out of the 75 normal cases, the model correctly predicted 72. Transfer learning was essential to attain these results because the approach extrapolates training models from other successful pre-trained data.

Transfer learning has also been used with InceptionV3 and ResNet50 models to predict COVID-19 based on X-ray images. The study by [27] developed a deep transfer learning (DTL) where they employed convoluted neural networks using X-ray data obtained from Kaggle. The dataset used comprised 160 COVID-19 X-ray images and another 160 normal X-ray images. The InceptionV3 model scored a 99.01% accuracy, while ResNet50 model managed to score an accuracy of 98.03%. The models' performance was slightly higher than other models against which the study was benchmarking its results. In [28], the study considered more than the two models encompassed in the study above. Specifically, the investigation considered DenseNet-121, SqueezeNet, ResNet18, and ResNet50. The dataset contained 5000 X-ray images. These neural networks were trained using the transfer learning approach on a subset of 2000 radiograms. 3000 images were used in validating the model. Findings suggested that the model's sensitivity rate was 98%, while its specificity rate was 90%.

Some studies have used the transfer learning approach to investigate the effectiveness of neural networks in predicting COVID-19 from X-ray images. The investigation by [20] examined VGG16 and VGG19 to establish which one maximizes the effectiveness of the model. Like many other studies, this investigation also used image data from public repositories, which had images classified into three groups, namely COVID-19, pneumonia, and normal. The highest AUC value was found to be 0.950 (95.0%) – VGG16. The VGG16 neural network achieved higher performance scores, where it obtained an accuracy of 95.9%, sensitivity of 92.5%, and specificity of 97.5%. Fig. 5 shows the accuracy level of the two neural networks across the number of fine-tuned convolutional blocks.

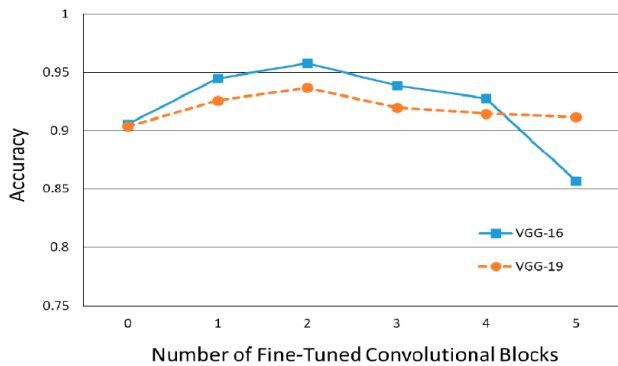


Fig. 5. Comparing the Accuracy of VGG16 and VGG19 Models [20].

Transfer learning can also be useful in building models that classify image data into more than three categories. In [29], the study employed this approach in classifying images into six diseases. The goal was to use X-ray data for known six diseases and determine whether or not the patients had COVID-19 too. The study used a dataset containing 3905 X-ray images. The specific neural network used in this investigation was MobileNetV2, which was trained using the data from patients suffering from the six diseases. Results showed that the classification accuracy was 87.66%. Other measures were accuracy (99.18%), sensitivity (97.36%), and specificity (99.42%). Table I shows the outcomes against the specific diseases.

TABLE I. CONFUSION MATRIX RESULTS [29]

	Actual classes						
	Covi d19	Ede ma	Effus ion	Emph ys ema	Fibr osis	Pneum onia	Nor mal
Predicted classes							
Covid19	21	0	1	1	0	1	0
Edema	270	254	210	199	155	171	136
Effusion	4	5	24	4	6	0	1
Emphysema	15	16	34	49	31	4	7
Fibrosis	46	17	35	50	78	3	18
Pneumonia	91	1	3	4	2	712	287
Normal	8	0	4	8	8	19	892

B. CNN with Support Vector Machines (SVMs)

Support vector machines have been in use to detect the likelihood of patients having the virus causing COVID-19. The study by [30] faults the generic means through which clinicians test for the virus, which is known as the real-time reverse transcription-polymerase chain reaction (RT-PCR) method. According to the source, the approach yields low positivity rates among persons who have recently contracted the virus. Hence, the study considers the method unreliable for such cases. Instead, the source suggests the use of CNN with support vector machines to conduct these tests. This method is

said to be effective because regardless of when one contracted the virus, chest X-rays of a normal person, that of a pneumonic person, and that of a COVID-19 infected person shall always be different. The dataset used for the analysis is from the first worldly available dataset on the same. The number of cases in the selected dataset was 71, where 48 were for COVID-19 infected persons, while the rest (23) were from normal people. The dataset also underwent augmentation to avoid possible overfitting by the model. This specific study reported an accuracy score of 90.5%. This value was acceptable but it was lower than that of using the CNN-SoftMax model. However, the selected approach scored a higher accuracy compared to the CNN-RF method. Table II compares the accuracy, sensitivity, specificity, and precision scores as reported in the study.

TABLE II. PERFORMANCE METRICS AGAINST DIFFERENT MODELS [30]

Classifier	Accuracy	Sensitivity	Specificity	Precision
CNN-Softmax	95.2%	93.3%	100%	100%
CNN-SVM	90.5%	86.7%	100%	100%
CNN-RF	81%	76.5%	100%	100%

The Support vector machines method has been used with kernel functions such as Gaussian, linear, cubic, and quadratic. In the study by [31], the goal was to establish the effectiveness of using support vector machines and neural networks in detecting COVID-19 in X-ray images. The model employed pre-trained models in training the data. The pretrained models that were used are the VGG16, the VGG19, the ResNet18, the ResNet50, and the ResNet101. The dataset contained 380 images data, 200 of which were for normally healthy persons, and the other 180 were from persons infected with the novel coronavirus. The ResNet50 fine-tuned model produced results with an accuracy of 92.6%. However, the ResNet50 when used with linear kernel produced an accuracy of 94.7%. The findings indicated that the deep learning methodologies are more efficient in detecting COVID-19 compared to the descriptors of local texture. These findings are also consistent with [32] and [33], which came to similar conclusions. Table III is a summary table comparing the performance of the selected neural network models in terms of their accuracy scores.

The confusion matrix below illustrates that out of the possible 45 COVID-19 cases, the model accurately predicted 43. On the other hand, out of the possible 50 non-COVID-19 cases, the model accurately predicted 45. Fig. 6 shows the confusion matrix associated with this analysis.

TABLE III. COMPARING ACCURACY SCORES ACROSS DEEP CNN MODELS [31]

Fine-tuning	Accuracy
VGG16	85.26%
ResNet18	88.42%
ResNet50	92.63%
ResNet101	87.37%
VGG19	89.47%

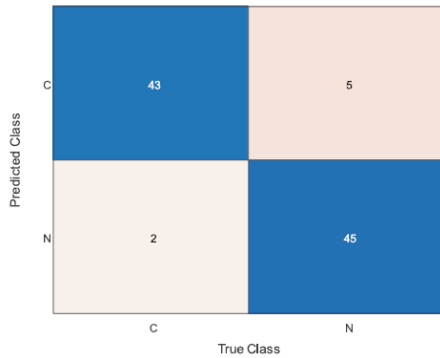


Fig. 6. Confusion Matrix [31].

At times, separating the classes into two (infected and not infected) can have a significant positive effect on the outcomes of models using the support vector matrix. In the study conducted by [34], the researchers used CNN to conduct feature extraction and support vector matrix as the classification method. Using InceptionV3, ResNet50, ResNet101, and Inception-ResNetV2 as the pre-trained models of choice, the study attempted to classify the data into two (infected versus not infected) and into three (COVID-19, pneumonia, and normal). The accuracy of the instrument was 97.33% when the researcher considered three classes, while it rose to 100% when the cases were separated into two. These findings suggest that the accuracy scores of a model can be significantly affected by the number of classification categories required. Fewer categories seem to produce more accurate results by the support vector-matrix model. Outcomes also suggested that the two top models were ResNet50 and ResNet101. Their confusion matrices as shown in Fig. 7.

C. CNN with Long Short-Term Memory (LSTM)

Some studies combined CNN with Long Short-Term Memory approach to predict the likelihood of a subject having COVID-19 based on their X-ray images. It is an architecture in the artificial recurrent neural network commonly used in deep learning [35]. It is different from conventional feedforward neural networks in that Long Short-Term Memory approach has feedback connections [36]. For this reason, the network can process entire data sequences as opposed to processing a single data sequence. Its name is inspired by the fact that programs use short term memory structures to generate long-term memory. The complexity of LSTM models has made them perfect candidates for solving complex machine learning problems such as speech recognition, machine translation, and many more. In image classification, LSTM has also been a formidable and reliable approach as noted in [37]. The study finds that the proposed classification method using LSTM is far more effective in classifying images than other state-of-the-art classification methods.

The use of CNN and LSTM has been found to result in high levels of accuracy. In [38], the study introduced a combined CNN-LSTM model of predicting the likelihood of COVID-19 infection given X-ray images. CNN was responsible for extracting features from the images, while LSTM was the method used to classify these images. The

research utilized 4575 X-rays from random subjects. Among the images, 1525 were for confirmed COVID-19 cases. Another 1525 were from patients with regular pneumonia, while the other 1525 from for normal patients without pneumonia and COVID-19. The outcome suggested that the accuracy of this model stands at 99.4%. Its AUC was 99.9%, F1-Score 98.9%, sensitivity 99.3%, and a specificity of 99.2%. The performance of the combined model was far more effective compared to if LSTM was not used. Fig. 8 shows the confusion matrices obtained from running the model on the data comparing the usage of LSTM and the lack of it. Evidently, using LSTM improved the model's performance by reducing incorrectly predicted COVID-19 cases from 3 to 2.

LSTM has been used alongside other methods to predict COVID-19 infection based on X-ray images. One study used CNN with LSTM, autoregressive integrated moving average (ARIMA), and the Prophet Algorithm (PA) [39]. Overall results suggest that the accuracy of the models ranged between 92.33% and 99.94% when predicting confirmed cases. The models seemed to perform relatively poor in predicting recovered and death cases. For the recovered cases, the best model attained an accuracy of 90.29%, while the worst model achieved an accuracy metric of 63.52%. Regarding death cases, the best model attained 94.18% as its accuracy value, while the worst model attained an accuracy value of 78.02%. Findings from the study established that while LSTM did well to predict confirmed and death cases, the model performed relatively poor in predicting recovered cases. All the same, LSTM seemed more effective in predictions compared to ARIMA. However, the Prophet Algorithm was the best model of the three in predicting all of confirmed, recovered, and death cases. Other studies that have affirmed the reliability of LSTM in COVID-19 prediction are [40] and [41]. Table IV compares the performance of the various models used in the study.

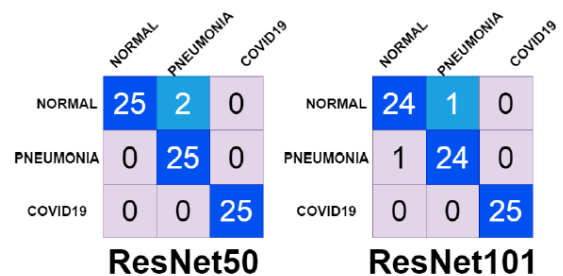


Fig. 7. Comparing Confusion Matrices ResNet50 and ResNet101 [34].

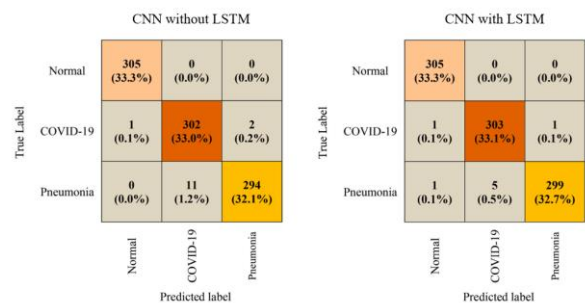


Fig. 8. Comparing Models with and without LSTM [38].

TABLE IV. PA, ARIMA AND LSTM PERFORMANCE SCORES [39]

Prediction Algorithm	Accuracy
PA (confirmed cases)	99.94%
PA (recovered cases)	90.29%
PA (death cases)	94.18%
ARIMA (confirmed cases)	92.33%
ARIMA (recovered cases)	63.52%
ARIMA (death cases)	78.02%
LSTM (confirmed cases)	94.16%
LSTM (recovered cases)	86.44%
LSTM (death cases)	92.76%

D. Other CNN Approaches

Many other studies utilized various approaches in reaching the same goal. The study by [42] found that by leveraging Auxiliary Classifier Generative Adversarial Network (ACGAN), the model's accuracy improved from 85% to 95%. In another study by [43], the researchers engage in a model utilizing depthwise convolution with fluctuating rates of dilation in a multi-class detection system. The COVID-normal test produced an accuracy score of 97.4%. In [44], the study considered 1215 images sourced online, which were taken through an augmentation process to end up with 1832 images. Furthermore, the study engaged in stage-I and stage-II deep network model designing. Using these methods and techniques, the ultimate model attained an accuracy of 97.7%, a precision value of 97.14%, and a recall value of 97.14%. The conclusion was that the model was effective in predicting COVID-19 infection from X-ray images. Another study reported in [45] developed a model that utilized the concatenation of Xception and ResNet50V2 networks. The researchers trained several deep convolutional networks, while leveraging 11,302 X-ray images sourced online. The proposed model achieved an accuracy of 99.5%. For this reason, the authors find the model effective and reliable in determining whether a patient is infected with COVID-19. Other studies that employed the Xception model and reported similar findings are [46, 47]. It underscores the importance of the pre-trained model in detecting COVID-19 infections.

Some studies have established that there is a big difference when considering binary class and multi-class situations in favor of binary. For example, classifying X-ray images into COVID-19 and non-COVID yields a higher accuracy value compared to if the classes are COVID-19, pneumonia, and healthy. The investigation reported in [48] used the DarkNet model in classifying the X-ray images. Findings from the investigation suggest that classification accuracy when using binary classes was 98.08%, while that obtained in a multi-class situation is 87.02%. Another study that utilized binary classification is [49], which assembled four classes, namely bacterial pneumonia, viral pneumonia, COVID-19, and healthy groups. Studies such as [50] use one pre-trained CNN model, the researchers adopted five pre-trained CNN-based models of ResNet101, ResNet50, ResNet152, Inception-ResNetV2, and InceptionV3. Findings indicated that ResNet50 was the most effective as it resulted in 99.7% in one of the datasets used. It indicates that this pre-trained model is also effective in detecting COVID-19.

In [51], the study used the ResNet101 CNN to examine the effectiveness of deep learning in detecting COVID-19 from X-ray images. The researchers used publicly available chest radiographs in the thousands, some of which were from confirmed COVID-19 patients. Findings established that the accuracy of the resultant model was 71.9%, while its sensitivity and specificity were 77.3% and 71.8%, respectively. The training process involved creating a model that would positively identify radiographs images with chest abnormalities. The study's strength is that it used mutually exclusive publicly available data and that it used labels with a strong clinical association with COVID-19 cases.

Multi-CNN is another approach used in modeling and classification of image data in artificial intelligence. The approach was used in [49], and it involved utilizing Bayesnet Classifier and Correlation-Based Feature Selection (CFS). Using two datasets, the multi-CNN method was tested. The first dataset contained 453 X-ray images from COVID-19 patients and 497 images from patients without the disease. The accuracy of the model on this dataset was 91.16% and an AUC of 96.3%. The second dataset contained 78 X-ray images; 71 of which were from COVID-19-infected patients. Findings on this data suggested that the accuracy score was 97.44% and an AUC of 91.1%. The study concluded that pre-trained multi-CNN was more effective in detecting the disease compared to using single-CNN approaches.

Some studies have utilized capsule neural networks in detecting COVID-19 from X-ray images. Capsule networks are a form of artificial neural networks, and they are known for their ability to fetch spatial information thereby exhibiting great performance. Some studies used the method CapsNet to detect COVID-19 and found that binary classes seem to perform better than multi-class approaches [52, 18]. An analysis of the model's performance on binary classes obtained an accuracy score of 97.24%, while in the multi-class, the score was 84.22% in [52]. The study concluded that it is a reliable model for physicians to use in conveniently detecting the COVID-19 status of their patients. Fig. 9 shows the confusion matrices comparing the results of the two analyses with binary and multi-class situations.

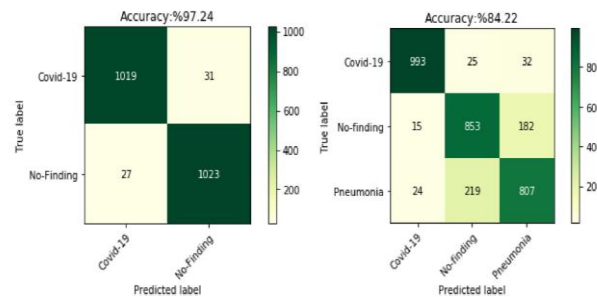


Fig. 9. Comparing Binary and Multi-Class Approaches [52].

The decision tree classifier has also been used in some studies alongside CNN to detect COVID-19 infection from X-ray images. The studies by [53, 54] find the RT-PCR test as inconvenient as it is not time-friendly and it is also not affordable to the populace. The researchers suggest a system that utilizes the decision tree algorithm to separate COVID-19

cases from the rest. The first separation occurs by isolating normal scans from abnormal ones. The second step in the decision tree classification involves telling between those that have signs of tuberculosis among the abnormal scans. The third step is similar to the second step only that this time it does so for COVID-19. The accuracy scores of these steps are 98%, 80%, and 95% for the respective steps.

V. DISCUSSION

Many of the studies adopted transfer learning as their preferred method in attempting to improve the effectiveness of the model. Findings have been quite consistent in establishing that this method boosts the performance scores across accuracy, sensitivity, precision, and F1-scores. According to [27], transfer learning improves model effectiveness by ensuring that the analyst does not spend too much time training new models. Instead, an analyst relies on previously trained models with some few improvements. The study by [23] finds that using transfer learning is a key consideration among many analysts when dealing with CNN. Some studies have reported increased accuracy values running up to 100%. It underscores the need for data analysts to embrace this approach in their endeavors, as it has proven to be reliable. Therefore, it is understandable why several studies settled for this approach. One important take-away from the review of transfer learning approach is that binary-class classification seems to be performing better than multi-class classification. Data augmentation was also prominent in this approach, which also contributed to the heightened effectiveness of the resultant models.

The use of support vector machines in classifying images to detect COVID-19 infections was also clear from this review. This approach has been lauded in [34] as a formidable supervised approach to image classification because of its ability to classify and regress too. When combined with functions such as Gaussian, linear, cubic, and quadratic, its performance increases even further. While it is a relatively new classification method, its adoption in this regard is a

testament to its effectiveness and reliability. The method is highly memory-efficient because its decision function uses a subset of training points. Perhaps, the only disadvantage with the SVM approach is that it is not efficient for large datasets because of the time it would take to train the model. For the case of COVID-19 detection, the required data does not have to be massive. Even here, data augmentation featured significantly, and it also positively affected the strength of the resultant models.

CNN with Long Short-Term Memory also featured prominently in this review. Findings were clear that combining CNN with LSTM significantly improves the accuracy of the trained models. This view is consistent with [36] where the researchers argue that this approach is an area of growing interest because of its effectiveness. The large range of parameters provided by LSTM and the input and output biases strongly argue the case for its adoption in CNN classification models. The method is also a bit insensitive to gap length, which is an advantage it holds against the RNN. Such advantages seem to give the LSTM approach an edge and explain why data scientists would prefer to work on models that encapsulate this approach. LSTM in binary classification seemed to be more accurate than in multi-class classification situations.

CNN has its pre-trained models that some studies have evidently taken advantage of to predict COVID-19 infections. Their usage is evident among the studies encapsulated in the 'other CNN approaches' subsection. Examples of common models are DenseNet-121, SqueezeNet, ResNet18, and ResNet50, among others [50]. They have proven to be highly effective in accurately predicting the disease based on X-ray images. Even here, binary-class classification seems to be performing better than multi-class classification. The use of decision tree classification was outstanding though it could not accurately predict recovery and death rates.

Table V summarizes the findings and limitations of articles consulted throughout this paper.

TABLE V. SUMMARY OF CONSULTED

#	Publication	Author Date	Accuracy	Sensitivity	Specificity	F1-Score	Purpose	Model or Approach	Limitation
1	[21]	(Bassi & Attux, 2021)	100.0%	100.0%	100.0%	100.0%	Detecting COVID-19 using X-ray images	Transfer Learning	Only 150 images
2	[22]	(Heidari, et al., 2020)	94.5%	98.4%	98.0%	-			Only investigates and tests two image preprocessing methods
3	[23]	(Apostolopoulos & Mpesiana, 2020)	96.8%	98.7%	96.5%	-			More patient data needed
4	[24]	(Makris, et al., 2020)	95.0%	-	-	-			None indicated
5	[25]	(Horry, et al., 2020)	86.0%	86.0%	86.0%	86.0%			Inadequate data
6	[26]	(Vaid, et al., 2020)	96.3%	-	-	-			Lack of publicly available and expert labeled images
7	[27]	(Benbrahim, et al., 2020)	98.03% - 99.01%	-	-	-		Transfer Learning, InceptionV3, ResNet50	---

8	[28]	(Minaee, et al., 2020)	-	98.0%	90.0%	-		Transfer Learning, ResNet18, ResNet50, SqueezeNet, and DenseNet-121	Limited number of COVID-19 images
9	[29]	(Apostolopoulos, et al., 2020)	99.18%	97.36%	99.42%	-		Transfer Learning, MobileNetV2	---
10	[30]	(Alqudah, et al., 2020)	95.2%	93.3%	100.0%	100.0%		SVM	The need for more classifier types
11	[31]	(Ismael & Şengür, 2021)	94.74%	91.0%	98.89%	94.79%		SVM, ResNet50	---
12	[32]	(Saraswati, Wardani, & Indradewi, 2020)	93.91%	98.75%	89.06%	91.26%		SVM	---
13	[33]	(Saygılı, 2021)	94.5%	92.25%	90.00%	-			---
14	[34]	(Novitasari, et al., 2020)	97.3% - 100.0%	-	-	-		SVM, ResNet50, ResNet101	Model time processing is long
15	[36]	(Sherstinsky, 2020)	-	-	-	-	Fundamentals of LSTM		---
16	[37]	(Öztürk & Özkaya, 2021)	-	-	-	-	Image Classification		---
17	[38]	(Islam, et al., 2020)	99.4%	99.3%	99.2%	98.9%		LSTM	Small sample size
18	[39]	(Alazab, et al., 2020)	95.0–99.0%	-	-	95.0-99.0%			---
19	[40]	(Demir, 2021)	100.0%	100.0%	100.0%	-			---
20	[41]	(Naeem & Bin-Salem, 2021)	98.94%	99.00%	99.00%	99.00%			Limited number of COVID-19 images
21	[42]	(Waheed, et al., 2020)	95.0%	90.0%	97.0%	-		ACGAN	Small dataset
22	[43]	(Mahmud, et al., 2020)	97.4%	97.8%	94.7%	97.1%		Inception, VGG-19	---
23	[44]	(Jain, et al., 2020)	98.9%	98.9%	98.7%	98.2%		ResNet50, ResNet101	Limited number of COVID-19 images
24	[45]	(Rahimzadeh & Attar, 2020)	99.5%	80.5%	-	-		ResNet50V2 and Xception	Small dataset
25	[46]	(Khan, et al., 2020)	89.6%	-	-	-	Detecting COVID-19 using X-ray images	Coro-Net, SVM	More testing required
26	[47]	(Singh, et al., 2020)	95.8%	95.6%	-	95.9%		XceptionNet	---
27	[48]	(Ozturk, et al., 2020)	98.1%	95.1%	95.3%	96.5%		DarkNet	Limited number of COVID-19 images
28	[49]	(Abraham & Nair, 2020)	91.2%	85.3%	98.5%	91.4%		Bayesnet Classifier	Not tested in a multi-class environment
29	[50]	(Narin, et al., 2021)	94.2%	95.4%	83.5%	74.8%		ResNet50, ResNet101, ResNet152	Limited number of COVID-19 images
30	[51]	(Che Azemin, et al., 2020)	71.9%	77.3%	71.8%	-		ResNet101	Inadequate data
31	[52]	(Toraman, et al., 2020)	97.4%	97.2%	97.0%	97.2%		CapsNet	Small dataset
32	[53]	(Yoo, et al., 2020)	95.0%	97.5%	90.0%	-		ResNet18	---
33	[54]	(Hassantabar, et al., 2020)	93.2%	96.1%	-	-		CNN-Softmax	---

VI. LIMITATIONS

One of the most significant limitations of this study is that the COVID-19 virus is still mutating. As such, it is difficult to tell whether the virus will mutate into a state that causes different patterns on the X-ray image. If this happens, there will be a need to redo the models to fit this new data. Another limitation is that the data sourced by the various studies is not the same. Some sourced it from public repositories, some did so from private sources, some combined the two, while some engaged in augmentation practices. It would be more valid and reliable if the studies had sourced their data from the same source and applied the different methods. In such a situation, it would be reasonable to compare the accuracy scores and determine which method is more effective. Thirdly, some studies applied multiple methods and approaches to their model building process. It is difficult to tell which of the component approaches contributed mostly to the model's effectiveness or whether they did not.

VII. CONCLUSION AND RECOMMENDATIONS

The study concludes that all the approaches reviewed in the discourse are valid and reliable. The slight differences in accuracy scores are not significant enough to warrant writing off some of the approaches. All of transfer learning, support vector machines, long short-term memory, and other CNN approaches delivered results that were basically above 90%. It explains the growing preference among physicians to use these technological methods in detecting COVID-19 early enough. The methods are all non-invasive, more affordable, and available almost everywhere because the only requirement is a chest X-ray of the subject. For the sake of improving the model's accuracy, the study makes the following recommendations.

1) Integrate transfer learning procedures in the model formulation process. The study has established that transfer learning boosts the formidability of models by allowing them to learn from previously trained models and data.

2) Engage in data augmentation practices. In the pre-processing segment of the data analysis phase, there is a need to augment data, especially where data is scarce. This study has found that data augmentation positively impacts the strength and viability of a CNN model.

3) Focus on classifying data based on binary classes. Throughout this review, whenever a study compared the accuracy scores between binary- and multi-class situations, the binary-class scenario produced better results. Hence, it is prudent to consider it the main focus of model formulation.

REFERENCES

- [1] T. Goel, R. Murugan, S. Mirjalili and D. K. Chakrabarty, "OptCoNet: an optimized convolutional neural network for an automatic diagnosis of COVID-19," *Applied Intelligence*, vol. 51, no. 3, pp. 1351-1366, 2021.
- [2] N. K. Chowdhury, M. M. Rahman and M. A. Kabir, "PDCOVIDNet: a parallel-dilated convolutional neural network architecture for detecting COVID-19 from chest X-ray images," *Health information science and systems*, vol. 8, no. 1, pp. 1-14, 2020.
- [3] WHO, "WHO Coronavirus (COVID-19) Dashboard," 17 December 2021. [Online]. Available: <https://covid19.who.int/>. [Accessed 17 December 2021].
- [4] D. Singh, V. Kumar and M. Kaur, "Classification of COVID-19 patients from chest CT images using multi-objective differential evolution-based convolutional neural networks," *European Journal of Clinical Microbiology & Infectious Diseases*, vol. 39, no. 7, p. 137, 2020.
- [5] M. Elgendi, M. U. Nasir, Q. Tang, R. R. Fletcher, N. M. C. Howard and S. Nicolaou, "The performance of deep neural networks in differentiating chest X-rays of COVID-19 patients from other bacterial and viral pneumonias," *Frontiers in Medicine*, vol. 7, no. 1, p. 550, 2020.
- [6] J. Civit-Masot, F. Luna-Perejón, M. Domínguez Morales and A. Civit, "Deep learning system for COVID-19 diagnosis aid using X-ray pulmonary images," *Applied Sciences*, vol. 10, no. 13, p. 4640, 2020.
- [7] M. Shorfuazzaman and M. S. Hossain, "MetaCOVID: A Siamese neural network framework with contrastive loss for n-shot diagnosis of COVID-19 patients," *Pattern recognition*, vol. 113, no. 1, p. 107700, 2021.
- [8] L. Li, T. Shim and P. E. Zapanta, "Optimization of COVID-19 testing accuracy with nasal anatomy education," *American journal of otolaryngology*, vol. 42, no. 1, p. 102777, 2021.
- [9] M. N. Esbin, O. N. Whitney, S. Chong, A. Maurer, X. Darzacq and R. Tjian, "Overcoming the bottleneck to widespread testing: a rapid review of nucleic acid testing approaches for COVID-19 detection," *Rna*, vol. 26, no. 7, pp. 771-783, 2020.
- [10] L. Wang, Z. Q. Lin and A. Wong, "Covid-net: A tailored deep convolutional neural network design for detection of covid-19 cases from chest x-ray images," *Scientific Reports*, vol. 10, no. 1, pp. 1-12, 2020.
- [11] M. Szmigiera, "Impact of the coronavirus pandemic on the global economy - Statistics & Facts," 23 November 2021. [Online]. Available: <https://www.statista.com/topics/6139/covid-19-impact-on-the-global-economy/#dossierKeyfigures>. [Accessed 17 December 2021].
- [12] S. A. Quadri, "COVID-19 and religious congregations: Implications for spread of novel pathogens," *International Journal of Infectious Diseases*, vol. 96, no. 1, pp. 219-221, 2020.
- [13] M. Lipsitch and N. E. Dean, "Understanding COVID-19 vaccine efficacy," *Science*, vol. 370, no. 6518, pp. 763-765, 2020.
- [14] M. A. Pettengill and A. J. McAdam, "Can we test our way out of the COVID-19 pandemic?," *Journal of clinical microbiology*, vol. 58, no. 11, pp. e02225-20, 2020.
- [15] F. M. Salman, S. S. Abu-Naser, E. Alajrami, B. S. Abu-Nasser and B. A. Alashqar, "Covid-19 detection using artificial intelligence," *First Journal of Biomedical Research*, vol. 1, no. 1, p. 1, 2020.
- [16] C. Shorten, T. M. Khoshgoftaar and B. Furht, "Deep Learning applications for COVID-19," *Journal of big Data*, vol. 8, no. 1, pp. 1-54, 2021.
- [17] T. B. Alakus and I. Turkoglu, "Comparison of deep learning approaches to predict COVID-19 infection," *Chaos, Solitons & Fractals*, vol. 140, no. 1, p. 110120, 2020.
- [18] G. Gilanie, U. I. Bajwa, M. M. Waraich, M. Asghar, R. Kousar, A. Kashif and H. Rafique, "Coronavirus (COVID-19) detection from chest radiology images using convolutional neural networks," *Biomedical Signal Processing and Control*, vol. 66, no. 1, p. 102490, 2021.
- [19] C. Ouchicha, O. Ammor and M. Meknassi, "CVDNet: A novel deep learning architecture for detection of coronavirus (Covid-19) from chest x-ray images," *Chaos, Solitons & Fractals*, vol. 140, no. 1, p. 110245, 2020.
- [20] K. S. Lee, J. Y. Kim, E. T. Jeon, W. S. Choi, N. H. Kim and K. Y. Lee, "Evaluation of scalability and degree of fine-tuning of deep convolutional neural networks for COVID-19 screening on chest X-ray images using explainable deep-learning algorithm," *Journal of Personalized Medicine*, vol. 10, no. 4, p. 213, 2020.
- [21] P. R. Bassi and R. Attux, "A deep convolutional neural network for COVID-19 detection using chest X-rays," *Research on Biomedical Engineering*, vol. 1, no. 1, pp. 1-10, 2021.
- [22] M. Heidari, S. Mirmiaharikandehi, A. Z. Khuzani, G. Danala, Y. Qiu and B. Zheng, "Improving the performance of CNN to predict the likelihood of COVID-19 using chest X-ray images with preprocessing algorithms," *International journal of medical informatics*, vol. 144, no. 1, p. 104284, 2020.

- [23] I. D. Apostolopoulos and T. A. Mpesiana, "Covid-19: automatic detection from x-ray images utilizing transfer learning with convolutional neural networks," *Physical and Engineering Sciences in Medicine*, vol. 43, no. 2, pp. 635-640, 2020.
- [24] A. Makris, I. Kontopoulos and K. Tserpes, "COVID-19 detection from chest X-Ray images using Deep Learning and Convolutional Neural Networks," in *11th Hellenic Conference on Artificial Intelligence*, Athens, City Publishers, 2020, pp. 60-66.
- [25] M. J. Horry, S. Chakraborty, M. Paul, A. Ulhaq, B. Pradhan, M. Saha and N. Shukla, "COVID-19 detection through transfer learning using multimodal imaging data," *IEEE Access*, vol. 8, no. 1, pp. 149808-149824, 2020.
- [26] S. Vaid, R. Kalantar and M. Bhandari, "Deep learning COVID-19 detection bias: accuracy through artificial intelligence," *International Orthopaedics*, vol. 44, no. 1, pp. 1539-1542, 2020.
- [27] H. Benbrahim, H. Hachimi and A. Amine, "Deep transfer learning with apache spark to detect covid-19 in chest x-ray images," *Romanian Journal of Information Science and Technology*, vol. 23, no. S, SI, pp. S117-S129, 2020.
- [28] S. Minaee, R. Kafieh, M. Sonka, S. Yazdani and G. J. Soufi, "Deep-covid: Predicting covid-19 from chest x-ray images using deep transfer learning," *Medical image analysis*, vol. 65, no. 1, p. 101794, 2020.
- [29] I. D. Apostolopoulos, S. I. Aznaouridis and M. A. Tzani, "Extracting possibly representative COVID-19 biomarkers from X-ray images with deep learning approach and image data related to pulmonary diseases," *Journal of Medical and Biological Engineering*, vol. 1, no. 1, p. 1, 2020.
- [30] A. M. Alqudah, S. Qazan, H. Alquran, I. A. Qasmieh and A. Alqudah, "Covid-19 detection from x-ray images using different artificial intelligence hybrid models," *Jordan Journal of Electrical Engineering*, vol. 6, no. 2, pp. 168-178, 2020.
- [31] A. M. Ismael and A. Şengür, "Deep learning approaches for COVID-19 detection based on chest X-ray images," *Expert Systems with Applications*, vol. 164, no. 1, p. 114054, 2021.
- [32] N. W. S. Saraswati, N. W. Wardani and I. G. A. A. D. Indradewi, "Detection of Covid Chest X-Ray using Wavelet and Support Vector Machines," *Int. J. Eng. Emerg. Technol*, vol. 5, no. 2, pp. 116-121, 2020.
- [33] A. Saygılı, "Computer-Aided Detection of COVID-19 from CT Images Based on Gaussian Mixture Model and Kernel Support Vector Machines Classifier," *Arabian Journal for Science and Engineering*, vol. 1, no. 1, pp. 1-19, 2021.
- [34] D. C. R. Novitasari, R. Hendradi, R. E. Caraka, Y. Rachmawati, N. Z. Fanani, A. Syarifudin and R. C. Chen, "Detection of covid-19 chest x-ray using support vector machine and convolutional neural network," *Commun. Math. Biol. Neurosci*, vol. 1, no. 1, p. 202, 2020.
- [35] G. Van Houdt, C. Mosquera and G. Nápoles, "A review on the long short-term memory model," *Artif. Intell. Rev*, vol. 53, no. 8, pp. 5929-5955, 2020.
- [36] A. Sherstinsky, "Fundamentals of recurrent neural network (RNN) and long short-term memory (LSTM) network," *Physica D: Nonlinear Phenomena*, vol. 404, no. 1, p. 132306, 2020.
- [37] Ş. Öztürk and U. Özkaya, "Residual LSTM layered CNN for classification of gastrointestinal tract diseases," *Journal of Biomedical Informatics*, vol. 113, no. 1, p. 103638, 2021.
- [38] M. Z. Islam, M. M. Islam and A. Asraf, "A combined deep CNN-LSTM network for the detection of novel coronavirus (COVID-19) using X-ray images," *Informatics in medicine unlocked*, vol. 20, no. 1, p. 100412, 2020.
- [39] M. Alazab, A. Awajan, A. Mesleh, A. Abraham, V. Jatana and S. Alhyari, "COVID-19 prediction and detection using deep learning," *International Journal of Computer Information Systems and Industrial Management Applications*, vol. 12, no. 1, pp. 168-181, 2020.
- [40] F. Demir, "DeepCoroNet: A deep LSTM approach for automated detection of COVID-19 cases from chest X-ray images," *Applied Soft Computing*, vol. 103, no. 1, p. 107160, 2021.
- [41] H. Naeem and A. A. Bin-Salem, "A CNN-LSTM network with multi-level feature extraction-based approach for automated detection of coronavirus from CT scan and X-ray images," *Applied Soft Computing*, vol. 113, no. 1, p. 107918, 2021.
- [42] A. Waheed, M. Goyal, D. Gupta, A. Khanna, F. Al-Turjman and P. R. Pinheiro, "Covidgan: data augmentation using auxiliary classifier gan for improved covid-19 detection," *Ieee Access*, vol. 8, no. 1, pp. 91916-91923, 2020.
- [43] T. Mahmud, M. A. Rahman and S. A. Fattah, "CovXNet: A multi-dilation convolutional neural network for automatic COVID-19 and other pneumonia detection from chest X-ray images with transferable multi-receptive feature optimization," *Computers in biology and medicine*, vol. 122, no. 1, p. 103869, 2020.
- [44] G. Jain, D. Mittal, D. Thakur and M. K. Mittal, "A deep learning approach to detect Covid-19 coronavirus with X-ray images," *Biocybernetics and biomedical engineering*, vol. 40, no. 4, pp. 1391-1405, 2020.
- [45] M. Rahimzadeh and A. Attar, "A modified deep convolutional neural network for detecting COVID-19 and pneumonia from chest X-ray images based on the concatenation of Xception and ResNet50V2," *Informatics in Medicine Unlocked*, vol. 19, no. 1, p. 100360, 2020.
- [46] A. I. Khan, J. L. Shah and M. M. Bhat, "CoroNet: A deep neural network for detection and diagnosis of COVID-19 from chest x-ray images," *Computer Methods and Programs in Biomedicine*, vol. 196, no. 1, p. 105581, 2020.
- [47] K. K. Singh, M. Siddhartha and A. Singh, "Diagnosis of coronavirus disease (covid-19) from chest x-ray images using modified xceptionnet," *Romanian Journal of Information Science and Technology*, vol. 23, no. 657, pp. 91-115, 2020.
- [48] T. Ozturk, M. Talo, E. A. Yildirim, U. B. Baloglu, O. Yildirim and U. R. Acharya, "Automated detection of COVID-19 cases using deep neural networks with X-ray images," *Computers in biology and medicine*, vol. 121, no. 1, p. 103792, 2020.
- [49] B. Abraham and M. S. Nair, "Computer-aided detection of COVID-19 from X-ray images using multi-CNN and Bayesnet classifier," *Biocybernetics and biomedical engineering*, vol. 40, no. 4, pp. 1436-1445, 2020.
- [50] A. Narin, C. Kaya and Z. Pamuk, "Automatic detection of coronavirus disease (covid-19) using x-ray images and deep convolutional neural networks," *Pattern Analysis and Applications*, vol. 1, no. 1, pp. 1-14, 2021.
- [51] M. Z. Che Azemin, R. Hassan, M. I. Mohd Tamrin and M. A. Md Ali, "COVID-19 deep learning prediction model using publicly available radiologist-adjudicated chest X-ray images as training data: preliminary findings," *International Journal of Biomedical Imaging*, vol. 1, no. 1, p. 1, 2020.
- [52] S. Toraman, T. B. Alakus and I. Turkoglu, "Convolutional capsnet: A novel artificial neural network approach to detect COVID-19 disease from X-ray images using capsule networks," *Chaos, Solitons & Fractals*, vol. 140, no. 1, p. 110122, 2020.
- [53] S. H. Yoo, H. Geng, T. L. Chiu, S. K. Yu, D. C. Cho, J. Heo and H. Lee, "Deep learning-based decision-tree classifier for COVID-19 diagnosis from chest X-ray imaging," *Frontiers in medicine*, vol. 7, no. 1, p. 427, 2020.
- [54] S. Hassantabar, M. Ahmadi and A. Sharifi, "Diagnosis and detection of infected tissue of COVID-19 patients based on lung X-ray image using convolutional neural network approaches," *Chaos, Solitons & Fractals*, vol. 140, no. 1, p. 110170, 2020.

Development of Mathematics Web-based Learning on Table Set-Up Activities

Gusti Ayu Dessy Sugiharni¹, I Made Ardana², I Gusti Putu Suharta³, I Gusti Putu Sudiarta⁴

Doctorate Program on Educational Science, Universitas Pendidikan Ganesha, Bali, Indonesia¹

Department of Mathematics Education, Universitas Pendidikan Ganesha, Bali, Indonesia^{2,3,4}

Abstract—This paper aimed to discuss product design and expert validation of the mathematics web-based learning table set up activities in the hospitality industry. This research was a type of Research and Development, which aimed to develop a new product. The experts involved in this study were four experts. There were two experts in the field of learning technology as media validators and two experts in the field of mathematics education as material validators. In the process of validating the mathematics web-based learning in this study, using a questionnaire that had been prepared to evaluate it as a research instrument. This research had produced mathematics web-based learning which consists of five parts, namely, the initial part to recall about the Cartesian coordinates; the translation sub-material section; the reflection sub-material section; the rotation sub-material section; and the dilatation sub-material section. In the review activity by experts, the average percentage of material validators was eighty five percent, its means is very good and the average percentage of media validators was ninety five its means is very good also. It showed that this mathematics web-based learning can be said to be proper to use.

Keywords—Development; web-based learning; mathematics; table set-up; activities

I. INTRODUCTION

Mathematics subjects have a quite unique and important part in the competence learning of the tourism department [1]-[2]. Understanding the right concepts in learning mathematics can train transcendental reasoning, range of thinking, and solving a case[3]-[4]. This will make students accustomed to completing case studies in tourism in a more analytical and realistic manner[5]. In general, this is in accordance with the statement which stated that mathematics shows outstanding skills in a person, both in terms of concretizing something abstract, finding the right solution in a case, as well as the power of thinking on an object[6]-[7].

In reality, mathematics is one of the subjects that are less attractive to Tourism Vocational School students[8]-[9]. This is because it is considered a difficult subject to learn and most students have not realized and understood the true meaning of mathematics[10]. This is in accordance with the opinion that most students do not want to focus on learning mathematics because of the assumption that mathematics is difficult, scary, boring and some people hate mathematics so that every time they take part in learning mathematics, someone immediately feels unwell[11]-[14].

Factors from students and teachers become the basis for the reason why many students are less interested in learning

mathematics[15]. The factor from the students that became the basis for the reason was the classical view of students, namely that mathematics is a difficult subject to learn[16]. The factor from the teacher that became the basis for the reason was the difficulty of the teacher in finding the right method to lead students to participate in mathematics learning voluntarily without feeling coercion directly[17]. This difficulty causes students to feel bored and not enthusiastic to take part in learning mathematics[18]. This is supported by the opinion which stated that the difficulty in selecting methods that can be used to make students understand in learning mathematics is a teacher difficulty[19]. Another factor that causes students' lack of interest in learning mathematics is because the form of teaching materials has not been able to raise awareness of the importance of mathematics[20]. Teaching materials that still feature algorithms and formula derivations, raise students' assumptions about solid material, feel less clear and it is difficult to understand the material because of a dislike for math subjects[21]. This is supported by the results of research showing that: 1) learning by using textbooks is not liked by students, because it creates a sense of being lost in dense material and emphasizes algorithms so that students have difficulty accepting mathematics learning[22]; 2) The presentation of learning that is commonly done by teachers has not been able to arouse students' desire to learn, so students are not quite ready to receive lessons [23]; 3) students do not feel challenged to work on the questions available in mathematics learning, because the examples of questions and practice questions provided are difficult to understand [24].

In addition, Tourism Vocational School students only focus on the competencies of the majors they choose[25]. Many students think that Mathematics is not so applied in Business World or Industrial World where they carry out On the Job Training or their place to find work after graduating from Vocational High School[26]. Some explorations have also been carried out by Mathematics teachers, but the number of students who have an interest can still be counted on the fingers[27]. Students' understanding of the many mathematical concepts that can be applied in solving problems related to the tourism sector is still so minimal[28]. This causes the sinking of students' desire to study mathematics voluntarily[29].

Overcoming these problems requires the development of teaching materials that can make Tourism Vocational Schools' students interested in learning mathematics. The teaching materials is able to developed can be in the form of mathematics web-based learning[30]-[31]. Applications in the form of colorful pictures with interesting characters and

mathematical material treats in it[33]-[32]. The reality in the field is that there are many mathematical learning applications that have been developed. Some even carry applications with the STEM concept[34]. However, there is no mathematics web-based learning that carries the theme of tourism practice, so that Tourism Vocational School students understand that mathematics learning is also used in the work practice of the tourism industry.

Based on this, this research was conducted to develop an application for learning mathematics that was raised in industrial work practices in one part of the food and beverage service. The material used in the development of this mathematics web-based learning is Transformation material. Where this Transformation material is raised in the table set up, that is the one of tourism practice activity.

II. METHOD

This research was a type of Research and Development (R&D), which aimed to develop a new product. The development activities carried out in this research were focused on product design and formative evaluation. The stages carried out consist of the Preliminary Research and Prototyping Stage.

A. Preliminary Research

The steps taken at this stage were literature studies to look for problems related in schools learning as well as deficiencies in existing mathematics learning. Field surveys to complement and strengthen the findings in the literature study also taken. This stage aimed to obtain information on problems in mathematics material and deficiency of previous instructional media. The field survey consisted of interviews with three teachers and distributing questionnaires to one hundred and eighteen students.

B. Prototyping Stage

The manufacture and improvement of product prototypes as a problem-solving medium obtained earlier was carried out at this stage, after finding problems in the learning process at the preliminary research stage. This stage consists of designing design guidelines, optimizing prototypes, formative evaluations. In the formative evaluation activity, it is the product evaluation stage (prototype) that had been made previously[35]. The prototype was tested in several stages of formative evaluation, including: 1) Research team members examined the design using a list of important characteristics from the intervention components; 2) A group of experts provide responses related to the intervention prototype. The experts involved in this study were 2 (two) experts in the field of learning technology as media validators and 2 (two) experts in the field of mathematics education as material validators. Usually this is done using open and closed questionnaires or interviews; 3) Walkthrough: through face-to-face researchers together with users (teachers and students) reviewing the intervention prototype; 4) Micro Evaluation was intended to evaluate a small group of users (students) to use the intervention section in normal situations; 5) Try-out a number of user groups (students) using the intervention. On the focus of effectiveness evaluation, evaluators did it by test.

Expert validation questionnaires, student response questionnaires, and teacher response questionnaires were analyzed using a multilevel scale. The data obtained was quantitative data which was then translated into qualitative data. Respondents did not answer one of the qualitative answers on the multilevel scale model, but answered one of the quantitative answers which were provided. Five alternative answers were provided on a graded scale with a range of values from 0 to 4, which are shown in Table I.

TABLE I. CRITERIA FOR GRADED SCALE

Score	Criteria
4	Very Good
3	Good
2	Enough
1	Bad
0	Very Bad

The percentage of answers for each question indicator can be calculated using the following formula.

$$\text{Percentage} = \frac{\sum \text{all respondents score}}{\sum \text{respondents} \times 4} \times 100\%$$

The percentage of answers to all aspects of the question can be calculated using the following formula.

$$\text{Percentage} = \frac{\sum \text{overall score of respondent criteria}}{\sum \text{respondents} \times \sum \text{item} \times 4} \times 100\%$$

In addition to using a multilevel scale in the expert validation questionnaire, the answers to the conclusions from the validation results used the Guttman scale. The Guttman scale yields an unequivocal “yes-no” answer. The “adequate-not eligible” scale was used in this questionnaire. Drawing conclusions about the properly of the media used the following formula.

$$\text{Percentage} = \frac{\sum \text{answers of proper from respondents}}{\sum \text{respondents}} \times 100\%$$

III. RESULT AND DISCUSSION

A. Preliminary Research

In the Preliminary Research stage, several potentials and problems faced by students were found based on the results of the preliminary research questionnaire presented in Table II. The potential and the problem was that students were less interested in learning mathematics because of the assumption that mathematics has nothing to do with tourism activities. According to them, productive learning activities are more important and more fun to carry out than learning mathematics. Students feel lazy and find it difficult to learn mathematical material contained in textbooks. And there was no mathematics learning media that can link productive learning with mathematics learning. This was supported by the results of interviews with mathematics subject teachers which can be concluded as follows. 1) Most students feel lazy and have

difficulty in learning mathematics; 2) Some students feel less helped by the teaching materials which they use in learning mathematics; 3) The teaching materials used in learning mathematics are quite varied, it's just that there are no learning media that can be collaborated with productive learning; 4) When applying mathematics learning media that can be downloaded from the internet, students play with their cellphones instead of studying; 5) The mathematics material

that they should have learned, especially in XI grade, was simply missed when they had carried out the On the Job Training program; 6) Educators expect mathematics material to be linked and collaborated with vocational practice activities; 7) Some students who think that mathematics is not important prefer to participate in vocational activities, even though they already know that they are lagging behind in learning mathematics.

TABLE II. RESULTS OF PRELIMINARY RESEARCH QUESTIONNAIRE

No.	Subject	Item											Total	Percentage (%)
		1	2	3	4	5	6	7	8	9	10	11		
1	PIS1	1	0	1	0	1	0	1	0	1	1	0	6	54.55
2	PIS2	1	0	1	1	0	0	1	1	1	0	1	7	63.64
3	PIS3	0	1	1	0	1	0	1	0	0	1	1	6	54.55
4	PIS4	0	1	0	0	1	1	1	0	1	1	1	7	63.64
5	PIS5	1	0	0	1	1	0	1	0	0	1	0	5	45.45
6	PIS6	0	1	0	1	1	1	1	1	1	0	0	7	63.64
7	PIS7	1	1	1	0	1	1	0	1	0	1	0	7	63.64
8	PIS8	0	0	0	1	0	1	1	1	1	0	0	5	45.45
9	PIS9	1	1	1	0	0	1	1	0	1	0	0	6	54.55
10	PIS10	0	1	0	1	0	0	0	1	0	0	1	4	36.36
11	PIS11	1	0	0	1	1	1	1	0	1	0	1	7	63.64
12	PIS12	0	1	0	1	0	1	1	1	0	1	1	7	63.64
13	PIS13	1	1	1	0	1	1	1	0	0	1	0	7	63.64
14	PIS14	0	1	0	1	0	1	0	1	1	0	0	5	45.45
15	PIS15	1	0	0	1	1	0	0	1	0	1	0	5	45.45
16	PIS16	0	1	0	1	0	1	0	0	1	1	1	6	54.55
17	PIS17	1	0	0	1	1	0	0	1	0	0	1	5	45.45
18	PIS18	0	1	1	1	0	1	1	0	0	1	1	7	63.64
19	PIS19	1	0	1	0	1	1	0	1	0	1	1	7	63.64
20	PIS20	1	1	0	0	1	0	1	1	1	1	1	8	72.73
21	PIS21	0	0	1	0	1	1	0	1	0	1	0	5	45.45
22	PIS22	1	0	1	0	1	1	1	0	1	0	1	7	63.64
23	PIS23	1	1	0	1	0	1	1	0	1	0	1	7	63.64
24	PIS24	0	1	0	1	1	1	1	1	0	0	0	6	54.55
25	PIS25	1	0	0	1	1	1	1	0	1	0	1	7	63.64
26	PIS26	0	1	0	1	0	1	0	1	0	1	1	6	54.55
27	PIS27	1	1	1	0	1	0	0	1	0	1	0	6	54.55
28	PIS28	1	1	0	1	0	1	0	1	1	0	0	6	54.55
29	PIS29	1	0	1	0	0	1	1	1	0	1	0	6	54.55
30	PIS30	1	1	0	1	0	1	1	0	0	1	1	7	63.64
31	P2S1	1	0	1	0	0	0	1	0	1	1	0	5	45.45
32	P2S2	1	1	0	0	1	1	0	0	1	1	1	7	63.64
33	P2S3	1	0	1	0	1	0	1	0	0	1	1	6	54.55
34	P2S4	1	1	1	0	0	1	0	0	1	0	1	6	54.55
35	P2S5	0	1	1	1	1	0	0	1	0	0	1	6	54.55
36	P2S6	1	1	1	1	0	1	0	0	1	0	0	6	54.55
37	P2S7	1	0	0	1	0	1	0	1	1	1	1	7	63.64
38	P2S8	0	1	1	0	0	1	1	0	1	0	1	6	54.55
39	P2S9	1	1	0	1	0	1	1	1	0	0	1	7	63.64
40	P2S10	1	1	0	1	1	0	1	0	1	0	1	7	63.64
41	P2S11	0	1	0	1	1	1	1	1	0	1	0	7	63.64
42	P2S12	1	0	0	0	1	1	1	1	1	0	0	6	54.55
43	P2S13	0	1	0	1	1	1	0	0	0	1	0	5	45.45
44	P2S14	0	1	0	1	0	1	1	1	1	0	1	7	63.64
45	P2S15	1	1	1	0	0	0	1	0	1	0	1	6	54.55
46	P2S16	1	0	0	1	0	1	1	1	0	0	0	5	45.45
47	P2S17	0	1	0	1	0	1	1	0	1	0	1	6	54.55
48	P2S18	1	0	0	1	1	1	0	1	0	1	1	7	63.64
49	P2S19	0	1	0	1	0	1	0	0	1	0	1	5	45.45
50	P2S20	1	1	1	1	1	0	0	1	0	1	0	7	63.64
51	P2S21	1	0	1	0	0	1	0	1	1	0	0	5	45.45
52	P2S22	1	1	1	1	0	0	1	0	0	1	0	6	54.55
53	P2S23	1	1	1	1	0	1	0	1	0	1	1	8	72.73
54	P2S24	1	0	0	1	1	0	0	1	1	0	1	6	54.55

55	P2S25	1	1	1	1	0	1	0	1	0	1	0	7	63.64
56	P2S26	0	1	0	0	1	1	1	1	1	0	0	6	54.55
57	P2S27	1	0	0	1	1	1	1	0	0	1	0	6	54.55
58	P2S28	0	1	0	1	1	1	0	0	1	0	1	6	54.55
59	P2S29	0	1	1	0	1	1	1	1	0	0	1	7	63.64
60	P2S30	1	0	1	0	1	0	1	0	1	0	1	6	54.55
61	P3S1	1	1	1	1	0	0	0	1	1	0	1	7	63.64
62	P3S2	0	1	1	0	1	0	1	1	0	1	1	7	63.64
63	P3S3	0	1	0	1	1	0	1	0	1	1	1	7	63.64
64	P3S4	1	0	0	1	1	1	0	0	1	0	1	6	54.55
65	P3S5	0	1	0	0	0	0	1	0	1	1	1	5	45.45
66	P3S6	1	1	1	1	1	1	0	1	0	0	1	7	63.64
67	P3S7	0	1	0	1	1	1	0	1	1	0	0	6	54.55
68	P3S8	1	1	1	0	0	1	0	1	0	1	0	6	54.55
69	P3S9	0	1	0	1	1	0	0	1	1	1	1	7	63.64
70	P3S10	1	0	0	1	0	1	0	1	1	1	1	7	63.64
71	P3S11	0	1	0	1	1	1	1	0	1	0	0	6	54.55
72	P3S12	1	1	1	1	1	0	0	1	0	0	1	7	63.64
73	P3S13	1	1	1	0	1	1	1	0	0	1	1	8	72.73
74	P3S14	0	1	1	1	1	1	0	1	0	1	0	7	63.64
75	P3S15	1	0	0	0	1	0	1	1	1	1	1	7	63.64
76	P3S16	1	1	1	1	0	0	1	1	0	1	1	8	72.73
77	P3S17	0	1	1	1	0	1	0	1	1	1	1	7	63.64
78	P3S18	0	1	0	0	0	1	1	1	1	1	1	7	63.64
79	P3S19	1	0	0	1	1	1	1	1	1	1	0	8	72.73
80	P3S20	0	1	0	1	1	1	0	1	1	0	1	7	63.64
81	P3S21	1	1	1	1	1	1	1	1	0	1	0	9	81.82
82	P3S22	1	0	0	1	1	1	1	0	1	0	0	6	54.55
83	P3S23	0	1	1	0	1	1	0	1	0	1	0	6	54.55
84	P3S24	1	1	1	1	0	1	1	1	1	1	1	10	90.91
85	P3S25	1	0	0	0	1	0	1	1	1	0	0	5	45.45
86	P3S26	1	1	1	1	0	0	1	1	1	1	1	9	81.82
87	P3S27	1	1	1	0	1	0	1	1	0	1	1	8	72.73
88	P3S28	0	0	1	0	1	0	1	0	1	1	1	6	54.55
89	P3S29	1	1	0	0	0	1	0	0	1	1	1	6	54.55
90	P4S1	1	0	1	0	1	0	1	0	1	1	1	7	63.64
91	P4S2	1	1	0	1	1	0	1	0	0	1	0	6	54.55
92	P4S3	1	0	1	0	1	0	1	1	1	0	0	6	54.55
93	P4S4	1	1	1	1	0	0	1	1	0	1	0	7	63.64
94	P4S5	0	1	0	0	1	0	0	1	1	1	1	6	54.55
95	P4S6	1	0	0	1	1	1	1	1	1	0	0	7	63.64
96	P4S7	0	1	0	1	1	1	1	0	0	1	0	6	54.55
97	P4S8	1	0	0	1	1	1	1	1	1	0	0	7	63.64
98	P4S9	1	1	1	0	1	0	1	1	0	1	0	7	63.64
99	P4S10	0	1	0	1	0	0	1	0	1	1	1	6	54.55
100	P4S11	1	0	0	0	1	0	1	1	1	1	1	7	63.64
101	P4S12	0	1	0	1	1	1	0	1	0	0	0	5	45.45
102	P4S13	1	1	0	1	0	1	1	0	0	1	1	7	63.64
103	P4S14	0	1	0	1	1	1	0	1	0	1	1	7	63.64
104	P4S15	1	0	0	0	1	1	0	1	1	1	0	6	54.55
105	P4S16	0	1	0	1	1	0	1	0	0	1	1	6	54.55
106	P4S17	1	1	1	1	1	1	0	1	0	0	1	8	72.73
107	P4S18	1	1	1	0	0	1	1	0	0	1	1	7	63.64
108	P4S19	1	1	0	1	0	1	0	1	0	1	1	7	63.64
109	P4S20	1	1	1	0	0	1	1	1	0	1	0	7	63.64
110	P4S21	1	0	0	1	0	1	1	1	1	0	0	6	54.55
111	P4S22	0	1	1	0	1	0	1	1	0	1	0	6	54.55
112	P4S23	1	1	0	1	0	0	0	1	1	1	1	7	63.64
113	P4S24	1	1	1	0	1	0	1	0	1	1	0	7	63.64
114	P4S25	0	0	1	0	1	1	1	1	0	1	1	7	63.64
115	P4S26	1	1	0	0	1	0	0	1	1	1	1	7	63.64
116	P4S27	1	0	1	0	1	0	1	0	1	0	1	6	54.55
117	P4S28	1	1	1	1	1	1	0	0	1	1	1	9	81.82
118	P4S29	1	1	1	0	0	0	1	0	1	1	1	7	63.64

B. Prototyping Stage

In the Prototyping stage, the researcher made a plan to determine the Basic Competence and Student Learning Experience and made a feasibility instrument. The selection of subject matter is done based on the consideration of the difficulties of teachers and students in learning mathematics. Transformation material in mathematics vocational high school XI grade was chosen because of the frequent delays in learning this material. This was because when these learning materials must have been given, students instead have to focus on vocational practice activities to face the On the Job Training (OJT) program. The students' too busy with vocational practice activities resulted in the Transformation material being missed and made students start to feel that mathematics was not important, the most important thing was a productive subjects.

This mathematics web-based learning was developed to make students more aware that mathematics can be found in productive subjects. And in order the cognitive load of students in learning mathematics can be reduced, so that students begin to feel that learning mathematics is interesting to understand. At this stage the researchers collaborated between vocational practice activities and mathematics learning, where mathematics learning material was inserted into several steps of vocational practice activities. The parts of the developed mathematics web-based learning can be explained as follows.

At the beginning section of the application before starting the Transformation lesson, students are invited to recall the Cartesian field. The initial part of this application can be seen in the form of Fig. 1.

In this section, students are led to imagine the Cartesian coordinates on the table-set up practice. Students are stimulated to determine the correct Cartesian coordinates for placing flower vases and other table-set up practice equipment.

The second part of the application is the part where learning mathematics begins to enter the sub-section of the translation material. The second of this application can be seen in the form of Fig. 2.

In this section, the table-set-up practice has reached the laying of plates. Here students are led to understand the concept of translation material with cases of shifting plates and shifting other table-set up practice equipment. Students are led to understand that shifts that occur in plates or other items will only change the point of position, not the size or shape of the item.



Fig. 1. Given the Cartesian Coordinates.

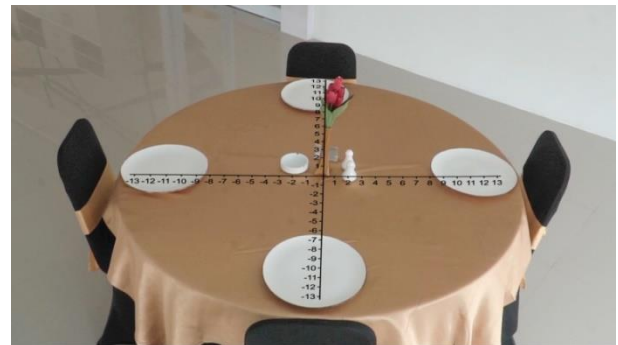


Fig. 2. Translation Sub-Material Section.

The third part of the application is the part where mathematics learning begins to enter the Reflection material sub-section. The third of this application can be seen in the form of Fig. 3.

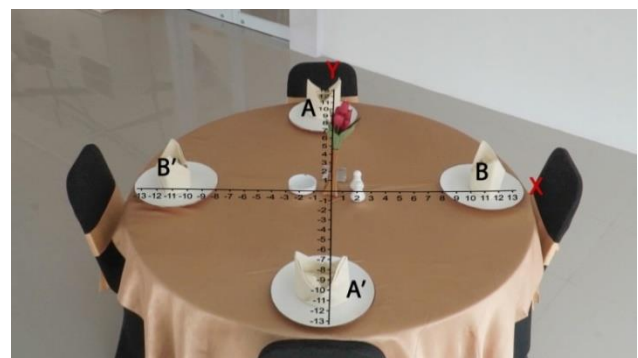


Fig. 3. Reflection Sub-Material Section.

In this section the table-set up practice has reached the laying of the napkin on the plate. Here students are led to understand the concept of Reflection material with the case of a flower vase as a mirror, where the distance from plate A to the flower vase is the same as the distance from plate A' to the flower vase. Students are led to understand the reflection that occurs on plate A and plate B and determine the position of the image according to the coordinates of the points. Students are also led to understand that the mirror in this reflection material can be a point and can also be a line.

The fourth part of the application is the part where mathematics learning begins to enter the Rotation material sub-section. The fourth of this application can be seen in the form of Fig. 4.

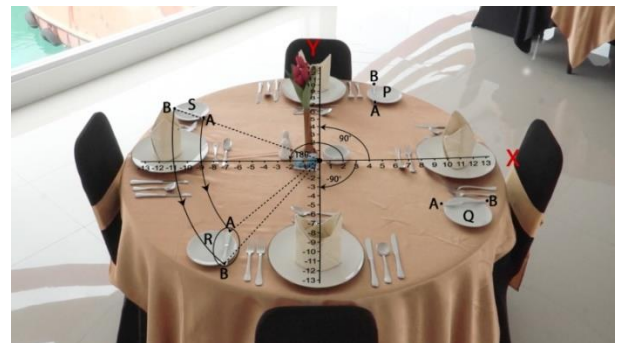


Fig. 4. Rotation Sub-Material Section.

In this section, the table-set up practice is equipped with cutlery placement. Here students are led to understand the concept of material Rotation with cases, rotation of the knife on the B&B plate marked with the letter "S" with the knife on the B&B plate marked with the letter "R". This rotation occurs with the flower vase as the axis. Students are led to understand the rotation that occurs if it is rotated clockwise or counterclockwise at a certain angle.

The fifth part of the application is the part where mathematics learning has entered the Dilatation material sub-section. The fifth of this application can be seen in the form of Fig. 5.



Fig. 5. Dilatation Sub-Material Section.

In this section the table-set up is complete, all the cutlery, crockery, glassware, and linen that are prepared on the table as a utensil to eat for a guest have been set up. Here students are led to understand the concept of Dilatation material with cases: replacement the show plate with B&B plate; And also with the replacement of other cutlery with the same shape but different sizes. Students are led to understand the enlargement or reduction that occurs if there is a replacement in the cutlery.

This developed mathematics web-based learning had been validated by educational technology experts and mathematics education experts. In the process of validating the application of mathematics learning in this study, using a questionnaire that had been prepared to evaluate it as a research instrument. Adjusting the objectives of each questionnaire was taken into consideration in the preparation of this instrument. The questionnaires were media expert evaluation questionnaires and material expert evaluation questionnaires. The activity of reviewing the mathematics web-based learning was carried out by distributing questionnaires to experts.

The results of the validation carried out by two material experts and two media experts on the mathematics web-based learning can be seen in Table III and Table IV.

TABLE III. VALIDATION RESULTS OF MATERIAL EXPERT VALIDATION ON MATHEMATICS WEB-BASED LEARNINGS

No.	Evaluated Aspect	Number of Items	Validators		Percentage (%)	Revision
			I	II		
1	Learning Design	16	11	14	78	No revision
2	Teaching Material	6	6	5	92	No revision
Mean					85	

TABLE IV. VALIDATION RESULTS OF MEDIA EXPERTS ON MATHEMATICS WEB-BASED LEARNING

No.	Evaluated Aspect	Number of Items	Validators		Percentage (%)	Revision
			III	IV		
1	Software engineering	10	10	10	100	No revision
2	Visual Communication	13	12	11	89	No revision
Mean					95	

The validation of the mathematics web-based learning was carried out by four experts, namely two experts in the field of Learning Engineering education and two experts in the field of Mathematics Education. The evaluation carried out on the mathematics web-based learning used several aspects to measure it, including: software engineering, visual communication, learning design and teaching materials. In the aspect of "software engineering", evaluator III assigned an assessment score "1 (proper)" on each indicator with the total number of indicators was 10. Evaluator IV also gave an assessment score "1 (proper)" on each indicator with the total number of indicators was 10. So that obtained a percentage of 100%. By matching the results of these percentages with the percentage level of achievement on a five scale, the "software engineering" aspect was included in very good qualifications, so there was no need to revise this aspect. In the aspect of "visual communication" there were 13 indicator items, evaluator III gave an assessment score "1 (proper)" on 12 indicator items and "0 (it was not proper)" on 1 indicator item. Evaluator IV gave an assessment score of "1 (proper)" on 11 indicator items and "0 (they were not proper)" on 2 indicator items. So that obtained a percentage of 89%. By matching the results of these percentages with the percentage level of achievement on a five scale, the "visual communication" aspect was included in the very good qualification, so there was no need to revise this aspect. In the aspect of "learning design" which consists of 16 indicator items, evaluator I gave an assessment score "1 (proper)" on 11 indicator items and "0 (they were not proper)" on 6 indicator items. Evaluator II gave an assessment score "1 (proper)" on 14 indicator items and "0 (they were not proper)" on 2 indicator items. So that obtained a percentage of 78%. By matching the results of these percentages with the percentage level of achievement on a five scale, the "learning design" aspect is included in good qualifications, so there is no need to revise this aspect. In the aspect of "teaching material" which consists of 6 indicator items, evaluator I gave an assessment score "1 (proper)" on all indicator items. Evaluator II gave an assessment score "1 (proper)" on 5 indicator items and "0 (it was not proper)" on 1 indicator item. So that the percentage obtained was 92%. By matching the results of these percentages with the percentage level of achievement on a five scale, the "teaching material" aspect is included in very good qualifications, so there is no need to revise this aspect.

In addition to the results of the expert validity test, walkthrough activities were also carried out. In this case the author used it as a guide for revising the mathematics web-based learning. The results of the walkthrough activities can be seen in Table V.

TABLE V. WALKTHROUGH RESULTS OF MATHEMATICS WEB-BASED LEARNINGS

No.	Evaluated Aspect	Students			Quantity	Percentage (%)	Note
		I	II	III			
1.	Content	4	4	3	11	92	Very Good
2.	Learning Design	4	4	3	11	88	Very Good
3.	Implementation	3	4	3	10	83	Very Good
4.	Technical Quality	4	4	4	12	94	Very Good
Mean						89	Very Good

The results of the pretest and posttest of students who were included in the Walkthrough activity can be seen in Table VI.

TABLE VI. PRETEST AND POSTTEST RESULTS ON WALKTHROUGH ACTIVITIES

No.	Students	Pretest	Posttest
1	SPW01	65	80
2	SPW02	70	85
3	SPW03	60	75
Mean		65	80

In the walkthrough activity involving 3 students, the average increase in student learning outcomes was obtained which in the pretest the average learning outcome was 65% and in the posttest the average learning outcomes increased to 80%. The average student response questionnaire results were also obtained by 89%. If the average value is matched with the percentage level of achievement on a five scale, the walkthrough activity was considered to be running very well. Based on the results of the expert validation and walkthrough activities, it can be concluded that the developed mathematics web-based learning is proper to be used. After the formative evaluation of mathematics web-based learning passed through expert validation and walkthrough activities, it was continued with Micro Group Evaluation with a larger number of students. The Micro Group Evaluation results of the Mathematics web-based learning can be seen in Table VII.

The results of the pretest and posttest of students who were included in the Micro Group Evaluation activity can be seen in Table VIII.

In the micro-evaluation activity that involved 15 students, it was found the average increase in student learning outcomes. The average learning outcome in the pretest was 69.3 and in the posttest the average learning outcomes increased to 79.6. The average student response questionnaire results of 97% also obtained. If the average value was matched with the percentage level of achievement on a scale of five, the micro-evaluation activity was considered to be running very well. Based on the results of the evaluation of the micro group, it can be concluded that the developed mathematics web-based learning was proper to be used. Furthermore, the flow of formative evaluation continues to the last part, namely the Try-out. The

Try-out results of the Mathematics web-based learning can be seen in Table IX.

TABLE VII. THE MICRO GROUP EVALUATION RESULT OF MATHEMATICS WEB-BASED LEARNING

Students	Efficiency	Content	Learning Design	Implementation	Mean
S1	4	4	3	4	3.75
S2	4	4	4	4	4.00
S3	3	3	4	4	3.50
S4	4	4	4	4	4.00
S5	3	4	4	4	3.75
S6	4	4	4	4	4.00
S7	4	4	4	3	3.75
S8	4	4	4	4	4.00
S9	4	4	3	4	3.75
S10	4	4	4	4	4.00
S11	4	4	4	3	3.75
S12	4	4	4	4	4.00
S13	4	4	3	4	3.75
S14	4	4	4	4	4.00
S15	4	4	4	4	4.00
Quantity	58	59	57	58	58.00
Percentage (%)	97	98	95	97	97
Note	Very Good	Very Good	Very Good	Very Good	Very Good

TABLE VIII. PRETEST AND POSTTEST RESULTS ON MICRO GROUP EVALUATION ACTIVITIES

No.	Students	Pretest	Posttest
1	SPEM01	60	75
2	SPEM02	75	82
3	SPEM03	70	80
4	SPEM04	70	84
5	SPEM05	65	76
6	SPEM06	75	84
7	SPEM07	70	78
8	SPEM08	65	80
9	SPEM09	65	75
10	SPEM10	75	85
11	SPEM11	60	76
12	SPEM12	70	79
13	SPEM13	75	81
14	SPEM14	75	84
15	SPEM15	70	75
Mean		69.3	79.6

TABLE IX. THE TRAY-OUT RESULT OF MATHEMATICS WEB-BASED LEARNING

Students	Evaluated Aspect			
	Implementat ion	Sustainabil ity	Appropria teness	Acceptance and attraction
S1	4	4	3	4
S2	4	3	4	4
S3	3	3	4	4
S4	4	3	4	4
S5	3	4	4	4
S6	4	4	4	4
S7	4	4	4	4
S8	4	4	4	4
S9	4	3	3	4
S10	4	3	4	4
S11	4	3	4	4
S12	4	4	4	4
S13	4	4	3	4
S14	4	4	4	4
S15	4	4	4	4
S16	4	4	4	3
S17	4	4	4	4
S18	4	3	3	3
S19	4	4	4	3
S20	4	3	4	4
S21	4	3	4	4
S22	3	4	4	4
S23	3	4	4	4
S24	3	4	4	3
S25	4	4	3	4
S26	4	3	4	4
S27	4	3	4	4
S28	3	3	4	3
S29	3	4	4	4
S30	3	4	4	4
Quantity	112	108	115	115
Percenta ge (%)	93	90	96	96
Note	Very Good	Very Good	Very Good	Very Good

The results of the pretest and posttest of students who were included in the Try-out activity can be seen in Table X.

In the Try-out activity involving 30 students, the average increase in student learning outcomes was obtained which in the pretest the average learning outcome was 67.8 and in the posttest the average learning outcome increased to 80.8. The average student response questionnaire results were also obtained by 93.8%. If the average value was matched with the percentage level of achievement on a five scale, the Try-out activity had been running very well. Based on the results of the Try-out activity, it can be concluded that the developed mathematics web-based learning was proper to use.

TABLE X. PRETEST AND POSTTEST RESULTS ON TRY-OUT ACTIVITIES

No.	Students	Pretest	Posttest
1	SPTO01	75	85
2	SPTO02	75	86
3	SPTO03	70	84
4	SPTO04	65	78
5	SPTO05	70	80
6	SPTO06	60	75
7	SPTO07	75	85
8	SPTO08	70	82
9	SPTO09	70	80
10	SPTO10	60	76
11	SPTO11	70	84
12	SPTO12	70	81
13	SPTO13	70	84
14	SPTO14	70	80
15	SPTO15	65	78
16	SPTO16	60	82
17	SPTO17	75	85
18	SPTO18	70	80
19	SPTO19	70	84
20	SPTO20	60	76
21	SPTO21	65	77
22	SPTO22	75	85
23	SPTO23	70	82
24	SPTO24	65	80
25	SPTO25	60	76
26	SPTO26	65	79
27	SPTO27	65	81
28	SPTO28	70	84
29	SPTO29	60	75
30	SPTO30	70	80
Mean		67.83	80.8

The results of this study support several previous studies. The following is the previous research. Bailey et al. with research title Finding Satisfaction: Intrinsic Motivation for Synchronous and Asynchronous Communication in the Online Language Learning Context. The results of the research showed that students' attention and motivation to learning arise when learning materials are associated with what students enjoy[36]. Ruder et al. with research title Getting Started with Team-Based Learning (TBL): An Introduction. The results of the research showed that stimulating student activity can be done by presenting learning challenges and direct involvement of students in learning practices[37]. Ardana et al. with the research title "The expansion of sociocultural theory-oriented mathematical learning model. The results of the study indicate that learning mathematics must consider 4 pillars (learning to know, learning to do, learning to be, and learning to live together in peace and harmony) [38]. Wares with research title A Gift Box Filled with Mathematics. The results of the research show that the relationship between feedback and reinforcement will be strengthened if it is used frequently and

REFERENCES

will decrease or even disappear if it is rarely or never used[39]. Therefore, activities related to repetition are very necessary in learning. Sudiarta et al. with the title Investigation on students' mathematical online discussion: A case study in grade 8 SMPN 1 Denpasar. The research result showed that online discussions are able to create very significant mathematical abilities (conceptual understanding, procedural fluency, strategic competence, adaptive reasoning, and productive disposition) and communication skills (clarification, advice). So in this case web-based learning is needed to support discussion activities. Furthermore, Chen et al. with research title Extending Cognitive Load Theory to Incorporate Working Memory Resource Depletion: Evidence from the Spacing Effect. The results of the research indicated that teachers must be able to regulate learning activities, starting from planning, the implementation process to the final stage, namely assessment or evaluation, so that students can participate in the learning process well without significant differences[40]. Based on the results of the research and several supporting theories, it can be concluded that in vocational mathematics learning there should be a collaboration of mathematics learning materials with vocational practice activities so that in addition to learning in theory students also get hands-on practical experience in learning mathematics.

IV. CONCLUSION

This research has succeeded in developing a prototype of a mathematics web-based learning that carries the theme of table set-up industry practice in the Food and Beverage Service department. In the expert test activities, the average percentage of material validators was 85% (very good) and the average percentage of media validators was 95% (very good). In the walkthrough activity, an average increase in student learning outcomes was obtained, which in the pretest was 65 and in the posttest increased to 80. The average student response questionnaire results were also obtained by 89% (very good). In the micro-evaluation activity, it was found that the average increase in student learning outcomes. The average in the pretest was 69.3 and in the posttest increased to 79.6. The average student response questionnaire results of 97% (very good) also obtained. In the Try-out activity, an average increase in student learning outcomes was obtained, which in the pretest was 67.8 and in the posttest increased to 80.8. The average student response questionnaire results were also obtained by 93.8% (very good). Thus it can be concluded that the mathematics web-based learning developed in this study has met the standards of validity, practicability and effectiveness to be said to be proper for use. Future work that can be done is to analyze the factors that are influenced by the use of this mathematics web-based learning and perform a comparative analysis with other equivalent learning applications.

ACKNOWLEDGMENT

The authors express gratitude to the Chancellor, Director of the Postgraduate Program, and Head of the Educational Sciences Study Program at Universitas Pendidikan Ganesha for their very useful support and encouragement.

- [1] S. Wilson, J. McChesney, and L. Brown, "Cultural Competencies and Planning for Teaching Mathematics: Preservice Teachers Responding to Expectations, Opportunities, and Resources," *J. Urban Math. Educ.*, vol. 10, no. 1, pp. 95–112, 2017.
- [2] J. Little, "Connecting Mathematics with Science to Enhance Student Achievement -- A Position Paper," in *Mathematics Education Research Group of Australasia*, 2019, pp. 452–459.
- [3] W. Sung and J. B. Black, "Factors to Consider When Designing Effective Learning: Infusing Computational Thinking in Mathematics to Support Thinking-Doing," *J. Res. Technol. Educ.*, vol. 53, no. 4, pp. 404–426, 2021.
- [4] N. Akhter and N. Akhter, "Learning in Mathematics: Difficulties and Perceptions of Students," *J. Educ. Res. Dept. Educ. IUB, Pakistan*, vol. 21, no. 1, pp. 147–163, 2018.
- [5] P. Rowlett, E. Smith, A. S. Corner, D. O'Sullivan, and J. Waldoock, "The Potential of Recreational Mathematics to Support the Development of Mathematical Learning," *Int. J. Math. Educ. Sci. Technol.*, vol. 50, no. 7, pp. 972–986, 2019.
- [6] Lambertus, "Developing Skills Understanding of Mathematical High School Student," *Int. J. Educ. Res.*, vol. 4, no. 7, pp. 315–319, 2016.
- [7] H. Stein, I. Gurevich, and D. Gorev, "Integration of Technology by Novice Mathematics Teachers -- What Facilitates Such Integration and What Makes It Difficult?," *Educ. Inf. Technol.*, vol. 25, no. 1, pp. 141–161, 2020.
- [8] H. Pathuddin, Kamariah, and M. I. Nawawi, "Buginese Ethnomathematics: Barongko Cake Explorations as Mathematics Learning Resources," *J. Math. Educ.*, vol. 12, no. 2, pp. 295–312, 2021.
- [9] A. Yulastri, H. Hidayat, Ganefri, S. Islami, and F. Edya, "Developing an Entrepreneurship Module by Using Product-Based Learning Approach in Vocational Education," *Int. J. Environ. Sci. Educ.*, vol. 12, no. 5, pp. 1097–1109, 2017.
- [10] J. Subrahmanyam, "Does Gender Play a Part in High School Students' Interest and Their Application of Cognitive Strategies in Learning Mathematics?," *Shanlax Int. J. Educ.*, vol. 9, no. 3, pp. 242–245, 2021.
- [11] K. Larkin and R. Jorgensen, "I Hate Maths: Why Do We Need to Do Maths? Using iPad Video Diaries to Investigate Attitudes and Emotions Towards Mathematics in Year 3 and Year 6 Students," *Int. J. Sci. Math. Educ.*, vol. 14, no. 1, p. 3, 2016.
- [12] N. Günbas, "Students Solve Mathematics Word Problems in Animated Cartoons," *Malaysian Online J. Educ. Technol.*, vol. 8, no. 2, pp. 43–57, 2020.
- [13] Tarzimah Tambychik and T. S. M. Meerah, "Students' Difficulties in Mathematics Problem-Solving: What do they Say?," *Procedia - Soc. Behav. Sci.*, vol. 8, no. 142–151, 2010.
- [14] J.-W. Lin, "The Impact of Team-Based Learning on Students with Different Self-Regulated Learning Abilities," *J. Comput. Assist. Learn.*, vol. 35, no. 6, pp. 758–768, 2019.
- [15] C. Whiteford, N. Kelly, and L. Dawes, "Why Become a Teacher? Exploring Motivations for Becoming Science and Mathematics Teachers in Australia," *Aust. J. Teach. Educ.*, vol. 46, no. 3, pp. 1–19, 2021.
- [16] Harun, B. Kartowagiran, and A. Manaf, "Student Attitude and Mathematics Learning Success: A Meta-Analysis," *Int. J. Instr.*, vol. 14, no. 4, pp. 209–222, 2021.
- [17] B. Liebech-Lien, "The Bumpy Road to Implementing Cooperative Learning: Towards Sustained Practice through Collaborative Action," *Cogent Educ.*, vol. 7, no. 1, pp. 1–17, 2020.
- [18] N. Guner, "Difficulties Encountered by High School Students in Mathematics," *Int. J. Educ. Methodol.*, vol. 6, no. 4, pp. 703–713, 2020.
- [19] W. Setyaningrum, A. Mahmudi, and Murdanu, "Pedagogical Content Knowledge of Mathematics Pre-service Teachers: Do they know their students?," *J. Phys. Conf. Ser.*, vol. 1097, pp. 1–8, 2018.
- [20] A. Asli and I. Zsoldos-Marchis, "Teaching Applications of Mathematics in Other Disciplines: Teachers' Opinion and Practice," *Acta Didact. Napocensia*, vol. 14, no. 1, pp. 142–150, 2021.

- [21] L. Luitel, "Exploring Teachers' Experiences on the Nature of Mathematics Based on Their Curricular and Pedagogical Practices: A Phenomenological Inquiry," *Int. Electron. J. Math. Educ.*, vol. 15, no. 3, pp. 1–12, 2020.
- [22] Salamia and U. Tisngati, "The Reflection Social-Cognitive Theory in Mathematics Education," in *International Conference on Educational Research and Innovation*, 2017, pp. 46–52.
- [23] P. Nugraheni and D. N. Mawardi, "The Crisis of Mathematical Learning," in *International Conference on Educational Research and Innovation*, 2017, pp. 68–71.
- [24] S. Hadi, "Authentic Assessment And Students' Mathematical Literacy," in *International Conference on Educational Research and Innovation*, 2017, pp. 53–60.
- [25] T. Hao and M. Pilz, "Attractiveness of VET in China: A Study on Secondary Vocational Students and Their Parents," *J. Educ. Work*, vol. 34, no. 4, pp. 472–487, 2021.
- [26] H. Ozdemir, "Maths Instruction in Vocational High School from Teachers and Students' Eyes: A Different Kettle of Fish," *REDIMAT - J. Res. Math. Educ.*, vol. 9, no. 2, pp. 196–214, 2020.
- [27] B. Küçük Demir, "The Opinions of Mathematics Teacher Candidates Who Have Received a STEM Training on STEM and the Activities They Designed in the Class," *Athens J. Educ.*, vol. 8, no. 4, pp. 401–416, 2021.
- [28] S. Osman, C. N. A. C. Yang, M. S. Abu, N. Ismail, H. Jambari, and J. A. Kumar, "Enhancing Students' Mathematical Problem-Solving Skills through Bar Model Visualisation Technique," *Int. Electron. J. Math. Educ.*, vol. 13, no. 3, pp. 273–279, 2018.
- [29] V. Manfreda Kolar and T. Hodnik, "Mathematical Literacy from the Perspective of Solving Contextual Problems," *Eur. J. Educ. Res.*, vol. 10, no. 1, pp. 467–483, 2021.
- [30] M. Simsek and N. Yazıcı, "Examining the Digital Learning Material Preparation Competencies of Pre-Service Mathematics Teachers," *Particip. Educ. Res.*, vol. 8, no. 3, pp. 323–343, 2021.
- [31] Q. A. Alajmi, A. Kamaludin, R. A. Arshah, and M. A. Al-Sharafi, "The Effectiveness of Cloud-Based E-Learning towards Quality of Academic Services: An Omanis' Expert View," *Int. J. Adv. Comput. Sci. Appl.*, vol. 9, no. 4, pp. 158–164, 2018.
- [32] A. Chaffai, L. Hassouni, and H. Anoun, "Real-Time Analysis of Students' Activities on an E-Learning Platform based on Apache Spark," *Int. J. Adv. Comput. Sci. Appl.*, vol. 8, no. 7, pp. 101–109, 2017.
- [33] S. Schutera et al., "On the Potential of Augmented Reality for Mathematics Teaching with the Application cleARmaths," *Educ. Sci.*, vol. 11, pp. 1–18, 2021.
- [34] J. Weidman and G. Wright, "Promoting Construction Education in K-12 by Using an Experiential, Student-Centered, STEM-Infused Construction Unit," *Technol. Eng. Teach.*, vol. 79, no. 1, pp. 8–12, 2019.
- [35] I. G. P. Suharta, N. N. Parwati, and I. G. N. Pujawan, "Integration of Ethnomathematics in Learning Geometry Transformation," in *5th Asian Education Symposium 2020 (AES 2020)*, 2020, pp. 107–110.
- [36] D. Bailey, N. Almusharraf, and R. Hatcher, "Finding Satisfaction: Intrinsic Motivation for Synchronous and Asynchronous Communication in the Online Language Learning Context," *Educ. Inf. Technol.*, vol. 26, no. 3, pp. 2563–2583, 2021.
- [37] P. Ruder, M. H. Maier, and S. P. Simkins, "Getting Started with Team-Based Learning (TBL): An Introduction," *J. Econ. Educ.*, vol. 52, no. 3, pp. 220–230, 2021.
- [38] I. M. Ardana, I. P. W. Ariawan, and G. A. D. Sugiharni, "The expansion of sociocultural theory-oriented mathematical learning model," *Cypriot J. Educ. Sci.*, vol. 16, no. 6, pp. 3016–3032, 2021.
- [39] A. Wares, "A Gift Box Filled with Mathematics," *Math. Teach. Learn. Teach. PK-12*, vol. 114, no. 4, pp. 318–324, 2021.
- [40] O. Chen, J. C. Castro-Alonso, F. Paas, and J. Sweller, "Extending Cognitive Load Theory to Incorporate Working Memory Resource Depletion: Evidence from the Spacing Effect," *Educ. Psychol. Rev.*, vol. 30, no. 2, pp. 483–501, 2018.

A Risk Management Framework for Large Scale Scrum using Metadata Outer Request Management Methodology

Rehab Adel¹, Hany Harb², Ayman Elshenawy³

Faculty of Engineering, Al-Azhar University, Cairo- Egypt^{1, 2, 3}

Faculty of Engineering and Technology, Egyptian, Chinese University, Cairo- Egypt³

Abstract—Recently, most software projects became naturally Distributed Agile Development (DAD) projects. The main benefits of DAD projects are cost-saving and being close to markets due to their distributed nature, such as in large-scale Scrum (LeSS). Developing LeSS projects leads to the emergence of challenges in risk management, especially the team collaboration challenges, where there is no standardized process for teams to communicate collaboratively. Team collaboration and the knowledge sharing is a vital resource for a large Scrum team's success. Hence, finding a dynamic technique that facilitates team collaboration in the LeSS environment is necessary. This paper proposes a risk management framework for LeSS using outer metadata requests. The proposed framework manages the outer requests amongst the distributed team. Therefore, it avoids missing team collaboration, risks, and threats to project completion. It also contributes to exchanging team skills and experience. The proposed framework is evaluated by applying it to two different case studies for large-scale Scrum projects. The evaluation results are given. The evaluation proved the effectiveness of the proposed framework.

Keywords—Distributed agile development; knowledge sharing; risk management; large scale scrum; metadata outer request management

I. INTRODUCTION

Agile is more robust than traditional software development methods. The agile manifesto formulation emphasizes customer involvement in the project, change request flexibility at any stage of the project, and delivers quality software at a cost-effective low and on time. Hence, there is a trend for software companies to globalize their agile development. A new type of agile software development has appeared in which team members work from various remote sites, referred to as distributed agile development (DAD) [1,2,3,4,5,6,7]. DAD incorporates many benefits, such as low production cost, the opportunity to involve the most developers around the world, and faster time to market [8].

Agile methodologies include Extreme Programming (XP), Scrum, Dynamic System Development (DSD), Lean Development (LD), etc. Most agile methods promote development iterations, working software, close collaboration between customers and developers, and process adaptability. The most widely used methodologies based on agile principles are XP and Scrum, where the most recently used agile methodology is Scrum [5, 7, 9, 10].

The Scrum framework comprises three components: roles, ceremonies, and artifacts. First, there are three distinct roles in the Scrum process (i) Scrum master: who organizes the Scrum process, review sessions, and meet with the team members, (ii) the product owner responsible for managing the project requirements, and (iii) the development team responsible for developing the validated requirements. The product owner and the development team can be grouped into feature teams. Secondly, the ceremonies have activities such as daily Scrum every day and sprint planning. A sprint is started, reviewed against the product owner's feedback, and possible changes are analyzed and completed retrospectively to suggest process improvements after sprint completion. Thirdly, there are three artifacts: (i) product backlog, (ii) sprint backlog, and (iii) burn down chart [7, 8, 11, 12, 13].

There is a shortage of highly skilled software development human resources in some software project locations. The migration of the skillful team from one physical location to another is a costly and challenging task. In this case, the IT projects are either challenged, impaired, or completed but failed due to a lack of IT human resources with the desired level of expertise [14,15]. Consequently, there is a need to improve software development infrastructure and human resources.

Organizations have to implement appropriate knowledge management practices. Previous studies have been analyzed proving that there are some problems of collaboration between distributed team members that affect knowledge sharing. Besides that, there are documentation obstacles like outdated documents and knowledge vaporization that result from much of the conversation and communication via chat [16].

In LeSS projects, Scrum team members can work from various remote sites to gain the maximum benefits of Scrum methodology. LeSS is a type of DAD. Many challenges are encountered when using Scrum methodology on LeSS projects, which are considered a primary source of emerging risks [7, 11]. These challenges related to daily Scrum meeting sessions based on team communication and customer involvement. The main difficulties result from: (i) geographical distances that cause many challenges in communication, (ii) Poor coordination between multiple teams, (iii) Conflict in requirements amongst the development team and numerous product owners, and (iv) Cultural differences such as language, religion, and social status between team members. These

difficulties reduce team cohesion and interdependence, besides causing a lack of collaboration and experience in managing distributed projects [2,3,4,7,17,19,20,21].

Such challenges lead to the appearance of some risks in LeSS. The potential risks are grouped into categories, each category contains several risk factors (RF). The most common RFs that significantly influence LeSS are:

1) *Communication*: There is no standardized process for the teams to communicate collaboratively [4].

2) *Collaboration and coordination*: due to the nature of LeSS, there are some difficulties in team coordination rules, plans, and feedback that cause misaligned software development activities during collaboration and iterative meetings among the teams [4].

3) *Project management*: One of its most essential tasks is risk management. Risk management implements several activities, such as (i) risk identification to identify and classify risks, (ii) risk evaluation to assess risks into three levels, such as (low, moderate, or high), and (iii) risk response to satisfy suitable actions and strategies to mitigate the impact of the risk, and (iv) risk monitoring to control and update the risk plan are all activities of project management [1,4,5,22,23]. IT project management activity includes all the structuring of the different phases of projects, so project objectives can be achieved optimally. As a result, there is a need to aggregate management methodologies into a single model, such as the approach to agile framework, Model-Driven Engineering (MDE) [24].

4) *Software development lifecycle (SDLC)*: SDLC is made up of several phases that must be completed during the software development process, such as planning, analysis, design, implementation, and testing. Agile principles emphasized the individual's involvement in all SDLC phases, which is difficult in LeSS team development [23].

The goal of the proposed framework can represent many issues that can be summarized as follows:

- Achieve a formal coordination strategy based on centralization: Each Scrum master on the sender side receives requests from his feature team and forwards them to the Scrum masters on the receiver side. Scrum masters on the receiver side communicate with their teams to find replies to these requests. They deliver these replies to the Scrum master on the sender side.
- Help the Scrum masters carry out their risk management activities by:(i) risk identification through using the meta-data outer request attributes, where any request point includes a request from one side to the other side, and each request statement can be classified into a certain risk factor attribute. Therefore, the proposal can accommodate any type of risk factor that is involved in a specific request. (ii) risk evaluation. The feature team on each side assesses the requests' points by assigning each request point a reward value. (ii) risk response. The main plan for risk mitigation is that each team should receive accepted replies to each request's points.

(iii) risk monitoring and control. This is achieved based on central management, where the Scrum masters can monitor the risks and their replies that are stored in the meta-data outer request attributes for all LeSS teams. Consequently, the Scrum masters successfully control these risks, ensuring that any emergence of new risks is covered.

- *Sharing knowledge and Exchanging experience*: The coordination process's results are used in building the knowledge repository, thereby contributing to increasing the team's learning process.

This paper is organized as follows: Section II represents related work and background. Section III introduces the LeSS development methodology. Section IV explains the metadata management. Section V presents the proposed model (the metadata outer request risk management framework). Section VI presents the implementation plan for the proposed model. Section VII introduces the discussion. Section VIII introduces the conclusion. Finally, the implications, limitations and future work are expressed.

II. RELATED WORK AND BACKGROUND

There are several studies related to DAD risk management. Some of these studies introduce many new agile risk strategies to identify risks in DAD projects. Other studies determine new risk management practices for DAD projects. Some researchers have focused on finding solutions for knowledge sharing problems in distributed team's environment and have suggested frameworks in large-scale practices.

First, in [17],Suprika et al. have identified and classified DAD risks into categories, each category is ranked numerically. In [18], Mohammad Shameem et al. have suggested three stages for defining DAD risks: (i) risk definition and categorization, (ii) verifying the validity of the risk's definition stage with expertise, and (iii) risk priorities according to their importance. In [21], Shrivastava et al. have proposed an approach to identify risks according to three goals: saving time, quality, and cost for DAD projects.

Secondly, in [23], S. Bick et al. have applied a grounded theory data analysis on various datasets to prove that a lack of dependency awareness causes ineffective inter-team coordination, leading to misaligned planning activities. In [25], FS Rahayu et al. have proposed a Scrum framework based on the perspective of Scrum's stakeholders; they have analyzed the risk breakdown structure, the root of which represents the risk category and its related subcategories. In [26],Breno Gontijo Tavares et al. have presented a survey on risk management practices in agile projects. In [27], Rizwan Qureshi et al. have proposed a novel framework to improve communication and coordination among the Scrum master and team in Scrum methodology. Also, the proposed framework is validated through a questionnaire. In [28], Hoda et al. have suggested a framework for multi-level project management to achieve the "self-organized team" principle. The framework levels are (task-individual-team-project) and represent the role involved at each level. In [13], Tavares et al. have analyzed survey data, suggested risk management practices, and explained how risk management is carried out in Scrum software projects. In [29],

Bruno Gontijo Tavares et al. have proposed the Rm4Am (risk management for agile methods) tool to rank the list of 127 risk management practices into 48 subcomponents and then into five components (artifacts, features, events, roles, and methods). According to large-scale agile frameworks, there are difficulties encountered by companies. In [30], Kieran Conboy et al. have presented the three frameworks with LeSS complex adoption processes: (i) Safe, adoption of SAFe provides a comprehensive view of projects while requiring no significant restructuring of the company's processes. It is also a well-documented framework, more complex compared to the other frameworks. Work is delivered by individual teams that collaborate and contribute to the larger whole, (ii) Scrum at Scale, it is a straightforward and effective framework for reducing and avoiding the introduction of new complexity. (iii) Spotify, which addresses short-term challenges effectively and responds quickly to changes. The success of the three frameworks depends on the effectiveness of cooperation between teams and the exchange of skills and experiences. There is also a need for management centralization to facilitate project management practices. Consequently, overcoming risks appears due to the nature of LeSS team and to be able to control all elements of management.

Thirdly, in [31], Sara Waheed et al. have focused attention on finding a solution for only the knowledge vaporization problem that is related to the documentation process. It has proposed a framework for the documentation process to avoid the knowledge vaporization. The framework is evaluated using a real-life case study for distributed team members. The team members are satisfied with the proposed framework. In [32], Agile enterprise architecture (AEA) has been introduced for reducing IT costs and skill variation. Using the AEA, artefacts or models can enhance DAD team performance. It accommodates agile principles, focuses on collaborative incremental development and sharing of team skills and business information.

There are some limitations to the previous studies. Each of the previous studies focused on solving a specific problem facing distributed teams. But to avoid distributed teams' risks, there is a need to develop a comprehensive solution to avoid risks and help the team develop as well. Especially this is due to the multiplicity of sources and reasons for the emergence of these DAD-related risks.

Some of the previous studies relied on gathering limited data and risk management practices suggestions either from analyzing previous data surveys or from risk management practitioners. The collected data is mainly based on personal human observations, which raised some doubts about the validity of the data. Some of these studies suffered from the absence of dynamic risk management. So, the control and data updating have been carried out manually as a traditional risk management technique. Contrary to these studies, this paper proposes a comprehensive solution to the DAD-related problems. This paper proposes a risk metadata outer request risk management framework for LeSS projects.

The proposed framework is embedded in the LeSS organization to manage four RFs in LeSS development: (i) communication, (ii) collaboration and coordination, (iii) project

management, and (iv) SDLC. The proposed framework also contributes to knowledge sharing amongst the LeSS distributed team to increase the team experience. It is applied to a case study of four user stories in a LeSS project sprint spread across three locations. Besides, being applied to two projects for a company, the proposed framework helps the Scrum master to manage the outer requests amongst the LeSS distributed team.

III. LARGE SCALE SCRUM PROCESS

The Scrum process has a management framework that manages complex software products and integrates many processes. The Scrum management methodology is applied to iterative and incremental life cycle models in software development. As presented in Fig. 1, the Scrum life cycle is divided into several stages. Each stage is called a "sprint", and the sprint period is usually from two to four weeks. It depends on five ceremonies; each ceremony has a short duration. If anyone's ceremony is not performed, they may lose an opportunity to complete a project.



Fig. 1. A Scrum Framework for Software Development [7].

Scrum, as a management framework, has the facility of monitoring the developed product and identifying project risks. Scrum teams are multifunctional teams in which every member has a good understanding of all the development functions. Also, Scrum teams are self-organized and can satisfy the best way to carry out their work without being led by anyone [7,13].

The Scrum process is suitable for small or medium-sized teams and projects. Nowadays, there is a trend toward using Scrum in large-scale projects with multiple and distributed teams, especially in multi-site projects. The main disadvantage of the Scrum process is the daily meeting ceremony sessions in LeSS that require a face-to-face meeting, which is challenging to use in large-scale projects[33,34].

In project planning, the product owner on the customer side prepares the product backlog, which is divided into chunks of small, desired functions. For sprint planning, a set of user stories are created from the ready items offered by the product owner. Each user story describes who uses the user story, its value to the customer, and its function [33,34].

The best management for the LeSS process has helped in solving this LeSS limitation. The workflow of LeSS is presented in Fig. 2, where the LeSS project development can be described as follows:

1) Each feature team in a location is assigned to one or several user stories from the planned sprint. They do the work plan and establish the sprint backlog to satisfy user interface (UI), code, unit tests, user acceptance tests, and task estimation time [33,34].

2) After the sprint development started, there was a daily stand-up meeting between the Scrum master and the feature team in each location. The Scrum master is responsible for ensuring that the team delivers value, helping to build a self-organizing team, and removing impediments [33,34].

3) After the sprint development is finished, a demo is prepared by the Scrum master to review the developed function with the development team. Then, sprint user stories in locations are integrated and thoroughly tested under the supervision of the product owner [33,34].

Finally, a retrospective meeting is conducted, and Scrum masters in each location integrate the results of their retrospective meeting [33,34].

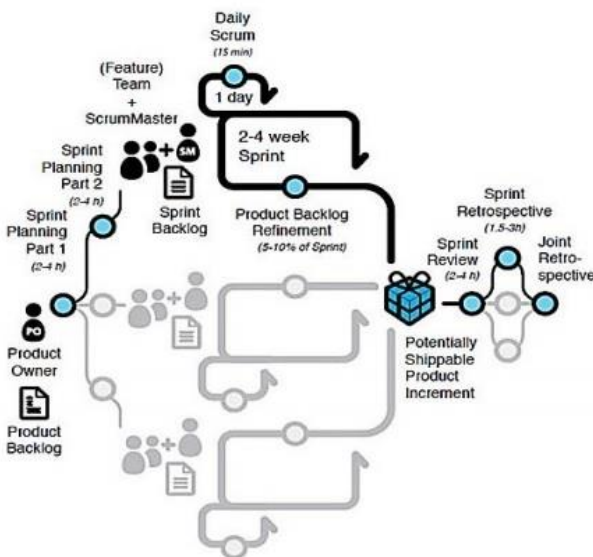


Fig. 2. A Large-Scale Scrum Framework [7].

IV. METADATA MANAGEMENT

The metadata management helps the project manager to perform all tasks related to project management by using data attributes. These data attributes carry the coordination and cooperation process of data through exchanging questions and dialogues among the project locations. The data recorded for these attributes facilitates the decision-making process.

In addition, these stored coordination's results are shared in building the team knowledge. Every organization can identify the data attributes of interest to them in the management or team coordination process.

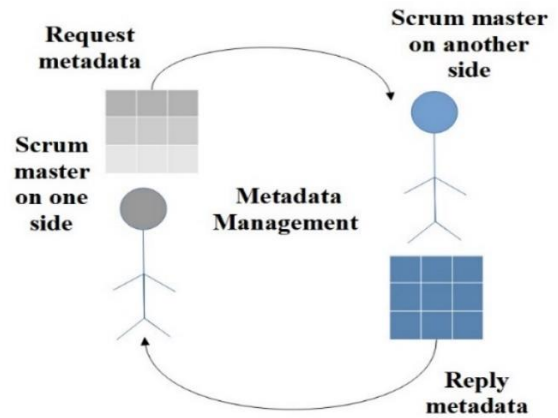


Fig. 3. Metadata Management on Two LeSS Sides.

This study applies metadata management to LeSS as a type of DAD project. Fig. 3 represents a metadata management process among two LeSS sides. The LeSS team coordination and the management process have been achieved through exchanging request points among the distributed team.

There are two types of metadata attributes needed:

1) *Request metadata attributes*: The request metadata attributes are request date, sprint number, point number, request description, risk factor (RF), and point reward ratio (PRR).

2) *Reply metadata attributes*: The reply metadata attributes are point number, reply date, reply description, reply status, reply content accepted, reply period status, and reply point reward ratio. Each Scrum master of a location is responsible for sending or receiving the exchanged request points. He also delivers the metadata to their featured team.

The request and reply metadata attributes will be explained in the next section.

V. METADATA OUTER REQUEST RISK MANAGEMENT FRAMEWORK FOR LESS

The architecture of the proposed metadata outer request risk management framework for LeSS is depicted in Fig. 4. It was applied to work on different sites in three locations. Each location has two roles, the feature team, and the Scrum master. Location A is for the sender's side, and locations B and C are for the receptor side. The framework consists of two main models: (i) the collaboration and coordination model and (ii) the knowledge sharing model.

A. Collaboration and Coordination Model

This model is responsible for collaborating and coordination between the sender and receiver sides by exchanging requests and replies for the shared tasks.

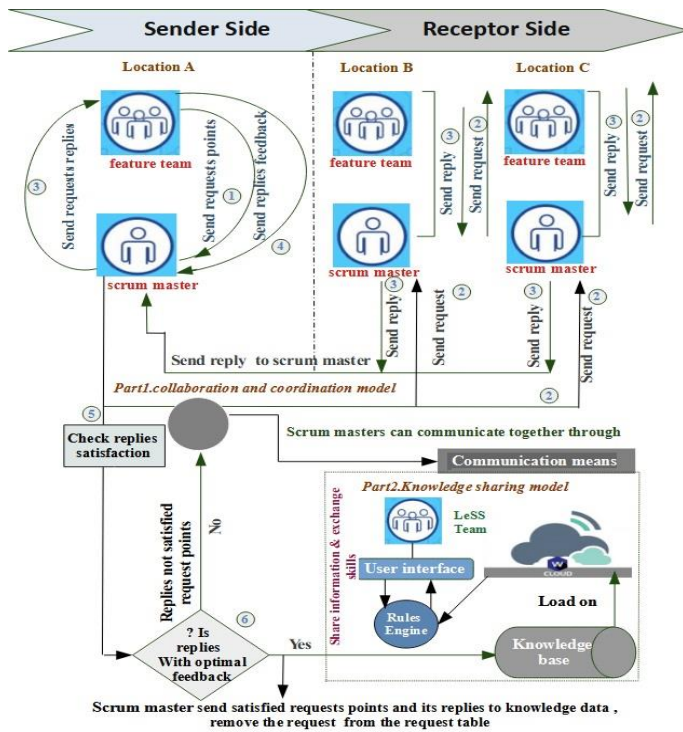


Fig. 4. Metadata Outer Request Risk Management Framework for LeSS.

Fig. 5 represents the flow sequence for a meta-outer request management from one location to the other locations, as, e.g., The process flow sequence for a request sent from side (A) to the different sides (B, C) can be summarized as follows:

1) At time t , the Scrum master on the sender side initializes the accumulative request reward at episode 0. The feature team on the sender side delivers the Scrum metadata request that contains the obstacles that arises during the development process. It also includes the required coordination data with other locations.

2) The Scrum master on the sender side conducts a meeting with the Scrum masters on the receptor side to discuss the metadata request that the sender team has received from the sender. Each receptor Scrum master sends the request to their feature team during their meeting together. Each feature team on the receptor side studies the metadata requests and prepares replies wherever there is a reply to each request point. Then, the feature team forwards the replies to the receptor Scrum master at time $t+1$. After that, the receptor Scrum master delivers the replies to the sender Scrum master.

3) The feature team at the sender side evaluates the received replies using the assessment attributes for each reply point shown in Table I. The request point reward is calculated using a point reward (PR) function illustrated as follows:

$PR = FRS * \text{Point Reward Ratio (PRR)}$. (1), and $FRS = RS * RCA * RPS$. The feature team at the sender side issues a new request state with the reset of un-replied request points.

4) Whenever request's replies are received, the sender Scrum master computes the Accumulative Reply Function

(ARF) as in (Eq.2) that illustrate as follow: $ARF = \text{Sum previous (TPR) value} + \text{Sum current (TPR) value}$. (2), and Total points reward $(TPR) = \text{sum (PR)}$ (3).

5) The Scrum master at the sender side checks if the request replies with optimal feedback rewards; if the optimal reward is not reached, the Scrum master resends the new request state to the receptor's Scrums and starts a new request action.

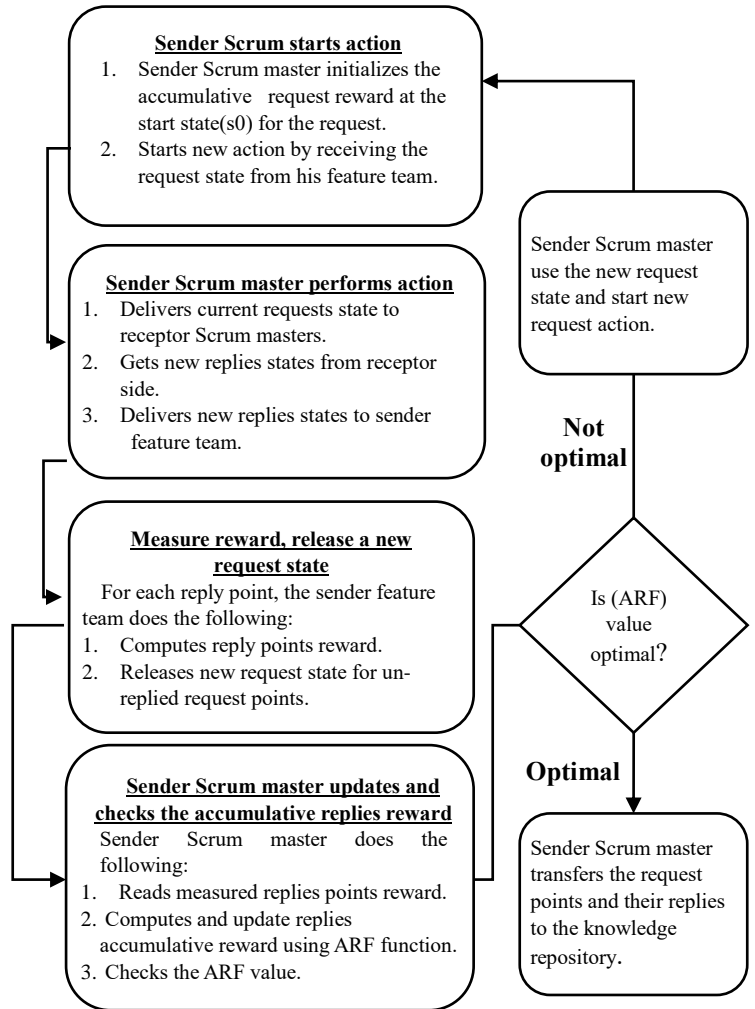


Fig. 5. Flow Sequence for Meta Outer Request Management.

TABLE I. REPLY ATTRIBUTES FOR THE ASSESSMENT REPLIES

Factor name	Factor description and related values
Reply Status (RS)	Indicate if there are a reply for the current request (value =1) point or not (value =0).
Reply Content Accept (RCA)	If the reply content is acceptable for the sender (value =1) If the reply content is not acceptable (value =0).
Reply Period Status (RPS)	Represents the reply to request points in time if the receptor responds to the request point in time less than or equal to 24 hours (value =1) else if greater than 24 hours (value =0).
Point Reward Ratio (PRR)	The reward ratio for each request point is according to the evaluation of the sender feature team.

B. Knowledge Sharing Model

The main objective of this model is to share information and exchange skills among the distributed team members. This can be achieved by building knowledge from the requests and replies to data exchanged amongst the LeSS teams. This knowledge is considered as a result of the coordination process. The scenario for building the knowledge repository is illustrated above at step (v) of the flow sequence. If a request-reply achieves the optimal reward, the Scrum master will send the complete information for the request and their replies to the knowledge sharing repository to be used by the LeSS team.

VI. IMPLEMENTATION

In this section, the proposed metadata outer request risk management framework is implemented and applied to two case studies. The first one is related to developing one sprint of a sales project using the LeSS developing method for only one request. The second one is related to developing several sales and purchase projects sprints in a medical service company using the LeSS developing method for many requests. The two case studies consist of many projects distributed in various locations. Many scenarios are applied to show the effectiveness of the proposed model.

A. Case Study 1: Sales Project

This section applies the proposed framework to one sprint of developing a sales project (project ID = P_sale1). First, the product owner and the Scrum masters fill the product backlog and highlight the high priority requirements to be developed first. The product owner discusses the highlighted user stories of one sprint and assigns user stories to suitable locations.

Table II shows the user stories assigned to locations A, B, and C in one sprint. User stories 1 and 4 are assigned to the development team in location A, user story 3 to the development team in location B, and user story 2 to the development team in location C. The sequence for managing the outer metadata request from one location to another can be described as the following:

1) The feature team in location A delivers the Scrum master metadata request state (s0) as shown in Table III with obstacles that faced them while completing their work. Initially, at time t, as shown in Table IV, the Scrum master at the sender side creates a reward table and initializes the replies' accumulative reward to zero. It also determines the reward ratio for each request point according to their job priority.

2) The Scrum master at location A executes an action a1 at time t+1 to change the request state. During their meeting, he delivers the request state to the receptor Scrum masters of locations B and C. Then, the receptor Scrum masters of locations B and C send the metadata replies, including the overall state of their locations. Finally, the Scrum master in location A passes these replies to his feature team. Tables V and VI include the reply states (s1) and (s2) for locations A and B.

3) The reward for reply state (s1) and (s2) for location A and location B is measured by the feature team in location A,

as shown in Tables V and VI. The reward is computed using Total Points Rewards (TPR) function, where $TPR \text{ for } s1 = \text{Sum} (PR \text{ for } s1) = (0 * 0.20) + (0 * 0.30) + (0 * 0.15) + (0 * 0.35) = 0$, $TPR \text{ for } s2 = \text{Sum} (PR \text{ for } s2) = (1 * 0.20) + (0 * 0.30) + (1 * 0.15) + (0 * 0.35) = 0.35$. The feature team sends rewards for s1, s2, and sends the new request state(s3) (with the reset un-replied request points as shown in Table VII) to their Scrum master.

TABLE II. A SPRINT WITH FOUR USER STORIES WERE DISTRIBUTED AMONGST THREE-TEAM LOCATIONS A, B, A, C

User story of Location A	User story of Location B
User story 1 As a system admin I want to add and control new users. So that I can control users and the user access to program components. Acceptance criteria 1- I can enter a new user 2-configure these users 3-Assign them accessing some functions	User story 3 As A salesman I want a review of the available quantity and last price for a product. I can carry out operation processes, I can review my sales daily So that I can do sales operation in a suitable way Acceptance criteria 1- Review available quantity and last price for a product? 2- Enter sales data for a customer contains? 3-Review our daily job is in excel formats
User story 4 As an account manager I want a sales report to be sent daily to my mailbox. So that I can review the sale progresses. Acceptance criteria 1- the report is sent daily to my mailbox 2-report contains important sales details 3-report is in excel formats	
User story of Location C	
User story 2 As A storekeeper I want to enter store item quantity and price; I want to withdraw an available quantity from the store item. So that I can do sales operation in a suitable way Acceptance criteria 1- I can enter store items, review the data for entered items? 2- if withdraw a quantity larger than available quantity, system refuse	

TABLE III. STATE (S0) IS THE INITIAL STATE FOR THE REQUEST

Metadata request from (A) for req. #1 for project (P_sale1)					
Request date	Sprint #	Point #	Request Description	RF	PRR
2020/01/01 01:12:00 PM	1	1	What are user data required to enter New user?	Communication With product owner	0.20
2020/01/01 01:12:00 PM	1	2	What are items balance attributes?	Coordination	0.30
2020/01/01 01:12:00 PM	1	3	What is UI and implementation to print excel report?	SDLC	0.15
2020/01/01 01:12:00 PM	1	4	What are the sales attributes?	Collaboration	0.35
Total Request Rewards					1

TABLE IV. INITIALIZE REQUEST REWARD

Request state	Request reward
s0 (Initial state for the request)	0

TABLE V. THE REPLY STATE (S1) FROM (B) AFTER ACTION A1

Metadata reply from (B) after action a1 at t for request #1							
Point #	Reply date	Reply description	RS	RPS	RCA	FRS	PR
1	2020/01/01 07:1:00PM	Rep: user attributes are name, job, phone no	1	1	0	0	0*0.20
2	2020/01/01 09:12:00 PM	Rep: Not mine	1	1	0	0	0*0.30
3		No reply	0	0	0	0	0*0.15
4	2020/01/01 03:12:00PM	Rep: Under construction	1	1	0	0	0*0.35
Total points rewards (TPR) = sum (RP)							0

TABLE VI. THE REPLY STATE (S2) FROM (C) AFTER ACTION A1

Metadata reply from (C) after action a1 at t for req. #1							
Point #	Reply date	Reply description	RS	RPS	RCA	FRS	PR
1	2020/01/01 07:1:00PM	Rep: user attributes are name, job, phone no	1	1	1	1	1*0.20
2	2020/01/01 09:12:00 PM	Rep: - Under construction	1	1	0	0	0*0.30
3	2020/01/01 05:12:00 PM	Rep: -Ok, we try to do it	1	1	1	1	1*0.15
4	2020/01/01 03:12:00PM	Rep: -Not mine	1	1	0	0	0*0.35
Total points rewards (TPR) = sum (RP)							0.35

4) Following action a1, the Scrum master at location A updates the reward table (as shown in Table VIII) with the replies accumulative reward using the accumulative reward (ARF) mentioned in (Eq. 2), where the sum of previous TPR = 0, and the sum of current TPR = 0.35. Then, ARF = 0 + 0.35 = 0.35, so the accumulative reward for initial request state is changed from 0 to 0.35.

5) The scrum master checks: if the replies' accumulative reward is with optimal feedback (equal 1), so all request points that are replied with acceptable content, the sender Scrum master transfers the request and their replies to the knowledge sharing repository. The Scrum master starts a new action with the new request state if the optimal reply is not reached. Now, the Scrum master checks the request ARF value. He finds that it equals 0.35, which is not an optimal reward, so he starts a new action with the new request state (s3) shown in Table VII.

TABLE VII. NEW REQUEST STATE (S3) AFTER ACTION A1

Metadata request from feature team in location A for request #1 for the project (P_sale1)					
Request date	Sprint #	Point #	Request description	RF	PRR
2020/01/01 01:12:00PM	1	2	What are item balance attributes?	Coordination	0.30
2020/01/01 01:12:00 PM	1	4	What are the sales attributes?	Collaboration	0.35
Total Request Rewards					0.65

TABLE VIII. REWARD TABLE AFTER ACTION A1

Request state	Action(a1)
s0 (Initial state for the request)	0.35
s1	0
s2	0.35

6) The scrum master performs action a2 at time t+2 and receives a new reply state (s4) and (s5) for locations A and B, respectively, as shown in Tables IX and X. He sends two reply states to his feature team.

TABLE IX. THE REPLY STATE (S4) FROM (B) AFTER ACTION A2

Metadata reply from B after action a2 at t+1for request #1							
Point #	Reply date	Reply description	RS	RPS	RCA	FRS	PR
2	2020/01/04 05:12:00PM	Not mine	1	1	0	0	0*0.30
4	2020/01/04 08:12:00PM	Customer attribute:- name, phone, address, Item attributes: code, qty, unit price	1	1	1	1	1*0.35
Total points rewards (TPR) = sum (RP)							0.35

TABLE X. THE REPLY STATE (S5) FROM (C) AFTER ACTION A2

Metadata reply from C after action a2 at t+1for request #1							
Point #	Reply date	Reply description	RS	RPS	RCA	FRS	PR
2	2020/01/04 05:12:00 PM	Reviewing with product owner	1	1	0	0	0*0.30
4	2020/01/04 08:12:00 PM	Not mine	1	1	0	0	0*0.35
Total points rewards (TPR) = sum (RP)							0

7) The feature team in location A measures the reward for reply state (s4) and (s5) for locations A and B, respectively, as shown in Table IX and X. The reward for reply state (s4) and (s5) for location A and location B is measured by the feature team in location A, as shown in Tables IX and X. Total points rewards (TPR) for s4 = Sum (PR for s4) = (0 *0.30) + (1 *0.35) = 0.35, TPR for s5 = Sum (PR for s5) = (0 *0.30) + (0 *0.35) =0. The feature team sends s4, s5 rewards and sends requests to state s6 (as shown in Table XI) to their Scrum master.

8) Following action a2, the Scrum master at location A updates the reward table (as shown in Table XII) with the replies accumulative reward using the accumulative reward (ARF) mentioned in (Eq. 2), where the sum of previous TPR = 0.35, and the sum of current TPR =0.35. Then, ARF =0.35 + 0.35 = 0.70, so the accumulative reward for initial request state is changed from 0.35 to 0.70.

9) The scrum master checks: if the replies' accumulative reward is with optimal feedback (equal 1). He finds that it equals 0.70, which is not an optimal reward, so he starts a new action with the new request state (s6) shown in Table XI.

10)The Scrum master performs an action a3 at time t+3 and receives a new reply state (s7) and (s8) for locations A and B, respectively, as shown in Tables XIII and XIV. He sends two reply states to his feature team.

11)The reward for reply state (s7) and (s8) for location A and location B is measured by the feature team in location A, as shown in Tables XIII and XIV. Total points rewards (TPR) for s7 = Sum (PR for s7) = (0 * 0.30) = 0, TPR for s8 = Sum (PR for s8) = (1 * 0.30) = 0.30. The feature team sends the rewards for s7 and s8 and the new request state (s9) (with the reset un-replied request points shown in Table XV) to its scrum master. There are no un-replied request points, so the sender feature team releases all request points and their replies to their scrum master.

12)Following action a3, the scrum master at location A updates the reward table with the replies accumulative reward, where the sum of the previous TPR = 0.70, and the sum of current TPR =0.30. Then ARF = 0.70 + 0.30 = 1, This means that the accumulative reward for the initial request state has been increased from 0.70 to 1(optimal reward). As shown in Table XVI, states s1, s2, s4, s5, s7, and s8 are real states for replies, whereas s0, s3, and s6 are transition states that serve as the starting point for the next state.

13)Now, the Scrum master checks the requested ARF value. He finds that the value equals 1, an optimal reward, so the goal is reached. The sender Scrum master transfers the request points and their replies that he accepted from his feature team (as shown in Table XV) to the knowledge repository state.

TABLE XI. NEW REQUEST STATE (S6) AFTER ACTION A2

Metadata request from feature team in (A) for request #1 for the project (P_sale1)					
Request date	Sprint #	Point #	Request description	RF	PRR
2020/01/01 01:12:00PM	1	1	What are user data required to enter new user?	Communication With product owner	0.30
Total Request Rewards					0.30

TABLE XII. REWARD TABLE AFTER ACTION A2

Request state	Action(a1)	Action(a2)
s0 (Initial request)	0.70	0
s1	0	0
s2	0.35	0
s3	0	0
s4	0	0.35
s5	0	0

TABLE XIII. THE REPLY STATE (S7) FROM (B) AFTER ACTION A3

Metadata reply from (B) after action a3 at t+2for request #1							
Point #	Reply date	Reply point description	RS	RPS	RCA	FRS	PR
1	2020/01/04 05:12:00 PM	Not mine	1	1	0	0	0*0.30
Total points rewards (TPR) = sum (RP)							0

TABLE XIV. THE REPLY STATE (S8) FROM (C) AFTER ACTION A3

Metadata reply from C after action a3 at t+2for request #1							
Point #	Reply date	Reply point description	RS	RPS	RCA	FRS	PR
1	2020/01/04 05:12:00 PM	Ok, will sent to your scrum master	1	1	1	1	1 *0.30
Total points rewards (TPR) = sum (RP)							0.30

TABLE XV. REWARD TABLE AFTER ACTION A3

Request state	a1	a2	a3
s0	1	0	0
s1	0	0	0
s2	0.35	0	0
s3	0	0	0
s4	0	0.35	0
s5	0	0	0
s6	0	0	0
s7	0	0	0
s8	0	0	0.30

TABLE XVI. THE GOAL STATE AFTER ACTION A3

Request date	Point #	Request description	PRR	Reply date	Reply description	Location
2020/01/01 01:12:00 PM	1	Communication with the product owner	What are user data required to enter new user?	2020/01/01 06:12:00PM	Rep: user attributes are name, job, phone no	C
2020/01/01 01:12:00 PM	2	Coordination	What are item balance attributes?	2020/01/04 05:12:00PM	Ok, will sent to your scrum master	C
2020/01/01 01:12:00 PM	3	SDLC	What is UI and implementation to print excel report?	2020/01/01 05:12:00PM	Rep: - Ok, we try to do it	C
2020/01/01 01:12:00 PM	4	Collaboration	What are the sales attributes?	2020/01/04 08:12:00 PM	Customer attribute:-name, phone, address, Item attributes : code, qty, unit price	B

B. Case Study 2: Sales and Purchase Project

In this section, the proposed model is implemented in real-time for developing a LeSS project of two sub-projects distributed physically in two locations. The LeSS team collaborated to develop two projects for a medical services company. The first project is a purchase project with a project ID = P_sale. This project belongs to a branch of the medical services company specialized in purchasing medicines and medical supplies. After the purchasing process, these items are stored in the company's warehouses. The second project is a sales project with ID= P_pur. It belongs to another branch of the medical services company for selling and marketing medical items.

Metadata attributes derived from team coordination after their development activities can be summarized as follows: (i) Request number; (ii) Request date; (iii) Project identifier; (iv) No sprint; (v) Number of request points sent from one location's development team to another location's development team; (vi) Number of replies to points; (vii) Total reward (Number of reply points/Number of request points); (viii) The number of episodes per request; (ix) Reliability (total reward/number of episodes); and (x) The number of risk factors covered in replies. Fig. 5 and 6 depict the data presented in Table XVII. The plot represents the relationship between reliability and the requests for the purchase project (P_pur) and the sales project (P_sale). The data plotted in Fig. 6 represents the reply points covered for each RF.

TABLE XVII. OUTER REQUEST DATA FOR PROJECT (P_SALE, P_PUR)

# Of req. and reply. points per project							Covered RF in replies			
Req. #	Sprint #	# Of req. points	# Of repl. points	Total reward	# Of episode per req.	Reliability =Tot. reward/# of episode	Communication	Coll.& Coord.	Project manag.	SDLC
Project ID = P_sale										
10	2	7	6	0.86	3	0.29	2	1	1	2
11	2	10	8	0.80	2	0.40		4	2	2
12	2	8	7	0.88	2	0.44	1	2	3	1
13	2	13	12	0.92	2	0.46	5	1	2	4
14	3	14	14	1	1	1		5	2	7
15	3	13	13	1	1	1	2		2	9
16	3	17	17	1	1	1	2	4	4	7
17	3	13	13	1	1	1	1	7	3	2
Project ID = P_pur										
19	1	13	12	0.92	4	0.46	3	2	4	3
20	2	15	14	0.93	3	0.33	2	9	2	1
21	3	8	7	0.87	1	0.87		1	3	3
22	4	11	11	1	1	1		4	5	1
23	4	7	7	1	1	1	1	3	1	2
24	5	20	20	1	1	1	1	5	8	6
10	2	7	6	0.86	3	# RF	20	48	42	50
		Sum = 169	Sum = 161			% RF	13 %	30 %	26 %	31 %

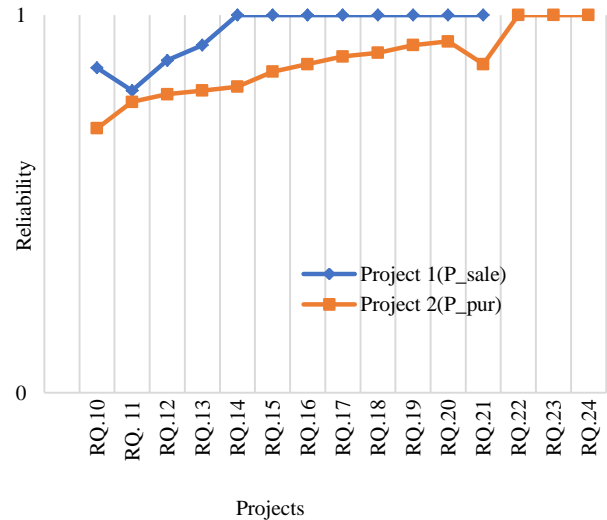


Fig. 6. Relation between Project Request and Reliability.

In Fig. 7, it is observed that the first two most frequent RFs are "Collaboration and Coordination" and "SDLC". On the other hand, the least frequent RFs are "Communication" and "Project management".

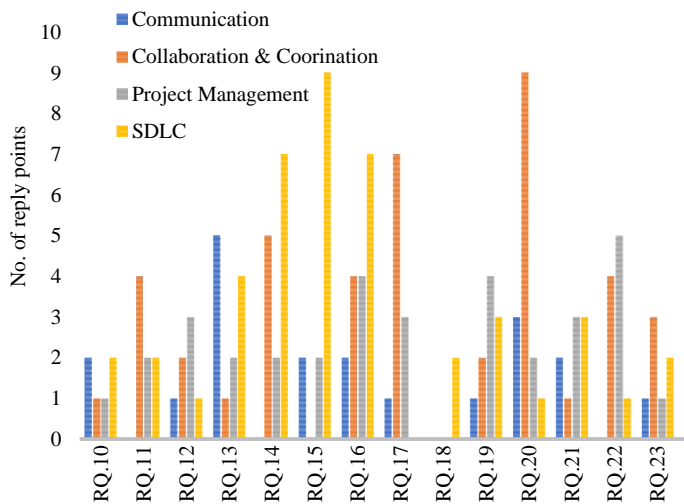


Fig. 7. Requests Points Numbers per each RF.

VII. DISCUSSION

The obtained results show that the total covered risks in the accepted replies are 161 points out of 168. 31% are related to risks in the SDLC, 30% are related to the risks resulting from collaboration and coordination, and 26% are related to risks resulting from project management. Finally, 13% is associated with the risk of results due to miscommunication between the teams. The proposed model achieves a success rate of 95% of replies to requests initialized by the teams. The reliability results indicate that two factors affect the reliability of any request: (i) the number of reply points per request. The number of reply points per request increases proportionally to the number of request points. (ii) The number of episodes per request. With a decreasing number of episodes per request, the reliability is increased, and the learning process occurs faster. The LeSS team experience will be rapidly improved.

VIII. CONCLUSION

A large-scale Scrum is a type of agile development project with a distributed team that faces several challenges. This study provides comprehensive suggestions for formal coordination strategies based on centralization. The suggested framework is embedded in the LeSS organization. So, it is successful in managing LeSS risk factors and highly centralized coordination has been achieved. The successful coordination results contribute to the sharing of information and knowledge amongst the LeSS distributed team, so success in increasing team experience is achieved, and the team becomes an agile mindset team. The paper has illustrated the methodology applied to overcome DAD risks in LeSS and how this framework can build experience and skills for a distributed team. Finally, the team is enabled to achieve openness and success in working in distributed agile environments.

IX. IMPLICATIONS

This framework contributes to increasing LeSS team cohesion and motivates the software professional team to work together to achieve the project's progress and performance. This framework is based on building a formal management

strategy. Therefore, the management organization can control LeSS software development practices. This can be achieved by concentrating project management on Scrum masters on each side of the dependent. Software professionals and managers should encourage members to share their skills and experience with their colleagues. The project manager should understand that knowledge sharing within the team provides clarity to members about the project and its deliverables. It is possible for researchers to apply the suggested framework to more LeSS projects and monitor the number of risk factors that are actually avoided. In this framework, the researchers can suggest different strategies to benefit from the knowledge data accumulated as a result of the coordination process. They can also observe any shortcomings in this proposal and try to suggest improvements.

X. LIMITATIONS AND FUTURE WORK

The proposed framework is evaluated via two case studies. It yields positive results in terms of increasing team collaboration and applying risk management through centralized management. The current study has two limitations. One of these limitations is clarifying the concept of central management using Scrum masters. This is due to applying the proposed framework to only two studies, especially the first case, which contains one request proposed by a team on the DAD project side. The second limitation arises because there are no methods satisfied for how to store the data and how to retrieve data from the knowledge repository. For further research, it will be exciting to apply the proposed framework to more real-life case studies for the LeSS team practices in distributed organizations. It is also interested in spreading the idea of centralization and studying suitable methods that can be applied to store the knowledge data in a knowledge repository. Searching for the required technique and learning how to retrieve the requests and their replies from the knowledge repository, it is an important issue that needs to be resolved.

REFERENCES

- [1] Torgeir Dingsøy, Nils Brede Moe1, Tor Erlend Fægri, Eva Amdahl Seim, "Exploring software development at the very large-scale: a revelatory case study and research agenda for agile method adaptation", *Empir Software Eng*, Vol. 23, No. 1, pp. 490–520,2018, Doi: 10.1007/s10664-017-9524-2.
- [2] Manasés Jesús Galindo Bello, Hochschule Fulda, Natarajan Meghana than et al, "SOFTWARE ENGINEERING IN GLOBALLY DISTRIBUTED TEAMS", *Computer Science & Information Technology*, pp. 01–16, CSCP2018, Doi: 10.5121/ csit .2018.81301.
- [3] Madan Singh, Naresh Chauhan, Rashmi Popli, "A Framework for M. Singh, N. Chauhan and R. Popli, "A Framework for Transitioning Of Traditional Software Development Method To Distributed Agile Software Development," 2019 International Conference on Issues and Challenges in Intelligent Computing Techniques (ICICT), 2019, pp. 1-4, Doi: 10.1109/ICICT46931.2019.8977654.
- [4] Wan Suzila Wan Husina, Yazriwati Yahyab, Nurulhuda Firdaus Mohd Azmib, Nilam Nur Amir Sjarifb, Suriyati Chupratb, Azri Azmib, "Risk Management Framework for Distributed Software Team: A Case Study of Telecommunication Company", *Procedia Computer Science*, Vol.161, pp. 178–186, 2019.
- [5] Abdelghany Salah Abdelghany, Nagy Ramadan Darwish, Hesham Ahmed Hefny , "Towards a Hybrid Approach for Software Project Management using Ontology Alignment", *International Journal of Computer Applications* Vol. 168, No. 6, pp. 0975 – 8887,2017,Doi: 10.5120/ijca2017914438.

- [6] Sinha, Richa, Shameem, Mohammad, Kumar, Chiranjeev, "SWOT: Strength, Weaknesses, Opportunities, and Threats for Scaling Agile Methods in Global Software Development", Innovations in Software Engineering Conference, Jabalpur, India, pp.27–29, 2020, Doi: 10.1145/3385032.3385037.
- [7] Mohammad Esteki, Taghi Javdani Gandomani, Hadi Khosravi Farsani, "A risk management framework for distributed scrum using PRINCE2 methodology", Bulletin of Electrical Engineering and Informatics, Vol.9, No. 3, pp. 1299–1310, 2020, Doi: 10.1109/ICISE.2019.00014.
- [8] Miloš Jovanović, Antoni-Lluís Mesquida, Antonia Mas, Ricardo Colomo-Palacios, "Agile transition and adoption frameworks issues and factors: A systematic mapping", IEEE Access, vol. 8, pp. 15711–15735, 2020.
- [9] Melaku Girma, Nuno M. Garcia, Mesfin Kifle, "Agile Scrum Scaling Practices for Large Scale Software Development", 4th International Conference on Information Systems Engineering, pp.1291–2160, 2020, Doi: 10.1109/ICISE.2019.00014.
- [10] Waqar Aslam, Farah Ijaz, "A quantitative framework for task allocation in distributed agile software development", IEEE Access, vol. 6, pp. 15380–15390, 2018.
- [11] Ayesha Khalid, Shariq Aziz Butt, Tauseef Jamal, Saikat Gochhait, "Agile Scrum Issues at Large-Scale Distributed Projects: Scrum Project Development At Large", International Journal of Software Innovation, Vol. 8, No. 2, pp. 85–94, 2020., Doi: 10.4018/IJSI.2020040106.
- [12] Gabriela Castro Flores, Ana M. Moreno, Lawrence Peters, "Agile and Software Project Management Antipatterns: Clarifying the Partnership" in IEEE Software, vol. 38, no. 05, pp. 39–47, 2021, Doi: 10.1109/MS.2020.3001030.
- [13] Tavares, Breno, Silva, Carlos, Diniz de Souza, Adler, "Risk management analysis in Scrum software projects", International Transactions in Operational Research, pp.1–22, 2017, Doi: 10.1111/itor.12401.
- [14] Hui Yi Chiang, Bertrand M. T. Lin, "A Decision Model for Human Resource Allocation in Project Management of Software Development," in IEEE Access, vol. 8, pp. 38073–38081, 2020, Doi: 10.1109/ACCESS.2020.2975829.
- [15] Prasad Sharma, Durga, Cloud-Based Outsourcing Framework for Efficient IT Project Management Practices (October 1, 2020). (IJACSA) International Journal of Advanced Computer Science and Applications, Vol. 11, No. 9, 2020, <https://thesai.org/Publications/ViewPaper?Volume=11&Issue=9&Code=IJACSA&SerialNo=18>, Available at SSRN: <https://ssrn.com/abstract=3703028>.
- [16] César France, Fabio Q. B. da Silva, Helen Sharp, "Motivation and Satisfaction of Software Engineers," in IEEE Transactions on Software Engineering, vol. 46, no. 2, pp. 118–140, 1 Feb. 2020, Doi: 10.1109/TSE.2018.2842201.
- [17] Suprika Vasudeva Srivastava, Urvashi Rathod b, "A risk management framework for distributed agile projects", Information and Software Technology Vol 85, pp. 1–15, 2017.
- [18] Mohammad Shameem, Rakesh Ranjan Kumar, Chiranjeev Kumar, Bibhas Chandra, Arif Ali Khan, "Prioritizing challenges of agile process in distributed software development environment using analytic hierarchy process", J Softw Evol Proc.30: e1979,16, 2018.
- [19] Yahia Ibrahim Alzoubi, Asif Qumer Gill a, Ahmed Al-Ani, "Empirical studies of geographically distributed agile development Communication challenges: A systematic review", Information & management, Vol.53, pp.22–37, 2016.
- [20] Muhammad Akil Rafeek, Adila Firdaus Arbain, Endah Sudarmilah, "Risk mitigation techniques in agile development processes", International Journal of Supply Chain Management, Vol. 8, pp. 1123–1129, No.2, 2019.
- [21] Shrivastava, Suprika, Rathod, Urvashi, "A Goal-driven Risk management approach for Distributed Agile Development Projects", Australasian Journal of Information Systems, Vol 23, pp. 4–29, 2019, Doi 10.3127/ajis.v23i0.1843.
- [22] Gu'nther Ruhe, Claes Wohlin, "Software Project Management in a Changing World", ISBN 978-3-642-55034-8 ISBN 978-3-642-55035-5 (eBook)- Doi:10.1007/978-3-642-55035-5.
- [23] Saskia Bick, Kai Spohrer, Rashina Hoda, Alexander Scheerer, Armin Heinz, "Coordination Challenges in Large-Scale Software Development: A Case Study of Planning Misalignment in Hybrid Settings," in IEEE Transactions on Software Engineering, vol. 44, no. 10, pp. 932–950, 1 Oct. 2018, Doi: 10.1109/TSE.2017.2730870.
- [24] Hamzane Ibrahim, Belangour Abdessamad, "Project Management Metamodel Construction Regarding IT Departments", (IJACSA) International Journal of Advanced Computer Science and Applications, Vol. 10, No. 10, 2019.
- [25] F S Rahayu, T Indrawan, S Kamarudin, "Risk Mitigation Strategies in Implementing Scrum Framework for Internet-Based IT Companies in Indonesia", Journal of Computer Information Systems", Indonesian Journal of Information Systems (IJIS)), Vol. 3, No. 1, ISSN 2623-0119, E- ISSN 2623-2308, August 2020.
- [26] Breno Gontijo Tavares, Carlos Eduardo Sanches da Silva, and Adler Diniz de Souza, "Practices to Improve Risk Management in Agile Projects", International Journal of Software Engineering, and Knowledge Engineering, Vol. 29, No. 3, pp. 381–399, 2019, Doi: 10.1142/S0218194019500165.
- [27] Rizwan Qureshi, Mohammed Bashiri, Ahmad A AL Zahrani, "Novel Framework to Improve Communication and Coordination among Distributed Agile Teams", IJ. Information Engineering and Electronic Business, Vol.4, No. 3, pp. 16–24, 2018, Doi: 10.5815/ijieeb.2018.04.03.
- [28] Hoda, Rashina, "Multi-Level Agile Project Management Challenges: A Self-Organizing Team Perspective", Journal of Systems and Software, Vol. 117, pp.245–257, Doi: 10.1016/j.jss.2016.02.049.
- [29] Breno Gontijo Tavares, Mark Keil, Carlos Eduardo Sanches da Silva & Adler Diniz de Souza (2020), "A Risk Management Tool for Agile Software Development", Journal of Computer Information Systems, Vol.61, Issue 4, Doi: 10.1080/08874417.2020.1839813.
- [30] Kieran Conboy, Noel Carroll, "Implementing Large-Scale Agile Frameworks: Challenges and Recommendations", IEEE Software, vol. 36, no. 2, pp. 44–50, 2019.
- [31] Sara Waheed, Bushra Hamid, NZ Jhanjhi, Mamoona Humayun, Nazir A Malik5, "Improving Knowledge Sharing in Distributed software Development", (IJACSA) International Journal of Advanced Computer Science and Applications, Vol. 10, No. 6, 2019.
- [32] Yehia Ibrahim Alzoubi, Asif Qumer Gill, "An Empirical Investigation of Geographically Distributed Agile Development: The Agile Enterprise Architecture is a Communication Enabler," in IEEE Access, vol. 8, pp. 80269–80289, 2020, doi: 10.1109/ACCESS.2020.2990389.
- [33] Apoorva Srivastava, Sukriti Bhardwaj, Shipra Saraswat, "SCRUM model for agile methodology," 2017 International Conference on Computing, Communication and Automation (ICCCA), 2017, pp. 864–869, Doi: 10.1109/CCAA.2017.8229928.
- [34] Muhammad Hammad, Irum Inayat, "Integrating Risk Management in Scrum Framework," 2018 International Conference on Frontiers of Information Technology (FIT), 2018, pp. 158–163, Doi: 10.1109/FIT.2018.00035.

Technique for Balanced Load Balancing in Cloud Computing Environment

Narayan A. Joshi

Department of Master of Computer Applications
Dharmsinh Desai University, Nadiad, India

Abstract—Resource sharing by means of load balancing in cloud computing environments helps for efficient utilization of cloud resources and higher overall throughput. However, implementation of poor load balancing algorithms may cause some virtual machines starving for additional cloud resources. Employing meagre crafted mechanism for priority-oriented load balancing may leave low-level priority virtual machines starving. We suggest an improved resource sharing mechanism for load balancing in the cloud computing environments. The suggested mechanism helps to provide efficient load balancing by avoiding starvation. In order to cater efficient load balancing, the proposed resource sharing technique takes respective virtual machines' priority levels into consideration. An implementation of the suggested load balancing algorithm in cloud environment provides reduction in waiting time of the starving virtual machines which are looking for additional resources in cloud platform. The implementation of our proposed algorithm has been deployed on a prototype cloud computing infrastructure testbed established with open source software OpenStack. The prototype cloud testbed is supported in backend by the open source CentOS Linux operating system's minimal setup. Experimental results of proposed load balancing mechanism in the prototype cloud computing infrastructure setup designate reduction in the waiting time of overloaded starving virtual machines. The proposed mechanism is beneficial to accomplish priority-oriented and starvation free resource sharing for load balancing in cloud computing environments. In future, the proposed technique can be further enhanced for implementing load balancing in collaborated cloud computing environments.

Keywords—Cloud environment; resource sharing; load balancing; starvation; priority oriented resource allocation

I. INTRODUCTION

Cloud computing is one of the most important and outstanding innovations in the 21st century. Amongst several technological innovations done in the 21st century, the cloud computing has seen the expeditious adoption into not only IT sector but also IT enabled services sectors. Nowadays majority of the computing solutions which are being used in various societal service sectors directly or indirectly bank upon cloud computing-based services in the backend. Various parameters such as progressions in mobile communication infrastructure technologies, computation technologies, data storage technologies and telecommunication technologies have increased the span of cloud computing environments in several countries. Apart from that, the ongoing global COVID pandemic have influenced a vital role in cloud computing based digital transformation of numerous organizations in both IT sector and IT-enabled services sectors around the world [1].

Moreover, in the last decade, establishment and utilization of cloud computing based various service models for offering virtual classrooms, distance learning and e-learning platforms has grown exponentially across urban and rural areas in developed and developing countries [2].

Moreover, advancements in virtualization, networking and storage technologies have enabled resource sharing by means of load balancing in cloud computing environments. Cloud load balancing distributes workloads and computing infrastructure across multiple servers in order to provide advantages such as: increased scalability, redundancy, reduced downtime, increased performance, increased flexibility and higher throughput [3]. However, effective resource management plays a vital role in the overall success of utilization of computing solutions which are based on cloud computing enabled IT services. End-user satisfaction highly depends on the quality of service and adequate fulfilment of service level agreement. For attaining the objective of efficient resource management, cloud service providers extensively bank upon resource allocation solutions by means of load balancing. The mechanism of load balancing in cloud computing systems involves reorganization of workload allocation amongst other nodes in a cloud computing platform. Load balancing process encompasses continuous identification of overburdened and lightly loaded machines in cloud and then migrate the workload from overburdened machines to suitable lightly loaded machine in cloud. It helps to attain optimum utilization of cloud resources by safeguarding virtual machines from becoming not only overloaded but also underloaded or idle [4].

Several load balancing approaches have been proposed so far in literature and many of them are being practiced extensively nowadays in various public and private cloud computing environments. A novel load balancing technique has been presented in this paper. The technique presented in this paper helps to avoid starvation and reduce waiting time for overburdened machines in the cloud.

In cloud computing environments, machines work at different priority levels for example, some of the priority values could be: high priority, standard priority or low priority. Priority-based resource allocation in cloud computing environments is advantageous, however it may often cause starvation for machines which work at low priority level. A priority-oriented and starvation free resource sharing mechanism suitable for cloud-based load balancing has been suggested here. The proposed algorithm reports reduction in the waiting time. Reduction in the waiting time of overloaded

virtual machines for additional cloud resources helps not only improve quality of service and performance but also better return on investment.

The sequence of this research paper is set out as follows: our observations on the related literature survey have been discussed in the Section 2 whereas the proposed load balancing mechanism has been presented in the Section 3. The Section 4 and the Section 5 represent the implementation details, observations and outcomes respectively. Concluding remarks and further research scope have been given in the Section 6.

II. LITERATURE REVIEW

Load balancing is primarily concerned with how the workload is distributed among machines in cloud computing environments. Inadequate and poor management of cloud resources at the cloud service provider layer may turn into poor quality of service. Often, such a deterioration in quality of service may further result into termination of service level agreements also. Excerpts and our observations about the relevant literature survey in the area of load balancing has been presented here.

A mechanism for resource sharing [5] carries out migration of tasks from overburdened virtual machines to the underloaded virtual machines. The load balancing decisions are taken dynamically. However, the technique evenly operates on each virtual machine irrespective of the VM's priority level. While taking load balancing decisions, the technique does not take individual VM's priority level into consideration. Hence, the mechanism may result into starvation causing reduction in performance of the load balancing virtual machines.

A task scheduling algorithm suggested in [6] is based on ant colony optimization. The simulation-based algorithm focuses on reducing the average waiting time and works to optimize the makespan of the system. Another task scheduling technique available in [7] offers load balancing. The technique implements modified particle swarm optimization task scheduling called LBMP SO to schedule tasks in cloud computing environment. The load balancing mutation particle swarm optimization technique aims to minimize makespan and maximize utilization of cloud resources.

A machine learning based task scheduling mechanism in cloud computing environment is present in [8]. The load balancing technique takes advantage of K-means algorithm in order to create clusters of jobs and the resources available based on their operating characteristics and processing behavior.

A load balancing technique based on Dynamic Data Replication Algorithms is available in [9]. The technique works on three phase data replication algorithms. The initial two phases work on finding appropriate node for the sake of achieving load balancing. On other side, the third phase focuses on achieving better access improved load balancing by means of the dynamic duplication deployment scheme.

A novel load balancing technique available in [10] incorporate big-ip into an experimental framework. The technique incorporates secure socket layer, local traffic manager and access policy manager. The approach promises to

offer high availability, redundancy and load balancing and data channel.

A load balancing technique based on Grey wolf optimization technique is available in [11]. The algorithm initially finds the unemployed or busy nodes. Then, the algorithm calculates such node's threshold and fitness function. The results obtained through the simulation indicate reduced cost and response time.

An integrated load balancing approach of Harries Hawks optimization and Pigeon inspired optimization algorithm is available in [12]. The cloudsim simulation-based load balancing technique ensures the optimal resource utilizations with task response time. A hybrid algorithm based on combining particle swarm optimization and genetic algorithm is available in [13]. The load balancing technique has a specific objective function.

A Weighted Signature based Load Balancing (WSLB) technique [14] aims on reducing users response time. The technique gathers the load assignment factor for each host and carries out mapping the virtual machines on the basis of the gathered factor value. A methodical review about load balancing techniques in software defined networks is available in [15]. The review mainly classified such techniques into deterministic and non-deterministic approaches. The paper discusses role, challenges and metric analysis in the domain of software defined networks. The study presented is based on single level classification.

In a load balancing approach based on software defined networking is available in [16]. The technique aims on optimizing traffic and data flow and reducing the delay. The resource sharing technique works on implementing FlowQoS mechanism like flow classifier and rate shaper with help of virtual queues.

An optimized resource management scheme known as MEMA is available in [17]. It splits the actual mechanism into two parts: load balancer for normal requests, and load balancer for urgent requests. The mechanism emphasizes on improving task allocation by means of providing quick services and servers to urgent requests. The technique works on lowering waiting time and maximizing fairness with help of a modified round robin technique. The technique entertains all nodes equally without discriminating their priority values.

A load balancing mechanism existing in [18] offers resource sharing suitable for cloud computing platform. A recommended load balancer software component EfficientLoadBalancer operates in coordination through various cooperating daemon threads: LoadBalancer, ManageState, OverLoadedVM and underLoadedVM. The load balancer operates differently in line with the various states of virtual machines. The technique maintains two values for representing VM's state: OVERLOAD_PASSIVE, UNDERLOAD_PASSIVE. The load balancer functions on the basis of shifting workload from the overburdened nodes to the unburdened nodes in cloud. However, the load balancer does not distinguish among the respective virtual machines' priority levels by operating all nodes equally for load balancing.

An improved technique for resource sharing has been suggested in [19]. The technique offers resource sharing in cloud computing environment and it balances workload as per the priority value of virtual machines. The load balancer module PriorityBasedLoadBalancer operates in coordination through various cooperating threads in background: PBLoadBalancer thread, ManageState thread, PBOverloaded VM thread and the thread PBUnderloadedVM thread. The priority-based load balancer module functions on transferring workload between virtual machines of the same priority level. However, in long run the load balancer may cause starvation in load balancing requests which involve low priority virtual machines.

A load balancing framework available in [20] works on attaining better performance on the parameters makespan and cost. The suggested framework is based on hybridization of heuristic technique with metaheuristic algorithm. The framework focuses on deadline constraints and improved resource provisioning in the Cybershake and Ligo workflows execution domain.

A load balancing technique based on genetic pso algorithm is available in [21]. The technique responsible for sharing resources in cloud computing, works over heterogeneous cloud infrastructure. The hybrid genetic pso based task distribution algorithm mainly works on optimizing cost of resource allocation and makespan. The technique works on improving load balancing of the workflow application over the heterogeneous resources in the cloud environment.

A honeybee algorithm-based load balancing technique is present in [22]. The task allocation technique aims to minimization of service makespan on the cloudsim and the workflow. The dynamic resource allocation mechanism works for both dependent and independent jobs. Moreover, the technique addresses to the task priorities and not the VM priorities.

An IMLDB mechanism for resource sharing [23] is based on Improved Modified Distribution Load Balancing and it aims to yield low cost for task migration. The mechanism eyes on the two facets overloading and under loading by means of maintaining profit of the capital gain during the process of task migration in the cloud computing environment.

Intercloud load balancing techniques are present in [24, 25]. The techniques work on resource sharing in collaborated cloud computing environments. The suggested techniques eye on offering not only optimized resource utilization but also continuous availability of cloud resources to stakeholders. However, the mechanisms do not discriminate among the respective virtual machines' priority levels. They treat all virtual machines at the same level.

A modified genetic based algorithm is available in [26]. The technique works on the optimization problem and strives to determine the fittest machines which are associated with various data centers for allocation of cloudlets into appropriate virtual machines. The technique reports lesser execution time consumption by the cloudlets.

In a view of the literature study presented above so far in this section, it is felt that some of the load balancing mechanisms are restricted to specific computation platforms only. Apart from it, few load balancing mechanisms focus on relocating entire overburdened virtual machines to some another host on the cloud infrastructure. Some of the load balancing techniques are static in nature, such techniques are inappropriate for the dynamic load balancing environments. On the other side, some available simulation-based load balancing mechanisms do require prior knowledge about various time variables such as the service time and the arrival time of workload. Often, there exist some closed source load balancing solutions of which no source code is available openly. Hence, it is difficult to extend such closed source solutions on open-source cloud computing frameworks such as the OpenStack. Whereas some of the existing open-source resource sharing techniques fail in controlling starvation problems arising due to their inability to tackle priority-oriented load balancing in particular way.

Hence, virtual machines' priority oriented and starvation free mechanism for dynamic resource sharing in cloud computing environments has been presented here. The load balancing technique presented here aims to overcome the starvation problem often faced by overloaded virtual machines. Furthermore, the technique takes the priority level of virtual machines before taking load balancing decisions. The suggested mechanism has been presented in the following Section 3.

III. MATERIALS AND METHOD

The resource sharing mechanism suggested in [18] provides load balancing functionality in cloud computing environment. However, the technique operates every virtual machine equally without discriminating the virtual machines according to their respective priority levels.

On the other side, the resource sharing technique available in [19] offers priority-based load balancing in cloud computing environment. The technique schedules resource sharing on basis of the preassigned priority value of the virtual machines. However, the technique may cause starvation for certain low priority virtual machines. Situations may arise such that the low priority and the standard priority virtual machines which are overloaded might not get necessary attention due to higher number of resource sharing demands made by the high priority virtual machines.

Hence, the constraints of the work available in [18] and [19] motivated us to extensively work the resource sharing problem. An extended mechanism of priority-based dynamic load balancing approach [19] for load balancing in cloud computing environments has been presented here in order to give adequate attention to such starving overloaded virtual machines. The block diagram our proposed methodology has been described in the Fig. 1. Working of various components of our proposed load balancer PBIImprovedLoadBalancer have been presented here:

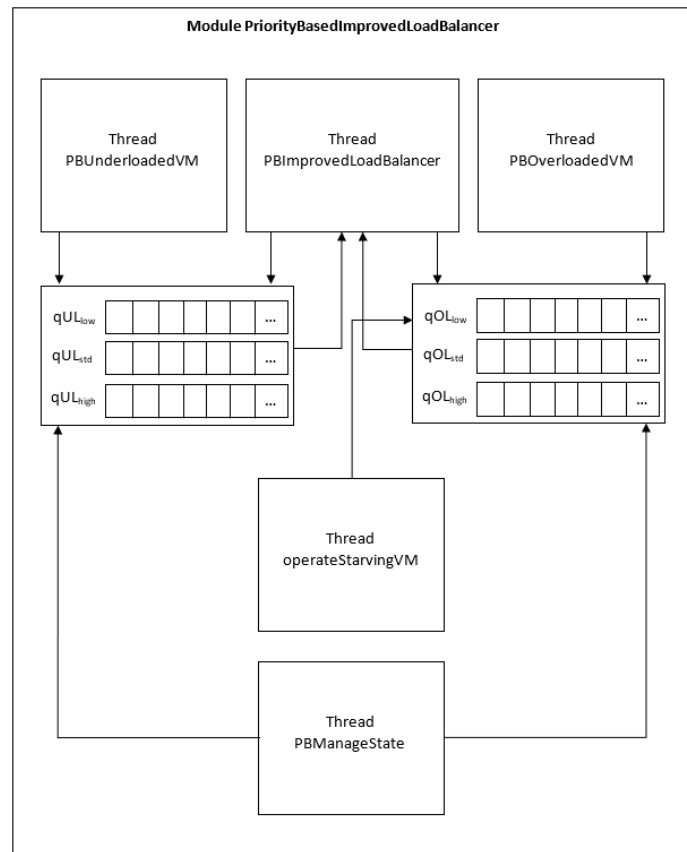


Fig. 1. Block Diagram of Proposed Load Balancing Technique Priority based Improved Load Balancer.

1) The mechanism maintains various state values for representing current state of a particular virtual machine. The AVAILABLE and UNAVAILABLE states indicate current availability and unavailability respectively of a particular virtual machine for load balancing. The UL_PASSIVE state is used to signal that a particular virtual machine was previously underloaded; but now it has already been considered for assigning additional workload and hence no more workload should be assigned to it. The OL_PASSIVE state is used to signal that a particular virtual machine was previously overloaded; but the virtual machine is currently under the process of unloading. The extended mechanism presented here offers one more state of virtual machines: OL_STARVING. The newly introduced state helps the mechanism to mark the overloaded virtual machines which are striving since considerable amount of time for availing additional resources by means of resource sharing in the cloud.

2) The three priority levels LOW, STANDARD and HIGH have been employed for representing current priority of machine. The mechanism permits resource sharing amongst the virtual machines at the same priority level.

3) Based on the current workload of the concerned virtual machines, the thread thread_PBUnderloadedVM puts the virtual machines with the underutilized resources in one of the respective priority queues: qULhigh, qULstd or qULlow. The daemon thread keeps fetching underutilized virtual machines

and drops them in the appropriate queue. For sharing the resources, the load balancer picks virtual machine from relevant priority queue of underloaded virtual machines. Empty queue indicates unavailability of underloaded virtual machine.

4) Based on the current workload of virtual machines, the thread PBOverloadedVM puts the overloaded virtual machines in one of the appropriate priority queues: qOLhigh, qOLstd or qOLlow. The daemon thread keeps fetching overloaded virtual machines and drops them in the appropriate queue. For obtaining the cloud resources, the load balancer picks virtual machines from relevant priority queue of overloaded virtual machines.

5) The resource sharing task is carried out by the thread PBImprovedLoadBalancer. The operation takes place between the overburdened virtual machine and the underburdened virtual machines at the same priority levels. The thread runs continuously. The thread may sleep for a while if there are no additional requirements available in the relevant overload queue.

6) In priority-based cloud computing environment, the suggested technique helps stay away from starvation. The technique periodically evaluates waiting time of concerned virtual machines in the LOW priority queue. The technique treats the starving LOW priority virtual machines with help of the continuously working thread operateStarvingVM.

7) To avoid multiple consecutive resource allocations on the same virtual machine, the load balancer module switches the state of concerned virtual machines to UL_PASSIVE state. Arrangement is such that the suggested resource sharing mechanism does not consider UL_PASSIVE virtual machines eligible for new load balancing requests. However, after completion of certain buffer time, such virtual machines should be automatically toggled back to the AVAILABALE state. Only AVAILABLE state virtual machines are considered eligible for making additional resource demands and sharing of resources.

8) A daemon thread PBImangeState is assigned the task of state management of virtual machine. It periodically keeps checking if the VM is currently passive or not. If the VM is found to be passive, then the thread toggles the VM state to AVAILABLE.

9) Finally, the enhanced module for priority-based resource allocation starts by initializing all time variables and all priority queues. The variables TSu, TSo and TSt represent sleeping time of various daemon threads PBIUnderloadedVM, PBIOverloadedVM, operateStarvingVM respectively.

10)Then the load balancer module launches various collaborating daemon threads PBIOverloadedVM, PBI UnderloadedVM, operateStarvingVM and PBEhancedLoad Balancer. The thread PBImangeState is responsible for VM state management. It also is launched during the starting phase of our load balancer module PBImprovedLoadBalancer.

11)The module maintains an enumerated data structure variable v_priority for maintaining the priority-level values of all virtual machines. At a time, the v_priority variable can have any one of the possible three VM priority values: LOW, STANDARD and HIGH.

12)The module maintains an enumerated data structure variable v_state for maintaining the current state values of all virtual machines. At a time, the v_state variable can have any one of the possible five state values: UNAVAILABLE, AVAILABLE, UL_PASSIVE, OL_PASSIVE and OL_STARVING.

Key segments of the recommended resource sharing algorithm with necessary explanation have been presented here:

```
Module PBImprovedLoadBalancer
{
// Algorithm for starvation free and priority oriented improved
// sharing of cloud resources
enum v_priority {LOW, STANDARD, HIGH};
// possible VM priority values

enum v_state {UNAVAILABLE, AVAILABLE,
UL_PASSIVE, OL_PASSIVE, OL_STARVING};
// Virtual machine state values: unavailable, available,
// underload passive, overload passive, overload starving

int TSt, TSo, TSu; //sleeping time for thread
```

```
struct VMachine
// Holds metadata of a VM
{
v_priority vm_priority;
v_state vm_state; // current state
// VM's resources' information
float vm_load;
unsigned int ncores;
unsigned long tot_mem, free_mem;
float bandwidth;
// Timestamp when VM's state was set as passive
unsigned long passive_set_time;
unsigned long WTUnder, WTOver;
// Threshold for waiting time in queues related to
// overloaded and underloaded virtual machines
char vmIP[40];
...
// getter and setter methods for accessing and
// setting VMachine structure members.
...
}
// Starvation time threshold
unsigned long OLVmStarvationThresholdTime;

// Queues for maintaining underloaded VMs
Queue <VM*> qUL_low, qOL_high, qUL_std;
// Queues for maintaining overburdened VMs
Queue <VM*> qOL_std, qUL_high, qOL_low;

// Keep detecting underloaded virtual machines and
// populate them in respective priority queue
Thread: thread_PBIUnderLoadedVM
{
VM* pVM_U = null;
void fetch_PBIUnderloaded_VM(){
//Thread method
while(true) {
pVM_U = null;
//Find out underloaded VM
pVM_U = determine_underloaded_VM();
if(qUL<pVM_U -> vm_priority>.find
(pVM_U) ||
pVM_U.passive_set_time < WTUnder)
continue;
if(!pVM_U) {
// At present there is no such VM.
// So, sleep thread for TSu sleep time.
sleep(TSu); continue;
}
qUL<pVM_U->
vm_priority>.append(pVM_U);
// Found underloaded VM.
// So, append it to relevant queue.
} //while
} //End of Thread method
}
```

```
// Keep detecting overloaded virtual machines and
// populate them in respective priority queue.
Thread: thread_PBIOverLoadedVM
{
    VM* pVMO = null;
    void fetch_PBIOverloaded_VM(){
    //Thread method
    while(true) {
        pVMO = null;
        // Find out overloaded VM
        pVMO = determine_overloaded_VM();
        if(qOL<pVMO->vm_priority>.find(pVMO) ||
        pVMO.passive_set_time<WTOver)
            continue;
        if(!pVMO) {
            // At present there is no such VM
            // So, sleep thread for TSo sleep time
            sleep(TSo); continue;
        }
        qOL<pVM->vm_priority>.append(pVMO);
        // Found overloaded VM.
        // So, append it to relevant queue.
    }//while
    }//End of thread method
}//Thread

// Procedure for starvation free and priority oriented load
// sharing
Thread: thread_PBImprovedLoadBalancer
{
    VMachine* pVMO, pVMU;
    void PBImprovedLoadBalance()
    {
        Thread sleep if there are no overloaded VMs
        Thread sleep if there are no resource sharing offers
        while(true) {
            pVMU=qUL<high,std,low>.fetch()
            if(!pVMU)
                // VM for resource sharing is unavailable at present.
                // So, search again.
                continue;
            if(pVMU->timeSincePassive() <
                MaxULTimeThreshold
                || !pVMU->isUnderloaded()
                || pVMU->vm_state== UL_PASSIVE)
                // Found VM but it is still passive or it has no
                // sharable resources
                continue;
            pVMO=qOL<pVMU.priority>.fetch()
            if(!pVMO)
                // Resource requirements unavailable at present.
                // So, search again.
                continue;
            if(pVMO->timeSincePassive() <
                MaxOLTimeThreshold
                || pVMU->isOverloaded()
                || pVMO->vm_state==OL_PASSIVE)
                // VM is still passive or it has no resource
                // requirements.
                continue;
            if(pVMU->vm_state == AVAILABLE &&
                pVMO->vm_state == AVAILABLE){
                // Both source and target VMs are available.
                // So, carry out resource sharing.
                // Make both VMs passive for further load
                // balancing requests and to protect them from
                // instantaneous overburdening.
                pVMU->vm_state=UL_PASSIVE;
                pVMO->vm_state=OL_PASSIVE;

                set passive_set_time for pVMO
                set passive_set_time for pVMU
                // Remove both VMs from respective wait queues
                qUL<pVMU.priority>.remove()
                qOL<pVMO.priority>.remove()
                // Load balance
                balance(pVMO,pVMU)
                ...
            }
        } // function PBImprovedLoadBalancer.
    } //while
} // thread thread_PBImprovedLoadBalancer.
// Keep detecting the starving virtual machines which are
// waiting for additional resource requirements in queue.
Thread: thread_operateStarvingVM
{
    void operateStarvingVM()
    {
        while(true){
            ...
            pVMO = qOL<low>.fetchLast()

            if(pVMO->timeSincePassive() >
                OLVmStarvationThresholdTime) {
                //VM is starving, so operate it.
                qOL<low>.shiftToFirst(pVMO)
                sleep(TSt);
                //Sleep thread for TSt Starvation sleep time.
                ...
            }
        } // while
    } // function operateStarvingVM
} // thread thread_operateStarvingVM

// Keep managing VM state
Thread: thread_PBImanageState
{
    void vmStateManager() {
        ...
        for all VMs: pVM
        if(pVM-> vm_state = UL_PASSIVE &&
            pVM->timeSincePassive()>=
            pVM->WTUnder)
            ||

```

```
(pVM-> vm_state = OL_PASSIVE &&
pVM->timeSincePassive(>=
pVM->WTOver)
// Time to remain in the passive state for a
// particular VM is over. So, now make it
// AVAILABLE for load balancing.
reset pVM's passive_set_time
// Make pVM as AVAILABLE for load balancing.
pVM->vm_state = AVAILABLE;
...
} // function thread_PBIManageState
} // thread thread_PBIManageState

// Launch module now.
void start()
{
...
Initialize times: TSu, Tso, TSt
Initialize time: OLVmStarvationThresholdTime

Initialize queue: qOL<low,std,high>
Initialize queue: qUL<low,std,high>

Spawn thread: thread_PBIOverLoadedVM

Spawn thread: thread_PBIUnderLoadedVM

Spawn thread: thread_PBImprovedLoadBalancer

Spawn thread: thread_operateStarvingVM

Spawn thread: thread_PBIManageState

...
} // function start
} // module PBImprovedLoadBalancer
```

The start() function in the suggested module PriorityBasedImprovedLoadBalancer starts with initializing various time intervals which are meant for making the thread sleep for certain time intervals. The module also sets the starvation time threshold in waiting queue for the overloaded virtual machines. Finally, the start() function launches the collaboratively working threads. The parallelly running threads thread_PBIOverLoadedVM and thread_PBIUnderLoadedVM keep finding those virtual machines which are in shortage of resources and the virtual machines which have excessive unutilized resources go wasted respectively. The priority based improved load balancer thread thread_PBImprovedLoadBalancer executes resource sharing. The collaboratively working thread thread_operateStarvingVM takes care of starving virtual machines which are waiting in queue.

IV. IMPLEMENTATION

The prototype cloud environment testbed was established on physical server and the entire setup was made run as suggested in the [19]. The private cloud computing environment was setup over a minimal setup of the open-

source CentOS Linux operating system platform. In order to facilitate the Infrastructure as a Service (IaaS) by means of offering cloud-based instances which are available on demand, the open-source cloud computing environment was established by installing OpenStack on top of the CentOS Linux platform.

V. RESULTS AND DISCUSSION

The mechanism begins with setting and initializing values of various data structures such as sleeping time of various threads, respective queues for maintaining information about overloaded and underloaded virtual machines. After initializing the data structures and queues, the algorithm spawns the collaborating daemon threads: PBIManageState, PBIOverLoadedVM, PBImprovedLoadBalancer PBIUnderLoadedVM and operateStarvingVM.

The daemon thread thread_operateStarvingVM keeps watching and operating the starving virtual machines. The Table I shows comparison of results obtained using our proposed method with the results of existing technique. For the low priority overloaded virtual machines, the experimental results have been presented in a Table I. The Table I represents the waiting times of various starving virtual machines in absence and presence of our suggested thread thread_operateStarving VM respectively. The function of the daemon thread thread_operateStarvingVM is to efficiently manage the starving overloaded virtual machines with a motive to reduce their waiting time.

The column A in the Table I represents the observed waiting time value of the overloaded virtual machines in absence of our suggested daemon thread thread_operateStarvingVM. The average of the waiting times mentioned in the column A is 9.62 milliseconds for such overloaded virtual machines [19].

The column B in the Table I represents the observed value of waiting time of the overloaded virtual machines in presence of our suggested daemon thread thread_operateStarvingVM. However, in presence of our suggested collaborative daemon thread thread_operateStarvingVM, the average value of the observed waiting times mentioned in the column B is found to be reduced to 7.1 milliseconds, which clearly designates performance improvement by means of reduction in waiting time of overloaded virtual machines in waiting queue.

TABLE I. TABLE SHOWING WAITING TIMES OF VIRTUAL MACHINES IN THE WAITING QUEUE IN ABSENCE AND PRESENCE OF THE THREAD THREAD_OPERATESTARVINGVM RESPECTIVELY

Virtual Machine (IP address)	Waiting time (milli seconds)	
	A. In absence of the thread_operateStarvingVM	B. In presence of the thread_operateStarvingVM
192.168.10.2	8.9 ms	6.4 ms
192.168.10.3	10.2 ms	7.6 ms
192.168.10.4	10.4 ms	7.9 ms
192.168.10.5	9.4 ms	6.9 ms
192.168.10.7	9.2 ms	6.7 ms

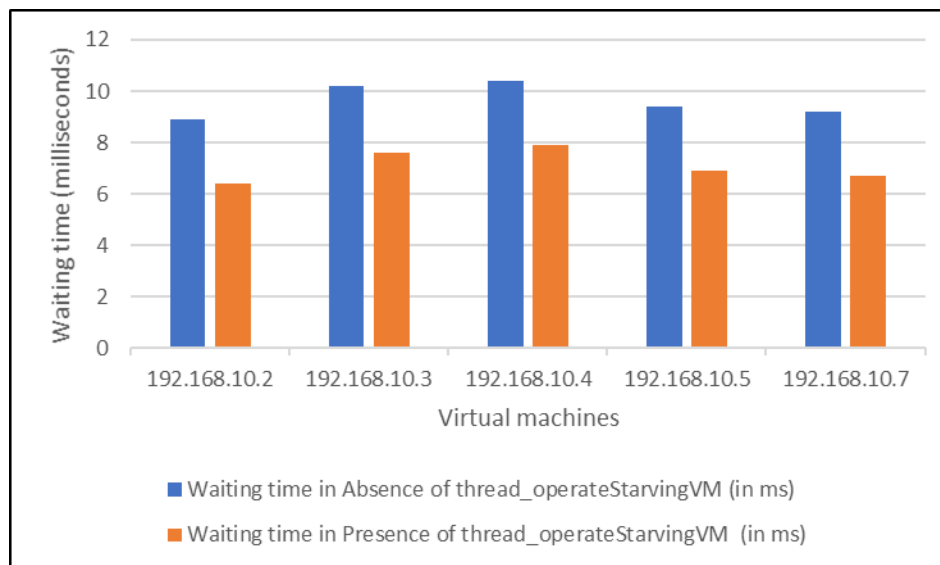


Fig. 2. Chart of Comparison of Waiting Times of Virtual Machines in Absence and Presence of the Thread thread_operateStarvingVM.

Moreover, a chart shown in a Fig. 2 also designates significant reduction in the waiting time of all concerned overloaded virtual machines for availing additional cloud resources for load balancing.

Such a reduction in the average waiting times is extremely beneficial to the low priority overloaded virtual machines in the cloud. The dropout in waiting time of a concerned starving overloaded virtual machine in a respective priority queue helps it to attain the required additional resources from cloud in lesser time. Hence, faster availability of additional cloud resources will cause faster execution of tasks. Quicker execution of tasks results into increased overall system performance and optimized utilization of cloud resources.

VI. CONCLUSION

An enhanced mechanism for priority-oriented resource sharing for cloud computing platform has been suggested in this paper. The mechanism prevents resource requirements on low priority virtual machines from starvation. Implementation of proposed algorithm clearly designates reduction in waiting time of concerned virtual machines. The technique is helpful in attaining efficient resource utilization and improved performance. The obtained results undoubtedly reveal reduction in the average waiting time of overloaded virtual machines in the waiting queue. Hence the technique helps overcome starvation. Thereby, the proposed technique helps achieving improved resource sharing for low priority virtual machines in cloud computing environment.

In future, this technique can be extended further on collaborated cloud computing environments for attaining improved resource utilization and getting better return on investment. Moreover, the suggested technique can be explored further for studying security aspects.

REFERENCES

[1] Alashhab Z, Anbar M, Singh M, Leau Y, Al-Sai Z, Alhayja S. Impact of coronavirus pandemic crisis on technologies and cloud computing applications, *Journal of electronic science and technology*. 2021; 19.

[2] Joshi N. Performance-centric cloud-based e-learning, *The IUP Journal of information technology*. 2014; 10(2).

[3] Afzal S, Kavitha G. Load balancing in cloud computing – A hierarchical taxonomical classification, *Journal of cloud computing*. 2019; 8.

[4] Mishra SK, Sahoo B, Parida PP. Load balancing in cloud computing: A big picture. *Journal of king saud university – computer and information sciences*. 2020; 32(2).

[5] Joshi N, Choksi DB, Kotecha K, Pandya S. Implementation of novel load balancing technique in cloud computing environment. *International conference on computer communication and informatics*. 2018.

[6] Amit D, Dinesh R. Design a novel technique for load balancing in cloud computing environment. *Solid State Technology*. 2021. 64(2).

[7] Arabinda P, Sukanata Kishoro B. A novel load balancing technique for cloud computing platform based on PSO. *Journal of king saud university – computer and information sciences*. 2020; In Press.

[8] Shivaprasada K, Sangameshwar, Rajesh S, Swasthika T. Machine learning aided scheduling on cloud computing, *International journal of emerging trends in engineering research*. 2020; 8(9).

[9] Hsieh HC, Ching M. The incremental load balance cloud algorithm by using dynamic data deployment. *Journal of grid computing*. 2019; 17.

[10] Bholanath M, Rajesh B, Sandip R. A novel approach to load balancing and cloud computing security using SSL in IaaS environment. *International journal of advanced trends in computer science and engineering*. 2020; 9(2).

[11] Sefati S, Mousavinasab M, Zareh Farkhady R. Load balancing in cloud computing environment using the Grey wolf optimization algorithm based on the reliability: performance evaluation. *Journal of supercomputing*. 2021; In press.

[12] Poornima G, Radhamani A. A hybrid meta-heuristic for optimal load balancing in cloud computing. *Journal of grid computing*. 2021; 19.

[13] Dhiraj K, Vijay D. Performance evaluation of new hybrid approach of load balancing in cloud computing. *Design engineering*. 2021; 2021(5).

[14] Ajit M, Vidya G. VM level load balancing in cloud environment. *International conference on computing, communications and networking technologies*. 2013.

[15] Neghabi AA, Navimipour NJ, Hosseinzadeh M, Rezaee A. Load balancing mechanisms in the software defined networks: a systematic and comprehensive review of the literature. *IEEE access*. 2018; 6:14159–14178.

[16] Gokilabharathi R, Deepalakshmi P. Efficient load balancing to enhance the quality of service (QoS) in Software Defined Networking (SDN). *International conference on trends in electronics and informatics*. 2018.

- [17] Manasser S, Alzghoul M, Mohmad M. An advanced algorithm for load balancing in cloud computing using MEMA technique. *International journal of innovative technology and exploring engineering.* 2019; 8 (3).
- [18] Joshi N. Efficient load balancing in cloud computing. *Research review international journal of multidisciplinary.* 2019; 4(6).
- [19] Joshi N. Priority based mechanism for resource sharing in cloud. *International journal of innovative technology and exploring engineering.* 2020; 9(3).
- [20] Kaur A, Kaur B. Load balancing optimization based on hybrid heuristic-metaheuristic techniques in cloud environment, *Journal of king saud university – Computer and Information Sciences.* 2019.
- [21] Manasrah A, Ali H. Workflow scheduling using hybrid GA-PSO algorithm in cloud computing. *Wireless communications and mobile computing.* 2018; 2018.
- [22] Gopinath G, Vasudevan SK. A novel improved honey bee based load balancing technique in cloud computing environment. *Asian journal of information technology.* 2016; 15(9).
- [23] Afzal S, Kavitha G. Optimization of task migration cost in infrastructure cloud computing using IMDLB algorithm. *International conference on circuits and systems in digital enterprise technology.* 2018.
- [24] Joshi NA. Optimized Mechanism for Resource Sharing in Cloud. *International journal of engineering and advanced technology.* 2019. 9(2).
- [25] Joshi N. Performance centric model for resource sharing in cloud. *Research review international journal of multidisciplinary.* 2018; 3(5).
- [26] Swarnakar S, Kumar N, Kumar A, Banerjee C. Modified genetic based algorithm for load balancing in cloud computing. *International conference for convergence in engineering.* 2020.

A Heuristic Feature Selection in Logistic Regression Modeling with Newton Raphson and Gradient Descent Algorithm

Samingun Handoyo¹, Nandia Pradianti², Waego Hadi Nugroho³, Yusnita Julyarni Akri⁴

Department of Statistics, Brawijaya University, Malang, Indonesia¹

Department of EECS-IGP, National Yang Ming Chiao Tung University, Hsinchu, Taiwan¹

Department of Statistics, Brawijaya University, Malang, Indonesia^{2,3}

Department of Midwifery, Tribuana Tungadewi University, Malang, Indonesia⁴

Abstract—Binary choices, such as success or failure, acceptance or rejection, high or low, heavy or light, and so on, can always be used to express decision-making. Based on the known predictor feature values, a classification model can be used to predict an unknown categorical value. The logistic regression model is a commonly used classification approach in a variety of scientific domains. The goal of this research is to create a logistic regression model with a heuristic approach for selecting input characteristics and to compare the Newton Raphson and gradient descent (GD) algorithms for estimating parameters. Among predictor traits, there were four that met the criterion for being both dependent on the target and independent of one another. Also, optional features In Malang, Indonesia, researchers used the Chi-square test to find four significant characteristics that increase the incidence of pregnant women developing preeclampsia: age (X1), parity (X2), history of hypertension (X3) and salty food consumption (X6). In the above work author proposed, the logistic regression model developed using the gradient descent approach had a lower risk of error than the logistic regression model generated using the Newton Raphson algorithm. The model with the gradient descent approach has a precision of 98.54 percent and an F1 score of 97.64 percent, while the model with the Newton Raphson algorithm has a precision of 86.34 percent and an F1 score of 72.55 percent.

Keywords—Classification model; feature selection; gradient descent; logistic regression; Newton Raphson

I. INTRODUCTION

In modern statistical modeling, there is a simple point of view in developing a statistical model, namely by observing the presence of a target feature in the data set. A descriptive model is developed if there is no target feature. On the other hand, if there is a target feature, a predictive model is developed. The clustering method is the most popular descriptive model. Marji et al [1] discussed topics related to fuzzy subtractive clustering, and Handoyo et al [2] discussed the performance of the optimal clustering method with a hybrid between subtractive fuzzy and c-mean fuzzy clustering. Another type of descriptive modeling is the method used as an assessment tool to generate a ranking of objects based on their features [3]. Predictive modelling is divided into 2 types based on the measuring scale of the target feature. The regression model is built when the target feature is continuous (interval or

ratio), while the classification model is built when the target feature is discrete (nominal or ordinal). In statistics, regression modeling is more emphasized to explore the causality relationship between the target and predictor features [4-5], but in the machine learning community, regression modeling is oriented to capture all existing patterns in a data set in order to obtain a model that is able to predict the unknown value of target feature with high accuracy [6]. Some examples of regression modeling for predictive purposes include Handoyo et al [7] have developed a model to predict the regional minimum wage, while Handoyo and Chen [8] have developed a model to predict daily soybean prices in Indonesia.

The application of the classification method gets more serious attention because a decision-making will be more measurable and easy to execute in the form of discrete choices, each continuous scale will also be simpler when it is transformed into a discrete scale [9]. Several researchers have compared the performance of classification models, including Widodo and Handoyo [10] compared logistic regression and Support Vector Machine, Nugroho et al [11] compared logistic regression and Learning Vector Quantization, and Handoyo et al [12] varied the threshold values to obtain the best performing logistic regression and linear discriminant models. A model involving only predictor features that have a significant contribution to the variability of the target feature is an ideal model for researchers [13-14]. Thus, feature selection is an important stage in model development. In general, the feature selection method is divided into 2 approaches, namely the wrapped and the filter approach. Wrapped approach features selection is computationally expensive because it involves the model with all of the possible feature combinations [15]. Feature selection with the filter approach method is more heuristic in nature, namely by evaluating both the dependency between predictor and target features, as well as independency among predictor features [16-17]. Chi-square test can be used for the above evaluation purposes if both features are categorical features [18].

Parameter estimation has an important role in producing the best model. In statistics, estimate parameters can be obtained by minimizing the sum of squared errors (SSE) known as the least square (LS) method [19] or by maximizing the log-likelihood function known as maximum likelihood estimation

[20-21]. The LS method is generally used for estimating parameters in linear systems, while the maximum likelihood estimation (MLE) method is used for estimating parameters in nonlinear systems. The complexity of the nonlinear model has also prompted researchers to lead using optimization methods such as Particle Swarm Optimization [22-23]. Newton Raphson algorithm works based on maximizing the likelihood function which is considered as an equation that is solved to find the equation root as the estimated parameters [24-25]. On the other hand, the gradient descent algorithm finds the estimated parameters by reducing the score function gradient and leads to be 0 which means the optimal solution has been reached [26-27].

In the field of public health, there are many problems that must be handled and controlled properly, one of which is the case of preeclampsia because it is the main cause of maternal death [28]. The immune system plays an important role in promoting the occurrence and development of preeclampsia. Wang et al [29] identified significant immune of the related genes for predicting the occurrence of preeclampsia. Women with preeclampsia are more likely to develop acute kidney injury, placental abruption, and postpartum hemorrhage syndrome before they give birth [30]. Reddy et al [31] evaluated the related application of a broader definition of hypertension and the most appropriate definition of end-organ dysfunction because there is still controversy over the definition that has been used so far.

Based on the description above, this study aims to obtain predictor features that are independent and have a significant effect on preeclampsia by using the Chi-square test, also to compare the performance of fitting the logistic regression model obtained using Newton Raphson algorithm and gradient descent by popular criteria used as classification model performance measure.

The paper consists of five sections. The remaining sections include Section 2 which described the proposed method in detail, namely the feature selection method with a filter approach using the Chi-square test, the cost function in predictive modeling, and both learning algorithms i.e. Newton Raphson and gradient descent. The presentation of empirical data, both of response and predictor features are given in Section 3, while in Section 4, the logistic regression model and its performance are discussed, both the model generated by the Newton Raphson and algorithm gradient descent. Conclusions and recommendations for further research are given in Section 5.

II. PROPOSED METHOD

A good model is simple and has high performance. One of the characteristics of the simple model is that it involves a small number of predictor features. Model parameters estimate are carried out in the training process using an optimization technique such as Maximum likelihood. When the log-likelihood function is non-linear in its parameters, a numerical iteration algorithm can be used to obtain an estimator of the model parameters. In this section, we will discuss the test of dependencies for feature selection, the score function in maximum likelihood, the Newton Raphson and gradient descent algorithm.

A. Chi Square Test for Feature Selection

In machine learning, the predictor and the response features are expected to have a relationship (dependency) while between two predictor features do not have a relationship [32]. The chi-square test is useful for evaluating the correlation between two categorical features. The chi-square (χ^2) statistical test has the null hypothesis i.e. two categorical features are independent versus the alternative hypothesis i.e. two categorical features are dependent [33]. The null hypothesis is rejected when the $P(\chi_{df}^2 > \chi^2 \text{ statistic})$ is less than 0.05 (the p-value is less than 0.05) and otherwise the null hypothesis not able be rejected.

The main idea of the chi-square test is to compare the observed values in the data with the theoretically expected values and test whether the values are related to each other. The contingency table associated with both categorical features is created to support the calculation of the chi-square value. The formula of chi square statistic is the following [34]:

$$\chi^2 = \sum_{i=1}^r \sum_{j=1}^c \frac{(O_{i,j} - E_{i,j})^2}{E_{i,j}} \quad (1)$$

Where χ^2 is Chi square statistic, $O_{i,j}$ is the observed value and $E_{i,j}$ is the expected value of two nominal variables. The Chi square statistic has a degree of freedom (df) of $(r - 1)(c - 1)$. The $E_{i,j}$ value can be calculated by formula:

$$E_{i,j} = \frac{\sum_{k=1}^c O_{i,j} \sum_{k=1}^r O_{k,j}}{N} \quad (2)$$

Where $\sum_{k=1}^c O_{i,j}$ is the sum of the i_{th} column, $\sum_{k=1}^r O_{k,j}$ is the sum of the k_{th} column, and N is the total instance.

When the evaluation of dependency between predictor and response feature, the expected decision is to reject the null hypothesis and the associated predictor feature is kept as the member of predictor variable. In other side, when the evaluation of dependency between 2 predictor features, the expected decision is to accept the null hypothesis that means both categorical features are kept as the member of predictor features.

B. Score Function in Maximum Likelihood Estimation

The goal of a predictive model is to make the correct prediction of the target value for a previously unseen data item. A score function is a function of the difference between the real answer $y^{(i)}$ and the predicted value $\hat{f}(x^{(i)}; \theta)$ [35]. Consider the n instances having the response feature $y^{(i)}$ and predictor feature $x^{(i)} = [x_1, x_2 \dots x_p]$ for $i = 1, 2, 3, \dots, n$. Assume $y^{(i)} = \theta^T x^{(i)} + \varepsilon^{(i)}$ is a regression model structure having as many as p unknown parameters. The $\varepsilon^{(i)}$ is a random noise (error) which is the un-modeled effect. By assuming $\varepsilon^{(i)} \sim NIID(0, \sigma^2)$, the probability density function of $\varepsilon^{(i)}$ can be stated such as the equation (3) following [36].

$$P(\varepsilon^{(i)}) = \frac{1}{\sqrt{2\pi}\sigma} \exp\left(\frac{-(\varepsilon^{(i)})^2}{2\sigma^2}\right) \quad (3)$$

The posterior probability with the unknown parameter θ is

$$P(y^{(i)}|x^{(i)}; \theta) = \frac{1}{\sqrt{2\pi}\sigma} \exp\left(\frac{-(y^{(i)} - \theta^T x^{(i)})^2}{2\sigma^2}\right) \quad (4)$$

The equation (4) means that $y^{(i)}|x^{(i)}; \theta \sim N(\theta^T x^{(i)}, \sigma^2)$ and it also is called the likelihood function. The following is the likelihood function of n instances:

$$\begin{aligned} \mathcal{L}(\theta) &= P(\vec{y}|X; \theta) \\ &= \prod_{i=1}^n P(y^{(i)}|x^{(i)}; \theta) \\ &= \prod_{i=1}^n \frac{1}{\sqrt{2\pi}\sigma} \exp\left(\frac{-(y^{(i)} - \theta^T x^{(i)})^2}{2\sigma^2}\right) \\ \ell(\theta) &= n \ln \frac{1}{\sqrt{2\pi}\sigma} + \sum_{i=1}^n \frac{-(y^{(i)} - \theta^T x^{(i)})^2}{2\sigma^2} \end{aligned} \quad (5)$$

The log likelihood is

$$\begin{aligned} \ell(\theta) &= \log \mathcal{L}(\theta) \approx \ln \mathcal{L}(\theta) \\ &= \ln \prod_{i=1}^n \frac{1}{\sqrt{2\pi}\sigma} \exp\left(\frac{-(y^{(i)} - \theta^T x^{(i)})^2}{2\sigma^2}\right) \\ &= \sum_{i=1}^n \left[\ln \frac{1}{\sqrt{2\pi}\sigma} + \ln \exp\left(\frac{-(y^{(i)} - \theta^T x^{(i)})^2}{2\sigma^2}\right) \right] \\ \ell(\theta) &= n \ln \frac{1}{\sqrt{2\pi}\sigma} + \sum_{i=1}^n \frac{-(y^{(i)} - \theta^T x^{(i)})^2}{2\sigma^2} \end{aligned} \quad (5)$$

Maximum Likelihood Estimation method is how to choose θ to maximize $\ell(\theta)$ in the equation (5) by the first derivative with respect to θ and set its to 0 [37]. All term in equation (5) involving the θ parameter is only the second part numerator i.e. the sum square of error which must be minimized to get the $\ell(\theta)$ maximum. In the other word, to obtain the optimum parameter θ through MLE is equivalence to minimize the equation (6) also called as the score function of regression model which is the negative of log likelihood $\ell(\theta)$.

Minimize

$$J(\theta) = \frac{1}{2} \sum_{i=1}^n (y^{(i)} - \theta^T x^{(i)})^2 \quad (6)$$

Where $J(\theta)$ is called as a loss or cost function of a regression model.

A binary classification model has the response feature of $y \in \{0,1\}$. In the logistic regression case, the classifier model structure is a sigmoid function which has a primary task to separate both classes or as a boundary curve between 2 classes. Suppose the sigmoid formula of an instance is stated in the following:

$$h_{\theta}(x) = g(\theta^T x) = \frac{1}{1 + e^{-\theta^T x}} \quad (7)$$

It is expected that $h_{\theta}(X) \in [0,1]$ with $P(y = 1|X; \theta) = h_{\theta}(X)$, and $P(y = 0|X; \theta) = 1 - h_{\theta}(X)$. The posterior

probability of a binary classification follows a binomial distribution as the following:

$$P(y|X; \theta) = h_{\theta}(X)^y (1 - h_{\theta}(X))^{1-y}$$

The n instances likelihood function is expressed as the following:

$$\begin{aligned} \mathcal{L}(\theta) &= P(\vec{y}|X; \theta) \\ &= \prod_{i=1}^n P(y^{(i)}|X^{(i)}, \theta) \\ &= \prod_{i=1}^n h_{\theta}(X)^{y^{(i)}} (1 - h_{\theta}(X))^{1-y^{(i)}} \end{aligned}$$

The log likelihood function for binary classification is

$$\begin{aligned} \ell(\theta) &= \log \mathcal{L}(\theta) \\ \sum_{i=1}^n [y^{(i)} \log h_{\theta}(X^{(i)}) + (1 - y^{(i)}) \log (1 - h_{\theta}(X^{(i)}))] \end{aligned} \quad (8)$$

The score function of a binary classification model is the negative of $\ell(\theta)$ which has the popular name called as cross entropy loss function as the following [38].

$$J(\theta) = - \sum_{i=1}^n [y^{(i)} \log h_{\theta}(X^{(i)}) + (1 - y^{(i)}) \log (1 - h_{\theta}(X^{(i)}))] \quad (9)$$

Machine learning model is trained by minimizing loss function to yield the estimate parameter θ .

C. Newton Raphson and Gradient Descent Algorithm

A way to obtain the estimate parameter θ is by maximizing the log likelihood function $\ell(\theta)$ through the first derivative with respect to θ and to be set 0. Because the $\ell'(\theta)$ has non linear form, the analytic (close form) solution can not be obtained. A numerical approach through the iterative method can be used to handle the problem. Newton's method was originally intended to find the roots of an equation by determining the value of the function to be 0 (to find the root of $f(\theta) = 0$) [39]. Consider that the gradient (slope) of a line equation is defined as the following:

$$f'(\theta^{(0)}) = \frac{\text{height}}{\text{base}} = \frac{f(\theta^{(0)})}{\Delta}, \text{ so } \Delta = \frac{f(\theta^{(0)})}{f'(\theta^{(0)})}$$

and the other hand $\Delta = \theta^{(0)} - \theta^{(1)}$ (i.e. base which is difference between 2 of x -coordinate values). For a stage t , a new x -coordinate can be expressed as the following.

$$\begin{aligned} \theta^{(t+1)} &:= \theta^{(t)} - \frac{f(\theta^{(0)})}{f'(\theta^{(0)})}, \text{ for } f(\theta) = \ell'(\theta) \text{ then it is obtained} \\ \theta^{(t+1)} &:= \theta^{(t)} - \frac{\ell'(\theta)}{\ell''(\theta)} \\ \theta^{(t+1)} &:= \theta^{(t)} + H^{-1} \nabla_{\theta} \ell(\theta) \end{aligned} \quad (10)$$

Where Hessian H is defined as $H_{ij} = \frac{\partial^2 \ell(\theta)}{\partial \theta_i \partial \theta_j}$ and $\nabla_{\theta} \ell(\theta) = \ell'(\theta)$. The equation (10) is the iterative formula of Newton Raphson algorithm [40]. The stopping criteria can be used

either a iteration number or a threshold value desired by user. So the solution of the Newton Raphson is a value that maximize the log likelihood function $\ell(\theta)$.

In the machine learning approach, a gradient descent (GD) is an algorithm that minimizes the cost function $J(\theta)$ such as stated in equation (9). The parameters that minimize $J(\theta)$ are obtained using a search algorithm that starts with a "initial guess" value by repeatedly changing it to make $J(\theta)$ smaller until it is expected to converge to a value. Here is the formula of the GD algorithm which starts with an initial value, and is repeatedly updated [41].

$$\theta_j = \theta_j - \alpha \frac{\partial}{\partial \theta_j} J(\theta) \quad (11)$$

The GD algorithm can be implemented when the partial derivative on the right-hand side of equation (9) has been known. Suppose there is 1 instance (x, y), so the summation term in the definition of $J(\theta)$ on the equation (8) can be negligible.

$$\begin{aligned} \frac{\partial}{\partial \theta_j} J(\theta) &= \frac{\partial}{\partial \theta_j} (-\ell(\theta)) \\ \frac{\partial}{\partial \theta_j} J(\theta) &= - \left(y \frac{1}{g(\theta^T x)} \right. \\ &\quad \left. - (1-y) \frac{1}{1-g(\theta^T x)} \right) \frac{\partial}{\partial \theta_j} g(\theta^T x) \\ &= - \left(y \frac{1}{g(\theta^T x)} - (1-y) \frac{1}{1-g(\theta^T x)} \right) g(\theta^T x) \left(1 - g(\theta^T x) \right) \frac{\partial}{\partial \theta_j} \theta^T x \\ &= - \left(y(1-g(\theta^T x)) - (1-y)g(\theta^T x) \right) x_j \\ &= - (y - g(\theta^T x)) x_j \end{aligned}$$

So, it is found that the first derivative of the loss function classification is

$$\frac{\partial}{\partial \theta_j} J(\theta) = -(y - h_{\theta}(x)) x_j \quad (12)$$

The gradient descent iterative formula is

$$\theta_j = \theta_j - \alpha \frac{\partial}{\partial \theta_j} J(\theta) \quad (13)$$

By substituting the equation (12) into the equation (13), It leads to the updating parameter final formula of the GD algorithm as the following:

$$\theta_j = \theta_j + \alpha \sum_{i=1}^n (y^{(i)} - h_{\theta}(X^{(i)})) X_j^{(i)} \quad (14)$$

Where α is a learning rate determined together with a stopping criteria value such as a threshold or iteration number before the training model is started.

III. DESCRIBING DATA

The data used in this study are the secondary data as many as 205 instances obtained from the Center of Child Development Studies at the Wira Husada Nusantara Midwifery

Academy Malang in 2021. The data set consist of a response feature, namely preeclampsia status, and 7 predictor features, namely the factors affecting preeclampsia include age, parity, history of hypertension, pregnancy interval, household harmony, consumption of salty foods, consumption of fruits, and vegetables. The description of features in the data set is stated in Table I.

TABLE I. CLASS LABEL DISTRIBUTION IN THE DATASET

Feature name	Class label	Label distribution
Preeclampsia (Y)	[No, Yes]	[140, 65]
Age (X1)	[No risk, Risk]	[133, 72]
Parity (X2)	[No risk, Risk]	[133, 72]
History of Hypertension (X3)	[No, Yes]	[135, 70]
Pregnancy Interval (X4)	[No risk, Risk]	[153, 52]
Household Harmony (X5)	[Yes, No]	[145, 60]
Salty Food Consumption (X6)	[No, Yes]	[116, 89]
Fruits and Vegetables Consumption (X7)	[Yes, No]	[141, 64]

All features in the data set are categorical consisting of 2 class labels, namely [No or No risk, Yes or Risk] except for X5 and X7 features which have class labels [Yes, No]. The class label in the first order is worth 0, while the class label in the second-order is worth 1. In the target feature y, the proportion of class 0 is 68% and the proportion of class 1 is 32%. The distribution of class labels on the predictor features is very similar to the distribution of class labels on the target features, except that the X6 feature has a distribution of class labels of 58% and 42% for class 0 and class 1. Imbalance class on the target feature should receive serious attention in building a classification model. Fortunately, in this data set, both the target and predictor features have a distribution of class labels that are classified as balanced.

IV. RESULT AND DISCUSSION

This section initially discusses feature selection by evaluating the dependencies between target and predictor features. The predictor features that have significant dependencies are preserved as the final candidate features that are evaluated for their independence. The final predictor features are selected from the final candidate features that are independent of each other. The classification model parameters associated with the final predictor feature are estimated using the Newton Rapson and Gradient descent algorithms. The performance of the two models is evaluated using several measures that are popularly used in classification.

A. Heuristic Feature Selection

Dependencies between two categorical features can be evaluated using Chi-square statistic which is calculated based on the contingency table formed from these two features. The contingency table between the target feature (Preeclampsia) and the Parity feature is presented in Table II.

The values in the cells of the contingency table are the observed values between the two categories (combination of 2

labels) derived from the two features. The observation values are compared with the expected values calculated using formula (2). Then the Chi-square statistic was calculated using formula (1). Table III presents the Chi-square statistic and associated p-value of the dependency measure between target and predictor feature.

All p-values in Table III are less than 0.05 (level of significance) which means that all predictor features have a significant dependence on the target feature. The evaluation between predictor features was based on the Chi-square statistic and the corresponding p-values which are presented in Table IV and Table V, respectively.

TABLE II. THE CONTINGENCY TABLE BETWEEN PARITY (X1) AND PREECLAMPSIA (Y)

Parity	Preeclampsia		
	No	Yes	Total
No Risk	108	25	133
Risk	32	40	72
Total	140	65	205

TABLE III. THE CHI SQUARE STATISTIC AND P VALUE OF DEPENDENCY BETWEEN PREDICTOR AND RESPONSE

Predictor	Chi square	P value
X1	136.59	0
X2	29.15	0
X3	166.76	0
X4	10.76	0.00104
X5	57.47	0
X6	98.53	0
X7	16.95	4.00E-05

TABLE IV. THE CHI SQUARE STATISTIC OF DEPENDENCY AMONG 2 PREDICTORS

Feature	X1	X2	X3	X4	X5	X6	X7
X1	205.0	1.842	2.168	10.73	37.06	2.316	13.23
X2	1.842	205.0	1.977	21.35	12.35	2.742	13.23
X3	2.168	1.977	205.0	12.01	79.30	2.386	17.47
X4	10.73	21.35	12.01	205.0	17.27	13.68	4.000
X5	37.06	12.35	79.30	17.27	205.0	34.44	13.94
X6	2.316	2.742	2.386	13.68	34.44	205.0	13.79
X7	13.23	13.23	17.47	4.000	13.94	13.79	205.0

TABLE V. THE P VALUE OF DEPENDENCY AMONG 2 PREDICTORS

Feature	X1	X2	X3	X4	X5	X6	X7
X1	0	0.117	0.092	0.001	0	0.082	0.000
X2	0.117	0	0.107	0	0.000	0.061	0.000
X3	0.092	0.107	0	0.001	0	0.078	0
X4	0.001	0	0.001	0	0	0.000	0.046
X5	0	0.000	0	0	0	0	0.000
X6	0.082	0.061	0.078	0.000	0	0	0.000
X7	0.000	0.000	0	0.0456	0.000	0.000	0

The independent features are obtained by using the grid search method. The first time the X1 feature is used as a search base i.e. to look for a p-value greater than 0.05 (significant level) in the X1 row, and the results show that the p-values of the X2, X3, and X6 features are greater than 0.05 that means features X1 are independent to features X2, X3, and X6. Next, feature X2 as the basis for searching and do checking whether the p-value of X3 and X6 in row X2 is greater than 0.05, lastly, feature X3 as the basis for searching and do checking whether the p-value of X6 in row X3 is greater than 0.05. The p-values in Table V which are greater than the significant level are marked with different colours. Thus the predictor features that have a significant dependence on the target feature and are also significantly independent of each other are features X1, X2, X3, and X6. These four features are finally used as predictor features of the logistic regression model to be built.

B. Model with the Newton Raphson Algorithm

The Newton Raphson algorithm is widely implemented in various statistical data analysis software, including R and SAS, which are statistical computing software that is popular among the statistician community. By setting the number of iterations = 1000 and the threshold value = 0.0001, the parameter estimators of the logistic regression model are presented in Table VI.

Based on the parameter estimator values in the second column of Table VI, the logistic regression model, namely the posterior probability of an instance as a member of class 0 is expressed in equation (15) as follows:

$$\pi(x) = \frac{\exp\left(\frac{-13.1080+4.3990X_{1(1)}+5.2480X_{2(1)}+7.9540X_{3(1)}+4.6360X_{6(1)}}{-13.1080+4.3990X_{1(1)}+5.2480X_{2(1)}+7.9540X_{3(1)}+4.6360X_{6(1)}}\right)}{1+\exp\left(\frac{-13.1080+4.3990X_{1(1)}+5.2480X_{2(1)}+7.9540X_{3(1)}+4.6360X_{6(1)}}{-13.1080+4.3990X_{1(1)}+5.2480X_{2(1)}+7.9540X_{3(1)}+4.6360X_{6(1)}}\right)} \quad (15)$$

If the coefficient is positive, it means that it contributes to support for class 0, on the other hand, a coefficient that is negative means that it contributes to support for class 1. All of coefficients except the intercept support for class 0 where the feature X3 has the highest contribution to support for class 0.

The ability of the model to predict the instances used to build the logistic regression model is determined based on the confusion matrix, which is a matrix whose elements state the number of instances that were predicted correctly or the number of instances that were predicted incorrectly by the logistic regression model in equation (15). The Table VII presents the confusion matrix of model in equation (15).

TABLE VI. THE ESTIMATE MODEL PARAMETERS RESULTED BY THE NEWTON RAPHSO AND GRADIENT DESCENT

Feature	$\hat{\beta}_j$ of Newton Raphson	$\hat{\beta}_j$ of Gradient descent
Intercept	-13.11	-10.02
X1	4.399	3.760
X2	5.248	3.688
X3	7.954	6.046
X6	4.636	3.575

TABLE VII. THE CONFUSION MATRIX WITH NEWTON RAPHSON ALGORITHM

Actual Class	Predicted Class	
	Class 0	Class 1
Class 0	140	0
Class 1	28	37

Based on Table VII, it can be seen that there is no instance of the class 0 which is predicted to be wrong. However, there are the 28 instances of the 65 instances of the class 1 which are predicted to be wrong. This logistic regression classification model with Newton Raphson algorithm turned out to produce a model that was only able to detect the sensitivity of the model in that the risk of misclassifying people with preeclampsia was very high, which was above 40%. The model performance is presented in Table VIII.

TABLE VIII. PERFORMANCE OF MODEL WITH NEWTON RAPHSON AND GRADIENT DESCENT ALGORITHM

Performance	Newton Raphson	Gradient descent
Accuracy	0.8634	0.9854
Precision	0.5692	0.9538
Recall	1	1
F1 Score	0.7255	0.9764

The model's accuracy performance is 86.34% meaning that the model is able to predict instances according to their actual class of 86.34%. While the performance of the F1 score of 72.55% means that the model is able to correctly predict the occurrence of preeclampsia cases by 72.35%.

C. Model with Gradient Descent Algorithm

As described in section 2, the gradient descent algorithm works based on the minimization of the cost function. In this research, the stochastic gradient descent method is applied by setting the learning rate hyper-parameter value = 0.015, and the number of iterations = 1000. After the training process is complete, the results of the cost function graph in Fig. 1, and the parameter estimator in the last column of Table VI.

Fig. 1 is the learning curve of the logistic regression model shows the curve of cross-entropy loss in which starting from the 200th iteration there is only a fairly small change and the curve tends to slope after the 800th iteration. This curve also illustrates that the selection of a learning rate of 0.015 is the right value, namely in the initial iterations, the curve does not experience a very sharp decrease (occurs when the learning rate value is too large) or the curve decreases very slowly (occurs when the learning rate is too small).

Based on the estimated parameter values which are in the last column of Table VI, the logistic regression model obtained with GD algorithm is as follows.

$$\pi(x) = \frac{\exp\left(\begin{matrix} -10.0160+3.7602X_{1(1)}+3.6878X_{2(1)}+ \\ +6.0457X_{3(1)}+3.5749X_{6(1)} \end{matrix}\right)}{1+\exp\left(\begin{matrix} -10.0160+3.7602X_{1(1)}+3.6878X_{2(1)}+ \\ +6.0457X_{3(1)}+3.5749X_{6(1)} \end{matrix}\right)} \quad (16)$$

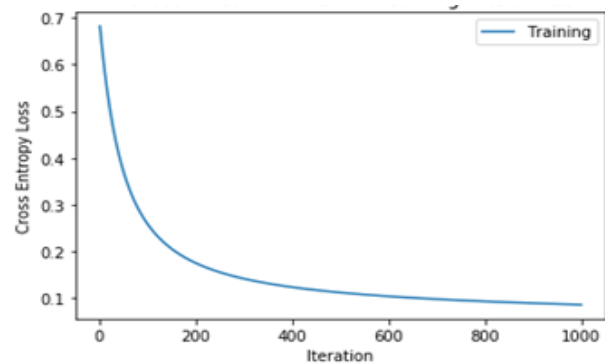


Fig. 1. The Learning Curve of the Logistic Regression Model.

In this logistic regression model, all of the coefficients except the intercept support for the class 0 where the X3 feature has the highest contribution to support for the class 0. Although the coefficients generated by the GD algorithm have a similar pattern to the coefficients generated by the Newton Rapson algorithm, the two models have different performances. The confusion matrix and performance measures of the logistic regression model with the GD algorithm are presented in Table VIII and Table IX.

TABLE IX. THE CONFUSION MATRIX WITH THE GRADIENT DESCENT ALGORITHM

Actual Class	Predicted Class	
	Class 0	Class 1
Class 0	140	0
Class 1	3	62

Table IX shows that only 3 instances of the 65 instances from the class 1 are predicted to be wrong and also all of instances from the class 0 are predicted to be correct. The Gradient descent method produces a logistic regression classification model that is able to detect the sensitivity of the model, namely the risk of misclassification of patients with preeclampsia case is very low, which is less than 5%.

The last column of Table VIII shows very clearly that the logistic regression classification model with gradient descent algorithm has superior performance than the one with Newton Raphson algorithm. It has the model's accuracy performance is 98.54% and the performance of the F1 score of 97.64%.

V. CONCLUSION

Feature selection using Chi-square test on factors that influence the incidence of pregnant women experiencing preeclampsia in Malang, Indonesia, obtained 4 significant features, namely consisting of age (X1), parity (X2), history of hypertension (X3), and consumption of salty foods (X6). The logistic regression model with the gradient descent algorithm has a lower risk of error in predicting cases of preeclampsia than the logistic regression model generated with the Newton Raphson algorithm. The model with the gradient descent algorithm has an accuracy performance of 98.54% and an F1 score of 97.64%, while the model with the Newton Raphson algorithm has an accuracy performance of 86.34% and an F1 score of 72.55%.

The dataset used in this study is too simple, which only consists of 7 predictor features, all of which are of binary categorical type. The comparison of the two algorithms will be more interesting if a dataset with a large number of predictor features is used and also involves both categorical and numeric features. Furthermore, the feature selection method used, not only involves the Chi-square test but also involves analysis of variance (F test) and also the Spearman correlation test.

REFERENCES

- [1] Marji, Handoyo S, Purwanto I N and Anizar M Y, "The Effect of Attribute Diversity in the Covariance Matrix on the Magnitude of the Radius Parameter in Fuzzy Subtractive Clustering" *Journal of Theoretical and Applied Information Technology*, vol. 96, no.12, pp. 3717-3728, 2018.
- [2] Handoyo S, Widodo A, Nugroho W H and Purwanto I N, "The Implementation of a Hybrid Fuzzy Clustering Public Health Facility Data" *International Journal of Advanced Trends in Computer Science and Engineering*, vol. 8, no.6, pp. 3549-3554, 2019.
- [3] Purwanto I N, Widodo A and Handoyo S, "System For Selection Starting Lineup of A Football Players by Using Analytical Hierarchy Process" *Journal of Theoretical & Applied Information Technology*, vol. 97, no. 1, pp. 19-31, 2018.
- [4] Utami H N, Candra and Handoyo S, "The Effect of Self Efficacy And Hope on Occupational Health Behavior in East Java of Indonesia" *International Journal of Scientific & Technology Research*, vol. 9, no.2, pp. 3571-3575, 2020.
- [5] Kusdarwati H and Handoyo S, "Modeling Treshold Liner in Transfer Function to Overcome Non Normality of the Errors" *IOP Conf. Series on The 9th Basic Science International Conferences*, vol. 546, no. 5, pp. 052039, 2019.
- [6] Kusdarwati H and Handoyo S, "System for Prediction of Non Stationary Time Series based on the Wavelet Radial Bases Function Neural Network Model" *Int J Elec & Comp Eng (IJECE)*, vol. 8, no. 4, pp. 2327-2337, 2018.
- [7] Handoyo S, Marji, Purwanto I N and Jie F, "The Fuzzy Inference System with Rule Bases Generated by using the Fuzzy C-Means to Predict Regional Minimum Wage in Indonesia" *International J. of Opers. and Quant. Management (IJOQM)*, vol. 24, no. 4, pp. 277-292, 2018.
- [8] Handoyo S and Chen Y-P, "The Developing of Fuzzy System for Multiple Time Series Forecasting with Generated Rule Bases and Optimized Consequence Part" *International Journal of Engineering Trends and Technology*, vol. 68, no. 12, pp. 118-122, 2020.
- [9] Handoyo S and Kusdarwati H, "Implementation of Fuzzy Inference System for Classification of Dengue Fever on the villages in Malang" *IOP Conf. Series on The 9th Basic Science International Conferences*, vol. 546, no. 5, pp. 052026, 2019.
- [10] Widodo A and Handoyo S, "The Classification Performance Using Logistic Regression And Support Vector Machine (Svm)" *Journal of Theoretical & Applied Information Technology*, vol. 95, no. 19, pp. 5184-5193, 2017.
- [11] Nugroho W H, Handoyo S and Akri Y J, "An Influence of Measurement Scale of Predictor Variable on Logistic Regression Modeling and Learning Vector Quantization Modeling for Object Classification" *Int J Elec & Comp Eng (IJECE)*, vol. 8, no. 1, pp. 333-343, 2018.
- [12] Handoyo S, Chen Y-P, Irianto G and Widodo A, "The Varying Threshold Values of Logistic Regression and Linear Discriminant for Classifying Fraudulent Firm" *Mathematics and Statistics*, vol. 9, no. 2, pp. 135 – 143, 2021.
- [13] Stalin S, Roy V, Shukla P K, Zaguia A, Khan M M, Shukla P K, & Jain A, "A machine learning-based big EEG data artifact detection and wavelet-based removal: an empirical approach" *Mathematical Problems in Engineering*, vol. 2021, pp. 2942808, 2021.
- [14] Shukla, P. K., Roy, V., Shukla, P. K., Chaturvedi, A. K., Saxena, A. K., Maheshwari, M., & Pal, P. R. "An Advanced EEG Motion Artifacts Eradication Algorithm" *The Computer Journal*, 2021.
- [15] Zhao Z, Li J, Fan C, Du Y, Zhou M, Zhang X, Zhao H, "Robust phase unwrapping algorithm for interferometric applications based on Zernike polynomial fitting and Wrapped Kalman Filter" *Optics and Lasers in Engineering*, vol. 152, pp. 106952, 2022.
- [16] Alkan Ö, Abar H, "Determination of factors influencing tobacco consumption in Turkey using categorical data analyses" *Archives of environmental & occupational health*, vol. 75, no.1, pp. 27-35, 2020.
- [17] Spiga O, Cicaloni V, Fiorini C, Trezza A, Visibelli A, Millucci L, Santucci A, "Machine learning application for development of a data-driven predictive model able to investigate quality of life scores in a rare disease" *Orphanet journal of rare diseases*, vol. 15, no. 1, pp. 1-10, 2020.
- [18] Thaseen I S, Kumar C, Ahmad A, "Integrated intrusion detection model using chi-square feature selection and ensemble of classifiers" *Arabian Journal for Science and Engineering*, vol. 44, no. 4, pp. 3357-3368, 2019.
- [19] Handoyo S and Marji, "The Fuzzy Inference System with Least Square Optimization for Time Series Forecasting" *Indonesian Journal of Electrical Engineering and Computer Science (IJECS)*, vol. 7, no. 3, pp. 1015-1026, 2018.
- [20] Lio W and Liu B, "Uncertain maximum likelihood estimation with application to uncertain regression analysis" *Soft Computing*, vol. 24, no. 13, pp. 9351-9360, 2020.
- [21] Orellana R, Bittner G, Carvajal R, Agüero J C, "Maximum Likelihood estimation for non-minimum-phase noise transfer function with Gaussian mixture noise distribution" *Automatica*, vol. 135, pp. 109937, 2021.
- [22] Handoyo S, Efendi A, Jie F, Widodo A, "Implementation of particle swarm optimization (PSO) algorithm for estimating parameter of arma model via maximum likelihood method" *Far East Journal of Mathematical Sciences*, vol. 102, no. 7, pp. 1337-1363, 2017.
- [23] Efendi A, Handoyo S, Prasjojo A P S, and Marji, "The Implementation of The Optimal Rule Bases Generated By Hybrid Fuzzy C-Mean And Particle Swarm Optimization" *Journal of Theoretical & Applied Information Technology*, vol. 97, no. 16, pp. 4453-4453, 2019.
- [24] Liu Z, Zhang X, Su M, Sun Y, Han H, Wang P, "Convergence analysis of newton-raphson method in feasible power-flow for DC network" *IEEE Transactions on Power Systems*, vol. 35, no. 5, pp. 4100-4103, 2020.
- [25] Feng Z, Ma N, Li W, Narasaki K, Lu F, "Efficient analysis of welding thermal conduction using the Newton-Raphson method, implicit method, and their combination" *The International Journal of Advanced Manufacturing Technology*, vol. 111, no. 7, pp. 1929-1940, 2020.
- [26] Farajtabar M, Azizan N, Mott A, Li A, "Orthogonal gradient descent for continual learning" *International Conference on Artificial Intelligence and Statistics*, pp. 3762-3773, 2020.
- [27] Fearnley J, Goldberg P W, Hollender A, Savani R, "The complexity of gradient descent: CLS= PPAD ∩ PLS" *Proceedings of the 53rd Annual ACM SIGACT Symposium on Theory of Computing*, pp. 46-59, 2021.
- [28] Pribadi A, "Zero mother mortality preeclampsia program: Opportunity for a rapid acceleration in the decline of maternal mortality rate in Indonesia" *International Journal of Women's Health and Reproduction Sciences*, vol. 9, no. 3, pp. 160-163, 2021.
- [29] Wang Y, Li Z, Song G and Wang J, "Potential of Immune-Related Genes as Biomarkers for Diagnosis and Subtype Classification of Preeclampsia" *Frontiers in genetics*, vol. 11, pp. 1481, 2020.
- [30] Novotny S, Lee-Plenty N, Wallace K, Kassahun-Yimer W, Jayaram A, Bofill J A and Martin J N, "Acute kidney injury associated with preeclampsia or hemolysis, elevated liver enzymes and low platelets syndrome Pregnancy hypertension, vol. 19, pp. 94-99, 2020.
- [31] Reddy M, Fenn S, Rolnik D L, Mol B W, da Silva Costa F, Wallace E M and Palmer K R, "The impact of the definition of preeclampsia on disease diagnosis and outcomes: a retrospective cohort study" *American Journal of Obstetrics and Gynecology*, vol. 224, no. 2, pp. 217-e1, 2021.
- [32] Shukla P K, Bhatele M, Chaturvedi A K, Sharma P, Rizvi M A, Pathak Y, "A Novel Machine Learning Model to Predict the Staying Time of International Migrants" *International Journal on Artificial Intelligence Tools*, vol. 30, no. 02, pp. 2150002, 2021.
- [33] Franke T M, Ho T, Christie C A, "The chi-square test: Often used and more often misinterpreted" *American Journal of Evaluation*, vol. 33, no. 3, pp. 448-458, 2012.

- [34] Adekpedjou A, De Mel W A, Zamba G K, "Data dependent cells chi-square test with recurrent events" Scandinavian Journal of Statistics, vol. 42, no. 4, pp. 1045-1064, 2015.
- [35] Du S, Lee J, Li H, Wang L and Zhai X, "Gradient descent finds global minima of deep neural networks" In International Conference on Machine Learning, pp. 1675-1685, 2019.
- [36] Luo Z, Li W, Gan Y, Mendu K and Shah S P, "Maximum likelihood estimation for nanoindentation on sodium aluminosilicate hydrate gel of geopolymer under different silica modulus and curing conditions" Composites Part B: Engineering, vol. 198, pp. 108185, 2020.
- [37] Liu Y, Liu B, "Estimating unknown parameters in uncertain differential equation by maximum likelihood estimation" Soft Computing, pp. 1-8, 2022.
- [38] Tripathi D, Edla D R, Bablani A, Shukla A K, Reddy B R, "Experimental analysis of machine learning methods for credit score classification" Progress in Artificial Intelligence, vol. 10, no. 3, pp. 217-243, 2021.
- [39] Ypma T J, "Historical development of the Newton–Raphson method" SIAM review, vol. 3, no. 4, pp. 531-551, 1995.
- [40] Gnetchejo P J, Essiane S N, Dadjé A, Ele P, "A combination of Newton-Raphson method and heuristics algorithms for parameter estimation in photovoltaic modules" Heliyon, vol. 7, no. 4, pp. e06673, 2021.
- [41] Fehrman B, Gess B, Jentzen A, "Convergence rates for the stochastic gradient descent method for non-convex objective functions" Journal of Machine Learning Research, vol. 21, pp. 136, 2020.

HEMClust: An Improved Fraud Detection Model for Health Insurance using Heterogeneous Ensemble and K-prototype Clustering

Shamitha S Kotekani¹, V Ilango²

Research Scholar (VTU Belgavi), CMR Institute of Technology, Bangalore¹
Professor, CMR Institute of Technology, Bangalore²

Abstract—Health insurance plays an integral part of society's economic well-being; the existence of fraud creates innumerable challenges in providing affordable health care support for the people. In order to reduce the losses incurred due to fraud, there is a need for a powerful model to predict fraud on the data accurately. The purpose of the paper is to implement a more sophisticated technique for fraud detection using machine learning: HEMClust (Heterogeneous Ensemble Model with Clustering). The first phase of the model aims in improving the quality of claims data by providing effective preprocessing. The second stage addresses the overlapping instances in provider specialties by grouping them using k-prototype clustering. The final stage includes building the model using a heterogeneous stacking ensemble that performs classification on multiple levels, with four base learners in level 0 and a meta learner in level 1. The results were assessed using evaluation metrics and statistical tests such as Friedman and Nemeyi to compare the performance of base classifiers against the proposed HEMClust. The empirical results show that the HEMClust produced 94% and 96% overall precision-recall rates on the dataset, which was an increase of 45% to 50% in the fraud detection rate for each class in the data.

Keywords—Fraud detection; health insurance; ensemble learners; meta-level learning; clustering; classification algorithms

I. INTRODUCTION

Health insurance has become a rapidly growing industry that plays a vital role in ensuring country's economic well-being. It provides us with much-needed cover during a financial crisis; it has benefitted many by reducing their healthcare expenditure burden, which otherwise jeopardizes their financial stability. The services provided by insurance industry can broadly be divided into two parts: life insurance and non-life insurance. This study considers life insurance, particularly health insurance. Many researchers have primarily administered claims data to be used extensively for healthcare data analytics[1]–[3]. The claims data include information related to medical examinations, diagnosis, drug-related information, doctor prescriptions along with medical diagnosis, it also contains financial data such as reimbursement amount, billing information etc. [4]. Claims are usually submitted from the patient's end or provider's end. A claim is processed when a policyholder submits a demand covering a particular treatment. Claims submitted to the facility will be validated further, and the request will be approved and reimbursed either to the practitioner (doctor / hospital) or the patient directly.

According to the study conducted by III (Insurance Information Institute); the overall net income (in billions) of the insurance industry over the last three years (2017-2019) was approximately 36.1, 59.6 and 61.4 billion [5]. This shows the growth of demand and dependence of people on the insurance sector. The rising demand for health cards has also increased the risk of fraudulent transactions. Health insurance fraud can be defined as intentional deception in which an insurance or medical provider provides false, misleading information to an insurer to obtain improper benefits from the policyholder's policy[6][7]. The studies state that around 10 per cent of healthcare expenditure is wasted on fraudulent transactions [8]. The fraudsters use several techniques to perpetrate fraud, such as altering the bills, forgery of documents or using powerful technologies for illegitimately collecting money from the consumers and the health providers. The main offenders of the health insurance sector can be broadly categorized into two providers and consumers [7]. Among the offenders, the study will concentrate on detecting providers fraud. The fraudulent activities involved by the providers include the following types of fraud:

- Phantom billing – This is a way of fabricating claims, it basically includes applying charges for treatment that has never been performed.
- Upcoding – This includes charging higher billed services when the patient might have received basic or recommending unnecessary procedures or test which is not required.
- Unbundling - This includes dividing a single procedure into many and providing multiple bills for each.
- Kickback fraud – This is a kind of bribery given to the provider for an improper service, for example, an inflated bill will be presented for reimbursement and the party of the difference amount will be paid to the provider as a reward.

There are two different ways to combat fraud, one way is detecting fraud (Fraud Detection) and the other one is to prevent fraud (Fraud Prevention) [9]. Fraud prevention involves stopping the fraud before it occurs by setting new rules or protocols. In health insurance, fraud prevention could be achieved in various ways, like denying policies for people by checking the risk possibilities or excluding providers from the authorized list of providers having malicious records. On

the other hand, fraud detection is applied when all the rules for preventing fraud fail, and a fraud transaction has already been committed. When any fraudulent transaction is detected, the aim will be to reverse it. To identify fraud for every incoming data, a fraud detection system will check every transaction to find any possibility of fraud. This will help the organization monitor or identify the fraudulent transactions quickly despite any change in the strategies adopted by the fraudsters.

As explained, claims data is a major source to retrieve information related to healthcare utilization and expenses, making it an appropriate database for our study in detecting fraud on health insurance. Though claims data have proved to be an attractive source of data for research, few challenges are associated while analyzing it like [10]–[12]:

1) Billers or coders with a lack of knowledge in medical terminologies tend to misinterpret the terminologies and end up entering incorrect information. Also, the way a particular data is fed into the system will vary from place to place.

2) Overlapping of codes, providers of different specialties will be referring to single code. This later causes code variability and sparsity in the data.

The above challenges demand that claims database needs efficient data preprocessing and a proper technique for dealing with misrepresented procedures or specialties.

There was a noted evolution seen in applications of analytical approaches in claims data, from simple record-based calculation to the use of machine learning (ML) techniques. Traditional fraud investigation on the data was time-consuming and also costly. Manually investigating fraud is not advisable in this era as fraudsters keep changing their way of committing fraud. Machine learning algorithms apply artificial intelligence techniques to help the fraud detection system learn from experience and improve its ability to see any fraud patterns [13]. Using ML techniques for fraud detection helps in executing entire data in a shorter period of time. All kinds of fraud could be detected more accurately, also with a slight variation applied in the analysis, the system could be used to anticipate new patterns of fraud. Since the insurance sector accumulates a large amount of data in the form of claims, the use of big data analytics will help in revealing complex claim patterns since more data leads to improving the predictive power of the model [14][15][16].

The study proposes a novel heterogeneous ensemble model with clustering to overcome the above challenges. The fundamental idea was to incorporate k-prototype clustering and an efficient preprocessing procedure to detect fraud from health insurance claims data. Finally, preprocessed and clustered subsets are obtained for training the base classifiers. The major contributions of the study are listed as below:

- To improve the data quality by applying effective preprocessing techniques.
- To group similar providers based on their specialties to reduce the overlapping procedures while detecting providers fraud.

- To provide a novel combination of heterogeneous ensembles through stacking framework for detecting fraud in health insurance using preprocessed and clustered data.

Paper uses distributed computing for handling the volume of data. Using the distributed environment, complex big data analysis can be performed in a second of time without any computational overheads. Traditionally, when the size of the data increase only solution lies was to upgrading or scaling up the machine, which is expensive as it doubles the cost. Instead, modern approaches have started focusing on scaling out. Scaling out increases the computational power by adding more machines to the network. Spark is one such distributed opensource framework where, big data applications could be easily distributed by its data structure called RDD (Resilient distributed dataset)[17], [18],[19]. Since spark is built on top of the Hadoop framework, it can perform the computations faster using in-memory primitives[19]. Distributed computing and scalability using spark is achieved using the following information in RDD:

- Data are partitioned into several sets; each partition contains an atomic piece of the database.
- The location of each partition will be included for providing faster access.
- Total number of dependencies are on the parent RDD.

The entire proceedings of the work are distributed as follows; Section 2 performs a detailed background review of the works and explains the gaps found in the research; Section 3 explains the proposed HEMClust model. Section 4 details the dataset and experimental setup used for implementation. Section 5 discusses the results obtained from the model finally, Section 6 concludes the work.

II. LITERATURE REVIEW

Many researchers used several complex learning algorithms in fraud detection, such as deep learning and ensemble learning, mainly because of their capability to learn complex relationships between the patterns. X. Zhou et al [20] developed a fraud detection model for online banking based on convolutional neural networks. The network consisted of six layers, including a feature sequencing layer, four convolutional layers, and a pooling layer. The model was used to verify and detect fraud on the online transactions that are performed in the bank. The model produced a good precision and recall rate.

Other than conventional classification algorithms, bagging and voting ensembles have been used as a state of the art techniques for fraud detection in several articles[9], [21], [22]. Most of the articles focused on bagging ensembles, which takes bootstrap samples, and training was concentrated on each chosen sample [23]. M. Zareapoor and P. Shamsolmoali [24] applied bagging classifier for detecting fraudulent transactions using credit card. The author combined three different learners such as Naïve Bayes (NB), kNearest Neighbours (knn), and a Bagging ensemble with a 10-cross validation for building a model.

David W.Fan et al. [25] had compared Stacked Generalization with other combiners to analyze using multiple algorithms for prediction. The results proved that stacked generalization had given impressive results than other base classifiers. Kerwin et al. [26] used stacking to deal with imbalanced class distribution for detecting fraud from the dataset. The author used different classification techniques and sampling techniques as a base learner and meta learner to improve the performance. Meta learner with Gradient Boosting Ensemble classifier produced a more excellent f1 score. It was observed that multiple algorithms have always been proved efficient in fraud detection from all these works.

The studies discussed above reveals that there is no comprehensive work related to health insurance fraud detection, mainly because of the lack of data availability. As far as our knowledge, CMS Medicare data [27] is the only available open-source data. CMS database consists of details regarding procedures and drug descriptions. There were few studies based on CMS Medicare data conducted by Mathew Herald et al. [28]–[31] using multiple data sets from CMS Medicare. Herald et al. [28] constructed a fraud detection model for big data by combining four datasets from CMS, resulting in 37,147,213 records. They applied neural networks and tree based ensembles such as random forest and gradient descent trees. The results were validated using cross-validation during learning, and the results showed that MLP learners outperformed GBT and RF with a ROC Score of 0.816. They further expanded their work by applying the deep learning model on big data sets with 4,692,370 instances, which improved the model's performance further.

The author also addressed the problem of imbalanced data learning in fraud detection. Data level sampling and algorithmic level techniques were applied on a given range of class ratios. The results showed that deep learning with oversampling and an ensemble of over and under sampling outperformed the baseline algorithmic models with an AUC score of 0.8505 and 0.8509, respectively. A similar dataset was used by L. K. Branting and F. Reeder [32] to calculate the fraud risk for 2012-2014. The author proposed a graph-based model for calculating the risk that appears on the dataset after combining the Part B and LEIE data. The whole aggregation was based on the NPI's, since the exclusions database contained missing entities, the author used the NPPES registry, which maintains the list of providers under Medicare. V. Chandola et al. [33] used Medicare claims data and LEIE exclusions database to find the hidden anomalies inside. The techniques used were social network analysis, spatial-temporal analysis and text mining. Later, weighted MLP was used to classify bad actors and produced an accuracy score from 71% to 81.4%.

In their paper, Mathew Herland et al. [29] concentrated on detecting upcoding fraud by finding providers who had procedural code other than one. It was also found that grouping the providers practicing on similar area had produced an improved prediction result.

A. Research Gap

Considering the above review, it was observed that Cart[34], RF [35], MLP [36] had been widely used in detecting

fraud in health insurance. It was observed that RF and Cart were good in classifying normal transactions, and MLP performed well in classifying fraudulent transactions. Studies conducted by M.Paz Sesmero et al. [37] Saurabh Tewari[38] proved that the hypothesis generated from varied classifiers on a space using stacking or voting would boost the overall predictions reduce the bias or variance than using homogeneous classifiers. Though several works reveal the dominance of ensemble learners over single learners for fraud detection on various domains[21], [24], [26], in health insurance, its implementation is minuscule. Overlapping of procedures between the specialties was also a major issue discussed in the literature, and the authors have grouped the classes manually considering the similarities [30], [39]. Since claims data contains hundreds of provider specialties with thousands of procedural codes, the current manual grouping to reduce the overlapping could not be considered as a feasible solution.

III. HETEROGENOUS ENSEMBLE CLASSIFIER WITH CLUSTERING (HEMCLUST) : PROPOSED TECHNIQUE

As emphasized, HEMClust incorporate stacking ensemble with an extension to the existing work of M. Herland et al. [30] by applying clustering to similar group providers based on their specialties. Data quality was also a significant concern during processing as the database contained lot of missing values. To overcome that, Feature-Wise Imputation (FWI) is applied. Using FWI, missing values are imputed using mean/mode/knn on each attribute by looking the severity and type of data. The proposed HEMClust works in three phases:

A. Phase 1: Data Pre-processing

As emphasized in Section 1, claims data contains many ambiguities caused by automated data entries, data redundancies, missing values and incorrect entries [12]. Enhancing data quality is inevitable as only perfect data could lead to a better model. The choice of methods was entirely dependent on the nature of our data. Following are the steps carried out to improve the data quality:

- To Identify and remove single-valued predictors as those attributes will not give any information for modelling.
- Cleaning incorrect data entry errors through fuzzy matching. Fuzzy matching finds the text that is very similar to the search given. It also lists the matches along with the matching ratio.
- Feature-wise imputation of missing values.
- Data normalization using a min-max scaler.

B. Phase 2 : Clustering Provider Specialties

The second phase of the model aims in reducing the overlapping instances and model variance. Here, clustering techniques are used to group provider specialties instead of manual grouping. Clustering finds groups in the data that are similar to each other. It divides the data into similar groups, such that the distance between two instances is identical if they belong to one cluster and far if they are from different clusters.

Before applying the clustering algorithm, the clustering tendency was measured using Hopkins's test.

The hypothesis generated from the test was used to find whether the data inherently contains any clusters. The statistic's null hypothesis(h_0) will state that the data has no meaningful clusters and is distributed uniformly. If the value of the results (H) is greater than $0.5 h_0$ will be rejected, and an alternate hypothesis (data is not uniformly distributed and it contains meaningful clusters) is accepted. Later, K-prototype (kproto) clustering will be applied for creating the groupings since it can efficiently handle large and heterogeneous data types[47], [48]. kproto clustering defines prototypes as centroids which is built from mean values of numerical and mode of categorical variables[49]. The whole procedure works similar to K-means clustering. It iteratively relocates the data based on partitioning to minimize the distance between a cluster and its prototype (similar to the centroid in K-means). Here, the distance between two points A and B is defined as[48].

$$f_n(A, B) = \sum_{j=1}^r (a_j - b_j)^2 + \gamma l \sum_{j=r+1}^s \delta(a_j, b_j) \quad (1)$$

Where r is the Euclidean distance applicable to numerical data, followed by hamming distance for dealing with categorical variable s . The variables γl and δ are user-defined values, which will be used avoid the influence of numerical and categorical variables when applied to the model.

C. Phase 3 : Heterogenous Ensemble Framework based on Stacking

Heterogenous ensembles possess the capability to generate varied results in a single space using different base classifiers. Individual classifiers used here will solve both binary class and multi-class classification problems. Following criteria was considered for the construction of base classifiers,

- Algorithms should be scalable for both large and small data sets.
- Algorithms should be able to provide quick predictions after training.

Multi-Layer Perceptron (MLP), Logistic Regression (LR), Cart and Random Forest (RF) were considered as the base pool of classifiers as it satisfies the above said criteria. Optimal set of parameters for all the base model was found by applying grid search optimization. Table I lists the parameters adopted throughout the study. A detailed explanation of these algorithms is out of the scope of this paper. Its explanation and implementation could be referred from the following articles [41], [23], [42], [43]. There are basically two types of ensembles Stacking ensemble and Voting ensemble. Though our model will be using stacking as the base classifier, it was evident to give a brief on voting ensemble. The voting ensemble combines predictions from different learners intending to attain the highest possible prediction accuracy. It uses majority voting or average voting techniques to combine the predictions generated from the base classifiers. During majority voting, the result of the final prediction of a sample will be based on the total number of times a class label predicted. The classifiers which get more than half of the vote against the test labels will be considered for final predictions. Whereas in average voting, every base classifier will be

assigned a weight. During the validation phase, prediction probabilities will be generated for each sample from all the classes. Finally, a product of weights assigned and their likelihood will be averaged. The class that scores the highest average will be considered [38], [44], [45].

TABLE I. PARAMETER LIST FOR THE BASE CLASSIFIERS

Acronym	Parameters
LR	Penalty: L2 (Ridge Regression), Solver: lbfgs, maxIter=150, regParam=0.3, elasticNetParam=0.2
Cart	criterion of split = gini, splitter = best, max_dept = 30 min_samples_leaf = 1, maxBins = 5000
RF	numTrees=100, maxBins = 5000
MLP	Learning_rate=0.1, No of epochs = 50.Momentum = 0.6, Batch_size = 256, No of hidden nodes = 5, Optimizer = adam

The stacked generalized model uses a meta learner on top of the base learners using stacking. Meta learners optimize the output or boost the predictions generated from the base learners. Stacking operates on multiple levels (Level 0 and 1). Level 0 learns with multiple classifiers, and these learners' weights (w_1, w_2, \dots, w_n) will be fed into a meta learner. Predictions made by each learning algorithm in the first phase become training data for the level 1 meta learner. The equation for stacking(stack) predictions from set of classifiers (x_1, x_2, \dots, x_n) with a linear combination of weights (w_1, w_2, \dots, w_n) is expressed in equation 1[37] [46].

$$f_{stack}(y) = \sum_{i=1}^n w_i f_i(x) \quad (2)$$

Algorithm 1: Procedure for building a stacking ensemble

Input: Preprocessed data $T = \{a_j, b_j\}_{j=1}^n$

Output: Ensemble model H

1. Learn level-0 classifier models
2. for $d=1$ to D do
learn h_d based on T
end for
3. Create new set of predictions from set T
for $j=1$ to n do
 $T_h = \{ a'_j, b_j \}$, where $a'_j = \{ h_1(a_i), h_2(a_i), \dots, h_D(a_i) \}$
end for
4. Learn meta classifier
learn H according to T_h
5. return H

So, for understanding the behaviour of the transaction, the level 0 classifiers will first classify the new data. Then the prediction results will be passed to the meta learner for making the final decision on a transaction to be fraud or non-fraud.

The basic structure of the stacking process used in this study is shown in Fig. 1. The model is applied to train and test data. k-cross validation(cv) is applied on the training data on level 0 to avoid chances of overfitting. Using cv a set of data is generated from each fold and creates a new portion of dataset for each of the four learners. In level 1, that particular dataset generated from the first level prediction is trained by the Random Forest, the meta classifier, and the final prediction

results will be generated. One more significant reason was that the time for prediction in RF is significantly faster than training the model as trees generated during the training are for future reference.

The conceptual architecture of the framework is explained in Fig. 2.

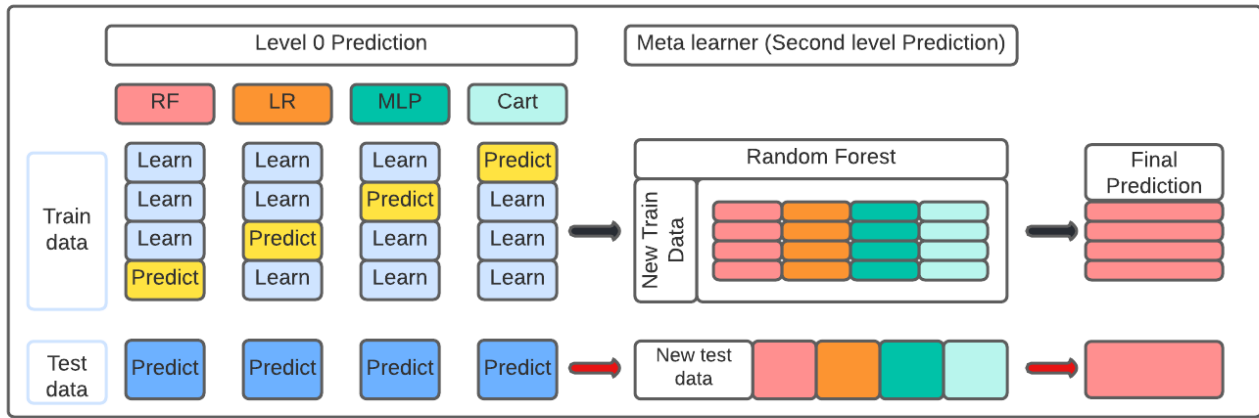


Fig. 1. Structure of Stacking Ensemble used in the Study.

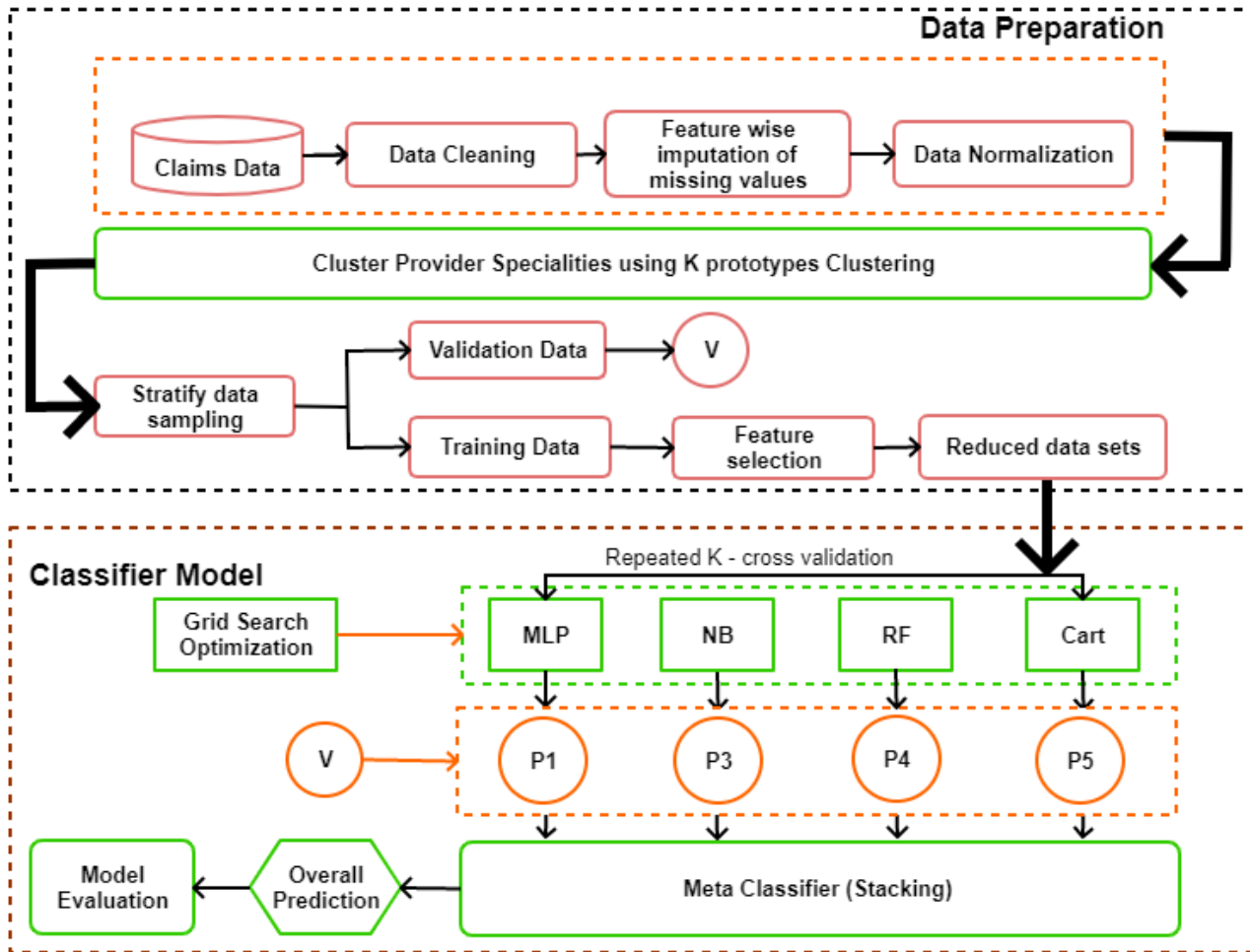


Fig. 2. Conceptual Framework of HEMClust Model.

IV. EXPERIMENTAL DESIGN

A. Experimental Data

The study uses Medicare Part B Providers data published on the CMS Medicare website for years 2014-2017[27]. CMS is a wing in the United States that manages national health care services. CMS collects all claims related data such as prescription, drug-related data, etc.- and analyses it to find and reduce fraud that occurs within the healthcare system. Study uses two datasets from Medicare healthcare for implementation of the model; the first is provider claims data. Providers claim data set which will be mentioned to as Part B, which provides information on all procedures performed by a physician in a particular year. Each physician has been given a unique identifier named NPI. NPI is used to represent a specific physician and procedure he performs for a particular disease. The procedures he performs against the details of the actual procedure could be found by matching the HCPCS code (Health care Common Procedure Code System). This database also provides necessary information about the total number of services performed by the physician, billed, submitted, and allowed charges for a particular service, place of service etc. The nature of the procedure also varies based on the location of the service.

The Second database used for the study is LEIE (List of Excluded Individuals and Entities), generally referred to as the LEIE database[40]. This database contains the list of providers who have been exempted from their service due to some reason. The exemption criteria are based on the crime they have performed, which matches the sections from the Social Security Act. The LEIE database is updated and maintained by the OIG (Office of Inspector General). OIG categorized exclusions into two types Mandatory exclusions and Permissive exclusions. So, example, Section 1128(a)(2) explains "Conviction based on doctor's behaviour towards the patient". Say, abuse or Neglect and the period of conviction is 5 years. Section 1128(b)(4) will be convicted if the provider has not renewed his license or if he is under suspension or surrender. the period of exclusions varies based on the kind of prohibitions. There are many kinds of coded reasons for exclusions, for Section 1128(b)(7), Providers will be convicted for kickback fraud etc. After combining Part B for 4 years (2013-2017), the total number of instances was 2740138. Overall dataset descriptions are available in Table II.

Labels for CMS Part B database were generated by joining with LEIE on NPI as a primary key, and the matching records were marked as fraud. While analyzing the LEIE database, around 93.7 percentage of NPI values were found missing, i.e., labelled "0". Out of 93.7 percentage of missing values, seven percentage had UPIN (Unique Physician Identifier Number). While matching this database, only 465 fraud classes could be found initially. This was quite disappointing that the proportion of fraud occurred and working data was contrastingly low. So, it became inevitable to find the NPI for the missing records. NPPES NPI Registry was used further in the study to refill the missing NPI's. Matching 72k records manually was a tedious task. To speed up the task, an "NPI Matching Algorithm" was developed and used further for matching the NPI's from the registry. Where NPI was not present, UPIN was used to

compare and match the records. After applying the algorithm, 9862 fraudulent records were matched.

B. Runtime Environment

The whole experiment was conducted in UBUNTU Linux Environment. The experiment setup was run on 2.8 GHz Intel Core i7-7700HQ, Quad-core CPU with 8 logical cores. NVIDIA beForce GTX 1050 with 4 GB dedicated GPU was also used along with 32GB RAM. Both Python and Spark was used for implementing the whole model. The spark ecosystem contains 5 significant components: Spark Core, Spark SQL, Spark Streaming, Spark MLlib, and GraphX. The Spark Core component serves as a basis for distributed processing of big data sets. Resilient Distributed Datasets (RDD) from spark core was applied, which helped save the execution time while loading and reusing the data because it provides distributed and in-memory computations. The machine learning model was implemented using Python Sklearn and Spark ML Library[50].

C. Post Processing or Validation of Results

For evaluating the efficiency of the framework on the fraud detection environment performance metrics such as Precision, Recall, f1 Score will be used. The metrics will check for each provider specialties in detecting upcoding fraud using multi-class classification and overall fraud detection using binary classification.

The model will also be evaluated using stratified repeated k fold cross-validation to ensure that it does not overfit the testing data. Table III explains the formulae for calculating the metrics used for evaluation.

TABLE II. DESCRIPTION OF DATASET USED FOR THE STUDY

Name of Data	Description of data	Features
Providers Data (Part B)	Information regarding claims a provider performs for a given procedure Oriented by Fields 1) National Provider Indicator (NPI) 2) Provider Speciality 3) Drug Description Code (HCPCS) 4) Place of Service	29
Exclusion Data (LEIE)	Information regarding providers that are exempted for committing fraud Oriented by Fields 1) National Provider Indicator (NPI) 2) Reason of Exclusion.	17

TABLE III. EVALUATION METRICS USED FOR THE STUDY

EM	Equation	Description
ACC	$ACC = \frac{TP + TN}{TP + FP + TN + FN}$	Explains the ratio of correctly predicted instances against the total number of instances
Pr	$Pr = \frac{TP}{TP + FP}$	Percentage of positive samples that are actually predicted correctly from the positive samples.
Re	$Re = \frac{TP}{TP + FN}$	Percentage of positive samples that are actually predicted from total number of samples
f1	$f1 = 2 * \frac{Pr * Re}{Pr + Re}$	Evaluate the balanced performance of classes in a model.
*EM,Evaluation Metrics *ACC,Accuracy; Pr,Precision;Re,Recall;f1,F1 score		

V. RESULTS AND DISCUSSION

A. Results

The section explains the outcomes from the experiments performed by using the proposed model. For a better understanding, the results are bifurcated into three parts.

- 1) Performance evaluation of heterogeneous ensemble learners over individual classifiers.
- 2) Validation of results on HEM model after applying the improvement strategies.
- 3) Validating the performance of proposed framework (HEMClust) over the baseline ensemble model (HEM model) using Friedman and Nemenyi tests.

The individual learners and HEM models were evaluated by comparing each model based on their performance criteria. The data was evaluated on the model in two different ways, binary classification (LEIE labelled data set which contains two classes, fraud and Non-fraud) and Multi-class classification (considering each provider specialties as class labels). Considering provider specialties as class labels were necessary to detect upcoding fraud because it could be detected by finding misclassified provider labels against their given specialties. Forty percent fragment of the data was kept aside for validation to see the generalization of the model on the unseen data. The result of the performance of each classifier on the data is shown in Table IV for fraud and Non-fraud class. It was evident that the heterogeneous stacking ensemble outperformed the individual classifiers and voting ensemble. Fig. 3(a) and 3(b) explains the learners' performance on each provider type. Displaying the results of all the specialties on one single plot was not feasible. To improve the readability, the entire plot was divided into two sections. The first section explains the lower performing specialties classes with an f1-score less than 35%, and the second describes the f1-score greater than 35% on the baseline model.

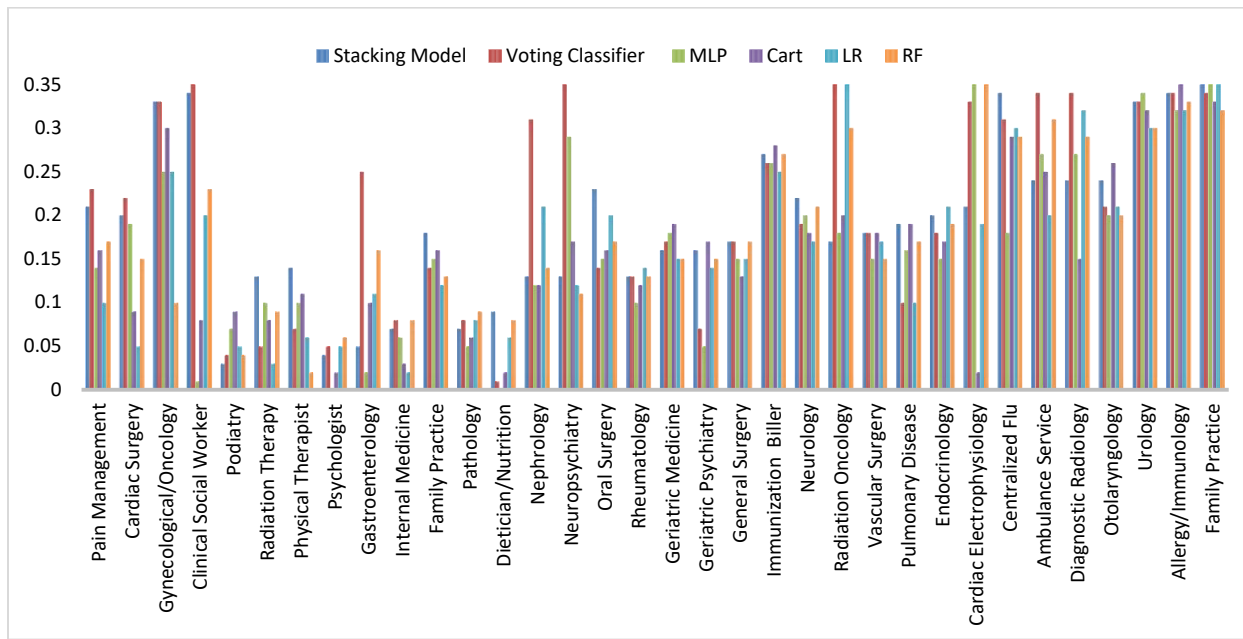
As emphasized earlier two improvement strategies were adopted in the study preprocessing and clustering. To begin with preprocessing, cleaning was performed on the data by identifying the variables which returns the variance zero, especially like single valued attributes as it can no way be influential for the predictor. As a result, attribute "CountryCode" was removed from the dataset. Columns HCPCS code and HCPCS description could be called duplicate columns because HCPCS code itself describes the drug code and its purpose. drug description feature was not found important as it just details the description provided in the feature HCPCS code. Cleaning the values inside the data was also mandatory. While observing "Provider Credentials"

column, it was found that a single value is interpreted several ways. For example, credentials "MD", on some places it is said as "M.D." and in some other places it is referred as "M D" and so on. So, necessary actions was taken to clean those values and make them similar. Data normalization is also considered an important part of designing a model. Normalization is used to bring down the features with varying scales to a similar scale [0-1 or $[-1,1]$]. Paper used min-max normalization which takes values of a feature and transforms it into a predefined interval between 0 and 1. It also tries to preserve the outlier relationship with scaling the data. In the second phase preprocessing was to deal with missing values, it was handled feature-wise by considering the rates of missing values on each attribute. Different approaches were applied to each attribute based on the severity of missing values on it. Following the work of Esra'a Alshdaifat [51], features were categorized based on certain categories. If 1-5% of data is missing in a column, it comes to the category of 'Manageable' or if 5-15% is missing, it will be categorized as 'Sophisticated' and anything above 15% will be categorized as 'Severe'. When the data sample falls under the category of manageable or sophisticated, missing values were handled by imputing it with the mean for numerical data. The values were replaced by any global constant or mode for categorical data. Normally imputing the missing values with mean or mode leads to bias by changing the correlations of the data. Since the amount of data that fall under this category is very small, it wouldn't affect much on the performance. If the category is above 15%, Knn was applied as a method of imputation. Using knn, missing values are filled with similar occurring instances or by finding its distance measure.

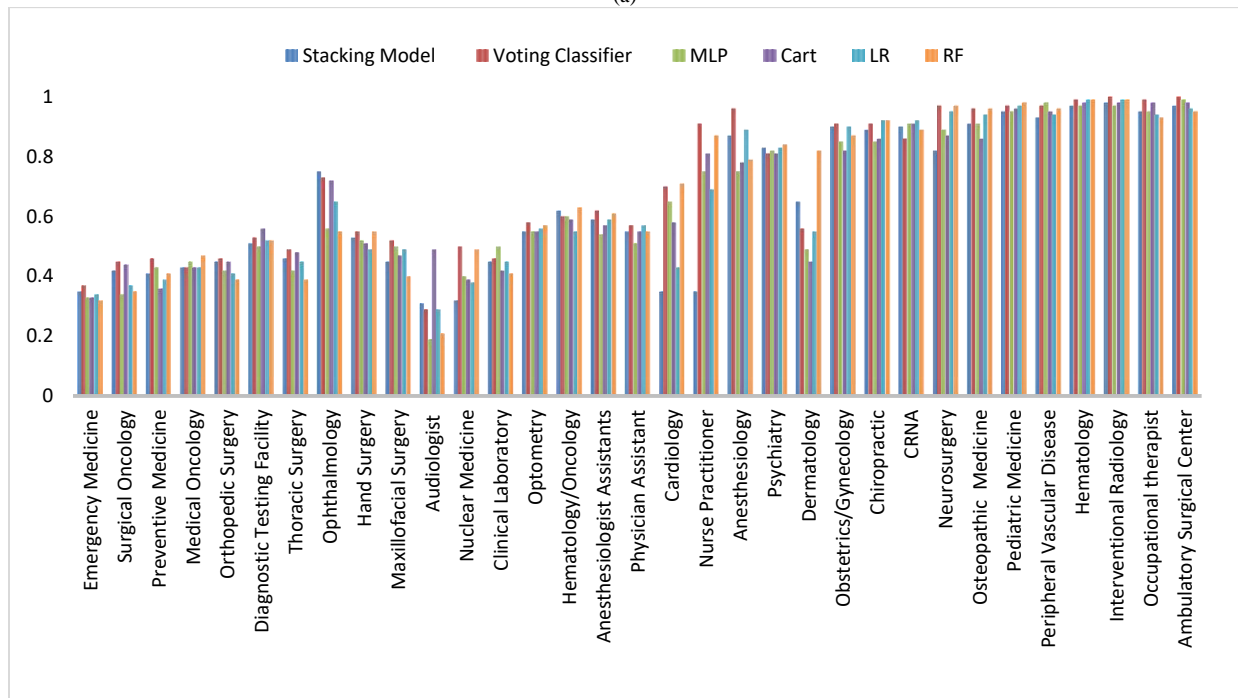
The feature selection was performed using the Extra tree classifier, a decision tree ensemble. Extra tree classifier is more reliable as it randomly selects the split. It is also computationally faster than any other classifier. Following are the discussion and conclusion on each feature's behaviour and importance after analyzing the results.

- From 26 features, 16 features have a value of importance greater than 0.
- Out of the 16 essential features, six numerical features hold 44.0% of the feature importance and 7 categorical features hold 49.0% of the feature importance and 3 features holds value less than 0.

It was found that the aggregated service, Billing information of the procedures, Provider Indicator and City are the most relevant features. Provider's Year of Service and Drug Indicator are less important features. After feature selection, the final number of attributes selected for further study was 15.



(a)



(b)

Fig. 3. (a). Performance of Dataset on each Classifier in Classifying Provider Specialities (f1 < 50), (b). Performance of Dataset on each Classifier in Classifying Provider Specialities (f1 > 50).

TABLE IV. FRAUD-NONFRAUD CLASSIFICATION RESULTS ON HEM MODEL AND INDIVIDUAL LEARNERS

Class	MLP		LR		Cart		RF		Heterogenous Voting		Heterogenous Stacking	
	NF	F	NF	F	NF	F	NF	F	NF	F	NF	F
Pr	1.0	0.50	0.99	0.50	1.0	0.73	1.0	0.92	0.99	1.0	1.00	0.96
Re	0.93	0.73	0.89	0.55	1.0	0.72	1.0	0.64	1.00	0.68	1.00	0.82
f1	0.96	0.68	0.94	0.53	1.0	0.72	1.0	0.75	0.99	0.77	1.00	0.88
Acc	0.92		0.88		0.99		0.99		0.99		0.99	

The most important step to be followed prior to clustering process is finding optimal number of clusters (i.e., the value of k). Determining appropriate value for k is important as different values lead to different conclusions and characteristics in the clusters. Also, it is important to find that the resultant value of k has the tendency to produce good clusters. Here, Hopkins's test is applied to measure cluster tendency and optimal k value. Basically, Hopkins value greater than 0.5 consisting of larger value of k shows the probability of grouping data into larger clusters[52]. The results revealed a higher degree of 0.99 value of clustering tendency in the data. Since, value obtained is (~0.99) which is greater than 0.50, null hypothesis is rejected and alternate hypothesis is concluded that the dataset is significantly clusterable. While determining the optimum value of k, there was a considerable decline in the value of statistic with the increase of parameters. The optimal value of k clusters against Hopkins's statistic is shown in Fig. 4. With 12 clusters good cluster tendency of 0.65 was achieved. So, with k value as 12 kproto clustering was applied on the PCA subspace. Partitioning clustering methods have proved to produce better results when applied with pca[53], [54]. Four principal components that explained a total variation of 98% was selected further for clustering. Overall mean accuracy of cluster wise provider specialties are cross-

validated, its characteristics and how each provider specialties are distributed in each cluster are shown in Fig. 5.

From the results on the boxplot of each cluster for provider specialties ranging from 0-76, Cluster 3 and 6 hold a maximum number of specialties. It was observed that cluster 3 contained specialties related to surgical procedures like, Vascular Surgery, Anesthesiology, Internal medicine and so on. Those procedures are formed in one group because of the common procedural code shared by these specialties for a particular treatment. The contents of clusters 1, 2 and 3 contained a smaller number of providers, and that group was dedicated to specialties with similar behaviour for example, cluster 4 had only 5 members such as Cardiology, Cardiac Surgery, Diagnostic Radiology, Anesthesiology and Internal Medicine. It can be said that these groups are related to cardiac surgery. It was also found that certain groups of providers like Anesthesiology, Ambulance providers, Internal medicine, Nurse Practitioner are included in more than 1 cluster. The reason might be that these providers are commonly included in many procedures. Further, the HEM model was applied on the clustered data, by considering each cluster as classes. Fig. 6 plots the confusion matrix using a color-encoded heatmap obtained from multi-class classification here, each class represents a cluster with grouping specialties.

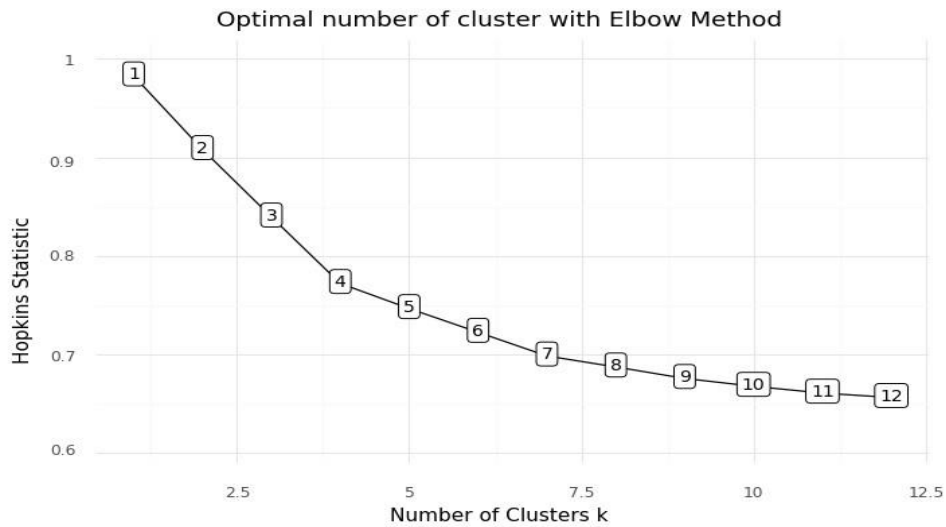


Fig. 4. Results of Hopkins Test Statistic for Measuring Clustering Tendency using k nearest Neighbour Distances.

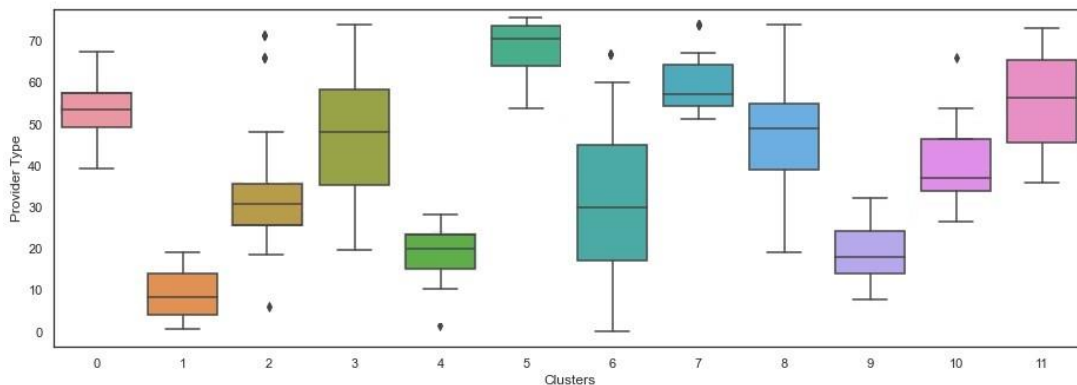


Fig. 5. Characteristics of each Cluster based on Provider Type.

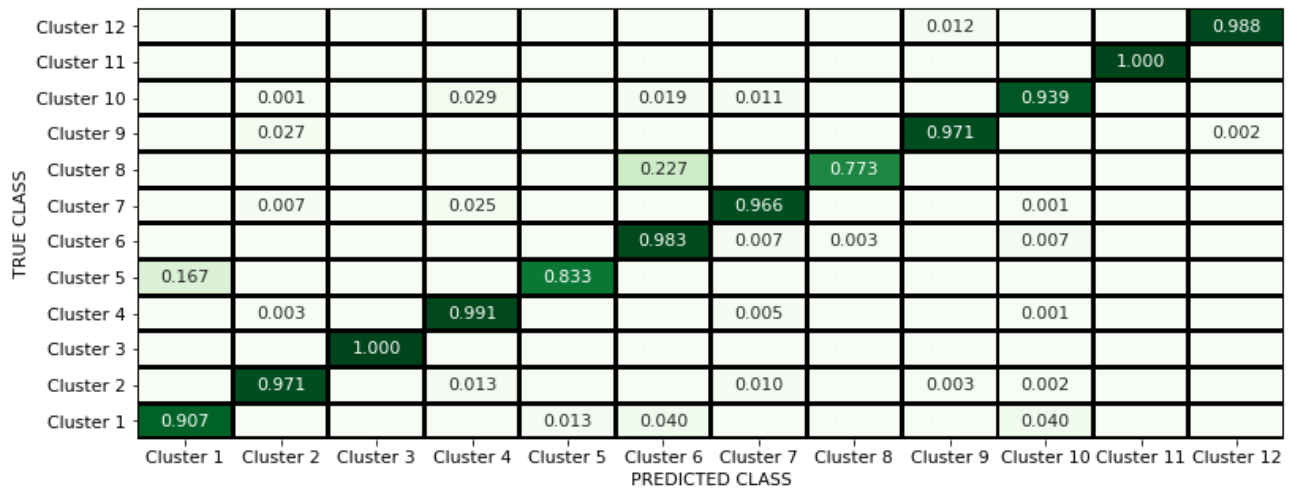


Fig. 6. Heatmap for Confusion Matrix Depicting the Multi Class Classification Results for each Cluster. Each Rows represents the True Class and Columns represents the Prediction done by the Classifier.

It was noticed that clusters 3 and 11 are detected with a higher TPR of 100% and cluster 8 is the least detected class compared to others with a TPR of 77.3%. There are also a few places where misclassified clusters were found from their original classes, although their percentage was tiny. A detailed description of results is plotted in Fig. 7. Heatmap is used to plot the overall key metrics such as precision-recall and f1-score for each class. The model produced an overall accuracy of 98%. Considering the weighted average precision, It could be noticed that almost 98% of data has been correctly classified only 2% was misclassified to wrong classes. All the above results prove that grouping strategies significantly increased the fraud detection ratio to at least 45-50%.

Further, for a more precise evaluation of the impact on the HEM model and the proposed improvement strategies, a comparison is made using two statistical tests Friedman and Nemeyi. Initial steps were to find whether there existed any significant difference between the mean models. A Friedman test is applied on all base classifiers, heterogeneous ensembles and HEMClust to determine whether or not these groups are statistically significant. The test statistic(X^2) and corresponding

p_value(p) from Friedman test was 11.04 & 0.026 respectively. Since obtained p_value is lesser than the default 0.05 here, null hypothesis can be rejected and the post-hoc Nemenyi test could be performed for finding an exact model that is different in performance from others. Results from Fig. 8, shows that LR, MLP, Cart, RF and Voting classifiers belong to one group. Also, LR performed significantly worse than other models, and Cart and RF seem to have similar performances. Though it is difficult to conclude a comparison concerning the Stacking ensemble because it belongs to two groups. Although it can be affirmed that HEMClust is significantly different from other groups, since HEMClust is built using a stacking ensemble, a few similarities in their performances could be seen.

B. Discussion

Basic aim for building HEMClust model is to identify provider fraud. So, the idea here was to detect misclassified provider specialties based on their respective procedural codes. Suppose a provider is classified into different group of class which it does not belongs to, that particular transaction could be alerted or further rechecked for fraud.

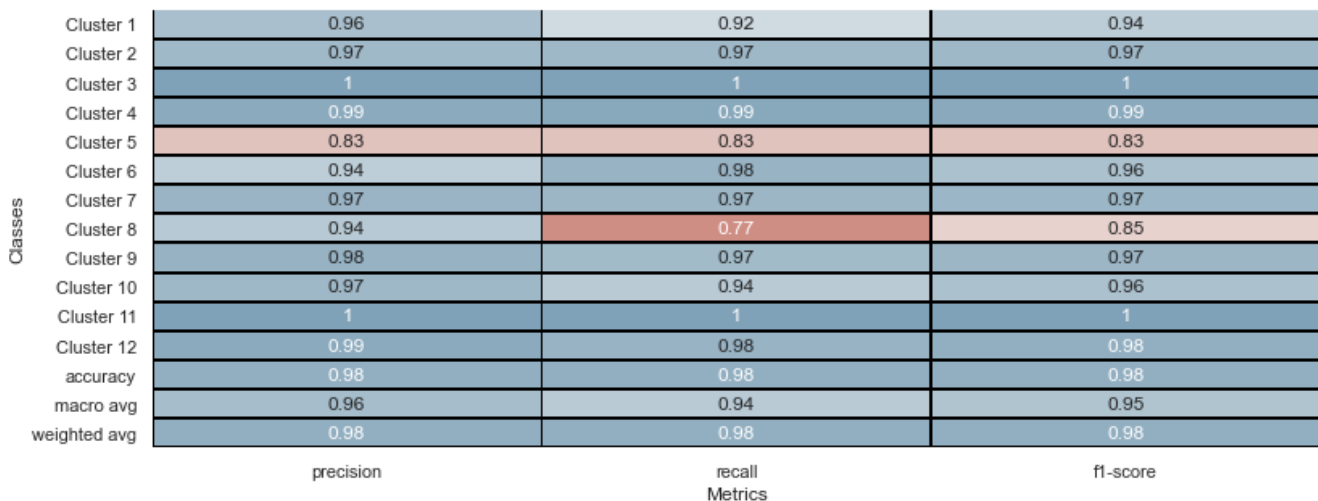


Fig. 7. Heatmap on Overall Performance Measures of HEMClustmodel on each Class.

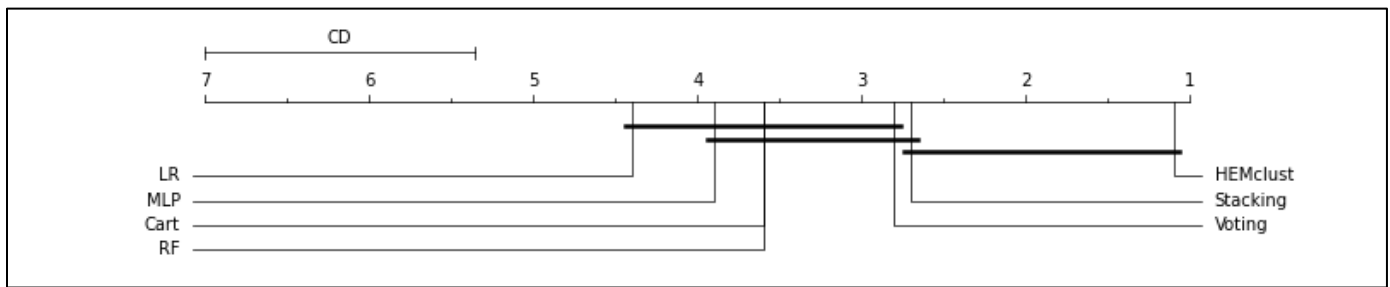


Fig. 8. Comparison of base Classifier against HEMClust with Nemenyi Test.

Attaining high accuracy was evident here as the risk of misclassification was very high. To build a better model all the areas related to claims data was studied in detail. Since the claims data is collected from various sources of healthcare sector it was evident to perform an appropriate preprocessing to improve the quality of data. Basically, detecting fraud is considered as a complex task as the boundary of separation between fraudulent and non-fraudulent classes is very noisy. Proposed model uses more sophisticated techniques for handling missing data to make it more convenient. feature engineering techniques were also used, which helped us select the essential feature that contributes in effective prediction. A varied performance result was observed from the initial experiment on each class when classified initially. It was found that the reason because of this was mainly due to the overlapping of procedures, which lead to the decrease in accuracy [30]. To improve the predictive accuracy, similar providers specialties were grouped using clustering. The results from clustering shows that providers performing similar kind of procedures were grouped in a single cluster. Further each cluster was considered as class labels and classified.

Following are the observations made from while implementing the classification model.

1) All the four learners, when individually applied, had an unstable performance. Though Cart and RF has good accuracy but there was high misclassification of classes.

2) Feature engineering and data cleaning had helped in improving the performance of the model also, the use of Spark Resilient distributed file system helped us in executing big data without time and memory overheads.

3) For selecting the meta learner, both RF and MLP was applied on base classifier separately. MLP as a Meta learner gave 83.9% precision score and 85.9% recall rate which states that the model could correctly classified only 83.9% of fraudulent samples. Random forest as a Meta learner gave 96% precision score and 94% recall rate and 98% of average f1 score, where the model could classify around 96% of fraudulent sample.

4) Statistical test like Friedman test and Nemenyi test was applied to know the differences in the performance of classifiers. Friend man test demonstrated a significant difference between the classifiers with the proposed method with a p_value of 0.02.

VI. CONCLUSION AND FUTURE WORK

The paper proposes a Heterogenous ensemble model with clustering (HEMClust) to detect fraud from claims data effectively. The model operates in three phases; first phase intends to apply preprocessing techniques to improve the data quality. The second phase aims to reduce the overlapping instances found in provider specialties using k-prototype clustering. The final step includes predicting fraudulent providers using a heterogenous ensemble model through stacking. The dataset used in the study was easily attributed to big data due to its voluminous nature. Spark framework was used on top of the Hadoop cluster to implement several model parts to avoid any computational overheads. Application of heterogeneous ensembles with meta learner helped in minimizing the error generated by these learners during prediction. It was found that the proposed HEMClust model showed the best overall fraud detection performance with an Average Precision-Recall Rate of 98%. During the study it was also observed that the fraud detection domain keeps evolving with the changing patterns of fraud. The problem is mainly referred as concept drift. The proposed model could also be extended to address the particular problem as ensemble learning has been used as state of the art to detect concept drift. However, interpretation of concept drift detection in fraud detection is out of this work's scope and could be considered for future work.

REFERENCES

- [1] H. Joudaki et al., "Improving fraud and abuse detection in general physician claims: A data mining study," *Int. J. Heal. Policy Manag.*, vol. 5, no. 3, pp. 165–172, 2016, doi: 10.15171/ijhpm.2015.196.
- [2] D. Thornton, M. Brinkhuis, C. Amrit, and R. Aly, "Categorizing and Describing the Types of Fraud in Healthcare," *Procedia Comput. Sci.*, vol. 64, pp. 713–720, 2015, doi: 10.1016/j.procs.2015.08.594.
- [3] K. E. Mues et al., "Use of the Medicare database in epidemiologic and health services research: A valuable source of real-world evidence on the older and disabled populations in the US," *Clin. Epidemiol.*, vol. 9, pp. 267–277, 2017, doi: 10.2147/clep.s105613.
- [4] E. Birman-Deych, A. D. Waterman, Y. Yan, D. S. Nilasena, M. J. Radford, and B. F. Gage, "Accuracy of ICD-9-CM codes for identifying cardiovascular and stroke risk factors," *Med. Care*, vol. 43, no. 5, pp. 480–485, 2005, doi: 10.1097/01.mlr.0000160417.39497.a9.
- [5] "Insurance Information Institute" <https://www.iii.org/fact-statistic/facts-and-statistics-insurance-fraud>.
- [6] FICCI, "Health Insurance Fraud."
- [7] H. Joudaki et al., "Using data mining to detect health care fraud and abuse: a review of literature.," *Glob. J. Health Sci.*, 2015, doi: 10.5539/gjhs.v7n1p194.

- [8] D. Erlangga, M. Suhrcke, S. Ali, and K. Bloor, "The impact of public health insurance on health care utilization, financial protection and health status in low: The middle-income countries: A systematic review(PLoS ONE (2019)14:8 (e0219731) DOI: 10.1371/journal.pone.0219731)," *PLoS One*, vol. 14, no. 11, pp. 1–20, 2019, doi: 10.1371/journal.pone.0225237.
- [9] I. Sohony, R. Pratap, and U. Nambiar, "Ensemble learning for credit card fraud detection," *ACM Int. Conf. Proceeding Ser.*, no. July, pp. 289–294, 2018, doi: 10.1145/3152494.3156815.
- [10] R. Konrad, W. Zhang, M. Bjarndóttir, and R. Proaño, "Key considerations when using health insurance claims data in advanced data analyses: an experience report," *Heal. Syst.*, vol. 9, no. 4, pp. 317–325, 2020, doi: 10.1080/20476965.2019.1581433.
- [11] K. Ferver, B. Burton, and P. Jesilow, "The Use of Claims Data in Healthcare Research," *Open Public Health J.*, vol. 2, no. 1, pp. 11–24, 2009, doi: 10.2174/1874944500902010011.
- [12] S. R. Sukumar, N. Ramachandran, and R. K. Ferrell, "Data Quality Challenges in Healthcare Claims Data : Experiences and Remedies," no. April 2014, p. 15, 2014.
- [13] S. K. Shamitha and V. Ilango, "A survey on machine learning techniques for fraud detection in healthcare," vol. 7, no. 4, pp. 5862–5868, 2018, doi: 10.14419/ijet.v7i4.15696.
- [14] R. A. Derrig, "Insurance fraud," *J. Risk Insur.*, vol. 69, no. 3, pp. 271–287, 2002, doi: <https://doi.org/10.1111/1539-6975.00026>.
- [15] J. M. Johnson and T. M. Khoshgoftaar, *Medicare fraud detection using neural networks*, vol. 6, no. 1. Springer International Publishing, 2019.
- [16] S. Dash, S. K. Shakyawar, M. Sharma, and S. Kaushik, "Big data in healthcare: management, analysis and future prospects," *J. Big Data*, vol. 6, no. 1, 2019, doi: 10.1186/s40537-019-0217-0.
- [17] Spark, "<http://spark.apache.org/>."
- [18] S. Salloum, R. Dautov, X. Chen, P. X. Peng, and J. Z. Huang, "Big data analytics on Apache Spark," *Int. J. Data Sci. Anal.*, vol. 1, no. 3–4, pp. 145–164, 2016, doi: 10.1007/s41060-016-0027-9.
- [19] M. Zaharia et al., "Resilient distributed datasets: A fault-tolerant abstraction for in-memory cluster computing," *Proc. NSDI 2012 9th USENIX Symp. Networked Syst. Des. Implement.*, pp. 15–28, 2012.
- [20] X. Zhou, Z. Zhang, L. Wang, and P. Wang, "A Model Based on Siamese Neural Network for Online Transaction Fraud Detection," *Proc. Int. Jt. Conf. Neural Networks*, vol. 2019-July, 2019, doi: 10.1109/IJCNN.2019.8852295.
- [21] S. Bagga, A. Goyal, N. Gupta, and A. Goyal, "Credit Card Fraud Detection using Pipeling and Ensemble Learning," *Procedia Comput. Sci.*, vol. 173, no. 2019, pp. 104–112, 2020, doi: 10.1016/j.procs.2020.06.014.
- [22] S. Liu, Y. Wang, J. Zhang, C. Chen, and Y. Xiang, "Addressing the class imbalance problem in Twitter spam detection using ensemble learning," *Comput. Secur.*, vol. 69, pp. 35–49, 2017, doi: 10.1016/j.cose.2016.12.004.
- [23] J. Novakovic and S. Markovic, "Classifier Ensembles for Credit Card Fraud Detection," 2020 24th Int. Conf. Inf. Technol. IT 2020, no. February, 2020, doi: 10.1109/IT48810.2020.9070534.
- [24] M. Zareapoor and P. Shamsolmoali, "Application of credit card fraud detection: Based on bagging ensemble classifier," *Procedia Computer Science*, vol. 48, no. C. pp. 679–685, 2015, doi: 10.1016/j.procs.2015.04.201.
- [25] D. W. Fan, P. K. Chan, and S. J. Stolfo, "A comparative evaluation of combiner and stacked generalization," *Proc. AAAI-96 Work. Integr. Mult. Learn. Model.*, no. June, pp. 40–46, 1996.
- [26] K. R. Kerwin and N. D. Bastian, "Stacked generalizations in imbalanced fraud data sets using resampling methods," *J. Def. Model. Simul.*, vol. 2628, pp. 0–2, 2020, doi: 10.1177/1548512920962219.
- [27] "Part B National Summary Data File (Previously known as BESS)," *Data base _ Medicare C.*, p. 21244, 2018, [Online]. Available: <https://www.cms.gov/Research-Statistics-Data-and-Systems/Downloadable-Public-Use-Files/Part-B-National-Summary-Data-File>.
- [28] M. Herland, T. M. Khoshgoftaar, and R. A. Bauder, "Big Data fraud detection using multiple medicare data sources," *J. Big Data*, vol. 5, no. 1, pp. 1–21, 2018, doi: 10.1186/s40537-018-0138-3.
- [29] R. A. Bauder, T. M. Khoshgoftaar, and T. Hasanin, "Data sampling approaches with severely imbalanced big data for medicare fraud detection," *Proc. - Int. Conf. Tools with Artif. Intell. ICTAI*, vol. 2018-Novem, pp. 137–142, 2018, doi: 10.1109/ICTAI.2018.00030.
- [30] M. Herland, R. A. Bauder, and T. M. Khoshgoftaar, "Approaches for identifying U.S. medicare fraud in provider claims data," *Health Care Manag. Sci.*, vol. 23, no. 1, pp. 2–19, 2018, doi: 10.1007/s10729-018-9460-8.
- [31] R. Bauder, T. M. Khoshgoftaar, and N. Seliya, "A survey on the state of healthcare upcoding fraud analysis and detection," *Heal. Serv. Outcomes Res. Methodol.*, vol. 17, no. 1, pp. 31–55, 2017, doi: 10.1007/s10742-016-0154-8.
- [32] L. K. Branting, F. Reeder, J. Gold, and T. Champney, "Graph Analytics for Healthcare Fraud Risk Estimation," pp. 845–851, 2016.
- [33] V. Chandola, S. R. Sukumar, and J. Schryver, "Knowledge discovery from massive healthcare claims data," *Proc. ACM SIGKDD Int. Conf. Knowl. Discov. Data Min.*, vol. Part F1288, no. August, pp. 1312–1320, 2013, doi: 10.1145/2487575.2488205.
- [34] J. R. Gaikwad, A. B. Deshmane, H. V. Somavanshi, S. V. Patil, and R. A. Badgular, "Credit Card Fraud Detection using Decision Tree Induction Algorithm," *Int. J. Innov. Technol. Explor. Eng.*, no. 6, pp. 2278–3075, 2014.
- [35] M. S. Kumar, V. Soundarya, S. Kavitha, E. S. Keerthika, and E. Aswini, "Credit Card Fraud Detection Using Random Forest Algorithm," 2019 *Proc. 3rd Int. Conf. Comput. Commun. Technol. ICCCT 2019*, no. March, pp. 149–153, 2019, doi: 10.1109/ICCCCT2.2019.8824930.
- [36] A. Gulati, P. Dubey, C. Mdfuzail, J. Norman, and R. Mangayarkarasi, "Credit card fraud detection using neural network and geolocation," *IOP Conf. Ser. Mater. Sci. Eng.*, vol. 263, no. 4, 2017, doi: 10.1088/1757-899X/263/4/042039.
- [37] I. K. Nti, A. F. Adekoya, and B. A. Weyori, "A comprehensive evaluation of ensemble learning for stock-market prediction," *J. Big Data*, vol. 7, no. 1, 2020, doi: 10.1186/s40537-020-00299-5.
- [38] S. Tewari and U. D. Dwivedi, "A comparative study of heterogeneous ensemble methods for the identification of geological lithofacies," *J. Pet. Explor. Prod. Technol.*, vol. 10, no. 5, pp. 1849–1868, 2020, doi: 10.1007/s13202-020-00839-y.
- [39] M. Herland, R. A. Bauder, and T. M. Khoshgoftaar, "Medical provider specialty predictions for the detection of anomalous medicare insurance claims," *Proc. - 2017 IEEE Int. Conf. Inf. Reuse Integr. IRI 2017*, vol. 2017-Janua, pp. 579–588, 2017, doi: 10.1109/IRI.2017.29.
- [40] "LEIE : Office of Inspector General LEIE Downloadable Databases." https://www.oig.hhs.gov/exclusions/exclusions_list.asp.
- [41] S. K. K. Asha RB, "Credit Card Fraud Detection using Artificial Neural Networks", *Global Transitions Proceedings*, pp. 35-41, Vol2, 2021, doi: 10.1016/j.glt.2021.01.006.
- [42] S. K. Shamitha and V. Ilango, "A hybrid technique for health insurance fraud detection on highly imbalanced dataset," *Int. J. Innov. Technol. Explor. Eng.*, vol. 8, no. 11, 2019, doi: 10.35940/ijitee.K2489.0981119.
- [43] A. Husejinović, "Credit card fraud detection using naive Bayesian and c4.5 decision tree classifiers," *Period. Eng. Nat. Sci.*, vol. 8, no. 1, pp. 1–5, 2020, doi: 10.21533/pen.v.
- [44] D. Gupta and R. Rani, "Improving malware detection using big data and ensemble learning," *Comput. Electr. Eng.*, vol. 86, p. 106729, 2020, doi: 10.1016/j.compeleceng.2020.106729.
- [45] N. Liu, H. Gao, Z. Zhao, Y. Hu, and L. Duan, "A stacked generalization ensemble model for optimization and prediction of the gas well rate of penetration: a case study in Xinjiang," *J. Pet. Explor. Prod. Technol.*, 2021, doi: 10.1007/s13202-021-01402-z.
- [46] R. Soleymanzadeh, M. Aljasim, M. W. Qadeer, and R. Kashef, "Cyberattack and Fraud Detection Using Ensemble Stacking," *Ai*, vol. 3, no. 1, pp. 22–36, 2022, doi: 10.3390/ai3010002.
- [47] R. Nooraeni, M. I. Arsa, and N. W. Kusumo Projo, "Fuzzy Centroid and Genetic Algorithms: Solutions for Numeric and Categorical Mixed Data Clustering," *Procedia Comput. Sci.*, vol. 179, no. 2020, pp. 677–684, 2021, doi: 10.1016/j.procs.2021.01.055.

- [48] G. Preud'homme et al., "Head-to-head comparison of clustering methods for heterogeneous data: a simulation-driven benchmark," *Sci. Rep.*, vol. 11, no. 1, pp. 1–14, 2021, doi: 10.1038/s41598-021-83340-8.
- [49] Z. Huang, "Extensions to the k-Means Algorithm for Clustering Large Data Sets with Categorical Values. *Data Mining and Knowledge Discovery* 2, 283-304," *Data Min. Knowl. Discov.*, vol. 2, no. 3, pp. 283–304, 1998.
- [50] K. D. L. Library, "<https://keras.io/>."
- [51] E. Alshdaifat, D. Alshdaifat, A. Alsarhan, F. Hussein, and S. M. F. S. El-Salhi, "The effect of preprocessing techniques, applied to numeric features, on classification algorithms' performance," *Data*, vol. 6, no. 2, pp. 1–23, 2021, doi: 10.3390/data6020011.
- [52] R. F. Lachlan, L. Verhagen, S. Peters, and C. ten Cate, "Are There Species-Universal Categories in Bird Song Phonology and Syntax? A Comparative Study of Chaffinches (*Fringilla coelebs*), Zebra Finches (*Taenopygia guttata*), and Swamp Sparrows (*Melospiza georgiana*)," *J. Comp. Psychol.*, vol. 124, no. 1, pp. 92–108, 2010, doi: 10.1037/a0016996.
- [53] F. Afrin and M. Tabassum, "Comparative Performance Of Using PCA With K-Means And Fuzzy C Means Clustering For Customer Segmentation," *Comp. Perform. Using PCA With K-Means Fuzzy C Means Clust. Cust. Segmentation*, vol. 4, no. 10, pp. 70–74, 2015.
- [54] C. Ding and X. He, "K-means clustering via principal component analysis," *Proceedings, Twenty-First Int. Conf. Mach. Learn. ICML 2004*, pp. 225–232, 2004, doi: 10.1145/1015330.1015408.

An Authorization Framework for Preserving Privacy of Big Medical Data via Blockchain in Cloud Server

Hemanth Kumar N P¹

Assistant Professor, Dept. of CSE
East Point College of Engineering and Technology
Bengaluru, India

Dr. Prabhudeva S²

Director, Dept. of MCA
Jawaharlal Nehru National College of Engineering
Shivamogga, India

Abstract—In recent years, cloud-based medical record sharing has greatly improved the process of researching the disease and patient diagnosis. However, since cloud systems are centralized, there is serious concern about data security and privacy. Blockchain technology is viewed as a promising method of dealing with privacy issues and data security because of its exclusive features of distributed ledgers, secrecy, verifiability, and enhanced security. The literature review has shown significant works on integrating blockchain technology with cloud system for managing and sharing healthcare data. It has been analyzed that previous works are primarily dependent on the centralized data storage approach, which raises privacy concerns. The previous works also do not emphasize handling big medical data and lack the reliability of the end-to-end security features system. This paper has presented an authorization framework for ensuring data security and privacy preservation using blockchain technology with IPFS as decentralized file storage and sharing system. The proposed study devises a proof of replication algorithm using smart contracts to provide a better access control mechanism. The implementation of the proposed framework is based on the symmetric encryption and Ethereum blockchain platform. The study outcome illustrates the efficiency and availability of the proposed scheme compared to the typical cloud-based blockchain method.

Keywords—Medical data; cloud; blockchain; data sharing; access control; security; privacy preservation

I. INTRODUCTION

Healthcare is a scientific field that refers to a multidimensional system that includes a range of services primarily concerned with preventing, diagnosing, and treating disease and injuries related to human health. Healthcare professionals need a variety of information to provide better patient treatment, such as a patient's medical history, clinical evidence (imaging and laboratory tests), and private and personnel information [1]. The traditional method of storing such medical records for patients was to handwrite notes or printed papers that are easy to lose and difficult to hold for the long run [2]. The advancement of information and communication technology (ICT) has enabled the creation of electronic medical records (EMR), which are easy to keep for a long time compared to handwritten notes or paper-based records. The boom in the digitization of medical records has led to the formation of big medical data, which can be used for a variety of purposes in the healthcare sector [3].

Medical experts and healthcare institutions need to compare and analyze big medical data containing similar or related clinical features to examine the disease and seek better treatments [4]. Furthermore, most often, the patients may not be able to recall in detail their past medical conditions and symptoms. EMR sharing can assist physicians in learning more about their patients' health, therefore enhancing accuracy in diagnosis and leading to an effective decision-making process towards increasing the success rate of the treatment. Despite these benefits, two major problems exist, i) the storage of big medical data and ii) the security aspects related to EMR sharing across a healthcare organization. The deep learning market report [5] states that approximately 90% of EMR generated in hospitals are images. Due to large EMRs being generated, more storage space and computing power are required to perform analytical tasks to benefit healthcare services for patient well-being. On the other hand, sharing EMRs raises a significant and noteworthy concern regarding privacy protection, data security, and interoperability [6]. Firstly, electronic medical records contain personal and sensitive information, so privacy protection is the shield of a patient's reputation. Next, only authentic or trustworthy medical data can be used to make accurate decisions on diagnosis and treatment. Conversely, the forged EMR reduces the importance of clinical aspects and mislead in effective treatment planning. Moreover, interoperability can enable patients to control access to their EMRs and enhance sharing of EMRs across healthcare facilities.

Cloud computing has emerged as a promising solution that offers flexible storage management and efficient sharing of big medical data in response to these problems. The cloud computing ecosystem adopts different cryptographic primitives to secure medical data or EMRs and access control mechanisms to ensure privacy-aware data sharing [7]. Despite the high emphasis on data security and privacy protection, few serious security concerns still remain. Firstly, cloud systems are assumed to be trusted when it comes to storing, managing, and distributing data. In this regard, the design of cloud systems for data management and sharing heavily relies on the involvement of third-party mechanisms, which are prone to leak, theft, and tampering due to lack of surveillance [8]. Unfortunately, there is no standard verification mechanism for existing schemes, and also there is no effective countermeasure to penalize a misbehaving server or cloud entity.

In recent years, blockchain technology has appeared as a potential solution to address security loopholes and ensure reliable sharing of EMRs using a distributed ledger [9]. Since the blockchain is open and transparent, blockchain-based medical data sharing can help patients to have better access control and monitor the use of medical data [10]. However, despite the many benefits of blockchain technology, most of the current work suffers from the following three major issues: i) How to design an effective mechanism for verifiable security of EMR in the blockchain. Another problem is that the blockchains are not meant for big EMR or medical data (like high dimensional medical images) as they are not scalable quickly. When data is stored on the blockchain, the information is available to everyone. Therefore, the second problem can be highlighted as follows: ii) How to ensure that only the authenticated person can access the EMR data; and iii) How to design a computationally-efficient mechanism, block structure, and fault-tolerant mechanism that can ensure system reliability and availability for a longer run. All these factors are not adequately addressed in the existing literature.

As a motivation, the proposed research work emphasizes developing a big medical data authorization framework that can maintain an effective balance between security, privacy, and scalability. Apart from this, it also ensures full-proof security for the seemly management and sharing of big medical data in the distributed environment. The major contribution of the proposed research work is highlighted as follows:

- The proposed study employed an Ethereum blockchain platform on an amazon cloud system to explore the effectiveness of smart contracts in user validation and access management.
- The study implements InterPlanetary File System (IPFS) as a peer-to-peer network system for storing medical, thereby eliminating issues associated with a centralized system.
- The study considers high dimensional medical images as big data further split into multiple and equal shards. Thereby, the study handles scalability issues in the blockchain system.
- A mechanism of key-pairing is employed using an asymmetric encryption algorithm to each shard of medical data. This mechanism ensures data security so that data is not visible to the user or IPFS nodes that store the data.
- A novel proof of algorithm is developed that handles each transaction related to data storage access and facilitates better management of data sharing.

The remaining sections of the proposed manuscript are described as follows: Section II presents the related work and highlights some significant issues explored based on the review analysis; Section III presents the proposed system model and methodology adopted; Section IV presents the system design implementation; Section V presents the result analysis and discusses the performance of the proposed system, and finally Section VI provides a conclusive remark on the entire contribution and findings of the proposed study.

II. REVIEW OF LITERATURE

This section briefly reviews the previous works on secure storage and sharing of medical data or EMR in digital healthcare systems using blockchain.

The first attempt towards medical data sharing using Ethereum blockchain is made by Yue et al. [11] to enable patients to control the access of their health-related information without compromising any privacy risk. Although this mechanism ascertains privacy preservation, it has some significant limitations: it does not provide access to patient family members, an essential concern in emergency situations. Apart from this, the model lacks the scalability feature. In a similar line of work, Jaiman and Urovi [12] suggested an access control framework for EMR sharing concerning patient consent. This work emphasizes joining data use ontology and access matrix that holds information about the data requestor. Considering these features, the data owner, i.e., patient or doctors makes EMR sharing rules, monitors its usage, and updates the access policy at any time. The existing approaches have not considered the efficiency factors in sharing medical data that continuously stream from bio-sensors and monitoring devices. In this regard, Shen et al. [13] presented an efficient scheme that combines peer-to-peer networking techniques with blockchain and digest chain to bring efficiency and flexibility in the sharing of medical data. The authors have introduced a scheme of the authorized network of participants to enable secure sharing of EMR between different healthcare departments, pharmacies, and patients. However, this approach has a security loophole because the storage of data in on-chain is vulnerable to scalability and privacy issues. Similarly, Dagher et al. [14] suggested a privacy-preserving scheme concentrating on the interoperability and access of the EMR using blockchain. This scheme adopted smart contracts stored on the Ethereum model, which holds hashing key of the EMR for ensuring interoperable. On the other hand, an advanced cryptography mechanism is employed to ensure secure sharing of EMR. Although this scheme is subjected to the high storage cost, it can't be applied to process big medical data and is open to vulnerability as it reveals information about the transactions. The above approaches lack off-chain policy and scalability, which is addressed in the proposed work using IPFS technology.

Zhang et al. [15] also aimed to address the issue of scalability by implementing the Ethereum model of blockchain technology. In this work, the ciphered data is stored on the on-chain system, which refers to the original medical records, while original medical records are kept over the off-chain system. The work of Madine et al. [16] has attempted to address the risk of single-point failover for the EMR stored on the cloud. The authors have applied the Ethereum model for devising smart contracts to enable patients to have full control over their data in various ways, such as transparency, traceability, undisputable, and security. IPFS system is employed as decentralized storage, and a re-encryption mechanism is adopted to provide data security. A blockchain-oriented digital healthcare system is presented in the work of Huang et al. [17] to attain robust security and traceability of the EMR sharing over the cloud system. An attribute re-encryption technique is applied to achieve complete access control for data

providers. An approach of a lightweight data sharing scheme is provided by Su et al. [18] using blockchain technology to achieve data privacy in the healthcare sector. The authors have applied an interleaving encoder to encrypt the medical data. Xu et al. [19] have given the mechanism of the health chain to support the requirement of privacy preservation for big medical data using blockchain and encryption to ensure a fine-grained access mechanism. This work also focuses on the key-management process to efficiently revoke or update keys for the authorized data requester.

Another significant work given by Wang and Song [20] adopted an attribute-based encryption technique combined with a blockchain mechanism for the cloud-assisted EMR sharing system. However, this approach failed to solve a problem related to the storage of big medical data and its sharing in an optimal way. Margheri et al. [21] introduced an information management model for monitoring EMR using modular blockchain system-based smart contracts. The work carried out by Guo et al. [22] modeled a hybrid system to enable better access control of EMR using blockchain. This scheme provides tamper-proof features by managing customized access policy, and off-chain nodes are employed to enforce attribute access mechanism on EMR data. Rajput et al. [23] suggested an approach of EMR access policy in an emergency based on Hyperledger fabric and composer. The authors have derived some customized policies under a smart contract for accessing emergency conditions for a specific time duration. The work carried out by Roehrs et al. [24] gave a prototype of the distributed blockchain to enhance the replication of data across nodes by combining medical records using blockchain and open interoperability. Another work of Guo et al. [25] have devised an attribute-oriented signature technique with blockchain, where a patient approves an EMR while providing no information other than evidence that he or she has substantiated it. The work carried out by Chen et al. [26] presented a conceptual design of a data storage system based on blockchain and a cloud system to manage personnel healthcare data. The study claimed that this storage system is independent of a third party and also does not allow a single party to have complete control over the access and processing of the data. However, none of the existing studies have provided standard management and sharing schemes for the medical data for pharmaceutical scientists. The work of Fan et al. [27] presented a clinical information management system using distributed ledger and consensus mechanism without much depending on the network resources. In a similar direction, a recent work carried out by Bataineh et al. [28] developed a security model for IoT-based healthcare systems using Ethereum Blockchain for surgical process management. Different from previous works, an application of fuzzy logic with blockchain is considered in another recent work by Zulkifli et al. [29] to provide an adaptive security mechanism for IoT-oriented healthcare.

For the management and sharing of medical data, different authors attempted to suggest solutions from different perspectives. There has been a huge development towards blockchain-based healthcare since 2016, which was the initial year till 2022. The analysis shows that most previous works adopted Ethereum or Hyperledger Fabric blockchain platform,

and most of them provided conceptual and experimental approaches. Table I summarizes the above-discussed literature concerning blockchain platforms and solution types.

It has been identified that many previous works failed to ensure maximum requirements of the security such as privacy, data security, access control, interoperability, storage, scalability, and system cost analysis for secure sharing of medical data or EMRs. Although, most of the existing works have emphasized efficient access control and privacy preservation mechanisms using attribute-based re-encryption before introducing medical data to the blockchain system. Few existing works suggested the implementation of smart contracts, and some have employed a chain-coding scheme for privacy-preserving of EMR. On the other hand, the hospital continuously generates massive data as the number of people coming to the healthcare center is countless. Among the literature which is being reviewed, it has been found that most of the works have not considered the issue associated with big medical data storage. The authors in [9] have considered the issue. However, it lacks details on the storage services. Moreover, there are few relevant works [14],[16],[23] [22] that have been considered IPFS as a medium of data storage. The solutions given by these works can overcome the big data issues; however, it needs more optimization to handle a considerable amount of EMR data especially high dimensional medical data. In particular, the previous scheme for sharing and storing EMR using blockchain is still in its infancy stage, involves high cost, lacks scalability, and needs more effort in the design and development. Table II highlights the finding of the review analysis.

TABLE I. SUMMARY OF THE PREVIOUS WORKS BEING REVIEWED

Citations	Blockchain Platform	Solution Type
[11]	Not Defined	Implementation
[12]	Ethereum	Experimental
[13]	Not Defined	Experimental
[14]	Ethereum	Experimental
[15]	Ethereum	Implementation
[16]	Ethereum	Experimental
[17]	Not Defined	Conceptual
[18]	Bitcoin	Conceptual
[19]	Doc-chain	Experimental
[20]	Not defined	Conceptual
[21]	Hyperledger Fabric	Implementation
[22]	Hyperledger Composer	Experimental
[23]	Hyperledger Fabric	Experimental
[24]	Customized	Experimental
[25]	Not Defined	Conceptual
[26]	Not Defined	Conceptual
[27]	Not Defined	Conceptual
[28]	Ethereum	Implementation
[29]	Hyperledger Fabric	Experimental

TABLE II. HIGHLIGHTS OF THE RESEARCH ISSUES

Issues	Addressed By	Not Addressed By
Privacy and Security	[11-12], [14-23], [25-29]	[13], [24]
Accessibility and Interoperability	[12-15], [17-24], [26], [27]	[11], [16],[25]
Scalability	[14-16] [18-19] [21] [23] [26-27]	[11-14], [17], [20], [22], [24-25], [28-29]
Cost Analysis	[12], [18-19], [25], [28-29]	[11] [13-17], [20], [23-24], [26-27]
Big medical data	[14], [16], [19], [22-23]	[11-13], [15-18], [24-26]

III. SYSTEM MODEL

The proposed study presents a novel model for medical data authorization towards security and privacy preservation using blockchain methodology. The study considers big data as a medical image. The rationale behind considering the medical image as input data to the system is that the medical images are of high dimensional data associated with significant storage and scalability, which is a big data problem. Fig. 1 depicts the high-level architecture of the system model for big medical data based on blockchain that includes data sharing and its management over the distributed healthcare environment.

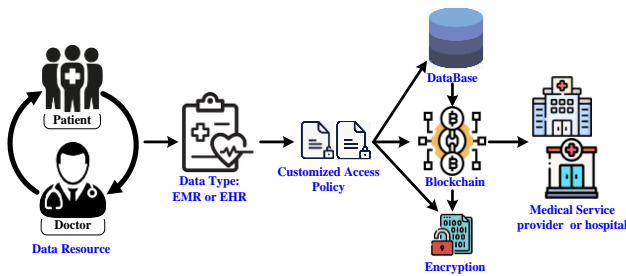


Fig. 1. High-level Architecture of the System Model.

A. System Model Components

As shown in Fig. 1, there are five main entities in the system model viz. i) data resource, ii) Data Type, iii) Access policy, iv) Database (medical data storage), and Security (encryption and blockchain), and v) medical service provider.

1) *Data resource*: The major medical data sources are the patient and the doctors. When patients interact with the physician, they share information consisting of previous records of the patient's health, drug history, current health issues, and other physiological symptoms.

2) *Data type*: The electronic health record (EHR) or electronic medical record (EMR) is built based on initial health information collected during the interaction between the patient and the doctors, after which the patient often undergoes other clinical examination such as laboratory tests, pre-operative assessment, and medical imaging. All these data are digital and stored in an electronic storage system. These digital records termed EMR or EHR, provide a holistic and long-term view of patient health.

3) *Customized access policy*: The patient he/she is the owner of their sensitive or private information in the EMR.

However, in real-world scenarios, medical data is available with both patients and healthcare organizations. Therefore, both entities can act as a medium of storing medical data to a cloud server. Therefore, a customized access policy is built for accessing the data by the doctors or the healthcare organization upon having the valid reason to share their data to the other healthcare organizations (data requester).

4) *Database and security*: This component of the system model involves the core part concerning data storage, security, and privacy. The data is stored in a distributed manner, either on a centralized or decentralized server. The integration of encryption with blockchain technology offers higher security privacy preservation and ensures the authenticity of the customized access policy. Blockchain is a system where there is no central authority to share the data, but even then, anyone can trust that the data is genuine.

5) *Medical service providers*: The medical service providers refer to healthcare facilities such as ad-hoc clinics, clinical laboratories, radiological centers, and hospitals interesting in accessing the medical data are treated as data requesters. According to the customized access policy, the data is provided to the data requester to decide the best strategy for surgery and treatment. Also, depending on the context, the patient can act as a data requester who requests to access the data stored on the cloud server. For example, sharing medical data to other healthcare facilities or organizations can facilitate better diagnosis, medical research, policy defining and effective treatment no matter where the patient is treated in the world if the healthcare records are available independent of time and place.

B. Need of the System

The proposed system model can address the following issues:

- 1) When the data is stored in a centralized server, there is a risk of a security issue, privacy leakage, and identity theft either by the creators of the system or by hackers.
- 2) The big medical data are not meant for blockchain as they are not scalable quickly.
- 3) When data is being stored on the blockchain, the data is available to everyone.
- 4) The solution on the blockchain is often subjected to higher costs as it requires a large processing time for the successful execution of the transactions.

C. Solution Strategy

1) The blockchain is a no-trust system where the code takes care of the issues associated with centralization and privacy.

2) The study considers the high dimensional medical image as the big data, which is further split into shards as 3 data copies of equal size and which handles the issue of big data into the blockchain. Therefore, the data become scalable.

3) The data is encrypted using an asymmetric algorithm that ensures data security and prevents unauthorized access.

4) The data is stored on a miner's device. The proof of replication algorithm is proposed to ensure that the miners are storing the data. While recovery, this algorithm ensures the file recovery with the least bandwidth.

5) In this work, the Ethereum blockchain provides secure and distributed sharing of medical records over the unsecured channel.

IV. SYSTEM IMPLEMENTATION

The proposed study devices an authorization framework for medical data, which provides access to data requester in a distributed environment using blockchain. The study considers a high-dimensional medical image of the patient-generated from the radiological department. Here, the patient must create a customized access policy and smart contract in the Ethereum blockchain. On the other hand, the radiologist is accountable for uploading data to the IPFS network. The uploading of this data requires sending accept file storage requests by IPFS to blockchain clients, and similarly, access to storage is also required for retrieving the data on their mobile phone or computer. The data can be retrieved by either patient or the doctors in the other hospital to download previous medical records and upload current or new medical reports. The IPFS network is a peer-to-peer network system, where the user as storage provider needs to create an account to become a blockchain client and provide storage of their computing nodes. Due to bandwidth and storage constraints, the user here uses a cloud server as a storage point rather than storing on the local computing nodes. Upon accepting request regarding accept file storage, the data is encrypted using asymmetric encryption (RSA) as primary level security for data protection at the location of the data storage provider (IPFS). The encrypted data is further introduced with the blockchain module. In this module, the sharing of the secret key information is carried out over blockchain, which automatically changes the private and public key pair so that the user has complete controller over either allowing or revoking access to the other user. Fig. 2 presents the process flow of the proposed authorization system for secure uploading and sharing of big medical data.

- The data service provider interacts with the IPFS network using the web3.0 interface and connects to the backend.
- The data service provider requests to accept file storage, blockchain client interacts with IPFS in the backend.
- IPFS network at cloud server verifies the blockchain client identity and reliability (bandwidth requirement, storage capacity) with proposed proof of replication algorithm (PoRA) and allows the file storage.
- On the blockchain client storage node, the medical data is encrypted and sent towards IPFS.

- MD5 hashes of medical data (image) are given to distributed hash tables (DHT) for protecting its integrity.
- The file storage transaction is verified by the transaction pool linked to Ethereum (Eth) blockchain. Gas price is paid at this time (miners in Eth1.0 validators in eth 2.0 in study 2.0 is used).
- Once the transaction gets updated, the response is given to the blockchain client, and the storage is used for the purpose of the application (storing patient data).
- Data requester, which can be patient or doctor either stores a new data or requests for access of a data.
- The request is forwarded to PoRA.
- PoRA checks the access policy (11) via smart contracts (PoRA is part of smart contracts).
- Access to storage is given to the Data requester.

A. Blockchain

In the present study, the Ethereum blockchain is being used, and the focus of this study is to build a medical image authorization system in a distributed environment. All transactions are logged in the blockchain. The transactions are of four types.

Fig. 3 presents a basic architecture of the medical data blocks over the blockchain (B.C.) with different components and transaction (T) records. The miner id refers to the identity of the transaction validators produced based on the proof of the work on the validator's computing devices or nodes. The second component, namely timestamp, refers to the first block created and the last transaction. The third component is the data hash value (H) SHA256 of the blocks for each transaction numerically represented as follows:

$$H_{12} = f(H_1 + H_2) \rightarrow f(T_1 \cdot H) + (T_2 \cdot H) \quad (1)$$

Where, $f(\cdot)$ denotes hashing function, and the validation and integrity check of the blocks are done based on the previous H of the block.

The next component, namely data_id is the unique identifier of the medical data that belongs to the particular patient id, whereas patient id denotes the unique identifier of the patient or the data owner. The data stored under the cloud server establishes trust between the requester or provider and the IPFS network. A smart contract is basically a computer program that runs on the blockchain. The smart contract includes all operations of the access policy used to validate and accept requests for data access. The operation involved in the smart contract is available to all blockchain users. The collection of smart contracts controls the entire storage and access mechanism in the proposed system. Hence, there won't be a centralized authority for limiting access and storing the files. The transactions done over a blockchain are organized in accept file storage, new file storage requests, give access to a file, and revoke access to a file.

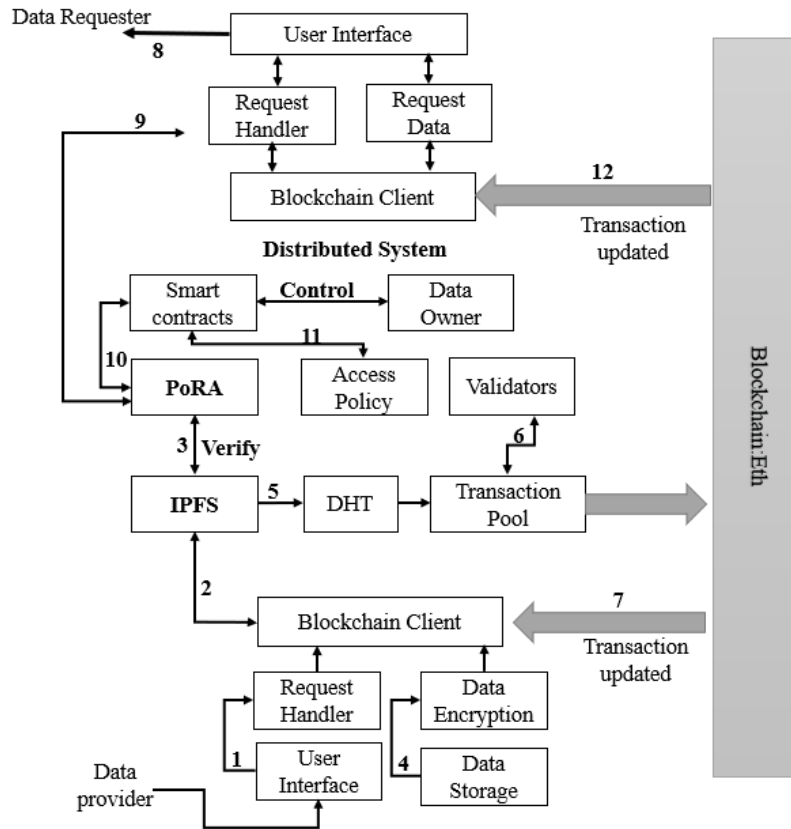


Fig. 2. System Implementation Process Flow for Secure Data Uploading and Sharing.

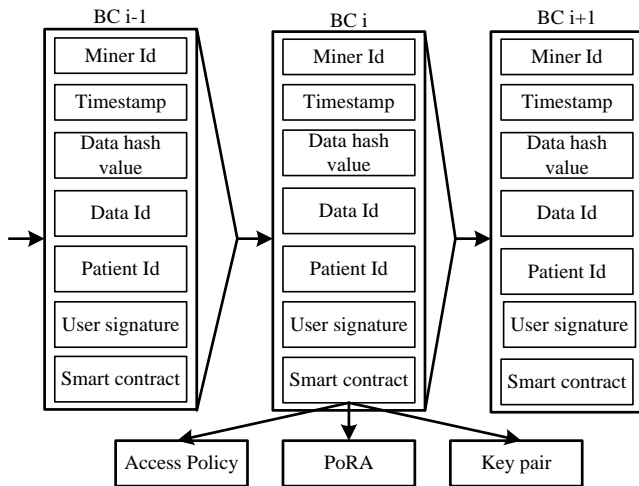


Fig. 3. Schematic Representation of Data Blocks.

B. Accept File Storage

The accept file storage transaction is subjected to the interaction of data service provider and data storage provider in the IPFS network. The data service provider needs a registration to have an account of blockchain, so that they can initiate a file storage request for uploading medical data to the IPFS distributed system meant for storing, sharing and accessing files. File storage request is typically accepted by the storage nodes. The storage nodes mean a user which is a part of blockchain client that facilitates their storage space either on

the local machine or cloud server. In the current study, the storage nodes of the IPFS network are the cloud server. Upon receiving the request, the blockchain client interacts with the IPFS network and confirms the storage request, (i.e., the user is ready to provide its storage space). The IPFS verifies the file storage request by creating accept file storage transaction. In this process, the IPFS validates the identity of storage provider and checks are reliability in terms of storage and bandwidth capacity with PoRA using smart contracts and allow the file storage. The mechanism of file storage consists of few core operations as shown in Fig. 4.

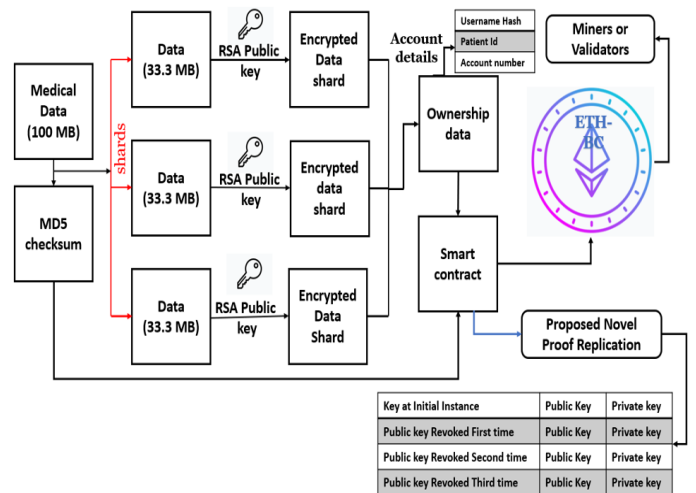


Fig. 4. Data Uploading and Storage Process.

1) In Fig. 4, the process of data storage on the blockchain client computing nodes in the IPFS network. The study considers medical data of size 100 MB, which is further split into the three shards with equal size. The ideology behind shards is that sharing and storing big data or high-dimensional data on the blockchain is challenging. Therefore, creating a set of equal-sized sub-images of the original image can provide a promising solution towards efficient file sharing operation in the blockchain. The study used an IPFS network, a decentralized file system based on the BitTorrent protocol, and the Distributed Hash Table (DHT). The IPFS system does not require a central server, and data can be stored in a network of distributed storage nodes, resulting in no single point of failure, higher storage throughput, and enhanced storage access and information retrieval mechanism over existing cloud storage systems. SHA256 hash values are calculated and stored in DHT to verify the integrity of medical images. At the same time, each shard is encrypted using the RSA asymmetric encryption algorithm and stored in IPFS storage nodes. As part of the study, smart contracts were integrated with the IPFS network to manage data access efficiently.

2) The patient metadata needs to be stored on the blockchain for the transaction; even though the medical data is stored on IPFS nodes, the metadata includes patient identification (I.D.), account numbers, smart contract details, hash values, and timestamps, among others. Mining pool transactions are conducted periodically by validators or blockchain miners. The fastest validators to verify a block of data will send the signature to the other validators for validation. After all, validators agree, valid blocks are added to the blockchain in consecutive order. Finally, the blockchain is synchronized by using the blockchain client to receive the identical copy of the blockchain. Furthermore, by storing hashes on the blockchain instead of raw data, the proposed model eliminates the risk of data leakage, ensuring high levels of data security.

C. New File Storage Request

This module of blockchain transactions is subjected to data access and storage updating with new data. The data requesters requested to access data or update the newly generated medical records of a particular patient in existing storage units of the IPFS network. A data requester is a patient or doctor in a medical facility. If the data requester is a patient, the system checks the blockchain record, verifies the patient's credentials, and allows access to the data store. On the other hand, if the data requester is a doctor or medical institution, the system using smart contracts verifies the requester's credentials. It authorizes access according to the access policy set by the patient. Fig. 5 shows the process of a new file storage request.

The data provider's entire process of data access and storage updating can be described in the following manner.

1) *Data storage access request (accomplished by data provider):* In order to access data on IPFS storage nodes in the cloud server, the data requester requires to execute a data access request transaction. If the data requester is a blockchain client, a key-sharing mechanism consisting of a pair of private and public keys is used for transaction authorization and its verification to access the blockchain. In addition, data requesters are required to provide a patient I.D. and account number when requesting access to the data. The transaction will then forward to PoRA for access request verification (refer to points 8 and 9 in Fig. 2).

2) *Approval to access storage (accomplished by PoRA) :* The data access request transaction is forwarded to the PoRA for the purpose of auditing and authorization. Then, the PoRA verify for this request based on the customized access policy and key sharing in the smart contract. Upon confirmation and authorization of the data requester's public key in the smart contract and access policy, permission is granted to the data requester to access the data storage on the IPFS network (refer to point 10 in Fig. 2). In addition, PoRA analyzes the authorized request identity, which contains the access request information related to the specific patient-ID and account number. It then searches for the hash value of the quarried medical data in the DHT to get the requested data on the IPFS storage node in the cloud server. The IPFS network then provides the requested data file in the ciphered form. PoRA uses a patient's private key to decrypt the ciphered medical data (image) and return the original plain medical data to the data requester (refer to point 11 in Fig. 2). Here, transactions will be clustered and introduced into the transaction pool for mining. All validated transactions will be enumerated and linked to the blockchain to be shared with data requesters.

3) *Updating data storage (accomplished by validators):* As long as the requester has access to the data collection, such as patients, doctors, or healthcare providers can access the data of their interest. Also, they can request new file storage access to upload newly generated medical data to existing data storage nodes via a blockchain client (refer to point 12 in Fig. 2).

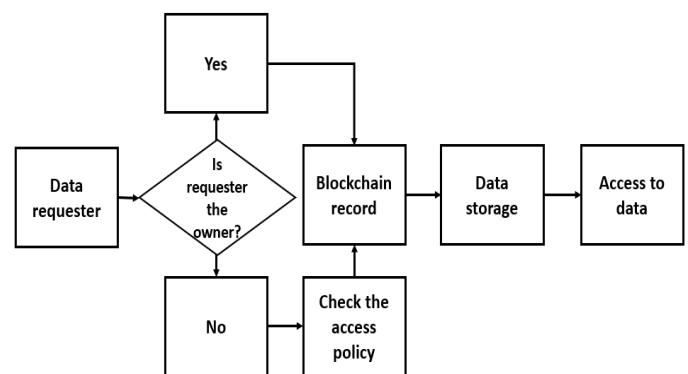


Fig. 5. Data Access and Storage Updating.

D. Give Access and Revoke Access to Data Storage

Upon verifying the data requester by the proposed PoRA, the requestor starts to make a transaction to access medical data by providing the unique identifier and account details of his patient to provide effective care accordingly. Once accessing data storage is completed, the transaction is updated and added to the blockchain by validators and acknowledged to all blockchain clients in the network. In this way, the patient can monitor their data sharing, thereby ensuring its ownership. However, to make the network reliable and ensure data security and privacy in the longer run, it is required to revoke the public and private key by updating to a new one after the purpose of data storage access is finished. Apart from managing the access control and sharing of medical data, the proposed PoRA also manages the key sharing process by securely revoking and updating the key that is known to the data requesters at each instance of data storage is accessed. Thus, eliminating the chances of key compromising and ensuring the trustworthiness of the network. The core procedure of the proposed PoRA algorithm is discussed in Algorithm 1.

Algorithm-1: Proof of Replication Algorithm (PoRA)

Input: file(F), Hash(H), Owner details(D), Access List(L)

Output: revoke key

1. $L' = \text{Old Copy of Access List}$
2. for each user (U) in access List(L)
3. if U not in L' :
4. $P, P' = \text{newKeyPair} () \# P$ (public) & P' (private) key
5. $[F1, F2, F3] = \text{sharding} (F)$
6. $F_e \leftarrow \text{ENC} (F1, F2, F3, P)$
7. Transfer (F1, F2, F3)
8. Share private key to U
9. For each user U' in old access list(L')
10. If U' not in L:
11. $P, P' = \text{newKeyPair} () \#$
12. Run $F_e = \text{ENC} (F, P)$
13. For U in L
14. Share private key with U

The algorithm takes input values as a medical data file (F), hash value (H) of the file, owner details (D), access list (L). After successful execution, it returns key revocation for each instance of access completion. The smart contract goes through the entire list when the access needs to be modified. L is the new access-list, whereas L' is the old access-list (line:1-2). In the new access list, if a user U is not present in the old access list, then the user's access needs to be given (line:3). This is done by generating a new keypair (P & P') (line:4). In the next step, the medical data file is divided into shards and encrypted using function ENC(), an asymmetric algorithm that takes shards and encryption key P(line:5-6). The encrypted file is then transferred to the IPFS storage nodes along with the private key to the user U (line:6-7). Further, the algorithm considers the users U' subjected to the old access list (L') and

do not belong to the new access-list L. The proposed algorithm PoRA again generates a new key pair that encrypts the file and shares the user's private key. In this way, at every instance of access and its completion, the proposed algorithm revokes the previous access list and re-encrypts the file in the new list with a new keypair (), which is further updated to the authorized user or doctor.

V. RESULTS

The design and development of the proposed system are carried out using Nodejs programming language installed on windows 10 Machine Intel(R)Core (T.M.)i7 16.0 GB RAM. Image dataset is used to validate the proposed model, and asymmetric encryption is used to protect the image. Ganache Simulator is used to simulate blockchain on the Local Machine. Kovan Testnet is used to simulate the entire program over the testing network with Keth (Ethereum with no real-world value) in order to test the gas price and processing time. Table III highlights configuration details of the system implementation.

A. System Parameters

TABLE III. SYSTEM MODEL CONFIGURATION DETAILS

Operating System	Windows 10
CPU	Intel(R) Core(TM) i7-9750H CPU @ 2.60GHz 2.59 GHz
RAM	16.0 GB
Programming Language	Nodejs
Compiler	Solodity 0.6.0(London)
Test Framework	Mocha 6.2.0
Ethereum Platform	Ganache
Performance Testing	Kovan Testnet
Storage nodes	AWS nano
Local network speed	100 mbps
Hard disk type	Solid State Drive
GPU	Nvidia GTX

B. Result and Analysis

Table IV presents the numerical outcome obtained for the proposed algorithm PoRA. The performance of the proposed scheme is compared with the cloud-based blockchain system. It must be noted that 1 unit of gwei is equal to 1 nano Ethereum. The parameter time for storage and recovery represents how fast a file can be uploaded and recovered under the ideal scenario. The ideal scenario is represented by the simulation parameters, i.e., 100 MB of the data file. Since the storage is decentralized, any one of the nodes is always available.

The performance analysis of Fig. 6 shows that the proposed system PoRA outperforms the cloud-based blockchain system. The graph trend exhibits that the time for storage is less, i.e., 0.8 milliseconds in the proposed system PoRA, compared to the cloud-based system, i.e., 1 millisecond. It is because the smart contract used in the proposed authorization scheme has a smaller number of steps.

TABLE IV. COMPARATIVE ANALYSIS

Parameters/Techniques	Cloud-Blockchain	PoRA [proposed]
Time for data storage 100 MB	1ms	800us
Time for Accessing data 100MB	5ms	2ms
Minimum gas price	10382 gwei	5202 gwei
Typical gas price	20481 gwei	8642 gwei
Uptime	99%	100%
Downtime	1%	0%(negligible)
Data loss	No loss	no loss
Data integrity with MD5 hash	97%	99%
Storage space	limited by cloud	limited by number of nodes [Virtually unlimited]
File system	Linux file system	distributed file system
Maximum size of individual file	2 G.B.	Unlimited (Maximum file size 2 G.B.)
Main storage type	Centralized (Only Storage, cloud	Decentralized

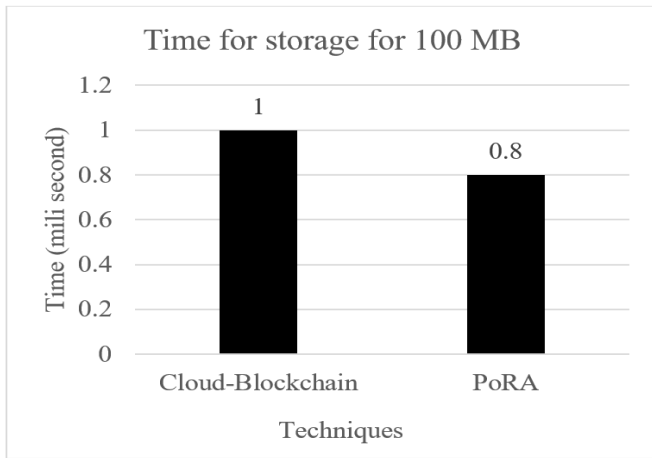


Fig. 6. Analysis of Storage Time.

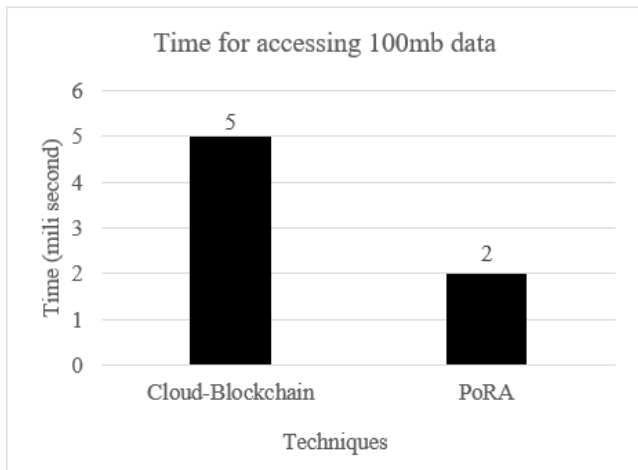


Fig. 7. Analysis of Access Time.

In Fig. 7, the performance analysis is shown for the time required for accessing the storage and recovering the file. The graph trend exhibits that the overall time is less for accessing the 100 MB of the file compared to the cloud-based system. The reason behind this is that, in the proposed system, the IPFS network is used as data storage nodes. The file is not stored in a central server but in a decentralized system where the system recognizes the nearest unit for the storage. As a result, this also reduces latency and the storage and recovery times of the data file. Apart from this, since more than one cloud is involved here, the storage space is virtually unlimited. The file size is limited by the md5 hash algorithm in the existing system since it is stored as a whole. However, in the proposed system, it is split into shards. Hence the file size is unlimited.

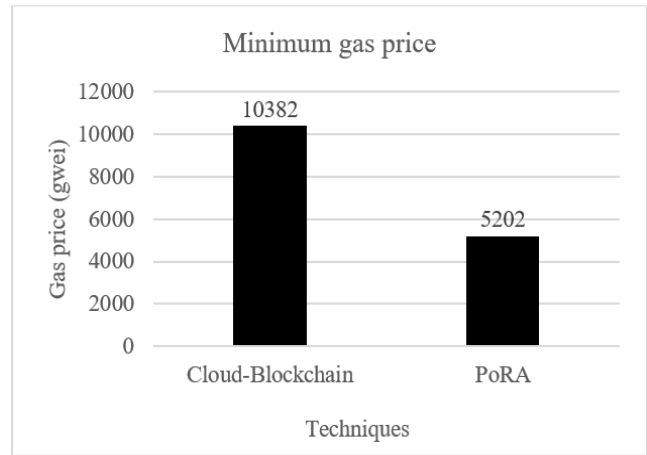


Fig. 8. Analysis of Minimum Gas Price.

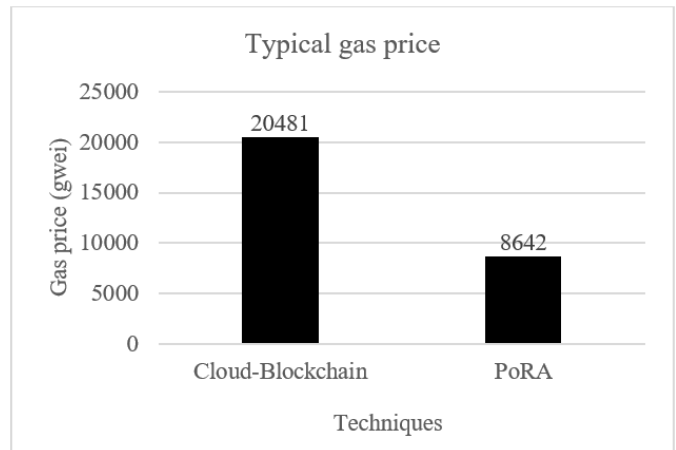


Fig. 9. Analysis of Typical Gas Price.

The blockchain client or any user pays the gas price in order to get his request accepted quickly by the blockchain. The gas price is decided by the number of times the smart contract updates a value in the blockchain. Fig. 8 and 9 present the performance analysis regarding the minimum gas price. The graph trend of both Fig. 8 and 9 exhibits that the proposed system has almost half of the gas price compared to the existing system. This means that using the proposed system is subjected to cost efficiency. In addition, the study has also carried out performance analysis regarding uptime and

downtime analysis. The analysis shows that the uptime is 100% in the proposed system, with a running time of 48 hours. The uptime might be lesser if the software runs for more hours. Also, data integrity is higher in the proposed system since the proposed design ensures the integrity of every shard of data rather than the entire file at once.

C. Discussion

The proposed system offers better flexibility compared to the existing approaches. The introduction of smart contract in the system design eliminates the trusted third entity's involvement in carrying out actions related to data processing. Therefore, cost-efficiency is introduced in the data-sharing process between organizations. The data scalability issue is narrowed down to a significant extent by introducing a mechanism of shards, which also leads to quick execution and fast processing with less delay. However, it may happen that when the user increases, the model faces some scalability issue over time. Future work will explore the scalability problem with the dynamic environment like IoT, and more optimization will be introduced to the model.

In the proposed system, the data owners, especially patients, are allowed to see their data being shared. They can change or customize the access policy for their data. They can also make a request regarding deleting and removing medical records if they want. In this way, the model ensures the agreement with privacy protection laws. The security of data is ensured with the encryption mechanism, and during the transaction, it will not reveal the patient information. The security and privacy features are the prime aspects in the proposed system modeling. Also, in future work, the study further explores the effectiveness of other variants of cryptographic approaches for securing the data-sharing platform.

VI. CONCLUSION

The core aim of the proposed work is to facilitate an efficient authorization framework based on blockchain technology for secure access of the patient medical data stored on the on-cloud server. Initially, the study has conducted a critical analysis of the existing literature and identified significant challenges associated with the previous works. To address the existing challenges, this work has suggested a novel approach of proof of replication algorithm to ensure the validation of each transaction on the blockchain and the key revocation mechanism. The study has established a reliable system using smart contracts to achieve an efficient access control and privacy-aware data sharing mechanism. The implementation of the proposed authorization framework study employed the Ethereum blockchain platform and IPFS network for the data storage on the AWS nano. Employing IPFS storage nodes in a cloud server eliminates the issues associated with a centralized system; the data is split into shards and stored in encrypted form, which leads to compensating the issue of scalability and data security. The outcome analysis shows the effectiveness of the proposed system regarding storage and access time, gas price, data integrity, and security compared to the typical cloud-blockchain-based systems. The proposed system can be applied in real-time scenarios to provide data security, privacy, and better medical data sharing process

management. In the future, the proposed work can be extended with more optimization approaches in system computational requirements, customized smart contracts and scalability enhancement for the IoT-assisted big data applications.

REFERENCES

- [1] Hassanalieragh, M., Page, A., Soyata, T., Sharma, G., Aktas, M., Mateos, G., Kantarci, B. and Andreescu, S., 2015, June. Health monitoring and management using Internet-of-Things (IoT) sensing with cloud-based processing: Opportunities and challenges. In 2015 IEEE international conference on services computing (pp. 285-292). IEEE.
- [2] Raghupathi, W. and Raghupathi, V., 2014. Big data analytics in healthcare: promise and potential. *Health information science and systems*, 2(1), pp.1-10.
- [3] Sood, S.P., Nwabueze, S.N., Mbarika, V.W., Prakash, N., Chatterjee, S., Ray, P. and Mishra, S., 2008, January. Electronic medical records: A review comparing the challenges in developed and developing countries. In Proceedings of the 41st Annual Hawaii International Conference on System Sciences (HICSS 2008) (pp. 248-248). IEEE.
- [4] Topol, E.J., 2015. The big medical data miss: challenges in establishing an open medical resource. *Nature Reviews Genetics*, 16(5), pp.253-254.
- [5] Report Linker "Deep Learning Market: Focus on Medical Image Processing", 2020-2030. Available online: <https://www.reportlinker.com/p05987918/Deep-Learning-Market-Focus-on-Medical-Image-Processing> (accessed on 16 December 2020).
- [6] Bhartiya, S., Mehrotra, D. and Girdhar, A., 2016. Issues in achieving complete interoperability while sharing electronic health records. *Procedia Computer Science*, 78, pp.192-198.
- [7] Zhang, R. and Liu, L., 2010, July. Security models and requirements for healthcare application clouds. In 2010 IEEE 3rd International Conference on cloud Computing (pp. 268-275). IEEE.
- [8] Chinnasamy, P. and Deepalakshmi, P., 2022. HCAC-EHR: hybrid cryptographic access control for secure EHR retrieval in healthcare cloud. *Journal of Ambient Intelligence and Humanized Computing*, 13(2), pp.1001-1019.
- [9] Shi, S., He, D., Li, L., Kumar, N., Khan, M.K. and Choo, K.K.R., 2020. Applications of blockchain in ensuring the security and privacy of electronic health record systems: A survey. *Computers & security*, 97, p.101966.
- [10] Sookhak, M., Jabbarpour, M.R., Safa, N.S. and Yu, F.R., 2021. Blockchain and smart contract for access control in healthcare: a survey, issues and challenges, and open issues. *Journal of Network and Computer Applications*, 178, p.102950.
- [11] Yue X, Wang H, Jin D, Li M, Jiang W. Healthcare data gateways: found healthcare intelligence on blockchain with novel privacy risk control. *Journal of medical systems*. 2016; 40(10):218.
- [12] V. Jaiman and V. Urovi, "A consent model for blockchain-based health data sharing platforms," *IEEE Access*, vol. 8, pp. 143734-143745, 2020.
- [13] B. Shen, J. Guo, and Y. Yang, "MedChain: Efficient healthcare data sharing via blockchain," *Appl. Sci.*, vol. 9, no. 6, p. 1207, Dec. 2018.
- [14] G. G. Dagher, J. Mohler, M. Milojkovic, and P. B. Marella, "Ancile: Privacy-preserving framework for access control and interoperability of electronic health records using blockchain technology," *Sustain. Cities Soc.*, vol. 39, pp. 283-297, May 2018.
- [15] Zhang P, White J, Schmidt DC, Lenz G, Rosenbloom ST. Fhirchain: applying blockchain to securely and scalably share clinical data. *Computational and structural biotechnology journal*. 2018; 16:267- 278.
- [16] M. M. Madine, A. A. Battah, I. Yaqoob, K. Salah, R. Jayaraman, Y. Al-Hammadi, S. Pesic, and S. Ellahham, "Blockchain for giving patients control over their medical records," *IEEE Access*, vol. 8, pp. 193102-193115, 2020.
- [17] H. Huang, X. Sun, F. Xiao, P. Zhu, and W. Wang, "Blockchain-based eHealth system for auditable EHRs manipulation in cloud environments," *J. Parallel Distrib. Comput.*, vol. 148, pp. 46-57, Feb. 2021.
- [18] J. Fu, N. Wang, and Y. Cai, "Privacy-preserving in healthcare blockchain systems based on lightweight message sharing," *Sensors*, vol. 20, no. 7, p. 1898, Mar. 2020.

- [19] J. Xu, K. Xue, S. Li, H. Tian, J. Hong, P. Hong, and N. Yu, "Healthchain: A blockchain-based privacy preserving scheme for large-scale health data," *IEEE Internet Things J.*, vol. 6, no. 5, pp. 8770–8781, Oct. 2019.
- [20] H. Wang and Y. Song, "Secure cloud-based EHR system using attributebased cryptosystem and blockchain," *J. Med. Syst.*, vol. 42, no. 8, p. 152, 2018.
- [21] Margheri A, Masi M, Miladi A, Sassone V, Rosenzweig J. Decentralised Provenance for Healthcare Data. *International Journal of Medical Informatics*. 2020; p. 104197.
- [22] H. Guo, W. Li, M. Nejad, and C.-C. Shen, "Access control for electronic health records with hybrid blockchain-edge architecture," in *Proc. IEEE Int. Conf. Blockchain (Blockchain)*, Jul. 2019, pp. 44–51.
- [23] A. R. Rajput, Q. Li, M. T. Ahvanooey, and I. Masood, "EACMS: Emergency access control management system for personal health record based on blockchain," *IEEE Access*, vol. 7, pp. 84304–84317, 2019.
- [24] Roehrs A, da Costa CA, da Rosa Righi R, da Silva VF, Goldim JR, Schmidt DC. Analyzing the performance of a blockchain-based personal health record implementation. *Journal of biomedical informatics*. 2019; 92:103140.
- [25] R. Guo, H. Shi, Q. Zhao, and D. Zheng, "Secure attribute-based signature scheme with multiple authorities for blockchain in electronic health records systems," *IEEE Access*, vol. 6, pp. 11676–11686, 2018.
- [26] Y. Chen, S. Ding, Z. Xu, H. Zheng, and S. Yang, "Blockchain-based medical records secure storage and medical service framework," *J. Med. Syst.*, vol. 43, no. 1, p. 5, Jan. 2019.
- [27] K. Fan, S. Wang, Y. Ren, H. Li, and Y. Yang, "MedBlock: Efficient and secure medical data sharing via blockchain," *J. Med. Syst.*, vol. 42, no. 8, p. 136, Aug. 2018.
- [28] M. R. Bataineh, W. Mardini, Y. M. Khamayseh and M. M. B. Yassein, "Novel and Secure Blockchain Framework for Health Applications in IoT," in *IEEE Access*, vol. 10, pp. 14914-14926, 2022.
- [29] Z. Zulkifl et al., "FBASHI: Fuzzy and Blockchain-Based Adaptive Security for Healthcare IoTs," in *IEEE Access*, vol. 10, pp. 15644-15656, 2022.

Dynamic and Optimized Routing Approach (DORA) in Vehicular Ad hoc Networks (VANETs)

Satyanarayana Raju K, Dr. Selvakumar K

Department of Information Technology
Annamalai University
Chidambaram, India

Abstract—Vehicular Ad hoc Networks (VANETs) are one of the significant areas of research and this is also a subfield in Ad Hoc Networks. This is mainly focused on improving the safety of roads and reducing the total number of accidents. There is no central coordination to this network, nodes are mobile, dynamic topology, the routing process is a big challenge, and this is most responsible for the delivery message to the small overhead and delay. Routing is a tedious task that occurs huge changes in network topology and delivers the data packets in a limited period. In VANETs many existing routing protocols are introduced to overcome various issues but these are not efficient to overcome all the issues in routing. Routing shows a huge impact on other parameters such as data transmission rate (DTR), packet delivery ratio (PDR), Packet Drop Ratio (PDRatio), Average Propagation Delay (APD) and throughput. In this paper, the dynamic and optimized routing approach (DORA) is introduced in VANETs to overcome the various issues and improve the performance of IP by measuring the DTR, PDR and PDRatio. Comparisons among the Ant Colony Optimization (ACO), improved distance-based ant colony optimization routing (IDBACOR), and DORA is shown.

Keywords—Data transmission rate (DTR); packet delivery ratio (PDR); packet drop ratio (PDRatio); throughput

I. INTRODUCTION

A vehicular ad hoc network (VANET) plays a major role in communication between the vehicles become smarter [1]. This network consists of two architectures as Vehicle-to-vehicle communication (V2V) ensures the communication between vehicles and Vehicle-to-infrastructure (V2I) which swaps the data between vehicles. VANET is one of the dynamic topologies that give the regular disconnected network. This contains limitless storage of battery, and the nodes in this network have the limitation of power. The transportation region should be improved with safety, this network ensures the development of many safety applications to prevent accidents, to improve the road capacity the applications are maximized and avoid traffic congestion, and real-time applications are used to access the internet.

From the past many years, huge data is created and transmitted through the network every time, which is called the explosion of data. Several approaches are developed and designed to fulfill the requirements of the users from all over the world. Due to the heavy traffic in the network and its high

usage in wireless networks, all systems are facing technical issues such as delay in the messages, huge packet drop ratio, throughput is very low, and communication cost is very high, and effect of these huge issues gives the overhead in the network.

VANETs are specifically the branch of MANETs. Compared with MANET, VANETS present with fast motion in vehicles which is fastly and dynamically changing the topology is extra advantage to the VANETS.

All these nodes are managed by the default roads layout. In VANETs, several levels control the node velocities such as limited speed, level of congestion, and traffic management systems such as traffic lights and top symbols, etc. In future, these nodes are used for high transmission ranges, storage of data, and all the energy sources are restored. These networks are more powerful to store and process the energy capacities that make workable and more reconcilable by measuring huge tasks [2, 3, 4, 5, 6].

Routing plays a significant role in this network based on the available properties of vehicles. Many existing approaches are incapable of deciding the optimal routes based on the inefficient communications among the VANETs. This will show an impact on packet delivery among the vehicular nodes. At this time, the local optimum situation may occur. The mobility nodes are facing traffic density on the streets and they are unable to find the nearest nodes. In this situation, the packets are kept in buffer by the nodes for long time.

If the data packets are in buffer for more time then the live path is terminated. This may show impact on network and leads to the end-to-end delay and packet delivery ratio (PDR). If the data packets are in buffer for more time then the live path is terminated. This may show impact on network and leads to the end-to-end delay and packet delivery ratio (PDR). Thus the proposed approach dynamic and optimized routing approach (DORA) in this paper is focused on solving these issues more effectively. DORA provides the optimal routing path based on multiple streets, and also proposed the intelligent packet delivery system based on other parameters such as data transmission rate (DTR), packet delivery ratio (PDR), Packet Drop Ratio (PDRatio), Throughput.

Fig. 1 shows the VANET network based on the vehicles movements at the junctions.

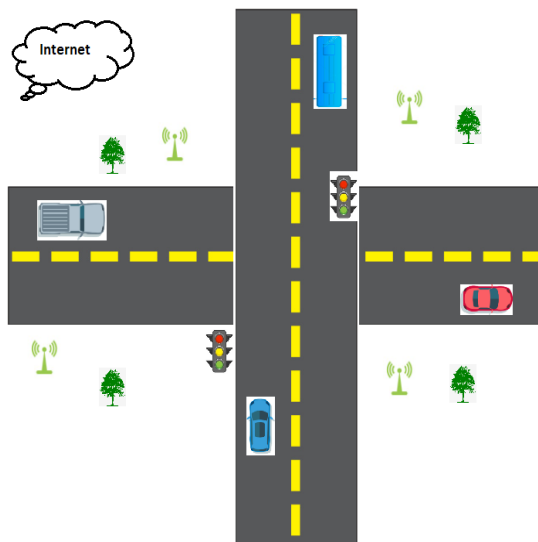


Fig. 1. VANET Networks.

II. LITERATURE SURVEY

Lo et al., [7] introduced a routing protocol called Enhanced Hybrid Traffic-Aware Routing (EHTAR) which is integrated with VANET in the urban platform. In this network, the functional nodes are placed at every junction which is used to observe the real-time vehicular and collect the traffic information for every road segment. This is called a Junction-Tracker. This is used to improve the communication and transmission among the nodes. Gazori et al., [8] proposed a unique model which utilizes the traffic lights as bridges for the help of routing in place of utilizing the mobile vehicles. In the route selection process this will prevent network failures. This protocol is mainly focused on swapping the data packets between bridge nodes. Among these, the path with the smallest hop count and the huge connection is selected. Wang et al., [9] introduced the Named Data Network (NDN) which is a new routing protocol. This is an improved routing protocol which is adopted the distance parameter to prevent defects in hop-count.

Nahar et al., [10] proposed the protocol integrated with cosine similarity-based selective broadcast routing protocol (CSBR). In this protocol, clustering plays a significant role in finding the suitable path to transfer the data to a destination. The proposed approach increases the packet delivery fraction (PDF) 5-10% and minimizes the average delay by 25%.

Brendha et al., [11] proposed the advanced VANET to improve road safety and minimize overall accidents. Because of the high mobility nodes, the routing is a difficult task, which causes a high impact on the topology to transfer the packets in very little time. Several existing approaches are discussed in this paper which is not reliable to solve the issues in routing.

Nazib et al., [12] study about various routing protocols in VANETs. These are divided into seven groups based on the implementation and developed concepts. Several advantages and disadvantages are also discussed by the author.

Qin et al., [13] study several VANETs routing protocols and introduced the new routing protocol is introduced to influence both densities of the vehicles and traffic lights based on network connectivity. The proposed approach follows the unicast packets to improve the traffic flow. Cardenas et al., [14] introduced the new protocol called probabilistic multimetric routing protocol (ProMRP) which is more suitable in VANETs. ProMRP is mainly focused on estimating the probability of every neighbor carrying the packet and successfully sending the packets to the destination. This is mainly calculating the four metrics such as distance to destination, the position of the nodes, node bandwidth and density, etc. Thus the author proposed the improved system called EProMRP. This shows the improved results based on the packet delivery.

Nazib et al., [15] introduced the reinforcement learning (RL)-based routing approaches that improve the quality-of-service (QoS) parameters in the VANETs routing. QoS parameters such as bandwidth, end-to-end delay, throughput, control overhead, and PDR. The proposed approach performed better compared with the existing approaches. Khan [16] proposed the new WSN which integrates the MANETS, VANETS, and other wireless networks that develop the intelligent transportation system which is focused on road safety and accurate vehicle movements according to the route change. Thus the performance improved. Zhenchang Xia et al., [17] discussed about various VANET approaches that are performed better. Several challenges such as low security, less reliability are to be overcome. R. Hussain et al., [18] discussed about the trust implementation in the VANET platform. The author mainly focused on providing the privacy and security for the data that is transmitted among the source and destination. H. Fatemidokht et al., [19] discussed about issues and overcome the issues by using Unmanned Aerial Vehicles (UAVs). This approach mainly worked on multiple tasks to increase the performance of proposed approach. N. B. Gayathri et al., [20] introduced the efficient scheme in the VANETS. This scheme mainly focused on implementing the pair-free platform that improves the transmission and computational efficiency. This approach also supports the batch checking that reduces the calculation overhead in VANETS.

III. DYNAMIC AND OPTIMIZED ROUTING APPROACH (DORA)

DORA is the dynamic and geographic routing approach that selects the nodes dynamically. The selection of paths can be done by analyzing the traffic and density of the vehicles in the junctions to select reliable routes in the network. The maps are used to find the actual positions of the nearest junctions. Based on the score given by the density of vehicles in traffic and distance among the metric curves are used to select the next destination, then the junction is selected. This works better on dense traffic platforms. The efficient selection of path is selected based on the packet travels. Every node in the network gives the information to the server (gateway) if it goes to its communication range. The gateway develops a various set of paths among itself and each node.

The algorithm is focused on various factors such as route discovery, route recovery, dynamic routing and maintaining the constant power at all the vehicles. The DORA develops the route by using the request of the route from the base stations (BS). The BS gives the route reply by using the messages. To find the efficient route, the distances between two vehicles are to be calculated. Distance factor plays the main role to measure the distance among the nearest vehicles are measure by using Euclidean distance is represented in (1).

$$\text{Dist} = \sqrt{(a_1 - a_2)^2 + (b_1 - b_2)^2} \quad (1)$$

Equation-1 (a1, b1) represents the neighbor nodes, and (a2, b2) represents the spatial region of the destination node. The data is sent to the destination node from source to find the accurate route. Various factors shows the huge impact on finding the route such as constant, lifespan and availability of buffer are measured. These factors are merged with reply packets to other general information. DORA is adopted with fitness function improves the more constant route, this results in increasing data PDR. This will also reduce the packet loss and more routes are added.

$$\text{route}(l) = \text{packets}(\text{transfer until the availability } t + \text{Predict } (P)_t | \text{available } t) \quad (2)$$

Predict (P)_t predicted time for the

link availability among two vehicles Va, Vb.

The reliability (R) is expressed as:

The link is available at the time. Hence L_{ab} the distance between two vehicles are represented in

$$L_{ab} = \sqrt{(a_1 - a_2)^2 + (b_1 - b_2)^2} \quad (3)$$

Hence, this will maintain the constant link among the vehicles and discover the accurate route and improves the performance of communication.

Algorithm Steps:

Input: Nodes (Vehicles) 95 with the initialize values at Nodes (N): 5 Joules

Functions (Route_Creation R_c, Route_Recovery R_{recovery}, Route_Diversion R_{diversion}, Mobility, Speed of Vehicles, vehicles position change)

N = {N₁, N₂, N₃ N_n}

Step 1: Select Source Node N_s and Destination Node N_d.

Step 2: Calculate the distance between two nodes using equation-1.

Step 3: If the N>1 //total nodes

Message ("Node Mobility and Communication started")

Else

Message ("Node Mobility and Communication not started")

Step 4: If N_s >1

Message ("Source Node transmits the data to destination node N_d)

Else

Message ("No transmission from source to destination node N_d and data loss occur")

Step 5: Now calculate the routing path duration from N_s to N_d

➤ Path duration is based on probability density function (pdf)

Step 6:

L₁, L₂, L₃, ... L_{E_H} defines the duration of links of 1,2,3, ... E_H nodes

E_H – Represents the average number of nodes required to reach the N_d.

Step 7: Path is expressed as:
 $T_{path} = \text{Min}(L_1, L_2, L_3, \dots L_{E_H})$

Step 8: Apply Bayes' theorem for pdf of T_{path} is $f(T_{path}) = E_H * E_Z * C_T^{E_H-1}$

Step 9: Based on the average duration the path is changed.

Step 10: Now data reached.

IV. SIMULATION

The following simulation parameters (Table I) are given below:

TABLE I. SIMULATION PARAMETERS

Simulation/Scenario	
Simulation Time (Sec)	120-140
MAC protocol	IEEE 802.11p
Range of Transmission	260 m
Total vehicles	95
Date packet sending rate PDR	4.5-14.5 packets/s
Data packet size	512 Bytes

V. EVALUATION RESULTS

To implement this protocol, the NS3 simulator is used to show better simulation and comparative results are shown by using ACO and IDBACOR routing protocol. The proposed approach DORA shows the high performance than other VANET protocols. This simulation consists of 95 vehicles. In general, the VANETS have a dynamic nature, with several fluctuations obtain in terms of data rates, speed of vehicles, etc. The initial value of each vehicle is 'Zero' and the mobility of the network is 120 km/h. Due to the boundless size of the network, huge mobility, and active topology. The proposed approach is more flexible to accept the variations in the vehicles. The experiments are conducted by using 95 vehicles and algorithms such as ACO, IDBACOR, and DORA. The simulation NS3 proves that the proposed model improves the performance in terms of DTR, PDR, PDRatio, APD, and throughput. Fig. 2 shows the vehicular network created by the NS3 simulator. Fig. 3 shows the communication among the nodes by sending request messages.



Fig. 2. Network with 95 Nodes. The Red Color nodes are considered as Vehicles.

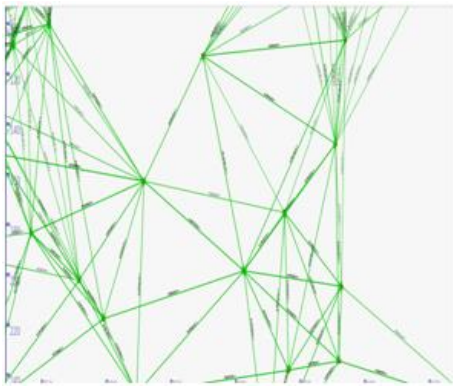


Fig. 3. Communication between 95 Nodes (Vehicles).

VI. PERFORMANCE METRICS

The efficiency and performance of DORA is shown with the comparison among the ACO and IDBACOR. The evaluation is calculated by using data transmission rate (DTR), packet delivery ratio (PDR), Packet Drop Ratio (PDRatio). Table II shows the performance of proposed approaches and existing approaches by showing the parameters:

A. Data Transmission Rate (DTR)

This parameter plays the major role in routing in VANETs. This defines the transmission time of the message to forward the vehicle to destination. This parameter shows the impact on various metrics such as traffic, collisions and mobility.

B. Packet Delivery Ratio (PDR)

PDR mainly focused on delivering the packets successfully to the destination. The PDR is calculated by using Eq. (4).

$$PDR = \frac{\sum_{a=1}^k \text{Packets Received}}{\sum_{a=1}^k \text{Packets originated}} \quad (4)$$

C. Packet Drop Ratio (PDRatio)

Packet Drop Ratio (PDRatio) is the fraction of the total transmitted packets that were not received at the destination. The PDRatio is calculated in Eq. (5) as follows:

$$PDRatio = \frac{(\sum_{a=1}^k \text{No of packets Sent} - \sum_{a=1}^k \text{No of packets received}) * 100}{\sum_{a=1}^k \text{No of packets Sent}} \quad (5)$$

TABLE II. PERFORMANCE OF ALGORITHMS BASED ON PARAMETERS

Algorithm	PDR (Bytes)	DTR (Bytes)	Packet Drop Ratio (Bytes)	Average Propagation Delay (APD) (Sec)	Throughput (Packet/Sec)
ACO	87.59	425.79	12.41	5.92	83.08
IDBACOR	90.25	455.25	9.75	5.43	87.14
DORA	91.96	493.19	8.04	5.02	88.47

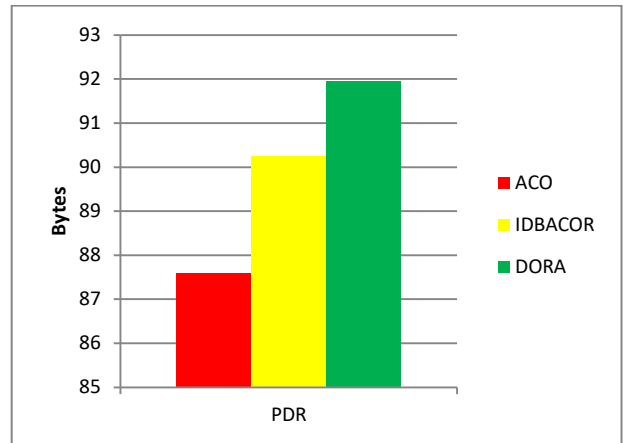


Fig. 4. Performance of Algorithms ACO, IDBACOR and DORA by showing PDR.

In Fig. 4 and Fig. 5 shows the performance of PDR by showing bar and line graphs. Compare with the existing approaches DORA performed better by transmitting data between nodes. DORA improves the CTP also for maintain the cumulative power according to the requirement at the nodes.

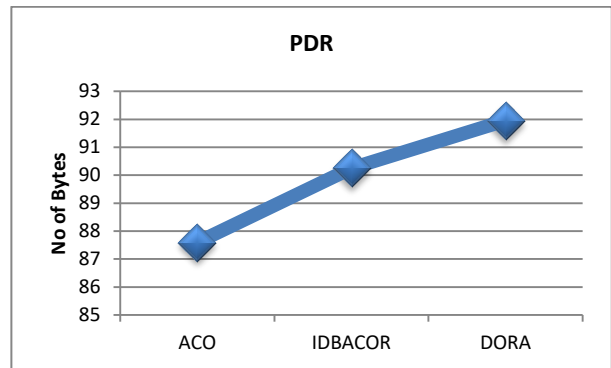


Fig. 5. Performance of Algorithms based on ACO, IDBACOR, and DORA by showing PDR.

In Fig. 6 and Fig. 7 shows DTR performance by calculating the transmission time for every message. This measures the transmitting time from source to destination.

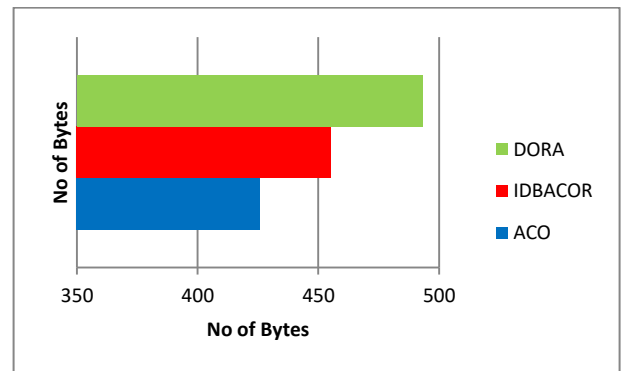


Fig. 6. Performance of Algorithms ACO, IDBACOR and DORA by showing DTR (Bytes).

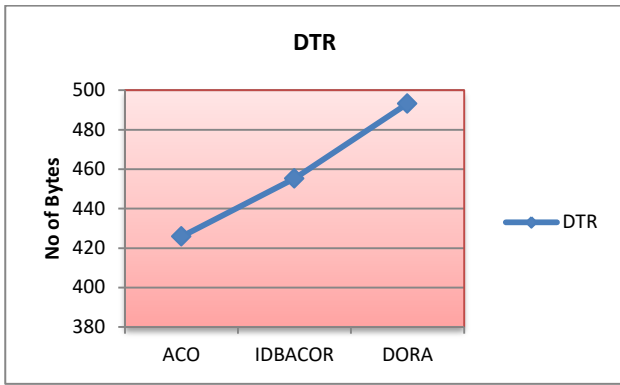


Fig. 7. Performance of Algorithms ACO, IDBACOR and DORA by showing DTR.

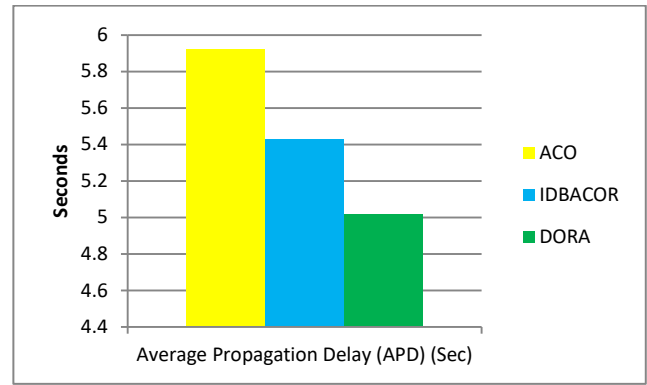


Fig. 10. Performance Representation of APD by using Bar Graphs.

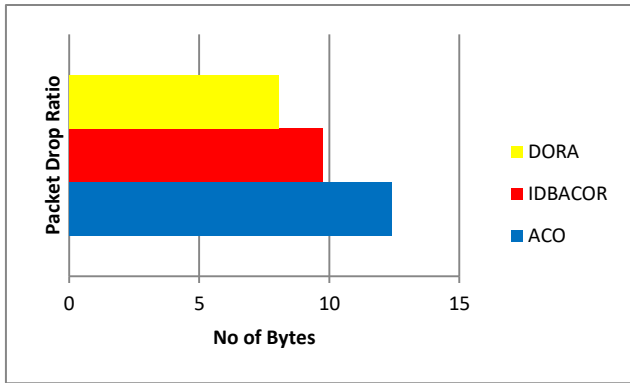


Fig. 8. Performance of Algorithms ACO, IDBACOR and DORA by showing Packet Drop Ratio represented by Line Graphs.

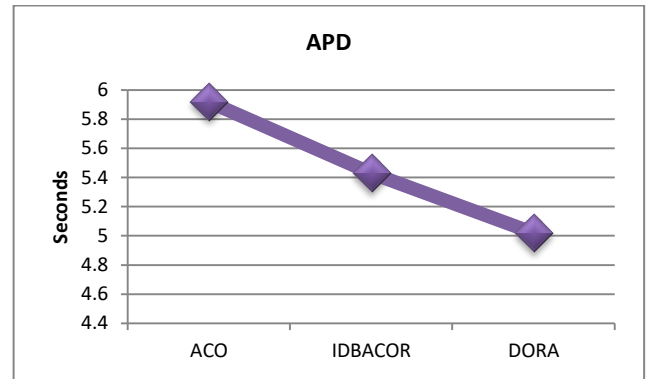


Fig. 11. Performance Representation of APD by using Line Graphs.

In Fig. 8, 9 show the packet drop ratio is measured. Compare with existing approaches DORA shows the very less drop rate. This is also based on the PDR.

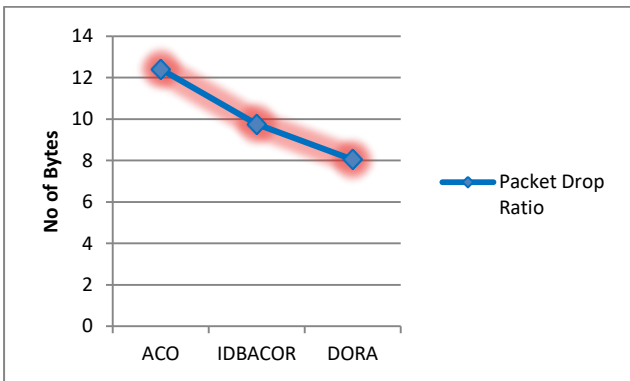


Fig. 9. Performance of Algorithms ACO, IDBACOR and DORA by showing Packet Drop Ratio.

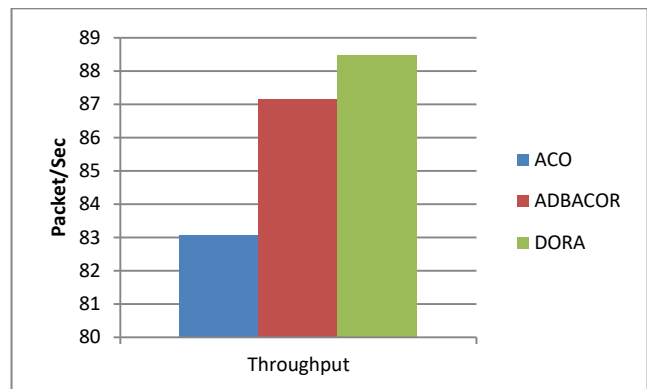


Fig. 12. Performance Representation of throughput by using Bar Graphs.

In Fig. 10, Fig. 11, Fig. 12 and Fig. 13 shows the performance of APD and throughput represented in the form of bar graphs and line graphs. The APD is reduced in DORA compare with existing approaches. The throughput is increased compare with ACO and IDBACOR.

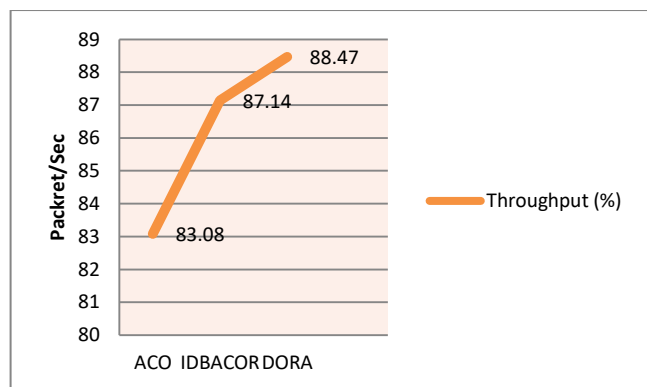


Fig. 13. Performance of Throughput.

The APD is used to measure the delay for the data transmission from source to destination. Compare with other approaches DORA shows the low APD.

VII. CONCLUSION

In this paper, dynamic and optimized routing approach (DORA) is developed to overcome the several issues such as dynamic routing in VANET's network. The proposed approach shows the optimal path from source to destination. This approach also overcomes very less packet loss which didn't show any impact on output. The DORA focused on data transmission and communication between the nodes (vehicles) in VANETs. DORA improves the performance by measuring the parameters such as DTR, PDR, PDRatio, APD and throughput. The experiments are conducted on 95 nodes (vehicles). The performance of the proposed approach achieved the better results compare with existing approaches such as ACO, IDBACOR. The performance of DORA is achieved the results such as PDR-91.96, DTR-493.19, PDRation-8.04, APD-5.02, throughput-88.47. In future, an improved simulation approach is to be developed to overcome the several obstacles present in dynamic routing.

REFERENCES

- [1] Melaouene, N., and Romadi, R. 2017. VANET's Applications and its systems based on RFID: state of the art. In proceeding of CoDIT 4th Interational conference on control, decision and information technologies (Barcelona, Spain, April 5-7, 2017).
- [2] I.A. Abbasi, B. Nazir, A. Abbasi, S.M. Bilal, S.A. Madani, A traffic flow oriented routing protocol for VANET. Springer EURASIP J Wireless Commun Netw 2014(121), 1–14 (2014).
- [3] B.T. Sharef, R.A. Alsaqour, M. Ismail, Review: vehicular communication ad hoc routing protocols: a survey. J. Netw. Comput. Appl. 5(4), 363–396 (2014).
- [4] A. Dahiya, R.K. Chauhan, A comparative study of MANET and VANET environment. J. Comput. Secur. 2(7), 87–91 (2010).
- [5] M. Jerbi, S.M. Senouci, R. Meraihi, Y.G. Doudane, in Communications, 2007. ICC '07. IEEE International Conference. An improved vehicular ad hoc routing protocol for city environments (2007), pp. 3972–3979.
- [6] J. Kumar, V. Mutneja, I.S. Gill, Behavior of position based routing in VANET. Int. J. Comput. Appl. 145(1), 49–52 (2016).
- [7] C. Lo and Y. Kuo, "Enhanced Hybrid Traffic-Aware Routing Protocol for Vehicular Ad hoc Networks," 2015 IEEE 82nd Vehicular Technology Conference (VTC2015-Fall), 2015, pp. 1-6, doi: 10.1109/VTCFall.2015.7390924.
- [8] R. Gazori and G. Mirjalily, "SBGRP as an Improved Stable CDS-Based Routing Protocol in Vehicular Ad Hoc Networks," 2019 27th Iranian Conference on Electrical Engineering (ICEE), 2019, pp. 1979-1983, doi: 10.1109/IranianCEE.2019.8786705.
- [9] X. Wang, W. Liu, L. Yang, W. Zhang and C. Peng, "A new content-centric routing protocol for Vehicular Ad Hoc Networks," 2016 22nd Asia-Pacific Conference on Communications (APCC), 2016, pp. 552-558, doi: 10.1109/APCC.2016.7581473.
- [10] A. Nahar, H. Sikarwar and D. Das, "CSBR: A Cosine Similarity Based Selective Broadcast Routing Protocol for Vehicular Ad-Hoc Networks," 2020 IFIP Networking Conference (Networking), 2020, pp. 404-412.
- [11] R. Brendha and V. S. J. Prakash, "A survey on routing protocols for vehicular Ad Hoc networks," 2017 4th International Conference on Advanced Computing and Communication Systems (ICACCS), 2017, pp. 1-7, doi: 10.1109/ICACCS.2017.8014615.
- [12] R. A. Nazib and S. Moh, "Routing Protocols for Unmanned Aerial Vehicle-Aided Vehicular Ad Hoc Networks: A Survey," in IEEE Access, vol. 8, pp. 77535-77560, 2020, doi: 10.1109/ACCESS.2020.2989790.
- [13] H. Qin and C. Yu, "A road network connectivity aware routing protocol for Vehicular Ad Hoc Networks," 2017 IEEE International Conference on Vehicular Electronics and Safety (ICVES), 2017, pp. 57-62, doi: 10.1109/ICVES.2017.7991901.
- [14] L. L. Cardenas, A. M. Mezher, P. A. B. Bautista and M. A. Igartua, "A Probability-Based Multimetric Routing Protocol for Vehicular Ad Hoc Networks in Urban Scenarios," in IEEE Access, vol. 7, pp. 178020-178032, 2019, doi: 10.1109/ACCESS.2019.2958743.
- [15] R. A. Nazib and S. Moh, "Reinforcement Learning-Based Routing Protocols for Vehicular Ad Hoc Networks: A Comparative Survey," in IEEE Access, vol. 9, pp. 27552-27587, 2021, doi: 10.1109/ACCESS.2021.3058388.
- [16] A. U. Khan, "Real time and Efficient Unicast Routing Protocols for Vehicular Ad Hoc Network: A Survey and Recommendations for efficiency enhancement," 2018 15th International Conference on Smart Cities: Improving Quality of Life Using ICT & IoT (HONET-ICT), 2018, pp. 117-121, doi: 10.1109/HONET.2018.8551330.
- [17] Zhenchang Xia, Jia Wu, Libing Wu, Yanjiao Chen, Jian Yang, and Philip S. Yu. 2021. A Comprehensive Survey of the Key Technologies and Challenges Surrounding Vehicular Ad Hoc Networks. ACM Trans. Intell. Syst. Technol. 12, 4, Article 37 (August 2021), 30 pages.
- [18] R. Hussain, J. Lee and S. Zeadally, "Trust in VANET: A Survey of Current Solutions and Future Research Opportunities," in IEEE Transactions on Intelligent Transportation Systems, vol. 22, no. 5, pp. 2553-2571, May 2021, doi: 10.1109/TITS.2020.2973715.
- [19] H. Fatemidokht, M. K. Rafsanjani, B. B. Gupta and C. -H. Hsu, "Efficient and Secure Routing Protocol Based on Artificial Intelligence Algorithms With UAV-Assisted for Vehicular Ad Hoc Networks in Intelligent Transportation Systems," in IEEE Transactions on Intelligent Transportation Systems, vol. 22, no. 7, pp. 4757-4769, July 2021, doi: 10.1109/TITS.2020.3041746.
- [20] N. B. Gayathri, G. Thumbur, P. V. Reddy and M. Z. Ur Rahman, "Efficient Pairing-Free Certificateless Authentication Scheme With Batch Verification for Vehicular Ad-Hoc Networks," in IEEE Access, vol. 6, pp. 31808-31819, 2018, doi: 10.1109/ACCESS.2018.2845464.

AUTHORS' PROFILE



K. Satyanarayana Raju, completed his graduation in Computer Science and Engineering in Swarnandhra college of Engineering and Technology affiliated to JNTU Hyderabad, and the Master's Degree in Information Technology SRKREC affiliated to Andhra University. He has 11 years of experience in teaching. His area of interest includes vehicular Ad-Hoc Networks, Machine Learning and Network Security.



Dr. K. Selvakumar, completed his graduation from Kongu Engineering College and Master's from NIT, Trichy and Ph.D in CSE from Annamalai University. Presently working as Professor in Annamalai University. His interested research area is WSN, NS and MC.

Comparative Analysis of RSA and NTRU Algorithms and Implementation in the Cloud

Bambang Harjito, Henny Nurcahyaning Tyas, Esti Suryani, Dewi Wisnu Wardani

Department of Informatics, Universitas Sebelas Maret
Jl. Ir. Sutami 36A Kentingan, Surakarta, Indonesia

Abstract—The emergence of cloud computing platforms makes it easier to connect and collaborate globally without setting up additional infrastructures such as servers and data centers. This causes the emergence of threats to data security against digital information. This security threat can be overcome by cryptography. Examples of cryptographic algorithms are RSA and NTRU. The main concern that arises in this research is how to perform a comparative analysis between asymmetric cryptographic algorithms, RSA (Rivest-Shamir-Adleman) and NTRU (Nth-Degree Truncated Polynomial Ring) algorithms and their implementation in cloud storage. Comparison of performance between the RSA and NTRU algorithms at security levels 80, 112, 128, 160, 192, and 256 bits by running 5 – 1000 data, the results obtained that the running time of the key generation process and encryption of the NTRU algorithm is more efficient than the RSA algorithm. Wiener's Attack test on the RSA algorithm and LLL Lattice Basis Reduction on the NTRU algorithm. NTRU algorithm has a more secure level of resilience, so that it can be said that the NTRU algorithm is more recommended for cloud storage security.

Keywords—Attacks; privacy; cryptography; RSA; NTRU; cloud storage

I. INTRODUCTION

Analysis of more than 135,000 organizations in 2020 shows that globally, cloud adoption has reached 81% as measured by the use of productivity platforms based on research from an information technology company and US research firm Gartner. Cloud services have become a significant industry. Cloud expects to grow from USD 50.1 billion in 2020 to USD 137.3 billion by 2025, with a Compound Annual Growth Rate (CAGR) of 22.3% research conducted Markets and Markets analysis. The increasing popularity of the cloud is also accompanied by several security problems in the cloud that are vulnerable to the possibility of being exposed to unwanted parties, especially security breaches in cloud storage [1]. Cryptography is one of the most effective and efficient components of network security in securing information. Cryptography ensures that only the party who has exchanged the keys can read the encrypted message (authentic party) [2]. The RSA (Rivest-Shamir-Adleman) and NTRU (Nth-Degree Truncated Polynomial Ring) algorithms are asymmetric cryptographic systems, however the NTRU algorithm is a lattice-based algorithm where the key selection is not only strong but also difficult to solve. Grid-based cryptography in general, is an improvement over classical number theory algorithms such as the RSA algorithm [3], [4]. This system is also known for its high level of security based

on worst-case hardness. Worst-case hardness is based on the complexity of the problem grids and the shortest vector problem (SVP). NTRU cryptosystem is a lattice-based cryptography known to withstand quantum computing attacks, and classical computing attacks [5], [6]. The RSA algorithm is more optimal for the encode process than the DES algorithm [7] besides that the RSA algorithm is superior to the ElGamal algorithm [8].

Each algorithm bases on a different problem, such as the security of the RSA algorithm, which is difficult to factor large numbers into prime factors [9]. The operation of the NTRU algorithm is based on objects in a truncated polynomial ring $R = \mathbb{Z}[X]/(X^N - 1)$ with convolution multiplication [10], [11]. The RSA algorithm, which is based on integer factoring, can be attacked using the Wiener's Attack algorithm, while the NTRU algorithm can be attacked with the well-known algorithm to find short vector, LLL (Lenstra-Lenstra-Lovasz) Lattice Basis Reduction algorithm, which is a lattice-based reduction algorithm [12]. In this research, a comparative analysis will be carried out between the RSA (Rivest-Shamir-Adleman) and NTRU (Nth-Degree Truncated Polynomial Ring) cryptographic algorithms and obtain the running time of key generation, encryption, decryption, and security level and see which algorithm is better and implementation on cloud storage using Flask.

II. RELATED WORK

The RSA algorithm is an algorithm that can be used to maintain the security and confidentiality of fingerprint data. Besides that, the RSA algorithm can be also applied to cloud computing security by using digital signatures combined with the AES algorithm [13], [14]. The NTRU algorithm is a lattice-based algorithm which refers to the lattice-based algorithm that makes the NTRU algorithm more resistant to quantum computing attacks [5], [6], [15], [16]. Cloud refers to a set of services and infrastructure accessed through the internet. Cloud service providers must use encryption algorithms to protect user data, such as the use of Advanced Encryption Standard (AES) algorithms, Rivest-Shamir-Adleman (RSA), Elliptic Curve Cryptography (ECC), and NTRU Encryption [17]–[19], in addition to the cloud, the application of the RSA and NTRU algorithms can implement in the IoT environment, the use of an accelerated IoT environment, the security of data collected and stored by devices becomes important [20]. NTRU's lattice-based cryptosystem has lattice problems in the form of grid problems and Shortest Vector Problem (SVP) and can be attacked using the LLL (Lenstra-Lenstra-Lovasz) algorithm, a well-known lattice-based reduction algorithm for grid-based

cryptographic grid problems [21]–[24]. The RSA cryptosystem is the most used in the SSL/TLS protocol that allows sensitive information to be sent via the internet. Wiener's Attack shows that the RSA algorithm can be attacked when the value of d is relatively small compared to the modulus of N [25].

III. PROPOSED WORK

In this section, we provide an overview of our solution comparative analysis of RSA and NTRU Algorithm and Implementation in the Cloud. The comparative analysis model is depicted in Fig. 1. According to the model, the model consist of five steps : (A) the key generation, encryption decryption process of RSA, (B) the key generation, encryption, decryption process of NTRU (C) Wiener attacks on the RSA (D) LLL attack on and NTRU, (E) Implemented in cloud storage. The process begins with the user who will upload the file to cloud storage, this file can be called plaintext. The encryption process will use the RSA and NTRU algorithm public keys. After the encryption process is finished, an encrypted message or ciphertext will be obtained, which will then be uploaded to cloud storage, then calculated and compared for the running time of the public key generation, the private key, and the running time of the encryption process, and the attack process on the public key. After the ciphertext file is uploaded to cloud

storage, a download process will be carried out, where this process will decrypt the encrypted message using a private key and will obtain a decrypted file or plaintext file, then compare the running time of the decryption process on the RSA and NTRU algorithms.

A. RSA (Rivest-Shamir-Adleman)

In this section, the key generation, encryption decryption process of RSA is the first step. It can be explained as follows:

1) *Key generation*: The key generation process in the RSA algorithm begins with selecting the prime numbers p and q , then looking for the value of $n = p * q$. Then select the e , $e < \phi$, where $\phi(n) = (p - 1) * (q - 1)$, must be a prime number. Select the encryption key ' e ', $1 < e < \phi(n)$,

$$gcd(e, \phi(n)) = 1 \tag{1}$$

e and $\phi(n)$ are coprime. By using the Expanded-Euclidean algorithm to calculate d , then:

$$ed \equiv 1(mod \phi(n)) \tag{2}$$

Or

$$ed \equiv k\phi(n) + 1 \tag{3}$$

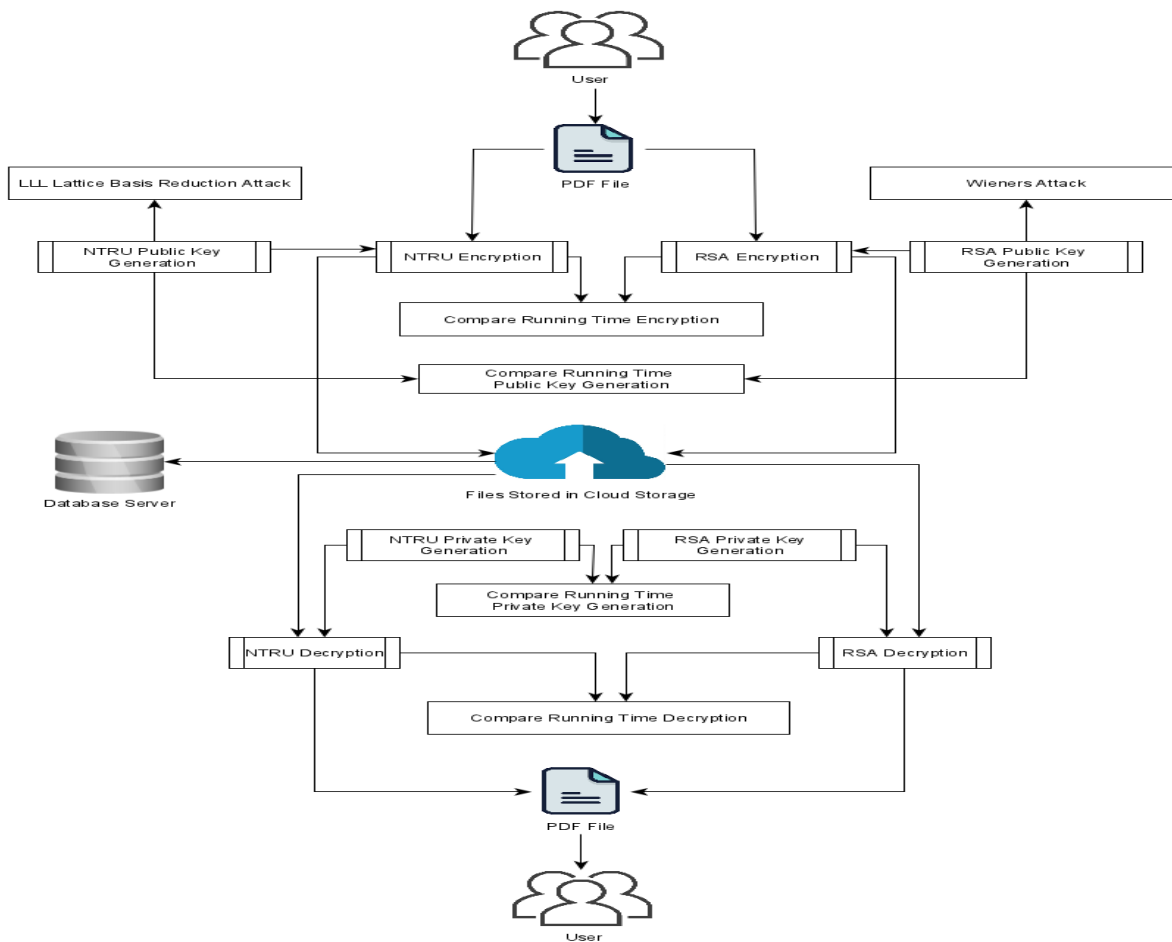


Fig. 1. Comparative Analysis of RSA and NTRU Algorithm and Implementation in the Cloud.

Testing a number with the Rabin-Miller algorithm. If $b_0 = 1$ or $b_0 = n - 1$, then n is a prime number.

$$b_0 = a^m \pmod{n} \quad (4)$$

If $b_0 \neq 1$ or $b_0 \neq n - 1$, do with Equation (9).

$$b_1 = b_0^2 \pmod{n} \quad (5)$$

If $b_1 = n - 1$, then b_1 validated probability as a prime.

2) *RSA encryption*: Plaintext is made into blocks of $m_1, m_2, m_3, \dots, m_n$ so that each block represents a value between $[0, n - 1]$ or $(0 < m_1 < n - 1)$. Where input message $m < n$. Then calculate the c_i ciphertext block for the plaintext block through the Equation (6).

$$c_i = m_i^e \pmod{n} \quad (6)$$

3) *RSA decryption*: Ciphertext c_i is processed using Equation (7) to get the original message, the plaintext message.

$$m_i = c_i^d \pmod{n} \quad (7)$$

B. NTRU (Nth-Degree Truncated Polynomial Ring)

The key generation, encryption decryption process of NTRU is the second steps. Before explaining further from the stage one to the next. We give the principle of NTRU.

The principle of the object used by the NTRU public-key cryptosystem is to use a polynomial of degree $N - 1$. If a and b are two polynomials in the ring R , they can be defined in Equation (8) and (11).

$$a = a_0 + a_1x + a_2x^2 + a_3x^3 + \dots + a_{N-2}x^{N-2} + a_{N-1}x^{N-1} \quad (8)$$

$$= \sum_{i=0}^{N-1} a^i x^i \quad (9)$$

Coefficient vector a will be represented as in the Equation (10).

$$a = (a_0, a_1, a_2, \dots, a_{n-2}, a_{N-1}) \quad (10)$$

$$b = b_0 + b_1x + b_2x^2 + b_3x^3 + \dots + b_{N-2}x^{N-2} + b_{N-1}x^{N-1} \quad (11)$$

$$= \sum_{i=0}^{N-1} b^i x^i \quad (12)$$

Coefficient vector b will be represented as the Equation (13).

$$b = (b_0, b_1, b_2, \dots, b_{n-2}, b_{N-1}) \quad (13)$$

The basic operations used in convoluted ring polynomials are addition, subtraction, and convolution multiplication. The polynomial coefficient $(a_0, a_1, \dots, a_{n-1})$ is an integer. Some coefficient values are 0. This set of polynomials is called R .

1) *Key generation*: NTRU Key Generation begins with selecting two polynomials $f \in \mathcal{L}_f$ and $g \in \mathcal{L}_g$ provided that f has an inverse modulo p and q , so f_p and f_q can writing in Equation (14), (15).

$$f * f_p \equiv 1 \pmod{p} \quad (14)$$

$$f * f_q \equiv 1 \pmod{q} \quad (15)$$

The private key consists of the polynomials f and f_p . After determining the polynomials f and g , the public key can be calculated by the Equation (16).

$$h \equiv pf_q * g \pmod{q} \quad (16)$$

2) *NTRU encryption*: To perform the encryption process, one chooses a polynomial m representing a message so that $m \in Lm$ and a random polynomial $r \in Lr$. The message must be converted to a polynomial m . Then select a small random polynomial, $r \in R$ used to shuffle the messages. Calculating the ciphertext e , with the Equation (17).

$$e \equiv r * h + m \pmod{q} \quad (17)$$

3) *NTRU decryption*: The decryption process begins by calculating the polynomial $a = f * e \pmod{q}$, then define the coefficient a between $-q/2$ and $q/2$, then calculating the polynomial $b = a \pmod{p}$ so that the private key f_p is obtained to calculate the value of d .

$$d = f_p * b \pmod{p} \quad (18)$$

Or

$$d \equiv f_p * [f * e]_q \pmod{p} \quad (19)$$

C. Wiener's Attack

In this section, Wiener's attack is a type of cryptographic attack against the RSA algorithm. This attack is the third steps. The attack uses an advanced fraction method (continued fraction). Continued Fraction of rational number $\frac{u}{v}$ is an expression of the form $x = a_0$, and we get Equation (20).

$$x = a_0 + \frac{1}{a_1 + \frac{1}{a_2 + \frac{1}{a_3 + \dots}}} \quad (20)$$

Where the coefficient a_0 is an integer and all other coefficients for a_i for $i \geq 1$ are positive integers. The coefficient a_i is called the partial quotients of the continued fraction. Generate unique continued fraction, with Euclidean algorithm, can efficiently determine all coefficients a_0, a_1, \dots, a_N .

D. LLL Lattice basis Reduction

LLL attack on and NTRU is the four steps. It can be depicted in Fig. 2.

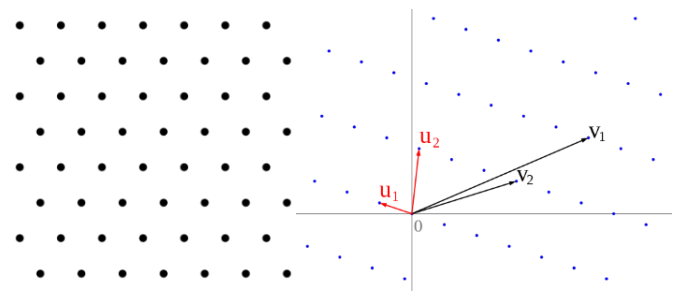


Fig. 2. Basis Lattice.

Fig. 2 shows an image of the vector lattice and lattice, which is the basis of the LLL algorithm. The LLL algorithm is a lattice basis reduction algorithm. The basis of a lattice $B = \{b_1, b_2, \dots, b_n\}$ will be defined as Gram-Schmidt basis $B = \{b_1^*, b_2^*, \dots, b_n^*\}$ by fulfilling the two conditions below:

(Size reduction) :

$$|\mu_{ij}| = \frac{|b_i \cdot b_j^*|}{\|b_j^*\|^2} \leq \frac{1}{2}, \text{ where } 1 \leq j < i \leq n. \quad (21)$$

(Lovasz Condition) :

$$\|b_i^*\|^2 \geq (c - \mu_{i,i-1}^2) \|b_{i-1}^*\|^2, \text{ for } \frac{1}{4} < c < 1 \text{ dan } 1 < i < n. \quad (22)$$

E. Cloud Storage

In this section, implemented in cloud storage is the five steps. Cloud storage is a cloud computing model that stores data on the internet through a cloud computing provider. *Cloud storage* is a cloud computing system that allows users to store and share data on the internet [26]. Cloud storage operates online, making it easier to retrieve and manage data. A cloud storage architecture, where a web browser will connect to a server that automatically accesses the database server. It can be depicted in Fig. 3.

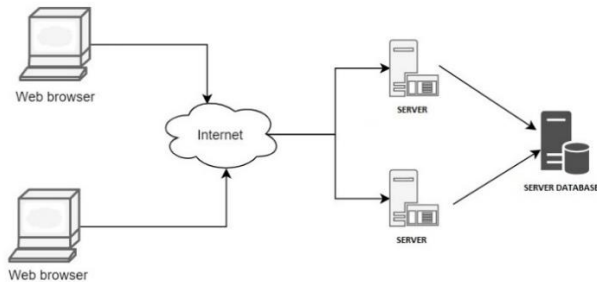


Fig. 3. Cloud Storage Architecture.

IV. PERFORMANCE ANALYSIS

In this section, we perform a comparative analysis of RSA and NTRU Algorithm and an Implementation in the Cloud.

A. Parameter

Security level algorithms RSA and NTRU are used in the Key Generation process. Table I shows the corresponding NTRU and RSA key sizes with equivalent security levels. Security level (k) 80, 112, 128, 160, 192, and 256 bits [27], [28].

The parameter used in the RSA algorithm is to take advantage of the number of bits selected, where the value of these bits will affect the length of the key. The parameter selection of the NTRU algorithm used in this study is the value of N, p, and q. This value will be used as a determinant of the length of the public key and private key which will later be used for the encryption and decryption process. The magnitude of this parameter is obtained from research [27], [28]. The

explanation of the parameter values for each security level is presented in Table II. As well as the results of the running time obtained based on the parameters used. It can be shown in Table III.

Table I and Fig. 4 show that NTRU's bandwidth usage is more efficient than RSA's when the level of security increases, from the same standard used in both RSA and NTRU algorithms, this security level will be used to compare the two algorithms so that we get a better result.

B. RSA (Rivest-Shamir-Adleman)

1) *Key generation*: From the process of key generation, encryption, and decryption of the RSA algorithm, the results are shown in Table II, showing the generation of public and private keys. The running time results are almost the same for low and moderate security, but public key generation is faster at the highest security. Private key generation on the RSA algorithm is faster at standard and high security.

2) *RSA encryption and decryption*: The RSA algorithm encryption process uses the solution $c_i = m_i^e \text{ mod } n$, to obtain an encrypted message in the form of a ciphertext message. The process of decrypting the ciphertext message is done using the solution $m_i = c_i^d \text{ mod } n$ to make the original message a plaintext message. The running time for the encryption and decryption of the RSA algorithm at each security level can be seen in Table II, showing that the results of the decryption process's running time are faster for each security level.

TABLE I. SECURITY LEVEL RSA, NTRU

Security Level (bits)	NTRU (bits)	RSA (bits)
80	2008	1024
112	3003	2048
128	3501	3072
160	4383	4096
192	5193	7680
256	7690	15360

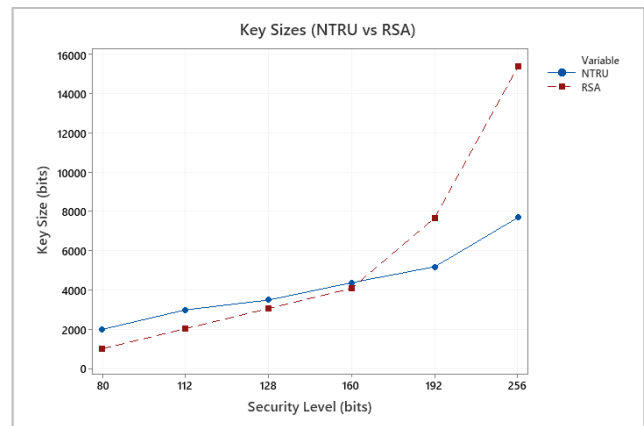


Fig. 4. Comparison of Security Level RSA, NTRU.

TABLE II. RUNNING TIME RSA

Security level	Security level (bits)	RSA (bits)	Public Key Generation (second)	Private Key Generation (second)	Encryption (second)	Decryption (second)
Low security	80	1024	0.62634	0.62634	0.0469	0.0153
Moderate security	112	2048	6.59910	6.59910	0.2594	0.0780
Standard security	128	3072	25.77820	25.77820	0.4458	0.1370
Standard security	160	4096	58.39774	58.39774	0.9420	0.2884
High security	192	7680	682.09213	682.09213	5.6284	1.7493
Highest security	256	15360	6920.16406	6920.16406	41.5171	12.5220

C. NTRU (Nth-Degree Truncated Polynomial Ring)

1) *Key generation*: The main parameters of the NTRU algorithm are integers N, p, q . This parameter value is used to determine polynomial rings. The results of the running time of the public key generation and the private key of the NTRU algorithm can be seen in Table III. Table III shows that the speed of the public key running time is faster than the private key at each security level.

2) *NTRU encryption and decryption*: The NTRU algorithm encryption process is carried out using the $e \equiv r * h + m_i \pmod q$ solution to obtain the ciphertext message. Ciphertext message can be processed with decryption using the NTRU algorithm to get plaintext message, with the solution $d \equiv f_p * [f * e]_q \pmod p$. The encryption and decryption process in the NTRU algorithm obtained results, as shown in Table III. It can be seen that the encryption and decryption process in the NTRU algorithm does not show a significant difference. However, it can be seen that the encryption process is faster for the low-security level and the highest security. Moderate, standard, and highest security

indicate that the decryption process is faster than the encryption process. The security level and the value of the NTRU parameter increase affect the running time speed.

D. Comparison of RSA and NTRU Algorithms

1) *Key generation*: Longer keys will provide higher security but will consume more computing time, so the value of security and speed will be inversely related. Generating a key with a long bit size can take from a few minutes to several hours, as shown in Tables II and III. From the two tables, Table II and Table III, the results are that private and public key generation in the NTRU algorithm is much faster than key generation in the algorithm RSA for security levels 80, 112, 128, 160, 192, 256 bits, as depicted in Fig. 5.

2) *Encryption*: The time required to encrypt files using both algorithms is compared to evaluate system performance. From the data obtained, the time for encryption using RSA is faster than NTRU with an average speed of RSA encryption of 2.3285 seconds and described in detail at different security levels as shown in Table II and Table III.

TABLE III. RUNNING TIME NTRU

Security level	Security level (bits)	Key Sizes (bits)	N	p	q	Public Key (second)	Private Key (second)	Encryption (second)	Decryption (second)
Low security	80	2008	251	3	2048	0.5719	0.6281	0.5478	0.74925
Moderate security	112	3033	401	3	2048	1.9941	2.1696	1.5158	1.4010
Standard security	128	3501	439	3	2048	2.4076	2.6754	1.7236	1.6765
Standard security	160	4383	487	3	2048	2.9953	3.4613	3.6976	3.4571
High security	192	5193	593	3	2048	4.4289	5.1424	6.3630	5.4323
Highest security	256	7690	743	3	2048	7.9426	9.0723	7.9774	9.1061

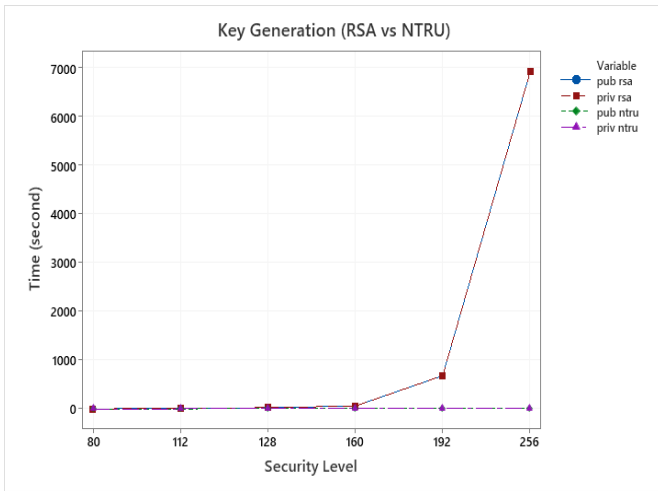


Fig. 5. Comparison of RSA, NTRU Key Generation.

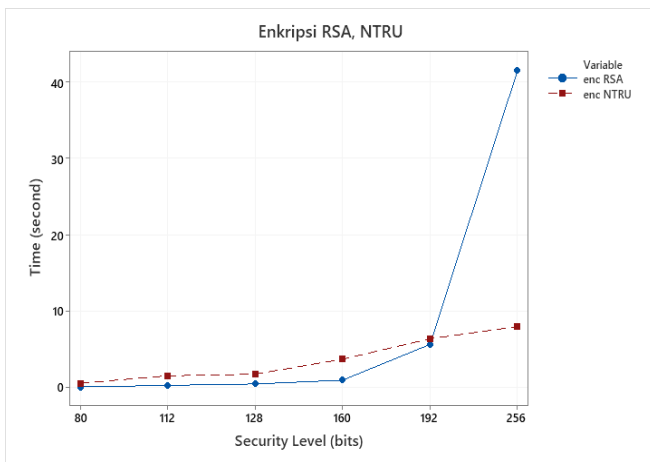


Fig. 6. Comparison of RSA, NTRU Encryption.

From Table II and Table III shows graphs of running time for the encryption process for the RSA and NTRU algorithms, as shown in Fig. 6. It can be seen that the encryption process for low-level RSA security is faster than NTRU, but when it reaches the security level of 256 bits, the NTRU algorithm is much faster than RSA.

3) *Decryption*: The average speed of the RSA algorithm decryption process is faster than the NTRU algorithm. RSA algorithm is more efficient in decrypting data than the NTRU algorithm. Table II and Table III show that when the security level is 80, 112, 128, 160, 192 bits, the RSA decryption process is faster, but when the security level is 256 bits, the NTRU process is faster than RSA decryption.

A comparison for the decryption process in Table II and Table III, a comparison chart is obtained for each security level as shown in Fig. 7. It can be seen that the RSA decryption process for low-security levels is faster than NTRU decryption, but when the security level is at the highest security level, which is 256 bits NTRU algorithm has a faster speed.

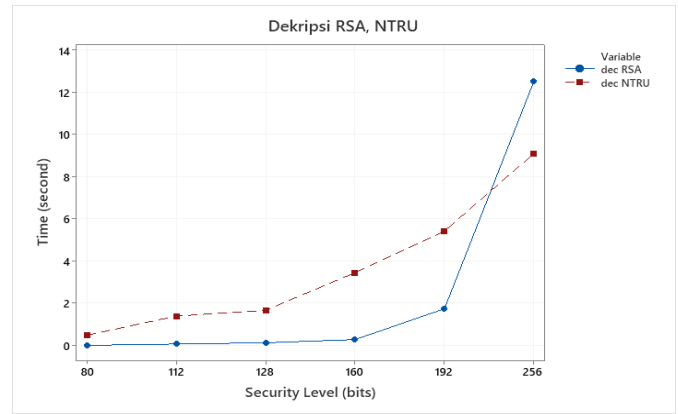


Fig. 7. Comparison of RSA, NTRU Decryption.

4) *Wiener's attack on RSA*: The security of the RSA algorithm depends on the difficulty of factoring large integers to obtain prime numbers, which is one of the mathematical computational problems that are difficult to solve. [29]. Wiener's Attack algorithm uses a continued fraction solution. Table IV is the result of the running time of the Wiener's attack process at different security levels, which shows that when the security level is increased, the time to carry out attacks will increase.

5) *LLL lattice basis reduction on NTRU*: The NTRU algorithm with parameters N, p, q can show each parameter's security level. The public key on the NTRU algorithm will be tested using an attack in the form of LLL (Lenstra-Lenstra-Lovasz) lattice basis reduction with the output obtained in the form of running time. This attack can show the strength of the NTRU algorithm. The strength of the NTRU algorithm is in the difficulty of finding a short vector of a lattice.

In Table V, it can be seen how the LLL lattice base reduction algorithm runs on different parameters. When the value of parameter N increases, the time to carry out an attack also increases, and when the value of N = 31, the time required to carry out an attack takes more than 9 hours. From Table V, it can be said that LLL can perform attacks on the NTRU algorithm but in small parameters and cannot find short vector problems (SVP) for a larger basis. When N's value is higher, the running time of the attack process using LLL tends to increase.

TABLE IV. RUNNING TIME WIENER'S ATTACK

Security level	Security level (bits)	RSA (bits)	Wieners Attack (second)
Low security	80	1024	0.09733
Moderate security	112	2048	0.35923
Standard security	128	3072	1.19537
Standard security	160	4096	1.46252
High security	192	7680	5.87838

TABLE V. RUNNING TIME LLL ATTACK

No	N	p	q	LLL Attack (second)
1	24	3	128	6780
2	25	3	128	7260
3	26	3	128	18600
4	27	3	128	15420
5	28	3	128	24060
6	29	3	128	28980
7	31	3	128	> 9 hours (32400 second)

E. Implementation on Cloud Storage

1) Upload process: Fig. 8 is a flow block diagram of the file upload process and when it is implemented to cloud storage, as shown in Fig. 9. Fig. 9 shows the results of file uploads using the RSA and NTRU algorithms applied to file storage. When the uploaded file has been selected, the uploaded file will be converted into a ciphertext message then sent to the database server.

2) Download process: Fig. 10 is a block diagram of the file download process that can be implemented in cloud storage. Fig. 9 shows the uploaded file can be downloaded and the file decryption process by pressing the download button.

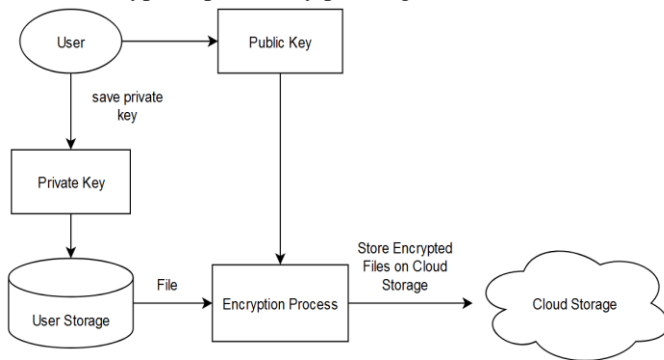


Fig. 8. Block Diagram Upload File.

Upload File (RSA)		
No	Nama File	Activity
2	lorem.pdf	Download Delete
3	henry.pdf	Download Delete
5	lorem.pdf	Download Delete
6	lorem.pdf	Download Delete
7	lorem.pdf	Download Delete

Upload File (NTRU)		
No	Nama File	Activity
3	henry.pdf	Download Delete
4	henry.pdf	Download Delete
5	henry.pdf	Download Delete
6	file.pdf	Download Delete

Fig. 9. File Storage.

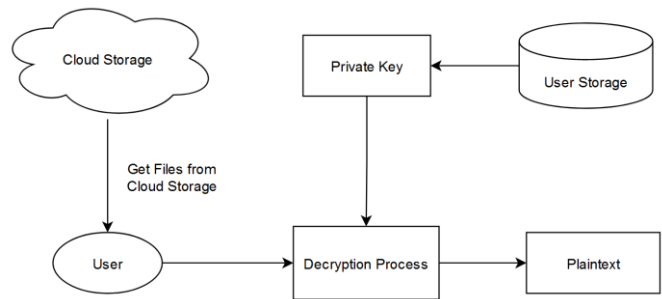


Fig. 10. Block Diagram Download File.

After pressing the download button, the program will download the file and do the decryption process. Then will get the result of a plaintext message.

V. CONCLUSION

The RSA algorithm (Rivest-Shamir-Adleman) and the NTRU algorithm (Nth-Dimensional Truncated Polynomial Ring) are algorithms to secure plaintext or original messages by encrypting messages. In this study, the two algorithms compared their performance in key generation, encryption, decryption, attack, and their implementation in cloud storage. Performance comparisons are made with two things, measuring running time and testing the security of attack attempts on both algorithms. From the results of this study, the results are as in Table II and Table III. The use of the selected parameter for the RSA bit, the higher the bit selected, the greater the time required. The greater the value of the N parameter in the NTRU algorithm, the greater the time required for the key generation, encryption, and decryption processes.

In terms of running time in the key generation and encryption process, the NTRU algorithm is more efficient than the RSA algorithm. In terms of security, by testing the Wiener's attack on the RSA algorithm and LLL Lattice Basis Reduction on the NTRU algorithm, it shows that the NTRU algorithm has a more secure level of resilience so that it can be said that the NTRU algorithm is more recommended for cloud storage security. In this paper, we have not discussed the comparison of the LLL algorithm attacks applied to the RSA algorithm and the NTRU algorithm. The comparison analysis of the RSA algorithm and the NTRU algorithm has proven successful, but it is hoped that in future research a different and updated implementation can be carried out using other algorithms, such as the comparison of the ECC and Elgamal algorithms.

REFERENCES

- [1] M. Ahmed and M. Hossain, "Cloud Computing and Security Issues in the Cloud," International Journal of Network Security & Its Applications, vol. 6, pp. 25–36, Jan. 2014, doi: 10.5121/ijnsa.2014.6103.
- [2] V. Mavroeidis, K. Vishi, M. D. Zych, and A. Jøsang, "The Impact of Quantum Computing on Present Cryptography," ijacsa, vol. 9, no. 3, 2018, doi: 10.14569/IJACSA.2018.090354.
- [3] E. Crockett, "Simply safe lattice cryptography," Jul. 2017, Accessed: Oct. 17, 2021. [Online]. Available: <https://smartech.gatech.edu/handle/1853/58734>.
- [4] L. Ducas, "Advances on quantum cryptanalysis of ideal lattices," undefined, 2017, Accessed: Oct. 17, 2021. [Online]. Available: <https://www.semanticscholar.org/paper/Advances-on-quantum->

- cryptanalysis-of-ideal-lattices-Ducas/bca6ef077421a07276f1b98623fe663e89e515da.
- [5] Z. Jing, C. Gu, Z. Yu, P. Shi, and C. Gao, "Cryptanalysis of lattice-based key exchange on small integer solution problem and its improvement," *Cluster Comput.*, vol. 22, no. 1, pp. 1717–1727, Jan. 2019, doi: 10.1007/s10586-018-2293-x.
- [6] Z. Liu, K.-K. R. Choo, and J. Grossschadl, "Securing Edge Devices in the Post-Quantum Internet of Things Using Lattice-Based Cryptography," *IEEE Communications Magazine*, vol. 56, pp. 158–162, Feb. 2018, doi: 10.1109/MCOM.2018.1700330.
- [7] M. N. A. Wahid, B. Esparham, A. Ali, and M. Marwan, "A Comparison of Cryptographic Algorithms: DES, 3DES, AES, RSA and Blowfish for Guessing Attacks Prevention," 2018, [Online]. Available: <https://symbiosisonlinepublishing.com/computer-science-technology/computerscience-information-technology32.pdf>.
- [8] Dr. M. Subhashini and Dr. R. Gopinath, "MAPREDUCE METHODOLOGY FOR ELLIPTICAL CURVE DISCRETE LOGARITHMIC PROBLEMS – SECURING TELECOM NETWORKS," 2020, doi: 10.34218/IJEET.11.9.2020.026.
- [9] W. Susilo and J. Tonien, "A Wiener-type attack on an RSA-like cryptosystem constructed from cubic Pell equations," 2021, Accessed: Feb. 05, 2022. [Online]. Available: <https://scihub.ee/https://doi.org/10.1016/j.tcs.2021.06.033>.
- [10] B. Santhiya and K. Anitha Kumari, "Analysis on DGHV and NTRU Fully Homomorphic Encryption Schemes," in *Proceedings of International Conference on Artificial Intelligence, Smart Grid and Smart City Applications*, Cham, 2020, pp. 669–678. doi: 10.1007/978-3-030-24051-6_61.
- [11] X. Shen, Z. Du, and R. Chen, "Research on NTRU Algorithm for Mobile Java Security," *Jan. 2009*, pp. 366–369. doi: 10.1109/EmbeddedCom-ScalCom.2009.72.
- [12] A. K. Lenstra, H. W. Lenstra, and L. Lovász, "Factoring polynomials with rational coefficients," *Math. Ann.*, vol. 261, no. 4, pp. 515–534, Dec. 1982, doi: 10.1007/BF01457454.
- [13] A. B. R. P. A. Putra, "Perbandingan Algoritma Rsa dan Elgamal pada Keamanan Data Sidik Jari," 2017, Accessed: Jan. 12, 2021. [Online]. Available: <https://digilib.uns.ac.id/dokumen/76770/Perbandingan-Algoritma-Rsa-dan-Elgamal-pada-Kemaman-Data-Sidik-Jari>
- [14] A. L. KHOIRULLOH, "KEAMANAN FILE DALAM CLOUD COMPUTING DENGAN DIGITAL SIGNATURE ALGORITMA RSA DAN ENKRIPSI FILE ALGORITMA AES," 2019.
- [15] D. J. Bernstein, J. Buchmann, and E. Dahmen, Eds., *Post-Quantum Cryptography*. Berlin Heidelberg: Springer-Verlag, 2009. doi: 10.1007/978-3-540-88702-7.
- [16] J. Hoffstein, J. Pipher, and J. H. Silverman, "NTRU: A ring-based public key cryptosystem," in *Algorithmic Number Theory*, Berlin, Heidelberg, 1998, pp. 267–288. doi: 10.1007/BFb0054868.
- [17] A. K. Bajwa and M. L. Sahi, "NTRU based Security in Cloud Computing," 2018, doi: 10.18535/IJECS/V7I6.09.
- [18] O. Pandithurai, S. Meena S., R. Shenbagalakshmi, and A. U. Sindujha, "A Novel Approach of Drops with NTRU in Cloud," in *2019 Fifth International Conference on Science Technology Engineering and Mathematics (ICONSTEM)*, Chennai, India, Mar. 2019, pp. 261–265. doi: 10.1109/ICONSTEM.2019.8918897.
- [19] N. Suba Rani, "A Novel Cryptosystem for Files Stored in Cloud using NTRU Encryption Algorithm," *IJRTE*, vol. 9, no. 1, pp. 2127–2130, May 2020, doi: 10.35940/ijrte.A2536.059120.
- [20] A. Nandanavanam, I. Upasana, and N. Nandanavanam, "NTRU and RSA Cryptosystems for Data Security in IoT Environment," in *2020 International Conference on Smart Technologies in Computing, Electrical and Electronics (ICSTCEE)*, Bengaluru, India, Oct. 2020, pp. 371–376. doi: 10.1109/ICSTCEE49637.2020.9277159.
- [21] X. Deng, "An Introduction to Lenstra-Lenstra-Lovasz Lattice Basis Reduction Algorithm," p. 11, 2016.
- [22] C. Peikert, "Lattice Cryptography for the Internet," in *Post-Quantum Cryptography*, vol. 8772, M. Mosca, Ed. Cham: Springer International Publishing, 2014, pp. 197–219. doi: 10.1007/978-3-319-11659-4_12.
- [23] D. Stehlé and R. Steinfeld, "Making NTRU as Secure as Worst-Case Problems over Ideal Lattices," in *Advances in Cryptology – EUROCRYPT 2011*, vol. 6632, K. G. Paterson, Ed. Berlin, Heidelberg: Springer Berlin Heidelberg, 2011, pp. 27–47. doi: 10.1007/978-3-642-20465-4_4.
- [24] D. Chi, J. W. Choi, J. S. Kim, and T. Kim, "Lattice Based Cryptography for Beginners," *IACR Cryptol. ePrint Arch.*, 2015.
- [25] W. Susilo, J. Tonien, and G. Yang, "A generalised bound for the Wiener attack on RSA," *Journal of Information Security and Applications*, vol. 53, p. 102531, Aug. 2020, doi: 10.1016/j.jisa.2020.102531.
- [26] P. Yang, N. Xiong, and J. Ren, "Data Security and Privacy Protection for Cloud Storage: A Survey," *IEEE Access*, vol. 8, pp. 131723–131740, 2020, doi: 10.1109/ACCESS.2020.3009876.
- [27] N. Howgrave-Graham, J. H. Silverman, and W. Whyte, "Choosing Parameter Sets for NTRUEncrypt with NAEP and SVES-3," in *Topics in Cryptology – CT-RSA 2005*, vol. 3376, A. Menezes, Ed. Berlin, Heidelberg: Springer Berlin Heidelberg, 2005, pp. 118–135. doi: 10.1007/978-3-540-30574-3_10.
- [28] S. Chandel, W. Cao, Z. Sun, J. Yang, B. Zhang, and T.-Y. Ni, "A Multi-dimensional Adversary Analysis of RSA and ECC in Blockchain Encryption," in *Lecture Notes in Networks and Systems*, 2020, pp. 988–1003. doi: 10.1007/978-3-030-12385-7_67.
- [29] C. Easttom, *Modern Cryptography: Applied Mathematics for Encryption and Information Security*. Springer International Publishing, 2021. doi: 10.1007/978-3-030-63115-4.

A Conceptual Framework for using Big Data in Egyptian Agriculture

Sayed Ahmed¹, Amira S. Mahmoud², Eslam Farg³, Amany M. Mohamed⁴
Marwa S. Moustafa⁵, Mohamed A.E. AbdelRahman⁶, Hisham M. AbdelSalam⁷, Sayed M. Arafat⁸
National Authority for Remote Sensing and Space Science (NARSS), Cairo, Egypt^{1, 2, 3, 4, 5, 6, 8}
Faculty of Computers and Artificial Intelligence, Cairo University, Giza, Egypt⁷

Abstract—Agriculture is a typical contributor to the Egyptian economy, which could benefit from the comprehensive capabilities of Big Data (BD). In this work, we review the BD role in the agriculture sector in responding to two main questions: 1) Which technique, frameworks and data types were adopted. 2) Identification of the existing gap associated with the data sources, modeling, and analysis techniques. Therefore, the contribution in this paper can be outlined in three main aspects. 1) Popular BD frameworks were briefed, and a thorough comparison was conducted between them. 2) The potential data sources were described and characterized. 3) A Conceptual framework for Egyptian agriculture practice based on BD analytics was introduced. 4) Challenges and extensive recommendations have been provided, which could guide future development.

Keywords—Agriculture; big data (BD); big data paradigm; BD processing framework; conceptual BD framework; geographical information systems (GIS); Hadoop; spark

I. INTRODUCTION

Climate change, water storage, and crop fluctuation are major issues in Egyptian agriculture. Variations in market prices and socio-cultural growth contribute to the volatility of food availability. Several challenges need to be tackled to improve agricultural productivity, such as low soil fertility, insect diseases, limited technical adaptation, and varied weather conditions. In the digital era, data become not only valuable but also intelligent. BD term has been introduced in mid-2011 to describe a broad set of heterogeneous large volumes of data that can hardly be managed and processed using conventional approaches [1, 2]. Massive amounts of data, rapid data generation and delivery, organized and unstructured data sources, validity, and value [3] are the five primary elements that define BD, as shown in Fig. 1.

The BD paradigm encompasses the tools, storage, processing, and security measures used [4]. An enormous quantity of data may be analyzed using BD paradigm. It has four parts: techniques, storage, processing, and representation (see Fig. 2). They seek to find hidden trends and patterns in vast amounts of data from several sources. The storage provides management methods and tools for storing organized and unstructured data.

A variety of cloud-based platforms are optimized for maximum processing power. Data value and accessibility for decision-makers are major BD challenges. Data quality, integrity, and legal concerns have recently been addressed by Egypt's government. Several private and public sector

endeavours to develop BD cyber-infrastructures. Recent academic research has focused on combining data and predictive analytics to assist governments better develop agricultural action plans. BD analytics and Remote Sensing (RS) can assist farmers manage their fields by extracting insights from acquired data.

Several attempts have been made to employ BD in agriculture [5]. BD is used by the business sector to increase large-scale commercial agriculture efficiency [5, 6]. Meanwhile, agribusiness makes better use of new communication and data sources. BD tools and approaches are utilized to successfully address and organize farm development difficulties [7, 8]. Governments must plan for the transition to digital agriculture. Several recent studies have explored BD in agriculture. Herein, we also introduce the conceptual design of BD in the Egyptian agriculture sector.

In this paper, we introduce a brief review of the potential BD role in agriculture to answer two main questions. The first question indicates the trending non-spatial and spatial BD Framework. The second question manifests the growing number data sources integrated within BD in agriculture. Therefore, A conceptual framework to adopt BD in Egyptian agriculture sector was presented and the main challenges and further directions were highlighted.

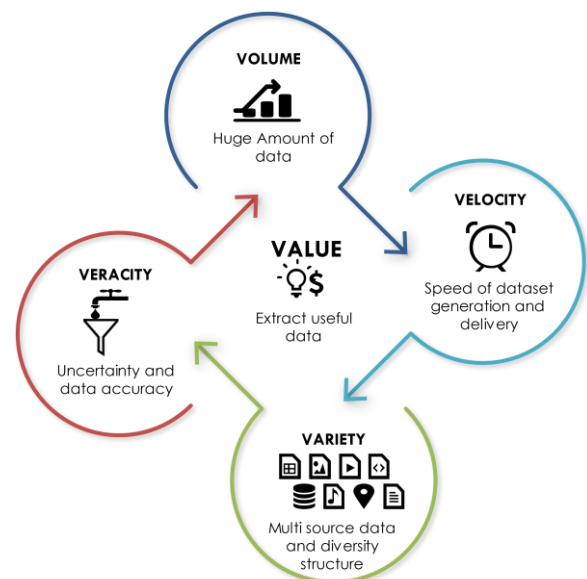


Fig. 1. Big data 5 V's Volume according to Fortune magazine.

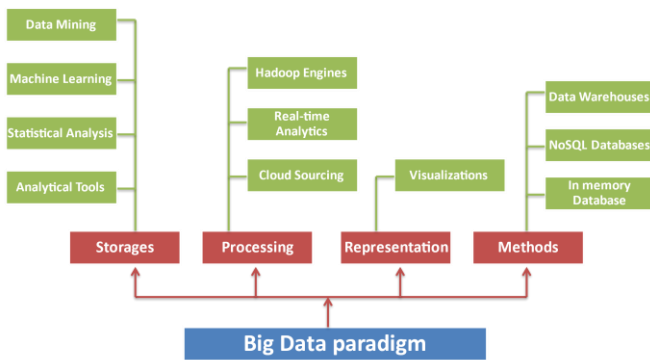


Fig. 2. The Big Data (BD) Paradigm.

The rest of this paper is organized as follows: Sections 2, and 3 briefly sum up the similarities of popular non-spatial and spatial BD framework. The potential BD data sources is discussed in Section 4. Section 5 presents the proposed conceptual framework for adopting BD in Egyptian agriculture sector. In Section 6, the BD challenges and future directions in the agriculture sector were discussed. Finally, Section 7 concludes the paper and provides future work.

II. NON-SPATIAL BD FRAMEWORKS

A. Batch BD Frameworks

The data had to pile up for hours or a few days to be processed in a batch setting. The data had to be loaded in memory processing time; otherwise, the data stored in database, or file system [9]. Examples of batch BD frameworks for large datasets include Hadoop Map Reduce and Spark. For smaller size, Informatica and Alteryx are widely used. For relational databases, Google BigQuery and Amazon Redshift are utilized.

Google introduced Hadoop framework [10], which comprised three elements, namely: Hadoop Distributed File System (HDFS), Yet Another Resource Negotiator (YARN), and MapReduce [11]. Typically, HDFS represents Hadoop's core component, which introduces reliable storage [11, 12]. HDFS has two architectures NameNode and DataNode [20]. YARN is considered the cluster management component in Hadoop framework [13]. Finally, MapReduce component performs two main functions, map and reduce. The users only define the map and reduce functions, and the framework is responsible for other administrative functions like parallelization and failover. Overall, Hadoop MapReduce employs HDFS for data storage, while YARN is employed for resources control and job scheduling [10, 13].

B. Stream BD Frameworks

Stream Frameworks process data as soon as it arrives at both micro-batches and real-time [9]. Examples of BD stream frameworks include Apache Storm and Apache Samza [11].

1) *Apache storm*: Twitter developed Apache Storm to process large-scale structured and non-structured data in real-time fashion [14-16]. A typical Apache storm topology [17] depends on a directed acyclic graph where the edge indicates the data exchange, and the node represents computation resources. A node is either a master node "Nimbus" or a

worker node "Supervisor." All nodes could accept streams (sequence of Tuples). In contrast, first nodes only accept Spouts, which can read messages from external sources and convert them to tuples and resend them to other bolts without any computation. Bolts receive, filter, compute, join, and create Tuples. The exchange protocol between bolts and spouts is defined by Stream grouping.

The Storm architecture [18] has three main components: Nimbus, Supervisor, and ZooKeeper. Nimbus oversees worker and slave nodes progress and assigns tasks in standard and failure cases. The supervisor is a stateless daemon responsible for initiating monitoring and restoring topologies execution [18]. ZooKeeper [19] maintains configuration information, distributed synchronization, and group membership.

Trident Application Programming Interfaces (APIs) were utilized in topology, which provides a wide range of high-level operators [14]. Trident APIs split the workload into micro-batches. The batch size is set as a parameter to control throughput and latency. However, their topologies are unfortunately inadequate to execute iterative algorithms due to their Directed Acyclic Graphs (DAGs) nature [20].

2) *Apache samza*: LinkedIn developed Apache Samza to tackle stream processing issues like scalability, resources allocation, etc. [21]. Apache Samza is built upon two other BD processing frameworks: Apache Kafka and Hadoop YARN [11, 21]. Apache Kafka is based on five main components: Producer, Topics, Consumer, Partitions, and Brokers. The Producer component is responsible for writing a topic for Kafka system. Every data stream entering Kafka system is called Topic. A consumer is an element with both reading ability to a Kafka topic and responsibility to maintain information with respect to its offset to be used in the case of failures. Brokers are the single nodes that form the Kafka cluster.

C. Hybrid BD Frameworks

Some applications require batch and stream processing frameworks. Therefore, it is mandatory to use hybrid processing frameworks in such cases. Apache Spark, as well as Apache Flink, are regarded as the most notable examples.

1) *Apache spark*: Apache Spark represents a hybrid framework constructed on top of Hadoop engine but optimizes processing through accelerating batch processing workloads using complete in-memory processing [11].

Apache Spark limited the creation of storage layer links to two cases: loading the data into memory to be processed and storing the final results. Unlike Apache MapReduce, Spark piles the intermediate results in memory. Resilient Distributed Datasets (RDDs) are the core data structure of Apache Spark, allowing developers to accumulate intermediate for reusability purposes. RDDs are fault-tolerant that could optimize partitions, maintaining the stored data [22].

Apache Spark framework [22] includes several main components combined with upper-level libraries such as Spark's MLlib for machine learning [23], GraphX [24] for

stream processing, and Spark SQL [25] for stream processing, and structured data processing.

Spark core is implemented in Scala and supports multi clusters. Spark supports upper-level APIs like Scala, Java, Python, and R and operates various data visualization and analysis algorithms. A cluster manager is utilized for requesting cluster resources for jobs' execution. Spark built-in cluster manager has many cluster managers used by Spark core, such as Hadoop YARN, Apache Mesos, and AmazonEC2. Besides, Spark enables data access in different data sources, such as HDFS, Cassandra, HBase, Hive, Alluxio, and many other data sources.

2) *Apache flink*: Apache Flink [26] is regarded as an open-source hybrid framework for applications such as real-time analytics, continuous data pipelines, batch processing, in addition to iterative algorithms. The main advantage is processing huge data volumes at an economic level of latency and high fault tolerance in a distributed environment. The DataSet API is used to process finite data sets and is often known as batch processing [26].

Finally, Table I compares the mentioned BD processing frameworks based on the following factors, including cluster architecture, data flow, data processing model, fault-tolerance, latency, scalability, back-pressure mechanism, programming languages, as well as different machine learning libraries.

TABLE I. A COMPARISON BETWEEN POPLAR NON-SPATIAL BD FRAMEWORKS

Framework	Hadoop	Storm	Trident Storm	Samza	Spark	Flink
Processing type	Batch	Stream	Stream	Stream	Hybrid	Hybrid
Computing cluster architecture	YARN	Nimbus	Nimbus	YARN and Kafka	YARN and Mesos	YARN and Kafka
Data Flow	MapReduce data flow	cyclic graph	DAGs	Kafka - Kafka job – Kafka	A queue of RDDs called DStream processed one-at-a-time using micro-batching cluster	stream -> system (operators) -> sinks
Data Processing Model	MapReduce	at-least-once	exactly-once	at-least-once	exactly-once	exactly-once
Fault-Tolerance	Yes	Yes	Yes	Yes	Yes (using lineage)	Yes (generating snapshots)
Latency	low	several milliseconds	several milliseconds for small batches	Several milliseconds	High	Low
Scalability	Yes	Yes	User-defined parallel processing	Yes	Yes (user demand)	Yes (only tasks that can be done in parallel)
Back-pressure Mechanism	No	Yes	Yes	No (buffering instead)	Yes	Yes
Programming Languages	Java mostly	Java API with adapters for Python, Ruby, and Perl	Java API with adapters for Python, Ruby, and Perl	Java mostly	API for Scala, Java, Python, and R	Java and Scala
Support for Machine Learning	Yes	compatible with SAMOA API	Trident-ML	compatible with SAMOA API	Yes (Spark MLlib)	Yes (FlinkML)

III. SPATIAL BD FRAMEWORKS

A. Hadoop-based

1) *Hadoop-GIS*: Hadoop-GIS is regarded as a MapReduce-based framework to process large-scale vector data, partitioning, as well as geographic queries [27]. Geographic (Spatial) queries can take many forms, such as descriptive, spatial relationship-based, distance-based queries, along with spatial mining and statistics techniques. In order to boost query performance, Hadoop-GIS utilize a spatial partitioning and local spatial indexing called SATO [41]. However, complex geometry forms, such as convex/concave polygons, line string, multi-point, as well as multi-polygon, are not supported. In fact, Hadoop-GIS supports only two-dimensional data and two query types over geometric objects, including box range as well as spatial joins.

2) *Spatial-Hadoop*: Spatial-Hadoop is a complete MapReduce framework that was introduced to overcome Hadoop-GIS limitations. It contains two new components for efficient and scalable spatial data processing: SpatialRecordReader and SpatialFileSplitter to support spatial data, spatial indexes, and operations [28].

Spatial-Hadoop supports different geometry types, such as points, multi-points, line strings, and polygons. In spatial indexes, spatial partitioning approaches were implemented, such as uniform grids, R-Tree, Quad-Tree, K-Dimensional Tree (KD-Tree), as well as Hilbert curves. Also, it supports many predefined spatial operations, such as box range queries, KNN queries, and spatial joins. Besides, it supports various geometric objects, including segments and polygons, and operations over them, producing convex hulls in addition to skylines. The mentioned capabilities are implemented in Spatial-Hadoop as distributed geometric data analytics framework.

B. Spark-based

1) *Spatial-Spark*: Spatial spark is a framework to process GIS data based on cluster computing. It was constructed on top of Spark RDD for providing a broad range of spatial operations, including range query, spatial join, spatial filtering, R-Tree index, and R-Tree partitioning to boost queries [29]. Spatial-Spark can be considered an in-memory BD framework intended for supporting two spatial join operators, including broadcast spatial join and partitioned spatial join [29].

2) *Geo-Spark*: Geo-Spark is regarded as an in-memory cluster computing framework constructed on Spark top to process large-scale GIS data faster than Spatial-Hadoop [30]. Geo-Spark expands the concept of RDDs as well as SparkSQL for supporting spatial data types, indexes, in addition to geometric operations at scale. It also helps spatial data partitioning systems, including a uniform grid, R-tree, Quad-Tree, KD B-Tree, as well as KNN queries. Geo-Spark is optimized to select a suitable join algorithm for achieving a balance in a cluster between run time as well as memory/CPU use [31]. Geo-Spark enables the Apache Spark developers for developing efficient spatial analysis applications utilizing operational quickly (for instance, Java and Scala) in addition to declarative (i.e., SQL) languages and spatial RDD APIs.

Toward more solid knowledge, principal differences and similarities among Hadoop-GIS, Spatial-Hadoop, Spatial-Spark, and Geo-Spark [30, 31] dependent on prevalent characteristics such as spatial partitioning, spatial indexing, DataFrame API, in-memory processing, etc., are summarized in Table II.

TABLE II. COMPARISON AMONG POPULAR BIG GIS DATA PROCESSING FRAMEWORKS

Feature	Hadoop-GIS	Spatial-Hadoop	Spatial-Spark	Geo-Spark
DataFrame API	×	×	×	√
In-memory processing	×	×	√	√
Spatial Partitioning	SATO	Multiple	Multiple	Multiple
Spatial Indexing	R-Tree	R-/Quad-Tree	R-Tree	R/Quad-Tree
KNN query	√	√	×	√
Query optimizer	×	×	×	√
Distance query	√	√	√	√
Distance join	√	√	√	√
Filter (Contains)	√	√	√	√
Filter (ContainedBy)	√	√	√	×
Filter (Intersects)	√	√	√	√
Filter (WithinDistance)	√	√	√	×

IV. BD MAJOR DATA SOURCES

A. Satellite Imagery

Satellite imagery is captured by active or passive sensors to study the Earth's surface [9]. The collected images using passive sensors estimate reflected sunlight emitted from the sun. In contrast, the images are usually acquired using active sensors. In heavy cloud cover, rain conditions, and at nighttime, active sensors, including the Synthetic Aperture Radar, are efficiently utilized to tackle limitations of passive sensors and increase the observational capability for agriculture applications.

B. Wireless Sensor Web and IoT

Wireless Sensor Network represents a collection of heterogeneous and sophisticated sensors responsible for collecting various data types, including temperature, humidity, wind, etc. WSW depends on Internet of Things technology (IoT), which integrates and deploys several heterogeneous spatially distributed sensors to enrich the identification and visualization capabilities of different agriculture areas [32]. The collected data [33] could facilitate the communication between the farmers, experts, and investors to maintain a closer day-to-day management when classical communication methods fail. Despite their wide usability in smart farming, WSW lacks the comprehensive coordination to different data sources as well as protocols from "Socio-techno-economic perspectives" [34].

C. Crowd-sourcing and Social-media

In the last few years, several platforms were developed to collect data from the public. These platforms either actively contributed where contributors are aware of the data collection [35], such as crowdsourcing, or passively contributed where contributors are not aware such as social media [36]. Unlike crowdsourcing platforms, social media are used to track pest and sharing weather information.

Social media is utilized in agriculture development for data gathering, information extraction, analytic workflow, geo-location pattern/image/text analytics, and information transferring over social media services [37]. Real-time analytics dependent on social media platforms [37] offer considerable chances for automatic detection and monitoring of plant disease, yield productivity, and forecasting [38]. For social media data, visual analytics can simplify Spatio-temporal analysis and generate a spatial-based decision for supporting environment, helping small farmers match end-user demand. Social media not only depends on text messages but also depends on posted videos and images by users. Analysis dependent on image/video, along with visual analytics, utilize social media posts to extract critical information.

D. Mobile CDRs and GPS Traces

GPS traces and mobile CDRs data are valuable resources, especially in natural disasters management such as landslide monitoring, Tsunami monitoring, earthquake management, forest fire, and flood management. GPS traces data had been a value-added in different agriculture applications [39], like identifying mobility patterns for agriculture machines and fuel consumption tracking.

E. Simulation

Numerical simulation, or referred to as forecasting, is regarded as one of the essential agricultural contributions to meteorological phenomena, land surface phenomena, and diverse pollutions kinds [40, 41]. Also, mechanistic modeling has helped estimate water spray [42] and parameter estimation of subsurface pipe [43].

The modeling and simulation tools for agriculture management focus on different aspects. Several mechanistic models were developed to enrich the scientific understanding of agriculture aspects to gain insights into physical, chemical, and biological control parameters in crop and animal production systems. Another group of simulation models was developed to plan and support decision-makers.

F. UAVS, Drones and LiDAR

UAVs, as well as drones, deliver images and videos with very high-resolution amenable to be utilized in various agriculture applications [44] such as live-stock monitoring, crop production, yield prediction, fertilizer, pesticide spraying, and soil mapping [45]. Many sensors can be embedded in a UAV or drone, such as weather sensors, cameras, and LiDAR sensors. The obtained sensors data can be integrated into real-time decision making in many fields such as spraying of pesticides through drone, plant phenotyping, and yield production estimation [46].

LiDAR technology [47] can create detailed topography maps and Digital Elevation Models (DEMs) necessary in crop architectural parameters, forests, and crop parameter analysis. LiDAR can also help in yield forecasting and monitoring, soil types, estimate and prevent soil erosion, land segmentation, and crop analysis field management [48]. LiDAR technology is highly valuable in geospatial community, with the massive data amounts amenable to utilization in a diversity of applications.

G. Vector-Based GIS Data

Vector-based GIS data provides powerful add-ons in agriculture management applications [49] like farmland suitability analysis, estimation fertilizer costs, and pesticide. Additional geospatial analysis for critical facilities (healthcare providers, schools, fire station, etc.) [52], estimation of the actual effect on human (age, gender, social and economic status, etc.), resources inventory (vehicles, supplies, equipment, etc.), and infrastructure (utility grids and transport networks) help and empower farmers community. Common GIS data sources enrich precision agriculture in developing countries [49].

In [49], the authors implemented a framework that integrated GIS with Multi-Criteria Decision Analysis (GIS-MCDA) to assess land suitability for irrigation with reclaimed water. In [53,54], the authors developed a GIS-based approach that studies the appropriate soil-site citrus features for enhancing productivity.

From the above discussion of various BD sources, it can be noted that satellite imagery, aerial imagery, crowdsourcing, social media records, simulation and GIS data could offer economic solution to enrich the Egyptian farming sector with valuable information. On the other hand, WSW, IoT, video and images from UAVs, GPS traces and CDRs, and LiDAR could be valuable and cost-effective data sources for private sector that could open new business opportunities.

V. A CONCEPTUAL FRAMEWORK FOR USING BD IN EGYPTIAN AGRICULTURE

In Egypt, agriculture's contribution of real GDP growth fell from 16.5% in 2002 to 11.4% in 2018 [1]. It employs 14.5 percent of the active population [1, 50] and supplies 91.5 percent of the population's requirements. It also only exports 8.7% of total commodities. BD analytics, the "new oil," can help the agriculture industry [51, 53]. According to a recent study, the internet's ubiquity and suitable communication technologies might assist evaluate enormous volumes of gathered data to address critical concerns like desertification and global food costs. Two significant reasons [51] often influence BD analytics adoption in Egypt:

- Push factor determines the motivation opportunities such as the new governmental investments in technology and infrastructure.
- Pull factor analyses business factors such data quality, security, and availability.

Egyptian agriculture issues fall into three categories: monitoring, management, and forecasting. As illustrated in Fig. 3, we developed a conceptual framework to address Egyptian agriculture difficulties using BD analytics. The next parts describe data collecting, data analysis, and issue solutions.

A. Data Collection

Data collection, the first and primary step of BD applications, aims to collect a variety of structured and unstructured data, including soil, yield, climate data, satellite images, and other information sources. The basic modules implemented in this stage include filtering and harmonizing the captured data and nullifying unnecessary data. Also, metadata is generated for each dataset to identify how the data is rendered and analyzed.

B. Data Analysis

The collected data had to be prepared by extracting the vital information for further analysis. The valuable information is extracted by cleaning, interpreting, integrating, mining, analyzing, and warehousing data in this stage. Different analysis approaches could be performed to improve data understanding, such as visual analysis, prescriptive, diagnostic, and predictive analysis.

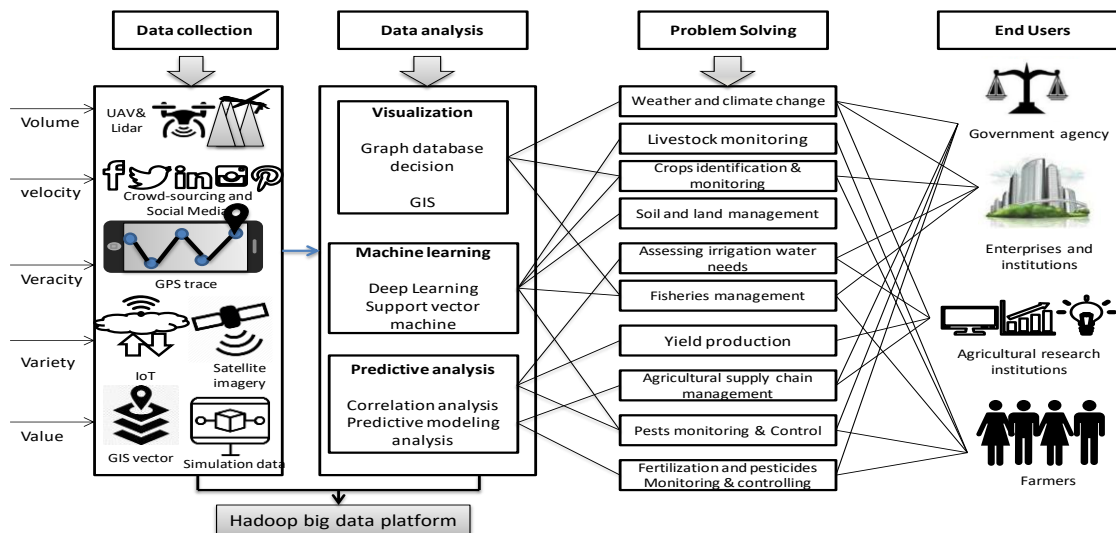


Fig. 3. The Proposed Conceptual Framework for BD in Egyptian Agriculture.

Generally, visual analysis can be utilized to gain insights about the uncovered relationships within massive datasets and empower investigators for obtaining more intuitive visual cognition as well as efficient decision-making assist. Now, government, as well as related policymakers, may utilize the aforementioned BD sources for conducting visual analysis of water resources monitoring, weather condition, soil condition, and close contact of scientific researchers for making decisions. Moreover, visualization is principally accomplished through GIS. By linking BD and GIS can help farmers, enterprises, and institutions better understand their spatial patterns as well as relationships. In this regard, GIS technology should first be provided with properly attained BD. The data collection is no longer restricted to conventional facilities and approaches, including stations, satellite RS, and field measurement. Besides, it still extends with IoT and UAV capabilities. For processing and analysis, this appears to happen primarily via batch processing technology like MapReduce and distributed system infrastructure like Hadoop.

The collected data is amenable to be transformed into an acceptable format for GIS systems. Decision-makers utilized tools such as GoogleEngine, which provide interactive digital maps with almost real-time visualization of much free satellite imagery and a continuous development platform for the intelligent integration of multi-sources information.

1) *Descriptive analytics*: Descriptive analytics enable visualization and interpreting of the collected data in order to answer the “what happened?” question [2, 7]. Several visualization tools and Ad-hoc were implemented for various data-related agriculture sources to tackle the complex nature of both structured and unstructured data. A basic summarization of these large volumes of data can be performed in diverse formats, including summaries, i.e., tables, charts, spreadsheets, etc.

2) *Diagnostic analytics*: Diagnostic analytics motivate analysts to perform a root cause analysis to discover key reasons for the events. A smart, well-designed dashboard combined with time-series data offers analysts mandatory

tools to quickly summarize an overview that matches the business objectives. The question answered using diagnostic analytics is, “why did it happen?”. Data mining, as well as correlation, can offer profound perception into defining the targeted problems and issues. DL is a full orientation shift in supervised machine learning, such as pattern recognition and natural language processing.

3) *Predictive analytics*: Predictive analytics aims to predict future by answering the “what is going to happen?” questions. Generally, ample statistical and machine learning approaches aim to correlate past and today data to assume the future.

4) *Prescriptive analysis*: Prescriptive analytics assess analysts for determining optimal actions and decisions on the basis of answers to a diversity of questions concerning “what might happen?”. For instance, analysts might possess numerous choices for dispatching maintenance actions towards a specific asset. For maintenance actions, the time-varying expense required items to be repaired or substituted, while the risk linked to each of such decisions is capable of determining the optimal dispatch. Prescriptive analytics synthesize the BD, diverse sciences’ principles, business rules, in addition to IoT disciplines for receiving the predictions merits, followed by taking the most optimal decisions. Prescriptive analytics goes beyond the prediction. Indeed, the “what will happen” and “when will happen” questions should be able to justify the “why it would happen” questions.

C. Problem Solving

Finally, the collected data is converted into actionable perceptions. Herein, the data captured from different sensors could be utilized to improve the monitoring, management, and prediction of agriculture sector activities in Egypt. Furthermore, BD is utilized to boost predictive insights in real-time for future outcomes in farming. Recently, the private Egyptian agricultural sector started implementing innovative technologies, particularly those requiring large scale of operations and costly initial investment. To implement new

technologies, this possesses a substantial influence on farmers' prospects. The modern visualization and analysis tools enable farmers, experts, and research institutions to easily connect and simplify data management in a cost-effective way. Such a shift to new technologies comes true by research as well as development in hardware and software services. Recently, agricultural innovation has caused auspicious new methods for boosting productivity. However, for Egyptian farmers, access to high quality and precise information at a reasonable expense is challenging.

Various efforts had been conducted to incorporate BD technologies in the agriculture sector. BD analytical help governments to establish policies and define mitigation plans toward climate change adaptation to secure food. BD integrated with IoT technology effectively supports a wide range of daily agriculture activities such as livestock monitoring, pest monitoring and fertilization control.

Several studies had investigated the power of BD in digital farming worldwide to effectively estimate the biophysical factors of different crops and yield prediction which adopted in crop monitoring, and the investigation of irrigation water needs.

VI. CHALLENGES AND FUTURE DIRECTION

This section discusses the open issues and challenges that face big data in agriculture sector. Some of the challenges were identified from the literature have been discussed previously.

A. Big Data Acquisition

Agriculture sector in Egypt requires different set of data from different sources in order to fill the gaps between current and required state by BD analytics. The integration of multiple data sources will improve data quality and data integrity, provided that individual data validation is conducted before data integration. In the context of agriculture management, data integration can benefit from the data semantics or properties related to the data itself. It is impossible to avoid noises and misinformation from big data as a lot of these are unintentional, especially from social media and crowdsourcing. Also, data privacy and accuracy issues associated with big data acquisition still represent significant challenges, despite the available protocols and analytical method which are crucially required during the acquisition process. One of the proposed solutions that can help to eliminate such noise and misinformation is to develop a framework that enables the integration of multiple sources of data, such as crowd-sourcing data sensor outputs. The framework could facilitate the detection to the anomaly or improper values caused by system failure or misleading data acquisition methods. Machine learning techniques can contribute to the integration filtration process to increase the data quality

B. Big Data Analytics

Due to the integration of multi-platform, multi-scale, and multi-discipline data, there is a must to enhance the predictive modeling capability for the farm management to become more efficient. Activities and research associated with using the integrated information and the results of predictive analysis are expected to better enhance our capability to efficiently handle

livestock, farm clinic, and supply and chain process. It has been noted that crowd-sourced data provided by affected farmers have significant value during the management and decision making. However, analytical methods are still strongly required to integrate these crowd-sourced data reliably and precisely into the physical sensing data (e.g., satellite, UAV) and official data (e.g., terrain data, census data). Only in this case, the smart farming can be effectively depicted in terms of pests control, livestock managements, and yield production. Hence, the decision-making processes can benefit from the analytical results and build food security system that benefits populations and communities

C. Cyber-infrastructures

There is a critical necessity for the design and development of cyber-infrastructures so that big data can be effectively integrated into agriculture sector management agencies for real-time decision making. These cyber-infrastructure capabilities provide shared knowledge and communicating platforms to the decision-makers and responders from different organizations to conduct the process required in agriculture in an effective way. Research efforts and related activities are still needed to overcome the challenges emerging from big, sensed data, including efficient data management, fast data transfer, and intuitive data visualization.

VII. CONCLUSION

This paper conducted a systematic literature review to inspect the recent cutting-edge research of BD in the agricultural and farming field. BD analytics can help the Egyptian agriculture sector overcome several challenges; however, it required a hefty investment to be integrated. Egyptian Farmers had to adopt modern and new technology to balance the food gap and supply concerns. This paper reviews 242 peer-reviewed articles on BD in agriculture, indicating BD's prominent role in tackling the agriculture sector's challenges. Therefore, ample conclusions were drawn:

- The up-raising trend in adopting BD in different agriculture applications, the availability of free satellite imagery, and the massive computational capabilities and efficient machine learning algorithms help researchers gain insights and recommend solutions to agriculture challenges.
- BD tackled a more comprehensive range of applications, even in the agriculture sector.
- Satellite imageries were specifically employed to produce different popular vegetation indices and land cover maps, especially Landsat and Sentinel-2 imagery.
- Extensive studies adopted different machine learning methods for RS data processing. In the last five years, deep learning had been adopted in several studies, especially in crop mapping and pests and disease identification.

ACKNOWLEDGMENT

This paper is based upon work supported by Science, Technology & Innovation Funding Authority (STDF) under grant (ESIP 2019) project ID (33547).

REFERENCES

- [1] W. Bank. (2020). World Development Indicators.
- [2] C. K. Emani, N. Cullot, and C. Nicolle, "Understandable big data: a survey," *Computer science review*, vol. 17, pp. 70-81, 2015.
- [3] A. Kamilaris, A. Kartakoullis, and F. X. Prenafeta-Boldú, "A review on the practice of big data analysis in agriculture," *Computers and Electronics in Agriculture*, vol. 143, pp. 23-37, 2017.
- [4] C. P. Chen and C.-Y. Zhang, "Data-intensive applications, challenges, techniques and technologies: A survey on Big Data," *Information sciences*, vol. 275, pp. 314-347, 2014.
- [5] S. Himesh, E. Prakasa Rao, K. Gouda, K. Ramesh, V. Rakesh, and G. Mohapatra, "Digital revolution and Big Data: a new revolution in agriculture," *CAB Rev*, vol. 13, no. 21, pp. 1-7, 2018.
- [6] C. Kempenaar et al., "Big Data analysis for smart farming: results of TO2 project in theme food security," Wageningen University & Research2016.
- [7] A. Krishnan, K. Banga, and M. Mendez-Parra, "Disruptive technologies in agricultural value chains," 2020.
- [8] S. Alkatheri, S. A. Abbas, and M. A. Siddiqui, "A Comparative Study of Big Data Frameworks," *International Journal of Computer Science and Information Security (IJCSIS)*, vol. 17, no. 1, 2019.
- [9] S. P. Cumbane and G. Gidófalvi, "Review of Big Data and Processing Frameworks for Disaster Response Applications," *ISPRS International Journal of Geo-Information*, vol. 8, no. 9, p. 387, 2019.
- [10] J. Dittrich and J.-A. Quiané-Ruiz, "Efficient big data processing in Hadoop MapReduce," *Proceedings of the VLDB Endowment*, vol. 5, no. 12, pp. 2014-2015, 2012.
- [11] V. Gurusamy, S. Kannan, and K. Nandhini, "The real time big data processing framework: Advantages and limitations," *International Journal of Computer Sciences and Engineering*, vol. 5, no. 12, pp. 305-312, 2017.
- [12] K. Shvachko, H. Kuang, S. Radia, and R. Chansler, "The hadoop distributed file system," in *2010 IEEE 26th symposium on mass storage systems and technologies (MSST)*, 2010, pp. 1-10: Ieee.
- [13] A. P. Kulkarni and M. Khandewal, "Survey on Hadoop and Introduction to YARN," 2014.
- [14] S. Kamburugamuve, G. Fox, D. Leake, and J. Qiu, "Survey of distributed stream processing for large stream sources," *Grids Ucs Indiana Edu*, vol. 2, pp. 1-16, 2013.
- [15] A. Toshniwal et al., "Storm@ twitter," in *Proceedings of the 2014 ACM SIGMOD international conference on Management of data*, 2014, pp. 147-156.
- [16] M. H. Iqbal and T. R. Soomro, "Big data analysis: Apache storm perspective," *International journal of computer trends and technology*, vol. 19, no. 1, pp. 9-14, 2015.
- [17] S. T. Allen, M. Jankowski, and P. Pathirana, *Storm Applied: Strategies for real-time event processing*. Manning Publications Co., 2015.
- [18] M. Ficco, R. Pietrantuono, and S. Russo, "Aging-related performance anomalies in the apache storm stream processing system," *Future Generation Computer Systems*, vol. 86, pp. 975-994, 2018.
- [19] S. Haloi, *Apache zookeeper essentials*. Packt Publishing Ltd, 2015.
- [20] W. Wingerath, F. Gessert, S. Friedrich, and N. Ritter, "Real-time stream processing for Big Data," *it-Information Technology*, vol. 58, no. 4, pp. 186-194, 2016.
- [21] S. A. Noghabi et al., "Samza: stateful scalable stream processing at LinkedIn," *Proceedings of the VLDB Endowment*, vol. 10, no. 12, pp. 1634-1645, 2017.
- [22] D. García-Gil, S. Ramírez-Gallego, S. García, and F. Herrera, "A comparison on scalability for batch big data processing on Apache Spark and Apache Flink," *Big Data Analytics*, vol. 2, no. 1, p. 1, 2017.
- [23] X. Meng et al., "Mllib: Machine learning in apache spark," *The Journal of Machine Learning Research*, vol. 17, no. 1, pp. 1235-1241, 2016.
- [24] R. S. Xin, D. Crankshaw, A. Dave, J. E. Gonzalez, M. J. Franklin, and I. Stoica, "Graphx: Unifying data-parallel and graph-parallel analytics," *arXiv preprint arXiv:1402.2394*, 2014.
- [25] M. Armbrust et al., "Spark sql: Relational data processing in spark," in *Proceedings of the 2015 ACM SIGMOD international conference on management of data*, 2015, pp. 1383-1394.
- [26] P. Carbone, A. Katsifodimos, S. Ewen, V. Markl, S. Haridi, and K. Tzoumas, "Apache flink: Stream and batch processing in a single engine," *Bulletin of the IEEE Computer Society Technical Committee on Data Engineering*, vol. 36, no. 4, 2015.
- [27] A. Aji et al., "Hadoop-GIS: A high performance spatial data warehousing system over MapReduce," in *Proceedings of the VLDB Endowment International Conference on Very Large Data Bases*, 2013, vol. 6, no. 11: NIH Public Access.
- [28] A. Eldawy and M. F. Mokbel, "Spatialhadoop: A mapreduce framework for spatial data," in *2015 IEEE 31st international conference on Data Engineering*, 2015, pp. 1352-1363: IEEE.
- [29] S. You, J. Zhang, and L. Gruenwald, "Large-scale spatial join query processing in Cloud," in *2015 31st IEEE International Conference on Data Engineering Workshops*, 2015, pp. 34-41.
- [30] R. K. Lenka, R. K. Barik, N. Gupta, S. M. Ali, A. Rath, and H. Dubey, "Comparative analysis of SpatialHadoop and GeoSpark for geospatial big data analytics," in *2016 2nd International Conference on Contemporary Computing and Informatics (IC3I)*, 2016, pp. 484-488: IEEE.
- [31] J. Yu, Z. Zhang, and M. Sarwat, "Spatial data management in apache spark: The geospatial perspective and beyond," *Geoinformatica*, vol. 23, no. 1, pp. 37-78, 2019.
- [32] M. Ben-Daya, E. Hassini, and Z. Bahroun, "Internet of things and supply chain management: a literature review," *International Journal of Production Research*, vol. 57, no. 15-16, pp. 4719-4742, 2019.
- [33] S. Rotz et al., "The politics of digital agricultural technologies: a preliminary review," *Sociologia Ruralis*, vol. 59, no. 2, pp. 203-229, 2019.
- [34] A. Khanna and S. Kaur, "Evolution of Internet of Things (IoT) and its significant impact in the field of Precision Agriculture," *Computers and electronics in agriculture*, vol. 157, pp. 218-231, 2019.
- [35] A. Stefanidis, A. Crooks, and J. Radzikowski, "Harvesting ambient geospatial information from social media feeds," *GeoJournal*, vol. 78, no. 2, pp. 319-338, 2013.
- [36] H. Qin, R. M. Rice, S. Fuhrmann, M. T. Rice, K. M. Curtin, and E. Ong, "Geocrowdsourcing and accessibility for dynamic environments," *GeoJournal*, vol. 81, no. 5, pp. 699-716, 2016.
- [37] T. Balan et al., "Smart Multi-Sensor Platform for Analytics and Social Decision Support in Agriculture," *Sensors*, vol. 20, no. 15, p. 4127, 2020.
- [38] P. Akulwar, "A Recommended System for Crop Disease Detection and Yield Prediction Using Machine Learning Approach," *Recommender System with Machine Learning and Artificial Intelligence: Practical Tools and Applications in Medical, Agricultural and Other Industries*, p. 141, 2020.
- [39] P. Debroy et al., "Characterization of the Soil Properties of Citrus Orchards in Central India using Remote Sensing and GIS," *National Academy Science Letters*, pp. 1-4, 2020.
- [40] J. W. Jones et al., "Brief history of agricultural systems modeling," *Agricultural Systems*, vol. 155, pp. 240-254, 2017/07/01/ 2017.
- [41] M. Langhammer, J. Thober, M. Lange, K. Frank, and V. Grimm, "Agricultural landscape generators for simulation models: A review of existing solutions and an outline of future directions," *Ecological Modelling*, vol. 393, pp. 135-151, 2019/02/01/ 2019.
- [42] C. G. Sedano, C. A. Aguirre, and A. B. Brizuela, "Numerical simulation of spray ejection from a nozzle for herbicide application: Comparison of drag coefficient expressions," *Computers and Electronics in Agriculture*, vol. 157, pp. 136-145, 2019.
- [43] Y. Qian, Y. Zhu, M. Ye, J. Huang, and J. Wu, "Experiment and numerical simulation for designing layout parameters of subsurface drainage pipes in arid agricultural areas," *Agricultural Water Management*, vol. 243, p. 106455, 2021/01/01/ 2021.
- [44] R. Raj, S. Kar, R. Nandan, and A. Jagarlapudi, "Precision Agriculture and Unmanned Aerial Vehicles (UAVs)," in *Unmanned Aerial Vehicle: Applications in Agriculture and Environment*: Springer, 2020, pp. 7-23.

- [45] P. Radoglou-Grammatikis, P. Sarigiannidis, T. Lagkas, and I. Moscholios, "A compilation of UAV applications for precision agriculture," *Computer Networks*, vol. 172, p. 107148, 2020.
- [46] U. S. Panday, A. K. Pratihast, J. Aryal, and R. B. Kayastha, "A Review on Drone-Based Data Solutions for Cereal Crops," *Drones*, vol. 4, no. 3, p. 41, 2020.
- [47] G. Haddeler, A. Aybakan, M. C. Akay, and H. Temeltas, "Evaluation of 3D LiDAR Sensor Setup for Heterogeneous Robot Team," *Journal of Intelligent & Robotic Systems*, 2020/08/12 2020.
- [48] L. Zhou, X. Gu, S. Cheng, G. Yang, M. Shu, and Q. Sun, "Analysis of Plant Height Changes of Lodged Maize Using UAV-LiDAR Data," *Agriculture*, vol. 10, no. 5, p. 146, 2020.
- [49] M. Paul, M. Negahban-Azar, A. Shirmohammadi, and H. Montas, "Assessment of agricultural land suitability for irrigation with reclaimed water using geospatial multi-criteria decision analysis," *Agricultural Water Management*, vol. 231, p. 105987, 2020.
- [50] FAO, "The future of food and agriculture – Trends and challenges," 2017.
- [51] E. D. Lioutas and C. Charatsari, "Big data in agriculture: Does the new oil lead to sustainability?," *Geoforum*, vol. 109, pp. 1-3, 2020.
- [52] Russ, M., 2021. Knowledge management for sustainable development in the era of continuously accelerating technological revolutions: A framework and models. *Sustainability*, 13(6), p.3353.
- [53] Fazelabdolabadi, B., Montazeri, M. and Pourafshary, P., 2021. A Data Mining Perspective on the Confluent Ions Effect for Target Functionality. *HighTech and Innovation Journal*, 2(3), pp.202-215.
- [54] Habeeb, N.J. and Weli, S.T., 2021. Combination of GIS with Different Technologies for Water Quality: An Overview. *HighTech and Innovation Journal*, 2(3), pp.262-272.

Design and Development for a Vehicle Tracking System

Tim Abe P. Andutan, Rosanna C. Ucat

College of Engineering, University of Southeastern Philippines, Davao City, Philippines

Abstract—In recent years, the drastic increase in the number of vehicle thefts brings about at an alarming rate around the world. However, existing vehicle tracking devices have certain limitations including the lack of ability to determine if the vehicle is on the right route. To address this problem, this study focused on the design and development of a vehicle tracking prototype with route detection, emergency button, and STATUS command to monitor the current location of the vehicle. Arduino Mega 2560, SIM900 Global System for Mobile communication (GSM) module, and NEO-6M Global Positioning System (GPS) module were used to develop the prototype. The GPS module, push buttons, and SMS command served as an input. The Arduino Mega 2560 was programmed using an algorithm to determine if the device deviated from its route, detect if the emergency button was pressed, and if STATUS command was received. The system sends a SMS if the vehicle deviated from its path, emergency button is pressed, and a STATUS command from the operator is received. Results showed that after several trials the prototype was successful in performing its functional objectives. The prototype was only limited to the use of a prototyping grade GPS module. The GPS used a built-in antenna and took time to connect to satellites. It is recommended to use an industrial grade GPS module and connect an external antenna to improve signal strength.

Keywords—Arduino; global positioning system; GPS; global system for mobile communications; GSM; vehicle tracking; route deviation detection

I. INTRODUCTION

As the number of automobiles in the road increases, the crime involving larceny or vehicle stealing also increases [1]. In recent years, the drastic increase in the number of vehicle thefts brings about at an alarming rate around the world [2]. The Interpol Statistics revealed that 4.2 million vehicles were reported to be stolen in 2008 from 149 countries [3]. In 2020, the National Insurance Crime Bureau (NICB) further revealed that the vehicle theft increased considerably which totaled up to 873,080 compared in 2019 [4].

Evidently, the scenario is also common in the Philippines with a highest record of 13.2 cases of vehicle theft per 100,000 population in 2014 [5]. The volume of vehicle theft has brought to a national concern which ranks third next to theft and robbery among all property crimes in the country [6]. Recently, the vehicle theft in the country was at 4.6 cases per 100,000 population in 2018 [5].

The application of this study could be significant to corporations such as the banking sector, logistics company, and food industry in improving vehicle security during

transportation of confidential materials, and accomplishing projects to avoid unwanted intrusions, delay, and theft. This study can also benefit the vehicle operators in terms of theft recovery and improvement of performance in vehicle security, tracking, and monitoring. This study can serve as a basis or foundation to future researchers in relation to vehicle monitoring and tracking system.

To address the growing concern in vehicle tracking, the proponent intended to design and develop an easy-to-use vehicle tracking and monitoring system with route deviation detection and SOS capability. The study also aimed to use the nature of Global System Monitoring – Short Message Service (GSM-SMS) Technology to effectively send notifications and location details of the vehicle when the vehicle deviated from its path, if the button was pressed during an emergency situation, and “<STATUS>” command was requested to determine the current status of the vehicle.

II. LITERATURE REVIEW

Khin and Oo [7] created a vehicle tracking system that utilizes GPS technology to determine a vehicle’s location. The study used GPS and GSM technology, in which the embedded GPS module retrieves the vehicle’s location. After which, the GPS continuously monitor the movement of the vehicle and plot the location using Google Map and displayed on a webpage. The vehicle’s position was also saved through MySQL databased using XAMPP platform.

Besides, Sharp, Cable, and Burns [8] used GPS technology for tracking the movements of the visitors in heritage sites. The research utilized GPS to understand the temporal and spatial distribution of the visitors’ movements. The findings were used to develop strategic opportunities to attract the visitors to the less visited areas of the heritage site and properly engage with the site.

The study of Shukla [9] incorporated GPS technology for landmine detection wherein GPS was attached to a rover and the rover was controlled using Dual Tone Multiple Frequency (DTMF). A landmine detection circuit was installed to the rover. When a landmine is detected, the rover returned the location from the GPS and directly sent to the operator and locate the landmine.

The recent studies mentioned above used GPS technology for tracking the movements of a robot, tourist, and vehicles. However, none of the studies utilized GPS to track the movement of a vehicle that identifies whether object of interest to be tracked deviated from its route or not. The studies also were not able to determine if the object being

tracked arrived to the specific location based on the coordinates from the GPS module.

The study of Reddy, Krishna, Chaitanya, and M. Neeharika [10] used GSM technology in developing a security alarm based on door knock patterns. Piezoelectric element was used to detect the door knocking pattern to detect possible intruder. When a correct knocking pattern is detected, the door unlocks, otherwise, the prototype sends a text message to the home owner indicating that possible intruder is present.

Sakthivel et al. [11] established the same concept, where they used a Vehicle Security System using embedded and GSM Technology. They designed a security system for automobiles by installing the device in the vehicle. Sakthivel et al. [11] created a password system before starting the host vehicle, alerting the owner of unauthorized persons attempt to drive the vehicle.

The concept about the use of GSM technology as a medium for sending a notification to the concerned personnel was used in the study. The GSM technology had provided various application in security and emergency purposes. Unlike the studies mentioned above, the study utilized the GSM technology to send an emergency alert notification whenever the SOS button is pressed. GSM was also used to monitor the current status of the vehicle when the operator sends a “<STATUS>” command, which were absent to those studies.

III. RESEARCH METHODOLOGY

A. Research Design

The research design used in the study was developmental research approach, which aimed to the design and development of both hardware and software components to produce a desired system that tracks the vehicle, check if the vehicle deviated from its path, and retrieve data from the GPS including the speed and the coordinates, button-trigger for emergency purposes. The system utilized the Global System for Mobile Communication (GSM) to transmit the data to a mobile phone. This study was non-experimental, since there were no manipulations of the variables.

Waterfall Method was used in this project; waterfall method is a sequential design process in which progress is seen as flowing straight downwards through a series of phases. Waterfall model was utilized since the proponents should complete each phase in order to proceed to the succeeding phase. Overlapping of the phases is not possible.

Fig. 1 showed the process started from the procurement of the materials. When the materials were already procured, the hardware, which includes the circuitry and the 3D printing were done. The programming phase under the software development commenced to test the functionality of the system based on the objectives of the study. When the prototype was already built, the proponents tested the prototype to various locations with the vehicle having the prototype attached to it. Data analysis was then carried out to discover the findings of the data obtained from the prototype sampling.

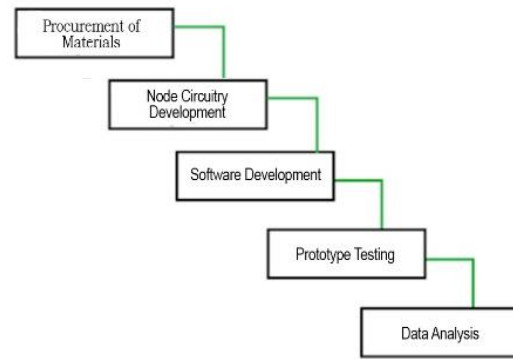


Fig. 1. Flow Diagram of the Study (Waterfall Method).

1) *Data sampling*: The proponent selected fourteen (14) distinct locations in Davao City. Four (4) locations were selected as the deviation route. While ten (10) locations were selected as the route. The prototype was put inside the vehicle and the vehicle travelled along the pre-determined route. The proponents then recorded if the prototype was able to record each location where the device traversed. Also, it was recorded if the prototype was able to detect the deviation route and if it successfully notified the user about the deviation. The SOS feature was also tested by pressing the SOS button repeatedly. Lastly, the “<STATUS>” command was also tested if the prototype was able to reply to the user the current location (coordinates), the current speed (kph), and the link to Google Maps.

The data for the deviation detection functionality was collected by recording whenever the coordinates from the GPS module were inside a specific area. If the coordinates were recorded in a specific area, the program then checked if that area was a deviation area. A success remark was recorded, which denotes that the prototype was able to identify the area correctly, and if successfully sent a SMS notification whenever the coordinates were inside the deviation area. Otherwise, no message was received.

The status command functionality was tested by giving ten alternating requests. Five requests for no status, and another five status requests. When the user sent a “<STATUS>” command, the prototype sent a SMS notification to the user. When no status request was sent, the prototype did not send any message. These two criteria were used to give a success remark. However, when the user sent a “<STATUS>” command to the prototype and no reply was received, or if the user did not request any status from the prototype but received an SMS, a failing remark was given.

Lastly, the same logic was applied to evaluate the SOS command. Whenever the driver pressed the emergency button on the device, the prototype sent an emergency notification on the dispatcher and a success remark was given. However, when the driver did not press the emergency button, and the prototype sent an emergency notification to the dispatcher, then, a failing remark was recorded.

B. Research Procedure

The research procedure focuses on the five major areas in the study, which included the materials used in the study, node circuitry development, software development, prototype testing, and data analysis. Procurement of materials discussed what materials were used in developing the study including material description and supplier. The node circuitry development discussed how the hardware counterpart of the prototype was built including the circuitry and the enclosure of the device, while the software development tackled the method on how the device was programmed. The prototype testing explained the method on which the data were collected. Lastly, the data analysis showed the tools to analyze the data and arrive with a comprehensive conclusion.

1) *Materials:* Prior to the development of the project, the following materials were procured, which included the Arduino Mega 2560 Rev 3, which served as the motherboard of the prototype. The SIM900 GSM module, was used to manage the SMS notification between the device and the receiver (driver and dispatcher). Ublox Neo 6M GPS module was used as GPS module that communicated to the satellites and acquired the coordinates. Stranded wires were used to manage the connection between the motherboard and other components, 5V 2A DC power supply to power the entire prototype and breadboard for testing the cricuity. The Arduino Mega 2560 Rev 3, SIM900 GSM module, and Ublox Neo 6M were procured from Makerlabs Electronics in Santa Cruz, Manila through Lazada Philippines, while the remaining components were procured in Davao Times Trading Incorporated in Palma Gil Street, Davao City.

2) *Node circuitry development:* The node of the data-gathering transceiver was developed. The following materials were integrated to the Arduino Mega 2560 board, which processed the input from the sensors and transmitted the data gathered to a smartphone via GSM. For the casing, 3D printed enclosure was designed using SketchUp: 3D Design Software 2018. The enclosure was made of Acrylonitrile butadiene styrene (ABS) polymer.

Fig. 2 showed the top view of the 3D design of the enclosure, the object on the left was the cover while, the object on the right was the body of the enclosure where the electronic components were attached.

Fig. 3 showed the right view of the body wherein the name of the prototype was engraved. Fig. 4 is the left view of the enclosure, Fig. 4 showed the thickness of the cover.

On the other hand, Fig. 5 showed the schematic diagram of the prototype. The prototype used Arduino mega 2560 as its main processor where the SOS button is connected to the digital pin 2 and ground pin, the GSM module RX pin was connected to the TX 16 pin while the TX pin was connected to the RX 17 pin of the Arduino mega. The GPS module RX pin is connected to TX 18 while the TX pin was connected to RX 19. The GSM and the GPS used a 5V logic levels from the Arduino.

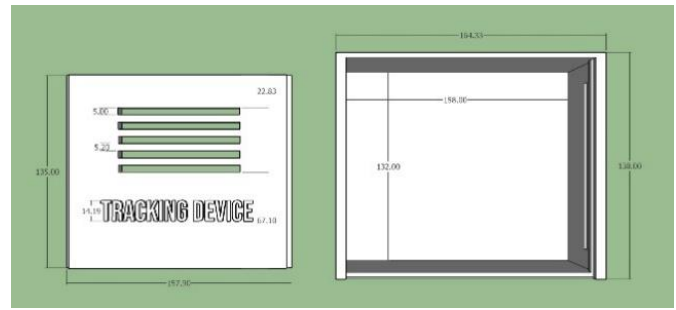


Fig. 2. Top View 3-dimensional Model.

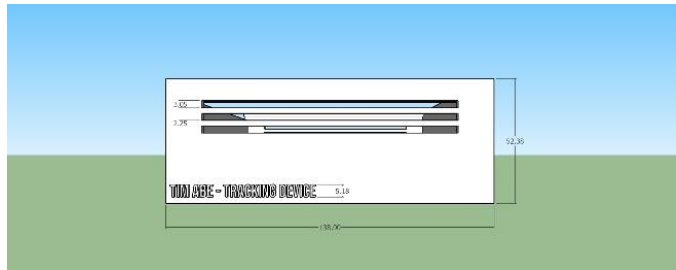


Fig. 3. Right View 3-dimensional Model.

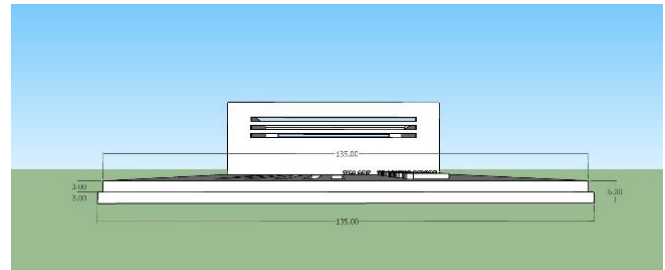


Fig. 4. Left View 3-dimensional Model.

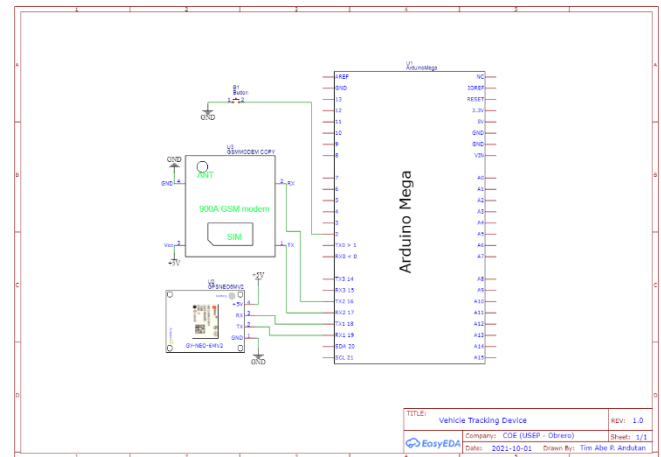


Fig. 5. Tracking Device Schematic Diagram.

Fig. 6 showed the list of all the components used in building the prototype and showed the placement of each component inside the 3D-printed ABS polymer enclosure.

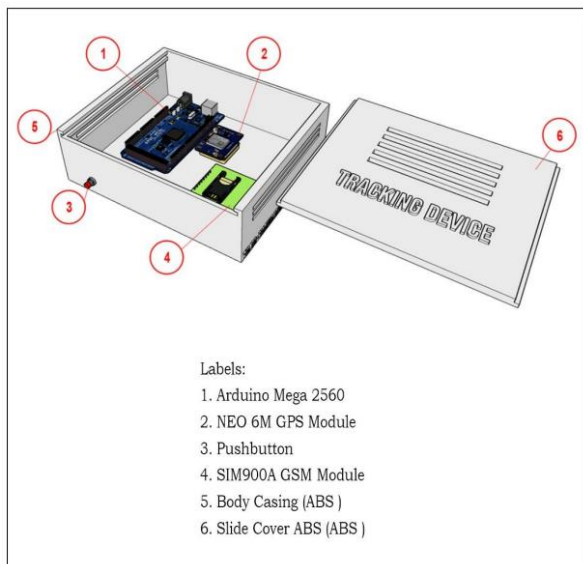


Fig. 6. Project Layout (Isometric Diagram).

3) *Software development:* The Arduino Mega board was programmed in Arduino Development Environment (Version 1.8.13) using C programming language. The Arduino Mega 2560 board was programmed to read the coordinates of a certain location and the speed (kph) on a real-time basis. The obtained coordinates were used to determine whether the coordinates were within the pre-determined route. These coordinates were used as a guide to determine if the current vehicle position deviated from its path. The coordinates of the pre-selected point were determined using Google Maps. If a deviation was recorded, the device automatically sent an alert message to the user. Moreover, the button served as an emergency button, in which it was programmed to send an emergency message to the user/owner when the button is pressed. On the other hand, the user can also send a message to determine the current status of the device by sending the keyword "<STATUS>." The device will then reply the following outputs: Current GPS coordinates, speed (kph), and a link directing to Google Maps to plot the location based on the coordinates received.

Fig. 7 showed the data flow diagram of how the prototype was programmed. It showed that when a signal was established for the GSM and GPS, the prototype started to read the coordinates and constantly checked whether the button is pressed, a status command was received, and if the coordinates is inside a specific preprogrammed location.

4) *Prototype testing:* Prior to the conduct of the data sampling, the prototype was tested initially. The prototype was tested within the residence of the proponent to check if the prototype was able to function accordingly. The code was revised several times to ensure the functionality of the whole system.

5) *Data analysis:* Prototype was analyzed and evaluated to the extent of the functionality of the whole system in terms of hardware and software development. The whole system

was analyzed according to three parameters: (1) Able to detect if the vehicle deviated from its route, (2) able to send SOS notification when the SOS button was pressed, and (3) able to send the current status of the vehicle in terms of speed (kph) and the current location (coordinates). Observation was done for each major functionality and tabulated. Percent error was computed for each major function of the prototype. Percent error was used to quantify how close the number of successes to an estimated total value in which in this case, the number of trials, it also denotes the accuracy of the test based on the data collected. It approximated the error percentage of the data (experimental) relative to the expected standard value (theoretical).

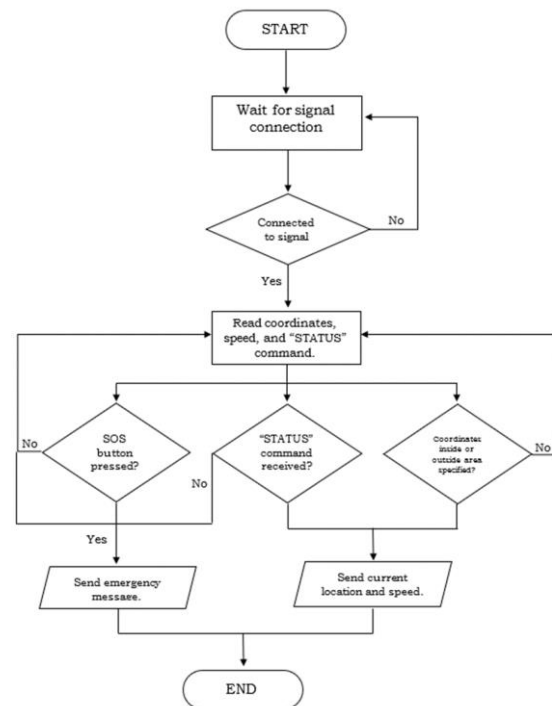


Fig. 7. Software Programming Flow Diagram.

IV. PRESENTATION, ANALYSIS AND INTERPRETATION OF RESULTS

A. Objective 1

The prototype was composed of both the hardware and software. For the hardware counterpart, the node of the data gathering transceiver was successfully developed using the four major components, which included the Arduino Mega 2560 board which managed the data processing, GSM SIM900A module for data transmission from the device to the mobile phone of the user, and the NEO 6M GPS module which facilitated the tracking of the location and the speed of the vehicle. For the software counterpart, the program for the route deviation detection, emergency command, command, tracking, and sending of SMS notifications was coded using the Arduino Integrated Development Environment (IDE) using the simplified C programming for Arduino boards. Fig. 8 presented the integration of the hardware and software of the prototype.

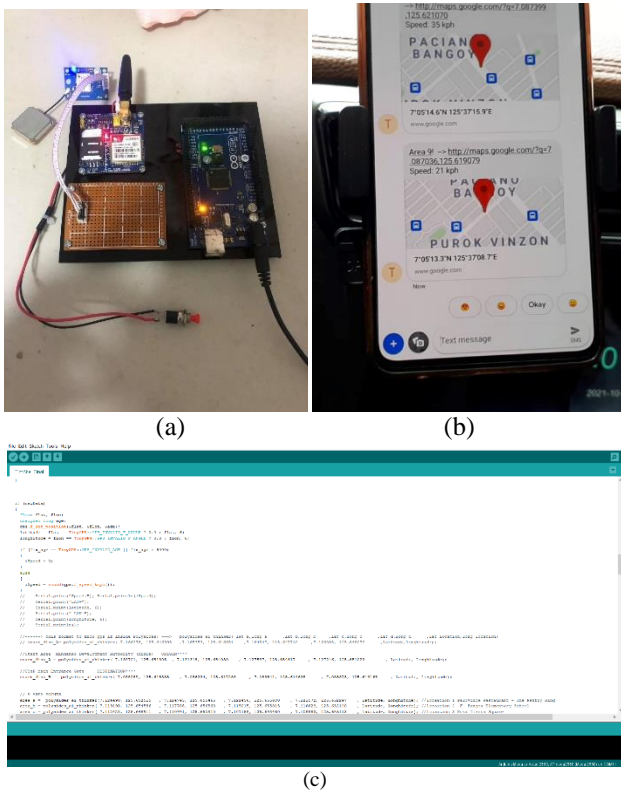


Fig. 8. Hardware and Software Integration of the Prototype (a) Node Circuitry Transceiver, (b) Received SMS from the Transceiver, (c) Arduino Mega 2560 Programming using Arduino IDE.

B. Objective 2

The prototype was tested to track the vehicles' location and speed through the use of the GPS module. The GPS module communicated to the satellites and to retrieve the vehicles' location using the coordinates. When the coordinates recorded by the GPS were inside a certain area, the prototype then sent an SMS notification to the driver and the dispatcher to locate the vehicles' current location.

Table I showed the results for tracking and speed monitoring. The prototype was tested in 14 distinct locations in Davao City, each location, the prototype successfully sent the specified area, its coordinates, and the speed of the vehicle. The mobile phone also successfully received an SMS, which contained the following mentioned details and the Google maps link. Table I also affirmed that the prototype sent a notification to the user when it traversed the correct path. Among the fourteen test locations, ten (10) locations were programmed as a correct path, while four (4) locations were programmed as the deviated path. It is shown that the prototype was successful in detecting the deviated path.

Fig. 9 showed the map for the entire testing. The red dotted line showed the restriction area, in the program, when the coordinates recorded by the GPS were inside the red area, the prototype sent a SMS to the user indicating that the vehicle deviated from its path. Within the Northern area, industrial companies were present and some portions of the area were used as a commercial space. In the Western part, residential spaces occupied most of the area. Commercial establishments

and schools were present. For the Eastern part, sea ports, beaches, and some commercial establishments were present. Lastly, for the Southern part, schools, commercial spaces, and residential areas were present.

TABLE I. RESULTS FOR LOCATION AND SPEED MONITORING

Area	Coordinates (Lat, Long)	Speed (kph)	Deviated? (Yes/No)	Received SMS? (Yes/No)	Description (Success/Fail)
1	7.124496,125.653671	38	No	Yes	Success
2	7.119050,125.654754	43	No	Yes	Success
3	7.111478,125.650077	24	No	Yes	Success
4	7.105888,125.645469	48	No	Yes	Success
5	7.099695,125.640449	34	No	Yes	Success
6	7.092534,125.634613	36	No	Yes	Success
7	7.085145,125.626663	42	No	Yes	Success
8	7.086773,125.621627	19	No	Yes	Success
9	7.087036,125.619079	21	No	Yes	Success
10	7.087199,125.616294	24	No	Yes	Success
11	7.082574,125.620010	36	Yes	Yes	Success
12	7.097366,125.614967	43	Yes	Yes	Success
13	7.132690,125.661613	31	Yes	Yes	Success
14	7.109219,125.649734	31	Yes	Yes	Success

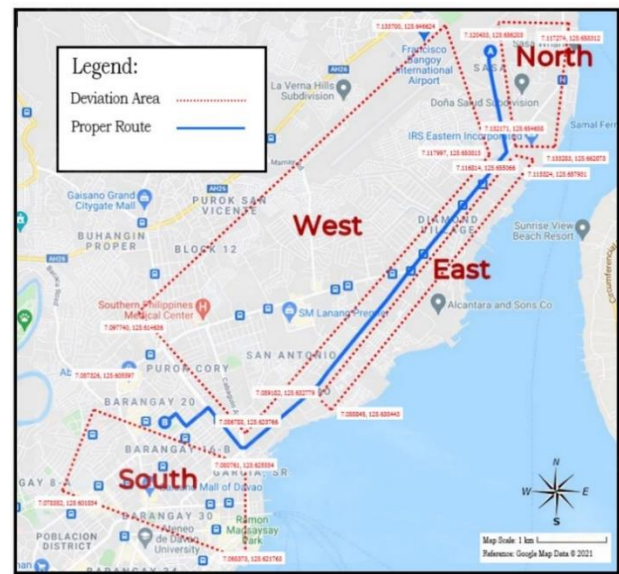


Fig. 9. Testing Route (Davao City).

C. Objective 3

The program showed the syntax on how the areas in the map were coded in the Arduino IDE. The numbers in the program were the coordinates of each corner of the area. There were four coordinates used to identify an area, since the area was identified by enclosing a specific location using a quadrilateral polygon. The highlighted line indicated the format of inputting the coordinates.


```
//-----> this format to know GPS if inside Polysides! --->
polysides_ai_thinker(lat a,long a ,lat b,long b ,lat c,long c ,lat d,long
d ,lat location,long location)

//Start Area Mindanao Development Authority (MinDa) ORIGIN****
start_dist_A = polysides_ai_thinker( 7.130701, 125.651305 , 7.131318,
125.654030 , 7.127597, 125.654617 , 7.127246, 125.651023 ,
latitude, longitude);

//UseP Main Entrance Gate DESTINATION****
start_dist_B = polysides_ai_thinker( 7.088289, 125.615335 , 7.086224,
125.617288 , 7.083541, 125.614638 , 7.085873, 125.613168 ,
latitude, longitude);

// Sample Area points
area_a = polysides_ai_thinker(7.124490, 125.652515 , 7.124745,
125.655465 , 7.122456, 125.655680 , 7.121572, 125.652247 , latitude,
longitude); //location 1 Palovince Restaurant - The Pakfry King
area_b = polysides_ai_thinker( 7.119198, 125.654586 , 7.117708,
125.656560 , 7.115015, 125.655015 , 7.116623, 125.652140 , latitude,
longitude); //location 2 F. Bangoy Elementary School
area_c = polysides_ai_thinker( 7.112428, 125.648911 , 7.110991,
125.650810 , 7.107158, 125.648460 , 7.108883, 125.645113 , latitude,
longitude); //location 3 Nova Tierra Square
area_d = polysides_ai_thinker( 7.107084, 125.643794 , 7.105274,
125.646347 , 7.099698, 125.643910 , 7.102839, 125.639050 , latitude,
longitude); //location 4 Caltex Lanang
area_e = polysides_ai_thinker( 7.100859, 125.638728 , 7.098911,
125.641829 , 7.095366, 125.638857 , 7.097048, 125.635092 , latitude,
longitude); //location 5 Diamond Hardware Republic
area_f = polysides_ai_thinker( 7.093535, 125.632753 , 7.091746,
125.636186 , 7.089095, 125.633579 , 7.091906, 125.628644 , latitude,
longitude); //location 6 Techno-Trade Resources Davao

//Deviation Area 1 West
deviation_a = polysides_ai_thinker( 7.133700, 125.646624 , 7.117997,
125.653815 , 7.086788, 125.623766 , 7.097740, 125.614636 ,
latitude, longitude);

//Deviation Area 2 East
deviation_b = polysides_ai_thinker( 7.116814, 125.655066 , 7.115324,
125.657931 , 7.088845, 125.638443 , 7.089182, 125.632779 ,
latitude, longitude);

//Deviation Area 3 South
deviation_c = polysides_ai_thinker( 7.080761, 125.625554 , 7.068373,
125.621763 , 7.078352, 125.601834 , 7.087326, 125.605597 ,
latitude, longitude);

//Deviation Area 4 North
deviation_d = polysides_ai_thinker( 7.132171, 125.654658 , 7.133283,
125.662873 , 7.117274, 125.658312 , 7.120433, 125.656203 ,
latitude, longitude);
```

The program and syntax for determining whether the point (longitude, latitude) from GPS module is inside a certain area enclosed by four points. A library has been made and was

used to easily code the Arduino program. Each location, the proponent should choose and enclose a specific area using the four points. The longitude and latitude of each point from the four points should be defined in the program with the use of Google Maps. If the longitude and latitude from the GPS was inside the enclosed area, the program returned a value of 1, otherwise, 0. An if-else statement have constructed whether the program returned 1 or 0, if the program returned a value of 1 (point is inside the area), an SMS notification will be sent, otherwise, the program will continue the loop.

- Route Deviation

It notified that the prototype was able to create distinction between the correct path and the deviated path. The 14 areas were identified strategically in which the proponent can easily traverse all the areas in a minimal time period and achieve the objectives. Also, the chosen areas were used, since these areas have known landmark for easier validation and documentation. For areas 1 to 10, the prototype did not receive an alert message that indicated that the vehicle deviated, since area 1-10 were programmed as a correct path. However, when the vehicle was in area 11 to 14, the driver and the dispatcher received an alert indicating that the vehicle deviated from its correct path. It was evident that for every area, the functional objective was satisfied; thus, a success remark was recorded and prototype was able to traverse all fourteen (14) locations. The prototype sent four (4) deviation notifications to the user as it traversed four (4) deviation routes.

Table II denoted that in fourteen (14) areas where the prototype was tested, the prototype was able to distinguish the four deviation areas that was programmed in the microcontroller and successfully notified the operator. Thus, all the testing from area 1 to area 14 yielded a successful remark.

TABLE II. RESULTS FOR ROUTE DEVIATION DETECTION (TRIAL 1)

Area	Coordinates (Lat, Long)	Speed (kph)	Speed Limit (kph)	Deviated? (Yes/No)	Received SMS?	Remarks (Success/Fail)
1	7.124496,125.653671	38	40	No	Yes	Success
2	7.119050,125.654754	43	40	No	Yes	Success
3	7.111478,125.650077	24	40	No	Yes	Success
4	7.105888,125.645469	48	30	No	Yes	Success
5	7.099695,125.640449	34	30	No	Yes	Success
6	7.092534,125.634613	36	30	No	Yes	Success
7	7.085145,125.626663	42	30	No	Yes	Success
8	7.086773,125.621627	19	30	No	Yes	Success
9	7.087036,125.619079	21	30	No	Yes	Success
10	7.087199,125.616294	24	30	No	Yes	Success
11	7.082574,125.620010	36	40	Yes	Yes	Success
12	7.097366,125.614967	43	40	Yes	Yes	Success
13	7.132690,125.661613	31	40	Yes	Yes	Success
14	7.109219,125.649734	31	40	Yes	Yes	Success

TABLE III. RESULTS FOR ROUTE DEVIATION DETECTION (TRIAL 2 – DRIVER)

Area	Coordinates (Lat, Long)	Speed (kph)	Speed Limit (kmh)	Deviated?	Driver Received SMS?	Remarks (Success/Fail)
1	7.124536,125.653678	51	40	No	Yes	Success
2	7.117696,125.654991	16	40	No	Yes	Success
3	7.111468,125.650077	38	40	No	Yes	Success
4	7.105462,125.645187	44	30	No	Yes	Success
5	7.098969,125.639831	32	30	No	Yes	Success
6	7.092573,125.634574	33	30	No	Yes	Success
7	7.085191,125.626670	31	30	No	Yes	Success
8	7.086732,125.621635	33	30	No	Yes	Success
9	7.087046,125.619064	28	30	No	Yes	Success
10	7.087119,125.616203	21	30	No	Yes	Success
11	7.109208,125.649772	18	40	Yes	Yes	Success
12	7.120164,125.657218	48	40	Yes	Yes	Success
13	7.084045,125.615516	25	40	Yes	Yes	Success
14	7.095824,125.616249	32	40	Yes	Yes	Success

TABLE IV. RESULTS FOR ROUTE DEVIATION DETECTION (TRIAL 2 – DISPATCHER)

Area	Coordinates (Lat, Long)	Speed (kph)	Speed Limit (kph)	Deviated?	Dispatcher Received SMS?	Remarks (Success/Fail)
1	7.124536,125.653678	51	40	No	Yes	Success
2	7.117696,125.654991	16	40	No	Yes	Success
3	7.111468,125.650077	38	40	No	Yes	Success
4	7.105462,125.645187	44	30	No	Yes	Success
5	7.098969,125.639831	32	30	No	Yes	Success
6	7.092573,125.634574	33	30	No	Yes	Success
7	7.085191,125.626670	31	30	No	Yes	Success
8	7.086732,125.621635	33	30	No	Yes	Success
9	7.087046,125.619064	28	30	No	Yes	Success
10	7.087119,125.616203	21	30	No	Yes	Success
11	7.109208,125.649772	18	40	Yes	Yes	Success
12	7.120164,125.657218	48	40	Yes	Yes	Success
13	7.084045,125.615516	25	40	Yes	Yes	Success
14	7.095824,125.616249	32	40	Yes	Yes	Success

Tables III and IV still showed the results for the route deviation detection for trial 2. In trial 2, there were two receivers that were involved in the trial, the driver and the dispatcher. It revealed that the prototype was still able to create distinction between the correct path and the deviated path. The prototype was able to traverse all fourteen (14) locations. The prototype sent four (4) deviation notifications to the driver and the dispatcher as it traversed four (4)

deviation routes. The selection of the locations was strategically chosen for it to be near and along the downtown area that have familiar landmarks for convenient validation of the results. Four locations were chosen for the deviation to enclose the preselected route used for the entire duration of the testing. The deviation areas were strategically positioned to the Eastern, Western, Southern, and Northern part relative to the proper route.

TABLE V. CONTENT COMPARISON

Test	Driver's Phone	Dispatcher's Phone	Remarks
Coordinates	Matched		Success
Received Message	Matched		Success

Table V showed the comparison between the driver's phone and the dispatcher's phone. The coordinates received by both the driver's phone and dispatcher's phone were the same, which indicated that the coordinates received by the GPS from the satellites were successfully fetched to both devices. Fig. 10 shows both the smartphones received identical messages indicating the coordinates, and the speed of the vehicle, which denoted that the message being received were not altered and manipulated.

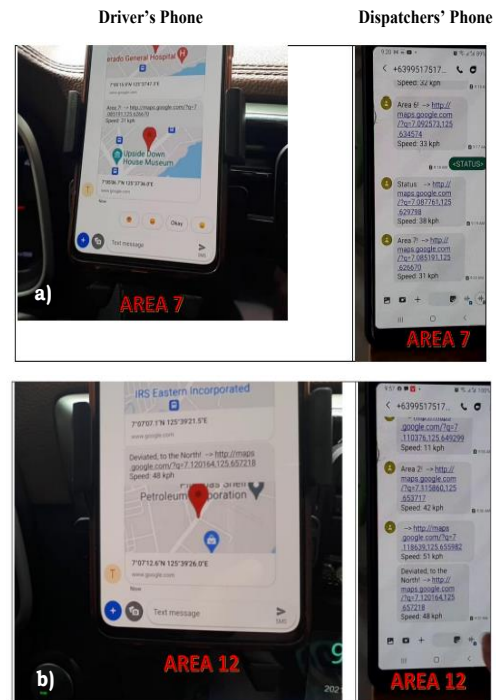


Fig. 10. (a) Route Tracking for Area 7 for both Driver and Dispatcher; (b) Deviation Detection (North) for both Driver and Dispatcher.

- Status Command

In Table VI, it revealed that the prototype was tested ten (10) times to evaluate the functionality of the status command. STATUS command was evaluated by sending a STATUS request to the prototype. The proponent sent five (5) requests to the prototype and the prototype sent its current location (coordinates), speed (kph), and a link to the Google Maps to

plot the location of the vehicle based on its coordinates. It affirmed that prototype was able to respond to the request five (5) times successfully.

TABLE VI. RESULTS FOR STATUS COMMAND

Entry	STATUS Requested? (Yes/No)	Received SMS (Yes/No)	Description (Success/Fail)
1	Yes	Yes	Success
2	No	No	Success
3	Yes	Yes	Success
4	No	No	Success
5	Yes	Yes	Success
6	No	No	Success
7	Yes	Yes	Success
8	No	No	Success
9	Yes	Yes	Success
10	No	No	Success

On the other hand, the proponent also did not send a message to the prototype five (5) times. Then, the prototype also did not respond, which indicated that the STATUS command was successful.

- Emergency Request (SOS Command)

Table VII showed the results for the SOS command. The SOS command was evaluated by pressing the SOS button five (5) times. It was expected as the user pressed the SOS button, the prototype should send SMS notification to the receiver (operator or main office) with the current location and an “Emergency Alert” phrase to indicate a distress signal. The proponent sent five (5) SOS command and the prototype was successful in sending five (5) emergency messages to the receiver. However, the proponent also did not press the SOS button, which indicated no emergency. Thus, the prototype also did not send an emergency message to the receiver; thereby, it suggested that the prototype worked.

TABLE VII. RESULTS FOR SOS (EMERGENCY ALERT BUTTON)

Entry	SOS Requested?	Coordinates	Received SMS?	Description (Success/Fail)
1	Yes	7.117279,125.654731	Yes	Success
2	No	-	No	Success
3	Yes	7.115866,125.653663	Yes	Success
4	No	-	No	Success
5	Yes	7.113910,125.652076	Yes	Success
6	No	-	No	Success
7	Yes	7.109687,125.648620	Yes	Success
8	No	-	No	Success
9	Yes	7.098881,125.639793	Yes	Success
10	No	-	No	Success

Furthermore, the algorithm of the program was to check if the coordinates from the GPS module were inside a certain area enclosed in a quadrilateral polygon. If the coordinates retrieved by the GPS module were inside a certain area, the device sent an SMS notification indicating the specific area where the coordinates were situated.

D. Objective 4

Table VIII showed the percent error of the three major functions of the prototype. For route deviation detection, out of 14 total number of trials, the prototype performed its functionality 14 times consecutively, which yielded to a percent error of 0%. For the status command, the functionality was assessed by sending five status requests and five no status requested (total of 10), in which the prototype was able to perform each function. The percent error yielded to 0%. Moreover, the route deviation was also tested for sending SMS notification for both driver and the dispatcher, in which the percent error still yielded to 0%. Lastly, for the emergency command, the SOS button was pressed five times and the prototype sent an SMS five times also. Moreover, the SOS button was not pressed five times. The button also did not send an SMS notification. Table VIII showed 0% of percent errors for all the major functions, which denoted that the prototype was able to perform its desired functions.

TABLE VIII. PERCENT ERROR OF MAJOR FUNCTIONS

Functionality	Number of Success	Total Number of Test	Percent Error
Route Deviation Detection (Driver)	14	14	0%
Route Deviation Detection (Driver & Dispatcher)	14	14	0%
Status Command	10	10	0%
Emergency Command (SOS)	10	10	0%

E. Interpretation of Results

The proposed vehicle tracking system using Arduino Mega 2560, NEO 6M GPS module, SIM900A GSM module, and push button was successful. Trials were conducted to assess the functionality of each major function, which included deviation detection, current status monitoring, and SOS SMS notification. Table I showed that out of the 14 distinct locations tested, all got a successful remark. The prototype was able to distinguish whether the area was proper route or deviation route. All ten proper routes and four deviation routes were successfully identified. Table VI showed that out of ten trials, the remarks were all successful. Five trials were performed to simulate a status request from the prototype and five trials were also conducted to request no status. Each trial that requested status report was successful as well as to the no status requested. Table VI also suggested that the STATUS command’s functionality was a success since no failure remark was recorded. In Table VII, the data showed that all ten trials for SOS command were successful. Five trials were conducted to simulate an emergency alert in which the prototype successfully sent five emergency notifications. Moreover, five trials were also done to test the no emergency

REFERENCES

(button not triggered), the data indicated that the prototype did not send emergency notification five times consecutively. Overall, all the tests recorded a successful remark and no failure.

Apparently, based on the reviews of previous literary works, there were no present prototypes, as of the date during the conduct of the study, were published that could detect if the vehicle deviated from its route, which is the primary feature developed in this study.

Lastly, during the conduct of the study, it was encountered that the device had taken time connecting to the satellite before acquiring the GPS coordinates that were needed to track the vehicle, which could identify if the vehicle deviated from its path and calculate the vehicles' speed.

V. CONCLUSION

Based on repeated testing and evaluation, the proponent can conclude that the study met its objective. The study proved that developing a vehicle tracking prototype with route deviation detection, emergency command, and current status command is possible using Arduino Mega 2560, uBlox NEO 6M GPS module, SIM900A GSM module and a pushbutton. The results showed that the prototype was able to distinguish the deviated path from the correct path. Moreover, the prototype also was able to distinguish whether the user pressed the SOS button or not, and if the user sent a "<STATUS>" command or not. The results also suggested that based on the actual testing, the prototype successfully performed its functional objective as a whole. There were issues encountered, such as the delay in receiving the text messages due to signal connectivity constraints, and the GPS module also had taken time connecting to the satellites due to buildings and walls that may block the signal and weather factor. Compared to the use of camera and any visual guidance system, the proposed prototype can detect deviation and deal with non-conventional factors, such as uneven road, too bright and/or too dim pathways.

- [1] T. Noman, S. Hossain, S. Islam, M. Islam, N. Ahmed and M. M. Chowdhury, "Design and implementation of microcontroller based anti-theft vehicle security system using GPS, GSM, and RFID," in 2018 4th International Conference on Electrical Engineering and Information Communication Technology (ICEEICT), 2018.
- [2] V. K. Sadagopan, U. Rajendran and A. J. Francis, "Anti-theft control system design using embedded system," in Proceeding of 2011 IEEE International Conference on Vehicular Electronics and Safety, 2011.
- [3] M. Abuzalata, M. Momani, S. Fayyad and S. Abu-Ein, "A Practical Design of Anti-theft Car Protection System Based on Microcontroller," American Journal of Applied Sciences, p. 709, 2012.
- [4] "Insurance Information Institute," February 2021. [Online]. Available: <https://www.iii.org/fact-statistic/facts-statisticsauto-theft>.
- [5] "World Data Atlas," February 2021. [Online]. Available: <https://knoema.com/atlas/ranks/Private-car-theft-rate>.
- [6] D. J. Barrera, R. M. Omaña, G. Alviola, R. Grapa, J. Ojales, K. Antonio and J. Montinod, "Motor Vehicle Theft in Negros Oriental, Philippines: Patterns Across Space, Time, and Targets," Prism, 2015.
- [7] J. M. M. Khin and N. N. Oo, "Real-Time Vehicle Tracking System Using Arduino, GPS, GSM and Web-Based Technologies," in International Journal of Science and Engineering Applications, Myanmar, 2018.
- [8] R. L. Sharp, T. T. Cable and A. Burns, "The Application of GPS Visitor Tracking Implications for Interpretation at Heritage Sites," in Journal of Interpretation Research, Manhattan, 2020.
- [9] R. M. Shukla, "Low-Cost DTMF Controlled Landmine Detection Rover," in International Research Journal of Engineering and Technology (IRJET), Maharashtra, 2019.
- [10] R. C. Reddy, P. Krishna, M. Chaitanya and M. Neeharika, "Security System Based on Knock-Pattern Using Arduino and GSM Communication," International Journal of Engineering and Techniques, pp. 154-157, 2018.
- [11] C. Sakhtivel, S. Umar Maktar, M. S, R. G and K. V, "Vehicle Security System using Embedded and GSM Technology," Global Research and Development Journal for Engineering, pp. 269-2743, 2018.

EMOGAME: Digital Games Therapy for Older Adults

Nita Rosa Damayanti, Nazlena Mohamad Ali

Institute of IR4.0 (IIR4.0), Universiti Kebangsaan Malaysia, Selangor, Malaysia

Abstract—EmoGame is a cognitive and emotional game useful for helping older adults who experience Mild Cognitive Impairment (MCI). EmoGame was developed with a memory therapy approach. This therapy can help cognitive and positive emotions and introduce objects through pictures, such as pictures of old objects and old music in old age. This study aims to build a game application for MCI older adults on the Android platform to support improved cognitive abilities and positive emotions for older adults. This app has two games which are memory puzzle and memory exploration. This study uses a mixture of quantitative and qualitative methods through data collection questionnaires, diary entries 3E (Expressing, Experiences and Emotions), and interviews. Respondents were selected aged 50 years and above through the Mini-Mental State Examination (MMSE). The findings found that memory therapy can help older adults increase positive emotions through digital games. Through diary entries and Diary 3E, respondents' feelings and experiences described positive emotions (happy, smile and like). The PANAS questionnaire (Positive and Negative Affect Schedule) was conducted for pre and post-testing to find positive emotions in EmoGame. Analysis of mean scores showed positive emotional factors at pre-interaction ($M = 3.39$, $SD = 0.89$) with post-interaction levels of positive emotions ($M = 4.02$, $SD = 0.97$), meaning there were significant differences in positive emotions of the older adults. The memory therapy applied in the EmoGame app is effective in helping to reduce the problem of memory decline and positive emotions for MCI older adults.

Keywords—Digital games; therapy; older adults; mild cognitive impairment

I. INTRODUCTION

A game is an electronic entertainment consisting of two elements, namely visual and audio. Games have many types, one of which is games for older adults. Games for older adults are made with a specific purpose to help the older adults train their minds. In the era of globalization, technological progress is developing so rapidly—one of these technological advances in information technology has given much goodness to human life. The health sector does not lag in integrating information technology and is developing so rapidly that many discoveries are being made. Information technology is also influencing changes in health services in the world to meet the needs of its practitioners, including older adults. Among the changes and advances that have taken place is information technology to solve various health problems, especially among older adults who suffer from mild cognitive impairment [28]. Mild Cognitive Impairment (MCI) will affect the way older adults think, behave, and do their regular daily work. Brain function will be disrupted, causing the older adult who suffers from it to face the problem of disorders in socialization and work. The

initial symptom of mild cognitive decline is that the older adult will experience an inability to perform daily activities due to the reduction in cognitive abilities experienced by the older adults [3].

Alzheimer's (AD) has become a severe health problem in society and has resulted in tremendous economic loss and social burden. By 2030 there will be 66 million people with Alzheimer's worldwide, and the number is likely to reach as many as 115 million people by 2050 [27] Before a person develops Alzheimer's, they will experience a cognitive decline called mild cognitive impairment (MCI). Something scary is that this cognitive decline can happen unnoticed. Alzheimer's in its early stages can act like most normal people. Seniors with mild cognitive impairment have a high risk of developing dementia at a percentage level of 10% to 15% per year. Cognitive impairment in older adults can be associated with the normal ageing process, or they may begin to experience symptoms of memory decline in the early stages. Memory changes affect the daily lives of older adults, such as difficulty receiving information, remembering, difficulty speaking, not understanding information, inability to comprehend movement space, inability to assess, and difficulty in paying attention [1]. Individuals with mild cognitive impairment are also more likely to have difficulty coping with questions and controlling their emotions. It is possible that they also experience personality changes. In addition, older adults who experience memory changes will also experience changes in social roles, family, feelings of shame, emotions, feelings of burden, frustration with memory problems resulting in loss of self-confidence and constant anxiety [2]. At an advanced age, emotions play a significant role in determining an individual's attitudes. Therefore, it is necessary to do mental preparation in managing emotions because a person at an advanced age is highly likely to experience changes and emotional decline, thus interfering with memory problems. Based on studies that have been done [5], seniors tend to show less stable and uncontrolled emotions. Feelings of anger occur due to negative thoughts that exist about something. To cope with the burden or stress experienced, positive emotional changes, especially among older adults, are essential [9].

Currently, therapy has been found to help older adults with mild cognitive impairment. According to Mosby's medical dictionary [7], therapy is defined as a rehabilitative treatment on a patient who has ever had any disease or experienced something. Therapeutic methods can help the problems and disabilities of older adults achieve cognitive, emotional and social development. In addition, the role of the game is one of the media that provides an atmosphere of thinking where the

player follows the set rules and strives to complete the game by following the rules. Games are an excellent technique for motivating players to understand concepts that are considered boring and use their minds [6]. One of the technological developments includes gerontechnology, which aims to apply technology that addresses the problems and difficulties arising from the symptoms of ageing so that seniors can use technology for a healthier and more independent life and can engage in social relationships [11]. Therefore, the solution from therapeutic technology is seen to help reduce the problem and improve emotional stability among older adults. This situation is in line with the increasing development of technology in the future, especially in health. Technology is seen to be able to enhance the impact of positive change. Game technology combined with therapy is proposed to increase positive emotions, especially among older adults [24]. This study aims to represent EmoGame as a therapy for older adults with Mild Cognitive Impairment.

II. BACKGROUND STUDY

A. Digital Games

Digital games mean interactive games for computers or computerized game machines requiring acting skills and play strategies. Players typically play using a selector device such as a projector, trackball, or buttons to control graphic display objects [10]. According to [30], digital gaming is entertainment that requires players to interact directly with a user interface on a screen or monitor using an electronic device. Most digital games provide in-game challenges that occur narratively with several pre-defined rules. Players are placed in competition to face obstacles on their own or with other players to succeed in the game [26]. Many media reports in digital gaming studies discuss the positive or negative effects of digital gaming activities on society.

Several studies attempt to generally examine whether digital gaming is a healthy activity or vice versa. Nevertheless, it is unfair to conclude whether digital games have a good or bad effect. Studies show that the effects of digital games are complex, unclear, and vary, depending on the context of the game and the player itself [16]. If one looks at the history of studies on the effects of other media, such as watching television, it has also produced similarly complex and vague results [22]. The following section will discuss research showing positive and negative effects on digital games to offset the complexity in considering the possible effects of digital games. Several studies show that digital games have had a positive impact on gamers in a familiar context or when used to achieve a specific purpose. These include the benefits of using games in specific contexts, such as education and healthcare, positively affecting cognitive skills, improving hand-eye coordination, and encouraging physical activity [20].

B. Aging and the Aging Process

Older adults refer to individuals over the age of 50 based on the aged standard set by the UN on ageing [17]. However, the World Health Organization (WHO), in its Aging Policy Framework published in [19], argues that age chronologically cannot be considered an accurate marker for physiological changes in the ageing process. There are many variations in

older adults' health status and quality of life. However, no matter how old an individual is, one thing is for sure is that the older adults' population is increasing over time, given the increased chances of survival and decreasing fertility rates. This group is categorized as older adults through the ageing process [25].

The ageing process can lower cognitive ability, chronic health problems and memory loss. Cognitive is a process of thought patterns that continually causes us to be alert or perceive something, covering all aspects of observation, thought, and memory. The phenomenon has led to a decline in cognitive function among older individuals, especially older adults. The process of healthy, fruitful, sensible and positive ageing are general terms that refer to the process of optimizing opportunities for health, participation and security in order to improve quality of life with age and enable them to realize the potential to earn physical, social and mental well-being in life [23]. However, the factors leading to the re-emergence of mental and emotional health resulting from memory changes in individuals, especially relatively older adults, remain little changed [14].

C. Reminiscence Therapy for the Older Adults

Reminiscence therapy is the desired process of recalling memories. Reminiscence therapy can be an event that may not be memorable or an event that has been forgotten directly experienced by the individual. Memory therapy (Reminiscence) can be a collection of personal experiences or "sharing" with others. [21] defines memory therapy (Reminiscence) as the process of cognitive recall of past events and experiences. [28] explains that memory therapy (Reminiscence) is a therapy in older adults who are encouraged (motivated) to discuss past events, identify the problem-solving skills and get positive emotions. According to [18], memory therapy (Reminiscence) aims to enhance positive, cognitive emotions and help individuals achieve self-awareness and understanding, adapt to stress and see their part in historical and cultural contexts. Reminiscence therapy also aims to create group togetherness and increase social intimacy. [15] stated that memory therapy (Reminiscence) aims to provide a pleasant experience to improve quality of life and improve socialization and relationships with others, provide cognitive stimulation, improve communication, and be an effective therapy for emotional symptoms get positive emotions. According to [29], memory therapy (Reminiscence) aims to increase self-esteem and increase self-esteem. Feeling worthless helps achieve self-awareness improves stress-coping skills by practising past problem-solving skills and improving social relationships.

D. Technology for the Older Adults

In the older adults a large number of studies have proven that the use of assistive technology and information communication technology in particular is able to address the effects of changes in physical, cognitive and social aspects as a result of the aging process. The use of assistive technology and information technology has great potential to induce positive emotional growth in the social environment of the older adults. The use of information and communication technology today is an aid tool in our lives and its use is also growing rapidly in the

field of health. Technology nowadays is the best tool that can be used to help the older adults. Previous studies have shown that the use of assistive technology and information communication technology has the potential to provide opportunities for older adults to increase their life satisfaction and in turn reduce the burden of health care payments (Auriane et al. 2016).

TABLE I. TECHNOLOGY GAMES OLDER ADULTS MILD COGNITIVE IMPAIRMENT

Author	Games and Technology used	Age Group	Findings
Suwicha Jirayucharoensa, (2019)	Nuerofeedback (computer)	50-74	Attention and Memory
Gorge Savulich (2017)	Games (IPAD)	51-64	Motivation and Confidencei
Gabriel Olievera (2017)	Egocentric Image (Ipad)	50 keatas	Memory
Nursyairah Azman (2017)	Dance game (computer)	50-80	Health
Karsten Gielis, (2017)	Card	55	Memory
Costas Boletsis (2016)	Smartkuber (Touch Screen)	Above 52	Motivation
Valeria Manera (2015)	Cooking games	50-84	Memory
Kim (2015)	Music Games	50	Memory Episodic
Stefani Fazi (2014)	Home interaction game (3D virtual reality)	50	Memory and motivation
Miradidic (2014)	DMS 48 (Object Image)	50-65	Memory
TF Hughes (2014)	Wii sports games (computer)	50-70	Health
Ballesteros (2014)	Lumosity	50	Processing speed, Attention, and episodic Memory
Dannhauser (2014)	Lumosity	50	Memory
Stelios Zygourisa (2014)	Supermarket (virtual reality)	50	Motivation
JA Anguera (2013)	Games Neuro Racer	50-85	Attention and Memory
Anguera (2013)	Neuro-racer	50	Attention and Memory
Franco (2013)	Nintendo wii fit for all	50	Memory
Man (2012)	Supermarket (virtual reality)	50	Memory
Rosen (2011)	Bowling (virtual reality)	50	Memory
Finn (2011)	Lumosity	50	Attention
Elizabeth H.Weybright (2010)	Nintendo	50-55	Memory
Stavros (2010)	Lumosity	50	Attention and memory
Bisson (2007)	Ball juggling	54	Health
Dustman (1992)	Games race (computer)	55	Memory speed reaction

The development of technological advances especially in game technology can help older adults who face symptoms of disability or mild cognitive impairment in training cognitive function. Nevertheless, studies on game technology to help mild cognitive impairment symptoms still need to be developed (George et al. 2017). Therefore, significant planning is needed to design technological game interfaces to support the skills and abilities of individuals who are going through the aging process especially the older adults.

From the existing literature review as shown in Table I, there are still few games using a reminiscence therapy approach to help cognitive and emotional. Therefore, the work was carried out in developing EmoGame application to support older adults with mild cognitive impairment problems.

III. METHODOLOGY

A. Participant

Twenty participants were categorized as MCI with the Mini-mental state examination (MMSE) test. The participants were recruited in a selected nursing home. The age group of participants is 50 years and older. We believe that this number of participants is considered significant for research trials like other studies [12], [13,4] The user study took two weeks. They were using the EmoGame app. Participants were given a 3E Diary and activity diary to evaluate the application and perform pre and post-play.

B. Procedure

We work directly with the participants to explain the research steps to be performed. The study will be conducted for two weeks. The first step taken by the researcher is to screen the study participants for their level of readiness to use the technology by using a questionnaire. Selected study participants will answer a Mini-Mental State Examination (MMSE) questionnaire to identify older adults with MCI.

Based on the results of the MMSE, a total of 20 respondents have been selected to participate in the study. The study participants were asked to fill in an activity diary in the first week. This diary aims to find about activities, technology, and how participants feel while doing daily activities. As a friendly reminder, for each study participant to fill in the daily activity diary, we will call and send a short message via Short Message Service (SMS). Participants were asked to record their daily activities in a written diary. Then in the second week, the participants will be asked to play the EmoGame application, and the participants are given the 3E (Expressing, Experiences and Emotions) Diary book. The purpose of giving this 3E Diary book is for participants to write about their feelings while playing the EmoGame game. Next, participants will be asked to fill in the Positive and Negative Effect Scale (PANAS) questionnaire and the System Usability Scale (SUS) questionnaire. Then the respondent will be asked to take the Mini-Mental State Examination (MMSE). The aim was to see if there was an increase in the level of cognitive ability of the respondents after undergoing memory or emotional therapy game training. After that, interviews will be conducted with older adults and experts to assess the effectiveness of cognitive or emotional therapy on study participants.

C. Games Application Development

We conducted interviews with older adults psychologists to get more insight. Based on the interviews, we found that memory therapy (Reminiscence) or emotion is excellent for developing positive emotions in an individual, especially among older adults. This statement is supported by the results of a study conducted by [8], who put forward the opinion that memory therapy (Reminiscence) is a process that is desired or not required to collect one's memories in the past. This means, memory therapy (Reminiscence) is a therapy, individuals will be encouraged or motivated to remember events in the past that helped create positive emotions.

D. Game Concept

The games developed are in the form of puzzle games, explorations of memories and musical melodies of memories, and pictures of old objects with nostalgia elements. We chose memory puzzles, memory exploration, and memory music because all of these things are easy to understand, especially for seniors. In addition, researchers argue that puzzle games, exploration of memories and musical melodies of memories, and pictures of old objects that have elements of nostalgia can attract the attention of the elderly and help create positive emotions in them. The game is made using two applications: Photoshop CS3 to create characters of old objects and cartoon characters and Unity 3D to compose the game patterns and graphics selected are 3D graphics. Next, we used Java SDK ver. 8 to support API (Application Programming Interface) while Android SDK rev. 21 is used for application development. Programming language: C# is used for game language programming. EmoGame app is an android-based game with a system of remembering the past that can contribute to the older adults MCI as an alternative medium to help improve cognitive and positive emotions.

EmoGame application is divided into four levels; the first is the Mini-Mental State Examination (MMSE) which serves to screen and identify seniors with mild cognitive impairment, while the second is the development of memory puzzle games. Memory puzzle games module are conceptualized puzzle games that use cards and are believed to improve a person's cognitive and emotional memory. A memory exploration game module with the concept of a village house has several parts of the house. The user will explore the village house and find old objects and reflective elements that can be navigated. Memories music was also used in the development of EmoGame. Through the music of memories, older adults can listen to memories, which are expected to give peace to their minds and emotions.

E. Research Framework

The research framework in Fig. 1 describes how the game is made and begins with the pre-production stage, where it prepares all the data to be used in the design, hardware requirements, software, flowcharts and storyboards. Then, the object is edited at the production stage, and the desired concept is applied via the method. The last step is the stage of testing and building the application into an application for Android and performing display testing, device testing, and testing.

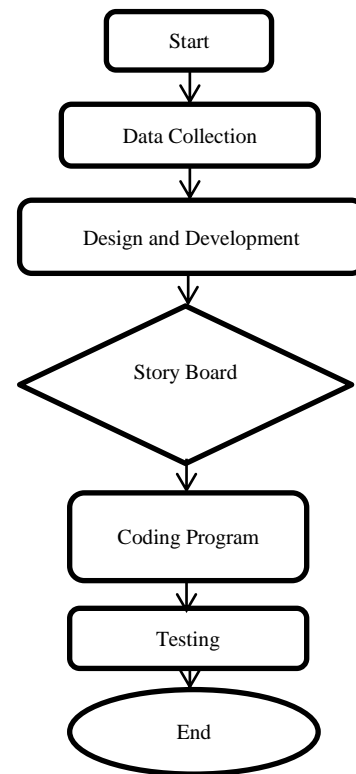


Fig. 1. Research Framework.

F. Application Interface

The screen interfaces of the developed application are shown in below.

1) *Home page*: Starting from the main menu, the user will enter the main page. To start the game, the user clicks the start button (Fig. 2).



Fig. 2. EmoGame Home Page.

2) *Mini-Mental State Examination (MMSE)*: Mini-Mental State Examination is used as a tool to detect the presence of cognitive impairment in a person/individual (Fig. 3).



Fig. 3. Mini Mental State Examination Page.

3) *Game puzzle memories*: Players of the memory puzzle game are presented with cards and open the picture, then find the same picture. If the card is open, it will go to the next game (Fig. 4).



Fig. 4. Games Puzzle Memories Page.

4) *Game exploration of memories*: A game of memory exploration exploring the village house and remembering the pictures which are in the house (Fig. 5).



Fig. 5. Games Exploration of Memories Page.

5) *Music of memories*: Music memories players can listen to music if they do not want to play (Fig. 6).



Fig. 6. Memory Music Page.

IV. FINDINGS

This section describes the cognitive findings, positive emotions and user experience when using the EmoGame application. Findings are presented before and after using the EmoGame application. The results are further divided into several separate sections for emotional and cognitive. Table II summarizes the demographic data of the participants. A total of twenty respondents consisted of older adults with MCI.

TABLE II. DEMOGRAPHIC DATA OF PARTICIPANTS

Demographic		No. (N)
Age	50 years and older	20
Citizen	Indonesian	20
Level of education	Primary school	-
	Diploma	11
	Degree	9

A. Mini Mental State Examination

The Mini-Mental State Examination (MMSE) results showed that 20 respondents suffered from MCI. Mini-mental state examination (MMSE) is a cognitive examination that is part of a routine examination to establish a diagnosis of dementia. This examination is indicated especially in elderly patients who have decreased cognitive function, thinking ability, and ability to perform daily activities. A mini-mental state examination (MMSE) is done by direct interviews with patients. The patient will be questioned and asked to follow the instructions. Of the 52 respondents tested using the Mini-mental state examination, 20 respondents experienced MCI based on the MCI score criteria. The MMSE is an examination consisting of 11 assessment items used to assess attention and orientation, memory, registration, recall, calculation, language skills, and the ability to draw complex polygons. MMSE value total scores range: Severe (0-9), Moderate (10-17), MCI (18-26) and Normal (27-30). The results obtained from 20 respondents have a score of 3 respondents with a score 18, 3 respondents with a score of 19, 4 respondents with a score of 20, 2 respondents with score 21, 3 respondents with a score 22, 3 respondents with score 24 and 2 respondents score 25. These 20 respondents were selected. Table III below shows the categories of levels of Mild Cognitive Impairment among the older adults who were selected to be in the study sample.

TABLE III. MINI-MENTAL EXAMINATION (MMSE) TEST SCORES OF STUDY PARTICIPANTS

No	Study Participant Code (Respondent)	Score (MMSE)
1	R1	18
2	R2	18
3	R3	18
4	R4	19
5	R5	19
6	R6	19
7	R7	20
8	R8	20
9	R9	20
10	R10	20
11	R11	21
12	R12	21
13	R13	22
14	R14	22
15	R15	22
16	R16	24
17	R17	24
18	R18	24
19	R19	25
20	R20	25

B. The Positive and Negative Affect Schedule (PANAS)

The Positive and Negative Affect Schedule (PANAS) which aims to look at how the emotional state among the elderly who are study participants. There are 20 PANAS questionnaire questions, ten positive PANAS questionnaire questions and ten negative PANAS questionnaire questions. Pre results in Fig. 7 and in Fig. 9 Pre and Post Analysis of EmoGame play is shown.

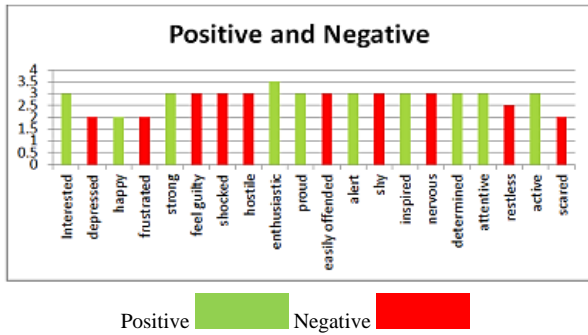


Fig. 7. Pre – Results Play EmoGame Application.

The study results at the pre-play stage mean positive effect values: attracted 3.5, happy 3.6, strong 2.8, enthusiastic 3.8, proud 3.4, alert 2.9, inspired 3.5, determined 3.4, attentive 3.6 and active 3.4. At the same time, post-play negative values mean showed depressed 2.0, frustrated 2.4. feeling guilty 2.7, shocked 2.7, hostile 2.6, easily offended 2.8, embarrassed 2.9, nervous 2.7, restless 2.6 and afraid 2.4. The following PANAS result after playing EmoGame (Fig. 8).

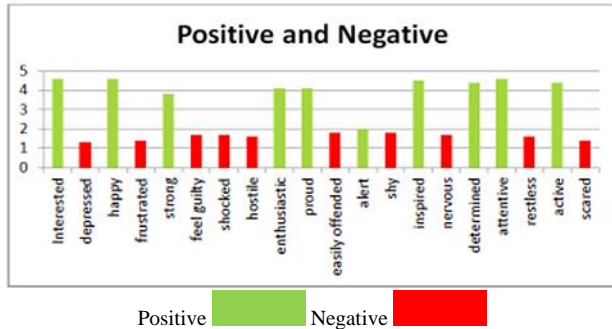


Fig. 8. Post – Results Play EmoGame Application.

The research results at the post-play stage the average value of positive emotions showed that the items were interested in playing 4.6, then happy 4.6, strong 3.8, enthusiastic 4.8, proud 4.1, alert 2.0, inspired 4.5, determined 4.4, attentive 4.6, active 4.4. Post-play positive emotions mean values showed depressed items at a value of 1.3, frustrated 1.4, guilty 1.7, shocked 1.7, hostile 1.6, easily offended 1.8, embarrassed 1.9, nervous 1.7, anxious 1.6 and afraid 1.4. Overall, the study results showed a significant difference between pre and post-play based on the results obtained from positive emotions pre with a mean value of 3 while post with a mean value of 4, for pre-negative emotions with a mean value of 2 while post with a mean value of 1. Researchers also measured the differences between two groups of pre and post paired data on an ordinal scale or interval so that the data obtained is more accurate. Here are pre and postpositive emotions (Fig. 9).

		N	Mean Rank	Sum of Ranks
Pasca_Bermain - Pra_Bermain	Negative Ranks	1 ^a	1.50	1.50
	Positive Ranks	9 ^b	5.94	53.50
	Ties	0 ^c		
	Total	10		

Fig. 9. Pre and Post-Play EmoGame.

The result obtained is negative rank 1. This level indicates that there is no decrease from pre-play to post-play. The next positive rank is the sample with the value of the second group (post-play) being higher than the value of the first group (pre-play); there are 9 data positive ranks. This means nine positive emotions are on the rise. Mean ranks are average at a negative level of 1.50, while the sum of ranks is at a value of 1.50 and positive ranks are 5.94, and the sum of ranks is 53.50, which means there is an increase from pre and post play. Then ties are the value of the second group (post-play) 0, which means there is a difference, and N is the total of pre and postpositive emotions consisting of 10 positive emotions. Next, the researcher performed an analysis. Analysis of mean scores showed positive emotional factors at pre-interaction (M = 3.39, SD = 0.89) with post-interaction levels of positive emotions (M = 4.02, SD = 0.97). The conclusions obtained as a result of the analysis prove an increase in positive emotions after playing the game EmoGame application.

C. Activity Diary

The study using diaries was conducted based on the method proposed by Jacelon and Imperio (2005). Thematic analysis was used to analyze the diaries and review the data collected from all study participants. Briefly, the researchers have done some of these analyzes: (i) Creating a sub-theme of spirituality and entertainment under the theme of Daily Activities, (ii) Creating a new theme, i.e. Social theme. Several themes are obtained by using a diary before playing. This diary aims to capture the results of daily activities, emotions, and the use of technology. Fig. 10 shows the theme Analysis.

From the diary results, spirituality is something that older adults must do. Older adults can then use technology like they use Youtube or Facebook. With technology, older adults can avoid negative emotions such as loneliness, irritability, sadness, forgetfulness in their daily activities. This is a severe problem in older adults with MCI.

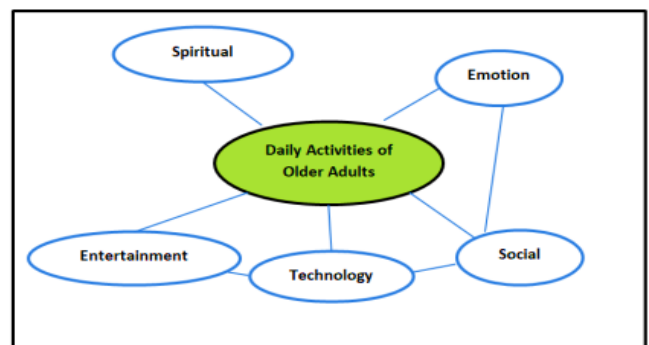


Fig. 10. Theme Analysis of Activity Diary.

D. 3 E Diary

A study found in the 3E diary discovered several related to the emotions of happiness, liking, pride, and excitement with the EmoGame app. Thematic visual maps describing the emotions of seniors involved in using EmoGame. Fig. 11 shows the Theme Analysis 3E Diary.

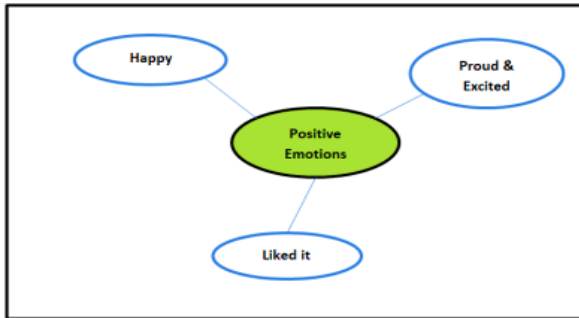


Fig. 11. Theme Analysis of 3E Diary.

Fig. 11 shows a thematic map showing the emotions involved in an EmoGame application. The thematic maps in the figure above are related to three themes of positive emotions while playing the EmoGame application obtained based on Diary 3E book data analysis. An explanation of the relevant emotional themes will be discussed as follows:

1) *Happy*: Emotions of joy were widely shared in Diary 3E by study participants. They stated that they wanted to play again and felt happy to play. The researchers hope that this game can help create a feeling of joy among older adults. The following are some of the posts that have been shared:

"I feel happy playing this game." (Diary R3)

"Happy and smiling to see the pictures and music in this game" (Diary R11).

Based on the notes or reports found in the 3E Diary it is clear that the EmoGame application is trendy among older adults and managed to create positive feelings and a sense of joy among them.

2) *Liking*: Positive emotion is defined as the user's interest or tendency to continue using the application (Charles, 2019). For seniors, the feeling of liking the game is an essential aspect. There were study participants who stated that they liked the EmoGame application. For example, there were study participants who consisted of older adults writing about their feelings of liking and interest in the EmoGame application as stated in the Diary 3E book entry:

"This game is exciting and easy to use. It is also fun to use" (Diary R4)

"Fun to use, very interesting" (Diary R9)

"I will play every day. I love this game" (Diary R11)

Although study participants in the early stages considered the EmoGame application difficult, that perception changed after playing it.

3) *Proud and excited*: The theme of Pride and Excitement is an emotion that is a sense of satisfaction resulting from obtaining a particular achievement (Chaplin., 2013). Based on the codes transcribed from the study participants' notes found in Diary 3E, older adults are excited about using gaming applications that provide new experiences using technology, thus creating a feeling of excitement among older adults. They also take pride in the easy to operate EmoGame application they provide. Examples of notes from study participants who used the EmoGame application that showed proud and excited emotions are as follows:

"The first time playing a game using a tablet is still a bit confusing, but I can play it" (Diary R3).

"Just have experience using tablets. After playing, I am very proud to play this game, I am thrilled." (Diary R4).

"I have started to be able to use this tablet, and I am good at playing." (Diary R16).

E. System Usability Scale (SUS)

Based on the results of user satisfaction using the application, it is found that the value given is an average of 82. Fig. 12 is as follows.

The evaluation results conclude that there is an overall value of 82, meaning that this EmoGame application is excellent and able to train the memory of older adults who suffer from Mild Cognitive Impairment.

F. Cognitive Analysis

Mini-mental state examination is carried out Pre and Post playing EmoGame. This research aims to find out the cognition of older adults. The test results using Wiloxcon analysis and SPSS 2.0 can be seen in Fig. 13.

Calculate Result Score										Amount	Score (Amount x 2.5)
Q1	Q2	Q3	Q4	Q5	Q6	Q7	Q8	Q9	Q10		
5	1	5	1	5	1	5	1	5	1	30	75
5	2	5	2	5	1	5	1	5	1	32	80
5	2	5	4	5	1	5	1	5	2	35	88
4	2	5	1	5	1	4	1	5	1	29	73
4	2	5	5	5	2	5	1	2	1	32	80
5	1	5	1	4	1	5	2	4	2	30	75
5	2	5	1	5	2	5	1	5	1	32	80
5	1	4	2	5	2	5	1	5	1	31	78
5	1	5	2	4	2	4	1	5	2	31	78
5	1	4	1	5	1	5	2	5	2	31	78
5	1	5	4	5	2	4	1	5	2	34	85
5	2	5	2	5	2	5	1	5	2	34	85
5	1	5	1	5	1	5	1	5	1	30	75
5	2	5	2	4	3	5	2	4	4	36	90
4	2	4	2	4	2	4	3	5	5	35	88
4	2	4	3	4	2	4	2	4	3	32	80
4	2	5	3	5	2	4	2	4	5	36	90
4	3	4	3	4	3	4	3	4	4	36	90
4	2	5	2	5	2	5	2	4	4	35	88
4	2	5	2	4	2	4	2	4	4	33	83
Average Score (Final Result)											82

Fig. 12. System Usability Score (SUS).

Ranks				
		N	Mean Rank	Sum of Ranks
Post Test - Pre Test	Negative Ranks	0 ^a	,00	,00
	Positive Ranks	22 ^b	11,50	253,00
	Ties	0 ^c		
Total		20		

Fig. 13. Mini-Mental State Examination Pre and Post Test Results.

The study results based on the Wilcoxon test clearly show that the negative ranks or negative difference between the results Pre and Post finishing playing the EmoGame application game is 0, whether it is at the value of N, mean, or sum rank. A value of 0 indicates no decrease from the pre-test and post-test values. The positive rank between results before and after play shows 20 positive N data which proves that there is a change among seniors before and after finishing playing the EmoGame application game with an increase of 11.50, while the total positive rank or sum of rank is 253.00. There is an equality value of ties here when the same value exists. We conduct hypothesis testing to establish a basis so that they can collect data to determine whether to reject or accept the statement. Fig. 14 shows the results of the MMSE Test using the Wilcoxon Analysis.

Test Statistics ^a	
	Post Test - Pre Test
Z	-4,109 ^b
Asymp. Sig. (2-tailed)	,000

a. Wilcoxon Signed Ranks Test
b. Based on negative ranks.

Fig. 14. The Results of the MMSE Test using the Wilcoxon Analysis.

Based on the findings of the statistical study test above, Asymp. sig. (2-tailed) p-value 0,000 is smaller than α 0.05 until the hypothesis is accepted. It can be concluded that H_a is accepted. This means there is a significant relationship between pre-playing and post- finishing playing the EmoGame application game. The EmoGame game application essentially involves brain exercise training consisting of memory puzzles and memory exploration that influence an effort to improve cognitive function among older adults with Mild Cognitive Impairment.

G. Expert Validation

The selection of the experts involved is based on purposive sampling. This type of sampling aims to require respondents with experience, expertise, skills and knowledge appropriate to the research topic. In this study, two experts were selected based on their expertise in elderly health and memory or emotional therapy. Table IV details the criteria of the participating experts.

TABLE IV. DETAILS AND CRITERIA FOR SELECTION OF EXPERTS

ID Expert	Expertise	criteria
E1	Older adults Health	Research in the field of MCI and Dementia.
E2	Memory or Emotion Therapy (<i>Reminiscence</i>) older adults	Research in the field of <i>Reminiscence</i> therapy

The assessments given by each expert are categorized to check their agreement in developing the game. Experts' opinions helped researchers evaluate applications developed and can be used for older adults with mild cognitive impairment. Among the aspects that have been emphasized are the aspects of the use of technology among older adults, the positive emotional effects, and the elements of memory therapy found in the EmoGame game application. Using simple technologies such as tablets and exposure to gaming technology to help seniors can evoke feelings of excitement and joy, creating positive emotions among them. One of the elderly health experts (Expert E1) agrees that games can stimulate positive emotions.

"It is essential because it can entertain and influence positive emotions to be happy. This game can entertain and train not to forget easily, and can improve memory because it is easy to use". (Expert E1).

In addition, the emotional or memory therapy approach (*Reminiscence*) is considered able to help the emotions and cognition of the elderly who have mild cognitive impairment. E2 experts give opinions on emotional or memory therapy (*Reminiscence*) that has been used in this research can help.

"The objects in the game are reminiscent of memories and past experiences such as those in emotional therapy or memories. Emotional or memory therapy can help lower the level of negative emotions in the elderly. I agree if games are developed for seniors with this therapeutic approach". (Expert E2).

In addition, E1 Expert also gave an opinion,

"The game is easy to play, and the objects in the game are reminiscent of memories and experiences." The games were developed to stimulate the emotions of the past and can provide positive emotions. This game also trains to improve memory and is easy to play". (Expert E1).

Based on the evaluation results and expert opinions, the game applications can help older adults with Mild Cognitive Impairment. Table V summarizes the results of the expert evaluation.

TABLE V. RESULTS OF EXPERT EVALUATION

EmoGame Gaming Application		Expert Assessment			
	Element		Yes	No	
1)	Digital Game Technology	Digital games Tablet platform	Games affect positive emotions and improve cognitive.	✓	
2)	Memory exploration game.	Elements of memory therapy (<i>Reminiscence</i>)	Emotional or memory therapy (<i>Reminiscence</i>) is recommended for the training of older adults.	✓	
3)	Puzzle Games	Cognitive elements	Games for older adults can help cognitive and positive emotions.	✓	

V. CONCLUSION

In general, research shows that play is an essential factor in training seniors with MCI. Although the research was conducted by developing game applications with a reminiscence memory therapy approach, the results showed that cognitive enhancement and affecting positive emotions are very significant where positive memories can cause positive emotions. In contrast, negative memories will contribute to emotional decline or failure (negative emotions).

Game applications that have been developed for seniors with MCI are expected to help seniors with positive emotions and improve their cognitive abilities. This game will be used to train the memory and emotions of older adults and solve their problems. The study results show that each factor of user involvement in the game can impact older adults. However, this factor's high or low impact is influenced by the duration of user engagement when playing EmoGame games application. The game development in this study bridges the gap in the literature review in-game engagement for seniors with every factor, feature, and correlation of game design capable of influencing and enhancing positive emotions among older adults. Researchers believe that the games that have been developed could be beneficial to older adults in the future.

ACKNOWLEDGMENT

We want to thank all respondents who participated in this study. This study was supported by the university research grant GUP-2019-066.

REFERENCES

- [1] Albert .2011. "The diagnosis of mild cognitive impairment due to Alzheimer's disease: recommendations from the National Institute on Aging Alzheimer's. "diagnosis Association workgroups on diagnostic guidelines for Alzheimer's disease".doi: 10.1016/j.jalz.2011.03.008.
- [2] Charlies katrine. 2014. "„Kitchen and cooking,“ a serious game for mild cognitive impairment and Alzheimer's disease: a pilot study. Journal Aging Neuro Science". doi: 10.3389/fnagi.2015.00024.
- [3] Annicka 2016. "How older adults with mild cognitive impairment relate to technology as part of present and future everyday life: a qualitative study". doi: 10.1186/s12877-016-0245-y.
- [4] Ann 2018. "Technology use to improve everyday occupations in older persons with mild dementia or mild cognitive impairment: A scoping review". <https://doi.org/10.1177/0308022618771533>.
- [5] Auriane 2016. "Recommendations for the Use of ICT in Elderly Populations with Affective Disorders". Jurnal frontiers in aging neuroscience. doi: 10.3389/fnagi.2016.00269.
- [6] Bjorg 2019. "Acceptance and Use of Innovative Assistive Technologies among People with Cognitive Impairment and Their Caregivers: A Systematic Review". <https://doi.org/10.1155/2019/9196729>.
- [7] Bree Chancellor 2013. "Art Therapy for Alzheimer's Disease and Other Dementias". doi: 10.3233/JAD-131295.
- [8] Brian D .2013. "Real-Time Strategy Game Training: Emergence of a Cognitive Flexibility Trait". <https://doi.org/10.1371/journal.pone.0070350>.
- [9] Ballesteros, 2014. "Brain training with non-action video games enhances aspects of cognition in older adults: A randomized controlled trial. Frontiers in Aging Neuroscience,". <http://dx.doi.org/10.3389/fnagi.2014.00277>.
- [10] Carmen M .2015. "Emotional processing in patients with mild cognitive impairment: The influence of the valence and intensity of emotional stimuli".doi: <https://doi.org/10.1016/j.jns.2015.07.034>.
- [11] Costas Boletsis et al 2016. "Smartkuber: A Serious Game for Cognitive Health Screening of Elderly Players". doi: 10.1089/g4h.2015.0107.
- [12] Elizabeth H Weybright 2010. "Effects of an interactive video game (Nintendo Wii) on older women with Mild Cognitive Impairment. Therapeutic recreation <https://www.researchgate.net/publication/260284248>.
- [13] Federica Pallavicini .2018. "Video Games for Well-Being: A Systematic Review on the Application of Computer Games for Cognitive and Emotional Training in the Adult Population". 2018. doi:10.3389/fpsyg.2018.02127.
- [14] Frank Knoefel 2018. "Implementation of a Brain Training Pilot Study For People With Mild Cognitive Impairment". doi: 10.5770/cgj.21.304
- [15] Ganguli 2013. "Mild cognitive impairment: incidence and vascular risk factors in a population-based. Neurology". doi: 10.1212/WNL.0b013e318295d776.
- [16] Gomez gallego. 2017. "Music therapy and Alzheimer's disease: Cognitive, psychological, and behavioural effects Alzheimer". 2018. <https://doi.org/10.1016/j.jrleng.2015.12.001>.
- [17] George Savulich .2017. "Cognitive Training Using a Novel Memory Game on an iPad in Patients with Amnesic Mild Cognitive Impairment (aMCI). International Journal of Neuropsychopharmacology". doi:10.1093/ijnp/pyx040.
- [18] I. Arevalo, et al.2015."Mini-Mental State Examination (MMSE) for the detection of Alzheimer's disease and other dementias in people with mild cognitive impairment (MCI)." Cochrane Database of Systematic Reviews". doi: 10.1002/14651858.CD010783.
- [19] Irene Lopatovska and Ioannis Arapaki. 2010. "Theories, methods and current research on emotions in library and information science, information retrieval and human-computer interaction". doi:10.1016/j.ipm.2010.09.001.
- [20] J. Skov Neergaard, et al. 2017. "Objective cognitive impairment and progression to dementia in women: the prospective epidemiological risk factor study." The Journal of Prevention of Alzheimer's Disease. vol. 4, no. 3, pp. 194–200, 2017.
- [21] K. Kakker, et al. 2017. "Association of chronic obstructive pulmonary disease with mild cognitive impairment and dementia." Current Opinion in Pulmonary Medicine. vol. 24, no. 2, pp. 173–178,2017.
- [22] Klein Koerkamp dan Baciu M, Hot P. 2012. Preserved and impaired emotional memory in Alzheimer's disease. Front Psychol. <http://dx.doi.org/10.3389/fpsyg.2012.00331>.
- [23] Liesbeth Joosten et al. 2011. "Group Therapy for Patients with Mild Cognitive Impairment and Their Significant Others: Results of a Waiting-List Controlled Trial". DOI: 10.1159/000315933.
- [24] Lucas Diener & Larsen .2006. "The contributions of positive and negative affect to emotional well-being]. ISSN 1849- 0395 (Electronic); 1332-0742 (Print).
- [25] Maaik Waanders.. 2015. "Perception of emotions in mild cognitive impairment and Alzheimer's dementia: does intensity matter?". doi: <https://doi.org/10.1515/tnci-2015-0013>.
- [26] R. C. Petersen, et al.2018, "Practice guideline update summary: mild cognitive impairment: report of the guideline development, dissemination, and implementation sub committee of the American Academy of Neurology". vol. 90, no. 3, pp. 126–135, 2018.
- [27] J.W. Sacre, 2018, "Mild cognitive impairment is associated with subclinical diastolic dysfunction in patients with chronic heart disease" European Heart Journal - Cardiovascular Imaging". vol. 19, no. 3, pp. 285–292.
- [28] Mickley KR dan Kensinger EA.2008. "Emotional valence influences the neural correlates associated with remembering and knowing". Vol 2008;8:143–152.
- [29] Michelle S Bourgeois. 2013. "Therapy Techniques for Mild Cognitive Impairment".doi: 10.1044/nnsld23.1.23.
- [30] Mo Li.2017. "The clinical mild-to-moderate Alzheimer disease". doi: 10.1097/MD.0000000000009381.

A Paradigm for DoS Attack Disclosure using Machine Learning Techniques

Mosleh M. Abualhaj¹, Ahmad Adel Abu-Shareha², Mohammad O. Hiari³
Yousef Alrabanah⁴, Mahran Al-Zyoude⁵, Mohammad A. Alsharaiah⁶

Department of Networks and Information Security^{1, 3, 5}
Department of Computer Science²
Department of Software Engineering⁴
Data Science and Artificial Intelligence⁶
Al Ahliyya Amman University, Amman, Jordan

Abstract—Cybersecurity is one of the main concerns of governments, businesses, and even individuals. This is because a vast number of attacks are their core assets. One of the most dangerous attacks is the Denial of Service (DoS) attack, whose primary goal is to make resources unavailable to legitimate users. In general, the Intrusion Detection and Prevention Systems (IDPS) hinder the DoS attack, using advanced techniques. Using machine learning techniques, this study will develop a detection model to detect DoS attacks. Utilizing the NSL-KDD dataset, the suggested DoS attack detection model was investigated using Naive Bayes, K-nearest neighbor, Decision Tree, and Support Vector Machine algorithms. The Accuracy, Recall, Precision, and Matthews Correlation Coefficients (MCC) metrics are used to compare these four techniques. In general, all techniques are performing well with the proposed model. However, The Decision Tree technique has outperformed all the other techniques in all four metrics, while the Naive Bayes technique showed the lowest performance.

Keywords—DoS attack; machine learning; NSL-KDD; IDPS systems

I. INTRODUCTION

The world is currently living in the digital era. This digital era has produced many services and applications to make life easier. One of the primary concerns of these services and applications is security [1]. Companies and even individuals live a nightmare due to the number of cyberattacks. At the same time, more than 61000 websites attack is blocked every day. In addition, around 24000 malicious mobile applications are blocked every day on the stores of the applications [2]. One of the most dangerous cyberattacks is a Denial of Service (DoS) attack. The main goal of the DoS attack is to make a resource unavailable to the intended users. DoS attack is increasing rapidly; it is expected that the number of worldwide DoS attack will reach 15.4 million by 2023 [3].

Intrusion Detection and Prevention Systems (IDPS) are among the techniques available to counteract a DoS attack. IDPS is software/hardware that observes and inspects system events in order to sense and warn of unauthorized efforts to access system resources in real-time or near real-time. IDPS detects intrusion by either searching for a pre-defined pattern in the traffic or by observing anomalies of what is considered normal traffic for the network or host [4]. IDPS should be

equipped with smart and self-learning techniques to detect zero-day DoS attacks. Machine learning is a subfield of artificial intelligence that encompasses a number of techniques for accomplishing this goal [5].

As the name implies, machine learning systems improve automaticity through experience and by using existing data, which makes it suitable to detect zero-day DoS attacks. Supervised, unsupervised, and semi-supervised machine learning are all types of machine learning. Generally, supervised learning algorithms operate on structured and labeled data similar to that used by the IDPS [6] [7]. Hence, the fundamental aim of this research is to suggest a paradigm for identifying suitable supervised machine learning algorithms for detecting DoS attacks via IDPS.

This paper is structured as follows. Section 2 covers the topics fundamental to this work. These topics include NSL-KDD dataset machine learning techniques, min-max scaler, and K-Fold Cross-Validation. Section 3 discusses related works that have employed machine learning approaches to detect DoS attacks. Section 4 discusses the proposed DoS attack detection model. Finally, Section 5 concludes the paper and discusses the scope for future work.

II. BACKGROUND

This section discusses the basic concepts that are related to this work. This includes a brief description of the NSL-KDD dataset used in this article. The Machine learning techniques used in this article will also be briefed. Finally, the algorithms used in the data pre-processing and to validate the result will be discussed.

A. NSL-KDD Dataset

NSL-KDD dataset is a processed version of the KDD-CUP99, in which the records that adversely impact the systems are removed. NSL-KDD dataset still has some problems; however, it is still considered an adequate benchmark dataset that helps security developers investigate intrusion detection techniques. The number of records in the NSL-KDD dataset is good to run the experiments and evaluate the results of different techniques. Table I shows the number of records in the NSL-KDD dataset according to the attack type. The NSL-KDD dataset has four different attack types. This paper is only interested in the DoS attack, and all records of the other attacks

are deleted during the pre-processing stage, as discussed below. Table II shows the main attributes of the NSL-KDD dataset [7][8][9].

TABLE I. NUMBER OF RECORD FOR EACH ATTACK

Attack Type	Number of records
DoS	53387
Probe	14077
U2R	119
R2L	3880
Normal	77055

TABLE II. THE FEATURES OF NSL-KDD DoS

No	Feature Name	Data Type	Feature Description	Lowest Value	Highest Value
1	duration	Numeral	The session's length	Zero	54451
2	protocol_type	Text	Session protocol	N/A	N/A
2	protocol_type	Text	Session protocol	N/A	N/A
3	service	Text	Destination service	N/A	N/A
4	flag	Text	The session's status flag.	N/A	N/A
5	src_bytes	Numeral	Bytes transmitted from sender to receiver	Zero	89581520
6	dst_bytes	Numeral	Bytes transmitted from receiver to sender	Zero	7028652
7	land	Numeral	1 If from/to the same host/port; else 0.	Zero	One
8	wrong_fragment	Numeral	The number of incorrect fragments.	Zero	Three
9	urgent	Numeral	Number of urgent packets	Zero	Three
10	hot	Numeral	Number of hot indicators	Zero	101
11	num_failed_logins	Numeral	Number of unsuccessful login in attempts	Zero	Four
12	logged_in	Numeral	1 If successfully logged in; else 0.	Zero	One
13	num_compromised	Numeral	The number of compromised conditions	Zero	7479
14	root_shell	Numeral	1 If a root shell is attained; else 0.	Zero	One
15	su_attempted	Numeral	1 If (su root) command tried; else 0.	Zero	Two

No	Feature Name	Data Type	Feature Description	Lowest Value	Highest Value
16	num_root	Numeral	Number of root accesses	Zero	7468
17	num_file_creations	Numeral	The total number of creation operations.	Zero	100
18	num_shells	Numeral	The total number of shell prompts.	Zero	Two
19	num_access_files	Numeral	The total number of operations on access control files.	Zero	Nine
20	num_outbound_cmds	Numeral	The total number of ftp session outbound commands.	Zero	One
21	is_host_login	Numeral	1 If the login belongs to the hot list; else 0.	Zero	One
22	is_guest_login	Numeral	1 If it's a guest login; else 0.	Zero	One
23	Count	Numeral	The number of sessions to the same host as the present session, in the last 2 seconds.	Zero	511
24	srv_count	Numeral	The number of connections to the same service as the current connection, In the last two seconds.	Zero	511
25	error_rate	Numeral	The ratio of connections in the same host connection that contain "SYN" errors	Zero	One
26	srv_error_rate	Numeral	The ratio of connections in the same-service connection that have "SYN" errors	Zero	One
27	error_rate	Numeral	The percentage of connections in the same-host connection that have "REJ" errors	Zero	One
28	srv_error_rate	Numeral	The ratio of connections in the same-service contain that contain "REJ" errors	Zero	One
29	same_srv_rate	Numeral	The percentage of connections to the same-service connection.	Zero	One
30	diff_srv_rate	Numeral	The percentage of connections to	Zero	One

No	Feature Name	Data Type	Feature Description	Lowest Value	Highest Value
			different services.		
31	srv_diff_host_rate	Numerical	The percentage of connections to various hosts in the same-service connection.	Zero	One
32	dst_host_count	Numerical	The percentage count of connections that contain the same receiver host.	Zero	255
33	dst_host_srv_count	Numerical	The percentage count of connections that contain the same receiver host and using the identical service	Zero	255
34	dst_host_same_srv_rate	Numerical	The percentage of connections that contain the same receiver host and using the identical service.	Zero	One
35	dst_host_diff_srv_rate	Numerical	The percentage of various services on the present host.	Zero	One
36	dst_host_same_src_port_rate	Numerical	The percentage of connections to the present host that contain the same port.	Zero	One
37	dst_host_srv_diff_host_rate	Numerical	The percentage of connections to the identical service coming from various hosts.	Zero	One
38	dst_host_serror_rate	Numerical	The percentage of connections to the present host that contain an "SO" error	Zero	One
39	dst_host_srv_serror_rate	Numerical	The percentage of connections to the present host and determined service that contain an "SO" error	Zero	One
40	dst_host_rerror_rate	Numerical	The percentage of connections to the present host that contain an "RST" error	Zero	One
41	dst_host_srv_rerror_rate	Numerical	The percentage of connections to the present host and determined service that contain an "RST" error	Zero	One

B. Machine Learning Techniques that are used in this Article

Supervised machine learning deals with data sets that contain both inputs and the corresponding desired outputs. The classification algorithms category is used within supervised learning when the outputs are discrete; restricted to a limited set of values. The most common classification algorithms are Naive Bayes, K-Nearest Neighbors (KNN), Decision Tree, and Support Vector Machines (SVM) [7][10][11][12].

1) *Naive bayes*: Naive Bayes is a simple technique based on the Bayes theorem and used to handle classification problems. The Naive Bayes assumption is that the features are independent of one another; existing of any feature is unrelated to any other feature. It is known as one of the best classification algorithms and creates fast machine learning models that predict quickly. In Naive Bayes, the features are making independent and equal contributions to the outcome. Equation 1 shows the probabilistic expressions used in Bayes' theorem [7][10].

$$P(X|Y) = \frac{P(Y|X)P(X)}{P(Y)} \quad (1)$$

2) *K-NN*: One of the most important and extensively used machine learning algorithms is K-NN. As the name implies, K-NN finds the closest K (number of neighbors) nearest neighbor points to the target point. Then, it predicts the output of the target point from these neighbor points. K can be constant or vary based on the local density of points. Typically, k equals the square root of the dataset's record count. Euclidean is one of the algorithms that are used to find the neighbor points by KNN. Equation 2 shows the formula of the Euclidean algorithm [7][11].

Euclidean Distance between X and Y =

$$\sqrt{(A_2 - A_1)^2 + (B_2 - B_1)^2} \quad (2)$$

3) *Decision Tree*: The decision tree technique creates an upside-down tree to represent the classification model. It is easy to understand, visualize, and requires little data preparation. The tree consists of nodes that symbolize a dataset's features, branches symbolize the decision rules, and leaves symbolize the class, as shown in Fig. 1. The decision tree is based on the if-else statements (True/False) to move to the next node till reaching the leaf [7][12].

4) *SVM*: SVM is a widely used supervised learning approach for classification. The SVM technique plots the data items as a space split into categories. Then, it finds the hyperplane that distinctly separates the points in space. The SVM technique should choose the hyperplane with the maximum distance between the target data points. This gives a more accurate classification for any new data points. Fig. 2 clarifies the SVM technique [7][10].

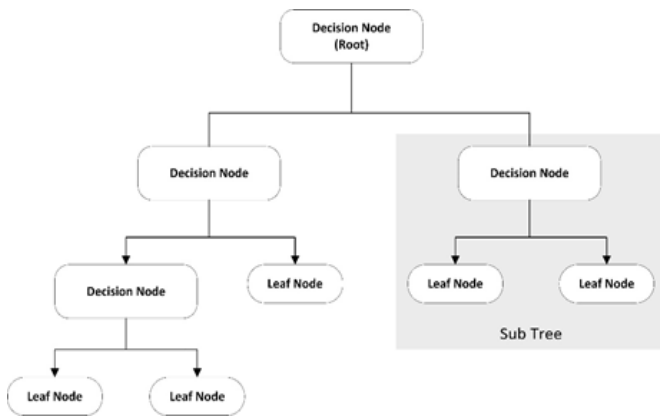


Fig. 1. Decision Tree Technique Scheme.

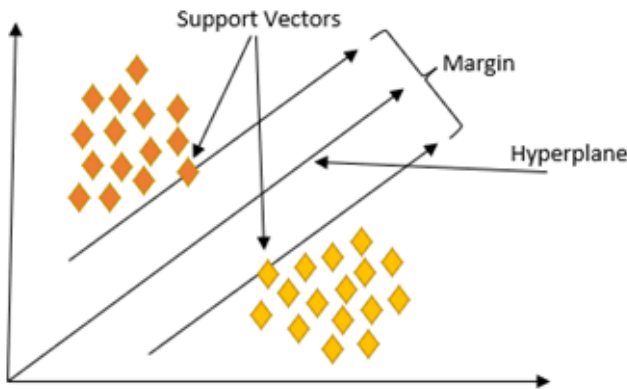


Fig. 2. SVM Technique Scheme.

C. Min-max Scaler

Most machine learning techniques perform better when the data are distributed similarly. In many cases, the data within the dataset is distributed on a wide-scale and, thus, the data should be scaled. Min-max scaler is one of the most used techniques to scale the data within the acceptable range for the machine learning techniques. By default, the Min-max scaler technique returns a value between 0 and 1, using Equation 3.

$$Z_{\text{new}} = (Z - Z_{\text{min}}) / (Z_{\text{max}} - Z_{\text{min}}) \quad (3)$$

Where Z_{new} is new derived value, Z is the original value, Z_{min} is the minimum value of the feature, Z_{max} is the maximum value of the feature [13].

D. K-Fold Cross-Validation

When it comes to machine learning, the approach known as K-Fold Cross-Validation is used to validate the results of a model. It is widely used because it is simple, easy to understand, and, more importantly, reduces the validated model's bias. Using the K-Fold Cross-Validation method, the data is split into various groups (k groups). The proposed machine learning is trained on $k-1$ groups, and the remaining group is used to validate the model [14].

III. RELATED WORK

This section discusses related work on detecting DoS attacks using machine learning approaches.

Peneti S. and Hemalatha E. have proposed a machine learning model to detect Distributed DoS (DDoS) attacks. The authors investigated four different machine learning techniques to design their model: XGBoost, AdaBoost, Random Forests, and Multilayer Perceptron. The CIC IDS 2017 dataset, which contains 83 additional features, has been used to evaluate the proposed model. The Recursive Feature Elimination method has been used to shrink the dataset to only the most relevant features to enhance the proposed model performance. The number of features has been set to six and after some experiments the number of features has been finalized to eight. The accuracy, precision, recall, and F1 score measures have been used to evaluate the suitable machine learning techniques for the proposed model. Among the investigated four techniques, Random Forests has outperformed the other techniques in detecting the DDoS attack, while the Multilayer Perceptron has performed less in this particular problem [5].

One of the recent articles that have been used the machine learning techniques for DoS attack detection was proposed by Wankhede S. & Kshirsagar D. Wankhede S. & Kshirsagar D have been used common machine learning techniques to detect DoS attack; namely Random Forest (RF) and Multi-Layer Perceptron (MLP) techniques. The suggested model is aimed at detecting DoS attacks at the application layer. The DoS attack that occurs at the other OSI layers has not been considered. The same CIC IDS 2017 dataset was used to evaluate the RF and MLP techniques for detecting DoS attacks at the application layer. The CIC IDS 2017 dataset is divided into distinct groups, and an appropriate group for each technique is identified. Weka tool has been used to evaluate the RF technique versus MLP technique in the proposed model. The results demonstrated that the RF outperforms the MLP in terms of accuracy [15].

Another article that used machine learning techniques for DoS attack detection was proposed by Zhe W., Wei C., and Chunlin L. However, the proposed model in this work is designed specifically for smart grid technology. The authors have investigated three different machine learning techniques to protect the smart grid: SVM, Decision Tree, and Naive Bayesian. After examining these three techniques on the KDD99 dataset, it is found that the SVM technique is the best for protecting smart grid technology from DoS attacks. The data is first collected from the network, then certain features are selected from the dataset, and the primary component analysis is used for dimensionality reduction. The accuracy, precision and recall, and F1 score measures have been used to evaluate the suitable machine learning techniques for the proposed model. Among the three techniques tested, SVM outperformed the others in detecting DoS attacks on smart grid technology. [16].

He Z., Zhang T., and Lee, R. B. have advocated the use of machine learning techniques to detect DoS attacks originating in the cloud. The proposed system has investigated four different DoS attack techniques: SSH brute-force, ICMP flooding, DNS reflection, and TCP SYN attacks. This method utilizes statistical data from the hypervisor of the cloud server and the virtual machines to prohibit network packages from being sent out to the external network. The authors have implemented a prototype of the proposed detection system

under natural cloud settings. The cloud is comprised of six servers (labeled S0 to S5), each of which hosts many virtual machines. Several machine learning techniques have been used in the proposed system, including SVM Linear Kernel, SVM RBF Kernel, SVM Poly Kernel, Decision Tree, Naive Bayes, and Random Forest. Among the investigated techniques, SVM Linear Kernel has outperformed other techniques in detecting the DoS attack sourced from the cloud [17].

IV. PROPOSED DOS ATTACK DETECTION MODEL

This section outlines the suggested model for detecting DoS attacks. First, the NSL-KDD dataset will be processed to be prepared for training and testing the proposed model. Then, the proposed DoS attack detection model will be introduced in detail.

A. Data Preprocessing

Data preprocessing is a set of operations applied to the data to prepare the dataset for machine learning. As discussed below, data transformation and normalization are two of these processes that have been applied to the NSL-KDD dataset in this paper [8][18].

1) *Data transformation:* NSL-KDD dataset contains numerical and nominal data, as shown in Table II. One of the first steps in data preprocessing is transformation, converting all data to numerical for the machine learning techniques to be applicable. Three nominal features in the NSL-KDD dataset have been transformed to numeric values: protocol type, service, and flag. These features have been converted using the label encoding method [19]. Label encoding changes the values to a number between zero and the number of classes minus one, as shown in Table III. Tables IV and V show samples of the NSL-KDD dataset before and after the transformation operation. Besides, the output column in the NSL-KDD dataset contains four different types of attacks, each of which has several sub-types. All the attack sub-types have been removed except for the DoS sub-types, which is our target in this paper. Then, all DoS sub-types have been replaced to be DoS attack, so that the output column contains only two outputs: DoS attack and normal data. Again, these two outputs have been converted to from nominal into numeric data using the label encoding method. Now, the output column contains 0 representing the DoS attack and 1 representing normal data.

2) *Data normalization:* An essential step in data preprocessing is normalization operation. Normalization techniques convert the large-scale values into a compatible scale. This enhances the performance of the machine learning techniques and leads to more accurate results. NSL-KDD dataset contains several features distributed at a large scale and needs to be normalized. This study has applied the Min-max scaler technique (as discussed above), which scales the

values of a feature between 0 and 1 [7][13]. Table VI shows a sample of the NSL-KDD dataset after normalization. Fig. 3 illustrates the NSL-KDD dataset data preprocessing steps.

TABLE III. TRANSFORMATION

Feature Name	Old Value	New Value
Protocol Type	Icmp	One
	Tcp	Two
	Udp	Three
Service	auth,bgp , X11, Z39_50	0-64
Flag	OTH	Zero
	REJ	One
	RSTO	Two
	RSTOS0	Three
	RSTR	Four
	S0	Five
	S1	Six
	S2	Seven
	S3	Eight
	SF	Nine
SH	Ten	

TABLE IV. BEFORE TRANSFORMATION

No	Instances	Output
1	0,tcp,ftp_data,SF,491,0,2,2,0,0,0,0,1,0,0,150,25,0.17,0.03,0.17,0,0,0,0,05,0	normal
2	0,udp,other,SF,146,0,13,1,0,0,0,0,0,08,0.15,0,255,1,0,0.6,0.88,0,0,0,0,0	normal
3	0,tcp,private,S0,123,6,1,1,0,0,0,05,0,07,0,255,26,0.1,0.05,0,0,1,1,0,0	DoS
4	0,tcp,private,REJ,0,121,19,0,0,1,1,0.16,0.06,0,255,19,0.07,0.07,0,0,0,0,1,1	DoS
5	0,tcp,private,S0,166,9,1,1,0,0,0,05,0,06,0,255,9,0,04,0,05,0,0,1,1,0,0	DoS

TABLE V. AFTER TRANSFORMATION

No	Instances	Output
1	0,1,19,9,491,0,0,0,0,0,0,0,0,0,0,0,0,0,0,0,0,0,0,2,2,0,0,0,0,1,0,0,150,25,0.17,0.03,0.17,0,0,0,0,05,0	1
2	0,2,40,9,146,0,0,0,0,0,0,0,0,0,0,0,0,0,0,0,0,0,0,13,1,0,0,0,0,0,0,08,0.15,0,255,1,0,0.6,0.88,0,0,0,0,0	1
3	0,1,44,5,0,0,0,0,0,0,0,0,0,0,0,0,0,0,0,0,0,0,0,123,6,1,1,0,0,0,05,0,07,0,255,26,0.1,0.05,0,0,1,1,0,0	0
4	0,1,44,1,0,0,0,0,0,0,0,0,0,0,0,0,0,0,0,0,0,0,0,121,19,0,0,1,1,0,0,16,0,06,0,255,19,0,07,0,07,0,0,0,0,1,1	0
5	0,1,44,5,0,0,0,0,0,0,0,0,0,0,0,0,0,0,0,0,0,0,0,166,9,1,1,0,0,0,05,0,06,0,255,9,0,04,0,05,0,0,1,1,0,0	0

V. PERFORMANCE EVALUATION

This section examines the suggested DoS attack detection model's performance. The proposed model was designed using the Python programming language. Python is easy to use and widely used with machine learning. It provides several built-in tools specifically for machine learning that simplify complex tasks. The device used for testing has Intel Core i7-9750H processor and 32GB RAM with 64 bit MS-Windows.

The confusion matrix contains four elements [20][21] that summarize the performance of a proposed machine learning model:

- 1) *True Positive (TP)*: indicates an attack and that the detection model successfully predicted this attack.
- 2) *True Negative (TN)*: indicates no attack and the detection model successfully predicted no attack.
- 3) *False Positive (FP)*: indicates no attack and the detection model wrongly predicted an attack.
- 4) *False Negative (FN)*: indicates an attack and the detection model wrongly predicted no attack.

Fig. 5 elaborates the confusion matrix. The target of the proposed model is to increase the TP and TN and decrease the FP and FN.

Four measures have been employed to evaluate the proposed system based on the elements of the confusion matrix. These measures are Accuracy, Recall, Precision, and Matthews Correlation Coefficients (MCC). Accuracy is the ratio of properly forecasted attacks to the total number of forecasted attacks. Accuracy can be calculated using Equation 4. The Recall is the number of samples in the attack class that is successfully predicted to the total number of the prediction of the attack class. Recall can be calculated using Equation 5. Precision is the number of attacks that are correctly predicted as an attack to the number of attacks that are predicted as an attack. Precision can be calculated using Equation 6. MCC is a measure of the quality of classification with two classes. The closer the value to 1 indicates a more accurate classification. MCC can be calculated using Equation 7 [7][9][20][21].

Fig. 6, 7, 8, and 9 show the Accuracy, Recall, Precision, and MCC of the proposed model with the four tested techniques: Naive Bayes, KNN, Decision Tree, and SVM. Fig. 6, 7, 8, and 9 show that the Decision Tree technique achieved the highest performance with all four metrics: Accuracy (99.891%), Recall (99.904%), Precision (99.912%), and MCC (99.964%). On the other hand, the Naive Bayes technique achieved the lowest performance with all four metrics: Accuracy (94.472%), Recall (98.114%), Precision (92.923%), and MCC (88.643%). In general, all techniques perform well with the proposed model, except for the Naive Bayes technique. However, the Decision Tree technique could be considered as the best among the four techniques because it outperforms the other techniques in all four metrics.

$$Accuracy = \frac{(TP+TN)}{(TP+TN+FP+FN)} \tag{4}$$

$$Recall = \frac{TP}{(TP+FN)} \tag{5}$$

$$Precision = \frac{TP}{(TP+FP)} \tag{6}$$

$$MCC = \frac{((TP*TN)-(FP*FN))}{\sqrt{(TP+FP)*(TP+FN)*(TN+FP)*(TN+FN)}} \tag{7}$$

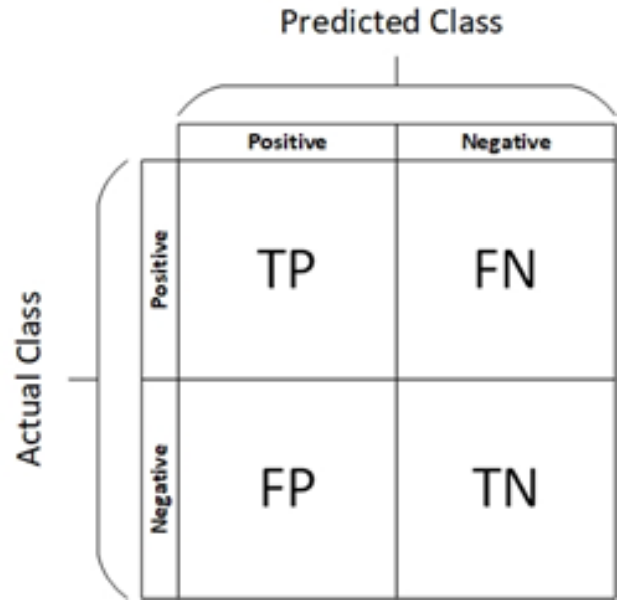


Fig. 5. Confusion Matrix.

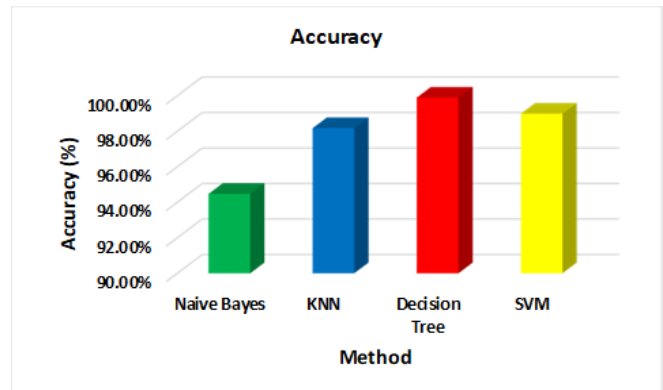


Fig. 6. Accuracy of the Proposed Model.

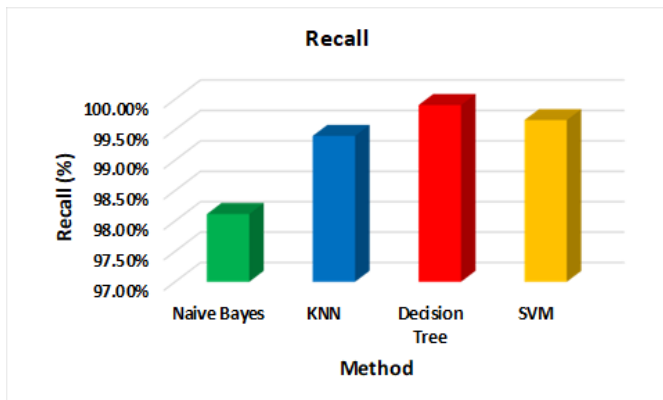


Fig. 7. Recall of the Proposed Model.

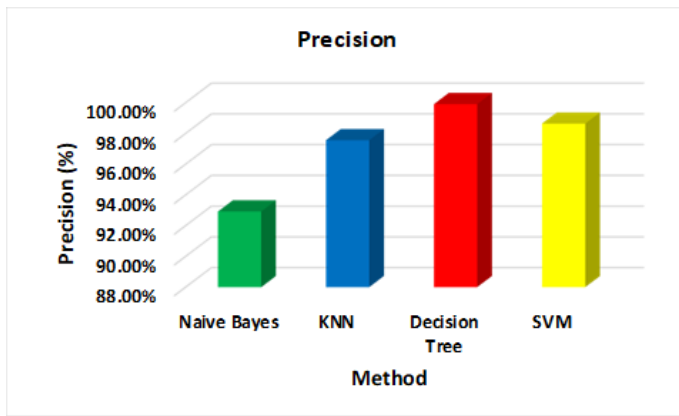


Fig. 8. Precision of the Proposed Model.

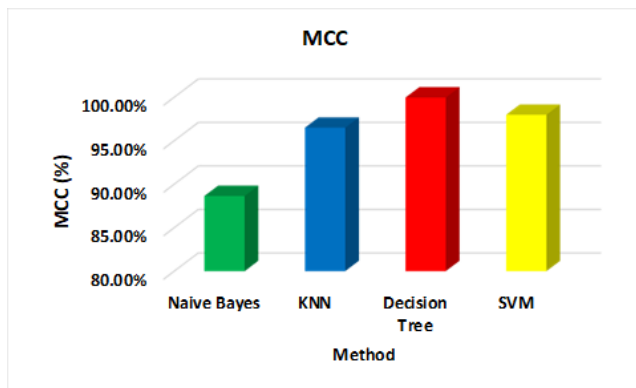


Fig. 9. MCC of the Proposed Model.

VI. CONCLUSION

DoS is a hazardous attack that threatens governments, businesses, and individuals. New techniques to launch DoS attacks emerge continuously. These techniques required an adaptive system to mitigate them. This paper developed a new paradigm for disclosing DoS attacks using machine learning approaches. The proposed model's primary objective is to mitigate existing and newly discovered DoS attack types. Several machine learning techniques were Naive investigated with the proposed model. Among these techniques, the Decision Tree technique has shown the highest performance. Whereas the Accuracy, Recall, Precision, and MCC, of the Decision Tree technique with the proposed model is 99.891%, 99.904%, 99.912%, and 99.964%, respectively. Therefore, the proposed detection model is promising for mitigating the newly emerged DoS attack types.

REFERENCES

- [1] M. Bang and H. Saraswat, "Building an effective and efficient continuous web application security program," 2016 International Conference On Cyber Situational Awareness, Data Analytics And Assessment (CyberSA), 2016, pp. 1-4, DOI: 10.1109/CyberSA.2016.7503287.
- [2] Symantec internet security threat report 2018 Volume 23, Symantec, 2018.
- [3] Cisco Annual Internet Report (2018–2023) White Paper, March 9, 2020, Cisco.
- [4] P. R. Chandre, P. N. Mahalle and G. R. Shinde, "Machine Learning Based Novel Approach for Intrusion Detection and Prevention System: A Tool Based Verification," IEEE Global Conference on Wireless

- Computing and Networking (GCWCN), 2018, pp. 135-140, DOI: 10.1109/GCWCN.2018.8668618.
- [5] S. Peneti and H. E, "DDoS Attack Identification using Machine Learning Techniques," International Conference on Computer Communication and Informatics (ICCCI), 2021, pp. 1-5, DOI: 10.1109/ICCCI50826.2021.9402441.
- [6] K. Hara and K. Shiimoto, "Intrusion Detection System using Semi-Supervised Learning with Adversarial Auto-encoder," NOMS 2020 - 2020 IEEE/IFIP Network Operations and Management Symposium, 2020, pp. 1-8, DOI: 10.1109/NOMS47738.2020.9110343.
- [7] Çavuşoğlu, Ü. (2019). A new hybrid approach for intrusion detection using machine learning methods. Applied Intelligence, 49(7), 2735-2761.
- [8] I. Abrar, Z. Ayub, F. Masoodi and A. M. Bamhdi, "A Machine Learning Approach for Intrusion Detection System on NSL-KDD Dataset," International Conference on Smart Electronics and Communication (ICOSEC), 2020, pp. 919-924, DOI: 10.1109/ICOSEC49089.2020.9215232.
- [9] Ravipati, Rama Devi, and Munther Abualkibash. "Intrusion detection system classification using different machine learning algorithms on KDD-99 and NSL-KDD datasets-a review paper." International Journal of Computer Science & Information Technology (IJCSIT) Vol 11 (2019).
- [10] T. M. Ma, K. YAMAMORI and A. Thida, "A Comparative Approach to Naive Bayes Classifier and Support Vector Machine for Email Spam Classification," 2020 IEEE 9th Global Conference on Consumer Electronics (GCCE), pp. 324-326, DOI: 10.1109/GCCE50665.2020.9291921.
- [11] P. Wang, Y. Zhang and W. Jiang, "Application of K-Nearest Neighbor (KNN) Algorithm for Human Action Recognition," IEEE 4th Advanced Information Management, Communicates, Electronic and Automation Control Conference (IMCEC), 2021, pp. 492-496, DOI: 10.1109/IMCEC51613.2021.9482165.
- [12] H. Elaidi, Y. Elhaddar, Z. Benabbou and H. Abbar, "An idea of a clustering algorithm using support vector machines based on binary decision tree," International Conference on Intelligent Systems and Computer Vision (ISCV), 2018, pp. 1-5, DOI: 10.1109/ISCV.2018.8354024.
- [13] Ahsan, Md Manjurul, et al. "Effect of data scaling methods on machine learning algorithms and model performance." Technologies 9.3 (2021): 52.
- [14] T. Wong and N. Yang, "Dependency Analysis of Accuracy Estimates in k-Fold Cross Validation," in IEEE Transactions on Knowledge and Data Engineering, vol. 29, no. 11, pp. 2417-2427, 1 Nov. 2017, DOI: 10.1109/TKDE.2017.2740926.
- [15] Wankhede, Shreekh, and Deepak Kshirsagar. "DoS attack detection using machine learning and neural network." Fourth International Conference on Computing Communication Control and Automation (ICCUBEA). IEEE, 2018.
- [16] Zhe, Wang, Cheng Wei, and Li Chunlin. "DoS attack detection model of smart grid based on machine learning method." IEEE International Conference on Power, Intelligent Computing and Systems (ICPICS). IEEE, 2020.
- [17] He, Zecheng, Tianwei Zhang, and Ruby B. Lee. "Machine learning based DDoS attack detection from source side in cloud." IEEE 4th International Conference on Cyber Security and Cloud Computing (CSCloud). IEEE, 2017.
- [18] A. K. B and M. M. Kodabagi, "Efficient Data Preprocessing approach for Imbalanced Data in Email Classification System," 2020 International Conference on Smart Technologies in Computing, Electrical and Electronics (ICSTCEE), 2020, pp. 338-341, DOI: 10.1109/ICSTCEE49637.2020.9277221.
- [19] B. -B. Jia and M. -L. Zhang, "Multi-Dimensional Classification via Decomposed Label Encoding," in IEEE Transactions on Knowledge and Data Engineering, DOI: 10.1109/TKDE.2021.3100436.
- [20] M. M. S. Pangaliman, F. R. G. Cruz and T. M. Amado, "Machine Learning Predictive Models for Improved Acoustic Disdrometer," IEEE 10th International Conference on Humanoid, Nanotechnology, Information Technology, Communication and Control, Environment and

- Management (HNICEM), 2018, pp. 1-5, DOI: 10.1109/HNICEM.2018.8666256.
- [21] N. Ajithkumar, P. Aswathi and R. R. Bhavani, "Identification of an effective learning approach to landmine detection," 1st International Conference on Electronics, Materials Engineering and Nano-Technology (IEMENTech), 2017, pp. 1-5, DOI: 10.1109/IEMENTECH.2017.8077018.

A Prediction Error Nonlinear Difference Expansion Reversible Watermarking for Integrity and Authenticity of DICOM Medical Images

David Muigai^{1*}, Elijah Mwangi², Edwell T. Mharakurwa³

Department of Electrical and Electronics Engineering, Dedan Kimathi University of Technology, Nyeri, Kenya^{1,3}
Faculty of Engineering, University of Nairobi, Kenya²

Abstract—It is paramount to ensure the integrity and authenticity of medical images in telemedicine. This paper proposes an imperceptible and reversible Medical Image Watermarking (MIW) scheme based on image segmentation, image prediction and nonlinear difference expansion for integrity and authenticity of medical images and detection of both intentional and unintentional manipulations. The metadata from the Digital Imaging and Communications in Medicine (DICOM) file constitutes the authentication watermark while the integrity watermark is computed from Secure Hash Algorithm (SHA)-256. The two watermarks are combined and compressed using the Lempel Ziv (LZ) -77 algorithm. The scheme takes advantage of the large smooth areas prevalent in medical images. It predicts the smooth regions with zero error or values close to zero error, while non-smooth areas are predicted with large error values. The binary watermark is encoded and extracted in the zero-prediction error using a nonlinear difference expansion. The binary watermark is concentrated more on the Region of non-interest (RONI) than the Region of interest (ROI) to ensure a high visual quality while maintaining a high capacity. The paper also presents a separate low degradation side information processing algorithm to handle overflow. Experimental results show that the scheme is reversible and has a remarkable imperceptibility and capacity that are comparable to current works reported in literature.

Keywords—Medical Image Watermarking (MIW); Digital Imaging and Communication in Medicine (DICOM); region of interest (ROI) and region of non-interest (RONI); prediction error (PE); nonlinear difference expansion (NDE); authenticity; integrity

I. INTRODUCTION

Medical images and patient data are often shared in e-diagnosis over open communication channels. The transmission of such data is prone to intentional and unintentional manipulations, affecting confidentiality, integrity and authenticity. Such manipulations can result in misdiagnosis and even lead to loss of life hence the need to ensure reliability [1-2].

Medical images and patient information are transmitted, stored, retrieved, printed, processed and displayed through Digital Imaging and Communications in Medicine (DICOM) standards [3]. In DICOM, metadata which is the patient report and information that connects to the image ensures reliability of medical images data. The metadata is saved in the image file header [3]. This technique is insecure as the metadata can be

easily modified, destroyed, or disconnected from the medical image [4].

Digital image watermarking, a branch of information hiding technology where a secret message is hidden in public data, can overcome these challenges. The secret message can be the metadata, a hospital logo, an electronic signature, or any other identifier in medical images. The requirements for medical image watermarking are reversibility, imperceptibility and reliability [2].

Digital image watermarking is classified into several classes based on the method of embedding the secret message, reversibility, application and region(s) used to encode the secret message [5]. It can be either frequency or spatial domain based on the method of encoding the secret message. Spatial domain techniques [4], [6] changes the pixel intensities of the image directly to implant the secret message. Frequency domain techniques [7-8] implants the secret message by changing the coefficient values of the transformed image. Digital image watermarking techniques are classified as reversible, semi-reversible or irreversible based on reversibility. In reversible techniques [9-10], the original image and the secret message are losslessly restored, while in irreversible techniques [11], the secret message and the original image cannot be losslessly restored. Semi-reversible techniques [12] restore some regions of the original image while others cannot be restored. Therefore, reversible techniques are preferred for watermarking medical images. Depending on the application of digital image watermarking, the schemes are classified as either fragile or robust. Robust watermarking techniques emphasize the robustness of the encoded message. The encoded watermark can resist legitimate and illegitimate attacks during image transmission in robust schemes. Therefore, robust watermarking strategies [13-14] are mainly used for copyright protection of images. Fragile watermarking methods emphasize on detection of manipulations during image transmission. Hence, fragile watermarking techniques [4], [6] are used to confirm the integrity of images. The watermarking can be further classified as ROI or RONI based. The anatomical details are contained in ROI whereas RONI carries the uninformative background usually black in color [15]. In ROI techniques [4],[16] the secret message is hidden in ROI while RONI techniques [17-18] hides it in RONI.

In this paper, a novel reversible MIW scheme based on prediction error nonlinear difference expansion for authenticity

*Corresponding Author.

and integrity of medical images is proposed. The scheme has the following objectives:

1) Predicting the medical image with zero error or values close to zero for smooth regions while non-smooth regions are predicted with large error values. Smooth regions are characterized by zero or slight differences in adjacent pixel intensities. Hiding the watermark in these regions is less visible.

2) Concentrating the watermark mainly in RONI to ensure excellent visual quality on the ROI while maintaining its security.

3) Determining an optimum point for trade-off between capacity and imperceptibility for prediction error nonlinear difference expansion watermarking.

4) Attaining good visual quality of watermarked images that supersede the benchmark value and the perceptual boundary.

5) Providing a low degradation approach to handle the overflow.

6) Lossless recovery of the medical image without the need of a location map.

The rest of this paper is organized as follows; The second section provides medical image watermarking schemes reported in the literature. The third section describes the proposed work. The fourth section presents the results and discussion. The fifth section, which is the final section, presents the conclusion and suggestion for further work.

II. RELATED WORK

Researchers have recently presented Medical Image Watermarking (MIW) techniques. This section analyzes some of these techniques. Roček *et al.* [12] presented a new MIW strategy that merges RONI watermarking method with zero-watermarking principle and reversibility features. The scheme uses a reversible watermarking in the RONI, which achieves a high capacity and implants data using the zero-watermarking principle. A Dual Tree Complex Wavelet Transform (DT-CWT) is used to merge these techniques. The limitation of the approach is the need for a location map at extraction to recover the image and the encoded watermark.

Gao *et al.* [19] presented a reversible MIW approach that achieves tamper detection and enhances ROI contrast. It utilizes Otsu's thresholding method to differentiate the RONI from the ROI. The scheme expands the peak-pairs of ROI histogram to achieve data encoding alongside a less distortion contrast enhancement. This approach creates a feature bit matrix from ROI and encodes it in the least significant bits of RONI to guarantee ROI reversibility. The limitations of the scheme are; (i) the scheme is semi-reversible as it can restore only the ROI at reception and (ii) the need for implanting the feature bit matrix.

Atta-ur-Rahman *et al.* [20] presented a reversible MIW approach for the integrity of medical images and the secrecy of patient data. The watermark is created chaotically and encoded using a chaotic key in selected pixels. The selected pixels are divided using a primitive polynomial of degree four and the

remainder appended to the secret message. At the reception, the computed remainder validates the watermark. In this approach, a high imperceptibility was exhibited. The approach's limitations were; the hiding capacity was not measured and the method is not region-based hence making it impossible to select hiding regions.

Liu *et al.* [21] presented a novel robust reversible MIW to protect the integrity and authenticity of medical images. This method addresses the challenge of losing information in watermark embedding due to image segmentation. It avoids biases during diagnosis by designing a recursive dither modulation (RDM) based watermarking. RDM is later combined with Singular Value Decomposition (SVD) and Slantlet Transform (ST) to protect image authenticity. The RONI and ROI are divided to generate the watermark encoded into the whole image, thus avoiding risk related to image segmentation.

Swaraja *et al.* [22] presented a MIW technique that conceals a dual watermark on RONI blocks for authenticity and tamper recognition in medical images. This procedure uses the lossless Lempel-Ziv-Welch compression algorithm to compress the dual watermark, thus increasing capacity. The embedding blocks are chosen based on the human visual systems characteristics, integrating Discrete Wavelet Transform (DWT) and Schur transform alongside Particle Swarm Bacterial Foraging Optimization Algorithm (PSBFO). The scheme is robust against signal attacks and compression and shows transparency from the simulation results.

Fares *et al.* [23] proposed a MIW approach based on Discrete Cosine Transform (DCT) and DWT for protecting patient data. The scheme proposes two approaches. The first approach combines DCT and Schur Decomposition (SD) and performs integration in medium frequencies thus achieving a good compromise between visual quality and robustness. The second approach combines SD and DWT to achieve a robust watermark distribution. The proposed schemes maintain good visual quality and are robust against attacks. The capacity of the first approach is 682 bits which correspond to 85 characters only. Therefore, the capacity of the first approach is limited. The second approach conceals 1024 bits equivalent to 128 characters. Therefore, the capacity of the second approach is certainly reduced.

III. METHODOLOGY

A fragile Medical Image Watermarking (MIW) scheme is presented for detecting both intentional and unintentional manipulations and ensuring the authenticity and integrity of DICOM medical images. The approach also presents a separate low degradation side information processing algorithm to handle overflow. The sub-sections are as follows.

A. Watermark Creation and Compression

There exist several ways for creating an authentication watermark [24]. The DICOM files consist of image data and metadata in a single *.dcm* file. The metadata contains patient information, image dimensions, parameters of modality acquisition and operator identification [24]. The scheme uses the metadata of DICOM images as the authentication watermark. It also employs the Secure Hash Algorithm (SHA)

-256 to compute the integrity watermark. This is a patent cryptographic hash function used in data integrity and digital certificates [25]. The output is a 64-digit hexadecimal number and is strong, and easy to compute [25]. The method detects manipulations by comparing the hidden and extracted integrity watermark. It also combines the authentication and integrity watermark to form the total watermark. The text string is compressed to a binary string using the Lempel Ziv -77 compression algorithm. Table I shows a summary of the watermark creation and compression data features.

TABLE I. WATERMARK CREATION AND COMPRESSION DATA FEATURE

Type of Watermark	Creation	Minimum size in bits	Maximum size in bits
Integrity	SHA-256	500	550
Authenticity	Metadata	22000	25000
Total Watermark	Authenticity + Integrity	22500	25550

B. Image Prediction

Any image pixel is predictable using an expression that constitutes its neighboring pixels [26]. The hiding capacity of prediction-error expansion depends on how close the predicted image resembles the original image. Medical images are characterized by a large smooth area, unlike other images and hiding the watermark in these areas is less distinguishable by the human visual system [4]. The scheme predicts the smooth areas of the medical image with zero error or values close to zero and non-smooth areas with large error values using (1). The predicted pixel is p_{ij} .

$$p_{ij} = \begin{cases} \frac{p_{i-1j}p_{ij-1}}{p_{i-1j-1}} & 0 \notin (p_{i-1j}, p_{ij-1}, p_{i-1j-1}) \\ p_{i-1j} + p_{ij-1} - p_{i-1j-1} & \text{otherwise} \end{cases} \quad (1)$$

C. Image Segmentation

There exist several techniques to segment medical images into ROI and RONI. The techniques can be manual, like use of polygons and freehand sketching, or automatic. A radiographer divides a medical image using a technique of his/her choice. The scheme automatically segments the medical image using a thresholding technique that utilizes the mean of pixels and morphological operations. The specific medical image segmentation procedure is as follows.

- 1) Load the medical image M_I .
- 2) Compute the mean of all pixels and consider it as the initial threshold T_0 .
- 3) Divide the pixels into two groups such that pixels greater than T_0 form the ROI, otherwise RONI.
- 4) Compute the mean of ROI M_{ROI} and RONI M_{RONI} separately.
- 5) Compute the new threshold T_1 as the average of M_{ROI} and M_{RONI} .
- 6) Repeat steps (iv) and (v) until the new threshold converges.
- 7) Convert the medical image into a binary image using the last threshold by making all pixels less than it black otherwise white.

- 8) Perform morphological filtering on the binary image obtained from step (vii).
- 9) Perform region filling on the binary image from step (viii).
- 10) Display the binary image.
- 11) Obtain the indices M_{I0} and M_{I1} corresponding to the pixels with values 0 and 1 of the binary image, respectively.
- 12) The RONI and ROI of the medical image correspond to M_{I0} and M_{I1} respectively.

D. Prediction Error Nonlinear Difference Expansion

The basic prediction error difference expansion first proposed by [27] is given as follows;

Let p_{ij} be the pixels of the original image and \hat{p}_{ij} be the predicted pixel. The prediction error is computed as;

$$e_{ij} = p_{ij} - \hat{p}_{ij} \quad (2)$$

Let b_i be a binary watermark. The watermark bits are embedded by expanding the prediction error as;

$$e'_{ij} = 2e_{ij} + b_i \text{ where } b_i = 0 \text{ or } 1 \quad (3)$$

Let $T > 0$, be the threshold to increase capacity and control degradation. It is directly proportional to degradation and capacity but inversely proportional to visual quality. The threshold T can be varied from 1 to the maximum possible gray intensity value of an image. The watermarked pixels are given by (4).

$$p'_{ij} = \hat{p}_{ij} + e'_{ij} \text{ if } e_{ij} < T \quad (4)$$

If $|e_{ij}| \geq T$, the pixels cannot carry a watermark bit and are shifted to provide a greater prediction error than the carrier pixels at detection using (5).

$$p'_{ij} = \begin{cases} p_{ij} + T & \text{if } e_{ij} \geq T \\ p_{ij} - (T - 1) & \text{if } e_{ij} < -T \end{cases} \quad (5)$$

The embedding threshold and the predicted image are transmitted as side information alongside the watermarked image to the receiver [26]. The problem of overflow and underflow is re-solved by creating a location map or using flag bits [26-28]. At detection, if the same predicted value for the original image is available, then the error is computed as in (6). \bar{p}_{ij} is the received image.

$$\bar{e}_{ij} = \bar{p}_{ij} - \hat{p}_{ij} \quad (6)$$

The prediction error differentiates the embedded and shifted pixels. If $-2T \leq \bar{e}_{ij} \leq 2T + 1$, then it is a carrier pixel and the error is computed as $\bar{e}_{ij} = 2e_{ij} + b$, where b is the least significant bit of \bar{e}_{ij} . The original and shifted pixels are recovered as in (7) and (8) respectively.

$$p_{ij} = \frac{\bar{p}_{ij} + \hat{p}_{ij} - b}{2} \quad (7)$$

$$p_{ij} = \begin{cases} \bar{p}_{ij} - T \\ \bar{p}_{ij} + (T - 1) \end{cases} \quad (8)$$

To overcome the challenge of high degradation caused by increasing T while increasing capacity, the transmission of the predicted image and T as side information, overflow and underflow in the basic prediction error linear difference expansion, the scheme uses a prediction error nonlinear difference expansion. It uses systematic multiple predictions and expansions of the zero - prediction error. The binary watermark is divided into sections equal to the number of expansions. The original image is predicted using (1). The error is computed using (2). The carrier and non-carrier pixels are embedded and shifted as in (9) and (10) respectively.

$$p'_{ij} = p_{ij} + b_i \text{ if } e_{ij} = 0 \text{ where } b_i = 0 \text{ or } 1 \quad (9)$$

$$p'_{ij} = \begin{cases} p_{ij} + 1 & e_{ij} \geq 1 \\ p_{ij} & e_{ij} \leq -1 \end{cases} \quad (10)$$

The first row and column are not used in embedding. The rest of the rows and columns are embedded in intervals of two pixels, with the initial pixels being P_{22} , P_{23} , P_{32} and P_{33} until all the other pixels are used in embedding the watermark. The image is predicted in each initial pixel embedding stage. This is the prediction error-linear difference expansion (PE-LDE) with a threshold $T=1$. To increase capacity with low distortion, unlike the basic prediction error difference expansion which increases T , the scheme uses a prediction error quadratic difference expansion (PE-QDE) considered as a cascade of the PE-LDE described as follows:

The image p'_{ij} is used again to perform PE-QDE and is predicted using (1) to obtain \hat{p}'_{ij} . The error is computed as;

$$e'_{ij} = p'_{ij} - \hat{p}'_{ij} \quad (11)$$

Let b'_i be the watermark to be embedded in PE-QDE. The carrier and non-carrier pixel are embedded and shifted as in (12) and (13) respectively.

$$p''_{ij} = p'_{ij} + b'_i \text{ if } e'_{ij} = 0 \text{ where } b'_i = 0 \text{ or } 1 \quad (12)$$

$$p''_{ij} = \begin{cases} p'_{ij} + 1 & e'_{ij} \geq 1 \\ p'_{ij} & e'_{ij} \leq -1 \end{cases} \quad (13)$$

The embedding in PE-QDE follows the same order as in PE-LDE. The process is repeated so as to increase the capacity at low distortion until saturation is reached.

The watermarked image is predicted at the reception using the same prediction technique used in embedding. During extraction, at any instance of image prediction that corresponds to an image prediction during embedding, the same predicted image is obtained. This guarantees reversibility. The error is computed as in (14). \check{p}_{ij} is the obtained predicted image.

$$\check{e}_{ij} = p''_{ij} - \check{p}_{ij} \quad (14)$$

The error obtained is the same as the expanded error in the last embedding stage of initial pixel P_{33} in PE-QDE. If the \check{e}_{ij} is either 0 or 1 then it is a carrier pixel, else a non-carrier pixel. For carrier pixels, the watermark is extracted as follows.

$$b = \check{e}_{ij} \quad (15)$$

The carrier and non-carrier pixels are recovered as;

$$p'_{ij} = \begin{cases} p''_{ij} - b & \text{if } \check{e}_{ij} \text{ is } 0 \text{ or } 1 \\ p''_{ij} - 1 & \text{if } \check{e}_{ij} > 1 \\ p''_{ij} & \text{otherwise} \end{cases} \quad (16)$$

The first row and column remain unaltered as it is not used in embedding. The rest of the rows and columns are extracted in intervals of two pixels with the initial pixels being P_{33} , P_{32} , P_{23} and P_{22} , an inverse order to that of embedding. This is the inverse PE-QDE. The inverse PE-LDE is as follows;

The image p'_{ij} is predicted using the same technique and the error is computed as in (17). \check{p}_{ij} is the obtained predicted image.

$$\check{e}_{ij} = p'_{ij} - \check{p}_{ij} \quad (17)$$

If \check{e}_{ij} is either 0 or 1 then it is a carrier pixel else a non-carrier pixel. For carrier pixels, the watermark is extracted as;

$$b = \check{e}_{ij} \quad (18)$$

The original carrier and non-carrier pixels are recovered as;

$$p_{ij} = \begin{cases} p'_{ij} - b & \text{if } \check{e}_{ij} \text{ is } 0 \text{ or } 1 \\ p'_{ij} - 1 & \text{if } \check{e}_{ij} > 1 \\ p'_{ij} & \text{otherwise} \end{cases} \quad (19)$$

The inverse PE-LDE follows the same order as inverse PE-QDE. Therefore, the binary watermark and the original image are restored.

E. Watermark Encoding

Fig. 1 shows the flow chart of the watermark embedding and the specific procedure is as follows:

- 1) Read the DICOM file.
- 2) Segment the image data using the segmentation procedure to obtain the binary mask.
- 3) Obtain the authentication watermark (AW) from the DICOM metadata.
- 4) Compute SHA-256 on the image data to get the integrity watermark (IW).
- 5) Concatenate the authentication and integrity watermark to form the total watermark.
- 6) Compress the total watermark using LZ-77 compression algorithm.
- 7) Divide the binary watermark into sections equal to the knee point less one.
- 8) Embed the first and second section of the binary watermark using the PE-LDE and PE-QDE respectively as described in section D to obtain the partial watermarked image.
- 9) Using the binary mask obtained in step (ii), segment the partial watermarked image such that the RONI and ROI region of the partial watermarked image corresponds to '0' and '1' of the binary watermark respectively.
- 10) Embed the third, fourth and fifth sections of the binary watermark using prediction error - third order difference

expansion (PE-TODE), prediction error -fourth order difference expansion (PE-FODE) and prediction error - fifth order difference expansion (PE-FIODE) respectively on RONI only. Consider these expansions as cascades of PE-LDE.

11) Obtain the watermarked image which may exhibit overflow.

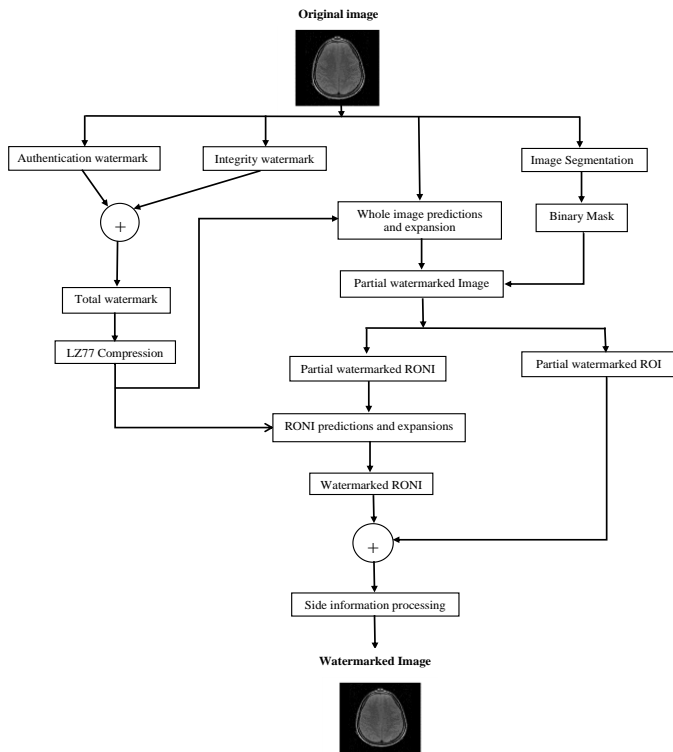


Fig. 1. Flowchart of Watermark Embedding.

F. Side Information Processing

Overflow and underflow problems in reversible watermarking are essential as it can lead to irreversibility or heavy distortion. Overflow occurs when the maximum gray level is exceeded, while underflow occurs when the minimum gray level is exceeded. The scheme does not exhibit underflow as pixel intensity are not decreased during processing. However, the approach can exhibit overflow. The maximum overflow is equals to the number of expansions used during embedding. The scheme preserves the last prediction error expansion to hide the side information. The scheme considers the length of the watermark, segmentation threshold, and locations of maximum gray level and overflowed pixels as side information. The procedure for Side Information Processing (SIP) can be described as follows:

- 1) Scan the watermark image and record the locations of maximum and overflowed gray levels.
- 2) Modify the maximum and overflowed gray pixels by subtracting the number of expansions used in embedding.
- 3) Concatenate the locations, segmentation threshold and length of the watermark and consider it as side information.
- 4) Compress the side information.

5) Hide the side information on the whole image using the last prediction error difference expansion.

6) Finally, obtain the watermarked image that carries the watermark and side information without exhibiting overflow for transmission.

G. Side Information Recovery

The side information is first recovered at extraction and the maximum and overflowed pixels are restored before extracting the watermark. The side information is recovered using the following steps.

- 1) Perform the sixth inverse prediction error difference expansion on the whole image to obtain the side information binary watermark.
- 2) Decompress the side information binary watermark.
- 3) Modify the locations obtained in step (ii) by adding the number of expansions used in embedding to restore the overflowed watermark image.

H. Watermark Extraction

Fig. 2 shows a flow chart of the watermark extraction and the specific procedure is as follows:

- 1) Using the side information recovery procedure, recover the side information and restore the maximum and overflowed pixels.
- 2) Separate the RONI and ROI of the watermarked image using the segmentation procedure. Use the recovered segmentation threshold
- 3) Extract the fifth, fourth and third sections of the binary watermark using inverse PE-FIODE, PE-FODE and PE-TODE respectively on the RONI only to recover the partial watermarked image
- 4) Extract the second and first sections of the binary watermark using inverse PE-QDE and PE-LDE respectively on the whole image to recover the original image
- 5) Concatenate the recovered sections of the binary watermark and decompress using LZ-77 decompression algorithm
- 6) Compare the recovered and hidden authenticity watermark for authentication verification
- 7) Compute the SHA-256 of the recovered image and compare it with the hidden integrity watermark to verify that the image has been transmitted without manipulation.

I. Performance Measures

The proposed scheme is evaluated in terms of capacity, imperceptibility, reversibility and robustness to provide a fair comparison with other relevant schemes. The capacity of the proposed scheme in bits per pixel (bpp) is computed using (20). The capacity of the scheme depends on the accurate prediction of the image. To increase capacity, systematic multiple predictions and expansions are employed.

$$capacity = \frac{\text{Number of pixels for embedding}}{\text{size of original image}} \quad (20)$$

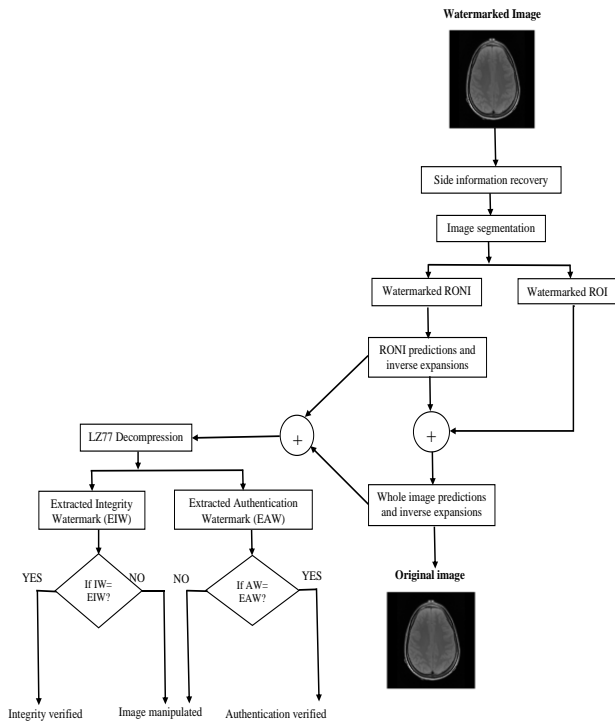


Fig. 2. Flowchart of Watermark Extraction and Verification.

The imperceptibility of the scheme is evaluated using PSNR, SSIM and Image Fidelity (IF) between the original and watermarked image. The PSNR, SSIM and IF are computed using (21), (22) and (23) respectively. The I and I' of the equations represent the original and watermarked image respectively and (i, j) are the coordinates of pixels in these images. The images are of dimensions $M \times N$.

$$PSNR(I, I') = 10 \times \log_{10} \frac{HP^2 \cdot M \cdot N}{\sum_{i=0}^{N-1} \sum_{j=0}^{M-1} (I(i, j) - I'(i, j))^2} \quad (21)$$

Where HP is the highest possible pixel value for the images. PSNR values range between 0 and $+\infty$. A higher PSNR value shows low image distortion and high visual quality.

$$SSIM(I, I') = \frac{(2\mu_I \mu_{I'} + C_1)(2\sigma_{II'} + C_2)}{(\mu_I^2 + \mu_{I'}^2 + C_1)(\sigma_I^2 + \sigma_{I'}^2 + C_2)} \quad (22)$$

Where $\mu_I, \mu_{I'}$ are the averages of I, I' respectively, $\sigma_I, \sigma_{I'}$ are variances of I, I' respectively, C_1, C_2 are balancing constants and $2\sigma_{II'}$ are the covariance for I, I' respectively. The SSIM is a quality measure based on Human Visual System to measure image distortion in structural information. Its values lie between 0 and 1. An SSIM of 1 indicates complete similarity.

$$IF = 1 - \frac{\sum_{i=1}^{N-1} \sum_{j=0}^{M-1} (I(i, j) - I'(i, j))}{\sum_{i=0}^{N-1} \sum_{j=0}^{M-1} (I(i, j))^2} \quad (23)$$

The IF parameter measures similarity between two images. An IF value of 1 between two images indicates that they are similar.

At extraction, the proposed scheme evaluates the reversibility of the image and the watermark. In evaluating the reversibility of the image, PSNR and Root Mean Square Error (RMSE) between the extracted and original image are used to verify that two images are 100% numerically identical. The RMSE is computed using (24).

$$RMSE(I, I') = \sqrt{\frac{\sum_{i=0}^{N-1} \sum_{j=0}^{M-1} (I(i, j) - I'(i, j))^2}{M \cdot N}} \quad (24)$$

A PSNR and RMSE of $+\infty$ and 0 respectively indicate that the image has been recovered without any loss else otherwise. In evaluating the watermark reversibility, Accuracy Ratio (AR) and Bit Error Rate (BER) between the embedded and extracted binary string is used. The BER and AR are computed as;

$$BER = \frac{\text{Number of error bits}}{\text{Total number of bits}} \quad (25)$$

$$AR = \frac{\text{Number of correct bits}}{\text{Total number of bits}} \quad (26)$$

A BER and AR value of 0 and 1 respectively indicate that the watermark has been recovered without any loss. The scheme also computes the BER between the original and extracted binary watermark as in (25) to evaluate robustness against attacks. A BER value closer to 0 indicate stronger robustness.

IV. RESULTS AND DISCUSSION

A. Experimental Setup

The experimental results were obtained using a PC with an Intel CPU of 2.6 GHz and 8GB RAM. The scheme was implemented in MATLAB 2021a to test the reversibility, imperceptibility, robustness and capacity. A set of 270 medical images in DICOM format comprising of 30 brain Magnetic Resonance Images (MRI) images, 30 cervix MRI images, 30 kidney Computed Tomography (CT) images, 30 lung CT images, 30 chest Digital Radiography (DX) images, 30 breast Mammography (MG) images, 30 liver Ultrasound (US) images, 30 chest Computed Radiology (CR) images and 30 headneck Positron emission tomography (PET) images were obtained from [29-30]. All images were 16 bpp and were re-sized to 512 x 512.

B. Imperceptibility

The imperceptibility of the scheme was evaluated using PSNR, SSIM and IF and the results given in Table II. The minimum PSNR value between the original and watermarked images is 83.0 dB, which is above the acceptable benchmark value of 40 dB [5] and the perceptual boundary of 82 dB [4] for the human visual system. Qasim *et al.* [4] conducted a relative Visual Grading Analysis (VGA) trial and determined that the modification of images to 82 dB or higher is unnoticeable to all observers. Therefore, the original and watermarked image are visually indistinguishable by the human eye. The SSIM and IF are either unity or close to unity indicating that the watermarked was hidden invisibly. A small set of the medical images and their corresponding watermarked images are shown in Fig. 3.

TABLE II. EVALUATION OF THE WATERMARKED IMAGES

Body Part Examined (Modality)	No of images used	Capacity (bpp)		PSNR		SSIM	IF	
		Minimum	Maximum	Minimum	Maximum		Minimum	Maximum
1. Brain (MRI)	30	0.47	0.93	84.5	85.5	1.00	0.93	0.99
2. Cervix (MRI)	30	0.98	1.21	83.8	85.0	1.00	0.96	0.98
3. Kidney (CT)	30	0.44	0.76	83.8	84.4	1.00	0.97	0.99
4. Lung (CT)	30	0.43	0.45	83.3	84.5	1.00	1.00	1.00
5. Chest (DX)	30	0.41	0.52	83.2	85.9	1.00	1.00	1.00
6. Breast (MG)	30	0.55	1.00	83.6	86.0	1.00	1.00	1.00
7. Liver (US)	30	0.62	0.85	83.8	85.6	1.00	0.95	0.99
8. Chest (CR)	30	0.41	0.53	83.8	86.2	1.00	1.00	1.00
9. Headneck(PT)	30	0.66	0.87	83.0	84.3	1.00	1.00	1.00
Overall Performance	270	0.41	1.21	83.0	86.2	1.00	0.93	1.00

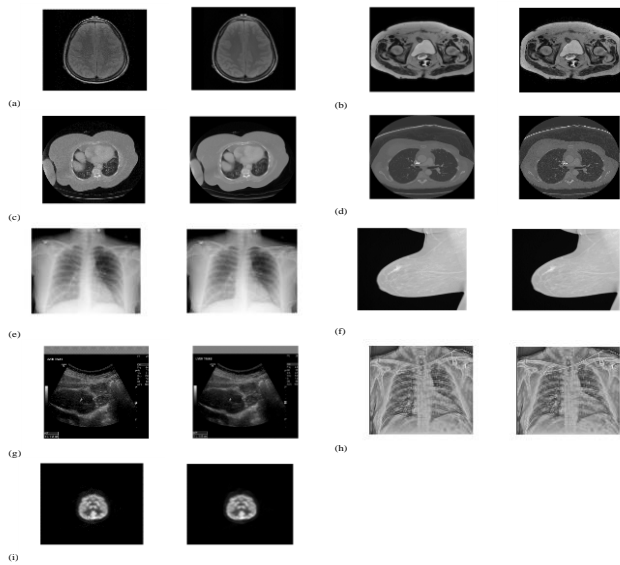


Fig. 3. Sample Medical Images and their Corresponding Watermarked Images. (a) MRI Brain, (b) MRI Cervix, (c) CT Kidney, (d) CT Lung, (e) DX Chest, (f) MG Breast, (g) US Liver, (h) CR Chest, (i) PT Headneck, [32-33].

C. Reversibility

The reversibility of the scheme was assessed at reception for both the extracted image and the watermark. The BER and AR values between the embedded and extracted binary watermark were used to evaluate the watermark reversibility. The values of zero and one respectively were obtained, demonstrating that the watermark was extracted without loss. This is a confirmation of the integrity and authenticity of the watermark. At the reception, the medical image is restored for diagnosis. The PSNR, RMSE, SSIM and IF between the original and extracted image were used to evaluate the image reversibility. The PSNR and RMSE values were positive infinity and zero respectively indicating that the two images are 100% numerically identical. The SSIM and IF were both unity demonstrating that the extracted image is identical to the original image.

D. Capacity

The binary watermark is encoded in the zero error pixels. To increase capacity, the number of iterations is increased. For the first and second iteration, that is the PE-LDE and PE-QDE, the binary watermark is encoded in the whole image, while for iterations above two, the binary watermark is encoded in the RONI only. A binary image obtained from the image segmentation procedure is used to distinguish the ROI from the RONI. This controls degradation in ROI as increasing capacity distorts the watermarked image. Fig. 4 shows the capacity of the scheme versus the number of iterations.

In Fig. 4, the capacity of the scheme increases steadily with an increase in the number of iterations until the knee point. After the knee point, increasing the number of iterations results in a low increase in capacity but still degrades the image due to the shifting of non-carrier pixels. The complexity of the approach and consequently the computational time increases with an increase in the number of iterations. After 30 iterations, an increase in the number of iterations increases capacity by less than 0.001bpp. This is the saturation point of the scheme. The scheme limits the number of iterations to 6 which correspond to the knee point. The capacity created in the 6th iteration hides the side information and is performed on both RONI and ROI. Fig. 5 shows PSNR as a function of capacity.

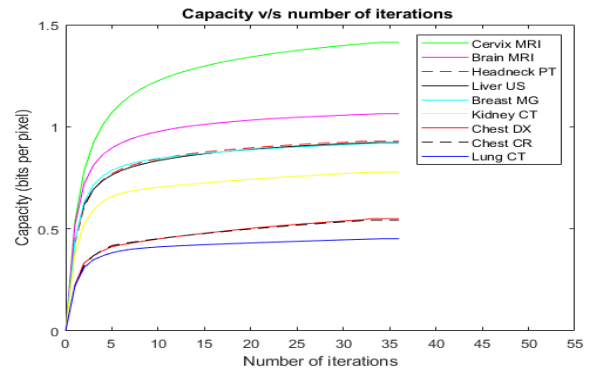


Fig. 4. Capacity v/s Number of Iterations.

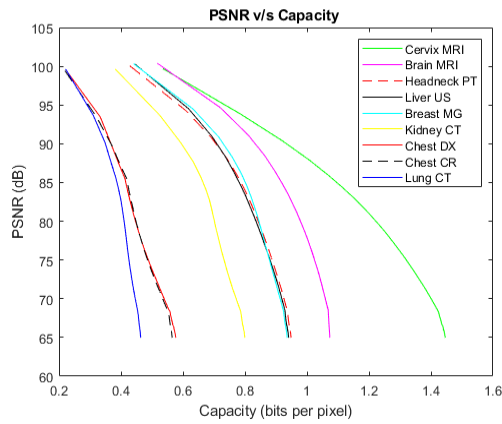


Fig. 5. PSNR v/s Capacity.

From Fig. 5, it can be noted that an increase in capacity distorts the watermarked image. An increase in capacity degrades the image until saturation. After saturation, increasing the number of iterations results in a negligible increase in capacity but continues to degrade the image due to the shifting of non-carrier pixels. Table III shows the specific number of bits in Kbytes hidden and the resultant PSNR for the images in Fig. 3. The cervix MRI image had the highest capacity of 36.57 Kbytes, while the lung CT had the lowest capacity of 12.87 Kbytes. Fig. 6 shows a sample binary image of MRI image (a) shown in Fig. 3.



Fig. 6. Binary Image of MRI Image in Fig. 3 (a).

E. Robustness

The robustness of the scheme was assessed using BER between the encoded and extracted binary watermark under various attacks. The average PSNR and BER of the scheme under various intentional and unintentional attacks are shown

in Table IV. In this table, adding or removing a region illustrate intentional attacks while the rest demonstrate unintentional attacks. The integrity and authenticity of the medical images are confirmed when the encoded and extracted watermark are completely identical. However, intentional and unintentional manipulations on the medical image result in a mismatch between the encoded and extracted watermark. The latter are malicious manipulations where a region is added or removed while the former are accidental manipulations occurring during transmission. The reversibility of the medical image under various attacks was also assessed using PSNR. The PSNR obtained for each image under attack was not positive infinity, indicating that the original medical image was not recovered. The BER obtained under various attacks for each image was non-zero, demonstrating a mismatch between the encoded and extracted watermark. Therefore, the authenticity and integrity of the medical images under attack is not confirmed. This shows that the approach is fragile to manipulations.

F. Comparison with Relevant Schemes

The developed scheme has been compared with other relevant MIW schemes as shown in Table V and Table VI.

The approaches are compared in terms of location map, reversibility, capacity and visual quality. The developed approach uses a non-linear difference expansion that does not need a location map at the extraction for recovery of the watermark and the image to guarantee reversibility thus is better than the approach [12]. The side information of the developed approach is hidden in the last iteration leading to a low degradation approach to handle the overflow. The developed scheme performs better than the scheme reported in [19] in terms of reversibility as it recovers the whole image while the former recovers only the ROI. The medical image is restored in its pristine state in the developed approach. Additionally, it gives a higher performance than schemes [19] and [22-23] in terms of capacity as it achieves a higher capacity at a lower degradation. Also, the developed scheme achieved the highest PSNR of 83.0 to 86.2 dB and a SSIM of unity compared to the scheme [12] and [19-23], demonstrating a better visual quality.

TABLE III. SPECIFIC NUMBER OF BITS HIDDEN IN EACH ITERATION AND THE RESULTANT PSNR FOR THE MEDICAL IMAGES SHOWN IN FIG. 3. ‘C’ REPRESENTS CAPACITY IN K BYTES

Body part examined	PE-LDE		PE-QDE		PE-TODE		PE-FODE		PE-FIODE		S I P		Total Bits Hidden
	C (kB)	PSNR (dB)	C (kB)	PSNR (dB)	C (kB)	PSNR (dB)	C (kB)	PSNR (dB)	C (kB)	PSNR (dB)	C (kB)	PSNR (dB)	
1. Brain (MRI)	16.96	100.3	6.67	94.6	2.96	91.0	1.70	88.4	1.08	86.4	0.79	84.8	30.16
2. Cervix (MRI)	17.53	99.6	8.20	93.8	4.47	90.3	2.86	87.8	2.00	85.9	1.51	84.3	36.57
3. Kidney (CT)	12.49	99.6	4.72	93.6	2.20	90.1	1.35	87.6	0.80	85.0	0.53	84.0	22.09
4. Lung (CT)	7.25	99.6	2.92	93.6	1.25	90.1	0.63	87.6	0.50	85.6	0.32	84.0	12.87
5. Chest (DX)	7.34	99.4	3.58	93.4	1.15	89.9	0.80	87.4	0.66	85.5	0.29	83.9	13.82
6. Breast (MG)	14.43	100.3	6.28	94.4	2.72	90.8	1.44	88.2	0.92	86.2	0.61	84.5	26.40
7. Liver (US)	14.57	100.3	5.68	94.5	2.47	90.9	1.41	88.3	0.91	86.3	0.69	84.7	25.73
8. Chest (CR)	7.19	99.4	3.34	93.4	1.55	89.9	0.70	87.4	0.73	85.4	0.26	83.9	13.77
9. Headneck (PT)	14.04	100.0	5.91	94.2	2.73	90.7	1.56	88.2	1.01	86.2	0.71	84.5	25.96

TABLE IV. AVERAGE PSNR AND BER OF THE PROPOSED SCHEME UNDER ATTACKS

Attack type	Parameter	PSNR	BER
Resizing	0.8	-	0.47
Rotation and cropping	-3°	51.9	0.46
Brightness adjustment	-	12.7	0.56
Histogram equalization	-	9.3	0.52
Gaussian noise	Mean=0.003 Variance=0.001	31.2	0.49
Salt and pepper noise	Density=0.09	19.1	0.58
JPEG compression	Quality factor=80	48.9	0.41
Median filter	Window= 5 x 5	68.7	0.48
Average filter	Window= 3 x 3	68.6	0.43
Adding a region	-	57.2	0.42
Removing a region	-	57.1	0.44

TABLE V. PERFORMANCE COMPARISON OF THE PROPOSED SCHEME WITH OTHER RECENT RELEVANT SCHEMES. RCSP STANDS FOR RESIDUE WITH CHAOTICALLY SELECTED PIXELS

Approach Year	Medical Image Segmentation	Hiding Region	Hiding Technique	Location map	Reversible	Capacity (bpp)	Visual Quality	
							PSNR	SSIM
Roček et al. [12]	Automatic	ROI RONI	DT-CWT LSB	YES	YES	ROI Dependent	Average = 81	Average = 1
Gao et al. [19]	Automatic	ROI RONI	HS LSB	NO	YES ONLY ROI	0.08 to 0.35	24.5 to 30.5	0.92 to 0.98
Atta-ur-Rehman et al. [20]	No segmentation	Whole Image	RCSP	NO	YES	---	Average = 71.1	---
Liu et al. [21]	Automatic	Whole Image	ST SVD	NO	YES	---	Average = 41.3	Average = 0.96
Swaraja et al. [22]	Automatic	ROI RONI	DWT PSBFO	NO	YES	0.76 to 1.00	Average = 34.5	---
Fares et al. [23]	No segmentation	Whole Image	DCT- Schur	NO	YES	6.50 x 10 ⁻⁴	Average = 48.0	Average = 1.
			DWT- Schur	NO	YES	9.77 x 10 ⁻⁴	Average = 49.2	Average = 1
Proposed Approach	Automatic	ROI RONI	PE NDE	NO	YES	0.41 to 1.21	83.0 to 86.2	Average = 1

TABLE VI. FURTHER COMPARISON OF THE PROPOSED SCHEME TO OTHER RELEVANT SCHEMES

Description	Jun [28]	Jaiswal [31]	Kang [32]	Proposed Scheme
Capacity (bpp)	0.25	0.48	1.00	0.70
PSNR	58.8489	49.4970	51.6190	84.34

The developed scheme is further compared to a linear difference expansion scheme [28], a prediction-error linear difference expansion scheme [31] and a fragile SVD with grouped block-based scheme [32]. The average performance in terms of PSNR and Capacity in bpp for the medical images shown in Fig. 3 are used for comparison. The scheme has a better performance than schemes in [28] and [31] in terms of capacity as it has a higher payload. The scheme has a better performance than the scheme [28] and [31-32] in terms of visual quality as it has the highest PSNR value.

V. CONCLUSION

An imperceptible and reversible watermarking scheme based on prediction error and non-linear difference expansion to ensure integrity, authenticity and detect manipulations on

DICOM medical images has been proposed. The experimental results obtained demonstrate that the approach is reversible and provides remarkable visual quality and capacity. The scheme yields PSNR values which are above the benchmark value and the perceptual boundary, demonstrating that it is imperceptible. The approach is fragile to manipulations making it suitable for detecting them. The approach also yields superior performance in terms of visual quality and compares favorably in terms of capacity to schemes available in the literature. It also yields superior results compared to other linear difference expansion-based schemes, demonstrating that the nonlinear difference expansion is superior to linear difference expansion in capacity and visual quality. The future work will involve developing a watermarking system that will not only detect manipulation but also restore the tampered regions.

REFERENCES

- [1] P. Aparna and P. V. Kishore, "A Blind Medical Image Watermarking for secure E-healthcare application using crypto-watermarking system," *Journal of Intelligent Systems*, vol. 29, no. 1, pp. 1558–1575, 2019, doi:10.1515/jisys-2018-0370.
- [2] S. M. Mousavi, A. Naghsh, and S. A. Abu-Bakar, "Watermarking techniques used in medical images: A survey," *Journal of Digital Imaging*, vol. 27, no. 6, pp. 714–729, 2014, doi: 10.1007/s10278-014-9700-5.

- [3] M. Larobina and L. Murino, "Medical Image File Formats," *Journal of Digital Imaging*, vol. 27, no. 2, pp. 200–206, 2013, doi: 10.1007/s10278-013-9657-9.
- [4] A. F. Qasim, R. Aspin, F. Meziane, and P. Hogg, "Roi-based reversible watermarking scheme for ensuring the integrity and authenticity of DICOM MR images," *Multimedia Tools and Applications*, vol. 78, no. 12, pp. 16433–16463, 2018, doi: 10.1007/s11042-018-7029-7.
- [5] N. A. Memon and A. Alzahrani, "Prediction-based reversible watermarking of CT scan images for content authentication and copyright protection," *IEEE Access*, vol. 8, pp. 75448–75462, 2020, doi: 10.1109/ACCESS.2020.2989175.
- [6] S-C Liew and J. M. Zain, "Reversible medical image watermarking for tamper detection and recovery," 2010 3rd International Conference on Computer Science and Information Technology, Chengdu, China, 2010, doi: 10.1109/ICCSIT.2010.5564078.
- [7] J. Liu, J. Huang, Y. Luo, L. Cao, S. Yang, D. Wei, and R. Zhou, "An optimized image watermarking method based on HD and SVD in DWT domain," *IEEE Access*, vol. 7, pp. 80849–80860, 2019, doi: 10.1109/ACCESS.2019.2915596.
- [8] O. M. Al-Qershi and B. E. Khoo, "Authentication and data hiding using a hybrid ROI-based watermarking scheme for DICOM images," *Journal of Digital Imaging*, vol. 24, no. 1, pp. 114–125, 2009, doi: 10.1007/s10278-009-9253-1.
- [9] B. Lei, E.-L. Tan, S. Chen, D. Ni, T. Wang, and H. Lei, "Reversible watermarking scheme for medical image based on differential evolution," *Expert Systems with Applications*, vol. 41, no. 7, pp. 3178–3188, 2014, doi:10.1016/j.eswa.2013.11.019.
- [10] T.-S. Nguyen, C.-C. Chang, and N.-T. Huynh, "A novel reversible data hiding scheme based on difference-histogram modification and optimal EMD algorithm," *Journal of Visual Communication and Image Representation*, vol. 33, pp. 389–397, 2015.
- [11] J. H. Wu, R.-F. Chang, C.-J. Chen, C.-L. Wang, T.-H. Kuo, W. K. Moon, and D.-R. Chen, "Tamper detection and recovery for medical images using near-lossless information hiding technique," *Journal of Digital Imaging*, vol. 21, no. 1, pp. 59–76, 2007, doi: 10.1007/s10278-007-9011-1.
- [12] A. Roček, K. Slavíček, O. Dostál and M. Javorník, "A new approach to fully-reversible watermarking in medical imaging with breakthrough visibility parameters", *Biomedical Signal Processing and Control*, vol. 29, pp. 44-52, 2016, doi: 10.1016/j.bspc.2016.05.005.
- [13] C. Gong, J. Li, U. A. Bhatti, M. Gong, J. Ma, and M. Huang, "Robust and secure zero-watermarking algorithm for medical images based on Harris-surf-DCT and chaotic map," *Security and Communication Networks*, vol. 2021, pp. 1–13, 2021, doi: 10.1155/2021/3084153.
- [14] K.-H. Chiang, K.-C. Chang-Chien, R.-F. Chang, and H.-Y. Yen, "Tamper detection and restoring system for medical images using wavelet-based reversible data embedding," *Journal of Digital Imaging*, vol. 21, no. 1, pp. 77–90, 2007, doi: 10.1007/s10278-007-9012-0.
- [15] F. Shih and Y. Wu, "Robust watermarking and compression for medical images based on genetic algorithms," *Information Sciences*, vol. 175, no. 3, pp. 200–216, 2005, doi: 10.1016/j.ins.2005.01.013.
- [16] H. L. Khor, S.-C. Liew, and J. M. Zain, "Region of interest-based tamper detection and lossless recovery watermarking scheme (ROI-DR) on Ultrasound Medical Images," *Journal of Digital Imaging*, vol. 30, no. 3, pp. 328–349, 2017, doi: 10.1007/s10278-016-9930-9.
- [17] Priyanka and S. Maheshkar, "Region-based Hybrid Medical Image Watermarking for secure telemedicine applications," *Multimedia Tools and Applications*, vol. 76, no. 3, pp. 3617–3647, 2016, doi: 10.1007/s11042-016-3913-1.
- [18] R. Eswarajah and E. Sreenivasa Reddy, "Robust medical image watermarking technique for accurate detection of tamper inside region of interest and recovering original region of interest," *IET Image Processing*, vol. 9, no. 8, pp. 615–625, 2015, doi: 10.1049/iet-ipr.2014.0986.
- [19] G. Gao, X. Wan, S. Yao, Z. Cui, C. Zhou, and X. Sun, "Reversible data hiding with contrast enhancement and tamper localization for medical images," *Inf. Sci.*, vols. 385–386, pp. 250–265, Apr. 2017, doi: 10.1016/j.ins.2017.01.009.
- [20] Atta-ur-Rehman, K. Sultan, N. Aldhafferi, A. Alqahtani, and M. Mahmud, "Reversible and fragile watermarking for medical images," *Comput. Math. Methods Med.*, vol. 2018, pp. 1–7, Jul. 2018, doi: 10.1155/2018/3461382.
- [21] X. Liu, J. Lou, H. Fang, Y. Chen, P. Ouyang, Y. Wang, B. Zou, and L. Wang, "A novel robust reversible watermarking scheme for protecting authenticity and integrity of medical images," *IEEE Access*, vol. 7, pp. 76580–76598, 2019, doi: 10.1109/ACCESS.2019.2921894.
- [22] K Swaraja, K Meenakshi, and P Kora, "An optimized blind dual medical image watermarking framework for tamper localization and content authentication in secured telemedicine," *Biomed. Signal Process. Control*, vol. 55, Jan. 2020, Art. no. 101665, doi: 10.1016/j.bspc.2019.101665.
- [23] K. Fares, A. Khaldi, K. Redouane, and E. Salah, "DCT & DWT based watermarking scheme for medical information security," *Biomedical Signal Processing and Control*, vol. 66, p. 102403, 2021, doi: 10.1016/j.bspc.2020.102403.
- [24] S. Padmanaban, K. Thiruvankadam, S. T. Padmapriya, and R. A. M. Kumar, "An medical image file formats and Digital Image conversion," *International Journal of Engineering and Advanced Technology*, vol. 9, no. 1S3, pp. 74–78, 2019, doi: 10.35940/ijeat.A1093.1291S419.
- [25] D. Rachmawati, J. T. Tarigan, and A. B. Ginting, "A comparative study of message digest 5(MD5) and sha256 algorithm," *Journal of Physics: Conference Series*, vol. 978, p. 012116, 2018, doi :10.1088/1742-6596/978/1/012116.
- [26] V. Kumar and N. V., "Hybrid local prediction error-based difference expansion reversible watermarking for medical images," *Computers & Electrical Engineering*, vol. 53, pp. 333–345, 2016, doi: 10.1016/j.compeleceng.2015.11.033.
- [27] D. M. Thodi and J. J. Rodriguez, "Prediction-error based reversible watermarking," 2004 International Conference on Image Processing, Singapore, 2004. ICIP '04, doi: 10.1109/ICIP.2004.1421361.
- [28] J. Tian, "Reversible data embedding using a difference expansion", *IEEE Transactions on Circuits and Systems for Video Technology*, vol. 13, no. 8, pp. 890-896, 2003, doi: 10.1109/TCSVT.2003.815962.
- [29] "TCIA collections," The Cancer Imaging Archive (TCIA). [Online]. Available: <https://www.cancerimagingarchive.net/collections/>. [Accessed: 20-Nov-2021].
- [30] "NBIA - National Biomedical Imaging Archive," National Institutes of Health. [Online]. Available: <https://imaging.nci.nih.gov/ncia/login.jsf>. [Accessed: 20-Nov-2021].
- [31] S. Jaiswal, O. Au, V. Jakhetiya, Y. Guo, A. Tiwari and K. Yue, "Efficient adaptive prediction based reversible image watermarking", 2013 IEEE International Conference on Image Processing, Melbourne, Australia, 2013.
- [32] Q. Kang, K. Li, and H. Chen, "An SVD-based fragile watermarking scheme with grouped blocks," *Proceedings of 2nd International Conference on Information Technology and Electronic Commerce*, Dalian, China, 2014, doi: 10.1109/ICITEC.2014.7105595.

Deep Learning Framework for Physical Internet Hubs Inbound Containers Forecasting

El-Sayed Orabi Helmi¹, Osama Emam², Mohamed Abdel-Salam³

Dept. of Business Information Systems, Faculty of Commerce and BA, Helwan University, Cairo, Egypt^{1,3}

Dept. of Computer Science, Faculty of Computing and AI, Helwan University, Cairo, Egypt²

Abstract—This article presents a framework for physical internet hubs inbound containers forecasting based on deep learning and time series analysis. The inbound containers forecasting is essential for planning, scheduling, and resources allocation. The proposed framework consists of three main phases. First, the inbound historical transaction has been processed to find out the training window size (lags) using auto correlation function (ACF) and partial autocorrelation function (PACF). Second, the framework uses convolutional neural network (CNN) and recurrent neural network (RNN) as training networks for the historical time series data in two techniques. The proposed framework uses univariate and multivariate time series analysis to explore the maximum forecasting outcomes. Last, the framework measures the accuracy and compares the forecasting output using mean absolute error matrix (MAE) for both approaches. The experiments illustrated that RNN forecasts univariate inbound transaction with total 5.0954 MAE rather than 5.0236 for CNN. The CNN outperforms multivariate inbound containers forecasting with 0.7978 MAE. All the results has been compared with autoregressive integrated moving average (ARIMA) and support vector machine (SVR).

Keywords—Physical internet hubs (π hubs); deep learning; convolutional neural network (CNN); recurrent neural network (RNN); time series forecasting

I. INTRODUCTION

All Physical internet (π) is a global logistics system first introduced by [1] in the early of this decade. The main objective of the physical internet is to connect all the logistics partners (customers, suppliers, shippers) in an intelligent way. π Hub is one of the main milestones in the future logistics network. π hub is responsible for distributing goods and items through the logistics network. These hubs should be managed and controlled in an intelligent manner to perform the complex logistics challenges. Scheduling and resources localization are two of these challenges. Also, moving items in and out the hub requires clear vision and scalable solutions [2]. Machine learning gives the researchers the ability to contribute solutions in different research fields. Machine learning, especially deep learning proposed research outperformed in classification, clustering, and regression analysis [2].

In 2012 [3] proposed the main functions that should be in any railway π hub. These functions have been measured using key performance indicators. These indicators measure the performance of the proposed design of the π hub through three perspectives. The first is from the customer's perspective. The second is suppliers' point of view. The last indicators measure the railway worker's satisfaction. The researchers in this case

study faced some challenges such as determining the number of containers that will be inbound in a certain π hub. They assumed that 30% of containers on each train will be unloaded and reloaded by others in stock containers. Then they calculated the estimated unload and reload time to this assumption. They also calculated the required time to unload and reload all the containers for the entire train. Starting from this challenge we tried to forecast the actual or near actual containers flow through the π hub. The objective of this research is to integrate two deep learning training networks with a physical internet providing framework for inbound containers forecasting. This framework will forecast the flow of goods and items through the π hub based on historical time series data. Based on time series analysis and deep learning techniques we propose this framework to be a guide for π hub resource management system aiming to achieve high accuracy with minimum inbound forecasting error.

The prediction process is one of the most difficult operations because it is subject to several variables, which makes choosing the appropriate algorithms to solve this problem very important. Some of the current prediction algorithms lack self-learning, such as linear and non-linear systems and moving average. And because of the strength in the field of deep learning in a number of areas, especially machine learning, drones, autonomous cars, computer vision and other fields, the research team decided to use deep learning algorithms in this research.

This article is divided into several parts. The first part provides an overview of some concepts, previous studies and some current analysis methods for time series. The researcher also presents in the first part of the article some methods of deep learning. As for the second part of the article, it presents the proposed framework for forecasting future inbound containers quantities in the short term, based on some previous data. As for the third part, it presents the results of the established experiments, their analysis and comparison with some of the current methods of prediction.

II. THEORETICAL BACKGROUND

The following section discusses briefly the main concept of physical internet, time series analysis, recurrent neural network, and convolutional neural network respectively. Some related studies will be discussed in section.

A. Physical Internet

Physical internet is a global open logistic system. Physical internet's main objective is to encapsulate interfaces and

protocols to manage physical, digital, and operational interconnectivity of the recent logistic functions through one global system. New containers, movers, nodes, and hubs have been proposed. Through a series of proposed standards and functions designs which replaced or integrated with the current logistics infrastructure that will replace the entire logistics system by 2050 [1]. The Physical Internet is structured in a similar way to data packets sent via the standard digital Internet. This notion fundamentally alters how commodities are designed, relocated, and distributed today. This approach, in which the items relocation process is known and implemented in an optimal and efficient manner at each relocation stage, is critical for all supply chain players. Prior to the start of the procedure, it was ensured that it would be transparent, efficient, and ecologically friendly [4]. The Physical Internet's goal entails enclosing commodities in smart, eco-friendly, and adaptable containers ranging in size from a shipping container to a little box. It therefore generalizes the marine container, which has shaped ships and ports to accommodate globalization, and extends containerization to logistical services in general. Instead of a warehouse or a truck, the Physical Internet relocates the private space's boundary to the inside of a container. These modular containers will be continuously monitored and directed using the Internet of Things to take advantage of their digital interconnection [1,4]. Each π container has a unique global identifier, such as the MAC address in the Ethernet network and the digital Internet, from an informational standpoint. This identifier is physically and digitally attached to each π container to ensure identification reliability and efficiency. Each π container has a smart tag attached to it that acts as its representative agent. Through the Physical Internet, it helps to ensure container identification, integrity, routing, conditioning, monitoring, traceability, and security. Smart tagging allows for the distributed automation of a wide range of handling, storage, and routing tasks.

B. Time Series Analysis

Before going further in our forecasting case study, it is essential to briefly illustrate the term time series data analysis which is the core foundation of our study. Time series data is recording of processes and observations varies over time. These observations can either be recorded in continuous points or as a set of discrete observations sequentially. These observations are exposed to trending, cyclical, seasonality and irregular variations. The trend of the observed data may be positive or negative in other word increasing or decreasing of data values over time. The cycle is a repetition of data behavior over a long time. The seasonality is a regular fluctuation of the observations at the same week, month or quarter every year. The irregularity in the time series data may happen for more than one reason. It could be because of noise, outliers, wrong data entry or sudden increase or decrease of observations value. Different analysis methods and techniques had been proposed over years. Time series consists of modeling mathematical descriptions estimating separately the four components independently. Time series analysis could be presented statistically in two approaches. The first approach is univariate analysis. The univariate approach is the analysis of single variable. The second approach is multivariate analysis approach. The multivariate approach is the analysis of two or

more variables. These variables may be dependent or independent variables. Univariate time series are subject to descriptive statistical analysis such as central tendency (mode, median, and median). It also, subject to dispersion analysis such as (variance, range and standard deviation). Multivariate analysis is more suitable for real life applications because of its high conclusion accuracy. Multivariate includes more than one factor of independent variables that influence the variability of dependent variables. Multivariate analysis is computational intensive. The researchers over years proposed significant methods and approaches. Those methodologies can be distinguished as ARIMA and nonARIMA methods. Several ARIMA stochastic models has been introduced, such as autoregressive (AR), moving average (MA), autoregressive moving average (ARMA), ARIMA, seasonal ARIMA (SARIMA), autoregressive fractionally integrated moving average (ARFIMA), and autoregressive conditional heteroscedasticity (ARCH) [5]. The ARIMA method has often been utilized for various types of univariate time series for many years. The ARIMA method has been well developed which made this method used in many research fields. Recently, many researchers developed nonARIMA methods with artificial intelligence [5, 6]. ARIMA model has some back draws such as it is computationally costly. It has poor performance in Long-term forecasting. Also, seasonal time series are not supported by ARIMA model. Today, the use of deep learning (DL) techniques has become the most popular approach for many machine learning problems, including time series forecasting. Deep neural networks have shown a great potential to map complex non-ARIMA feature interactions. Deep learning models are an alternative solution for forecasting because of their accuracy [7, 8].

Other researcher used support vector machine in regression analysis despite of it has some major disadvantages such as it is ineffective for large datasets. The SVM will underperform if the number of features for each data point exceeds the number of training data samples [9].

C. Recurrent Neural Network

A recurrent neural network (RNN) is a class of artificial neural networks (ANN) connections between nodes. RNN is made up of a set of nodes connected by edges, where the edges have a direction associated with them along with a temporal sequence. This allows it to exhibit temporal dynamic behavior. Derived from feed forward neural networks, RNNs can use their internal state (memory) to process variable length sequences of inputs [3]. RNNs are one of the most frequently utilized ANN architectures for time series prediction problems. They also become popular in natural language processing research. RNNs feedback architecture allows cells inherent the temporal sequence order and variables dependencies [9]. Long Short-Term Memory (LSTM) cell, Elman RNN cell, and the Gated Recurrent Unit (GRU) are the most popular RNN network architectures in time series modeling and forecasting [10].

D. Convolutional Neural Networks

A convolutional neural network (CNN, or ConvNet) is a type of deep neural network that is most commonly used for image analysis [11]. Based on the shared-weight architecture of

the convolution kernels that scan the hidden layers and translation invariance properties, they are also known as shift invariant or space invariant artificial neural networks (SIANN). Multilayer perceptron are regularized variants of CNNs. Multilayer perceptron are completely linked networks in which each neuron in one layer communicates with all neurons in the subsequent layer. These networks' "complete connectivity" makes them vulnerable to data over fitting. Regularization methods commonly used include adjusting weights as the loss function is minimized and randomly trimming connections. CNNs take a different method to regularization: they take advantage of the hierarchical pattern in data and use smaller and simpler patterns embossed in the filters to assemble patterns of increasing complexity. As a result, CNNs are at the bottom end of the connectedness and complexity spectrum [12]. This is accomplished by running a filter (or weight matrix) over the input and computing the dot product between the two at each location (i.e. a convolution between the input and filter). Because of this structure, the model can learn filters that recognise specific patterns in the incoming data. The idea behind using CNNs to anticipate time series values is to learn filters that reflect certain recurrent patterns in the series and use them to forecast future values. CNNs may function well on noisy series because of their layered structure, which allows them to eliminate noise in each subsequent layer and extract just the important patterns, comparable to neural networks that use wavelet transformed time series [13].

III. PROPOSED FRAMEWORK

This framework consists of three phases. The first phase is data collection and preprocessing. In this task the framework collects, integrates, and preprocesses all the previous inbound transactions that have been made in the π hub. This task checks the data stationary. If the data is non-stationary data, the framework will use the difference technique to convert the data to be in stationary status. Section 4 discusses this phase. Deep learning is the second phase with 70% of the inbound transactions. In this phase the framework feeds the stationary data to the learning network (NN, RNN, and CNN) and computes the learning rate. The training happens with two approaches (univariate, multi-variate). The univariate approach is suitable for independent variables. The multi-variate is suitable for highly dependent dimensions. Testing and validation are the third phase. This phase tests and validates the inbound flow prediction against 30% off the collected data. Therefore, the framework calculates the accuracy of each learning network using mean absolute error technique. Fig. 1 illustrates the phases of the proposed framework.

As in Fig. 1, the entire data values must be stationary data to avoid the impact of the abnormal and outliers. Also, the framework calculates the statistical auto-correlation function (ACF) and partial auto-correlation function (PACF) to find out the target lag length. Those lags indicate the most appropriate forecasting window size, for example predicts 10 days flow ahead. Also, the framework ignores the calculation of variables independency by making the training in two techniques using univariate or multivariate analysis. Despite of the time consuming, the use of both techniques make the framework suitable for any time series analysis.

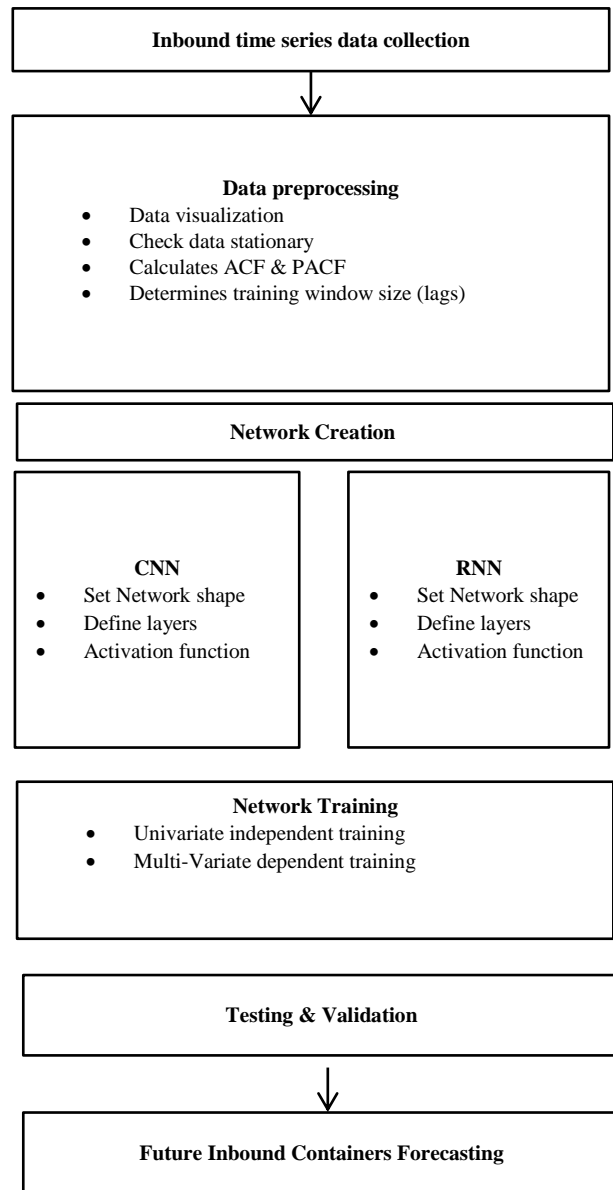


Fig. 1. Physical Internet Hubs Inbound Containers Forecasting Proposed Framework.

IV. DATA PRE-PROCESSING

Regarding the lack of real-life π hubs, we use a store item demand forecasting challenge dataset offered by Kaggle [14]. Then we select 6 random variables from the dataset to be present container volume. Some data preprocessing has been made to meet the proposed design of [3] which proposed a design for railway π hub. The inbound containers in their proposed π hub had 6 main volumes. The container volumes are (1.2, 2.4, 3.6, 4.8, 6 and 12 meters). These containers are the current intermodal containers. Table I shows the number of data points (count), the arithmetic mean, the standard deviation, the 1st quartile, the 2nd quartile, the 3rd quartile, the minimum, the maximum, interquartile range (IQR) and outlier values for each container volume used in this study.

TABLE I. THE INBOUND HUB CONTAINERS TIME SERIES DATASET SUMMARY (NUMBERS IN 1000S)

	Container size in meter					
	1.2 m	2.4 m	3.6 m	4.8 m	6 m	12 m
Count	2922	2922	2922	2922	2922	2922
Mean	30.95	57.43	36.99	35.6	32.4	55.23
S.D	17.38	16.67	11.96	23.2	22.9	15.46
Min	4	13	8	4	3	17
Q1	18	45	28	18	15	44
Q2	25	56	36	25	21	55
Q3	42	68	44	54	52	65
Max	100	115	81	120	113	108
IQR	24	23	16	36	37	21
outlier	>78	>102.5	>68	>108	>107.5	>96.5

As shown in Table I, the training data set contains time series data for 6 different containers. Each container has 2922 observations. It also, shows that the training data is normally distributed for all variables with different IQRs and outlier values. Although the training dataset is normally distributed, it is non-stationary data. Fig. 2 illustrates the non-stationary status of the training dataset.

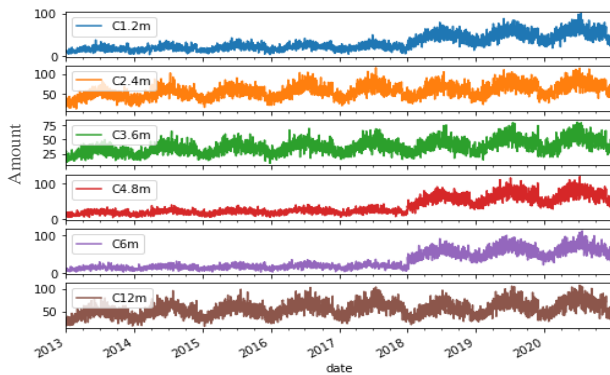


Fig. 2. Non-stationary Time Series Historical Inbound Containers Data.

As shown in Fig. 2, some fluctuations were observed in the training data. It also shows that some repeat behavior (cycle) in the data especially for the 2.4 meters, 3.6 meters and 12 meters volume containers.

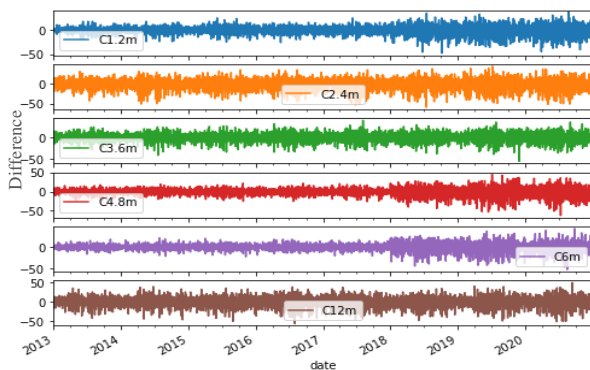


Fig. 3. Time Series Stationary Training Dataset.

Fig. 2 illustrates regular and predictable changes that recur every calendar year (seasonality) in the time series dataset. It also shows trend fluctuation at some data point. The difference technique has been used to convert the time series to stationary status. Fig. 3 shows the stationary data which has been used for training the proposed framework. The data was converted to the stationary status using the difference method. This phase was essential to avoid any bias in the training data, which gives better judgment of the forecasting output.

The proposed framework uses an 8 years stationary dataset to perform the learning phase. The network uses 70% of the dataset for training, 20% for testing and 10% for validation. Furthermore, the autocorrelation function and partial autocorrelation function had been used to determine the lags length. Although this step can be dispensed with, the researcher believes that it may be a good start and is governed by a statistical basis that enables the proposed framework to start the training process effectively. According to the results of ACF and PACF, the lags length of our training was 7, 24 days for narrow and wide window forecasting, respectively. The next section discusses the network learning, testing and validation experiments for CNN and RNN in two approaches. These approaches are univariate and multivariate time series forecasting.

V. EXPERIMENTS AND RESULTS

This section discusses in detail the performed experiments. The framework has been implemented using python and TensorFlow. The learning networks have been developed for both univariate and multivariate with two different input sizes to maximize the forecasting outcomes of the proposed framework. Also, this section discusses the different shapes of the implemented neural networks for narrow and wide input window as deep learning univariate and multivariate time series forecasting.

A. Narrow Window Univariate Inbound Containers Forecasting

Univariate time series refers to a time series that consists of single (scalar) observations recorded sequentially over equal time increments. The proposed implementation of CNN uses the previous 6 days to predict the 7th day in the time series inbound transaction. Fig. 4 and 5 show the building structure of CNN and RNN in the proposed framework experiments.

As shown in Fig. 4, the implemented CNN consists of 4 fully connected dense layers and 1 convolutional layer. Each layer uses the relu activation function. The relu function has been used to maximize the non-linearity behavior of the proposed network. This implementation forecasts the container's flow for each container volume one by one independently. The proposed implementation of RNN uses the long-short term memory (LSTM) for prediction. Fig. 5 illustrates the 6 layers RNN structure.

As shown in Table II, the total absolute error for the 4 algorithms is almost the same. But RNN (LSTM) outperforms with total MAE 5.0236. It also performs the training of 6 meters volume container better than SVR by 6 % and CNN by 10%.

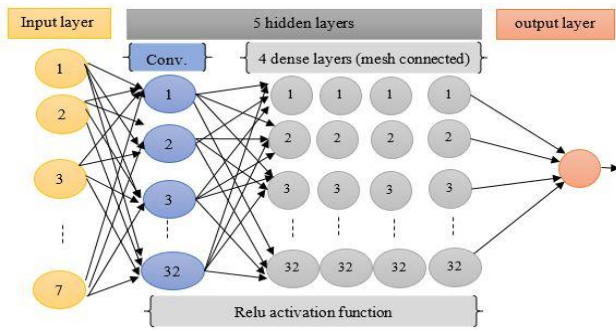


Fig. 4. CNN Structure for Multi Layers Forecasting Model.

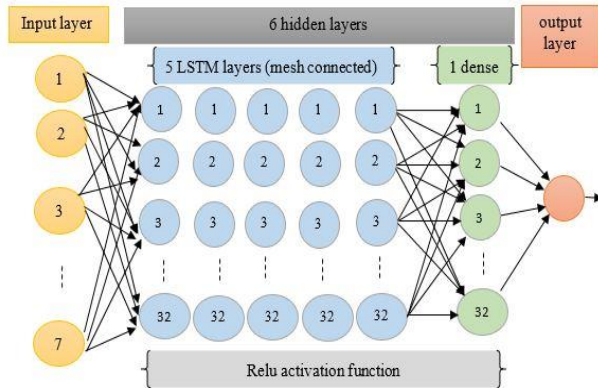


Fig. 5. RNN Proposed Multilayer Model Implementation.

TABLE II. UNIVARIATE INDEPENDENT INBOUND NARROW WINDOW FORECASTING NETWORKS MEAN ABSOLUTE ERROR

Container volume	Algorithm			
	ARIMA	SVR	CNN	RNN (LSTM)
1.2m	1.2321	0.9522	0.9073	1.0219
2.4m	1.1201	0.7816	0.8157	0.8055
3.6m	1.3210	0.8194	0.8504	0.8207
4.8m	1.2421	0.9451	0.9316	0.8458
6m	1.4124	0.8414	0.8794	0.7902
12m	1.3410	0.7470	0.7110	0.7395
Sum of (MAE) error	7.6687	5.0867	5.0954	5.0236

B. Univariate Wide Window Inbound Containers Forecasting

In this series of experiments, the framework uses multi-steps output forecasting. Those experiments had been carried out with the same CNN and RNN previous architecture as in Fig. 4 and 5. The only difference in these experiments is that we predict 24 days in future rather than one day. The network shape is (32, 24, 1). Where 32 are number of neurons is the input layers, 24 is output size and 1 is number of features to be predicted. These experiments use the historical inbound transaction of the 6 container sizes independently to predict the flow of each container size individually. Table III illustrates the forecasting accuracy measurement.

C. Multivariate Narrow Window Inbound Containers Forecasting

The possibility of a dependency relationship that could exist between different container volumes, especially as stated in the proposed design of railway warehouses and the method of transporting containers using trains. In order to, give the proposed framework realistic and relevant real-life applications and our desire to improve the forecast. In these experiments series, we used a multivariate time series analysis technique. We used the same lag length of narrow univariate forecasting window and the structure of CNN and as in Fig. 6. The only difference here was using the entire day observations of the 6 containers volume as one input vector. Also, the output was a vector of 6 features each feature represent one of the containers volume. The experiments showed that, MAEs were 0.8921, 0.7934 & 0.9231 for CNN, RNN and SVR model respectively.

D. Multivariate Wide Window Inbound Containers Forecasting

The framework has been trained to forecast the future flow dependently at the same time. The output shape for both CNN and RNN is (32, 24, 6). Fig. 7 shows the structure of RNN-LSTM network.

As shown in Fig. 7, the RNN (LSTM) network consists of 6 hidden fully connected feed forward layers. The performed experiments proved that CNN outperformed. The mean absolute error for SVR, CNN and RNN (LSTM) multivariate forecasting is 0.9176, 0.7978 and 0.9151, respectively. These experiments showed that CNN proposed architecture performs multivariate forecasting better than RNN.

TABLE III. UNIVARIATE INDEPENDENT WIDE WINDOW INBOUND FORECASTING NETWORKS MEAN ABSOLUTE ERROR

Container volume	Algorithm			
	ARIMA	SVR	CNN	RNN (LSTM)
1.2m	1.3251	0.9904	0.89105	0.8802
2.4m	1.2134	1.014	0.9003	0.8605
3.6m	1.3421	0.9948	0.9102	0.7912
4.8m	1.1012	0.9853	0.8807	0.8014
6m	1.2115	0.9947	0.8904	0.8114
12m	1.2341	0.9862	0.8926	0.7812
Sum of (MAE) error	7.4274	5.9654	5.36525	4.9259

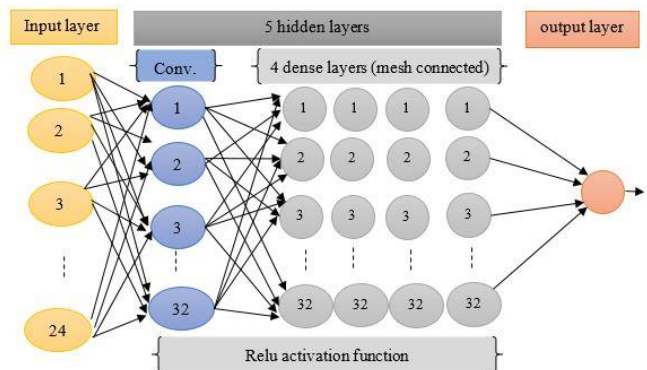


Fig. 6. CNN Multivariate Inbound Forecasting Structure.

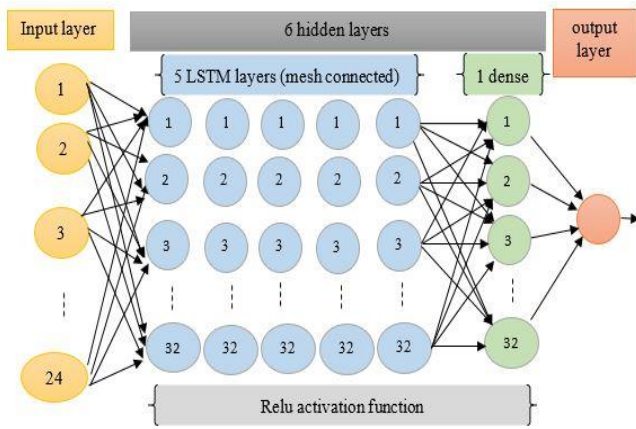


Fig. 7. Multivariate RNN (LSTM) Forecasting Network Structure.

VI. CONCLUSION

The proposed framework forecasts π_{hub} inbound containers using CNN and RNN deep learning networks for both univariate and multivariate forecasting approaches. ACF and PACF have been used to determine better forecasting window size based on the status of the training data. The difference technique has been used to overcome the non-stationary training data. All the forecasting results have been compared to time series forecasting ARIMA and SVR algorithms. It has been found that RNN forecasts the univariate independent container flow for short term rather than CNN. While CNN performs univariate independent containers flow better than RNN and SVR for long term forecasting. On other hand in has been found that CNN outperforms forecasting for multivariate analysis for both short and long time forecasting.

REFERENCES

[1] Montreuil, Benoit, "toward a Physical Internet: meeting the global logistics sustainability grand challenge", Springer, Vol. 3, pp. 71-87, 2, 2011.
[2] Martin Christopher, Logistics and supply chain management (5th Ed.). London: Pearson Education 2016.

[3] Dupond, Samuel, "A thorough review on the current advance of neural network structures", Annual Reviews in Control, Annual Reviews in Control, Vol. 14, pp. 200-230, 2019.
[4] Eric Ballot, Benoit Montreuil, Collin Thivierge, "Functional Design of Physical Internet Facilities: A Road-rail Hub". Gardanne, France : s.n.12th IMHRC Proceedings. pp. 13, 2012.
[5] Kolinski Adam, "The Impact of Eco-efficiency in Production on Availability of Machines and Equipment", Efficiency in Sustainable Supply Chain, springer, pp. 161-177, 2017.
[6] Hendikawati1, "A survey of time series forecasting from stochastic method to soft computing", Journal of Physics: Conference Series, pp. 20-30, 2020.
[7] Anggraeni W, Boga K and Mahananto F., "The Performance of ARIMAX Model and Vector Autoregressive (VAR) Model in Forecasting Strategic Commodity Price in Indonesia", Procedia Computer Science , pp. 189-196, 2018.
[8] Pedro Lara-Ben'itez, Manuel Carranza-Garc'ia, " An Experimental Review on Deep Learning Architectures". International Journal of Neural Systems, Vol. 31, pp. 201, 2021.
[9] Najafi G, Ghobadian B, Moosavian A, Yusaf T, Mamat R, Kettner M , Azmi W H. (2016). SVM and ANFIS for prediction of performance and exhaust emissions of a SI engine with gasoline ethanol blended fuels. Applied Thermal Engineering, pp.186-203, 2016.
[10] Hansika Hewamalage, Christoph Bergmeir, Kasun Bandara, "Recurrent Neural Networks for Time Series Forecasting: Current Status and Future Directions", Elsevier, pp. 1-56, 2020.
[11] Cho, K., van Merriënboer, B., Gulcehre, C., Bahdanau, D., Bougares, F., Schwenk, H., Bengio, Y. "Learning phrase representations using RNN Encoder-Decoder for statistical machine translation". Stroudsburg, PA, USA: Proceedings of the 2014 Conference on Empirical Methods in Natural Language Processing (EMNLP). Association for Computational Linguistics. pp. 1724-1734, 2014.
[12] Zhang, Wei. "Shift-invariant pattern recognition neural network and its optical architecture". Proceedings of Annual Conference of the Japan Society of Applied Physics, pp. 90, 1988.
[13] T. Fisher, C. Krauss, "Deep learning with Long Short-Term Memory networks for financial market predictions". FAU Discussion papers in Economics, pp. 102, 2017.
[14] Store Item Demand Forecasting Challenge. Kaggle. Online|12 June 2021 [Cited: 18 March 2022 .]https://www.kaggle.com/c/demand-forecasting-kernels-only.

An Intelligent Anti-Jamming Mechanism against Rule-based Jammer in Cognitive Radio Network

Sudha Y, Dr. Sarasvathi V

Visvesvaraya Technological University
PESIT-Bangalore South Campus and affiliated to VTU, Belgavi, India

Abstract—Cognitive Radio Network (CRN) has become a promising technology to overcome the problem of insufficient spectrum utilization. However, the CRN is susceptible to the well-known jamming attack, which reduces its spectrum utilization efficiency. Existing jamming identification schemes and their countermeasure typically require prior statistical information about the communication channel and jamming pattern. This is quite an impractical assumption in the real context. The prime research problem is that the existing schemes are mainly associated with higher computational costs and communication overhead. Hence, the proposed manuscript presents a non-device-centric and efficient anti-jamming mechanism in the form of higher spectrum utilization driven by reinforcement learning techniques to address this above-stated problem. The proposed anti-jamming mechanism is modeled in two phases of implementation. First, the design of the customized environment is introduced as a single wideband cognitive-communication channel where a jammer signal sweeps transversely in the entire band of interest. Secondly, an intelligent agent is designed based on a model-free off-policy algorithm that operates over the same spectrum band. The agent uses its frequency-band knowledge discovery capability to learn frequency band selection and preference strategies to detect and avoid jamming signals, maximizing its successful transmission rate. The simulation results show that the proposed anti-jamming mechanism can effectively eliminate interference and is efficient in power usage and Signal to Noise Ratio (SNR) compared to other existing advanced algorithms.

Keywords—Anti-jamming; agent; cognitive radio network; reinforcement learning

I. INTRODUCTION

Cognitive Radio (CR) is a communication system that perceives its environment and autonomously adjusts according to its radio operating parameters. It has been introduced to address the contradiction between the constrained spectrum resource and the growing demand for spectrum [1]. CR dynamically proposes access to the spectrum, thereby making opportunistic and intelligent use of the spectrum to both Primary User (PU) and Secondary User (SU) [2]. However, a significant security concern arises due to Cognitive Radio Networks (CRNs) openness and dynamic nature [3]-[4]. Since many research studies have been presented in literature towards spectrum sensing and accessing techniques, SU is acquisitive for spectrum holes to collaborate with other SUs to achieve their objectives. However, the previous works ignore that the SUs are vulnerable to different security threats, which can interrupt or block the information flow in CRN. The major security threat in CRN is the jamming attacks that severely

degrades network performance [5]-[6]. Jammers can restrict or block the communication channels by introducing unremitting signals, thereby reducing the Signal-To-Noise Ratio (SNR), which may also degrade the throughput of the active communication flow and data transmissions [7]. Many anti-jamming solutions and schemes were introduced in the existing literature to mitigate jamming attacks. The existing anti-jamming solution based on frequency hopping offers a better approach against jamming attacks but introduces higher energy costs to the users [8]-[9]. The researchers have extensively adopted the game theory approach with Direct-Sequence Spread Spectrum (DSSS) technology to counter the impact caused by jamming attacks in CRN [10]-[11]. Although these schemes could deal with jamming effectively, these schemes require prior information about the jamming strategies and communication model, which is quite an impractical assumption considering the real scenario. With the upsurge of Artificial Intelligence (AI) technology, Machine Learning (ML) mechanisms have been extensively utilized in developing anti-jamming models. A class of ML, namely Reinforcement Learning (RL), has received widespread attention to address decision-making problems in recent years. In the context of the anti-jamming solution, RL can be efficiently utilized to explore the characteristics of jamming attacks and build an optimal policy to mitigate the jamming effect. For instance, many researchers applied the Q-learning based RL approach as an anti-jamming solution to choose an appropriate transmission power and optimal frequency hopping channel [12]-[14]. However, the Q-learning-based anti-jamming solution is prone to computational overhead due to the wide expansion in the size of the Q-table in the direction of deriving optimal policy. The researchers also applied a Deep Q-network (DQN) value-based learning mechanism [15]-[16]. DQN is a robust algorithm, and the limitation is, its slow learning rate. It is suitable only for a low-dimensional and discrete action space. Whereas, in the context of CRN anti-jamming, the action space is often both high-dimensional and continuous.

This paper proposes an efficient anti-jamming mechanism using the RL technique. Firstly, a customized environment is designed that mimics the communication scenario and sweep jammer. On the other hand, an agent modeled will operate over the same spectrum band. The training of the agent is carried out using a Deep Deterministic Policy Gradient (DDPG) algorithm. The proposed mechanism does not require any knowledge about the communication model and jamming strategy in the environment. The agent senses the spectrum and takes action in the continuous action space to distinguish whether the current carrier frequency is appropriate based on a

deterministic policy gradient. SNR and low power cost are considered as a basis for the reward for each agent's action. Table I shows some of the short forms and its abbreviations used throughout this paper. The remaining sections of this paper are planned as follows: Section II presents a review of existing works in the context of anti-jamming mechanisms in wireless networks. Section III presents the problem description based on the review analysis. Section IV presents the proposed system design and methodology adopted. Section V presents implementation strategies adopted in the proposed system of anti-jamming. Section VI discusses the outcome and performance analysis, and finally, the overall contribution of this paper is concluded in Section VII.

TABLE I. ABBREVIATION USED

CR	Cognitive Radio
PU	Primary User
SU	Secondary User
CRN	Cognitive Radio Networks
SNR	Signal-To-Noise Ratio
DSSS	Direct-Sequence Spread Spectrum
AI	Artificial Intelligence
ML	Machine Learning
RL	Reinforcement Learning
DDPG	Deep Deterministic Policy Gradient
UAV	Unmanned Aerial Vehicle
BPSK	Binary Phase Shift Keying
SSID	Service Set Identifier
DQN	Deep Q-network

II. RELATED WORK

The existing literatures has extensively studied an anti-jamming problems to enhance the communication and information flow in the severe electromagnetic spectrum of wireless networks. At present, there is less work being carried out towards a rule-based implementation strategy to thwart jamming attacks on cognitive radio networks. The preliminary discussion carried out by Ahmed and Ismail [17] has constructed a rule-based game theory to develop an anti-jamming model. The researcher has developed a Stackelberg framework that uses a rule mechanism to assign an incentive to the defender to protect the channel. Another work carried out by Ye et al. [18] has constructed a rule system using swarm intelligence that emphasizes the allocation of jammer tasks. The study mainly formulates a rule system for making a precise decision for cooperative jamming in the cognitive network.

The work carried out by Singh and Trivedi [19] has integrated game theory with decision-making theory using Markov decision process and zero-sum game. The study has used the reinforcement learning concept to formulate rules that assist in maximizing the gain of anti-jamming. The Q-learning-based concept was adopted by Liu et al. [20], where a rule-based system is constructed. The work carried out by Ibrahim et al. [21] has used game theory to resist jamming attacks in the

cognitive radio network. The presented machine learning approach is constructed to develop anti-jamming features, while Markov-Game is used for modeling jamming and anti-jamming processes.

The study of Wang et al. [22] introduces an approach of the dynamic spectrum jamming mitigation scheme based on intelligent algorithms. The presented scheme is adaptive to the dynamic environment and offers effective anti-jamming capability. The work towards optimizing the different jamming parameters such as modulation mode, jamming signal power, and the duty cycle is conducted by Amuru et al. [23]. In this study, the authors have used a multi-arm gambling machine to determine optimal parametric values to guarantee an optimal jamming scheme. The work of Furqan et al. proposed an interference detection scheme based on sparse coding [24], in this study, the sparse coding of the compressed signal is considered, and the convergence mode with machine learning technique is used to distinguish spectrum holes, legitimate primary users, and jammers. Huang et al. [25] introduced channel-hopping technology robust to various jamming attacks. This proposed technology can operate without a pre-assignment role and has a limited time to rendezvous on available channels. Quan et al. [26] presented a multi-pattern frequency hopping scheme to mitigate follower and partial-band jammer. The authors have applied their frequency modes to the data channel to enhance the randomness of the transmission frequency, and the system can effectively suppress jamming. The jamming and jamming mitigation can be regarded as a game process. The rise of advancement in CRN game theory has been extensively studied to mitigate interference attacks. The authors in the study of Wu et al. [27] suggested a scheme of power distribution considering Colonel Blotto's game to resist jamming attacks. Similar works have been carried out by Jia et al. [28]-[29], where Stackelberg's game theory is employed to develop an efficient anti-jamming scheme in the wireless communication channel. The researchers in the work of Wang et al. [30] studied the selection of suitable frequency channels. This study adopts a stochastic game strategy to explore optimal data and control channels to obtain higher throughput under a high-power jamming effect. The work carried out by Hanawal et al. [31] studied joint frequency hopping and transmission adaptation rate to mitigate the reactive-sweep effect. The authors have presented a model that interacts with the user and the jammer as a zero-sum gaming approach, providing a resilient strategy against jamming. The study of Chang et al. [32] presented an anti-jamming model, which adopts a channel hopping mechanism to mitigate the interference effect caused by the jammer. Gao et al. [33] suggested a bi-matrix game model interacting among the user and the jammer. Also, the study derived optimal conditions for Nash Equilibrium under linear constraints. Though the game theory concepts have been successfully employed to model anti-jamming solutions, these methods require prior information such as jamming strategy and communication model, which is quite impractical in real-time scenarios. The adoption of RL technology in anti-jamming modeling is significant against jamming attacks. The RL agent enables the anti-jamming system to get optimal strategy through seamless interaction with the communication environment without depending on the prior information about

the jamming strategies. The work carried out by Gwon et al. [34] suggested a mechanism to cope with the jamming attacks based on the Q-learning to determine the suitable strategy for channel access. Similarly, Liu et al. [35] suggested an anti-jamming scheme oriented on the deep RL technique, enabling users to get optimal decision strategy after exploring different actions through spectrum sensing. The authors in the study of Bi et al. [36] presented a multiuser anti-jamming model by utilizing an advanced version of the Q-learning technique to attain efficiency and optimality in the network resources and communication process. In the work of Liu et al. [37], a consecutive deep RL technique is discussed to deal with dynamic jamming attacks. Table II below shows some of the strengths and limitations of the existing approaches in the above studied literatures.

TABLE II. COMPARISON OF EXISTING APPROACHES

Approach	Authors	Strength	Limitation
Game theory	[17] [21] [27][28] [29][30] [33]	Good for modeling jamming attack.	Need apriori information of the attack. Complications towards designing complex networks.
Machine learning	[20][23] [24][34] [36][37] [38][39] [40]	Higher accuracy of detection.	Training dependencies, Higher resource involved in the detection, instantaneous attack response is limited.
Swarm Intelligence	[18]	Easier modeling of attack.	Highly iterative, leading to computational complexity.
Adaptive Approach	[22]	Higher scalability.	Needs well-defined attack environment.
Channel-hopping	[25][32]	Effective for spectrum utilization, no dependency of apriori attack information.	Drains more resources from cognitive radio nodes.
Frequency hopping	[26][31]	Effectively suppress jamming.	Not benchmarked with other frequency modes.

The use of the RL technique is also found in the application of Unmanned Aerial Vehicle (UAV) systems. In the study of Gao et al. [38], the RL approach of DQN is implemented to derive optimal policy against jamming attacks. The researchers in Han et al. [39] have introduced a 2D anti-interference model where the SINR of the user's signal is improvised based on the spread spectrum and user mobility. A DQN is used to achieve an optimal strategy for the anti-jamming system. The adoption of RL is carried out by Chen et al. [40] to build an anti-jamming system in the application of wireless body area network. In this work, an RL-driven power control mechanism is developed where Q-learning with transfer-learning technique is used to attain optimality in the policy and learning rate. In the work of Lu et al. [41], the anti-jamming technique is presented for UAV-based cellular networks, where a deep RL technique is implemented to determine the best relay strategy. In addition, an approach of transfer learning is used to provide additional support to the anti-jamming system to defend jammers without depending on any form of statistical

knowledge about the jamming pattern and the communication model. In addition, various other studies offer a similar form of solutions [42]-[50]. These studies have mainly used game theory and another optimization-based approach. The adoption of game theory offers a good modeling aspect towards the set of actions of the cognitive radio nodes or access points. It also offers the inclusion of static and dynamic scenarios to be modeled in an anti-jamming framework. However, the approaches used are quite dependent on apriori information of the attack or based on a limited set of attack characteristics. This situation in modeling doesn't assist if one node starts exhibiting differential malicious behavior in the cognitive radio network. Hence, they potentially suffer from a lack of strategy towards prevention approach.

III. RESEARCH GAP

From the prior section, it has been seen that not many studies have used rule-based anti-jamming mechanisms. The study carried out by Ibrahim et al. [21], and other researchers have mainly used game-based logic which has its pitfalls. Unfortunately, such studies can only be modeled considering a limited set of actions of jamming, which is then subjected to the machine learning approach. The inclusion of network parameters, especially frequency and bandwidth, are less modeled in such studies, which could offer a prime indicator. Further, other models discussed in the prior section are mainly inclined towards the progressive exploration of jamming points, and hence, the delay could rise. This section discusses some significant open issues explored based on the literature discussed above.

1) *No Standard technique*: After reviewing different anti-jamming schemes in existing literature, it has been analyzed that there is currently no universal anti-jamming mechanism that can handle both static and dynamic jamming attacks. It has also been analyzed that designing an efficient technique for detecting and mitigating jamming attacks is quite more challenging than executing and implementing jammers in the communication channel of wireless network systems.

2) *Lack of effectiveness and efficiency*: The existing anti-jamming approaches are ineffective or have limited scope when the jammer covers the entire frequency spectrum. As a result, the wireless communication channel does not recover effectively to provide its services. Another significant issue is how to achieve efficiency in the anti-jamming mechanisms. The frequency hopping-oriented anti-jamming technique can withstand narrowband jamming attacks but at the cost of compromised and degraded spectral efficiency. Similarly, the jamming mitigation based on retransmission protocol can recover communication channels, but it also degrades efficiency and affects the overall communication performances. Most of the schemes in the literature do not consider a trade-off between communication efficiency and the effectiveness of jamming mitigation techniques.

3) *Impractical assumption*: The existing solutions against jamming attacks based on the model-based analysis are impractical in the real-time implementation scenario. The model-based analysis like game theory and cross-layer

optimization often adopts prior knowledge regarding global channel information and jamming strategy, which is an unrealistic assumption. Also, these approaches are subjected to high computational complexity in the modeling. The jamming mitigation solutions in the existing literature also lack novelty in the design and modeling. It has been found that a similar kind of design consideration and modeling strategy is adopted in most of the studies, which needs optimization in their solution design to meet the requirement of the real-time networking scenario.

4) *Curse of high-dimensionality*: Recently, reinforcement learning has been extensively studied to design adaptive anti-jamming schemes. However, existing schemes based on Q-learning suffer from the huge dimensionality problem in a complex environment because to achieve optimal policy, the amplitude of actions needs to increase. As a result, the size of the Q-table of Q-learning also increases, which causes slow learning and restricts application scenarios.

5) *Lack of suitable environment*: Most of the RL-based solutions in the existing studies lacks modeling of a suitable networking environment to assess the RL agent. To validate the scope of the RL agent-based solution, the researchers must design and implement a suitable environment.

Therefore, the prominent research gap identified in existing studies are that, there are few available standard methodologies to deal with jamming issues in complex network system. Further, the formulation of the presented solution is carried out using impractical assumptions that doesn't work on ground reality. Hence, there is a big research gap between the demands to be met in resisting the jamming due to the ineffectiveness of existing solutions. Therefore, the problem statement is stated as "it is challenging to develop a lightweight, robust, and cost-effective computational solution towards mitigating jamming attack in communication environment". Hence, the motivating factor towards adopting the proposed research scheme is due to the rise of security-critical applications for securing the real-world's wireless communication technologies such as Bluetooth, Wi-Fi, and cellular technologies like 3G, 4G, and 5G that demands an intelligent design in the anti-jamming techniques by considering the constraints associated with the network. In this regard, the above factor motivates for an efficient and intelligent jamming scheme that can effectively balance communication efficiency and anti-jamming capabilities. The next section discusses the proposed system to address above discussed research problem.

IV. PROPOSED SYSTEM

This section will discuss the proposed system of intelligent anti-jamming mechanisms based on the RL technique. The prime aim of the proposed study is to present an effective and efficient strategy to counter the jammer in the cognitive wireless networking system. Therefore, a model-free and off-policy scheme is employed to design the anti-jamming mechanism. The proposed mechanism does not require or depend on the prior information of jammer signature and channel models. The off-policy algorithm in RL agent design offers a better scope of accurate prediction of the jamming frequency and evades it in advance.

Another significant contribution of the current research study is modeling a customized environment synchronized with Open AI-Gym functions. This is the novel contribution of the current study, where the proposed customized environment imitates the scenario of the communication channel and jammer under consideration. The proposed anti-jamming mechanism operates in this environment over the same set of channels and uses its ability to learn sub-band selection strategies to avoid jamming signals. The objective of the proposed work is to offer a better solution that can meet the requirement of a real-time scenario. The schematic diagram and workflow of the proposed model are shown in "Fig. 1".

A. Scope of the Study

The transmission method considered in the present study is the Binary Phase Shift Keying (BPSK) modulation. The BPSK is popularly used in many modern communication systems like Wi-Fi, Bluetooth, and even car locking systems. Jamming of these systems can have a devastating effect on the company's overall image, which is offering the service. Such jamming might also result in the theft of valuable physical or digital assets. Since the communication protocols like Wi-Fi have a band defined for itself and agreed between the gateway and the end node, the system will always know when a particular channel is busy.

The system which is being proposed will help the communication system to shift the frequencies dynamically between the available channels and the band. It is assumed here that the band which can be observed in the simulation is always free since there is always an understanding between the various transceivers present in the system, and every other transceiver knows the channel and the band being used by another transceiver. Hence, when a foreign attacker element like jammer is introduced, a particular frequency that is known to be free by all the transceivers will get blocked.

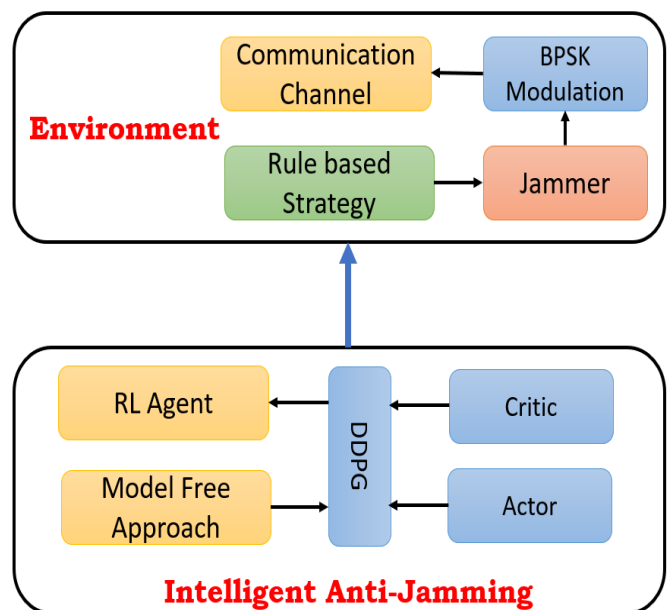


Fig. 1. The Schematic Architecture of the Proposed Anti-Jamming System.

B. System Design

The development of the proposed system is carried out in two implementation phases 1) Environment modeling and 2) agent-based intelligent anti-jamming. In the first phase of implementation, the study presents a design of environment considering a single communication channel with a transmitter, receiver, and rule-based jammer. In particular, the study considers the case scenario of a sweep jamming attack that uses a digital modulation scheme, viz. BPSK, in which the carrier frequency varies according to the modulating digital signal. The phase transition of the BPSK digital modulation is characterized by the π radian, and it has the lowest spectral efficiency at least 1 bit/s/Hz. The signal $s_k(t)$ can be expressed as follows:

$$s_k(t) = f(t) \quad (1)$$

The expression (1) represents a signal concerning the function of time i.e., $f(t)$, which is meant for constructing the signal in the simulation model. The variable t denotes time in the range $[0, \infty]$ and $s_k(t)$ in the range $[0, 1]$. A signal $s(t)$ modulated using BPSK during k time interval can be represented as follows:

$$s_k(t) = \sqrt{2R} \cos\left(2\pi f_0 t + d_k \frac{\pi}{2}\right), (k-1)T \leq t < kT \quad (2)$$

where R refers to the mean signaling power, the term $d_k \in \{+1, -1\}$ regulates the data bit, f_0 denotes base frequency, and T denotes symbol period. Furthermore, the communication frequency is the unit of frequency between the sender (transmitter module) and the recipient (receiver module). The unit of the frequency used to create interference is referred to as the jamming frequency. The proposed study considers single-channel continuous frequency band and jamming frequencies in the simulation environment. RL techniques involve environment and agent mechanisms that require feedback (reward/penalty) from the environment. In the present work, the SNR obtained at the recipient is considered as the basis of the award. Later sections discuss the jamming model and the relationship between the environment and the RL agent.

C. Sweep Jamming

The jammer forwards a forged signal with a power (P_j) on the target frequency channel to intentionally intrude the information flow or the active communication process. In some cases, the jammer also introduces jamming by reducing the SNR of the data signal received by the recipient with less interference power. The current research work considers the Sweep jamming scenario in the communication channel.

A sweep jammer sequentially blocks N_j adjacent channels with power P_j / N_j from N communication channels in each time slot. In this jamming attack scenario, a narrowband frequency of the jammer's power is recurrently swept over a comparatively wideband frequency with a sweeping rate such that there is enough time to complete its jamming function at any given frequency. Before the jammer terminates, it comes back to that frequency again. The communication channel (C) selected by the jammer (J) at instance (k) can be represented as $C_j^k \in \{1, 2, 3, \dots, N\}$. The study considers a simple scenario,

where the set of jamming actions (J) at a different position such that $C^K \rightarrow [C_j^K]_{1 \leq j \leq J}$. It is also believed that the jammer can jam all communication channels if the transmitter or receiver resides within the proximity of the jammer.

D. Reinforcement Learning

RL is an explicit type of ML technique that is concerned with the function of the agent and the environment. The agent is a programmed AI function that interacts with the unknown environment, learns the behavior, and decides to solve the task. The agent operates in the environment and gets rewards for each operation. The agent's goal is to maximize the expected cumulative reward by selecting the best action for its current situation. "Fig. 2", depicts a typical relationship between the RL agent and the environment.

The environment refers to the program or task that the agent needs to perform. It takes the current state and operation of the agent as input and returns the Reward/Punishment and the next state as output. The agent is the programmed entity that refers to the learner and decision-maker that executes an action in the environment. The agent gets observation and reward and sends an action to the environment. An action can be described as a set of possible moves that the agent can perform in the environment to solve a given problem. Observation is the state of the current situation that is returned by the environment. A reward/punishment is the feedback return given to the agent for each specific move or action. An agent is designed based on the policy to decide the agent's next move according to the current state of observation.

The RL entails a programmed decision-maker algorithm as an agent learning the behavior through repeated trial and error interaction with the task scenario, i.e., environment. Moreover, the success and failure rate of the agent is decided based on its reward, which indicates how better the action was. Generally, RL is implemented using episodes, a set of time steps during which the agent learns the optimal strategy towards deciding actions to achieve the cumulative reward. During these time steps, the state in the environment may vary, which may also impact the actions learned by the agent. However, the agent attempts to maximize its reward by choosing an optimal action according to the current state of observation and, at the same time, automatically updating the corresponding strategy.

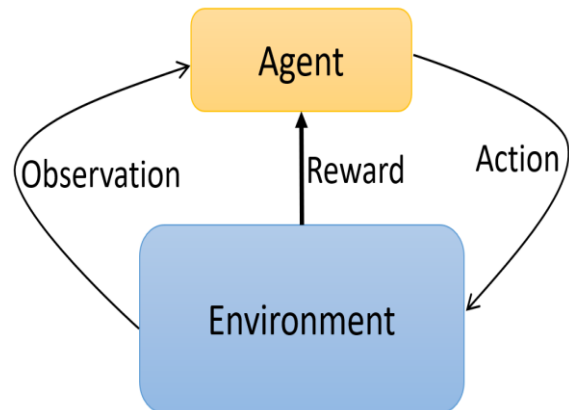


Fig. 2. Relationship between Environment and RL Agent.

V. METHODOLOGY AND ALGORITHMS

This section discusses the implementation strategies adopted in the environment modeling and development of the anti-jamming system using the RL mechanism.

A. Environment Modeling

The environment consists of the communication model and the jammer. The communication model is designed by considering Wi-Fi communication channels. However, with changing the base frequency and band frequency, any of the following technologies can be considered 5G, 3G, 4G, and Bluetooth. As mentioned, the jammer used here is a sweep jammer that will keep increasing and decreasing the frequency of jamming over time, which means that jamming frequency keeps sweeping the communication spectrum. Fig. 3 shows the modeling of the environment, which mimics the communication scenario. As shown in “Fig. 3”, the current research work considers a scenario of CRN communication as an environment that consists of two users (sender and recipient), including one transmitter (T_x), and receiver (R_x), and a jammer (J). The transmitter is accountable for the signal modulation, and the receiver is accountable for demodulating and receiving the signal from the transmitter.

The signal (S) can be jammed by producing noise or interference in the same frequency band. The study considers the base signal using BPSK modulation in the simulation process, as shown in “Fig. 4”. The block of a random integer is meant to model the wireless channel's noise before subjecting it to the BPSK block.

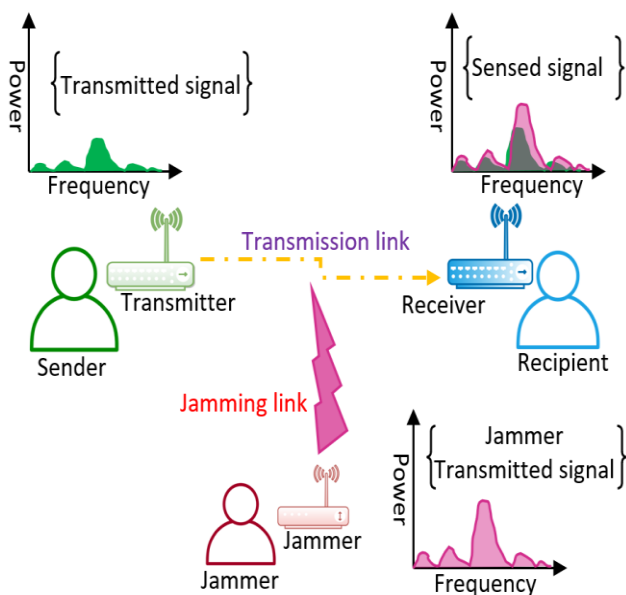


Fig. 3. Environment Model.

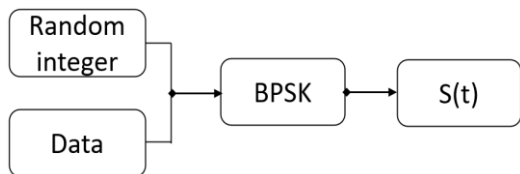


Fig. 4. Signal Construction Process.

B. Design Consideration

The proposed study in the environment modeling considers the processing of signals in continuous time instead of the processing of signals in discrete time-slots. This is because the current work focuses on overcoming jamming at the physical layer. The jammer works continuously, and the proposed anti-jamming overcomes the interference effect caused by jammer (J) on the entire signal of interest instead of the data. Under this consideration, both J and sender (T_x) share the same continuous-time signal. The T_x opts transmission channel frequency (f_s) from the pre-determined set of frequencies such that $f = \{f_1, f_2, f_3 \dots f_N\}$ of the communication (WiFi) band to forward or carry out the transmission of the data packets to the recipient (R_x) with power P_s . In the case of jamming, the jammer chooses the random transmission channel frequency (f_j) of the same communication band, attempting to impede transmission between T_x and R_x with power P_j .

The proposed system constructs a condition for a jamming attack towards the ongoing communication. According to this condition, the power variable P_j associated with the channel frequency of jammer f_j is required to be potentially higher than the power variable P_s associated with transmission channel frequency f_s that is received at the receiver end. Moreover, the study in the phase of environment modeling also considers the bandwidth (b) factor, which is equal for both f_s and f_j such that:

$$b_s = b_j \quad (3)$$

$$b \in f_s \rightarrow b_s \quad (4)$$

$$b \in f_j \rightarrow b_j \quad (5)$$

According to the above expressions (3)-(5), it states that bandwidth b_s should be similar to the bandwidth required for jamming b_j as per expression (3) which bears a predefined set of frequency f_s as per expression (4). At the same time, bandwidth b also carries jamming frequency b_j as per expression (5). Hence, expression (3)-(5) will mean that bandwidth consideration in the proposed model bears characteristic of both a predefined set of frequency as well as jamming frequency. This consideration makes the system model difficult to assess the network parameters. This problem becomes more difficult in cognitive radio networks as several secondary users are compared to primary users over a wide spectrum band. Apart from this, it will also become a challenging aspect to distinguish between the busy channel and jammed channel. This research challenge is further solved as follows: The proposed study considers that if the T_x forwards data in a transmission medium which is also designated by the J, then the SNR of the signal at R_x is corrupted severely. Considering above discussed scenario and notions, the SNR at R_x can be numerically expressed as follows:

$$SNR = \frac{P_s h_s}{P_j h_j F(f_s=f_j)} \quad (6)$$

In the above equation (6), the term h_s refers to channel gain from T_x to R_x and the term h_j indicates channel gain from J and R_x . Here, $F(x)$ refers to characteristics function that defines the

probability distribution of the received signal based on the condition numerically expressed as follows:

$$\begin{cases} 1 & \text{if } f_j = f_i; \text{ True} \\ 0 & \text{Otherwise} \end{cases} \quad (7)$$

The above expression (7) represents that if input argument (x) of this function is true, the value of this function is equal to 1; otherwise, 0. The study also considers demodulation cutoff value, where data transmission fails when the SNR is lower than this cutoff value. Since at the beginning, the agent (A_g) may not be able to recognize the channel or transmission medium chosen by the J. In this regard, the A_g has to sense the frequencies of channel f_s continually and store the sensing results in the form of a vector. In the proposed modeling, this vector is considered as environment state (S_t) for the corresponding action (A_t) carried out by the A_g (an anti-jamming mechanism). The A_t carried out by A_g is decided based on observed S_t of environment and A_g gets immediate feedback as a reward R_w which is characterized according to the selection of channel and channel switching power cost. In the proposed study, the output of A_g is an un-jamming of transmission medium or communication channel based on its A_t towards channel selection strategies. Therefore, the A_g tries to attain successful communication with a minimal channel switching power cost. Considering this factor R_w for A_g towards its corresponding A_t can be numerically expressed as shown in equation 8:

$$R_w = R_{SNR}(A_t) - c(A_t) \quad (8)$$

In the above equation 8, the first term $R_{SNR}(A_t)$ refers to R_w achieved $A_g \forall$ successful transmission. The success of transmission is considered when the SNR of the signal at R_x surpasses demodulation cutoff value, and in this case, the R_w will be equal to 1; otherwise, it would mean that the transmission has failed, and then the value of R_w will be -1, as expressed in equation 9 as follows:

$$A_g \leftarrow R_w = \begin{cases} 1 & \text{if } SNR_{R_x} \geq SNR_{cutoff} \\ -1 & \text{Otherwise} \end{cases} \quad (9)$$

In equation 9, the term SNR_{R_x} refers to the SNR of the signal at R_x (received signal) considered as a basis for computing R_w . The proposed study considers a control channel that conveys signals in transient to R_x is secure, which the jammer cannot influence. The second term $c(A_t)$ in the above equation 9 refers to the communication cost factor associated with A_t regarding the channel switching. The T_x and R_x in environment performs transmission of information on the fixed channel with stable power. But during the channel switching process the A_g tries to succeed by taking into account the low power cost. Otherwise, it will be penalized. Hence, the proposed study considers the $c(A_t)$ term in the computation of R_w for each A_t .

C. Algorithmic Principle

The prime challenge is creating a difference between busy and jammed channels using an intelligent anti-jamming mechanism. The complete idea is implemented on the

cognitive radio node and not on the access point. The prime justification behind this is that cognitive radio nodes create a bridge of communication between the base station and access point; therefore, they are more prone to jamming attacks. If the access point experiences a jamming attack, it can easily be rectified by switching over to the next access point, but this is not the case with cognitive radio nodes. If the jamming attack intrudes on cognitive radio nodes, then it will directly affect the primary users. The modeling of the environment contains three significant functions such that i) `__init__` function, ii) reset function, and iii) step function.

1) *init__function*: This function creates and initializes the environment, as demonstrated in Fig. 5. The environment is built to scan the available channels over the given Service Set Identifier (SSID) tries to block it in this function. Since the proposed study considered a WiFi communication channel, the terms SSID used here are just for recognizing which signal is being blocked. The SSID here is not a real one, but it is simulated. Also, the jamming frequency is set to the first available channel.

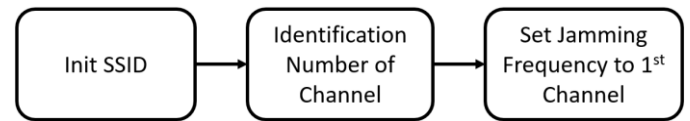


Fig. 5. Process of Environment Initialization.

2) *Reset function*: The reset function sets the environment back to its original setting. The reset function sets the jamming frequency back to the first available frequency in the channel, the reward is reset to zero, the signal is turned on, and communication channels are observed. The process of the resetting environment is shown in “Fig. 6”.

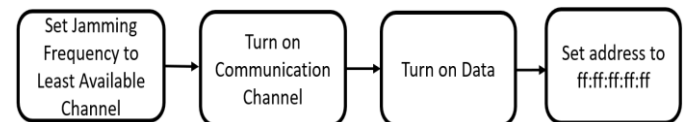


Fig. 6. Process of Environment Setting.

3) *Step function*: This is the main function of the environment. In this function, the packet of data is tried to be transferred. If the jamming frequency is equal to the base frequency, then the data either gets corrupted or does not pass. Based on this, the environment either gives a positive or negative reward. The process flow of the step function is shown in “Fig. 7”.

- Agent (A_g): The agent itself is an anti-jamming system that deals with the decision-making process. Initially, the agent interacts with the environment, senses the frequency spectrum, and instructs the transmitter to select a jamming-free communication channel.
- State (S_t): State refers to the perceived observation of the environment. Here, the state is the agent's frequency spectrum explored and sensed.

- Action (A_t): action refers to the strategic decision taken by the Agent. In the proposed study, the action changes communication band frequency and channel selection.
- Reward (R_w): Reward is the agent's feedback for the action taken for the observation in the environment. The term Reward is the higher SNR and low communication cost in the proposed system.

The proposed intelligent anti-jamming system is based on the function of the RL agent and its interaction with the environment. The environment responds to the agent via SNR so that the agent can inevitably distinguish whether the currently used carrier frequency is appropriate. Concurrently, the output strategy/policy can be further optimized, thereby circumventing surplus and redundant losses from frequency hopping. In the current work, the modeling of the agent is carried out based on the DDPG RL technique, which offers better interaction with the environment and automatically constructs a policy regarding observation and action state. However, the DDPG method involves two functions parameterized with a neural network, namely the Critic and the actor, to derive the best strategy or optimal policy. The actor's job is to specify a decision strategy towards deciding the optimal action for each state of observation. The Critic is responsible for estimating the value functions characterizing how well the actor takes action. The critic function generates the Q-value, representing the expected cumulative long-term reward that the agent receives from the environment for its action towards the current state of observation.

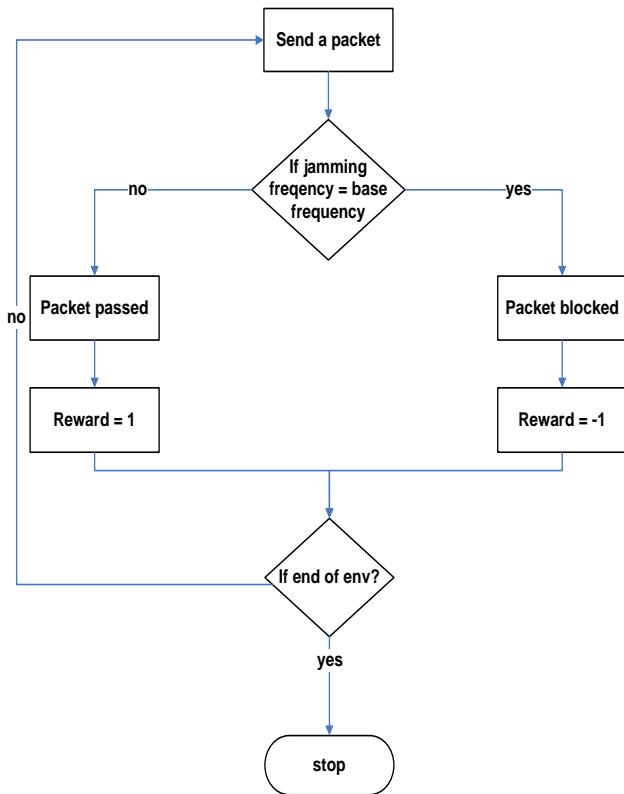


Fig. 7. Process of a Step Function.

The core principle of DDPG is to combine and get the benefits of both deterministic policy gradient mechanism and Q-learning function. The key aspect of the deterministic policy gradient mechanism is that it can handle continuous actions space while minimizing learning time. The mathematical representation of the DDPG is as shown in “Fig. 8”.

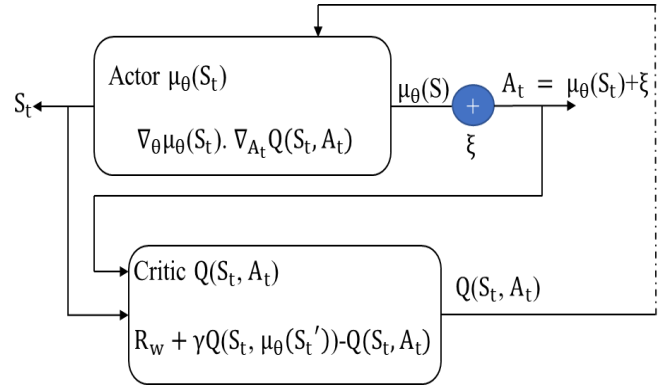


Fig. 8. Schematic Representation of DDPG.

Above Fig. 8 shows the building block of the DDPG with actor $\mu_\theta(S_t)$ and critic $Q(S_t, A_t)$ representation. However, to estimate the optimal policy and Q-value function, a DDPG algorithm maintains two networks i) current network and ii) target network. The current network consists of two function approximators such as current actor $\mu_\theta(S_t)$ and Critic $Q_\theta(S_t, A_t)$. The target network consists of two similar function approximators such as target actor $\mu_{\theta'}(S_t)$ and target critic $Q_{\theta'}(S_t, A_t)$, both the current network and target network have similar configuration, function, and parameterization. The target network is the copy of the main network (current) that helps to maintain stability in the training process of the main network.

1. Algorithmic Principle for Agent Modelling

Init Param
 Param = [E, BS, BL, ξ]
 Agent = f (Current, Target, Param)

The modeling of agent considers three major procedures such as i) building actor-network, ii) building critic network and iii) initialization of target actor-critic network. In the agent modeling, the algorithm also considers parameters (Param) such as ξ random process for initial state observation, batch size (BS) buffer length (BL), and E episode.

Procedure-1: Building Current Network

Input layer (S_t)
 denselayer1 (size =100, connect=inputlayer, activation=relu)
 denselayer2 (size =100, connect= denselayer1, activation=relu,)
 denselayer3 (size =100, connect= denselayer2, activation=relu)
 Actor = f_1 (actor_Network, S_t)

The above-discussed procedure is mentioned for actor configuration with input layers and multiple dense layers connected in a feed-forward manner. A $f_1(x)$ refers to the deterministic policy actor function used to construct an actor model with input arguments of actor_network, which includes all configured layers, and observation state S_t from the environment and returns the corresponding action that is expected to maximize the long-term cumulative reward.

Procedure-2: Building Critic_Network

Config \rightarrow StatePath
inputlayer (S_t , 'state')
denselayer (size = 100, connect = input, activation=relu)
Config \rightarrow ActionPath
inputlayer (A_t , 'action')
denselayer (size = 100, connect = input, activation=relu)
Config \rightarrow State_Action
Netlayers (dim= (1,2))
Add activation_function: relu
denselayer (size = 100, connect = state_action)
Add activation_function: relu
Critic= $f_2(\text{StatePath}, \text{ActionPath}, \text{State_Action path})$

The above-discussed procedure is mentioned for Critic configuration with state path, action path, and state action path. The Critic takes S_t and A_t as inputs and returns the Q-value representing the expected long-term reward. The $f_2(x)$ refers to the value function used to construct Critic network, which maps input value consisting of S_t and A_t to an expected and cumulative output value as reward based on the Q-value

Procedure-3: Building Target network

Actor_target= $f_1(\text{Actor}, S_t)$
Critic_target = $f_2(\text{Critic}, \text{StatePath}, \text{ActionPath}, \text{State_Action path})$

To achieve stability in the training phase of the current network, the algorithm initializes the target network with the same configuration as the current network. Therefore, the proposed RL agent adopts a four-function estimator (i.e., two from the current network and two from the target network) to perform the anti-jamming operation by sensing the spectrum without relying on any kind of statistical information about the jamming pattern and communication mode. The proposed anti-jamming mechanism has the advantage that it is suitable for continuous action space and overcomes the limitation associated with Q-learning and model-based jamming mitigation approaches. Thus, it can meet the requirement of a real-time deployment scenario. The algorithm for anti-jamming based on the proposed off policy and model-free Agent is discussed as follows:

2. Algorithmic Principle for Anti-jamming

Input: $E_p, A_t, T, \gamma, \mu_\theta, \mu_{\theta'}, Q_\theta, Q_{\theta'}, B_s, A_g$

Output: Unjammed signal

Start

1. Init random θ for the current network: $[\mu, Q]$
 2. Init random θ' for target network: $[\mu', Q']$
 3. For episode = 1: E_p do
 4. Init ξ for A_t exploration
-

5. Sense frequency spectrum
6. get initial state S_t
7. For $i = 1:T$ do
8. select action $A_t = \mu(S)$
9. select channel $f_s \in C_i$ and (P_s) according to current policy
10. Execute: $A_t \leftarrow$ initiate communication
11. Sense new spectrum S_{t+1}
12. Compute R_w
13. Using equation 8
14. store experience: $[S_t, A_t, R_w, S_{t+1}]$ into experience pool ψ
15. Check $|\psi| \geq B_s$ do
16. random selection of B_s from ψ
17. For each experience in B_s
18. Compute target actor and critic value
19. Using equation 14
20. Update current Critic by minimizing the loss
Using equation 15
21. Update the current actor using policy gradient
Using equation 16
22. Update target actor and target critic
Using equation 17 & 18

End

The above-mentioned algorithmic steps describe the working principle of the agent to perform un-jamming based on the interaction with the environment where it senses the spectrum and takes the action by exploring and learning the channel switching pattern. Concurrently, the agents get rewarded and observe the next state. The proposed algorithm takes a set of inputs such as number of episodes (E), number of iterations (T), Set of Action (A_t), discount factor (γ), current-actor (μ_θ), target-actor ($\mu_{\theta'}$), current Critic (Q_θ), target critic ($Q_{\theta'}$) and batch size (B_s). In the beginning steps, the algorithm randomly initializes the weighting parameters (θ and θ') for both current and target network, respectively (Step:1-2). In the next step, the algorithm initializes ξ a random process for A_t exploration based on the initial S_t perceived by sensing the spectrum frequency (Step:3-6). In these steps, the A_g interacts with the environment (the communication scenario and jammer). In the communication scenario, the study considers channel link such that $C_i \in \{1,2,3, \dots N\}$. The A_g senses the C_i and for each C , the proposed algorithm considers value 1 if C is in a good state, otherwise, 0. Therefore, the A_g gets feedback (R_w) +1 if a C with a good state is selected, otherwise R_w will be -1. When A_g interacts with the environment, it gets the initial S_t such that $S_t = \{1,2,3, \dots N\}$, and performs current A_t . Here, N denotes the number of channels (C). According to policy (i.e., current A_t) the channel $f_s \in C_i$ with transmitter power P_s is selected to launch the communication (Step:8-10). The proposed algorithm also considers that the A_g keeps sensing the spectrum and gets set of states such that $S_t \in M$, where M is the n -dimension vector the holds most recent observations S_t space. At every instance t , the recent state S_t will be added to the M , and the previous S_t (S_{t-M}) will be ignored (Step:11). The recent S_t at next instance, $t + 1$ can be represented as follows:

$$S_{t+1} \leftarrow \{S_t, S_{t-1}, S_{t-2}, \dots, S_{t-(N-1)}\} \quad (10)$$

In the next step of the algorithm, a set of $A_t \in K$, where K is the n -dimension vector space that holds distinct A_t sets such that $K \in \{1,2,3, \dots N\}$, where each genuine A_t in the K denotes the channel index. Hence, in this regard, when an A_t is selected, the A_g will guide the transmitter to access the corresponding C and subsequently A_g gets the R_w which exposes the state-selected C (Step 12). It is to be noted that the A_g is allowed to access a single channel to sense the spectrum and learn the channel selection strategy in each iteration. According to numerical expression 8, attaining higher R_w meant getting a higher possibility of successful transmission. Therefore, in this regard, the core objective of the A_g to get an optimal policy or strategy π , that maps the S_t to the K , towards maximizing the long-term cumulative R_w for the decisions choosing anti-jamming action towards accessing un-jammed channel such that:

$$R_{wK} = \sum_{i=0}^{\infty} \gamma^i R_{w+i+1} \quad (11)$$

The agent mechanism meets this objective by computing the ideal action-value such that:

$$Q^*(S_t, A_t) = \max_{\pi} \chi [R_{wK} | S_t = M, A_t = K, \pi] \quad (12)$$

From the above numerical expression, the objective of the maximizing cumulative R_w is achieved to increase the χ (expectation) on all S_t accessible by the policy of the R_w achieved after each A_t , where $Q^*(S_t, A_t)$ refers to the optimal action-value function and π refers to policy rule (i.e., policy mapping sequences to A_t). Therefore, the optimal policy for a precise A_t in any accessible S_t can be achieved by solving the following numerical equation as follows:

$$\pi^* = \arg(\max_{\pi} Q^*(S_t, A_t)) \quad (13)$$

Where π^* refers to the optimal decision policy regarding precise action in any given state of the environment. Therefore, A_t with maximum $Q^*(S_t, A_t)$ have maximum cumulative R_w and a higher probability of being selected. Thus, the agent A_g can choose the action A_t with maximum action-value to effectively overcome the impact of jamming attacks. Since the action space is continuous, computing max in the action-value function $\max_{\pi} Q^*(S_t, A_t)$ value is extremely a difficult task because the algorithm is required to be executed every time the A_g interacts environment to perform an A_t which is unacceptable in the real-time scenario. But adopting the DDPG algorithm in the proposed anti-jamming modeling, the agent perceives a value function (by Critic network) and action strategy (by actor-network) synchronously. The Critic uses off-policy and the Bellman equation to learn the value functions ($Q^*(S_t, A_t)$) and exploiting this information, the actor learns the action strategy (π^*) in such a way that it works particularly well for continuous action spaces in the environment. In this process, it is considered that derivative of function ($Q^*(S_t, A_t)$) exists at all points in its domain concerning the A_t argument. This enables to derive an optimal gradient-based learning protocol the policy $\mu(S_t)$, i.e., a function of the actor towards deciding optimal action. In this regard, estimation of the action value can be done by approximating $Q(S_t, A_t, \theta) \approx Q^*(S_t, A_t)$ instead of executing complex and iterative optimization procedures every time to compute $\max_{\pi} Q^*(S_t, A_t)$. But to

achieve stability in the agent learning process, the algorithm maintains two networks, i.e., the current actor-critic network and target actor-critic network. The current network performs a selection of action and evaluation of action-value, and the target network is used to maintain stability in the training process of the current network. The training of the current network requires experience pool ψ to approximate $Q^*(S_t, A_t)$. The experience pool ψ is a set of transitions obtained via interaction between the current actor-network and the environment which is stored in the experience pool $\psi \in \{S_t, A_t, R_w, S_{t+1}\}$ (Step:14). In this next step, the algorithm performs a sampling process by taking a random B_S (minibatches) of transitions from the ψ to update the parameters of current Critic and current actor networks (Step:15-16). The process of sampling B_S splits the transition data into small batches to compute error and update network parameters. To stabilize the performance of the agent mechanism, the algorithm then computes the target actor value and target Critic value for the next S_t . Q-value (Step:18) numerically obtained through Bellman equation as follows:

$$y_k = R_w + \gamma Q_{\theta'}((S_t', \mu_{\theta'}(S_t')) \quad (14)$$

In the next step of the algorithm (Step:20), the training of the current Critic network is accomplished by updating its parameter based on the loss function numerically expressed as follows:

$$\mathcal{L}(\theta) = \frac{1}{B_S} \sum_k (y_k - Q_{\theta}(S_t, A_t))^2 \quad (15)$$

In the above equation (15), MSE (mean-squared-error) is used as a loss function that computes the sum of squared distances between the updated target Critic (action-value) and current Critic (action-value). Further, in the next step of the algorithm (Step:21), an iterative optimization algorithm (gradient descent) is used to update and rejuvenate the weights θ of the current actor towards determining appropriate A_t decision strategy that maximizes the R_w numerically expressed as follows:

$$\nabla_{\theta} J(\theta) = \frac{1}{B_S} \sum_k \nabla_{\theta} \mu_{\theta}(S_k) \times \nabla_{A_t} Q_{\theta}(S_t, A_t) |_{A_t=\mu_{\theta}(S_k)} \quad (16)$$

In the above numerical expression, the current-actor network is updated with the average of the sum of gradients in an off-policy manner with B_S of transitions. Finally, the target actor and target Critic network is updated to provide better stability in the learning process of the current actor and Critic network numerically expressed in equation 17 and 18 (Step:22):

$$\mu_{\theta'} \leftarrow \phi \theta + (1 - \phi) \mu_{\theta'} \quad (17)$$

$$Q_{\theta'} \leftarrow \phi \theta + (1 - \phi) Q_{\theta'} \quad (18)$$

Where ϕ refers to the hyperparameter between [0,1]. In this operation, a sliding averaging mechanism is used to update the parameters of the target network once per update of the current network. As a result, the target network slowly tracks the learned networks, thereby significantly improving stability in learning the action values. "Fig. 9", illustrates the architecture of the proposed anti-jamming mechanism based on the above-discussed algorithm.

From the Section II of this paper, it can be seen that there was previous technique to solve the problem, however, DQN and Q-Learning is the extensively used methodologies that offers better guidelines towards proposed problem mitigation. Therefore, the outcome of the proposed technique is compared with DQN and Q-Learning which represents the frequently adopted solution.

“Fig. 11” shows the performance analysis of the proposed system regarding the power cost factor. The graph trend exhibits that the proposed system performs much better than the other two RL techniques regarding reduction in the fluctuation of the power consumption during data transmission. The performance of the Q-learning technique is worse than DQN based anti-jamming process. This is because state space is so huge that it suffers in finding an optimal policy. The Q-learning depends on the Q-table, which is discrete, and also it uses a simple Bellman algorithm to perform the frequency hopping, which directly depends on Q-function. The agent algorithm tries to choose the frequency which gives the highest reward. In the case of Q-learning, the agent algorithm uses a Q-table to decide the optimal reward; hence the frequency needs to keep changing. Therefore, more frequency hopping leads to more power consumption. The DQN exhibited little fluctuation in the power consumption and has achieved closer performance to the proposed system. The DQN is more efficient than Q-learning, tries to optimize action-value for the present scenario. The Q-learning is discrete and has a limited number of rows and columns in Q-Table, whereas in DQN, one neural network decides the best action and state pair for the given scenario. The proposed system uses the DDPG algorithm suitable to continuous action space and has less randomness than Q-learning and DQN. The proposed system converges to less fluctuation and achieves lower power consumption.

In “Fig. 12”, it can be analyzed that both proposed and DQN exhibits similar performance regarding SNR. However, in the case of Q-learning, the graph trend exhibits lower SNR compared to the others. The SNR refers to the overall number of useful packets received over the total number of packets transmitted. In the transmission scenario, two things are possible once the packet is transmitted, i) the packet will not receive at the receiver side, and ii) the packet may corrupt by the time it is received. If the packet is corrupt in practicality, there will be syndrome bits that can be used to correct the corrupted packets. However, the proposed study does not consider the syndrome bits, but the study considers the communication channel whether the packets transferred are intact or not. Thereby, the system has only one control variable, i.e., whether the signal is being jammed or not. The Q-learning algorithm always considers discrete frequencies. Since the discrete hopping frequency of Q-learning is always much higher than sweeping width, the communication gets blocked more often in Q-learning than in a continuous system like DQN and the proposed agent algorithm. Hence, while DQN and proposed show a similar SNR ratio, Q-learning shows a much lower SNR ratio. Even if DQN and proposed show a similar SNR ratio, the proposed method consumes less power compared to DQN. Hence, the proposed algorithm is deemed to be better than the other Q-learning and DQN methods. It could be also noted that in order to develop an anti-

jamming mechanism over complex network environment, there is a need to fine tune the proposed scheme. However, interestingly, there are just a need of amending the communication topology as well as constraint information within the model. Hence, no reengineering technique is required to ensure that proposed system does operate over complex network environment. The primary reason behind this claim is that proposed system harnesses learning functions using low epoch to generate the optimal result, whereas the existing approaches do demands higher dependency of resource leading to degradation of signal quality in its outcome.

Further, Table IV highlights that the proposed system offers better improvement of power reduction, higher signal quality, and lower processing time in contrast to frequently used Q-Learning and DQN approach. Similar trend is expected with any other existing approach toward problem solution and hence better consistency is noted.

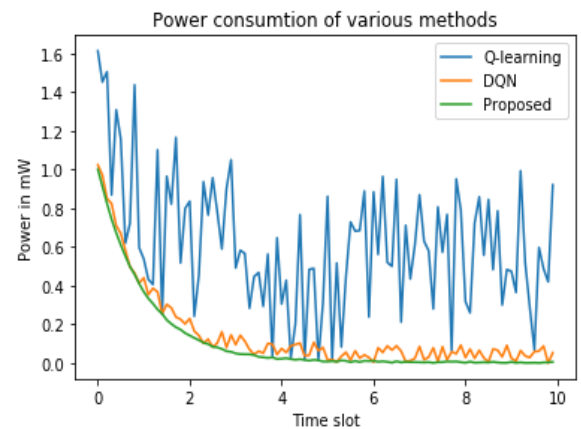


Fig. 11. Analysis of the Power.



Fig. 12. Analysis of the SNR.

TABLE IV. COMPARISON OF OUTCOMES

Techniques	Improvement in Power Reduction	Improvement in Signal Quality	Processing Time
Q-Learning	87.57%	98.41%	0.26619s
DQN	76.29%	82.63%	0.59851s
Proposed	35.81%	81.59%	0.98791s

VII. CONCLUSION

The previous works on anti-jamming mechanisms for wireless communication have concentrated on how to prevent jamming attacks but neglected the possibility that jammers could obtain frequency action. However, existing anti-jamming methods can guarantee a solution on a temporary basis. They may fail to ensure efficient performance for the long run, especially where intelligent jammers are deployed. Aiming at this issue, the proposed system has been presented as an efficient and intelligent anti-jamming scheme based on the model-free and off-policy agent mechanism. Overall implementation of the proposed work is carried out in a multi-fold manner, such as 1) Building a customized RL environment for evaluating agent mechanism 2) designing the intelligent anti-jamming agent algorithm to perform the anti-jamming process. The proposed system is more intelligent than the existing works, it has robust environmental applicability, and avoids the additional overhead caused by continuous action space. The simulation results show the proposed system's effectiveness compared to the widely adopted Q-learning and DQN based anti-jamming system. Moreover, the proposed work is limited to modeling the intelligent anti-jamming scheme, and it is not evaluated against intelligent anti-jamming techniques. The current research work will be extended with intelligent jamming scheme, which will be introduced against the proposed anti-jamming solution.

REFERENCES

- [1] Rehmani MH, Dhaou R, editors. The cognitive radio, mobile communications and wireless networks. Springer International Publishing; 2019.
- [2] Marinho J, Monteiro E. Cognitive radio: survey on communication protocols, spectrum decision issues, and future research directions. *Wireless networks*. 2012 Feb;18(2):147-64.
- [3] N. Mansoor, A.M. Islam AM, M. Zareei, S. Baharun, T. Wakabayashi, S. Komaki. Cognitive radio ad-hoc network architectures: a survey. *Wireless Personal Communications*, vol. 81, Iss.3, pp.1117-42, 2015.
- [4] Y. Sudha and V. Sarasvathi, "Evolution of the Security Models in Cognitive Radio Networks: Challenges and Open Issues," 2020 International Conference on Innovation and Intelligence for Informatics, Computing and Technologies (3ICT), pp. 1-6, 2020, doi: 10.1109/3ICT51146.2020.9311956.
- [5] S.B. Nanthini SB, M. Hemalatha, D. Manivannan, L. Devasena, "Attacks in cognitive radio networks (CRN)-A survey". *Indian Journal of science and Technology*, vol.1, Iss.7, pp.530, 2014.
- [6] S. Bhattacharjee, R. Rajkumari, N. Marchang, "Cognitive radio networks security threats and attacks: a review". *International Journal of Computer Applications*. 2014; 975:8887.
- [7] DK. Jasim, S.B. Sadkhan, "Cognitive Radio Network: Security and Reliability trade-off-Status, Challenges, and Future trend". *IEEE 1st Babylon International Conference on Information Technology and Science (BICITS)*, Apr 28 pp. 149-153, 2021.
- [8] M.K. Hanawal, M.J. Abdel-Rahman, M. Krunch, "Joint adaptation of frequency hopping and transmission rate for anti-jamming wireless systems", *IEEE Transactions on Mobile Computing*, vol.15, Iss.9, pp.2247-59, 2015.
- [9] Di Pietro, R. and G. Oligeri, "Jamming mitigation in cognitive radio networks", *IEEE Network*, vol.27, Iss.3, pp.10-15, 2013.
- [10] Xiao L. Spread spectrum-based anti-jamming techniques. In *Anti-Jamming Transmissions in Cognitive Radio Networks 2015* (pp. 5-9). Springer, Cham.
- [11] K. Ibrahim K, Qureshi IM, Malik AN, Ng SX. Bandwidth-Efficient Frequency Hopping based Anti-Jamming Game for Cognitive Radio assisted Wireless Sensor Networks. In *2021 IEEE 93rd Vehicular Technology Conference (VTC2021-Spring)* 2021 Apr 25 (pp. 1-5). IEEE.
- [12] L. Xiao, Y. Li, J. Liu, and Y. Zhao, "Power control with reinforcement learning in cooperative cognitive radio networks against jamming," *The Journal of Supercomputing*, vol. 71, no. 9, pp. 3237–3257, 2015.
- [13] L. Xiao, Y. Li, C. Dai, H. Dai, and H. V. Poor, "Reinforcement learning based noma power allocation in the presence of smart jamming," *IEEE Transactions on Vehicular Technology*, vol. 67, no. 4, pp. 3377–3389, 2018.
- [14] Lmater MA, Haddad M, Karouit A, Haqiq A. Smart Jamming Attacks in Wireless Networks During a Transmission Cycle: Stackelberg Game with Hierarchical Learning Solution. *International Journal of Advanced Computer Science and Applications (IJACSA)*. 2018 Apr 1;9(4).
- [15] G. Han, L. Xiao, and H. V. Poor, "Two-dimensional anti-jamming communication based on deep reinforcement learning," in *Proc. IEEE International Conference on Acoustics, Speech and Signal Processing (ICASSP)*, 2017, pp. 2087–2091.
- [16] Han, Guoan & Xiao, Liang & Poor, H. Vincent. (2017). Two-dimensional anti-jamming communication based on deep reinforcement learning. 2087-2091. 10.1109/ICASSP.2017.7952524.
- [17] S. Ahmed, Ismail, "Stackelberg-Based Anti-Jamming Game for Cooperative Cognitive Radio Networks", University of Calgary's Digital Repository, Doctorial Thesis, 2017.
- [18] F. Ye, F. Che and H. Tian, "Cognitive cooperative-jamming decision method based on bee colony algorithm," 2017 Progress in Electromagnetics Research Symposium - Fall (PIERS - FALL), 2017, pp. 531-537, doi: 10.1109/PIERS-FALL.2017.8293195.
- [19] TS. Singh, A. Trivedi, "Anti-jamming in cognitive radio networks using reinforcement learning algorithms", Ninth International Conference on Wireless and Optical Communications Networks, DOI:10.1109/WOCN.2012.6331885, 2012.
- [20] H. Liu, H. Zhang, Y. He, and Y. Sun, "Jamming Strategy Optimization through Dual Q-Learning Model against Adaptive Radar", *MDPI*, vol.22, Iss.145, 2022, <https://doi.org/10.3390/s22010145>.
- [21] K. Ibrahim, S. X. Ng, I. M. Qureshi, A. N. Malik and S. Muhaidat, "Anti-Jamming Game to Combat Intelligent Jamming for Cognitive Radio Networks," in *IEEE Access*, vol. 9, pp. 137941-137956, 2021, doi: 10.1109/ACCESS.2021.3117563.
- [22] Wang, X., Wang, J., Xu, Y., et al.: 'Dynamic spectrum anti-jamming communications: challenges and opportunities', *IEEE Commun. Mag.*, 2020, 58, (2), pp. 79–85.
- [23] Amuru, S., Tekin, C., Schaar, M.V., et al.: 'Jamming bandits—A novel learning method for optimal Jamming', *IEEE Trans. Wirel. Commun.*, 2016, 15, (4), pp. 2792–2808.
- [24] Furqan HM, Aygül MA, Nazzal M, Arslan H. Primary user emulation and jamming attack detection in cognitive radio via sparse coding. *EURASIP Journal on Wireless Communications and Networking*. 2020 Dec;2020(1):1-9.
- [25] Huang JF, Chang GY, Huang JX. Anti-jamming rendezvous scheme for cognitive radio networks. *IEEE Transactions on Mobile Computing*. 2016 May 3;16(3):648-61.
- [26] Quan, H., Zhao, H. & Cui, P. Anti-jamming Frequency Hopping System Using Multiple Hopping Patterns. *Wireless Pers Commun* 81, 1159–1176 (2015).
- [27] Y. Wu, B. Wang, K. J. R. Liu, and T. C. Clancy, "Anti-jamming games in multi-channel cognitive radio networks," *IEEE J. Sel. Areas Commun.*, vol. 30, no. 1, pp. 4–15, Jan. 2012.
- [28] L. Jia, Y. Xu, Y. Sun, S. Feng, and A. Anpalagan, "Stackelberg game approaches for anti-jamming defence in wireless networks," *IEEE Wireless Commun.*, vol. 25, no. 6, pp. 120–128, Dec. 2018.
- [29] L. Jia, F. Yao, Y. Sun, Y. Xu, S. Feng, and A. Anpalagan, "A hierarchical learning solution for anti-jamming stackelberg game with discrete power strategies," *IEEE Wireless Commun. Lett.*, vol. 6, no. 6, pp. 818–821, Dec. 2017.
- [30] B. Wang, Y. Wu, K. J. R. Liu, and T. C. Clancy, "An anti-jamming stochastic game for cognitive radio networks," *IEEE J. Sel. Areas Commun.*, vol. 29, no. 4, pp. 877–889, Apr. 2011.
- [31] Hanawal MK, Abdel-Rahman MJ, Krunch M. Joint adaptation of frequency hopping and transmission rate for anti-jamming wireless

- systems. *IEEE Transactions on Mobile Computing*. 2015 Oct 19;15(9):2247-59.
- [32] G.-Y. Chang, S.-Y. Wang, and Y.-X. Liu, "A jamming-resistant channel hopping scheme for cognitive radio networks," *IEEE Transactions on Wireless Communications*, vol. 16, no. 10, pp. 6712–6725, 2017.
- [33] Gao, Y., Xiao, Y., Wu, M., Xiao, M. and Shao, J., 2018. Game theory-based anti-jamming strategies for frequency hopping wireless communications. *IEEE Transactions on Wireless Communications*, 17(8), pp.5314-5326.
- [34] Y. Gwon, S. Dastango, C. Fossa, and H. T. Kung, "Competing mobile network game: Embracing anti-jamming and jamming strategies with reinforcement learning," in *Proc. IEEE Conf. Commun. Netw. Secur. (CNS)*, Oct. 2013, pp. 28–36.
- [35] Liu, X., Xu, Y., Jia, L., et al.: 'Anti-jamming communications using spectrum waterfall: a deep reinforcement learning approach', *IEEE Commun. Lett.*, 2018, 22, (5), pp. 998–1001.
- [36] Y. Bi, Y. Wu, and C. Hua, "Deep reinforcement learning based multiuser anti-jamming strategy," in *Proc. IEEE Int. Conf. Commun. (ICC)*, May 2019, pp. 1–6.
- [37] S. Liu, Y. Xu, X. Chen, and, "Pattern-aware intelligent anti-jamming communication: A sequential deep reinforcement learning approach," *IEEE Access*, vol. 7, pp. 169204–169216, 2020.
- [38] N. Gao, Z. Qin, X. Jing, Q. Ni, and S. Jin, "Anti-intelligent UAV jamming strategy via deep Q-Networks," *IEEE Trans. Commun.*, vol. 68, no. 1, pp. 569–581, Jan. 2020.
- [39] G. Han, L. Xiao, and H. V. Poor, "Two-dimensional anti-jamming communication based on deep reinforcement learning," in *Proc. IEEE Int. Conf. Acoust., Speech Signal Process. (ICASSP)*, New Orleans, LA, USA, Mar. 2017, pp. 2087–2091.
- [40] G. Chen, Y. Zhan, Y. Chen, L. Xiao, Y. Wang, and N. An, "Reinforcement learning based power control for in-body sensors in WBANs against jamming," *IEEE Access*, vol. 6, pp. 37403–37412, 2018.
- [41] X. Lu, L. Xiao, C. Dai, and H. Dai, "UAV-aided cellular communications with deep reinforcement learning against jamming," *IEEE Wireless Commun.*, vol. 27, no. 4, pp. 48–53, Aug. 2020.
- [42] Jiang, S. and Xue, Y., 2011. Providing survivability against jamming attack for multi-radio multi-channel wireless mesh networks. *Journal of Network and Computer Applications*, 34(2), pp.443-454.
- [43] Xiao, L., Li, Q., Chen, T., Cheng, E. and Dai, H., 2015, December. Jamming games in underwater sensor networks with reinforcement learning. In *2015 IEEE Global Communications Conference (GLOBECOM)* (pp. 1-6). IEEE.
- [44] Xiao, L., Xie, C., Chen, T., Dai, H. and Poor, H.V., 2016. A mobile offloading game against smart attacks. *IEEE Access*, 4, pp.2281-2291.
- [45] Zhang, H., Qi, Y., Wu, J., Fu, L. and He, L., 2016. DoS attack energy management against remote state estimation. *IEEE Transactions on Control of Network Systems*, 5(1), pp.383-394.
- [46] Al Mamoori, S., Nizampatnam, M. and Jaekel, A., 2019. Optimal attack-aware RWA for scheduled lightpath demands. *SN Applied Sciences*, 1(11), pp.1-12.
- [47] Xie, C. and Xiao, L., 2016, October. User-centric view of smart attacks in wireless networks. In *2016 IEEE International Conference on Ubiquitous Wireless Broadband (ICUWB)* (pp. 1-6). IEEE.
- [48] Tu, S., Waqas, M., Meng, Y., Rehman, S.U., Ahmad, I., Koubaa, A., Halim, Z., Hanif, M., Chang, C.C. and Shi, C., 2020. Mobile fog computing security: A user-oriented smart attack defense strategy based on DQL. *Computer Communications*, 160, pp.790-798.
- [49] Qin, J., Li, M., Wang, J., Shi, L., Kang, Y. and Zheng, W.X., 2020. Optimal Denial-of-Service attack energy management against state estimation over an SINR-based network. *Automatica*, 119, p.109090.
- [50] Zhao, C., Wang, Q., Liu, X., Li, C. and Shi, L., 2021. Reinforcement learning based a non-zero-sum game for secure transmission against smart jamming. *Digital Signal Processing*, 112, p.103002.

Rainfall Forecasting using Support Vector Regression Machines

Lemuel Clark Velasco^{1*}, Johanne Miguel Aca-ac², Jeb Joseph Cajes³, Nove Joshua Lactuan⁴, Suwannit Chareen Chit⁵

Premier Research Institute of Science and Mathematics¹
MSU-Iligan Institute of Technology, Iligan City, The Philippines^{1, 2, 3, 4}
Universiti Utara Malaysia, UUM Sintok, Kedah, Malaysia⁵

Abstract—Heavy rainfall as a consequence of climate change have immensely impacted the ecology, the economy, and the lives of many. With the variety of available predictive tools, it is imperative that performance analysis of rainfall forecasting models is properly conducted as a measure for disaster preparedness and mitigation. Support Vector Regression Machine (SVRM) was utilized in predicting the rainfall of a city in a tropical country using a 4-year and 17-month rainfall dataset captured from an automated rain gauge (ARG) in Southern Philippines, involving parameter cost and gamma identification to determine the relationship between past and present values, determining optimal cost and gamma parameters to improve prediction accuracy, and forecasting model evaluation. The SVRM model that utilized Radial Basis Function (RBF) kernel function having the parameters of $c=100$; $g=1$; $e=0.1$; $p=0.001$ and the lag variable which used 12-hour report with lags up to 672-timesteps (i-672) demonstrated a Mean Square Error (MSE) of 3.461315. With close to accurate forecast between the predicted values and the actual rainfall values, the results of this study showed that SVRM has the potential to be a viable rainfall forecasting model given the proper data preparation, model kernel function selection, model parameter value selection and lag variable selection.

Keywords—Support vector regression machines; support vector machines; rainfall forecasting

I. INTRODUCTION

Climate change is a widespread and growing threat to biodiversity and ecosystems globally. One of the disasters caused by climate change is heavy rainfall and its frequency is noticeable among tropical countries resulting to catastrophic disasters such as landslides and flood which led to loss of lives, property, and livestock. Rainfall forecasting has received immense attention in recent years due to heightened emphasis on minimizing life and property losses through proper conduct of mitigation and preparedness in disaster risk reduction [1]–[3]. Rainfall forecasting models need to be evaluated and optimized for efficient performance in order for these predictive models to be utilized as disaster risk management tools that can serve as decision-making tools to alert individuals on incoming natural disasters through advance notice for the tactical planning of activities and approach [2]. Support Vector Machines (SVM) with a specific forecasting variant known as Support Vector Regression Machines (SVRM) is an emerging high performing machine learning algorithm used for natural phenomena such as rainfall forecasting [4], [5]. SVRM finds a hyperplane in a n-

dimensional space with n-number of features that specifically classifies the data points into classes, applying structural risk minimization elementary principles to obtain quality generalization on a finite number of learning patterns [3], [5]–[8]. Since SVRM first plots the inputs into a high-dimensional space and looks for a parting hyperplane that maximizes the margin between the classes which then uses kernels to find the optimal hyperplane, various SVRM models can be developed, evaluated and optimized in order to be efficiently used as forecasting models to be effectively used disaster risk reduction.

Iligan City in Southern Philippines, has recently been in the pathway of typhoons due to climate change. Local authorities led by the Iligan City Disaster Risk Reduction Management Council (CDRRMC) need to develop decision support tools in disaster mitigation, preparedness, response and recovery. Despite availability of historical rainfall data, there is a lack of a forecasting model to determine rainfall which is essential in the resource and mitigation planning in times of disasters. Additionally, proper rainfall data preprocessing as well as optimal parameter configuration of forecasting models are needed to utilize rainfall forecasting tools that yields reliable predictive results [2], [7]. This study attempted to conduct performance analysis of SVRM models by conducting rainfall data preparation, kernel selection, SVRM parameter selection, lag variable selection, and implementation of SVRM models. Through model verification in terms of error computation, an assessment on the predictive performance of these SVRM models was conducted to determine the reliability of the forecasting model. By conducting performance analysis, this study hopes to contribute in the on-going efforts to evaluate and optimize efficient performance of rainfall forecasting models that can be used as decision-making tools to save both lives and property.

II. METHODOLOGY

A. Rainfall Data Preparation

The rainfall data preparation phase of this study involves three activities namely data selection, data correction and data representation. Data selection is the process of determining the appropriate dataset input variable along with its corresponding time-range as input layer data [3], [9]. The researchers considered rain, rain rate, air temperature, humidity, air pressure, water level and solar radiation as candidate meteorological data that can be possible datasets to be selected [1], [2], [9]. Input data for this study were obtained from the

*Corresponding Author.

Philippine Department of Science and Technology - Advance Science and Technology Institute (DOST-ASTI) which were collected rainfall data from Automated Rain Gauges (ARG) having 15-minute intervals with a unit of measurement in millimeters. The acquired dataset may have incomplete, inconsistent, and noisy values which can be due to incomplete data lacking attribute values, lacking certain attributes of interest. Thus, data correction by finding, checking, or eliminating corrupt and inaccurate records from the rainfall dataset was then conducted to discriminate incomplete, incorrect, or irrelevant parts of the dataset. Manual visual inspection of the raw rainfall data from the obtained spreadsheet file was initially conducted to determine the extent of the data cleaning as well as data recording anomalies such as missing rainfall data brought about by ARG limitations. Further examination of the dataset was performed that examined aggregate data, noisy data containing errors or outliers, and inconsistent data containing discrepancies in codes or names [3], [10].

As shown in Fig. 1, the acquired rainfall data is device-dependent that is why data representation which involved representation processing of key variables and attributes was then conducted. The raw dataset also contains the location of the ARG (LOCATION), latitude of the ARG (LATITUDE), longitude of the ARG (LONGITUDE), elevation of the ARG (ELEVATION), date of installation of the ARG (DATE INSTALLED) and date of reading and amount of rainfall (DATE/TIME READ; RAINFALL AMOUNT). The rainfall data captured in 15-minute observations in terms of millimeters along with its date of reading was considered in this study as the training, testing and validation data sets following the data partitioning process.

```
@relation RogongonOriginal
@attribute Date date "MM/dd/yyyy HH:mm"
@attribute RAINFALL_ROGONGON numeric
@data '03/01/2013 0:00',0
'03/01/2013 0:15',0
'03/01/2013 0:30',0
'03/01/2013 0:45',0
'03/01/2013 1:00',0
```

Fig. 1. Sample Raw Data from the ARG.

B. SVRM Model Design

The design of an SVRM forecasting models depends on a set of specific selection processes which includes kernel selection, parameter selection, and architecture selection [2], [3], [6], [10]–[12]. As shown in Fig. 2, SVRM utilizes kernel functions to transform and map training data from an input space into a high dimensional feature space in which it searches for an optimal classification hyperplane that separates the data into different categories [10], [12]–[14]. Configured by the researchers, the kernel function is the component of the SVRM that plays a central part in the assimilation of data and transforming such data for pattern discovery and general types of relations such as classifications, rankings, cluster, and regressions [13], [14]. Kernel selection as conducted by the researchers involves the testing of different kernel functions to determine the optimal parameters needed to build the SVRM model. The data set was tested with Linear Function Kernel—which excels in linearly separable data, and Radial Basis

Function (RBF) Kernel—which is excellent with nonlinear data sets. The study followed proposed the methodology to come up with the best fitted kernel function for an SVRM rainfall forecasting model [15]. The process involved utilizing the grid search method to produce an optimal parameter which was used as a reference parameter for the kernel selection process in an integrated development environment (IDE) using the entire training set and evaluated on the testing set. The kernel functions were then observed for their forecasting accuracy and behavior with the model having the lowest Mean Squared Error (MSE) adopted and used in the parameter selection phase.

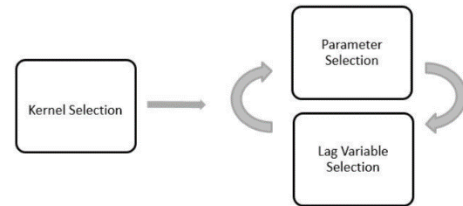


Fig. 2. Model Design Flow.

As supported by studies which used the MSE error metric in assessing the accuracy of the SVRM models, the selection for which parameters was included in model revolved around the selected kernel [16], [17]. The researchers then conducted parameter selection where optimal values of key parameters are selected for forecasting unknown data [4], [11], [12], [16], [17]. The process involves utilizing the Grid Search method to find an optimal combination value of the key parameters Cost (C), Gamma (g), and Epsilon (e). Table I shows that the key parameter (C) defines the penalty for errors, the parameter (g) influences the hyper-line flexibility, while the parameter (e) defines the upper and lower bound of the fractions of the support vectors relative to the total number of training examples [3], [6], [10]–[12], [17].

Utilizing the selected kernel from the kernel selection process, testing of different parameter values were determined with the use of Grid Search and an Exhaustive Parameter Search methodology using the data training and testing sets. This is to validate the reliability of Grid Search in searching for optimal parameter values and to also find the best fitted parameters for the final model [3], [15]. The study also utilized a feature space which was used in both Grid Search and Exhaustive Parameter Search methodologies. The parameter values were evaluated and observed for their forecasting accuracy. Parameter values with the lowest MSE were selected as the optimal parameter values for the kernel function and final forecasting model. The kernel adopted along with the selected parameter values were used to select the lag variable that were used in the final model.

TABLE I. PARAMETERS AND ITS FUNCTION

PARAMETERS	FUNCTION
Cost Penalty (C)	Defines the penalty for errors
Gamma (g)	Influences the hyper-line flexibility
Insensitive Loss Function (e)	Width of ε-insensitive zone/tube
Epsilon (p)	The set of epsilon function in epsilon SVR

Lag variable selection, where optimal value for the lagged variables were selected, was used by the researchers to determine the relationship between past and current values of the series which can be captured by a propositional learning algorithm like the SVRM algorithm. Fundamentally, the value of the lagged variables created regulates the size of the time window [6], [10]. This step involves evaluating 2 lag variable values wherein each lag value utilized 4 years, 7 months, and 30 days' worth of rainfall data in periods of 15 minutes. The first lag variable value (Lag Variable I) had a per-12-hour report with lags up to 672-time steps ($i-672$) in the past, wherein i represents the current date of the model. The configuration of the first lag variable value was considered since the heuristic standard for weather forecasting is on a weekly basis. The second lag variable value (Lag Variable II) had a per-12-hour report with lags up to 2976-time steps ($i-2976$) in the past. The configuration of the second lag variable value was considered since rainy season in countries like the Philippines starts in June and last till November, wherein the months of September and October are often the typhoon season in the entire archipelago. The forecasted values were validated using the remaining month of the data. Using the selected kernel function, kernel parameter values, and the data set, architectures determined were used through a determined IDE. The lag variables were observed for its forecasting accuracy and behavior with the lag variable having the lowest MSE was selected for the final model.

C. SVRM Model Evaluation

The researchers integrated and constructed an SVRM model utilizing the LIBSVM library for SVRM processes to improve efficient and effective management of the rainfall forecasting process. It is necessary that the computing environment settings befit for developing SVRM model and the needed libraries and IDE should be ready before the development start. Computer running on Mac OS, Windows, or Ubuntu is necessary, with an IDE, preferably the Waikato Environment for Knowledge Analysis (WEKA). Few WEKA packages or extension were installed like grid search that handled optimization of the parameters and enhance the specific values for the parameters. The SVRM programme stimulates the training, validating, and forecasting of the data after creating the data and environment in which the system was constructed. The specification of parameters, kernel, lag variable, and training of the prepared dataset was then referred to as training. Furthermore, the trained model was validated by using an error metric until an output was finally generated.

Using the testing set, SVRM model evaluation examined each model in the training process for its accuracy in forecasting 12 hour-ahead rainfall values in 672-time or 2976-time lagged steps in the past. The predicted result was compared to the testing set's actual rainfall data. For the rainfall forecasting system, the model with the lowest MSE was then chosen as the final model. The computation of the measure of error is an important aspect of evaluating a forecasting model's prediction accuracy. The forecasting error, which is the difference between the anticipated and actual rainfall levels, is a measure of a forecasting model's accuracy [17]. The MSE shown in Equation (1) was used in this study since the actual values of the data are in the denominator of the equation and

will produce undefined or infinite results when the actual demand is zero.

$$MSE = \frac{1}{n} \sum_{i=1}^n (Y_i - \hat{Y}_i)^2 \quad (1)$$

where Y_i are the observed values of the variable being predicted and \hat{Y}_i are the predicted values.

The MSE, the model's consistency will be indicated by a minimal error. The rainfall data from the testing set was then used to test the selected SVRM models. The data was fed into the chosen SVRM models, which generated anticipated results for the next 12 hours. In a 15-minute cycle, 80% of the rainfall data was loaded into the selected models to anticipate rainfall for the next 12 hours. The predicted values were then compared to the testing set's actual rainfall value. The anticipated rainfall values were evaluated using MSE after the evaluation phase was completed. Error assessment was then conducted where the validation results were converted and compared to the actual results to see if they are accurate in terms of the actual rainfall data [3], [11]. In this process, the validation set was utilized to generate validation findings throughout the month of October in 2017. The accuracy of the forecasting was then tested by comparing these findings. Following the selection of the best performing model, the forecasted values were graphed into a line graph and compared to the actual rainfall levels. For charting, the values of each iteration of each model were aligned with the real values of the same week. Visual inspection was then carried out by watching it on a weekly basis. Every day in October, for example, the next seven days were gathered and graphed. As a result, the full validation set was observed for a total of 31 days. The t-score shows the differences of the two groups, the larger values specify the difference between the two samples while the smaller values specify the similarity of the two samples. The t-score t , gave the means of the first and second samples, X_1 and X_2 , with n being the sizes of both X_1 and X_2 with S_p , the pooled standard deviation is shown in Equation (2).

$$t = \frac{x_1 - x_2}{s_p \sqrt{\frac{2}{n}}} \quad (2)$$

In this study, X_1 and X_2 are the means of the forecasted and actual values for rainfall in each week. The pooled standard deviation S_p provided the standard deviations in samples S_1^2 and S_2^2 , with n_1 and n_2 representing the sample size of the first and second group as provided by Equation (3).

$$S_p = \sqrt{\frac{(n_1-1)S_1^2 + (n_2-1)S_2^2}{n_1 + n_2 - 2}} \quad (3)$$

III. RESULTS AND DISCUSSION

A. Rainfall Data Preparation Results

In the preparation of the rainfall data for the SVRM model design, the rainfall data used in the study was selected, cleaned, represented and partitioned. Rainfall Data from 2013 to 2017 was exported as a .csv file from the ARG installed in Rogongon, Iligan City (Latitude: 8.232697, Longitude: 124.419372) on February 12, 2013. The attributes referring to location (LOCATION), latitude (LATITUDE), longitude (LONGITUDE), elevation (ELEVATION), and date of

installation (DATE INSTALLED) were removed since it plays insignificant contribution to the learning process. A delimiter on semicolon was then used to separate the attribute of a single data unit for the date, time of reading and the rainfall amount (DATE/TIME READ; RAINFALL AMOUNT). Shown in Table II is the format for the 163, 777 rows of data having its respective date, time, and rainfall. The dataset was partitioned into 80% training set and 20% testing set and was then converted into .arff to be suited for WEKA.

TABLE II. FORMAT OF THE DATASET

DATE / TIME	RAINFALL
NN/NN/NNNN 00:15	NN
NN/NN/NNNN 00:30	NN
NN/NN/NNNN 00:45	NN
NN/NN/NNNN 01:00	NN

B. SVRM Model Design Results

Kernel functions plays a central part in the assimilation of data and transforming such data for pattern discovery. Thus, which kernel would be most suitable depends upon the data that the kernel would use [13], [18]. The study evaluated the Linear Function kernel, which is an excellent kernel function for linearly separable data sets, and the RBF kernel, which excels with nonlinear data sets [3], [6], [13]. To determine if a Linear or RBF kernel function will be used in the final model, the researchers evaluated the MSE value the function kernels were able to yield. Table III shows the results of the kernel selection process which the study utilized the parameter values produced by Grid Search as reference parameter values.

TABLE III. GRID SEARCH RESULT

COST	GAMMA	ACCURACY
100	10	91%

As shown in Table IV, the Cost value of 100 and the Gamma value of 10 were obtained through the Grid Search procedure. The accuracy was calculated using an 80/20 split, with 80% of the training set and 20% of the testing set yielding a 91% accuracy on the testing set. To calculate the MSE of the Linear and RBF kernels, the Cost and Gamma values obtained during the Grid Search procedure were then used as reference parameter values.

TABLE IV. COMPARISON BETWEEN LINEAR AND RBF KERNELS

LINEAR PARAMETER	LINEAR MSE VALUE	RBF PARAMETERS	RBF MSE VALUE
Cost (C) = 100	MSE > 100	Cost (C) = 100 Gamma (g) = 10 Loss Function (e) = 0.1 Epsilon (p) 0.001	3.6377

Kernel parameters were employed in nonlinear feature mapping to govern the trade-off between margin maximization and error minimization. The hyper parameters regulate the model's training process and have a significant impact on the SVRM forecasting model's development and test performance [12], [18]. The hyper parameters control the training process of the model and have an extensive effect in the development and

resulting test performance of the SVRM forecasting model. The results shows that RBF kernel yielded an MSE of 3.6377 while the linear kernel yielded an extensive MSE value of greater than 100. This could only mean that the data set was not linearly separable but is nonlinear in nature. In the behavior of the data used in this study, RBF was found to be more accurate. As such, RBF kernel function was the choice for the SVRM modelling.

This study compared Grid Search and Exhaustive Search methodologies to determine the best fit parameter combination and to validate Grid Search methodology's reliability and compatibility with the LibSVM library and WEKA forecasting software. After conducting Grid Search and Exhaustive Search testing, the parameter combination values MSE's were recorded, and the results are presented in Table V and VI. The performance of an SVRM forecasting model relies on three key parameters. The key parameter (C) is a parameter that allows the trade-off between training error and model complexity, parameter (C) defines the penalty for errors. If the value of parameter (C) is too big there would be the likelihood of overfitting a model. Whilst having a smaller (C) parameter value may result to the underfitting of a model and increase the number of training errors. The parameter (g) influences the hyper-line flexibility while parameter (e) controls the width of the ϵ -insensitive zone, used to fit the training data. If the value of parameter (e) is big, this will result in having fewer support vectors selected, and will result in a flatter or less complex regression estimates. Results of the Grid Search produced a Cost of 100 and a Gamma of 10 and yielded an MSE of 3.637. While Exhaustive Search produced a Cost of 100 and a Gamma of 1 and yielded an MSE of 3.6377 as observed in Table IV. Although Exhaustive Search yielded the lower MSE among the two methodology's the difference between the two is only 0.0004, a small difference. From the tested models shown, it can be noted that both parameters set values can be applied in the final model. The researchers opted for the parameter results yielded by the exhaustive search with $c=100$; $g=1$; $e=0.1$; $p=0.001$ for the final model.

TABLE V. CONSTANT PARAMETER VALUES

INSENSITIVE LOSS (e)	EPSILON (p)
0.1	0.001

TABLE VI. GRID SEARCH RESULT

COST	GAMMA	MSE
100	10	3.637

The researchers provided a feature range of exponents for the Grid Search. For Cost (C) = {0.0001, 0.001, 0.01, 0.1, 1, 10, 100} and for Gamma (g) = {0.0001, 0.001, 0.01, 0.1, 1, 10, 100, 1000}. The search was tested for all 56 combinations of Cost and Gamma. Grid Search is tested for each combination, evaluating for each of the combinations MSE. The Grid Search process ended with the parameter combination of Cost (C) = 100 and Gamma (g) = 10, with an MSE of 3.637, the lowest MSE determined by the Grid Search process out of the 56 possible combinations. The researchers also tested tuning the parameter using a more practical approach to the process. Like Grid Search, the researchers tested all 56 combinations for

Cost and Gamma ($C=\{10^{-4}, 10^{-3} \dots 10^1, 10^2\}$; $g=\{10^{-4}, 10^{-3} \dots 10^2, 10^3\}$) manually using MSE to find the combination with the lowest MSE. The search ended with parameter combination of Cost (C) = 100 and Gamma (g) = 1, with an MSE of 3.6366. The procedure entails analyzing two lag variable values, each of which will use rainfall data from the previous four years, seven months, and thirty days in 15-minute intervals. The first lag variable value (Lag Variable I) produced a per-12-hour report with lags up to 672-time steps (i-672) in the past, with I representing the model's current date. The second lag variable value (Lag Variable II) provided a per-12-hour report with lags as far back as 2976-time steps (i-2976). The testing set was used to determine the lag values. The MSE result for each lag variable value in each 15-minute cycle is shown in Table VII for each 12-hour report. The accuracy of Lag Variable I is better. Although Lag Variable I had the lower MSE score, it is worth noting that the difference between it and Lag Variable II is only about 0.00247.

TABLE VII. 12 HOUR-AHEAD MSE VALUES

DATE / TIME	LAG VARIABLE I	LAG VARIABLE II
10/31/2017 0:00	3.6387	3.6388
10/31/2017 0:15	3.6387	3.6389
10/31/2017 0:30	3.6387	3.639
10/31/2017 0:45	3.639	3.6391
---	---	---
---	---	---
10/31/2017 23:15	3.6436	3.6436
10/31/2017 23:30	3.6437	3.6437
10/31/2017 23:45	3.6438	3.6439
MSE	3.64129	3.64154

C. SVRM Model Evaluation

The optimal lagged variable was chosen after thorough test and comparison. The results show that Lag Variable I with the value of i-672 yields slightly better results than Lag Variable II (i-2976) making it a viable option for a model. The lowest MSE is achieved after tuning the cost value to 100 and gamma value to 1 which is optimal based on the training set used. The test shows a 0.0247 difference between Grid Search using RBF kernel with 3.6377 MSE value compared to 3.6366 MSE value of manual tuning. The training set produced an average of 3.641315 MSE value with minimum and maximum value 3.6387 and 3.6439 respectively using Lag Variable I. The values produced were relatively high for MSE due to the nature of the training set. As shown in Table VIII, the data yielded a t-value of 3.95426E-74. The p-value $p = 0.05$ by default which means the forecasted data is acceptable if the margin of error is less than 5%. The researchers used a total of 58 data points by using 29 data points from forecasted and actual data sets. The degrees of freedom $df = 56$ (degrees of freedom is number of datapoints minus 2) with its critical value 1.673 is used in assessing the H_0 where H_0 is not rejected since the t-value is less than the critical value. This shows that the predicted values have no statistically significant difference from the actual values. The low t-value also means that the difference between the actual and forecasted values is extremely small and the error becomes insignificant.

TABLE VIII. SNAPSHOT OF THE STUDENT'S T-TEST

DATE / TIME	ACTUAL	PREDICTED
10/01/2017 0:00	2.434331	2.3236
10/01/2017 0:15	2.434833	2.3235
10/01/2017 0:30	2.435335	2.3235
10/01/2017 0:45	2.435837	2.3234

Visual representation of the rainfall data exhibits the minimal differences between the actual and forecasted values from the validation set with the lines of the graphs overlapping except for the time intervals with the values equal to 0. The pattern being generated in Fig. 3 shows that the average predicted rainfall values were close to the actual rainfall values. This indicates that the model was able to create an accurate prediction result for the average rainfall value for the validation set [3], [9], [10], [15]. However, having an accurate prediction result in the first and middle half of the data set does not mean that the prediction accuracy will not drop. It is worth noting the fact that regardless of the magnitude of the error, an error will still propagate further errors which will eventually drop the prediction accuracy further down the timeline, especially when the number of units of the predicted values are overstretched. Shown in Fig. 4, the pattern generated shows that a significant error ensued in the beginning of the prediction result. The error continued along the timeline further dropping the accuracy of the result. The model was not able to accurately predict the maximum rainfall value for the data set. This indicate that the model was not able to predict certain change in the data value which in this case are the sudden increase in the value of rainfall due to sudden heavy rain down pour.

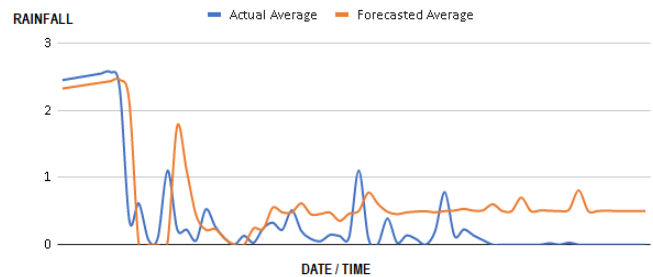


Fig. 3. Average Actual and Forecasted Rainfall.

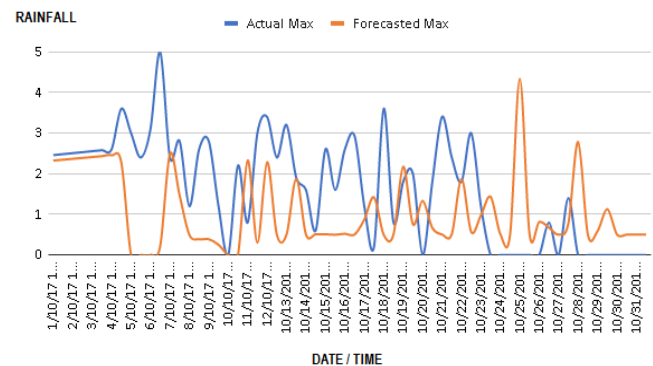


Fig. 4. Maximum Actual and Forecasted Rainfall.

IV. CONCLUSION AND RECOMMENDATIONS

This study attempted to implement a rainfall forecasting strategy using SVRM by performing data preparation, SVRM model design, model implementation and testing the forecasted results for performance evaluation and model validation. On the data preparation process, data correction and representation of the dataset greatly affects the outcome of the data being predicted. Manual vision inspections were conducted and were able to remove irrelevant dates with missing values which results into a number of 163,777 rows. In SVRM model design, it was found out that in order to produce a good forecasting outcome, the right values must be identified for parameters cost and gamma, along with a kernel function that will fit the data set along with a lag variable value that can optimally determine the relationship between the past and current values of the data set. The rainfall dataset was tested with both linear and RBF kernel functions. The data set was first tested with RBF kernel function with temporary base parameter values for cost and gamma identified with the use of Grid Search, the temporary base parameter values were Cost (C) = 100 and Gamma (g) = 10 with an accuracy of 91% resulting to a MSE value of 3.6377. The data set was then tested with the linear kernel function using the same base parameter values and resulted in an MSE value greater than 100. The researchers concluded that the data set was non-linear in nature and is not linearly separable. Thus, the model utilized RBF as its selected kernel function. The second phase of the selection involved selecting the best parameter values for cost and gamma. The study utilized two tuning techniques for the selection process; the following were the Grid Search and Exhaustive Search techniques. Tuning was first tested using Grid Search, the search produced values of Cost (C) = 100 and Gamma (g) = 10 with an MSE value of 3.637. The second tuning was then tested using Exhaustive Search with a feature space range for Cost (C) = {0.0001, 0.001, 0.01, 0.1, 1, 10, 100} and Gamma (g) = {0.0001, 0.001, 0.01, 0.1, 1, 10, 100, 1000}. Exhaustive search produced the lower MSE value of 3.6366 with values for Cost (C) = 100 and Gamma (g) = 1. The results yielded in only an MSE value difference of 0.0004, a very small difference. It can be concluded that both tuning techniques can be utilized for tuning parameters in the creation of the SVRM model design. However, the researchers opted for the parameter set values yielded by Exhaustive Search parameter tuning in the final model. The last phase of the selection process involved the selection of a lag variable value. The lag variable determines the past and current relationship of a data series in a particular timeframe. The study tested two variable values; Lag Variable I and Lag Variable II. Lag Variable I have a per-12-hour report with lags up to 672-timesteps (i-672) in the past, while Lag variable II has a per-12-hour report with lags up to 2976-time steps (i-2976) in the past. Lag variable I was first tested and produced an MSE value of 3.641315, while Lag variable II produced an MSE value of 3.651315 in the second test. Though Lag Variable I yielded the lower MSE score, it is also worth noticing that it only differs by a small variance of approximately 0.00247 when compared with Lag Variable II. This is an indication that Lag Variable II is also a promising Lag Variable value for the SVRM forecasting model. The final model utilized Lag variable I for the final model.

It is recommended that a different rainfall dataset from a non-tropical country be used to validate the SVRM models presented in this study. Having datasets with a vast difference of rainfall values is expected affect the performance of the model which in turn affects the accuracy, behavior and performance of the SVRM. Tropical climate like that of the Philippines having only wet and dry seasons anytime within the year records a different rainfall behavior from geographies having four seasons. The researchers would also like to recommend for further studies on the aspect of kernel, lag variable and architecture selection. Further studies on these processes will help optimize the performance of the SVRM in rainfall forecasting. Aside from WEKA, other SVRM development frameworks could also be used to expand model performance analysis conducted in this research. One or more SVRM development frameworks can be compared with the model results of presented in this study as well as conducting a contrast if other development frameworks have better or the same performance with that of WEKA. Overall, the results of this study showed that SVRM has the potential to be a viable rainfall forecasting model given the proper data preparation, model kernel function selection, model parameter value selection and lag variable selection.

ACKNOWLEDGMENT

The authors would like to thank the support of the Mindanao State University-Iligan Institute of Technology (MSU-IIT) Office of the Vice Chancellor for Research and Extension for their assistance in this study. This work is supported by MSU-IIT as an internally funded research under the Premier Research Institute of Science and Mathematics (PRISM)- Applied Mathematics and Statistics (AMS) Research Group. The authors would also like to thank the Philippines Department of Science and Technology - Advance Science and Technology Institute (DOST-ASTI) for the data used in this study.

REFERENCES

- [1] J. M. West et al., "U.S. Natural Resources and Climate Change: Concepts and Approaches for Management Adaptation," *Environmental Management*, vol. 44, no. 6, p. 1001, 2009, doi: 10.1007/s00267-009-9345-1.
- [2] R. Muhammad and J. Mahmmud, "Rainfall Event Analysis for Urban Flooding Study Using Radar Rainfall Data," 2015. [Online]. Available: www.jzs.uos.edu.krd.
- [3] N. Hasan, N. C. Nath, and R. I. Rasel, "A support vector regression model for forecasting rainfall," in 2015 2nd International Conference on Electrical Information and Communication Technologies (EICT), 2015, pp. 554–559. doi: 10.1109/EICT.2015.7392014.
- [4] M. Mokhtarzad, F. Eskandari, N. Jamshidi Vanjani, and A. Arabasadi, "Drought forecasting by ANN, ANFIS, and SVM and comparison of the models," *Environmental Earth Sciences*, vol. 76, no. 21, p. 729, 2017, doi: 10.1007/s12665-017-7064-0.
- [5] A. Pozdnoukhov, G. Matasci, M. Kanevski, and R. S. Purves, "Spatio-temporal avalanche forecasting with Support Vector Machines," *Natural Hazards and Earth System Sciences*, vol. 11, no. 2, pp. 367–382, 2011, doi: 10.5194/nhess-11-367-2011.
- [6] D. Boswell, "Introduction to Support Vector Machines," 2002.
- [7] Y. Lin, Y. Lee, and G. Wahba, "Support Vector Machines for Classification in Nonstandard Situations," *Machine Learning*, vol. 46, no. 1, pp. 191–202, 2002, doi: 10.1023/A:1012406528296.
- [8] C.-H. Wu, J.-M. Ho, and D. T. Lee, "Travel-time prediction with support vector regression," *IEEE Transactions on Intelligent*

- Transportation Systems, vol. 5, no. 4, pp. 276–281, 2004, doi: 10.1109/TITS.2004.837813.
- [9] A. El-Shafie, M. Mukhlisin, A. A. Najah, and M. R. Taha, “Performance of artificial neural network and regression techniques for rainfall-runoff prediction,” *International Journal of Physical Sciences*, vol. 6, no. 8, pp. 1997–2003, Apr. 2011, doi: 10.5897/IJPS11.314.
- [10] J. Du, Y. Liu, Y. Yu, and W. Yan, “A prediction of precipitation data based on Support Vector Machine and Particle Swarm Optimization (PSO-SVM) algorithms,” *Algorithms*, vol. 10, no. 2, Jun. 2017, doi: 10.3390/a10020057.
- [11] E. G. Ortiz-García, S. Salcedo-Sanz, and C. Casanova-Mateo, “Accurate precipitation prediction with support vector classifiers: A study including novel predictive variables and observational data,” *Atmospheric Research*, vol. 139, pp. 128–136, 2014, doi: <https://doi.org/10.1016/j.atmosres.2014.01.012>.
- [12] J. Zhang, X. Qiu, X. Li, Z. Huang, M. Wu, and Y. Dong, “Support Vector Machine Weather Prediction Technology Based on the Improved Quantum Optimization Algorithm,” *Computational Intelligence and Neuroscience*, vol. 2021, p. 6653659, 2021, doi: 10.1155/2021/6653659.
- [13] J. July, D. Ben, A. Mezghani, S. Zribi Boujelbene, and N. Ellouze, “Evaluation of SVM Kernels and Conventional Machine Learning Algorithms for Speaker Identification.”
- [14] H. Fizazi Izabatene, W. Benhabib, and S. Ghardaoui, “Contribution of Kernels on the SVM Performance,” *Journal of Applied Sciences*, vol. 10, no. 10, pp. 831–836, 2010.
- [15] G. Adhani, A. Buono, and A. Faqih, “Optimization of Support Vector Regression using Genetic Algorithm and Particle Swarm Optimization for Rainfall Prediction in Dry Season,” *TELKOMNIKA Indonesian Journal of Electrical Engineering*, vol. 12, no. 11, Nov. 2014, doi: 10.11591/telkomnika.v12i11.6518.
- [16] M. v Shcherbakov, A. Brebels, A. Tyukov, T. Janovsky, and V. Anatol, “A Survey of Forecast Error Measures,” 2013.
- [17] H. Wang and D. Xu, “Parameter Selection Method for Support Vector Regression Based on Adaptive Fusion of the Mixed Kernel Function,” *Journal of Control Science and Engineering*, vol. 2017, p. 3614790, 2017, doi: 10.1155/2017/3614790.
- [18] A. Villa, M. Fauvel, J. Chanussot, P. Gamba, and J. A. Benediktsson, “Gradient Optimization for multiple kernel’s parameters in support vector machines classification,” in *IGARSS 2008 - 2008 IEEE International Geoscience and Remote Sensing Symposium*, 2008, vol. 4, pp. IV-224-IV-227. doi: 10.1109/IGARSS.2008.4779698.

Using Decision Tree Classification Model to Predict Payment Type in NYC Yellow Taxi

Hadeer Ismaeil, Sherif Kholeif, Manal A.Abdel-Fattah
Information Systems Department, Faculty of Computers and Artificial Intelligence
Helwan University, Cairo, Egypt

Abstract—The taxi services are growing rapidly as reliable services. The demand and competition between service providers is so high. A billion trip records need to be analyzed to raise the spirit of competition, understand the service users, and improve the business. Although decision tree classification is a common algorithm which generates rules that are easy to understand, there is no implementation for classification on taxi dataset. This research applies the decision tree classification model on taxi dataset to classify instances correctly, build a decision tree, and calculate accuracy. This experiment collected decision tree algorithm with Spark framework to present the good performance and high accuracy when predicting payment type. Applied decision tree algorithm with different aspects on NYC taxi dataset results in high accuracy.

Keywords—Big data analytics; apache spark; decision tree classification; taxi trips; machine learning

I. INTRODUCTION

Big data describes the large volume of data, but there's no rule strictly defines the size of data. What really determines that the data is big, is the need for multiple physical or virtual devices to process this data as fast as possible. In [1], this data is generated by everything around us like systems, digital devices, and remote sensors. Big data is used for collecting and analyzing large and complex data sets to produce knowledge. In the past, storing, processing, and analyzing this volume of data were a problem; but new technologies solved this problem [2].

One of the tools that are used to analyze data is Apache Spark, which is open-source data analytics tools. Spark is based on MapReduce, but it's faster as it stores the data in the memory into RDD (Resilient Distributed Databases) [3]. Fig. 1 represents the difference between Spark and Hadoop performance.

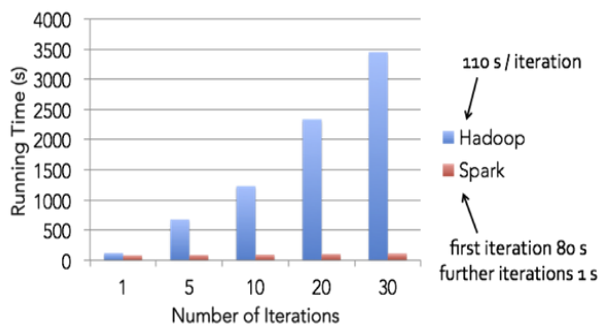


Fig. 1. Spark and Hadoop Performance. [3].

When talking about machine learning, Spark has two types of machine learning libraries: Spark MLlib, and Spark ML. Spark MLlib is the original API and it is based on RDD API, so it has more features than the new API (Spark ML). Spark ML provides high-level API, and it is based on data frames and dataset; it supports pipeline and easier to construct. Spark MLlib focuses on the basics of the algorithm leaving data preparation and pipelines to the user, but Spark ML works on all those aspects from data preparation to model training. Spark MLlib is the best choice when dealing with a stream of data. The new features will be added to Spark ML and this why this research will use Spark ML. [4].

Spark ML is based on pipeline concept which uses different stages to perform separate tasks from data cleaning to feature selection and applying machine learning algorithm. Pipeline stages consist of two basics transformers and estimators. Transformers use transform method which takes a data set as input and returns an enhanced dataset as a result. Estimators, when fit, returns a transform, it uses the fit method on data set to produce a model. A decision tree is an estimator that trains dataset to produce a model [4].

Classification is an important technique for assigning a data object to predefined class or category. One of the most commonly used algorithms, used to apply a classification technique, is the Decision tree algorithm. Decision tree one of the important algorithms in Classification technique. It builds a tree model. Decision tree algorithm is popular because it's easy to implement and understand. In addition, it is simple and fast to construct compared to other classification algorithms.

Decision tree algorithms extract knowledge from data, present it graphically and produce a clear and understandable rule. It is one of the most powerful and popular algorithms that can handle continuous and categorical variables using less computation. The most common used decision tree algorithms are ID3, C4.5, and CART. C4.5 is an improved version of ID3. [5][6].

Transportation plays a vital role in human life especially Taxi and Car services. As a business, it is a huge industry. Every minute there is a hundred of trips from just a single zone, which create a huge amount of data [7] [8]. NYC Taxi and Limousine commission provides an open Dataset that includes detailed trip record from NYC yellow taxi through 2017. Predicting payment method is considered important to business. Customers add their credit card only in trusted services. The greater the number of registered or used credit cards, the higher the service reliability is. It is also important to

the driver to know the payment method as some drivers prefer cash and others prefer credit for guaranteed payment. This dataset can be used to predict a lot of things like passenger count, Hotspot to reduce peak factor, Rush hour for extra charges and high demand at a specific time.

II. BACKGROUND

A. Big Data Analytics

The concept of big data has been around for years, and most firms now realize that if they capture all the data that flows into their operations, they can use analytics to extract tremendous value. Big data analytics assists businesses in harnessing their data and identifying new opportunities. As a result, smarter business decisions, more effective operations, higher profits, and happier consumers are the result. Big data analytics is the often-difficult process of analyzing large amounts of data to identify information such as hidden patterns, correlations, market trends, and customer preferences that can assist businesses in making better decisions. Data analytics tools and approaches provide organizations with a way to evaluate data sets and obtain new information on a large scale. Basic questions regarding business operations and performance are answered by business intelligence (BI) queries. Big data analytics is a type of advanced analytics that entails complicated applications that use analytics systems to power aspects like predictive models, statistical algorithms, and what-if analyses [9].

Without the right tools, methods, and techniques, big data analytics can be time-consuming, difficult, and computationally demanding. When the amount of data is too large to analyze and analyze on a single machine, Apache Spark and Apache Hadoop can help by using parallel and distributed processing. It is critical to first comprehend the concept of "big data" to comprehend the significance of parallel and distributed processing. The fast rate at which big data is generated necessitates that it be processed quickly, and the variety of big data implies that it contains several data kinds, including structured, semi-structured, and unstructured data. Because of the amount, velocity, and variety of big data, new, novel methodologies, and frameworks for collecting, storing, and analyzing the data were developed, which is why Apache Hadoop and Apache Spark were formed.[10].

B. Big Data Analytics Tools

Understanding parallel and distributed processing helps in understanding big data analytics tools and how they are used. Because both parallel processing and distributed processing entail breaking down computation into smaller sections, the two can be confused. The memory architecture distinguishes parallel computing from distributed computing. Parallel computing is the use of several processors to solve a problem at the same time. Distributed computing is the use of multiple computers to solve a problem at the same time. Because distributed computing is disk-based rather than memory-based, parallel computing processes have access to the same memory space as distributed computing workloads. Some distributed computing operations are performed on a single computer, while others are performed on multiple computers. Apache Hadoop and Apache Spark are both open-source systems for

big data processing, although they differ in important ways. Hadoop processes data using MapReduce, whereas Spark employs resilient distributed datasets (RDDs). Hadoop uses a distributed file system (HDFS), which allows data files to be stored on several machines. Because servers and machines may be added to accommodate increasing data quantities, the file system is scalable. Because Spark lacks a distributed file storage system, it is mostly utilized for computation on top of Hadoop. Spark does not require Hadoop to run, although it can be used with Hadoop because it can construct distributed datasets from HDFS files. Spark does not provide a distributed file storage system; it is mostly utilized for computation on top of Hadoop. Spark does not require Hadoop to run, although it can be used with Hadoop because it can construct distributed datasets from HDFS files. The performance gap between Hadoop and Spark is significant. UC Berkeley researchers noticed that Hadoop is wonderful for batch processing but inefficient for iterative processing, so they invented Spark to address this. Spark program iteratively run 100 times quicker in memory than Hadoop and 10 times faster on disc. Spark's quickness is attributed to its in-memory processing. Instead, Hadoop MapReduce sends data to disc, which is read on the next iteration. It is substantially slower than Spark because data is reloaded from disc after each iteration [11].

C. Apache Spark MLlib

MLlib, an Apache Spark machine learning library, covers the major machine learning methods such as classification, clustering, regression, dimensionality reduction, transformers, and collaborative filtering. Some machine learning techniques can be applied to streaming data, which is useful for Spark Streaming applications [12].

D. Classification

Classification is a method of locating models that describe multiple data classes or concepts. By performing analysis, The class labels that are known for a set of training data or data objects during this model can be obtained. The primary goal of this model is to properly anticipate an unknown object's class label. The classification problem should include some input that is regarded as training data with class labels and is utilized to determine the class label for unlabeled test data or instances.

The primary challenge for categorization is data preparation. This procedure includes the following steps: selecting, pre-processing, data cleaning, data integration and transforming.

Decision Trees are the most common classification algorithms. A decision tree is described as a flow chart with a tree structure that includes a root node, non-leaf nodes, and leaf nodes. Each non-leaf node describes a test attribute, each branch describes a test outcome, and each leaf node retains the class label. The basic idea behind the decision tree is to divide the data recursively into subsets with the final goal of having each subset contain nearly homogeneous states of the target variable. The attribute selection measure must choose a splitting criterion that "best" separates the given dataset. Some well-known decision tree algorithms include ID3, C4.5, and CART, which use the Information Gain, Gain Ratio, and Gini Index as attribute selection measures, respectively. C5 is also a decision tree-based algorithm that is an improved version of

C4.5. When the decision tree is built, it is used to categorize another new instance by traversing from the root node to the leaf node and applying the test criteria at each non-leaf node. Each instance's class is the class of the leaf node [6].

III. RELATED WORK

In [6], B. Charbuty, et. al. studied and compared the most popular decision tree algorithms, ID3, C4.5, CART, CHAID, and QUEST as the most common data classifier. Literature review related to Decision Tree was presented. The literature review compared different research papers work in terms of year of study, dataset, techniques, or algorithms used on the predefined dataset, and the resulted accuracy. The literature reviews the most recent research papers applied in different areas/datasets like medical, text classification, user smartphones classification, etc. this study proves the efficiency of decision tree in creating efficient and understandable rules and achieving high accuracy.

In [13] B. Roy, et. Al. applied a set of machine learning algorithm to predict trip duration between two locations. One of the algorithms used in this research was Decision tree Regression Model with varying max depth parameter and default values for other hyperparameters. Decision tree regression model with the biggest max depth achieved the best accuracy compared to the lower max depth. But other regression achieved better accuracy than decision tree regression model with different max depth.

In [14], S. Singh, et. al. studied and compared the most popular decision tree algorithms, ID3, C4.5, and CART. The survey described the advantage and disadvantage of each algorithm. The survey also contains a comparison between characteristics of each algorithm like the type of data suitable for each algorithm, speed, dealing with missing values and splitting formula. It also shows some application of decision tree such as business, industry, medicine and so on. Common datasets, tools, and problems of decision tree were introduced. The final observation of the survey was the dependency of splitting formula and dataset feature with the performance of the algorithm.

In [15], H. Sun, et. al. described how taxi data was collected through sensors and GPS. They analyzed taxi data to extract and filter data to get a valuable information and results. The results from analysis helped them propose a new application that adds new benefits to the taxi passengers and drivers. They described data attributes and how they used big-data tools to extract useful information, so they can notice relations between attributes. The analysis steps were described briefly to produce analysis results and patterns that was helpful to their mobile service.

In [16], X. Meng, et. al. discussed MLlib (machine learning library) and the need of this library to benefit from the great wealth of data nowadays. They described how spark is efficient with machine learning algorithms as it is iterative in nature. They also discussed other advantages of integrating MLlib with Spark. They presented the history of spark and MLlib development. They discussed briefly core features, performance, Scalability, and continuous improvements of MLlib library.

In [17], S. Salloum, et. al. presented the importance of big data analytics, Spark framework, and how Spark was initiated. They also presented the core features of Spark, Spark Components, how Apache Spark is perfect when dealing with iterative analysis and algorithms, and Apache Spark case studies in industry. They described Spark API's and Libraries and compared different libraries, compared machine learning packages (spark.ml and spark. MLlib), and the use of each of them. Other features and packages were introduced like Graph analysis, stream processing, batch streaming, and interactive analytics.

IV. DATASET

The dataset describes yellow taxi trips throughout January 2017. NYC Taxi and Limousine Commission (TLC) shares a billion of data through their website [18].

This data was collected by technology providers authorized under the Taxicab & Livery Passenger Enhancement Programs (TPEP/LPEP) and provided to NYC Taxi and Limousine Commission. This data was not generated but collected from real life. This dataset contains 1048575 trip records. Each trip record contains a timestamp for pickup and drop-off, the id of the vendor that provided the record, pickup and drop-off location, passenger count, trip distance, payment type and detailed information about the amount paid by the passengers. Data dictionary was illustrated in Table I.

TABLE I. DATA DICTIONARY

Attribute Name	Description
Vendor ID	A code indicating the TPEP provider that provided the record. 1= Creative Mobile Technologies, LLC. 2= VeriFone Inc.
pickup Date Time	The date and time when the meter were engaged, it was categorized based on hour interval 0:3 = a; 4:7=b; 8:11=c; 12:15=d; 16:19=e; 20:23=f.
Dropoff Date Time	The date and time when the meter were disengaged, it was categorized based on hour interval 0:3 = a; 4:7=b; 8:11=c; 12:15=d; 16:19=e; 20:23=f.
Passenger Count	The number of passengers in the vehicle. The driver enters this value.
Trip Distance	The elapsed trip distance in miles reported by the taximeter.
PULocation ID	TLC Taxi Zone in which the taximeter was engaged
DOLocation ID	TLC Taxi Zone in which the taximeter was disengaged
Rate Code ID	The final rate code in effect at the end of the trip. 1= Standard rate 2=JFK 3=Newark 4=Nassau or Westchester 5=Negotiated fare 6=Group ride
Store and Fwd. Flag	This flag indicates whether the trip record was held in vehicle memory before it is sent to the vendor, aka "store and forward," because the vehicle did not have a connection to the server. Y= store and forward trip

	N= not a store and forward trip
Payment Type	A numeric code signifying how the passenger paid for the trip. 1= Credit card 2= Cash 3= No charge 4= Dispute 5= Unknown 6= Voided trip
Fare Amount	The time-and-distance fare calculated by the meter.
Extra	Miscellaneous extras and surcharges. Currently, this only includes the \$0.50 and \$1 rush hour and overnight charges.
MTA Tax	\$0.50 MTA tax that is automatically triggered based on the metered rate in use
Improvement Surcharge	\$0.30 improvement surcharge assessed trips at the flag drop. The improvement surcharge began being levied in 2015
Tip Amount	Tip amount – This field is automatically populated for credit card tips. Cash tips are not included, this column was categorized: 0.0 = no tips; 1.0 = tips
Tolls Amount	Total amount of all tolls paid in trip.
Total Amount	The total amount charged to passengers (Does not include cash tips).

In Fig. 2, a 2D correlation matrix was presented to declare the relations between the data variables.

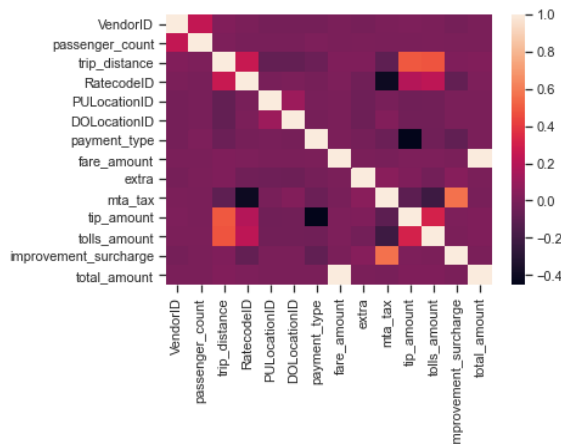


Fig. 2. Covariance Heatmap.

V. DATA PREPARATION

In the dataset, first, the total amount column was removed because this column has a high correlation with other columns. Second, The Improvement surcharge column were removed because it has a constant value. Third, pickup-Date-Time and drop-off-Date-Time is timestamp column with thousands of unique instances, so dividing it into categories was the best solution for this research and each category has a range of hours. Fig. 3 introduces the framework of applying decision tree algorithm on taxi dataset.

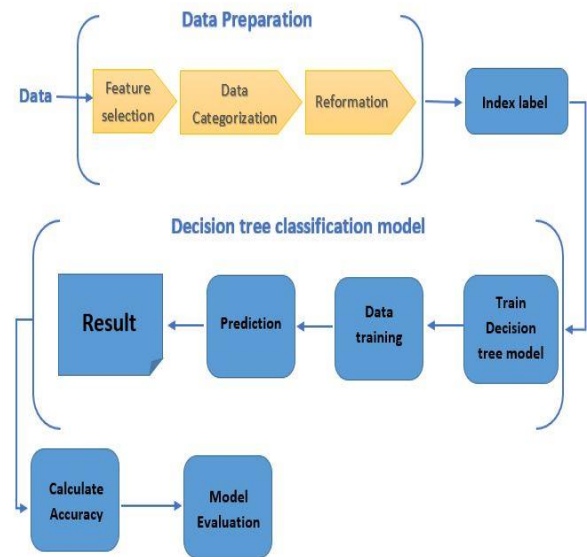


Fig. 3. The Framework of Applying Decision Tree Algorithm on Taxi Data.

VI. CLASSIFICATION ON SPARK

In [19] K. Zhao, et. al. they analyzed Uber and yellow taxi samples in NYC using three predictors: Neural Network, Markov predictor, and Lempel-Ziv-Welch predictors. They calculated accuracy based on different features; Neural Network was the only machine learning based method used in this comparison. Until now, there are not enough research papers applied in this dataset. Although Classification achieved good accuracy when applied in different applications like healthcare and business [20] [21] [22], and also decision tree was used in different applications and achieved high accuracy [5] [23], decision tree classification was not applied on taxi dataset yet. Based on those previous researches, decision tree classification was used with Apache Spark tool to calculate the accuracy of prediction. This research used Java language to apply classification algorithm on Apache Spark. This research used Spark version 2.2.1. When applying classification algorithm on taxi dataset, some issues appeared; some are related to the data as it needs some preparation before executing the algorithm and the others are related to the algorithm. After data preparation, the following steps were taken to apply the classification algorithm to NYC taxi dataset:

- 1) Load the data stored in JSON format.
- 2) Use “String Indexer Model” to index labels and add metadata to the label column.
- 3) Identify and index categorical feature.
- 4) Split the data into training and test sets of data.
- 5) Set Decision tree model.
- 6) Convert Indexed Labels to original labels.
- 7) Use Pipeline to chain indexer and tree.
- 8) Start training model and make prediction.
- 9) Compute test errors and accuracy.

VII. RESULTS

This model was executed in 5 minutes and 7.823 seconds. The algorithm was applied on 8GB Ram and 2 GHz processor core i7. The resulted accuracy of this model is 96.5%.

This research will use another evaluation metrics to evaluate this algorithm. There are four main categories that are used to calculate these metrics. In a supervised classification problem, there exists a true output and a predicted or model generated output. Therefore, the result of each data point will be assigned to one of the following categories:

- True Positive (TP): label is positive, and prediction is positive.
- True Negative (TN): label is negative, and prediction is negative.
- False Positive (FP): label is negative, but prediction is positive.
- False negative (FN): label is positive, but prediction is negative.

These four categories are the basics for most classification evaluation metrics. Metrics like precision and recall consider the type of error, while F-measure captures the balance between precision and recall and combine them to calculate F-measure. Precision (Positive Predictive Value) measures how many selected items from the dataset are relevant, while recall (True Positive Rate) measure how many relevant items are selected. For Example, if dataset contains 100 taxi trips containing 75 trips that were paid by credit cards and 25 trips were paid in cash. And let's suppose an algorithm for detecting credit card payment type identifies 60 trips paid with credit card, 55 were actually paid with a credit card (true positive) while the rest was paid in cash (false positive). Using the following formula, precision could be calculated as (PPV = $55/60 = 0.92$) and recall (TPR = $60/75 = 0.8$). High precision means that the algorithm returned relevant results more than irrelevant ones (from 60 trips the returned 55 that are really paid with credit card). High recall means that the algorithm returns most of the relevant results (there were 75 trips paid with a credit card in the dataset, but the algorithm identified only 55 trips).

$$PPV = \frac{TP}{TP+FP} \quad (1)$$

$$TPR = \frac{TP}{P} = \frac{TP}{TP+FN} \quad (2)$$

$$F = 2 \cdot \frac{\text{precision} \cdot \text{recall}}{\text{precision} + \text{recall}} \quad (3)$$

In binary classification, there are only two possible class labels. However, in Multiclass classification there are many class labels as in this research dataset, payment type are classified from 1 to 6 digits having 6 possible classes. Precision and recall were calculated for each class label then weighted precision, recall, and F-measure were calculated. The following table compares accuracy, test error, weighted precision, weighted recall, and weighted F-measure when changing the splitting criteria of the data into training and

testing set. In the first case, 10% of data was held for testing. In the Second case, 20% of data was held for testing and so on.

The decision tree is a gradual algorithm which performs a recursive partitioning for the feature. Each partition is selected gradually by selecting the best split from several possible splits to maximize the information gain of a tree node. The node impurity is a measure of dividing the training data of the labels at the node into relatively homogenous subsets. There are two impurity measures for classification: Gini impurity and Entropy. Next Graphs compares evaluation metrics in terms of different node impurity. The node impurity measures the labels homogeneity at the node with two main impurity measures for classification. Table III illustrates the Gini impurity and Entropy formulas.

This research will use splitting criteria (0.8, 0.2) 80% for the training set and 20% held for the testing set as it gets the best results compared to other splitting criteria in Table II. Table IV compare time and number of evaluation metrics when using different impurity measures. Fig. 4, Visualize the difference between accuracy of Gini impurity and accuracy of Entropy, Entropy achieves the best Accuracy. Fig. 5, Visualize the difference between precision of Gini impurity and precision of Entropy, Gini impurity achieves highest precision with a slight difference of 0.03. Fig. 6, Visualize the difference between recall of Gini impurity and recall of Entropy, Entropy achieves the highest recall. Fig. 7, Visualize the difference between f-measure of Gini impurity and f-measure of Entropy, Entropy achieves the highest f-measure.

TABLE II. EVALUATION METRICS FOR DIFFERENT SPLITTING CRITERIA

	Splitting criteria [0.9,0.1]	Splitting criteria [0.8,0.2]	Splitting criteria [0.7,0.3]
Accuracy	96.5%	96.6%	96.6%
Test error	3.5%	3.4%	3.4%
Weighted precision	96.47%	96.57%	96.52%
Weighted recall	96.53%	96.6%	96.56%
Weighted F-measure	96.3%	96.4%	96.3%

TABLE III. NODE IMPURITY FORMULAS

Impurity	Formula	Description
Gini impurity	$\sum_{i=1}^c f_i(1 - f_i)$	f_i is the frequency of label i at a node and C is the number of unique labels.
Entropy	$\sum_{i=1}^c -f_i \log(f_i)$	

TABLE IV. EVALUATION METRICS FOR NODE IMPURITY

	Gini impurity	Entropy
Time	5:45s	5:58s
Accuracy	96.53%	96.6%
Test error	3.5%	3.4%
Weighted precision	96.55%	96.52%
Weighted recall	96.52%	96.57%
Weighted F-measure	96.29%	96.34%

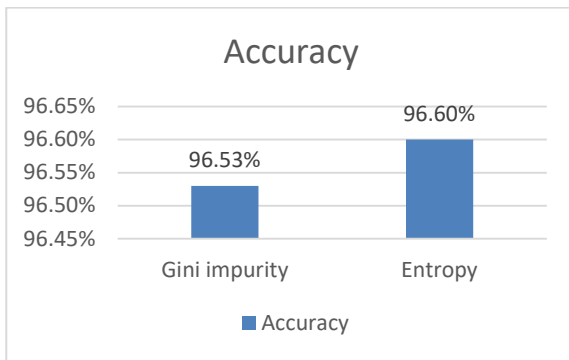


Fig. 4. Accuracy for Node Impurity.

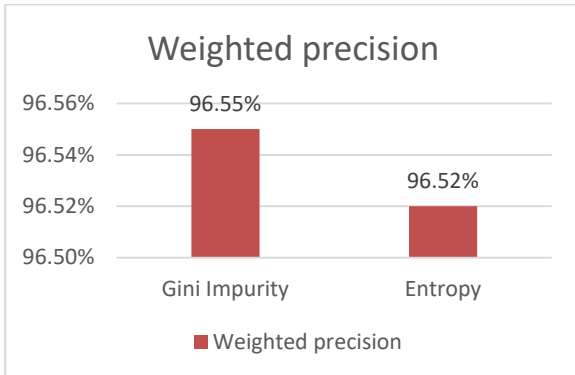


Fig. 5. Precision for Node Impurity.

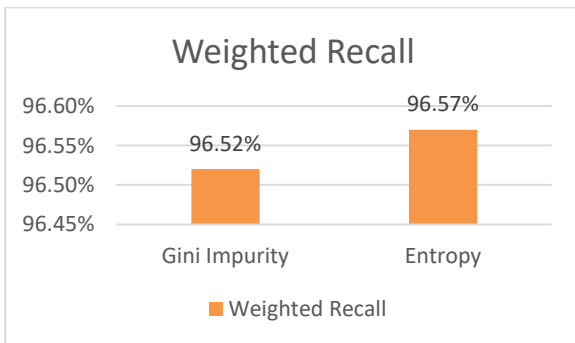


Fig. 6. Recall for Node Impurity.

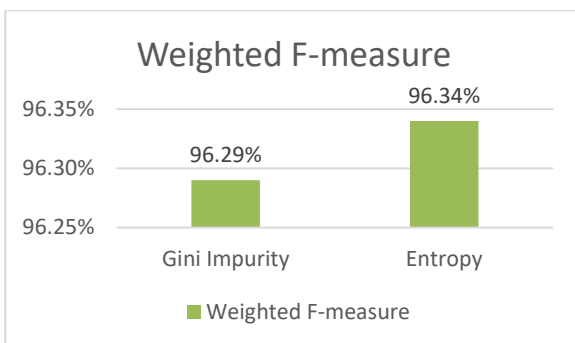


Fig. 7. F-measure for Node Impurity.

VIII. CONCLUSION

This research applied a decision tree classification model on NYC Taxi and Limousine Commission dataset to predict

payment type with varying hyperparameters. The dataset contains detailed taxi trips, and each trip record describes the vendor of the data record, passenger count, pickup and drop-off location and timestamp and detailed receipt. Accuracy, precision, recall and f-measure were calculated with different splitting criteria and different node impurity. The experiment shows a promising result as the accuracy and other evaluation metrics is higher than 96%. For future work, the Decision tree classification model can be applied to the same dataset to predict passenger count, rush hour to predict extra charges, and high demand in a specific time zone. Also, this model can be applied to car services in Egypt like Uber and Careem. An application of Grid search cross validation can be applied too to get the best hyperparameters for this dataset.

REFERENCES

- [1] An introduction to big data", *Opensource.com*, 2018. [Online]. Available: <https://opensource.com/resources/big-data>. [Accessed: 13-Sep-2018].
- [2] Che, D., Safran, M. and Peng, Z. (2013). From Big Data to Big Data Mining: Challenges, Issues, and Opportunities. *Database Systems for Advanced Applications*. 7827, 1-15.
- [3] L. Joseji, "6 Sparkling Features of Apache Spark! - DZone Big Data", *dzone.com*, 2014. [Online]. Available: <https://dzone.com/articles/6-sparkling-features-apache>. [Accessed: 24-Sep-2018].
- [4] H. Karau and R. Warren, High performance Spark. O'Reilly Media, 2017, pp. 219 - 251.
- [5] H. Sharma and S. Kumar, "A Survey on Decision Tree Algorithms of Classification in Data Mining", *International Journal of Science and Research (IJSR)*, vol. 5, no. 4, pp. 2094-2097, 2016.
- [6] B. Charbuty and A. Abdulazeez, "Classification Based on Decision Tree Algorithm for Machine Learning", *Journal of Applied Science and Technology Trends*, vol. 2, no. 01, pp. 20-28, 2021.
- [7] F. Wang, "Analysis of NYC Yellow Taxi data", NYC Data Science Academy Blog, 2016. [Online]. Available: <https://nycdatascience.com/blog/student-works/analysis-of-nyc-yellow-taxi-data/>. [Accessed: 11-Nov-2018].
- [8] M. Yazici, C. Kamga and A. Singhal, "A Big Data Driven Model for Taxi Drivers' Airport Pick-up Decisions in New York City", *2013 IEEE International Conference on Big Data*, pp. 37-44, 2013.
- [9] A. Kushwaha, A. Kar and Y. Dwivedi, "Applications of big data in emerging management disciplines: A literature review using text mining", *International Journal of Information Management Data Insights*, vol. 1, no. 2, p. 100017, 2021.
- [10] J. Wang, C. Xu, J. Zhang and R. Zhong, "Big data analytics for intelligent manufacturing systems: A review", *Journal of Manufacturing Systems*, 2021.
- [11] S. Kumar and M. Singh, "Big data analytics for healthcare industry: impact, applications, and tools", *Big Data Mining and Analytics*, vol. 2, no. 1, pp. 48-57, 2019.
- [12] M. Juez-Gil, Á. Arnaiz-González, J. Rodríguez, C. López-Nozal and C. García-Osorio, "Approx-SMOTE: Fast SMOTE for Big Data on Apache Spark", *Neurocomputing*, vol. 464, pp. 432-437, 2021.
- [13] B. Roy and D. Rout, "Predicting Taxi Travel Time Using Machine Learning Techniques Considering Weekend and Holidays", *Proceedings of the 13th International Conference on Soft Computing and Pattern Recognition (SoCPaR 2021)*, pp. 258-267, 2022.
- [14] S. Singh and M. Giri, "Comparative Study Id3, Cart and C4.5 Decision Tree Algorithm: A Survey", *International Journal of Advanced Information Science and Technology (IJAIST)*, vol. 3, no. 7, pp. 47-52, 2014.
- [15] H. Sun and S. McIntosh, "Big Data Mobile Services for New York City Taxi Riders and Drivers", *IEEE International Conference on Mobile Services*, pp. 57-64, 2016.
- [16] X. Meng, J. Bradley, B. Yavuz, E. Sparks, S. Venkataraman, D. Liu, J. Freeman, D. Tsai, M. Amde, S. Owen, D. Xin, R. Xin, M. J. Franklin, R.

- Zadeh, M. Zaharia and A. Talwalkar, "MLlib: Machine Learning in Apache Spark", *Journal of Machine Learning Research*, vol. 17, pp. 1235-1241, 2016.
- [17] S. Salloum, R. Dautov, X. Chen, P. Peng and J. Huang, "Big data analytics on Apache Spark", *International Journal of Data Science and Analytics*, vol. 1, no. 3-4, pp. 145-164, 2016.
- [18] [Dataset] "NYC Taxi & Limousine Commission - Trip Record Data", *Nyc.gov*, 2018. [Online]. Available: http://www.nyc.gov/html/tlc/html/about/trip_record_data.shtml. [Accessed: 22- Sep- 2018].
- [19] K. Zhao, D. Khryashchev, J. Freire, C. Silva and H. Vo, "Predicting Taxi Demand at High Spatial Resolution: Approaching the Limit of Predictability", *IEEE International Conference on Big Data (Big Data)*, pp. 833-842, 2016.
- [20] V. Chaurasia and S. Pal, "A Novel Approach for Breast Cancer Detection using Data Mining Techniques", *International Journal of Innovative Research in Computer and Communication Engineering*, vol. 2, no. 1, pp. 2456 - 2465, 2014.
- [21] A. Linden and P. Yarnold, "Using data mining techniques to characterize participation in observational studies", *Journal of Evaluation in Clinical Practice*, vol. 22, no. 6, pp. 839-847, 2016.
- [22] T. Bahari and M. Elayidom, "An Efficient CRM-Data Mining Framework for the Prediction of Customer Behaviour", *International Conference on Information and Communication Technologies*, vol. 46, pp. 725-731, 2015.
- [23] Y. SONG and Y. LU, "Decision tree methods: applications for classification and prediction", *Shanghai Arch Psychiatry*, pp. 130-135, 2015.

An Extended DBSCAN Clustering Algorithm

Ahmed Fahim

Department of Computer Science, Prince Sattam Bin Abdulaziz University, Aflaj, Saudi Arabia
Department of Computer Science, Faculty of Computers and Information, Suez University, Suez, Egypt

Abstract—Finding clusters of different densities is a challenging task. DBSCAN “Density-Based Spatial Clustering of Applications with Noise” method has trouble discovering clusters of various densities since it uses a fixed radius. This article proposes an extended DBSCAN for finding clusters of different densities. The proposed method uses a dynamic radius and assigns a regional density value for each object, then counts the objects of similar density within the radius. If the neighborhood size \geq MinPts, then the object is a core, and a cluster can grow from it, otherwise, the object is assigned noise temporarily. Two objects are similar in local density if their similarity \geq threshold. The proposed method can discover clusters of any density from the data effectively. The method requires three parameters; MinPts, Eps (distance to the k^{th} neighbor), and similarity threshold. The practical results show the superior ability of the suggested method to detect clusters of different densities even with no discernible separations between them.

Keywords—Cluster analysis; density-based clustering; varied density clusters; data mining; extended density-based spatial clustering of applications with noise (E-DBSCAN)

I. INTRODUCTION

Cluster analysis is used for knowledge discovery rather than prediction. It aims to discover the groups of similar data in a given dataset. In other words, the objective of clustering is to divide a set of objects into some subsets such that similar objects are collected together in a subset and dissimilar objects are assigned to different subsets. Every subset is known as a cluster. Clustering is an unsupervised machine learning task because it requires neither a training set nor known labels for the discovered clusters. The resulting clusters depend on what the cluster is. A fine clustering algorithm should have the ability to discover clusters of different forms, sizes, densities, and handle noise in data. It should not be sensitive to the ordering of input data, and the parameters given by the user. In addition, the number of parameters should be as very small as possible. Most of the mentioned factors may be satisfied in a density-based method called DBSCAN “Density-Based Spatial Clustering of Applications with Noise” [1]. It is considered the leader in discovering clusters based on regions' density in data space. It defines the density of an object as the count of its neighbors in a given radius. But this idea does not apply to a dataset having different densities. So many modified versions of it and new methods have been proposed to overcome this drawback. OPTICS [2] algorithm is an extension for DBSCAN and doesn't deliver clusters explicitly. It estimates an arrangement of points in a dataset based on the core distance and reachability distance. DENCLUE [3] is a density-based approach that uses influence functions (maybe parabolic functions, square wave function, or the Gaussian function). It

applies the influence function on each object in the dataset and specifies the density attractors that are the regional maxima of the overall density function. It fails to find clusters of various densities because it employs two input parameters σ and ζ which are equivalent to Eps and Minpts in DBSCAN.

This paper introduces an extended DBSCAN algorithm, wherein in this version the neighborhood radius (Eps) is not fixed for all objects as in the basic version. Eps will be equal to the distance to the k^{th} neighbor. Thus, the Eps will vary from one object to another. MinPts parameter controls the regional density of objects; where the regional density of an object is equal to the sum of distances to its MinPts-nearest neighbors. For each object, the algorithm counts the objects in its k-nearest neighbors that have a similar regional density to it. Certainly, this number will be less than or equal to the value of k-nearest neighbors. If the object has more than or equal to MinPts similar objects then it is a core object and the cluster can grow from it otherwise the object is noise temporarily. So, the algorithm requires another parameter to judge the similarity of local densities among objects. The practical results show the superior ability of the suggested method in handling various density clusters.

The main contribution of this research is that it presents a way to overcome the main problem of the DBSCAN. It allows the Eps to vary from one object to another. It redefines the density of an item as the number of similar items within its neighborhood, in addition to the sum of the distances to the MinPts-nearest neighbors. This technique made the DBSCAN able to detect clusters of different densities.

The article is arranged as follows; subsection A presents the DBSCAN algorithm and its main problem. Section II demonstrates several related techniques. The suggested method is shown in Section III. Section IV illustrates the efficacy of the suggested technique and explains the outcomes. Finally, the concluding section brings the paper to a close.

A. DBSCAN Algorithm

The DBSCAN technique is the head technique in the density-based class. It counts the objects in a fixed neighborhood radius (Eps) of the current object. If the count of objects in this radius is larger than or equal to a threshold (MinPts), then this object is a dense (core) object, and the cluster can be grown from it otherwise, the object is considered temporarily as a noise object. So, the objects in the dataset are classified into cores, borders, or noises, as shown in Fig. 1. A border object is not a core; it belongs to a core object's neighborhood. A noise object is neither a core nor a border object.

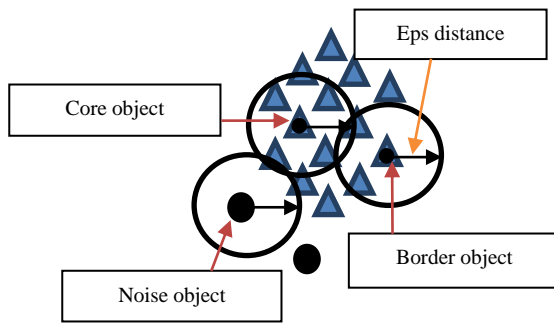


Fig. 1. Concept of the Core, Border and Noise Object where Minpts = 3.

The following definitions are used by DBSCAN [1]:

Definition 1: Eps-neighborhood of an object x is denoted by $N_{Eps}(x) = \{y \mid dis(x,y) \leq Eps\}$, where $dis(x,y)$ is the Euclidean distance.

Definition 2: Directly density-reachable, an object x is directly density-reachable from an object y wrt. Eps, and MinPts if

- 1) $x \in N_{Eps}(y)$ is part of the neighborhood of y .
- 2) y is a core object ($|neighborhood\ of\ y| \geq MinPts$).

Definition 3: Density-reachable, an object x is density-reachable from an object y wrt. Eps and MinPts if there is a chain of objects where each object is directly density-reachable from the previous one in the chain.

Definition 4: Density-connected, two objects are density-connected wrt. Eps and MinPts, if there is an object z such that both objects are density-reachable from z .

Definition 5: A cluster C is a non-empty subset of objects satisfying:

- 1) $\forall x, y: \text{if } x \in C \text{ and } y \text{ is density-reachable from } x, \text{ then } y \in C.$
- 2) $\forall x, y \in C: x \text{ is density-connected to } y.$

Definition 6: Noise is the collection of objects that are not assigned to any cluster.

DBSCAN works as follows:

```

DBSCAN (dataset D, Eps, MinPts)
// all points in the dataset are Unclassified
ClusId = 0 // -1 Unclassified, 0 Noise
For i = 1 to D.size
    Point = D.get(i)
    IF Point.ClusId <> -1
        Neighbors = D.regionQuery(Point, Eps)
        If Neighbors.size ≥ MinPts
            ClusId = ClusId + 1
            Point.ClusId = ClusId
            ExpandCluster(D, Neighbors, ClusId, Eps, MinPts)
        Else
            Point.Clus_Id = 0 // point is noise temporarily
        End If
    End If
End For
End // DBSCAN
    
```

```

ExpandCluster(D, Neighbors, ClusId, Eps, MinPts)
For Each point in Neighbors
    Point.ClusId = ClusId
End For
While Neighbors.size < > 0
    CurrPoint = Neighbors.first();
    Res = D.regionQuery(CurrPoint, Eps)
    If Res.size ≥ MinPts
        For i = 1 to Res.size
            ResPoint = Res.get(i);
            If ResPoint.ClusId = -1
                ResPoint.ClusId = ClusId
                Neighbors.append(ResPoint)
            Else If ResPoint.ClusId = 0 // point is noise
                ResPoint.ClusId = ClusId // point is a border point
            End If
        End For
    End If
    Neighbors.delete(CurrPoint)
End While
End // ExpandCluster
    
```

The Expand_cluster function collects the density-connected core objects and the border objects that are connected directly to any core in the cluster. This approach discovers clusters of varied shapes and sizes efficiently, but it has trouble detecting bunches of different densities because it uses global values for its parameters; the Eps, and the MinPts threshold that represents the minimum density for any core object.

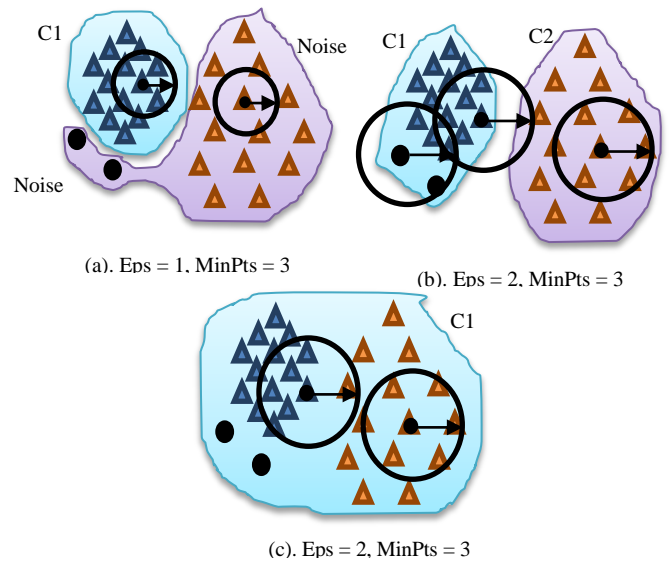


Fig. 2. Eps Value is not Suitable for all Clusters in Data.

Fig. 2 explains the problem of using a single value for the Eps parameter in DBSCAN. In Fig. 2(a), the assigned value for the Eps is small. So, the DBSCAN discovers the dense cluster C1 that contains all the blue triangles, and classifies the other objects as noises -orange triangles and the two black circles-. In Fig. 2(b), the value of Eps is increased, and the clusters are well separated, so the DBSCAN discovers the clusters C1, C2 but it merges the noise objects (the two black circles) with the dense cluster C1. That means its ability to handle noise

decreased. In Fig. 2(c), the value of Eps is the same as in Fig. 2(b), but the clusters are closer to each other. So, the DBSCAN places all the objects in one cluster. From Fig. 2, we see that a global value for the Eps is unsuitable at all for a dataset that contains clusters of different densities.

II. RELATED METHODS

Because clustering techniques play a significant role in data mining and knowledge discovery, they are used in various applications like image processing, search engine, bioinformatics, pattern recognition, market research, social network analysis, and so many others. The clustering strategies may be categorized into four classes: partitioning, hierarchical, density-based, and grid-based methods.

A. Partitioning Methods

Algorithms that are belonging to partitioning class such as k-means [4], PAM "Partitioning Around Medoids" [5], CLARA "Clustering LARge Applications" [5], and CLARANS "Clustering Large Applications based on RANdomized Search" [6], [7] describe a cluster as a collection of objects with the least variance from the mean or the medoid of the cluster; where the mean is the center of the objects in the cluster and A medoid is a cluster representative object with the least amount of dissimilarity to the other objects in the cluster. Convex-shaped clusters are favorable by this definition. If the data contain clusters of different shapes, then; this definition is not suitable, and the clustering technique does not find the actual clusters; it may divide some clusters or merge some of them. These methods are unable to discover overlapped clusters or clusters of different shapes. Also, these strategies necessitate knowing the number of clusters in advance. The DBSCAN method was used to solve this problem, as well as a suitable selection for the initial centers [8]. The k-means method works as follows: -

```
k-means(dataset D, k)
  For i=1 to k
    x = 1+ rand()% (D.size -1)
    means[i] = D[x] //select the initial means randomly
  End For
  Assign_object_to_nearest_cluster_and_update_means()
  //given below
do
  oldmse = mse
  Assign_object_to_nearest_cluster_and_update_means()
  While mse < oldmse
Return means
//-----
Assign_object_to_nearest_cluster_and_update_means()
  For i=1 to k
    npc[i] = 0 // npc refers to number of points in each cluster
    oldmeans[i] = means[i]
    means[i] = 0
  End For
  mse = 0
  For i = 1 to D.size
    dis[j] = 0    min=1
    For j = 1 to k
      dis[j] = dis(oldmeans[j], D[i])
```

```
      If dis[j] < dis[min]
        min = j
      End If
    End For
  End For
  clusid[i] = min // assign point to the closest cluster
  mse = mse + dis[min] // update mean square error
  means[min] = means[min]+D[i]
  npc[min] = npc[min]+1 //update the number of points
                        in the cluster
  End For
  For j= 1 to k
    means[j]= means[j]/ npc[j] // update the means
  End For
End // Assign_object_to_nearest_cluster_and_update_means
```

B. Hierarchical Methods

In the second category, hierarchical techniques create a hierarchical dendrogram like a tree structure. These techniques are classified into agglomerative and divisive methods. Agglomerative methods build the dendrogram from the bottom-up, while divisive methods build it from the top-down. The agglomerative methods are more familiar than the divisive methods. A hierarchical method starts with initial clusters that may be singleton clusters. In each step, it picks to combine two clusters based on a metric measure as in the single link method [9], complete link [10], and the average link method. There are several techniques in the hierarchical class such as CURE "Clustering Using Representatives" [11] that selects representatives for each cluster and uses these representatives in cluster calculations. BIRCH "Balanced iterative reducing and clustering using hierarchies" [12] is another model of hierarchical methods, which introduced the idea of the cluster feature tree. Where each cluster feature holds the count of objects in the cluster, their linear sum, and their square sum. These cluster features are arranged in a height-balanced cluster feature tree. But it uses the centroid of a cluster as a representative and redistributes the objects to the closest seed. This means that it prefers convex-shaped clusters.

C. Density-based Methods

This category introduces another description of what a cluster is. This description depends on a density concept, where a cluster is a collection of density-connected objects. A dense object is known as a core object which has not less than a specified number of objects within its neighborhood of a specified radius. This term was introduced in the DBSCAN method [1]. It is the main founder for the density-based methods to find clusters of different forms and sizes. It does not demand to know the number of clusters in advance. Also, it can treat noise objects. Unfortunately, this method fails to detect clusters of different densities since it uses a fixed value for its parameters; Eps and MinPts. This limitation motivated many researchers to propose ideas to overcome this problem. So, it has attracted the interest of researchers from all over the world.

In [13], The author presented a concept that allows Eps to change from one cluster to the next while maintaining control over the density of each core object within the cluster. The method needs two input parameters; MinPts and MaxPts. The

minimum density for core objects in the cluster is controlled by MinPts, and the maximum density is controlled by MaxPts. The method arranges the objects in the dataset based on the distance to the MaxPts neighbor, and it starts to create a cluster from the core that has the minimum distance to the MaxPts neighbor. When there is a very tiny difference in density within the cluster, this approach yields good quality clusters. Because this method focuses on homogenous clusters, if the variance in density inside the cluster grows, the method will divide the cluster.

In K-DBSCAN [14], the authors developed a two-step algorithm. To begin, the method computes each object's density as the average distances to its k-nearest neighbors and sorts the objects based on their densities; from the density curve, they can see how many levels (k) of density are present in the dataset; and finally, the method divides the dataset into k different levels of density using the k-means. Second, each density level is subjected to a modified version of DBSCAN. The number of density levels derived from the curve determines the final output. The average distance to the k-nearest neighbors is similar to the k-dist plot, but the algorithm may see incorrect levels of density, causing some clusters to split. Using the k-means to partition the data into different levels of density leads to a problem because they consider each level of density as a new dataset and apply a modified version of DBSCAN on it. Surely, the objects in the same level do not have the same density there will be variance in the density of objects and their modified version of DBSCAN does not consider this. If the dataset has a single density level this means $k=1$ in k-means and all objects are assigned the same level of density, the modified version of DBSCAN that is used in this method may assign all objects the same cluster unless clusters are well separated. Since the method assigns an object and all its k-nearest neighbors -that are in the same level of density- the same cluster.

In [15], the author presented a new paradigm to deal with different density clusters. The approach gives each object a local density value equal to the sum of its k1-nearest neighbors' distances. Then, it divides objects into attractors and attracted objects by counting the objects in the object's k-nearest neighbors that are denser. The clusters evolve from denser to sparser objects. This approach requires four input parameters, which is a significant number. Furthermore, the fine-tuning setting is a difficult operation.

In [16], to enlarge the cluster, the authors recommended using a mutual k-nearest neighborhood to establish k-deviation density of points and a deviation factor to locate direct density reachable neighbors for core points. This procedure yields inaccurate results. The method tends to split the clusters since it allows a very small density deviation within a cluster. The problem in this method comes from the computational way of the k-deviation density.

GMDBSCAN [17] is a grid-based technique. It is based on a spatial index (sp-tree). It allows the Minpts to vary from one cell to the next based on the density of each grid cell, uses the same Eps value in each grid cell, and runs DBSCAN on the data in each grid cell. This approach employs several parameters that have an impact on the clusters that produce.

The problem with GMDBSCAN is that it takes a long time to run on large datasets.

GMDBSCAN-UR [18] is a GMDBSCAN algorithm adaptation. It selects as representative objects some well-scattered points that form the shape and extent of the dataset in each grid cell. GMDBSCAN's time-consuming difficulty is solved using this solution. It permits one DBSCAN parameter (Minpts or Eps) to vary from one cell to the next, and it performs better than GMDBSCAN. With varying density clusters, however, it does not yield reliable results. VDBSCAN [19] separates the k-dist plot based on the curve's sharp change. It chooses an appropriate Eps value for each partition and runs DBSCAN on it. When the dataset comprises clusters of varied uniform densities, it works well. When there is a density gradient, however, erroneous clusters result. Unless the clusters are well separated, it may split dense clusters or merge sparser ones.

DBSCAN-DLP [20] splits the input data into distinct density levels based on some statistical characteristic of density variation, then estimates the Eps value for each density level before applying DBSCAN clustering to each density level with corresponding Eps. This approach works best with clusters of uniform density; the variance in density of objects inside a cluster should be very minimal and below a certain threshold. The authors of [21] proposed a mathematical method for selecting various Eps values from the k-dist plot and running the DBSCAN algorithm on the data, advancing from least to biggest Eps while disregarding previously clustered elements. To discover inflection points on the curve when the curve alters its concavity, the method employs spline cubic interpolation. Some clusters are divided as a result of this procedure. DSets-DBSCAN [22] applies DSets clustering first, with DBSCAN's input parameters derived from the original cluster extracted by DSets. Most earlier methods calculated Eps based on some local density criteria and used DBSCAN to find clusters in a dataset with several density levels.

CMDD (Clustering Multi-Density Dataset) [23] combines DBSCAN with k-nearest neighbors to generate k local density values for each object in the dataset, this method uses two parameters MinPts and k for k-nearest neighbors, where MinPts represents the lowest density for a core object, and k represents the highest density for a core object in the cluster. It begins by clustering the densest unclassified objects, it is based on the same definitions of DBSCAN and computes k values for each object and needs to arrange the objects in the dataset based on their density to the kth neighbor. So, it consumes more time than the proposed method. It produces good clusters of varied densities, but the denser cluster may take some objects from the adjacent cluster as shown in experiments. The proposed method only computes one value for each object and does not need to arrange the objects in the dataset. So, it starts creating clusters from any object. CMDD method uses cluster initiator or reference. The proposed method does less computation than CMDD.

In [24], the author introduced a clustering method that requires only two intake parameters, uses all k-nearest neighbors to compute the thickness of objects which leads to an increase in the effects of noise on density, and this leads the

method to merge clusters with a smooth gradient in density. The density of object x is compared with the density of its k -nearest neighbors y_1, y_2, \dots, y_k , then the object x with its similar neighbors are assigned the same cluster-id, how many objects are similar to x is not matter, to expand this cluster; each object y is compared with its k -nearest neighbors p_1, p_2, \dots, p_k . i.e there is no cluster initiator. The proposed method compares between the object x and all objects that are a candidate to be in its cluster using the k -nearest neighbors, there must be $MinPts$ similar object to object x , otherwise, the object x is noise temporally.

EXDBSCAN "an Extension of DBSCAN to detect Clusters in Multi-Density Datasets" [25] requires a single parameter ($MinPts$), and it assumes that ϵ (Eps) has a small value, how to select the initial value for ϵ is not specified, also when creating the next cluster if the point p is an outlier then ϵ is increased by $\Delta\epsilon$, how to compute $\Delta\epsilon$ is not specified, the process of increasing ϵ by $\Delta\epsilon$ may be executed k times before p becomes a core point. The cluster is generated as soon as p becomes a core, and the algorithm then tests whether p is an outlier. If p is an outlier, all points in the cluster are assigned unclassified and p assigned outlier. If the initial value of ϵ is very small and the first checked point is a core, the method will split this cluster. Since the method starts the creation of the next cluster with the first initial value of ϵ , this may lead to dividing some clusters.

The authors of [26] presented a clustering technique based on density peaks (DPC). DPC is a new density and distance-based clustering technique. The concept behind this strategy is that cluster centers have high local densities and are spread out. It calculates an object's local density by counting its neighbors over a defined distance termed dc (as Eps in DBSCAN). After locating the centers, clusters are established by allocating each object to the cluster that contains the object's nearest neighbor with a higher density. However, the dc distance has an impact on clustering outcomes, and this approach requires the user to input the number of clusters. This approach can find clusters of various sizes and forms but does not perform well in the presence of varied density clusters, and it does not handle noise well.

In [27], the authors presented "a shared-nearest-neighbor-based clustering by fast search and find of density peaks algorithm" (SNN-DPC). SNN-DPC has some faults. To begin, manually setting the number of shared-nearest neighbors k is required. Second, SNN-DPC still selects cluster centers using a decision graph or requires the number of required clusters as an input. Nonetheless, these center-based algorithms have trouble clustering datasets with a variety of clusters [28].

D. Grid-based Methods

Grid-based clustering is mainly oriented towards spatial datasets. The quantization of the data space into multiple cells is the central principle of these methods. Grid-based approaches do not operate directly with objects; instead, they work with objects in the same grid cell as a single unit, and

they merge the cells to build clusters using statistical information. Many algorithms are belonging to this family of clustering algorithms like STING (Statistical Information Grid) [29], wave cluster [30], and CLIQUE (Clustering in Quest) [31].

III. PROPOSED METHOD (AN EXTENDED DBSCAN CLUSTERING ALGORITHM)

This section describes the details of the suggested approach that is based on DBSCAN but controls the density permitted within each cluster. The proposed technique finds the k -nearest neighbors for each object, and computes the local density (LD) of each object as the sum of lengths to the $MinPts$ -nearest neighbors; where $MinPts$ is the minimum density for a core object. The maximum density for a core object is less than or equal to k since the proposed method relies on the k -nearest neighbors. The Eps value is varied from one object to another since Eps equals the distance to the k^{th} neighbor. For any object x , the method finds its k -nearest neighbors and counts the number of similar objects to object x . If the count of similar objects to object x is larger than or equal to $MinPts$, object x is a core and the cluster starts to grow, otherwise, object x is assigned noise temporarily. The proposed method counts similar objects within a dynamic radius instead of counting all objects within a fixed radius as in the basic DBSCAN. The method relies on the next mathematical formulas:

Equation (1) defines the set of k -nearest neighbors $knn(x)$ for an object x .

$$knn(x) = \{y_i | dis(x, y_i) \leq dis(x, y_k), i = 1, 2, \dots, k\} \quad (1)$$

where $dis(x, y_i)$ is the Euclidean distance.

Equation (2) defines the Local Density (LD) of an object x as the total of lengths to its $MinPts$ -nearest neighbors.

$$LD(x) = \sum_{i=1}^{MinPts} dis(x, y_i) \quad (2)$$

Equation (3) computes the Density Similarity (DS) between two neighbors.

$$DS(x, y) = \begin{cases} \frac{LD(x)}{LD(y)} * 100 & LD(y) \geq LD(x) \\ \frac{LD(y)}{LD(x)} * 100 & LD(x) > LD(y) \end{cases} \quad (3)$$

Equation (4) checks whether two neighbors are Similar Neighbor (SN) or not.

$$SN(x, y) = \begin{cases} 1 & DS(x, y) \geq Similarity_Level \\ 0 & DS(x, y) < Similarity_Level \end{cases} \quad (4)$$

Where, $Similarity_Level$ is an input parameter.

Equation (5) counts the number of similar neighbors to an object x .

$$|SN(x, y_1, y_2, \dots, y_k)| = \begin{cases} \geq MinPts & x \text{ is Core} \\ < MinPts, x \notin knn(core) & x \text{ is Noise} \\ < MinPts, x \in knn(core) & x \text{ is Porder} \end{cases} \quad (5)$$

The proposed method is based on the following definitions:

Definition 1: Directly density-reachable, an object y is directly density-reachable from an object x wrt. $knn(x)$ and $MinPts$ if

- 1) $y \in knn(x)$ and
- 2) $|SN(x, y_1, y_2, \dots, y_k)| \geq MinPts$ (core object condition).

Definition 2: Density-reachable, an object x is density-reachable from an object y wrt. $knn(y)$ and $MinPts$ if there is a chain of objects x_1, \dots, x_n where $x_1 = y$, and $x_n = x$ such that each object is directly density-reachable from the previous object in the chain.

Definition 3: Density-connected, an object x is density-connected to an object y wrt. $knn(z)$ and $MinPts$ if there is an object z such that both objects are density-reachable from z wrt. $knn(z)$ and $MinPts$.

Definition 4: A cluster C is a non-empty subset of objects meeting the next needs:

- 1) $\forall x, y$: if $x \in C$ and y is density-reachable from x wrt. $knn(x)$ and $MinPts$, then $y \in C$.
- 2) $\forall x, y \in C$: x is density-connected to y wrt. $knn(z)$ and $MinPts$.

Definition 5: Noise is the collection of objects that are not assigned to any cluster.

The method works as follow:

Input: dataset D , k , $MinPts$, SL (Similarity Level)

Output: set of clusters

E-DBSCAN(dataset D , k , $MinPts$, SL)

```
All objects are unclassified
For each object  $x$  in dataset  $D$ 
    Find the  $knn(x)$  as in (1)
    Compute  $LD(x)$  as in (2)
    Compute  $DS(x,y)$  as in (3)
    Count  $SN(x)$  as in (4)
End for
clusterId=0
for  $i= 1$  to  $D.size()$ 
    If  $SN(x_i) \geq MinPts$  and  $unclassified(x_i)$  then
        clusterId = clusterId + 1
        Grow_Cluster( $x_i$ , clusterId)
    End if
End for
End // E-DBSCAN
//*****
Grow_Cluster( $x$ , clusterId)
```

Assign x clusterId

Add all unclassified $SN(x,y)$ to seedList and assign them clusterId

While seedList is not empty

$X=getTop()$

If $SN(X) \geq MinPts$

append all unclassified $SN(X, y_j)$ to seedList and

assign them clusterId

End if

seedList.Remove(X)

End while

End //Grow_Cluster

The variable $SN(x)$ stores the number of similar neighbors for the object x and the function $SN(X, y_i)$ returns the objects y_i which are similar to the object X . The function Remove deletes the top element from the seedList after classifying its similar neighbors so the algorithm reaches a terminate point. Cluster creation is started from any core object by calling the function $Grow_Cluster(x,id)$, where x is the first core object in the cluster that has the label id . The next section presents some results that show the ability of the suggested approach in finding clusters of various densities even without separation between clusters.

IV. RESULTS AND DISCUSSION

This section explains the outcomes of running the suggested method E-DBSCAN to many datasets, which reflects its superior ability to detect clusters of diverse densities. We also compared the suggested method's findings to those of DBSCAN [1], CMDD [23], and the method in [24]. Two dimensions datasets were chosen for easy visualization. Each black circle represents a noise object in all next figures. The first dataset is pictured in Fig. 3. It has 476 objects that form clusters of varied shapes, sizes, and densities. There are six noise objects in total.

The right section of this dataset is the most complex, as it comprises a low-density cluster with three high-density clusters, one of which has two denser clusters. The algorithm discarded the noise objects accurately. The proposed method (E-DBSCAN) discovers 8 clusters and 8 noise objects as displayed in Fig. 3(a). When the similarity level is increased from 71 to 73, the red triangles cluster is divided into two clusters, also the magenta squares cluster is divided into two clusters and two more objects are assigned noise as shown in Fig. 3(b). When the similarity level is increased from 73 to 75, the blue stars cluster is divided into two clusters and three more objects are assigned noise as shown in Fig. 3(c).

DBSCAN fails to handle this data as shown in Fig 3(d), it returned the smallest cluster as noise, and the right region is returned as a single cluster. There is no proper Eps value to detect the correct clusters in this dataset.

In CMDD method, the denser cluster may take some objects from the adjoining cluster as shown in Fig. 3(e) where the cyan crosses cluster and red pluses cluster take six objects from the green triangles cluster. In addition, this method returns noise as small or singleton clusters as displayed in Fig. 3(e), Fig. 3(f).

The method in [24] returned the right region as three clusters as shown in Fig. 3(g). It merged the denser cluster with its low-density surrounding cluster since it does not use the concept of a core object as in the proposed method. Also, this method discards the very small (less than 0.006 of the dataset size) clusters as outliers.

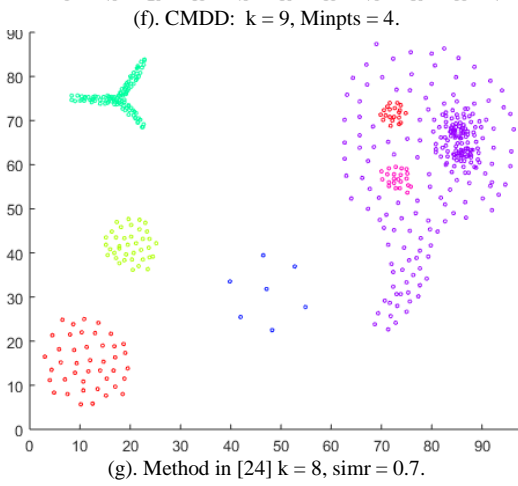
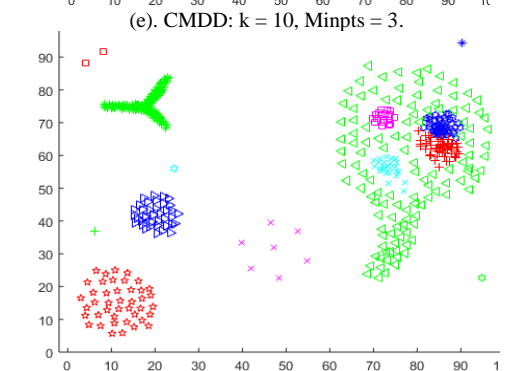
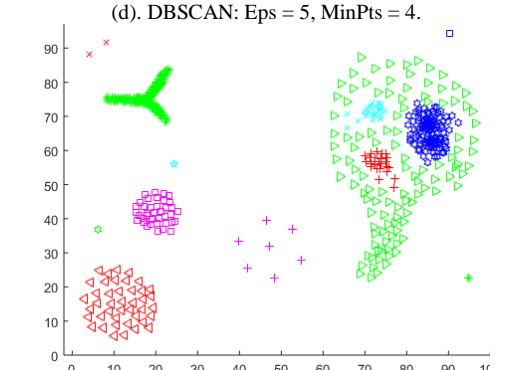
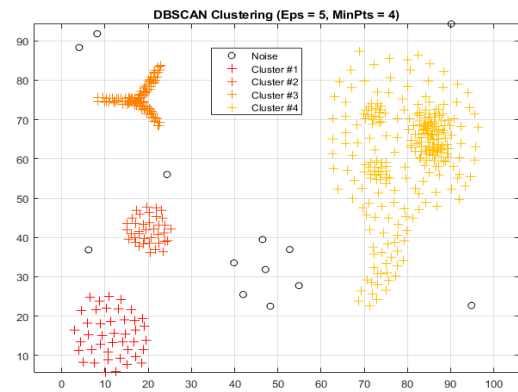
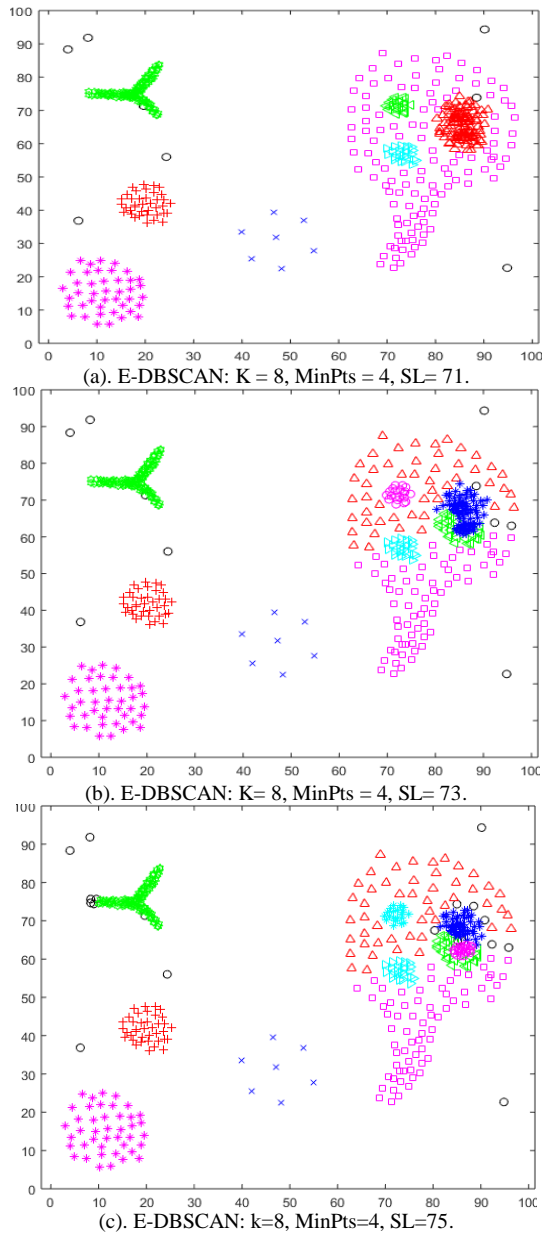


Fig. 3. Dataset 1 and the Resulting Clusters.

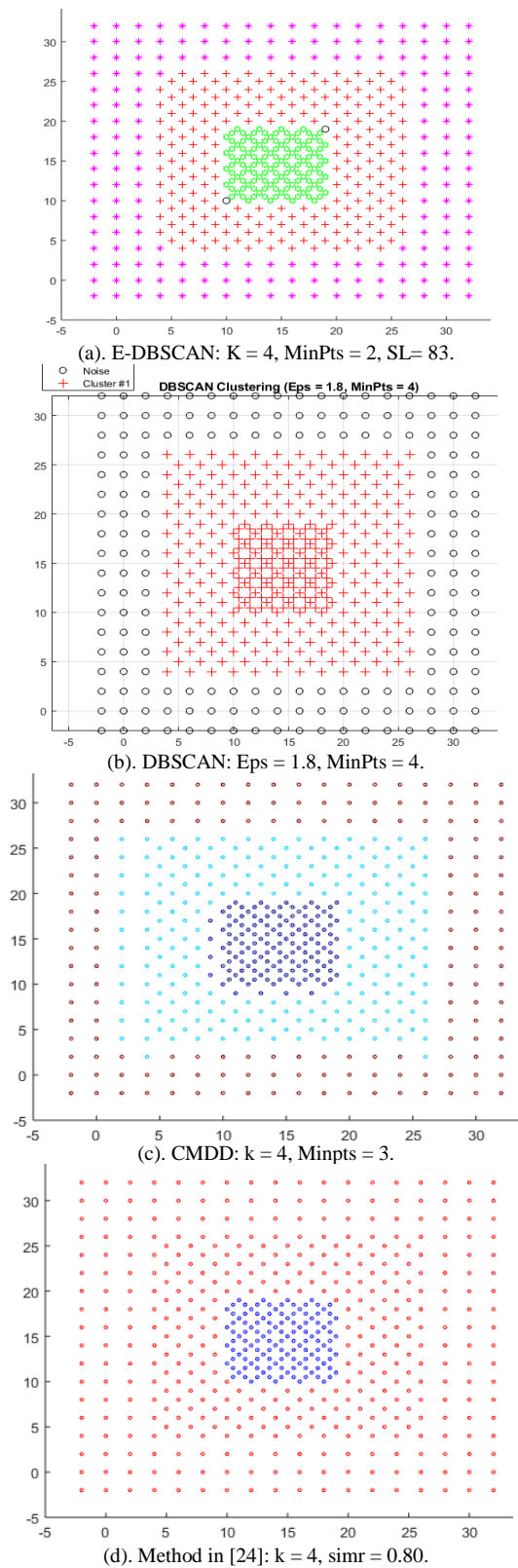
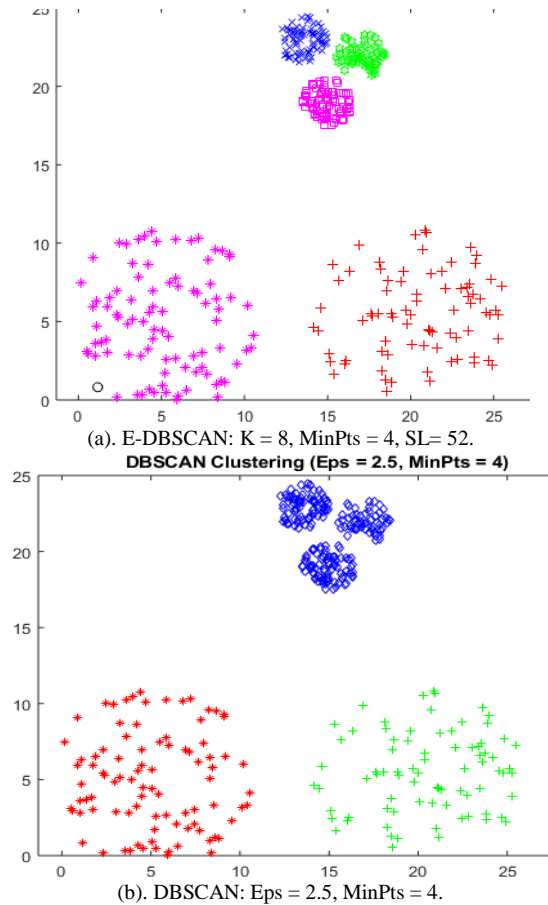


Fig. 4. Dataset 2 and the Resulting Clusters.

Dataset 2 has 526 objects, which is pictured in Fig. 4. The consistent density gradient in this data poses a hurdle. The outer cluster has the lowest density, with two interlaced inner more dense clusters. The E-DBSCAN discovered the clusters correctly and assigned two objects noise as shown in Fig. 4(a). DBSCAN merged the two inner clusters and assigned the outer cluster noise as displayed in Fig. 4(b). So, there is no single Eps value to find the correct clusters from this dataset. CMDD has trouble that is shown in Fig. 4(c) where the inner densest cluster took some objects from the middle dense cluster and the middle cluster took some objects from the outer less density cluster. The method in [24] returned two clusters as shown in Fig. 4(d). It merged the outer cluster with the middle one.

Dataset 3 has 383 objects constituting five convex clusters with two levels of density as presented in Fig. 5. The E-DBSCAN discovered the actual five clusters from data as displayed in Fig. 5(a). DBSCAN cannot detect the correct clusters using a single Eps value as portrayed in Fig. 5(b). It merged the three dense clusters since they are close to each other. CMDD returned a good result, but it assigned the two cyan objects a new cluster as shown in Fig. 5(c). The method in [24] returned a good result, but it has one misclassified object (the yellow cluster takes one object from the magenta cluster) as depicted in Fig. 5(d).



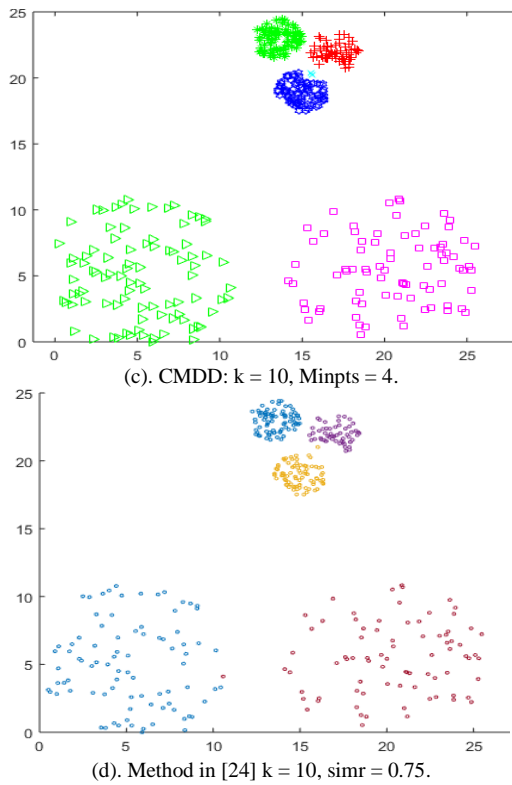
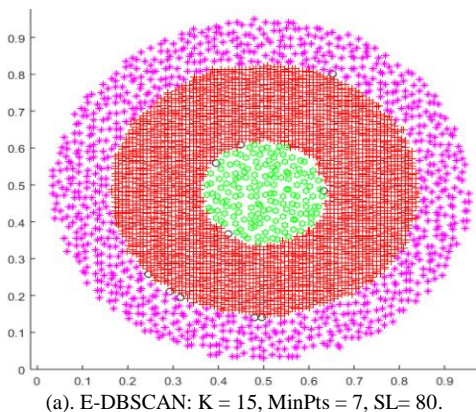
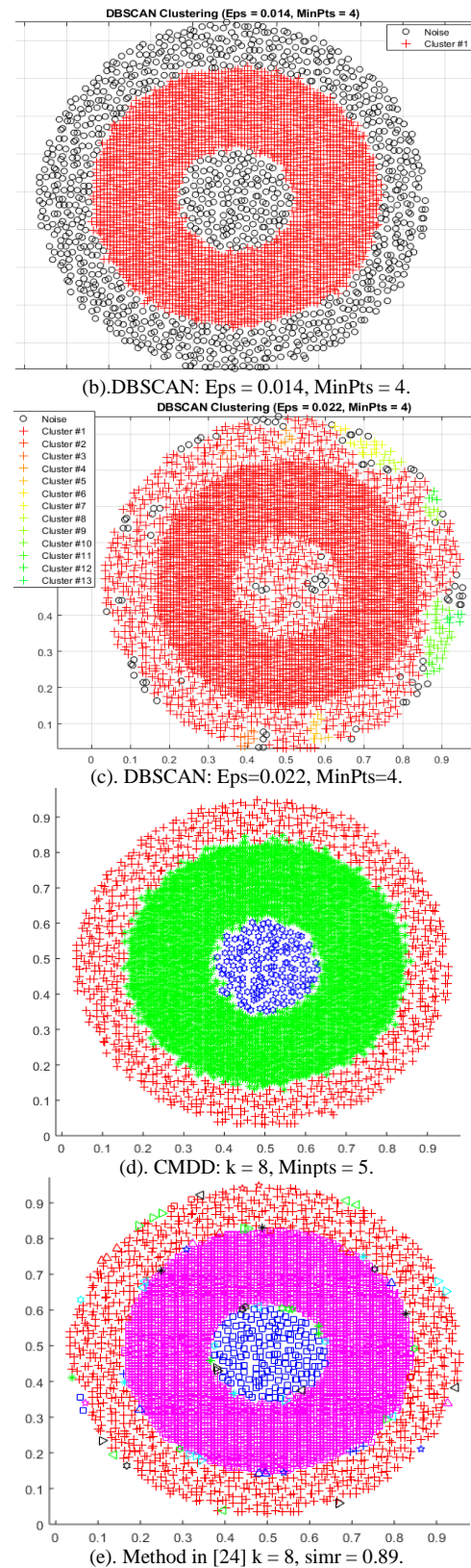
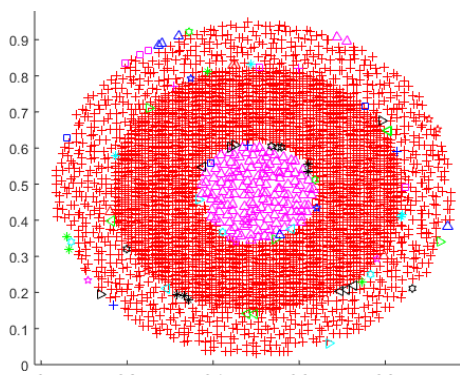


Fig. 5. Dataset 3 and the Resulting Clusters.

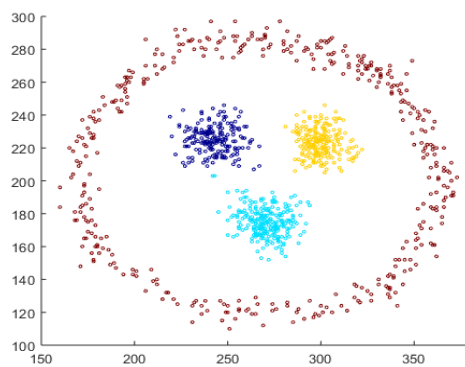
Dataset 4 contains 4600 objects that form three clusters as shown in Fig. 6. The challenge here there is no separation between clusters. Each cluster touches its nearest cluster. The proposed method discovered the accurate clusters and assigned ten objects noise as displayed in Fig. 6(a). Using a small value for Eps, DBSCAN detected the densest cluster and returned the others as noise as shown in Fig 6(b). Increasing the Eps, DBSCAN divided the dataset into 13 clusters. Since objects in the outer and the inner cluster are not of the same density as shown in Fig. 6(c). The problem of CMDD appeared again where the densest green cluster took some border objects from the inner and the outer cluster as shown in Fig. 6(d). This problem emerges when clusters are in touch. The method in [24] produced three clusters as appeared in Fig. 6(e), Fig. 6(f), but it returned 95, 82 objects outlier, respectively.





(f). Method in [24] $k = 8$, $\text{simr} = 0.88$.

Fig. 6. Dataset 4 and the Resulting Clusters.



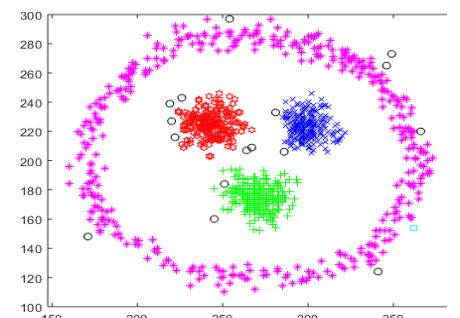
(d). Method in [24]: $k = 12$, $\text{simr} = 0.6$.

Fig. 7. Dataset 5 and the Resulting Clusters.

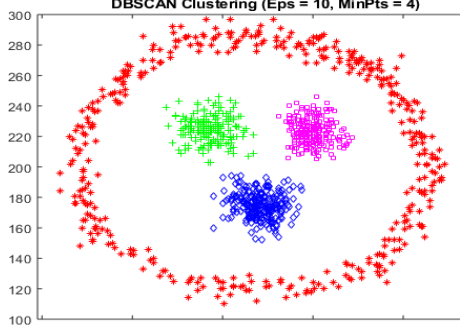
As seen in Fig. 7, Dataset 5 has 1016 objects. As demonstrated in Fig. 7(a), the suggested technique successfully locates the four accurate clusters as well as the noise objects. Other methods failed to discard the noise objects well. But all of them returned good results as shown in Fig. 7(b), (c), (d).

Fig. 8 depicts Dataset 6, which has 399 objects. Because it comprises interconnected clusters that are quite close to one other, this dataset is extremely difficult to analyze. The suggested method returned five clusters as shown in Fig. 8(a). In the upper left cluster, there is a smooth gradient in density in this group. Furthermore, the right cluster contains an inner high dense cluster with no separation between them, which the method effectively detects.

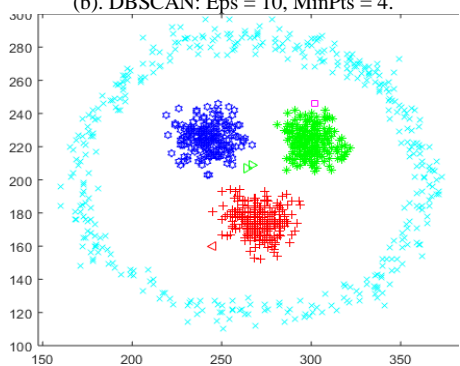
DBSCAN returned five clusters and considered the low-density cluster as noise besides discarding five objects as noises from the two upper left clusters, and two objects are misclassified as shown in Fig 8(b). Raising the Eps value implies decreasing the quality of the outcome as displayed in Fig. 8(c) by combining the two lower left clusters into one and simultaneously merging the two upper left clusters.



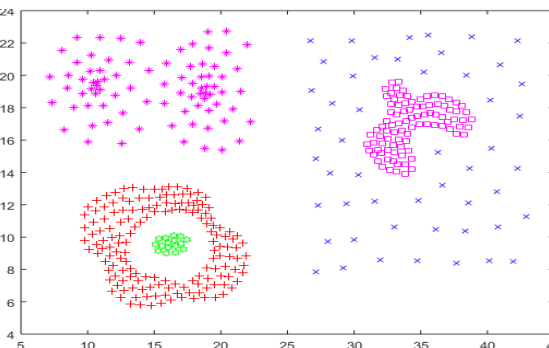
(a). E-DBSCAN: $K = 7$, $\text{MinPts} = 3$, $\text{SL} = 50$.
DBSCAN Clustering ($\text{Eps} = 10$, $\text{MinPts} = 4$)



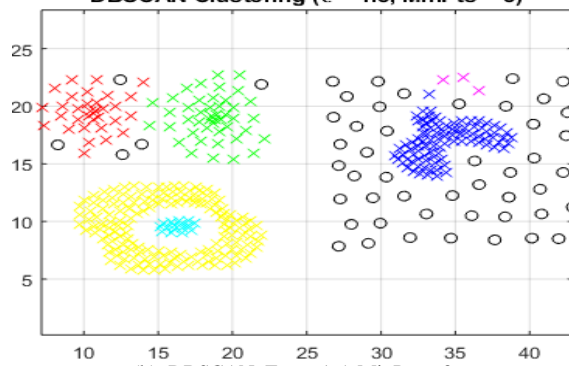
(b). DBSCAN: $\text{Eps} = 10$, $\text{MinPts} = 4$.



(c). CMDD: $k = 17$, $\text{Minpts} = 4$.



(a). E-DBSCAN: $k = 9$, $\text{MinPts} = 3$, $\text{SL} = 70$.
DBSCAN Clustering ($\epsilon = 1.5$, $\text{MinPts} = 3$)



(b). DBSCAN: $\text{Eps} = 1.5$, $\text{MinPts} = 3$.

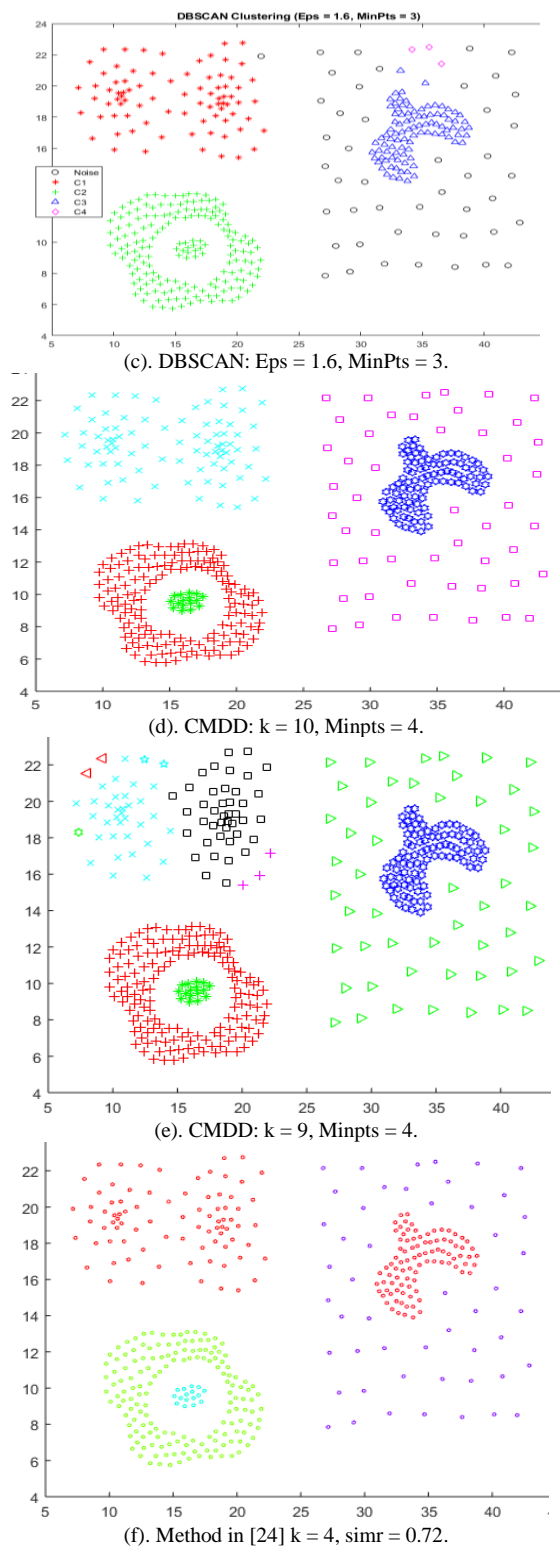
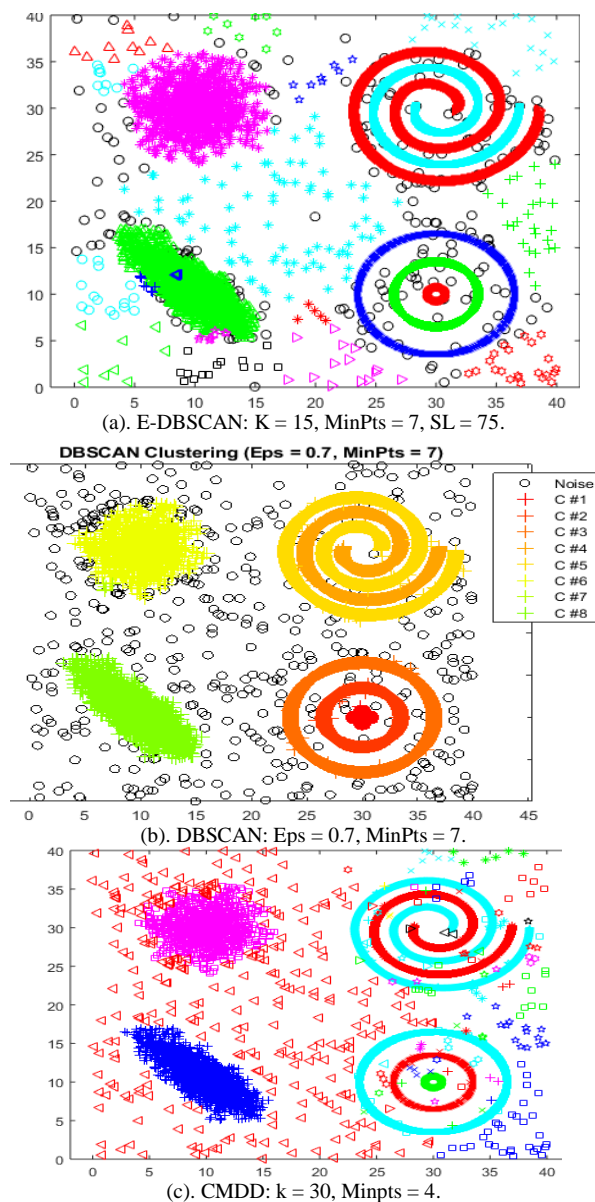


Fig. 8. Dataset 6 and the Resulting Clusters.

CMDD removed five objects from the upper left cluster and three objects from the black cluster as displayed in Fig. 8(e). The suggested method, CMDD, and the method in [24] returned the same result as displayed in Fig. 8(a), (d), (f).

Dataset 7 contains 8537 objects, which is displayed in Fig. 9. The suggested approach discovered the basic seven clusters, some noise objects, and the other objects are allocated to different fifteen clusters as displayed in Fig. 9(a). These fifteen clusters are considered noise in DBSCAN as displayed in Fig. 9(b), but the suggested technique treated them as clusters as depicted in Fig. 9(a). DBSCAN discovered 8 clusters, the eighth cluster is tiny and can be considered noise. The other objects are treated as noise, as shown in Fig. 9(b). CMDD discovered the basic seven clusters, but it can't handle noise, there are many singleton clusters as displayed in Fig. 9(c). The technique in [24] discovered eight clusters as displayed in Fig. 9(d), but some sparser objects are assigned to the top left cluster. Also, this method does not handle noise. Comparing the results in subfigures a, b, c, and d, you find that the result in a is more accurate than the others.



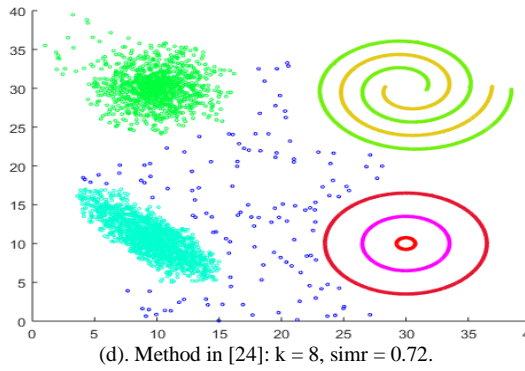


Fig. 9. Dataset 7 and the Resulting Clusters.

Dataset 8 contains 373 objects that form two clusters of various sizes, forms, and densities. The suggested approach produces the correct clusters accurately as displayed in Fig. 10(a). DBSCAN divided the upper cluster into two clusters and merged one of them with the lower cluster in addition to discarding one noise object as displayed in Fig. 10(b). CMDD and the technique in [24] discovered the correct clusters as displayed in Fig. 10(c), and Fig. 10(d).

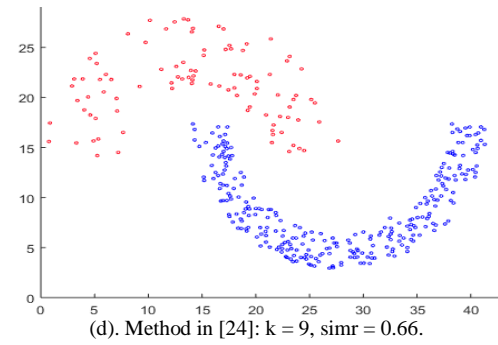
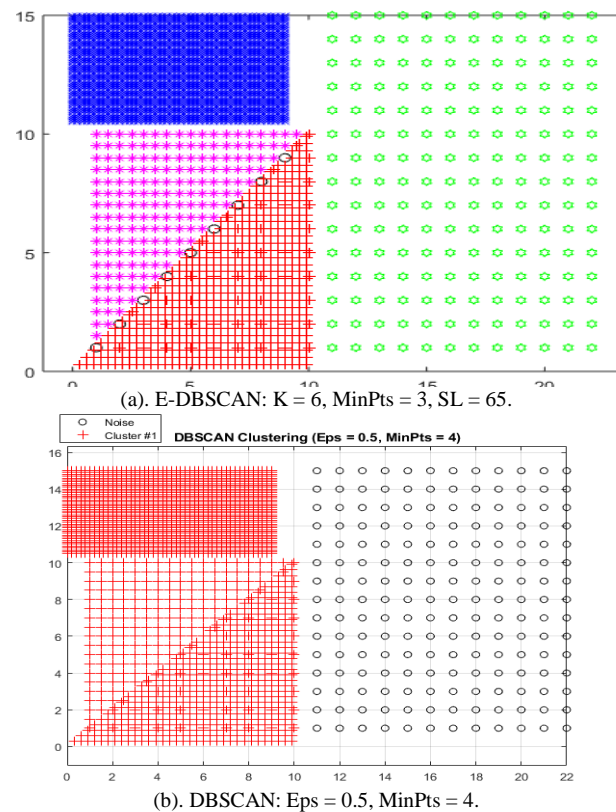
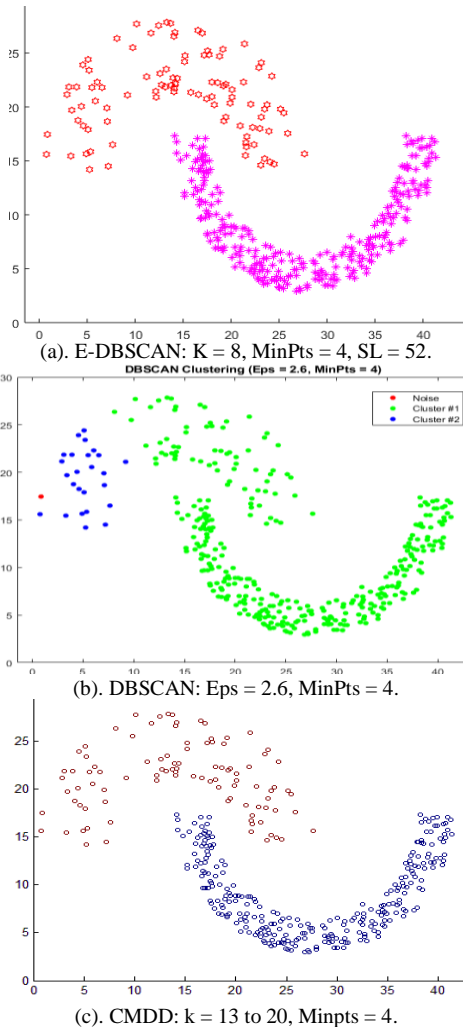


Fig. 10. Dataset 8 and the Resulting Clusters.

Dataset 9 contains 3147 objects as shown in Fig. 11. It contains four clusters of different sizes, forms, and densities. The suggested method discovered the four clusters from data accurately and nine noise objects as displayed in Fig. 11(a). DBSCAN failed to locate the clusters from this dataset when $\text{Eps} = 0.5$, it merged three clusters into one and treated the fourth cluster as noise as displayed in Fig. 11(b). The same problem of CMDD appeared again where the cyan cluster took 12 objects from the red cluster. These objects are treated as borders for the cyan cluster as shown in Fig. 11(c). The method in [24] produced a better result than that of CMDD, but it has 2 misclassified objects and has removed one object from the lower-left corner of the red cluster as displayed in Fig. 11(d).



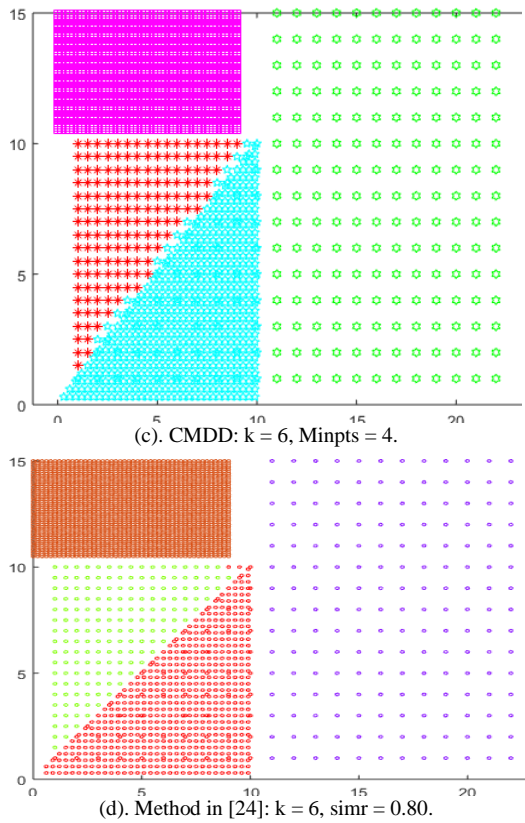


Fig. 11. Dataset 9 and the Resulting Clusters.

Dataset 10 contains 300 objects as displayed in Fig. 12. The suggested technique discovered the correct three clusters from data in addition to two small clusters (the red and cyan) and assigned eighteen objects noise as displayed in Fig. 12(a). DBSCAN failed to locate the correct clusters. There is no appropriate Eps value to discover the clusters in this data as displayed in Fig. 12(b) and Fig. 12(c). CMDD discovers the three main clusters, it does not distinguish noise objects as in DBSCAN, see Fig. 12(d). The method in [24] failed to discover the correct clusters as displayed in Fig. 12(e).

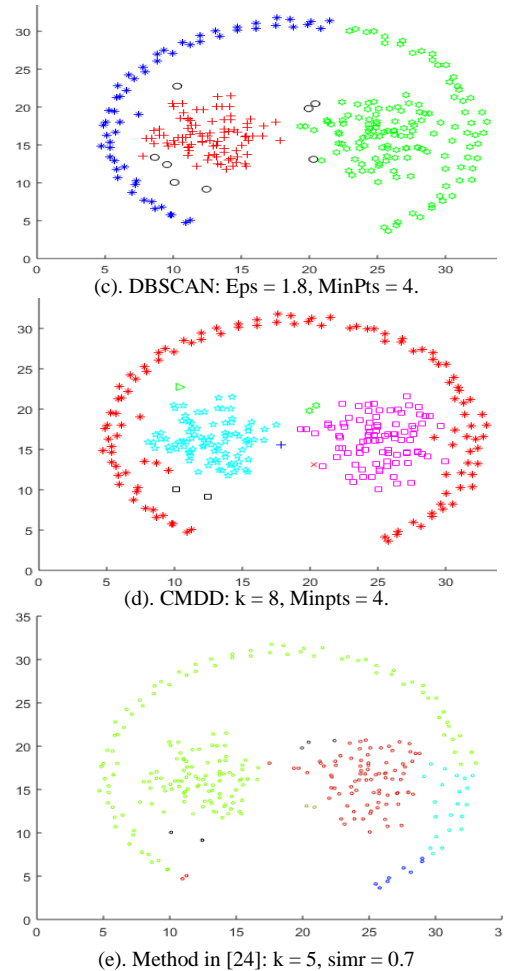


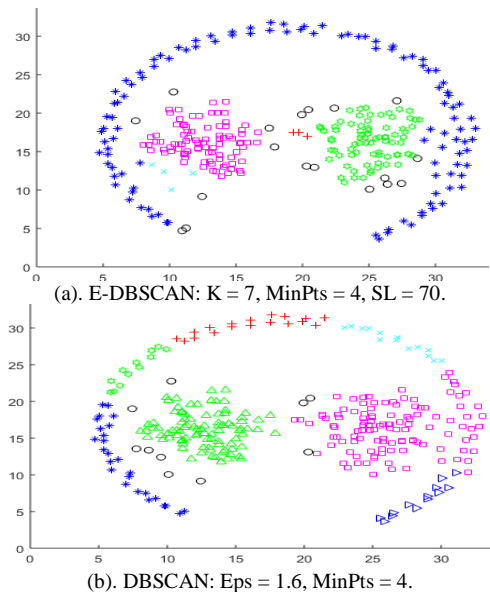
Fig. 12. Dataset 10 and the Resulting Clusters.

V. CONCLUSION

In this work, we have introduced an extended version of the DBSCAN method, the proposed method can handle clusters of diverse densities. This method uses the distance to the k^{th} neighbor to be Eps, this idea makes the Eps vary from one object to another. So, this solves the problem of fixed Eps in the basic DBSCAN. In the proposed method, MinPts is used as in the basic DBSCAN and it must be smaller than the value of k in k -nearest neighbors. Since the suggested approach uses k -nearest neighbors it needs a termination condition for cluster expansion, it uses similarity level (SL) as a termination condition. The similarity between two objects relies on their local density. The local density of an object is equal to the total of the lengths to its MinPts-nearest neighbors.

The practical results indicate that the suggested approach (E-DBSCAN) can find clusters of diverse sizes, forms, and densities. All of these qualities for clusters prompted the researchers to propose several changes to the DBSCAN algorithm to handle these challenges jointly, particularly clusters of varying densities.

MinPts parameter ranges from 2 to 7, as a general rule it is near from half of the k -nearest neighbor, k for k -nearest neighbors ranges from 4 to 15. The value of SL (similarity level) ranges from 52 to 83.



ACKNOWLEDGMENT

The author extends his appreciation to the Deputyship for Research & Innovation, Ministry of Education in Saudi Arabia for funding this research work through the project number (IF-PSAU-2021/01/17758).

REFERENCES

- [1] M. Ester, H.-P. Kriegel, J. Sander, and X. Xiaowei, "A Density-based algorithm for discovering clusters in large spatial databases with noise," in Proceedings of 2nd International Conference on Knowledge Discovery and Data Mining (KDD-96), 1996, pp. 226–231.
- [2] M. Ankerst, M. M. Breunig, H. Kriegel, and J. Sander, "OPTICS: Ordering Points To Identify the Clustering Structure," in ACM SIGMOD Record, 1999, vol. 28, no. 2, pp. 49–60.
- [3] A. Hinneburg and D. A. Keim, "An Efficient Approach to Clustering in Large Multimedia Databases with Noise," in Proceedings of the Fourth International Conference on Knowledge Discovery and Data Mining, 1998, vol. September, pp. 58–65.
- [4] A. M. Fahim, A. M. Salem, F. A. Torkey, and M. A. Ramadan, "Efficient enhanced k-means clustering algorithm," J. Zhejiang Univ. Sci., vol. 7, no. 10, pp. 1626–1633, 2006, doi: 10.1631/jzus.2006.A1626.
- [5] J. E. Gentle, L. Kaufman, and P. J. Rousseeuw, Finding Groups in Data: An Introduction to Cluster Analysis., vol. 47, no. 2. 1991.
- [6] R. T. Ng and J. Han, "Efficient and effective clustering methods for spatial data mining," Proc. 20th Int. Conf. Very Large Data Bases, pp. 144–155, 1994.
- [7] R. T. Ng and J. Han, "CLARANS: A method for clustering objects for spatial data mining," IEEE Trans. Knowl. Data Eng., vol. 14, no. 5, pp. 1003–1016, 2002, doi: 10.1109/TKDE.2002.1033770.
- [8] A. Fahim, "K and starting means for k-means algorithm," J. Comput. Sci., vol. 55, no. October, p. 101445, 2021, doi: 10.1016/j.jocs.2021.101445.
- [9] R. Sibson, "SLINK: an optimally efficient algorithm for the single-link cluster method," Comput. J., vol. 16, no. 1, pp. 30–34, 1973.
- [10] D. Defays, "An efficient algorithm for a complete link method," Comput. J., vol. 20, no. 4, pp. 364–366, 1977, doi: https://doi.org/10.1093/comjnl/20.4.364.
- [11] S. Guha, R. Rastogi, and K. S. Cure, "An efficient clustering algorithm for large databases," Proc. ACM SIGMOD Int. Conf. Manag. Data, vol. 2, no. 1, pp. 73–84, 1998, [Online]. Available: https://dl.acm.org/citation.cfm?id=276312.
- [12] T. Zhang, R. Ramakrishnan, and M. Livny, "BIRCH: an efficient data clustering method for very large databases," in ACM SIGMOD int. conference on Management of data, 1996, pp. 103–114, doi: 10.1093/nq/s9-II.32.108-a.
- [13] A. Fahim, "Homogeneous Densities Clustering Algorithm," Int. J. Inf. Technol. Comput. Sci., vol. 10, no. 10, pp. 1–10, 2018, doi: 10.5815/ijitcs.2018.10.01.
- [14] M. Debnath, P. K. Tripathi, and R. Elmasri, "K-DBSCAN: Identifying spatial clusters with differing density levels," in Proceedings - 2015 International Workshop on Data Mining with Industrial Applications, DMIA 2015: Part of the ETyC 2015, 2015, pp. 51–60, doi: 10.1109/DMIA.2015.14.
- [15] A. Fahim, "A Clustering Algorithm based on Local Density of Points," Int. J. Mod. Educ. Comput. Sci., vol. 9, no. 12, pp. 9–16, 2017, doi: 10.5815/ijmecs.2017.12.02.
- [16] C. Jungan, C. Jinyin, Y. Dongyong, and L. Jun, "A k-Deviation Density Based Clustering Algorithm," Math. Probl. Eng., vol. 2018, 2018, doi: 10.1155/2018/3742048.
- [17] C. Xiaoyun, M. Yufang, Z. Yan, and W. Ping, "GMDBSCAN: Multi-density DBSCAN cluster based on grid," in IEEE International Conference on e-Business Engineering, ICEBE'08 - Workshops: AiR'08, EM2I'08, SOAIC'08, SOKM'08, BIMA'08, DKEEE'08, 2008, pp. 780–783, doi: 10.1109/ICEBE.2008.54.
- [18] M. A. Alhanjouri and R. D. Ahmed, "New Density-Based Clustering Technique: GMDBSCAN-UR," Int. J. Adv. Res. Comput. Sci., vol. 3, no. 1, pp. 1–9, 2012.
- [19] P. Liu, D. Zhou, and N. Wu, "Varied Density Based Spatial Clustering of Application with Noise," Proc. IEEE Conf. ICSSSM 2007 pg 528, vol. 531, pp. 528–531, 2007.
- [20] Z. Xiong, R. Chen, Y. Zhang, and X. Zhang, "Multi-density DBSCAN algorithm based on Density Levels Partitioning," J. Inf. Comput. Sci., vol. 9, no. 10, pp. 2739–2749, 2012.
- [21] S. Louhichi, M. Gzara, and H. Ben Abdallah, "A density based algorithm for discovering clusters with varied density," 2014 World Congr. Comput. Appl. Inf. Syst. WCCAIS 2014, no. 1, 2014, doi: 10.1109/WCCAIS.2014.6916622.
- [22] J. Hou, H. Gao, and X. Li, "DSets-DBSCAN: A Parameter-Free Clustering Algorithm," IEEE Trans. Image Process., vol. 25, no. 7, pp. 3182–3193, 2016, doi: 10.1109/TIP.2016.2559803.
- [23] A. Fahim, "Clustering Algorithm for Multi-density Datasets," Rom. J. Inf. Sci. Technol., vol. 22, no. 3–4, pp. 244–258, 2019, doi: 10.1007/978-3-030-38501-9_2.
- [24] A. Fahim, "A Clustering Algorithm for Varied Density Clusters based on Similarity of Local Density of Objects," in Proceedings of the International Conference on Intelligent Computing and Control Systems, ICICCS 2020, 2020, no. Iccics, pp. 26–31, doi: 10.1109/ICICCS48265.2020.9121008.
- [25] A. Ghanbarpour and B. Minaei, "EXDBSCAN: An extension of DBSCAN to detect clusters in multi-density datasets," 2014 Iran. Conf. Intell. Syst. ICIS 2014, pp. 1–5, 2014, doi: 10.1109/IranianCIS.2014.6802561.
- [26] A. Rodriguez and A. Laio, "Clustering by fast search and find of density peaks," Science (80-.), vol. 344, no. 6191, pp. 1492–1496, 2014, doi: 10.1126/science.1242072.
- [27] R. Liu, H. Wang, and X. Yu, "Shared-nearest-neighbor-based clustering by fast search and find of density peaks," Inf. Sci. (Ny), vol. 450, pp. 200–226, 2018, doi: 10.1016/j.ins.2018.03.031.
- [28] X. X. Wang, Y. F. Zhang, J. Xie, Q. Z. Dai, Z. Y. Xiong, and J. P. Dan, "A density-core-based clustering algorithm with local resultant force," Soft Comput., vol. 24, no. 9, pp. 6571–6590, 2020, doi: 10.1007/s00500-020-04777-z.
- [29] W. Wang, J. Yang, and R. Muntz, "STING: A statistical information grid approach to spatial data mining," Proc. 23rd Int. Conf. Very Large Databases, VLDB 1997, pp. 186–195, 1997.
- [30] G. Sheikholeslami, S. Chatterjee, and A. Zhang, "Wavecluster: A multi-resolution clustering approach for very large spatial databases," Proc. Int. Conf. Very Large Data Bases, no. 24, pp. 428–439, 1998.
- [31] R. Agrawal, J. Gehrke, D. Gunopulos, and P. Raghavan, "Automatic Subspace Clustering of High Dimensional Data for Data Mining Applications," ACM SIGMOD International Conf. Manag. Data, vol. 27, no. 2, pp. 94–105, 1998.

Unsupervised Chest X-ray Opacity Classification using Minimal Deep Features

Mohd Zulfaezal Che Azemin¹, Mohd Izzuddin Mohd Tamrin², Mohd Adli Md Ali³, Iqbal Jamaludin⁴
Kulliyyah of Allied Health Sciences, International Islamic University Malaysia, Kuantan, Pahang, Malaysia^{1,4}
Kulliyyah of ICT, International Islamic University Malaysia, Gombak, Kuala Lumpur, Malaysia²
Kulliyyah of Science, International Islamic University Malaysia, Kuantan, Pahang, Malaysia³

Abstract—Data privacy has been a concern in medical imaging research. One important step to minimize the sharing of patient’s information is by limiting the use of original images in the workflow. This research aimed to use minimal deep learning features in detecting anomaly in chest X-ray (CXR) images. A total of 3,504 CXRs were processed using a pre-trained deep learning convolutional neural network to output ten discriminatory features which were then used in the k-mean algorithm to find underlying similarities between the features for further clustering. Two clusters were set to distinguish between “Opacity” and “Normal” CXRs with the accuracy, sensitivity, specificity, and positive predictive value of 80.9%, 86.6%, 71.5% and 83.1%, respectively. With only ten features required to build the unsupervised model, this would pave the way for future federated learning research where actual CXRs can remain distributed over multiple centers without sacrificing the anonymity of the patients.

Keywords—Unsupervised classification; minimal deep features; convolution neural network; chest x-ray; airspace opacity

I. INTRODUCTION

A key ingredient of anonymity in the development of machine learning models does not have to use original data in the learning process. Chest X-ray (CXR) is one of the most common modalities used in deep learning research where the images need to be labelled for further classification steps [1]. While the identity of the subjects is normally stripped from the data, it was shown that the CXRs may still contain details that could be used to identify the patients [2].

Supervised learning in radiology has grown rapidly in recent years. The applications, among others, include identifying abnormalities only from radiology reports [3], pneumonia detection using deep neural network ensemble [4], transfer learning for COVID19 classification [5], and multimodal strategy to increase the model performance [6]. Models constructed using supervised methodology requires labels annotated by experts as ground truth during training and testing phases. The problem is aggravated when the concordance rate among the radiologists is not optimal [7].

To address the problems with lack of ground truth, unsupervised approach has been proposed in recent research. The works range from the use of feature engineering based on pixel values and texture features [8] to the use of generative adversarial network (GAN) to detect anomaly in the CXRs [9]. GAN-based methods have shown promising results in

identifying abnormal images but disease-free CXRs are still required in the training stage where the confirmation of experts is still needed.

This research work aims to address the problems of hyperparameters fine-tuning and lack of labels inherent in a supervised learning architecture by using minimal deep features from a pre-trained deep learning convolutional neural network applied on the k-means algorithm, which is used to find underlying similarities in the features for classification of CXRs.

II. MATERIALS AND METHODS

The images were downloaded from ChestX-ray14 [1], a representative collection of CXRs for thoracic disorders for a general population, curated by the National Institutes of Health (NIH) Clinical Centre, USA, which primarily consist of all frontal CXRs in the centre. A total of 2,166 “airspace opacity” labels were obtained from previously published Google Health study [7]. This abnormality constitutes the most common finding in the dataset. “No findings” were assigned to the 1,388 CXRs when the original NIH and Google Health labels did not reveal any abnormality. Fig. 1 summarizes the classification used in this study.

As shown in Fig. 2, a pre-trained GoogLeNet deep learning convolutional neural network (CNN) was adopted to extract features from the CXRs [10]. The CNN was pretrained on more than a million images publicly available data set (<http://www.image-net.org>) which can classify image classes of everyday objects including pencil, coffee mug, keyboard, and animals. Each CXR resulted in 1,024 deep features which uniquely characterized the image. The features were extracted using MATLAB R2021a (MathWorks Inc., MA).

The deep features were fed into RapidMiner Studio Educational Version 9.10 (RapidMiner Inc., MA) as illustrated in Fig. 3. Forward selection was employed to increase the relevance and minimize features redundancy, which reduced the features to ten. k-Means algorithm was applied on the feature pool to determine a set of 2 clusters (i.e., “Opacity” vs “No Findings”) and assigned each CXR to a cluster. Opacity is the term used in radiology to describe the presence of whiteness region in the lungs. It was chosen because this type of anomaly is considered as one of the most prevalent in CXRs [11]. The clusters comprised CXRs with similar features with the similarity determined based on a distance measure between them. “Map Clustering on Labels” module estimates a

Supported by Ministry of Higher Education of Malaysia under the Fundamental Research Grant Scheme (ID: FRGS19-181-0790 / FRGS/1/2019/ICT02/UIAM/02/4.)

mapping between the given clustering and prediction by adjusting the given clusters with the given labels to estimate the best fitting pairs. Table I summarizes the algorithms used for the distance measure. The algorithms were chosen based on their availability in RapidMiner.

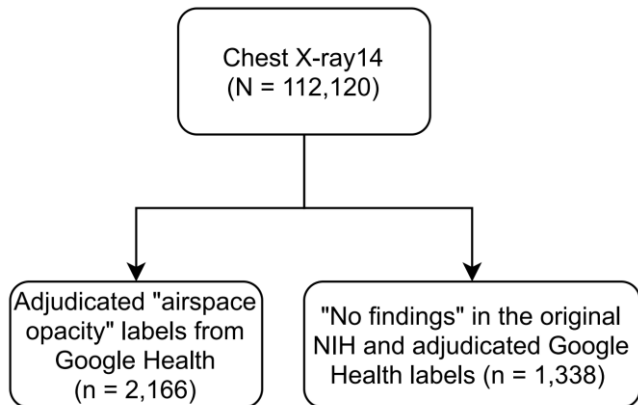


Fig. 1. CXR Images used in this Study, “Opacity” = 2,166 vs “No findings” = 1,388.

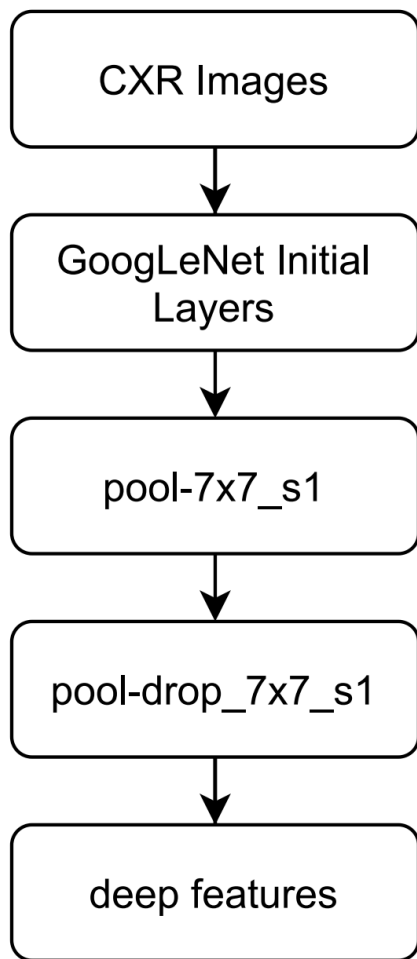


Fig. 2. Deep Features Extracted from GoogLeNet Convolution Neural Network Implemented in MATLAB.

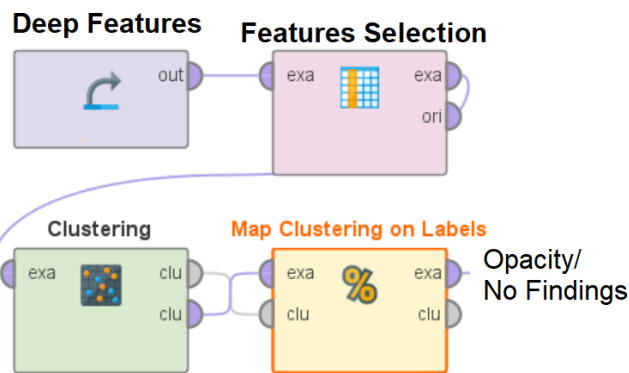


Fig. 3. Unsupervised Clustering using Deep Features on RapidMiner.

TABLE I. BRIEF DESCRIPTION OF THE DISTANCE MEASURES USED WITH THE K-MEANS ALGORITHMS

Distance Measure	Brief Description
Euclidean Distance	<p>The Euclidean distance, d between the CXR image and centroid, x and y are represented by this formula:</p> $d(x, y) = \sqrt{\sum_{k=1}^{10} (x_k - y_k)^2}$ <p>Where 10 is the total number of features, whereby x_k and y_k, are the k^{th} feature of the CXR image and the centroid respectively.</p>
Camberra Distance	<p>The Camberra distance, d between the CXR image and centroid, x and y are represented by this formula:</p> $d(x, y) = \sum_{k=1}^{10} \frac{ x_k - y_k }{ x_k + y_k }$ <p>Where 10 is the total number of features, whereby x_k and y_k, are the k^{th} feature of the CXR image and the centroid respectively.</p>
ChebychevDistance	<p>The Chebychev distance, d between the CXR image and centroid, x and y are represented by this formula:</p> $d(x, y) = \max_k x_k - y_k $ <p>Where 10 is the total number of features, whereby x_k and y_k, are the k^{th} feature of the CXR image and the centroid respectively.</p>
Correlation Similarity	<p>The correlation similarity between CRX image and centroid, x and y are represented by this formula:</p> $\text{corr}(x, y) = \frac{\sum_{k=1}^{10} (x_k - \bar{x})(y_k - \bar{y})}{\sqrt{\sum_{k=1}^{10} (x_k - \bar{x})^2} \sqrt{\sum_{k=1}^{10} (y_k - \bar{y})^2}}$ <p>Where 10 is the total number of features, whereby x_k and y_k, are the k^{th} feature of the CXR image and the centroid respectively.</p>
Cosine Similarity	<p>The cosine similarity between CRX image and centroid, x and y are represented by this formula:</p> $\text{cos}(x, y) = \frac{\sum_{k=1}^{10} x_k y_k}{\sqrt{\sum_{k=1}^{10} x_k^2} \sqrt{\sum_{k=1}^{10} y_k^2}}$ <p>Where 10 is the total number of features, whereby x_k and y_k, are the k^{th} feature of the CXR image and the centroid respectively.</p>
Dice Similarity	<p>The dice similarity between CRX image and centroid, x and y are represented by this formula:</p> $\text{sim}(x, y) = \frac{2 \sum_{k=1}^{10} x_k y_k}{\sum_{k=1}^{10} x_k^2 + \sum_{k=1}^{10} y_k^2}$ <p>Where 10 is the total number of features, whereby x_k and y_k, are the k^{th} feature of the CXR image and the centroid respectively.</p>

III. RESULT AND DISCUSSION

The performance of classification model was evaluated by its accuracy, sensitivity, specificity, and precision. The analysis of performance was expressed in true positive (TP), true negative (TN), false positive (FP), and false negative (FN). The measurements of each performance parameter were calculated as follows:

$$\text{Accuracy} = (\text{TP} + \text{TN}) / (\text{TP} + \text{TN} + \text{FP} + \text{FN})$$

$$\text{Sensitivity} = \text{TP} / (\text{TP} + \text{FN})$$

$$\text{Specificity} = \text{TN} / (\text{TN} + \text{FP})$$

$$\text{Positive Predictive Value (PPV)} = \text{TP} / (\text{TP} + \text{FP})$$

Table II provides the summary of the performance of the k-Means algorithm implemented using various distance measures. Generally, Mahalanobis Distance outperforms all other distance metrics with an accuracy, sensitivity, specificity, PPV of 80.9%, 86.6%, 71.5%, and 83.1%, respectively. This can be due to its ability to handle outliers and consideration of correlation between the features [12].

The unsupervised model with the highest accuracy shows higher sensitivity compared to specificity, which implies fewer opacity cases would be missed with the trade-off of higher false-positive results. Having a higher sensitivity is arguably more important than a higher specificity in the context of a disease screening. This is because the missed disease cases are more severe than falsely diagnosed with the disease, which can be further ruled out with a more accurate modality.

TABLE II. PERFORMANCE OF THE UNSUPERVISED CXR OPACITY CLASSIFICATION USING DEEP FEATURES WITH VARIOUS DISTANCE MEASURES

Distance Measure	Accuracy	Sensitivity	Specificity	PPV
Euclidean Distance	75.3	81.6	65.2	79.1
Camberra Distance	71	63.7	82.9	85.8
Chebychev Distance	73.9	80.1	63.8	78.2
Correlation Similarity	61.8	45.3	88.4	86.4
Cosine Similarity	71.7	64.9	82.7	85.8
Dice Similarity	51.3	24.4	94.8	88.3
Inner Product Similarity	61.8	100	0	61.8
Jaccard Similarity	61.8	100	0	61.8
Kernel Euclidean Distance	75.2	81.3	65.4	79.2
Manhattan Distance	76.6	79.4	72	82.1
Max Product Similarity	52.4	77.1	12.2	58.7
Overlap Similarity	68.7	57.2	87.4	88
KL Divergence	60.8	44.6	87	84.7
Mahalanobis Distance	80.9	86.6	71.5	83.1
Squared Euclidean Distance	75.2	81.6	64.9	79

Inner Product Similarity	<p>The inner product similarity between CRX image and centroid, x and y are represented by this formula:</p> $\text{sim}(x, y) = \sum_{k=1}^{10} x_k y_k$ <p>Where 10 is the total number of features, whereby x_k and y_k, are the k^{th} feature of the CXR image and the centroid respectively.</p>
Jaccard Similarity	<p>The Jaccard similarity between CRX image and centroid, x and y are represented by this formula:</p> $\text{sim}(x, y) = \frac{\sum_{k=1}^{10} x_k y_k}{\sum_{k=1}^{10} x_k^2 + \sum_{k=1}^{10} y_k^2 - \sum_{k=1}^{10} x_k y_k}$ <p>Where 10 is the total number of features, whereby x_k and y_k, are the k^{th} feature of the CXR image and the centroid respectively.</p>
Kernel Euclidean Distance	<p>The kernel Euclidean distance, k between the CXR image and centroid, x and y are represented by this formula:</p> $k(x, y) = e^{-\gamma D(x,y)^2}$ <p>Where gamma is a parameter that can be configured and $D(x,y)^2$ is the squared Euclidean distance between CXR image and the centroid.</p>
Manhattan Distance	<p>The Manhattan distance, d between the CXR image and centroid, x and y are represented by this formula:</p> $d(x, y) = \sum_{k=1}^{10} x_k - y_k $ <p>Where 10 is the total number of features, whereby x_k and y_k, are the k^{th} feature of the CXR image and the centroid respectively.</p>
Max Product Similarity	<p>The maximum product similarity between CRX image and centroid, x and y are represented by this formula:</p> $\text{sim}(x, y) = \max x_k^{10} x_k y_k$ <p>Where 10 is the total number of features, whereby x_k and y_k, are the k^{th} feature of the CXR image and the centroid respectively.</p>
Overlap Similarity	<p>The overlap similarity between CRX image and centroid, x and y are represented by this formula:</p> $\text{sim}(x, y) = \frac{\sum_{k=1}^{10} x_k y_k}{\min(\sum_{k=1}^{10} x_k^2, \sum_{k=1}^{10} y_k^2)}$ <p>Where 10 is the total number of features, whereby x_k and y_k, are the k^{th} feature of the CXR image and the centroid respectively.</p>
KL Divergence	<p>The Kullback-Leibler divergence, D_{KL} between the CXR image and centroid, x and y are represented by this formula:</p> $D_{KL}(x, y) = \sum_{k=1}^{10} x_k \log \frac{x_k}{y_k}$ <p>Where 10 is the total number of features, whereby x_k and y_k, are the k^{th} feature of the CXR image and the centroid respectively.</p>
Mahalanobis Distance	<p>The Mahalanobis distance between the CXR image and centroid, x and y are represented by this formula:</p> $\text{mahalanobis}(x, y) = (x - y)^T C^{-1} (x - y)$ <p>Where x is the vector of CXR image, y is the vector of the centroid, and C^{-1} is the inverse covariance matrix of the CXR image and the centroid.</p>
Squared Euclidean Distance	<p>The squared Euclidean distance, d^2 between the CXR image and centroid, x and y are represented by this formula:</p> $d(x, y)^2 = \sum_{k=1}^{10} (x_k - y_k)^2$ <p>Where 10 is the total number of features, whereby x_k and y_k, are the k^{th} feature of the CXR image and the centroid respectively.</p>

It is evident that without any training data for parameters fine-tuning, unsupervised approach results in a decent performance compared to the previously published state-of-the-art supervised classification method with the sensitivity, specificity and PPV of 86.1%, 89.7% and 91.6%, respectively [7]. It is important to highlight that while the supervised approach yields better performance, it requires dataset labelled by experts which is less cost effective.

Dice Similarity shows the lowest overall performance with an accuracy of 51.3%. Even though the specificity and PPV imply a good performance with more than 80%, the specificity is significantly lower than the average results of all distance measures.

For unsupervised opacity classification, previously published work based on GAN reported an area under the receiver operating characteristic of 0.838 [9]. However, this unsupervised algorithm still requires training dataset from normal CXRs to determine the anomaly score by calculating the pixel variation between the original and reconstructed images.

Deep features enable the use of standard patterns and image features with a high degree of correlation with human perception in a different context [10]. In this paper, we have shown that using unsupervised classification, the features with similar characteristics could be grouped to classify x-ray images.

Irrelevant features were effectively discarded using a feature selection technique, with less than 1% of the total of 1,024 features were eventually used in the classification. The high compression rate demonstrates the possibility of a high throughput screening with lower hardware requirements.

Another advantage of using minimal features is the privacy preservation of the patients. It is almost impossible to reconstruct the original images using compact features. The importance of using minimum information is highlighted in the previous research [2]. The study demonstrated a potential attack might cross-reference the CXR images to obtain classified information even when all the personal identifiers were removed.

IV. CONCLUSION

To the best of our knowledge, this is the first attempt to report the use of unsupervised CXR opacity classification with minimal deep features. With only ten features required to build the unsupervised model without hyperparameters fine-tuning, this would pave the way for future federated learning research

where actual CXRs can remain distributed over multiple centers without sacrificing the patients' anonymity.

ACKNOWLEDGMENT

This work was supported by the Ministry of Higher Education of Malaysia under the Fundamental Research Grant Scheme with identification number FRGS19-181-0790 / FRGS/1/2019/ICT02/UIAM/02/4.

REFERENCES

- [1] X. Wang, Y. Peng, L. Lu, Z. Lu, M. Bagheri, and R. M. Summers, "ChestX-ray8: Hospital-scale chest X-ray database and benchmarks on weakly-supervised classification and localization of common thorax diseases," 2017. doi: 10.1109/CVPR.2017.369.
- [2] K. Packhäuser, S. Gündel, N. Münster, C. Syben, V. Christlein, and A. Maier, "Is Medical Chest X-ray Data Anonymous?," CoRR, vol. abs/2103.08562, 2021, [Online]. Available: <https://arxiv.org/abs/2103.08562>.
- [3] S. Towfighi, A. Agarwal, D. Y. F. Mak, and A. Verma, "Labelling chest x-ray reports using an open-source NLP and ML tool for text data binary classification," medRxiv, 2019, doi: 10.1101/19012518.
- [4] I. Sirazitdinov, M. Kholiavchenko, T. Mustafaev, Y. Yixuan, R. Kuleev, and B. Ibragimov, "Deep neural network ensemble for pneumonia localization from a large-scale chest x-ray database," Computers & Electrical Engineering, vol. 78, pp. 388–399, 2019, doi: <https://doi.org/10.1016/j.compeleceng.2019.08.004>.
- [5] S. G. Sundaram, S. A. Aloyuni, R. A. Alharbi, T. Alqahtani, M. Y. Sikkandar, and C. Subbiah, "Deep Transfer Learning Based Unified Framework for COVID19 Classification and Infection Detection from Chest X-Ray Images," Arabian Journal for Science and Engineering, 2021, doi: 10.1007/s13369-021-05958-0.
- [6] G. Zamzmi, S. Rajaraman, and S. Antani, "UMS-Rep: Unified modality-specific representation for efficient medical image analysis," Informatics in Medicine Unlocked, vol. 24, p. 100571, 2021, doi: <https://doi.org/10.1016/j.imu.2021.100571>.
- [7] A. Majkowska et al., "Chest radiograph interpretation with deep learning models: Assessment with radiologist-adjudicated reference standards and population-adjusted evaluation," Radiology, vol. 294, no. 2, 2020, doi: 10.1148/radiol.2019191293.
- [8] P. Ghosh, S. K. Antani, L. R. Long, and G. R. Thoma, "Unsupervised segmentation of lungs from chest radiographs," in Medical Imaging 2012: Computer-Aided Diagnosis, 2012, vol. 8315, pp. 884 – 889. doi: 10.1117/12.911574.
- [9] T. Nakao et al., "Unsupervised Deep Anomaly Detection in Chest Radiographs," Journal of Digital Imaging, vol. 34, no. 2, pp. 418–427, 2021, doi: 10.1007/s10278-020-00413-2.
- [10] C. Szegedy et al., "Going deeper with convolutions," in Proceedings of the IEEE Computer Society Conference on Computer Vision and Pattern Recognition, 2015, vol. 07-12-June-2015. doi: 10.1109/CVPR.2015.7298594.
- [11] J. T. Wu et al., "AI Accelerated Human-in-the-loop Structuring of Radiology Reports," AMIA Symposium, vol. 2020, pp. 1305–1314, Jan. 2021, [Online]. Available: <https://pubmed.ncbi.nlm.nih.gov/33936507>
- [12] S. Ana-Maria Ramona, C. Marian Pompiliu, and M. Stoyanova, "Data Mining Algorithms for Knowledge Extraction," 2020. doi: 10.1007/978-3-030-43449-6_20.

IoT based Speed Control for Semi-Autonomous Electric On-Road Cargo Vehicle

P. L. Arunkumar¹

Research Scholar, Dept. of Electrical Engineering, Faculty of Engineering
Annamalai University, Annamalai Nagar, Chidambaram, Tamilnadu, India

M. Ramaswamy²

Professor, Dept. of Electrical Engineering
Faculty of Engineering, Annamalai University
Annamalai Nagar, Chidambaram, Tamilnadu, India

T. S. Muruges³

Associate Professor, Dept. of ECE
Government College of Engineering Srirangam
Tiruchirappalli, Tamilnadu, India

Abstract—The paper develops an investigative GSM enabled IoT based speed control scheme suitable for electric On-Road cargo vehicles. The design involves the bounding of the parameters that include the vehicle speed, motor speed, Truck payload, battery SoC (State of Charge), battery SoH (State of Health), real time navigation points using GPS, tire pressure, motor temperature and current consumption, driver fatigue detection and vehicle proximity detection which enters the system using GSM enabled wireless sensors and IoT based maps for arriving at the recommended speed. It engages a state-of-the-art Microcontroller based embedded system to govern the operation of the three-phase induction motor in accordance with the changes that the vehicle either experiences or becomes necessary for it to negotiate. It incorporates a close monitoring methodology for evolving a sequence of steps that enable the system to remain in operation over scheduled time frames. The results obtained from a simulation process carried out using embedded-c firmware code on ARM Core STM32 micro-controller exemplify the merits and illustrate the performance of the chosen vehicle in terms of its ability to be used in real world systems.

Keywords—Electric vehicle; IoT; speed control; battery SoC; battery SoH; micro-controller; embedded system; GSM; proximity sensor; payload; real time navigation; GPS

I. INTRODUCTION

The emerging development in the vehicular technology refurbishes measures to confront pollution in numerous ways with a perspective to ensemble cleaner alternatives particularly with a need for improving the performance of the cargo traffic. The advances in the communication technology bring in a need to explore autonomous vehicles (AV) as an inevitable option and as a vital business archetype.

The amalgamation of high-speed, durable, low-latency connectivity, and IoT technologies facilitate the transformation towards the fully smart Autonomous Vehicle (AV). A few of the implausible benefits of the AVs include enhancing the performance by lowering the fuel consumption, increasing the transport accessibility, reducing emission levels, and lowering congestion with the use of large-scale data/information from the connected sensors and devices [1].

The challenges involved in integrating the sensor technology with the transportation infrastructure for achieving a sustainable Intelligent Transportation System (ITS) augur efforts in enabling a fully operational and cooperative ITS environment [2].

Off late the cargo segment invites a greater attention and the related vehicle systems consider the on-road traffic on a larger framework. It demands the electric vehicles to be operated at an optimal recommended speed with a purpose to ensure the safe and secure state of the battery over a longer period [3].

There can be one or more intelligent autonomous systems in the case of unmanned, fully automatic intelligent vehicles, which continuously monitor the vehicles and control the speed of the vehicle, this paper explores the semi-automatic multi-modal speed control within the recommended limits for employing their usage in real world systems, following a structured flow with Related Works, Research Gap, Proposed Work with its methodology, simulation and unite testing with results and conclusion.

II. RELATED WORK

The new and upcoming technologies in the transportation and power sector of Electric vehicles that offer huge benefits in terms of the economic and environmental factors have been reviewed by Ayob et al. (2014). A comprehensive review and evaluation of several types of electric vehicles and its associated equipment in particular battery charger and charging station has been outlined and a comparison on the commercial and prototype electric vehicles in terms of the electric range, battery size, charger power and charging time carried out [4].

A study to shed light on future opportunities and the possible hurdles associated with autonomous vehicle (AV) technologies has been studied by Bagloee et al. (2016)[5]. The evolution of the Internet of Things (IOT) relating to its use in the automotive sector has been discussed by Bajaj et al. (2018) to provide a perspective on the various areas that include the connected car services/applications, Vehicle communications, IoT in Intelligent Transportation, IoT based Supply Chain

Management in Automotive Industry and New Generation Cars, where reports reveal tangible progress [6].

The need for introducing the electric vehicles with IoT based technology to monitor the battery life of electric vehicles has been brought out by Urooj et al. (2021). The parameters in the form of the distance covered cost and capacity of battery which in turn contribute towards the smooth function of the electric vehicles have also been monitored [7].

Though a host of issues have been addressed, still there needs to be enough literature around how the firmware side of speed controller can be developed and tested at test benches before integration into real vehicle for manufacturability. The scope extends on a wide front and demands further studies to accomplish a new dimension in the field of cargo transportation.

III. PROBLEM DEFINITION

The focus accentuates to extradite a GSM enabled IoT-based speed control scheme of a battery-operated on-road vehicle with different parameters in the form of the vehicle speed, engine speed, proximity, and driver fatigue detection with the battery SoC (state of charge), battery SoH (state of health), tire pressure remaining within limits to forge real time navigation needs. It attempts to involve the use of sensors and GSM enabled IoT network through an ARM based STM32 micro controller for enabling the vehicle to operate at the recommended speed. It evaluates the algorithm's adaptability using bench testing-based simulation and orients to demonstrate its real time adoption to production lines.

IV. PROPOSED WORK

The block schematic of the system seen in the Fig. 1 includes the battery-operated power source to the vehicle along with the associated auxiliary circuits. It explains the basic philosophy relating to the control of speed for the chosen vehicle across the operating range on the guidelines of the parametric considerations. Designing an Intelligent system to maintain optimum speed can help to derive the maximum efficiency of the on-road vehicles.

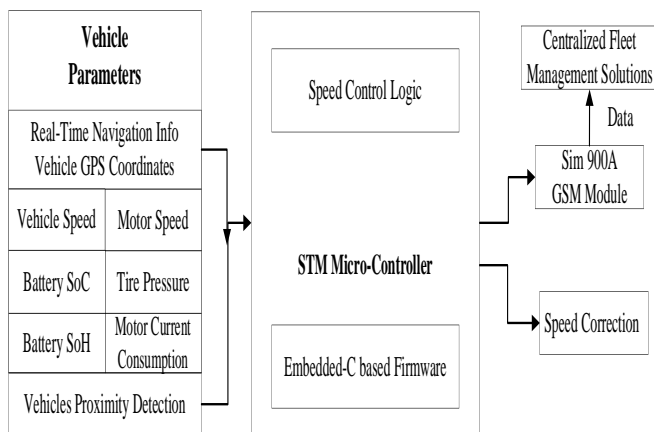


Fig. 1. Block Diagram for On-Road Electric Cargo Vehicle Speed Control.

The hardware consists of STM32 micro controller that offers advanced and flexible multi-core architecture, graphic support with power-efficient real-time control and high feature

integration, ATMEGA 16 based PWM generators, DIP switches to select multiple enabling wireless technologies for IoT, powered by a standard 12 volts system, with GSM module operating at a voltage less than 4.5 volts [8].

V. PROPOSED METHODOLOGY

The optimum performance of an on-road cargo electric vehicle, measured in terms of the control of its speed may be obtained by tuning the parameters of the vehicle. The parameters that entail to be monitored include the vehicle speed, motor speed, tire Pressure, Battery SoC, Battery SoH, real time navigation points using GPS coordinates, motor current consumption, driver fatigue detection and the vehicle proximity detection.

An autonomous vehicle (AV) in general relies on the devices and components that exchange, share and construe data. Interoperability of the devices and components guarantee that they augur to shape an integrated ecosystem within the vehicle, effortlessly communicating with each other without forfeiting the performance [9].

The AVs experience inimitable capricious circumstances often and testing the on-road prototypes may be perilous and hence as an alternative, testing and validating AVs can be done using simulation for swift and cost-effective results. The guaranteed approach may be to explore the AV domain validity by means of parameterization and simulation by employing a sub-system-based test approach at the unit level in the developer bench [9].

While the AVs can reduce the burden on the driver and make the industry driverless, the march towards autonomous vehicles remains only in research for a while due to the consideration of dynamic changes in environment where the vehicle operates, bringing in many real-time unexpected factors outside its control. It may or may not require the presence of the driver, while the semi-autonomous vehicles can partially take few decisions based on the programmed intelligence at the IoT Smart Edge Nodes and enable/aid the driver with adequate recommendations [10].

The transition from manual to autonomous mode may take time to become reality, while the transition can be enabled by an interim option of the Semi-Autonomous Vehicle. It offers a realistic, pragmatic, and swift solution to necessitate mobility on-demand which refers to a vehicle operated by a human, not being self-driven. The solutions may serve to automate the driving functions under ideal conditions and can conduct the same task in a sustainable and convenient fashion.

The methodology informs the system of any circumstances that may curtail or disable the automated driving system in accordance with the demand, where in it requires the driver to perform the tasks. It involves the sensor fusion element, where the inputs from an onboard sensor that holds the semantic knowledge of the perceived environment becomes crucial for ensuing interpretation, prediction, planning and decisive action [11]. The priority on the entities considers the highest associated risk of collision with few sample entities including dynamic instances (e.g. (vulnerable) road users), static instances (e.g., road boundaries) and the obstacles on the path that surpass a specific size.

The monitoring of the electric vehicle state includes the status of the energy storage system that include the electric battery's state of Health (SoH) a figure of merit that indicates the battery level of degradation, state of Charge (SoC) providing information about the current amount of energy stored in the battery [12], the tire pressure which holds a high impact on the tire-road contact as it influences the characteristics of the tire forces [13], regulating the speed and movement of the electric vehicle by adjusting the PWM value on the DC motor thereby attaining vehicle Speed and motor speed control [14], real time navigation points using GPS coordinates that uses real time geographical data received from quite a few GPS satellites to determine the longitude, latitude, speed and route that aids in navigating the vehicle [15], motor current consumption, driver fatigue detection system that alerts the driver across multiple stages depending on the severity of the drowsiness symptoms [16] and the vehicle proximity detection which can probably reduce the fatality rate.

The monitoring of the parameters under consideration is conducted by using appropriate sensors at regular periodic intervals incessantly during the entire duration of the vehicle operation commencing from ignition ON to OFF that also includes the idle time with a periodicity of 10 ms maintained through a RTOS (real-time operating system).

The GSM for data monitoring mutually with GPS for live positioning facilitates secure and periodic monitoring of the parameters to initiate the STM32F746NG micro-controller, being the central backbone of the vehicle/system that offers reliability, performance calculating power, accessibility, real-time support, automotive bus interfaces, high speed data interfaces, digital and analog pins as well as low-power mode.

The SIM 900A, a readily available GSM/GPRS module for communication, operates with a mobile SIM card that provides internet connectivity to moving vehicles and systems. The process uses the SIM 900A to interface with the STM micro-controller by means of the serial data connection with the data

being sent from SIM 900A to the centralized server at regular intervals. The receiving interface system validates the data and upon receiving the command from the centralized server of the fleet management, when transferred to the STM controller can control the speed of the vehicle.

The highly configurable and quite versatile STM32 micro controller ensures edge processing when it conducts the computation of data directly in the smart sensor node or at the gateway, to save power consumption, guaranteeing data confidentiality, allowing analysis of the critical information at the node level, and reducing anomaly detection time [17].

The ARM interfaced to ATMEGA 16 based PWM generators simulate the vehicle speed, motor speed at the test bench. On receiving the commands, it processes the user sent instructions to operate the vehicle at its synchronized speed. However, based on the user commands, the processor simultaneously sends PWM signals for operating the motor at the desired speed to attain the desired movement.

The DIP Switch in the hardware system of the Fig. 2 facilitates to select connectivity in case of the scalable implementation across various enabling wireless technologies for IoT with the system employing two separate potentiometers for simulating the vehicle and motor speeds [19]. The hardware system as seen from the same figure receives the data from the IoT based intelligent embedded edge nodes and the sensors to allow the micro-controller for recommending the speed based on the software intelligence reflected through the Flow Chart depicted in the Fig. 3.

It operates together with the various vehicle parameters and facilitates the control implementation by means of actuators [20]. The speed correction arrives at the actuator and vehicle speed control recommendation is obtained either from the intelligence in micro-controller present within the vehicle or from the vehicle owner based on the data communicated through IoT mechanisms via SIM900A GSM Module.

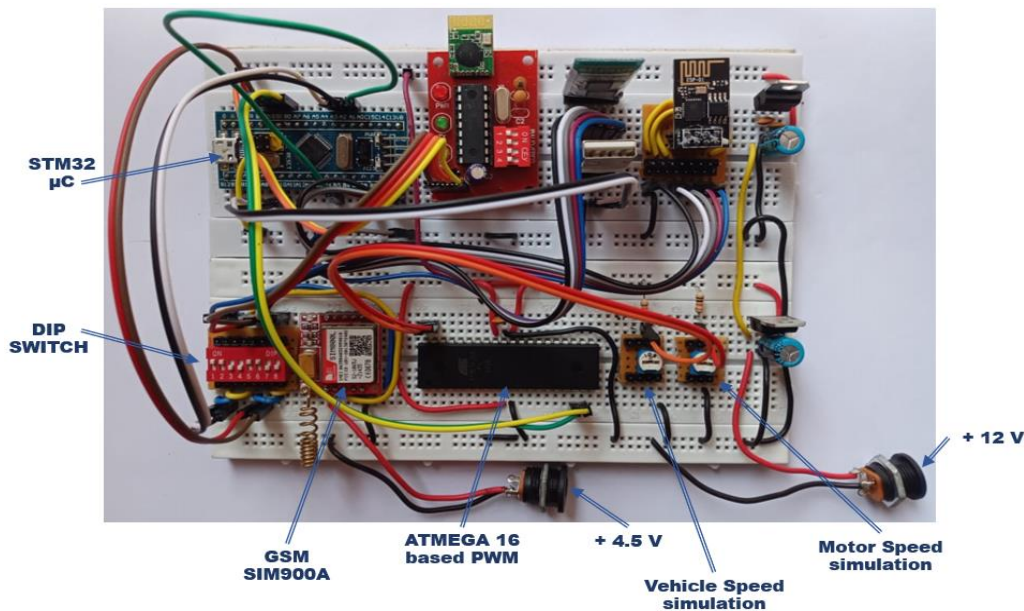
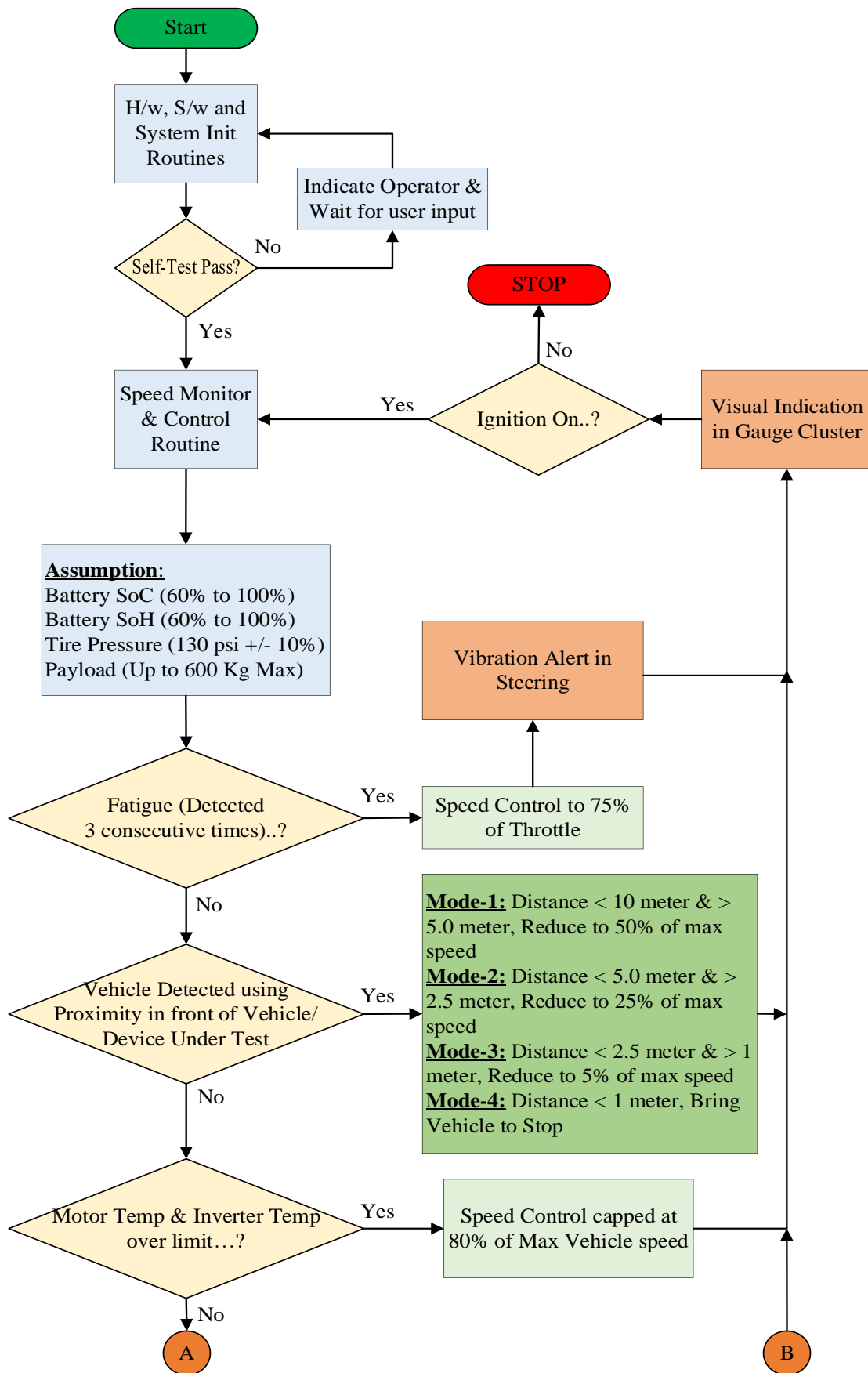


Fig. 2. Simulated Hardware Test System for On-Road Electric Cargo Vehicle Speed Control.



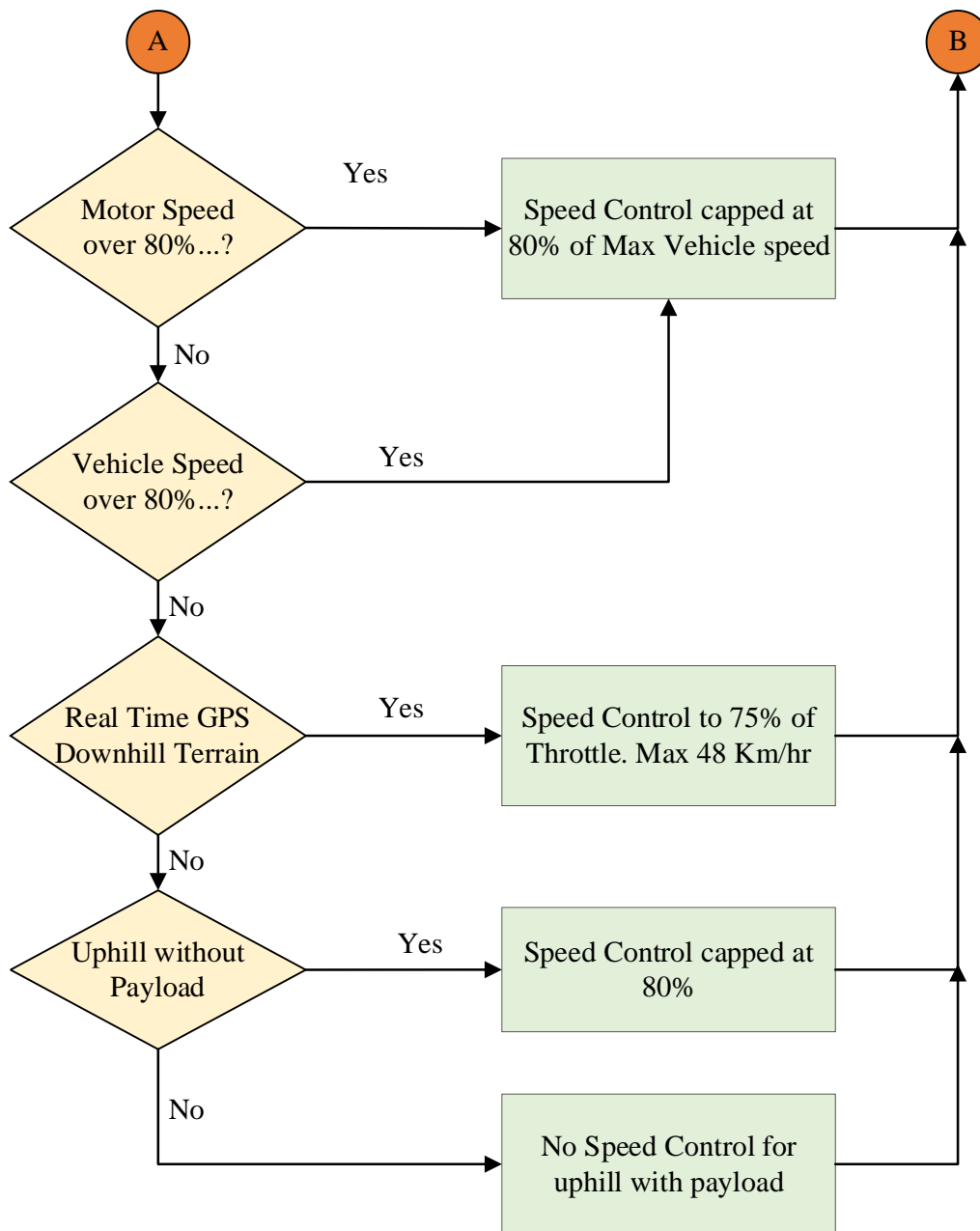


Fig. 3. Algorithmic Flow Chart for On-Road Electric Cargo Vehicle Speed Control.

The IDE can be used as a development environment and the cross compiler together with the skeleton infra-structure is created with the required minimal base reset codes, initializing routines and hardware abstraction layer codes. It avails the FreeRTOS as the real time operating system functions to prioritize the task and events with embedded-C-based multi-function multi-file implementation along with the occasional assembly language instructions for accessing several registers and timing critical functions.

VI. SIMULATION AND TESTING

Understanding the accuracy offered by a simulation paves way for the means to determine its efficacy during development and validation activities. The

automated/autonomous vehicles envisage the roads to be safer and operate cohesively using robust networks and powerful IoT based solutions being essential to reduce significant human errors [18].

The 'Supro, a stylish and spacious van launched by Mahindra & Mahindra Ltd, offers a whole new concept in cargo transportation in the sense it brings emissions down to absolute zero levels and proffers to be the first of its kind in India [18]. The benefits include being eco-friendly, direct drive transmission with a single speed gearbox and sophisticated speed management of the motor that allows to cruise through traffic effortlessly without shifting gears, home charging option that goes from 0 to 100% through a 15 amp plug point in just 8 hours 45 mins*.

The electric drive motor with an exceptional power of 25kW & 90 Nm torque gathers smooth drive with a top speed of 60kms/hr and on full charge it can run up to 110 kms. The revolutionary regenerative braking technology helps it to literally recover the energy it dispenses. A unique instrument cluster provides valuable information in the form of the Status of Charge (Battery %), Distance to Empty (DTE), Speed, Gear Engaged, Total Running and E-gen efficiency. With a 72V lithium-ion battery, long-life, maintenance-free options are entrusted.

The boost mode provides the vehicle with additional power to manage steep inclines and the Revive® emergency feature gives an extra 7 kms range once the vehicle goes out of charge to reach the nearest charging point destination [21].

The Table I given below provides all the Technical Specifications for the chosen electric vehicle Mahindra eSupro and the Cargo Van Specifications for the same is furnished in Table II along with the input parameters and the simulation values in the Table III.

The testing adopts a simulation procedure explained using the Fig. 4 that entails generating the sensor signal using appropriate instruments to check the embedded firmware code implemented for the vehicle speed control. The process engages to simulate the engine and vehicle speed with 2 separate ATMEGA 16 based function generators and predicts the vehicle tire pressure, Battery SoC, Battery SoH, while providing information on real time navigation and payload as serial data over the bus.

The vehicle parameters on being simulated with the preconditional assumption that the vehicle continues to be fully functional with the IoT connectivity. The Intelligent Edge Node Smartness aids only in controlling while it relies on the IoT infra-structure for data monitoring and assumes that the SoC, SoH, Payload, Tire Pressure remain within the permissible limits.

TABLE I. MAHINDRA eSUPRO TECHNICAL SPECIFICATION

Battery and Electric Motor		Warranty	
Battery Pack Rating	200Ah	Vehicle	2yrs / 40,000kms**
Electric Motor	3-ph, AC induction	Battery	3yrs / 40,000kms**
Max Power	25kW @ 3000 rpm	Vehicle Dimensions	
Max Torque	90Nm @ 1500 rpm	Length	3798 mm
Suspension		Width	1540 mm
Front	McPherson Strut with Coil Spring	Height	1922 mm
Rear	Leaf Spring	Wheelbase	1950 mm
Wheels & Tires		Ground Clearance	130 mm
Wheels	4.5J x 13	Performance	
Tire Size	155/80 R13 Radial Tubeless	Top Speed	60 km/hr
Brakes		Battery Range	115* kms (Cargo Van)
Front	Hydraulic, Disc	Charge Time (0 to 100% @ 25°C)	8 hours 30 minutes
Rear	Hydraulic, Drum		

TABLE II. MAHINDRA eSUPRO CARGO VAN SPECIFICATION

Specifications	Cargo Van
Seating Capacity	Driver + Co-Driver
Loading Bay (L x W x H in ft)	6 x 4 x 4
Loading Volume (litre)	2330
Payload (kg)	600
Gross Weight (kg)	1920
Kerb Weight (kg)	1320

It simulates the proximity of the other vehicles through the variable power supply (PoT), with the consideration that higher voltages relate to the objects being closer. Even though the object detection on the four directions becomes realizable, it recognizes precedence for the frontal detection.

The system, with the prioritized parameters in the Table IV attaches the highest priority to the Battery SoC & SoH and provides control over the speed only if both the parameters remain within the permissible limits, in addition to the tire pressure and payload. However, a change of the parameters together with its priority persuades the commendation of the requisite speed to be set and thus administers the accurate operational requirements to eventually achieve the desired speed control objective.

TABLE III. INPUT PARAMETERS AND SIMULATION VALUES

S.No.	Parameter	Max. Value Observed in Vehicle	Ideal / Optimum Value	Sensor Output		Simulation Range
				O/p Signal	Value (with unit)	
1	Motor Speed	3000 rpm	2400 rpm	PWM	Hz	0 to 150 kHz
2	Vehicle Speed	60 km/hr	48 km/hr	PWM	Hz	0 to 150 kHz
3	Truck Payload	600 kg	600 kg	Raw Data	Ton (kg)	N/A
4	Tire Pressure	130 psi	130 psi	Raw Data	Psi	N/A
5	Battery SoC	100 %	60% < SoC < 100%	Raw Data	%	N/A
6	Battery SoH	100 %	60% < SoH < 100%	Raw Data	%	N/A
7	Driver Fatigue (Eye) Detection	No	No	Boolean	Yes/No	Yes/No
8	Motor Temperature	70 deg cel	70 deg cel	ADC	Voltage	0 to 100 deg cel
9	Real Time Navigation points using GPS	20.04 deg, 20.04 deg	Non-Zero Number	Latitude, Longitude	Number	Random Values
10	Motor Current Consumption	2.1 Amp	2.1 Amp	Current Reading	Amp	0 to 10 Amp

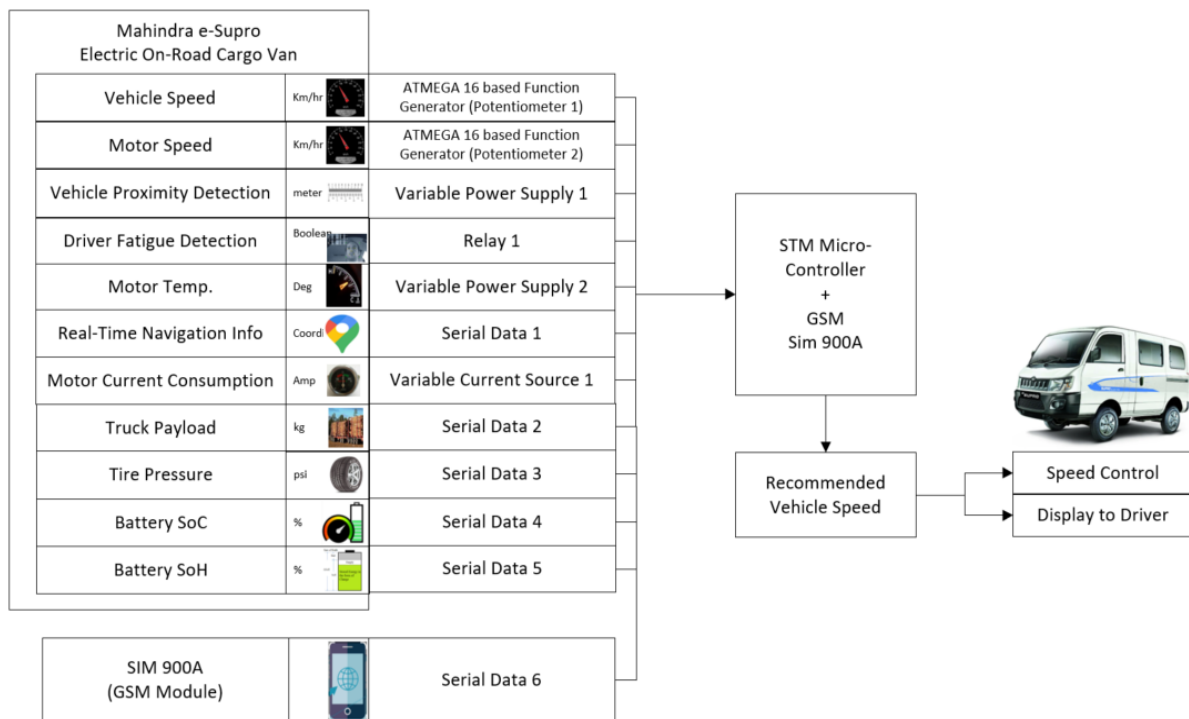


Fig. 4. Simulation and Testing Block Diagram for On-Road Electric Cargo Vehicle Speed Control.

TABLE IV. PRIORITIZED PARAMETERS

Parameter	Priority
Battery SoC	1
Battery SoH	2
Driver Fatigue (Eye) Detection	3
Vehicle Proximity Detection	4
Real Time Navigation points using GPS	5
Vehicle Speed	6
Motor Speed	7
Motor Current Consumption	8
Motor Temperature	9
Truck Payload	10
Tire Pressure	11

VII. RESULTS AND DISCUSSION

The target owes to examine the use of the IoT for the speed control of a battery operated on road electric vehicle across the standard operating ranges of the SoC, SoH, payload and tire pressure as detailed in the Table V. It operates on the etiquettes of the ARM microcontroller from where it controls the speed in tune with the demands over specific time frames. It monitors the other parameters with the relative sensor inputs being simulated and evaluates the vehicle for the control of the speed through the feedback mechanism from the micro controller.

The scheme rallies to vary the pulse widths to realize the change in the speed using the controller module in the ATMEGA-16 based function generator. It simulates various cases of speed ranging from 0 to 100% of the vehicle top

speed, which corresponds from 0 to 60 km/hour over a span of 20 minutes rehearsing an emulation of the actual vehicle under stable operating conditions.

Fig. 5 depicts the input pulse and the output response where the vehicle when operated up to 80% of the max speed yields higher life for the battery and provides better mileage. When the vehicle crosses the expected speed, the controller reacts by reducing the speed with a deviation of $\pm 5\%$ which enables to extend the life- time of the battery.

The variations in the speed of the motor seen from the Fig. 6 show that the motor speed remains at an optimum of 70% to 80% of its max capacity to ensure its smooth functioning. It further explains that when the motor speed attempts to go above 80%, the micro-controller recommends the vehicle speed to be reduced.

The graph in the Fig. 7 relates to restricting the motor to operate within an ideal temperature range of around 70 deg Celsius with a view to achieve the maximum power output and a long lifespan for the battery. Since the temperature of the motor can be reduced by lowering the load on the motor, in case the temperature exceeds 70 deg Celsius, the micro-controller allows reducing the load to bring the vehicle speed within a minimal deviation of $\pm 5\%$.

TABLE V. OPERATING RANGE OF VEHICLE PARAMETERS

Parameter	Values
Battery SoC	60% to 100%
Battery SoH	60% to 100%
Tire Pressure	130 psi \pm 10%
Payload	Up to 600 kg (max)

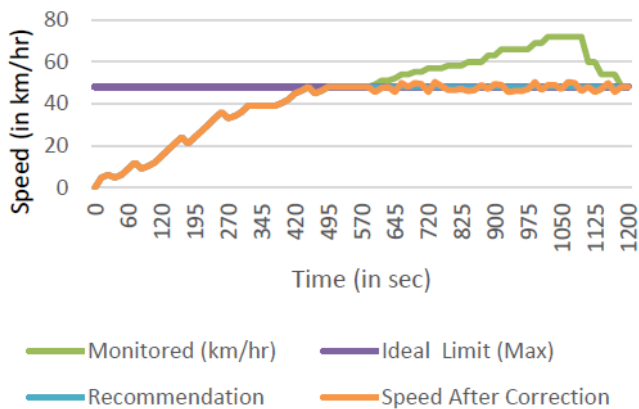


Fig. 5. Speed Control based on Vehicle Speed.

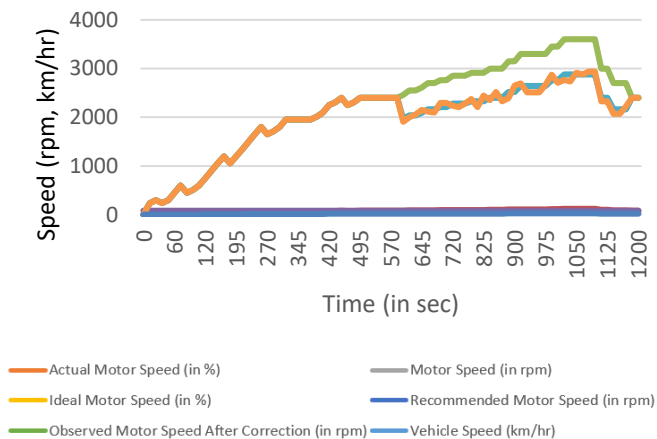


Fig. 6. Speed Control based on Motor Speed.

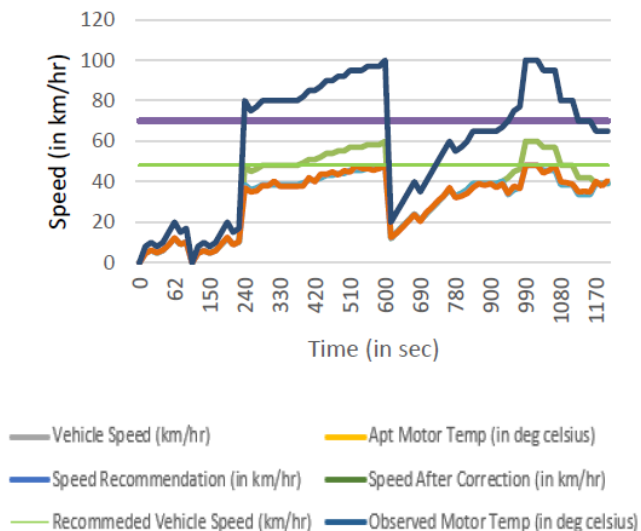


Fig. 7. Speed Control based on Motor Temperature.

The driver's fatigue detection constitutes to significant criterion for manual and semi-autonomous vehicles for enabling the speed control from an increased safety

perspective. The fatigue detection as shown in Fig. 8 returns a Boolean value to indicate the safe operating conditions and in any case without the fatigue being detected, the speed of the vehicle depends only on the other parameters. Whereas in case of fatigue detection, identified by three or more consecutive repeated occurrences, considering the safety of the driver, irrespective of the vehicles speed being within or above limits, the driver receives a visual warning through the dashboard, vibrational warning through the steering system to reduce the vehicle speed to 75% of the current speed and then regulates it to be not above the recommended max of 42 km/hr.

The speed control based on Real Time GPS input coordinates underscores further study under two different cases that include the uphill and downhill terrain travel without payloads. When the vehicle travels uphill as shown in Fig. 9 or downhill as shown in Fig. 10, it does not travel a straight path with predefined fixed inclinations. However, with an empty on road electric cargo vehicle travelling upwards with no payload, the speed restrictions can be functional. With payload, limiting the speed may not provide the vehicle with required momentum, pulling power and traction to climb uphill.

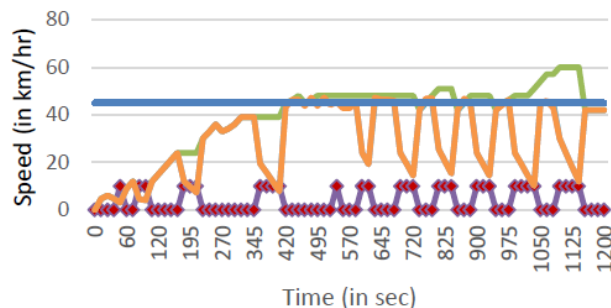


Fig. 8. Speed Control Due to Fatigue Detection.

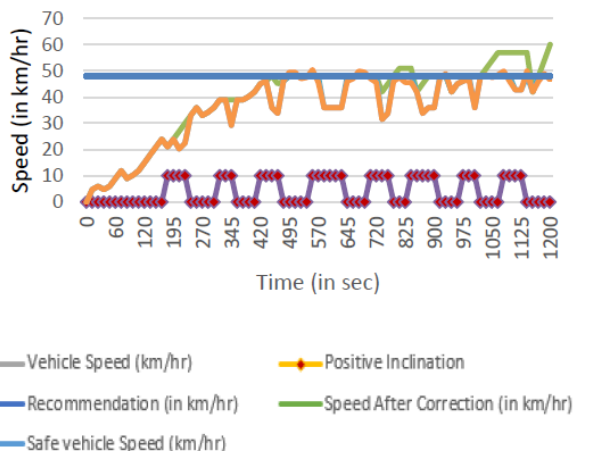


Fig. 9. Speed Control based on Uphill terrain Movement (without Payload).

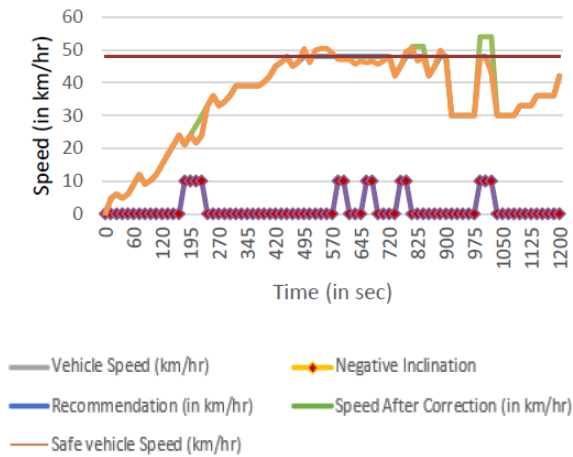


Fig. 10. Speed Control based on Downhill Terrain Movement.

The speed control in the case of the vehicle travelling downhill may be very tight considering the safety of the driver, as control can be lost easily travelling downhill. The test results illustrate that the speed requires to be maintained/reduced to 80% of the driver’s acceleration input, besides ensuring that it does not exceed the max speed of 48 km/hr.

It employs a proximity sensor deployed appropriately on the front grill to circumvent a crash and attempts to discern the obstructions in the frontal path of the vehicle. It orients to report the distance at which it detects the obstruction or the vehicle and follows a four-stage classification based on the distance to estimate the proximity from the frontal side of the vehicle and allow the speed reduction appropriately in the four different modes as noted in the Table VI.

It simulates the obstructions detected along with its distance from the vehicle, with the distance as the key parameter for determining on speed control. The Fig. 11 derives the resultant output enabling the speed control based on the distance reported between the vehicle and the nearest obstruction.

The intelligent microcontroller monitors the requisite parameters and elicits a decision based on more than one criterion. The results also show that the algorithm either maintains or reduces the speed of the vehicle automatically and notifies the driver that the speed reduces to the recommended level with a deviation of 5% and accuracy of 95%, as observed from the simulated results. Future research can be envisaged to validate the base parameters considered for speed control with its priorities, experiment with a different RTOS, test the same system and at integration level or system level, integrate with a real vehicle and so-on.

TABLE VI. SPEED CONTROL AS PER THE PROXIMITY RANGE

	Distance between the vehicles frontal end and Obstruction	Speed reduction (% of applied throttle)
Mode 1	> 5 to < 10 meters	50%
Mode 2	> 2.5 to < 5 meters	25%
Mode 3	> 1 to < 2.5 meter	5%
Mode 4	< 1 meter	0% (Stop)

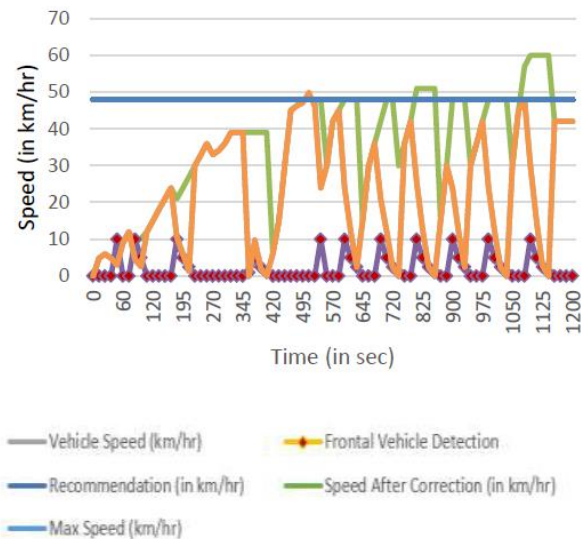


Fig. 11. Speed Control based on Frontal Vehicle Detection.

VIII. CONCLUSION

An IoT based methodology suitable for controlling the speed of a battery operated on road ‘Supro cargo vehicle within the prescribed parametric range has been developed. The firmware design has been articulated using an ARM microcontroller through which it obtains the variation in the width of the PWM pulse for the converter interface that in turns controls the motor operating the vehicle. It has been formulated using the real time input from the GPS for controlling the speed based on the location services and a proximity sensor suitably deployed on the front grill. The test bench of the algorithm has been laid from a real time python-based coding to provide the varying requirements to the microcontroller through the inputs to the interface. The simulation results have been presented to foster the suitability of the scheme for use in on road cargo vehicular systems.

REFERENCES

- [1] Khayyam, H., Javadi, B., Jalili, M., & Jazar, R. N. (2020). Artificial intelligence and internet of things for autonomous vehicles. In *Nonlinear approaches in engineering applications* (pp. 39-68). Springer, Cham.
- [2] Guerrero-Ibanez, J., Zeadally, S., & Contreras-Castillo, J. (2018). Sensor technologies for intelligent transportation systems. *Sensors*, 18(4), 1212.
- [3] Mol, C., O’Keefe, M., Brouwer, A., & Suomela, J. (2010). Trends and insight in heavy-duty vehicle electrification. *World Electric Vehicle Journal*, 4(2), 307-318.
- [4] Ayob, A., Mahmood, W. M. F. W., Mohamed, A., Wanik, M. Z. C., Siam, M. M., Sulaiman, S., ... & Ali, M. A. M. (2014). Review on electric vehicle, battery charger, charging station and standards. *Research Journal of Applied Sciences, Engineering and Technology*, 7(2), 364-373.
- [5] Bagloee, S. A., Tavana, M., Asadi, M., & Oliver, T. (2016). Autonomous vehicles: challenges, opportunities, and future implications for transportation policies. *Journal of modern transportation*, 24(4), 284-303. <https://doi.org/10.1007/s40534-016-0117-3>.
- [6] Bajaj, R. K., Rao, M., & Agrawal, H. (2018). Internet of things (IoT) in the smart automotive sector: a review. In *IOSR Journal of Computer Engineering (IOSR-JCE)*, conference on recent trends in computer engineering (CRTCE) (pp. 36-44).
- [7] Urooj, S., Alrowais, F., Teekaraman, Y., Manoharan, H., & Kuppusamy, R. (2021). IoT Based Electric Vehicle Application Using Boosting Algorithm for Smart Cities. *Energies*, 14(4), 1072.

- [8] <https://www.st.com/en/microcontrollers-microprocessors/stm32-arm-cortex-mpus.html>.
- [9] <https://www.electronicsforu.com/tech-zone/test-measurement/parameters-evaluate-autonomous-vehicles>.
- [10] <https://www.automotiveworld.com/articles/semi-autonomous-vehicles-the-short-term-solution-to-restart-ride-sharing-innovation/>, <https://www.brookings.edu/blog/techtank/2017/01/30/semi-autonomous-vehicles-must-watch-the-road-and-the-driver/>.
- [11] Weller, G., Sohr, S., Alt, D. et al. Comprehensive Safety Concept for Automated Driving. *ATZ Worldw* 122, 26 – 31(2020). <https://doi.org/10.1007/s38311-019-0167-3>, <https://www.daimler.com/documents/innovation/other/safety-first-for-automated-driving.pdf>.
- [12] Noura, Nassim, LoïcBoulon, and Samir Jemeï. "A review of battery state of health estimation methods: Hybrid electric vehicle challenges." *World Electric Vehicle Journal* 11.4 (2020): 66.
- [13] Hegedűs, Tamás, et al. "Handling of tire pressure variation in autonomous vehicles: an integrated estimation and control design approach." 2020 American Control Conference (ACC). IEEE, 2020.
- [14] Wibawa, I. P. D., and C. Ekaputri. "Speed and steering control system for self-driving car prototype." *Journal of Physics: Conference Series*. Vol. 1367. No. 1. IOP Publishing, 2019. <https://doi.org/10.1088/1742-6596/1367/1/012068>.
- [15] Rahiman, Wan, and Zafariq Zainal. "An overview of development GPS navigation for autonomous car." 2013 IEEE 8th Conference on Industrial Electronics and Applications (ICIEA). IEEE, 2013.
- [16] Chellappa, Yogesh, Narendra Nath Joshi, and Vaishnavi Bharadwaj. "Driver fatigue detection system." 2016 IEEE International Conference on Signal and Image Processing (ICSIP). IEEE, 2016.
- [17] <https://www.st.com/en/applications/factory-automation/edge-processing.html>.
- [18] Vermesan, O., Bahr, R., Falcitelli, M., Brevi, D., Bosi, I., Dekusar, A., Velizhev, A., Alaya, M.B., Firmani, C., Simeon, J.F. and Tcheumadjeu, L.T., (2020). IoT technologies for connected and automated driving applications. In *Internet of Things-The Call of the Edge: Everything Intelligent Everywhere* (pp. 306-332). River Publishers.
- [19] P.L.Arunkumar, M. Ramaswamy, C.Sharmeela (2021), "IoT Based Multi-Modal Speed Controller for an Off-Road open port Electric Double Cab Vehicle", *International Journal of Engineering Trends and Technology*, Vol. 69, Issue 12, pp. 127-135.
- [20] P.L.Arunkumar, M. Ramaswamy, C.Sharmeela (2022), "Internet of Things Based Speed Control for an Industrial Electric Vehicle Using ARM Core", *Ecological Engineering & Environmental Technology*, Vol. 23, Issue 2, pp. 113-121.
- [21] <https://www.mahindrasupro.com/esupro/>.

A Novel Approach of Hyperspectral Imaging Classification using Hybrid ConvNet

Soumyashree M Panchal¹

Assistant Professor

Department of Information Science & Engineering
HKBK College of Engineering, Bangalore, India

Shivaputra²

Assistant Professor

Electronics and Communication Engineering
Dr. AIT, Bangalore India

Abstract—In recent years, remote sensing applications have been booming, and with this hyperspectral imaging (HSI) has been used in many real-life applications. However, the classification of HSI is a significant problem due to the complex features of the captured hyperspectral scene. Moreover, the HSI is often inherently nonlinear and has very high-dimensional data. Recent years have seen a rise in deep learning applications for addressing nonlinear problems. However, deep learning tends to overfit when sparse or less training data is available. In this paper, the proposed work focuses on addressing the trade-off problem between classification performance and less training samples for classifying hyperspectral image data in a single training process. Thus, the study presents a hybrid multilayer learning system based on the joint approach of 2D and 3D convolutional kernels. The main reason is to utilize the spectral-spatial and spatial correlations in the learning process to achieve improved generalization of features in the training process for better HSI classification. The study outcome exhibits higher precision, recall rate, and F1-score performance. The overall accuracy is 99.9%, with a better convergence rate. The results prove that the proposed model is effective for HSI classification even with fewer training data samples.

Keywords—Hyperspectral image; convolution neural network; classification; spatial feature; spectral feature

I. INTRODUCTION

Hyperspectral imaging (HSI) consists of hundreds of narrow bands with rich spectral and spatial data in remote sensory applications. These spatial and spectral characteristics of hyperspectral remote sensing images can provide useful information for detecting and classifying objects [1]. Since the early 1990s, HSI has been widely applied in a variety of real-world contexts, including precision agriculture [2] and land management to healthcare and military target identification [3]. HSIs are high-dimensional data with a high correlation between adjacent spectral bands, making it more complex in time and space context and leading to the Hughes phenomenon [4]. Thus, reducing the amount of redundancy in HSI processing is a crucial concern. In the literature, most of the existing studies have focused on exploring the role of spectral features of HSI in classification. Indeed, HSIs also typically have spatial features where the adjacent pixels tend to be part of the same class. Because of these characteristics, two significant challenges encountered related to HSI processing viz. i) the high spatial inconsistency concerning spectral features and ii) constraints samples and the high dimensionality data. Several factors are usually responsible for the challenges

mentioned above, such as changes in lighting conditions, environment, surroundings impact, and temporal circumstances [5]. These challenges often result in problems for most traditional methods and reduce their classification accuracy [6]. To overcome these problems, the analysis of spatial features has been reported to be valuable in improving object identification and classification performance. According to recent literature, classification of the HSI object based on spectral-spatial information, incorporating spatial attributes into pixel-wise cataloging processes [7] using mathematical morphological operations, Artificial Neural Networks (ANN), and machine learning methods such as support vector machines (SVMs), Logistic Regression, and many others [8]. Moreover, existing researches have also tried to address the problem associated with feature engineering, using principal component analysis (PCA) and linear discriminant analysis (LDA) [9][10]. Despite this, the previous works heavily rely on shallow and manual feature descriptors and are usually created for specific purposes, limiting their effectiveness in real-time situations [11].

Several deep learning models, including ConvNet convolution neural networks (CNNs), recurrent neural networks (RNNs), and deep autoencoders, have recently made significant breakthroughs in computer vision tasks, such as image classification [12] object recognition [13], and language processing [14]. These applications have inspired HSI analysis, and deep learning has proved to be highly effective in detecting and classifying objects. In contrast to traditional manual methods, deep learning can extract valuable insights from input data samples through a sequence of hierarchical layers [15]. In the literature, deep learning-based research works for HSI classification have few flaws and rely on substantial labeled samples [16]. However, feature generalization can be fully automated, making deep learning more appropriate for various situations. Furthermore, the previous deep learning models adopt a very complex structure, lack the ability for the input data to be spatially invariant, and are prone to overfitting problems due to the high dimensionality and small sample size of HSI. Therefore, there is a need to develop an effective model that can perform precise feature analysis to classify HSI objects with data samples without posing an overfitting issue. Hence, the factor of motivation is to understand the fact the wider scope of usage of HSI could be more leveraged if these impending problems are addressed where the existing solution encounters problems associated with computational complexities and non-inclusion of various constraints. This

results in evolution of proposed solution towards addressing this point for classifying HSI objects. In this paper, the proposed work addresses the HSI classification issue by using a new hybrid deep learning mechanism to identify the object category of each pixel with a limited number of data samples. Specifically, the study emphasizes feature learning aspects of the proposed hybrid learning model, which uses both 2D ConvNet and 3D ConvNet to process hyperspectral cube structure. The proposed hybrid ConvNet assembles 2D and 3D convolution layers as complementary operations to attain rich contextual information in the learning process concerning both spatial feature and mixed feature (i.e., spatial-spectral) to achieve maximum possible accuracy. The significant contribution of this paper is highlighted as follows:

- The proposed research work enhances the function of deep learning techniques with stochastic data treatment and feature selection process for the optimal performance in HSI classification.
- Unlike previous schemes, the proposed work emphasizes balancing overall accuracy and computational efficiency.
- A hybridization is introduced in the learning model, providing less dependency on the training sample and quick convergence.
- The design of the proposed model for HSI classification is adaptive to different HSI data, thus meeting the requirement of the real-time deployment scenario.

The remaining sections of this paper are organized as follows: Section II presents a brief review of the existing works done in the context of HSI classification; Section III highlights the significant issue and the research gap explored based on the review analysis; Section IV discusses the proposed system design and methodology adopted; Section V focuses on the detailing the implementation procedures for processing hyperspectral cube and classifying the objects from the HSI; in Section VI results and discussion is carried out for the validation of the proposed work and finally Section VII concludes the real contribution of this paper.

II. REVIEW OF LITERATURE

This section briefly reviews the existing solutions in this context and highlights the significant problem explored based on the review analysis. Although the HSI classification has been extensively studied in the past recent years. The existence of noise seriously affects the classification accuracy of the model. The work carried out by Lu et al. [17] suggested a different technique named penalized linear discriminant (PLD) with principal components to address the issue of noise in HSI data. PLD analysis is implemented to determine the optimal covariance matrix of noisy data, and then it is eliminated using a principal component transformation scheme. The study outcome shows that this method removed noise significantly without losing spectral fidelity. Hou et al. [18] presented a supervised dimensionality reduction scheme based on the kernel-based possibilistic clustering mechanism in the same line of work. The fundamental principle of this kernel-based possibilistic clustering scheme is the construction of the

weights to generalize effective transformation directions for executing HSI classification. However, deciding a suitable kernel is quite tricky, and similar performance may not be achieved on the other HSI dataset. In this direction, Hang et al. [19] reported the suitability of applying local graph discriminant (LGD) embedding. However, this lacks consideration of the spatial features of the HSI data. The authors have developed a regularization scheme that considers the spatial information in LGD embedding, thereby boosting classification performance. The study has also shown that implementing this method can improve the performance of the kernel-based methods. Jia et al. [20] emphasized addressing the problem of labeling data samples in the classification task. This study suggests an unsupervised model based on the combined approach of Gabor filters and LAD to extract the most revealing and refined features for classification. However, LDA is quite popular, but it ignores the local structure of the data, which limits the applicability of LDA in real-time HSI classification. To address this problem, Wang et al. [21] presented a locality adaptive LDA method to generalize an illustrative subspace of data sample and determine the points closely associated with spectral and spatial domains. LDA heavily relies on certain assumptions, limiting its scope to a specific context. In this regard, another most popular method is principal component analysis (PCA), which is an unsupervised dimensionality reduction technique. The application of PCA is used in the study of Tu et al. [22] for the HSI dimensionality reduction. The authors have extracted sub-cubes in the further steps, which is then decomposed into texture and background layers. The obtained texture layer is introduced to the pixel-wise classifier. The result shows the effectiveness of the presented approach under fewer training samples. In the work of Chen et al. [23], PCA is integrated with a feature engineering process based on the local binary pattern that produces multifeatured vectors. Further, a kernel extreme learning mechanism is employed for the classification task, and its parameter is optimized using the gray wolf optimization algorithm. However, due to a complex implementation strategy, the method may pose a huge computational complexity issue while executing the model training process. Despite many works, the kernel-based methods suffer convex problems and adequate selection of an adequate kernel. Recently, multilayer learning models have been recognized as advanced classification methods for HSI classification. For example, deep ConvNet via hashing semantic attribute is presented by Yu et al. [24]. In this study, a series of hash functions are produced to improve the generalization of classes and discriminative learning mechanisms into the input HSI. A large CNN is configured to perform HSI classification task. However, the presented CNN model is complex and lacks a trade-off between precise feature generalization and network complexity. The work in the context of effective feature learning is carried out by Zhang et al. [25], where the authors have presented an unsupervised learning-based feature extraction mechanism. The presented mechanism is devised using a recursive autoencoder that considers both spatial and spectral information to construct a high-level features vector for the learning model. The authors in the study of Liu et al. [26] have tried to enhance the performance of extreme learning machines by introducing the concept of transfer learning for

HSI classification. Transfer learning introduces weights and concealed biases by using instances in the source domain. The application of the feedback attention technique in CNN is presented in the work of Yu et al. [27] for HSI classification. The feedback attention is integrated to improve the feature extraction process with the semantic information from the top dense layer. This model considers spatial-spectral information for the feature analysis. Also, the computational complexity is controlled band attention technique is incorporated in the learning model. Dong et al. [28] focused on addressing the problem caused by the small training sample size by designing pixel cluster CovNet with a spatial-spectral synthesis mechanism. A co-occurrence matrix is created to store spatial attributes, and band superposition is then applied to fuse the spatial attributes with spectral features. The authors have devised a certain policy to increase the training sample size, which is then subjected to the Covnet model for the classification. However, increasing sample size may introduce non-linearity and redundancy in the training data sample, which may impact the real performance of the learning model. Different from the other works, Zhang et al. [29] presented graph convolution networks that produce operative local spectral-spatial attributes for effective HSI classification.

Hence, various research works have been done to date for the HSI classification using different approaches. However, there is still a substantial problem concerning the model complexity, overfitting issue, learning, and classification performance that needs further effort by the researchers with evolved solutions. The next section highlights significant research problems explored based on the above discussion.

III. RESEARCH PROBLEM

The prominent research gap explored in existing solution is associated with narrowed classification performance for HSI which demands more lightweight feature extraction technique using machine learning. Further, the significant research issues explored based on the review of existing literature.

- HSI data is high-dimensional, which makes supervised classification techniques very difficult to implement. In this case, the complexity of the HSI data and the limited number of training samples are the major challenges.
- Space and spectral information are essential for applying effective classification mechanisms to HSI data but are not considered in most existing studies.
- Most machine learning methods implement the recursive nature of algorithms that do not consider the characteristics and quality of the data.
- The existing deep learning-based solution is often subjected to the overfitting issue due to the lack of proper labeled and large data samples. Such a model also requires multiple attempts of training and tuning to meet the targeted requirements of the performance.
- HSSI requires higher computing resources and longer execution times which are not as prominently emphasized in the previous works. Such existing solution is not much suitable for time-sensitive and mission-critical applications.

Hence, there is a requirement to evolve up with good solution that leads towards an effective processing and classifying HSI.

IV. SYSTEM DESIGN

This section illustrates the design of the proposed system for the HSI classification using a unique and hybrid multilayer learning model. Therefore, the proposed study's ultimate goal is to extract the comprehensive and precise feature concerning 2D spatial information and 1D spectral information with neighbor pixels in the center that needed to be classified. However, it is well known that the constraint of training sample heavily impacts the learning model performance with increase in feature dimension. To this end the modelling of the proposed system aims to address Hughes phenomenon problem, pixel mixing and achieve a good trade-off between the number of limited or unbalanced training samples, and model performance, and control overfitting. The design of the proposed system for HSI classification is demonstrated in Fig. 1.

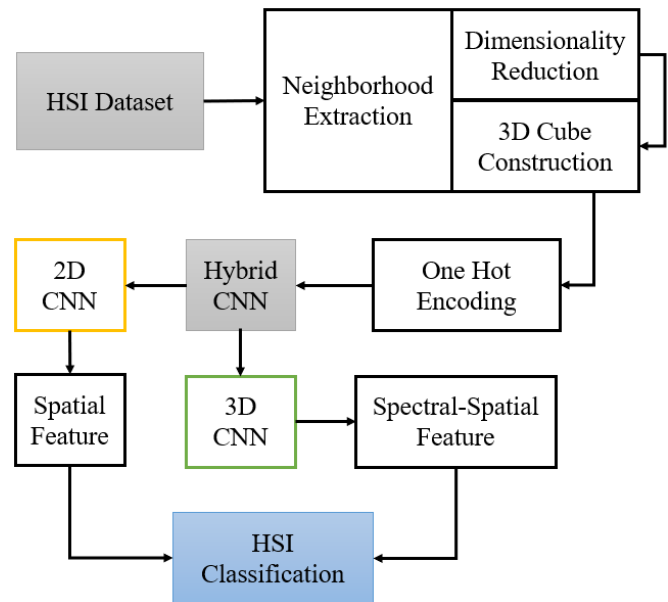


Fig. 1. Schematic Architecture of the Proposed System.

The HSI classification dataset is considered the Indian pine data collected through “airborne visible/infrared imaging spectrometer sensor” in north-western Indiana. Further, the system modelling process emphasizes on the neighborhood extraction process that incorporates two distinct operations. The first operation is subjected to dimensionality reduction as the HSI data exhibit the mixing pixel property, introducing the high intra-class variability and inter-class similarity. To this end, the study implements principal component analysis (PCA), which leads in reduction of redundant spectral information without losing spatial information for the object identification and classification. On the other hand, the second operation is executed to construct 3D cube using frequency and spatial domain information. This operation leads to generation of HSI into several images of 5x5 pixel (5 neighboring pixel) visualization with respect to spectral analysis, spatial analysis and spectral-spatial analysis in transform domain. The obtained

3D cubes are vectorized using one-hot encoding mechanism, to make it suitable for the proposed deep learning model. The study proposes hybrid deep learning model which is a combined implementation of 2D ConvNet and 3D ConvNet that synchronizes both spectral both spatio-spectral feature concerning 2D and 3D convolution operation for processing 3D HSI cube to extract precise attributes closely related to objects of the HSI. In this way, the proposed system is computationally efficient, and can achieve better HSI classification performance without posing overfitting problem.

A. 2D ConvNet

The design of Convnet is inspired by the visual system that does not need human involvement in the feature extraction process. The 2D ConvNet utilizes 2D kernels to extract spatial features map followed by convolution operation to map input observation to the output prediction class. Essentially, the convolution is an algebraic operation executed based on the summation of the scalar product between input HSI and filter (kernel) employed to extract features from the 3D HSI cube. This kernel is a matrix that moves or strides over the input HSI data, executes scalar product with the sub-region of spatial dimension. Further, a non-linearity is introduced to the model by passing the obtained feature map through the activation function given as follows:

$$v_{i,j}^{x,y} = f \left(b_{i,j} + \sum_{m=1}^{d_{l-1}} \sum_{\rho=0}^{\gamma_{i-1}} \sum_{\sigma=0}^{\delta_{i-1}} w_{i,j,m}^{\sigma,\rho} \times v_{i-1,m}^{x+\rho,y+\sigma} \right) \quad (1)$$

Equation (1) exhibits activation $v_{i,j}^{x,y}$ of convolution operation in 2D ConvNet, with spatial positions (x, y) in j^{th} feature map at every i^{th} layer under consideration, where $f(\cdot)$ denotes activation function, $b_{i,j}$ denotes bias term at i^{th} layer and for j^{th} feature map, d_{l-1} denotes the number of feature map in $(l-1)^{\text{th}}$ layer and the kernel depth $w_{i,j}^{m,\sigma,\rho}$ at position (ρ, σ) for the j^{th} feature map of i^{th} layer, γ_i represents the width of kernel, δ_i indicates height of kernel and $w_{i,j}$ represents weight term for j^{th} feature map of i^{th} layer. In the proposed model 2D ConvNet, Relu is considered as the activation function numerically expressed as follows:

$$f(x) = f_{max}(0, x) \quad (2)$$

In the proposed 2D ConvNet only 1 convolution layer is configured and pooling layers are not taken under consideration to keep significant attributes of each pixel. The 2D ConvNet is implemented before the flattening layer and 3 fully connected layers. The reason is that with 2D ConvNet, the spatial attributes within the different spectral bands can be captured powerfully without losing vital spectral features, which is a crucial for the effective classification of HSI data.

B. 3D ConvNet

The configuration of the 3D Covnet is quite similar to the 2DCovnet. The significant difference is that it has additional layer of reordering where convolution operation is carried out using 3D kernel with multiple contagious spectral bands in the input layer using 3D information. It preserves their correlations under a spectral context by sequentially ordering images of similar bands. The operation of the 3D Covnet can be expressed as follows:

$$v_{i,j}^{x,y,z} = f \left(b_{i,j} + \sum_{m=1}^{d_{l-1}} \sum_{\rho=0}^{\gamma_{i-1}} \sum_{\sigma=0}^{\delta_{i-1}} \sum_{n=0}^{n_{i-1}} w_{i,j,m}^{\sigma,\rho,n} \times v_{i-1,m}^{x+\rho,y+\sigma,z+n} \right) \quad (3)$$

Where, n_i denotes the size of the 3-D kernel along the spectral dimension and remaining parameters are similar as expressed in equation (1). In the proposed 2D ConvNet 3 convolution layer is configured and Relu is used as activation function.

V. SYSTEM IMPLEMENTATION

Mathematically, the HSI data considered in the study expressed as $I = (I_1, I_2, I_3 \dots I_D)^T \in R^{D \times (M \times N)}$, where D indicates number of spectral bands containing $(M \times N)$ images per band subjected to the output class $Y = (Y_1, Y_2, Y_3 \dots Y_C) \in R^{1 \times 1 \times C}$, where C indicates object classes. The major operation in HSI classification is assign an exclusive label to each pixel according to the both spatial and spectral features. Therefore, the classification of HSI can be considered as domain mapping problem, where mapping function $f(x)$ takes input data I and after applying some transformation operation, the function should provide matching class Y given as follows:

$$Y = f(I, \theta)$$

Where θ denotes learning adjustable parameter required in the feature learning and mapping process. The following are the steps carried out for implementing proposed hybrid Covnet for processing 3D HSI data.

Step: 1 Load the HSI dataset $\rightarrow I \in R^{D \times (M \times N)}$. The input data contains a dimension of $145 \times 145 \times 200$, where (145×145) is the dimension of the image and 200 is the number of spectral bands. Fig. 2 presents a sample visualization of image at random bands under range of 200.

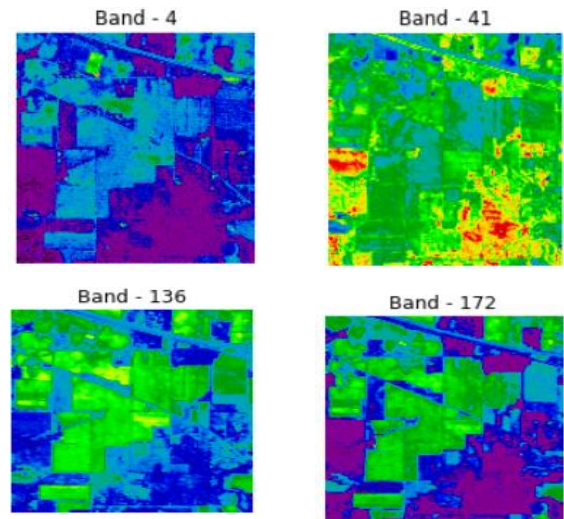


Fig. 2. Sample Visualization of HSI Bands.

Step: 2 Since, the HSI is of high dimension and often contains mixed pixel posing huge inter-class similarity and intra-class variability. Therefore, the study applies a PCA technique to overcome these issues to an extent by reducing redundant spectral information. As a result, reduced spectral band is attained while preserving spatial information. Mathematically, this operation can be given as follows:

$$I \in \mathbb{R}^{B \times (M \times N)} \leftarrow f_{PCA}(I \in \mathbb{R}^{D \times (M \times N)})$$

The processing of input data (I) using PCA returns a reduced number of spectral bands (B) such that $D \rightarrow B$, while keeping spatial information ($M \times N$) same for carrying out object classification.

Step: 3 The next operation is to perform neighborhood extraction which is subjected to construction of set of 3D cubes each representing 3D images, where object class is decided by its centering pixel. Numerically, this operation given as follows

$$I \in \mathbb{R}^{B \times (M \times N)} \rightarrow I' \in \mathbb{R}^{B \times (w \times w)}$$

Where, ($w \times w$) denotes window size covering all ‘B’ at centering pixel at spatial location (p, q). In the proposed system the size of window ($w \times w$) is considered equal to (5×5). The constructed 3D cubes from input data $I \in \mathbb{R}^{B \times (M \times N)}$ is the $(M - w + 1) \times (N - w + 1)$. Therefore, the 3D data cubes (D) with spatial location (p, q) denoted as $D_{(p,q)}$ covers width $p - (w - 1)/2$ to $p + (w - 1)/2$ and height from $q - (w - 1)/2$ to $q + (w - 1)/2$ and all ‘B’ of the dimensionality reduced data i.e., $\in \mathbb{R}^{B \times (M \times N)}$.

Step: 4 Split the obtained set of 3D data cubes into training and testing set. Further, apply one hot encoding operation to vectorize the 3D data cubes in the training samples.

Step: 5 Develop a hybrid Covnet model using 3D Covnet and 2D Covnet. Since, it has been discussed that 2D Covnet does not process spectral information and 3D Covnet is able to process both spectral and spatial data simultaneously.

In order to attain comprehensive and precise feature learning, the proposed study performs hybridization of the 3D CovNet and 2D CovNet to leverage capability of both model in the HSI classification task. The configuration details of the proposed hybrid CovNet is mentioned in Table I. The flow procedure of the proposed system using hybrid CovNet is illustrated in Fig. 3. The proposed system comprises of many operational steps. In the first step the HSI data is loaded, and further it is subjected to the PCA for the dimensionality reduction. As a result, the original HSI data of dimension ($145 \times 145 \times 200$) is reduced to the ($145 \times 145 \times 30$). In the next process, neighborhood windowing is carried out with window size (5×5) followed by zero padding operation. This operation leads to generation of 10249 number of data cubes having dimension of ($25 \times 25 \times 30$) where 30 is the number of spectral bands and 25×25 is the spatial resolution. The next vital operation is executed to perform modelling of hybrid ConvNet which comprises of total 3 layer of 3D ConvNet and 1 layer of 2D ConvNet. The first layer of 3D ConvNet comprises kernel size of ($3 \times 3 \times 7$) with filter size 8 which after convolving provides feature map of size ($23 \times 23 \times 24 \times 8$) where (23×23) is the resolution size of 3D data cube (two spatial information) with (24) spectral bands (one spectral information) and filter size 8 subjected for the further convolving operation at next layer of 3D ConvNet. The convolution operation in Covnet is most critical process. For example, at the first layer of 3D ConvNet the input data cube

convoluted with learnable filters such as filters and 3D kernel, characterized by the weighting and bias parameter resulting in generation of the feature map. Already activation of this operation is shown in equation (3). Similarly, the second layer of the 3D ConvNet takes feature map of first layer and after convolution it provides a feature map ($21 \times 21 \times 20 \times 16$) with two spatial information (21×21) and one spectral information (20) with filter size 16. This layer comprises a kernel size of ($3 \times 3 \times 5$). On the other hand, the third layer of 3D ConvNet comprises kernel size of ($3 \times 3 \times 3$) with filter size equal to 32 which after convolving provides a feature map of size ($19 \times 19 \times 18 \times 32$) where (19×19) is the resolution size of 3D data cube (two spatial information) with (18) spectral bands (one spatial information) and filter size 32. On the sub-sequent layer 2D ConvNet is implemented with single layer which comprises kernel size of (3×3) with filter size 64 which after convolving provides feature map of size ($17 \times 17 \times 64$) where (17×17) is the spatial resolution of 3D data cube and filter size 64. As it has been already discussed that 2D ConvNet are not able to process spectral information, whereas 3D ConvNet efficiently processes spatial-spectral information. Furthermore, the reason behind implementing 3D ConvNet at three layers is due to the fact that it increases spectral-spatial feature maps for better feature generalization process. Also, 2D ConvNet is implemented at single layer is due to the fact that it efficiently recognizes spatial attributes from different spectral information without compromising the spectral information. Further, flattening layer is introduced after 2D ConvNet to flatten the multi-dimensional feature map to a single dimension vector for further processing at fully connected layers used to extract more precise features by reshaping feature maps into an n-dimension vector. The last layer of proposed Hybrid ConvNet is the classification layer which uses SoftMax classifier for the classification of HSI objects. The training of model is carried out using back-propagation algorithm with Adam optimizer.

TABLE I. CONFIGURATION DETAILS OF PROPOSED HYBRID COVNET

Layers	Shape
InputLayer	25,25,30,1
Conv3D_L1	23,23,24,8
Conv3D_L2	21,21,20,16
Conv3D_L3	19,19,18,32
Reshape	19,19,576
Conv2D_L1	17,17,64
Flatten	18496
Dense_L1	256
Dropout	256
Dense_L1	128
Dropout	128
Dense_L1	16

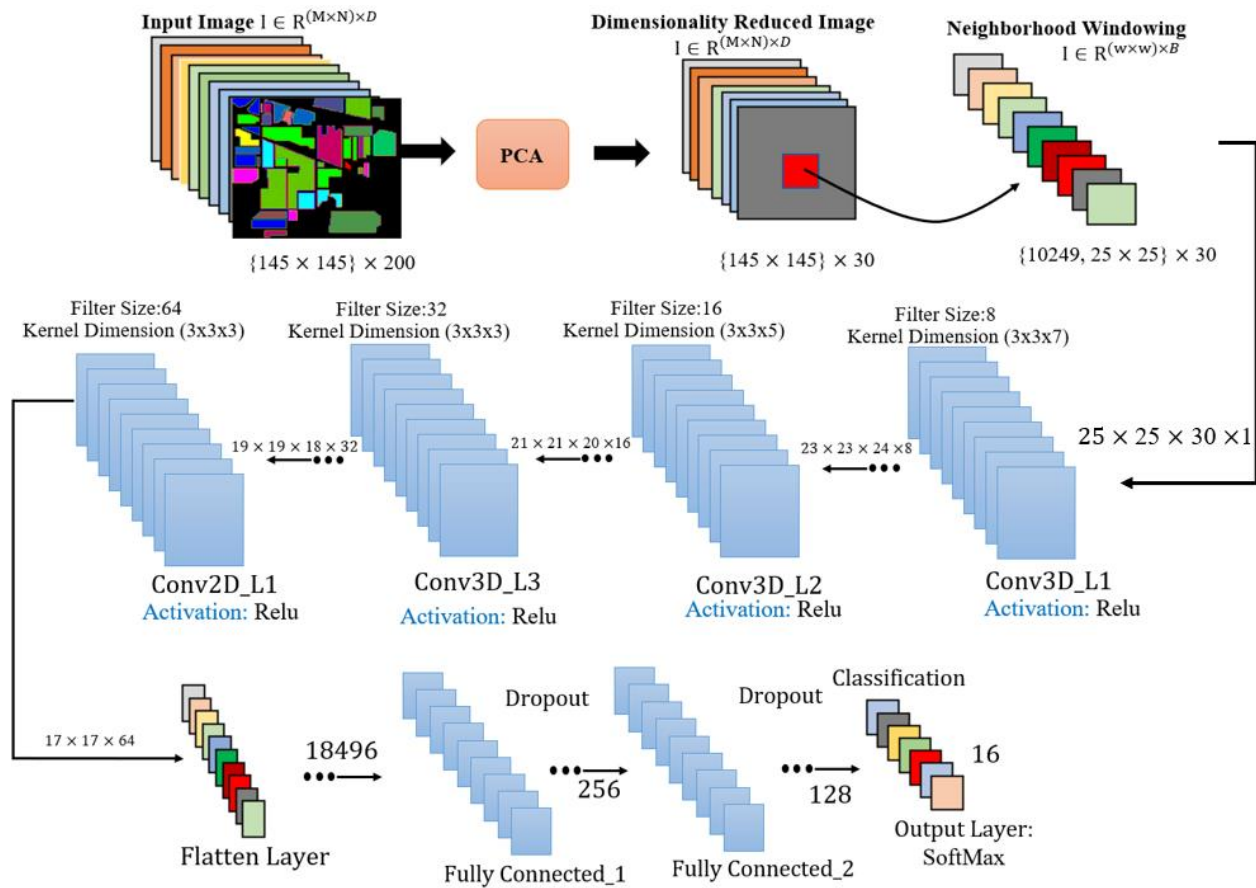


Fig. 3. Process Flow of the Proposed Hybrid CovNet.

VI. RESULT AND ANALYSIS

The implementation of the proposed system is carried out using Python programming language. The study considers Indian pine HSI dataset for the model execution. The proposed hybrid ConvNet model is trained using assignment of random weights at initial process, mini-batch size is kept equal to 256 after empirical analysis, the model is trained for 100 epochs. This section discusses the outcome obtained and performance analysis of the proposed system to justify the proposed contribution in the field of HSI processing.

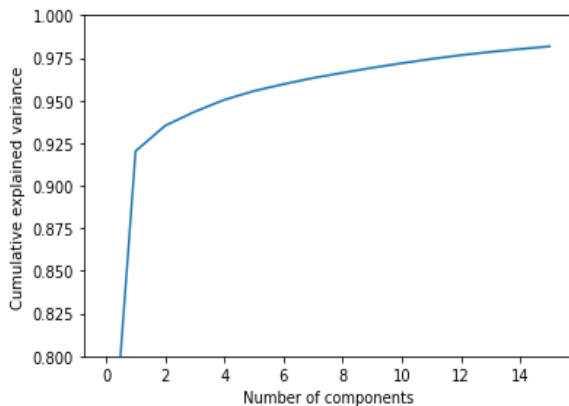


Fig. 4. Analysis of Cumulative Variance (%).

Fig. 4 shows the performance of the PCA applied for dimensionality reduction. The graph trend exhibits slightly a linear trend in the percentage variance explained by each component.

Fig. 5 shows performance analysis of proposed model regarding its loss curve in training. The graph trends lower value of loss is maintained for 80% epochs. However, at initial the loss rate is high but after 10 epochs the loss gets lower and stabilized from 20 epochs to 100 epochs.

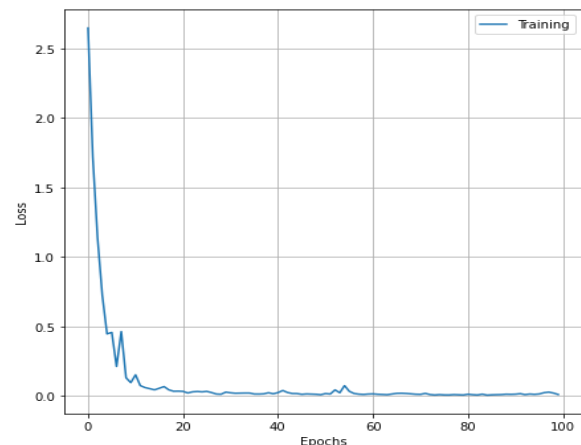


Fig. 5. Analysis of Training Loss.

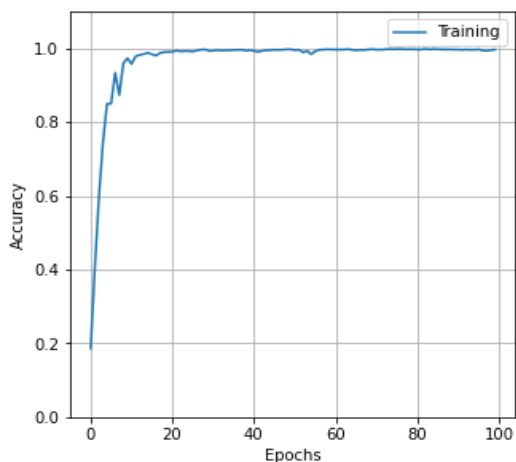


Fig. 6. Analysis of Training Accuracy.

Similar, observation can be found in Fig. 6 for the training accuracy analysis. The graph trend shows constantly higher training accuracy from 20th epoch to 100 epochs.

It can be seen from Table II that the proposed system has achieved good performance for the classification of the HSI objects. The results show a 100% precision score obtained for each class of HSI dataset. Similarly, the outcome exhibits 100% recall rate for each class except one class namely ‘Buildings-Grass-Trees-Drive’ that exhibits 99% recall rate. On the other hand, the result shows 100% F1-score for 14 classes of HSI data, and 99% for two classes namely ‘Grass-trees’ and ‘Buildings-Grass-Trees-Drive’. The performance in terms of overall accuracy is 99.9%. Therefore, the proposed model proved to be efficient and effective for the processing of the HSI data without compromising the classification performance which also evident through the confusion plot shown in Fig. 7. The performance analysis from the human visual system perspective, the ground truth of input HSI data is shown in Fig. 8 and the visualization of predictive classified outcome is presented in Fig. 9. The comparison of both figure shows that the predictive outcome is almost similar to the ground truth data, thereby exhibiting the effectiveness of the proposed system using a hybrid learning model. A closer look into the existing system showcase that proposed system is capable enough to be processed on varied number of HSI with better classification performance with respect to accuracy. Further, the learning method involved the proposed study is of hybrid form that can be used for identifying and localizing multiple form of standard land area in the HSI image.

The findings of this study based on simulation analysis also show that the proposed model has a better convergence rate. The reason behind this is that the features extracted by the proposed Hybrid ConvNet consist of fine and precise contextual attributes of HSI images. The implementation of multilayer 3D ConvNet effectively exploited both spatial and spectral information and the single-layer 2D ConvNet, exploiting rich spatial context analysis without losing spectral information. Finally, it has been found that the proposed multilayer hybrid deep learning model effectively synchronizes correlation between spatial and spectral features and provides better classification results with less training data samples.

TABLE II. ANALYSIS OF CLASSIFICATION OUTCOME

HSI classes	Precision	Recall	F1-Score
Alfalfa	1.00	1.00	1.00
Corn-notill	1.00	1.00	1.00
Corn-mintill	1.00	1.00	1.00
Corn	1.00	1.00	1.00
Grass-pasture	1.00	1.00	1.00
Grass-trees	1.00	1.00	0.99
Grass-pasture-mowed	1.00	1.00	1.00
Hay-windrowed	1.00	1.00	1.00
Oats	1.00	1.00	1.00
Soybean-notill	1.00	1.00	1.00
Soybean-mintill	1.00	1.00	1.00
Soybean-clean	1.00	1.00	1.00
Wheat	1.00	1.00	1.00
Woods	1.00	1.00	1.00
Buildings-Grass-Trees-Drive	1.00	0.99	0.99
Stone-Steel-Towers	1.00	1.00	1.00
Over all Accuracy (%)	99.9 %		

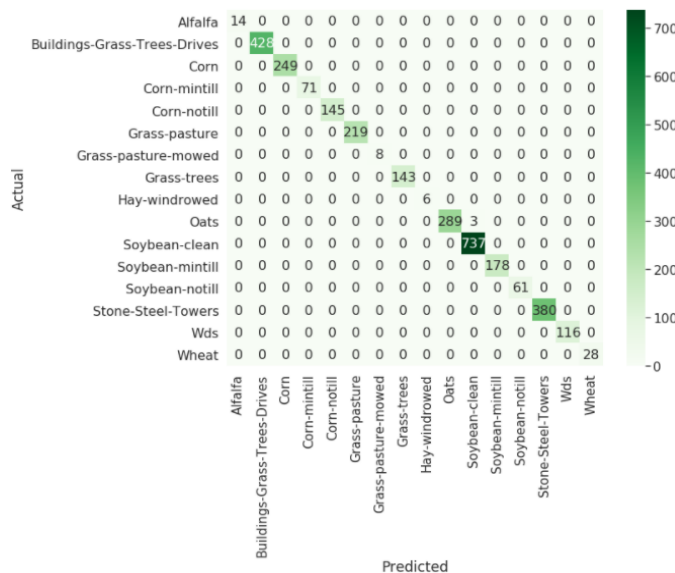


Fig. 7. Analysis of the Confusion Plot.



Fig. 8. Visualization of the Ground Truth of Input HSI Data.

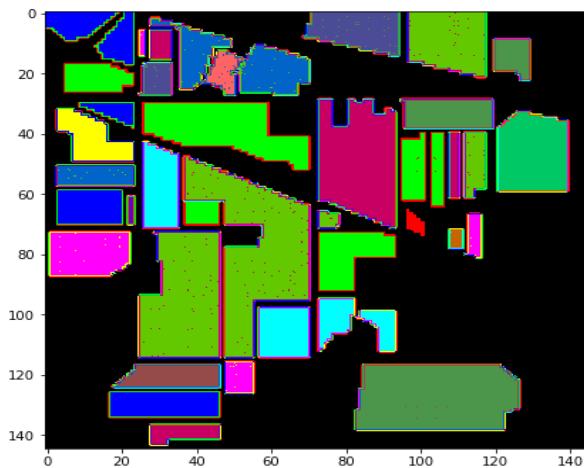


Fig. 9. Visualization of the Predicted Classified Objects.

VII. CONCLUSION

In this paper, the proposed study has explored the effectiveness of deep learning techniques for addressing issues associated with HSI classification. The proposed study has suggested modeling of hybrid learning mechanism emphasizing the trade-off between the classification performance and model overfitting problem due to the limited training data samples. The hybridization is carried out considering the application of 3D ConvNet and 2D ConvNet, which are good at exploring the spatial-spectral and spatial features. The study outcome exhibits superiority of the proposed system regarding classification performance and convergence rate. The proposed hybrid model is computationally inexpensive compared to the conventional or standalone complex 3D ConvNet. Despite the effectiveness of the proposed system, it has been realized that more optimization is required in the proposed deep learning mechanism to make it more adaptive and flexible to meet the requirement of real-time implementation. The proposed model can be introduced with other data modeling process like different preprocessing and data reduction mechanism that suits most of HSI dataset. Accordingly, it will be also very interesting to explore the application of transfer learning in future research work. The limitation of the study is associated with more extensive analysis of the outcome, which at present is restricted to Indian pine HSI dataset.

REFERENCES

- [1] Wang, C.L.; Ren, J.; Wang, H.W.; Zhang, Y.; Wen, J. Spectral-spatial classification of hyperspectral data using spectral-domain local binary patterns. *Multimed. Tools Appl.* 2018, 77, 29889–29903.
- [2] C. M. Gevaert, J. Suomalainen, J. Tang, and L. Kooistra, "Generation of spectral-temporal response surfaces by combining multispectral satellite and hyperspectral uav imagery for precision agriculture applications," *IEEE Journal of Selected Topics in Applied Earth Observations and Remote Sensing*, vol. 8, no. 6, pp. 3140–3146, June 2015.
- [3] Tiwari, K.C.; Arora, M.K.; Singh, D. An assessment of independent component analysis for detection of military targets from hyperspectral images. *Int. J. Appl. Earth Obs. Geoinf.* 2011, 13, 730–740.
- [4] Hidalgo, D.R., Cortés, B.B. and Bravo, E.C., 2021. Dimensionality reduction of hyperspectral images of vegetation and crops based on self-organized maps. *Information Processing in Agriculture*, 8(2), pp.310-327.
- [5] Stuart, Mary B., Andrew JS McGonigle, and Jon R. Willmott. "Hyperspectral imaging in environmental monitoring: a review of recent developments and technological advances in compact field deployable systems." *Sensors* 19, no. 14 (2019): 3071.
- [6] Zhang, T., Fu, Y., Wang, L. and Huang, H., 2019. Hyperspectral image reconstruction using deep external and internal learning. In *Proceedings of the IEEE/CVF International Conference on Computer Vision* (pp. 8559-8568).
- [7] Borzov, S.M. and Potaturkin, O.I., 2017. Efficiency of the spectral-spatial classification of hyperspectral imaging data. *Optoelectronics, instrumentation and data processing*, 53(1), pp.26-34.
- [8] Gewali, U.B., Monteiro, S.T. and Saber, E., 2018. Machine learning based hyperspectral image analysis: a survey. *arXiv preprint arXiv:1802.08701*.
- [9] Koonsanit K., Jaruskulchai C., Eiumnoh A. (2012) Band Selection for Hyperspectral Imagery with PCA-MIG. In: Bao Z. et al. (eds) *Web-Age Information Management. WAIM 2012. Lecture Notes in Computer Science*, vol 7419. Springer, Berlin, Heidelberg.
- [10] D. M. S. Arsa, H. R. Sanabila, M. F. Rachmadi, A. Gamal and W. Jatmiko, "Improving Principal Component Analysis Performance for Reducing Spectral Dimension in Hyperspectral Image Classification," *2018 International Workshop on Big Data and Information Security (IW BIS)*, 2018, pp. 123-128, doi: 10.1109/IWBIS.2018.8471705.
- [11] Q. Hou, Y. Wang, L. Jing and H. Chen, "Linear Discriminant Analysis Based on Kernel-Based Possibilistic C-Means for Hyperspectral Images," in *IEEE Geoscience and Remote Sensing Letters*, vol. 16, no. 8, pp. 1259-1263, Aug. 2019, doi: 10.1109/LGRS.2019.2894470.
- [12] Guo, Y., Liu, Y., Bakker, E.M., Guo, Y. and Lew, M.S., 2018. CNN-RNN: a large-scale hierarchical image classification framework. *Multimedia tools and applications*.
- [13] Zhao, Z.Q., Zheng, P., Xu, S.T. and Wu, X., 2019. Object detection with deep learning: A review. *IEEE transactions on neural networks and learning systems*, 30(11), pp.3212-3232.
- [14] Attardi, G., 2015, June. Deepnl: a deep learning nlp pipeline. In *Proceedings of the 1st Workshop on Vector Space Modeling for Natural Language Processing* (pp. 109-115).
- [15] Ahmad, M., Shabbir, S., Roy, S.K., Hong, D., Wu, X., Yao, J., Khan, A.M., Mazzara, M., Distefano, S. and Chanussot, J., 2021. Hyperspectral Image Classification-Traditional to Deep Models: A Survey for Future Prospects. *IEEE Journal of Selected Topics in Applied Earth Observations and Remote Sensing*.
- [16] Li, Y., Zhang, H., Xue, X., Jiang, Y. and Shen, Q., 2018. Deep learning for remote sensing image classification: A survey. *Wiley Interdisciplinary Reviews: Data Mining and Knowledge Discovery*, 8(6), p.e1264.
- [17] M. Lu et al., "Penalized Linear Discriminant Analysis of Hyperspectral Imagery for Noise Removal," in *IEEE Geoscience and Remote Sensing Letters*, vol. 14, no. 3, pp. 359-363, March 2017, doi: 10.1109/LGRS.2016.2643001.
- [18] Q. Hou, Y. Wang, L. Jing and H. Chen, "Linear Discriminant Analysis Based on Kernel-Based Possibilistic C-Means for Hyperspectral Images," in *IEEE Geoscience and Remote Sensing Letters*, vol. 16, no. 8, pp. 1259-1263, Aug. 2019, doi: 10.1109/LGRS.2019.2894470.
- [19] R. Hang and Q. Liu, "Dimensionality Reduction of Hyperspectral Image Using Spatial Regularized Local Graph Discriminant Embedding," in *IEEE Journal of Selected Topics in Applied Earth Observations and Remote Sensing*, vol. 11, no. 9, pp. 3262-3271, Sept. 2018, doi: 10.1109/JSTARS.2018.2847042.
- [20] S. Jia et al., "Flexible Gabor-Based Superpixel-Level Unsupervised LDA for Hyperspectral Image Classification," in *IEEE Transactions on Geoscience and Remote Sensing*, vol. 59, no. 12, pp. 10394-10409, Dec. 2021, doi: 10.1109/TGRS.2020.3048994.
- [21] X. Wang and F. Liu, "Weighted Low-Rank Representation-Based Dimension Reduction for Hyperspectral Image Classification," in *IEEE Geoscience and Remote Sensing Letters*, vol. 14, no. 11, pp. 1938-1942, Nov. 2017, doi: 10.1109/LGRS.2017.2743018.
- [22] B. Tu, J. Wang, G. Zhang, X. Zhang and W. He, "Texture Pattern Separation for Hyperspectral Image Classification," in *IEEE Journal of Selected Topics in Applied Earth Observations and Remote Sensing*,

- vol. 12, no. 9, pp. 3602-3614, Sept. 2019, doi: 10.1109/JSTARS.2019.2924930.
- [23] H. Chen, F. Miao, Y. Chen, Y. Xiong and T. Chen, "A Hyperspectral Image Classification Method Using Multifeature Vectors and Optimized KELM," in IEEE Journal of Selected Topics in Applied Earth Observations and Remote Sensing, vol. 14, pp. 2781-2795, 2021, doi: 10.1109/JSTARS.2021.3059451.
- [24] C. Yu et al., "Hyperspectral Image Classification Method Based on CNN Architecture Embedding With Hashing Semantic Feature," in IEEE Journal of Selected Topics in Applied Earth Observations and Remote Sensing, vol. 12, no. 6, pp. 1866-1881, June 2019, doi: 10.1109/JSTARS.2019.2911987.
- [25] X. Zhang, Y. Liang, C. Li, N. Huan, L. Jiao and H. Zhou, "Recursive Autoencoders-Based Unsupervised Feature Learning for Hyperspectral Image Classification," in IEEE Geoscience and Remote Sensing Letters, vol. 14, no. 11, pp. 1928-1932, Nov. 2017, doi: 10.1109/LGRS.2017.2737823.
- [26] X. Liu, Q. Hu, Y. Cai and Z. Cai, "Extreme Learning Machine-Based Ensemble Transfer Learning for Hyperspectral Image Classification," in IEEE Journal of Selected Topics in Applied Earth Observations and Remote Sensing, vol. 13, pp. 3892-3902, 2020, doi: 10.1109/JSTARS.2020.3006879.
- [27] C. Yu, R. Han, M. Song, C. Liu and C. -I. Chang, "Feedback Attention-Based Dense CNN for Hyperspectral Image Classification," in IEEE Transactions on Geoscience and Remote Sensing, vol. 60, pp. 1-16, 2022, Art no. 5501916, doi: 10.1109/TGRS.2021.3058549.
- [28] S. Dong, Y. Quan, W. Feng, G. Dauphin, L. Gao and M. Xing, "A Pixel Cluster CNN and Spectral-Spatial Fusion Algorithm for Hyperspectral Image Classification With Small-Size Training Samples," in IEEE Journal of Selected Topics in Applied Earth Observations and Remote Sensing, vol. 14, pp. 4101-4114, 2021, doi: 10.1109/JSTARS.2021.3068864.
- [29] X. Zhang, S. Chen, P. Zhu, X. Tang, J. Feng and L. Jiao, "Spatial Pooling Graph Convolutional Network for Hyperspectral Image Classification," in IEEE Transactions on Geoscience and Remote Sensing, doi: 10.1109/TGRS.2022.3140353.

Non-Repudiation-based Network Security System using Multiparty Computation

Divya K.S¹

Research Scholar, GSSS Institute of
Engineering and Technology for
Women, Mysuru, India

Roopashree H.R²

Associate Professor, GSSS Institute
of Engineering and Technology for
Women, Mysuru, India

Yogeesh A C³

Assistance Professor
Government Engineering College
Kushalnagar, India

Abstract—Security has always been a prominent concern over the network, and various essential requirements are required to cater to an efficient security system. Non-repudiation is a requirement about the non-deniability of services acting as a bridge between seamless relaying of service/data and efficient security implementation. There have been various studies carried out towards strengthening the non-repudiation system. There are certain pitfalls that render inapplicability on dynamic cases of vulnerability. The conventional two-party non-repudiation schemes have been widely explored in the existing literature. But this paper also advocates the adoption of multi-party computation, which has better feasibility toward strengthening a distributed security system. The current work presents a survey on the existing approaches of non-repudiation to investigate its effectiveness in the multi-party system. The prime aim of the proposed work is to analyze the current research progress and draw a research gap as the prominent contribution of the proposed study. The manuscript begins by highlighting the issues concerning multi-party strategies and cryptographic approaches, and the security requirements and standardization are briefly discussed. It then describes the essentials of non-repudiation and examines state-of-the-art mechanisms. Finally, the study summarizes and discusses research gaps identified through the review analysis.

Keywords—Future network; multiparty computation; nonrepudiation; security

I. INTRODUCTION

The computational infrastructure has evolved from desktop computing to distributed architecture of computing. To elaborate further, it can be said that the ecosystem of the computation has evolved periodically from desktop computation to the client-server, and after the event of the internet, the model of the web-server-based applications. The new dimension of a highly scalable infrastructure includes cloud computing and the Internet of Things (IoT) [1][2]. The various applications are running on these distributed architectures, which are critical for different walks of life, including defense, government, e-commerce, e-hospitals, education, etc., in the form of context-oriented pervasive and ubiquitous manner. In any computing model, reliability becomes a primary requirement once it matures because the system has various vulnerabilities, and those vulnerabilities pose multiple threats to the system [3]. A direct attack on the system introduces the failure of the entire system; therefore, appropriate security measures must be researched and developed according to the changing dynamics of the

computing environment. The reliable security system must comply with the essential consideration of practical aspects for Confidentiality, Integrity, Authentication, Availability, Authorization, Access Control, and Non-repudiation [4][5]. The robust security in such distributed architecture means that multiple parties or entities must collaborate to generate security attributes. One such popular technique is "Multiparty Computation," which collects the inputs from various participating entities to preserve or isolate their privacy from the other parties [6]. A function generates the output based on these inputs. The focus of the current paper is to study the research trend on the non-repudiation aspects. The common word meaning of repudiation is to deny. In digital security systems, the transaction occurs between the stakeholder or the different parties for the authentication or the security protocol requirements. Therefore, both parties cannot deny that the sender does not send either message and is not received by the receiver. The guarantee of non-denial is the authentication of the signature or message or the document or, in general, any attributes defined as non-repudiation. Various network architectures, including wireless vehicle network, Wireless Sensor Networks (WSN), Internet of Things (IoT), etc., demand customized security solutions. The popular techniques used in the security domain include Public Key Cryptography (PKC), Digital Signature (D.S.), digital certificate (D.C.), hashing, and critical public infrastructure (PKI). Symmetric Key Cryptography (SKC), etc. [7]-[10]. There is a challenge that the method adopted should be suitable for most of the essential requirements of the security protocols, or at least the process for non-repudiation should also complement another security requirement. This paper critically analyses the various approaches used for the non-repudiation protocol design in general and specific to the different networks. Further, this paper focuses on the research approaches adopted for designing a non-repudiation scheme using multi-party computation. The proposed manuscript offers updated information about multi-party security solutions towards non-repudiation. Therefore, it is essential to gather research trends in this direction and make the information available to the researchers interested in security protocol design, especially for non-repudiation using multi-party computation. The contribution of this paper is as follows: The initial Section II of the paper provides conclusive information from the journal of Onieva et al. [11], and then in Section III, the methodology for the literature data collection is described. Section IV discusses

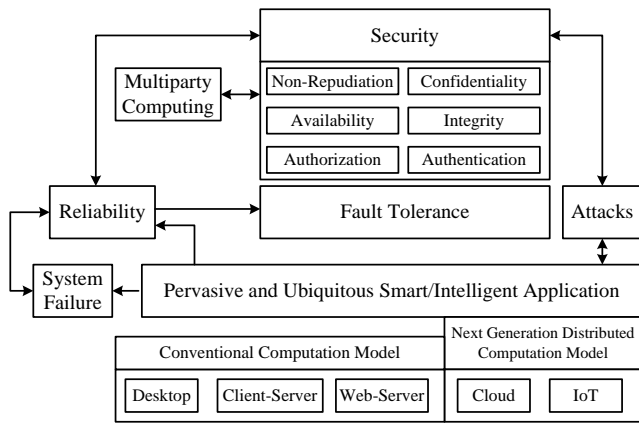


Fig. 2. Conceptual Computing Model and Security Requirements.

III. METHODOLOGY FOR DATA COLLECTION

The scope of the digital security system is very vast; therefore, in the initial stage of the study, the keyword-based on the 'non-repudiation' provides the following statistics. Although there are many other reputed journals like Springer, Elsevier, Inder- science Wiley, IGI, NCBI, etc. However, IEEE digital library offers an easy-to-use digital library to find the appropriate problem statement after understanding the current research trend and gap analysis. The data from the IEEE is considered during this initial phase of the study. The timeline of these publications was found from 1994 till 2022, which shows that the research in the field of non-repudiation is always active as throughout the time, The various new networks and communication-based applications evolves on the digital platform and that make the system dynamics. Therefore, the legacy solutions to non-repudiation do not fit the newly developed system. Therefore, to understand the current trend, the literature of only the last five years' publications of the conference and journals is segregated. The statistics found for the same are as tabulated in Table I.

Generally, the IEEE journals and transactions papers are of exceptionally high reputation, so the '34' reports are initially analyzed, whose time stamping from 2015 till 2022 as seen in Table II. The next section discusses about the existing studies toward non-repudiation followed by multiparty-based non-repudiation techniques.

TABLE I. STATISTICS OF PUBLICATION ON NON-REPUDIATION

Type	Number
Conference	785
Journal	87
Magazine	9
Early Access	6

TABLE II. STATISTICS OF SELECTED PUBLICATIONS

Type	Number
Conference	305
Journal	69

IV. STUDY TOWARDS NON-REPUDIATION

This section discusses the existing approaches carried out in different areas of implementation towards addressing the non-repudiation problem.

A. Securing Adhoc Networks Scheme

The ad-hoc technology, Smart On-Board Units (s-OBUs) and Smart Road Side Units (s-RSUs) make the realization of the Vehicular ad-hoc Network (VANETs), where the infotainment system that provides data communication of all types, either sensor data, images, or the video takes place seamlessly and provides passengers conform and safety application and fulfill the vision of intelligent transport system. There has been a tremendous effort towards building such an ecosystem of the network, but there are many security challenges, and the existing security mechanism is ineffective. The work carried out by Pan et al. [13] has presented a secure data sharing methodology using edge computing. The security of the data is offered using the encryption approach of ciphertext policy attributes. Further study towards ensuring non-repudiation was carried out by Bae et al. [14], where an authentication framework is presented. The author has also discussed the significance of using key management and encryption-based approach for securing communication systems in vehicular networks. The existing system mainly emphasizes an authentication scheme towards ensuring a non-repudiation system. Work in such direction was reported by Alfadhi et al. [15], where a hash-based function is developed to perform authentication that further reduces redundancy of authentication. Further, the study implementation of Abbasi et al. [16] has presented a clustering approach using trust and reputation to offer better non-repudiation in vehicular networks. Another study carried out by Fang et al. [17] has emphasized using blockchain and digital signature. The repudiation attacks occur in the VANET, where the attacker denies the participation of sending and receiving the messages. Due to this, the trusted authority gets confused about the audit. The authors, Azees et al. [18], have surveyed the research work towards the non-repudiation in the VANET, and the key finding of those works is tabulated in Table III. In the mechanism suggested by Jie Li et al. [19], whenever the malicious vehicle transmits a fraudulent message and denies the transmission of that message, the trusted authority opens the signature in the message to reveal the actual identity of the vehicle. Though this method provides a cost-effective solution, certificate management is quite challenging in this method. To overcome the problem of the overhead of the certificate management in the PKI-based cryptosystem, the authors Choi and Jung [20] proposes an ID-based cryptosystem to provide non-repudiation. In this scheme, a timestamp is encoded with the date and the time of the message encoded and defines the message validity time. The biggest challenges in all these approaches are that they must be supported by the mobility-prone network, which is not offered with evidence Table III highlights the advantages and issues associated with all these approaches. This scheme cannot ensure strong non-repudiation because of the critical escrow problem of the I.D.-based systems. The authors Biswas and Misic [21] designed a scheme for the non-repudiation of the privacy-preserving authentication in VANET to prevent the repudiation attack. In

their system, a signature is created for each message, and to sign the message, each sender needs to have a unique secret key and a session parameter. Once the sender signs the message and sends it, then they cannot deny the signature for the broadcast message. Table III summarizes the important implementation work towards securing an ad-hoc network scheme to ensure non-repudiation.

TABLE III. KEY FINDINGS FOR NON-REPUDIATION IN VANET

Ref	Problem	Technologies Used	Pros	Cons
Pan [13]	Delay due to Data sharing	Edge computing	Offers confidentiality	Induce network overhead
Bae et al. [14]	Secure communication	Authentication	Generalized architecture	Not benchmarked
Alfadh i et al. [15]	Privacy protection	Hash-based authentication	Reduced computational cost	Not resistive for physical attacks
Abassi et al. [16]	Transmission reliability	Clustering algorithm	Robust and validated scheme	Not applicable for dynamic attackers
Li et al. [19]	ACPN	PKC, Digital Signature	Cost-effective	manage certificate
Choi et al. [20]	Certificate overhead	ID-based Cryptos	Time validity	non-repudiation, key escrow problem
Biswas [21]	N.R. privacy	Message signature	Repudiation attack	Overhead of signature

1) *Identified research gap:* The VANET is a dynamic network where the system works in a decentralized manner; therefore, a method is required to mitigate the effect of the repudiation attack that should have significantly less computational overhead and yet be very effective supports the distributed computing paradigms. Therefore, a multi-party computation-based non-repudiation protocol is advised.

B. Certificateless Scheme

This form of scheme targets to resist the critical escrow issue in network security. A dedicated module called certificate authority generates secret keys that possess complete trust factors within it [22]. For adequate security, this mechanism uses a key generation center and user where the splitting of the secret key is carried out. The work carried out by Zhang et al. [23], Li et al. [24], Won et al. [25], and Islam et al. [26] has used certificates scheme with a different focus on implementation, viz. securing 5G communication, access control on a wearable device, smart city, and enhancing encryption, respectively.

1) *Identified research gap:* Although this scheme is claimed to offer security concerning non-repudiation, it fails to fully optimize the information associated with the identity of the nodes to generate the public key. It also introduces

dependency towards the publishing process for the user's public key. Another significant issue in this approach is that this scheme offers too many usages of encrypting information; however, the decryption process depends on only one private key. Hence, such a mechanism cannot provide resiliency against forged third-party users.

C. Conventional Cryptographic Measures

The conventional cryptographic measures make use of key-based approaches as well as encryption approaches. Existing systems offer many schemes that only emphasize these approaches to provide non-repudiation. The work carried out by Shim et al. [27], and Lin et al. [28] have used key-based methods while the work carried out by Li et al. [29], Amerimehr et al. [30], Zia et al. [31], Randriamasy et al. [32], and Tseng et al. [33] have used encryption-based method. All these approaches are meant for different research problems associated with strengthening the security scope of the application.

1) *Identified research gap:* The significant issue in adopting conventional cryptographic measures is that none of the mentioned studies have considered device-related complexity issues. Implementing key management will also demand storage, processing, and updating of the key, which consumes extra buffer in resource-constrained devices that have not been addressed. Further usage of encryption has not been testified for its capability towards resisting different forms of threats.

D. Privacy and Authentication Measures

Privacy and authentication are highly connected. The communicating nodes should be secured to prevent their private information from being vulnerable. One way to offer better security is to provide privacy preservation approaches and authentication techniques. Approaches towards privacy preservation are seen in the work of [34]-[35], while some authentication approaches are seen in the creation of [36]-[37]. These studies have strengthened non-repudiation; however, it was not the only focus.

1) *Identified research gap:* These approaches focus more on privacy and authentication; however, no claim was found to offer faster response time. Response time is required for ensuring a lightweight encryption approach. Existing approaches are also proven to be scalable for the extensive communication environment. Apart from this, there are also various other miscellaneous approaches, e.g., blockchain [38], [39], [40], and various other analytical approaches [41]-[42]. All these approaches are focused on the split form of problems in a wireless network as well as they are also found to be quite specific towards solving methodologies. They cannot leverage any form of flexibility and scalability when different network conditions are applied. Hence, there is a broader scope of improvement towards these approaches for strengthening the non-repudiation issue. The next section discusses existing methods to multi-party non-repudiation schemes.

V. STUDY TOWARDS MULTI-PARTY SCHEMES

The multi-party based non-repudiation process is widely used in the context of the applications like online auction/bidding systems, business to business/business to consumer, e-commerce, multicast-based collaborative applications, secure cloud storage, secure group encrypted e-mail, securing tender information from the bidders, contract signed by multiple organizations, securing keys in the authentication system, e-mail system, certified notification, etc. The popular methods and technologies used for these systems include PKI, Hash, group encryption, TTP-free methods, source authentication, and schemes to mitigate the effect of non-repudiation attacks. Blockchain has been found to design a multi-party non-repudiation scheme in recent times. The section below describes the researcher's various approaches in this context.

Electronics bidding is one process that mandatory require efficient security. The method proposed by Curtis et al. [43] provides a scalable system designed with essential cryptographic functions. The method isolated the bidder's identities among two core units of the scheme with the assumption that they could not collude. The registration process uses PKI with hash and is controlled by the registration authority to guarantee non-repudiation between all the participants as an auctioneer and the actual winner of the bid. This approach of a registration authority is helpful in many other applications as a framework for the design of effective, secure multi-party transactions.

The basic design of the cryptosystem always considers the hardness of the Discrete Logarithm Problem (DLP), and a typical DLP is described as if a group 'G' such that 'g' is the generator of the group and 'h' is the element of 'G', then the discrete logarithm to the base 'g' of 'h' in a group 'G'. This problem becomes more challenging if the Pohlig-Hellman algorithm cannot solve the DLP very quickly, and it can happen only if DL-cryptosystem Z_p , where p is a prime number such that $p-1=2q$ {significant prime factor}. The authors Yanping and Liaojun [44] propose an MPNR protocol based on DLP and group encryption. In any of the online platforms of the enterprises, either in the form of business to business or business to consumer, there are the different digital processes involved, including 1) item request, 2) documents transaction for agreements, 3) payment, 4) different contracts and 5) acknowledgment in a single batch or a group.

In the designed scheme, the stakeholder can direct another message to multiple distinguished recipients to remove exchanges of the same message. It also utilizes the offline Trusted Third Party (TTP), which alleviates the cons of the use of the online TTP and provides better efficiency. The Alternative Time Temporal Logic (ATL) is a variant of the Computational Tree Logic (CTL), used in many contexts where multiple parties are involved for controllability. One of the MPNR methods based on ATL is proposed by Wang et al. [45] to make it useful in e-commerce by adding time limits to each stakeholder so that it acquires a time-independent and fair transaction. Another approach applicable for commencing is proposed by the authors, Wang and Wang [46], use group encryption to design MPNR without using a TTP and validate

the model using a popular cryptographic model validation method, namely SVO logic. In the era of collaboration, a scalable architecture based on multicast communication provides a platform to build business models involving multi-party as a stakeholder.

To secure such frameworks, a Secure Multicast Communication (SMC) is desired where the packet overhead and computational efficiency is to be optimal. The most significant problem for SMC is designing an authentication model for the sources. The authors Eltaief and Youssef [47] propose a model for SMC in the context where the communication channel is compromised by the attackers who work on the integrity of the data. The model exploits a multi-layer connected chain structure to build secure multicast authentication. It adjusts the effect of the packet loss but ensures non-repudiation of the origin of the source.

In the era of globalization, where the global network concept is emerging, the role of cloud systems is most important. There is always a hiccup to migrate their data to the cloud system unless they are not assured of the strength and guarantee of security. The authors, Feng et al. [48], highlight their work related to the different issues of security, including 1) fairness, 2) roll-back attack, and 3) repudiation. The method suggested by them for MPNR protocol ensures proper storage in the cloud system with non-repudiation and handles the roll-back attacks. Another model told by Feng et al. [49] focuses on the data integrity aspect during cloud storage by identifying vulnerabilities in popular cloud storage providers. Based on identifying the repudiation problem, a novel MPNR scheme fixes the issue and justifies mitigation of the effect of various network attacks [33].

To design a robust system of authentication schemes, the security of keys plays a vital role. Mandal and Mohanty [50] propose a TTP method to generate the keys and distribute them to respective groups. The security analysis reveals its strength against various attacks, including 1) the non-repudiation attack, 2) replay attack, 3) chosen cipher attack, and 4) man-in-the-middle attack. The protocol can use for various applications like a) group encrypted e-mail multicast in the defense sector, b) securing tender information from the bidders, c) contract signed by multiple organizations, etc.

The traditional benchmarked approaches of the multi-party fair exchange protocol demand more communication cost if applied to other networks' topologies different than mesh topology. The authors Shiraishi et al. [51] found that if the mesh topology strategy is used for the line topology, its performance degrades. To overcome this issue, they propose an N-party certified e-mail protocol for line topology with fairness, non-repudiation, trusted third party invisibility, and timeliness in less communication cost. An application like certified notification requires a fair exchange with strong proof and non-repudiation of the message's origin and exchange. The authors Payeras-Capellà et al. [52] introduce a Multiparty Fair Certified Notification (MFCN)-scheme based on blockchain. The system allows to sending simultaneously certified notifications to the group of receivers. It validates the strategy to achieve better security properties, including a) confidentiality, b) fairness, and c) timeliness with a stateless

TTP. Table IV highlights research towards multi-party non-repudiation schemes along with the associated research gap being explored.

TABLE IV. RESEARCH TOWARDS MULTI-PARTY NON-REPUDIATION SCHEME

Citation	Application	Problem	Approaches
Curtis et al. [43]	Securing Bidding system	Registration authority	PKI, Hash
Yanping et al. [44]	B2C and B2B	DLP Model	Group encryption, offline TTP
Wang et al. [45]	e-commerce	ATL	Adding time limit
Wang et al. [46]	e-commerce	SVOL	Group encryption
Wang et al. [47]	Multicast communication	chain structure	Source authentication
Feng et al. [49]	Cloud Storage	vulnerabilities for repudiation	Overcome non-repudiation
Mandal et al. [50]	Authentication system	Key security	Resistive to non-repudiation attack
Shiraishi et al. [51]	e-mail system	Line topology	Less communication cost without TTP
Payeras et al. [52]	Certified notification	stateless TTP	Blockchain

1) *Identified research gap:* There are various schemes towards multi-party non-repudiation schemes, where authentication is the prime focus. However, most of the deployed security techniques towards this don't consider the dynamic attribute of the user/node present in the network. This form of implementation can successfully stop one specific form of attack; however, they fail to identify when the attacker changes their attack strategy. The validation of different parties involved in this process is checked only once during the entire simulation. In contrast, there is a fair possibility of inclusion of new kinds of intrusion, or one of the nodes could possibly go rogue. Hence, the existing multi-party non-repudiation system is highly symptomatic and operational over a smaller network and with a priori information of types of attackers.

The next section discusses the open-end research problems identified from the existing review work.

VI. OPEN RESEARCH ISSUES

After reviewing the existing approaches, it has been seen that it has addressed various security problems associated with the different network variants. Therefore, each technique has its scope of implementation while also related to multiple pitfalls. Although all the approaches are liked with the usage of encryption measures, key-based procedures, Certificateless schemes, privacy and authentication schemes, etc., all of these techniques have been specifically meant to address a particular set of problems. The multiparty-based approach is one of the best options; however, they still suffer from various issues concerning non-repudiation as well as it also requires inclusion. The significant problems that are found to be yet an open-end are as follows.

A. Network-Specific Solution

It has been noticed that existing schemes for non-repudiation have been mainly carried out toward specific groups of networks viz. convention network, 5G, Big Data, IoT, vehicular network, cloud environment, wireless sensor network, etc. It should be noted that each network form has its way of incorporating security, which is unique from each other. However, some security protocols may be quite common in this form. A closer look into Table III highlights that maximum work has been attempted to date in the vehicular network. In contrast, many works are carried out on sensory application and IoT (5G). It is well-known that 5G, IoT, and cloud are future technologies and require more security strength to offer better non-repudiation. However, multi-party is not equally focused on these networks.

B. Authentication Flexibility on Different Networks

Existing approaches have used authentication within a significantly narrower scope of its applicability. It should be noted that authentication approaches for different network forms have other dependencies. There is less work to address authentication among massive devices present in IoT. The majority of the applications currently in upcoming times will use IoT, and hence there is a drastic need to incorporate robust authentication measures.

C. Strengthening Multiparty-based Approach

Multiparty-based authentication approach is one of the most robust techniques to offer security. However, existing studies have not provided any form of evidence toward assuring the resiliency of the trusted third party involved in this process. There is a need to incorporate a secure encryption mechanism that can offer robust privacy and non-repudiation while using a multi-party-based approach. A lightweight encryption policy with a faster key management mechanism is the most effective mechanism that can be opted for strengthening non-repudiation issues in dynamic networks.

D. Mechanism of Validation

The majority of the existing approaches towards multiparty-based schemes have not witnessed any standard validation approach. There is a possibility of including any number of multi-party-based authentication systems; hence, there is a need for a cost-effective solution towards a validation approach using unique performance parameters.

E. Computational Complexity

The inclusion of a multiparty-based solution could also offer a potential computational complexity when it comes to validating the stream of data or service requests. In such a case, including an encryption mechanism will further elevate the problem over a wireless network. Apart from this, encryption is a highly iterative operation. At the same time, it is required to offer a good balance between communication and computation, which is not found in existing approaches.

VII. CONCLUSION

This paper has presented a review of the non-repudiation system where the investigation is mainly to check the effectiveness score in involving a multi-party system. After

reviewing all the related research approaches, there are various conclusive remarks. It has been identified that the existing studies towards security have a splitting form of implementation towards non-repudiation. Some models a direct non-repudiation system, while others implement a different technique to ascertain non-repudiation. The frequencies of former approaches are comparatively less in contrast to later forms of policies. Also, very few works have implemented the multi-party mechanism to perform validation or security authentication. Besides, multi-party mechanisms developed in the existing system are too specific to network type. Unfortunately, they offer a reduced scope of practical implementation. It should be noted that techniques, e.g., cloud and IoT, integrate multiple forms of other networking systems. A closer look into Table III shows that studies were not focused on cloud and IoT systems, which is required in the existing approach.

More studies on authentication mechanisms have been carried out, but they are not entirely using multi-party computation systems. On the other hand, multi-party computation/validation studies have lacked novel authentication mechanisms. On the other hand, the existing studies where both multi-party authentication systems have been addressed do not deploy a computationally cost-effective technique. There is no report of practical scenario if it runs over resource-constrained devices.

Therefore, our future work will develop a comprehensive model of a multi-party computational system that can offer a superior form of non-repudiation in a dynamic network. The study will consider the use case of IoT systems hosted over a cloud environment. It will be meant towards bridging the gap in current research work.

REFERENCES

- [1] B. Nayak, M. Mangla, S. N. Mohanty, S. Satpathy, Integration of Cloud Computing with Internet of Things Foundations, Analytics and Applications, Wiley, ISBN: 9781119769309, 1119769302, 2021.
- [2] A. Nagaraj, Introduction to Sensors in IoT and Cloud Computing Applications, Bentham Science Publishers, ISBN: 9789811479335, 981147933X, 2021.
- [3] H. Pham, Reliability and Statistical Computing Modeling, Methods and Applications, Springer International Publishing, ISBN: 9783030434120, 3030434125, 2020.
- [4] D. C. Wilson, Cybersecurity, MIT Press, ISBN: 9780262542548, 0262542544, 2021.
- [5] B. Gordijn, M. Christen, M. Loi, The Ethics of Cybersecurity, Springer International Publishing, ISBN: 9783030290535, 3030290530, 2020.
- [6] D. Evans, V. Kolesnikov, M. Rosulek, A Pragmatic Introduction to Secure Multi-Party Computation, Now Publishers, ISBN: 9781680835083, 1680835084, 2019.
- [7] M.E. Whitman, H.J. Mattord, Principles of Information Security, Cengage Learning, ISBN: 9780357506561, 0357506561, 2021.
- [8] D. Chatterjee, Cybersecurity Readiness-A Holistic and High-Performance Approach, SAGE Publications, ISBN: 9781071837351, 1071837354, 2021.
- [9] L. Bock, Modern Cryptography for Cybersecurity Professionals-Learn how You Can Leverage Encryption to Better Secure Your Organization's Data, Packt Publishing, ISBN: 9781838647797, 1838647791, 2021.
- [10] M. Chapple, Access Control and Identity Management, Jones & Bartlett Learning, ISBN: 9781284198355, 1284198359, 2020.
- [11] Onieva, Jose A., Jianying Zhou, and Javier Lopez. "Multi-party non-repudiation: A survey." ACM Computing Surveys (CSUR) 41, no. 1 (2009): 1-43.
- [12] I. Symeonidis, D. Rotaru, M. A. Mustafa, B. Mennink, B. Preneel and P. Papadimitratos, "HERMES: Scalable, Secure, and Privacy-Enhancing Vehicular Sharing-Access System," in IEEE Internet of Things Journal, vol. 9, no. 1, pp. 129-151, 1 Jan.1, 2022, doi: 10.1109/IJOT.2021.3094930.
- [13] J. Pan, J. Cui, L. Wei, Y. Xu & H. Zhong, "Secure data sharing scheme for VANETs based on edge computing", Springer-EURASIP Journal on Wireless Communications and Networking volume 2019.
- [14] M.A.R. Bae, L. Simpson, X. Boyen, E. Foo, & J. Pieprzyk, "Authentication strategies in vehicular communications: a taxonomy and framework", Springer-EURASIP Journal on Wireless Communications and Networking, 2021.
- [15] S.A. Alfadhli, S. Lu, A. Fatani, H. Al-Fedhly, & M. Ince, "SD2PA: a fully safe driving and privacy-preserving authentication scheme for VANETs", Springer-Human-centric Computing and Information Sciences, volume 10, Article number: 38, 2020.
- [16] R. Abassi, A. B. C. Douss & D. Sauveron, "TSME: a trust-based security scheme for message exchange in vehicular Ad hoc networks" Springer-Human-centric Computing and Information Sciences volume 10, Article number: 43, 2020.
- [17] W. Fang, W. Chen, W. Zhang, J. Pei, W. Gao & G. Wang, "Digital signature scheme for information non-repudiation in blockchain: a state of the art review", Springer-EURASIP Journal on Wireless Communications and Networking volume 2020, Article number: 56, 2020.
- [18] M. Azees, P. Vijayakumar and L. Jegatha Deborah, "Comprehensive survey on security services in vehicular ad-hoc networks," in IET Intelligent Transport Systems, vol. 10, no. 6, pp. 379-388, 8 2016. doi: 10.1049/iet-its.2015.0072.
- [19] Jie Li, Huang Lu, et al.: 'ACPN: A Novel Authentication Framework with Conditional Privacy-Preservation and Non-Repudiation for VANETs', IEEE Transactions on Parallel and Distributed Systems, 2014, 26, (4), pp- 938 – 948.
- [20] Choi, J., Jung, S., 'A security framework with strong non-repudiation and privacy in VANETs'. In Proceedings of the 6th IEEE Conference on Consumer Communications and Networking Conference table Las Vegas, NV, USA, 2009, pp: 835-839.
- [21] Biswas, S., Mistic, J., 'A cross-layer approach to privacy-preserving authentication in WAVE-enabled VANETs, IEEE Transactions on Vehicular Technology, 2013, 62, (5), pp. 2182–2192.
- [22] Rezaeibagha, Fatemeh, Yi Mu, Xinyi Huang, Wenjie Yang, and Ke Huang. "Fully secure lightweight certificateless signature scheme for IIoT." IEEE Access 7 (2019): 144433-144443.
- [23] Y. Zhang, F. Ren, A. Wu, T. Zhang, J. Cao and D. Zheng, "Certificateless Multi-Party Authenticated Encryption for NB-IoT Terminals in 5G Networks," in IEEE Access, vol. 7, pp. 114721-114730, 2019. doi: 10.1109/ACCESS.2019.2936123.
- [24] F. Li and J. Hong, "Efficient Certificateless Access Control for Wireless Body Area Networks," in IEEE Sensors Journal, vol. 16, no. 13, pp. 5389-5396, July1, 2016. doi: 10.1109/JSEN.2016.2554625.
- [25] J. Won, S. Seo and E. Bertino, "Certificateless Cryptographic Protocols for Efficient Drone-Based Smart City Applications," in IEEE Access, vol. 5, pp. 3721-3749, 2017. doi: 10.1109/ACCESS.2017.2684128.
- [26] S. Hafizul Islam and F. Li, "Leakage-Free and Provably Secure Certificateless Signcryption Scheme Using Bilinear Pairings," in The Computer Journal, vol. 58, no. 10, pp. 2636-2648, Oct. 2015. doi: 10.1093/comjnl/bxv002.
- [27] K. Shim, "A Survey of Public-Key Cryptographic Primitives in Wireless Sensor Networks," in IEEE Communications Surveys & Tutorials, vol. 18, no. 1, pp. 577-601, Firstquarter 2016. doi: 10.1109/COMST.2015.2459691.
- [28] J. Lin, W. Zhu, Q. Wang, N. Zhang, J. Jing and N. Gao, "RIKE+ : using revocable identities to support key escrow in public key infrastructures with flexibility," in IET Information Security, vol. 9, no. 2, pp. 136-147, 3 2015. doi: 10.1049/iet-ifs.2013.0552.

- [29] F. Li, D. Zhong and T. Takagi, "Efficient Deniably Authenticated Encryption and Its Application to E-Mail," in *IEEE Transactions on Information Forensics and Security*, vol. 11, no. 11, pp. 2477-2486, Nov. 2016.
- [30] A. Amerimehr and M. H. Dehkordi, "Quantum Symmetric Cryptosystem Based on Algebraic Codes," in *IEEE Communications Letters*, vol. 22, no. 9, pp. 1746-1749, Sept. 2018. doi: 10.1109/LCOMM.2018.2844245.
- [31] M. Zia and R. Ali, "Cryptanalysis and improvement of blind signcrypton scheme based on elliptic curve," in *Electronics Letters*, vol. 55, no. 8, pp. 457-459, 18 4 2019. doi: 10.1049/el.2019.0032.
- [32] M. Randriamasy, A. Cabani, H. Chafouk and G. Fremont, "Formally Validated of Novel Tolling Service With the ITS-G5," in *IEEE Access*, vol. 7, pp. 41133-41144, 2019. doi: 10.1109/ACCESS.2019.2906046.
- [33] Y. Tseng, T. Tsai and S. Huang, "Leakage-Free ID-Based Signature," in *The Computer Journal*, vol. 58, no. 4, pp. 750-757, April 2015. doi: 10.1093/comjnl/bxt116.
- [34] C. Hu and Y. Huo, "Efficient privacy-preserving dot-product computation for mobile big data," in *IET Communications*, vol. 11, no. 5, pp. 704-712, 30 3 2017. doi: 10.1049/iet-com.2016.0782.
- [35] C. Sun, J. Liu, X. Xu and J. Ma, "A Privacy-Preserving Mutual Authentication Resisting DoS Attacks in VANETs," in *IEEE Access*, vol. 5, pp. 24012-24022, 2017. doi: 10.1109/ACCESS.2017.2768499.
- [36] M. A. Sahi *et al.*, "Privacy Preservation in e-Healthcare Environments: State of the Art and Future Directions," in *IEEE Access*, vol. 6, pp. 464-478, 2018. doi: 10.1109/ACCESS.2017.2767561.
- [37] F. Wang, Y. Xu, H. Zhang, Y. Zhang and L. Zhu, "2FLIP: A Two-Factor Lightweight Privacy-Preserving Authentication Scheme for VANET," in *IEEE Transactions on Vehicular Technology*, vol. 65, no. 2, pp. 896-911, Feb. 2016. doi: 10.1109/TVT.2015.2402166.
- [38] K. Shim, "Security Analysis of Various Authentication Schemes Based on Three Types of Digital Signature Schemes," in *IEEE Access*, vol. 6, pp. 68804-68812, 2018. doi: 10.1109/ACCESS.2018.2879961.
- [39] W. Huang, Y. Liao, S. Zhou and H. Chen, "An Efficient Deniable Authenticated Encryption Scheme for Privacy Protection," in *IEEE Access*, vol. 7, pp. 43453-43461, 2019. doi: 10.1109/ACCESS.2019.2907250.
- [40] M. A. Alazzawi, H. Lu, A. A. Yassin and K. Chen, "Efficient Conditional Anonymity With Message Integrity and Authentication in a Vehicular Ad-Hoc Network," in *IEEE Access*, vol. 7, pp. 71424-71435, 2019. doi: 10.1109/ACCESS.2019.2919973.
- [41] C. Sun, J. Liu, Y. Jie, Y. Ma and J. Ma, "Ridra: A Rigorous Decentralized Randomized Authentication in VANETs," in *IEEE Access*, vol. 6, pp. 50358-50371, 2018. doi: 10.1109/ACCESS.2018.2868417.
- [42] J. Li, H. Lu and M. Guizani, "ACPN: A Novel Authentication Framework with Conditional Privacy-Preservation and Non-Repudiation for VANETs," in *IEEE Transactions on Parallel and Distributed Systems*, vol. 26, no. 4, pp. 938-948, April 2015. doi: 10.1109/TPDS.2014.2308215.
- [43] B. Curtis, J. Pieprzyk and J. Seruga, "An Efficient eAuction Protocol," *The Second International Conference on Availability, Reliability and Security (ARES'07)*, Vienna, 2007, pp. 417-421. doi: 10.1109/ARES.2007.37.
- [44] L. Yanping and P. Liaojun, "Multi-party Non-repudiation Protocol with Different Message Exchanged," *2009 Fifth International Conference on Information Assurance and Security*, Xi'an, 2009, pp. 491-494. doi: 10.1109/IAS.2009.329.
- [45] X. Wang, "Formal Analysis and Improvement of Multi-Party Non-Repudiation Protocol," *2009 5th International Conference on Wireless Communications, Networking and Mobile Computing*, Beijing, 2009, pp. 1-4. doi: 10.1109/WICOM.2009.5302343.
- [46] X. Wang and X. Wang, "Formal Analysis Of Multi-party Non-repudiation Protocols Without TTP," *2010 International Conference on Communications and Intelligence Information Security*, Nanning, 2010, pp. 96-99. doi: 10.1109/ICCIS.2010.33.
- [47] H. Eltaief and H. Youssef, "Efficient sender authentication and signing of multicast streams over lossy channels," *ACS/IEEE International Conference on Computer Systems and Applications - AICCSA 2010*, Hammamet, 2010, pp. 1-7. doi: 10.1109/AICCSA.2010.5586962.
- [48] J. Feng, Y. Chen, D. Summerville, W. Ku and Z. Su, "Enhancing cloud storage security against roll-back attacks with a new fair multi-party non-repudiation protocol," *2011 IEEE Consumer Communications and Networking Conference (CCNC)*, Las Vegas, NV, 2011, pp. 521-522. doi: 10.1109/CCNC.2011.5766528.
- [49] J. Feng, Y. Chen and D. H. Summerville, "A fair multi-party non-repudiation scheme for storage clouds," *2011 International Conference on Collaboration Technologies and Systems (CTS)*, Philadelphia, PA, 2011, pp. 457-465. doi: 10.1109/CTS.2011.5928724.
- [50] S. Mandal and S. Mohanty, "Multi-party Key-Exchange with Perfect Forward Secrecy," *2014 International Conference on Information Technology*, Bhubaneswar, 2014, pp. 362-367. doi: 10.1109/ICIT.2014.30.
- [51] Y. Shiraishi, M. Mohri, H. Miyazaki and M. Morii, "A Three-Party Optimistic Certified Email Protocol Using Verifiably Encrypted Signature Scheme for Line Topology," *2015 IEEE 2nd International Conference on Cyber Security and Cloud Computing*, New York, NY, 2015, pp. 260-265. doi: 10.1109/CSCloud.2015.64.
- [52] M. Payeras-Capellà, M. Mut-Puigserver and M. À. Cabot-Nadal, "Smart Contract for Multiparty Fair Certified Notifications," *2018 Sixth International Symposium on Computing and Networking Workshops (CANDARW)*, Takayama, 2018, pp. 459-465. doi: 10.1109/CANDARW.2018.00089.

An Algorithm based on Convolutional Neural Networks to Manage Online Exams via Learning Management System Without using a Webcam

Lassaad K. SMIRANI¹

Umm al-Qura University, Deanship of e-Learning and
Distance Education KSA
InnoV'COM Lab, University of Carthage, Tunisia

Jihane A. BOULAHIA²

Umm al-Qura University, College of Computer and
Information Systems KSA
InnoV'COM Lab, University of Carthage, Tunisia

Abstract—Cheating attempts in educational assessments have long been observed. Because students today are characterized by their great digital intelligence, this negative conduct has intensified throughout the emergency remote teaching time. First, this article discusses the most innovative methods for combating cheating throughout the online evaluation procedure. Then, for this aim, a Convolutional Neural Networks for Cheating Detection System (CNNCDS) is presented. The proposed solution has the advantage of not requiring the use of a camera, it recognizes and identifies IP addresses, records and analyzes exam sessions, and prevents internet browsing during exams. The K-Nearest Neighbor (K-NN) has been adopted as a classifier while the Principal Component Analysis (PCA) was used for exploratory data analysis and for making predictive models. The CNNCDS was learned, tested, and validated by using data extracted from a face-to-face exam session. Its main output is a binary students' classification in real-time (normal or abnormal). The CNNCDS surpasses the fundamental classifiers Multi-class Logistic Regression (MLR), Support Vector Machine (SVM), Random Forest (RF), and Gaussian Naive Bayes (GNB) in terms of mean accuracy (98.5%). Furthermore, it accurately detected screen pictures in an acceptable processing time, with a sensitivity average of 99.8 percent and a precision average of 1.8 percent. This strategy has been shown to be successful in minimizing cheating in several colleges. This solution is useful for higher education institutions that operate entirely online and do not require the use of a webcam.

Keywords—Artificial intelligence; convolutional neural network; learning assessment; online cheating; online examination; higher education; emergency remote teaching

I. INTRODUCTION

Evaluation is the most important stage of the teaching process [1][2][3][4]. Indeed, assessment is at the heart of the learning service, providing faculty members with important information about what students understand, allowing them to plan and manage lessons and providing relevant feedback [5]. The evaluation stage allows students to become aware of their learning methods and use this knowledge to improve and develop their acquaintance by taking on more responsibility [6]. Additionally, data analyses as a result of the assessment allow students, faculty members, and parents, as well as the broader educational community, to be informed about the teaching outcomes achieved at a specific time to highlight

success, plan interventions, and continue to foster accomplishment [7].

In the case of face-to-face or online evaluation, completing this phase is critical to the overall success of the teaching and learning procedure [8][9]. In all cases, some students try to well evaluate by their proper efforts, but some others look for violating academic integrity [10]. When students are evaluated face to face, the traditional method of cheating is for any of them to try to chat to their colleagues, pass a note around, or bring a cheat sheet. To avoid this type of cheating, a supervisor is required, and sufficient spacing between student tables is provided to make his job easier. However, there are several new techniques to cheat on online exams [11][12][13][14][15]. The access to the Internet is the most common method of cheating [16][17][18]. Cheating with Internet access provides students endless sources of information as well as the opportunity to speak with others about how to provide unlawful services to students while they are taking the exam [18][19][20]. Additionally, Internet access enables screen sharing, remote desktop access, and the ability for someone other than the candidate to access the exam via the student's computer [18].

The first solution to minimize online cheating is using applications to block the internet navigation that can be used in combination with the Learning Management System (LMS) like Blackboard [20]. When running this special application, students will have no access to any other resource on the device. The second solution is screen recording; some applications record and store the screens of the student's device while taking the exam [20][21]. The faculty member will use these recordings to ensure that the exam ran perfectly, and that the student did not cheat [22]. The third option is to use surveillance cameras to film the students' behavior and gaze throughout the exam. However, this technique is not completely effective, particularly when the number of students is large, as it will be difficult to control their behavior [22][23]. Many faculty members claim that it is difficult to organize an electronic evaluation without the risk of cheating, but efforts are still being made to reduce the number of possible fraudulent attempts [20-26]. As a result, it is necessary to be equipped with tools to prevent cheating, as well as to properly select the test options provided by the LMS and to accurately determine the periods for online exams [27][28].

Several approaches are possible to reduce cheating during remote exams. Depending on the student's input. The problem can be divided into three sub-parts: i) video, ii) voice, and iii) handwriting/mouse clicks. As a result, deep learning methods can be efficient for completing each of these subtasks [29-35].

This paper discusses new research on smart techniques for reducing cheating on higher education online exams. This study will provide an overview of the main techniques. It investigates the impact of artificial intelligence in preventing attempted cheating during an online exam, as well as the best way to reduce the risk of cheating. The controller's task is greatly aided by the opening of the cameras during the passage of the examinations at a distance. However, the use of a webcam is not permitted in some faculties, where educators are not permitted to ask candidates to turn on the camera. In this case, it is more difficult to detect cheating. As a result, our main contribution is to present a solution without filming the candidate. Several parameters will be implemented to complete this mission, such as the identification of the IP address and the candidates' academic and personal information, as well as the capture of navigation screen images, that will be processed by Convolutional Neural Networks (CNN).

This paper is organized as follows: Section 2 presents the study background; we'll give a brief review of the most important techniques based on AI for detecting and reducing cheating behaviors in electronic online assessments. Section 3 offers solutions for managing online exams in the absence of a camera and based on LMS options. Section 4 presents the CNNCDS, its architecture, and its main components such as the K-Nearest Neighbor (K-NN); and the Principal Components Analysis (CPA). In Section 5 the experimentations and the results are offered before the conclusion section.

II. STUDY BACKGROUND

In their evaluation methods, online education models try to emulate the traditional teaching way which remains without any doubt the most reliable method for evaluation [17][18][19], indeed the world's largest virtual universities and online training institutions always rely on presential evaluation in specially designed testing centers. Remarkably, some online evaluations do not pose any cheating problem, but for other types of evaluation, cheating is possible [17][19][20][22]. Indeed, the most important questions that arise at the beginning of this study: What types of solutions can be adopted to prevent cheating in an online exam? And, what are the means to further disseminate the notion of academic integrity?

Academic integrity is an important aspect of higher education. These values safeguard a university's reputation, as well as the scientific value and meaning of degrees, and they also provide a framework for professional and academic work. In [23], the authors attempt to answer an important question that arises when discussing online education: why does academic dishonesty occur? And, why some students are compelled to engage in these behaviors while learning online. They present the most commonly used methods for promoting academic integrity. The authors in [24] state that it is possible to uncover cases of identification of cheating behaviors through the strengthening of the faculty member-student

relationship and real-time discussions between them. As a result, the proposal is to expand student-faculty member discussions similar to those that have traditionally occurred in the classroom. The authors present Intelligent Discussion Comments (IDC), using a scalable asynchronous system to engage students in real-time discussions to extract authentic student understanding. To enrich the discussion process and supporting the educational team in their supervisory, two AI services are used such as voice recognition and transcription.

Online exams have emerged on the surface on various types of academic misconduct, including plagiarism. In addition, academic misconduct and plagiarism represent a barrier to the development of students' critical thinking and analytical skills [24]. In [25] the researchers analyze various forms of academic misconduct and propose strategies applicable in higher education, but the rapid evolution of technology has made it difficult to well detect cheating attempts, so other methods of detecting cheating must be used.

In the following section, we will first present biometric authentication, and then we discuss the most important research that dealt with smart techniques and various methods and tools for detecting and preventing cheating.

A. Biometric Authentication

Biometric authentication verifies an individual's identity and ensures secure access to an electronic system by utilizing an individual's unique biological characteristics. Biometric technologies are based on the notion that each individual can be uniquely identified by one or more biological characteristics such as fingerprints, hand morphology, retina and iris physiognomy, voice waves, typing dynamics, DNA, or signatures. The use of these identity proofs as part of a validation process for a user wishing to access a system is known as biometric authentication [26]. Biometric technologies are being used to secure a wide range of digital communications, whether for a business, an e-commerce site, internet payments, or simply connecting to a computer or a smartphone. Biometric authentication systems compare the provided biometric data to the confirmed authenticated data in a database. Authentication is confirmed and access is granted if the two samples match. This procedure is occasionally used as part of a multi-factor authentication system. Thus, the user of a smartphone can connect using his secret pin code and add an iris scan to it. Many types of biometric authentication technologies like the retinal scan produce an image of the arrangement of blood vessels on the photosensitive surface of a person's eye. Iris recognition identifies an individual based on the unique patterns of their iris, which is the ring of color around the pupil. Furthermore, the finger scan (a digital version of the fingerprint created with an ink pad and paper) analyzes the patterns drawn by ridges and creases on a finger image. The recognition of finger veins is based on the individual's unique pattern of finger veins. Also, facial recognition systems employ digital codes known as "faceprints" to identify 80 nodal points on the human face. Finally, rather than more variable conditions, voice identification systems rely on characteristics generated by the shape of the speaker's mouth and throat. The world has progressed from the oldest known biometric verification method, to modern biometric verification methods that are almost instantaneous. It is also becoming

more precise as a result of the introduction of computerized databases, the digitization of analog data, and AI techniques. AI concerns the conception of an artificial machine capable of possessing or exhibiting the capacities and characteristics of a human brain [29][30]. It is in fact about teaching the machines to think. There are two types of approaches for AI, the first is strong, called the cognitive approach when the machine must think like a man. The second is weak, called the pragmatist approach when the machine must lead to the same solutions as humans. AI remains difficult to define because we do not know how to define the notion of Intelligence. Intelligent methods proliferate, and there is a relationship between them "Fig. 1". We are attempting to focus on those who can contribute to the administration of online exams.

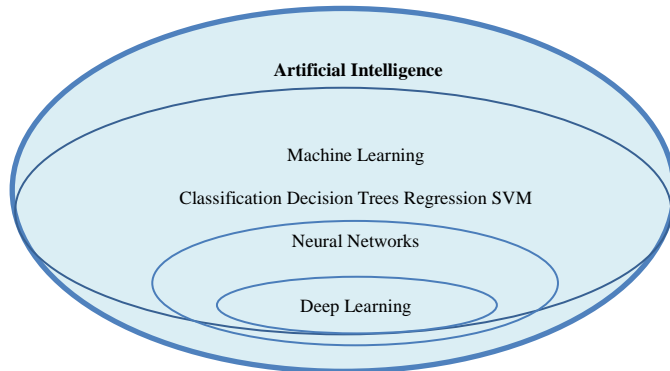


Fig. 1. The Relationship between Different Types of Machine Learning Methods.

B. Related Work based on the Role of Intelligent System

In the literature, several possible definitions of AI. In general, AI is a methodology that makes computers more intelligent, so they show characteristics normally associated with intelligence in human behavior, i.e. language comprehension, learning, problem-solving, and reasoning [29].

1) *Natural language processing*: Natural Language Processing (NLP) is a multidisciplinary field that combines linguistics, computer science, and artificial intelligence to develop natural language processing tools for a variety of applications. It should not be confused with computational linguistics, which uses computer tools to understand languages. NLP emerged from research labs to be gradually implemented in computer applications that required the incorporation of human language into the machine. As a result, NLP is also known as linguistic engineering. Some researchers have used NLP to detect cheating such as [32-34].

2) *Machine learning*: Machine Learning is an AI technology that gives the possibility to machines to learn without having previously been programmed. Machine Learning is explicitly linked to Big Data since to learn and grow, computers need data streams to analyze and train on [35]. The greatest advantage offered by machine learning is analyzing a very huge volume of data much more efficiently in terms of speed and precision than other traditional methodologies. Machine Learning can detect cheating in a millisecond, just by basing itself on data introduced, as well as

on other historical and social information Machine Learning is the ideal science to take advantage of Big Data and its opportunities [36]. This technology can extract valuable data from immense and complex sources of information without involving humans. Entirely driven by data, Machine Learning is therefore perfectly suited to the complexity of Big Data, from which it is truly inseparable. Traditional analytical tools often come up against a maximum volume of data that can be analyzed. Machine learning reveals its full potential when data sources are growing, allowing it to learn and refine insights with precision always improved. Some researchers have used Machine Learning to find solutions against cheating in online exams [35-38]. In [37], the authors introduced a new way which consists in authenticating the student, it is a question of analyzing the answers and verifying that the student is the author of them. The researchers present FLEXauth, which is an application for discovering cheating in digital exams and based on AI techniques with the assumption that each student has an individual style to answer certain types of homework. then they made comparisons with reference material for which the author is verified. In [38], the authors present a chapter on intelligent methods of cheating detection using machine learning, and they review some scientific articles from various disciplines that address the challenges of cheating detection. They use machine learning to detect anomalies, errors, and cheatings by emphasizing numerous empirical considerations critical in developing cheating prediction models. The authors in [28] focus on the modeling of activities to prevent cheating problems, they present the RIVA method which considers the face-to-face activities undertaken at the faculty. Next, the author proposed a model for supervising an online exam that contains substantial improvements.

In [21], the authors dealt with intelligent preventive systems on neural networks and took into consideration two main modules: The Internet Protocol (IP) detector and the behavior detector. Student behavior is monitored to prevent and detect any malicious practices. They proposed an e-cheating intelligence agent that is based on the relationship model for detecting online cheating using AI technique by monitoring IP and student behavior as well as creating a new dataset for this study. The proposed method used Long Short-Term Memory (LSTM) network with a densely connected concept, namely DenseLSTM to detect online cheating. The proposed method was examined on different data groups confirming its effectiveness. The Deep Neural Network (DNN), LSTM, DenseLSTM, and Recurrent Neural Network (RNN) achieved accuracy rates of 68%, 92%, 95%, and 86%, respectively [21].

In [20], Man and Harring proposed a new method to try to prevent cheating by using an eye-tracker. The proposed method was created by integrating visual fixation and eye-tracking indication into a traditional psychometric modeling framework and investigating pattern differences in the trade-offs of visual attention. Sangalli and his colleagues in [22], suggested some measures based on co-occurring events and measures of interaction with the course to distinguish between two kinds of

cheating. They used K-means clustering and Support Vector Machine (SVM). They gained good results with an accuracy of over 95%.

In [39], the authors designed a Convolutional Neural Network (CNN) model for users to enter text by looking at the on-screen keyboard and blinking. A method that divides the human gaze into nine directions. The CNN model accurately estimates how people look under different lighting conditions.

The authors in [38] used the online m-learning course sessions to design and propose a robust method of variations in pose and lighting for facial verification using a camera-based on CNN.

In [42], the authors propose students' performance evaluation examining on the computer using a new approach based on process exploration. Their approach consists of two phases: process extraction and similarity analysis. They apply a real-life application in an Enterprise Resource Planning (ERP) course to present the practicality, usefulness, and validity of the proposed approach. Fifteen student responses are evaluated by the instructor. This work proved a very good match between the automatic evaluation system and the instructor.

In the context of assessment control, the most intelligent methods used for cheating detection are based on CNN "Fig. 2". CNN are widely applied in image and video recognition, recommender systems, and natural language processing. A CNN is a type of feed-forward artificial neural network, in which the connection pattern between neurons is inspired by the visual cortex of animals [35]. The arrangement of the neurons in this region of the brain is so that they overlap when paving the visual field. Their operation is inspired by biological processes, they consist of a multilayer stack of perceptron's, the purpose of which is to preprocess small amounts of information [37]. A major advantage of convolutional networks is the use of a single weight associated with the signals entering all the neurons of the same convolutional nucleus [42]. This method reduces the memory footprint, improves performance, and allows translation processing invariance. This is the main advantage of the CNN over the multilayer perceptron, which considers each neuron independent and therefore assigns a different weight to each incoming signal [44]. When the input volume varies over time, it becomes interesting to add a parameter along the time scale in the parameterization of the neurons. In this case, we will speak of a time-delayed neural network. Compared to other image classification algorithms, convolutional neural networks use relatively little pre-processing. This means that the network is responsible for changing without supervision, which is not the case with other more traditional algorithms. The absence of initial settings and human intervention is a major advantage of CNN. A first approach would be to use a simple Machine Learning algorithm, such as logistic regression or a random forest. Although these approaches obtain relatively correct results, this type of algorithm will not be able to be generalized to images whose item ends up in a corner of the image rather than in the center of it. In other words, the spatial character of the characteristic elements of certain categories is not considered. To well achieve the goals, we need to use an algorithm capable of detecting relative shapes regardless of

their position in the image: this is what CNN allow. Yann LeCun [40] was one of the first to apply this type of neural network on a large scale, to detect amounts on checks in the 1990s.

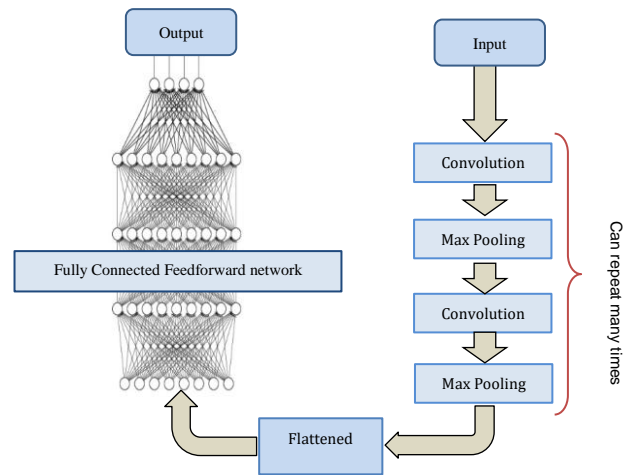


Fig. 2. Convolutional Neural Networks.

3) Using artificial neural networks for webcam analysis methods: To monitor an online exam, we only had the student's microphone, webcam, and input devices (keyboard/mouse). In this section, we will focus on video and detecting student keyboard/mouse input rather than audio. The aim of this section is to explain the method used to generate a database of synthetic student videos. When a student takes the exam online, a stream of videos is sent to the teaching team. Indeed, since the student's computer boots to a live image, it gives us greater control of their machine and allows us to gain access to the webcam, microphone, and keyboard. The aim is to give the possibility to supervise several students in parallel during the exam. The goal is therefore to annotate a video and notify the supervisor at the right time. We might think that to monitor more students, no automation is required and that it would suffice to employ more people to monitor students remotely. While this is theoretically achievable, it is not possible to scale it for a course with a larger number of students taking their exams online. This would require complex logistics. Indeed, for a small course, it is still possible for several members of the teaching team to supervise a few students at a time, but today online courses have several hundred students, it is therefore difficult to have the logistics to allow so many exams online simultaneously. These data would allow passing judgment a priori on the most diligent students, but do not help with the direct supervision of the exam. Therefore, the overall goal of the system that we wish to achieve is to flag times of suspicious activity to aid supervisors by guiding their attention helping them to supervise more students at a time. Action detection is already achievable if you have the data. This would only be based on the pre-trained actions of the network [41][42]. On the process of face images generation, the data is the basis of these types of intelligent methods. Monitoring by video is based on the

notion of normality. The idea is to learn neural network normal behavior, then anything that does not fit into this normality is classified as abnormal and requires supervision by a human. This has already been done by [22] which makes it possible to obtain such a classification space. This method uses a database of videos, each with a normal or abnormal tag. More formally, it is necessary to encode the data in a vector space of greater dimension which will be used for the training. The network will then learn a decision boundary among this data, to obtain a better representation for classification. The network will therefore be able to discriminate any element belonging to this space. The boundary will classify behaviors considered normal on one side and all abnormal elements on the other. It is, therefore, necessary to provide enough normal behaviors so that the network can learn and generalize about the behavior of students during the exam period. The rest is up to human empathy to decide whether cheating is suspected. However, many researchers such as [43][44][45] had shown that we can learn and manipulate image spaces: transferring their contents and representations to others.

III. PROPOSED SOLUTIONS

At the onset of the pandemic, and through other challenges associated with distance education, student online evaluation became the most important issue for faculty members.

The first experience of many students and faculty members with online learning was urgent and unprepared. In the spring of 2020 [13], it was discovered that the rate of cheating on online exams had increased. The peculiarity of the educational environment in some faculties is characterized by the interdiction of using the camera. Faculties cannot require students to use a camera while taking an online test, so this study considered alternatives without using a camera during the remote electronic assessment.

A. Solutions in the absence of a Camera

From a legal standpoint, the University's policies must address the subject of digital examination monitoring, whether through biometrics and/or AI or simply recorded video surveillance (Blackboard, WebEx). This is only permissible if the students consent to it explicitly, freely, and informedly.

In the absence of a video of the student taking the exam from home, e-learning management systems like Blackboard provide a multitude of options that the faculty member should be familiar with to make the remote exam more reliable and secure "Fig. 3".

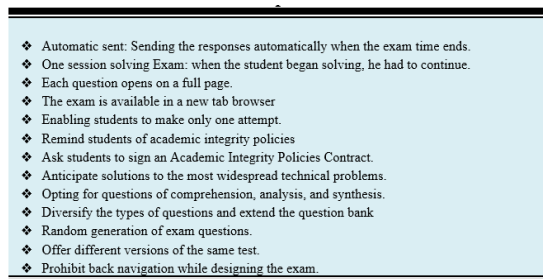


Fig. 3. Tips for Secure Exams.

B. Attribute Classes

When performing online exams, the most important attribute is candidate authentication. The main attribute classes can be classified as follows:

1) Verification of normal behavior: this is a continuous verification of the candidate's normal behavior: The detection of abnormal behavior in online exams should not be done at the start of the exam only; periodic and continuous verification is needed.

2) Security: Here we are dealing with the subject of access to the exam which must be completely secure, and no foreign person can access it.

3) A rich and diversified question bank: The richer the question bank, the easier it will be to generate the exam and the more secure the evaluation.

4) LMS conviviality: The LMS should be simple and accepting.

C. Check the IP Address

Faculty members use different methods to verify the identity of students. The IP address is a way of locating the student with good precision. To ensure that they do not have students taking the exam together, the network allows each student's IP address to be communicated when connecting to the LMS. It is the main condition for sending the exam key. A trick is also to send the exam key in the video conference chat and close the exam key as soon as all students have entered. Then it is difficult for the students to pass the exam key to someone else. The exam key only controls the entrance to the exam. Students can continue to take the exam when the instructor closes the exam key.

D. Blocking the Browser

Several applications make it possible to block the browsing of students on the Internet during the examination.

E. Recording the Exam Session

All student activities while taking the exam can be recorded and saved by the instructor.

F. Use of CNN Model

CNN was the first approach suggested and used for high-dimensional image analysis. It is composed of convolutional filters that convert 2D to 3D. The major benefit of CNN over author models is that it automatically identifies important features without the need for human intervention. In our framework, we will use the CNN model for cheating detection by analyzing the stored students' sessions. During the exam cycle, each student's computer screen is registered and processed in the database for remote proctoring. When an unexpected event occurs, the evaluation results provide alerts for exam coordinators/online surveyors. The main objective of this work is to focus on cheating and plagiarism in online exams.

IV. CONVOLUTIONAL NEURAL NETWORK FOR CHEATING DETECTION SYSTEM

Many projects have investigated and detected abnormal files using smart models [30-35]. All these projects

investigated the video sequences emitted by the student's webcam. Our solution treats the images from the student's navigation screens as the second stage. While the first stage focuses on the student's academic and personal information, as well as his IP address.

In the absence of a camera, our solution sought to capitalize on all data that could be recovered directly relating to the student. The data in Table I. are of three types: data provided by the student once entering the university, data provided by the administration concerning the academic results of the student, and data provided by the LMS and exactly the report established by Analytic for Learn (A4L).

TABLE I. PERSONAL AND ACADEMIC STUDENT DATA

	Var1	Var2	Var3	
1. Personal student Data	First Name	Middle Name	Last Name	
	Day of Birth	Month of Birth	Year of Birth	
	Place of Birth	City of Birth		
2. University Data	Department	Faculty	Id	
3. Student Level	Instant student level	The average level in the course	Overall average	
4. Student Location	Country	City	Street	
5. Ip address	Block One	Block Two	Block Three	Block Four
6. Student activity on LMS	Access Operations	LMS Time Spent	Degree of Student Interactions	School Assignments Submission

Before delivering the exam key to the candidate, we use personal and geographical information as the first step in our solution. This is a method of knowing the seriousness of the student by ensuring that there is only one student in a small geographical area and the other information gives an idea of the diligently and performance level of the student. In Addition to these sources of students' information, we have data provided from our proposed CNNCDS classification model which checks whether the student cheated in the exam or not. The CNNCDS requires a set of human-defined goals to forecast, make recommendations, or make decisions affecting real or virtual environments. This is accomplished using both machine and human input. CNNCDS are intended to operate with varying degrees of autonomy. The designed framework is based on specialized knowledge and data derived from the student, as well as his history in the faculty and his behavior either in person (exam session recording) or virtually via the LMS.

A. CNNCDS' Architecture

CNNCDS's architecture is comprised of three types of layers: Convolutional layers, grouping layers, and classification layers. Convolution is the most important operation in the formation of a convolutional network. By applying a filter to a matrix representation of an image, it generates a series of small images, which are then passed to a grouping layer. This sequence can be repeated multiple times throughout the network until the vector containing the abstract properties reaches the flattening layer and passes to the dense layer. CNN is still being used to improve computer vision in terms of

precision. The common CNN architecture contains many layers for continuously extracting appropriate image characteristics and feeding them to the classification module.

The goal of designing a CNN is to analyze the images of the screenshots, received during the online blackboard exam, and predict fraud. When designing CNNCDS, three main parameters were considered: image size, number of cores, number of layers. according to the minimum learning error obtained by each neural network of a specific number of layers ranging from 1 to 5, it is observed that the network with 2 layers corresponds to the error minimum. Concerning the number of filters, we note that we did not vary the size of a filter, we took the usual sizes used (5*5) and (3*3). For picture size, choosing a large size will make it hard to learn because the CNN input layer will be so big and therefore, we will need more hidden layers which will lead to memory shortage or long calculations.

From the previous sections, we combine the best parameters to design our CNN: 4 hidden layers, 32 filters, and 256 * 256 images. A convolutional layer can be made up of several conv2d layers followed by a grouping layer and may be dropped. Consequently, we have several conv2d layers grouped into two convolution layers. Flattening layers are used to transform the output into a long vector and then process it by a classification layer.

B. The K-Nearest Neighbor (K-NN)

This classifier has been adopted because of its best performance compared to (Multi-class Logistic Regression (MLR), Support Vector Machine (SVM), k-Nearest Neighbor (kNN), Random Forest (RF), and Gaussian Naive Bayes (GNB)).

The kNN uses the majority rule to assign the right class of membership to each non-labeled input by considering the distance between its k-nearest neighbors nearest to the training sample. To measure the differences between examples represented as vector inputs, many kNN classifiers employ simple Euclidean metrics. The Euclidean distance is calculated by (1).

$$d(x, x_T) = \sqrt{\sum_{i=1}^n w_i ((a_i(x) - a_i(x_T)))} \tag{1}$$

N represents the dimension of the entry vector $u=(a_1, a_2, \dots, a_n)$, the weight of each attribute is represented by w . k-nearest neighbor determines the class label by (2).

$$Y(d_i) = argmax_k \sum_{x_j \in kNN} y(x_j, c_k) \tag{2}$$

Equation (2) means the class prediction that has the most members in the k-nearest neighbor. d_i represents the test example. In the training set, the k-nearest neighbor is represented by x_j . $y(x_j, c_k)$ is binary and indicates if x_j belongs to the class c_k .

C. Principal Components Analysis (CPA)

CPA is used in exploratory data analysis and predictive modeling. It is commonly used for dimensionality reduction by projecting each data point onto only the first few principal components to obtain lower-dimensional data while preserving

as much of the data's variation as possible. The first component was calculated by (3), to maximize variance:

$$w_1 = \arg \max_{\|w\|=1} \left\{ \sum_i (t_1)_{(i)}^2 \right\} \quad (3)$$

Written in matrix form, we obtained (4).

$$w_1 = \arg \max_{\|w\|=1} \{ \|Xw\|^2 \} = \arg \max_{\|w\|=1} \{ W^T X^T X w \} \quad (4)$$

Rayleigh's quotient is defined as the quantity to be maximized.

The n-th component will be obtained by subtracting the first n-1 principal components from X:

$$\hat{X}_n = X - \sum_{s=1}^{n-1} X w_s w_s^T \quad (5)$$

Then we obtain the weight vector that extracts the maximum variance. The selection of KNN and CPA is based on the literature, these two modules have provided satisfaction in many research projects.

D. Input Data

The entries are the raw bytes of an image file to generate a matrix. The byte stream of an image will be placed in an array and then transformed into a matrix. Images are symbolized in a variety of ways, the most frequent of which is as a grid of small squares known as pixels. In a very simple image with only black and white pixels, each pixel could be represented by a 0 (black) or 1 (white).

We can represent $2^8=256$ different colors or shades of gray with 8 bits per pixel. This is adequate for a black-and-white photograph but does not allow for subtle color shades in a photograph. For full-color images, 32 bits per pixel are typically used, allowing for $2^{32}=4294967296$ possibilities.

E. Output Data

The network output is binary, either normal or abnormal behavior. Because any file that is not identified as an exam screen page is considered a fraudster.

F. Data Preprocessing

The CNNCDS recognizes images from a dataset placed in a folder, and a Python program using the Keras and Tensorflow libraries was invoked to use these images. There are numerous deep learning frameworks available today. Keras was chosen because it helps to lower cognitive load, it provides a unified and simple Application Programming Interface, it reduces the number of user activities needed for common use cases, and it offers clear and actionable feedback in the event of operator error. Keras is completely embedded with low-level TensorFlow functionality, facilitates the creation of highly configurable workflows with the ability to customize any piece of features.

G. The CNNCDS Learning Process

The CNNCDS learning process began with the creation of a database during the administration of electronic exams on Blackboard in a presentable manner. The exam control has been well established, ensuring that the students' monitors are not obstructed. The images of the screen captured during the examination session are the CNNCDS network entries. The

output of the network is binary and represents the student's normal or abnormal state. During the training process, CNNCDS "Fig. 4" learns the values of the filters on its own. The proposed framework consists of using general and personnel student data to carry out a secure online exam on LMS.

The faculty member is called to take advantage of the options provided by Blackboard to further secure the exam by i) Establishing a bank of diversified and numerous questions and ii) Providing the exam with a password iii) Controlling Students behavior using a CNN model as described in the flowchart "Fig. 5".

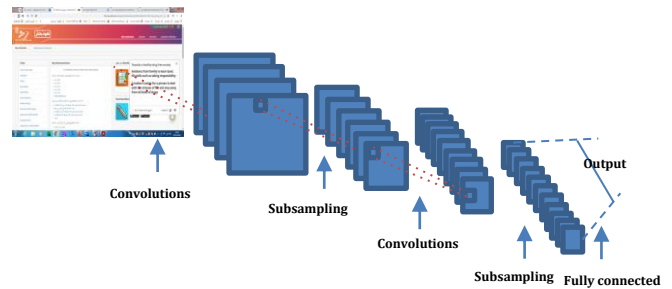


Fig. 4. The CNNCDS Structure.

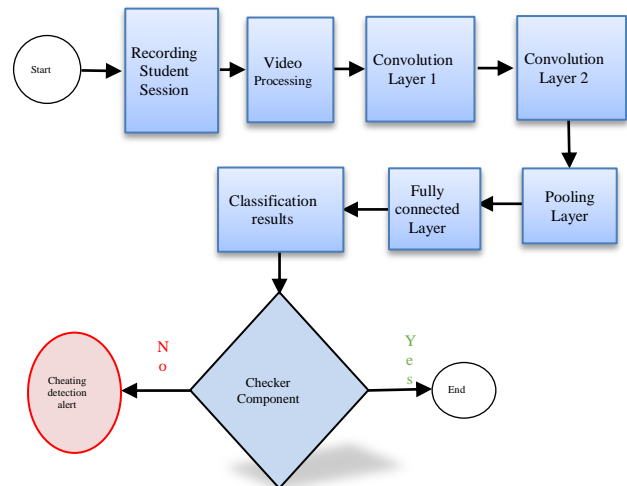


Fig. 5. Flowchart of the Proposed Video Sessions' Management by the CNN Model.

V. EXPERIMENTATIONS AND RESULTS

At the beginning of the academic year, an application form will be completed by the students which contains general and personal questions.

This application will be saved in the form of quizzes in the blackboard question bank tool. At any time during the exam, the faculty member can ensure the authentication of any student by launching polling from this question base. In this case, the student will have only 10 seconds to reply (Table II).

The online exam management procedure is divided into four steps: In the first step, the student had to run the program Myipaddress on his browser before connecting to Blackboard;

and he communicated it to the instructor. The instructor used a python application called IpControl to ensure that all the addresses are different and that there is only one student per address to avoid corporation between students while solving the exam. In the second step, the student launches two programs before receiving the exam key, the first to block navigation and the second to record the session. In the third step, the instructor sends the exam key to the students. The fourth step is to launch the CNNCDS program.

TABLE II. MONITORING SEQUENCE OF THE ONLINE EXAM

Students	Instructor	Time
	Preparing an application form	At the beginning of the academic year
Filling in the application form		At the beginning of the academic year
Launching My Ip Address Command		Before the beginning of the Exam
Sending Ip Address to the instructor		Before the beginning of the Exam
	Receiving Ip Addresses from all students	Before the beginning of the Exam
	Launching IpControl application	Before the beginning of the Exam
	Launching user authentication Application	Before the beginning of the Exam
	Sending confirmation to appropriate students	Before the beginning of the Exam
Blocking the navigation browser		Before the beginning of the Exam
Begin session registration		Before the beginning of the Exam
Informing the instructor		Before the beginning of the Exam
	Sending the exam key	Before the beginning of the Exam
Begin the exam		During the exam session,
	Sending a polling	During the exam session
Responding to the polling in 10 seconds		During the exam session
	Checking the results given by the CNNCDS	During the exam session
	Final classification of the student	During the exam session

To evaluate our proposed CNNCDS model at different levels, it was compared with four based classifiers. For given input data, a binary classifier generates output with two class values 1/0. The one of interest is typically represented as "positive," while the other is denoted as "negative". The observed labels for all data instances are contained in a test dataset used for performance evaluation. Having followed classification, the observed labels are compared to the predicted labels to determine performance. If a binary

classifier's performance is perfect, the predicted labels will be identical, but it is relatively rare to be able to develop an ideal binary classifier that is useful in a variety of situations.

The confusion matrix is constructed from the three components of binary classification. A binary classifier predicts whether all data instances in a test dataset are positively or negatively. True positive, true negative, false positive, and false negative are the four outcomes of this classification.

- True positive (TP): correct positive prediction.
- False positive (FP): incorrect positive prediction.
- True negative (TN): correct negative prediction.
- False negative (FN): incorrect negative prediction.

Accuracy is the percentage of correct predictions that a learner has achieved. It is computed by dividing the number of correct estimates by the total number of predictions (6).

$$Accuracy = \frac{TN+TP}{TN+FP+FN+TP} \quad (6)$$

- Precision, also known as the positive predictive value, is the ratio of the pertinent instances to the retrieved instances (7).

$$Precision = \frac{TP}{FP+TP} \quad (7)$$

- Recall, also called sensitivity, is a fragment of the retrieved relevant instances (8).

$$Recall = \frac{TP}{FN+TP} \quad (8)$$

- The F1-score is a statistical measure that combines precision and recall with rate performance (9).

$$F1 - score = \frac{precision*recall}{precision + recall} \quad (9)$$

As we had mentioned above, during an electronic face-to-face exam on Blackboard, a database of examples was created in the eLearning. A list of images for normal files was created as well as a list of images for abnormal files. CNNCDS was compared to the other classifiers on two levels: the first with 70% of the base of examples reserved for learning and 30% for testing. The second test was conducted with 90% of the resources allocated to learning and 10% to testing (Table III).

TABLE III. THE PERFORMANCE OF CNNCDS

	Accuracy		Error		Sensitivity		Pr. time	
	70.30	90.10	70.30	90.10	70.30	90.10	70.30	90.10
Random Forest algorithm	95	96	5.0	4.0	95	96	4.0	5.0
Multi-class Logistic Regression	97	98	2.5	1.9	96	97.5	6	7
Gaussian Naïve Bayes	91	92.5	9	8	95.5	97	1	0.95
Support Vector Machine	97.1	98.0	3	2.50	96.5	97.5	10	13
CNNCDS	98.2	98.5	2	1.8	99.2	99.8	4	6

CNNCDS outperforms the basic classifiers (Multi-class Logistic Regression (MLR), Support Vector Machine (SVM), Random Forest (RF), and Gaussian Naive Bayes (GNB) in terms of mean accuracy (98.5%). Furthermore, it correctly identified screen images with an acceptable processor time, with a sensitivity average of 99.8% and a precision average of 1.8 %.

Following validation, the proposed method was tested in many sections at the first preparatory year college during the 2020-2021 academic year. The results were brilliant and provided great satisfaction except that the students found this method strange and comes to limit their activities during exams especially in the context of the covid-19 pandemic. The efficiency of the method is 100%. No fraud operation has been detected once the method is applied. The advantage of this method is the use of diverse Dataset and it does not rely on video sequences but rather on navigation sequences of students taking exams, the limitations are that the base of learning materials is specific to Umm al-Qura University.

VI. CONCLUSION

Dishonest students' actions reflect poorly on them and the Institute. Although copying is the most common form of dishonest, fraudulent students invent a variety of other forms of cheating. Outside the exam sessions, students should be aware that collaborative work is acceptable, but copying works against them and violates academic integrity principles.

Cheating attempts have increased, particularly with distance learning and online exams, as many faculty members seek new ways to combat the problem.

The purpose of this article is to prevent cheating and to find appropriate solutions to detect more complex types of cheating. It should also be a major concern for faculty members who want to maintain academic integrity. The document proposes new solutions to these problems to create more resilient and intelligent future systems. This work identifies intelligent methods for cheating detection in online education exams. The emphasis is placed on steps that faculty members had to undertake to secure electronic assessments. To accomplish this aim, the authors have defined the following four main objectives: i) Identify the latest technologies on cheating detection, ii) Identify the role of intelligent methods and their advantages on cheating detection and prevention, iii) Present a new model for online proctored exam process and determine its effectiveness, and iv) Apply this new model and identify the limitations of this study and recommend further work.

The most important approach is the prevention of cheating and finding appropriate solutions without using webcam. Research shows that most anti-cheating services can be hacked by various methods set up by very smart and connected students. AI techniques can help improve the performance of the detection procedure. The use of the webcam is always the most adequate solution to better overcome the problem of cheating. Not relying on the webcam made the mission difficult but possible.

The proposed method is based on i) IP address, ii) Personnel Student Data, iii) Blocking the browser, iv) Recording and analyzing the exam session. Also, when

passing the exam, an authentication method is proposed to avoid cheating. Using a database specific to each student, polling questions will be sent to ensure that the student is himself and not another person who is taking the exam. A delay of 10 seconds only will be reserved for the student to respond.

The proposed method's main component is CNNCDS which classifies screenshots of students' computers while taking online exams and detects abnormal navigation. The CNNCDS was learned using a dataset created in the same environment as students took face-to-face electronic exams on Blackboard. CNNDCS was used on online electronic exams after it had been learned, tested, and validated. Its output is binary in order to alert the faculty member to unusual behavior.

In terms of mean accuracy, CNNCDS outperforms the basic classifiers (Multi-class Logistic Regression (MLR), Support Vector Machine (SVM), Random Forest (RF), and Gaussian Naive Bayes (GNB) (98.5%). Furthermore, with a sensitivity average of 99.8 % and a precision average of 1.8%, it correctly identified screen images in an acceptable processor time. This method is effective in reducing cheating in some universities where using the camera is not allowed.

ACKNOWLEDGMENT

The authors would like to thank the Deanship of Scientific Research at Umm al-Qura University for supporting this work by Grant Code: 19-EDU-1-03-0001.

REFERENCES

- [1] Crooks, T. J. (1988). The impact of classroom evaluation practices on students. *Review of educational research*, 58(4), 438-481.
- [2] Entwistle, N., & Ramsden, P. (2015). *Understanding student learning* (routledge revivals). Routledge.
- [3] Astin, A. W. (2012). *Assessment for excellence: The philosophy and practice of assessment and evaluation in higher education*. Rowman & Littlefield Publishers.
- [4] Alruwais, N., Wills, G., & Wald, M. (2018). Advantages and challenges of using e-assessment. *International Journal of Information and Education Technology*, 8(1), 34-37.
- [5] Dumford, A. D., & Miller, A. L. (2018). Online learning in higher education: exploring advantages and disadvantages for engagement. *Journal of Computing in Higher Education*, 30(3), 452-465.
- [6] White, A. M. J. (2021). Information literacy and critical thinking in higher education: Some considerations. In *Research Anthology on Developing Critical Thinking Skills in Students* (pp. 111-124). IGI Global.
- [7] H. M. Alakrash and N. A. Razak, "Education and the fourth industrial revolution: Lessons from COVID-19," *Computers, Materials and Continua*, pp. 951-962, 2021.
- [8] L. W. Anderson, "Objectives, evaluation, and the improvement of education," *Studies in Educational Evaluation*, vol. 31, (2-3), pp. 102-113, 2005.
- [9] Büchele, S. (2021). Evaluating the link between attendance and performance in higher education: the role of classroom engagement dimensions. *Assessment & Evaluation in Higher Education*, 46(1), 132-150.
- [10] Ahsan, K., Akbar, S., & Kam, B. (2021). Contract cheating in higher education: a systematic literature review and future research agenda. *Assessment & Evaluation in Higher Education*, 1-17.
- [11] García-Morales, V. J., Garrido-Moreno, A., & Martín-Rojas, R. (2021). The transformation of higher education after the COVID disruption: Emerging challenges in an online learning scenario. *Frontiers in Psychology*, 12, 196.

- [12] Khenkitisack, P., & Reidt, E. The Learning Process of Students in Creating Video as an Exam Format in Higher Education—an Evaluation in an Economics Course.
- [13] Bautista-Puig, N., Aleixo, A. M., Leal, S., Azeiteiro, U., & Costas, R. (2021). Unveiling the Research Landscape of Sustainable Development Goals and Their Inclusion in Higher Education Institutions and Research Centers: Major Trends in 2000–2017. *Frontiers in Sustainability*, 2, 12.
- [14] Felix, J. J. (2021). Higher education in times of instability and disruption: Rethinking notions of values, value creation and instructional practices in Vietnam and beyond. *Frontiers in Communication*, 6, 22.
- [15] Hamdan, K. M., Al-Bashaireh, A. M., Zahran, Z., Al-Daghestani, A., Samira, A. H., & Shaheen, A. M. (2021). University students' interaction, Internet self-efficacy, self-regulation and satisfaction with online education during pandemic crises of COVID-19 (SARS-CoV-2). *International Journal of Educational Management*.
- [16] Almomani, E. Y., Qablan, A. M., Atrooz, F. Y., Almomany, A. M., Hajjo, R. M., & Almomani, H. Y. (2021). The Influence of Coronavirus Diseases 2019 (COVID-19) Pandemic and the Quarantine Practices on University Students' Beliefs about the Online Learning Experience in Jordan. *Frontiers in Public Health*, 8, 997.
- [17] Joseph, D., Nethsinghe, R., & Cabedo-Mas, A. (2021). Online teaching and learning during Covid-19: Flexible harmonies in higher education. In *Online Teaching and Learning in Higher Education during COVID-19* (pp. 50-68). Routledge.
- [18] Holden, O. L., Norris, M. E., & Kuhlmeier, V. A. (2021). Academic integrity in online assessment: a research review. In *Frontiers in Education* (p. 258). Frontiers.
- [19] M. E. M. Amer, "Effectiveness of Using Electronic Exams in Assessment in Saudi Universities: Empirical Study," *International Journal of Educational Technology and Learning*, vol. 8, (2), pp. 61-69, 2020.
- [20] K. Man and J. R. Harring, "Assessing preknowledge cheating via innovative measures: A multiple-group analysis of jointly modeling item responses, response times, and visual fixation counts," *Educational and Psychological Measurement*, vol. 81, (3), pp. 441-465, 2021.
- [21] L. C. O. Tiong and H. J. Lee, "E-cheating Prevention Measures: Detection of Cheating at Online Examinations Using Deep Learning Approach--A Case Study," *arXiv Preprint arXiv: 2101.09841*, 2021.
- [22] V. A. Sangalli, G. Martinez-Muñoz and E. P. Cañabate, "Identifying cheating users in online courses," in *2020 IEEE Global Engineering Education Conference (EDUCON)*, 2020, pp. 1168-1175.
- [23] O. Popoola, "Marker detection of contract cheating: An investigative corpus linguistic approach," in *European Conference on Academic Integrity and Plagiarism 2021*, pp. 131.
- [24] K. Rundle, G. J. Curtis and J. Clare, "Why students do not engage in contract cheating," *Frontiers in Psychology*, vol. 10, pp. 2229, 2019.
- [25] M. Paechter and B. Maier, "Online or face-to-face? Students' experiences and preferences in e-learning," *The Internet and Higher Education*, vol. 13, (4), pp. 292-297, 2010.
- [26] X. Zhu and C. Cao, "Secure Online Examination with Biometric Authentication and Blockchain-Based Framework," *Mathematical Problems in Engineering*, vol. 2021, 2021.
- [27] H. J. Bullock, A. Luccioni, K. H. Pham, C. S. N. Lam and M. Luengo-Oroz, "Mapping the landscape of artificial intelligence applications against COVID-19," *Journal of Artificial Intelligence Research*, vol. 69, pp. 807-845, 2020.
- [28] R. Ismail, V. Osmanaj and A. Jaradat, "Moving towards E-university: Modelling the online proctored exams," *AICMSE-AICSSH 2019 August (Oxford) | 12th-14th August 2019 Conference 2019*.
- [29] L. author, J. Boulahia and R. Bouallegue, "A semi blind channel estimation method based on hybrid neural networks for uplink LTE-A," *International Journal of Wireless & Mobile Networks* Vol, vol. 8, 2017.
- [30] K. Muthumayil, M. Buvana, K. R. Sekar, A. E., Amraoui, I. Nouaouri, and R. F. Mansour, "Optimized convolutional neural network for automatic detection of COVID-19," *Computers, Materials and Continua*, pp. 1159-1175, 2021.
- [31] P. Dawson, W. Sutherland-Smith, and M. Rickson. "Can software improve marker accuracy at detecting contract cheating? A pilot study of the Turnitin authorship investigate alpha." *Assessment & Evaluation in higher education*, 45(4), 473-482.
- [32] T. Lancaster, "Academic Dishonesty or Academic Integrity? Using Natural Language Processing (NLP) Techniques to Investigate Positive Integrity in Academic Integrity Research." *Journal of Academic Ethics*, 1-21, 2021.
- [33] S. K. Kim, and J.H. Huh, "Blockchain Agreement for Self-identification of Online Test Cheating: Improvement of Algorithm Performance," In *2020 20th International Conference on Control, Automation and Systems (ICCAS)*, 2020, pp. 1124-1133.
- [34] I. Đ Babić, "Machine learning methods in predicting the student academic motivation," *Croatian Operational Research Review*, pp. 443-461, 2017.
- [35] F. Kamalov, H. Sulieman and D. Santandreu Calonge, "Machine learning based approach to exam cheating detection," *Plos One*, vol. 16, (8), pp. e0254340, 2021.
- [36] M. Geetha, R. S. Latha, S. K. Nivetha, S. Hariprasath, S. Gowtham et al, "Design of face detection and recognition system to monitor students during online examinations using machine learning algorithms," in *2021 International Conference on Computer Communication and Informatics (ICCCI)*, 2021, pp. 1-4.
- [37] J. Opgen-Rhein, B. Küppers and U. Schroeder, "An application to discover cheating in digital exams," in *Proceedings of the 18th Koli Calling International Conference on Computing Education Research*, 2018, pp. 1-5.
- [38] H. S. Asep and Y. Bandung, "A design of continuous user verification for online exam proctoring on M-learning," in *2019 International Conference on Electrical Engineering and Informatics (ICEEI)*, 2019, pp. 284-289.
- [39] J. Huang, G. Shen and X. Ren, "Connotation Analysis and Paradigm Shift of Teaching Design under Artificial Intelligence Technology." *International Journal of Emerging Technologies in Learning*, vol. 15, (5), 2021.
- [40] Y. LeCun, Y. Bengio and G. Hinton, "Deep learning," *Nature*, vol. 521, (7553), pp. 436-444, 2015.
- [41] T. M. Tashu, J. P. Esclamado and T. Horvath, "Intelligent on-line exam management and evaluation system," in *International Conference on Intelligent Tutoring Systems*, 2019, pp. 105-111.
- [42] F. A. Abubakar and S. Boukari, "A Convolutional Neural Network with K-Nearest Neighbor for Image Classification," *International Journal of Advanced Research in Computer and Communication Engineering*, vol. 7, pp. 1-7, 2018.
- [43] C. Zhang, R. Yao and J. Cai, "Efficient eye typing with 9-direction gaze estimation," *Multimedia Tools Appl*, vol. 77, (15), pp. 19679-19696, 2018.
- [44] S. Minaee, M. Minaei and A. Abdolrashidi, "Deep-emotion: Facial expression recognition using attentional convolutional network," *Sensors*, vol. 21, (9), pp. 3046, 2021.
- [45] D. Canedo, A. Trifan and A. J. Neves, "Monitoring students' attention in a classroom through computer vision," in *International Conference on Practical Applications of Agents and Multi-Agent Systems*, 2018, pp. 371-378.

A Cubic B-Splines Approximation Method Combined with DWT and IBP for Single Image Super-resolution

Victor Kipkoech Mutai^{1*}, Elijah Mwangi², Ciira wa Maina³

Department of Electrical and Electronic Engineering, Dedan Kimathi University of Technology, Nyeri, Kenya¹

Faculty of Engineering, University of Nairobi, Kenya²

Centre for Data Science and Artificial Intelligence, Dedan Kimathi University of Technology, Nyeri, Kenya³

Abstract—The process of converting low-resolution images into high-resolution images by removing noise and estimating high-frequency information is known as image super-resolution. Aliased and decimated versions of the actual scenes are considered low-resolution images. The edges of high-resolution images produced by super-resolution from a single image are typically blurred. This paper proposes an approach to generate high-resolution image with sharp edges by combining a cubic B-Splines approximation, a discrete wavelet transform (DWT), and an iterative back-projection (IBP) edge-preserving weighted guided filter. A two-stage cubic B-Splines approximation, which includes pre-filtering and interpolation, is employed to up-sample the low-resolution image. The pre-filtering approach is used to transform pixel values to B-Splines coefficients. This approach minimizes blurring in the up-sampled image. The lost high-frequency information is then estimated using a one-level discrete wavelet transform based on the db1 wavelet. Finally, using a weighted guided filter, the resulting image is subjected to back-projection to obtain a high-resolution image. The proposed single-image super-resolution approach is applied on RGB colour images. The proposed method outperforms other selected approaches for comparison objectively in terms of PSNR and SSIM and also in visual quality.

Keywords—Single-image super-resolution; pre-filtering; cubic B-Splines approximation; discrete wavelet transform (DWT); iterative back-projection (IBP); B-Splines coefficients

I. INTRODUCTION

In many fields of digital imaging, there is usually a need for images of a higher resolution in a pre-processing stage for other subsequent operations. The main applications include diagnosis of medical conditions, pattern recognition, remote sensing, and surveillance [1]-[3]. The details that can be obtained from an image depends on its resolution. The capture of high-resolution images is not always feasible in surveillance systems because of limitations in terms of storage requirements, bandwidth for transmission of high-resolution images, power, and the cost of the image capturing device [4], [5]. Therefore, the image acquisition and transmission systems limit the resolution of the captured images, leading to constraints on the quality of the images available for interpretation and perception. As a result, image super-resolution (SR) is required to improve the information content in order to gain more details from the images. Multi-frame image reconstruction [6]-[8] and single-image super-resolution (SISR) [9]-[13] are the two types of super-resolution image reconstruction.

Image super-resolution aims at the recovery of the lost high-frequency information and preservation of the edges [14]. In this paper, an approach that combines cubic B-Splines approximation, discrete wavelet transform and iterative back-projection is proposed to achieve super-resolution from a single image. This is the first attempt to integrate the pre-filtering in cubic B-Splines approximation for image super-resolution. The key contributions of the proposed methodology over the current approaches are as follows:

- 1) Design and integration of the pre-filtering to improve the up-scaling performance of the cubic B-Splines approximation.
- 2) Comparative analysis of wavelet image reconstruction to determine the best-performing wavelet among the three wavelet families (Daubechies, Symlets and Coiflets) in terms of the recovery of the lost frequency information.
- 3) Localization of the edges of the image using a weighted guided filter in back-projection to preserve and enhance details of the edges while avoiding widening of those edges.
- 4) Attaining good objective performance and visual quality with low computation time.

The rest of the paper is organized as follows. Section 2 presents the previous related works and contributions of this research paper. Section 3 presents the detailed proposed methodology. Experimental results and discussion are given in Section 4. Summary of the findings and suggestions for further work are presented in Section 5.

II. RELATED WORK

Single-image super-resolution is an inverse optimization problem without a unique solution and thus very challenging because multiple solutions can be achieved based on the texture details. Direct interpolation using interpolation kernels [14], [15], wavelet transforms [16],[17], use of statistical approaches to estimate missing pixel values [18],[19], and example-based approaches [20], [21] are the sub-categories of single-image super-resolution. Bicubic interpolation is widely used in up-scaling [22], [23]. However, it exhibits non-uniform gain which leads to distortions and larger lobes which introduces artifacts. The cubic B-Splines has been found to perform better than the widely used Keys' bicubic interpolation. However, it is an approximating function requiring a two-stage process [24]. Chen *et al.* [25] proposed an example-based approach that employs local multi-gradient level pattern prediction. The method results in high-quality

*Corresponding Author.

output images compared to approaches selected for comparison. The approach is however limited by; (i) high computation requirements and (ii) high storage requirements for databases for training images.

The low-resolution (LR) image is used as the low-frequency sub-band, (LL), of the high-resolution image in the wavelet-based approach for super-resolution. The task is to estimate the high-frequency sub-bands in order to obtain a HR image. Demirel and Anbarjafari [26] proposed using a dual-tree complex wavelet transform (DT-CWT) for resolution enhancement of satellite images. They interpolated the input LR images using a bicubic interpolation function and the subsequent high-frequency sub-bands, and combined them to form a super-resolved image using the inverse DT-CWT. To improve image quality, Lidong *et al.* [27] combined the DWT and contrast limited adaptive histogram equalization (CLAHE) in their approach. The low-resolution image is decomposed into four sub-bands. After that, the CLAHE is applied to the low-frequency sub-bands. Demirel and Anbarjafari [28] proposed an algorithm to improve image resolution using the DWT and SWT decompositions. To preserve the image's high-frequency information content, DWT based on the Daubechies 9/7 wavelet family is used. These approaches were however limited by (i) blurring in the highly textured areas and (ii) lack of comparison among the wavelets used in order to determine the wavelet that produce higher quality images.

In addition to estimating the high-frequency components, various methods have been employed to improve the super-resolved images quality further. Iterative back-projection [29]-[32] is one such process that minimizes the reconstruction error. Bareja and Modi [33] proposed a SISR based on IBP with an infinite symmetric exponential filter (ISEF) to preserve the edges. Ngocho and Mwangi [34] proposed back-projection using the Laplacian of Gaussian (LoG) kernel to enhance the edges and reduce noise in the resulting image. Makwana and Mehta [35] proposed an approach that combines IBP method with the Canny Edge detector and Gabor Filter for retrieval of the high-frequency information. They applied this method to grayscale images and compared them with existing algorithms. Despite the improvement in objective performance with these approaches, they employed global filters which leads to widening of the edges of the super-resolved images leading to reduced visual quality.

Motivations behind the proposed approach. In the previous works it was noted that despite the better performance of the cubic B-Splines than other interpolation kernels, direct interpolation using cubic B-Splines on the pixel values of an image leads to over-smoothing especially in the regions having high local variances [12],[13]. The proposed approach attempts to rectify this issue by employing a pre-filter to compute the B-Splines coefficients which are then subjected to cubic B-Splines interpolation. In addition, various wavelets have been employed in estimation of the lost high-frequency information. However, no comparison among the wavelets used was tested. This investigation seeks to perform comparative analysis of various wavelet families to determine best performing wavelet in image-reconstruction [26]-[28]. Lastly, all the previous approaches employing iterative back-projection used global

filters resulting in images with wider edges which is undesirable [31]-[35].

III. PROPOSED METHODOLOGY

The flowchart for the proposed single-image super-resolution approach is shown in Fig. 1. The proposed method combines a two-stage cubic B-Splines approximation, DWT, and iterative back-projection.

A. Cubic B-splines Approximation

1) *Pre-filtering*: The pre-filtering step is used to compute the coefficients of an image using a direct B-splines filter. This method employs a recursively moving average filter to reduce the computational cost. The cubic B-Splines approximation is a two-stage process which begins with the estimation of the B-Splines coefficients, $c(k)$ from the pixel values of an image, $f(k)$. The challenge is to determine the coefficients such that the interpolation kernel passes through the pixel values exactly. The desired values $f(k)$ are obtained from the coefficients, $c(i)$ as in (1).

$$\sum_{i \in \mathbb{Z}} c(i) \beta^n(x - i)|_{x=k} = f(k) \quad \forall k \in \mathbb{Z} \quad (1)$$

Where n is the degree of B-Splines kernel.

Using discrete B-Splines kernel, (1) can be rewritten as in (2).

$$f(k) = b^n(k) * c(k) \quad (2)$$

Where $*$ is the convolution operator and $b^n(k) = \beta^n(x)|_{x=k}$.

The B-Splines coefficients, $c(k)$ can be obtained as in (3)

$$c(k) = f(k) * (b^n(k))^{-1} \quad (3)$$

$(b^n(k))^{-1}$ is the direct B-Splines filter. By sampling the discrete cubic B-splines interpolating kernel, (4) is obtained. The kernel is non-zero in the interval $-1 \leq k \leq 1$.

$$b^3(k) = \left(\frac{1}{6}, \frac{4}{6}, \frac{1}{6}\right) \quad -1 \leq k \leq 1 \quad (4)$$

By taking a z-transform of (4), (5) is obtained.

$$\beta^3(z) = \sum_{k=-1}^1 b^3(k) z^{-k} = \frac{z+4+z^{-1}}{6} \quad (5)$$

The direct cubic B-splines filter is obtained as in (6)-(9).

$$(b^3(k))^{-1} \stackrel{z}{\leftrightarrow} \frac{1}{\beta^3(z)} \quad (6)$$

$$\begin{aligned} \frac{1}{\beta^3(z)} &= \frac{6}{z+4+z^{-1}} = 6 \left(\frac{1}{1-\alpha z^{-1}} \right) \left(\frac{-\alpha}{1-\alpha z} \right) \\ &= 6 \left(\frac{-\alpha}{1-\alpha^2} \left(\frac{1}{1-\alpha z^{-1}} + \frac{1}{1-\alpha z} - 1 \right) \right) \end{aligned} \quad (7)$$

$$6 \left(\frac{-\alpha}{1-\alpha^2} \alpha^{|k|} \right) \stackrel{z}{\leftrightarrow} 6 \left(\frac{-\alpha}{1-\alpha^2} \left(\frac{1}{1-\alpha z^{-1}} + \frac{1}{1-\alpha z} - 1 \right) \right) \quad (8)$$

$$(b^3(k))^{-1} = 6 \left(\frac{-\alpha}{1-\alpha^2} \alpha^{|k|} \right) \quad (9)$$

Where $\alpha = -2 + \sqrt{3}$.

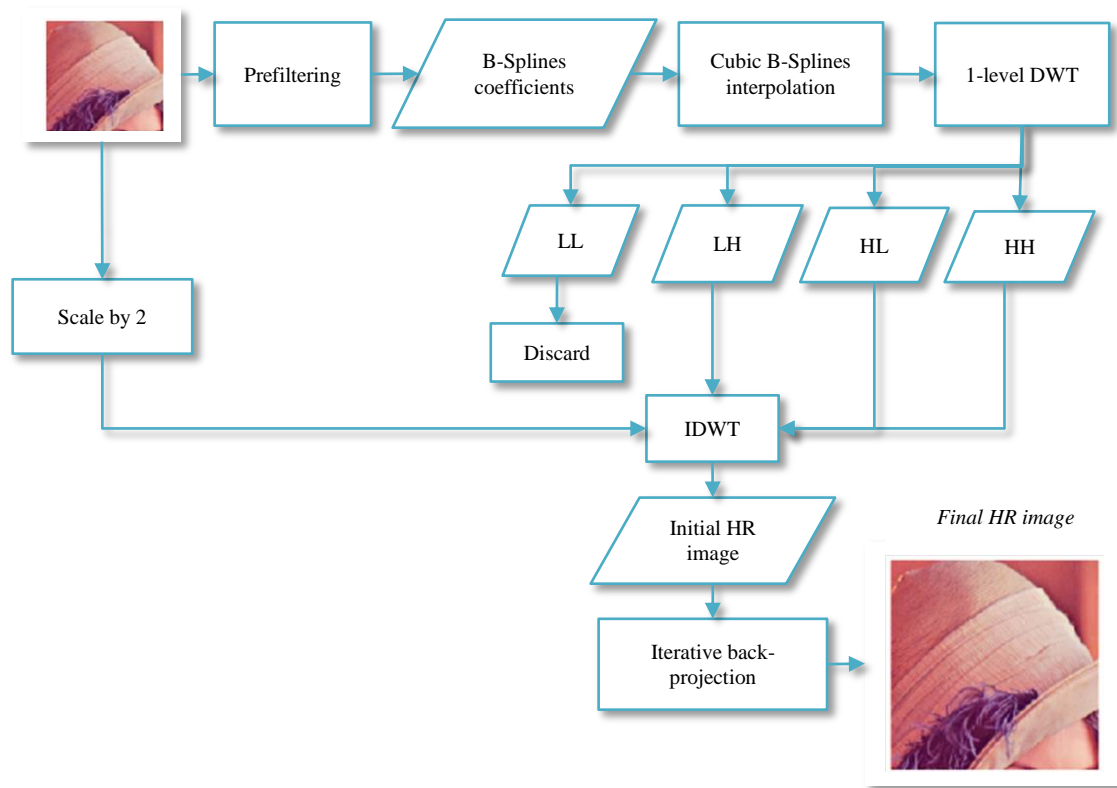


Fig. 1. Proposed Methodology.

$(b^3(k))^{-1}$ is a direct cubic B-Splines filter having alternating sign change. The filter in (9) can be implemented using a causal filter in (10) and an anti-causal filter in (11). The cubic B-Splines coefficients are then obtained as in (12).

$$c^+(k) = f(k) + \alpha c^+(k-1) \quad k = 1, \dots, J-1 \quad (10) \quad c^-(k) = \alpha(c^-(k-1) - c^+(k)) \quad k = J-2, \dots, 0 \quad (11)$$

$$c(k) = \frac{c^-(k)}{6} \quad (12)$$

$f(k)$ are the signal values, $c^+(k)$ is the causal filter, $c^-(k)$ is the anti-causal filter, J is the signal length, and $c(k)$ are the B-splines coefficients. The starting points for the two filters in (10) and (11) are given in (13) and (14) as follows.

$$c^+(0) = \sum_{k=0}^{k_0} f(k) \alpha^k \quad (13)$$

$$c^-(J-1) = \frac{-\alpha}{1-\alpha^2} (c^+(J-1) + \alpha c^+(J-2)) \quad (14)$$

2) *Cubic B-Splines interpolation*: The cubic B-Splines is based on the one-dimensional approximation kernel given in (15):

$$u(x) = \frac{1}{6} \begin{cases} 4 - 3|x|^2(2 - |x|) & 0 \leq |x| < 1 \\ (2 - |x|)^3 & 1 \leq |x| < 2 \\ 0 & 2 \leq |x| \end{cases} \quad (15)$$

This approximation kernel is applied in (16) to obtain new pixel values of the interpolated image, $f(x)$, from the B-splines coefficients, $c(k)$. Since the kernel is separable, for

images, it is first applied along the rows and then along the columns sequentially.

$$f(x) = \sum_k c(k)u(x-k) \quad (16)$$

The condition for the kernel to be interpolating is given in (17):

$$u(x) = \begin{cases} 1 & x = 0 \\ 0 & |x| = 1, 2, \dots \end{cases} \quad (17)$$

It is noted that for cubic B-Splines, $u(0) \neq 1$ and hence does not satisfy the condition for being directly interpolating. Therefore, if it is applied directly to the pixel values of an image, it may lead to over-smoothing, especially in the regions with high local variances. This investigation seeks to determine whether pre-filtering will improve the performance of the cubic B-Splines approximation.

B. One-level Discrete Wavelet Transform

One level DWT is used to estimate the high-frequency sub-bands of the super-resolved image by passing the signal through a low-pass filter (LPF) and high-pass filter (HPF) [36]. It is used to decompose a signal to approximation and detail coefficients, each with half-the frequency components from the original signal. The decomposition is done in two stages for images, first along the rows and then along the image columns. The output of the operation is four sub-bands (*LL*, *LH*, *HL* and *HH*). This study will investigate which wavelet will produce higher quality super-resolution images better among the three wavelet families: Daubechies, Symlets and Coiflets.

C. Iterative Back-Projection (IBP)

Super-resolution is an inverse problem without a unique solution. A number of possible results can be limited by applying additional constraints leading to outputs closer to the ground truth images. The IBP is one such process to minimize the reconstruction error by projecting back the error difference, $e^{(n)}$ between the input LR image, and the low-resolution image from the resolution enhancement process, $SR^{(n)} \downarrow$. The process is repeated until convergence is achieved. The IBP process can be summarized as in (18) and (19).

$$e^{(n)} = LR - SR^{(n)} \downarrow \quad (18)$$

$$SR^{(n+1)} = SR^{(n)} + (e^{(n)} * p) \uparrow \quad (19)$$

Where n denotes the n^{th} iteration, \uparrow is the up-sampling operator and \downarrow is the down-sampling operator, p is the back-projection filter and $*$ is the convolution operator. In this paper, the weighted guided image filter [37],[38] has been selected as the back-projection filter. The weighted guided image filter combines the benefits of both the global and the local image filters. It incorporates edge-aware weighting that depends on whether the pixel values are on the edges or in smooth areas. Because of this weighting, the weighted guided filter maintains the sharpness of the edges of the image. Its complexity is also independent of the size of the kernel. Thus, we can use the larger kernel sizes can be employed with a negligible increase in computation times.

D. Proposed Single Image Super-resolution Process

The proposed image super-resolution process is given in steps (i) to (vii) as follows:

Step (i) The input LR image is subjected to a two-stage cubic B-Splines approximation with an up-sampling factors of 2 and 3. The LR image is subjected to a direct B-Splines filter (pre-filtering) in the first stage to transform the pixel values to coefficients in the B-Splines domain. In the second stage, the B-Splines coefficients are up sampled by integer factors of 2 and 3 using the cubic B-Splines approximation kernel.

Step (ii) The output image from the cubic B-Splines approximation is then decomposed into approximation coefficients (LL) and detail coefficients (LH, HL and HH) using one-level discrete wavelet transform based on the selected db1 wavelet.

Step (iii) The pixel values of the LR image are scaled by a factor of 2. The factor of 2 corresponds to the normalization factor for a one-level DWT. The scaled LR image and the detailed coefficients are subjected to one-level Inverse Discrete Wavelet Transform (IDWT) to get the initial HR image.

Step (iv) The initial HR image, $SR^{(0)}$ is down-sampled by a factor of 2 and 3 depending on the decimation factor used. The result is a low-resolution image, $LR^{(1)}$

$$LR^{(1)} = SR^{(0)} \downarrow \quad (20)$$

Step (v) The low-resolution image, $LR^{(1)}$ is subtracted from LR to obtain an error image $e^{(1)}$.

$$e^{(1)} = LR - LR^{(1)} \quad (21)$$

Step (vi) The error image, $e^{(1)}$ is then convolved with a back-projection filter, p , and up-sample it. The results are then added to the initial HR image.

$$SR^{(1)} = SR^{(0)} + (e^{(1)} * p) \uparrow \quad (22)$$

Step (vii) Steps (iv) to (vi) are repeated until the convergence is achieved.

IV. RESULTS AND DISCUSSION

In this section, the experimental settings are first introduced, then performance of the proposed super-resolution algorithm and the comparison to other proposed approaches is reported.

A. Experimental Settings

A total of 74 images were used in the super-resolution approach. The images are obtained from the public databases. The first set. The second image set contains the 24-bit RGB colour images from Signal and Processing Institute from University of California, Los Angeles, USA [41]. The dataset contains 36 high altitude aerial images of dimensions 512×512 and 1024×1024 pixels. The format is Tagged Image Format File (TIFF). The second set was obtained from Eastman Kodak Company [42]. It contains 24 RGB colour images of dimensions 512×768 pixels and 256×256 pixels. The last dataset was obtained from Deep AI [43]. It contains 14 images of dimensions 512×768 pixels commonly used for testing SR models. The test image sets contain images with significantly different frequency content and variations in texture and edges. The simulations were conducted in MATLAB R2020a environment. Fig. 2 illustrates a sample of 16 images from the databases.

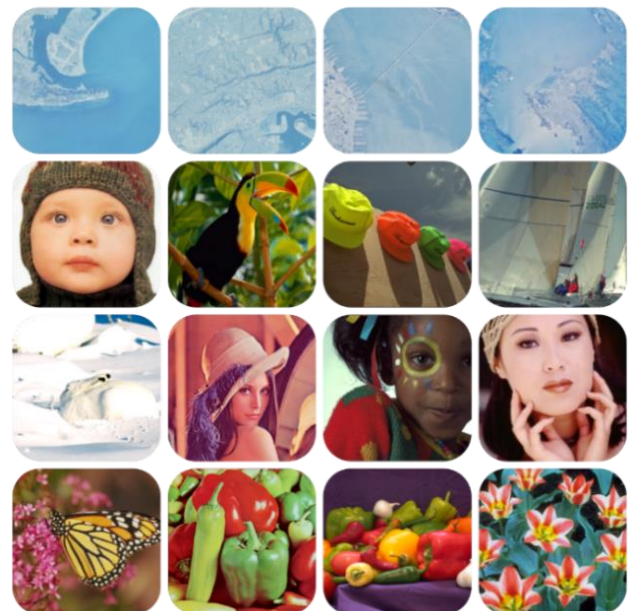


Fig. 2. Sample Test Images from the Selected Databases. From the Left to the Right and Top to the Bottom: Aerial1 (1024×1024), Aerial2 (1024×1024), Aerial3 (1024×1024), Aerial4 (1024×1024) Baby (768×512), Bird (768×512), Kodim03 (768×512), Kodim10 (768×512), Arctic hare (256×256), African girl (768×512), Lena (512×512), Monarch (768×512), peppers1(512×512), peppers2 (768×512) and tulips (768×512).

For comparison, three single-image super-resolution methods have been used: LoG IBP [34], VDSR [39], NEDI [40], and bicubic interpolation as the baseline.

B. Experimental Results

The Peak Signal-to-Noise Ratio (PSNR) based on Mean Square Error (MSE) and Structural Similarity Index Measure (SSIM) are used to quantify the performance of the algorithm. The MSE measures the amount of lost frequency information in the image through pixel-by-pixel comparison. SSIM on the other hand considers effects of luminance and brightness of the image. The higher the PSNR and SSIM, the better the quality of the super-resolved image.

1) *Investigation of the importance of pre-filtering in cubic B-splines approximation:* Two sets of experimental approaches were conducted to validate the effectiveness of the pre-filtering incorporated in cubic B-splines approximation. Grayscale version of the test images were used in this investigation. The test images were decimated by a factor of 2 to obtain LR

images. In the first approach, the cubic B-splines interpolation was applied directly to the pixel values of the LR images. In the second approach, the proposed pre-filter was first used to transform the pixel values of the LR images to B-Splines coefficients. The cubic B-Splines interpolation was then applied to the B-Splines coefficients. Table I shows the results for the PSNR and SSIM comparison between the cubic B-Splines approximation which integrates the pre-filtering approach and direct interpolation using cubic B-Splines interpolation kernel. From Table I, the results indicates that cubic B-Splines approximation achieves better performance with the average PSNR and SSIM improvement of 3.43 dB and 0.05 respectively from direct interpolation. The other test images also gave similar results. These results indicates that applying a pre-filter to pixel values of an image before performing up-sampling with cubic B-Splines produces significantly better results than otherwise.

TABLE I. COMPARISON BETWEEN CUBIC B-SPLINES APPROXIMATION (WITH PRE-FILTERING) AND DIRECT INTERPOLATION (WITHOUT PRE-FILTERING)

Image Labels ↓	PSNR (dB)			SSIM		
	Without Pre-filtering	With Pre-filtering	Improvement	Without Pre-filtering	With Pre-filtering	Improvement
Aerial1	29.39	30.66	1.28	0.72	0.77	0.05
Aerial5	31.41	33.99	2.58	0.74	0.79	0.05
Baby	32.21	35.26	3.05	0.90	0.95	0.04
Bird	30.19	34.39	4.11	0.92	0.97	0.05
Kodim03	30.20	32.59	2.39	0.87	0.91	0.04
Kodim10	29.02	30.82	1.80	0.84	0.89	0.05
Arctic hare	33.03	37.66	4.63	0.94	0.97	0.03
Lena	32.21	35.34	3.13	0.89	0.93	0.04
Peppers2	32.83	36.18	3.35	0.93	0.96	0.03
Tulips	29.50	33.52	3.26	0.86	0.92	0.06
AVERAGE	30.99	34.42	3.43	0.85	0.90	0.05

TABLE II. PSNR COMPARISON OF THE PERFORMANCE OF SELECTED WAVELETS IN IMAGE RECONSTRUCTION

Image Labels ↓	Daubechies				Symlets			Coiflets		
	db1	db2	db3	db4	sym2	sym3	sym4	coif2	coif3	coif4
Aerial1	33.49	31.10	28.85	27.78	31.50	29.40	30.74	27.91	26.82	26.08
Aerial2	34.00	31.37	28.36	27.01	31.60	29.20	28.64	27.27	26.09	25.44
Aerial5	35.65	32.62	29.54	28.23	32.69	29.67	30.32	27.89	27.10	26.67
Baby	32.86	27.90	23.48	21.22	29.00	25.00	23.92	20.21	17.92	16.44
Bird	31.49	26.52	22.00	19.77	26.70	22.45	23.04	19.58	17.64	16.62
Kodim03	31.74	29.38	26.48	24.89	29.40	26.97	27.57	24.43	22.82	21.79
Arctic hare	35.10	28.95	24.11	21.73	29.70	24.15	26.13	21.33	19.14	17.98
Lena	31.21	27.41	23.20	21.03	28.00	23.56	24.66	21.12	18.97	17.75
Peppers2	34.28	30.96	26.54	24.05	31.40	26.89	27.04	24.27	21.58	19.93
Tulips	30.24	26.05	21.76	19.50	29.00	21.99	22.72	19.35	17.10	15.76
AVERAGE	33.01	29.23	25.43	23.52	29.90	25.93	26.48	23.34	21.52	20.45

2) *Comparative analysis for wavelet image reconstruction:*

The performance of the three wavelet families: Daubechies (db1, db2, db3 and db4), Coiflets (coif2, coif3 and coif4) and Symlets (sym2, sym3 and sym4) is evaluated in this subsection. The test images were converted to grayscale. They were then down-sampled followed by up-sampling by a factor of 2 using cubic B-Splines approximation. High-resolution images were then reconstructed based on the wavelets above. The results for a sample of ten images are shown in Table II. From the results obtained, the db1 wavelet achieves the best performance among the selected wavelets for all images. db1 wavelet has therefore been chosen in the proposed approach to estimate the missing frequency information in one-level DWT.

3) *Convergence of the iterative back-projection (IBP):*

In this subsection, the convergence of the IBP based on the weighted guided filter is analyzed. Fig. 3 indicates the PSNR values for the four selected test images versus the number of iterations. The convergence is achieved when the difference between the PSNR values for the consecutive iterations is less than 0.01dB. From Fig. 3, the PSNR values increase gradually with the number of iterations, and convergence is achieved within five steps. The other test images gave similar results.

With the convergence achieved within five steps of IBP, the number of iterations in the proposed super-resolution approach was set to 5.

4) *Comparison with recently proposed approaches*

a) *Objective performance:* In this subsection, the proposed approach's SR performance in comparison with

other approaches is analyzed on 16 test images from the specified databases, as shown in Fig. 3. The performance metrics used for this comparison are PSNR and SSIM. The objective performance results in terms of PSNR and SSIM with an upscaling factor of 2 are shown in Tables III and IV respectively. The proposed approach outperformed the selected approaches in 13 out of the 16 sample images.

In terms of SSIM, the proposed approach outperformed the selected approaches in all the selected images. The algorithm achieved highest average PSNR and SSIM. The best performance is highlighted in red.

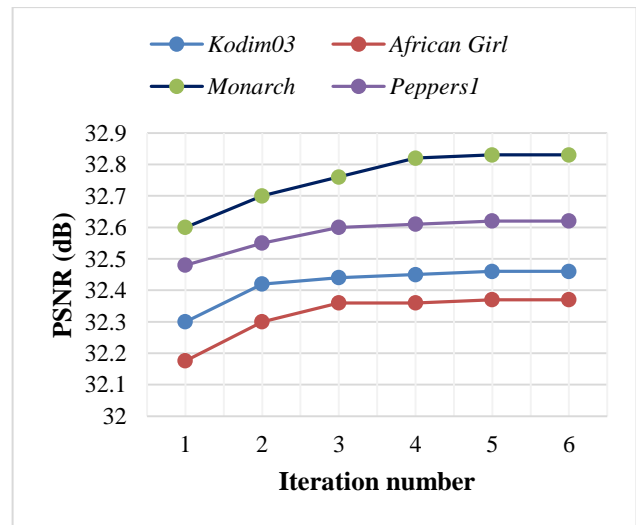


Fig. 3. PSNR Variations against Iterations for IBP.

TABLE III. PSNR RESULTS WITH AN UP-SAMPLING FACTOR OF 2

Image Labels ↓	Proposed			VDSR [39]			Bicubic			LoG IBP [34]			NEDI [40]		
	R	G	B	R	G	B	R	G	B	R	G	B	R	G	B
Aerial1	31.4	34.6	40.1	31.0	34.4	39.3	30.5	33.7	39.2	30.4	33.6	38.9	29.5	33.0	38.9
Aerial2	33.1	36.1	39.9	32.4	35.7	38.3	32.0	35.1	39.0	32.5	35.4	38.8	29.5	33.3	38.2
Aerial5	34.7	35.1	35.5	34.3	34.9	35	33.6	34.1	34.6	33.6	34.0	34.2	32.5	33.4	34.7
Aerial8	29.9	33.8	41.3	29.5	33.6	40.1	29.0	32.9	40.4	29.0	32.8	40.2	28.2	32.1	39.8
Baby	36.5	36.6	36.5	34.9	35.1	34.9	35.4	35.6	35.5	36.0	36.2	36.0	31.6	32.0	32.3
Bird	36.2	36.5	36.3	34.8	35.2	34.3	34.7	35.1	34.8	36.2	36.5	36.1	29.7	30.2	30.0
Woman	31.8	31.8	31.9	32.4	32.4	32.4	30.6	30.7	30.7	31.5	31.6	31.7	27.2	27.2	27.3
Kodim03	33.7	33.5	33.4	34.0	33.9	33.6	32.6	32.5	32.6	33.0	32.9	32.7	31.2	31.2	31.7
Kodim10	32.0	31.9	31.8	32.7	32.7	32.5	31.1	31.0	31.0	31.5	31.5	31.3	29.1	28.8	29.1
Arctic hare	40.1	42.3	43.2	36.7	36.7	36.2	38.1	40.4	41.3	40.1	42.2	43.1	32.3	34.6	35.3
African girl	32.1	32.4	32.3	32.0	32.4	32.4	31.3	31.5	31.5	31.4	31.9	31.7	29.8	29.7	30.0
Lena	36.7	33.3	32.2	35.2	33.0	31.7	35.4	32.1	31.2	36.1	32.7	31.3	31.6	29.1	29.8
Monarch	33.0	32.7	32.6	33.6	33.6	33.5	31.8	31.6	31.5	32.7	32.4	32.3	28.6	28.4	28.6
Peppers1	31.8	30.3	31.9	31.0	30.2	31.0	30.4	29.0	30.9	30.4	29.4	31.0	29.5	27.0	29.4
Peppers2	37.8	37.5	37.2	36.6	37.2	35.5	36.5	36.3	36.1	37.5	37.2	36.7	32.2	32.5	32.7
Tulips	34.9	34.9	33.9	34.0	34.1	33.7	33.4	33	32.4	34.4	34.1	33.6	29.8	28.9	28.3
AVERAGE	34.5	34.6	35.6	33.5	33.8	34.6	32.9	33.4	34.5	33.5	33.7	35.0	30.1	30.7	32.3

TABLE IV. SSIM RESULTS WITH AN UP-SAMPLING FACTOR OF 2

Image Labels ↓	Proposed			VDSR [39]			Bicubic			LoG IBP [34]			NEDI [40]		
	R	G	B	R	G	B	R	G	B	R	G	B	R	G	B
Aerial1	0.84	0.88	0.92	0.78	0.85	0.90	0.77	0.83	0.91	0.77	0.83	0.91	0.74	0.82	0.90
Aerial2	0.89	0.89	0.92	0.86	0.88	0.90	0.85	0.87	0.9	0.87	0.88	0.9	0.76	0.81	0.88
Aerial5	0.89	0.89	0.88	0.80	0.81	0.78	0.80	0.81	0.78	0.79	0.79	0.76	0.76	0.77	0.77
Aerial8	0.85	0.89	0.95	0.83	0.88	0.94	0.82	0.86	0.94	0.83	0.87	0.94	0.78	0.84	0.93
Baby	0.96	0.96	0.95	0.95	0.95	0.93	0.95	0.95	0.93	0.96	0.95	0.94	0.91	0.91	0.89
Bird	0.98	0.98	0.96	0.97	0.96	0.93	0.97	0.97	0.95	0.98	0.98	0.96	0.92	0.92	0.91
Woman	0.95	0.96	0.96	0.95	0.95	0.95	0.94	0.95	0.94	0.95	0.95	0.95	0.90	0.91	0.90
Kodim03	0.95	0.93	0.92	0.93	0.93	0.92	0.91	0.92	0.9	0.92	0.92	0.91	0.89	0.89	0.88
Kodim10	0.94	0.95	0.91	0.92	0.92	0.92	0.90	0.90	0.89	0.90	0.91	0.90	0.86	0.86	0.86
Arctic hare	0.98	0.98	0.98	0.96	0.96	0.96	0.98	0.98	0.98	0.98	0.98	0.98	0.95	0.95	0.96
African girl	0.91	0.92	0.90	0.90	0.91	0.90	0.89	0.9	0.88	0.9	0.91	0.89	0.86	0.87	0.85
Lena	0.96	0.94	0.85	0.93	0.91	0.81	0.93	0.88	0.80	0.93	0.88	0.80	0.90	0.84	0.78
Monarch	0.96	0.96	0.95	0.96	0.95	0.95	0.96	0.95	0.94	0.96	0.96	0.95	0.93	0.93	0.92
Peppers1	0.85	0.88	0.85	0.79	0.86	0.82	0.78	0.84	0.82	0.78	0.84	0.82	0.78	0.83	0.8
Peppers2	0.97	0.97	0.95	0.96	0.97	0.93	0.96	0.97	0.94	0.96	0.97	0.94	0.94	0.94	0.91
Tulips	0.94	0.96	0.95	0.93	0.95	0.95	0.92	0.94	0.94	0.93	0.95	0.95	0.88	0.89	0.89
AVERAGE	0.93	0.94	0.93	0.90	0.92	0.91	0.88	0.89	0.89	0.90	0.91	0.91	0.86	0.87	0.88

For the high-altitude aerial images obtained from [41], the PSNR was found to differ by as much as 9 dB between the colour channels – Aerial1 (Red=31.4 dB, Blue= 40.1 dB). This difference arises because the aerial images are almost one colour, with some colour channels containing very little information. The channel with low information returns very high PSNR values. In aerial1 image, the red channel contains highest information followed by the green channel and lastly the blue channel.

The test image sets have images with significantly different frequency content and variations in texture and edges. The performance is therefore different for each image with images having high-frequency content achieving low PSNR and SSIM values when compared to images with low-frequency content. This is evident by peppers1 (Red=31.8dB, Green=30.3dB and Blue=31.9dB) and Arctic Hare (Red=40.1dB, Green=42.3dB and Blue=43.1dB). Arctic Hare is a significantly smooth image thus low frequency content while peppers1 image has high frequency content.

Interpolation approaches performs better in smooth images as observed in Arctic Hare where the proposed algorithm, LoG IBP [34], and Bicubic interpolation all achieved the highest SSIM of 0.98 for an up-scaling factor of 2 compared to the VDSR [39] algorithm, which gave 0.96.

The VDSR algorithm achieves better image quality in those images with patterns, for example, Monarch, where it achieved a PSNR improvement of over 0.9dB from the proposed algorithm in the blue and green colour channels.

For up-scaling factor of 3, the high-resolution images from the selected databases were decimated by a factor of 3 to obtain

the low-resolution images. The images were then up-scaled by 3 using the proposed approach to obtain high-resolution images. The results were then compared to VDSR [39] and bicubic interpolation. LoG IBP [34] and NEDI [40] only up-scales the image by a factor of 2 and were therefore not compared for up-scaling factor of 3. Table V shows the PSNR and SSIM results for this comparison.

The approach with the best performance is highlighted in red. The selected approaches were applied independently to the three colour channels in RGB colour space in order to ensure the same treatment is applied in the colour images.

From Table V, the proposed approach outperforms the selected approaches in 15 out of the 16 test images from the sample. It also achieves highest SSIM for all the test images from the selected databases.

b) Visual quality comparison: Fig. 4 shows two images used for visual comparison. The blue rectangular box in the two selected images in shows the regions of interest to evaluate the performance of the super-resolution algorithms.

c) Computational complexity: To evaluate the computational complexity, a total of 10 images were used: Aerial1, Aerial2, Aerial5, Aerial8, Kodim03, Kodim10, Lena, Monarch, Baby and Bird. Despite this measure not being a scientific method of computing execution time, it however serves as an indicator of the computational complexity of each algorithm. The elapsed time it takes to super-resolve each image using the start and stop watch timers in MATLAB environment. Table VI and Table VII shows the results for the up-scaling factor of 2 and 3 respectively.

TABLE V. PSNR AND SSIM RESULTS FOR AN UP-SCALING FACTOR OF 3

Image Labels ↓	PSNR (dB)									SSIM								
	Proposed			VDSR [39]			Bicubic			Proposed			VDSR [39]			Bicubic		
	R	G	B	R	G	B	R	G	B	R	G	B	R	G	B	R	G	B
Aerial1	29.1	32.8	39.1	28.5	32.8	39.0	27.3	30.9	37.0	0.75	0.83	0.91	0.74	0.82	0.91	0.71	0.79	0.89
Aerial2	26.9	31.1	37.1	26.9	31.1	36.7	25.8	29.8	35.4	0.63	0.78	0.87	0.61	0.72	0.86	0.61	0.70	0.84
Aerial5	30.9	32.4	35.3	30.9	32.4	35.2	29.5	30.7	32.9	0.75	0.79	0.84	0.74	0.77	0.79	0.70	0.73	0.75
Aerial8	26.8	30.8	38.7	26.8	30.4	38.3	25.1	29.1	36.9	0.74	0.81	0.92	0.71	0.79	0.91	0.70	0.77	0.90
Baby	30.5	31.0	31.3	30.1	30.7	31.0	29.9	30.3	30.5	0.88	0.88	0.86	0.88	0.88	0.86	0.88	0.88	0.85
Bird	30.3	30.8	30.8	29.6	30.5	29.6	30.2	30.6	30.5	0.91	0.91	0.93	0.90	0.91	0.87	0.92	0.92	0.89
Woman	26.8	28.5	26.9	26.8	26.9	26.9	26.3	26.4	26.4	0.87	0.87	0.87	0.87	0.87	0.87	0.87	0.87	0.87
Kodim03	30.2	30.5	31.0	30.3	30.4	31.1	28.4	28.5	28.9	0.86	0.86	0.85	0.86	0.86	0.85	0.85	0.85	0.84
Kodim10	28.1	28.3	28.1	28.0	27.6	28.0	26.6	26.3	26.4	0.83	0.83	0.82	0.84	0.83	0.83	0.82	0.82	0.81
Arctic hare	29.5	32.2	33.3	29.3	31.6	32.5	29.1	31.8	33.0	0.91	0.92	0.95	0.90	0.91	0.91	0.90	0.91	0.90
African girl	28.2	28.4	28.6	28.1	28.8	28.1	27.1	27.3	27.3	0.82	0.86	0.85	0.82	0.84	0.81	0.81	0.82	0.81
Lena	30.6	28.3	29.7	30.2	28.2	29.7	30.1	27.6	28.3	0.89	0.83	0.81	0.87	0.82	0.77	0.87	0.81	0.75
Monarch	27.5	27.4	27.8	27.4	27.4	27.8	27.1	26.9	27.2	0.91	0.92	0.89	0.90	0.90	0.90	0.90	0.90	0.88
Peppers1	29.2	26.4	29.1	28.0	26.2	28.7	27.5	24.8	27.4	0.82	0.88	0.82	0.80	0.83	0.81	0.76	0.79	0.77
Peppers2	32.0	32.2	32.8	31.5	32.1	32.0	31.7	31.8	32.2	0.92	0.93	0.90	0.92	0.92	0.87	0.92	0.92	0.88
Tulips	28.9	28.2	27.5	29.0	28.2	27.3	28.4	27.8	27.2	0.84	0.85	0.84	0.85	0.85	0.84	0.82	0.82	0.82
AVERAGE	29.9	30.0	32.7	28.8	29.1	31.4	28.1	28.8	30.5	0.85	0.87	0.89	0.81	0.83	0.87	0.82	0.83	0.84

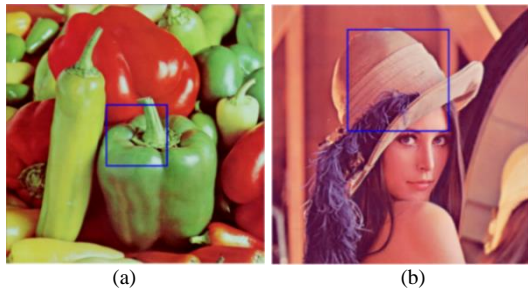


Fig. 4. Two Test Images used for Visual Comparison (a) Peppers1 Image and (b) Lena Image.

TABLE VI. EXECUTION TIME FOR UP-SCALING BY 2

Execution Time	METHOD				
	Bicubic	Proposed	VDSR [39]	LoG IBP [34]	NEDI [40]
Total time in seconds	6.21	16.18	238.21	20.61	982.1
Time per image in seconds	0.62	1.62	23.82	2.06	98.21

TABLE VII. EXECUTION TIME FOR UP-SCALING BY 3

Execution Time	METHOD		
	Proposed	VDSR [39]	BICUBIC
Total time in seconds	24.68	311.82	10.01
Time per image in seconds	2.47	31.18	1.00

From the results in Table VI and Table VII, it can be observed that: Bicubic interpolation has the shortest execution across the two up-scaling factors each taking less than 1 second to up-scale an image, The VDSR requires more than 20s per image and 4. The NEDI algorithm is computationally intensive requiring almost 100 seconds per image.

The proposed approach is second only to bicubic interpolation showing its computational efficiency with higher objective and visual performance.

V. CONCLUSION

This paper proposes a single image super-resolution approach that combines the cubic B-Splines approximation and discrete wavelet transform. The results demonstrated that the performance of the cubic B-splines can be significantly improved by first transforming the pixel values of an image to coefficients in the B-Splines domain before performing interpolation. The db1 wavelet was also found to recover the lost high-frequency information than other wavelets. In order to further enhance the sharpness of the edges of the super-resolved images a weighted guided filter has been added into the proposed approach as a back-projection filter. The proposed algorithm was tested on a set of 74 RGB colour images. The results for a sample of 16 images from the set have been reported for up-scaling factors of 2 and 3. The approach was applied independently to the three colour channels. It outperformed bicubic interpolation and the other selected super-resolution algorithms in visual quality.

In terms of the visual comparison, Fig. 5 and Fig. 6 shows the zoomed extracts obtained from peppers1 and Lena image in Fig. 4 for the up-scaling factor of 2. From the zoomed extracts, the ground truth image has clear and sharper edges. The proposed method recovers the sharpness of the edges partially and maintains the natural texture of the images. The bicubic interpolation causes blurring of the output images NEDI, LoG IBP and VDSR maintains the edges but clearly smoothen out the highly textured areas. Other images also show similar results.

The suggestions for further work are:

1) Development of a 2-dimensional cubic B-Splines kernel. In this paper, a 1-dimensional kernel has been applied sequentially along the rows and the columns of the test images.

2) Up-scaling by a rational number e.g., $3/2$. The up-scaling by integer factors of 2 and 3 were used in this paper.

3) Further work could also constitute improvement of the resolution of noisy images.

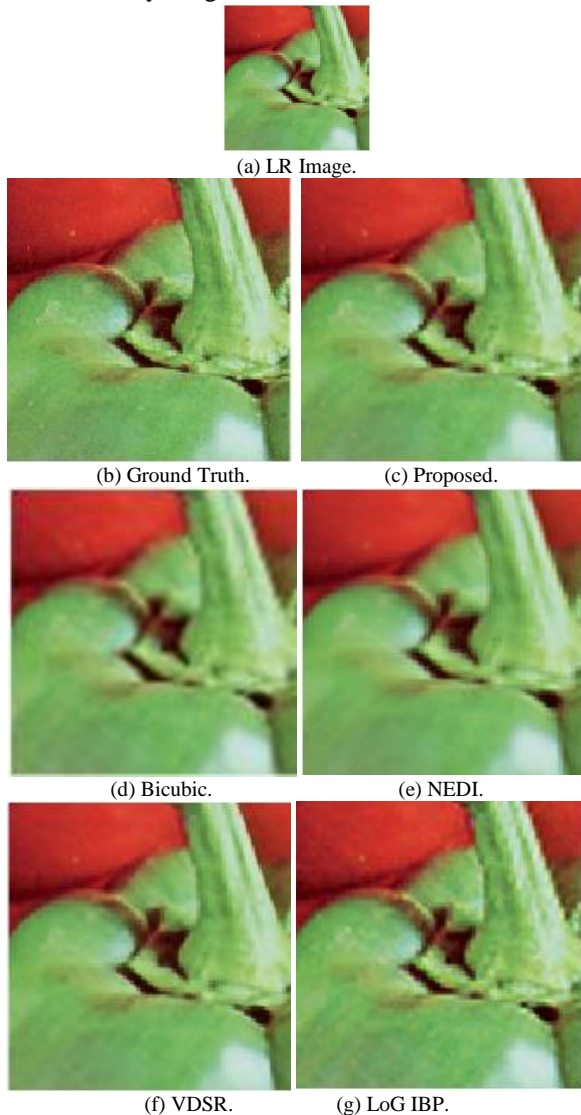


Fig. 5. Visual Comparison for the Zoomed Extracts Obtained from Peppers1 Image with an Upscaling Factor of 2.

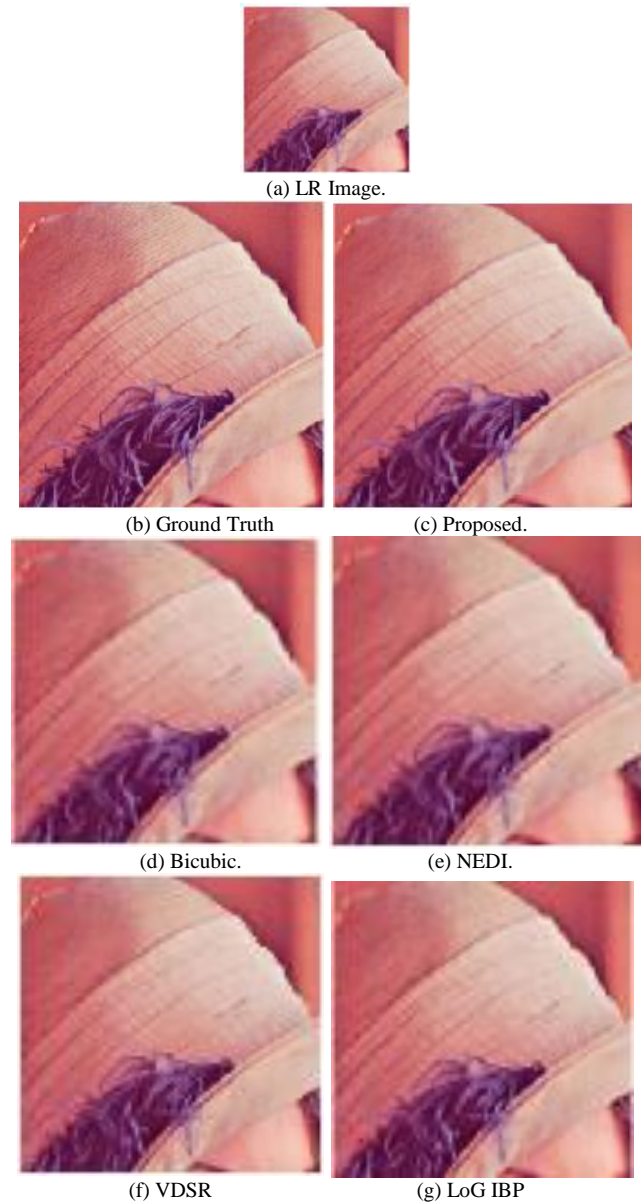


Fig. 6. Visual Comparison for the Zoomed Extracts Obtained from Lena Image with an Upscaling Factor of 2.

REFERENCES

- [1] L. Yue, H. Shen, J. Li, Q. Yuan, H. Zhang, and L. Zhang, "Image super-resolution: The techniques, applications, and future," *Signal Processing*, vol. 128, pp. 389–408, Nov. 2016, doi: 10.1016/j.sigpro.2016.05.002.
- [2] H. Wang, X. Gao, K. Zhang, and J. Li, "Single-Image Super-Resolution Using Active-Sampling Gaussian Process Regression," *IEEE Trans. on Image Process.*, vol. 25, no. 2, pp. 935–948, Feb. 2016, doi: 10.1109/TIP.2015.2512104.
- [3] Lizhe Wang, Ke Lu, and Peng Liu, "Compressed Sensing of a Remote Sensing Image Based on the Priors of the Reference Image," *IEEE Geosci. Remote Sensing Lett.*, vol. 12, no. 4, pp. 736–740, Apr. 2015, doi: 10.1109/LGRS.2014.2360457.
- [4] L. An and B. Bhanu, "Face image super-resolution using 2D CCA," *Signal Processing*, vol. 103, pp. 184–194, Oct. 2014, doi: 10.1016/j.sigpro.2013.10.004.
- [5] M.-C. Yang, C.-P. Wei, Y.-R. Yeh, and Y.-C. F. Wang, "Recognition at a long distance: Very low-resolution face recognition and hallucination," in *2015 International Conference on Biometrics (ICB)*, Phuket, Thailand, May 2015, pp. 237–242. doi: 10.1109/ICB.2015.7139090.

- [6] M. M. Khattab, A. M. Zeki, A. A. Alwan, A. S. Badawy, and L. S. Thota, "Multi-Frame Super-Resolution: A Survey," in 2018 IEEE International Conference on Computational Intelligence and Computing Research (ICIC), Madurai, India, Dec. 2018, pp. 1–8. doi: 10.1109/ICIC.2018.8782382.
- [7] N. L. Nguyen, J. Anger, A. Davy, P. Arias, and G. Facciolo, "Self-supervised multi-image super-resolution for push-frame satellite images," in 2021 IEEE/CVF Conference on Computer Vision and Pattern Recognition Workshops (CVPRW), Nashville, TN, USA, Jun. 2021, pp. 1121–1131. doi: 10.1109/CVPRW53098.2021.00123.
- [8] J. I. Delgado-Centeno, P. J. Sanchez-Cuevas, C. Martinez, and M. A. Olivares-Mendez, "Enhancing Lunar Reconnaissance Orbiter Images via Multi-Frame Super Resolution for Future Robotic Space Missions," *IEEE Robot. Autom. Lett.*, vol. 6, no. 4, pp. 7721–7727, Oct. 2021, doi: 10.1109/LRA.2021.3097510.
- [9] Y. Zhang, Q. Fan, F. Bao, Y. Liu and C. Zhang, "Single-Image Super-Resolution Based on Rational Fractal Interpolation," in *IEEE Transactions on Image Processing*, vol. 27, no. 8, pp. 3782–3797, Aug. 2018, doi: 10.1109/TIP.2018.2826139.
- [10] H. Kim and G. Kim, "Single Image Super-Resolution Using Fire Modules With Asymmetric Configuration," *IEEE Signal Process. Lett.*, vol. 27, pp. 516–519, 2020, doi: 10.1109/LSP.2020.2980172.
- [11] Y. Yan, W. Ren, X. Hu, K. Li, H. Shen, and X. Cao, "SRGAT: Single Image Super-Resolution With Graph Attention Network," *IEEE Trans. on Image Process.*, vol. 30, pp. 4905–4918, 2021, doi: 10.1109/TIP.2021.3077135.
- [12] T. Briand and P. Monasse, "Theory and Practice of Image B-Spline Interpolation," *Image Processing On Line*, vol. 8, pp. 99–141, Jul. 2018, doi: 10.5201/ipol.2018.221.
- [13] F. Champagnat and Y. Le Sant, "Efficient Cubic B-spline Image Interpolation on a GPU," *Journal of Graphics Tools*, vol. 16, no. 4, pp. 218–232, Oct. 2012, doi: 10.1080/2165347X.2013.824736.
- [14] R. Lan et al., "Cascading and Enhanced Residual Networks for Accurate Single-Image Super-Resolution," *IEEE Trans. Cybern.*, vol. 51, no. 1, pp. 115–125, Jan. 2021, doi: 10.1109/TCYB.2019.2952710.
- [15] Y. Li, F. Qi, and Y. Wan, "Improvements On Bicubic Image Interpolation," in 2019 IEEE 4th Advanced Information Technology, Electronic and Automation Control Conference (IAEAC), Chengdu, China, Dec. 2019, pp. 1316–1320. doi: 10.1109/IAEAC47372.2019.8997600.
- [16] P. Megha, M. Swarna, V. Sowmya, and K. P. Soman, "Low contrast satellite image restoration based on adaptive histogram equalization and discrete wavelet transform," in 2016 International Conference on Communication and Signal Processing (ICCSP), Melmaruvathur, Tamilnadu, India, Apr. 2016, pp. 0402–0406. doi: 10.1109/ICCSP.2016.7754166.
- [17] T. D. Gadhiya, A. K. Roy, S. K. Mitra, and V. Mall, "Use of discrete wavelet transform method for detection and localization of tampering in a digital medical image," in 2017 IEEE Region 10 Symposium (TENSYP), Cochin, India, Jul. 2017, pp. 1–5. doi: 10.1109/TENCONSpring.2017.8070082.
- [18] X.-L. Tian and J.-Q. Chen, "A Fast Algorithm for Single Image Super-Resolution Reconstruction via Revised Statistical Prediction Model," in 2016 International Conference on Information System and Artificial Intelligence (ISAI), Hong Kong, China, Jun. 2016, pp. 305–309. doi: 10.1109/ISAI.2016.0071.
- [19] T. Peleg and M. Elad, "A Statistical Prediction Model Based on Sparse Representations for Single Image Super-Resolution," *IEEE Trans. on Image Process.*, vol. 23, no. 6, pp. 2569–2582, Jun. 2014, doi: 10.1109/TIP.2014.2305844.
- [20] K.-W. Hung, Z. Zhang, and J. Jiang, "Real-Time Image Super-Resolution Using Recursive Depthwise Separable Convolution Network," *IEEE Access*, vol. 7, pp. 99804–99816, 2019, doi: 10.1109/ACCESS.2019.2929223.
- [21] T. Lu, Y. Wang, J. Wang, W. Liu, and Y. Zhang, "Single Image Super-Resolution via Multi-Scale Information Polymerization Network," *IEEE Signal Process. Lett.*, vol. 28, pp. 1305–1309, 2021, doi: 10.1109/LSP.2021.3084522.
- [22] R. Li and Q. Lv, "Image sharpening algorithm based on a variety of interpolation methods," in 2012 International Conference on Image Analysis and Signal Processing, Huangzhou, China, Nov. 2012, pp. 1–4. doi: 10.1109/IASP.2012.6425043.
- [23] W. Zhang, K. Jiang, L. Wang et al., "A Wavelet-Based Asymmetric Convolution Network for Single Image Super-Resolution," *IEEE Access*, vol. 9, pp. 28976–28986, 2021, doi: 10.1109/access.2021.3058648.
- [24] P. Thevenaz, "Image Interpolation and Resampling," in *Handbook of Medical Image Processing and Analysis*, Elsevier, 2009, pp. 465–493. doi: 10.1016/B978-012373904-9.50037-4.
- [25] C.-W. Chen, F.-K. Hsu, D.-W. Yang, J. Wang, and M.-D. Shieh, "Effective model construction for enhanced prediction in example-based super-resolution," in 2016 IEEE Asia Pacific Conference on Circuits and Systems (APCCAS), Jeju, South Korea, Oct. 2016, pp. 156–159. doi: 10.1109/APCCAS.2016.7803921.
- [26] H. Demirel and G. Anbarjafari, "Satellite Image Resolution Enhancement Using Complex Wavelet Transform," *IEEE Geosci. Remote Sensing Lett.*, vol. 7, no. 1, pp. 123–126, Jan. 2010, doi: 10.1109/LGRS.2009.2028440.
- [27] H. Lidong, Z. Wei, W. Jun, and S. Zebin, "Combination of contrast limited adaptive histogram equalization and discrete wavelet transform for image enhancement," *IET Image Processing*, vol. 9, no. 10, pp. 908–915, Oct. 2015, doi: 10.1049/iet-ipr.2015.0150.
- [28] H. Demirel and G. Anbarjafari, "Image Resolution Enhancement by Using Discrete and Stationary Wavelet Decomposition," *IEEE Trans. on Image Process.*, vol. 20, no. 5, pp. 1458–1460, May 2011, doi: 10.1109/TIP.2010.2087767.
- [29] S. Lei, X. Liao, and Z. Tao, "Content-aware Up-sampling for Single Image Super-resolution," in 2020 Asia-Pacific Conference on Image Processing, Electronics and Computers (IPEC), Dalian, China, Apr. 2020, pp. 213–217. doi: 10.1109/IPEC49694.2020.9115143.
- [30] F. Deeba, S. Kun, F. Ali Dharejo, and Y. Zhou, "Wavelet-Based Enhanced Medical Image Super Resolution," *IEEE Access*, vol. 8, pp. 37035–37044, 2020, doi: 10.1109/access.2020.2974278.
- [31] E. Castro, M. Nakano, G. Sanchez, and H. Perez, "Improvement of Image Super-resolution Algorithms using Iterative Back Projection," *IEEE Latin Am. Trans.*, vol. 15, no. 11, pp. 2214–2219, Nov. 2017, doi: 10.1109/TLA.2017.8070429.
- [32] J.-S. Yoo and J.-O. Kim, "Noise-Robust Iterative Back-Projection," *IEEE Trans. on Image Process.*, vol. 29, pp. 1219–1232, 2020, doi: 10.1109/TIP.2019.2940414.
- [33] M. N. Bareja and C. K. Modi, "An Improved Iterative Back Projection Based Single Image Super Resolution Approach," *Int. J. Image Grap.*, vol. 14, no. 04, p. 1450015, Oct. 2014, doi: 10.1142/S0219467814500156.
- [34] B. M. Ngocho and E. Mwangi, "Single image super resolution with guided back-projection and LoG sharpening," in 2016 18th Mediterranean Electrotechnical Conference (MELECON), Lemesos, Cyprus, Apr. 2016, pp. 1–6. doi: 10.1109/MELCON.2016.7495419.
- [35] R. R. Makwana and N. Mehta, "Single Image Super-Resolution VIA Iterative Back Projection Based Canny Edge Detection and a Gabor Filter Prior," undefined, 2013, Accessed: Dec. 21, 2021. [Online]. Available: <https://www.semanticscholar.org/paper/Single-Image-Super-Resolution-VIA-Iterative-Back-a-Makwana-Mehta/3fab67d595249b485bf3e0b76e7749ff68695c45>.
- [36] C . Vonesch, T. Blu, and M. Unser, "Generalized Daubechies Wavelet Families," *IEEE Trans. Signal Process.*, vol. 55, no. 9, pp. 4415–4429, Sep. 2007, doi: 10.1109/TSP.2007.896255.
- [37] Z. Li, J. Zheng, Z. Zhu, W. Yao, and S. Wu, "Weighted Guided Image Filtering," *IEEE Transactions on Image Processing*, vol. 24, no. 1, pp. 120–129, Jan. 2015, doi: 10.1109/TIP.2014.2371234.
- [38] H. Geethu, S. Shamna, and J. J. Kizhakkethottam, "Weighted Guided Image Filtering and Haze Removal in Single Image," *Procedia Technology*, vol. 24, pp. 1475–1482, 2016, doi: 10.1016/j.protcy.2016.05.248.
- [39] J. Kim, J. K. Lee, and K. M. Lee, "Accurate Image Super-Resolution Using Very Deep Convolutional Networks," in 2016 IEEE Conference on Computer Vision and Pattern Recognition (CVPR), Las Vegas, NV, USA, Jun. 2016, pp. 1646–1654. doi: 10.1109/CVPR.2016.182.

- [40] Xin Li and M. T. Orchard, "New edge-directed interpolation," *IEEE Trans. on Image Process.*, vol. 10, no. 10, pp. 1521–1527, Oct. 2001, doi: 10.1109/83.951537.
- [41] "Test Images." <https://homepages.cae.wisc.edu/~ece533/images/> (accessed Oct. 15, 2020).
- [42] R. Franzen, "Kodak Lossless True Color Image Suite", Eastman Kodak, 27 January 2020. [Online]. Available: <http://r0k.us/graphics/kodak/>. (accessed Feb. 06, 2022).
- [43] "Set14 Super Resolution Dataset", DeepAI. <https://deepai.org/dataset/set14-super-resolution> (accessed Feb. 06, 2022).

Supervised Learning Techniques for Intrusion Detection System based on Multi-layer Classification Approach

Machine Learning and Intrusion Detection System

Mansoor Farooq

Department of Management Studies
University of Kashmir
Srinagar, India

Abstract—The goal of this study is to discover a solution to two problems: first, the signature-based intrusion detection system SNORT can identify a new attack signature without human intervention; and second, signature-based IDS cannot detect multi-stage attacks. The interesting aspect of this study is the growing ways to address the aforementioned issues. We introduced a multi-layer classification strategy in this study, in which we employ two layers, the first of which is based on a decision tree, and the second of which includes machine learning technique fuzzy logic and neural networks. If the first layer fails to identify fresh attacks, the second layer takes over and detects new signature assaults, updating the SNORT signature automatically.

Keywords—IDS; SNORT; fuzzy logic; neural networks; decision tree; Naïve Bayes

I. INTRODUCTION

According to information technology, a network intrusion is a sequence of attacks against network-based security measures [13]. Network traffic is monitored by the Intrusion Detection System (IDS), which alerts information security personnel when harmful activity is discovered [10].

Because of their effectiveness in blocking assaults on network resources, IDSs are not able to adapt to scenarios where new attacks are being carried out, requiring human intervention [13]. On the other hand, if the IDS is used on an overloaded network, it might constitute a bottleneck. For the IDS to be launched to production, it needs time to analyse network data [13].

Using an existing IDS, SNORT would be used to compare packet signatures to the criteria set out by SNORT. Packets that are thought to be malicious will be run through an intelligent model that has been trained to look for harmful content [14][9]. Using an intelligent model, SNORT might be used as the initial step of a strainer to limit traffic for unnecessary exploration, to put it another way: SNORT's workload is reduced, which in turn reduces human mediation since the intelligently trained model is responsible for determining whether or not a certain group of packets is harmful. SNORT will establish an automatic signature if a malicious group of packets is detected.

For the first time, a training model is being combined with a reasoning model to detect abuse of network data packets [9]. IDS on a production level device may then utilize the rule generated by the justification model to identify and block malicious data packets of the kind just described.

To address some of SNORT's inadequacies, this study proposes a new technique to intrusion detection that works in combination with it. In order to address these issues, a variety of data mining approaches are being presented in the answer. The following goals must be accomplished in order to attain the goal:

- Make sure the data set for training and assessment is appropriate since certain machine learning techniques are involved in the solution.
- For new threats, the first line of defence will be a classifier module, built using machine learning algorithms.
- The second layer of classification is needed for traffic that cannot be accurately classified by the first layer, is based on a reasoning module.

II. METHODOLOGY AND RESULTS

The goal of the comparison research for algorithm classification is to develop a training model for detecting abuse. The results of this comparative study are offered in the form of a perplexity matrix and metrics such as true-positives, false-positives, true-negatives, and false-negatives. It also provided links between expected and predicted classes of KDD'99 intrusion detection data, with an arbitrary split of 66% for training model development and 34% for training model testing for abuse detection

A. Data Set: KDD '99

KDD'99's intrusion detection data collecting is employed. Researchers have tested several intrusion detection methods using this data collection, which is based on a DARPA programme from 1998. Using raw TCP/IP dumps, Sniffer was able to capture all network traffic.

Each instance in the dataset has been assigned to one of 22 assault classes or 1 normal class based on the data set's 41

distinct and continuous properties [6]. This includes the DoS attack, which is also known as a "user of root attack," as well as the "remote to user attack" (Probe).

Feature Selection (CFS) was used to identify the most important data points in the network. The value of each feature is determined by the search algorithm and the classifier function, and a subset of features is provided by CFS (Hall 1999).

B. Classifier Module

Both Nave Bayes and Decision Tree may be used to build a training model that can be used to identify abuse.

1) *Naïve Bayes*: Using probabilistic inference, Bayesian reasoning may be used in decision-making in situations where previous occurrences are utilised to predict future events [2]. Using the Bayes Theorem, we can calculate the posterior likelihood using the formulas $P(q|c)$, $P(c)$, and $P(s|y)$. According to the Naive Bayesian Classifier, one predictor's influence on a given class (c) is independent of the effect of another predictor (y) [12]. Conditional freedom is granted in this way.

The Bayes algorithm explains the following:

$$P(s|y) = \frac{P(q|c)P(c)}{P(y)} \quad (1)$$

$$P(s|Y) = P(q1 | c)*P(q2 | c)*...P(qn | c)*P(c) \quad (2)$$

2) *Decision tree*: In a decision tree, the current node's choice promotes the next node's decision in a sequence of decisions [4] Open-source version of the C4.5 decision tree method – J48 [4]– is accessible through Weka [7]. J48 accepts a wide range of data kinds as input, including nominal, textual, and numeric, but it is also quite inefficient.

The algorithm constructs a decision tree starting from a training set T S, which is a set of cases, or tuples in the database terminology. Each case specifies a value for a collection of attributes and for a class [5]. Each attribute may have either discrete or continuous values. Moreover, the special value unknown is allowed, to denote unspecified values. The class may have only discrete values."

The algorithm works as

- The algorithm operates over a collection of training instances, T.
- If all occurrences of T is in class K.
 - Then create a T and an end node.
 - Select a characteristic S. Create a division node as well.
- Instant T's value for attribute S is divided into a subset (U1..n).
- Recursively apply the method to each of the T subgroups.

3) *Experiment*: Data from the KDD'99 intrusion detection training set was utilised in our investigation, and a complete KDD dataset was supplied. 34% of the data gathering, approximated at 150,000 of the famed classified insitences, was utilised for the persistence of these prototypes' effectiveness testing.

Using a two-model development technique, we created the training mode

- All classes in the IDS have been considered as a training model in this approach.
- Malicious and natural classifications are created for the data set of training models in this method.

a) *All-Classes Based Model Creation Strategy*: [4] Bhargava claim that Decision Tree findings outperform Naive Bayes [2]. Table I shows a Naive Bayes and Decision Trees training model.

The Decision Tree classifiers and Naive Bayes respectively, provide different projected and expected classes, as seen in the Fig. 1 and Fig. 2.

Table II displays the cumulative relative impacts for each classifier using TP and FP measures. The FP findings skew Naive Bayes' TP. However, the Decision Tree regularly produces low FP and high TP.

TABLE I. INCLUDES ALL CLASS MODEL BASED ON THE RESULT OF NAIVE BAYES AND DECISION TREE

Instances Classified	Naïve Bayes	Decision Tree
Correctly	92.45 % (145321)	99.95% (146756)
Incorrectly	7.17% (12543)	0.04% (66)

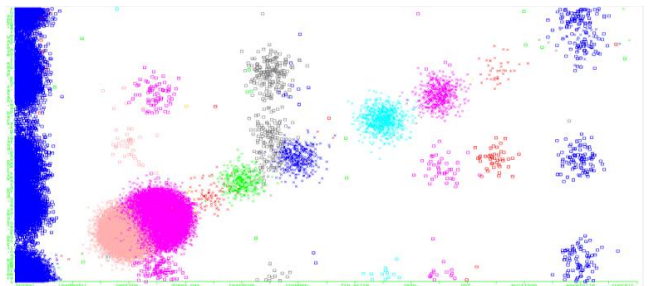


Fig. 1. Shows Naïve Bayes all Class Model Strategy, Predicted vs. Expected Class, Variances.

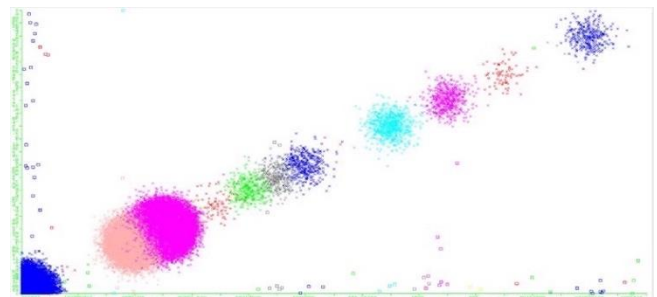


Fig. 2. Shows Decision Tree all Class Model Strategy, Predicted vs. Expected Class, Variances.

TABLE II. ALL-CLASSES MODEL CREATION STRATEGY FOR NAÏVE BAYES AND DECISION TREE

	True-Positive		False-Positive	
	Naïve Bayes	Decision Tree	Naïve Bayes	Decision Tree
Normal	0.617	0.999	0	0
Buffer Overflow	0.462	0.615	0.001	0
Load Module	0.4	0.2	0.001	0
Perl	0	0	0	0
Neptune	0.999	1	0.001	0
Smurf	0.998	1	0	0
Guess Password	0.952	1	0.025	0
Pod	0.987	1	0	0
Teardrop	0.988	0.997	0	0
Portsweep	0.111	0.979	0.01	0
IPsweep	0.97	0.993	0.007	0
FTP Write	0	0.5	0.002	0
Back	0.984	0.996	0	0
IMAP	1	0.4	0	0
Satan	0.894	0.986	0.002	0
PHFF	1	0	0.011	0
Rootkit	0.667	0	0.012	0
Spy	0	0	0	0
Land	0.75	1	0	0

b) *Two-Classes based Model Creation Strategy*: For a two-class model approach, the results of the Naive Bayes and Decision Tree algorithms are shown in Table III. The usage of Decision Tree-generated training models has been shown to be superior than Naive Bayes.

A comparison of Nave Bayes and Decision Tree Classifiers utilizing a two-class modelling technique shows the difference between predicted and anticipated classes.

Fig. 3 shows the band in the top-left and bottom-right quadrants of the graph shows that the number of incorrectly categorised cases has decreased, resulting in a more reliable model for instance projection.

TABLE III. RESULTS OF TWO-CLASSES MODEL FORMATION STRATEGY USING NAÏVE BAYES AND DECISION TREE

Instances Classified	Naïve Bayes	Decision Tree
Correctly	97.98% (148788)	99.97% (149888)
Incorrectly	1.5 % (2430)	0.03% 70

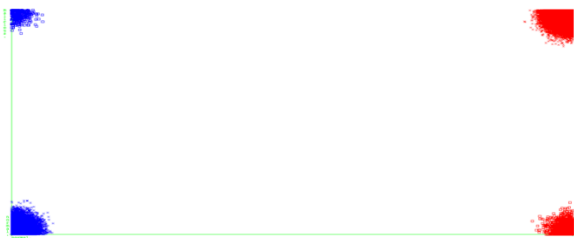


Fig. 3. Naïve Bayes Two Class Model Strategy, Predicted vs. Expected Class, Variances.

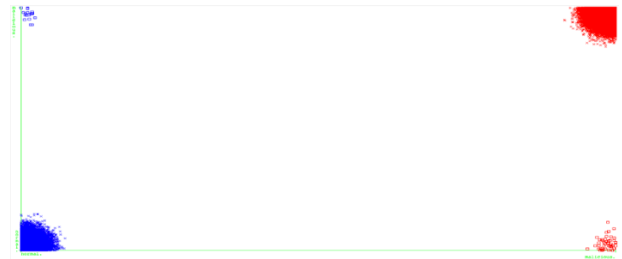


Fig. 4. Shows Decision Tree Two Class Model Strategy, Predicted vs. Expected Class, Variances.

Although the model construction technique changed, the Decision Tree was always attained. In Fig. 4, the number of erroneously identified occurrences decreases in the upper left and lower right quadrants.

TABLE IV. TWO-CLASSES MODEL CREATION STRATEGY ACCURACY / CLASS FOR NAÏVE BAYES AND DECISION TREE

Class	True-Positive		False-Positive	
	Naïve Bayes	Decision Tree	Naïve Bayes	Decision Tree
Normal	0.989	0.999	0.017	0
Malicious	0.983	1	0.011	0.001

Table IV displays the cumulative relative results per classifier for the TP and FP measurements. The Decision Tree has a high true-positive rate and a low false-positive rate.

C. Reasoning Module

In the event that the first stage of classification fails, this mechanism steps in to offer a backup classification stage. A hybrid model of neural network (MLP) and fuzzy logic is used in the reasoning process [8]. This module's output will be a signature, which will be included in the rule base as an addition.

The suggested reasoning tool in this study categories network traffic into two categories: normal (1) and attack (0). To put it another way, the hybrid model is built around two modules neural networks and a fuzzy logic module. It will categorize network traffic as normal if both modules classify it as such, but it will classify it as an attack if either module does so. The neural network has the benefit of being able to operate with both poor and correct data [3]. Fig. 5 shows the hybrid model. When employed in the IDS context, this capability may be used to identify attack patterns that have been provided throughout the training.

It is possible that certain assaults will not be detected by one of the modules, but they may be detected by the other one when utilizing a hybrid method. Furthermore, one module will compensate for weaknesses in other modules' anti-malware detection capabilities. As a result, the false-positive rate for malicious traffic might rise.

1) *Neural network*: As a computational model of the central nervous system, it can learn and recognise patterns. It has been described as a system that adapts to overt or covert information flows during learning [1].

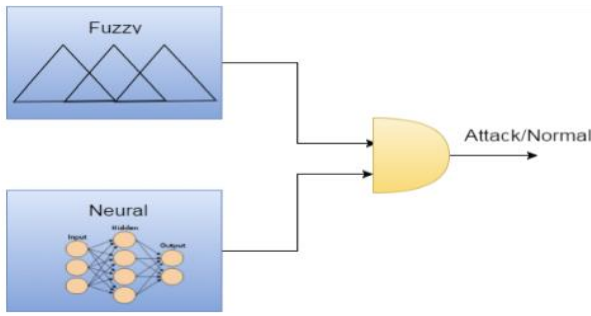


Fig. 5. Hybrid Model Overview.

This design has various tiers (one input layer, several hidden layers, and one output layer). Each layer has neurons, which are processing units. It connects to the mass of the next stratum. In the training phase, back-propagation is used. The input data is given to the neural network, and the output is compared to the intended output. This error is used to alter the weights. The error estimations and weight adjustments follow [1].

$$f_j(n) = h_j(n) - u_j(n) \tag{3}$$

$$\epsilon(n) = \frac{1}{2} \sum_j f_j^2(n) \tag{4}$$

$$\Delta b_{ji}(n) = -\mu \frac{\partial \epsilon(n)}{\partial v_j(n)} a_i(n) \tag{5}$$

2) *Fuzzy logic:* To be a computer model based on human language concepts. Rule-based systems are converted to their mathematical equivalents by fuzzy systems [11]. The fuzzifier, inference engine, rule basis, and defuzzifier are all represented in Fig. 6. The following is how fuzzy systems work: [11].

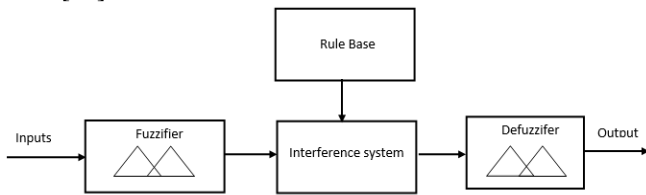


Fig. 6. Fuzzy Logic Components.

- Each input is transformed into a fuzzy input set using the appropriate membership methods.
- The inference engine creates a fuzzed performance based on the criteria supplied.
- The defuzzification membership functions are used to turn the fuzzy output into a crisp value.

Table V lists the inputs that the reasoning module gets from the ip info finder module.

The rule base includes the reasoning for generating the output. The inference engine will employ this set of (if... then) rules to get a fuzzier result. Table VI demonstrates the reasoning module's criteria for predicting malicious traffic.

On the basis of information gathered, the reasoning module determines whether or not an IP address may be

sending malicious traffic. This may be done using a data mining approach, such as clustering or regression. Many factors led to the selection of fuzzy logic for this module. The "if-then" rule form, which is supported by fuzzy logic, may be used to represent the analysis of the acquired data. Aside from that, determining whether or not an IP address is malicious might be tricky in certain cases.

The final output will be considered malicious if it is higher than 0.5, otherwise, it will be considered normal.

3) *Experiment:* A three-layer neural network module (MLP) is used in our experiment. Whereas the input layer has one neuron, the hidden layer has eight, and the output layer has 10. 10% of the whole KDD'99 IDS and the starting weights were used to train the neural network segment, and the module was trained by constraining the overall mean square to .01 and the maximum number of epochs to 3000.

The KDD'99 IDData collection was used to construct the fuzzy module system:

1) With the exception of 'support,' all of the specified features have been stabilized such that each property has the same range of values (between 0 and 1). This action contributes to the streamlining of the rule-generation process.

2) We have defined three values: U1, U2, U3, where: U1=0.45, U2=0.376, U3=0.76.

3) All features except service were transformed from numerical values into descriptions throughout the iteration through the training data.

$0 \leq \text{attribute value} < U1 \rightarrow \text{Very Low (UL)}$.

$U1 \leq \text{attribute value} < U2 \rightarrow \text{Low (L)}$.

$U2 \leq \text{attribute value} < U3 \rightarrow \text{High (H)}$.

$U3 \leq \text{attribute value} \leq 1 \rightarrow \text{Very High (UH)}$.

TABLE V. THE REASONING MODULE INPUTS

Input Name	Description
IP Geographic Location	Specifies which country the IP is based at
Is IP in a block list	Specifies whether the IP is found in a block list or not
Is IP an anonymous proxy	Specifies whether the IP is an anonymous proxy or not
IP Rating	An array that shows the IP rating on different DNSBL

TABLE VI. IF THEN RULES USED IN THE REASONING MODULE

If Condition	Statement
(IP in a block list)	Possible malicious traffic
(IP country in a black list) AND (IP is an anonymous proxy)	Possible malicious traffic
(IP country in a black list) AND (IP is a TOR exit node)	Possible malicious traffic
(IP Rating is low)	Possible malicious traffic

The performance might be categorized as either normal or offensive. The rule was then written down as follows. The rule was then created in the following form:

if (feature1 is feature_desc AND feature2 is feature2_desc AND feature10 is feature10_desc) then output is output_desc

4) If the previous phase's rule was added to the rule base, it will not be applied to the rule base again. There are a total of 1248 rules applied to the fundamental rule. As illustrated in Fig. 7 and 8, the last stage in the implementation of the fuzzy module was to pick relationship functions for both inputs and outputs.

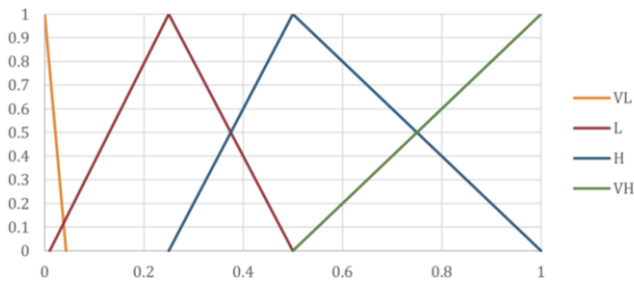


Fig. 7. Shows Relationship Function Excluding 'Service' Feature.

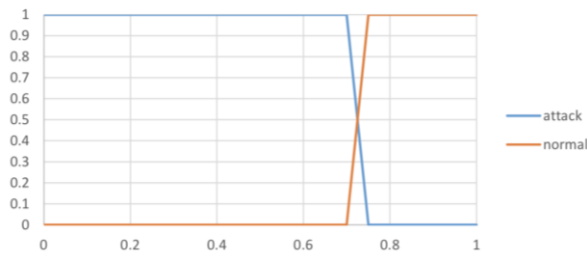


Fig. 8. Shows the Output's Relationship.

Table VII displays the hybrid model's assessment results after neural network training, rule development, and fuzzy module membership function selection.

TABLE VII. INCLUDES A HYBRID MODEL WITH NEURAL NETWORK AND FUZZY LOGIC RESULTS

Class	True-Positive			False-Positive		
	Neural Network	Fuzzy Logic	Hybrid Model	Neural Network	Fuzzy Logic	Hybrid Model
Normal	0.972	0.978	0.952	0.029	0.022	0.048
Malicious	0.966	0.9995	0.9997	0.034	0.0005	0.0003

III. CONCLUSION

Despite the fact that SNORT monitors and detects an attack, the reality is that it is not designed to identify new threats and, as a result, generates a large number of false alarms at a rapid pace. For the first time, data mining approaches have been employed to bring new stages into the solution of previously existing IDS. The suggested model's initial phase accurately detects the vast majority of data. According to Decision Tree, a comparison of two distinct training models using the Naive Bayes and the Decision Tree algorithms shows that the most effective outputs have a higher true-positive score and a greater degree of granularity.

The second stage of the proposed model (reasoning mechanism) was built using a hybrid approach. used a neural network and fuzzy logic to identify new attacks. The rate of intrusion detection rose after deployment.

REFERENCES

- [1] Anthony, M. and Bartlett, P. "Neural Network Learning: Theoretical Foundations" 2009, Cambridge University.
- [2] Altawajry, H., Bayesian-based intrusion detection system, in IAENG Transactions on Engineering Technologies 2013, Springer. p. 29-44.
- [3] Borah, S. and A. Chakraborty, Towards the Development of an Efficient Intrusion Detection System. International Journal of Computer Applications, 2014. 90.
- [4] Bhargava, N., et al., Decision Tree Analysis on J48 Algorithm for Data Mining. International Journal, 2013. 3(6).
- [5] Davis, J.J., and A.J. Clark, Data preprocessing for anomaly-based network intrusion detection: A review. Computers & Security, 2011. 30(6): p. 353-375.
- [6] Hall, M. (1999) Correlation-based Feature Selection for Machine Learning. The University of Waikato.
- [7] Hall, M., et al., The WEKA Data Mining Software: An Update. SIGKDD Explorations, 2009. 11(1).
- [8] Kukielka, P. and Kotulski, Z. (2010) "Adaptation of the neural network-based IDS to new attacks detection," Available from <http://arxiv.org/abs/1009.2406> (Access Date: 17 Oct 2014).
- [9] Kim, G., S. Lee, and S. Kim, A novel hybrid intrusion detection method, integrated anomaly detection with misuse detection. Expert Systems with Applications, 2014. 41(4): p. 1690-1700.
- [10] Kang, D.-K., D. Fuller, and V. Honavar. "Learning misuse and anomaly detection classifiers using a bag of device calls representation." In Information Assurance Workshop, 2005. IAW'05. Proceedings from the Sixth Annual IEEE SMC. 2005. IEEE.
- [11] Rajasekaran, S. and Pai, G. "Neural Networks, Fuzzy Logic, and Genetic Algorithm: Synthesis and Applications" 2003, PHI Learning Pvt. Ltd.
- [12] Rawat, R. and A. Jain, Review: Boosting Classifiers for Intrusion Detection. International Journal of Scientific & Engineering Research, 2013. 4(7): p. 1-5.
- [13] Roesch, M. SNORT: Lightweight Intrusion Detection for Networks. in LISA. 1999.
- [14] Shanmugam, B. "Improved Intrusion Detection System Using Fuzzy Logic for Detecting Anomaly and Misuse Type of Attacks" in Proceedings of the Conference of Soft Computing Pattern Recognition. 2009, pp.212-217.

A Comprehensive Study of Different Types of Deduplication Technique in Various Dimensions

G.Sujatha¹, Dr.Jeberson Retna Raj²

Department of Computer Science and Engineering

School of Computing, Sathyabama Institute of Science and Technology, Chennai, India^{1,2}

Department of Networking and Communications, School of Computing

SRM Institute of Science and Technology, Chennai, India¹

Abstract—In the current digital era, the growth of digital data is highly exceptional. There are various sources available for these digital data. The quantity of digital data being produced rose exponentially with time because of organizations and even by individuals, finally end up in the need of huge storage space. Cloud storage provides the storage space for such requirement. Since the storage space is utilized by many different users, having the duplicate data cannot be avoided. So it is necessary to make use of some storage optimization technique to handle such duplicate contents. Deduplication is a technique which is used to evade redundant data get stored. Among the various digital data, the possibility of having duplicate copies is high for data. In this research work, we review the benefits of having deduplication in optimizing the usage of storage space and study about the various types of deduplication techniques in different dimensions which can be used for data. It helps to select the appropriate data deduplication technique to increase their effective storage utilization and reduce the wastage of memory space because of duplicate data.

Keywords—Digital data; deduplication; storage optimization; cloud storage service; duplicate copies; bandwidth utilization

I. INTRODUCTION

The growth of information in the current period is very massive as shown in the Table I and Fig. 1. Many organizations and even individuals face lot of issues in storing and securing their huge volume of data.

The best way out for these issues is Cloud storage. Cloud storage is the service offered by the cloud to their users on demand [1]. It is nothing but a collection of data storage servers which can be located in different geographical locations. It can support any type of digital data like text, audio, video and image. The cloud storage providers takes the complete responsibility of data protection and also provide reliable data access. Apart from this, there are many other benefits in using cloud storage service [2]. There are many cloud storage providers existing like Microsoft Onedrive, Google drive, Dropbox, Box, Amazon Drive, and Apple icloud. Eventhough the cloud provides the storage space for their user as a service, it is not efficiently utilized because of duplicate copies of data. Such duplicate copies will occupy storage space unwantedly. This will decrease the efficient utilization of storage space. There are many storage optimization techniques which are employed to increase the better utilization of storage space. They are data compression, thin provisioning, snapshots, clones and Data deduplication.

Among these techniques data deduplication [3,4] is widely used for efficient utilization of cloud storage by preventing the wastage of storage space due to duplicate copies.

The result of deduplication is shown in the Fig. 2. With the help of deduplication technique, nearly 60% of storage space wastage can be controlled.

TABLE I. DATA GROWTH RATE

Year	Data volume (ZB)
2006	0.16
2007	0.28
2008	0.48
2009	0.8
2010	1
2011	1.8
2015	8
2020	40

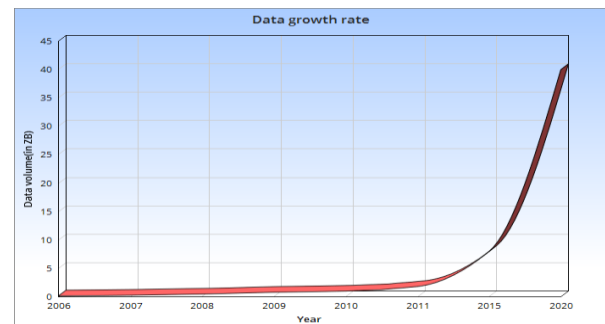


Fig. 1. Growth Rate of Data.

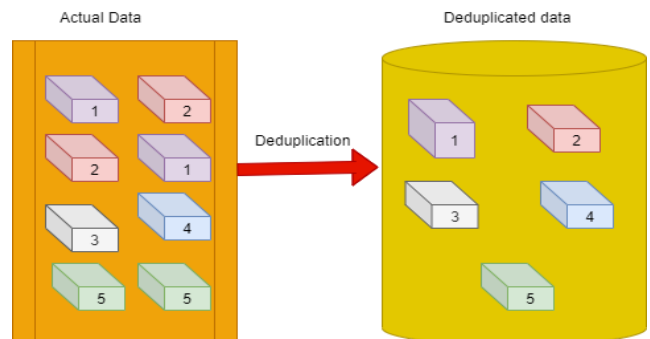


Fig. 2. Process of Deduplication.

The size of storage space prevented from redundant copies will depend upon the dataset or volume of the data. When the size of the data is very huge, then the possibility of having duplicate copies can also be very high. And it also depends upon the type of data. A sample for the same is represented in the below Table II.

TABLE II. COMPARISON OF DIFFERENT TYPES OF APPLICATION WITH RESPECT TO THEIR STORAGE SPACE PREVENTION FROM DUPLICATE COPIES

Type of Application	Type of content	Approximate space saving
User documents	Official documents, Images, Entertainment data	30-50%
Deployment shares	Software binaries, Cab files, symbols	70-80%
Virtualization libraries	ISOs, virtual hard disk files, etc.	80-95%
General File share	All types of content	50-60%

The major benefits of data deduplication are as follows:

- 1) Cost effective.
- 2) Clear storage space.
- 3) Clever replication.

Among the multimedia data types, audio, image and video occupy huge storage space when compared to text. Audio deduplication [5,6] is a process of finding and removing duplicate copies of audio data. This will reduce the wastage of memory due to duplicate copies of audio data. In cloud storage, storing cinema songs and favourite dialogues from movies are very common. And the possibility of having duplicate copies in such cases is also very high. If we apply deduplication techniques to avoid such duplication, it is possible to improve the utilization of storage space effectively. Data deduplication can be done in various ways. And all of the techniques we are going to discuss in the further sections is not with respect to the usage of any analytics algorithm or any of the classifier to identify the duplicate copies. In this study, we discuss about the process of deduplication and perform a comprehensive study on different digital data deduplication techniques in various dimensions that can be applied to data.

The rest of the paper flows as literature survey in Section II, Section III explain the architecture of the data deduplication process, Section IV discuss the various data deduplication techniques, Section V describes the comparison and analysis of various data deduplication techniques, and Sections V and VI briefs the conclusion and future work.

II. RELATED WORK

The various types of storage optimization techniques are categorized as Location based deduplication, Time based deduplication and Chunk based deduplication [7]. The

characteristics and performance of various deduplication techniques under these categories are analysed and the author concluded that variable sized deduplication technique is comparatively better than other techniques. They also suggested to carry out the future work in optimizing the processing time of variable sized deduplication techniques.

The various chunking algorithms like Rabin fingerprint, Two Divisors, MAXP, Bimodal, MCDC, Leap-Based, AE algorithms [8] are compared and analysed their advantages and disadvantages. The authors concluded that AE algorithm is more efficient and mentioned that there is a space on chunking size variance issue for future work.

The deduplication in primary storage can be done by the following ways. They are inline, offline, Post processing and cache based algorithm [9]. The author analyzed the performance of inline, offline and cache based algorithm with respect to various criteria. They mentioned the future work as concentrating on deduplication techniques in backup storage system.

III. ARCHITECTURE OF DATA DEDUPLICATION

Image, Video and Audio data are most frequently handled by many users and even many users store their digital data in cloud storage space. And the possibility of having duplicate files from same user or from different user is also very high. For example, duplicate copies of songs or favorite dialogues of movie. This will actually decrease the effectual utilization of cloud storage space. To overcome this problem, we have the concept called data deduplication.

Fig. 3 represents the architecture of data deduplication. The following are the steps which are followed in the process of Data deduplication:

- 1) When an input data is to be uploaded in the storage space, the user initially raises the request for the storage provider to do the same.
- 2) The cloud storage provider has to decide the deduplication technique.
- 3) Then the respective deduplication technique will be carried out to find the duplicate copy.
- 4) When it finds a match, then it is considered as a duplicate data and it should not be stored again in the storage space.
- 5) But reference to access the data will be shared with the user.
- 6) The user can get the data whenever it is required.
- 7) When there is no match, the input data will be uploaded in the storage space.

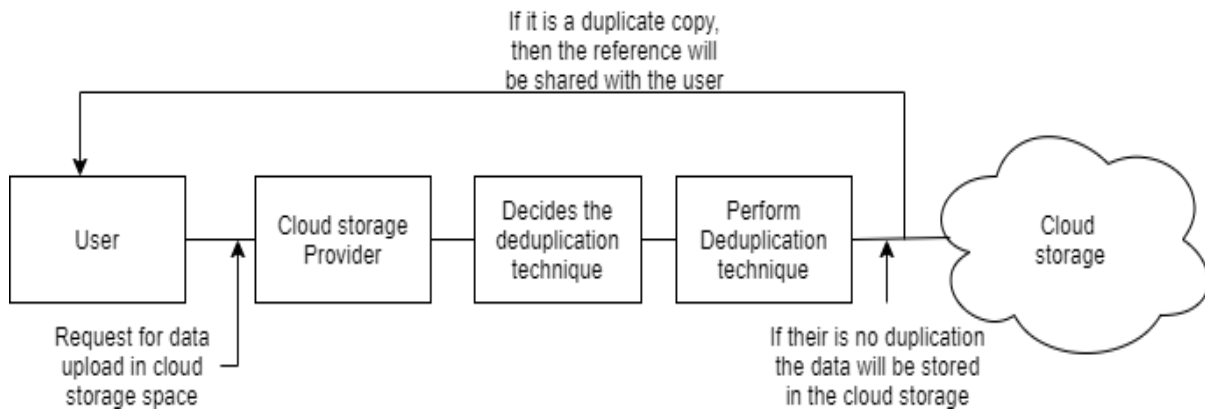


Fig. 3. Architecture of Data Deduplication.

IV. TYPES OF DIGITAL DATA DEDUPLICATION

Data deduplication will reduce the cost of storage space to be spent by the organisation. And it is comparatively better than compression technique. There are various types of deduplication exists as shown in the Fig. 4 and we can also view this process in different dimensions. They are where, when and how. The Different types of Data Deduplication in various dimensions are:

- 1) Source deduplication.
 - a) Local source deduplication.
 - b) Global source deduplication.
- 2) Target deduplication.
- 3) Inline deduplication.
- 4) Post-process deduplication.
- 5) Content-based/hash based deduplication.
- 6) Content-aware deduplication.
- 7) Chunk-level deduplication.
 - a) Fixed sized deduplication.
 - b) variable sized deduplication.
- 8) File-level deduplication.

A. Source Deduplication

Source deduplication [10] is the method of identification and removal of duplicate copy before the data is getting transmitted to the backup storage system. It does the data deduplication in the client side as shown in the Fig. 5. This will work with the help of client software which is used to communicate with the storage device to check whether the data to be stored is already present in the backup storage space. The advantage of using source deduplication is utilization of low bandwidth for data transmission but the disadvantage is, it uses client resources for the entire deduplication process. This includes generation of fingerprint for the comparison and the process of identifying the duplicate copy. This source deduplication can be done by two ways. They are local deduplication and global deduplication. In local-level deduplication, the duplicate copy will be initially identified locally, then proceed with the backup process which may depends upon the presence of that particular data in the backup storage. Here the deduplication will be done at that device only. In case of global deduplication, the fingerprint of the data is calculated in the client side and that is getting transferred to the target storage system to compare with the existing data fingerprint. And the data will be stored only when it does not already exist in the storage space. So the deduplication is done across all the users and their devices.

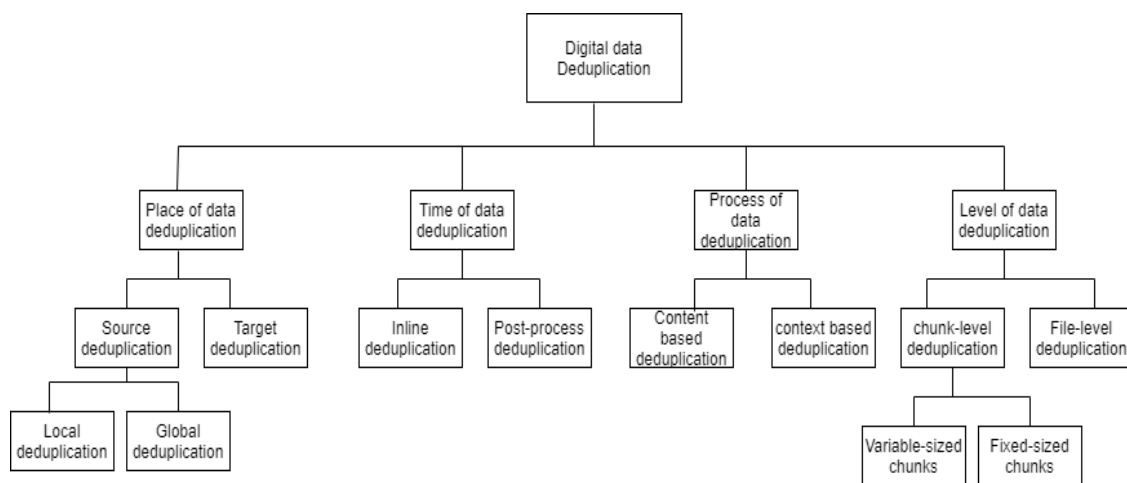


Fig. 4. Different Types of Data Deduplication in Various Dimensions.

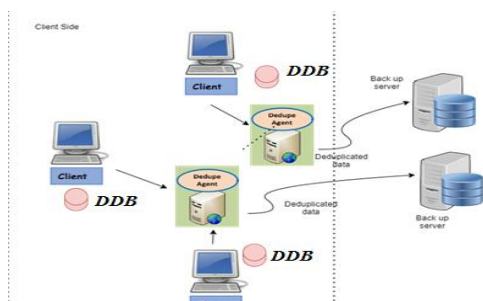


Fig. 5. Client-Side Data Deduplication.

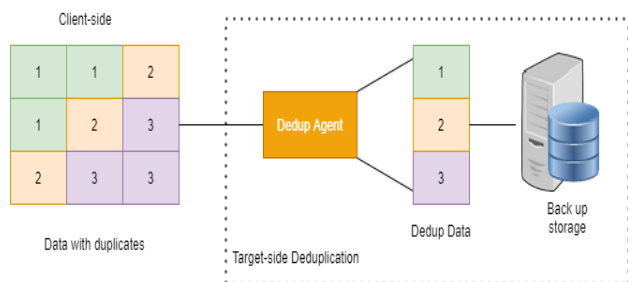


Fig. 6. Target-Side Data Deduplication.

B. Target Data Deduplication

The method of target data deduplication is shown in the Fig. 6. In Target data deduplication [11], the deduplication process is done in the backup server storage system. In the backup side, a dedicated device is employed to carry out the deduplication process. This will reduce the overhead in client side. But the disadvantage is, it requires more bandwidth for data transmission since it may contains duplicate data too.

C. Inline Data Deduplication

The inline data deduplication [12,13,14] can be otherwise called as synchronous deduplication as it allows the data can be stored only when it is unique and not already present in the storage. Not all the data is getting written in the storage space, but only the unique. It is shown in the Fig. 7.

D. Post-process Data Deduplication

In Post-process data deduplication [15], the data is initially written in the storage space as it comes as shown in the Fig. 8. Then the deduplication process will optimize the storage space with unique data. The time of performing this deduplication process is varied with various systems. It can be in seconds, minutes or even hours after the data got stored in the storage space.

E. Content-based or Hash-based Deduplication

The deduplication is performed by considering the content of the digital data [16]. A hash value is generated for the content and that hash value is used to check for the duplication. Any hashing algorithm like MD5, SHA-5256, SHA-512 can be used to calculate the hash value for the digital data and it is shown in the Fig. 9.

F. Content-aware Deduplication

Content-aware deduplication [17] considers the data as an object for the deduplication process. It does the process by comparing object with the other objects. For example if the

input file is word document, then it restricts its comparison only with all other word documents existing in the storage. It achieves byte-level deduplication. This content-aware technique tries to find the similar segments or bytes and those bytes which are really changed or unique will alone be stored in the storage space. The steps in the content-aware deduplication are shown in the Fig. 10.

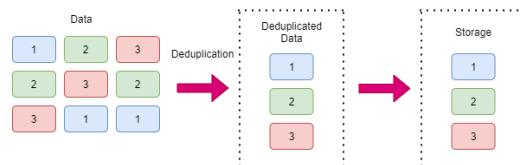


Fig. 7. Inline Data Deduplication.

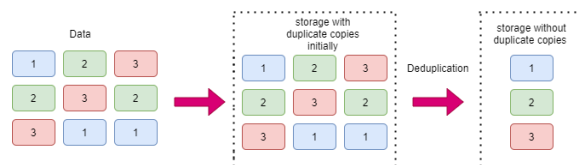


Fig. 8. Post-process Data Deduplication.

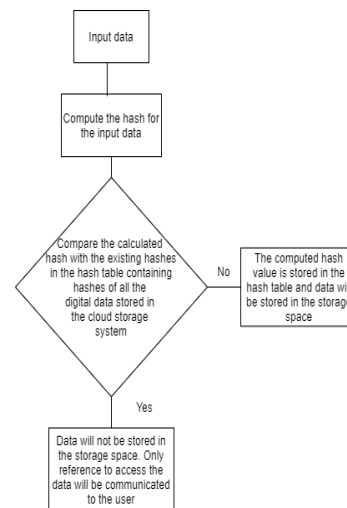


Fig. 9. Content-based Data Deduplication.

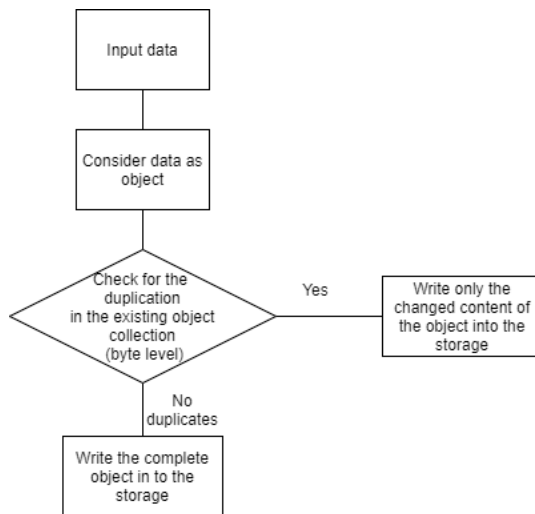


Fig. 10. Content-aware Data Deduplication.

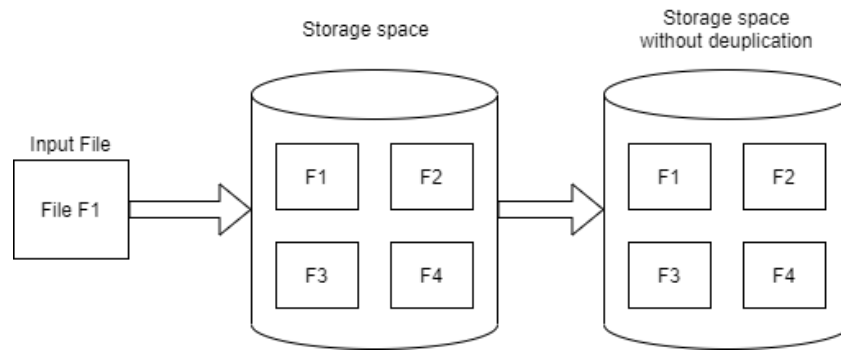


Fig. 11. File-level Deduplication.

G. File-level Deduplication

In file-level deduplication [18] as shown in the Fig. 11, the complete file is taken for comparison. According to the process of deduplication, for example, if hash-based deduplication is decided, then the hash value is calculated for the complete file and the calculated hash value is used to compare the hash values of the existing files stored in the hash table.

H. Chunk Level Deduplication

In chunk level deduplication technique [19,20] the entire content of the digital data is splitted into various chunks. The data upload process involves the following steps. Initially the entire content is divided into chunks. There are many algorithms existing for chunk creation. Then the hash value will be calculated for each and every chunk. Using those hash values duplicity of particular chunk can be identified. This will increase the granularity or degree of deduplication. Which means the wastage of memory is even reduced due to this chunk level deduplication. The chunk level deduplication can be done in two ways. They are Fixed-size chunking [21] and variable-size chunking. In fixed-size chunking, the entire content is divided into equal size chunks. But in variable-size chunking, it is not mandatory that all the chunks will be in the same size. But it requires additional computation for each byte [22]. Fig. 12 and Fig. 13 show the process of chunk-level-Fixed size and Variable size deduplication process.

1) *Chunk level - fixed size deduplication:* In Fixed-size chunk-level deduplication technique, the entire content is divided into equal size chunks. The duplicate copy of chunk-level data can be identified with the help of this technique. For example, if a user wants to upload their data in the cloud storage space, then the data must be divided into chunks and the duplicity of each chunk will be checked before storing the chunk in the storage space. When any of the chunks is already present in the storage space, then that particular chunk alone not gets stored again. This will improve the utilization of storage space.

2) *Chunk level- variable sized deduplication:* In variable-size chunk-level deduplication technique, the entire content is divided into variable size chunks. Which means, each chunk of any size and not compulsorily same. The system will decide the boundary of the each chunks. It also divides the data in content-based strategy. Actually because of this variable-size

chunks, the process of deduplication yield very good results in the finding of duplicate copies.

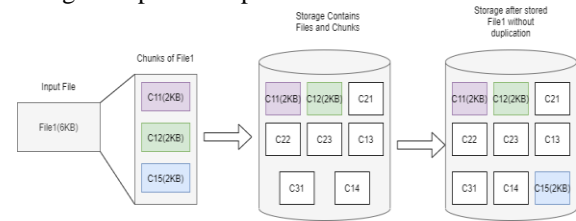


Fig. 12. Chunk-level -Fixed Size Deduplication.

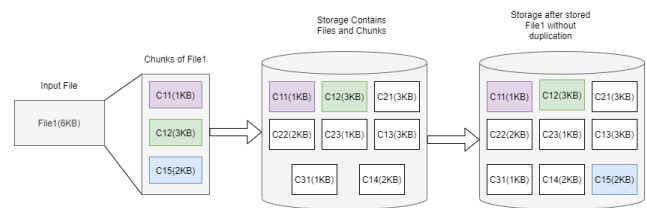


Fig. 13. Chunk-level -Variable Size Deduplication.

V. COMPARISON AND ANALYSIS OF VARIOUS DEDUPLICATION TECHNIQUES

A. Source vs Target based Deduplication Techniques

Table III shows the comparison of Source and Target deduplication techniques in various metrics. The source based deduplication requires less LAN bandwidth as it has the deduplication process in the client-side itself. But it requires more client resources for handling deduplication. In target based deduplication the process overhead in the client-side is less and comparatively fast in process.

TABLE III. SOURCE VS TARGET BASED DEDUPLICATION TECHNIQUES

Metrics	Source based Deduplication	Target based Deduplication
Place of deduplication	Deduplication occurs at client side	Deduplication occurs at backup medium.
Utilization of Bandwidth	Requires Less LAN bandwidth	Required more LAN bandwidth
Client resources	Requires more client resources	Required less client resources
Process overhead at client	More	Less
Speed	Comparitively slow	Fast

B. Inline vs Post-process Deduplication Techniques

Table IV shows the comparison of Inline and Post-process deduplication techniques. Inline deduplication has better storage throughput when compared to post-process deduplication. The Post-process deduplication is faster than in-line process in terms of storage performance.

TABLE IV. INLINE VS POST-PROCESS DEDUPLICATION TECHNIQUES

Metrics	InlineDeduplication	Post-process Deduplication
Time of deduplication	Deduplication occur at the time of data flow	Deduplication occur after it has been written
Storage performance	Slow	Fast. Since the hash calculation is deferred.
Storage requirement and network traffic	Less	Comparatively more
Storage throughput	Reduced storage throughput	Better comparatively
Temporary storage space	Not required	Required

C. Content-aware vs Content-based Deduplication Techniques

Table V shows the comparison of Content-aware and Content-based deduplication techniques. It shows that Content-aware deduplication process has more efficiency.

TABLE V. CONTENT-AWARE VS CONTENT-BASED DEDUPLICATION TECHNIQUES

Metrics	Content-aware Deduplication	Content-based Deduplication
Granularity of deduplication	Even Byte level is possible	Chunk/Block level is possible
Efficiency	More when compared to content-based deduplication	Better
Execution time	Fast. Since it handles data in the form of object. The comparison will be done with the same type of objects only and not with all.	Slow. Since it has to check for all the chunks individually
Metadata overhead	Additional metadata is required to store the type of the object.	Usual details required to handle chunk-based informations.

D. File Level vs Chunk Level Deduplication Techniques

Table VI shows the comparison of File-level and chunk-level deduplication techniques. The chunk-level deduplication process has good efficiency since it does the deduplication at chunk level. And it requires more resource and also it has high computational complexity.

Consider in the storage space, it has audio file F1 already and the new request comes to store another audio file F2. The contents of the file F2 is a part of the File F1.

The MD5 hash value calculated for File F1 is 34195925cbe68a7dc78859b93e13e33e and the hash value calculated for File F2 is 09fd1195ba1c83e51966feb33faa4a80.

In File-level deduplication technique, the files will be considered as different files since their hash values are different. But actually the content of File F2 is the part of the File F1 content. But both are considered as different files in

File-level deduplication technique. In chunk-level deduplication technique, the files will be divided into chunks and hash value will be calculated for each chunks. Then the chunk-level duplication can be checked.

Using this chunk-level deduplication technique, the content of F2 can be identified as duplicate copy. So the content of File F2 will not get stored again in the storage space. This will improve the utilization of storage space. Assume, if the size of the File F1 is 9.85KB and size of file F2 is 9.78KB (without compression). The memory consumption for these two files in storage space is as shown in the Table VII and Fig. 14.

From the observation, using chunk-level deduplication technique, the storage space utilization can be improved without storing duplicate copies of data.

E. Fixed-size vs Variable-size Chunk Level Deduplication Techniques

From the Table VIII, it is observed that Variable-size chunk-level deduplication is a better choice since it does the chunking meaningfully and it also yields good level of efficiency in terms of storage space utilization.

TABLE VI. FILE LEVEL VS CHUNK LEVEL DEDUPLICATION TECHNIQUES

Metrics	File level Deduplication	Chunk level Deduplication
Granularity of deduplication	File level	Chunk level
Resource utilization	Less	More
Execution time	Fast. Since comparison is done for entire file only once.	Slow. Since it has to check for all the chunks individually
Metadata overhead	Little metadata overhead	More metadata overhead
Computational complexity	Low	High
Level of efficiency in terms of storage space utilization	Less	High. Since the deduplication is chunk level. Avoid the duplicate copy of even part of the data.

TABLE VII. MEMORY REQUIREMENT IN STORAGE SPACE

Deduplication Technique	Memory required (in KB)
File-level	19.63
Chunk-level	9.85

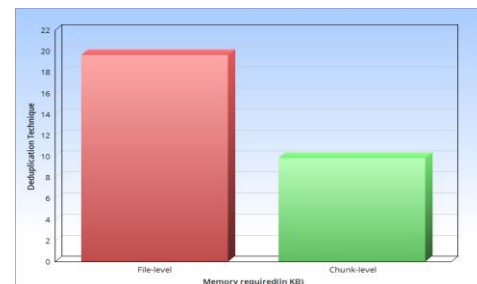


Fig. 14. Memory Requirement in Storage Space using File-level and Chunk-Level Deduplication Techniques.

TABLE VIII. FIXED-SIZE VS VARIABLE-SIZE CHUNK LEVEL DEDUPLICATION TECHNIQUES

Metrics	Fixed-size Chunk level Deduplication	Variable-size Chunk level deduplication
Granularity of deduplication	Chunk level	Chunk level
Size of the chunk	Fixed	Variable
Execution time	Fast. Since the content is to be divided into fixed size without any constraints.	Slow. Since it has to divide the content into variable size in a content-based manner.
Boundary shift problem	It has boundary shift problem even if one byte is either added or deleted in their boundary.	It does not have any boundary shift problem.
Generating indexes	More	Few
Throughput	Low	High
Computational complexity	Low	High
Level of efficiency in terms of storage space utilization	Less	High.

REFERENCES

- [1] KamalaKannan, T., Sharmila, K., Shanthi, M. C., & Devi, M. R.(2019) Study on Cloud Storage and its Issues in Cloud Computing, International Journal of Management, Technology And Engineering, Volume IX, Issue I, 2019, P(976-981).
- [2] R. Arokia Paul Rajan , S. Shanmugapriyaa (2012) Evolution of cloud storage as cloud computing infrastructure service. IOSR Journal of Computer Engineering, Volume 1, Issue 1, PP 38-45.
- [3] Tang, Y., Yin, J., & Wu, Z. (2016, June). Try Managing Your Deduplication Fine-Grained-ly: A Multi-tiered and Dynamic SLA-Driven Deduplication Framework for Primary Storage. In 2016 IEEE 9th International Conference on Cloud Computing (CLOUD) (pp. 859-862). IEEE.
- [4] Paulo, J., & Pereira, J. (2014). A survey and classification of storage deduplication systems. ACM Computing Surveys (CSUR), 47(1), P(1-30).
- [5] Nurshafiqah, M. Z., Yoshii, H., Enomoto, F., Koike, I., & Kinoshita, T. (2017, April). Data Deduplication for Audio Data Files. In Proceedings of 32th International Conference on Computers and Their Applications (CATA2017) (pp. 17-21).
- [6] Sawant, A. A., & Game, P. S. (2018, August). Deduplication of Audio Files to Remove Redundancy in Cloud storage. In 2018 Fourth International Conference on Computing Communication Control and Automation (ICCUBEA) (pp. 1-4). IEEE.
- [7] Manogar, E., & Abirami, S. (2014, December). A study on data deduplication techniques for optimized storage. In 2014 Sixth International Conference on Advanced Computing (ICoAC) (pp. 161-166). IEEE.
- [8] Anand Bhalerao, Ambika Pawar(2017), A survey: On data deduplication for efficiently utilizing cloud storage for big data backups on International Conference on Trends in Electronics and Informatics ICEI 2017.
- [9] D.Viji, Dr.S.Revathy(2019) , Various data deduplication techniques of primary storage on Proceedings of the Fourth International Conference on Communication and Electronics Systems (ICCES 2019) IEEE Conference Record # 45898; IEEE Xplore ISBN: 978-1-7281-1261-9.
- [10] Fu, Y., Jiang, H., Xiao, N., Tian, L., & Liu, F. (2011, September). AA-Dedupe: An application-aware source deduplication approach for cloud backup services in the personal computing environment. In 2011 IEEE International Conference on Cluster Computing (pp. 112-120). IEEE.
- [11] Deepu, S. R. (2014). Performance Comparison of Deduplication techniques for storage in Cloud computing Environment. Asian Journal of Computer Science And Information Technology, 4(5) (pp. 42-46).
- [12] Kim, Y., Kim, C., Lee, S., & Kim, Y. (2016). Design and Implementation of Inline Data Deduplication in Cluster File System. KIISE Transactions on Computing Practices, 22(8), 369-374.
- [13] Wildani, A., Miller, E. L., & Rodeh, O. (2013, April). Hands: A heuristically arranged non-backup in-line deduplication system. In 2013 IEEE 29th International Conference on Data Engineering (ICDE) (pp. 446-457). IEEE.
- [14] Srinivasan, K., Bisson, T., Goodson, G. R., & Voruganti, K. (2012, February). iDedup: latency-aware, inline data deduplication for primary storage. In Fast (Vol. 12, pp. 1-14).
- [15] Kathpal, Atish, Matthew John, and Gaurav Makkar. "Distributed duplicate detection in post-process data de-duplication." HiPC. 2011.
- [16] Pal, S., More, K., & Pise, P. (2018, February). Content-Based Deduplication of Data Using Erasure Technique for RTO Cloud. In 2018 International Conference On Advances in Communication and Computing Technology (ICACCT) (pp. 109-113). IEEE.
- [17] <https://pibytes.wordpress.com/2013/02/17/deduplication-internals-content-aware-deduplication-part-3/>.
- [18] Jyoti Malhotra, JagdishBakal "FiLeD: File Level Deduplication Approach". International Journal of Computer Trends and Technology (IJCTT) V44(2):74-79, February 2017. ISSN:2231-2803.
- [19] Bhalerao, Anand, and AmbikaPawar. "Two-Threshold Chunking (TTC): Efficient Chunking Algorithm For Data Deduplication For Backup Storage.", International Journal of Scientific and Technology Research Volume 8, Issue 09, September 2019 ISSN 2277-8616.

The various deduplication techniques are analysed using various parameters and metrics. From the above results it is seen that applying in-line deduplication with chunk-level technique may result with good efficiency in the deduplication process.

VI. CONCLUSION

The cloud storage provides the storage space for the individual and the organization that are all in need of storage space. The cloud storage can be efficiently utilized with the help of deduplication techniques. There are various types of deduplication techniques and every technique has its own advantages and disadvantages and that can be efficiently utilized for suitable applications. In this paper we analysed the benefits of applying deduplication technique for efficient utilization of cloud storage space and discussed about the different deduplication techniques in various dimensions. Among various techniques, In-line with variable-sized chunk level deduplication will help us to achieve efficient utilization of cloud storage space since it does not require additional storage space as it is required in Post-process method, because it does not store any duplicate data and in case of variable – sized chunk level deduplication, it looks for even the part of the data is duplicate or not instead of checking the duplication for complete data. The major reason of this research work is to compare the various available deduplication technique. So that the various groups of cloud storage providers can be benefitted by applying the suitable deduplication techniques in their respective scenarios.

VII. FUTURE WORK

The limitation of our work is, we did not consider various types of digital data for comparing the deduplication techniques. In future research work, we are interested in analyzing the various techniques of deduplication with the respect to the different types of digital data.

- [20] Venish, A., &Sankar, K. S. (2016). Study of chunking algorithm in data deduplication. In *Proceedings of the International Conference on Soft Computing Systems* (pp. 13-20). Springer, New Delhi.
- [21] Sharma, N., AV, K. P., &Kakulapati, V. (2019). Data deduplication techniques for big data storage systems. *Int. J. Innov. Technol. Explor. Eng.*, 8(10), 1145-1150.
- [22] Yoon, M. (2019). A constant-time chunking algorithm for packet-level deduplication. *ICT Express*, 5(2), 131-135.

PLA Mechanical Performance Before and After 3D Printing

Houcine SALEM¹, Hamid ABOUCHADI², Khalid ELBIKRI³

M2SM, Research Center STIS, Dep. of Mechanical Engineering, ENSAM, Mohammed V University, Rabat, Morocco^{1,3}
PCMT, Research Center STIS, Dep. of Mechanical Engineering, ENSAM, Mohammed V University, Rabat, Morocco²

Abstract—PLA or polylactic acid is a thermoplastic made from renewable sources. Thanks to its environmental value compared to petroleum sourced materials, it is widely used in 3D printing industry. Due to the advantages of additive manufacturing in terms of cost and time consumption, many industries are using these technologies to re-engineer parts or assemblies to optimize their products. However, the properties given by the supplier are not conforming to the final printed product. This issue can be dangerous, especially when these products are used in the biomedical fields or toys for children or other sensitive areas. The aim of this paper is to outline the difference between the final properties and the primary ones. The samples are tested in traction following the ASTM D638 Standard. The specificities of the standard in terms of specimen dimensions and test methodologies have been respected. The results demonstrated that there is a difference between the performance of the material before and after using a 3d printer.

Keywords—Additive manufacturing; PLA; test sample; traction; 3D printing

I. INTRODUCTION

With the affordable price of 3D printers and the rise of local and industrial Fablabs (fabrication laboratory), the study of the mechanical behavior of the material becomes important. People start printing any broken object in their homes and replace it without thinking in the possible damage that it can do to the assembly. Even the industries start prototyping products to replace missing pieces using the technical data sheet of the material as reference. These technical sheets of commercial plastics are available on the internet and give the mechanical, physical and thermal properties [1]. These properties may vary depending on the supplier and the specific grade of the resin in question. They may also vary depending on the process and manufacturing parameters during the implementation of the products. For example, the morphology/structure of semi-crystalline used in 3D printing can be very sensitive to small variations in implementation parameters such as build plate temperature, temperature of the nozzle, etc. Therefore, manufacturers of products made of plastic materials are led to carry out their own mechanical tests when developing a new product to make sure it meets the design parameters. Mechanical tests are essential to determine the mechanical properties [2] of materials needed for a given application or for other reasons such as quality control or research and development.

The most common thermoplastics used in 3D printing are ABS (acrylonitrile butadiene styrene) and PLA (poly lactic

acid) [3][4]. Due to its environment friendly properties [5] and its performances [6], PLA is the subject of our research.

The study targets the following objectives:

- Test in traction the targeted material PLA (polylactic acid).
- Determine the effect of movement speed on the mechanical properties in traction.
- Compare the mechanical behavior of the material before and after being processed on a 3D printing machine.

The first step was to analyze the technical data sheet of the used PLA before printing it. Then the test conditions of an ASTM Standard were followed, which resulted in the shape and dimensions of the test samples, in addition to all the details of the test machining and procedure.

The 3D printer and the test machine used in the study are adequate to the scope of the standard, thus, a specific methodology was followed to test the samples and to calculate the mechanical performance after 3D printing. Then the results were compared to the original data of the supplier.

The rest of the paper contains information about the tested material, the test methodology and the manufactured test specimens. The following section is about the results of the mechanical properties [7] before and after 3D printing. Then, a discussion is presented to analyze the results.

II. TESTED MATERIAL: PLA

PLA or Polyactid acid is thermoplastic polyester “Fig. 1” widely used in 3D printing. Thanks to the fact that it is produced from renewable resources (such as corn starch, tapioca roots or sugar cane), it is the second most used bio plastic in the world [8], even if it’s not a commodity polymer. In 3D printing it’s by far the most used plastic filament, especially for the FDM (Fused Deposition Modeling) processes [9]. The main applications are the proof of concept in architecture, games or cinema.

PLA polymers range from amorphous glassy polymer to semi-crystalline and highly crystalline polymer with a glass transition 60–65 °C, a melting temperature 130-180 °C, and a tensile modulus 2.7–16 GPa [10][11]. Heat-resistant PLA can withstand temperatures of 110 °C.[12] The basic mechanical properties of PLA are between those of polystyrene and PET.

The PLA is used in food packaging and in many objects injected, extruded or thermoformed. It is also used in surgery

as the stitches are made of biodegradable polymers to decompose under water and enzymes. In addition to being one of the most used material in 3D printing, thanks to its affordability and performance.

Physical Properties

Property	Testing Method	Typical Value
Density(g/cm ³ at 21.5 °C)	ASTM D792 (ISO 1183, GB/T 1033)	1.17-1.24
Glass transition temperature(°C)	DSC, 10 °C/min	50-60
Softening temperature of filament(for 1.75 mm; °C)	Custom method	146-150
Melt index(g/10 min)	210 °C, 2.16 kg	7-11
Moisture content(%)	Thermogravimetric	≤0.1%
Odor	/	Almost odorless
Solubility	/	Insoluble in water; soluble in chloroform, toluene, and tetrahydrofuran(THF)

Mechanical Properties¹

Property	Testing Method	Typical Value
Young's modulus(MPa)	ASTM D638 (ISO 527, GB/T 1040)	2636±330
Tensile strength(MPa)	ASTM D638 (ISO 527, GB/T 1040)	46.6±0.9
Elongation at break(%)	ASTM D638 (ISO 527, GB/T 1040)	1.90±0.21
Bending modulus(MPa)	ASTM D790 (ISO 178, GB/T 9341)	3283±132

Fig. 1. Technical Data Sheet of the used PLA.

III. TEST CONDITIONS

A. ASTM D638

The official name of the standard is “D638 – 10 Standard Test Method for Tensile Properties of Plastics” “Fig. 2”.

This test method covers the determination of tensile properties of reinforced and unreinforced plastics in the form of dumbbell-shaped test samples standards. These samples are tested under defined condition in terms of pretreatment, temperature, humidity and movement speed.

It is used to test materials with a thickness up to 14mm. However, for the analysis of samples in the form of thin sheets less than 1.0 mm thick, the ASTM D882 is the preferred test method. If the thickness is greater than 14mm, it must be reduced by machining.

1. Scope 2. Referenced Documents 3. Terminology 4. Significance and Use 5. Apparatus 6. Test Specimens 7. Number of Test Specimens 8. Speed of Testing 9. Conditioning 10. Procedure 11. Calculation 12. Report 13. Precision and Bias ⁵ 14. Keywords	ANNEXES (Mandatory Information) A1. TOE COMPENSATION A2. DEFINITIONS OF TERMS AND SYMBOLS RELATING TO TENSION TESTING OF PLASTICS A3. MEASUREMENT OF POISSON'S RATIO A3.1 Scope A3.2 Referenced Documents A3.3 Terminology A3.4 Significance and Use A3.5 Apparatus A3.6 Test Specimen A3.7 Number of Test Specimens A3.8 Conditioning A3.9 Procedure A3.10 Calculation A3.11 Report A3.12 Precision and Bias A3.13 Keywords SUMMARY OF CHANGES
---	--

Fig. 2. Scope and Content of the ASTM Standard.

This standard is designed to provide tensile properties of plastic material, in order to characterize it in a research and development aim.

All the samples must be made in exactly the same environment with the same printing conditions.

The testing machine must respect the following details:

- A fixed or a stationary grip.
- A Movable member with a second grip.
- Valid grips to ensure that the specimen is correctly inserted and aligned with the z axis so that no rotary motion in necessary to avoid slippage. The grips must be held clean at all time.
- A drive mechanism with a regulated speed.
- A load indicator to follow and retrieve the stress data.
- The material of the grips must be adaptable to the thermoplastic samples.
- An extension indicator to show the strain.
- A micrometer to measure the width and thickness of the specimen.

The specimens used in this standard are also normalized following these criteria:

- There are five types of dumbbell shaped specimens. The shape and the dimensions are determined for a specific material with a specific thickness range. It also depends on how does the material break. For example, if it's in the narrow section a specific type is advised.
- The standard has different dimension criteria for rigid plastics, non-rigid ones and reinforced composites.
- The standard also gives preparation methods, depending on the process [13] used to manufacture the specimen.
- The gage marks on the specimen must be done in a way that does not affect the material behavior.

The number of test specimens is five for each sample for isotropic materials.

The speed of testing depends on the type of material; a table is given by the standard to choose within a range.

The test procedure is also detailed in the standard, starting with the measures of width and thickness of the specimen before testing it. This procedure also depends on the machining used to manufacture the test, and the shape and dimensions of the specimen.

All specimens must be held by the grips in the same way and shall be tightened firmly, but without crushing the sample. Then, the record of the load-extension curve must be done with a specific extension indicator.

The calculation takes into account the toe compensation that occur in the beginning of the test, then the calculation method is specified in the norm to determine the adequate data.

B. Test Machine

The universal tensile test machine (DELTALAB EM 550) “Fig. 3” used in this study is shown below. It has a load cell capacity of 50kN. It submits test samples to efforts and measures the deformation in order to establish constitutive laws of the sample’s material. The machine is designed to be used in many materials and structural testing applications. It performs tensile test, compression, bending, fatigue, creep, hardness, friction as well as tests on assemblies and structures.

The machine is connected to a control part consisting of a computer, a printer, DELTALAB software and a software / machine interface to control, acquire and process data.

General characteristics

- Maximum force on the cross member: 50 kN.
- Maximum stroke: 1 m.
- Drive: Direct current servomotor with tachometric generator.
- Transmission: Wheel and worm gear reducer, pulleys, toothed belt and ball screw.
- Displacement measurement: Optoelectronic encoder for resolution 500 positions per revolution.
- Force measurement: Sensor with deformation gauges.
- Power supply: 240 V single phase / 50 Hz at 1 kW max.
- Maximum servomotor torque: 3 N.m.
- Load range: 0 to 50 kN in tension and compression.
- Height under cross member: 1000 mm.
- Distance between columns: 400 mm.
- Travel speed of the cross member: 0.5 mm / min at 350 mm / mn.
- Drive device by 2 screws with double row of balls.
- Resolution of the displacement measurement sensor: 0.01 mm.
- Resolution of the force sensor of 50 kN: 25 N.
- Display of force and displacement on screen DC electric motor with tacho generator.



Fig. 3. Test Machine DELTALAB Serie EM550.

C. Test Samples

For our study, the ASTM D638 standard for tensile testing of plastics is used. Here is the geometry “Fig. 4” determined from the standard:

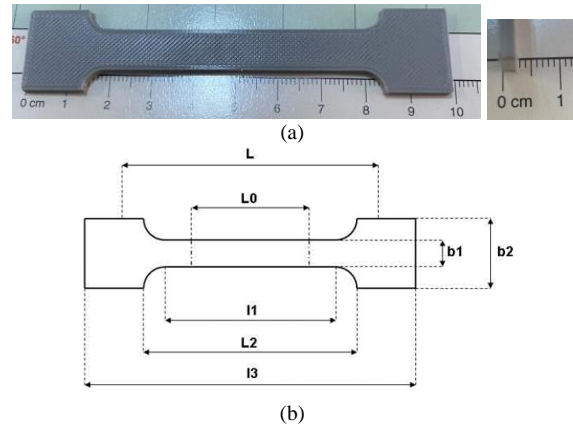


Fig. 4. Test Sample from the ASTM Standard: a-Printed Sample b-ASTM Standard.

Among the samples geometries proposed by the ASTM D638, the dumbbell shaped geometry shown above was chosen. To facilitate the results analysis, the necessary dimensions were listed for the requested calculations “Table I”. These dimensions are necessary to transform the load into stress. The effective length is the length which is assumed to take the entire measured displacement. Thus, in dividing the displacement on this length, the strain can be estimated and consequently, the data displacement (mm) – load (Newtons) can be transformed into strain (%) – stress (MPa).

The sample has been designed using SOLIDWORKS 2018, following the ASTM D638 dimensions.

The process parameters “Fig. 5” have been set using Ultimaker Cura, with an infill pattern of 100% to respect the volume of a sample made by injection molding.

TABLE I. TEST SAMPLE DIMENSIONS FROM THE ASTM STANDARD

Dimension	Symbol	Value[mm]
Thickness	T	3
Width in the reference length area	b1	10±0.5
Length of the narrow calibrated part	l1	60 ± 0.5
Width in the shoulder area	b2	20±0.5
Reference length	L0	50±0.25
Distance between tools	L	115±5

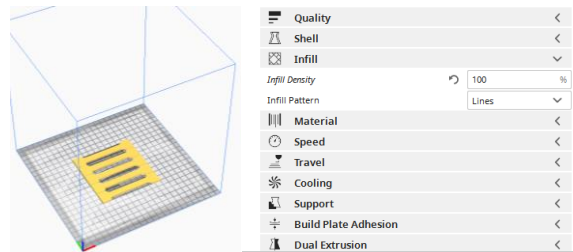


Fig. 5. 3D Printing Parameters.

D. 3D Printer

The 3D printer used “Fig. 6” to manufacture the samples in the ENDER-3.



Fig. 6. 3D Printing Machine ENDER-3.

The chosen printer is one of the best fused deposition modeling with a low price range, thanks to its performance and polyvalence. Its functionalities are comparable with high cost printers. The print volume is 220*220*250mm, with a heated build plate, a pick-up detector and a tight filament path that facilitates printing of flexible filaments.

The Ender-3 is an open-source printer is commonly used in local fabrication laboratories to manufacture small parts or to learn about robotics and mechanics. This technology is mature and stable, which allow a 200 hour work flow. In addition, it allows completing a print after a power outage for example, with thermal runaway protection. Thanks to this stability and a high precision pulley, this printer affords more resistance and lower noise. With an extrusion mechanism MK8, it reduces the clogging risk and it can print almost any filament in the market. The rails made with CNCs provide precise positioning and a solid frame to ensure a good quality and a high printing precision. The build plate can reach 110°C in 5 minutes.

This is the technical specifications of the printer:

- Modeling Technology: FDM (Fused Deposition Modeling).
- Printing Size: 220x220x250mm.
- Printing Speed: 180mm/s.
- Filament: 1.75mm PLA, TPU, ABS.
- Working Mode: Online or SD offline.
- File Format: STL,OBJ,G-code.
- Machine Size: 440x440x465mm.
- Net Weight: 8KG.
- Power Supply: 100-265V 50-60HZ.
- Output: 24V 15A 270W.
- Layer Thickness: 0.1-0.4mm.

- Nozzle Diameter: 0.4mm.
- Printing Accuracy: ± 0.1 mm.
- Nozzle Temperature: 255°C.
- Hotbed Temperature: 110°C.

IV. METHODOLOGY

A. Test Method

Here are the followed steps to test the sample “Fig. 7”, according to the ASTM standard:

- Measure the width and thickness of each sample at 0.025 mm near.
- Place the sample in the handles of the test machine.
- Tighten the handles evenly as necessary to prevent the sample from slipping during the test.
- Adjust the test speed.
- Perform the test and record the results.

Five tests were carried out for two different speeds, which give us a total of 10 test specimens tested.



Fig. 7. Tested Samples after Traction.

B. Calculation Method

The calculation method used is simple and systematic. First of all, the raw data of the results were analyzed and then converted it into more practical units in terms of stress and strain.

Due to the initial clearance in the assembly, the first portion of the graph curve before the linear domain must be discarded since it is not representative of displacement as a function of force. Indeed, this small part of the curve very often represents the movement of the sample in the jaws of the universal traction machine. Thus, to normalize the curves, the linear domain is extended up to the intersection with the abscissa and the graph is shifted to obtain the point of intersection of the extension with the x axis at the origin.

In this case, in order to find the yield point, only the point where the applied force is maximum is determined. Then a conversion to MPa is necessary to obtain the yield point.

There are two types of conversions required, converting force to stress and converting displacement to strain.

Force (kN) to Stress (MPa)

$$\sigma(\text{MPa}) = \frac{\text{Force (N)}}{\text{Surface (mm}^2\text{)}} \quad (1)$$

Surface = $T_i W_i$

“ T_i ” represents the thickness and “ W_i ” the width of the specified sample “ i ”.

Once the coordinate of the first maximum stress found, the associated displacement in mm are found and transformed it into strain.

$$\epsilon(\%) = \frac{\text{Displacement (mm)}}{\text{length (mm)}} \quad (2)$$

V. RESULTS

A. Data

After realizing the ten tensile tests for the two travel speeds, the calculations explained above were carried out and the obtained curves and the results are shown in the following tables and graphs: “Fig. 8”, “Table II”, “Fig. 9”, and “Table III”.

B. Speed Test Effect

The bibliographical analysis shows that the stress rate modifies the mechanical properties [14][15] of the material tested. Young's modulus and elastic limit increase with increasing stress speed. The deformation of the material at the elastic limit is lower. However, the resistance to flow is higher with increasing speed.

This is explained by the fact that when the speed is higher, the material spends less time to deform elastically and therefore begins its plastic deformation more quickly. As the speed is faster, there is less time for the polymer chains to move through the material under tension. On the other hand, the mechanical properties [16][17] at the yield point are increased, in particular since a greater load can be applied due to the resistance which is stronger.

However, the results obtained in our case are almost identical between the speed of 50 mm / min and 25 mm / min. This is explained by the difference between these speeds which is not very large. In the research cited [18], the ratio between the speeds is 1/10 while in our case the ratio is 1/2.

C. Mechanical Properties

The equations are an exception to the prescribed specifications of this template. You will need to determine whether or not your equation should be typed using either the Times New Roman or the Symbol font (please no other font). To create multileveled equations, it may be necessary to treat the equation as a graphic and insert it into the text after your paper is styled.

The table “Table IV” shows the comparison of the data provided by the supplier and the data found experimentally.

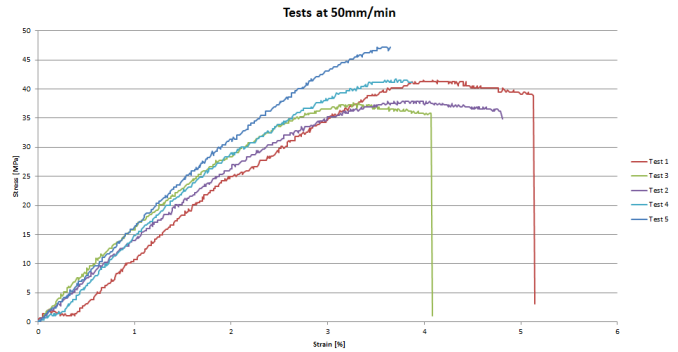


Fig. 8. Stress / Strain Graph for the 5 Tests at 50mm/min.

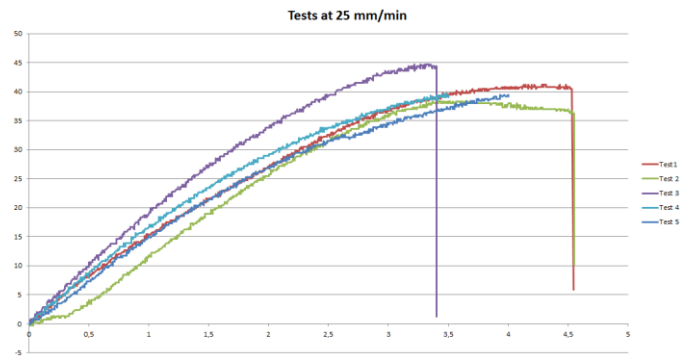


Fig. 9. Stress / Strain Graph for the 5 Tests at 25mm/min.

TABLE II. RESULTS OF THE 5 TESTS AT 50 MM/MIN

Measured properties	Symbol	Unit	Test1	Test2	Test3	Test4	Test5	Average	SV	CV
Thickness	T	mm	2,86	2,9	2,92	2,88	2,88	2,888	0,023	0,008
Length	L	mm	60,45	59,7	59,7	60,45	59,8	60,02	0,395	0,007
Width	W	mm	10,095	10,095	10,02	10,05	10,07	10,07	0,032	0,003
Surface	S	mm ²	28,872	29,276	29,258	28,94	29	29,07	0,185	0,006
Load at yield point	Py	N	1190	1110	1100	1210	1370	1196	108,5	0,09
Load at elastic limit	Pe	N	1180	1010	1070	1170	1290	1144	108,1	0,094
Travel to Py	dy	mm	2,61	2,42	1,98	2,24	2,1	2,27	0,251	0,111
Displacement to Pe	de	mm	2,32	1,78	1,76	2	1,88	1,95	0,229	0,117
Elastic modulus in tension	E	MPa	1147,3	1277,3	1394,7	1344	1455	1324	118,3	0,089
Resistance to yield point	sy	MPa	41,21	37,9	37,6	41,8	47,2	41,14	3,88	0,094
Elastic limit	se	MPa	40,87	34,5	36,6	40,4	44,5	39,37	3,91	0,099
Strain at yield point	ey	%	4,33	4,054	3,317	3,706	3,512	3,78	0,41	0,108
Strain at the elastic limit	ee	%	3,83	2,982	2,948	3,309	3,144	3,24	0,36	0,111

TABLE III. RESULTS OF THE 5 TESTS AT 25 MM/MIN

Measured properties	Symbol	Unit	Test1	Test2	Test3	Test4	Test5	Average	SV	CV
Thickness	T	mm	2,89	2,925	2,4	2,845	2,857	2,78	0,21	0,078
Length	L	mm	60,3	59,951	60,251	60,841	60,24	60,30	0,32	0,005
Width	W	mm	10,1	10,078	10,245	10,095	10,11	10,12	0,06	0,007
Surface	S	mm ²	29,2	29,478	24,588	28,72	28,90	28,16	2,02	0,072
Load at yield point	Py	N	1200	1130	1100	1130	1140	1140	36,74	0,032
Load at elastic limit	Pe	N	1160	1120	1030	1080	1010	1080	62,04	0,057
Travel to Py	dy	mm	2,49	2,22	2,02	2,12	2,41	2,25	0,19	0,087
Displacement to Pe	de	mm	2,19	2,01	1,73	1,86	1,88	1,93	0,17	0,09
Elastic modulus in tension	E	MPa	1257	1223	1543	1317,4	1271,9	1322,4	127,9	0,097
Resistance to yield point	sy	MPa	41,2	38,333	44,752	39,345	39,43	40,60	2,53	0,062
Elastic limit	se	MPa	39,8	37,994	41,904	37,604	34,93	38,44	2,59	0,068
Strain at yield point	ey	%	4,13	3,703	3,3526	3,4845	4,00	3,73	0,33	0,089
Strain at the elastic limit	ee	%	3,63	3,3527	2,8713	3,0571	3,12	3,20	0,29	0,092

The first observation is that the young modulus of the tested specimens is 50% compared to that given by the supplier.

As regards the tensile strength, it is 12.3% lower for the test specimens tested.

As for the deformation at break, it is greater for the material tested by 200% compared to the supplier's data.

D. Synthesis

From the results detailed in the previous section, it is shown that the mechanical properties of the test specimens are completely different from those given by the supplier. The mechanical strength of 3D printed specimens is significantly lower than that of the material before it is printed (50% lower Young's modulus, 12% lower tensile strength, and 200% higher strain).

This difference is explained by the micrographic structure "Fig. 10" of the material after printing. Indeed, despite entering 100% infill in the printer management software, this rate is not achievable with this type of process. In Fig. 10, the micrographic structure of a sectional view of a 3D printed test specimen is shown. This structure clearly shows voids between the printed filaments. This implies two changes in mechanical performance.

The first is that the strain is greater because the cracks propagate less quickly inside the specimen. This is because the crack stops when it encounters a void, so the specimen continues to deform until a new crack appears which in turn stops etc.

The second change is in the mechanical resistance which is significantly lower. Indeed, because of the voids, the density of the material is less important, which implies a lower resistance compared to a solid specimen made by injection molding.

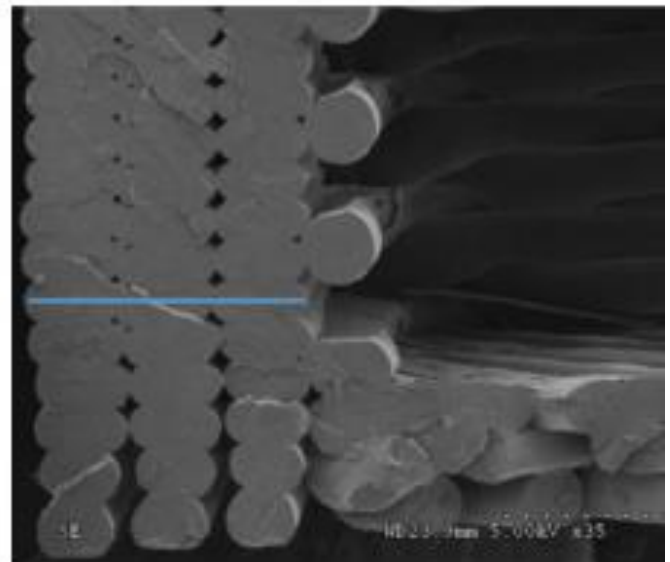


Fig. 10. Scanning Electron Micrograph of the 3D Printed Samples Perimeters [19].

TABLE IV. PROPERTIES COMPARISON BETWEEN THE TECHNICAL DATASHEET AND THE TESTED PLA

Property	PLA datasheet	Tested PLA
Young's modulus (MPa)	2636 ± 330	1323±123
Tensile strength (MPa)	46.6±0.9	40.87±3.2
Elongation at break (%)	1.9±0.21	3.75±0.37

VI. CONCLUSION

PLA is the most used material in 3D printing, especially for the fused deposition modeling process, which is the most used process because it is the cheapest and easiest process to use. Knowledge of the mechanical properties of parts printed in PLA is very important, as these parts are increasingly used in proof of concept for important applications, especially in the biomedical field, such as implants etc.

This study allowed to test in traction specimens designed in PLA with a 3D printer, all while following the details of ASTM D638 [20]. Then was a comparison between the results obtained and the data provided by the supplier was detailed. The results have shown that there is a huge lag in the mechanical performance of the specimen before and after printing. This information is very important because most researchers use the data provided by the material supplier to justify the strength of manufactured parts. This can be dangerous especially for applications in the biomedical or industrial field.

This study therefore allowed outlining the importance of testing parts after manufacture to ensure their mechanical properties. That said, other studies can be carried out to enrich the latter. In particular by using different types of filling to find which type provides better resistance. Studies can also be carried out on other manufacturing parameters such as printing direction to study the influence of each parameter.

REFERENCES

- [1] Carrasco, F., P. Pagès, J. Gámez-Pérez, O. O. Santana et M. L. Maspoch. 2010. « Processing of poly(lactic acid): Characterization of chemical structure, thermal stability and mechanical properties ». *Polymer Degradation and Stability*, vol. 95, no 2, p. 116-125.
- [2] Anderson, Kelly S., Kathleen M. Schreck et Marc A. Hillmyer. 2008. « Toughening Poly(lactide) ». *Polymer Reviews*, vol. 48, no 1, p. 85-108.
- [3] Mikula, K.; Skrzypczak, D.; Izydorczyk, G.; Warchoł, J.; Moustakas, K.; Chojnacka, K.; Witek-Krowiak, A. 3D Printing Filaments as a Second Life of Waste Plastics—A Review. *Environ. Sci. Pollut. Res.* 2021, 28, 12321–12333.
- [4] Shah, J.; Snider, B.; Clarke, T.; Kozutsky, S.; Lacki, M.; Hosseini, A. Large-Scale 3D Printers for Additive Manufacturing: Design Considerations and Challenges. *Int. J. Adv. Manuf. Technol.* 2019, 104, 3679–3693.
- [5] Agüero, A.; Morcillo, M.D.C.; Quiles-Carrillo, L.; Balart, R.; Boronat, T.; Lascano, D.; Torres-Giner, S.; Fenollar, O. Study of the Influence of the Reprocessing Cycles on the Final Properties of Poly(lactide) Pieces Obtained by Injection Molding. *Polymers* 2019, 11, 1908.
- [6] Arrieta, P.M.; Samper, D.M.; Aldas, M.; López, J. On the use of PLA-PHB Blends for Sustainable Food Packaging Applications. *Materials* 2017, 10, 1008.
- [7] Sin, Lee Tin, A. R. Rahmat et W. A. W. A. Rahman. « 5. Mechanical Properties of Poly(Lactic Acid) ». In *Poly(lactic Acid) – PLA Biopolymer Technology and Applications*. Elsevier.
- [8] Ceresana. "Bioplastics - Study: Market, Analysis, Trends - Ceresana". www.ceresana.com. Archived from the original on 4 November 2017. Retrieved 9 May 2018.
- [9] O. a. Mohamed, S.H. Masood, J.L. Bhowmik, Optimization of fused deposition modeling process parameters: a review of current research and future prospects, *Adv. Manuf.* (2015) 42–53. doi:10.1007/s40436-014-0097-7.
- [10] A One Dimensional Meshfree-Method for Solving Thermal Problems of Selective Laser Sintering Process of Polymer Powders Yaagoubi, H., Abouchadi, H., Janan, M.T. 2019 International Conference on Optimization and Applications, ICOA 2019, 2019, 8727660.
- [11] A New Method to Analyze the Quality Characteristics of 3D Printing Technologies: Production, Time, Cost Yaagoubi, H., Abouchadi, H., Janan, M.T., Souetre, M. 2020 International Conference on Electrical and Information Technologies, ICEIT 2020, 2020, 9113198.
- [12] Mathematical study on the relation of energy density and other parameters in the selective laser sintering of polyamide12 and their influences on the quality of the final produced part Yaagoubi, H., Abouchadi, H., Janan, M.T. 6th International Conference on Optimization and Applications, ICOA 2020 - Proceedings, 2020, 9094498.
- [13] A. Lanzotti, M. Martorelli, G. Staiano, Understanding Process Parameter Effects of RepRap Open-Source Three-Dimensional Printers Through a Design of Experiments Approach, *J. Manuf. Sci. Eng.* 137 (2014) 011017. doi:10.1115/1.4029045.
- [14] B.M. Tymrak, M. Kreiger, J.M. Pearce, Mechanical properties of components fabricated with open-source 3-D printers under realistic environmental conditions, *Mater. Des.* 58 (2014) 242–246. doi:10.1016/j.matdes.2014.02.038.
- [15] A. Bagsik, V. Schöppner, Mechanical Properties of Fused Deposition Modeling Parts Manufactured with ULTEM 9085, in: Antec, Boston, 2011.
- [16] Y. Song, Y. Li, W. Song, K. Yee, K.Y. Lee, V.L. Tagarielli, Measurements of the mechanical response of unidirectional 3D-printed PLA, *Mater. Des.* 123 (2017) 154–164. doi:10.1016/j.matdes.2017.03.051.
- [17] V.E. Kuznetsov, A.N. Solonin, O.D. Urzhumtsev, R. Schilling, A.G. Tavittov, Strength of PLA components fabricated with fused deposition technology using a desktop 3D printer as a function of geometrical parameters of the process, *Polymers (Basel)*. 10 (2018) 313. doi:10.3390/polym10030313.
- [18] Lunt, James (3 January 1998). "Large-scale production, properties and commercial applications of polylactic acid polymers". *Polymer Degradation and Stability*. 59 (1–3): 145–152. doi:10.1016/S0141-3910(97)00148-1. ISSN 0141-3910.
- [19] Effect of Infill Patterns on the Mechanical Performance of Lightweight 3D-Printed Cellular PLA Parts Christian Lubombo and Michel Huneault Department of Chemical and Biotechnological Engineering, Université de Sherbrooke, Sherbrooke, Canada.
- [20] ASTM D638-14, Standard test method for tensile properties of plastics, West Conshohocken, PA, 2014. doi:10.1520/D0638-14.1.

Detecting Hate Speech on Twitter Network using Ensemble Machine Learning

Raymond T Mutanga¹, Nalindren Naicker², Oludayo O Olugbara³

Department of Information Technology, Durban University of Technology, Durban, South Africa^{1,3}
Department of Information Systems, Durban University of Technology, Durban, South Africa²

Abstract—Twitter is habitually exploited now-a-days to propagate torrents of hate speeches, misogynistic, and misandry tweets that are written in slang. Machine learning methods have been explored in manifold studies to address the inherent challenges of hate speech detection in online spaces. Nevertheless, language has subtleties that can make it stiff for machines to adequately comprehend and disambiguate the semantics of words that are heavily dependent on the usage context. Deep learning methods have demonstrated promising results for automatic hate speech detection, but it requires a significant volume of training data. Classical machine learning methods suffer from the innate problem of high variance that in turn affects the performance of hate speech detection systems. This study presents a voting ensemble machine learning method that harnesses the strengths of logistic regression, decision trees, and support vector machines for the automatic detection of hate speech in tweets. The method was evaluated against ten widely used machine learning methods on two standard tweet data sets using the famous performance evaluation metrics to achieve an improved average F1-score of 94.2%.

Keywords—Classical learning; deep learning; ensemble learning; hate speech; social media; twitter network; voting ensemble

I. INTRODUCTION

Twitter is a popular microblogging social networking service platform invented for the central purpose of connecting geographically dispersed people to seamlessly collaborate, communicate, microblog, network, socialise and share information. It is recently used for fostering business entities as a way of reaching out to a throng of clients and retaining them. However, despite its popularity and usefulness, there is a rapid rise in its usage for propagating hateful speeches and aiding torrents of invectives against innocent people. The level of anonymity of the accounts granted by social media networking platforms has made them havens for promoting hateful, discriminating, and vulgar speeches. Considering that Twitter generates a high volume of tweets daily, hate speech propagation should be curbed to avoid people deactivating their accounts and quitting the network platform. Human annotators are currently employed by Twitter and Facebook to delete nocuous tweets perceived to be hateful in curtailing the excessiveness of hate speech propaganda on social media platforms. In addition, the public is requested to report nocuous tweets to the service providers. However, these manual methods are laborious, sentimental, and susceptible to a subjective human judgement of what truly constitutes hate speech [1].

The repercussions of hateful tweets, limitation of legislation, and ineffectiveness of human annotators have created the necessity to apply machine learning methods for automatic hate speech detection. Classical and deep machine learning methods can be employed to automatically detect hate speech in text documents. The classical machine learning methods mostly use the vector-based representation of handcrafted features, which is time-consuming to craft and is typically incomplete [2]. Moreover, the vector space model often fails to effectively capture the semantic and syntactic representations of text. Deep learning methods generally allow for more accurate prediction through auto-generation of suitable feature representations. Recurrent neural networks (RNN) are deep learning methods that can preserve the sequence information over time. The contextual information can be considered in the task of object classification using deep learning methods [3]. However, deep learning requires a large chunk of data to obtain accurate results. Furthermore, the end-to-end mechanism through which deep learning methods make decisions may not be suitable for text processing in the discipline of natural language processing because of the lack of interpretability. This is particularly pertinent to hate speech detection, where a manual appeal process is needed for a system that censors the speech of a person [4].

Research studies in machine learning have evolved to ensemble learning methods that agglutinate multiple learning methods to improve the performance of a detection system. This allows for harnessing the strengths of multiple learning methods and optimisation of classical machine learning methods in an object classification task. In general, ensemble learning methods can be classified appositely into four main categories of bagging, boosting, stacking, and voting [5]. The predictions from many decision trees are combined in a bagging ensemble learning method. Boosting involves correcting the performances of prior classifiers and adding them sequentially to the ensemble. Since every classifier is obliged to fix the errors in the predecessors, boosting is sensitive to outliers which are considered a disadvantage. Learning how to best combine the predictions from several inducers is achieved through a stacking meta-learning method. Like all meta-model ensemble methods, stacking is simply not feasible in many real-world situations because of a lot of reasons [6]. Predicting a class with the most votes by adding the votes of crisp class labels is called a voting ensemble that works by combining the predictions from multiple classifiers. The majority vote in the task of classification is predicted by

summing the prediction for each label, which makes it suited for complex multiclass problems [7].

Different ensemble machine learning methods have been effectively applied to diverse application domains such as speech emotion recognition [8, 9], product image classification [10], and lung cancer prediction [11]. However, it is more challenging to process highly unstructured text documents with the orthodox machine learning methods that are well developed for numerical data processing. Consequently, a voting ensemble machine learning method that agglutinates logistic regression, support vector machines, and decision trees is proposed in this study for hate speech detection in tweets. Logistic regression has shown positive results on binary text classification because of its ability to be easily tuned to accommodate new data. Support vector machines are widely used for many types of classification problems because of their ability to work in high dimensional spaces to address the overfitting logjam. Decision trees have shown promising results in dealing with highly unstructured data because they do not require data scaling.

In general, tweets are short messages, and their meanings are often rife with idioms, onomatopoeias, homophones, phonemes, and acronyms [12]. Hence, the work reported in this paper agglutinates the strengths of logistic regression, support vector machines, and decision trees in a voting ensemble learning method for hate speech detection in tweets. It is envisaged that support vector machines will bring stability to the voting ensemble because it is not influenced by outliers in a data set. The process of carefully choosing and configuring the parameters for an ensemble learning method is still an open area. The parameter configuration in the proposed voting ensemble learning was carefully fine-tuned for optimal performance. This research study is aimed at enhancing the performance of hate speech detection systems using the method of voting ensemble learning and testing its performance against numerous baseline methods.

This paper is compactly structured as follows. In Section II, the related literature on hate speech detection is briefly reviewed. In Section III, the materials and methods of the study are discussed. In Section IV, the experimental results and discussion are explicated. The concluding statements are delineated in Section V of this paper.

II. RELATED LITERATURE

Hate speech detection is an automated task of determining whether a given piece of text content contains hateful utterances or not. It is a difficult problem in the fields of natural language processing (NLP) and artificial intelligence (AI) for which the classical or deep learning methods experimented. The classical machine learning methods heavily depend on a complex process of feature engineering where features from an input text are rigorously extracted. Deep learning methods eliminate the need for feature engineering by automatically learning features from the input text [7]. There is ongoing research to increase the accuracy of text classification methods owing to the unstructured and complex nature of NLP problems. The review of related literature is planned under the themes of classical learning, deep learning, and ensemble learning as explicated in this section.

A. Classical Learning

The classical machine learning approach uses the established vector-based model such as n-grams and bag of words for text representation, while support vector machine (SVM), decision tree (DT), and logistic regression (LR) are traditionally deployed for text classification. The SVM was originally designed for binary classification tasks [7], but its usage has long been extended to a multiclass classification problem by breaking a given classification problem into several binary sub problems. The binary classification method divides n-dimensional space features into distinct regions that correspond to two specified output classes [13]. Its performance is attributed to the ability to model nonlinear decision boundaries and it is robust against overfitting [14]. DT can achieve a good performance in several classification tasks while producing easily interpretable decisions. The knowledge learned by a DT during the training session is represented in a hierarchical structure that allows for easy comprehension and interpretation by non-experts. LR method uses a probability function or a sigmoid cost function whose output is limited to values between 0 and 1 to make it well suited for binary classification problems. Davidson et al. [15] used a crowd-sourced hate speech lexicon to collect and label tweets containing hate speech. They trained six classical learning methods to distinguish three classes of hate speech as contained in their data set. Their best result was an F1-score of 90.00%.

B. Deep Learning

Deep learning methods learn through a series of interconnected network layers wherein each layer receives input from a prior layer and provides input to a subsequent layer [2]. The raw data in a deep learning text classification task are vectorised to produce the desired input sequence [14]. The size of the input layer is defined by the number of inputs. The additional layers improve the learning capability to obtain a stable output. The output layer provides a result in the form of probabilities of the output classes and has the same number of neurons as the output classes [16]. The long-short term memory (LSTM) can model an ordered sequential input such as textual data [17]. The LSTM was specifically developed to address the vanishing gradient problem faced by the vanilla version of recurrent neural network (RNN) [14] and it has been used in many classification tasks [1, 16, 18, 19]. It has been proven to work well with text data, but it requires a large amount of data for training and validation [17]. Convolution neural network (CNN) uses the pooling technique to minimise the outputs of network layers, but it is prone to high dimensionality in a text processing task. Mutanga et al. [20] explored the use of a transformer method to detect hate speech to obtain the best accuracy of 92.00% and F1-score of 75.00% using DistilBERT.

C. Ensemble Learning

It is promising to harness the strengths of different machine learning methods through the framework of ensemble learning for improving the performance of hate speech detection systems. Popular ensemble learning methods include bagging, boosting, and stacking. Bagging minimises variance by combining the verdicts from different decision trees [21,

22]. It has led to the development of many other decision tree-based ensemble learning methods. The idea behind the bagging ensemble is to create numerous subsets of data from the training sample picked arbitrarily with replacement. Each of the subsets created is used to train its decision trees, resulting in an ensemble of different models. However, the bagging approach does not necessarily lead to improved performance. It can result in performance declination, for example, when a model already has low variance. In addition, empirical evidence has suggested that bagging can push an unstable method towards an optimal performance [23-25]. Conversely, it may lead to a declination in the performance of stable methods. Models are sequentially added to an ensemble in boosting, where each model rectifies the error made by the prior method in the sequence [26, 27]. However, one apparent hiccup of boosting is that it is highly responsive to outliers because each method is required to address errors in the predecessor method. The stacking ensembles are generally used to learn how to best combine predictions from multiple inducers. Stacking ensembles, like all meta-model ensemble learning methods, are not feasible in many real-world applications because they can be expensive to train, deploy and maintain.

There are relatively few studies conducted on hate speech detection using ensemble machine learning methods. In their work, MacAvaney et al. [4] evaluated the efficacy of support vector machines, bidirectional encoder representations from transformers, and an ensemble of neural networks for detecting hate speech. They trained their model on four hate speech data sets to achieve the best F1-score of 91.18% obtained using an ensemble of neural networks on a hate speech tweet data set. Ahluwalia et al. [19] used an ensemble learning method of LR, SVM, random forest (RF), and gradient boosting machine (GBM) to detect English hate speech against women. They trained their model on a data set of binary classes and a data set of multiple classes to achieve the best accuracy of 65.10% for binary classification and an F1-score of 40.60% for multiclass classification. The said works have employed ensemble learning methods for hate speech detection, but it should be noted that none of them has combined logistic regression, decision trees, and support vector machines in an ensemble architecture despite the efficacy shown by the algorithms when used solitarily [4, 15, 19]. The contribution of this paper is the development of a new robust voting ensemble method that harnesses the capabilities of LR, DT, and SVM [14, 15] to address overfitting, accommodate new data, and allow for interpretability of a hate speech detection system.

The review of the related literature has generally indicated that relatively few studies have focused on using ensemble learning for hate speech detection in online spaces. Most of these few studies have reported performance results that require further improvement. The current method based on voting ensemble learning gave the state-of-the-art results of 94.20% accuracy and an F1-score of 94.21% surpassing the results of earlier studies that used the same data set. The results have reflected an improvement over the F1-score of 90.00% reported in [15] and the highest benchmarked accuracy result of 92.00% reported in [20].

III. MATERIALS AND METHODS

The materials and methods used in this study are lucidly presented in this section based on experimental data sets with baseline methods, and essential steps of the proposed voting ensemble method.

A. Experimental Materials

The publicly available data sets of hate speech offensive (HSO) language and Kaggle were used for experimentation in this study. The HSO data set comprised of 11310 tweets that were labelled as 'Hate' or 'Neutral' as made available on the GitHub repository [15]. The Kaggle data set is made up of 8778 neutral tweets and 1155 hate tweets. The data set was grossly imbalanced, and it was important to measure the performance of machine learning methods on a smaller data set. Consequently, the data set was reduced programmatically to 2300 tweets to test the performance of the experimental methods on a smaller data set. The balanced version of the data set consisted of 1150 hate tweets and 1150 neutral tweets that were used for experimentation in this study.

The baseline experimental methods and the proposed voting ensemble method were all implemented using the Python programming language. The Keras library was used to implement the deep learning methods, while the scikit-learn Python library was used to implement the baseline classical and ensemble learning methods. Specifically, `sklearn.tree`, `sklearn.linear_model`, and SVM submodules were used to implement DT, LR, and SVM respectively. All the baseline ensemble learning methods were implemented using the `sklearn.ensemble` submodule. The Keras library was used to implement the CNN and LSTM deep learning methods. Several experiments were faithfully conducted on a computer machine running Windows 10 operating system with configuration of Intel (R) Core (TM) i5-8250U CPU @ 1.60GHz (8 CPUs), 1.8GHz, 8 GB RAM, and 500 Gigabytes of a hard disk drive.

B. Proposed Method

The proposed voting ensemble method comprises the phases of pre-processing, feature representation, and feature classification. The essential steps of the pre-processing include the removal of special characters and punctuations, normalisation of hashtags, lowercasing of the characters of the input text, removal of short words, and text tokenisation. The feature representations were based on the widely used bag of words and word embedding. They were applied after pre-processing to convert the raw tweets data into a useful form amenable to machine learning processing. The bag of words representation converts a text document into a fixed-length vector of occurrence of words in the input text and it was used to implement the classical learning methods. The regularity presented by specific keywords has provided a solid foundation for a bag of words representation to focus on specific words in a data set [28]. Since hate speech is generally expressed through largely homogenous words, it is envisaged that a bag of words representation can effectively capture and represent the vocabulary of known hate words such as black, white, Indian, Jews, foreigners, strangers, enemies, and so on.

Word embedding is a more promising text vocabulary representation that is used by deep learning methods to encode meanings of words into a real value vector such that highly similar words are closer in the vector space. It is a foundation for sentence embedding that presents a huge advantage over the bag of words vector model. It can capture word context, syntactic and semantic relationships with words in a text document. Moreover, it eliminates the sparse representation hiccup often associated with the bag of words representation. The word embedding approach follows the distributional hypothesis, where semantically similar words are found in the same context [2]. The word embedding layer for text classification is usually the first data processing layer of a deep learning model and word embedding methods have been demonstrated to perform well in different NLP tasks [29-31]. In this study, word embedding was implemented using the Keras embedding layer of deep learning because of its ability to capture contextual words and syntactic similarities to enhance the interpretation of tweet meanings.

The basic idea behind the proposed method of this study lies in the selection of an optimal bias-variance trade-off. The presence of high variance can lead to the problem of overfitting, while high bias may result in underfitting. Due to the nature of tweets, variance is likely to occur, particularly in fora that focus on a specific type of hate speech. The Islamophobic for instance may express hate speech in largely similar terms that are difficult to detect using a learning method. The proposed voting ensemble method aggregates the decisions from three classical inducers, which are LR, DT, and SVM to obtain accurate classification decisions. Fig. 1 shows the architecture to illustrate the steps of the proposed voting ensemble learning method.

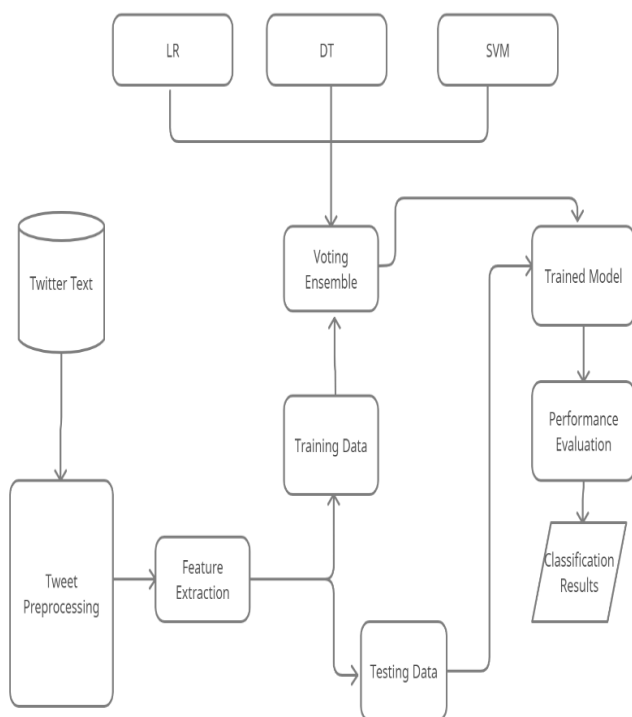


Fig. 1. The Architecture of the Proposed Voting Ensemble Learning Method.

The base inducer of DT is used when the dependent variable is qualitative as in the episode of a text classification task. DT is highly interpretable, fast to train, and works well with decision boundaries [14]. The inclusion of the DT method in the proposed ensemble is based on its appropriateness when dealing with categorical data such as distinguishing hate tweets from innocuous tweets. Earlier studies have investigated the use of DT methods in hate speech detection tasks and recorded satisfactory performance [32]. The important parameters in DT to perform the grid search cross-validation technique are `max_depth` and `random_state`. The `max_depth` parameter determines the depth of a tree. The deeper the tree, the more splits it has, and it captures more information about the data. In our experiments, the `max_depth` value for optimal searching was 10 trees. The depth parameter is also used as a regularisation scheme to prevent overfitting. This step is crucial in our study because tweets are generally regarded as noisy and highly dimensional. The `random_state` parameter that controls the random choices for the training sample was set at 42.

The LR inducer attempts to find a probability-based relationship between the independent variable and class label in each data set. It aims to create a probability function that uses features as inputs and returns the probability of that instance belonging to a given class [33, 34]. The LR does not require scaling of input features and it requires comparatively fewer computation resources [14]. The regularisation parameter (`L2`), and 'squared magnitude' of coefficient as a penalty to the loss function were used for optimisation. The 'fit_intercept' parameter was set to 'True' to incorporate the intercept value to the LR method. The 'Solver' parameter that defines the method to be used in the optimisation problem was set to 'sag' which is compatible with the L2 penalty.

The optimisation of the SVM inducer employed the grid search cross-validation scheme to come up with the best parameters for model fitting. The optimal value for parameter C that defines the tolerance threshold for misclassification was set at 0.1. Moreover, the linear kernel that works on the assumption that input data is linear was applied. Thereafter, the auto deprecated gamma setting, which is the recommended default value was used in conjunction with the linear kernel. The optimal value of the degree parameter was set at 3. The learning rate for the proposed ensemble learner was specified in the Python program before training. The low learning rate specified in Table I was used for preventing the ensemble model from converging to an undesirable optimum [35]. The tolerance setting is a stopping technique that stops the iteration process once the specified value is reached and it affects the training time of a model [36]. The parameters for the inducers and voting ensemble (VE) method are succinctly summarised in Table I.

The results computed by the voting ensemble learning method can be based on either hard or soft voting. The class probability score for each classification method that the current sample belongs to, is considered soft voting [34]. At that point, soft voting criteria determine the class with the highest probability by averaging the individual values of the inducers [37]. Hard voting involves summing the votes for crisp class labels from the other inducers and predicting the class with the

most votes. The class label Y can be decided by the majority voting of each classifier C as in the following example.

$$Y = \text{mode}(c1(x), c2(x), \dots, cm(x)) \quad (1)$$

If the predictions from $c1$, $c2$, and $c3$ are 'hate', 'neutral', and 'hate', respectively, the final prediction will be 'hate' according to the principle of majority voting. Consequently,

$$Y = \text{mode}[\text{hate}, \text{neutral}, \text{hate}] = \text{hate} \quad (2)$$

The hard voting scheme is suited for predicting distinct class labels, while soft voting is appropriate for predicting continuous values. This study was based on tweets labelled under distinct categories. Hence, it implies that hard voting is more desirable for this study as compared to soft voting.

TABLE I. CONFIGURATION SETTINGS FOR THE PROPOSED VOTING ENSEMBLE METHOD

Parameter	DT	LR	SVM	VE
max_depth	10			10
learning_rate				0.4
n_estimators				3
random_state	42		None	
C		0.1	0.1	1.0
cache_size			200	200
degree			3	3
gamma			auto_deprecated	
kernel			linear	linear
max_iterations		100	-1	-1
shrinking			True	True
tolerance (tol)		0.0001	0.001	0.001
penalty		L2		
fit_intercept		True		
solver		sag		

IV. RESULTS AND DISCUSSION

This section presents a discussion of the comparative results of the proposed voting ensemble learning method against ten widely used machine learning methods. The baseline methods are AdaBoost, AdaBoost-DT, Bagging, Bagging-SVM, CNN, DT, LR, LSTM, RF, and SVM. The experimental data sets of Kaggle and HSO were each split into training and testing data in the ratios of 80:20 and 70:30. Although the proposed voting ensemble learning method is comprised of LR, SVM, and DT inducers, each inducer was implemented separately to establish a comparison with the proposed voting ensemble learning method. In addition, other widely used machine learning methods were evaluated against the proposed method. The performances of the learning methods were analysed and discussed in terms of four functional metrics of accuracy, precision, recall, and F1-score. In addition, the performances of the learning methods were evaluated and discussed in terms of non-functional metrics of kappa, hamming loss, Jaccard similarity, and execution time.

A. Accuracy Results

This section presents the analysis of the accuracy of the experimental results of the proposed voting ensemble method along with several baseline methods. The accuracy scores calculated for the two experimental data sets are listed in Table II. It can be observed that accuracy scores computed by the proposed voting ensemble learning method are consistently higher than the scores computed by other learning methods across the two experimental data sets. The proposed ensemble learning method recorded the highest average accuracy score of 94.212% across both data sets, irrespective of the test split. It is worth mentioning that the voting ensemble learning method had the highest accuracy scores across the two data sets under the different train and test splits. Expectedly, all methods performed better with the larger HSO data set as compared to the smaller Kaggle data set, with the proposed voting ensemble learning method giving the highest accuracy score of 96.739% under the bigger data set using the 80:20 train test split. This trend is attributable to the fact that bigger data sets allow methods to learn data patterns more comprehensively during training, thereby impacting overall performance, particularly in the case of deep learning methods, which generally require large data sets to perform well.

TABLE II. ACCURACY SCORES OF LEARNING METHODS USING DIFFERENT TRAIN-TEST SPLITS

Data set	Kaggle		HSO		Average
	80:20	70:30	80:20	70:30	
Train: test split	80:20	70:30	80:20	70:30	Average
AdaBoost	87.887	87.883	91.304	90.870	89.486
AdaBoost-DT	90.539	90.448	93.043	89.855	90.972
Bagging	90.318	90.566	92.174	89.275	90.583
Bagging-SVM	91.468	90.654	95.217	94.493	92.958
CNN	88.240	88.031	95.000	94.493	91.441
Decision Tree	90.097	90.301	91.739	89.275	90.353
Logistic Regression	91.689	91.509	95.435	94.493	93.281
LSTM	91.202	90.890	95.435	94.638	93.041
Random Forest	89.434	90.065	93.478	93.478	91.614
Support Vector Machine	89.788	88.709	92.391	92.464	90.838
Voting Ensemble	92.042	91.834	96.739	96.232	94.212

Fig. 2 shows the plot of average accuracy scores computed by the learning methods across the experimental data sets to visually illustrate the extent to which one learning method gives better accuracy than another. This result implies that the voting ensemble method can detect all the correct cases better than any other method, while AdaBoost performed worst in this case. The voting ensemble method is therefore the most useful when all classes are equally important while AdaBoost is not useful in this scenario.

B. Precision Results

This section presents the precision scores computed by the proposed voting ensemble learning method against the baseline learning methods explored in this study. It can be observed in Table III that the voting ensemble learning method

outperformed other learning methods across the two experimental data sets. The proposed voting ensemble learning method recorded the highest average precision score of 93.779%. The LSTM performed relatively well, scoring the second-highest precision score of 93.457%. The exceptional performance of the LSTM may be linked to its ability to capture long-term dependencies. This property makes it suitable for text classification tasks such as hate speech detection, where the semantics of a tweet can be derived from the arrangement of words in the tweeted document.

The least average precision score of 89.743% was recorded by the AdaBoost method with the default parameter setting. The combination of AdaBoost with another classifier in ensemble learning improves the system performance. The AdaBoost method with DT as base learner outperformed the default AdaBoost because it gave an average precision of 91.006%, which is higher than 89.743% recorded by the default AdaBoost method. Most methods performed better with the 80:20 train test split as compared to the 70:30 split. However, only RF and DT performed better with a 70:30 split. The precision computed by DT and RF fell when the training data set was increased by 10% on the larger HSO data set. The drop-in performance may be the result of overfitting because both DT and RF are susceptible to overfitting [17]. Table III shows the precision scores of all the learning methods experimentally compared in this study.

Fig. 3 shows the plot of the average precision scores computed by the learning methods across the experimental data sets to visually illustrate the extent to which one method gives better precision than another. This result implies that the voting ensemble method can correctly detect hate speeches from the predicted class of hate speeches better than any other method, while AdaBoost performed worst in this case. The voting ensemble method is therefore the most useful when the cost of false positives is high while AdaBoost is not useful in this scenario.

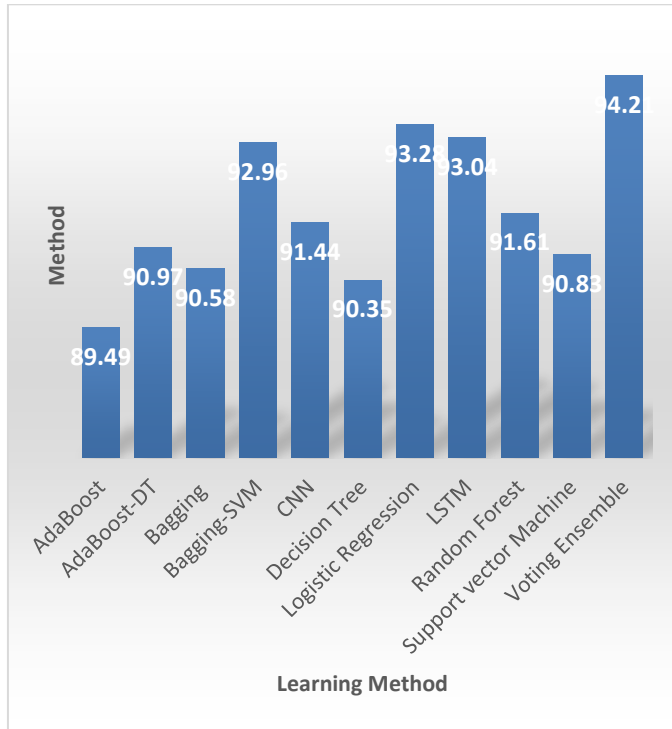


Fig. 2. The Average Accuracy of Learning Methods.

TABLE III. PRECISION SCORES OF LEARNING METHODS USING DIFFERENT TRAIN-TEST SPLITS

Data set	Kaggle		HSO		Average
	80:20	70:30:00	80:20	70:30	
AdaBoost	88.093	88.011	91.686	91.182	89.743
AdaBoost-DT	90.523	90.436	93.096	89.970	91.006
Bagging	90.306	90.562	92.495	89.550	90.728
Bagging-SVM	91.519	90.723	95.248	94.489	92.995
CNN	88.495	88.315	95.042	94.674	91.631
Decision Tree	90.083	90.288	91.790	89.342	90.376
Logistic Regression	91.680	91.508	95.539	94.538	93.316
LSTM	91.207	90.919	95.477	96.224	93.457
Random Forest	89.418	90.053	93.508	93.478	91.614
Support Vector Machine	89.804	88.702	92.488	92.475	90.868
Voting Ensemble	92.030	91.830	96.747	94.507	93.779

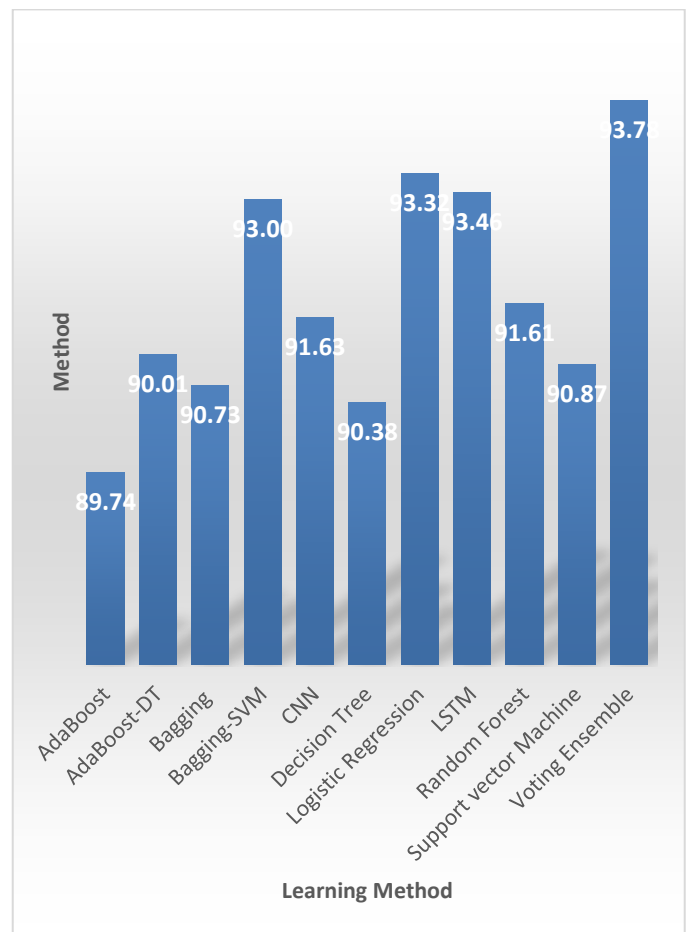


Fig. 3. The Precision of Learning Methods.

C. Recall Results

This section presents an evaluation of the learning methods investigated in this study based on the recall metric. Results from Table IV show that the proposed voting ensemble learning method gave an average recall value of 94.210%, which is superior to that of baseline learning methods used in this study. In addition, it can be noted that default meta classifiers of Bagging and AdaBoost were outperformed by their ensemble variants, which used different learning methods as base learners. The recall score for the default AdaBoost is 89.408%, while the recall score for the AdaBoost-DT is 90.959%. In addition, the recall score for the bagging method is 90.552%, while bagging-SVM had a recall score of 92.937%. It is obvious from these results that combining meta classifiers with different learning methods can lead to improved performance as shown in Table IV.

TABLE IV. RECALL SCORES OF LEARNING METHODS USING DIFFERENT TRAIN-TEST SPLITS

Data set	Kaggle		HSO		Average
	80:20	70:30	80:20	70:30	
AdaBoost	87.767	87.801	91.304	90.761	89.408
AdaBoost-DT	90.549	90.457	93.043	89.788	90.959
Bagging	90.312	90.553	92.174	89.170	90.552
Bagging-SVM	91.414	90.599	95.217	94.519	92.937
CNN	88.384	88.160	95.000	94.534	91.520
Decision Tree	90.119	90.310	91.739	89.223	90.348
Logistic Regression	91.680	91.496	95.435	94.550	93.290
LSTM	91.177	90.854	95.435	94.691	93.039
Random Forest	89.447	90.068	93.478	93.508	91.625
Support Vector Machine	89.749	88.695	92.391	92.444	90.820
Voting Ensemble	92.040	91.823	96.739	96.237	94.210

Fig. 4 shows the plot of average recall scores computed by the learning methods across the experimental data sets to visually illustrate the extent to which one learning method gives a better recall than another. This result implies that the voting ensemble method can correctly detect cases of hate speeches from all the actual classes of hate speeches better than any other learning method, while AdaBoost performed worst in this case. The voting ensemble method is therefore the most useful when the cost of false negatives is high while AdaBoost is not useful in this scenario.

D. F1-score Results

This section presents the results of the overall F1-score for the learning methods explored in this study. Table V shows that the proposed voting ensemble method consistently outperformed the baseline learning methods investigated by recording the highest average F1-score of 94.208%. The solitary bagging ensemble learning method recorded an average F1-score of 90.564%, while the bagging-SVM ensemble method recorded an average F1-score of 92.948%. Furthermore, the mean score of 89.897% of the average F1-scores for both AdaBoost and Decision tree learning methods is inferior to the average F1-score of 90.692% for AdaBoost-

DT ensemble learning method. The analysis of the F1-score for LSTM and CNN deep learning methods has shown that LSTM consistently outperforms CNN. It can be perceived in Table V that LSTM recorded an average F1-score of 93.035%, while CNN recorded an average F1-score of 91.439%. This difference in performance may come from the capability of LSTM to capture long-term dependencies that are necessary when extracting word meanings in a text. The superior performance of the ensemble learning methods as compared to any solitary methods, including deep learning has illustrated that agglutinating multiple learning methods through ensemble learning is highly promising for reducing the error rate of the final learner in a hate speech detection system.

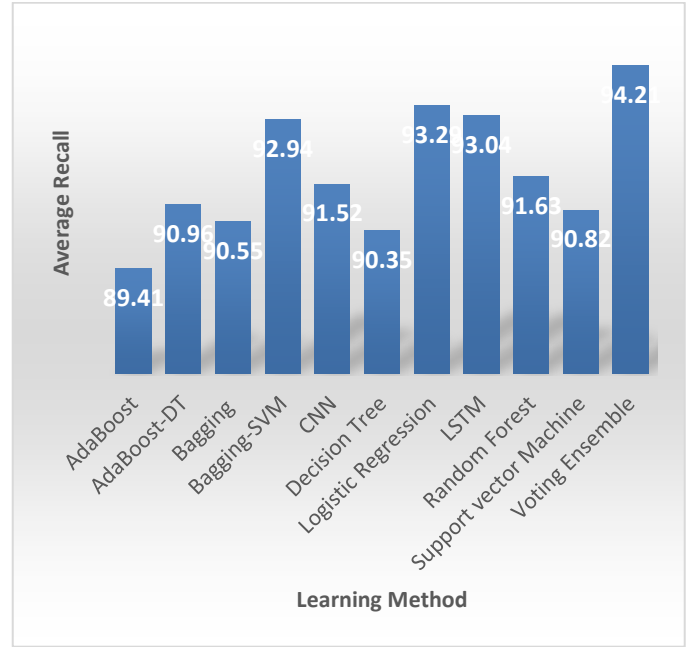


Fig. 4. The Average Recall of Learning Methods.

TABLE V. F-MEASURE SCORES OF LEARNING METHODS USING DIFFERENT TRAIN-TEST SPLITS

Data Set	Kaggle		HSO		Average
	80:20	70:30	80:20	70:30	
AdaBoost	87.835	87.848	91.284	90.831	89.449
AdaBoost-DT	90.533	90.443	93.041	89.830	90.962
Bagging	90.309	90.557	92.159	89.232	90.564
Bagging-SVM	91.449	90.635	95.217	94.492	92.948
CNN	88.238	88.026	94.999	94.492	91.439
Decision Tree	90.092	90.296	91.737	89.255	90.345
Logistic Regression	91.680	91.501	95.432	94.493	93.277
LSTM	91.190	90.877	95.434	94.638	93.035
Random Forest	89.427	90.059	93.477	93.477	91.610
Support Vector Machine	89.771	88.699	92.387	92.456	90.828
Voting Ensemble	92.035	91.826	96.739	96.230	94.208

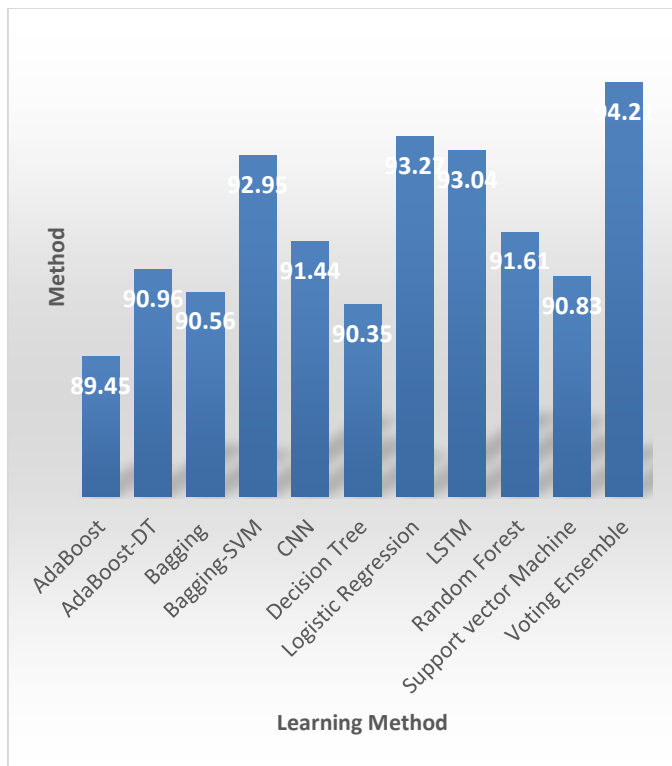


Fig. 5. The Average F-Measure Score of Learning Methods.

Fig. 5 shows the plot of average F1-scores computed by the learning methods across the experimental data sets to visually illustrate the extent to which one method gives a better F1-score than another. This result implies that the proposed voting ensemble method can better detect incorrectly classified cases better than any other learning method, while AdaBoost performed worst in this case. The voting ensemble is therefore the most useful when the classes are imbalanced while AdaBoost is not useful in this scenario.

Results from the functional metrics used in this study indicate that the voting ensemble outperformed the benchmark algorithms used in the study. It is worth noting that the individual performance of the meta classifiers was inferior to that of the proposed voting ensemble model. This superior performance of the proposed model may be attributed to the minimal overfitting, model extensibility, and interpretability features from each of the base learners [14, 15]. These results confirm the literature position that ensemble learning outperformed individual classifier algorithms in hate speech detection [38, 39].

E. Non-functional Results

This section presents the evaluation of all the learning methods investigated using the non-functional metrics of Hamming loss, Jaccard, Kappa, and execution time. The proposed voting ensemble method recorded the best Hamming loss, Jaccard, and Kappa scores as shown in Table VI. This result shows that the proposed ensemble learning method can maximise predictive capability while concomitantly minimising misclassification errors better than any of the baseline learning methods investigated. However, the proposed voting ensemble learning method recorded the second-highest

training time of 0.095 hours, which is a tradeoff decision to consider between efficiency versus accuracy. The long execution time taken by the proposed ensemble method was because each inducer was trained separately, and the final aggregated decision was achieved through the principle of majority voting.

It can be observed from Table VI that SVM recorded the lowest Kappa score indicating a low level of inter-annotator agreement. This may be the result of minimal parameter tuning applied to the SVM method. The learning method recorded the worst Hamming loss of 10% to suggest a poor selection of parameters for the method. It is interesting to observe that ensemble learning methods such as bagging-SVM and voting ensemble took more time to train than the deep learning methods. This implies that although they perform better, ensemble learning methods are computationally expensive. However, the benefits of an improved performance can outweigh the need for increased resources in critical applications like hate speech detection.

TABLE VI. NON-FUNCTIONAL PERFORMANCE OF LEARNING METHODS

Method	Hamming loss	Jaccard	Kappa	Execution Time
AdaBoost	8.696	91.304	82.609	0.013
AdaBoost-DT	7.174	92.826	85.652	0.010
Bagging	6.739	93.261	86.522	0.064
Bagging-SVM	4.565	95.435	90.870	0.353
CNN	5.000	95.000	90.000	0.001
Decision Tree	6.087	93.913	87.826	0.009
Logistic Regression	4.565	95.435	90.870	0.003
LSTM	4.565	95.435	90.870	0.082
Random Forest	6.522	93.478	86.957	0.076
Support Vector Machine	10.000	90.000	80.000	0.011
Voting Ensemble	3.261	96.739	93.478	0.095

V. CONCLUSION

The primary contribution of this study is the construction and validation of a voting ensemble learning method to improve the automatic detection of hate speech in tweets. This is challenging open research because of the anaphoric, synonymy, and polysemy nature of the slang of tweets that make the interpretation of hate speech ambiguous, difficult, and controversial. The voting ensemble learning method has been demonstrated in this study to yield the best performance when compared to other learning methods.

However, one apparent curb of this study is the bag of words representation of features that suffers from the anaphoric, synonymy, and polysemy nature of words. In addition, a bag of words representation presents the inability to capture important information about interdependencies that exist among words. Moreover, word embedding representation can fall short in making machines draw adequate inferences from certain classes of sentences.

In the future, a knowledge-based method with sentence embedding will be introduced for tweet hate speech detection and compared the results against those of the existing word embedding learning methods. This envisioned novel method will circumvent the intrinsic curbs of the bag of words and word embedding representations. It will significantly increase the confidence level of social media prosecutors to genuinely regulate whether a given tweet is of hate speech or not.

REFERENCES

- [1] K. Pitsilis, H. Ramampiaro, and H. Langseth, "Effective hate-speech detection in Twitter data using recurrent neural networks," *Applied Intelligence*, vol. 48, no. 12, pp. 4730-4742, 2018.
- [2] T. Young, D. Hazarika, S. Poria, and E. Cambria, "Recent trends in deep learning based natural language processing," *IEEE Computational Intelligence Magazine*, vol. 13, no. 3, pp. 55-75, 2018.
- [3] S. Sohangir, D. Wang, A. Pomeranets, and T. M. Khoshgoftaar, "Big data: Deep learning for financial sentiment analysis," *Journal of Big Data*, vol. 5, no. 1, p. 3, 2018.
- [4] S. MacAvaney, H.-R. Yao, E. Yang, K. Russell, N. Goharian, and O. Frieder, "Hate speech detection: Challenges and solutions," *PLoS one*, vol. 14, no. 8, 2019.
- [5] R. Polikar, "Ensemble learning," in *Ensemble Machine Learning*: Springer, pp. 1-34, 2012.
- [6] M. Graczyk, T. Lasota, B. Trawiński, and K. Trawiński, "Comparison of bagging, boosting and stacking ensembles applied to real estate appraisal," in *Asian Conference on Intelligent Information and Database Systems*, Springer, pp. 340-350, 2010.
- [7] U. Abubakar, S. A. Bashir, M. B. Abdullahi, and O. S. Adebayo, "Comparative study of various machine learning algorithms for tweet classification," *i-manager's Journal on Computer Science*, vol. 6, no. 4, p. 12, 2019.
- [8] K. Zvarevashe and O. O. Olugbara, "Recognition of cross-language acoustic emotional valence using stacked ensemble learning," *Algorithms*, vol. 13, no. 10, p. 246, 2020.
- [9] K. Zvarevashe and O. Olugbara, "Ensemble learning of hybrid acoustic features for speech emotion recognition," *Algorithms*, vol. 13, no. 3, p. 70, 2020.
- [10] S. Oyewole and O. Olugbara, "Product image classification using Eigen Colour feature with ensemble machine learning," *Egyptian Informatics Journal*, vol. 19, no. 2, pp. 83-100, 2018.
- [11] E. Adetiba and O. O. Olugbara, "Lung cancer prediction using neural network ensemble with histogram of oriented gradient genomic features," *The Scientific World Journal*, vol. 2, 2015.
- [12] A. Modupe, O. O. Olugbara, and S. O. Ojo, "Filtering of mobile short messaging service communication using latent Dirichlet allocation with social network analysis," in *Transactions on Engineering Technologies*: Springer, pp. 671-686, 2014.
- [13] C. J. Burges, "A tutorial on support vector machines for pattern recognition," *Data Mining and Knowledge Discovery*, vol. 2, no. 2, pp. 121-167, 1998.
- [14] K. Kowsari, K. J. Meimandi, M. Heidarysafa, S. Mendu, L. Barnes, and D. Brown, "Text classification algorithms: A survey," *Information*, vol. 10, no. 4, p. 150, 2019.
- [15] T. Davidson, D. Warmsley, M. Macy, and I. Weber, "Automated hate speech detection and the problem of offensive language," in *Eleventh International AAAI Conference on Web and Social Media*, 2017.
- [16] L. Gao and R. Huang, "Detecting online hate speech using context aware models," *arXiv preprint arXiv:1710.07395*, 2017.
- [17] Q. Liu, F. Zhou, R. Hang, and X. Yuan, "Bidirectional-convolutional LSTM based spectral-spatial feature learning for hyperspectral image classification," *Remote Sensing*, vol. 9, no. 12, p. 1330, 2017.
- [18] I. Kwok and Y. Wang, "Locate the hate: Detecting tweets against blacks," in *Twenty-Seventh AAAI Conference on Artificial Intelligence*, 2013.
- [19] R. Ahluwalia, H. Soni, E. Callow, A. Nascimento, and M. De Cock, "Detecting hate speech against women in English tweets," *EVALITA Evaluation of NLP and Speech Tools for Italian*, vol. 12, pp. 194-199, 2018.
- [20] R. T. Mutanga, N. Naicker, and O. O. Olugbara, "Hate speech detection using transformer methods," *International Journal of Advanced Computer Science and Applications*, vol. 11, no. 9, 2020.
- [21] I. Siloko and C. Ishiekwe, "Boosting and bagging in kernel density estimation," *The Nigerian Journal of Science and Environment*, vol. 14, no. 1, pp. 32-37, 2016.
- [22] A. Kadiyala and A. Kumar, "Applications of python to evaluate the performance of bagging methods," *Environmental Progress & Sustainable Energy*, vol. 37, no. 5, pp. 1555-1559, 2018.
- [23] F. Li, J. Fan, L. Wang, H. Zhang, and R. Duan, "A method based on manifold learning and Bagging for text classification," in *2011 2nd International Conference on Artificial Intelligence, Management Science and Electronic Commerce (AIMSEC)*, 2011.
- [24] L. Xinqin, S. Tianyun, L. Ping, and Z. Wen, "Application of bagging ensemble classifier based on genetic algorithm in the text classification of railway fault hazards," in *2019 2nd International Conference on Artificial Intelligence and Big Data (ICAIBD)*, 2019: IEEE, pp. 286-290.
- [25] H. ALSaif and T. Alotaibi, "Arabic text classification using feature-reduction techniques for detecting violence on social media," *Work*, vol. 10, no. 4, 2019.
- [26] J. Prusa, T. M. Khoshgoftaar, and D. J. Dittman, "Using ensemble learners to improve classifier performance on tweet sentiment data," in *2015 IEEE International Conference on Information Reuse and Integration*, 2015.
- [27] D.-S. Cao, Q.-S. Xu, Y.-Z. Liang, L.-X. Zhang, and H.-D. Li, "The boosting: A new idea of building models," *Chemometrics and Intelligent Laboratory Systems*, vol. 100, no. 1, pp. 1-11, 2010.
- [28] K. Wang, Y. Wang, Q. Zhao, D. Meng, X. Liao, and Z. Xu, "SPLBoost: An improved robust boosting algorithm based on self-paced learning," *IEEE Transactions on Cybernetics*, 2019.
- [29] E. Cambria, S. Poria, A. Gelbukh, and M. Thelwall, "Sentiment analysis is a big suitcase," *IEEE Intelligent Systems*, vol. 32, no. 6, pp. 74-80, 2017.
- [30] R. Socher, C. C. Lin, C. Manning, and A. Y. Ng, "Parsing natural scenes and natural language with recursive neural networks," in *Proceedings of the 28th International Conference on Machine Learning (ICML-11)*, pp. 129-136, 2011.
- [31] P. D. Turney and P. Pantel, "From frequency to meaning: Vector space models of semantics," *Journal of Artificial Intelligence research*, vol. 37, pp. 141-188, 2010.
- [32] P. Fortuna and S. Nunes, "A survey on automatic detection of hate speech in text," *ACM Computing Surveys (CSUR)*, vol. 51, no. 4, pp. 1-30, 2018.
- [33] R.-E. Fan, K.-W. Chang, C.-J. Hsieh, X.-R. Wang, and C.-J. Lin, "LIBLINEAR: A library for large linear classification," *Journal of Machine Learning Research*, vol. 9, no. Aug, pp. 1871-1874, 2008.
- [34] A. Genkin, D. D. Lewis, and D. Madigan, "Large-scale Bayesian logistic regression for text categorization," *Technometrics*, vol. 49, no. 3, pp. 291-304, 2007.
- [35] A. Vaswani et al., "Attention is all you need," in *Advances in Neural Information Processing Systems*, 2017, pp. 5998-6008.
- [36] S. Liu, "A survey on fault-tolerance in distributed optimization and machine learning," *arXiv preprint arXiv:2106.08545*, 2021.
- [37] D. Agnihotri, K. Verma, P. Tripathi, and B. K. Singh, "Soft voting technique to improve the performance of global filter based feature selection in text corpus," *Applied Intelligence*, vol. 49, no. 4, pp. 1597-1619, 2019.
- [38] S. A. Kokatnoor and B. Krishnan, "Twitter hate speech detection using stacked weighted ensemble (SWE) model," in *2020 Fifth International Conference on Research in Computational Intelligence and Communication Networks (ICRCICN)*, 2020.
- [39] M. K. A. Aljero and N. Dimililer, "A novel stacked ensemble for hate speech recognition," *Applied Sciences*, vol. 11, no. 24, p. 11684, 2021.

Methodology for Infrastructure Site Monitoring using Unmanned Aerial Vehicles (UAVs)

Cristian Benjamín García Casierra¹, Carlos Gustavo Calle Sánchez²
Javier Ferney Castillo García³, Felipe Muñoz La Rivera⁴

Faculty of Engineering, Electronics Engineering Program, Universidad Santiago de Cali, Cali, Colombia^{1, 2, 3}
School of Civil Engineering, Pontificia Universidad Católica de Valparaíso, Valparaíso, Chile⁴
School of Civil Engineering, Universitat Politècnica de Catalunya, Barcelona, Spain⁴

Abstract—Monitoring a work of infrastructure allows one to know the state of this and the efficiency of the workers. The follow-up is a work carried out by the auditor, which sails to correspond with the design in planes. It takes fulfillment in the budgeted one and complies with the established times. This work uses classical topography elements, which demand time and money and the implications on the safety issue of non-construction personnel. To avoid this, this project implements a methodology capable of carrying out the task of monitoring civil work. An unmanned aerial vehicle or drone is used, which are small remotely controlled flying devices that in recent years have become an extremely useful tool in activities that human beings cannot perform or that threaten their integrity. For the realization of this work, a drone Quadcopter Phantom 3 Standard is used, responsible for taking photographs; these are loaded in the software Agisoft Metashape Professional that by photogrammetry techniques allows digital processing of images, generating a 3D vision, cloud of dots, digital surface model and distance measurement. By obtaining this information, it is possible to make a match with the work schedule and detect delays or advances in a precise way.

Keywords—Topography; unmanned aerial vehicle; infrastructure work monitoring; digital image processing component; construction site

I. INTRODUCTION

The construction industry is relevant to the development of countries. This industry is related to the development levels of each government and is an important source of jobs. Despite its relevance, the sector is characterized by low productivity levels. Construction projects often exceed planned costs and times [1]. This situation is associated with a series of factors specific to the working conditions, such as the worksite, the multiple teams, the fragmentation of the sector, and the low industrialization and digitalization of its processes [2]. Thus, project management and incorporating new technologies are key to improving these indicators. Construction 4.0 is a new paradigm that promotes the sector's digitalization, automation, and industrialization. Thus, working with digital models of projects, tools for capturing the territory, and sensorization are key aspects [3].

Monitoring the progress of a project is key to its effective control. The constant review of the project's progress according to the planning and the supervision of the quality and scope are aspects of interest for project managers [4]. This activity is regularly performed based on the observation of the project

managers, supported by traditional surveying tools. In the surveys of infrastructure works with classic topographic elements and visual inspections, the personnel must be inside the worksite to collect data. This displacement takes time and presents discontinuity since there are areas of impossible or difficult access, exposing possible accidents [5].

Site surveys have benefited from technological advances, currently using instruments for measuring different terrain variables, 3D scanners, and technology that uses GNSS systems are some examples. Unmanned aerial vehicles (UAVs) are presented as an efficient alternative for job site surveillance and inspection within these new technologies [6]. They have been used for military, agricultural, and urban management purposes. The use of drones for construction site surveys offers a series of benefits that reduce the risks and problems of traditional methods. It is possible to obtain continuous, accurate, real, and fast data of the entire surface under construction without accidents [7], [8].

While there are existing works that use drones for job site monitoring, it is necessary to advance in the establishment of methods and workflows to systematize these applications and increase the number of success stories to demonstrate the benefits [9]. To meet these objectives, the methodology presented in this research is a tool aimed at efficiently and accurately streamlining the work of construction site monitoring. It reduces the presence of experts within the construction, reducing the time in data collection and the risks of a possible accident. In addition, it provides digital elevation models for a complete analysis, using as base instruments a Phantom 3 standard drone and Agisoft Metashape Professional software. The information must be collected to recognize the differences between surveys with classic elements and surveys using drones for its creation. Based on this, a detailed methodology is designed, which has the final objective to compare the data collected and the data provided by the intervenor in an estimated time of 7 months.

This article is organized as follows: Section I is the introduction, describing the research problem, Section II presents the background and a contextual framework for a better understanding of the topic addressed. Section III contains the research methodology developed in this work. Section IV describes the proposed solution. Section V presents the results and analysis, and finally our conclusions in

Section VI are shown. Translated with www.DeepL.com/Translator (free version).

II. BACKGROUND

Topographic surveys can contribute greatly to identifying previously unseen surface features and can be used to produce three-dimensional computer models of the surveyed area, which can be manipulated in a variety of ways. *Surveying* is the science that studies the set of procedures for determining the positions of points on the earth's surface using measurements according to the three elements of space. These elements can be two distances and an elevation, or a distance, a direction, and an elevation [10]. This plan is essential for the correct location of any work to be carried out and for the elaboration of any technical project. To know the position of points in the area of interest is necessary to determine their location using three coordinates: latitude, longitude, and elevation [11]. We will analyze two site surveys for this methodology: surveys with classic elements and surveys using a drone.

A. Inspection of the Construction Site with Classical Methods

To carry out the site inspection, it is very necessary and indispensable to have a topographic map of the site of the work project, to make a respective marking of points on the ground, in order to make measurements for the calculation of soil movements, to have a record of measurements to check the situation of sections of work already done and to determine the volumes of soil moved (excavated and transported) and of course to have at hand the chronogram of the work.

Topographic maps or charts are the results of a cartographic projection, which are mathematical transformations that allow representing (project) the sphere on the plane, and converting the geographic coordinates (latitude and longitude) into Cartesian coordinates (X and Y). This process entails distortions of the original three-dimensional surface, which is converted to a flat two-dimensional surface [12].

B. Drone Inspection

To perform surveys with drones, a technique (or collection of techniques) called photogrammetry is used to determine objects' geometric and spatial properties in a given area from aerial images. The main objective is to convert two-dimensional data into cartographic information. To obtain a faithful reconstruction of the data, the objects in the reconstruction area must appear in a sufficient number of images [13]. This information is the one that allows extracting its structure. To obtain this extra information, an overlap is made between consecutive images. The UAV pilot must plan the route or mission so that in each image, there is an element that also appears in the previous, following images [14].

The flight of a remotely piloted aircraft (Drone) is performed at an altitude that must be calculated taking into account the desired scale and the focal distance of the camera, but also must take into account the parameter of "correlation," which indicates that a certain territory must be covered with images. Each photo must have an area in common with the photograph taken previously. To comply with this, the RPAS must have an absolute flight altitude and a constant speed to

perform shots with regular intervals that correspond to equal paths and thus ensure a percentage of correlation between the succession of images. To obtain excellent results, it is necessary to ensure that the longitudinal overlap is greater than 80% and the transverse overlap is greater than 60% [8].

Some elements are relevant to understand for the correct use of drones. Focal length is the basic description of a photographic lens. It is not a measure of the actual distance of a lens but "is a calculation of the optical distance from the point where the rays converge to form a sharp image of an object for the digital sensor of the camera's focal plane". On the other hand, the pixel is the smallest unit of the pictorial elements that constitute a digital image, projecting the color spectrum. Color pixels are generally believed to have red, green, and blue components. A digital image is obtained from a matrix of pixels distributed in rows and columns. As a result, the sum of all the pixels distributed in the rows and columns is its size in pixels. The greater the number of pixels in an image, the higher its resolution. In addition, the ground sampling distance (GSD) is the distance between two consecutive pixel centers measured on the ground. The higher the value of the image GSD, the lower the spatial resolution of the image and the less visible details [15].

The GSD is related to the flight altitude: the higher the flight altitude, the higher the GSD value. Even when flying at a constant altitude, images from one project may not have the same GSD. This is due to differences in terrain elevation and changes in camera angle while shooting. Since the orthomosaic is created using the 3D point cloud and camera positions, an average GSD will be calculated and used. Finally, in photogrammetry and Drone flights, the scale is a parameter of great importance, this is data that in many of the cases is known before the flight is performed, but it can also be known after the flight has been performed. It is required to find the appropriate height at which the Drone should take the photographs when the scale at which the work is required is known, in case if the height is known. However, not the scale [16]. We must find it using a calculation between the focal distance and the flight height (later on, we will detail how to calculate the flight heights) [17], [18].

C. Digital Image Processing

Digital image processing can extract useful information from images and build digital models. The decreasing costs of computer equipment, the increasing amount of image digitizing equipment available on the market, and new technologies that tend to promise great advances in image processing are factors that combine to indicate the future trend of digital image processing. Image processing aims to improve the appearance of images and make certain details more evident in them that are desired to be noticed [19]. The image may have been generated in many ways, such as photographically, electronically, or through television monitors. The processing of the images can, in general, be done by optical methods or by digital methods on a computer [20].

Photogrammetry is the process of generating a 3D model from 2D images; the resulting model can be scaled and used to measure distances between objects. Since archaeologists have used the early 1980s terrestrial photogrammetry, the high cost

of hardware and processing equipment meant that it was not a viable technique for most projects. In the 2000s, with the advent of low-cost digital cameras and improved computer processing, photogrammetry became a more viable option for small-scale site analysis and assessment. With the rapid development of drones in recent years, architects and archaeologists have benefited greatly, as photogrammetry has become easier [21], [22].

III. RESEARCH METHODOLOGY

To develop this research, Design Science Research Method (DSRM) is used as a basis. Thus, the research methodology contains five stages: 1) identification of problems and motivations; 2) definition of objectives and potential solution; 3) design and development; 4) demonstration; and 5) evaluation. Fig. 1 shows the activities and tools for each stage.

In the first stage, a literature review was conducted to identify construction site inspection issues, along with the advantages of using drones and technical specifications for their use. Web of Science and Scopus databases were used. With this, in the second stage, the research team defined the objective of a potential solution: the use of drones and photogrammetry can improve construction site inspection processes. Thus, in the third stage, a workflow was proposed. It contains the stages, characteristics, technical elements, and processes to perform the inspections. A series of recommendations are given so that the method can be replicated. With this, the fourth stage demonstrates the method's usefulness in a case study. Finally, in the fifth stage, the results are analyzed, and the effectiveness of the proposed method compared to the traditional method is discussed first.

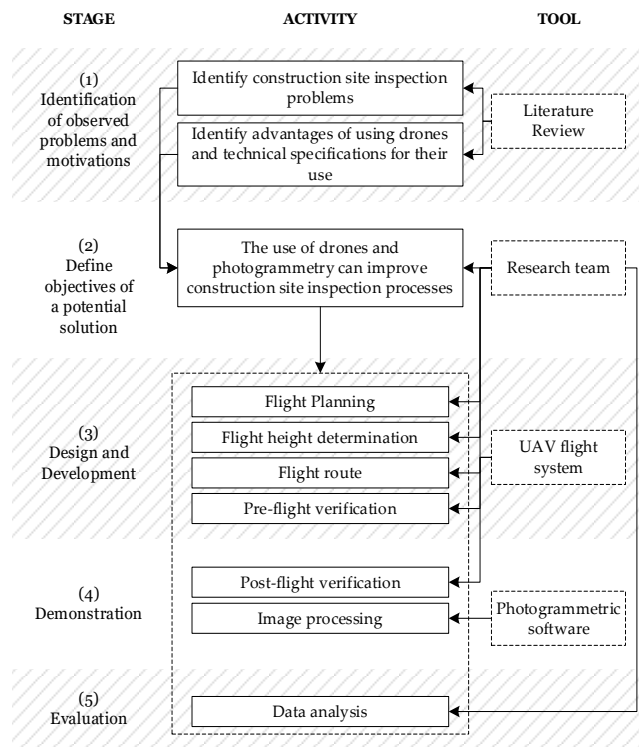


Fig. 1. Research Methodology.

TABLE I. APPLICATIONS OF UAV IN CONSTRUCTION

Applications	Methodology processing	Methodology Aircraft	References
monitoring construction progress	Change detection using point clouds	No defined	Huang et al.2022 [23]
Comparison modeling software	3D reconstruction modeling techniques	No defined	Keyvanfar et al, 2022 [24]
Monitoring road base	3D reconstruction modeling techniques	No defined	Lo et al, 2022 [25]
construction progress monitoring and inspection	3D reconstruction modeling techniques	No defined	Amir et al, 2022 [26]
Dynamic site layout planning	3D reconstruction modeling techniques	No defined	Ahmed et al 2021 [27]
Impact on workers' health and safety	No defined	Define safety operation, and describe potential risks	Jeelani & Gheisari [28]
safety inspections in construction	Image capture	For manual flight using check list pre and post flight	Oliveira et al., 2021 [29]
Monitoring the work cycles of earthmoving excavators	Video	No defined	Yiguang et al, 2021 [30]
monitoring work in a construction project	3D reconstruction modeling techniques	No defined	Kaamin et al, [31]

Table I indicates some applications of UAV technology utilized by civil engineering in the construction process. As shown in the table, since only two studies define the methodology for aircraft and the other studies realize 3d reconstruction modeling techniques for several applications.

IV. PROPOSED METHODOLOGY

In order to achieve the research goals, a methodology is proposed. Fig. 2 shows the proposed workflow. It considers seven stages: A) Flight Planning, B) Flight height determination, C) Flight route, D) Pre-flight verification, E) Post-flight verification, F) Image processing, and G) Data analysis.

A. Flight Planning

It is important to know the place where the flight will take place. The orography, branch of the study of the physical geography that is in charge of studying and describing the relief of a region in particular, forces to value the opportunities and risks. Depending on this, the way of carrying out the work will be defined. To do so, we will start working with a small-

scale cartographic map and a real survey of the terrain. It is necessary to determine whether it is legal to fly in the chosen area (whether or not it is controlled airspace, restricted airspace, photographic flight prohibition, etc.).

Then, a take-off and landing point is defined, this must be a relatively flat place, far from the frequent passage of people and without obstacles around it, since, in case of any failure, an RTH manoeuvre (Return to the point of origin) must be

executed, and it is likely that the landing of the aircraft will not be in the precise point.

B. Flight Height Determination

The main natural and artificial obstacles found on the route to and from the site are explored in this stage. It is important to know the heights of these obstacles since the drone may not have sensors to avoid collisions.

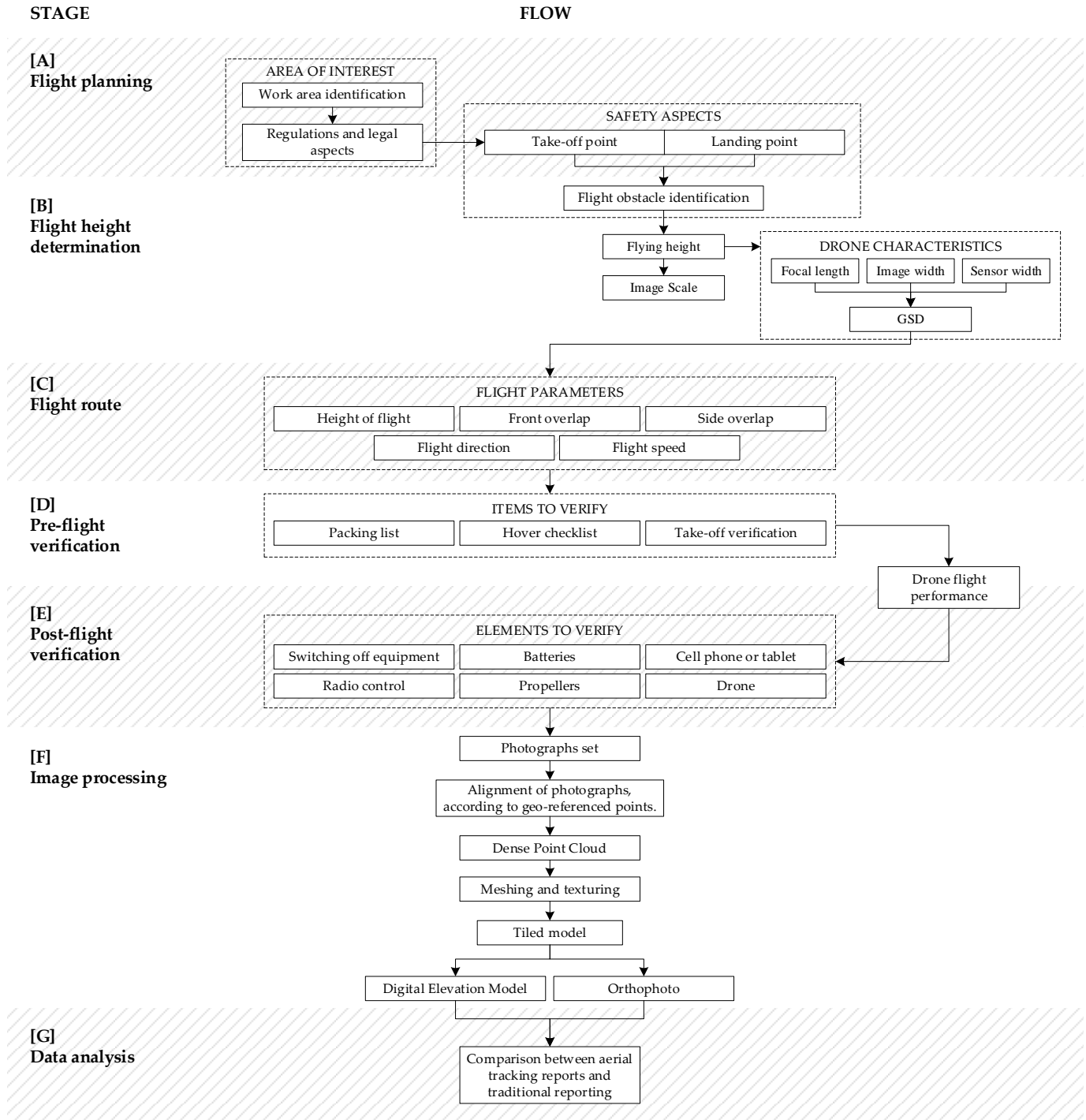


Fig. 2. Proposed Workflow.

The structure with the highest height is the construction site crane, 35 meters high for the case study. Therefore, a safe flight height of $H=75$ meters is defined. It is possible to determine the flight height to respond to a given scale. Equation (1) allows us to choose the average flight height, where Zm is the mean flight height, f is the focal length, and Em is the Image scale.

$$Zm = f \times Em \quad (1)$$

In addition, the scale of a photograph is determined by equation (2), where f is the focal length, H is the height of flight over the ground, ab is the distance over the frame, and AB is the distance over the ground.

$$E = \frac{ab}{AB} = \frac{f}{H} \quad (2)$$

On the other hand, the ground sample distance (GSD) is calculated by equation (3).

$$GSD = \frac{\text{Flying height } (H) \times \text{Sensor width}}{\text{Focal length } (f) \times \text{Image width}} \quad (3)$$

Table II shows the parameters used according to the DJI Phantom 3 Standard drone.

TABLE II. FLIGHT HEIGHT PARAMETERS

E	Image width	Sensor width	Focal length	Flying height	GSD
-	[px]	[mm]	[mm]	[m]	[cm/px]
1/3750.93	4,000	6.17	20	75	0.578

C. Flight Route

The flight route to be flown must be planned. The Waypoint flight mode is proposed. This consists of recording a series of geo-located points that the aircraft will fly autonomously, freeing the pilot from its control and allowing him to focus his capabilities on other aspects such as battery level, remote connection status, and altitude number photos taken. This step is carried out for the case study using the DroneDeploy mobile application. The following flight parameters used are shown in Table III.

TABLE III. FLIGHT PARAMETERS

Height of flight	Correlation zone (Front overlap)	Correlation zone (Side overlap)	Flight direction	Flight speed (mapping)
[m]	[%]	[%]	[°]	[m/s]
75	75	65	6	15

Providing this data in the DroneDeploy application automatically displays a calculation of flight time, area to be covered, number of photos to be taken, and how many batteries will be needed. Similarly, if the pilot prefers, a manual flight can be performed to maintain the flight parameters. Before making the flight, several aspects must be taken into account, such as:

- The time range (10:00 am - 3:00 pm). It is recommended to perform the flight at noon because the sun's position avoids excessive shadows.

- To be within the operating temperature range of the drone (0° to 40° C).
- Not to exceed the maximum service ceiling above sea level (6000m).
- Have optimal battery charge level (Drone, remote control, and cell phone).
- To establish a connection with enough satellites.
- Ensure that there is no interference between the Drone-Control connection.
- It is not recommended to fly the drone if the wind speed is 8-10 m/s or more.

Also, avoid proceeding if weather conditions are not suitable (Rain, thunderstorm, fog). It is recommended to monitor weather measurement data, temperature, wind speed and direction, precipitation probability, cloud cover percentage, visibility distance, available satellites, and KP level. The latter measures the geomagnetic disruption caused by solar activity, with 0 being the minimum level, nine being the maximum, and 3 or 4 being safe to fly. If this index is high, it generates inaccuracy in the global positioning system and a decrease or fluctuation in the number of blocked satellites.

D. Pre-flight Verification

Before starting the flight, a checklist should be considered to certify that the initial variables guarantee a safe flight. This process is facilitated by using the DJI mobile application for the case study. The following aspects should be verified:

- Packing list: this starts by checking the application update, downloaded maps, cell phone, and radio control battery charged, SD card with enough space, propeller condition, lens cloths, and UAV pilot license.
- Hover checklist: The drone is inspected for defects, battery correctly positioned and sufficiently charged, propellers adjusted, camera protector removed, SD card in position, monitor brightness at maximum, and antennas in position.
- Take-off verification: Check for the presence of other drones in the area, warn the spectators that the drone is going to take off, look for/listen for defects in the drone, monitor battery power, and signal strength.

E. Post-flight Verification

After landing, the drone should be turned off. Place the camera protector, put the batteries away, recharge them, and remove the cell phone or tablet. In addition, the radio control should be turned off and put away. The propellers should be removed, cleaned, and put away. Cables should be disconnected, the photographs taken should be downloaded to the computer, and, finally, the drone should be cleaned and put away.

F. Image Processing

Photogrammetry techniques are used to reconstruct the 3D model from photographs. In the case study, Agisoft Metashape Professional software was used to process the images taken. In

the first instance, these are aligned, a process consisting of joining each photograph's geo referenced points. The result is dependent on the correlation percentages used in the flight. The "Dense Point Cloud" is created, a set of vertices in a three-dimensional coordinate system. These vertices are identified as X, Y, and Z coordinates and represent the external surface of an object. It is possible to make the "Mesh", which is the basis for generating a texture completely created in the next process called "Texture", now the three-dimensional model is obtained. If a detailed texture is required, the process called "Tiled model" is applied, created from the dense point cloud. This 3D model is useful to observe structures that are not accurately detailed in a simple photograph. Finally, the "Digital Elevation Model" and the "Orthophoto" are generated. The first one provides information about the different heights presented in the terrain, being an important tool to assess the vertical evolution of the work. At the same time, the second tool is the pairing of all the photographs represented in a new composite image. Because these maps accurately illustrate the land, it is possible to measure real distances.

G. Data Analysis

In the case under study, at the beginning of the monitoring of the work indicated, it was provided by those in charge, the schedule called "Construction of mixed superstructure" of the Postgraduate Building, which began on August 15, 2018, and ended on July 8, 2019, with a duration of 266 days. Based on this, the analysis and comparison with the software-generated models were started. This process consists of taking each item, specifying whether it is built within the defined dates, and then writing a report.

Finally, a comparison was made between the aerial monitoring reports and those provided by the construction supervisor to determine whether the proposed methodology is more efficient than the one used traditionally.

V. RESULTS AND ANALYSIS

This section presents the results obtained with the applied methodology. Fig. 3 shows a comparison between the initial day of aerial monitoring to the site (August 2, 2018) and the last day (May 24, 2019). A total of 8 months were considered in the investigation, excluding December 2018 and January 2019.

Table IV shows the activities corresponding to the work development processes.

The analysis of the processed models and their comparison with the work schedules are presented in Table V. In addition, observations of the status of each activity are shown with their respective dates.

The success cases presented in [9] show applications in the construction industry of RPAS in passive mode, i.e. only the images are acquired and the reconstruction of the site is performed. In our work, in addition to delivering the orthophotomosaic, an on-site measurement of the quantities of executed work is performed.

In [11] was described basic method for photogrammetry orientation. This paper is result of case study to automate the whole process of construction project. In our job was considered characteristics of vehicle and flight conditions, safety and chronograph actualization used measurements from flight data, this information beyond automate monitoring construction process.

As shown in Table IV, the construction site presents some delays observed in the photographic records obtained in the proposed methodology. In addition, a contrast can be made between what was built (an aerial photogrammetric record) and what was established in the schedule.

Due to these delays in phase 1 of the work (Underground), the contractor reprogrammed times and presented a new schedule of the same stages initially exposed (Construction of composite superstructure). The stakeout began on March 18, 2019, and ended on July 15, 2019. This generated that part of the data obtained in the aerial monitoring did not present the construction of the items. In addition, the new dates exceeded the estimated monitoring time range (8 months). The weather is against the methodology presented, but it is also against the construction progress, so the monitoring process is not affected.

Some of the reasons for the delays were: Restricted hours of use of the crane tower due to its noise and proximity to a residential area. The rains, the water table, and shallow water that drained over the excavation caused flooding. Based on the results obtained and the comparisons made with the supervision reports of the work, it can be deduced that the methodology created is efficient, safe, fast, and accurate, facilitating the preparation of reports and other supervision activities.



Fig. 3. Research Methodology.

TABLE IV. WORK DEVELOPMENT PROCESSES ACTIVITIES

Activity	Description
1	Columns-screens in concrete LEVEL +1.50 to LEVEL +6.00. SOUTH SIDE.
2	Concrete columns-screens LEVEL +1.50 to LEVEL +6.00. NORTH SIDE
3	Beams and solid mezzanine slab. LEVEL +6.00. SOUTH SIDE - Metal structure slab and classrooms LEVEL +6.00. SOUTH SIDE
4	Concrete columns-screens LEVEL +6.00 to LEVEL +9.70. SOUTH SIDE.
5	Beams and solid mezzanine slab LEVEL +9.70. SOUTH SIDE. - Metal structure slab and classrooms LEVEL +9.70. SOUTH SIDE.
6	Beams and solid mezzanine floor slab LEVEL +6.00 NORTH SIDE - Metal structure slab and classrooms LEVEL +6.00 NORTH SIDE - Circulations and bridges LEVEL +6.00.
7	Concrete columns-screens LEVEL +6.00 to LEVEL +9.70 NORTH SIDE - Metal structure slab and classrooms LEVEL +9.70 NORTH SIDE
8	South side stage 1: Beams axes 4, 5, 6 and 7.
9	South side stage 1: IP profiles, classroom metal structure, classroom connectors axes 7-6, 6-5, and 5-4.
10	South side stage 1: Casting of classroom slabs axes 7-6, 6-5, 5-4.
11	South side stage 1: Screens MP-1 level + 8.30 to +11.20
12	South side stage 1: Screens CP-1 level +9.70 to +11.20
13	South side, stage 2: Beams axes 2, 3 and 8.
14	South side, stage 2: IP Profiles, Classroom collaborating sheet, Classroom connectors axes 8-7, 4-3, and 3-2.
15	South side stage 2: Casting of classroom slab axes 7-6, 6-5, 5-4
16	South side stage 2: Screens MP-1 level + 8.30 to +11.20
17	South side stage 2: Screens CP-1 level +9.70 to +12.60
18	Stage 3: Bridges and circulations
19	North side stage 1: Beams axes 7, 6, 5 and 4
20	North side stage 1: IP Profiles, Collaborating sheeting classroom, Connectors classrooms axes 8-7, 4-3, and 3-2
21	North side stage 1: Casting of classroom slab axes 7-6, 6-5, 5-4
22	North side stage 1: Screens MP-1 level + 8.30 to +11.20
23	North side stage 1: Screens CP-1 level +9.70 to +12.60

TABLE V. ANALYSIS OF PROCESSED MODELS AND COMPARISON WITH SCHEDULED

Activity	Schedule		Observations
	Start date	End date	
1	15/08/18	8/09/18	In the model produced from the photographs of the September 19, 2018 photogrammetric flight, it can be seen that 12 of the 14 concrete screens have been constructed.
2	25/09/18	19/10/18	On September 28, 2018, the placement of the +1.50m level metal structure is being completed. Between October 9 and October 18 of the same month, the established in this topic was built.
3	10/09/18	3/10/18	On September 19, construction had not yet started. This started on October 9, 2018 and was completed between March 12 and March 21, 2019.
4	4/10/18	29/10/18	On October 9, construction had not yet started. According to the photogrammetric record of February 22, 2019, this item is completed.
5	30/10/18	24/11/18	On March 21, 2019, the start of the beam work was observed. On April 25, the assembly of the metallic structure is being done and on May 3, the casting of the mezzanine slab will start.
6	20/10/18	15/11/18	On October 23, 2018, the construction of the columns-screens from +1.50m to +6.00m started. On November 16, 2018, i.e. one day after the completion of items 1, 2 and 3, the column-screens were completed. Between February 22 and March 28, 2019, items 1 and 2 were completed, item 3 is completed on April 25, 2019, in these items the work had an approximate delay of 3 months.
7	16/11/18	11/12/18	On November 16, 2018, despite being the same day that this topic should be started, the work presents a delay, due to the fact that on that day they were just finishing the +1.50m level screens. This item was completed between March 28 and April 3, 2019.
8	26/03/19	10/04/19	This issue in general includes the whole process of construction of the beams in shafts 4, 5, 6 and 7, it is concluded that the construction of these was completed on time.
9	10/04/19	23/04/19	On April 25, 2019, the work presents a delay due to the fact that only the metallic structure of axes 4-5 and 5-6 is finished, and that of axes 7-6 were implemented between April 25 and 28.

10	17/04/19	25/04/19	On April 25 (the same day that this item should have been completed), the metallic structure is being placed, generating a backlog in this item. The casting of the classroom slabs begins between April 28 and May 3, 2019.
11	10/04/19	25/04/19	Item completed within the time established in the schedule.
12	15/04/19	29/04/19	Topic completed within the time stated in the schedule.
13	29/03/19	15/04/19	This topic in general includes the whole process of construction of the beams in axes 2, 3 and 8, from the photogrammetric analysis, it is concluded that the construction of these was performed in the established time.
14	15/04/19	27/04/19	On May 3, 2019, the work presents a delay due to the fact that only the metallic structure of axes 3-4 is finished.
15	24/04/19	29/04/19	On May 3, the slab of the classroom that composes axes 8-7 is being cast, this should have been cast 4 days ago.
16	15/04/19	27/04/19	Item completed within the time established in the schedule.
17	27/04/19	07/05/19	Item done in the time established in the schedule.
18	27/04/19	09/05/19	On May 3, 2019, it can be observed that the circulation of the south side, which compose axes 8, 7, 6, 5 and 4, are being finished, which generates that the work has a delay.
19	03/04/19	09/04/19	This issue includes the whole process of construction of the beams in axes 7, 6, 5 and 4, the elaboration of the beams started on May 3, 2019.
20	09/04/19	23/04/19	On May 3, 2019, only the profiles of axes 5-6 have been located.
21	16/04/19	23/04/19	Performing the photogrammetric analysis, it is observed that the work presents delay in this subject.
22	09/04/19	24/04/19	Item completed within the time established in the schedule.
23	13/04/19	29/04/19	Item completed within the time established in the schedule.

VI. CONCLUSION

This paper deals with the monitoring of infrastructure works using aerial photogrammetry. The use of the drone becomes an active tool in the task of monitoring the evolution of the work, since, with an overflight combined with image processing software, it is possible to evaluate the entire structural construction area, which reduces the displacement of personnel within it and the taking of specific photographs for each work activity. The methodology presented in this research is efficient and suitable for construction site monitoring. The management of the aircraft requirements, the identification of the flight zone, the safety conditions and the photogrammetry requirements allowed obtaining the final objective of comparing the data collected and the data provided by the supervisor in a civil construction. The data obtained showed the delay in the construction and there was a need to make modifications in the construction schedule of the work. Validation of the methodology is not achieved with a single case of application, so the conclusions presented here are limited to this study. To have an external validation, it is suggested the application of the proposed development and tested in different conditions.

REFERENCES

- [1] M. Nasrun, M. Nawi, N. Baluch, and A. Y. Bahauddin, "Impact of Fragmentation Issue in Construction Industry: An Overview 3 Discussions: Fragmentation Issue," in MATEC Web of Conferences, 2014, vol. 15.
- [2] R. Navon and R. Sacks, "Assessing research issues in Automated Project Performance Control (APPC)," *Autom. Constr.*, vol. 16, no. 4, pp. 474–484, 2007, doi: 10.1016/j.autcon.2006.08.001.
- [3] F. Muñoz-La Rivera, J. M. Serrano, I. Valero, and E. Oñate, "Methodological - Technological Framework for Construction 4 . 0," *Arch. Comput. Methods Eng.*, vol. 28, no. 2, pp. 689–711, 2021, doi: 10.1007/s11831-020-09455-9.
- [4] B. J. Yap Hui, I. N. Chow, and K. Shavarebi, "Criticality of Construction Industry Problems in Developing Countries: Analyzing Malaysian Projects," *J. Manag. Eng.*, vol. 35, no. 5, 2019, doi: 10.1061/(ASCE)ME.1943-5479.0000709.
- [5] J. J. Lin and M. Golparvar-Fard, "Proactive Construction Project Controls via Predictive Visual Data Analytics," *Congr. Comput. Civ. Eng. Proc.*, vol. 2017-June, pp. 147–154, 2017, doi: 10.1061/9780784480830.019.
- [6] M. W. Park, C. Koch, and I. Brilakis, "Three-Dimensional Tracking of Construction Resources Using an On-Site Camera System," *J. Comput. Civ. Eng.*, vol. 26, no. 4, pp. 541–549, 2012, doi: 10.1061/(asce)cp.1943-5487.0000168.
- [7] K. K. Han and M. Golparvar-Fard, "Potential of big visual data and building information modeling for construction performance analytics: An exploratory study," *Autom. Constr.*, vol. 73, pp. 184–198, 2017, doi: 10.1016/j.autcon.2016.11.004.
- [8] Q. F. M. Dupont, D. K. H. Chua, A. Tashrif, and E. L. S. Abbott, "Potential Applications of UAV along the Construction's Value Chain," *Procedia Eng.*, vol. 182, no. 3, pp. 165–173, 2017, doi: 10.1016/j.proeng.2017.03.155.
- [9] S. Dastgheibifard and M. Asnafi, "A Review on Potential Applications of Unmanned Aerial Vehicle for Construction Industry," *Sustain. Struct. Mater.*, vol. 1, no. July, pp. 44–53, 2018, doi: 10.26392/SSM.2018.01.02.044.
- [10] T. Rakha and A. Gorodetsky, "Review of Unmanned Aerial System (UAS) applications in the built environment: Towards automated building inspection procedures using drones," *Autom. Constr.*, vol. 93, no. September, pp. 252–264, 2018, doi: 10.1016/j.autcon.2018.05.002.
- [11] Z. A. Memon, M. Z. Abd. Majid, and M. Mustaffar, "The Use Of Photogrammetry Techniques To Evaluate The Construction Project Progress," *J. Teknol.*, no. June, 2012, doi: 10.11113/jt.v44.358.
- [12] H. P. Tserng, S. P. Ho, and S. H. Jan, "Developing BIM-assisted as-built schedule management system for general contractors," *J. Civ. Eng. Manag.*, vol. 20, no. 1, pp. 47–58, 2014, doi: 10.3846/13923730.2013.851112.
- [13] M. Gheisari and B. Esmaceli, "Applications and requirements of unmanned aerial systems (UASs) for construction safety," *Saf. Sci.*, vol. 118, no. December 2017, pp. 230–240, 2019, doi: 10.1016/j.ssci.2019.05.015.
- [14] W. W. Greenwood, J. P. Lynch, and D. Zekkos, "Applications of UAVs in Civil Infrastructure," *J. Infrastruct. Syst.*, vol. 25, no. 2, p. 04019002, 2019, doi: 10.1061/(asce)is.1943-555x.0000464.
- [15] N. Snavely, S. M. Seitz, and R. Szeliski, "Modeling the world from Internet photo collections," *Int. J. Comput. Vis.*, vol. 80, no. 2, pp. 189–210, 2008, doi: 10.1007/s11263-007-0107-3.
- [16] M. Prosser-Contreras, E. Atencio, F. Muñoz La Rivera, and R. F. Herrera, "Use of Unmanned Aerial Vehicles (UAVs) and Photogrammetry to

- Obtain the International Roughness Index (IRI) on Roads,” *Appl. Sci.*, vol. 10, no. 24, p. 8788, 2020, doi: 10.3390/app10248788.
- [17] S. Harwin and A. Lucieer, “Assessing the accuracy of georeferenced point clouds produced via multi-view stereopsis from Unmanned Aerial Vehicle (UAV) imagery,” *Remote Sens.*, vol. 4, no. 6, pp. 1573–1599, 2012, doi: 10.3390/rs4061573.
- [18] E. Romero-Chambi, S. Villarroel-Quezada, E. Atencio, and F. M. La Rivera, “Analysis of optimal flight parameters of unmanned aerial vehicles (UAVs) for detecting potholes in pavements,” *Appl. Sci.*, vol. 10, no. 12, pp. 1–33, 2020, doi: 10.3390/APP10124157.
- [19] I. K. Hung, D. Unger, D. Kulhavy, and Y. Zhang, “Positional Precision Analysis of Orthomosaics Derived from Drone Captured Aerial Imagery,” *Drones*, vol. 3, no. 2, p. 46, 2019, doi: 10.3390/drones3020046.
- [20] D. Moon, S. Chung, S. Kwon, J. Seo, and J. Shin, “Comparison and utilization of point cloud generated from photogrammetry and laser scanning: 3D world model for smart heavy equipment planning,” *Autom. Constr.*, vol. 98, no. July, pp. 322–331, 2019, doi: 10.1016/j.autcon.2018.07.020.
- [21] M. G. Fard and F. Peña-Mora, “Application of visualization techniques for construction progress monitoring,” *Congr. Comput. Civ. Eng. Proc.*, vol. 40937, no. January, pp. 216–223, 2007, doi: 10.1061/40937(261)27.
- [22] H. A. Mesa, K. R. Molenaar, and L. F. Alarcón, “Comparative analysis between integrated project delivery and lean project delivery,” *Int. J. Proj. Manag.*, vol. 37, no. 3, pp. 395–409, 2019, doi: 10.1016/j.ijproman.2019.01.012.
- [23] R. Huang, Y. Xu, L. Hoegner, U. Stilla, U. “Semantics-aided 3D change detection on construction sites using UAV-based photogrammetric point clouds”. *Automation in Construction*, vol. 134, 2022, doi: 10.1016/j.autcon.2021.104057.
- [24] A. Keyvanfar, A. Shafaghat, M.S.F. Rosley, M.S.F. “Performance comparison analysis of 3D reconstruction modeling software in construction site visualization and mapping”. *International Journal of Architectural Computing*, 2022, doi:10.1177/14780771211066876
- [25] Y. Lo, C., Zhang, Z., Ye, C., Cui, “Monitoring road base course construction progress by photogrammetry-based 3D reconstruction”. *International Journal of Construction Management*, 2022, doi:10.1080/15623599.2022.2040078.
- [26] A. Ibrahim, M. Golparvar-Fard, K. El-Rayes. “Metrics and methods for evaluating model-driven reality capture plans”. *Computer-Aided Civil and Infrastructure Engineering*, vol. 37, pp. 55-72, 2022, doi:10.1111/mice.12693.
- [27] A. W. A. Hammad, B.B.F. da Costa, C.A.P. Soares, A.N. Haddad. “The use of unmanned aerial vehicles for dynamic site layout planning in large-scale construction projects”. *Buildings*, vol. 11, issue 12, 2021, doi:10.3390/buildings11120602.
- [28] L. Jeelani, M. Gheisari. “Safety challenges of UAV integration in construction: Conceptual analysis and future research roadmap”. *Safety Science*, vol. 144, 2021, doi:10.1016/j.ssci.2021.
- [29] R. O. Rey, R.R.S. de Melo, D.B. Costa. “Design and implementation of a computerized safety inspection system for construction sites using UAS and digital checklists 欵?Smart Inspects ” . *Safety Science*, vol. 143, 2021, doi: 10.1016/j.ssci.2021.105430.
- [30] Y. Wu, M. Wang, X. Liu, Z. Wang, T. Ma, Z. Lu, D. Liu, Y. Xie, X. Li, X. Wang. “Monitoring the work cycles of earthmoving excavators in earthmoving projects using UAV remote sensing”. *Remote Sensing*, vol. 13, issue 19, 2021, doi: 10.3390/rs13193853.
- [31] M. Kaamin, A.S. Sarif, N.A. Mustafa, R.A. Rahman, M.A.A Kadir, N.H. Abdullah, A.H.M. Nor, P. Luo. “Accurate and Precision Monitoring using Unmanned Aerial Vehicle in Construction Engineering”. *International Journal of Nanoelectronics and Materials*, vol. 14, issue:Special Issue ISSTE, pp. 51-58, 2021, <https://www.scopus.com/inward/record.uri?eid=2-s2.0-85126130176&partnerID=40&md5=1055c889c7aafaa5eb5904deee2823fb>.

Development of Pipe Inspection Robot using Soft Actuators, Microcontroller and LabVIEW

Mohd Aliff¹, Mohammad Imran², Sairul Izwan³, Mohd Ismail⁴

Quality Engineering Research Cluster, Malaysian Institute of Industrial Technology
Universiti Kuala Lumpur, 81700, Johor, Malaysia

Nor Samsiah⁵

Center for Artificial Intelligence Technology
Universiti Kebangsaan Malaysia
Selangor, Malaysia

So Shimooka⁹

Faculty of Engineering, Academic Field of Natural Science
and Technology, Okayama University
3-1-1 Tsushima-naka, Kita-ku, Okayama, Japan

Tetsuya Akagi⁶, Shujiro Dohta⁷, Weihang Tian⁸

Department of Intelligent Mechanical Engineering
Okayama University of Science, Okayama, Japan

Ahmad Athif¹⁰

Center for Artificial Intelligence and Robotics (CAIRO)
Universiti Teknologi Malaysia, Skudai, Johor, Malaysia

Abstract—Pipeline transportation is particularly significant nowadays because it can transfer liquids or gases over a long distance, usually to a market area for use, using a system of pipes. The pipeline's numerous fittings, such as elbows and tees, as well as the various sizes and types of materials utilized, make routine inspection and maintenance challenging for the technician. Therefore, the compact and portable pipe inspection robots with pneumatic actuators are required for use in industry especially in hazardous areas. Flexible pneumatic actuators with clean and safe pneumatic energy have high mobility to move in complex pipelines. High safety features such as no oil or electrical leakage, which would be dangerous if used in an explosive environment are a major factor it is widely used nowadays. As a result, the goal of this study is to propose and present the development of pipe inspection robot that employ soft actuators and are monitored by LabVIEW for usage in a variety of pipe sizes and types. This research focuses on the movement of robots in the pipeline by proposing some important mechanisms such as sliding mechanism, holding mechanism, and bending unit to move easily and effectively in the pipeline. Experiments show that with an appropriate pneumatic pressure source of 4 bar, a flexible robot using the soft pneumatic actuator can bend and move in a 2-inch diameter pipe smoothly and efficiently. It has been discovered that the proposed mechanism may readily travel pipe corners while bending in any required direction.

Keywords—Soft pneumatic actuator; pipe inspection robot; flexible actuator; microcontroller; sliding and holding mechanism

I. INTRODUCTION

Robotic development is currently one of the most important concerns of the twenty-first century, as robotics is widely used in a range of fields, including engineering, medical, agriculture, education, art, and more [1-4]. Robots have been built in a variety of ways in the industrial world to eliminate or limit human involvement in forced labor and hazardous working conditions [5-9]. Water and gas pipelines are extremely complicated due to the sizing and type of piping utilized, as

well as the presence of massive numerical corners and joints. Furthermore, pipelines are the most frequent technique of transporting oil and gas from one location to another in the oil and gas business since they are more cost effective than other modes of transportation. Corrosion, fluid leakage, inefficiency, and other factors necessitate frequent maintenance of these pipelines. Furthermore, most pipelines are located underground or undersea, making direct inspections of the pipes difficult for technicians. As a result, robotic inspection has been created using a variety of pipe inspection technologies to accommodate varied pipeline configurations [10]. There have been various varieties of inspection robots produced, including the wheel type, walking type, inchworm type, pig type, and caterpillar type [11]. In pipe inspection, the robot must have good mobility to carry out the inspection operation, and it is even better if the robot has a flexible body that can alter naturally without causing any disruption or getting caught in the middle of the inspection.

Pneumatic actuators, sometimes called air actuators, are low-cost and safe motion control devices that convert energy from pressurized gas or air into linear or rotational motion [12, 13, 14]. The scientific community has recently become more interested in appropriate and adaptable systems to investigate pneumatic actuation capabilities for increasingly complex occupations [15, 16, 17]. It is deemed feasible and safe for use in pipe inspection because it does not rely on electricity as its primary source of energy. Pneumatic actuators have been shown to be suitable for pipe inspection in different research situations [18, 19, 20] due to their ability to prevent explosions and short circuits. Furthermore, today's researchers have developed a variety of pneumatic actuators, one of which is the soft pneumatic actuator, which is widely employed in the rehabilitation sector [16]. This study used a soft pneumatic actuator on the front of the robot known as a bending unit to navigate the robot in the desired direction through the pipe. The inspection robot must include a specific mechanism, such

as a holding and sliding mechanism, to stimulate robot movement during the inspection process [20]. In order to accomplish smooth and effective movement when operating inside the pipe, the pipeline inspection robot with a holding and sliding mechanism that utilizes flexible soft pneumatic actuators was designed and tested in this study.

II. METHODOLOGY

The pipe inspection robot's prototype design is shown in Fig. 1. The gripping mechanism, bending unit, and sliding unit make up the pipe inspection robot. The robot prototype is about 500 mm in length.

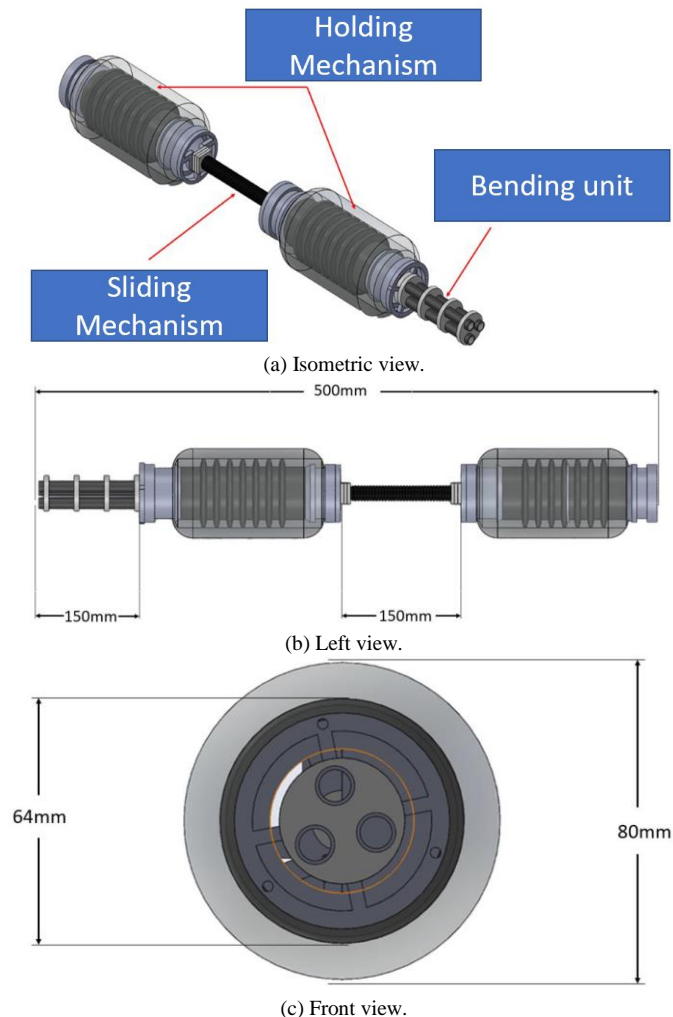


Fig. 1. Prototype Design of Pipe Inspection Robot.

The robot's prototype is shown in Fig. 2. As a navigator, this robot has a pneumatic soft actuator bending unit mounted on the front of the robot. The soft actuator can bend in any direction and adjust depending on the angle of the pipe's tees and elbows. The inspection robot's body is also equipped with soft actuator sliding and holding mechanisms. Because of its modest size, this flexible actuator is suited for use, allowing the flexible body to move organically in accordance with the soft actuator. The robot requires 6 ports for air pressure to be delivered to three primary parts: the bending unit, sliding

mechanism, and holding mechanism. Because the bending unit needs to bend and regulate the direction of the robot on the X, Y, and Z axes, it has three air supplies. The holding mechanism requires two airports for the upper and lower bodies to keep the robot inside the pipe, whereas the operating and sliding mechanism only requires one port to push and pull the robot. However, as compared to the holding unit, the sliding and bending units employ different amounts of pressure. This is since the sliding and bending units are made of different materials and have different structures than the holding mechanism. The air pressure provided to the holding mechanism is lower than that to the sliding and bending unit. Only the holding mechanism component employed a 6 mm pneumatic fitting, whereas the rest of the pneumatic fittings were 4 mm.

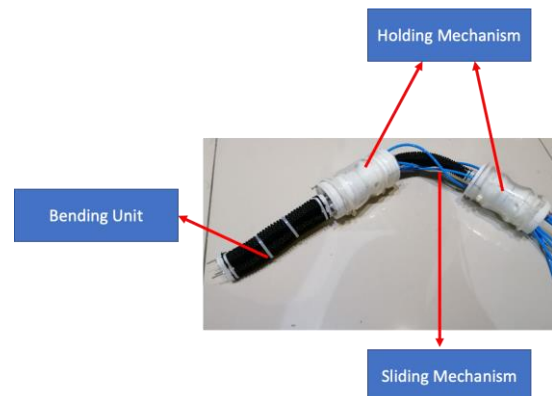


Fig. 2. Prototype of Robot.

III. CONTROL SYSTEM

Fig. 3 depicts the robot control system in block diagram. A sliding mechanism, six on/off control valves, an Arduino microcontroller (MEGA 2560 REV3), and a personal computer are used to build control system programming and send commands to the Arduino in the moving process.

The working principle of the proposed robot is shown in Fig. 4. First, the pipe holding mechanism at the end of the pipe robot expands so that it can hold the pipe (1). Next, actuators in the sliding mechanism are pressurized, then, the sliding mechanism extends (2). When the actuators reach at maximum length, the top of pipe holding mechanism expands to hold the robot inside the pipe (3). Next, pipe holding mechanism at the end of robot contracts (4). Then, the compressed air in chambers of three actuators is exhausted. At the same time, the sliding mechanism contracts and end holding mechanism moves forward (5). By repeating these processes from (1) to (5), the robot will move forward as an inchworm. On the other hand, the backward motion can be realized by using the opposite operation mentioned above. In the case to steer the robot toward desired direction in pipe joint, first, bending actuator of the sliding mechanism is generated by pressurizing one or two extension type flexible actuators. Next, from this condition of bending motion, three actuators in the sliding mechanism are pressurized. Then, the robot can move forward while changing moving direction. The robot can move to six directions by pressurized one or two extension type flexible pneumatic actuators on the sliding mechanism.

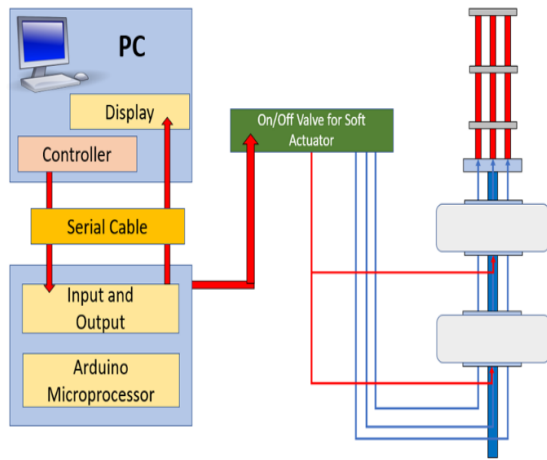


Fig. 3. Block Diagram of the Control System.

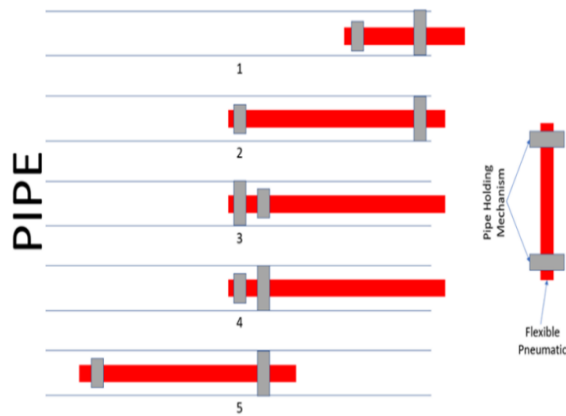


Fig. 4. Operating Principle of the Inspection Robot.

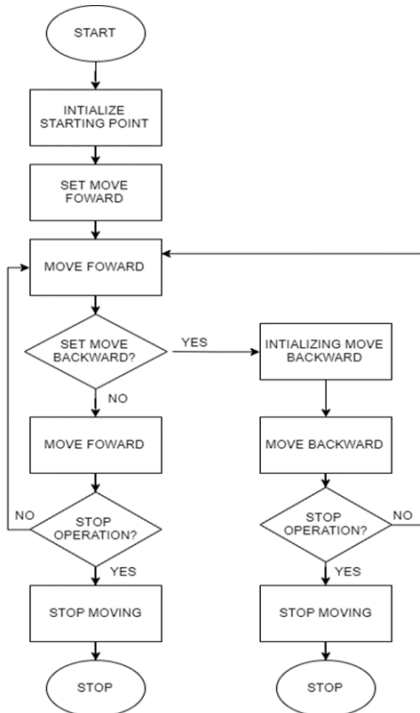


Fig. 5. Prototype Flow Chart.

The control system's flow chart is shown in Fig. 5. The operator can manually control and monitor the inspection robot in this investigation via a graphical interface. The Arduino will receive and process all input data from the interface before sending the output to the pneumatic valve. The pneumatic valve regulates the flow of pneumatic pressure into and out of the soft actuators and silicone rubber tube. The inspection robot can travel forward or backward, as well as bend left or right, while functioning in the pipe, due to the pneumatic valve's control system.

IV. RESULT AND DISCUSSION

The controller's interface is shown in Fig. 6. Each component that must be controlled by the operator is shown on the LabVIEW interface. The gear in Fig. 6 determines whether to move the robot forward or backward when operating inside the pipeline. Toggle up for forward movement and down for backward movement. The program's block diagram alters as a result of the operator's instructions. When a component is turned on, the light turns green, as seen in the Fig. 7.

All robotic systems are started using the start pushbutton as a switch mechanism. The system will not function unless this button is pressed. Head (H), Body (B), and Tail (T) indicators are key components for the holding and sliding mechanism. Holding mechanisms that utilise silicone rubber tubes as holdings between pipes and robots are designated by the letters H and T. For push and pull approaches, B is for the sliding mechanism that uses a soft actuator to extend forward or backward. The 3-axis controls X, Y, and Z in Fig. 6 are used to control the robot's direction. This controller can move in six directions: X, Y, Z, XY, XZ, and YZ. When the robot reaches the pipeline intersection, this navigation system is required.

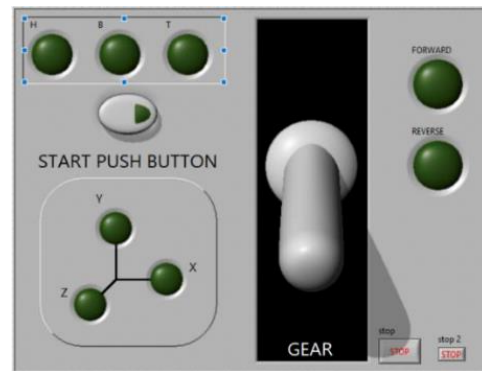


Fig. 6. LabVIEW Controller Interface.

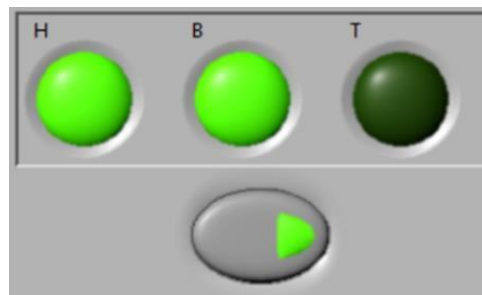


Fig. 7. Light Green Colour on Interface.



Fig. 8. View of the Curving Movement using a Bending Unit.

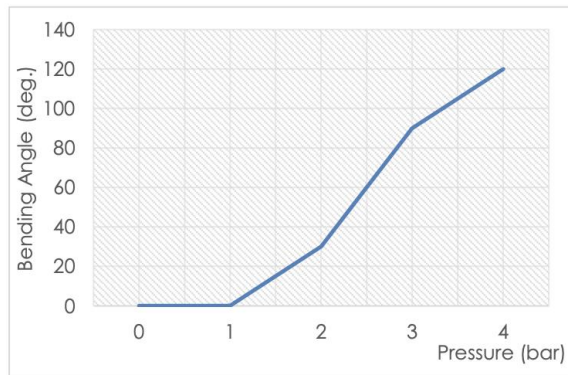


Fig. 9. Graph Bending Angle against Pressure.

For the bending unit, it consists of three pneumatic soft actuators that are joined together and can bend when pressure is applied to it. A silicone rubber tube with a diameter of 2 mm on the inside and 4 mm on the outside makes up these soft actuators. The soft actuators are placed parallel every 120 degrees from the center of the disc. By placing three soft actuators in the X, Y, and Z axis positions, the bending unit can generate 6 directions to bend in the X, Y, Z, XY, XZ, and YZ axes. The bending motion was caused by a combination of artificial muscle contraction and expansion concepts. When air pressure is applied to the soft actuator, the resulting force increases as the air pressure is increased. Fig. 8 depicts the use of a bending unit to create a curved movement. Fig. 9 depicts a bending angle graph when pressure is applied to a bending unit. Based on Fig. 9, with a pressure of 4 bar, the maximum bending angle can be achieved up to 120 degrees. However, if the air pressure is less than 1 bar, the bending unit will not have enough pressure to move and bend in the appropriate direction.

The diagram of the holding mechanism when expanding and contracting outside and within the pipe is shown in Fig. 10. The mechanism is made from a single silicon rubber tube that may expand and shrink. The device has a 50 mm exterior diameter and a 100 mm length. The following is the working theory for pipe holding. As supply pressure is applied to the tube, it can expand until it reaches the inside diameter of the pipeline. A maximum outer diameter of 80 mm can be attained with a supply pressure of 2 bar. When the input pressure is withdrawn, the mechanism returns to its previous shape by restoring the force of the rubber. This device can prevent the robot from slipping in the pipe by using silicone rubber as the main material and repeating the processes specified. Because of the robotic mechanism's ability to expand to meet piping

sizes, the robot can be employed in a variety of piping systems. Robots with the ability to work in several dimensions of the piping system will cut inspection costs and make the operation easier to complete.

An experiment was carried out to assess the consistency of the tested flexible sliding mechanism. The sliding mechanism is made up of a single soft actuator that connects the robot's head and tail. To archive a maximum movement, this actuator will extend to its maximum length. After the upper body robot grips the pipe, the pressure is released, and the robot's lower body is pulled, and the process is repeated. The experiment of extending a soft actuator in pushing and pulling action is shown in Fig. 11. The movement of the robot can be viewed using a ruler as a reference, and if the pressure is maintained, the soft actuator will continue to stretch. Because the actuator may burst, the maximum pressure supplied must not exceed 5 bars. The greatest extension, as indicated in Fig. 11(4), can be seen.

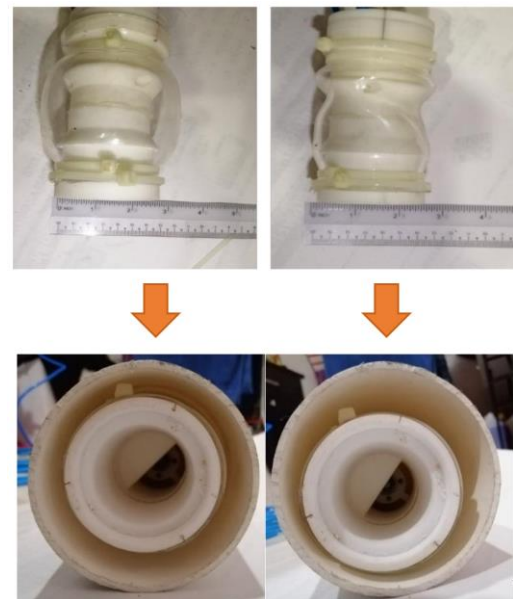


Fig. 10. Diagram of the Holding Mechanism when Expanding and Contracting Outside and Inside the Pipe.

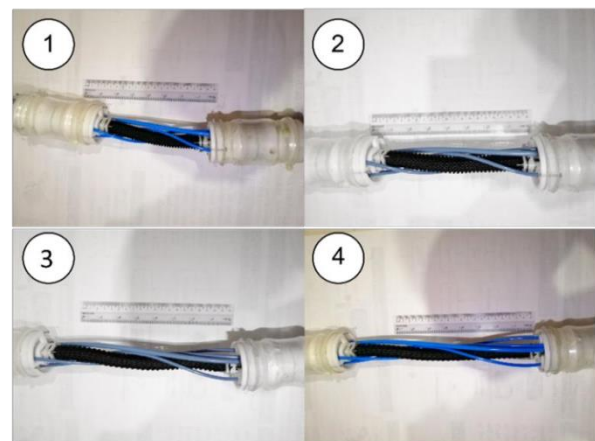


Fig. 11. Extension Testing of Soft Actuator.

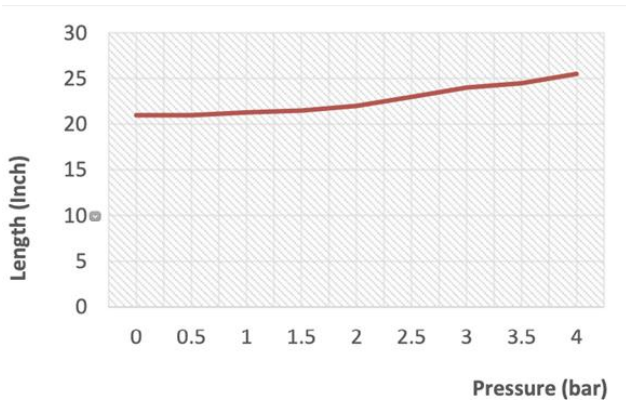


Fig. 12. Extension (Inch) against Pressure (Bar).

The extension of the sliding mechanism against pressure is shown in Fig. 12. During extension testing, we discovered that when the air pressure is below 2 bar, only minor movement is visible. As a result, the air pressure provided to the actuator must be greater than 2 bar in order to see some physical change on the soft actuator. Data was logged from the soft actuator's initial length (150 mm) to its maximum extension (180 mm). We can determine the amount of pressure required to move the robot at the ideal speed and length using this graph.

Fig. 13 shows the prototype moving effectively through the 2-inch pipe. According to the statistics, depending on the air pressure, the time necessary for the prototype to flow through the pipeline will grow or decrease. The prototype moves more quickly at high pressure than at low pressure because high pressure air allows the sliding mechanism to expand further and reach its full length. From the experimental results, with a supply pressure of 4 bar, the proposed robot can move through a 2 -inch diameter pipe as far as 3 meters for 37.8 s. As a result, the suggested inspection robot is particularly efficient in terms of speed relative to size, thanks to its compact and lightweight body size and ability to move fast inside the pipe.

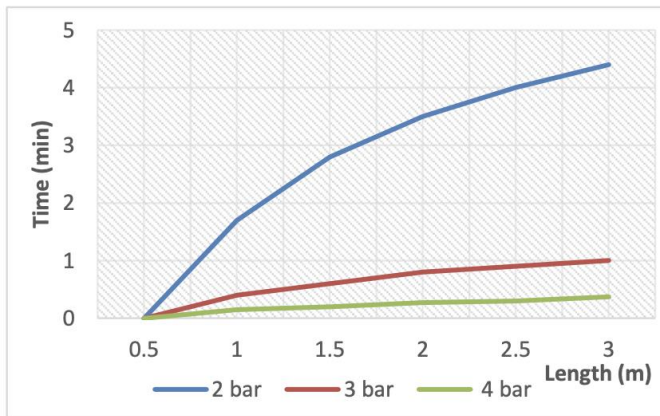


Fig. 13. The Graph of Distance Compared to Time (Min).

Fig. 14 shows a picture of the holding mechanism being tested when the applied pressure is 0 kPa and 200 kPa. When the applied pressure is 200 kPa, the holding system can hold 3 inch-diameter PVC pipe, as can be seen on the right side of Fig. 14. The radial orientation of the rubber tube expands when the input pressure is applied to it. When a supply pressure of

200 kPa is applied, a peak exterior diameter of 80 mm can be attained. The device returns to its previous condition when the input pressure is released.

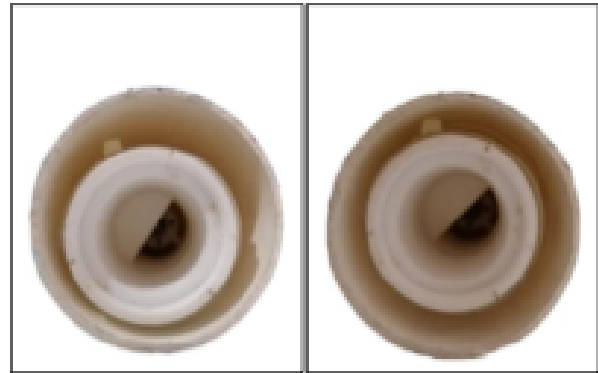


Fig. 14. Holding Mechanism Testing.

The holding mechanism has no effect on the robot's speed because it just serves to grab the pipeline. The holding mechanism can assist the robot in moving inside the pipe more efficiently with proper movement operation and steps. Furthermore, when fed with a pressure of 200 kPa, the holding mechanism may adjust the size of the rubber tube up to a maximum of 80 mm in diameter, preventing the robot from slipping inside the pipe. This will enable the inspection robot travel more smoothly in the pipe with many tees, elbows, and sockets, in addition to the robot configuration that includes a bending unit and sliding mechanism.

V. CONCLUSION

The purpose of the project is to develop the soft actuator inspection robot that can move smoothly and efficiently in different pipe sizes. The proposed inspection robot is equipped with a bending unit, sliding mechanism, and holding mechanism to help it move inside the pipe more quickly and smoothly. To control its navigation, the project has also built an interface using LabVIEW to operate the robot more easily and securely. This interface can also instruct the robot to bend in 6 predetermined directions in addition to moving forward or backward. From the experimental results, with a supply pressure of 4 bar, the proposed robot can move through a 2 -inch diameter pipe as far as 3 meters for 37.8 s. Moreover, by supplying a pressure of 4 bar, the bending unit can produce a maximum bending angle of 120 degrees. Then, when supplied with a pressure of 200 kPa, the holding mechanism can change the size of the rubber tube to a maximum of 80 mm in diameter and can prevent the robot from slipping inside the pipe. In conclusion, the aims of this project have been accomplished with a soft actuator robot that can travel smoothly in the pipe and the proposed control system can control the path of the robot using the constructed interface.

ACKNOWLEDGMENT

This research work is supported by the Universiti Kuala Lumpur through Short Term Research Grant (STR18039). The authors would like to thank the research management center of Universiti Kuala Lumpur, for managing the project.

REFERENCES

- [1] W. Tian, Y. Suzuki, T. Akagi, S. Dohta, W. Kobayashi, T. Shinohara, S. Shimooka and M. Aliff, "Development of Wrist Rehabilitation Device Using Extension Type Flexible Pneumatic Actuators with Simple 3D Coordinate Measuring System," *International Journal of Automotive and Mechanical Engineering*, 18(4), 2021, pp. 9158–9169.
- [2] M. Aliff, M. Dinie, M. I. Yusof, and N. S. Sani, "Development of Smart Glove Rehabilitation Device (SGRD) for Parkinson's Disease," *International Journal of Innovative Technology and Exploring Engineering (IJITEE)*, 9(2), 2019, pp. 4512 – 4518.
- [3] M. Aliff, F. Danieal, M. F. Mohamed, A. 'Athif, T. Akagi and N. Samsiah, "Development of Flexible Pneumatic Rehabilitation Actuator for Knee Injury," *TEST Engineering & Management*, 83, 2020, pp. 12849 – 12855.
- [4] M. Aliff, S. Dohta and T. Akagi, "Control and Analysis of Robot Arm using Flexible Pneumatic Cylinder," *Mechanical Engineering Journal*, Vol. 1, No. 5, dr0051, 2014, pp. 1-13.
- [5] M. S. A. M. Nor, M. Aliff and N. Samsiah, "A Review of a Biomimicry Swimming Robot using Smart Actuator," *International Journal of Advanced Computer Science and Applications (IJACSA)*, 12(11), 2021, pp. 395– 405.
- [6] M. Aliff, A. R. Mirza, M. Ismail and N. Samsiah, "Development of a Low-Cost Bio-Inspired Swimming Robot (SRob) with IoT," *International Journal of Advanced Computer Science and Applications (IJACSA)*, 12(7), 2021, pp. 452–457.
- [7] M. Aliff, N. S. Sani, M. I. Yusof, and A. Zainal, "Development of Fire Fighting Robot (QRob)," *International Journal of Advanced Computer Science and Applications (IJACSA)*, 10(1), 2019, pp. 142 – 147.
- [8] M. Aliff, N. Firdaus, N. Rosli, M. I. Yusof, N. Samsiah, and S. Effendy, "Remotely Operated Unmanned Underwater Vehicle for Inspection," *International Journal of Innovative Technology and Exploring Engineering (IJITEE)*, 9(2), 2019, pp. 4644 – 4649.
- [9] M. Aliff, I. S. Amry, M. I. Yusof, A. Zainal, A. Rohanim, and N. S. Sani, "Development of Smart Rescue Robot with Image Processing (iROB-IP)," *International Journal of Electrical Engineering and Technology*, 11(9), 2020, pp. 08-19.
- [10] Q. Liu, T. Ren, Y. Chen, "Characteristic analysis of a novel in-pipe driving robot," *Mechatronics*, vol. 23(4), 2013, pp. 419-428.
- [11] A. Nayak, and S. K. Pradhan, "Design of a New In-Pipe Inspection Robot," *Procedia Engineering*, 97, 2014, pp. 2081-2091.
- [12] M. Aliff, S. Dohta, and T. Akagi, "Control and analysis of simple-structured robot arm using flexible pneumatic cylinders," *International Journal of Advanced and Applied Sciences*, 4(12), 2017, pp. 151-157.
- [13] T. Morimoto, M. Aliff, T. Akagi, and S. Dohta, "Development of Flexible Pneumatic Cylinder with Backdrivability and Its Application," *International Journal of Materials Science and Engineering*, 3(1), 2015, pp. 7-11.
- [14] M. Aliff, S. Dohta, T. Akagi and H. Li, "Development of a Simple-structured Pneumatic Robot Arm and its Control Using Low-cost Embedded Controller," *Journal of Procedia Engineering*, Vol. 41, 2012, pp. 134-142.
- [15] N. Kato, S. Dohta, T. Akagi, W. Kobayashi, and M. Aliff, "Improvement of Wearable Wrist Rehabilitation Device Using Flexible Pneumatic Cylinders," *MATEC Web of Conferences*, 82, 2016, 02006. doi:10.1051/mateconf/20168202006.
- [16] S. Shimooka, T. Akagi, S. Dohta, T. Shinohara, M. Aliff, "Development of Reinforced Extension Type Flexible Pneumatic Actuator with Circumferential Restraints and Its Application for Rehabilitation Device," *International Journal of Automotive and Mechanical Engineering* 17(3), 2020, pp. 8116 – 8127.
- [17] H. Obayashi, T. Akagi, S. Dohta, W. Kobayashi, Y. Matsui, S. Shimooka, T. Shinohara and M. Aliff, "Development of Portable Rehabilitation Device Driven by Low-Cost Servo Valve Using Tap Water," *International Journal of Mechanical Engineering and Robotics Research*, 9(3), 2020, pp. 353 – 359.
- [18] K. Hayashi, T. Akagi, S. Dohta, W. Kobayashi, T. Shinohara, K. Kusunose and M. Aliff, "Improvement of Pipe Holding Mechanism and Inchworm Type Flexible Pipe Inspection Robot," *International Journal of Mechanical Engineering and Robotics Research*, 9(6), 2020, pp. 894 – 899.
- [19] Y. Hua, M. Konyo, and S. Tadokoro, "Design and analysis of a pneumatic high-impact force drive mechanism for in-pipe inspection robots," *Advanced Robotics*, 30(19), 2016, pp. 1260-1272. doi:10.1080/01691864.2016.1205511.
- [20] K. Kusunose, T. Akagi, S. Dohta, W. Kobayashi, T. Shinohara, Y. Hane, K. Hayashi, and M. Aliff, "Development of Inchworm Type Pipe Inspection Robot using Extension Type Flexible Pneumatic Actuators," *International Journal of Automotive and Mechanical Engineering* 17(2), 2020, pp. 8019 – 8028.

Deep Learning-based Detection System for Heavy-Construction Vehicles and Urban Traffic Monitoring

Sreelatha R¹

Department of Information Science
BMS College of Engineering
Bangalore, Karnataka, India

Dr. Roopa Lakshmi R²

Department of Computer Science
Manipal Institute of Technology
Manipal, Karnataka, India

Abstract—In this intelligent transportation systems era, traffic congestion analysis in terms of vehicle detection followed by tracking their speed is gaining tremendous attention due to its complicated intrinsic ingredients. Specifically, in the existing literature, vehicle detection on highway roads are studied extensively while, to the best of our knowledge the identification and tracking of heavy-construction vehicles such as rollers are not yet fully explored. More specifically, heavy-construction vehicles such as road rollers, trenchers and bulldozers significantly aggravate the congestion in urban roads during peak hours because of their deadly slow movement rates accompanied by their occupation of majority of road portions. Due to these reasons, promising frameworks are very much important, which can identify the heavy-construction vehicles moving in urban traffic-prone roads so that appropriate congestion evaluation strategies can be adopted to monitor traffic situations. To solve these issues, this article proposes a new deep-learning based detection framework, which employs Single Shot Detector (SSD)-based object detection system consisting of CNNs. The experimental evaluations extensively carried out on three different datasets including the benchmark ones MIO-TCD localization dataset, clearly demonstrate the enhanced performance of the proposed detection framework in terms of confidence scores and time efficiency when compared to the existing techniques.

Keywords—Intelligent transportation systems; heavy-construction vehicles detection; traffic monitoring and SSD-based CNN component; deep learning

I. INTRODUCTION

Now-a-days, Machine-learning based transportation systems are gaining more popularity due to the incorporation of deep-learning technology for various traffic domains such as traffic monitoring, speed measurement, density estimation and so on [1]. Further, due to the presence of upgraded visual surveillance systems along with GPS, makes it possible to generate enormous volume of traffic information, which can be used for future processing. As a result, traffic monitoring by means of analyzing traffic congestion using movement of vehicles is acquiring enormous attention in the recent years due to its complicated intrinsic factors. Specifically, the state-of-the-art highly sophisticated traffic surveillance cameras are capturing traffic flow along with rich-set of traffic parameters, which in turn can be effectively employed for detection followed by tracking of targeted vehicles in the given traffic environment.

Generally speaking, the performance of any traffic monitoring system is primarily dependent on two critical factors -speed of moving vehicle and density of road-traffic, which may vary from minimum to a greater extent. Specifically, in the present literature, urban traffic monitoring is implemented by means of analyzing traffic congestion of roads based on vehicle speed and road category aspects [1]. It is possible to detect the slow moving vehicles in urban traffic using Robust Visual Features. Authors have proposed a new visual feature to detect the vehicles using SURF based Features [2]. However, in the real-world road scenarios, the speed of the given vehicle mainly depends upon the type of vehicle such as slow-moving Excavator vs fast moving sports car. Due to these reasons, the classification followed by the exact identification of target moving vehicles in given traffic scenarios is very much important, so that the reliability of given traffic monitoring system can be guaranteed to a greater extent [3]. In addition to that accurate identification of target moving vehicles is very much essential in order to reduce the false alarms in target vehicle classification systems.

From another perspective, in the existing road traffic situations, one of the critical factors for heavy-traffic congestion is the presence of construction vehicles such as Front-end loaders and Rollers, which generally move at dead-slow speed. Precisely, the construction vehicles while moving dominate a huge portion of road due to their bigger size when compared with other vehicles such as cars. Further, the construction vehicles generally move at a low-paced manner and fail to follow with the average speed of other moving vehicles, due to which they affect the flow of moving traffic to a greater extent. In other words, on road construction vehicles are becoming a main hindrance in the present urban traffic situations, due to their severe impact in terms of reducing the average traffic flow on the specified urban roads. In this way, the existence of heavy construction vehicles on the urban traffic scenes significantly affects the traffic flow characteristics to a larger extent. In order to solve these issues, the accurate detection followed by tracking of heavy-construction vehicles in urban traffic roads are very much compulsory so that the traffic in congested urban roads can be controlled as well as monitored up to certain extent on-road traffic situations. The organization of the article is described as follows. Section I gives the introduction of the topic. Section II explains the existing literature survey. Section III gives the methodology frame work of the proposed Single Shot Detector (SSD)-based object detection framework, which can detect the

construction vehicles in traffic. Section IV shows the results and discussion. Section V concludes the paper with future work.

II. RELATED WORK

From the past few decades, a huge number of attempts is made in the literature towards identification and tracking of moving vehicles in urban traffic scenarios. For instance, Wang et al. [1] presented spatio-temporal features-based system for vehicle detection followed by the type classification of vehicles. In this approach, first moving objects are detected using spatio-temporal features-based algorithm, which then classifies type of detected objects by utilizing features fusion methods. Though this method performs better in general scenes; yet, it fails for identifying complex vehicle models as well as poorly illuminated traffic scenes. Further, Song et al. [3] introduced a visual feature-based vehicle detection and counting system, which can be employed in highway traffic scenarios. Precisely, in this framework, the defining of the road surface area consists of a remote area and also a proximal area. In each frame, the two road areas are sequentially detected in order to get reasonable detection results in the monitoring field. The authors employed ORB feature extraction algorithm, to predict the position of the object in the image, which is further analysed, so that the vehicle trajectory of different objects can be calculated.

Iwasaki et al. [4] proposed a robust vehicle detection framework, which uses IR thermal camera based thermal images for detecting vehicle positions followed by their respective movements. Praveen et al. [5], introduced a Gaussian mixture models-based approach for vehicle tracking followed by the speed estimation of the moving vehicles in various traffic surveillance kind of applications. However, this approach fails to attempt towards the detection of construction vehicles in traffic-prone urban roads. Further, very recently in 2020, Afrin and Yodo [6] presented a summative survey of various road traffic congestion measures that primarily contribute towards resilient and also sustainable transportation systems. According to their study, it is suggested that the management of traffic in the work zone areas are very much important in order to control congestion especially at peak hours of movements. In this aspect, they suggest that, the work zone should be planned cautiously in terms of ramp meters, computerized lane usage systems, coordinated traffic control plans and controlling traffic signals, which in turn could be useful to reduce the traffic congestions during peak hours.

Recently, Ankit Gupta et al. [3] in 2019, presented a detailed study, which indicated the impact of slowly moving vehicles on the capacity of crowded urban roads. Specifically, in their study, the authors utilized various road links from the urban arterial network of Varanasi, which though having widened road lanes, yet poses congestion challenges regularly due to the poor traffic management aspects in the Varanasi city. Further, they considered passenger car units as the basic unit of measuring highway capacity in terms of experimental and also direct empirical approaches and thereby performed an analysis on the impact of dynamic behavior of passenger car units. However, this study mainly concentrates on different modes of corrosion-induced failures in the reinforced concrete

structures and their impacts on service life of the simple rectangular beams. Furthermore, Ji et al. [7] presented a video-based construction vehicles detection framework, which can detect hydraulic excavators and dump trucks on state-owned land areas. Precisely, the authors introduce detection techniques using ROI of inverse valley features of mechanical arm as well as spatial-temporal reasoning for identifying hydraulic excavators. However, their system employs videos captured from stationary cameras and focuses mainly on traffic scenes on state-owned land areas.

To summarize, the existing state-of-the art techniques are focusing primarily towards the detection and tracking the speed of moving vehicles in urban traffic roads [8], [9], yet not much efforts are done for the detection of heavy construction vehicles in traffic-prone roads. From another perspective, construction vehicles such as road rollers, trenchers and bulldozers significantly aggravate the congestion in urban roads during peak hours because of their deadly slow movement rates accompanied by their occupation of majority of road portions. Due to these reasons, promising frameworks are very much important, which can identify the heavy-construction vehicles moving in urban traffic-prone roads so that appropriate congestion evaluation strategies can be adopted to monitor traffic situations. Further, though vehicle detection on highway lanes are studied extensively on the literature, yet to the best of our knowledge, detection frameworks for identifying heavy-construction vehicles on urban traffic scenes are not fully explored.

A. Motivation and Contributions

This article presents a deep-learning based detection framework, which identifies the heavy construction vehicles from the urban traffic scenes by making use of Single Shot Detector[10](SSD)-based object detection using convolutional neural networks. Specifically, the proposed construction vehicle detection framework is named as, "Deep-Learning Based Detection Framework", abbreviated as DLDF, employs SSD technique in order to accurately identify the construction vehicles present in the moderate to heavily congested traffic environments. More specifically, the main contributions of the proposed DLDF are given by,

- A brand-new SSD-based deep learning network with feature extraction and detection modules is created by the combination of SSD and convolutional layers. Precisely, a new SSD network of size 122 layers starting from input layer to till softmax layers is generated in order to detect heavy construction vehicles from traffic scenes.
- The proposed SSD-based DLDF is trained and tested by employing a rich set of databases (app. 137743 images+) of moving vehicles, which consists of traffic scenes collected from three different datasets including benchmark MIO-TCD localization dataset [11], VISAL Dataset [12] and so on.
- The performance evaluations of the proposed DLDF with state-of-the art technique to demonstrate the better predictions along with time efficiency comparisons.

III. METHODOLOGY OF PROPOSED FRAMEWORK

Fig. 1 shows the block diagram of proposed Single Shot Detector (SSD)-based object detection framework, which can detect the construction vehicles in traffic scenes by making use of deep learning based automatically learned image features. Specifically, the proposed construction vehicle detection framework is named as, “Deep-Learning Based Detection Framework”, abbreviated as DLDF, employs SSD technique in order to accurately identify the construction vehicles present in the heavily congested traffic environments. More specifically, the proposed DLD framework consists of two stages namely, training as well as testing stages as shown in Fig. 1.

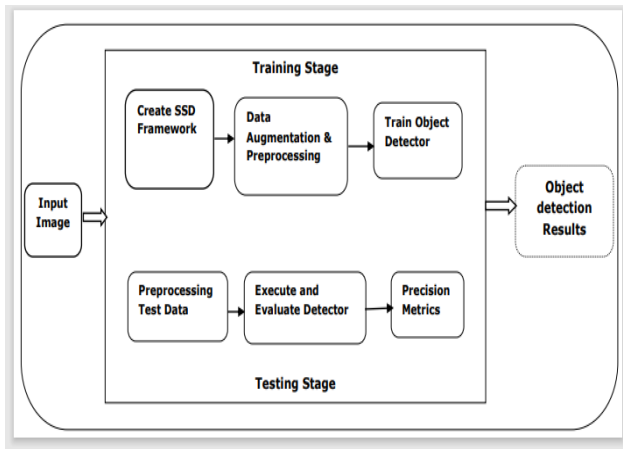


Fig. 1. Block Diagram of Proposed DLDF Framework.

Initially the input image is fed in to the training stage of the framework, which starts with creation of SSD framework module. Precisely, the SSD object detection network is created which consists of two sub-networks namely, a feature extraction network and a detection network. More precisely, the feature extraction network is generated by employing a pretrained CNN such as Mobile Net whereas detection sub-network is developed by composing SSD-specific layers and few convolutional layers. The SSD layers are used in order to specify the several significant input parameters to the proposed SSD network including input size, number of classes, size of training images and so on. After the SSD network is created, data augmentation and preprocessing is carried out in order to enhance the network accuracy by randomly transforming the original training data. Precisely, the transformations such as random flipping, random scaling and jittering image color are carried out during data augmentation and preprocessing module, in order to increase the variety of training samples. After the preprocessing module is completed, the SSD detector is trained as per the training parameters such as max epochs and initial learning rate as specified during the network creation stage.

In the testing stage, initially the preprocessing transformations are applied followed by the execution of detector on the test images. Then the resultant detection results are evaluated by means of precision and recall metrics. Then the object detection results are indicated in the form of outputs containing the bounding boxes, scores, and the labels for vehicles detected in the image.

IV. EXPERIMENTAL SETUP AND DATABASE CREATION

The performance of the proposed DLD framework is evaluated on three different datasets as given by.

- The 2017 MIO-TCD localization dataset [11].
- VISAL Dataset [12].
- Web-source Traffic videos, which are illustrated as follows.

1) *2017 MIO-TCD localization dataset [11]:* Miovision traffic camera dataset” (MIO-TCD) is one of the bench-mark dataset widely used in traffic analysis incorporating motor vehicles. It includes 11 traffic object classes such as buses, trucks, pickup trucks, work vans and pedestrians. It contains 7,86,702 annotated images captured at different timings of the day by hundreds of traffic surveillance cameras that are deployed in Canada and the United States. The 2017 MIO-TCD localization dataset contains 137,743 high resolution images each consisting of one or more foreground objects among the predefined object classes. Specifically, the 110,000 training images and 27,743 testing images from this dataset are utilized in order to evaluate the performance of the proposed framework.

2) *VISAL dataset [12]:* This Video, Image, and Sound Analysis Lab (VISAL) dataset is created for highway traffic video classification purpose, which consists of set of highway traffic videos ranging from low, medium, or high traffic scenes.

3) *Openly available traffic videos:* Different images of construction vehicles are extracted from web-based traffic videos are considered for the experimentation purpose in the proposed framework. Specifically, 10+ categories of construction vehicles dumping truck, bulldozers, Excavators, grader and front-end loader images from low-density as well as high-density traffic roads are considered for evaluation purposes.

Fig. 2 shows the snapshot of sample database images that are considered for training and testing stages of the proposed DLD framework as given below. The proposed DLD framework is evaluated in HP -Pro laptop of Intel Core i5-2.71 GHz processor, 8 GB RAM, 64-bit OS with MATLAB environment. Initially, the performance of proposed SSD framework for detecting construction vehicles from traffic scenes is evaluating by means of creation of SSD-based deep learning network with feature extraction and detection modules. Specifically, in the proposed DLD framework, SSD network of size 122 layers starting with input to focalloss and softmax layers is generated in order to detect construction vehicles from traffic scenes. More specifically, Fig. 3(a) shows the snapshot of Layer-Graph (Lgraph) generated by the proposed DLD framework, which clearly indicates the first few layer’s pictorial version, name of each layer along with type, activation function, weight and bias values. Similarly, Fig. 3(b) illustrates the snapshot of last few layers along with all other specifications of each layer.



Fig. 2. Snapshot of Sample Database Images.

V. RESULT AND DISCUSSION

For evaluation purpose, the proposed deep-learning based Detection framework DLDF is compared with state-of-the art approach introduced by Ji et al. [4] by considering similar kind of experimentation scenarios. Specifically, the efficiency and effectiveness of the proposed DLDF framework is compared with that of the reference method, which are mentioned in subsequent discussions as follows:

- 1) *Method 1*: proposed DLDF method -indicated as DLDF Method.
- 2) *Method 2*: ROI-based method by Ji et al. [4] - indicated as Ref.Method illustrated as follows.

Fig. 3 and 4 shows the snapshot of the last few layers used in Lgraph with specifications for the analysis used for training. Fig. 5 shows the detection results of proposed DLDF method by means of bounding box and label. Specifically, the heavy construction vehicle named 'Excavator' moving in a field-side road is exactly detected by proposed DLDF technique in terms of bounding box with suitable dimensions as well as confidence level scores. More specifically, the proposed DLDF framework accurately identifies the Excavator vehicle by means of bounding box of dimensions (101, 53,147,114) and confidence level score of value 75.56%. Further the total time taken by the DLDF framework for detection of this vehicle is 7.872 seconds including feature extraction and mapping stages.

Fig. 6 presents the detection results of proposed DLDF method in terms of yellow-colour two bounding boxes and labels. Specifically, the heavy construction vehicle named 'Roller' moving in a field-side road is exactly detected by proposed DLDF technique in terms of two bounding boxes of dimensions (91,28,141,139) and (23,26,177,150) respectively

whereas confidence level scores of corresponding boxes are 83.05% and 67.01% respectively. However, the size of Roller vehicle seen in the input image is more than the threshold boundary of detection boxes; therefore, the complete vehicle is mapped into two bounding boxes, with the primary box indicating higher confidence results when compared with that of secondary bounding box.

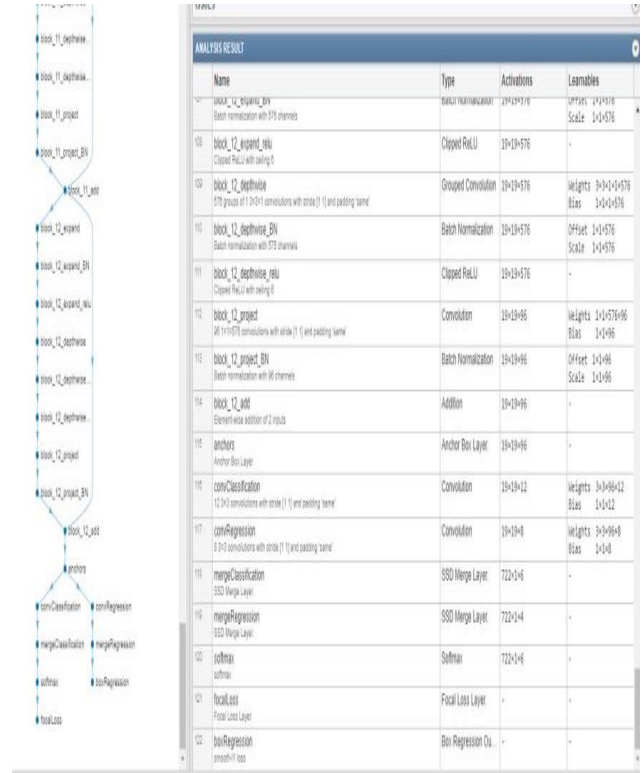


Fig. 3. Snapshot of Layer-Graph (Lgraph).

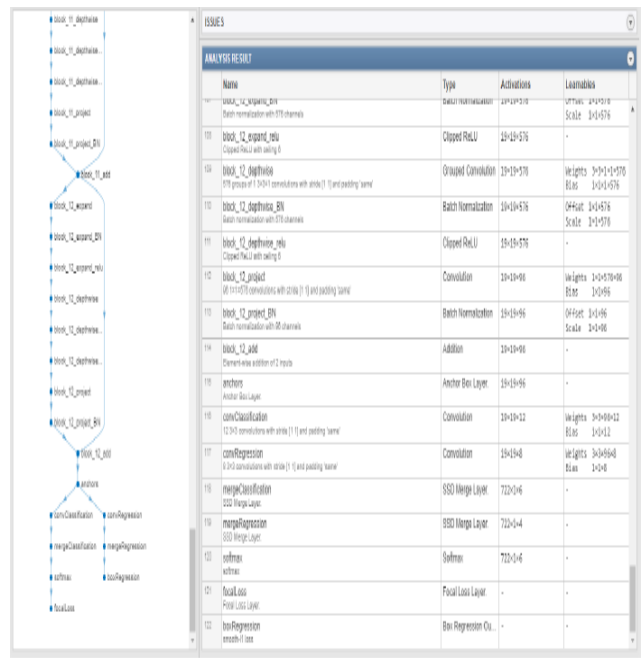


Fig. 4. Snapshot of Last Few Layers of Lgraph with Specification.



Fig. 5. Detection Results for Excavator Vehicles.

Fig. 7 indicates the construction vehicle detection results of proposed DLDF framework in terms of 'Vehicle' label followed by a bounding box. Precisely, the heavy construction vehicle named UNAC 'Trencher' moving on road-side is exactly detected by proposed DLDF technique in terms of bounding box with suitable dimensions as well as confidence level scores. More precisely, the proposed DLDF framework accurately identifies the Trencher vehicle by means of Bounding box of dimensions (32, 43,156,128) and confidence score of value 64.02%. There is a slight decrease in confidence scores are due to the presence of external objectives within scope of observation and also the movement of vehicle at considerably farther distance.



Fig. 6. Detection Results for Roller Vehicles.



Fig. 7. Detection Results of UNAC Trencher Vehicles.



(a)

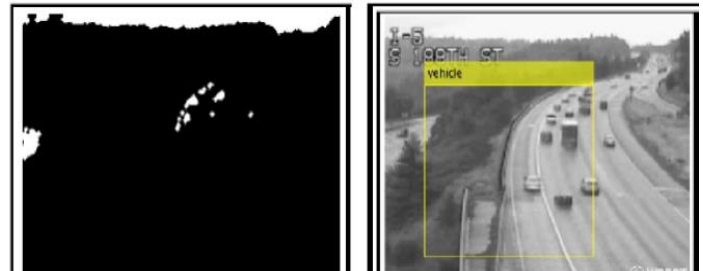


Fig. 8. (a) Ground Truth Traffic Scene (b) Detection Results of Ref.Method (c) Detection Results of DLDF Method.

Fig. 8 illustrates detection performance of the proposed Deep-learning based detection framework (DLDF) by comparing with the corresponding results of ROI-based method reference method [4]. Specifically, Fig. 8(a) shows the ground truth traffic scene taken from the experimental dataset, which depicts slightly busy traffic road with various kinds of moving vehicles including cars and a construction truck vehicle. Fig. 8(b) indicates the detection results of reference method in terms of White-colored regions on the resultant image. Fig. 8(c) shows the detection results of the proposed DLDF method, in which the construction vehicle is exactly detected, even though it is moving at a quite reasonably at a farther distance. In this way, the better detection results of proposed DLDF method can be clearly observed when compared with the reference method by means of labeling and bounding boxes.

Further, the efficiency of the proposed DLDF framework is evaluated by considering the total time consumption of all activities followed by the subsequent comparisons with the reference method, which is detailed Table I. Table I results are indicated as follows, the time taken by the proposed DLDF method for feature extraction is 2.480 seconds followed by total prediction time is 4.875 seconds whereas the time taken by Ref. method for feature extraction is 2.466 seconds followed by total detection time is 4.553 seconds respectively. Though, the time taken by the proposed DLDF method is slightly high when compared with that of Ref. method, yet it shows considerably better performance in terms of detection results as shown in Fig. 8(c). Furthermore, the confidence level of proposed framework scores 50.93% for the given traffic scene, even capturing at a faraway distance, while the ref. method achieves only 35.60% for the same scene. In this way, it is observed from the detection results that the proposed framework performs reasonably better compared to the reference technique in terms of good confidence scores.

TABLE I. TIME EFFICIENCY COMPARISON RESULTS (IN SECONDS)

Task	Proposed DLDF	Ref. Method
Features extraction	2.480	4.875
Total Time	2.466	4.553

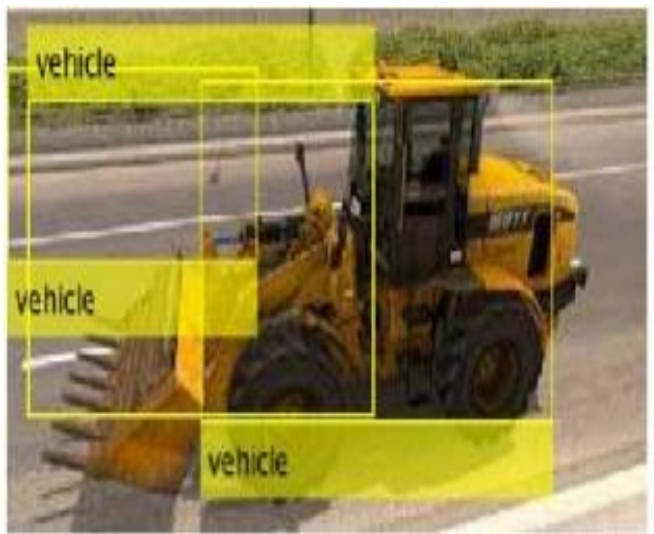


Fig. 9. Detection Results of Front-End Loader Vehicle.

Fig. 9 shows the vehicle detection results of proposed DLDF framework in terms of 3 'Vehicle' labels followed by a respective bounding box. Specifically, the heavy construction vehicle named 'Front End Loader' moving on road-side is exactly detected by proposed DLDF technique in terms of 3 bounding boxes with suitable dimensions and confidence level scores as shown in Table II. More specifically, it is observed in Table II results that the bounding box with dimensions [11,29,167,99] identifies larger portion of the vehicle, which results in confidence score of 66.98%, whereas remaining two boxes cover slightly lesser portions of vehicle, hence result in lesser confidence scores respectively. Since in the middle bounding box, the vehicle coverage is more due to which the detection confidence scores are also increased as shown in Table II.

Fig. 10 indicates the vehicle detection results of proposed DLDF framework by means of a label followed by the respective bounding box. Precisely, clustered scene with two different construction vehicles named - 'Bulldozer' and 'TLB', which are moving on a hilly-road side is considered for evaluation purpose. Though the test image includes two different construction vehicles, yet the proposed DLDF method is able to identify the vehicles at a reasonably good confidence level of 63.97%. However, it can be observed that, since the input image is slightly cluttered in terms of including body parts of two different Vehicles, which may complicate the detection process. Due to these reasons, the proposed DLDF detects it as single vehicle, since it combines the front portion of one vehicle with side portion of another type vehicle.

Fig. 11 shows the vehicle detection results of proposed DLDF framework for the test image, in which blurred version of vehicle can be observed. Precisely, it can be noticed that, in the test image, the image quality is very low followed by a lot

of occurrence of overlapping on the construction vehicle, due to which the proposed DLDF fails to detect the construction vehicle present in the image. If noise and overlapping are eliminated from the test image, then the proposed DLDF can be employed to detect the presence of vehicle.

TABLE II. DETECTION RESULTS

Bounding boxes- dimensions	Confidence scores (in %)
[1 19 121 61]	54.40
[11 29 167 99]	66.98
[94 23 171 107 99]	54.55



Fig. 10. Detection Results of Bulldozer, TLB Vehicles.



Fig. 11. Detection Results of Blurred Version of Vehicles.

VI. CONCLUSION AND FUTURE WORK

In this article, a new deep-learning based detection framework, which employs Single Shot Detector (SSD)-based object detection system consisting of CNNs is proposed for detecting heavy-construction vehicles on urban traffic scenes. The experimental results carried out on three different datasets including the benchmark ones, clearly demonstrate the enhanced performance of the proposed detection framework in terms of confidence scores and time efficiency when compared to the existing techniques. In future, the proposed framework can be successfully employed on intelligent transportation systems for monitoring congested conditions of urban traffic situations.

REFERENCES

- [1] Yu Wang, X. Ban, H. Wang, DI Wu, Hao Wang, Shouqing Yang, Sinuo Liu and Jinhui Lai, Detection and Classification of Moving Vehicle from Video Using Multiple Spatio-Temporal Features, in IEEE Access, special section on recent Advances in Video Coding and Security, Vol.7, Pages 80287-80299, <https://doi.org/10.1109/ACCESS.2019.2923199> 2019.
- [2] Sreelatha R and Roopa Lakshmi R, A Novel Framework for Detecting Slow Moving Vehicles in Urban Traffic Using Robust Visual Features, R, Sreelatha and R, Roopa Lakshmi, A Novel Framework for Detecting Slow Moving Vehicles in Urban Traffic Using Robust Visual Features, in proc. ICSDMI 2021- available at SSRN digital library: <http://dx.doi.org/10.2139/ssrn.3854305>, pages 1-10, 2021.
- [3] H. Song, H. Liang, H. Li, Z. Dai and X. Yun, "Vision-based vehicle detection and counting system using deep learning in highway scenes", in European Transport Research Review Journal, Vol. 11:51, Pages 1-16, <https://doi.org/10.1186/s12544-019-0390-4>, 2019.
- [4] Y. Iwasaki, M. Misumi and T. Nakamiya, Robust Vehicle Detection under Various Environments to Realize Road Traffic Flow Surveillance Using an Infrared Thermal Camera, The Scientific World Journal, Hindawi Publishing Corporation, Vol.1, Pages 1-12, <https://doi.org/10.1155/2015/947272>, 2015.
- [5] Praveen M Dhulavvagol, Abhilash Desai and Renuka Ganiger, Vehicle Tracking and Speed Estimation of Moving Vehicles for Traffic Surveillance Applications, in proc. of ICCTCEEC-2017, Pages73-377, <https://doi.org/10.1109/CTCEEC.2017.8455043> 2017.
- [6] Tanzina Afrin and Nita Yodo," A Survey of Road Traffic Congestion Measures towards a Sustainable and Resilient Transportation System", in MDPI journal of sustainability, Vol 12, Pages 1- 23, <https://doi.org/10.3390/su12114660>, 2020.
- [7] Wenyang Ji, Lingjun Tang, Dedi Li, Wenming Yang, Qingmin Liao," Video-based construction vehicles detection and its application in intelligent monitoring system", in proc. of Elsevier CAAI Transactions on Intelligence Technology, vol.1, pages 162-172, <https://doi.org/10.1016/j.trit.2016.09.001>, 2016.
- [8] Kahlil Muchtar, Nasaruddin, Afdhal and IndraNugraha, "Attention-based Approach for Efficient Moving Vehicle Classification", in proc. of Elsevier Procedia computer science, ICCSCI-2019,Pages683-691, doi /10.1016/j.procs.2019.08.217, 2019.
- [9] Huansheng Song, Haoxiang Liang, Huaiyu Li, Zhe Dai and Xu Yun, Vision-based vehicle detection and counting system using deep learning in highway scenes, in the journal of European Transport Research Review, 2019.
- [10] Liu, Wei, Dragomir Anguelov, Dumitru Erhan, Christian Szegedy, Scott Reed, Cheng Yang Fu, and Alexander C. Berg." SSD: Single shot multibox detector." In 14th European Conference on Computer Vision, ECCV 2016. Springer Verlag, 2016.
- [11] Zhiming Luo, Frdric Branchaud-Charron, Carl Lemaire, Janusz Konrad, Shaozi Li, Member, Akshaya Mishra, Andrew Achkar, Justin Eichel, and Pierre-Marc Jodoin, MIO-TCD: A New Benchmark Dataset for Vehicle Classification and Localization, in IEEE Trans. on Image Processing, Vol. 27, No.10,pages5129-5141, doi.org/10.1109/TIP.2018.2848705 2018.
- [12] Antoni B. Chan and Nuno Vasconcelos, Probabilistic Kernels for the Classification of Auto-regressive Visual Processes, In IEEE Conference on Computer Vision and Pattern Recognition(CVPR), San Diego, Jun 2005

Classification of Autism Spectrum Disorder and Typically Developed Children for Eye Gaze Image Dataset using Convolutional Neural Network

Ms. Praveena K N, Dr. Mahalakshmi R

Department of Computer Science and Engineering
Presidency University, Itkalpur, Rajanukunte, Bengaluru, India

Abstract—Autism is a neurobehavioral problem that hinders to interact with others. Autistic Spectrum Disorder (ASD) is a psychological disorder that hampers procurement of etymological, communication, cognitive, social skills and Stereotypical motor behaviors and capabilities. Recent research revealing that Autism Spectrum Disorder can be diagnosed using gaze structures which has opened up a new field where visual focus modelling could be highly used. Diagnosis of ASD becomes a difficult task due to wide range of symptoms and severity of ASD. Deep neural networks have been widely employed and have shown to perform well in a variety of visual data processing applications. In this paper, typically developed (TD) or ASD is classified using Convolution neural Networks (CNN) for the fixation maps of the corresponding observer's gaze at a given image. The objective of this paper is to observe whether eye-tracking data of fixation map could classify children with ASD and typical development (TD). We further investigated whether features on visual fixation would attain better classification performance. The proposed CNN model achieves 75.23% accuracy for validation.

Keywords—Autism spectrum disorder; classification; fixation maps; eye expression; visual focus; gaze pattern; CNN

I. INTRODUCTION

Currently, the world is facing lot of difficulties in medical field to diagnose the diseases in early stage. Doctors and specialists did not have the benefit of technology to identify a disease in prior in order to take precautionary measures to predict the diseases in early stage [26]. Once the condition is in risky level and becomes too late for treatments, it couldn't help to diagnose the disease. Therefore, by using data science algorithms, the data can be analysed efficiently to gain meaningful knowledge about the status of a person's health. This increase in figuring technologies for the presentation of deep learning techniques in numerous grounds of learning. Here in this research I have taken ASD Eye gaze patterns image dataset for classifying autistic and typically developed children.

Humans have an amazing tendency to focus on certain aspects of an image rather than viewing the whole scene in its entirety. Simulating the Visual Focus Modelling (VFM) selective focus function, also known as visual focus prediction or visual saliency detection. In the fields of computer vision and neuroscience, this is a well-known research subject. Visual attention helps observers to recognise the essential

regions of a scenario, which is a critical aspect in many applications. Various This research is useful in the development of visual attention models such as bottom-up and top-bottom saliency models, saccadic models, and models for identifying items of interest.

Recently, several studies have shown that gaze characteristics can be used to recognize emotional conditions, perceptive processes, and neuropathology particularly in persons with Autism Spectrum Disorder (ASD). This has opened up a new field in which visual focus modelling can be beneficial in a variety of ways, including assisting in the early identification of ASD and building Computer-Human Interfaces (CHIs) that are suited for people with ASD.

It has been found that youngsters with ASD can have uncommon examples in gaze perception, which is affected by the kid's essential visual handling being unfocussed.

In this paper, the fixation maps which represents the locations of the gaze pattern responding to the given stimuli which is useful to decide whether the observer has ASD or not [3]. Therefore, a Grand Challenge named "Saliency4ASD: Visual centre demonstrating for Autism Spectrum Disorder" will be held at IEEE ICME'19 Grand challenge. It is one of the Dataset Repository and the key goal of this initiative is to coordinate and guide the visual focus modelling community's activities toward a social challenge in healthcare. The dataset containing fixation maps of children with ASD and TD for 300 images were shared as part of the Saliency4ASD grand challenge in 2019.

This paper builds a classification model using deep learning technique called convolutional neural networks (CNNs) model for determining if an observer is typical developed (TD) or has ASD based on the fixation maps of the associated observer's gaze at the captured image. The objective of this paper is to observe whether eye-tracking data of fixation map could classify children with ASD and typical development (TD). We further investigated whether features on visual fixation would attain better classification performance. The rest of the paper is organized as follows: Section 1 deals with introduction, Second Section gives a detailed literature review on classification of ASD, in particularly, the works connected to the visual attention study from a cognitive perception. Section 3 briefing about Autism Spectrum Disorder. Autism is a neurobehavioral problem that hinders to interact with others. Autistic Spectrum Disorder

(ASD) is a psychological disorder that hampers procurement of etymological, communication, cognitive, social skills and Stereotypical motor behaviours and capabilities. Section 4 describes the thorough overview of the Grand Challenge "Saliency4ASD operation. Sections 5 and 6 discuss the datasets, its types, methods & metrics used in the proposed work. Section 7 and 8 represent the proposed model for classifying ASD/TD and Results respectively.

II. RELATED WORK

Almost all the people with ASD are experiencing more challenges with social communication and association, and finding difficulty in showing confined examples of behaviour, interests, or exercises in any given task [9]. The drawn out related issues, may incorporate troubles in performing every day works, making and keeping connections, and looking after a basic work. ASD isn't just perhaps the most confounded mental issues, yet additionally it is quite possibly the most effortlessly acquired. A more experienced parent, an ASD family history, and some inherited disorders are all risk factors for ASD. Because of the mind boggling quality to-quality and quality to-climate cooperation systems, some basic investigations demonstrated that the genetic and atomic premise of the people with ASD include in excess of 100 qualities [23]. There is a reasonable differential between those with ASD and those with Typical Development (TD), particularly as far as neighbourhood wisdom instead of worldwide perception.

People with ASD pay more attention to neighbourhood details with a more grounded tactile capacity, according to certain related works as well as improved perceptual discrimination along with an extraordinary tactile reactivity, such as eruption or under reaction to the climate [1].

At the moment, the most common methods for detecting ASD are conducting interviews with guardians or family members of ASD affected children, as well as observation and examination of their behaviour. Nonetheless, these finding methods are not just powerless against the inclination of the abstract clarification, yet in addition are time-devouring and costly. Furthermore, due to numerous limits and blockages, more than a third of ASD testing does not follow the precise and accurate diagnosis pathway [24]. A few recent research have recommended for the use of the aggregate technique to overcome the difficulties of genotyping investigations on complex mental diseases such as schizophrenia. The Broad Autism Phenotype (BAP) was proposed by few other studies few surveys have discovered that the parents of children with ASD are gifted individuals. At the same time, these parents were experiencing ASD symptoms unknowingly.

Dataset serves as a substantial aggregate to aid in the diagnosis of ASD development. Eye tracking data comprises vast data of visual consideration, neurological control, and individual psychology. Furthermore, eye development data has been successfully employed to assist with several other mental turmoil conclusion tasks, such as mental state acknowledgment and neuropathology determination [24]. In contrast to old-style quantization table-based determination procedures, eye development information-based strategies are

unbiased, dependable, efficient, and logical due to the programmed assortment and quantitative processing. As a result, image statistics on eye development can greatly aid in ASD diagnosis. Few studies have discovered that people with ASD have different personality's eye movement behaviours than people with normal. In terms of preference predispositions, the study and evaluation of eye development records may afford a technique to identify between people with ASD and those with TD [25]. ASD kid's, for example, give a smaller amount of attention towards the frontal area entertainers and pay more attention to the ground districts when viewing a movie. Young people by ASD give a smaller amount of attention towards the eyes of human faces than those with TD. While watching recordings, Jones et al. [13] used technology of eye tracking to investigate the dispersal of optical obsessive information in people with TD and those with ASD. According to examinations, people with ASD give a smaller amount of attention to the entertainer's eyes and give extra responsiveness to their mouths [18]. Additionally, there have been current research improving this problem that use AI propels and a deep learning method has been taken to anticipate where children with ASD will glance in various settings [5], with a focus on human looks. Fang et al. [8] also recommended using gaze following associated visual enhancements for autism analysis.

Advances in eye-development information studies show that people with ASD have different eye-development behaviour than those with TD.

III. AUTISM SPECTRUM DISORDER

Mental imbalance range issue is an assortment of multipart issues of the mind advancements remember trouble for social connections, dreary practices and interchanges. These issues root at youthful age of 2-3 years and thusly, indications of ASD might be acknowledged at a youthful age [6] Autism Spectrum Disorders are multiple times regular in young men than in young ladies [5].

A. The Causes of Autism

The causes of autism are as follows:

- 1) It can be happened in children of any race, civilization, or communal family.
- 2) Chemical imbalance may cause because of specific blends of qualities which may build a youngster's danger in chemical imbalance.
- 3) Chemical imbalance is more likely in a child with a more experienced parent.
- 4) On the off chance that a pregnant lady is presented to specific drugs or engineered synthetic substances, like liquor or hostile to seizure prescriptions, her kid is probably going to be therapeutically contemplative.
- 5) Other danger factors incorporate maternal metabolic issues like as diabetes and obesity. Untreated phenylketonuria (otherwise called PKU, a metabolic contamination affected by the shortfall of a synthetic and rubella) has additionally been connected to psychological instability (German measles).

B. Autism Screening and Diagnosis

It is hard to get a definite conclusion of chemical imbalance. The specialist will accentuation on exercises and development of youngsters. Diagnosis of Autism can takes place in two methods:

- A progressive screening will verbalize the specialist whether the youngster is on target with rudimentary capacities, for example, schooling, talking, exercises, and moving. Pros suggest that kids be screened for these formative deferrals all through their precise registration at 9 months, year and a half, and 24 or 30 months old enough. Kids are constantly checked decisively for mental imbalance at their 18-month and two year registration.
- In the event that the youth exhibits signs of an issue on these screenings, they will require an additional an unmistakable appraisal. This might incorporate hearing and vision appraisals or inherited tests. The expert might need to bring somebody who has useful involvement with mental awkwardness issues, like a developmental pediatrician or an adolescent clinician. Picked investigators can other than give a test called the Autism Diagnostic Observation Schedule (ADOS) [21].

C. Autism Treatment

Here is certainly not remedy aimed at chemical imbalance. However, initial determination be able to gain an extraordinary change in the ground for a kid with mental imbalance. There are two main treatments of autism. They are:

- Behavioural and open treatment are two sorts of treatment. One of these medications is Applied Behaviour Analysis (ABA), which advances positive conduct while restraining negative conduct.
- Behavioural and open treatment are two sorts of treatment. One of these medications is Applied Behaviour Analysis (ABA), which advances positive conduct while restraining negative conduct.
- Sensory joining treatment can assist the individuals who with having issues with being reached or with seeing or hearing things.
- Speech treatment creates social limits.

IV. SUMMARY OF THE DATASET

During ICME'19, Dell, Invensun, and "Quest Industries Creative" co-supported the Grand Challenge "Saliency4ASD [1]: Visual thought introducing for Autism Spectrum Disorder," which was directed by Shanghai Jiao Tong University and the University of Nantes (a Research, Education and Innovation gathering of the Region Pays de la Loire, France).

Major points of these events existed as follows:

- Change visual consideration nearby district to a clinical consideration social issue, just as to help field experts in building a first benchmark of models that might be used in the analysis of ASD and the progression of gainful

apparatuses for people with ASD. This Grand Challenge's underlying technique focused exclusively on cutting edge youngsters with ASD and kids with TD, disregarding the chance of comorbidities (i.e., when no less than two issues co-happen in a comparative subject, like Attention Deficit Hyperactivity Disorder) and the different degrees of ASD inside the synthetic awkwardness range [9]. By taking a dataset of pictures, cover a wide-ranging scope of substance and together with total eye-following data got through visual thought tests with kids with ASD and with TD [1]. This dataset will take into account the preparation and tuning of visual thought calculations, just as a reasonable correlation of their shows.

- Standard models used for saliency and grouping, given that devices, and determining appropriate measurements are all available in this grand challenge [1].
- Identify probable concerns from the datasets that can aid in the identification of individual look examples using autism, for instance the impact of the content (like photographs with humans, without humans, some human faces, and so on).
- Given that a pattern of exhibiting methodologies on behalf of ASD [1], which give intuitions of the essential highlights powerful optical consideration of persons with ASD [8], along with thoughts for probable demonstrating systems (like machine learning, training techniques, network models [8], and so forth).
- Considering this, the proposed experiments meant for the observers mounted as:
 - Track 1: Assumed an image, calculate the saliency maps that [1] correspond to people with ASD's gaze behaviour.
 - Track 2: Given an image and one observer's fixation sequence, classify whether he or she has ASD or TD.

V. DESCRIPTION OF THE DATASET AND THE PROCESSED EYE GAZE DATA

The dataset made for the Saliency4ASD Grand Challenge, which contains pictures and eye tracking information of youngsters with ASD and TD, is displayed in this section.

A. Experiment with Subjectivity

To create a dataset for analysing observation forms in kids with ASD, a one-on-one experiment was conducted with kids with ASD and TD [20], in which they were educated to openly observe pictures however their eye movements were captured using an eye-tracker [1].

We procured 300 pictures from, which is an enormous public data base that contains pictures with different scenes [4], to concentrate on the characteristics and changes in eye movements among kids with ASD and ordinary children under various visual improvements. The test boosts incorporate 40 pictures of different animals, 88 pictures of structures or articles, 20 pictures of typical scenes, 36 pictures of numerous

people in a solitary picture, 41 pictures of different individuals and items in a solitary picture, 32 pictures of a solitary person in one picture, and 43 pictures of a single individual and things in a single picture [4].

Images were displayed and eye movements were recorded using a Tobii T120 Eye Tracker [17]. This eye tracker has a 17-inch display with a 1280*1024 (width*height) resolution [4]. The eye tracker's sampling rate is defined as 120 Hz, and the tracking range is 50 to 80 cm [4]. Subjects are positioned at a viewing distance of 65 cm from the eye tracker [4] in our studies.

B. Subjects

Twenty exceptionally effective kids with ASD who satisfied DSM-V [4] analytical principles for autism [10] were included in the dataset of eye movements for kids with Autism Spectrum Disorder (ASD) [19][13][14]. Amongst 20 members with ASD, just 14 subjects might finish the adjustment stage then get active eye development information [15]. The average age for the participants were 8 years. Along with this ASD, 14 healthy kids were recruited as controls, whose average age is 8 years [4]. In the dataset, gender, race and education were matched with two groups to guarantee the speculation of the data set. In the given dataset, parents gave written consent.

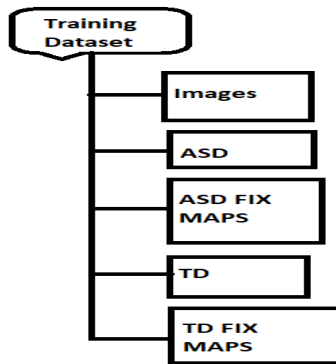


Fig. 1. Training Dataset Structure.

The Grand Challenge participants were given a training dataset in response to their request [1]. It indicates that this dataset is freely accessible for research scholars [1].

This dataset was provided to members after they requested it in order to construct and tune models. It contains 300 images as well as eye tracking data from 14 children with ASD and 14 children with Typical Development (TD) [16]. As may be seen in [2] this dataset is open to the research community. Fig. 1 represents the structure of Training dataset which is described as follows:

- Images: Images are in the form of “png” format.
- ASD: Text documents containing children with ASD's fixation sequences. Each document is a single image with fixations from all individuals [1]. It shows the index of fixation, as well as the A and B coordinates [1] and fixation time [1]. The fixation index [1] (Idx) goes from 0 to 1 [1].

- ASD Fixmaps: This record contains the saliency maps (in "png" documents) of each picture got from fixations of youngsters with ASD [1], following separating with a 1-degree Gaussian channel [1].
- TD: Manuscript documents that contain the fixation structures of children with TD.
- TD Fixmaps: This record has the saliency maps [1] (in "png" documents) of every picture obtained from TD fixations [1].

VI. METHODS AND METRICS

The methodologies and metrics used to assess the models performance are discussed in this section. The following metrics could be used for comparing saliency maps to predict gaze pattern of ASD children.

Accuracy: Accuracy is defined as the number of correct predictions divided by the total number of input samples [11].

Accuracy = (Correct number of guesses) / (Number of total predictions made)

F1 score: It is used to assess the test's precision. The Harmonic Mean of recall and precision is the F1 Score. F1 Score has a range of [0, 1] [5]. It lets you know how explicit and robust your classifier is (the number of occurrences it accurately arranges) (it doesn't miss a critical number of examples).

Mathematically, it is written as:

$$F1=2* 1/((1/precision)+(1/recall))[17]$$

The F1 score determines the stability of precision and recall [5].

Precision: The number of correct positive results divided by the number of positive results predicted by the classifier is the precision [5].

Mathematically, it is written as:

$$Precision=True\ positive/(True\ positive+False\ positive)[16][11][22]$$

Recall: It is calculated by dividing the number of correct positive results by the total number of relevant samples [5] (all samples that should have been classified as positive) [5].

$$Recall=True\ positive / (True\ positive+False\ Negative) [8]$$

VII. PROPOSED MODEL FOR CLASSIFYING ASD AND TD

A. Methodology

Fig. 2 depicts the flow chart of research methodology and it tells about the data collection, data pre-processing & augmentation and classification. The approach describes the method that will be used to carry out the experiment. It entails data preparation and enhancement, classification, prediction using CNN model and performance evaluation.

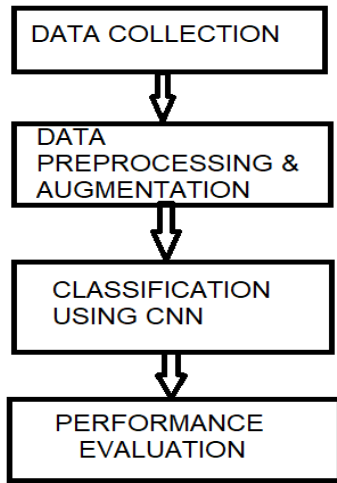


Fig. 2. Flow Chart of Research Methodology.

Fig. 3(a) and (b) denotes sample image of ASD and TD fixation map respectively. This research involved the automatic detection and classification of ASD and TD for ASD and TD fixation maps [2]. First the input pictures are pre-processed and features are extracted automatically using Convolution Neural Networks (CNN). The CNN architecture is used to classify the ASD and TD. Sample example of ASD and TD fixation maps are as follows:

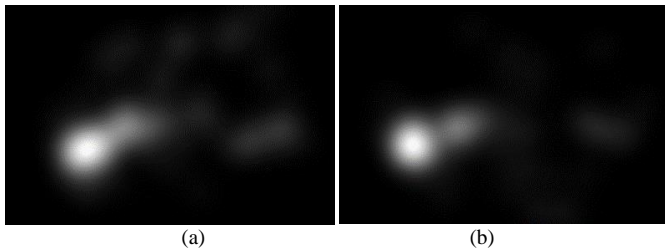


Fig. 3. Sample Image of (a) ASD Fixation Map (b) TD Fixation Map.

ASD Fixmaps: This record contains the saliency maps (in "png" documents) of each picture got from fixations of youngsters with ASD [1], following separating with a 1-degree Gaussian channel [1].

TD Fixmaps: This record has the saliency maps [1] (in "png" documents) of every picture obtained from TD fixations [1].

For classification challenges, deep learning technology is applied. When compared to traditional architecture, it processes a huge number of hidden layers. It learns features by consuming a huge quantity of labelled data without using any feature extraction methods [2]. CNN is a core deep learning algorithm that gives the best results on a variety of databases, including Cifar-10, MS-coco Mnist, and others. CNN is utilised in this study to classify ASD and TD using fixation maps.

B. Convolutional Neural Network (CNN)

CNN is a feed forward neural network [17][6] that is mostly used to analyse computer vision problems.

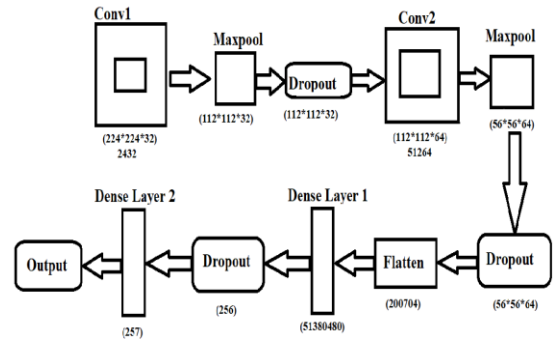


Fig. 4. Flowchart for CNN Implementation.

Fig. 4 depicts the CNN implementation flowchart. It consists of Convolution layer followed by Maxpool layer, dropout layer, flatten layer which is followed by dense layers. The architecture is represented by a multi-layered perceptron with shift invariant properties. Multiple layers are interconnected and constructed based on the human visual brain. The input layer, hidden layer, and output layer are the three main layers that make up the CNN architecture [3]. The input layer [3] represents about the image that will be entered, it pre-processes the image to make it uniform in height, width, and channel count. Convolution is depicted in the second major layer. With stride and padding, an array of uniform filters is convoluted to the input images in this layer. The equation defines the convolution layer for this work.

$$D_{i,i,j} = \sum_{k=0}^{k-1} \sum_{p=0}^{H-1} \sum_{q=0}^{H-1} I_{i+p,j+q,k}^{l-1} h_{pqkm} + b_{ijm} \quad (1)$$

Where $D_{i,i,j}$ is the convolution's output, and F_{pqkm} represents weight applied to the convolution, and b_{ijm} represents bias applied to the convolution [3]. $I=1...m$ and $j=1...n$ represents row and column indexes of input image [3], F_{pqkm} represents weight applied to the convolution [3], and b_{ijm} represents bias applied to the convolution [3]. Equation (1) is used to calculate striding and padding.

$$((W-F+2P)/S)+1 \quad (2) [11]$$

Where:

W is the number of input volume size [11],

F is the size of filters to be [11] convoluted with input,

P is the padding and.

S is the stride.

In deep learning approaches, the Rectified linear unit (ReLU) [7] is a widely used activation function [15] [7]. It is complex to enhance weight through the gradient descent if the input has narrow derivative, ReLU allows to reduce the vanishing gradient problem. ReLU activation function is derived by the following equation (3).

$$(d_{i,k}) = \max(0, D_{i,k}) \quad (3)$$

$$(x) = ax \text{ for } x < 0$$

$$x \text{ for } x \geq 0$$

Where $\sigma(x)$ denotes ReLU parametric function and (i) denotes convolutional output from the filter and diseased image. Pooling layer serves to reduce the spatial resolution of convolutional outcome on each dimension. Pooling has designed using maximum, minimum or mean values of the kernel in an image. Max pooling is widely used for convolutional neural network.

Let $K \times K$ block is taken from the $N \times N$ image. Maximum value is selected from $K \times K$ block and placed it in a pool. Commonly 2×2 window is preferred for pooling layer.

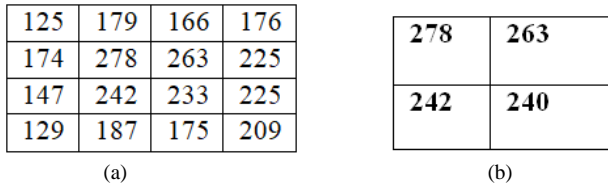


Fig. 5. Pooling Layer (a) 4×4 Convolved Output (b) 2×2 Max Pooled Output.

The values from the convolution layer are shown in Fig. 5(a), and the max pooled values from the specified convolution layer are shown in Fig. 5(b).

After collecting features from the convolutional layer, the outputs are processed through a pooling layer before being flattened into a single-dimensional vector. A $2 \times 2 \times 64$ convolved 2D vector is converted to a 256 flat vector using the flatten filter. The flattened layer's output is connected to the activation function by the dense layer. Each input node is connected to its corresponding output node. The data in the dense layer is normalised using the ReLU activation function, where w_k is the weight function present in the k th node of [3] the flattened layer. In this study, CNN is used to do binary classification of ASD and TD. The trained model for ASD classification was created using the Keras model's prediction class, which accepts trained data as Numpy Arrays as input. Binary classes are employed in this study, hence binary inputs have been converted to arrays as dictionaries. Class weights are assigned to [3] each sample's keys in the training [3] phase. For each label, the sigmoid activation function is utilised to categorise the probability distribution and which is shown in Fig. 6.

Sigmoid function is given by:

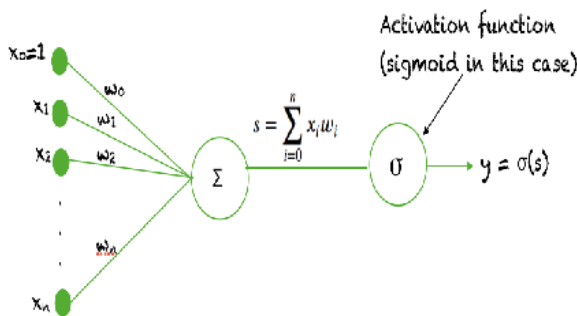


Fig. 6. Sigmoid Activation Function.

At the point when the activation function for a neuron is a sigmoid function, it is an assurance that the yield of this unit will consistently be somewhere in the range of 0 and 1. Likewise, as the sigmoid is a non-linear function, the yield of this unit would be a non-direct function of the weighted amount of data sources. Such a neuron that utilizes a sigmoid function as an activation work is named as a sigmoid unit.

C. Proposed Model for Classifying ASD and TD

Fig. 7 represents the CNN implementation for the proposed model. By using ASD/TD fixation maps as an input image, the proposed methodology explains how to classify ASD and TD. Deep neural networks are used to extract hidden information from fixation maps and make decisions in this case [3]. Our proposed classification model, which is based on the CNN architecture [2] and uses the fixation maps, is shown in Fig. 6. Fig. 6 shows our proposed categorization model based on eye tracking fixation maps. Fixation maps are incorporated into a proposed model to classify whether the person is having autism or not [2] [3]. The eye movement dataset [2] for ASD children [2] provided by the Saliency4ASD grand challenge organiser is used to train the ASD classification networks [2] [3].

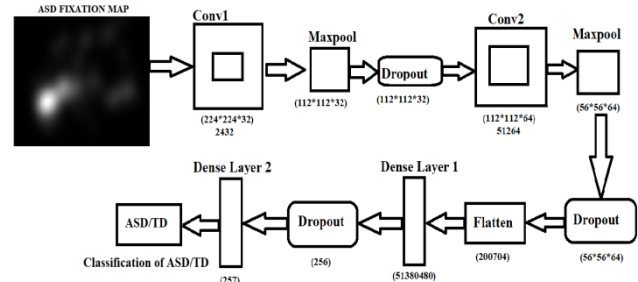


Fig. 7. Proposed Model for CNN Implementation.

VIII. EXPERIMENT

A. Dataset Usage

The training dataset comprises 300 images, where every image is observed by 14 TD youngsters and 14 ASD kids [3]. Meanwhile a few of the youngsters probably won't take a gander at the areas inside the pictures, a portion of the pictures have under 14 fixation maps from the ASD or TD gatherings.

The first 70% of images (images 1-210) and their associated fixation maps are used for training the proposed model [2] in the Saliency4ASD grand challenge, while images 211-300 and their associated fixation maps are utilised as the validation dataset to [2] choose the model for testing [2].

B. Experimental Setup

The proposed ASD classification model's training process is carried out in Google colab. The Adam optimizer [2] is utilized to train any deep learning model [2], with a learning rate [2] of 0.001 and a batch size of 20. The model is prepared for [2] 60 epochs, then the model that performs best on the validation dataset [2] is picked for testing. In the time of the evaluation, the model's weights are stable [2], and dropout is [2] utilized.

IX. RESULTS

The major goal of this research is to use Fixation maps to automatically detect and classify ASD. 300 ASD fixation maps and 300 TD fixation maps are used for classification. Each image is converted to grayscale and resized with 224 X 224 dimension for processing.

A. Classification of ASD using CNN Training and Testing Phase

The detected section of ultrasound is scaled to 224 x 224 height and breadth for training purposes. The initial convolution for the input image is made up of 32 3X3 filters, yielding 2432 parameters. The activation function for this convolution is ReLU [3]. The convolution layer's 2-dimensional vector is max pooled with a 2X2 matrix [3]. The 2nd convolution of the generated data employs 64 filters with a kernel size of [3] 3X3 array [3], ReLU activation, and yields 51264 parameters [2]. For this convolution, the max pooling filter size is 2X2 [2]. The second convolution produces 51264 parameters. These 51264 data are converted to a single dimension vector using a flattened layer. The first dense layer uses 51380480 parameters to execute nonlinear operations on the flattened input vector. The output of the second dense layer is 257 params. Due to binary level disease classification, sigmoid activation is used in this study; it processes single dimension data as input from a flattened layer [2]. From the input images, this architecture generates 257 features using metrics, loss, and learning rate algorithms. Fit complied data from architecture is utilized to train the model [12]. The training and validation accuracy is 74.33% and 75.23% respectively which is shown in Table I.

TABLE I. CNN TRAINING IMPLEMENTATION WITH OUTPUT PARAMETERS USING PYTHON

Training Accuracy	Validation Accuracy
74.33%	75.23%

Two categories of images with sizes of 224X224 have been added to the batch for testing. The corresponding classes are recognised by the prediction matrix which is given by:

Prediction Matrix =

148	25
20	168

Performance Analysis: The confusion matrix [2] is used to calculate the performance analysis for the estimated matrix [3] which is shown on Table II. True positive, true negative, false positive, and false negative [14] scores for the confusion matrix [14] are obtained from the prediction matrix on the ASD validation [2]. Table III represents the performance analysis for classification of ASD on training and validation data. Table IV depicts the performance analysis for classification Accuracy on testing data. The performance methods are designed by using below mentioned formulae:

$$\text{Accuracy} = \text{TP} + \text{TN} / (\text{TP} + \text{TN} + \text{FP} + \text{FN}) [9][10]$$

$$\text{Precision} = \text{TP} / (\text{TP} + \text{FP}) [9][10]$$

$$\text{Recall} = \text{TP} / (\text{TP} + \text{FN}) [9][10][21]$$

$$\text{F score} = 2 * \text{Precision} * \text{Recall} / (\text{Precision} + \text{Recall}) [9][10][21]$$

TABLE II. CONFUSION MATRIX

Testing samples	Training samples	
	148	25
	20	168

TABLE III. PERFORMANCE ANALYSIS FOR CLASSIFICATION OF AUTISM SPECTRUM DISORDER (ASD) ON TRAINING AND VALIDATION DATA

Layer (type)	Output Shape	Param #
Conv2d (Conv2D)	(None, 224, 224, 32)	2432
max_pooling2d (MaxPooling2D)	(None, 112, 112, 32)	0
dropout (Dropout)	(None, 112, 112, 32)	0
Conv2d_1 (Conv2D)	(None, 112, 112, 64)	51264
max_pooling2d_1 (MaxPooling2D)	(None, 56, 56, 64)	0
dropout_1 (Dropout)	(None, 56, 56, 64)	0
flatten (Flatten)	(None, 200704)	0
dense(Dense)	(None, 256)	51380480
dropout_2(Dropout)	(None, 256)	0
dense_1(Dense)	(None, 1)	257
Total params: 51,434,433		
Trainable params: 51,434,433		
Non-Trainable params: 0		

TABLE IV. PERFORMANCE ANALYSIS FOR CLASSIFICATION ACCURACY ON TEST DATA

FN	FP	TP	Precision	Accuracy	Recall	F1
0.00	0.00	93.00	0.73	0.75	0.75	0.74
1.00	0.00	92.00	0.73	0.75	0.75	0.74
1.00	1.00	91.00	0.73	0.75	0.75	0.74
2.00	0.00	91.00	0.73	0.75	0.75	0.74
2.00	1.00	90.00	0.73	0.75	0.75	0.74
2.00	2.00	89.00	0.73	0.75	0.75	0.74
3.00	0.00	90.00	0.73	0.75	0.75	0.74
3.00	1.00	89.00	0.73	0.75	0.75	0.74
3.00	2.00	88.00	0.73	0.75	0.75	0.74
3.00	3.00	87.00	0.73	0.75	0.75	0.74
4.00	0.00	89.00	0.73	0.75	0.75	0.74
4.00	1.00	88.00	0.73	0.75	0.75	0.74
4.00	2.00	87.00	0.73	0.75	0.75	0.74
4.00	3.00	86.00	0.73	0.75	0.75	0.74
4.00	4.00	85.00	0.73	0.75	0.75	0.74

FN: False Negative

FP: False Positive

TP: True Positive

The above Tables II, III and IV depicts confusion matrix, performance metrics for classification of ASD using CNN and Performance Analysis for Classification Accuracy on test data, respectively.

Loss function: It is used to calculate model error. The training and validation loss is depicted in Fig. 8. While training neural networks and machine learning models in general [9], thorough going Possibility delivers a structure for selecting a loss function [9]. While training neural network models, the two primary types of loss functions to use are cross-entropy [9] and mean squared error [7][9].

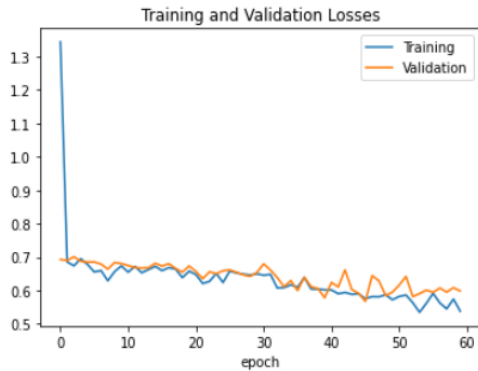


Fig. 8. Training and Validation Loss.

Trainig and validation accuracy: It is the metric for evaluating classification models. Fig. 9 represents the training and validation accuracy.

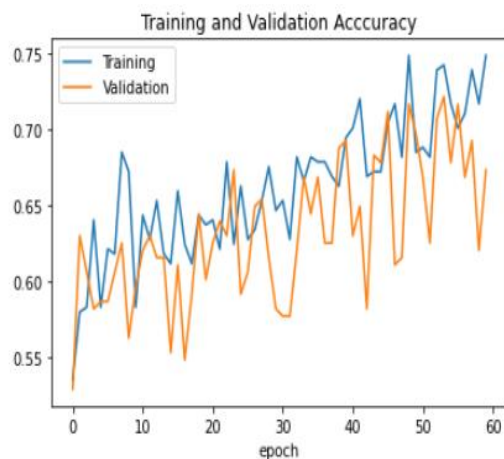


Fig. 9. Training and Validation Accuracy.

X. CONCLUSION

The major goal of this paper is to classify ASD based on observer's Fixation maps is proposed. The CNN architecture is used to extract the features from fixation maps. 300 ASD fixation maps and 300 TD fixation maps are used for classification. Each image is converted to grayscale and resized with 224 X 224 dimension for processing. The proposed model achieves 75.23% accuracy on the validation dataset.

The objective of this paper is to observe whether eye-tracking data of fixation map could classify children with ASD and typical development (TD). We further investigated whether features on visual fixation would attain better classification performance. In future work, the perceptive

technique would be examined and incorporated with the model to enhance the accuracy and other metrics. And also we will try to examine different features of images and can be integrated in our future model. A comprehensive analysis on the dissimilarities in the fixation maps among TD and ASD children will also be accompanied.

ACKNOWLEDGMENT

I would like to express my deep gratitude to my professor Dr. Mahalakshmi R, my research supervisor, for her patient guidance, enthusiastic encouragement and useful critiques of this research work. Finally, I wish to thank my parents for their support and encouragement throughout my study.

DECLARATION OF CONFLICTING INTERESTS

The author(s) declared no potential conflicts of interest with respect to the research, authorship, and/or publication of this article.

FUNDING

The author(s) declared no funding.

COMMUNITY INVOLVEMENT

It is acknowledge that community involvement is not applicable/required.

REFERENCES

- [1] Gutiérrez, Jesús, Zhaohui Che, Guangtao Zhai, and Patrick Le Callet. "Saliency4ASD: Challenge, dataset and tools for visual attention modeling for autism spectrum disorder." *Signal Processing: Image Communication* 92 (2021): 116092.
- [2] Duan, Huiyu, Guangtao Zhai, Xiongkuo Min, Zhaohui Che, Yi Fang, Xiaokang Yang, Jesús Gutiérrez, and Patrick Le Callet. "A dataset of eye movements for the children with autism spectrum disorder." In *Proceedings of the 10th ACM Multimedia Systems Conference*, pp. 255-260. 2019.
- [3] H. Duan, G. Zhai, X. Min, Y. Fang, Z. Che, X. Yang, C. Zhi, H. Yang N. Liu, Learning to predict where the children with ASD look, in: 2018 25th IEEE International Conference on Image Processing (ICIP), 2018, pp. 704–708.
- [4] A. Borji, L. Itti, State-of-the-Art in visual attention modeling, *IEEE Transactions on Pattern Analysis and Machine Intelligence* 35 (1) (2013) 185–207. doi:10.1109/TPAMI.2012.89.
- [5] Condy, Emma E et al., "Maternal Affect during a Challenging Mother–Child Interaction: The impacts of Broad Autism Phenotype and Respiratory Sinus Arrhythmia Reactivity in Mothers of Children with and Without Autism Spectrum Disorder." *Journal of autism and developmental disorders* 49, no. 12 (2019): 4891–4900.
- [6] Ibrahim, Izaida. "Specific Learning Disorder in Children with Autism Spectrum Disorder: Current Issues and Future Implications." *Advances in Neurodevelopmental Disorders* (2019): 1-10.
- [7] Duan, Huiyu, Xiongkuo Min, Yi Fang, Lei Fan, Xiaokang Yang, and Guangtao Zhai. "Visual attention analysis and prediction on human faces for children with autism spectrum disorder." *ACM Transactions on Multimedia Computing, Communications, and Applications (TOMM)* 15, no. 3s (2019): 1-23.
- [8] Y. Fang, H. Duan, F. Shi, X. Min, G. Zhai, Identifying children with autism spectrum disorder based on gaze-following, in: 2020 IEEE International Conference on Image Processing (ICIP), 2020, pp. 423–427.
- [9] Le Meur, Olivier, Alexis Nebout, Myriam Chere, and Elise Etchamendy. "From Kanner Autism to Asperger Syndromes, the Difficult Task to Predict Where ASD People Look at." *IEEE Access* 8 (2020): 162132-162140.

- [10] Tilke Judd, Krista Ehinger, Frédo Durand, and Antonio Torralba. 2009. Learning to predict where humans look. In Proceedings of the IEEE International Conference on Computer Vision (ICCV).2106–2113.
- [11] American Psychiatric Association et al. 2013. Diagnostic and statistical manual of mental disorders (DSM-5). American Psychiatric Pub.
- [12] W. Jones, K. Carr, A. Klin, “Absence of preferential looking to the eyes of approaching adults predicts level of social disability in 2-year-old toddlers with autism spectrum disorder”, *Archives of general psychiatry* (2008) 946–954.
- [13] A. Klin, W. Jones, R. Schultz, F. Volkmar, D. Cohen, “Visual fixation pat-terns during viewing of naturalistic social situations as predictors of social competence in individuals with autism”, *Archives of general psychiatry* (2002) 809–816.
- [14] Z. Bylinskii, T. Judd, A. Oliva, A. Torralba, F. Durand, What Do Different Evaluation Metrics Tell Us About Saliency Models?, *IEEE Transactions on Pattern Analysis and Machine Intelligence* 41 (3) (2019) 740–757. doi:10.1109/TPAMI.2018.2815601.
- [15] Peter C. Pantelis and Daniel P. Kennedy, “Deconstructing atypical eye gaze perception in autism spectrum disorder”, *Scientific reports*, vol. 7, no. 14990, pp. 1–10, 2017.
- [16] Startsev, Mikhail, and Michael Dorr. "Classifying autism spectrum disorder based on scanpaths and saliency." In 2019 IEEE International Conference on Multimedia & Expo Workshops (ICMEW), pp. 633-636. IEEE, 2019.
- [17] Tao, Yudong, and Mei-Ling Shyu. "SP-ASDNet: CNN-LSTM based ASD classification model using observer scanpaths." In 2019 IEEE International conference on multimedia & expo workshops (ICMEW), pp. 641-646. IEEE, 2019.
- [18] Rahman, Shafin, Sejuti Rahman, Omar Shahid, Md Tahmeed Abdullah, and Jubair Ahmed Sourov. "Classifying Eye-Tracking Data Using Saliency Maps." In 2020 25th International Conference on Pattern Recognition (ICPR), pp. 9288-9295. IEEE, 2021.
- [19] Wang, Wenguan, and Jianbing Shen. "Deep visual attention prediction." *IEEE Transactions on Image Processing* 27, no. 5 (2017): 2368-2378.
- [20] Elbattah, Mahmoud, Romuald Carette, Gilles Dequen, Jean-Luc Guérin, and Federica Cilia. "Learning clusters in autism spectrum disorder: Image-based clustering of eye-tracking scanpaths with deep autoencoder." In 2019 41st Annual international conference of the IEEE engineering in medicine and biology society (EMBC), pp. 1417-1420. IEEE, 2019.
- [21] Startsev, Mikhail, and Michael Dorr. "Classifying autism spectrum disorder based on scanpaths and saliency." In 2019 IEEE International Conference on Multimedia & Expo Workshops (ICMEW), pp. 633-636. IEEE, 2019.
- [22] Ahmed, Zeyad AT, and Mukti E. Jadhav. "Convolutional Neural Network for Prediction of Autism based on Eye-tracking Scanpaths." *International Journal of Psychosocial Rehabilitation* 24, no. 05 (2020).
- [23] Wu, Chongruo, Sidrah Liaqat, Sen-ching Cheung, Chen-Nee Chuah, and Sally Ozonoff. "Predicting autism diagnosis using image with fixations and synthetic saccade patterns." In 2019 IEEE International Conference on Multimedia & Expo Workshops (ICMEW), pp. 647-650. IEEE, 2019.
- [24] Arru, Giuliano, Pramit Mazumdar, and Federica Battisti. "Exploiting visual behaviour for autism spectrum disorder identification." In 2019 IEEE International Conference on Multimedia & Expo Workshops (ICMEW), pp. 637-640. IEEE, 2019.
- [25] Goldberg, Joseph H., and Jonathan I. Helfman. "Visual scanpath representation." In Proceedings of the 2010 Symposium on Eye-Tracking Research & Applications, pp. 203-210. 2010.
- [26] Praveena K.N., Mahalakshmi R. (2022) A Survey on Early Prediction of Autism Spectrum Disorder Using Supervised Machine Learning Methods. In: Rana N.K., Shah A.A., Iqbal R., Khanzode V. (eds) Technology Enabled Ergonomic Design. Design Science and Innovation. Springer, Singapore. https://doi.org/10.1007/978-981-16-6982-8_2.

Technological Affordances and Teaching in EFL Mixed-ability Classes during the COVID-19 Pandemic

Waheed M. A. Altohami¹

Department of English, College of Science & Humanities
Prince Sattam Bin Abdulaziz University
Alkharj, Saudi Arabia
Faculty of Education, Department of Foreign Languages,
Mansoura University, Egypt

Mohamed Elarabawy Hashem²

College of Science & Arts in Tabarjl, Jouf University, KSA
Al-Azhar University, Cairo, Egypt

Abdulfattah Omar³

Department of English, College of Science & Humanities
Prince Sattam Bin Abdulaziz University
Alkharj, Saudi Arabia
Faculty of Arts, Port Said University, Egypt

Mohamed Saad Mahmoud Hussein⁴

Faculty of Education
Assiut University, Assiut
Egypt

Abstract—With the widespread of COVID-19 in Saudi Arabia, the educational authorities issued firm directions to convert to virtual classes exploiting the available Learning Management System (LMS). However, during the academic year 2020-2021, the researchers observed that writing EFL instructors at Prince Sattam bin Abdulaziz University (PSAU), Saudi Arabia, faced diverse challenges due to having online mixed-ability classes, i.e. those classes where students have varying levels of readiness, motivation, and academic caliber. Though many previous studies explored the influence of the COVID-19 pandemic on teaching and learning practices, very few studies addressed the way technological affordances pose challenges for instructors teaching mixed-ability classes. Therefore, the present study, using mixed quantitative and qualitative research methods, sought to explore challenges that evolved due to the technological affordances of LMS to spot the persistent problems and to offer relevant solutions for upgrading, writing teaching and learning practices. The basic research design relied on an online questionnaire followed by semi-structured interviews. Findings showed that differentiated instruction proved to be the most successful strategy for teaching writing in mixed-ability online classes as it allowed the adaptation of materials, teaching and learning practices, and assessment tools to motivate low-achievers. In addition, the collaborative tools offered by the Blackboard such as the White Board, Discussion Board, Blogs, and Breakout Groups helped to meet the preferences of visual, auditory, and kinesthetic learners. Finally, further studies are recommended to explore the affordances of educational technologies regularly to identify potential benefits and limitations for offering the best teaching and learning practices.

Keywords—Technological affordances; blackboard; writing teaching; EFL mixed-ability classes; differentiation instruction; COVID-19

I. INTRODUCTION

Recent years have witnessed great advances in the use of technology in the area of distance teaching and learning. These technological advancements acquired more significance

during the time of worldwide crises such as COVID-19. Indeed, the outbreak of COVID-19 at the end of 2019 caused all aspects of life to go dramatically as it forced the largest lockdown and precautionary measures ever known. As the whole world became under the COVID-19 siege, there was a great demand for educational technologies such as Virtual Laboratories, Augmented Reality, Wearable Technology, Cloud Computing, LMS where virtual classrooms have turned out to be the only available avenue of communication through which teaching is channeled. That is, online teaching/learning became the representative of the new pandemic pedagogy [9]. It turned out to be the only legitimate heir to the throne of the long-lasting traditional teacher-centered pedagogy. Though its advent has been unplanned, it seems that the new pedagogy is here to stay and higher education institutions should be ready to deal with the new scenario for a longer time [10]. In the Saudi context, the Saudi government saved no efforts to make all the necessary technical support available to the students and teachers alike for the new change to take effect. LMS, represented mainly by the Blackboard, which was already in use before the coronavirus outbreak, was assigned as the official portal for education. In a short time, teachers had to adjust themselves to the new situation and shape their professional practice in a way that fits the new paradigm [12].

Though educational technologies were principally devised to simulate physical teaching/learning environments, many issues and challenges still render their usage questionable. Indeed, before the breakout of the pandemic, online learning was at its best a trendy practice, but it has never been inclusively adopted as the main system of education [11]. Yet recently, online teaching/learning became the norm. Taking into consideration that the online teaching is learner-centered [7], one major challenge is having students with different abilities and diverse competencies due to their diverse backgrounds, learning styles, personal traits, goals, and motivations, all grouped in one class [1, 2]. Such kind of

classes is referred to as 'mixed-ability class'. Having students with different learning styles and speed means that they are expected to respond differently to the teaching methods across diverse classroom situations [3]. Accordingly, teachers are requested to adapt their materials as well as their teaching styles and strategies to cope with such varied levels, especially in electronic platforms where many privileges of face-to-face communication are markedly missing. This issue becomes more complicated while teaching productive skills, writing and speaking.

The present study is mainly concerned with highlighting the challenges that face instructors in teaching writing courses at Prince Sattam bin Abdulaziz University (PSAU) with special reference to the strategies they individually develop to overcome the challenges caused by students' mixed abilities in online classes. Indeed, writing is a very crucial skill that all students need in their academic study to fulfill most of the academic duties, especially doing assignments and exams. The English Department at PSAU offers four writing courses targeting the instruction of writing short paragraphs to writing researched essays. In all writing courses, instructors are conventionally required to help students to improve their skills and to become good writers [5], and they usually depend on student's writing proficiency in order to test their knowledge and abilities [6] as it provides tangible evidence for learners' progress in language learning [8]. Still, teaching writing for students in mixed-ability classes forms a great challenge for many instructors since they are required to meet students' needs, design multi-level tasks, implement different teaching strategies, and build on students' previous experiences.

Taking into consideration the four writing courses taught at PSAU, the present study seeks to answer one major research question: What is the impact of technological affordances on teaching writing in mixed-ability online EFL classes during the COVID-19 pandemic? Under this overarching question, three sub-questions are subsumed: (a) What are the major challenges that face instructors during online teaching of writing for mixed-ability classes? (b) What are the strategies that can be employed online to help instructors to teach writing effectively in online mixed-ability classes? and (c) To what extent are the online mediated strategies effective in teaching writing in mixed-ability classes? By answering these questions, the present study aims at (a) exploring how COVID-19 imposed a new pedagogy making full use of educational technology, (b) identifying the major challenges that face writing instructors in online mixed-ability classes, (c) outlining the online mediated strategies that would help instructors in teaching writing in online mixed-ability classes, and (d) helping instructors of writing courses at PSAU to evaluate the advantages of virtual mixed-ability classes that they could build on to promote their students' writing skill. Towards fulfilling these objectives, we use qualitative and quantitative research methods in the form of an online questionnaire combining closed and open. It moves from a description or an assessment of the current situation of teaching writing at PSAU to the analysis of the demanding challenges. Complementarily, all instructors representing the research community are engaged in semi-structured online

interviews via zoom to discuss such challenges as well as instructors' views and assessments of the teaching strategies used in physical and virtual mixed-ability classes.

The remainder of the article is organized as follows. Section 2 is a brief survey of the previous studies that mapped the terrains of teaching writing to mixed-ability classes via technologically-led platforms. Section 3 outlines the theoretical underpinnings underlying the present study as it identifies mixed-ability classes, discusses the major differences between physical and virtual classes, delineates the rationale behind using educational technologies to facilitate teaching/learning at the time of emergency, and highlights how the tools offered by LMS could be efficiently used for teaching writing for mixed-ability classes. Section 4 offers the study methodology in terms of data collection instruments and the procedure of analysis. Section 5 reports on the findings of the study. Section 6 summarizes the main findings, discusses relevant pedagogical implications for teaching writing in mixed-ability virtual classes, and offers recommendations for future research.

II. LITERATURE REVIEW

Teaching language skills in mixed-ability classes have received notable scholarly attention due to the diversity of challenges that affects instructors' and learners' performance. However, to the authors' best knowledge, the current study is the first to explore the best EFL teaching and learning practices despite the challenges offered by technological affordances, especially those marking LMS. Iloanya [38] explained teacher's role in mixed-ability classes as they integrate students with learning disabilities and outstanding students in the same class to achieve the desired learning results. Ten people were interviewed, namely four primary school teachers, four secondary school teachers, and two members of the Education Department. The objective of the interview was to learn how teachers manage their teaching in mixed-capacity classes. Findings showed that some teachers faced many challenges while teaching students in mixed-ability classes, whereas some other teachers were much concerned with innovating new strategies to ensure that students help each other. That is, they were quite persuaded that teachers have to provide new techniques to ensure that students have an access to quality education.

Other studies focused on the teaching strategies for meeting students' diverse needs in mixed-ability classes. Aftab [19] highlighted the importance of teachers' beliefs about differentiated instruction in teaching mixed-ability classrooms. An online open-ended questionnaire was distributed to 120 teachers at private middle schools in order to understand their perspectives and beliefs around the use of differentiated instruction in teaching mixed-ability classes. Findings showed that 95 % of the teachers wished to use differentiated instruction, while 40.8% of the teachers already used differentiated instruction in their classes. Teachers recognized that using differentiated instruction would develop and improve students' academic progress, increase their participation in the class, and cover their different needs; however, there is still dereliction in implementation.

Based on a semi-structured interview, Reyes and Rodríguez [39] explored EFL teachers' views regarding how to fulfill students' needs in mixed-ability classes. Findings showed that fulfilling students' needs in mixed-level classes requires having diverse instruction methods that adopt more materials that suit both low and high-level students. In addition, teachers have to pay more attention to individualized and continuous assessment because they have played an important role in fulfilling students' needs in mixed-ability classes. The study affirmed that there was not "a magic strategy" that fulfills every student's needs in mixed-ability classes. Similarly, Svård [2] aimed at exploring the perceptions of the EFL teachers in Botswana about teaching mixed-level classes focusing on the way teachers intervene to satisfy learners' needs in light of persistent difficulties. Findings revealed that teachers have mixed feelings as some envisaged having mixed-ability classes as natural and therefore they tried to work out solutions for common challenges. Other teachers thought it is the government's responsibility to classify learners based on their abilities to create homogenous learning groups.

Al-Shammakhi and Al-Humaidi [40] compared the perceptions of 180 male and female EFL teachers in Oman teaching mixed-ability classes with a special focus on the challenges involved. Findings showed that both male and female teachers faced the same challenges and they worked out the same solutions to overcome these challenges. Yet, female teachers have been proved as more efficient in motivating their students. Similarly, Alsubaiei [4] explored the challenges encountered and the strategies adopted in mixed-ability classes and by thirty female EFL teachers in English Language Institute (ELI). The basic research instrument was an online questionnaire. Findings revealed that the major challenges encountered by most teachers were mainly related to three basic areas: students' motivation, teaching and learning practices, and the courses materials. Furthermore, the level of teachers' training proved to have no relationship with the effectiveness of their teaching strategies.

Due to the strict precautionary measures imposed on the educational settings worldwide because of the outbreak of COVID-19, online classes became a much safer channel. Such emerging practices drew the attention of researchers for exploring teaching and learning practices as well as readiness for converting to online learning. Coman, *et al.* [41] analyzed data collected from 762 students representing two major Romanian universities. Data reflected students' perceptions concerning online learning during the COVID-19 pandemic. Results showed that the Romanian universities were not yet completely ready for the exclusive application of the online learning. A similar study was conducted by Farrah and al-Bakry [26] who investigated the potential challenges and benefits of online learning practices applied during the COVID-19 pandemic in the Palestinian universities as perceived by six university students. Findings affirmed that the experience is not up to the expectations and needed further improvements in terms of the technological infrastructure and training of teachers.

Given the focus of the present study, another array of research examined how to cope with the mixed-ability classes'

challenges while teaching writing. Aljahdali and Alshakhi [42] explored the benefits and challenges resulting from teaching writing to Saudi university students using the integrated skills approach. Results indicated that students' performance in writing improved albeit considerations of the multi-level students and the highly crowded classrooms. Similarly, Bantis [43] used task-based learning (TBL) as a communicative portal to teach writing to mixed-level students. Results showed that TBL has been proved to be an effective tool in differentiated learning for meeting students' different individual needs.

Likewise, a pool of research investigated the potential horizons and applications of online learning. In her study, Hakim [44] aimed to probe the different perspectives of the currently imposed state of teaching caused by the COVID-19 pandemic that imposed a completely technology-mediated mode of learning. Results accrued from 50 instructors working for the King Abdulaziz University, Saudi Arabia, pointed out that some technical issues related to the quality of the internet, demotivated students, and attention deficit rendered the process of online learning quite immature. Conversely, findings also highlighted many advantages for integrating technology in the classroom. In the same vein, Alpala and Peña [45] examined the effectiveness of using virtual resources in secondary school for upgrading students' performance in writing. Results showed that virtual resources positively affected the learning process and enhanced communication among students.

Teaching writing in virtual classrooms for mixed-ability students received equal scholarly attention. For example, Yusof, *et al.* [46] examined the effect of using Facebook Note to afford students to provide feedback on their peers' writing within the framework of the process-oriented approach to writing. The aim was to cope with the diversity of levels through providing timely feedback. Results highlighted the effectiveness of the peer review in dealing with mixed-ability class challenges. Equally important, Pennington [48] suggested a four-step approach based on the use of assistive technology to teach writing at the sentence level to students with moderate to severe disabilities. The selection of the digital tool among the many available ones was based on the individual needs of the students. Similarly, Fonseca [49] investigated the effect of using Google Classroom as an assistive tool to teach writing to university students at Universidad Nacional. Findings illuminated many benefits of the application of the virtual classroom as it facilitates the acquisition of the skill in an enjoyable and attractive atmosphere.

More specifically, online collaborative platforms proved to be highly effective in mediating writing instruction. Jeong and Hmelo-Silver [25] affirmed the positive impact of using online collaboratively-employed Google Docs on university students' performance in academic writing. Likewise, Yunus, *et al.* [50] investigated the advantages and disadvantages of using social networking tools in teaching writing to TESL Malaysian university students. Results showed that such integration enriched students' knowledge, enhanced their motivation, and promoted confidence in learning writing. Furthermore, Wu, *et al.* [51] examined the effect of using online flipped writing

instruction on the EFL writing performance of English majors in Taiwan. Findings indicated that the suggested method was effective in improving the writing skill and mitigating demotivating factors.

Based on this literature review, it could be stated that despite the diversity of the educational technologies and tools manipulated for teaching in general and for teaching writing in particular, they were used sided with physical classes. The quick turn to online teaching/learning because of the COVID-19 pandemic in the Saudi context imposed new teaching and learning pedagogy. However, scarce studies have been conducted to investigate the issue of writing teaching in mixed-ability classes exclusively via electronic platforms. Therefore, we feel a need to explore the challenges that face EFL writing instructors in mixed-ability classes, and the strategies worked out to overcome them.

III. THEORETICAL FRAMEWORK

Writing, especially for EFL students, is an instrumental skill that they require for both academic and personal purposes such as expressing ideas and identities, convincing their audience, offering inputs and knowledge [13] in addition to other daily activities such as emailing and networking. To be fully accomplished, the process of writing is commonly planned to go through a set of stages: being excited and motivated to write, prewriting, making an outline, writing notes, drafting, and finally revising and editing [14]. Among the several problems that might occur during the process of writing are spelling mistakes, wrong use of punctuation marks, run-on and fragmentary sentences, and dangling modifiers. Since these mistakes are common, writing teachers are usually required to devote enough time and to offer a healthy environment in classrooms for developing better writing skills [15]. This could be done through adopting the teaching strategies that best suit learners' interests and needs. Also, students ought to be granted enough chances to practice their writing skills since the ultimate goal of learners is to learn to produce well-written documents.

Relevant literature asserts that writing difficulties are related to some psychological, linguistic and cognitive problems on the part of learners. Psychologically speaking, writing requires students to write independently without getting immediate feedback and without interacting with peers; therefore, it is largely claimed to be the most complex language skill [8]. Equally important, beginners often face many problems regarding the application of grammatical rules to writing well-formed sentences. Such problems are related to spelling, grammatical patterns, well-formedness, word choice, coherence, etc. [16]. Relatedly, Alfaki [17] argues that some of the cognitive problems that students face during writing process include problems of punctuation, organization, capitalization, content and spelling. All of these problems get much complicated in mixed-ability classes as students learn at different rates and require different types of feedback.

By definition, a mixed-ability class is the one where learners clear great difference in achievement, understanding, linguistic repertoire, and learning. It covers a broad set of variations among students in different language learning competencies in addition to classroom practices [18]. Indeed,

teaching students with different personalities, desires, intelligences, backgrounds, and learning styles is a very big challenge for many EFL teachers because they have to design their lesson plans and even materials to meet students' needs [19, 20]. Another term that is quite similar to mixed-ability classes is 'heterogeneous classes' in which students have different abilities, learning styles, language knowledge, and cultural background [21]. They also include differences in gender and age.

Indeed, teaching mixed-ability classes is challenging and demanding for both learners and teachers who always plan to ensure efficient learning for students. Yet, teachers sometimes fail to realize the benefits of mixed-ability classes [23]. One benefit is that the interaction between the high achievers and the low achievers, under the teacher's guidance, is likely to get students to feel responsible for their learning [2]. Furthermore, such interaction often brings about a sense of belonging and achievement [3], and supports mutual scaffolding, feedback, and sharing of experiences thereby enhancing understanding [24]. Despite these advantages, teaching mixed-ability classes remains a hard job that needs a resourceful teacher. With the existence of varying levels of skills, interests and linguistic repertoire in the same class, teachers stand uncertain as to how to teach the whole class without doing injustice to gifted, struggling, and average students [4].

The gamut of the in-class practices and the efforts that teachers exert to meet the learning needs of each learner came to be known as 'differentiated instruction' or 'responsive teaching'. Principally, differentiated instruction aims at achieving equity in educational opportunities between high and low achievers by pushing low achievers to move from their comfort zones [31]. For Orr [34], differentiation is "all about making the learning engaging, empowering, investigative, explorative and open ended" (vii). To do so, teachers are required to design their teaching in response to what their students competence by altering the content, the instructional method, learning activities and assessment tools [47]. In this regard, Tomlinson [52] and Valiande [31] argue that differentiation covers three important features of the instructional situation: (a) input/content, the content is what student is meant to learn, (b) process, how students critically make sense of the presented knowledge, and (c) output/product, the manifestation of what students already learned.

Teachers worldwide have been trained to use similar instruction approaches in physical classrooms. Yet, virtual classes represent another story. As mentioned earlier, the high mortality rates and the widespread of COVID-19 forced academic officials to convert to the online teaching/learning mode [27]. It started at a slow rate and gradually blended learning paved the way to the complete shift to the online learning [28, 29]. However, countries responded varyingly to the COVID-19 pandemic with regard to its aftermaths for education due to differences in the technical infrastructure that accommodate online teaching and learning practices [30]. Indeed, the accelerating advances in the Information and Communication Technology (ICT) have smoothed the way for the successful application of Technology-Enhanced Learning and Teaching (TELL) [25]. In this regard, the UNESCO [22]

reported that online education is expected to catch up with face-to-face education and soon technology will characterize the universities and become the mainstream medium of delivering education. Still, the whole experience of using educational technologies should be evaluated in light of the affordances of ICT. Affordances refer to the actual properties of a thing, primarily those functional properties that determine just how the thing could be used [36]. The major affordances of ICT included the accessibility of rapid-changing information, the diversity of experiences, the communication and collaborative abilities of technology, reflection and critiquing potentials, immediacy, multimodality.

Now with the newly imposed pandemic pedagogy in which online learning has become the mainstream system of education, the instructional practices that deal with mixed-ability writing classes should adjust to the new situation. Although writing is commonly perceived of as an individual work, students can gain substantial benefits out of their collaboration with their peers through the different tools offered by diverse educational technologies. Many of these technologies are integrated in the Blackboard system that is used widely in Saudi universities (see Fig. 1). For instance, online collaborative technologies like wiki, blogs, Google Doc and online word processors provide common space enabling students to work simultaneously on the same writing project and trade mutual feedback on their work [25]. Facebook might be also used as a collaborative tool in teaching the writing skill [38].

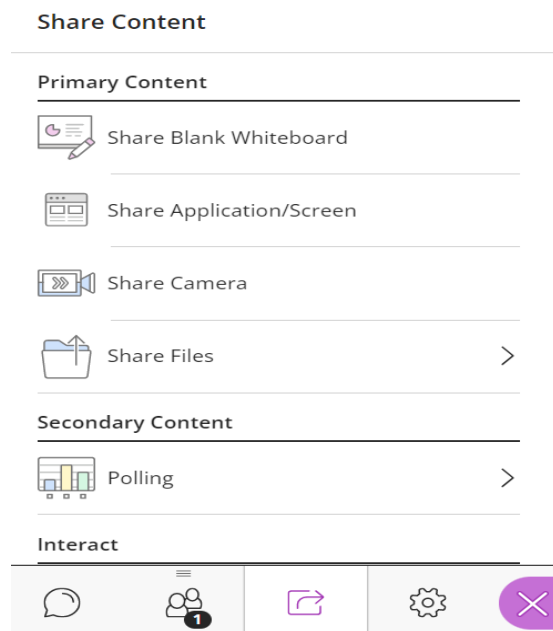


Fig. 1. The basic Tools for Sharing Content via the Blackboard.

Such collaboration can be actualized by different means including sharing written texts for peer review in addition to sharing the writing experience itself [32]. Hyland [32] argues that online learning affords a communicative atmosphere that makes for the unattainable interaction achieved in the physical classroom. The main disadvantages that were always ascribed to the computer-assisted language learning were the isolation the learners experience while they interact only with the

technological device. However, this drawback is mitigated through the collaborative activities that the online learning has considerably facilitated. In the context of teaching and learning writing online, collaborative learning has been proved as a positive approach in which students learn through small groups supporting each other to develop and improve their education [33]. Zurita, *et al.* [35] claim that collaborative learning in mixed-ability classes helps low achievers to accomplish writing tasks better and faster. Simultaneously, high achievers in mixed-ability classes perform writing tasks more strongly, whether in a homogeneous or a heterogeneous group. Despite the many studies that applauded the horizons of collaboration, Bower *et al.* argue that collaborative activities flow more seamlessly in the traditional classroom than is the case in the virtual classroom [37].

IV. METHODOLOGY

The research design adopted in the present study integrates both quantitative and qualitative methods with the aim of (a) identifying their attitudes towards writing online teaching with a particular reference to the technological affordances that mark LMS represented by the Blackboard system at PSAU, (b) exploring the challenges that face EFL instructors teaching writing courses online for mixed-ability classes compared to physical classes, and (3) discussing the best teaching strategies that have been proved as efficient in overcoming these challenges. For more effective use of the questionnaire, two types of validity have been fulfilled: content validity and face validity. Regarding content validity, a jury of English language teaching professors as well as professors of educational technology has verified the questionnaire for clarity, readability and comprehensibility. Furthermore, regarding face validity, since we targeted a stratified sample to ensure that all strata of EFL writing instructors at PSAU are represented, an online questionnaire is administered to 15 instructors teaching the four writing courses in Department of English (male and female sections), College of Science and Humanities, PSAU. Those instructors have been teaching writing both offline and online over three years. This rubric has been made in order to ensure that they experienced both the benefits and challenges of online and offline writing teaching for mixed-ability students. The researchers made sure that each class included students with different levels in writing. Their grades in the different writing courses formed the major standard for such classification.

The questionnaire includes four areas of investigation: (a) manageability of diversity in online writing mixed-ability classes (4 statements), (b) the major challenges encountered in such classes (7 statements), (c) online writing teaching and learning practices (6 statements), and (d) perceptions regarding the integration or exclusion of online teaching technologies (4 statements). Participants' responses would be distributed over Likert's five-point scale: (5) Strongly Agree [SA], (4) Agree [A], (3) Neutral [N], (2) Disagree [D], and (1) Strongly Disagree [SD]. The questionnaire has been initially administered to a group of five instructors to make sure that all statements are readable and understandable. Some modifications are made accordingly. Complementary to the questionnaire, semi-structured interviews with all writing instructors are carried out via the Blackboard. Such interviews

are intended for participants to provide more detailed and in-depth information about the specific challenges they faced and the particular strategies and activities they employed to respond to these challenges taking into consideration the quick transition to the use of the Blackboard system.

V. DATA ANALYSIS

A. The Questionnaire

The questionnaire administered to the target research community at PSAU was intended to record writing instructors' responses and perceptions regarding four major areas: (1) manageability of diversity in online writing mixed-ability classes, (2) the major challenges encountered in such classes, (3) online writing teaching and learning practices, and (4) perceptions regarding the integration or exclusion of online teaching technologies. Regarding the first issue of the manageability of diversity in online writing mixed-ability classes, Table I offers raw statistics.

Statistics in Table I show that most instructors (82%) agreed that teaching writing in mixed-ability online classes is manageable due to the facilities provided via the Blackboard system. Students' roles are identified by the instructor either simply as attendees or moderators. Also, instructors can control students' participations during the virtual class by nominating who can participate. Still, a considerable number of instructors (74%) affirmed that they feel pressured during the writing virtual class due to the fact that available resources (such as the White Board) do not allow writing clearly and neatly to offer proper illustrations and writing models to students. Based on a real experience of two of the authors, many students are not properly motivated to participate in answering the target activities and drills. One reason is that high achievers usually outshine low achievers who finally get frustrated. Still, instructors argued that it is not necessary to divide the class into homogenous groups. That is, heterogeneity could be exploited for enhancing teamwork in writing assignments during the virtual class. In addition, most instructors (87%) agreed that having students with diverse writing levels is natural in physical and virtual classrooms. The Blackboard system offers user-friendly assessment tool though it requires considerable customization.

The second issue addresses the challenges that emerge owing to students' diverse levels in writing online classes (see Table II).

Indeed, diversity is acknowledged by nearly half instructors (47%) as a persistent challenge in online writing classes. The major challenge that students' diverse levels provoke is that low achievers got stuck in most writing activities due to lack of motivation. Taking into consideration that writing is a productive language skill, most instructors (86%) affirmed that linguistic diversity is more prevailing and even problematic when compared to cultural diversity. Here, we affirm that students at PSAU share a similar cultural context. Minor cultural differences are believed as causing no individual core differences in students' writing performance with special reference to the topics offered for writing. Equally important, students' writing performance is rather affected by a set of psychological factors including anxiety

during the online class, the pressure caused by poor internet connection, and inability to handle the tools offered by the Blackboard system, personality traits, and lack of motivation. Despite all these challenges, instructors differed with respect to the notion of tailoring the content, teaching style, and teaching strategies to meet a particular proficiency level set in light of students' writing actual performance. Rather, nearly all instructors (96%) affirmed that they had to vary their teaching methods, writing course materials, and assessment tools to meet students' diverse levels.

The third issue concerns online teaching and learning practices as shown in Table III.

TABLE I. INSTRUCTORS' RESPONSES REGARDING THE MANAGEABILITY OF DIVERSITY IN ONLINE WRITING MIXED-ABILITY CLASSES

No.		SA	A	N	D	SD
1. Manageability of diversity						
1.1	Teaching writing in mixed-ability online classes in manageable	63	19	7	11	0
1.2	I feel overwhelmed upon teaching writing in mixed-ability online classes	51	23	14	12	0
1.3	I think the only practical method to teach mixed-ability online classes is that students are grouped homogenously	22	10	49	6	5
1.4	Having students with diverse writing levels is a natural occurrence inside online EFL classroom	87	0	13	0	0

TABLE II. INSTRUCTORS' RESPONSES REGARDING THE CHALLENGES OF DIVERSITY

No.		SA	A	N	D	SD
2. Challenges of diversity						
2.1	Diversity in online writing classes is not a serious problem and usual classroom dynamics can manage it	19	12	22	14	33
2.2	Students' diverse levels cause low achievers to be demotivated to write	66	19	15	0	0
2.3	Linguistic diversity is the most widely prevailing feature of diversity inside EFL writing class	86	14	0	0	0
2.4	Cultural diversity is not a serious issue in my writing classes	95	5	0	0	0
2.5	Psychological factors do not intervene with students' academic performance online writing classes	0	0	22	35	43
2.6	Taking students' diverse levels into consideration, I always opt for a particular proficiency level and tailor my teaching style and strategies accordingly	7	36	23	34	0
2.7	I vary my writing teaching methods, materials and assessment tools to cope with the varying levels in the online class	87	0	4	0	0

TABLE III. INSTRUCTORS' RESPONSES REGARDING ONLINE TEACHING AND LEARNING PRACTICES

No.		SA	A	N	D	SD
3. Online teaching and learning practices						
3.1	Challenge emerging due to mixed-ability classrooms can be addressed effectively online	66	17	0	10	7
3.2	All you need to teach in mixed-ability classrooms in online environments is to replicate the effective remedies employed in the physical classroom	12	15	33	27	3
3.3	There are peculiarities that render online writing classes as relatively distinct from physical classes	87	13	0	0	0
3.4	Students respond positively to the procedures taken to cope with diversity in online environments	5	57	16	22	0
3.5	Online teaching provides easier route for enriching the teaching setting with various presentation modes that meet students' different learning styles	27	52	11	10	0
3.6	Collaborative online tools can make up for the lack of physical co-presence	30	45	13	12	0

Responses showed that the majority of instructors (83%) agreed that many of the challenges emerging from traditional mixed-ability classes could be effectively addressed online. Still, the common writing remedial work targeting low achievers in physical classrooms has been proved as effective in online teaching platforms including the Blackboard. Furthermore, all instructors affirmed that online classes do not have some of the privileges found in physical classes where face-to-face communication usually helps to provide prompt feedback to students' writing performance. As affirmed by about 60% of the instructors, low achievers in the different writing courses showed positive tendency toward all the procedures taken to upgrade their writing level. Equally important, around 80% of the instructors agreed that the online teaching setting provided by the Blackboard is markedly rich as it offers various presentation modes through the tools of Share Blank Whiteboard, Share Application/Screen, Share Files, Blogs, Discussion Board, and Breakout Groups. Furthermore, the facility of recording sessions provides students with a living reference that they can check anytime. Finally, 75% of the instructors affirmed that such collaborative tools help to bridge the lacuna caused by lack of physical presence.

The final issue addressed in the questionnaire concerns instructors' tendency toward blended learning which integrates face-to-face communication and online tutoring (see Table IV).

About 60% of the instructors were not explicit about the impact of the technological affordances characteristic of different LMS platforms on their – as well as their learners' – performance. Similarly, they were not decisive regarding continuing only with online classes. That is why most of them (99%) opted for the integration of virtual and physical classrooms for more effective learning since electronic

teaching platforms, represented by the Blackboard in the present study, offer the three basic components of the traditional learning process: content, communication, and assessment. Still, in light of such affordances, a considerable number of the instructors (66%) requested much training for a better use of electronic teaching platforms as they affirmed that they are not fully competent in using all of the tools provided by such platforms.

TABLE IV. INSTRUCTORS' RESPONSES REGARDING INTEGRATING PHYSICAL AND ONLINE TEACHING

No.		SA	A	N	D	SD
4. Exclusion or integration						
4.1	The technological affordances marking the use of LMS affect teachers'/learners' performance	2	17	57	4	20
4.2	I prefer to continue exclusively online as online teaching could fully replace face-to-face teaching	7	13	54	20	6
4.3	Virtual classrooms should be blended with physical classrooms if applicable	87	12	1	0	0
4.4	Much training should be available for a better use of electronic teaching and learning platforms for both teachers and learners	42	24	34	0	0

B. The Interview

Complementary to the quantitative method in the form of the questionnaire, semi-structured interviews are conducted to elicit a clearer and detailed vision about the challenges that writing instructors' at PSAU encountered while teaching students with diverse achievement levels as well as the strategies they empirically found as effective in overcoming such challenges. Despite their affirmation that teaching writing in online mixed-ability classes is manageable, the instructors argued that as long as there is a large gap among students' writing proficiency levels, crucial customizations have to be made. In online mixed-ability classes, the input/content, processes and output/products should be diversified and offered through different audiovisual modes. They used to teach the prerequisite content allowing high achievers to proceed and adapting the content for low achievers. According to most instructors, this is perfectly achieved through the mechanisms of differentiated instruction. One successful strategy is homogenous grouping by classifying students in light of their readiness (i.e., attitudes, experiences, and knowledge), interest (preferences and passions), and learning profile (learning style, type of intelligence, group orientation, and culture-based preferences). With students homogeneously grouped, instructors can tailor their teaching both quantitatively and qualitatively providing that intensive teaching is delivered to those who need more support. However, the learning outcomes should remain the same for all students.

As for differentiating teaching for the online writing class, instructors emphasized that much of the teaching and learning practices marking physical classes are adapted to the new

web-based dynamics and tools offered by the Blackboard. In this regard, instructors highlighted that students' diverse learning styles represent a common challenge in EFL writing classes where multiple intelligences abound. In the context of virtual classes, the instructors considered the resources offered by the Blackboard as perfect for empowering students to use their unique learning styles to achieve better performance in the different writing skills. That is, the multimedia tools, including the White Board, Discussion Board, Blogs, Share Files and Share Screen/Application, made it easy for the instructors to satisfy the preferences of visual, auditory, and kinesthetic learners. Similarly, the designing of instruction so that a student works individually, in pairs and in groups also helped meet the needs of intrapersonal and interpersonal intelligence, exploiting the tool of Breakout Group on the Blackboard. However, instructors affirmed that it took them much time to use all such tools adequately and professionally. To be more familiar with all such technological affordances, the instructors affirmed that much training is required.

One more challenge in online mixed-ability writing classes is the demotivated students who are reluctant to participate being so anxious about writing due to their low self-image. Low achievers used to feel unwilling to embark on interaction with their peers, thereby depriving themselves of developing their potential. To address this challenge, instructors put forth some insightful solutions. This might be addressed by assigning them easy, yet challenging, tasks that are one step beyond their proficiency level. The point is that these tasks keep students on track to achieve the target learning outcomes, usually in the form of writing projects. Some of the strategies that have been proved to be successful in motivating students in writing online classes include providing easy access to available resources usually offered on the content of the course on the Blackboard. These resources include PowerPoint presentations, YouTube channels with relevant educational material, and links to web-based exercises with self-correction. Furthermore, instructional methods could be diversified into visual, auidial, and textual formats providing concrete and clear examples. The ultimate goal of such strategies is to help them gain a sense of accomplishment hopefully transforming them into more motivated writers.

Additionally, instructors suggested a more humanistic approach to deal with the different online writing assignments given to students by relating them to their schemata and eliciting their relevant background knowledge and experience so that a sense of intimacy and relevance is ignited gearing their motivation positively. Furthermore, participants encourage low achievers in online writing classes through publishing their work in front of their mates, reinforcing their strengths, and choosing topics that are highly interesting to them. In addition, some instructors stated that they interact with students and come down to their level in order to understand their problems and simplify the process of writing to them. To motivate students and at the same time differentiate assessment tools, students were encouraged to practice self-correction through different websites such as www.grammarly.com and <https://languagetool.org/>. Instructors also highlighted that the emphasis on product (i.e. Students' output) rather than the process causes less capable

students to have an inferior self-image about themselves when comparing their final products with the more capable ones. In response to this challenge, instructors mostly contended that online writing instruction encourages participation from reluctant students and provide equal opportunities for students. In addition, encouraging students to learn autonomously making use of available online resources render the teacher as simply a facilitator.

Another related challenge highlighted by the instructors is the quality of students' participation in the various writing activities and drills. Many of the students' responses were said to be hasty and imprecise. They even used to copy directly from the internet sources, thereby offering a false reflection of their real progress in writing. To buffer against short, undeveloped responses, a specific length of response was set by instructors beforehand. Feedback is offered asynchronously to mitigate the pressure naturally experienced when students are required to respond in real time and to give them more time to reflect on the writing assignment. As for the plagiarism problem, students were notified that final works are to be scanned for plagiarism. Furthermore, taking into consideration students' tendency to provide perfect – albeit falsework, the instructors suggested assessing students' writings from a process-oriented, rather than a product-oriented, prospect. In this regard, peer reviewing and editing could relieve many of the pressures of low achievers. Instructors also stressed the importance that assessment should span all proficiency levels and uniquely addresses students' diverse levels. In other words, a proper assessment the one that reflects the extent of progress achieved across all levels. This essentially required teachers to identify students' profiles by making a record of their linguistic proficiency through placement tests for homogenous grouping.

The inability to provide instant feedback on students' contributions, due to the fact that students' inputs are posted at the same time, constituted another challenge to instructors. Lack of in-time feedback is likely to allow for immature contributions and to render students' primary inputs undeveloped. Teachers suggested sorting responses by students and then determining which ones are in need of instant feedback to develop their input and to pay them due attention in later discussions.

VI. CONCLUSION AND FUTURE RESEARCH

The present study aimed at identifying the perceptions and attitudes of writing instructors at Prince Sattam bin Abdulaziz University towards teaching mixed-ability classes via learning management systems after the quick transition to online learning after the outbreak of COVID-19. The major focus was the challenges that faced them during virtual classes with regard to the content preparation, teaching and learning practices, and assessment methods. It is also thought to reveal how the technological affordances marking the use of the Blackboard system have been customized for offering equal learning opportunities for students with diverse learning styles, intelligence, preferences, and linguistic caliper. Towards the fulfillment of these objectives, both quantitative and qualitative methods have been implemented, represented by an online questionnaire and semi-structured interviews

respectively. Both of them targeted four major areas: (a) manageability of diversity in online writing mixed-ability classes, (b) the major challenges encountered in such classes, (c) online writing teaching and learning practices, and (d) perceptions regarding the integration or exclusion of online teaching technologies.

Results obtained from the questionnaire and the interviews pointed out that writing instructors at PSAU do not have the luxury to use or not use online platforms. For educational systems to adapt to worldwide changes, they have to be ready with efficient technological infrastructure and well-trained instructors and educators. The challenges expressed by the instructors are serious, but using online resources is simultaneously unavoidable. The very simple fact of diversity, demotivation, quality of feedback and participation and copying from the internet resources were the most common challenges that instructors highlighted. They suggested that differentiated instruction was the main approach to deal with such challenges making full use of the collaborative tools offered by available educational technologies. The rationale behind differentiation is to reach to teach. Importing traditional teaching and activities used in physical classrooms is not enough. Instructors stressed that the peculiarities of the online class should be respected and necessary adjustments to the traditional class-based methods should be made. The adaptation of the face-to-face activities to the e-learning environment surely requires instructors to be armed with the virtual teaching-specific competencies that, in turn, require relevant training courses.

In accordance with the findings of the present study, it is recommended to administer a placement test at the beginning of each semester in order to divide students in writing classes into groups based on their writing skill level. This would help teachers to target each group based on their abilities which in turn will help them to focus well on weaker groups. Also, it is recommended to provide workshops targeting the best teaching strategies for teaching writing in online mixed-ability classes. This would help instructors to tailor assignments and to offer help in different writing subskills in accordance with students' competence. Training should also target the best practices of educational technologies to maximize educational outcomes. Furthermore, it should be noted that the continuous evaluation and clear understanding of the affordances of educational technologies would help to inform practitioners of the potential benefits and limitations of different technologies to improve future teaching and learning practices.

The current research design can inform further studies addressing other potential challenges in teaching other language skills in online mixed-ability classes, especially speaking. In addition, further studies are recommended to evaluate students' writing skills before and after the implementation of some of the strategies discussed in the present study.

REFERENCES

- [1] M. Gurgenzidze, "Methodology: Teaching mixed ability classes," *GESJ: Education Science and Psychology*, vol. 1, no. 20, pp. 56-63, 2012.
- [2] A. C. Svärd, "The challenge of mixed-ability classes: How should upper secondary English teachers work in large mixed-ability classes in order to help the weaker students?," *Högskolan för lärande och kommunikation*, Jönköping, Sweden, 2006.
- [3] A. Šímanová, "Dealing with mixed ability classes," Department of English Language and Literature, Masaryk University, Brno: Czech Republic, 2010.
- [4] M. S. Alsubaiei, "Challenges in mixed ability classes and strategies utilized by ELI teachers to cope with them," *English Language Teaching*, vol. 10, no. 6, pp. 182-189, 2017.
- [5] M. Cain, *Teaching for Mastery in Writing: A strategy for helping children get good at words*. Bloomsbury Publishing, 2018.
- [6] J. Harmer, *How to teach writing*. Essex, UK: Stenton Associates, 2007.
- [7] M. Debattista, "A comprehensive rubric for instructional design in e-learning," *The International Journal of Information and Learning Technology*, vol. 35, no. 2, pp. 93-104, 2018.
- [8] D. Byrne, *Teaching writing skills*. London; New York: Longman 1988.
- [9] A. N. Miller, D. Sellnow, D. Sellnow, and M. G. Strawser, "Pandemic pedagogy challenges and opportunities: instruction communication in remote, HyFlex, and BlendFlex courses," *Communication Education*, vol. 70, no. 4, pp. 1-3, 2021.
- [10] T. Muthuprasad, S. Aiswarya, K. S. Aditya, and G. K. Jha, "Students' perception and preference for online education in India during COVID - 19 pandemic," *Social Sciences & Humanities Open*, vol. 3, no. 1, p. 100101, 2021/01/01/ 2021.
- [11] M. Adnan and K. Anwar, "Online Learning amid the COVID-19 Pandemic: Students' Perspectives," *Online Submission*, vol. 2, no. 1, pp. 45-51, 2020.
- [12] R. Khalil et al., "The sudden transition to synchronized online learning during the COVID-19 pandemic in Saudi Arabia: a qualitative study exploring medical students' perspectives," *BMC medical education*, vol. 20, no. 1, pp. 1-10, 2020.
- [13] L. Q. Troyka and D. Hesse, *Simon & Schuster handbook for writers*, 5th ed. Toronto: Pearson Prentice Hall, 2010.
- [14] T. Hedge, *Writing*. Oxford: Oxford University Press, 2005.
- [15] J. Cole and J. Feng, "Effective strategies for improving writing skills of elementary English language learners," presented at the Chinese American Educational Research and Development Association Annual Conference, Chicago, IL, Apr 15-16, 2015.
- [16] E. Tyner, *College writing basics: A progressive approach*. Belmont: Wadsworth Publishing Company, 1987.
- [17] I. M. Alfaki, "University students' English writing problems: Diagnosis and remedy," *International Journal of English Language Teaching*, vol. 3, no. 3, pp. 40-52, 2015.
- [18] S. Ainslie, *Teaching Language to Adults. Mixed ability teaching: meeting learners' needs* (Australian Journal of Teacher Education). Britain: Bourne Press Ltd, 1995.
- [19] J. Aftab, "Teachers' beliefs about differentiated instructions in mixed ability classrooms: A case of time limitation," *Journal of Education and Educational Development*, vol. 2, no. 2, pp. 94-114, 2015.
- [20] J. Ireson and S. Hallam, *Ability Grouping in Education*. London: SAGE Publications, 2001.
- [21] P. Ur, *A course in Language Teaching: Practice and Theory*. Cambridge: Cambridge University Press, 1996.
- [22] The UNESCO. Global Education Monitoring Report Team. *Global education monitoring report, 2020: Inclusion and education: all means all, 2020* available at <https://unesdoc.unesco.org/ark:/48223/pf0000373718>.
- [23] D. Nusrat, "Overcoming the Challenges Faced in a Mixed Ability Classroom," *IOSR Journal Of Humanities And Social Science (IOSR-JHSS)*, vol. 22, no. 7, pp. 9-14, 2017.
- [24] L. Heltemes, *Social and Academic Advantages and Disadvantages of Within-class Heterogeneous and Homogeneous Ability Grouping (Mathematical and Computing Sciences Masters)*. St. John Fisher College: Fisher Digital Publications, 2009.
- [25] H. Jeong and C. E. Hmelo-Silver, "Seven Affordances of Computer-Supported Collaborative Learning: How to Support Collaborative Learning? How Can Technologies Help?," *Educational Psychologist*, vol. 51, no. 2, pp. 1-19, 2016.

- [26] M. Farrah and G. H. al-Bakry, "Online learning for efl students in palestinian universities during Corona Pandemic: advantages, challenges, and solutions," *Indonesian Journal of Learning and Instruction*, vol. 3, no. 2, pp. 65-78, 2020.
- [27] U. N. C. T. Development, *World Investment Report 2020: International Production Beyond the Pandemic*. United Nations, 2020.
- [28] H. Singh, "Building effective blended learning programs," in *Challenges and Opportunities for the Global Implementation of E-Learning Frameworks*: IGI Global, 2021.
- [29] T. Driscoll, *Designing Effective Distance and Blended Learning Environments in K-12*. Information Science Reference, 2021.
- [30] E. J. Sintema, "Effect of COVID-19 on the performance of grade 12 students: Implications for STEM education," *Eurasia Journal of Mathematics, Science and Technology Education*, vol. 16, no. 7, p. em1851, 2020.
- [31] S. Valiande, "Application and evaluation of differentiation instruction in mixed ability classrooms," Paper presented at the 4th Hellenic Observatory PhD Symposium, London, LSE, 25-26 June, 2009.
- [32] K. Hyland, *Second Language Writing*. Cambridge: Cambridge University Press, 2019.
- [33] W. Jolliffe, *Cooperative learning in classroom: Putting it into practice*. Thousand Oaks, United States: SAGE Publications In, 2007.
- [34] R. Orr, "100 ideas for primary teachers: Differentiation". London: Bloomsbury Education, 2017.
- [35] G. Zurita, M. Nussbaum, and R. Salinas, "Dynamic Grouping in Collaborative Learning Supported by Wireless Handhelds," *Educational Technology & Society*, vol. 8, no. 3, pp. 149-161, 2005.
- [36] G. Salomon. (Ed.), *Distributed cognitions—psychological and educational considerations*: Cambridge: Cambridge University Press, 1993.
- [37] M. Bower, B. Dalgarno, and G. Kennedy, *Blended Synchronous Learning: A Handbook for Educators*. Australian Government - Department of Employment, 2014.
- [38] J. Iloanya, "How Mixed-Ability Grouping Works in Botswana's Schools?," *International Journal of Technology and Inclusive Education (IJTIE)*, vol. 1, no. 3, pp. 462-467, 2014.
- [39] P. Reyes and J. Rodríguez, "Teaching English in Mixed-ability Classrooms: Some teachers' thoughts on responding to the needs of all learners," *Malmö högskola University*, 2005.
- [40] F. Al-Shammakhi and S. Al-Humaidi, "Challenges Facing EFL Teachers in Mixed Ability Classes and Strategies Used to Overcome Them," *World Journal of English Language*, vol. 5, no. 3, pp. 33-45, 2015.
- [41] C. Coman, L. G. Țiru, L. Meseșan-Schmitz, C. Stanciu, and M. C. Bularca, "Online teaching and learning in higher education during the coronavirus pandemic: students' perspective," *Sustainability*, vol. 12, no. 24, p. 10367, 2020.
- [42] W. Aljahdali and A. Alshakhi, "Exploring EFL Writing Teaching Through the Integrated Skills Approach: A Case Study in the Saudi Context," *Journal of Language Teaching and Research*, vol. 12, no. 5, pp. 800-809, 2021.
- [43] A. M. Bantis, *Using task based writing instruction to provide differentiated instruction to English language learners*. University of Southern California, 2008.
- [44] B. Hakim, "Technology Integrated Online Classrooms and the Challenges Faced by the EFL Teachers in Saudi Arabia during the COVID-19 Pandemic," *International Journal of Applied Linguistics and English Literature*, vol. 9, no. 5, pp. 33-39, 2020.
- [45] D. P. O. Alpala and N. M. Peña, "A Virtual Room to Enhance Writing Skills in the EFL Class," *HOW Journal*, vol. 21, no. 1, pp. 62-81, 2014.
- [46] J. Yusof, N. Manan, A. A. Alias, and A. Pandian, "Guided peer feedback via Facebook Notes for mixed-ability ESL learners in in the Process Writing classroom: An Exploratory Study .," *Voice of Academia*, vol. 7, no. 1, pp. 14-33, 2012.
- [47] E. Bearne (Ed.), *Differentiation and diversity in the primary school*. London: Routledge, 1996.
- [48] R. C. Pennington, "Write on! Using Assistive Technology and Systematic Instruction to Teach Sentence Writing to Students With Moderate to Severe Disability," *Journal of Special Education Technology*, vol. 31, no. 1, pp. 50-57, 2016.
- [49] K. A. B. Fonseca, "Google Classroom: An Effective Virtual Platform to Teach Writing in an EFL Composition Course," *International Journal of English Language Teaching*, vol. 6, no. 1, pp. 27-35, 2019.
- [50] M. M. Yunus, H. Salehi, and C. Chenzi, "Integrating Social Networking Tools into ESL Writing Classroom: Strengths and Weaknesses," *English Language Teaching*, vol. 5, no. 8, pp. 42-48, 2012.
- [51] W. C. V. Wu, J. C. Yang, J. Scott Chen Hsieh, and T. Yamamoto, "Free from demotivation in EFL writing: the use of online flipped writing instruction," *Computer Assisted Language Learning*, vol. 33, no. 4, pp. 353-387, 2020/05/03 2020.
- [52] C. A. Tomlinson, *How to differentiate instruction in mixedability classrooms* (2nd ed.). Alexandria, VA: Association for Supervision and Curriculum Development.

Deep Learning Applications in Solid Waste Management: A Deep Literature Review

Sana Shahab¹, Mohd Anjum², M. Sarosh Umar³

Department of Business Administration, College of Business Administration¹
Princess Nourah bint Abdulrahman University, P.O. Box 84428, Riyadh 11671, Saudi Arabia¹
Department of Computer Engineering, Aligarh Muslim University, Aligarh, India^{2,3}

Abstract—Solid waste management (SWM) has recently received more attention, especially in developing countries, for smart and sustainable development. SWM system encompasses various interconnected processes which contain numerous complex operations. Recently, deep learning (DL) has attained momentum in providing alternative computational techniques to determine the solution of various SWM problems. Researchers have focused on this domain; therefore, significant research has been published, especially in the last decade. The literature shows that no study evaluates the potential of DL to solve the various SWM problems. The study performs a systematic literature review (SLR) which has compiled 40 studies published between 2019 and 2021 in reputed journals and conferences. The selected research studies have implemented the various DL models and analyzed the application of DL in different SWM areas, namely waste identification and segregation and prediction of waste generation. The study has defined the systematic review protocol that comprises various criteria and a quality assessment process to select the research studies for review. The review demonstrates the comprehensive analysis of different DL models and techniques implemented in SWM. It also highlights the application domains and compares the reported performance of selected studies. Based on the reviewed work, it can be concluded that DL exhibits the plausible performance to detect and classify the different types of waste. The study also explains the deep convolutional neural network with the computational requirement and determine the research gaps with future recommendations.

Keywords—Solid waste management; systematic literature review; deep learning; convolutional neural networks

I. INTRODUCTION

In recent years, waste generation around the globe has increased multi-folds due to population growth, fast urban settlement, economic development, and advancement in lifestyle [1]. The World Bank statistics indicate that the worldwide solid waste (SW) generation was approximately 2.01 billion tons per annum in 2016. It is predicted that the world will produce 2.01 and 3.40 billion tons annually by 2030 and 2050 [2]. The statistics indicate the significant increase in the SW generation around the globe [3]. More than 33 per cent of the total generated MSW are not handled in an environmentally safer manner, with the waste dumped illegally on roadsides or abandoned lands [2]. This poorly handled and openly dumped waste directly affects the environment, constitutes health risks of inhabitants, and engenders water and air pollution and land deterioration [4]. Therefore, this massive quantity of SW has become a significant threat to the

ecosystem of the city and surrounding areas [5]. It has also given birth to illegal dumping [6]. It also substantially obstructs the sustainable growth of the city/region [7]. Nowadays, countries are more serious about a healthier and more sustainable environment. Several studies evidence that the leading causes of poor SWM are inadequate planning and improper operations [8], [9]. SWM bodies lack funds, infrastructure, and advanced technology in most developing countries. After the emergence of smart cities and sustainable urban development, researchers have put a lot of effort into transforming the SWM industry using current technologies and intelligent systems [10]. SW is a natural product from daily life activities and per capita waste generation significantly more in urban regions than rural areas due to high income and urban lifestyle [11]. SWM has emerged as a crucial environmental issue around the globe, especially in developing countries [12], [13]. Therefore, it is strongly demanded to create an effective SWM system for conserving resources protecting environmental and public health [14]. The environmental problems of SWM are very complex to resolve because of their heterogeneous nature [15].

The background analysis concludes that the SWM has focused on utilizing cutting-edge technologies to improve and automate the services. Advanced technologies such as the internet of things (IoT), information technology, machine learning (ML) have drastically improved the efficiency of various SWM processes, namely waste forecasting, collection, transportation, sorting and recycling [16], [17]. DL subset of ML methods has been significantly implemented in diverse areas of the environment, such as pollution control, wastewater, SWM services [18]. The SWM system encompasses various interconnected processes which contain numerous complex operations. This system also involves many non-linear parameters, including highly inconstant influencing factors, namely socioeconomic and demographic [19]. It is challenging to optimize the performance of these systems without affecting the health of inhabitants and the environment [20]. Therefore, DL techniques are supposed to involve in all stages of the SWM system. In earlier review studies, Ye et al. (2020) has thoroughly analyzed the 85 papers published in 2004 - 2019 and demonstrated the different applications of artificial intelligence (AI) models in the SWM service framework. In [21], the author has reviewed approximately 200 studies published during the last two decades and summarized the applications of ML methods in different stages of SWM from waste inception to final disposal. In parallel with these extensive studies, this SLR study primarily concentrates on the

applications of DL models in SWM services and interpret it in view of overall process of SWM.

The main goal of this SLR study is to motivate the researchers more to apply DL techniques for solving various SWM problems involving waste detection, classification, prediction etc. It compares the performance of DL models and uncovers the best models for different tasks. It also highlights some gaps in applications of DL for SWM tasks and discusses some aspects for future priority. This information will help the researchers to choose the better model for their studies. The overall benefits of DL are encouraging for its further use towards developing an innovative and sustainable SWM system.

The survey study is structured in the following sections. Section II draws the picture of applications of various DL models in SWM. Section III comprises the methodology of the SLR architecture, which involves systematic review protocol, review questions, searching process and selection criteria, screening, article quality assessment, and data extraction. Section IV explains the overview of survey findings which includes descriptive statistics of review: country of the author academic's affiliation, mainstream journals and their publishing areas, and thematic analysis: major DL models, their applications, data set used, performance evaluation and comparison with other DL/conventional method, and depicts the detail description of CNN models. Section V illustrates the concept of DL, the design of a CNN architecture and computational requirements to implement the CNN models. Section VI identifies the Research gaps and priorities, demonstrating data acquisition, data preprocessing, model selection and architecture definition, and model comparison. Section VII comprises the summary of the SLR, important observations with shortcomings and the reason for the popularity of DL in SWM. Finally, the conclusion of the SLR study is displayed in Section VIII.

II. SKETCH OF DL IN CONTEXT OF SWM

The literature demonstrates that emerging DL models can be effectively applied in the SWM field [17]. DL is a large subset of ML techniques that comprises various computational methods and algorithms that implements artificial neural networks (ANN) with feature learning. DL techniques have significantly transformed the field of computer vision and image processing. Therefore, DL has emerged as the most attention-drawing branch of ML in recent years and has gradually reached the top. The convolutional neural network (CNN) is an epoch-making category of deep neural networks with huge potential and tremendous image recognition growth with reliable outcomes. CNN can be recognized as fundamental building blocks in diverse tasks such as photo tagging, medical imaging, and self-driving cars. A typical workflow of the DL models is depicted in Fig. 1. Generally, it comprises four main steps: (1) Data collection and preparation (2) Choosing or designing model and hyperparameters (3) Training, testing, and performance evaluation (4) Tuning hyperparameters if needed and deployment. Table VII lists the

DL models applied in the SWM with research objectives/goals.

They are also exhibiting significant growth in everything from security to environment and waste management. Many eminent researchers around the globe have made remarkable contributions in SWM using DL. In SWM, DL models have been extensively implemented to solve various problems such as waste identification and segregation, real-time bin level detection, and prediction of waste generation. DL models have abilities to recognize and learn features directly from the image. This distinct feature has substantially enhanced image detection and classification. The transfer learning technique is implemented using a combination of three pre-existing CNNs, namely VGG19, DenseNet169, and NASNetLarge, to classify the waste into six categories [22]. Many CNN architectures have been proposed with different layers to categorize the different types of waste, such as recyclable: metal, paper, plastic, cardboard, nonrecyclable, medical, biodegradable, inorganic, trash, etc. [23], [24].

The pre-existing CNNs, namely enhanced ResNext [25], YOLOv2 and YOLOv3 [26], ResNet-50 and Auto Encoder network with support vector machine as classifier [27], [28], MobileNet-V2 [29] and Hybrid of CNN and multilayer perceptron [30] have also been performed above type classification tasks. Waste classification is an important activity to separate different types of waste, which significantly improves the recycling efficiency of the process. Various types of CNN with different layers have also been substantially used in many tasks of SWM other than waste detection and classification. A Long Short Term Memory (LSTM) CNN has been implemented to predict the amount of waste generation [31], [32], and carbon dioxide concentration in the waste bin [33]. Additionally, a deep CNN has been designed that consider various waste generation influencing factors to forecast the per capita waste generation [34] and demolition waste for three categories reusable, recyclable, and landfill [35]. A waste bin equipped with a camera, microcontroller, and servo motor has been built to separate the different types of waste materials automatically. The hardware of the bin is controlled by custom software based on the ResNet-34 algorithm with multi-feature fusion and a new activation function [17], [36].

Moreover, different CNN models have been implemented to identify and locate the illegal dumps using street-level image data and high-resolution satellite imagery [37], [38]. Based on the analysis of selected research papers for SLR, DL models have been extensively utilized in SWM, from waste inception to final disposal. They have been implemented in SWM processes such as waste generation prediction, bin level detection, material identification, illegal dump detection and location identification, and waste classification (refer to Tables VII and VIII). This can help to develop sustainable SWM service infrastructure through efficient resource utilization. DL has significantly impacted the recycling process as it has the power to detect different types of material and items to segregate. This has made the recycling process very effective and efficient in material recovery. Fig. 2 displays the application of the DL models in different stages of the SWM processes.

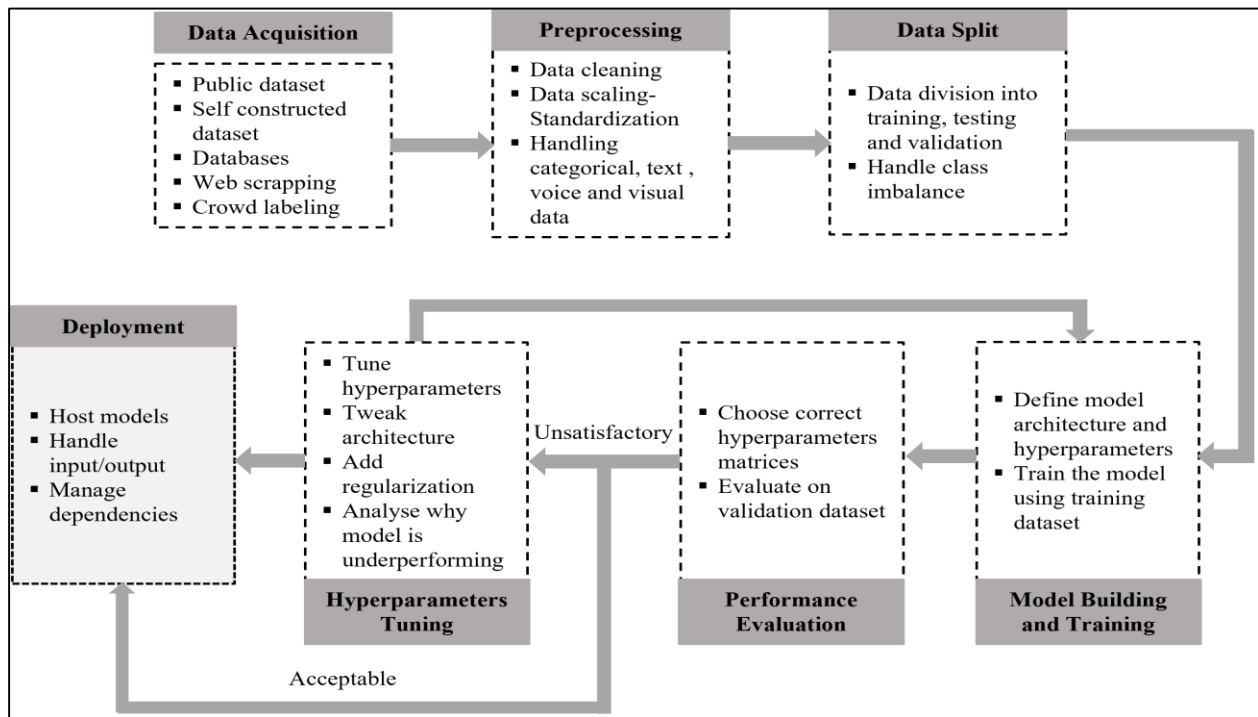


Fig. 1. Schematic Picture of DL Models Workflow.

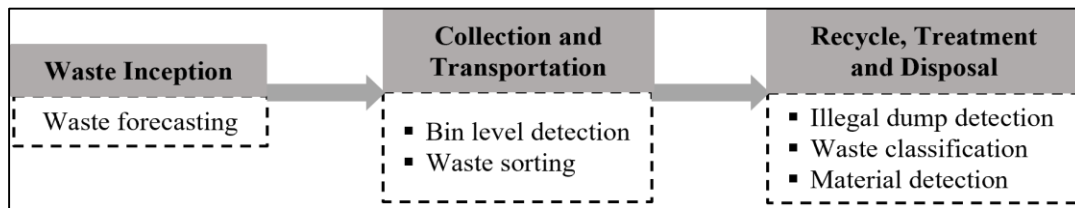


Fig. 2. Application of DL Model in SWM Processes.

To explore the potential applications of various CNNs models to provide the effective and efficient solution of different tasks involved in SWM, a thorough analysis of recently published studies is necessary to increase more advanced developments in this field. The survey demonstrates the comprehensive SLR and elaborates the various DL models implemented to enhance existing SWM techniques involved in its distinct stages, from inception to the final disposal. Some hybrid DL based approaches and performance comparison of implemented DL models with other DL/conventional models are explained to present an in-depth understanding of different models. The review study aims to provide SWM, and allied researchers are keen to apply DL approaches in their respective areas of study using major research aspects such as DL models, applications, efficiency, and accuracy. The major contribution of the survey study is to add the SLR of applications of DL in SWM, which was not previously figured out in the knowledge pool of existing literature.

III. METHODOLOGY

An SLR is carried out to examine the application of DL in SWM research published from 2019 to 2021. The SLR is defined as a systematic procedure to summarize the

experimental results of the studies related to an investigation or technology, determine the gaps in current research, and develop the background for new research. The content of SLR is motivated and structured according to two systematic review studies, namely, [39], [40]. The SLR presents a comprehensible view of various DL techniques implemented in SWM. Following typical steps are conducted to enhance the credibility and reliability of the review.

A. Systematic Review Protocol

The SLR is performed to identify, evaluate, and interpret potential studies applying DL models in various SWM domains [40]. The study extensively follows the SLR methodology, which provides equitable review procedures, ensures quality to credibility, and understands results and conclusions. The SLR has a standard protocol comprising three phases: planning, execution, and reporting [40], [41]. The systematic review protocol defines the methodology of locating, studying, analyzing, and evaluating the research articles. Fig. 3 demonstrates the proposed review prototype based on the SLR guidelines. The SLR protocol describes the review process and is generally explained in technical reports.

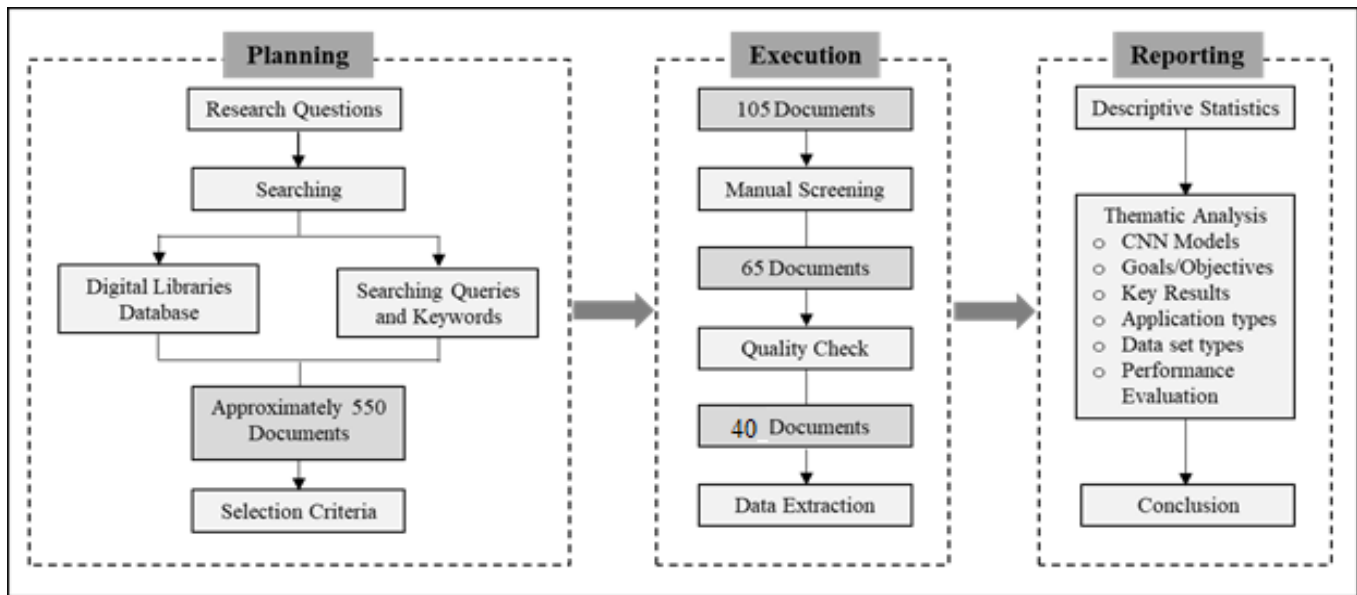


Fig. 3. Flowchart Displaying the SLR Procedure.

B. Review Questions

The primary objective of the SLR is to recognize and assess the published literature that implements the DL model in SWM. The following typical review questions are formulated and addressed to execute the proposed methodology.

RQ1: What are the different applications of the DL model in SWM?

RQ2: What are the DL models implemented to solve SWM problems?

RQ3: How is the performance of different models with respect to other algorithms and techniques?

C. Searching Process and Selection Criteria

The methodology considers an individual research paper or article as a review unit, called a document. All the documents are retrieved from a global digital libraries database, namely Scopus, Elsevier, Google Scholar, Springer, IEEE, Wiley, Emerald, and Web of Science. These are the top libraries that contain peer-reviewed global research from multiple disciplines and are widely accessed by authors to perform SLR. The preliminary search retrieved numerous articles associated with the SWM, DL and CNN but did not exhibit the direct implementation of the DL model in SWM. Additionally, many publications were also in top search, applying the conventional model (such as statistical model) in SWM. This initial search retrieved approximately 550 documents from 2019 to 2021 from the digital search libraries. Then, structured query searches with inclusion and exclusion criteria were executed to retrieve relevant literature and restrict the number of documents. These search queries included some keywords for accepting and rejecting the documents [42]. In SLR, the application of DL was the main keyword, and SWM was the context in the query string. Therefore, all searched queries were around two aspects, (a) application of DL (b) context: SWM. Table I depicts the matrix of retrieved documents for chosen keywords from afore mentioned digital libraries.

TABLE I. THE COUNT OF RELEVANT PAPERS FOR DIFFERENT SEARCH STRINGS FROM VARIOUS DIGITAL LIBRARIES

Key-word	Waste	MSW	Garbage	Trash	Litter	Rubbish	Dump
CNN	149	87	17	12	3	1	2
DL	163	78	20	8	2	5	3

Additionally, the inclusion keywords were “waste management”, “garbage”, “litter”, “trash”, “dump”, “rubbish”, “deep learning”, “convolutional neural network”, and “deep neural network” while exclusion keywords were “waste recycling”, “wastewater treatment”, “waste-to-energy”, “sewer systems”, “waste incineration”, and “vehicle routing”. The gathered literature was analyzed and evaluated in a methodology context covering the studies that implemented the DL techniques to address the SWM issues. After executing the search as mentioned above procedure, 105 studies were uncovered as pertinent to the search topic for 2019-2021.

D. Screening

Manual scrutiny was carried out to ensure the completeness, reliability, and quality of SLR. Inclusion and exclusion criteria were set to make the scrutiny process straightforward, manageable, and objective. Table II displays the chosen inclusion and exclusion criteria to select the papers under four categories for further review. These categories were publication type, document language, accessibility, and subject/title. Then, all selected documents in the searching and data collection process were reviewed according to the attributes set in Table II. The journal or conference research was selected in the first screening, completely accessible and available in English. Generally, conference papers lack quality; therefore, their use in SLRs is uncommon [43]. But few good qualities conference papers were considered in the study. Moreover, their title / subject was also analyzed to determine and choose the most competent research.

TABLE II. ATTRIBUTES, INCLUSION AND EXCLUSION CRITERIA USED TO SELECT THE RELEVANT STUDIES FOR ANALYSIS OF SLR

Attribute	Inclusion criteria	Exclusion criteria
Publication type	Journal articles and conference papers	Book chapters, Patents, Magazines articles, Conference posters, Thesis, Editorials, Industry and Market reports etc.
Document Language	English	Other than English such as Chines, Spanish, Russian etc.
Accessibility	Full text of document accessible	Abstract, partially accessible, or inaccessible
Title/Subject	The main topic was solid waste management. The research applied pre-trained or designed CNN model	The main topic was related to any technology or a specific area such as the IoT, AI, and ML. The research applied any ANN other than deep neural networks.

Additionally, the abstract and conclusion were also rigorously inspected and analyzed in the context of the search topic to determine the more suitable papers and eliminate the duplicate documents having different titles but identical content. It was also investigated that the selected documents were concentrated on applying DL models in the context of SWM. After accomplishing the entire screening process, 65 studies out of 105 were promoted for further process.

E. Quality Assessment

After conducting the screening process, a quality check was performed for all selected studies. The quality assessment checklist was formulated to assess individual research and prune the insignificant and irrelevant research [40]. Ten quality criteria were determined to develop the checklist, and each study was evaluated qualitatively. A questionnaire was formulated to represent the criteria in the form of questions answered on the Likert scale of 5. The Likert scale and designed questions are presented in Table III and Table IV. The overall score of each paper was calculated by adding the points achieved in all questions stated in Table IV. The article was chosen for review if it had an overall score of more than or equal to 25 points. The top 40 papers out of 105 were picked after performing the quality assessment process.

F. Data Extraction

The pertinent data is extracted from all selected studies and summarized in Tables VI and VII to determine the consolidated outcomes. This extracted data includes the items, namely implemented DL model/technique, study goal/objective, key findings, application domains, dataset utilized in model evaluation, and performance comparison with other benchmark studies.

TABLE III. LIKERT SCALE TO EVALUATE QUALITY ASSESSMENT QUESTIONS

Criteria fulfilled	Completely	Substantially	Partially	Poor	Not
Assigned Score	5	4	3	2	1

TABLE IV. QUALITY ASSESSMENT CRITERIA AND CORRESPONDING QUESTIONS TO SELECT THE HIGH-QUALITY RESEARCH STUDIES

Criteria	Questions
Problem definition	Q1: Examine that the problem is clearly stated and has well-defined objectives.
Credibility	Q2: Justify that the problem is well formulated and the proposed approach is practically implemented on actual and sufficient data.
Methodology	Q3: Determine the applicability of the research methods and software platform in the context of the study.
Analysis and conclusion	Q4: Investigate that the accuracy is computed and critically discussed in conclusion.
Argumentation	Q5: Determine those results are compared them with other benchmark studies.
Scope	Q6: Confirm that the application area and scope of research are figured out.
Significance	Q7: Validate that the research has a remarkable contribution to the knowledge pool and/or enhanced the technology.
Structure and writing	Q8: Verify that the study comprises smooth articulation among sections with appropriate academic writing language.
Presentation	Q9: Assess the clarity of the content in the context of research goals.
Referencing	Q10: Verify the reliability and relevance of the cited references in the context of the study.

IV. OVERVIEW OF SURVEY FINDINGS

A. Descriptive Statistics of Review

In the SLR study, 40 research studies were considered published globally in the recent three years, i.e., 2019(7), 2020(22) and 2021(11). All the studies were reviewed according to the country of the academic's affiliation to analyze the contribution of various regions in the subject area. Asia published the most significant number of studies that focused on the review subject area (57.5%), and most of these studies were performed in China (22.5%). 35 % of total studies were contributed from the European region, and 7.5% were from Australia and Africa. Researchers from developing countries conducted 60% of the total studies. At the same time, the remaining 40% belonged to the developed countries, with the categorization of developing/developed countries according to the Human Development Report [44]. The statistics exhibited that researchers from developing countries focused more on SWM than developed countries. The literature evidenced that SWM was a crucial problem in developing countries; therefore, authors gave more attention to SWM research and published more studies. Motivated by the SLR study in [45], all the selected studies were analyzed by publication to determine the mainstream journals and their publishing areas. Table V depicts the list of journals and conferences. The best journals of studies subject with documents count were IEEE Access (5) and Waste Management (5). These results concluded that electronics and computer science researchers focused on applying the current state of the art of their field and invested more effort to solve the SWM issues by developing automatic and intelligent systems. Additionally, Waste Management was dedicated to SW Management, Disposal, Policy, Education, Economic and Environmental assessment. According to the analysis of

publishing areas of each journal, it was deduced that SWM research was strongly related to the environmental sciences.

B. Thematic Analysis of Review

After the emergence of the various computational model of DL, no review study consolidated the applications of DL models in SWM and allied fields. The analysis of compiled studies unveiled four major applications of DL in SWM, namely waste detection, identification, bin level detection, and forecasting of waste generation. Additionally, DL was also applied to perform tasks such as demolish material prediction, custom software development for robot control, defect detection in potatoes, and different types of polythene material.

Table VI displays the applications of DL models identified in considered studies and implemented model performance evaluation for the used data set. All the studies except one had applied the proposed model on an actual data set which showed the experimental performance of the models. Only one study had performed the experiments on simulated data to evaluate the model performance. A significant number of studies had compared the performance of the implemented model with other DL/conventional models. Moreover, most studies had a sufficiently large data set to train, validate and test the proposed model. Therefore, it could be concluded that the performance of the models was reliable and could be utilized for comparison in further studies.

TABLE V. THE LIST OF PAPERS CHOSEN FOR THIS SLR ACCORDING TO JOURNALS / CONFERENCES WITH THEIR PUBLICATION AREAS

Publisher	Journal/Conference	Focused Areas
Elsevier (13)	Automation in Construction (1)	Computer-aided design and engineering, Product modelling and process simulation, Automated inspection, and robotics
	Case Studies in Chemical and Environmental Engineering (1)	Environmental and chemical engineering applications- Water, Air, soil, waste, resource recovery, energy
	Journal of Cleaner Production (2)	Cleaner Production, environmental, and sustainability
	Journal of KSU – Computer and Information Sciences (1)	Computer science and applications, Information science
	Journal of the International Measurement Confederation (1)	Sensors, Data processing, Fusion algorithms, Mathematical modelling, processes, and algorithms
	Resources, Conservation & Recycling (1)	Sustainable production, consumption and management, Resources conservation and recycling
	Waste Management (5)	SWM generation, collection, transportation, segregation, recycling, composition, policy, environment assessment
Hindawi (2)	Applied Computational Intelligence & Soft Computing(1)	AI, Fuzzy and soft computing, Operations research, Mathematical modelling, and programming
	Computational Intelligence and Neuroscience (1)	AI, Fuzzy system, Neural network, Neuro-biologically inspired evolutionary designs, Genetic algorithm
IEEE (6)	IEEE Access (5)	Multidisciplinary from science and engineering
	IEEE Transactions on Consumer Electronics (1)	Concept, design, development, production of electronics, systems, software, and services for the consumer market
MDPI (9)	Applied Sciences (2)	Engineering, environmental, earth, material, and pure science
	Applied System Innovation (1)	Computer and human-machine interaction, Applications of the IoT, Smart and intelligent system
	Electronics (1)	AI, Computer science and engineering, Systems and control engineering, control and system
	Energies (1)	Energy and environment, sustainable energy, AI systems design and control, Smart cities
	Future Internet (1)	IoT, Smart Cities and urban development, human-computer interaction, and usability
	International Journal of Environmental Research and Public Health (1)	Environmental science and engineering, Digital health, Environmental health, and ecology
	Remote sensing (1)	Remote sensing applications, Image processing and pattern recognition, Data fusion and data assimilation
	Sustainability (1)	Air pollution and climate change, Water pollution and sanitation, Sustainable development
Springer (2)	International Journal of Environmental Science and Technology (1)	Environmental science and technology, Solid and hazardous waste management, Air, water, and soil pollution
	Multimedia Tools and Applications (1)	Air traffic and online control, Real-time system, Computer-aided instruction, Remote home care, Smart system
Wiley (1)	Concurrency Computation Practice and Experience (1)	AI and ML, Big data applications, algorithms, and systems, Data science
World Scientific (1)	International Journal of Software Engineering and Knowledge Engineering (1)	Application software, Knowledge management and engineering, Smart system design
Conferences (6)	Held by Elsevier (2), Springer (2), IOP Press (1), and other (1)	AI, Computer and information science, System development, environment, and material science

TABLE VI. TABULATION OF APPLICATION TYPE, DATA SET TYPE AND PERFORMANCE EVALUATION

Reference	Application type	Data set type	Performance evaluation
[22]	Identification and classification	Real (5000 images)	The combined model classification accuracy is compared with standard pre-trained models VGG19, DenseNet169, and NASNetLarge.
[25]	Identification and classification	Real (two datasets 2527 and 5904 images)	Performance is shown with respect to the ResNext model, which is applied to different datasets.
[36]	Intelligent hardware design	Real (4168 images)	ResNet-34: 98.59%, ResNet-34-A: 99.41%, ResNet-34-B: 99.95%, ResNet-34-C: 99.28% and proposed model: 99.96%.
[46]	Smart bin hardware design	Real (565 images)	The garbage level inside the bin is monitored accurately in real-time.
[16]	Electrical and electronic item recognition	Real (210 images)	R-CNN accuracy (90% - 96.7%) is compared with respect to CNN (maximum 90%).
[47]	Intelligent robot design	Real (47000 images)	The robot picked garbage efficiently, and no comparison is shown.
[35]	Material prediction	Real (2280 demolition)	No comparison is shown.
[26]	Real-time detection	Real (375 images)	Manual verification is performed for test images.
[23]	Identification and classification	Real (2527 image)	Accuracies of CNN with various fusions are compared with AlexNet, GoogleNet, VGGNet, and ResNet-101.
[17]	Smart bin design and waste sorting	GITHUB 2020 dataset	There are shown the comparison of existing CNN models ResNet-34, VGG16, AlexNet, and ResNet50.
[24]	Identification and classification	Real (400 images)	Statistical analysis is performed after manual verification.
[48]	Defect detection	Real (images not defined)	No comparative study is performed.
[30]	Waste sorting	Real (100 images)	Improved accuracy is shown with CNN.
[31]	Forecasting	Real (weekly observation of 1000 households, 2011-2018)	Displayed 85% improved results with respect to the traditional ARIMA model.
[49]	Waste segregation	Real (2527 images)	Compared with various CNN models.
[28]	Identification and classification	Real (25077 images)	Compared with other current states of the art studies.
[50]	Garbage detection	Real (4795 and 12346 images)	No comparison, different classes accuracies are compared.
[51]	Garbage detection	Real (8000 images)	No comparison is shown, but the prediction is manually verified.
[52]	Polythene type identification	Simulated (33000 images per class)	Performance is compared with 23 layers networks with different image sizes.
[32]	Forecasting	Real (730 data samples)	Compared with ARIMA and conventional ANN.
[33]	Prediction	Real (9358 data points)	No comparative analysis is shown.
[34]	Prediction	Real (2827 data point)	No comparison with other studies is shown.
[53]	Waste classification	Real (7724 images)	YOLOv3 results are compared with YOLOv3-tiny.
[27]	Waste classification	Real (1989 images)	No comparative analysis is presented.
[29]	Waste classification	Real (2527 images)	Performance is compared with MobileNet, InceptionV4, InceptionResnetV2, Xception, DenseNet121 & 169.
[17]	Waste classification	Real (4163 images)	Performance comparison is shown among four models DenseNet169, ResNet50, VGG16, and AlexNet.
[54]	Localization and recognition	Real (56,964 images)	Performance is compared with BNInception and ResNet-50.
[55]	Real-time waste identification	Real (2527 images)	Various models based on MobileNetV2, InceptionV2, & V4 are tested to obtain optimal accuracy.
[56]	Construction and demolition waste classification	Real (Two data sets of 525 and 1758 images)	No comparison with other studies is shown.
[57]	Waste classification	Real (More than 25000 images)	The performance of VGG19 is compared with ResNet50 and InceptionV3.
[58]	Glass and metal detection	Real (2000 images)	Performance comparison analysis of three models is shown.
[59]	Classification	Real (6640 images)	Accuracies of Resnet101, EfficientNet-B0, B1 and ensemble are compared to determine the optimal model.
[60]	Classification	Real (500 images)	No comparison with other studies is shown.
[61]	Detection and classification	Real (369 images)	No comparison with other studies is shown.
[62]	Detection and recognition	Real (546 images)	No comparison with other studies is shown.
[63]	Waste dump detection	Real (5000 images captured by UAV)	No comparison with other studies is shown.
[64]	Plastic classification	Real (109820 images)	Proposed CNN accuracy is compared with AlexNet, MobileNet v.1 and MobileNet v.2
[65]	Waste classification	Real (2527 images)	Multilayer hybrid CNN accuracy is compared with AlexNet, ResNet50, and Vgg16.
[38]	Illegal dump detection	Real (3000 images)	No comparison with other studies is shown.
[66]	Classification	Real (5416 images)	Various state-of-arts models are compared.

TABLE VII. TABULATION OF DL MODELS, OBJECTIVES AND KEY RESULTS

Reference	DL Model/Technique	Goal/Objective	Key results
[22]	Transfer learning: proposed a combination of pre-trained models VGG19, DenseNet169, and NASNetLarge	Waste classification into six categories	Classification accuracy: more than 92% for all distinct classes with an average of 96.5%
[25]	DNN-TC: an improved version of ResNext	Waste classification into organic, inorganic, and medical waste	Applied on two data sets and obtained accuracies 94% and 98%, respectively
[36]	ResNet-34 incorporating input images with multi features, reuse of the residual unit and a new activation function	Developed hardware of automatic garbage classification system	Identified 14 subcategories of recyclable and nonrecyclable with an accuracy of 99.96%
[46]	IoT and Tensor flow	Smart bin with real-time waste object detection and classification features	Obtained hardware of automated segregation and monitoring system
[16]	CNN and faster region CNN	E-waste recognition and classification	Acquired e-waste equipment identification accuracy between 90% - 96.7%
[47]	SegNet and ResNet	Robot for waste picking from grass	Attained waste recognition accuracy up to 95% without path planning
[35]	Deep neural network	Prediction of demolition waste for reusable, recyclable, and landfill	Prediction accuracy recyclable: 95%, reusable: 98%, and landfill: 99%
[26]	YOLOv2 and YOLOv3 CNN	Garbage container detection and classification	Identified and classified the garbage and its type with an accuracy of more than 90%
[23]	DL models using the feature and score-level fusion	Waste categorization into five classes	Obtained accuracies 94.11% and 94.58% for double fusion PSO and GA, respectively
[17]	Integration of IoT and ResNet-34, VGG16, AlexNet, and ResNet50	Sorting of digestible and non-digestible along with smart trash bin	Exhibited maximum accuracy of 95.31% and successfully real-time bin monitoring
[24]	Two Deep CNN with four and five layers	Waste classification into four categories	Computed accuracies of four and five layers DCNN 61.67% and 70%, respectively
[48]	CNN with nine layers	Real-time defect detection into potato	Achieved 83.3% accuracy in real-time
[30]	Hybrid of CNN and multilayer perceptron	Waste sorting as recyclable and others	Determined the accuracy more than 90%
[31]	Multi-site LSTM CNN	Waste forecasting	Reported RMSE, MAE and MAPE as 0.5, 0.41 and 0.74
[49]	DenseNet121 optimized by genetic algorithm	Recyclable waste segregation	Highest accuracy demonstrated 99.6%
[28]	Auto Encoder network, CNN, Ridge Regression and Support vector machine as a classifier	Waste Classification	Achieved 99.6% accuracy
[50]	Fast region CNN	Street litter detection and classification	Achieved accuracies between 73.4% and 97.3% for different classes
[51]	Fast region CNN with edge computing	Garbage detection for street cleanliness assessment	Achieved accuracies between 81% and 93% for different classes
[52]	CNN with fifteen layers	Polythene Classification	Input image size 120x120 pixels, report accuracy for 15 layers network 99.2%
[32]	LSTM CNN	Waste forecasting	Reported R2 and MAPE as 0.96, 6, and 63.66 (Training), 0.92 and 114.05 (Testing)
[33]	Simple and modified LSTM CNN	Prediction of carbon mono oxide concentration inside the bin	Prediction accuracies exhibited by simple and modified models were 88% and 90%
[34]	CNN with three hidden layers of eighty neurons	Per capita waste generation prediction	Forecasted accuracy 94.6%
[53]	YOLOv3 and YOLOv3-tiny	Waste segregation for disposal and recycling	Mean average precision of implemented network is 94.99%
[27]	ResNet-50 and Support Vector Machine	Waste categorization into four classes	Obtained the classification accuracy of approximately 87%
[29]	MobileNet-V2	Waste categorization into six classes	The accuracy of the implemented network is 96.57%
[17]	DenseNet169, ResNet50, VGG16, and AlexNet	Waste categorization into six classes	Accuracies of all four models are 94.9%, 93.4%, 91.7%, and 89.3% respectively
[54]	Multi-task learning architecture-based CNN	Simultaneous waste localization and recognition	Shown F1 score 95.12% to 95.88%, with a 95% confidence interval
[55]	Single Shot Detector and Faster R-CNN based on MobileNetV2 and Inception-ResNet	Identification of six types of waste	Reported the accuracy for both models 97.63% and 95.76%, respectively
[56]	Two Deep CNN with multiple layers	Construction and demolition waste classification	Single and multi-waste classification accuracies are obtained 91.88% and 96.17%, respectively
[57]	VCG-19, ResNet50, and InceptionV3	Waste categorization into fifty classes	Obtained the accuracy 86.19% for fifty classes
[58]	Three CNN with different number of layers	Metal and glass detection into a waste bag	Determined the maximum accuracy for metal and glass 100% and 96.28, respectively
[59]	Resnet101, EfficientNet-B0, EfficientNet-B1 and ensemble	Waste categorization into seven classes	Overall accuracies 92.43%, 91.53%, 90.02%, and 94.11%
[60]	Faster Region CNN	Biodegradable and non-degradable waste segregation	Computed average accuracy 84.34%
[61]	RetinaNet	Waste pollutant detection and classification inside water	Obtained average precision 0.8148

[62]	YOLOv2	Classifying battery-containing devices, detecting batteries, and recognizing battery-structures	100% is demonstrated for classifying battery-containing from non-battery-containing devices
[63]	Deep CNN using Single Shot Detector	Waste dump identification on the riverbank	Masks generated on waste by the model are compared with the original image.
[64]	CNN with twenty-three layers	Different types of plastic material detection	Demonstrated the average accuracy of 74%
[65]	Multilayer hybrid CNN model	Waste classification into six categories	Shown classification accuracy up to 92.6%
[38]	Combination of ResNet50 and Feature Pyramid Network	Waste dump identification and classification	Achieved classification precision 94.5%
[66]	Seven state-of-the-art CNNs like MobileNetV3, AlexNet, ResNet	Waste classification into nine categories	Obtained accuracy from 91.9% to 94.6%

Table VII demonstrates the proposed DL models, objectives, and key results of compiled studies. A significant number of studies had implemented pre-existing CNN for self-constructed data set. In contrast, the remaining studies had designed their own CNN and applied it to their data set to demonstrate the experimental results. The deeper analysis of compiled studies deduced that most studies concentrated on the different waste identification and classification types. At the same time, some focused on the prediction of waste generation with various influencing factors. Few studies developed the smart bin using the IoT, and the DL model was used to build the custom software to control the bin hardware. One study constructed the waste picking robot from the grass ground, using DL-based custom software to manage the robot hardware. Moreover, objectives such as detecting different types of polythene materials and defects in potatoes were also obtained successfully. The key results of complied studies are discussed in detection precision and classification accuracy. The evaluation of results exhibits that the reported accuracies were more than 90%.

The comprehensive analysis of considered studies indicates that a significant number of studies had implemented pre-existing CNNs such as AlexNet, MobileNet-v2, YOLOv3, ResNet-50, NASNetLarge while remaining studies applied manually constructed CNNs which are built through a different number of neural layers. Pre-existing CNNs are developed by various researchers from academic and industry backgrounds. The CNNs have already demonstrated remarkable performance on image recognition benchmarks. These networks are trained, so only top layers, called fully connected layers, are retrained and fine-tuned according to the data set. Conceptually, these networks reutilize the weights and structure of a prior model from the convolutional layers. The construction and training of a CNN based new image recognition from scratch involve a lot of time and computational power. Therefore, the utilization of pre-existing networks increases computational efficiency.

V. DEEP LEARNING

In the last decade, AI has completely transformed and shifted into the era of computation, and DL is the only reason for this cutting-edge development. It has a very interesting and unique feature to 'self-learn' distinctive patterns directly from the data. It has the ability to extract features automatically without hand crafting them. It has emerged as the most promising computing method to automate the categorization of

visual and spatial data in the context of SWM. Nowadays, SWM and allied field researchers are getting huge amounts of street or city-level data from various systems such as city surveillance systems, unmanned aerial vehicles, high-resolution satellite imagery, or online platforms where many people participate in data collection [67]. However, conventional AI methods have limited capacity to analyze this huge amount of data which is a bottleneck for researchers [68]. DL computing techniques have the extensive power to overcome this condition through automatic analysis of a massive dataset.

DL theoretical concepts are not developed recently; it has been published as far back as the 1980s [69]. This approach has become more prevalent, understandable, and practically possible in the last decade due to tremendous growth in computer hardware, the development of exceptional computational tools, and the accessibility of massive preprocessed and annotated data necessary to implement this methodology [70]. The literature analysis evidence that it has been implemented in automation of complex data computation tasks, object detection and location in visual data, photo tagging, self-driving car, speech recognition etc., across a wide range of industries [70]. The authors strongly believed that this methodology could achieve similar remarkable advantages in SWM. It potentially saves a lot of time for manual data analysis; therefore, DL enables the SWM and allied researchers to concentrate on more crucial tasks and could develop improved features for large scale and real-time monitoring SWM systems [16], [17].

A subset of ML, DL consists of utilizing the data structures named 'deep ANN', interchangeably DL. It is fundamentally consecutive arrangements of non-linear functions or several layers of digital neurons. These multiple layers of neurons construct the deeper the network. These networks learn hidden patterns automatically from the input data without explicit construction of distinct features to categorize the data. This drives the AI to be widely understandable and usable to non-expert users. DL models are trained to perceive and learn these patterns by labelled inputs and corresponding outputs. After learning, the model predicts data that was never seen earlier [70]. This AI model, where labelled data is given in training of deep ANN, is termed supervised DL. Fig. 4 displays DL workflow using supervised learning through classification of e-waste items.

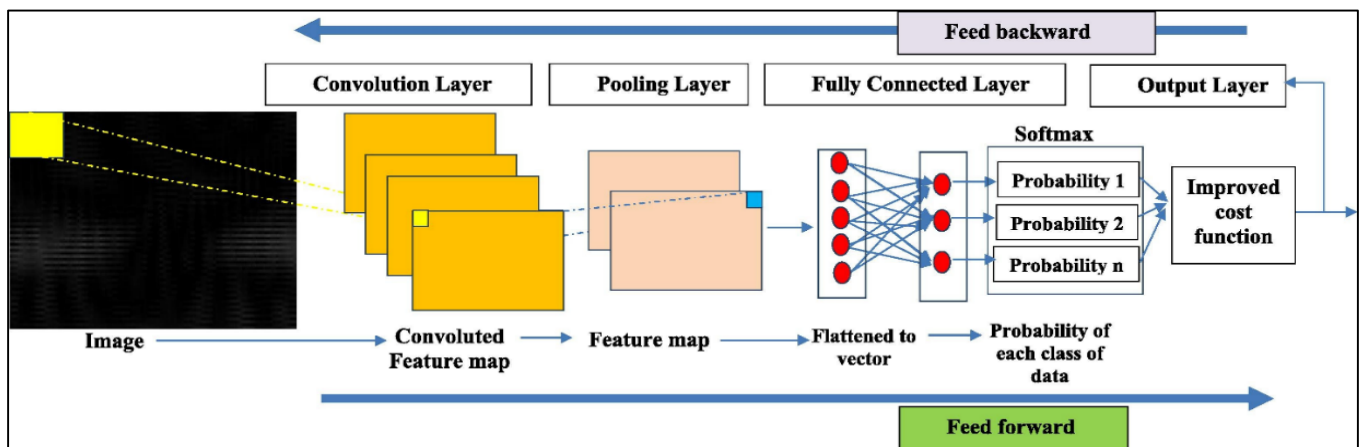


Fig. 4. A Typical Architecture of CNN.

A. Convolutional Neural Network

The CNN is an essential class of deep neural networks, more precisely, DL, a subset of ML and inherently re-branding ANN. CNN has exhibited massive growth in image recognition, so they are specially implemented to analyze visual data and perform tasks beyond classification. The CNN allows to extract the features from the image and conducts its training from these features. It is different from a conventional neural network in processing and extracting features. Image features are handcrafted to implement image recognition using a conventional neural network while CNN receives the image's raw pixels as input data, trains the proposed model, then automatically extracts the features to perform the better classification. Fig. 4 depicts the general architecture of a CNN [71]. A typical CNN has comprised an input layer, followed by the alternate combination of convolutional layer and pooling layer, and top of the network fully connected layer followed by classification output layer.

The input layer defines the size of the input image and holds the values of raw pixels extracted from the image. The input image dimensions are represented by the height, width, and the number of colour channels (1 and 3 for grayscale and colour images, respectively) in the image. This layer also carries out input data preprocessing such as simple rescaling or normalization, mean subtraction, normalization and principal component analysis and whitening.

The convolution layer is the core element of CNN building which comprises filter and stride. A filter is a small size two-dimensional layer of neurons mapped over a small segment of the input image and covers the whole image through shifting. The convolution operation is performed by the computing dot product between the filter and image pixel, added over the filter area. After that, the filter is shifted in the horizontal and vertical direction to perform similar computation in each area of the whole image. The step size of shifting is called stride. When the filter moves over the input image or output of the preceding layer, it uses the same set of weights to carry out the convolution operation to create the feature maps. Therefore, feature maps and filters are equal in number. All feature maps comprise a different set of weights and neurons of the same map using similar weights for different input regions. Initially,

all these filters have random values and become network parameters that will be learned subsequently.

The pooling layer decreases output data size from the convolution layer, called down sampling operation. Various types of pooling functions occur, but max pooling is generally utilized. It reduces the count of connections to the following layer, the typically fully connected layer. It also decreases the count of parameters learnt in the previous layer and does not perform any learning. The max-pooling filter gives the maximum value for every sub-region.

A fully connected layer is called a hidden layer, like an ANN. It connects each neuron of the preceding layer with every neuron of the successive layer. It determines the patterns to categorize the images by incorporating the features learned in the preceding layers and usually learns the non-linear function.

B. Computational Requirements

Generally, deep CNN models are implemented in several programming languages: Python, R, MATLAB, Java, and C/C++. Many open-source software libraries such as TensorFlow, PyTorch, OpenCV, Theano and Microsoft CNTK (Cognitive Toolkit) provide a diverse range of functions for most of the programming languages, including Python and R [72][73]. Moreover, software libraries like Keras provide a highly simplified interface for the DL libraries like TensorFlow.

The physical resources required to execute DL models are either Graphical Processing Unit (GPU) or Central Processing Unit (CPU). Generally, a CPU comprises only 2 to 16 cores, which are the smallest computation unit in a computer. A GPU consists of thousands of more simplified cores than CPU cores, optimized to execute parallel arithmetic operations, and is best for executing DL models [74]. Therefore, GPU decreases the program execution time in significant orders of magnitude and makes physical implementation possible [70]. Nowadays, an alternative is available for computation, which does not need the local computer hardware resources, is called cloud computing. It provides online on-demand computing and storage resources for computation without user management. Platforms like Google Cloud Platform Microsoft Azure provide a subscription to execute DL models online at cloud.

VI. RESEARCH GAPS AND PRIORITIES

Even though DL models have been extensively implemented in recent years to solve various SWM problems, they are still in the early phase of evolution and application. This SLR study has uncovered some gaps in applying DL models to SWM, and some aspects must be prioritized in the future.

A. Data Acquisition

DL models perceive insights and uncover hidden patterns from a massive amount of data applying various techniques. Reliable and enough data are the most fundamental and core elements of DL models applications. The quality and quantity of historical waste data are extremely crucial for the reliable performance of the DL model [75]. However, most of the studies deal with small or medium datasets, which could be attributed to SWM infrastructure and practices [16], [47]. Generally, SWM associated data are collected and organized by distinct channels encompassing various stakeholders. This hybrid management structure makes the data gathering and compilation extremely hard and complex [76]. Due to the lack of SWM related data, precise DL models are tough to implement. Furthermore, authors have analyzed that most research studies have utilized self-constructed data set for training, validation, and testing purposes. Therefore, it implies that the data set for DL model implementation is not available in the public domain. The scarcity of open benchmark data set is a major obstacle in implementing DL models in SWM and allied fields.

Now-a-days, many techniques are available to construct a large data set from a smaller one. For example, data augmentation is one of the most prevalent methods in fields such as data analysis to increase data size for effective and accurate model implementation. In SWM tasks such as waste classification material detection, the data augmentation technique is utilized to increase the amount of sample data for better performance of the DL model [52], [64]. Additionally, the collection of waste generation data is growing due to extensive waste monitoring, and some constructive data set are accessible freely [77]. Currently, city monitoring data is collected using remote sensing, geographic information system, unmanned aerial vehicle photography, satellite imagery, and modern technologies like IoT, sensors, and radio frequency identification to develop the SWM monitoring system. These sources generate a massive amount of data; therefore, it is highly demanded to develop a system for combining these existing data resources and constructing a data management platform with a unified protocol for distinct formats and types. Data fusion technology can also be applied to analyze and monitor the interconnection between distinct systems, databases and data types. Furthermore, data sharing mechanisms must be flexible and open to develop the reliable and quality data opening environment.

B. Data Preprocessing

Data preprocessing is not a vital phase for the AI, ML and DL models, but it is the highly consequential phase. If the collected data are processed correctly, it significantly impacts the training phase and predicted outcomes. Generally, it decreases the training time of DL model and sometimes

enhances the model performance. Besides this, it is also instrumental in transforming the collected data into an appropriate form for the subsequent model phases. Missing values and noise are common in data collection and recording. Mostly linear interpolation or mean value replacement are applied to fix missing data points [31], [78]. But these methods have one major drawback of information loss. In [79], the author applied the ANN to reconstruct the missing values in methane generation data and showed a significant decrease in mean square error. This leads to the novel direction for constructing MSW data missing value to future researchers.

In addition, the selection of suitable input variables for the DL model can extensively control the performance of the training phase and the robustness of DL models. These appropriate variables would improve the performance and reduce the modelling complexity. The SWM system is very complex contains various interconnected processes with numerous complex operations. This system also involves many non-linear parameters, including highly inconstant influencing factors, namely socioeconomic and demographic and operating control parameters [80]. The labelling of visual data is also highly consequential on supervised DL model learning performance and predicted results. An inaccurate label can significantly confuse the model learning, which will lead to erroneous results [81]. The survey analysis has uncovered that most of the existing studies have applied the DL algorithm on a selected set of labelled data that is correct in real-world applications. Furthermore, precise data labelling is cumbersome and time-consuming [81]. In [81], the author has demonstrated a DL technique to select the most appropriate data for labelling cost-effectively. This active labelling of data can focus on attaining the best training and testing performance for waste classification and illegal dump detection using the DL model with limited data. This can also be used to create the benchmark data set for different categories of waste.

C. Model Selection and Architecture Definition

Now-a-days, numerous DL models are available for implementation, but there is no specific rule to choose the best model. Generally, CNNs are applied to imagery or spatially related data, while LSTM/RNN are performed best on sequential data. Table VIII demonstrates the strengths and drawbacks of the DL models used in SWM and can help select the appropriate model. The DL model selection in SWM depends on the types of input data and tasks performed. The right accuracy selection also plays a crucial role in choosing a suitable DL model. Defining DL model architecture is a critical step for successfully executing model over studies data set with acceptable accuracy. There is no clear set of instructions to build the model, but the following two things help to develop model architecture. The model must possess satisfactory accuracy on the studies data set and must be easily trainable or exist as a pre-trained model. The practical aspect associated with accuracy is the speed versus accuracy tradeoff. DL communities have currently constructed a diverse range of architectures for distinct use cases that can be applied in real-world problems. For example, if someone has a constraint of computing resources, then one must choose fast architecture such as MobileNetv2 [29], [55], [66], and if someone does not have the above constraint, then one can go state-of-art model

which promises then best accuracy. Furthermore, some architectures are lighter and faster as they cut down the layers, making them faster and slimmer.

Additionally, different existing or pre-trained models can be applied to the same data set to obtain the best model to perform the target task. Based on Table VI and Table VII, CNNs have been widely applied in waste classification with remarkable accuracy [28]. However, these are rarely implemented in other SWM processes. Therefore, researchers have opportunities to develop new CNN architectures or can apply existing CNN in other processes. LSTM/RNN models have been implemented to forecast waste generation, but these models can have potential applications in other sequential data related to SWM [31]–[33].

TABLE VIII. STRENGTH AND DRAWBACK OF DL MODEL APPLIED IN SWM WITH THEIR APPLICATIONS

Model	Strength	Drawback	Applications in SWM
CNN	Capable of extracting features automatically; therefore, no explicit crafting of features. They have been used effectively for imagery data. Perform well with data that has spatial relationships.	Require massive sample data for training Require parameters tuning	Waste detection and classification- Glass, Metal, Trash, Cardboard, Plastic, Medical, Recyclable, Nonrecyclable, e-Waste, Polyethylene, Organic, Inorganic etc. Object detection- Battery, Defects in potatoes, Waste bags etc. (refer to Table VI)
LSTM /RNN	They have been efficiently used for sequence data like text, speech etc.	Require massive computation	Waste forecasting, Gas prediction inside the bin [31]–[33]

D. Model Comparison

It must be conducted to evaluate the effectiveness and performance of the DL model. This SLR analysis has uncovered that many studies have applied on one model with showing any comparative performance with other model [27], [33], [61]–[63], [34], [35], [38], [47], [48], [50], [51], [56]. In some studies, the outcomes from different models have been compared and analyzed to choose the best one while they lack in comparison to similar models from different studies [24], [26], [31], [32]. However, these studies have shown good results, but this comparison does not provide evidence for the best model selection. Very few studies have utilized the results of other studies as a baseline for comparison, but both results are Computer using the different data set; therefore, this type of comparison does not seem very meaningful and convincing [15], [28]. In waste classification and similar tasks, a significant number of studies have demonstrated the comparison with a similar type of model on the same data set and shown better accuracy (refer to Table VI). This SLR has also undermined that the current studies do not explain more about the model description, such as hyperparameters setting and fine-tuning. Therefore, it is extremely difficult to reproduce the results from implemented DL model. Consequently, the author has suggested explaining the DL model description with minor detail that will help advance

scientific research with previous outcomes and fast development and applications in SWM.

VII. DISCUSSION

The overall discussion about the SLR study can be partitioned into three subsets. The first subset describes the summary of the study. The second subset discusses an important observation with a shortcoming. The third subset explains why applications of DL models in SWM is growing with remarkable momentum.

First, the comprehensive SLR concentrates on analyzing and evaluating the various DL models and their applications in SWM, obtained from 40 research studies published in reputed journals and reliable conferences between 2019 and 2021. The reported key results of all complied studies are displayed, and performance comparisons shown within the study are also manifested. The outcomes of the SLR study indicates that various types of CNNs, manually constructed, pre-existing, and hybrid with other approaches, have been implemented to perform various tasks. Generally, waste identification and classification problems are fundamentally complex as waste have ill-defined features readable to the machine. Therefore, traditional ML and image process algorithms do not have sufficient capabilities to provide a reasonable solution in terms of effectiveness and efficiency. Other than waste classification, DL models have also been applied to predict waste generation, gas concentration and illegal waste dump detection.

Second, the in-depth analysis of the literature unveils that all the studies used self-constructed data set. Therefore, it can be confidently concluded that no benchmark data set exists, which is a major drawback for the researchers comparing their model performance with benchmark results. So, firstly it can be strongly recommended that an annotated benchmark data set be constructed for each waste category for future research. Secondly, it also seems clear that DL models provide more cutting-edge techniques in SWM, which are significantly effective and efficient compared to traditional ML and image process approaches. Therefore, DL models have gained sufficient momentum in the SWM research community to solve a wide variety of problems.

Third, the field of DL has got popular recently, so researchers from SWM research communities are increasing interest in applying DL models for SWM services. The SLR evidence that applications of DL models in SWM have started recently, especially in the last three years. The literature in this field is growing at a significant pace with novel applications in different SWM tasks. Therefore, the SLR study has focused on the research published in the last three years. The maturity of DL applications in this field can take a long time as the SWM system has highly complex interconnected components. It has been practically applied in many applications, namely intelligent waste identification and classification. For example, SpotGarbage, an Android App and robot for waste picking over grass, has successfully applied the DL models to detect, localize, and classify the waste automatically. Furthermore, most of the chosen studies for SLR are exploratory, so it can also be anticipated that more applications will be in practice soon.

VIII. CONCLUSION

Various AI and image processing approaches have been implemented for solving the SWM problems, such as waste generation prediction and waste level detection in the bin over the years. But in the last decade, DL has been successfully applied in diverse domains. Even though the main focus of DL (especially unsupervised learning) is in the image processing domain, this study has performed the SLR of the emerging research relating to the DL applications in the SWM. Furthermore, these approaches are popularly known to conquer the vanishing gradient problem, which was an acute limitation on the depth of ANN. In the last few years, lots of research efforts have been made to apply DL in the SWM domain. This study performs an SLR of published research that applies the DL models for SWM. Forty relevant research studies are uncovered after executing the rigorous SLR procedure. These research studies are analyzed and examined based on the SWM problem they focused, type of data set utilized, implemented models comparison, and performance evaluation according to the performance matrices used by individual papers. The performance of DL models is compared with other existing techniques. The overview of findings implies that DL exhibits better performance and outperforms as compared to other prevalent ML and image processing techniques.

Significance of this SLR: The identified DL learning techniques have been effectively applied to model the complex processes in SWM. Therefore, DL is drawing the attention of researchers from around the world and has emerged as a foundation for SWM problem-solving. This SLR study also provides evidence that DL in SWM is the most active research field. Furthermore, it is observed that DL models consist of cutting-edge techniques to solve the SWM problems. These techniques are remarkably efficient and do not need hand crafted features as traditional ML and image process approaches. Hence, DL models have obtained significant popularity in the SWM research community to solve a wide range of problems. The main goal and significance of this SLR provide the background about different DL models with their performance in a variety of SWM tasks and gaps for future research on this particular topic. It also elaborates the basic DL model (CNN architecture) design and provides comprehensive information about DL in SWM, which could be highly useful to SWM practitioners.

For future work, it is recommended to implement the general concepts and best practices of DL, as illustrated through this SLR, to problems of SWM where this cutting edge approach has not yet been significantly applied. One crucial suggestion is to construct the annotated benchmark data set for public use. It is strongly needed to compare and enhance the performance of the DL models. It will also provide a boost to the applications of models in SWM.

ACKNOWLEDGMENT

This research was supported by the Princess Nourah bint Abdulrahman University Researchers Supporting Project number (PNURSP2022R259), Princess Nourah bint Abdulrahman University, Riyadh, Saudi Arabia.

REFERENCES

- [1] C. Mukherjee, J. Denney, E. G. Mbonimpa, J. Slagley, and R. Bhowmik, "A review on municipal solid waste-to-energy trends in the USA," *Renewable and Sustainable Energy Reviews*, vol. 119, Elsevier, Mar. 01, 2020, doi: 10.1016/j.rser.2019.109512.
- [2] S. Kaza, L. C. Yao, P. Bhada-Tata, and F. Van Woerden, *What a Waste 2.0: A Global Snapshot of Solid Waste Management to 2050*, vol. 1. Washington: World Bank Publications, The World Bank Group, 1818 H Street NW, Washington, DC 20433, 2018.
- [3] C. Magazzino, M. Mele, and N. Schneider, "The relationship between municipal solid waste and greenhouse gas emissions: Evidence from Switzerland," *Waste Manag.*, vol. 113, pp. 508–520, Jul. 2020, doi: 10.1016/j.wasman.2020.05.033.
- [4] M. Triassi, R. Alfano, M. Illario, A. Nardone, O. Caporale, and P. Montuori, "Environmental pollution from illegal waste disposal and health effects: A review on the 'triangle of death,'" *Int. J. Environ. Res. Public Health*, vol. 12, no. 2, pp. 1216–1236, Jan. 2015, doi: 10.3390/ijerph120201216.
- [5] D. Demirbilek, A. Öztüfekçi Önal, V. Demir, G. Uslu, and H. Arslanoglu-Isik, "Characterization and pollution potential assessment of Tunceli, Turkey municipal solid waste open dumping site leachates," *Environ. Monit. Assess.*, vol. 185, no. 11, pp. 9435–9449, 2013, doi: 10.1007/s10661-013-3263-7.
- [6] D. H. F. da Paz, K. P. V. Lafayette, M. J. de O. Holanda, M. do C. M. Sobral, and L. A. R. de C. Costa, "Assessment of environmental impact risks arising from the illegal dumping of construction waste in Brazil," *Environ. Dev. Sustain.*, vol. 22, no. 3, pp. 2289–2304, Mar. 2020, doi: 10.1007/s10668-018-0289-6.
- [7] A. S. Nagpure, "Assessment of quantity and composition of illegal dumped municipal solid waste (MSW) in Delhi," *Resour. Conserv. Recycl.*, vol. 141, pp. 54–60, Feb. 2019, doi: 10.1016/j.resconrec.2018.10.012.
- [8] M. A. Hannan, M. Arebey, R. A. Begum, A. Mustafa, and H. Basri, "An automated solid waste bin level detection system using Gabor wavelet filters and multilayer perception," *Resour. Conserv. Recycl.*, vol. 72, pp. 33–42, Mar. 2013, doi: 10.1016/j.resconrec.2012.12.002.
- [9] A. Malakahmad and N. D. Khalil, "Solid waste collection system in Ipoh city Solid Waste Collection System In Ipoh City:A Review," 2011 *Int. Conf. Business, Eng. Ind. Appl.*, no. March, pp. 174–179, 2016, doi: 10.1109/ICBEIA.2011.5994236.
- [10] M. A. Hannan, M. Arebey, R. A. Begum, and H. Basri, "Radio Frequency Identification (RFID) and communication technologies for solid waste bin and truck monitoring system," *Waste Manag.*, vol. 31, no. 12, pp. 2406–2413, 2011, doi: 10.1016/j.wasman.2011.07.022.
- [11] K. Kawai and T. Tasaki, "Revisiting estimates of municipal solid waste generation per capita and their reliability," *J. Mater. Cycles Waste Manag.*, vol. 18, pp. 1–13, Jan. 2016, doi: 10.1007/s10163-015-0355-1.
- [12] M. Haraguchi, A. Siddiqi, and V. Narayanamurti, "Stochastic cost-benefit analysis of urban waste-to-energy systems," *J. Clean. Prod.*, vol. 224, pp. 751–765, Jul. 2019, doi: 10.1016/j.jclepro.2019.03.099.
- [13] K. L. P. Nguyen, Y. H. Chuang, H. W. Chen, and C. C. Chang, "Impacts of socioeconomic changes on municipal solid waste characteristics in Taiwan," *Resour. Conserv. Recycl.*, vol. 161, Oct. 2020, doi: 10.1016/j.resconrec.2020.104931.
- [14] Z. Ceylan, S. Bulkan, and S. Elevli, "Prediction of medical waste generation using SVR, GM (1,1) and ARIMA models: a case study for megacity Istanbul," *J. Environ. Heal. Sci. Eng.*, vol. 18, no. 2, pp. 687–697, Dec. 2020, doi: 10.1007/s40201-020-00495-8.
- [15] M. Bagheri, R. Esfilar, M. S. Golchi, and C. A. Kennedy, "A comparative data mining approach for the prediction of energy recovery potential from various municipal solid waste," *Renew. Sustain. Energy Rev.*, vol. 116, Dec. 2019, doi: 10.1016/j.rser.2019.109423.
- [16] P. Nowakowski and T. Pamuła, "Application of deep learning object classifier to improve e-waste collection planning," *Waste Manag.*, vol. 109, pp. 1–9, 2020, doi: 10.1016/j.wasman.2020.04.041.
- [17] M. W. Rahman, R. Islam, A. Hasan, N. I. Bithi, M. M. Hasan, and M. M. Rahman, "Intelligent waste management system using deep learning with IoT," *J. King Saud Univ. - Comput. Inf. Sci.*, Sep. 2020, doi: 10.1016/j.jksuci.2020.08.016.

- [18] Z. Ye, J. Yang, N. Zhong, X. Tu, J. Jia, and J. Wang, "Tackling environmental challenges in pollution controls using artificial intelligence: A review," *Science of the Total Environment*, vol. 699, Elsevier, Jan. 10, 2020, doi: 10.1016/j.scitotenv.2019.134279.
- [19] L. Chhay, M. A. H. Reyad, R. Suy, M. R. Islam, and M. M. Mian, "Municipal solid waste generation in China: influencing factor analysis and multi-model forecasting," *J. Mater. Cycles Waste Manag.*, vol. 20, no. 3, pp. 1761–1770, 2018, doi: 10.1007/s10163-018-0743-4.
- [20] M. Z. Joharestani, C. Cao, X. Ni, B. Bashir, and S. Talebiesfandarani, "PM2.5 prediction based on random forest, XGBoost, and deep learning using multisource remote sensing data," *Atmosphere (Basel)*, vol. 10, no. 7, p. 373, Jul. 2019, doi: 10.3390/atmos10070373.
- [21] W. Xia, Y. Jiang, X. Chen, and R. Zhao, "Application of machine learning algorithms in municipal solid waste management: A mini review," *Waste Management and Research*. SAGE Publications, Sage UK: London, England, pp. 1–16, Jul. 16, 2021, doi: 10.1177/0734242X211033716.
- [22] G. L. Huang, J. He, Z. Xu, and G. Huang, "A combination model based on transfer learning for waste classification," *Concurr. Comput.*, vol. 32, no. 19, pp. 1–12, 2020, doi: 10.1002/cpe.5751.
- [23] K. Ahmad, K. Khan, and A. Al-Fuqaha, "Intelligent Fusion of Deep Features for Improved Waste Classification," *IEEE Access*, vol. 8, pp. 96495–96504, 2020, doi: 10.1109/ACCESS.2020.2995681.
- [24] A. A. A. G. S. Altikat, "Intelligent solid waste classification using deep convolutional neural networks," *Int. J. Environ. Sci. Technol.*, pp. 1–8, 2021, doi: 10.1007/s13762-021-03179-4.
- [25] A. H. Vo, L. Hoang Son, M. T. Vo, and T. Le, "A Novel Framework for Trash Classification Using Deep Transfer Learning," *IEEE Access*, vol. 7, pp. 178631–178639, 2019, doi: 10.1109/ACCESS.2019.2959033.
- [26] M. Valente, H. Silva, J. M. L. P. Caldeira, V. N. G. J. Soares, and P. D. Gaspar, "Detection of waste containers using computer vision," *Appl. Syst. Innov.*, vol. 2, no. 1, pp. 1–13, 2019, doi: 10.3390/asi2010011.
- [27] O. Adedeji and Z. Wang, "Intelligent waste classification system using deep learning convolutional neural network," *Procedia Manuf.*, vol. 35, pp. 607–612, 2019, doi: 10.1016/j.promfg.2019.05.086.
- [28] M. Toğaçar, B. Ergen, and Z. Cömert, "Waste classification using AutoEncoder network with integrated feature selection method in convolutional neural network models," *Meas. J. Int. Meas. Confed.*, vol. 153, 2020, doi: 10.1016/j.measurement.2019.107459.
- [29] D. Ziouzos, D. Tsiktisiris, N. Baras, and M. Dasygenis, "A Distributed Architecture for Smart Recycling Using Machine Learning," *Futur. Internet*, vol. 12, no. 9, p. 141, 2020, doi: 10.3390/fi12090141.
- [30] Y. Chu, C. Huang, X. Xie, B. Tan, S. Kamal, and X. Xiong, "Multilayer hybrid deep-learning method for waste classification and recycling," *Comput. Intell. Neurosci.*, vol. 2018, pp. 1–9, 2018, doi: 10.1155/2018/5060857.
- [31] M. Cubillos, "Multi-site household waste generation forecasting using a deep learning approach," *Waste Manag.*, vol. 115, pp. 8–14, 2020, doi: 10.1016/j.wasman.2020.06.046.
- [32] D. Niu, F. Wu, S. Dai, S. He, and B. Wu, "Detection of long-term effect in forecasting municipal solid waste using a long short-term memory neural network," *J. Clean. Prod.*, vol. 290, pp. 1–8, 2021, doi: 10.1016/j.jclepro.2020.125187.
- [33] A. Hussain et al., "Waste Management and Prediction of Air Pollutants Using IoT and Machine Learning Approach," *Energies*, vol. 13, no. 15, pp. 3930–3951, 2020.
- [34] F. Fasano, A. S. Addante, B. Valenzano, and G. Scannicchio, "Variables Influencing per Capita Production , Separate Collection , and Costs of Municipal Solid Waste in the Apulia Region (Italy) : An Experience of Deep Learning," *Int. J. Environ. Res. Public Health*, vol. 18, no. 2, pp. 752–774, 2021.
- [35] L. A. Akanbi, A. O. Oyedele, L. O. Oyedele, and R. O. Salami, "Deep learning model for Demolition Waste Prediction in a circular economy," *J. Clean. Prod.*, vol. 274, no. 2020, 2020, doi: 10.1016/j.jclepro.2020.122843.
- [36] Z. Kang, J. Yang, G. Li, and Z. Zhang, "An Automatic Garbage Classification System Based on Deep Learning," *IEEE Access*, vol. 8, pp. 140019–140029, 2020, doi: 10.1109/ACCESS.2020.3010496.
- [37] M. Anjum and M. S. Umar, "Garbage localization based on weakly supervised learning in Deep Convolutional Neural Network," in *Proceedings - IEEE 2018 International Conference on Advances in Computing, Communication Control and Networking, ICACCCN 2018*, Oct. 2018, pp. 1108–1113, doi: 10.1109/ICACCCN.2018.8748568.
- [38] R. N. Torres and P. Fraternali, "Learning to identify illegal landfills through scene classification in aerial images," *Remote Sens.*, vol. 13, no. 22, pp. 1–21, Nov. 2021, doi: 10.3390/rs13224520.
- [39] F. Zhang, C. Cao, C. Li, Y. Liu, and D. Huisingh, "A systematic review of recent developments in disaster waste management," *J. Clean. Prod.*, vol. 235, pp. 822–840, 2019, doi: 10.1016/j.jclepro.2019.06.229.
- [40] B. Kitchenham and S. Charters, "Guidelines for performing systematic literature reviews in software engineering," in *Technical report, Ver. 2.3 EBSE Technical Report*. EBSE, 2007, p. 65.
- [41] M. Abdallah, M. Abu Talib, S. Feroz, Q. Nasir, H. Abdalla, and B. Mahfood, "Artificial intelligence applications in solid waste management: A systematic research review," *Waste Manag.*, vol. 109, pp. 231–246, 2020, doi: 10.1016/j.wasman.2020.04.057.
- [42] M. Staples and M. Niazi, "Systematic review of organizational motivations for adopting CMM-based SPI," *Inf. Softw. Technol.*, vol. 50, no. 7–8, pp. 605–620, 2008.
- [43] W. Reim, V. Parida, and D. Örtqvist, "Product-Service Systems (PSS) business models and tactics - A systematic literature review," *J. Clean. Prod.*, vol. 97, pp. 61–75, Jun. 2015, doi: 10.1016/j.jclepro.2014.07.003.
- [44] United Nations, *Human Development Report 2020*. 2020.
- [45] A. Annarelli, C. Battistella, and F. Nonino, "Product service system: A conceptual framework from a systematic review," *Journal of Cleaner Production*, vol. 139, Elsevier Ltd, pp. 1011–1032, Dec. 15, 2016, doi: 10.1016/j.jclepro.2016.08.061.
- [46] T. J. Sheng et al., "An Internet of Things Based Smart Waste Management System Using LoRa and Tensorflow Deep Learning Model," *IEEE Access*, vol. 8, pp. 148793–148811, 2020, doi: 10.1109/ACCESS.2020.3016255.
- [47] J. Bai, S. Lian, Z. Liu, K. Wang, and D. Liu, "Deep learning based robot for automatically picking up garbage on the grass," *IEEE Trans. Consum. Electron.*, vol. 64, no. 3, pp. 382–389, 2019.
- [48] S. Jagtap, C. Bhatt, J. Thik, and S. Rahimifard, "Monitoring potato waste in food manufacturing using image processing and internet of things approach," *Sustain.*, vol. 11, no. 11, pp. 1–12, 2019, doi: 10.3390/su11113173.
- [49] W. L. Mao, W. C. Chen, C. T. Wang, and Y. H. Lin, "Recycling waste classification using optimized convolutional neural network," *Resour. Conserv. Recycl.*, vol. 164, no. August 2020, p. 105132, 2021, doi: 10.1016/j.resconrec.2020.105132.
- [50] P. Ping, G. Xu, E. Kumala, and J. Gao, "Smart Street Litter Detection and Classification Based on Faster R-CNN and Edge Computing," *Int. J. Softw. Eng. Knowl. Eng.*, vol. 30, no. 4, pp. 537–553, 2020, doi: 10.1142/S0218194020400045.
- [51] P. Zhang, Q. Zhao, J. Gao, W. Li, and J. Lu, "Urban Street Cleanliness Assessment Using Mobile Edge Computing and Deep Learning," *IEEE Access*, vol. 7, pp. 63550–63563, 2019, doi: 10.1109/ACCESS.2019.2914270.
- [52] K. M. Bobulski J, "Waste classification system using image processing and convolutional neural networks," *Int. Work. Artif. Neural Networks*, 2019 Jun 12, Springer, Cham., pp. 350–361, 2019, [Online]. Available: http://dx.doi.org/10.1007/978-3-030-20518-8_30.
- [53] S. Kumar, D. Yadav, H. Gupta, O. P. Verma, I. A. Ansari, and C. W. Ahn, "A novel yolov3 algorithm-based deep learning approach for waste segregation: Towards smart waste management," *Electron.*, vol. 10, no. 1, pp. 1–20, 2021, doi: 10.3390/electronics10010014.
- [54] S. Liang and Y. Gu, "A deep convolutional neural network to simultaneously localize and recognize waste types in images," *Waste Manag.*, vol. 126, pp. 247–257, 2021, doi: 10.1016/j.wasman.2021.03.017.
- [55] D. O. Melinte, A. M. Travediu, and D. N. Dumitriu, "Deep convolutional neural networks object detector for real-time waste identification," *Appl. Sci.*, vol. 10, no. 20, pp. 1–18, 2020, doi: 10.3390/app10207301.

- [56] P. Davis, F. Aziz, M. T. Newaz, W. Sher, and L. Simon, "The classification of construction waste material using a deep convolutional neural network," *Autom. Constr.*, vol. 2021, 2021, doi: 10.1016/j.autcon.2020.103481.
- [57] H. Wang, Y. Li, L. M. Dang, J. Ko, D. Han, and H. Moon, "Smartphone-based bulky waste classification using convolutional neural networks," *Multimed. Tools Appl.*, vol. 79, no. 39–40, pp. 29411–29431, 2020, doi: 10.1007/s11042-020-09571-5.
- [58] O. I. Funch, R. Marhaug, S. Kohtala, and M. Steinert, "Detecting glass and metal in consumer trash bags during waste collection using convolutional neural networks," *Waste Manag.*, vol. 119, pp. 30–38, 2021, doi: 10.1016/j.wasman.2020.09.032.
- [59] M. H. Huynh, P. T. Pham-Hoai, A. K. Tran, and T. D. Nguyen, "Automated Waste Sorting Using Convolutional Neural Network," *Proc. - 2020 7th NAFOSTED Conf. Inf. Comput. Sci. NICS 2020*, pp. 102–107, 2020, doi: 10.1109/NICS51282.2020.9335897.
- [60] V. P. Brintha, R. Rekha, J. Nandhini, N. Sreekaarthick, and B. Ishwaryaa, "Automatic Classification of Solid Waste Using Deep Learning," in *Proceedings of International Conference on Artificial Intelligence, Smart Grid and Smart City Applications*, 2019, pp. 881–889, doi: 10.1007/978-3-030-24051-6_83.
- [61] H. Panwar et al., "AquaVision: Automating the detection of waste in water bodies using deep transfer learning," *Case Stud. Chem. Environ. Eng.*, vol. 2, Sep. 2020, doi: 10.1016/j.cscee.2020.100026.
- [62] W. Sterkens, D. Diaz-Romero, T. Goedemé, W. Dewulf, and J. R. Peeters, "Detection and recognition of batteries on X-Ray images of waste electrical and electronic equipment using deep learning," *Resour. Conserv. Recycl.*, vol. 168, May 2021, doi: 10.1016/j.resconrec.2020.105246.
- [63] O. Youme, T. Bayet, J. M. Dembele, and C. Cambier, "Deep Learning and Remote Sensing: Detection of Dumping Waste Using UAV," in *Procedia Computer Science*, Jan. 2021, vol. 185, pp. 361–369, doi: 10.1016/j.procs.2021.05.037.
- [64] J. Bobulski and M. Kubanek, "Deep Learning for Plastic Waste Classification System," *Appl. Comput. Intell. Soft Comput.*, vol. 2021, pp. 1–7, 2021, doi: 10.1155/2021/6626948.
- [65] C. Shi, C. Tan, T. Wang, and L. Wang, "A waste classification method based on a multilayer hybrid convolution neural network," *Appl. Sci.*, vol. 11, no. 18, pp. 1–19, Sep. 2021, doi: 10.3390/app11188572.
- [66] C. Wang, J. Qin, C. Qu, X. Ran, C. Liu, and B. Chen, "A smart municipal waste management system based on deep-learning and Internet of Things," *Waste Manag.*, vol. 135, pp. 20–29, Nov. 2021, doi: 10.1016/j.wasman.2021.08.028.
- [67] B. M. Allan, D. G. Nimmo, D. Ierodiaconou, J. VanDerWal, L. P. Koh, and E. G. Ritchie, "Futurecasting ecological research: the rise of technoecology," *Ecosphere*, vol. 9, no. 5, May 2018, doi: 10.1002/ecs2.2163.
- [68] J. J. Valletta, C. Torney, M. Kings, A. Thornton, and J. Madden, "Applications of machine learning in animal behaviour studies," *Animal Behaviour*, vol. 124, Academic Press, pp. 203–220, Feb. 01, 2017, doi: 10.1016/j.anbehav.2016.12.005.
- [69] I. Goodfellow, Y. Bengio, and A. Courville, *Deep learning*. 2016.
- [70] Y. Lecun, Y. Bengio, and G. Hinton, "Deep learning," *Nature*, vol. 521, no. 7553, pp. 436–444, 2015, doi: 10.1038/nature14539.
- [71] A. Kumar, C. P. Gandhi, Y. Zhou, R. Kumar, and J. Xiang, "Improved deep convolution neural network (CNN) for the identification of defects in the centrifugal pump using acoustic images," *Appl. Acoust.*, vol. 167, p. 107399, Oct. 2020, doi: 10.1016/j.apacoust.2020.107399.
- [72] F. Seide, A. A.-P. of the 22nd A. SIGKDD, and U. 2016, "CNTK: Microsoft's open-source deep-learning toolkit," in *Proceedings of the 22nd ACM SIGKDD international conference on knowledge discovery and data mining*, 2016, pp. 2135–2135, [Online]. Available: <https://dl.acm.org/doi/abs/10.1145/2939672.2945397>.
- [73] C. J. Abadi, Martín, Barham P, "{TensorFlow} A system for large-scale machine learning," in *12th USENIX symposium on operating systems design and implementation (OSDI 16)*, 2016, pp. 265–283, [Online]. Available: <https://www.usenix.org/conference/osdi16/technical-sessions/presentation/abadi>.
- [74] J. Nickolls and W. J. Dally, "The GPU computing era," *IEEE Micro*, vol. 30, no. 2, pp. 56–69, 2010, doi: 10.1109/MM.2010.41.
- [75] S. Majchrowska et al., "Deep learning-based waste detection in natural and urban environments," *Waste Manag.*, vol. 138, pp. 274–284, Feb. 2022, doi: 10.1016/j.wasman.2021.12.001.
- [76] M. Abbasi and A. El Hanandeh, "Forecasting municipal solid waste generation using artificial intelligence modelling approaches," *Waste Manag.*, vol. 56, pp. 13–22, 2016, doi: 10.1016/j.wasman.2016.05.018.
- [77] H. Niska and A. Serkkola, "Data analytics approach to create waste generation profiles for waste management and collection," *Waste Manag.*, vol. 77, pp. 477–485, Jul. 2018, doi: 10.1016/j.wasman.2018.04.033.
- [78] C. Birgen, E. Magnanelli, P. Carlsson, Ø. Skreibeberg, J. Mosby, and M. Becidan, "Machine learning based modelling for lower heating value prediction of municipal solid waste," *Fuel*, vol. 283, Jan. 2021, doi: 10.1016/j.fuel.2020.118906.
- [79] B. Fallah, K. T. W. Ng, H. L. Vu, and F. Torabi, "Application of a multi-stage neural network approach for time-series landfill gas modeling with missing data imputation," *Waste Manag.*, vol. 116, pp. 66–78, Oct. 2020, doi: 10.1016/j.wasman.2020.07.034.
- [80] J. Soto-Paz et al., "A New Approach for the Optimization of Biowaste Composting Using Artificial Neural Networks and Particle Swarm Optimization," *Waste and Biomass Valorization*, vol. 11, no. 8, pp. 3937–3951, Aug. 2020, doi: 10.1007/s12649-019-00716-8.
- [81] D. Wang and Y. Shang, "A new active labeling method for deep learning," in *Proceedings of the International Joint Conference on Neural Networks*, Sep. 2014, pp. 112–119, doi: 10.1109/IJCNN.2014.6889457.

Proposal of an Automated Tool for the Application of Sentiment Analysis Techniques in the Context of Marketing

Gabriel Elías Chanchí Golondrino¹, Manuel Alejandro Ospina Alarcón², Wilmar Yesid Campo Muñoz³
Faculty of Engineering, Systems Engineering Program, University of Cartagena, Cartagena de Indias, Colombia^{1,2}
Faculty of Engineering, Electronics Engineering Program, University of Quindío, Armenia, Colombia³

Abstract—Currently, the opinions and comments made by customers on e-commerce portals regarding different products and services have great potential for identifying customer perceptions and preferences. Based on the above, there is a growing need for companies to have automated tools based on sentiment analysis through polarity analysis, which allow the examination of customer opinions to obtain quantitative indicators from qualitative information that enable decision-making in the context of marketing. In this article, we propose the construction of an automated tool for conducting opinion mining studies, which can be used in a transparent way to the algorithmic process by the marketing units of companies for decision making. The functionality of the proposed tool was verified through a case study, in which the opinions obtained from electronic commerce website concerning one of the best-selling technological products were investigated.

Keywords—E-commerce; marketing; opinion mining; polarity analysis; sentiment analysis

I. INTRODUCTION

The opinions and comments made in various digital media by customers regarding different products and services, being subjective and descriptive, have great potential for identifying the perception and preferences of the user regarding the products and services offered by companies to formulate appropriate marketing strategies [1]–[4]. In the same way, from the rapid growth of e-commerce platforms and social networks, potential buyers of products and services take into consideration the evaluations or reviews made by other clients before buying a product from a given company [5]–[8].

By the above, with the current evolution of artificial intelligence methods and the wide dissemination of machine learning models, one of the emerging areas of computer science is affective computing, which through techniques such as opinion mining or sentiment analysis allows obtaining quantitative indicators from subjective information that includes emotional content, such as opinions [9]–[13]. Sentiment analysis techniques correspond to a subdomain of natural language processing (NLP), and their objective is to identify how sentiments are expressed in a text through the determination of the polarity value (positive, negative, neutral) that are present in an opinion [7], [14]–[17]. In this way, considering the advantages of sentiment analysis techniques in terms of the analysis of qualitative information such as the opinion of customers on social networks and electronic

commerce portals, these become useful tools for decision-making in the context of marketing by companies [14], [18], [19].

Based on the advantages provided by opinion mining techniques, in companies and organizations, there is a growing need for automated tools, which from structured and unstructured qualitative data extracted from different sources (social networks, electronic commerce, marketing campaigns, perception surveys, among others) make it possible to identify the individual and group perception of customers concerning a product or service more objectively and make decisions regarding marketing campaigns [6], [20]–[23].

This article proposes the design and implementation of an automated tool for the application of sentiment analysis or opinion mining techniques in the context of marketing and specifically in the analysis of reviews made on e-commerce portals by clients regarding the perception or degree of satisfaction with a product or service. In this sense, the tool receives as input, in a .CSV file, the opinions or reviews of the clients regarding a product or service and obtains as output, the polarity (positive, negative, neutral) associated with each of the opinions, as well as the statistical analysis of the polarities, the average percentage distribution of the polarities, and the percentage distribution of the dominant polarities of the total opinions. The proposed tool was implemented in the Python language using machine learning models associated with sentiment analysis techniques provided by the Python-compatible Paralleldots library. The proposed automated tool is intended to serve as a reference for conducting sentiment analysis studies in the context of marketing, to evaluate the impact and promote decision-making regarding the products and services offered by companies through digital media.

The rest of the article is organized as follows: Section 2 shows different studies that are relevant to the problems faced and the objectives to be achieved. Section 3 describes the methodology considered for the development of this research. Section 4 presents the results obtained in this work, which includes the description of the design and implementation of the automated tool and its application in a case study in the context of marketing. Section 5 gives a discussion that summarizes the data and facts obtained to support the purpose of this investigation. Finally, section 6 presents the conclusions and future work derived from this research.

II. RELATED WORK

Different studies have been carried out regarding the application of the sentiment analysis theme and/or opinion mining in the business context. Thus in [24], a study on the perception of users regarding airport service in 10 main airports in the world was executed based on the application of sentiment analysis on the comments of 1224 passengers extracted from the Skytrax portal. In [25], a sentiment analysis study was developed on the opinions of tourists on social networks regarding the behavior and performance of this sector (airlines, tourism organizations, news, and tourism events) during the first months of the COVID-19 pandemic. In [26], a context-sensitive recommendation system was proposed, which extracted people's food preferences from their comments using sentiment analysis techniques for suggesting restaurants according to these preferences. In [27], a comparative study was carried out on the effectiveness of the application of sentiment analysis techniques and the stars rating with a total of 900 customer reviews of different products and services. It was obtained that the sentiment analysis techniques are effective in detecting the underlying tone of the analyzed content. In [28], a new sentiment analysis method supported by a knowledge-based lexicon is proposed, which was used to evaluate the polarity of customer opinions after the launch of new products in the videogame industry. In [29], a study of sentiment and text analysis after posts on Twitter related to Halal tourism was developed to identify the perception of users and the most popular tourist destinations. In [30], a sentiment analysis study was carried out on the opinions and comments of the inhabitants of India in relevant news articles regarding the economy and the financial market to identify their perception of the volatility of the stock market. In [23], an analysis of the perception of customers of energy companies in the United Kingdom was done based on the opinions expressed by them on Twitter, using a sentiment analysis approach supported by a knowledge-based lexicon. In [31], a sentiment analysis study was developed on the opinions of Twitter users regarding autonomous vehicles and their related promotional events.

Although the aforementioned works present a case of application of the sentiment analysis theme in the business context, they have focused on a few of the challenges of this topic, such as the improvement in precision and the optimization of supervised learning models or polarity classification [5], without addressing the development of tools that automate the process of opinion mining or sentiment analysis to facilitate their extrapolation and use transparently in different application contexts by stakeholders to obtain objective indicators of the perception of clients or potential clients from subjective information [6], [20]–[23].

III. METHODOLOGY

For the development of this work, 4 methodological phases were considered: exploration and selection of technologies, design of the automated tool, construction of the automated tool, and case study (see Fig. 1).

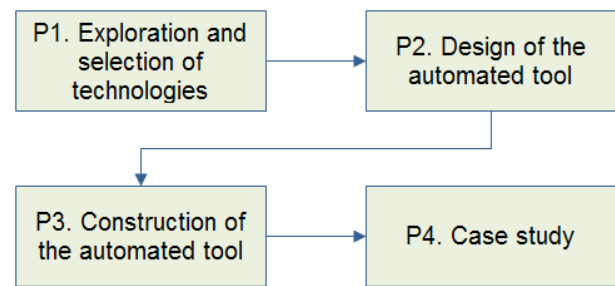


Fig. 1. Methodology Phases.

In phase 1 of the methodology, a set of tools and technologies were explored to carry out the processes of word processing, sentiment analysis, and/or polarity in text, statistical analysis, and data visualization. Thus, the Python pandas library was selected for obtaining and processing the text of opinions from .CSV or excel files. Regarding sentiment analysis, the Python Paralleldots library was selected, which enables the extraction of the value or distribution of the polarities (positive, negative, and neutral) associated with the text of an opinion. For the analysis through descriptive statistics of the polarities obtained in the sentiment analysis process, the NumPy Python library was selected. Regarding the visualization of statistical and graphic results, the Python libraries Tkinter and matplotlib were selected. In phase 2 of the methodology, the functional modules of the tool were defined, as well as the processes associated with these modules and that allowed text processing, obtaining polarities in opinions, and statistical and graphical analysis of the results. Additionally, from the defined modules and processes, the high-level interfaces of the automated tool were designed. In phase 3 of the methodology, based on the high-level interfaces defined in phase 2, the automated tool for the application of sentiment analysis techniques in the context of marketing was implemented using the Python language and the libraries selected in phase 1, which allows performing on a dataset of opinions, the functional processes mentioned in phase 2 (text processing, determination of the polarities of the opinions and graphical and statistical analysis of the results). Finally, in phase 4, based on the use of the proposed automated tool, a case study was developed on a dataset made up of comments made to a technological producer offered in the Latin American e-commerce portal "Mercado Libre". This case study was carried out in order to demonstrate the ease with which the tool can process and analyze opinion datasets obtained from different e-commerce portals.

IV. RESULTS

This section describes the development of the different phases considered in the methodology presented in section 2, which includes the design and implementation of the proposed automated tool, as well as the case study developed through the tool. At the tool design level, the functional modules and the processes developed in each of these modules are presented. Regarding the implementation, the interfaces and/or tabs that make up the applied tool are described. Regarding the case study, the results obtained from the sentiment analysis study performed on the opinions or reviews of a product offered on the "Mercado Libre" website are presented.

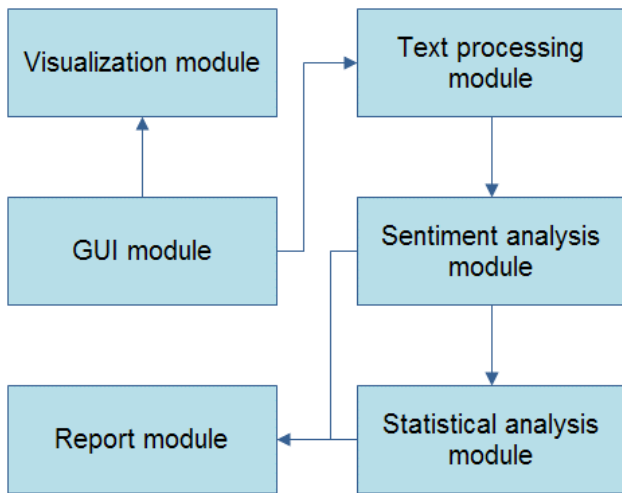


Fig. 2. Functional Modules of the Tool.

Based on the above, Fig. 2 presents the six functional modules that make up the proposed automated tool: the GUI module, text processing module, sentiment analysis module, statistical analysis module, visualization module, and report module.

The GUI module was implemented through the Python Tkinter library, which was in charge of managing the different components, controls, and events that make up the graphical interface of the tool, in such a way that it allowed the interaction with the user and the presentation of the results of the study of sentiment analysis at the statistical and graphical level. The text processing module was implemented using the pandas library, and it was responsible for making it possible to access the opinion data stored in a .CSV or excel file. The sentiment analysis module was implemented through the Paralleldots library that oversees obtaining the polarity values (positive, negative, and neutral) of the different opinions extracted from the file attached to the tool. The statistical analysis module was implemented through the NumPy library, and it was responsible for the application of descriptive statistics techniques on the polarities obtained in the different opinions. The visualization module was implemented using the Python matplotlib library which allowed displaying the results of the percentage distribution of the polarities in each one of the opinions and the total of opinions. Finally, the report module was implemented through the Python file management functionalities that allowed generating a report in .CSV format with the polarities calculated for each of the opinions and the statistical analysis obtained from those polarities.

Taking into consideration the modules that make up the automated tool, Fig. 3 illustrates the different functional processes that the tool performs and that comprise those modules through a flow diagram. Thus, once the file with the opinions was loaded either in .CSV or excel format, the tool obtained each of the opinions through the pandas library and proceeded with the calculation of the polarities (positive, negative, and neutral) associated with them, using the Paralleldots library while these polarities were stored in a floating NumPy array. Once the polarities of the opinions of the file were obtained, the tool performed the analysis through descriptive statistics using the NumPy library. In the same way,

the automated tool generated a set of graphs with the distribution of polarities on every single opinion and overall. Finally, the tool allowed generating a report in .CSV format with the polarities calculated for each opinion and their statistical analysis.

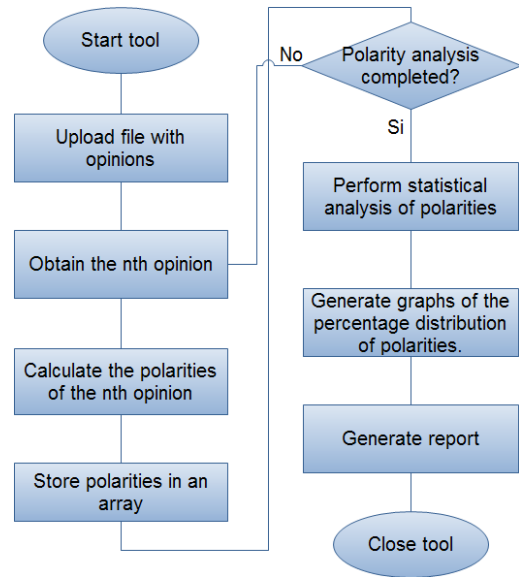


Fig. 3. Flow Diagram of the Tool's Functional Processes.

Considering the processes defined and presented in Fig. 3, Fig. 4 shows the graphical interface of the implemented tool, which consists of five tabs labeled as "Opinion Analysis", "Statistical Analysis", "Polarities per Opinion", "Average Polarity Distribution", "Dominant Polarities".

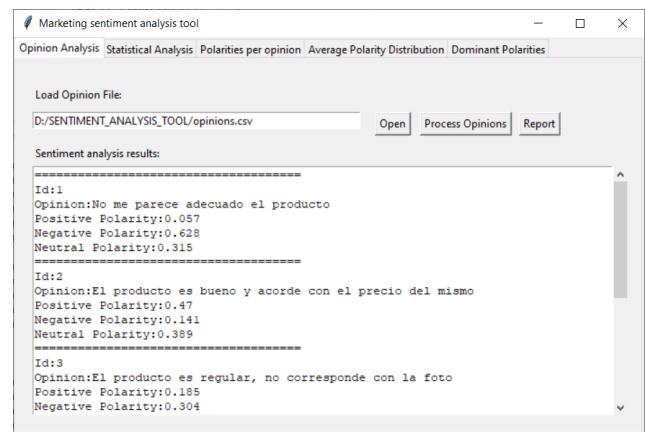


Fig. 4. "Opinion Analysis" Tab of the Tool.

By pressing the "Open" button in the "Opinion Analysis" tab, it is possible to load a .CSV or excel file with the opinions or reviews of a product taken from an electronic commerce website. By pressing the "Process Opinion" button once the file was loaded into the tool, it calculated the polarity associated with each of the opinions while the results were presented in the text area of this tab. In the same way, it was possible to generate a report in a .CSV file in this tab with the polarities obtained for each opinion and their statistical analysis. As an example, Fig. 4 presents the results obtained for an example file, which has 5 test opinions. Thus, for the first opinion, the

result was a positive polarity of 0.057, a negative polarity of 0.628, and a neutral polarity of 0.315. On the other hand, Fig. 5 shows the "Statistical Analysis" tab of the automated tool, in which it is possible to calculate the average, the percentage distribution, the standard deviation, the maximum value, and the minimum value from the total of the opinions and for the 3 polarities (positive, negative, neutral). Likewise, the tool allowed obtaining, for the consolidation of the polarities, the percentage of dominant polarities, which was calculated by counting the polarity with the highest value in the different opinions.

To illustrate this, Fig. 5 shows how for the 5 test opinions loaded in the example file from Fig. 4, the polarity that presented a greater average in the total of opinions is the neutral one with an average value of 0.376 and with a percentage distribution in the total of opinions of 37.6%. In the same way, the minimum and maximum values for the neutral polarity are 0.315 and 0.511 respectively. On the other hand, if only the dominant polarities in each of the opinions are considered, the positive and negative polarities are dominant with 40% each. Continuing with the tabs of the automated tool, Fig. 6 shows the "Polarities per opinion" tab, in which it is possible to graphically obtain the distribution of the 3 polarities (positive, negative, and neutral) in each of the opinions uploaded to the file uploaded in the "Opinion Analysis" tab that added together result in 1.

As an example, Fig. 6 presents the distribution of the polarities for the 5 test opinions loaded in the example file of Fig. 4 in a way that it is possible to see how in two out of five opinions (1, 4) the dominant polarity is negative, the other two (2, 5) have a positive dominant polarity while in the remaining one (3), the dominant polarity is neutral. On the other hand, Fig. 7 shows the "Average Polarity Distribution" tab of the automated tool, in which it is possible to obtain the average percentage of the distribution of polarities over the total opinions of the file loaded in the "Opinion Analysis" tab. Thus, Fig. 7 shows the percentage of distribution of the polarities corresponding to the 5 test opinions loaded in the example file of Fig. 4. Then, it is possible to appreciate how the polarity with the percentage of greater distribution in the total of the opinions is the neutral one with 37.6%, while the polarity with a smaller percentage of distribution in the total of the opinions is the positive one with 27.4%.

Finally, Fig. 8 shows the "Dominant Polarities" tab of the automated tool, in which it is possible to obtain the percentage of dominant polarities over the total opinions in the file loaded in the "Opinion Analysis" tab. Thus, it is possible to observe in Fig. 8 the percentage of dominant polarities for the 5 test opinions of the example file loaded in Fig. 4; both the negative and positive polarities are each one dominant with 40% of the opinions while the neutral polarity is presented as dominant in the remaining 20% of the opinions.

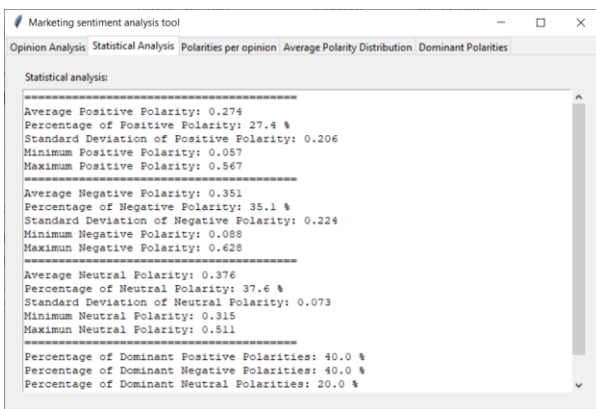


Fig. 5. "Statistical Analysis" Tab of the Tool.

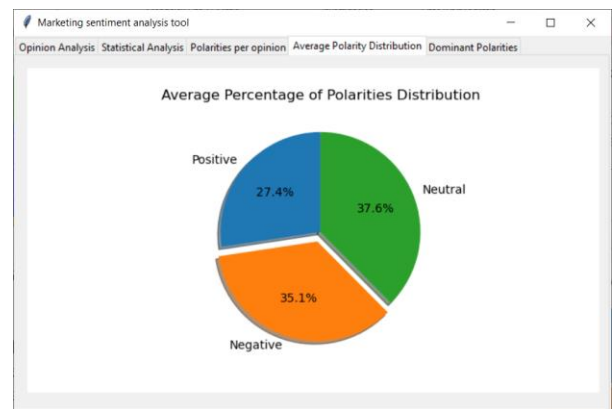


Fig. 7. "Average Polarity Distribution" Tab of the Tool.

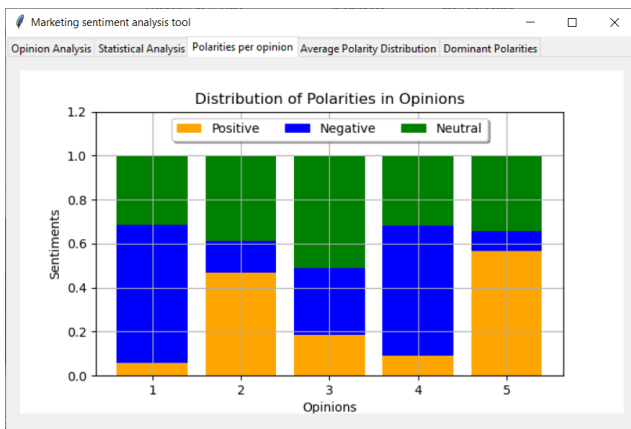


Fig. 6. "Polarities per Opinion" Tab of the Tool.

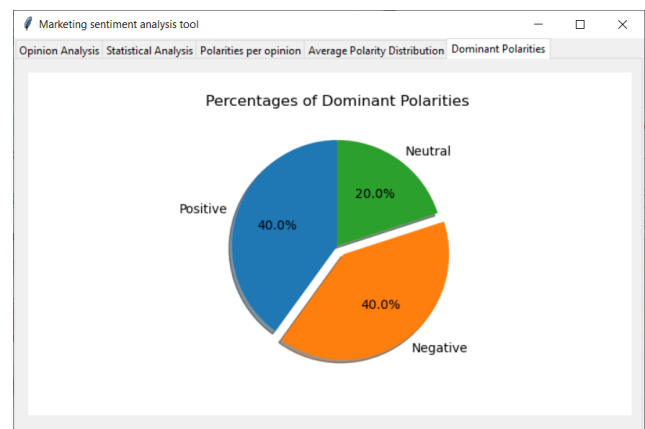


Fig. 8. "Dominant Polarities" Tab of the Tool.

Once the different tabs of the tool proposed in this article have been presented to verify its usefulness, the case study developed from the opinions made by users of a Latin American electronic commerce website is presented below. The opinions were made on a specific technological product. In this way, a total of 26 opinions were collected by a group of users of the "Mercado Libre" portal about the experience of buying and using one of the best-selling cell phones in the virtual store (Motorola Moto E7). Thus, a .CSV file with the 26 opinions was generated after eliminating unnecessary spaces and spelling correction in some opinions, to improve the precision of the results. Thus, Fig. 9 shows the polarity distribution obtained for the 26 opinions of the case study considered.

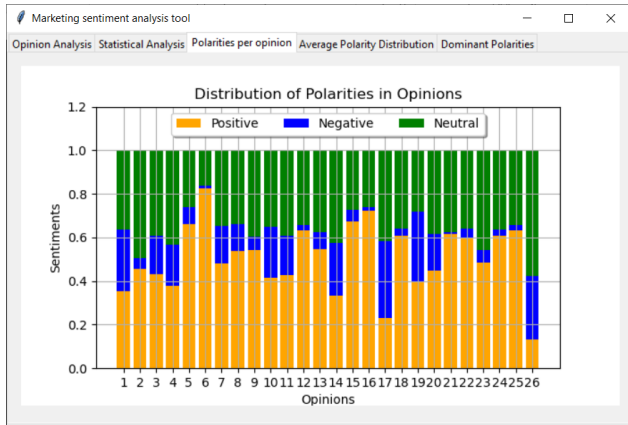


Fig. 9. Distribution of Polarities in the Case Study.

From the results obtained in Fig. 9, it is possible to observe how the polarity that has a higher percentage of presence in the different opinions of the case study is the positive polarity, followed by the neutral polarity, which can be seen more clearly in the statistical results shown in Table I, which were extracted from the results that the tool throws in the "Statistical Analysis" tab.

TABLE I. STATISTICAL RESULTS OBTAINED

Polarity	Statistical results
Positive	Average: 0.507
	Percentage of distribution: 50.7 %
	Standard Deviation: 0.152
	Minimum Value: 0.131
	Maximum Value: 0.826
Negative	Average: 0.128
	Percentage of distribution: 12.8 %
	Standard Deviation: 0.106
	Minimum Value: 0.009
	Maximum Value: 0.354
Neutral	Average: 0.366
	Percentage of distribution: 36.6 %
	Standard Deviation: 0.008
	Minimum Value: 0.161
	Maximum Value: 0.577

Then, according to the results of Table I, the polarity with a higher percentage of distribution in the 26 opinions of the case study is positive with 50.7%, followed by the neutral polarity with a percentage of 36.6%, and the negative one with a distribution percentage of 12.8%, which indicates that the distribution percentage of the positive polarity is four times the percentage of distribution of the negative one. In the same way, the polarity with the highest maximum value is the positive one with a value of 0.826, followed by the neutral polarity with a maximum value of 0.577. These results can be explained by the fact that most of the opinions highlighted the good relationship between the price and the quality of the product. On the other hand, if only the dominant polarities in each of the 26 opinions of the study case are quantified, the results presented in Table II are obtained.

TABLE II. RESULTS OF DOMINANT POLARITIES

Polarity	Percentage of dominant polarity
Positive	76.923%
Negative	0%
Neutral	23.077%

According to the results of Table II, the positive polarity is dominant in 76.923% of the opinions while the neutral polarity is dominant in 23.077% of the opinions. In the same way, the negative polarity is not dominant in any of the opinions of the case study.

V. DISCUSSION

The tool proposed in this article allows the automation of the process of sentiment analysis on datasets made up of customer reviews of products available on e-commerce portals. Thus, from the opinions contained in a .CSV file or in an excel file, the proposed tool allows to load and process this file in order to obtain the degree of polarity of each opinion, as well as the total polarity. Similarly, through the proposed tool it is possible to perform an analysis based on descriptive statistics to obtain the average, minimum value, maximum value and standard deviation of each of the polarities, as well as the percentage of opinions in which each of the polarities is dominant or greater. Finally, the proposed tool allows generating a graphic analysis, by means of which two pie charts are obtained showing the percentage distribution of polarities in the opinions and the percentage distribution of dominant polarities.

The advantages provided by the tool can be seen more clearly in the case study developed on a dataset of product reviews from the "Mercado Libre" portal, in which the percentage of the positive distribution of reviews is four times the percentage of the negative distribution. In this way, the tool, through sentiment analysis techniques, makes it possible to obtain quantitative value enclosed in qualitative data, which complements and enriches the results of traditional valuation methods based on star ratings. In this sense, the application of these sentiment analysis techniques contributes to decision making by service providers with respect to marketing campaigns.

Finally, it should be noted that one of the major challenges and/or limitations of this study is to automate the correction of typographical and orthographic errors in the opinions to improve the accuracy in obtaining the polarities. In this sense, in the case study developed, this process was performed manually, considering that it was a dataset of 26 opinions, so that a future work derived from this work is to automatically perform the pre-processing of the opinions.

VI. CONCLUSION

Based on the growing need for companies to have tools that take advantage of the opinions of customers regarding the products and services offered by them to obtain quantitative indicators of customer perception, this article proposed an automated tool for the application of sentiment analysis techniques on the opinions of customers in electronic commerce portals, which can be used in a transparent way to the algorithmic process by the marketing units of the companies for the taking of decisions.

The proposed tool allows to load a .CSV or excel file with the opinions of the clients and obtain the distribution of the 3 polarities in each one of the opinions and overall, in an automated way. Also, the results of the application of the techniques of descriptive statistics on the consolidation of the polarities. In the same way, the tool obtains the percentage of the dominant polarities in the consolidated opinions. Through the statistical and graphical results, the automated tool provides quantitative indicators based on customer opinions that can be considered for decision-making in the context of marketing.

The Python language libraries used for the construction of the proposed automated tool proved to be adequate for the different processes associated with access to the text of opinions, analysis of sentiments and/or polarities, statistical analysis of polarities, and visualization of the results of the analysis. In this sense, this tool aims to serve as a reference to be replicated in other contexts in which it is intended to quantitatively identify the perception of a person, user, or client through the analysis of their opinion.

The case study developed from the use of the automated tool allowed the researchers to conclude that the 26 opinions made on the "Mercado Libre" website about the cell phone show a positive percentage distribution that is four times the negative percentage distribution. Likewise, it was possible to conclude that at the level of the dominant polarities, none of the 26 opinions had the negative polarity as dominant. The above is explained by the fact that in most of the comments the good relation between quality and price of the analyzed product stands out.

To enrich the functionality of the proposed tool, link the functionality of frequent words analysis in the text to identify the most common terms with which users or customers describe the products is a must. In the same way, a comparative study is intended to be carried out in the future between the results of sentiment and/or polarity analysis and the star ratings provided by customers on electronic commerce websites.

ACKNOWLEDGMENT

The authors would like to thank the Universidad de Cartagena-Colombia and the Universidad del Quindío-Colombia for their support in the development of this research.

REFERENCES

- [1] K. B. Vamshi, A. K. Pandey, and K. A. P. Siva, "Topic Model Based Opinion Mining and Sentiment Analysis," 2018 Int. Conf. Comput. Commun. Informatics, pp. 1–4, Jan. 2018, doi: 10.1109 / ICCCI.2018.8441220.
- [2] C. Chauhan and S. Sehgal, "Sentiment analysis on product reviews," Proceeding - IEEE Int. Conf. Comput. Commun. Autom. ICCCA 2017, vol. 2017-Janua, pp. 26–31, Dec. 2017, doi: 10.1109/CCAA.2017.8229825.
- [3] L. F. Chaparro et al., "Sentiment Analysis of Social Network Content to Characterize the Perception of Security," 2020 IEEE/ACM Int. Conf. Adv. Soc. Networks Anal. Min., pp. 685–691, Dec. 2020, doi: 10.1109 / ASONAM49781.2020.9381434.
- [4] Y. Sharma, V. Mangat, and M. Kaur, "A practical approach to Sentiment Analysis of Hindi tweets," Proc. 2015 1st Int. Conf. Next Gener. Comput. Technol. NGCT 2015, pp. 677–680, Jan. 2016, doi: 10.1109/NGCT.2015.7375207.
- [5] S. S. Sharma and G. Dutta, "SentiDraw: Using star ratings of reviews to develop domain specific sentiment lexicon for polarity determination," Inf. Process. Manag., vol. 58, no. 1, p. 102412, Jan. 2021, doi: 10.1016/J.IPM.2020.102412.
- [6] H. C. K. Lin, T. H. Wang, G. C. Lin, S. C. Cheng, H. R. Chen, and Y. M. Huang, "Applying sentiment analysis to automatically classify consumer comments concerning marketing 4Cs aspects," Appl. Soft Comput., vol. 97, p. 106755, Dec. 2020, doi: 10.1016/J.ASOC.2020.106755.
- [7] T. Daudert, "Exploiting textual and relationship information for fine-grained financial sentiment analysis," Knowledge-Based Syst., vol. 230, p. 107389, Oct. 2021, doi: 10.1016/J.KNOSYS.2021.107389.
- [8] A. Giachanou, J. Gonzalo, and F. Crestani, "Propagating sentiment signals for estimating reputation polarity," Inf. Process. Manag., vol. 56, no. 6, p. 102079, Nov. 2019, doi: 10.1016/J.IPM.2019.102079.
- [9] O. O. Rudovic, "Machine learning for affective computing and its applications to automated measurement of human facial affect," 2016 Int. Symp. Micro-NanoMechatronics Hum. Sci., pp. 1–1, Nov. 2016, doi: 10.1109 / MHS.2016.7824242.
- [10] M. Ishizuka, "Textual affect sensing and affective communication," 2012 IEEE 11th Int. Conf. Cogn. Informatics Cogn. Comput., pp. 2–3, Aug. 2012, doi: 10.1109 / ICCI-CC.2012.6311136.
- [11] K. Hulliyah, N. S. A. A. Bakar, and A. R. Ismail, "Emotion recognition and brain mapping for sentiment analysis: A review," Proc. 2nd Int. Conf. Informatics Comput. ICIC 2017, vol. 2018-Janua, pp. 1–6, Feb. 2018, doi: 10.1109/IAC.2017.8280568.
- [12] M. Li, Q. Lu, Y. Long, and L. Gui, "Inferring Affective Meanings of Words from Word Embedding," IEEE Trans. Affect. Comput., vol. 8, no. 4, pp. 443–456, Oct. 2017, doi: 10.1109/TAFFC.2017.2723012.
- [13] E. Cambria, S. Poria, A. Gelbukh, and M. Thelwall, "Sentiment Analysis Is a Big Suitcase," IEEE Intell. Syst., vol. 32, no. 6, pp. 74–80, Nov. 2017, doi: 10.1109 / MIS.2017.4531228.
- [14] P. Mukherjee, Y. Badr, S. Doppalapudi, S. M. Srinivasan, R. S. Sangwan, and R. Sharma, "Effect of Negation in Sentences on Sentiment Analysis and Polarity Detection," Procedia Comput. Sci., vol. 185, pp. 370–379, Jan. 2021, doi: 10.1016/J.PROCS.2021.05.038.
- [15] F. H. Khan, U. Qamar, and S. Bashir, "eSAP: A decision support framework for enhanced sentiment analysis and polarity classification," Inf. Sci. (Ny), vol. 367–368, pp. 862–873, Nov. 2016, doi: 10.1016/J.INS.2016.07.028.
- [16] C. A. Melton, O. A. Olusanya, N. Ammar, and A. Shaban-Nejad, "Public sentiment analysis and topic modeling regarding COVID-19 vaccines on the Reddit social media platform: A call to action for strengthening vaccine confidence," J. Infect. Public Health, vol. 14, no. 10, pp. 1505–1512, Oct. 2021, doi: 10.1016/J.JIPH.2021.08.010.

- [17] S. Zirpe and B. Joglekar, "Polarity shift detection approaches in sentiment analysis: A survey," Proc. Int. Conf. Inven. Syst. Control. ICISC 2017, Oct. 2017, doi: 10.1109/ICISC.2017.8068737.
- [18] R. Ren and D. Wu, "An Innovative Sentiment Analysis to Measure Herd Behavior," IEEE Trans. Syst. Man, Cybern. Syst., vol. 50, no. 10, pp. 3841–3851, Oct. 2020, doi: 10.1109/TSMC.2018.2864942.
- [19] K. Mishev, A. Gjorgjevikj, I. Vodenska, L. T. Chitkushev, and D. Trajanov, "Evaluation of Sentiment Analysis in Finance: From Lexicons to Transformers," IEEE Access, vol. 8, pp. 131662–131682, 2020, doi: 10.1109/ACCESS.2020.3009626.
- [20] S. M. Mohammad, "Sentiment analysis: Automatically detecting valence, emotions, and other affectual states from text," Emot. Meas., pp. 323–379, Jan. 2021, doi: 10.1016/B978-0-12-821124-3.00011-9.
- [21] U. Kryva and M. Dilai, "Automatic Detection of Sentiment and Theme of English and Ukrainian Song Lyrics," Int. Sci. Tech. Conf. Comput. Sci. Inf. Technol., vol. 3, pp. 20–23, Sep. 2019, doi: 10.1109/STC-CSIT.2019.8929732.
- [22] P. Kadmateekarun and S. Nuanmeesri, "Automatic sentiment analysis from opinion of Thais speech audio," Proc. 2015 Int. Conf. Sci. Technol. TICST 2015, pp. 288–291, Dec. 2015, doi: 10.1109/TICST.2015.7369372.
- [23] V. Ikoro, M. Sharmina, K. Malik, and R. Batista-Navarro, "Analyzing Sentiments Expressed on Twitter by UK Energy Company Consumers," in 2018 5th International Conference on Social Networks Analysis, Management and Security, SNAMS 2018, Nov. 2018, pp. 95–98, doi: 10.1109/SNAMS.2018.8554619.
- [24] S. Kiliç and T. O. Çadirci, "An evaluation of airport service experience: An identification of service improvement opportunities based on topic modeling and sentiment analysis," Res. Transp. Bus. Manag., p. 100744, Nov. 2021, doi: 10.1016/J.RTBM.2021.100744.
- [25] D. Obembe, O. Kolade, F. Obembe, A. Owoseni, and O. Mafimisebi, "Covid-19 and the tourism industry: An early stage sentiment analysis of the impact of social media and stakeholder communication," Int. J. Inf. Manag. Data Insights, vol. 1, no. 2, p. 100040, Nov. 2021, doi: 10.1016/J.JJIMEI.2021.100040.
- [26] E. Asani, H. Vahdat-Nejad, and J. Sadri, "Restaurant recommender system based on sentiment analysis," Mach. Learn. with Appl., vol. 6, p. 100114, Dec. 2021, doi: 10.1016/J.MLWA.2021.100114.
- [27] S. Al-Natour and O. Turetken, "A comparative assessment of sentiment analysis and star ratings for consumer reviews," Int. J. Inf. Manage., vol. 54, p. 102132, Oct. 2020, doi: 10.1016/J.IJINFOMGT.2020.102132.
- [28] F. Chiarello, A. Bonaccorsi, and G. Fantoni, "Technical Sentiment Analysis. Measuring Advantages and Drawbacks of New Products Using Social Media," Comput. Ind., vol. 123, p. 103299, Dec. 2020, doi: 10.1016/J.COMPIND.2020.103299.
- [29] S. Ainin, A. Feizollah, N. B. Anuar, and N. A. Abdullah, "Sentiment analyses of multilingual tweets on halal tourism," Tour. Manag. Perspect., vol. 34, p. 100658, Apr. 2020, doi: 10.1016/J.TMP.2020.100658.
- [30] R. N. Paramanik and V. Singhal, "Sentiment Analysis of Indian Stock Market Volatility," Procedia Comput. Sci., vol. 176, pp. 330–338, Jan. 2020, doi: 10.1016/J.PROCS.2020.08.035.
- [31] Y. Ding, R. Korolov, W. (Al) Wallace, and X. (Cara) Wang, "How are sentiments on autonomous vehicles influenced? An analysis using Twitter feeds," Transp. Res. Part C Emerg. Technol., vol. 131, p. 103356, Oct. 2021, doi: 10.1016/J.TRC.2021.103356.

Affinity Degree as Ranking Method

Rosyazwani Mohd Rosdan¹, Wan Suryani Wan Awang², Samhani Ismail³

Faculty Informatics and Computing, University Sultan Zainal Abidin, Besut Campus, Terengganu, Malaysia^{1,2}
Faculty Medicine, Medical Campus, University Sultan Zainal Abidin, Medical Campus, Terengganu, Malaysia³

Abstract—In machine learning, ranking is a fundamental problem that attempts to rank a list of things based on their relevance in a certain task. Ranking can be helpful, especially for future decision making. The framework for ranking has been classified into three primary approaches in machine learning: pointwise, pairwise, and listwise. However, learning to rank in all three approaches still lacks continuous learning ability, particularly when it comes to determining the degree of relevancy of ranking orders. In this paper, an affinity degree technique for ranking is proposed as another potential machine learning framework. The definition and attributes of the affinity degree technique are discussed, as well as the results of an experiment adopting the affinity degree approach as a ranking mechanism. The experiment's performance is measured using assessment metrics such as Mean Average Precision (MAP).

Keywords—Affinity; affinity degree; rank; machine learning

I. INTRODUCTION

Learning to rank is a machine learning framework that aims to organise things in a particular order according to preference and relevance. Due to its emerging use in domains like information retrieval (IR) and recommender systems, learning to rank has drawn the attention of many machine learning researchers in the recent decade. The main reasons for the machine learning framework for ranking shared the exact nature of classification and regression methods. Also, the machine learning method can tune the parameters to overcome the disadvantages in the IR model, such as low precision and rigidity [1]. Learning to rank can be another predictive analytic technique under machine learning that presents learning to rank approaches [2]. Thus, learning to rank can be categorised as supervised learning with training and testing phases [3] and solving evaluation problems in search relevancy ranks [4]. Similar to other machine learning frameworks, the performance of learning to rank models is measured using the loss function that computes the difference between prediction and ground truth [5].

Dong, Chen, Guan, Li, and Xu mentioned the issues of learning to rank as a lack of continual learning ability and complicated tasks to construct a large-scale and resourceful training set [1]. Falah also mentioned the deficiency of current learning to rank approaches as lacking continual learning ability [4]. Therefore, this paper aims to incorporate the affinity degree classification algorithm into the rank technique as part of the learning ability for learning to rank issues. Since the ranking methodology also used classification and regression to rate the variables, the affinity degree classification algorithm might better fit the ranking system.

An affinity degree is a calculation for determining the degree of relationship and classification of the correlated data. Affinity degree has been established in peer-to-peer network data replication [6] as the calculation to define the similarity between two or more correlated data. The study used an affinity degree to find the correlation between files from different nodes. The correlation data is calculated to find the most binding factors contributing to the similarity between files. The results obtained from the calculation then will be ranked based on parameters. Therefore, affinity degree calculation has been implemented as one of the machine learning classification techniques in predictive analytic [7]. Thus, this paper will explore the affinity degree technique to rank as a machine learning framework.

The rest of the paper is organised as follows; Section 2 introduces the learning-to-rank theoretical background. After that, Section 3 describes more about affinity degree. Section 4 experiment for adopting the affinity degree into the learning-to-rank framework. Section 5 discussed the details of the experiment to validate the proposed idea. Finally, section 6 concludes the paper.

II. THEORETICAL BACKGROUND

In traditional IR approaches, machine learning techniques were booming for the ranking problem, in which the learning-based method aimed to use labelled data for practical ranking function [8]. Learning to rank encompasses mainly supervised algorithms where the method uses machine learning techniques to train the model in a ranking task. Learning to rank was successfully applied to defect prediction to rank modules based on their defectiveness in software engineering. In test prioritization, this method can rank test targets based on a testing objective [9].

Learning to rank can be categorised into pointwise, pairwise, or listwise. For pointwise procedures, the approaches formed the model from the score assigned by users to individual objects. The yield rank is a collection of records with conventional scores. There is no reliance between training reports since the training reports are utilised independently [1], [10]. The simplest form, pointwise ranking, can be treated as classification or regression by learning the numerical rank views of documents as an absolute quantity [11].

The pairwise procedure learns by comparing two training objects and their given ranks or ground truth [12]. Trained by training samples as object pairs with independent variables and learning the classification (regression) model, two records are doled out in each pair with two relevance scores by individuals.

Nonetheless, only the match report dependence is considered, which implies that dependence between each report within the total rank cannot be considered entirely [1], [11]. The applicability of such methods is limited by the high computational cost of pairwise comparisons of user rated items in generating the training samples for the binary classifier [10].

The third procedure, listwise approaches, learn from the list of records. The records are relegated to a query in each list with diverse pertinence scores. Typically, this approach optimises a smooth approximation of a loss function that measures the distance between the references list of ranked items in the training data and the ranked list of items produced by the ranking model [10]. One common advantage is that more reliance between records is considered than pointwise and pairwise models with unreliable flexibility [1]. Meanwhile, Hass points out that the pairwise and the listwise approaches usually perform better than the pointwise approach [12].

Finding a suitable algorithm for a specific data set is significant for extracting the best information. Therefore, comparing the algorithm and ranking them into order will help indicate which algorithm should be applied. For selecting the best algorithm for a problem given, Carlos presents combination techniques called Zoomed ranking, which analyses the given data set and compares it with the relevant data set that has been processed by an algorithm using the "distance" concept for calculation [13]. Also, Bradzil presented three ranking methods: average rank, success rate ratio and significance win for algorithm selection [14]. The ranking methods eventually were being evaluated by average weighted correlation measures.

The ranking system has several different frameworks besides machine learning. Thus, there are various studies about the application of machine learning in ranking challenges and the importance and advantage of ranking in the machine learning framework. Yongyao Jiang addresses the ranking challenge in geospatial data discovery and proposes a system architecture to combine existing search-oriented open-source software, semantic knowledge base, ranking feature extraction, and machine learning algorithm [15]. Results show that the machine learning approach outperforms other methods in terms of both precision at K and normalised discounted cumulative gain.

Besides, the importance of machine learning rank or learning to rank in the construction of the IR system has been pointed out in [16]. Because each query has a set of associated documents represented by feature vectors that reflect the relevance of the documents to the query, it is a goal to build a model to predict the ground truth label of test data as accurately as possible in terms of the loss function. Also, it can be used to explore multiple ranking algorithms across different approaches in the item of accuracy and efficiency. Also, Hong Li specifically discussed exploring the fundamental problems existing approaches and future work in learning to rank [13]. Document retrieval is a task where the system maintains a collection of documents. The system retrieves the query words from the collection, ranks the document and returns the top-ranked documents.

Although ranking systems are most common in the IR environment, recent studies prove that the system can be applied in different environments, such as the medical field. The ranking system was used for ranking the Multimodal Features extracted from Congestive Heart Failure (CHF) and Normal Sinus Rhythm (NSR) subjects. Use high ranking features for detection of CHF and normal subjects. The findings indicate that the proposed approach with feature ranking can be beneficial for automatic detection of congestive heart failure patients and can be very helpful for clinicians and physicians' further decision-making to decrease the mortality rate [17]. A case study from Iran in which A Rad used the AHP algorithm and data mining to cluster and rank university majors [18]. Also, in the data mining field, D. Scully proposes an effective and efficient combined regression and ranking method that optimises the regression and objectives simultaneously [19]. Koshti used the learning to rank pairwise approach to making faster and better decisions for recruiting football players and having a list of options ranked on given criteria [2].

Nevertheless, regarding the affinity definition that is proposed to be used in this paper as a ranking technique, there is a study presenting a novel ranking scheme, Affinity Rank, which utilises two metrics [20]. The focus of the study is to evaluate the diversity of information retrieval performance. Measures the topic coverage of a group of documents, and information richness, which measures the amount of information contained in a document. Although the affinity in the rank system is not entirely new, there are not many of them.

III. AFFINITY DEGREE METHOD

Affinity is a notion that has received widespread attention in domains such as chemistry, biology, physics, social networks, security, and computer science. Affinity can hold a different meaning based on various concerns. Here, affinity is defined as a relationship, similarity, dependency and closeness between variables. Following is the affinity notation used in data replication by Awang [6]. The study proposed combining popularity and affinity files as the most critical parameters in replica selection. Affinity files were defined as the similarity between two or more correlated files before the system replicated the file. The affinity set is a set of any data that creates an affinity between files. Thus, the affinity between sets A and B consists of the intersection of elements between A and B plus the target and is not a null set. The equation can define the target in set B as $fid(B)$, where f is a file and id refer to the file id.

$$aff_{AB} = \{x|x \in (A \times B + \{f_T(B)\}) \neq \emptyset\} \quad (1)$$

Definition 1: Let $A = \{f_{a1}, f_{a2}, \dots, f_{an}\}$ and $B = \{f_{b1}, f_{b2}, \dots, f_{bn}\}$, T is a targeted class. The sets A and B are said affinity denoted by (1); where $f_T(B)$ is the target class in B.

$$aff_{AB}^A = \frac{aff_{AB}}{A + f_T(B)} \quad (2)$$

Definition 2: The affinity degree between A and B concerning A is defined as (2). The value expresses the degree of affinity between the data set A, and the affinity sets AB concerning A.

IV. EXPERIMENT

The main idea of affinity degree implementation is to measure the dependency or correlation between cause and particular effect. Measurement results might predict the set with the highest affinity degree as the leading cause of that effect. Therefore, this experiment focused on defining the risk of which symptoms can lead to a heart disease diagnosis. Through the affinity degree results, where the value of affinity degree was classified into five classes based on a specific indicator, the experiment could analyse the probability by ranking the affinity strength or assuming the correlation between dependent and independent variables.

This experiment was conducted according to KDD process in Fig. 1 [21]. Start with data selection, preprocessing and transformation data as the process results were shown in Table I, then affinity degree implementation. The ranking results were displayed in Tables II, III, IV and V by categories before the evaluation process.

In this experiment, MAP will be used as an evaluated method. MAP stands for the mean of the average precisions for each query computed. Average precision is computed as the sum of precisions for each found and relevant document, divided by the number of relevant documents. Using this construction, relevant but not found objects receive a precision of zero [22].

A. Heart Disease Data

The heart disease datasets used in this research were obtained from the Heart Disease Databases in the UCI Machine Learning Repository [23]. This data set dates from 1988 and consists of four databases contributed by the Cleveland Clinic Foundation (CCF), Hungarian Institute of Cardiology (HIC), Long Beach Medical Center (LBMC), and University Hospital in Switzerland (SUH), respectively. Each heart disease database has the same clinical instance format for each patient with 76 attributes, including the target attribute. It consists of 1025 patients with 499 patients ruled with heart disease while 526 were healthy. The target field refers to the presence of heart disease in the patient. It is an integer, valued at 0 or 1, indicating the absence or presence of coronary heart disease in patients. For other attributes, the integer, valued from 0 to 4, stated heart disease's absence, presence, and severity. Several risk factors can be controlled and cannot be controlled. The risk factors that can be controlled are blood pressure, blood cholesterol level, smoking, diabetes, obesity, inactivity and stress.

Meanwhile, a risk factor that could not be altered was age, gender, family history, and race. As part of preprocessing, this paper's attributes were compared to significant risk factors mentioned in the previous study for simplicity. Pre-processing focused on the handling of missing values, discretisation of numeric attributes and removal of instances with missing values [24]-[25]. Later, the attribute was compared with Hajar [26], Berg Gundersen, Sørliie and Bergvik [27], Mack and

Gopal [28] and McClelland et al. [29]. For the age attribute, the age class was divided through class interval where the highest age minus the lowest age before was divided with the number of classes. Table I shows the reduced attribute details used in this experiment. Also, to get a better analysis, the data then were clustered into four categories: male older, male younger, female older, and female younger.

The experiment then implemented the adaptive equation in Section 3 defined as (2) into the data set. The affinity degree value then was ranked from highest to lowest displayed in Tables II, III, IV and V. The rank results show that the symptoms for each category were different. So, gender and age might greatly influence indicating the risk factor for heart disease diagnosis. For evaluating, this experiment used MAP as a tool, where the results will be discussed more in the next section.

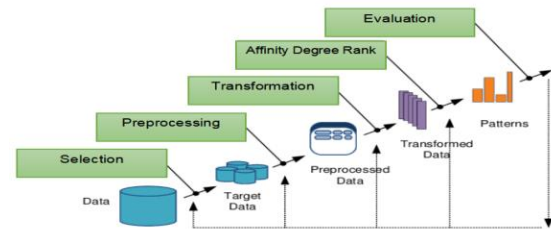


Fig. 1. Diagram of KDD Process.

TABLE I. HEART DISEASE ATTRIBUTE LIST AND DESCRIPTION

Attribute	Descriptions
age	0 = (<40)
	1 = (40-59)
	2 = (60-79)
	3 = (≥80)
gender	0 = female
	1 = male
Chest pain type (cp)	0 = typical angina
	1 = atypical angina
	2 = non-angina
	3 = asymptomatic
Resting blood pressure in mm Hg (restbtps)	0 = (<120)
	1 = (120-129)
	2 = (130-139)
	3 = (≥140)
Total cholesterol in mg/dL (chol)	0 = (<200)
	1 = (200-239)
	2 = (≥240)
Fasting blood sugar > 120 mg/dL (fbs)	0 = false
	1 = true
Maximum heart rate (thalach)	0 = (<60)
	1 = (60-100)
	2 = (>100)
Presence of heart disease	0 = absence
	1 = presence;

Table II displays the affinity degree rank for the female who is an older category. There are only 9 patients in this category with 0.811 for the highest and 0.801 for the lowest affinity degree values. Meanwhile, the younger female category shown in Table III has 0.858 for the highest and 0.802 for the lowest with 45 patients in this category. Table IV shows the affinity degree values for an older male category with 19 patients. The highest value for affinity degree in this category is 0.814, while the lowest is 0.802. Last, Table V with 90 patients for the younger male category shows the highest affinity degree values are 0.873, and the lowest is 0.802.

TABLE II. AFFINITY DEGREE RANK FOR OLDER FEMALE CATEGORY

age	gender	cp	trestbps	chol	fb	thalach	Class	AffinityDegree
O	F	0	Hyper 2	Border	1	C	Abs	0.811638591
O	F	2	Hyper 2	High	0	C	Pre	0.808306709
O	F	2	Normal	High	0	C	Pre	0.808306709
O	F	1	Elevated	High	0	C	Pre	0.806709265
O	F	3	Hyper 2	Border	0	C	Pre	0.806709265
O	F	0	Normal	Desirable	0	C	Pre	0.803514377
O	F	0	Normal	Border	0	C	Pre	0.801916933
O	F	2	Elevated	Border	0	C	Pre	0.801916933
O	F	2	Hyper 2	Desirable	0	C	Pre	0.801916933

TABLE III. AFFINITY DEGREE RANK FOR YOUNGER FEMALE CATEGORY

age	gender	cp	trestbps	chol	fb	thalach	Class	AffinityDegree
Y	F	0	Hyper 2	High	0	C	Abs	0.858
Y	F	0	Hyper 2	High	0	C	Pre	0.851
Y	F	0	Hyper 1	High	0	C	Abs	0.839
Y	F	0	Hyper 1	High	0	C	Pre	0.832
Y	F	0	Normal	High	0	C	Abs	0.825
Y	F	2	Elevated	Border	0	C	Pre	0.821
Y	F	1	Hyper 1	Border	0	C	Abs	0.821
Y	F	0	Normal	High	0	C	Pre	0.818
Y	F	0	Elevated	Border	0	C	Abs	0.818
Y	F	2	Hyper 2	High	0	C	Pre	0.816
Y	F	2	Normal	High	0	C	Pre	0.816
Y	F	0	Hyper 1	High	1	C	Abs	0.816
Y	F	1	Hyper 1	High	1	C	Abs	0.816

Y	F	1	Hyper 1	Border	0	C	Pre	0.813
Y	F	1	Hyper 1	High	0	C	Pre	0.813
Y	F	0	Hyper 2	Border	0	C	Abs	0.812
Y	F	0	Hyper 2	Border	1	C	Abs	0.812
Y	F	0	Hyper 3	High	1	C	Abs	0.812
Y	F	2	Hyper 1	High	0	B	Abs	0.812
Y	F	2	Hyper 1	High	0	C	Pre	0.812
Y	F	0	Elevated	Desirable	0	C	Abs	0.810
Y	F	0	Hyper 2	Desirable	0	C	Abs	0.810
Y	F	0	Elevated	Border	0	C	Pre	0.810
Y	F	0	Hyper 1	Desirable	0	C	Pre	0.810
Y	F	1	Hyper 1	High	1	C	Pre	0.808
Y	F	3	Hyper 2	High	1	C	Pre	0.808
Y	F	0	Elevated	High	0	C	Pre	0.807
Y	F	0	Hyper 1	Border	0	C	Pre	0.807
Y	F	1	Elevated	High	0	C	Pre	0.807
Y	F	1	Normal	Border	0	C	Pre	0.807
Y	F	1	Normal	Desirable	0	C	Pre	0.807
Y	F	2	Elevated	High	0	C	Pre	0.807
Y	F	2	Normal	Desirable	0	C	Pre	0.807
Y	F	2	Hyper 1	Border	0	C	Pre	0.804
Y	F	1	Hyper 2	Desirable	0	C	Pre	0.802
Y	F	1	Hyper 2	High	0	C	Pre	0.802
Y	F	2	Elevated	Desirable	1	B	Pre	0.802
Y	F	2	Hyper 1	Desirable	0	C	Pre	0.802
Y	F	2	Hyper 1	High	1	C	Pre	0.802
Y	F	2	Hyper 1	High	1	C	Pre	0.802
Y	F	2	Hyper 1	High	1	C	Pre	0.802
Y	F	2	Hyper 2	Border	0	C	Pre	0.802
Y	F	2	Hyper 2	Desirable	0	C	Pre	0.802
Y	F	2	Hyper 2	High	1	C	Pre	0.802
Y	F	2	Normal	Border	0	C	Pre	0.802

TABLE IV. AFFINITY DEGREE RANK FOR OLDER MALE CATEGORY

age	gender	cp	trestbps	chol	fb	thalach	Class	AffinityDegree
O	M	0	Elevated	High	0	C	Abs	0.814701378
O	M	1	Hyper2	High	0	C	Abs	0.814701378
O	M	2	Hyper2	High	0	C	Abs	0.814701378
O	M	0	Elevated	Border	0	B	Abs	0.811638591
O	M	0	Elevated	Border	0	C	Abs	0.811638591
O	M	0	Hyper1	High	0	C	Abs	0.811638591
O	M	0	Hyper2	Desirable	0	C	Abs	0.811638591
O	M	0	Hyper2	High	0	C	Abs	0.811638591
O	M	0	Normal1	Border	0	C	Abs	0.811638591
O	M	2	Hyper2	Border	0	C	Abs	0.811638591
O	M	0	Elevated	High	1	C	Abs	0.810107198
O	M	0	Hyper2	Desirable	1	C	Abs	0.810107198
O	M	0	Normal1	High	0	C	Abs	0.810107198
O	M	2	Hyper2	High	1	C	Abs	0.810107198
O	M	0	Elevated	High	0	C	Pre	0.806709265
O	M	1	Hyper2	High	0	C	Pre	0.806709265
O	M	0	Hyper2	Border	0	C	Pre	0.803514377
O	M	2	Normal1	High	0	C	Pre	0.801916933
O	M	3	Hyper2	Border	1	C	Pre	0.801916933

TABLE V. AFFINITY DEGREE RANK FOR YOUNGER MALE CATEGORY

age	gender	cp	trestbps	chol	fb	thalach	Class	AffinityDegree
Y	M	0	Hyper2	High	0	C	Abs	0.873
Y	M	0	Hyper2	High	0	C	Pre	0.867
Y	M	0	Elevated	High	0	C	Abs	0.862
Y	M	0	Hyper2	Border	0	C	Abs	0.859
Y	M	0	Normal1	Border	0	C	Abs	0.859
Y	M	0	Elevated	High	0	C	Pre	0.856
Y	M	0	Hyper2	Border	0	C	Pre	0.853
Y	M	0	Normal1	Border	0	C	Pre	0.853
Y	M	1	Elevated	High	0	C	Abs	0.848

Y	M	0	Normal1	High	0	C	Abs	0.842
Y	M	1	Elevated	High	0	C	Pre	0.842
Y	M	0	Hyper1	High	0	C	Abs	0.839
Y	M	0	Normal1	High	0	C	Pre	0.835
Y	M	0	Elevated	Desirable	0	C	Abs	0.833
Y	M	0	Hyper1	High	0	C	Pre	0.832
Y	M	2	Hyper1	Border	0	C	Abs	0.830
Y	M	0	Hyper1	High	1	C	Abs	0.828
Y	M	0	Elevated	Desirable	0	C	Pre	0.826
Y	M	1	Hyper1	Border	0	C	Pre	0.826
Y	M	3	Hyper2	High	0	C	Abs	0.825
Y	M	2	Hyper2	Border	0	C	Abs	0.824
Y	M	2	Hyper1	Border	0	C	Pre	0.823
Y	M	0	Elevated	High	0	B	Abs	0.822
Y	M	0	Hyper2	Desirable	0	C	Abs	0.822
Y	M	2	Elevated	High	0	C	Abs	0.822
Y	M	2	Normal1	Border	0	C	Abs	0.822
Y	M	0	Elevated	Border	0	C	Abs	0.821
Y	M	0	Hyper1	Border	0	C	Abs	0.821
Y	M	0	Hyper1	Desirable	0	C	Abs	0.821
Y	M	0	Normal1	Desirable	0	C	Abs	0.821
Y	M	2	Normal1	High	0	C	Abs	0.821
Y	M	2	Hyper1	High	0	C	Pre	0.818
Y	M	3	Hyper2	High	0	C	Pre	0.818
Y	M	2	Elevated	Border	0	C	Abs	0.818
Y	M	3	Hyper1	Border	0	C	Abs	0.818
Y	M	2	Hyper1	Desirable	0	C	Pre	0.816
Y	M	2	Hyper2	Border	0	C	Pre	0.816
Y	M	0	Normal1	Border	1	C	Abs	0.816
Y	M	1	Hyper2	Border	0	C	Abs	0.816
Y	M	1	Normal1	Border	0	C	Abs	0.816
Y	M	2	Elevated	Desirable	0	C	Abs	0.816

Y	M	2	Hyper 1	High	1	C	Abs	0.816
Y	M	2	Hyper 2	High	0	C	Abs	0.816
Y	M	2	Norma 1	Desira ble	0	C	Abs	0.816
Y	M	3	Elevat ed	Border	0	C	Abs	0.816
Y	M	2	Hyper 2	Desira ble	0	C	Abs	0.815
Y	M	0	Hyper 2	Desira ble	0	C	Pre	0.815
Y	M	1	Elevat ed	Border	0	C	Pre	0.815
Y	M	2	Elevat ed	High	0	C	Pre	0.815
Y	M	2	Norma 1	Border	0	C	Pre	0.815
Y	M	0	Elevat ed	Border	0	C	Pre	0.813
Y	M	0	Hyper 1	Border	0	C	Pre	0.813
Y	M	2	Norma 1	High	0	C	Pre	0.813
Y	M	0	Elevat ed	Border	1	C	Abs	0.812
Y	M	0	Elevat ed	High	1	C	Abs	0.812
Y	M	0	Hyper 2	Border	1	C	Abs	0.812
Y	M	0	Hyper 2	High	1	C	Abs	0.812
Y	M	2	Elevat ed	Border	1	C	Abs	0.812
Y	M	3	Hyper 1	High	1	C	Abs	0.812
Y	M	1	Hyper 1	High	0	C	Pre	0.812
Y	M	2	Elevat ed	High	1	C	Pre	0.812
Y	M	0	Hyper 2	Desira ble	1	B	Abs	0.810
Y	M	0	Hyper 2	High	0	B	Abs	0.810
Y	M	1	Hyper 3	High	0	C	Abs	0.810
Y	M	3	Norma 1	High	0	C	Abs	0.810
Y	M	1	Elevat ed	Desira ble	0	C	Pre	0.810
Y	M	2	Elevat ed	Border	0	C	Pre	0.810
Y	M	0	Norma 1	Border	1	C	Pre	0.808
Y	M	1	Hyper 2	Border	0	C	Pre	0.808
Y	M	1	Norma 1	Border	0	C	Pre	0.808
Y	M	2	Elevat ed	Desira ble	0	C	Pre	0.808
Y	M	2	Hyper 1	High	1	C	Pre	0.808
Y	M	2	Hyper 2	Border	1	C	Pre	0.808

Y	M	2	Hyper 2	High	0	C	Pre	0.808
Y	M	2	Norma 1	Desira ble	0	C	Pre	0.808
Y	M	3	Elevat ed	Border	0	C	Pre	0.808
Y	M	3	Norma 1	Desira ble	0	C	Pre	0.808
Y	M	1	Elevat ed	Border	1	C	Pre	0.807
Y	M	2	Hyper 2	Desira ble	0	C	Pre	0.807
Y	M	2	Hyper 2	Desira ble	1	C	Pre	0.807
Y	M	1	Norma 1	High	0	C	Pre	0.804
Y	M	3	Hyper 2	Border	0	C	Pre	0.804
Y	M	1	Norma 1	Desira ble	1	C	Pre	0.802
Y	M	2	Hyper 1	Desira ble	1	C	Pre	0.802
Y	M	2	Hyper 2	High	1	C	Pre	0.802
Y	M	3	Elevat ed	Desira ble	0	C	Pre	0.802
Y	M	3	Hyper 2	Border	1	C	Pre	0.802
Y	M	3	Hyper 2	Desira ble	0	C	Pre	0.802
Y	M	3	Hyper 2	High	1	C	Pre	0.802
Y	M	3	Hyper 2	High	1	C	Pre	0.802
Y	M	3	Norma 1	Border	0	C	Pre	0.802

V. EVALUATION AND DISCUSSION

The experimental results reveal a variance of affinity degree that shows the relations or correlation between data with various affinity degree values. Shown in Fig. 2, the affinity degree rank differs in mean average precision between each category, and the differences are just a small gap. With 0.39 for the male and older category, the second category for female and older had 0.40, 0.27 for the third category, male and younger, and the last category for female and younger, with 0.29 in value of mean precision. For overall mean average precision, the value is 0.34.

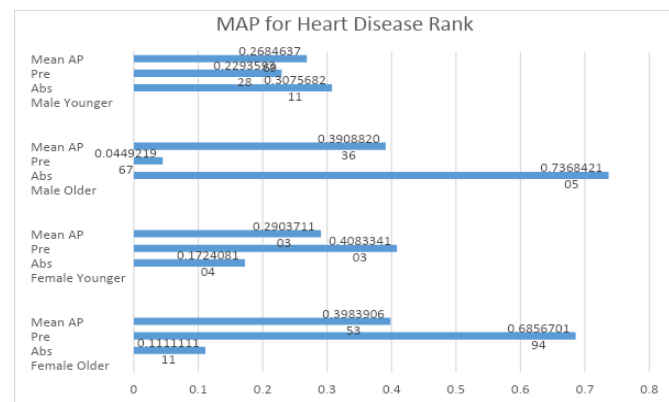


Fig. 2. The Evaluation Result of MAP for Heart Disease Rank.

All the value for mean average precision in each category were less than 0.5. The number of instances in each category might influence the evaluation results. For example, in male and older category, there are 14 instance of presence and only 5 for absence instances. Therefore, the gap between these two instances were small. Same goes to male and younger category, although the total instances were 90, but the gap between two instances were only 6. The small gap between instances does influence the mean average precision calculation.

The affinity degree is calculated to determine the relationship between heart disease symptoms and the diagnosis. From the coronary heart disease data sets, all 1025 records of patients were taken for calculation purposes. The data set was clustered into four groups according to the patient's gender and age. From the affinity degree calculated in this experiment, the highest score of degree or rank can be the most potential attribute for the patient to be diagnosed with heart disease or not. The limitation in this experiment were the results are not verified as there is no domain expert were involved. In future, more experiments with with variance data volumes need to be done along with the domain expert verified the results.

VI. CONCLUSION

This paper implemented the notion of affinity as another alternative technique for the ranking system. Heart disease experiments with an enhancement of the affinity degree equation have been done. The experiment defines the strength of correlation or dependency between data then ranks them based on affinity degree value. The experiment was evaluated by the MAP method, which uses the mean of average precision to compute for a set of queries. The results have shown the potential of affinity degree as one of the rank techniques. More experiments for diverse data samples with larger data volumes could be used to validate and verify the equation in the future.

ACKNOWLEDGMENT

Thanks to the internal grant of UNISZA (UniSZA/2021/DPU2.0/08) for financially supporting our work. Also, thanks to all team members for reviewing for spelling errors and synchronisation consistencies and for the constructive comments and suggestions.

REFERENCES

- [1] X. Dong, X. Chen, Y. Guan, S. Li and Z. Xu, "An overview of learning to rank for information retrieval," in 2009 WRI World Congress on Computer Science and Information Engineering, IEEE, March 2009, vol. 3, pp. 600-606, doi: 10.1109/CSIE.2009.1090.
- [2] A. V. Koshti, "Learning to Rank Model Performance and Review with Pairwise Transformations," M.S. thesis, Creative Components, 757, Iowa State Univ., Ames, Iowa, 2021.
- [3] H. Li, "A short introduction to learning to rank," IEICE TRANSACTIONS on Information and Systems, vol. 94(10), pp. 1854-1862, Oct. 2011, doi: 10.1587/transinf.E94.D.1.
- [4] F. Al-akashi, "Learning-to-Rank: A New Web Ranking Algorithm using Artificial Neural Network," International Journal of Hybrid Innovation Technologies, vol.1(1), pp.15-32, 2021, doi: http://dx.doi.org/10.21742/ijhit.2021.1.1.02.
- [5] A. Rahangdale and S. Raut, "Machine learning methods for ranking," International Journal of Software Engineering and Knowledge Engineering, vol. 29(06), pp. 729-761, 2019, doi: 10.1142/S021819401930001X.

- [6] W. S. W. Awang, M. M. Deris, O. F. Rana, M. Zarina and A. N. M. Rose, "Affinity replica selection in distributed systems," in International Conference on Parallel Computing Technologies. Springer, Cham, Aug. 2019, pp. 385-399, doi: https://doi.org/10.1007/978-3-030-25636-4_30.
- [7] R. M. Rosdan, W. S. W. Awang and W. A. W. A. Bakar, "Comparison of affinity degree classification with four different classifiers in several data sets," International Journal of Advanced Technology and Engineering Exploration, vol. 8(75), pp. 247, 2021, doi: http://dx.doi.org/10.19101/IJATEE.2020.762106.
- [8] M. F. Tsai, T. Y. Liu, T. Qin, H. H. Chen and W. Y. Ma, "Frank: A ranking method with fidelity loss," in Proceedings of the 30th annual international ACM SIGIR conference on research and development in information retrieval, Jul. 2007, pp. 383-390.
- [9] A. Bertolino, A. Guerriero, B. Miranda, R. Pietrantuono and S. Russo, "Learning-to-rank vs ranking-to-learn: strategies for regression testing in continuous integration," in Proceedings of the ACM/IEEE 42nd International Conference on Software Engineering, June 2020, pp. 1-12, doi: https://doi.org/10.1145/3377811.3380369.
- [10] J. Liang, J. Hu, S. Dong and V. Honavar, "Top-N-Rank: A Scalable List-wise Ranking Method for Recommender Systems," in 2018 IEEE International Conference on Big Data (Big Data), IEEE, Dec. 2018, pp. 1052-1058.
- [11] H. Valizadegan, R. Jin, R. Zhang, and J. Mao, "Learning to Rank by Optimising NDCG Measure," NIPS Vol. 22, pp. 1883-1891, Jan 2009.
- [12] R. Haas and B. Hummel, "Learning to rank extract method refactoring suggestions for long methods," in International Conference on Software Quality, Springer, Cham, Jan. 2017, pp. 45-56, doi: 10.1007/978-3-319-49421-0_4.
- [13] C. Soares and P. B. Brazdil, "Zoomed ranking: Selection of classification algorithms based on relevant performance information," in European conference on principles of data mining and knowledge discovery, Springer, Berlin, Heidelberg, Sept. 2000, pp. 126-135.
- [14] P. B. Brazdil and C. Soares, "A comparison of ranking methods for classification algorithm selection," in European conference on machine learning, Springer, Berlin, Heidelberg, May 2000, pp. 63-75.
- [15] Y. Jiang, Y. Li, C. Yang, F. Hu, E. M. Armstrong, T. Huang,... and C. J. Finch, "Towards intelligent geospatial data discovery: a machine learning framework for search ranking," International journal of digital earth, vol. 11(9), pp. 956-971, 2017, doi: http://dx.doi.org/10.1080/17538947.2017.1371255.
- [16] Learning to rank. Retrieved from https://www.cs.purdue.edu/homes/liu1740/report.pdf.
- [17] L. Hussain, W. Aziz, I. R. Khan, M. H. Alkinani and J. S. Alowibdi, "Machine learning based congestive heart failure detection using feature importance ranking of multimodal features," in Mathematical Biosciences and Engineering, vol. 18(1), pp. 69-91, 2020, doi: 10.3934/mbe.2021004.
- [18] A. Rad, B. Naderi and M. Soltani, "Clustering and ranking university majors using data mining and AHP algorithms: A case study in Iran," in Expert Systems with Applications, vol. 38(1), pp. 755-763, 2011, doi: 10.1016/j.eswa.2010.07.029.
- [19] D. Sculley, "Combined regression and ranking," in Proceedings of the 16th ACM SIGKDD international conference on Knowledge discovery and data mining, Jul. 2010, pp. 979-988.
- [20] Y. Liu, B. Zhang, Z. Chen, M. R. Lyu and W. Y. Ma, "Affinity rank: a new scheme for efficient web search," in Proceedings of the 13th international World Wide Web conference on Alternate track papers & posters, May 2004, pp. 338-339.
- [21] Monitoring Online Tests through Data Visualization - Scientific Figure on ResearchGate. Retrieved from: https://www.researchgate.net/figure/The-Steps-of-a-KDD-process_fig7_220073492 [accessed 24 Mar, 2022].
- [22] Trotman, A. (2005). Learning to rank. Information Retrieval, 8(3), 359-381.
- [23] UCI Machine Learning Repository. Heart disease data set. Retrieved from https://archive.ics.uci.edu/ml/machine-learning-databases/heart-disease.
- [24] R. Rosly, M. Makhtar, M. K. Awang, M. I. Awang, and M. N. A. Rahman, "Analysing performance of classifiers for medical

- datasets,” International Journal of Engineering & Technology, vol. 7(2.15), pp. 136-138, 2018, doi: 10.14419/ijet.v7i2.15.11370.
- [25] M. Makhtar, R. Rosly, M. K. Awang, M. Mohamad and A. H. Zakaria, “A Multi-Classifer Method based Deep Learning Approach for Breast Cancer,” Int. J. Eng. Trends Technol. (1), pp. 102-107, 2020, doi: 10.14445/22315381/CATI3P217.
- [26] R. Hajar, “Risk factors for coronary artery disease: historical perspectives,” Heart views: the official journal of the Gulf Heart Association, vol. 18(3), pp. 109, 2017.
- [27] A. E. Berg Gundersen, T. Sørli and S. Bergvik, “Women with coronary heart disease—making sense of their symptoms and their experiences from interacting with their general practitioners,” Health Psychology and Behavioral Medicine, vol. 5(1), pp. 29-40, 2017.
- [28] M. Mack, A. Gopal, “Epidemiology, traditional and novel risk factors in coronary artery disease,” Heart failure clinics, vol. 12(1), pp. 1-10, 2016.
- [29] R. L. McClelland, N. W. Jorgensen, M. Budoff, M. J. Blaha, W. S. Post, R. A. Kronmal and A. R. Folsom, “10-year coronary heart disease risk prediction using coronary artery calcium and traditional risk factors: derivation in the MESA (Multi-Ethnic Study of Atherosclerosis) with validation in the HNR (Heinz Nixdorf Recall) study and the DHS (Dallas Heart Study),” Journal of the American College of Cardiology, vol. 66(15), pp. 1643-1653, 2015, doi: <http://dx.doi.org/10.1016/j.jacc.2015.08.035>.

Developing a Credit Card Fraud Detection Model using Machine Learning Approaches

Shahnawaz Khan¹

Faculty of Engineering
Design and Information & Communications Technology
Bahrain Polytechnic
Isa Town, Bahrain

Abdullah Alourani²

Department of Computer Science and Information
College of Science in Zulfi
Majmaah University
Al-Majmaah, 11952
Saudi Arabia

Bharavi Mishra³

Department of Computer Science & Engineering
The LNM Institute of Information Technology
Jaipur, Rajasthan, India

Ashraf Ali⁴

Faculty of Computer Studies
Arab Open University, Kingdom of Bahrain

Mustafa Kamal⁵

College of Science & Theoretical Studies
Saudi Electronic University, Dammam, Saudi Arabia

Abstract—The growing application and usage of e-commerce applications have given an exponential rise to the number of online transactions. Though there are several methods for completing online transactions, however, credit cards are most commonly used. The increased number of transactions has given the opportunity to the fraudsters to mislead the customers and make them execute fraudulent transactions. Therefore, there is a need for such a method that can automatically classify detect fraudulent transactions. This research study aims to develop a credit-card fraud detection model that can effectively classify an online transaction as fraudulent or genuine. Three supervised machine learning approaches have been applied to develop a credit-card fraud classifier. These techniques include logistic regression, artificial intelligence and support vector machine. The classification accuracy achieved by all the classifiers is almost similar. This research has used the confusion matrix and area under the curve to demonstrate the score of the different performance measures and evaluate the overall performance of the classifiers. Several performance measures such as accuracy, precision, recall, F1-measure, Matthews correlation coefficient, receiver operating characteristic curve have been computed and analysed to evaluate the performance of the credit-card fraud detection classifiers. The analysis demonstrates that the support vector machine-based classifier outperforms the other classifiers.

Keywords—Credit card fraud detection; neural network; support vector machine; logistic regression; performance measures

I. INTRODUCTION

With the increased use of financial technology, the use of online transactions has increased manifolds in recent years. This expansion and use of electronic commerce have increased the trust of customers in online transactions. There are several kinds of financial fraud such as credit card fraud, securities fraud, insurance fraud, etc. that use online methods to accomplish the fraud. Most online transactions utilize credit cards. Therefore, the most common type of fraud among all the frauds types is credit card fraud [17]. Credit card frauds can be

further categorized into offline fraud, application fraud, bankruptcy fraud, internal fraud, behavioural fraud, counterfeit fraud, cardholder-not-present fraud, etc. Online transactions are providing new opportunities for fraudsters. Frauds are activities by the fraudsters that are intended to yield the fraudster personal or financial gain [23]. These activities are often criminal or wrongful. Credit card frauds cause problems and losses to financial institutions as well as individuals. There are hundreds of transactions every second for any financial institution [2]. Manual fraud detection and prevention is not a feasible solution. There has been a tremendous amount of effort by the research community in developing efficient detection techniques for credit card frauds. So that the trust of the customers can increase in e-commerce and online transactions and the losses that occurred due to the frauds can be minimized.

Digital transactions can take place over the phone or on the internet. For executing a transaction, very basic information is required such as expiry date, card number, card verification number etc. Cardholders provide this information through phone or the internet. Fraudsters apply several techniques and attempt to steal the credit card information of the customers so that they can use it for doing fraudulent transactions. It is a very serious, and costly problem for financial service providers. Billions of dollars are subject to fraudulent transactions every year [22]. The fraudulent transaction is an issue of concern for all the credit card providers or by expansion for all the financial systems that provide the facilities for online transactions to their customers. It is usually the result of someone stealing the credit card information of the customers which also impact the brand value of the credit card service providers and the merchants.

The worldwide cost of fraudulent transactions is projected to be 38.5 billion U.S. dollars by 2027 and it was 32 billion dollars in 2021 [26]. The fraudulent transactions cause a huge

loss for the merchants also because they usually have to bear all the related costs such as administrative charges, issuer fees etc. The number of digital transactions is huge, therefore, verifying each transaction for its genuineness is not an easy task for the financial service providers. Consequently, credit card providers often only investigate the cases when they are reported by the customers. The literature highlights several other issues in which the primary issue is the imbalance amount of the cases in the available historical data. The number of actual fraud cases in the data is usually very small in comparison to the number of genuine transactions. The imbalance of the training data creates the problem of biases in the classification accuracy of the classifier. The presence of the dominating class corners the other classes. Thus, the classifier keeps predicting the dominating class. Therefore, even if the classifier is predicting wrong, the accuracy of the classifier will not be impacted by large.

Therefore, there is a need for a system that can detect fraudulent transactions efficiently and raise an alarm as soon as the transaction is made, so that the credit card provider can take immediate action and reduce the risk of capital loss. Several researchers have utilized multiple machine learning and other computational methods to detect credit card frauds. This research aims to tackle the issue of data imbalance and develop a credit card fraud detection system. There are several techniques that aim to minimize the effect of the data imbalance. This research applies such techniques for data preparation and during the model evaluation phase. Because the researchers are in the view that only measuring the accuracy will not be a proper evaluation of the classifier.

Various researchers have applied several machine learning and hybrid methods for detecting fraudulent transactions and have developed classifiers that can detect fraudulent transactions. Several researchers have used standalone methods [7], [8], [13], [17], [27] while many researchers have also applied hybrid approaches [3], [22] for detecting credit card frauds. The issue of the presence of the highly imbalanced amount of data samples is the primary challenge in developing an effective credit-card fraud detection model. Several approaches have been applied such as feature selection, feature engineering, sequence classification, supervised and unsupervised machine learning methods, data pre-processing to balance the data classes.

Credit card fraud detection methods discussed in this research focus on identifying if a transaction on a credit card is fraudulent or not by applying several machine learning techniques such as logistic regression, artificial neural networks, and support vector machines. Credit card fraud detection systems use historical transaction data to train. The decision of these systems relies on the spending behavioural patterns learned during the training process from historical transaction data. The system aims to develop an efficient credit-card fraud detection model that can effectively classify the transactions into genuine transactions or fraudulent transactions efficiently. Several performance measures such as accuracy, precision, recall, F1-measure, Matthews correlation coefficient, receiver operating characteristic curve have been calculated to evaluate the performance of different

classification models. Among the implemented models, the support vector machine model performs better.

This paper has been organized into five sections. The second section of the paper examines the literature review and presents the background work briefly. Section three discusses machine learning techniques, data and pre-processing. Section four presents the results obtained from different classifiers implemented by this research study and also exhibits the various performance measures and evaluates the performance of the credit card fraud detection models. The last section presents the conclusion.

II. RELATED WORK

In binary classification, the basic concept is to find the threshold value that enables the classifier to assign a particular label to the case or instance being predicted. There have been conducted several research studies on detecting credit card frauds based on the spending behaviour of the customer. However, sometimes the customer spending behaviour changes during certain conditions such as holidays or other special occasions. This might create an issue for supervised machine learning systems. Research by [3] proposes a hybrid approach for managing customer abnormal spending behaviour. The proposed approach combines supervised and unsupervised machine learning approaches and presents effective results in case of abnormalities of the spending behaviours.

A research study [7] applies a generative adversarial network (GAN) to detect credit card frauds. As the credit card transaction data is usually highly imbalanced, the proposed framework by the research study [7] has a higher false-positive rate if the sensitivity is improved. Research [22] applies and compares several machine learning techniques such as Naïve Bayes, random forest, logistic regression, decision tree, AdaBoost, multiple layer perceptron etc. The research demonstrates that the AdaBoost with majority voting produces the best results among all the alternatives. There is an interesting fact to consider for this research [22], that the transactions data used for developing the classifier has only 0.0355% fraudulent transactions. The data used is highly imbalanced and no measures have been taken to counter the imbalances of the data. In the research study presented by [17], several machine learning methods have been applied for credit card fraud detection. The study illustrates that SVM, ANN, C5.0 decision tree, and LR performs better among the tested criteria. However, the number of false positives is high among all the implemented methods.

A random forest algorithm is an effective method for developing supervised classification models. A research study by [27] implements random forest supervised machine learning techniques to detect the behavioural patterns for genuine transactions and fraudulent transactions. A similar research study by [13] proposes a random forest algorithm-based machine learning model for detecting credit card frauds. The model presented by the research [13] exhibits good accuracy. Though, the performance measure is based on the statistics obtained from the confusion matrix only. As has been discussed above by several researchers the credit card fraud detection problem poses the challenge of the imbalance data classes. Therefore, there should have been some other

performance measure such as the receiver operating characteristic (ROC) curve that could have been employed for a better performance measure. In a similar domain, the research study by [18] focuses on minimizing the number of incorrect fraud classifications. Actually, that's the primary target of any researcher working in this domain. The research study by [18] employs multiple algorithms for anomaly detection and implements algorithms such as isolation forest and local outlier factor algorithms. The results presented by the study are sensitive to the quantity of the data and face the challenge of imbalanced data for the classification classes.

A research study by [20] presents an interesting perspective on credit card fraud detection and infer that there is no constant pattern for fraud. Therefore, supervised machine learning techniques are not efficient in credit card fraud detection. It [20] proposes an unsupervised machine learning approach using a restricted Boltzmann machine (RBM) and deep Auto-encoder. However, the results achieved are less promising than some of the supervised machine learning approaches. A Bayesian network classifier-based approach presented by [6] in a research study uses a hyper-heuristic evolutionary algorithm to detect the patterns. The presented solution like the other approaches discussed in this section targets the class imbalance and misclassification issues of the credit card fraud detection problem. Research by [2] introduces a real-time fraud detection system using machine learning and big data. This solution primarily focuses on the detection speed of the transactions, use of big data and scalability.

The research study by [4] considers the spatial and temporal features among others and presents a 3D convolutional neural network for credit card fraud detection. The present approach [2] implements the model on the real-world data collected from multiple locations. The research by [15] proposes a hidden Markov model-based approach for automated feature engineering to improve the performance of the classifier and to model temporal feature correlation. A similar research study [28] that focus on the features of the transactional data, develops a deep learning-based solution that uses homogeneity-oriented behaviour analysis for feature engineering. A research study [1] proposes an optimized light gradient boosting based machine learning technique for predicting credit card frauds. This research [1] relies on parameter optimization for improving the performance of the classifier.

An interesting approach to solving the credit card detection problem is sequence classification or prediction problem. Research [8] formulates credit card fraud detection as a sequence classification problem. It applies long short-term memory neural network to identify the fraudulent transaction. The research concludes that articulating the fraud detection task as a sequence-learning problem leads to an increased number of false positives. As a matter of fact, online transactions should not be considered a sequential classification problem, because the amount, time, and point of the online transactions usually change randomly. It will require a highly disciplined spending behaviour to express online transactions as a sequence learning problem.

III. METHODOLOGY

A. Dataset and Pre-processing

One of the primary issues for data preparation for credit-card fraud transaction data is the labelling of the data. Often the fraudulent label of the transactional data can only be decided posterior the transaction has been executed and reported by the customer. The dataset used in this research study consists of transactions made by European cardholders in September 2013 [14]. The dataset contains 284,807 transactions made during two days. The fraudulent transactions made during this time were 492 which is just 0.172% of all transactions made during this time. As it is evident that the data is imbalanced, therefore, this research uses the resampling technique and makes an effort to oversample the fraudulent transactions and to remove the genuine transactions. The dataset was transformed using principal component analysis to maintain the confidentiality of the transactions [14] and the principal components are used as features for training the classifiers. The dataset contains 30 input features such as transaction time, transaction amount and 28 principal components. The output classes have two labels 1 and 0. The fraudulent transactions are assigned label 1 and the genuine transactions are labelled as 0.

B. Modelling for Credit Card Fraud Detection

Several approaches and algorithms have been implemented for credit card fraud detection. Some of these solutions have been discussed in the related work section. Several features and affairs have been taken into consideration for credit card fraud detection classifiers. One of the common issues that are discussed throughout the literature in credit card fraud detection is the presence of class data imbalance. However, none of the algorithms or approaches discussed precisely tackle the class imbalance issue. Therefore, this research implements a two-step process for handling the issue. The first phase is data pre-processing. In the data pre-processing phase, the study aims to reduce the class data imbalance by increasing the number of cases for the minority class, and by reducing the number of cases for dominating class. This section discusses the approaches used in this study.

1) *Logistic regression*: Logistic regression is a probabilistic modelling process that produces the probability of the discrete output variables based on the input variables. Often logistic regression is applied for binary classification when the input variable is single or multiple. However, logistic regression can be applied to classify more than two output classes, which is known as multinomial logistic regression. Furthermore, it can be used for ordering the level of the output variable classes which is known as ordered logistic regression. However, logistic regression is often used for binary classification problems. Credit card fraud detection is a binary classification problem in which the output of the transaction is either fraud or a genuine transaction given the input features for the transactions. Therefore, logistic regression can be used as a credit card fraud detection technique.

Credit card detection can be performed by computing the probability of the given transaction using the given features and comparing it with a threshold value such as 0.5. If the computed probability is more than 0.5 then it will be classified as fraud if less than the threshold then it will be classified as a genuine transaction. Let us assume that the probability of the fraudulent transaction based on the transaction features x is $P(y = 1|x)$ or simply $P(x)$. To compute the probability-estimate log-odds can be computed. Log-odds are directly proportional to the probability of the transaction label. Higher the odds, the higher the probability of the given label for the transaction.

$$\text{It can be defined as: } \frac{P(x)}{1-P(x)} \tag{1}$$

For modelling and simplifying the computational process, natural logarithm was applied as follows:

$$\text{logit}(x) = \log\left(\frac{P(x)}{1-P(x)}\right) \tag{2}$$

$$\text{Let's consider, } \log\left(\frac{P(x)}{1-P(x)}\right) = w'x + b \tag{3}$$

Here, w' is the transpose of the weight vector and b is the offset variable. The above equation (Eq. 3) can be further simplified by applying exponential on both sides:

$$P(x) = \frac{e^{w'x+b}}{1+e^{w'x+b}} \tag{4}$$

Therefore, the probability of the fraudulent $P(x)$ can be estimated using the above equation (Eq. 4) in which x are the features of the transaction. The aim is to optimize the values of w and b based on the transactional data. It can be learnt by converting the above problem into maximum likelihood estimation problem and optimizing it for w and b using the transactional data.

The log-likelihood from the equation (eq 4) can be derived as following (Eq 5):

$$\log(w, b) = \sum_1^n [y_i \log P(x_i) + (1 - y_i) \log(1 - P(x_i))] \tag{5}$$

The optimized values of w and b are estimated by maximizing the log-likelihood (Eq. 5) or by converting the above problem into minimization problem after multiplying with a negative sign.

2) *Artificial neural network:* Artificial neural network (ANN) is one of the most powerful machine-learning techniques. ANN aims to simulate the behaviour of biological organisms. In the human nervous system, neurons are connected to other neurons through connections which are known as axons and dendrites. The strength of the connections is subject to change in accordance with the external stimuli which are referred to weights in ANN. The computational units in ANN are termed as neurons. Though, the ANN simulation of the biological organism is very basic still, the complexity and computation capabilities of the artificial neural network is very powerful. Artificial neural networks have been applied to solve complex computational problems for example in machine translation [9], [10], [11], [24], [25], image processing [12], time series forecasting [21], classification etc. There are several neural network

architectures that are employed in machine learning for various different tasks. The following diagram (Fig. 1) presents a general feed-forward neural network architecture. This study employs a feed-forward neural network. Input layer is the first layer and works as input to the neural network. The input layer of the neural network used in this study contains 25 neurons corresponding to the features of a transaction. Two middle layers, popularly known as hidden layers, have been used each of which contains 10 neurons. The output layer has 2 neurons corresponding to each class. The network uses the backpropagation algorithm for learning. The layers are fully connected layers. The activation function used is rectified linear units (ReLU).

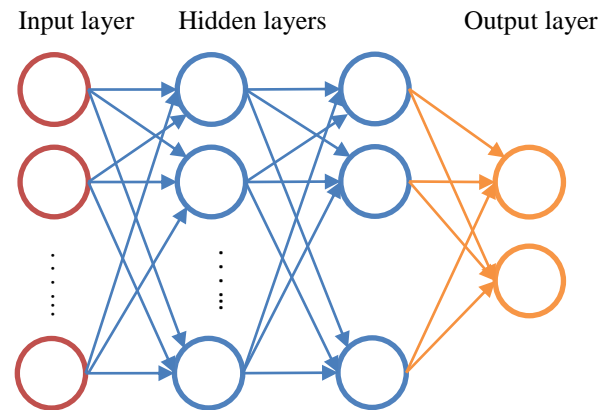


Fig. 1. Feed-forward Neural Network General Architecture.

The ReLU activation function is a very simple but effective activation function. It returns a zero if the input received by the activation function is negative, otherwise, no change is applied on the input and the input values is returned as it is if the input is positive. It can be simply stated as:

$$f(x) = \begin{cases} 0, & x \leq 0 \\ x, & x > 0 \end{cases} \tag{6}$$

3) *Support vector machines:* Support vector machines like artificial neural networks have been among the most popular machine learning algorithms. SVMs are commonly applied in solving supervised machine learning problems such as regression, classification and outlier detection. Though, the number of samples for this research study is ample, but, SVMs can also be applied in a scenario where the number of dimensions is more than the sample size. SVMs, for classification, functions by finding the best hyperplanes that separate the data points in accordance with the classes. The hyperplanes set apart the data points of one class from the data points of other classes. The optimization is applied for finding the best hyperplane that can find the maximum margin among the data points of one class from the data points of the other class. The support vectors are the closes data points to the hyperplane. SVMs can be implemented using different types of kernel functions. Kernel methods are a set of algorithms that are used in machine learning techniques for pattern analysis and detection. Kernel functions, transforms the data

into higher dimensions, expecting to find clearer decision boundaries for data separation. Kernel functions aids in efficiently transforming high dimensional data for creating optimal boundaries for decision making. The kernel function used in this research is the quadratic kernel function.

A quadratic kernel is a non-stationary and special form of the polynomial kernel. The general form of the polynomial function looks as follows:

$$K(f, g) = (f^T g + c)^d \tag{7}$$

Here, f and g are the computed vectors of features from the input data samples, c is a free parameter and has a value of $c \geq 0$, and d is the degree of polynomial. When the degree $d = 2$. Then, the kernel function is called quadratic kernel function and can be presented as follows:

$$K(f, g) = (f^T g + c)^2 \tag{8}$$

IV. RESULTS AND DISCUSSION

This research study implements several machine learning methods for credit card fraud detection. The selected methods are logistic regression, artificial neural network and support vector machines. Three models were trained using the above-mentioned machine learning technique on the selected training data. The training process has applied five-cross validation. Test data samples were randomly selected before applying resampling techniques to evaluate the performance of the system on real-world data. The accuracy achieved for the logistic regression method is 99.92% and the prediction speed is around 300 thousand predictions per second. The accuracy for the neural network-based model is 99.92% while the prediction speed is 650 thousand predictions per second. Support vector machines model has the prediction speed of about 350 thousand predictions per second and the accuracy of 99.94%. The prediction speed of the artificial neural network-based model is the fastest among the tested models, but the application of the model on big data has yet to be tested [2]. As the accuracy achieved by all the developed models is similar, therefore, some other evaluation metrics must be used to measure the performance of the developed models. The confusion matrix for classification models demonstrates the true positive (TP), true negatives (TN), false positives (FP), and false negatives (FN). It illustrates how many of the instances have been classified to their actual class and how many have been misclassified. The following Tables I to III illustrate the confusion matrix and several performance metrics for the three classification models:

1) *Accuracy*: Accuracy is the primary performance evaluation metric and measures the ratio of correct prediction over the total number of predictions by the classifier. It can be presented as:

$$Accuracy = \frac{True\ Positive + True\ Negative}{Total\ Predictions}$$

The models (logistic regression, artificial neural network and support vector machines) achieved an accuracy of 99.91%, 99.91% and 99.94% respectively.

2) *Precision*: Precision is also known as the positive predictive value and is the ratio of the true positive predictions over the total positive predictions:

$$Precision = \frac{True\ Positive}{True\ Positive + False\ Positive}$$

The models (logistic regression, artificial neural network and support vector machines) achieved a precision of 87.32%, 76.91% and 87.67% respectively.

3) *Recall*: Recall measures the true positive rate of the classifier and is also known as sensitivity in binary classification. It is calculated as the fraction of the true positive predictions over all the positive cases that were retrieved for the testing:

$$Recall = \frac{True\ Positive}{True\ Positive + False\ Negative}$$

The sensitivity or recall measured for logistic regression classifier is 61.59%, recall for the artificial neural network is 75.81% and for support vector machines is 78.05%.

TABLE I. CONFUSION MATRIX AND PERFORMANCE METRICS FOR LOGISTIC REGRESSION

		Logistic Regression		
		Predicted Class		
		Genuine	Fraud	
True Class	Genuine	284271	44	99.98%
	Fraud	189	303	61.59%
			87.32%	99.92%

TABLE II. CONFUSION MATRIX AND PERFORMANCE METRICS FOR ANN

		Artificial Neural Network		
		Predicted Class		
		Genuine	Fraud	
True Class	Genuine	284203	112	99.96%
	Fraud	119	373	75.81%
			76.91%	99.92%

TABLE III. CONFUSION MATRIX AND PERFORMANCE METRICS FOR SVM

		Support Vector Machine		
		Predicted Class		
		Genuine	Fraud	
True Class	Genuine	284261	54	99.98%
	Fraud	108	384	78.05%
			87.67%	99.94%

4) *Specificity*: To measure the true negative prediction rate of the classifier, specificity is calculated as the proportion of the true negative predictions over the total negative cases that were retrieved for the testing:

$$\text{Specificity} = \frac{\text{True Negative}}{\text{True Negative} + \text{False Positive}}$$

The negative prediction rate or the specificity of the logistic regression is 99.98%, specificity for the artificial neural network is 99.96%, and the specificity for the support vector machines-based classifier was measured as 99.98%.

5) *F1-Score*: F1-score or F-measure considers the importance of true positive and true negative. It is the harmonic mean of the two performance measures calculated earlier which are precision and recall:

$$F1 - \text{score} = 2 * \frac{\text{Precision} * \text{Recall}}{\text{Precision} + \text{Recall}}$$

F1-score measured for logistic regression classifier is 72.23%, 76.36% for artificial neural network classifier, and 82.58% for support vector machines.

6) *Matthews Correlation Coefficient (MCC)*: Matthews correlation coefficient [19] calculates the correlation between the actual classes and predicted classes of the cases. Matthews correlation coefficient (MCC) provides a more accurate evaluation of the overall performance of the binary classifier than other performance measures such as precision, recall, F1-score, and accuracy [5]. MCC is the ration of the covariance of the actual classes of the cases and the predicted labels over the product of the standard deviations of the true classes (σ_t) and the predicted classes (σ_p). MCC is measured as following:

$$MCC = \frac{\text{Cov}(t,p)}{\sigma_t \cdot \sigma_p} \\ = \frac{TP \cdot TN - FP \cdot FN}{\sqrt{(TP + FP)(TN + FN)(TP + FN)(TN + FP)}}$$

MCC has been calculated for all the three classifiers. The value of the Matthews correlation coefficient remains between -1 and +1. Higher the value of MCC, better the model is. The MCC value for logistic regression is 0.733 or 73.3%, 76.32% for the artificial neural network classifier and 82.69% for the support vector machine classifier.

7) *Receiver operating characteristic curve*: Another important criterion to consider is the highly imbalanced amount of data points in the training data. Highly imbalanced data introduces several issues in developing machine learning models. One of such issues is biasness. In the case of highly imbalanced data, the prediction accuracy is usually biased. In the case of imbalanced data, the accuracy calculated based on the confusion matrix might be misleading because it will not address the issue of biased classification. Therefore, some other evaluation measure should also be considered while

evaluating the performance of the classification model. This research has considered the Receiver Operating Characteristic (ROC) curve as an additional performance measure for the classifiers. ROC curve was initially developed and applied during the world war II for detecting the enemy objects [16]. ROC is fundamentally a graphical representation or a plot that illustrates the accuracy of the classification capability of a binary classifier (Lusted, 1971). ROC curve is a widely used performance measure to evaluate the performance of the binary classifiers. ROC curve plots the sensitivity of the classifier against the false positive rate. False positive rate can be obtained by subtracting the specificity of the classification model from one. The graph is drawn on a 1x1 space which means that the scale on each of the x and y-axis is in the range of 0 to 1. The line connecting the coordinates (0, 0) and (1, 1) will represent a random classifier. An ideal classifier would score a point on the upper left corner (0, 1) which represents the case of zero false positives and zero false negatives.

The following Fig. 2 demonstrates the ROC curve for logistic regression model. The logistic regression classification model yields a point (0.38, 1) and the area under curve is 0.97.

The following Fig. 3 demonstrates the ROC curve for artificial neural network classifier. The artificial neural network model yields the threshold point (0.24, 1) and the area under the curve for artificial neural network model is 0.90. The following Fig. 4 illustrates the ROC curve for support vector machine model. The support vector machine classification model yields a point (0.22, 1) and the area under curve is 0.94. It can be seen that the point yield by the support vector machine vector model is the closest to the point of the best classification model.

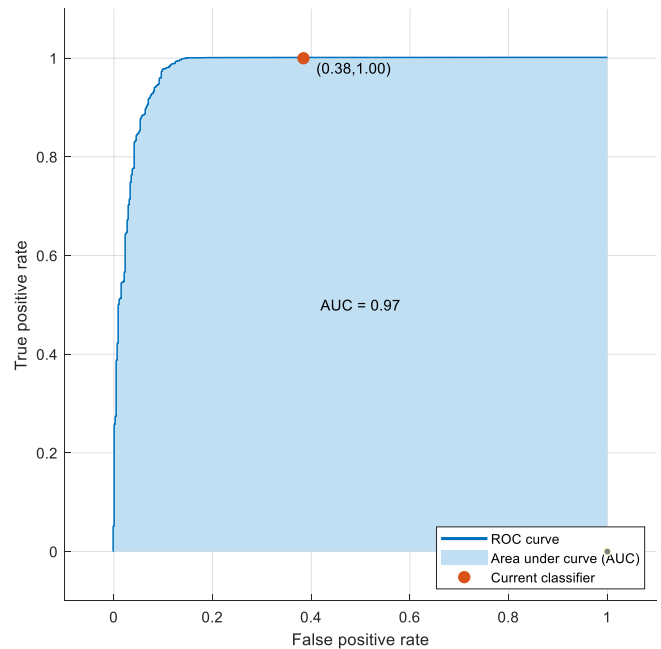


Fig. 2. ROC Curve for Logistic Regression Model.

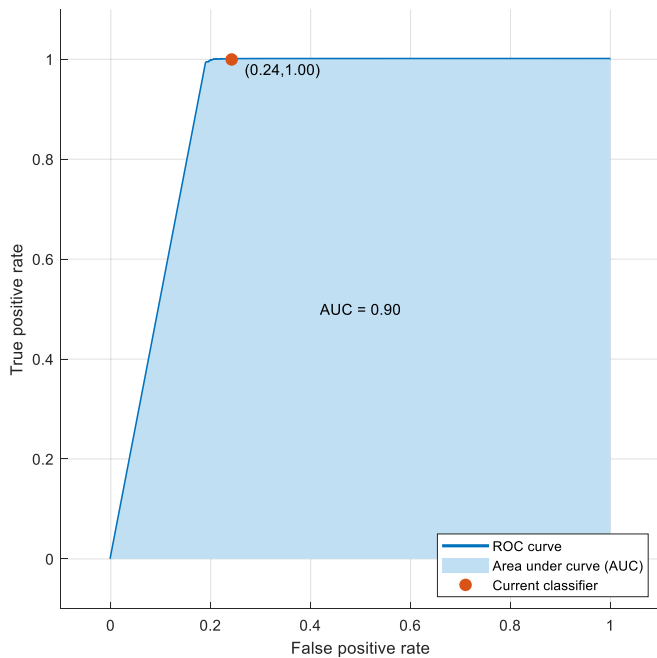


Fig. 3. ROC Curve for Artificial Neural Network Model.

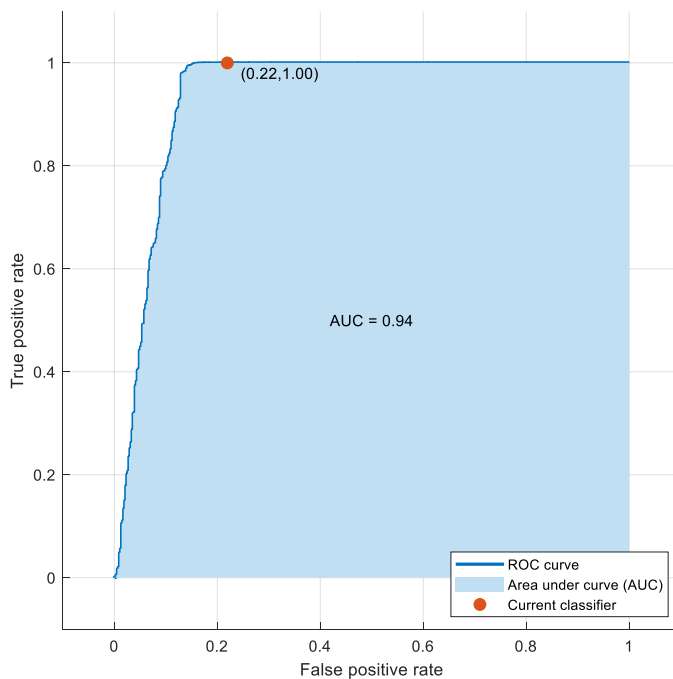


Fig. 4. ROC Curve for Support Vector Machine Model.

V. CONCLUSION

Credit card fraud is an issue of concern among financial institutions and causes huge financial losses for service providers. Fraudulent transactions have cost over 32 billion United States dollars worldwide in 2021. This amount is projected to increase by over 38 billion dollars in the next 5 years by 2027. Several computational approaches have been employed to develop an effective model for credit card fraud detection. Researchers have employed supervised and unsupervised machine learning approaches. However, the

supervised machine learning approaches have produced better results. There are several issues while developing the credit-card fraud detection model. Availability of the highly imbalanced class data is the issue of major concern. The presence of the dominating class corners the other classes. Thus, the classifier keeps predicting the dominating class. Therefore, even if the classifier is predicting wrong, the accuracy of the classifier will not be impacted by large. This research study has applied a resampling technique to counter the effect of imbalanced class data. However, due to the nature of the problem, it is neither feasible nor practical to completely ignore and eliminate the gap of imbalanced data classes. This research study has implemented three machine learning techniques which are logistic regression (LR), artificial neural network (ANN), and support vector machines (SVM).

The models have been evaluated thoroughly using different performance evaluation measures and matrices. Though based on the accuracy computed from the confusion matrix, all the model scores same. But, further analysis using different performance measures demonstrates that the support vector machines classification model outperforms the other models. The prediction accuracy and specificity are almost the same for all the classification models, while the precision is almost 12% lower for the ANN model than the other two models. While the SVM model has slightly higher precision than the LR model. Recall of the SVM model is almost 21% higher than the LR model and almost 3% higher than the ANN model. Similarly, the MCC value and F1-score for the SVM model are over 12% higher than the LR model and 7% higher than the ANN model. Receiver operating curve yields a point (0.38, 1) for the LR model, (0.24, 1) for the ANN model, and (0.22, 1) for the SVM model. The best-case scenario for the classifier on the ROC curve is to yield a point on the upper left corner (0, 1) which represents the case of zero false positives and zero false negatives. Among, the three tested models, SVM is the closest classification model to the best point (0, 1). Therefore, it can be concluded based on the various performance measures that the SVM model outperforms the other models for credit card detection.

ACKNOWLEDGMENT

The authors would like to thank the Deanship of Scientific Research at Majmaah University for supporting this work under project no: R-2022-50.

REFERENCES

- [1] Altyeb, A. A., & Malebary, S. J. (2020). An Intelligent Approach to Credit Card Fraud Detection Using an Optimized Light Gradient Boosting Machine. *IEEE Access*, 1–1. doi:10.1109/access.2020.2971354.
- [2] Carcillo, F., Dal Pozzolo, A., Le Borgne, Y.-A., Caelen, O., Mazzer, Y., & Bontempi, G. (2018). SCARFF: A scalable framework for streaming credit card fraud detection with spark. *Information Fusion*, 41, 182–194. doi:10.1016/j.inffus.2017.09.005.
- [3] Carcillo, F., Le Borgne, Y.-A., Caelen, O., Kessaci, Y., Oblé, F., & Bontempi, G. (2019). Combining Unsupervised and Supervised Learning in Credit Card Fraud Detection. *Information Sciences*. doi:10.1016/j.ins.2019.05.042.
- [4] Cheng, D., Xiang, S., Shang, C., Zhang, Y., Yang, F., & Zhang, L. (2020). Spatio-Temporal Attention-Based Neural Network for Credit Card Fraud Detection. *Proceedings of the AAAI Conference on Artificial Intelligence*, 34(01), 362–369. doi:10.1609/aaai.v34i01.5371.

- [5] Chicco, D., & Jurman, G. (2020). The advantages of the Matthews correlation coefficient (MCC) over F1 score and accuracy in binary classification evaluation. *BMC genomics*, 21(1), 1-13.
- [6] De Sá, A. G., Pereira, A. C., & Pappa, G. L. (2018). A customized classification algorithm for credit card fraud detection. *Engineering Applications of Artificial Intelligence*, 72, 21-29.
- [7] Fiore, U., De Santis, A., Perla, F., Zanetti, P., & Palmieri, F. (2017). Using generative adversarial networks for improving classification effectiveness in credit card fraud detection. *Information Sciences*. doi:10.1016/j.ins.2017.12.030.
- [8] Jurgovsky, J., Granitzer, M., Ziegler, K., Calabretto, S., Portier, P.-E., He-Guelton, L., & Caelen, O. (2018). Sequence classification for credit-card fraud detection. *Expert Systems with Applications*, 100, 234–245. doi:10.1016/j.eswa.2018.01.037.
- [9] Khan, S. N., & Usman, I. (2019). A model for English to Urdu and Hindi machine translation system using translation rules and artificial neural network. *Int. Arab J. Inf. Technol.*, 16(1), 125-131.
- [10] Khan, S., & Mishra, R. B. (2011). Translation rules and ANN based model for English to Urdu machine translation. *INFOCOMP Journal of Computer Science*, 10(3), 36-47.
- [11] Khan, S., & Mishra, R. B. (2012). A neural network based approach for English to Hindi machine translation.
- [12] Khan, S., Thirunavukkarasu, K., Hammad, R., Bali, V., & Qader, M. R. (2021). Convolutional neural network based SARS-CoV-2 patients detection model using CT images. *International Journal of Intelligent Engineering Informatics*, 9(2), 211-228.
- [13] Kumar, M. S., Soundarya, V., Kavitha, S., Keerthika, E. S., & Aswini, E. (2019). Credit Card Fraud Detection Using Random Forest Algorithm. 2019 3rd International Conference on Computing and Communications Technologies (ICCCT). doi:10.1109/iccct2.2019.8824930.
- [14] Le Borgne, Yann-A., and Gianluca Bontempi. "Machine Learning for Credit Card Fraud Detection - Practical Handbook" Universit'e Libre de Bruxelles, 2021, https://www.researchgate.net/publication/351283764_Machine_Learning_for_Credit_Card_Fraud_Detection_-_Practical_Handbook.
- [15] Lucas, Y., Portier, P. E., Laporte, L., He-Guelton, L., Caelen, O., Granitzer, M., & Calabretto, S. (2020). Towards automated feature engineering for credit card fraud detection using multi-perspective HMMs. *Future Generation Computer Systems*, 102, 393-402.
- [16] Lusted, L. B. (1971). Signal detectability and medical decision-making. *Science*, 171(3977), 1217-1219.
- [17] Makki, S., Assaghir, Z., Taher, Y., Haque, R., Hacid, M.-S., & Zeineddine, H. (2019). An Experimental Study with Imbalanced Classification Approaches for Credit Card Fraud Detection. *IEEE Access*, 1–1. doi:10.1109/access.2019.2927266.
- [18] Maniraj, S. P., Saini, A., Ahmed, S., & Sarkar, S. (2019). Credit card fraud detection using machine learning and data science. *International Journal of Engineering Research and*, 8(09).
- [19] Matthews, B. W. (1975). Comparison of the predicted and observed secondary structure of T4 phage lysozyme. *Biochimica et Biophysica Acta (BBA) - Protein Structure*, 405(2), 442–451. [https://doi.org/https://doi.org/10.1016/0005-2795\(75\)90109-9](https://doi.org/https://doi.org/10.1016/0005-2795(75)90109-9).
- [20] Pumsirirat, A., & Yan, L. (2018). Credit card fraud detection using deep learning based on auto-encoder and restricted boltzmann machine. *International Journal of advanced computer science and applications*, 9(1), 18-25.
- [21] Qader, M. R., Khan, S., Kamal, M., Usman, M., & Haseeb, M. (2021). Forecasting CO2 Emissions Due To Electricity Power Generation In Bahrain.
- [22] Randhawa, K., Loo, C. K., Seera, M., Lim, C. P., & Nandi, A. K. (2018). Credit Card Fraud Detection Using AdaBoost and Majority Voting. *IEEE Access*, 6, 14277–14284. doi:10.1109/access.2018.2806420.
- [23] Sahin, Y., Bulkan, S., & Duman, E. (2013). A cost-sensitive decision tree approach for fraud detection. *Expert Systems with Applications*, 40(15), 5916-5923.
- [24] Shahnawaz, & Mishra, R. B. (2015). An English to Urdu translation model based on CBR, ANN and translation rules. *International Journal of Advanced Intelligence Paradigms*, 7(1), 1-23.
- [25] Shahnawaz, M. R. (2011). ANN and rule based model for English to Urdu-Hindi machine translation system. In *Proceedings of National Conference on Artificial Intelligence and agents: Theory & Application, AIAIATA* (pp. 115-121).
- [26] Szmigiera, M. (2021). Value of fraudulent card transactions worldwide 2021-2027, Statista.com, accessed on 15-Jan-2022. <https://www.statista.com/statistics/1264329/>.
- [27] Xuan, S., Liu, G., Li, Z., Zheng, L., Wang, S., & Jiang, C. (2018). Random forest for credit card fraud detection. 2018 IEEE 15th International Conference on Networking, Sensing and Control (ICNSC). doi:10.1109/icnsc.2018.8361343.
- [28] Zhang, X., Han, Y., Xu, W., & Wang, Q. (2019). HOBA: A Novel Feature Engineering Methodology for Credit Card Fraud Detection with a Deep Learning Architecture. *Information Sciences*. doi:10.1016/j.ins.2019.05.023.

Bayesian Hyperparameter Optimization and Ensemble Learning for Machine Learning Models on Software Effort Estimation

Robert Marco^{1*}, Sakinah Sharifah Syed Ahmad², Sabrina Ahmad³

Department of Informatics, Universitas Amikom Yogyakarta, Yogyakarta, Indonesia¹

Faculty of Information & Communication Technology, Universiti Teknikal Malaysia Melaka, Malaysia, Melaka, Malaysia^{2,3}

Abstract—In recent decades, various software effort estimation (SEE) algorithms have been suggested. Unfortunately, generating high-precision accuracy is still a major challenge in the context of SEE. The use of traditional techniques and parametric approaches is largely inaccurate because they produce biased and subjective accuracy. Meanwhile, none of the machine learning methods performed well. This study applies the AdaBoost ensemble learning method and random forest (RF), on the other hand the Bayesian optimization method is applied to determine the hyperparameters of this model. The PROMISE repository and the ISBSG dataset were used to build the SEE model. The developed model was comprehensively compared with four machine learning methods (classification and regression tree, k-nearest neighbor, multilayer perceptron, and support vector regression) under 3-fold cross validation (CV). It can be seen that the RF method based on AdaBoost ensemble learning and bayesian optimization outperforms this approach. In addition, the AdaBoost-based model assigns a feature importance rating, which makes it a promising tool in software effort prediction.

Keywords—Bayesian optimization; adaboost ensemble learning; random forest; software effort estimation

I. INTRODUCTION

Software effort estimation (SEE) is a method of estimating the amount of time it will take to build a software system in person-months or person-hours [1][2]. Uncertainty and imprecision characterize software effort estimation environments [3][4]. The topic of SEE, on the other hand, has been characterized as a regression problem in general [5]. Various SEE models in the literature still show considerable performance deviations and are extremely dataset-dependent.

SEE has previously been accomplished via expert judgment, analogy, decomposition and recomposition, and parametric techniques [6]. Meanwhile, standard SEE methodologies can produce erroneous estimates due to human bias and subjectivity [7]. The Machine learning (ML) algorithm is very effective in modeling uncertainty as a better decision-making process [8]. However, no single learning method is ideal for all supervised learning tasks [9]. However, a single sophisticated algorithm may not be a consideration for building current SEE models, as the performance of any model mainly depends on the characteristics of the data set used, such as data set size, outliers, categorical features, and missing values.

Several machine learning techniques have been widely applied in the SEE context which have been considered as necessary steps, such as: Case-Based Reasoning (CBR), Artificial Neural Networks (ANN), Support Vector Regression (SVR) [10], while for other ML methods, such as Random Forest (RF), Classification And Regression Tree (CART) and K-Nearest Neighbor (kNN), they are still ignored. RF is a powerful, easy-to-train ensemble learner with big data [11]. RF is widely used in the data mining domain and has achieved good performance when dealing with regression and classification problems [12]; this method can overcome overfitting and is less affected by outliers [13]. On the other hand, RF improves prediction accuracy without significant computational improvement, and is not sensitive to multicollinearity [14]. Some researchers have also applied RF to solve regression problems in the context of SEE, for example [15][16][17]. Unfortunately, the RF model can only be extended horizontally because decision trees exist in parallel and these decision trees have equal weight in voting for the final prediction even though some of these trees may underperform.

The use of Ensemble learning combines several algorithms that process different hypotheses to make their predictions perform well [18]. According to Lessmann et al. (2015), the ensemble method is better than the single ML and other statistical method [19]. While, Kocaguneli et al. (2012), the proper use of the ensemble method can outperform the performance of single learners on the ML model [20], as well as being one of the best methods in increasing the accuracy and stability of the most influential estimation [21]. Averaging, voting, and bagging are three common broad ensemble approaches that have piqued the interest of machine learning researchers. Meanwhile, developing ensemble methods such as stacked generalization, AdaBoost algorithm, Gradient tree boosting have not been widely tried/ignored [22].

Ren et al. (2016) investigated the use of ensembles in classification and regression and the success of AdaBoost about regression behaviour [23]. AdaBoost, as a popular boosting algorithm, combines weak estimators and implements them on an improved version of the data with the help of weighted majority voting/hard voting [24]. However, AdaBoost may not offer high accuracy when the dataset is heavily contaminated with noise [25]. In contrast to, Martin-Diaz et al. (2017), AdaBoost is also known to achieve a

*Corresponding Author.

significant reduction in bias as well [26], and low error variance [24]. Also, it is not easy to overfit during training [27].

Unfortunately, the method will need to be fine-tuned to fit the scenario at hand. Automatic hyperparameter adjustment saves time and effort when experimenting with different machine learning model configurations, improves algorithm accuracy, and increases reproducibility. Hyperparameter tuning is a well-known approach for achieving optimal performance in machine learning models [28][29]. Several other studies have shown that the accuracy dimension in SEE is strongly influenced by choice of information estimation using parameter tuning techniques [30]. Because determining the best hyperparameter combination can improve the ML model's performance [28][31]. However, much of the work seems to implicitly assume that tuning the parameters will not significantly change the results [32]. In the worst case, improper parameter setting may lead to inferior performance results [33]. However, the default hyperparameter setting may not produce consistent results depending on the data set used [34]. Based on the work by [35], there is still limited work investigating the impact of parameter setting for SEE methods in improving prediction accuracy.

Manual search, grid search, and random search are some of the most used hyperparameter optimization strategies [36]. When the hyperparameter space is large, however, this method is time consuming and impractical [6]. Manual search necessitates a higher level of professional knowledge, is difficult to implement without prior experience, and takes time [37]. Meanwhile, grid search suffers from a dimensional curse, which means that as the number of hyperparameters set or the complexity of the search space and the range of values of the hyperparameters increases, the algorithm's efficiency declines dramatically [37]. Random search, on the other hand, is more effective in high-dimensional space [38], but this method is not reliable for training complex models [38]. Despite the fact that this method provides automatic tuning, it can acquire the optimization goal function's ideal global importance.

Among other classic hyperparameter optimization techniques, Bayesian optimization is a very successful optimization algorithm for solving computationally expensive functions [39]. Bayesian hyperparameter optimization technique to further promote generalization accuracy [40]. Bayesian optimization is effective for problems with fewer hyperparameters and that are difficult to parallelize [6]. Therefore, it promises to encourage the use of hyperparameter tuning for further applications in SEE.

Motivated by the benefits mentioned above, the AdaBoost RF-based method of ensemble learning was developed to capture the relationships between features in an SEE context. To reduce time dependence and impracticality, Bayesian optimization method is used to find suitable hyperparameter models. The datasets in the PROMISE and ISBSG repositories have built the model in this paper. Based on literature review, there is still a limited use of the AdaBoost and RF ensemble learning methods adopted to build the SEE model. The remainder of this paper begins with related work, followed by

experimental design. Then, the results and discussion containing the comparison of models. At the end, discuss the conclusions and future work.

II. RELATED WORK

Meanwhile, the literature on offline learning does not have a supervised procedure for automatic parameter setting. In the context of offline SEE, the use of Classification and Regression Tree (CART) with the addition of more innovative features can improve accuracy [28], the researchers used a grid search strategy to obtain optimal parameters for five machine learning techniques (KNN, Regression Trees (RT), Multilayer Perceptrons (MLP), Bagging+RT, and Bagging+MLP) without used generating ensembles. The results revealed that while RT, Bagging+RT, and KNN were unaffected by tuning settings, MLP and Bagging+MLP were. Minku (2019) Linear Regression in Logarithmic Scale (LogLR) results in a more stable prediction performance [41]. Meanwhile, Minku and Yao (2013) investigated the RT, Bagging+MLP, and Bagging+RT techniques shown to perform well across several data sets. This suggests that the best parameters to use with a machine learning approach may change over time [35]. In the context of SEE, parameter tuning in Support Vector Regression (SVR) is critical. A tabu search has been proposed in particular to find the best SVR parameter tuning [42]. Elish (2013) conducted an empirical study based on five machine learning approaches (KNN, SVR, MLP, Decision Tree (DT), and Radial Basis Function Network (RBFN)) that suggested a heterogeneous ensemble. Due to its irregular and unstable performance across the specified data set, the single approach is unreliable. Furthermore, across all data sets, five machine learning approaches were trained using the same configuration, but no explanation for parameter tuning was supplied [43].

Meanwhile, Villalobos-Arias and Quesada-López (2021) investigated CART, SVR, and ridge regression (RR) using random search and grid search with six bio-inspired algorithms. The results demonstrate that the Flash+Log+SVR model is the most accurate in the most data sets, while the Hyperband+Log+RR model is the most stable in the most datasets [44]. In particular, the stacked ensemble that offers the best overall accuracy in this study takes the average of the estimated effort values generated by Bagging, RF, ABE, AdaBoost, Gradient boosting machine, and Ordinary least squares regression which are optimized using grid search techniques [25]. Meanwhile, Zakrani et al. (2018) used the grid search (GS) method to improve SVR. The results show that this approach can help improve the SVR technique's performance [45]. Stacking ensemble learning uses two hyperparameter tuning (Particle Swarm Optimization and Genetic Algorithms) while base learners (linear regression, MLP, RF, and Adaboost regressor). Experimental results reveal that the estimation accuracy is higher when hyperparameters are set using PSO [6]. ROME (Rapid Optimizing Methods for Estimation) is a configuration technique that uses sequential model-based optimization (SMO) to identify configuration settings for KNN, SVR, RF, and CART techniques. For both traditional and current tasks, ROME outperforms sophisticated approaches [46]. The accuracy and stability of SVR in SEE were tested to see how a

random search hyperparameter tuning strategy affected them. According to the findings, the SVR set for random search performed similarly to the SVR set for grid search [47].

Based on the findings of previous empirical investigations in the context of SEE. This paper is different from previous research. The RF-based AdaBoost ensemble learning method reinforced by the Bayesian optimization method was used to find the appropriate hyperparameter model. Meanwhile, four ML techniques, such as: classification and regression tree (CART), k-nearest neighbor (k-NN), multilayer perceptron (MLP), and support vector regression (SVR) were used to compare the performance results of the proposed SEE model.

III. EXPERIMENTAL DESIGN

The data sets, ensemble learning, hyperparameter tuning, parameter setting ML, and evaluation measures utilized in this paper are described in depth in this section.

A. Datasets

The most widely used datasets related to the SEE context are the Repositories on PROMISE and ISBSG, among the most popular datasets. In 9 datasets from the public PROMISE repository (also known as SEACRAFT), as well as two sub-datasets from the ISBSG10 and ISBSG18-IFPUG repositories.

Table I lists the data set that was used in paper, including the number of projects, features, and categorical features. This paper uses eleven datasets (china, albrecht, maxwell, nasa93, cocomo81, kitchenham, kemerer, desharnais, and ISBSG10) and the preprocessing rules used in the study by [28][1], and the UCP dataset according to the regulations [48]. Meanwhile, ISBSG18-IFPUG refers to research [44].

B. Data Preprocessing

The Data Preprocessing approach in study was used to improve prediction accuracy in the end. The Data Preprocessing technique is an effective option for effort estimation [50], is a crucial step in improving machine learning performance [51]. According to Famili et al. (1997) the first step by removing features on the dataset that is not relevant. Machine learning algorithms will perform better if irrelevant features are removed [52]. Subsequent processing converts information on categorical data into numeric. Ordinal coding assigns a unique number code to each category [53], the advantage is that the dimensions of the problem space do not increase because each category is displayed as a single input [54]. Handling missing data by using kNNI (K-Nearest Neighbor Imputation). This method proved to be efficient for estimating missing attribute values in various software engineering datasets [55]. In this study, data normalization was used as a scale of values 0 and 1. For all datasets, Mensah et al. (2018) discovered that the normalized Z-score [0,1] generated the best prediction accuracy when compared to box-cox and log transformation [56]. This research will utilize two subsets at random: training (80%) and testing (20%) as a predicted evaluation of the training procedure.

C. Random Forest Algorithm

For regression purposes, the random forest is a set of tree predictors $h(x; \theta_k), k = 1, 2, \dots, K$ where x represents the observed input vector (covariate) of length p with a random vector associated with X and θ_k is independent and identically distributed (iid) random vector. A regression setting where has a numeric result, Y , but makes multiple points of contact with the classification problem (categorical results). The observed (training) data are assumed to be taken independently of the combined distribution (X, Y) and consist of $n(p + 1) - tuples (x_1, y_1), \dots, (x_n, y_n)$.

For regression, the random forest prediction is the unweighted mean of the collection $\bar{h}(x) = (\frac{1}{K}) \sum_{k=1}^K h(x; \theta_k)$. For $k \rightarrow \infty$ the Law of Large Numbers ensures [57].

$$E_{X,Y}(Y - \bar{h}(X))^2 \rightarrow E_{X,Y}(Y - E_{\theta}h(X; \theta))^2 \quad (1)$$

The quantity on the right is the prediction (or generalization) error for a random forest, designated PE_f^* . Convergence in Eq. (1) implies that the random forest is not overfit [57]. Determine the mean prediction error for the individual tree $h(X; \theta)$ as:

$$PE_t^* = E_{\theta}E_{X,Y}(Y - h(X; \theta))^2 \quad (2)$$

Assume that for all θ the tree is unbiased, eg $EY = E_X h(X; \theta)$, then yields:

$$PE_f^* \leq \bar{\rho} PE_t^* \quad (3)$$

Where $\bar{\rho}$ is the weighted correlation between residuals $Y - h(X; \theta)$ and $Y - h(X; \theta')$ for independent θ, θ' .

D. Adaboost Ensemble Learning

AdaBoost is a popular variation of the original Boosting scheme [27]. AdaBoost is a robust ensemble approach for fitting a poor collection of learners to a enhanced data set. The predictions of the weak learner are merged using weighted summation, to reproduce the final prediction [58]. The Adaboost regressor is a high-accuracy ensemble learner that is used to tackle regression issues [59], Adaboost.R2, a modified version of Adaboost.R, is used for regression [27].

TABLE I. THE STUDY'S DATA SET

Dataset	Size [49]	Proj	N	Cat.
China	large	499	17	0
Albrecht	small	24	7	0
Cocomo81	small	63	17	0
Desharnais	medium	81	8	0
IFPUG	large	36	12	11
ISBSG10	large	952	11	6
Kemerer	small	16	6	0
Kitchenham	large	145	4	0
Maxwell	small	62	26	0
Nasa93	small	93	18	16
UCP	small	71	5	0

Given w_1, w_2, \dots, w_N , which is applied to the training set, seeks to improve the training data in each boosting iteration, using different weights. The first update iteration uses the same weights and training data as before. The learner's algorithm is then re-applied to the new weighted data, after each initial weight is updated. If the weights for the training data that were predicted incorrectly in the previous phase are increased, the weights for the training data that were successfully predicted will be reduced. Finally, each weak learner is compelled to concentrate on the sample that the preceding one missed in the sequence [27]. In the following, Adaboost.R2 steps according to the rules [60][61]:

- Set the initial weight (w_i) to the training set.
- As the training set, define the original data's input (x) and target (y) variables.
- Install the regression model (h_t) to the training set with the notation $h_t: x \rightarrow y$.
- Get the predicted training target value: $y_i^{(p)}(x_i)$.
- Use the following equation to find the loss value for the i -th training sample (\mathcal{L}_i).

$$\mathcal{L}_i = \delta \left[\left| y_i^{(p)}(x_i) - y_i \right| \right] \quad (4)$$

Any function that is $\mathcal{L}_i \in [0,1]$, can be used as the loss function (δ). Calculate the average loss ($\bar{\mathcal{L}}$) for v_i using the following formula:

$$\bar{\mathcal{L}} = \sum_{i=1}^N \mathcal{L}_i \frac{w_i}{\sum w_i} \quad (5)$$

When $\bar{\mathcal{L}}$ is smaller than 0.5, an appropriate forecast is produced.

- If $\bar{\mathcal{L}}$ is more than 0.5, the weights should be updated using the equation below.

$$w_i \rightarrow w_i \beta^{[1-\mathcal{L}_i]} \quad (6)$$

$$\beta = \frac{\bar{\mathcal{L}}}{1-\bar{\mathcal{L}}} \quad (7)$$

- To get the required loss function range, repeat steps 4-7.

E. Bayesian with Gaussian Process Optimization of Model Hyperparameters

Bayesian optimization is a useful strategy for locating the by extremes of computationally expensive functions [39]. In this paper, Bayesian optimization is used in this research to discover the maximum value at the sampling point for the unknown function f in model hyperparameter configuration problem [62][63]. The objective function is computationally $f: X \rightarrow \mathbb{R}^+$ over the compact hyperparameter domain X^1 , which aims to minimize f without using gradient information.

Thus, the hyperparameter mapping in Bayesian depends on the objective function. The target value is predicted with the historical result X . A series of steps to find the hyperparameter

as follows: 1) Define the historical model, 2) Find the optimal parameter, 3) Apply the detected hyperparameter to the objective function, 4) Update the model with new result, and 5) 2-4 steps are repeated until the threshold value is reached or the process exceeds the limited time.

Determines a previously small sample of n points $x_i \in X$ uniform at random, and computes the value of the function at those locations $f(x_1), \dots, f(x_n)$. Then, model f using a probabilistic model for the function. We'll take f as a Gaussian process. Because the Gaussian process is so flexible and simple to use, Bayesian optimization uses it to fit the data and update the posterior distribution [37]. For only a finite collection of points x_1, \dots, x_n , posterior delivers a probability distribution over a particular function. The Gaussian process posits that the probabilities $p(f(x_1), \dots, f(x_n))$ form a multivariate Gaussian distribution that is specified by the mean function $\mu(x)$ and the covariance function $\kappa(x_i, x_j)$, where κ is a positive definite kernel function (such as: the squared exponential kernel, the rational quadratic kernel, and the Matern kernel). The posterior predictive mean function $\mu(x)$ and the posterior predictive marginal variance function $\sigma^2(x)$, both specified across the X , domain and calculated in closed form, are obtained by modeling f using the Gaussian process [62].

Then determine the sampling point, x_{n+1} , from X to find the location of the minimum function. Controlled by the optimization proxy of the acquisition function, $u: X \rightarrow \mathbb{R}^+$.

$$x_{n+1} = \arg \max_x u(x) \quad (8)$$

This paper, will use the expected enhancement algorithm which is defined as follows [64]:

$$u_{EI}(x) = E[\max(0, f(x^*) - f(x))] \quad (9)$$

The minimum observation value of f is $f(x^*)$, while $E[\cdot]$ which expresses the expectation of a random variable at $f(x)$. Thus, we receive the same reward as "fixing" $f(x^*) - f(x)$ there is no alternative reward when $f(x)$ is less than $f(x^*)$. The right-hand side of Eq. (9) can be written as given the Gaussian Process predicted mean and variance functions:

$$u_{EI}(x) = (f(x^*) - \mu(x))\Phi(Z) - \phi(Z) \quad (10)$$

Where, ϕ is its derivative, and Φ is the standard normal cumulative distribution function, while $Z = \frac{f(x^*) - \mu(x)}{\sigma(x)}$.

Based on the above analysis, the basic framework of Random Forest and AdaBoost embedded in Bayesian Optimization is formulated in Fig. 1.

F. Parameter Settings ML

Classification And Regression Tree (CART), Multilayer Perceptron (MLP), Support Vector Regression (SVR), K-Nearest Neighbor (KNN), and Random Forest (RF) were employed in the experiment. Table II shows the hyperparameter search space for setting the parameter values of a single approach using Bayesian Optimization.

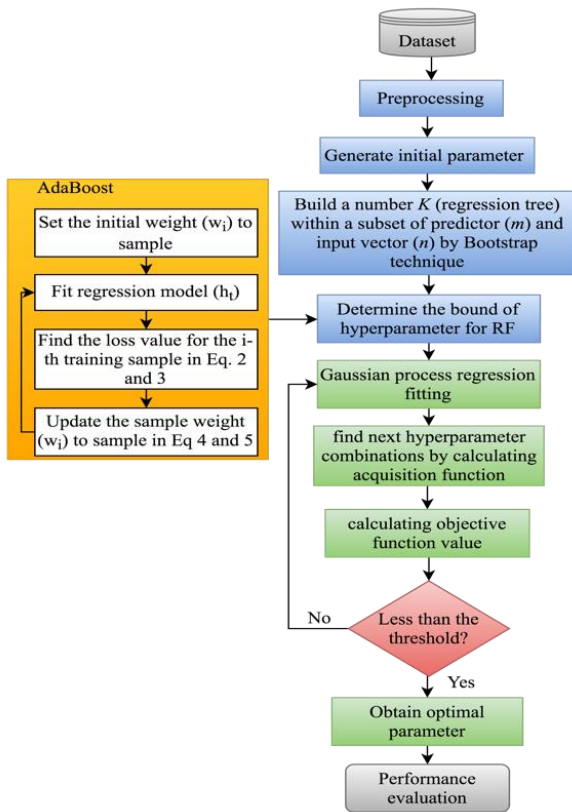


Fig. 1. The Flow Chart of the Proposed RF-Adaboost with Bayesian Optimization.

TABLE II. ML TECHNIQUE PARAMETER VALUES

ML	Parameter Values
CART	criterion: {mse, mae} max_depth: {2, 6, 7, 8} min_samples_split: {10, 20, 40} max_leaf_nodes: {5, 20, 100} min_samples_leaf: {20, 40, 100} max_features: {auto, log2, sqrt, None}
MLP	hidden_layer_sizes: {(50,50), (100,50)} solver: {adam, sgd} activation: {'relu', 'tanh'} learning_rate: {constant, adaptive} alpha: {0.0001, 0.05}
SVR	kernel: {sigmoid, poly, rbf} degree: {3, 4, 5, 6, 7, 8, 9} kernel parameter: {0.0001, 0.001, 0.01, 0.1} learning rate: {0.01, 0.02, 0.03, 0.04, 0.05} deviation tolerated: {0.001, 0.01, 0.1}
k-NN	K: {1, 2, 3, 4, 5, 6} weights: {uniform, distance}
RF	number of trees: 125 criterion: {mse, mae} n_estimators: {10, 20, 30, 50, 100} min sample leaf: {3, 4, 5, 6, 7} min samples split: {3, 5, 7, 9} max_features: {1, 13} max_depth: {5, 15, 20, 30, 50} max depth of the tree: {100, 200, 300}

G. Cross-Validation

The cross-validation methodology is a widely known method for revealing the model's true performance, and it is highly recommended by researchers [58]. For the PROMISE and ISBSG R10/R18-IFPUG datasets, will apply ten times 3-fold cross-validation. This paper divided the data into three folds or groups at random. The test set is chosen, and the remaining two folds are joined to form the train set. For each schema, the model is based on a train set (a combination of machine learning algorithms, ensemble learning, and hyperparameter tuners). Within this framework, AdaBoost functions as a meta-regressor for ensemble and Bayesian optimization to provide automatic tuning that functions as an appropriate hyperparameter model optimization objective. Sub-partitioning is done via 3-fold cross-validation because the tuner does not have access to the test set. The model is retained on the entire set with these parameters once the optimal hyperparameter values have been identified. Finally, an assessment matrix will be used to assess the model. The flowchart of the framework in the proposed regression scheme based on AdaBoost and bayesian hyperparameter tuning is summarized in Fig. 2.

H. Evaluation Metrics

Mean absolute error (MAE), root mean square error (RMSE), and R-squared (R^2) are the metrics that are used in the evaluation. If the MAE and RMSE are low, and the R^2 is high, the model is better.

$$MAE = \frac{1}{m} \sum_{i=1}^m |X_i - Y_i| \tag{11}$$

$$RMSE = \sqrt{\frac{1}{m} \sum_{i=1}^m (X_i - Y_i)^2} \tag{12}$$

$$R^2 = 1 - \frac{\sum_{i=1}^m (X_i - Y_i)^2}{\sum_{i=1}^m (\bar{Y} - Y_i)^2} \tag{13}$$

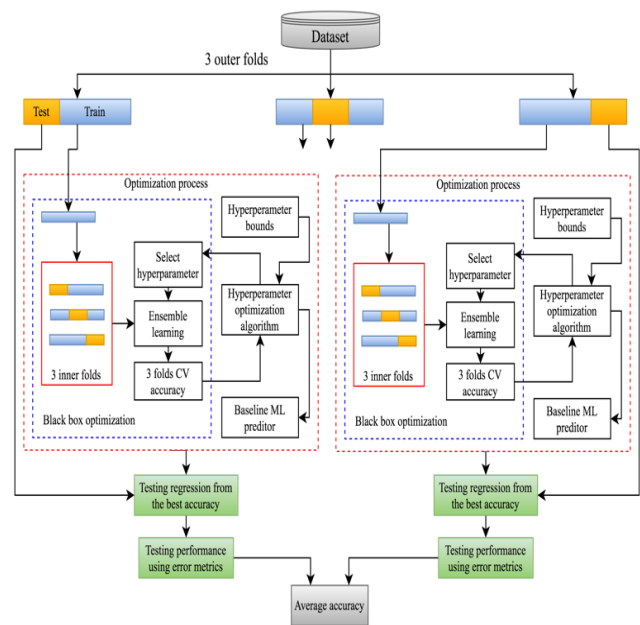


Fig. 2. Procedure Training and Testing Scheme.

IV. RESULT AND DISCUSSION

This section will address the issues raised in section 1 by conducting three sets of experiments to determine the accuracy of the SEE: 1) without hyperparameters tuning (default), 2) hyperparameters tuning, and 3) SEE model using Adaboost ensemble learning with Bayesian hyperparameters.

In this paper describe the experiments in depth and offer the findings of each experiment in this section. All of the tests were run in a Python environment. In this study, eleven software engineering repository data sets with various dimensions and attributes were employed. Table I lists the dataset's details, including the number of samples, characteristics, and target value. In the first step, carried out the data preprocessing stage, which was used to overcome missing data by Missing Data Treatment (MDT) using k-NNI and converting categorical data into numeric using the ordinal encoder. In the next step, will normalize the data with a scale of 0 and 1. The data has been converted to a format where powerful machine learning algorithms may be deployed to create accurate predictions in the SEE context using various data preprocessing approaches.

A. Model with Default Parameter Tuning

After passing through the data preprocessing stage, the next step will be to compare 5 ML methods (namely, CART, MLP, SVR, KNN, and RF) without setting the hyperparameters using the default parameters tuning. The purpose of the ML algorithm comparisons is to assess which algorithm is more likely to have the best performance without tuning in to different problems. The default settings in the training data are used to train the machine learning technique. More exact findings are obtained by using the ML approach with the lowest MAE and RMSE. When it comes to the R^2 value, the greater the number, the better the accuracy. For the performance of the ML method, which considers the values of MAE, RMSE, and R^2 . Where the best value is marked in bold, otherwise the worst value is marked in italics.

Tables III to V list the best possible performance values for each model and dataset, as well as the tuner who achieved them (without tuning where the parameters are set randomly within the range). Each model's performance changes depending on the dataset. For the PROMISE and ISBSG datasets, the dataset used with small/medium/large effect sizes [49]; in the first experimental stage, the default settings for the base learners model will yield the most accurate predictions. Based on the experimental results in this paper, it can be seen that RF almost usually outperforms other methods. In particular, when measured in MAE (Table III), RF achieved the best average rating, CART performed second, followed by k-NN and SVR with a slightly worse average rating, and MLP performed the worst among all related methods. Nonetheless, no significant differences could be found concerning the three methods: k-NN, MLP, and SVR. RF has advantages over other methods in most datasets with medium/large effect sizes but performs worse than CART, k-NN, and SVR in many datasets with small effect sizes. In terms of RMSE (Table IV) and R^2 (Table V), the results are almost similar to the MAE values.

TABLE III. COMPARISON MAE USING DEFAULT PARAMETER TUNING

Dataset	MAE				
	CART	KNN	MLP	SVR	RF
Albrecht	0.0534	0.1016	0.0888	<i>0.1694</i>	0.1217
China	0.0178	0.0244	0.0284	<i>0.0567</i>	0.0115
Cocomo81	0.0934	0.0466	<i>0.0949</i>	0.1230	0.0681
Desharnais	0.0228	0.0594	<i>0.0678</i>	0.0522	0.0161
IFPUG	0.2557	0.1591	0.1853	<i>0.1923</i>	0.1698
ISBSG10	0.0174	0.0268	0.0228	<i>0.0568</i>	0.0132
Kemerer	0.1167	0.2732	0.2442	<i>0.3319</i>	0.2326
Kitchenham	0.0065	0.0068	0.0074	<i>0.0823</i>	0.0044
Maxwell	0.0667	0.0718	0.0638	<i>0.0982</i>	0.0544
Nasa93	0.0433	0.0492	0.0451	<i>0.0945</i>	0.0213
UCP	0.1146	0.1367	<i>0.2307</i>	0.0960	0.1012

TABLE IV. COMPARISON RMSE USING DEFAULT PARAMETER TUNING

Dataset	RMSE				
	CART	KNN	MLP	SVR	RF
Albrecht	0.0776	0.1538	0.1238	<i>0.2379</i>	0.1702
China	0.0479	0.0479	0.0567	<i>0.0730</i>	0.0400
Cocomo81	<i>0.1911</i>	0.0745	0.1139	0.1528	0.1396
Desharnais	0.0321	0.0656	<i>0.0861</i>	0.0654	0.0248
IFPUG	<i>0.3762</i>	0.2290	0.2379	0.2382	0.2271
ISBSG10	0.0387	0.0455	0.0309	<i>0.0624</i>	0.0280
Kemerer	0.1964	0.2934	0.2680	<i>0.3673</i>	0.2674
Kitchenham	0.0129	0.0156	0.0150	<i>0.0831</i>	0.0098
Maxwell	0.1049	0.0982	0.0855	<i>0.1120</i>	0.0959
Nasa93	0.1102	<i>0.1223</i>	0.0717	0.1179	0.0457
UCP	0.2655	0.1801	<i>0.2932</i>	0.1206	0.1961

TABLE V. COMPARISON R^2 USING DEFAULT PARAMETER TUNING

Dataset	R^2				
	CART	KNN	MLP	SVR	RF
Albrecht	0.9524	0.8135	0.8791	<i>0.5536</i>	0.7714
China	0.7954	0.7956	0.7131	<i>0.5246</i>	0.8570
Cocomo81	<i>-0.6659</i>	0.7467	0.4075	-0.0650	0.1108
Desharnais	0.9284	0.7014	<i>0.4870</i>	0.7032	0.9572
IFPUG	<i>-2.7883</i>	-0.4036	-0.5145	-0.5186	-0.3807
ISBSG10	0.6840	0.5636	0.7984	<i>0.1795</i>	0.8344
Kemerer	0.8173	0.5926	0.6599	<i>0.3614</i>	0.6616
Kitchenham	0.7354	0.6119	0.6429	<i>-9.8874</i>	0.8474
Maxwell	0.5269	0.5848	0.6853	<i>0.4590</i>	0.6043
Nasa93	0.2071	<i>0.0227</i>	0.6643	0.0928	0.8635
UCP	0.3484	0.7003	0.2054	0.8656	0.6445

Based on the study results in the table, it shows that the algorithm with the best performance in almost all datasets is RF. RF obtained the highest accuracy in china, desharnais, IFPUG, ISBSG10, kitchenham, Maxwell, and Nasa93. With the best accuracy value in the kitchenham dataset with MAE (0.0044), RMSE (0.0098), and R^2 (0.8474), although Desharnais owns the best R^2 value. Furthermore, the second position is obtained by CART, which has the best accuracy value on albrecht and kemerer. Meanwhile, KNN, MLP, and SVR have almost similar performance.

The lack of parameter adjustment in this situation can result in worst performance of CART, KNN, MLP, and SVR. This is due to SVR's ability to perform effectively with limited data sets. However, it is unsuccessful in dealing with outliers in training data, which is a common occurrence in real-world applications. As a result, some outliers cause regression to be poor. Meanwhile, MLP, with a small data set without any appropriate parameter tuning, can reduce the number of hidden nodes which causes a decrease in its approximation ability [65]. KNN is extremely sensitive to characteristics that are irrelevant or redundant. Because it is unclear which sort of distance and which attribute are employed in distance-based learning KNN to give the best results, and because must calculate the distance of each query instance to all training samples, the computational cost is relatively large [66]. CART performs badly on smaller data sets compared to bigger data sets. As a result, using this CART approach without considering the data's magnitude is not recommended [67].

B. Comparison Model with Hyperparameter Tuning and Ensemble Learning

Next, this model will use hyperparameter tuning based on the Bayesian-based Gaussian process. The ML method is trained with hyperparameter tuning on the training data in the training process. All tuners are used as an optimization method combined with a cross-validation procedure. Configure using cross-validation (i.e. cv: 3), verbose: 3, scoring: 'mean_squared_error', and 10 iterations. Because the datasets in this scenario are small, will narrow the search space to the most promising values based on previous research.

Next, the same experiment was repeated using Adaboost ensemble learning. With repeat the experiment to find the best convergence with 10 iterations. Configure the Adaboost ensemble learning using the maximum number of estimators at which the algorithm is terminated (n_estimator: 200), learning_rate: 1, and random_state: 0. After that, will compare the algorithms have done, aiming to assess which algorithm is more likely to be efficient and how this efficiency varies by hyperparameters tuning and reinforcement using ensemble learning on different problems. Fig. 3 shows the performance of Bayesian hyperparameter and Adaboost ensemble learning on the ML model concerning the error function based on MAE, RMSE, and R^2 .

The performance of each model varies depending on the dataset. Base learners model with parameter tuning using

Bayesian which produces the most accurate predictions. In Fig. 3, it shows that the algorithm that has the best performance in almost all datasets is RF. RF achieved the highest accuracy in cocomo81, ISBSG10, kitchenham, maxwell, nasa93, and UCP. Meanwhile, CART, KNN, MLP, and SVR have almost similar performance. These results show that CART, KNN, MLP, and SVR are not very sensitive to parameters tuning, while RF is very sensitive to parameters tuning which results in stable prediction performance. This suggests that the best parameters to use with a machine learning approach may change over time.

As for the base learner model with Adaboost ensemble learning, it shows different results. Where the algorithm that has the best performance is CART, followed by RF as the second algorithm that has the best performance. While KNN, MLP, and SVR have almost similar performance. For CART, obtain the highest accuracy in albrecht, china, cocomo81, ISBSG10, IFPUG, kemerer, and UCP. This analysis of different optimization approaches reveals that the Adaboost ensemble learning optimization is the clear victor, as it can create a model with the highest test accuracy for eleven data sets. To summarize, the meta-parameter analysis for Adaboost, which was used to strengthen the basic CART model, significantly outperforms other models (on this dataset).

C. The Best Model using Adaboost with Bayesian Hyperparameter Optimization

The same experiment used the ML algorithm to set the Adaboost Ensemble learning parameters using Bayesian hyperparameter optimization. In this paper, will repeated the experiment to find the best convergence with iterations from 10 to 200. The effect of the ML model on setting the Bayesian hyperparameter values of the Adaboost ensemble model is presented in Table VI to VIII.

In particular, when measured in MAE, RMSE, and R^2 (Table VI to VIII), RF and SVR achieve the best average ratings, followed by MLP, and CART, while k-NN with slightly worse average ratings among all related methods. In this respect, RF, SVR, and MLP have advantages over other methods in most datasets with medium/large effect sizes but perform worse than CART and k-NN in many datasets with small effect sizes. CART and k-NN perform best on data sets with small effect sizes. No significant differences could be found among the three methods RF, SVR, and MLP had similar overall performance and were superior to CART and k-NN with medium/large effect sizes depending on the data set. Nonetheless, the RF method is more consistent among the best methods regardless of the metric.

This experiment shows that overall, the five machine learning models that are strengthened by the Bayesian gaussian process and Adaboost ensemble learning have almost the same performance in all datasets used. However, it can be determined that RF, SVR, and MLP have the best results in this area.



(a) Baseline ML with Bayesian gaussian Process (MAE, RMSE, and R^2). (b) Baseline ML with Adaboost ensemble learning (MAE, RMSE, and R^2).

Fig. 3. Comparison Algorithm: (a) Baseline ML with Bayesian Gaussian Process; (b) Baseline ML with Adaboost Ensemble Learning.

TABLE VI. COMPARISON MAE USING BAYESIAN HYPERPARAMETER TUNING WITH ADABOOST ENSEMBLE LEARNING

Dataset	MAE (Bayesian optimization-Adaboost ensemble learning)				
	CART	KNN	MLP	SVR	RF
Albrecht	0.1463	<u>0.1888</u>	0.1694	0.0490	0.1070
China	0.0396	0.0436	<u>0.0528</u>	0.0243	0.0359
Cocomo81	0.0557	0.1462	0.1563	<u>0.1603</u>	0.1600
Desharnais	0.0166	<u>0.0482</u>	0.0277	0.0081	0.0210
IFPUG	0.2431	0.1849	0.1771	<u>0.2713</u>	0.1842
ISBSG10	0.0326	0.0452	<u>0.0476</u>	0.0436	0.0241
Kemerer	<u>0.4681</u>	0.2340	0.2317	0.3388	0.3521
Kitchenham	0.0079	0.0130	<u>0.0663</u>	0.0195	0.0068
Maxwell	0.1114	0.0753	0.0909	0.0924	<u>0.1431</u>
Nasa93	0.0653	0.1101	0.0729	<u>0.8203</u>	0.0456
UCP	0.1131	0.1612	<u>0.1969</u>	0.1460	0.1574

TABLE VII. COMPARISON RMSE USING BAYESIAN HYPERPARAMETER TUNING WITH ADABOOST ENSEMBLE LEARNING

Dataset	RMSE (Bayesian optimization-Adaboost ensemble learning)				
	CART	KNN	MLP	SVR	RF
Albrecht	0.1463	<u>0.1888</u>	0.1694	0.0490	0.1070
China	0.0396	0.0436	<u>0.0528</u>	0.0243	0.0359
Cocomo81	0.0557	0.1462	0.1563	<u>0.1603</u>	0.1600
Desharnais	0.0166	<u>0.0482</u>	0.0277	0.0081	0.0210
IFPUG	0.2431	0.1849	0.1771	<u>0.2713</u>	0.1842
ISBSG10	0.0326	0.0452	<u>0.0476</u>	0.0436	0.0241
Kemerer	<u>0.4681</u>	0.2340	0.2317	0.3388	0.3521
Kitchenham	0.0079	0.0130	<u>0.0663</u>	0.0195	0.0068
Maxwell	0.1114	0.0753	0.0909	0.0924	<u>0.1431</u>
Nasa93	0.0653	0.1101	0.0729	<u>0.8203</u>	0.0456
UCP	0.1131	0.1612	<u>0.1969</u>	0.1460	0.1574

TABLE VIII. COMPARISON R² USING BAYESIAN HYPERPARAMETER TUNING WITH ADABOOST ENSEMBLE LEARNING

Dataset	R ² (Bayesian optimization-Adaboost ensemble learning)				
	CART	KNN	MLP	SVR	RF
Albrecht	0.8311	<u>0.7190</u>	0.7737	0.9810	0.9096
China	0.8602	0.8301	<u>0.7517</u>	0.9473	0.8847
Cocomo81	0.8582	0.0247	-0.1146	<u>-0.1723</u>	-0.1677
Desharnais	0.9807	<u>0.8386</u>	0.9468	0.9954	0.9693
IFPUG	-0.5819	0.0844	0.1600	<u>-0.9702</u>	0.0913
ISBSG10	0.7758	0.5687	<u>0.5220</u>	0.5987	0.8772
Kemerer	<u>-0.0370</u>	0.7408	0.7458	0.4566	0.4133
Kitchenham	0.9006	0.7320	<u>-5.9438</u>	0.3952	0.9264
Maxwell	0.4667	0.7561	0.6448	0.6329	<u>0.1194</u>
Nasa93	0.7216	0.2077	0.6527	<u>-42.901</u>	0.8639
UCP	0.8818	0.7597	<u>0.6418</u>	0.8030	0.7710

V. CONCLUSION

An enhanced hyperparameter tuning approach on an ensemble learning algorithm will be evaluated for its impact on model accuracy and stability in this study. The parameters of five machine learning models trained on eight datasets from the PROMISE repository and two subsets of data from the ISBSG R10/R18-IFPUG dataset are adjusted using this tuner. This study applies a state-of-the-art method by combining Bayesian-based gaussian processes with Adaboost ensemble learning to improve ML performance in a SEE context. Tuning, training, evaluation, and cross-validation will all be used in this project. The findings of this study show that optimizing machine learning models can considerably improve their performance. The implementation of AdaBoost ensemble learning and Bayesian hyperparameter optimization can improve the performance of the RF method. RF outperformed other methods in almost all datasets. As such, AdaBoost ensemble learning is the optimization that impacts machine learning model performance across all data sets in

this scenario. On the other hand, the Bayesian optimization approach based on the Gaussian process to improve the performance of machine learning prediction models can achieve high accuracy in some cases.

More empirical research could be conducted in the future to support the conclusions of this study and to acquire knowledge utilizing different data sets. Additionally, compared or investigated various different optimization strategies, particularly for classification issues. It's also crucial to test the efficacy of various feature selection approaches, as well as increase with optimization tuning, when estimating software effort.

REFERENCES

- [1] L. Song, L. L. Minku, and X. Yao, "A novel automated approach for software effort estimation based on data augmentation," ACM on Eur. Soft. Eng. Conf. and Symp. on the Found. of Soft. Eng., pp. 468–479, November 2018.
- [2] S. S. Gautam and V. Singh, "The state-of-the-art in software development effort estimation," J. of Software: Evolution and Process, Vol. 30, No. 12, May 2018.
- [3] M. Usman, K. Petersen, J. Börstler, and P. Santos Neto, "Developing and using checklists to improve software effort estimation: A multi-case study," J. of Systems and Software, Vol. 146, pp. 286–309, September 2018.
- [4] S. Ezghari and A. Zahi, "Uncertainty management in Software effort estimation using a consistent fuzzy analogy-based method," J. of Appl. Soft. Comp., Vol. 67, pp. 540–557, 2018.
- [5] M. Azzeh, "Software Effort Estimation Based on Optimized Model Tree," PROMISE, 2011.
- [6] S. K. Palaniswamy and R. Venkatesan, "Hyperparameters tuning of ensemble model for software effort estimation," J. of Amb. Intell. and Human. Comp., No. 0123456789, 2020.
- [7] P. Pospieszny, B. Czarnacka-Chrobot, and A. Kobylinski, "An effective approach for software project effort and duration estimation with machine learning algorithms," J. of Systems and Software, Vol. 137, No. January, pp. 184–196, 2018.
- [8] R. Alizadehsani et al., "Handling of uncertainty in medical data using machine learning and probability theory techniques: a review of 30 years (1991–2020)," Springer US, 2021.
- [9] J. Novaković, P. Strbac, and D. Bulatović, "Toward optimal feature selection using ranking methods and classification algorithms," J. of Op. Res., Vol. 21, No. 1, pp. 119–135, 2011.
- [10] Y. Mahmood, N. Kama, A. Azmi, A. S. Khan, and M. Ali, "Software effort estimation accuracy prediction of machine learning techniques: A systematic performance evaluation," J. of Soft. Pract. and Exp., 2021.
- [11] S. K. Palaniswamy and R. Venkatesan, "Hyperparameters tuning of ensemble model for software effort estimation," J. of Amb. Intell. and Human. Comp., Vol. 12, No. 6, pp. 6579–6589, 2021.
- [12] H. Zhao, X. Chen, T. Nguyen, J. Z. Huang, G. Williams, and H. Chen, "Stratified over-sampling bagging method for random forests on imbalanced data," Springer Int. Pub. Switzerland, Vol. 9650, pp. 63–72, 2016.
- [13] G. W. Cha, H. J. Moon, and Y. C. Kim, "Comparison of random forest and gradient boosting machine models for predicting demolition waste based on small datasets and categorical variables," Int. J. of Env. Res. and Pub. Heal. MDPI, Vol. 18, No. 16, 2021.
- [14] X. Ren et al., "A Dynamic Boosted Ensemble Learning Method Based on Random Forest," arXiv preprint, 2018.
- [15] Z. Abdelali, H. Mustapha, and N. Abdelwahed, "Investigating the use of random forest in software effort estimation," Procedia Computer Science, Vol. 148, pp. 343–352, 2019.
- [16] A. Zakrani, M. Hain, and A. Namir, "Software development effort estimation using random forests: An empirical study and evaluation," Int. J. of Int. Eng. and Sys., Vol. 11, No. 6, pp. 300–311, 2018.

- [17] S. M. Satapathy, B. P. Acharya, and S. K. Rath, "Early stage software effort estimation using random forest technique based on use case points," *IET Software*, Vol. 10, No. 1, pp. 10–17, 2016.
- [18] W. Zhang, C. Wu, H. Zhong, Y. Li, and L. Wang, "Prediction of undrained shear strength using extreme gradient boosting and random forest based on Bayesian optimization," *Geo. Front.*, Vol. 12, No. 1, pp. 469–477, 2021.
- [19] S. Lessmann, B. Baesens, H. V. Seow, and L. C. Thomas, "Benchmarking state-of-the-art classification algorithms for credit scoring: An update of research," *Eur. J. of Oper. Res.*, Vol. 247, No. 1, pp. 124–136, 2015.
- [20] E. Kocaguneli, T. Menzies, and J. W. Keung, "On the value of ensemble effort estimation," *IEEE Trans. on Soft. Eng.*, Vol. 38, No. 6, pp. 1403–1416, 2012.
- [21] M. Fernández-Delgado, E. Cernadas, S. Barro, and D. Amorim, "Do we need hundreds of classifiers to solve real world classification problems?," *J. of Mach. Learn. Res.*, Vol. 15, pp. 3133–3181, 2014.
- [22] S. Shukla, S. Kumar, and P. R. Bal, "Analyzing effect of ensemble models on multi-layer perceptron network for software effort estimation," *IEEE World Cong. on Serv.*, Vol. 2642–939X, pp. 386–387, 2019.
- [23] Y. Ren, L. Zhang, and P. N. Suganthan, "Ensemble Classification and Regression – Recent Developments, Applications and Future Direction," *IEEE Comput. Intell. Mag.*, Vol. 11, No. 1, pp. 41–53, 2016.
- [24] F. Pedregosa et al., "Scikit-learn: Machine Learning in Python," *J. of Mach. Learn. Res.*, Vol. 12, pp. 2825–2830, 2011.
- [25] P. Phannachitta and K. Matsumoto, "Model-based software effort estimation - A robust comparison of 14 algorithms widely used in the data science community," *Int. J. of Inn. Comp.*, Vol. 15, No. 2, pp. 569–589, 2019.
- [26] I. Martin-Diaz, D. Morinigo-Sotelo, O. Duque-Perez, and R. J. De Romero-Troncoso, "Early Fault Detection in Induction Motors Using AdaBoost with Imbalanced Small Data and Optimized Sampling," *IEEE Trans. on Ind. App.*, Vol. 53, No. 3, pp. 3066–3075, 2017.
- [27] R. E. Schapire, Y. Freund, P. Bartlett, and W. S. Lee, "Boosting the margin: A new explanation for the effectiveness of voting methods," *Annals of Statistics*, Vol. 26, No. 5, pp. 1651–1686, 1998.
- [28] T. Xia, R. Krishna, J. Chen, G. Mathew, X. Shen, and T. Menzies, "Hyperparameter Optimization for Effort Estimation," *arXiv preprint*, Vol. 4, 2018.
- [29] M. Hosni, A. Idri, A. Abran, and A. B. Nassif, "On the value of parameter tuning in heterogeneous ensembles effort estimation," *J. of Soft Comp.*, pp. 1–34, 2017.
- [30] A. Kumar, B. D. . Patro, and B. K. Singh, "Parameter Tuning for Software Effort Estimation Using Particle Swarm Optimization Algorithm," *Int. J. of App. Eng. Res.*, Vol. 14, No. 2, pp. 139–144, 2019.
- [31] P. Phannachitta, "On an Optimal Analogy-based Software Effort Estimation," *Inf. and Soft. Tech.*, Vol. 125, No. June 2019, p. 106330, 2020.
- [32] L. Song, L. L. Minku, and X. Yao, "The impact of parameter tuning on software effort estimation using learning machines," *ACM Int. Conf. Proc. Ser.*, Vol. Part F1288, 2013.
- [33] A. Arcuri and G. Fraser, "Parameter tuning or default values? An empirical investigation in search-based software engineering," *Int. Sym. on Sear. Bas. Soft. Eng.*, pp. 33–47, 2011.
- [34] M. M. Ozturk, "The impact of parameter optimization of ensemble learning on defect prediction," *Comp. Sci. J. of Mol.*, Vol. 27, No. 1, pp. 85–128, 2019.
- [35] L. L. Minku and X. Yao, "An analysis of multi-objective evolutionary algorithms for training ensemble models based on different performance measures in software effort estimation," *ACM Int. Conf. Proc. Ser.*, Vol. Part F1288, 2013.
- [36] R. Shu, T. Xia, J. Chen, L. Williams, and T. Menzies, "Improved Recognition of Security Bugs via Dual Hyperparameter Optimization," *arXiv*, 2019.
- [37] J. Wu, X. Y. Chen, H. Zhang, L. D. Xiong, H. Lei, and S. H. Deng, "Hyperparameter optimization for machine learning models based on Bayesian optimization," *J. of Elect. Sci. and Tech.*, Vol. 17, No. 1, pp. 26–40, 2019.
- [38] J. Bergstra, R. Bardenet, Y. Bengio, and B. Kégl, "Algorithms for hyper-parameter optimization," *Ann. Conf. on Neu. Inf. Proc. Sys.*, pp. 1–9, 2011.
- [39] E. Brochu, V. M. Cora, and N. de Freitas, "A Tutorial on Bayesian Optimization of Expensive Cost Functions, with Application to Active User Modeling and Hierarchical Reinforcement Learning," *arXiv preprint*, 2010.
- [40] J. C. Lévesque, C. Gagné, and R. Sabourin, "Bayesian hyperparameter optimization for ensemble learning," *Conf. on Uncer. in Art. Intell., UAI 2016*, pp. 437–446, 2016.
- [41] L. L. Minku and X. Yao, "A Principled Evaluation of Ensembles of Learning Machines for Software Effort Estimation Categories and Subject Descriptors," *Proc. of Int. Conf. on Pred. Mod. in Soft. Eng.*, Banff Alberta, Canada, 2011.
- [42] A. Corazza, S. Di Martino, F. Ferrucci, C. Gravino, F. Sarro, and E. Mendes, "Using tabu search to configure support vector regression for effort estimation," *Emp. Soft. Eng.*, Vol. 18, No. 3, pp. 506–546, 2013.
- [43] M. O. Elish, "Assessment of voting ensemble for estimating software development effort," *Proc. of the IEEE Sym. on Comp. Intell. and Dat. Min.*, SSCI 2013, pp. 316–321, 2013.
- [44] L. Villalobos-Arias and C. Quesada-López, "Comparative study of random search hyper-parameter tuning for software effort estimation," *Ass. for Comp. Mach.*, Vol. 1, No. 1, 2021.
- [45] A. Zakrani, A. Najm, and A. Marzak, "Support Vector Regression Based on Grid-Search Method for Agile Software Effort Prediction," *Coll. in Inf. Sci. and Tech.*, Vol. 2018-October, pp. 492–497, 2018.
- [46] T. Xia, R. Shu, X. Shen, and T. Menzies, "Sequential Model Optimization for Software Effort Estimation," *IEEE Trans. on Soft. Eng.*, Vol. 5589, No. c, pp. 1–16, 2020.
- [47] L. Villalobos-Arias, C. Quesada-López, J. Guevara-Coto, A. Martínez, and M. Jenkins, "Evaluating hyper-parameter tuning using random search in support vector machines for software effort estimation," *ACM Int. Conf. on Pred. Mod. and Dat. Analy. in Soft. Eng.*, pp. 31–40, 2020.
- [48] M. Azzeh, A. B. Nassif, and S. Banitaan, "Comparative analysis of soft computing techniques for predicting software effort based use case points," *IET Software*, Vol. 12, No. 1, pp. 19–29, 2018.
- [49] L. Song, L. L. Minku, and Y. A. O. Xin, "Software effort interval prediction via Bayesian inference and synthetic bootstrap resampling," *ACM Trans. on Soft. Eng. and Meth.*, Vol. 28, No. 1, 2019.
- [50] J. Huang, Y. F. Li, J. W. Keung, Y. T. Yu, and W. K. Chan, "An empirical analysis of three-stage data-preprocessing for analogy-based software effort estimation on the ISBSG data," *Proc. of Int. Conf. on Soft. Qual. Relia. and Sec.*, Prague, Czech Republic, pp. 442–449, 2017.
- [51] J. Huang, Y. Li, and M. Xie, "An empirical analysis of data preprocessing for machine learning-based software cost estimation," *J. of Inf. and Soft. Tech.*, Vol. 67, pp. 108–127, 2015.
- [52] A. Famili, W. M. Shen, R. Weber, and E. Simoudis, "Data preprocessing and intelligent data analysis," *Intell. Dat. Analy.*, Vol. 1, No. 1, pp. 3–23, 1997.
- [53] S. Viaeane, G. Dedene, and R. A. Derrig, "Auto claim fraud detection using Bayesian learning neural networks," *J. of Exp. Sys. with App.*, Vol. 29, No. 3, pp. 653–666, 2005.
- [54] E. Fitkov-Norris, S. Vahid, and C. Hand, "Evaluating the Impact of Categorical Data Encoding and Scaling on Neural Network Classification Performance: The Case of Repeat Consumption of Identical Cultural Goods," *J. of Comm. in Comp. and Inf. Sci.*, Vol. 311, pp. 343–0352, 2012.
- [55] I. Abnane, M. Hosni, A. Idri, and A. Abran, "Analogy Software Effort Estimation Using Ensemble KNN Imputation," *Proc. of Int. Conf. On Soft. Eng. and Adv. App.*, Kallithea, Greece, pp. 228–235, 2019.
- [56] S. Mensah, J. Keung, S. G. MacDonell, M. F. Bosu, and K. E. Bennin, "Investigating the Significance of the Bellwether Effect to Improve Software Effort Prediction: Further Empirical Study," *IEEE Trans. on Relia.* Vol. 67, No. 3, pp. 1176–1198, 2018.

- [57] M. R. Segal, "Machine Learning Benchmarks and Random Forest Regression," *Biostatistics*, pp. 1–14, 2004.
- [58] Z. Zhang, J. T. Kwok, and D. Y. Yeung, "Parametric distance metric learning with label information," *IJCAI Inte. Joint Conf. on Art. Intell.*, pp. 1450–1452, 2003.
- [59] R. Polikar, "Ensemble based systems in decision making," *IEEE Cir. and Sys. Mag.*, Vol. 6, No. 3, pp. 21–44, 2006.
- [60] A. Sharafati, S. B. H. S. Asadollah, and M. Hosseinzadeh, "The potential of new ensemble machine learning models for effluent quality parameters prediction and related uncertainty," *Proc. Saf. and Env. Prot.*, Vol. 140, pp. 68–78, 2020.
- [61] D. L. Shrestha and D. P. Solomatine, "Experiments with AdaBoost.RT, an improved boosting scheme for regression," *Neu. Comput.*, Vol. 18, No. 7, pp. 1678–1710, 2006.
- [62] M. T. Young, J. Hinkle, A. Ramanathan, and R. Kannan, "HyperSpace: Distributed Bayesian Hyperparameter Optimization," *Proc. Int. Sym. on Comp. Arch. and Hig. Perfor. Comput., SBAC-PAD 2018*, No. 1, pp. 339–347, 2019.
- [63] J. Snoek, H. Larochelle, and R. P. Adams, "Practical Bayesian Optimization of Machine Learning Algorithms," *Adv. in Neu. Inf. Proc. Sys.*, 2012.
- [64] M. Feurer and F. Hutter, "Hyperparameter Optimization," *Auto. Mach. Lear.*, The Springer Series, pp. 3–34, 2019.
- [65] R. Marco, S. S. S. Ahmad, and S. Ahmad, "Empirical Analysis of Software Effort Preprocessing Techniques Based on Machine Learning," *Int. J. of Intell. Eng. and Sys.*, Vol. 14, No. 6, pp. 554–567, 2021.
- [66] S. B. Imandoust and M. Bolandraftar, "Application of K-Nearest Neighbor (KNN) Approach for Predicting Economic Events: Theoretical Background," *Int. J. of Eng. Res. and App.*, Vol. 3, No. 5, pp. 605–610, 2013.
- [67] E. Kocaguneli, T. Menzies, J. Hihn, and B. H. Kang, "Size doesn't matter? On the value of software size features for effort estimation," *Proc. of Int. Conf. On Pred. Mod. in Soft. Eng.*, Lund, Sweden, pp. 89–98, 2012.

A Robust Reversible Data Hiding Framework for Video Steganography Applications

Manjunath Kamath K¹

Assistant Professor
Dept. of Computer Science and Engineering
Canara Engineering College
Benjanapadavu, India

Dr. R. Sanjeev Kunte²

Professor
Dept. of Information Science and Engineering
J.N.N College of Engineering
Shivamogga, India

Abstract—Reversible Data Hiding (RDH) is a special form of data hiding approach for data integrity and confidentiality protection where the secret image bits (SI) are embedded into Cover Media (CM) by altering its intrinsic pixel attributes. However, in RDH the CM along with the secret message is recovered at the end of computing phase. However, despite of its potential use-cases for enhancing the embedding performance, when it comes to security for various network standards, the traditional RDH mechanisms cannot fully comply with the standards for different set of attacks during the bit-stream transmission scenarios. Therefore, the proposed study contributes towards a computational framework of a robust RDH framework for Video Steganography (VS) which is modeled and simulated under various attack effects and the observation outcome are produced in before and after attack situations to justify the improvement over Embedding Capacity (EC) and Peak Signal-to-Noise Ratio (PSNR) performance for both CM and secret message unlike traditional difference expansion-based methods (DE). The outcome of the study shows that the formulated RDH method not only achieves better reversibility at lower cost of computing but also ensures effective PSNR and imperceptibility outcome for both CM and secret image.

Keywords—Reversible data hiding; data integrity; embedding capacity; video steganography

I. INTRODUCTION

The underlying principle of Data Hiding (DH) has been extensively explored and the scope of evolution in research advancement for practical solutions still being nurtured. The prime agenda of this area is to provide better level of security solutions in communication scenarios for various network applications [1][2]. This area has got wide range of applications starting from civil, military to critical healthcare domains. However, DH has come as a substitution for the traditional data security mechanisms of crypto-graphic solutions where the prime challenge persists in dealing with bit-stream pattern vulnerability for textual and image data in transit [3]-[8]. In conventional approaches of DH, the secret message is embedded into a Cover Media (CM) as a hidden data so that the privacy of the data can be protected while in wireless transmission and this approach has been found as a promising security measure as the bit stream patterns are not easily noticeable by the malicious users. Exposing the data requires a high technical and tactical computing process which is not a trivial task to be carried out by the malicious user

during network transmission [9] [10]. However, in some cases of DH such as steganography and watermarking the secret message while embedded into CM alters its intrinsic properties which result in distortion during the data embedding operations and the restoration of CM in acceptable form while extracting the message is highly required in some sensitive cases. Thereby distortion of CM is strictly forbidden in some critical scenarios [11][12][13]. The reversible data hiding (RDH) has gained attention from researchers for solving this problem to a greater extent in the field of DH and also ensures protection of the content ownership and authenticity of data. Unlike digital watermarking the prime concern of RDH is to conceal the data into cover medium in such a way so that the embedded data remains unnoticeable which refers to imperceptibility [14]-[17].

However, traditional RDH techniques lacks efficiency while restoring the CM in the original form as the process of secret image bits extraction often affects the signal quality of both the message and the CM. In many cases most of the RDH techniques are also found shrouded with computing complexity problems and do not ensure robustness against different forms of network attacks in video steganography [18][19][20]. This study explores various attack scenarios and their impact on the concealed data and introduces a simplistic and robust RDH framework for uncompressed video formats. This model intends to design the framework in such a way where it measures the performance of EC in terms of marked image quality and the capacity of payload metric considering the optimized execution flow of H.264/AVC encoding standard. The framework enables two model executions such as DWT and DWPT in conditional bases prior performing the embedding process for the uncompressed CM. However, it also creates a test environment to observe the outcome of EC and PSNR without attacks and even if the marked image undergoes through any of the most popular attacks such as a) Speckle noise, b) Gaussian noise, c) Histogram Equalization etc. in transit, then how the attacks affect the CM and secret image quality in the reconstruction phase. Also, the study observes the outcome with respect to EC in the measure of Normalized Correlation (NC) and assesses visual perception metric from the extraction of secret image quality before and after the attack is performed. The numerical assessment produces the promising outcome correspond to PSNR for both CM and secret image in the presence of attacks and without performing attacks which are comparable to the

existing approach of DE. This also shows that the proposed RDH attains good reversibility with enhancement in the EC aspects with the measure of imperceptibility for Normalized Correlation (NC) metric as $NC(Ow/Rw)$. Here Ow refers to original video frame and Rw refers to reconstructed video frame index. The prime novelty of this formulated approach is as follows:

- It addresses the overflow/underflow problem of intrinsic pixel attributes for secret image during the numerical computing which maintains the range of pixel values for frames with upper bound of 255 and lower bound of 0.
- Another contributory aspect of the proposed method of RDH is it addresses the design limitations of existing Difference Expansion (DE) approach in RDH, where the difference value between pixel pairs is computed and this computed difference values are used to embed the secret data. The traditional DE based approaches ensure better hiding capacity of secret message but do not ensure better reconstruction of signals for CM and secret image in or without the presence of attack effects. This indicates that the distortion effects remain present in the restored signal too.
- The system model of RDH here not only balances the EC and PSNR performance but also ensures robustness against different types of popular attacks.
- It also exhibits that in the presence of attacks also the system attains considerable optimized reversibility with good PSNR performance.
- It also ensures higher imperceptibility while maintaining better computing performance for embedding scenario considering H.264/AVC.
- The simplistic design format for the H.264/AVC based embedding solutions also optimizes the time complexity for operations which is not much addressed in the existing systems.

Owing to the above stated contributory points of novelty, the proposed system of RDH evolves up with a solution to address impending problems towards data hiding scheme that was not solved before. The paper is further organized as follows: here Section II analyses the related studies correspond to RDH and its implications on the futuristic research prospects of video steganography. Section III further implies exhibiting the problem formulation for the study where the scope of improvement of the RDH method is also discussed followed by research method explanation in Section IV. Further Section V discusses the core numerical design modeling for the proposed RDH framework and in Section VI discusses the proposed algorithm modeling followed by in Section VII the produced comparable outcomes for performance assessment are observed to show the improvement in the aspects of EC, security, and reconstructed signal quality. And finally, Section VIII remarks conclude the overall research.

II. REVIEW OF LITERATURE

In the past two decades RDH advances with its widespread methodical approaches. This aspect of RDH has been studied and reflected in more and more publications to strengthen the research scope from futuristic perspectives. This section critically reviews the related literatures from the recent publications and its primary concern lies in finding the current state-of-the-art approaches, their strength factors, and design limitations. Moreover, it also extracts the gap that persists in RDH research, clarifying the possible research needed in this domain. The implications of futuristic communication systems over 4G and 5G although provides idea for seamless way of data streaming but the security loopholes remain open research problems for various concern. However, the traditional RDH approaches also encounters a challenge while increasing the EC as it affects the visual perception of CM, once the signal is recovered during secret message extraction process. This condition also remains as vulnerability for the present communication systems and provides intruder the opportunity to target the secret information. A set of studies have explored the trade-off for RDH that remains between Visual Perception (VP) and Embedding Capacity (EC). The relationship that exists between VP and EC that can be expressed with a maximization problem, and realized as follows:

$$EC \propto \frac{1}{VP} \quad (1)$$

This Equation (1) indicates that a major concern of the current research trend is to maximize the EC in RDH without sacrificing the considerable of VP at the receiver end as reconstruction of CM and embedded message is also required in acceptable forms in some of the critical cases. Thereby, the prime motive of the current research evolves towards balancing this trade-off. The study of Cao et al. [21] has suggested that no matter in which domain of RDH procedure is concerned either 1) Plaintext Domain or 2) Encrypted Domain, but in both the domains proper restoration of CM and secret image bits has to be carried out irrespective of EC and its dependency on the size of the secret image [21]. It also explores that reason behind the justifications for the type of SM which has be embedded inside the CM. So here lies a question that what kind of form of SM is to be embedded inside CM so that maximum level of security can be retained throughout the transmission. Here security refers to protection of data confidentiality and integrity. However, the challenge in imposing the security arises as it also has to maintain the minimum threshold of human visual perception for acceptable form of reconstructed media. The study suggests from its crucial findings that optimization can be a better approach to deal with this aspect of RDH which can be of two different types such as i) Single objective optimization problem and ii) Multi-objective optimization problem. The study of Qi et al. [22], Wang et al. [23] and Ou et al. [24] considers single-objective based optimization considering the technique Multiple Histogram Modifications (MHM) where the bin selection approach has been referred extensively to attain better EC performance. However, the study of Ke et al. [25] studies the encrypted domain of RDH and introduces a fully Homomorphic encryption and Difference Expansion (DE)

based RDH based on single objective optimization solution. The study also attempts to minimize the Rate Distortion (RD) effects on the CM while also attain better EC for data hiding and also claims that the outcome produced show effective security outcome.

However, it is observed that the above studies have not extensively discussed about different types of attack scenarios and the also the conventional HS based approaches do not ensure better utilization of CM during the embedding scenario. And also, often exploits the texture characteristics of image for correlation purpose which could degrade the quality of the CM.

The multi-level optimization based solutions also have been referred in various studies; the study of Yin et al. [26] introduced a multi-objective optimization based theory to develop a solution approach for RDH. However, one limitation of the approach is that it can only operate in JPEG images for combination of non-overlapping parts. However, this approach also attempts to attain a proper balance between EC and RD. The study in this research specific context does not talk about the inclusion of videos as CM for video steganography applications. On the other hand the study of Mohammadi et al. [27] also emphasizes on multi-objective problem formulation for local difference predictor. The labeling during the prediction scenario also helps in effective extraction of the embedded data. The study not only ensures better performance for signal quality aspects of the reconstructed cover video but also attain high EC from the point of view of data hiding and security. The limitation of the study lies within the fact that it doesn't considers video object as a cover media. There exist other related studies such as Roy et al. [28], Peng et al. [29] and Wang et al. [30] which have also incorporated the multi-objective optimization based solutions and also talk about its scope in the futuristic methods of RDH. The study of Li et al. [31] also talked about the problem context of variation in statistical features of shifting histograms and introduced an improved version of difference histogram shifting based algorithms. However, another improved version of DE based approach was seen in the study of Kim et al. [32] which also utilizes the features of location map and Laplace distribution. The DE based approaches also observed for lossless compression which can be observed in the studies of [33-37].

The study by Liu et al. [38] provides a solution approach of combination of art image generation and data hiding for image security aspect. The outcome assessed from this approach shows that, the algorithm's computational complexity is quite higher and data hiding performance is also not considerable for different images. There are studies by Wang et al. [39], Yao et al. [40], and Ke et al. [41], where the prime concern was laid on digital data security considering RDH techniques. However, most of studies consider RDH on encrypted domain however most of the techniques are not assessed for color images and computational complexity aspects are also not much explored. The study of Rahman et al. [42] also introduces a RDH technique for the authentication of source for biological signals. Similar problem context for RDH is also explored in, Wu et al. [43] and Xie et al. [44]. Here one critical observation exhibits the matter of fact that

majority of the techniques are majorly concerned about enhancing the EC of the image signal. The study of Weng et al. [45] addresses the problem of higher embedding distortion considering the approach of invariability and adjustment in the pixel attributes. However, this approach of RDH is found not suitable for the high dimensional image matrix. The study of Wang et al. [46] explores various DE based RDH mechanisms and presented their design models for VQ-based data hiding. The study also refers another significant research, the study basically introduces a novel DE based embedding solutions to enhance the EC without compromising with the distortion aspect. Apart from this, various recent work towards RDH has been carried out by Zhou et al. [47], Dragoi et al. [48], Li et al. [49], and Sheidani et al. [50]. Although, these techniques are quite robust from security perspective, but a computationally extensive process has been implemented towards data hiding that increases complexity on the long run. The next section outlines the identified research problems in this perspective.

III. RESEARCH PROBLEM

The prime motive behind the design solutions for RDH is to enhance the quality of data security so that the contribution in this domain could make this research track more worthy for different purposeful use cases. Another primary concern of RDH is to overcome the constraints of privacy protection offered by the traditional cryptographic and DH methods. From the previous segment of the study, a set of observations are outlined which helps in generalizing the problem statement of this research specific context. It should be noted that the advancement of embedded and computing systems has brought so many changes in the existing communication scenarios and also network protocol integrations for artificial intelligence (AI) based systems aims to serve more and more consumers for streaming services. However, RDH since many years have extensively applied on digital images whereas later various communication standards from the business and security perspectives of data protection have enabled the seamless video transmission over wireless channels and with this a consistent evolution on standard frame formats is also witnessed. Hence, various video frame formats of CIF, QCIF, WVGA and HD have been explored for different streaming applications. The study mostly focuses on video steganography-based applications where data security from the point of view of privacy protection plays a crucial role. However, the study realizes that those traditional RDH systems are evolving but still lacks improvement in many areas. Prime objective of this section is to illustrate those key findings which cover the areas where RDH requires improvement. The following are the key aspects for research problem:

- Most of the critical vision-based systems require effective and secure transmission of secret message embedded in a video and henceforth require robustness in security implementations.
- It is also observed that the traditional approaches of HS/MHM and DE in RDH mostly focuses on images for transmission but do not talk much about the videos as CM. This has become a core motivating factor for this research.

- Most of the existing popular approaches of DE attains better EC along with adequate data hiding but lacks computing efficiency along with high distortion problem of images. However, RDH on encryption domain even though achieve higher EC factor but also do not ensure better reversibility and not evaluated for color videos or other forms of images. It can also be seen the reconstruction of CM and secret message do not ensure better PSNR range for uncompressed videos when entropy encoding is concerned.
- Very lesser studies have actually revealed the potential factors of H.264/AVC towards performing embedding of secret image in an uncompressed video which opens up more VS based applications deployment opportunities for security concern.
- The existing MHM and DE based approaches do not ensure robustness against different security attacks rather JPEG compression. This restricts their deployment in futuristic critical use-cases where proper reconstruction of CM and message is required.
- It is also observed that not much emphasize has been given on the assessment of computational complexity for the traditional RDH solutions for videos. Videos are formed through a sequence of frames which creates a larger form of complex data and needs efficient processing, storage indexing and transmission schema to meet the requirements of effective embedding operations of RDH.

Thereby the study formulates its problem statement as “To design and develop a secure and robust RDH framework for uncompressed videos which should comply with the futuristic network constraints while maintaining better embedding performance in the measure of imperceptibility while maintaining efficient reversibility of the reconstructed CM and the secret image”.

IV. RESEARCH METHOD

The study adopts analytical research modeling for the design of H.264/AVC based embedding solution to comply with the requirements of formulated RDH framework. The core functional block-based execution shows that initially the framework enables model selection of customized blocks under the conditional cases of discrete wavelet transform (DWT) and discrete Wavelet Packet Transform (DWPT) to make the uncompressed video (C_m) suitable for embedding operation. The mode of DWT exploits the high correlation between the adjacent temporal frames and also deals with high frame rate video constraints. This helps in efficient computing of C_m from both storage and processing point of view. The incorporation of DWT while performing the embedding operation also maximizes the capacity of ownership protection. The DWT model here also helps in decomposing the Y components for YUV color-space during the embedding operation for H.264/AVC. During the embedding process the workflow for the DWT model also insert the secret image into the resulting sub-bands using extracted low level coefficient values. The DWT decomposition here also makes the video suitable for the embedding operations considering a

customized function of principal component analysis (PCA) and also enhances the security of the algorithm. Finally, the embedding operation considering UC-Video Cover and secret data generates the H.264/AVC based encrypted video. The Fig. 1 shows the overall design of the system model for proposed solution of RDH.

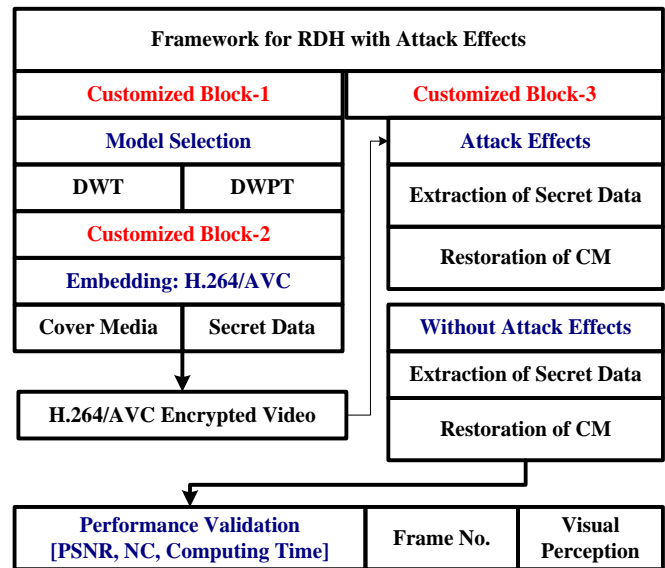


Fig. 1. Framework for RDH.

The system further also assesses the performance outcome in the measure of visual perception for the original frame index, reconstructed frame index of both CM and secret image message for two different types of scenarios. Here one scenario indicates extraction of secret data after performing a set of attacks such as – i) Speckle noise, ii) Gaussian noise, iii) Histogram equalization, iv) Salt and pepper noise, v) Poisson noise, vi) Frame averaging, v) JPEG compression, vi) Gamma correction and vii) Median Filtering. On the other hand, another scenario considers assessment of the model without attack effects. In both the scenarios the visual perception for the reconstructed CM and secret image bits are computationally assessed with the metrics of PSNR. Here the NC refers to the performance index to justify the metric for embedding capacity and shows how the formulated approach attains better data hiding as compared to the traditional RDH mechanisms. The study further also assessed the computing time for embedding and to generate the encrypted video sequence of H.264/AVC for C_m which is also referred as embedded video. The next section further shows the numerical modeling for the execution operations of the proposed RDH framework.

V. NUMERICAL DESIGN IMPLEMENTATION

The numerical design and modeling of the proposed system has been implemented over a computing environment and subjected to cover most of the executable operations for RDH and H.264/AVC based embedding. The study impels the design requirements to make the RDH numerical framework model robust and considers a set of hypothetical assumptions to make it more realistic for the futuristic video steganography-based applications.

A. Assumption for System Design

The study considers a set of hypothetical assumptions during the design and research modeling of the formulated approach. The prime reason behind taking these assumptions is to develop a sophisticated numerical model for the research specific purposes. The primary assumption considers that both S_{msg} to be embedded and the video file in the form of C_m are not distorted and restore its original form after a set of computation. The video file $v_i \rightarrow C_m$ is considered to be uncompressed in the initial phase of the system modeling and further subjected to embedding process. The secondary assumption of the research is that the formulated RDH approach offers better embedding capacity along with robustness, perceptibility and security measures which is needed to be validated under different conditions of parametric numerical evaluation. The tertiary assumption in the context of the formulated study considers that the embedded secret information msg in C_m to be transmitted over a wireless medium to a specified terminal under different operating conditions.

B. Model Selection and Embedding Process

1) *Uncompressed video: C_m processing:* The system initially considers two different mode of selection that is either DWT or DWPT in the form of analytical model and further enables the proposed effective embedding operations with respect to potential form of computing aspect. Further customizes a function to read and process the cover media that is- $f(x): f \leftarrow C_m$. This function considers uncompressed video file (v_i) in the form of cover medium $v_i \rightarrow C_m$. To process the uncompressed v_i for i number of frame sequence, the system initially locates the file v_i with two distinct attributes, the expression to denote the C_m with these two attributes can be expressed in Equation (2) as:

$$C_m \leftarrow [f_n(v_i), floc(v_i)] \quad (2)$$

Here the first attribute in the vector $f_n(v_i)$ indicates the particular file naming string, whereas the second attribute $floc(v_i)$ denotes the locator of the v_i within the disk drive file system structure. Finally, the system process both the attributes $f_n, floc \in v_i$ to generate an object $Obj(v)$ as follows:

$$V_{obj}(i) \leftarrow [floc \parallel f_n] \in v_i \quad (3)$$

The Equation (3) shows a concatenation operation of these string attributes in order to generate an object file of $V_{obj}(i)$. The method further converts the yuv4mpeg media object form of $V_{obj}(i)$ into numerically compatible movie format M . The system here also applies another custom functional module $f(x): f \leftarrow V_{obj}(i)$, to generate the numerically compatible format M and associative fields after as set of computing procedure. The numerical conversion of the yuv4mpeg (C_m) is shown with the following flowchart as shown in Fig. 2.

The process flow in the Fig. 2 shows that in this procedure initially the system enables the function to load the object form of video sequence $V_{obj}(i)$. In the further stage the system computes the structure of data and its corresponding

color map $[d, C_m]$ from the $V_{obj}(i)$ which is in the form of YUV structure of data. The system further computes the file size on the disk in bytes and process the file in the read only mode followed by computation of the headers (h) and last position of headers $e(h)$. Finally, the process computes the headers and start computing the frame length (f_i) for each frame i . The computation of the f_i takes place with the following mathematical Equation (4).

$$f_i(i) = f_h(i) \times f_w(i) \quad (4)$$

Here in the Equation (4) the system computes frame length for each frame $i \in V_{obj}(i)$. Further, the process flow enables conditional statement to check the color space from the fields, if color space is found to be 'C420' then the system computes the frame length as shown in Equation (5):

$$f_i(i)_{C420} = (f_i(i) \times \lambda) / \rho \quad (5)$$

However, in another case if the color space in the fields match with 'C422' then the system computes the frame length as below:

$$f_i(i)_{C422} = (f_i(i) \times \lambda) \quad (6)$$

In the case of color space 'C444' the frame length is computed as shown in Equation (7).

$$f_i(i)_{C444} = (f_i(i) \times \rho) \quad (7)$$

Further the process flow execution computes the frame count (f_c) before proceeding to the reading of YUV-frame sequence. The Equation (8) shows the numerical expression for frame count.

$$f_c = (f_b - e(h)) / \sum (\alpha + f_i(i)) \quad (8)$$

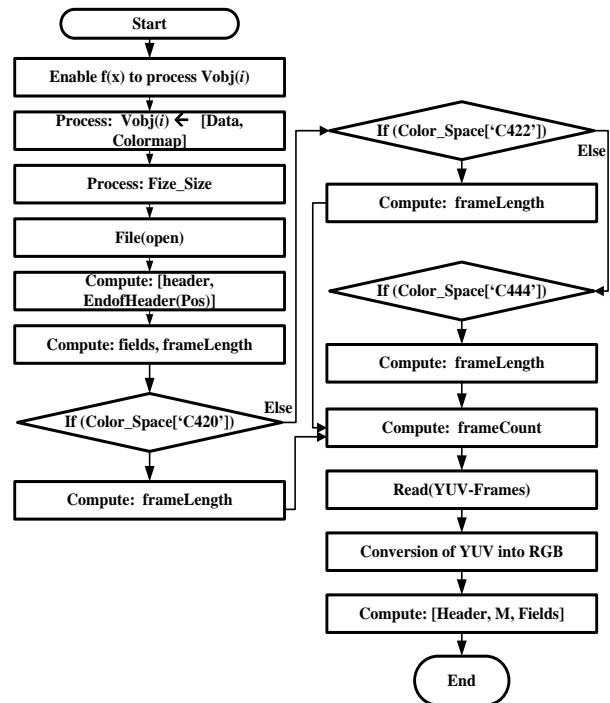


Fig. 2. Process-flow of the Conversion Operation of $[V_{obj}(i) \rightarrow M]$.

Here f_b refers to the file size in bytes and α is a system constant. After computing the frame length, the system further read the YUV-frame sequence from the video object and converts it into final sequence of RGB which is in the numerically compatible format. Finally the system generates the computed header, M and fields for the consecutive part of the process execution.

C. Uncompressed: Smsg Processing

Further the system process in this phase of modeling also considers S_{msg} in the form of secret image bits ($S_{msg} \rightarrow w$) and digitize it in the compatible numerical form. For this process the system initially locates the specific w with two distinct attributes $wLoc$ and wN . The secret message is further generated with the following numerical expression Equation (9).

$$S_{msg}(i) \leftarrow [wLoc \parallel wN] \in w \quad (9)$$

Further the system computes the numerical form of S_{msg} by performing digitization of the matrix and generates secret image bits type-1 ($w1$) followed by computation of secret image bits type-2 ($w2$) in binary form based on thresholding.

D. Formulated H.264/AVC based Embedding Procedure

The system further extends its workflow on the formulated embedding procedure of the secret message msg in the form of secret image bits $w2$. The system designs the embedding procedure with two stages of execution with invoking custom function. Initially it considers nf , M for f_i . The system furthers also constructs a cell structure of $M\{f_i\}$. The system performs numerical vectorization of the $msg \rightarrow w2$ with the following mathematical expression.

$$R1, C1 \leftarrow Rf(msg \rightarrow w2) \\ w2 \leftarrow Rf(w2t)R1xC1 \quad (10)$$

In the above equation (10), the system here computes the resizing operations with respect to a transpose operation for the dimension of $R1$, $C1$ correspond to $w2$ matrix. Further the computation, converts the RGB component of $M\{f_i\}$ into YCbCr color space as $YCbCr[i] \leftarrow M\{f_i\}$. It also computes the individual frame matrix for YUV such as $y \leftarrow y(r,c,1)$, $u \leftarrow u(r,c,2)$ and $v \leftarrow v(r,c,3)$ from the converted YCbCr[i]. The computation further applies N-level wavelet decomposition procedure on the $y \leftarrow y(r,c,1)$ component with "haar" wavelet transformation. The wavelet decomposition here takes place with the following mathematical Equation (11).

$$C1, C2 \leftarrow Wd(\text{Matrix}[y(r,c,1)]N) \quad (11)$$

The wavelet decomposition is carried out on the matrix form of $y(r,c,1)]_N$ at level-N. The outcome produced by the function generates two distinct coefficients of $C1$ and $C2$ which are further subjected to approximation stage of two-dimensional signal vector. The function $LL \leftarrow Acoeff(C1, C2)$ performs basically approximation of the coefficients and generates sub-band of LL . The final coefficient approximation stage further extensive analysis the $C1$, $C2$, N and generates other sub-band components of LH , HL , HH components. These two stages of execution modeling can be expressed as shown in Equation (12).

$$LL \leftarrow Acoeff(C1, C2) \\ LH, HL, HH \leftarrow Ecoeff(C1, C2, N) \quad (12)$$

The system further performs wavelet decomposition for respective channel (ch) of bands which can be formed as $[LL \rightarrow 1, LH \rightarrow 2, HL \rightarrow 3, HH \rightarrow 4]$.

$$Cb1, Cb2 \leftarrow Wd(\text{Matrix}[ch]N) \\ LLd \leftarrow Acoeff(Cb1, Cb2) \\ LHd, HLd, HHd \leftarrow Ecoeff(Cb1, Cb2, N) \quad (13)$$

In the above Equation (13), the system computes the coefficient extraction process for different bands with conditional execution of ch which ranges between $1 \rightarrow 4$. The system further computes sub-blocks correspond to the matrix form of LLd for each row and col vectors as $sub(i,j,n) \leftarrow LLd((i,r),(j,c))$. The model here also exploits the standard principle of H.264/AVC encoding operations to complement the embedding operation and further the computed sub-blocks are then further processed under a custom function of $PCA(x)$ which generates the final data ($Fdata$) from the covariance matrix ($CovM$). This final data is referred to the H.264/AVC encrypted data.

E. Formulated RDH with Extraction Procedure

The extraction procedure in the context of RDH for the formulated approach also constructs a custom function of f : $f_{ex}(x) \leftarrow Sub^*w, R_f(RGB) C_m$. The custom function in this case considers encrypted video object with H.264/AVC coding standard with $Sub^*w, R_f(RGB)$ and also considers nf , wavelet name, the dimension factor of $R(i), C(i)$. The system reconstructs the video sequence here for $Tm: [m1/m2]$. In the initial phase of computation, the system constructs the cover from the $Sub^*w, R_f(RGB)$ for different f_i which is represented as shown in Equation (14):

$$ReCov(i) \leftarrow Sub^*w:Rf(RGB)x,y,z,I \quad (14)$$

The reconstructed cover for particular f_i further undergoes thorough secret image extraction procedure for two different modes of operations. Here the system initially again converts the $R_f(RGB) \rightarrow YCbCr[i]$ with the numerically compatible format of YUV. And further computes the frame indexes for $y \leftarrow y(r,c,1)$, $u \leftarrow u(r,c,2)$ and $v \leftarrow v(r,c,3)$. The system further again performs wavelet decomposition and computes the coefficient attributes for this extraction operation of w as shown in Equation (15),

$$Cexb1, Cexb2 \leftarrow Wd(\text{Matrix}[y]N) \\ LL \leftarrow ExAcoeff(Cexb1, Cexb2, N) \\ LH, HL, HH \leftarrow Excoeff(Cexb1, Cexb2, N) \quad (15)$$

Further the system performs a sub-blocking operation with H.264 to generates sub-blocks $sub(i, j, n)$. Finally, the $PCA(x)$ algorithm generates the reconstructed $w2$ after set of operations.

VI. ALGORITHM DESIGN

The algorithm design for the formulated embedding operations for two different mode of embedding operations is shown as follows:

Numerical Algorithm-I: Formulated Embedding Process in RDH technique

Input: $M, f_i, nf, w2$

Output: Reconstructed cover media $[Re(V_i)]$

Start

1. Init $\rightarrow M, f_i, nf, w2, nf \in M$ for f_i
2. Enable $Tm: [m1/m2]$
3. Construct \rightarrow cell structure of $M\{f_i\}$
4. Enable : $f_{en1}(x)$. pass in: $M\{f_i\}, msg \rightarrow w2$
5. $R1, C1 \leftarrow R_f(msg \rightarrow w2)$
6. $w2 \leftarrow R_f(w2)_{R1 \times C1}$
7. $C1, C2 \leftarrow Wd(\text{Matrix}[y(r,c,1)]_N)$
8. $LL \leftarrow \text{Acoeff}(C1, C2)$
9. $LH, HL, HH \leftarrow \text{Ecoeff}(C1, C2, N)$
10. $Cb1, Cb2 \leftarrow Wd(\text{Matrix}[ch]_N)$
11. $LLd \leftarrow \text{Acoeff}(Cb1, Cb2)$
12. $LHd, HLd, HHd \leftarrow \text{Ecoeff}(Cb1, Cb2, N)$
13. Select $ch: 1 \rightarrow 4$
14. $n \leftarrow 1$
15. Compute sub-blocks correspond to LLd
 For $i \leftarrow 1$ to r
 i. For $j \leftarrow 1$ to c
 1. $\text{sub}(i,j,n) \leftarrow LLd((i,r),(j,c))$
 $n \leftarrow n+1$
 End
 End
16. Enable custom function of $\text{PCA}(x)$: pass in $\text{sub}(i,j,n)$
17. $\text{PCA}(x)$: pass out $Fdata \leftarrow \text{Eign}(\text{CovM})^T * \text{Adjst}$ // here
 $Adata \leftarrow \text{sub}_{\text{double}} - \text{Sub}_{\text{mean}}$
18. $R_f(\text{Sub} * w)$
19. Reconstruct $Odata \leftarrow \text{Sub} * w(i)$
20. Apply Flip-array up \rightarrow down on $Odata$
21. construct
22. $\text{new_y}(r,c,1) \leftarrow \text{IDWT2}(LLd, LHd, HLd, HHd)$
23. $\text{new_y}(r,c,1) \leftarrow \text{IDWT2}(\text{new_y}(r,c,1), LH, HL, HH)$
24. $y(r,c,1), u(r,c,2), v(r,c,3)$
25. compute numerical form of y
26. Perform reconstruction from $YCbCr \rightarrow R_f(\text{RGB})$

End

The computation of the formulated embedding approach for mode type-1 in DWT model whole perform the PCA analysis for component of $\text{sub}(i,j,n)$ further generates Final data attributes considering the following Equation (16).

$$Fdata \leftarrow \text{Eign}(\text{CovM})^T * \text{Adjst} \quad (16)$$

Further it reconstructs the $\text{Sub} * w$ with resizing factor and generates the original form of data $Odata$. It also enhances the embedding efficiency by performing flip-array up-down approach. Further the system constructs the $\text{new_y}(r,c,1)$ followed by reconstruction of $R_f(\text{RGB})$. The extensive analysis of the formulated approach shows that the embedding efficiency has significantly increased owing to the involvement of PCA. The numerical outcome is further shown in the result and analysis section.

The algorithm for extraction procedure is shown as follows:

Numerical Algorithm-II: The w Extraction Procedure

Input: $\text{Sub} * w, R_f(\text{RGB}) \quad C_m$

Output: $\text{ReCov}(i)$

Start

1. Init $\rightarrow \text{Sub} * w, R_f(\text{RGB}), nf, Dim \leftarrow (R, C)$
2. $Tm: [m1/m2], f_{ex}(x)$
 a. For each frame f_i
 i. Enable : $\text{ReCov}(i) \leftarrow \text{Sub} * w : R_f(\text{RGB})_{x,y,z,i}$
 ii. Convert: $(\text{RGB}) \rightarrow YCbCr[i]$
 b. End
3. $\text{Cexb1}, \text{Cexb2} \leftarrow Wd(\text{Matrix}[y]_N)$
4. $LL \leftarrow \text{ExAcoeff}(\text{Cexb1}, \text{Cexb2}, N)$
5. $LH, HL, HH \leftarrow \text{Excoeff}(\text{Cexb1}, \text{Cexb2}, N)$
6. Perform Sub-block operation with H.264/AVC
7. $\text{sub}(i,j,n)$
8. $R_f(w2) \leftarrow \text{PCA}(x)$

End

The secret image bits extraction procedure has been verified for before attack and under the attack's scenario with the simplified computing steps. Here the system basically considers 9 different set of attacks in the form forms of $AS = \{AS1, AS2, AS3, AS4, AS5, AS6, AS7, AS8, AS9\}$. The performance of imperceptibility along with the signal quality evaluation is further done in the numerical outcome section. The performance estimation of signal quality considers PSNR as a metric to justify the outcome.



VII. RESULT AND ANALYSIS

The study outcome to justify the performance of the formulated embedding approach in RDH process is shown and discussed in this section. The study in this section not only estimates the PSNR, NC outcome but also assess the time complexity for above two algorithms of embedding and extraction with respect to CPU time. The analysis clearly shows that the experiments are conducted for a cover media named Akiyo.CIF of type Y4M, where the frame size is considered to be CIF (288 x 352). The size on the disk for the CM found to be approximately 43.5 MB (44,552 KB). The message media is considered as a single image file of TIF and its size on the disk is approximately 5KB. The numerical experiments are further realized in a computing environment of MATLAB R2015a environment on a PC with CPU Intel(R) Core (TM) i5-3470 @ 3.2 GHZ with 4-GB of RAM. The numerical computing is carried out considering a set of explicit custom functions invoked during the simulation of the above-mentioned numerical modeling of i) Uncompressed cover media and secret image processing, ii) Formulated approach of embedding and iii) Extraction process in RDH. The simulation outcome from the numerical modeling takes a set of observation of each frame and its visual perception measures correspond to the input CM and the embedded secret data in the form of image. To justify the reversibility and proper data hiding performance the system model considers two different scenarios. Here in one scenarios secret image is simply extracted considering Algorithm-II from the embedded





CM and the visual perception with respect to frame number is obtained for both CM and w . In another scenario the study considers w extraction after performing a set of attacks on the embedded CM. The similar sort of observations are carried during the reconstruction process of the original CM frame along with the reconstructed frame after embedding and also the visual perception of frame after performing a set of attacks conditionally.




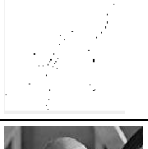

The visual perception score for the original image (Table I(A)) and the extracted image on shows higher similarity score in the absence of attacks which shows that the proposed RDH model attains good reversibility while fulfilling the requirements of PSNR for the reconstruction scenario. However, the experiments for VP are further also extended to generalize the robustness of the system in the presence of nine different types of attacks AS = {AS1, AS2, AS3, AS4, AS5, AS6, AS7, AS8, AS9}. The visualization to show the attack effect on the extracted secret image bits is provided in Table I(B). It considers embedding process and a specific type of attack at a time performed on the embedded CM.

TABLE I. (A): VISUALIZATION OF ORIGINAL SECRET IMAGE, EXTRACTED SECRET IMAGE FROM BITSTREAM (BEFORE ATTACK)

Original Secret Image (w_2)	Extracted Secret Image (w_2) from the Bitstream (Before Attack)
	

(B): VISUALIZATION OF ORIGINAL SECRET IMAGE, EXTRACTED SECRET IMAGE FROM BITSTREAM (AFTER ATTACK EFFECTS)

Types of attacks performed on w_2	Visualization of the extracted w_2 (After Performing Attack)
1. Speckle noise	
2. Gaussian noise	
3. Histogram Equalization	
4. Salt and pepper noise	

5. Poisson noise	
6. Frame averaging	
7. JPEG compression	
8. Gamma correction	
9. Median Filtering	

The interpretation of the visual outcome here shows that how the extracted secret image looks like while the embedded CM of Akiyo.CIF undergoes through a set of attacks conditionally. The outcome obtained clearly shows that in all the cases of attacks the system attains considerable outcome of visual perception for secret image bits. However, the effects of Gamma correction are found more on the extracted secret image. The system further also performs analysis on the visual perception and the parameters for embedding efficiency for data hiding aspects for the CM which is further shown in the following Table II.

TABLE II. NUMERICAL OBTAINED FOR PSNR, NC FOR CM= AKIYO.CIF AFTER EMBEDDING AND EXTRACTION PROCESS

Original frame from C_m	Frame after Embedding Process	Frame After Attack
AS-1: PSNR(Ov/Rv) = 47.0357	AS-1: NC(Ow/Rw) = 0.72456	AS-1 NC(Ow/Rw)=0.767
AS-2: PSNR(Ov/Rv) = 48.77	AS-2: NC(Ow/Rw) = 0.55514	AS-2 NC(Ow/Rw)=0.57004
AS-3: PSNR(Ov/Rv) = 50.4078	AS-3: NC(Ow/Rw) = 0.36798	AS-3 NC(Ow/Rw)=0.574
AS-4: PSNR(Ov/Rv) = 44.4851	AS-4: NC(Ow/Rw) = 0.6484	AS-4 NC(Ow/Rw)=0.68499
AS-5: PSNR(Ov/Rv) = 50.77	AS-5: NC(Ow/Rw) = 0.545	AS-5 NC(Ow/Rw)=0.5654
AS-6: PSNR(Ov/Rv) = 48.7379	AS-6: NC(Ow/Rw) = 0.44532	AS-6 NC(Ow/Rw)=0.67
AS-7: PSNR(Ov/Rv) = 43.13	AS-7: NC(Ow/Rw) = 0.5364	AS-7: NC(Ow/Rw)=0.39645
AS-8: PSNR(Ov/Rv) = 50.41	AS-8: NC(Ow/Rw) = 0.476	AS-8: NC(Ow/Rw)=0.697
AS-9: PSNR(Ov/Rv) = 52.41	AS-9: NC(Ow/Rw) = 0.486	AS-9: NC(Ow/Rw)=0.687

The study incorporates numerous performance metrics to validate the system such as PSNR and NC. Here the PSNR performance is obtained considering the following standard form of mathematical Equation (17) as below.

$$\text{PSNR} = 10 \times \log\left(\frac{\text{MAX}^2}{\text{MSE}}\right) \quad (17)$$

Here MSE refers to mean square error computation for the original frame and the embedded frame of CM. And also, MAX refers to the maximum possible pixel range of each frame. The system also considers another performance metric of NC which is attributed as a measure to assess the embedding efficiency and the robustness of the proposed H.264/AVC based embedding operations against different forms of attacks. It measures the similarity index between the frame after embedding and the frame after attack. It is also applicable to the original secret image and extracted secret image similarity measures. The standard form of numerical model to evaluate this NC is given as below.

$$\text{NC} = \frac{\sum[\text{Ow}(i,j) \times \text{Rw}(i,j)]^2}{\left(\sqrt{\sum \text{Ow}(i,j)^2}\right) \times \left(\sqrt{\sum \text{Rw}(i,j)^2}\right)} \quad (18)$$

The performance metric of NC here evaluates the robustness and embedding efficiency accomplished by the proposed algorithm (P-RDH). The analysis of imperceptibility from the PSNR outcome for the original frame of C_m and the embedded frame shows that the system accomplishes considerable PSNR during the reconstruction of original CM of Akiyo, CIF even though in the presence of different types of attacks. The average PSNR (dB) outcome for CIF (288 x 352) is obtained as 52.7379dB which is comparable to the conventional baselines of RDH (C-RDH). The visual outcome of the PSNR is also shown with the following Fig. 3. The system outcome is further assessed for NC to justify the efficiency of encoding process in terms of embedding efficiency and robustness for different conditions. The NC computation here also justifies the robustness of the system modeling during the attack scenario.

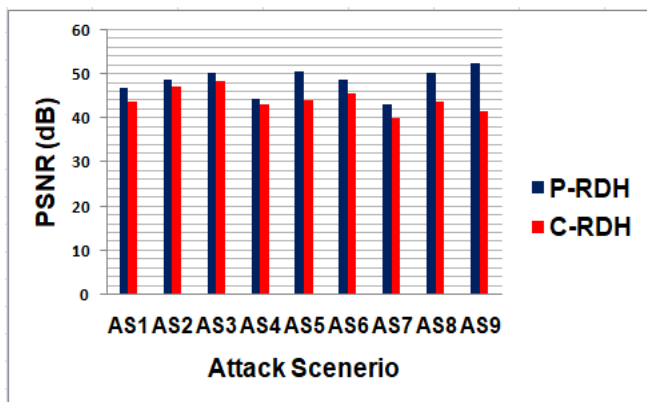


Fig. 3. Analysis of PSNR Outcome for CM Reconstruction.

The analysis of the outcome of NC shows that with the variation of embedding strength the system achieves better normalized correlation not only in the case of secret image of Lena but also in the case of reconstructed frames of CM. This indicates that the proposed approach P-RDH outperforms C-RDH to a greater extent under different operational conditions

and also ensures higher reconstructed signal quality. The system performance in this chapter also shows that the P-RDH attains superior performance from the viewpoint of computing too. It attains CPU execution time of overall 143.166324 seconds during the computing process of embedding whereas in the existing system it is quite higher. The reconstruction process accomplishes the CPU time of 30.7447secs for each frame which is also found significant as compared to the existing baselines.

The prime reason behind this is the proposed encoding applies PCA based component analysis is to generate significant coefficient attributes from both the secret image bits and cover-media which in extraction process helps. Thereby to a greater extent the system outperforms the C-RDH by means of PSNR and CPU computing for embedding. It also enhances the embedding capacity irrespective of the message size.

VIII. RESULT AND DISCUSSION

The outcome obtained from the current study showcase that proposed scheme is highly resilient to different forms of attacks which the existing schemes didn't have reported for [21]-[25]. A simplified assessment towards the optimal data hiding scheme presented in [22] has claimed about higher reversibility degree, however it fails to identify the threat on dynamic scenarios. The system of proposed RDH is found to offer higher robustness towards attack of various forms (i.e., Speckle noise, Gaussian noise, Histogram equalization, salt and pepper, Poisson noise, jpeg compression and frame averaging, Gamma correction and median filtering), hence attain efficient imperceptibility from data security viewpoint and this critical aspect has not much explored in the existing studies [30]-[36]. Further, it is also noted that the outcome of this RDH in this research aspect is also found comparable with the existing baseline solution for PSNR, NC and computing time. From the perspective of the computational efficiency, the study outcome is also found to support the claim that it balances the trade-off between EC and the visual perception while accomplishing faster CPU execution with PCA based solution for H.264/AVC. Similarly, the attack analysis has been carried out for the CM too where it shows higher PSNR efficiency in post embedding phase of reconstruction of the signal whereas in the after-attack scenario the signal quality in the measure of PSNR got slightly affected in case-8. Such case was not evident in the recent work too [44]-[50]. However, in the other cases the system found higher PSNR outcome with good reversibility of both secret message and the CM. Therefore, from the overall perspective of study outcome, it shows that proposed system offers better performance in data hiding compared to majority of the related existing models.

IX. CONCLUSION

This research study introduces a novel computing framework of RDH mechanism which ensures better embedding capacity under both attack and un-attack scenarios. The simplistic design approach of the embedding ensures better flow of execution and also retains higher PSNR with imperceptivity for extraction process of both secret image and cover media. The outcome also shows that in 1-2 cases of

attack scenario the PSNR performance got affected for the reconstructed signals but still higher imperceptibility is achieved. The system is not only robust against different form of attacks as on an average the NC score is obtained towards 1 but also it can be seen that it balances the trade-off between EC and CPU computing time while maintaining acceptable PSNR range for the reconstructed frames of CM. This indicates the performance efficiency of the H.264/AVC based system. It also further ensures that the good reversibility is happening for both Akiyo.CIF and Lena.TIF. The system performance of embedding still has a scope to be improvised despite its robustness against different form of attacks for that reason the study in the future work of this research targets to enhance the optimization procedure to strengthen the embedding procedure of RDH so that it can ensure better EC, PSNR and execution time trade-off for different range of cover media types and secret image. Apart from this, the prime significance of the proposed study is that it offers an efficient computational model towards framing up RDH, which can be applied over any form of video steganography application owing to its robustness. Without losing potential quality of the video, the proposed system is capable of leveraging better embedding capacity without using any iterative scheme or sophisticated operation involved in it. Hence, the scope of adopting the proposed RDH model is quite higher in multimedia application to a large extent.

REFERENCES

- [1] Barton JM, inventor; Barton, James M., assignee. Method and apparatus for embedding authentication information within digital data. United States patent US 5,646,997. 1997 Jul 8.
- [2] J. Fridrich, *Steganography in Digital Media: Principles, Algorithms, and Applications*. Cambridge, U.K.: Cambridge Univ. Press, 2009.
- [3] Y. Q. Shi, Z. Ni, D. Zou, C. Liang, and G. Xuan, "Lossless data hiding: Fundamentals, algorithms and applications," in *Proc. IEEE Int. Symp. Circuits Syst.*, vol. 2, May 2004, pp. 3336.
- [4] Y. Q. Shi, "Reversible data hiding," in *Proc. Int. Workshop Digit. Watermarking*, 2004, pp. 112.
- [5] R. Caldelli, F. Filippini, and R. Becarelli, "Reversible watermarking techniques: An overview and a classification," *EURASIP J. Inf. Secur.*, vol. 2010, 2010, Art. no. 134546.
- [6] J. M. Barton, "Method and apparatus for embedding authentication information within digital data," U.S. Patent 5 646 997, Jul. 8, 1997.
- [7] C. W. Honsinger, P. W. Jones, M. Rabbani, and J. C. Stoffel, "Lossless recovery of an original image containing embedded data," U.S. Patent 6 278 791, Aug. 21, 2001.
- [8] F. Bao, R.-H. Deng, B.-C. Ooi, and Y. Yang, "Tailored reversible watermarking schemes for authentication of electronic clinical atlas," *IEEE Trans. Inf. Technol. Biomed.*, vol. 9, no. 4, pp. 554563, Dec. 2005.
- [9] G. Coatrieux, C. Le Guillou, J.-M. Cauvin, and C. Roux, "Reversible watermarking for knowledge digest embedding and reliability control in medical images," *IEEE Trans. Inf. Technol. Biomed.*, vol. 13, no. 2, pp. 158165, Mar. 2009.
- [10] K. L. Chung, Y. H. Huang, P. C. Chang, and H. Y. M. Liao, "Reversible data hiding-based approach for intra-frame error concealment in H.264/AVC," *IEEE Trans. Circuits Syst. Video Technol.*, vol. 20, no. 11, pp. 16431647, Nov. 2010.
- [11] D. Coltuc and I. Caciula, "Stereo embedding by reversible watermarking: Further results," in *Proc. Int. Symp. Signals, Circuits Syst.*, Jul. 2009, pp. 14.
- [12] X. Tong et al., "Stereo image coding with histogram-pair based reversible data hiding," in *Proc. Int. Workshop Digital-Forensics Watermarking*, 2014, pp. 201214.
- [13] X. Wang, C. Shao, X. Xu, and X. Niu, "Reversible data-hiding scheme for 2-D vector maps based on difference expansion," *IEEE Trans. Inf. Forensics Security*, vol. 2, no. 3, pp. 311320, Sep. 2007.
- [14] F. Peng, Y.-Z. Lei, M. Long, and X.-M. Sun, "A reversible watermarking scheme for two-dimensional CAD engineering graphics based on improved difference expansion," *Comput.-Aided Design*, vol. 43, no. 8, pp. 10181024, 2011.
- [15] K. Hwang and D. Li, "Trusted cloud computing with secure resources and data coloring," *IEEE Internet Comput.*, vol. 14, no. 5, pp. 1422, Sep. 2010.
- [16] J. Fridrich, M. Goljan, and R. Du, "Invertible authentication," *Proc. SPIE*, vol. 4314, pp. 197208, Aug. 2001.
- [17] M. Goljan, J. J. Fridrich, and R. Du, "Distortion-free data embedding for images," in *Proc. 4th Inf. Hiding Workshop*, 2001, pp. 2741.
- [18] J. Fridrich, M. Goljan, and R. Du, "Lossless data embedding paradigm in digital watermarking," *EURASIP J. Adv. Signal Process.*, vol. 2002, no. 2, pp. 185196, 2002.
- [19] G. Xuan, J. Zhu, J. Chen, Y. Q. Shi, Z. Ni, and W. Su, "Distortionless data hiding based on integer wavelet transform," *Electron. Lett.*, vol. 38, no. 25, pp. 16461648, Dec. 2002.
- [20] G. Xuan, J. Chen, J. Zhu, Y. Q. Shi, Z. Ni, and W. Su, "Lossless data hiding based on integer wavelet transform," in *Proc. IEEE Int. Workshop Multimedia Signal Process.*, Dec. 2002, pp. 312315.
- [21] X. Cao, Y. Zhou and J. -M. Guo, "Guest Editorial Introduction to Special Section on Modern Reversible Data Hiding and Watermarking," in *IEEE Transactions on Circuits and Systems for Video Technology*, vol. 30, no. 8, pp. 2297-2299, Aug. 2020. doi: 10.1109/TCSVT.2020.3002109.
- [22] W. Qi, X. Li, T. Zhang and Z. Guo, "Optimal Reversible Data Hiding Scheme Based on Multiple Histograms Modification," in *IEEE Transactions on Circuits and Systems for Video Technology*, vol. 30, no. 8, pp. 2300-2312, Aug. 2020, doi: 10.1109/TCSVT.2019.2942489.
- [23] J. Wang, X. Chen, J. Ni, N. Mao and Y. Shi, "Multiple Histograms-Based Reversible Data Hiding: Framework and Realization," in *IEEE Transactions on Circuits and Systems for Video Technology*, vol. 30, no. 8, pp. 2313-2328, Aug. 2020, doi: 10.1109/TCSVT.2019.2915584.
- [24] B. Ou and Y. Zhao, "High Capacity Reversible Data Hiding Based on Multiple Histograms Modification," in *IEEE Transactions on Circuits and Systems for Video Technology*, vol. 30, no. 8, pp. 2329-2342, Aug. 2020, doi: 10.1109/TCSVT.2019.2921812.
- [25] Y. Ke, M. -Q. Zhang, J. Liu, T. -T. Su and X. -Y. Yang, "Fully Homomorphic Encryption Encapsulated Difference Expansion for Reversible Data Hiding in Encrypted Domain," in *IEEE Transactions on Circuits and Systems for Video Technology*, vol. 30, no. 8, pp. 2353-2365, Aug. 2020, doi: 10.1109/TCSVT.2019.2963393.
- [26] Z. Yin, Y. Ji and B. Luo, "Reversible Data Hiding in JPEG Images With Multi-Objective Optimization," in *IEEE Transactions on Circuits and Systems for Video Technology*, vol. 30, no. 8, pp. 2343-2352, Aug. 2020, doi: 10.1109/TCSVT.2020.2969463.
- [27] Mohammadi, Ammar, Mansor Nakhkash, and Mohammad Ali Akhaee. "A high-capacity reversible data hiding in encrypted images employing local difference predictor." *IEEE Transactions on Circuits and Systems for Video Technology* 30.8 (2020): 2366-2376.
- [28] A. Roy and R. S. Chakraborty, "Toward Optimal Prediction Error Expansion-Based Reversible Image Watermarking," in *IEEE Transactions on Circuits and Systems for Video Technology*, vol. 30, no. 8, pp. 2377-2390, Aug. 2020, doi: 10.1109/TCSVT.2019.2911042.
- [29] Peng, Fei, et al. "Separable robust reversible watermarking in encrypted 2D vector graphics." *IEEE Transactions on Circuits and Systems for Video Technology* 30.8 (2020): 2391-2405.
- [30] Wang, Xiang, Xiaolong Li, and Qingqi Pei. "Independent embedding domain based two-stage robust reversible watermarking." *IEEE Transactions on Circuits and Systems for Video Technology* 30.8 (2019): 2406-2417.
- [31] J. Tian, "Reversible data embedding using a difference expansion," *IEEE Trans. Circuits Syst. Video Technol.*, vol. 13, no. 8, pp. 890-896, Aug. 2003.

- [32] L. Kamstra and H. J. A. M. Heijmans, "Reversible data embedding into images using wavelet techniques and sorting," *IEEE Trans. Image Process.*, vol. 14, no. 12, pp. 2082–2090, Dec. 2005.
- [33] W. L. Tai, C. M. Yeh, and C. C. Chang, "Reversible data hiding based on histogram modification of pixel differences", *IEEE Trans. Circuits Syst. Video Technol.*, vol. 19, no. 6, pp. 906-910, Jun. 2009.
- [34] J. Tian, "Reversible data embedding using a difference expansion", *IEEE Trans. Circuits Syst. Video Technol.*, vol. 13, no. 8, pp. 890-896, Aug. 2003.
- [35] A. M. Alattar, "Reversible watermark using the difference expansion of a generalized integer transform", *IEEE Trans. image Process.*, vol.13, no. 8, pp. 1147-1156, Aug. 2004.
- [36] L. Kamstra and H. J. A. M. Heijmans, "Reversible data embedding into images using wavelet techniques and sorting", *IEEE Trans. Image Process.*, vol. 14, no. 12, pp. 2082-2090, Dec. 2005.
- [37] H. J. Kim, V. Sachnev, Y. Q. Shi, J. Nam and H. Choo, "A Novel Difference Expansion Transform for Reversible Data Embedding," in *IEEE Transactions on Information Forensics and Security*, vol. 3, no. 3, pp. 456-465, Sept. 2008.
- [38] S. Liu and W. Tsai, "Line-Based Cubism-Like Image—A New Type of Art Image and its Application to Lossless Data Hiding," in *IEEE Transactions on Information Forensics and Security*, vol. 7, no. 5, pp. 1448-1458, Oct. 2012.
- [39] Wang, H. Lin, X. Gao, W. Cheng and Y. Chen, "Reversible AMBTC-Based Data Hiding With Security Improvement by Chaotic Encryption," in *IEEE Access*, vol. 7, pp. 38337-38347, 2019.
- [40] H. Yao, X. Liu, Z. Tang, Y. Hu and C. Qin, "An Improved Image Camouflage Technique Using Color Difference Channel Transformation and Optimal Prediction-Error Expansion," in *IEEE Access*, vol. 6, pp. 40569-40584, 2018.
- [41] Y. Ke, J. Liu, M. Zhang, T. Su and X. Yang, "Steganography Security: Principle and Practice," in *IEEE Access*, vol. 6, pp. 73009-73022, 2018.
- [42] M. S. Rahman, I. Khalil and X. Yi, "Reversible Biosignal Steganography Approach for Authenticating Biosignals Using Extended Binary Golay Code," in *IEEE Journal of Biomedical and Health Informatics*, vol. 25, no. 1, pp. 35-46, Jan. 2021.
- [43] Wu, J. Dugelay and Y. Shi, "Reversible Image Data Hiding with Contrast Enhancement," in *IEEE Signal Processing Letters*, vol. 22, no. 1, pp. 81-85, Jan. 2015.
- [44] X. Xie, C. Chang and K. Chen, "A High-Embedding Efficiency RDH in Encrypted Image Combining MSB Prediction and Matrix Encoding for Non-Volatile Memory-Based Cloud Service," in *IEEE Access*, vol. 8, pp. 52028-52040, 2020.
- [45] S. Weng, Y. Zhao, J. Pan and R. Ni, "Reversible Watermarking Based on Invariability and Adjustment on Pixel Pairs," in *IEEE Signal Processing Letters*, vol. 15, pp. 721-724, 2008.
- [46] W. Wang, C. Huang and S. Wang, "VQ Applications in Steganographic Data Hiding Upon Multimedia Images," in *IEEE Systems Journal*, vol. 5, no. 4, pp. 528-537, Dec. 2011.
- [47] N. Zhou, M. Zhang, H. Wang, Y. Ke and F. Di, "Separable Reversible Data Hiding Scheme in Homomorphic Encrypted Domain Based on NTRU," in *IEEE Access*, vol. 8, pp. 81412-81424, 2020. doi: 10.1109/ACCESS.2020.2990903.
- [48] I. C. Dragoi and D. Coltuc, "On the Security of Reversible Data Hiding in Encrypted Images by MSB Prediction," in *IEEE Transactions on Information Forensics and Security*, vol. 16, pp. 187-189, 2021. doi: 10.1109/TIFS.2020.3006382.
- [49] S. Li, L. Hu, C. Sun, L. Chi, T. Li and H. Li, "A Reversible Data Hiding Algorithm Based on Prediction Error With Large Amounts of Data Hiding in Spatial Domain," in *IEEE Access*, vol. 8, pp. 214732-214741, 2020. doi: 10.1109/ACCESS.2020.3040048.
- [50] S. Sheidani, A. Mahmoudi-Aznavah and Z. Eslami, "CPA-Secure Privacy-Preserving Reversible Data Hiding for JPEG Images," in *IEEE Transactions on Information Forensics and Security*, vol. 16, pp. 3647-3661, 2021. doi: 10.1109/TIFS.2021.3080497.

Automated Feature Extraction for Predicting Multiple Sclerosis Patient Disability using Brain MRI

Ali M. Muslim¹, Syamsiah Mashohor², Rozi Mahmud³, Gheyath Al Gawwam⁴, Marsyita binti Hanafi⁵
Department of Computer and Communication System Engineering, Universiti Putra Malaysia, Serdang, Malaysia^{1, 2, 5}
Department of Imaging, Universiti Putra Malaysia, Serdang, Malaysia³
Department of Neurology, Baghdad University, Baghdad, Iraq⁴

Abstract—Predicting Multiple Sclerosis (MS) patient's disability level is an important issue as this could help in better diagnoses and monitoring the progression of the disease. Expanded Disability Status Scale (EDSS) is a common protocol used to manually score the disability level. However, it is time-consuming requires expert knowledge and exposure to inter-and intra-subject variation. Many previous studies focused on predicting patients' disability from multiple MRI scans and manual or semi-automated features extraction. Furthermore, all of them are required patient follow up. This study aims to predict MS patients' disability using fully automated feature extraction, single MRI scan, single MRI protocols and without patient follow-up. Data from 65 MS patients were used in this study. They were collected from multiple centers in Iraq and Saudi Arabia. Automated brain abnormalities segmentation, automated brain lobes, and brain periventricular are segmentation have been used to extract large scan features. A linear regression algorithm has been used to predict different types of MS patient disability. Initially, weak performance was found until MS patients were divided into four groups according to the MRI-Tesla model and the condition of the patient with a lesion in the spinal cord or not. The best performance was with an average RMSE of 0.6 to predict the EDSS with a step of 2. These results demonstrate the possibility of predicting with fully automated feature extraction, single MRI scan, single MRI protocols and without patient follow-up.

Keywords—Multiple sclerosis; expanded disability status scale prediction; multiple sclerosis disability; magnetic resonance imaging

I. INTRODUCTION

Multiple Sclerosis (MS) is a chronic, progressive autoimmune condition that affects the central nervous system (brain and spinal cord). MS occurs when the immune system attacks the myelin that protects the nerve fibres in the brain and spinal cord [1]. The exact cause of MS is still unknown. However, there are several risk factors that have been suggested as possible causes of MS such as genes, lack of sunlight, lack of vitamin D, smoking, race, climate, teenage obesity, viral infections and being female [4]. MS is considered a rare disease in Asia [2–4] with a prevalence estimated between 0 and 35 per 100,000 [2, 3, 5, 6, 8], resulting in a lack of a high number sample size. Brain and spinal cord MRI are one of the most significant paraclinical tests that aid the diagnosis of MS and can help to substitute for clinical findings. MRI has a key feature for investigation, diagnosis, treatment decisions, monitoring treatment response, and monitoring disease progression of MS. The most significant finding within the

MRI related to MS is location, type, size, and the number of MS lesions [8]. Almost all MS lesions can be seen in Fluid-attenuated inversion recovery (FLAIR) MRI. FLAIR MRI is one of the most commonly MRI protocols that has been used for MS diagnoses and monitoring the progression of the disease. MS-lesions in FLAIR MRI are typically hyperintense.

Expanded Disability Status Scale (EDSS) is a gold standard to score MS clinical patient disability levels [9]. EDSS is a clinician-administered assessment scale used to evaluate the functional systems of the central nervous system. EDSS scores range from 0, which indicate no disability, to 10, which indicate death due to MS, with an increment interval of 0.5. Fig. 1 shows the EDSS scores range with its corresponding disability level and with the progression of the disease. To assist EDSS, eight neurological Functional Systems (FS) should be scored by an expert. The scoring range for these eight neurological FS examinations is between 0-4 to 0-15 [9]. The lowest score means normal FS, while the highest score means complete loss of function in a particular neurological FS. Scoring the MS patient's disability level using EDSS is time-consuming requires expert knowledge and inter-and intra-subject variation.



Fig. 1. EDSS Scores Range with its Corresponding Disability Level and the Progression of the Disease [9].

An automated method to predict MS-patient disability level using a fully automated feature extraction is challenging due to the high variety of MRI inhomogeneous of different image sizes, brain size, image density range, MRI Tesla, and MS type. Some of the MS patients have lesions in the brain, the spinal cord, or both. Furthermore, some MS-lesions are

clinically silent, or they can consider as silent inflammation that makes the prediction of MS-patients disability level using brain MRI is not an easy task.

Each side of the brain contains four lobes, and each brain lobe is responsible for controlling specific human activities and tasks. The frontal lobe is significant for cognitive functions and voluntary movement or activities control. The parietal lobe processes temperature, taste, touch, and movement information. While the occipital lobe is primarily responsible for vision. The temporal lobe processes memories, integrating them with sensations of taste, sound, sight, and touch [1]. Brain abnormalities such as MS-lesion in each of the brain lobes may directly affect the FS that is related to its brain lobes. Thus, classifying brain abnormalities based on brain lobes can help to predict which human activities or tasks can be affected by the abnormalities. Furthermore, it clinically proved that the MS lesions near the periventricular brain area significantly correlate to the patient's disability [22, 21, 23]. Hence, identifying the MS lesion based on the brain periventricular area is significant for MS disability prediction.

This study aims to predict clinical MS patients' disability levels using a fully automated feature extraction, single MRI scan, single MRI protocols and without patient follow-up.

Furthermore, this study seeks to identify the most correlated MRI features to the MS patients' disability levels.

The structure of this paper is as follows. Section II will present a summary for the recent related work. Section III will explain the dataset, pre-processing, feature extraction and method used in this study. Section IV will present the results of the method we used. Sections V will present the discussion, conclusion and main limitations of this study.

II. RELATED WORK

Multiple Sclerosis disability prediction has been active research in the last few years. MS is a clinically heterogeneous disease. Furthermore, traditionally MRI and patient disabilities have a weak correlation. Thus, most of the previous studies used supporting non-raw MRI data to support MS disabilities prediction. The supporting data include general patient information such as age and gender, clinical information such as MS types and treatment plans, radiological information such as lesion type, lesion location and manual lesion segmentation. Table I, summarises the recent previous studies on MS disability prediction. As a consequence of using supporting non-raw MRI data, all previous studies can consider using manual or semi-automatic feature extraction [10,11,13,14,16,17].

TABLE I. SUMMARIES THE RECENT PREVIOUS STUDIES ON MS DISABILITIES PREDICTION

Author, year	Type of disability prediction	Type of required data				Study duration (years)	Required patient follow up	Performance
		Raw MRI	Radiological	Clinical	General patient information			
Tommasin, 2021 [12]	Disability progression	Yes	Yes	Yes	Yes	2-6	Yes	Accuracy of 0.79
Pellegrini, 2020 [13]	Disability progression	No	Yes	Yes	Yes	2	Yes	All C-indices ≤ 0.65
Pinto 2020 [18]	Disability progression	No	Yes	Yes	Yes	1-10	Yes	Best AUC=0.89 ± 0.03 within two years
Law,2019 [15]	Disability progression	No	Yes	Yes	Yes	2	Yes	AUC of 61.8%
Dekker 2019 [19]	Disability progression	Yes	Yes	Yes	Yes	6-12	Yes	$R^2 = 0.56$ for 6-year and $R^2 = 0.38$ for 12- Year
Zhao 2017 [20]	Disability progression	No	Yes	Yes	Yes	5	Yes	Best accuracy of 75%
Colato,2021 [14]	Future disability progression	Yes	Yes	Yes	Yes	3.25	Yes	C-index of 0.72
Tousignant 2019 [21]	Future disability progression	Yes	Yes	Yes	Yes	1	Yes	AUC of 0:66.
Colato,2021 [14]	Cognitive worsening	Yes	Yes	Yes	No	3.25	Yes	C-index of 0.72
Dekker 2019 [19]	Cognitive worsening	Yes	Yes	Yes	Yes	6-12	Yes	$R^2 = 0.26$ for 6-year and $R^2 = 0.14$ for 12- Year
Barile, 2021 [22]	Predict three EDSS groups prediction: low, medium, and high	Yes	Yes	No	Yes	7	Yes	RMSE of 0.92 ± 0.28
Roca, 2020 [16]	Predict EDSS groups with a step of 1 EDSS	Yes	Yes	No	Yes	2	Yes	MSE score of 3 and EDSS score error of 1.7
Marzullo , 2019 [17]	EDSS prediction	Yes	Yes	No	No	2.5-6	Yes	Average RMSE of $1:08 \pm 0:09$

The main limitations of previous studies can be summarized as follow: First, using radiological or clinical data which require human interaction and expert knowledge. Second, using a huge amount of input data. Third, all are cohort studies and require patient follow-up. Fourth, neglecting spinal cord lesions. Fifth use more than MRI protocols. Sixth, using manual or semi-automated feature extraction which required human interaction [12,15,18].

Compared to the related work, this study is using a single brain MRI protocol and without patient follow up with full automated feature extraction.

III. MATERIALS AND METHODS

A. Patients

2D FLAIR MRI for 65 patients from two datasets was used in this study. All patients had confirmed diagnosis of MS with an EDSS scored by an expert. The first dataset was collected at MS-Clinic, Baghdad Teaching Hospital, Medical City Complex, Baghdad, Iraq. It consists of 48 patients, 36 females and 12 males, with an average age of 33 years ranging from 15 to 55 years. The MRI scan was collected between 2016 and 2021. 1.5 Tesla came from more than 20 centers, average EDSS score of 2 ranged from 0 to 5. The second dataset consists of 17 patients, 11 females and 6 males, with an average age of 33 years ranging from 22 to 46 years. The MRI scan was collected between 2017 and 2018. 3 Tesla came from two centers, average EDSS score of 1 ranged between 0 and 6. It was collected at King Fahad General Hospital, Medina, Saudi Arabia.

Typically, MS-lesion considers as a gold standard of brain abnormalities. The MS-lesion in FLAIR MRI is defined as an area of focal hyperintensity. Moreover, the MS-lesions are round to ovoid in shape and range in size from a few millimeters to more than one or two centimeters in diameter [23]. Lesion type, location, size, and lesion number are the most important characteristics that describe brain abnormality for MS lesions. From normal visual observation, it can be seen that the lesion has a weak correlation with the EDSS score. Fig. 2 shows an example of FLAIR MRI for patients with different EDSS scores. It is clear that the size, shape, and number of focal hyperintensity areas are weakly correlated to the EDSS. The yellow circles circulate the focal hyperintensity areas, mostly considered as MS lesions.

B. Methodology

The proposed methodology can be divided into six stages: input data, pre-processing, feature extraction, feature selection, disability prediction algorithm and performance evaluation. The overall proposed methodology is summarized in Fig. 3.

- Input data: Single brain MRI and single MRI protocols (FLAIR) have been used in this study. Due to the different behaviours of MS disease between patients with a lesion at spinal cord or not. A small portion of radiological data has been used to discrimination between patients with a lesion at the spinal cord or not. No patient follow-up is required.
- Pre-processing: To transform the raw data into a useful and efficient format, five stages of the pre-processing

processes have been used. They are explained in detail in the next paragraph.

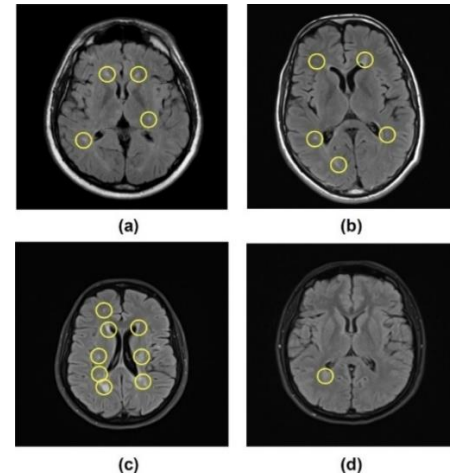


Fig. 2. FLAIR MRI for MS Patients with different EDSS Scores. (a) 29 Years Old Patient with EDSS = 0, (b) 31 Years Old Patient with EDSS = 1, (c) 39 Years Old Patient with EDSS = 2, (d) 35 Years Old Patient with EDSS = 4.

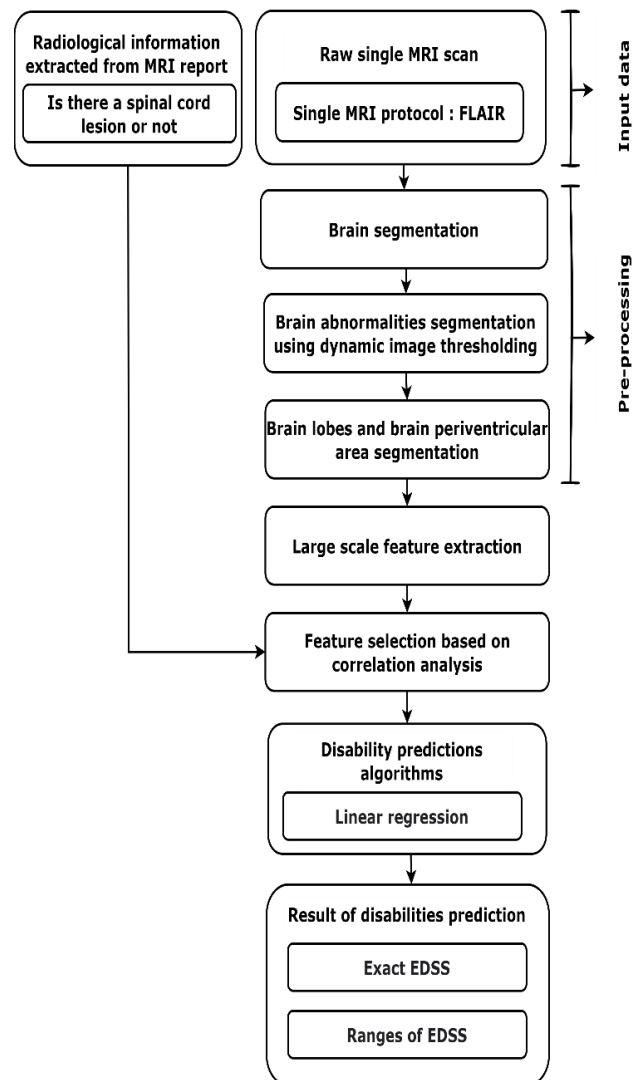


Fig. 3. Flowchart for the Overall Proposed Methodology.

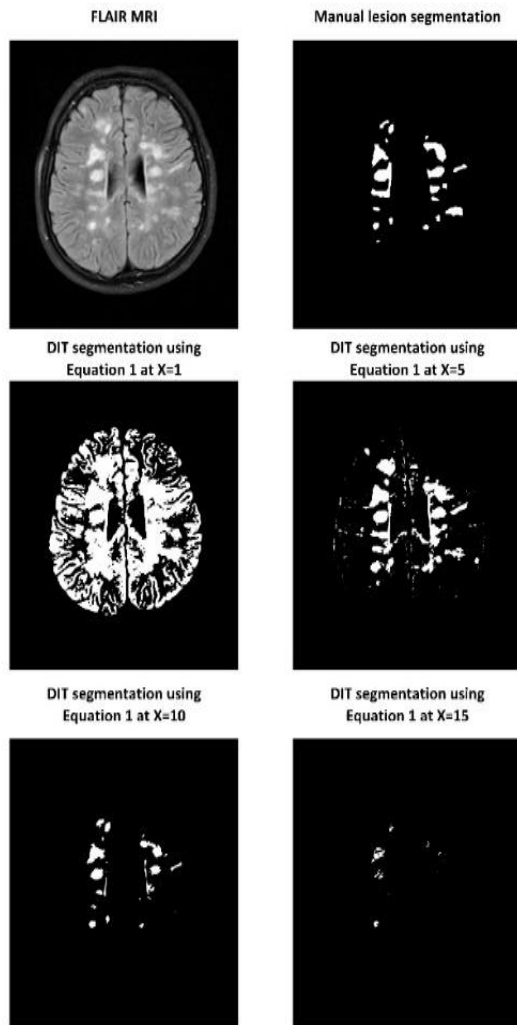


Fig. 4. Examples of Dynamic Image Thresholding (BIT) Segmentation using (1) in Comparison with Manual Lesion Segmentation.

The brain segmentation process is used to segment the brain area by removing the skull from an MRI image, keeping only the area occupied by the brain, the dark space between the skull and brain which is occupied by the CSF used to segment the brain area. Brain Extraction Tool (BET) [20] has been used for this purpose.

Segment brain abnormalities areas associated with MS disabilities are significant for disability prediction. Multiple sclerosis is a clinically heterogeneous disease. MS brain abnormalities had high variations in size, shape, number, and location. In addition to the high variation of MRI scans in size, quality, Tesla, and density among MS patients. Thus, brain abnormalities segmentation is challenging. Our proposed Dynamic Image Thresholding (DIT) method based on the mean and standard deviation of brain volume has been proposed to segment brain abnormalities. Based on the characteristic of FLAIR MRI, the brain abnormalities in FLAIR MRI are typically hypertension. To identify which level of brain hypertension has the highest correlation to the MS disability. Different values of image thresholding have been performed using (1) and (2) to investigate which level has

the highest correlation to the patient's disabilities. The image thresholding was performed with a different thresholding level increment by a step value of 0.05 of the mean and standard deviation above the mean. The step value of 0.05 was chosen to be small enough to investigate the effect of every small change in brain hypertension level. Typically, the standard deviation of brain volume has a much smaller value than the mean value. Thus, the increment value of (2) is much smaller than (1). Fig. 4 and Fig. 5 show examples of BIT segmentation using (1) and (2), respectively, at different values of X.

$$Th_1 = \mu + 0.05 * X * \mu \quad (1)$$

$$Th_2 = \mu + 0.05 * X * \sigma \quad (2)$$

Where μ = mean density value of whole-brain volume.

X=1,2, 3, until the image thresholding value segment nothing.

σ = patient-based density standard deviation for whole-brain volume.

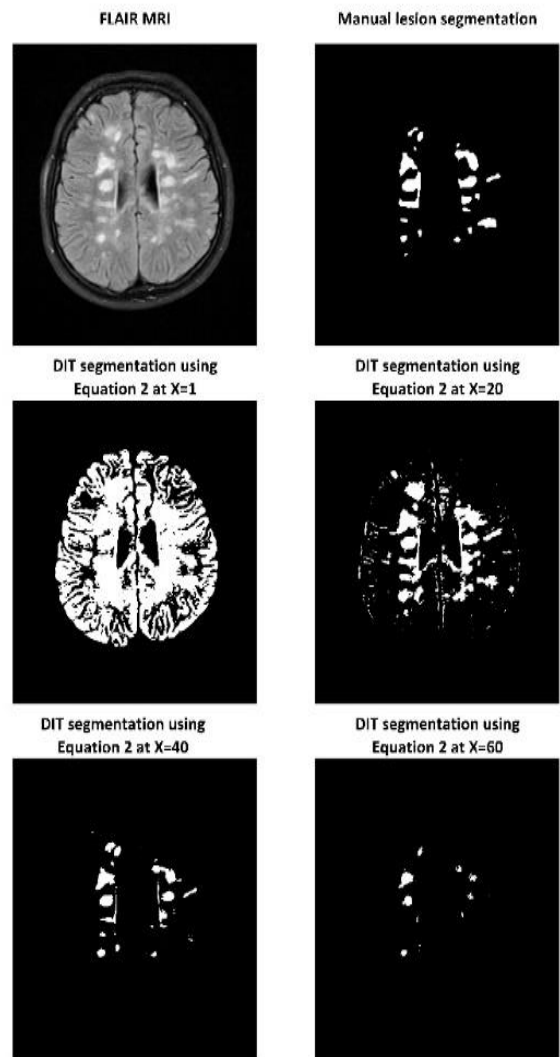


Fig. 5. Examples of Dynamic Image Thresholding (BIT) Segmentation using (2) in comparison with Manual Lesion Segmentation.

The segmented areas in Fig. 4 at X=10 represent brain abnormalities areas that are very close to the seen brain abnormalities (seen lesion). In other words, the segmented area in Fig. 4 at X=10 segments the brain areas, which have a very close level of image hyperextension to the seen lesion. Moreover, it is clear that the segmented area in Fig. 4 at X<10 segments brain abnormalities at a level of image hyperextension less than the level of the seen lesion, while at X>10 is the opposite, the levels of image hyperextension, which represent brain abnormalities at X<10 and X>10 are hard or impossible to detect by human eyes.

Automated segmentation of brain lobes and periventricular brain area is challenging due to the following: First, high variation of the human brain in shape, size and abnormalities. Second, high variation of brain MRI in quality, size and number of slices. Third, segmentation of brain lobes and periventricular brain area is usually performed using 3D MRI. Thus, using a 2D MRI with a small number of MRI slices is not an easy task.

three main steps: First, resize the 3D brain model as same as the 2D brain volume. Second, segment both brain volume and 3D brain model into sixteen identical sections. Third, label each section in the brain volume to it is corresponding 3D brain model lobes. An example of the brain lobes segmentation is shown in Fig. 7(b), (d) and (f) for the axial, sagittal and coronal brain plan, respectively.

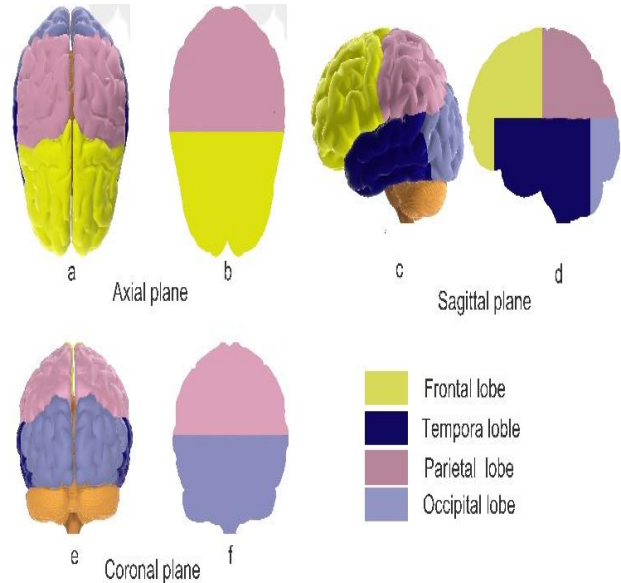


Fig. 7. 3D Brain Model with Lobes Labeled Compared to the Output of our Proposed Automated Lobes Segmentation for Axial, Sagittal, and Coronal Planes. a), c) and e) Represent the 3D Brain Model with Lobes Labeled, While b), d) and f) Represent the Output of the Same 3D Brain Model with Lobes Labeled by our Proposed Automated Lobes Segmentation.

Furthermore, the periventricular brain area is segmented by masking the central 75% of brain volume that can approximately cover the whole brain periventricular area. The periventricular lesions are located adjacent to the brain ventricles system, the periventricular lesion and ventricles system shown in Fig. 8. The output of our proposed brain periventricular is segmentation also shown in Fig. 8.

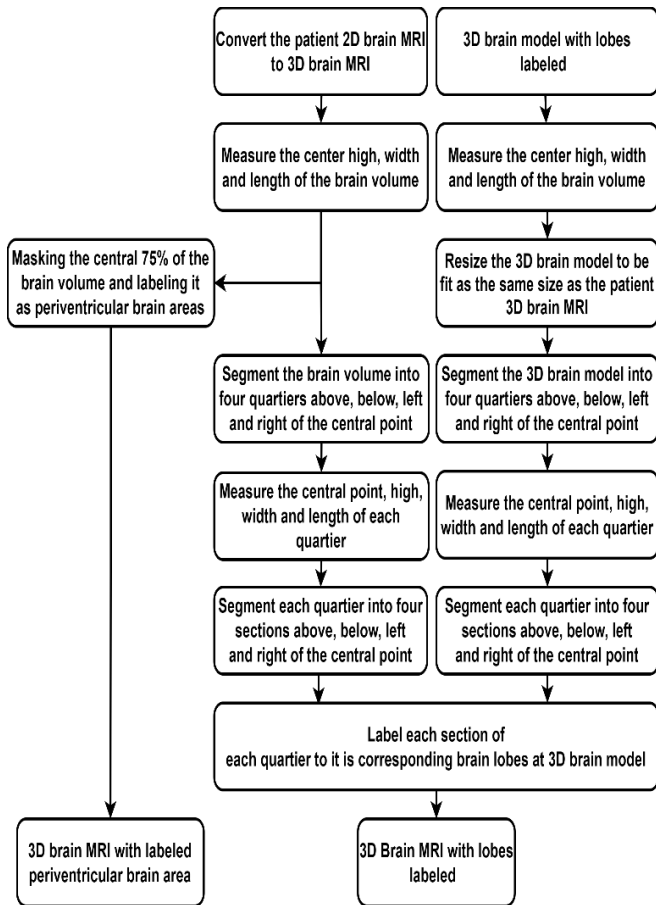


Fig. 6. Flowchart for the Automated Brain Lobes and Brain Periventricular Area Segmentation.

However, an automated method to approximately segment brain lobes and periventricular brain area for 2D MRI has been proposed. A flowchart for the overall process is shown in Fig. 6. The brain lobes segmentation was performed based on 3D brain model with lobes labelled. The axial, sagittal and coronal brain plan of 3D model is shown in Fig. 7(a), (c), and (e), respectively. The brain lobes segmentation is based on

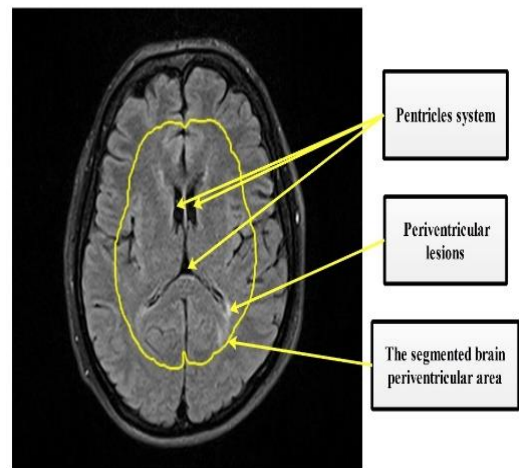


Fig. 8. Axial MRI Cross-Section Slice is Shown Periventricular Lesion and Ventricles System with the Segmented Brain Periventricular Area inside the Yellow Line.

- Feature extraction: Due to the high level of MRI inhomogeneous, a large-scale ratio-based feature extraction has been used. The features were extracted from brain abnormalized areas which were segmented automatically using our proposed DIT method.

Based on McDonald diagnostic criteria [9], FLAIR MRI features and disease characteristics for certain types of features have been extracted based the types of features are lesion locations, shape, size, number and density [7]. All previously extracted features were classified based on the location of brain lobes and brain periventricular areas.

Then, 3D based ration features have been generated based on the above-mentioned extracted features using (3), (4) and (5). The features have been generated for all possibilities of F, L and V. Total of 8200+ features have been extracted for every patient. All features are extracted automatically and without human interaction against the related work using manual or semi-automated feature extraction [10,11,13,14,16,17].

$$\frac{\text{The value of (F) located at (L) of whole brain volume}}{\text{The value of (F) at whole brain volume}} \quad (3)$$

$$\frac{\text{The value of (F) located at (L) of brain periventricular area}}{\text{The value of (F) at (V)}} \quad (4)$$

$$\frac{\text{The value of (F) of (V)}}{\text{The value of (F) at whole brain volume}} \quad (5)$$

Where $F=$ could be one of the following: size, number, mean, maximum, minimum and standard deviation.

$L=$ could be one of the brain lobes: frontal, parietal, temporal and occipital.

$V=$ could be whole brain volume or periventricular brain area.

- Feature selection: To reduce the dimension of the extracted features a filter-based features selection based on correlation analysis has been used to select the highest correlated features using Pearson correlation. Pearson correlation has been used based on try and error.
- Disability prediction: A linear regression algorithm has been used to predict patient disabilities. All prediction algorithms have been performed using the MATLAB 2019a software environment. The linear regression parameters settings are listed in Table II.

TABLE II. LINEAR REGRESSION PARAMETER SETTINGS

Model Type	Model Parameters
Regression	Model name: Linear regression Preset: linear Terms: linear Robust option: off

The linear regression algorithm has been used for the following reasons: First, the linear regression algorithm shows a good performance in predicting both exact EDSS and different ranges of EDSS. Second, able to predict the EDSS value even if it does not exist in the training data. Third, more suitable to work with an unbalanced dataset. Due to the

rareness of the disease, most of the MS datasets are leaking of class balance.

- Performance evaluation: The performance of different types of disabilities predictions has been tested for disabilities prediction, including a different range of EDSS and exact EDSS. The EDSS has been used as a golden standard to score patient disabilities. 5-fold cross-validation has been used. The evaluation metrics that have been used are RMSE, R-Squared, MSE and MAE.

IV. RESULTS

More than 8200 features were automatically extracted from the brain abnormalities area segmented by DIT to predict MS patient disabilities. Normally, the EDSS step value is 0.5. However, to investigate the ability of disability prediction, the performance was tested for five levels of EDSS steps starting from 0.5, representing normal EDSS steps to an EDSS step of 2.5. A significant correlation between the extracted feature and the EDSS was found for MS patients after splitting them into four groups based on MRI Tesla and MS lesion location in the spinal cord. Furthermore, no significant correlation was found before patient grouping.

Tables III and IV present the EDSS prediction performance for exact EDSS and different ranges of EDSS. The best performance was with an average RMSE of 0.6 and for the EDSS step of 2. In comparison with the performance of previous studies which predicted exact EDSS and range of EDSS using manual or semi-automated feature extraction and required patient follow-up, the result shows a promising result to predict MS disabilities using full automated features extracted and without patient follow-up.

TABLE III. THE PREDICTION RESULTS FOR PATIENTS WITH A LESION AT BRAIN ONLY

Step value (EDSS)	1.5 MRI Tesla				3 MRI Tesla				Average RMSE
	RMSE	R-Squared	MSE	MAE	RMSE	R-Squared	MSE	MAE	
0.5*	1.071	0.38	1.146	0.917	1.783	0.15	3.179	1.2	1.427
1	1.1397	0.32	1.299	1.001	1.296	0.28	1.276	1.015	1.217
1.5	0.772	0.38	0.596	0.679	1.043	0.42	1.088	0.979	0.907
2	0.536	0.39	0.286	0.431	0.806	-0.9	0.650	0.626	0.671
2.5	0.493	0.72	0.246	0.307	0.778	-0.2	0.605	0.619	0.641

*Normal EDSS step

TABLE IV. THE PREDICTION FOR PATIENTS WITH LESIONS AT BRAIN AND SPINAL CORD

Step value (EDSS)	1.5 MRI Tesla				3 MRI Tesla				Average RMSE
	RMSE	R-Squared	MSE	MAE	RMSE	R-Squared	MSE	MAE	
0.5*	1.03	0.52	1.06	0.84	0.51	0.68	0.25	0.42	0.77
1	1.03	0.56	1.07	0.83	0.70	0.28	0.49	0.58	0.87
1.5	0.76	0.64	0.58	0.58	0.64	0.31	0.41	0.60	0.70
2	0.61	0.46	0.37	0.50	0.50	-0.08	0.25	0.45	0.55
2.5	0.56	0.36	0.31	0.47	0.55	-0.24	0.31	0.49	0.55

*Normal EDSS step

V. DISCUSSION AND CONCLUSION

MS-lesion location and MRI Tesla play an important role to predict patient disability levels. MS-lesion can be found on the brain or spinal cord or both of them. Lesion locations have a high impact on the MS patient's disability level. In this study, a single brain MRI was used to predict EDSS value for those with a lesion in the brain and spinal cord. In addition, a small portion of radiological data extracted from MRI reports has been used to identify the location of the lesion in the spinal cord or not. It is clear that the image quality of MRI affects the performance since MRI Tesla of 3 outperformed the results of MRI Tesla of 1.5. This is due to the differences between the image quality of MRI Tesla of 1.5 and 3. Therefore, increasing the magnet strength will improve the qualities of extracted features to represent brain abnormalities resulting in better prediction performance. From the result, it is clearly shown that by grouping MS patients according to MRI Tesla and lesion location in brain MRI, the performance was improved. It is due to two reasons. First, different MRI Tesla provides different image characteristics in terms of clarity, details, and noise reduction and provides different amounts of signal received from the human body during an MRI scan [24]. Second, different brain and spinal cord lesion locations led to different behaviors of different disease symptoms and progression [23].

The performance of EDSS prediction algorithms was tested with different EDSS steps from 0.5 to 2.5 to investigate which EDSS step the algorithms provide higher performance. EDSS step of 0.5 represents the traditional scoring of disability level using the clinical physical examination. From Tables III and IV, the overall best performance has been obtained with EDSS step of 2.

The proposed EDSS prediction based on DIT shows a promising result to predict the level of EDSS on the tested datasets. Consequently, the DIT have a good representation of brain abnormalities.

The study's main limitations are the lack of high sample size due to the rareness of the disease. It is highly recommended to group MS patients based on MRI Tesla and the location of lesions in the brain only or brain and spinal cord. The proposed method presents promising results for future studies to predict patient disability levels with fully automated feature extraction using single MRI scan without non-MRI data, which may contribute to shorter diagnosis time. Furthermore, this can help better understand and monitor the progression of MS disease.

ACKNOWLEDGMENT

We would like to express our thanks to MS-Clinic, Baghdad Teaching Hospital, Medical City Complex, Baghdad, Iraq, and King Fahad General Hospital, Medina, Saudi Arabia for their help and support in terms of collecting data.

REFERENCES

- [1] Ridler, "New biomarker predicts disability in MS.," *Nat. Rev. Neurol.*, vol. 14, no. 7, p. 380, 2018.
- [2] B. Nourbakhsh and E. M. Mowry, "Multiple Sclerosis Risk Factors and Pathogenesis.," *Continuum (Minneapolis, Minn.)*, vol. 25, no. 3, pp. 596–610, Jun. 2019.
- [3] J. Correale and M. I. Gaitán, "Multiple sclerosis and environmental factors: the role of vitamin D, parasites, and Epstein-Barr virus infection.," *Acta Neurol. Scand.*, vol. 132, no. 199, pp. 46–55, 2015.
- [4] S. M. K. Gamage et al., "Multiple Sclerosis Patients with Markedly Low Intrathecal Antibody Response in Sri Lanka," *Mult. Scler. Int.*, vol. 2018, p. 5342936, 2018.
- [5] S. Nguengang Wakap et al., "Estimating cumulative point prevalence of rare diseases: analysis of the Orphanet database," *Eur. J. Hum. Genet.*, vol. 28, no. 2, pp. 165–173, 2020.
- [6] W. L. Cheong, D. Mohan, N. Warren, and D. D. Reidpath, "Multiple Sclerosis in the Asia Pacific Region: A Systematic Review of a Neglected Neurological Disease," *Front. Neurol.*, vol. 9, p. 432, 2018.
- [7] P. Browne et al., "Atlas of multiple sclerosis 2013: a growing global problem with widespread inequity," *Neurology*, vol. 83, no. 11, pp. 1022–1024, 2014.
- [8] M. Filippi et al., "Assessment of lesions on magnetic resonance imaging in multiple sclerosis: practical guidelines," *Brain*, vol. 142, no. 7, pp. 1858–1875, 2019.
- [9] J. F. Kurtzke, "Rating neurologic impairment in multiple sclerosis: an expanded disability status scale (EDSS).," *Neurology*, vol. 33, no. 11, pp. 1444–52, 1983.
- [10] E. Martínez-Heras et al., "Characterization of multiple sclerosis lesions with distinct clinical correlates through quantitative diffusion MRI," *NeuroImage Clin.*, vol. 28, p. 102411, 2020.
- [11] A. D. Almutairi et al., "Lesion load assessment among multiple sclerosis patient using DIR, FLAIR, and T2WI sequences," *Egypt. J. Radiol. Nucl. Med.*, vol. 51, no. 1, p. 209, 2020.
- [12] S. Tommasin et al., "Machine learning classifier to identify clinical and radiological features relevant to disability progression in multiple sclerosis," *J. Neurol.*, 2021.
- [13] F. Pellegrini et al., "Predicting disability progression in multiple sclerosis: Insights from advanced statistical modeling," *Mult. Scler. J.*, vol. 26, no. 14, pp. 1828–1836, 2020.
- [14] E. Colato et al., "Predicting disability progression and cognitive worsening in multiple sclerosis using patterns of grey matter volumes," *J. Neurol. Neurosurg. Psychiatry*, vol. 92, no. 9, pp. 995–1006, 2021.
- [15] M. T. Law et al., "Machine learning in secondary progressive multiple sclerosis: an improved predictive model for short-term disability progression.," *Mult. Scler. J. - Exp. Transl. Clin.*, vol. 5, no. 4, p. 2055217319885983, 2019.
- [16] P. Roca et al., "Artificial intelligence to predict clinical disability in patients with multiple sclerosis using FLAIR MRI," *Diagn. Interv. Imaging*, 2020.
- [17] A. Marzullo et al., "Prediction of Multiple Sclerosis Patient Disability from Structural Connectivity using Convolutional Neural Networks," in 41st Annual International Conference of the IEEE Engineering in Medicine and Biology Society, EMBC 2019, 2019, pp. 2087–2090.
- [18] M. F. Pinto et al., "Prediction of disease progression and outcomes in multiple sclerosis with machine learning.," *Sci. Rep.*, vol. 10, no. 1, p. 21038, Dec. 2020.
- [19] I. Dekker et al., "Predicting clinical progression in multiple sclerosis after 6 and 12 years.," *Eur. J. Neurol.*, vol. 26, no. 6, pp. 893–902, Jun. 2019.
- [20] Y. Zhao et al., "Exploration of machine learning techniques in predicting multiple sclerosis disease course.," *PLoS One*, vol. 12, no. 4, p. e0174866, 2017.

- [21] A. Tousignant, P. Lemaître, D. Precup, D. L. Arnold, and T. Arbel, "Prediction of Disease Progression in Multiple Sclerosis Patients using Deep Learning Analysis of MRI Data," in *Proceedings of The 2nd International Conference on Medical Imaging with Deep Learning*, 2019, vol. 102, pp. 483–492.
- [22] B. Barile, A. Marzullo, C. Stamile, F. Durand-Dubief, and D. Sappey-Marinier, "Ensemble Learning for Multiple Sclerosis Disability Estimation Using Brain Structural Connectivity," *Brain Connect*, 2021.
- [23] M. Filippi et al., "Assessment of lesions on magnetic resonance imaging in multiple sclerosis: practical guidelines," *Brain*, vol. 142, no. 7, pp. 1858–1875, Jul. 2019.
- [24] J. M. Wardlaw et al., "A systematic review of the utility of 1.5 versus 3 Tesla magnetic resonance brain imaging in clinical practice and research," *Eur. Radiol.*, vol. 22, no. 11, pp. 2295–2303, 2012.

Random and Sequence Workload for Web-Scale Architecture for NFS, GlusterFS and MooseFS Performance Enhancement

Mardhani Riasetiawan, Nashihun Amien

Department of Computer Science and Electronics
Faculty of Mathematics and Natural Sciences, Universitas Gadjah Mada, Yogyakarta, Indonesia

Abstract—The problem in the data storage method that can support the data processing speed in the network is one of the key problems in big data. As computing speed increases and cluster size increases, I/O and network processes related to intensive data usage cannot keep up with the growth rate and data processing speed. Data processing applications will experience latency issues from long I/O. Distributed data storage systems can use Web scale technology to assist centralized data storage in a computing environment to meet the needs of data science. By analyzing several distributed data storage models, namely NFS, GlusterFS and MooseFS, a distributed data storage method is proposed. The parameters used in this study are transfer rate, IOPS and CPU resource usage. Through testing the sequential and random reading and writing of data, it is found that GlusterFS has faster performance and the best performance for sequential and random data reading when using 64k block data storage. MooseFS uses 64k power storage blocks to obtain the best performance in random data read operations. Using 32k data storage blocks, NFS achieves the best results in random writes. The performance of a distributed data storage system may be affected by the size of the data storage block. Using a larger data storage block can achieve faster performance in data transmission and performing operations on data.

Keywords—Component; network storage; container; NFS; GlusterFS; MooseFS; random workload; sequence workload

I. INTRODUCTION

The current digital era is driven by data derived from a variety of information, both individuals, companies and governments, which is more available than ever before. Currently, various information technology-based companies produce big data [1]. Large volumes in big data require large data storage. Digital products such as Twitter can generate 7 Terabytes (TB) a day of data, while Facebook produces 10 TB of data a day. Several similar enterprise companies have the same tendency to produce data per day [2].

Big data storage and processing needs require huge resources [9]. The gap between computing and data storage is quite large. With multicore technology in the processor, the ability of the CPU has increased for big data needs. However, the ability of data storage to serve data processing and storage still experiences its obstacles. The characteristics of the physical storage media account for most of the slow data storage performance. Even though optimization has been carried out in the Input / Output (I/O) layer in data storage, the

I/O layer remains volatile. Problems related to the inefficiency in data management in storage media become more visible when multi-tasking big data in a shared resource environment [3].

An architecture is needed that can match resources with storage and data processing needs [8]. The web-scale architecture can handle the fast-growing processing and storage needs efficiently without rearranging the existing architecture [4]. As computation speed increases and cluster size increases, the I/O and network processes associated with intensive data use cannot keep up with the growth and data processing speed. Data processing applications will experience latency problems from long I/O [5].

Problems in data storage methods in the network that can support data processing speed are one of the crucial issues in big data. The research was conducted by analyzing the results of observations and exploration of storage performance by comparing architectures and file systems by considering parameters such as I/O performance, seek time, memory, and network usage. The results of data analysis from this study are expected to be a reference in building a data storage center for big data needs.

II. LITERATURE REVIEW

Research on measuring the performance of data storage was conducted [10]. This study measures the performance of high-performance data storage systems on baremetal clouds such as AWS, Azure, CGE, and OCI that run Hadoop. The test parameters in this research are I/O, CPU, memory and throughput. Researchers run the method for benchmarking I/O with TestDFSIO, Flexible I/O tester (fio). To test the use of CPU resources using the K-means, Terrasort, Pagerank, and Wordcount algorithms which are run on the server to be tested. Another test was the use of network resources running K-means and Terrasort using 10TB of data. The results indicate that Hadoop systems running on high-performance data storage are a good choice for building high-performance virtual clusters to process shared workloads. In the results of this study, high-performance storage performance makes a significant impact on HDFS-based workloads with a large number of virtual cores. Non-RAID storage performs six times better with increased volume and CPU per server compared to clusters containing a large number of low-end servers. With a model like the one developed by researchers,

we can get better scalability and efficiency on high-capacity servers and bare metal servers suitable for seeking increased performance and cost savings [10].

The research performed a statistical analysis of the variability of write and read operations on parallel file systems [11]. This study uses six factors to be tested, namely Application Programming Interface (API), I/O strategy, request size, access pattern, stripe size, and stripe count. The researcher used the ANOVA F-test method to generate a comprehensive model from the observations that had been made. The results of this study indicate that these various factors within the range of values evaluated affect performance in a way that is indistinguishable from the presence of errors in the experiments performed. It should be noted that the conclusions of this study are only statistically valid for the range of values considered. For other values and a different set of other significant factors can emerge.

One of the earliest and most successful distributed systems was developed by Sun Microsystems and is known as the Sun Network Filesystem (or NFS) [12]. To define NFS, Sun developed an open protocol that simply defines the message format used to communicate by the client and server so that other groups outside Sun Microsystems can develop their own NFS.

Gluster is an open source, software-only file-based NAS scale-out platform. This enables enterprises to combine a large number of commodity data storage devices and compute resources into a single storage pool resulting in high performance and centrally managed storage. Both capacity and performance can scale independently on demand, from a few terabytes to several petabytes, using on-premises hardware and public cloud storage infrastructure. Combining affordable hardware with a scaling approach, users get radically better price and performance, in an easy-to-manage solution that can be configured for the most demanding workloads.

GlusterFS is designed for several purposes such as elasticity, linear scaling, and scale-out. The elasticity in GlusterFS is the idea that an enterprise should be able to flexibly adapt to data growth (or reduction) and add or remove resources to the storage pool as needed, without disrupting existing systems.

Linear Scaling is that twice the amount of system storage will provide twice the performance. What is observed in this case is twice with the same average response time for each event in the external file system I/O system i.e., how long the NFS client waits for the file server to return the information associated with each NFS client request. Traditional filesystem models and architectures cannot be scalable in this way and therefore can never achieve performance at true linear scale.

Gluster is designed to provide a scale-out architecture for performance and data storage capacity requirements. This implies that the system must be able to increase (or decrease) along some dimensions. By combining the data storage, CPU, and I/O resources of a large number of systems with affordable hardware. If you want to add more capacity to your

scale-out system, you can add more disks at a lower cost. In practice, both performance and data storage capacity can be linearly increased in Gluster.

As a distributed file system, Moose File System (MooseFS) has been widely used in industry. As the architecture built by MooseFS becomes more efficient to increase the level of data handling, companies such as Douban (a Chinese social networking service website) and Lenovo have benefited greatly from using MooseFS. MooseFS has just been released as an open-source project in the GitHub repository since 2016, and some research has been done on MooseFS [7].

MooseFS consists of four main parts: client, chunk server, master server and metalogger. The master server maintains all the metadata of the system files. The server chunk is the storage unit in MooseFS. The basic unit in data storage is called a chunk, and all chunks are managed by the chunk server. When a client wants to get services from MooseFS, the server and client first interact with the master server for metadata information retrieval operations, and then communicate with the chunk server to read or write data. Metaloggers are backups of the master server. Its main function is to periodically download metadata from the master server to be promoted as new in case of failure. In the general case, a single metalogger is sufficient to handle failures.

Metalogger stores metadata (such as permissions and last access of data) and file and directory hierarchies in master main memory and then performs a permanent copy of the metalogger. With this, MooseFS gives users the global namespace of the system. The MooseFS client accesses the file system by mounting the namespace in the local file system. The client can perform the operation by communicating to the master server which directs the client to the chunk server.

In MooseFS, each file has a purpose, namely a certain number of copies that must be preserved. When the client writes data, the master server sends it a list of server chunks where the data will be stored. Then, the client sends data to the first chunk server which instructs the other chunk servers to replicate the files synchronously. MooseFS uses `msfmount` to communicate between users and `msfmount` itself is based on Filesystem Userspace (FUSE) which means MooseFS can work with operating systems that use this mechanism such as Linux, FreeBSD, OSX and others.

III. METHODOLOGY

This section introduces the methods of studying network storage services. The method is developed around a test platform that allows us to run specific benchmarks. First, we aim to test client capabilities and network attaches storage design decisions. Then, use the test platform to measure the impact of these two aspects on performance under different workloads.

A. Overview

The environment that will be created for this research can be used as a prototype for centralized data storage and computing services. Users will be connected to the

environment via a wireless network. Docker has a non-permanent nature of data storage, so Docker needs to be integrated with external data storage methods so that data is permanently stored and accessed in a cluster. In this study, the availability of datasets prepared for computational purposes will be stored in an external file system (in this study is DFS) which is connected to the research environment created.

The data service in the environment to be built is expected to be able to produce dynamic data storage and processing. Storage and dynamic data processing in this research are that when a user accesses the service, the system will run Docker and create a directory automatically which will be tied to Docker that is running and used by the user. It is expected that by using data storage like this, the data in Docker will always be in its position when one user accesses the same data.

B. Goal

The aim of this research is to evaluate and analyse which file system is best among NFS, GlusterFS and MooseFS for big data storage and processing based on I/O performance, network transfer rate and CPU usage inside network storage cluster for data science environment.

In this study, we are using the black-box testing approach. We instrument a testbed in which one more test computers run the desired application-under-test. The Testing running several workloads inside Docker for reading and writing specific files to defined directory attached into network storage. In the meantime, testing tool writing an output file for collected data during testing execution.

We require tests to be repeatable and automated run testing scenario sequentially to get an average number of data at one time. Since we target three various network storage with write and read scenario using four different storage block, we need all scenario able to be performed without supervision and logged automatically.

C. Testbed

This study utilizes three storage clients connected for each network storage and mounted like local directory and using Docker to creating workloads. We are using three storage clients to simulate concurrent workloads running at the same time. Our test application receives benchmark test parameters,

which describe the sequence of operations to be performed. Then, the test application is operated remotely through Docker to generate workloads. Network storage clusters synchronize in the background and each client detect updated file listing generated from Docker workload. Once benchmark tools running from Docker, every parameter is going generated and written in the output file and processed to measure performance metrics. The testing runs workloads thirty times for each scenario with different block size.

We plan the testbed using Linux virtual server explain in Fig. 1. The server controls the experiments by running network storage clusters and clients installed with Docker container and host benchmark tools. Both clients and network storage clusters are attached to the virtual network interface. With this setup allow the server easily to manage and observe from the virtual server host. Linux virtual servers connected with 10Gbps network link.

D. Benchmark Performance

After knowing the design choices of network storage types, we use our testbed to check their influence on performance. We plan a methodology to calculate metrics related to read and write workloads. A workload is generated by the testing application based on a benchmark definition. A variable of reading and write workload with different storage block size. Besides, workload type can be specified to random or sequential to test how service reacts to different I/O.

Performance is calculated. We calculate (i) transfer rate between clients and storage server (ii) IOPS during random and sequential workload (iii) CPU usage in operating system user-space.

E. Network Attached Storage (NAS) under Test

This study comparing three network storage and limiting the analysis to the native client using Docker workload. Table I list considered technology specification of three network storages. Each network storage using different technologies, architecture and method to work with data and metadata. In such allow us to compare the impact of the technology design and architecture to handling different data workloads.

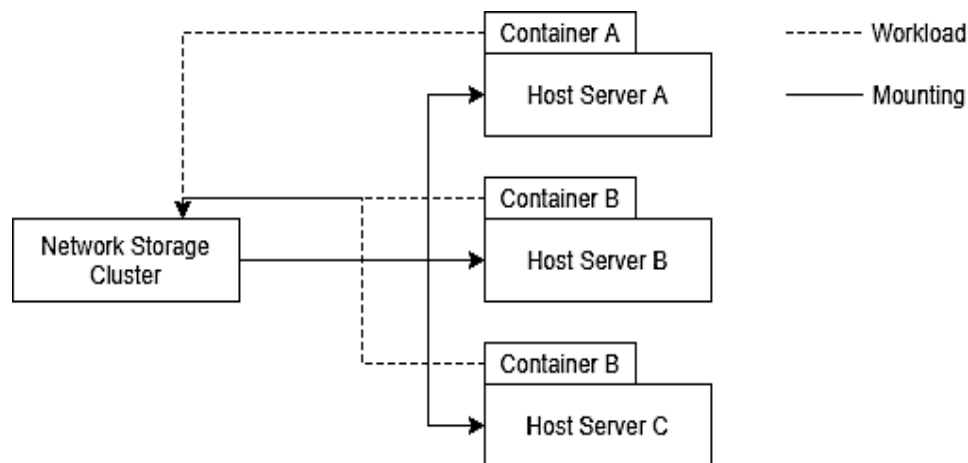


Fig. 1. Testbed Environment for Network Storage Workload Testing.

TABLE I. THE TECHNOLOGY SPECIFICATION

	NFS	GlusterFS	MooseFS
API Access	Remote Procedure Call (RPC), NFS Client	libglusterfs, Fuse, NFS, SMB, Swift, libgfapi	POSIX, FUSE MooseFS clients.
High Availability	Need additional softwear and hardware	Mirroring	Master – Slave
Architecture	Client – Server	Client – Server without metadata	Using master server to manage server
Metadata	Data and metadata are saving inside NFS	Using Elastic Hashing Algorithm instead of saving metadata	Saving metadata inside master server
Cache	Client side	Not usning cache	Using RAM inside storage server
Fault Tolerant	Need additional softwear and hardware	Eliminates server that is in status not available	Do quarantine against the server machine who can't perform I/O operations
Replication and Synchronization	Need additional software and hardware	Not replicating directly	Keep some copy of data.

IV. RESULT AND DISCUSSION

We evaluate the testing parameter with different storage block and network storages. Workload running from Docker to read or writing test file with random or sequential to write 10GB files for each task. Our experiment checks how the network storage will handle batches workload for reading and write using four different storage block: (i) 8k, (ii) 16k, (iii) 32k, dan (iv) 64k.

A. Transfer Rate

In data storage transfer rate can represent how many data can be transferred during the reading or writing process in one time. In general, with a higher transfer rate meaning the storage system able to process big data faster. In our methodology, we are trying to process 10 GB data with random and sequential data to be processed and transferred from the client into the storage cluster network. In Fig. 2, we can see the average result from transfer rate benchmark. In

random read and sequence read, GlusterFS having better transfer rate compared to NFS and MooseFS. GlusterFS transfer rate for random read workload increase with bigger storage block size. However, GlusterFS transfer rate performance for sequential read workload not affected by the storage block size. MooseFS with sequential read workload affected with the changes in block size with 32k and the performance in 64k quite same with 32k block size.

The result for random write, MooseFS having significant performance result with 64k storage block size with reaching 300MiB/s transfer. GlusterFS and NFS transfer rate for random write performance is not affected by the block size. In Sequence read workload the NFS having better performance than GlusterFS and MooseFS. The NFS performance reaching a peak with 32k storage block size and able to be reaching 1200MiB/s. However, the performance is dropping with a 64k block size. We believe in NFS performance dropping because of the bottleneck in the networks.



Fig. 2. Average Transfer Rate from Read and Write for Sequence and Random Workloads.

B. IOPS

IOPS refers to the maximum number of reads and writes to non-contiguous storage locations. These operations are typically dominated by seeking time, or the time it takes a disk drive to position its read/write heads to the correct location. We are trying to measure IOPS to identify IOPS between three network storages as shown in Fig. 3.

The result for this test showing IOPS affected with storage block. In random read and sequence read workload GlusterFS having the best performance with 8k storage block size. However, the IOPS performance dropping in 16k, 32k and 64k. MooseFS with random write having a better performance with 16k but it gradually decreases in 32k and 64k block size.

In random read, sequence read, and random write with MooseFS able to reach better performance. However, IOPS performance degraded with 32k and 64k block size. NFS having same degrade performance with 16k and 32k. However, in 64k block size NFS having better result than GlusterFS and MooseFS.

C. CPU Usage

The equations are an exception to the prescribed CPU usage in user space is part of this. A user-space program is any process that doesn't belong to the kernel. Shells, compilers, databases, web servers, and the programs associated with the desktop are all user space processes. If the processor isn't idle, it is quite normal that the majority of the CPU time should be spent running user space processes. This scenario able to crash the system or the environment and we need to restart the system.

Higher CPU usage causing process stuck in the system and causing a bottleneck in the data processing. In this study we

measure how efficient the network-attached storage using the processing resources.

Result in Fig. 4 showing the average result of CPU usage in userspace. We found CPU usage in the three network storage affected with different storage block size. NFS showing low CPU usage in random read, random write, and sequence read workloads. However, NFS in sequence writes using high CPU resources.

GlusterFS having high usage CPU resources when running sequence read workloads with around 25% - 30% CPU usages. GlusterFS with random read, random write and sequence write are affected with storage block size as we can see in Fig. 4 GlusterFS CPU usage lower with bigger storage block size. GlusterFS and NFS having a similar pattern with CPU usage is decreasing with bigger storage block size. In the meantime, MooseFS having increase CPU usage in 32k block size workload and CPU usage dropped with bigger storage block size.

D. NFS Performance

The results of the random read scenario transfer rate performance test on NFS show that 64k blocks have the highest yield, 32k in second place, then 16k and 8k in third and fourth place, as shown in Fig. 5. The results of the random write scenario transfer rate performance test on NFS show that 16k blocks have the highest yields, 32k in second place, then 64k and 8k in third and fourth place. The results of the transfer rate performance test for the sequence read scenario on NFS show that 64k blocks have the highest yield, 16k in second place, then 32k and 8k in third and fourth place. The results of the transfer rate performance test for the sequence write scenario on NFS show that 32k blocks have the highest yield, 64k in second place, then 16k and 8k in third and fourth place.

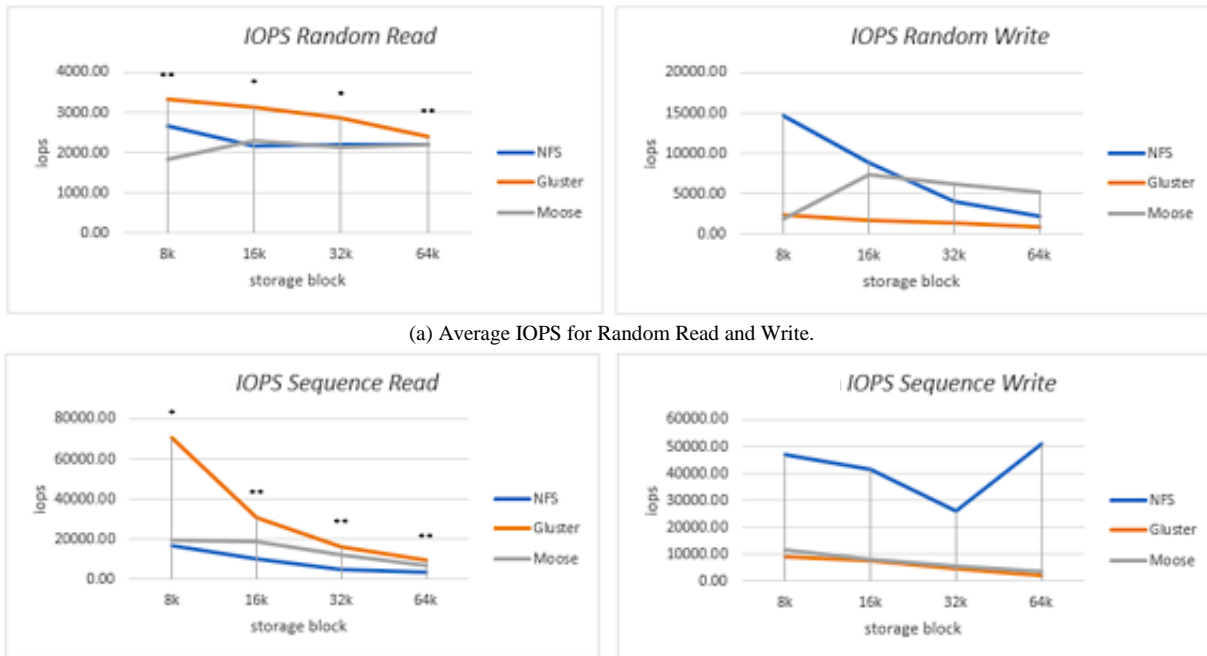
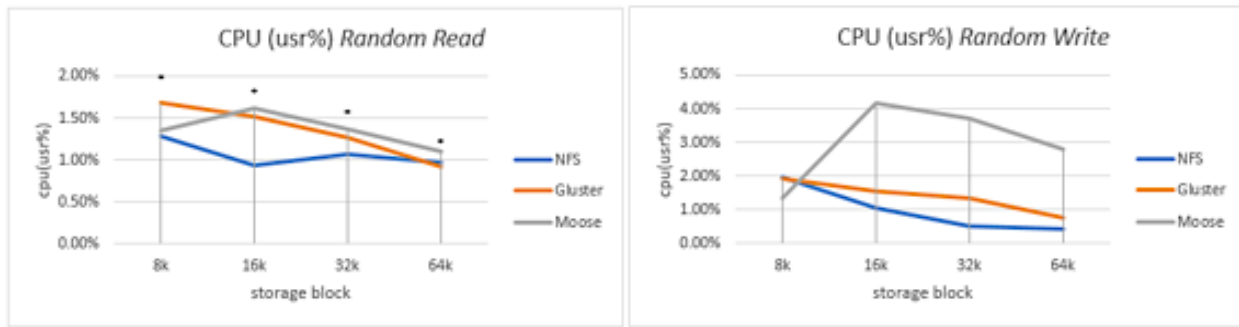
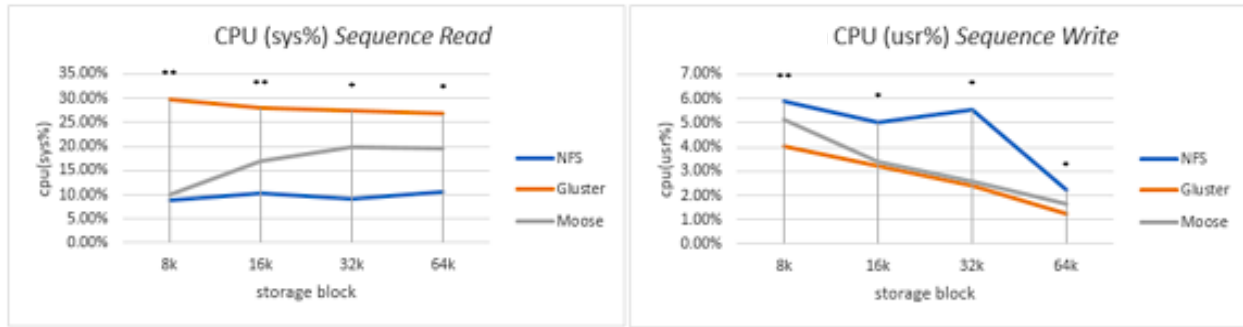


Fig. 3. Average IOPS from Read and Write for Sequence and Random Workloads.



(a) Average CPU (usr%) for random read and write



(b) Average CPU (usr%) for sequence read and write

Fig. 4. Average CPU usage in Network Storage Performance with different Block Size.

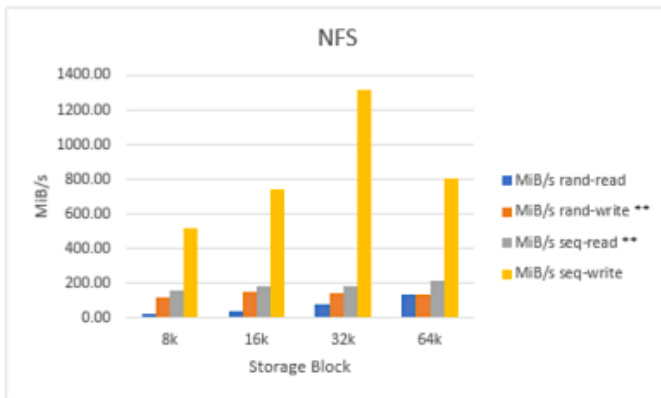


Fig. 5. Transfer Rate Performance from NFS Benchmark.

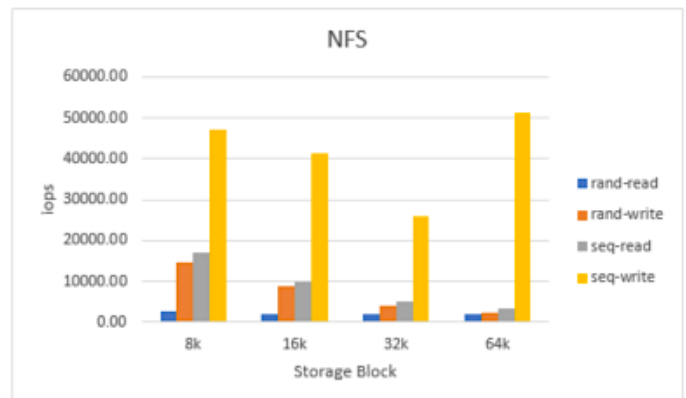


Fig. 6. IOPS Performance in NFS Workload.

The results of the random read scenario IOPS performance test on NFS show that 8k blocks have the highest results, 64k in second place, then 32k and 16k in third and fourth place. The results of the IOPS performance test in the random write scenario on NFS show that 8k blocks have the highest yield, 16k in second place, then 32k and 64k in third and fourth place, as shown in Fig. 6.

The IOPS performance test results in the sequence read scenario on NFS show that 8k blocks have the highest yields, 16k in second place, then 32k and 64k in third and fourth place. The IOPS performance test results in the sequence write scenario on NFS show that 64k blocks have the highest yield, 8k is in second place, then 16k and 32k are in third and fourth place.

The results of the CPU performance test (usr%) for the random read scenario on NFS show that the 16k block has the lowest results, 64k is in second place, then 32k and 8k are in the third and fourth place. The results of the cpu performance test (usr%) for the random write scenario on NFS show that the 64k block has the lowest yield, 32k is in second place, then 16k and 8k are in the third and fourth place. The results of the CPU performance test (usr%) in the sequence read scenario on NFS show that 64k blocks have the lowest results, 32k are in second place, then 16k and 8k are in the third and fourth places. The results of the CPU performance test (usr%) in the sequence write scenario on NFS show that 64k blocks have the lowest results, 16k are in second place, then 32k and 8k are in the third and fourth places, as shown in Fig. 7.

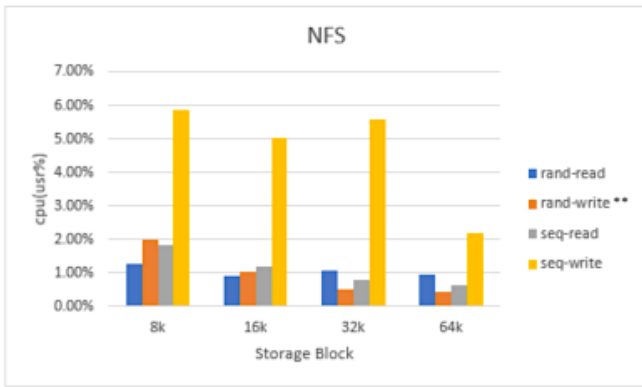


Fig. 7. CPU (usr%) Performance in NFS Benchmark.

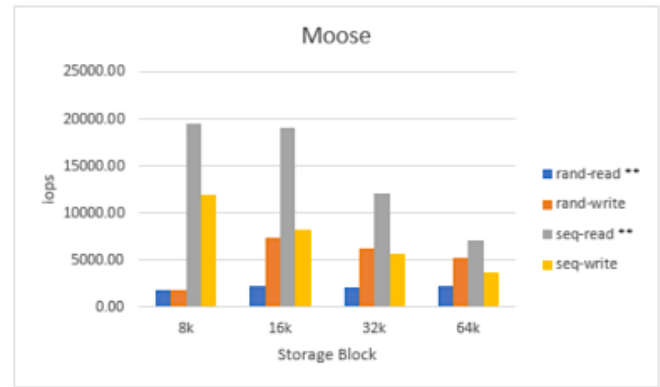


Fig. 9. Average IOPS in MooseFS with different Block Size and Workload.

E. MooseFS

Benchmark of the random read scenario transfer rate performance test on MooseFS show that the 64k block has the highest yield, 32k is in second place, then 16k and 8k are in the third and fourth place. The results of the random write scenario transfer rate performance test on MooseFS show that 64k blocks have the highest yield, 32k in second place, then 16k and 8k in third and fourth place, as shown in Fig. 8.

The results of the transfer rate performance test for the sequence read scenario on MooseFS show that 32k blocks have the highest yield, 64k in second place, then 16k and 8k in third and fourth place. The results of the transfer rate performance test for the sequence write scenario on MooseFS show that 64k blocks have the highest yield, 32k are in second place, then 16k and 8k in third and fourth place.

The results of the random read scenario IOPS performance test on MooseFS show that the 16k block has the highest yield, 64k in second place, then 32k and 8k in third and fourth place. The results of the IOPS performance test in the random write scenario on MooseFS show that 16k blocks have the highest yield, 32k in second place, then 64k and 8k in third and fourth place. The IOPS performance test results in the sequence read scenario on MooseFS show that 8k blocks have the highest yields, 16k in second place, then 32k and 64k in third and fourth place. The IOPS performance test results in the sequence write scenario on MooseFS show that 8k blocks have the highest results, 16k are in second place, then 32k and 64k are in third and fourth places, as shown in Fig. 9.

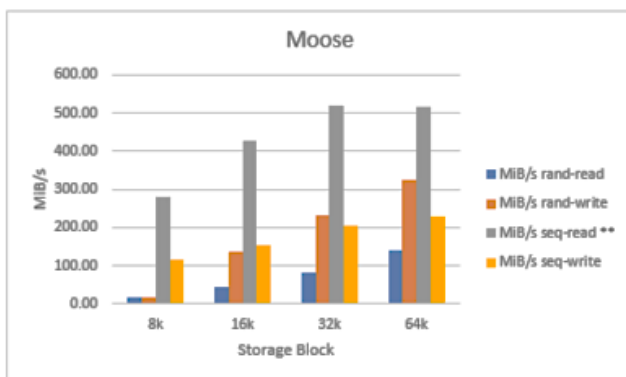


Fig. 8. Average Performance Transfer Rate in MooseFS with different Blocksize and Workload.

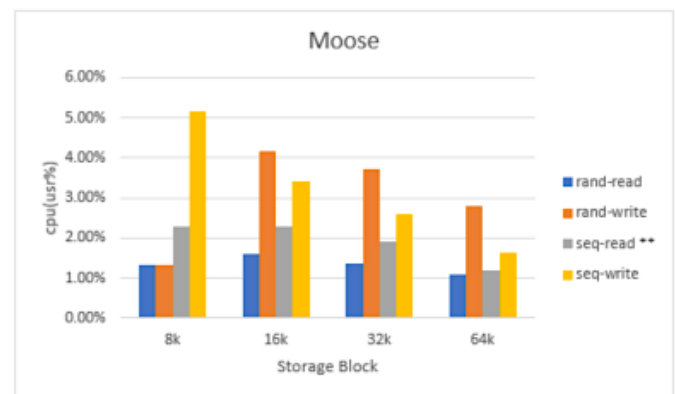


Fig. 10. Average CPU (usr%) in MooseFS with different Block Size and Workload.

The results of the CPU performance test (usr%) for the random read scenario on MooseFS show that 64k blocks have the lowest results, 8k is in second place, then 32k and 16k are in third and fourth place. The results of the cpu performance test (usr%) of the random write scenario on MooseFS show that the 8k block has the lowest result, 64k is in second place, then 32k and 16k are in the third and fourth place. The results of the CPU performance test (usr%) in the sequence read scenario on MooseFS show that the 64k block has the lowest results, 32k is in second place, then 16k and 8k are in the third and fourth place. The results of the CPU performance test (usr%) in the sequence write scenario on MooseFS show that 64k blocks have the lowest results, 32k are in second place, then 16k and 8k are in the third and fourth places, as shown in Fig. 10.

F. Random Read Workload in NFS, GlusterFS and MooseFS

In the random read test, GlusterFS has good performance at data transfer speed and bandwidth, resulting in higher iops than NFS and MooseFS. The high performance of iops causes the runtime value to be smaller, which means that in jobs that require random data reading, GlusterFS can complete it quickly. GlusterFS's speed in handling reading work can be influenced by the GlusterFS architecture that propagates metadata and breaks data files into smaller data on all machines in one cluster of distributed storage systems [6]. The performance results from NFS and MooseFS in the random data reading test produce almost the same values in blocks of 16k, 32k, and 64k except for CPU usage.

The use of CPU resources in the random read test shows that NFS uses the least amount of CPU resources on both the user CPU and the CPU system. GlusterFS experienced a decrease in user and system CPU resource usage according to the larger block being tested. MooseFS in this study experienced an increase in CPU user usage in 16k blocks and after that experienced a decrease in CPU user usage on 32k and 64k blocks. The use of the CPU system on NFS, GlusterFS and MooseFS tends to increase in proportion to the larger the data storage block.

G. Random Write Workload in NFS, GlusterFS and MooseFS

In the random write test on MooseFS, the transfer rate and bandwidth performance always increase for each block tested, resulting in a small runtime. The lowest performance on the random write test is GlusterFS. On the performance of NFS IOPS, the performance decreases on each block.

MooseFS on random write testing with high bandwidth and transfer rate performance results in high CPU system and user usage. In the random write test on MooseFS, it is carried out in parallel which is synchronized by the master server and therefore must be sequential so that writing data requires a lot of processing. So the CPU load depends on the number of operations and RAM on the total number of files and folders, not the total size of the files themselves. RAM usage is proportional to the number of entries in the file system because the master server process stores all metadata in memory [7].

H. Sequence Read in NFS, GlusterFS and MooseFS

Testing on a distributed file system on sequence read performance resulted in different performance from the random read. The results of this test show that GlusterFS has the best performance for sequential file reading. The value of GlusterFS bandwidth and transfer rate in the sequence read test results in high-performance values. GlusterFS has decreased performance on IOPS with each increase in the block size of data storage so that GlusterFS tends to experience a decrease in the system and user CPU resource usage.

In MooseFS, the transfer rate and bandwidth performance increase with each increase in the block being tested so that it affects the CPU resource usage which also increases for each block tested. In the NFS test results, the performance is below GlusterFS and MooseFS. The bandwidth performance and transfer rate appear to decrease in each block. The decline in performance on NFS is caused by a bottleneck that occurs in each block. When multiple NFS clients read data from an NFS server, there may be a winner-lose pattern in which the network bandwidth is unfairly distributed among clients. This winner-lose pattern is included in an unexpected scenario because in this experiment using the same tools and operations in running the test.

I. Sequence Write in NFS, GlusterFS and MooseFS

In the sequence write test, NFS has better performance when compared to MooseFS and GlusterFS which produce almost the same test value. Based on the results of the NFS test data, performance has decreased when writing data to data storage with 64k blocks. Average CPU usage across all

distributed file systems tends to decrease as the data storage block under test gets larger. The use of the CPU system on NFS has increased along with the increase in bandwidth and data transfer performance.

In MooseFS and GlusterFS, the performance of almost all parameters is below that of NFS. In this experiment, the performance of GlusterFS and MooseFS is below NFS possible because of the metadata function that needs to be processed and distributed in GlusterFS and MooseFS to all servers so that there is a possibility of increasing execution on the server to write data.

V. CONCLUSION

In this paper, a studied network attaches storage for web-scale infrastructure proposed for data science environment. Distributed data storage systems can assist in centralized data storage for data science needs with a computing environment with webscale technology. The distributed data storage method has proposed by analyzing several distributed data storage models, namely, NFS, GlusterFS, and MooseFS. The parameter used in this study is the transfer rate, IOPS, and CPU resource usage.

By testing the work of reading and writing data sequentially and randomly, it found that GlusterFS's performance was faster in reading data both sequentially and randomly with the best performance using 64k block data storage. MooseFS achieves the best performance on random data read jobs using 64k blocks of power storage. NFS gets the best results in random writing using 32k blocks of data storage.

Performance of the distributed data storage system can be affected by each size of the data storage block. With larger data storage block used, faster the performance can be in terms of data transfer and execution of operations on the data. However, this also implies greater use of resources.

Based on the test results, it can be concluded that each distributed data storage system has its advantages in every job. GlusterFS can achieve good performance on data reading jobs, NFS can obtain the best performance on data writing jobs in order, and MooseFS achieves the best performance at reading data sequentially.

ACKNOWLEDGMENT

The research has supported from Magister Program of Computer Science, Department of Computer Science and Electronics, Faculty of Mathematics and Natural Sciences, Universitas Gadjah Mada. The work one part of the research on GamaCloud infrastructures in the thesis work.

REFERENCES

- [1] P. China Venkanna Varma, K. Venkata Kalyan Chakravarthy, V. Valli Kumari, and S. Viswanatha Raju, "Analysis of a Network IO Bottleneck in Big Data Environments Based on Docker Containers," *Big Data Res.*, vol. 3, pp. 24–28, 2016, doi: 10.1016/j.bdr.2015.12.002.
- [2] P. Zikopoulos and C. Eaton, *Understanding Big Data: Analytics for Enterprise Class Hadoop and Streaming Data*, 1 st. McGraw-Hill Osborne Media ©2011.
- [3] Mishra and A. K. Somani, "Host managed storage solutions for Big Data," no. February, 2018, doi: 10.13140/RG.2.2.19115.90406.

- [4] A. Leibovici, "Understanding Web-Scale Properties," 2014.
- [5] J. Wang, J. Yin, D. Han, X. Zhou, and C. Jiang, "ODDS- Optimizing Data-locality Access for Scientific Data Analysis," IEEE Trans. Cloud Comput., 2017, doi: 10.1109/TCC.2017.2754484.
- [6] B. Depardon, L. Mahec, S. Cyril, B. Depardon, L. Mahec, and S. Cyril, "Analysis of Six Distributed File Systems," 2013.
- [7] Y. Fang, H. Zhu, and G. Lu, "Modeling and Verifying MooseFS in CSP," 2018 IEEE 42nd Annu. Comput. Softw. Appl. Conf., pp. 270–275, 2018, doi: 10.1109/COMPSAC.2018.00043.
- [8] E. Mohammed Mahmoud Nasef, and N Azaliah Abu Bakar, "Enterprise Architecture "As-Is" Analysis for Competitive Advantage", International Journal of Advanced Computer Science and Application (IJACSA), vol 11, issue 7, 2020.
- [9] I. Shabani, E. Meziu, B. Berisha, and T. Biba, "Design of Modern Distributed Systems based on Microservices Architecture", International Journal of Advanced Computer Science and Application (IJACSA), vol 12, issue 2, 2021.
- [10] Lee, H. & Fox, G.C., 2019, Big Data Benchmarks of High-Performance Storage Systems on Commercial Bare Metal Clouds, 2019 IEEE 12th International Conference on Cloud Computing (CLOUD), 1–8.
- [11] Inacio, E.C., Barbeta, P.A., Systems, A., Inacio, C., Barbeta, P.A. & Dantas, A.R., 2017, A Statistical Analysis of the Performance Variability of Statistical Analysis of the on Performance Variability of Read / Write Operations Parallel File Systems, Procedia Computer Science, 108, 2393–2397. <http://dx.doi.org/10.1016/j.procs.2017.05.026>.
- [12] Sandberg, R., 2000, The Sun Network Filesystem: Design , Implementation and Experience, , 1–16.

A Data Security Algorithm for the Cloud Computing based on Elliptic Curve Functions and Sha3 Signature

Sonia KOTEL
ISITCom of Hammam Sousse
University of Sousse
Sousse, Tunisia

Fatma SBIAA
Faculty of Sciences of Monastir
University of Monastir
Monastir, Tunisia

Abstract—The rapid development of distributed system technologies enforces numerous challenges. For example, one of the most critical challenges facing cloud computing is ensuring the security of confidential data during both transfer and storage. Indeed, many techniques are used to enhance data security on cloud computing storage environment. Nevertheless, the most significant method for data protection is encryption. Thus, it has become an interesting topic of research and different encryption algorithms have been put forward in the last few years in order to provide data security, integrity, and authorized access. However, they still have some limitations. In this paper, we will study the security concept in Cloud Computing applications. Then, an ECC (Elliptical Curve Cryptography) based algorithm is designed and tested to ensure cloud security. The experimental results demonstrate the efficiency of the proposed algorithm which presents a strong security level and reduced execution time compared to widely used existing techniques.

Keywords—Cloud; IaaS simulation upon SimGrid (SCHIAas); elliptic curve encryption; one-time pad symmetrical encryption method (OTP); confidentiality; integrity

I. INTRODUCTION

Nowadays, cloud computing is satisfying the huge need for operating the large amounts of data that is stored and exchanged daily in cloud servers. Cloud storage covers the requirement of the growing demand for storage and decreases the charge of maintaining huge volumes of data. Despite the various benefits of the cloud, security remains the main problem. Indeed, the cloud storage server can be untrusted while the transmitted data includes sensitive information. Therefore, any transmitted information can be captured or modified by a malicious user. In this context, the Cloud poses security problems [1], mainly for confidentiality and data integrity since the data are managed outside the governance framework of the cloud users and the service provider can access the data at any time [2]. In order to ensure the data confidentiality, it is crucial to use an efficient encryption scheme to achieve secure control in the cloud storage server. Various cloud data security schemes have been developed and proposed to address data privacy and integrity issues [3-5], including RSA-based cryptosystems, elliptic curves [6], and hash functions [7]. In fact, all encryption systems are based on complex mathematical functions. The symmetric cryptosystem is based on the Secret Key using simple mathematical functions such as substitution and permutations. However, asymmetric cryptosystem requires likewise factoring big

prime numbers (RSA) or it used the discrete log problems (DLP). Moreover, the public key cryptosystem is also famous as a holomorphic encryption scheme. Key size raises a plenty in public key cipher. Because of this huge key size, asymmetric cryptosystem needs much computational power. Recently, hybrid cryptosystems based on asymmetric cipher for key exchange and symmetric cipher for data confidentiality. Therefore, Elliptic curve encryption has settled the issue of big key size. ECC employs small key size to decrease the computational power and this can be performed in a cloud environment or IoT devices [6]. Moreover, the cloud provider service should ensure the secret data authentication and guarantee the robustness of the proposed cryptosystem against any process to reveal or change the data. Otherwise, there are an important requirement of a digital signature to ensure the data integrity.

The main contribution in this work is to propose a new security design for cloud computing architecture that reviews the different security deficiencies. Compared with related works, the proposed design offers a new hybrid technique which is faster and more secure. The present approach combines both the elliptic curve cryptographic (confidentiality issue) and the hash function SHA3(integrity issue).

This paper is organized as follows. The first section will introduce the cloud security issues. In the second section, we will study the cloud computing security overview. Section 3 will describe the proposed hybrid cryptosystem. Finally, we will discuss the experimental results and the security analysis results by comparing them to related works.

II. CLOUD SECURITY ISSUES

Commonly speaking, there are various kinds of security attacks in a cloud. This section presents an overview of the most important ones. Therefore, there are novel security requirements in the cloud compared to traditional environments. In fact, NIST is accountable for preserving security over the cloud computing environment and developing standards and rules which provides a precious involvement that gives a better knowledge of cloud applications and computing techniques [4]. The famous three cloud user service models in cloud architecture are: Infrastructure as a Service (IaaS), Platform as a Service (PaaS), and Software as a Service (SaaS). These service models required various levels of security over the cloud environment. The cloud service provider is compiled to gives

services, resource distribution management, and security. The cloud computing architecture, shown in Fig. 1, details the five essential modules which are composed of services that are employed in the cloud. Cloud security is a large and complicated task when the data is transferred to the cloud among the client-server frameworks. Indeed, the principle of trust in the cloud architecture can be overfed as the clients ensure the capacities of the infrastructure that it offers the essential services reliably and faithfully.

There are various issues in cloud computing security as listed below [9-13]. The main contribution deals with data integrity and data confidentiality issues.

- Confidentiality: Confidentiality in cloud data storage relates to ensuring the user's data is secret and only the approved users can manipulate the data [1]. Indeed, the data is ciphered before it is deployed. The service provider obtains ciphered data. Then, it is deemed insignificant. But the user is responsible for processing the access control rule, ciphering the data, deciphering it, and exploiting the encryption keys. The traders of cloud computing are widely used the two basic techniques such as physical isolation and cryptography to reach the confidentiality [2].
- Integrity: data integrity is the preservation of the data to check that is not modified or missed by using the services of the third party. Hence, the Cloud service provider must put forward protection against insider attacks on data. Therefore, any modification to the stored data must be identified using techniques having higher visibility to define what or who can edit the data that possibly impact their integrity. Further, computation integrity should be verified at the data stage and computation stage. Also, the data integrity service could assist in picking up lost data or detecting if there is data exploitation.
- Trust: The cloud service provider is required to put forward an adequate security policy to reduce the threat of information loss or data management [3].
- Privacy: is specified as the forwardness of a user to have power over the disclosure of secret information. An illegal admittance to client's confidential data will make security issues [5] [13].
- Reliability and Availability: Trustworthiness of cloud service provider declines when a client's data get dripped [8].
- Authentication and Authorization [14]: To inhibit unauthorized access, software is needed beyond the organization's firewall.

In the next section, we will present an overview of existing encryption schemes over cloud computing.

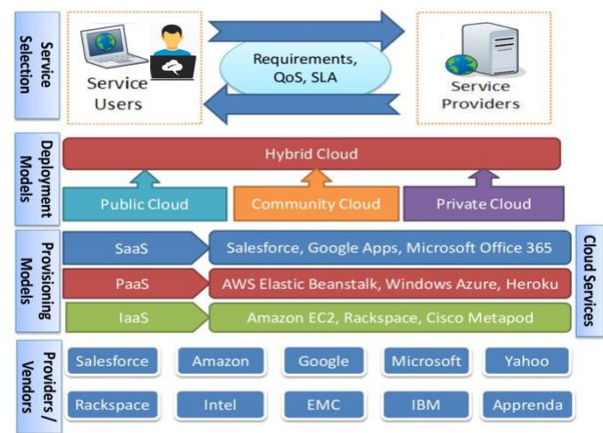


Fig. 1. Cloud Computing Infrastructure.

III. RELATED WORK

Various related works about improvement the infrastructure security issues through data sharing in cloud computing have been proposed. Precisely, we select the methods that have been proposed to secure data transaction, access management and user authentication in the cloud. Indeed, authors in [15] presented virtual private storage services that gratify the standard requirements (authentication, integrity confidentiality, etc.). Most of these requirements are done by ciphering the files stocked in the cloud. But similar ciphering drives to complicate the search operation through documents and to harden the collaboration operation in real-time modification. Furthermore, Farash MS and Attari, MA proposed in [16] an enhanced authentication design based on elliptic curve cryptographic functions (ECC) to offer a password authenticated key for swapping authentication method. The major drawback of this design is that it does not ensure the anonymity of clients and it does not resist against the man-in-the-middle attack.

Moreover, in [17] Xie Q et al. proposed an authenticated key exchange method using a two-factor anonymous dynamic identification. This suggested protocol is suitable to smart card repudiation and password update unless centralized memory space. This solution does not ensure security against man-in-the-middle attack.

Furthermore, in [18] Chang CC et al. put forward a security method that would satisfy basic security requirements and offer mutual authentication among the cloud and its hardware equipment. This proposed method was mainly based on ECC functions to offer secure communication among the cloud and its linked machines. The main limitation of this method is that is vulnerable to the known-key-security attack, and it does not provide a good forward secrecy feature.

In addition, the authentication scheme proposed in [19] would satisfy the security demands and resist different attacks. The suggested method connects the cloud with its devices using ECC cryptographic functions. The principal drawback of this proposed scheme is that it does not ensure client untraceability and it is not secure against the known-key attack.

Also, the approach presented in [20] is based on an unidentified and efficient two-factor authentication protocol that correctly authenticates employers to the mobile cloud service. The proposed approach uses the ECC cryptographic method to offer mutual authentication among mobile phones devices and cloud services. However, it does not ensure user untraceability.

Our work is notably different from the existing schemes. We focus on both data storage confidentiality and integrity in Cloud Computing services. Indeed, the contribution is based on proposing a hybrid design using both the ECC functions and SHA-3 algorithm to ensure data security and integrity. The proposed design is presented in the next section.

IV. PROPOSED CRYPTO-SYSTEM

In this section, we will describe the proposed encryption scheme. Indeed, in order to resolve the data security problems in the Cloud’s data centers, we will study the two fundamental services which are confidentiality and integrity. We propose three different scenarios: the first one uses the simple mapping method (M1) while the second implements the double mapping architecture (M2). The main contribution consists in the hybrid approach that combines the simple mapping method to the OTP process. The final comparison will allow us to validate the appropriate scenario.

Thus, the third scenario of the proposed crypto-system is based on the combination of elliptic curve cryptography and the one-time pad symmetrical encryption method (OTP) as well as the hash function SHA3. For the data privacy, we will use a list of elliptic curve points which represent the OTP encryption keys. Therefore, each block of the confidential data will be ciphered using a different key. Moreover, to guarantee the integrity of the treated data we will apply the SHA3 hash function on the encrypted data in order to have a signature which can be verified during the data deciphering. The following Fig. 2 illustrates the proposed crypto-system.

In the following subsections, we will describe the elementary functions that constitute the designed system.

A. Elliptic Curve Cryptography

Cloud computing confidentiality can be ensured using encryption schemes based on Elliptical curve cryptography (ECC). This public key encryption technique is based on elliptic curve theory. It is used in order to design faster, smaller, and more efficient cryptographic keys. Indeed, the best assured group of new public key methods is built on the arithmetic of elliptic curves. It has been contended that elliptic curves are a foundation for future internet security, given the relative security level and the performance of these algorithms. Moreover, according to some researchers, ECC based schemes are more computationally efficient than the first-generation public key systems, RSA and Diffie-Hellman. It can provide an efficient security level with a 164-bit key while other systems require above 1024-bit key [3]. Therefore, ECC helps to establish equivalent security with lower computing power and battery resource usage. Thus, it is becoming widely used in various domains such as mobile applications.

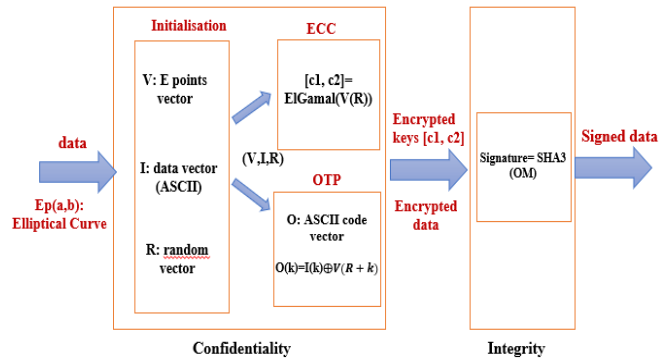


Fig. 2. Proposed Crypto-System Architecture.

B. OTP Encryption Technique

OTP is a symmetric cryptography technique, which uses randomly generated keys (see Fig. 3). It was created by G.Vemam in 1917. The encryption and decryption process uses XOR operators on the keys and secret messages. This technique is very powerful and resists brute force attacks under duress of using a random key just once.

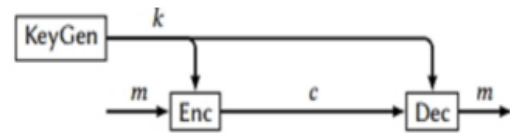


Fig. 3. OTP Encryption.

C. SHA3 Function

Hash functions produce a reduced and unique digest (of fixed size) as representation of data of any size. They calculate a message identification code which is called a hash value.

$$H: \{0,1\}^* \rightarrow \{0,1\}^n$$

$$M \rightarrow H(M)$$

The most common hash functions are MD52, SHA1, SHA2, SHA3. These algorithms are usually very fast since the generated hash value can be very small while ensuring that the transmitted message has not been altered or modified by a third party by sending the message along with its signature. The SHA-1 and SHA-2 hashing algorithms are very essential and widely used to secure communications such as wireless communications. But, they present many weaknesses and limitations which necessitated finding another replacement. NIST held a three-round competition to find a new secure hashing algorithm. This new algorithm “SHA3” exceeds the limits of the security presented in the previous hashing algorithms. Thus, SHA-3 is a cryptographic hash function that has four versions which allow to calculate signatures of different sizes: 224, 256, 384 and 512 bits. It is not intended to replace SHA-2 because until now no attack on SHA-2 has been demonstrated, but to provide another solution following the possibilities of attacks against MD5 standards, SHA-0 and SHA-1. Moreover, it is totally different since it is built on a completely different principle.

The Keccak algorithm is a cryptographic hash function designed by Guido Bertoni, Joan Daemen, Michaël Peeters, and Gilles Van Assche. It is the best algorithm among all applicants that was chosen for the SHA3 hash function. Thus, the SHA-3 (Keccak) scheme consists in two main stages which are the absorbing and the squeezing phases (see Fig. 4). During absorption, the original message M is subjected to the permutation f . In the squeezing phase, the output hash value is truncated from the first r -bit and further transformations are done if the required output bit is not obtained. Thus, it calculates the output of the resulting permutations of the value Z . The main objectives of using this construct are to have effective security against generic attacks and to make the use of the compression function simpler and more flexible.

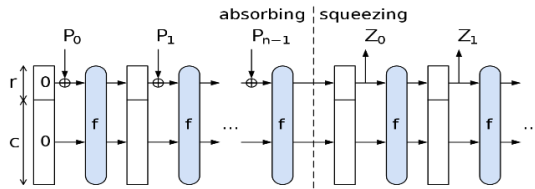


Fig. 4. Hashing Algorithm.

D. Proposed Hybrid Crypto-System Design

We propose, in the present paper, a hybrid crypto-system which is based on the combination of the elliptical curve cipher, the symmetric "OTP" encryption method and the SHA3 hash function. Fig. 5 illustrates the activity diagram that describes the data encryption process.

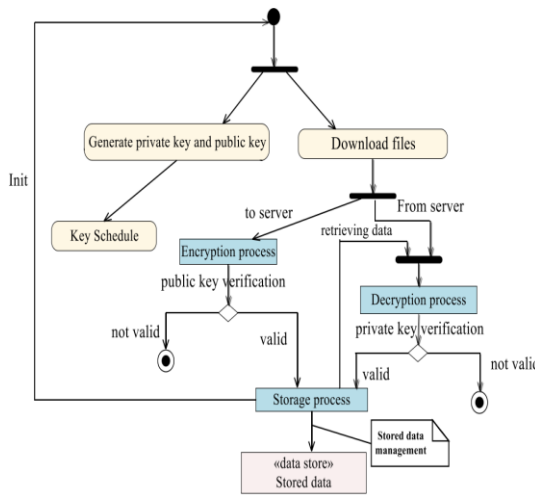


Fig. 5. Activity Diagram.

The proposed crypto-system based on the elliptical curve cryptography. In particular, we used ElGamal for data encryption and decryption. The public key PK is the result of multiplication of PrK with the generating point of the curve G .

Each user must generate its own private and public key couple. The private key PrK is just an integer chosen such that $PrK \leq P$. The public key PK is the result of multiplying PrK with the generating point of the curve G . Algorithm 1 details the generation function of these two keys. Considering that:

$$E_P(a,b) \text{ an elliptic curve in the form } y^2 = x^3 + ax + b$$

$G(x,y)$ the generating point of the curve E

Algorithm 1. Couple Key Generation (Private, Public)

- 1: Output {PrK, PK}
- 2: PrK: private key random value (between 0 and P)
- PK: public key a point of the curve E
- 3: $PK = PrK * G$
- 4: Return (PrK, PK)

In order to use the points of the curve as the encryption key for the OTP method, the system starts by generating a vector that contains these points. Algorithm 2 details the curve points generator process.

Algorithm 2. Curve Points Generator

- 1: Output V: points vector of the curve E
- 2: For $i=0$ to P do
- 3: $y2 = i^3 + a * i + b \text{ mod } P$
- 4: if $y2$ is perfect square then
- 5: add $y2$ to V
- end if
- end for
- 6: Return V

Algorithms 3 and 4 illustrate the ElGamal encryption and decryption processes respectively.

Algorithm 3. ElGamal-Encryption

- 1: Input: Plain Data , PK
- with Plain: point to encrypt
- 2: Output: $\{c1, c2\}$
- with $c1, c2$ two points of the curve
- 3: k random value (between 0 and P)
- 4: $c1 = k * G$
- with G : the generating point of the curve
- 5: $c2 = \text{Plain} + k * PK$
- 6: Return $\{c1, c2\}$

Algorithm 4. ElGamal-Decryption

- 1: Input: Data $\{c1, c2\}$, PrK
- 2: Output: Decrypted point
- 3: Sub point = $Prk * c1$
- 4: Decrypted = $c2 - \text{Sub}$
- 5: Return Decrypted

In Simple Mapping technique, for an elliptic curve E , the cipher generates a vector V containing the list of points of this curve. For a message $m (m_1, m_2, \dots, m_n)$ and for each block m_i , the crypto-system looks for the corresponding point P in the vector V where $P = V[m_i] + 256 * i$. The encrypted message is the set of all the founded points where each is encrypted by ElGamal encryption. When encrypting a message M of n blocks (m_1, m_2, \dots, m_n) , for each block m_i is associated a point of the curve so Encrypted value of m_i is only the result of encryption of the associated point.

The Double Mapping method is a simple optimization of the previous method where instead of encrypting a block salt at a time; we perform the encryption of two blocks. Hence for a message $m (m_1, m_2, \dots, m_n)$ and for each pair of points (m_i, m_{i+1}) , the crypto-system looks for the point that corresponds to the value $C = m_i + m_{i+1} * 256$ in vector V . The encrypted

message is only the set of found points where each one is encrypted by ElGamal encryption.

V. EXPERIMENTAL RESULTS

We implemented the proposed crypto-system using the Java language as well as the “Bouncy Castle” library which provides a set of classes and methods for different fields of cryptography such as elliptic curves and hash functions.

In order to evaluate the proposed solution, we used the SCHIaaS simulation environment that provides the IaaS model simulation with the SimGrid library which implements hypervisor level functionalities (see Fig. 6) [21]. SCHIaaS implements cloud-level functionality such as running and stopping instances. It also supports the main management functions of virtual machines (VMs), namely, run, terminate, suspend, resume and describe instances. Moreover, it allows the description of available resources, the management of image and instance types and the management of cloud storage. The SimSchlounder was used for the assessment since it supports the main cloud agent management functions for scientific computing. The type of application can be the execution of tasks and workflows. There is no limit to the number of tasks that can be simulated. These tasks can be heterogeneous and may require heavy CPU or I/O usage.

For both Calculation and Storage interface, SCHIaaS provides two implementations of both calculation and storage engines: these are RICE (Reduces Implementation of Compute Engine) and RISE (Reduces Implementation of Storage Engine). Fig. 7 describes how we can add simulation entity in SCHIaaS environment.

In order to realize the simulation, the RISE storage engine has been modified while allowing data to be encrypted before storage and decrypted before loading. For storing or loading data the "Storage" interface uses the RISE storage engine. The latter uses the "Encryption Task" task to encrypt or decrypt the processed data.

We took into consideration the execution time which represents a fundamental criterion for the Cloud applications. So to verify the reliability of the proposed crypto-system in terms of security, we carried out so many security tests on images such as the histogram analysis, the calculation of correlation and entropy, PSNR, NPCR and UACI.

In order to verify the reliability of the proposed crypto-system, we carried out several security analyzes. Thus, we

calculated entropy, PSNR and correlation values between adjacent pixels on standard images. We have also taken into consideration the execution time which represents a fundamental criterion in the evaluation of such a technology. In this context, we compared the execution times obtained for different file sizes.

A. Execution Time

In this section, we will evaluate the speed of the selected encryption methods using images sized 1.2 Mo. All tests are performed on an HP PC with CPU: Intel (R) Core (TM) i7-4500U @ 1.80GHz, 2401 MHz, 2 core (s), 4 logic processor (s), installed memory (RAM): 8 GB. We will compare two different mapping methods (M1, M2) with the hybrid approach that combines mapping and OTP method. Table I represents the encryption and decryption execution time.

The execution time is computed in milliseconds. We note that the used elliptical curve “secp256k1” is tested using the following parameters (previously detailed in section IV.D) described in Table II.

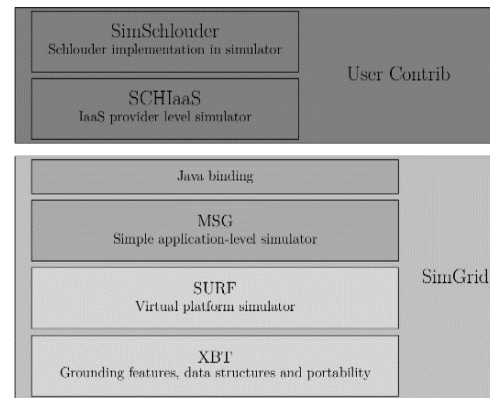


Fig. 6. SCHIaaS Simulation Environment.

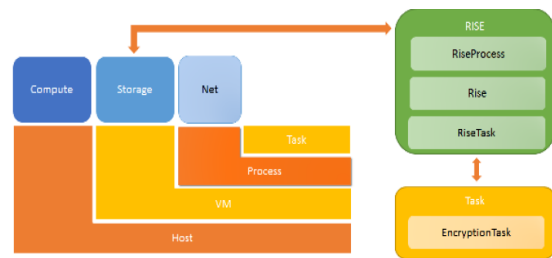


Fig. 7. SCHIaaS Simulation Entity Added.

TABLE I. EXECUTION TIME RESULTS (MS)

Encrypted image (512x512)	simple mapping E.T		double mapping E.T		simple mapping combined to OTP E.T		SHA-3 Encryption
	Encryption	Decryption	Encryption	Decryption	Encryption	Decryption	
Lena	10256	10556	9614	9955	291	240	72
Baboone	9652	10215	8649	8896	323	235	68
Barbara	9577	11994	9073	10790	346	250	75
Peppers	10125	10869	9399	10260	332	231	76

TABLE II. “SECP256K1” ELLIPTICAL CURVE PROPERTIES

Elliptical Curve parameters	Values
a	00000000 00000000 00000000 00000000 00000000 00000000 00000000 00000000
b	00000000 00000000 00000000 00000000 00000000 00000000 00000000 00000007
P	$2^{256}-2^{32}-2^9-2^8-2^7-2^6-2^4-1$
Gx	0x79BE667E F9DCBBAC 55A06295 CE870B07 029BFCDB 2DCE28D9 59F2815B16F81798
Gy	0x483ADA77 26A3C465 5DA4FBFC 0E1108A8 FD17B448 A6855419 9C47D08FFB10D4B8
N	FFFFFFFF FFFFFFFF FFFFFFFF FFFFFFFF BAAEDCE6 AF48A03B BFD25E8CD0364141
H	01

It is clear that the execution times of the simple and the double mapping methods are very high, which means that they cannot be used for Cloud applications. However, hybrid method is faster. This approves its use for cloud computing security. In addition, we note that the execution time can vary, for the same processed data, from one encryption or decryption operation to another. This is due to the random variable generated during the ElGamal encryption operation.

B. Discussion

Here, in this section, we will compare the experimental results analysis with related works. Fig. 8 and Fig. 9 illustrate the encryption time analysis for the proposed hybrid cryptosystem. Here, the evaluation experiments are based on 400 kb size of data. Authors in [23] proposed a new data security algorithm based on RSA and HMAC. The data is encrypted using RSA and the HMAC code was generated for integrity check when the data is transferred to the cloud server. Moreover, Amalarethinam, I. George, and H. M. Leena presented in [24] an enhanced RSA algorithm. In addition of the two large prime numbers P and Q two other prime numbers are selected. So, the private key and the public key are composed of a distinct couple of numbers. Therefore, in [25] proposed a secured storage algorithm for cloud and IoT based on elliptic curve-based key generation algorithm.

From Fig. 7 and Fig. 8, it can be observed that the proposed cryptosystem takes less encryption and decryption time than the existing schemes in [23], [24] and [25].

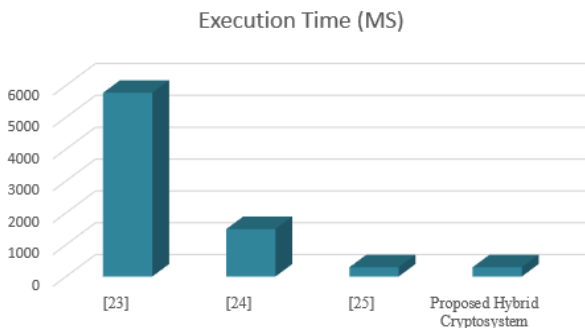


Fig. 8. Encryption Time Comparative Analysis.

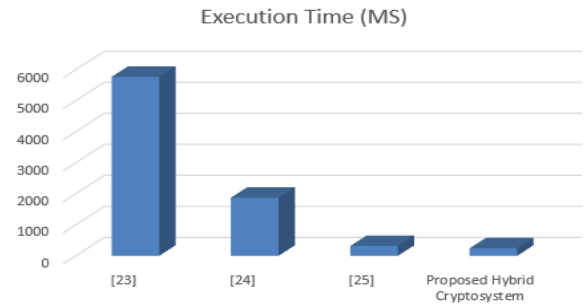


Fig. 9. Decryption Time Comparative Analysis.

C. Security Analysis

According to Claude Shannon, if the cryptographer has information on the statistics of the plain message (frequency of letters or sequence of letters), he can break the encryption method. Thus, to analyze the security level of the ECC algorithm against this category of attacks, we will apply different tests on encrypted standard images [22]. Considering the similarity between the methods M1 “simple mapping” and M2 “double mapping”, we limit ourselves to analyzing the results resulting from the methods M2 and M3.

1) *Histogram analysis:* A histogram shows how the pixels in an image are distributed; it represents the distribution of the intensities of the image by associating each intensity value with the number of pixels taking this value. The analysis of the histograms of the original and encrypted images is shown in the Fig. 10.

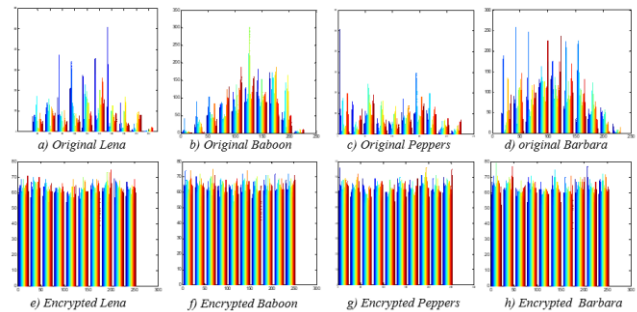


Fig. 10. Histograms of Plain Images and Ciphred Images (Image à Traduire).

As illustrated in Fig. 10, the pixels in the histogram of the encrypted image are uniformly distributed; each intensity is almost the same. Hence, the encrypted image does not reflect any information about the original image.

2) *Correlation coefficient analysis:* It is well proven that the less correlation value between two adjacent pixels the higher ability to resist to statistical attacks. In this sub-section, we computed the correlation coefficient between two adjacent pixels in plain image and ciphred image. The correlation between horizontally, vertically, and diagonally adjacent pixels is calculated using the following equations:

$$E(x) = \frac{1}{N} \sum_{i=1}^N x_i \tag{1}$$

$$D(x) = \frac{1}{N} \sum_{i=1}^N (x_i - E(x))^2 \quad (2)$$

$$\text{cov}(x, y) = \frac{1}{N} \sum_{i=1}^N (x_i - E(x))(y_i - E(y)) \quad (3)$$

$$r_{xy} = \frac{\text{cov}(x, y)}{\sqrt{D(x)}\sqrt{D(y)}} \quad (4)$$

Where x and y are the intensities of two adjacent pixels in the image and N is the total number of pixels.

Table III represents the obtained results of horizontal, vertical and diagonal correlation coefficients between two adjacent pixels in the original and encrypted test images using the crypto-system.

Obtained results indicate that the correlation coefficients for the various encrypted images are very close to zero. This means that the two methods M1 and M2 are good at hiding the details of the original images.

3) *Entropy analysis*: Information entropy is the most significant property of randomness. In practice, the probability p_i is approximated by a statistical count, which obviously leads to approximations of the amount of information. The average amount of information in an image can be calculated by taking a weighted arithmetic average of the amounts of information provided by each level (with p_i coefficients). The result is called the entropy of the image:

$$H(m) = \sum_{i=0}^{2^n-1} p(m_i) \log_2 \frac{1}{p(m_i)} \quad (5)$$

Where m is the information source, $p(m)$ defines the probability of symbol m . Considering that there are 2^8 information source states and they perform with the same probability, using Equation (5), we achieve the best entropy value when $H(m) = 8$, which illustrates that the origin is certainly random. Therefore, the encrypted image information entropy should be close to 8. The closest value to 8, the smaller chance for the crypto-system to disclose information.

Table IV details results of the encrypted images entropy using the two encryption methods M1 and M2. Obtained entropy values using M2 are closer to the ideal value than those obtained using M. Hence, the probability of fortuitous information leakage is minor.

4) *Peak Signal-to-noise ratio (PSNR)*: The most common measure used to assess the confidentiality of an image is the peak signal-to-noise ratio (PSNR) which is a criterion for measuring image distortion given by the following formula:

$$PSNR = 10 \log_{10} \left(\frac{P_{max}^2}{MSE} \right) \quad (6)$$

Where P_{max} is the maximum pixel value of the image and the MSE is the pixel-to-pixel mean squared error which presents the error between the original image and the encrypted one.

As illustrated in Table V, PSNR values, using the two encryption methods, between the encrypted image and the plain image are small. Indeed, the lower value of PSNR denotes better cipher quality. Therefore, obtained results prove that the encryption quality of each test image is quite good.

TABLE III. CORRELATION COEFFICIENTS RESULTS OF ORIGINAL AND ENCRYPTED TEST IMAGES USING M1 AND M2 METHODS

	Plain Image (512×512)				Encrypted Image (512×512)			
	Lena	Baboon	Barbara	Peppers	Lena	Baboon	Barbara	Peppers
Horizontal M1	0.9719	0.8665	0.8597	0.9792	0.0009	0.0031	0.0012	0.0009
Horizontal M2					0.0021	0.0014	0.0027	0.0013
Vertical M1	0.9850	0.7586	0.9591	0.9826	0.0034	0.0065	0.0048	0.0051
Vertical M2					0.0032	0.0028	0.0024	0.0072
Diagonal M1	0.9593	0.7261	0.8418	0.9680	0.0001	0.0002	0.0018	0.0006
Diagonal M2					0.0013	0.0007	0.0031	0.0010

TABLE IV. THE INFORMATION ENTROPY OF ORIGINAL IMAGES AND CIPHERED IMAGES

	Plain Image (512×512)				Encrypted Image (512×512)			
	Lena	Baboon	Barbara	Peppers	Lena	Baboon	Barbara	Peppers
H-M1	7.4456	7.3579	7.4664	7.5715	7.9217	7.9224	7.9219	7.9201
H-M2					7.993	7.9993	7.9992	7.9992

TABLE V. PSNR VALUES BETWEEN PLAIN IMAGE AND CIPHERED IMAGE

	Lena	Baboon	Barbara	Peppers
PSNR-M1	9.2302	9.5219	9.1636	8.4925
PSNR-M2	9.2481	9.5384	9.1628	9.2813

VI. CONCLUSION AND PERSPECTIVES

Although, several initiatives had been made in order to provide a secured Cloud environment, Elliptic Curve Cryptography (ECC) is considered to be one of the most efficient solutions with improved performance in computing power and battery resource requirements. Recently, ECC had provided a robust and secured model for the development and deployment of secured application in the Cloud. In the present work, we proposed an efficient crypto-system to ensure the data security in cloud Datacenters. The main contribution of the present work consists in designing a hybrid scheme using a new implementation of ECC functions combined with OTP and SHA-3 algorithm. Finally, the proposed cryptosystem was implemented on the SCHIaaS Cloud simulator to better test its performances. We evaluated the execution time of the proposed crypto-system and we noticed that by increasing the size of the elliptical curve parameters the execution time increases while remaining an acceptable time. Moreover, the security level ensured by the designed system has been proven with a set of security tests which were applied on standard images. As future work, we propose to implement several attacking scenarios in order to evaluate the efficiency of the proposed approach that should meet all security requirements.

REFERENCES

- [1] C. Wang, Q. Wang, K. Ren, N. Cao, Wenjing, "Toward Secure and Dependable Storage Services in Cloud Computing", IEEE Transactions on Services Computing, vol. 5, no. 2, pages 220–232, April 2012.
- [2] A. Alharbi, H. Zamzami and E. Samkri "Survey on Homomorphic Encryption and Address of New Trend", International Journal of Advanced Computer Science and Applications (IJACSA), Vol. 11, No. 7, 2020.
- [3] D. Adrian, S. Creese, M. Goldsmith, "Insider attacks in cloud computing. Trust", Security and Privacy in Computing and Communications (TrustCom) IEEE 11th International Conference, 2012.
- [4] Getov, Vladimir. "Security as a service in smart clouds--opportunities and concerns." 2012 IEEE 36th Annual Computer Software and Applications Conference. IEEE, 2012.
- [5] Abuhussein, Abdullah, et al. "Evaluating security and privacy in cloud services." 2016 IEEE 40th annual computer software and applications conference (COMPSAC). Vol. 1. IEEE, 2016.
- [6] R. Yadav, S. Srinivasan, S. Gupta, "Security Analysis of RSA and ECC in Mobile Wimax", International conference on Signal Processing, Communication, Power and Embedded System (SCOPEs), 2016.
- [7] National Institute of Standards & Technology (NIST), "Secure Hash Standard (SHS)", FEDERAL INFORMATION PROCESSING STANDARDS PUBLICATION, 2015.
- [8] Mushtaq, M. Faheem, et al. "Cloud computing environment and security challenges: A review", International Journal of Advanced Computer Science and Applications (IJACSA), 8.10 (2017): 183-195.
- [9] Aldossary, Sultan, and William Allen. "Data security, privacy, availability and integrity in cloud computing: issues and current solutions", International Journal of Advanced Computer Science and Applications (IJACSA), 7.4 (2016): 485-498.
- [10] Victor S. Miller, "Use of Elliptic Curves in Cryptography", Conference on the Theory and Application of Cryptographic Techniques, 1985.
- [11] B.Thirumala, R. Naresh, "A Study on Data Storage Security Issues in Cloud Computing", International Conference on Intelligent Computing, Communication & Convergence (ICCC-2016), pages 128–135, 2016.
- [12] A. Mohammed, A. Ben Soh, E. Pardede, "A Survey on Data Security Issues in Cloud Computing : From Single to Multi-Clouds", JOURNAL OF SOFTWARE, vol. 8, no. 5, May 2013.
- [13] Sherman S. M. ChowYi-Jun HeLucas C. K. HuiSiu Ming Yiu. SPICE–Simple Privacy-Preserving Identity-Management for Cloud Environment, In International Conference on Applied Cryptography and Network Security, volume 7341, pages 526–543, 2012.
- [14] H. Guiqiang, D. Xiao, T. Xiang, S. Bai, Y. Zhang, "A Compressive Sensing Based Privacy Preserving Outsourcing of Image Storage and Identity Authentication Service in Cloud", Information Sciences, September 2016.
- [15] Kamara and Lauter . CS2: A Searchable Cryptographic Cloud Storage System,IJSIR,2012.
- [16] Farash MS, Attari,MA (2014) A secure and efficient identity-based authenticated key exchange protocol for mobile client-server networks. J Supercomput 69(1):395–411.
- [17] Xie Q, Wong DS, Wang G, Tan X, Chen K, Fang L (2017) Provably secure dynamic ID-based anonymous two-factor authenticated key exchange protocol with extended security model. IEEE Trans Inf Forensics Secur 12(6):1382–1392.
- [18] Chang CC, Wu HL, Sun CY (2017) Notes on "secure authentication scheme for IoT and cloud servers". Pervasive Mob Comput 38:275–278.
- [19] Kumari S, Karupiah M, Das AK, Li X, Wu F, Kumar N (2018) A secure authentication scheme based on elliptic curve cryptography for IoT and cloud servers. J Supercomput 74(12):6428–6453.
- [20] Mo J, Hu Z, Chen H, Shen W (2019) An efficient and provably secure anonymous user authentication and key agreement for mobile cloud computing. Wireless Commun Mob Comput. <https://doi.org/10.1155/2019/4520685>.
- [21] Schiaas. SCHIaaS : IaaS simulation upon SimGrid. <http://schiaas.gforge.inria.fr/simschlouder.html>, June 2017.
- [22] S. Somaraj, M. Ali Hussain, "Performance and Security Analysis for Image Encryption using Key Image", Indian Journal of Science and Technology, vol. 8, no. 35, December 2015.
- [23] Sharma, Tejinder. "Proposed hybrid RSA algorithm for cloud computing." 2018 2nd international conference on inventive systems and control (ICISC). IEEE, 2018.
- [24] Amalarethinam, I. George, and H. M. Leena. "Enhanced RSA algorithm with varying key sizes for data security in cloud." 2017 World Congress on Computing and Communication Technologies (WCCCT). IEEE, 2017.
- [25] Malarvizhi Kumar, Priyan, et al. "Cloud-and IoT-based deep learning technique-incorporated secured health monitoring system for dead diseases." Soft Computing 25.18 (2021): 12159-12174.

Sentiment Analysis on Customer Satisfaction of Digital Banking in Indonesia

Bramanthyo Andrian, Tiarna Simanungkalit, Indra Budi, Alfani Farizki Wicaksono
Faculty of Computer Science, University of Indonesia, Jakarta, Indonesia

Abstract—Southeast Asia, including Indonesia, is seeing an increase in digital banking adoption, owing to changing customer expectations and increasing digital penetration. The pandemic Covid-19 has hastened this tendency for digital transformation. However, customer satisfaction should not be left unmanaged during this transition. This research aims to obtain customer satisfaction of digital banking in Indonesia based on sentiment analysis from Twitter. Data collected were related to three digital banks in Indonesia, namely Jenius, Jago, and Blu. Total of 34,605 tweets were collected and analyzed within the period of August 1st 2021 to October 31st 2021. Sentiment analysis was conducted using nine standalone classifiers, Naïve Bayes, Logistic Regression, K-Nearest Neighbours, Support Vector Machines, Random Forest, Decision Tree, Adaptive Boosting, eXtreme Gradient Boosting and Light Gradient Boosting Machine. Two ensemble methods were also used for this research, hard voting and soft voting. The results of this study show that SVM among other stand-alone classifiers has the best performance when used to predict sentiments with value for F1-score 73.34%. Ensemble method performed better than using stand-alone classifier, and soft voting with 5-best classifiers performed best overall with value for F1-score 74.89%. The results also show that Jago sentiments were mainly positive, Jenius sentiments mostly were negative and for Blu, most sentiments were neutral.

Keywords—Sentiment analysis; ensemble method; customer satisfaction; digital bank

I. INTRODUCTION

The Covid-19 global pandemic has wreaked havoc on economies, people, and societies [1]–[4]. With more individuals staying at home and working from home, the banking industry is seeing how the global health crisis has prompted clients to adopt digital services to cope with lockdown measures. Indonesia is well suited for digital banking due to its large unbanked population and high mobile penetration rate [5]–[8]. Traditional banks with legacy models, on the other hand, are facing a pressing need to digitally convert their services in order to keep up with increased demand, as the pandemic increases both consumers' and businesses' need for digital banking services availability, access, and control [9].

Because of digital banking, the competitive dynamics in banking industry of Asia Pacific are growing fiercer. Newly licensed indigenous digital banks, worldwide virtual-only banks, and digitized traditional banks are all fueling competition. In the long run, digital banking will almost probably lead to more ratings dispersion between banking systems and institutions in Asia Pacific [10]. The rise of digital banking in Asia was recently charted by McKinsey. As the

region's authorities raise license allocations and establish standards for the next generation of digital banks, there will be chances for both incumbents and new entrants to enter the digital banking sector [11]. Fig. 1 shows growth of digital banking in Asia. Indonesia, however, has yet to establish a legal framework for digital banks. The prerequisite to establish a digital bank can only be met with the acquisition of a banking license. It differs from its two neighbors, Singapore and Malaysia [12]. Currently there are several digital banks operated in Indonesia such as Jenius, Jago, and Blu. Customer satisfaction will be one of the important factors for the success of digital banks.

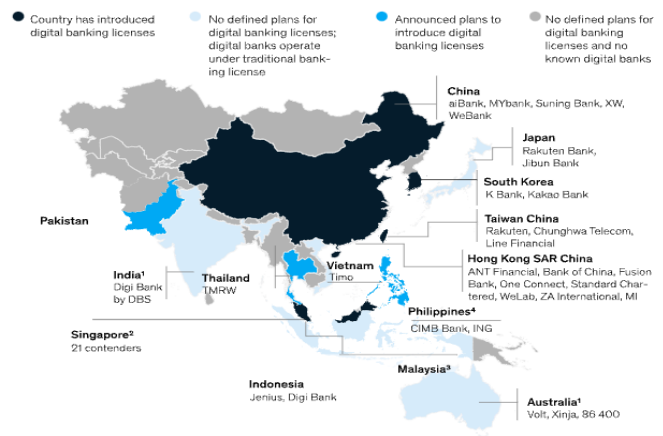


Fig. 1. Mapping the Growth of Digital Banking in Asia [11].

Text mining technique such as sentiment analysis had been used by researchers to examine users' opinion through social media. Previous study by Wisnu et al. [13] used sentiment analysis using Twitter data to obtain customer satisfaction of digital payment in Indonesia, and compare K-Nearest Neighbor (KNN) and Naïve Bayes classifier algorithm accuracy. KNN has superior accuracy than Naïve Bayes, according to their research, and clients are nearly satisfied with the services offered. Another study by Effendy et al. [14] used sentiment analysis to analyze public opinion on Twitter for City Public Transportation using Support Vector Machine (SVM). Their study showed that the public has mixed feelings for public transport services.

This study employed sentiment analysis to determine customer satisfaction with digital banking in Indonesia from Twitter data collected for three digital banks in Indonesia, namely Jenius, Jago, and Blu, based on previous research. Sentiment analysis was carried out utilizing two ensemble approaches, hard voting and soft voting, as well as several

well-known standalone classifiers. This research aims to answer the following three research questions:

RQ1. How is the demographic distribution of public opinion of tweets?

RQ2. How is the performance of ensemble method compared to standalone classifiers?

RQ3. What is the customer satisfaction of digital banks in Indonesia namely Jenius, Jago, and Blu based on sentiment of tweets?

By answering these research questions, we hope that the result of this study may enrich previous research in the use of text mining for analyzing customer satisfaction in banking industry.

This study is structured in several sections: in Section II, the relevant literature regarding digital banking and sentiment analysis is discussed here. In Section III, the research process used in this study is explained here, while in Section IV and V, result of data analysis and discussion are presented. The last section, that is Section VI and VII, concludes with conclusion and future work recommended based on this study.

II. LITERATURE REVIEW

A. Digital Bank

Digital banking, often known as branchless banking, is the delivery of financial services outside of traditional bank branches by information and communication technology (ICTs), according to [15]. To some extent, most major banks throughout the world have gone digital. For everything from checking their balances to making complex payments, consumers have grown accustomed to having the option of visiting a local branch or banking via their home phone, mobile phone, or computer. Digital banks, on the other hand, are a more recent and disruptive branch of banking. Digital banks are distinct from other types of digital banking in that they can only be accessed via the internet. Within a city or a country, they do not have any branch offices. Consumers assume that digital banks' infrastructure and personnel savings will be immediately translated into higher savings rates and lower lending rates. Some clients, on the other hand, may miss the emotional comfort of going to a neighborhood branch office, renting a safe deposit box, getting advice from a banker, or dealing with neighborly activities [16].

Currently there are several digital banks operated in Indonesia such as Jenius, Jago, and Blu. Bank Tabungan Pensiunan Nasional (BTPN) established Jenius, Indonesia's first digital bank in 2016, and released a mobile banking app that allows clients to manage their money using their mobile phones, bringing smooth banking to the Indonesian new generation's fingertips [17]. Whereas Bank Artos, in 2020, changed their name to Bank Jago and start providing digital banking and digital finance service that boast integration with various digital ecosystem in Indonesia [18]. In 2021, Bank Central Asia (BCA), Indonesia's biggest private bank, through their subsidiary, now named Bank Digital BCA launched their digital bank apps Blu [19].

B. Sentiment Analysis

In recent years, sentiment-based opinion mining has been investigated to better understand the attitudes and features of demographic or market groupings, as well as the trustworthiness of content and reasons for submitting evaluations [20]. Diverse sentiment analysis approaches have been produced in a variety of disciplines, resulting in modest number of publications [20]–[22]. Sentiment analysis is based on the assumption that information presented through text (e.g., a review) is either subjective (i.e., opinionated) or objective (i.e., factual) (i.e., factual). Personal sentiments, beliefs, and judgments are used to make subjective assessments of entities or events. To develop objective reviews, facts, evidence, and measurable observations are used [23]. Customer evaluations and social media posts commonly convey happiness, dissatisfaction, disappointment, delight, and other emotions [24].

Sentiment analysis is a polarity classification challenge in terms of methodology. Depending on the number of classes involved, sentiment polarity categorization might be binary, ternary, or ordinal. In a binary categorization, we assume that a given customer evaluation is subjective. In other words, a binary categorization assumes that a text is mostly negative or positive, and then assigns the review a polarity of "negative" or "positive". The negative and positive poles of sentiment are defined differently depending its domain and application. In the context of tourism, "negative" and "positive" may relate to "unsatisfied" and "satisfied" respectively, although additional research is needed to connect theoretical frameworks of satisfaction to sentiment polarity.

Because reviews aren't always subjective, a ternary classification with a third, "objective" category is required. In the ternary classification problem, the classifier performs an implicit classification to distinguish between objective and subjective statements, assigning a "negative", "positive", or "neutral" class label. Negative and positive polarity are sometimes confused with neutral polarity. To tackle sentiment analysis, a cascaded technique can be utilized, consisting of a binary classifier to discriminate between subjective and objective evaluations and a binary polarity classifier to further categorize subjective reviews into two groups, negative or positive. In objective assessments, words that are clearly defined as negative or positive in a dictionary are rarely seen. They may also comprise polarities that are blended without a distinct sense of direction. Ordinal classification can be done utilizing a sentiment strength rating system in addition to binary and ternary classification (e.g., one to five stars) [25].

C. Feature Inference and Extraction

Following the study done by Lyu et al. [26], Face++ API could be used to infer demographic information such as age and gender of users using their profile pictures. Face++ API will return zero or more faces based on profile picture URL provided. In this study, missing picture URL or invalid URL and result with 0 faces are excluded, the rest were inferred. Based on study by Lyu et al. [26], Face++ API provides good accuracy when used to infer age and gender information paired with Twitter data.

In addition, the TF-IDF (Term Frequency - Inverse Document Frequency) approach was applied to extract features in this work. The TF-IDF method combines the concepts of Term Frequency (TF) and Inverse Document Frequency (IDF). The TF approach counts the number of times a word appears in a document. Meanwhile, the IDF approach calculates the word's importance throughout the whole list of documents. TF-IDF is a statistical methodology for determining the relevance of a word in relation to a document in a collection of documents that combines the TF and IDF methodologies. The TF-IDF approach [27] has the potential to increase sentiment analysis performance.

III. METHODOLOGY

This research aims to find customer satisfaction of digital banking using sentiment analysis from tweets related to three digital banks in Indonesia, namely Jenius, Jago, and Blu. This research is done using Python, a general-purpose programming language used in many applications such as education, scientific and numeric computing. Tweets were collected through Twitter API using snsrape library.

Fig. 2 shows the overall outline of the sentiment analysis process. The steps are as follows.

A. Data Collection

Data was collected from social media site Twitter through Twitter API. Tweets data were scrapped from between August 1st 2021 to October 31st 2021. Subset of the data collected will be annotated manually by two researchers and used for training and evaluating the classifier model.

B. Pre-processing

Data obtained from Twitter needs to be cleansed before feeding it to the classifier model. Pre-processing is needed to remove noise, unwanted or unnecessary data and make it predictable and analyzable for next task. The text pre-processing steps in this research are described as follows.

- Case Folding – First process was converting all the characters in a tweet into the same case, in this case lower case is used.
- Sentence Normalization – Second process was identifying what type of text is there and then, removing special (non-alphanumeric) characters, and trimmed excess spaces.
- Word Tokenize – Third process was splitting sentence into words to be subjected for further analysis like stop word removal and stemming.
- Stop Words Removal – Fourth process was removing stop words from given text so that other words which define overall meaning could be focused more. NLP-id library was used in this process and later in stemming process.
- Stemming – Fifth process is reducing a word to its word stem that affixes to suffixes and prefixes. Lemmatizer was used in the process to get the root word from every word in a tweet.

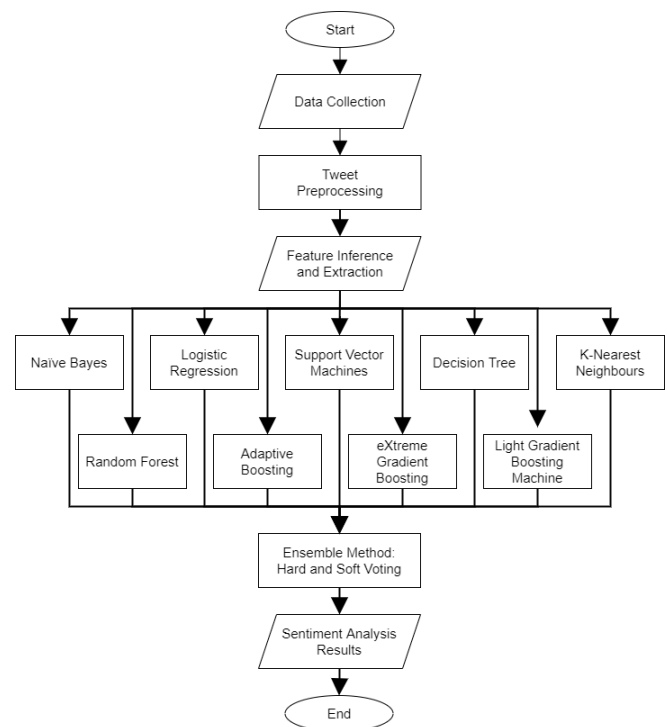


Fig. 2. Research Process.

C. Feature Inference and Extraction

Face++ API was used to infer demographic information such as age and gender of Twitter users using their profile pictures. Demographic was inferred using faceplib library. TF-IDF utilized in this study to extract features. It determines if a word is related to a document in a collection of documents. sklearn library is used for this and later subsequent process.

D. Training Standalone Classifiers

In this step, we trained several popular classifiers namely Naïve Bayes (NB), Logistic Regression (LR), K-Nearest Neighbors (KNN), Support Vector Machines (SVM), Random Forest (RF), Decision Tree (DT), Adaptive Boosting (AdaBoost), eXtreme Gradient Boosting (XGB) and Light Gradient Boosting Machine (LGBM). We utilized multinomial distribution for the NB classifier because it has been shown to perform well in text classification based on [28]. Meanwhile, we used the linear kernel for SVM for the same reason. The classification model is then assessed for accuracy, precision, recall, and F1-Score using K-fold cross validation with K-Fold=10.

E. Ensembling Classifiers

In this step, several best classifiers from the previous step were combined or ensembled to obtain better predictive performance. Hard voting and soft voting were the two types of ensemble voting procedures we employed. In hard voting, each stand-alone classifier has one vote, and the winner was determined by a majority vote. Meanwhile, average category probabilities were utilized as voting scores in soft voting, and the winner was chosen based on each classifier's greatest vote score or average probability.

F. Sentiment Analysis Result

In the last step, we take best classifier model from previous two steps and used it to analyze the sentiment for rest of the data. We used sentiment analysis to identify sentiment polarity of given tweet whether it's positive, negative, or neutral towards selected digital banks. Then, result of sentiment analysis will be discussed further.

IV. RESULTS

A. Data Collection

Data collected from Twitter by using Python sncrape library yielded total of 34,605 tweets in Indonesian language related to three digital banks in Indonesia, namely Jenius, Jago, and Blu. We removed duplicate tweets based on tweet ID and excluded tweets coming from each bank official account as we would like to find bank's customer satisfaction sentiment and that left us with a total of 24,672 tweets. We sampled 2100 tweets and manually annotated their sentiment. Process of manual annotation yielded 813 tweets with positive polarity, 585 tweets with neutral polarity, and 702 tweets with negative polarity. Table I shows three samples of manually annotated tweets.

TABLE I. SAMPLE OF MANUALLY ANOTATED TWEETS

Tweet	Label
@PrincesAinhy @blubybcadigital Fiturnya yaa...bikin happy Karena so simple dan memudahkan usernya banget.	Positive
@Tanyajago Halo kak, aku kan udah buat kartu fisik jago nih. Nah, kartunya udah nyampe jugak, kan ada pilihan kartu digital tuh. Kita bisa ngga buat juga kartu digitalnya?	Neutral
@JeniusConnect Woi aplikasi ngaco...web g bsa dibuka...krim email lama..uang gue di jenius g bsa diapa2in woi..	Negative

B. Pre-processing

After data collection and manual annotation steps, next step was to prepare the data for building classifier model. The text pre-processing used are case folding, sentence normalization, word tokenize, stop words removal and stemming with the help of Python NLP-id library. Table II describes visualization of preparation steps.

TABLE II. SAMPLE OF PRE-PROCESSED TWEET

Procedure	Tweet
Case Folding	@radenrauf @jeri72550254 @jadijago keren nih, buruan daftar nikmati untungnya dengan buat akun jago#jagoramerame
Sentence Normalization	keren nih buruan daftar nikmati untungnya dengan buat akun jago
Word Tokenize	['keren', 'nih', 'buruan', 'daftar', 'nikmati', 'untungnya', 'dengan', 'buat', 'akun', 'jago']
Stop Words Removal	['keren', 'buruan', 'daftar', 'nikmati', 'untungnya', 'akun', 'jago']
Stemming	['keren', 'buru', 'daftar', 'nikmat', 'untung', 'akun', 'jago']

C. Feature Inference and Extraction

After data pre-processing, next step was feature inference and extraction. Face++ API was used to infer demographic information such as age and gender of tweets' users using their profile picture. Out of 24,672 tweets, we found 9,515 valid

unique users that have profile pictures to be inferred. But unfortunately, only 61 users age and gender information could be inferred and a total of 103 accompanying tweets. Age information was found between range of 21 years old and 68 years old and we simplify it based on these age group, young adult (21-25), adult (26-35), middle aged adult (36-55) and senior (>55).

TF-IDF was used for feature extraction which gave weights to words based on its frequency and importance. The result will be used to fit classifier model algorithm for prediction. We used scikit-learn machine learning toolkit for this process to extract both unigram and bigram word features. Furthermore, we only retained 50,000 most frequently occurring words in the dataset. The word must occur in at least 2 documents and must not occur in more than 50 percent of the documents. Table III shows the result of TF-IDF.

The higher the TF-IDF score, the rarer the term is in the document and vice versa. For example, the more common the word across documents, the lower the score is (e.g., "dapet" and "biaya"). The more unique a word to the first document (e.g., "dapet cashback" and "jenius appsnya"), the higher the score is.

TABLE III. TF-IDF FEATURE EXTRACTION RESULT

#	Term	Score	#	Term	Score
1	dapet cashback	0.240403	11	appsnya	0.202075
2	jenius appsnya	0.240403	12	cashback	0.199040
3	admin transfer	0.231245	13	money	0.196270
4	registrasi	0.231245	14	link	0.183363
5	jago pindah	0.231245	15	gratis	0.181641
6	referral	0.224141	16	rekening bank	0.181641
7	gratis biaya	0.224141	17	buka rekening	0.180008
8	appsnya lot	0.224141	18	biaya admin	0.176974
9	nyari	0.218337	19	dapet	0.146667
10	pindah jenius	0.209178	20	biaya	0.143481

D. Model Training

After feature extraction steps, next process was to train and evaluate selected classifier models using scikit-learn machine learning toolkit. In the process, we compared 9 standalone classifiers with 2 ensemble classifiers built from 5-best standalone classifiers. For model testing, we employed 10-fold cross validation. The tweets dataset was first separated into ten equal parts. Tweets from 9 folds were used as train set in each iteration of cross validation, while the remaining fold was used as test set. In the procedure, accuracy, precision, recall, and F1-score were assessed. Table IV shows the results of each classifier model's performance.

As shown in Table IV, SVM outperforms all other standalone classifiers in terms of overall performance, with values of 74.29%, 74.58%, 73.13%, and 73.34% for accuracy, precision, recall, and F1-score, respectively. LR performed below RF with similar F1-score of 73.30% with RF, NB and LGBM are the next best three after. It was clear that KNN performed worst overall with accuracy, precision, recall, and F1-score

respectively 40.52%, 46.65%, 38.25% and 32.56%. Meanwhile, AdaBoost and XGB performed better than KNN by 65.72% and 70.63% F1-score respectively. All the ensemble methods with 5-best classifiers (SVM, LR, RF, NB, LGBM) have higher performance overall over stand-alone classifiers. Soft voting ensemble method with 5-best classifiers perform best overall with value for accuracy, precision, recall, and F1-score respectively 75.86%, 76.18%, 74.67% and 74.89%.

TABLE IV. CLASSIFIERS PERFORMANCE RESULT

Classifier	Accuracy	Precision	Recall	F1-Score
Naïve Bayes	73.81%	74.87%	71.87%	71.88%
Logistic Regression	74.48%	74.68%	73.14%	73.30%
SVM	74.29%	74.58%	73.13%	73.34%
Decision Tree	66.33%	65.95%	65.17%	65.11%
KNN	40.52%	46.65%	38.25%	32.56%
Random Forest	74.19%	74.36%	72.78%	72.90%
AdaBoost	66.95%	66.78%	65.91%	65.72%
XGB	72.24%	73.29%	70.52%	70.63%
LGBM	71.33%	71.48%	70.82%	70.72%
5-Best Hard Voting	75.43%	75.74%	74.01%	74.19%
5-Best Soft Voting	75.86%	76.18%	74.67%	74.89%

E. Sentiment Analysis

In this last step, we used best performing classifier model from previous step which was soft voting ensemble method with 5-best classifiers to predict sentiment automatically for the rest of tweets dataset. Out of 22,572 tweets, 12,504 tweets have positive sentiment, 5,603 tweets have neutral sentiment, and 4,465 tweets have negative sentiment. Result of predicted sentiment then combined back with manual sentiment for result discussion. Table V shows the combined result of manual and predicted sentiment mapped to each digital bank, namely Jenius, Jago and Blu.

TABLE V. SENTIMENT ANALYSIS RESULT BY DIGITAL BANK

Digital Bank	Tweets			
	Total	Positive	Neutral	Negative
Jenius	10,094	2,115	3,588	4,391
Jago	12,639	10,442	1,738	459
Blu	1,939	760	862	317
Total	22,572	13,317	6,188	5,167

TABLE VI. SENTIMENT ANALYSIS RESULT BY DEMOGRAPHIC GROUP

Demographic Group	Tweets			
	Total	Positive	Neutral	Negative
Age:				
young adult (21-25)	32	19	7	6
adult (26-35)	48	24	14	10
middle aged adult (36-55)	21	7	9	5
senior (>55)	2	2	0	0
Gender:				
Male	40	16	11	13
Female	63	36	19	8

Result of sentiment analysis was also combined with demographic information inferred from users' profile picture to find sentiment polarity distribution in different age group and gender. Out of 9,515 valid unique users, we were only able to infer 63 users with a total of 103 accompanying tweets. Table VI shows the demographic group of successfully inferred users and their tweets sentiment.

V. DISCUSSION

This research aims to obtain customer satisfaction of digital banking in Indonesia based on sentiment analysis from Twitter related data collected for three digital banks in Indonesia, namely Jenius, Jago, and Blu. The result displayed in Table IV shows that SVM has the best performance overall compared to the other stand-alone classifiers with value for accuracy, precision, recall, and F1-score respectively 74.29%, 74.58%, 73.13% and 73.34% compared to research done by [28], SVM performance was second best behind NB by small margin. This research showed similar result with previous research that KNN perform worst compared to the other stand-alone classifiers accuracy, precision, recall, and F1-score respectively 40.52%, 46.65%, 38.25% and 32.56% for text classification.

Both ensemble methods, hard voting and soft voting with 5-best classifiers performed better overall compared to stand-alone classifiers. Soft voting with 5-best classifier being the best with overall performance of accuracy, precision, recall, and F1-score respectively 75.86%, 76.18%, 74.67% and 74.89%. Ensemble method is a technique that combines several stand-alone classifiers model to produce one optimal classifier model. Thus, the performance is dependent to the classifiers that composed it. Then, by using only the 5-best classifiers, the ensemble method's likelihood of achieving greater performance might be improved. Between hard voting and soft voting, hard voting has a lower performance compared to soft voting because they dependent to individually predicted labels of each classifier, low performance from one of the classifiers could affect the result more. Soft voting, on the other hand, performs better because it uses a more robust technique to forecast labels formulated by the average probability value from all classifiers, which reduces overfitting and creates a smoother model [28].

This research also produced classification of sentiment with positive, neutral and negative polarity for each digital bank as seen in Table V. Bank Jago has most tweets compared to the other two digital banks with value of 12,639 tweets, Bank Jenius and Bank Blu have 10,094 and 1,939 tweets respectively. Small number of tweets for Bank Blu might be contributed to the fact that they are relatively a new player in digital banking industry in Indonesia. Fig. 3 displayed distribution of tweets and their sentiment for each digital bank. Positive sentiment was dominant for Bank Jago with value of 82.62% compared with neutral sentiment of 13.75% and negative sentiment of only 3.63%. Meanwhile, sentiment for Bank Jenius mostly was negative with value of 43.50% compared with neutral sentiment of 35.55% and positive sentiment of 20.95%. For Bank Blu, most sentiment was neutral with value of 44.46% compared with positive sentiment of 39.20% and negative sentiment of only 16.35%.

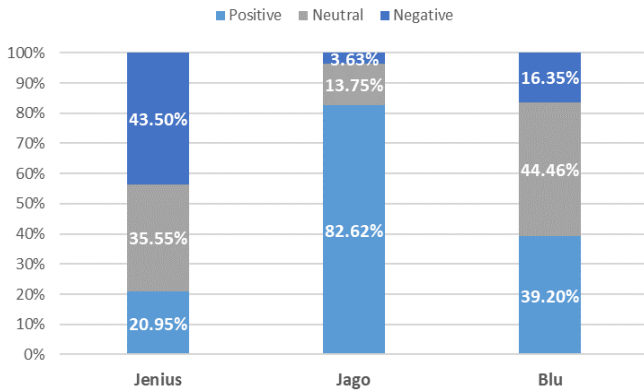


Fig. 3. Sentiment Analysis result grouped by Digital Bank.

For demographic distribution result, based on age group, adult and young adult tend to express their opinion more in social media and as they get older, they are less inclined to voice their opinion. Middle aged adult tends to give opinion with varying polarity, on contrary young adult and adult tend to give opinion with positive polarity. Meanwhile, based on gender group, female tend to express their opinion more than male and they have tendencies to give positive opinion as their counterpart, male tends to give opinion with mixed polarity. But this result needs to be confirmed further as population of successfully inferred users for demographic information is very less compared to total population of valid unique users. This low inferred rate may be contributed due to small resolution and low quality of profile pictures. Image preprocessing is recommended for future studies to improve success rate of inferred profile pictures such as interpolation technique to increase low image resolution and image filtering and segmentation technique to improve image quality.

The sentiment of the digital banking in Indonesia could be further analyzed using word cloud to view most frequently appeared word in the tweets, which were represented by its size and color hue. Fig. 4 displayed word cloud related to three digital banks in Indonesia. Green word cloud represents positive sentiment, yellow word cloud represents neutral sentiment and red word cloud represents negative sentiment. The result showed that most tweets contained comments related to digital banks apps and its features, user experience, bank policies, and running promotions.

Most positive sentiment that mostly coming from Bank Jago were related to appreciation of promotional events such as giveaways that were held by Bank Jago. Other things that the users being appreciative were related to Bank Jago policies related to low admin fee and high interest rate compared to other digital banks. Some users also praised Bank Jago apps for its simple user interface and fast user experience. Meanwhile, for negative sentiments that mostly coming from Bank Jenius were related to complaint of slow responding apps, login issues and other bad user experiences when using the apps. Other things that user complaints related to Bank Jenius policy, Feasible, whereby additional subscription fee is charged to customers to unlock services or features, but without significant improvements to its apps. Complaints also raised for their complicated process to unlink connected device.



Fig. 4. Word Cloud of the Sentiment.

Most neutral sentiments observed were related to inquiry of services and features offered by respective digital banks. Inquiries also included new prospective users asking for information, user experience and comparison of digital banks before deciding to open an account. Users also curious for new player in the digital bank space, Bank Blu, as it was often mentioned together with other digital banks comments. This was often true when users asked for comparison of digital banks. This showed that word of mouth and user testimony from social media like Twitter is one of deciding factor for user in choosing digital banks. Based on this, digital banks should pay more attention to the sentiments and user voices on social media, and make sure that their needs are being heard and improvements done are based on user feedbacks. They can leverage automatic sentiment analysis in their customer service tools to increase respond time in complaints handling or identifying most requested improvements from user feedbacks or targeting specific demographic group for promotions.

VI. CONCLUSION

Sentiment analysis is useful in social media analysis as it allows us to gain an insight in public opinion for certain topics. This research aims obtain customer satisfaction of digital banking in Indonesia through sentiment analysis using Twitter data for three digital banks in Indonesia, namely Jenius, Jago, and Blu with sentiment analysis approach. Sentiment analysis was conducted using nine stand-alone classifiers, namely, Naive Bayes, Logistic Regression, K-Nearest Neighbors, Support Vector Machines, Random Forest, Decision Tree, Adaptive Boosting, eXtreme Gradient Boosting and Light Gradient Boosting Machine, and two ensemble methods were also used for this research, hard voting and soft voting.

Results of classifier models evaluation showed that SVM among other stand-alone classifiers has the best performance when used to predict sentiments compared to the other stand-alone classifiers with value for accuracy, precision, recall, and F1-score respectively 74.29%, 74.58%, 73.13% and 73.34%. Meanwhile, ensemble method performed better than using stand-alone classifier, and soft voting with 5-best classifiers

perform best overall with value for accuracy, precision, recall, and F1-score respectively 75.86%, 76.18%, 74.67% and 74.89%.

Results of sentiment analysis showed that positive sentiments were dominant for Bank Jago with the value of 82.62%, Bank Jenius sentiment mostly were negative with the value of 43.50% and for Bank Blu, most sentiment were neutral with the value of 44.46%. Based on findings, user tweets revolved around digital banks apps and its features, user experience, bank policies, and running promotions. Positive sentiments came in form of appreciation toward promotional events, customer centric policies, user friendly apps and fast user experience. Meanwhile, negative sentiments came in form of complaints toward bad user experience when using apps and complicated policies. Lastly, neutral compliments came in form of information or inquiry related to digital banks services and service comparison between them. Furthermore, demographic distribution shows that based on age group, adult and young adult tend to voice their opinion more on social media compared to other age groups. Meanwhile based on gender group, female tend to voice their opinion more compared to their male counterpart. Based on this, digital banks should pay more attention to the sentiments and user voices on social media and improve their services and offering accordingly.

VII. FUTURE WORK

Based on findings in this study, there are several suggestions for the future works that can be explored to improve classifier performance and feature inference. First, adding more data pre-classification and pre-processing steps could be considered, such as part-of-speech (POS) tagging. Second, instead of using only TF-IDF feature, another type of features could be considered, such as Word2Vec or Paragraph2Vec. Success rate of feature inference based on profile picture may be improved by image preprocessing technique to increase image resolution and quality such as interpolation, image filtering and segmentation technique. Finally, study related to customer satisfaction of digital banking in Indonesia could be expanded beyond text classification and opinion mining using different set of methodology.

REFERENCES

- [1] J. Torales, M. O'Higgins, J. M. Castaldelli-Maia, and A. Ventriglio, "The outbreak of COVID-19 coronavirus and its impact on global mental health," *Int. J. Soc. Psychiatry*, vol. 66, no. 4, pp. 317–320, Mar. 2020, doi: 10.1177/0020764020915212.
- [2] L. Votintseva, M. Andreeva, I. Kovalenin, and R. Votintsev, "Digital transformation of Russian banking institutions: assessments and prospects," *IOP Conf. Ser. Mater. Sci. Eng.*, vol. 497, p. 12101, Apr. 2019, doi: 10.1088/1757-899X/497/1/012101.
- [3] N. Salari et al., "Prevalence of stress, anxiety, depression among the general population during the COVID-19 pandemic: a systematic review and meta-analysis," *Global. Health*, vol. 16, no. 1, p. 57, 2020, doi: 10.1186/s12992-020-00589-w.
- [4] BAI, "BAI Banking Outlook: COVID-19 Digital Banking Update," 2020. <https://www.bai.org/research/bai-banking-outlook/covid19-digital-banking-update/> (accessed Oct. 25, 2021).
- [5] Komite Stabilitas Sistem Keuangan, "Sinergi Menjaga Momentum Pemulihan Ekonomi dan Stabilitas Sistem," 2021. [https://www.bi.go.id/id/publikasi/ruang-media/news-release/Documents/siaran-pers-nomor-4-kssk-pres-2021.pdf#search=%22bank digital%22](https://www.bi.go.id/id/publikasi/ruang-media/news-release/Documents/siaran-pers-nomor-4-kssk-pres-2021.pdf#search=%22bank%20digital%22) (accessed Oct. 31, 2021).
- [6] Investor Daily, "Demam Bank Digital," 2021. <https://investor.id/editorial/256483/demam-bank-digital> (accessed Oct. 25, 2021).
- [7] I. Harjanti et al., "IT Impact on Business Model Changes in Banking Era 4.0: Case Study Jenius," in 2019 2nd International Conference of Computer and Informatics Engineering (IC2IE), 2019, pp. 53–57, doi: 10.1109/IC2IE47452.2019.8940837.
- [8] Y. Yulita, M. Apriza, S. Wulandari, D. Isnaini, and Y. Arisandy, "Management level of using digital services Bank Syariah Indonesia (BSI) KCP ipuh," *BIMA J. Business, Manag. Account. J.*, vol. 2, no. 2, pp. 200–211, 2021, doi: 10.37638/bima.2.2.200-211.
- [9] A. Beatty, "COVID-19 Proves Digital Banking Is No Longer Optional," 2020. <https://www.finextra.com/blogposting/18870/covid-19-proves-digital-banking-is-no-longer-optional> (accessed Oct. 25, 2021).
- [10] G. Gunning, "The Future Of Banking: Virtual Banks Chase the Dream in Asia-Pacific," 2019. <https://www.spglobal.com/en/research-insights/articles/the-future-of-banking-virtual-banks-chase-the-dream-in-asia-pacific> (accessed Oct. 25, 2021).
- [11] R. Bick, D. Bugrov, H. Gerson, A. McFaul, and A. Pariyskiy, "Joining the next generation of digital banks in Asia," 2021. <https://www.mckinsey.com/industries/financial-services/our-insights/joining-the-next-generation-of-digital-banks-in-asia> (accessed Oct. 25, 2021).
- [12] M. Nabila, "Welcoming the Digital Bank in Indonesia," 2020. <https://dailysocial.id/post/welcoming-the-digital-bank-in-indonesia> (accessed Oct. 25, 2021).
- [13] H. Wisnu, M. Afif, and Y. Ruldevyani, "Sentiment analysis on customer satisfaction of digital payment in Indonesia: A comparative study using KNN and Naïve Bayes," *J. Phys. Conf. Ser.*, vol. 1444, no. 1, p. 012034, Jan. 2020, doi: 10.1088/1742-6596/1444/1/012034.
- [14] V. Effendy, "Sentiment Analysis on Twitter about the Use of City Public Transportation Using Support Vector Machine Method," *Int. J. Inf. Commun. Technol.*, vol. 2, no. 1, p. 57, Jul. 2016, doi: 10.21108/IJOICT.2016.21.85.
- [15] C. Herington and S. Weaven, "E - retailing by banks: e - service quality and its importance to customer satisfaction," *Eur. J. Mark.*, vol. 43, no. 9/10, pp. 1220 - 1231, Jan. 2009, doi: 10.1108/03090560910976456.
- [16] IBM, "Asia Virtual Banking," 2019. [Online]. Available: <https://www.ibm.com/downloads/cas/AD8DOBR2>.
- [17] A. Arshad, "Covid-19 paves the way for digital banking in Indonesia," 2021. <https://www.straitstimes.com/asia/se-asia/covid-19-paves-the-way-for-digital-banking-in-indonesia> (accessed Oct. 25, 2021).
- [18] R. D. Kurnia, "Bank Jago: Sejarah, Gojek Akuisisi Saham, dan Fakta Lainnya," 2021. <https://www.goala.app/id/blog/bisnis/bank-jago-sejarah-gojek-akuisisi-saham-dan-fakta-lainnya/> (accessed Oct. 25, 2021).
- [19] CNN Indonesia, "Aplikasi Bank Digital BCA 'blu' Resmi Dirilis Hari Ini," 2021. <https://www.cnnindonesia.com/ekonomi/20210702161202-78-662380/aplikasi-bank-digital-bca-blu-resmi-dirilis-hari-ini> (accessed Oct. 25, 2021).
- [20] F. N. Ribeiro, M. Araújo, P. Gonçalves, M. André Gonçalves, and F. Benevenuto, "SentiBench - a benchmark comparison of state-of-the-practice sentiment analysis methods," *EPJ Data Sci.*, vol. 5, no. 1, p. 23, 2016, doi: 10.1140/epjds/s13688-016-0085-1.
- [21] P. Gonçalves, M. Araújo, F. Benevenuto, and M. Cha, *Comparing and combining sentiment analysis methods*. 2013.
- [22] J.-L. Seng and H.-F. Yang, "The association between stock price volatility and financial news - a sentiment analysis approach," *Kybernetes*, vol. 46, no. 8, pp. 1341–1365, Jan. 2017, doi: 10.1108/K-11-2016-0307.
- [23] R. Feldman, "Techniques and Applications for Sentiment Analysis," *Commun. ACM*, vol. 56, no. 4, pp. 82–89, Apr. 2013, doi: 10.1145/2436256.2436274.
- [24] D. E. O'Leary, "Blog mining-review and extensions: 'From each according to his opinion,'" *Decis. Support Syst.*, vol. 51, no. 4, pp. 821–830, 2011, doi: <https://doi.org/10.1016/j.dss.2011.01.016>.

- [25] J. Broß, "Aspect-Oriented Sentiment Analysis of Customer Reviews Using Distant Supervision Techniques," 2013.
- [26] H. Lyu et al., "Social media study of public opinions on potential COVID-19 vaccines: Informing dissent, disparities, and dissemination," *Intell. Med.*, Aug. 2021, doi: 10.1016/j.imed.2021.08.001.
- [27] E. Haddi, X. Liu, and Y. Shi, "The Role of Text Pre-processing in Sentiment Analysis," *Procedia Comput. Sci.*, vol. 17, pp. 26–32, 2013, doi: 10.1016/j.procs.2013.05.005.
- [28] M. Fauzi and A. Yuniarti, "Ensemble Method for Indonesian Twitter Hate Speech Detection," *Indones. J. Electr. Eng. Comput. Sci.*, vol. 11, pp. 294–299, Jul. 2018, doi: 10.11591/ijeecs.v11.i1.pp294-299.

System Architecture for Brain-Computer Interface based on Machine Learning and Internet of Things

Shahanawaj Ahamad

Department of Information and Computer Science
College of Computer Science and Engineering
University of Hail, Hail City
Saudi Arabia

Abstract—Brain functions are required to be read for curing neurological illness. Brain-Computer Interface (BCI) connects the brain to the digital world for brain signals receiving, recording, processing, and comprehending. With a Brain-Computer Interface (BCI), the information from the user’s brain is fed into actuation devices, which then carry out the actions programmed into them. The Internet of Things (IoT) has made it possible to connect a wide range of everyday devices. Asynchronous BCIs can benefit from an improved system architecture proposed in this paper. Individuals with severe motor impairments will particularly get benefit from this feature. Control commands were translated using a rule-based translation algorithm in traditional BCI systems, which relied only on EEG recordings of brain signals. Examining BCI technology’s various and cross-disciplinary applications, this argument produces speculative conclusions about how BCI instruments combined with machine learning algorithms could affect the forthcoming procedures and practices. Compressive sensing and neural networks are used to compress and reconstruct ECoG data presented in this article. The neural networks are used to combine the classifier outputs adaptively based on the feedback. A stochastic gradient descent solver is employed to generate a multi-layer perceptron regressor. An example network is shown to take a 50% compression ratio and 89% reconstruction accuracy after training with real-world, medium-sized datasets as shown in this paper.

Keywords—Brain-computer interface; machine learning; internet of things; EEG; system architecture

I. INTRODUCTION

Brain-Computer Interface (BCI) also known as Mind Machine Interface (MMI), is a technology that connects the brain to a computer or other electronic device in order to investigate the normal brain’s functioning, including its original output level and muscle pathway [1]. In order to create a link between the brain and the computer, two requirements must be met:

- Various states of the brain should be distinguished.
- Detection and classification of similar features practically.

It is possible to monitor brain activity using a variety of methods, the most common of which being Electroencephalograms (EEG), Electrocardiograms, Magnetic Resonance Imaging, Magneto-Encephalograms, and Positron Emission Tomograms (PET) [2].

A variety of approaches can be used to detect or measure these electrical and chemical impulses. There are issues and advancements to be made, just like with any other system, so it works on them. Both the efferent and afferent systems may be affected. The brain can be connected directly to its environment if the neurological system is effectively bypassed [3-5]. This can be done through BCI. While first designed to provide alternative methods of communication for those with disabilities, these devices now have the potential to provide “other sensations” for those who are unable to do so. Brain-computer interfaces (BCIs) provide direct communication between the brain and the world around it.

A patient can use a BCI to control a specific computer application, such as a computer cursor or a robotic limb. Patients with lock-in syndrome, for example, can benefit from developing a communication network even when they are paralyzed. Many researchers have been working on BCIs to capture and analyze EEG patterns associated with mental states throughout the past few years [6, 7, 8, 9, 10]. EEG activity in the left side of the motor cortex is associated with visualizing a change in the posture of the right hand. Other often employed mental exercises include moving the left hand, toes, and tongue around the mouth and feet. The block diagram for BCI can be shown in Fig. 1.

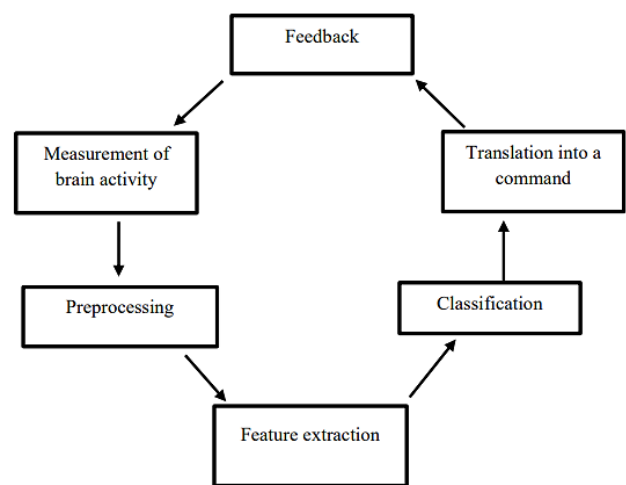


Fig. 1. BCI Framework.

A Brain-Computer Interface (BCI) based on electroencephalography (EEG) is used in this study. Depending on where the electrode is placed, there are two main approaches to collecting EEG data. Non-invasive electrodes are attached to the scalp while invasive electrodes are attached directly to the cerebral cortex [11]. The non-invasive approach is less intrusive and more portable than fMRI, making it suited for performance arts.

Improvements in biomedical signal processing have led to Electroencephalography (EEG) signals being utilized to diagnose brain illnesses and widely used in Brain-Computer Interface (BCI) devices. In order to operate external equipment like a wheelchair or a computer, BCI employs electrical impulses from the brain, in the form of EEG waves, as an input. Electroencephalography (EEG) is a method for recording electrical brain wave activity along the scalp as a result of neural activation in the brain. An electroencephalogram (EEG) is a short-term recording of the electrical activity of the brain for a short period of time (usually 20–40 minutes), which is accomplished by attaching electrodes to the scalp of the subject. EEG can be used to diagnose a variety of neurological illnesses, although it is most commonly used to treat epilepsy. EEG can be useful in the early stages of some serious disorders, such as coma, brain death, and encephalopathies. There are various different diseases for which electroencephalography (EEG) can be used as a first-line diagnostic approach. EEG is still the most commonly used method for diagnosing even if MRI and CT scans are increasingly prevalent currently. In the EEG approach, evoked potentials (EP) are utilized to average the EEG activity to stimulus responses in visual, auditory, or somatosensory activity. In addition, event-related potentials (ERPs) are employed in cognitive sciences, psychophysiology, and cognitive psychology for averaging EEG responses to complicated stimuli.

This paper has been organized in five sections. Section 1 is introduction that refers the basics and contexts of research with introduction to various ongoing and future aspects. Section 2 is for background study and research that mentions the contributions of significant research in the field, their relevance and reference to this research work. Section 3 is about research methodologies that specify the adopted research processes and methods to carry out this research work. Section 4 and Section 5 are about implementation and results, and conclusion, respectively.

II. BACKGROUND STUDY AND RESEARCH

In order to identify changes in the surface of the head as a result of electrical activity in the brain, EEG is largely used in neuroscience and clinical neurological procedures. Wet (gelled) silver/silver chloride electrodes (Ag/AgCl), typically with the help of an EEG cap, are used in the state-of-the-art approach. It takes a long time and a lot of effort to get ready for an event like this. Electrolyte stability also limits the wear time (gels). Brain-computer interfaces (BCIs) are a new field of application for EEG [12-15]. Silver-chloride-coated metal discs, often composed of stainless steel, tin, gold, or silver, are applied to the scalp in specific places. The International 10/20 system is used to specify the positions. All electrodes are

numbered, and a letter is assigned to each one. The letter identifies the location of the electrode in relation to the brain. Examples include the F-Frontal lobe and T-temporal lobe.

Dry contact electrodes must have acceptable hair layer penetration, biocompatibility, electrochemical stability, and signal quality comparable to typical wet electrodes in order to be viable. Aside from the long-term applicability and patient comfort that we strive for, we also want to ensure compatibility with bio-signal amplifiers, ease of use, and preparation time for patients [16]. As a result, three major types of electrodes have been created: Titanium nitride covers the first two gold multi-pin electrodes as well as (ii) polyurethane multi-pin electrodes. In order to make gold multi-pin electrodes, the electrical precision brass pins are gold-coated and soldered to an epoxy baseplate.

Fig. 2 depicts the four stages of the BCI configuration for this project, from data collection via EEG and analog-to-digital conversion to digital signal processing, feature selection, and control of external mechatronic devices [17]. In the first step, non-invasive EEG data is collected, and in the second step, digital EEG signals are processed with filters. Custom algorithms and mechatronics have been developed in the second and third phases to monitor the appearance of individual brain waves and produce the desired sounds. For PDR detection, a unique feature selection technique is used in the third phase. In the final stage, eight wirelessly connected modules of custom percussion instruments produce synchronized sounds [18]. As a result, the BCI system generates repetitive noises that prompt the performer to record reliable EEG data.

OpenBCI's high-quality open-source BCI solution is employed in this research. The system architecture is built using frameworks that are commonly used to run BCIs. OpenBCI's STL files are used to 3D print the headgear used for the initial round of EEG data collecting [19, 20, 21, 22]. A Cyton board, an Arduino-compatible, eight-channel neural interface with a 32-bit processor, is attached to the headwear's rear. For example, the OpenBCI GUI can analyze the digitized EEG data from this board to remove artifacts and identify certain features.

Analog signals are detected by placing electrodes on one's scalp for EEG-based BCI. For use with the Ultra-Cortex Mark III-Nova and Ultra-Cortex Mark IV 3D-printed EEG headgear, electrodes are mounted according to International 10-20 system specifications [23]. Conductive silver chloride (AgCl) is used to coat the dry electrode, making it easier for the performer to use and more durable for long-term performances.

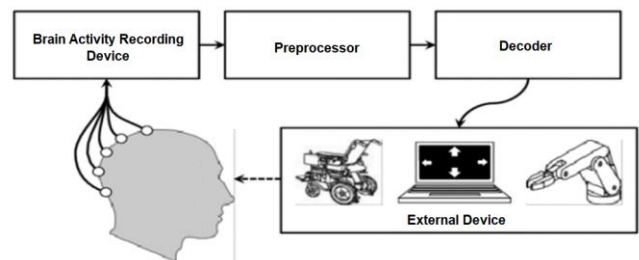


Fig. 2. System Architecture for Four Stages of the BCI Configuration.

III. RESEARCH METHODOLOGY

The Welch method uses windowed Fourier transformations of signal segments to calculate the Fourier spectral characteristics. Using only frequency data is the fundamental shortcoming of the method, as it does not use time-domain data [24]. However, studies have shown that EEG signals can be improved by combining frequency and time-domain data. The band power in multiple frequency bands is calculated from the AR spectrum and the power sum is used as independent parameters. Fig. 3 shows the block diagram of the proposed methodology for this research work.

A. Classification

Research on BCI-specific machine learning models using data from children with impairments is few, to our knowledge. It was in 2020 that Aydin applied LDA, KNN, and SVM to two fNIRS datasets containing typical developing adults (average age 28.5 3.7 years). For motor imagery fNIRS-BCI signals, LDA showed the maximum classification accuracy, while SVM had the best performance for mental arithmetic. The best KNN outcomes were achieved with a low k. It was determined that the number of features should be proportional to the value of k in this investigation [25]. When compared to a single powerful learner, ensemble classifiers have improved classification accuracy. SVM, LDA, and rLDA were compared against bagging using four different data sets involving motor imagery, mental arithmetic, and word production tasks. There were no significant differences in bitrate or classification accuracy between bagging and alternative algorithms across the datasets. According to their last remarks, they urged the development of novel ensemble classification methods. Seven models were chosen in this work because of the lack of research on classifying learners for a fNIRS-BCI. Based on past research, we chose KNN, SVM, LDA, and Bagging as our top four models. Random Forests, AdaBoost, and Extra Tree were introduced to the ensemble of classifiers. 10-fold stratified cross-validations were conducted on each model's hyperparameters to measure classification accuracy [26, 27, 28]. Accuracy, sensitivity, and specificity were used to measure classification performance.

B. Feature Selection

Spontaneous electrical activity in neurons, as measured by EEG, is examined in general for its amplitude and frequency. Using scalp EEG, the experiment collects data and focuses on the frequency of the scalp EEG in the visual cortex. EEG data is transformed from the time domain to the frequency domain using the fast Fourier transform (FFT) technique. To monitor PDR and control sound mechanisms, the Open Sound Control protocol uses a special algorithm that analyses the frequency information from the digitalized EEG data after the FFT method is applied in the GUI of OpenBCI (OSC). However, EEGs can vary greatly depending on the individual, their age, their gender, and their overall health. There is a 7.5-15Hz PDR tolerance. As we get older, the EEG slows down, and this development is more pronounced for males than for women. Young people's EEG data isn't yet mature because they're under the age of 26. Children under the age of 8 Hz can have a PDR that is slower than 8Hz. As a result, it's critical to check the performer's PDR scope before running the function.

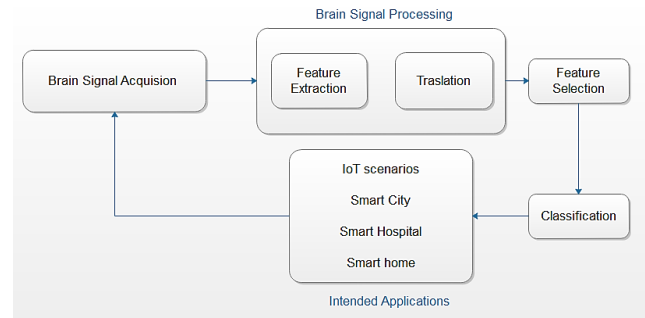


Fig. 3. Block Diagram for the Proposed Methodology.

C. Dataset

The proposed approaches are evaluated using the ECoG recordings from Dataset I of the BCI Competition III, as depicted in Fig. 4. BCI experiment participants conducted hypothetical motions of their left little finger or tongue to record motor imagery signals. Recorded ECoG signals were sampled at 1000 Hz. Amplification and storage at microvolt values made it easier to classify the recorded potentials. Sample recordings of either imaginary finger or tongue movement were recorded for three seconds. To avoid visual evoked potentials, the recording began 0.5 seconds after the visual round ended.

D. Auto-Regressive Features

Automatic regression (AR) models are used to represent random processes in statistics and signal processing, and they are particularly useful for modeling time-varying processes. Output variables are modeled by the AR to be reliant on their prior values. AR denotes an autoregressive model with order p. To put it another way, the AR (p) model is

$$X_t = C + \sum_{i=1}^p \varphi_i X_{t-i} + \varepsilon_t \quad (1)$$

The backshift operator B can be used to write this in the same way:

$$X_t = C + \sum_{i=1}^p \varphi_i B^i X_t + \varepsilon_t \quad (2)$$

$$\text{So that, } \varphi(B)X_t = C + \varepsilon_t \quad (3)$$

Thus, an AR model can be thought of as the output of a white noise-inputted all-pole infinite impulse response filter.

E. Data Acquisition

To ensure accuracy and quality, it compares the target signal to background noise. Once this digital brain data has been decoded into the intended action, it can be classified, and the necessary attributes calculated and selected from the neural data.

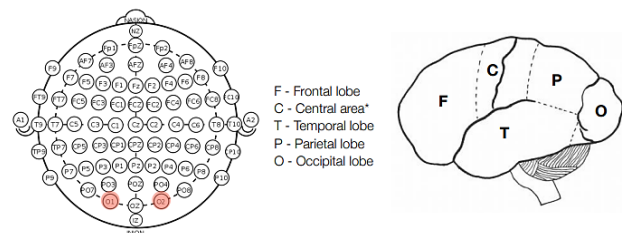


Fig. 4. The ECoG Recordings from Dataset I of the BCI Competition III.

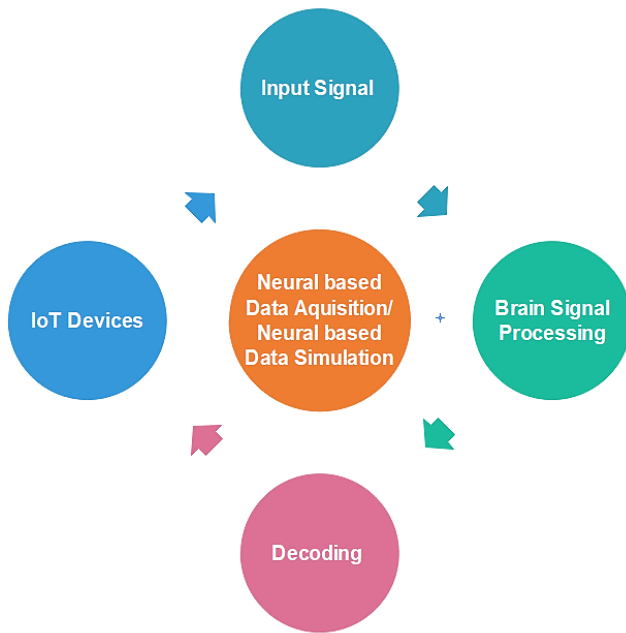


Fig. 5. Neural based Data Acquisition for Machine Learning.

In addition, optional feedback is sent to BCI users (which generates brain signals) and the cycle is again repeated. An anti-clockwise motion (as seen in Fig. 5) stimulates the simulation of data to begin.

The input from the stimulation data decoder is processed using various machine learning (ML) methodologies (neural networks). It's important to note that the generated input provides high-level information about the multimedia devices that will be triggered, their frequencies, and the timing of their activation.

BCI technology-related parameters were subsequently specified using thresholding patterns that received neural input in the intended action and generalized form have been shown in the Fig. 6. To display multimedia-based actions, the process moves from brain data simulation to user interface and interactivity.

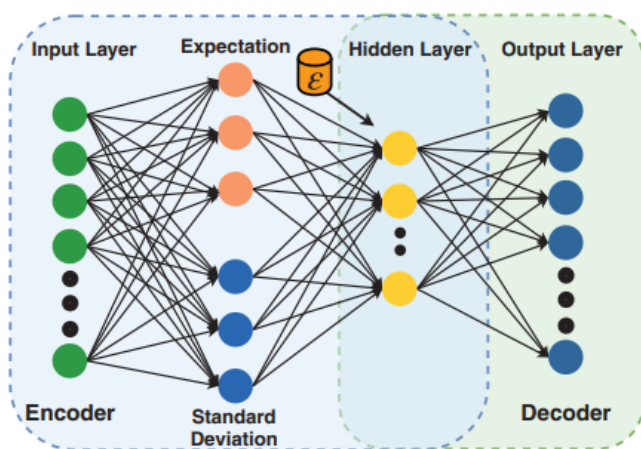


Fig. 6. Neural Networks based Threshold or Firing Pattern.

IV. IMPLEMENTATION AND RESULTS

The computer-based assessment test of visuomotor skills was divided into two blocks, one standard, and one non-standard for participants. This necessitated the use of cognitive-motor integration in order to treat the condition (CMI). Participants had to navigate a cursor as quickly and accurately as possible from the tablet's center to one of four peripheral goals using their dominant index finger (up, down, left, or right). Users clicked on an 8 millimeter wide solid green circle in the middle of the screen to begin their experiment. Upon seeing an open green 10 mm diameter peripheral target after a 200ms center hold period, the participant was given the "Go" signal and was free to begin moving. A green cursor was positioned over an open green target by sliding the touch screen with one's fingers.

Upon reaching the peripheral goal and remaining there for 500 milliseconds, the experiment was over. Next, the central target was presented after a 200-ms intertrial interval. At 37.5 millimeters from the tablet's central starting point, the tablet's peripheral targets were (center-to-center distance). Overall, there were 20 trials per task, with five trials for each goal. Participants used their fingers to move the cursor under their fingers to engage directly with the target in the conventional condition. As a result of the non-standard CMI scenario, a white line separated the display into two halves. Participants had to pay attention to the tablet's upper half for the targets and cursor. Participants had to glide their fingers along the tablet screen's bottom to move the cursor.

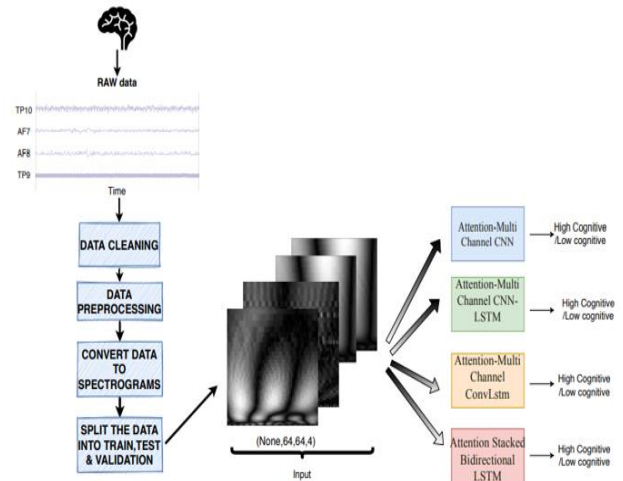


Fig. 7. Proposed Methodology for the Classification of Cognitive Load using EEG Data.

The collected data will be used to improve classification accuracy on IVa datasets in our experimental assessment. Fig. 7's SCU architecture is modified to categorize these images using an SSVEP-based model. As a data reference channel, we employed the frontal cortex (Fz) instead of the nine sensor channels originally used to simplify SSVEP classification training. They demonstrated that this model outperformed both standard approaches and time-series specialized models like Recurrent Neural Networks when it came to recognize SSVEP EEG signals (RNN). All tests utilize one-dimensional convolutional layers as depicted in Fig. 8,

batch normalization, and maximum pooling. After applying a bandpass filter between 9 and 60 Hz, as well as another filter at 50 Hz, the EEG channels are initially pre-processed before the data is eventually normalized between 0 and 1.

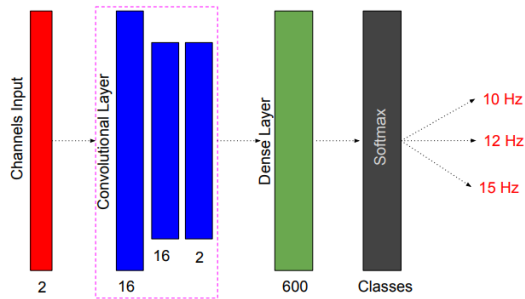


Fig. 8. Layer Representation of Neural Networks.

For the experiments, dataset IV has been used from the BCI competition. The accuracy is the actual fraction of the samples that are correctly classified from the samples obtained in (4):

$$\text{Accuracy} = \frac{TP+TN}{TP+TN+FP+FN} \quad (4)$$

The Precision is the percentage of relevant samples, evaluated as in (5):

$$\text{Precision} = \frac{TP}{TP+FP} \quad (5)$$

The Recall measures the positives identified correctly as in (6):

$$\text{Recall} = \frac{TP}{TP+FN} \quad (6)$$

Where, TP-True Positive, TN-True Negative, FP-False Positive and FN-False Negative.

Based on the findings provided in Table I, it appears that the Random Forest method outperformed the Neural Network and Gradient Boosting classifier. An individual’s maximum level of accuracy was 70.2 percent, which was a reasonable improvement above the random guess accuracy of 33 percent. Because we used to leave one out cross-validation in this situation, the inter-subject accuracy of 56.8% was also quite encouraging. It was shown that training a model on an individual’s data yielded better results for intra-class classification than utilizing data from various persons, which could raise concerns about privacy.

The use of the supervised forward feature selection method resulted in considerable improvements to our results. Reducing 60 feature set from 60 to 10 was done by removing unnecessary and distracting features. We were able to enhance our performance on the validation set as a result of our methodology’s ability to reduce overfitting. This method had a 10 percent improvement in average accuracy and the maximum accuracy we could achieve with wearable devices was 80.6 percent, well above the accuracy of any previous method for EEG classification based on RGB colors. Fig. 9 and 10 represent the graphs for accuracies at 200ms time window using all and 10 features respectively. The classifier was able to correctly classify 72% of the subjects on average. The accuracy went up to 95% of the time Intra-subject

classification was likewise superior to inter-subject classification in this situation. The accuracy of inter-subject classification was raised by 1.3 percent. In this situation, the Random Forest approach outperformed both the neural network and the gradient boosting techniques. Table II shows the results.

TABLE I. ACCURACY USING ALL FEATURES AT 200MS

Metrix	SVM	KNN	Gradient Boost	Random Forest	Logistic Regression	Neural Network
Inter-Subject Accuracy	0.456	0.446	0.572	0.668	0.508	0.590
Average-Subject Accuracy	0.574	0.514	0.708	0.725	0.606	0.623
Best-Subject Accuracy	0.678	0.613	0.769	0.802	0.700	0.800

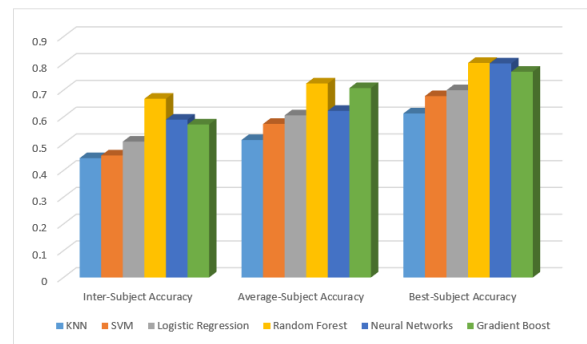


Fig. 9. Graph for accuracy using all features at 200ms

TABLE II. ACCURACY WITH 10 FEATURES AT 200MS TIME WINDOW

Metrix	SVM	KNN	Random Forest	Gradient Boost	Logistic Regression	Neural Network
Inter-Subject Accuracy	0.466	0.477	0.681	0.511	0.488	0.575
Average-Subject Accuracy	0.587	0.592	0.820	0.697	0.592	0.613
Best-Subject Accuracy	0.678	0.613	0.906	0.820	0.690	0.866

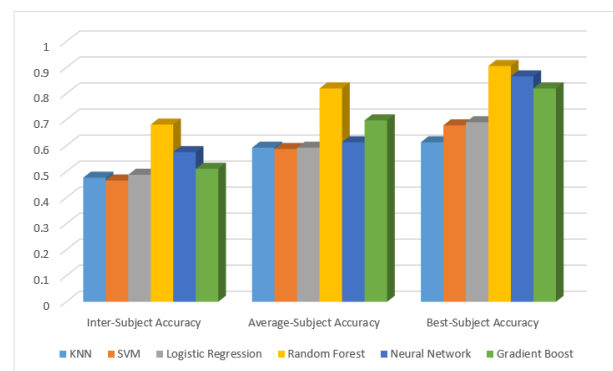


Fig. 10. Graph for Accuracy with 10 Features at 200ms Time Window.

Two types of classification were carried out: intra-subject and inter-subject. We used to leave out one subject cross-validation for the second classification, where we trained the model using seven subjects' data and validated it using a single subject's data, then repeated it for all subjects. The average cross validation accuracy, ROC-AUC, and MCC of our model were used to assess its performance. The original and condensed datasets are also included in our results. Fig. 11 and 12 show the average accuracy, the average AUC score, and the average MCC score for both intra-subject and inter-subject categorization. Our greatest results were achieved in a 200ms time frame. A total of 200ms of experimentation was placed throughout this time. All peak frequencies and its harmonics have been shown in the Fig. 13 for fast Fourier transform (FFT) method that has an important role in processing for the discrete signals.

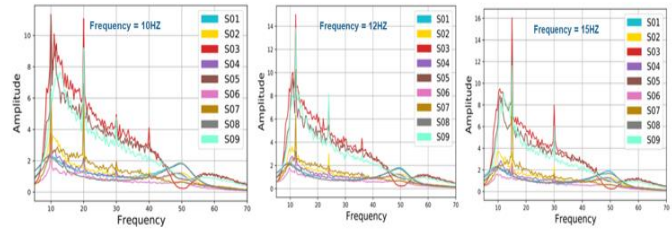


Fig. 13. Peak Frequency and its Harmonics for FFT throughout all Nine Disciplines.

V. CONCLUSION

To help people with disabilities, brain-computer interfaces (BCI) have been developed. However, new uses for this technology have emerged, such as the expansion of human potential. This work presented novel system architecture for the BCI, and this article has shown to be easily configured and modular to access the different EEG signals. Locked-in individuals have no other way to communicate or exert control over their surroundings but through the use of a Brain-Computer Interface (BCI). When conducting a BCI, electrocorticography (ECoG) gives superior resolution to non-invasive methods. EEG signals, on the other hand, have a limited range of signal amplitude and bandwidth. ECoG can identify gamma activity more quickly than EEG because these high frequencies are more closely linked to specific sections of the motor, linguistic, and intellectual functions. Classification is done using a variety of machine learning algorithms. So, SVMs can be used to make generalizations that are good out of sample, if the parameters are specified correctly. This suggests that SVMs can be robust, even if the training sample has some bias, by selecting an acceptable generalization grade.

REFERENCES

- [1] J. D. Cunha, S. Perdakis, S. Halder and R. Scherer, "Post-Adaptation Effects in a Motor Imagery Brain-Computer Interface Online Coadaptive Paradigm," in IEEE Access, vol. 9, pp. 41688-41703, 2021, doi: 10.1109/ACCESS.2021.3064226.
- [2] B. S. Lin, H. A. Wang, Y. -K. Huang, Y. L. Wang and B. S. Lin, "Design of SSVEP Enhancement-Based Brain Computer Interface," in IEEE Sensors Journal, vol. 21, no. 13, pp. 14330-14338, 1 July1, 2021, doi: 10.1109/JSEN.2020.3033470.
- [3] J. D. Simeral et al., "Home Use of a Percutaneous Wireless Intracortical Brain-Computer Interface by Individuals With Tetraplegia," in IEEE Transactions on Biomedical Engineering, vol. 68, no. 7, pp. 2313-2325, July 2021, doi: 10.1109/TBME.2021.3069119.
- [4] S. Samejima et al., "Brain-Computer-Spinal Interface Restores Upper Limb Function after Spinal Cord Injury," in IEEE Transactions on Neural Systems and Rehabilitation Engineering, vol. 29, pp. 1233-1242, 2021, doi: 10.1109/TNSRE.2021.3090269.
- [5] L. Ferrero, M. Ortiz, V. Quiles, E. Iáñez and J. M. Azorín, "Improving Motor Imagery of Gait on a Brain-Computer Interface by Means of Virtual Reality: A Case of Study," in IEEE Access, vol. 9, pp. 49121-49130, 2021, doi: 10.1109/ACCESS.2021.3068929.
- [6] D. R. Deo, P. Rezaei, L. R. Hochberg, A. M. Okamura, K. V. Shenoy and J. M. Henderson, "Effects of Peripheral Haptic Feedback on Intracortical Brain-Computer Interface Control and Associated Sensory Responses in Motor Cortex," in IEEE Transactions on Haptics, vol. 14, no. 4, pp. 762-775, 1 Oct.-Dec. 2021, doi: 10.1109/TOH.2021.3072615.
- [7] X. Zhao, C. Liu, Z. Xu, L. Zhang and R. Zhang, "SSVEP Stimulus Layout Effect on Accuracy of Brain-Computer Interfaces in Augmented Reality Glasses," in IEEE Access, vol. 8, pp. 5990-5998, 2020, doi: 10.1109/ACCESS.2019.2963442.

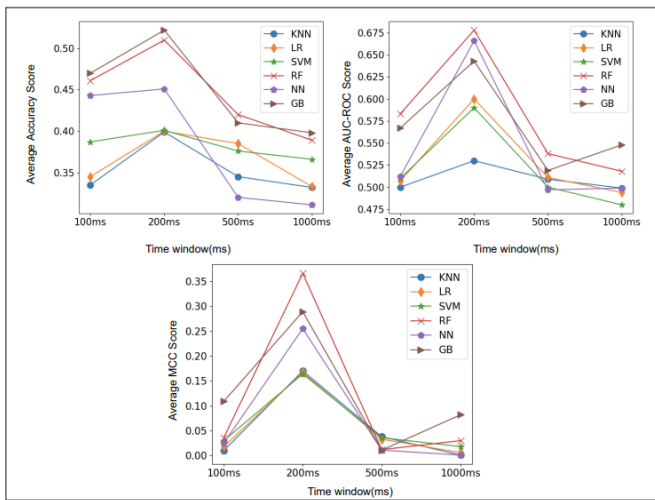


Fig. 11. Average Accuracy, ROC-AUC and MCC Scores for Inter-Subject Categorization.

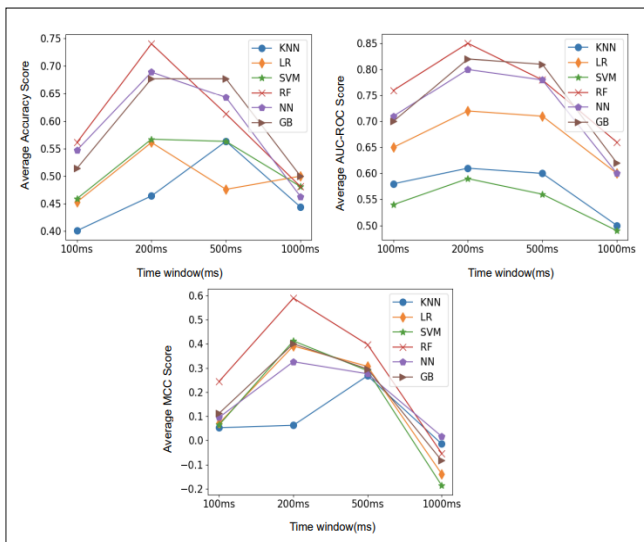




Fig. 12. Average Accuracy, ROC-AUC and MCC Scores for Intra-subject Categorization.

- [8] M. Xu, J. Han, Y. Wang, T. P. Jung and D. Ming, "Implementing Over 100 Command Codes for a High-Speed Hybrid Brain-Computer Interface Using Concurrent P300 and SSVEP Features," in *IEEE Transactions on Biomedical Engineering*, vol. 67, no. 11, pp. 3073-3082, Nov. 2020, doi: 10.1109/TBME.2020.2975614.
- [9] J. Jin et al., "Bispectrum-Based Channel Selection for Motor Imagery Based Brain-Computer Interfacing," in *IEEE Transactions on Neural Systems and Rehabilitation Engineering*, vol. 28, no. 10, pp. 2153-2163, Oct. 2020, doi: 10.1109/TNSRE.2020.3020975.
- [10] Z. Lv, L. Qiao, Q. Wang and F. Piccialli, "Advanced Machine-Learning Methods for Brain-Computer Interfacing," in *IEEE/ACM Transactions on Computational Biology and Bioinformatics*, vol. 18, no. 5, pp. 1688-1698, 1 Sept.-Oct. 2021, doi: 10.1109/TCBB.2020.3010014.
- [11] C. Easttom et al., "A Functional Model for Unifying Brain Computer Interface Terminology," in *IEEE Open Journal of Engineering in Medicine and Biology*, vol. 2, pp. 91-96, 2021, doi: 10.1109/OJEMB.2021.3057471.
- [12] L. Carmona, P. F. Diez, E. Laciár and V. Mut, "Multisensory Stimulation and EEG Recording Below the Hair-Line: A New Paradigm on Brain Computer Interfaces," in *IEEE Transactions on Neural Systems and Rehabilitation Engineering*, vol. 28, no. 4, pp. 825-831, April 2020, doi: 10.1109/TNSRE.2020.2979684.
- [13] C. H. Han, K. R. Müller and H. J. Hwang, "Enhanced Performance of a Brain Switch by Simultaneous Use of EEG and NIRS Data for Asynchronous Brain-Computer Interface," in *IEEE Transactions on Neural Systems and Rehabilitation Engineering*, vol. 28, no. 10, pp. 2102-2112, Oct. 2020, doi: 10.1109/TNSRE.2020.3017167.
- [14] M. Bevilacqua, S. Perdakis and J. D. R. Millán, "On Error-Related Potentials During Sensorimotor-Based Brain-Computer Interface: Explorations With a Pseudo-Online Brain-Controlled Speller," in *IEEE Open Journal of Engineering in Medicine and Biology*, vol. 1, pp. 17-22, 2020, doi: 10.1109/OJEMB.2019.2962879.
- [15] Y. Zhou, S. He, Q. Huang and Y. Li, "A Hybrid Asynchronous Brain-Computer Interface Combining SSVEP and EOG Signals," in *IEEE Transactions on Biomedical Engineering*, vol. 67, no. 10, pp. 2881-2892, Oct. 2020, doi: 10.1109/TBME.2020.2972747.
- [16] V. K. Benzy, A. P. Vinod, R. Subasree, S. Alladi and K. Raghavendra, "Motor Imagery Hand Movement Direction Decoding Using Brain Computer Interface to Aid Stroke Recovery and Rehabilitation," in *IEEE Transactions on Neural Systems and Rehabilitation Engineering*, vol. 28, no. 12, pp. 3051-3062, Dec. 2020, doi: 10.1109/TNSRE.2020.3039331.
- [17] O. Y. Kwon, M. H. Lee, C. Guan and S. W. Lee, "Subject-Independent Brain-Computer Interfaces Based on Deep Convolutional Neural Networks," in *IEEE Transactions on Neural Networks and Learning Systems*, vol. 31, no. 10, pp. 3839-3852, Oct. 2020, doi: 10.1109/TNNLS.2019.2946869.
- [18] Z. Gu, Z. Chen, J. Zhang, X. Zhang and Z. L. Yu, "An Online Interactive Paradigm for P300 Brain-Computer Interface Speller," in *IEEE Transactions on Neural Systems and Rehabilitation Engineering*, vol. 27, no. 2, pp. 152-161, Feb. 2019, doi: 10.1109/TNSRE.2019.2892967.
- [19] A. Kumar, L. Gao, E. Pirogova and Q. Fang, "A Review of Error-Related Potential-Based Brain-Computer Interfaces for Motor Impaired People," in *IEEE Access*, vol. 7, pp. 142451-142466, 2019, doi: 10.1109/ACCESS.2019.2944067.
- [20] D. Kim, W. Byun, Y. Ku and J. H. Kim, "High-Speed Visual Target Identification for Low-Cost Wearable Brain-Computer Interfaces," in *IEEE Access*, vol. 7, pp. 55169-55179, 2019, doi: 10.1109/ACCESS.2019.2912997.
- [21] V. Kartsch, G. Tagliavini, M. Guermandi, S. Benatti, D. Rossi and L. Benini, "BioWolf: A Sub-10-mW 8-Channel Advanced Brain-Computer Interface Platform With a Nine-Core Processor and BLE Connectivity," in *IEEE Transactions on Biomedical Circuits and Systems*, vol. 13, no. 5, pp. 893-906, Oct. 2019, doi: 10.1109/TBCAS.2019.2927551.
- [22] B. Lei et al., "Walking Imagery Evaluation in Brain Computer Interfaces via a Multi-View Multi-Level Deep Polynomial Network," in *IEEE Transactions on Neural Systems and Rehabilitation Engineering*, vol. 27, no. 3, pp. 497-506, March 2019, doi: 10.1109/TNSRE.2019.2895064.
- [23] A. Jafarifarmand and M. A. Badamchizadeh, "EEG Artifacts Handling in a Real Practical Brain-Computer Interface Controlled Vehicle," in *IEEE Transactions on Neural Systems and Rehabilitation Engineering*, vol. 27, no. 6, pp. 1200-1208, June 2019, doi: 10.1109/TNSRE.2019.2915801.
- [24] M. E. M. Mashat, C. T. Lin and D. Zhang, "Effects of Task Complexity on Motor Imagery-Based Brain-Computer Interface," in *IEEE Transactions on Neural Systems and Rehabilitation Engineering*, vol. 27, no. 10, pp. 2178-2185, Oct. 2019, doi: 10.1109/TNSRE.2019.2936987.
- [25] S. Ge et al., "SSVEP-Based Brain-Computer Interface with a Limited Number of Frequencies Based on Dual-Frequency Biased Coding," in *IEEE Transactions on Neural Systems and Rehabilitation Engineering*, vol. 29, pp. 760-769, 2021, doi: 10.1109/TNSRE.2021.3073134.
- [26] S. Ahamad, "Evolutionary Computing Driven Extreme Learning Machine for Objected Oriented Software Aging Prediction", *International Journal of Computer Science and Network Security (IJCSNS)*, ISSN: 1738-7906, Vol. 22, No. 1, pp. 781-789, January 2022, doi: 10.22937/IJCSNS.2022.22.1.100.
- [27] M.A.Bari and S. Ahamad, "Managing Knowledge in Development of Agile Software " *International Journal of Advanced Computer Science and Applications (IJACSA)*, 2(4), 2011, ISSN: 2156-5570 (Online), 2158-107X (Print), pp. 72-76. doi: 10.14569/IJACSA.2011.020411.
- [28] S. Ge, Y. Jiang, P. Wang, H. Wang and W. Zheng, "Training -Free Steady-State Visual Evoked Potential Brain-Computer Interface Based on Filter Bank Canonical Correlation Analysis and Spatiotemporal Beamforming Decoding," in *IEEE Transactions on Neural Systems and Rehabilitation Engineering*, vol. 27, no. 9, pp. 1714-1723, Sept. 2019, doi: 10.1109/TNSRE.2019.2934496.

Wave Parameters Prediction for Wave Energy Converter Site using Long Short-Term Memory

Manzoor Ahmed Hashmani¹, Muhammad Umair²

High Performance Cloud Computing Center (HPC3)
Department of Computer and Information Sciences
Universiti Teknologi PETRONAS, Seri Iskandar, Malaysia

Horio Keiichi³

Graduate School of Life Science and Systems Engineering
Kyushu Institute of Technology
Fukuoka, Japan

Abstract—Forecasting the behaviour of various wave parameters is crucial for the safety of maritime operations as well as for optimal operations of wave energy converter (WEC) sites. For coastal WEC sites, the wave parameters of interest are significant wave height (H_s) and peak wave period (T_p). Numerical and statistical modeling, along with machine and deep learning models, have been applied to predict these parameters for the short and long-term future. For near-future prediction of H_s and T_p , this study investigates the possibility of optimally training a Long Short-Term Memory (LSTM) model on historical values of H_s and T_p only. Additionally, the study investigates the minimum amount of training data required to predict these parameters with acceptable accuracy. The Root Mean Square Error (RMSE) measure is used to evaluate the prediction ability of the model. As a result, it is identified that LSTM can effectively predict H_s and T_p given their historical values only. For H_s , it is identified that a 4-year dataset, 20 historical inputs, and a batch size of 256 produce the best results for three, six, twelve, and twenty-four-hour prediction windows at half-hourly step. It is also established that the future values of T_p can be optimally predicted using a 2-year dataset, 10 historical inputs, and a 128-batch size. However, due to the much dynamic nature of the peak wave period, it is discovered that the LSTM model yielded relatively low prediction accuracy as compared to H_s .

Keywords—Wave energy converter; significant wave height; peak wave period; LSTM

I. INTRODUCTION

Ocean or sea waves carry a tremendous amount of kinetic energy and are considered an important source of renewable energy [1]. These waves have the highest energy density among available renewable energy sources [2]. Among the different types of ocean waves, it is the wind-generated wave that is almost always visible on the sea surface [3]. Maritime navigation, commercial, renewable power generation, and non-commercial activities are thus subject to prevailing wind-wave conditions and their future forecast. To describe the nature of wind-waves, the complex association of various wave and weather parameters needs to be studied. Due to their stochastic nature, modelling and forecasting of wind-waves using deterministic equations is considered a challenging task [4].

Numerical wave modelling [5][6][7], statistical modelling [8] [9], as well as machine and deep learning methods [10][11][12][13] have been applied to study and forecast the nature of wind-waves for short-term and long-term time

periods. Despite its wide application, it has been reported that numerical modelling requires high computation power and a large amount of data [14]. As an alternative, machine learning models that have outperformed statistical models [9] and execute faster than numerical wave models [15] can be used as a surrogate for numerical modelling [14].

In this study, a deep learning model, specifically long short-term memory (LSTM), is evaluated to forecast the future values of two important wave parameters, i.e., significant wave height (H_s) and peak wave period (T_p) [16] for the near-shore WEC site.

The paper is divided into the following sections: Section II reviews the literature on wave energy converter, and recent machine and deep learning studies on wave parameters prediction. In Section III, the problem statement is defined. Section IV describes the methodology by explaining the study area selection criteria, dataset preprocessing and arrangement steps, hardware and software setup, the LSTM model and its parameters, and evaluation criteria. Results and related discussion are presented in Section V. Finally, in Section VI, the conclusion and future work is discussed.

II. LITERATURE REVIEW

A. Wave Energy Converter

A wave energy converter (WEC) generates electric energy by converting the kinetic energy of sea waves into mechanical energy, which subsequently runs the electric generators to generate electricity. Based on their design principles, a wave energy converter can be divided into three categories [17]:

- 1) *Attenuator*: This type of WEC rides the waves in parallel to the predominant wave direction to generate energy.
- 2) *Point absorber*: The point absorber WEC is a floating or submerged structure. It heaves up and down relative to the incident wavelength to generate energy.
- 3) *Terminator*: The terminator WEC produces energy by physically intercepting a wave by having its principal axes parallel to the wave direction.

The power generation efficiency of a WEC is highly dependent on prevailing wave conditions and mostly affected by significant wave height (H_s), peak energy wave period (T_p) and wave energy period (T_e) [16]. The prediction of these parameters plays an important part in forecasting energy potential and generation, and as well as the operational safety

of the WEC site. In a recent study, it has been reported that the commercial deployment of WECs still remains low [18]. Hence, there is still a lot of room for research and development in various aspects of the WEC echo system, including wave parameter forecasting using alternative approaches such as machine and deep learning.

B. Wind-Wave Parameters Forecasting using Machine Learning Models

Recently, various machine learning techniques have been applied to forecast wind-wave parameters and sea weather. One of such studies conducted by Ali et. al. [19] forecasted half-hourly peak energy wave period (T_p) using the extreme learning machine (ELM), which is a training algorithm for single hidden layer feedforward neural network (SLFN). The study compared the results of ELM with five other deep learning and linear regression models, including recurrent neural network (LSTM). A six-year record of peak energy wave period was used to train and test the models. An interesting finding was presented, which indicates that for T_p forecasting, deep learning models (i.e., CNN and LSTM) didn't perform well as compared to ELM. For example, in the North Moreton Bay region, the study reported that ELM produced a higher R value as compared to CNN and RNN (i.e., ELM = 0.963, CNN = 0.932, and RNN = 0.928). Similarly, the ELM model resulted in a lower RMSE value as compared to CNN and RNN (i.e., ELM = 0.52, CNN = 0.98, and RNN = 1.24). This study has established that ELM is the better choice for half-hourly T_p forecasting. However, the study did not go beyond the half-hourly forecast of T_p and how LSTM might perform in such a case. Additionally, the study's scope was limited and didn't consider forecasting another important wave parameter of interest, i.e., significant wave height.

In the work presented by Fan, Xiao, and Dong [11], an LSTM network was proposed to predict near-future significant wave height. The study trained the proposed model on wave datasets acquired from ten different locations across the globe. Keeping in consideration the gradual development of wave height, six parameters were chosen as inputs to the LSTM model. These parameters were wind direction, wave height one hour ago, and wind speed at 1, 2, 3, and 4 hours ago. The study proposed a simple LSTM model with one hidden layer and one output layer. The results of the LSTM model were compared with five other machine and deep learning models. The study reported superior prediction performance when compared to the back propagation neural network, extreme learning machine, support vector machine, residual network, and random forest algorithm. The study suggests using one year of data for one-hour forecasting and two years of data for six-hour forecasting. Additionally, the study advocates the inclusion of wind speed data as a factor to improve the forecasting efficiency of significant wave height. However, this study has not considered prediction of an important parameter of interest, i.e., the peak wave period.

A long-term (i.e., up to two years) significant wave height and peak wave period prediction method based on XGBoost and LSTM models was presented by Hu et. al. [15]. The study trained and tested the models on hourly data collected for H_s , T_p and surface wind over a span of 24 years. The surface wind

parameters (i.e., speed and direction) were used as inputs for each model. The models then predicted H_s and T_p values over a span of two years. When compared to the numerical wave model WAVEWATCH III (WW3), the results showed that machine learning models exhibited an edge over numerical model in terms of faster execution. As compared to LSTM and WW3, the study reported lower Mean Absolute Percentage Error (MAPE) values for XGBoost for both target parameters. The study also reported that a tree-based model (i.e., XGBoost) came to saturation on the training data beyond 5 years. Additionally, it was found that the LSTM model yielded improved prediction performance on larger dataset. The study concludes that XGBoost is preferable if limited training data is available.

Kim et. al. [13] proposed an interesting technique to predict ocean weather by converting 1D ocean data into a 2D image and applying convolutional LSTM (ConvLSTM) to predict eight ocean weather parameters after one week. The method uses the AutoEncoderis for its effectiveness in removing noise from data, thus optimizing the training process of ConvLSTM. The model took eight parameters as an input. Six of the parameters have 20-year of data, while the remaining two have 4-year of data. The study predicted ocean weather for a window of one week with an average error of 6.7%. However, this study does not include significant wave height and peak energy wave period as target prediction parameters.

It has been observed in these studies that

- 1) Generally, datasets covering various wave and weather parameters across multiple years are used to train and test the models [19][15][13].
- 2) LSTM and its variants have shown superior forecasting accuracy across different time frames and on various sizes of training dataset [11] [15] [13].

Given the recent applications of LSTM in wave parameters forecasting problems, for a near-shore wave energy converter site, this study proposes to identify the wave parameters (i.e., H_s and T_p) prediction capability of an LSTM model using historical values of target parameters only. Hence, a problem statement is formulated and discussed in succeeding section.

III. PROBLEM STATEMENT

Sea surface waves, or wind-waves, are generally produced by the wind blowing over large stretches of water [3]. These waves carry a tremendous amount of kinetic energy, which can be converted into electricity by using a wave energy converter (WEC). Due to its stochastic nature, forecasting various parameters of wind-waves is a challenging task that requires high computational power and a large amount of time-series data. For wave energy converter sites, the wave parameters of interest are identified as being significant wave height (H_s), peak wave period (T_p), and wave energy period (T_e) [16]. For near-coast wave energy converter sites, the parameters of interest are significant wave height (H_s) and peak wave period (T_p). Presented studies have shown that machine learning-based prediction of these parameters (i.e., H_s and T_p) requires a large dataset consisting of various wave and weather parameters to train the model. Contrary to this approach, in this study, we attempt to answer the following research questions.

RQ1: For a near-shore wave energy converter site, can the stochastic nature of significant wave height and peak wave period be predicted using an LSTM model which is trained on their historical values only?

RQ2: What is the minimum dataset size required to optimally train an LSTM model for the wave parameters (i.e., H_s and T_p) prediction problem?

The following research objectives are hence defined.

RO1: To develop, train and evaluate an LSTM model which predicts significant wave height and peak wave period given it is trained on their historical values only.

RO2: To identify the minimal dataset size required to optimally train an LSTM-based model for wave parameters prediction.

IV. METHODOLOGY

A. Study Area

The coastal areas of east Australia have a high potential for wave energy generation [19]. For this reason, this study has been designed on the data collected by a moored wave monitoring buoy (i.e., the Datawell 0.9m GPS Waverider buoy) deployed off the eastern coast of Australia at a latitude of $26^{\circ} 33.960' S$, and longitude of $153^{\circ} 10.870' E$. The location of the buoy is shown in Fig. 1. The buoy is approximately 8 km off the coast of Coolum Beach, Queensland, Australia, and the reported water depth at this site is 36 meters. The dataset is available under a Creative Commons Attribution 4.0 license and can be accessed at the Queensland Government's open data portal (<https://www.data.qld.gov.au/dataset/coastal-data-system-waves-mooloolaba>) [20].

B. Dataset Description

To train and test the LSTM model, the wave parameters dataset from the years 2000 to 2014 was initially selected as a source dataset (D_{src}). The dataset has a temporal resolution of 30 minutes and consists of 235,708 readings for six parameters, namely significant wave height (H_s), maximum wave height (H_{max}), zero upcrossing wave period (T_z), peak energy wave period (T_p), peak direction related to true north (P_{dir}) and sea surface temperature (SST). However, upon initial investigation, it was found that D_{src} suffers from missing values in continuity (i.e., from March 2nd, 2009, till September 30th, 2009). In this case, as shown in Fig. 2., the application of data interpolation technique to such a long missing series resulted in undesirable values. Thus, a subset (D_{sub}) of D_{src} was identified for further investigation such that D_{sub} has a smaller number of missing data points in continuity. The features of D_{src} and D_{sub} are given in Table I.

C. Data Preprocessing

Since one of the objectives of this study is to investigate the forecasting of H_s and T_p based on their historical values only, thus as a first step, irrelevant parameters are dropped from the dataset (D_{sub}).

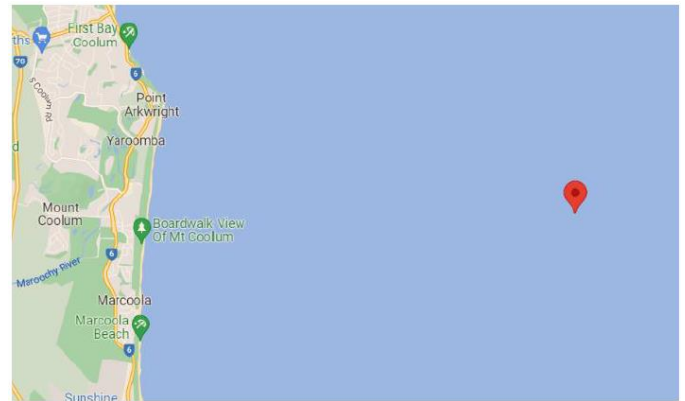


Fig. 1. The Buoy's Location off the Coast of Coolum Beach. (Source: Google Maps).

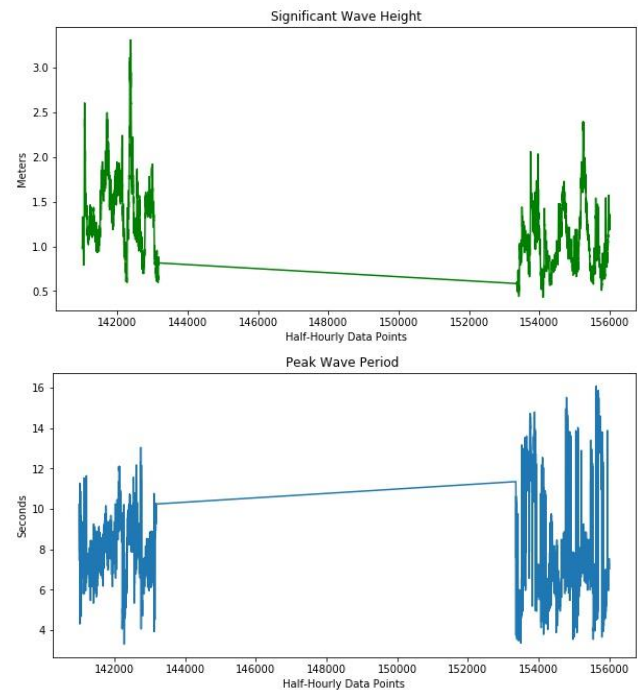


Fig. 2. Examples of Linear Trend in Interpolated Values due to the Large Number of Missing Data Points in Continuity.

TABLE I. FEATURES OF BUOY DATASETS

Dataset	Location	Latitude	Longitude	Water Depth	Dataset Fields	Time Period	Data Instances	Missing or Abnormal Values
D_{src}	Mooloolaba, Australia	$26^{\circ} 33.960'$	$153^{\circ} 10.870'$	36 meters	Date, Time, H_s , H_{max} , T_z , T_p , P_{dir} , SST	20-Apr-2000 31-Dec-2014	235,708	22,003
D_{sub}	Mooloolaba, Australia	$26^{\circ} 33.960'$	$153^{\circ} 10.870'$	36 meters	Date, Time, H_s , T_p	1-Jan-2001 31-Dec-2008	136,481	3,774

In the second step, it is important to identify the magnitude of data anomalies and gaps at both temporal scale and parameter level. Thus, at the parameter level, a statistical analysis for data anomalies, such as negative or extremely large values, is conducted. The results of this investigation are presented in Table II, which indicates the absence of any such anomalies.

TABLE II. SUMMARY OF THE DATASET (2001-2008)

Measure	Significant Wave Height	Peak Wave Period
Instances Count	136,481	136,481
Mean	1.15	8.88
Standard Deviation	0.49	2.50
Minimum Value	0.22	2.05
Maximum Value	5.88	19.22
25%	0.81	7.02
50%	1.05	8.74
75%	1.39	10.55

In the third step, to identify missing values on a temporal scale, a series at a half-hourly step size is generated for each day for 8 years starting from January 1st, 2001, to December 31st, 2008. A date and time-based one-to-one mapping of values from D_{sub} is completed on the generated series. This step identified 3,774 missing values in D_{sub} . The magnitude of missing values was smaller than the magnitude of missing values in the dataset D_{src} . Interpolation is not applied to the segment in which a large series of missing data points is identified. For the rest of the data, the linear interpolation technique is applied to fill in the missing values. Some examples of the interpolated values are presented in Fig. 3.

At this stage, as per recommendation of a previous study [11] and to answer RQ2, three datasets of 2,4 and 8-year data are created. These datasets are used to train, validate, and test the LSTM model.

D. Hardware and Software Setup

For the experiment, the LSTM model is written in the Python programming language using the Keras framework. For data processing, NumPy and the Pandas libraries are used. The programming environment is built on a Windows 10 Pro system running on an Intel (R) Core (TM) i7-9750H CPU at a clock speed of 2.60 GHZ. All experiments are executed on an

NVIDIA GeForce RTX 2070 with a Max-Q Design GPU with 8 GB of RAM.

E. Long Short-Term Memory Model

Long short-term memory (LSTM) is a variant of RNN that with the help of a forget gate solves the RNN’s problems of exploding and vanishing gradient [21]. In an LSTM, each time step is represented by an identical neural network cell, which by passing its non-linear activation to the next cell builds a system memory. This system memory is used to model time series data. In Fig. 4, the LSTM network cell is depicted. The equations for LSTM cell are given in equations 1-6.

$$f_t = \sigma(W_{xf}x_t + W_{hf}h_{t-1} + b_f) \tag{1}$$

$$i_t = \sigma(W_{xi}x_t + W_{hi}h_{t-1} + b_i) \tag{2}$$

$$o_t = \sigma(W_{xo}x_t + W_{ho}h_{t-1} + b_o) \tag{3}$$

$$g_t = \tanh(W_{xg}x_t + W_{hg}h_{t-1} + b_g) \tag{4}$$

$$c_t = f_t \otimes c_{t-1} + i_t \otimes g_t \tag{5}$$

$$h_t = o_t \otimes \tanh(c_t) \tag{6}$$

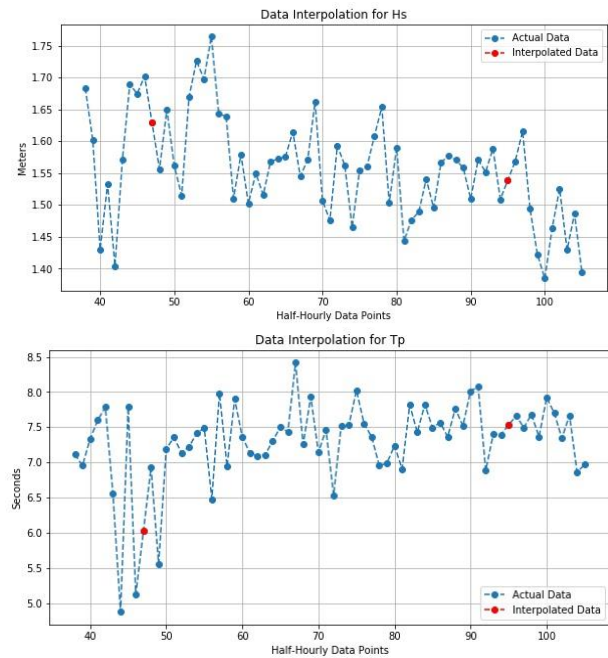


Fig. 3. Examples of Interpolation Results (Dataset 2001-2008).

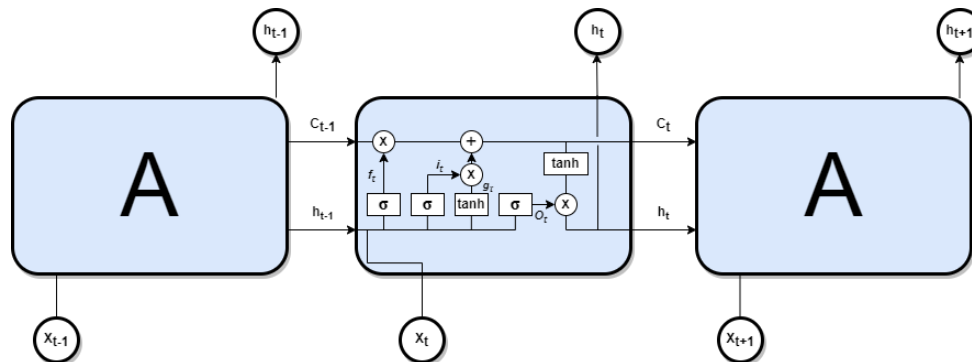


Fig. 4. Long Short-Term Memory Configuration.

Where, σ = sigmoid function, W = weight for each layer, x_t = input in time step t , b = bias, \tanh = hyperbolic tangent function, \otimes = element-wise product, c_t = main message passed between the steps, f_t = forget gate, and h_t = value passed to the next cell.

An LSTM model is designed to predict half-hourly forecasts for significant wave height (H_s) and peak wave period (T_p) at four different forecast windows. The model takes historical values of H_s and T_p as input. The model has three layers (L_1 , L_2 , and L_3). A dropout layer (D) is added after the L_2 layer. For its better performance, Adaptive Moment Estimation (ADAM) is employed [13]. The parameters of the LSTM model are provided in Table III.

TABLE III. LSMT MODEL PARAMETERS

Parameters	Value
L_1	32
L_2	16
L_3	8
D	0.2
Activation Functions	Hyperbolic Tangent
Optimizer	ADAM
Learning Rate	0.001
Patience	5

F. Evaluation Criteria

To evaluate the prediction efficiency of the model, the root mean square error (RMSE) measure is used. The formula to calculate RMSE is presented in equation 7.

$$RMSE = \sqrt{\frac{1}{n} \sum_{i=1}^n (o_i - p_i)^2} \quad (7)$$

Where o_i = observed value and p_i = predicted value.

TABLE V. PREDICTION RESULTS (RMSE)

Datasets	H_i	BS	Significant Wave Height				Peak Wave Period			
			3H	6H	12H	24H	3H	6H	12H	24H
2 Years	10	128	0.0356	0.0417	0.0701	0.0693	0.1260	0.1713	0.2369	0.4094
	10	256	0.0338	0.0411	<u>0.0720</u>	0.0705	0.1653	0.1973	0.2569	0.4123
	20	128	0.0361	0.0401	0.0693	0.0690	0.2223	0.2574	0.2972	0.4157
	20	256	0.0374	0.0421	0.0696	<u>0.0708</u>	0.1901	0.2311	0.2777	0.4200
4 Years	10	128	0.0356	0.0315	0.0467	0.0444	<u>0.9196</u>	1.6406	1.6669	2.0899
	10	256	0.0306	0.0286	0.0461	0.0426	0.8620	1.7244	1.7385	2.0853
	20	128	0.0470	0.0427	0.0537	0.0499	0.8360	1.7622	1.7986	2.1027
	20	256	0.0279	0.0268	0.0334	0.0327	0.8545	<u>1.8000</u>	<u>1.8334</u>	<u>2.1314</u>
8 Years	10	128	0.0623	0.0546	0.0484	0.0463	0.2872	0.4008	1.1169	0.8585
	10	256	0.0595	0.0558	0.0534	0.0542	0.3865	0.4624	1.1541	0.9006
	20	128	<u>0.0734</u>	<u>0.0624</u>	0.0559	0.0518	0.3668	0.4501	1.1378	0.9234
	20	256	0.0582	0.0543	0.0516	0.0516	0.4556	0.5137	1.1858	0.9310

V. RESULTS AND DISCUSSION

To predict significant wave height and peak wave period for the WEC site, four experiments are designed for each dataset in which a combination of historical inputs (H_i) and batch sizes (BS) are used to train the LSTM model. The validation data split of 20% remains constant across experiments. The evaluated combinations are presented in Table IV. The model is tested on its half-hourly prediction accuracy at four near-future windows, i.e., three, six, twelve, and twenty-four hours, and their results, in the form of RMSE values, are presented in Table V.

The RMSE values for the near-future prediction of significant wave height indicate that the model trained on 4 years of data, 20 historical inputs, and a batch size of 256 outperformed all other H_s prediction experiments. The RMSE values for the half-hourly 3, 6, 12, and 24-hour forecasts are 0.0279, 0.0268, 0.0334, and 0.0327, respectively. It is also observed that the lowest RMSE values for half-hourly 3, 6, 12, and 24-hour forecasts are produced by model trained on either 2 or 8-year of data. This indicates that the optimal prediction efficiency of the LSTM model is related to the dataset size, which in this case is 4 years. Hence, to predict the complex behaviour of H_s optimally, 4-year significant wave height historical data is sufficient. The best-performing prediction results for significant wave height are shown in Fig. 5(a).

TABLE IV. EXPERIMENTAL COMBINATIONS

Dataset	Historical Inputs (H_i)	Batch Size (BS)	Forecast Windows
2-year 4-year 8-year	10	128	3-hour 6-hour 12-hour 24-hour
	10	256	
	20	128	
	20	256	

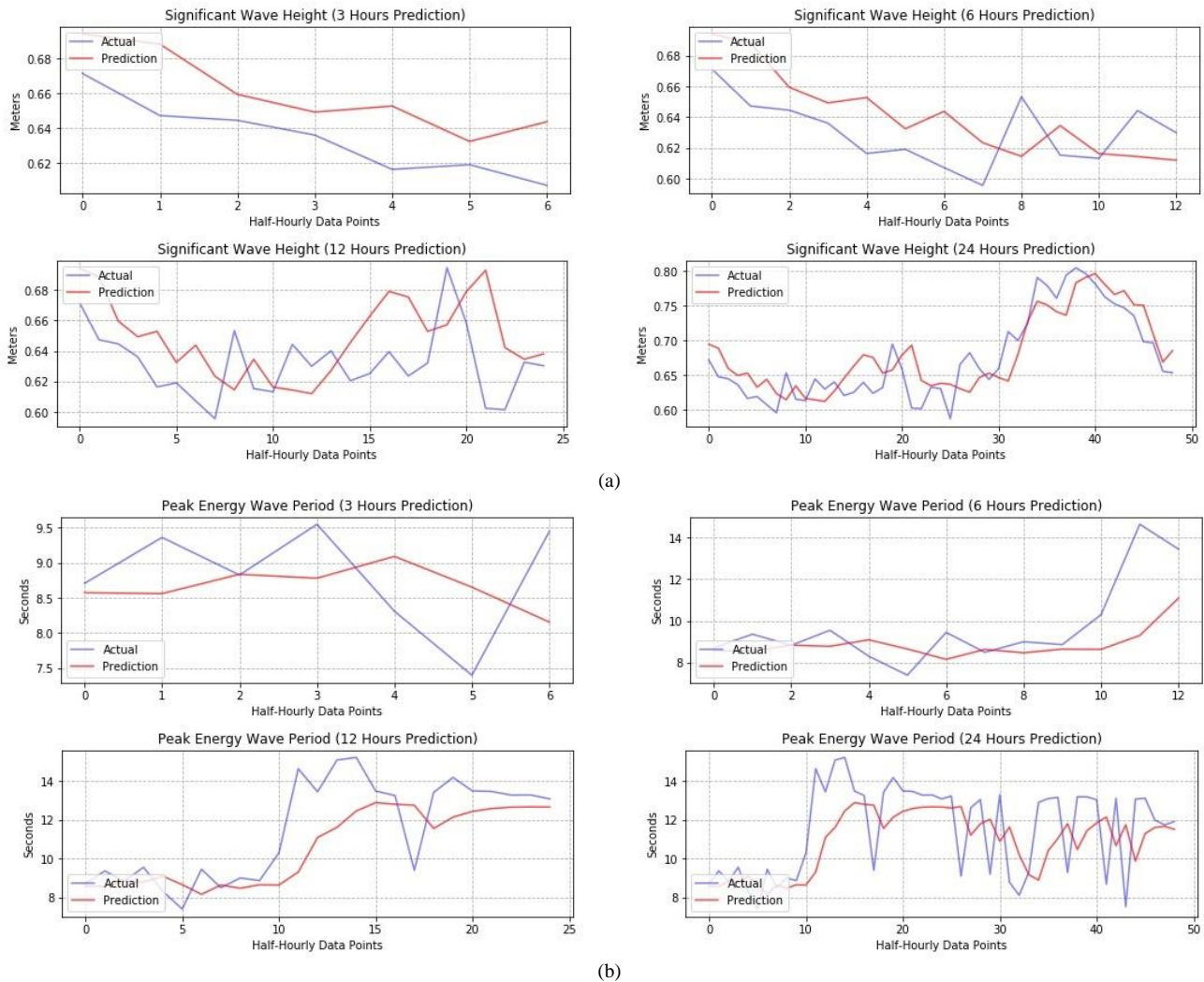


Fig. 5. Best Prediction Results for, (a) Significant Wave Height, (b) Peak Wave Period.

For all near-future forecast windows, the forecast for the peak wave period is best produced by the smallest dataset and with the minimum historical inputs and batch size (i.e., 2-year dataset, $H_i=10$, $BS=128$). The RMSE values for half-hourly 3, 6, 12, and 24-hour forecasts are 0.126, 0.1713, .2369, and 0.4094, respectively. However, when compared to the model's forecasting ability for significant wave height, these values remain high. This indicates that for T_p prediction, the model is not efficiently identifying the trend for a relatively much dynamic pattern of T_p . It is also observed that the model trained on a larger dataset, i.e., an 8-year dataset, performed well as compared to the model trained on a 4-year dataset. The worst performing RMSE values for T_p are generated by the model trained using 4-year data. Fig. 5(b) depicts the best-performing prediction results for the peak wave period.

VI. CONCLUSION AND FUTURE WORK

A wind wave is a type of ocean wave that is generally present on the sea surface and affects navigation, commercial, power generation, and non-commercial activities taking place in a maritime environment. Thus, the study of wind-wave state

prediction plays a pivotal role in the planning, execution, and safety of these activities.

In this study, from the point of view of a near-shore wave energy converter site, the effect of minimal training parameters and dataset size on the LSTM-based significant wave height and peak wave period prediction model is investigated.

Three datasets with variable temporal length were prepared, and on each dataset, four experiments were conducted to investigate the prediction ability of LSTM based on the target parameter's historical inputs and batch sizes. In addition, the study investigated the minimum dataset size required for the training of the LSTM model.

It was found that for significant wave height, the LSTM model generated better results using a 4-year dataset, 20 historical inputs, and a 256-batch size. It was also observed that for the peak wave period forecast, the model didn't perform as well as compared to the significant wave height forecast. However, it was identified that a 2-year dataset with 10 historical inputs and a 128-batch size yielded the best results for T_p prediction. Based on the presented results, the study concluded that future values of H_s and T_p can be predicted by

training an LSTM model on their historical values only. Additionally, the study also identified the minimum size of the dataset (4 years for H_s and 2 years for T_p) required to train and predict the future values of H_s and T_p .

Development of a LSTM model which can forecast both H_s and T_p with a similar sized dataset and accuracy can be considered as future work of this study.

ACKNOWLEDGMENT

This research work is a part of an ongoing research project jointly funded by Universiti Teknologi PETRONAS, Malaysia and Kyushu Institute of Technology, Japan (Grant Number: 015ME0-123).

REFERENCES

- [1] M. Satriawan, Liliyasi, W. Setiawan, and A. G. Abdullah, "Unlimited energy source: a review of ocean wave energy utilization and its impact on the environment," *Indones. J. Sci. Technol.*, vol. 6, no. 1, pp. 1–16, 2021, doi: 10.17509/ijost.v6i1.31473.
- [2] A. Clément et al., "Wave energy in Europe: Current status and perspectives," *Renew. Sustain. Energy Rev.*, vol. 6, no. 5, pp. 405–431, 2002, doi: 10.1016/S1364-0321(02)00009-6.
- [3] A. K. Laing et al., *Guide to Wave Analysis and Forecasting*. 1998.
- [4] J. Mahjoobi and A. Etemad-Shahidi, "An alternative approach for the prediction of significant wave heights based on classification and regression trees," *Appl. Ocean Res.*, vol. 30, no. 3, pp. 172–177, 2008, doi: 10.1016/j.apor.2008.11.001.
- [5] T. W. Group, "The WAM model—A third generation ocean wave prediction model," *J. Phys. Oceanogr.*, vol. 18, no. 12, pp. 1775–1810, 1988.
- [6] N. Booij, L. H. Holthuijsen, and R. C. Ris, "The SWAN" wave model for shallow water," in *Coastal Engineering 1996, 1997*, pp. 668–676.
- [7] H. L. Tolman et al., "Development and implementation of wind-generated ocean surface wave models at NCEP," *Weather Forecast.*, vol. 17, no. 2, pp. 311–333, 2002, doi: 10.1175/1520-0434(2002)017<0311:DAIOWG>2.0.CO;2.
- [8] G. Reikard, P. Pinson, and J. R. Bidlot, "Forecasting ocean wave energy: The ECMWF wave model and time series methods," *Ocean Eng.*, vol. 38, no. 10, pp. 1089–1099, 2011, doi: 10.1016/j.oceaneng.2011.04.009.
- [9] R. Kalra, M. C. Deo, R. Kumar, and V. K. Agarwal, "Artificial neural network to translate offshore satellite wave data to coastal locations," *Ocean Eng.*, vol. 32, no. 16, pp. 1917–1932, 2005, doi: 10.1016/j.oceaneng.2005.01.007.
- [10] S. C. James, Y. Zhang, and F. O'Donncha, "A machine learning framework to forecast wave conditions," *Coast. Eng.*, vol. 137, no. February, pp. 1–10, 2018, doi: 10.1016/j.coastaleng.2018.03.004.
- [11] S. Fan, N. Xiao, and S. Dong, "A novel model to predict significant wave height based on long short-term memory network," *Ocean Eng.*, vol. 205, no. December 2019, p. 107298, 2020, doi: 10.1016/j.oceaneng.2020.107298.
- [12] K. Osawa, H. Yamaguchi, M. Umair, M. A. Hashmani, and K. Horio, "Wave Height and Peak Wave Period Prediction Using Recurrent Neural Networks," 2020 Int. Conf. Comput. Intell. ICCI 2020, no. October, pp. 1–4, 2020, doi: 10.1109/ICCI51257.2020.9247805.
- [13] K. S. Kim, J. B. Lee, M. Il Roh, K. M. Han, and G. H. Lee, "Prediction of ocean weather based on denoising autoencoder and convolutional LSTM," *J. Mar. Sci. Eng.*, vol. 8, no. 10, pp. 1–24, 2020, doi: 10.3390/jmse8100805.
- [14] M. Umair, M. A. Hashmani, and M. H. B. Hasan, "Survey of Sea Wave Parameters Classification and Prediction using Machine Learning Models," *Proc. - 2019 1st Int. Conf. Artif. Intell. Data Sci. AiDAS 2019*, pp. 1–6, 2019, doi: 10.1109/AiDAS47888.2019.8970706.
- [15] H. Hu, A. J. van der Westhuysen, P. Chu, and A. Fujisaki-Manome, "Predicting Lake Erie wave heights and periods using XGBoost and LSTM," *Ocean Model.*, vol. 164, no. November 2020, p. 101832, 2021, doi: 10.1016/j.ocemod.2021.101832.
- [16] M. Umair, M. A. Hashmani, and H. Keiichi, "Optimal Feature Identification for Machine Prediction of Wind-Wave Parameters at Wave Energy Converter Site," 2020 Int. Conf. Comput. Intell. ICCI 2020, no. October, pp. 185–189, 2020, doi: 10.1109/ICCI51257.2020.9247677.
- [17] B. Drew, A. R. Plummer, and M. N. Sahinkaya, "A review of wave energy converter technology," *Proc. Inst. Mech. Eng. Part A J. Power Energy*, vol. 223, no. 8, pp. 887–902, 2009, doi: 10.1243/09576509JPE782.
- [18] T. Aderinto and H. Li, "Ocean Wave energy converters: Status and challenges," *Energies*, vol. 11, no. 5, pp. 1–26, 2018, doi: 10.3390/en11051250.
- [19] M. Ali et al., "Advanced extreme learning machines vs. deep learning models for peak wave energy period forecasting: A case study in Queensland, Australia," *Renew. Energy*, vol. 177, pp. 1031–1044, 2021, doi: 10.1016/j.renene.2021.06.052.
- [20] T. S. of Queensland, "Coastal Data System - Waves (Mooloolaba)." <https://www.data.qld.gov.au/dataset/coastal-data-system-waves-mooloolaba> (accessed Feb. 01, 2022).
- [21] S. Hochreiter and J. Schmidhuber, "Long Short-Term Memory," *Neural Comput.*, vol. 9, no. 8, pp. 1735–1780, Nov. 1997, doi: 10.1162/neco.1997.9.8.1735.

Dynamic User Activity Prediction using Contextual Service Matching Mechanism

M. Subramanyam¹

Department of Electronics and Communication Engineering
PES College of Engineering, Mandya
Karnataka, India

S. S. Parthasarathy^{2*}

Professor, Department of Electronics and Communication
Engineering, PES College of Engineering, Mandya
Karnataka, India

Abstract—The significance of context-based services is significantly increasing with the advancement of integrated technologies of sensors and ubiquitous technologies. The existing approaches are reviewed to find out that identification of user's activity has more scope of improvement. After reviewing the current literature towards context-based methodologies, it is found that existing methods are devoid of considering dynamic context; while the modelling perspective is mainly towards considering predefined and static contextual information. Further, existing models doesn't have any inclusion of potential belief system nor any incorporation of service matching. Further, practical world case-studies is characterized by complex activity of user while it is quite challenging to extract the accurate contextual information associated with complex user activity. From the practical deployment scenario, the existing system offers less supportability toward collaborative network, which is highly essential to be considered for constraint modelling for user activity detection. Therefore, the proposed manuscript contributes a solution towards existing research problems by introducing a Dynamic User Activity Prediction using Contextual Service Matching Mechanism. A mixed research methodology is used to prove how service matching mechanism is important in contextual service discovery using multimodal activity data. The first contributory solution towards addressing the research problem is by introducing a novel and simplified belief system that considers both static contextual parameters as well as dynamic activity-based contextual parameter. The second contributory solution towards existing problem is to develop a novel service matching module that takes the input from service reposit, user calendar events, and collaborative units for assisting in similarity-based recommendation system. The model considers Hidden Markov Model for activity determination considering states of activity. With a combined usage of user activity context, feature management, and collaborative model, the proposed system offers better granularity in investigating user activity. The experimental and simulation analysis of the proposed outcome shows the enhanced accuracy performance of proposed system under different test environment. The study also investigates the impact of the service matching mechanism as well as relevance feedback on the accuracy to find that the proposed system excels better accuracy.

Keywords—Contextual information; service discovery; prediction; ubiquitous computing; user activity

I. INTRODUCTION

With the significant advancement in Information and Communication Technology (ICT) in various fields e.g. mobile network, cloud computing, Internet-of-Things (IoT), etc. there

is abundant information in multiple forms [1][2]. However, such raw information is never directly useful for anyone and hence this leads to the birth of contextual information [3]. The usage of contextual information is found in the human-centric application, community-based application, and opportunistic application. They are further found in various classified applications e.g. user tracking, identification of human activity, social network, environmental monitoring, healthcare sector, etc. The majority of the identification of the human-based activity is carried out using smartphones, wearable sensors, development boards, etc. A context can be defined as sensed data utilized for representing the specific state/circumstances of a defined entity [4]. Contextual information is closely associated with sensory data. It is quite evident that there are various sources of origination of contextual information where the major complexity is to represent the accurate context in presence of higher uncertainty [5]. Various forms of reasoning approach, as well as dynamic interpretation, is essential for modeling contextual information from abstraction process at high-level [6][7]. The robustness of the contextual modeling must be minimized to enhance their technology adoption as well as to ensure better compatibility with the upcoming application of ubiquitous computing. Effective modeling of contextual-based services also calls for the inclusion of heterogeneity as well as comparability, which is highly essential in framing up the application of user activity detection. At present, there have been various research work being carried out towards context-based application, where different methodologies and environment has been considered [8]-[12].

However, irrespective of such research work, various challenges still exist in the area of contextual modeling. Various researchers have reported various levels of difficulties as well as technical challenges associated with contextual information [13]-[17]. Out of various challenges, some of the challenges associated with contextual information modeling are the complicated relationship among the context along with ambiguity in the dependencies of various internal factors [18]. If the model suffers from inaccurate reasoning then it fails to offer a significant conclusive interpretation of the queried context. To improve the accuracy of user activity detection from contextual information, existing research approaches are found to adopt supervised learning techniques (e.g. k-nearest neighbor, Support Vector Machine, etc.), fuzzy logic, naïve Bayesian, Decision tree, and stochastic approach. The prime issues in such algorithms are i) hardcoded thresholding, ii) no

*Corresponding Author.

preference to quality, iii) problematic validation scheme, iv) less computationally efficient, v) accuracy depends on the size of the dataset, etc. All these issues have not yet been solved in the present state of research work and only some of them have been addressed concerning user activity. From the viewpoint of user-activity detection, one of the most challenging aspects is to perform prediction of upcoming user activity as well as intention. This research problem is less emphasized in the existing system and hence this manuscript introduces context-based solution to address this problem.

The proposed system also implements a novel mechanism of Markov modeling for enhancing the predictive operation of dynamic user activity using contextual service mechanism. Section II discusses the existing research approaches towards using contextual information followed by outlining problem identification in Section III. The adopted research methodology is briefed in Section IV followed by a discussion of the analytical model in Section V. The discussion of the predictive approach is illustrated in Section VI. The simulation approach is discussed in Section VII while the discussion of obtained results is discussed in Section VIII. Finally, Section IX summarizes the finding as well as the contribution of the proposed study.

II. RELATED WORK

Usage of context has always been proven to be an essential factor for extracting certain latent traits when the information is quite bulky and unorganized. Existing research work has a different mechanism to use the service factor for catering to the demands of the developed design.

Most recently, the formulation of the context factor is implemented by Ehatisham-UI-Haw [19] towards an activity recognition system. In this approach, the granularity of the context is obtained from the behavioral aspects of the user where a classification modeling is carried out to identify fine and course-grained activity. Yachir et al. [20] have introduced a framework for service discovery followed by service selection in IoT applications. However, less evidence is shown to prove that the selection process offers higher reliability. Other authors e.g. Guo and Ma [21] and Yao [22] offer to construct a ubiquitous system with an aid of context. The uniqueness in the study of Guo and Ma [21] is that a scheduler system is designed for context-awareness based on activity data obtained from wearables. This system makes use of a smartphone that acts as a gateway for data aggregation from multiple wearables as well as it also carries out scheduling operations to implement a context-aware engine.

The work carried out by Klimek [23] has developed an intelligent mechanism for context-awareness associated with a use case of mountain hikers. The data is obtained from various sensors as well as mobile networks followed by data processing and analysis of human activity. The work carried out by Shen et al. [24] have developed a model where activities of human are assessed for understanding its gesture. The data is captured from the wristband followed by applying classification technique to determine the activity context. The performance of such monitoring-based applications could be further enhanced using ontology as seen in the work of Ni et al. [25]. Pahlevan et al. [26] have harnessed the potential of

contextual information for developing a dynamic algorithm using financial data captured from web services. Although such an approach assists in the identification of activity to some extent there was no inclusion of a classification approach for further enhancing the performance of detection of user activity. There are various studies to prove that the process of identification of various activities can be further enhanced using the clustering approach. Existing studies have witnessed the usage of extreme learning mechanisms for activity recognition systems as seen in the work of Chen et al. [27]. The study has used a neural network for identifying the activity of humans based on sensory data. Study on classifier design for a similar purpose is also seen in the work of Wang et al. [28].

Various studies are being explored towards user activity prediction. The work carried out by Alam et al. [29] has presented an algorithm that can predict user activity using the Markov model of finite order to ensure the prediction accuracy of 88%. The sensor-based contextual data can be also used for developing an application for identifying user activity. The work carried out by Pham et al. [30] has used a sophisticated machine learning scheme for recognition of human activity motivated by Long Short Term Memory and Convolution Neural Network. The activity data used in the study bears the characteristic of spatial and temporal aspects using capsule networks. A study towards a prediction-based approach was also presented by Huang et al. [31] that takes the contextual information for forecasting the most probable mobile application using time and location information as the context. The study outcome is benchmarked with linear and Bayesian network models. However, the limitation of this model is its higher dependency on manual setting of threshold that is not feasible in many of the smart applications. The work carried out by Kim et al. [32] has used a Bayesian network for predicting using historical contextual data showing 90% of accuracy performance. Lawal and Bano [33] have used a convolution neural network with two streams to localize human activity.

Elmalaki et al. [34] presented a framework that can significantly discretize between decision-making and application logic. The authors have presented a system to configure sensitivity using a java package for discovering the level of upcoming sensitivity. Implemented using the prototype, the study outcome has proven reduced overhead and reduced processing time. However, the model significantly misses analysis of any significant behavior as it is too dynamic. Xu et al. [35] have used q-networks to localize the human activity from the video sequence using Spatio-temporal aspects. At present context-based research work is also studied concerning ubiquitous and pervasive computing for better compatibility with upcoming wearable devices. A learning approach with a higher degree of activeness can superiorly assist in exploiting the power of context factors as shown in the study of Hsu et al. [36]. A development environment is designed for building navigation systems with better efficiency in learning. However, the model misses various essential functional tracks important in ubiquitous learning as well as it doesn't discuss any form of synchronization/communication among multiple devices for sharing context. Most recently, Kamberov et al. [37] have performed an investigation about the

significance of device integration for contextual sharing. However, the idea presented is without any numerical proof despite its potential thought. Popescu et al. [38] have developed an automated machine learning system for human activity recognition systems.

Xu [39] has also presented a study towards context-based services towards mobile data associated with activity detection. According to Khalid et al. [40], a better optimization principle can upgrade the performance of predictive accuracy that can be used for recommendation systems as well. Hence, the author applied swarm intelligence on the contextual information aggregated from the social network to perform recommendations. The recommender also maps various cloud-based services for the users to offer better precision. A similar form of study has also been carried out by Kim and Yoon [41] by additionally using probabilistic-based graphical structure. Study towards recommendation system is also carried out by Neto and Sales [42] in the context of the education system. Therefore, this section offers evidence that there has been considerable work being carried out towards using context-based information for curving activity detection by multiple means. Apart from these, there are some recent studies that has been carried out towards similar direction viz. classification system of activity (Singh et al. [43]), activity modelling using behavioral context (Asim et al. [44]), adaptive model of intervention using user-centric approach (Bilal et al. [45]), recognition of human activity (Siddiqi et al. [46]).

Therefore, various studies have evolved out to address the problems in activity detection and analysis characterized by benefits as well as issues. The next section outlines the research problems extracted from existing studies.

III. RESEARCH PROBLEM

The previous section has briefed that various research-based approaches do exist to offer to the model of the user activity. However, there are following open-end issues that are required to be addressed for further improving context-based user activity identification-based services. The open end problems captured after reviewing the existing literature in the prior section are as follows:

- **Lack of Considering Dynamic Context:** Existing studies mainly consider the static context where the information is either from a dataset or from a synthetic approach without the inclusion of any time-based properties in it. Hence, modeling of user activity detection based on static context is less reliable when exposed to the real-time environment of deployment.
- **Doesn't include Robust Belief System:** A robust belief system is always dependent on the deciding factor as well as dynamic observation. Normally, information related to belief is considered to be stored in an information server that is used for matching the queried user identity. Hence, the normal (or static) belief system is not in a condition to offer stable specificity performance and very often its accuracy degrades exponentially.

- **Non-Inclusion of Service Matching:** Existing system has less potential contributions towards an effective service discovery for assisting multiple numbers of users with heterogeneous context. Developing a service matching system is yet a computationally challenging problem in the case of the availability of dynamic context. At present, there is no such research work that has proven cost-effective service matching based on dynamic contexts.
- **Complex User Activity Detection:** At present, there are large numbers of studies in the last decade corresponding to user activity detection. But the major pitfalls are i) considering less number of features (or context), ii) less change of environmental parameters during the collection of context, and iii) usage of available optimization techniques that use an iterative process. It should be known that such a model of user activity detection is not in support of low-powered devices in mobile networks.
- **Less Supportability of Collaborative Network:** The absence of a collaborative network is another significant loophole that doesn't support the application to support ubiquitous computing. Although there are many research works claiming to support ubiquitous computing, none of the research work at present is reported to offer the supportability of a collaborative network that is an essential backbone of any ubiquitous application.

Apart from the above highlighted research problem, an essential observation is that there is a potential research gap where the core limitation of an existing literatures that considers static context. However, the practical applications of user activity determination demands inclusion of dynamic context. Hence, the prime motivation is to develop a scheme which can be practically validated where dynamic context modelling can be carried out with a potential and simplified belief system. With an upcoming smart and intelligence applications, services, and robots [47]-[49], there is a need to include the dynamic context as well as service modelling to make it properly functional. Hence, this acts a prime motivation factor to carry out development of proposed system. The proposed system considers the adoption of dynamic context, includes a comprehensive belief processing system using the CIOB model [50], develops a novel service matching mechanism with higher supportability of a collaborative network, and offers cost-effective user activity detection. The above-mentioned points of research problems are addressed in the proposed system as discussed in the next section.

IV. PROPOSED METHODOLOGY

The present work is an extension of the prior contextual model named CCSS [51] that uses a Context Collection and Request analysis Unit (CCRU) for refining the user request at the first level using beliefs and further refines the request using Collaboration Unit (CU) to match the service requirement of the user. The use of user activity as a context in Ubiquitous computing has been shown in many studies, by using inefficient service matching in the service discovery model.

This motivated us to address the use of user activities as one of the important contexts in the service matching process of the service delivery model.

The main aim of the proposed model DUAP is to incorporate the additional context of multiple user activities along with user profile and another context into the CIOB model [50] to get the best possible match of the desired service for the user in the ubiquitous application.

The idea is also to extract significant features from the activity context to generate dynamic belief and predict the most appropriate service. Referring to Fig. 1, the Service Matching Mechanism (SMM) exploits both static and dynamic context as multi-modal context along with recommendations and relevance feedback mechanism. The mechanism functionality is as described. The basic CIOB model takes multi-modal static context parameters such as user profile, location context, environmental context, etc. There is the inclusion of additional context information in the CIOB model namely activity context. The activity is dynamic as well every activity context holds certain hidden intentions. Getting the context as an intention from users' activity may assist SMM, service discovery, and customization of service. If the accurate activity and their respective features of the user are known then it is possible to determine the multi-modal user activities such as the status of different gestures like walking, sitting, running, etc. This is feasible by computing from linear and angular acceleration in x, y, and z planes given by accelerometer and gyro meter fixed with the portable mobile devices. These gestures along with their other context can be mapped to their probable intentions by behavioral pattern analysis. For example, if a person is running from the past one hour from one location to another in the early morning then the system predicts his behavior or intention as the user is jogging. This user may look for some health drinks, so that the health drink service discovery may notify and collaborate both the user and the service content. If the past pattern of the user is captured and the system has a continuous learning mechanism then the ultimate goal of the context-based service tailoring may be achieved.

The research methodology adopted for the study is a mixed-mode where experimental, analytical, and simulation have been carried out. Fig. 2 shows the flow adopted in designing the research methodology. The contribution of the proposed system are as follow:

- Capturing Data from Wearable Device Module: A prototype is developed for a wearable device using a microcontroller and Smartphone. It can capture the sensory signals and split the signals into two forms of features i.e. time domain and frequency domain feature. This offers better granularity in numerical analysis resulting in enhanced accuracy.
- Context Formulation: A significant mathematical modeling is carried out for formulating the context of the user activity. The prior CCSS model is used as well as the CIOB model where the context parameters are directly fed to the belief model to formulate a belief system regarding the queried activity tracked from wearable devices.

- Similarity Matching Mechanism: This block mainly takes the input of belief and along with service deposits, user event calendar, and the collaborative unit, it performs matching of the queried user activity to understand its intention. The term intention could be also related to any emergent action undertaken by the user owing to certain critical conditions in either positive or negative aspects. It performs further operations:
 - User Activity Modeling: This block is responsible for allocating mathematical variables for defining user activity concerning time instances and contextual information.
 - Model Fitness: This block maintains a check on the goodness of the proposed model in presence of uncertainties. This is mainly used for ensuring prediction of the next level of activity also.
 - Anticipation Function: As the proposed system performs predictive analysis hence this function is used for retaining the anticipated outcomes for analysis of the correctness of the identified user's intention.
 - HMM Incorporation: Hidden Markov Model (HMM) is mainly used for modeling the proposed analytical model and it is explicitly used for determining the upcoming user activity based on the higher probability value of the user context.

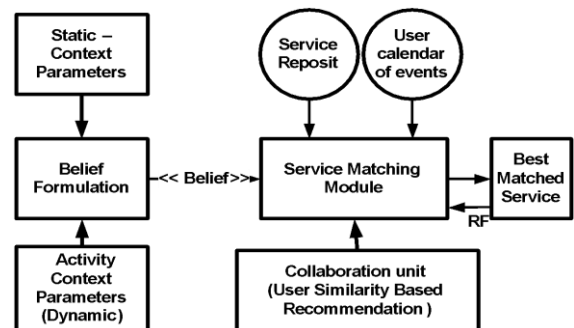


Fig. 1. Schema of Proposed System of DUAP.

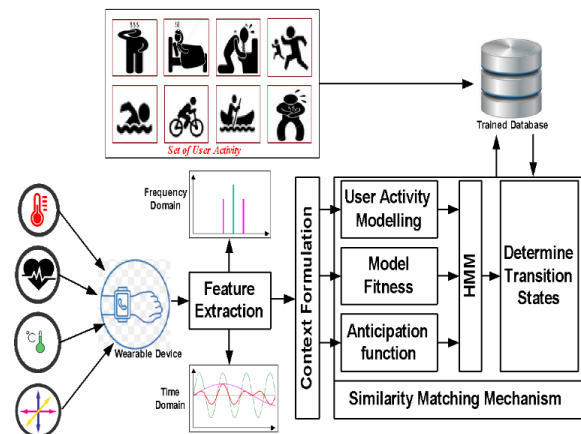


Fig. 2. Top Level Architecture DUAP.

The complete modeling is carried out in two stages i.e. training stage and the validation stage. The training stage consists of capturing the real-time multiple dynamic activities from multiple users to build a trained dataset using the main block of SMM. In the validation stage, the inputs are taken from different users to formulate a query for testing the effective predictive capability of DUAP. The contribution of the proposed methodology is that it offers discrete set of information that assists in analyzing the model more effectively. For this purpose, the experimental approach is used for aggregating data while the analytical approach is used for the complete implementation of the predictive approach based on contextual user activity. Finally, the simulation method is used for assessing the final trends of research outcomes. The next section illustrates the analytical modeling of DUAP. Hence, adoption of all the three research methodologies, unlike any existing system reported in Section II, assists to accomplish the target aim of proposed model.

V. ANALYTICAL MODELING

This section presents an elaborated discussion of the proposed analytical modeling meant for signifying the importance of the service matching mechanism towards contextual service discovery. For effective analytical modeling, the study consider a situation where heterogeneous sensors were deployed in the embedded form to extract dynamic user activity-based information. Consider that variable I to represent set of information captured from the wearable device where the study considers different sets of user activity as u_1, u_2, u_3, u_4 , and u_5 . Consider that a variable S represents problem space where different contextual information about the features resides corresponding to all the instances of sensory data collected. Empirically, it can be expressed in Equation (1) as,

$$S = \alpha_1 + \alpha_2 + \alpha_3 + \dots + \alpha_N \quad (1)$$

The study considers that $A: S \times I$ is an analytical model that is responsible for mapping all the test order o such that $o \in I$ as well as $S \times I \rightarrow \beta$, where the variable β may consider as service decision in terms of problem space. To check the significance of user activity in proposed model, a function ϕ is deployed to check the mode fitness. It can be expressed in the form of Equation (2):

$$\phi(x): y \times \beta \quad (2)$$

In the above equation, the argument x of the function ϕ represents $[o, A(\psi_o, o)] \subseteq x$ while the variable y should represent $m.I$ and the variable m represents times of information being relayed from the sensor. Therefore, it can say that service decision β is nearly equivalent to the problem space of the information instance. The model fitness of the work initiates by considering instances of the test say δ ; hence, δ will be a subset of $m.I$ consider that $\gamma(o)$ be the probability factor where the order o is a part of δ itself. The anticipation of the assessment function $\phi(x)$ is represented mathematically as,

$$\phi \rightarrow \sum_{o \in I} (\gamma(o) \cdot \phi(x)) \quad (3)$$

In above Equation (3), the numerical outcome of ϕ is required to be emphasized for enhancing the service discovery as well as service matching mechanism to obtain best-matched

services. Therefore, considering that A_{op} is the optimized analytical model representing best-matched service, the above expression (3) is reformulated as follows:

$$A_{op} \cdot \text{Max}_i [\phi(\delta, A)] \quad (4)$$

Although, there are various forms of context-based information associated with belief formation. Different forms of user activity will also have different forms of context and hence, it is not possible to give a shape of every discrete morphology of all contexts. Therefore, the study considers that there are two cases of context say α_a and α_p that corresponds to the active context and passive context respectively. The proposed model will also consider that these two forms of context (active/passive) will be evaluated based on the corresponding analytical model's A_a and A_p respectively for formulating a better predictive model. The inclusion of probability is considered in this i.e. $\gamma(\alpha_a)$ and $\gamma(\alpha_p)$ corresponding to type α_a and α_p respectively. Lemma-1 illustrates this operation as follows:

Lemma-1: Consider that A_{op} is the best service model on instance δ i.e. $A_{op} = A_{op}(a) + A_{op}(p)$, which will mean that $A_{op}(a)$ is the best-matched service for δ_a and $A_{op}(p)$ is the best-matched service for δ_p .

Proof: It is obvious that despite the presence of different forms of context viz. $\alpha_1, \alpha_2, \alpha_3, \dots, \alpha_n$, which will mean that there are n -number of context information about the user activity, then,

$$\alpha = \alpha_1 + \alpha_2 + \alpha_3 + \dots + \alpha_n \quad (5)$$

Consider that $\alpha_a = \{ \alpha_1, \alpha_7, \alpha_9, \dots \}$ and $\alpha_p = \{ \alpha_2, \alpha_4, \alpha_{10}, \dots \}$ than it can be said that,

$$\alpha = \alpha_a + \alpha_p \quad (6)$$

where, $(\alpha_a + \alpha_p) \leq n$. Similar fact discussed above is also applicable to the time instance δ with respect to δ_a and δ_p . Hence, it can also be written as,

$$A_{op}(a) = \text{Max}_{A(a)} \phi[\delta_a, A_a] \quad (7)$$

$$A_{op}(p) = \text{Max}_{A(p)} \phi[\delta_p, A_p] \quad (8)$$

The above expression also assists to offer the conditions e.g. $\gamma(\alpha_a) \cdot \phi[\delta_a, A_{op}(a)]$ is greater than $\gamma(\alpha_a) \cdot \phi[\delta_a, A_{op}]$. Similarly, the next condition will be $\gamma(\alpha_p) \cdot \phi[\delta_p, A_{op}(p)]$ is greater than $\gamma(\alpha_p) \cdot \phi[\delta_p, A_{op}]$. The concatenation of these will yield,

$$\gamma(\alpha_a) \cdot \phi[\delta_a, A_{op}(a)] + \gamma(\alpha_p) \cdot \phi[\delta_p, A_{op}(p)] \quad (9)$$

and the above expression (9) is always greater than $\phi[\delta, A_{op}]$. However, logically, as $A_{op} = \text{Max}_A \phi[\delta, A]$. Therefore, from Equation (9), it can be mathematically presented that,

$$\phi[\delta, A_{op}] = \gamma(\alpha_a) \cdot \phi[\delta_a, A_{op}(a)] + \gamma(\alpha_p) \cdot \phi[\delta_p, A_{op}(p)] \quad (10)$$

However, in simpler meaning, it can be said that $A_{op} = A_{op}(a) + A_{op}(p)$.

The advantage of using the Lemma-1 is that the proposed system can apply its process of service matching mechanism for all the time instances of context data by exploring the optimized composition of the time instances itself within the scope of contextual forms. Hence, the inference of the term active and passive is highly flexible and extensible too and can be fine-tuned as per any application-level deployment. However, still, it is quite a challenging task for exploring the best service associated with the obtained belief from dynamic data of user activity. Hence, Hidden Markov Model (HMM) is applied over the various instances of information I . Once the system develops the belief factor considering both static as well as dynamic context (user activity context parameters), the service matching model will be responsible for predicting the form of the context based on the input of user activity. Hence, HMM can be significantly used for determining the consecutive probable activities and it can potentially assist in user activity prediction based on its corresponding contextual information. Therefore, the variable I is considered as training data that will be used for computing the HMM parameters and hence it splits the variable I in such a way that $I=[I_1 I_2]$, where a subset of information I_1 is used for training purposes for implementing the predictive operation of HMM while I_2 could be used for enhancing the contextual performance during comparative analysis with the trained data. Hence, better training using HMM could be used for contextual prediction of user intention.

VI. HMM-BASED ACTIVITY DETERMINATION

This section presents the mechanism of determination of consecutive probable activity with the help of HMM. The concept of the analytical model is presented in the prior section to develop a similar HMM-based model for user activity determination. For this purpose, a matrix mU is considered to denote all feasible dynamic activity of user such that consists of elements as $u_1, u_2 \dots u_N$. The algorithm takes an input of user activity (Line-1) and performs extraction of the features f concerning time (f_t) and frequency (f_f) domain (Line-2). For all the values of service reposit and user calendar events (Line-3) to assess the user activity u , Markov model A , transition state, and anticipated outcome of the prediction. Further elaboration is as follows: Here, the variable A is considered to be a Markov chain for assisting in determining the transition state in the form of probability $\gamma(u_j | u_i)$. This denotes the transition of user activity u_i to u_j . The algorithmic steps for this purpose is shown as following:

Algorithm for User Activity Determination

Input: u (user activity)

Output: ϑ (expected outcome), $trans_state$ (transition state)

Start

1. *get* $U(t) = \{u_1, u_2, \dots, u_N\}$

2. $f \rightarrow [f_t, f_f]$

3. **For** $i=1:p$

4. Obtain $\alpha = \{\alpha_a, \alpha_p\}$ & $A = \{A_a, A_p\}$

5. $trans_state = [\gamma_a(u_j | u_i), \gamma_p(u_j | u_i)]$

6. $\vartheta[\delta, A_a, A_p] = \gamma(\alpha_a) \cdot \vartheta[\delta_a, A_a] + \gamma(\alpha_p) \cdot \vartheta[\delta_p, A_p]$

7. **End**

8. **End**

End

Hence, it can be said that $u \subseteq mU$. Hence, the maximum probability of transition associated with user activity can be denoted as $a(u)$ corresponding to the user activity u . Mathematically, it can be represented as,

$$a(u) \rightarrow \text{Max}_{v \in M} \gamma(v|u) \quad (11)$$

According to the principle of HMM, the Markovian characteristics can be depicted for $a(u)$ that is considered to be an elite forecast for the consecutive activity of the user. This condition is only valid if u is considered to be the present form of activity (or state). Therefore, a better form of user intention can be formulated from multiple dynamic activities where a selection of the most elite transition state is carried out for the consecutive state in the predictor design. Considering arbitrary samples from the δ instances of the HMM, the model can easily compute the accuracy of the HMM prediction as following:

$$\vartheta_{\delta, A} \rightarrow \sum_{u \subset mU} \gamma \quad (12)$$

As the presented model is all about probability for computing the next transition state, hence, the right-hand side of Equation (12) will signify probability γ as $\gamma(u)$. $\gamma(a(u)|u)$. The model uses similar contextual parameter $\alpha = \alpha_a + \alpha_p$ where A_a and A_p is considered as similar chain parameters for HMM corresponding to context form of α_a and α_p respectively. It will also mean that the system implements A_a and A_p Markov chains for determining the contextual form of u_a and u_p respectively. Therefore,

Transition state of $A_a = \gamma_a(u_j | u_i)$

Transition state of $A_p = \gamma_p(u_j | u_i) \quad (13)$

Therefore, equation (10) in Lemma-1 can be now remodeled concerning A_a and A_p HMMs corresponding to instances of δ_a and δ_p respectively as follows,

$$\vartheta[\delta, A_a, A_p] = \gamma(\alpha_a) \cdot \vartheta[\delta_a, A_a] + \gamma(\alpha_p) \cdot \vartheta[\delta_p, A_p] \quad (14)$$

The above-mentioned formulation is only valid if a selection of δ_a and δ_p is carried out based on arbitrary order to A_a and A_p . In the above Equation (14), the variable $\gamma(\alpha_a)$ and $\gamma(\alpha_p)$ represent test order in terms of probability whose scope resides within the two contextual categories. It will eventually mean that $\vartheta[\delta_a, A_a]$ and $\vartheta[\delta_p, A_p]$ is empirically equivalent to $\gamma_a(u)$. $\gamma_a(a_a(u) | u)$ and $\gamma_p(u)$. $\gamma_p(a_p(u) | u)$ respectively. One interesting fact about this model is that it suits very well with the CIOB model [43] in the decision generation module which consistently interacts with the belief processing module, where both update the information server. Therefore, the suitability of this predictive model is better justified using HMM approach over the contextual user's activity data.

The Lemma-2 discussed above exhibits the significance of retaining HMM features only in the cases when the information includes the inherent characteristics of the Markov principle. Therefore, this provides the evidence that incorporating HMM significantly assists in the prediction of user activity as a next probable states. However, the complete accuracy is directly depending on the size of the data. The significant *contribution* of this model of HMM is that it splits the data (to be trained or already trained) into multiple smaller parts to extract the

context of the user's intention, unlike any existing approaches reported in literature. The next section discusses the outcome accomplished from the proposed study.

Lemma-2: The significance of user activity and service matching mechanism for a model A is developed on the basis of on trained information I where A_a and A_p and designed depending upon I_a and I_p respectively. Therefore, the significance of service matching is maximum only when $\vartheta[\delta_a, A_a]$ is found greater than $\vartheta[\delta_a, A]$. Similarly, it is also valid for $\vartheta[\delta_a, A_a]$ is found greater than $\vartheta[\delta_a, A]$

Proof: In this case, the model considers that the initial contextual form α_a has the probability of $\gamma(a(u), u|\alpha_a)$ representing its present user activity being u and consecutive user activity being $a(u)$. Hence, it can be stated that updated anticipation function $\vartheta[\delta_a, A]$ is equivalent to the summation of $\gamma(a(u), u|\alpha_a)$, where $u \subseteq mU$. The overall sum is also said to be equivalent to the summation of $\gamma(a(u)|u, \alpha_a)$. $\gamma(u|\alpha_a)$. The generalized structure of this summation then becomes the summation of $\gamma(a(u)|u, \alpha_a)$. $\gamma(u)$. Therefore, a closer look at this logic will show that the expression $\gamma(a(u)|u, \alpha_a)$. $\gamma(u)$ is very much lesser than $\gamma_a(a_a(u)|u, \alpha_a)$. $\gamma_a(u)$, which can be shortly written as $\vartheta[\delta_a, A_a]$. Hence, this will prove that $\vartheta[\delta_p, A]$ is significantly less than $\vartheta[\delta_p, A_p]$.

VII. EXPERIMENTAL ANALYSIS

The analysis is carried out by capturing real-time data with multiple forms of bio-signals to understand the significance of user activity. The purpose is to predict user intention based on the computed contextual data. This section outlines the application environmental parameters as well as the performance assessment process undertaken to discuss the simulation settings considered for the study.

A. Application Environment

The application considered for the proposed system is a pervasive context-awareness system exclusively generated for predicting the user's intention related to their health. The model assumes that a user is equipped with a wearable device that has 4 different forms of sensors e.g. i) ambient temperature sensor, ii) heartbeat sensor, iii) body temperature sensor, and iv) accelerometer. The analysis uses an ambient temperature sensor TF41 that is cost-effective and can perform tracking of temperature under all forms of environmental conditions. A readily available heartbeat sensor circuit is used that works quite well with the 8051 microcontrollers. The heartbeat sensor is integrated into the board using amplifier LM358 OP-AMP. MAX30205 is used as the body sensor that is found to be directly under the compliance of ASTE E1112 with 16-bit resolution in temperature reading. Finally, ADXL335 is used as the 3-axis accelerator that works on low-power devices. An android application is developed that is wirelessly integrated with the transceiver module. The data captured by the temperature sensor will be related to both room and body. The corresponding inference is coded to identify certain standard situations e.g. hot ($>40^\circ\text{C}$), cold ($<10^\circ\text{C}$), fire ($>100^\circ\text{C}$), normal ($10\text{-}30^\circ\text{C}$), etc. Similarly, an inference system is developed for heat beats i.e. normal (60-100 beats per minute), tachycardia

(>100 beats per minute), and bradycardia (< 60 beats per minute). Usage of the accelerometer can be used for identifying the states/gait patterns e.g. walking, sitting, running, climbing up/down, etc.

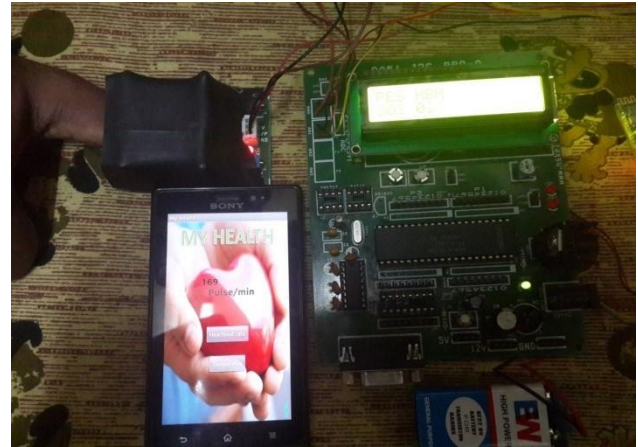


Fig. 3. Laboratory Prototype of DUAP.

The proposed prototype shown in Fig. 3 has been tested on 25 subjects to capture the data related to the user's activity. The raw data of user activity is then subjected to the proposed analytical model, where the prediction is carried out. Following are the steps to summarize the prototype implementation viz.

- Step-1: A hardware model is developed with 8051 microcontrollers and android application connected in the wireless medium.
- Step-2: The prototype of the wearable device is tested on 25 subjects to capture the raw data about user activity.
- Step-3: All the captured data of 25 subjects are subjected to training operation as discussed in HMM implementation in algorithm section. The captured trained data is exported to MATLAB for effective analysis, although any data analytic software can also be used.
- Step-4: The model considers new 10-15 subjects to captured the raw signal (untrained data).
- Step-4: The prediction algorithm is applied to understand the user's intention.

The final processing of the algorithm in MATLAB gives the predictive outcome to show the effectiveness of the proposed service matching mechanism. The next section discusses the performance assessment to validate the outcome.

B. Performance Assessment

The study outcome of the proposed system is assessed using standard parameters of True Positive (P_1), False Negative (P_2), False Positive (P_3), and True Negative (P_4). The model defines P_1 as the number of all the captured data of user activity that is precisely identified. P_2 is defined as several all the computed user activity that is captured with a higher degree of error. P_3 is the number of non-event-based data that has not been identified correctly, while P_4 represents several non-

event-based data that are precisely identified. The assessment of the proposed system is carried out using True Positive Rate (P_5), False Positive Rate (P_6), and Accuracy (P_7). Following are the expression for the same:

$$P_7 = \frac{(P_1 + P_4)}{\sum_{i=1}^4 P_i} \quad (14)$$

$$P_5 = \frac{P_1}{P_2 + P_1} \quad (15)$$

$$P_6 = \frac{P_3}{P_3 + P_4} \quad (16)$$

Equation (14), (15), and (16) represents the computation of True Positive Rate (P_5), False Positive Rate (P_6), and Accuracy (P_7). The proposed system also uses precision (P_8), recall (P_9), and accuracy (P_{10}) for finally assessing the outcome using the following expression:

$$P_8 = \frac{\sum_i P_i(i)}{\sum_i (P_1 + P_3)(i)} \quad (17)$$

$$P_9 = \frac{\sum_i P_i(i)}{\sum_i (P_1 + P_2)(i)} \quad (18)$$

$$P_{10} = \frac{\sum_i (P_1 + P_4)(i)}{\sum_i n(i)} \quad (19)$$

VIII. RESULTS ANALYSIS

The study outcome of the proposed system is initially assessed using Receiver Operating Characteristics (ROC) curve where P_5 and P_6 are the dependable characteristics' (Fig. 4). The trend for the empirical ROC is computed from the obtained numerical outcomes and the outcome that is further normalized using the binormal model. However, there are all the possibilities that there are certain levels of inaccuracies owing to the impartial or irregular distribution of data. Hence, for effective analysis of data, a smoother estimation of parametric ROC trend is applied by implementing a binormal model which shows dependencies on Gaussian distribution. It is also observed that the reliability of the ROC trend has higher dependencies on the threshold factor. If the threshold factor of P_3 is configured to 0.1 then the numerical value of P_5 will be approximately 80% in the trials. A closer look into the Area Under Curve (AUC) shows maximum coverage that directly interprets that the proposed system has the enhanced capability to perform efficient identification of the user's intention in the presence of the increasing value of the P_3 threshold.

The ROC performance in Fig. 4 highlighted the better performance of the proposed system while it is essential to understand various other parameters e.g. recall, precision, and accuracy. Table I highlights the numerical outcomes to show that the proposed system offers approximately 89% of recall, 91.78% of precision, and 91.33% of accuracy for 10 different trials. By trials, it will mean that different subjects being used in the prototypes and tested for consistency in the outcomes at least 5-6 times. The observations against all the test cases are recorded as a single trial.

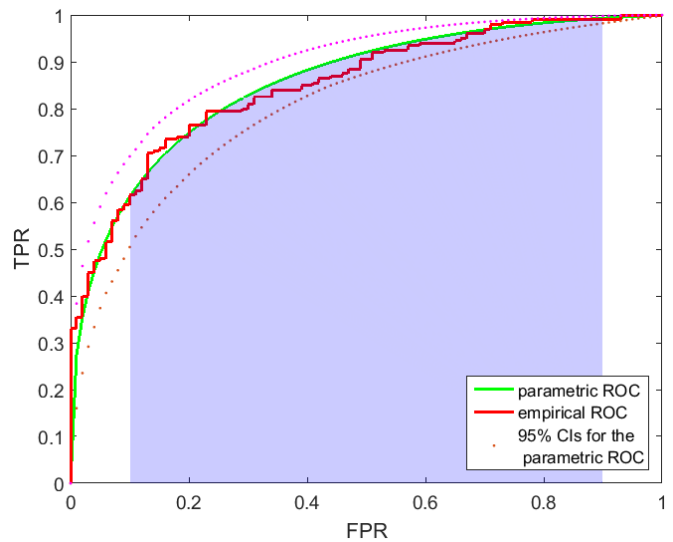


Fig. 4. Analysis of ROC Trend.

TABLE I. SUMMARIZED NUMERICAL OUTCOMES

Trials	Recall	Precision	Accuracy
Trial-1	81.6%	83.8%	89.7%
Trial-2	87.8%	86.9%	91.6%
Trial-3	86.2%	91.7%	93.5%
Trial-4	82.8%	95.7%	87.9%
Trial-5	89.8%	98.6%	98.7%
Trial-6	90.6%	87.9%	91.6%
Trial-7	91.7%	89.2%	87.9%
Trial-8	97.6%	96.5%	91.4%
Trial-9	87.9%	89.7%	89.5%
Trial-10	95.9%	97.8%	91.5%
Average	89.19%	91.78%	91.33%

The effectiveness of the proposed model is assessed if the component block for Service Matching Module SMM is used or removed. Fig. 5 shows that the proposed study offers better accuracy on an increasing number of observations if the SMM block is considered. In absence of an SMM block, the accuracy drops, and thereby it shows the significance of the proposed SMM block in identifying the user's intention based on the HMM-based approach as well as contextual-based approach.

It is quite clear from Fig. 5 that the proposed system offers significantly better accuracy; however, a relevant feedback is applied to understand the self-sustainability towards accuracy performance. Relevance feedback is a mechanism where the outcome is once again cross-checked by the user. It is the cross to increase the probability of identification in presence of uncertainties. Fig. 6 showcases the impact of relevance feedback towards accuracy.

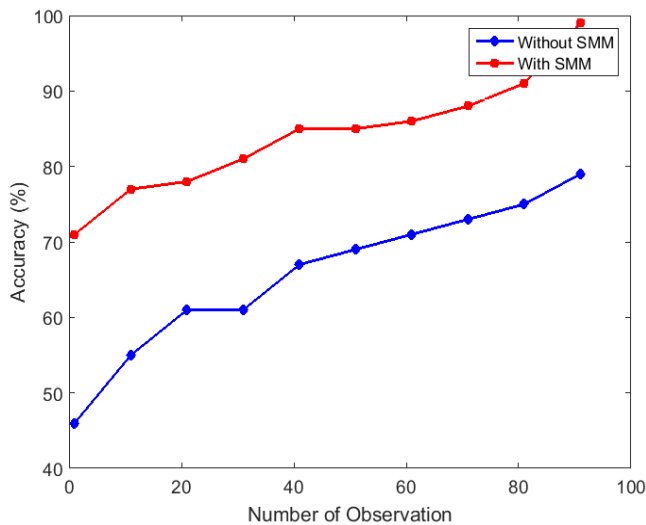


Fig. 5. Accuracy Observation.

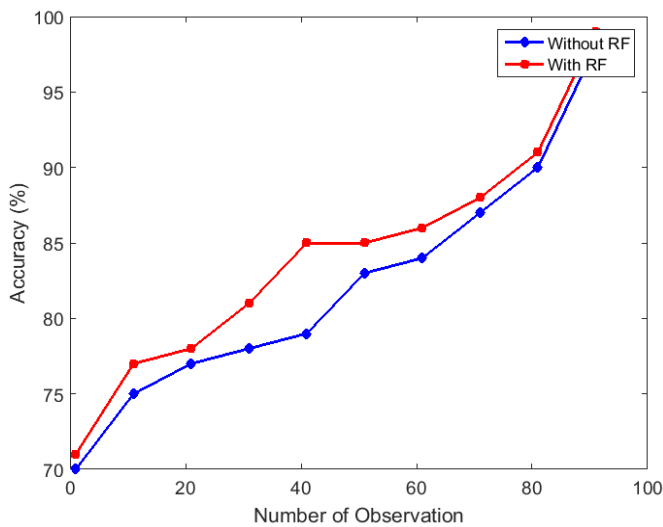


Fig. 6. Analysis with Relevance Feedback.

The graphical outcome in Fig. 6 shows that relevance feedback has the least significant impact on accuracy. Both the curve has a nearly similar performance of accuracy towards 100 observations. The prime reason behind this is the algorithm of the analytical modeling possesses the capability to perform uncertainty modeling while applying HMM for detecting the next state of transition. This phenomenon significantly reduces all the possible errors to a large extent in increasing time series analysis giving more stochastic characteristics to the accuracy curve. Hence, this states that the proposed system is highly reliable and requires lesser dependencies from a human user.

Discussion: From the outcome obtained in proposed study, it has been observed that the model offers better accuracy performance over increasing number of observation. The contribution as well as novelty of the proposed system, are as follows:

- With an aid of mathematical modeling, the proposed framework is highly capable of making a reliable prediction compared to existing approaches. The complete model is assessed for increasing number of trials to find the consistency of the prediction accuracy over multiple iterations.
- The proposed study adopts HMM in a very unique way, unlike existing system, that is reported to suit very well with any form of collaborative units. One of the essential contributory points observed from the numerical outcomes is that proposed system offers an efficient contextual learning operation, where sequence of raw data can be directly used for learning with potential statistical foundation. Adoption of HMM will permit consistency towards adding or deleting penalties while it offers more potential towards managing any form of inputs with variable length. Better flexibility in modelling the proposed scheme is therefore ensured.
- The overall runtime of the proposed system is approximately 0.56227 seconds in core i7 machine to make a prediction (or recommendation). The performance in this regards is nearly similar over other test environment too.
- The outcome of the study shows that proposed system can offer the clear establishment of a complex relationship with the complicated context captured from the wearable devices.

IX. CONCLUSION

The model presented in this manuscript is associated with the design of an activity-based context-awareness system where multimodal activity data is considered followed by feature extraction while the learning mechanism is applied further to develop to support an intelligent recommendation system. This paper discusses the significance of SMM in identifying the dynamic user activity using mixed-mode research analysis. The applicability of such an approach in the wearable device is designed keeping healthcare applications in mind due to its faster response time. At the same time, there is significant algorithm complexity of DUAP under several rounds of observation. This proves that the proposed algorithm offers cost-effective identification of user identity.

REFERENCES

- [1] A. McEwen, Hakim Cassimally, Designing the Internet of Things, John Wiley & Sons, 2013.
- [2] Samuel Greengard, The Internet of Things, MIT Press, 2015.
- [3] Gregory Vert, S. Sitharama Iyengar, Vir V. Phoha, Introduction to Contextual Processing: Theory and Applications, CRC Press, 2016.
- [4] K. Hwang, M. Chen, Big-Data Analytics for Cloud, IoT and Cognitive Computing, John Wiley & Sons, 2017.
- [5] L. Snidaro, J. García, J. Llinas, E. Blasch, Context-Enhanced Information Fusion: Boosting Real-World Performance with Domain Knowledge, Springer, 2016.
- [6] W. Zhu, Z. Wang, G. Hou, and M. Yu, "Capability-based context ontology modeling and reasoning for C4ISR communication," *Journal of Systems Engineering and Electronics*, vol. 27, no. 4, pp. 845-857, Aug. 2016.

- [7] S. Irene and R. Pitchiah, "Distributed and scalable context reasoning in a home environment," *12th Annual IEEE International Conference on Sensing, Communication, and Networking (SECON)*, Seattle, WA, 2015, pp. 157-159.
- [8] Y. Cao, T. Jiang, and Z. Han, "A Survey of Emerging M2M Systems: Context, Task, and Objective," *IEEE Internet of Things Journal*, vol. 3, no. 6, pp. 1246-1258, Dec. 2016.
- [9] P. Makris, D. N. Skoutas and C. Skianis, "A Survey on Context-Aware Mobile and Wireless Networking: On Networking and Computing Environments' Integration," *IEEE Communications Surveys & Tutorials*, vol. 15, no. 1, pp. 362-386, First Quarter 2013.
- [10] C. Perera, A. Zaslavsky, P. Christen and D. Georgakopoulos, "Context-Aware Computing for The Internet of Things: A Survey," *IEEE Communications Surveys & Tutorials*, vol. 16, no. 1, pp. 414-454, First Quarter 2014.
- [11] O. Yurur, C. H. Liu and W. Moreno, "A survey of context-aware middleware designs for human activity recognition," *IEEE Communications Magazine*, vol. 52, no. 6, pp. 24-31, June 2014.
- [12] Ö. Yürür, C. H. Liu, Z. Sheng, V. C. M. Leung, W. Moreno, and K. K. Leung, "Context-Awareness for Mobile Sensing: A Survey and Future Directions," *IEEE Communications Surveys & Tutorials*, vol. 18, no. 1, pp. 68-93, First quarter 2016.
- [13] M. Gaved, P. Luley, S. Efremidis, I. Georgiou, A. K-Hulme, A. C. Jones, and E. Scanlon, "Challenges in Context-Aware Mobile Language Learning: The MASELTOV Approach", Communication in Computer and Information, In mLearn, *13th World Conference on Mobile and Contextual Learning At: Istanbul* pp. 351-364, 2014.
- [14] C. Gurrin, D. Byrne, N. O'Connor, G. J. F. Jones and A. F. Smeaton, "Architecture and challenges of maintaining a large-scale, context-aware Human Digital Memory," *5th International Conference on Visual Information Engineering (VIE 2008)*, Xian China, 2008, pp. 158-163.
- [15] J. Pauty, D. Preuveneers, P. Rigole, and Y. Berbers, "Research challenges in mobile and context-aware service development", In Future Research Challenges for Software and Services Conference, pp. 141-148. 2006.
- [16] M. Satyanarayanan, "Challenges in implementing a context-aware system", *IEEE pervasive computing*, vol.1, no. 3, 2002.
- [17] Z. Yujie and W. Licai, "Some challenges for context-aware recommender systems," *5th International Conference on Computer Science & Education*, Hefei, pp. 362-365, 2010.
- [18] S. Mohammadi, S. Kylasa, G. Kollias and A. Grama, "Context-Specific Recommendation System for Predicting Similar PubMed Articles," *IEEE 16th International Conference on Data Mining Workshops (ICDMW)*, Barcelona, pp. 1007-1014, 2016.
- [19] M. Ehatisham-Ul-Haq, M. A. Azam, Y. Amin, and U. Naem, "C2FHAR: Coarse-to-Fine Human Activity Recognition With Behavioral Context Modeling Using Smart Inertial Sensors," *IEEE Access*, vol. 8, pp. 7731-7747, 2020, doi: 10.1109/ACCESS.2020.2964237.
- [20] A. Yachir, Y. Amirat, A. Chibani, and N. Badache, "Event-Aware Framework for Dynamic Services Discovery and Selection in the Context of Ambient Intelligence and Internet of Things," *IEEE Transactions on Automation Science and Engineering*, vol. 13, no. 1, pp. 85-102, Jan. 2016.
- [21] A. Guo and J. Ma, "Context-Aware Scheduling in Personal Data Collection From Multiple Wearable Devices," *IEEE Access*, vol. 5, pp. 2602-2614, 2017, doi: 10.1109/ACCESS.2017.2666419.
- [22] C. B. Yao, "Constructing a User-Friendly and Smart Ubiquitous Personalized Learning Environment by Using a Context-Aware Mechanism," *IEEE Transactions on Learning Technologies*, vol. 10, no. 1, pp. 104-114, Jan.-March 1 2017.
- [23] R. Klimek, "Exploration of Human Activities Using Message Streaming Brokers and Automated Logical Reasoning for Ambient-Assisted Services," in *IEEE Access*, vol. 6, pp. 27127-27155, 2018, doi: 10.1109/ACCESS.2018.2834532.
- [24] C. Shen, Y. Chen, G. Yang, and X. Guan, "Toward Hand-Dominated Activity Recognition Systems With Wristband-Interaction Behavior Analysis," *IEEE Transactions on Systems, Man, and Cybernetics: Systems*, vol. 50, no. 7, pp. 2501-2511, July 2020, doi: 10.1109/TSMC.2018.2819026.
- [25] Q. Ni, A. B. G. Hernando, and I.P.d.I. Cruz, "A Context-Aware System Infrastructure for Monitoring Activities of Daily Living in Smart Home", *Journal of Sensors*, 2016.
- [26] A. Pahlevan, J-L. Duprat, A. Thomo, and H. Müller, "Dynamics: Effective Context-Aware Web Service Selection Using Dynamic Attributes", *Future Internet*, vol.7, no. 2, pp.110-139, 2015.
- [27] M. Chen, Y. Li, X. Luo, W. Wang, L. Wang, and W. Zhao, "A Novel Human Activity Recognition Scheme for Smart Health Using Multilayer Extreme Learning Machine," *IEEE Internet of Things Journal*, vol. 6, no. 2, pp. 1410-1418, April 2019, doi: 10.1109/JIOT.2018.2856241.
- [28] S. Wang, Z. Zheng, Z. Wu, Q. Sun, H. Zou, and F. Yang, "Context-aware mobile service adaptation via a Co-evolution eXtended Classifier System in mobile network environments", *Mobile Information Systems*, vol.10, no. 2, pp.197-215, 2014.
- [29] M. R. Alam, M. B. I. Reaz, and M. A. Mohd Ali, "SPEED: An Inhabitant Activity Prediction Algorithm for Smart Homes," *IEEE Transactions on Systems, Man, and Cybernetics-Part A: Systems and Humans*, vol. 42, no. 4, pp. 985-990, July 2012.
- [30] C. Pham et al., "SensCapsNet: Deep Neural Network for Non-Obtrusive Sensing Based Human Activity Recognition," *IEEE Access*, vol. 8, pp. 86934-86946, 2020, doi: 10.1109/ACCESS.2020.2991731.
- [31] K. Huang, C. Zhang, X. Ma, and G. Chen, "Predicting mobile application usage using contextual information", *Proceedings of the 2012 ACM Conference on Ubiquitous Computing*, pp. 1059-1065, 2012.
- [32] B. Kim, S. Kang, J-Y. Ha, and J. Song, "Agatha: predicting daily activities from place visit history for activity-aware mobile services in smart cities", *International Journal of Distributed Sensor Networks*, Vol.11, No. 12, pp.867602, 2015.
- [33] I. A. Lawal and S. Bano, "Deep Human Activity Recognition With Localisation of Wearable Sensors," *IEEE Access*, vol. 8, pp. 155060-155070, 2020, doi: 10.1109/ACCESS.2020.3017681.
- [34] S. Elmalaki, L. Wanner, and M. Srivastava, "Caredroid: Adaptation framework for android context-aware applications", *Proceedings of the 21st Annual International Conference on Mobile Computing and Networking*, pp. 386-399, 2015.
- [35] W. Xu, J. Yu, Z. Miao, L. Wan, and Q. Ji, "Spatio-Temporal Deep Q-Networks for Human Activity Localization," *IEEE Transactions on Circuits and Systems for Video Technology*, vol. 30, no. 9, pp. 2984-2999, Sept. 2020, doi: 10.1109/TCSVT.2019.2919064.
- [36] T. Y. Hsu, C. K. Chiou, J. C. R. Tseng, and G. J. Hwang, "Development and Evaluation of an Active Learning Support System for Context-Aware Ubiquitous Learning," *IEEE Transactions on Learning Technologies*, vol. 9, no. 1, pp. 37-45, Jan.-March 1 2016.
- [37] R. Kamberov, C. G. Canut, and V. Santos, "Sociology Paradigms for Dynamic Integration of Devices into a Context-Aware System", *Journal of Information System Engineering & Management*, vol.2, Iss.1, pp1-11, 2017. DOI:10.20897/jisem.201702.
- [38] A. -C. Popescu, I. Mocanu and B. Cramariuc, "Fusion Mechanisms for Human Activity Recognition Using Automated Machine Learning," *IEEE Access*, vol. 8, pp. 143996-144014, 2020, DOI: 10.1109/ACCESS.2020.3013406.
- [39] T. Xu, Y. Zhou, B. David, and R. Chalon, "Supporting Activity Context Recognition in Context-Aware Middleware", In *Proceedings of Activity Context-Aware System Architectures Workshop in AAAI*, vol. 13. 2013.
- [40] O. Khalid, M. U. S. Khan, S. U. Khan, and A. Y. Zomaya, "OmniSuggest: A Ubiquitous Cloud-Based Context-Aware Recommendation System for Mobile Social Networks," *IEEE Transactions on Services Computing*, vol. 7, no. 3, pp. 401-414, July-Sept. 2014.
- [41] Y-H. Kim and Y. Yoon, "Context prediction of mobile users based on time-inferred pattern networks: a probabilistic approach", *Hindawi-Mathematical Problems in Engineering*, Article ID 106139, 2013. DOI: https://doi.org/10.1155/2013/106139.
- [42] F. M. Mendes Neto and A. Farias Azevedo Sales, "A Recommendation System for Ubiquitous Learning in the Context of Formal and Informal Education," *IEEE Latin America Transactions*, vol. 13, no. 4, pp. 1061-1067, 2015.

- [43] G. Singh, M. Chowdhary, A. Kumar and R. Bahl, "A Personalized Classifier for Human Motion Activities With Semi-Supervised Learning," *IEEE Transactions on Consumer Electronics*, vol. 66, no. 4, pp. 346-355, Nov. 2020, doi: 10.1109/TCE.2020.3036277.
- [44] Y. Asim, M. A. Azam, M. Ehatisham-ul-Haq, U. Naeem and A. Khalid, "Context-Aware Human Activity Recognition (CAHAR) in-the-Wild Using Smartphone Accelerometer," *IEEE Sensors Journal*, vol. 20, no. 8, pp. 4361-4371, 15 April 2020, doi: 10.1109/JSEN.2020.2964278.
- [45] H. S. M. Bilal et al., "Towards User-Centric Intervention Adaptiveness: Influencing Behavior-Context Based Healthy Lifestyle Interventions," *IEEE Access*, vol. 8, pp. 177156-177179, 2020, doi: 10.1109/ACCESS.2020.3026688.
- [46] M. H. Siddiqi et al., "A Unified Approach for Patient Activity Recognition in Healthcare Using Depth Camera," *IEEE Access*, vol. 9, pp. 92300-92317, 2021, doi: 10.1109/ACCESS.2021.3092403.
- [47] M. Takeda, K. Sato, Y. Hirata, T. Katayama, Y. Mizuta and A. Koujina, "Standing, Walking, and Sitting Support Robot Based on User State Estimation Using a Small Number of Sensors," *IEEE Access*, vol. 9, pp. 152677-152687, 2021, doi: 10.1109/ACCESS.2021.3127275.
- [48] H. Abdelkawy, N. Ayari, A. Chibani, Y. Amirat and F. Attal, "Spatio-Temporal Convolutional Networks and N-Ary Ontologies for Human Activity-Aware Robotic System," *IEEE Robotics and Automation Letters*, vol. 6, no. 2, pp. 620-627, April 2021, doi: 10.1109/LRA.2020.3047780.
- [49] S. Sambolek and M. Ivasic-Kos, "Automatic Person Detection in Search and Rescue Operations Using Deep CNN Detectors," *IEEE Access*, vol. 9, pp. 37905-37922, 2021, doi: 10.1109/ACCESS.2021.3063681.
- [50] P. Venkataram and M. Bharath, "Context-based service discovery for ubiquitous applications," *The International Conference on Information Networking 2011 (ICOIN2011)*, Barcelona, 2011, pp. 311-316.
- [51] M. Subramanyam and P. Venkataram, "A context-aware collaborative service provisioning system for Mobile-Commerce," *2012 National Conference on Communications (NCC)*, Kharagpur, pp. 1-5, 2012.

Progressive 3-Layered Block Architecture for Image Classification

Munmi Gogoi, Shahin Ara Begum
Department of Computer Science
Assam University Silchar (A Central University)
Silchar Assam, India

Abstract—Convolutional Neural Networks (CNNs) have been used to handle a wide range of computer vision problems, including image classification and object detection. Image classification refers to automatically classifying a huge number of images and various techniques have been developed for accomplishing this goal. The focus of this article is to enhance image classification accuracy implemented on CNN models by using the concept of transfer learning and progressive resizing with split and train strategy. Furthermore, the Parametric Rectified Linear Unit (PReLU) activation function, which generalizes the standard traditional rectified unit, has also been applied on dense layers of the model. PReLU enhances model fitting with almost little significant computational cost and low over-fitting hazard. A “Progressive 3-Layered Block Architecture” model is proposed in this paper which considers the fine-tuning of hyperparameters and optimizers of the Deep network to achieve state-of-the-art accuracy on benchmark datasets with fewer parameters.

Keywords—CNN; transfer learning; progressive resizing; PReLU; deep network

I. INTRODUCTION

Image classification methods using convolution neural networks (CNNs) have recently achieved remarkable success in the field of computer vision, compared to other classic machine learning techniques [1-3]. Many Computer Vision tasks, such as image segmentation and object identification, can be simplified to image classification, thereby enhancing accuracy of classification can have a broad impact across a variety of application domains. The automatic feature extraction capability of the CNN network replaces the conventional feature extraction methods (e.g., SIFT, HOG, GIST), etc., as the deep learning network does not require hand-engineered feature design [4].

We have seen remarkable advancements in the image classification domain in the last several years, owing primarily to advances in two technical directions: creating more sophisticated network architectures and designing efficient techniques to handle overfitting. As neural networks become more complex (e.g., increased depth [1, 2], increased width [5, 6], as well as the utilization of shorter strides [5, 6, 2], new non-linear activations emerge [7-12], and as more complex layer designs emerge [1, 13]), the ability of neural networks to fit training data is improving. On the other hand, effective regularization approaches [12,14-16], active data augmentation [1, 2, 17, 18], and large-scale data [19, 20] lead to greater generalization. Considering the factors which affect

the performance of deep models, this paper proposes a "Progressive 3-Layered Block architecture" for image classification by implementing transfer learning and progressive resizing concept. Transfer learning technique not only reduces the problem of network overfitting but also reduces the training time and addresses the issue of insufficient training data in deep models [21]. Progressive Resizing is a technique for resizing all of the images in a sequential manner while training CNN models on lower to larger image sizes, which results in fine-tuning the final model as well as increasing the accuracy score. Furthermore, on the dense layers of the proposed model, we have employed the Parametric Rectified Linear Unit (PReLU) activation function [22], which generalizes the standard rectified unit. PReLU enhances model fitting at a low computational cost with little possibility of overfitting. The developed model is trained under optimized hyper-parameters and experimental evaluation is carried out on benchmark datasets. The proposed model achieves higher accuracy and leads to better performance with fewer parameters as compared to previously developed models.

The rest of the paper is organized as follows: Section II describes the theoretical background of the concepts used in developing the model. Section III presents the related research on image classification using deep learning models, focusing on three aspects *viz.* model development based on parameter efficiency, progressive training and improvement on datasets, optimization strategies and developmental platforms. Section IV deals with the proposed architecture and implementation setup. Section V reports the results obtained on benchmark dataset and Section VI presents concluding remarks.

II. THEORETICAL BACKGROUND

The theoretical background used in the proposed “Progressive 3-Layered Block and developmental platforms Architecture for image classification” is described in this section

A. Transfer Learning

Deep learning suffers from the problem of data dependence as it requires a massive amount of training data to understand the latent patterns in the data. Deep learning has a linear relationship between the model and the size of the data set. It is not feasible in deep learning to train an entire Convolutional Neural Network (CNN) from the beginning as it is very challenging to obtain a large enough dataset.

Therefore, it is common to pre-train a CNN on a very large dataset like ImageNet and then reuse the CNN either as a starting point or as a feature extractor for the second target task. This technique has gained huge success in particularly the computer vision field because of its extraordinary setting [46]. Transfer learning addresses the problem of insufficient training data and training time but also it reduces the problem of network overfitting [21]. The proposed work implements the EfficientnetB5 as a pretrained model which has been trained on the popular imageNet dataset.

EfficientNet is a recent CNN architecture developed by Google. EfficientNet sets new records for both accuracy and computational efficiency in image classification and it outperforms the present state of the art. Mingxing Tan and Quoc V. Le of the Google Research Brain team introduced the EfficientNet model in [54]. According to the paper, optimizing the depth, width, and resolution of networks helps to improve classification performance. The family of EfficientNet is scaled up in multiple block layers (from B0 to B7 through compound scaling formula i.e., all three dimensions such as depth, width and resolution are scaled up together to make it more accurate and effective, and there is an optimal balance between all the dimensions. Compared to other previously developed pretrained networks EfficientNet is more effective because it follows the compound scaling formula. Fig. 1 depicts a visualization of the compound scaling method of EfficientNet [54].

A comparison of EfficientNet's performance on the ImageNet dataset with other sophisticated transfer learning models is also documented in the literature. The most recent version of EfficientNet, EfficientNet-B7, has been shown to have the highest accuracy of all with the fewest parameters as depicted in Fig. 1.

B. Progressive Re-Scaling

The notion of progressively re-scaling image datasets has been introduced into Deep Learning Networks to improve accuracy [33]. Super-resolution [47] and GAN training [48] have both leveraged progressive re-scaling approaches.

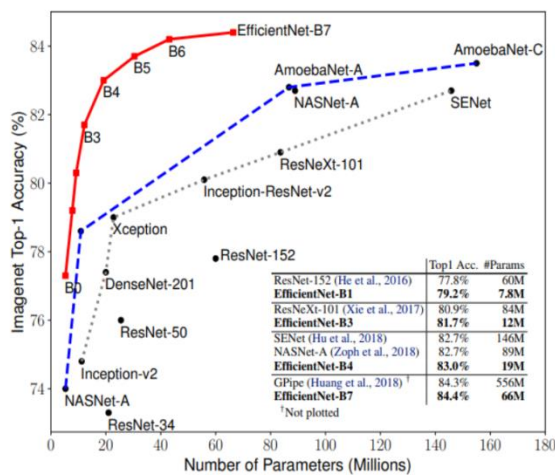


Fig. 1. Recent Version of EfficientNet and their Accuracy and Parameters with respect to other Networks [54].

The progressive training of image data begins with low-resolution images and incrementally changes the image resolution as training continues. In general Progressive Image resizing is a strategy for resizing the image dataset successively while the CNN models are trained on lower to larger image sizes as shown in Fig. 2.

One way to apply this technique is to train a model on smaller image sizes, such as 128 by 128 pixels, and then use the weights of this model to train another model on larger images, and so forth. Larger models use layers and weights from earlier smaller models in their architecture, which allows them to fine-tune their models and improve their accuracy scores. To the human eye, resizing images from (64 x 64) to (128 x 128) is an insignificant change. However, to CNN models, it provides a whole new dataset to train on.

Image size is vital in improving model accuracy, and several studies have been published in which researchers dynamically modify image sizes throughout training [34]. Three image sizes have been input into the system in the proposed “Progressive 3-Layered block Architecture”, while the regularization parameter has been considered to combat over-fitting of the deep model during training (Algorithm 2). The pipeline of progressive resizing of images in all three blocks of images is shown in Fig. 3.

C. Parametric ReLU (PReLU) Approach

The activation function of a neural network can be defined as in equation 1.

$$f(y_i) = \begin{cases} y_i & \text{if } y_i > 0 \\ a_i y_i & \text{if } y_i \leq 0 \end{cases} \quad (1)$$

Where y_i denotes the input to the nonlinear activation function f on the i^{th} channel, and a_i is a coefficient which governs the negative part's slope. The subscript i in a_i denotes that we enable nonlinear activation to vary across channels. When the value of the coefficient ($a_i = 0$), the activation function is denoted as ReLU; and when a_i is a learnable parameter, the (1) is referred to as Parametric ReLU (PReLU) [13]. A Parametric Rectified Linear Unit, or PReLU can be defined as an activation function that generalizes the traditional rectified unit by adding a slope for negative values as shown in Fig. 4.

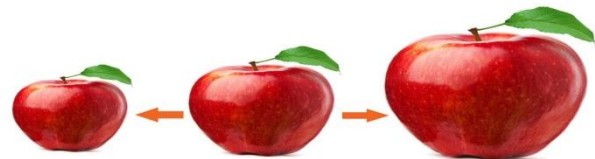


Fig. 2. Progressive resizing of Image.

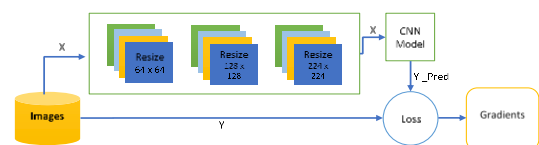


Fig. 3. Progressive resizing Pipeline.

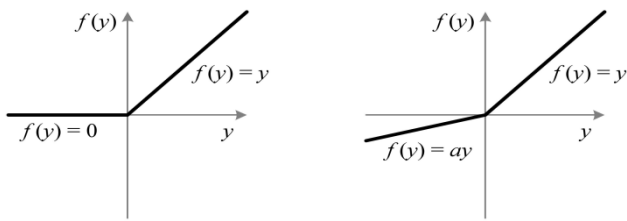


Fig. 4. ReLU Vs PReLU (In PReLU the Coefficient is Not Constant in the Negative Part and is Adaptively Learned).

Different layers may have different forms of nonlinearities. According to the literature, the PReLU for the initial layers have more positive slopes while investigates with convolutional neural networks (CNNs), i.e., closer to linear. Because the initial layers' filters are Gabor-like filters like edge or texture detectors, this demonstrates a situation in which positive and negative filter responses are respected.

In contrast, the authors find deeper layers have smaller coefficients, suggesting the model becomes more discriminative at later layers (while it wants to retain more information in earlier layers).

III. RELATED WORK

There has been a lot of research work in the literature to improve deep learning models for image classification. In recent years, with the growth of deep learning, in the realm of image classification, various deep architectures, including CNNs, R-CNN, Caps Net, ResNet, etc., have been introduced through which deep-level features can be obtained [23,24]. This section presents the related work on image classification using deep learning into three aspects viz. model development based on parameter efficiency, progressive training and improvement on data-set, optimization techniques and developmental platforms.

A. Model Development based on Parameter Efficiency

In recent years, Convolutional Neural Networks (CNNs) have considerably improved performance on a variety of computer vision applications. [1-3]. Many studies, including DenseNet [25] and EfficientNet [26], concentrate on parameter efficiency, with the goal of achieving higher accuracy with fewer parameters. In the present day, the variations of ResNet such as EffNet-L2 (SAM (Sharpness Aware Minimization)), PyramidNet (SAM) [27] BiT-L (ResNet), BiT-M (ResNet) [28], TRResNet-L-V2 [29], etc. with their improvements have gained huge success in the image classification domain over various benchmark datasets.

B. Progressive Training and Improvement on Dataset

Progressive training relies on dynamically changing the setting of the network during training. Some new techniques such as transfer learning [30], adversarial learning [31], and language models [32] have recently gained popularity. Introducing Progressive rescaling of image data in a deep learning network is one of the major factors which can improve accuracy of the model [33]. Image size is a vital component for CNN models accuracy, and several studies have been published in which throughout training, researchers dynamically change the image size to improve model performance. However, accuracy and training speed both are

influenced by progressive rescaling of image data and related works such as Mix & Match [34] has been found in the literature on resizing of image data where similar regularization is applied to all image sizes resulting in a decrease in model accuracy. There is another work on regularization where both training speed and accuracy can be improved by adjusting regularization in an adaptive manner [26].

C. Optimization Techniques and Developmental Platforms

Increasing the number of layers in a network raises the network's complexity, necessitating the use of optimization techniques. SGD, Adam [35], AdaGard [36] and AdaDelta [37] are some of the different optimization strategies implemented in the deep architectures such as CNN model along with hyperparameter optimization [38], of the deep network which is vital for better performance as well as network optimization. The advancement of deep learning techniques with GPU processing in combination with a vast dataset enables researchers to solve research issues across different application domains. Many popular frameworks for deep learning applications viz. Tensorflow, Caffe, Torch, Theano, CNTK, and libraries like Pydrive, Cuda, OpenCL, OpenCV, OpenMP, Keras, etc. allow the development of deep learning applications rapidly [39] [40] [41]. Image categorization [42] and object detection [43] are examples of applications where neural architecture search (NAS) has been applied in network architecture optimization. NAS initiatives in the past have primarily focused on increasing the efficiency of FLOPs [44, 45].

This paper aims to improve model accuracy, training speed, and parameter efficiency significantly over the state of the art by taking into account the aforementioned factors.

IV. PROPOSED ARCHITECTURE

The proposed "Progressive 3-Layered Block Architecture" model for image classification is presented here. The model has three phases as shown in Fig. 5, the model uses the pre trained architecture of EfficientNet5 as a transfer learning model and constructs the model by adding layers with the concept of compound scaling. The proposed architecture applies the PReLU activation in the dense layers which adaptively learns the parameter from the data. As in (1), the controlling coefficient a_i controls the slope of the negative part by adaptively learning the parameters. The total amount of additional parameters introduced by PReLU is negligible while considering the total weights. In the proposed "Progressive 3-Layered Block Architecture", progressive rescaling technique on images has been implemented to improve the accuracy while considering the regularization parameter along with image size. As an improvement on the progressive learning, the split and train strategy has been implemented which speeds up training along with improved resizing dataset.

The "Progressive 3-Layered Block Architecture" contains three phases:

Phase I: In the phase I, we build a base model for 64X64 image size:

Step 1: Load the pre-trained model

Step 2: Load image dataset for training

Step 3: Set the parameters and add layers implementing compound scaling

Step 4: Set PReLU activation for model layers

Algorithm 1(PReLU activation on model layers)

Step i: Initialize the value of PReLU (a_i) for equation 1, where a_i is the controlling coefficient.

Step ii: Update the value of a_i for one layer as in equation 2,

$$\frac{\partial \varepsilon}{\partial a_i} = \sum_{y_i} \frac{\partial \varepsilon}{\partial f(y_i)} \frac{\partial f(y_i)}{\partial a_i} \quad (2)$$

Where, ε is the objective function and $\frac{\partial \varepsilon}{\partial f(y_i)}$ is the gradient

that has been propagated from a deeper layer.

Step iii: The summation \sum_{y_i} runs all the positions of the feature map to update the value of all the layers.

Step iv: Adopt momentum as in equation 3 while updating a_i

$$\Delta a_i = \mu \Delta a_i + \epsilon \frac{\partial \varepsilon}{\partial a_i} \quad (3)$$

Where μ denotes momentum and ϵ denotes learning rate.

Step v: Repeat step (1-4) for all the layers.

Step 5: The network takes a set of training images as input, performs feed forward propagation (convolution, PReLU, and pooling operations, as well as forward propagation in the Fully Connected layer), and calculates the output probabilities for each class..

Step 6: Calculate the output layer’s total error by, Total Error= $\sum \frac{1}{2} (\text{target probability} - \text{output probability})^2$

Step 7: The CNN model goes through several convolutions and pooling phases during training and updates the weights with a backpropagation algorithm to minimize the output error.

Finally, save the model weights of the first phase.

Phase II: Build a model for 128x128 image size where the output of the first block is the input of the second block. The progressive resizing on images is performed considering adaptive regularization.

Algorithm 2 (Progressive rescaling on images considering regularization)

Step i: Initialize image size S_0 , set regularization $\{\phi_0^k\}$, where k is dropout.

Step ii: Set target image size S_t , set regularization $\{\phi_t^k\}$.

Step iii: Total model training has N steps and P stages

Where, for every stage $1 \leq i \leq P$,

Now, for $i=0$ to $P-1$ do

Size of the input image:

$$S_i \leftarrow S_0 + (S_t - S_0) \cdot \frac{i}{P-1}$$

Regularization parameter:

$$R_i \leftarrow \{\phi_i^k\} = \{\phi_0^k\} + (\{\phi_t^k\} - \{\phi_0^k\}) \cdot \frac{i}{P-1}$$

Train the model for $\frac{N}{P}$ steps with S_i and R_i .

End for

Now, train the model by following the steps of **Phase I** and save the model weight of the **Phase II**.

Phase III: The third block loads the weights of block 2 as an input and builds a model for image size 224X224 by repeating all the steps of Phase I and Phase II

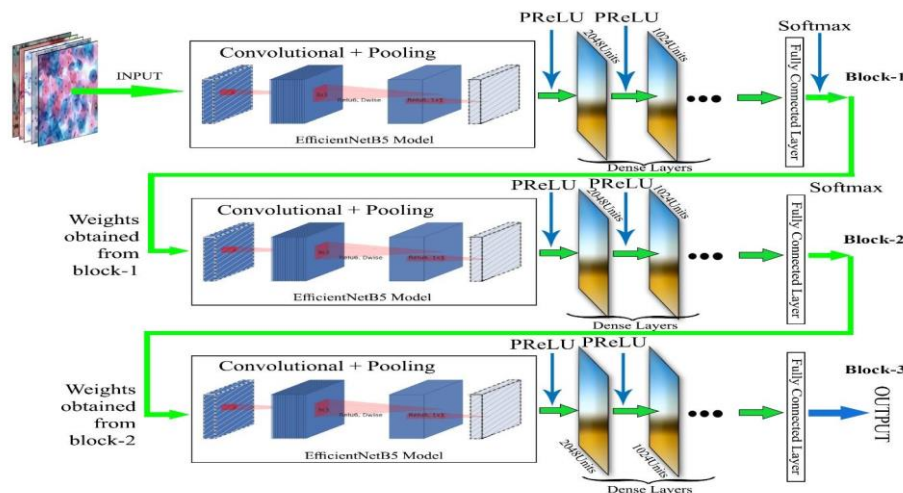


Fig. 5. The “Progressive 3-Layered Block Architecture” for Image Classification.

V. DATASET AND EXPERIMENTAL SETUP

A. Dataset

To ensure the robustness of the proposed “Progressive 3-Layered Block Architecture”, the network is trained and evaluated on three publicly available datasets: CIFAR-10, CIFAR100, and CALTECH 101. The datasets were randomly split into 90:10 (CIFAR-10), (CIFAR100) and 80:10:10 (CALTECH101) proportions for training and validation respectively. The CIFAR-10 dataset comprises 60,000 color images from diverse objects with and categorized into 10 classes (airplane, bird, dog, frog, deer, dog, horse, ship, and truck, automobile) for a total of 6000 images per class [49] Fig. 6. During the training of the proposed method, the datasets were automatically split into 50000 training images and 10000 test images. CIFAR100 is similar to CIFAR10, with the exception that it has 100 classes, each with 600 images. Each class has 500 training images and 100 testing images. The CIFAR-100's 100 categories are divided into 20 super classes. Fei-Fei Li et. al gathered the CALTECH101 dataset in September 2003.

It is made up of images of objects from 101 different classes, as well as one backdrop clutter class. Each class has approximately 40 to 800 images, for a total of approximately 9000 photographs. Images come in a variety of sizes, with common edge lengths ranging from 200 to 300 pixels. The detail of datasets used for the experiment is presented in Table I.



Fig. 6. Data Set of CIFAR10 and CALTECH1.

TABLE I. DETAILS OF DATASETS FOR EXPERIMENT

Name of the Dataset	Training Images	Validation Images	Classes
CIFAR-10 [49]	50,000	10,000	10
CIFAR-100 [49]	50,000	10,000	100
CALTECH101	60,000	15,000	101

B. Implementation Setup

The network architecture is implemented in Python using Keras [50], a deep learning framework, with TensorFlow [51] as the backend. The experiments for image classification are conducted using model and data-parallelism. The setup includes a GPU environment running the Linux operating system which comprises over 2,000 CPU cores, 1.5TB memory, and GPU accelerators (NVIDIA Tesla V100 32GB) using Google collab pro version. By using the GPU configuration platform, a pretrained network has been implemented on ImageNet and the network has been re-trained on the CIFAR10, CIFAR100, and CALTECH101 dataset using fine-tuning approaches. Moreover, an adaptive learning schedule has been considered where each iteration of the learning process uses 150 epochs with a decreasing learning rate schedule of 5% for every 10 epochs.

VI. RESULT AND DISCUSSION

The experimental setup and outcomes of the proposed network model on benchmark data sets are presented in this section. This section compares and contrasts recent deep model progress with the proposed model of “Progressive 3-Layered Block Architecture” for Image Classification.

Accuracy and error rate is calculated to compare various models [55]. Models attaining the lowest error rate and the highest possible accuracy are usually the most desirable.

The accuracy and the error rate is defined as follows:

$$Accuracy = \frac{TP + TN}{TP + TN + FP + FN}$$

$$Error = \frac{FP + FN}{TP + TN + FP + FN}$$

TN, FN, TP, FP are the number of true negatives and false negatives, true positives and false positives respectively.

A. The PReLU Setup and Comparison Experiment

An improved accuracy of PReLU over ReLU is observed in the “Progressive 3-Layered Block Architecture” for Image Classification over benchmark datasets. The training implementation gained 96.15% accuracy and 96.47% accuracy on CIFAR10 and CIFAR100 using 10 view testing respectively. The model has been trained with ReLUs in all layers by implementing progressive training on different blocks without loading the weight of the previous block which gains average 3% accuracy in all three blocks. Later the model is trained by replacing all ReLUs with PReLUs and also performs progressive training by loading weights from the previous block. Table II details the result obtained where PReLU gains 3.2% accuracy over ReLU in CIFAR10, 3.73% accuracy gain over ReLU in CIFAR100 and 2.67% accuracy gain over ReLU in CALTECH101. The better value for each dataset is denoted in boldface.

TABLE II. THE PERFORMANCE COMPARISON OF PReLU AND ReLU ON THREE BENCHMARK DATASETS

Datasets	Activation Function	Image size(Progressive scaling)	Performance Metric (Accuracy)
CIFAR 10	ReLU	64 X 64	79.70
		128 X 128	83.96
		224 X 224	93.66
	PReLU	64 X 64	81.26
		128 X 128	87.26
		224 X 224	96.15
CIFAR 100	ReLU	64 X 64	54.90
		128 X 128	86.69
		224 X 224	92.99
	PReLU	64 X 64	59.78
		128 X 128	88.44
		224 X 224	96.47
CALTECH101	ReLU	64 X 64	63.31
		128 X 128	85.91
		224 X 224	93.95
	PReLU	64 X 64	64.88
		128 X 128	86.94
		224 X 224	95.39

Table II presents the performance comparison of PReLU and ReLU on three benchmark datasets where experimentation is carried out considering the three image sizes viz., 64x64, 128x128, and 224x224. Since implementation of Parametric Rectified Linear Unit (PReLU) activation function on model layers generalizes the classic rectified unit and enhances model fitting with almost no additional computing cost and no risk of overfitting, it shows better performance on all the datasets with rescaled images. In CIFAR10 the model obtained 96.15% accuracy compared to ReLU (93.66%) in 224x224 image data. In CIFAR100 and CALTECH101, the model obtained 96.47% and 95.39% accuracy respectively on PReLU which was higher than ReLU at 92.99% and 93.95 % in both the cases. Fig. 7. further compares the training and validation curve of this approach where ReLU is 93.66% and PReLU is 95.17% on 50 epochs on CIFAR10 dataset. These results suggest that the “Progressive 3-Layered Block Architecture” for Image Classification model generalized well in all three datasets while implementing PReLU with a progressive approach.

B. Progressive Learning Setup and Experiment

The size of the image has a significant impact on the effectiveness of training and accuracy improvement of Deep Neural Networks (DNN). This experimentation considers three parameters while training the network with resized images as presented in Table III.

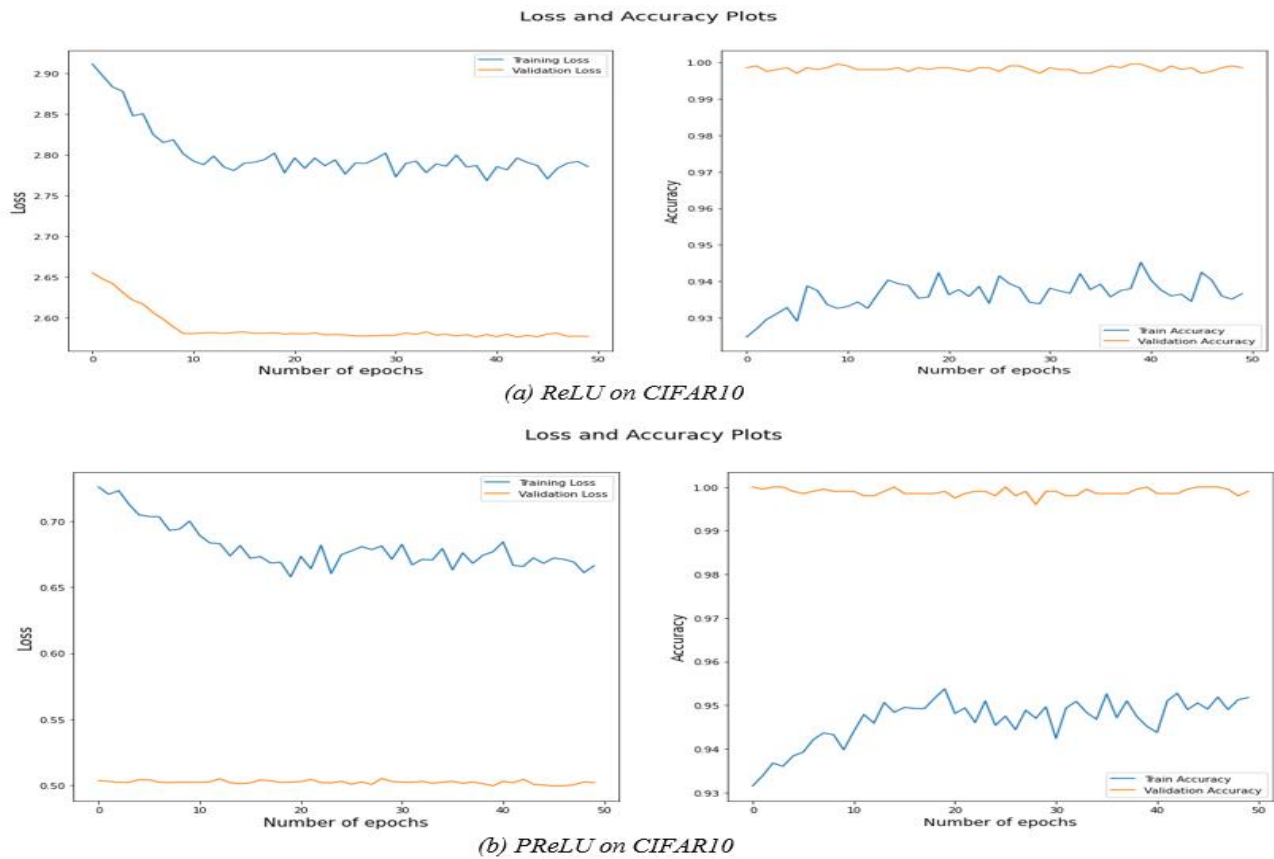


Fig. 7. Accuracy Plot of PReLU over ReLU on CIFAR 10 (a) Loss and Accuracy Plots of ReLU on CIFAR10 where ReLU is 93.66 (b) Loss and Accuracy Plots of PReLU on CIFAR10 where PReLU is 95.17 on 50 Epoch.

TABLE III. PROGRESSIVE RESCALING SETUP PARAMETERS

Parameters	First training stage		Second training stage		Third training stage	
	Min	Max	Min	Max	Min	Max
Image Size	64	244	64	244	64	244
RandAugm-ent	5	10	5	15	5	20
Dropout rate	0.1	0.3	0.2	0.5	0.1	0.5

In literature, it is found that the accuracy of deep models depends on the regularization parameters of the model while implementing progressive rescaling on image data, it is recommended to adjust the regularization parameters for better accuracy instead of keeping fixed regularizations. In [43] it is mentioned that, to combat overfitting in large models, stronger regularization is required: EfficientNet-B7, for example, employs larger dropout rates and stronger data augmentations than EfficientNet-B0. In the present experimentation, Dropout [15] and RandAugment [52] regularization has been considered with progressive training of images for three training stages for different image sizes.

This experimentation presents the performance over three benchmark datasets with the experimental setup presented as in Table III where for each stage 100 epoch is set.

Through Table IV, we observe that the accuracy is 79.28% in CIFAR10 while the image size is 64X64 with weaker regularization (RandAugment =5, Dropout 0.1) and on the other hand the accuracy is increased to 93.17 after the third training stage with bigger image size and stronger regularization. For CIFAR100 and CALTECH101 datasets, we observe that the accuracy increases as well to 93.99 and 92.72% respectively with a larger image size and stronger regularization parameters. The progressive rescaling of the dataset improves the model's accuracy as well as its training time.

From the experiments conducted it is observed that, in a high-accuracy regime, scaling up data size is more effective than merely scaling up a model size, where it can be concluded that, for instance, when the accuracy of CIFAR100 is beyond 96.47, it is quite challenging to further increase its accuracy by simply increasing model size and so in other image datasets used in this experiment. Fig. 8, further illustrates the training and validation accuracy of CIFAR10 and CIFAR100 on progressive rescaling setting where we observed that the model obtained 96.15% accuracy on CIFAR10 and 96.47% accuracy on CIAFR100 after certain set of training on each stage while implementing progressive rescaling setting.

TABLE IV. PROGRESSIVE LEARNING FOR DIFFERENT IMAGE SIZES AND THEIR ACCURACY WHILE CONSIDERING REGULARIZATION PARAMETERS IN CIFAR10, CIFAR100 AND CALTECH101

Dataset	Image size	RandAug-ment	Dropout rate	Accuracy
CIFAR10	64	5	0.1	79.28
	224	20	0.5	93.17
CIFAR100	64	5	0.1	57.89
	224	20	0.5	93.99
CALTECH 101	64	5	0.1	62.19
	224	20	0.5	92.72

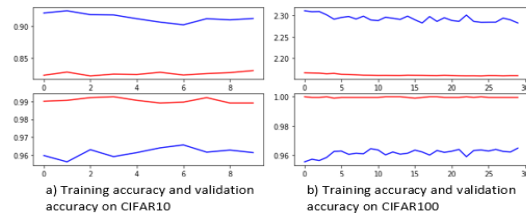


Fig. 8. Plotting the Training and Validation Accuracy of CIFAR10 and CIFAR100.

C. Performance Comparison

This section presents the comparative results on ImageNet, and the performance comparison of the proposed “Progressive 3-Layered Block Architecture” with other models on CIFAR-10, CIFAR-100, and CALTECH 101.

The proposed model uses the pre-trained transfer learning model Efficientnet-B5 trained on ImageNet, ILSVRC2012 and fine-tuned with the same ImageNet setting as in [53]. A smaller batch size of 512, and small initial learning rate of 0.001 with cosine decay has been used. Table V demonstrates the performance comparison of the proposed "Progressive 3-Layered Block architecture" with other models where the top-1 Accuracy is 86.52 %, 2.49%, 2.52 % and 3.51% improvement compared to EfficientNet (2019), ResNet-RS (2021), and DeiT/ViT (2021) respectively. At the same time, the proposed model has fewer FLOPs and fewer parameters compared to other models, which implies that scaling up image size seems more effective than increasing model size by adding layers over the considered datasets.

Table VI presents the performance comparison of the proposed model with other models on all three datasets.

The “Progressive 3-Layard Block architecture” model for image classification combines the progressive rescaling setting with transfer learning technique and PReLU activation where better optimizers and fine-tuning of hyperparameters improve the model accuracy. The model is trained for 65 hrs.’ 70 hrs.’, and 71 hrs.’ respectively for all three datasets which are comparatively less than other benchmark models in the literature. The accuracy on CIFAR10 is 98.79%, CIFAR100 is 96.47% and CALTECH101 is 95.39% for 224X224 images while loading the previous weight of images during training and follows the split and training strategy while training. Fig. 9. further compares the loss and accuracy of CIFAR100 and CALTECH101 where the accuracy is 96.47 % and 95.39% respectively on 224x224 images where the proposed model outperforms the accuracy of CIFAR100 and CALTECH101 with other benchmark models.

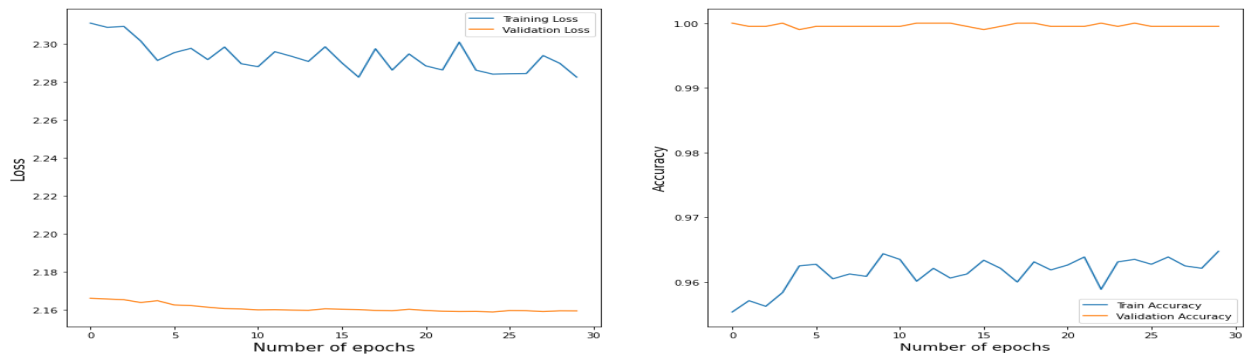
TABLE V. PERFORMANCE COMPARISON AND RESULTS OF THE PROPOSED MODEL IN TERMS OF ACCURACY, PARAMETERS, AND FLOPS ON IMAGENET

Name of the Network	EfficientNet 2019	ResNet-RS 2021	DeiT/ViT (2021)	Progressive 3-Layered Block Architecture
Top 1 Accuracy	84.3%	84.0 %	83.1%	86.52%
Parameters	43 M	164 M	86 M	36 M
FLOPs	19 B	64 B	56 B	20 B

TABLE VI. PERFORMANCE COMPARISON AND RESULTS ON CIFAR10, CIFARR100 AND CALTECH101

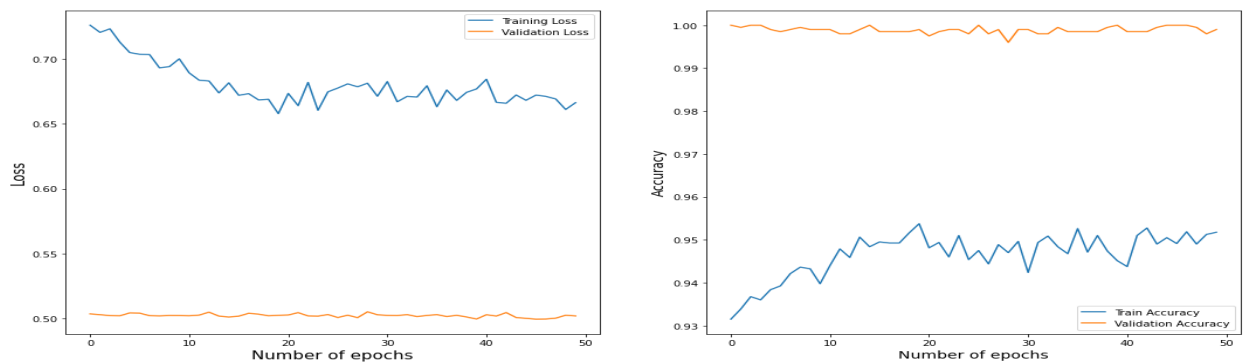
Datasets	Network Models	Accuracy	PARAM	Flops	Training time(Hours)
CIFAR 10	AlexNet (Doan Cong Danh 2019)	89.67%	27.31M	---	144
	BiT-L(ResNet)Kolesnikov, A et al., 2019	98.91	928	---	----
	EfficientNet-B7 (Tan & Le 2019)	98.9	64 M	38B	139
	EffNet-L2(SAM)	99.70	0.575114	--	
	Progressive 3-Layered Block Architecture	98.79	36 M	20 B	65
CIFAR100	AlexNet(KP) Akrou, M et.,al 2019	66.78	61 M	-----	146
	BiT-L(ResNet)Kolesnikov, A et al., 2019	93.51		-----	
	EfficientNet-B7 (Tan & Le 2019)	91.7	64M	38B	138
	EffNet-L2(SAM) Foret, P et al., 2020	96.08	56 M		
	Progressive 3-Layered Block Architecture	96.47	36 M	20 B	70
CALTECH101	Alexnet	-----		-----	
	ResNet34	95	60.5 M	----	
	EfficientNet-B7 (Tan & Le 2019)	93.0	64 M	38 B	139
	EffNet-L2 (SAM) Foret, P et al., 2020	94.32	56 M		
	Progressive 3-Layered Block Architecture	95.39	36 M	20 B	71

Loss and Accuracy Plots



(a) CIFAR100 (96.47%)

Loss and Accuracy Plots



(b) CALTECH101 (95.39)

Fig. 9. Plotting the Loss and Accuracy Plot of CIFAR100 and CALTECH101 on 224x224 Images.

VII. CONCLUSION AND FUTURE WORK

Accuracy improvement in image classification has a wide ranging impact on various application domains and deep convolution neural networks (CNNs) have gained remarkable success in this area. This paper proposed a “Progressive 3-Layered Block Architecture” for image classification by implementing transfer learning and progressive resizing concept. The proposed architecture applies the PReLU activation in the dense layers which adaptively learns the parameters from the data. The efficiency of the proposed architecture is established by its superior performance, low execution time and fewer parameters compared to other models in literature. We evaluate the model in tensorflow environment using three benchmark datasets viz. CIFAR10, CIFAR100 and CALTECH101. The evaluation of proposed “Progressive 3-Layered Block Architecture” is carried out in three different experimental setup viz. PReLU setup, progressive rescaling setup and performance comparison with other CNN models. At the same time, our proposed model has fewer FLOPs and fewer parameters compared to other models. From the results obtained it may be concluded that enhancement in learning strategies, adopting standard activation functions, fine-tuning of hyper-parameters and optimizers and scaling up image size is more effective than increasing model size by adding layers in high accuracy regime. With increased performance, less execution time, and fewer parameters, the suggested architecture outperforms the competition in all three benchmark datasets. However, more testing on multiple datasets with different image sizes and training samples is required for general applicability.

REFERENCES

- [1] Szegedy, C., Liu, W., Jia, Y., Sermanet, P., Reed, S., Anguelov, D., Rabinovich, ..., and A (2015) Going deeper with convolutions. Proceedings of the IEEE conference on computer vision and pattern recognition, pp. 1–9.
- [2] Simonyan, K., Zisserman, A. et al. (2014) Very deep convolutional networks for large-scale image recognition.
- [3] Girshick, R. (2015) Fast r-cnn. Proceedings of the IEEE international conference on computer vision, pp. 1440–1448.
- [4] Liu, X., Zhang, R., Meng, Z., Hong, R., and Liu, G. (2019) On fusing the latent deep CNN feature for image classification. World Wide Web, 22 (2), 423–436.
- [5] P. Sermanet, D. Eigen, X. Zhang, M. Mathieu, R. Fergus, and Y. LeCun. Overfeat: Integrated recognition, localization and detection using convolutional networks. 2014.
- [6] M. D. Zeiler and R. Fergus. Visualizing and understanding convolutional neural networks. In ECCV, 2014.
- [7] V. Nair and G. E. Hinton. Rectified linear units improve restricted boltzmann machines. In ICML, pages 807–814, 2010.
- [8] A. L. Maas, A. Y. Hannun, and A. Y. Ng. Rectifier nonlinearities improve neural network acoustic models. In ICML, 2013.
- [9] M. D. Zeiler, M. Ranzato, R. Monga, M. Mao, K. Yang, Q. V. Le, P. Nguyen, A. Senior, V. Vanhoucke, J. Dean, and G. E. Hinton. On rectified linear units for speech processing. In ICASSP, 2013.
- [10] M. Lin, Q. Chen, and S. Yan. Network in network. arXiv:1312.4400, 2013.
- [11] R. K. Srivastava, J. Masci, S. Kazerounian, F. Gomez, and J. Schmidhuber. Compete to compute. In NIPS, pages 2310–2318, 2013.
- [12] I. J. Goodfellow, D. Warde-Farley, M. Mirza, A. Courville, and Y. Bengio. Maxout networks. arXiv:1302.4389, 2013.
- [13] K. He, X. Zhang, S. Ren, and J. Sun. Spatial pyramid pooling in deep convolutional networks for visual recognition. arXiv:1406.4729v2, 2014.
- [14] G. E. Hinton, N. Srivastava, A. Krizhevsky, I. Sutskever, and R. R. Salakhutdinov. Improving neural networks by preventing co-adaptation of feature detectors. arXiv:1207.0580, 2012.
- [15] N. Srivastava, G. Hinton, A. Krizhevsky, I. Sutskever, and R. Salakhutdinov. Dropout: A simple way to prevent neural networks from overfitting. The Journal of Machine Learning Research, pages 1929–1958, 2014.
- [16] L. Wan, M. Zeiler, S. Zhang, Y. L. Cun, and R. Fergus. Regularization of neural networks using dropconnect. In ICML, pages 1058–1066, 2013.
- [17] A. G. Howard. Some improvements on deep convolutional neural network based image classification. arXiv:1312.5402, 2013.
- [18] A. Krizhevsky, I. Sutskever, and G. Hinton. Imagenet classification with deep convolutional neural networks. In NIPS, 2012.
- [19] J. Deng, W. Dong, R. Socher, L.-J. Li, K. Li, and L. FeiFei. Imagenet: A large-scale hierarchical image database. In CVPR, 2009.
- [20] O. Russakovsky, J. Deng, H. Su, J. Krause, S. Satheesh, S. Ma, Z. Huang, A. Karpathy, A. Khosla, M. Bernstein, et al. Imagenet large scale visual recognition challenge. arXiv:1409.0575, 2014.
- [21] Tan, C., Sun, F., Kong, T., Zhang, W., Yang, C., & Liu, C. (2018, October). A survey on deep transfer learning. In International conference on artificial neural networks (pp. 270-279). Springer, Cham.
- [22] He, K., Zhang, X., Ren, S., & Sun, J. (2015). Delving deep into rectifiers: Surpassing human-level performance on imagenet classification. In Proceedings of the IEEE international conference on computer vision (pp. 1026-1034).
- [23] Wang, Y. and Wang, Z. (2019) A survey of recent work on fine-grained image classification techniques. Journal of Visual Communication and Image Representation, 59, 210–214.
- [24] Krizhevsky, A., Sutskever, I., and Hinton, G.E. (2017) ImageNet classification with deep convolutional neural networks. Communications of the ACM, 60 (6), 84–90 .
- [25] Huang, G., Liu, Z., Van Der Maaten, L., and Weinberger, K. Q. Densely connected convolutional networks. CVPR, 2017.
- [26] Tan, M. and Le, Q. V. Efficientnet: Rethinking model scaling for convolutional neural networks. ICML, 2019a.
- [27] Foret, P., Kleiner, A., Mobahi, H., and Neyshabur, B. (2020), Sharpness-Aware Minimization for Efficiently Improving Generalization.
- [28] Kolesnikov, A., Zhai, X., and Beyer, L. (2019) Revisiting self-supervised visual representation learning. Proceedings of the IEEE/CVF Conference on Computer Vision and Pattern Recognition, pp. 1920–1929.
- [29] Ridnik, T., Lawen, H., Noy, A., Baruch, E.B., Sharir, G., and Friedman, I. (2021) Tresnet: High performance gpu-dedicated architecture. Proceedings of the IEEE/CVF Winter Conference on Applications of Computer Vision, pp. 1400–1409.
- [30] Karras, T., Aila, T., Laine, S., and Lehtinen, J. Progressive growing of gans for improved quality, stability, and variation. ICLR, 2018.
- [31] Yu, H., Liu, A., Liu, X., Li, G., Luo, P., Cheng, R., Yang, J., and Zhang, C. Pda: Progressive data augmentation for general robustness of deep neural networks. arXiv preprint arXiv:1909.04839, 2019.
- [32] Press, O., Smith, N. A., and Lewis, M. Shortformer: Better language modeling using shorter inputs. arXiv preprint arXiv:2012.15832, 2021.
- [33] Howard, J. Training imagenet in 3 hours for 25 minutes <https://www.fast.ai/2018/04/30/dawnbench-fastai/>, 2018.
- [34] Hoffer, E., Weinstein, B., Hubara, I., Ben-Nun, T., Hoefler, T., and Soudry, D. Mix & match: training convnets with mixed image sizes for improved accuracy, speed and scale resiliency. arXiv preprint arXiv:1908.08986, 2019.
- [35] Kingma, Diederik P., and Jimmy Ba. "Adam: A method for stochastic optimization." arXiv preprint arXiv:1412.6980 (2014).
- [36] Duchi, John, Elad Hazan, and Yoram Singer. "Adaptive subgradient methods for online learning and stochastic optimization." Journal of Machine Learning Research 12.Jul (2011): 2121-2159.

- [37] Zeiler, Matthew D. "ADADELTA: an adaptive learning rate method." arXiv preprint arXiv:1212.5701 (2012).
- [38] Dong, X., Tan, M., Yu, A. W., Peng, D., Gabrys, B., and Le, Q. V. Autohas: Efficient hyperparameter and architecture search. arXiv preprint arXiv:2006.03656, 2020.
- [39] Bahrampour, S., Ramakrishnan, N., Schott, L., Shah, M. et al. (2015) Comparative study of deep learning software frameworks. Comparative study of deep learning software frameworks.
- [40] Akiba, T. (2018), Performance of distributed deep learning using ChainerMN.
- [41] Karmanov, I., Salvaris, M., Fierro, M., and Dean, D. (2018) Comparing deep learning frameworks: a Rosetta stone approach. Machine Learning Blog.
- [42] Zoph, B., Vasudevan, V., Shlens, J., and Le, Q. V. Learning transferable architectures for scalable image recognition. CVPR, 2018.
- [43] Tan, M., Pang, R., and Le, Q. V. Efficientdet: Scalable and efficient object detection. CVPR, 2020.
- [44] Tan, M. and Le, Q. V. Mixconv: Mixed depthwise convolutional kernels. BMVC, 2019b.
- [45] Tan, M., Chen, B., Pang, R., Vasudevan, V., and Le, Q. V. Mnasnet: Platform-aware neural architecture search for mobile. CVPR, 2019.
- [46] Huh, M., Agrawal, P., & Efros, A. A. (2016). What makes ImageNet good for transfer learning? arXiv preprint arXiv:1608.08614.
- [47] Bee Lim, Sanghyun Son, Heewon Kim, Seungjun Nah, and Kyoung Mu Lee. Enhanced Deep Residual Networks for Single Image Super-Resolution. In 2017 IEEE Conference on Computer Vision and Pattern Recognition Workshops, CVPR Workshops 2017, Honolulu, HI, USA, July 21-26, 2017.
- [48] Tero Karras, Timo Aila, Samuli Laine, and Jaakko Lehtinen. Progressive Growing of GANs for Improved Quality, Stability, and Variation. In 6th International Conference on Learning Representations, ICLR 2018, Vancouver, BC, Canada, April 30 - May 3, 2018, Conference Track Proceedings.
- [49] Krizhevsky, A., & Hinton, G. (2009). Learning multiple layers of features from tiny images.
- [50] Keras (2018), Keras-high-level neural networks API. URL <https://keras.io/>.
- [51] Tensorflow (2018). URL <https://www.tensorflow.org/>. Accessed 20.
- [52] Cubuk, E. D., Zoph, B., Shlens, J., and Le, Q. V. Randaugment: Practical automated data augmentation with a reduced search space. ECCV, 2020.
- [53] Dosovitskiy, A., Beyer, L., Kolesnikov, A., Weissenborn, D., Zhai, X., Unterthiner, T., Dehghani, M., Minderer, M., Heigold, G., Gelly, S., Uszkoreit, J., and Houtsby, N. An image is worth 16x16 words: Transformers for image recognition at scale. ICLR, 2021.
- [54] Tan, M., & Le, Q. (2019, May). Efficientnet: Rethinking model scaling for convolutional neural networks. In International Conference on Machine Learning (pp. 6105-6114). PMLR.
- [55] T. Pan-Ning, M. Steinbach, and V. Kumar, "Classification: Basic Concepts, Decision Trees, and Model Evaluation," Introduction to data mining 1 (2006): 145-205.

Face Recognition using Principal Component Analysis and Clustered Self-Organizing Map

Jasem Almotiri

Department of Computer Science
College of Computers and Information Technology
Taif University, Makkah, Saudi Arabia

Abstract—Face recognition is one of the cornerstones of the face processing schemes that composed the contemporary intelligent vision-based interactive systems between computers and humans. Instead of using neurons of the Self-Organized Map (SOM) neural network to cluster the facial data, in this work, we applied an agglomerative hierarchical clustering to cluster the neurons of the SOM network, which in turns, used to cluster the facial dataset. In prior, Principal Component Analysis (PCA) is employed to reduce the dimension of the facial data as well as to establish the initial state of SOM neurons. The design of the clustered-SOM recognition engine involves post-training steps that labeled the clustered SOM neurons resulting in a supervised SOM network. The effectiveness of the proposed model is demonstrated using the well-known ORL database. Using five images per person for SOM training, the proposed recognizer results in a recognition rate of 94.7%, whereas using nine images raise the recognition rate up to 99.33%. The facial recognizer has attained a notable reliability and robustness against the additive white Gaussian noise, where increasing the level of noise variance from 0 to 0.09, the recognition rate decreased only by 8%. Furthermore, time cost is analyzed, where using 200 images for training takes less than 4 seconds to be performed, whereas testing using a new set of 200 images takes less than 0.013 seconds which is competitive to many artificial intelligence and machine learning based schemes.

Keywords—Artificial intelligence; machine learning; clustering; agglomerative hierarchical clustering; face recognition; neural network; self-organizing map; principal component analysis

I. INTRODUCTION

As a basic definition, facial recognition is the process that utilizes techniques and algorithms to match the physical characteristics against the photos of peoples' faces where face identification allows faster and more accurate face identification rather than that is carried out by the naked human eye. Face recognition can take variants spheres of face recognition-related activities and operations to new ambits. For example, in the fields of security, face recognition can do a lot more to enhance security extends from street crime to airport security where these issues have been dominated the headlines in many countries all over the world. The limited information in security cases opens the doors for a wide band of accusations related to bias or discrimination.

Face recognition systems open the counterpart door that entails no antecedent information related to age, race, or gender especially face recognition that is carried out based on classical techniques that adapt prior saved databases composed of the

faces of persons of interest or persons who are suspected to involve in a serious violent crime. In the nutshell, face recognition systems offer up a further intelligence in people identification, especially in situations where it is considered a tedious task to be done by human staff alone as encountered in the large, crowded areas and establishments.

This recent surge of facial recognition usage increases the demands on recognition performance metrics included: (1) recognition accuracy and (2) the speed of response. The majority of facial recognition methods and schemes in literature have been built based on two major cascaded engines: (1) facial data representation (facial features/characteristics extraction) engines (2) Facial classification engines.

Facial representation engines can be either supervised such as Linear Discriminative Analysis (LDA) [1][2] or unsupervised such as Principal Component Analysis (PCA) [1][3], Locality Preserving Projection (LPP) [4], Discrete Wavelet Transform (DWT) [5] and other sparsity-based techniques [6] [7] or it can be a merged of supervised and unsupervised techniques as proposed in [8].

Facial classification engines can also be categorized as unsupervised [9], [10] or supervised such as using group sparsity representation-based classification [11], or using techniques that built based on deep learning [12] such as artificial neural networks [13], [14],[15], [16][17],[18], Support Vector Machine (SVM) [19], [20], or Decision Tree and Random Forest [21]. Furthermore, the classification engines can be built based on a hybrid of supervised and unsupervised techniques [22].

A considerable portion of artificial intelligent and machine learning based schemes is simple to be implemented, however the recognition performance is moderate, or the reliability of the facial recognizer show dramatic changes against changes occur in the number of training images used per person, or against additive white Gaussian noise.

The other portion of techniques, that adapt complex frameworks (such as complex-structured neural networks) show high to moderate recognition performance associated with high computational overhead and time cost that lessen the applicability of these techniques.

In this work, we aim to design an intelligent facial recognizer model that can be deployed with low computational overhead and time cost yet have competitive facial recognition

rate. Furthermore, we aim a high level of reliability in our designed model through a high robustness against sizeable change in the volume of available training data as well as against high levels of additive Gaussian noise.

To achieve these goals, in this work, we use an effective combination of the simple standard PCA algorithm that modified mathematically to suit the high dimensionality of the facial data and to dramatically lower the computational overhead. Then, we designed a special variant of SOM, denoted as clustered SOM to perform the classification step, where instead of using the converged SOM neurons as our classifiers, we applied an agglomerative clustering algorithm, to obtain a set of clusters composed of SOM neurons, afterwards, these clusters are labeled based on the training dataset yields a supervised version of clustered SOM. The training data with labeled exemplars are used to label the different generated clusters by measuring the distance between the facial vectors that composed the training data and the neurons that play the role of "cluster members". Then, the different labeled SOM clusters used to classify the new coming facial data into their corresponding classes.

This hybrid framework has the ability to learn and response fast due to the flexibility of the supervised clustered SOM, where it can learn easily and with low computational overhead as well as it has a high detection performance where the operational neurons undergo two cascaded refinement one during raw SOM neural network training and the other one during the agglomerative clustering applied on these converged neurons. Thus, we can summarize the contribution of this work in five-fold:

- We present the design and implementation of a human facial recognition system based on PCA as a feature extractor (facial representation) and the agglomerative hierarchical clustered SOM as the recognition engine. Moreover, we study the recognition performance of the system using a benchmark ORL dataset.
- The proposed system shows supremacy in terms of time-cost and computational overhead to perform either training or test stages where the processing time per image in the training stage is as low as 0.0182 sec per training image whereas it expends less than $7e-5$ sec per test image.
- The system shows robustness against the noise addition, where the recognition performance can tolerate high levels of Gaussian noise with zero mean and different levels of variations.
- We compare the performance of the PCA-clustered SOM model with other methods that either involved SOM or SOM-variants, where our proposed method show supremacy in terms of recognition rate. However, it shows comparable or underperformance with nuance differences to other schemes that built using other techniques, where these methods show vast inferiority in other aspects of recognition performance such as time cost, complexity overhead, and robustness especially against adding white Gaussian noise.

- Based on the several performance analyses that conducted to measure the reliability and the robustness of the proposed recognition model, it can be implemented in the real time applications where the high robust against noisy signal as well as the fast time response and fast learning of new coming images, make the model mostly appropriate for security systems that utilized the personal biometric features.

The rest of this paper is organized as follows: related works that constructed based on SOM network is discussed in Section 2. Section 3 details the proposed method. Section 4 presents the experimental results and analysis. Section 5 presents the results discussion and Section 6 concludes the paper.

II. RELATED WORK

One of the efficient yet robust unsupervised neural networks is Self-Organizing Map (SOM) as it can play a dual role in the field of face recognition, where it can be used either to represent the facial data (as a feature extractor and dimensionality reduction tool), or it can be used as a classification engine. SOM network can be even integrated with other dimensionality reduction techniques such as PCA as proposed by Kumar et al. [23]. SOM network can be used as a dimensionality reduction as well as facial data representation as proposed by Lawrence et al. [24].

As a pre-processing step applied to the SOM network before the output of the network can be fed to the classification engine, Ruiz and Jaime [25] applied Fourier transform to the output of the SOM network (optimal weight vectors of the SOM neurons) to attain a translation invariance to the feature map generated by applying a two-dimensional Gabor filter to the input raw facial images. Afterwards, backpropagation neural network was used for sake of classification.

In a facial recognition scheme uses K-Nearest Neighbor (KNN) as a classification engine, Yodkhad et al. [26] used the clustering capability of the SOM network to group the training data and extract the representative prototype of each group, which, accelerate the classification duty of KNN algorithm.

Using SOM network as the major classifier engine of the face recognition system is proposed by Neagoe and Stanculescu [22], where PCA, LDA, and ICA techniques of data representation and feature extraction were used for comparison purposes cascaded by a SOM-variant scheme called concurrent SOM (CSOM) which was proposed and developed by the first author of [22]. In this scheme, the training data is partitioned into multiple sub datasets (partitions), each partition represents one class of data. Then, multiple SOM networks are generated and each one is trained by one partition of training data. In the testing stage, the Euclidean distance between the testing vectorial image and each trained SOM network is calculated, and the winner "SOM network" with the minimum distance gives the class to the input testing image.

Besides the eigenfaces that can be generated by the PCA method and the fisher face that can be generated by LDA (or Fishers' Linear Discriminant), SOM network can be used to generate what is called SOM-face as proposed in [27] where an

enhanced version of SOM network, called as kernel-based SOM network is used to extract the representative features of the facial data, where authors called it as SOM-face [27].

Based on SOM-face, Zhi and Meng [28] proposed a face recognition method based on multiple training images, where, in addition to the topological shape-feature vector generated by SOM network, a wavelet-feature vector is generated by a wavelet-network, then both feature vector representations fed to the classification engine.

Instead of training the SOM network via the individual vector facial images as a holistic, Tan *et al.* [29], partitioned each facial image into equal-sized nonoverlapping subblocks. Then, the resulted subblocks used to train the SOM map or multiple SOM maps in a step called by the authors as the localizing step. The major goal of this step is to generate the local vector representation of facial data to be fed to a soft KNN-ensemble classifier for sake of facial recognition.

Using the SOM network as a classifier engine, Monteiro *et al.* [30] proposed four schemes of SOM/SOM-variant-based classifiers. Since SOM is used as a classifier, all four classifiers' engines that implemented by the authors use either SOM grid neurons pre-training labeling or post-training labeling step. The first proposed classifier used the labeled

training data for SOM neurons labeling which, in turn, used as the classification engine of the recognition system. The second classifier uses the centroids of the labels available for each class of facial data to label the SOM neurons after the training process, where the centroids of labels of each class are pre-computed. The third classification engine is built by turning SOM into a supervised classifier by augmenting each input vector with its corresponding class label, where these vectors are used to adjust the corresponding augmented weight-vectors of SOM neurons. The fourth SOM-based classifier was built by using an entire SOM network to represent one single class of the available facial data. Afterwards, these networks are trained separately using the corresponding input facial vectors for each class. During the testing phase, however, the best-matched neuron (winner) is chosen via all the available trained SOM networks and the winner trained SOM network assigns its class to the incoming test vector.

III. METHOD

The high-level block diagram of the proposed method is shown in Fig. 1. Seeking an optimal representative subspace of the input facial data, classical PCA is applied as a first step. Then, facial data is projected on the resulting PCA-subspace and split into projected training and projected testing datasets.

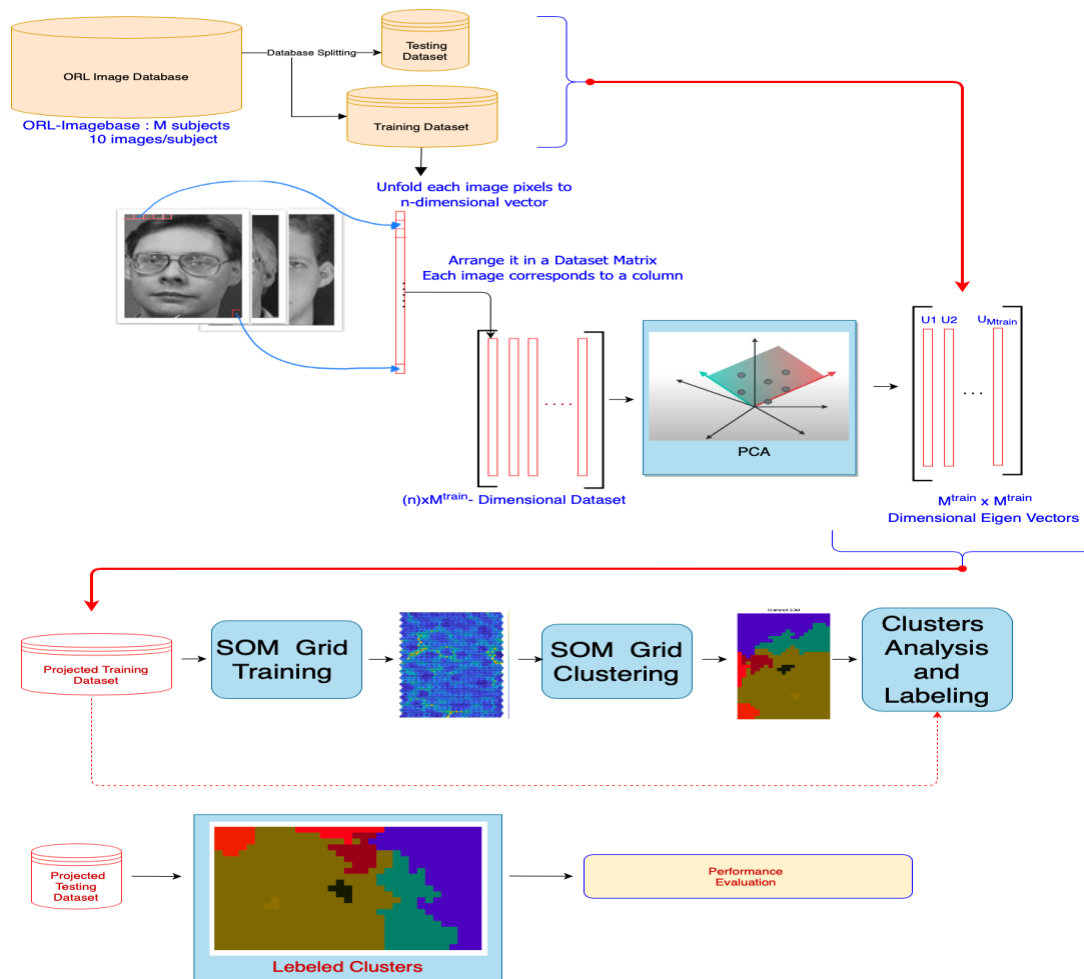


Fig. 1. High-level Block Diagram of the Proposed Face Recognition System Work Flow.

The projected training dataset is used to establish the topological space of the SOM neural grid. Then, the best-matched units of the SOM network undergo a hierarchical clustering for sake of optimal robust and compact representation of facial data. As a post-training step, the projected labeled training data used in analyzing and labeling SOM clusters based on the majority occurrence voting of a specific subject (face image belongs to a specific person in the training dataset). Then, new coming facial data is classified by the proposed facial recognizer into their corresponding classes.

In subsequent sections, each step of the recognition model is explained in detail.

A. Principal Component Analysis (PCA)

Formally, the ORL database is composed of J gray-scale images, that can be represented by the matrix $X_{c,r}^{j,p}$, where $c \times r$ corresponds to the vertical and horizontal dimensions of the j^{th} image (in our case, $r = 92, c = 112$) of the p^{th} person (subject/class). As a first step, the pixels of $X_{c,r}^{j,p}$ are vectorized into an n -dimensional vector: $I_j^p \in \mathbb{R}^n$ where $n = c \times r$ by reading the pixel values in the image $X_{c,r}^{j,p}$ in a raster-scan manner, in our case, $n = 10,304$.

Thus, the set of images in the ORL database can be represented as a rectangular matrix Y of columns $Y = [I_1, I_2, \dots, I_J]$ where J index represents the total number of images in the raw dataset.

The dimensionality of these images is too large to be fed and efficiently analyzed by the recognition engine of the proposed model. For sake of obtaining a more compendious representation of data, the regular form of the principal component analysis technique is used.

Given as input, a rectangular matrix Y whose columns are seen as variables, the main objective of the principal component analysis is to create a new set of variables (called principal components) that have a linear combination of the input variables in such a way that the variance between the principal components (resulted basis vectors) and each of the original variables is maximized.

As a first step, the vectorized dataset Y is split into two sub-datasets: the first one is the training dataset $Y^{train} = [I_1, I_2, \dots, I_M]$ which used to produce the principal components basis vector used to establish and train the SOM network, and to label the clusters of the clustered SOM, M represents the total number of involved images in the training stage. The other sub-dataset is the testing dataset $Y^{test} = [I_1, I_2, \dots, I_m]$ which is used to test the recognition performance of the proposed model, m represents the testing images involved in the testing stage, where $m = J - M$. Fig. 2 shows the pipeline of the facial data representation stage using the PCA method.

As PCA is a variance optimization process, if some variables (vectors of matrix Y) show a large variance compared to other variables, then, during variance maximization, PCA will load on the ones of large variances. Therefore, as a prior step to PCA, is to normalize the data in two succeeded steps. First, the average of vectorized training images $I_j \in Y^{train}$ is obtained as in (1):

$$I_{mean} = \frac{1}{M} \sum_{j=1}^M I_j \quad (1)$$

Each vectorized image vector $I_j \in Y^{train}$ is subtracted from the average image vector I_{mean} to obtain the normalized training dataset as elaborated in (2) and (3):

$$\xi_j^{train} = I_j^{train} - I_{mean} \quad (2)$$

$$\xi_j^{test} = I_j^{test} - I_{mean} \quad (3)$$

Let the set of all standardized image vectors $\xi_j^{train}; j = 1:M$ compose the standardized training dataset matrix $\Xi^{train} = [\xi_1, \xi_2, \dots, \xi_M]$, whereas $\Xi^{test} = [\xi_1, \xi_2, \dots, \xi_m]$ represents the standardized testing dataset matrix composed of all standardized image vectors $\xi_j^{test}; j = 1:m$. $\xi_j, I_j, I_{mean} \in \mathbb{R}^n$.

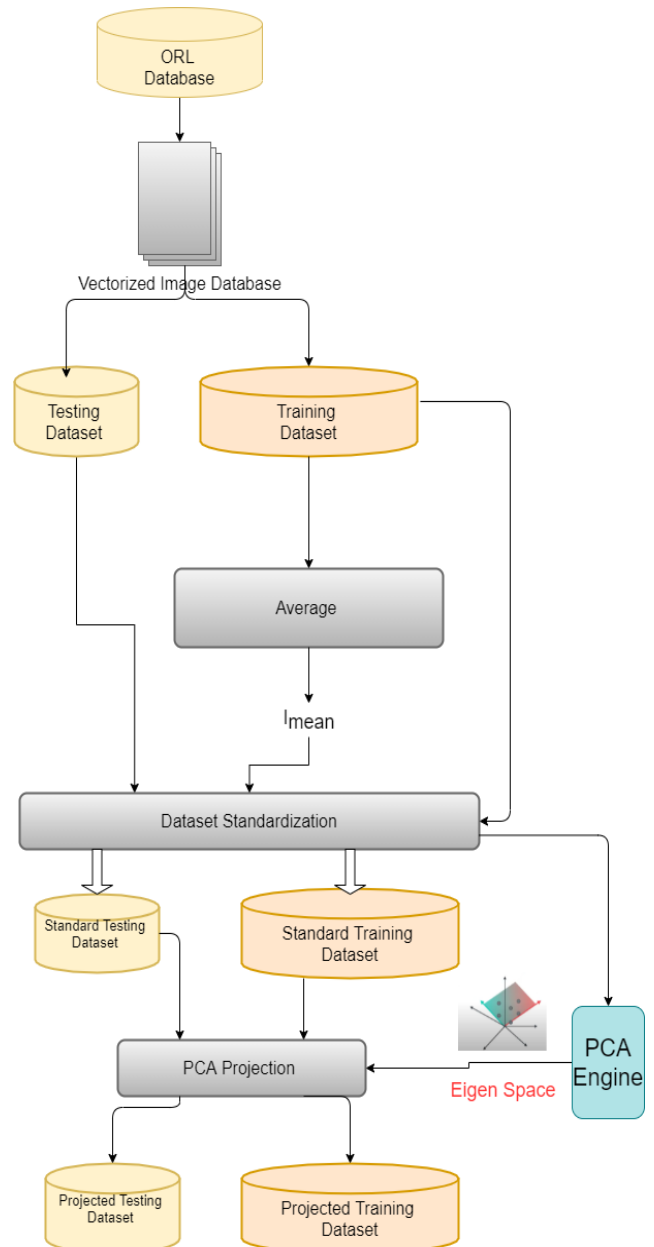


Fig. 2. Flowchart of the PCA-based Feature Reduction Scheme.

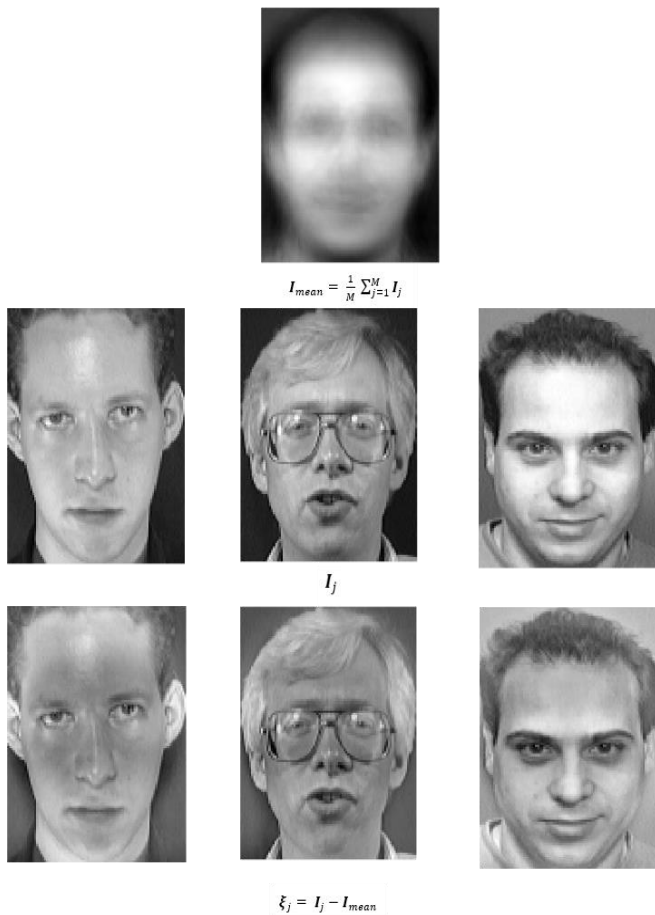


Fig. 3. Average Image I_{mean} and the Deviation of a Randomly Selected Set of Training Images I_j^{train} from the Average Image ξ_j .

As a visual illustration of the outputs of (2) and (3). Fig. 3 shows the average image and the deviation of a randomly selected set of training images from the average image I_{mean} .

Let U be defined as a linear transformation that maps the standard version of n -dimensional Ξ^{train} matrix onto a feature subspace of f -dimensional feature vectors, where $f \ll n$. By projecting Ξ^{train} on U space, the new formed feature vectors $\mathfrak{F}_j^{train} \in \mathbb{R}^f$ are defined as in (4):

$$\mathfrak{F}^{train} = U^T \Xi^{train}, j = 1, 2, \dots, M. \quad (4)$$

Based on (4) we can define the matrix $\mathfrak{F}^{train} = [\mathfrak{F}_1^{train}, \mathfrak{F}_2^{train}, \dots, \mathfrak{F}_M^{train}]$ as that represents the projected training dataset that will be used to train the neurons of the SOM network in the recognition stage of the proposed model.

Same wise is applied on the standardized testing dataset as defined in (5):

$$\mathfrak{F}^{test} = U^T \Xi^{test}, j = 1, 2, \dots, m. \quad (5)$$

Based on (5), we define, $\mathfrak{F}^{test} = [\mathfrak{F}_1^{test}, \mathfrak{F}_2^{test}, \dots, \mathfrak{F}_m^{test}]$, as the result of projecting the standardized testing data Ξ^{test} on

the eigenspace defined by U^T . The columns of U matrix are the eigenvectors e_i that represent the eigenstructure decomposition of the covariance matrix C that can be defined as in (6) and (7):

$$\lambda_i e_i = C e_i, i = 1, 2, \dots, M \quad (6)$$

$$C = \Xi^{train} \Xi^{train^T} \quad (7)$$

where, the scalars λ_i are the eigenvalues of the covariance matrix C .

The covariance matrix C is of high dimensionality to be computationally processed by the PCA engine for sake of finding the eigenvectors e_i in an efficient manner. To solve this problem, many previous works had handled this difficulty via different tactics. In this work, we adapted the solution proposed by [31].

First, let e_i^C be the eigenvectors correspond to the covariance matrix C that defined in (7) and let e_i^K be the eigenvectors corresponds to the new-defined matrix K that constructed by switching the order of the transpose in (7) as illustrated in (8):

$$K = \Xi^{train^T} \Xi^{train} \quad (8)$$

The eigenvectors e_i^K and the eigenvalues λ_i^K corresponds to the matrix K are given as in (9):

$$K e_i^K = \lambda_i^K e_i^K, i = 1, 2, \dots, M \quad (9)$$

Pre-multiplying both sides of (9) by matrix Ξ^{train} , we have (10):

$$\Xi^{train} K e_i^K = \Xi^{train} \lambda_i^K e_i^K \quad (10)$$

Substitute the value of K of (8) and rearrange the terms, yields (11):

$$\Xi^{train} \Xi^{train^T} \Xi^{train} e_i^K = \lambda_i^K \Xi^{train} e_i^K \quad (11)$$

based on the basic definition of the covariance matrix C in (7) we have (12):

$$C \Xi^{train} e_i^K = \lambda_i^K \Xi^{train} e_i^K \quad (12)$$

It can be noted from (12), that the terms “ $\Xi^{train} e_i^K$ ” and λ_i^K represent the eigenvectors and the eigenvalues of the covariance matrix C respectively. Thus, based on (12), to find the eigenvalues and the eigenvectors of the matrix C , we first construct the matrix K and then find the corresponding eigenvalues λ_i^K and eigenvectors e_i^K . Then, the eigenvalues of C are set to λ_i^K whereas the eigenvectors of C are obtained by multiplying the standardized training matrix Ξ^{train} by the eigenvectors of the matrix K as summarized in (13) and (14):

$$e_i^C = \Xi^{train} e_i^K \quad (13)$$

$$\lambda_i^C = \lambda_i^K \quad (14)$$

Fig. 4 shows the first nine eigenfaces U_j corresponding to the first nine eigenvalues λ_j^C for $i = 1, 2, 3, \dots, 9$.

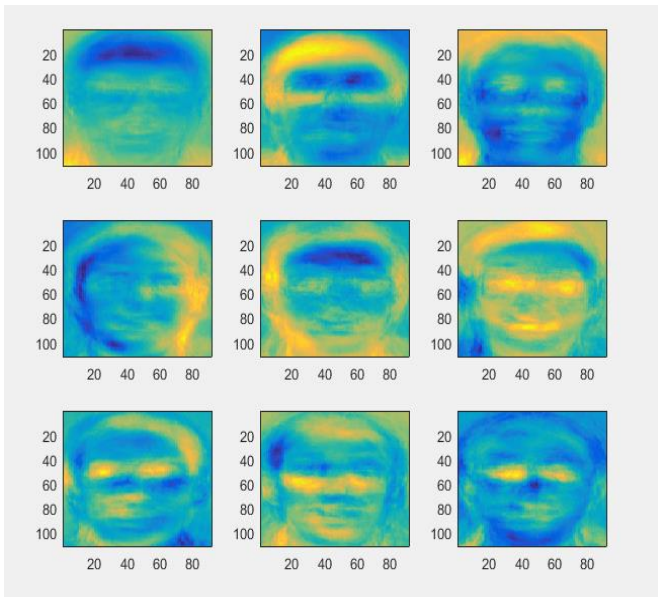


Fig. 4. First Nine Eigenfaces U_j Corresponding to the First Nine 2D - Eigenvalues λ_j^f for $i = 1, 2, 3, \dots, 9$.

B. Hierarchical Clustered SOM Network

The second stage in our proposed model is the recognition engine. The hierarchical agglomerative clustering was applied on the well-trained neurons of the self-organizing map (converged map) yields clusters that were labeled by training data and used as the classification engine of the system.

As illustrated in Algorithm I, the first step of the classification engine is to establish the SOM grid which is used as a second layer of dimensional reduction and facial data representation. SOM networks belong to the family of topographic maps, represents a type of competitive unsupervised learning systems where the input space, which in our case is \mathfrak{F}^{train} is “mapped” in a less-dimensional output space with the following principle: the similar feature vector $\mathfrak{S}_i^{train} \in \mathfrak{F}^{train}$ will be projected into the same neuron or, at least, in the neighborhood of it, in the output space of the SOM grid.

As can be shown in Fig. 1, in our proposed model, we have two cascaded projections: first projection is when the standardized training data Ξ^{train} and the standardized testing data Ξ^{test} projected onto the eigenvectors of the U space producing \mathfrak{F}^{train} and \mathfrak{F}^{test} . The second projection, \mathfrak{F}^{train} is projected onto the SOM grid to construct the output space of the SOM neural network.

Typically, the incremental-learning algorithm of SOM networks proceeds as follows [32]: Let the codebooks of the SOM neurons modeled by the vectors $W_k \in \mathbb{R}^f$ whereas $\mathfrak{F}^{train} \in \mathbb{R}^f$ represents the observation vectors (input space). Then, we can define the regression of a set of weight vectors codebooks $w_k \in W$ into the input space \mathfrak{F}^{train} by the following mathematical relation (15):

$$W_k^{t+1} = W_k^t + h_{win}(\mathfrak{F}_j^{train})(\mathfrak{F}_j^{train} - W_k^t) \quad (15)$$

where:

t : is the sample index.

where, $h_{win}(t)$ is called the neighborhood function, which is often, chosen to be as Gaussian defined by (16):

$$h_{win}(t) = \alpha^t \exp\left(-\frac{\|l_j - l_w\|^2}{2\sigma_t^2}\right) \quad (16)$$

Algorithm I: SOM Training Algorithm

Input : Specify the size (number of grid units) and the dimensions (width, Height) of SOM map.
Initialize wights vectors, Initialize $\sigma(t)$.
Normalize training data $\mathfrak{F}^{train} \in \mathbb{R}^f$
define value for the maximum number of epochs as N^{epoch}
 K : total number of SOM neurons on the grid
 M : total number of training input vector presentations.

$h_{num}^{accum} = 0$ // the accumulated value of the numerator of equation (18)
 $h_{den}^{accum} = 0$ // the accumulated value of the denominator of equation (18)

Output : Converged 2D SOM grid.

- 1 : FOR ($epoch = 1, \dots, N^{epoch}$)
- 2 : Specify a new value for $\sigma(t)$
- 3 : //for each data item \mathfrak{F}^{train}
- 4 : FOR ($t = 1, \dots, M$)
- 5 : $t = t + 1$
- 6 : //for each neuron k on SOM grid.
FOR ($k = 1, \dots, K$)
- 7 : Compute the distances $\mathfrak{D}_k(t)$ using:
$$\mathfrak{D}_k(t) = \|\mathfrak{F}_j^{train} - w_k(t)\|^2$$
- 8 : END FOR
- 9 : Compute winning (BMU) neuron using:
$$\mathfrak{D}_{k,win}(t) \triangleq \min(\mathfrak{D}_k(t))$$
- 10 : //for each neuron k on SOM grid.
FOR ($k = 1, \dots, K$)
- 11 : compute the neighborhood function value for j presentation of input as:
$$h_{k,win}(t) = \exp(-\|r_k - r_{win}\|/\sigma(t)^2)$$
- 12 : accumulate h_{num}^{accum} as:
$$h_{num}^{accum} = h_{num}^{accum} + h_{k,win}(t)\mathfrak{F}_t^{train}$$

accumulate h_{den}^{accum} as:
$$h_{den}^{accum} = h_{den}^{accum} + h_{k,win}(t)$$
- 13 : END FOR
- 14 : END FOR
- 15 : // Weight Update at the end of each Epoch
- 16 : FOR ($k = 1, \dots, K$)
- 17 : Update weight vectors w_k using:
$$w_k = \frac{h_{num}^{accum}}{h_{den}^{accum}}$$
- 18 : END FOR
- 19 : END FOR

where, “win” refers to the “winner” neurons on the SOM grid, where the weight vectors W_{win}^t of winner neurons are defined by the condition (17):

$$\|\mathfrak{F}_t^{train} - W_{win}^t\| \leq \|\mathfrak{F}_t^{train} - W_k^t\| \forall k \in K \quad (17)$$

where, K represents the total number of neurons of SOM grid, $k = 1, 2, \dots, K$.

α^t : represents the learning rate which decreases in a monotonic manner according to learning steps (iterations) and has the value of: $0 < \alpha^t < 1$.

σ_t : represents the width of the neighborhood function which decreases monotonically with learning steps.

l_j, l_w : represent the 2D vectorial locations in the display SOM grid, where $l_j \in \mathbb{R}^2$ and $l_w \in \mathbb{R}^2$.

In the incremental (online) learning described by (15) The unsupervised learning is accomplished recursively for each presentation of the t^{th} training feature vector \mathfrak{F}_t^{train} . However, in our work, we use batch SOM [33] instead of an online SOM variant. Thus, weight updating takes place at the end of each epoch. Mathematically, let's define t_o and t_f as the start and finish of each epoch, then, weight updating is given by (18):

$$w_k(t_f) = \frac{\sum_{t_o}^{t_f} h_{win,k}(t) \mathfrak{F}_t^{train}}{\sum_{t_o}^{t_f} h_{win,k}(t)} \quad (18)$$

A self-organizing map in its raw version described in equations (15) to (18), serves as a dimensional reduction and facial representation analysis scheme and the next step of the recognition stage is to predict the SOM neuron's membership of a new (testing) facial feature vector matrix \mathfrak{F}^{test} that is presented to the output layer of the SOM network.

This process yields a set of contiguous neurons in correspondence to a particular facial pattern in the testing dataset. As a consequence, a set of facial patterns might belong to different persons mapped to the same set of contiguous neurons in the output layer of the SOM network. However, in our model, the SOM network is required to serve as a facial recognition engine that can recognize among 40 classes represents the subjects (person labels) of the original dataset. This entails SOM-nodes to be highly subject-oriented (high dependable on the person class). To enhance the uniqueness of SOM response, we apply a hierarchical agglomerative clustering on the SOM neurons themselves successively.

There are two main schemes of hierarchical cluster analysis: Agglomerative Hierarchical Clustering (HAC) and Divisive Hierarchical Clustering (DAC). In our proposed model, we used the agglomerative hierarchical clustering scheme as illustrated in Algorithm II. This type is of a bottom-up approach where each SOM codebook neuron is treated as a singleton cluster at the outset, then it agglomerates each pair of clusters successively. This process continues until clusters are merged into a pre-specified number of clusters that are specified at the beginning of the process. The prespecified number of clusters, in turn, represents the different target classes of the recognition process.

Algorithm II: Agglomerative Hierarchical Clustering (AHC) Algorithm

Input	:	Converged SOM network (weight vectors) with K neurons. \mathcal{M} : pre-specified number of clusters resulted from AHC.
Output	:	Clustered SOM
1	:	Let each neuron on SOM grid form one cluster NO clusters _initial = K // each cluster contain a single SOM Neuron. $\mathcal{M} = K, \text{ where } \mathcal{M} \ll K$
2	:	$I = K$ // initialize the index of while loop.
3	:	WHILE ($I \geq \mathcal{M}$)
4	:	Find a pair of clusters with the smallest cluster-to-cluster distance (linkage) that given by : $\mathcal{D}_{average}(cluster^A, cluster^B)$ $= \frac{1}{n_A n_B} \left(\sum_{i=1}^{n_A} \sum_{j=1}^{n_B} dist(x_{Ai}, x_{Bj}) \right)$ where, n_A, n_B : are the number of elements in $cluster^A$ and $cluster^B$ respectively. x_A and x_B represents the members of $cluster^A$ and $cluster^B$ respectively.
5	:	Based on a distance computed. Merge the two clusters of least distance into one cluster. Update while loop index: $I = K - 1$
6	:	ENDWHILE

As a post-training step, the projected labeled training data used in analyzing and labeling the resulted SOM clusters based on the majority occurrence voting of a specific subject (face image belongs to a specific person in the training dataset). Then, new coming facial data is classified by the proposed facial recognizer into their corresponding classes.

IV. EXPERIMENTAL RESULTS

In this section, the facial recognition performance of our proposed system as well as a comparison to other facial recognition systems are represented. Moreover, a series of experiments are carried out to evaluate the efficiency and the robustness of the proposed facial recognition model.

A. Experimental Setup

All experiments are performed using the ORL (Olivetti Research Lab) [34] dataset, which is a classical dataset composed of 400 sample images, each of 92×112 grayscale pixel resolution with 256 intensity levels. The dataset contains images for 40 persons (subjects), 10 images for each person (subject). As shown in Fig. 5, The images were taken at different lighting conditions, even for some subjects they are taken at different sessions, which adds kind of facial distortions such as different facial expressions (smiling, nonsmiling, open eyes, and closed eyes) and different facial details (wearing glasses or no glasses).



Fig. 5. Examples of Raw Facial Images of ORL Database show the different Lighting Conditions, different Facial Expressions and different Facial Details.

Although all images are taken in an upright position in the frontal view, it exhibits a slight left-right rotation in the pose angle and alignment, which, in turn, can be exploited to examine the robustness of the proposed system against imprecise facial alignment.

We measured the performance based on the recognition rate criterion basically, which required setting up an experimental protocol same as used in several previous works in this field, where the images per person are randomly permuted. Then, five images of each person are used for the training stage whereas the other five images are used for testing purposes. Moreover, for sake of examining the efficiency and the reliability of the proposed system, we experimented with different sizes of training dataset per person. The results for 30 runs of the experiment were recorded and the average is taken and analyzed in the following experiments.

B. Experiment 1

The performance of our proposed model as well as the recognition performance of other recognition schemes are shown in Table I and Table II.

TABLE I. COMPARATIVE RESULTS OF THE PROPOSED TECHNIQUE WITH OTHER EXISTING SOM-BASED FACIAL RECOGNITION SCHEMES BASED ON THE ORL DATASET.

Author	Year	Method	train to test ratio	Recognition Rate
Lawrence <i>et al.</i> [24]	1997	SOM + Convolutional ANN	5:5	94.25%
		PCA	5:5	89.5%
Zhi and Ming [35]	2005	SOM + Wavelet Network	7:3	92.5
		Regular SOM	7:3	84
		RBF-Kernel SOM	7:3	85
Kumar <i>et al.</i> [36]	2005	PCA + SOM	5:5	62.64
Neagoe and Anton [38]	2010	PCA+ Concurrent SOM	5:5	93
		Comon ICA + Concurrent SOM	5:5	88
		INFOMAX PCA + concurrent SOM	5:5	94
Proposed Model	2022	PCA + Hierarchical Agglomerative Clustered SOM	5:5	94.7

TABLE II. COMPARATIVE RESULTS OF THE PROPOSED TECHNIQUE WITH OTHER EXISTING FACIAL RECOGNITION SCHEMES BASED ON THE ORL DATASET

Author	Year	Method	train to test ratio	Recognition Rate
Tan <i>et al.</i> [37]	2009	Partial Similarity	5:5	97.3
Feng <i>et al.</i> [6]	2016	Fast Superimposed Parameter Classifier	5:5	94.5
Hamdan and Mukhtar [19]	2016	Moments-based Angular Radial Transform	5:5	87.7
Abuzneid <i>et al.</i> [13]	2018	LBPH + multi-KNN + Backpropagation ANN	5:5	98
Kong <i>et al.</i> [39]	2018	CSGF(2D) 2 PCA Net + Linear SVM	5:5	97.5
Sun <i>et al.</i> [17]	2020	Gradient Number Pattern +Fuzzy Convex-Concave Partition + CNN	4:6	95.69
			6:4	98.28
Qin <i>et al.</i> [40]	2020	Collaborative Representation (CR)+ Enhanced Nearest Neighbour	5:5	92.5
Gupta <i>et al.</i> [21]	2020	Combination of SIFT (64-components) and SURF (64-components) + Random Forest	8:2	94.7
			8:2	86.2
Proposed Model	2022	PCA + Hierarchical Agglomerative Clustered SOM	5:5	94.7

In Table I, we compared favorably with other facial recognizers which were built using either SOM or SOM-variants. However, based on a recently published survey, the SOM network has limited usage [41] in face recognition systems either using SOM as a feature extractor, data representative or using it as a face recognition engine. Therefore, to better discuss and interpret the results obtained from our proposed method, a comparison with other existing schemes that used different machine learning and artificial neural networks other than SOM network are shown in Table

II. It is worth to mention that all schemes listed in Table I and Table II are built based on ORL dataset.

C. Experiment 2: Impact of Training Dataset Volume

In this experiment, the impact of increasing the ratio of the size of facial data involved in the training stage to that used for testing purposes is demonstrated. Fig. 6 and Fig. 7 show the relationship between increasing the ratio of training to testing data versus the achieved recognition performance. The experiment is set up by varying the number of involved training images from 5 to 9 images. The characteristic curve between the recognition rate and the number of training images involved is computed for every case.

Obviously, as the size of training data increases, the principal components analysis algorithm generates more representative eigenvectors which, in turn, reflects in more accurate dataset projection and further enhanced dataset presentation enabling clustered SOM network to recognize better.

D. Experiment 3: Impact of Adding Noise

To discuss the robustness of our model against additive noise, we have conducted noise sensitivity experiments on the ORL dataset where the noisy testing images were generated by adding Gaussian additive noise of zero mean and different values of variation to each test image as illustrated in Fig. 8.

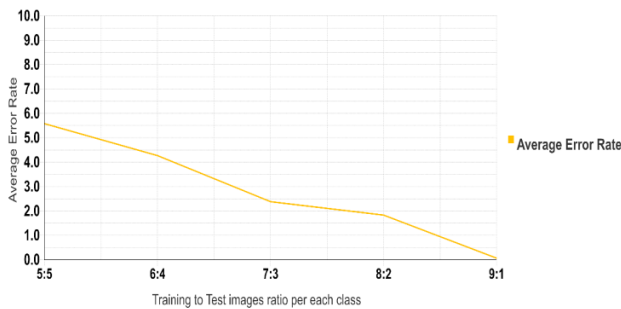


Fig. 6. Impact of Increasing the Size of Training Dataset on the Achieved Recognition Performance of our Proposed System in Terms of Average Recognition Error.

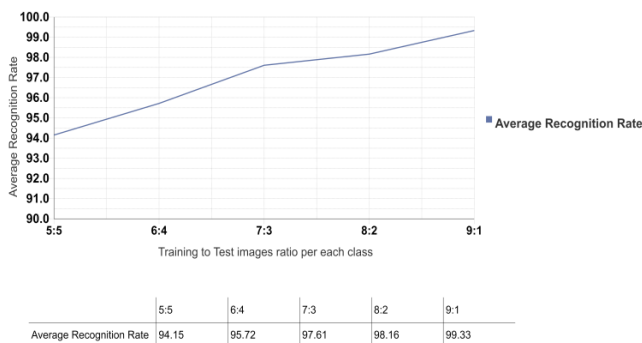


Fig. 7. Impact of Increasing the Size of Training Dataset on the Achieved Recognition Performance of our Proposed System in Terms of Average Recognition Rate.

TABLE III. AVERAGE RATE RECOGNITION RATE (OVER 30 ITERATIONS WITH 5:5 TRAINING TO TEST DATA VOLUME RATIO) OF OUR PROPOSED PCA-CLUSTERED SOM MODEL AGAINST ORL TEST IMAGES DISTORTED BY ADDING GAUSSIAN NOISE OF ZERO MEANS AND FIVE DIFFERENT VALUES OF VARIATIONS σ

Variations (σ)	Average Recognition Rate (%)	Average Recognition Error (%)
0.00	94.15	5.58
0.01	94.15	5.85
0.02	93.88	6.11
0.05	91.95	8.05
0.09	86.88	13.11

We run the experiment at five levels of deviation σ and the corresponding average recognition rate over 30 iterations using 200 images of the ORL dataset as training images (training to test ratio is 5:5) was reported as shown in Table III. In addition to using the raw images of the ORL dataset without any type of pre-processing.

TABLE IV. TIME COST OF PROPOSED PCA-CLUSTERED SOM MODEL AVERAGED OVER 30 RUNS WITH DIFFERENT TRAINING TO TESTING DATASET VOLUMES USING ORL DATASET

Size of Training Dataset	$v^{train} : v^{test} *$ Ratio	Average Training Time (sec)	Average Test Time (sec)
200	5:5	3.65	0.0129
240	6:4	4.389	0.0120
280	7:3	5.128	0.0114
320	8:2	5.98	0.0102
360	9:1	7.00	0.0085

* $v^{train} : v^{test}$: ratio of training dataset volume to testing dataset volume.

E. Experiment 4: Time Cost

The objective of this experiment is to verify the proposed model in terms of overhead complexity where the average training and average testing time corresponding to different sizes of training to test ratios were recorded in Table IV. Simulations are done on MATLAB 2021a, executed on an Intel Core (TM) i7-4500U CPU, 8 GB RAM in Windows 10 platform using customized code developed for this model and using SOM toolbox [42].

V. DISCUSSION

It can be noted from Table I and Table II, our proposed model shows supremacy against most of the different methods that used SOM/SOM-variants network either as a classifier or as a feature extractor as in using the regular SOM in [23] or as RBF-kernel based SOM presented in [42] or concurrent SOM-based technique proposed in [22].

The system proposed by Tan *et al.*[11] has about 3.15% average improvement over our proposed method, however, this improvement comes with a computational cost as a normal result to portioning each image into sub-block for sake of extracting local-features of facial data, although Tan *et al.*[11] didn't refer to the time expended, extensive computations always reflect as time-consuming and power-hungry face recognition style. The same scenario repeated for [24] where SOM is used as a feature extractor that fed a CNN network with optimal facial data representation.

Zhi and Ming [35] had achieved comparable performance to our method, however, the training data size used is large than that used in our method. Moreover, for the same training data size used by [35], our proposed system can achieve an average performance reaches up to 97.61% as elaborated in Fig. 7. Although superior results are reported in Table I for methods that used techniques other than PCA and SOM, these methods have underperformance in contrary to our proposed system in other aspects of recognition performance.

Abuzneid et al. [13] combined different types of machine learning methods that led to a computationally intensive solution including increasing the system latency resulted from by recognizing facial images in the test phase of the system.

On the other hand, authors [13] had conducted image-preprocessing including cropping, resizing, and histogram equalization and it took 25 hours to perform the backpropagation network training, where nothing was recorded about the time required for the testing stage. The proposed method proposed by Abuzneid et al. [13] has several cascaded computational blocks as LBPH, BBNN representation, and multi-KNN which is considered a huge computational overhead.

As another example, in the proposed system by Sun et al. [43], two types of descriptors, Local Gradient Number Pattern (LGNP) and Fuzzy Convex-Concave Partition (FCCP) were used to represent facial data. Moreover, a deep neural network was used as a classification engine which represents a recognition system with high complexity.

Lawrence et al. [24] reported in their experimental results that without preprocessing step, the resultant error yielded two times greater error rate which means that the average recognition rate will decrease down to 88.5%.

The authors reported that the training time required to train the CNN network was approximately 4 hours. Although Gupta et al. [21] achieved a comparable recognition performance using SIFT-64 and SURF-64 facial data representation that cascaded by random forest as a classifier, authors [21], as can be noted from Table II used 80% of the ORL dataset to train their model. However, as shown in Table III, our model can achieve a higher recognition performance reached up to 98.16% for using this percentage of training data.

As a typical example of image pre-processing that can enhance the overall performance but at the same time can blur many of the facial recognition performance drawbacks is that proposed by Qin et al [44] where down sampling algorithm is used to resize the facial image down into 46×56 pixel matrix proceeded by a non-linear transformation stretching gray image enhancement as a pre-processing step. Collaborative Representation (CR) was used as a feature extractor whereas an enhanced KNN was used as a classification engine. In our case, we have used raw images for training and testing to test the robustness of our system against different facial effects in one hand and to keep the computational cost down to the minimum in the other hand.

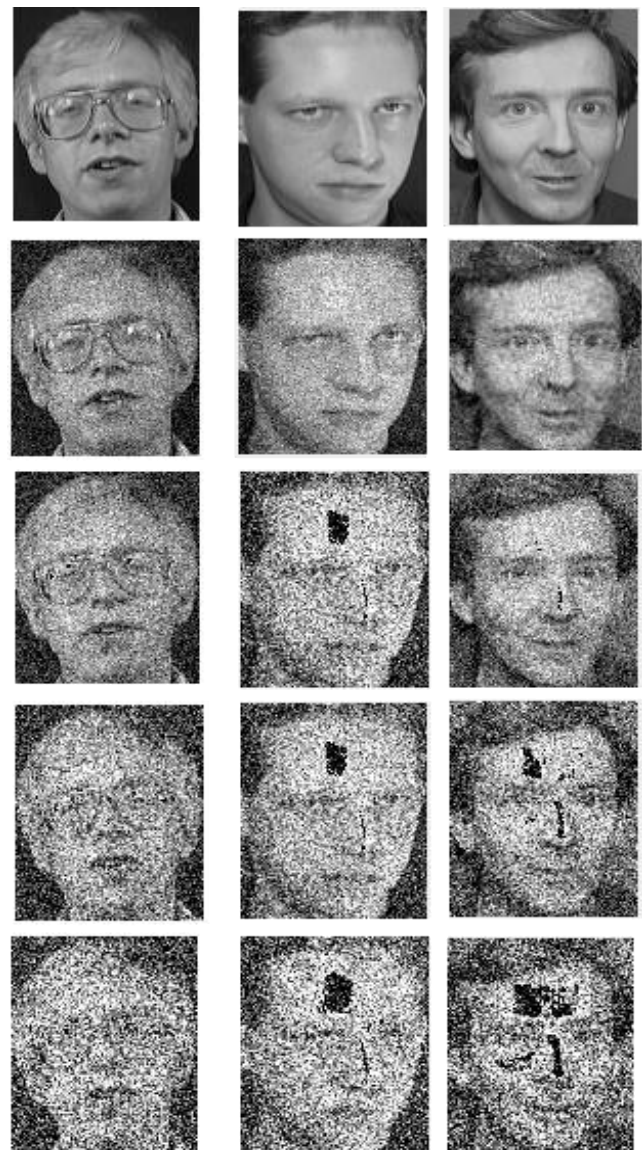


Fig. 8. Subset of Original Test ORL Dataset and the Corresponding Noisy Ones after Adding Gaussian Noise with Zero mean $\mu = 0$ and different Levels of Variations σ . First Row Represents the Original ORL Test Dataset. Second Row Represents Noisy Test Images using $\sigma = 0.01$. Third Row Represents the Noisy Test Image using $\sigma = 0.02$. Forth Row Represents the Noisy Test Images using $\sigma = 0.05$. Fifth Row Represents the Noisy Test Images using $\sigma = 0.09$.

As shown in Fig. 8 and as revealed in Table III, our proposed system can handle adding additional white Gaussian noise at different levels of variations and beyond that can occur in real-time photo capturing.

As with all face recognizers that built on the machine learning techniques, one major limitation to our proposed model is the need to re-train in case of a new persons (subjects) are added to the database. However, as shown in Table IV, the time cost required for training 200 images is less than 4 seconds and that required for 360 images is less than 8 seconds which is substantially low if it is to be used in real-time applications.

VI. CONCLUSION

This paper has presented an agglomerative clustered SOM-based face recognition model where regular PCA was used to extract the eigenfaces of the facial data for purpose of facial data representation whereas supervised clustered SOM was used as the recognition engine of the proposed model. The proposed model is found to be efficient in terms of time cost for both training and testing stages where it takes less than 3.7 seconds to train the model using 200 training images whereas identifying one single image takes less than $7e-5$ seconds. Therefore, the online training version of the system can be used efficiently for real-life applications where the cost of training and testing is as important issue same as the recognition accuracy. The proposed model is rigorously validated using the ORL dataset and based on the comparative analysis conducted in this work, the recognition performance is superior to methods that used SOM/SOM-variants. Moreover, the system shows robustness against adding Gaussian noise at different levels of variations as well as robustness against using the raw facial data without the need for an image pre-processing step. Using the clustered SOM with features processors other than PCA or using an ensemble of SOM networks are a possible extension for our future work.

REFERENCES

- [1] M. Martinez and A. C. Kak, "PCA versus LDA," *IEEE Transactions on Pattern Analysis and Machine Intelligence*, vol. 23, no. 2, pp. 228–233, 2001, doi: 10.1109/34.908974.
- [2] A. Eleyan and H. Demirel, "PCA and LDA Based Face Recognition Using Feedforward Neural Network Classifier," in *Multimedia Content Representation, Classification and Security*, vol. 4105, B. Günsel, A. K. Jain, A. M. Tekalp, and B. Sankur, Eds. Berlin, Heidelberg: Springer Berlin Heidelberg, 2006, pp. 199–206. doi: 10.1007/11848035_28.
- [3] C. L. Chowdhary and D. Acharjya, "Singular Value Decomposition–Principal Component Analysis-Based Object Recognition Approach," in *Bio-Inspired Computing for Image and Video Processing*, Chapman and Hall/CRC, 2018, pp. 323–341.
- [4] J. Pan, X.-S. Wang, and Y.-H. Cheng, "Single-Sample Face Recognition Based on LPP Feature Transfer," *IEEE Access*, vol. 4, pp. 2873–2884, 2016, doi: 10.1109/ACCESS.2016.2574366.
- [5] K. Sett et al., "Face recognition using fusion of spatial and temporal features," in *2018 Emerging Trends in Electronic Devices and Computational Techniques (EDCT)*, Kolkata, India, Mar. 2018, pp. 1–4. doi: 10.1109/EDCT.2018.8405063.
- [6] Q. Feng et al., "Superimposed Sparse Parameter Classifiers for Face Recognition," *IEEE Trans. Cybern.*, vol. 47, no. 2, Art. no. 2, Feb. 2017, doi: 10.1109/TCYB.2016.2516239.
- [7] J. Sun, Y. Lv, C. Tang, H. Sima, and X. Wu, "Face Recognition Based on Local Gradient Number Pattern and Fuzzy Convex-Concave Partition," *IEEE Access*, vol. 8, pp. 35777–35791, 2020, doi: 10.1109/ACCESS.2020.2975312.
- [8] B. Jyostna Devi, N. Veeranjanyulu, and K. V. K. Kishore, "A novel face recognition system based on combining eigenfaces with fisher faces using wavelets," *Procedia Computer Science*, vol. 2, pp. 44–51, 2010, doi: 10.1016/j.procs.2010.11.007.
- [9] Lying Ma, Yegui Xiao, K. Khorasani, and R. K. Ward, "A new facial expression recognition technique using 2-D DCT and K-means algorithm," in *2004 International Conference on Image Processing*, 2004. ICIP '04., Singapore, 2004, vol. 2, pp. 1269–1272. doi: 10.1109/ICIP.2004.1419729.
- [10] C. Cifarelli, G. Manfredi, and L. Nieldu, "Statistical Face Recognition via a k-Means Iterative Algorithm," in *2008 Seventh International Conference on Machine Learning and Applications*, San Diego, CA, USA, 2008, pp. 888–891. doi: 10.1109/ICMLA.2008.146.
- [11] S. Tan, X. Sun, W. Chan, L. Qu, and L. Shao, "Robust Face Recognition With Kernelized Locality-Sensitive Group Sparsity Representation," *IEEE Trans. on Image Process.*, vol. 26, no. 10, pp. 4661–4668, Oct. 2017, doi: 10.1109/TIP.2017.2716180.
- [12] J. Kong, M. Chen, M. Jiang, J. Sun, and J. Hou, "Face Recognition Based on CSGF(2D)2PCANet," vol. 6, p. 13, 2018.
- [13] M. A. Abuzneid and A. Mahmood, "Enhanced Human Face Recognition Using LBPH Descriptor, Multi-KNN, and Back-Propagation Neural Network," *IEEE Access*, vol. 6, pp. 20641–20651, 2018, doi: 10.1109/ACCESS.2018.2825310.
- [14] A. Bouzalmat, N. Belghini, A. Zarghili, and J. Kharroubi, "Face Detection and Recognition Using Back Propagation Neural Network and Fourier Gabor Filters," *SIPIJ*, vol. 2, no. 3, pp. 15–21, Sep. 2011, doi: 10.5121/sipij.2011.2302.
- [15] S. Lawrence, C. L. Giles, and A. D. Back, "Face Recognition: A Convolutional Neural-Network Approach," *IEEE TRANSACTIONS ON NEURAL NETWORKS*, vol. 8, no. 1, p. 16, 1997.
- [16] S. Almadby and L. Elrefaei, "Deep Convolutional Neural Network-Based Approaches for Face Recognition," *Applied Sciences*, vol. 9, no. 20, p. 4397, Oct. 2019, doi: 10.3390/app9204397.
- [17] J. Sun, Y. Lv, C. Tang, H. Sima, and X. Wu, "Face Recognition Based on Local Gradient Number Pattern and Fuzzy Convex-Concave Partition," *IEEE Access*, vol. 8, pp. 35777–35791, 2020, doi: 10.1109/ACCESS.2020.2975312.
- [18] T. Goel and R. Murugan, "Classifier for Face Recognition Based on Deep Convolutional - Optimized Kernel Extreme Learning Machine," *Computers & Electrical Engineering*, vol. 85, p. 106640, Jul. 2020, doi: 10.1016/j.compeleceng.2020.106640.
- [19] B. Hamdan and K. Mokhtar, "Face recognition using Angular Radial Transform," *Journal of King Saud University - Computer and Information Sciences*, vol. 30, no. 2, pp. 141–151, Apr. 2018, doi: 10.1016/j.jksuci.2016.10.006.
- [20] J. Kong, M. Chen, M. Jiang, J. Sun, and J. Hou, "Face Recognition Based on CSGF(2D) 2 PCANet," *IEEE Access*, vol. 6, pp. 45153–45165, 2018, doi: 10.1109/ACCESS.2018.2865425.
- [21] S. Gupta, K. Thakur, and M. Kumar, "2D-human face recognition using SIFT and SURF descriptors of face's feature regions," *Vis Comput.*, vol. 37, no. 3, pp. 447–456, Mar. 2021, doi: 10.1007/s00371-020-01814-8.
- [22] V.-E. Neagoe, A.-C. Mugioiu, and I.-A. Stanculescu, "Face Recognition using PCA versus ICA versus LDA cascaded with the neural classifier of Concurrent Self-Organizing Maps," in *2010 8th International Conference on Communications, Bucharest, Romania*, Jun. 2010, pp. 225–228. doi: 10.1109/ICCOMM.2010.5509041.
- [23] D. Kumar, C. S. Rai, and S. Kumar, "Face Recognition using Self-Organizing Map and Principal Component Analysis," in *2005 International Conference on Neural Networks and Brain*, Beijing, China, 2005, vol. 3, pp. 1469–1473. doi: 10.1109/ICNNB.2005.1614908.
- [24] S. Lawrence, C. L. Giles, Ah Chung Tsoi, and A. D. Back, "Face recognition: a convolutional neural-network approach," *IEEE Trans. Neural Netw.*, vol. 8, no. 1, pp. 98–113, Jan. 1997, doi: 10.1109/72.554195.
- [25] J. Ruiz and R. Jaime, "Backpropagation and SOM for face feature recognition," in *Proceedings of 3rd IEEE International Conference on Image Processing*, Lausanne, Switzerland, 1996, vol. 3, pp. 487–490. doi: 10.1109/ICIP.1996.560537.
- [26] P. Yodkhad, A. Kawewong, and K. Patanukhom, "Approximate nearest neighbor search using self-organizing map clustering for face recognition system," in *2014 International Computer Science and Engineering Conference (ICSEC)*, Khon Kaen, Thailand, Jul. 2014, pp. 151–156. doi: 10.1109/ICSEC.2014.6978186.
- [27] X. Tan, S. Chen, Z.-H. Zhou, and F. Zhang, "Robust face recognition from a single training image per person with kernel-based som-face," 2004, pp. 858–863.
- [28] Yang Zhi and Gu Ming, "A SOM-Wavelet Networks for Face Identification," in *2005 IEEE International Conference on Multimedia and Expo*, Amsterdam, The Netherlands, 2005, pp. 852–855. doi: 10.1109/ICME.2005.1521557.

- [29] Xiaoyang Tan, Songcan Chen, Zhi-Hua Zhou, and Jun Liu, "Face Recognition Under Occlusions and Variant Expressions With Partial Similarity," *IEEE Trans. Inform. Forensic Secur.*, vol. 4, no. 2, pp. 217–230, Jun. 2009, doi: 10.1109/TIFS.2009.2020772.
- [30] I. Q. Monteiro, S. D. Queiroz, A. T. Carneiro, L. G. Souza, and G. A. Barreto, "Face recognition independent of facial expression through SOM-based classifiers," in *2006 International Telecommunications Symposium, Fortaleza, Ceara, Brazil, Sep. 2006*, pp. 263–268. doi: 10.1109/ITS.2006.4433281.
- [31] A. Eleyan and H. Demirel, "PCA and LDA Based Face Recognition Using Feedforward Neural Network Classifier," in *Multimedia Content Representation, Classification and Security*, vol. 4105, B. Günsel, A. K. Jain, A. M. Tekalp, and B. Sankur, Eds. Berlin, Heidelberg: Springer Berlin Heidelberg, 2006, pp. 199–206. doi: 10.1007/11848035_28.
- [32] T. Kohonen, *Self-Organizing Maps*, 2nd ed., vol. 30. Berlin: Springer-Verlag Berlin Heidelberg, 1997.
- [33] R. D. Lawrence, "A Scalable Parallel Algorithm for Self-Organizing Maps with Applications to Sparse Data Mining Problems," . . . , p. 25.
- [34] AT & T Laboratories Cambridge, "ORL: The Database of Faces." <https://cam-orl.co.uk/facedatabase.html> (accessed Jul. 01, 2021).
- [35] Yang Zhi and Gu Ming, "A SOM-Wavelet Networks for Face Identification," in *2005 IEEE International Conference on Multimedia and Expo, Amsterdam, The Netherlands, 2005*, pp. 852–855. doi: 10.1109/ICME.2005.1521557.
- [36] D. Kumar, C. S. Rai, and S. Kumar, "Face Recognition using Self-Organizing Map and Principal Component Analysis," p. 5.
- [37] S. Tan, X. Sun, W. Chan, L. Qu, and L. Shao, "Robust Face Recognition With Kernelized Locality-Sensitive Group Sparsity Representation," *IEEE Trans. on Image Process.*, vol. 26, no. 10, Art. no. 10, Oct. 2017, doi: 10.1109/TIP.2017.2716180.
- [38] V.-E. Neagoe, A.-C. Mugioiu, and I.-A. Stanculescu, "Face Recognition using PCA versus ICA versus LDA cascaded with the Neural Classifier of Concurrent Self-Organizing Maps," p. 4.
- [39] J. Kong, M. Chen, M. Jiang, J. Sun, and J. Hou, "Face Recognition Based on CSGF(2D)2PCANet," vol. 6, p. 13, 2018.
- [40] Y. Qin, L. Sun, and Y. Xu, "Exploring of alternative representations of facial images for face recognition," *Int. J. Mach. Learn. & Cyber.*, vol. 11, no. 10, Art. no. 10, Oct. 2020, doi: 10.1007/s13042-020-01116-4.
- [41] G. Guo and N. Zhang, "A survey on deep learning based face recognition," *Computer Vision and Image Understanding*, vol. 189, p. 102805, Dec. 2019, doi: 10.1016/j.cviu.2019.102805.
- [42] "SOM toolbox programming team," SOM Toolbox. <http://www.cis.hut.fi/projects/somtoolbox/>.
- [43] J. Sun, Y. Lv, C. Tang, H. Sima, and X. Wu, "Face Recognition Based on Local Gradient Number Pattern and Fuzzy Convex-Concave Partition," *IEEE Access*, vol. 8, pp. 35777–35791, 2020, doi: 10.1109/ACCESS.2020.2975312.
- [44] Y. Qin, L. Sun, and Y. Xu, "Exploring of alternative representations of facial images for face recognition," *Int. J. Mach. Learn. & Cyber.*, vol. 11, no. 10, Art. no. 10, Oct. 2020, doi: 10.1007/s13042-020-01116-4.

Performance Evaluation of Safe Avoidance Time and Safety Message Dissemination for Vehicle to Vehicle (V2V) Communication in LTE C-V2X

Hakimah Abdul Halim¹, Azizul Rahman Mohd Shariff^{2*}, Suzi Iryanti Fadilah^{3*}, Fatima Karim⁴
School of Computer Sciences, University Sains Malaysia, Malaysia, Penang, Malaysia

Abstract—VANET has many opportunities to manage vehicle safety on the road efficiently. The standards from European Telecommunications Standards Institute (ETSI) for Intelligent Transport System (ITS) provide necessary upper-layer specifications for safety message dissemination between vehicles using Cooperative Aware Messages (CAM) and Decentralized Event Notification Message (DENM). Besides, mobile radio technology of Long-Term Evolution (LTE) in Release-14 comes with two modes of communication, which is mode 3 and mode 4 to support vehicle to vehicle communications. The relationship between vehicle time gap, speed, and UE transmit power significantly impacts the Packet Delivery Ratio (PDR) and throughput. With higher vehicle moving speeds, longer safe distances must be kept in ensuring safety. However, at longer safe distances, we have proven that communication may be lost because CAM messages cannot be exchanged successfully. As a result, no vehicle safety can be guaranteed using V2V communication. This may get worse in urban or cities environment where interference is dominant. Simulation results provide evidence that variable distance between vehicles cannot be ignored to ensure vehicle safety with successful message communication among them.

Keywords—Time gap; safe distance; collision; VANET; CAM

I. INTRODUCTION

In recent years, vehicular systems have gotten a ton of consideration from specialists, mainly communicating a message for improving vehicle [1]. VANET is an exceptional and conceivably the most significant class of Mobile Ad hoc Networks (MANETs). The transmission of messages between vehicles within VANET is not enough to prevent vehicle collisions. Therefore, this research aims to study the safe distance between the vehicle and the message disseminate within a safe distance. Collisions between vehicles occur on roads on daily basis. Vehicle collisions occurred on roads because of human factors. For example, due to human behaviors tending to drive at high speeds, vehicles could not brake safely to avoid a collision with other vehicle because there is no sufficient braking time maintained. The time gap is the safe distance required for the vehicle to press the brake before a collision occurs. Based on the human factors driving with different speeds of the vehicle, the time gap is significant. Different vehicle speeds also require different time gaps because they have a proper distance between them before they stop. During braking, the vehicle must maintain a safe time gap for a safe distance to avoid the collision happen [21].

In this research, the focus is on vehicle communications in a mode 3 environment. The two major problems for moving vehicles are maintaining safe distances or safe time gaps between them to avoid collisions at the desired speeds. These are done by periodically exchanging safety messages using the CAM message as specified in the ETSI standards. Maintaining safe distances between any vehicles is paramount in avoiding collisions and ensuring safety. However, even with the dissemination of CAM messages between vehicles, a message that is received by any moving vehicle does not guarantee safety as it still does not meet the Safety Avoidance Time (AT) or safe time gap. A collision is still highly probable even if vehicles at the time of successful CAM message receptions, do not keep safe distances between them. There is a potential trade-off between safe time gap and vehicle safety, influenced by the transmit power. At higher speeds, the time gap required increases, hence the safe distances that must maintain between vehicles get larger, potentially leading to loss of communication. This research will study the relationship between vehicle time gap, speed, and UE transmit power significantly impacts the Packet Delivery Ratio (PDR), throughput. Simulation results provide evidence that variable distance between vehicles cannot be ignored to ensure vehicle safety with successful message communication among them.

The rest of the paper is organized as follows. Background is overviewed in Section II. Section III describes research methodology using avoidance time. Section IV addresses result and discussion. Finally, conclusions are given in last section of the paper.

II. BACKGROUND

The smart transportation system has become a new factor for the economic development. Intelligent Transport Industry has made great investment and dedicated development resources for the vehicle-to-everything technology, autonomous vehicles. One of the smart transportation systems is already in use that is Dedicated-short-distanced-communication (DSRC) and now next level for this is cellular-V2X by using IEEE 802.11p and 3GPP-LTE/5G NR which is being deployed as a new emerging smart transportation technology. The author described all the positive, negative factors and the challenges faced by these two technologies and how IoT technology can well collaborate and integrate with DSRC and Cellular-V2X to cope with the new economic challenges [21][23]. One of the smart transportation techniques in order to increase safety and efficiency along with decreased

*Corresponding Author.

fuel consumption is to move vehicles in squad. In this situation, vehicles communicate with each other through radio signals in send any alert/safety messages while moving on road. The author [23] described that emergency message communication between vehicles-to-everything can be more efficient by redesigning platooning-application for vehicles along with considering the communication with 3GPP scheduled mode. There is not a single authorized algorithm for administration of resources. Therefore, vehicles forming a squad can communicate with one data packet at a time to occupy the communication medium. For platooning, the real time message packet delivery using 3GPP, can only be possible with distributed time slots for communication using IEEE 802.11p. Reliability and throughput of message packet delivery was simulated under variable traffic of data packets using cellular-V2X factors. In [25], the authors presenting an analytical survey regarding the new emerging cellular vehicle-to-vehicle and cellular vehicle-to-everything technologies and how the standard 3GPP wireless communication network is struggling to cope with the real time emergency communication and reliability challenges associated with C-V2V and C-V2X in both homogeneous and heterogeneous smart transport systems. The authors are mainly focusing with the challenges associated with the typical and more advanced reliable and secure traffic system by evaluating the wireless technologies for inter-connected vehicle communication. In this survey, different types of wireless communication methods and the applications used are classified along with the challenges faced by radio technology for inter-vehicle communication [27]. As the 5G network promises massive communication with reliable connection, it has brought a dynamic progressive change in wireless communications. As in Internet-of-vehicles, quick, safe and reliable message communication is required in order to meet requirements for the end-user as well as for the business purposes and 5G technology can well facilitate this purpose when it comes to vehicle-to-everything and autonomous-vehicle applications. The authors [27] describes that 5G technology advancement not only facilitate users in terms of vehicle communication but also provides us reliable and correct traffic alerts along with helping the environment by decreased pollution and mishap ratio. Therefore, this survey paper well advocates how 5G technology advancement and its communication protocols can facilitate vehicle-to-everything and internet-of-vehicles cellular networks by protecting the environment. In this era, everything related to vehicle-to-everything demands a safe, secure, reliable, trustworthy, environment and fuel friendly smart transportation system not only for the vehicles driven by humans but more needed for the autonomous vehicles [28]. To ensure all these economical, humanitarian and environment friendly requirements and to cope with the challenges associated with them, newly developed European and American technologies named "Europe-ITS-G5" and "DSRC (US-WAVE) are ready to be used on vast dimensions based on IEEE 802.11p. Other technologies like "C-V2X (LTE)" have less capability to integrate well with 5G technology in order to meet the new emerging future requirements for smart transportation system and inter-vehicle communication. The authors [28] presented a detailed analysis for the existing technologies and how vehicle industry is facing the challenges

along with its positive and negative effects on transportation system. Internet-of-Vehicles is an emerging technology which needs a lot of development and improvements as it involves real time communication among heterogeneous vehicles [29]. Vehicles can be both human-driven and autonomous ones, but the challenge is to broadcast massive and instantly changing messages among vehicles to ensure safety along with ever changing over the time vehicle volume is another factor to be considered. Different studies have been done to understand the response spectrum and message communication using IEEE 802.11p of vehicle-to-vehicle single-hop communication along with resource distribution time slots among heterogeneous especially in traffic congestion. For multi-hop V2V message transmission, not only vehicles on road broadcast signals but also if they get disconnected then radio broadcasters along roadside were also being analyzed [29].

A. Safety Message Dissemination

VANET is a distinctive sort of portable correspondence where topology changes powerfully because of vehicles' high portability. Vehicles utilize two sorts of messages to refresh their status and to disseminate a message to other vehicles. Security message scattering in VANETs has been tended to in vast numbers of the distributed articles. The issues related to the congestion control with regards to VANETs. The essential issue brought about by the congestion control is the communicated storm issue that prompts organize clog and bundle crashes bringing about parcel misfortune. It examines a few varieties of direct flooding and different kinds of forwarding protocols to moderate this issue [5]. The cross-layer communication, known as Cross-Layer Broadcast Protocol (CLBP), for crisis message dispersal in VANETs. CLBP utilizes a measurement, considering physical channel conditions and the moving vehicles' speed to choose many messages handing-off hubs towards the goal. The creators of CLBP perform recreations to approve their plan. The other exploration paper [6] proposes a direction-based plan for security message dispersal and contrasts its presentation and the direct flooding [7]. Based on all the research from this current paper, it does not mention a safety avoidance model for message dissemination. Furthermore, most recent research does not mention a safety message successfully sent within a safe distance. Therefore, to ensure maximum data packet delivery, focusing on finding the optimal combination of Beacon Generation Interval and transmission range [18]. The author described that previous research work in VANET focused on uniform vehicular networks and they totally ignored the presence/interruption of other broadcasting or radio signals from wireless devices. Therefore, multi-variant wireless signals increase the complexity of inter-vehicle communication. The author presented critical review of two types of heterogeneous wireless communication technologies which are DSRC and C-V2X, afterwards suggested an approach for reliable communication between heterogeneous vehicles having multiple radio access devices. It claims that the proposed Quality-of-service-aware-Relaying algorithm (QR) provide efficient results for message broadcasting and relaying-count in contrast of other standard-protocols [18]. In this paper [19], author is focused only on V2V communication comprising on heavy vehicles like trucks by using platooning to ensure safe distances between heavy vehicles on road which

increases traffic safety along with decreased fuel consumption. Cooperative-Adaptive-Cruise-Control is one of the devices to ensure safe V2V communication. The paper presented a comparison between two types of radio/wireless technologies which are IEEE 802.11p and 3GPP-Cellular-V2X. The later radio technology being used in proposed framework for V2V communication which consists of two modes that are Mode3 which is base-station-scheduled and Mode4 which is autonomously scheduled. Simulation results advocates that minimum feasible vehicle spacing between trucks in extra over-crowding of multiple radio message distribution by heterogeneous vehicles was more efficiently achieved with Cellular-V2X radio technology as compared to IEEE 802.11p [20]. In this paper the authors [6] described that by improving cellular-systems, V2X can be more efficient with increased throughput and decreased response time. It is acquired by replacing Long-term-Evolution-V2X with New-Radio-V2X as the prior one can provide primary road-safety-applications and later one can provide more enhanced smart road safety application systems. The author of this paper introduced Cellular-V2X as an essential technology either in terms of centralized or distributed network system to ensure primary and enhanced road safety applications with the development of Long-term-Evolution-V2X to New-Radio-V2X. Smart transportation system cannot rely on smart-single-vehicle system but it requires inter-connected smart heterogeneous vehicle system and to ensure this smart heterogeneous vehicle system, integration of Cellular-V2X and 5G smart technology has become crucial for autonomous and smart transportation. Moreover, it analyzed the possible issues to cope with the combination of 5G radar and Cellular-V2X communication system. The authors [26] advocates that the importance of vehicle-to-everything applications can never be ignored as they made drastic improvements in terms of traffic safety and reliability and lessen fuel consumption but due to high cost of smart vehicle applications, developers must test these through simulation before the release of actual application in market. They used ns3 simulator to test their proposed vehicle communication model using an open-sourced easier to configure, quick and simple simulation model to combine multiple communication heaps instead of single communication stack using IEEE 802.11p, C-V2X mode4, 3GPP and LET-transmission models. To handle emergency, speed and space alerts using ETSI standards, sample applications were presented.

B. Collision Avoidance in VANET

VANET uses several various safety applications for safety purposes. VANET is owned by a Cooperate Collision Avoidance System (CCAS) class which is also called Intelligent Transport Systems (ITS). Most of the collision avoidance systems in VANET research consists of two different approaches: proactive and reactive [8]. Proactive approach uses data through neighboring vehicles to prevent a collision. While reactive approach is activated when a vehicle sends emergency warnings messages to neighboring vehicles and an irrational behavior happens such as instant hard and strong braking and mechanical failures in the vehicle.

Based on the research, most of the system and design were proposed to use the same fundamental technologies, which are

the Global Positioning System (GPS) wireless communication devices. However, when DSRC wireless technologies have been introduced, all the designs based on preventing rear-end collision scenarios have become one of the significant research areas [10]. An algorithm used to prevent a collision at the scenarios of road intersection has been proposed by the researchers [11]. This proposed significant concept is mainly focused on the scenarios of road intersection where an algorithm is implemented to prevent a collision occurred. By improving the ready used roadsides' infrastructures with an improved communication coverage and another traffic signal, it could significantly avoid collisions at the intersections. These researchers utilized an estimator that consolidates the measurement from in-vehicle sensor and GPS. Moreover, authors [9] also proposed an improved algorithm that is suitable for the curve's environments. Apart from that, there are several works have been designed to enhance the warning system. As such, assistant of lane changing, forwarding collision, and intersection warning systems are designed to operate in different types of function. Now a days, safe and reliable method for massive vehicle transportation is vehicle patrolling able to communicate with each other using radio technology. Communicating emergency safety messages with each other ensures an improved traffic reliability and decreased fuel consumption. The authors [24] described that to ensure message delivery from the leading vehicle in a patrol to other vehicles to improve safety messages regarding geographical positioning of vehicles and to maintain safe distances among them, separating message broadcasting by using relays is the proposed method from the leading vehicle to other vehicles. In order to align variable information origins and restrict parameters for the reported vehicle squad positioning, an adaptive distributive-model-predictive-control (DMPC) was proposed in the research to avoid errors regarding vehicle geographical positioning. Therefore, consequently provides an effective framework for collision avoidance in V2V. In automatic vehicle driving, vehicles are programmed to understand its local commands and there is a great lack of understanding the emergency messages sent by other vehicles [30]. Therefore, relying on local radio environment is not useful and there should be other techniques for vehicle-to-network message transmission by using 5G technology or any Wi-Fi. Therefore, author presented an approach for make learning pattern better for autonomous vehicles in response in efficient manner using V2X learning system for better collision avoidance system.

C. Packet Delivery Rate in V2V Safety Communication

Most of the research does not mention and claim that the time gap(s) must be considered when sending and receiving a message. It is very crucial in order to ensure the rate of data packet delivery is maximum in vehicle-to-vehicle (V2V) safety (broadcast) communication. A beacon message is also called a CAM (Cooperative Awareness Message), where it broadcasts the position, the vehicle direction, the speed, and the other information or forms the backbone of the analysis done by the ITS Stations in range [15]. This paper also only focuses on PDR results on clustering head to sending and receiving a message. The cluster head of each cluster member will receive the forwarded packet from its cluster member. All the forwarded packets by the cluster members are probability

calculated which is associated with the number of times the same packet is received during one interval [9]. The elected cluster head will continue to distribute it towards the transmission direction upon receiving the sent packet by the cluster member. In the conventional way of multi-hop broadcasting, every vehicle requires to disseminate the received data by simple re-broadcasting. However, this broadcasting method will create redundant data in re-transmissions, resulting in an unused radio channel occupation and interfering with the radio channel. Therefore, decreasing redundancy and at the same time to ensure its reachability is very crucial in order to improving data delivery in a VANET. Hence, the simple way and efficient approach to achieve this goal is to re-broadcast the probabilistically [12]. A lot of research is going on integration of vehicle-to-everything and device-to-device communication with the development of 5G technology but still many challenges are to be coped with integration of vehicle-to-everything and device-to-device communication. The author is presenting an approach for quality enhancement of message delivery over VANET by dealing with all possible antecedent issues. Considering vehicles as clusters by using adaptive-mobility-aware-path-similarity algorithm. Cluster head selection was proposed on numerous factors, one of them was future-path sameness. It used Bayesian-rule-based-fuzzy-logic algorithm for vehicle-to-vehicle and device-to-device communication. It used two kinds of safety messages which are “accident” and “traffic” for safe message distribution. The author [17], modeled the projected cellular-5G VANET in OMNET++ simulator and was aimed to increase packet delivery ratio, turnout and to decrease communication and distribution time of message in vehicle ad hoc networks [17]. The author [22] has described the undeniable importance of cellular-vehicle-to-everything(C-V2X) in today’s 5G technology for the Intelligent Transportation System (ITS). Undoubtedly, it played a vital role in providing increased turnout, faster message communication along with decreased waiting time but there are still challenges to be coped with. Some of them are heterogeneous vehicles and frequent radio signal losses between them in emergency situations to avoid vehicle collision or any damage. The author suggested an approach to deal with such emergency message communication links between vehicles along with assuring the Quality of Service by first selecting the best device for message broadcasting in order to avoid node-to-node delay with the help of a dedicated similarity-based communication link. In case, if it fails to search and select any such device to broadcast emergency message then alternate selection will be a pedestrian 5G base-station. To reduce bulk-messages, author suggested Chaotic-Crow-Search-Algorithm and simulation results via Omnet++4.6 simulator showed a little improved output and packet delivery ratio in emergency message communication along with a minor decrease in node-to-node message delay [16].

III. OVERVIEW OF METHODOLOGY

Fig. 1 shows the difference between lane 1, lane 2, and lane 3 with varying speeds V_1 , V_2 , and V_3 . Vehicle in all lanes must maintain different safe AT time [4] to avoid any rear-end collisions. To ensure the safe AT time is maintained, all vehicles will exchange safety messages to know each other’s exact road positions. In lane 1, vehicles A, B and C is assumed to be able to maintain safe distances by exchanging the safety message because at 40km/hr, the safe distances (or AT time) are small. Due to that reason, the amount of transmit power needed is also small and may not reach the maximum permitted transmit power level. When the received power is equal or larger than the received power threshold ($Prx \geq Prx(th)$), an exchanged safety message can be received, and a vehicle can ensure safe distance be maintained. In lane 3 for vehicle D and F, when the speed is increased to 100km/hr, the required safe distance (or AT time) to be maintained is large. Transmission of a vehicle safety message by vehicle F may not be received by vehicle D simply because received power is lower than received power threshold $Prx < Prx(th)$. Due to this reason, communication between vehicle D and F is lost. A safety message might not be received because the distance to be kept is large.

Fig. 2 shows the broadcast safety message between Vehicle A and Vehicle B. For any vehicle moving speed [4], the AT safe parameter is x (s) and actual AT parameter between these two vehicles is y (s). Vehicle A and Vehicle B will exchange a safety message, both will be sending and receiving. However, if at the time of successful message reception for both vehicles, $y < x$, there is no sufficient avoidance time maintained, a crash might still happen between these two-vehicles. This fundamentally means that even if a message is successfully received by a vehicle (vehicle A) from another vehicle (vehicle B), vehicle safety still cannot be guaranteed since no maintenance a proper safe distance (AT safe).

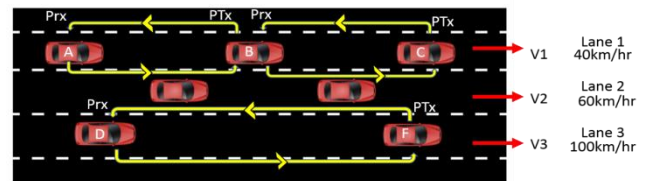


Fig. 1. V2V Message Dissemination within the AT time within difference Speed.

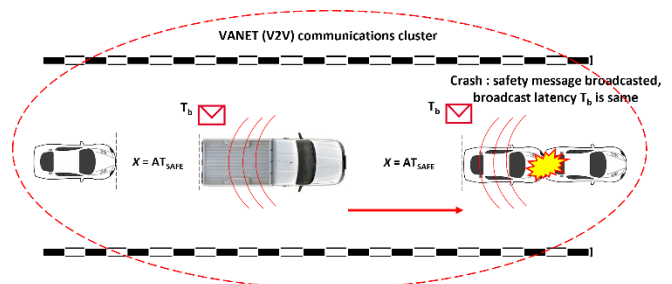


Fig. 2. V2V Communication with Safe AT (Avoidance Time).

A. Avoidance Time Concept

As indicated by the research and exploration on the delay of passenger vehicle, the analyst vehicle based on the security on passenger vehicle, time gap has been used instead of time headway. It is proved that the time gap represents the actual time which is only appears to the following vehicle to prevent collision of rear-end with a leading vehicle performing a uniform deceleration in a VANET. [2] It is fundamental for an after the vehicle to hold a protected after separation to the primary vehicle to consider enough opportunity to slow down upon the leading vehicle plays out a uniform deceleration to a halt. VANET time-gap approach could be used as a warning system to the following vehicles to avoid collision with the leading vehicles in a high traffic density area. Thus, TGFD is characterized as the accompanying vehicle's base time to decelerate and safely break without crashing the primary vehicle when both apply to the emergency breaks due to unexpected conditions. The time-gap following distance is defined as car speeding calibration and maintaining a pre-selected time-gap in between both vehicles, the leading vehicle and the following vehicle. The researchers discovered that time-gap is specified as the critical factor for safety, and proper time-gap calculations which could lead to a better performance and give allowances for in-vehicle distraction [2]. TGFD model for passenger vehicles must consider the passenger vehicle braking time and the time factors which are time perception, time decision, time broadcast, and time propagation in the VANET environment [3]. The Standards for Cooperative Awareness Message (CAM) and a Decentralized Environmental Notification Message (DENM) defines that communication should be delivered with the expected service requirement of maximum 100ms end-to-end latency (Final draft ETSI, 2014-09). The safety time gap was calculated by reference the VANET AT model for autonomous passenger vehicle as per below [4];

$$(auto) = Tb + Ts + Tpr + 0.28 \quad (1)$$

T_s is the reaction time of an autonomous vehicle system, and reaction time can be set in the range between 0.011s to 0.2s. The best time reaction is 0.011s since it is the fastest. The reaction time set for this study is 0.2s. T_b is the broadcast time, and T_{pr} is propagation time; the value of 0.28.

The braking time T_{br} for a straight road can be calculated by converting to the time component. "v" is the speed in km/hr, and "a" is the deceleration m/s². The value of 0.28 is a fixed value for the AT model [2]. By referencing from the $AT_{prv}(auto)$ model, the reaction time was set to 0.2s, and deceleration (it is the variable) was set to -8.8 m/s² and input the overall stopping distance in the unit meter(m), that must be set in OMNET++ while running the simulation.

IV. SIMULATION AND RESULTS

In this research, Veins (Vehicles in Network Simulation) is used as a simulation tool which is a built-in simulation framework on OMNeT++ simulation environment. Veins recruits OMNeT++ simulation kernel for a discrete event simulation whereas all the simulation controls and data collections are performed by OMNeT++. Veins instantiate SUMO to model a vehicle movement to provides a modular

framework for the custom applications simulation. An example to abstract away from a discrete event simulation of wireless channels is by controlling event routing between nodes and modeling signal processing. In this case, dedicated model libraries are used for simulating such as Internet protocols (IPs) or cellular network communications. Veins build on this basic concept to provide a suite of model that can be served as a framework in modular type for simulating applications. Based on the suite of IVC models, the implementation of custom and application-specific data generation and dissemination protocols could be done referring to the IVC models suite available in OMNET++, such as the safety and efficiency of traffic. Such application simulations and all Veins modules used are consolidated and connected to be executable. This executable application could be run as a GUI application or as a command-line batch simulation. The combination of precise channel and access models, behavior, and mobility feedbacks enables wide range captures of necessary factors to investigate intersection collision avoidance approaches. The running simulation of the vehicle shows in Fig. 3 that running via OMNET ++. This simulation will be running within the time that was already setting in the code.

A separate instance simulates the SUMO, as mentioned above, a road traffic simulator's vehicle movement, which started and controlled by the running simulation. Veins utilize the object subscriptions integrated with SUMO to improve its efficiency. When vehicles are generated or their states are changed, Veins allow it to call updates and push notifications from a running simulation. Fig. 4 shows the workspace for SUMO. This file of sumo will be integrated with OMNET++ when running the simulation.

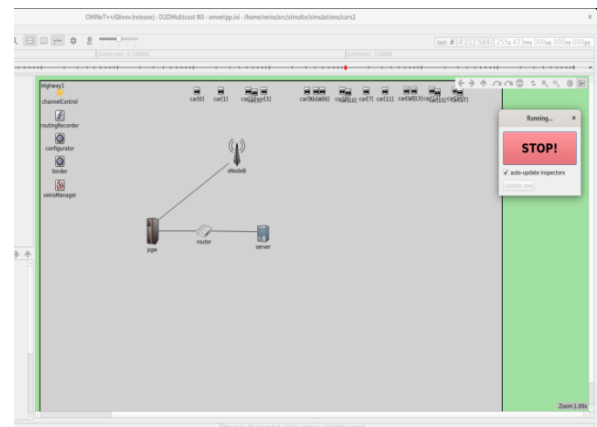


Fig. 3. Simulation Running in OMNET++.

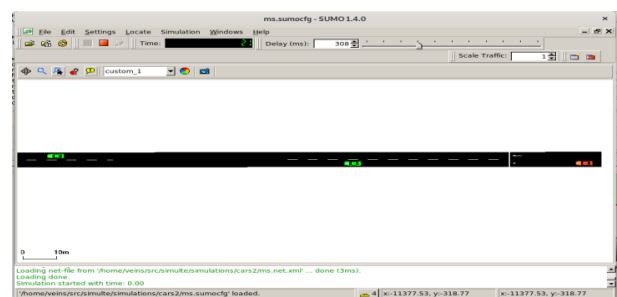


Fig. 4. SUMO Workspace.

The results were evaluated based on the time gap setting with different speed measures and vehicle density.

A. Packet Delivery Ratio (PDR) and Time Gap

Fig. 5 shows the graph for the results PDR with Time Gap setting. The PDR was decreasing when the density was an increase. The density set to 30 vehicles with a 50km/hr speed shows that highly PDR slowly decreases when the speed was increased. The density 100 of the vehicle shows that low PDR starts at the beginning 36 of 50km/hr until 120km/hr. This has happened because PDR does not been successfully sent when the density is increasing. The higher density, PDR will be affected, and message dissemination could not be successfully disseminated. Even the distance between vehicle to vehicle maintained it does not measure the message was successfully disseminated. This result meets this research objective, investigating the relationship between the safe vehicle time gap and the broadcast message's speeds. When vehicles maintain a safe time gap to ensure safety, which is to avoid collisions, the results show that this impacts the PDR and the distances between vehicles increases affecting message reception. The average difference PDR between densities 30 and 100 with 8 points of difference time gap setting is 5%. From Fig. 6 also while setting time gap(s) to the default value, the high of PDR was achieve. The results show that with a minimum time gap(s) setting, which is 4meter = 0.774s, the PDR slightly increases to 80% of PDR with low density 30. For the high density 100, the PDR slightly drop 40%, which means that in high density, the vehicular communication is dropping while sending and received message, and some communication is loss. Fig. 5 and Fig. 6 can be described that the time gap(s) setting affected the PDR. The larger and smaller distance was affected the vehicular communication when broadcasting a message.

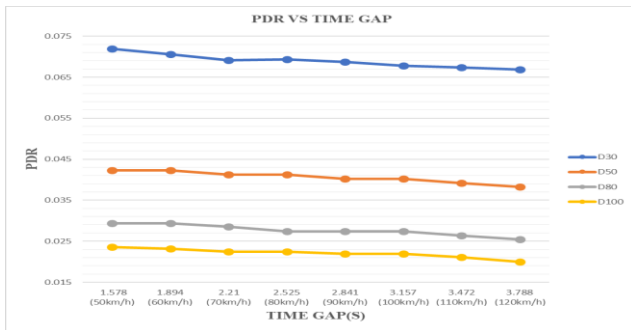


Fig. 5. PDR with Time Gap(s) Setting based on the Converted Time Gap(s) Speed.

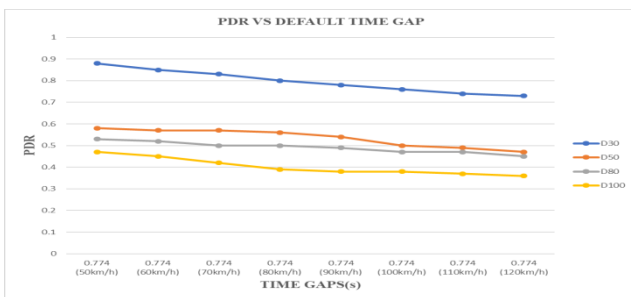


Fig. 6. PDR with Time Gap(s) Setting based on default Time Gap(s) Speed.

B. Throughput with Time Gap(s) Analysis Result

Fig. 7 shows the Throughput and Time Gap. For these results, the simulation was tested with the difference in speed and safety time gap. This figure shows that the throughput was decreased when the velocity and time gap is high. The successful message delivery rate over communication between V2V decreased when the simulation was run in high densities and velocity vehicles. This might be because the larger distance-time gap setting affected the packet arrive at their destinations successfully. This can be seen at time gap settings of 3.788s for vehicle speeds 120km/hr, respectively. Furthermore, these results meet with a problem statement discussed in Section 1, which is the communication between vehicles to the vehicle might be a loss of communication, even maintaining the safety distance. The average throughput between densities 30 and 100 is 213.72bps. From the average results, the successful CAM delivery over communication between V2V was decreased when the simulation was run in high densities and velocity vehicles.

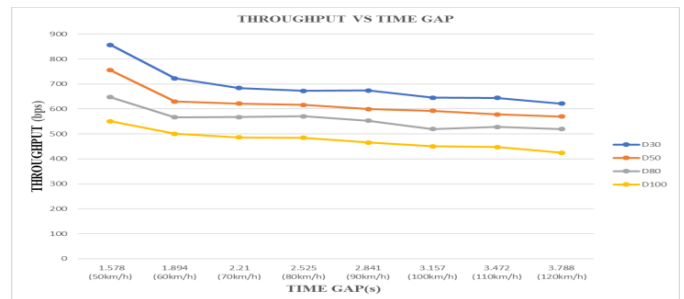


Fig. 7. Throughput and Time Gap(s).

C. Different UE Transmit Power with PDR and Time Gap(s) Analysis Result

Other simulation results were measured to investigate the packet delivery ratio (PDR) under different time gap settings with different vehicle speeds. The setting also under different vehicle densities and UE transmit power, as shown in Fig. 8. This figure shows that within 19dBm, the PDR was decreasing, which means that they send a packet of the message that was decreased and did not have been received successfully. The higher densities and speed with the high time gap, the PDR slowly decreases based on the different densities, the higher densities. The UE transmit power also affects the reception of messages shown with lower PDR. Higher mobility for vehicles, i.e., higher vehicle velocity, has a more substantial impact on PDR. This can be seen at time gap settings of 3.472s and 3.788s for vehicle speeds of 110Km/hr and 120km/hr, respectively. For UE transmit power was set to 27dBm above the standard also affected the message reception and slightly decrease when vehicle speed increase with higher mobility. Again, this result show that time gap settings with a difference of UE transmit power affects PDR and potentially vehicle safety.

D. Different UE Transmit Power with Throughput and Time Gap(s) Analysis Result

Fig. 9 shows the performance throughput with different speeds, densities, and UE transmits power 27dBm, 23dBm, and 19dBm. The 27dBm UE transmit power was set above the

standard in ETSI. The rate of successful message delivery over communication between the vehicle to vehicle slowly decreased when the high densities have been tested. This can be seen at time gap settings of 3.472s and 3.788s for vehicle speeds of 110Km/hr and 120km/hr, respectively. This result shows that time gap settings with a difference of UE transmit power affect throughput and slightly decrease when vehicle speed increase with higher mobility and potentially affects vehicle safety. This result shows that in the highest safety time gap, 3.788s with 120km/hr, the throughput is in the lowest value for densities set to 30 and 50. When a vehicle to vehicle broadcast a message with high speed and the distance is more significant between the vehicles, some of the messages were not successfully sending and received by the vehicle.

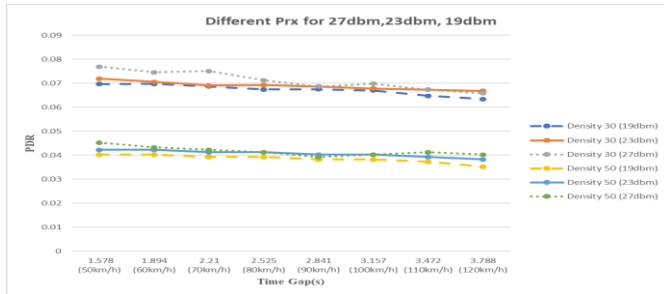


Fig. 8. Different Prx for 27dBm, 23dBm and 19dBm.

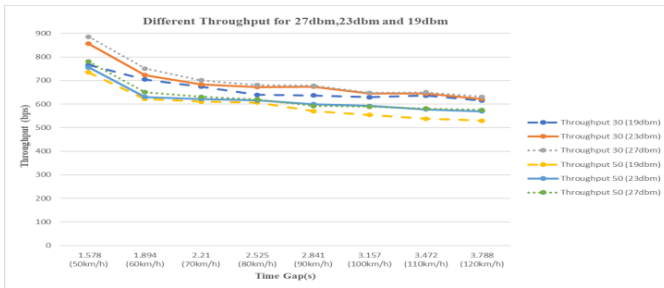


Fig. 9. Different Throughput for 27dBm, 23dBm and 19dBm.

E. PDR for each of Vehicle with Different Speed, Time Gap, and UE Transmit Power

This figure shows that the performance PDR per vehicle with different speed and time gap settings transmit power 23dBm. The rate of successful message delivery over communication between the vehicle to vehicle slowly decreases. This result shows that the distance between the vehicle affected the performance of PDR. The performance of PDR with the time gap formula shows that the lowest than the default time gap setting in veins simulation. The average difference between 60km/hr with default time gap setting and formula is 51%, and for 100km/hr is 53%. This can confirm that the distance between vehicles was affected by the CAM message.

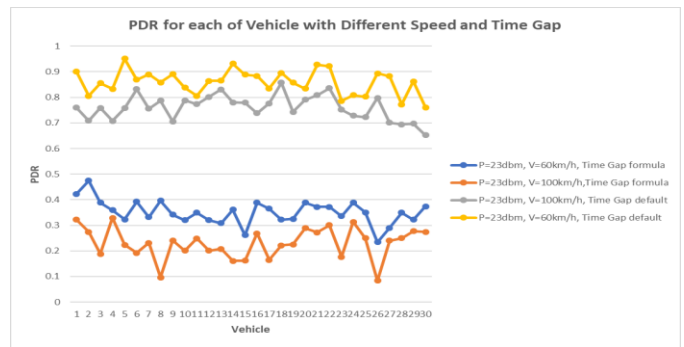


Fig. 10. PDR for each Vehicle with Different Speed, Time Gap, and UE Transmit Power.

V. CONCLUSION

The message dissemination between vehicle-to-vehicle communications impacts the packet delivery ratio and throughput based on the setting with different speed, time gap, and UE transmit power. Based on the findings, the relationship between vehicle time gap and speed impacted the packet delivery ratio (PDR), throughput, and UE power transmission. For the different speed and time gap, PDR's performance decreases while the speed was increase and while the vehicle's densities are increasing. It can be shown from the results that for vehicles to maintain safety on the road avoiding collisions, keeping a desired safe distance between them is essential, which means maintaining a proper time gap. However, the time gap is proportional to vehicle speed. As vehicle speed increases, the time gap also increases. The increasing time gap means increasing safe distances, and with the increase in safe distance, potential messages exchanged between all vehicles cannot be received. This will ultimately affect vehicle safety severely. It can also be shown that the Tx power of UEs also affects PDR, using a lower UE Tx power, while maintaining safe distances caused smaller message reception. Finally, it can be shown that even when vehicles exchanged safety messages between them to ensure safety, this does not necessarily guarantee safety as the distances between them grow apart (although safe), messages still cannot be received. The future work for this research is to evaluate the vehicle safety message dissemination performance under the influence of interference in an urban radio environment, the relationship and trade-off between PDR (successful CAM reception), UE transmit power, SNR and safe distances.

ACKNOWLEDGMENT

The project is fully funded by Universiti Sains Malaysia (USM) and Ministry of Higher Education Malaysia under FRGS Grant Scheme (FRGS/1/2018/ICT03/USM/03/1).

REFERENCES

- [1] Xu, Q., Mak, T., Ko, J., & Sengupta, R. (2004). Vehicle-to-vehicle safety messaging in DSRC.VANET '04: Proceedings of The 1St ACM International Workshop On Vehicular Ad Hoc Networks, 19–28.
- [2] Fadilah, S., & Mohd Shariff, A. (2014). A Time Gap Interval for Safe Following Distance (TGFDD) in Avoiding Car Collision in Wireless Vehicular Networks (VANET) Environment. IEEE 5Th International Conference On Intelligent Systems, Modelling, And Simulation, 683-689.
- [3] Green, M. (2000). " How long does it take to stop?" Methodological analysis of driver perception-brake times. Transportation human factors, Transportation Human Factors 2(3);,195-216.
- [4] Jaiyeoba, O., Mohd Shariff, A., & Fadilah, S. (2019). Passenger Vehicle Avoidance Time Model For Connected and Autonomous Vehicles. 7Th International Conference On Information And Communication Technology (Icoict).
- [5] Giang, A. T., Busson, A., & Vèque, V. (2013). Message dissemination in VANET: Protocols and performances. In Wireless vehicular networks for car collision avoidance (pp. 71-96). Springer, New York, NY.
- [6] Bi, Y., Cai, L., Shen, X., & Zhao, H. (2010). A cross-layer broadcast protocol for multihop emergency message dissemination in inter-vehicle communication. , IEEE International Conference On Communications (ICC), 1–5.
- [7] Ababneh, N., & Labiod, H. (2010). Safety message dissemination in VANETs: Flooding or trajectory-based?. IEEE The 9Th IFIP Annual Mediterranean Ad Hoc Networking Workshop (Med-Hoc-Net), 1-8.
- [8] Diakaki, C., Papageorgiou, M., Papamichail, I., & Nikolos, I. (2014). Overview and analysis of Vehicle Automation and Communication Systems from a motorway traffic management perspective.
- [9] Lei, C., & Englund, C. (2016). Cooperative Intersection Management: A Survey. IEEE Transactions On Intelligent Transportation Systems, 570-586.
- [10] Kenney, J. (2011). Dedicated short-range communications (DSRC) standards in the United States. Proceedings Of The IEEE, 99(7), 1162-1182.
- [11] Huang, Q., & Miller, R. (2002). An adaptive peer-to-peer collision warning system. Vehicular Technology Conference. IEEE 55Th Vehicular Technology Conference. VTC Spring 2002.
- [12] Lei, C., & Englund, C. (2016). Cooperative Intersection Management: A Survey. IEEE Transactions On Intelligent Transportation Systems, 570-586.
- [13] Intelligent Transport Systems (ITS); Vehicular Communications; Basic Set of Applications; Part 3: Specifications of Decentralized Environmental Notification Basic Service. (2014). Final Draft ETSI EN 302 637-3 V1.2.1 (2014-09).
- [14] Intelligent Transport Systems (ITS); Vehicular Communications; Basic Set of Applications; Part 2: Specification of Cooperative Awareness Basic Service. (2014). Final Draft ETSI EN 302 637-2 V1.3.1 (2014-09).
- [15] Veitas, V., & Delaere, S. (2018). In-vehicle data recording, storage, and access management in autonomous vehicles.
- [16] Mughal, B., Low, T., & Wagan, A. (2018). Single-hop Packet Delivery Rate in V2V Safety Communications for Worst-case Highway Scenarios. IEEE 4Th International Conference On Computer And Information Sciences (ICCOINS).
- [17] Alghamdi, S. A. (2020). Novel path similarity aware clustering and safety message dissemination via mobile gateway selection in cellular 5G-based V2X and D2D communication for urban environment. Ad Hoc Networks, 103, 102150.
- [18] Ghafoor, K. Z., Guizani, M., Kong, L., Maghdid, H. S., & Jasim, K. F. (2019). Enabling efficient coexistence of DSRC and C-V2X in vehicular networks. IEEE Wireless Communications, 27(2), 134-140.
- [19] Vukadinovic, V., Bakowski, K., Marsch, P., Garcia, I. D., Xu, H., Sybis, M., ... & Thibault, I. (2018). 3GPP C-V2X and IEEE 802.11 p for Vehicle-to-Vehicle communications in highway platooning scenarios. Ad Hoc Networks, 74, 17-29.
- [20] Chen, S., Hu, J., Shi, Y., Zhao, L., & Li, W. (2020). A vision of C-V2X: Technologies, field testing, and challenges with chinese development. IEEE Internet of Things Journal, 7(5), 3872-3881.
- [21] Kiela, K., Barzdenas, V., Jurgo, M., Macaitis, V., Rafanavicius, J., Vasjanov, A., ... & Navickas, R. (2020). Review of V2X–IoT standards and frameworks for ITS applications. Applied sciences, 10(12), 4314.
- [22] Alghamdi, S. A. (2021). Cellular V2X With D2D Communications for Emergency Message Dissemination and QoS Assured Routing in 5G Environment. IEEE Access, 9, 56049-56065.
- [23] Nardini, G., Viridis, A., Campolo, C., Molinaro, A., & Stea, G. (2018). Cellular-V2X communications for platooning: Design and evaluation. Sensors, 18(5), 1527.
- [24] Hong, C., Shan, H., Song, M., Zhuang, W., Xiang, Z., Wu, Y., & Yu, X. (2020). A joint design of platoon communication and control based on LTE-V2V. IEEE Transactions on Vehicular Technology, 69(12), 15893-15907.
- [25] Soto, I., Calderon, M., Amador, O., & Urueña, M. (2022). A survey on road safety and traffic efficiency vehicular applications based on C-V2X technologies. Vehicular Communications, 33, 100428.
- [26] Malinverno, M., Raviglione, F., Casetti, C., Chiasserini, C. F., Mangués-Bafalluy, J., & Requena-Esteso, M. (2020, November). A multi-stack simulation framework for vehicular applications testing. In Proceedings of the 10th ACM Symposium on Design and Analysis of Intelligent Vehicular Networks and Applications (pp. 17-24).
- [27] Storck, C. R., & Duarte-Figueiredo, F. (2020). A survey of 5G technology evolution, standards, and infrastructure associated with vehicle-to-everything communications by internet of vehicles. IEEE access, 8, 117593-117614.
- [28] Costandou, A., & Leba, M. (2019, February). Convergence of V2X communication systems and next generation networks. In IOP Conference Series: Materials Science and Engineering (Vol. 477, No. 1, p. 012052). IOP Publishing.
- [29] Ni, Y., Cai, L., He, J., Vinel, A., Li, Y., Mosavat-Jahromi, H., & Pan, J. (2019). Toward reliable and scalable internet of vehicles: Performance analysis and resource management. Proceedings of the IEEE, 108(2), 324-340.
- [30] Magdum, S. S., Franklin, A., & Tamma, B. R. A Cooperative Federated Learning Mechanism for Collision Avoidance using Cellular and 802.11 p based Radios Opportunistically.

Design and Implementation of a Low-cost CO₂ Monitoring and Control System Prototype to Optimize Ventilation Levels in Closed Spaces

Ramcés Cavallini-Rodríguez
Facultad de Ingeniería
Universidad Tecnológica del Perú
Lima, Peru

Jesús Espinoza-Valera
Facultad de Ingeniería
Universidad Tecnológica del Perú
Lima, Peru

Carlos Sotomayor-Beltran
Facultad de Ingeniería
Universidad Tecnológica del Perú
Lima, Peru

Abstract—High concentrations of CO₂ levels are significantly present in closed environments that do not have proper ventilation. Such high concentrations generate negative health consequences such as dizziness, headaches and various respiratory problems. For this reason, the design and implementation of a low-cost CO₂ monitoring and control prototype is proposed to optimize ventilation levels in closed spaces. The parameters that the proposed device measures are concentration of carbon dioxide, humidity and temperature. A digital PID controller was implemented, with the use of C++ programming language and an exhaust fan to stabilize carbon dioxide levels within a closed space. The aforementioned parameters can be viewed in two ways: The first way is locally through a LCD screen and LED indicators, and the second one, remotely using the free Arduino IoT Cloud platform. The closed environment was emulated using a cardboard box and in the tests it was obtained that the prototype manages to keep the CO₂ concentration levels below the established limit. However, this can be further improved by using more precise sensors for more accurate results. It is expected that this model can be successfully scaled to closed spaces such as classrooms and offices.

Keywords—CO₂ Monitoring; IoT; Low-cost Indoor Ventilation System; NodeMCU; Open Source Software

I. INTRODUCTION

Currently, outdoor air pollution has increased in all countries due to the growth of automotive fleets and industrial companies. This affects indoor environments with a significant increase in CO₂ levels in a proportion between 2 to 5 times more than outdoors [1]. An example of this is reflected inside different environments such as classrooms, offices, bedrooms, etc; where the CO₂ concentration has values that exceed the maximum levels recommended by international standards. These places do not have an adequate mechanical ventilation system to dissipate the polluting gases that are generated inside, and even in many cases the doors and windows are kept closed. Likewise, despite the fact that they have been designed to accommodate a limited number of people, the maximum capacity allowed is exceeded on a daily basis.

Different CO₂ monitoring systems have been developed for closed spaces that do not directly control this parameter. A CO₂ prediction model has been developed based on the history of measurements [2]. A user alert system has been also proposed by means of text messages to the cell phone and an email notification [3]. The information obtained is even shown

through an LCD screen and warns us with an audible alarm when the maximum levels established are exceeded [4]. The aforementioned studies [2], [3], [4] defend the importance of monitoring the levels of polluting gases, such as CO₂, existing inside a closed space. This, with the aim of analyzing indicators that allow reducing the spread of diseases in the short and long term. The tendency of the authors in this regard is to develop portable prototypes that determine the concentration of harmful agents to health within the environment using low-cost sensors that provide information in real time, which seeks to maintain adequate ventilation levels below the recommended limit.

CO₂ is a gas that is released by human respiration and this is adequate to measure ventilation levels [5]. Because people exhale predictable levels of CO₂, a direct connection to air pollution can be made [3]. This parameter is extremely important, since high concentrations of CO₂ have very harmful effects on health [6]. On the other hand, the measurement of other parameters of air quality, such as particulate matter, relative humidity and temperature, are very important as well. Environmental parameters, temperature and humidity, also influence people's well-being [7], [8] and these are necessary to have a correct indoor air quality index [2].

Some devices that has been previously designed to measure different parameters from air quality have shown data in real time through the uses of displays. For example, an open source web platform was developed to display the information provided by the sensors using a MySQL server for data storage [7]. ThingSpeak was also used, which is a free web platform for the collection and representation of the measured variables [3]. On the other hand, a mobile phone application called Dataplicity was used to remotely access the pollutant indicators [9], whereas in another study only a 16x2 LCD screen was used to fulfill the same purpose [10].

When considering the methodology used by some studies to develop devices that measure air quality, diverse ones were followed. For instance, a quantitative experimental investigation was applied in 10 schools and in 2 training centers for 8 days and between 5 to 10 hours a day taking measurements from different air quality sensors [11]. A similar methodological approach is applied using pollutant weighted calculation tools and the test is performed in 2 environments. The first is a laboratory at the University of Warwick (England) during 1

hour of classes with a number of 100 students. The second environment is a kitchen of the same school, with a single person preparing the food for 1 hour [1]. On the other hand, in one study [8] a qualitative methodology based on surveys was used as an instrument to understand the experience of discomfort and evaluate the environment from the participants own point of view. Then, a statistical analysis was performed based on census data for 8 hours a day in 4 scenarios. Similarly, in another study [12] a systemic perspective of the model designed with a smoothing algorithm to reduce sensor errors caused by power failures and a data aggregation algorithm that minimizes network traffic and saves time was developed. In a research carried out in India [10], empirical methods were used to know the level of gases harmful to health using the designed prototype, but they did not specify the place or conditions where it was used.

A research carried out in Spain [11], presents as a result a very precise device whose data had a value $R^2 = 0.902$ in a simple linear regression test, and $S = 143$ and $p = 0.1348$ in the Moses test comparing it with the commercial Perfect Prime CO2000 device. Similarly, researchers in Portugal [13] presented a very reliable proposal, showing sensors with R^2 values between 0.73 and 0.87, obtained from linear regression tests. Another work in India [3] explained a system with good sensitivity, which although it was not compared with another device, had a sensor which was experimentally calibrated for 24 hours.

Some studies have concluded that portable devices are reliable to measure the quality of the air inside closed environments and also confirm that the use of IoT sensors is favorable for these equipments. For example, the use of IoT technology simplifies access to the information provided by the different sensors installed in the environment in order to have a better quality of air [14]. With the information collected by sensors interconnected by means of IoT technology, it was possible to develop an anticipated model based on CO₂ concentrations to improve ventilation at any time [2]. On the other hand, Interaction with a wireless sensor network that provides real-time pollutant gas indices is also affordable for everyone. Mounting a network of wireless sensors is easier and more efficient and naturally, it reduces the amount of wiring used from the end devices to the central monitoring station [15]. Finally, the Raspberry Pi development board facilitates the connection with other IoT sensors and not only with analog or digital sensors to collect information on the contamination rates in a closed area [12].

In view of this global problem, which is detrimental to people's health, of not having an adequate CO₂ monitoring and control system, it is necessary to design and implement one that optimizes the level of ventilation in closed spaces [7].

II. METHODOLOGY

A. Electronic Components

The prototype is divided into five operating stages and uses the following electronic components, with the aim of achieving a low-cost system that can be implemented in closed environments.

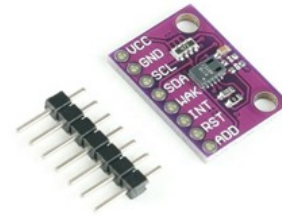


Fig. 1. CCS 811 Sensor.

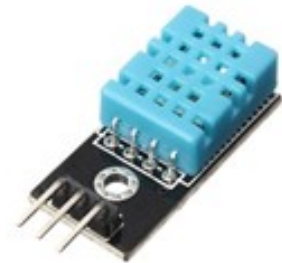


Fig. 2. DHT11 Sensor.

1) *Acquisition Stage*: Two types of sensors were implemented in this stage.

- CCS 811 Sensor (Fig. 1): It is an air quality sensor that allows us to obtain the equivalent concentration of CO₂ from the measurement of Total Volatile Organic Compounds (VOC) in a very precise way. This sensor was chosen as a main parameter for CO₂ measurement due to its low economic value compared to other types of air quality sensor on the market that cost up to 6 times more.
- DHT11 sensor (Fig. 2): It is a sensor that measures temperature and humidity parameters. It is a digital type that can be powered with 3.5 to 5V. Its temperature measurement range is 0 to 50° C, with an accuracy of 2° C. It allows to measure the relative humidity of 20-80% with a maximum sampling period of 1 second.

2) *Control Stage*: It is made up solely of the NodeMCU module.

- NodeMCU v3 module (Fig. 3): This module has an ESP8266 processor at a speed of 80 to 160 MHz. It has 1 analog port, 17 general purpose ports, 4 PWM outputs and allows I2C, UART, SPI type communication and Wifi. This device was chosen because it is a very popular and cheap module to carry out electronic projects that are synchronized with a free service in the cloud every second, due to its low consumption and high performance.

3) *Communication Stage*: It will be done wirelessly through the Wifi technology of the NodeMCU module. This communication was chosen because this technology is incorporated into the NodeMCU development board and that it has a free server called Arduino IoT Cloud to be able to view the



Fig. 3. NodeMCU v3 Module.



Fig. 5. AC Digital Dimmer.



Fig. 4. 16X2 LCD + I2C Module.



Fig. 6. 220V Air Extractor.

KPI control indicators remotely, both on the web and on the cell phone.

4) *Display Stage*: It is made up of a 16X2 LCD screen with I2C module and 3 LEDs.

- 16X2 LCD Screen + I2C Module (Fig. 4): This component is a small screen that allows information to be displayed. It has 2 rows and in each row you have the possibility of observing up to 16 alphanumeric characters.
- It consists of 3 light emitting diodes of green, yellow and red respectively. They will allow to show visually based on a color of the led a range of the CO₂ sensor to indicate if the ppm values are low, medium or high, respectively.

5) *Actuator Stage*: It is made up of 1 pre-actuator and 1 actuator.

- AC 220V / 2A digital dimmer (Fig. 5): Provides alternating current voltage regulation in order to achieve different levels of voltages that are located within the voltage range, while varying the power delivered to the load. This is controlled by a PWM signal. : This device was chosen as a pre-actuator to gradually vary the speed of the extractor motor, due to the effect of the PID controller established to maintain the optimal CO₂ concentration at an approximate value of 1000 ppm.
- 220V Extracting fan (Fig. 6): It is that device that extracts the air through its rotating blades in a direction from inside to outside of an enclosure. It works with voltages of 220-240 VAC and at frequencies of 50 and 60 Hz. In addition, they have a protection impedance. This device was chosen to extract the concentrated gas into the environment when CO₂ levels exceed a dangerous value for human health and thus dissipate it.

A diagram of the five stages working together in the design of the prototype is show in Fig. 7.

B. Mechanical Structure

Fig. 8 shows the design of the structure through the CAD Solidworks 2020 program, with general dimensions of 102 x 50 x 110 mm and 2 mm thick, which will contain the system components (LCD screen, sensors and plate development) so that they fit perfectly. After that, a 3D printing can be made using Acrylonitrile Butadiene Styrene (ABS) as a material, to protect the elements of the system. ABS material was chosen because it has sufficient protection against dust and splashes of water.

The front, side, rear and bottom views are seen in Fig. 9, Fig. 10, Fig. 11, and Fig. 12, respectively.

C. Software

The programming of the NodeMCU v3 module was done through the Arduino IDE platform, since the module has compatibility with that development environment. The goal is to keep the CO₂ concentration at 1000 ppm through the use of a digital PID controller. Likewise, the temperature and humidity parameters were considered in order to compensate for the variations in CO₂.

First, the readings of the temperature and humidity sensor were taken to be able to introduce them to the CO₂ sensor and improve the variation of the reading of its concentration. The PID controller is activated when the carbon dioxide concentration exceeds the value of 1500 ppm, because from this concentration it begins to be very harmful to health. With the establishment of the desired level of CO₂ and the correct tuning of the controller, the output value of the control signal is calculated. The power that will be delivered to the air extractor is the output of the PID controller, therefore a restriction of its maximum value was established at 100 and minimum at 0.

This rectified output signal will be sent to the dimmer, which will regulate the power that will be sent to the extractor. Finally, when the carbon dioxide concentration is less than 900 ppm, the PID controller will stop working, since the

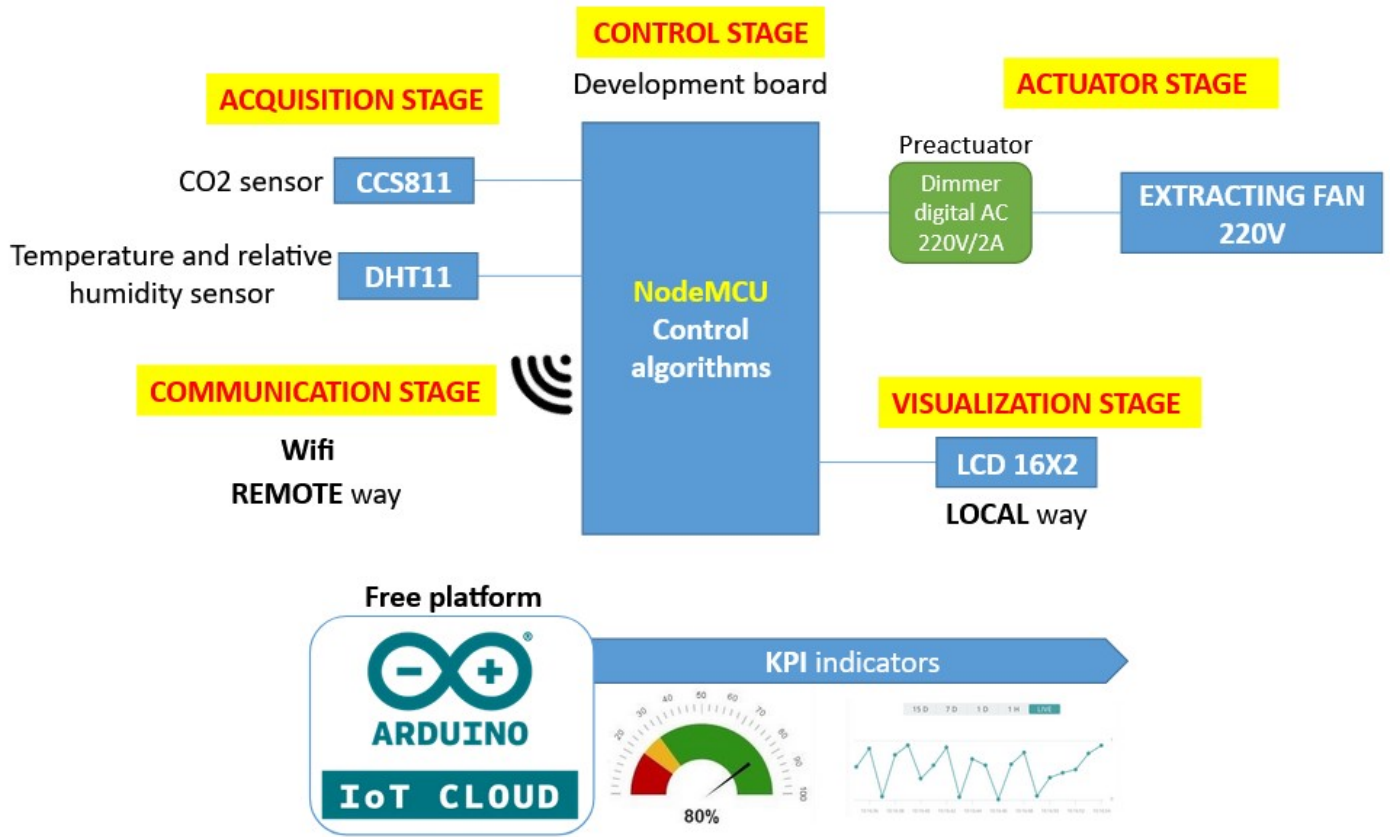


Fig. 7. Interconnection of the 5 Stages of the System.

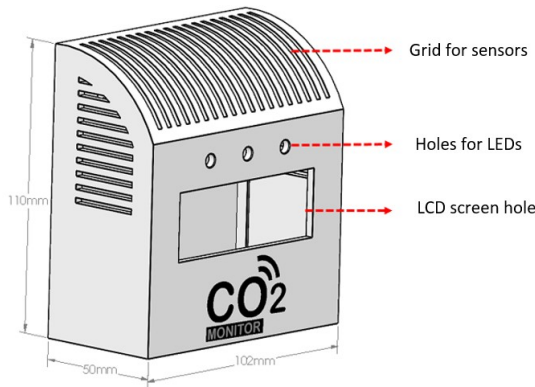


Fig. 8. Design View of the Exterior Structure.

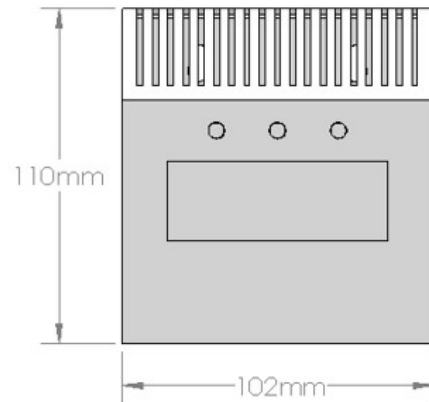


Fig. 9. Front View of the Exterior Structure.

ventilation level of the place will be safe. The values of temperature, humidity and CO₂ concentration will be sent to the cloud, displayed on the LCD screen and there will be 3 LED indicators: green when the CO₂ concentration is less than 1000 ppm, yellow when it is between the range 1000 - 1500 ppm and red when higher than 1500 ppm. Fig. 13 shows the logic used for programming the entire system.

D. Data Transmission to the Cloud

The measurements from the sensors are sent to the Arduino IoT Cloud platform. This platform is free, easy to use and all standards are open source. In addition to being compatible with all Arduino boards, it also has compatibility with the ESP8266 microcontroller, which is used by the NodeMCU module. This platform uses the MQTT protocol for data transmission and allows other interaction methods such as command line tools,

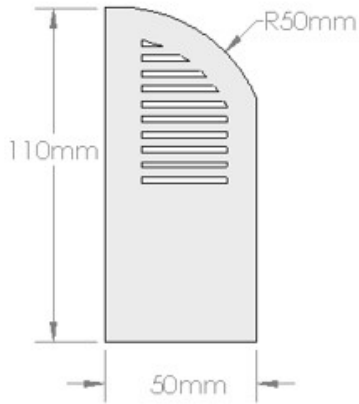


Fig. 10. Side View of the Exterior Structure.

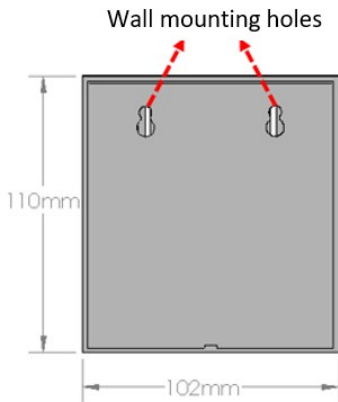


Fig. 11. Rear View of the Exterior Structure.

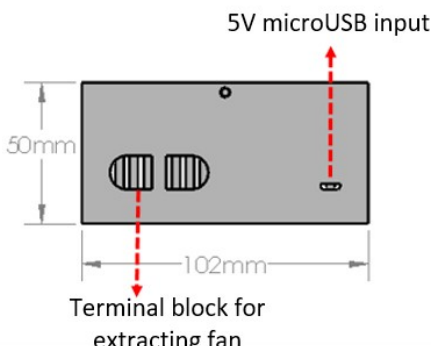


Fig. 12. Bottom View of the Exterior Structure.

JavaScript, and WebSockets. It even has a data storage of up to 2 days.

In this platform, 3 variables corresponding to each of the parameters that are obtained from the sensors were created and it was established that they are updated when their value changes. An interface called “CO₂ Monitoring and Control System” was also designed and added a percentage progress

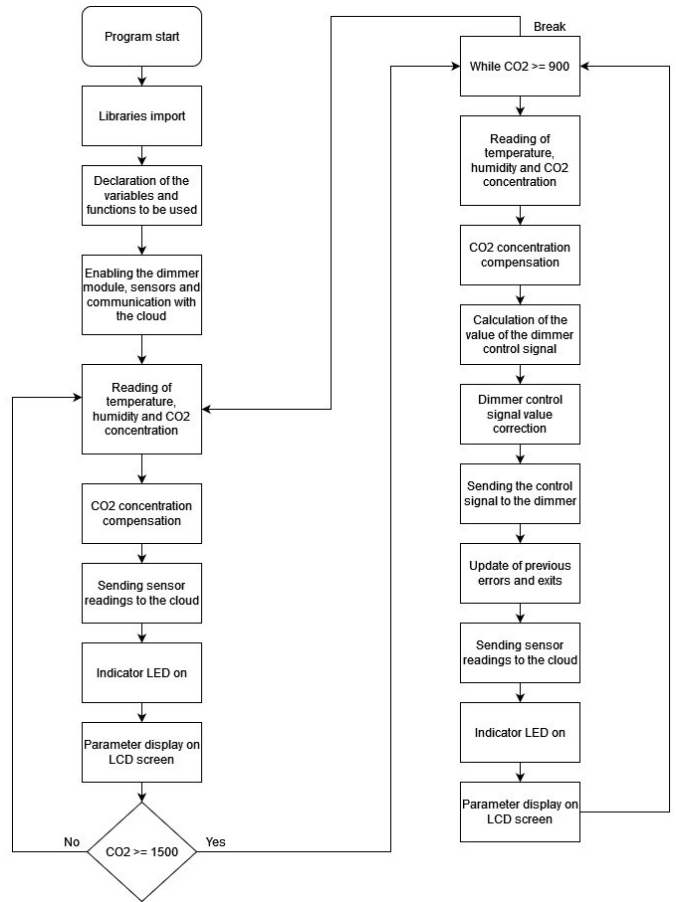


Fig. 13. Flow Diagram of System Operation.

indicator for the humidity value, a nominal progress indicator for the temperature value and a trend graph for the value of CO₂ concentration in ppm, as shown in Fig. 14.

III. RESULTS AND DISCUSSION

For the tests of the designed prototype, in Fig. 15 we have emulated a closed environment based on a cardboard box measuring 41x55x38 cm, in which 27 small holes were made, with an approximate diameter of 2 cm, on both sides and in the back of the box so that the air can circulate when the extractor is turned on, since otherwise there would not be an exchange of the flow of clean and polluted air inside the box. The cardboard box was chosen because of its low price and that it allowed to accumulate carbon dioxide in such a way as it would be done in a real closed space. However, the use of other materials such as resin or glass, as in the case of the research carried out in Algeria [16], would have allowed to observe the total operation of the system and to obtain a more natural behavior of the CO₂ due to a better permeability. Also, a plastic box with IP56 protection could be used to protect the system components and be the external structure of the prototype, as was done in England [17] and Indonesia [7].

As can be seen in Fig. 16, a hole with a diameter of 11.5 cm was made in the front of the box so that the air extractor can be installed outside of it. Likewise, 4 small holes were

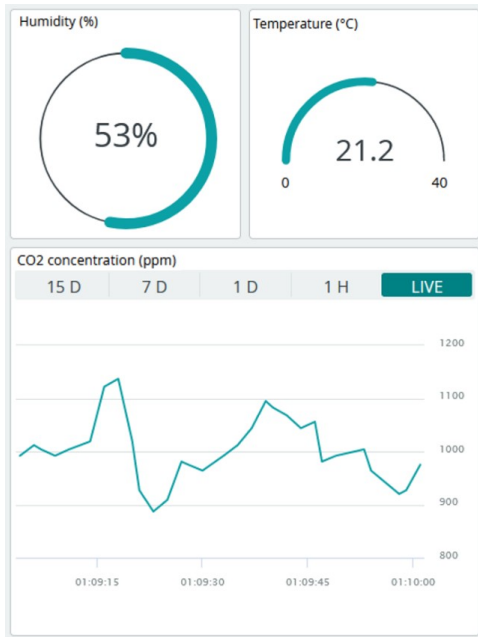


Fig. 14. KPI Indicators of the Cloud Interface.



Fig. 15. View of the Cardboard Box where the Prototype was Tested.

made in the corners to hold the extractor with screws and washers. This extractor will circulate the air from the inside to the outside of the box when the CO₂ levels are not within the allowed ranges. One type of exhaust fan that should be used in a real room is the AC180 model from the Broan brand, which works at 200 VAC 50Hz. In addition, it consumes 18W of power with an extraction capacity of 163 m³ / h and a noise level of 45 Db, being indicated for residential environments such as rooms, offices and classrooms. In a study conducted in a city in India (Durgapur), 6 conventional "cooler" type air extractors were used to ventilate the CO₂ produced in the small environment [8]. Also, in an office space in the same country, generic mechanical ventilation was used, producing a lot of noise [18], as well as a conventional extractor that was activated when the carbon dioxide limits were exceeded [19].

It can be seen in Fig. 17 that inside the box the breadboard was placed with the different components that intervene in the system, such as the NodeMCU development board, the CO₂ sensor, the temperature and humidity sensor, the LEDs and the screen. LCD coupled to its I2C module. The LCD screen and

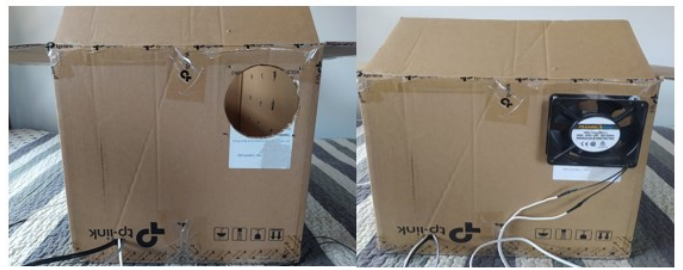


Fig. 16. Hole for Extractor Installation.

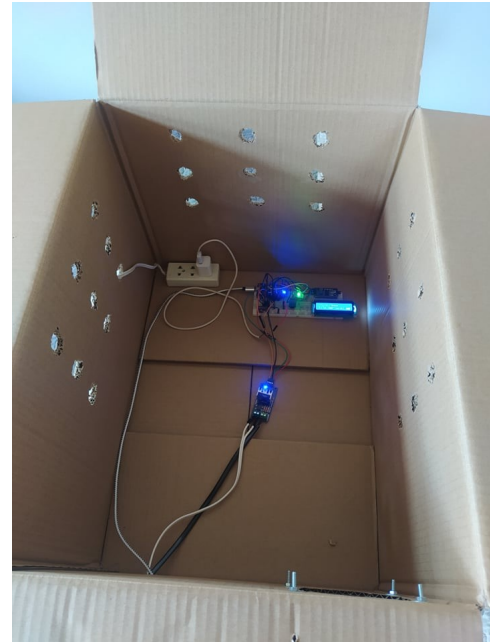


Fig. 17. Distribution of the Components within the Cardboard Box.

its module are powered with 5V DC through an adapted cell phone charger, the Node MCU, through a microUSB cable connected to the laptop and the other components use 3V DC provided by the development board. In the middle part of the box it can be seen the dimmer that will function as a pre-actuator, regulating the power delivered and enabling the connection between the control stage led by the NodeMCU and the power stage where the air extractor is located.

Fig. 18 shows the local display stage made up of the 16x2 LCD screen, which provides us with information about the values obtained from the CO₂ concentration through the CSS811 sensor in ppm measurements, and the temperature and relative humidity through the DHT11 sensor in ° C and % measurements, respectively.

In Fig. 19, we roughly mimic the CO₂ exhaled by people through smoke generated by burning paper in order to perform the tests. A quarter of rolled paper is set on fire and immediately placed inside the box on a metal container, to finally close it. The exhaust fan would be located in a real environment at least 2.3 meters from the ground, embedded in the wall. In the same way, the prototype that contains the CO₂ sensor must be mounted on the wall with the correct orientation, because CO₂

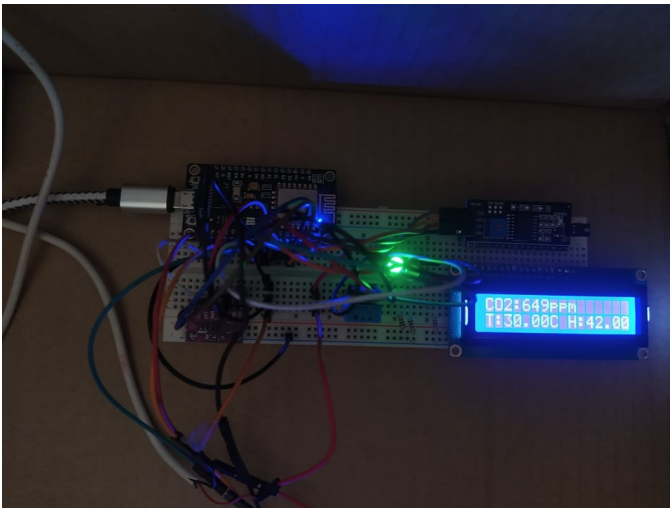


Fig. 18. Local Display Stage.



Fig. 19. CO₂ Generation within the Cardboard Box.

is denser than air, it tends to fall to the ground and with this it would absorb the CCS 811 sensor located at the interior of the structure, which has ventilation grills that will allow the access of this gas. A research work has used the MQ135 sensor to measure the CO₂ concentration and have located this at ground level [12]. Also, in a study in India, the MQ2 gas sensor is used interconnected with Arduino and installed on top of a desk [20]. Similarly in another work, an all-in-one prototype is designed, which is installed on the wall [17].

Fig. 20 shows the result of test 1 represented with a trend graph of CO₂ concentration (ppm) vs. time (seconds), sampled in 5 second intervals. At the beginning, an establishment is observed at approximately 8000 ppm, since it was the initial moment where the smoke was generated and accumulated. Also, it should be noted that an important factor is the size of

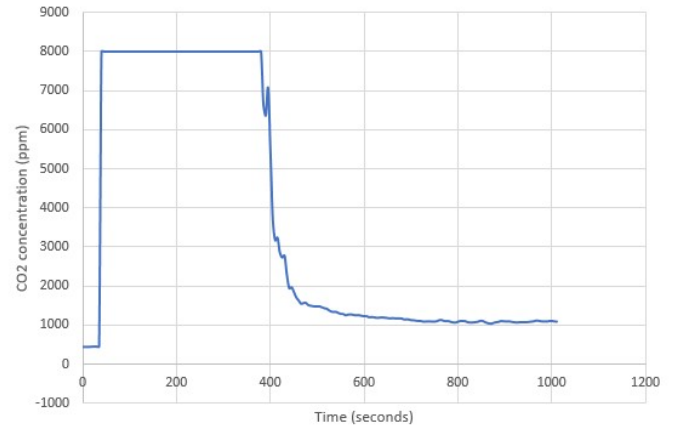


Fig. 20. Test Result 1.

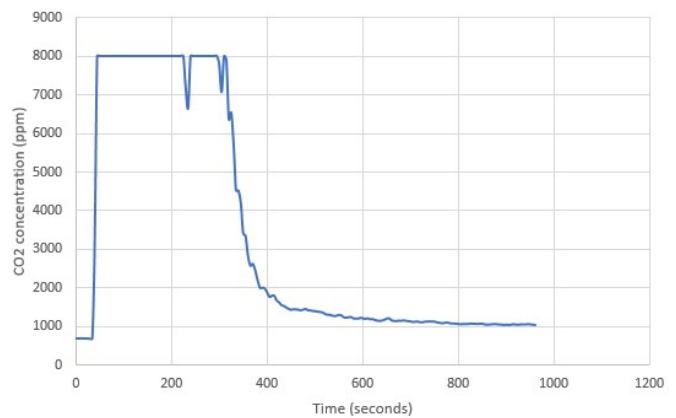


Fig. 21. Test Result 2.

the environment since, being a small box, the smoke generates a CO₂ concentration inside the box much higher than in a natural and conventional scenario. After some time, a decrease in the CO₂ concentration occurs as a result of the action of the air extractor, thus achieving an approximate establishment of 1000 ppm after 800 seconds.

In Fig. 21 the result of test 2 is shown, in addition to the initial establishment period at 8000 ppm, some downward peaks are observed since being a non-natural environment and only simulated, the generated CO₂ conditions are not constant, as if they would be in a traditional environment. Despite this, in general a similar behavior is observed with respect to the results of test 1, stabilizing at approximately 1000 ppm after 800 seconds, thus generating a clean and safe environment. In both tests carried out, the correct extraction of carbon dioxide inside the box can be observed, through the exponential decay of its concentration seen in both graphs. This behavior is repeated in some studies carried out in Italy [21] and the United States [22] inside classrooms, varying the number of people and ventilation elements. This was also observed in an investigation conducted in two laboratories in Indonesia [23].

In Fig. 22 the remote viewing stage is shown through the free Arduino IoT Cloud platform that can be monitored through the web or its free software for Android and iOS.

CO₂ monitoring and control system

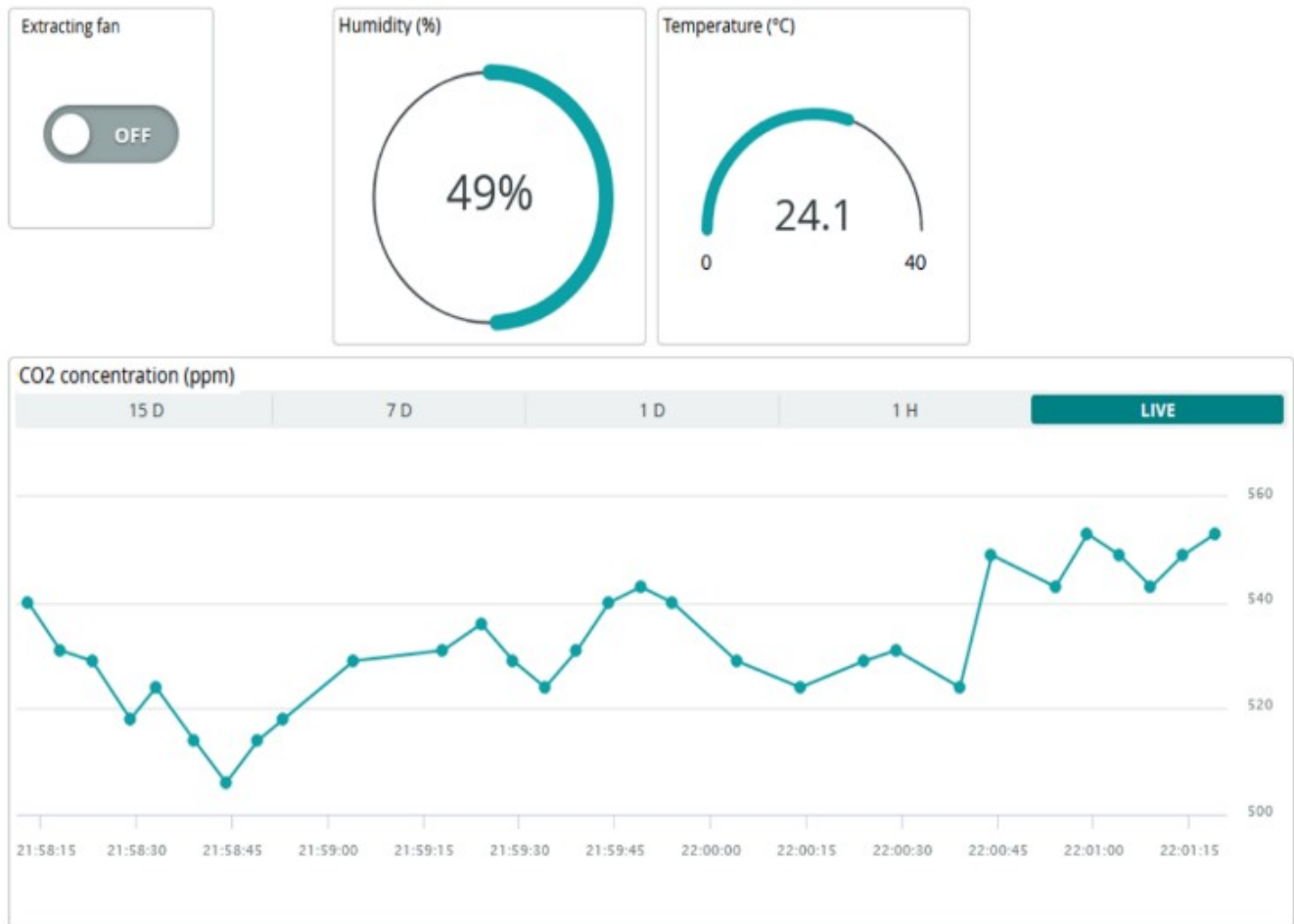


Fig. 22. Remote Viewing Stage.

In either of these two media, KPI indicators for humidity, temperature and CO₂ concentration are displayed in real time with a history of up to 2 days.

IV. CONCLUSION

In the present research work, a monitoring and control system of CO₂ concentration in closed rooms has been developed using low-cost components and a free software application to view the data remotely through smartphones, laptops and desktop computers. The results demonstrate its effectiveness compared to other studies, since after approximately 800 seconds of having detected the high levels of CO₂ concentration, it reaches adequate levels, less than 1000 ppm, thus producing a healthy area for the exchange of air of the people who inhabit it. The finished prototype would be located on the side of the room for the correct detection of the parameters described above.

As a future work, it is suggested that the development of

the prototype be located within a structure with a degree of protection IP (Ingress Protection), with the aim of resisting dust and humidity found in the environment. Likewise, it is recommended to use CO₂ sensors of the NDIR (Non Dispersive Infrared Detector) type, since they are more accurate for gas detection, easier to calibrate and have minimal error percentages. Take into account the number of occupants and the volume of the room, since the precision of the sensors to be used and the number of air extractors to install depends on this. Finally, to obtain accurate measurements it is recommended to install the structure approximately 1 meter from the ground.

REFERENCES

- [1] S. Esfahani, P. Rollins, J. P. Specht, M. Cole y J. W. Gardner, "Smart City Battery Operated IoT Based Indoor Air Quality Monitoring System", en 2020 IEEE SENSORS, Rotterdam, 25–28 october 2020. 2020.
- [2] R. Xiahou, J. Yi, L. He, W. He y T. Huang, "Indoor air monitoring system based on internet of things and its prediction mode'l", Proceedings of

- the International Conference on Industrial Control Network and System Engineering Research (ICNSER), vol. 2019, pp. 58–63, 2019
- [3] R. K. Kodali, S. Pathuri y S. C. Rajnarayanan, “Smart Indoor Air Pollution Monitoring Station”, en 2020 International Conference on Computer Communication and Informatics (ICCCI), Coimbatore, India, 22–24 january 2020. IEEE, 2020.
- [4] C. Calvin Adrianto, Y. Calvinus y P. B. Mardjoko, “Design Of CO, CO2, Temperature, Humidity, And Weather Monitoring System Based On Internet of Things (IoT) & Android”, IOP Conference Series: Materials Science and Engineering, vol. 1007, p. 012175, december 2020
- [5] D. Thomas, B. Mistry, S. Snow y M. C. Schraefel, “Indoor Air Quality Monitoring (IAQ): A Low-Cost Alternative to CO2 Monitoring in Comparison to an Industry Standard Device”, Advances in Intelligent Systems and Computing, vol. 858, n. 1, pp. 1010–1027, 2018
- [6] G. Marques y R. Pitarma, “IAQ Evaluation Using an IoT CO2 Monitoring System for Enhanced Living Environments”, en Advances in Intelligent Systems and Computing, Cham: Springer International Publishing, 2018, pp. 1169–1177
- [7] A. A. Hapsari, A. I. Hajamydeen, D. J. Vresdian, M. Manfaluthy, L. Prameswono y E. Yusuf, “Real Time Indoor Air Quality Monitoring System Based on IoT using MQTT and Wireless Sensor Network”, en 2019 IEEE 6th International Conference on Engineering Technologies and Applied Sciences (ICETAS), Kuala Lumpur, Malaysia, 20–21 december 2019. IEEE, 2019.
- [8] P. K. Sharma, B. Poddar, S. Dey, S. Nandi, T. De, M. Saha, S. Mondal y S. Saha, “On detecting acceptable air contamination in classrooms using low cost sensors”, 9th International Conference on Communication Systems and Networks (COMSNETS), vol. 2017, pp. 484–487, 2017
- [9] D. Suriano, G. Cassano y M. Penza, “Design and Development of a Flexible, Plug-and-Play, Cost-Effective Tool for on-Field Evaluation of Gas Sensors”, Journal of Sensors, vol. 2020, pp. 1–20, august 2020.
- [10] P. Satyanarayana y R. Narmadha, “Implementation of Wireless Sensor Network Based Indoor Air Quality Monitoring System using GSM”, International Journal of Engineering and Advanced Technology, vol. 8, n. 6, pp. 4885–4889, august 2019.
- [11] M. D. Fernández-Ramos, F. Moreno-Puche, P. Escobedo, P. A. García-López, L. F. Capitán-Vallvey y A. Martínez-Olmos, “Optical portable instrument for the determination of CO2 in indoor environments”, Talanta, vol. 208, p. 120387, february 2020.
- [12] J.-Y. Kim, C.-H. Chu y S.-M. Shin, “ISSAQ: An Integrated Sensing Systems for Real-Time Indoor Air Quality Monitoring”, IEEE Sensors Journal, vol. 14, n. 12, pp. 4230–4244, december 2014.
- [13] M. Lopes, J. Reis, A. P. Fernandes, D. Lopes, R. Luorenco, T. Nunes, C. H. G. Faria, C. Borrego y A. I. Miranda, “Indoor air quality study using low-cost sensors”, en AIR POLLUTION 2020, 8–10 june 2020. Southampton UK: WIT Press, 2020.
- [14] F. Tahsiin, L. Anggraeni, I. Chandra, R. A. Salam y H. Bethaningtyas, “Analysis of Indoor Air QualityBased on Low-Cost Sensors”, International Journal on Advanced Science, Engineering and Information Technology, vol. 10, n. 6, pp. 2627–2633, december 2020.
- [15] A. K. Kanal y T. Kovacsazhy, “IoT Solution for Assessing the Indoor Air Quality of Educational Facilities”, en 2019 20th International Carpathian Control Conference (ICCC), Krakow-Wieliczka, Poland, 26–29 may 2019. IEEE, 2019.
- [16] A. Mellit, M. Benghanem, O. Herrak y A. Messalaoui, “Design of a Novel Remote Monitoring System for Smart Greenhouses Using the Internet of Things and Deep Convolutional Neural Networks”, Energies, vol. 14, n. 16, p. 15, august 2021.
- [17] T. Pietrucha, “Ability to Determine the Quality of Indoor Air in Classrooms without Sensors”, E3S Web of Conferences, vol. 17, p. 00073, 2017.
- [18] S. N. Mabdeh, A. Al-Zghoul, T. Alradaideh, A. Bataineh y S. Ahmad, “Simulation study for natural ventilation retrofitting techniques in educational classrooms – A case study”, Heliyon, vol. 6, n. 10, october 2020
- [19] O. A. Postolache, J. M. D. Pereira y P. M. B. S. Girao, “Smart Sensors Network for Air Quality Monitoring Applications”, IEEE Transactions on Instrumentation and Measurement, vol. 58, n.º 9, pp. 3253–3262, september 2009
- [20] K. Shahzad y B. Oelmann, “A comparative study of in-sensor processing vs. raw data transmission using ZigBee, BLE and Wi-Fi for data intensive monitoring applications”, en 2014 11th International Symposium on Wireless Communications Systems (ISWCS), Barcelona, Spain, 26–29 august 2014.
- [21] A. Zivelonghi y M. Lai, “Mitigating aerosol infection risk in school buildings: the role of natural ventilation, volume, occupancy and CO2 monitoring”, Building and Environment, vol. 204, p. 13, October 2021.
- [22] J. Allen, J. Spengler, E. Jones, J. Cedeno-Laurent, “5-step guide to checking ventilation rates in classrooms”. Reporte tecnico, Harvard. https://schools.forh.earth.org/wp-content/uploads/sites/19/2021/01/Harvard-Healthy-Buildings-program-How-to-assess-classroom-ventilation-10-30-2020-EN_R1.8.pdf, 2020.
- [23] L. V. de Abreu-Harbich, V. L. A. Chaves y M. C. G. O. Brandstetter, “Evaluation of strategies that improve the thermal comfort and energy saving of a classroom of an institutional building in a tropical climate”, Building and Environment, vol. 135, pp. 257–268, may 2018

BCSM: A BlockChain-based Security Manager for Big Data

Hanan E. Alhazmi¹, Fathy E. Eassa²

Department of Computer Science, Faculty of Computing and Information Technology
King Abdulaziz University (KAU), Jeddah, Saudi Arabia^{1,2}
Computer Science Department, Umm Al-Qura University, Makkah 21955, Saudi Arabia¹

Abstract—The amount of data generated globally is increasing rapidly. This growth in big data poses security and privacy issues. Organizations that collect data from numerous sources could face legal or business consequences resulting from a security breach and the exposure of sensitive information. The traditional tools used for decades to handle, manage, and secure data are not suitable anymore in the case of big data. Furthermore, most of the current security tools rely on third-party services, which have numerous security problems. More research must investigate protecting user-sensitive information which can be abused and altered from several sides. Blockchain is a promising technology that provides decentralized backend infrastructure. Blockchain keeps track of transactions indefinitely and protects them from alteration. It provides a secure, tamper-proof database that may be used to track the past state of the system. In this paper, we present our big data security manager based on Hyperledger Fabric, which provides end-to-end big data security, including data storage, transmitting, and sharing as well as access control and auditing mechanisms. The manager components and modular architecture are illustrated. The metadata and permissions related to stored datasets are stored in the blockchain to be protected. Finally, we have tested the performance of our solution in terms of transaction throughput and average latency. The performance metrics are provided by Hyperledger Caliper, a benchmark tool for analyzing Hyperledger blockchain performance.

Keywords—Big data security; blockchain; access control; hyperledger fabric

I. INTRODUCTION

Since 2011, five Exabytes (10^{18}) of data have been generated every two days. Nowadays, this is done in less than ten minutes [1]. Social media data, videos, server logs, and sensor data are among the many types of data that have been generated. Compared to a traditional relational database management system, big data technologies are more equipped to deal with large volumes and diverse types of data. Large amounts of information can be gathered from various big data applications. For instance, these massive amounts of data always contain sensitive information that might disclose a person's identity. Although all of the information required to identify a person may not be present in the same dataset, a combination of data sources may be able to reveal their identity. Because of this, these sensitive data must be protected. When it comes to storing large amounts of data, distributed storage like Hadoop Distributed File System (HDFS) [2] is commonly used. Multiple nodes must cooperate to complete a single task in distributed storage. Consequently, the reliability of computing results will be affected if an attack targets one or more nodes. Distributed data storage significantly raises the

storage node's obligation to protect the data. Key management becomes more difficult in the case of encrypted data storage. As a result, the traditional symmetric and asymmetric encryption techniques cannot be directly applied in big data schemes [3]. In the existing Hadoop implementation [4], the Portable Operating System Interface (POSIX) architecture is used to enable access to folders and files stored in HDFS where users may or may not be granted access to a whole dataset. However, this does not prevent authorized users from misusing or abusing the data. It also provides system security auditing [5]; however, there is no standard format for this auditing, making it difficult to read and analyze. Our previous work [6] presented the way for implementing a security framework in Hadoop. We proposed integrating blockchain technology with new fragmentation and encryption techniques to increase big data security. We have tested the performance of our techniques which imposed negligible computation overhead in contrast to the security and privacy improvements. Once the data are fragmented and stored, the next step is to test the performance when integrated with blockchain. This paper presents a new security solution for big data, called BCSM, that leverages the unique security by design and tamper-proof properties of blockchain technology in contemporary domains[7], [8]. Data is stored in HDFS, and the related metadata and permissions will be held as assets inside the blockchain. We used Hyperledger Fabric [9], a permissioned blockchain with a distributed ledger that allows smart contracts [10]. Unlike other public blockchains like Ethereum, Bitcoin, or Monero, the data in Fabric can only be accessed by those who have been authorized. Paper contributions are summarized below: 1) proposing a new architecture of integrating big data (Hadoop) with blockchain (Hyperledger fabric); 2) enforcing access control policies based on data permissions; 3) protecting metadata and permissions to be stored and accessed by blockchain. 4) evaluating the performance of the proposed solution in terms of throughput and latency for reading and writing operations. The remainder of the paper is structured as follows. Section 2 is a compilation of related work. The proposed BCSM manager is presented in depth in Section 3. Section 4 presents the findings of the BCSM manager's testing and evaluation. The conclusion is addressed in Section 5.

II. STATE OF THE ART

A. Blockchain Technology

Blockchain is a decentralized system for exchanging digital currencies that were first introduced by bitcoin [11]. Blockchain is managed by a peer-to-peer network. It is a

distributed ledger that records and stores transactions in blocks that are linked using cryptography. An untrusted party submits a transaction block, which is then confirmed by the other participants in the chain of transactions without any central authority. The chain expands indefinitely from the first block, the genesis block, as each subsequent block ties to the previous one via its hash value. In other words, the hash value of the preceding block is considered when calculating the hash value of a new block. As a result, any attempt to alter the hashes of connected blocks will cause the shared ledger to be tampered with, making the blockchain tamper-resistant. All members of the blockchain will have access to a shared ledger. Each peer will have access to the latest version of the blockchain after being updated to its unique state.

Tractability is one of the important features of the blockchain. Transactions on the blockchain are tagged with a timestamp once they've been validated. Thus, allowing users to track the history of all transactions to facilitate auditing, which is essential in data management and applications that need access to a tamper-proof log history.

1) *Consensus Algorithms:* Consensus algorithms are used to obtain consensus on the new state of the blockchain. A consensus algorithm uses a group of participants who are directly participating in the system to make agreements instead of using third-party decision-making. Practical Byzantine Fault Tolerance (PBFT), PBOT, Proof of work (PoW), and proof of stake (PoS) are some of the most well-known examples of consensus algorithms on the blockchain. They differ in identity management mechanisms, adversary power, and energy savings [12].

2) *Smart Contract:* The smart contract is stored on a blockchain which is a piece of code executed when some conditions are fulfilled. Smart contracts are often used to automate the execution of business logic. All participants are instantly receiving the outcome without the engagement of an intermediary or the loss of time. On the other hand, smart contracts eliminate the need for a centralized authority. Aside from just exchanging digital currency, smart contracts can also be used to build applications in the supply chain, business process management (BPM), and healthcare, all of which are areas where blockchain technology has the potential to have a significant influence.

3) *Blockchain Types:* Bitcoin was the first public blockchain. That is, anyone with an anonymous identity can join and read the blockchain, submit transactions, and participate in the consensus process. Although public blockchains have the advantage of being accessible to anyone with unknown identities, the rise of private blockchains is more suited from an intra-organizational viewpoint to incorporating blockchain into several products. Users who want to join the private or permissioned blockchain must be authenticated by an additional permission layer. As a result, the main distinction between public and private blockchain is participating in the system. Furthermore, there is a third form of blockchain known as a consortium blockchain, which can be considered a hybrid because only certain nodes can participate in consensus, and access to read or write on the blockchain [13]. Fabric, Sawtooth, Burrow, and Iroha are examples of open-source industrial blockchain frameworks under the Hyperledger projects hosted by Linux. In order to build permissioned blockchain

platforms, Hyperledger Fabric provides a modular design and contains a Membership component. It contains the "chain-code" which is used to implement the application logic, and transaction functionalities in several programming languages. The Fabric uses an execute-order-validate approach instead of an order-execute [14] to solve the drawbacks of permissioned blockchains, like the non-deterministic execution of concurrent transactions, inflexible trust model, execution on all nodes, and hard-coded consensus. The Transaction Log and the World State are parts of Fabric's ledger. All transactions are recorded in a transaction log. By utilizing the world state, a program may obtain the current value of a state without searching through the entire transaction log. Key-value pairs are the default representation for ledger states. When a transaction updates any value that was previously entered in the ledger or adds new data, this is a new state for the blockchain that will be preserved in everlasting; it is impossible to return the last state of the blockchain [13].

B. Big Data Security and Privacy Issues

1) *Access Control:* Access Control is a critical aspect of big data. Organizations and users working with Big Data must implement access control policies. An access control mechanism governs the connectivity of various nodes to the system. A weak access control method can enable attackers to get unauthorized access to data storage, bringing security and privacy concerns [15]. Access control lists (ACL) and policies help protect data by granting nodes and devices privacy and security permissions. Although numerous research studies have focused on access control mechanisms, specific difficulties still need to be solved. For example in cloud, data owners who outsource their data to the cloud may selectively seek to make it visible/accessible to other users. Such a feature necessitates access control in order to enforce the authorizations provided by the data owners properly [16], [17]. For instance, these authorizations cannot be implemented in a cloud either by the data owners or cloud service providers (CSPs). However, making the outsourced data self-enforce the access permissions is a promising solution to this problem. The automation provided by smart contract will make this feasible [18].

2) *Data Integrity:* Data integrity is another consideration in maintaining big data privacy and security. Data integrity entails ensuring the consistency and accuracy of data. In the big data era, data must ensure its integrity properties from origination to final destination in analysis reports to provide valuable outcomes for business and decision-making.

3) *Metadata and Policy Protection:* Metadata is a type of data that describes other data with information that makes it easier to find, use and manage. Policies are sets of rules that are used to regulate data access. One of the attack methods is when attackers access or alter metadata and policies to compromise or get unauthorized access to data. Most of the time, data owners are unaware of whether these metadata or policies are accessed and changed by attackers. As few prior research discuss metadata and policy protection, thus there is a critical need to focus on this issue.

4) *Data Privacy:* Data privacy guarantees that only those with authorization may access the data. Big data may contain person sensitive data. Thus these data must not be revealed

without the person permission. Obtaining approval from a person is also restricted to specific causes. Consequently, protecting people sensitive attributes such as social security numbers and addresses is necessary to guarantee data privacy.

5) *Data Auditing*: Data integrity is not always possible to be guaranteed. Data loss due to malicious activity or system failure poses a significant security risk. For instance, numerous cloud-based big data auditing approaches have been proposed to maintain the integrity of big data stored in cloud storage [19], [20]. A third-party auditor (TPA) is commonly used in these approaches to perform auditing tasks on behalf of data owners. Although TPA is considered a trustworthy entity that always acts honorably, it may not be as trustworthy as it appears. Cloud service providers (CSPs) may even hire a TPA to assist them in concealing data corruption incidents. Furthermore, because of centralization, the single point of failure might have disastrous impacts. TPA system disruptions can be caused by external attacks and internal abuses flaws. Decentralized schemes are more reliable and robust than TPA-based ones.

Our research proposes a decentralized big data security manager based on blockchain technology to address all the above issues.

C. Related Work

Several research studies have explored the use of blockchain technology in healthcare to allow patients to own and control their medical information. Blockchain technology has the potential to enable secure electronic health record (EHR) sharing in which patients are the real owners. The authors of [21] suggested that the blockchain simply stores metadata relevant to medical events to avoid overwhelming blockchain limited storage due to storing the entire health records.

In the work of [22] authors presented a privacy-preserving framework for EHR by using blockchain technology with a zero-knowledge proof cryptographic protocol named Identity Mixer. Their solution aims to protect private data and maintain anonymity.

L. Yue et al. [23] introduced a blockchain-based big data-sharing architecture and used smart contracts to facilitate big data sharing. The Access control mechanism is used for addressing big data's privacy and security issues.

A supply chain is a network that transfers products from suppliers to customers, generating a huge amount of data in the process. Authors in [24] proposed integration of blockchain-based supply chain management with big data technology. However, their contribution is limited to protecting the consumers from the risk of food fraud, and they used big data to enhance the analysis process for business profits.

I. Makhdoom et al. [25] suggested a "privacy sharing" on a blockchain system for the secure and private preservation of IoT data in smart city environments. Data privacy is managed by blockchain, and some limited users have access to the blockchain data, which is encrypted and governed by an embedded access control mechanism.

To overcome blockchain synchronization time and storage space limitations, authors in [26] proposed a blockchain-based

personnel management system that provides a new on-chain and off-chain data storage model to address the problem of insufficient storage space. However, they used a central database for out-of-chain storage, which has a risk of a single point of failure.

To improve Hadoop security, authors in [27] presented a big data access control approach that maintains metadata security by enhancing the heartbeat model.

Adopting blockchain technology by means of big data security and management necessitates more efforts. Previous research exploited blockchain for limited big data applications, for example, data sharing and access control. Furthermore, there is a lack in the state of the art to provide end-to-end big data security solutions based on blockchain technology which integrates data security at rest while transmitting and offering auditing and access control mechanisms. This research intends to solve the above constraints by presenting a comprehensive and general blockchain-based security manager for big data.

III. PROPOSED SECURITY MANAGER

In this section, the proposed security manager for big data is presented. First, we describe the architecture of the proposed solution, then the details of the components and processes of our manager are provided.

A. Manager Architecture

As shown in Fig. 1, the manager elements consist of the following:

- **Data Owner (DO)** is the entity that owns the data and wants to access or store it. DO has full control over his data. DO needs to define policy for his data access, including data access permissions for others.
- **User (U)** is the entity that grants access to request data.
- **BlockChain-based Security Manager (BCSM)** ensures the legitimacy of the system events. The events involve storing big data and metadata and accessing the ledger's assets and logs. In addition, the BCSM is responsible for managing blockchain. BCSM will communicate with other entities via a secured SSL/TLS connection.
- **Big data Distributed Storage (BDS)** BDS is in charge of storing big data after fragmentation and encryption.
- **The BlockChain (BC)** is responsible for recording security events on the blockchain ledger. It includes the following:
 - Smart Contract: represents the following logic:
 - 1) creating MD and PL and inserting them as assets into ledger DB
 - 2) managing and accessing these assets according to user or data owner actions.
 - 3) managing the ACL rules used for the authorization process. The smart contract is used to interact with the ledger to read or modify the assets (MD and PL).

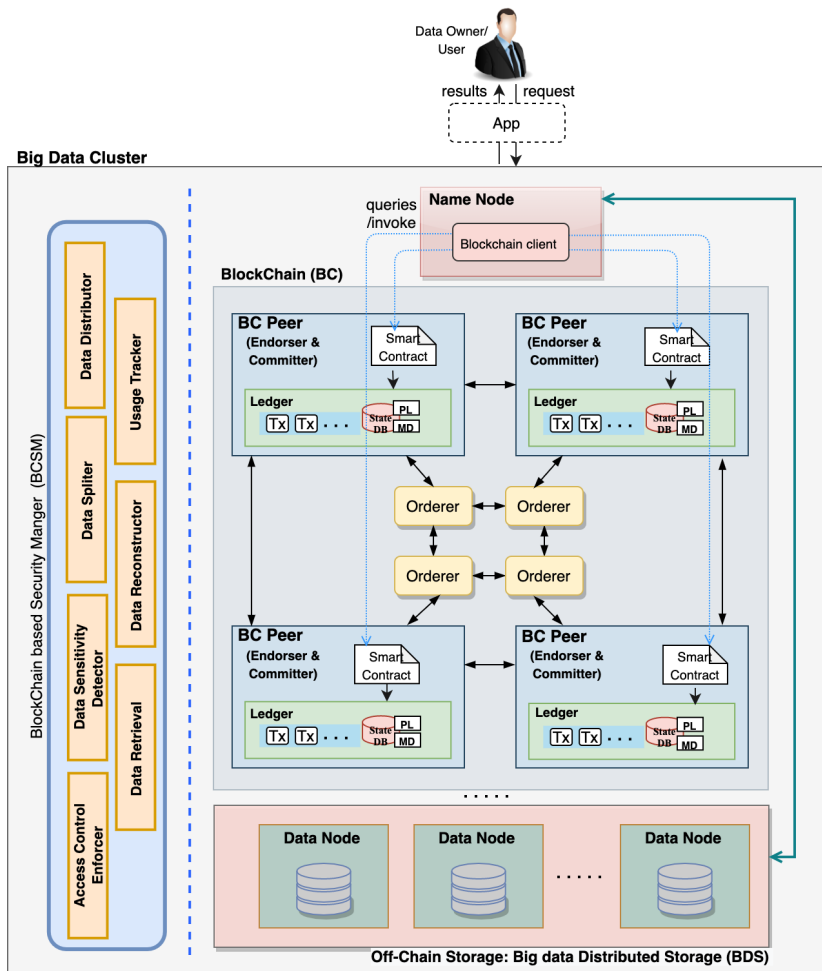


Fig. 1. Manager Architecture.

- **BC Peers:** There are two types of peers endorser which hold the smart contract and committer; both peers host a copy of blockchain ledger.
- **Orderers:** are a collection of many nodes in charge of generating an ordered list of transactions and creating blocks. Orderer is responsible for transaction hashing and block creation. The separation of smart contract execution and ordering transactions derived from Fabric architecture provides better performance and solves scalability issues compared to other blockchain platforms.

Furthermore, BC is responsible for keeping track of the system auditing logs.

- **On-chain and Off-chain Storage** Recent studies advocate storing the highly critical transactions that must be approved via blockchain consensus in order to avoid overwhelming the blockchain ledger[28]. Due to the limitations in blockchain storage, it is recommended to store the necessary critical data which require tamper-proof. These blockchain difficulties can be improved by using additional mechanisms applied on off-chain data such as fragmentation, scrambling,

and calculating the hash of the dataset to preserve it on blockchain for checksum purposes.

Specifically, there are the following components that make up the proposed Security Manager BCSM:

1) **Data Sensitivity Detector (DSD):** The approaches of sensitivity detection are classified as automated, semi-automated, or manual. Our sensitivity detection relies on the data owner's (DO) policies and requirements. DO needs to specify the level of data sensitivity (high, low, or none) and indicate the sensitive attributes that must be protected.

2) **Data Splitter (DS):** We take advantage of fragmentation techniques to give an extra layer of data security. According to the user requirements, data is divided into sensitive and non-sensitive collections. By computing the SHA-256 for the original file and comparing the hashing result to the result of the file after the reconstruction process, the checksum is utilized to confirm data integrity. The security of sensitive data is handled by our manager based on the level of sensitivity. Scrambling is used to harden the fragmentation process for low-sensitive data, and this is complemented with distributed big data storage partitioning. Furthermore, to minimize the enormous cost of encrypting the entire data volume, our method performs encryption on the high-sensitive part of the

dataset. The details of our fragmentation algorithm is presented in [6].

3) *Data Distributor (DD)*: DD assigns dataset-id for each uploaded dataset to be referred to in merged files. It creates MD and PL based on a specific structure and inserts the merged files into big data storage. Moreover, DD sends MD and PL to be kept on the blockchain ledger and managed by the smart contract.

4) *Data Retrieval (DR)*: DR gets data-hash and metadata from the blockchain using dataset-id. After that, it requests merged files from the BDS. Finally, the DR decrypts the metadata and sends it to the Data Reconstructor.

5) *Data Reconstructor (DRE)*: DRE returns the data to its original version according to the metadata stored in the blockchain. This component applies decryption and defragmentation techniques in order to reconstruct the original data. Furthermore, the data-hash is retrieved to perform the checksum needed to check data integrity.

6) *Access Control Enforcer (ACE)*: ACE handles data owner and user authentication and authorization processes. Once the ACE has authenticated the client, the authorization process is started. To verify the identity of a user, ACE employs multi-factor authentication. Data can only be accessed with the privileges specified in PL using ACL rules defined in the blockchain smart contract. Under the PL, only a selected group of users have access to the required data.

7) *Usage Tracker (UT)*: This component is responsible for responding to data owner/auditor requests of acquiring auditing information. Auditing information related to data access and usage is retrieved from the blockchain utilizing the traceability feature given by the blockchain.

Fig. 2 illustrates the communication flow during the write operation, highlighting the interactions between different components starting from the Data Owner's request to upload the dataset to inserting in big data distributed storage. Fig. 3 illustrates the communication flow between several components throughout the reading process for sensitive data.

IV. EXPERIMENTAL RESULTS AND ANALYSIS

A. Performance Measurement Tool

The process of performance evaluation means measuring the system performance, which is under test. This basically includes measuring what occurs when dependent variables are changed. Measuring blockchain network performance has been a significant concern among researchers and developers. The blockchain network consists of several peers that communicate with each other in order to collaborate to perform transactions.

We used Hyperledger Caliper v0.4.2 [29] to evaluate our solution performance. Hyperledger Caliper is a unified blockchain benchmark tool that integrates with different blockchain platforms. It allows us to test the performance of our manager components running under blockchain when interacting with client application requests for dataset read and write operations

TABLE I. EXPERIMENTS SETUP

Components	Values
Number of Organizations	2
Number of Endorsor Peers	2
Ordering Service	RAFT
Endorsement Policy	"OR('Org1MSP:peer')" "OR('Org1MSP:peer', 'Org2MSP:peer')"
Block Size	10 transactions per block
Programming Language for smart contract	Nodejs
Ledger Database	CouchDB
Number of clients	2
Transaction duration	30s
Send Rates	50-650 tps

B. Performance Metrics

- **Transaction Throughput** is not measuring only at one node but across all nodes in the network. It is the rate at which the blockchain commits valid transactions in a specific time period, represented in transactions per second (tps).

- **Transaction Latency** is the time it takes for the whole network to validate a transaction, including broadcasting and allocation time used by the consensus algorithm.

- **Fail Rate** is described as the amount of failed transactions performed out of the total transactions

C. Experiment Environment Setup

Our blockchain platform is Hyperledger Fabric v2.3.3. The experiments were conducted on a host machine equipped with Intel Core i9 2.3 GHz, 16GB DDR6 memory, and a 1TB SSD hard disk. Table 1 discusses the default Fabric experiment setup. In this experiment, read or write operation is performed to virtual Hadoop cluster based on our previous study experiment [6]. The Hadoop cluster consists of one Name node and three Data nodes using the virtual machine manager VirtualBox 6.1.26.

D. Experiments Profile

To conduct our experiments, we have developed a Fabric Chaincode (smart contract), which is in charge to represent some functions of our manager components, including the authorization process of ACE, Data Distributor (DD), and Data Retrieval (DR). Moreover, the client application sending write and read requests is also implemented as part of the Caliper workload module to submit the transactions. Our previous experiment [6] started with preparing the dataset by fragmentation and encryption to ensure the efficiency of using the off-chain data storage security. Along with each operation, there is a call to blockchain to handle the management of that operation. In this paper, our concern is to test the performance of blockchain network during reading and writing operations.

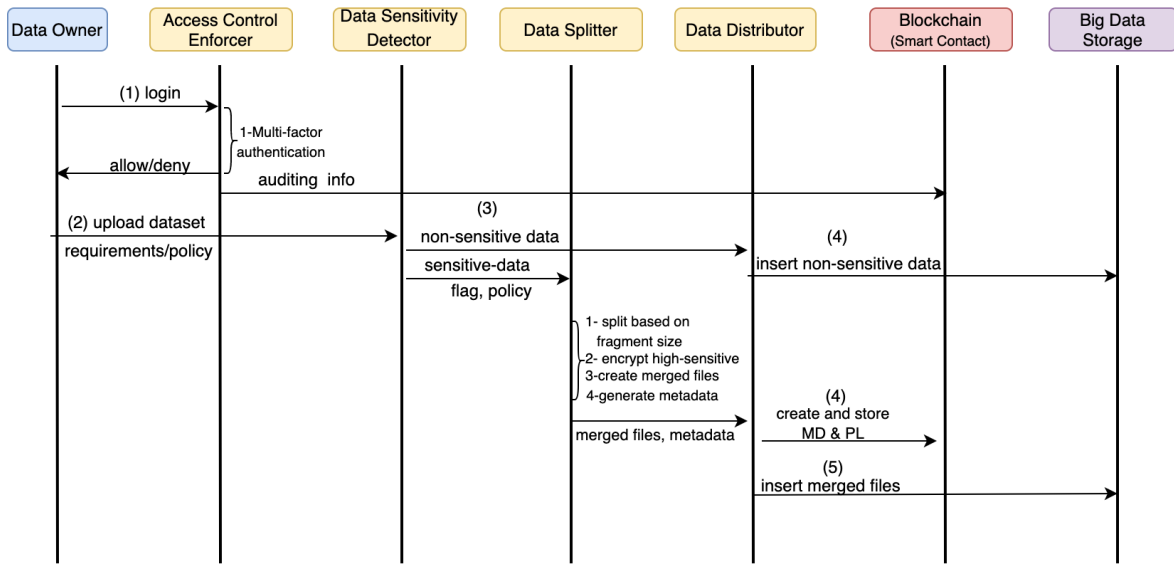


Fig. 2. Sequence Diagram for Writing Operation.

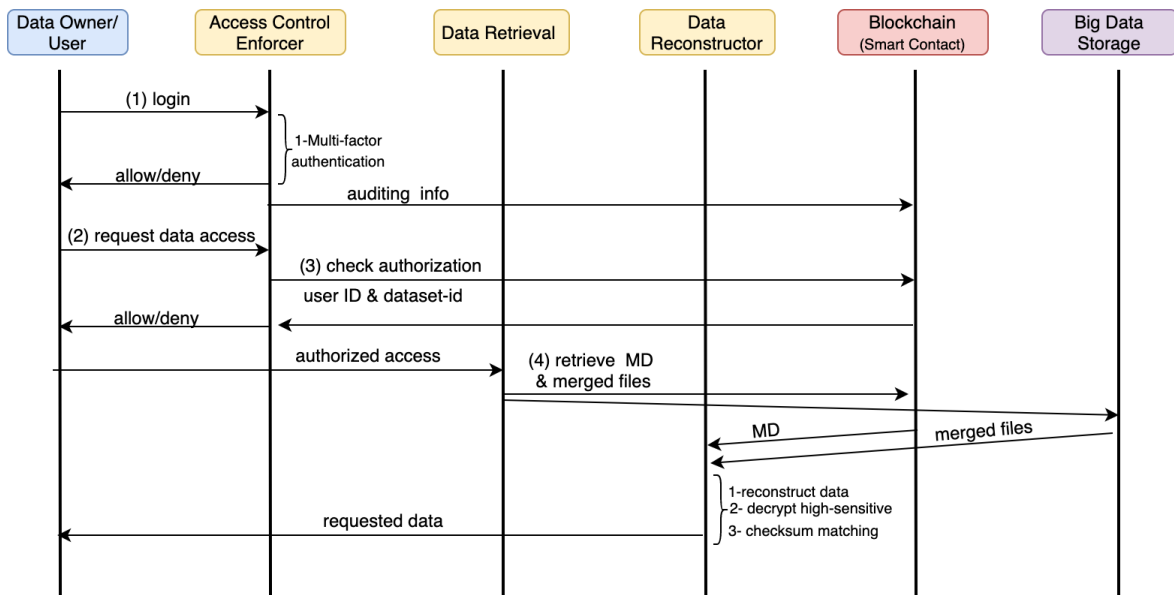


Fig. 3. Sequence Diagram for Reading Operation.

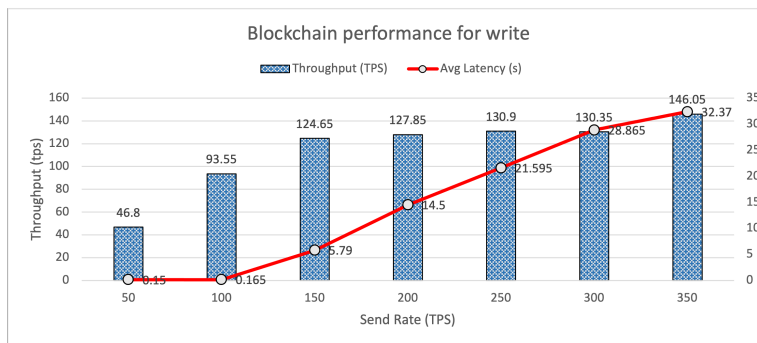


Fig. 4. Write Experiments Results.

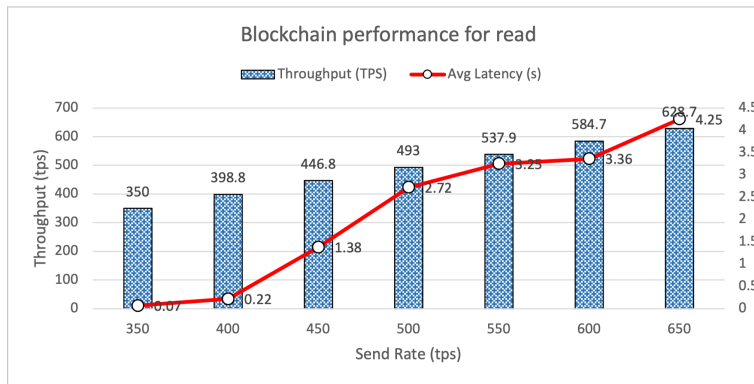


Fig. 5. Read Experiments Results.

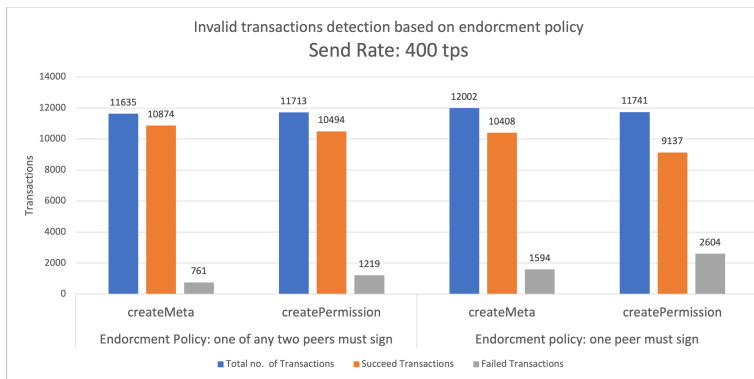


Fig. 6. Failed Transactions with Different Endorsement Policies.

E. Results and Analysis

Write Experiments: Fig. 4 plots the experimental results in terms of transaction throughput and latency for write operation. This operation involves two functions which are creating the metadata and permission lists to be stored in ledger CouchDB. The throughput increased linearly with the increase in send rate. The results show a remarkable drop in throughput when the send rate reaches 150 tps. However, the growth of transaction throughput had significant decreased approximately to half of the send rate value when the send rate was above 250 tps. Also, the figure plots the experimental results of transaction latency. When the send rate was above 150 tps, the latency had a significant increase.

Read Experiments: We evaluated the performance of our manager by varying transaction send rates (350 tps to 650 tps) to measure transaction throughput and latency. The Fabric has robust performance for reading and accessing assets stored in its ledger. In our read experiment scenarios, the results show no impact on throughput and average latency for send rates from 50 to 300 tps. The throughput reaches the same value as send rate with the same latency equals 0.01 seconds. Consequently, we started our performance evaluation for reading experiments from 350 tps when the performance showed a significant impact. We configured the test with a different number of transactions in each round of testing. Even though the average latency grows with the number of transactions, the rise is not sharp and growing very slowly. Fig. 5 plots the experimental results in terms of average transaction throughput. As shown in Fig. 5, the solution can process a throughput of around

350 to 628 transactions per second (authorization decisions) with an average latency of 0.07 to 4.25 seconds. Fig.5 shows the transaction throughput increased linearly with the increase in send rate. However, the transaction throughput increased until the send rate reached around 500 tps. The transaction throughput growth decreased when the send rate was above this point. Fig. 5 also shows the results of transaction latency. The transaction latency increases with the increase in the send rate. There is a small growth of latency for send rates from (350 tps to 400 tps). However, the growth of latency is increased from (450 tps to 650 tps).

Endorsement Policy in Write Experiments: Moreover, we evaluate our solution with different endorsement policies. Write experiments include the execution of two functions: (1) createMeta, which creates and inserts metadata into the ledger state (2) createPermission, which creates the permission list then inserts it into the ledger state. As depicted in Fig. 6, the experiment shows an impact on the number of failed transactions. In the case of "OR('Org1MSP.peer')", the peer from organization1 must sign. In the other case, "OR('Org1MSP.peer', 'Org2MSP.peer')", one of any two peers can sign. This experiment indicates that the choice of endorsement policy has a significant impact on the number of invalid transactions.

V. CONCLUSION

This study presents our proposed manager BCSM, which aims to enhance big data security and privacy. Our security manager is based on blockchain technology, and we have

developed a prototype manager using Hyperledger Fabric and Hadoop to test the feasibility of this solution. We have defined several big data security and privacy issues and proposed our manager to address these issues. Moreover, our solution takes into account the limitation of blockchain insufficient data storage. This solution can effectively solve problems such as big data leakage and tampering. Blockchain technology is still in its early stages. There is a limitation in state of the art to leverage blockchain for improving security for large-scale data application scenarios, particularly in the big data industry. The non-tampering and traceability of blockchain are expected to have significant benefits in the field. Our manager provides a secure environment for big data sharing, storage, and transmission. The blockchain is in charge of ensuring the security of big data storage and retrieval procedures, as well as access control and auditing mechanisms. Previous studies have not sufficiently addressed big data security issues; for example, they mainly focused on access control, data sharing, and auditing for specific big data applications such as smart homes and healthcare. We believe that almost all big data fields can refer to our suggested solution, which better solves big data security problems and the potential of blockchain technology in the future.

REFERENCES

- [1] D. Laffly, "Big data in geography," *TORUS 1-Toward an Open Resource Using Services: Cloud Computing for Environmental Data*, pp. 45–54, 2020.
- [2] "The apacheTM hadoop® project." [Online]. Available: [https://hadoop.apache.org/docs/ \(2022/02/20\)](https://hadoop.apache.org/docs/ (2022/02/20)).
- [3] D. Lv, S. Zhu, H. Xu, and R. Liu, "A review of big data security and privacy protection technology," in *2018 IEEE 18th International Conference on Communication Technology (ICCT)*, pp. 1082–1091, 2018.
- [4] T. A. Kumar, H. Liu, J. P. Thomas, and X. Hou, "Content sensitivity based access control framework for hadoop," *Digital Communications and Networks*, vol. 3, no. 4, pp. 213–225, 2017.
- [5] P. Koopman, "Embedded system security," *Computer*, vol. 37, no. 7, pp. 95–97, 2004.
- [6] H. E. Alhazmi, F. E. Eassa, and S. M. Sandokji, "Towards big data security framework by leveraging fragmentation and blockchain technology," *IEEE Access*, vol. 10, pp. 10768–10782, 2022.
- [7] A. Yazdinejad, R. M. Parizi, A. Dehghantanha, H. Karimipour, G. Srivastava, and M. Aledhari, "Enabling drones in the internet of things with decentralized blockchain-based security," *IEEE Internet of Things Journal*, vol. 8, no. 8, pp. 6406–6415, 2021.
- [8] S. Yaqoob, M. M. Khan, R. Talib, A. D. Butt, S. Saleem, F. Arif, and A. Nadeem, "Use of blockchain in healthcare: A systematic literature review," *International Journal of Advanced Computer Science and Applications*, vol. 10, no. 5, 2019.
- [9] E. Androulaki, A. Barger, V. Bortnikov, C. Cachin, K. Christidis, A. De Caro, D. Enyeart, C. Ferris, G. Laventman, Y. Manevich, *et al.*, "Hyperledger fabric: a distributed operating system for permissioned blockchains," in *Proceedings of the thirteenth EuroSys conference*, pp. 1–15, 2018.
- [10] I. Mokdad and N. M. Hewahi, "Empirical evaluation of blockchain smart contracts," in *Decentralised Internet of Things*, pp. 45–71, Springer, 2020.
- [11] S. Nakamoto, "Bitcoin: A peer-to-peer electronic cash system." [Online]. Available: <https://bitcoin.org/bitcoin.pdf> (2019/07/02).
- [12] X. Li, P. Jiang, T. Chen, X. Luo, and Q. Wen, "A survey on the security of blockchain systems," *Future Generation Computer Systems*, vol. 107, pp. 841–853, 2020.
- [13] L. S. Sankar, M. Sindhu, and M. Sethumadhavan, "Survey of consensus protocols on blockchain applications," in *2017 4th international conference on advanced computing and communication systems (ICACCS)*, pp. 1–5, IEEE, 2017.
- [14] M. Vukolić, "Rethinking permissioned blockchains," in *Proceedings of the ACM Workshop on Blockchain, Cryptocurrencies and Contracts*, pp. 3–7, 2017.
- [15] P. Centonze *et al.*, "Security and privacy frameworks for access control big data systems," *Comput. Mater. Continua*, vol. 59, no. 2, pp. 361–374, 2019.
- [16] S. D. Capitani di Vimercati, P. Samarati, and S. Jajodia, "Policies, models, and languages for access control," in *International Workshop on Databases in Networked Information Systems*, pp. 225–237, Springer, 2005.
- [17] E. Damiani, S. D. C. Di Vimercati, and P. Samarati, "New paradigms for access control in open environments," in *Proceedings of the Fifth IEEE International Symposium on Signal Processing and Information Technology, 2005.*, pp. 540–545, IEEE, 2005.
- [18] Y. Xiao, N. Zhang, J. Li, W. Lou, and Y. T. Hou, "Privacyguard: Enforcing private data usage control with blockchain and attested off-chain contract execution," in *European Symposium on Research in Computer Security*, pp. 610–629, Springer, 2020.
- [19] C. Wang, S. S. Chow, Q. Wang, K. Ren, and W. Lou, "Privacy-preserving public auditing for secure cloud storage," *IEEE transactions on computers*, vol. 62, no. 2, pp. 362–375, 2011.
- [20] F. Zafar, A. Khan, S. U. R. Malik, M. Ahmed, A. Anjum, M. I. Khan, N. Javed, M. Alam, and F. Jamil, "A survey of cloud computing data integrity schemes: Design challenges, taxonomy and future trends," *Computers & Security*, vol. 65, pp. 29–49, 2017.
- [21] A. J. N. Gupta and P. Roy, "Adopting blockchain technology for electronic health record interoperability," tech. rep., Cognizant Technology Solutions, New Jersey, U.S, 2016.
- [22] C. Stamatellis, P. Papadopoulos, N. Pitropakis, S. Katsikas, and W. J. Buchanan, "A privacy-preserving healthcare framework using hyperledger fabric," *Sensors*, vol. 20, no. 22, p. 6587, 2020.
- [23] L. Yue, H. Junqin, Q. Shengzhi, and W. Ruijin, "Big data model of security sharing based on blockchain," in *2017 3rd International Conference on Big Data Computing and Communications (BIGCOM)*, pp. 117–121, IEEE, 2017.
- [24] M. R. Amin and M. F. Zuhairi, "Review of fscm with blockchain and big data integration," *Indian J. Comput. Sci. Eng.*, vol. 12, pp. 193–201, 2021.
- [25] I. Makhdoom, I. Zhou, M. Abolhasan, J. Lipman, and W. Ni, "Privysharing: A blockchain-based framework for privacy-preserving and secure data sharing in smart cities," *Computers & Security*, vol. 88, p. 101653, 2020.
- [26] J. Chen, Z. Lv, and H. Song, "Design of personnel big data management system based on blockchain," *Future Generation Computer Systems*, vol. 101, pp. 1122–1129, 2019.
- [27] C. Zhang, Y. Li, W. Sun, and S. Guan, "Blockchain based big data security protection scheme," in *2020 IEEE 5th Information Technology and Mechatronics Engineering Conference (ITOEC)*, pp. 574–578, IEEE, 2020.
- [28] J. Eberhardt and S. Tai, "On or off the blockchain? insights on off-chaining computation and data," in *European Conference on Service-Oriented and Cloud Computing*, pp. 3–15, Springer, 2017.
- [29] "Hyperledger caliper—a blockchain benchmark tool." [Online]. Available: <https://www.hyperledger.org/use/caliper> (2021/12/02).

A Review-based Context-Aware Recommender Systems: Using Custom NER and Factorization Machines

Rabie Madani, Abderrahmane Ez-zahout
Intelligent Processing and Security of Systems Team
Computer Sciences Department
Faculty of Sciences
Mohammed V University
Rabat, Morocco

Abstract—Recommender Systems depend fundamentally on user feedback to provide recommendation. Classical Recommenders are based only on historical data and also suffer from several problems linked to the lack of data such as sparsity. Users' reviews represent a massive amount of valuable and rich knowledge information, but they are still ignored by most of current recommender systems. Information such as users' preferences and contextual data could be extracted from reviews and integrated into Recommender Systems to provide more accurate recommendations. In this paper, we present a Context Aware Recommender System model, based on a Bidirectional Encoder Representations from Transformers (BERT) pretrained model to customize Named Entity Recognition (NER). The model allows to automatically extract contextual information from reviews then insert extracted data into a Contextual Machine Factorization to compute and predict ratings. Empirical results show that our model improves the quality of recommendation and outperforms existing Recommender Systems.

Keywords—Recommender systems; context aware recommender systems; factorization machines; bidirectional encoder representations from transformers; named entity recognition

I. INTRODUCTION

In the last few years, the number of services and items offered and produced by businesses and websites have increased quickly, which makes the choice of products and services meeting customers' needs more difficult.

Recommender systems (RS) tackle this problem by helping users to find suitable resources, based on their past behaviors and preferences. Today, companies use RS in several domains to assist users, enhance customer experience and make it easier for them to satisfy their needs by speeding up searches.

Whereas, traditional Recommender systems such as Collaborative Filtering techniques [1] are based on two dimensions (User X Item) and on numeric rating (e.g., 5 stars rating) to compute similarities between users and items and produce recommendations. Context Aware Recommender Systems [2] use other dimensions beside the two classical dimensions, namely contextual information dimensions (User X Item X Context) to enhance the accuracy. The contextual information represents the environmental factors that influence the user's decision. In general, numeric rating expresses whether a user likes or dislikes an item, however, it does not allow us to

understand why, when or where he/she makes this choice and reasons behind it.

Where sparsity and the lack of information represent big challenges to Recommender Systems, customers' reviews could be a good resource to solve these problems and help companies to well understand decisions made by users. In fact, many models have been proposed to extract valuable information from reviews like sentiment analysis and rating extraction, but only few works have been presented to extract contextual information from users' reviews.

In this article, we present a new model for contextual information extraction based on a pre-training language representation method trained on large amounts of data like Wikipedia called BERT and a custom Named Entity Recognition. The extracted data is used by a Contextual Machine Factorization algorithm to predict the user's interest.

This paper is organized as follows.

The remainder of this paper is presented as follows. In Section 2, we give a review of related works. In Section 3, we define the context dimension and we present the Named Entity Recognition and BERT. We introduce Factorization Machine algorithm and its use in Context-Aware Recommender Systems in Section 4. In Section 5, we present the proposed work in detail. In Section 6 we discuss obtained results. Finally, a conclusion of the work is presented in the last section.

II. RELATED WORK

Recently, many works have been proposed for extracting precious data from reviews and integrating them into recommendation process. This section presents recent applications of reviews-based Recommender systems.

Zheng et al. [3] presented a Deep Cooperative Neural Networks (DeepCoNN) model based on word embedding techniques and two convolutional neural networks (CNNs). The first network extracts user behaviors from users' reviews and the second network extracts item properties from reviews written on items. The model merges network outputs and transmits it to a factorization machine algorithm for the prediction.

Similarly to DeepCoNN [3], R. Catherine and W. Cohen [4] proposed a model called Learning to Transform for

Recommendation (TransNets) based on two parallel CNNs, one to process the target review and the other to process the texts of the user and item pair and Factorization Machine to predict rating. The difference between the two models is that the transnet model integrates an additional Transform layer to represent the target user-target item pair.

McAuley and Leskovec [5], introduced a Hidden Factors and Hidden Topics (HFT) model that merges reviews written by users and ratings to provide recommendations. The model uses Latent-Factor Recommender Systems to predict ratings and the Latent Dirichlet Allocation to discover hidden dimensions in review text.

Tan et al. [6], introduced a Rating-Boosted Latent Topics (RBLT) framework which models item features and user preferences by combining textual information extracted from reviews and numeric ratings. The RBLT model represents users item as a latent rating factor distribution, and repeats reviews with rating n time to dominate topics. To perform predictions outputs are introduced into a Latent Factorization Machine (LFM).

Zhang et al. [7], proposed an Explicit Factor Models (EFM) to produce explainable recommendations. EFM extracts user sentiments from reviews and explicit item features, then recommends or not recommends items based on hidden features learned, items features and users' interest. All previously cited works have exploited reviews to boost recommender systems, but they ignore contextual information which could significantly improve recommendations.

Other researchers succeeded in integrating context in recommendation tasks such as Aciar, [8] proposed a Mining Context Information method based on classification rules text mining techniques to automatically identify user's preferences and contextual information inside reviews, extract it and integrate it in recommendation. However, this method identifies sentences containing context but it can not extract contextual information from these sentences.

Hariri et al. [9] which proposed a Context Aware Recommender system that models user reviews to obtain contextual data and combines it with rating history to compute the utility function and suggest items to users. The model handles the context like a supervised problem of topic modeling and builds the classifier of context using a labeled-LDA. The system uses conventional recommendation algorithms to predict ratings. However, this work predicts the utility function not the rating.

Levi et al. [10] introduced a Cold Start Context-Based Hotel Recommender System based on context groups extracted from reviews. This approach uses many elements, including a weighted algorithm for text mining, an analysis to understand hotel features sentiment, clustering to build a hotel's vocabulary and nationality groups. Despite this study tackling the cold start issue, it doesn't show how to integrate extracted context in recommendation adequately.

Compos et al. [11] introduced an approach to extract contextual information from user reviews using large-scale and generic context taxonomy based on semantic entities obtained from DBpedia. In this approach a software tool builds the taxonomy by exploring DBpedia automatically, and also allows for manual adjustments of the taxonomy. Despite this work

presenting a semi-automatic method to extract context from reviews, it does not explain how to use extracted data to predict ratings.

Lahlou et al. [12] proposed a review aware Recommender system based on users' reviews to build a contextual recommendation. The proposed architecture allows to automatically exploit contextual information from reviews to build recommendations. They also presented a Textual Context Aware Factorization Machines (TCAFM) which is tailored to context. This work shows good performances in terms of accuracy, but it considers the whole review as a context instead of extracting contextual data, and in the real world datasets only few reviews contain this kind of data.

III. CONTEXT EXTRACTION

To extract contextual information from reviews, we should firstly define context dimensions (a.k.a. categories of context). In the literature, many context modeling approaches have been introduced, but the most commonly used context representation is [13], the major of these approaches use ontologies to build context taxonomy. For instance, Castelli et al. [14] use the W4 model (a.k.a. Who, When, Where, What) as components of context, "Who" is linked to the Person, "When" is associated to the Time, "Where" refers to the Location and "What" refers to the Fact. Similarly, Kim et al. [15] instantiate the 5W1H model (a.k.a. Who, Why, Where, What, When, How) as contextual components associated respectively to Status, Goal, Location, Role, Time, Action. Chaari et al. [16] proposed a basic context descriptor to describe contextual components as Service, User, Activity, Location, Device, Resource, Network. Table I resumes some principle modeling techniques of context. After revising and analysing proposed works, we choose to use four contextual dimensions, Time, Location, Companion and Environmental dimensions.

TABLE I. MAIN CONTEXT MODELING APPROACHES

Ref	Context categories
[14]	The W4 model (Who, When, Where, What): Person, Time, Location, Fact.
[15]	The 5W1H model (Who, Why, Where, What, When, How): Status, Goal, Location, Role, Time, Action.
[16]	Basic context descriptor: Service, User, Activity, Location, Device, Resource, Network.
[17]	Agent, Action, Time, Space, Policy, Event, Person, Geo-spatial
[11]	Location, Time, Environmental context, Social context

A. Named Entity Recognition (NER)

NER is one of the most important tasks of information extraction in Natural Language Processing. The aim of NER is to identify named entities in unstructured text then classify them into predefined categories (locations, organisations, monetary values, percentages, time, persons, etc.) The Named Entity Recognition is considered as a sequence labeling task

where a given sentence is presented as a tokens sequence $w = (w_1, w_2, w_3, \dots, w_n)$, and transformed to a token labels sequence $y = (y_1, y_2, y_3, \dots, y_n)$ [18], the neural model is generally composed from three elements : word embedding layer, context encoder layer and decoder layer [19].

Bidirectional long short-term memory networks (Bi-LSTM) [20][21] is widely applied in Natural Language Processing tasks and adopted by most of NER, due to its sequential characteristic and its capacity to learn contextual word representations. Despite NER having been employed in several application domains, many application fields are still not discovered, such as in Context Aware Recommender Systems.

B. BERT

BERT (Bidirectional Encoder Representations from Transformers) As its name indicates, it is a model of language representation that relies on a module called "Transformer". A transformer is a component which relies on attention methods and which is built on the basis of an encoder and a decoder. In opposition with directional and shallow-bidirectional models (OpenAI GPT [22], ELMo [23]), BERT pre-trains deep bidirectional representations from unstructured text on both left and right context in all layers [24]. It has been pre-trained on large corpus such as the entire BookCorpus and Wikipedia.

Fig. 1 represents BERT architecture, The arrows show the flow of information from layer to layer. E_1, T_r, m and T_1 respectively represent the embedding representation, the intermediate representations and the final output for a given word.

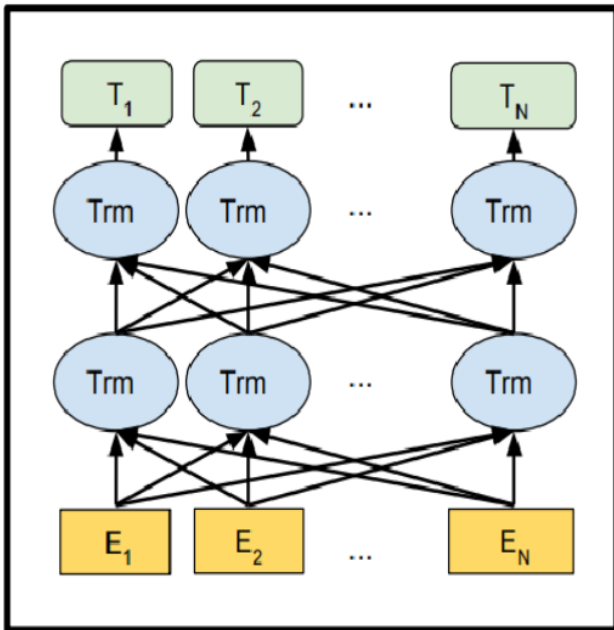


Fig. 1. BERT Architecture.

Language Modeling is a usual NLP task of predicting the next word given the start of the sentence. The Masked Language Model (MLM) allows to BERT to learn in an unsupervised way, the entry is sufficient on its own, no need to

label anything. The principle of Masked Language Modeling is to predict "masked" tokens from the other tokens in the sequence. In the first step of BERT's pre-training, 15% of the tokens of each sequence are masked, randomly. This step is very essential because BERT gets its deep bidirectionality from it.

IV. MACHINE FACTORIZATION FOR CONTEXT AWARE RECOMMENDER SYSTEMS

Factorization machines (FM) proposed by Rendle [25], a general-purpose supervised learning algorithm that could be used in regression and classification tasks. It rapidly became one of the most popular algorithms for recommendation and prediction. It is a generalization of the linear model that is able to capture interactions between variables and also it can significantly reduce the polynomial complexity to linear computation time. FM is very efficient especially within high dimensional sparse datasets.

Let $x \in \mathbf{R}^d$ be the feature vectors and y be the corresponding label. The model equation for a factorization machine is defined as:

$$y(x) = w_0 + \sum_{i=1}^d w_i x_i + \sum_{i=1}^d \sum_{j=i+1}^d \langle v_i, v_j \rangle x_i x_j \quad (1)$$

Where $w_0 \in \mathbf{R}$ is the bias term, $w \in \mathbf{R}^d$ are weights corresponding to each feature vector, $V \in \mathbf{R}^{d \times k}$ the interaction matrix, v_i is the i^{th} row of the V matrix, $\langle v_i, v_j \rangle$ the interaction between the i^{th} and j^{th} variable. It is important to point out that this factorization has the ability to compute all pairwise interactions, even hidden feature interactions which can significantly reduce engineering efforts.

Context Aware Factorization Machines is an application of the origin FM algorithm without any tuning. In effect, it is easy for the algorithm to incorporate the additional dimensions without making any changes, since it uses a sparse vector representation. Fig. 2 represents how to transform the contextual dimensions into a prediction problem from real-valued features using Sparse Feature Vector Representation.

We used FM for two main reasons. The First reason is that the algorithm is designed to support sparse data, and the extracted contextual information will make the matrix more sparse. The second reason is that the computation cost of FM is a linear time complexity ($O(kd)$), even for additional contextual dimensions.

V. METHODOLOGY

The implementation of our model is a two-steps process. The first step is for context extraction from reviews using a custom NER and BERT model. As shown in Fig. 3, in this step we aim to switch from the two-dimensional mode used by classic Recommender Systems to multi-dimensions mode used by Context-aware Recommenders. In the second step a contextual Factorization Machine is applied to predict ratings and generate recommendations based on outputs from the previous step.

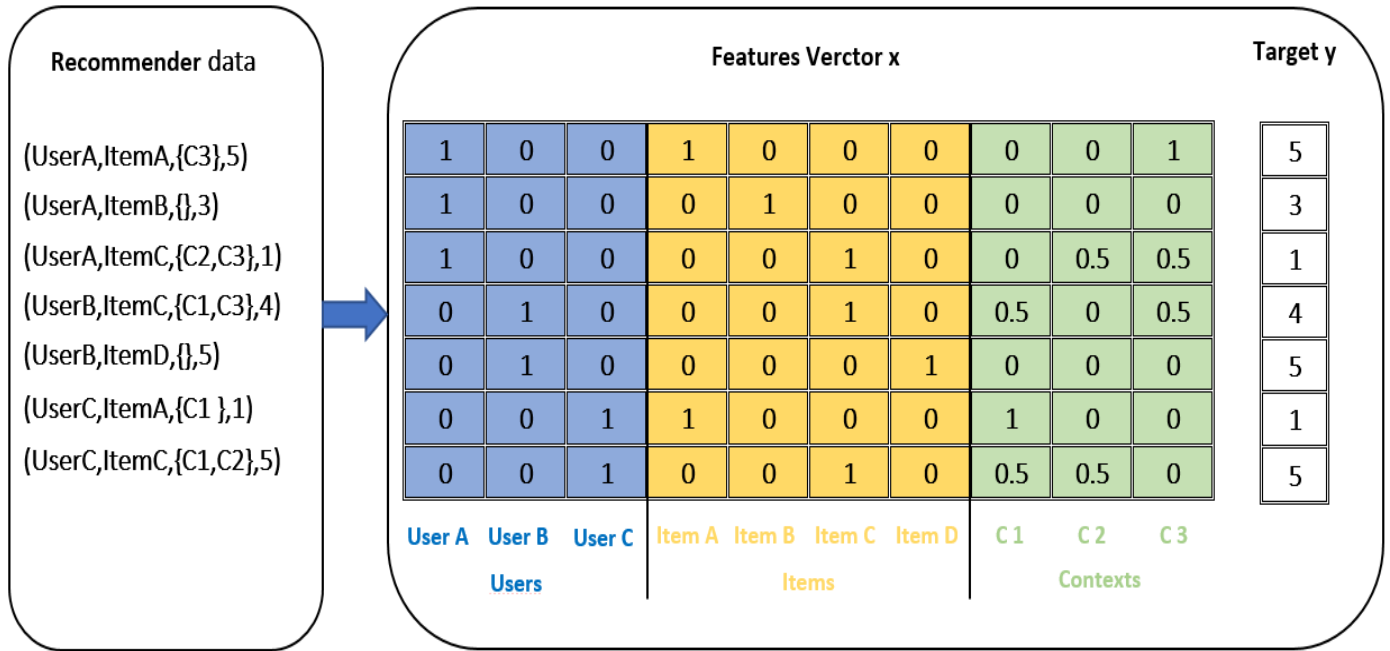


Fig. 2. Recommendation Data is Transformed to a Prediction Problem, where the First Three Columns Refer to users, the Next Four Columns Refer to Items and the Last Three Column Represent the Context.

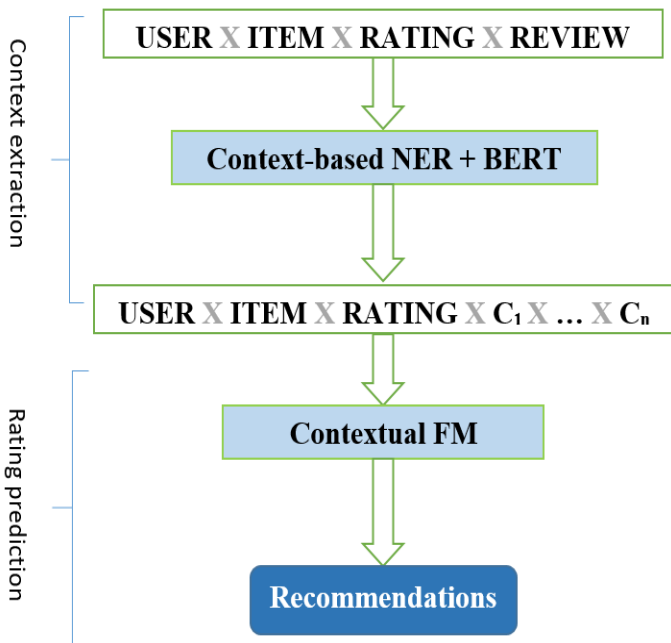


Fig. 3. The Global Architecture of our Model.

A. Context Extraction Step

In this step, The Named Entity Recognition is treated as a sequence labeling problem. Our model consists of three layers as shown in Fig. 4 namely, word embedding layer, BiLSTM layer and CRF layer. In the first layer, the BERT pre-trained model takes a sequence of n words (w_1, w_2, \dots, w_n),

then outputs a contextual embedding vector representation of each word. In contrast to context independent word embedding techniques such as Word2Vec [26], BERT is a powerful model, highly bidirectional and utilizes contextual information to learn word's context. BERT has two variants:

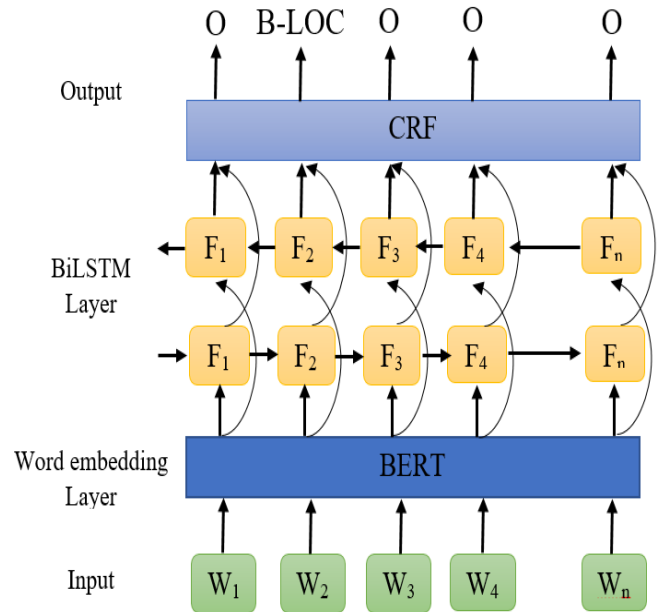


Fig. 4. The Architecture of the Custom NER.

- **BERT Base:** 12 layers (transformer encoders), 768 hidden layers, 12 attention heads and 110M parameters.

- **BERT Large**: 24 layers (transformer encoders), 1024 hidden layers, 16 attention heads and 340M parameters.

In this work we use the BERT Base model [27].

In the second layer, the Bidirectional Long Short-Term Memory (Bi-LSTM) took part. Bi-LSTM is an extension of LSTM proposed by [28] that uses forward and backward networks to process sequences. It is designed to avoid gradient vanishing and exploding and also escape the problem of long term dependency.

The output from the embedding layer is sent to the Bidirectional Long Short-Term Memory (Bi-LSTM) to extract vector features from words. Bi-LSTM concatenates the forward and the backward networks as a final result $[H_l, H_r]$. In the last layer, Conditional Random Fields (CRF) [28] outputs the most probable tag sequences. CRF is a probabilistic discriminative model that is used to label sequences. The use of CRF helps the model to learn labels and constraints that ensure the validity of the sequence. For example, the BIO format (Beginning, Inside, Outside) is a common tagging format for tagging tokens, the first word label must begin by "B" or "O" not by "I", this constraint is learned automatically by CRF.

Let X be the input sequence and Y the corresponding tag sequences, P the matrix obtained from the previous layer and T the transition matrix which represents the probability from label y_i to label y_{i+1} . The score of the tags sequence is computed as follow :

$$Score(X, Y) = \sum_{i=1}^n P_{i, y_i} + \sum_{i=1}^n T_{y_i, y_{i+1}} \quad (2)$$

B. Rating Prediction Step

In this step, a Contextual Factorization Machine (CFM) takes the output from the previous step and predicts the rating. CFM is similar to MF except that a matrix of weights is added to capture the importance of contextual dimensions. the CFM equation is given as follow:

$$y(x) = w_0 + \sum_{i=1}^d w_i b_i x_i + \sum_{i=1}^d \sum_{j=i+1}^d \langle v_i, v_j \rangle b_i b_j x_i x_j \quad (3)$$

where $w_0 \in \mathbf{R}$ is the global bias, $w \in \mathbf{R}^d$ are weights corresponding to each feature vector, $V \in \mathbf{R}^{d \times k}$ the interaction matrix, v_i i th row of the V matrix, $\langle v_i, v_j \rangle$ the interaction between the i -th and j -th variable and $B \in \mathbf{R}^p$ the matrix of weights of the importance. The parameter b_i equal to 1 for item and user and $b_i x_i$ for other dimensions.

VI. EXPERIMENT AND RESULTS

A. Corpora and Dataset

We use three corpora to pre-train our custom NER :

- **Corpus 1** is the CoNLL-2003 [29] NER dataset which consists of 18,453 sentences, 254,983 tokens and four entities namely persons, locations, organizations and miscellaneous.

- **Corpus 2** is the Groningen Meaning Bank (GMB) [30] for name entity classification, developed at the University of Groningen. It comprises 63,256 sentences, 1,388,847 tokens and eight entities (Geographical Entity, Organization, Person, Geopolitical Entity, Time, Artifact, Event, Natural Phenomenon).

- **Corpus 3** is a custom corpus that we build to face some lake in the two aforementioned corpus. In fact, after training our custom NER, it is still not able to extract some categories such as Companion context and Environmental context, e.g., "I watched the movies with my friend at the cinema" friend and cinema should be annotated as companion and location, but it's not the case. The new corpus allows us to fine-tune our custom NER, and tackle this problem. It is created in a BIO(Beginning, Inside, Outside) format and consists of 3500 sentences, 43,565 tokens and three entities.

To evaluate our model, we have selected Amazon Customer Reviews Dataset [31] and Yelp dataset [32]. Amazon dataset consists of customer reviews, ratings and product metadata(price, brand, descriptions, ...). It includes more than 233.1M reviews collected between 1996 and 2018 and 21 categories of products. This dataset is considered as the largest public dataset for rating. The Yelp dataset is a free to use dataset for academic and personal purposes, it contains more than 8.5M reviews and more than 160K businesses.

We adopted three metrics to evaluate our custom NER namely Precision, F1 and Recall:

$$Precision(P) = \frac{TP}{TP + FP} \quad (4)$$

$$Recall(R) = \frac{TP}{TP + FN} \quad (5)$$

$$Precision(P) = \frac{Precision \times Recall}{Precision + Recall} \quad (6)$$

And we use the Mean Square Error (MSE) to evaluate the performance of the CFM algorithm. The corresponding equation of the MSE is introduced as follow:

$$MSE = \frac{1}{N} \sum_{i=1}^n (r_n - \hat{r})^2 \quad (7)$$

B. Experimental Setting

As previously mentioned the proposed approach consists of two steps: the context extraction step and the rating prediction step. In the first step, the custom NER is trained using the FLAIR library, an open source NLP framework for state-of-the-art text classification and sequence labeling. We use Google Colab to train the model (GPU 12GB). In order to not exceed the available GPU memory, we fix the mini-batch to 32 and the maximum sequence length 512. We use a Bi-LSTM with a single layer with a hidden size of 256 to process input sequences and a learning rate to 0.1.

In the second step, We build our CFM using Tensorflow framework [33], our implementation is inspired from [34][35]. We split the data into 80% for training and 20% for test. As we are dealing with a regression problem, the model

parameters are learned by minimizing the loss function, we also prevent overfitting by adding a L2 regularization term. Since it is efficient with sparse data, we use a gradient-based optimizer. We fix the number of iteration to 1000 since the CFM algorithm needs more time to converge.

C. Results and Discussion

1) Custom NER: Results of the custom NER for different corpus are represented in Fig. 5. As we can see, the custom NER achieves the best F1 score of 91.59% for Corpus1, 89.92% for Corpus3 and the worst F1 score of 80.17% for Corpus2. The disparity in results can be explained by the fact that the quality of data from Corpus to another. The GMB Corpus gets the worst performance because it is not perfect. It is not completely human, the corpus is built using existing annotation and must be corrected manually by humans.

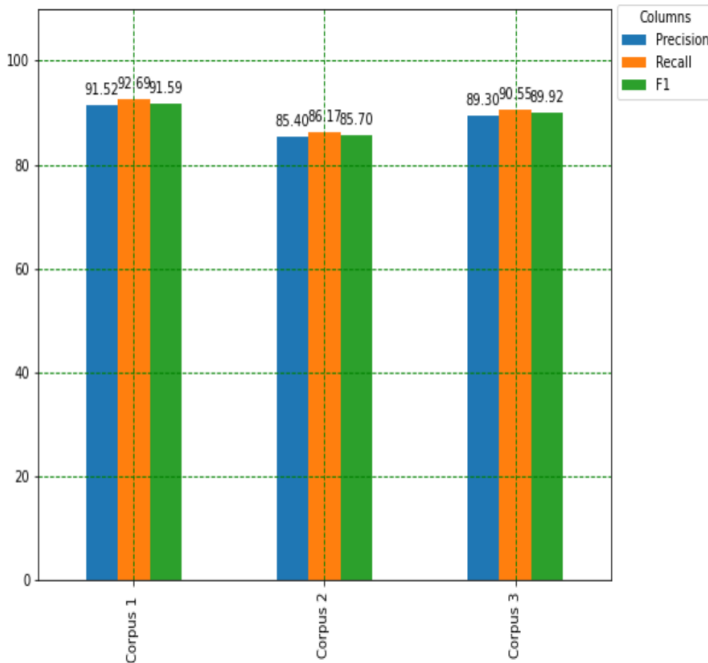


Fig. 5. Results of Three Corpus using F1 Score, Precision and Recall.

Table II shows the obtained results for each entity. The model gets a F1 score of 94.34% for Companion, 90.70% for location, 85.90% for environmental entity and 77.04% for Time. We can explain the difference in obtained results by the difference in the degree of difficulty encountered during the extraction of each entity. For instance it is less difficult to extract location (i.e., name of city) from unstructured text than extract time entity which can be written in different ways (i.e, 5pm, 5p.m, 5 p.m, Five pm ,). Even ContextNER does get good performance on Corpus 2 it still competitive compared with other recent models.

2) Contextual Factorization Machine: To validate the effectiveness of CFM we compare it with five competitive baselines:

- **FM [25]:** Factorization Machine is the famous Collaborative filtering RS method. It takes the matrix of rating and transforms it to two low-rank matrices.

TABLE II. OBTAINED RESULTS FOR EACH ENTITY

Entity	Precision	Recall	F1 score
Location	91.47%	87.23%	90.70%
Time	77.74%	76.35%	77.04%
Companion	92.59%	96.15%	94.34%
Environmental	86.37%	85.43%	85.90%

- **PMF [36]:** Probabilistic Matrix Factorization uses Gaussian distributions to estimate users and items latent factors.

- **HFT [37]:** Hidden Factor as Topic extracts latent factors from reviews by employing topic distributions.

- **CDL [38]:** Collaborative Deep Learning is a hierarchical Bayesian model which performs deep representation learning for Collaborative filtering RS.

- **DeepCoNN [3]:** Deep Cooperative Neural Networks model extracts user behaviours and item properties from reviews.

All works already mentioned have incorporated reviews except FM and PMF.

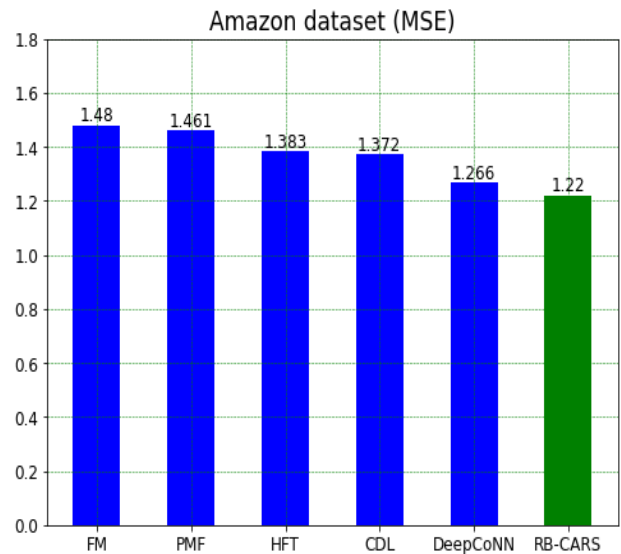


Fig. 6. Obtained Results for Amazon Dataset.

In Fig. 6, results for the Amazon dataset are reported in terms of MSE. We can definitely notice that our model significantly improves the quality of recommendation passing from 1.480 for FM to 1.22 which means an improvement of 12.9% over FM model and 5.3% over DeepCoNN.

By the same way, our model shows good performance over the other models for the Yelp dataset. As we can see in Fig. 7, the model gets a MSE 1.382 over 1.792 for FM model

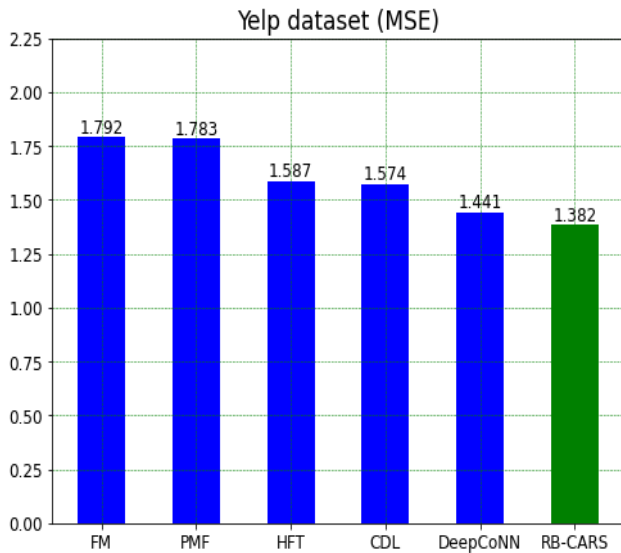


Fig. 7. Obtained Results for Yelp Dataset.

and 1.441 for DeepCoNN, equivalent to 13.4% and 4.9% of improvement respectively for both models.

TABLE III. OBTAINED RESULTS FOR EACH ENTITY

Datasets	Amazon	Yelp	All datasets average
FM	1.480	1.792	1.636
PMF	1.461	1.783	1.622
HFT	1.383	1.587	1.485
CDL	1.372	1.574	1.473
DeepCoNN	1.266	1.441	1.353
DeepCoNN	1.220	1.382	1.301
Improvement (%)	12.9	13.4	13.15

The difference in results is mainly related to the sparsity of the two datasets and it is worth to note that with other datasets less sparse than the two datasets used in these experiments our model can perform better. Table III represents all obtained results.

VII. CONCLUSION

This article presented an automatic method to extract contextual information from users' reviews, then use it to improve recommendation quality with less time spent in feature engineering. This work is divided into two main steps:

The first for context extraction using a custom NER, where the model used in this step consists of three layers, namely

word embedding layer which takes a sequence of words and outputs a contextual embedding vector representation of each word using BERT model, the Bi-LSTM layer which extracts vector features from words generated by the previous layer and the last layer called the CRF layer which helps to automatically learn labels and constraints and guarantee the sequence validity. The second step is for ratings prediction. The CFM algorithm takes the output from the first step and computes the ratings. In contrast to the generic FM, the CFM is able to capture the importance of the contextual dimensions and incorporate them into the process of recommendation.

To evaluate the performance, the proposed model was compared with five models and obtained results show that the model achieves good results. For future work, the proposed model will be improved in both steps, namely the data extraction step and techniques utilized for this end and also for ratings prediction.

REFERENCES

- [1] "GroupLens: applying collaborative filtering to Usenet news: Communications of the ACM: Vol 40, No 3." <https://dl.acm.org/doi/10.1145/245108.245126>.
- [2] U. Panniello, A. Tuzhilin, and M. Gorgoglione, "Comparing context-aware recommender systems in terms of accuracy and diversity," *User Model User-Adap Inter*, vol. 24, no. 1, pp. 35–65, Feb. 2014, doi: 10.1007/s11257-012-9135-y.
- [3] L. Zheng, V. Noroozi, and P. S. Yu, "Joint Deep Modeling of Users and Items Using Reviews for Recommendation," arXiv:1701.04783 [cs], Jan. 2017, Accessed: Nov. 11, 2021. [Online]. Available: <http://arxiv.org/abs/1701.04783>.
- [4] R. Catherine and W. Cohen, "TransNets: Learning to Transform for Recommendation," in *Proceedings of the Eleventh ACM Conference on Recommender Systems*, New York, NY, USA, Aug. 2017, pp. 288–296. doi: 10.1145/3109859.3109878.
- [5] J. McAuley and J. Leskovec, "Hidden factors and hidden topics: understanding rating dimensions with review text," in *Proceedings of the 7th ACM conference on Recommender systems*, New York, NY, USA, Oct. 2013, pp. 165–172. doi: 10.1145/2507157.2507163.
- [6] Y. Tan, M. Zhang, Y. Liu, and S. Ma, "Rating-Boosted Latent Topics: Understanding Users and Items with Ratings and Reviews," 2016.
- [7] Y. Zhang, G. Lai, M. Zhang, Y. Zhang, Y. Liu, and S. Ma, "Explicit factor models for explainable recommendation based on phrase-level sentiment analysis," in *Proceedings of the 37th international ACM SIGIR conference on Research & development in information retrieval*, New York, NY, USA, Jul. 2014, pp. 83–92. doi: 10.1145/2600428.2609579.
- [8] A. Levi, O. Mokryn, C. Diot, and N. Taft, "Finding a needle in a haystack of reviews: cold start context-based hotel recommender system," in *Proceedings of the sixth ACM conference on Recommender systems*, New York, NY, USA, Sep. 2012, pp. 115–122. doi: 10.1145/2365952.2365977.
- [9] S. Aciar, "Mining Context Information from Consumer's Reviews." <https://www.semanticscholar.org/paper/Mining-Context-Information-from-Consumer-%E2%80%99-s-Aciar/3c0977e396849c345ff5283772ecd5c1b7097c08>.
- [10] N. Hariri, B. Mobasher, R. Burke, and Y. Zheng, "Context-Aware Recommendation Based On Review Mining," 2011.
- [11] P. Campos, N. Rodríguez-Artigot, and I. Cantador, "Extracting Context Data from User Reviews for Recommendation: A Linked Data Approach," 2017.
- [12] F. Z. Lahlou, H. Benbrahim, and I. Kassou, "Review Aware Recommender System: Using Reviews for Context Aware Recommendation," *IJDAI*, vol. 10, no. 2, pp. 28–50, Jul. 2018, doi: 10.4018/IJDAI.2018070102.
- [13] G. Adomavicius, B. Mobasher, F. Ricci, and A. Tuzhilin, "Context-Aware Recommender Systems," *AI Magazine*, vol. 32, no. 3, Art. no. 3, 2011, doi: 10.1609/aimag.v32i3.2364.

- [14] G. Castelli, A. Rosi, M. Mamei, and F. Zambonelli, "A Simple Model and Infrastructure for Context-Aware Browsing of the World," in Fifth Annual IEEE International Conference on Pervasive Computing and Communications (PerCom'07), Mar. 2007, pp. 229–238. doi: 10.1109/PERCOM.2007.4.
- [15] J. D. Kim, J. Son, and D. K. Baik, "CA 5W1H Onto: Ontological context-aware model based on 5W1H," International Journal of Distributed Sensor Networks, vol. 2012, no. 247346, 2012, doi: 10.1155/2012/247346.
- [16] T. Chaari, E. Dejene, F. Laforest, and V.-M. Scuturici, "A Comprehensive Approach to Model and Use Context for Adapting Applications in Pervasive Environments," Int. Journal of Systems and software, vol. 80, pp. 1973–1992, Dec. 2007, doi: 10.1016/j.jss.2007.03.010.
- [17] H. Chen, T. Finin, and A. Joshi, "The SOUPA Ontology for Pervasive Computing," in Ontologies for Agents: Theory and Experiences, Basel, 2005, pp. 233–258. doi: 10.1007/3-7643-7361-X10.
- [18] B. Y. Lin, F. Xu, Z. Luo, and K. Zhu, "Multi-channel BiLSTM-CRF Model for Emerging Named Entity Recognition in Social Media," in Proceedings of the 3rd Workshop on Noisy User-generated Text, Copenhagen, Denmark, Sep. 2017, pp. 160–165. doi: 10.18653/v1/W17-4421.
- [19] H. Yan, B. Deng, X. Li, and X. Qiu, "TENER: Adapting Transformer Encoder for Named Entity Recognition," arXiv:1911.04474 [cs], Dec. 2019, Accessed: Nov. 14, 2021. [Online]. Available: <http://arxiv.org/abs/1911.04474>
- [20] S. Hochreiter and J. Schmidhuber, "Long Short-Term Memory," Neural Computation, vol. 9, no. 8, pp. 1735–1780, Nov. 1997, doi: 10.1162/neco.1997.9.8.1735.
- [21] Z. Huang, W. Xu, and K. Yu, "Bidirectional LSTM-CRF Models for Sequence Tagging," arXiv:1508.01991 [cs], Aug. 2015, Accessed: Nov. 14, 2021. [Online]. Available: <http://arxiv.org/abs/1508.01991>
- [22] A. Radford and K. Narasimhan, "Improving Language Understanding by Generative Pre-Training," undefined, 2018, Accessed: Nov. 14, 2021. [Online]. Available: <https://www.semanticscholar.org/paper/Improving-Language-Understanding-by-Generative-Radford-Narasimhan/cd18800a0fe0b668a1cc19f2ec95b5003d0a5035>
- [23] M. E. Peters et al., "Deep contextualized word representations," arXiv:1802.05365 [cs], Mar. 2018, Accessed: Nov. 14, 2021. [Online]. Available: <http://arxiv.org/abs/1802.05365>
- [24] J. Devlin, M.-W. Chang, K. Lee, and K. Toutanova, "BERT: Pre-training of Deep Bidirectional Transformers for Language Understanding," arXiv:1810.04805 [cs], May 2019, Accessed: Nov. 14, 2021. [Online]. Available: <http://arxiv.org/abs/1810.04805>
- [25] S. Rendle, "Factorization Machines," in 2010 IEEE International Conference on Data Mining, Dec. 2010, pp. 995–1000. doi: 10.1109/ICDM.2010.127.
- [26] T. Mikolov, I. Sutskever, K. Chen, G. Corrado, and J. Dean, "Distributed Representations of Words and Phrases and their Compositionality," arXiv:1310.4546 [cs, stat], Oct. 2013, Accessed: Nov. 16, 2021. [Online]. Available: <http://arxiv.org/abs/1310.4546>
- [27] Wolf et al., "HuggingFace's Transformers: State-of-the-art Natural Language Processing," arXiv:1910.03771 [cs], Jul. 2020, Accessed: Nov. 16, 2021. [Online]. Available: <http://arxiv.org/abs/1910.03771>
- [28] J. D. Lafferty, A. McCallum, and F. C. N. Pereira, "Conditional Random Fields: Probabilistic Models for Segmenting and Labeling Sequence Data," in Proceedings of the Eighteenth International Conference on Machine Learning, Jun. 2001, pp. 282–289.
- [29] E. F. T. K. Sang and F. De Meulder, "Introduction to the CoNLL-2003 Shared Task: Language-Independent Named Entity Recognition," arXiv:cs/0306050, Jun. 2003, Accessed: Nov. 20, 2021. [Online]. Available: <http://arxiv.org/abs/cs/0306050>
- [30] "Home - Groningen Meaning Bank." <https://gmb.let.rug.nl/> (accessed Nov. 20, 2021).
- [31] "Amazon review data." <https://jmcauley.ucsd.edu/data/amazon/> (accessed Nov. 20, 2021).
- [32] "Yelp Dataset." <https://www.yelp.com/dataset> (accessed Nov. 20, 2021).
- [33] M. Abadi et al., "TensorFlow: A system for large-scale machine learning," arXiv:1605.08695 [cs], May 2016, Accessed: Nov. 20, 2021. [Online]. Available: <http://arxiv.org/abs/1605.08695>
- [34] S. Rendle, "Factorization Machines with libFM," ACM Trans. Intell. Syst. Technol., vol. 3, no. 3, p. 57:1–57:22, May 2012, doi: 10.1145/2168752.2168771.
- [35] F. Z. Lahlou, Textual context Aware Factorization Machines. 2019. Accessed: Nov. 20, 2021. [Online]. Available: <https://github.com/fzlahlou/TCAFM/blob/2beb2e73a28f2f577c05d4d77122bf26225e0dd1/TCAFM%20and%20FM%20Code.py>
- [36] R. Salakhutdinov and A. Mnih, "Probabilistic Matrix Factorization," in Proceedings of the 20th International Conference on Neural Information Processing Systems, Red Hook, NY, USA, Dec. 2007, pp. 1257–1264.
- [37] J. McAuley and J. Leskovec, "Hidden factors and hidden topics: understanding rating dimensions with review text," in Proceedings of the 7th ACM conference on Recommender systems, New York, NY, USA, Oct. 2013, pp. 165–172. doi: 10.1145/2507157.2507163.
- [38] H. Wang, N. Wang, and D.-Y. Yeung, "Collaborative Deep Learning for Recommender Systems," arXiv:1409.2944 [cs, stat], Jun. 2015, Accessed: Nov. 22, 2021. [Online]. Available: <http://arxiv.org/abs/1409.2944>

A Computer Vision-based System for Surgical Waste Detection

Md. Ferdous, Sk. Md. Masudul Ahsan
Dept. of Computer Science and Engineering (CSE)
Khulna University of Engineering & Technology (KUET)
Khulna, Bangladesh

Abstract—The world population is going through a difficult time due to the pandemic of COVID-19 while other disasters prevail. However, a new environmental catastrophe is coming because surgical masks and gloves are putting down anywhere, leading to the massive spreading of COVID-19 and environmental disasters. A significant number of masks and gloves are not properly managed. They are scattered around us such as roads, rivers, beaches, oceans and other places. Since these types of waste are turned into microplastics and chemicals are deadly harmful to the environment, human health and other species, especially for the aquatic animals on this planet. During the outbreaks of corona pandemic, surgical waste in the open place or seawater can create a fatal contagious environment. Putting them in a particular area can protect us from spreading infectious diseases. This study proposed a system that can detect surgical masks, gloves and infectious/biohazard symbols to put down infectious waste in a specific place or a container. Among the various types of surgical waste, this study prefers mask and gloves since it is currently the most widely used element due to the COVID-19. A novel dataset is created named MSG (Mask, Biohazard Symbol and Gloves), containing 1153 images and their corresponding annotations. Different versions of the You Only Look Once (YOLO) are applied as the architecture of this study; however, the YOLOX model outperforms.

Keywords—COVID-19; You Only Look Once (YOLO); surgical waste; deep learning; image dataset; real-time detection

I. INTRODUCTION

Plastics have become a severe hazard to natural habitats and human health. Moreover, some of them are recyclable e.g. PET bottles. During the COVID-19 pandemic, surgical masks and gloves have increased extensively to reduce coronavirus spread. They are not reusable for being medical waste and infectious. People throw masks and gloves everywhere as a general waste due to the lack of planning and unconsciousness. Therefore, it is our prime duty to manage them properly. Otherwise, we will have to face extreme catastrophes. This hazard will likely be accelerated because of excessive use and exhaustion of plastic for example surgical masks, surgical gloves, face shields and personal protective equipment (PPE). A disposal system that can accurately identify masks, gloves, and biohazard symbols may participate in managing such type of terrible waste safely. This study preferred the biohazard symbol because symbols are unique all over the world than language. The outline is such that the system will identify masks and gloves as waste and keep these waste in a particular place/container/waste bin where the biohazard symbol is drawn. In this case, Computer Vision (CV) may help us a lot. There are different object detection models available right

now. The YOLO models have the highest popularity because of their speed and auspicious performance. Although, in recent years many anchor-free object detection models [1] [2], Non-maximum Suppression (NMS) free i.e. end to end models [3] [4] [5] has been deployed. Training the model based on anchor creates a problem at the time of initialization of anchors. Rather, the anchor-free strategy does not face such types of problems. YOLO family always tries to execute the latest technology (e.g. YOLOv2 [6] anchor mechanism, YOLOv3 [7] Residual Net) to enhance speed and optimized implementation within a desirable time. Additionally, YOLO architecture has two mechanism-based models, one is anchor-based and the other is anchor-free training strategy. YOLOv3, YOLOv4, and YOLOv5 depend on anchor technology, whereas YOLOX relies on an anchor-free training mechanism. YOLOv3 is a mainly used model for industrial purposes and still exists many versions. YOLOv3 [7] focuses on layer-wise feature extraction and does not pay any attention to the sequential impact among the layers. Feature extraction performs using Darknet-53. YOLOv3-spp is another version of YOLOv3, which uses the spatial pyramid pooling (spp) module into the model and produces better performance than the other. YOLOv4 [8] and YOLOv5¹ are two newly published architectures and both of them show comparable performance in many applications. There are different versions of YOLOv5 based on the model size such as small, medium, large and extra-large. The model architecture for each version remains the same. However, the only difference is the model depth and width. This theory also applies to YOLOX's different version. In this study, the authors explore a novel dataset and apply different CV models to determine which model yields the best performance to achieve the goal. In particular, four models are presented to identify surgical waste and biohazard symbols accurately. Finally, one of them is selected as the proposed model. Additionally, collecting relevant images, creating annotations and preparing the dataset are also discussed. The remaining sections of the paper are organized as follows: Section II describes the literature review of surgical waste detection. Dataset preparation and methods are discussed in Section III. The model's training process is expressed in Section IV. The performance measurement of the architecture is illustrated in Section V. Section VI represents the experimental result of the architectures. Deliberation of this study and limitations are enlightened in Section VII. Section VIII consists of concluding remarks with the future direction.

¹<https://github.com/ultralytics/yolov5>

II. LITERATURE REVIEW

Scientists and Researchers have strongly advised us to wear masks for preventing coronavirus. However, the widespread use of these protective gear makes a terrible situation to the environmental system due to human insensibility. Many people consciously or unconsciously put down such dangerous waste in our surroundings which may cause a severe health hazard for any species on this globe. As a result, infectious waste (surgical masks and gloves) increases day by day. In 2020, about 150 million masks will go to the sea. Meanwhile, some countries face problems with this type of waste. Approximately the demand for surgical masks is 28 million per day all over the world [9]. Furthermore, every day 1.6 million tons of waste are generated due to the corona pandemic [10]. It is terrifying that this horrible rubbish is scattered around us. Hence, there is a possibility to spread coronavirus rather than resistance. Our primary purpose is to develop a system to detect infectious waste and infectious symbols as if it can detect and manage such dangerous malicious material from our environment. Object detection is a well-known research area. AquaVision [11] represents an automatic detection system that can detect waste bodies from the water. The authors try to use different transfer learning models to conduct their work. Floating plastic liter detection using Sentinel-2 imagery from space illustrated in [12]. A system that can detect marine life and plastic waste in underwater environment is shown in [13]. Different deep learning methods e.g. Single Shot Detector (SSD), MobileNet are used to detect aquatic animals and waste. In this study, we have dealt with surgical waste detection, which has rarely been done before. A disposal system that can identify waste from the environment and biohazard symbol for keeping the waste in a particular place. From this motivation, a novel dataset is created and named after the MSG dataset to detect the surgical mask, gloves and biohazard symbol. Surgical masks and gloves are detected as waste and biohazard symbols to detect place/container/waste bin to put these types of waste there. Several CV models are trained and tested using the MSG dataset to conduct this work as if more precise detection is generated within an acceptable time. YOLO models (YOLOv3-spp, YOLOv4, YOLOv5 and YOLOX) are selected as the detection architecture.

III. MATERIALS AND METHODS

A. Dataset Preparation (MSG Dataset)

Realistic criteria are applied to the model at the training and testing time to swear the model's robustness. Among the criteria are taken into account is:

- 1) Real-time condition.
- 2) Lighting variations.
- 3) Multiclass.
- 4) Underwater condition.
- 5) Waste floating on the water.

The MSG dataset is built based on real-time images from our surroundings including roads, beaches, water, maintenance holes and so on. Several images of the dataset are synthetic. Moreover, most of them are natural. Some images are taken using the Samsung Galaxy A51 smartphone camera and the rest of the images are taken from internet mining. Images are chosen from close range and distance range to make the

dataset a distance variant. The angle variation left, right, back and top angle images are taken. The dataset comprises diverse gesture conditions such as curling and kneeling. At the time of image collection, this study tries to take different types of colored masks and gloves. The color variation of the mask is white, sky blue, pink, black and others. Different types of masks are included surgical, N95, Cone-style, KN95 and so on. Surgical gloves also have blue, white, black and pink colors. Transparent gloves are included with more eagerness to make the system as robust and reliable underwater as well as an object floating on the water condition. According to the above criteria, 1153 images are collected from different internet sources and smartphones camera. Completing the collection of the images, our next step is to annotate the collected images. All the image annotations are handcrafted. The annotations process are done in a graphical image annotation tool called LabelImg [14]. Three types of annotation classes are there:

- Surgical mask as mask.
- Surgical gloves as gloves.
- Biohazard symbol as biohazard.

The dataset is available at <https://github.com/Md-Ferdous/Surgical-waste-dataset>. The MSG dataset contains 1153 images and 1990 instances where 80% of them (923 images) are selected as the training dataset, 8% (92 images) for validation and the remaining 12% (138 images) for the test dataset. There are three combinations of the MSG dataset keeping the same amount of images into the training, testing and validation set. A validation dataset is provided into the model for an unbiased evaluation and fine-tuning during training. Moreover, the validation process at the training time tells us about the model's training condition such as whether the model is going on the right path? The test dataset is used to evaluate the model's performance. The testing dataset contains ambiguous images for example a paper looks relative to a mask, a plastic/polythene similar to gloves. Creating this ambiguity is to see how well the model performs in real-world conditions. Fig. 1 shows the number of images of every class. There are 568 masked images and 251 images that contain both masks and gloves instances. 10 images contain three classes altogether. The rest is the same. The MSG dataset consists of 1133, 598 and 259 instances of mask, gloves and biohazard symbols, respectively.

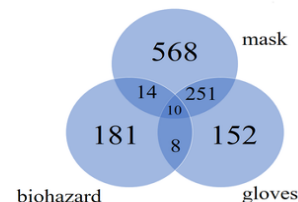


Fig. 1. Number of Images of every Class.

Fig. 2, exhibits the number of instances in the training, testing and validation set of a combination of the dataset. The training set contains 831, 492 and 217 instances of mask, gloves and biohazard symbols, respectively. The total number of masks, gloves and biohazard symbols in the validation set

are 117, 46 and 16. At last, the testing set consists of 184, 60 and 26 instances of the mask, gloves and biohazard symbol, respectively.

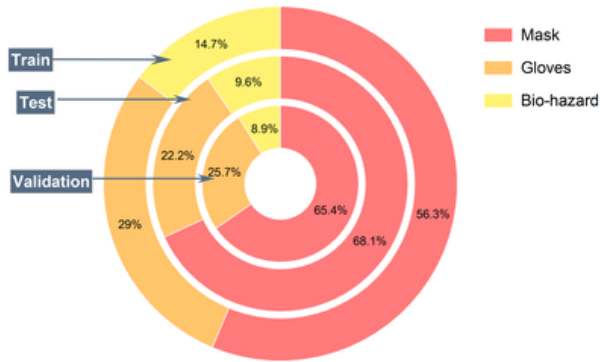


Fig. 2. Number of Instances in the Training, Testing and Validation Set.

B. Framework

A pictorial is shown in Fig. 3, which provides an overview of how the objects are detected from an image. First, an image is fed into the YOLO architecture; differential features are extracted from the network’s backbone. Next, the backbone network uses the extracted features and emits a feature pyramid to the head network. After that, the head regresses the bounding boxes and classifies objects. Output from the prediction portion could be any combination of the desired three classes (mask, gloves, biohazard). Moreover, a novel dataset is created to detect and manage infectious waste from our surroundings. Finally, different variations, angles, states and textured images are selected from the real-time condition to accelerate the system robustness.

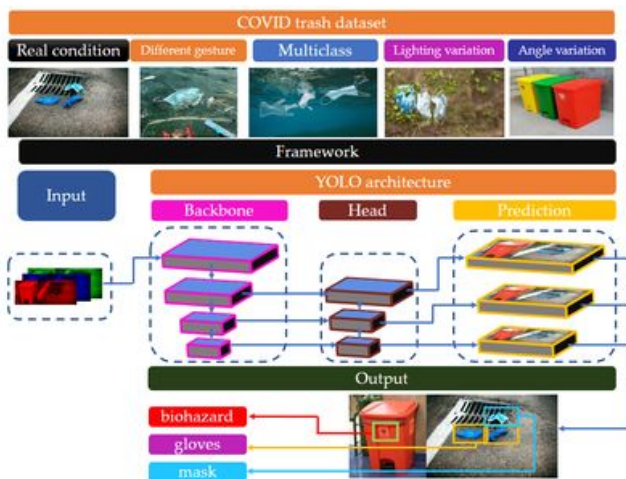


Fig. 3. Framework.

C. Objective of Experiment

This study aims to detect surgical waste and bio-hazard symbols correctly within a reasonable time interval. Therefore, different types of YOLO architectures are examined to achieve different objectives. Additionally, two types of YOLO models

are chosen, one is anchor-based and the other is anchor-free training mechanism. Three types of anchor-based and one anchor-free object detection models are shown in Table I.

There are four different versions of YOLOv5 (YOLOv5-s, YOLOv5-m, YOLOv5-l and YOLOv5-x) and YOLOX (YOLOX-s, YOLOX-m, YOLOX-l and YOLOX-x) architecture. Here s, m, l and x denote small, medium, large and extra-large, respectively. According to the theory, a greater model size has better accuracy than a smaller one. On the other hand, a smaller model size is faster than a larger one. It is a dilemma and the solution lies in the perspective or application type you want to build. Therefore, it is essential to evaluate all versions of the YOLOv5 and YOLOX for giving a comprehensive description of their performance. Another notable subject is to see the performance between the anchor-based and anchor-free detectors.

TABLE I. OBJECTIVE OF EXPERIMENTS

Training mechanism	Model
Anchor-based	YOLOv3-spp
	YOLOv4
	YOLOv5-s
	YOLOv5-m
	YOLOv5-l
Anchor-free	YOLOv5-x
	YOLOX-s
	YOLOX-m
	YOLOX-l
	YOLOX-x

D. YOLOX

1) *Decoupled Head*: In object detection, two egregious tasks are performed in parallel, one is object classification and the other is bounding box regression. These two tasks share almost the same parameters [15] [16]. Hence, there is an impingement between two tasks and it is a sensitive issue in computer vision. Classification confidence is the probabilities of class levels. At the same time, localization confidence is inexistent. In repetitive regression or even non-maximum suppression, correctly aligned bounding boxes are misaligned. This issue was initially discovered by IoU-Net [17]. They discovered that the characteristic that produces a high classification score for object classification invariably predicts a coarse bounding box. The IoU calculation between ground truth and predicted bounding boxes might be a solution to solve this problem. To forecast the IoU, they first add head to the network as if it can emit the localization score. Then, the final classification score is calculated by combining the localization confidence score and the classification confidence score. This method does help to alleviate the problem of dislocation. Based on this formula, two certain branches, one for classification and the other for localization i.e. double-headed network, was proposed in Double head R-CNN [18] to untangle the head of siblings. In a double-headed network, classification is performed using a fully connected head network and box regression is performed using another convolution head network [15]. Due to having facilities in a double-headed network for object classification and localization many one-stage and two-stage object detection models follow dual-headed architecture [19] [20] [16] [18]. If we divide YOLO families architecture, it has three portions:

backbone, head, and prediction. Backbone (e.g. PAN [20] and FPN [21]) continuously emit feature pyramids to the head. The head classifies objects and localizes the bounding boxes using this feature. Still (YOLOv3-spp, YOLOv4 and YOLOv5) no YOLO family model used double-headed architecture where YOLOX uses double-headed architecture. YOLOX [22] shows that coupled heads may destroy the performance of object detection. The YOLOX architecture is shown in Fig. 4.

2) *Exceptional Data Enhancement*: Many data augmentation techniques have been proposed in recent years mosaic is one of them. Mosaic is an effective and efficient augmentation technique proposed by a company named ultralytics in their YOLOv3². For boosting the performance of the YOLOX mosaic and MixUp augmentation strategies were applied in [22]. The YOLOv4 [8], YOLOv5 and other object detectors [23] used the mosaic augmentation technique. MixUp [24] is another augmentation strategy that is primarily designed for the image classification task. Modifying it into BoF [23] it is used for the training of objection detection tasks also. In YOLOX, mosaic augmentation is accomplished. A random affine transformation is performed where rotation is done on both axis using a value in the range of -10 deg to +10 deg, translation is done a value between (0.4, 0.6), scaling is attained on both axis within a value of (0.1, 2), the same amount of shear is done on both axis by a value of (-2 to +2). All values are taken from the author’s perspective.

3) *Anchor-free Mechanism*: Although anchor-based training mechanism is well known and famous for object detection model, it has some handicaps. The drawback can be categorized as follows:

- 1) Selection: Before training an anchor-based model needs to choose an optimal set of anchors for the optimal performance. A clustering analysis needs to be conducted on anchors to choose an optimal set.
- 2) Complexity: Anchors may create complexity on detection heads for prediction. Besides, it may increase perplexity for the number of predictions for an image.
- 3) Memory inefficient: For edge computation, in terms of total latency, this might constitute a bottleneck for transferring a massive number of predictions (anchors) across devices (e.g. NPU to CPU) [22]. Recently published YOLO family (YOLOv3-spp, YOLOv4 and YOLOv5) follows the anchor-based training mechanism.

Megvii company³ released a version named YOLOX, which is based on anchor-free training mechanism. Although YOLOv1 [25] may be the most common anchor-free detector. YOLOv1 predicts bounding boxes at points near the center of objects rather than utilizing anchor boxes. This strategy was done to achieve high performance. Furthermore, low recall problems suffered from YOLOv1. For this reason, YOLOv2 [6] went back to the anchor-based mechanism. In the last two years, Anchor-free detectors have grown at a breakneck pace e.g. FCOS [26], CornerNet [2], object as points [1]. Another type of anchorless detector is the [27] which is adopted on DenseBox [28]. The number of design parameters that require heuristic tuning and the number of tricks such as anchor

clustering [6] and grid sensitive [29] requires less amount when using an anchor-free system. Anchor-free detectors enhance the model performance and simplify it especially at the training and decoding phase.

4) *Multi Positives*: Another aspect of YOLOX is it selects a center point and considers it as positive while ignoring the other predictions, although there is a high probability of being positive [22]. A 3×3 area is chosen around the center point, which is called center sampling in FCOS [26].

IV. TRAINING PROCESS

The entire training and testing process is carried out on the Google cloud platform. The entire training process can be divided into three stages:

- 1) Prefer a model for training and refashioning its corresponding configuration file as the target.
- 2) Set initial parameters into the network using pre-trained weights.
- 3) Start the learning process by setting the training parameters. For training, the Stochastic Gradient Descent (SGD) approach was employed.

The learning rate is adopted using $lr \times \text{batchsize}/64$ [30]. The initial learning rate is set to 0.01 and it changes over time according to the cosine learning rate schedule. The cosine learning rate can be calculated using Equation 1. Generalized Intersection over Union (GIoU) [31] is calculated for bounding box regression loss is shown in Equation 2. The weight decay is 0.0005 and the SGD momentum is 0.9. NMS threshold is set to 0.65. The first five epochs were warm-up epochs. These warm-up epochs help the network train gradually, making a basic sense of the dataset. Training is done up to 180 epochs. Input image size was 640×640. YOLOX is trained according to Megvii company’s GitHub repository in the PyTorch environment. YOLOv5 is also trained in the PyTorch environment and trained according to the construction of a company named Ultralytics.

$$lr = 0.5 \times \left(1.0 + \cos \left(\pi \times \frac{\text{iteration}}{\text{total iteration}} \right) \right) \quad (1)$$

$$IoU = \frac{\text{Intersection}}{\text{Union}} = \frac{G \cap D}{G \cup D} \quad (2)$$

$$GIoU = IoU - \frac{|C \setminus \text{Union}|}{|C|} \quad (3)$$

Where G and D are the prediction and ground truth bounding boxes respectively. C is the smallest convex object for G and D. All models are trained in the PyTorch environment and an SGD optimizer is used. Table II represents the training hyperparameters.

TABLE II. TRAINING HYPERPARAMETERS

Model	Initial learning rate	Decay	Momentum	Batch size
YOLOX	0.01	0.0005	0.9	32/16/12
YOLOv5	0.01	0.0005	0.9	32
YOLOv3-spp	0.001	0.000484	0.937	32
YOLOv4	0.001	0.0005	0.9	2

²<https://github.com/ultralytics/yolov3>

³<https://github.com/Megvii-BaseDetection/YOLOX>

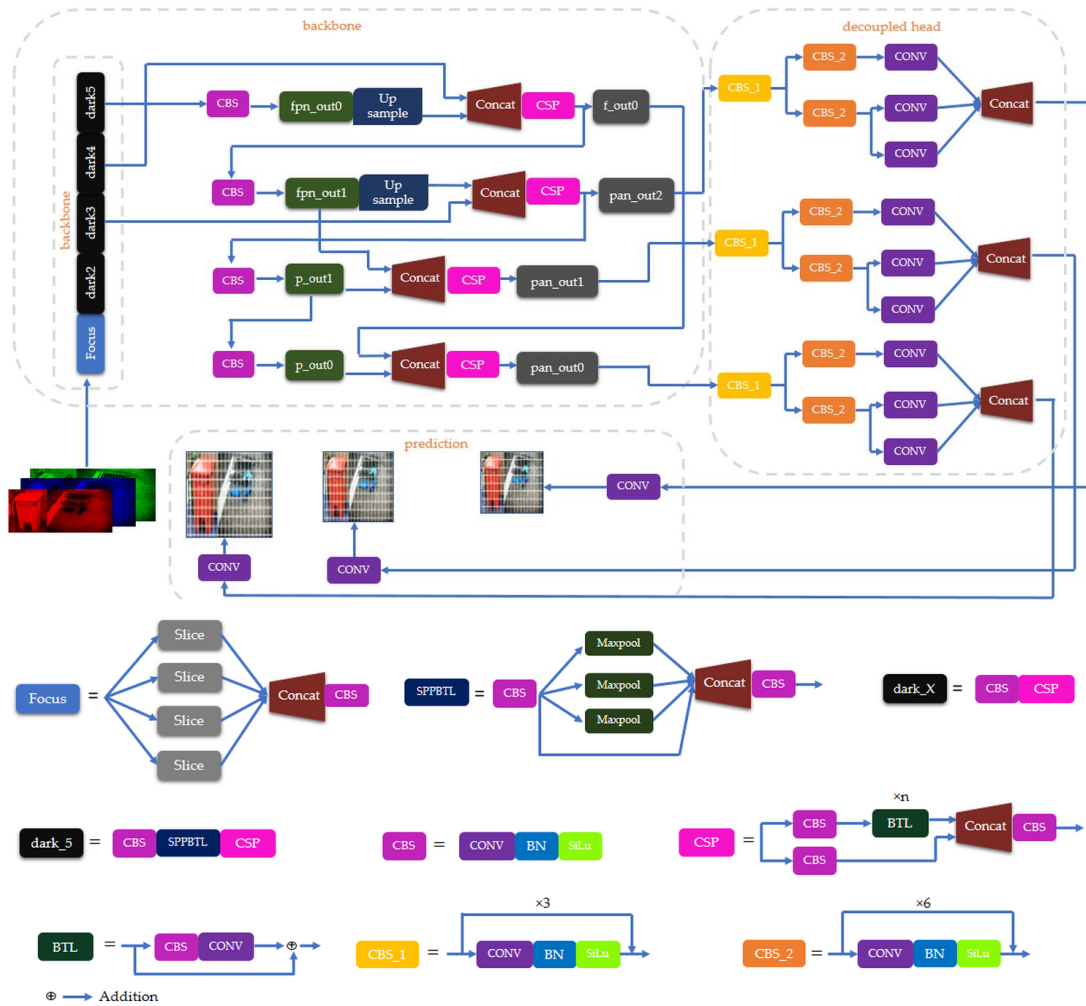


Fig. 4. Architecture of YOLOX.

V. EVALUATION METRICS

Intersection over Union (IoU) is shown in Fig. 5. Though the IoU is used in non-maximum suppression, it can also be used in evaluating a model as a performance metric. When evaluating an object detection model, we try to determine whether the predicted class is like the desired class—simultaneously investigating the perfect alignment of the bounding boxes that exist around the object into the image. Using the ground truth bounding boxes (G) and predicted/detected bounding boxes (D), one can calculate the IoU. The IoU calculation tells us how much the predicted bounding boxes are related to the ground truth bounding boxes i.e. the percentage of overlap between two bounding boxes. The bigger the overlap area, the higher the IoU. Equation 2 [32] is used to calculate the IoU between two the bounding boxes. True Positive (TP), False Positive (FP) and False Negative (FN) are calculated according to [33] [34] [35]. TP, FP and FN are the confusion matrix criteria. Table III represents if the model predicts true class and its IoU is greater than 50%, then the detection would be considered as TP. Inversely, FP is considered if the IoU is smaller than 50% and detection tell the right class according to ground truth. FP detects a ground

truth class, but its bounding box position is not correct like the ground truth box. FP yields an improper detection case. In the case of FN, the system will not be able to detect any class where ground truth boxes exist.

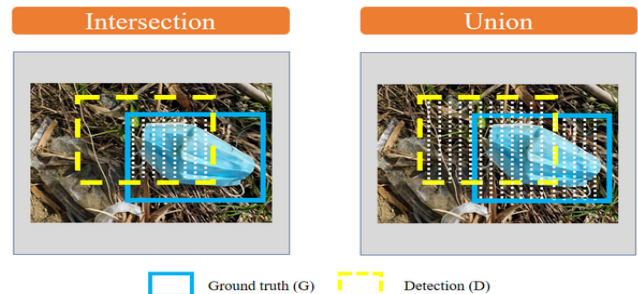


Fig. 5. IoU Calculation Mechanism

If the TP is omitted from the total positives, we will get the FN. Therefore, the object confidence score is set to greater than 50% for calculating the TP, FP and FN. In object detection, every position of an image will be True Negative (TN) without

desired class. Hence, TN is not so important to measure the performance of an object detection model.

TABLE III. CALCULATION PROCESS OF THE TP, FP AND FN

IoU (%)	Class	TP	FP	FN
>=50	true	✓	✗	✗
>=50	false	✗	✓	✗
<50	true/false	✗	✗	✓

Precision is a metric that depicts the capability of a model to identify its relative objects correctly. It is the proportion of positive predictions that are correct across all detections. The recall is a metric that delineates the power of a model to find all relevant examples. It is the proportion of positive predictions subject to the entire ground truth. Precision and recall are calculated as [33] [36]. This study evaluates the model’s performance using the Average Precision (AP). AP is a scheme to encapsulate the Precision-Recall (PR) curve. Higher precision is clear evidence that a model is confident when classifying examples among the detections. On the other hand, higher recall is an indicator of the power of a model. It tells us how many correct detections are performed among all the ground truths. Moreover, precision and recall are primary metrics of an object detection model. If a model has high recall yet low precision is an obvious referential that the model emits maximum positive example truly, but it has many false positives i.e. classify many negative examples as positive. On the contrary, low recall yet high precision indicates that the model appropriately classifies positive examples; however, it may contain only a few positive examples. Hence, it is necessary to choose a threshold, as if both the precision and recall will be maximized. The PR curve helps us to select the appropriate threshold among the different threshold values. Using the precision and recall value, the PR curve can be plotted [33] [36]. AP is the Area Under the Curve (AUC) of the PR curve. AP can be calculated using the Equation 4. According to Equation 4, n is the number of thresholds. For every value of recall or precision, find the difference between the current and next to recall value, then multiply the difference with the Interpolated Precision (IP) value. IP are the maximum precision value at a recall value R where the corresponding recall value is greater than or equal to R . At each threshold, AP is the weighted sum of all precision where the recall value accelerates the weight.

$$AP = \sum_{k=0}^{k=n-1} [R(k) - R(k+1)] \times IP(k) \quad (4)$$

Different IoU marginal values are used to test the model in object detection. Therefore, different IoU values yield different performances. Furthermore, Mean Average Precision (mAP) is another metric that is calculated using the AP’s of every class shown in Equation 5 where n is the number of classes.

$$mAP = \frac{1}{n} \sum_{k=1}^{k=n} AP_k \quad (5)$$

Evaluation metrics are calculated according to [33] [35] [36]. This study tests the model in both cloud-based and

local environments. The local environment with CPU is not capable enough for training. We test the model in a local environment with a CPU to see its performance on user label equipment. The training phase is conducted on a cloud-based platform. A 15GB sized Tesla T4 GPU is used for high speed and performance for training and testing. Parameter description of two platforms is given in Table IV. At the time of speed calculation of the model, only the processing time is considered except the loading time of an image. The bottom-most speed is the mean of all testing images.

TABLE IV. PLATFORM PARAMETERS

Purpose	Platform	GPU	GPU size	CPU core	RAM
Training and testing	Cloud	Tesla T4	15GB	2	12GB
Testing	Local	None	None	4	32GB

VI. RESULTS

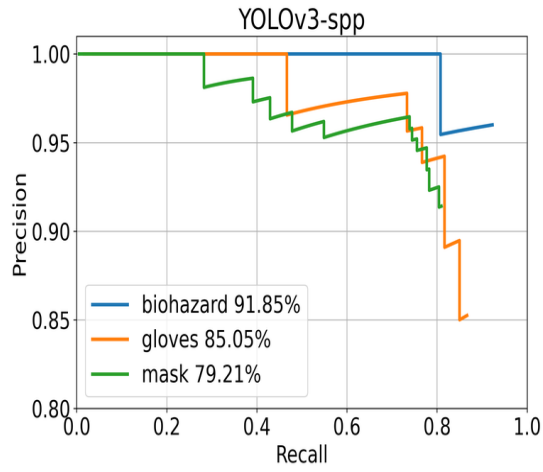
In the PR curve, precision and recall are plotted in Y-axis and X-axis respectively. Moreover, detection ability would be better when the precision is higher with the increase of the recall value. Therefore, according to this theory, better performance would be in the right up corner of the PR curve. To check the robustness of the model, training and testing are done using three different dataset combinations.

A. Anchor-based Method

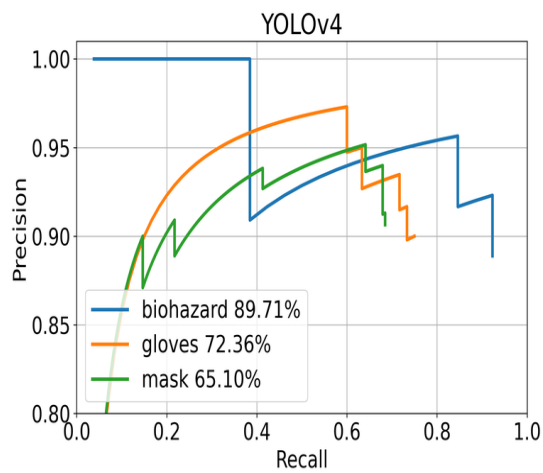
The average precision of the three classes for the anchor-based method is shown in Table V. YOLOv3-spp emits the highest mAP of 85.37% among the other methods. YOLOv5-1 generates a better mAP of 84.78% among different versions of YOLOv5. For a dataset combination, for mask objects, 149 are truly detected, 14 objects are false detection and 35 are undetected. For the gloves object, 52 gloves are detected accurately, 9 are false and 8 are undetected. The number of true positive, false positive, and false negative are 24, 1 and 2 for the biohazard symbol. Fig. 6 represents the PR curves of several anchor-based methods for a dataset combination. Well performed models PR curve is shown here. Fig. 7 exhibits some qualitative measures of the anchor-based methods. YOLOv3-spp produces better generalization than the other tested models. YOLOv4 depicts some under-detected and false detection results. YOLOv5 yields better generalization even after having many false detection outputs than YOLOv4.

TABLE V. PERFORMANCE OF ANCHOR BASED MODEL

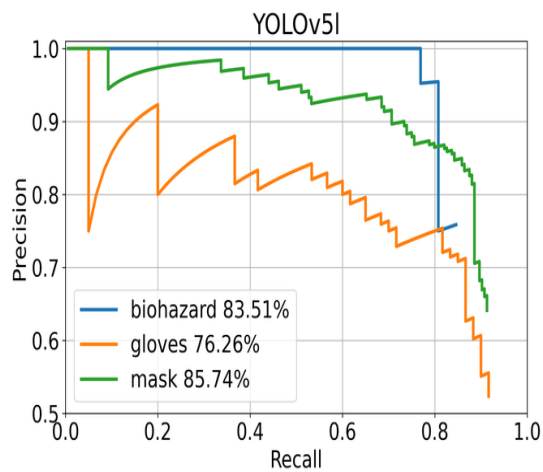
Model	mask AP	gloves AP	biohazard AP	mAP
YOLOv3-spp	79.21	85.05	91.85	85.37
YOLOv4	64.69	73.51	89.11	75.77
YOLOv5-s	84.21	79.36	82.19	81.92
YOLOv5-m	83.29	80.42	84.45	82.72
YOLOv5-1	86.84	77.69	89.81	84.78
YOLOv5-x	85.36	76.12	88.75	83.41



(a)



(b)



(c)

Fig. 6. Precision-recall Curve of the Anchor-based Model.

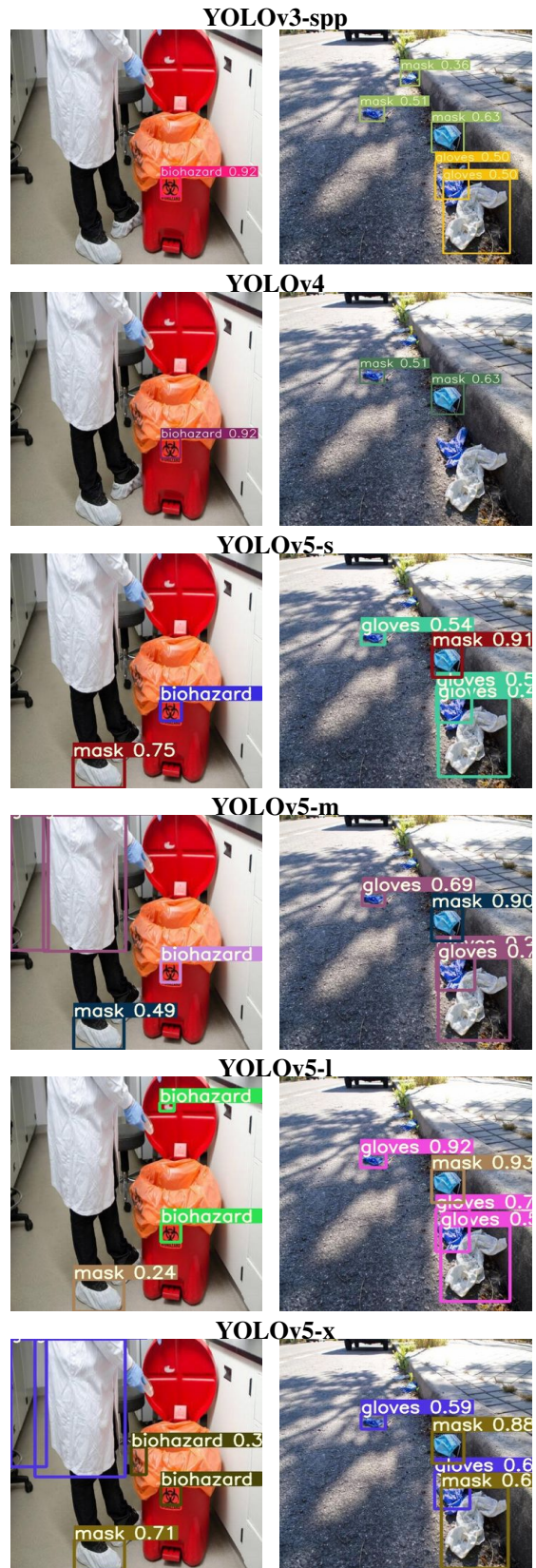


Fig. 7. Qualitative Measures of Anchor-based Methods.

B. Anchor-free Method

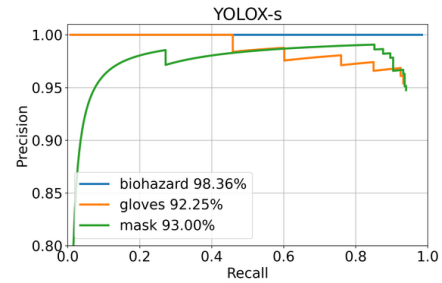
The YOLOX is trained and tested using three different combinations of the dataset shown in Table VI. Averaging of the mAP of each combination of datasets, the YOLO-l architecture delivers the highest mAP than the other models. For example, the ground truth of the mask, gloves and bio-hazard symbol are 184, 60, and 26, respectively, in a dataset combination. Accurate detection of masks, gloves and symbols is 169, 55 and 26; false detection is 8, 6 and 0; under detected objects are 15, 5 and 0, respectively for YOLOX-l. Due to easy examples, the model generates 100.00% AP for bio-hazard objects for a combination of the dataset.

TABLE VI. PERFORMANCE OF YOLOX IN THE DIFFERENT DATASET COMBINATIONS

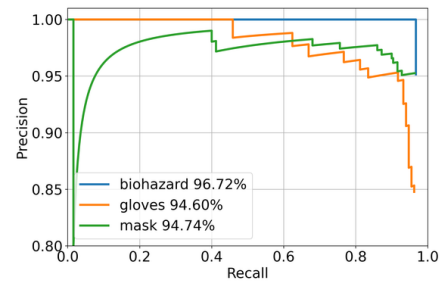
Combination	mask AP	gloves AP	biohazard AP	mAP	Avg. of the mAP
YOLOX-s					
1	85.99	81.60	100.00	89.20	90.1
2	93.00	92.25	98.36	94.54	
3	88.57	82.35	88.00	86.30	
YOLOX-m					
1	89.30	86.55	100.00	91.95	91.38
2	96.74	94.60	96.72	95.36	
3	87.91	83.69	90.99	87.53	
YOLOX-l					
1	89.47	87.05	100.00	92.17	92.49
2	95.64	96.23	96.72	96.20	
3	92.15	81.01	94.20	89.12	
YOLOX-x					
1	86.44	79.75	100.00	88.73	90.86
2	95.64	93.97	95.03	94.88	
3	90.56	85.47	90.88	88.97	

Fig. 8 represents the PR curve of tested anchor-free architecture of different versions for a dataset combination. Per image inference time on both GPU and CPU versus mAP is shown in Fig. 9, where it is clearly seen that CPU inference time is greater than the GPU time. Models mAP differs a little amount according to the model size. In GPU, the YOLOX-s needs 0.06s time to infer an image, whereas YOLOX-x takes 0.12s time, two times more than YOLOX-s. On the other hand, in CPU the YOLOX-s needs 0.70s time to infer an image, whereas YOLOX-x takes 4.01s time, which is approximately five times more than YOLOX-s. Hence, it is said that increasing model size CPU requires more time to infer an image than GPU. Additionally, GPU time maybe differ on the criteria of the GPU architecture. Fig. 10 displays several qualitative measures of anchor-free architecture—the different versions of the YOLOX architecture yield approximately the same results. The input combinations of the dataset are responsible for the performance. In this case, remarkable improvement may happen for the different training and testing dataset combinations, although their averaging produces the conventional results. Since different dataset combinations have been used, YOLOX-l architecture provides the highest individual mAP than others. Additional testing is conducted using the test dataset of the second combination because, among the three combinations, these combination generates the highest mAP. Furthermore, the test dataset of the second combination is divided into two portions, one is relatively easy to guess and the other is relatively hard to guess for the model. A relatively complex sub-division is created using several criteria that are listed below. These criteria are done from the author’s perspective.

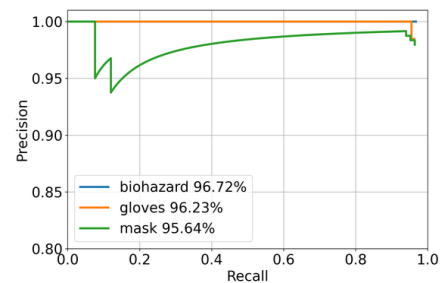
- 1) Objects and the image background color are approximately the same.
- 2) Excess or inadequate light into the images.
- 3) Complex image background compares to objects.
- 4) Occlusion and small objects into the images.



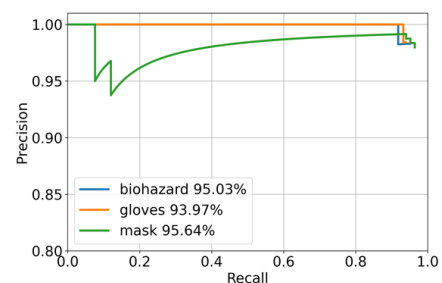
(a)



(b)



(c)



(d)

Fig. 8. Precision-recall Curve of the Anchor-free Model.

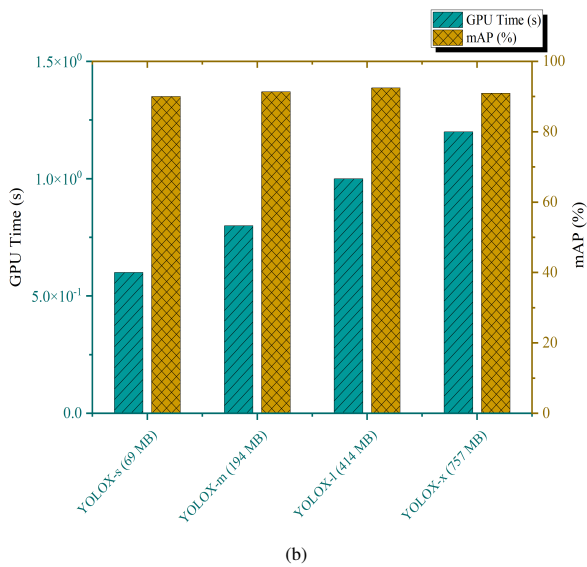
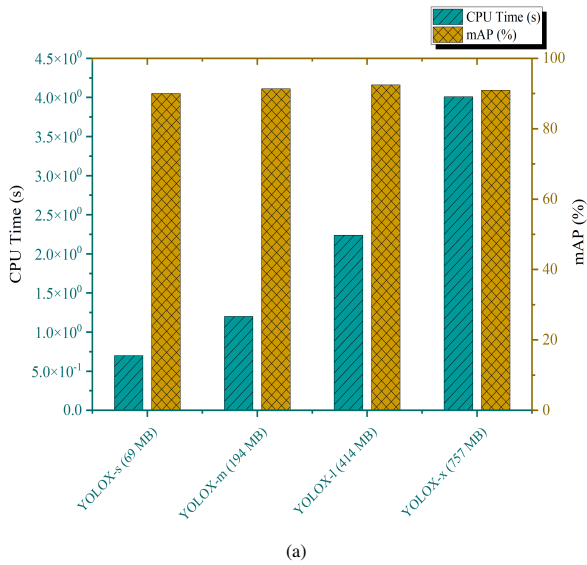


Fig. 9. Inference Time of GPU vs mAP in (a) and CPU vs mAP in (b) of all Version of the YOLOX.

Table VII displays the performance of YOLOX-l models for relatively easy and hard samples of the second combination of test dataset where, for easy and challenging examples, 95.71% and 94.04% mAP are encountered, respectively. The average precision of both the anchor-free and anchor-based architecture is shown in Fig. 11, where anchor-free models mAP is larger than anchor-based models.

TABLE VII. PERFORMANCE OF YOLOX-L FOR RELATIVELY EASY AND HARD CASES

case	mask AP	gloves AP	biohazard AP	mAP
Relatively easy	97.91	94.79	100.00	97.57
Relatively hard	93.78	92.87	97.62	94.76

1) *Where is the Milestone?:* Fig. 12 shows several satisfactory results. According to the Fig. 12, images are natural and most wanted phenomena for waste. Fig. 12a, 12b, 12c, 12d and 12f objects are correctly detected even after complex background; despite being small objects in Fig. 12e, 12g, and 12i objects are well-identified; into the Fig. 12h are some underwater images where obscurity, different lighting condition may happen, still objects are recognized properly.

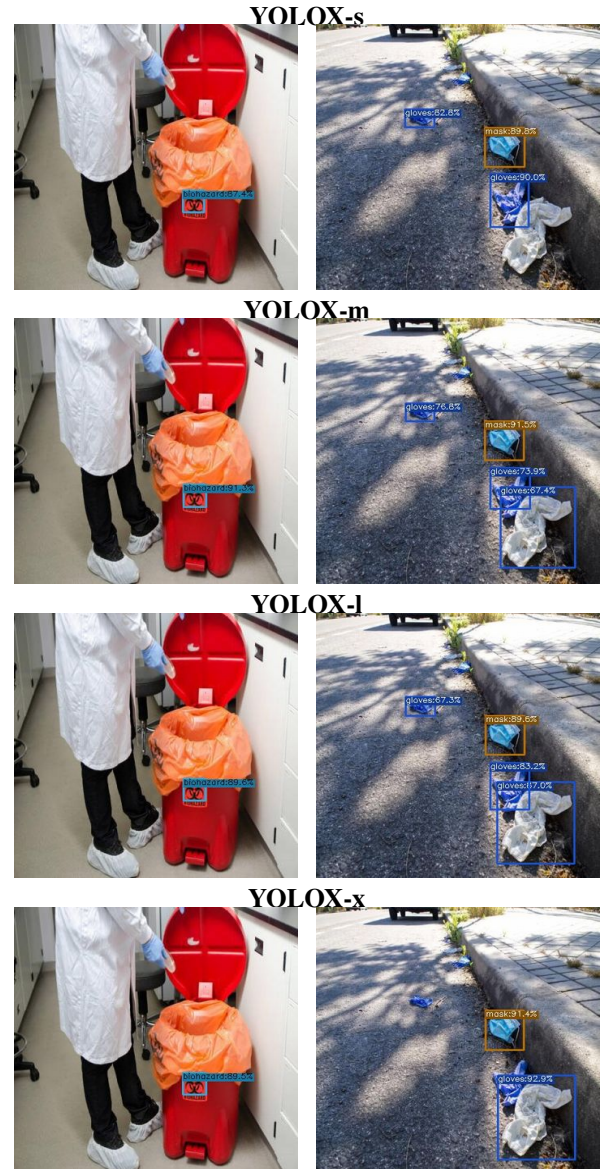


Fig. 10. Several Qualitative Measures of Anchor-free Methods.

2) *Where is Incorrect Detection?:* According to the dataset combination, the FP rate is 4.34%, 10%, and 0.0% for masks, gloves, and biohazards, respectively. FN occurs when the model is unable to detect an object despite its presence in the image. FN rate of mask, gloves, and biohazard class is 8.15%, 8.33%, and 0.0%, respectively. Fig. 13 shows some false detection of the YOLOX-l model. FP detection occurs when objects have crowded situations into the images. When the objects are blurred, they are under-detected by the model in

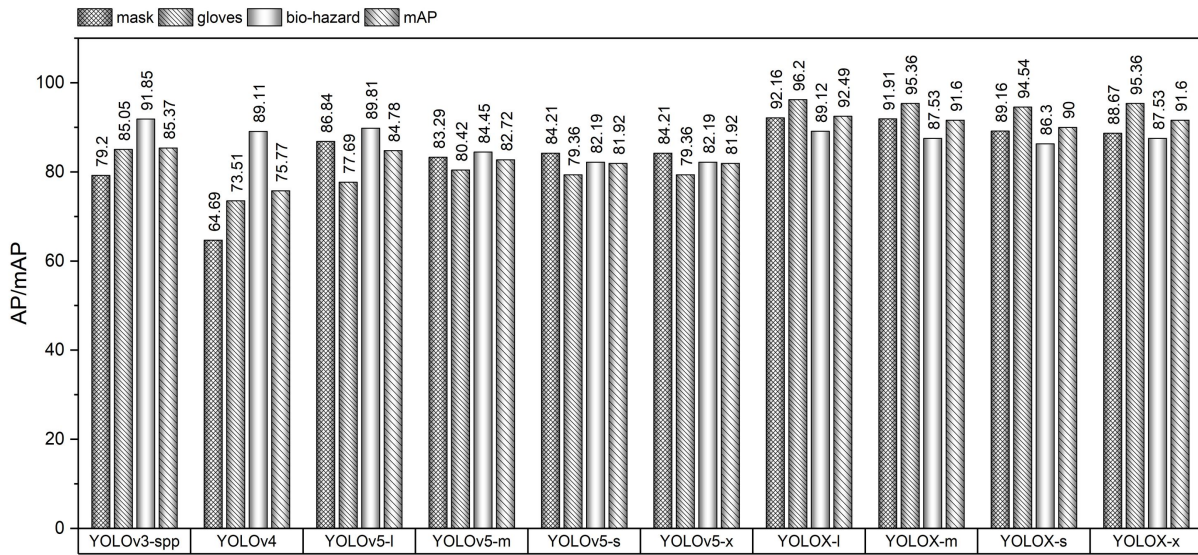


Fig. 11. Average Precision of Each Model.

most cases. Fig. 13a additional gloves and masks are detected. Crowded masks and gloves are there. In Fig. 13b contains small and occluded gloves and mask objects perhaps for this reason they are under detected, in Fig. 13c perhaps objects may not be detected because there are exists some blurriness on the gloves and mask.

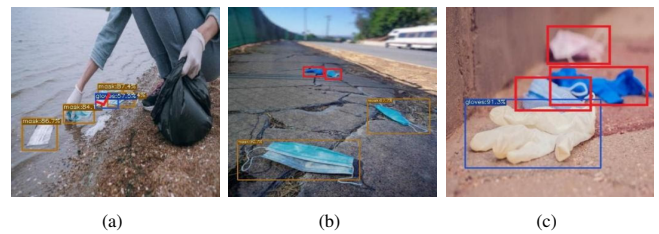


Fig. 13. Incorrect Detection of YOLOX-l Architecture.



Fig. 12. Satisfactory Result of YOLOX-l Architecture.

VII. DISCUSSION

This study examined four different types of object detectors from the YOLO family. The models are trained, tested, and evaluated to attain different goals. The gist contribution and findings are listed below:

- 1) A novel dataset is created to detect and manage surgical waste (mask, gloves and biohazard symbol) from our surroundings including roads, beaches, underwater as well as floating on the water condition.
- 2) Experiment is conducted using two different training mechanisms, one is anchor-based and the other is an anchor-free mechanism. Anchor-based models (YOLOv3-spp, YOLOv4 and YOLOv5) highest mAP 85.27% is lower than the anchor-free models (YOLOX-l) mAP 92.49%. Among the anchor-based model, YOLOv3-spp (mAP 85.27%) performs better than others.
- 3) Additional exploration is performed using all versions of the YOLOX to find TP, FP and FN. In most cases, satisfactory results are yielded by the model. False detection produces when objects are occluded, blurred and crowded. False-negative (misdetection) generates when objects are small and complex to attain minimum feature selection.

Additionally, several limitations exist in this study that can be explored in future work. First, the dataset size may be increased for system robustness. This study detects only three types of classes; hence integrating more classes would be a good exploration. The YOLO architectures are fast and accurate in detecting objects from images. Additionally, YOLO models have the sensitiveness of small objects. Therefore, other anchor-free object detection models may be investigated to evaluate the dataset.

VIII. CONCLUSION

Plastic waste is going to be a threat to humankind and other species day by day. This type of waste is scattered worldwide only for the unconsciousness of humankind. If the proper steps are not taken, it will be dangerous for us in the days ahead. Surgical waste is a kind of plastic waste. Nowadays, the number of this type of waste is also increasing alarmingly, which is responsible for serious health hazards. In this study, authors try to create a novel dataset with surgical waste (mask and gloves) and biohazard symbols to detect such waste from our surroundings and appropriately manage them in certain places. Two types of training mechanism-based YOLO models are chosen to conduct this work. One is anchor-based (YOLOv3-spp, YOLOv4 and YOLOv5) and the other is anchor-free (YOLOX) architecture. This study found that anchor-free architecture performs better generalization than anchor-based architectures. More clearly, YOLOX yields the highest mAP of 92.49% and YOLOv3-spp generates the highest mAP of 85.27%. Satisfactory performance comes up even if there are some limitations. Dataset explorations would be reasonable for future work. Applying the other anchor-free architecture in this area will be a future direction.

REFERENCES

- [1] Xingyi Zhou, Dequan Wang, and Philipp Krähenbühl. Objects as points. *arXiv preprint arXiv:1904.07850*, 2019.
- [2] Hei Law and Jia Deng. Cornernet: Detecting objects as paired keypoints. In *Proceedings of the European conference on computer vision (ECCV)*, pages 734–750, 2018.
- [3] Nicolas Carion, Francisco Massa, Gabriel Synnaeve, Nicolas Usunier, Alexander Kirillov, and Sergey Zagoruyko. End-to-end object detection with transformers. In *European Conference on Computer Vision*, pages 213–229. Springer, 2020.
- [4] Jianfeng Wang, Lin Song, Zeming Li, Hongbin Sun, Jian Sun, and Nanning Zheng. End-to-end object detection with fully convolutional network. In *Proceedings of the IEEE/CVF Conference on Computer Vision and Pattern Recognition*, pages 15849–15858, 2021.
- [5] Qiang Zhou, Chaohui Yu, Chunhua Shen, Zhibin Wang, and Hao Li. Object detection made simpler by eliminating heuristic nms. *arXiv preprint arXiv:2101.11782*, 2021.
- [6] Joseph Redmon and Ali Farhadi. Yolo9000: better, faster, stronger. In *Proceedings of the IEEE conference on computer vision and pattern recognition*, pages 7263–7271, 2017.
- [7] Joseph Redmon and Ali Farhadi. Yolo3: An incremental improvement. *arXiv preprint arXiv:1804.02767*, 2018.
- [8] Alexey Bochkovskiy, Chien-Yao Wang, and Hong-Yuan Mark Liao. Yolo4: Optimal speed and accuracy of object detection. *arXiv preprint arXiv:2004.10934*, 2020.
- [9] Organisation for Economic Co-operation and Development. *The Face Mask Global Value Chain in the COVID-19 Outbreak: Evidence and Policy Lessons*. OECD Publishing, 2020.
- [10] Nsikak U Benson, David E Bassey, and Thavamani Palanisami. Covid pollution: impact of covid-19 pandemic on global plastic waste footprint. *Heliyon*, 7(2):e06343, 2021.
- [11] Harsh Panwar, PK Gupta, Mohammad Khubeb Siddiqui, Ruben Morales-Menendez, Prakhar Bhardwaj, Sudhansh Sharma, and Iqbal H Sarker. Aquavision: Automating the detection of waste in water bodies using deep transfer learning. *Case Studies in Chemical and Environmental Engineering*, 2:100026, 2020.
- [12] Kyriacos Themistocleous, Christiana Papoutsas, Silas Michaelides, and Diofantos Hadjimitsis. Investigating detection of floating plastic litter from space using sentinel-2 imagery. *Remote Sensing*, 12(16):2648, 2020.
- [13] Rahul Hegde, Sanobar Patel, Rosha G Naik, Sagar N Nayak, KS Shiv-aprakasha, and Rekha Bhandarkar. Underwater marine life and plastic waste detection using deep learning and raspberry pi. In *Advances in VLSI, Signal Processing, Power Electronics, IoT, Communication and Embedded Systems*, pages 263–272. Springer, 2021.
- [14] Tzu-Ta Lin. Labelimg, 2015.
- [15] Yue Wu, Yinpeng Chen, Lu Yuan, Zicheng Liu, Lijuan Wang, Hongzhi Li, and Yun Fu. Rethinking classification and localization for object detection. In *Proceedings of the IEEE/CVF conference on computer vision and pattern recognition*, pages 10186–10195, 2020.
- [16] Guanglu Song, Yu Liu, and Xiaogang Wang. Revisiting the sibling head in object detector. In *Proceedings of the IEEE/CVF Conference on Computer Vision and Pattern Recognition*, pages 11563–11572, 2020.
- [17] Borui Jiang, Ruixuan Luo, Jiayuan Mao, Tete Xiao, and Yuning Jiang. Acquisition of localization confidence for accurate object detection. In *Proceedings of the European conference on computer vision (ECCV)*, pages 784–799, 2018.
- [18] Yu-Wei Chao, Sudheendra Vijayanarasimhan, Bryan Seybold, David A Ross, Jia Deng, and Rahul Sukthankar. Rethinking the faster r-cnn architecture for temporal action localization. In *Proceedings of the IEEE Conference on Computer Vision and Pattern Recognition*, pages 1130–1139, 2018.
- [19] Tsung-Yi Lin, Priya Goyal, Ross Girshick, Kaiming He, and Piotr Dollár. Focal loss for dense object detection. In *Proceedings of the IEEE international conference on computer vision*, pages 2980–2988, 2017.
- [20] Shu Liu, Lu Qi, Haifang Qin, Jianping Shi, and Jiaya Jia. Path aggregation network for instance segmentation. In *Proceedings of the IEEE conference on computer vision and pattern recognition*, pages 8759–8768, 2018.
- [21] Seung-Wook Kim, Hyong-Keun Kook, Jee-Young Sun, Mun-Cheon Kang, and Sung-Jea Ko. Parallel feature pyramid network for object detection. In *Proceedings of the European Conference on Computer Vision (ECCV)*, pages 234–250, 2018.
- [22] Zheng Ge, Songtao Liu, Feng Wang, Zeming Li, and Jian Sun. Yolox: Exceeding yolo series in 2021. *arXiv preprint arXiv:2107.08430*, 2021.
- [23] Qiang Chen, Yingming Wang, Tong Yang, Xiangyu Zhang, Jian Cheng, and Jian Sun. You only look one-level feature. In *Proceedings of the IEEE/CVF Conference on Computer Vision and Pattern Recognition*, pages 13039–13048, 2021.
- [24] Hongyi Zhang, Moustapha Cisse, Yann N Dauphin, and David Lopez-Paz. mixup: Beyond empirical risk minimization. *arXiv preprint arXiv:1710.09412*, 2017.
- [25] Joseph Redmon, Santosh Divvala, Ross Girshick, and Ali Farhadi. You only look once: Unified, real-time object detection. In *Proceedings of the IEEE conference on computer vision and pattern recognition*, pages 779–788, 2016.
- [26] Zhi Tian, Chunhua Shen, Hao Chen, and Tong He. Fcos: Fully convolutional one-stage object detection. In *Proceedings of the IEEE/CVF international conference on computer vision*, pages 9627–9636, 2019.
- [27] Wei Yin, Yifan Liu, Chunhua Shen, and Youliang Yan. Enforcing geometric constraints of virtual normal for depth prediction. In *Proceedings of the IEEE/CVF International Conference on Computer Vision*, pages 5684–5693, 2019.
- [28] L Huang, Y Yang, Y Deng, and Y Densebox Yu. Unifying landmark localization with end to end object detection. *arXiv 2015. arXiv preprint arXiv:1509.04874*.
- [29] Xin Huang, Xinxin Wang, Wenyu Lv, Xiaying Bai, Xiang Long, Kaipeng Deng, Qingqing Dang, Shumin Han, Qiwen Liu, Xiaoguang Hu, et al. Pp-yolov2: A practical object detector. *arXiv preprint arXiv:2104.10419*, 2021.

- [30] Priya Goyal, Piotr Dollár, Ross Girshick, Pieter Noordhuis, Lukasz Wesolowski, Aapo Kyrola, Andrew Tulloch, Yangqing Jia, and Kaiming He. Accurate, large minibatch sgd: Training imagenet in 1 hour. *arXiv preprint arXiv:1706.02677*, 2017.
- [31] Hamid Rezaatofighi, Nathan Tsoi, JunYoung Gwak, Amir Sadeghian, Ian Reid, and Silvio Savarese. Generalized intersection over union: A metric and a loss for bounding box regression. In *Proceedings of the IEEE/CVF Conference on Computer Vision and Pattern Recognition*, pages 658–666, 2019.
- [32] Rafael Padilla, Sergio L Netto, and Eduardo AB da Silva. A survey on performance metrics for object-detection algorithms. In *2020 International Conference on Systems, Signals and Image Processing (IWSSIP)*, pages 237–242. IEEE, 2020.
- [33] Rafael Padilla, Wesley L Passos, Thadeu LB Dias, Sergio L Netto, and Eduardo AB da Silva. A comparative analysis of object detection metrics with a companion open-source toolkit. *Electronics*, 10(3):279, 2021.
- [34] Md Ferdous and Sk Md Masudul Ahsan. Multi-scale safety hardhat wearing detection using deep learning: A top-down and bottom-up module. In *2021 International Conference on Electrical, Communication, and Computer Engineering (ICECCE)*, pages 1–6. IEEE, 2021.
- [35] Jimin Yu and Wei Zhang. Face mask wearing detection algorithm based on improved yolo-v4. *Sensors*, 21(9):3263, 2021.
- [36] Haidi Zhu, Haoran Wei, Baoqing Li, Xiaobing Yuan, and Nasser Kehtarnavaz. A review of video object detection: Datasets, metrics and methods. *Applied Sciences*, 10(21):7834, 2020.

Human-Computer Interaction in Mobile Learning: A Review

Nurul Amirah Mashudi¹, Mohd Azri Mohd Izhar², Siti Armiza Mohd Aris³
Razak Faculty of Technology and Informatics
Universiti Teknologi Malaysia (UTM), Kuala Lumpur, Malaysia

Abstract—Mobile learning mainly concerns mobility and high-quality education, regardless of location or time. Human-computer interaction comprises the concepts and methods in which humans interact with computers, including designing, implementing, and evaluating computer systems that are accessible and provide an intuitive user interface. Some studies showed that mobile learning could help overcome multiple limitations and improve learning in educational systems. The study investigates the HCI design challenges, including the guidelines and methods in mobile HCI for education. An existing mobile learning tool was discussed on the current and future design enhancements of Udemy. Next is the further discussion on future mobile learning to provide the possible improvements for learners based on the challenges of mobile HCI in education.

Keywords—Human-computer interaction; education technology; digital technology; mobile learning; e-learning

I. INTRODUCTION

In the rapidly evolving field of mobile learning, education has served as the key emphasis. Various initiatives have shown that mobile learning helps overcome numerous limitations that affect educational systems and make learning more convenient [1]. This has led to a distinct sub-community of experts with extensive experience and skills in developing and delivering mobile learning. Mobile learning is also a kind of e-learning that uses the number of specific features available on computers, devices, and bandwidth and the characteristics of the networks [2]. E-learning is described as applying digital electronic tools and media to support learning.

In contrast, mobile learning refers to the same concept but in the context of mobile devices and wireless transmission [3]. In short, mobile learning is a word to describe the usage of a mobile device to help facilitate learning. Furthermore, mobile learning has been recommended to be applied in any educational system using portable devices as the prominent technology [4]. Moreover, research on mobile learning has been performed in the last decade on many occasions. Each research played an essential role in providing researchers with knowledge on effectively using mobile devices in education. However, some of these studies were non-educational studies whose findings could not identify the research design. According to the researchers, their results were published without making any reference to the educational levels of the learners [5].

The mobile learning interaction is supported by pedagogical requirements and technological characteristics to provide and support user needs. There is a strong consensus that mobile learning is mutually dependent on the technology that

facilitates learning, as shown in many studies [6], [7], [8]. Mobile learning mainly concerns mobility and high-quality education, regardless of location or time. Academic disciplines related to human-computer interaction (HCI) are interested in researching all forms of human-technology interaction, along with its design processes, software, and technology tools. The primary goal of mobile HCI is to investigate various motivations and approaches used by mobile device users to engage with the devices and data accessibility [1], [9], [10]. Historically, the main priority of HCI has been humans and how technology must fulfill their needs to guarantee that it does so effectively. This viewpoint, it is argued, also describes the objective of the new intelligent technological world. As a result, HCI has developed tremendously, broadened the scope of inquiry, and made significant breakthroughs. However, the use of new technologies continues to grow and demand higher levels of complexity.

Moreover, humans' counterpart to technology is changing; as a result, individuals are more conscious and concerned but also less optimistic and demanding [11]. There are several challenges to implementing HCI in education based on how students prepared for their class, how they interacted with users during the class, and what the students thought of the interactions. Educators have been encouraged to innovate by these challenges, which has led them to explore other methods of interacting with the target users in educational contexts. The context can be viewed as an interactional issue instead of a representation issue [12]. In addition, the mobile context can be denoted as data linked to the interaction between the user of the application, the application itself, and the users' surroundings.

Despite advocating creating learning environments that enable students to have hands-on experiences dealing with real users, educators highlight several limitations that prevent students from interacting with others [13]. Establishing relationships between students and prospective users requires time and effort. According to the study in [14], the most prevalent thing related to mobile HCI is the user's mobility. There is a great distinction in the literature regarding mobility and interaction between extremely mobile, somewhat mobile, and stationary interactions [14]. Mobile HCI researchers claimed that the user's movement influences the physical environment of the interaction in a significant way that they identify mobility as one of the most significant challenges. In addition, connections to remote information and mobile device interactions can develop social relationships and communication. According to an interactive activities viewpoint, the study results are not mutually exclusive, as both are integrated [15]. Thus, the user

accomplishes the objective by utilizing and interacting with the technology. Students vary in their abilities and development speed regarding design thinking. Many of those were found to have difficulty analyzing their results and problems out with fresh ideas [16].

This article provides a review of mobile HCI in education. The study's objective is to determine the challenges and importance of HCI in education, including the current platforms or tools in developing mobile learning based on the HCI framework. Furthermore, future mobile learning is discussed to identify the issues regarding mobile HCI that can be improved effectively and efficiently. The following sections structure the paper: Section II provides the importance of mobile HCI in education. The HCI design for mobile learning tools is presented in Section III, followed by the existing mobile learning tools or platforms in Section IV. Next, the discussion on the future of mobile learning is clarified in Section V. Lastly, we conclude the paper in Section VI.

II. THE IMPORTANCE OF MOBILE HCI IN EDUCATION

HCI comprises the concepts and methods humans interact with computers, including designing, implementing, and evaluating computer systems [17]. The main focus of the HCI is on the usability of software applications in which software technology is accessible and provides an intuitive user interface. One of the factors affecting technology adoption is the usability of the technology. When people choose to adopt a new system, they desire to utilize it. Mobile devices usage provides an incentive for informal learning in which learners are free to pick up other tasks depending on the situation [18]. The additional benefit of mobile HCI is that outdoor learning more exciting and enriching. Research shows that learning outdoors benefits the development of learners' knowledge and hands-on learning as long as the activity is conceived, organized, and followed up properly [19]. The integration of mobile HCI will benefit students and enhance their learning experience by providing contextual learning [20]. The mobile HCI aims to offer contextual information to students to enhance their learning environment and location.

Smartphones have been considered tools or devices for gaining access to information and services [21]. Besides that, smartphones are provided a significant way of getting information, but it also promotes interactions between people involved in various activities. Generally, educators encourage students to use search engines and other apps that provide news feed and language learning and use social media to communicate with others. Mobile devices are particularly beneficial for learners looking to search and access documents and perform various other tasks, such as survey-taking, summarizing material, reading books, taking pictures, and sharing information [22]. Researchers discovered that mobile website usability is influenced by many factors, including the lighting, the number of people around, movement, and the environment's sounds [23]. According to Korn and Zandar, the experiment sparked intriguing discussions and reflections among the 64 participants.

Apart from the contextual information, video creation can create a new way for the student to develop creative ideas for communication while ensuring effective presentation of

knowledge and abilities. Some researchers have found that students engaged in collaborative video creation demonstrated and improved strong media literacy and digital skills [24]. Moreover, creating a video presentation can help create a fair, competitive environment for various materials, including paper prototypes and software prototypes. In response to these sentiments, students will obtain a better experience in video creation than written reports and presentation slides for sharing information. The effectiveness and accessibility of video are growing with the ubiquity and efficiency of smartphone cameras, and thus, it is recommended that instructors utilize video in the assessments. However, the most reliable human memory can be prone to error [25]. The importance of mobile HCI in education can show the difference between how designers recall the interaction and what occurred during the interaction. Students who utilize mobile HCI in the learning process will remember their interactions and user-centered design process completely different from the recorded videos. The mobile HCI approach in education seems to be a kind of organized learning in which students can extract information from the interaction sessions.

III. THE HCI DESIGN FOR MOBILE LEARNING TOOLS

This section explained the HCI design for mobile learning tools. The challenges in HCI design based on human technology, interactions, security and privacy, well-being, accessibility, and creativity [11] are described in Section III(A). Furthermore, it is challenging to determine the critical factors to concentrate on and identify the necessary or critical boundaries to teach. The guidelines and methods on mobile HCI are then clarified according to the design challenges that comprise the interface guidelines as a starting point and collection of realistic design principles for mobile device interfaces in Section III(B).

A. HCI Design Challenges

New challenges for human-computer interaction experts examine how HCI helps solve significant social problems, emphasize the necessity for multidisciplinary approaches, and identify sixteen main challenges for society-oriented and technology-oriented problems [26]. The aim is to probe into the significant problems in modern-day fast technological advancement, leading to smarter interactive technologies and increased social demands, with individual and community expectations. The challenges of HCI design consist of six challenges: an integration of human technology, an interaction between humans and the environment, privacy and security, health and well-being, universal accessibility, and creative learning.

Live and working peacefully with technology is defined as part of human technology integration. This technological feature will include language comprehension, learning, thinking, and creative thinking. It has become necessary due to the emergence of smart ecosystems, composed of smart devices, services, materials, and environmental conditions that collaborate seamlessly and transparently. Smart ecosystems have an intricate web of symbiotic relationships with humans, extending well beyond technological limits and involving many diverse disciplines to resolve complicated ethical, social, and philosophical matters. There are many ways involved, such as

combining human values into design elements and exchange. For instance, automation comes second to human control or strategizing around increasing our focus on humanistic problems instead of solely being driven by deterministic ones [27]. Many practical aspects must be integrated with the criteria mentioned to form a comprehensive design strategy that addresses meaningful human control, system accountability and transparency, and intelligent system transparency and volatility.

Interaction between humans and the environment describes how humans interact with many technological systems that have become more intelligent and interactive, not only with a single object [28]. Interactions in technologically enhanced, autonomous, and smart settings are likely to be more implicit and unspoken. Additionally, issues dealing with the challenges and opportunities surrounding human interaction in these settings result in new implications and applications. Digital content will combine with and support the physical structure, and information will naturally flow from one entity to another. The difficulties laid out before us will guide us to evolve our current design and assessment methods and approaches to keep pace with the continually evolving technology environment—understanding how the increased interaction possibilities impact humans [29].

The capability of users to maintain control over data collection and distribution and what that data may be used for is at the core of privacy. While computing security relates to protecting the computer systems' hardware, software, electronic information, and services. Intelligent systems must benefit people beyond just being functional to empower individuals and protect their privacy and security. The introduction of new dimensions concerning technologically enhanced and intelligent settings implies privacy, trust, and security all take on more importance in the digital realm [30]. To understand this concept, the key aspects to consider are privacy and the difficulties it creates in the new digital world, and the problems it presents on a societal level as they emerge in various environments. Privacy should be protected even further because the new technology landscape features advanced information processing and artificial intelligence to gather a large amount of data about the user and a substantial amount of information about user behavior that may result in developing conclusions. Hence, the findings of HCI research should contribute to regulating government policies on privacy, security, and safety in the context of the new intelligence period.

Health includes both the absence of illness or disability and a condition of full physical, mental, and social well-being. An abundance of well-being also involves a feeling of purpose and pleasure and comfortable living standards. Opportunities for medical advancements with new technological developments make it possible to live healthier and cheaper methods of helping people have a long and healthy life. Technology may also help people reach their personal and emotional well-being objectives, encompassing both health elements and a chance to become happier. Healthcare technology is now extensively used, yet unsolved research questions remain. However, the larger problem is that since technology is ubiquitous, the question becomes how it can be maximized to enhance well-being, particularly when it comes to questions of how to improve interaction difficulties and remain human-centered.

With the development of devices, services, products, or

environments more accessible, designers have to think about accessibility. The idea of universal access to information society technologies means that everyone may use information society technologies wherever and at any time. Innovative environments present new difficulties related to accessibility and universal access, especially due to the rising technical complexity [31], which significantly affects daily life. As technology-augmented settings have historically focused on human beings, HCI initiatives will be expanded to the well-being of other groups, including those with disabilities. The idea of accessibility and universal access has been around for some time, but now, concerning demographics and growing technical complexity, these concepts are necessary and critical for future civilizations. While certainly, it introduces universal access concerns, the introduction of intelligent environments presents new possibilities that should be taken advantage of. Methods that seek to address accessibility only based on reactivity will lack design complexity and scalability needs. Therefore, HCI research demands more comprehensive solutions, demanding a significant place in the foreseeable future.

The concept of learning suggests any of these: taking in new information, learning a skill, or experiencing something new. The act of being creative has to do with the capacity to generate unique and original ideas or to create something entirely new or innovative. This will allow individuals from different backgrounds, abilities, and interests to work together to discover, understand, and develop new knowledge to tackle difficult issues. Innovative and developing technologies may aid with emerging and distinct learning styles since they have developed due to new and emerging technologies permeating into daily life for the new generations. To address the question, 'What is the proper role of technology in the learning context?'. In this age of evolving technology, the debate is more relevant than ever, touching on such themes as privacy and ethics, learning concepts, and pedagogical factors. Regardless, problems concerning Human-Computer Interaction have a huge impact on the performance of the technology in education. While creativity has a prominent responsibility for future society, cultivating and exploring ways to be supported are essential. The revolution will influence various learning styles and how educational technologies are used.

B. Guidelines and Methods

1) *Mobile Human-Computer Interaction*: There are various ways humans engage with computers, and it is thus necessary to provide the proper interface between humans and computers, as shown in Fig. 1. Since people first started interacting with computers, the development in the HCI area has occurred in terms of interaction quality and various points of history. Several research centers have instead focused on ideas like multimodality, intelligent adaptive interfaces, and active interfaces despite using conventional interfaces. Human-computer interaction is defined as a field dedicated to developing, testing, and implementing interactive computing for human use and studying the key human-computer interaction aspects [32]. It utilizes the information on both machines and humans in its field of study. Applying the methods of computer graphics, operating systems, programming languages, and application frameworks in the design and construction of new technology is of primary concern. While the human aspects such as computer user satisfaction are an important

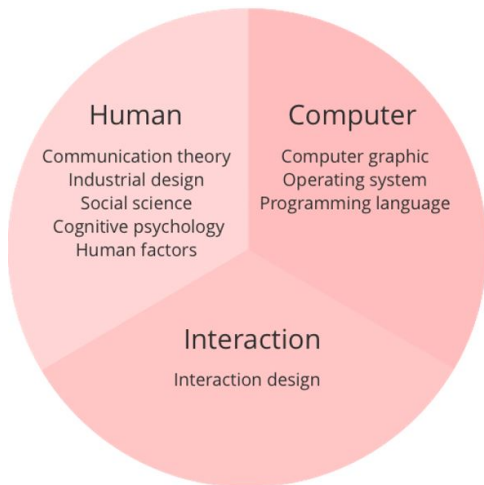


Fig. 1. Overview of Human, Computer and Interaction.

consideration, communication theory, graphic design, industrial design, languages, social sciences, cognitive psychology, and social psychology are essential when interacting with humans. HCI is multidisciplinary, resulting in individuals from many backgrounds being involved in its progress. The interface between humans and computers is known as human-machine interaction (HMI), machine-machine interaction (MMI), or computer-human interaction (CHI) [33], [34].

Various methods for human-computer interaction design had appeared since the 1980s when human-computer interaction design (HCI) as a discipline began to gain popularity. The concept of interaction between users, designers, and technical systems serves as the foundation for most design methods. Early methods regarded user cognitive processes as predictable and measurable, which enabled design practitioners to draw inspiration from cognitive science findings in domains including memory and cognitive when creating user interfaces [35]. The activity theory, a tool employed in HCI, describes and analyzes the physical, social, and technical environment in which human-computer interactions occur. Activity theory establishes a framework and defines a process for analyzing and designing activities. In addition, it offers checklists for researchers to plan the interface design and helps designers structure the interaction designs around activities [36].

Besides that, user-centered design (UCD) is a contemporary and widely implemented design philosophy based on the concept that people should be spotlighted in any computer system [37]. There are several roles inside a project, including the roles of the user, the designer, and the technical experts. These roles need to work together to comprehend the user's needs, requirements, and constraints. The participatory design does include methods of facilitating the participation of end-users in designing new products and services. However, it does not quite mirror the approach used in participatory design, which stresses collaboration between design partners, customers, and end-users. The user interface design has seven principles: tolerance, simplicity, visibility, affordance, consistency, structure, and feedback [38]. In addition, it encompasses many concepts that can be conceived of at any point throughout the development of user interfaces.

VSD, known as the value-sensitive design, is a method for developing technologies that reflect the values of individuals who use the technology and those whose well-being is affected by the technology [39]. A three-tiered method for developing VSD includes conducting conceptual, empirical, and technical studies. Conceptual studies seek to grasp and elucidate all users who will be using the technology along with the various values and the possible values conflicts that could emerge due to its usage. Empirical studies focus on understanding the target users' values, needs, and behaviors based on qualitative and quantitative research studies that aid in this process. Finally, technical studies should include research into how users utilize technology with systems development to serve the best values established in both the research and development process [40].

The challenge of accessibility guidelines for mobile applications has not been extensively researched, although it is almost as essential as websites. Mobile applications are sophisticated and have to work in many different form factors and interaction methods, making it impossible to make them completely accessible [41], [42]. As a consequence of comparing the mobile HCI guidelines, a richer set of recommendations for mobile design will be produced, such as removing cluttering, producing good navigation, creating a user-friendly touch screen, readable text, and elements visible on the interface, and many more. In addition, a valuable asset called user attention must be allocated appropriately. According to Babich, when interfaces are cluttered, it makes information such as extra buttons, images, and text difficult to extract [43].

2) *Mobile Learning*: Implementing a systematic approach to the design process for mobile learning sources and materials will be highly effective once we use the concepts of HCI [44], as illustrated in Fig. 2. Learners must be able to gather data, regardless of any ambiguous circumstances. Also, learners need to be provided with opportunities to reduce risks in the user interfaces and limit the dangers of mistakes and other unexpected moves. The design of the e-learning application must assist the user in acquiring information with ease [45] and without putting a lot of effort in [46]. The design must comply with the specifications such as subject content should have a pleasing visual appearance, easy-to-use navigation structure, animated and graphical presentations can potentially transform learning into an enjoyable experience to achieve everyone's expectations.

Research is performed to discover which issues need help from mobile learning. An interactive approach can be used for effective learning where the topic is fully recognized [47]. A broad range of solutions is available to solve the problem depending on what has to be solved [48]. The development team must consider if the topic can be delivered in a video or other instructional medium [49]. A certain kind of learning material to be used is selected during the solution recognition. The actual design process begins at the mobile learning application design phase. HCI concepts control this to ensure that the solution conforms to industry-standard recommendations and guidelines [50]. Furthermore, some design strategies are adapted to meet the situation depending on the learner. This consists of all options, such as design, layout, font, and color.

After the design process, the learning resource is evaluated for different technical and non-technical aspects [46]. Then, the testing phase is HCI-controlled, which follows the

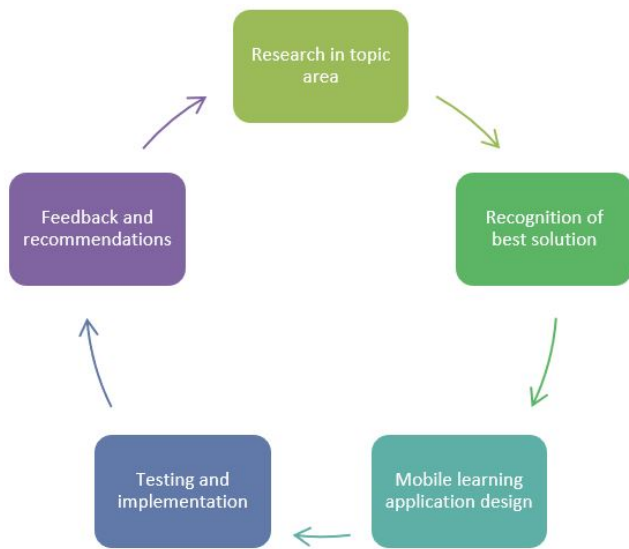


Fig. 2. HCI Guideline Concepts in Mobile Learning.

requirements' rules and standards. Once it is shown that the solution works by the conclusion of the testing process, it is deployed to end-users which are the learners [51]. Finally, a customer survey helps assess the product's strengths. The feedback resulted in recommendations on what to improve, making the process again.

IV. EXISTING MOBILE LEARNING TOOLS / PLATFORMS

Although e-learning on a personal computer enables an exciting learning experience, it is valuable to include mobile learning in digital learning apps. Various benefits have been discovered in mobile learning, such as accessing anytime and anywhere, requiring low-cost requirements, and having interval warranties. In this section, the types of mobile learning tools or platforms are briefly explained in Section IV(A). The examples and design evaluation of two mobile learning tools or platforms are described subsequently in Section IV(B).

A. Types of Mobile Learning Tools / Platforms

The Internet has hundreds of educational opportunities, yet each can be learned in many different ways. Mobile learning has revolutionized the industry of e-learning. For the most part, mobile learning tools tend to concentrate on one objective: studying for an assessment or learning a new language [52]. However, educational institutions, businesses, and almost every other organization use mobile learning platforms to bring learning to life and enable people to learn effectively. Several types of mobile learning tools will be discussed in this section: online courses tools, memorization tools, assessment preparation tools, and supporting tools.

- 1) Online courses tools: Students prefer using e-learning courses rather than traditional ones since online ones are prevalent and accessible. In general, videos are the backbone of many online courses, including text materials [53]. In addition, online courses and education platforms, such as Udemy and Coursera, provide various educational programs and courses for

professionals and instructors to use. Also, students can engage with online courses like Duolingo, an app that offers language lessons. While it is common for language courses to provide students with video-based lectures, Duolingo has a different method. Students take quizzes, type in words, and repeat words or phrases upon listening to the recordings. In addition, a rationale exists in Duolingo to help keep track of their progress and remind them to practice what they have already learned based on the mistakes that most frequently arise.

- 2) Memorization tools: All modern memorization methods are used to create memorization tools. In learning applications, the visual display of information is one of the primary benefits. A common and long-known strategy for memory is using flashcards [54]. Educators use flashcards in physical classrooms to encourage students to memorize vocabulary, historical figures, or technical terminology. The idea of using flashcards provides an effective and efficient learning process as a memorization tool.
- 3) Assessment preparation tools: A software application that aids students with their academic preparation often comes equipped with large databases of assignments collected from various disciplines and schedule and evaluation systems. There are a variety of applications that vary by kind, including flashcards, databases containing information, and online quizzes. This kind of app includes SAT Up, ExamPrep, and GradeUp. Assessment and scheduling are fundamental in these applications to make preparation as successful as possible. It is essential to work on an examination application with push notification functionality and continuous assessment systems. Students will benefit from learning how to prepare and remember things effectively. Some of these assessment preparation aids also offer supplementary resources. Having all the necessary resources on hand is advantageous for most people, particularly if your study app focuses on a certain kind of assessment. Preparing students for exams by including supporting resources such as a database with relevant terminology is simpler when the resources are related to the assessment.
- 4) Supporting tools: Additional applications that aid students in learning are supporting tools [55] such as online dictionaries like Oxford Dictionary, online databases like Scribd, and note-taking applications like EverNote. These applications are not intended to provide academic support by themselves, but they assist students in their educational endeavors.

B. Examples and Design Evaluation of Mobile Learning - Udemu

According to the findings, a large majority of the students chose Udemu due to its affordability, plentiful course options, and good accessibility [56]. Learning through Udemu is an essential online educational practice nowadays. A variety of categories offered by Udemu includes development, IT and software, business, design, marketing, others. An analysis has been done to identify the user experience of Udemu and another competitive platform, namely Coursera. Based

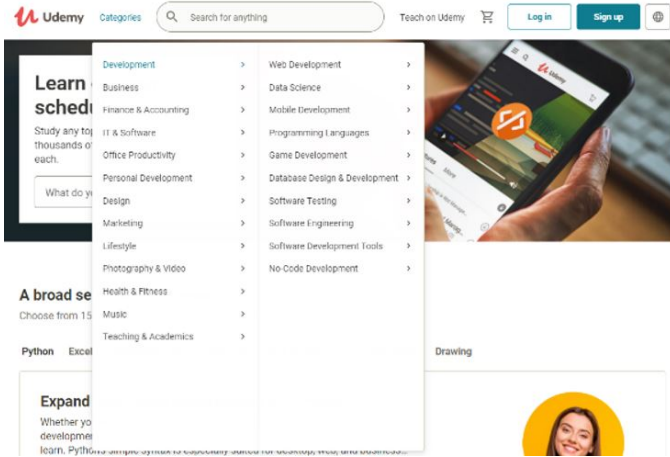


Fig. 3. Categories Offered on Udemey.

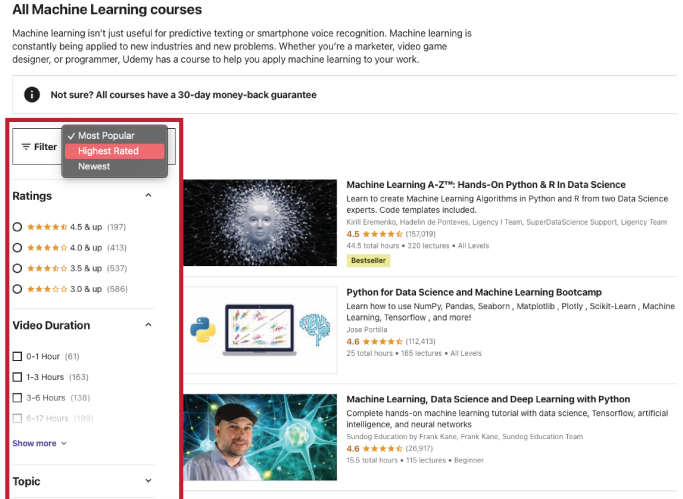


Fig. 5. A Filter Feature Provided on Udemey.

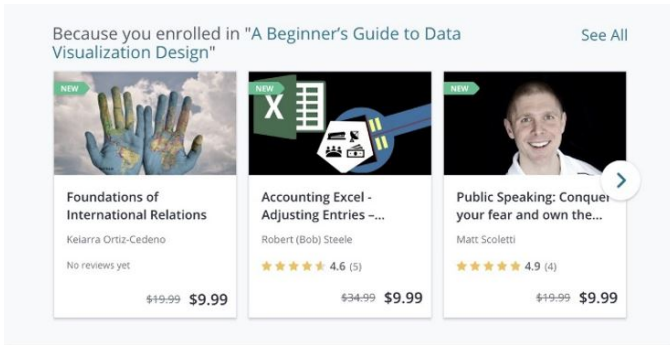


Fig. 4. The Course Suggested based on users' Enrollment.

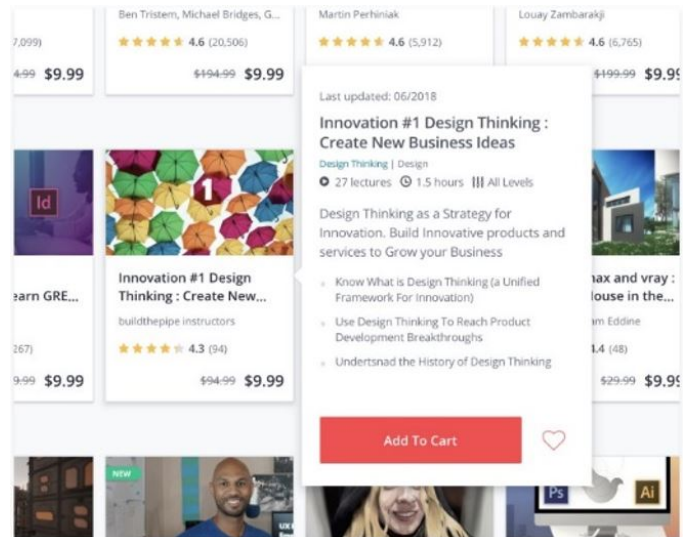


Fig. 6. The Tooltip to Display Perceptible Information about the Course.

on the analysis, students have highlighted that Udemey has various courses, including those specifically for hobbies, which allowed them to feel as if they could learn anything virtually. Additionally, over a hundred thousand courses in sixty-five different languages were provided on Udemey, which were readily accessible [56]. Students loved Udemey's teaching style, which allowed extensive learning in a practical context.

Udemey was deemed to be simple to use in the study. The landing page style is immaculate and straightforward, with a large categories button located on the top to provide easy access to the thirteen main areas, as shown in Fig. 3. Search tools that can find anything on the site (a global list of courses with links on the homepage) would have simplified locating a class and made the experience intuitive [57]. The website also offers several features, including courses that users are currently watching, courses recently added to the platform, and courses popular in broad subject areas wherein users have joined, as in Fig. 4. Every class includes a description of the course, prerequisites, criteria for ratings and reviews, and biographical information about the educator. The instructional objectives, the teacher's expectations, and the topics covered are made abundantly evident [58].

From the Category menu, a user may navigate to the Category page. The featured posts are only the beginning in which users can further explore and filter down to particular categories and popular subjects. As users enter the list of

courses belonging to the selected category, the filter feature is performed again in Fig. 5. The filter feature provides a hide and unhide function to create a compact and comfortable view. Apart from that, the tooltip is particularly beneficial on the platform. When users hover to a course card, the tooltip will be displayed in Fig. 6. This tool only applies to desktop users and only on specific pages, but it assists those who have signed up for the course predict what to expect. Additionally, the Add to Cart button and Favorite button have made the widget more discoverable for users.

An onboarding wizard that helps people quickly get up and running on an information platform like the mobile app might be included in that kind of platform, as shown in Fig. 7. The website can filter out new users' interests before users search on courses by questioning what subjects and categories the top Udemey learners are interested in. The questions users like may vary. If users choose not to complete the onboarding process, they can simply skip it. We have seen successful

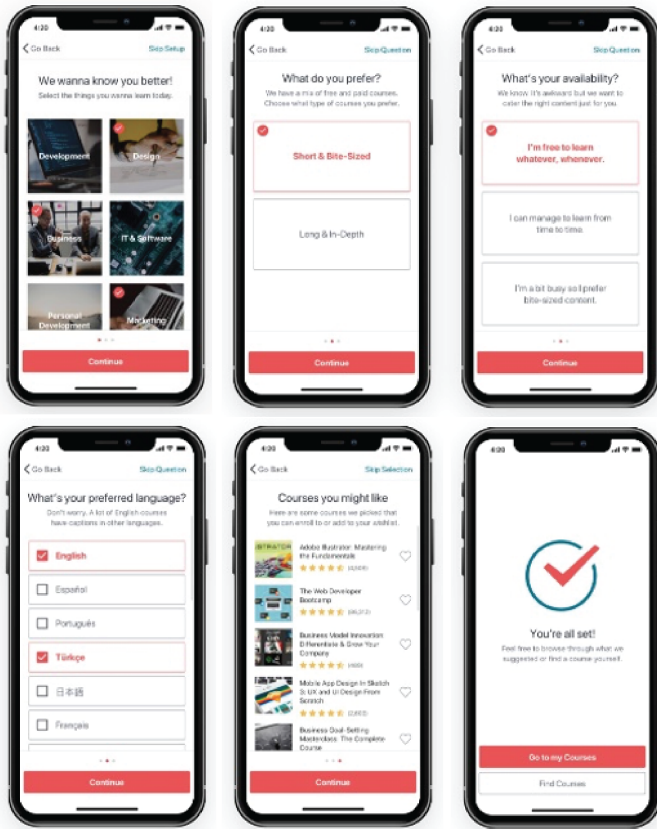


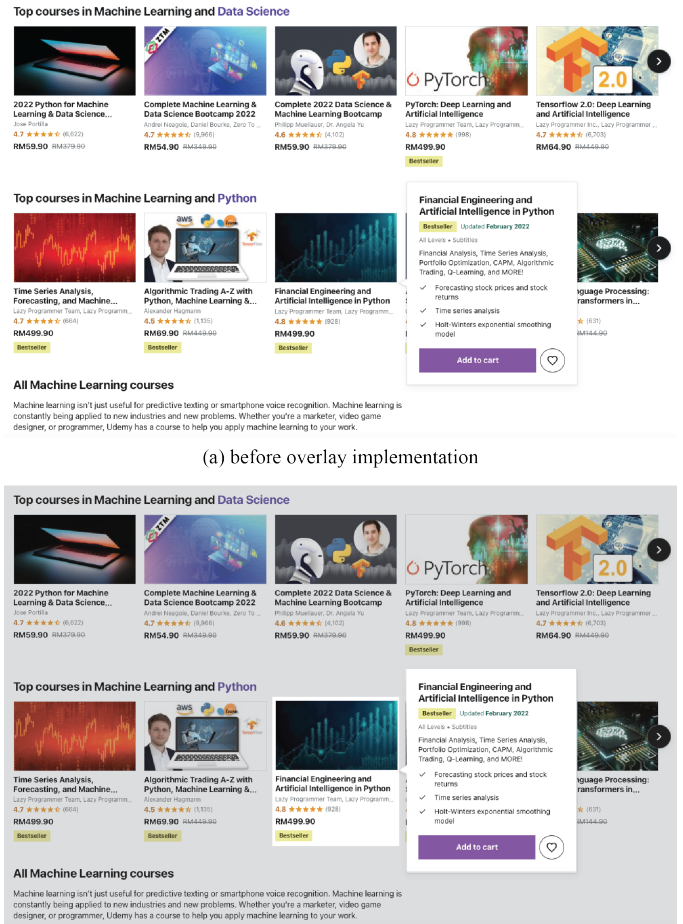
Fig. 7. Onboarding Wizard on Mobile Platform.

onboarding processes that involve both Netflix and Canva in which fonts, colors, images, everything says precisely. We wanted to accomplish this by using this method to change the course of Udemy's marketing strategy. Although these advertisements claim that Udemy members can access the material anywhere, this statement is inaccurate. It is indeed possible that they're attempting to increase user activity by encouraging mobile content consumption.

Furthermore, one critical key consideration in typefaces is isolating the topic of the text. Other than shadows, the tooltip feature merges on the cards may benefit from an overlay to focus, as illustrated in Fig. 8. The overall design is critical to ensure that the reader pays attention to essential information. Thus, the background of the tooltip feature must be a little darker to emphasize the content inside the tooltip feature.

V. FUTURE OF MOBILE LEARNING

This article reports on the findings of a comprehensive review which showed that smartphones not only assist the learning process; they also need research to identify effective learning methods and activities for lifelong learning. Java-enabled phones are becoming more popular since many phone manufacturers are producing these phones at a low price and with an extensive range of features. Students are advised to use Java-enabled smartphones in the future for educational initiatives [59]. With the information provided, students will perform a broad scope of sophisticated and fun learning activities such as revising for a test, answering multiple-choice



(a) before overlay implementation

(b) after overlay implementation

Fig. 8. Overlay Implementation for the Tooltip Feature.

questions, or watching short videos on lectures. Besides that, many learners have difficulty using free Wi-Fi in public areas, subject to security risks [60]. Some learners reported challenges with the UI or other device issues [61]. Some learners noticed difficulties, including shorter battery life caused by accessories [60], [62]. Future-proofing devices and networks to serve mobile learning requirements will resolve these issues. Parents must provide a suitable device for mobile learning, and some service providers must provide a better mobile plan to avoid learners using risky public Wi-Fi.

The communication, social expectations, and reflections highlight how important it is to pay attention to the under elements of HCI education. As such, there is a potential for future HCI education research to offer learners real-world user experience and use reflective HCI as an essential pedagogical strategy [63]. A well-built platform provides instruction consistent with the existing pedagogical ideas, making future educational technology advancements possible. In addition, there are numerous learning and teaching tools on the platform, including ready-made lecture notes that educators can utilize and specific course materials that students can have access to as needed [64]. This also enhances the efficiency of education by integrating teaching and learning. The platform's layout is quite convenient to use and pleasant to look at. Educators

and learners can benefit from using the platform since it will allow them to access as much information as possible. More is still to be assessed to validate effective computer-assisted language learning methodologies [65], and advanced mobile learning platforms are needed; thus, further work is still required. The datasets of online learning activity could be utilized to glean insights about the course behavior of learners and assist educators in the development of teaching methods [66].

VI. CONCLUSION

Human-computer interaction studies all aspects of HCI, including design processes, software, and tools. The mobile device promotes informal learning, in which learners are allowed to take on extra activities as necessary. The importance of mobile HCI in education can show the difference between how designers recall the interaction and what occurred during the interaction. New challenges for human-computer interaction experts examine how HCI helps solve significant social problems and emphasize the necessity for multidisciplinary approaches. The challenges in HCI design include human technology, interactions between humans and computers, privacy and security, well-being, universal accessibility, and creative learning. Additionally, this study discussed current mobile learning resources, such as online courses, memorizing tools, assessment preparation tools, and supporting tools. Udemy was selected as one of the learning platforms to explore the design and possible improvements. Some students mentioned issues with the user interface or other aspects of the device, while others highlighted drawbacks, such as shorter battery life caused by accessories. Thus, future-proofing devices and networks to support mobile learning needs will likely entail resolving these issues, and parents are then required to supply an appropriate device for mobile learning.

ACKNOWLEDGMENT

This research was supported in part by the Ministry of Higher Education (MoHE) of Malaysia through the Fundamental Research Grant Scheme (FRGS/1/2021/TK0/UTM/02/67), and in part by UTMSPACE through the UTMSPACE Contract Research Grant UTMSPC1.16 (R.K130000.7756.4J554).

REFERENCES

- [1] A. Botha, D. Van Greunen, and M. E. Herselman, "Mobile human-computer interaction perspective on mobile learning," in *International Conference on Computing and ICT Research, Kampala, Uganda*, 2010, Conference Proceedings.
- [2] A. Stone and K. U. Thames, "Designing scalable, effective mobile learning for multiple technologies," *Learning with mobile devices: research and development*, pp. 145–154, 2004.
- [3] M. Milrad, *Mobile Learning: Challenges, perspectives and reality*. na, 2003.
- [4] Y.-S. Chen, T.-C. Kao, and J.-P. Sheu, "A mobile learning system for scaffolding bird watching learning," *Journal of computer assisted learning*, vol. 19, no. 3, pp. 347–359, 2003.
- [5] H. Crompton and D. Burke, "The use of mobile learning in higher education: A systematic review," *Computers & Education*, vol. 123, pp. 53–64, 2018.
- [6] Y. Laouris and N. Eteokleous, "We need an educationally relevant definition of mobile learning," in *Proceedings of mLearn*, vol. 2005, 2005.
- [7] C. Quinn, "mlearning: Mobile, wireless, in-your-pocket learning," *LiNE Zine*, vol. 2006, pp. 1–2, 2000.
- [8] M. Sharples, I. Arnedillo-Sánchez, M. Milrad, and G. Vavoula, *Mobile learning*. Springer, 2009, pp. 233–249.
- [9] B. Bauer and A. S. Patrick, "A human factors extension to the seven-layer osi reference model," *Retrieved January*, vol. 6, 2004.
- [10] S. Love, *Understanding mobile human-computer interaction*. Elsevier, 2005.
- [11] C. Stephanidis, G. Salvendy, M. Antona, J. Y. Chen, J. Dong, V. G. Duffy, X. Fang, C. Fidopiastis, G. Fragomeni, and L. P. Fu, "Seven hci grand challenges," *International Journal of Human-Computer Interaction*, vol. 35, no. 14, pp. 1229–1269, 2019.
- [12] P. Dourish, "What we talk about when we talk about context," *Personal and ubiquitous computing*, vol. 8, no. 1, pp. 19–30, 2004.
- [13] J. S. Hui, E. M. Gerber, and S. P. Dow, "Crowd-based design activities: helping students connect with users online," in *Proceedings of the 2014 conference on Designing Interactive Systems*, 2014, Conference Proceedings, pp. 875–884.
- [14] A. Oulasvirta, S. Tamminen, and K. Höök, "Comparing two approaches to context: realism and constructivism," in *Proceedings of the 4th decennial conference on Critical computing: between sense and sensibility*, 2005, pp. 195–198.
- [15] V. Kaptelinin and B. A. Nardi, *Acting with technology: Activity theory and interaction design*. MIT press, 2006.
- [16] A. Alnuaim, P. Caleb-Solly, and C. Perry, *A mobile location-based situated learning framework for supporting critical thinking: A requirements analysis study*. Springer, 2014, pp. 139–158.
- [17] B. A. Kumar and P. Mohite, "Usability of mobile learning applications: a systematic literature review," *Journal of Computers in Education*, vol. 5, no. 1, pp. 1–17, 2018.
- [18] A. Jones, K. Issroff, E. Scanlon, G. Clough, P. McAndrew, and C. Blake, "Using mobile devices for learning in informal settings: is it motivating?" in *IADIS International Conference on Mobile Learning*. IADIS Press, 2006, pp. 251–255.
- [19] J. Dillon, M. Rickinson, and K. Teamey, *The value of outdoor learning: evidence from research in the UK and elsewhere*. Routledge, 2016, pp. 193–200.
- [20] H. Ryu and D. Parsons, "A learner-centred design of a location-aware learning reminder," *International Journal of Mobile Learning and Organisation*, vol. 2, no. 2, pp. 187–200, 2008.
- [21] L.-H. Wong, M. Milrad, and M. Specht, *Seamless learning in the age of mobile connectivity*. Springer, 2015.
- [22] S. McQuiggan, J. McQuiggan, J. Sabourin, and L. Kosturko, *Mobile learning: A handbook for developers, educators, and learners*. John Wiley & Sons, 2015.
- [23] A. S. Tsaiousis and G. M. Giaglis, "An empirical assessment of environmental factors that influence the usability of a mobile website," in *2010 Ninth International Conference on Mobile Business and 2010 Ninth Global Mobility Roundtable (ICMB-GMR)*. IEEE, 2010, Conference Proceedings, pp. 161–167.
- [24] A. Vasilchenko, D. P. Green, H. Qarabash, A. Preston, T. Bartindale, and M. Balaam, "Media literacy as a by-product of collaborative video production by cs students," in *Proceedings of the 2017 ACM conference on innovation and technology in computer science education*, 2017, Conference Proceedings, pp. 58–63.
- [25] E. Tulving and F. I. Craik, *The Oxford handbook of memory*. Oxford University Press, 2000.
- [26] B. Shneiderman, C. Plaisant, M. Cohen, S. Jacobs, N. Elmqvist, and N. Diakopoulos, "Grand challenges for hci researchers. interactions 23, 5 (aug. 2016), 24–25," *Google Scholar Google Scholar Digital Library Digital Library*, 2016.
- [27] S. E. Bibri, "The human face of ambient intelligence," *Atlantis Ambient and Pervasive Intelligence*. Atlantis Press, 2015.
- [28] Y. Li and O. Hilliges, *Artificial Intelligence for Human Computer Interaction: A Modern Approach*. Springer, 2021.
- [29] D. Norman, *Things that make us smart: Defending human attributes in the age of the machine*. Diversion Books, 2014.
- [30] S. Sophonhiranrak, "Features, barriers, and influencing factors of mobile learning in higher education: A systematic review," *Heliyon*, vol. 7, no. 4, p. e06696, 2021.

- [31] B. Curum and K. K. Khedo, "Cognitive load management in mobile learning systems: principles and theories," *Journal of Computers in Education*, vol. 8, no. 1, pp. 109–136, 2021.
- [32] T. T. Hewett, R. Baecker, S. Card, T. Carey, J. Gasen, M. Mantei, G. Perlman, G. Strong, and W. Verplank, *ACM SIGCHI curricula for human-computer interaction*. ACM, 1992.
- [33] G. A. Boy, *Human-systems integration: from virtual to tangible*. CRC Press, 2020.
- [34] Y. Chen, O. Yang, C. Sampat, P. Bhalode, R. Ramachandran, and M. Ierapetritou, "Digital twins in pharmaceutical and biopharmaceutical manufacturing: a literature review," *Processes*, vol. 8, no. 9, p. 1088, 2020.
- [35] P. Vallejo-Correa, J. Monsalve-Pulido, and M. Tabares-Betancur, "A systematic mapping review of context-aware analysis and its approach to mobile learning and ubiquitous learning processes," *Computer Science Review*, vol. 39, p. 100335, 2021.
- [36] G. Paul, "Iterative design. lecture presented in industrial and operations engineering 436," in (*Human Factors in Computer Systems, University of Michigan, Ann Arbor, MI*, 2008, Conference Proceedings.
- [37] S. Tabrizi and N. Cavus, "Hci standards for developing mobile learning applications in education," in *INTED2017 Proceedings, IATED, 11th international technology, education and development conference*, 2017, Conference Proceedings, pp. 6507–6513.
- [38] C. Ghaoui, *Encyclopedia of human computer interaction*. IGI Global, 2005.
- [39] M. Sapraz and S. Han, "Implicating human values for designing a digital government collaborative platform for environmental issues: A value sensitive design approach," *Sustainability*, vol. 13, no. 11, p. 6240, 2021.
- [40] A. Braham, F. Buendía, M. Khemaja, and F. Gargouri, "User interface design patterns and ontology models for adaptive mobile applications," *Personal and Ubiquitous Computing*, pp. 1–17, 2021.
- [41] M. Ballantyne, A. Jha, A. Jacobsen, J. S. Hawker, and Y. N. El-Glaly, "Study of accessibility guidelines of mobile applications," in *Proceedings of the 17th international conference on mobile and ubiquitous multimedia*, 2018, Conference Proceedings, pp. 305–315.
- [42] S. Criollo-C, A. Guerrero-Arias, Á. Jaramillo-Alcázar, and S. Luján-Mora, "Mobile learning technologies for education: Benefits and pending issues," *Applied Sciences*, vol. 11, no. 9, p. 4111, 2021.
- [43] N. Babich, "Mobile ux design: Key principles," *UX Planet*, 2016.
- [44] Z. Al Mahdi, V. R. Naidu, and P. Kurian, *Analyzing the Role of Human Computer Interaction Principles for E-Learning Solution Design*. Springer, 2019, pp. 41–44.
- [45] E. McKay, *Enhancing learning through human computer interaction*. Igi Global, 2007.
- [46] B. Mehlenbacher, L. Bennett, T. Bird, M. Ivey, J. Lucas, J. Morton, and L. Whitman, "Usable e-learning: A conceptual model for evaluation and design," in *Proceedings of HCI International*, vol. 2005, 2005, p. 11th.
- [47] A. Al-Hunaiyyan, A.-S. Salah, and N. Al-Huwail, "Blended e-learning design: Discussion of cultural issues," *International Journal of Cyber Society and Education*, vol. 1, no. 1, pp. 17–32, 2008.
- [48] M. Berry, *Enhancing learning through mobile computing*. Igi Global, 2007, pp. 57–74.
- [49] T. Gross, "Human-computer interaction education and diversity," in *International Conference on Human-Computer Interaction*. Springer, 2014, pp. 187–198.
- [50] M. Kurosu, *Human-Computer Interaction. Theories, Methods, and Tools: 16th International Conference, HCI International 2014, Heraklion, Crete, Greece, June 22-27, 2014, Proceedings, Part I*. Springer, 2014, vol. 8510.
- [51] L. Zhang, X. Zhang, Y. Duan, Z. Fu, and Y. Wang, "Evaluation of learning performance of e-learning in china: A methodology based on change of internal mental model of learners," *Turkish Online Journal of Educational Technology-TOJET*, vol. 9, no. 1, pp. 70–82, 2010.
- [52] J. A. Swanson, "Assessing the effectiveness of the use of mobile technology in a collegiate course: A case study in m-learning," *Technology, Knowledge and Learning*, vol. 25, no. 2, pp. 389–408, 2020.
- [53] A. Dirin and M. Nieminen, "User experience evolution of m-learning applications," in *CSEDU 2017. Proceedings of the 9th International Conference on Computer Supported Education-Volume 1, April 21-23, 2017, in Porto, Portugal*. SCITEPRESS Science And Technology Publications, 2017, Conference Proceedings.
- [54] M. Zakaria, S. Maat, and F. Khalid, "A systematic review of m-learning in formal education," *Int. J. Innov. Creat. Chang.*, vol. 7, no. 11, 2019.
- [55] S. Kumar Basak, M. Wotto, and P. Belanger, "E-learning, m-learning and d-learning: Conceptual definition and comparative analysis," *E-learning and Digital Media*, vol. 15, no. 4, pp. 191–216, 2018.
- [56] A. Nurhudatiana and A. S. Caesarion, "Exploring user experience of massive open online courses (moocs) a case study of millennial learners in jakarta, indonesia," in *Proceedings of the 2020 9th International Conference on Educational and Information Technology*, 2020, Conference Proceedings, pp. 44–49.
- [57] D. Selmanovic, A. Sayar, and P. O. Durdu, "Cross cultural usability testing of mooc platform," in *2021 5th International Symposium on Multidisciplinary Studies and Innovative Technologies (ISMSIT)*. IEEE, 2021, pp. 409–414.
- [58] E. A. Rodwell, "A pedagogy of its own: Building a ux research program," *Practicing Anthropology*, vol. 43, no. 2, pp. 17–21, 2021.
- [59] N. Cavus and D. Ibrahim, "m-learning: An experiment in using sms to support learning new english language words," *British journal of educational technology*, vol. 40, no. 1, pp. 78–91, 2009.
- [60] K. Masters, R. H. Ellaway, D. Topps, D. Archibald, and R. J. Hogue, "Mobile technologies in medical education: A mee guide no. 105," *Medical teacher*, vol. 38, no. 6, pp. 537–549, 2016.
- [61] J. A. Frank and V. Kapila, "Mixed-reality learning environments: Integrating mobile interfaces with laboratory test-beds," *Computers & Education*, vol. 110, pp. 88–104, 2017.
- [62] M. H. Jarrahi, S. B. Nelson, and L. Thomson, "Personal artifact ecologies in the context of mobile knowledge workers," *Computers in human behavior*, vol. 75, pp. 469–483, 2017.
- [63] W. Roldan, X. Gao, A. M. Hishikawa, T. Ku, Z. Li, E. Zhang, J. E. Froehlich, and J. Yip, "Opportunities and challenges in involving users in project-based hci education," in *Proceedings of the 2020 CHI Conference on Human Factors in Computing Systems*, 2020, pp. 1–15.
- [64] Y. Zhonggen, Z. Ying, Y. Zhichun, and C. Wentao, "Student satisfaction, learning outcomes, and cognitive loads with a mobile learning platform," *Computer Assisted Language Learning*, vol. 32, no. 4, pp. 323–341, 2019.
- [65] J. Burston and K. Arispe, "Looking for a needle in a haystack: Call and advanced language proficiency," *calico journal*, 2018.
- [66] A. Gelan, G. Fastré, M. Verjans, N. Martin, G. Janssenswillen, M. Creemers, J. Lieben, B. Depaire, and M. Thomas, "Affordances and limitations of learning analytics for computer-assisted language learning: a case study of the vital project," *Computer Assisted Language Learning*, vol. 31, no. 3, pp. 294–319, 2018.

A Secure and Trusted Fog Computing Approach based on Blockchain and Identity Federation for a Granular Access Control in IoT Environments

Samia EL HADDOUTI
ENSIAS
Mohamed V University in Rabat

Mohamed Dafir ECH-CHERIF EL KETTANI
ENSIAS
Mohamed V University in Rabat

Abstract—Fog computing is a new computing paradigm that is an extension of the standard cloud computing model, which can be adopted as a cost effective strategy for managing connected objects, by enabling real-time computing and communication for analytical and decision making. Nonetheless, even though Fog-based Internet of Things networks optimize the standard architecture by moving computing, storage, communication, and control decision closer to the edge network, the technology becomes open to malicious attackers and remains many business risks that are not yet resolved. In fact, access control, privacy as well as trust risks present major challenges in Internet of Things environments based on Fog computing due to the large scale distributed nature of devices at the Fog layer. In addition, the traditional authentication methods are not adequate in Fog-based Internet of Things contexts since they consume significantly more computation power and incur high latency. To deal with these gaps, we present in this paper a secure and trusted Fog Computing approach based on Blockchain and Identity Federation technologies for a granular access control in IoT environments. The proposed scheme uses Smart Contract concept and Attribute-Based Access Control model to ensure the level of security and scalability required for data integrity without resorting to a central authority to make an access decision.

Keywords—Access control; blockchain; fog computing; identity federation; IoT; smart contracts

I. INTRODUCTION

The Internet of Things (IoT) is fueling significant advances and smart services in various areas such as home automation, smart city, smart healthcare, intelligent transportation, etc; adding thereby value to businesses and increasing users convenience [1]. In fact, the rapid advance of communication and networking technologies, such as Bluetooth, WiFi, ZigBee, and GSM, enable connectivity among heterogeneous IoT subjects (e.g., smartphones, laptops, sensors, game consoles, etc.) to the Internet, which significantly accelerates data collection, aggregation and sharing in the IoT [2]. Yet, with expansion of IoT systems associated with big data from smart applications that require unlimited computing and storage resources, serious constraints with cloud-based solutions have been arisen due to real-time and reliable transport of enormous IoT traffic. Indeed, classical IoT infrastructures rely on centralized cloud computing paradigms to process and interpret large amounts of data sets, which include high latency and limited capacity with the increase of the latter. In addition, integrated Cloud Computing becomes a potential target for numerous security threats [3]. To address these technological gaps, Fog-based

IoT network, which integrates network edge and cloud core, is recommended in recent years as a more effective solution to fulfill IoT requirements more positively [4], by extending the IoT network and expand its scope. The principle is making use of Fog Computing approach [5], [6] to offload network tasks (e.g., computing, storage, etc.), by moving computing and caching resources and analytical services closer to the edge network where data is generated [7]. Thus, data no longer needs to be sent in its entirety to data centers, which ultimately contributes to improving the quality of service. Fig. 1, illustrates the basic three-layer of a Fog-based IoT network.

While fog computing solves the aforementioned issues, new concerns arise in terms of security, privacy and trust that become more complex due to device heterogeneity, distributed management and mobility [8]. Moreover, to ensure mutual access control between Fog devices in such a distributed and unreliable environment, traditional authentication mechanisms, such as password-based authentication or certificate-based authentication methods, are no longer suitable. At the outset, several access control systems have been proposed but most of them are static for closed environment and they did not completely meet the dynamic Fog-based IoT requirements in term of scalability, data privacy and identity management. To deal with these downsides, the emerging Blockchain technology is seen as a new philosophy for building a truly decentralized, trust-less and secure access control structure for the Fog-based IoT networks [9]. From these perspectives, this work introduces with the aim of overcoming the current Fog-based IoT limitations, by proposing a secure and trusted Fog Computing approach based on Blockchain and Identity Federation technologies for a granular access control in IoT environments. The given scheme aims to enhance typical Fog-based IoT networks as a result of a combination of strengths of two technologies: Identity Federation [10] to retrieve additional attributes from different Identity Providers; within a trust circle; for granting access to an end user, and a consortium Blockchain to govern particular Smart Contracts to automate access control policies relied on Attribute-Based Access Control (ABAC) model [11], by providing far greater privacy and security and nullify the need for a third party. In particular, the proposed approach protects IoT devices by defining access control policies, which state the conditions of an end user's attributes to regulate the access to these IoT devices via a smart contract. The users' attributes are provided by Identity Providers members of an Identity Federation. In the aim to

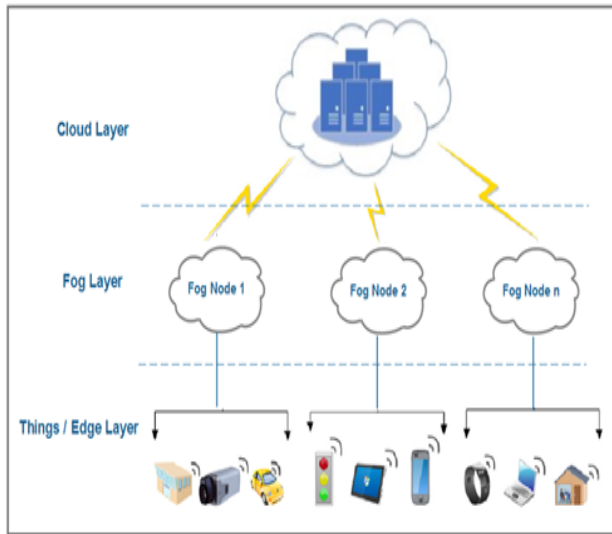


Fig. 1. Fog-based IoT Architecture.

elaborate a trusted environment, the nodes of the consortium Blockchain act as Service Providers within the given Identity Federation. The fog layer interacts with the given consortium Blockchain to check the relevant smart contract if a subscriber tries to apply the resources of a fog node.

The remainder of the paper is organized as follows: Section 2 reviews the existing approaches for the access control and authentication in Fog Computing environments. Section 3 presents the main security challenges in Fog-based IoT networks. Section 4 deals with properties of the Blockchain technology as a focal element for the proposed paradigm. Section 5 introduces the model by outlining its key features, followed by a detailed description of its components' architecture. Indeed, the section gives a system overview, architectural and main interactions among key components and actors. Section 6 is devoted to assessing the proposed approach. Finally, Section 7 is dedicated to conclusion and future work.

II. RELATED WORKS

Several works and initiatives have proposed various access control methods for Fog-based IoT networks.

In [12], Ibrahim et al. proposed a secure and mutual authentication model that allows any fog user to authenticate mutually with any fog server. This mutual authentication is under the registration authority (RA) at the cloud level. The main drawbacks of this approach, is the centralization of the RA that is considered as a Single Point of Failure. In fact, if the central RA is compromised, a negative impact would be felt in the whole system. In addition, the proposal did not consider the privacy aspect, by protecting the users' anonymity.

Similarly, Amor et al. [13] presented a solution of a mutual authentication between fog users and fog servers, by establishing a session key without disclosing user's real identity. The proposed scheme relies on various authentication methods and mechanisms such as bi-linear pairing, the elliptic curve discrete logarithm problem and pseudonym-based cryptography to enhance security aspects. However, the centralization feature of the given approach remains as a serious problem to deal with.

In [14], Imine et al. introduced an authentication method based on Blockchain technology and secret sharing technique to verify the authenticity of any fog node in the architecture, and to allow fog nodes to establish mutual authentication with each other. The major weakness of this method was its relationship with a centralized cloud. In fact, if the latter is compromised, there would be a negative impact on the whole system.

In recent years, there have several initiatives whose work was based on Blockchain and Identity Management for Fog-based IoT technology [15],[16],[17],[18]. Most of the features of these works are satisfied by our proposal. Furthermore, the latter is specially designed to added more features that enhance security and privacy aspects, by introducing Identity Federation technology as a crucial brick to ensure trusted interactions between different stakeholders to aggregate user's attributes from different Identity Providers for granting access to the requested IoT devices. In addition, the adoption of Blockchain technology, as a decentralized and distributed network, may be the most suitable environment for carrying out the authentication and authorization processes; through a smart contract; without resorting to a central authority and enhancing thereby the security and trustworthiness aspects. Thus, the proposed scheme will certainly pave the way to a wider adoption of the proposed paradigm by different industries.

III. SECURITY CHALLENGES IN FOG-BASED IOT NETWORKS

There have been immense efforts in recent years to cope with security issues in Fog-based IoT environments at different levels of gateways; though Identity Management, authentication and access control are the pillar security features that play a major role in establishing trust between Fog-based IoT components, by preventing malicious objects being easily connected to the network.

A. Identity Management

Generally speaking, Identity Management (IdM) aims to facilitate the management of identities in the digital world by decreasing extra administration costs. An integrated system that is in charge of ensuring IdM process is known as an Identity Management System (IdMS). It is generally made up of the following bricks [19]: (i) *Identity Provider (IdP)*, the structure that creates, manages, and maintains digital identities. Likewise, it generates assertions about identity attributes. (ii) *Service Provider (SP)*, it is also known as a Relying Party, corresponding with organizations that are providing resources and services to end users. (iii) *Control Party* refers typically to a regulatory body that uses identity information for investigations and access monitoring. The IdM models are mainly classified as conventional or isolated, centralized, federated and user centered [20],[21]. Nevertheless, Identity Federation model is more appropriate for ensuring a trust context between the different stakeholders; by optimizing the exchange of information related to user authentication on the basis of the establishment of agreements between IdPs and SPs [22].

There are currently several frameworks and standardization initiatives of IdMS in different phases of developments, and each of them has its own distinguishing features. In [23], the

authors present a comparative analysis of the most popular IdMSs against a set of identity requirements. It is worth emphasizing the fact that even when there are many IdMS proposals in the literature; nevertheless; they do not meet the fog paradigm requirements. In this sense, establishing an IdM approach in the Fog-based IoT networks can be a challenging task to get a successful set up of an appropriate IdMS, which should take into account the highly dynamic network conditions expected in fog computing contexts and the large amount of computing resources required for a given operation.

B. Authentication

To access protected resources and services, entities need to be identified and authenticated as a part of information security. Authentication is the process by which a legitimate entity (e.g., a person, an organization or a device) proves a claim about holding specific identities. There are a variety of methodologies that can be used to authenticate entities. Existing authentication schemes are generally built on three main concepts that are based on the following [24]: (i) *Something an entity knows*; known as a knowledge-based authentication, this method involves the transmission of a secret, which is specific to an individual, by means of a password, code word, Personal Identification Number (PIN) and the like [25]. Despite its traditional and wide use, the level of risk protection afforded by these schemes is far from being adequate to ensure the required security level [26]. (ii) *Something an entity has*; is based on the possession of physical or digital private objects, referred to generally as a token, that the end user has. Examples of something an entity possesses include, among many others, digital certificates, smart cards, tokens and so on [27]. Although the security enhancement provided by this method, is useless in uncontrolled environments where a valid token may have been stolen. (iii) *Something an entity is*; referred to as a biometric-based authentication. This approach allows the authentication of entities based on either the human physiology or behavioural characteristics including fingerprint, iris, retinal, hand geometry, facial voice recognition, etc [28].

There are several approaches that have been started to implement authentication on IoT. However, traditional authentication schemes that exist in the web world will not be directly effective in fog computing due to the requirements of large computing power and real-time processing. Hence, new authentication techniques in fog computing have been proposed, each one with its strengths and weaknesses [29].

C. Access Control Models

After a successful authentication of an entity, an access control is required as the core of information security and shared data protection. It states policies and measures by which a Relaying Party determines whether an already authenticated entity has sufficient privileges to access the requested resource, and thus limits the actions that the legitimate entity can perform in such a way that only authorized access is possible. Access control models can be implemented in many places and at different levels [30].

1) *Access Control Matrix*: the Access Control Matrix (ACM) was the first theoretical access control model that defines access permissions between specific subjects and objects [31]. In this model, an access matrix, also known as a protection matrix, is designed with two-dimensional array, where the matrix rows are indexed by subjects, while matrix column are labelled by objects. This matrix acts as a lookup table for operating systems, where the context of each cell states the set of actions of a particular object that are allowed for a particular subject.

2) *Role Based Access Control*: David Ferraiolo and Rick Kuhn have elaborated on the RBAC model in 1992 [32], in which system permissions are assigned to users based on their roles so that security management costs are reduced. Indeed, the idea behind this model is that there will be fewer roles than users since users change frequently and roles do not. According to job functions, roles are created with privileges that are granted to users on the basis of their jobs or roles in the system. In other words, roles act as links between end users and resources. Despite its many benefits, the RBAC model could only be useful and suitable for organization whose trades and missions know little involvement.

3) *Attribute Based Access Control*: the Attribute Based Access Control (ABAC) model has been designed and developed ultimately to reduce the complexities of previous models within distributed and dynamic environments [33]. Under ABAC, the access to a protected resource is granted on the basis of the individual's attributes, of a resource, or of an environment. Access rules are created without the establishment of relationships between subjects and objects, which significantly increases the flexibility feature that is actually required in modern applications based on the emergence of the Service Oriented Architecture (SOA). For expressing access control policies, ABAC implementations are based on the eXtensible Access Control Markup Language (XACML) developed by the Advancing Open Standards for the Information Society (OASIS) [34]. Even though there are particular advantages of ABAC, a consensus definition of this approach is needed, and work remains to be done in assuring attribute accuracy and reliability.

IV. BLOCKCHAIN TECHNOLOGY: FEATURES AND WORKING PRINCIPLES

A. Overview

Blockchain [35] is a tamper resistant distributed database “Distributed Ledger” of recording transactions occurring within a network without the need for a central authority or third party (i.e., a bank, company, or government). A Blockchain contains a set of blocks, and every block contains a hash of the previous block, creating a chain of blocks from the *genesis* block to the current block as depicted in Fig. 2.

In 2008, Blockchain technology was combined with other computing concepts to create modern cryptocurrencies, and the first such Blockchain based cryptocurrency was Bitcoin [36]. The latter, along with certain cryptographic mechanisms, stores information representing electronic payments that are attached to digital addresses. Users use public and private keys to securely sign transactions within the system, allowing all participants to independently verify the validity of these

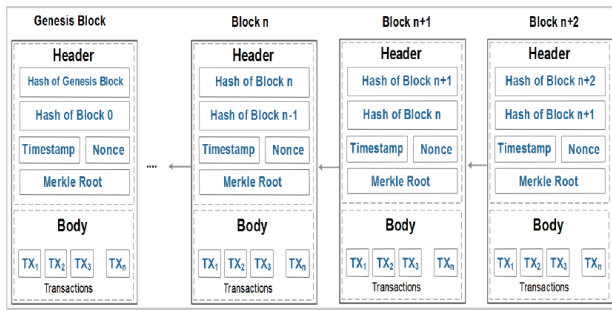


Fig. 2. High Level Structure of Blocks in a Blockchain System.

transactions through a consensus algorithm. After Bitcoin’s success and growing visibility since its launch, Blockchain applications are gaining massive momentum in the last few years, and are wide used in fields of supply chain, financial, medical, IoT, and so on, where extensive research attention has been received [37].

B. Classification of Blockchain

Broadly, Blockchains are classified into three categories [38]:

1) *Public Blockchain*: is also termed *permissionless* Blockchain, and are perfectly represent decentralized systems, where everyone is allowed to participate in the network by reserving rights to publish blocks, access contents, maintain a copy of the distributed ledger, and participate in the validation of new blocks with the same authority like other participants. The conception of public Blockchain aims to host a large number of anonymous peers, which makes the tamper of its contents too costly, and thus the immutability and security of transactions are kept intact. However, in terms of infrastructure, public Blockchain require significant resources with more energy and power for their function and achieving validation consensus, which may also impact the speed of transactions.

2) *Private Blockchain*: unlike public Blockchain, private Blockchain are *permissioned*, by restricting members that can participate in the network. The access control is entrusted to one entity, and blocks are published by delegated peers within the network. The number of transactions per second is increased since the number of peers is less in a private Blockchain, which also speed up the performance of transactions. However, private Blockchain are not resistant enough to tampering, and are more prone to potential malicious behaviors.

3) *Consortium Blockchain*: Consortium Blockchain are also known as *Federated Blockchain*. They are hybrid of the previous two types, but they are closer to Private Blockchain since both of them are permissioned. The prime idea behind the adoption of a consortium Blockchain is to intensify the effect of cooperation in order to overcome the challenges of a particular industry. Indeed, by joining a consortium Blockchain, organizations will benefit from shared resources, decreased development time and cost, and increased consensus trust. This type of collaboration helps members of a consortium Blockchain to build business solutions with economies of scale.

C. Cryptographic Mechanisms

Besides the hashing mechanism that is used to represent the current state of a Blockchain, by guarantying that no transactions in history can be tampered with, digital signatures [39] are another cryptographic concept that underpins the security of Blockchain technology. Indeed, in a Blockchain network, data transactions must be maintained by only approved parties. To that end, private keys are generated randomly and used in digital signatures required to spend transactions as proofs of ownership. Blockchain uses different types of cryptography including the Elliptic Curve Digital Signature Algorithm (ECDSA) [40] to authenticate transactions. However, it does not require digital certificates for its users to trust the integrity of the network because the Blockchain miners have already verified the transfer of digital values. Hence, they are not dependent on central authorities and servers as is the case with traditional Public Key Infrastructures (PKI) [41]. The whole process of a transaction signing in Blockchain is illustrated in Fig. 3.

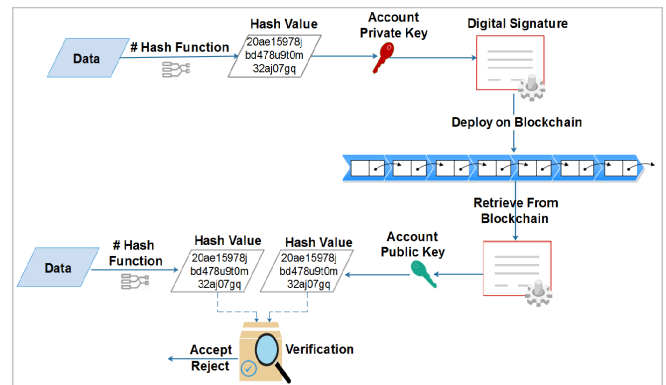


Fig. 3. Digital Signature Scheme on Blockchain.

D. Consensus Algorithms

Consensus algorithms are considered as the backbones and key elements in the working principles of Blockchains, by ensuring the network’s security, integrity, and performance. Basically, consensus algorithms aim to reach a common assent and unanimity on the synchronized state of a distributed ledger among all participant peers, in order to find some measure of trust between unknown peers, achieving thus the integrity and reliability of information stored on Blockchain, while preventing tampering and the double spending problem in distributed environments. The most widely utilized consensus algorithms throughout public and private Blockchain infrastructures are:

1) *Proof-of-Work (PoW) Algorithm*: is the first consensus algorithm that was established with Blockchain. In PoW [42], peers compete against each other to be selected as a leader to add blocks to the chain, by performing computationally expensive amount of work to resolve a mathematical challenge in a predefined time (10 minutes for the Bitcoin Blockchain). Publishing new blocks is more widely known under the name of “mining”.

2) *Proof-of-Stake (PoS) Algorithm*: following concerns due to the increase of energy consumption in Blockchains based on

the PoW consensus, researchers have thought of alternatives for the said algorithm. Proof of Stake (PoS) [43] is one of the main candidates that have been proposed to solve the energy and resources expenditure problem created by the PoW. In fact, instead of the power of solving a computationally expensive puzzle, in the PoS participants have to prove the ownership of blocked money (i.e. stake) in their cryptocurrency wallets. The greater the stake, the more likely the peer is selected as a validator to generate the next block. Although the clear advantages of PoS over PoW to reach a consensus on a Blockchain network, PoS possesses several potential security issues. These include a lack of initial coin distribution, a threat to decentralization, and an increased chance of double-spending when forks occur due to identical node verification [44].

3) *Delegated Proof-of-Stake (DPoS) Algorithm:* in this algorithm [45], a group of nodes are elected by stakeholders to produce and publish blocks. These nodes are called producers or witnesses. The number of elected witnesses is defined in such a way that at least 50% of nodes trust there is enough decentralization. Typically, witnesses take turns generating a block within a fixed time interval. For each block generation, the corresponding witness is rewarded. However, in the case where a witness has not generated any block within the fixed schedule, it is removed from the elected group until its notification of the intention to start generating blocks again.

4) *Practical Byzantine Fault Tolerance (PBFT) Algorithm:* is specifically intended for permissioned Blockchains where the number of participants is usually lower than public Blockchains. By this virtue, reaching a consensus therefore does not require costly proofs. The PBFT is based on state machine replication approach [46]. It aims to reduce transmission errors, while introducing considerable optimizations that improve the response time of previous algorithms.

E. Smart Contract Concept

The concept of Smart Contracts was introduced by Szabo in 1997 [47], where he defined the Smart Contract as a computer code including terms and clauses of a traditional contract that is executing automatically. With the emergence of Blockchain technology, this approach has become feasible and viable. Indeed, the combination of Smart Contracts with Blockchain technology has changed the way businesses are currently done since “contracts” can be utilized and executed easily and quickly. As a matter of course, this innovative approach might replace traditional legal and economic contracts that are enforced by centralized entities such as lawyers, insurance agencies, and banks. The execution of a Smart Contract within a Blockchain network does not require intermediaries to verify and validate its terms and clauses. From a technical point of view, a Smart Contract performs the function of carrying out transactions via the execution of a related code, with predefined rules, that is stored on a distributed ledger and is identified by a unique address. Deploying Smart Contracts has undoubtedly brought considerable benefits to business and customers as is already mentioned. Nevertheless, advantages of the adoption of Smart Contracts could not come up without challenges. In fact, security vulnerabilities can occur to make a series of attacks against any network possible in the case of existing bugs or loopholes in deployed codes, which become more complex to

manage with the immutable feature of the Blockchain system [48].

V. PROPOSED FOG-BASED IOT SCHEME

In this section, we present the detailed methodology of our proposed access control model based on Blockchain and Identity Federation technologies to enhance security, privacy and trust aspects within Fog-based IoT networks.

A. System Architecture

The proposed architecture of the system is depicted in Fig. 4. It consists of five main components and these are as follows:

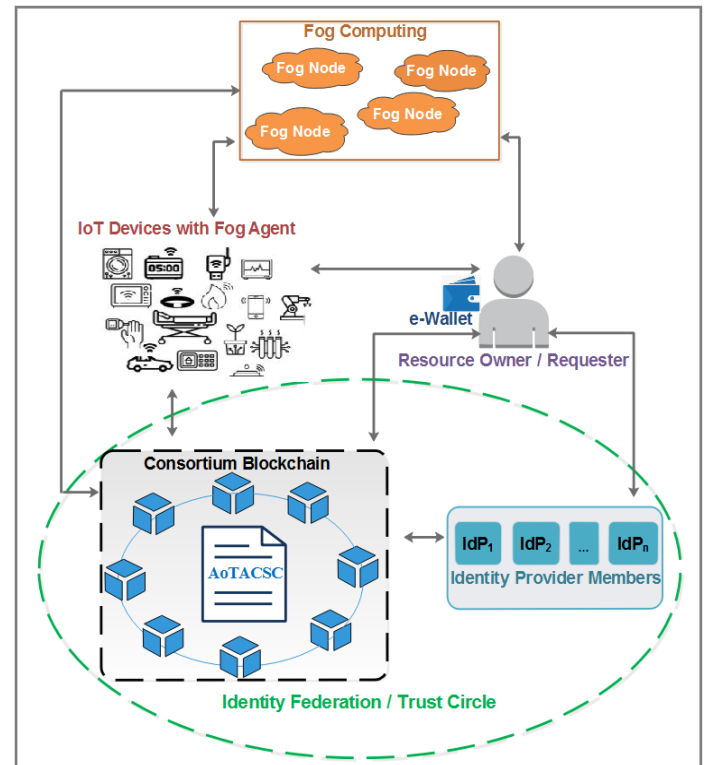


Fig. 4. Proposed System Architecture.

1) *End Users:* an end user can play the role of a resource owner who protects his resources by defining access over it, or a resource requester who aims to access protected resources. It is worth emphasizing that every end user has at least one electronic wallet that includes his credentials, addresses and all the keys needed to sign and validate transactions, and ask for resources access. In the proposed paradigm, we consider a wallet as a Distributed Application through which an end user could interact with the Blockchain platform to register his resources that need to be protected and to define his access control policies.

2) *Fog Nodes:* these nodes are hosting fog services, by providing a real-time execution of services at the edge of the network and performing effectively and efficiently computation and communication. However, unlike the previous proposed approaches of access control in Fog Computing in which

access policies is usually conferred to fog nodes, thereby malicious intruders can gain the possibility of compromising these policies; the given proposed solution delegates the access control process to a consortium Blockchain. The motivation behind this approach is essentially to establish efficient access control policies by ensuring confidentiality, accountability and integrity. In this way, if an end user tries to apply the resources of a fog node and in order to make data driven decisions, the fog node retrieves securely information from the consortium Blockchain by triggering the execution of a Smart contract, which will generate an output with information including the authentication assertion in addition to the access profile that indicates the number of leased resources, their duration, and their scale authorized for the given end user.

3) *Consortium Blockchain*: is the focal point of the proposed architecture to ensure the access control for IoT devices. Indeed, this consortium Blockchain is made up of nodes able to successfully process authentication and authorization functions via a smart contract called *IoT Access Control Smart Contract (IoTACSC)*, which is a representation of the access control policies for each pair (resource, end user) on the basis of the ABAC model. Nodes of the Consortium Blockchain act as Service Providers within an Identity Federation and interact with end users, Identity Providers and fog computing nodes. The execution outcome of the IOTACSC is validated by all Blockchain nodes before being recorded in a distributed ledger that is obviously only shared, replicated and synchronized among the nodes of the Consortium Blockchain to increase consensus trust with economies of scale, thereby providing data security and network privacy in the Fog Computing environments. It is noteworthy that every fog node submits its IOTACSC onto the consortium Blockchain, and if an end user tries to request a resource of a fog node, the latter checks the relevant contract from the Consortium Blockchain.

4) *Identity Providers*: to enhance the privacy aspect and come into line with the typical approach of Identity Federation, digital identities of end users still remains the involvement of their home organizations via trusted IdPs. The latter provide identity attributes of end users to get fog resources access according to access control policies described in IOTACSC. As external entities, IdPs interact with the IOTACSC through *Application Program Interfaces (API)*.

5) *IoT Devices*: these devices are in the form of wireless sensors constrained in their computational power and energy availability. Those limitations restrict them to be part of the consortium Blockchain, since being part of the Blockchain network implies keeping a copy of the Blockchain locally and a track of the network transactions. Nevertheless, all the devices are uniquely identified in the consortium Blockchain by creating automatically a public key for every device. Thus, each IoT device will have a unique identifier illustrated on the Access Control Policy. To interact with the consortium Blockchain and fog computing nodes, a fog agent may be deployed on access devices to help end users to request fog resources.

B. System Interactions

this section explains the different interactions between the different components of the proposed architecture. These interactions can be divided into two different phases:

1) *Registration Phase*: this phase relates to the establishment of access control policies regulating the access to IoT devices. Before putting forward the registration process, it should be noted that resource owners are the only entities with the ability to interact with the Consortium Blockchain in order to define new policies to access the relevant IoT device. Thus, a resource owner is always asked for authentication prior being able to interact with the nodes of permissioned Blockchain. The authentication protocol is composed of two processes, including registration and login. In essence, the identity of a resource owner within the consortium Blockchain is built up by binding his *Wallet's Public Key (WPubKey)* with a unique *user identifier (UsrID)*, and then uploading the said identity on the Consortium Blockchain in form of an identity transaction. The components of the latter are shown in Table I. The workflow of the registration phase is as follow: after

TABLE I. COMPONENTS OF AN IDENTITY TRANSACTION

Information	Description
TransactionType	Identity
User	Resource Owner
UserID	Alice001
WPubKey	fc4a1f566d1e0aa06436098c09d35d9762bf240
UserName	Alice001
Password	@lice001!!
Timestamp	The time the transaction occurs, i.e., 177131cee76
Signature	0xc3373d3bd1d4edc089001fd330920c303e95c51b131c22bc91b2f9f9f56e0de9

a successful authentication, the resource owner is invited to register the resource under his control. After the registration of the IoT device, the resource owner has to outline how access is authorized to the resource device by defining an access policy with corresponding access rights to specify which group of resource requesters can perform what actions to the given IoT device. For that end, the given access policies have to state the conditions of attributes that need to be satisfied to grant the access resource. The predefined access policy is translated to an AoTACSC, which is then broadcasted to all the nodes of the consortium Blockchain. These nodes reach agreement about the received smart contract and the validated data is added to the ledger of the Consortium. This registration flow is clearly illustrated through the sequence diagram in Fig. 6.

2) *Resource Access Phase*: The resource requester attempts to access a protected resource managed by a fog node within fog computing. In this stage, we assume that the requester is already aware of the access control policy regulating the access to the protected device. Referring to Fig. 7, a detailed view illustrating the resource access phase is provided. The resource requester sends a resource request to the fog agent on IoT device. The latter search the relevant IOTACSC address on consortium Blockchain, then communicate the found address to the requester. The resource requester submits his access request through his wallet to the consortium Blockchain. The relevant transaction is broadcasted to all nodes that evaluate the transaction, by executing the IOTACSC already deployed by the owner of the requested resource. For that end, the resource requested is asked to select trusted IdPs that are members of the Identity Federation system, and are managing the attributes required by IOTACSC. The end user is then redirected to the chosen IdP for authentication. In the case of a successful authentication, Blockchain nodes send an

attribute query combined with an authentication assertion to the given IdP, which prepares an attribute assertion and return the result to the consortium Blockchain. At this step, the end user may be asked to select another IdP, and the previous process is repeated till nodes get the set of attributes defined in IoTACSC. Afterword, based on a set of attribute assertions, the execution of IoTACSC makes an authorization decision about the end user's request. In fact, if it was successfully executed, the IoTACSC generates a secret access key and assigns an access token, which indicates the access rights for the resource requester. This access token is broadcasted to every node in the consortium Blockchain. Nodes reach agreement about the received access token, which is then recorded into the consortium Blockchain. An access token contains a unique identifier (ID), the address of the resource requester, the policy that must be satisfied, a list of access rights and the current status. An example of an authorisation token is illustrated in Fig. 5. The resource requester uses the authorization token to

```

{
  "id": "MNut98Are07",
  "issuer": "ResourceOwner1",
  "status": "ACTIVE",
  "address": "cf4a1f566d1e0aa06436098c09d35d9762bf240",
  "policy": "Division:IT AND Role:Administrator",
  "rights": [
    {
      "resource": "camera1/power",
      "action": "TURN_ON"
    },
    {
      "resource": "camera1/power",
      "action": "TURN_OFF"
    }
  ]
}

```

Fig. 5. Example of an Authorisation Token.

access the targeted resource. When a Fog node is receiving requests with an access token, it will check and verify its validity, by referring to the consortium Blockchain. If this access token was delivered by the IoTACSC corresponding to the IoT device, it allows access else it denies.

C. Design of IoT Access Control Smart Contract (IoTACSC)

As mentioned above, to realize automation, efficiency and credibility of transactions corresponding to access control process, the proposed approach consists of a smart contract (IoTACSC) which implements predefined access control policies; based on ABAC model; to control the access requests from subjects, by expressing conditions over a set of attributes paired to the latter. More broadly, IoTACSCs of the proposed system allow object owners to conduct a registration process by implementing access control policies. We designed the registration of IoT devices corresponding to access control policies as in Algorithm 1, which receives the identifier of IoT device (Id_{IoT_Device}) as input, and returns an address of this IoT device ($Address_{IoT_Device}$) and an address of the IoTACSC ($Address_{IoTACSC}$).

On the other hand, IoTACSCs endorse the permission decision process, by determining whether an end user is allowed to perform the access operation on an IoT device according to the exclusive access control policy deployed

by the resource owner. We designed the permission decision policy as in Algorithm 2, which receives the identifier of resource requester (EU_Id), the address of the requested IoT device ($Address_{IoT_Device}$) and the address of the IoTACSC ($Address_{IoTACSC}$) as input, and returns an access token ($Access_TKN$), then the judgment result ("Grant" or "Deny").

Algorithm 1: Registering a New IoT Device.

```

/* This algorithm translates an
access control policy in form of
IoTACSC and records the latter on
the consortium Blockchain */
Input :  $Id_{IoT\_Device}$ : is the identifier of a target
device.  $AC\_Policy_{IoT\_Device}$ : is an Access
Policy related to a target device.
Output:  $Address_{IoT\_Device}$ ,  $Address_{IoTACSC}$ 
1 Auth_ControlBC: Authentication Control at the
Consortium Blockchain level
/* A boolean function that checks if
a given Device Owner is well
authenticated at the Consortium
Blockchain */
2 DO_BCCheckAuthentication : REQ ×
Auth_ControlBC = {true, false}
3 H: is a hash function.
/* A boolean function that makes a
decision on whether an end user
may access a device resource in a
particular environment */
4  $AC\_Policy\_Rules(eu, d_r, e) \leftarrow$ 
 $f(ATT(EU), ATT(D_r), ATT(E))$ 
5 if DO_BCCheckAuthentication = true then
/* Generate an address of the IoT
device */
6  $H(IoT\_Device_{PubKey}) \leftarrow Address_{IoT\_Device}$ 
/* Create an IoTACSC and
generate its address */
7  $AC\_Policy(eu, d_r, e) \leftarrow$ 
 $ATT(EU) \wedge ATT(D_r) \wedge ATT(E)$ 
 $Address_{IoTACSC} \leftarrow$ 
 $add.IoTACSC(AC\_Policy(eu, d_r, e))$ 
8 else
9 | return a rejection notification
10 end
11 return  $Address_{IoT\_Device}$ ,  $Address_{IoTACSC}$ 

```

VI. ANALYSIS AND EVALUATION

A. Potential Advantages

It is clear that the proposed approach can actually added significant and considerable values for Fog-based IoT environments, by providing an access control layer, while promoting the decentralization aspect and preserving security and privacy requirements. Indeed, the main offered advantages of the proposed paradigm are highlighted as follows: noitemsep

- Access control processes are managed through IoTACSC, which conduct faster transactions at lower

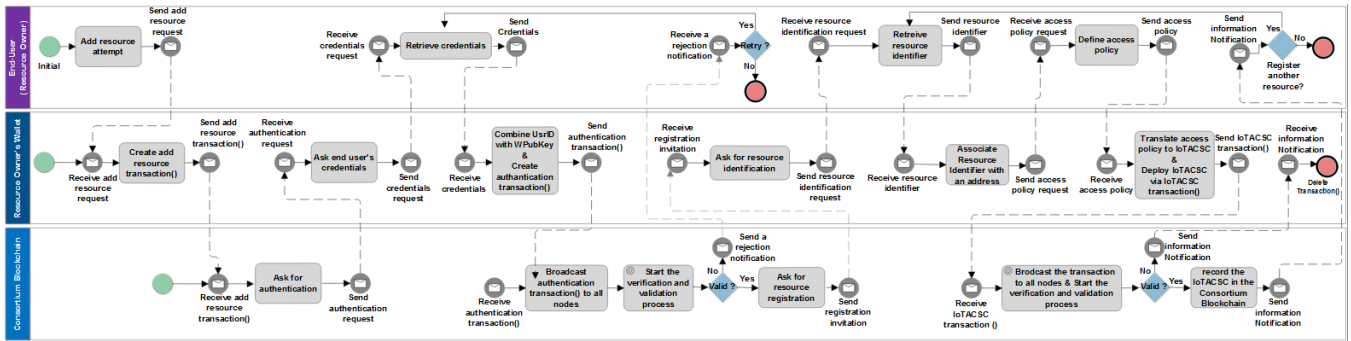


Fig. 6. Registration Workflow.

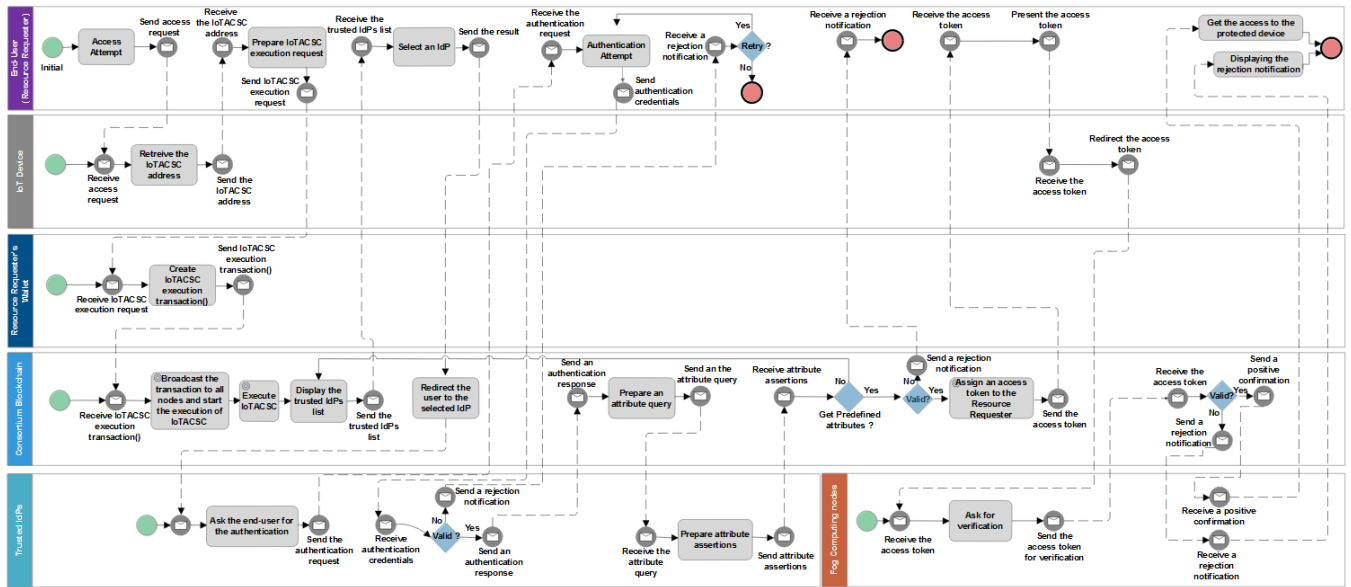


Fig. 7. Resource Access Workflow.

costs, improve its secrecy and achieve greater control over exchanged data.

- By combining the features of the Identity Federation and federated Blockchain, it is possible to take advantage of the benefits of both technologies regarding the trust management.
- The adoption of the consortium Blockchain instead of a public Blockchain speeds up transaction handling, by limiting the number of participant nodes needed to validate transactions during the permission decision process, without leading to the risk of centralization;
- The proposed approach preserves and promotes the privacy requirement while linking identities across different trust domains. In fact, identities are always maintained by related home IdPs. Only the corresponding attributeIDs are stored on the Consortium Blockchain and their values are known to home IdPs managing identity attributes.
- Since the majority of fog nodes will not be able to store Blockchain information due to their constrained nature, our architecture does not include fog nodes in

the Blockchain. Consequently, the given may be easily and widely adopted by reaching a wider audience.

B. Open Issues

Although several advantages of the proposed scheme led us to positive statements, there are some open problems which are interesting to investigate further. In fact, it is wise to be aware of the following limitations: noitemsep

- The proposed model presents latency issues due to the time taken to mining transactions on Consortium Blockchain.
- As every node needs to process and verify transactions and maintain the updated copy of the distributed ledger, the inter-node latency increases. Thus, the system needs to improve the default consensus algorithm, while maintaining security and avoiding double spending issues;
- It is harder for the nodes to maintain the full copy of the ledger with the increase of data. Thus the nodes should be equipped with powerful hardware.

Algorithm 2: Resource Access Process

Input : EU_Id : is the identifier of an Resource Requester. $Address_{Resource}$: is the address of the target device resource. $Address_{IoTACSC}$: is the address of IoTACSC.

Output: $Access_TKN$: is an access token.
ACD: an access control decision regarding a protected device resource {Grant, Deny}

- 1 P_D : is a set of permissions associated to atarget device D.
- 2 $P_DExpectedAttributes: P_D \rightarrow \{Att\}$, a function returning the set of attributes related to the P_D .
- 3 IDF_F : is a set of IdPs members of an Identity Federation F.
- 4 $AuthAssertion(Uid)_{IdP_i}$: is an authentication assertion of an end user (Uid) at a home IdP_i .
/* A set of home IdPs supposed to provide attributes required by P_D */
- 5 $ExpectedIdPs: \{P_DExpectedAttributes\} \rightarrow \{IdPs\}$
/* The set of aggregated attributes from different IdPs */
- 6 $aggregatedAttributesList \leftarrow \{\}$
- 7 **foreach** $IdP_i \in ExpectedIdPs$ **do**
- 8 | **if** $AuthAssertionA(Uid)_{IdP_i} = OK$ **then**
| /* Get attribute values corresponding to $attributeIDs$ for Uid according to $P_DExpectedAttributes$ */
- 9 | **foreach**
| $attributeID \in \{P_DExpectedAttributes\}$ **do**
- 10 | | $aggregatedAttributesList.append$
11 | | $(IdP_i.getAttributeValue$
| | $(AuthAssertion(Uid)_{IdP_i}, attributeID))$
- 12 | **end**
- 13 | **return** $ExpectedAttributes$
- 14 **end**
- 15 **end**
/* Generate a token ACC_TKN */
- 16 **if** $aggregatedAttributesList.hasReqAttributeID()$ **then**
- 17 | $(result, ACC_TKN) \leftarrow returnResult()$
- 18 **else**
- 19 | **return** a rejection notification
- 20 **end**
/* Access Decision */
- 21 **if** $IoTACSC_D.CheckIoTACSC_D(ACC_TKN) = Allow$ **then**
- 22 | ACD \leftarrow "Grant"
- 23 **else**
- 24 | ACD \leftarrow "Deny"
- 25 **end**
- 26 **return** ACD

VII. CONCLUSION AND FUTURE WORK

Fog-based IoT networks have been designed as a solution to efficiently manage the resource continuum from the edge up to the cloud, by providing enormous opportunities and also bringing remarkable challenges. Access control considered one

of the main challenges introduced by IoT devices and fog nodes that are not able to protect themselves due to their limited processing and storage capabilities. Several models and approaches have been proposed with a lack of scalability and vulnerabilities to cyberattacks.

In this paper, we propose a new scheme that combines the ABAC model with Blockchain and Identity Federation technologies. The proposed approach can solve the introduced issues in the open Fog-based IoT environments. Indeed, by adopting the Smart Contract principle, our proposed model provides secure, dynamic, reliable and scalable access control and authentication policies. The operating principle relies on the conception of an IoT Access Control Smart Contract deployed on a consortium Blockchain, where an object owner defines an access control policy managing the exploitation of the given object, by referring to a set of attribute aggregated from different Identity Providers belonging to an Identity Federation, enhancing thereby the trust management.

At this step, we have designed the approach. In our future work, we will implement the latter to demonstrate the feasibility of using Blockchain technology to manage access control process for IoT devices within Fog Computing environments. Moreover, we intent to design a lightweight consensus algorithm, which is expected to be more effective and well suited for the philosophy of the conceptual model, reducing the computational power and latency.

REFERENCES

- [1] I. Yaqoob, E. Ahmed, I. A. T. Hashem, A. I. A. Ahmed, A. Gani, M. Imran, and M. Guizani, "Internet of things architecture: Recent advances, taxonomy, requirements, and open challenges," *IEEE wireless communications*, vol. 24, no. 3, pp. 10–16, 2017.
- [2] L. Da Xu, W. He, and S. Li, "Internet of things in industries: A survey," *IEEE Transactions on industrial informatics*, vol. 10, no. 4, pp. 2233–2243, 2014.
- [3] M. Kazim and S. Y. Zhu, "A survey on top security threats in cloud computing," *International Journal of Advanced Computer Science and Applications*, vol. 6, no. 3, 2015.
- [4] H. R. Abdulqadir, S. R. Zeebaree, H. M. Shukur, M. M. Sadeeq, B. W. Salim, A. A. Salih, and S. F. Kak, "A study of moving from cloud computing to fog computing," *Qubahan Academic Journal*, vol. 1, no. 2, pp. 60–70, 2021.
- [5] Y. PAN and G. LUO, "Cloud computing, fog computing, and dew computing," *ZTE COMMUNICATIONS*, vol. 15, no. 4, pp. 1–2, 2017.
- [6] T. H. Luan, L. Gao, Z. Li, Y. Xiang, G. Wei, and L. Sun, "Fog computing: Focusing on mobile users at the edge," *arXiv preprint arXiv:1502.01815*, 2015.
- [7] J. He, J. Wei, K. Chen, Z. Tang, Y. Zhou, and Y. Zhang, "Multitier fog computing with large-scale iot data analytics for smart cities," *IEEE Internet of Things Journal*, vol. 5, no. 2, pp. 677–686, 2017.
- [8] P. Zhang, M. Zhou, and G. Fortino, "Security and trust issues in fog computing: A survey," *Future Generation Computer Systems*, vol. 88, pp. 16–27, 2018.
- [9] A. Baouya, S. Chehida, S. Bensalem, and M. Bozga, "Fog computing and blockchain for massive iot deployment," in *2020 9th Mediterranean Conference on Embedded Computing (MECO)*. IEEE, 2020, pp. 1–4.
- [10] D. Rountree, *Federated identity primer*. Newnes, 2012.
- [11] C. Hu *et al.*, "Nist special publication 800-162. guide to attribute based access control (abac) definition and considerations. national institute standards and technology," 2016.
- [12] M. H. Ibrahim, "Octopus: An edge-fog mutual authentication scheme." *Int. J. Netw. Secur.*, vol. 18, no. 6, pp. 1089–1101, 2016.

- [13] A. B. Amor, M. Abid, and A. Meddeb, "A privacy-preserving authentication scheme in an edge-fog environment," in *2017 IEEE/ACS 14th International Conference on Computer Systems and Applications (AICCSA)*. IEEE, 2017, pp. 1225–1231.
- [14] Y. Imine, D. E. Kouicem, A. Bouabdallah, and L. Ahmed, "Masfog: an efficient mutual authentication scheme for fog computing architecture," in *2018 17th IEEE International Conference On Trust, Security And Privacy In Computing And Communications/12th IEEE International Conference On Big Data Science And Engineering (TrustCom/BigDataSE)*. IEEE, 2018, pp. 608–613.
- [15] A. Ouaddah, A. Abou Elkalam, and A. Ait Ouahman, "Fairaccess: a new blockchain-based access control framework for the internet of things," *Security and communication networks*, vol. 9, no. 18, pp. 5943–5964, 2016.
- [16] G. Liu, J. Wu, and T. Wang, "Blockchain-enabled fog resource access and granting," *Intelligent and Converged Networks*, vol. 2, no. 2, pp. 108–114, 2021.
- [17] M. J. Baucas, P. Spachos, and K. N. Plataniotis, "Public key reinforced blockchain platform for fog-iot network system administration," *IEEE Internet of Things Journal*, 2021.
- [18] Y. Zhang, R. Nakanishi, M. Sasabe, and S. Kasahara, "Combining iota and attribute-based encryption for access control in the internet of things," *Sensors*, vol. 21, no. 15, p. 5053, 2021.
- [19] E. Bertino and K. Takahashi, *Identity management: Concepts, technologies, and systems*. Artech House, 2010.
- [20] A. Jøsang and S. Pope, "User centric identity management," in *AusCERT Asia Pacific information technology security conference*, vol. 77. Citeseer, 2005.
- [21] A. Bhargav-Spantzel, J. Camenisch, T. Gross, and D. Sommer, "User centrality: a taxonomy and open issues," *Journal of Computer Security*, vol. 15, no. 5, pp. 493–527, 2007.
- [22] M. Gaedke, J. Meinecke, and M. Nussbaumer, "A modeling approach to federated identity and access management," in *Special interest tracks and posters of the 14th international conference on World Wide Web*, 2005, pp. 1156–1157.
- [23] S. E. Haddouti and M. D. E.-C. E. Kettani, "Towards an interoperable identity management framework: a comparative study," *arXiv preprint arXiv:1902.11184*, 2019.
- [24] L. Müller, "Authentication and transaction security in e-business," in *IFIP International Summer School on the Future of Identity in the Information Society*. Springer, 2007, pp. 175–197.
- [25] A. Conklin, G. Dietrich, and D. Walz, "Password-based authentication: a system perspective," in *37th Annual Hawaii International Conference on System Sciences, 2004. Proceedings of the*. IEEE, 2004, pp. 10–pp.
- [26] Z. Zhao, Z. Dong, and Y. Wang, "Security analysis of a password-based authentication protocol proposed to ieeec 1363," *Theoretical Computer Science*, vol. 352, no. 1-3, pp. 280–287, 2006.
- [27] S. Zhao and W. Hu, "Improvement on otp authentication and a possession-based authentication framework," *International Journal of Multimedia Intelligence and Security*, vol. 3, no. 2, pp. 187–203, 2018.
- [28] V. Matyas and Z. Riha, "Toward reliable user authentication through biometrics," *IEEE Security & Privacy*, vol. 1, no. 3, pp. 45–49, 2003.
- [29] J. Ni, K. Zhang, X. Lin, and X. Shen, "Securing fog computing for internet of things applications: Challenges and solutions," *IEEE Communications Surveys & Tutorials*, vol. 20, no. 1, pp. 601–628, 2017.
- [30] E. Bertino, S. Das, K. Kant, and N. Zhang, "Policies, access control, and formal methods," 2012.
- [31] M. A. Harrison, W. L. Ruzzo, and J. D. Ullman, "Protection in operating systems," *Communications of the ACM*, vol. 19, no. 8, pp. 461–471, 1976.
- [32] R. Sandhu, D. Ferraiolo, and R. Kuhn, "American national standard for information technology—role based access control," *ANSI INCITS*, vol. 359, p. 1, 2004.
- [33] V. C. Hu, D. Ferraiolo, R. Kuhn, A. R. Friedman, A. J. Lang, M. M. Cogdell, A. Schnitzer, K. Sandlin, R. Miller, K. Scarfone *et al.*, "Guide to attribute based access control (abac) definition and considerations (draft)," *NIST special publication*, vol. 800, no. 162, pp. 1–54, 2013.
- [34] T. Moses, "Extensible access control markup language (xacml) version 2.0," *OASIS standard*, 2005.
- [35] D. Yaga, P. Mell, N. Roby, and K. Scarfone, "Blockchain technology overview," *arXiv preprint arXiv:1906.11078*, 2019.
- [36] S. Nakamoto, "Bitcoin: A peer-to-peer electronic cash system," *Decentralized Business Review*, p. 21260, 2008.
- [37] T. T. A. Dinh, R. Liu, M. Zhang, G. Chen, B. C. Ooi, and J. Wang, "Untangling blockchain: A data processing view of blockchain systems," *IEEE transactions on knowledge and data engineering*, vol. 30, no. 7, pp. 1366–1385, 2018.
- [38] G. Hileman and M. Rauchs, "2017 global blockchain benchmarking study," *Available at SSRN 3040224*, 2017.
- [39] A. Shamir, "New directions in cryptography," in *International Workshop on Cryptographic Hardware and Embedded Systems*. Springer, 2001, pp. 159–159.
- [40] D. Johnson, A. Menezes, and S. Vanstone, "The elliptic curve digital signature algorithm (ecdsa)," *International journal of information security*, vol. 1, no. 1, pp. 36–63, 2001.
- [41] J. Buchmann, E. Karatsiolis, A. Wiesmaier, and E. Karatsiolis, *Introduction to public key infrastructures*. Springer, 2013, vol. 36.
- [42] B. Sriman, S. Ganesh Kumar, and P. Shamili, "Blockchain technology: Consensus protocol proof of work and proof of stake," in *Intelligent Computing and Applications*. Springer, 2021, pp. 395–406.
- [43] F. Saleh, "Blockchain without waste: Proof-of-stake," *The Review of financial studies*, vol. 34, no. 3, pp. 1156–1190, 2021.
- [44] P. Vasin, "Blackcoin's proof-of-stake protocol v2," *URL: <https://blackcoin.co/blackcoin-pos-protocol-v2-whitepaper.pdf>*, vol. 71, 2014.
- [45] D. Larimer, "Dpos consensus algorithm-the missing white paper," *Bitshare whitepaper*, 2017.
- [46] F. B. Schneider, "The state machine approach: A tutorial," *Fault-tolerant distributed computing*, pp. 18–41, 1990.
- [47] N. Szabo, "Formalizing and securing relationships on public networks," *First monday*, 1997.
- [48] N. Atzei, M. Bartoletti, and T. Cimoli, "A survey of attacks on ethereum smart contracts (sok)," in *International conference on principles of security and trust*. Springer, 2017, pp. 164–186.

Intraday Trading Strategy based on Gated Recurrent Unit and Convolutional Neural Network: Forecasting Daily Price Direction

Nabil MABROUK¹, Marouane CHIHAB²
Computer Sciences Laboratory
Ibn Toufail University
Kenitra, Morocco

Zakaria HACHKAR³
Fundamental and Applied Physics Laboratory
Cadi Ayyad University
Safi, Morocco

Younes CHIHAB⁴
Computer Sciences Laboratory
Ibn Toufail University
Kenitra, Morocco

Abstract—Forex or FX is the short form of the Foreign Exchange Market, it is known as the largest financial market in the world where Investors can buy a certain amount of currency and hold it on until the exchange rate moves, then sell it to make money. This operation is not easy as it looks; due to the forte fluctuation of this market, investors find it a risky area to trade. A successful strategy in Forex should reduce the rate of risks and increase the profitability of investment by considering economic and political factors and avoiding emotional investment. In this article, we propose a trading strategy based on machine learning algorithms to reduce the risks of trading on the forex market and increase benefits at the same time. For that, we use an algorithm that generates technical indicators and technical rules containing information that may explain the movement of the stock price, the generated data is fed to a machine-learning algorithm to learn and recognize price patterns. Our algorithm is the combination of two deep learning algorithms, Gated Recurrent Unit “GRU” and Convolutional Neural Network “CNN”; it aims to predict the next day signal (BUY, HOLD or SELL) The model performance is evaluated for USD/EUR by different metrics generally used for machine learning algorithms, another method used to evaluate the profitability by comparing the returns of the strategy and the returns of the market. The proposed system showed a good improvement in the prediction of the price.

Keywords—Forex; trading; machine learning; deep learning; random forest; technical indicators; technical rules; convolutional neural network; gated recurrent unit

I. INTRODUCTION

The price of a currency changes over time due to many macroeconomics and political factors. This price variation creates a rate of exchange; investors use it to make money by buying a certain amount of currency and holding it on until the exchange rate moves, then selling it. This type of market is called Foreign Exchange Market (FOREX or FX), and it is known as the largest financial market in the world [1], [2], [3], [4]. Because of geographical dispersion, the FX market is characterized by high liquidity, a large volume of trades, and continuous trades, as the market is open 24 hours a day [5]. Many national and international companies and financial institutions rely on exchange rate volatility for their benefits [3]; They are exposed to exchange rates risk, which poses a severe threat to international trade flows [6]. Traders, who represent over 90% of FX market volume, must be conscious and aware of the uncertainty since it significantly

influences their investment decisions. However, we can notice the cyclical nature of the Forex market by using a large-scale analysis [7]. In the last few decades, the common research stream was on reducing the rate of risks and increasing the profitability of investment in the forex [8]; different types of analyses were employed, such as (i) technical analysis and (ii) fundamental analysis. According to [9], [10], both approaches are considered practical tools in forecasting the price movement.

(i) technical analysis has existed since [11], this method is based on the use of historical data such as prices, trading volumes, and other data to predict price trends that are expected to persist in the future [12], [11].

(ii) Fundamental analysis is a method for forecasting market trends and price movements based on analyzing a set of economic factors. These indicators include various activities related to the macroeconomic condition (e.g., government policies, bank policies, natural disasters, social stability, and economic trends) [13].

Investors always aim to get an idea of the future price’s movement; this leads many researchers to propose different strategies to forecast the price movement by applying several techniques and methods. One of these methods is technical analysis, which is based on mathematical calculations of historical data, which may help investors in trading. [14] provided a remarkable literature that shows how to estimate the equity risk premium using technical indicators such as the moving-average rule, momentum rule, and volume-based indicators. Despite their widespread use among practitioners, technical indicators have received significantly less attention in the literature [15]. The technical indicators repose on past data (price and volume) to identify price patterns and trends believed to persist into the future [14]. Currently, many types of indicators may help in identifying trends. Many successful professional traders and academics have recommended that instead of depending on a single rule, they combine a variety of technical trading rules to increase the accuracy of their forecasting models [16], [17], [9], [18].

In this article, we propose a trading strategy based on technical indicators and machine learning especially deep learning. The goal is to forecast the next day’s price direction, in each prediction the model is fed with specific sequence

of observation as slid-window, the experiment was done on different slid-widows; firstly an algorithm generates technical indicators and target variable called signal (buy, hold, or sell); after that, the stage of features selection to reduce the high dimensionality and improve the performance of the model; prepare the dataset for the model using the sliding-window approach.

II. RELATED WORK

Recently, new techniques of algorithm trading have come into existence; thanks to computer and technological progress [19], a lot of research has been established in several areas, especially algorithms and finance. However, most transactions are done electronically thanks to electronic markets, which helped collect a vast volume of data. Many studies suggested that the high evolution of global markets requires more and complex and developed techniques. Researchers have become interested in resolving electronic financial market problems using algorithms, especially machine learning algorithms, thanks to the enormous available volume of historical data. In the past, much research was carried on forecasting currency exchange rate, and several techniques and methodologies have been applied in this field. However, when it comes to successful trading strategies, fundamental analysis has gotten a lot of attention in this sector in the past; In this article, we are interested in machine learning and technical analysis, which is based on mathematical calculation and technical indicators.

The prediction of currency movements using technical indicators has been discovered firstly by [20] and [21]. According to Poole's viewpoint, currency exchange traders' expectations are shaped by the historical data of past price trends. Poole proved that based on specific rules, traders could make profits. According to these rules, traders can make a decision to buy or sell. Dooley & Schafar have worked on historical data from March 1975 to October 1975 trying to predict the next price direction based on seven different filter rules; they have proved that information about past exchange rate fluctuations is profitable when we use the correct filter rules. Traditional trading methods only use one approach [22]; on the other hand, algorithmic trading is a process in which a computer, rather than a human makes a specific investment. These methods can handle the complicated, non-linear, and dynamic properties of financial markets and the high frequency of data. Using appropriate non-linear approaches, such as neural networks, the suggested economic models could correctly anticipate future currency fluctuations for periods more extended than one year [23], [24].

Many studies proposed combining diverse approaches to improve regression and classification accuracy and performance [25]. Numerous researchers have applied machine learning to build trading strategies, among the machine learning algorithms, such as Random Forest (RF), support vector machine (SVM), Logistic regression (LR), Neural Network (NN). [25] have built numerous models using a bootstrap approach based on neural networks and combined the output of these models to forecast currency exchange rates. As a result, they found that their strategy significantly improved forecasting accuracy compared to the methodologies as mentioned earlier. A random forest algorithm has been introduced by [26], which made use of bagging to increase classification

accuracy. [27] have described the random forest algorithm as the top-performing algorithm to predict stock price directions accurately. A small number of studies have been carried on forecasting currency exchange rate by using random forest algorithm; one of these studies was done by [28], they have used the random forest algorithm in forecasting currency exchange rates, and according to Them: random forest algorithm surpassed the SVM and Multiple Linear Regression methods predicting the Chinese Yuan correctly.

Intelligent machine learning systems played an important role and showed impressive performance in modeling and forecasting data, such as Bitcoin high-frequency price time series. [29] have employed three different sets of models of Artificial Intelligence systems in order to forecast high-frequency Bitcoin price time series, i.e., statistical machine learning approaches, algorithmic models, and finally, artificial neural network topologies. They have reported that the BRNN has exceptional forecasting accuracy as a result. Its convergence is unobstructed and very rapid; on the other side, artificial neural networks can imitate human decision-making thanks to the parallel processing features, even in the presence of underlying nonlinear input-output relationships in noisy signal environments. In the pre-market-efficiency era (i.e., pre- 1960s), several practitioners and researchers believed that predictable patterns in stock returns might lead to "abnormal" profits for trading techniques [30].

[31], have proposed a theoretical Multi-Agent System for stock market Speculation. They used four agents: the Meta-heuristic Algorithm agent, technical indicators, Text Mining agent, and Fundamental Factor agent. The final decision is made based on combining the four agent's results. To forecast the future trend of the Forex market, [32] has applied deep neural network techniques. This study aims to help traders determine if there will be an uptrend or a downtrend, or a neutral trend in the future. The model performance is examined over various input data sizes and different window lengths. Besides, Different threshold values of exchange rate percentage change are tested to signal an uptrend or downtrend to find a good decision. The results show that deep neural networks can correctly predict market direction. Furthermore, according to the results, the model's accuracy is maintained throughout a range of input lengths and threshold values. Another approach was proposed by [33], to forecast the future price in the next week; the study showed impressive results to improve the prediction accuracy by using Random forest. Several recent research from other domains of application has demonstrated that the Long-Short Term Memory (LSTM), which is a type of deep learning that can be utilized to model time series, outperforms typical machine learning methods.[34] have developed a predictive model based on LSTM to forecast the next day's currency price. The results showed that the appropriate sequence input length for developing an accurate LSTM model should be between 9 and 12 periods. Also, training the model using data from a short period is preferable then training it with data from an extended period. Finally, re-training the model regularly with a new dataset can improve the model's accuracy. Also [35] used too LSTM to build their trading strategy, but instead of predicting the next day's currency price, they tried to forecast the next day's price direction, which facilitated the problem. However, their approach is based on feeding the model with two different datasets; the first is macroeconomic



data and the second is technical indicator data; their approach tries to combine two techniques in one hybrid model, the fundamental analysis and technical analysis. As a result, their proposed hybrid model had the best performance in terms of profit _accuracy for predictions in all periods. It reduced the number of transactions compared to the baseline models.

III. OUR PROPOSITION

A. Datasets

In this research, the dataset used is of the two most-traded currencies in the world: the United States Dollar (USD) and the Euro (EURO); the EUR/USD currency pair is the quotation of two currencies USD and EUR; when trading a currency pair, the first currency (base currency) is used to buy the second one (quote currency). The dataset covers the period, from January 01, 2014, until January 30, 2021. we have segregated the datasets into two parts, the first part is for training the model, and the second is for the test phase. However, to conserve the temporal order, we have segregated the dataset non-randomly because the collected data is a time-series dataset; it is sequential data obtained through repeated measurements over time, for example, hourly, daily, or weekly.

The goal of this work is to create a good strategy for day trading, and for that, we have used an OLHCV data, indexed on the timestamp one day; each row is a one-day observation of five variables: Open, High, Low, close, and Volume (OLHCV).

1) *The Target Variable:* In this article, we are trying to predict the next price direction, but the price feature in the collected dataset is a continuous variable. To formulate the problem as a classification problem, we created a new variable that indicates the decision as a signal (Buy Signal, Sell Signal, and Hold Signal). First, we determinate a positive number as a threshold called α . the goal is to compare this parameter with the log return. When the log return of the current day is inferior to $-\alpha$, it indicates that it is an uptrend, so it is a SELL signal, and when the log return is superior to α , it indicates that's a downtrend, so it is a BUY signal; otherwise, it is a HOLD signal. However, in this case, the type of this variable is categorical; that is why We have converted this feature using one-hot encoding, so it can be provided to our algorithms and fit our model. The threshold (α): α is between 0 and 1. . Due to the forte fluctuation of the markets, there will always be a difference between the prices of the current and the next day. However, not each movement of the prices should be an uptrend or downtrend; the operation costs of buying or selling could be more expensive than the returns. To reduce the noise and identify the real trends, we compare the log-returns with a threshold called α to avoid the problem of unbalanced classes in the datasets, which happen in our case when α is too much

low or too high. However, balancing the dataset artificially will affect the sequential datasets. We decided to run our algorithm using different thresholds starting from zero (which led us to a binary classification problem) to 0.001. when we go with a threshold higher than 0.001, we are stuck with unbalanced datasets

2) *Technical Indicators:* The collected dataset consists only of five features, Open, High, Low, close, and Volume (OLHCV). To add additional information to the original datasets, we created an algorithm that generates new features based on mathematical calculations, this type of feature is known as "technical indicators".

In general, technical analysts use technical indicators to understand and analyze the price movement in a specific market and avoid emotional investments. However, technical indicators give an idea of where the price might go next in a given market at a specific time.

In this research, we have used the most-used technical indicators:

- The Weighted Moving Average (WMA)
- The Exponential Moving Average (EMA)
- The simple moving average (SMA)
- The Relatively Strength Index (RSI)
- The average directional index (ADX)
- The Commodity Channel Index (CCI)
- The Rate-of-Change (ROC)
- The Bollinger Band (BB)
- The Moving Average Convergence Divergence (MACD)
- The Moving Polynomial trending

Technical analysts may get different results depending on the chosen parameters, even using the same technical indicators. So, to train our model with the best parameters of technical indicators, in our strategy, we generate each technical indicator on multiple periods, as shown in Table I. The goal is for our algorithm to identify the best subset of relevant characteristics predictors and determine the optimal combination of parameters (features).

TABLE I. TECHNICAL INDICATORS AND THEIR PARAMETERS

Technical Indicators (TI)	Intervals for TI parameters
SMA	Period: [5, 30]
WMA	Period: [5, 100]
EMA	Period: [5, 100]
RSI	Period: [5, 30]
ADX	Period: [5, 30]
ROC	Period: [15, 30]
MACD	Period: Fast [15, 30] Period: Slow: [20, 35] Period: Signal: [5, 10]
CCI	Period: [5, 30]
BB	Period: [5, 30]

3) *Simple Technical Trading Rules*: In general, for technical analysts generating technical indicators is not enough to build a trading strategy; to reach their goal, they convert technical indicators into trading rules. In our research, to enrich our datasets and get the best results, we will use some simple trading rules such as:

- Simple Moving Average (10) Rule "SMA(10) signal"
$$\begin{cases} \text{Buy, if } PRICE_t > SMA(10)_t \& price_{t-1} < SMA(10)_{t-1} \\ \text{Sell, if } PRICE_t < SMA(10)_t \& price_{t-1} > SMA(10)_{t-1} \\ \text{Hold, otherwise} \end{cases}$$
- Simple Moving Average Crossover-Trading Rule "SMA Crossover Signal"
$$\begin{cases} \text{BUY, if } sma(10)_t > sma(50)_t \& sma(10)_{t-1} < sma(50)_{t-1} \\ \text{SELL, if } sma(10)_t < sma(50)_t \& sma(10)_{t-1} > sma(50)_{t-1} \\ \text{HOLD, otherwise} \end{cases}$$
- The Relative Strength Index Signal "RSI signal"
$$\begin{cases} \text{Buy, if } RSI < 30 \\ \text{Sell, if } RSI > 70 \\ \text{Hold, otherwise} \end{cases}$$
- the Average True Range rule "ATR signal"
$$\begin{cases} \text{Buy, if } price_{t-1} + ATR < Price_t \\ \text{Sell, if } price_{t-1} - ATR > Price_t \\ \text{Hold, otherwise} \end{cases}$$

B. Our Approach

1) *Feature Selection*: In machine learning, adding more features improves the accuracy of the model, but using a large number of features could lead to opposite effects due to noisy variables, this last reduce the model performance; The solution is to reduce the high dimensionality of the dataset by selecting the features that can add more information and contribute most to the prediction. The authors in [36] have specified the goal of features selection in three parts: improving the prediction speed, interpretation of predictors easily, and providing a better understanding of them, improving the prediction performance by eliminating the noisy features. The authors in [37], [38], [39] have categorized most existing feature selection algorithms into four main classes: similarity-based, information-theoretical-based, sparse-learning-based, and statistical-based methods. In our research, we used feature selection techniques to reduce the number of inputs from more than 150 variables to less than 30, we kept just the most important features.

2) *Convolutional Neural Network*: A convolutional neural network (CNN, or ConvNet) is a type of deep neural network; its name is taken from mathematical linear operation between matrixes called convolution. The connectivity patterns between its neurons are inspired by the organization of the animal visual cortex. The convolution technique allows for recognizing visual patterns in input data [40]. As with any Artificial Neural Network, CNN has Multiple layers, and the convolutional layer is the most important. Each convolutional layer looks for features by sliding several filters over the input matrix and comparing it piece by piece [41]. In [42], they specified the most important and beneficial aspect of a convolutional neural network in two parts: the first is solving complex tasks by

reducing the number of parameters in ANN; the second is obtaining abstract features when going forward and deeper.

3) *Gated Recurrent Unit*: GRU is an abbreviation of Gated Recurrent Unit, and it is a Recurrent neural network unit, which is a type of deep neural network. GRU was proposed by [43] to have each recurrent unit record dependencies on multiple time scales in an adaptable way. In many machine-learning tasks, recurrent neural networks have lately shown promising results, especially when the input and/or output are of variable duration [44]. The GRU is known by its good performance in dealing with sequence learning tasks. When learning long-term dependencies, GRU overcomes the challenges of vanishing and explosion of gradients in traditional recurrent neural networks (RNNs).

4) *Gated Recurrent Unit and Convolutional Neural Network Approach*: In this article, our proposition to create a good trading strategy is based on combining two deep neural network approaches: the gated recurrent network and the convolutional neural network. As shown in Fig. 2, our model is composed of four layers:

- the first layer is the input layer; it takes a two-dimensional matrix as input; the number of rows is the same number of days to look back. Each row represents the observation of all variables on a specific day. The number of variables determines the number of columns; each column represents the values of a specific variable on the days to look back.

- the second layer is the convolutional layer, it is fed directly by the input layer; it looks for features by sliding multiple filters over the input matrix to recognize patterns.

- the third layer is the GRU layer; it is implemented on many-to-one architecture, as shown in Fig. 4 because the goal of our model is to predict the next day's price direction, not multiple days. This layer is added to deal with the sequential data nature.

- The last layer is the dense layers/output layer, reduce the number of features and get one decision (BUY, SELL or HOLD).

5) *Sliding-Window Approach*: The noisy part of the time-series datasets may negatively affect the RNN's memory, then the ability to learn patterns. To avoid this problem, we used the sliding-window approach, which consists of including previous time-steps as input. For example, a window of size four means it will take as input the current time-step and the previous three time-steps as shown in Fig. 5. Market forecasting, weather forecasting, and network traffic forecasting are all examples of this approach [45], [46], [47]. In our article, to choose the best window length, we experimented with our model on different windows length starting from 1 to 20. The results are shown in Table II

C. Our Investment Strategy

To develop an effective trading strategy, we must first determine the goal of our strategy, identify a personal risk profile, and finally evaluate the available time and resources.

Usually, in forex trading, the currency exchange rate is meager. This fact impacts the profitability of the investment when the invested amount of money is not so significant,

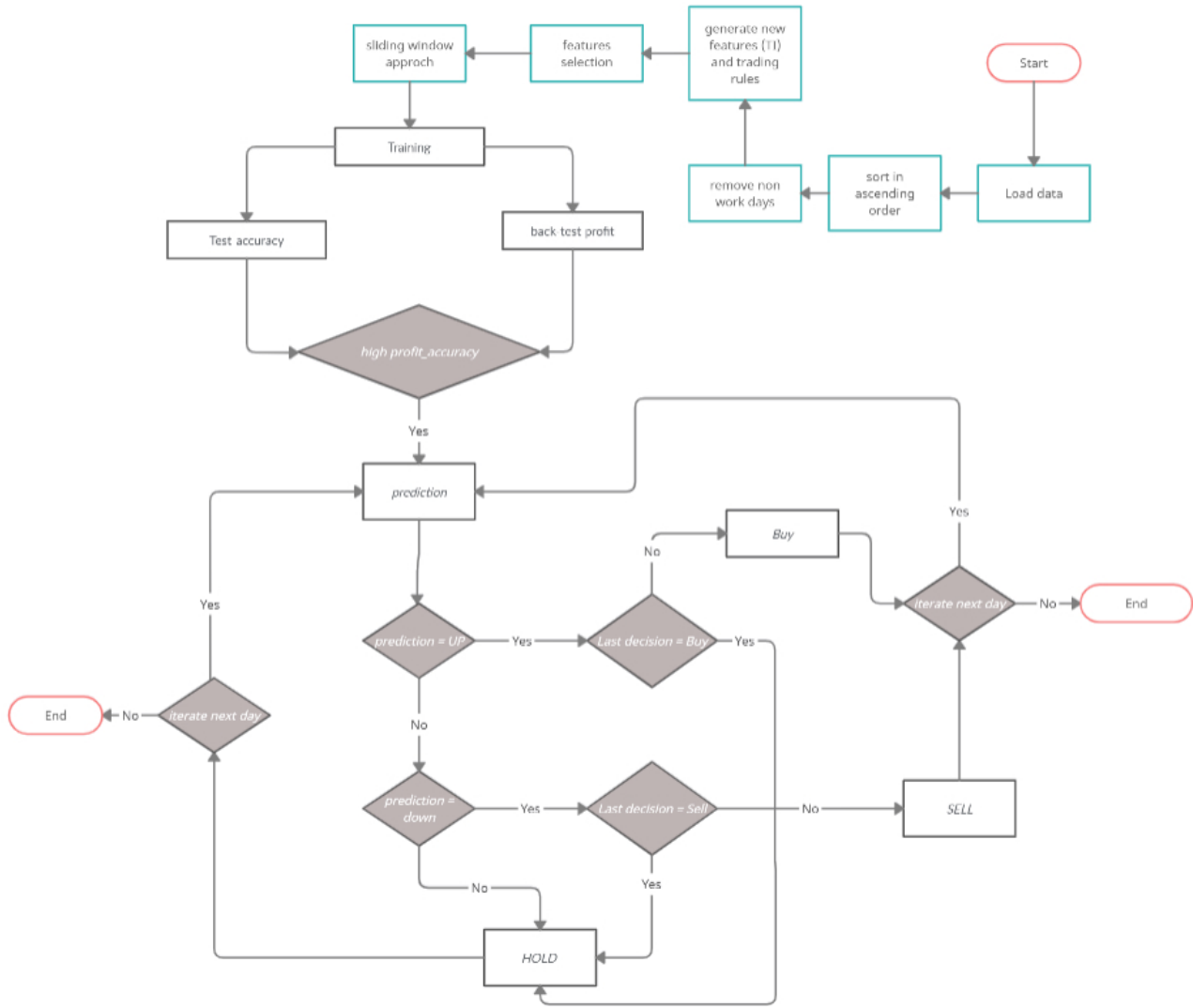


Fig. 1. Our Investment Strategy for Intraday Foreign Exchange.

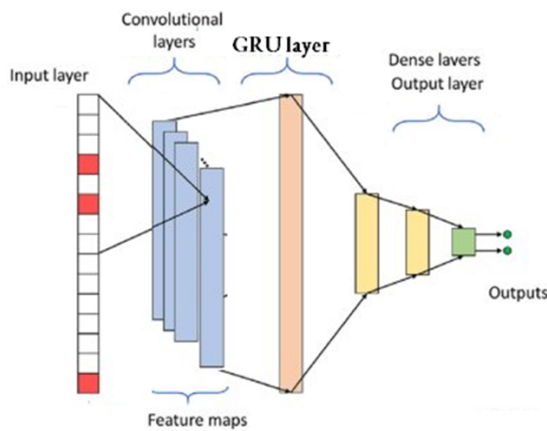


Fig. 2. GRU and CNN Approach.

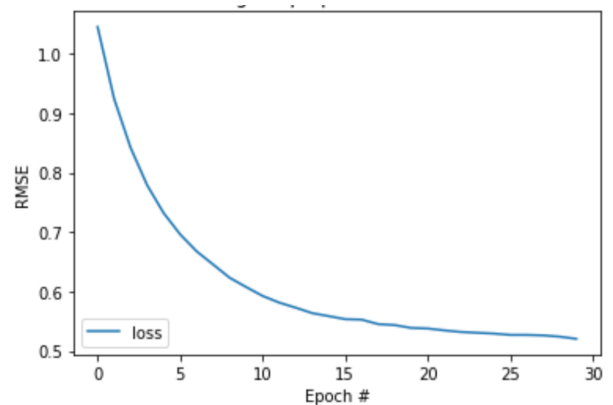


Fig. 3. Training Loss Per Epochs on Forex Dataset.

and the benefits could be lower than the transaction costs. However, in forex investments, a third intervening part called

TABLE II. MODEL ACCURACY BY WINDOW-SIZE VS THRESHOLD

Threshold \ window size [inputs]	1 [31x1]	2 [31x2]	3 [31x3]	4 [31x4]	5 [31x5]	6 [31x6]	10 [31x10]	15 [31x15]	20 [31x20]
0	0.635	0.686	0.704	0.704	0.726	0.713	0.741	0.739	0.693
0.0001	0.627	0.694	0.699	0.695	0.699	0.703	0.695	0.712	0.730
0.0002	0.582	0.683	0.684	0.695	0.7160	0.726	0.695	0.726	0.703
0.0003	0.603	0.669	0.688	0.683	0.709	0.718	0.711	0.696	0.709
0.0005	0.609	0.660	0.678	0.682	0.685	0.704	0.713	0.712	0.707
0.001	0.543	0.594	0.621	0.640	0.633	0.639	0.650	0.659	0.638

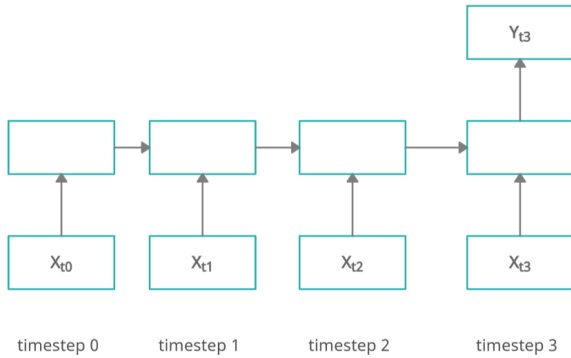


Fig. 4. Many-to-One GRU Architecture.

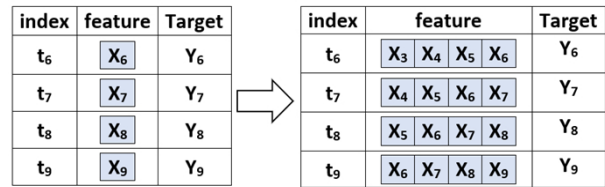


Fig. 5. Example of Sliding-Window Approach.

brokers proposes a technique called "leverage" to resolve this issue; it is based on borrowing funds to purchase an asset. In our strategy, we used the leverage of 1:100, which is the equivalence of an investment of 1000\$, and we can tread up to 100000\$.

Our investment strategy is explained in Fig. 1; we buy only when the price is low, and we sell when the price is higher, which means that the machine learning model should predict the direction of trade in the future. For that, we have created an algorithm that compares the log return of the current day with the threshold α ; if it is superior to α , we buy; if it is inferior to $-\alpha$, we buy; otherwise, we HOLD. However, in this case, the type of this variable is categorical, and we converted it using one-hot encoding to be provided to our algorithms and fit our model.

IV. DISCUSSION AND RESULTS

Table II summarizes the overall results of our study; the experiments showed that, in general, the model reached a much higher accuracy in forecasting the next-day price direction, especially when the window length is between 6 and 10. We can notice a slight improvement in the accuracy when the window length goes larger until reaching 10 days; then, after this window length, it starts going down.

The experiment also was done on several thresholds, from 0 to 0.001. Unlike the window length, each increment of threshold has a reverse influence on the accuracy, significantly when it surpasses 0.001. In this case, the model tends to predict a HOLD signal more than other signals due to the unbalanced dataset so that the accuracy could be more than 65%; the back-test showed that the profit_accuracy is lower than 40%. On

average, the model showed its best results when the threshold was limited between 0 and 0.0002 and the window length was between 6 and 10. However, in forex trading, the machine learning metrics are not enough to evaluate the strategy's profitability; we used another back-test to evaluate it based on the log returns. After back-testing the results, we found a proportionality relation between the model accuracy and the profit_accuracy.

To improve the performance of our model in terms of accuracy and running time at the same time, we need to fine-tune the model with the best parameters and the optimal number of epochs to train our model. Figure 3 shows the training loss in each number of epochs; we notice that the plot of training loss decreases to the point of stability, which is 25. We can conclude that the optimal number of epochs to train our model is 25.

The proposed strategy may not be effective 100% due to the fort fluctuations of the market, and in some cases, the prediction could fail, because the market is related to the macroeconomic and political situation; in this case, we should take into consideration two parameters before taking a decision. The first one is the exchange rate: if the loss is too high, the algorithm stops investing until this value become positive. The second one is the number of successive fails. If the algorithm keeps failing in predicting the right price direction, then it should stop investing until it starts getting good results.

V. CONCLUSION

The proposed CNN-GRU model is a novel forecasting approach to forecast the daily price directions of USD/EUR.

It's based on technical analysis and deep learning algorithms. We used the original time series data to generate new features called technical indicators, and fed it to our model in a specific window; each timestep includes previous time steps as input. Our proposed approach allowed us to reduce the noisy part of the data and improve the trading results compared to samples algorithms such as SMV and logistic regression, which are impacted by the high-frequency fluctuation of the market and the noisy nature of time-series data. The experiments showed promising results in forecasting the daily price directions.

In the forex, many factors may impact the state of the market in different ways, making it too complex to develop the best trading strategy. In this study, we have proposed a trading strategy to trade the EUR/USD pair; this solution is developed and back-tested in a specific period, it may not stay helpful and profitable in the future. In this case, our proposed solution must be adapted to the current situation. Of course, previous success is no guarantee of future outcomes, but a strategy that has proven to be dependable in a variety of market situations may, continue to be so in the future.

REFERENCES

- [1] O. DAVID and B. LEUSTEAN, "Forex and the liberalized financial market," vol. 71, Jan. 2009.
- [2] M. Amiri, M. Zandieh, B. Vahdani, R. Soltani, and V. Roshanaei, "An integrated eigenvector-dea-topsis methodology for portfolio risk evaluation in the forex spot market," *Expert systems with applications*, vol. 37, no. 1, pp. 509–516, 2010.
- [3] J. Kamruzzaman and R. Sarker, "Ann-based forecasting of foreign currency exchange rates," vol. 3, Jan. 2004.
- [4] K. Tanamarttayarat, "The world's largest financial market: Forex," Available at SSRN 3109245, 2018.
- [5] H. Law, S. Aghabozorgi, S. Lim, Y. Teh, and T. Herawan, "Processing of kuala lumpur stock exchange resident on hadoop mapreduce," in *Proceedings of the International Conference on Data Science (ICDATA)*. Proceedings of the International Conference on Data Science (ICDATA), 2014, p. 1.
- [6] J. Yao and C. L. Tan, "A case study on using neural networks to perform technical forecasting of forex," *Neurocomputing*, vol. 34, pp. 79–98, 2000.
- [7] S. Borenstein, J. Bushnell, F. A. Wolak, and M. Zaragoza-Watkins, "Report of the market simulation group on competitive supply/demand balance in the california allowance market and the potential for market manipulation," *Energy Institute at Haas Working Paper*, vol. 251, 2014.
- [8] M. R. E. Shazly and H. E. E. Shazly, "Comparing the forecasting performance of neural networks and forward exchange rates," *Journal of Multinational Financial Management*, vol. 7, pp. 345–356, 1997.
- [9] J. J. Murphy, *Charting made easy*. John Wiley & Sons, 2012, vol. 149.
- [10] R. J. Sweeney, *Foreign exchange markets*. Edward Elgar, 2005.
- [11] A. Cowles, "Can stock market forecasters forecast?" *Econometrica*, vol. 1, p. 309, 1933.
- [12] L. Menkhoff and M. P. Taylor, "The obstinate passion of foreign exchange professionals: technical analysis," *Journal of Economic Literature*, vol. 45, pp. 936–972, 2007.
- [13] M. R. Adarjani, "Evaluation of the profitability of technical analysis for asian currencies in the forex spot market for short-term trading," *AU-GSB e-JOURNAL*, vol. 5, 2012.
- [14] C. Neely, D. Rapach, J. Tu, and G. Zhou, "Forecasting the equity risk premium: The role of technical indicators," *Management Science*, vol. 60, Apr. 2011.
- [15] J. D. Schwager, *Market Wizards*. New York Institute of Finance, 1989.
- [16] K. Calhoun, "Forex volatility patterns," *TECHNICAL ANALYSIS OF STOCKS AND COMMODITIES-MAGAZINE EDITION-*, vol. 25, p. 22, 2007.
- [17] C. Lento, N. Gradojevic, and C. S. Wright, "Investment information content in bollinger bands?" *Applied Financial Economics Letters*, vol. 3, pp. 263–267, 2007.
- [18] Z. Liu and D. Xiao, "An automated trading system with multi-indicator fusion based on ds evidence theory in forex market," in *2009 Sixth International Conference on Fuzzy Systems and Knowledge Discovery*, vol. 3. IEEE, 2009, pp. 239–243.
- [19] R. Moscinski and D. Zakrzewska, *Building an Efficient Evolutionary Algorithm for Forex Market Predictions*. Springer, 2015.
- [20] W. Poole, "Speculative prices as random walks: An analysis of ten time series of flexible exchange rates," *Southern Economic Journal*, vol. 33, pp. 468–478, 1967.
- [21] M. P. Dooley and J. R. Shafer, "Analysis of short-run exchange rate behavior : March 1973 to november 1981," *Board of Governors of the Federal Reserve System*, 1975.
- [22] G. Fusai and A. Roncoroni, *Implementing Models in Quantitative Finance: Methods and Cases*. Springer International Publishing, 2008.
- [23] L. Kilian and M. P. Taylor, "Why is it so difficult to beat the random walk forecast of exchange rates?" *Journal of International Economics*, vol. 60, pp. 85–107, 2003, empirical Exchange Rate Models.
- [24] M. Frömmel, *Portfolios and investments*. BoD–Books on Demand, 2013.
- [25] H. He and X. Shen, "Bootstrap methods for foreign currency exchange rates prediction," in *2007 International Joint Conference on Neural Networks*. IEEE, 2007, pp. 1272–1277.
- [26] L. Breiman, "Random forests," *Machine Learning*, vol. 45, pp. 5–32, 2001.
- [27] M. Ballings, D. Van den Poel, N. Hespels, and R. Gryp, "Evaluating multiple classifiers for stock price direction prediction," *Expert Systems with Applications*, vol. 42, pp. 7046–7056, 2015.
- [28] W. Lv and R. Zhang, "A regression model on effective exchange rate of rmb based on random forest," in *2011 International Conference on E-Business and E-Government (ICEE)*. IEEE, 2011, pp. 1–3.
- [29] S. Lahmiri and S. Bekiros, "Intelligent forecasting with machine learning trading systems in chaotic intraday bitcoin market," *Chaos, Solitons & Fractals*, vol. 133, p. 109641, 2020.
- [30] J. Conrad and G. Kaul, "An anatomy of trading strategies," *The Review of Financial Studies*, vol. 11, pp. 489–519, 1998.
- [31] Y. Chihab, Z. Bousbaa, H. Jamali, and O. Bencharef, "An approach based on heterogeneous multiagent system for stock market speculation," *Journal of Theoretical and Applied Information Technology*, vol. 97, no. 3, pp. 835–845, 2019.
- [32] H. Hassanpour, "Evaluation of deep neural network in directional prediction of forex market," 2020.
- [33] Y. Chihab, Z. Bousbaa, M. Chihab, O. Bencharef, and S. Ziti, "Algo-trading strategy for intraweek foreign exchange speculation based on random forest and probit regression. applied computational intelligence and soft computing, p 2019," 2019.
- [34] W. Pongsena, P. Sitsayabut, N. Kerdprasop, and K. Kerdprasop, "Development of a model for predicting the direction of daily price changes in the forex market using long short-term memory," *International Journal of Machine Learning and Computing*, vol. 11, pp. 61–67, Jan. 2021.
- [35] D. C. Yıldırım, I. H. Toroslu, and U. Fiore, "Forecasting directional movement of forex data using lstm with technical and macroeconomic indicators," *Financial Innovation*, vol. 7, no. 1, pp. 1–36, 2021.
- [36] G. Chandrashekar and F. Sahin, "A survey on feature selection methods," *Computers & Electrical Engineering*, vol. 40, no. 1, pp. 16–28, 2014, 40th-year commemorative issue.
- [37] J. Li, K. Cheng, S. Wang, F. Morstatter, R. P. Trevino, J. Tang, and H. Liu, "Feature selection: A data perspective," *ACM Computing Surveys (CSUR)*, vol. 50, no. 6, pp. 1–45, 2017.
- [38] J. Li and H. Liu, "Challenges of feature selection for big data analytics," *IEEE Intelligent Systems*, vol. 32, no. 2, pp. 9–15, 2017.
- [39] Z. Kiala, O. Mutanga, J. Odindi, and K. Peerbhaya, "Feature selection on sentinel-2 multispectral imagery for mapping a landscape infested by parthenium weed," *Remote Sensing*, vol. 11, no. 16, p. 1892, 2019.
- [40] Y. LeCun, L. Bottou, Y. Bengio, and P. Haffner, "Gradient-based learning applied to document recognition," *Proceedings of the IEEE*, vol. 86, no. 11, pp. 2278–2324, 1998.

- [41] C. Szegedy, W. Liu, Y. Jia, P. Sermanet, S. Reed, D. Anguelov, D. Erhan, V. Vanhoucke, and A. Rabinovich, "Going deeper with convolutions," in *Proceedings of the IEEE conference on computer vision and pattern recognition*, 2015, pp. 1–9.
- [42] S. Albawi, T. A. Mohammed, and S. Al-Zawi, "Understanding of a convolutional neural network," in *2017 International Conference on Engineering and Technology (ICET)*. Ieee, 2017, pp. 1–6.
- [43] K. Cho, B. Van Merriënboer, D. Bahdanau, and Y. Bengio, "On the properties of neural machine translation: Encoder-decoder approaches," *arXiv preprint arXiv:1409.1259*, 2014.
- [44] A. Graves, *Supervised Sequence Labelling with Recurrent Neural Networks*. Springer, 2012.
- [45] S. Bengio, F. Fessant, and D. Collobert, "A connectionist system for medium-term horizon time series prediction," in *Proc. Intl. Workshop Application Neural Networks to Telecoms*. Proc. Intl. Workshop Application Neural Networks to Telecoms, 1995, p. 308–315.
- [46] D. W. Patterson, K. H. Chan, and C. M. Tan, "Time series forecasting with neural nets: a comparative study," in *Proc. the international conference on neural network applications to signal processing*. Proc. the international conference on neural network applications to signal processing, 1993, p. 269–274.
- [47] T. Edwards, D. S. W. Tansley, R. J. Frank, and N. Davey, "Traffic trends analysis using neural networks," in *Proceedings of the International Workshop on Applications of Neural Networks to Telecommunications*, vol. 3. Proceedings of the International Workshop on Applications of Neural Networks to Telecommunications, 1997, p. 157–164.

Remote Healthcare Monitoring using Expert System

Prajoona Valsalan, Najam ul Hasan, Imran Baig, Manaf Zghaibeh
College of Engineering
Dhofar University, Salalah, Oman

Abstract—With the introduction of the novel coronavirus and the ensuing epidemic, health care has become a primary priority for all governments. In this context, the best course of action is to implement an Internet of Things (IoT)-based remote health monitoring system. As a result, IoT systems have attracted significant attention in academia and industry, and this trend is likely to continue as wearable sensors and smartphones become more prevalent. Even if the doctor is a substantial distance away, IoT health monitoring enables the prevention of illness and the accurate diagnosis of one's current state of health through the use of a portable physiological monitoring framework that continually monitors the patient's systolic blood pressure, blood glucose, oxygen saturation, and diastolic blood pressure. The expert system generates a diagnosis of the patient's health status based on the sensor data. Once the patient's sensor data is transmitted to the cloud via a WiFi module, the expert system uses it to diagnose the patient's health status in order to facilitate any medical attention or critical care that may be required for his condition. The simulation is carried out in Matlab, and the results of the study are presented to demonstrate the suggested system's significance.

Keywords—Internet of Things (IoT); remote health care monitoring; wearable sensors; fuzzy logic

I. INTRODUCTION

Every time the human species makes technological advancements, health is always a major worry [1]. In recent years, both the academic community and the financial markets have placed a premium on the healthcare services sector. This industry has amassed substantial wealth as a result of its research potential [2]. Inadequate resources, skyrocketing healthcare expenditures, and ineffective hospital resource management are just a few of the problems plaguing the healthcare business [3]. Additional logistical challenges exist, such as the volume of medical treatment required by patients, the limited availability of beds and equipment, and the shortage of healthcare specialists. Patient monitoring is often passive, meaning that medical practitioners modify medications in response to changes in the patient's health situation [4]. The current Corona virus outbreak, which has wreaked havoc on the global economy, demonstrates how health care has become increasingly vital in today's world. In this case, it is always preferable to monitor patients in locations where the virus has spread using remote health monitoring devices. The Internet of Things' most major application is in healthcare management, where it is used to track health issues using the remote health monitoring technique. The Internet of Things (IoT) is a process that involves linking computers to the internet via sensors and networks [5]. These connected components can be included into health-monitoring devices. The data is then transmitted to remote computers, providing a simple, energy-efficient, significantly smarter, scalable, and interoperable method of tracking and optimizing care for any health concern. To

aid people in living smarter lives, modern technologies now include a customisable interface, assistant gadgets, and tools for managing mental health [6]. Numerous attempts have been made to remotely send patient data without requiring an in-person hospital visit, utilizing recent advancements in IoT and wireless sensor networks. This enables doctors to decide on the most appropriate course of action or to summon specialized medical aid. In an emergency, the transmission of critical patient data can have a significant impact on the patient's life. The Internet of Things-based health monitoring systems have devised a novel method of tracking patients who live in remote locations.



Fig. 1. Proposed System.

Oman had 346K confirmed COVID-19 infections as of February 20, 2022, with 4K coronavirus fatalities [7]. A fever, shortness of breath, poor oxygen saturation, irregular blood pressure, and an elevated blood glucose level are all indications of risk. Patients who have elevated systolic and diastolic blood pressure are said to be in a hypertensive crisis, whereas those who have elevated blood glucose levels are said to be in a diabetic crisis. A patient who is hypertensive, diabetic, or hypoxemic has a decreased chance of survival and will require urgent care. Patients may be unaware of their condition. As a result, they perish due to a lack of therapy or medical attention. As a result, the current answer is a health monitoring system based on the Internet of Things (IoT) [8]. The response time is critical since the patient's health state may deteriorate in certain instances. Therefore, a continuous remote monitoring system via the Internet of Things presents significant opportunities in the field of e-health [9]. This technology has the ability to significantly improve healthcare and pave the way for numerous improvements using remote health care monitoring techniques. The Internet of Things serves as a catalyst for healthcare and is critical to healthcare services [9]. The body sensor network detects aberrant and unexpected situations by assessing physiological traits and symptoms and giving vital signals for medical investigation [10]. As a result, interim medications can be delivered immediately to avert potentially

life-threatening conditions.

In this study, we designed an expert system to enable remote patient monitoring to assess whether a patient is healthy or requires nutritional control, medical attention, or critical care. As depicted in Figure 1, the built expert system can be divided into two subsystems. The first subsystem is in charge of data collection. The patient is fitted with wearable sensors that monitor vital signs such as blood pressure, blood glucose, and oxygen saturation level. Bluetooth-enabled sensors connect to his smartphone. The smartphone is equipped with an app that records sensor readings and patient data and transmits them to the cloud via the internet. This subsystem is located at the patient end. The second subsystem is utilized to diagnose the patient's health status by utilizing cloud-based data. Expert systems that are based on fuzzy logic use this information to determine if the patient is healthy or need medical attention. The second subsystem is at the hospital end to diagnose the patient health state. The main contribution of this study can be summarized as follows:

- 1) The architecture of the remote health monitoring system was designed with the objective of monitoring patients' health status on a frequent basis.
- 2) Physicians and patients have access to the system's recommended system outcome at any time and from any location.
- 3) Using artificial intelligence logic, the proposed system runs health diagnostics to decide whether or not the patient is healthy or in need of medical assistance.
- 4) MATLAB simulations are utilized to illustrate the suggested system's study outcomes.

The paper is organized as follows: Section II highlights similar research on IoT-based health monitoring systems. Section III goes into the suggested expert system's system concept and architecture for diagnosing a patient's health condition based on body vital data collected from sensors and the fuzzy logic mechanism to suggest the patient's health state and appropriate recommendations. In Section IV, the experimental setup is detailed, in Section V, the simulation results are displayed, and in Section VI, the article is concluded.

II. RELATED WORK

While significant effort has been made in the past to provide medical care outside of traditional hospital grounds, this has become much more critical in light of the present COVID-19 pandemic scenario [11], as seen by an increase in the number of publications. However, as several recent survey papers have highlighted, more work remains to be done in terms of providing medical diagnosis and care to patients at home [12]. For instance, as detailed in [13], a remote patient monitoring system tries to efficiently manage hospital resources by monitoring patients at home. It is an Internet of Things-based patient monitoring technology that automates the collection and transmission of patient data to remote databases. This data is accessible via the a web system, which features an intuitive user interface. The author in [14] describes a home monitoring and decision support system that is intended to assist clinicians in the diagnosis, remote monitoring, treatment, prescription, rehabilitation, and progression of individuals with Parkinson's disease. This is

a data-collection expert system that supports clinicians in diagnosing and treating tremors. The author in [15] offers a Smart Architecture for In-Home Healthcare System, which is a healthcare solution that monitors patients and the elderly with special needs using photographs and facial expressions. The author in [16] did an extensive investigation of many Internet-of-Things-based technologies that could be employed for telemedicine and illness preventive services. A study was done to monitor children's health using a wireless system powered by the Internet of Things and capable of providing real-time notifications to parents and guardians [17]. The author in [18] delivers an IoT-based health monitoring solution for children with autism. A head-worn sensor is used to collect health information from autistic patients. The data acquired from these patients' brains is subsequently transmitted in real time to a monitoring server. If there are any discrepancies in the information read, an alarm is generated and an email is sent to the carer. Additionally, the physician is notified in the event of an emergency. Additionally, for scalability and security, personal information about patients can be stored in the cloud. Other researchers have developed a remote COVID-19 patient monitoring system that incorporates the examination of critical biological data such as PPG, ECG, and temperature to evaluate the patient's health status. Additionally, they discuss the challenges associated with security threats in IoT-based smart health systems [19]. Another Internet of Things system was developed to identify prospective COVID-19 patients by utilizing eight distinct learning algorithms that aid in the differentiation of cold symptoms from COVID-19 symptoms [20]. A study examines the use of IoT systems to monitor patients in smart cities in order to ensure that ambulances and other assistance can reach them swiftly [21]. The author in [22] developed a wearable Internet of Things health monitoring system with its own network, nicknamed the body area network, in which several sensors continuously monitor and record parameters. The author in [23] developed an Internet-of-Things-based health monitoring system capable of tracking a patient's basic symptoms such as heart rate, oxygen saturation percentage, body temperature, and eye movement. The capturing elements included heartbeat, SpO₂, temperature, and eye blink sensors, while the processing device was an Arduino-UNO. Although the developed system has been implemented, no specified performance measures have been established for any of the patients. The author in [24] demonstrated an IoT-enabled healthcare monitoring kit. The developed system monitored fundamental health parameters such as heartbeat, electrocardiogram, body temperature, and respiration. The primary hardware components used in this project are the pulse sensor, temperature sensor, blood pressure sensor, ECG sensor, and Raspberry Pi. The author in [25] outlines an Internet of Things-based healthcare system in which ECGs and other healthcare data are recorded and securely transmitted to the cloud, where specialists can access them. Signal augmentation techniques, encryption, and other appropriate analysis are used to prevent identity theft or clinical error. The author in [26] discusses the health care monitoring system and IoT-based analyses. This research successfully built a new IoT-based framework for health applications. Three vital signs, including body temperature, heart rate, and blood pressure, may be precisely measured by the device. Physicians may view and monitor data in real time, even if patients complete their medical tests outside of the clinical setting.

III. PROPOSED EXPERT SYSTEM

A. System Architecture

The primary objective of this project is to develop a smart IoT-based health monitoring system capable of diagnosing a patient's health state based on sensor-read bodily vital statistics. The proposed system's initial section is implemented at the patient's end. A variety of body sensors are implanted in the patient, including a blood pressure sensor that detects both systolic and diastolic pressures, an oxygen saturation sensor, and a blood glucose sensor. These three vital signs of the body are frequently altered, especially when the patient is infected with COVID 19. These measurements must be reviewed frequently for such patients to avoid undesirable repercussions. However, it is difficult to visit the hospital on a frequent basis. As a result, this sensor data is transmitted to the cloud via a gateway and stored on a medical support service's data server.

The second section of the proposed system applies fuzzy logic to process on the sensor data received from the first subsystem and to diagnose the patient's health status. The patient health status is summarised as healthy, requiring only dietary supervision, or requiring medical attention or critical care.

B. Fuzzy Based Health Diagnosis System

The suggested system utilizes wearable sensors on the patient to monitor systolic and diastolic blood pressure, oxygen saturation level, and blood glucose level. As illustrated in Fig. 2, these are the inputs to our diagnosis expert system at the medical care service center.

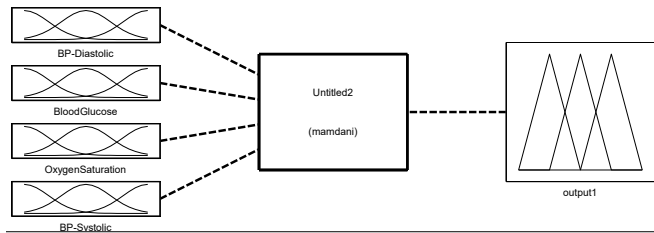


Fig. 2. Overview of Diagnostic System.

The inputs to the system has to be considered as membership function. The Blood pressure diastolic values are divided into four ranges: Normal, Stage 1 Hypertension, Stage 2 Hypertension, Hypertensive Crisis [27]. The Blood glucose input is divided as Low, Normal, Prediabetic, Diabetic. The oxygen saturation level is divided as Crisis, Hypoxemia, Normal. The Blood pressure Systolic values are divided as Normal, Elevated, Stage 1 Hypertension, Stage 2 Hypertension, Hypertensive Crisis.

The pressure in the arteries when the heart rests between beats is measured by the diastolic reading. This is when the heart receives oxygen and fills with blood. The input Blood Pressure Diastolic is measured in mmHg and the membership function is shown in Fig. 3. It is divided into four ranges : Normal (<80 mmHg), Stage 1 Hypertension (80mmHg - 89mmHg), Stage 2 Hypertension (90mmHg - 120mmHg), Hypertensive Crisis (>120mmHg).

The characteristic of Blood Pressure Diastolic is as follows:

$$Normal = \begin{cases} 1 & \text{if } x \leq 79 \\ \frac{80-x}{80-79} & \text{if } 79 < x < 80 \\ 0 & \text{if } x \geq 90 \end{cases} \quad (1)$$

$$Stage1HT = \begin{cases} 1 & \text{if } 80 \leq x \leq 89 \\ \frac{x-79}{80-79} & \text{if } 79 < x < 80 \\ \frac{90-x}{90-89} & \text{if } 89 < x < 90 \\ 0 & \text{if } x \leq 79; x \geq 90 \end{cases} \quad (2)$$

$$Stage2HT = \begin{cases} 1 & \text{if } 90 \leq x \leq 120 \\ \frac{x-89}{90-89} & \text{if } 89 < x < 90 \\ \frac{121-x}{121-120} & \text{if } 120 < x < 121 \\ 0 & \text{if } x \leq 89; x \geq 121 \end{cases} \quad (3)$$

$$Crisis = \begin{cases} 1 & \text{if } x \geq 121 \\ \frac{x-120}{121-120} & \text{if } 120 < x < 121 \\ 0 & \text{if } x \leq 120 \end{cases} \quad (4)$$

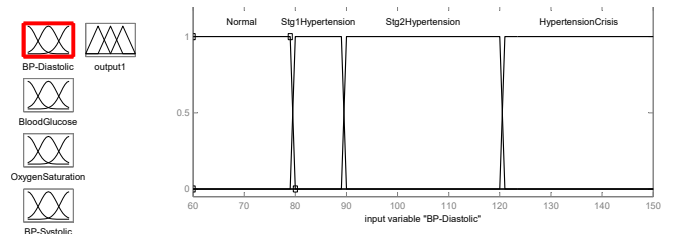


Fig. 3. Blood Pressure Diastolic Membership Function.

Diabetes is defined as a blood glucose level that is higher than normal. And if a diabetic patient's blood glucose level isn't controlled, it can lead to death [28]. As a result, there's a big need to keep track of blood glucose levels and make sure you're getting the right amount of insulin. Blood glucose is another input considered, which is measured in mmol / L and the membership function is shown in Fig. 3. It is divided into four ranges : Low(0 mmol / L - 3.9 mmol / L), Normal(4.0 mmol/L - 5.4 mmol/L), Prediabetic(5.5 mmol/L - 6.9 mmol/L) and Diabetic(>7.0 mmol/L) as shown in Fig. 4.

The characteristic of Blood Glucose is as follows:

$$Low = \begin{cases} 1 & \text{if } x \leq 3.9 \\ \frac{4-x}{4-3.9} & \text{if } 3.9 < x < 4 \\ 0 & \text{if } x \geq 4 \end{cases} \quad (5)$$

$$Normal = \begin{cases} 1 & \text{if } 4 \leq x \leq 5.4 \\ \frac{x-3.9}{4-3.9} & \text{if } 3.9 < x < 4 \\ \frac{5.5-x}{5.5-5.4} & \text{if } 5.4 < x < 5.5 \\ 0 & \text{if } x \leq 3.9; x \geq 5.5 \end{cases} \quad (6)$$

$$Prediabetic = \begin{cases} 1 & \text{if } 5.5 \leq x \leq 6.9 \\ \frac{x-5.4}{5.5-5.4} & \text{if } 5.4 < x < 5.5 \\ \frac{7-x}{7-6.9} & \text{if } 6.9 < x < 7 \\ 0 & \text{if } x \leq 5.4; x \geq 7 \end{cases} \quad (7)$$

$$Diabetic = \begin{cases} 1 & \text{if } x \geq 7 \\ \frac{x-6.9}{7-6.9} & \text{if } 6.9 < x < 7 \\ 0 & \text{if } x \leq 6.9 \end{cases} \quad (8)$$

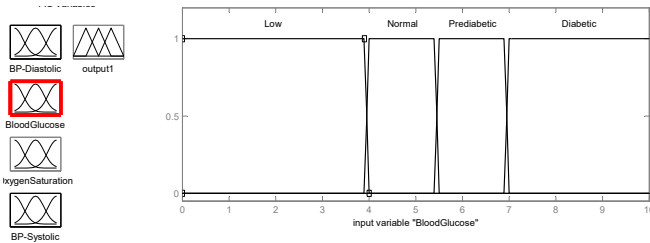


Fig. 4. Blood Glucose Membership Function.

The percentage of oxygen in a person’s blood is known as oxygen saturation. A pulse oximeter is a gadget that medical practitioners frequently use for fast tests or continuous monitoring [29]. The oxygen saturation level in a healthy person ranges from 95% to 100%. If a person’s levels go below this range, they may feel symptoms including difficulty breathing and confusion, which are signs of a shortage of oxygen. The input Oxygen Saturation is divided into three ranges: Critical Crisis (<90%), Hypoxemia (90% - 94%) and Normal (95% - 100%) as shown in Fig. 5.

The characteristic of Oxygen Saturation is as follows:

$$Crisis = \begin{cases} 1 & \text{if } x \leq 89 \\ \frac{90-x}{90-89} & \text{if } 89 < x < 90 \\ 0 & \text{if } x \geq 90 \end{cases} \quad (9)$$

$$Hypoxemia = \begin{cases} 1 & \text{if } 90 \leq x \leq 92 \\ \frac{x-89}{90-89} & \text{if } 89 < x < 90 \\ \frac{94-x}{94-92} & \text{if } 92 < x < 94 \\ 0 & \text{if } x \leq 89; x \geq 94 \end{cases} \quad (10)$$

$$Normal = \begin{cases} 1 & \text{if } x \geq 95 \\ \frac{x-94}{95-94} & \text{if } 94 < x < 95 \\ 0 & \text{if } x \leq 6.94 \end{cases} \quad (11)$$

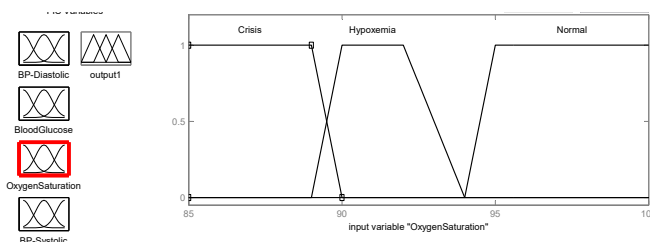


Fig. 5. Oxygen Saturation Membership Function.

When your heart beats, it squeezes and pushes blood to the rest of your body through your arteries. Your systolic blood pressure is the result of this force exerting pressure on those blood vessels[27].The input systolic blood pressure is divided into five ranges: Normal (<121 mmHg), Elevated (121mmHg - 129mmHg), Stage1 Hypertension (130mmHg - 139mmHg),

Stage2 Hypertension (140mmHg- 80mmHg) and Hypertensive Crisis (>180) as shown in Fig. 6.

The characteristic of Blood Pressure Systolic is as follows:

$$Normal = \begin{cases} 1 & \text{if } x \leq 120 \\ \frac{121-x}{121-120} & \text{if } 120 < x < 121 \\ 0 & \text{if } x \geq 121 \end{cases} \quad (12)$$

$$Elevated = \begin{cases} 1 & \text{if } 121 \leq x \leq 129 \\ \frac{x-120}{121-120} & \text{if } 120 < x < 121 \\ \frac{130-x}{130-129} & \text{if } 129 < x < 130 \\ 0 & \text{if } x \leq 120; x \geq 130 \end{cases} \quad (13)$$

$$Stage1HT = \begin{cases} 1 & \text{if } 130 \leq x \leq 139 \\ \frac{x-129}{130-129} & \text{if } 129 < x < 130 \\ \frac{140-x}{140-139} & \text{if } 139 < x < 140 \\ 0 & \text{if } x \leq 129; x \geq 140 \end{cases} \quad (14)$$

$$Stage2HT = \begin{cases} 1 & \text{if } 140 \leq x \leq 179 \\ \frac{x-139}{140-139} & \text{if } 139 < x < 140 \\ \frac{180-x}{180-179} & \text{if } 179 < x < 180 \\ 0 & \text{if } x \leq 139; x \geq 180 \end{cases} \quad (15)$$

$$Crisis = \begin{cases} 1 & \text{if } x \geq 180 \\ \frac{x-179}{180-179} & \text{if } 179 < x < 180 \\ 0 & \text{if } x \leq 179 \end{cases} \quad (16)$$

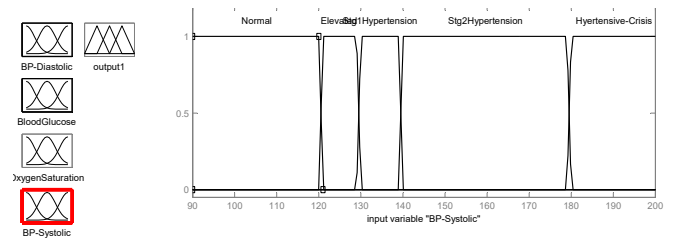


Fig. 6. Blood Pressure Systolic Membership Function.

The output of the expert system is the diagnosis of health state of the based on the data obtained from the sensors. In the pandemic situation, it is recommended to get hospitalised if the condition of the patient is critical and needs medical care. So here the output membership function is divided into four ranges: Healthy (<40), Diet Control (40 - 59), Medical Attention (60-79), Critical Care (80-99) as shown in Fig. 7.

The characteristic of Output health state is as follows:

$$Healthy = \begin{cases} 1 & \text{if } x \leq 39 \\ \frac{40-x}{40-39} & \text{if } 39 < x < 40 \\ 0 & \text{if } x \geq 40 \end{cases} \quad (17)$$

$$DietControl = \begin{cases} 1 & \text{if } 40 \leq x \leq 59 \\ \frac{x-39}{40-39} & \text{if } 39 < x < 40 \\ \frac{60-x}{60-59} & \text{if } 59 < x < 60 \\ 0 & \text{if } x \leq 39; x \geq 60 \end{cases} \quad (18)$$

$$MedicalAttention = \begin{cases} 1 & \text{if } 60 \leq x \leq 79 \\ \frac{x-59}{60-59} & \text{if } 59 < x < 60 \\ \frac{80-x}{80-79} & \text{if } 79 < x < 80 \\ 0 & \text{if } x \leq 59; x \geq 80 \end{cases} \quad (19)$$

$$CriticalCare = \begin{cases} 1 & \text{if } 80 \leq x \leq 99 \\ \frac{x-79}{80-79} & \text{if } 79 < x < 80 \\ \frac{100-x}{100-99} & \text{if } 99 < x < 100 \\ 0 & \text{if } x \leq 79; x \geq 100 \end{cases} \quad (20)$$

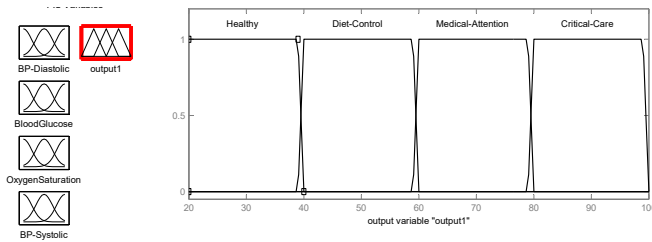


Fig. 7. Output Health State Membership Function.

The expert system’s fuzzy rules are defined as a set of all conceivable input combinations. When the normal range of the input Systolic Blood Pressure is considered first, it can be combined with the other input ranges of oxygen saturation (3 ranges: crisis, hypoxemia, normal), blood glucose (4 ranges: low, normal, prediabetic, and diabetic), and diastolic blood pressure (4 ranges: normal, stage 1 hypertension, stage 2 hypertension, and hypertensive crisis) to create a total of 48 rule sets. As a result of the input Systolic Blood Pressure having five ranges (Normal, Elevated, Stage 1 Hypertension, Stage 2 Hypertension, and Hypertensive Crisis), the total number of rule sets for the fuzzy system will be $48 \times 5 = 240$, as illustrated in Fig. 8. The combination of the four input sensors specified ranges results in a total of 240 rules. These rules produce a person’s health state, which may be healthy, diet-controlled, medically attended, or severely cared for. If all sensor input values are within the usual range, the patient is termed healthy. If any of these inputs—Systolic Blood Pressure, Diastolic Blood Pressure, or Blood Glucose level—is found to be slightly elevated above the usual range, the patient is advised as to have Diet Control. If more than one or two input values are outside the normal range or within critical ranges, the patient is referred to a critical care unit or advised for official medical attention. To facilitate comprehension, few rules are further described as follows:

RULE: IF Systolic Blood Pressure == Normal AND Oxygen Saturation == Normal AND Blood sugar == Normal AND Diastolic Blood Pressure == Normal then output health state = Healthy

RULE: IF Systolic Blood Pressure == Elevated AND Oxygen Saturation == Normal AND Blood sugar == Prediabetic AND Diastolic Blood Pressure == Normal then output health state = Diet Control

RULE: IF Systolic Blood Pressure == Normal AND Oxygen Saturation == Hypoxemia AND Blood sugar == Normal

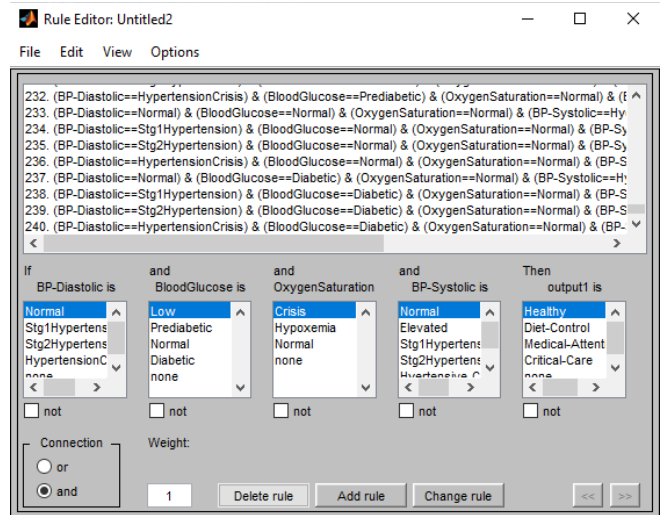


Fig. 8. Rules for Fuzzification.

AND Diastolic Blood Pressure == Normal then output health state = Medical Assistance

RULE: IF Systolic Blood Pressure == Stage 2 Hypertension AND Oxygen Saturation == crisis AND Blood sugar == Normal AND Diastolic Blood Pressure == Stage 1 Hypertension then output health state = Critical Care

IV. EXPERIMENTAL SETUP

Matlab is used to simulate the suggested expert system. The implementation makes use of the fuzzy logic tool. A four-input, single-output fuzzy logic system was developed for diagnosing a patient’s health status. The blood glucose level, the diastolic blood pressure value, the oxygen saturation level, and the systolic blood pressure value are all inputs. As discussed previously, four inputs have distinct ranges: oxygen saturation (3 ranges: crisis, hypoxemia, and normal); blood glucose (4 ranges: low, normal, prediabetic, and diabetic); diastolic blood pressure (4 ranges: normal, stage 1 hypertension, stage 2 hypertension, and hypertensive crisis); and systolic blood pressure (5 ranges: normal, elevated, stage 1 hypertension, stage 2 hypertension, and hypertensive crisis). The output of the fuzzy logic system is the patient’s state of health, which is classified into four categories: healthy, diet control, medical attention, and critical care. As illustrated in Fig. 9, the fuzzy logic rules are programmed. The output health status of any set of input values is calculated by the use of fuzzy logic, which adheres to fuzzy principles.

Fig. 9 illustrates the outcome of the centroid method defuzzification. The output health state of a patient can be determined using any combination value of inputs of diastolic blood pressure, blood glucose level, oxygen saturation level and systolic blood pressure values. As indicated, the diastolic blood pressure is 74.3, which is within the normal range of the input. Blood glucose level is 5, which is likewise within the usual range. The oxygen saturation level is 90.6, which is within the range of hypoxemia, and the systolic blood pressure is 108, which is within the normal range. The output health state value derived using the centroid approach is 69.4, indicating that the patient requires medical intervention.

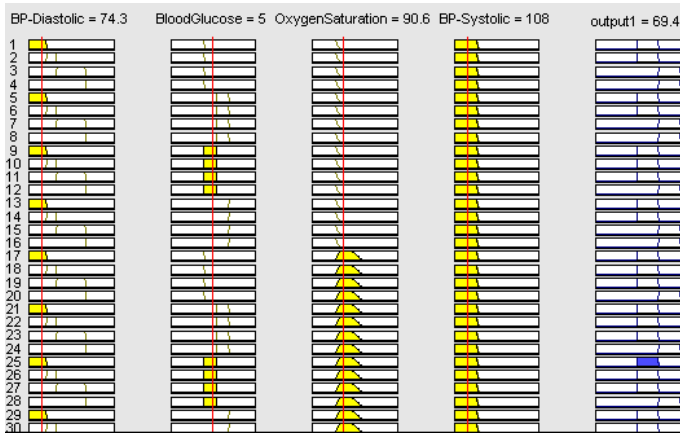


Fig. 9. Simulation Result.

V. SIMULATION RESULTS

Matlab's fuzzy logic toolbox provides a platform for solving any system defined by an input and output set and guided by particular rules. As a result, we chose Matlab's fuzzy toolbox for this project's simulation platform. The simulation result shown in Fig. 10 depicts the patient's output health condition for all possible combinations of the two inputs Blood glucose and Diastolic Blood Pressure. For example it can be easily understood that when the Diastolic Blood Pressure is in Hypertensive Crisis range ($>120\text{mmHg}$) and Blood Glucose is in Diabetic Range ($>7.0\text{mmol/L}$), then the output health state is in Critical Care (80-99). If the Diastolic Blood Pressure is Normal ($<80\text{mmHg}$) and the Blood Glucose is Normal ($4.0\text{mmol/L} - 5.4\text{mmol/L}$), then the output state is in the healthy range Healthy (<40).

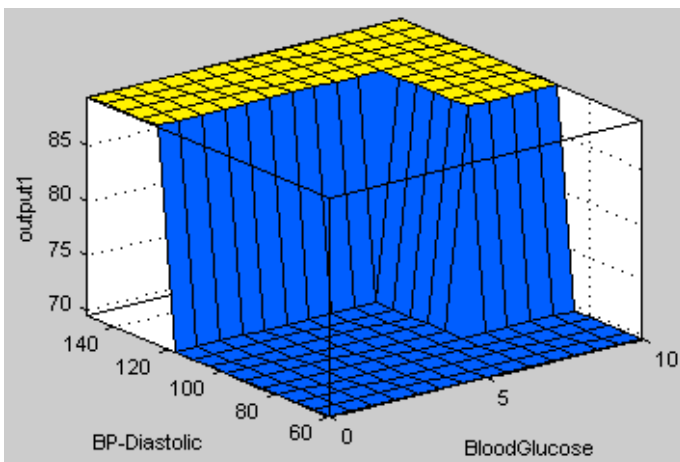


Fig. 10. Diastolic BP and Blood Glucose Surface View.

Fig. 11 shows the surface view output for the input combination of all ranges of Blood glucose and Systolic Blood Pressure. For example it is also observed that if the Blood glucose is in the normal range ($4.0\text{mmol/L} - 5.4\text{mmol/L}$) and Systolic Blood Pressure is also normal ($<121\text{mmHg}$) then the output health state is in the range Healthy (<40).

The output surface view of Oxygen Saturation level and Blood Glucose is shown in Fig. 12. The output health state

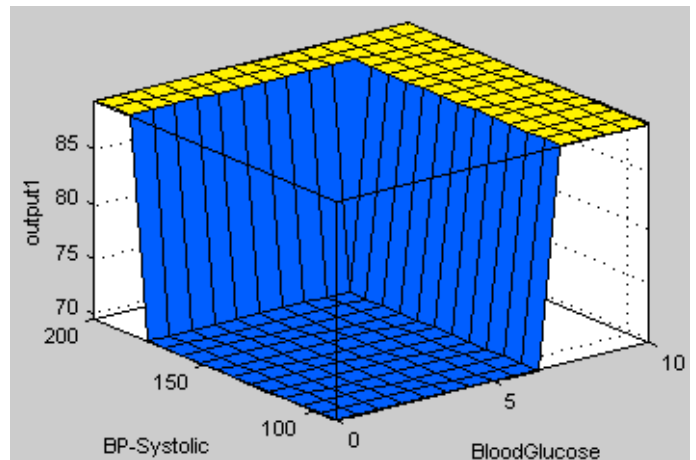


Fig. 11. Systolic BP and Blood Glucose Surface View.

for all input combination of the inputs Oxygen Saturation level and Blood Glucose can be easily calculated. For example if the Oxygen level is in Hypoxemia range ($90\% - 94\%$) and Blood glucose is in Normal range ($4.0\text{mmol/L} - 5.4\text{mmol/L}$), then the output Health state is in Medical Attention range ($60-79$). If the oxygen saturation level is in Critical Crisis ($<90\%$) and the Blood Sugar Diabetic ($>7.0\text{mmol/L}$) then the output health state is in critical care ($80-99$).

Fig. 13 shows the output health state for all the input range combination of systolic and diastolic blood pressure. For example it is also observed that if Systolic Blood Pressure is in Hypertensive Crisis range (>180) and the Diastolic Blood Pressure is in Hypertensive Crisis range ($>120\text{mmHg}$) then the output health state is in the critical care range.

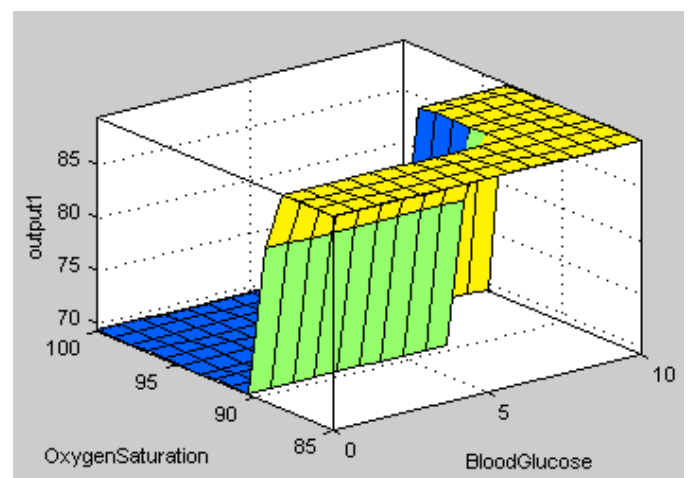


Fig. 12. Oxygen Saturation and Blood Glucose Surface View.

VI. CONCLUSION

The suggested smart health monitoring system enables healthcare practitioners to quickly identify particular patients' health vital information and give the appropriate service based on their health status. This monitoring system will become more adaptive and updatable in the future as a result of

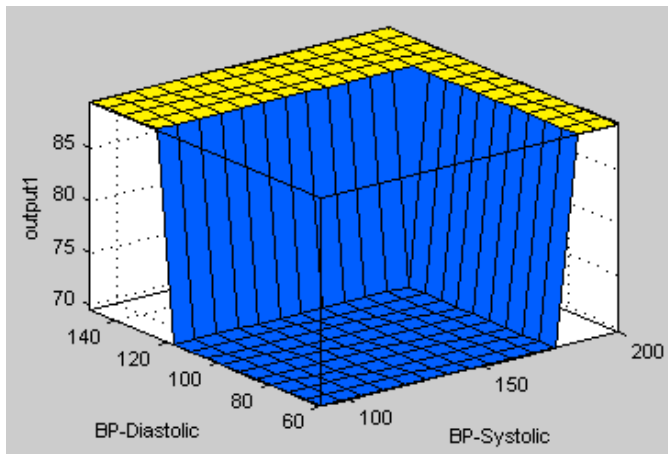


Fig. 13. Systolic and Diastolic Blood Pressure Surface View.

IoT technology. By monitoring diastolic blood pressure, blood glucose level, oxygen level, and systolic blood pressure level, we have made diagnosis and treatment easier with this proposed expert system. Contactless tracking and treatment of patients, particularly COVID-19 patients, is now possible with the use of a specifically developed IOT smart health monitoring device. The output health state is diagnosed using the fuzzy approach based on the sensor data obtained. The proposed system generates the following outputs for the four input sensor data received: healthy, diet control, medical attention, and critical care. When the patient's sensor data falls within the ranges wherein the output is judged to be necessary for medical attention or critical care, the patient can be hospitalized immediately. The Matlab simulation results demonstrate the significance of the expert system in enabling the remote health monitoring process. The proposed approach will enhance the current healthcare system, potentially saving a large number of lives during this pandemic situation.

ACKNOWLEDGMENT

This work is supported by Dhofar University Research Grant Project code: DU-AY-2020-21-DURG-002.

REFERENCES

- [1] M. M. Islam, A. Rahmanand, and M. R. Islam, "Development of smart healthcare monitoring system in IoT environment," SN Computer Science, vol. 1, no. 3, 2020.
- [2] V. Tamilselvi, S. Sribalaji, P. Vigneshwaran, P. Vinu, and J. GeethaRamani, "IoT based health monitoring system,," in 2020 6th International Conference on Advanced Computing and Communication Systems (ICACCS), Coimbatore, India, 2020.
- [3] Bhardwaj, V., Joshi, R. & Gaur, A.M. IoT-Based Smart Health Monitoring System for COVID-19. SN COMPUT. SCI. 3, 137 (2022). <https://doi.org/10.1007/s42979-022-01015-1>.
- [4] Iranpak, S., Shahbahrami, A. & Shakeri, H. Remote patient monitoring and classifying using the internet of things platform combined with cloud computing. J Big Data 8, 120 (2021). <https://doi.org/10.1186/s40537-021-00507-w>
- [5] Islam, M.M., Rahaman, A. & Islam, M.R. Development of Smart Healthcare Monitoring System in IoT Environment. SN COMPUT. SCI. 1, 185 (2020). <https://doi.org/10.1007/s42979-020-00195-y>
- [6] Mamdiwar, S.D.; R, A.; Shakruwala, Z.; Chadha, U.; Srinivasan, K.; Chang, C.-Y. Recent Advances on IoT-Assisted Wearable Sensor Systems for Healthcare Monitoring. Biosensors 2021, 11, 372. <https://doi.org/10.3390/bios11100372>

- [7] <https://covid19.who.int/region/emro/country/om>
- [8] Ali I. Siam, Mohammed Amin Almaiah, Ali Al-Zahrani, Atef Abou Elazm, Ghada M. El Banby, Walid El-Shafai, Fathi E. Abd El-Samie, Nirmeen A. El-Bahnasawy, "Secure Health Monitoring Communication Systems Based on IoT and Cloud Computing for Medical Emergency Applications", Computational Intelligence and Neuroscience, vol. 2021, Article ID 8016525, 23 pages, 2021. <https://doi.org/10.1155/2021/8016525>
- [9] H. Bhardwaj, K. Bhatia, A. Jain and N. Verma, "IOT Based Health Monitoring System," 2021 6th International Conference on Communication and Electronics Systems (ICCES), 2021, pp. 1-6, doi: 10.1109/ICCES51350.2021.9489207
- [10] P. S. Akram, M. Ramesha., S. A. S. Valiveti, S. Sohail and K. T. S. S. Rao, "IoT based Remote Patient Health Monitoring system," 2021 7th International Conference on Advanced Computing and Communication Systems (ICACCS), 2021, pp. 1519-1524, doi: 10.1109/ICACCS51430.2021.9441874
- [11] Nor Shahanim Mohamad Hadis et al 2020 J. Phys.: Conf. Ser. 1535 012004
- [12] Mohammad Monirujjaman Khan, Safia Mehnaz, Antu Shaha, Mohammed Nayem, Sami Bourouis, "IoT-Based Smart Health Monitoring System for COVID-19 Patients", Computational and Mathematical Methods in Medicine, vol. 2021, Article ID 8591036, 11 pages, 2021. <https://doi.org/10.1155/2021/8591036>
- [13] Suryandari, Y. (2020). Survei IoT Healthcare Device. Jurnal Sistem Cerdas, 3(2), 153 - 164. <https://doi.org/10.37396/jsc.v3i2.55>
- [14] Chiuchisan, I. U. L. I. A. N. A., O. A. N. A. Geman. An approach of a decision support and home monitoring system for patients with neurological disorders using internet of things concepts. WSEAS Trans Syst. 13.1 (2014): 460-469
- [15] Mano LY, et al. Exploiting IoT technologies for enhancing Health Smart Homes through patient identification and emotion recognition. Comput Commun. 2016;89:178-90.
- [16] Albahri AS, et al. IoT-based telemedicine for disease prevention and health promotion: State-of-the-Art. J Netw Comput Appl.;173:102873; 2021
- [17] Hong-tan L, et al. Big data and ambient intelligence in IoT-based wireless student health monitoring system. Aggress Violent Behav. 2021. <https://doi.org/10.1016/j.avb.2021.101601>.
- [18] Sundhara Kumar KB, Krishna B. IoT based health monitoring system for autistic patients. In: Proceedings of the 3rd International Symposium on Big Data and Cloud Computing Challenges (ISBCC-16'). Springer, Cham, 2016.
- [19] Sharma N, et al. A smart ontology-based IoT framework for remote patient monitoring. Biomed Signal Process Control. 2021;68:102717.
- [20] Otoom M, et al. An IoT-based framework for early identification and monitoring of COVID-19 cases. Biomed Signal Process Control. 2020;62:102149.
- [21] Poongodi M, et al. Smart healthcare in smart cities: wireless patient monitoring system using IoT. J Supercomput. 2021;7(11):12230-55.
- [22] Wan J, et al. Wearable IoT enabled real-time health monitoring system. EURASIP J Wirel Commun Netw. 2018;2018(1):298.
- [23] Tamilselvi V, Sribalaji S, Vigneshwaran P, Vinu P, GeethaRamani J. IoT based health monitoring system. In: 2020 6th International conference on advanced computing and communication systems (ICACCS). IEEE; 2020. p. 386-9.
- [24] Acharya AD, Patil SN. IoT based health care monitoring kit. In: 2020 Fourth international conference on computing methodologies and communication (ICCMC). IEEE; 2020. p. 363-8.
- [25] Shamim Hossain M, Ghulam M. Cloud-assisted industrial internet of things (iiot)-enabled framework for health monitoring. Comput Netw. 2016;101:192-202.
- [26] Tan ET, Abdul HZ. Health care monitoring system and analytics based on internet of things framework. IETE J Res. 2019;65.5:653-60.
- [27] <https://www.webmd.com/hypertension-high-blood-pressure/guide/diastolic-and-systolic-blood-pressure-know-your-numbers>
- [28] <https://www.diabetesselfmanagement.com/managing-diabetes/blood-glucose-management/blood-sugar-chart/>
- [29] "Hypoxemia: Symptoms, Causes, Treatments. Cleveland Clinic," 2020, <https://my.clevelandclinic.org/health/diseases/17727-hypoxemia>.

An End-to-End Method to Extract Information from Vietnamese ID Card Images

Khanh Nguyen-Trong

Department of Software Engineering

Posts and Telecommunications Institute of Technology

Hanoi, Vietnam

Abstract—Information extraction from ID cards plays an important role in many daily activities, such as legal, banking, insurance, or health services. However, in many developing countries, such as Vietnam, it is mostly carried out manually, which is time-consuming, tedious, and may be prone to errors. Therefore, in this paper, we propose an end-to-end method to extract information from Vietnamese ID card images. The proposed method contains three steps with four neural networks and two image processing techniques, including U-Net, VGG16, Contour detection, and Hough transformation to pre-process input card images, CRAFT, and Rebia neural network for Optical Character Recognition, and Levenshtein distance and regular expression to post-process extracted information. In addition, a dataset, including 3.256 Vietnamese ID cards, 400k manual annotated text, and more than 500k synthetic text, was built for verifying our methods. The results of an empirical experiment conducted on our self-collected dataset indicate that the proposed method achieves a high accuracy of 94%, 99.5%, and 98.3% for card segmentation, classification, and text recognition.

Keywords—Optical character recognition; U-Net network; VGG16 network; CRAFT network; rebia network

I. INTRODUCTION

The ID card is the most widely used identity document of Vietnamese citizens. It provides crucial information used for many business processes, such as ID number, name, address, and date of birth. However, extracting information from such cards is usually carried out manually, which is time-consuming, tedious, and can prone to errors. In this context, methods that automatically analyze and extract information, such as Optical Character Recognition (OCR) are frequently used.

However, there have been several challenges in reading information from cards captured in natural scenes, including difficulties in scene text recognition, lacking training data, and the complexity of Vietnamese language. According to *et al.* [1], the diversity of scene text, the complexity of the background, and the interference factors are the most difficulties for scene text detection and recognition. The first difficulty is caused by diversities in fonts, colors, scales, and text orientations. For example, a Vietnamese ID card can contain three or four different fonts and colors. Moreover, there are four types of cards, as illustrated in Fig. 1, which have several formats for the same field. Especially for the 9-digit ID card, it can contain handwriting text or old fonts created by typewriters. The complexity of background leads to difficulty to clearly distinguish texts from backgrounds. For instance, the Vietnamese ID card background is usually incorrectly detected as

text. As shown in Fig. 2a, the bounding box, the detected text region, also contains the pattern background. The interference factors, such as noise, blur, distortion, low resolution, non-uniform illumination, and partial occlusion make the detection and recognition harder, as illustrated in 2b.

Due to sensitive information, researchers have faced many difficulties in collecting Vietnamese ID cards for model training. This lack of data can easily lead to bad results in extracting information. Moreover, the Vietnamese alphabet is a Latin-based alphabet, but with many additional characters, including five accent symbols (\acute{a} , \grave{a} , \hat{a} , \tilde{a} , \grave{q}) and derivative characters, such as \hat{e} , \grave{a} , \acute{u} ... [2]. Therefore, we cannot apply available OCR methods and pre-trained models, usually for English, to this language.

There have already been a few studies on similar cards, for example, Egyptian ID [3], Indonesian ID [4], or even Vietnamese ID cards [5], [6]. Most of them are deep learning-based due to the outstanding performance in OCR [7]–[9]. However, the proposed methods focus either on different languages, like English or on sub-tasks, such as text recognition [5], [6]. They cannot be used for the Vietnamese language or to directly deal with raw images captured in natural scenes.

Therefore, this paper presents an end-to-end method for information retrieval from Vietnamese ID card images. The method consists of 3 consecutive steps (Pre-processing, Text detection and recognition, and Post-processing) with four neural networks, two image processing techniques, and two basic Natural language processing to deal with raw card images captured in natural scenes. We also created four datasets to deal with the lack of data. In summary, the major contributions of this work are as follows::

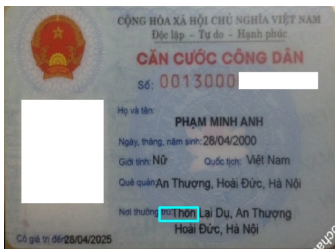
- We proposed an end-to-end deep learning-based method to extract information from the Vietnamese ID card, which is based on state-of-the-art methods in related fields.
- We introduced four neural networks (U-NET, VGG16, CRAFT, and Rebia) to analyze the card and extract its content. To assure the correlation among models, we based on the output of the previous step to train models for the subsequent one.
- We applied (i) Contour detection and Hough transformation at the pre-processing step to align and crop the card; (ii) Levenshtein distance and regular expression at the post-processing step to correct extracted information.



Fig. 1. Front Side of Vietnamese ID Card.



(a) Pattern background as text



(b) Occlusion text

Fig. 2. Complexity of Background and Interference Factors.

- We built four datasets for Vietnamese OCR, including two manual (ID Cards and manually annotated text) and two synthetic (synthetic image and text) datasets. The datasets contain more than 400k manual labeled text from 3.256 Vietnamese ID Card. Furthermore, we evaluated our proposed method on these datasets and highlighted the experimental results thus obtained.
- We proposed a microservice architecture to deploy our method on a real system, which allows balancing the information flow between each step of the end-to-end method.

The remainder of this paper is structured as follows. Section 2 discusses relevant previous studies. Section 3 provides the details regarding our proposed networks. The experimental evaluation is presented in Section 4, and finally, some concluding remarks and a brief discussion are provided in Section 5.

II. RELATED WORKS

In general, information retrieval from ID card images relates to the OCR of semi-structured documents, such as receipts [10], bank cards [11], business cards [12], [13], invoices [14], [15], and so on. It typically contains several

common steps, including pre-processing, text detection, text recognition, and layout analysis [5], [10], [16]–[18].

Clearly, in the context of Scene Text Recognition (STR), where document images can be affected by many factors, pre-processing is necessary to improve the quality and normalize the input data. This step can include a series of sub-tasks, such as document detection, segmentation, alignment, and basic image processing techniques. For example, with a raw image captured in natural scenes, we must check the existence of documents, and then extract their position. The latter usually produces information about the top-left and bottom-up corners of the box that covers the object. To have a stable result in further steps, the document can be aligned vertically, in which the text direction is from left to right.

The output of pre-processing is passed to the next step, where the text detection is essentially performed [5], [16]. Then, at the layout analysis step, these ROIs are extracted and classified into corresponding fields, for example, ID number, name, date of birth, address. At the final step, where the main principle of what is usually called optical character recognition happens, we predict the potential string of extracted text areas.

Regarding the order of these steps, the pre-processing is usually performed first, while the remaining can be varied. For example, text detection and recognition can be performed together, as in the stepwise methodologies or step-by-step like integrated methodologies [19]. The layout analysis is typically done after recognizing, which determines the corresponding label of ROI and so on.

Recently, with the development of deep learning, many methods have been proposed for these steps with potential accuracy. For the pre-processing step, they usually applied both traditional image processing techniques [20] and deep neural networks such as the canny edge detection algorithm [10], Otsu's method [5], U-Net [21], and VGG [22]. Applying deep learning to OCR also achieved higher performance and low processing time than traditional machine learning. Regarding text detection, for example, Baek *et al.* [23] presented a character-based method, Character Region Awareness for Text Detection (CRAFT) that effectively detects text areas by exploring each character region and affinity between them. Liao *et al.* [24] proposed another method that can detect the character in real-time. Similarity these are also many models in the literature for text recognition, such as CHAR model [25], CTPN [26], TRBA [27], Shi *et al.* [28] and so on. They can be categorized into character-level and word-level. The first approach firstly locates the position of each character, then

recognizes them by a classifier, and groups characters into the final text. Meanwhile, the second method, which outperforms the first one, considers the text line as a whole and focuses on mapping the entire text into a target string sequence [29].

These methods are applicable to many language types, such as English, Korean, Chinese. However, it is impossible to directly apply to Vietnamese that contain additional accent and diacritical marks. Additional training is needed to learn its specific features. Moreover, they usually focus on sub-steps or a specific problem, e.g., only pre-processing [5], or text detection [23]. We cannot simply juxtapose these steps for an end-to-end method to extract information from the Vietnamese ID card. To achieve high and stable performance, they need to correlate with each other. The output of the previous step should be used as the input to train models for the subsequent step.

III. PROPOSED METHOD

Due to the variety of captured images and types of ID cards, the proposed method contained three steps with four neural networks, as shown in Fig. 3. It consisted of a set of deep learning and traditional machine learning techniques in Computer Vision and Natural Language Processing, as follows:

- We performed several pre-processing steps, including segmentation, alignment, and identification, to determine and normalize the card. First, we detected and segmented cards from input images. Next, they were vertically aligned and cropped, with text from left to right. Then, we determined their type (9-digit, 12-digit, or the new 12-digit ID Card). Two deep learning methods, and two image processing algorithms were applied for this step: U-Net model for the detection, and segmentation, VGG16 model for the classification, Contour Detection, and Hough Transformation for the alignment.
- We applied the word-level approach to detect and recognize Vietnamese optical texts on the cards, including the CRAFT method [23] for text detection, the Attn method with ResNet, and BiLSTM for text recognition.
- Lastly, to correct text errors and identify text fields (Named Entity Recognition), such as names, date of births, we performed two main tasks, including layout analysis and text correction. The Levenshtein distance, regular expression, and two pre-defined dictionaries were applied.

The input of the first step is images containing Vietnamese ID cards, while the output is the ID cards that were cropped, aligned from the background. The type of card is an important output of this step. Then, the cropped ID is used as input for the next step (text detection and text recognition), which produces two lists: a list of predicted texts, and a list of bounding boxes. The last step takes these lists and the type of cards, from the first step, to analyze and results in a list of texts with their field. More detail description of these steps will be presented in the following subsections.

A. Preprocessing: Segmentation, Normalization, and Identification

Owing to the unconstrained nature of captured images, three preprocessing steps were applied to make them available for the next steps, including segmentation, normalization, identification. These tasks allowed us to separate the cards from background images, vertically align them, and identify their type.

Thanks to its efficiency in image segmentation, we trained a U-Net model to segment Vietnamese ID cards. The network has the same architecture as the work of Ronneberge *et al.* [30]. But, instead of using 512 x 512 input images, we down-scaled to 256 x 256 pixels. The output was a 128 x 128 image that is used then as a mask to segment the card.

The model allows us to determine a binary mask of cards. Thus, we combined two basic image-processing techniques to align and crop cards: Contour Detection, and Hough Transformation. The first algorithm was applied to the binary image to detect the boundaries of cards. Then, we transformed these lines to Hough coordinate to find two interacted parallel lines that bound the card. It allows us to determine four corner coordinates of the card. From these corners, we applied a perspective transformation to align and crop the card to 600x400 pixel images.

Lastly, we identified the type of cropped cards by fine-tuning the VGG16 network trained on ImageNet [31]. This network consisted of sixteen layers: thirteen convolutional and three fully connected layers. Each layer contained convolutional layers, max-pooling layers, and fully connected layers. We fine-tuned the model with our dataset to classify eight classes: the front, the back, the reversed front, and back of the 9-digit, 12-digit cards. Therefore, the feature extractor of VGG16 was kept as the original network. To adapt to our dataset, we updated the classifier section with a new fully-connected layer that adjusts to 8 classes only.

B. Text Detection and Recognition

Vietnamese is a Latin-based language that has several additional accents and diacritical marks [32]. The language has more than 250 characters. Among twenty-nine alphabetic scripts, the language consists of twenty-two Latin letters ('f', 'j', 'w', and 'z' letters are eliminated). The remaining are created by combining these letters with diacritics located just at the top or bottom of letters, with or without a small gap between them.

Therefore, instead of training a new model which requires many manual labeled datasets, we adapted models trained on English datasets to detect text. Thanks to its performance in dealing with the low-quality dataset, we applied the CRAFT text detector to localize the text in cropped cards. The model supports *effectively detect text area by exploring each character and affinity between characters* [23].

CRAFT has three detection levels: (i) individual character; (ii) individual word; and (iii) connected words or sentences. The processing time of the first level is long, while the third level is unstable. Thus, we applied only the second level to detect individual words on the cards.

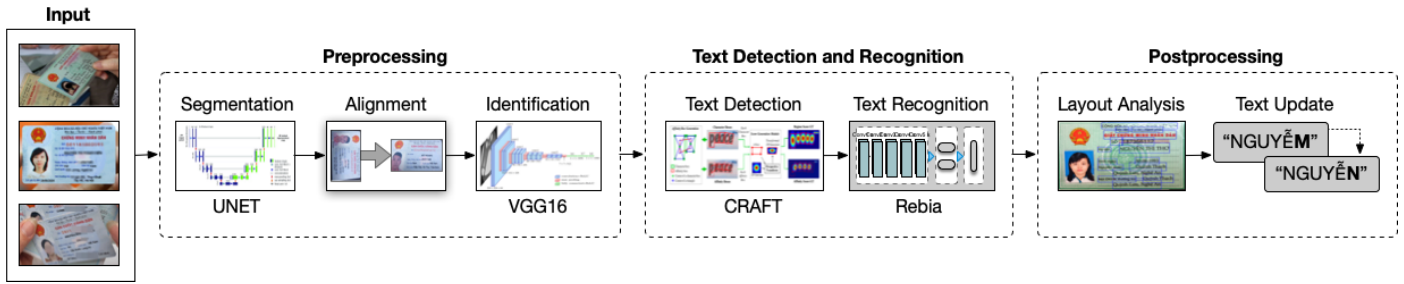


Fig. 3. Information Retrieval from Vietnamese ID Card Images.

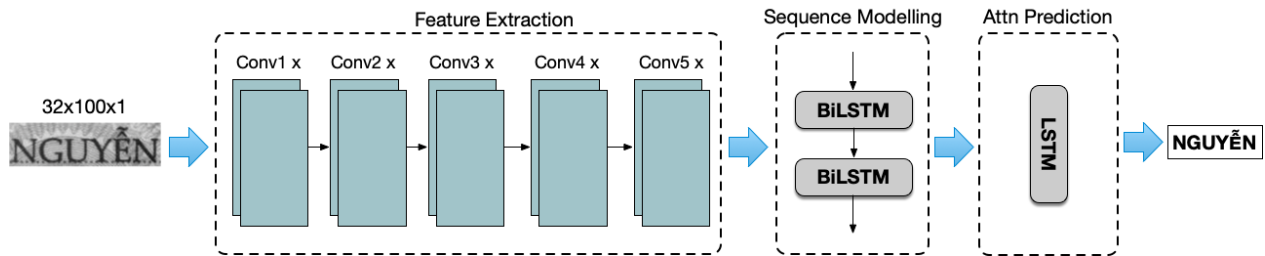


Fig. 4. Rebia Neural Network for Text Recognition.

The model allows detecting only the alphabet word without the tone marks, such as the grave accent, hook above, tilde, acute accent, and dot below. Therefore, we adapted the detector to cover the tone marks by enlarging bounding boxes of detected areas.

The input of this step is 600x400 pixel images that were segmented and aligned previously. The output is a list of bounding boxes that contains cropped words.

For text recognition, we propose a deep neural network, namely Rebia, to recognize the optical words on Vietnamese ID cards. Unlike most existing methods in the field, we didn't apply the rectification step before extracting the feature. Since these texts have a similar orientation and shape, rectification, which is used to normalize different types of texts (i.e., curved and tilted texts), is not necessary. The proposed network contained three blocks, as shown in Fig. 4 and detailed in Table I. First, the feature map that focuses on the word level was extracted by ResNet neural network. The network contained five layers. We converted all text images to gray-scale of size 100 x 32 pixels, to normalize the input data.

Next, we reshaped the extracted features to a sequence feature used for prediction. Thanks to its capability of capturing contextual information within a sequence [33], we used two Bidirectional Long Short-Term Memory (BiLSTM) at this step. The two networks have the same hidden unit that is 256.

Lastly, an attention-based decoder was employed to predict the sequence feature. It contained an LSTM layer with 256 hidden units.

We applied the ReLu activation for three blocks. After each convolution, a batch normalization was used to standardize its outputs. The objective function was the negative log-likelihood of the probability of label sequence.

C. Post-processing: Layout Analysis and Text Update

After recognizing, we categorized the text to the corresponding fields, such as the name, ID, address, and date of birth. Due to the lack of a training dataset, we combined natural language processing, regular expression techniques, and dedicated layout analysis algorithms to determine field types.

The front of a Vietnamese ID card is typically organized from left to right, top to bottom, and line by line, while the back is more complicated. But for the back, we are interested only in the issued date and place, which has the same structure. Therefore, we first sorted bounding boxes of detected words from left to right and line by line.

Next, we evaluated and updated the recognized text by the Levenshtein distance with the help of several domain-specific dictionaries. We combined these texts with results from the above step to identify different fields. Furthermore, for fixed-format fields, such as the date, number, and ID, we also applied the regular expression and algorithms, as follows:

- For the ID number: By experiment, we found that one of the most common issues for this field was the overlap of the caption and content (ID number). It made the recognized ID numbers have several additional characters at the beginning. Therefore, for a text line that was determined as the ID number, we took only a fixed number of digits, starting from the end of the text (9 for the old card, 12 for the new card).
- For the date of birth, expired, and issued date: Each card type has its format to represent the date, so we applied a rule-based mechanism and the regular expression to check the text.

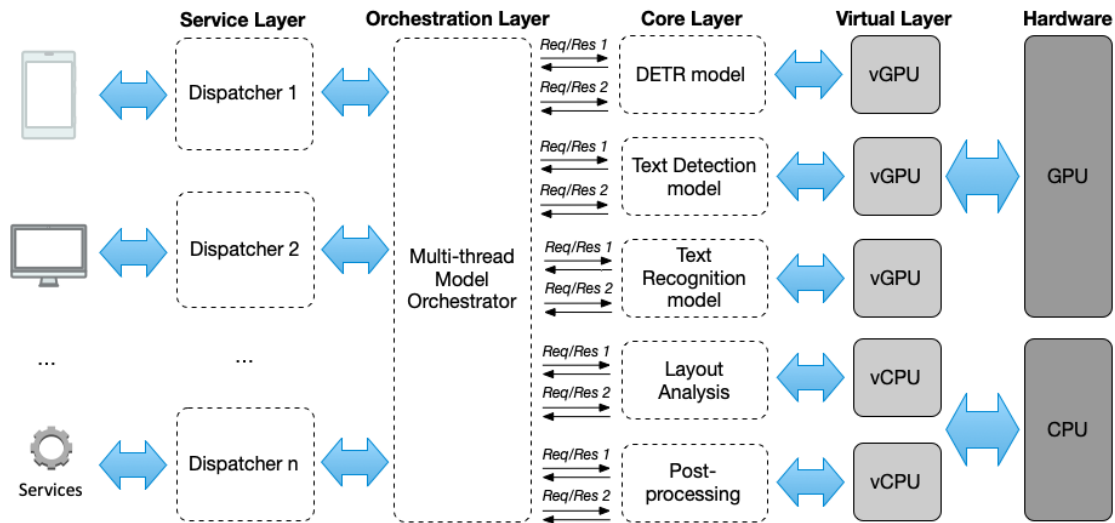


Fig. 5. Multi-layer Architecture for Load Balancing of Model Execution.

TABLE I. DETAILED ARCHITECTURE OF REBIA FOR TEXT RECOGNITION

Feature Extraction - Resnet		
Layer	Configuration (kernel, stride, padding, channel)	Output
conv1 x	Conv1: 3x3, 1x1, 1x1, 32 Conv2: 3x3, 1x1, 1x1, 64 MaxPool: 2x2, 2x2, 0x0	100x32
conv2 x	01 BasicBlock: 3x3,128 3x3,128 Conv3: 3x3,1x1,1x1,128 MaxPool: 2x2, 2x2, 0x0	50x16
conv3 x	02 BasicBlock: 3x3, 256 3x3, 256 Conv4:3x3, 1x1,1x1,256 MaxPool:2x2, 2x2, 0x0	25x18
conv4 x	05 BasicBlock: 3x3, 512 3x3, 512 Conv5:3x3, 1x1,1x1,512	26x4
conv5 x	03 BasicBlock: 3x3,512 3x3,512 Conv6:2x2,1x2,1x0,512 Conv7:2x2,1x1,0x0, 512	26x1
Sequence Modelling - BiLSTM		
BiLSTM	Hidden units:256	256
BiLSTM	Hidden units:256	256
Prediction - Attn decoded		
LSTM	Hidden units:256	256

- For the name and address: First, we built three dictionaries containing common Vietnamese family names, middle names, and addresses. Then we applied the Levenshtein algorithm and regular expression to correct the text, if necessary.

D. Multi-layer Architecture for Load Balance of Model Execution

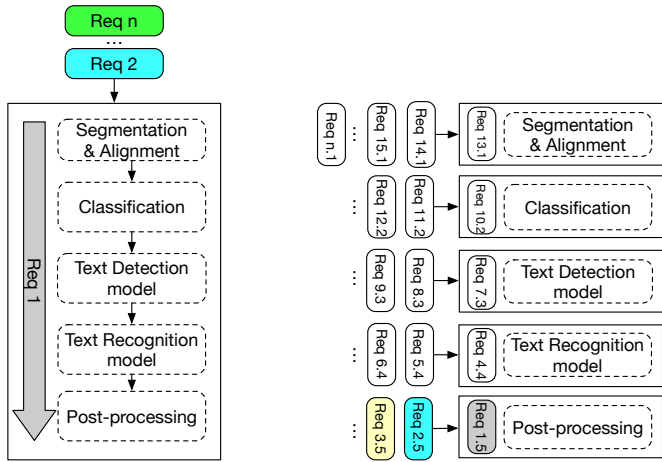
In this study, we propose a multi-layer system architecture to deploy the end-to-end method, which supports load balancing of model execution. We considered each model as an independent and parallel process, which can serve different ID cards at the same time, as shown in Fig. 6. It eliminated the bottleneck at some models due to high memory consumption, especially text detection and recognition.

Therefore, we deployed the proposed end-to-end method into five sub-tasks and processed them separately. Each one consists of a model/orchestrator with different input and output. Owing to model orchestrators and API gateways, the proposed architecture can coordinate the input and output of these sub-tasks, as presented in 5.

Thus, each information extraction request was split into five sub-requests, as shown in Fig. 6. On the left figure (single request invocation), all models are blocked until the last sub-task (post-processing) finishes, while on the right (multi-request supports), models are free if they finish their jobs. (A request n was split into five sub-requests ($Req\ n.x$); x denotes the sub-task that corresponds to different steps of the proposed method.)

We applied the FIFO (First In, First Out) technique to handle multi-sub-requests. The complete architecture of our system is presented in Fig. 5, which contains three layers and is based on the virtual technique to maximize infrastructure using, as follows:

- The orchestration layer contains the model orchestrators that are responsible to coordinate different steps.
- The gateway layer includes different API gateways that interact with the corresponding micro-services at each step.
- The micro-services layer is composed of different micro-services that support API to interact with models.



(a) Single request end-to-end invocation (b) Multi-requests end-to-end invocation

Fig. 6. Single (a) and Multi Request (b) End-to-end Services.

Check/Order	File Name	Image	Predict	Correct	
<input type="checkbox"/> 1	1/orginin_img/front_001925.jpg		Nguyễn	Nguyễn	Update
<input type="checkbox"/> 2	1/orginin_img/front_001926.jpg		dat	dat	Update
<input type="checkbox"/> 3	1/orginin_img/front_001927.jpg		Hoa	Hoa	Update
<input type="checkbox"/> 4	1/orginin_img/front_001928.jpg		Long	Long	Update
<input type="checkbox"/> 5	1/orginin_img/front_001929.jpg		Nguyễn	Nguyễn	Update
<input type="checkbox"/> 6	1/orginin_img/front_001930.jpg		Ninh	Ninh	Update
<input type="checkbox"/> 7	1/orginin_img/front_001931.jpg		Nam	Nam	Update
<input type="checkbox"/> 8	1/orginin_img/front_001932.jpg		Kiên	Kiên	Update
<input type="checkbox"/> 9	1/orginin_img/front_001933.jpg		quán	quán	Update
<input type="checkbox"/> 10	1/orginin_img/front_001934.jpg		Nam	Nam	Update
<input type="checkbox"/> 11	1/orginin_img/front_001935.jpg		quán	quán	Update
<input type="checkbox"/> 12	1/orginin_img/front_001936.jpg		Chợ	Chợ	Update

Fig. 7. Dedicated Annotation Tool.

- The infrastructure layer applied virtual techniques to share physical hardware (GPU, CPU, and different virtual GPU and CPU) among micro-services.

IV. EXPERIMENTS

A. Dataset

We used four datasets in this study, including two manual (ID Cards and manually annotated text) and two synthetic (synthetic image and text) datasets for training U-Net, VGG16, and Rebia. The following steps were performed to prepare our datasets:

- **ID cards:** we collected 3.256 Vietnamese ID cards from volunteers and public images on the internet. It contains 1.530 samples for the 9-digit card, 935 for the 12-digit card, and 783 for the new 12-digit (since the chip-based ID card has just been released in 2021, in this study we focused only on the three other cards). We then used the labelImg¹ tool to annotate this dataset.
- **Synthetic images:** we extracted ID cards from the above dataset and randomly put them on background images containing different objects (i.e., papers, business cards, license cards, and so on). We thus generated a total of 60k synthetic images.
- **Manually annotated text:** We first applied the CRAFT model on extracted ID cards to detect individual words. Next, Tesseract OCR was applied to predict the text. Then, we developed a dedicated tool to correct the texts manually, as shown in Fig. 7. This process is illustrated as in Fig. 8, phase 3. Lastly, we obtained a total of 400k manually annotated texts.
- **Synthetic text:** This dataset consists of more than 500k synthetic texts generated from popular Vietnamese names, addresses, numbers, etc. We used a

tool, namely Synthetic Data Generator² to generate this dataset.

For the manually annotated and synthetic text, we also applied data augmentation methods to balance and increase samples, including rotation, blur, noise, and so on. Finally, we obtained a total of 8M samples. The first two datasets were used to train U-Net and VGG16, while the last two datasets were applied to train Rebia.

B. Model Training Setup

The proposed method is a continuous process, in which the output of the previous step is the input of the subsequent step. The used models should correlate with each other. Therefore, we based on the previous model to train the next model.

As detailed in Fig. 8, the model training contains three phases:

- 1) *Phase 1 - Segmentation model training:* we trained and validated the U-Net model on ID cards and synthetic image datasets.
- 2) *Phase 2 - Classification model training:* we used the trained U-NET model to extract ID cards from the first dataset and vertically align them. To preserve consistency between the segmentation and identification step, we combined these cards with those manually extracted from the same dataset to train the VGG16 model.
- 3) *Phase 3 - Recognition model training:* similarly, we used the trained VGG16 and CRAFT model to detect and crop text areas. Based on these areas, we created the manually annotated text (as presented in the previous subsection). This dataset was then combined with the systemic text to train the Rebia model.

All models were implemented using the TensorFlow Framework 2.3.0 and Python 3.6.9, on an NVIDIA Tesla K80 GPU with a 12 GB memory and an Intel(R) 2.3Ghz

¹<https://github.com/tzutalin/labelImg>

²<https://github.com/Belval/TextRecognitionDataGenerator>

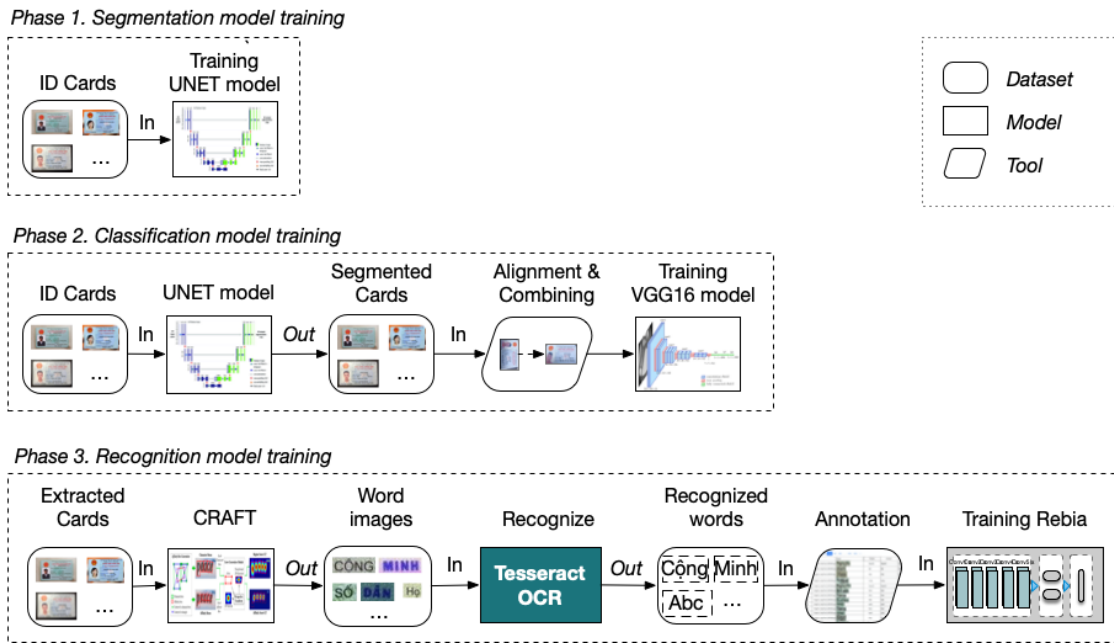


Fig. 8. Model Training Setup.

Xeon(R) micro-processor. We used the following parameters and techniques to train the models:

- To prevent bias, we divided all datasets into two subsets for training (80% randomly sample) and testing (20% randomly sample).
- For the loss function, we used a binary cross-entropy, categorical cross-entropy, and attention loss function to train the U-NET, VGG16, and Rebia models, respectively.
- For the optimization, we applied an Adam optimizer with $\beta_1 = 0.9$, $\beta_2 = 0.999$, and $e = 10^{-7}$. The initiated learning rate was 10^{-4} , and a self-adjusting learning rate technique (lr) to train U-NET and VGG16; while, Rebia was used an Adadelta optimizer with $\beta_1 = 0.9$, $\rho = 0.95$, $\epsilon = 10^{-8}$, and $lr = 1$.
- To minimize the cost function, we applied a mini-batch with a size of 192 for Rebia, 128 for U-NET and VGG16.
- The early stop technique was employed to increase the training speed and reduce over-fittings. It makes the three models stop learning if they have reached their maximum accuracy.
- The shuffle data were used, such that the models could learn randomly and provide more objective results. Before selecting the batches, we conducted a shuffling process to balance the dataset, in which fifty percent of samples were randomly chosen from each one.

After successfully training and validating the models, we deployed the end-to-end method on the same hardware configuration. To support the proposed multi-layer architecture, we implemented four Docker containers. Instance segmentation,

text detection, and text recognition were hosted by three separated dockers, while both layout analysis and post-processing were hosted by only one docker.

V. RESULTS AND DISCUSSION

Owing to the early stop technique, the U-NET and VGG16 training were stopped after 48 and 15 epochs, as shown in Fig. 9a and 9b. The two figures also show that the gap between training loss and test loss is tiny, which means that the model operated accurately, without any overfitting. The accuracy of U-NET and VGG16 is 94% and 99.5% on the test set, respectively, as shown in Table II. For the Rebia model, the training was converged at 60 epochs. The model achieves a high accuracy of 98.3% on the validation test, as shown in Fig. 11.

TABLE II. ACCURACY OF THE PROPOSED MODELS ON THE TESTING SET

Model	Accuracy
U-NET (Segmentation model)	94.0%
VGG16 (Classification model)	99.5%
Rebia (Recognition model)	98.3%

Thanks to transfer learning, U-Net, and VGG16 models quickly reached a high accuracy after several initial steps/iterations. They improved only 2 – 5% of accuracy during the remaining time. It can be explained by the fact that the pre-trained models were trained on a large dataset (the ISBI dataset for U-NET, ImageNet for VGG16).

We used U-Net to segment the cards, as shown in Fig. 10. The figure presents an example of using the U-Net model to detect the binary mask of a 12-digit card. We then cropped the card from background images and vertically aligned it, as presented in Fig. 12.

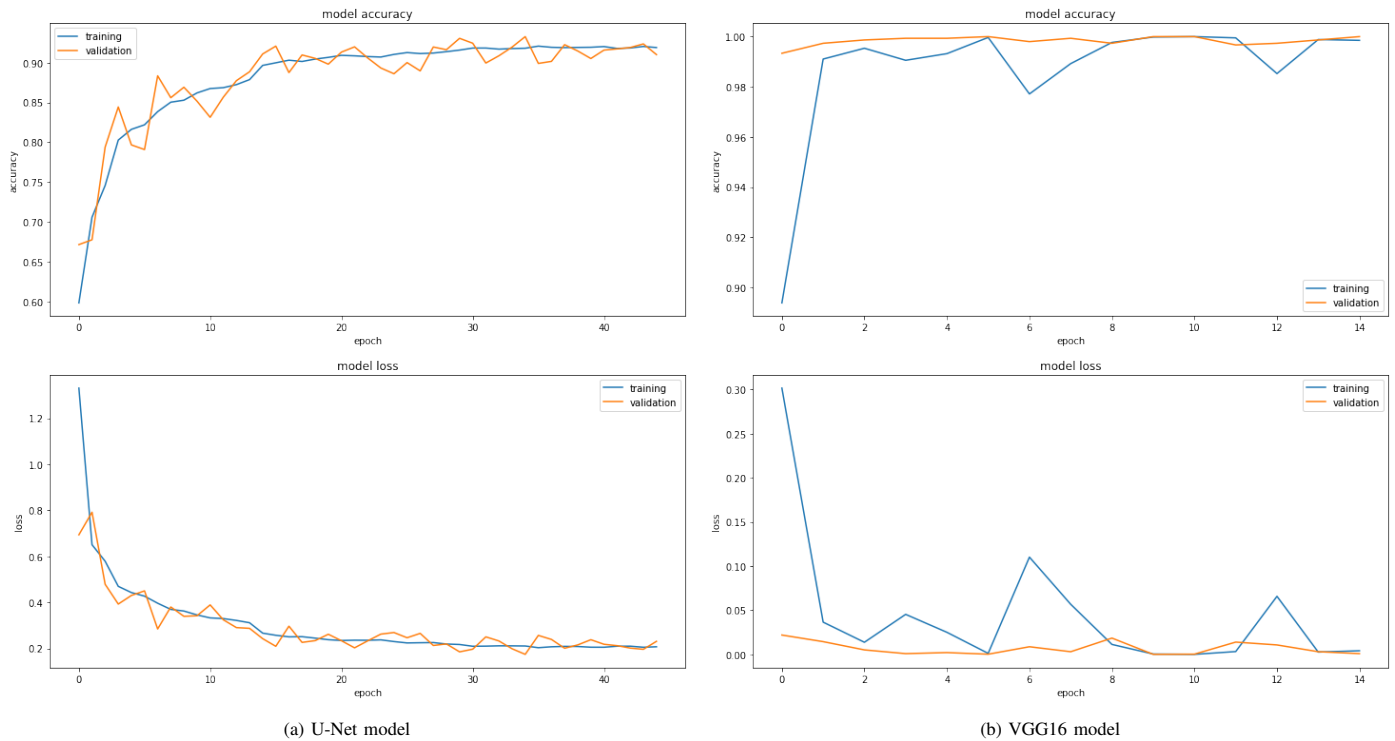


Fig. 9. Progress of Loss and Accuracy for Training and Testing U-Net and VGG16.

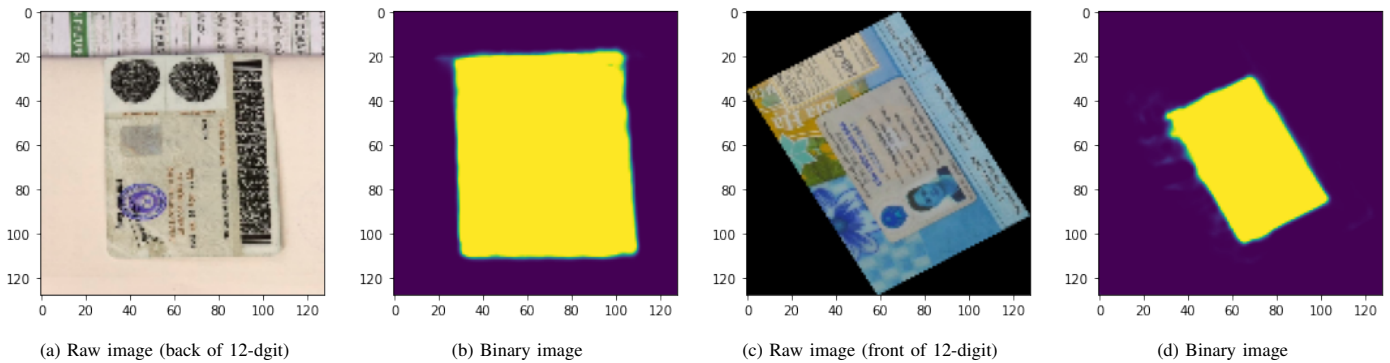


Fig. 10. Segmentation Step (a, b: the Back of a 12-Digit Card and Its Binary Image; c and the Front of a 12-Digit Card and Its Binary Image.)

Experimental results have shown that the proposed methods outperformed similar works in extracting information from the Vietnamese ID card. At the pre-processing step, our method (combination of U-Net, and traditional machine learning) provides more stable results than the work presented in [5], [34]. These methods usually work well in controlled environments, e.g., enough light, clear cards [5], or existence of four corners of cards [34]. For unstable environments, which are very common in many practice applications, they failed in pre-processing the input images, e.g., ID card detection and classification. For this task, thanks to the U-Net model and a rich dataset, our method can respond to unstable situations with high accuracy of 94.0%.

The type of card is important information, but to our

knowledge, no existing works presented the way to identify this information. Based on the VGG16 network, we can classify different types of ID cards with high accuracy of 99.5%. Therefore, our method is capable to deal with input images that have many ID cards. Furthermore, this information was very useful at the post-processing step. Regarding text recognition, we obtained a higher accuracy than recent works, such as Hoai *et al.* [6] (98.3% compared with 89.7%) and Viet *et al.* [35] (98.3% compared with 91%).

Besides, owing to the proposed multi-layer architecture, the end-to-end method took an average of 2.5 seconds to extract information from a raw image, as illustrated in Fig. 13. The figure also shows a typical example of the input image that contained similar cards, such as student, business, or license

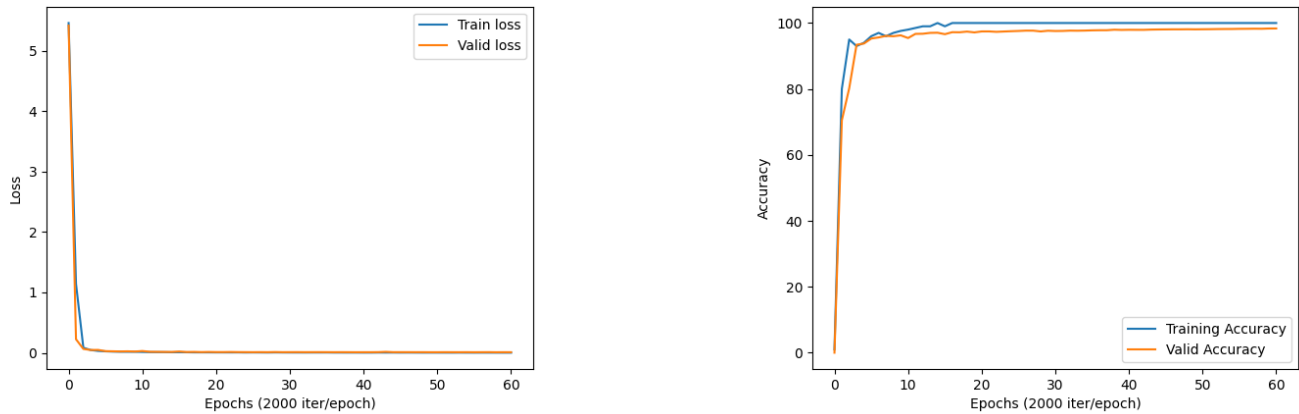
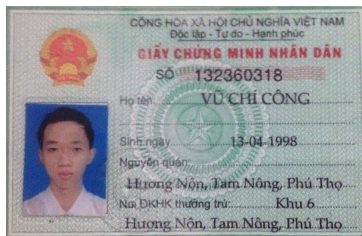


Fig. 11. Progress of Loss and Accuracy for Training and Testing Rebia Network.



(a)



(b)

Fig. 12. An Old ID Card before (a) and after (b) the Pre-processing Step.

cards. With the help of the trained models and algorithms, our method can extract important information accurately.

VI. CONCLUSION

In this paper, we have presented an end-to-end method to extract information from the Vietnamese ID card. The proposed method contains three consecutive steps: Pre-processing, text detection and recognition, and post-processing. Four neural networks were proposed and trained, which allows us to extract information efficiently, including U-NET for segmentation, VGG16 for classification, CRAFT for text detection, and Rebia for text recognition. We also applied a natural language processing technique (the edit distance) and two image process algorithms (Contour detection and Hough transformation) for layout analysis, text correction, and card alignment.

In addition, a dataset including 3.256 Vietnamese ID cards, 400k manually annotated texts, and more than 500k synthetic

texts, was built to validate the proposed methods. We conducted an empirical experiment on our self-collected dataset to demonstrate the effectiveness of the proposed method, which achieved a high accuracy of 94%, 99.5%, and 98.3% for segmentation, classification, and text recognition. These results indicate the promise of the proposed method in the information extraction of similar semi-structured documents. In the future, we will focus on the chip-based ID card and improve the performance of our model, especially the text detector.

REFERENCES

- [1] Y. Zhu, C. Yao, and X. Bai, "Scene text detection and recognition: Recent advances and future trends," *Front. Comput. Sci.*, vol. 10, p. 19–36, Feb. 2016.
- [2] N. Nguyen, T. Nguyen, V. Tran, T. Tran, T. Ngo, T. Nguyen, and M. Hoai, "Dictionary-guided scene text recognition," in *Proceedings of the IEEE Conference on Computer Vision and Pattern Recognition (CVPR)*, 2021.
- [3] A. Nousseir and O. Adel, "Automatic extraction of arabic number from egyptian id cards," in *Proceedings of the 7th International Conference on Software and Information Engineering, ICSIE '18*, (New York, NY, USA), p. 56–61, Association for Computing Machinery, 2018.
- [4] F. M. Rusli, K. A. Adhiguna, and H. Irawan, "Indonesian ID card extractor using optical character recognition and natural language post-processing," *CoRR*, vol. abs/2101.05214, 2021.
- [5] T. N. T. Thanh and K. N. Trong, "A method for segmentation of vietnamese identification card text fields," *International Journal of Advanced Computer Science and Applications*, vol. 10, no. 10, 2019.
- [6] D. Hoai, H.-T. Duong, and V. Truong Hoang, "Text recognition for vietnamese identity card based on deep features network," *International Journal on Document Analysis and Recognition (IJDAR)*, vol. 24, 06 2021.
- [7] R. Soni, B. Kumar, and S. Chand, "Text detection and localization in natural scene images based on text awareness score," *Applied Intelligence*, vol. 49, pp. 1376–1405, 2018.
- [8] A. Hazra, P. Choudhary, S. Inunganbi, and M. Adhikari, "Bangla-meitei mayek scripts handwritten character recognition using convolutional neural network," *Applied Intelligence*, vol. 51, pp. 2291–2311, 2021.
- [9] X. Ma, K. He, D. Zhang, and D. Li, "Pieed: Position information enhanced encoder-decoder framework for scene text recognition," *Applied Intelligence*, vol. 51, pp. 6698–6707, 2021.
- [10] X. Wang, X. Zhang, S. Lei, and H. Deng, "A method of text detection and recognition from receipt images based on CRAFT and CRNN," *Journal of Physics: Conference Series*, vol. 1518, p. 012053, apr 2020.

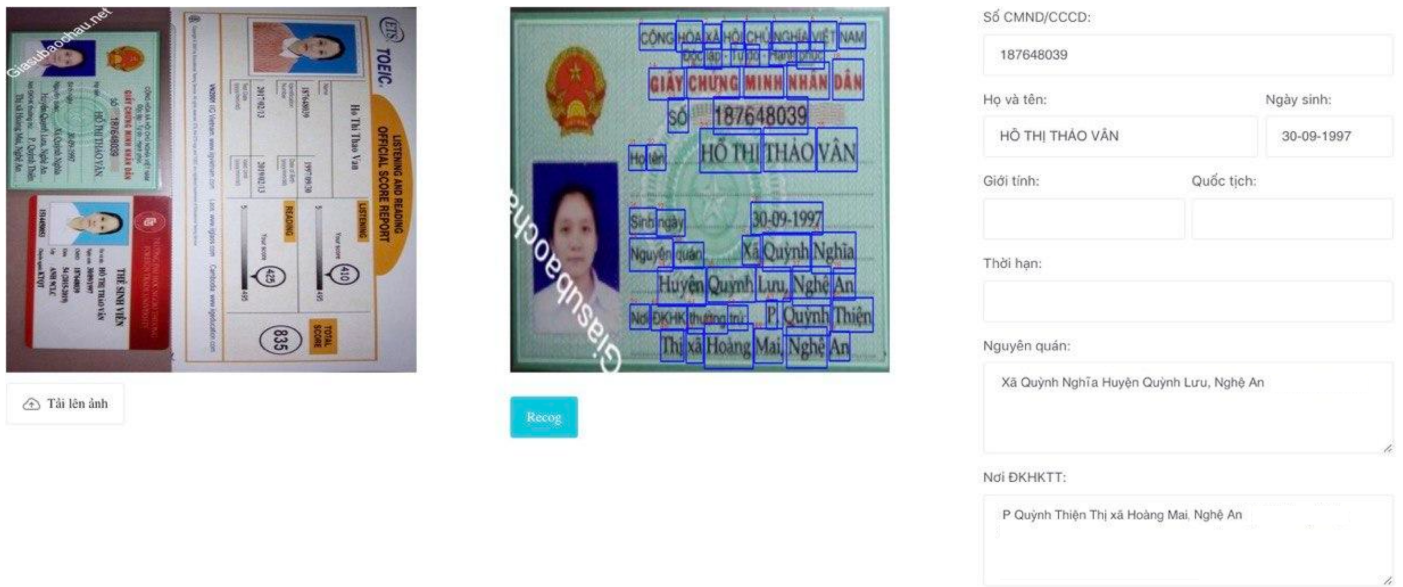


Fig. 13. Extracted Information (the Left Image) from a Raw Image Captured with Several Similar Cards (the Right Image). The Card and Texts were Successfully Segmented, Cropped, Aligned and Detected, as in the Middle Image.

- [11] Y. Gao, C. Xu, Z. Shi, and H. Zhang, "Bank card number recognition system based on deep learning," (New York, NY, USA), Association for Computing Machinery, 2019.
- [12] M.-C. Ko and Z.-H. Lin, "Cardbot: A chatbot for business card management," in *Proceedings of the 23rd International Conference on Intelligent User Interfaces Companion, IUI '18 Companion*, (New York, NY, USA), Association for Computing Machinery, 2018.
- [13] S. Srivastava, S. Sahay, D. Mehrotra, and V. Deep, "Automation of business cards," in *Advances in Interdisciplinary Engineering* (M. Kumar, R. K. Pandey, and V. Kumar, eds.), (Singapore), pp. 371–380, Springer Singapore, 2019.
- [14] H. T. Ha, M. Medved, Z. Neverilová, and A. Horak, "Recognition of ocr invoice metadata block types," in *TSD*, 2018.
- [15] P. Kumar and S. Revathy, "An automated invoice handling method using ocr," in *Data Intelligence and Cognitive Informatics* (I. Jeena Jacob, S. Kolandapalayam Shanmugam, S. Piramuthu, and P. Falkowski-Gilski, eds.), (Singapore), pp. 243–254, Springer Singapore, 2021.
- [16] M. Ryan and N. Hanafiah, "An Examination of Character Recognition on ID card using Template Matching Approach," *Procedia Computer Science*, vol. 59, no. Iccsci, pp. 520–529, 2015.
- [17] R. Valiente, M. T. Sadaiké, J. C. Gutiérrez, D. F. Soriano, and G. Bressan, "A process for text recognition of generic identification documents over cloud computing," *IPCV'17 International Conference on Image Processing, Computer Vision, and Pattern Recognition*, no. April 2017, p. 4, 2016.
- [18] A. Alnefaie, D. Gupta, M. H. Bhuyan, I. Razzak, P. Gupta, and M. Prasad, "End-to-end analysis for text detection and recognition in natural scene images," in *2020 International Joint Conference on Neural Networks (IJCNN)*, pp. 1–8, 2020.
- [19] Q. Ye and D. Doermann, "Text detection and recognition in imagery: A survey," *IEEE Transactions on Pattern Analysis and Machine Intelligence*, vol. 37, no. 7, pp. 1480–1500, 2015.
- [20] K. Karthick, K. B. Ravindrakumar, R. Manikandan, and R. Cristin, "Consumer service number recognition using template matching algorithm for improvements in OCR based energy consumption billing," *ICIC Express Letters, Part B: Applications*, vol. 10, no. 10, pp. 895–901, 2019.
- [21] Z. Zeng, W. Xie, Y. Zhang, and Y. Lu, "Ric-unet: An improved neural network based on unet for nuclei segmentation in histology images," *IEEE Access*, vol. 7, pp. 21420–21428, 2019.
- [22] K. Simonyan and A. Zisserman, "Very deep convolutional networks for large-scale image recognition," 2015.
- [23] Y. Baek, B. Lee, D. Han, S. Yun, and H. Lee, "Character region awareness for text detection," *CoRR*, vol. abs/1904.01941, 2019.
- [24] M. Liao, Z. Wan, C. Yao, K. Chen, and X. Bai, "Real-time scene text detection with differentiable binarization," *CoRR*, vol. abs/1911.08947, 2019.
- [25] M. Jaderberg, K. Simonyan, A. Vedaldi, and A. Zisserman, "Synthetic data and artificial neural networks for natural scene text recognition," 2014.
- [26] Z. Tian, W. Huang, T. He, P. He, and Y. Qiao, "Detecting text in natural image with connectionist text proposal network," 2016.
- [27] J. Baek, G. Kim, J. Lee, S. Park, D. Han, S. Yun, S. J. Oh, and H. Lee, "What is wrong with scene text recognition model comparisons? dataset and model analysis," *CoRR*, vol. abs/1904.01906, 2019.
- [28] B. Shi, M. Yang, X. Wang, P. Lyu, C. Yao, and X. Bai, "Aster: An attentional scene text recognizer with flexible rectification," *IEEE Transactions on Pattern Analysis and Machine Intelligence*, vol. 41, no. 9, pp. 2035–2048, 2019.
- [29] X. Chen, L. Jin, Y. Zhu, C. Luo, and T. Wang, "Text recognition in the wild: A survey," 2020.
- [30] O. Ronneberger, P. Fischer, and T. Brox, "U-net: Convolutional networks for biomedical image segmentation," in *Medical Image Computing and Computer-Assisted Intervention – MICCAI 2015* (N. Navab, J. Hornegger, W. M. Wells, and A. F. Frangi, eds.), (Cham), pp. 234–241, Springer International Publishing, 2015.
- [31] J. Deng, W. Dong, R. Socher, L.-J. Li, K. Li, and L. Fei-Fei, "Imagenet: A large-scale hierarchical image database," in *2009 IEEE Conference on Computer Vision and Pattern Recognition*, pp. 248–255, 2009.
- [32] T.-H. Pham, X.-K. Pham, and P. Le-Hong, "On the use of machine translation-based approaches for vietnamese diacritic restoration," in *2017 International Conference on Asian Language Processing (IALP)*, pp. 272–275, 2017.
- [33] B. Shi, X. Bai, and C. Yao, "An end-to-end trainable neural network for image-based sequence recognition and its application to scene text recognition," 2015.
- [34] H. D. Liem, N. Minh, N. B. Trung, H. T. Duc, P. H. Hiep, D. V. Dung, and D. H. Vu, "Fvi: An end-to-end vietnamese identification card detection and recognition in images," *2018 5th NAFOSTED Conference on Information and Computer Science (NICS)*, pp. 338–340, 2018.
- [35] H. T. Viet, Q. Hieu Dang, and T. A. Vu, "A robust end-to-end information extraction system for vietnamese identity cards," in *2019 6th NAFOSTED Conference on Information and Computer Science (NICS)*, pp. 483–488, 2019.

A New Text Summarization Approach based on Relative Entropy and Document Decomposition

Nawaf Alharbe¹, Mohamed Ali Rakrouki², Abeer Aljohani³
Applied College
Taibah University
Saudi Arabia

Mashaal Khayyat⁴
College of Computer Science and Engineering
University of Jeddah
Saudi Arabia

Abstract—In the era of the fourth industrial revolution, the rapid relay on using the Internet made online resources explosively grow. This revolution emphasized the demand for new approaches to utilize the use of online resources such as texts. Thus, the difficulty to compare unstructured resources (text) is urging the demand of proposing a new approach, which is the core of this paper. In fact, text summarization technology is a vital part of text processing, therefore, the focus is on the semantic information not just on the basic information. It requires mining topic features in order to obtain topic-words and topic-sentences relationships. This automatic text summarization is document decomposition according to relative entropy analysis; which means measuring the difference of the probability distribution to measure the correlation between sentences. This paper introduced a new method for document decomposition, which categorizes the sentences into three types of content. The performance demonstrated the efficiency of using the relative entropy of the topic probability distribution over sentences, which enriched the horizon of text processing and summarization research field.

Keywords—Natural language processing; text summarization; extractive methods; relative entropy

I. INTRODUCTION

At present, the rapid popularization of the Internet makes resources explosively growth. On the one hand, rich information resources bring great convenience. On the other hand, it also makes people difficult to select suitable resources. From the view of network information resources, the proportion of unstructured resources has been growing rapidly, and the processing of this type of data is more difficult compared to structured data. A text is a typical unstructured data, its effective analysis and processing has practical significance for Internet users.

Text summarization technology is a very important part of text processing. From a technical point of view, the techniques based on slight semantic features are different from those based on word features. The focus of this paper is not the basic information that can be observed in the composition of a document, such as words or sentences, but the deeper semantic information behind. By mining topic features, we can get topic-word features and topic-sentence features. Based on the relationship between sentences, it is possible to measure the ability to express the topic of a document, and then choose a sentence as a text summarization.

In this context, this paper proposes a new method of automatic text summarization based on relative entropy and document decomposition. The relative entropy is used to

measure the difference of the probability distribution in order to measure the correlation between sentences. Also, a new document decomposition method is introduced for categorizing sentences as three types of content.

The remainder of this paper is organized as follows. In Section II, some important related works to text summarization are presented. A brief review of the LDA model is presented in Section III. Section IV is devoted to the presentation of probability distribution of topics over sentences. An improved sentence similarity calculation method is proposed in Section V. In Section VI, a candidate abstract sentence selection method based a greedy algorithm is proposed. The experimental results are presented in Section VII. Finally, Section VIII summarizes this research work.

II. LITERATURE REVIEW

In the 1950s, the rise of statistics prompted the germination of text summarization techniques, and statistical methods were limited to the surface features of documents. For example, according to the position of the sentence in the paragraph, the position of the paragraph in the article, the word frequency and the inverse text word frequency, the similarity between the sentence and the title and other characteristics to evaluate the importance of the sentence. Lunh [1] believed that words with a large number of occurrences are relatively closely related to the topic of the document, so the weight of words can be calculated according to the number of times they appear in the document, and sentence weights can be obtained based on the weight of words. Select sentences with higher weights as the abstract of the document. This idea has also become a cornerstone of the subsequent development of text summarization technology. Although the principle seems simple, the implementation results have a high accuracy rate, even surpassing many later more complex algorithms. Later, Baxendale [2] proposed that some summary words in the document also represent the topic of the document and should be given a higher weight. Edmundson [3] measures the importance of sentences according to three factors: clue words, keywords, and location, and selects sentences with greater weight as abstracts. In statistics, text is a linear sequence of sentences, and a sentence is a linear sequence of words. When analyzing text, it can finally be attributed to the analysis of words, and the weight of sentences can be obtained by analyzing the characteristics of words. In recent years, the academic community has further proposed methods based on integer linear programming [4]–[6] and methods of maximizing sub-

modular functions, which can consider sentence redundancy in the process of sentence selection [7], [8].

In the 1990s, with the rise of the Internet, the number of documents increased exponentially. At the same time, the rise of machine learning has made great progress in natural language processing, which has given new inspiration to text summarization technology. On the basis of statistics, Kupiec et al. [9] proposed a Naive Bayes classification model to select document summary sentences. With the development of machine learning, more advanced algorithms have been applied to text summarization techniques, such as decision tree model, hidden Markov model, conditional random field model, neural network, etc. Conroy and O'leary [10] calculated the correlation between words based on the hidden Markov model and on mutual dependencies, Goularte et al. [11] used linear regression model modeling, Svore et al. [12] proposed a neural network-based abstract method. Machine learning methods mainly focus on how to convert text summarization problems into machine learning problems. Although the text summarization obtained by the machine learning method has achieved good results, the lack of corpus in this aspect greatly restricts the training effect. In some recent work, the summarization is represented as a word or sentence level classification problem based on neural network architectures, and it is addressed by computing sentence representations [13]–[17]. Zhong et al. [18] reranked extractive summaries using document-level features.

A recent comprehensive and consistent review of text summarization for papers published between 2008 and 2019 can be found in Widyassari et al. [19]. Some in-depth investigation and analysis of automatic text summarization techniques have been provided by [20]–[22].

III. TEXT SUMMARIZATION BASED ON LDA MODEL

Since the LDA (Latent Dirichlet Analysis) [23] model was proposed, it has been widely used in the literature. It can be seen that the effect of the LDA model in the field of text topic extraction has been extremely recognized, and it has become a popular technology in the direction of text mining.

LDA is a hierarchical Bayesian model, in order to represent topics in each document in the form of a probability distribution. It is a "bag of words" model that treats the document as a set of words. There is no order of words, each one in the document is selected according to a certain probability from the thesaurus of the input document topic.

From a topology perspective, the LDA model assumes that the text consists of several randomly selected topics, and each topic is expressed by several randomly selected words in the corresponding thesaurus. This is an assumption that obeys objective reality. Based on this document composition method, the topic can be regarded as the probability distribution on the vocabulary (topic-word), and the document can be regarded as the probability distribution on the topic (doc-topic). This assumption can also be applied to large-scale data processing, that is, mapping documents to the subject space, so as to achieve the effect of dimensionality reduction.

A. Model Solving

The solution for the LDA model is a very complex optimization solution process, and it is very difficult to solve it optimally. For solving this model approximately, heuristic methods are used. There are roughly three types: One is an approach based on expectation advancement, one is based on variational EM solving, and one is based on Gibbs sampling [24]. Generally speaking, Gibbs sampling method is simpler than the other two types and works well. Therefore, for most computing tasks, this method is used to solve the LDA model.

B. Determination of the Number of Topics

A parameter that needs to be specified manually is the number of topics in the training corpus. The determination of the number of topics is a process of selecting models corresponding to different numbers of topics, which is a difficult problem to solve. There are generally two ways to determine the number of topics:

- 1) **Experience setting:** In the process of text mining, the corpus usually used as training needs to be relatively comprehensive, and the corpus can be basically determined in several aspects. For example, it is known in advance that these topics are about: culture, news, sports, politics, entertainment, then the number of topics can be clearly set to 5. However, for most of the training corpus, it is not known in advance which topics it contains, which requires repeated debugging or the use of enumeration methods. Since there is no model that can evaluate the results well, the debugging process needs to observe the correspondence between words and topics in the results to judge in the way of human understanding, and then determine a reasonable number of topics.
- 2) **Perplexity-based determination method:** This metric represents the uncertainty in predicting data. If a topic model obtains a low perplexity degree on the test corpus, then the model is considered to be very expressive, and the number of topics determined by the model is considered reasonable.

The characteristic of the LDA model is that the more accurate the model is, the narrower the scope of use is. Therefore, for different corpora, the size of the number of topics cannot be set completely by experience. Instead, the number of topics is determined by two methods: experience setting and perplexity calculation. The number of topics needs to be continuously set, and the number of topics with the lowest perplexity is taken as the training parameter.

IV. PROBABILITY DISTRIBUTION OF TOPICS OVER SENTENCES

From the analysis in Section III, it can be seen that the LDA model represents the document in the form of a topic by representing the document as a certain probability distribution of the topic. Similarly, the topic is also represented as a certain probability distribution of words, thus forming a hierarchical structure: document-sentence-topic-word. Since we know the probability distribution of topic-words, we can use this hierarchical model to calculate the probability distribution of sentences-topics.

In Arora and Ravindran [25], three methods (generative, semi-derivative, and derivation) are proposed to estimate the probability distribution of sentences given a topic based on a hierarchical Bayesian model, and there is a strong assumption about the calculation: All sentences of a document express a topic, and each word in each sentence corresponds to only one topic. The performance of these methods has been verified, and in this paper, the derivation method with relatively good performance is selected for improvement.

Let assume that S_i ($i \leq \text{length}(D)$) are the sentences in a document D , W_j ($j \leq n$, where n is the number of words) is a word in the document, and T_k ($k \leq K$, where K is the number of all topics) are the topics contained in the document. We calculate the probability $P(T|S)$ of topic T given a sentence S , thereby calculating the probability that the topic T_k belongs to the sentence S_i .

To find the topic probability distribution over a sentence, it can be given by the Bayesian formula:

$$P(T|S) = \frac{P(S|T) \cdot P(T)}{P(S)} \quad (1)$$

From the output of the LDA model, the topic probability $P(T)$ of the document can be obtained, so that:

$$P(T) = \sum_{k=1}^K P(T_k|D) \quad (2)$$

For the probability $P(S)$ of a sentence, it can be calculated according to the words contained in the sentence. Similarly, it can be calculated by the known $P(W_i|S)$ as follows:

$$P(S) = \sum_{j=1}^n P(W_j|S) \quad (3)$$

where n is le length of the sentence S .

In order to calculate $P(S|T)$, we assume that each sentence in the document contains only one topic, and each word expresses only one topic. Then, in the case of known topics, we calculate the probability that the sentence belongs to each topic.

From Arora and Ravindran [25], three methods are pointed out for computing $P(S|T)$ for multiple documents. Since the text summarization of a single document is similar to the text summarization of multiple documents, we propose an explicit improvement using partially generated derivation as follows:

$$P(S_i|T_k) = P(D|T_k) \cdot \sum P(T_k|W_j) \quad (4)$$

where $P(S_i|T_k)$ represents the probability that sentence S_i expresses topic T_k ; $P(D|T_k)$ represents the probability that document D generates topic T_k ; $P(T_k|W_j)$ represents the probability that topic T_k generates word W_j .

From the Bayesian generation formula, the above formula can be rewritten as:

$$\begin{aligned} P(S_i|T_j) &= \frac{P(T_k|D)P(D)}{P(T_k)} \cdot \frac{P(\prod W_j|T_k)}{P(\prod_{W_j \in S_i} W_k)} \\ &= \prod_{W_j \in S_i} P(W_j|T_k) \cdot \frac{P(T_k|D)}{\prod_{W_j \in S_i} W_j} \end{aligned} \quad (5)$$

In order to calculate $P(W_j)$, it can be calculated according to the output data of LDA:

$$P(W_j) = \sum_{k=1}^K P(W_j|T_k) \cdot P(T_k) \quad (6)$$

Combining the above Eq. 1 - 6, we can get the representation of $P(T|S)$ as follows.

$$P(T_k|S_i) = \frac{P(T_k|D)^2 \prod_{W_j \in S_i} P(W_j|T_k)}{\sum_{j=1}^n P(W_j|S_i) \cdot \prod_{W_j \in S_i} \sum_{k=1}^K P(W_j|T_k)P(T_k|D)} \quad (7)$$

V. IMPROVEMENT OF SENTENCE SIMILARITY CALCULATION METHOD

The goal of extraction-based text summarization is to use a good method to calculate the weight of each sentence as a basis for measuring their importance. Among several methods used for automatic text summarization, machine learning methods use sentences and words of documents as learning features. Statistical methods measure sentence weights according to word frequency, position of sentences in paragraphs, and similarity of sentences and topics on words. In graph model, the same words are used as the basis for establishing edges between nodes (sentences). The vector space model uses the words as the vector dimension, and each document forms a matrix to calculate keywords through singular value decomposition. All these methods build models based on the features of sentences or words in sentences.

A big drawback of modeling based on word features is that it cannot solve semantic associations well. Different words may express the same topic. In this case, how to determine the semantic association between words is a key point that needs to be improved. The characteristics of topic model can just make up for the shortcomings of the semantic relationship that cannot be mined in word-based modeling. This paper combines the characteristics of the topic model to calculate the similarity of two sentences in the semantic dimension.

Combined with the computational model presented in Section IV, the probability distribution of topic over sentence is transformed into sentence-to-sentence, sentence-to-document similarity through relative entropy, so the calculation method of sentence weight is obtained.

A. Relative Entropy Definition

Relative Entropy (also known as Kullback–Leibler Divergence, KLD for short) is a measure of the difference between two probability distributions P and Q . It can be expressed

in the form of $D_{KL}(P||Q)$, where Q is the probability distribution of theoretical data, as a measurement standard, and P is the probability distribution of real data, as the object of estimation. $D_{KL}(P||Q)$ represents the loss, or difference, when fitting the probability distribution P of real data with the probability distribution Q of theoretical data. The biggest feature of relative entropy is asymmetry, that is to say $D_{KL}(P||Q) \neq D_{KL}(Q||P)$, and relative entropy does not satisfy the triangle inequality relation.

In Shannon's information theory, if the probability distribution of the character set is given, then a way to encode the character set with the least number of bits can be designed according to this probability distribution. Assuming that the character set is X , and the probability of one character x is $P(x)$, then the average number of optimally encoded bits of character x is equal to the entropy set of the character set:

$$H(x) = \sum_{x \in X} P(x) \log \left(\frac{1}{P(x)} \right) \quad (8)$$

On the same character set, there is also another probability distribution $Q(x)$, if the optimal encoding based on $P(x)$ is used to encode characters conforming to $Q(x)$. Due to the difference in probability distribution, the number of bits required for encoding will be higher. In this case, the concept of relative entropy is proposed, which measures the average number of bits used to encode each character. According to this relationship, the divergence between two probability distributions P and Q is measured as follows.

$$\begin{aligned} D_{KL}(P||Q) &= \sum_{x \in X} P(x) \log \left(\frac{1}{Q(x)} \right) - \sum_{x \in X} P(x) \log \left(\frac{1}{P(x)} \right) \\ &= \sum_{x \in X} P(x) \log \left(\frac{P(x)}{Q(x)} \right) \end{aligned} \quad (9)$$

Relative entropy is greater than zero and has a value of 0 if and only if the two probability distributions are the same. From Eq. (9), it can be concluded that when the probability distributions P and Q are discrete random variables, the calculation method of relative entropy is as follows.

$$D_{KL}(P||Q) = \sum_{x \in X} P(x) \ln \left(\frac{P(x)}{Q(x)} \right) \quad (10)$$

B. Application of Relative Entropy to Distance Metrics

Since relative entropy is based on a probability distribution, it is tested against another probability distribution, and the difference between test distribution and reference distribution is not an absolute method to measure the distance, because it does not have symmetry and transitivity.

It is generally believed that if the topic distribution on a sentence is closer to the topic distribution on the document than the topic distribution on other sentences is closer to the topic distribution on the document, then it can be considered that the ideas expressed in this sentence can more comprehensively

include the theme of the entire document. For a sentence, what you want to get is the similarity of the sentence relative to the article on the topic, without calculating the similarity of the document relative to a sentence on the topic. Therefore, the asymmetric nature of relative entropy will not have any effect on the content that needs attention.

Based on the above ideas, the topic distribution on the document is regarded as a theoretical probability distribution, and the probability distribution on the sentence is regarded as the actual probability distribution. Then, with the help of relative entropy, a method to measure sentence similarity and sentence weight is obtained.

The similarity between the topic probability distribution on the sentence and the document can be expressed as:

$$D_{KL}(P(T|S_i)||P(T|D)) = \sum_{k=1}^K P(T_k|S_i) \log \left(\frac{P(T_k|S_i)}{P(T_k|D)} \right) \quad (11)$$

At the same time, the similarity of two sentences S_r and S_t can be calculated:

$$D_{KL}(P(T|S_r)||P(T|S_t)) = P(T|S_r) \log \left(\frac{P(T|S_r)}{P(T|S_t)} \right) \quad (12)$$

VI. SELECTION OF CANDIDATE ABSTRACT SENTENCES

The strategy usually used for the selection of the center is to uniformly calculate the weight of the sentences in the document. After the weights of all sentences are obtained, several sentences with larger weights are selected as text summaries, and then subsequent semantic modification is performed.

Although this strategy has the ability to better express the main idea of the document, but through the understanding of the writing characteristics, we can know that an expository writing usually has some general statements to describe the summary of all central points described in the document. Then it will be expanded according to the specific content of each center point, and this will be clearly explained. So, a document can be seen as three levels of content:

- 1) The central sentence that describes all the ideas of the document, referred here as the general thesis.
- 2) The general situation described by each central idea of the document becomes a sub-thesis here.
- 3) Other auxiliary sentences describing each central idea become general descriptive sentences.

For a good abstract, it should include two levels of content: general thesis and sub-thesis, including sentences describing all the central ideas of the document, as well as sentences explaining what each central idea is, but not the content of general descriptive sentences. That is, it does not include examples or analytic sentences to demonstrate a central idea, which are redundant information for the abstract.

We believe that this paper is the first work considering the decomposition of sentences that constitute a document according to three levels, by observing their characteristics.

Three kinds of sentences make up a document: sentences that express the general thesis (first-level sentences), sentences that express the sub-thesis (second-level sentences), and general descriptive sentences (third-level sentences). The sentences describing the general thesis are concise and comprehensive, including the most important topics of the document, which appear most often in expository texts or news. It is the most needed content in the summarizing task of this document. The sub-thesis is used to illustrate or enrich the general thesis. The topics of the general thesis are scattered and included in different sub-theses, with relatively more length. It is usually argued from several different aspects and is the composition of an ideal summary. For general descriptive sentences, which are the lengthiest and contain the largest number of topics but are all irrelevant and don't appear many times throughout the document.

In order to select a sentence set that contains all the topics of the document, that is, when selecting the general thesis sentence and the sub-thesis sentence, it is only necessary to consider the number of topics contained in the sentence. The more topics are included, the more topics are included in the candidate set. Although feasible, this method ignores the importance of the narrative in the document itself.

For example, let a document containing only three central ideas. The document introduces these three central ideas in different proportions, respectively 20%, 30%, and 50%. If both sentences contain these three topics, but the topic probability distribution is different, one is 15%, 35%, 40%, and the other is 40%, 30%, 30%. Obviously the first sentence is more in line with the content of the document, and they state the same central idea in "similar" proportions. This coincides with the application of relative entropy to the distance measure mentioned above. Based on the concept of relative entropy, a summary sentence that is more representative of the document can be found.

A. Selection of Candidate Sentences for General Thesis

The first-level sentences are used in order to more accurately clarify all the points of view in the document. Thus, it is necessary to express more topics in a sentence as short as possible, i.e. playing the role of an outline. These sentences contain relatively few and important topics that will not only appear in the general thesis of the document, but also in the sub-thesis and general descriptive sentences. So, the number of occurrences in the entire document will be much more than other topics. The high frequency of such topics coincides with the relative entropy characteristics introduced in Section IV. Therefore, a strategy is proposed: For each sentence in the document, the relative entropy of the probability distribution between this sentence and the document topic is calculated. If a sentence has a high degree of coincidence with the topic of the document, it means that the content of its expression is closer to the overall document. In this way, using relative entropy, a sentence that is as similar as possible to the topic of the document is selected as the sentence that expresses the general thesis of the document. The implementation of this strategy is presented in Algorithm 1.

Algorithm 1 General thesis candidate sentences selection algorithm

Input: Document sentences $S = \{S_1, S_2, \dots, S_m\}$; number of abstracts L ; number of topics K

Output: General thesis candidate sentences Θ

```
1: Candidate sentences set  $\psi = \emptyset$ ; General thesis sentences set  $\Theta = \emptyset$ ; Topics  $T = \{T_1, T_2, \dots, T_K\}$ ;  $L = K$ 
2: while  $i < m$  do
3:   if  $length(\psi) < L$  then
4:      $\psi = \psi \cup S_i$ 
5:   else if  $D_{KL}(P(T|S_i)||P(D)) < \text{argmax}(\psi)$  then
6:      $\psi = [\psi - \text{argmax}(\psi)] \cup S_i$ 
7:   end if
8: end while
9: while  $|\Theta| < K$  do
10:   $\Theta = \Theta \cup \max(\psi)$ 
11: end while
12: return  $\Theta$ 
```

The basic idea of Algorithm 1 is based on the greedy algorithm. The most similar sentences to the topic of the document are selected as candidate sentences. The process of the proposed algorithm can be stated as follows.

- 1) First of all, it is necessary to determine the size of the candidate sentence. Since the LDA model requires the user to input the number of topics, and the text summarization model requires the user to input the number of abstracts, the size of the candidate sentence can be jointly determined according to the required number of abstracts and the number of topics of the article. Here, it is set to be the same as the number of abstract sentences, and further selections will be made in the last step.
- 2) Based on the idea of a greedy algorithm, the topic similarity of each sentence to the document (relative entropy-based method) is calculated, and sentences with a high degree of similarity with the document topic are selected. If the number of current candidate sentences is less than the target number, the current sentence will be added. Otherwise, the sentence will be used as a candidate sentence only when the current sentence has a high degree of similarity with the topic of the document.
- 3) Again, based on the greedy algorithm, from the candidate sentences selected in the second step, the smallest set of sentences that can cover all topics is selected. We end up with the smallest set of sentences that cover the most topics.

B. Selection of Candidate Sentences for Sub-thesis

Sub-thesis candidate sentences refer to a certain length of description in a document in order to clearly describe a certain point of view, and select sentences that can summarize the sub-thesis. These sentences are sub-thesis candidate sentences. A notable feature of sub-thesis writing is that each sentence describing the relevant content expresses the same content to a large extent, and the topics contained in the sentences are basically the same. But it will also be mixed with some third-level content, that is, general construction sentences, which

will cause the deviation of the topic center. Therefore, how to eliminate the influence of the topic of the general construction sentence as much as possible, and choose the sentence that really expresses the point of view, needs further analysis.

For a paragraph in a document that expresses a sub-thesis as the object of analysis, in order to clarify an idea, it is usually necessary to use other sentences to explain and supplement, and usually the sub-thesis will appear in each sentence. For example, for the paragraph analysis of a document during the two sessions on "people's livelihood", the author will illustrate through examples of environmental protection, food, safety, etc. Through the topic analysis of LDA, three topics of environment, food and life will be obtained, and the most of the content is related to the topic of "life".

Based on this writing habit, this paper proposes a selection strategy of candidate sentences for sub-thesis based on topic selection: Taking the paragraph as the basic unit of analysis, after the LDA model analysis, the topic distribution of the paragraph is obtained, and several topics with the highest probability are selected as the target probability distribution. After that, the relative entropy of each sentence with this distribution is calculated. Then, the sentence with the smallest entropy value is selected as the candidate sentence for sub-thesis.

Algorithm 2 Sub-thesis candidate sentences selection algorithm

Input: Document $D = \{C_1, C_2, \dots, C_m\}$

Output: The sub-thesis candidate sentences θ

```
1: Abstract sentences set  $\theta = \emptyset$ ; Topics  
    $T = \{T_1, T_2, \dots, T_K\}$ ;  $L = K$ ; Paragraph  
    $C_i = \{S_{i1}, S_{i2}, \dots, S_{im}\}$   
2: Divide sentences according to paragraphs, taking sentences  
   of the same paragraph as a unit of analysis  
3: while  $i < m$  do  
4:   Count topics included in paragraph  $C_i$   
5:   Calculate the probability distribution  $P(T|C_i)$  of the  
   topic on the paragraph  
6:   while  $j < \text{length}(C_i)$  do  
7:     if  $|\theta_i| = \emptyset$  or  $D_{KL}(P(T|S_{ij})||P(T|C_i)) < \text{value}(\theta_i)$   
     then  
8:        $\theta_i = S_{ij}$   
9:     end if  
10:  end while  
11: end while  
12: return  $\theta$ 
```

In Algorithm 2, the input text D consists of m paragraphs of text. For each paragraph C_i , first count the topics contained in the paragraph and the probability distribution of the topics. Then for each sentence S_{ij} in the paragraph C_i , we calculate the relative entropy of the topic probability distribution over the sentence and the paragraph. If the paragraph C_i has no candidate, that is, $|\theta_i| = \emptyset$ or the current relative entropy is greater than the relative entropy of the most similar sentence in the paragraph, that is, $D_{KL}(P(T|S_{ij})||P(T|C_i)) < \text{value}(\theta_i)$, set the current sentence as the candidate center sentence of the current paragraph, i.e. $\theta_i = S_{ij}$. In this way, until the calculation of all paragraphs is completed, the sentence saved

in the θ_i array is the central sentence of each paragraph, that is, the sub-thesis of the document.

VII. EXPERIMENTAL RESULTS AND ANALYSIS

The purpose of this experiment is to use the relative entropy method on the basis of the topic model to verify the correctness of the general thesis and sub-thesis summary methods, and how to set the parameters to maximize their accuracy.

A. Dataset and Evaluation Method

This paper uses the NLPCC 2015 [26] corpus as the experimental object. NLPCC2015 has three tasks. The third one is to perform news text summarization task for Weibo. The dataset consists of 250 news predictions that have been sentenced, completely sourced from Sina.com. The model training data uses the Internet corpus provided by Sogou Lab, involving 1761 articles in 9 aspects of recruitment, tourism, military, health, IT, sports, finance, market, and culture.

The evaluation method used for scoring is ROUGE [27] adapted to Chinese¹. It's a recall-based calculation method adopted by most works as an automatic evaluation tool for the quality of text summaries. ROUGE measures the quality of automatic text summarization by calculating the degree of overlap between automatic summaries and expert summaries on various evaluation criteria. Usually, the degree of overlap between automatic summarization and expert summarization in N -grams or the length of the maximum co-occurrence subsequence is used. Among them, $N = \{1, 2, 3, 4\}$, indicating the coverage ability of automatic summarization on the content of expert summarization. It is generally believed that the 1-gram-based ROUGE score (ROUGE-1) reflects the closeness of automatic summarization and expert summarization [28], while ROUGE-2 reflects the smoothness of automatic summarization. The value range of the ROUGE score is $[0, 1]$. The closer to 1, the closer the automatic abstract to the expert abstract.

B. Experimental Results

The LDA model is used for model training on the training dataset. Since the main categories contained in the dataset are known, the number of topics of the LDA model is artificially set to 9. The output model of LDA is a two-dimensional array representing the corresponding probability of word-topic. Since the number of vocabulary is too large, the top ten words with the highest probability under each category are selected for display here. The output results are presented in Table I.

From Table I, we can see that the categories corresponding to the nine topics are: recruitment, tourism, military, health, IT, sports, finance, market, and culture.

1) *Experiment of General thesis Abstract Method:* Based on the output results of the LDA model, Algorithm 1 is used to extract the sentences expressing the general thesis in the text, and compare the accuracy with the manual summary. The accuracy of the result is only about 30%, and the effect is very poor. Although there are many topics that may be

¹All experiments were re-run by ourselves since our algorithm did not participate in the NLPCC.

TABLE I. SOME OUTPUT RESULTS OF THE LDA MODEL

Topic 0:	Topic 1:	Topic 2:
Major=0.0083278164279716	Travel=0.013141023064702821	USA=0.007125444347199101
Student=0.007842661514385616	Visitors=0.004266203667474156	Japan=0.004809696664837551
Work=0.00733710875165395	Culture=0.004019739964102812	Plane=0.003791742025381582
School=0.0062748712404097975	City=0.0028504078737947554	Training=0.0037772489295390833
Education=0.005451361658338121	World=0.00240451233961009	System=0.003626238305766903
University=0.005270162961600818	Travel agency=0.0021930419407089076	Troop=0.003605801384330944
Candidate=0.005198484819478605	Chengdu=0.001931720410524329	Military=0.0035635128929766818
Exam=0.005015208574173687	Active=0.001658761327230168	Combat=0.0033607386032706472
Occupation=0.0035060068912367887	Park=0.0016147225498504244	Equipment=0.003248380941722047
Admissions=0.003493704451970437	Passenger=0.0015058548118690985	Progress=0.0032425202170355927
Topic 3:	Topic 4:	Topic 5:
Hospital=0.0059093508141070915	Computer=0.0020919139266127283	Match=0.00949530427474704
Sohu=0.005476764815671471	Internet=0.002007672796693706	Team member=0.0036720771812709914
Treatment=0.004703755393063685	iPhone=0.0017364146623097224	League=0.0032591843413982942
Live member=0.00459868303471546	Index=0.0015133078417762656	Team=0.0029232011897390537
Patient=0.0031455965425699617	Big data = 0.0013829300513194772	Reporter=0.002426053667587339
Health=0.0025964168608791265	System=0.0013096471915589481	Champion=0.0023930186697693075
Surgery=0.002488186684299358	Mobile=0.001085641175064798	Club=0.00237514767051908
Female=0.002363139272183045	BAT=0.0010612095334178121	Players=0.0022026031092450336
Found=0.0022240460467755595	AI=0.001029019868443202	Final=0.0021788234475517664
Occurrence=0.0021507363034214463	Understanding=9.899805996801138E-4	Season=0.002021560606839102
Topic 6:	Topic 7:	Topic 8:
Company=0.01909300611739068	China=0.009771496614544694	Interest=0.008119586724125997
Shareholder=0.008083219805765936	Company=0.007841044022748052	Life=0.004442234745400481
Shares=0.006859302052065136	Market=0.007116032951475622	Work=0.0037912371185839034
Ltd = 0.005513593668215	Enterprise=0.0067178444904189465	Child=0.0036027960884871127
Investment=0.004954318183600884	Development=0.006082827574448052	Know=0.0033194226653292082
Equity=0.004667721949358522	Current=0.0043594695781138115	Problem=0.0031881717400462665
Item=0.004523799009845025	Reporter=0.004117429660299634	AC=0.0030608909613718408
Securities=0.004491724613939593	Already=0.0037238429854752793	Man=0.0030123506377184076
Funding=0.004018111411489305	Product=0.003661836682905302	China=0.0027328446003346604
Reform=0.003952631004273419	Country=0.003587531849997642	Culture=0.0026000345127893025

expressed in a document, most of them have nothing to do with the main thesis expressed, so the topics in the document are ordered in non-ascending order of probability, and the topics with relatively small probability are gradually removed. The relative entropy of the topic distribution in the document and the topic distribution of each sentence is calculated, and the accuracy is calculated for different reduction rates (the interval between two reductions is 3%).

Observing Fig. 1, we can see that although there are some fluctuations (caused by the reduction of the interval), it can be observed that when the subject of a document is reduced to between 26% and 33%, the accuracy rate is the highest, that is, the calculation is performed at this time. The resulting automatic summary is the most likely to be a manual summary. Based on this conclusion, this paper sets the text topic reduction rate as 30% as the calculation parameter for the subsequent experiments.

The requirement of NLPCC2015 for text summarization is for Sina Weibo [29]. Given a document, it needs to be summarized into an abstract that can be used as a Weibo (up to

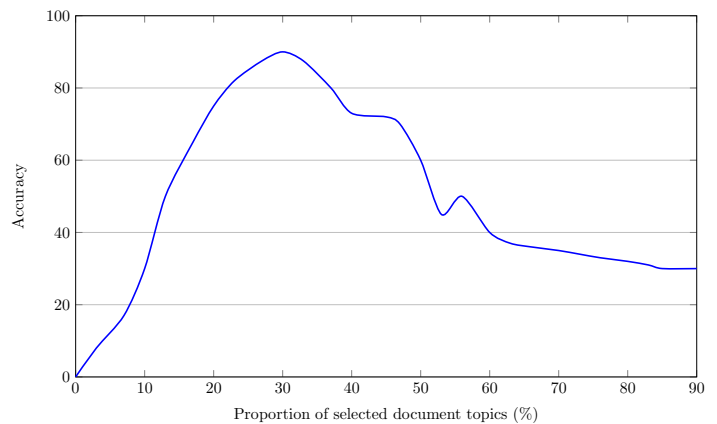


Fig. 1. The Impact of Document Topic Selection Ratio on Abstract.

140 words), so the summary needs to be as short as possible. This is in line with the concept of the general thesis presented

TABLE II. ROUGE SCORE OF EACH ALGORITHM WHEN THE ABSTRACT LENGTH IS 80

Algorithm	ROUGE-1	ROUGE-2	ROUGE-3	ROUGE-4	ROUGE-L
WUST-1	0.563	0.322	0.234	0.189	0.624
WUST-2	0.572	0.331	0.239	0.191	0.631
Team-Best	0.542	0.312	0.229	0.178	0.610
FMAS	0.483	0.297	0.211	0.164	0.601
SentenceRank	0.470	0.308	0.226	0.175	0.598
GenSubE	0.571	0.328	0.232	0.198	0.637

TABLE III. ROUGE SCORE OF EACH ALGORITHM WHEN THE ABSTRACT LENGTH IS 140

Algorithm	ROUGE-1	ROUGE-2	ROUGE-3	ROUGE-4	ROUGE-L
WUST-1	0.586	0.395	0.275	0.206	0.650
WUST-2	0.599	0.409	0.290	0.218	0.653
Team-Best	0.587	0.413	0.264	0.212	0.639
FMAS	0.511	0.332	0.217	0.201	0.621
SentenceRank	0.535	0.386	0.283	0.207	0.582
GenSubE	0.532	0.351	0.254	0.203	0.631

in this paper. Our proposed algorithm (denoted GenSubE) is compared to the following algorithms:

- SentenceRank [30]: It evaluates the importance of sentences by measuring the relationship between them.
- Team-Best [25]: It's based on a super-edge sorting method, first find the subject word, calculate the sentence weight, and then use the edge-based random walk algorithm.
- WUST-1 and WUST-2 [26]: The best systems from the NLPCC 2015.
- FMAS as the baseline on the dataset. It's a pure statistical-based summarization method, considering TF-IDF (Term Frequency Inverse Document Frequency), sentence position, sentence length, and sentence similarity to calculate sentence weights.

The comparative results of the performance of the compared algorithms are presented in Tables II and III in terms of ROUGE evaluation indicators, when the target abstract lengths are 80 and 140 characters, respectively.

From Table II, it can be seen that for the 80-word abstract, the score of our proposed algorithm is almost similar as the best competition algorithms (WUST-1 and WUST-2) with the highest scores in the dataset, which are higher than the commonly used SentenceRank algorithm and the statistics-based FMAS algorithm. The ROUGE-1 evaluation index is usually regarded as the best criterion for judging automatic summaries and manual summaries. It can be seen that the recall rate achieved on ROUGE-1 is close to the best results. On the 140-word abstract, in Table III, the results of our proposed algorithm are not particularly outstanding. Only higher than the FMAS algorithm, and there is no advantage in the ROUGE score compared to the other text summarization methods. This is because the sentences extracted by the general thesis abstract method are usually not very long, usually only two sentences, so it has a good performance on the 80-word abstract. In the comparison of the 140-word abstract, it only maintains an above-average level.

2) *Experiment of Sub-thesis Abstract Method:* In this section, the general thesis and sub-thesis abstracting methods are used, and only the 140-word text abstract task is compared with other algorithms to observe the performance results. Algorithms 1 and 2 are combined to extract the sentences of the document's general thesis and sub-thesis, respectively. The performance of our method is compared with the other summary algorithms on the 140-word summary task. The performance results are presented in Fig. 2.

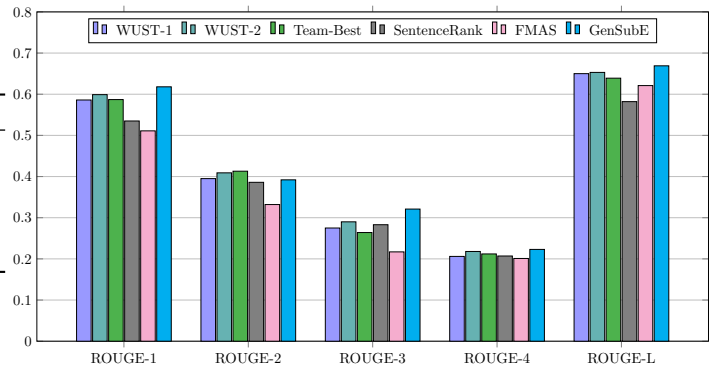


Fig. 2. ROUGE Value of Each Algorithm when the Abstract Length is 140 Words.

Fig. 2 shows that after extending the length of the abstract to 140 words, the score of our proposed method has been greatly improved compared with the method of simply extracting the general thesis. Compared with the SentenceRank algorithm and the statistics-based FMAS algorithm, it has great advantages in the all ROUGE evaluation indicators. The results show that our algorithm outperforms the best competition algorithms on all scores except on ROUGE-2 which is very close. Compared with the general thesis method, the text summaries obtained by the combined method have a great improvement in sentence fluency and comprehensive coverage. At the same time, compared with the other algorithms, it has obtained better than the best competition algorithms. The method proposed in this paper performs very well on the NLPCC2015 dataset.

VIII. CONCLUSION

In this paper, we propose a new method for document summarization. After processing the document through the LDA model, the probability distribution of the word-topic can be obtained. Firstly, we convert the probability distribution of word-topic into the probability distribution of topic-sentence to extract sentences in the document based on semantic analysis. After that, in order to measure the relationship between two sentences or sentences and document, relative entropy is introduced to measure the similarity of two probability distributions. The relative entropy of the topic probability distribution of the sentence over the document, and of the sentence over the paragraph are calculated, respectively. The smallest entropy value indicates that the difference is relatively small, and can be used as the central sentence of the paragraph. Also, this paper introduces a new document decomposition method based on relative entropy analysis. Through experiments and analysis on the NLPCC 2015 dataset, it can be known that when the

number of document topics is reduced to 30%, the probability distribution of abstract sentences and document topics are the most similar. At the same time, the results obtained on the 80-word abstract task and the 140-word abstract task are compared with other method. The performance results demonstrated the efficiency of using the relative entropy of the topic probability distribution over sentences to measure sentence relations.

REFERENCES

- [1] H. P. Luhn, "The automatic creation of literature abstracts," *IBM Journal of Research Development*, vol. 2, pp. 159–165, 1958.
- [2] P. B. Baxendale, "Machine-made index for technical literature—an experiment," *IBM Journal of Research and Development*, vol. 2, pp. 354–361, 1958.
- [3] H. P. Edmundson, "New methods in automatic extracting," *Journal of the ACM (JACM)*, vol. 16, pp. 264–285, 1969.
- [4] R. McDonald, "A study of global inference algorithms in multi-document summarization," in *Lecture Notes in Computer Science (including subseries Lecture Notes in Artificial Intelligence and Lecture Notes in Bioinformatics)*, vol. 4425 LNCS, 2007, pp. 557–564.
- [5] D. Gillick and B. Favre, "A scalable global model for summarization," in *Association for Computational Linguistics (ACL)*, 2009, pp. 10–18.
- [6] C. Li, X. Qian, and Y. Liu, "Using supervised bigram-based ilp for extractive summarization," in *ACL 2013 - 51st Annual Meeting of the Association for Computational Linguistics, Proceedings of the Conference*, vol. 1, 2013, pp. 1004–1013.
- [7] H. Lin and J. Bilmes, "Multi-document summarization via budgeted maximization of submodular functions," in *NAACL HLT 2010 - Human Language Technologies: The 2010 Annual Conference of the North American Chapter of the Association for Computational Linguistics, Proceedings of the Main Conference*, 2010, pp. 912–920.
- [8] —, "A class of submodular functions for document summarization," in *ACL-HLT 2011 - Proceedings of the 49th Annual Meeting of the Association for Computational Linguistics: Human Language Technologies*, vol. 1, 2011, pp. 510–520.
- [9] J. Kupiec, J. Pedersen, and F. Chen, "Trainable document summarizer," in *SIGIR Forum (ACM Special Interest Group on Information Retrieval)*, 1995, pp. 68–73.
- [10] J. M. Conroy and D. P. O'leary, "Text summarization via hidden markov models," in *SIGIR Forum (ACM Special Interest Group on Information Retrieval)*, 2001, pp. 406–407.
- [11] F. B. Goularte, S. M. Nassar, R. Fileto, and H. Saggion, "A text summarization method based on fuzzy rules and applicable to automated assessment," *Expert Systems with Applications*, vol. 115, pp. 264–275, 2019.
- [12] K. M. Svore, L. Vanderwende, and C. J. Burges, "Enhancing single-document summarization by combining ranknet and third-party sources," in *EMNLP-CoNLL 2007 - Proceedings of the 2007 Joint Conference on Empirical Methods in Natural Language Processing and Computational Natural Language Learning*, 2007, pp. 448–457.
- [13] J. Cheng and M. Lapata, "Neural summarization by extracting sentences and words," in *54th Annual Meeting of the Association for Computational Linguistics, ACL 2016 - Long Papers*, vol. 1, 2016, pp. 484–494.
- [14] R. Nallapati, B. Zhou, C. dos Santos, Çağlar Gulçehre, and B. Xiang, "Abstractive text summarization using sequence-to-sequence rnns and beyond," in *CoNLL 2016 - 20th SIGNLL Conference on Computational Natural Language Learning, Proceedings*, 2016, pp. 280–290.
- [15] R. Nallapati, F. Zhai, and B. Zhou, "Summarunner : A recurrent neural network based sequence model for," *The Thirty-First AAAI Conference on Artificial Intelligence*, pp. 3075–3081, 2017.
- [16] J. Xu and G. Durrett, "Neural extractive text summarization with syntactic compression," in *EMNLP-IJCNLP 2019 - 2019 Conference on Empirical Methods in Natural Language Processing and 9th International Joint Conference on Natural Language Processing, Proceedings of the Conference*, 2020, pp. 3292–3303.
- [17] D. Anand and R. Wagh, "Effective deep learning approaches for summarization of legal texts," *Journal of King Saud University - Computer and Information Sciences*, 2019.
- [18] M. Zhong, P. Liu, Y. Chen, D. Wang, X. Qiu, and X. Huang, "Extractive summarization as text matching," in *Proceedings of the 58th Annual Meeting of the Association for Computational Linguistics*, 2020, pp. 6197–6208.
- [19] A. P. Widyassari, S. Rustad, G. F. Shidik, E. Noersasongko, A. Syukur, A. Affandy, and D. R. I. M. Setiadi, "Review of automatic text summarization techniques & methods," *Journal of King Saud University - Computer and Information Sciences*, 2020.
- [20] M. Gambhir and V. Gupta, "Recent automatic text summarization techniques: a survey," *Artificial Intelligence Review*, vol. 47, pp. 1–66, 2017.
- [21] W. S. El-Kassas, C. R. Salama, A. A. Rafea, and H. K. Mohamed, "Automatic text summarization: A comprehensive survey," *Expert Systems with Applications*, vol. 165, 2021.
- [22] J. Li, C. Zhang, X. Chen, Y. Hu, and P. Liao, "Survey on automatic text summarization," *Jisuanji Yanjiu yu Fazhan/Computer Research and Development*, vol. 58, pp. 1–21, 2021.
- [23] D. M. Blei, A. Y. Ng, and M. I. Jordan, "Latent dirichlet allocation," *Journal of Machine Learning Research*, vol. 3, pp. 993–1022, 2003.
- [24] G. Heinrich, "Parameter estimation for text analysis (based on gibbs sampling)," *Technical Report, Fraunhofer IGD*, 2009.
- [25] R. Arora and B. Ravindran, "Latent dirichlet allocation based multi-document summarization," in *Proceedings of SIGIR 2008 Workshop on Analytics for Noisy Unstructured Text Data, AND'08*, 2008, pp. 91–97.
- [26] X. Wan, J. Zhang, S. Wen, and J. Tan, "Overview of the nlpcc 2015 shared task: Weibo-oriented chinese news summarization," in *Lecture Notes in Computer Science (including subseries Lecture Notes in Artificial Intelligence and Lecture Notes in Bioinformatics)*, vol. 9362, 2015, pp. 557–561.
- [27] C. Y. Lin, "Rouge: A package for automatic evaluation of summaries," *Proceedings of the workshop on text summarization branches out (WAS 2004)*, 2004.
- [28] C. Y. Lin and E. Hovy, "Automatic evaluation of summaries using n-gram co-occurrence statistics," in *Proceedings of the 2003 Human Language Technology Conference of the North American Chapter of the Association for Computational Linguistics, HLT-NAACL 2003*, 2003.
- [29] C. SINA. (2009) Sina weibo. www.weibo.com. [Online]. Available: www.weibo.com
- [30] R. Mihalcea and P. Tarau, "Textrank: Bringing order into texts," in *Proceedings of the 2004 Conference on Empirical Methods in Natural Language Processing, EMNLP 2004 - A meeting of SIGDAT, a Special Interest Group of the ACL held in conjunction with ACL 2004*, 2004, pp. 404–411.

A Game Theory-based Virtual Machine Placement Algorithm in Hybrid Cloud Environment

Nawaf Alharbe
Applied College, Taibah University,
Saudi Arabia

Mohamed Ali Rakrouki
Applied College, Taibah University, Saudi Arabia
Business Analytics and DEcision Making Lab (BADEM)
at Tunis Business School, Tunisia

Abstract—This paper deals with the problem of virtual machine placement in hybrid cloud situation from an economic and QoS perspectives. Because excessive investment of resources in cloud computing environment will result in resources waste, and too few resources can generate QoS issues. This paper uses a game theory model to describe the problem and find the balance between these contradictions. Based on this model, a virtual machine placement algorithm for scheduling virtual resources is proposed. Compared to the traditional game theory, our LBOGT algorithm proposes a game between tripartite sides: users, individual providers and provider groups. Experiments show that our proposed algorithm reduces physical machines energy consumption by 6.16%, and increases by 10.6% in profit provider under the premise of users' QoS.

Keywords—Cloud computing; virtual machine placement; game theory; quality of service; load balancing; energy consumption

I. INTRODUCTION

From the point of view of security and cost, if a small and medium-sized enterprise only needs to meet the needs of its internal personnel, and its business on the data center does not need to be open to the public, this company can build its own private cloud. However, sometimes high-intensity workload for some reason can suddenly usher, and the local private cloud resources cannot normally meet the needs of all the new requests. At this time, the solution for this company is to rent cloud resources from other cloud providers in order to complete their tasks. In this way, the company uses both its own private cloud and the public cloud of other providers, thus combining into a hybrid cloud.

Over time, cloud computing develops more towards the direction of hybrid cloud and cloud alliance [1]. A single cloud provider is largely constrained by the market because of limited cloud resources, limited market radiation range, and limited system throughput. The cloud computing model as an economic model is dependent on the market, so small and medium cloud computing providers join forces with each other to form an alliance [2], [3]. Due to the change of this model, the game participants in the traditional game model are limited to users or a single cloud computing provider, and fail to reflect the collective interests of the entire hybrid cloud, which is flawed from the perspective of game theory. At the same time, as a hybrid cloud collective, it cannot reflect the collective interests well. The income of a collective is not simply to ensure the income of all the individual units to meet the maximum collective revenue.

Therefore, this paper proposes an improved game theory model: taking cloud computing users, a single cloud computing

provider, and an aggregate of multiple providers as game theory participants, each representing its own interests. At the same time, under certain conditions, the two are also conflicting interests, and they need to fight for their own interests through games. Among them, cloud users hope that the response time of services is short and the quality of task completion is high, so they need more cloud resources. From the one hand, a single cloud computing provider hopes that its own interests are high, so it needs to reduce the investment of resources and maintenance costs. On the other hand, a provider group hope that cloud users will be satisfied with the service, and hope to increase the income of the entire group and reduce expenditure.

To sum up, this paper focuses on developing a virtual machine (VM) placement algorithm in a hybrid cloud environment. This scheme can describe the relationship between users, cloud resource providers and hybrid cloud systems composed of providers. The scheme comprehensively considers the QoS requirements of users and the benefits obtained by the provider, as well as energy consumption of the system. Finally, this paper proposes a VM placement algorithm based on this game theory to ensure user QoS and improve resource utilization.

II. LITERATURE REVIEW

From the perspective of providers and users, cloud computing is a dynamic process, and its management is a very important issue. For cloud computing providers, the management of cloud resources is very important for the 3 levels of services (IaaS, PaaS, SaaS) to ensure service-level agreements (SLA) [4], standardization, security, high availability, high energy consumption ratio, and resources utilization maximization.

From user's point of view, cloud computing services are divided into two stages [5]. The first one is the pre-processing stage, in which users are faced with the selection of cloud computing services. The second stage is a stage of continuous interaction with providers or cloud computing management, where users need to monitor the performance of their own services. Users will consider whether to continue to use the service or purchase other services according to their own evaluation results. User's QoS and system performance are considered by Calheiros et al. [6]. They designed a predictive load balancing model using queuing theory, and the virtual machine deployment is determined by using QoS target and predicted load. Different QoS requirements analysis for various users is provided by Xu et al. [7]. They proposed a multi-dimensional QoS scheduling strategy based on multi-workflow in cloud environment. According to this model, the task flow

is scheduled to meet the preferences of different users. Starting from the needs of users, Bardsiri and Hashemi [8] designed various QoS indicators for service providers, and established a user QoS evaluation model according to these QoS indicators. The similarity of trustworthiness in the cloud environment is studied by Pan et al. [9] to find trusted adjacent services and predict missing QoS values by enhancing similarity of trusted services. Recently, Farzai et al. [10] considered the bandwidth as QoS indicator and proposed a hybrid genetic algorithm for minimizing power consumption, resource wastage, and bandwidth. The proposed method demonstrated high potential of scalability for large problem instances. In order to meet QoS requirements, Jing et al. [11] proposed a QoS-aware scheme based on a Particle Swarm Optimization (PSO) algorithm. Recently, Aloufi et al. [12] This paper discusses how cloud computing provides users with QoS by presenting the concept and characteristics of cloud computing and how machine learning techniques can be applied to resource management. In particular, this survey highlighted the advantages of utilizing machine learning to schedule forthcoming requests in order to achieve QoS and save energy. Edinat et al. [13] reviewed several previously proposed models that have been utilized in the literature to improve QoS and proposed a model based on Deep Reinforcement Learning and an enhanced DRL agent.

Load balancing is a difficult and an important problem in cloud computing. It's directly affects resource utilization, thereby affecting the profitability of cloud computing providers. References [14], [15] used live migration of virtual machines as an optimization goal to reduce energy consumption. A multi-objective ant colony optimization algorithm has been proposed by Fang and Qu [16] in order to balance simultaneously the load among the physical machines and the internal load of machines. Recently, a machine learning-based approach has been proposed by Ghasemi and Haghghat [17] for the same problem. A survey on load balancing algorithms and their classification is provided by Xu et al. [18].

Currently, there are currently two main methods to reduce the energy consumption of cloud computing: Dynamically adjust power consumption of physical server CPUs to save power; Turn off unnecessary services or energy-consuming resources in the cloud computing system to save power. In this way, Sotomayor et al. [19] suspended relatively low-priority tasks to reduce power consumption. Chen et al. [20] proposed power saving approaches by shutting down unnecessary virtual machines according to server load balancing. Recently, energy consumption in cloud computing environment has attracted more researchers [21]–[25].

III. METHODOLOGY

A. Member Interests in Hybrid Cloud

Due to the internal heterogeneity of the hybrid cloud system, resource management and scheduling difficulties of this system are greatly increased. There are many different cloud providers in a hybrid cloud system. After analyzing users needs, it is also difficult for the hybrid cloud to submit the analysis results to different providers. Furthermore, each provider must satisfy user's QoS requests. In order to ensure these requests, it is necessary to limit or even reduce the number of user task requests per unit time. However, the reduction

of the number of processing tasks will reduce the profit of the provider. To deal with this contradictory relationship between user and provider, we need to build a game model.

This paper assumes that a provider in the hybrid cloud virtualizes physical resources through the hypervisor, and virtual resources will be provided to users in the form of virtual machines. The provider accepts a user's task application and finds that the remaining local resources are not enough to meet the user's needs, and cannot suspend or close tasks and virtual machines using local resources. At this time, the provider will have to follow some scheduling rules. Forcibly shut down some virtual machines, or the provider can transfer this local request to other providers in the hybrid cloud through the hybrid cloud management system, and use resources of other providers in order to complete the local request by outsourcing [26]. The final benefits are managed and distributed uniformly by the hybrid cloud system.

B. Solution Design

Hybrid cloud faces security, price, benefit distribution and other issues [27], [28]. To build a stable hybrid cloud system, we first need to establish a stable provider portfolio, then conduct business modeling, and finally develop a virtual machine deployment solution. Therefore, the design focus of this paper is divided into three parts:

- 1) Hybrid cloud group member selection model: A stable system must be stable internally, and all internal members of the system can bring benefits to the group. Therefore, the benefits of members in the group are greater than the benefits of running alone.
- 2) A game model: It is an economic model that can reflect the interests of multiple parties, can quantify and describe the relationship between QoS problem, interest problem and energy consumption problem of the hybrid cloud system. In addition, it can participate in solving the virtual machine deployment and revenue problems of the hybrid cloud. This paper adds a player to the traditional game-theoretic model, the individual resource provider, in order to make the model more flexible and able to safeguard the interests of all providers.
- 3) A virtual machine placement algorithm: It's an optimization algorithm proposed according to the game model. The purpose is to satisfy the user's QoS and improve resource utilization.

The overall design of the system is depicted in Fig. 1.

IV. GAME MODEL BUILDING

A. Metrics used by the Model

1) *Stable Hybrid Cloud Membership - Pareto Optimization*: Pareto optimization is an economic concept proposed by the Italian economist Vilfredo Pareto. Pareto optimization means that there are no losers in a change in a model, and at least one member can profit.

A cooperative game needs to meet a precondition, that is, to follow the principle of Pareto optimization. For game participants, the global benefit of the entire game must be

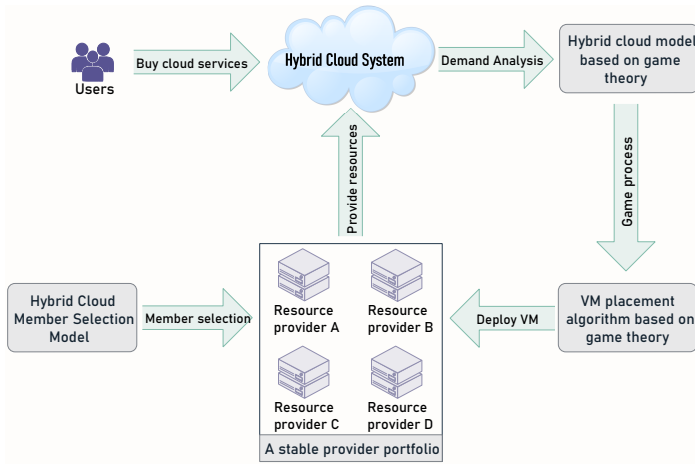


Fig. 1. Hybrid Cloud Virtual Machine Deployment Diagram.

greater than the benefit obtained by each player acting alone. Considering the stability of the hybrid cloud, there is a similar nature. Members of a stable team portfolio will not gain higher benefits if they leave the team to act alone or join a new team.

2) *Hybrid Cloud Member Benefit Distribution Principle - Shapley Value*: Shapley value refers to the fair distribution of the overall benefit according to the contribution value of members to the group. The Shapley value of a member represents the average expected contribution value of the member to the group.

Let $I = \{1, 2, \dots, n\}$ be a set, any subset S of I corresponds to a function $V(S)$, if it satisfies:

$$\begin{cases} V(\emptyset) = 0 \\ V(S_i \cup S_j) \geq V(S_i) + V(S_j) \\ S_i \cap S_j = \emptyset \\ \forall S_i, S_j \in I \end{cases} \quad (1)$$

Then $[I, V]$ is called the n -player cooperative game, and V is the characteristic function of the game. $V(S)$ is the payoff of the cooperative strategy.

Here, $X_i (i = 1, 2, \dots, n)$ is used to denote the income that member i in I should get from the maximum benefit $V(I)$ of cooperation, and $X = (X_1, X_2, \dots, X_n)$ is the allocation of the maximum benefit in the cooperative strategy and satisfy:

$$\begin{cases} \sum_{i=1}^n X_i = V(I) \\ X_i \geq V(i); \forall i = (1, 2, \dots, n) \end{cases} \quad (2)$$

Then, the Shapley value can be written as $X = (X_1, X_2, \dots, X_n)$ where:

- $X_i = \sum_{s \in S_i} W(|s|)[V(s) - V(s/i)]$
- $W(|s|) = \frac{(n - |s|)! (|s| - 1)!}{n!}$
- S_i is all subsets of I that contain i

- $|s|$ is the number of elements in the subset
- $W(|s|)$ is the weighting factor.

Shapley value is used in this paper to measure the provider's contribution to the team, that is, how much the game player can add to the entire team combination when the game player joins the provider combination scheme. The higher the contribution value, the higher the benefit value allocated to the cloud provider. If the Shapley value is negative, it means that the provider's joining cannot increase the benefits of the alliance, and its joining will not be considered. The Shapley value of the cloud provider can be calculated by Eq. 3.

$$\varphi_i(v) = \sum_{S \subseteq RP} \frac{|S|!(|RP| - |S| - 1)!}{|RP|!} [v(S \cup \{RP_i\}) - v(S)] \quad (3)$$

where the cloud provider set is denoted by $RP = \{RP_1, RP_2, \dots, RP_n\} (n \in \{1, 2, \dots, N\})$, v corresponds to the characteristic function V of the game in the Shapley value, and the calculation method is shown in formula Eq. 4. A hybrid cloud is defined as a combination of providers, denoted by S , where $S \subseteq RP$ and $S > 1$.

B. Principles of Member Selection in Hybrid Cloud

The cloud computing service provider in this paper is not a single one, but a combination of several cloud computing providers. The choice between a group of providers and a single provider outside the group is a two-way street, with a single provider choosing whether to join the group, and the group considering whether to allow a single provider to join. The specific selection model of a single provider is not considered in this paper. This is because a single provider considers whether to join or not, and needs to integrate its own situation and whether the agreement between the two parties is beneficial to itself. There are too many variables to discuss. Therefore, the group composed of cloud computing providers needs to be stable, and the average revenue of a single provider is beneficial to the team, mainly satisfying the following points:

- 1) First, determine whether the resources owned by all providers in the provider team can meet the constraints of the system on resources.
- 2) For all providers in the group, the benefits obtained by joining the group must be higher than the benefits obtained by operating alone. In this way, during the operation of the group, no provider will consider withdrawing the group, so that this group is a stable combination.
- 3) If the team's combination scheme is optimal, on the premise of satisfying the above two points, a combination of providers needs to be selected. The average income obtained by this combination scheme is the highest, which can not only satisfy resource constraints and user QoS, but also guarantee the maximum benefit of members.

Users need to pay according to their own tasks and QoS preferences when purchasing cloud computing services. When providers consider service pricing, they need to price each

resource used by users separately. The final price is calculated from the price of resources offered by a single provider. The price of k -type resources in the hybrid cloud S can be calculated by Eq. 2, where δ is a price correction parameter.

$$price_S^k = e^{\delta|S|} \cdot \overline{price_p^k} \quad (4)$$

Let R_k be the number of various resources in a hybrid cloud S , then the total profit $profit(S)$ per unit time of the cloud S can be calculated by Eq. 5.

$$profit(S) = \sum_k price_S^k \cdot R_k \quad (5)$$

Assume a stable hybrid cloud combination scheme $S = \{RP_1, RP_2, \dots, RP_S\}$, the physical machine of all available resources is $\{m_1^1, \dots, m_{M^1}^1, \dots, m_i^k, \dots, m_1^S, \dots, m_{M^S}^S\}$, a physical machine can be represented by m_i^k , where $1 \leq i \leq M^k$, M^k is the number of available physical machines provided by the cloud provider RP_k , the remaining available resources on each physical machine m_i^k can be represented by a resource vector $\vec{R}(m_i^k)$. The tasks submitted by users $\{1, 2, \dots, U\}$ are numbered from 1 to N , and each task corresponds to a virtual machine. The set $A = \{A_1^1, \dots, A_x^u, A_y^u, \dots, A_N^U\}$ represents all virtual machine allocation policies of the resource scheduling center, where $A_n^u = (A_n^u(m_1^1), \dots, A_n^u(m_{M^1}^1), \dots, A_n^u(m_i^k), \dots, A_n^u(m_1^S), \dots, A_n^u(m_{M^S}^S))^T$, $v(S) = (a_{n1}^u(m_i^k), \dots, a_{n2}^u(m_i^k), \dots, a_{nZ}^u(m_i^k))$ represents the number of resources allocated to task n on the physical machine m_i^k .

C. Hybrid Cloud Group Member Selection Model

The cloud resource provider in the hybrid cloud is a set, and there are multiple providers. Therefore, according to this set, multiple different subsets can be formed. These subsets are different composition methods of multiple providers, which means that some providers can be included in the hybrid cloud, and some cannot be included. So, we need to judge which providers can be included in the hybrid cloud and bring benefits to the whole. There are two main ways to judge:

- 1) **Stability:** A hybrid cloud is called stable, when any provider in the hybrid cloud benefits more if it leaves the cloud [29]. It can also be said that this hybrid cloud is the best choice for this provider. Generally speaking, the providers in a stable hybrid cloud should be mutually beneficial, and the providers should exist more in the form of cooperation rather than competition, and their competitors are outside the cloud system. A stable hybrid cloud should also bring more user resources to all providers, and users are more inclined to use the hybrid cloud rather than the system resources provided by a single provider. Fig. 2 shows the filtering process of a stable hybrid cloud combination scheme, in which Pareto optimization means that each member of the combination scheme brings positive benefits to all other members. At the same time, the income obtained in the group is also higher than from not participating in the group.

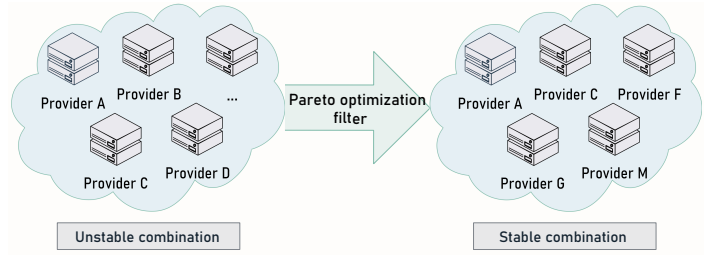


Fig. 2. Filter a Stable Provider Portfolio.

- 2) **Fairness:** A provider in the hybrid cloud hopes that the system is fair, which refers to the fairness of processing user requests, that is, the fairness of scheduling, and the fairness of benefit distribution. Each member should be fairly assigned tasks, and then the corresponding benefits should be distributed according to the completion of the tasks. The distribution of benefits in this paper is based on the Shapley value.

A hybrid cloud cooperation game can be expressed as $G = aP, v$, where aP is all available providers RP in the hybrid cloud, v is the characteristic function, for a provider combination S . Then, this paper defines its characteristic function as $v(S)$ as follows.

$$v(S) = \begin{cases} 0; & \text{(insufficient total resources)} \\ profit(S); & \text{(total resources met)} \end{cases} \quad (6)$$

When $v(s)$ is 0, it means that the hybrid cloud combination S is not feasible. Firstly, according to Eq. 6, we select the provider combinations that satisfy resource constraints, and then judge the overall benefits of these hybrid cloud combinations. The final total benefit is uniformly distributed by the contribution value calculated by the Shapley value. The contribution ability of the provider, that is, the ratio of $\varphi_i(v)$ to the total contribution is the measure. Then, the benefit value that each provider can obtain in the hybrid cloud combination scheme S is calculated as follows.

$$value_i(S) = \frac{\varphi_i(v)}{\sum_{RP_x \in S} \varphi_x(v)} \cdot v(S) \quad (7)$$

The value of each provider's benefits when not participating in the group is:

$$value_i = \begin{cases} 0 & ; \text{(Available resources meet demand)} \\ \sum_k price_S^k \cdot R_k & ; \text{(Available resources don't meet demand)} \end{cases} \quad (8)$$

The hybrid cloud combination scheme S is said to be stable, if $value_i(S) > value_i; \forall RP_i \in S$

D. User QoS Indicators in Game Model

Since the primary goal of cloud computing services is to ensure user QoS, it is necessary to model and evaluate user QoS preferences. Therefore, the user QoS indicators in this

paper consist of the following five elements: Response time, cost, system availability, reliability and trustworthiness.

The user QoS indicators in a hybrid cloud environment are represented by a vector $\{Q_1, Q_2, Q_3, Q_4, Q_5\}$, in which all QoS indicators are in the $[0, 100]$ interval. Each indicator corresponds to a weight, which is determined according to the user's QoS preference and the type of service purchased when the user signs an SLA with the provider. The user's QoS preference and the type of service purchased will affect the division of QoS indicators. The weight value of QoS is also represented by a set of vectors $\{w_1, w_2, w_3, w_4, w_5\}$. Therefore, according to the above analysis, the overall QoS index of the service purchased by the user can be expressed by Eq. 9, where $\{q_1, q_2, q_3, q_4, q_5\}$ corresponding to the response time, cost, system availability, reliability, and trustworthiness, respectively.

$$QoS = \sum_{i=1}^5 w_i \cdot q_i \quad (9)$$

One of the most important QoS indicators is service response time [30]. The computation amount of a task can be estimated from the task type submitted by the user and the environment variables combined with the historical data. It is then calculated according to the computing power $PC(m_i^k)$ of the virtual machine assigned to the user. The response time estimation for the user task is as follows.

$$RT_n = \frac{W_n}{PC(m_i^k)} \quad (10)$$

From the user's point of view, the shorter the response time, the better. This paper unifies the response time $q_1 = 100 - RT_n/Q_1$. It can be seen that the longer the response time, the less q_1 .

From the provider's point of view, the provider hopes to maximize its own benefits, but high cost will affect the user experience. The resource pricing in this paper is represented by $price_k^S$, from which the cost required by the user is:

$$Cost(r_n) = \sum_{k=1}^K r_{nk} \cdot price_k^S \quad (11)$$

In this paper, in order to reflect the cost problem of the provider, when the resource price is less than a certain value, the user's QoS experience is certain and will not increase because of this. Therefore, the user service cost is divided into two levels. In the interval $[0, mark_u]$, the user QoS index q_2 is set to 100, and in $[mark_u, Q_2]$, the higher the service charge, the lower the q_2 value. The normalized q_2 can be represented by Eq. 12.

$$q_2 = \begin{cases} 100 & ; \text{if } Cost(r_n) \leq mark_u \\ \frac{100 - Cost(r_n) - mark_u}{Q_2 - mark_u} & ; \text{if } mark_u < Cost(r_n) \leq Q_2 \end{cases} \quad (12)$$

Since there are no specific data studies on effectiveness, reliability and trustworthiness in QoS, these three are not

studied in depth in this paper. The three settings are as follows: The availability and reliability are mainly obtained by referring to the running status of the server in the historical data. The credibility can use the user's historical evaluation and the system itself to set the evaluation of the previous service completion.

The above three parameters q_3, q_4, q_5 give QoS ratings respectively according to the evaluation results. Then, the three indicators are unified according to the first two parameters, respectively, corresponding to a certain value in the interval $[0, 100]$, representing the scoring result of this attribute.

E. The Proposed Game Theory Model

The game theory model in this paper mainly considers the relationship between the following three in the cloud computing environment: cloud service users, a single provider, and a group of multiple providers. The purpose of using game theory is to use a model that can describe the interests of the three parties at the same time. This model must be objective, and can adapt to different applicable occasions through parameters adjustments. For example, in some occasions, it favors user QoS, and in some cases, it favors resource utilization, that is, multiple providers. Based on the above analysis, the game theory model in this paper establishes three optimization goals according to three stakeholders: user QoS optimization, server resource utilization optimization, and system maintenance cost optimization.

According to the relevant introduction above, we first establish the resource constraints of a hybrid cloud combination, and then establish the combination model of resource providers, and calculate the optimal provider combination through the constraints and the overall revenue value. Then a tripartite game model is established to calculate the overall total revenue of the system. The hybrid cloud game model in this paper is represented by a quadruple $\{Players, Req, A, Utility\}$ as follows:

- 1) *Players* are players in the game, that is, users who submit resource requests, the hybrid cloud, and the providers in the hybrid cloud.
- 2) *Req* is the resource request matrix formed by the task submitted by the user.
- 3) $A = \{A^u | u = 1, 2, \dots, U\}$ represents the deployment placement scheme of virtual machines allocated to users in the system.
- 4) *Utility* is a global revenue function. The utility describes the total revenue that can be obtained by the entire system of a virtual machine deployment solution. The larger the value, the better.

Utility is divided into three parts according to three stakeholders, the first part is user QoS and has been introduced above. Then, the calculation method of the revenue value representing the resource utilization of the provider group is introduced. For a stable provider combination S , there are N tasks ready to be allocated at a certain time, and the virtual machine resource vector corresponding to the task is \vec{r}_n . The initial total resource vector on physical machine m_i^k is $\vec{M}(m_i^k)$, $util_t^{(m_i^k)}$ (calculated as in Eq. 13) is the utilization rate of resources of type t on physical machine m_i^k , and

the average utilization rate of the resources on the physical machine is $utl_t^{(m_i^k)}$.

$$utl_t^{(m_i^k)} = 1 - \frac{R_t(m_i^k) - \sum_n x_{nt}^{(m_i^k)}}{PM_t(m_i^k)} \quad (13)$$

where $R_t(m_i^k)$ represents the number of resources available on physical machine m_i^k , $x_{nt}^{(m_i^k)}$ is the number of resources of type n allocated to the task on physical machine m_i^k , and $PM_t(m_i^k)$ represents the total number of resources t on physical machine m_i^k .

The portion of the global benefit that represents the provider's interests is:

$$MT_i = \sum_{k=1}^K \omega_k^P \cdot N_k^P \cdot value_k^P \quad (14)$$

where $value_k^P$ represents the unit price of the corresponding resource, N_k^P represents the usage of the corresponding resource, and ω_k^P represents the price correction parameter of the corresponding resource. So the global revenue of the game is calculated by Eq. 15.

$$Utility = \alpha \cdot \frac{\sum_{n=1}^N QoS_n}{N} + \beta \cdot \frac{\sum_{y=1}^{M_N} MT_y}{M_N} + (1-\alpha-\beta) \cdot \frac{\sum_{i=1}^{M_N} utl^{(m_i^k)}}{M_N} \quad (15)$$

where MT_y is the revenue of a single cloud resource provider.

In order to ensure the fairness of the three benefits, the three parts of the above equation can be normalized. From Eq. 15, it can be seen that the relationship between the three optimization objectives can be balanced by adjusting the value of the tripartite interest weights α and β .

V. VIRTUAL MACHINE PLACEMENT ALGORITHM

A. Load Balancing Optimization in Physical Servers

When a cloud computing system creates a virtual machine on a physical server, because both are multi-dimensional resources, it cannot guarantee that the proportion of virtual machine resources matches the resource ratio of the physical machine. For example, the CPU resources may have been fully occupied by the virtual machine, but there are still a lot of memory resources left; or the memory resources are fully allocated but the CPU resources are still left. This part of the remaining resources will not be able to continue to be allocated, resulting in resource fragmentation and waste of resources. Therefore, for the sake of load balancing, the proportion of resources allocated to virtual machines should preferably be similar, so that resource fragmentation is not easy to generate. Thus, ensuring balanced operation of each physical server, reducing energy and resource waste, and improving utilization. Thereby, the system throughput can be increased at the same cost.

Because cloud users have various needs, in general, cloud resource providers will also provide virtual machine customization functions for cloud users, so the virtual machine requests of cloud users received by the hybrid cloud system will be various. The proportion of various resources in the machine is also uneven. First of all, if it is assumed that the resource ratio of all virtual machines is the same, then each physical server can ensure the load balancing of virtual machine resources. Therefore, this paper proposes an algorithm for load balancing optimization as follows:

- 1) When the hybrid cloud system is initialized, virtual machines with large difference in resource ratio are preferentially allocated, so that virtual machines with different resource ratios can complement each other's deficiencies.
- 2) When the hybrid cloud is running, if there is a new virtual machine assignment task, the Nash equilibrium of game theory is used to calculate whether to start a new physical server or not.
- 3) When the hybrid cloud is running, if a virtual machine needs to be shut down, the Nash equilibrium of the same calculation game theory determines whether to carry out the migration work and migration target of other virtual machines.

We calculate the average resources \overline{Res} of physical servers as a reference standard for the proportion of virtual machine resources as follows.

$$\begin{aligned} \overline{Res} &= \{\overline{PE}, \overline{Mem}, \overline{Store}\}^T \\ &= \left\{ \frac{\sum_{i=1}^n PE_i}{n}, \frac{\sum_{i=1}^n Mem_i}{n}, \frac{\sum_{i=1}^n Store_i}{n} \right\}^T \end{aligned} \quad (16)$$

where PE represents the number of processor cores corresponding to the physical server, Mem represents the amount of memory, and $Store$ represents the number of external storage memory. The amount of resources required by a virtual machine can also be expressed as $VRes$.

The skewness of virtual machine resources is calculated from the Euclidean distance between virtual machine resources and physical machine resources as follows.

$$\begin{aligned} VVari_t &= \sqrt{(VPE_i - \overline{PE})^2 + (VMem_i - \overline{Mem})^2 + (VStore_i - \overline{Store})^2} \\ \forall i &= (1, 2, \dots, n) \end{aligned} \quad (17)$$

The first step of the optimization algorithm is initialization. In this step, for each virtual machine to be created and its corresponding candidate physical machine, the utility value $Utility$ is calculated and sorted. All physical machines are initially marked as inactive. This optimization problem is solved using a greedy algorithm. Assuming that an optimal deployment scheme for $n - 1$ virtual machines has been obtained, the optimal deployment scheme for the n virtual machine is to find a corresponding running state physical machine to ensure that the available resources are sufficient to create the virtual machine, and the benefits value is maximized.

The best physical machine that satisfies the conditions is directly enabled at the beginning. After several iterations of creation, the available resources on the best physical machine selected may not be enough to create the n virtual machines. At this time, the physical machine needs to make a decision, to determine whether it is necessary to delete some received virtual machines to make room to create new ones. The selection order is to delete from the maximum skewness between the virtual machine resource type and the total resources of the physical machine until the available resources are sufficient to create a new virtual machine.

The decision on whether to choose to replace a virtual machine is based on the utilization rate corresponding to the least used resource type (Eq. 18) on the physical machine before and after replacement. If the utilization rate increases after replacement, it means that the replacement is beneficial and the virtual machine can be replaced.

$$\begin{aligned}
 utl_{\min}^{(m_i^k)} &= \min_t \{ utl_t^{(m_i^k)} \} \\
 &= \min_t \left\{ 1 - \frac{R_t(m_i^k) - \sum_n x_{nt}^{(m_i^k)}}{PM_t(m_i^k)} \right\} \quad (18)
 \end{aligned}$$

B. Algorithm Flow

Based on the above analysis, this paper proposes a game theory-based load balancing optimization algorithm (LBOGT). The idea of the algorithm: When placing virtual machines in the hybrid cloud system, it first obtains the resource information of the applied virtual machines from the application list. Next, the resource skewness of each virtual machine is calculated according to the resource information, and sorted in descending order of skewness. Then, put them in the *vmlist* table and wait for the system to schedule. The system sequentially fetches the virtual machines to be scheduled from the *vmlist*, and calculates the virtual placement position with the greatest benefit according to the global revenue *Utility*. When the virtual machine is placed, there may be insufficient physical machine resources. At this time, calculate whether to migrate the virtual machine according to Eq. 18. If the virtual machine needs to be migrated, it is treated as a new virtual machine to be deployed. Otherwise, apply for new physical resources.

The detailed process of the LBOGT algorithm is given in Fig. 3.

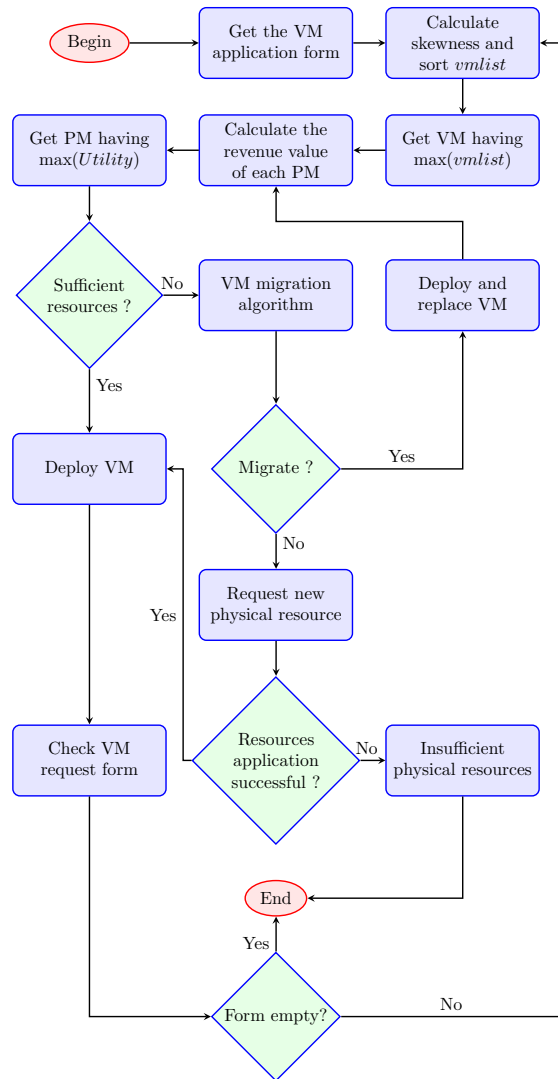


Fig. 3. LBOGT Algorithm Flowchart.

VI. EXPERIMENTAL RESULTS

This section will validate the aforementioned provider team member selection model and our proposed virtual machine placement algorithm based on load balancing optimization (LBOGT). This paper uses CloudSim [31] to build a cloud computing simulation experimental environment, and uses JAVA programming to test the algorithm. CloudSim is an open and extensible simulation framework that integrates modeling, simulation and experimentation into one cloud computing environment for experiments. The physical machine configuration in this paper is shown in Table I. Then, simulate 24 hours of data from a hybrid cloud data center. Our proposed algorithm LBOGT is compared to Inter Quartile Range (IQR), Median Absolute Deviation (MAD), Static Threshold (THR) and Game Theory (GT) algorithms.

A. Selection of Hybrid Cloud Group Members

TABLE I. HYBRID CLOUD SYSTEM RESOURCE CONSTRAINTS

Attributes	Ranges
Number of physical machines (host)	[400, 1000]
Number of processor (CPU) cores	[1600, 32000]
Processor (CPU) frequency	[0.50GHz, ∞]
Physical machine memory size	[6400GB, 128000GB]
Physical machine external memory size	[400TB, 10000TB]

There are currently 5 providers to be selected. The processor of the providers are Intel Xeon of the following models: E5-2620, E5-2603, E5-2609, E7-4807, E7-8837. The number of virtual machine requests is 800, and other configurations are shown in Table II.

TABLE II. THE CANDIDATE PROVIDERS OF THE HYBRID CLOUD SYSTEM

Provider	Number of CPU cores	CPU frequency	RAM size	External storage size	CPU unit price	RAM unit price	External storage unit price	Price correction parameter δ
1	1680	2.10GHz	8960GB	560	0.01	0.004	0.06	1.02140275
2	1280	1.80GHz	10240GB	640	0.008	0.003	0.06	1.16487403
3	1560	2.40GHz	8320GB	520	0.008	0.002	0.07	1.05145024
4	1680	1.86GHz	8960GB	560	0.015	0.003	0.05	1.13123516
5	1920	2.66GHz	15360GB	480	0.015	0.004	0.05	1.19472345

Based on the constraints shown in Table I, the configuration properties made up of all provider combinations are now calculated. There are a total of 5 providers, excluding the 5 possibilities of a single provider, then a total of 26 different provider combinations are possible.

From Table III, it can be seen that it is not that the more providers, the greater the average revenue value. This is because when a provider with a poorly configured physical server joins, the team will have an evaluation of the newly added provider's configuration, and a poorly configured server may affect all user experiences. Therefore, it is necessary to select an optimal combination among all combinations. This combination needs to meet the resource constraints of the team, and the average host revenue should be the highest. The average host revenue value refers to the team's total revenue evenly distributed to each host.

TABLE III. RESTRICTIONS RESULTS

Provider combination	Total number of hosts	Total core	Total memory	Total external storage	Restrictions
1,2	600	2960	19200	1200	-
1,3	540	3240	17280	1080	Insufficient hosts
1,4	560	3360	17920	1120	Insufficient hosts
1,5	520	3600	24320	1040	Insufficient hosts
2,3	580	2840	18560	1160	Insufficient hosts
2,4	600	2960	19200	1200	-
2,5	560	3200	25600	1120	Insufficient hosts
3,4	540	3240	17280	1080	Insufficient hosts
3,5	500	3480	23680	1000	Insufficient hosts
4,5	520	3600	24320	1040	Insufficient hosts
1,2,3	860	4520	27520	1720	-
1,2,4	880	4640	28160	1760	-
1,2,5	840	4880	34560	1680	-
1,3,4	820	4920	26240	1640	-
1,3,5	780	5160	32640	1560	-
1,4,5	800	5280	33280	1600	-
2,3,4	860	4520	27520	1720	-
2,3,5	820	4760	33920	1640	-
2,4,5	840	4880	34560	1680	-
3,4,5	780	5160	32640	1560	-
1,2,3,4	1140	6200	36480	2280	-
1,2,3,5	1100	6440	42880	2200	-
1,2,4,5	1120	6560	43520	2240	-
1,3,4,5	1060	6840	41600	2120	-
2,3,4,5	1100	6440	42880	2200	-
1,2,3,4,5	1380	8120	51840	2760	-

In order to calculate the total revenue for each provider group, firstly we calculate the pricing of all system resources according to Eq. 4. The price correction parameter δ in the

formula are obtained according to the resource evaluation of the resource provider as shown in Table II. The total value of the group's income is calculated by Eq. 5, and the final calculation results are shown in Table IV.

TABLE IV. GROUP INCOME STATEMENT

Provider combination	CPU pricing	Memory pricing	External storage pricing	Total team revenue	Average hosting revenue
1,2	0.00982699	0.00377042	0.06587525	180.53017618	0.30088363
1,3	0.00934619	0.00313097	0.06721474	156.97679288	0.29069776
1,4	0.01189442	0.00373966	0.05892296	172.97365957	0.30888153
1,5	0.01432433	0.00452347	0.06056971	224.57098009	0.43186727
2,3	0.00882057	0.00287075	0.07155513	161.33542275	0.27816452
2,4	0.01173446	0.00344753	0.06367146	177.33228943	0.29555382
2,5	0.01448011	0.00426519	0.06553975	228.92960995	0.40880287
3,4	0.01108883	0.00277221	0.06476609	153.77890613	0.28477575
3,5	0.01365808	0.00383868	0.06694615	205.37622665	0.41075245
4,5	0.01589270	0.00426856	0.05802687	221.37309333	0.42571749
1,2,3	0.00933849	0.00326628	0.06821110	249.42119591	0.29002465
1,2,4	0.01118396	0.00365055	0.06291186	265.41806259	0.30161143
1,2,5	0.01301146	0.00421863	0.06412122	317.01538311	0.37739927
1,3,4	0.01079012	0.00322069	0.06357714	241.86467929	0.29495693
1,3,5	0.01253676	0.00390646	0.06491364	293.46199981	0.37623333
1,4,5	0.01408585	0.00421931	0.05916692	309.45886649	0.38682358
2,3,4	0.01058763	0.00304101	0.06667357	246.22330915	0.28630617
2,3,5	0.01249127	0.00373481	0.06809592	297.82062967	0.36319589
2,4,5	0.01416845	0.00403925	0.06254709	313.81749636	0.37359226
3,4,5	0.01363980	0.00371653	0.06321842	290.26411306	0.37213348
1,2,3,4	0.01048640	0.00329758	0.06534985	334.30908231	0.29325358
1,2,3,5	0.01189721	0.00380811	0.06636202	385.90640283	0.35082400
1,2,4,5	0.01315573	0.00404879	0.06223136	401.90326952	0.35884220
1,3,4,5	0.01279173	0.00379602	0.06270749	378.34988622	0.35693385
2,3,4,5	0.01277394	0.00366354	0.06515995	382.70851608	0.34791683
1,2,3,4,5	0.01224430	0.00373649	0.06437356	470.79428924	0.34115528

It can be seen from Table IV that the best combination that meets the constraints is the provider combination (1, 4, 5). The revenue of the host unit reached 0.38682358, and the average revenue of team members was the largest.

B. QoS Performance Test

The QoS performance test mainly compares IQR, MAD, THR, GT and LBOGT algorithms. In the comparison process, this paper sets the parameters α and β of Eq. 15 to 0.8 and 0.1, respectively, which can clearly reflect the QoS improvement of LBOGT algorithm. IQR, MAD, and THR algorithms are all built-in algorithms in CloudSim simulation software, which are used as reference in this paper.

THR algorithm is a short-answer threshold algorithm with fast algorithm speed and poor optimization results. Since IQR algorithm only tries to optimize the discrete degree of the deployment results during the virtual machine deployment process, the interquartile range of the deployment results is as small as possible, so that the load balance of the virtual machines can be guaranteed to a certain extent. IQR algorithm is a rough state optimization of the overall result, it is not specific to each physical machine, so the result is still far from the optimal solution. MAD algorithm weakens the individual extreme values in the deployment process, thereby ensuring the load balancing effect of most virtual machines. It is a deployment scheme that sacrifices a few and satisfies the overall deployment scheme. MAD sacrifices the performance of a few virtual machines. The optimization result also has a certain distance from the optimal solution.

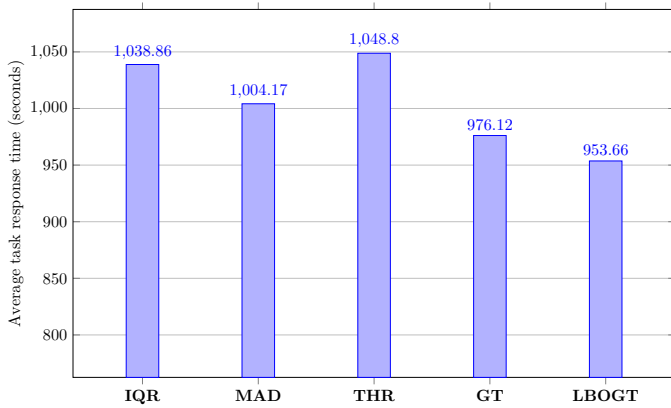


Fig. 4. Task Response Time Comparison.

From Fig. 4, it can be seen that the response time of LBOGT and GT algorithms is shorter, because compared with other reference algorithms, LBOGT and GT consider all QoS preferences of users, including five preference attributes of QoS, so the response time is better. Compared to GT, LBOGT increases the optimization of virtual machine deployment. Therefore, the performance of LBOGT's response time is slightly better than that of GT, and the effect is increased by 2.3%, because the response time of the system to tasks when there is not too much pressure is similar.

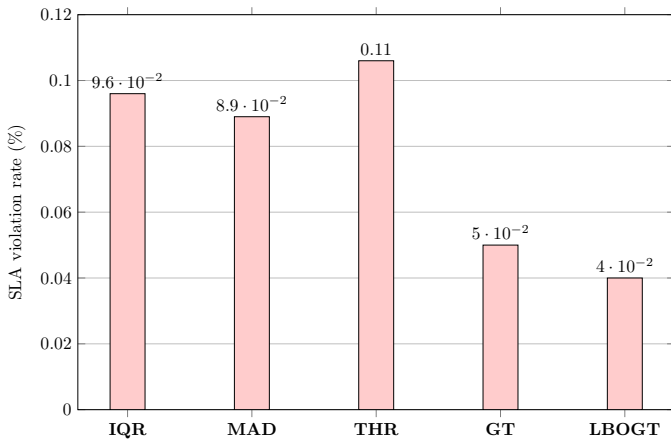


Fig. 5. SLA Violation Rate Comparison.

From Fig. 5, it can be seen that the SLA violation rate of the LBOGT model is 0.01% lower than that of GT model. This is because when the virtual machine placement algorithm is executed, there is an optimization process for LBOGT to select a virtual machine. The algorithm first selects virtual machines with larger resource skewness for deployment. In this way, virtual machines whose skewness can compensate each other can be deployed to a server as much as possible during the deployment process, so that the server can achieve load balancing. It reduces server resources waste, optimizes resource allocation, and allows users' tasks to be better executed. The higher the value of α in the utility function (Eq. 15), the higher the user's QoS weight is, so the game model will consider the user's QoS more. The smaller the α , the higher the individual provider's income, because the provider and the user have conflict of interest to a certain extent. The provider expects low cost and high income, while the user expects low

consumption and high QoS. In the utility function, the lower the α and β , the higher the resource utilization of the hybrid cloud system, which can reduce resources waste and reduce maintenance costs. The other three algorithms have higher SLA violation rate values because they do not consider too much user QoS.

C. Power Consumption Performance Test

Before testing the power consumption performance of the LBOGT algorithm, it is necessary to set α and β parameters of Eq. 15 to 0.1. The performance of the algorithms in term of power consumption is presented in Fig. 6.

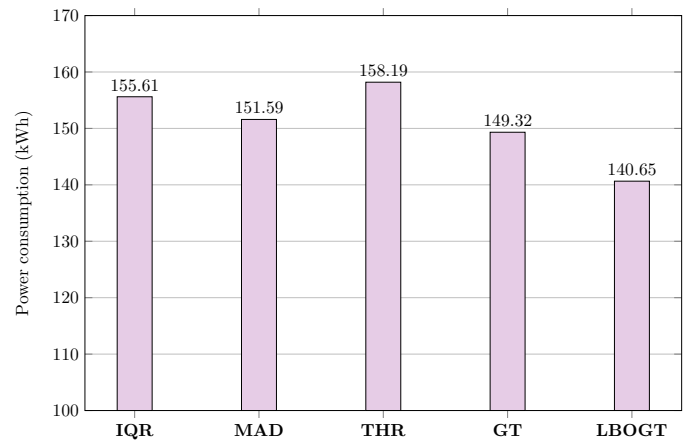


Fig. 6. Power Consumption Comparison.

Fig. 6 shows that LBOGT has great advantage in power consumption, saving 6.16% of energy than GT algorithm. Because there is a virtual machine optimization selection step in the process of LBOGT algorithm compared to GT. The virtual machine deployment order can be optimized to achieve better load balancing effect, thus reducing the waste of resources. On the other hand, LBOGT considers that there will be new requests during the operation of the hybrid cloud system, so there will be dynamic addition of virtual machines. LBOGT will also optimize the newly added virtual machine requests, so it is also conducive to the best deployment.

In the following, it is the comparison of the benefits of our proposed LBOGT algorithm and the traditional game theory-based algorithm GT. The comparison here refers to the income value obtained after pricing various resources when modeling the provider's interests. The income value is not added to the unit when setting it. It is a relative value and is used as the global income of the game theory. For judgment and comparison, see Table IV for details. Since the LBOGT algorithm has made improvements to the deficiencies of GT algorithm in the management of virtual machines to be deployed, and the provider's profit has been considered when formulating the global profit function of the game, it can be seen from Fig. 7 that the improved LBOGT algorithm can bring greater benefits. This benefit is more obvious when the task request is larger. Indeed, when the number reaches 1600, the benefit value increases by 10.6%.

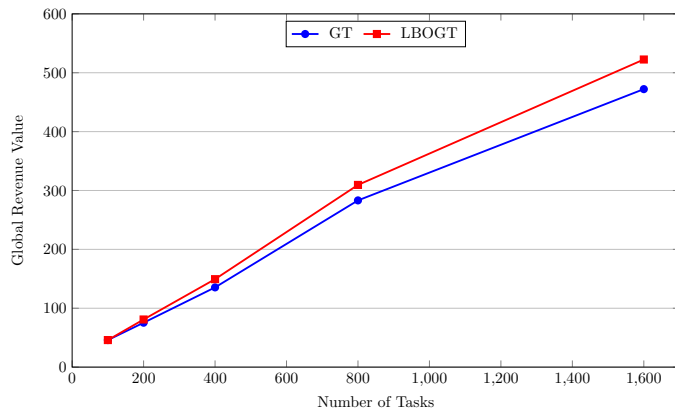


Fig. 7. Global Revenue Comparison.

VII. CONCLUSION

This paper considers the problem of virtual machine placement problem in hybrid cloud situation from the perspective of economics and QoS. In order to coordinate user QoS and cloud resource utilization, a game theory model of a three-party game is established, and the relationship between the three parties is reflected through a game's profit function. Finally, a virtual machine placement algorithm based on game theory and load balancing optimization is proposed. The algorithm mainly selects the virtual placement position through the game theory revenue function, and optimizes the placement order of the virtual machine through its resource application ratio. The experimental results show that our proposed LBOGT algorithm can coordinate and balance user QoS and cloud computing resource utilization. When the number of executed tasks reaches 1600, the cloud computing revenue is 10.6% higher than that obtained by the traditional game theory method.

Several various adjustments, testing, and experiments have been left to be completed in the future. More virtual machine placement objectives can be investigated in the future, in particular SLA-aware placement schemes.

REFERENCES

- [1] R. Moreno-Vozmediano, R. S. Montero, and I. M. Llorente, "IaaS cloud architecture: From virtualized datacenters to federated cloud infrastructures," *Computer*, vol. 45, pp. 65–72, 2012.
- [2] H. Zhang, G. Jiang, K. Yoshihira, H. Chen, and A. Saxena, "Intelligent workload factoring for a hybrid cloud computing model," in *Proceedings - 5th 2009 World Congress on Services*, 2009, pp. 701–708.
- [3] Z. Wu and H. V. Madhyastha, "Understanding the latency benefits of multi-cloud webservice deployments," *ACM SIGCOMM Computer Communication Review*, vol. 43, pp. 13–20, 2013.
- [4] V. C. Emeakaroha, M. A. Netto, R. N. Calheiros, I. Brandic, R. Buyya, and C. A. D. Rose, "Towards autonomic detection of sla violations in cloud infrastructures," vol. 28, pp. 1017–1029, 2012.
- [5] Z. ur Rehman, O. K. Hussain, F. K. Hussain, E. Chang, and T. Dillon, "User-side qos forecasting and management of cloud services," *World Wide Web*, vol. 18, pp. 1677–1716, 2015.
- [6] R. N. Calheiros, R. Ranjany, and R. Buyya, "Virtual machine provisioning based on analytical performance and qos in cloud computing environments," in *Proceedings - the International Conference on Parallel Processing*, 2011, pp. 295–304.
- [7] M. Xu, L. Cui, H. Wang, and Y. Bi, "A multiple qos constrained scheduling strategy of multiple workflows for cloud computing," in *Proceedings - 2009 IEEE International Symposium on Parallel and Distributed Processing with Applications*, 2009, pp. 629–634.

- [8] A. K. Bardsiri and S. M. Hashemi, "Qos metrics for cloud computing services evaluation," *International Journal of Intelligent Systems and Applications*, vol. 6, pp. 27–33, 2014.
- [9] Y. Pan, S. Ding, W. Fan, J. Li, and S. Yang, "Trust-enhanced cloud service selection model based on qos analysis," *PLoS ONE*, vol. 10, 2015.
- [10] S. Farzai, M. H. Shirvani, and M. Rabbani, "Multi-objective communication-aware optimization for virtual machine placement in cloud datacenters," *Sustainable Computing: Informatics and Systems*, vol. 28, 2020.
- [11] W. Jing, C. Zhao, Q. Miao, H. Song, and G. Chen, "Qos-dpso: Qos-aware task scheduling for cloud computing system," *Journal of Network and Systems Management*, vol. 29, 2021.
- [12] O. F. Aloufi, K. Djemame, F. Saeed, and F. Ghaban, "A survey on predicting workloads and optimizing qos in the cloud computing," in *Proceedings - 2021 International Congress of Advanced Technology and Engineering, ICOTEN 2021*. Institute of Electrical and Electronics Engineers Inc., 2021.
- [13] A. Edinat, R. Al-Sayyed, and A. Hudaib, "A survey on improving qos in service level agreement for cloud computing environment," *International Journal of Interactive Mobile Technologies*, vol. 15, pp. 119–143, 2021.
- [14] X. Wang and Y. Wang, "Coordinating power control and performance management for virtualized server clusters," *IEEE Transactions on Parallel and Distributed Systems*, vol. 22, pp. 245–259, 2011.
- [15] G. Jung, M. A. Hiltunen, K. R. Joshi, R. D. Schlichting, and C. Pu, "Mistral: Dynamically managing power, performance, and adaptation cost in cloud infrastructures," in *Proceedings - International Conference on Distributed Computing Systems*, 2010, pp. 62–73.
- [16] F. Fang and B.-B. Qu, "Multi-objective virtual machine placement for load balancing," *ITM Web of Conferences*, vol. 11, p. 01011, 2017.
- [17] A. Ghasemi and A. T. Haghghat, "A multi-objective load balancing algorithm for virtual machine placement in cloud data centers based on machine learning," *Computing*, vol. 102, pp. 2049–2072, 2020.
- [18] M. Xu, W. Tian, and R. Buyya, "A survey on load balancing algorithms for virtual machines placement in cloud computing," *Concurrency and Computation: Practice and Experience*, vol. 29, 2017.
- [19] B. Sotomayor, K. Keahey, I. Foster, and T. Freeman, "Enabling cost-effective resource leases with virtual machines," in *Proceedings - 2007 ACM/IEEE International Symposium on High Performance Distributed Computing*, 2007.
- [20] Y. Chen, A. Sivasubramaniam, A. Das, Q. Wang, W. Qin, and N. Gautam, "Managing server energy and operational costs in hosting centers," *Performance Evaluation Review*, vol. 33, pp. 303–314, 2005.
- [21] A. S. Abohamama and E. Hamouda, "A hybrid energy-aware virtual machine placement algorithm for cloud environments," *Expert Systems with Applications*, vol. 150, 2020.
- [22] C. Wei, Z. H. Hu, and Y. G. Wang, "Exact algorithms for energy-efficient virtual machine placement in data centers," *Future Generation Computer Systems*, vol. 106, pp. 77–91, 2020.
- [23] S. Azizi, M. Zandsalimi, and D. Li, "An energy-efficient algorithm for virtual machine placement optimization in cloud data centers," *Cluster Computing*, vol. 23, pp. 3421–3434, 2020.
- [24] H. Feng, Y. Deng, and J. Li, "A global-energy-aware virtual machine placement strategy for cloud data centers," *Journal of Systems Architecture*, vol. 116, 2021.
- [25] R. B. Madhumala, H. Tiwari, and V. C. Devaraj, "Virtual machine placement using energy efficient particle swarm optimization in cloud datacenter," *Cybernetics and Information Technologies*, vol. 21, pp. 62–72, 2021.
- [26] B. Rochwerger, D. Breitgand, E. Levy, A. Galis, K. Nagin, I. M. Llorente, R. Montero, Y. Wolfsthal, E. Elmroth, J. Caceres, M. Ben-Yehuda, W. Emmerich, and F. Galan, "The reservoir model and architecture for open federated cloud computing," *IBM Journal of Research and Development*, vol. 53, pp. 1–11, 2009.
- [27] G. Chen, H. V. Jagadish, D. Jiang, D. Maier, B. C. Ooi, K. L. Tan, and W. C. Tan, "Federation in cloud data management: Challenges and opportunities," *IEEE Transactions on Knowledge and Data Engineering*, vol. 26, pp. 1670–1678, 2014.

- [28] D. C. Erdil, "Autonomic cloud resource sharing for intercloud federations," *Future Generation Computer Systems*, vol. 29, pp. 1700–1708, 2013.
- [29] F. Palmieri, L. Buonanno, S. Venticinque, R. Aversa, and B. D. Martino, "A distributed scheduling framework based on selfish autonomous agents for federated cloud environments," *Future Generation Computer Systems*, vol. 29, pp. 1461–1472, 2013.
- [30] C.-T. Fan, Y.-S. Chang, W.-J. Wang, and S.-M. Yuan, "Execution time prediction using rough set theory in hybrid cloud," in *Proceedings - 2012 9th International Conference on Ubiquitous Intelligence and Computing and 9th International Conference on Autonomic and Trusted Computing*. IEEE, 2012, pp. 729–734.
- [31] R. Buyya, R. Ranjan, and R. N. Calheiros, "Modeling and simulation of scalable cloud computing environments and the cloudsim toolkit: Challenges and opportunities," in *Proceedings - 2009 International Conference on High Performance Computing and Simulation*, 2009, pp. 1–11.

Ensuring Privacy Preservation Access Control Mechanism in Cloud based on Identity based Derived Key

Suresha D
Research Scholar, VTURRC
Associate Professor, Dept. of CSE
Dr. AIT, Bangalore, Karnataka

Dr. K Karibasappa
Professor, Dept. of CSIT
Graphic Era Deemed To Be University
Dehradun, Uttarakhand

Dr. Shivamurthy
Associate Professor, VIAT,
Muddenahalli, Bangalore,
Karnataka, India

Abstract—Cloud computing is a dominant technology that involves massive amounts of data storage and access via the internet. Because there is a large amount of data stored in data centers, it is critical to implement appropriate access control mechanisms over data stored in a cloud. Today, there are numerous access control mechanisms available to provide confidentiality, privacy, and data origin authentication in a cloud environment. The available access control techniques may have a higher computational overhead and lack security concerns. In this paper, we designed and implemented a privacy-preserving access control in cloud computing using derived key identity-based encryption. The proposed method may reduce computational overhead while generating the key while also increasing the robustness of cryptographic keys. During the key generation process, the trusted key center (TKC) is involved. The experimental results show that the proposed method reduces computational overhead and provides an easy way to implement an access control mechanism in a cloud environment.

Keywords—Access control; cloud storage; confidentiality; data origin authentication; key derivation

I. INTRODUCTION

The exponential growth of cloud services allows data owners and cloud users to store and access large amount of data in cloud data centers. When huge volume of data is stored and accessed, raises number of security concerns. One of the cloud's security concerns is providing reliable access control over cloud data. To improve data access control, a set of access control mechanisms has been implemented. Identity-based access control is a popular method for data owners to store data in the cloud. In this mechanism, the cloud user requests access to data from the cloud that has been uploaded by the specific data owner. The data owner receives the user's request and generates the public key using the cloud user's data credentials. The user's public key is used to encrypt the data, which is then shared with a cloud user. The trusted key center (TKC) is involved in the generation of the cloud user's private key using the TKC's secret value and the user's public key. The first major concern with identity-based encryption is the higher computational cost of obtaining the cloud user's public and private keys. The second major concern with this mechanism is that data origin authentication may fail. In this context, the proposed scheme is intended to reduce the limitations of identity-based encryption while also addressing key robustness effectively. The proposed scheme is purely based on Identity-

Based Encryption (IBE). In IBE approach, the data owner encrypts the data using the public key which is derived from cloud user and the decryption at the cloud user is carried out using private key. The TKC is required whenever the private key is derived. The IBE which simplifies the management of public key certificates at the public key infrastructure (PKI) and this can be the alternative approach to public key encryption.

However, one main important drawback of IBE is that the computational overhead at key pair generation. The proposed work definitely overcome the limitations of Identity-Based Encryption. Instead of generating public-private key pair, pair of secret keys are generated for encryption/decryption as well as data origin authentication. The Trusted Key Center (TKC) is involved for secure communication between the data owner and the cloud user. The proposed approach can increase the comparability of data sharing, cloud user authentication and increases key robustness.

II. LITERATURE SURVEY

Khalid Albulayhi et al. [1] conducted an analytical review on fine-grained access control mechanisms in cloud computing. They have analyzed existing access control methods such as traditional access control mechanisms (ACMs), encryption based ACMs and the modern ACMs and their limitations in the field of cloud computing to improve data access control in the cloud environment. Ajay Kumar Dubey et al. [2] proposed a attribute-based credit computation method to access the data in a withe help of access control mechanism form the cloud. Cloud services are essential and demanded in today's information technology for sharing and accessing data over the internet. The primary responsibility of the cloud service provider is to ensure the scalability, dependability, and security of cloud data. This paper emphasizes on the working of different types of access control mechanisms to control the aceeing of data. An algorithmic namely crowd review and attribute-based credit computation system has been proposed and the cloudsim tool has been used for simulating the results to demonstrate the credit value for the cloud environment.

Jialu Hao et al. [3] proposed a fine-grained attribute hiding policy for cloud-based internet of things (IoT). The attribute information is completely hidden using a randomizable technique and a fuzzy-based Bloom filter mechanism. A system has been proposed that achieves effective policy

privacy preservation with the minimal storage and computation overhead. According to the experimental results, valuable attribute information is not disclosed to unauthorized parties. Shengmin Xu et al. [4] proposed fine-grained bilateral access control for secure cloud-fog computing. A new concept has been proposed that is cloud-fog computing which allow them to provide a variety of on-demand services over the network. The identification and retrieval of useful data from a large volume of cipher text data without the use of expensive decryption mechanisms remains a difficult problem. A system has been created that provides confidentiality as well as data origin identification by utilizing a new cryptographic technique known as matchmaking attribute-based encryption (MABE).

Sana Belguith et al. [5] proposed a privacy-preserving attribute-based framework for cloud access control. To distribute keys among cloud users, existing cryptographic techniques for access control impose a high computational cost on the data owner's site. A system has been created that combines attribute-based encryption and attribute-based signature mechanisms to allow the secure sharing of outsourced data via the public cloud. Mahender Kumar and Satish Chand [6] proposed a secure key issuing identity-based encryption in a cloud environment. Because of the high cost of storage, traditional public key cryptosystems are impractical in real-time environments. To overcome the limitations of traditional public key cryptography, the author has proposed a mechanism for generating the user's private key that eliminates the need for a key generation center (KGC) and to secure communication over a public channel, the ECC-based blind technique is used.

Shengmin Xu et al. [7] proposed fine-grained access control mechanism for dynamic groups in a cloud environment. Cloud computing is a new trend in which users can store data and access the data based on scalable on-demand services. At the same time, cloud computing introduces numerous security issues because cloud service providers (CSPs) doesn't share the same trusted domain for all the users. Yi Liu et al. [8] proposed a secure and fine-grained access control mechanism for storing electronic health care records in mobile cloud computing. To access the e-health care records in a controlled manner, the bilinear Diffie-hellman exponent assumption is used. The simulation results have been generated and the model proved to be suitable for mobile cloud computing.

Fangbo Cal et al. [9] conducted a survey on various access control techniques to protect information and system resources and to limit unauthorized users accessing information in the cloud environment. The paper provides the summary of the benefits and drawbacks of various access control mechanisms and suggested some future research directions. Shivanna K et al. [10] proposed a double encryption method for cloud computing privacy preservation. The author proposed a double encryption mechanism to improve the privacy of data stored on cloud, one for storing data and the other for accessing data from the cloud server.

Rashad Elhabob et al. [11] proposed identity-based encryption with an authorized equivalence test for cloud-aided IoT. A system has been proposed to collect the data using different sensors, encrypt the data and store the data on the cloud and the identity-based encryption with authorized equivalence test (IBE-AET) has been proposed to test the equivalence of two messages encrypted with the same or different identities

and simulated the results and theoretical analysis has been done. Kwangsu Lee [12] proposed a revocable identity-based encryption method based on the subset difference method rather than the complete subtree (CS) method. A system has been proposed by combining identity-based and hierarchical identity-based encryption.

Hongbing Cheng et al. [13] proposed a method for accountable privacy preservation based on identity-based encryption. The system architecture for accountable privacy preservation, as well as a detailed security analysis, is presented. The system is designed to defend against various types of attacks, and the simulation results in increased efficiency. Chandrashekar Meshram et al. [14] proposed an identity-based encryption technique based on fuzzy technique for data sharing in cloud environment. To reduce key disclosure, a technique has been implemented that protects against a chosen ciphertext attack and a chosen sub-tree attack and it has the proficiency to overcome the limitations of currently available methods in terms of security and public key length.

Hua Deng et al. [15] [16] [17] proposed Identity-Based Encryption for cloud data security with flexible data sharing among the users. They proposed two different kind of algorithms such as Identity-based Encryption (IBE) and Identity-Based broadcast encryption (IBBE). The main aim of this work is to tackle the critical issue of revocation of identity and propose a revocable IBE scheme in the server-aided setting. Nishat Farjana et al. [18] [19] [20] [21] secure identity-based data sharing scheme for social networks in cloud computing. The main aim of this scheme is to provide secure data sharing over authorized users. This approach is able to resist the keywords guessing attack as well as reduced computational cost.

Sharma et al. [22] [23] [24] proposed a blockchain based architecture using identity-based encryption. In today's world, blockchain and Internet of Things (IoT) are two dominant areas of information technology. These technologies are widely used in supply chain, logistic and automotive industry. They proposed a blockchain technology in order to improve the data sharing as well as security. The reliable sharing of health records can enhance the treatment process with a help of diagnosis accuracy, security and privacy. The architecture what they developed is purely based on Identity-Based Encryption (IBE) algorithm.

III. DESIGN CONSIDERATION

The proposed scheme is envisioned to ensure flexible access control mechanism with reduced computational cost and storage overheads. The scheme has the following notations and their meanings as illustrated in Table I.

A. Design Goals

The proposed method can be summarized as the following design goals:

- 1) The design of the system is to construct two distinct secret keys from the single master key in which $SecKey^1$ is used to achieve data confidentiality and $SecKey^2$ is used to achieve data origin authentication.

TABLE I. NOTATIONS AND MEANINGS

Notations	Descriptions
$MasKey^1$	Master key^1
$SecKey^1$	Secret key^1
$SecKey^2$	Secret key^2
$AuthTag^1$	Authentication tag^1
$AuthTag^2$	Authentication tag^2
TKC	Trusted Key Center
$Stkc$	Secret value of TKC
X	Original data
Y	Encrypted data
E	Encryption
D	Decryption
HMAC	Hash message authentication code
SHA_1	Secure hash $algorithm^1$
CSP	Cloud Service Provider

- 2) The TKC (Trusted Key Center) is used for semi key generation such that TKC has given an authority to generate the $SecKey^2$ for checking data origin authentication.
- 3) The system is designed to construct the secret keys using randomly selected characters from the master key with the random bits that increases the key robustness in such a way that adversary will not have a chance to capture the copy of the master key or even secret keys.
- 4) The $SecKey^1$ will be sent to the cloud user from the data owner in a secure channel and the $SecKey^2$ is generated by the TKC and the secret key 2 will be sent to the cloud user if required by the cloud user to check the authenticity of the data owner.

IV. PROPOSED METHODOLOGY

From the point of view of the data owner, the following points are considered:

- 1) The data owner must register with the CSP before storing data in cloud storage.
- 2) The data owner derives the $MasKey^1$ using standard Blowfish algorithm.
- 3) Extract part1 and part2 of the $MasKey^1$ and send part2 to the trusted key center (TKC). The part1 of the $MasKey^1$ is retained its own.
- 4) Data owner computes $SecKey^1$ using SHA1 hashing technique and receives $SecKey^2$ from the TKC and encrypt the data using $SecKey^1$ and perform the data origin authentication using $SecKey^2$.

From the point of view of the TKC, the following points are considered:

- 1) If TKC accepts the credentials of the cloud user then send those credentials to the data owner.
- 2) The TKC receives the part2 of $MasKey^1$ from the data owner, derives the $SecKey^2$.
- 3) The part2 of the $MasKey^1$ is concatenated with a secret value $Stkc$ known only by the TKC.
- 4) The $SecKey^2$ is derived using SHA_1 hashing function. The SHA_1 algorithm takes input as a concatenated result and produces the 160 bit hash code.
- 5) The TKC sends secret key2 to the cloud user through a secure channel if required by the cloud user to the authenticity of the data owner.

Algorithm 1	Deriving Master key^1 ($MasKey^1$) at the data owner site
Input:	Key generator algorithm (Blowfish)
Output:	Master key^1
1:	generate key using Blowfish algorithm
2:	initialize key with 128 bits
3:	initialize master key^1 ($MasKey^1$) \leftarrow key
4:	convert master key^1 into a string
5:	record master key^1 for further processing

From the point of view of the cloud user, the following points are considered:

- 1) Whenever the cloud user requested for accessing the data from the CSP, cloud user identifies himself to the TKC by presenting appropriate credentials and request a $SecKey^1$ that corresponds to the data owner.
- 2) The cloud user receives the $SecKey^1$ from the data owner and decrypts the data.
- 3) The cloud user also receives the $SecKey^2$ from the TKC if required and verifies the data origin authentication.

In the following section, a set of algorithms have been proposed for accomplishing the privacy preservation using entity-based key derivation. The parameters used for configuring each of the algorithm are key generation, key derivation and Trusted Key Center (TKC) for information exchange, encryption/decryption and data origin authentication through signature verification. However, each cloud user receives two different secret keys in which one key is used for encryption/decryption and another key is used for data origin authentication. The proposed system is designed in such a way that two derived keys belongs to a specific user and those keys can not be breakable by the unauthorized users.

At the data owner's site, **Algorithm 1** is designed to generate master key^1 ($MasKey^1$). The standard Blowfish algorithm is used to generate the master key^1 of 128 bits. This master key is converted into a string of characters that is needed for subsequent processing.

The proposed work's main goal is to extract characters randomly from the $MasKey^1$. **Algorithm 2** is intended to split $MasKey^1$ into two parts, such as $part^1$ and $part^2$. $MasKey^1$ is initially made up of 128 bits, which are then converted into 16 characters, each of which stores 8 bits of data. In the first pass, extract 8 characters randomly from the master key and store it in $part^1$. Another set of 8 characters are extracted randomly and store it in $part^2$ in the second pass. The data owner keep $part^1$ for generating the secret key^1 ($SecKey^1$) and send $part^2$ to the TKC to generate secret key^2 ($SecKey^2$).

Algorithm 3 TKC is used in the proposed work for semi-key generation that is TKC receives the data credentials from the cloud user such as user e-mail and contact information, and then send the credentials to the data owner. The data owner generates the $SecKey^1$ using the standard SHA_1 algorithm which concatenates the $part^1$ of the $MasKey^1$ and the user e-mail id and the output of the SHA_1 function is 160-bit hash code.

Algorithm 4 is used to derive secret key^2 ($SecKey^2$) at TKC (Trusted Key Center). The TKC is only involved in

Algorithm 2	Extract $part^1, part^2$ from $MasKey^1$ at data owner site
Input:	$MasKey^1$
Output:	$part^1, part^2$
1:	receives $MasKey^1$ Algorithm 1
2:	if $MasKey^1$ is string then
	compute length of the $MasKey^1$
3:	randomly extract half amount of the characters from $MasKey^1$ store extracted characters into $part^1$
4:	randomly extract half amount of characters from $MasKey^1$ store extracted characters into $part^2$
5:	$part^1$ is kept in its own and $part^2$ is sent to the TKC for further processing

Algorithm 3	Derive secret $key^1 (SecKey^1)$ at the data owner site
Input:	$part^1$, email-ID of the cloud user
Output:	$SecKey^1$
1:	if TKC accepts the cloud user credentials then
2:	TKC sends user credentials to the data owner
3:	data owner computes $string^1 \leftarrow (part^1 \text{ --- } email_1 D)$
4:	compute $SecKey^1 \leftarrow SHA_1(string^1)$
5:	initialize $SecKey^1 \leftarrow 160$ bits

generating $SecKey^2$ using $part^2$ of $MasKey^1$ and secret value S_{tkc} . To generate $SecKey^2$, the TKC receives the $part^2$ of the master key from data owner and concatenates part2 with S_{tkc} value is know only to TKC. The $SecKey^2$ is computed using SHA_1 algorithm, which takes input as concatenated result and produces 160 bit hash code. The hash code of 160 bits is used as a $SecKey^2$ which is used for signature verification.

Algorithm 5 is designed for encrypting data at the data owner's site. The data owner encrypts the original data using $SecKey^1$ and generates encrypted data, which is then stored in the cloud.

To perform a reliable communication in cloud computing, the data owner who stored data in the cloud must be authenticated. **Algorithm 6** describes the construction of the authentication tag at the data owner's site.

Algorithm 7 is designed for decrypting encrypted data stored in the cloud environment at the cloud user site. To decrypt the data, the cloud user must obtain $SecKey^1$ from the data owner. The cloud user decrypts the data with the $SecKey^1$ obtained from the data owner.

Algorithm 8 describes signature verification via authentication tag at the cloud user site. Using $SecKey^2$, the cloud

Algorithm 4	Derive secret $key^2 (SecKey^2)$ at TKC
Input:	$part^2$, secret value of TKC (S_{tkc})
Output:	$SecKey^2$
1:	receives $part^2$ of the $MasKey^1$ from the data owner
2:	compute $string^2 \leftarrow (part^2 \text{ --- } S_{tkc})$
3:	compute $SecKey^2 \leftarrow SHA_1(string^2)$
4:	initialize $SecKey^2 \leftarrow 160$ bits
5:	establish $SecKey^2$ to data owner for signature computation
	establish $SecKey^2$ to the cloud user if required

Algorithm 5	Encryption (E) at the data owner site
Input:	Original data (X), $SecKey^1$
Output:	Encrypted data (Y)
1:	receives $SecKey^1$ from the TKC
2:	initialize $SecKey^1$ for encryption and decryption of data
3:	compute $Y \leftarrow E(SecKey^1 (X))$
4:	store encrypted data (Y) on CSP

Algorithm 6	Generate authentication tag at the data owner site
Input:	Original data (X), $SecKey^2$
Output:	Authentication $tag^1 (AuthTag^1)$
1:	receives $SecKey^2$ from the TKC
2:	initialize $SecKey^2$ for data origin authentication
3:	compute $AuthTag^1 \leftarrow HMAC(X, SecKey^2)$
4:	store $AuthTag^1$ on CSP

Algorithm 7	Decryption at cloud user site
Input:	Encrypted data (Y), $SecKey^1$
Output:	Original data (X)
1:	receives $SecKey^1$ from the data owner via secure channel
2:	compute $X \leftarrow D (SecKey^1 (Y))$
3:	utilize X

user can validate the data owner's authentication. In this case, the cloud user uses the HMAC algorithm to compute authentication $tag^2 (AuthTag^2)$ of the original data. The HMAC algorithm takes original data and the $SecKey^2$ as input and produces the $AuthTag^2$. The data owner receives $AuthTag^1$ from CSP and compares it to $AuthTag^2$. If both authentication tags are successfully compared, the cloud user may confirm that data was sent by an authenticated party; otherwise, do not.

1) *Implementation:* The proposed scheme is implemented using a Java-based JSP web application. The scheme is being tested in a physical cloud environment such as Amazon Web Services. Device setup includes Tomcat 8.5 with Corretto 11 running on 64bit Amazon Linux 2/4.1.2.

V. EXPERIMENTAL RESULTS

The proposed scheme is based on the identity-based encryption. The $MasKey^1$ is generated using standard blowfish algorithm and its size is 128 bits which is then converted into 16 characters. In the first pass, 8 characters are extracted randomly from the master key and store it in $part^1$ and in the second pass another set of 8 characters are extracted randomly and store it in $part^2$. The data owner keeps $part^1$ for generating the secret $key^1 (SecKey^1)$ and send $part^2$ to the TKC to generate secret $key^2 (SecKey^2)$. The $SecKey^1$ is generated by concatenating $part^1$ of the $MasKey^1$ and the unique attribute of the cloud user which was collected by the TKC and the concatenated result will be given as input to the SHA_1 algorithm and it produces 160 bit hash code. The hash code of 160 bits is used for encrypting data at data owner side. TKC generates the $SecKey^2$ using $part^2$ of $MasKey^1$ and secret value S_{tkc} . To generate $SecKey^2$, the TKC receives the $part^2$ of the master key from data owner and concatenates part2 with S_{tkc} value is known only to TKC. The $SecKey^2$ is computed using SHA_1 algorithm, which takes input as

Algorithm 8	Validate authentication tag at the cloud user site
Input:	Original data (X), $SecKey^2$
Output:	True or False
1:	receives $SecKey^2$ from the TKC if required
2:	compute Authentication $tag^2 (AuthTag^2)$ such that $AuthTag^2 \leftarrow HMAC(X, SecKey^2)$
3:	receives $AuthTag^1$ from CSP
4:	if $AuthTag^2 == AuthTag^1$ then return true ie authentication successful
5:	else return false ie authentication unsuccessful
	end if

concatenated result and produces 160 bit hash code. The hash code of 160 bits is used as a *SecKey*² which is used for signature verification. The computation cost for generating two secrete keys is reduced when compared to having two separate master keys is shown in Table II. The memory requirement also reduces when compared to the *MasKey*² is shown in the Table III.

The Fig. 1 depicts the time required to derive the *MasKey*² and the proposed method of key derivation. The graphical representation demonstrates that the proposed method has a low processing overhead when calculating the key.

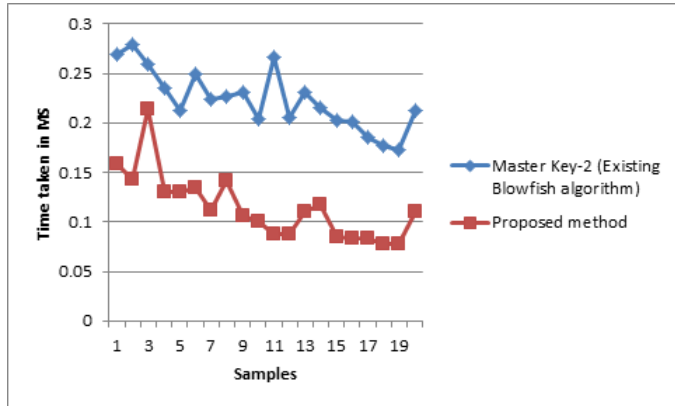


Fig. 1. Time Taken in ms (Master *key*² vs. Proposed Method)

The Fig. 2 depicts the time required to derive the *MasKey*¹ and the proposed method of key derivation. In this paper, the proposed scheme is compared to the existing solution's *MasKey*¹. The Fig. 2 shows that the computational cost of deriving the keys used in the proposed method is significantly lower than the existing key derivation technique.

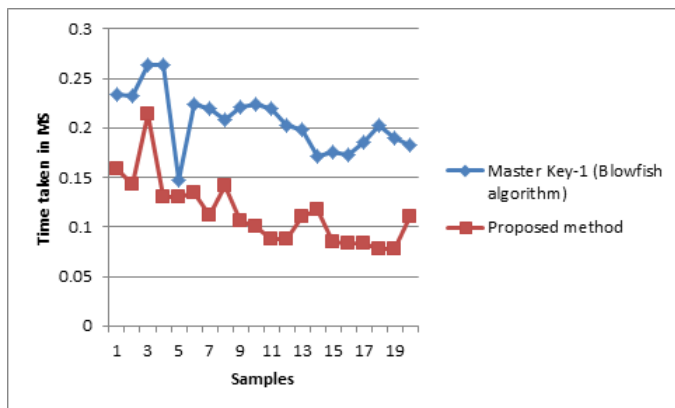


Fig. 2. Time Taken in ms (Master *key*¹ vs. Proposed Method).

Memory utilization is also a major concern during key generation in order to increase the efficiency of the cloud environment. The Table III compares the proposed scheme's memory utilization in megabytes to existing cryptographic keys such as *MasKey*¹ and *MasKey*². The Fig. 3 and 4 show a graphical representation of the memory utilization of

the proposed method of key derivation and the *MasKey*¹. The proposed method's memory utilization of key derivation and *MasKey*¹ is nearly identical to the experimental data.

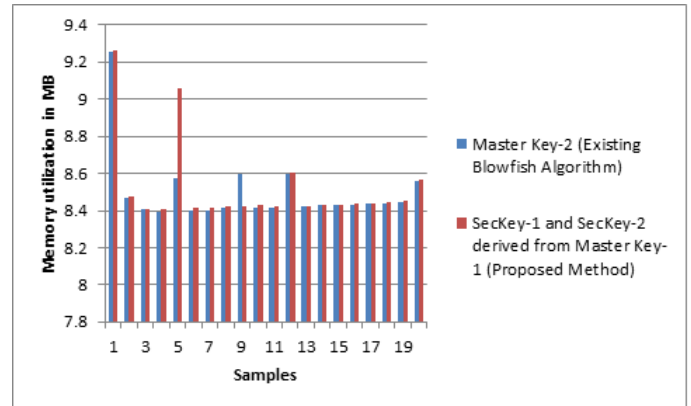


Fig. 3. Memory Utilization in MB (Master *key*² vs. Proposed Method).

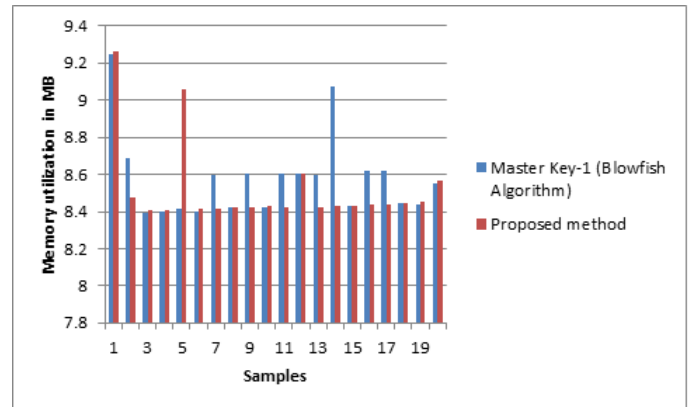


Fig. 4. Memory Utilization in MB (Master *key*¹ vs. Proposed Method).

VI. EXPERIMENTAL ANALYSIS

The experimental analysis is made in this paper to tackle the following issues:

A. Key Derivation

In this paper, a system is proposed for deriving secret keys from a single master key, with the goal of limiting the number of master key generations. Jialu Hao et al. [3]proposed a cloud-based IoT device access control policy in which the author considered the system public key, master secret key, and an attribute set for generating the secret key. As the system public key and master key are considered for key generation, the computational overhead can easily increase. In this paper, we designed an algorithm that generates secret keys from a single master key in order to greatly reduce computational overhead.

B. Enhancement of Data Security

In the proposed system, we first computed a 128-bit master key using the standard Blowfish algorithm. The secret keys

TABLE II. TIME TAKEN (MS) FOR KEY DERIVATION (EXISTING VS. PROPOSED METHODOLOGY)

Sample	<i>MasKey</i> ¹ (Blowfish Algorithm)	<i>MasKey</i> ² (Existing: Blowfish Algorithm)	<i>SecKey</i> ¹ , <i>SecKey</i> ² derived from <i>MasKey</i> ¹ (Proposed methodology)
1	0.234	0.269	0.159
2	0.232	0.279	0.143
3	0.263	0.259	0.214
4	0.263	0.235	0.130
5	0.147	0.212	0.130
6	0.224	0.250	0.134
7	0.219	0.224	0.112
8	0.208	0.227	0.142
9	0.221	0.231	0.106
10	0.224	0.204	0.100
11	0.220	0.266	0.088
12	0.203	0.206	0.087
13	0.198	0.231	0.110
14	0.171	0.215	0.118
15	0.176	0.203	0.085
16	0.173	0.201	0.083
17	0.185	0.185	0.083
18	0.202	0.177	0.078
19	0.190	0.173	0.078
20	0.183	0.212	0.111
Avg.	0.206	0.222	0.114

TABLE III. MEMORY UTILIZATION IN MEGABYTES (EXISTING VS. PROPOSED METHODOLOGY)

Sample	<i>MasKey</i> ¹ (Blowfish Algorithm)	<i>MasKey</i> ² (Existing: Blowfish Algorithm)	<i>SecKey</i> ¹ , <i>SecKey</i> ² derived from <i>MasKey</i> ¹ (Proposed methodology)
1	9.247	9.255	9.259
2	8.685	8.466	8.475
3	8.395	8.404	8.405
4	8.399	8.396	8.407
5	8.412	8.575	9.057
6	8.402	8.398	8.413
7	8.594	8.403	8.415
8	8.425	8.414	8.425
9	8.602	8.597	8.424
10	8.420	8.416	8.431
11	8.604	8.414	8.423
12	8.602	8.599	8.601
13	8.600	8.424	8.422
14	9.072	8.432	8.432
15	8.434	8.431	8.430
16	8.620	8.433	8.441
17	8.623	8.436	8.440
18	8.445	8.440	8.443
19	8.441	8.447	8.450
20	8.553	8.558	8.568
Avg.	8.578	8.496	8.518

are derived from the master key by using randomly selected characters, the cloud user's data credential, and the trusted key center's secret value. During key generation, the *SHA*₁ hashing technique is used to generate a 160 bit hash code, which is then used as a secret *key*¹ and secret *key*². In this context, the secret key size is increased from 128 bits to 160 bits, which improves data security because increasing the key size automatically improves data security.

C. Semi Key Generation

The trusted key center (TKC) is involved in this paper for semi key generation in collaboration with the data owner. The TKC is only in charge of creating the secret *key*², which is only used for data origin authentication via signature verification. The TKC does not have complete control over the generation of secret *key*¹.

D. Key Robustness

The main goal of this paper is to improve the robustness of the derived keys. The system is designed in such a

way that secret keys are generated using randomly selected characters and the cloud user's credential. In this context, the randomly selected characters and cloud user's credential should be required whenever the adversary attempts to crack the secret key. Even if the adversary captures the e master key, extracting the actual random characters for the next time is extremely difficult. Table IV shows a functional comparison of the proposed method with related research work.

VII. CONCLUSION

The proposed method has been put into practice in order to improve computational efficiency and data origin authentication. In order to increase the computational efficiency, secret keys are derived from the single master key so that processing overhead of key derivation is comparatively less compared with another master key. The trusted key center (TKC) is involved in the proposed method for secure communication between data owner and cloud user. The TKC play a major role for key generation and key establishment. The TKC validates the data credentials of the cloud user and the unique identity of the

TABLE IV. FUNCTIONAL COMPARISON

Parameters	Jialu Hao et al. [3]	Sana Belguith et al. [5]	Mahender Kumar et al. [6]	Rashad Elhabob et al. [11]	Proposed Method
Flexible Access Control	Yes	Yes	Yes	Yes	Yes
Privacy policy	Yes	Yes	Yes	Yes	Yes
Computation cost for key derivation	High	High	High	High	Low
Non-Repudiation	No	No	No	No	Yes
Storage overhead for key derivation	High	High	High	High	Low
Key robustness	Medium	Medium	Medium	Medium	High

cloud user is sent to the data owner to derive the secret key1 in order to provide the confidentiality. This leads to identity based key derivation that reduces the unauthorized access. It means that secret key1 generated for a specified user will not be used for another cloud user. At the same time the secret key2 has been generated by the TKC for data origin authentication. Since, the TKC is a trusted third party so that entire control for secret key2 generation is handed over to the TKC can able to make a mutual authentication between data owner and cloud user. The experimental results are compared to existing solutions, and the proposed scheme is capable of being deployed in a real-world cloud environment.

Compliance with Ethical Standards

The proposed methodology is designed under the guidance of eminent personalities and it is found that the proposed methodology is not available in the prior art search.

REFERENCES

- [1] K. Albulayhi, A. Abuhussein, F. Alsubaei, and F. T. Sheldon, "Fine-grained access control in the era of cloud computing: An analytical review," in *2020 10th Annual Computing and Communication Workshop and Conference (CCWC)*. IEEE, 2020, pp. 0748–0755.
- [2] A. K. Dubey and V. Mishra, "Crowd review and attribute-based credit computation for an access control mechanism in cloud data centers," *International Journal of Computers and Applications*, pp. 1–8, 2020.
- [3] J. Hao, C. Huang, J. Ni, H. Rong, M. Xian, and X. S. Shen, "Fine-grained data access control with attribute-hiding policy for cloud-based iot," *Computer Networks*, vol. 153, pp. 1–10, 2019.
- [4] S. Xu, J. Ning, Y. Li, Y. Zhang, G. Xu, X. Huang, and R. Deng, "Match in my way: Fine-grained bilateral access control for secure cloud-fog computing," *IEEE Transactions on Dependable and Secure Computing*, 2020.
- [5] S. Belguith, N. Kaaniche, A. Jemai, M. Laurent, and R. Attia, "Pabac: a privacy preserving attribute based framework for fine grained access control in clouds," in *SECRYPT 2016: 13th International Conference on Security and Cryptography*, vol. 4. SciTePress, 2016, pp. 133–146.
- [6] M. Kumar and S. Chand, "Eski-ibe: Efficient and secure key issuing identity-based encryption with cloud privacy centers," *Multimedia Tools and Applications*, vol. 78, no. 14, pp. 19753–19786, 2019.
- [7] S. Xu, G. Yang, Y. Mu, and R. H. Deng, "Secure fine-grained access control and data sharing for dynamic groups in the cloud," *IEEE Transactions on Information Forensics and Security*, vol. 13, no. 8, pp. 2101–2113, 2018.
- [8] Y. Liu, Y. Zhang, J. Ling, and Z. Liu, "Secure and fine-grained access control on e-healthcare records in mobile cloud computing," *Future Generation Computer Systems*, vol. 78, pp. 1020–1026, 2018.
- [9] F. Cai, N. Zhu, J. He, P. Mu, W. Li, and Y. Yu, "Survey of access control models and technologies for cloud computing," *Cluster Computing*, vol. 22, no. 3, pp. 6111–6122, 2019.
- [10] K. Shivanna, S. P. Deva, and M. Santoshkumar, "Privacy preservation in cloud computing with double encryption method," in *Computer Communication, Networking and Internet Security*. Springer, 2017, pp. 125–133.
- [11] R. Elhabob, Y. Zhao, N. Eltayieb, A. M. Abdelgader, and H. Xiong, "Identity-based encryption with authorized equivalence test for cloud-assisted iot," *Cluster Computing*, vol. 23, no. 2, pp. 1085–1101, 2020.
- [12] K. Lee, "A generic construction for revocable identity-based encryption with subset difference methods," *PLoS one*, vol. 15, no. 9, p. e0239053, 2020.
- [13] H. Cheng, C. Rong, M. Qian, and W. Wang, "Accountable privacy-preserving mechanism for cloud computing based on identity-based encryption," *IEEE Access*, vol. 6, pp. 37869–37882, 2018.
- [14] C. Meshram, C.-C. Lee, S. G. Meshram, and M. K. Khan, "An identity-based encryption technique using subtree for fuzzy user data sharing under cloud computing environment," *Soft Computing*, vol. 23, no. 24, pp. 13127–13138, 2019.
- [15] H. Deng, Z. Qin, Q. Wu, Z. Guan, R. H. Deng, Y. Wang, and Y. Zhou, "Identity-based encryption transformation for flexible sharing of encrypted data in public cloud," *IEEE Transactions on Information Forensics and Security*, vol. 15, pp. 3168–3180, 2020.
- [16] H. Li, Y. Dai, and B. Yang, "Identity-based cryptography for cloud security," *Cryptology ePrint Archive*, 2011.
- [17] J. Li, J. Li, X. Chen, C. Jia, and W. Lou, "Identity-based encryption with outsourced revocation in cloud computing," *Ieee Transactions on computers*, vol. 64, no. 2, pp. 425–437, 2013.
- [18] N. Farjana, S. Roy, M. Mahi, J. Nayeem, and M. Whaiduzzaman, "An identity-based encryption scheme for data security in fog computing," in *Proceedings of International Joint Conference on computational intelligence*. Springer, 2020, pp. 215–226.
- [19] Q. Huang, W. Yue, Y. He, and Y. Yang, "Secure identity-based data sharing and profile matching for mobile healthcare social networks in cloud computing," *IEEE Access*, vol. 6, pp. 36584–36594, 2018.
- [20] X. Zhang, Y. Tang, H. Wang, C. Xu, Y. Miao, and H. Cheng, "Lattice-based proxy-oriented identity-based encryption with keyword search for cloud storage," *Information Sciences*, vol. 494, pp. 193–207, 2019.
- [21] P. Mishra and V. Verma, "Study of identity-based encryption for cloud data security," in *Decision analytics applications in industry*. Springer, 2020, pp. 401–408.
- [22] P. Sharma, N. R. Moparthy, S. Namasudra, V. Shanmuganathan, and C.-H. Hsu, "Blockchain-based iot architecture to secure healthcare system using identity-based encryption," *Expert Systems*, p. e12915, 2021.
- [23] D. Unal, A. Al-Ali, F. O. Catak, and M. Hammoudeh, "A secure and efficient internet of things cloud encryption scheme with forensics investigation compatibility based on identity-based encryption," *Future Generation Computer Systems*, vol. 125, pp. 433–445, 2021.
- [24] N. Vaanchig, Z. Qin, and B. Ragchaasuren, "Constructing secure-channel free identity-based encryption with equality test for vehicle-data sharing in cloud computing," *Transactions on Emerging Telecommunications Technologies*, p. e3896, 2020.

Multiple Hydrophone Arrays based Underwater Localization with Matching Field Processing

Shuo Jin, Xiukui Li

School of Information and Communication Engineering
Dalian University of Technology

Abstract—Matched field processing technology (MFP) is a general passive localization method for underwater sound source due to its advantages in ultra-long distance positioning. In this paper, assume the total number of hydrophones remains unchanged, a single hydrophone array is divided into multiple hydrophone sub-arrays for independent positioning, and the positioning results of sub-arrays are fused to reduce the impact of noise and improve the robustness of the positioning system. Based on the traditional Bartlett processor, we derive the formula for average positioning error which varies with signal to noise ratio (SNR) and the number of hydrophones. The formula is used to decide the optimal structure of sub-arrays, i.e., the number of sub-arrays and the number of hydrophones in each sub-array. Experiments and simulations prove that multiple sub-arrays can improve the positioning accuracy compared with the single hydrophone array in the noisy environment. The average positioning errors produced by the experiments are consistent with the numerical ones based on the theoretical analysis.

Keywords—Matched Field Processing (MFP); hydrophone array; source localization; underwater acoustic

I. INTRODUCTION

After decades of development, underwater acoustic positioning technology is the primary means for underwater positioning and tracking in various applications and fields. Underwater positioning can be divided into active and passive positioning. Active positioning usually can be categorized into three basic techniques: ultra short baseline location (USBL), short baseline location (SBL) and long baseline location (LBL). Those techniques can be combined to create complex positioning system including long ultra short baseline location (LUSBL) and short and long ultra short baseline location (SLUSBL), etc. Passive positioning implements the positioning by processing noise or signal generated by the target source without actively generating wave; thus it can achieve high concealment. Passive positioning mainly includes four methods: ternary method, target motion analysis (TMA), matched field processing (MFP) and focused beamforming. In various underwater positioning methods, MFP takes advantages of the characteristics of acoustic field propagation to obtain the source position, and it is an important means of underwater long-distance positioning, particularly for ultra long distance positioning.

Matched field processing technology is a general means of underwater passive positioning due to its advantages in ultra-long distance positioning. Considering the marine environment parameters and acoustic communication channel characteristics, MFP estimates the acoustic field amplitude and phase of receive array by using the underwater acoustic field

model. The amplitude and phase estimates form replica vectors which is matched with receiving data in hydrophone arrays. This realizes the passive positioning of underwater targets and accurate estimation of marine environmental parameters.

The waveguide propagation theory is applied to underwater acoustic propagation analysis by Clay in 1966 [1], and it is widely used in MFP [2–6]. The positioning error are mainly produced by environmental mismatch and underwater noise. Inaccurate environmental parameters will cause errors in sound field calculation, resulting in positioning errors [7–11]. When the noise power is high, the signal to noise ratio(SNR) of the receiving signal will reduce, and the positioning error will increase. Debever *et al.* designs a coherent wide-band white noise constrained processor to reduce the effect of noise on the positioning [12]. Collins *et al.* proposes a processor to eliminate the noise in the signal [13]. Lee *et al.* investigates a robust adaptive positioning algorithm used in shallow water [14]. Seong *et al.* designs an optimal processor for motion source localization with correlation noise based on the normal mode propagation mode [15].

Single array MFP is evolving into multiple array MFP. Nicholas *et al.* studies the performance of coherent and incoherent positioning with underwater L-shaped array which consists of a horizontal and a vertical array. The results show that coherent and incoherent positioning results are not of much difference [16]. Zurk *et al.* uses the received signals at three vertical arrays in Santa Barbara Channel Experiment (SBCX) to localize the mobile source with known motion information which is obtained through adaptive MFP algorithm [17]. Tollefsen *et al.* designs three different processors for multi-array MFP, and proves that coherent processor can achieve the best performance when the synchronization error is small [18].

The design of hydrophone array involves multiple aspects. Tracey *et al.* discusses the prediction of the sidelobe level of matched results in conventional MFP, and proposes a method to analyze and predict the relationship between the output power distribution of traditional MFP fuzzy surface and array aperture [19]. Bogart *et al.* investigates the MFP performance of several horizontal line array apertures and compares to a full water column vertical array in a simulated range-independent shallow water environment [20]. It is demonstrated that a horizontal array of sufficient length can equal or exceed the water column vertical array in range–depth localization performance. Tantom *et al.* proposes a general guideline for designing matched field processing arrays using normal mode propagation model, and evaluates the performance of various line array configurations [21].

Compared with single array, multiple sub-arrays structure can improve the robustness of the localization system in dealing with environment mismatch and large noise. Due to sound directivity, if only one array is used for positioning, the positioning result may have a large error when the array is located at the direction where the received sound signal is with low energy. However, when multiple arrays are used, certain arrays may be in the direction where the received sound signal is with high energy even if some arrays are receiving low-power signals. The underwater white noise can be considered almost equal at different positions. We use the received SNR as the weighting coefficient in the final positioning result fusion, and the positioning error will be reduced. When the power of the sound source is low which yields a low received SNR, the positioning accuracy yielded by multiple arrays is higher than that of single array.

In this paper, we propose multiple sub-arrays joint positioning method. Assume the total number of hydrophones remains unchanged, a single hydrophone array is divided into multiple hydrophone sub-arrays for independent positioning, and the positioning results of sub-arrays are fused to obtain the sound source location. This will reduce the impact of noise and improve the robustness of the positioning system. Based on the traditional Bartlett processor, we derive the formula for average positioning error which varies with SNR and the number of hydrophones. The formula is used to decide the optimal structure of sub-arrays, i.e., the number of sub-arrays and the number of hydrophones in each sub-array. Experiments and simulations proves that multiple sub-arrays can improve the positioning accuracy compared with the single hydrophone array in the noisy environment. The average positioning errors produced by the experiments are consistent with the numerical ones based on the derived formula.

The remainder of this paper is organized as follows. Section II introduces the system model of traditional MFP and the signal propagation model. In Section III, the positioning principle of multiple sub-arrays are introduced. In Section IV, the formula that the average positioning error varies with different hydrophone allocation methods is derived. Section V presents the performance of multiple sub-arrays joint positioning by underwater real data and simulations, and Section VI concludes this paper.

II. SYSTEM MODEL

Matching field processing is a general technology for long-distance underwater positioning. Its principle is to match the actual signal received by hydrophones with the acoustic field which is calculated at the position of hydrophone array. The position with the largest matching result is considered to be where the sound source is located.

The matching result of traditional processor is the power weighted sum of each hydrophone,

$$B_a(\mathbf{x}) = \frac{1}{L} \sum_{l=1}^L |\mathbf{W}(\mathbf{x}, l)^H \mathbf{Y}(\mathbf{x}_R, l)|^2 \quad (1)$$

where L is the number of segments selected for matching at the receiving hydrophone; $\mathbf{x} = (r, h)$ is the position point to be matched, where r is the horizontal distance between the sound source and the array, and h is the depth of the sound

source, $\mathbf{W}(\mathbf{x}, l) = \frac{\mathbf{G}(\mathbf{x}, l)}{|\mathbf{G}(\mathbf{x}, l)|}$ is the weight of the sound pressure calculated by using the underwater acoustic channel model, where $\mathbf{G}(\mathbf{x}, l) = (g_1(\mathbf{x}, l), g_2(\mathbf{x}, l), \dots, g_N(\mathbf{x}, l))^H$. $g_i(\mathbf{x})$ is the sound pressure received by the i th hydrophone when the sound source transmits the signal in unit power, and N is the number of hydrophones. $\mathbf{Y}(\mathbf{x}_R, l)$ is the actual received signal,

$$\mathbf{Y}(\mathbf{x}_R, l) = (1 + J)P_s \mathbf{G}(\mathbf{x}_R, l) + \mathbf{T} \quad (2)$$

where J is the attenuation factor of the acoustic signal in the propagation channel; P_s is the power of the source; \mathbf{x}_R represents the sound source position. \mathbf{T} is the additive white Gaussian noise, and $\mathbf{T} = (N_1(\mu_1, \sigma_1^2), N_2(\mu_2, \sigma_2^2), \dots, N_N(\mu_N, \sigma_N^2))^H$. It can be considered that the additive noise in each hydrophone follows the same Gaussian distribution $N(\mu, \sigma^2)$, where μ can be regarded as 0.

In the actual marine environment, the underwater noise may be large, and when the transmitting power of the sound source is low, the SNR at the receiver will be low. In addition, most underwater sound sources are mobile, and the transmission power of the source in a certain direction is high, and it is low in other directions. Therefore, when the sound source is in the moving state, if the sound wave propagation direction of the source changes, the SNR of some positions at the receiver may reduce, which may result in serious deviation of the positioning result.

In this situation, dividing a single array into multiple independent arrays and implementing jointly localization will improve the positioning accuracy. When the hydrophone arrays are placed in different positions, the hydrophone arrays with low SNR will be assigned a lower weight in deciding the location of sound source. This will reduce the environment influence, particularly in low SNR scenario, and improves the fault tolerance of the system.

III. MULTIPLE SUB-ARRAYS JOINT LOCATION

Compared with the single array, the advantage of multiple sub-arrays joint localization is its strong adaptability in the complex and varied underwater environments. When the sound source radiates the sound wave outward in the free field, the sound pressure level presents an uneven property with different directions, which is called the directivity of the sound source. The directivity of the sound source is related to the scale of the sound source and the radiation wavelength. When the sound source is small enough to be regarded as the point sound source, the sound wave diverges evenly outward in the form of approximately spherical surface with the sound source as the center. Thus, the sound pressure levels are equal at the points which are of equal distances to the source center. When the scale of the sound source is much larger than the wavelength of the sound wave, the sound wave propagates in a concentrated direction in the form of a sound beam, the sound wave can be considered to have strong directivity. Therefore, for this kind of sound source, the horizontal distribution range of multiple sub-arrays is wider, and it is easier to realize the full utilization of acoustic signal.

The system model and array structure of multiple sub-arrays based positioning are shown in Fig. 1 and Fig. 2 respectively. Ar_i is the i th array.

In the proposed positioning system, we can adopt different positioning methods for different arrays (see Fig. 1). The specific method can be determined according to the noise intensity and the environments where the arrays are situated. Finally, the positioning results of different arrays are averaged with different weights which will be determined by the number of hydrophones and noise intensity of each array.

Assume N hydrophones are available. Those N hydrophones are divided into m groups, and each group has $\frac{N}{m}$ hydrophones, called sub-array (see Fig. 2). Different sub-arrays can be placed in different positions according to the actual environment to form a spatial pattern, and the distance between different arrays is set accordingly. The vertical positions of different sub-arrays can be different. The horizontal distance between each sub-array and the sound source is denoted by $r_i, i = 1, 2, \dots, m$. The m hydrophone sub-arrays are used to localize the sound source independently, and the location results produced by m sub-arrays are fused to determine the location of sound source. Take one array as the reference array, such as Ar_1 . Assume that the horizontal distance between Ar_i and Ar_1 is s_i , and the positioning result of the i th array is denoted by (r_i, h_i) , where h_i is the depth of the sound source obtained by the i th sub-array. Then the final sound source location is

$$\begin{aligned} r_1 &= \Omega \cdot \mathbf{R} \\ h_1 &= \Omega \cdot \mathbf{H} \end{aligned} \quad (3)$$

where

$$\begin{aligned} \Omega &= (\omega_1, \omega_2, \dots, \omega_m) \\ \mathbf{R} &= (r_1 - s_1, r_2 - s_2, \dots, r_m - s_m)^T \\ \mathbf{H} &= (h_1, h_2, \dots, h_m)^T \end{aligned} \quad (4)$$

where ω_i represents the weight of the i th sub-array. Hence, when the position of Ar_1 is known, the distance and depth between the sound source and Ar_1 can be inferred.

In Fig. 2, when the sound source is in some directions, due to the spatial structure of multiple arrays, the receiving power of the sound source signal at the array will be increased and the received SNR can be improved.

The challenging work for the multiple sub-arrays joint localization includes techniques of forming the hydrophone array pattern, weight assignment of different hydrophones array, and synchronization of array hydrophones.

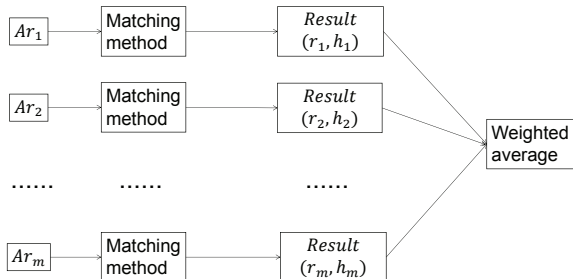


Fig. 1. System Model.

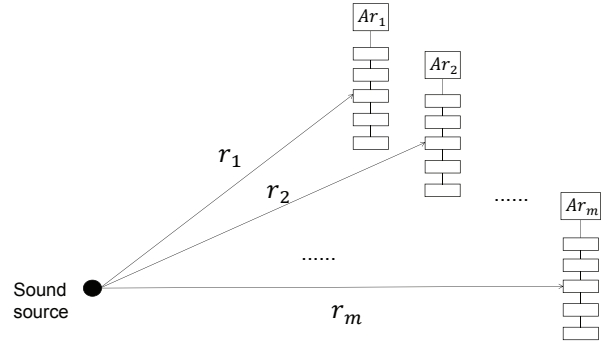


Fig. 2. Array Structure.

IV. DISTRIBUTION OF HYDROPHONE ARRAY AND PERFORMANCE ANALYSIS

If l is set as a constant value, then (2) can be written as

$$\mathbf{Y}(\mathbf{x}_R) = (1 + J)P_s \mathbf{G}(\mathbf{x}_R) + \mathbf{T} \quad (5)$$

To analyze the influence of different parameters on the matching results, function $F(\mathbf{x})$ is assumed to be the product of $\mathbf{W}(\mathbf{x})$ and $\mathbf{Y}(\mathbf{x}_R)$.

$$\begin{aligned} F(\mathbf{x}) &= \mathbf{W}(\mathbf{x})^H \mathbf{Y}(\mathbf{x}_R) \\ &= (1 + J)P_s \sum_{i=1}^N \frac{g_i(\mathbf{x}_R)g_i(\mathbf{x})}{\sqrt{\sum_{k=1}^N g_k^2(\mathbf{x})}} + n \sum_{i=1}^N \frac{g_i(\mathbf{x})}{\sqrt{\sum_{k=1}^N g_k^2(\mathbf{x})}} \end{aligned} \quad (6)$$

where n follows the normal distribution $\mathcal{N}(0, \sigma^2)$.

From (6), for each \mathbf{x} , $F(\mathbf{x})$ is a normal distribution. Its mean is $(1 + J) \sum_{i=1}^N \frac{g_i(\mathbf{x}_R)g_i(\mathbf{x})}{\sqrt{\sum_{k=1}^N g_k^2(\mathbf{x})}}$, and variance is $\sigma^2 \sum_{i=1}^N \frac{g_i^2(\mathbf{x})}{\sum_{k=1}^N g_k^2(\mathbf{x})}$, where $(1 + J)P_s$ is a constant value and can be set as k .

Let

$$M(\mathbf{x}) = k \sum_{i=1}^N \frac{g_i(\mathbf{x}_R)g_i(\mathbf{x})}{\sqrt{\sum_{k=1}^N g_k^2(\mathbf{x})}} \quad (7)$$

be the mean of $F(\mathbf{x})$ and it is a function of position \mathbf{x} .

From (7),

$$\frac{M(\mathbf{x})}{\sqrt{\sum_{k=1}^N g_k^2(\mathbf{x}_R)}} = k \sum_{i=1}^N \frac{g_i(\mathbf{x}_R)g_i(\mathbf{x})}{\sqrt{\sum_{k=1}^N g_k^2(\mathbf{x}_R)} \sqrt{\sum_{k=1}^N g_k^2(\mathbf{x})}} \quad (8)$$

Obviously, (8) is the formula for calculating the cosine value between two vectors. Thus when $\mathbf{x} = \mathbf{x}_R$, $\frac{M(\mathbf{x})}{\sqrt{\sum_{k=1}^N g_k^2(\mathbf{x}_R)}}$ has

the maximum value of k . $\sqrt{\sum_{k=1}^N g_k^2(\mathbf{x}_R)}$ is a constant value.

Hence $M(\mathbf{x})$ has a maximum value of $k \sqrt{\sum_{k=1}^N g_k^2(\mathbf{x}_R)}$ at $\mathbf{x} = \mathbf{x}_R$. The value of $M(\mathbf{x})$ is related to N ; thus $M(\mathbf{x})$ can be written as $M(\mathbf{x}, N)$. Then the value of $F(\mathbf{x})$ is also related

to N .

$$F(\mathbf{x}, N) = M(\mathbf{x}, N) + n \sum_{i=1}^N \frac{g_i(\mathbf{x})}{\sqrt{\sum_{k=1}^N g_k^2(\mathbf{x})}} \quad (9)$$

For each position \mathbf{x} , $F(\mathbf{x}, N)$ is a Gaussian distribution with mean $M(\mathbf{x}, N)$ and variance $\sigma^2 \sum_{i=1}^N \frac{g_i(\mathbf{x})}{\sqrt{\sum_{k=1}^N g_k^2(\mathbf{x})}}$. In the calculation of the variance, N appears in both the numerator and denominator. However it is obvious that the values of the numerator and denominator do not increase in proportion with the increase of N ; thus the value of variance is also related to N , which can be written as $\sigma^2(\mathbf{x}, N)$.

Set a total of d location points on the ambiguity surface. Denote the probability that point $\mathbf{x}_t (1 \leq t \leq d)$ can reach the maximum value by $\mathbb{P}_t(\mathbf{x}_t, N)$ and the absolute distance between the potential location point and the true position by $|\mathbf{x}_t - \mathbf{x}_R|$. The positioning error of \mathbf{x}_t is defined as $\mathbb{P}_t(\mathbf{x}_t, N) \times |\mathbf{x}_t - \mathbf{x}_R|^2$ if point \mathbf{x}_R is considered as the position of the sound source.

The average positioning error can be given by

$$E(N) = \frac{\sum_{t=1}^d \mathbb{P}_t(\mathbf{x}_t, N) \times |\mathbf{x}_t - \mathbf{x}_R|^2}{d} \quad (10)$$

For the position point \mathbf{x}_t , the value of $F(\mathbf{x}_t, N)$ follows the Gaussian distribution. Hence $(\bar{x} - 3\sigma(\mathbf{x}_t, N), \bar{x} + 3\sigma(\mathbf{x}_t, N))$ can be considered as the range of $F(\mathbf{x}_t, N)$, where \bar{x} is the mean of $F(\mathbf{x}_t, N)$, i.e., the value of $M(\mathbf{x}_t, N)$. Hence the Euclidean distance between the mean of $F(\mathbf{x}, N)$ and $F(\mathbf{x}_R, N)$ is $|M(\mathbf{x}_R, N) - M(\mathbf{x}_t, N)|$.

To find $\mathbb{P}_t(\mathbf{x}_t, N)$, the continuous probability density function is discretized. We can divide the possible values of $F(\mathbf{x}_t, N)$ into $\alpha (\alpha \in \mathbb{N}^*)$ segments, where \mathbb{N}^* represents the set of positive integers. The length of each segment is denoted by β , and $\beta = \frac{6\sigma^2(\mathbf{x}_t, N)}{\alpha}$. Therefore, the probability that $F(\mathbf{x}_t, N)$ reaches the maximum is the sum of the probabilities of all segments of $F(\mathbf{x}_t)$ reaching the maximum. Let the start and end values of segment i of $F(\mathbf{x}_t, N)$ be $C_i(\mathbf{x}_t, N)$ and $C_{i+1}(\mathbf{x}_t, N)$, respectively. Then

$$\begin{aligned} \mathbb{P}_t(\mathbf{x}_t, N) &= \mathbb{P}(F_{max}(\mathbf{x}, N) = F(\mathbf{x}_t, N)) \\ &= \sum_{i=1}^{\alpha-1} \mathbb{P}(F_{max}(\mathbf{x}, N) \in (C_i(\mathbf{x}_t), C_{i+1}(\mathbf{x}_t))) \\ &= \sum_{i=1}^{\alpha-1} \frac{\prod_{j=1}^d \mathbb{P}(L_1(i, j, t) | L_2(i, t))}{\mathbb{P}(F(\mathbf{x}_t, N) < C_i(\mathbf{x}_t, N))} \end{aligned} \quad (11)$$

where $L_1(i, j, t)$ represents $F(\mathbf{x}_j, N) < C_i(\mathbf{x}_t, N)$, and $L_2(i, t)$ represents $F(\mathbf{x}_t, N) \in (C_i(\mathbf{x}_t, N), C_{i+1}(\mathbf{x}_t, N))$.

$L_1(i, j, t)$ and $L_2(i, t)$ are independent of each other, then

$$\begin{aligned} \mathbb{P}(F_{max}(\mathbf{x}, N) = F(\mathbf{x}_t, N)) &= \sum_{i=1}^{\alpha-1} \frac{\prod_{j=1}^d \mathbb{P}(L_1(i, j, t)) \mathbb{P}(L_2(i, t))}{\mathbb{P}(F(\mathbf{x}_t, N) < C_i(\mathbf{x}_t, N))} \\ &= \sum_{i=1}^{\alpha-1} \frac{\prod_{j=1}^d A_1(\mathbf{x}_t, i, j) A_3(\mathbf{x}_t, i)}{A_2(\mathbf{x}_t, i)} \end{aligned} \quad (12)$$

where

$$A_1(\mathbf{x}_t, i, j) = \int_{-3\sigma^2(\mathbf{x}_j, N)}^{C_i(\mathbf{x}_t)} f(M(\mathbf{x}_j, N), \sigma(\mathbf{x}_j, N)) dz \quad (13)$$

$$A_2(\mathbf{x}_t, i) = \int_{-3\sigma^2(\mathbf{x}_t, N)}^{C_i(\mathbf{x}_t)} f(M(\mathbf{x}_t, N), \sigma(\mathbf{x}_t, N)) dz \quad (14)$$

$$A_3(\mathbf{x}_t, i) = \int_{C_i(\mathbf{x}_t)}^{C_{i+1}(\mathbf{x}_t)} f(M(\mathbf{x}_t, N), \sigma(\mathbf{x}_t, N)) dz \quad (15)$$

where $f(\mu, \xi)$ represents the probability density function of normal distribution $\mathcal{N}(\mu, \xi)$. If the maximum value $M(\mathbf{x}_k, N) + 3\sigma^2(\mathbf{x}_k, N)$ of point \mathbf{x}_k is not greater than the minimum value $C_i(\mathbf{x}_t, N)$ of segment i , then the $\mathbb{P}_k(\mathbf{x}_k, N)$ is considered to be 0. Therefore, for each potential location point, the smaller the $\sigma(\mathbf{x}_t, N)$ is, the larger the distance between $M(\mathbf{x}_t, N)$ and $M(\mathbf{x}_R, N)$ is. This means the a smaller positioning error will be produced, particularly for the position points close to the true position of the sound source.

Because the matching result information of all other location points need to be considered when calculating the probability that a location point obtain the maximum value of matching result, the computational complexity of this method increases with the number of location points to be matched. Therefore, in the actual positioning process, if there are many location points to be matched, the following simple method can be used to calculate $\mathbb{P}_t(\mathbf{x}_t, N)$.

Interval (u_1, u_2) can be regard as the value range of $F(\mathbf{x}, N)$ at the true position point \mathbf{x}_R , where $u_1 = M(\mathbf{x}_R, N) - 3\sigma^2(\mathbf{x}_R, N)$ and $u_2 = M(\mathbf{x}_R, N) + 3\sigma^2(\mathbf{x}_R, N)$. Therefore, for the position point \mathbf{x}_t , $\mathbb{P}_t(\mathbf{x}_t, N)$ can be approximately expressed by the integral of the probability density function of $F(\mathbf{x}_t, N)$ in the interval (u_1, u_2) ,

$$\begin{aligned} \mathbb{P}_t(\mathbf{x}_t, N) &= \mathbb{P}_e(F_{max}(\mathbf{x}, N) = F(\mathbf{x}_t, N)) \\ &= \int_{u_1}^{u_2} \frac{1}{\sqrt{2\pi}\sigma(\mathbf{x}_t, N)} \exp\left(-\frac{(z - M(\mathbf{x}_t, N))^2}{2\sigma^2(\mathbf{x}_t, N)}\right) dz \end{aligned} \quad (16)$$

The positioning accuracy can be expressed as the reciprocal of the mean error,

$$Q(N) = \frac{1}{E(N)} = \frac{1}{\sum_{t=1}^d \mathbb{P}_t(\mathbf{x}_t, N) \times |\mathbf{x}_t - \mathbf{x}_R|^2} \quad (17)$$

The positioning results of all arrays will be averaged with weights. A hydrophone array will be divided into multiple hydrophone sub-arrays. If the total number of hydrophones remains unchanged, the number of hydrophones in each hydrophone sub-array will decrease. Assume there are N

hydrophones and m hydrophone sub-arrays. The number of hydrophones in the i th hydrophone sub-array is denoted by N_i ; thus $N = \sum_{i=1}^m N_i$. The weight coefficient depends on the SNR and the number of hydrophones at each receiving sub-array. The weight coefficient increases with the SNR. If the received signal power is P_r and the noise power is P_n at each sub-array, the signal-to-noise ratio is $SNR = \frac{P_r - P_n}{P_n}$.

Thus $Q(N, m, SNR)$ definition

$$Q(N, m, SNR) = \frac{\sum_{i=1}^m \omega_i Q_i}{m} \quad (18)$$

where

$$\omega_i = \frac{SNR_i \times N_i}{\sum_{k=1}^m SNR_k \times N_k} \quad (19)$$

Therefore, when the noise power at the receiving array is known, the signal power can be obtained by subtracting the noise power from the received signal power, and then the positioning error can be calculated by (18). When the actual SNR of the received signal is small, the optimal number of hydrophones can be determined to improve the positioning accuracy by calculating the positioning error of the array.

V. MARINE DATA PROCESSING AND SIMULATION EXPERIMENT

A. Experimental Environment

The environmental parameters of SwellEx-96 are used in these experiments [22]. As shown in Fig. 3, the topmost layer is water with a depth of 216.5 meters and a density of $1g/m^2$. The seafloor first consists of a 23.5m thick layer of sediment with a density of $1.76g/m^2$ and a decay of $0.2dB/mkHHz$. The sound speed at the top of the sedimentary layer is $1572.368m/s$, and the sound speed at the bottom is $1593.016m/s$. At the bottom is a 800m-thick mudstone layer with a density of $2.06g/m^2$ and an attenuation of $0.06dB/mkHHz$. The upper and lower speed of mudstone is $1881m/s$ and $3245m/s$, respectively. At the bottom is an infinite half space with a density of $2.66g/s$, an attenuation of $0.020dB/mkHHz$, and a sound speed of $5200m/s$.

B. Marine Data Processing

The SwellEx-96 experiment includes S5 and S59 experiments. We use the S5 experimental data. The test sound source of S5 is dragged at the speed of $2.5m/s$ at the depth of 54m for 75 minutes. The sound source randomly selects 13 frequencies between 49Hz and 388Hz, and the hydrophone array contains 21 hydrophones. The depth of each hydrophone is shown in Table I. In this test, the 75-minute data are processed, and the signal frequency is 388Hz. The sound field is considered to be independent of the distance, and the kraken normal wave model is used for calculation acoustic field [15]. The matching method adopts the minimum mean square error method. The signal sampling frequency at the hydrophone is 1500Hz. The first 1s data are matched. The experimental results are shown in Fig. 4.

In Fig. 4, the horizontal axis represents the time (minutes), and the vertical axis represents the horizontal distance matching result. The curve with sign o represents the matched sound source trajectory, and the curve with sign $*$ represents

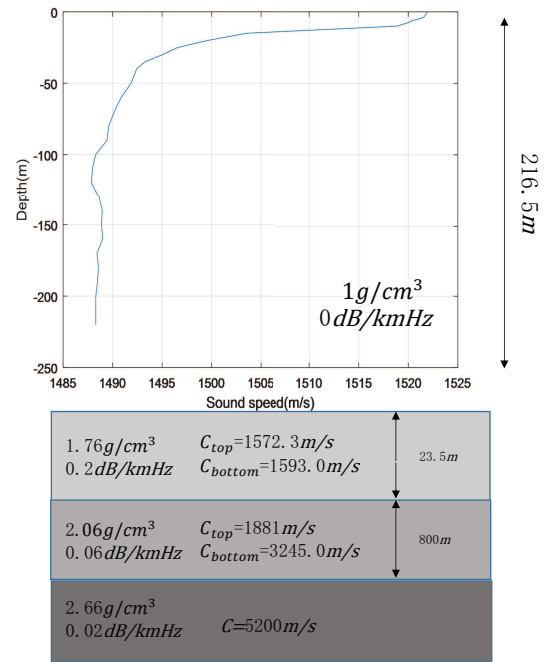


Fig. 3. Experimental Environment.

the motion trajectory of the actual sound source. Obviously there is a large error in the matching result.

Because there is only a single vertical array in this experiment, the positioning results of the same array at different times are used to replace the positioning results of different arrays at the same time, and then the positioning results are fused. The number of hydrophones in each sub-array of multiple arrays is the same as that in the single array. The positioning results are shown in Fig. 5.

Fig. 5 shows average positioning result error with respect to the number of hydrophones. It is observed that the overall positioning result error decreases with the increase of the number of hydrophones, and the average error with two arrays is around 400-600m which is less than that of single array positioning.

TABLE I. HYDROPHONE INDEX NUMBER AND DEPTH

Element Number	Depth(m)	Element Number	Depth(m)
1	212.25	34	150.38
4	206.62	37	144.74
7	200.99	40	139.12
10	195.38	46	127.88
13	189.76	49	122.25
16	184.12	52	116.62
19	178.49	55	111.00
22	172.88	58	105.38
25	167.26	61	99.755
28	161.62	64	94.125
31	155.99		

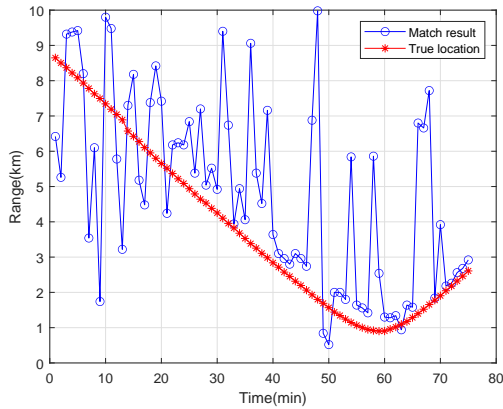


Fig. 4. 75-min Horizontal Distance Matching Results.

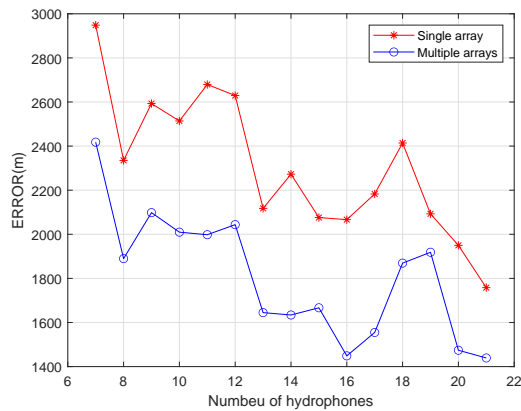


Fig. 5. The Average Positioning Error Varies with the Number of Hydrophones.

C. Simulation for Performance Comparison of The Single Array and Multiple Sub-array System

The environment for the SwellEx-96 experiment is relatively ideal, and it is with low noise, high transmission power and high SNR. Thus in such situation the advantages of multiple arrays are not obvious. To verify the performance of the algorithm in low SNR, instead of experimental data, we use simulation data to evaluate the positioning error by dynamically varying the noise power.

The signal transmitting frequency is 388Hz. The sound field is considered to be independent of the distance. The normal mode is used to calculate acoustic field, and the kraken is used to calculate the acoustic field [15]. A single hydrophone array consists of 20 hydrophones, ranging from 94.125 meters to 206.62 meters in depth. Set $x_R = (r_0, h_0) = (3000m, 60m)$. In the simulation, the horizontal search range is 0-10km, and the step size is 20m; The vertical search interval is 0-100m and the step length is 2m. Then the 20 hydrophones are divided into four groups, and each group has five hydrophones, called sub-array, which are located in the same depth as that of the first five hydrophones of the single hydrophone array. The horizontal distance between sub-arrays and the sound source are $r_1 = 1km$, $r_2 = 3km$, $r_3 = 7km$ and $r_4 = 8km$, respectively. The positioning error is defined as the Euclidean distance between the estimated position and the true one, i.e., $E_R = \sqrt{(r_m - r_0)^2 + (h_m - h_0)^2}$,

where (r_m, h_m) is the estimated position. Since (r_m, h_m) represents the center point of the matching position, when the positioning error is less than the search step, the positioning error is regarded as 0. The received SNR is defined as $SNR = 10 \log_{10} \frac{P_s \sum_{i=1}^N |g_i(x)|^2 / N}{\sigma^2}$, where P_s is the power of the signal source, and σ^2 is the noise power. For the multiple sub-array system, different sub-arrays are placed at different locations, and the signal array system is placed in a different location. Considering the sound wave directivity, we assume the transmission power of sound source for the signal array system is $P_{s,0}$, and the transmission power of sound source for a sub-array is $P_{s,k}, k = 1, 2, \dots, 4$. Set $P_{s,0}=0.65W$, $P_{s,1} = 0.25W$, $P_{s,2} = 0.5W$, $P_{s,3} = 0.75W$, and $P_{s,4} = 0.1W$, respectively. Four hydrophone sub-arrays are used to localize the sound source independently, and the final localization results are fused to determine the location of sound source. The mean value of noise is 0W, and the standard deviation is $\sigma = 0.001 - 0.01W$. With 5000 trials, the positioning results are shown in Fig. 6.

From Fig. 6, when the SNR is between -5dB and -19dB, the positioning error of the single array is 0, and this proves that low noise power has slight influence on the positioning result of the single array. The positioning error of multiple sub-arrays increases from 11m to 60m. Obviously the positioning error of multiple sub-arrays is higher than that of single arrays. However, when the SNR is between -25dB and -21dB, the positioning error of the single array system increases rapidly when the SNR decreases, which is from 3m to 124m. The positioning error of multiple arrays increases slowly from 65m to 67m.

Set $\sigma = 0.01 - 0.1$. The average positioning errors with respect to SNR are shown in Fig. 7. It is observed that the positioning error does not increase with the decrease of SNR, and there is a threshold effect in the positioning result. The positioning error of the single array remains around 145m after -30dB, while the positioning error of the multiple sub-arrays remains around 67m, which is 78m less than that of the single array. With low SNR, the positioning accuracy of the multiple sub-arrays is much higher than that of the single array.

When the number of hydrophones is set to 15, the positioning results of the single array and multiple sub-arrays are shown in Fig. 8. It is observed that the positioning error of the

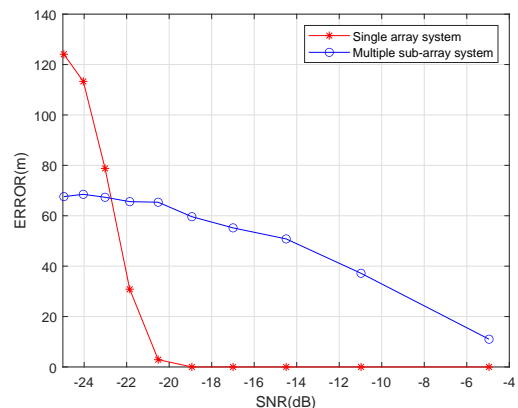


Fig. 6. When $SNR = -25 \sim -5dB$, the Positioning Errors of the Single Array System with 20 Hydrophones and the Four Sub-arrays, Each with 5 Hydrophones.

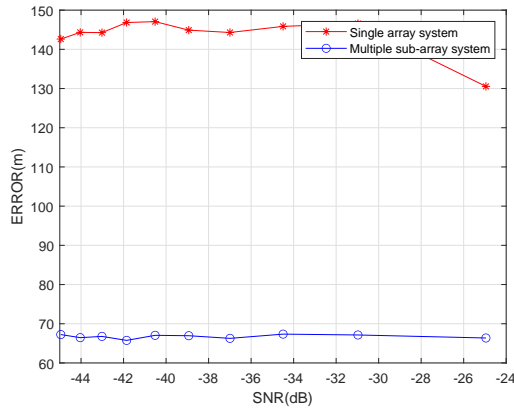


Fig. 7. When $SNR = -46 \sim -25dB$, the Positioning Errors of the Single Array System with 20 Hydrophones and the Four Sub-arrays, Each with 5 Hydrophones.

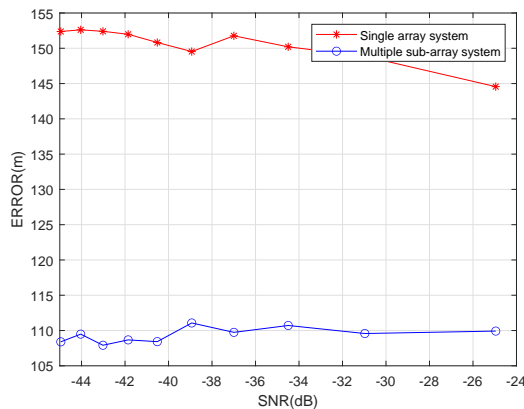


Fig. 8. When $SNR = -46 \sim -25dB$, the Positioning Errors of the Single Array System with 15 Hydrophones and the Three Sub-arrays, Each with 5 Hydrophones.

single array is about 151m and that of multiple sub-arrays is about 109m. Hence, when 5 hydrophones are added, the single array positioning error is reduced by 6m, while the multiple sub-array positioning error is reduced by 42m, which shows that the multiple sub-array positioning accuracy is improved significantly.

The effect of the number of hydrophones in each hydrophone array on the positioning accuracy is shown in Fig. 9. Set $\sigma = 0.1$ and $m = 1$. The average positioning error decreases with the number of hydrophones. When the number of hydrophones changes from 5 to 10, the positioning error decreases with a higher rate, whereas when the number of hydrophones changes from 10 to 20, the positioning error decrease with a slower rate. Note that, $E(N)$ jumps to a higher value when the number of hydrophones is 12, 13 and 16, respectively, in that situation the hydrophones are in a high noisy environment and the positioning accuracy decreases.

D. Simulation for Optimal Structure of Multiple Sub-arrays

To find the optimal number of hydrophones in each sub-array for high-accuracy positioning, 20 hydrophones are divided into multiple groups to form different sub-array structures which are decided by the number of hydrophones in each sub-array and the total number of sub-arrays. Each hydrophone

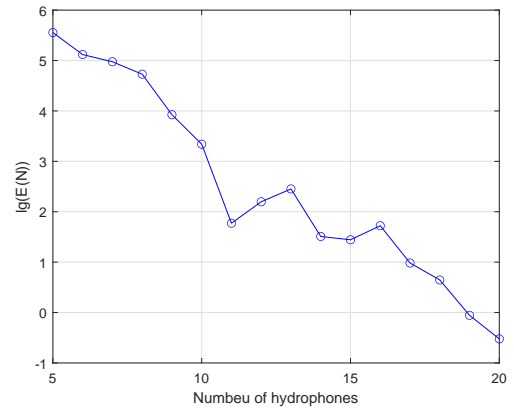


Fig. 9. When the $\sigma = 0.1$, the $\log_{10} E(N)$ Changes with the Number of Hydrophones.

sub-array contains at least 5 hydrophones. Herein we consider 4 sub-array structures to verify the positioning performance. Structure 1: the structure of sub-arrays is same as that defined in Section V-C; Structure 2: The 20 hydrophones are divided into two sub-arrays, and each array has 10 hydrophones. Set $P_{s,0} = 0.75W$, $P_{s,1} = 0.5W$ and $P_{s,2} = 1$, respectively. Set $r_1 = 3km$ and $r_2 = 8km$, respectively, where r_j represents the horizontal distance between the j th sub-array and the sound source; Structure 3: 20 hydrophones are divided into 3 sub-arrays, and the number of hydrophones in each array is 6, 7, and 7, respectively. Set $P_{s,0} = 0.725W$, $P_{s,1} = 0.5W$, $P_{s,2} = 0.75W$, and $P_{s,3} = 1W$, respectively. Set $r_1 = 3km$, $r_2 = 7km$, and $r_3 = 8km$, respectively; Structure 4: 20 hydrophones are divided into 3 sub-arrays, and the number of hydrophones in each array is 6, 6, and 8, respectively. Set $P_{s,0} = 0.775W$, $P_{s,1} = 0.5W$, $P_{s,2} = 0.75W$, and $P_{s,3} = 1W$ respectively. Set $r_1 = 3km$, $r_2 = 7km$, and $r_3 = 8km$, respectively. The positioning results of multiple sub-arrays for Structure 2-4 and the corresponding positioning results of the single array are shown in Fig. 10-15.

Let E_{rs} represent the average positioning error of the single array and E_{rm} represent the average positioning error of multiple sub-arrays. From Fig. 10 and Fig. 11, when the SNR is less than $-30dB$, E_{rs} is around 145m, while E_{rm} is around 97m. The positioning error of the multiple sub-arrays

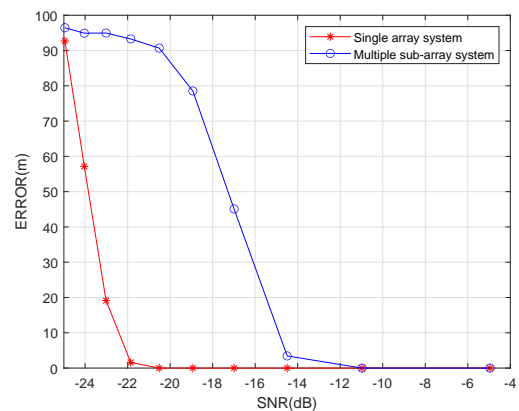


Fig. 10. When $SNR = -25 \sim -5dB$, the Positioning Results of the Single Array System and Multiple Sub-array System of Structure 2.

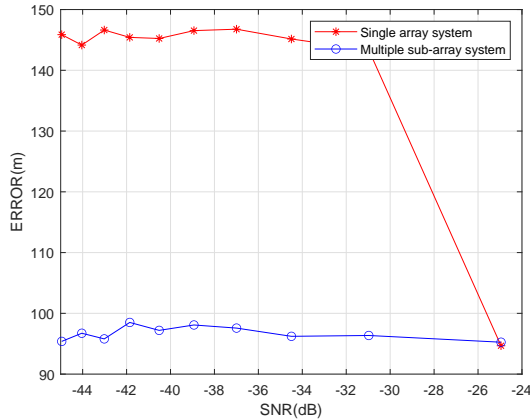


Fig. 11. When $SNR = -46 \sim -25dB$, the Positioning Results of the Single Array System and Multiple Sub-array System of Structure 2.

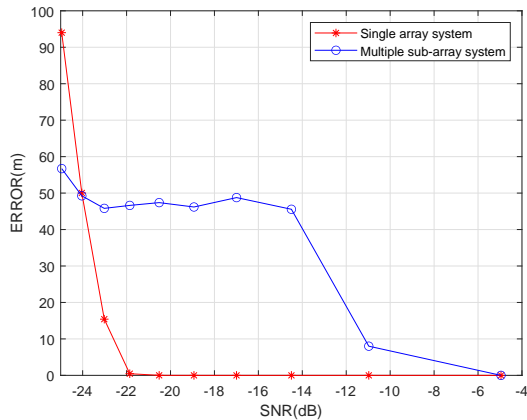


Fig. 12. When $SNR = -25 \sim -5dB$, the Positioning Results of the Single Array System and Multiple Sub-array System of Structure 3.

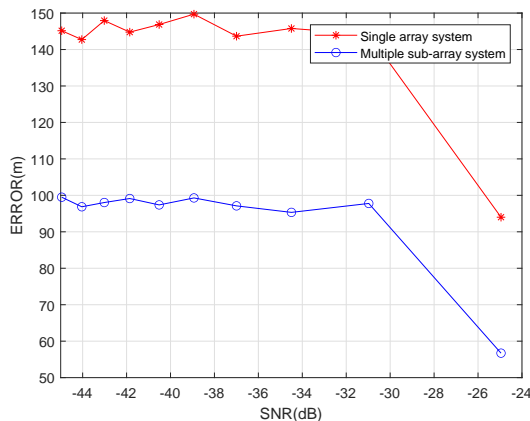


Fig. 13. When $SNR = -46 \sim -25dB$, the Positioning Results of the Single Array System and Multiple Sub-array System of Structure 3.

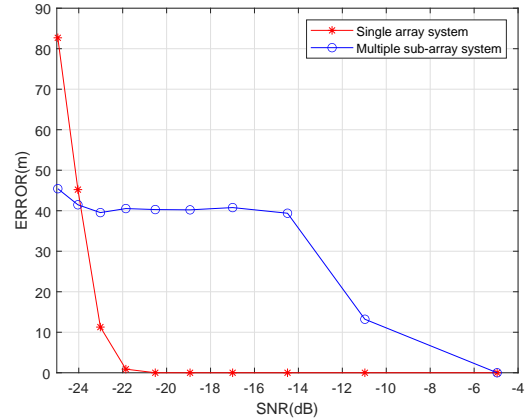


Fig. 14. When $SNR = -25 \sim -5dB$, the Positioning Results of the Single Array System and Multiple Sub-array System of Structure 4.

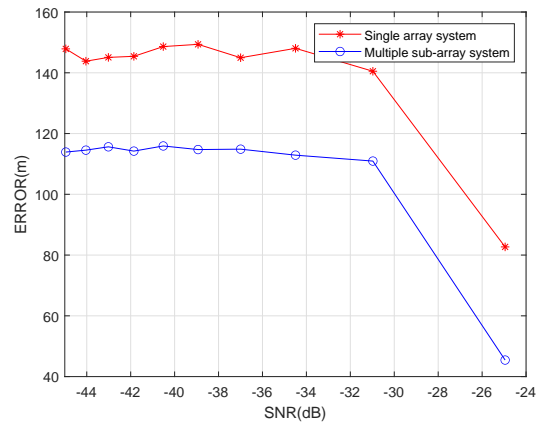


Fig. 15. When $SNR = -46 \sim -25dB$, the Positioning Results of the Single Array System and Multiple Sub-array System of Structure 4.

is 48m less than that of the single array. For the Structure 3, E_{rs} is around 146m, and E_{rm} is around 98m. For the Structure 4, E_{rs} is around 146m and E_{rm} is around 114m. In summary, for the positioning errors produced by the four structures, $E_{rm,1} < E_{rm,2} < E_{rm,3} < E_{rm,4}$, where $E_{rm,k}$ is the positioning error produced by Structure k . With the configured parameters of the four structures, the numerical results $\hat{E}_{rm,k}$ yielded by (18) are $\hat{E}_{rm,1} = 4.32$, $\hat{E}_{rm,2} = 7.62$, $\hat{E}_{rm,3} = 8.08$, and $\hat{E}_{rm,4} = 9.35$, respectively, and $\hat{E}_{rm,1} < \hat{E}_{rm,2} < \hat{E}_{rm,3} < \hat{E}_{rm,4}$. Those are consistent with the simulation results. Hence, under the current experimental conditions, when the SNR is lower than $-30dB$, the Structure 1 achieves the highest positioning accuracy.

VI. CONCLUSION

The experimental results show that when the SNR is higher than a threshold, the positioning error of the multiple sub-array system is slightly higher than that of the single array system. However, when the SNR decreases, the positioning error of the single array decreases faster than that of the multiple sub-array system, and will exceed that of the multiple sub-array system. When the SNR reduces to a certain threshold, the positioning error will not increase with the decrease of SNR , and the positioning error of the single array system is around twice

that of the multiple sub-array system. In addition, by designing different multiple sub-array structures, the simulation results of positioning errors of the multiple sub-array system are obtained, and they are consistent with the theoretical analysis.

In this paper, a multiple sub-arrays joint positioning method is proposed based on the MFP technology. Assume the total number of hydrophones remains unchanged, a single hydrophone array is divided into multiple hydrophone sub-arrays for independent positioning, and the positioning results of sub-arrays are fused to obtain the sound source location. Average positioning error of the multiple hydrophone sub-array system is derived and then the number of sub-arrays and the number of hydrophones in each sub-array are discussed. Experiments and simulations show that the multiple sub-array system can improve the positioning accuracy compared with the single hydrophone array in the noisy environment. The average positioning errors produced by the experiments are consistent with the numerical ones based on the derived formula.

ACKNOWLEDGMENT

This research did not receive any specific grant from funding agencies in the public, commercial or nonprofit sectors. My sincere acknowledgment goes to Dr. Li Xiukui.

REFERENCES

- [1] Clay, C.S. Use of arrays for acoustic transmission in a noisy ocean. *Reviews of Geophysics*. 4(4), 475–507, 1966.
- [2] Hinich, M.J. Maximum likelihood estimation of the position of a radiating source in a waveguide. *The Journal of the Acoustical Society of America*. 66(2), 480–483, 1979.
- [3] David, R. Dowling, R. Incomplete acoustic time reversal, frequency shifting, and matched field processing. *The Journal of the Acoustical Society of America*. 150, A193-A193, 2021. <https://doi.org/10.1121/10.0008096>
- [4] Scripps, UCSD, L.A., Jolla, C.A. Localizing a quiet moving source with range-coherent matched field processing. *The Journal of the Acoustical Society of America*. 150, A277-A277, 2021. <https://doi.org/10.1121/10.0008283>
- [5] Capon, J., Greenfield, R.J., Kolker, R.J. Multidimensional maximum-likelihood processing of a large aperture seismic array. *Proceedings of the IEEE*. 55(2), 192–211, 1967.
- [6] Tran, P.N., Trinh, K.D. Adaptive matched field processing for source localization using improved diagonal loading algorithm. *Acoust Aust*. 45, 325–330, 2017. <https://doi.org/10.1007/s40857-017-0089-4>
- [7] Shang, E.C. Source depth estimation in waveguides. *The Journal of the Acoustical Society of America*. 77(4), 1413–1418, 1985.
- [8] Shang, E.C., Clay, C.S., Wang, Y.Y. Passive harmonic source ranging in waveguides by using mode filter. *The Journal of the Acoustical Society of America*. 78(78), 172–175, 1985.
- [9] Yang, T.C. A method of range and depth estimation by modal decomposition. *The Journal of the Acoustical Society of America*. 82(5), 1736–1745, 1987. .
- [10] Yang, T.C. Effectiveness of mode filtering: A comparison of matched-field and matched-mode processing. *The Journal of the Acoustical Society of America*. 87(5), 2072–2084, 1987.
- [11] Battle, D.J., Gerstoft, P., Hodgkiss, W.S. Bayesian model selection applied to self-noise geoacoustic inversion. *The Journal of the Acoustical Society of America*. 116(4), 2043–2056, 2004.
- [12] Debever, C. Investigation of the Limits of Broadband Robust Matched-field Processing. University of California, San Diego, 2011.
- [13] Collins, M.D., Makris, N.C., Fialkowski, L.T. Noise cancellation and source localization. *The Journal of the Acoustical Society of America*. 96(3), 1773–1776, 1994.
- [14] Lee, Y.P. Multiple-frequency robust adaptive matched-field processing(mfp) in shallow water. *The Journal of the Acoustical Society of America*. 97(5), 3290–3290, 1995.
- [15] Song, H.C., Seong, W. Localization of a moving source in oceanic waveguide using a vertical array in the presence of correlated noise. *The Journal of the Acoustical Society of America*. 95(5), 2981–2981, 1994.
- [16] Nicholas, M., Perkins, J.S., Orris, G.J.: Source motion mitigation for adaptive matched field processing. *The Journal of the Acoustical Society of America*. 113, 2719–2731, 2003. <https://doi.org/10.1121/1.1561817>
- [17] Zurk, L.M., Lee, N., Ward, J. Environmental inversion and matched-field tracking with a surface ship and an l-shaped receiver array. *The Journal of the Acoustical Society of America*. 116, 2891–2901, 2004. <https://doi.org/10.1121/1.1802755>
- [18] Tollefsen, D., Gerstoft, P., Hodgkiss, W.S. Multiple-array passive acoustic source localization in shallow water. *The Journal of the Acoustical Society of America*. 141(3), 1501–1501, 2017.
- [19] Tracey, B.H. Statistical description of matched field processing ambiguity surfaces. *The Journal of the Acoustical Society of America*. 118, 1372–1380, 2005. <https://doi.org/10.1121/1.2000750>
- [20] Bogart, Christopher, W. Source localization with horizontal arrays in shallow water: Spatial sampling and effective aperture. *The Journal of the Acoustical Society of America*. 96(3), 1677–1686, 1994.
- [21] Tantom, S.L., Nolte, L.W. On array design for matched-field processing. *The Journal of the Acoustical Society of America*. 107, 2101–2101, 2000. <https://doi.org/10.1121/1.428492>
- [22] Murray, J., Ensberg, D. The swellex-96 experiment[eb/ol], 1996. <http://swellex96.ucsd.edu/>

High-quality Voxel Reconstruction from Stereoscopic Images

Arturo Navarro

Department of Computer Science
Universidad Católica San Pablo, Peru

Manuel Loaiza

Department of Computer Science
Universidad Católica San Pablo, Peru

Abstract—Volumetric reconstruction from one or multiple RGB images has shown significant advances in recent years, but the approaches used so far do not take advantage of stereoscopic features such as distance blur, perspective disparity, textures, etc. that are useful to shape the object volumes. Our study is to evaluate a convolutional neural network architecture for reconstruction of 128^3 voxel models from 960 pairs of stereoscopic images. The preliminary results show an 80% of coincidence with the original models in 2 categories using the Intersection over Union metric. These results indicate that good reconstructions can be made from a small dataset. This will reduce the time and memory usage for this task.

Keywords—Voxel reconstruction; stereoscopy; convolutional neural networks; disparity maps

I. INTRODUCTION

Voxel Reconstruction is a wide field of research within computer vision. It is currently getting more attention thanks to the appearance of high-resolution RGB-D and stereo cameras. This field has benefitted from the development of machine learning neural networks, which have allowed volumetric reconstruction to obtain promising advances both for single-image and multiple-image cases. This reconstruction takes pictures from real or synthetic 3D objects and obtains a model made of voxels. Voxels are the 3D equivalent of the 2D pixels; this means that voxels are mainly indivisible blocks of position and color data, that can be put together and broken down. Such properties are important for applications like robotic vision, particle simulation, or volume comparison.

Computer vision itself offers multiple opportunities for further development since it is still a budding topic to deal with due to the gap between the information provided by the pixels and the interpretation that can be given to that information. Current volumetric reconstruction methods based on Convolutional Neural Networks (CNN) have achieved significant progress in the quality of the results, however reconstructions are made usually under good conditions that are rarely replicated in reality: multiple views, good lighting, and definition, or extensive datasets. They also don't make any use of depth information provided by stereoscopic vision. Stereoscopy is a vital function for human beings for depth perception. It gives good information about volume and depth mainly from depth cues like accommodation, focus, occlusion, linear and aerial perspective, relative size, density, and motion parallax [1]. Much of this information is present in only one of the ocular perspectives through the so-called monocular depth, but it is the complementation that allows a better perception, through the binocular depth.

Current approaches for 3D reconstruction tasks have been obtained mainly under optimal conditions and multiple view-points, which is often not possible in real situations. On the other hand, while single-image reconstruction methods have also made improvements, they rely on intensive pretraining and large datasets to estimate the hidden parts and fill in the volume. These datasets are usually formed by images with simple and unique objects; this is good for techniques testing but it has limited practical applications. Reconstructed voxel meshes also tend to be low-resolution (32^3 voxels), losing important details that could be significant to some applications.

This study aims to validate a deep learning model for stereo 3D reconstruction, to get a good resolution model of 128^3 voxels from 960 couples of stereoscopic images. For that purpose, The architecture proposed by [7] was implemented. This generated more detailed voxel models for the applications previously mentioned. The dataset used for this study will be kept small due to limited computational resources. We aimed to prove that a 3D reconstruction is feasible from a small dataset of detailed images and limited computational resources that could be use for practical applications, where optimal image capture is not ideal.

The rest of this document is as follows: chapter two will include the related work to this study. Methodology and dataset is presented in chapter three. The results will be shown in chapter four. Chapter five will review the discussion and the final chapter will include the conclusions.

II. STEREOSCOPY

It is a technique of depth artificial representation from two stereographic images, where each of them represents the vision from one of the human eyes, thus imitating the real vision. Depth is reconstructed in the brain from the 2D images captured by the retina, and from certain signals or cues present in those images [2]. Much of this information is present in only one of the ocular perspectives through the so-called monocular depth, but it is the vision complementation that allows a better perception, through the binocular depth.

Main cues:

- Occlusion: Visual obstruction of a near object on a more distant one.
- Linear Perspective: Phenomenon by which parallel lines seem to get closer the further they are apart.

- Aerial perspective: Perception of distance through the absorption of light. Closer objects appear more colorful and brighter than distant objects in general.
- Relative size: Related to perspective. Nearby objects appear larger.
- Density: The denser an object's texture appears, the farther away it is assumed to be. It is also known as texture gradient.
- Adequacy: It is the adjustment of the muscle and the ocular lens to focus an image. The further away the object is, the more relaxed the muscle and the more circular the lens.
- Focus: It is the rotation of the eyes, to focus together on an object at a certain distance. The eyes converge on near objects and diverge on distant ones.
- Motion Parallax: When the viewer (human, camera, etc.) is in motion, nearby objects appear to move faster than distant objects.

Fig. 1 shows the main binocular cues for depth perception.

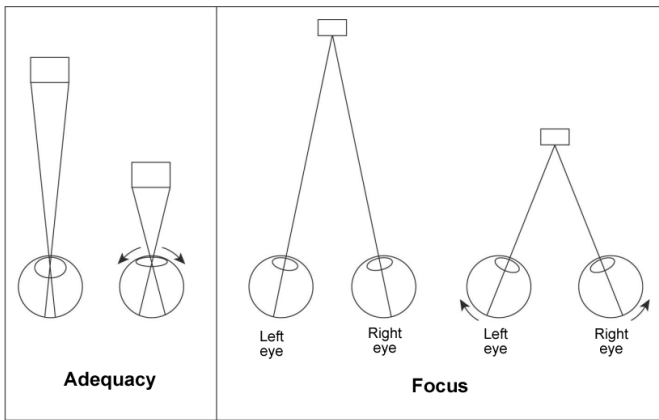


Fig. 1. Binocular Cues. [1]

III. CONVOLUTIONAL NEURAL NETWORKS

They are supervised learning neural networks, based on multilayer perceptrons, where the hidden layers are specialized to detect certain shapes, starting from simple lines and curves, up to more specialized layers capable for complex figures detection. [3]. These networks are especially used for artificial vision since they are biologically inspired by the functioning of the human visual cortex.

The input for the convolutional network is a normalized set of image pixels, where each input neuron corresponds to a pixel, separated by channels (red, blue, green). A group of nearby pixels is then convolved with a filter matrix called kernel. These kernels are applied one by one to each neuron input, which are previously trained. The result of that convolution is a matrix that feeds the next network layer. For this first layer, the output of each neuron is calculated as:

$$Y_j = f \left(b_j + \sum_{i=1} K_{ij} * Y_i \right) \quad (1)$$

Where Y_j is the output of each neuron, Y_i are its inputs, K_{ij} is the kernel, b_j is the bias, and $f()$ is an activation function, commonly the Rectified Linear Function or ReLu; which is defined as $f(x) = \max(0, x)$.

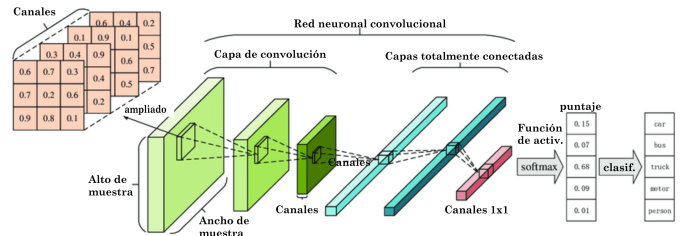


Fig. 2. Example of Convolutional Neural Network [4].

The next step is sampling, which is reducing the size of the output matrix of the previous layer, thus reducing the computational cost of the convolutions. The most common reduction method is Max Pooling which selects the max value from $m \times n$ group of neighbour cells. This also helps to reduce noise from the extracted images. On the reduced outputs a new set of kernels is applied to perform a finer detail extraction followed by another sampling process. This is repeated as necessary.

Finally, as shown in Fig. 2, the outputs of the last convolution-sampling process are sent to a fully connected supervised learning network that is responsible for classifying the details to a previously established category [5].

IV. RELATED WORK

In [6], the authors made a classification for 3D reconstruction approaches, focusing on shape representations, the network architectures, and the training mechanisms, stating specific issues such as limited datasets, fine-scale reconstruction, and unseen objects. Recently, Xie et al. [7] proposed to reconstruct synthetic 3D models into a low-quality voxel mesh and a point cloud using a dataset of couples of RGB images and their correspondent disparity maps to feed a 3 CNN pipeline (Fig. 3), this work is the first to use stereo images for reconstruction based on deep learning. It obtained similar results to reconstruction from multiple-image-based reconstructions.

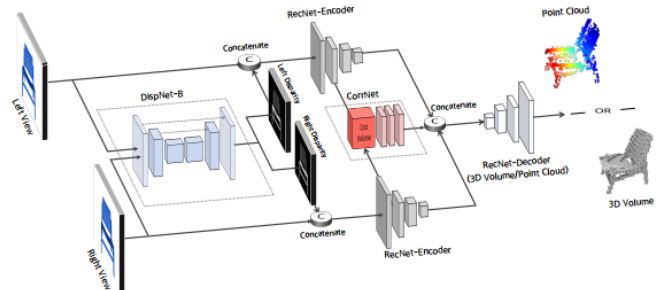


Fig. 3. CNN Architecture for 3d Mesh and Point Cloud Reconstruction from RGB and Disparity Stereoscopic Images. [7]

Similarly, Xie worked also on a point view and voxel reconstruction approach for single and multiple views named

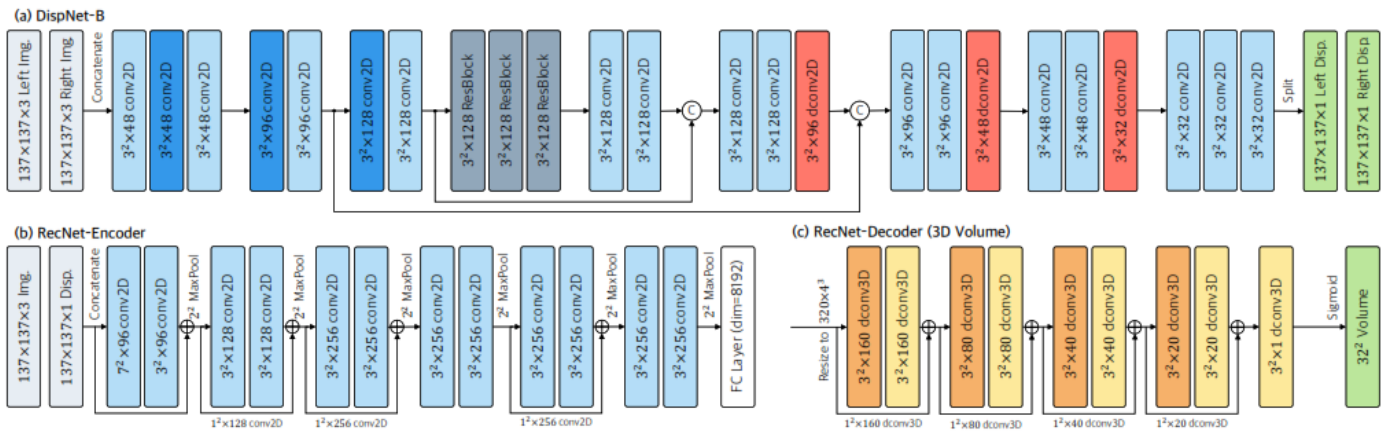


Fig. 4. DispNet and RecNet Architecture. [7]

Pix2Vox [8] [9]. For the voxel mesh upscaling task, Wang et al. [10] presented a long-term recurrent CNN and Generative Adversarial Network (GAN) combination to complete and improve resolution for voxel volumes. These works generate low-resolution 32^3 meshes and get small and simple images as inputs, our work starts from complex and detailed images from a small dataset to get similar results in completion.

A relatively recent study to improve recognition by CNNs is that of Qi et. al [11] which improves the results on both volumetric and multiview-based reconstructions by using two CNNs with specialized jobs. These architectures produce also low-quality voxel meshes. Dryanovski et al [12] using mobile devices and the *Google Tango* platform to achieve a low computational cost and low memory consumption reconstruction of large scenes by using a hash table to store the volumetric information. The method also includes a fusion process to improve the quality and completeness of reconstructions. Kar, Häne, and Malik [13], propose a stereo reconstruction system based on projective geometry to transfer from 2D to 3D elements from multiple images joined by a CNN to a volumetric mesh of 32^3 and a depth point map. Riegler et al [14] present a CNN fusion architecture for multiview reconstruction, based on truncated signal distance function (TSDF) and octree data structures for simple objects. The efficiency of representation is addressed by Liu et al. [15], where the authors propose a point-voxel convolution to reduce the memory cost of voxel models. Multiple-view approaches rely on large datasets, camera poses and costly 3D fusion processes. Moreover, getting many views for a scene is not always feasible. Stereo-based reconstruction uses only two images; therefore, partial 3D mesh fusion is less costly.

In [16], Firman et al. start from a trained set of decision trees in a random forest to complete a scene making predictions about the reconstructed geometry in *voxlets* or groups of voxels, for a low-resolution mesh, using only a single input depth image. Yang et al. [17], seek a higher resolution also starting from a single image, but applying Generative Adversarial Networks (GANs) to identify a specific set of objects (benches, chairs, armchairs, and tables) from a single image, but with meshes of 256^3 voxels. In contrast, Häne et al. used Convolutional Neural Networks (CNN), [18] to achieve a hierarchical prediction by subdividing an initial 16^3

mesh into a 256^3 voxel to refine the result. For that purpose, they use also a single image, but the framework is prepared to work with more inputs. More recently, Tatarchenko et al. [19] proposed two new methods in the recognition task that is based on the Intersection over Union (IoU) metric: Clustering and Recovery, although also pointing to low-resolution meshes. TSDF volumes and regression instead of depth maps are used by Choe [20] and Murez [21], making their reconstructions based on camera poses. Jadhav [22], worked on a homography multiview image correspondence to complete voxel meshes. Addressing the limitation of single image perspective, Watson et al. [23] introduces a process for obtaining stereo images from a single RGB input, adding depth on key information for reconstruction. Volumen completion from single image input is made by Varley et al. [24], which work consists of a fast voxel mesh completion method applied to robot grasping. One-image-based reconstructions require semantic labeled datasets and they are restricted to specific domains, since they complete occluded parts from similar preprocessed scenes. Stereo reconstruction obtains their depth information from the very input, and our work relies only in the ground truth model for refinement. Other approaches like TSDF volumes and homography need also camera poses and multiple images which are not always available.

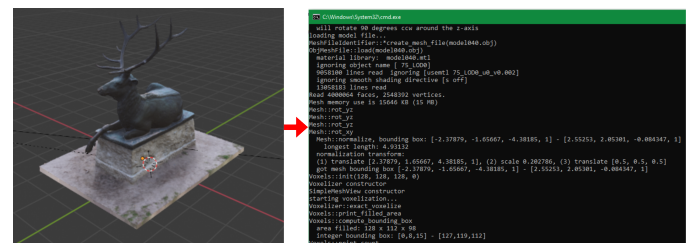


Fig. 5. Voxelization Process on Binvox.

Stereo image inputs carry enough depth information to obtain a suitable 3D voxel mesh model that can be used in practical applications. Our work starts from a small dataset of detailed images, so the computational cost is small both in image processing and 3d mesh fusion. To overcome domain-restricted limitations, we tested two different categories of objects: complex low-res scenes and single high-detailed objects.

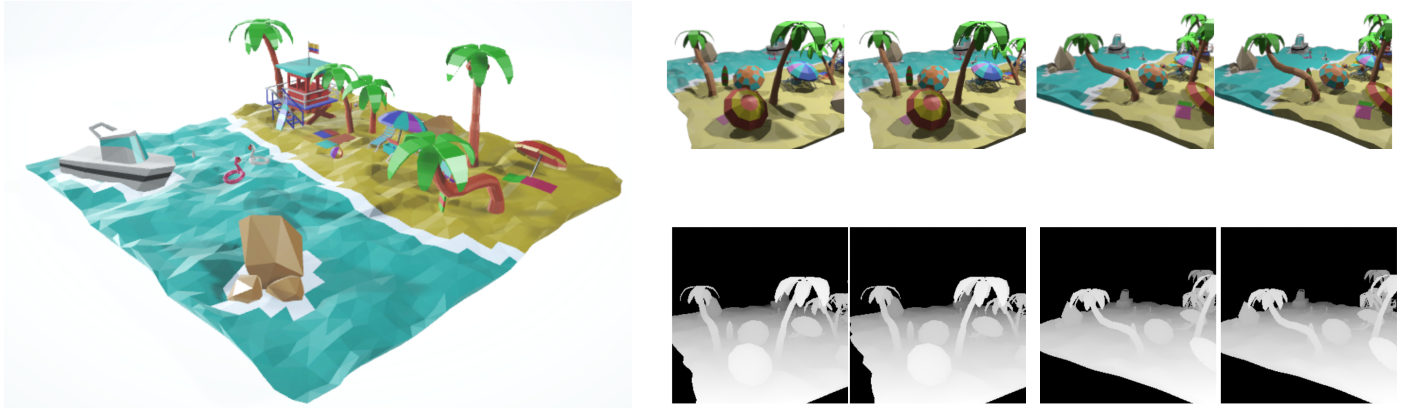


Fig. 6. Left: Original Model. Right up: Pairs of Left-Right RGB Images. Right Down: Pairs of Left-Right Disparity Maps.

V. METHODOLOGY

We use the DispNet, and RecNet architecture from [7] for high-quality volumetric reconstruction from a dataset of pairs of stereoscopic images with details that recreate real conditions, such as a Gaussian blur or low lighting. This dataset was generated from 3D models that could be found on <https://sketchfab.com>. The Blender tool was used to create the RGB and depth images according to the procedure described in [9]. The dataset is extended by adding the same images with a depth of field of 3m.

The tested architecture includes interconnected convolutional and residual neural networks of the encoder-decoder type, as can be seen in Fig. 4. DispNet includes 5 convolution and 4 deconvolution layers to deliver the two disparity images. RecNet includes 6 convolution layers, one fully connected layer, and 7 deconvolution layers to finally build the volumetric mesh. Two modifications were made to the original RecNet decoder architecture to produce 128^3 voxel grids. Several residual blocks are included in both networks. CorrNet .. is a three-dimensional convolutional network with nine convolutional layers and a final fully connected layer; Although it was implemented, due to limitations of the development platform it could not be tested with more than 500 images.

A comparison of the refinement of the volumetric mesh was obtained by training the current convolutional network to obtain higher resolution meshes; specifically 128^3 voxels. This will be useful for models belonging to taxonomies with more complex shapes. For the validation of the results, a voxelization process will be used from the tested models to obtain ground truth meshes with Blender and Binvex (Fig. 5). The results were measured using the IoU metric against the previously obtained *ground truth* reconstructions.

A. Implementation Details

The architecture was implemented with Kaggle Notebook, using a NVIDIA Tesla P100 GPU with 13 GB of GDDR5 memory, an Intel(R) Xeon(R) 2.30GHz CPU, 16 GB of RAM, and 359 GB of disk space. The implementation has been carried out with the Python programming language and the Keras *deep learning* library, which is already equipped with all

the types of convolutional layers required to build the proposed models. Due to limitations in space and use time, the number of epochs for both networks are limited to 100, which we found was enough to achieve good results.

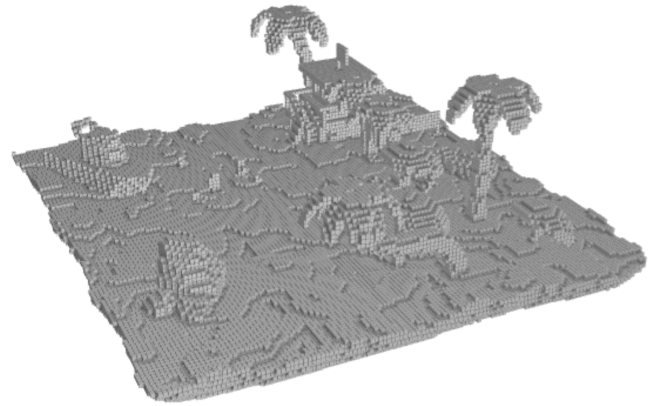


Fig. 7. Binvex Mesh Sample.

B. Data set

Dataset has been built with pairs of stereoscopic images in RGB and their correspondent disparity maps captured from 40 3d objects selected from 2 categories of free models obtained from sketchfab.com: complex scenes with low polygon count and high poly count statues. A production pipeline for these images has been created in the **Blender** (<https://www.blender.org/>) tool, where a stereoscopic camera with azimuth angle $\theta_{az} \in [0,360)$ and elevation angle $\theta_{el} = 30$, with a 35mm focal length, 32mm sensor size, and a 130mm [7] stereo baseline. The camera is positioned at 12 different angles with an angular increment of 30° . The RGB images obtained are 256×256 pixels. In the case of disparity images, these are obtained by applying a depth filter which is then color inverted to generate the disparity details. These images also have 256×256 pixels. Fig. 6 shows some images in RGB and disparity. Each model has been voxelized with the **binvox** tool (<https://www.patrickmin.com/binvox/>), since this format

is more compatible with Keras (Fig. 7). A three-dimensional mesh of occupancy (binary values) is obtained, loaded, and stored for use. The size of the dataset is then increased by applying a 6-pixel neighborhood Gaussian blur effect to the RGB images.

VI. RESULTS

A. DispNet Results

The DispNet network received two RGB stereoscopic images concatenated as a 6-channel array for a set size of 960 pairs. As output, it generated two stereoscopic grayscale disparity images (1 channel), which are also concatenated in a 2-channel array with a set size of 960 pairs. The network is configured as shown in Fig. 4. The Dispnet class includes a minimum square error loss function, Adam optimizer, 100 training epochs, batch of size 6, and validation set equal to 30%. After training, the following metrics are obtained:

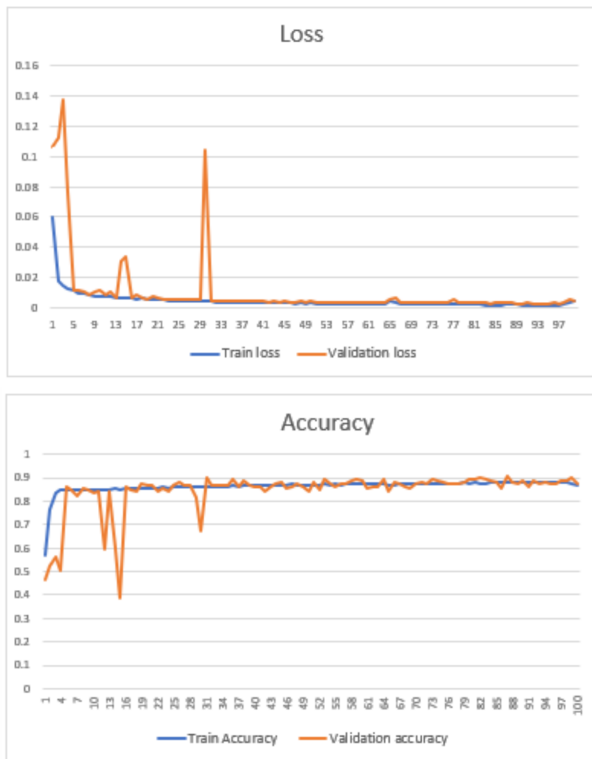


Fig. 8. Dispnet Loss and Accuracy during 100 Epochs of Training.

TABLE I. TRAINING RESULTS FOR DISPNET AFTER 100 EPOCHS

Metric	Train	Validation
loss	0.0016	0.0027
accuracy	0.8634	0.8431

Table I shows an error value below of 0.01% for both sets and an accuracy of about 86% for the training set and 84% for the validation set. The training progress can be seen in Fig. 8. These results are quite acceptable, even though it is a small dataset. Visually the disparity images produced by Dispnet are

very similar to the original in shape and color. This can be seen in Fig. 9. These generated images are feasible to use as input for RecNet.

B. RecNet Results

Two inputs are used for RecNet: the left RGB image and disparity pair merged into 4 channels, and the corresponding right side RGB-disparity merge, as output; the occupancy maps are given by *binvox* with each of the 40 models multiplied 12 times. Unlike DispNet, RecNet is implemented with a binary entropy loss function. Adam optimizer, 100 epochs and batch of 6 are also used. The metrics shown in Table II and Fig. 10 indicate a very low precision that could not be corrected either. with CorrNet aggregation [9]. The generated models are acceptable in both categories as seen in Fig. 11. There is usually a loss of fine detail such as thin lines or small extremities.

TABLE II. RECNET TRAINING METRICS FOR 100 EPOCHS

Metric	Train	Validation
loss	0.007	0.0128
accuracy	0.1256	0.1139

C. Intersection over Union Metric

The IoU metric calculates the total number of matches between two 3D meshes produced by an intersection or coincidences in both arrays over the total number of occupied cells of both meshes. This is represented in the following equation

$$IoU = \frac{\sum_{i,j,k} I(\hat{V}^{(i,j,k)} > t)I(V^{(i,j,k)})}{\sum_{i,j,k} [I(\hat{V}^{(i,j,k)} > t) + I(V^{(i,j,k)})]} \quad (2)$$

Where $\hat{V}^{(i,j,k)}$ is the generated mesh, $V^{(i,j,k)}$ the original mesh; t is a limit (threshold) applied to the values of the mesh produced to approximate the values to 0 or 1 respectively. The I function is a limit function to obtain only binary values before performing the summations. The IoU result is a percentage value indicating the matches between arrays.

For both categories with normal and blurred variants on each one; the resulting IoU metric is shown in Table III. Fig. 12 indicates the comparison of metric values for each category, as well as the IOU frequencies for grouping entries with an interval of 0.05.

TABLE III. AVERAGES IOU VALUES FOR EVERY CATEGORY TRAINED

Category	Value
Scenes	0.896
Statues	0.815
Blurred scenes	0.895
Blurred statues	0.816
Average	0.856

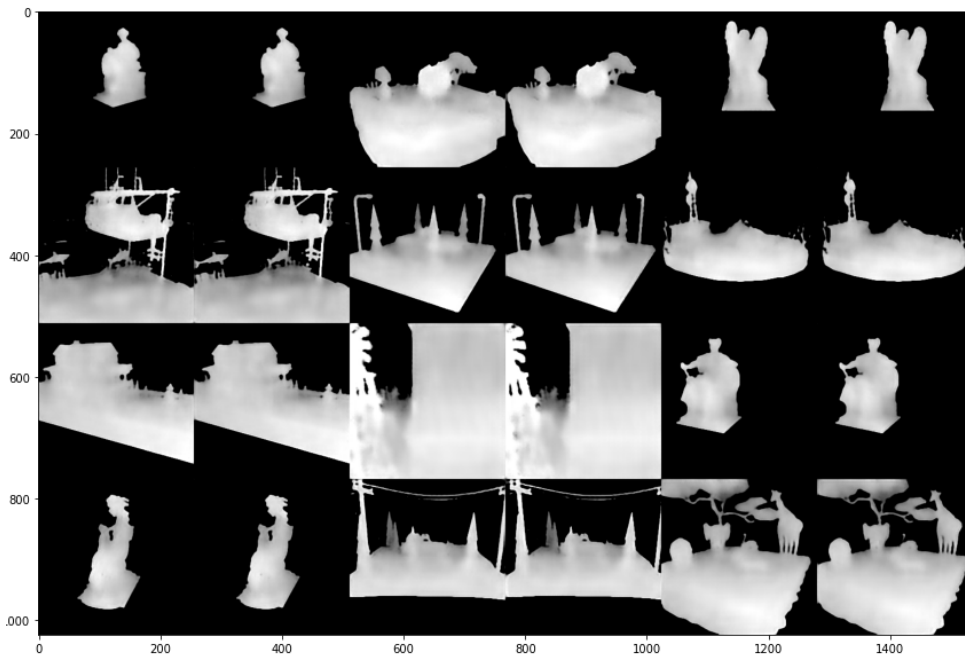


Fig. 9. Disparity Maps Generated by DispNet.

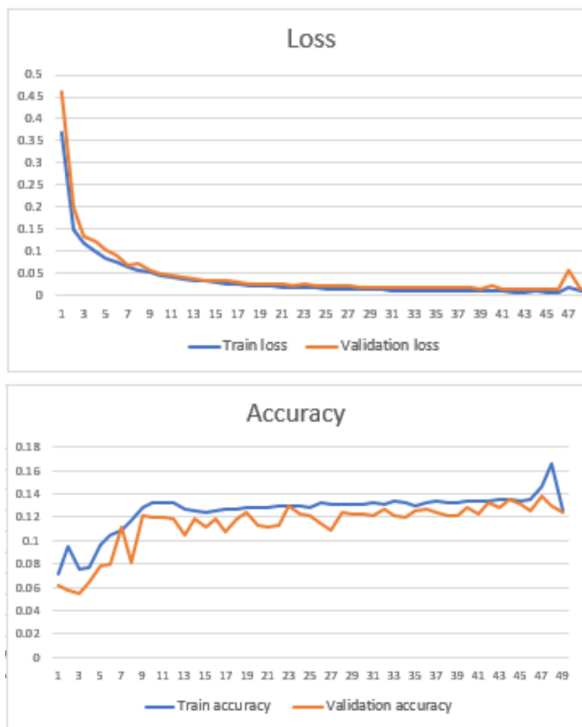


Fig. 10. RecNet Loss and Accuracy during 100 Epochs of Training.

VII. DISCUSSION

Our research shows that a 3D volumetric reconstruction can be achieved from a small set of pairs of stereoscopic images. The metrics get values of 80% for a small dataset compared to [7], where the author uses more than a million pairs of images,

with values between 65% and 70% for model precision. The additional information given by the depth maps helps to get more accurate reconstructions. A smaller set of better quality images requires less computational power and less time consumption, which is ideal for applications on free GPU developing platforms like Google Colab or Kaggle Notebook. It is possible that the balance of quality of inputs and the size of the set leads to good reconstructions with fewer resources. This is related to the main limitations faced during this study: the time and size constraints of GPU use and the access to bigger datasets. Our CNN architecture wasn't specially modified for a 128^3 voxel model, apart from a stride modification on the final layer of the pipeline. Therefore, a more precise model could be achieved with additional configurations on the architecture.

The quality of inputs has been established as an important variable to reconstruction accuracy. The author in [7] used 137×137 RGB pictures, relying more on the number of inputs given. 256×256 or even bigger RGB and depth pictures have shown similar results for this CNN architecture as smaller pictures. This could be extended for reconstruction research on single and multiple RGB images, which usually use low-quality pictures. These results could be extended for real good-quality pictures taken with stereo and depth cameras. Better tuned CNNs based on this architecture can be made for these real pictures, the model resolution could also be extended with extra steps in the pipeline.

VIII. CONCLUSION

In this work, we have developed a two-step convolutional network architecture for 3d reconstruction from a small dataset of pairs of stereoscopic images with complex scenes and detailed objects. Our work is influenced by depth perception cues noticed as disparity maps which are generated in the first step and then used to feed the reconstruction step. Re-

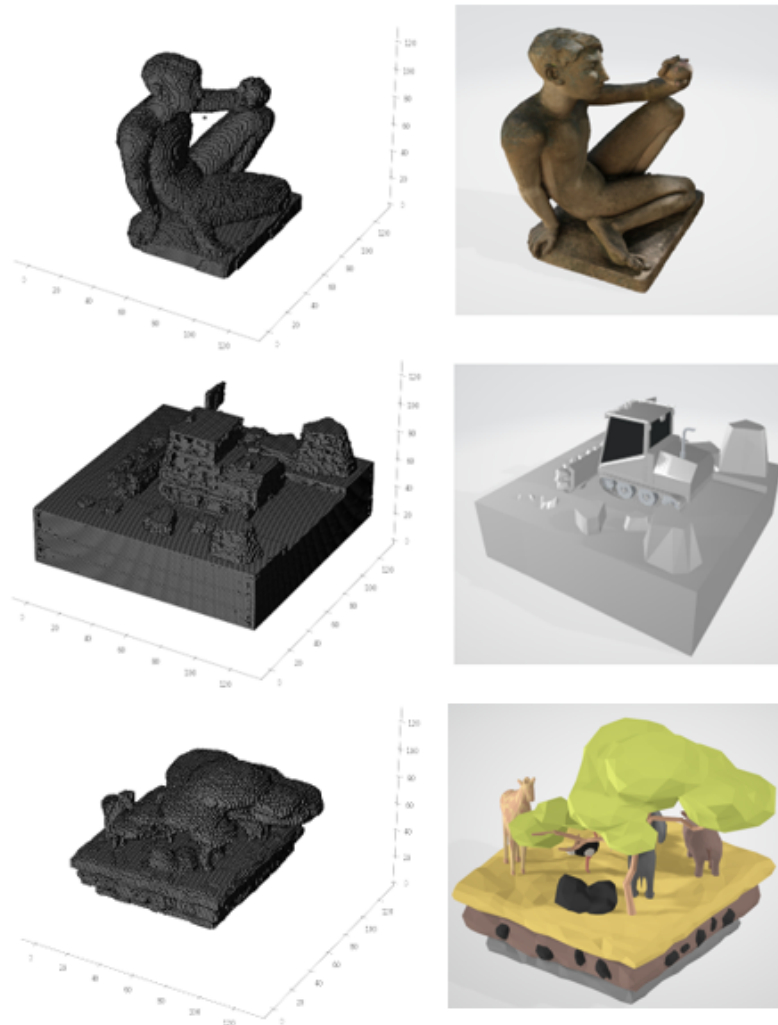


Fig. 11. RecNet Result Meshes (Left) Compared to Ground Truth Meshes (Right).

constructed models have on average 80% on the intersection over union metric. This percentage is similar to state-of-the-art proposals with bigger datasets. The models also have better resolution (128^3) than previous works. This suggests that a set of hundreds of rich and detailed stereoscopic images could be enough for the reconstruction of these volumetric models. The dataset was enlarged with a blurred version of the RGB images as input. Future work will focus on refining the final result with bigger datasets, applying another transformations to images like rotation and contrast; and tuned networks settled for this task that could overcome low accuracy levels on network training and validation.

ACKNOWLEDGMENT

We acknowledge the financial support of the "Proyecto Concytec - Banco Mundial", through its executing unit "Fondo Nacional de Desarrollo Científico, Tecnológico y de Innovación Tecnológica (Fondecyt)", for their research work entitled "Reconstrucción y modelado 3D de las superficies de componentes y piezas de maquinaria pesada usada en Minería,

con nivel de precisión milimétrica, para su aplicación en un nuevo proceso optimizado de mantenimiento especializada".

The authors would like to thank EdwinRC (<https://sketchfab.com/Edwin3D>), noe-3d.at (<https://sketchfab.com/www.noe-3d.at>), and VIMUNE (<https://sketchfab.com/vimune>), for the fantastic models used in this study.

REFERENCES

- [1] J. LaViola Jr., E. Kruijff, R. McMahan, D. Bowman, I. Poupyrev, *3D User interfaces, theory and practice*, 2017.
- [2] E. Abbott, *Chapter 2 Principles of Stereoscopic Depth Perception and Reproduction*, 2004
- [3] J.I. Bagnato, *¿Cómo funcionan las Convolutional Neural Networks? Visión por Ordenador*, 2018, <https://www.aprendemachinelearning.com/como-funcionan-las-convolutional-neural-networks-vision-por-ordenador/>, retrieved on 17/02/2022.
- [4] X. Kang, B. Song and F. Sun, *A deep similarity metric method based on incomplete data for traffic anomaly detection in IoT*, Applied Sciences, 01, 2019.

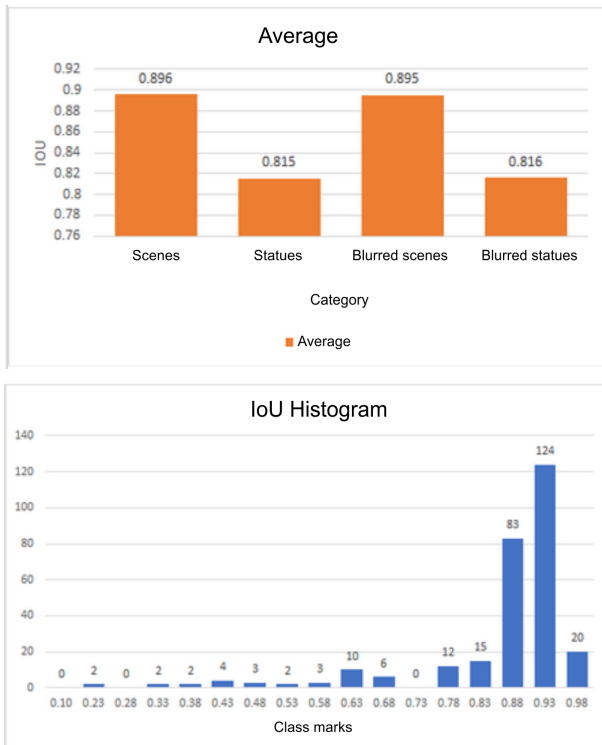


Fig. 12. Left: IOU Metric Average for Each Category. Derecha: IoU Histogram with 0.05 Interval Width.)

[5] S. Saha, *A comprehensive guide to Convolutional Neural Networks — the ELI5 way*, 2018, <https://towardsdatascience.com/a-comprehensive-guide-to-convolutional-neural-networks-the-eli5-way-3bd2b1164a53?gi=c6d122c7b4c>, retrieved on 17/02/2022.

[6] X.F. Han, H. Laga and M. Bennamoun, *Image-based 3D Object reconstruction: state-of-the-Art and trends in the Deep Learning era*, 11 2019.

[7] H. Xie, H. Yao, S. Zhou, S. Zhang, X. Sun, and W. Sun, *Toward 3d object reconstruction from stereo images*, 10 2019.

[8] H. Xie, H. Yao, X. Sun, S. Zhou and S. Zhang, *Pix2Vox: Context-aware 3D reconstruction from single and multi-view images*, 01 2019.

[9] H. Xie, H. Yao, S. Zhang, S. Zhou, and W. Sun, *Pix2vox++: Multi-scale context-aware 3d object reconstruction from single and multiple images*, International Journal of Computer Vision, 2020.

[10] W. Wang, Q. Huang, S. You, C. Yang and U. Neumann, *Shape inpainting using 3D Generative Adversarial Network and Recurrent Convolutional Networks*, 11 2017.

[11] C.R. Qi, H. Su, M. Niessner, A. Dai, M. Yan, and L. Guibas, *Volumetric and multi-view CNNs for object classification on 3d data*, 04 2016.

[12] I. Dryanovski, M. Klingensmith, S. Srinivasa, and J. Xiao, *Large-scale, real-time 3d scene reconstruction on a mobile device*, Autonomous Robots, vol. 41, 02 2017.

[13] A. Kar, C. Häne, and J. Malik, *Learning a multi-view stereo machine*, 08 2017.

[14] G. Riegler, A.O. Ulusoy, H. Bischof and A. Geiger, *OctNetFusion: learning depth fusion from data*, 10 2017.

[15] Z. Liu, H. Tang, Y. Lin and S. Han, *Point-Voxel CNN for efficient 3D Deep Learning*, 07 2019.

[16] M. Firman, O. Aodha, S. Julier, and J. Gabriel, *Structured prediction of unobserved voxels from a single depth image*, pp. 5431–5440, 06 2016.

[17] B. Yang, S. Rosa, A. Markham, N. Trigoni, and H. Wen, *3d object dense reconstruction from a single depth view*, IEEE Transactions on Pattern Analysis and Machine Intelligence, vol. PP, 02 2018.

[18] C. Häne, S. Tulsiani, and J. Malik, *Hierarchical surface prediction for 3d object reconstruction*, pp. 412–420, 10 2017.

[19] M. Tatarchenko, S. Richter, R. Ranftl, Z. Li, V. Koltun, and T. Brox, *What do single-view 3d reconstruction networks learn?*, pp. 3400–3409, 06 2019.

[20] J. Choe, S. In, F. Rameau, M. Kang and I. S. Keon, *VolumeFusion: deep depth fusion for 3D scene reconstruction*, 08 2021.

[21] Z. Murez et al., *Atlas: end-to-end 3D scene reconstruction from posed images*, ECCV 2020: Computer Vision – ECCV 2020 pp 414-431, 11 2020.

[22] T. Jadhav, K. Singh and A. Abhyankar, *Volumetric 3D reconstruction of real objects using voxel mapping approach in a multiple-camera environment*, Turk J Elec Eng & Comp Sci (2018) 26: 755 – 767, 03 2018.

[23] J. Watson, O. Mac Aodha, D. Turmukhambetov, G.J. Brostow and M. Firman, *Learning stereo from single images*, 08 2020.

[24] J. Varley, C. DeChant, A. Richardson, J. Ruales and Peter Allen, *Shape completion enabled robot grasping*, 03 2017.

Structural Information Retrieval in XML Documents: A Graph-based Approach

Imane Belahyane, Mouad Mammass, Hasna Abioui, Assmaa Moutaoukkil, Ali Idarrou
IRF-SIC Laboratory
Ibn Zohr University, Agadir, Morocco

Abstract—Although retrieval engines are becoming more and more functional and efficient, they still have the drawback of not being able to locate the relevant documentary granularity, which results in ignoring the structural aspect. In the context of XML document, Information Retrieval Systems allow to return the user's documentary granules. Several studies have used graphs to represent XML documents. However, in the scope of this research, the semi-structured document's structure and that of a user's query can be seen as arborescences composed of a hierarchy of nested elements. By using graph theory, by calculating the structural proximity and especially the intersection between these two arborescences. The article presents a model for structural information retrieval based on graphs. A collection of multimedia documents are randomly extracted from INEX (Initiative for the Evaluation of XML Retrieval) 2010 to validate the approach. The first results shows the interest of such an approach.

Keywords—Semi-structured document; XML document; largest common sub-graph; structural Information retrieval

I. INTRODUCTION

Due to the digital revolution in terms of documentary masses and their exhaustiveness as well as heterogeneity, it is becoming more difficult to access information. Saying so, this requires a lot of efforts to respond to a user's queries. In this respect, it is necessary to use an accurate tool to facilitate Information Retrieval (IR) in order to increase the performance of an Information Retrieval System (IRS). The research falls within the context of IR in Semi-Structured Documents (SSD) which are characterized by a flexibility. The latter overshadows the limitations of using structured documents (DBMS - Database Management System).

Indeed, the semi-structured document has organizational properties that facilitate their analysis. In literature, XML (eXtensible Markup Language) documents are often referred to as SSD. As a result, XML is becoming the preferred format for information exchange [1]. In the sense, it is used today by ERP (Enterprise Resource Planning) suppliers, middleware editors and database providers. It is also used in e-commerce and libraries. Evidently, an XML documents are complex objects because they are heterogeneous in terms of type, size, format, content (image, text, video, etc), structure, etc. In fact, a structural IR facilitates access to the documentary granule (fine information) [2]. The paper is concerned with structural IR, while taking into account the structural information (relations between documentary components). For this purpose, it is required to compare the structure of the user's query with that of the document. The underlying idea of the approach to structural IR in XML documents is to:(1) Return the fragments

(document parts) that are relevant to the user's query and (2) Return the ordered results by order of relevance.

Otherwise, XML documents are composed of nested tags, which enable their representation in the form of graphs. The work is mainly interested in the representation of document structures using graphs. Comparing two documents structurally is therefore the same as comparing the graphs that represent them [3]. The multi-structurality generated by graphs induces complex and multiple relations between two similar components of a document. It is therefore necessary to use a rich representation model in order to perform IR in documents with complex structures. Indeed, graphs are used in several works and several domains, and are efficient to model structured objects [4].

The paper is divided into the following sections. While Section 2 provides some approaches that have addressed the problem of IR in XML documents using graph theory, Section 3 introduces the approach on structural IR. Section 4 reports the first results. Finally, Section 5 presents some perspectives.

II. A GRAPH-BASED STRUCTURAL IR APPROACHES: THE STATE-OF-ART

The XML documents exploitation requires the use of a rich representation. Indeed, graph theory is widely used to represent complex objects. This section presents a brief overview of the studies that used graphs in the field of structural IR, and then introducing the mathematical formalism of graph theory.

In [5], the authors proposed an IR approach based on the edit distance and the structural summary of the trees (representing SSD). Based on two scores, it propagates the first one (content score) at the tree level in order to extract the sub-trees containing the relevant leaves. The trees' relevant leaves' extraction, representing the XML document, are performed by an algorithm based on the TF-IDF technique [6]. The second score's calculation (structure score) of the previously extracted sub-trees is based on the edit distance algorithm [7]. The structure score adapts an optimal coverage strategy [8] based on the edit distance [7] through the heavy path [9]. In this work [10], IR in XML documents is based on a model that takes the DTDs set forming the document collection and merges them into an un-oriented graph. The approach is based on the edit distance [7] and the shortest path model inspired by [11]. The selection of relevant leaves is established according to the existing nodes in the query, from the leaves to the root. These relevant node paths are merged into a sub-tree.

In these works [12], the integration of the document structure enhances the performance of a graph matching system.

The method is based on the trees' abstract from which a set of vectors are extracted. Hence, the process consists of a structural analysis phase. To build the content of each tree, a linguistic analysis phase and the application of the weighting function are calculated. This is done by adapting the formulas TF-IDF and TF-IEF [2], in order to attribute to each node a weight reflecting its importance in the collection where it belongs.

For this work [13], it deals with the problem of finding the largest common sub graph applied to the compatibility graph. Indeed, a compatibility graph of two graphs is the one where its nodes belong to the nodes union of these two graphs, and are linked by compatible edges. This means that these edges are preserved. The suggested approach involves combining RT-composition with the PC (Constraint Programming) model defined in [14]. The latter is an optimization problem based on soft constraints and the generalization of hard constraints (CSP - Constraint Satisfaction Problems), by optimizing the objective function. The approach is also based on heuristics following this work [15], in order to eliminate sub-problems and look for maximal cliques in the initial compatibility graph. In fact, the TR-decomposition, introduced in [16] seeks to reduce the CSP to instantaneous problems for the detection of a clique of n size. TR-decomposition includes a triangulation process, where a given graph is transformed into a triangulated graph by adding edges. By definition, a graph is triangulated if each of its cycles of length is greater than or equal to 4 and has at least one chord. A chord of a cycle is any edge whose extremities are two consecutive nodes of the cycle. Triangulation is applied in order to take advantage of their maximal clique number limit. The search for the largest common sub graph is therefore equivalent to finding a maximal clique of the triangulated graph.

III. GRAPHS' BASICS

A. Definition

A graph is a pair of sets $G = (V, E)$, in which V is the non-empty set of nodes, of cardinality $|V|$ and E is the non-empty set of edges between nodes, of cardinality $|E|$. A graph is mainly characterized by its ability to represent multiple relationships between the same nodes. While the tree is an undirected, acyclic and a connected graph, the arborescence is totally the opposite. It has a tree structure when ignoring the direction of the arcs.

B. Graphs' Inclusion

Inclusion is an order relation between graphs. Indeed, inclusion is designed to judge a sub-graph's belonging to a given graph. G_1 Graph is included in G_2 graph, if all the nodes and edges connecting the nodes of G_1 graph belong to G_2 graph.

$$G_1 \subset G_2 \iff V_{(G_1)} \subset V_{(G_2)} \text{ and } E_{(G_1)} \subset E_{(G_2)}$$

The inclusion of graphs has been used in specific contexts. To evaluate the inclusion between two objects, represented by X and Y graphs, several works have used the function of Tversky [17] (1), Cosine (2) or Jaccard (3):

$$Tversky(X, Y) = \frac{|X \cap Y|}{|X \cup Y|} \quad (1)$$

$$Cosine(X, Y) = \frac{|X \cap Y|}{\sqrt{|X| \times |Y|}} \quad (2)$$

$$Jaccard(X, Y) = \frac{|X \cap Y|}{|X \cup Y|} \quad (3)$$

avec:

- $|X|$: Cardinality of the object X
- $|Y|$: Cardinality of the object Y

IV. STRUCTURAL INFORMATION RETRIEVAL APPROACH

Graphs are widely used to model structural and complex data in different application domains: in imaging [18], in pattern recognition [19] [20] [21] and in chemistry [22] [23] [24]. In all these works, the problem is about looking for a relation between graphs (inclusion, intersection, etc). For example, the inclusion of graphs is used to compare graphs. More generally, the objective is to find the best match between the compared graphs, by finding the maximum number of similar nodes and edges [3].

As indicated before, this work introduces a new approach to structural IR. The underlying SSD allows to manipulate the documentary granularity in order to properly answer user's needs, expressed by a query. To optimize the IR and return the most relevant results, the approach takes into account the following remarks:

- Representing the queries and the document using graphs;
- Retaining only the relevant fragments (parts of documents);
- Using the order of relevance to order the results

The following section details the approach on structural IR. Indeed, the proposed approach is composed of three steps as shown in Fig. 1.

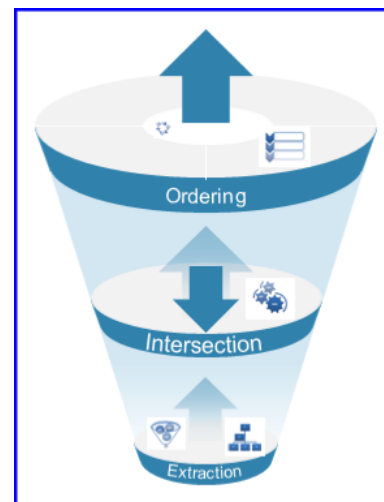


Fig. 1. General Process of the Approach on Structural IR.

A. Structure Extraction Phase

This phase consists of:

- 1) Extracting the structure of the document and representing it as an arborescence;
- 2) Extracting the structure of the query and representing it as an arborescence;
- 3) Extracting the paths of the arborescence representing the document;
- 4) Extracting the paths of the arborescence representing the query.

In the first and second steps, the structure of the document (respectively of the query) is extracted and an arborescence of the document is presented.

In the third and fourth steps, the approach adapts an arborescence linearization technique. The latter system automatically reduces one of the well-known problems in graph theory which is the combinatorial cost. Proposing to consider a graph as a set of paths. Thus, comparing two graphs is equivalent to comparing the paths composing them [3]. In [3]:

- A path of k length is defined as: a series of nodes u_0, u_1, \dots, u_k , such as:
 $\forall i \in [0, k - 1]$, u_i and u_{i+1} are adjacent, u_0 is the path's origin and u_k is its extremity.
- **The path of G graph is a G sub-graph.**
- The depth of an arc in a path is the length of the path from the root to this arc. In the example of Fig. 2, the depth of the A/C arc is 3 when considering the $doc/E/A/C$ path.
- B/M relation is defined from B node to M node if there is an arc that associates the former with the latter (Fig. 2).

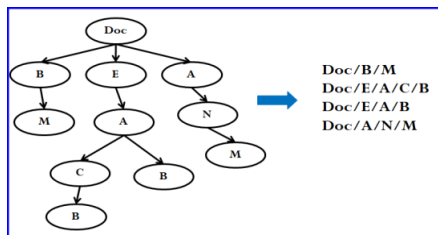


Fig. 2. Example of Path Extraction from a given Arborescence.

B. The Intersection Between the Query and the Document

In this phase, calculation of the inclusion $DegIn(p_q, p_d)$ between the query and the document paths is implemented. This inclusion (according to the proposed approach) enables the evaluation of the intersection between p_q and p_d paths.

$$DegIn(p_q, p_d) = \frac{|NCR(p_q, p_d)|}{|p_q|} \quad (4)$$

with;

- p_d : a path of the document;

- p_q : a path of the query;
- $|NCR(p_q, p_d)|$: The number of the common relations that exists between p_q and p_d ;
- $|p_q|$: number of relations in p_q .

If all relations of the query's path p_q exist in the document's path p_d , the value of equation (4) is equal to 1. The value of (4) reflects the ratio of the number of common relations between the document's path and the query's one.

In the arborescence structure representing the structure of a document (respectively of the query), it is interesting to take into account the depth of a relation (arc) because it expresses the context of this relation in the path.

C. Ordering Results

This phase presents results in order of relevance. Hence, it is composed of three main steps:

- 1) Considering the depth of common relations between the query and document paths;
- 2) Applying the smoothing function;
- 3) Ordering the results according to the $score(p_q, p_d)$.

The final score $score(p_q, p_d)$ is defined by:

$$score(p_q, p_d) = DegIn(p_q, p_d) \times smooth(p_q, p_d) \quad (5)$$

This shows that taking into account the depth of common relations between the query and document paths is effective. In this case, the smoothing technique is established as follows.

$$smooth(p_q, p_d) = \log_{10}\left(e + \frac{1}{1 + |dist(p_q, p_d)|}\right) \quad (6)$$

The smoothing function takes into consideration the distance $dist(p_q, p_d)$ (see Fig. 3).

$$dist(p_q, p_d) = depLast(p_d) - depCom(p_q, p_d) \quad (7)$$

- $dist(p_q, p_d)$: the distance between the last relation of the document path and the last common relation between p_q and p_d ;
- $depLast(p_d)$: depth of the last relation of the document path;
- $depCom(p_q, p_d)$: depth of the last common relations between p_q and p_d .

Moreover, this logarithm shows that a significant increase in the distance $dist(p_q, p_d)$ does not generate a large increase in the final score $score(p_q, p_d)$. Several studies have used the smoothing function to reduce irregularities. Smoothing is a technique that consists in reducing irregularities and singularities of a curve in mathematics.

Fig. 3 introduces a computational application to calculate the final score.

TABLE I. COMPARING THE PROPOSED METHOD WITH OTHER APPROACHES

Tversky method	Cosine method	Jaccard method	The proposed method
$Tve(R, G_1) = 1$	$Cos(R, G_1) = 1$	$Jac(R, G_1) = 1$	$DegIn(R, G_1) = 0.25$
$Tve(R, G_2) = 1$	$Cos(R, G_2) = 1$	$Jac(R, G_2) = 1$	$DegIn(R, G_2) = 0.5$
$Tve(G_0, G_3) = 1$	$Cos(R, G_3) = 1$	$Jac(R, G_3) = 1$	$DegIn(R, G_3) = 0$

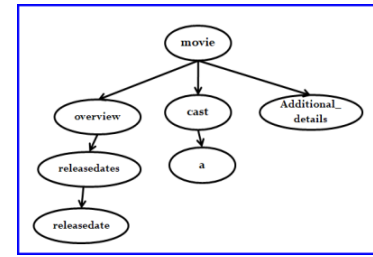


Fig. 5. Arborescence of the Query.

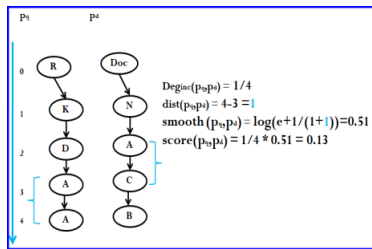


Fig. 3. Numerical Application for Score Calculation.

V. EVALUATING THE PROPOSED APPROACH

A. Comparing the Proposed Approach with that of Tversky, Jaccard and Cosinus

Through the example illustrated in Fig. 4 , it is demonstrated in Table I that Tversky, Jaccard and Cosine methods do not take into account the distribution of the graph’s component. G_1, G_2 and G_3 arborescences represent the structure of the four SSD, and R stand for the query’s structure.

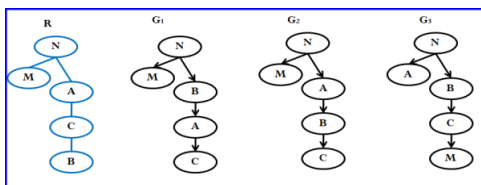


Fig. 4. Example of Arborescences representing the Documents and the Query.

In the proposed approach, the information conveyed by the document structure is unavoidable. The relations constitute the backbone of the graph since they make explicit the nature of the links and add contextual, structural and semantic information [4].

In [3], the methods of Jaccard, Cosine, Tversky and more broadly the surface measures do not take into consideration the information conveyed by the structure. However, the same components (image, text, audio, etc) may not play the same role in two different documents.

This is explained through the exploitation of the different

arcs connecting the nodes of the graph that represents the document.

B. Experimentation and Discussion

To evaluate the approach, collections of multimedia documents extracted from INEX (Initiative for the Evaluation of XML Retrieval) 2010 ¹ and a corpus of queries are used.

Table II and III presents the description of the corpus of queries and documents.

TABLE II. DESCRIPTION OF THE CORPUS INCLUDING THE DOCUMENTS

	Characteristics
Corpus size	10,5 Go
Number of documents in the corpus	4 418 083
Number of documents in the sample	1000
Total number of nodes in the sample	47882
Average depth/document	3.63

TABLE III. DESCRIPTION OF THE CORPUS CONTAINING THE QUERIES

	Characteristics
Queries’ number in the corpus	5
Total number of nodes in the corpus	21
Average depth /queries	3.18

The paper have designed a prototype using Python language which is composed of two modules: the first one relies on SAX (Simple API for XML) API (Application Programming Interface), to carry out the first parsing. This module provides an intermediate file intercepted by a second module to refine the query and order the results according to their relevance.

Next, an extract of the results obtained by applying a query on all the documents of the corpus is presented. Fig. 6 presents an extract of obtained results, when applying the query represented by the arborescence structure in Fig. 5 on the documents of the corpus. The approach allows to return the fragments (parts of documents) considered relevant to the user’s query.

¹It focuses on rich structures in which classical IR models are not sufficient. In other words, it is about the labels of structural elements that carry essential information that the textual content does not specify. This new task is based on a corpus extracted from the IMDB website which contains 1,590,000 movies and several million actors, producers, directors, etc.

For example, the results of the ordering of the **document** 1 in Fig. 6 are all correct, according to the proposed approach: The path `[/movie, /overview, /releasedates, /releasedate]` is ordered first in the retrieval, while `[/movie, /additional_details, /aliases, /alias]` is ordered second in the retrieval.

For the third ordering, it is taken by the path `/movie, /cast, /composers, /composer]`, because, it provides a score value of 0.24.

The fourth position is taken by `[/movie, /overview, /rating]`, because, it presents a value of 0.17 for the score value.

The fifth position is taken by `[/movie, /overview, /writers, /writer]`, because, it presents a value of 0.16 for the value of the score.

While analyzing the displayed results, it is noted that the system privileges the paths composed of the relations closest to the leaves, specifically, where two paths of a document have the same number of relations in common with a given path of the query. The proposed approach privileges the paths with relations that are (in common) relatively close to the leaf (Fig. 6).

```
Fragments of the document 1:./input/1000elt/10900.xml
Fragment 1 -> [/movie, /overview, /releasedates, /releasedate] avec un score de: 0.57
Fragment 2 -> [/movie, /additional_details, /aliases, /alias] avec un score de: 0.48
Fragment 3 -> [/movie, /cast, /composers, /composer] avec un score de: 0.24
Fragment 4 -> [/movie, /overview, /rating] avec un score de: 0.17
Fragment 5 -> [/movie, /overview, /writers, /writer] avec un score de: 0.16

Fragments of the document 2:./input/1000elt/82300.xml
Fragment 1 -> [/movie, /overview, /releasedates, /releasedate] avec un score de: 0.57
Fragment 2 -> [/movie, /additional_details, /aliases, /alias] avec un score de: 0.48
Fragment 3 -> [/movie, /cast, /composers, /composer] avec un score de: 0.24
Fragment 4 -> [/movie, /overview, /rating] avec un score de: 0.17
Fragment 5 -> [/movie, /overview, /writers, /writer] avec un score de: 0.16

Fragments of the document 5:./input/1000elt/354000.xml
Fragment 1 -> [/movie, /overview, /releasedates, /releasedate] avec un score de: 0.57
Fragment 2 -> [/movie, /additional_details, /aliases, /alias] avec un score de: 0.48
Fragment 3 -> [/movie, /cast, /actors, /actor, /name] avec un score de: 0.47
Fragment 4 -> [/movie, /actors, /actor, /name, /cast, /actors] avec un score de: 0.28
Fragment 5 -> [/movie, /cast, /composers, /composer] avec un score de: 0.24
Fragment 6 -> [/movie, /cast, /actors, /actor, /name] avec un score de: 0.23
Fragment 7 -> [/movie, /overview, /rating] avec un score de: 0.17
Fragment 8 -> [/movie, /overview, /writers, /writer] avec un score de: 0.16
....

Fragments of the document 1000:./input/1000elt/91900.xml
Fragment 1 -> [/movie, /overview, /releasedates, /releasedate] avec un score de: 0.57
Fragment 2 -> [/movie, /additional_details, /aliases, /alias] avec un score de: 0.48
Fragment 3 -> [/movie, /cast, /actors, /actor, /name] avec un score de: 0.47
Fragment 4 -> [/movie, /actors, /actor, /name, /cast, /actors] avec un score de: 0.28
Fragment 5 -> [/movie, /cast, /composers, /composer] avec un score de: 0.24
Fragment 6 -> [/movie, /cast, /actors, /actor, /name] avec un score de: 0.23
Fragment 7 -> [/movie, /overview, /rating] avec un score de: 0.17
Fragment 8 -> [/movie, /overview, /writers, /writer] avec un score de: 0.16
```

Fig. 6. Results Extract.

VI. CONCLUSION AND PERSPECTIVES

This work comes in the context of IR in SSD that uses more particularly XML documents. With respect to the works studied in section 2, the proposed approach is a part of the approaches using graphs to represent objects. The proposed approach seeks to improve the automation of IR, by facilitating access to the document granule (while preserving the characteristics of each document: content and structure). For instance, this enables to optimize the access to relevant information. it has been proven that: (1) The approach is based on graphs,

taking into account the relations between the components of the documents and proving that this is a crucial parameter in the proposed structural IR approach. As a matter of fact, the content of a multimedia document does not only depend on the content of its components, but also on the relations between these components. (2) To overcome the combinatorial problem (well-known in graph theory), by conceiving a graph as a set of paths. The correspondence of the paths of the graphs allows to preserve both the contextual and hierarchical aspects of the components. (3) It has shown that the so-called surface measures cannot answer the problem. Hence, the first results obtained are encouraging.

In future research, a comparative study with other works will be done. Finally, to make the proposed approach more complete, it is important to take into account both the documentary content and the structure that conveys a significant amount of information.

REFERENCES

- [1] Martin Bryan et al. Guidelines for using xml for electronic data interchange. *SGML Centre*, 1998.
- [2] Karen Sauvagnat. *Modèle flexible pour la recherche d'information dans des corpus de documents semi-structurés*. PhD thesis, Université Paul Sabatier-Toulouse III, 2005.
- [3] Ali Idarrou. *Entreposage de documents multimédias: comparaison de structures*. PhD thesis, Toulouse 1, 2013.
- [4] Hasna Abioui Assmaa Moutaoukkil Ali Idarrou Imane Belahyane, Mouad Mammass. Comparative study on graph-based information retrieval: the case of xml document. *International Journal of Advanced Engineering, Management and Science*, 2021.
- [5] Cyril Laitang, Mohand Boughanem, and Karen Pinel-Sauvagnat. Xml information retrieval through tree edit distance and structural summaries. In *Asia Information Retrieval Symposium*, pages 73–83. Springer, 2011.
- [6] Gerard Salton and Christopher Buckley. Term-weighting approaches in automatic text retrieval. *Information processing & management*, 24(5):513–523, 1988.
- [7] Erik D Demaine, Shay Mozes, Benjamin Rossman, and Oren Weimann. An optimal decomposition algorithm for tree edit distance. In *International Colloquium on Automata, Languages, and Programming*, pages 146–157. Springer, 2007.
- [8] Serge Dulucq and Hélène Touzet. Analysis of tree edit distance algorithms. In *Annual Symposium on Combinatorial Pattern Matching*, pages 83–95. Springer, 2003.
- [9] Philip N Klein. Computing the edit-distance between unrooted ordered trees. In *European Symposium on Algorithms*, pages 91–102. Springer, 1998.
- [10] Cyril Laitang, Karen Pinel-Sauvagnat, and Mohand Boughanem. Dtd based costs for tree-edit distance in structured information retrieval. In *European Conference on Information Retrieval*, pages 158–170. Springer, 2013.
- [11] Robert W Floyd. Algorithm 97: shortest path. *Communications of the ACM*, 5(6):345, 1962.
- [12] Samaneh Chagheri, Catherine Roussey, Sylvie Calabretto, and Cyril Dumoulin. Classification de documents combinant la structure et le contenu. In *8ème Conférence en Recherche d'Information et Applications CORIA 2012*, pages p–261, 2013.
- [13] Maël Minot, Samba Ndojh Ndiaye, and Christine Solnon. Recherche d'un plus grand sous-graphe commun par décomposition du graphe de compatibilité. *Onzièmes Journées Francophones de Programmation par Contraintes (JFPC)*, pages 1–11, 2015.
- [14] Samba Ndojh Ndiaye and Christine Solnon. Cp models for maximum common subgraph problems. In *International Conference on Principles and Practice of Constraint Programming*, pages 637–644. Springer, 2011.

- [15] Christine Solnon and Serge Fenet. A study of aco capabilities for solving the maximum clique problem. *Journal of Heuristics*, 12(3):155–180, 2006.
- [16] Philippe Jégou. Decomposition of domains based on the micro-structure of finite constraint-satisfaction problems. In *AAAI*, volume 93, pages 731–736, 1993.
- [17] Amos Tversky. Features of similarity. *Psychological review*, 84(4):327, 1977.
- [18] Imane Belahyane, Mouad Mammass, Hasna Abioui, and Ali Idarrou. Graph-based image retrieval: State of the art. In *International Conference on Image and Signal Processing*, pages 299–307. Springer, 2020.
- [19] Pasquale Foggia, Gennaro Percannella, and Mario Vento. Graph matching and learning in pattern recognition in the last 10 years. *International Journal of Pattern Recognition and Artificial Intelligence*, 28(01):1450001, 2014.
- [20] Xavier Cortés, Donatello Conte, and Hubert Cardot. Learning edit cost estimation models for graph edit distance. *Pattern Recognition Letters*, 125:256–263, 2019.
- [21] Luc Brun, Pasquale Foggia, and Mario Vento. Trends in graph-based representations for pattern recognition. *Pattern Recognition Letters*, 134:3–9, 2020.
- [22] Samuel Wieczorek. *Une mesure d’inclusion entre objets structurés. Application à la classification de molécules*. PhD thesis, Université Joseph-Fourier-Grenoble I, 2009.
- [23] Frédéric Suard and Alain Rakotomamonjy. Mesure de similarité de graphes par noyau de sacs de chemins. In *21 Colloque GRETSI, Troyes, FRA, 11-14 septembre 2007*. GRETSI, Groupe d’Études du Traitement du Signal et des Images, 2007.
- [24] Angiras Menon, Nenad B Krdzavac, and Markus Kraft. From database to knowledge graph—using data in chemistry. *Current Opinion in Chemical Engineering*, 26:33–37, 2019.

Dynamic Support Range based Rare Pattern Mining over Data Streams

Sunitha Vanamala^{1*}, L. Padma Sree², S. Durga Bhavani³

Lecturer, Department of CS, TSWRDCW, Warangal East, Warangal Telangana, India¹

Professor, Department of ECE, VNR Vignana Jyothi Institute of Technology and Science, Hyderabad, Telangana, India²

Retd. Professor, School of Information Technology, JNTU, Hyderabad, Telangana, India³

Abstract—Rare itemset mining is a relatively recent topic of study in data mining. In certain application domains, such as online banking transaction analysis, sensor data analysis, and stock market analysis, rare patterns are patterns with low support and high confidence that are extremely interesting when compared to frequent patterns. Numerous applications generate large amounts of continuous data streams. We require efficient algorithms capable of processing data streams in order to analyze them and find unique patterns. The strategies developed for static databases cannot be used to data streams. As a result, we require algorithms created expressly for data stream processing in order to extract critical unique patterns. Rare pattern mining is still in its infancy, with only a few ways available. To address this is developed the Dynamic Support Range-based Hybrid-Eclat Algorithm (DSRHEA), an Eclat-based technique for mining unique patterns from a data stream using bit-set vertical mining with two item-based optimizations. The detected patterns are kept in a prefix-based rare pattern tree that uses double hashing to maintain the unusual pattern in the data stream. Testing showed that the proposed method did well in terms of how long it took to run, how many rare patterns it made and accuracy.

Keywords—Depth first search; Hybrid-Eclat algorithm; SRP-tree; itemset; frequent-pattern support; rare-pattern support; pivot; data stream; rare itemset; infrequent itemset

I. INTRODUCTION

Information systems play a vital role in identifying trends, making decisions, and adapting to the emerging changes in the market. In the current global scenario, wherein the organisations have to be sharp in its analysis of trends, there is a need for entities to be adaptable to new and dynamic solutions that can provide insights in effective ways. Utility mining and pattern detection solutions play a big role in the FMCG market [1].

Many of the earlier studies focusing on the application of business intelligence solutions in the pattern mining or utility mining space have discussed leveraging the data from information systems for analysis. However, there are very few systems among the explored models that exhibit the scope for dynamic analysis models. It is imperative that the current condition in the competitive scenario requires entities to focus on conditions wherein dynamic selection of data is targeted for informed decisions. In an illustrative scenario of a supermarket environment, the frequent mining set possibilities keep emerging over time and could lead to a paradigm shift in how each pattern or itemset billing happens periodically.

Thus, there is a need for consistent follow-up of emerging trends and periodic analysis that shall help in covering the process effectively. In this manuscript, the focus is on developing a linear and systematic approach for dynamic analysis of the pattern set designs, which shall help in accomplishing the requisite tasks. The goal of this paper is to make a dynamic model of how items are classified into different labels based on the patterns that appear in the data systems over a certain amount of time.

To speed up the process of discovering new association rules, it is crucial to identify common patterns in a dataset. Because association rules presume that every record in the database has the same occurrence frequency, they can only utilize one min-SUP per record. There are several drawbacks of mining frequent itemsets (as well as frequent patterns) with a simple min-SUP constraint in a non-uniform database. Finding patterns involving uncommon items will be impossible if min-SUP is set very high. In order to recognize patterns that include both common and unique things, we need to reduce min-SUP to a lower value. A combinatorial explosion may happen because these common objects are linked together in all possible ways. This could lead to too many patterns depending on the needs of the individual and the application.

The model proposed in this study is adapted on the basis of pivot, support, for the itemset conditions emerging in the domain. In the further sections of this report, the emphasis is on related work review, wherein key studies in the domain are explored to understand the critical success factors and constraints to consider in developing a comprehensive solution. Followed by, in the further section, the methods adapted for the model are discussed, that can help in accomplishing the proposed model. Experimental study is discussed in Section 4 and conclusion discussed in Section 5.

A. Motivation

Because rare situations represent considerable obstacles for data mining methods [2], they deserve special attention. The fundamental mining difficulties, on the other hand, have not yet been adequately investigated. Indeed, much of the literature in this area is devoted to adapting the Apriori [3]-based generic itemset mining framework to various exemptions of the frequent-itemset as well as frequent association ideas [4]. Whereas these methods often cover a considerable amount of the search-space for uncommon itemsets and relationships, they are nevertheless insufficient because several rare-associations are ignored owing to excessive computational

*Corresponding Author

ISSN 2156-5570 (Online); ISSN 2158-107X (Print)

costs or unnecessarily restricted definitions. As an outcome, these strategies will be unable to collect a large amount of potentially good itemsets that are interesting in particular domains such as fraud detection, etc.

B. Problem Statement

The technique of evaluating previously unknown datasets for classifying into usable information is known as data mining. This data is collected and accumulated in common places, such as data warehouses, for efficient investigation, data-mining algorithms, helping financial decisions, as well as other information needs, effect on cost savings as well as profit improvements. Data mining is often referred to as information discovery as well as actionable insights. An itemset is a group of connected events/features in a dataset. Frequent-itemset mining is important in data mining since it uncovers latent, intriguing relationships among items in the dataset depending on the specific user-defined support and confidence levels. The Association-Rule Mining approach uncovers incredibly useful itemsets that are crucial in decision-making. The problem of frequent itemset mining, which entails mining only those itemsets that appear frequently in the input data, has dominated previous study in the topic. As a result, unusual events/features aren't captured in item sets. Those itemsets, also known as uncommon itemsets, are more intriguing than frequent itemsets in particular sectors, such as the detection of computer intrusions and fraudulent transactions in financial institutions. As a result, current study will focus on the other side of the ARM approach, which should be given equal weight in decision-making, as rare itemsets can be more valuable than regular itemsets. The same basic technique that may be used to find common itemsets can also be used to find rare itemsets. The goal of this paper is to create a collection of algorithms for mining-rare itemsets from datastream.

II. RELATED WORK

Several frequency-related data mining techniques based on Apriori [5] have been developed, with mining outputs typically relating to common or expected events. Approach, rare-pattern mining (RPM) [6-8], was created to solve this issue, and numerous RPM methods have been suggested in the recent past. Rare-patterns, as opposed to frequent as well as common patterns, may be more beneficial in some circumstances (e.g., itemsets as well as association rules) that are vital for real-world applications. The most common types of static rare itemset mining techniques are support-threshold, no-support-threshold, and limitations are well discussed in [7]. Since the support-threshold of rare-itemsets is lesser than that of frequent itemsets, establishing lesser or different support thresholds makes it easier to generate uncommon itemsets. Darrab et al. [9] presented the multiple-support approach, which successfully discovered unusual itemsets by using various minimal support thresholds. Koh et al., [10] presented the Apriori-reverse approach to find unusual rules in totally scattered itemsets, which only includes items underneath the maximal support level. Szathmary et al. [11] later suggested a "rare-itemset mining approach (ARIMA)". The rarity method, which is a top-down rare-itemset mining automated system, was introduced by Troiano et al. [12]. Until now, a variety of RPM algorithms, such as CFP-growth++ [13], have been

widely proposed. Several of them [14-16] are focused on dealing with variable data streams. Several algorithms relying on the Apriori method have a large number of candidates.

Tanbeer et al. [17] established a two-phase technique. First, a compact forest architecture CPS tree is used to keep the sliding window's contents in a predetermined sequence. All closed, frequent patterns are discovered in the second step of the tree reconstruction. An item must be constructed for each time it is used during the time period in order to use this approach, which takes further time and distance to compute.

The three processes described in Deypir et al. [18] involve the startup of the window, the updating of the window, and the production of patterns. The sequence is an interesting paradigm for tackling typical pattern mining issues since it doesn't need to examine the entire history of team and handling and could just handle a restricted range of recent events. It took a lot of memory and processing time to use sliding window techniques in the past, on the other hand.

One scan reads the databases and loads the transactions to find the most current frequent itemsets using the sliding window concept, but they were using an FP-like tree that requires more time, the model's clustering algorithm is limited, thus the different method is used to address the problem [19].

Sets of rare itemsets (SRP) were created by David Huang [20]. The new transaction's components are added to a tree data structure using the FP tree technique. Most FP trees are formed by placing all transactions' components in decreasing order of support count. As a result, it is impossible to organize data streams in a logical sequence. An architecture known as a connections table is utilized to maintain track of the sliding window's components in canonical order in order to overcome this problem. Rare items are made when a product or service path doesn't have enough support.

To save time and money, pruning is used in RP-Tree [21]. Patterns based on FP-Tree are stored in a Tree based hierarchical file system.

According to Sunitha et al [22], using bitsets as well as vertical pattern mining, different minimum item support (MIS) values are employed to overcome the problem of missing uncommon pattern sets with significant support but high confidence.

Using the approach developed by Sunitha et al. [23], researchers were able to uncover beneficial atypical association rules. Such an unusual association rule mining technique is carried out using a sliding window technique with a vertical bit sequence structure. When doing a search, a sliding window strategy is a good way to find connections that aren't obvious.

Multiple data streams and stream data are classified by an adaptive learner employing named time frames in the methodology provided by Manal Almuammar et al [24], [25].

The Éclat RP-growth approach suggested by Sunitha et al [26], [27] is developed from Zaki's Eclat [28]. Bit set mining in the form of a vertical pattern. This solution relies heavily on an effective pruning strategy and the construction of linear trees. Rahul et al. [29] suggested a compact feature extraction tree structure with better weight requirements to find common

patterns in a centralized database scanning over a continuous data stream. Outliers from incremental datasets may be identified using a single-pass rare pattern mining approach suggested by Anindita et al. [30].

III. METHODS IN MODEL

The model employs two supports, frequent-pattern Support (*fps*) and rare-pattern support (*rps*), as well as the Sliding Window size, which is the maximum number of blocks that can be present in each window. Because blocks may overlap between windows, the processed blocks data is reused in each window, and modifications are required based on newly arrived blocks and the oldest block that is about to expire upon the arrival of the new block. From steam data and a correlation measure, the model can detect both frequent and unusual Itemsets. Lift can be used to filter the rules.

A. Basic Terminology

Let $\{i_1, i_2, i_3, \dots, i_n\}$, in be the list of Items I in the database. The data stream is a continuous stream $\{t_1, t_2, \dots, t_n, t_{n+1}, \dots\}$, with each transaction containing a subset of I items. A nonempty itemset with one or more items from items list I is called an item set. A k-itemset is an itemset that contains k items. The percentage of transactions in the database that have the itemset X marked as $|X|$ is known as support for an itemset X .

Each block is a series of transactions, and the total number of transactions in the block reflects the block size $|B|$ which is time sensitive and may change across blocks.

1) *Frequent itemset*: The given itemset X is considered to as frequent-pattern support if and only if $s_x > fps$ the support s_x exceeds the frequent-pattern Support *fps*.

2) *Rare itemset*: A pattern X is a rare pattern if ($rps \leq s_x < fps$), the support s_x of the corresponding pattern X is lesser than frequent-pattern Support (*fps*) but greater than or equal to rare-pattern support (*rps*).

3) *Rare-pattern support and frequent-pattern support*: The support of an itemset represents the frequency of corresponding itemset towards the set of records (buffered from data stream). The default range of support is in between 0 and 1 that includes 1, and standard measure of the support is 0.5. The default rare pattern support *rps* represents as $0 < rps \leq 0.5$, the default frequent pattern support *fps* represents as $0.5 < fps \leq 1$.

4) *Buffered Records' Time Frame (brtf)*: The amount of buffering time threshold of the recent transactions of the data stream, which should be greater than zero time units and having minimum transactions streamed from the corresponding data stream, which shall be greater than records' count threshold *rct*.

5) *Pivot points*: Maximum and minimum soft margins are the support average considered for developing the key points

which can stand critical for the estimation of rare patterns and frequent patterns. Soft margins estimation is a statistical approach, which denotes the disparity between mean and deviation as well as the aggregate of mean and deviation as minimum and maximum soft margins in respective order.

B. Dynamic Support Range Assessment Process

For a given Buffered Records' Time Frame (*brtf*), find the number of records $\{brc \exists brc \geq rct\}$ buffered as a set R .

Find all possible patterns of diversified sizes from the records listed as a set R , which represents as a set P .

Discover support of each pattern $\{p_i \exists p_i \in P \wedge 1 \leq i \leq |P|\}$ as follows.

Let the notation S be the set, such that each i^{th} entry represents the support s_i of i^{th} pattern $\{p_i \exists p_i \in P\}$.

$\forall_{i=1}^{|P|} \{p_i \exists p_i \in P\}$ Begin

$$s_i = \frac{1}{|R|} \left(\sum_{j=1}^{|R|} \{1 \exists (p_i \subseteq r_j) \wedge (r_j \in R)\} \right)$$

$S \leftarrow s_i$

End

1) *Estimating minimum and maximum supports by soft margins*: The fundamental objective of using the soft margins is to track the corresponding ranges of a metric in the learned transactions. The Soft margin values estimated from the learned transactions shall remain standard measures for the present transactions [31]. The estimation of the minimum and maximum supports of the proposed mining rare patterns from data stream is follows:

$$\mu = \frac{1}{|S|} \left(\sum_{i=1}^{|S|} \{s_i \exists s_i \in S\} \right)$$

$$\delta = \frac{1}{|S|} \sum_{i=0}^{|S|} \left\{ \sqrt{(\mu - s_i)^2} \exists s_i \in S \right\}$$

$$fps = sm + \delta$$

// Finding the standard measure of the supports listed in set S

// Find the standard deviation of the supports listed in set S

// rare-pattern support (*rps*)

Algorithm1: Algorithmic Description of Calculating Dynamic Min and Max support ranges

```
//finding supports of each pattern from initial block//  
For each record  $r$  of the initial block  $B_1$ , Begin  
Find all possible patterns of count  $2^{n-1}$ , here  $n$  represents the  
number of elements in the record  $\{r \exists r \in B_1\}$   
Move the discovered patterns count  $2^{n-1}$  to the set  $P$ , if the  
corresponding patterns do not exists in the set  $P$   
End  
For each pattern  $p$  of the set  $P$  Begin  
Find the support  $s_p$  of pattern  $p$  as
```

$$s_p = \frac{\text{no of records having the pattern } p}{\text{total number of records}}$$

```
Move the support  $s_p$  to the set  $S$ 
```

```
End
```

```
Find the average  $\mu$  of supports listed in set  $s$  as
```

$$\mu = \frac{\text{sum of supports of all patterns}}{\text{total number of patterns}}$$

```
Find the root mean square deviation  $\delta$  of the supports listed in  
set  $S$  as,
```

$$\delta = \frac{\text{sum of absolute difference of average from each support listed in set } S}{\text{total number of supports}}$$

```
Find the pivot  $P$  of the supports  $S$  of all patterns as follows
```

```
Find the frequent pattern coefficient  $fps$  as,
```

$$fps = \mu + \delta$$

```
Find the rare pattern support  $rps$  as
```

$$rps = \mu - \delta$$

C. Dynamic Support Range based Hybrid-Eclat Algorithm (DSRHEA)

DSRHEA is referred as hybrid Éclat because it uses the BFS (Breadth First Search) and DFS (Depth First Search) algorithms. The algorithm's characteristics are listed below.

The algorithm is based on Éclat and instead of *tid - set*, it uses bit-set to represent the transaction set of an itemset. The significant feature of this format is that it only scans data once to extract unusual patterns, which is necessary for stream data processing because it cannot be stored.

The support of one itemset is found by scanning the transaction block once. As explained in Algorithm1, a rare item in the current block may become frequent or vice versa in the data stream, hence all items with $support \geq fps$ are examined and used to construct higher order items.

Prefix Node is used to store itemset since it saves memory. The prefix is stored once for all suffix items in the node, and the itemset is generated by concatenating prefixes and suffix items. The prefix is the first (n-1) item in an itemset, while the suffix is the nth item. *PrefixBvList* is also utilized, which initially has a two-item *prefixbvnnode* that must be expanded to generate huge 'n' items, where n is a user-defined number.

The intersection of bit-sets of related parent one itemsets is used to generate two itemsets using BFS. The prefix items, with the exception of the suffix item, should all be the same to intersect any two items. *Abd* and *acd*, for example, can be intersected but not *abd* and *acd* since the initial (n-1) items of *Abd* and *acd*, (*ab* and *ac*) are not the same. The same criterion should be applied to higher order itemsets. A *prefixbvnnode* is constructed for each one item, with the supplied *oneitem* as the prefix, and suffix items are generated for eligible two items, with an array list containing all *prefixbvnodes* generated. For example, if the provided window has four items, let's call them *a,b,c,d*, then the three *prefixbvnodes* are constructed and added to the Array List. List of nodes *a*, *b*, and *c*, their respective suffix items.

To generate higher order item sets, the proposed algorithm uses an optimization based on two item sets. As mentioned in Algorithm2, the generated huge objects are kept in a two-level *hashmap*. Algorithms 3 and 4 are used to update the *hashtable* with the infrequent itemsets in the prefix node. The Stack data structure is used to implement DFS.

Algorithm 2: Dynamic Support Range based Hybrid-Eclat Algorithm (DSRHEA)

```
DSRHEA()  
blockid = 0;  
pefrefixBvNodeList pbvlist; //holds oneitems  
BlockSupports bsup; // block wise parameters  
Globals gb; //support parameters of datastream  
While(datastream)  
Begin  
blocksize = 0;  
While (currenttimeunit)  
Begin updateitemslistwithnewtransaction();  
Blocksize ++;  
End  
bsup = updateSupportthresholdsArrays(); filteroneitemslist(bsup);  
generateLargeItemsWithPrefixBasedBFSDFS(rpt, gb, bsup);  
Blockid ++;  
displayRarepatterns();  
End
```

1) *Optimization based on bigram itemsets*: To generate two items, the algorithm uses breadth first search, all two items are generated and stored into a *hashtable*, these two itemsets are used to prune the number of candidates while generating large item sets for eg: itemset $\{abcd\}$ is joined with $\{abcd\}$ to generate large item $\{abcde\}$ of size 5, however, if the itemset $\{de\}$ doesn't satisfy the support criteria for rare itemset, then obviously itemset $\{abcde\}$ will not satisfy the support criteria, so before joining itemsets, support $(n-1)^{th}$ item of the first itemset, $(n-1)^{th}$ item of the second itemset) is checked in two itemsets *hashtable* to prune the unfruitful candidate rare itemsets. This pruning strategy reduces the number of candidate itemsets and intersection operations while generating large itemsets, hence the algorithm's efficiency is improved in terms of execution time.

Algorithm 3: Discovering

n- Itemsets

Method: generateLargeItemswithPrefixBasedBFSnDFS

Input: one Item list, *fps* root potential Items, *rpt, gb, bsup* .

Output: Set of *frequent pattern support* > *fps* .

```
numOfOneitems < -oneitemsList.size();  
rpt.insertOrUpdateOneItems(this.oneItemsList, gb, bsup);  
oneItemI = 0;
```

```
While(oneItemI < numOfOneitems)
```

```
Create a prefixnode(pbv1)
```

```
for a prefix oneItemI;
```

```
For each remaining oneitem oneItemJ
```

```
Perform inter section(oneItemI, oneItemJ), calculate  
support and generate all two
```

```
Items using vertical mining in BFS that satisfy support  
criteria(bsup.currentsupport2) and Append to pbv1
```

```
twoItemspbvnodeList.add(pbv1)
```

```
rpt.insertOrUpdateLargeItems(pbv1, gb); //update  
hashtable with two items of current oneitem
```

```
For each prefixbvnode pbv1 in twoItems pbv node list  
If(isExtendible(pbv1)) //extendible if node has more than  
one suffix items
```

```
Pbvstack.push(pbv1)
```

```
While(!pbvstack.empty())
```

```
pbvcurrentnode = pbvstack.peak();
```

```
If(!isExtendible(pbv1))
```

```
rpt.insertorupdatelargeitem(pbvstack.pop())
```

```
//the items in popped prefixbvnode are inserted into  
hashtable of largeitems
```

Continue;

Else

```
Create pbvnewNode; //for storing generated large items  
Pbvnewnode.prefixitem.addall(pbvcurrentnode, prefixitemset)
```

```
Generate and update Largeitems //two itemset o  
optimization.
```

```
Push the generated node onto the stack if numberof  
suffixitems in the node > 0
```

2) *Structure of two level hash-table*: To store and maintain the patterns generated from the data stream, The tree is implemented as a Linear tree, implemented using array list, each entry in the array list is a *hashmap* (level map), the level map keeps itemsets of same size, n level maps are to be created to store itemsets of n length, *n* is the *max* itemset size maintained. The structure of two-level *hashmap* is shown in Fig. 1. The rare patterns are extracted from *hashtable* that satisfy support criteria as given in rare item definition.

3) *Discounting*: When the number of blocks in window exceeds, the discounting of old block supports is performed, then the support of newly arrived block are added as described in algorithms 3,4 and 5.

Algorithm 4: insertOrUpdateOneItems

```
1. If(globals.Blockid == 0)
```

```
2. Create a levelwisepreixmap and suffixmap with items  
in one items list
```

```
3. Else
```

```
4. If(globals.Blockid >= gb.windowSize)
```

```
5. Begin
```

```
6. discountOldBlockSupports(bsup);
```

```
7. End
```

```
8. Insert or update
```

```
levelwisepreixmap and suffixmap with items in  
oneitems list
```

Algorithm5: insertOrUpdateLargeItems

```
1. For(; rootSize <= pfxLength; rootSize ++)
```

```
2. {
```

```
3. rootpt.add(new LevelWisePrefixMap(rootSize, 200));
```

```
4. If(globals.Blockid == 0)
```

```
5. Create a levelwisepreixmap and suffixmap with  
items in prefixnode
```

```
6. Else
```

```
7. If(globals.Blockid >= gb.windowSize)
```

```
8. DiscountOldBlockSupports(bsup);
```

```
9. Create or update levelwisepreixmap and suffixmap  
with items in prefixnode
```

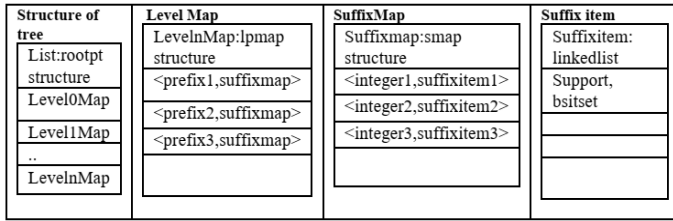


Fig. 1. Hash based Two Level Tree Structure.

IV. EXPERIMENTAL RESULTS

Experiments have been carried on different datasets listed in FIMI repository [32].The implementation has been done using Java, which is interpreted on Intel core i5 2.4 GHz computer running Windows 10 and equipped with 8GB of RAM. To establish the performance significance of the DSRHEA, the rare patterns count and speed of execution have been compared with contemporary model SRPTREE. The details of the dataset, window size, and dynamic supports observed, as well as resultant values of the performance indicators are listed in Table I.

The above stated Fig. 2 to 4 demonstrates the rare patterns discovered by both proposed DSRHEA, and contemporary model SRPTREE. Fig. 2 to 4 states that the contemporary model SRPTREE having significant count of missing rare patterns that compared to the DSRHEA. It is noting that marginal ratio of missing patterns as 24%, 24%, and 1% in the respective order of datasets T10I4D100K, T40I10D100K, and Kosark (250K). According to these statistics, the missing pattern ratio of SRPTREE that compared to DSRHEA is proportionate to the number of rare patterns discovered.

Fig. 5 illustrates the process time observed from DSRHEA and SRPTREE to discover rare patterns from different datasets. The statistics related to process time indicating that DSRHEA is outperforming SRPTREE with minimal process time, which has observed as 22.807%, 47.466%, and 10.052% in the respective order of datasets T10I4D100K, T40I10D100K, and Kosark (250K).

TABLE I. STATISTICS OF INPUTS AND OUTCOMES OF THE EXPERIMENTAL STUDY

Dataset details		Dynamic supports		Rare Patterns Count		Process time in mille seconds	
Dataset	Block Size	FPS	RPS	DSRHEA	SRPTREE	DSRHEA	SRPTREE
T10I4D100K	25K	0.00116	0.00054	16532	12539	22.807	129.602
T40I10D100K	25K	0.00899	0.00147	732166	557045	47.466	70.825
Kosark (250K)	25K	0.00492	0.00175	21075	21055	10.052	41.55

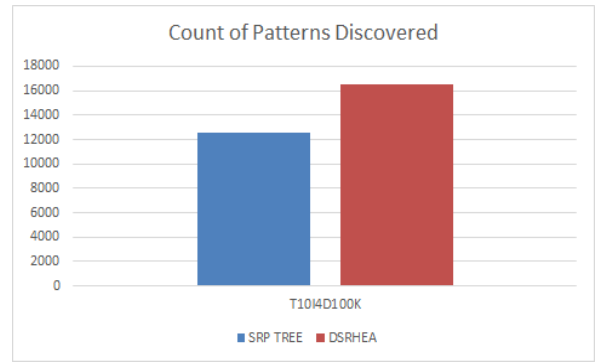


Fig. 2. Performance Comparison of DSRHEA and SRP Tree towards Rare Pattern Discovery from T10I4D100K Data Set.

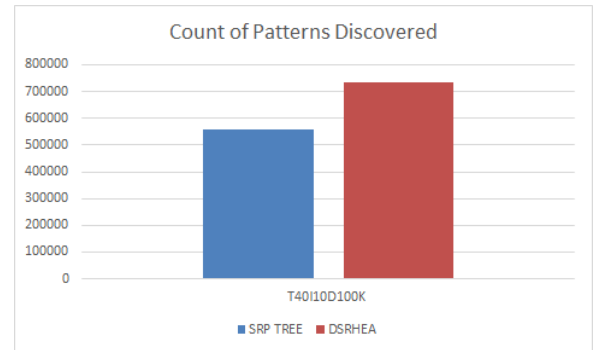


Fig. 3. Performance Comparison of DSRHEA and SRP Tree towards Rare Pattern Discovery from T40I10D100K Data Set.

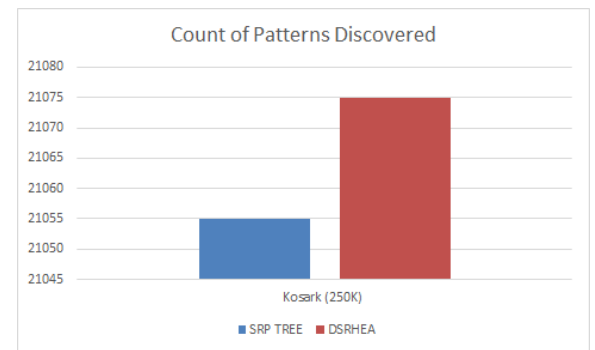


Fig. 4. Performance Comparison of DSRHEA and SRP Tree towards Rare Pattern Discovery Kosark Data Set.

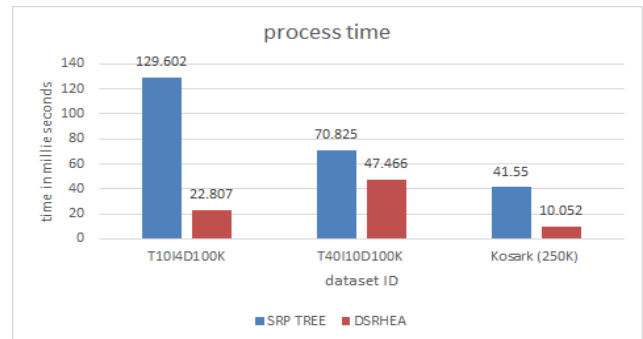


Fig. 5. Performance Comparison of DSRHEA and SRP Tree towards Processing Time.

A. Cross Validation

The performance study was carried out using cross-validation. The DSRHEA cross-validation metrics were compared to the values obtained in an experimental investigation on the same dataset utilizing modern models HECLAT RPStream and SRPTree [20] with static and dynamic supports. The comparison investigation is presented in full in the following cross-validation metric examination.

Human annotation was used to identify high utility itemsets with changeable values of the six items in order to undertake cross-validation. Human annotation partitioned the total itemsets identified into two, reflecting positive and negative labels in descending order. There are a total of 21794 rare itemsets that have been considered. Among these itemsets, 14206 have been labeled as positive (really uncommon itemsets), whereas 7588 have been designated as negative (falsely rare itemsets). Positive itemsets have limited support (rare support) and maximal confidence, while negative itemsets have confidence less than the threshold and redundant itemsets. The experimental statistics (cross-validation metrics) are provided in the following performance analysis.

The DSRHEA model outperformed the other alternatives significantly, as illustrated by the figurative illustration in Fig. 6.

The metric accuracy denotes the positive predictive value, which is the ratio of true positives to the total of true positives and false negatives. The metric precision values for DSRHEA, HECLAT RPStream, and SRPTree with static and dynamic support were 0.997, 0.9584, 0.8976, and 0.9175, respectively. According to these results, the DSRHEA model exceeds the other models in terms of positive pattern predictive value, as determined by precision.

The measure specificity can be used to calculate the real detection rate of negatively labeled uncommon patterns, which is derived as the ratio of true negatives to the sum of true negatives and false positives. The specificity shows the best method for removing patterns that aren't actually unusual (having negative label). The metric specificity values for DSRHEA, HECLAT RPStream, and SRPTree with static and dynamic support were 0.9836, 0.9657, 0.8836, and 0.9136, respectively. These numbers suggest that the DSRHEA model surpasses the other models in spotting patterns that aren't actually infrequent, as shown by specificity.

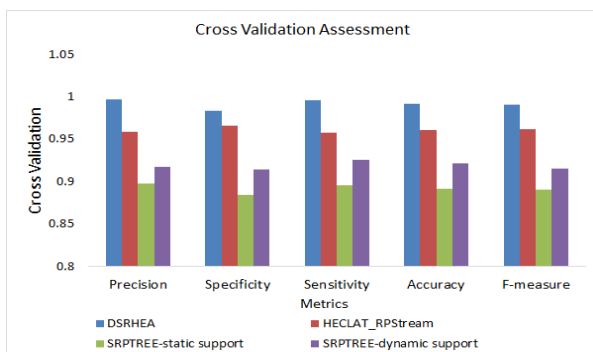


Fig. 6. The Related Performance Metric Values of the Models DSRHEA, HECLAT_RPStream, and SRPTree with Static and Dynamic Support Discovered from Cross-Validation.

The true positive rate is calculated using sensitivity, which is the ratio of true positives to the sum of true positives and false negatives (rate of truly rare patterns discovered). The metric sensitivity values for DSRHEA, HECLAT RPStream, and SRPTree with static and dynamic support were 0.9957, 0.9577, 0.8957, and 0.9257, respectively. These values suggest that the DSRHEA model surpasses the other models in terms of detecting truly unusual patterns, as measured by sensitivity.

The metric accuracy used to characterize measurement approximations towards true-value is the ratio of the count of actually discovered rare patterns, truly discarded patterns that are not unusual, to the total count of patterns discovered and rejected (discovering truly rare patterns and discarding truly not the rare patterns). The metric accuracy values for DSRHEA, HECLAT RPStream, and SRPTree with static and dynamic support were 0.9915, 0.9605, 0.8915, and 0.9214, respectively. As assessed by accuracy, these values reveal that the model DSRHEA beats the other models in terms of detecting actually unusual patterns and eliminating those that aren't.

The metric F-measure, which is the reciprocal of the ratio of "product of precision and sensitivity" to "sum of the corresponding precision and sensitivity," represents the consistency of accuracy and sensitivity values displayed in the rare pattern mining process. The metric f-measure for DSRHEA, HECLAT RPStream, and SRPTree with static and dynamic support was 0.9903, 0.962, 0.8905, and 0.9155, respectively. In terms of consistency of values depicted for accuracy and sensitivity, which is represented by the f-measure, the model DSRHEA obviously beats the other models.

V. CONCLUSION

This article demonstrates how to implement rare pattern mining from data streams using a time-sensitive sliding window. The methods are éclat-based and implemented using bit-sets. The approach makes use of two-level hash tables to store newly formed large rare patterns. An optimization based on the support of two item sets is also a critical element of the method, as it increases the overall efficiency of the program in terms of time complexity by lowering the number of candidates and their join. In this application is used a range of input support criteria to do data analysis. Support is calculated dynamically. The proposed method has been proved to be more effective than earlier relevant algorithms. The essential points are as follows: 1) Two-item optimization, 2) Prefix node-based massive item generation, 3) Vertical mining with bit-sets instead of TID-sets are two ways to make more items, and 4) Calculation of dynamic support. The cross validation results indicating that the proposed DSRHEA is outperforming the other contemporary models in regard to identify truly rare patterns. The DHREA has shown 99% accuracy to discover truly rare patterns. The evolutionary techniques such as fuzzy reasoning can be used to discover rare patterns under variable contexts, which will be the future research.

REFERENCES

[1] H. T. Nguyen, L. P. Phan, H. H. Huynh, and H. X. Huynh. (2021). "Collaborative Recommendation based on Implication Field," Int. J.

- Adv. Comput. Sci. Appl., vol. 12, no. 10, 2021, doi: 10.14569/IJACSA.2021.0121003.
- [2] Ngai, E. W., Hu, Y., Wong, Y. H., Chen, Y., & Sun, X. (2011). The application of data mining techniques in financial fraud detection: A classification framework and an academic review of literature. *Decision support systems*, 50(3), 559-569.
- [3] Liu, Y. (2010, January). Study on application of apriori algorithm in data mining. In *2010 Second international conference on computer modeling and simulation (Vol. 3, pp. 111-114)*. IEEE.
- [4] Kruse, S., & Naumann, F. (2018). Efficient discovery of approximate dependencies. *Proceedings of the VLDB Endowment*, 11(7), 759-772.
- [5] T. Slimani and A. Lazzez, "Efficient analysis of pattern and association rule mining approaches," *International Journal of Information Technology and Computer Science*, 6(3), pp. 70–81, 2014.
- [6] Yanqing Ji, Hao Ying, John Tran, Peter Dews, Ayman Mansour, and R Michael Massanari. (2012). A method for mining infrequent causal associations and its application in finding adverse drug reaction signal pairs. *IEEE Transactions on Knowledge and Data Engineering*, 25(4):721–733, 2012.
- [7] Yun Sing Koh and Sri Devi Ravana. (2016). Unsupervised rare pattern mining: a survey. *ACM Transactions on Knowledge Discovery from Data*, 10(4):1–29, 2016.
- [8] Kanimozhi SC Sadhasivam and Tamilarasi Angamuthu (2011). Mining rare itemset with automated support thresholds. *Journal of Computer Science*, 7(3):394, 2011.
- [9] Darrab S, Ergenic B (2017) Vertical pattern mining algorithm for multiple support thresholds. In: *International conference on knowledge based and intelligent information and engineering (KES)*. *Procedia computer science*, vol 112, pp 417–426.
- [10] Yun Sing Koh and Nathan Rountree. (2005). Finding sporadic rules using aprioriinverse. In *Pacific-Asia Conference on Knowledge Discovery and Data Mining*, pages 97–106. Springer, 2005.
- [11] Laszlo Szathmary, Amedeo Napoli, and Petko Valchev. (2007). Towards rare itemset mining. In *19th IEEE International Conference on Tools with Artificial Intelligence*, pages 305–312. IEEE, 2007.
- [12] Luigi Troiano, Giacomo Scibelli, and Cosimo Birtolo. (2009). A fast algorithm for mining rare itemsets. In *Ninth International Conference on Intelligent Systems Design and Applications*, pages 1149–1155. IEEE, 2009.
- [13] R Uday Kiran and P Krishna Reddy. (2011). Novel techniques to reduce search space in multiple minimum supports-based frequent pattern mining algorithms. In *Proceedings of the 14th International Conference on Extending Database Technology*, pages 11–20, 2011.
- [14] C Sweetlin Hemalatha, Vijay Vaidehi, and R Lakshmi. (2015). Minimal infrequent pattern based approach for mining outliers in data streams. *Expert Systems with Applications*, 42(4):1998–2012, 2015.
- [15] M.A. Thalor and S. Patil, "Incremental Learning on Non-stationary Data Stream using Ensemble Approach," *International Journal of Electrical and Computer Engineering*, Aug 1;6(4):1811, 2016.
- [16] David Tse Jung Huang, Yun Sing Koh, Gillian Dobbie, and Russel Pears. (2014). Detecting changes in rare patterns from data streams. In *Pacific-Asia Conference on Knowledge Discovery and Data Mining*, pages 437–448. Springer, 2014.
- [17] Tanbeer, S. K., Ahmed, C. F., Jeong, B. S., & Lee, Y. K. (2009). "Efficient single-pass frequent pattern mining using a prefix-tree", *Information Sciences*, vol. 179(5), pp. 559–583, 2009.
- [18] Deypir, M., Sadreddini, M. H., & Hashemi, S., (2012). "Towards a variable size sliding window model for frequent item set mining over data streams", *Computers & industrial engineering*, Vol. 63(1), pp. 161–172, 2012.
- [19] Gangin Lee, Unil Yun , Keun Ho Ryu, (2014). "Sliding window based weighted maximal frequent pattern mining over data streams", *Expert Systems with Applications*, vol. 41, pp. 694–708, 2014.
- [20] David Huang, Yun Sing Koh, Gillian Dobbie. (2012). "Rare Pattern Mining on DataStream" *Data Warehousing and Knowledge Discovery Lecture, Notes in Computer Science Volume 7448*, 2012, pp 30.
- [21] Tsang, S., Koh, Y.S., Dobbie, G. (2011). RP-Tree: Rare Pattern Tree Mining. In: Cuzzocrea, A., Dayal, U. (eds.) *DaWaK 2011. LNCS*, vol. 6862, pp. 277–288. Springer, Heidelberg (2011).
- [22] Sunitha Vanamala, L.Padma Sree, S.Durga Bhavani. (2013). "Efficient rare association rule mining algorithm " *Int. J. of Engineering Research and Applications (IJERA)* , Vol. 3, Issue 3, pp.753-757 , 2013.
- [23] Vanamala, S., Sree, L., & Bhavani, S. (2014). Rare association rule mining for data stream. *International Conference on Computing and Communication Technologies*, 1-6.
- [24] Manal Almuammar, Maria Fasli. (2018). "Learning Patterns from Imbalanced Evolving Data Streams", *Big Data (Big Data) 2018 IEEE International Conference on*, pp. 2048- 2057, 2018.
- [25] Manal Almuammar, Maria Fasli. (2017). "Pattern discovery from dynamic data streams using frequent pattern mining with multi-support thresholds", *the Frontiers and Advances in Data Science (FADS) 2017 International Conference on*, pp. 35-40, 2017.
- [26] Vanamala S., Padma Sree L., Durga Bhavani S. (2021) *Eclat_RPGrowth: Finding Rare Patterns Using Vertical Mining and Rare Pattern Tree*. *Computer Networks, Big Data and IoT. Lecture Notes on Data Engineering and Communications Technologies*, vol 66. Springer, Singapore. https://doi.org/10.1007/978-981-16-0965-7_14.
- [27] W. A. W. A. Bakar, M. Man, Z. Abdullah, and M. B. Man. (2021). "CRS-iEclat: Implementation of Critical Relative Support in iEclat Model for Rare Pattern Mining," *Int. J. Adv. Comput. Sci. Appl.*, vol. 12, no. 7, 2021, doi: 10.14569/IJACSA.2021.0120722.
- [28] Zaki M (2000) Scalable algorithms for association mining. *IEEE Trans Knowl Data Eng* 12(3):372–390.
- [29] Rahul Anil Ghatage. (2015). *Frequent Pattern Mining Over Data Stream Using Compact Sliding Window Tree & Sliding Window Model (IRJET)* , Volume: 02, July-2015, eISSN: 2395 -0056 p-ISSN: 2395-0072 15.
- [30] Anindita Borah, Bhabesh Nath. (2019). Incremental rare pattern based approach for identifying outliers in medical data, *Applied Soft Computing*, Volume 85, 2019.
- [31] <https://www.investopedia.com/trading/using-pivot-points-for-predictions/>.
- [32] Frequent itemset mining dataset repository. <http://fimi.untwerpen.be/data/>.

Energy Efficient Hop-by-Hop Retransmission and Congestion Mitigation of an Optimum Routing and Clustering Protocol for WSNs

Prakash K Sonwalkar¹

Research Scholar, Dept. of Computer Science and Engineering, Jain College of Engineering Belagavi, India

Vijay Kalmani²

Professor, Dept. of Computer Science and Engineering Jain College of Engineering Belagavi, India

Abstract—In the past few decades, wireless sensor networks, which take a growing number of applications in the surroundings further than the human reach, have risen in popularity. Various routing pseudo codes have been suggested for network optimization, emphasizing energy efficiency, network longevity, and clustering processes. To the existing load balancing energy-efficient sleep awake, aware smart sensor network routing protocol, the modified load-balancing efficient-energy sleep active alert smart routing system for wireless sensor networks is presented in this paper, which takes network homogeneity into account. The modified protocol is the optimum clustering and routing protocol in wireless sensor networks (OCSRN), which simulates an enhanced network coupled node pair model. Our suggested modified approach studies and enhances factors such as network stability, network lifetime, and cluster monitor mechanism choice. The significance of typically combining sensor endpoints is applied to maximize energy efficiency. The proposed protocol significantly improved network parameters in simulations, showing that it could be a valuable option for WSNs. In wireless sensor networks, in addition to memory considerations and dependable transportation, this paper presents a hop-by-hop re-transmission strategy and congestion mitigation, which is the major contribution of this paper. It is a very consistent method based on a pipe flow model. After performing additional optimized overhead to improve the network lifespan of wireless sensors networks, the current algorithm can be paralleled to the less energy adaptive clustering hierarchy protocol. The optimal clustering in multipath and multihop technique intends to minimize the energy consumption highlighted for a circular area enclosed by a sink by replacing one-hop communication with efficient multihop communication. The optimum quantity of clusters is determined, and the energy consumption is reduced by splitting the network into clusters of nearly equal size. The obtained simulation results will demonstrate the increase in the network lifetime compared to previous clustering strategies such as Low Energy Adaptive Clustering Hierarchy.

Keywords—Wireless sensor network; network lifetime; clustering strategies; clustering process

I. INTRODUCTION

In recent years, a great deal of research has been done on low power protocols, network setup, routing protocols, and analysis issues in sensor networks. Several routing protocols can be used to accomplish optimal routing in the context of

energy, such as proximity, multipath, and so on. Battery power is a critical component in the algorithm design for extending the network's endpoint lifespan [1]. To enhance overall network performance, it is ideal for increasing the lifespan of sensor endpoints. The numerous energy consumption sources in WSNs can be divided into "constituent" - "practical" pairs. The practical consists of the native foundations of energy dissipation required to complete the prescribed task at each endpoint. The energy wastage is due to inefficient medium access, routing, or topology control in the latter category [2]. Depending on the application environment, each consumer contributes to overall energy consumption. Energy control in WSNs was first classified into conservation and supply of energy. The former refers to providing energy to each endpoint during runtime to fully (or partially) power the sensor endpoints [3]. Outward power supply bases currently display non-continuous behavior in many circumstances, which can cause system failure [4]. Energy harvesting and conservation to be integrated into a unified ecosystem to avoid degeneration of the collected energy. From a data-centric standpoint, WSN applications can be classified into periodic sampling, event-driven, or hybrid situations based on convergent validity [5].

In the first group, the measured data must be transferred to the gateway regularly for processing. As a result, data traffic will be exceedingly dense, especially if acquisition durations are short [6]. As a result, the likelihood of errors, passive listening, and suboptimal routing increases. Unlike the previous classification, data transfer is less frequent in event-driven operations. Other sources of energy use, on the other hand, may be dominant. Finally, heterogeneous WSNs are considered in the third category of WSN applications, wherein the measured data is regularly communicated [7]. Simultaneously, the network samples the environment regularly to detect predetermined events. The energy-saving approaches can be classified into three categories: Data-oriented methods: Time-driven methods, and event-driven methods are classified into this category based on WSN applications. The first subcategory concerns the communication module, accounting for most energy usage in time period-centric scenarios. The latter group includes methods for reducing the strain of frequent data collecting or resource sensors [8 & 9]. In addition, local mechanisms for modifying components of each endpoint are included.

TABLE I. SUMMARY OF RELATED PAST RESEARCH WORK FOR CLUSTERING IN COMPARISON WITH PROPOSED WORK

Peer to Peer Network connection	Year	Methodology	Classification	Advantages	Disadvantages
Proposed Protocol	2022	C.H. voting technique with hop-by-hop re-transmission strategy and congestion mitigation	Synthesis clustering strategy	Simple, reliable, efficient, and easy to use	Fails to identify the voting of dead C.H. node during node selection
CFFB Protocol [29]	2019	Fuzzy – Neuro method	Adaptable strategy	Deep Learning-based technique for voting optimum C.H.	adds more load to the network
Optimized routing protocol with cluster-based energy-efficient large area WSNs [30]	2019	Derivative Independent Simplex Technique	Synthesis clustering strategy	Lessens the effective consumption of energy	Typical number of clusters in single round effects in a large delay of operations
C.H.E.S. – D.L.F. protocol [31]	2018	G.A./Fuzzy predictive strategy	Adaptable strategy	Efficient CH voting that improves time span of network	Extensive calculation such as hop count, density results in fast energy reduction
Multi-Criteria selection analysis strategy protocol [32]	2016	The algorithm scales the transmission rate, residual energy, distance to B.S.	Combined – Scaling technique	Enhances the network lifetime	Mathematical complexity
K-Means – Clustering method in WSN [33]	2015	Residual Energy scaling strategy and value of threshold node	Adaptable strategy	Enhanced are nodes deployed in the network	Power consumed in residual energy computed with threshold data is an extra burden on the network
Energy Efficient multihop clustering Protocol [34]	2014	Scaling the energy level	Synthesis clustering strategy	Enhanced connectivity and stability	With some nodes dead, the delay is caused
LEACH [35]	2004	A randomized voting of cluster heads, formation of C.H.'s are self-configured	Deterministic techniques	Fast, simple, low overhead	Large redundant data, limitations due to random data

The approaches in this domain are combined with event-driven and time-driven WSN applications such as memory overflow and reliable transport with memory considerations, as illustrated in Table I, which depicts the summary and compares the past research works with the proposed work. The network-based techniques mainly aim for energy consumption for retaining network functionality.

The key contributions of this research work are as follows:

- 1) With new green algorithms and technologies, this research presents a hop-by-hop re-transmission and congestion mitigation, a very consistent method in WSN based on a pipe flow model [10, 11].
- 2) This research further attempts to create an efficient-energy framework for ad-hoc clustered routing while protecting edge devices from attacks that drain their batteries [12].

II. LITERATURE REVIEW

A survey of efficient-energy hierarchical cluster-based routing in wireless sensor networks was conducted. The research investigated several elements: low power protocols, network topologies, routing protocol, and wireless sensor network coverage issues. Different routing protocols can be used to accomplish optimal routing in the context of energy, such as location-aided, multipath, data center, mobility, QoS [13]. Next, a cluster routing method, DECSA, provided an efficient-energy clustering routing algorithm based on energy residual and distance for wireless sensor networks. The improved algorithm properly balances energy consumption, extends the lifetime by 31%, helps conserve by 40%, and performs better than the original LEACH procedure [14]. However, additional performance characteristics such as

quality of service constraints and performance level were overlooked. The research was performed on a clustering routing protocol for the energy balance of wireless sensor networks based on simulated annealing and genetic algorithm. In this protocol, the simulated annealing and genetic algorithm were used to cluster the sensor endpoints while also considering the residual energy of the endpoints and the average energy of the cluster to obtain a more reasonable cluster head distribution in the lower level of the network [15]. A study on network load balancing and its application to the lifecycle of wireless sensor networks was neglected here. The efficient-energy hierarchical unequal clustering in wireless sensor networks was proposed, using an unequal clustering strategy for even energy distribution [16]. It also lowers overall energy usage, which extends the network's lifespan. The model assumes that all endpoints are immobile after deployment, that they can determine their location using GPS receivers, and that the network is homogeneous. A WSN-assisted IoT strategy was developed using an adaptive fuzzy rule-based efficient-energy clustering and immune-inspired routing protocol [17]. A bio-inspired optimization technique is applied for routing to improve data transmission dependability. Cluster-based routing is an effective method of lowering energy use. Compared to existing clustering and routing approaches, it improves QoS characteristics. The limitation was an optimum routing with large residual energy for multihop communication within the clusters, deploying many base stations to reduce the burden on cluster monitors near each base station to increase energy efficiency. Overall, network lifetime in wireless sensor networks was not explored. The proposed method uses simple fuzzy rule-based neural networks combined with clustering to properly exploit energy while avoiding the wastage caused during the head and cluster patterning selection. The practiced

system allows cluster patterning and routing to make better decisions about which endpoints to send data to, resulting in a transmission system that is faster, more efficient energy, and less prone to failure. But only the placement of the base station at the center of the network will reduce the number of hops for data transmission. Hence, the minimum energy consumption is one of the limitations identified in this research work. In addition, an efficient-energy clustered gravitational and fuzzy-based routing algorithm in WSNs was proposed [18]. This paper omitted the impact of effective communication among endpoints on the availability of residual energy, which is a drawback noted here. The swarm intelligence-based efficient-energy clustering with multihop routing algorithm for maintainable wireless sensor networks is proposed. The study developed a unique wireless sensor network clustering and multihop routing protocol based on swarm intelligence [19]. An improved particle swarm optimization technique selects cluster heads and efficiently organizes clusters. The optimization-based routing procedure is then used to identify the network's best pathways. The research significantly improved particle swarm optimization—the optimization approach takes advantage of both the clustering and routing processes, resulting in optimal energy efficiency and network longevity. Sensor endpoints can operate in sensing mode to detect physical variables or communication mode to send information to the base station. Each endpoint's connectivity manages traffic, and each endpoint is assigned to a location index. The connection between endpoints is similar, and the distance between them may be determined by measuring the signal power received. An efficient-energy smart routing in WSN employing a dominant genetic algorithm is provided, and a heuristic-based efficient-energy communication strategy is used [20, 21]. To find the best efficient-energy routing channel between sensor endpoints and define the best efficient-energy trajectory for mobile data gathering endpoints, a novel development in the genetic algorithm known as Dominant Genetic Algorithm (DGA) has been proposed. Because of its natural occurrence, the dominance of high fitness solutions has been integrated into the Genetic algorithm [22]. The constraint here is that it is assumed that there is no sensor mobility in the first situation, whereas in the second case, cluster heads are already present. Clusters have already formed, and the amount of energy expended to determine the route of a mobile data gathering endpoint is calculated using DGA.

III. METHODOLOGY ADOPTED

In this research, developing a modified load-balancing efficient-energy sleep active alert intellectual routing system for wireless sensor networks, the endpoints send location data to the base station, and the base station uses central coupling at minimum distance. All endpoints are combined with random neighbors, and the base station transmits their position data if they are coupled. The endpoints receive status updates and come to be alert of the attached endpoint [23]. Each attached endpoint compares its distance from a base station to its partner distance to the base station endpoint remains active if there is a reduced distance than a neighbor endpoint. If there is an awake mode, all the endpoints are in active mode, and else all the endpoints switch to sleep mode. Next, transmit network advertisement, listen and wait to the selection medium and

receive the awake request from the endpoints. If the mode is not active, receive the channel advertisement and relate with the received strength signal indicator, quality, link, and variant node. Finally, send a request to cluster head with energy information, receive TDMA slot, and transmit detected data in the allocated slot.

Further, the PCHs allocated the TDMA slot for transmission by transmitting the TDMA list, receiving data from endpoints, and aggregating received data from member endpoints. The active nodes are considered during the selection of the cluster heads. All the nodes have the same initial energy in the first round. The nodes in active mode will select themselves as cluster heads based on the probability of selecting cluster head with distributed algorithm 1 and each node select the random number between 0 and 1 and compares it to a threshold A_H is as illustrated in equation (1) as follows.

$$A_H = \begin{cases} \frac{P_D}{1 - P_D * (\text{Initial Round}) \bmod \frac{1}{P_D}}; & \text{if } n \in T \\ 0; & \text{Otherwise} \end{cases} \quad (1)$$

Where T is the set of active nodes in the first round. If a node's random number is smaller than the threshold (A_H), the node will elect itself as a cluster head and is referred to as Root-Cluster-Heads (RCHs). When a node is designated as an RCH, it sends an advertisement message to the entire network. Active-mode nodes only hear the broadcast messages from different RCHs. They choose their RCHs based on the advertising 'Received Signal Strength Indication (RSSI). To avoid collisions, when an Active-mode node determines which cluster it wants to join, it sends a request to that RCH via the Carrier Sensed Multiple Access (CSMA) M.A.C. protocol. Active-mode nodes additionally send their energy statistics to RCH along with their requests. The RCH calculates the remaining energy and its distance from each node, then chooses a C.H. for the following round, known as Sub-Cluster-Head (S.C.H.). In the network transmission phase, if there are M amount of nodes and L are the optimum quantity of cluster heads, then the average nodes in one cluster will be,

$$\left(\frac{M}{L} - 1\right) \quad (2)$$

For the data transmission to begin, the transceiver of the non-cluster head node dissipates $Energy_{(TX)}$ to run the transmission circuit and $TX_{(Amp)}$ to achieve an acceptable signal to noise ratio (SNR), therefore for the transmission of the message bit M_{BIT} a non-cluster head node will expand to equation (3).

$$Energy_{non-CH} = \left(\frac{M}{L} - 1\right) (Energy_{(TX)} * M_{BIT} * TX_{(Amplifier)} * M_{BIT} * d_{to-CH}^2) \quad (3)$$

To receive the data from a non-cluster head node on by the transceiver on cluster head expands in each cluster by equation (4) as follows:

$$E_{Recieve} = (E_{RX} * M_{BIT}) \left(\frac{M}{L} - 1\right) \quad (4)$$

Where the dissipated energy by each circuitry is denoted by E_{RX} for data receive and dissipated energy by cluster head to

total data is data received ($E_{Receive\ Data}$) from its nodes associated is illustrated in equation (5) as follows.

$$E_{Total} = (E_{Receive\ Data} * M_{BIT}) * \left(\frac{M}{L}\right) \quad (5)$$

The energy of transmission (E_{Trans}) dissipated by cluster heads to transmit the total data D_{Total} to the base station is given by equation (6) as follows

$$E_{Trans} = Energy_{(TX)} * D_{Total} * TX_{(Amp)} * d_{to-BS}^2 \quad (6)$$

Here d_{to-BS}^2 is the distance between a base station and the cluster head. The total energy dissipated by the cluster head in one round is given by equation (7) as follows

$$E_{CH-Total\ Energy} = E_{Receive} + E_{Total} + E_{Trans} \quad (7)$$

The dissipated total energy by cluster head is the dissipated energy in data reception from the nodes associated. The following Algorithm 1 describes this approach:

Algorithm 1: Algorithm for EESAA protocol

Start

The endpoints transmit position data to a base station
Base station uses significant combination at a minimum distance

If coupled:

- All nodes are coupled with any of the neighbors
- B.S. Broadcast their status information
- Nodes receive status updates
- Nodes become aware of coupled partner
- Every coupled node compares its distance to B.S. ->
- > to its partner distance to B.S.
- The endpoint remains active if distance < partner endpoint

If (Alert mode):

Yes: All endpoints are active

Else if:

- a. **No:** Endpoints switch to sleep mode
- If (C.H.):**
- b. **Yes:** Transmit cluster head
- c. Delay and eavesdrop to the intermediate endpoint until a certain range.
- d. Obtain requests from endpoints
- Else if:**
- e. **No:** Active mode
- f. **If (in RCHs range):**
- g. **Yes:** loop over to step c
- Else if:**
- h. **No:** Receive C.H.s advertisement
- If (S.C.H.s)**
- i. **No:** loop over to step h and compare RSSI, Link, quality, and type
- Else if:**
- Yes:**
- Transmit request to cluster head with energy statistics
- Receive TDMA slot and transmit detected data in the assigned slot
- Switch** (to step (e)):
- Case 1:**
- j. **If (RCHs):** C.H.s assign TDMA space for transmitting data
- Broadcast TDMA list and Receive endpoint data
- Aggregate received data from member endpoints
- (Go To): Base Station

End

Next, we perform the setup phase for LEACH, and in this, we assign node_(i) as the monitor of the cluster and the corresponding broadcast status of the cluster monitor. Then with delay for link communication request, next produce TDMA time slot and transmit to cluster points (t=0) with a stable-state operation for t=T_(round) seconds [24]. In the next step, wait for broadcasts from the monitor of the cluster, with transmitting for join-request to chosen cluster heads and pause for cluster monitor (t=0) schedule. This approach is presented in the following Algorithm 2.

Algorithm 2: Algorithm for setup phase for LEACH protocol

Start

If cluster monitor Endpoint_(i)

Yes:

- a. broadcast cluster monitor status
- b. Wait for link request communications
- c. Create a TDMA schedule and send it to cluster members (t=0)
- d. balanced-state operation for t=T_(round) seconds

Else if:

No:

- e. Wait for messages from the cluster monitor
- f. Transmit for link-request to selected cluster monitors
- g. pause for cluster monitor (t=0) schedule
- h. Loop over to step d

End

In the optimum clustering and routing protocol in the wireless sensor networks (OCSRN) stage, the Input number of endpoints is defined and generates a random position of each endpoint. An endpoint neighbor discovery cluster head selection cluster creation and routing table creation [25, 26]. Further, there is time slot assignment along with communication to the base station, and finally, the data tracing process is done in this stage. Algorithm 3 describes this approach as follows.

Algorithm 3: Algorithm for setup phase for LEACH protocol

Start

Input number of endpoints
Generate random position of each endpoint
Endpoint neighbor discovery
Cluster head selection
Cluster creation and routing table creation
Time Slot assignment
Communication to the base station and data tracing
Display the result

End

The methodology is further extended to the flow pipe strategy, a robust transport method in wireless sensor networks, as illustrated in Fig. 1.

The reliable transport with memory considerations is as shown in Fig. 2.

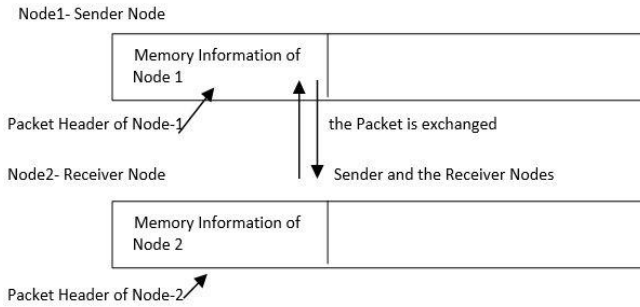


Fig. 1. Memory Overflow Prevention Strategy.

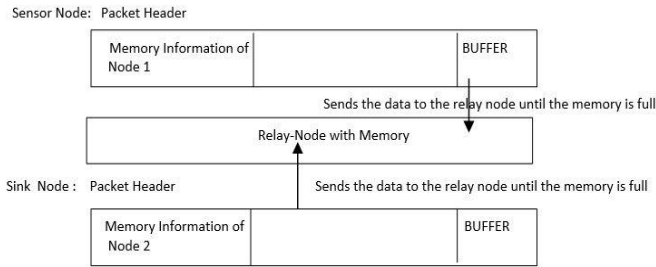


Fig. 2. Reliable Transport with Memory Consideration.

The transmitter node obtains the receiving node's memory information in this manner. As a result, the solution described can prevent memory overflow [28]. The local variables linked with each node help in transmission in the nodes. As the source adjusts its transmission rate, the throughput can be enhanced using the memory information contained in each node's packet header. The techniques described above are effective on low-memory nodes and good use of the channel. Inter-segment data can be transferred from source to sink at a reasonable cost and with great reliability using the abovementioned approach.

The next section illustrates the results from the study performed in the existing load balancing intellectual sensor network routing protocol, modified in terms of load balancing efficient-energy sleep active alert routing protocol, which considers network homogeneity [27].

IV. RESULTS OBTAINED

The packet delivery ratio (PDR) is obtained by considering the homogeneous network into the account and is compared with the existing load balancing protocol concerning the modified load-balancing efficient-energy sleep active alert smart routing protocol is, as illustrated in Fig. 3. The comparison is made by considering the sensor radius of WSN. The end-to-end delay is achieved by allowing for the homogeneous network into consideration. It is related to the existing load balancing efficient-energy sleep awake, aware smart sensor network routing protocol concerning the modified load-balancing efficient-energy sleep active alert smart routing protocol is illustrated in Fig. 4. The results are compared by considering the WSN endpoint's sensor radius vs. round trip delay (in seconds).

It is related to the existing routing protocol for varied load-balancing efficient-energy sleep active alert smart routing

protocol, as illustrated in Fig. 5. The results are compared by considering the WSN endpoint's C.H. formation delay (milliseconds).

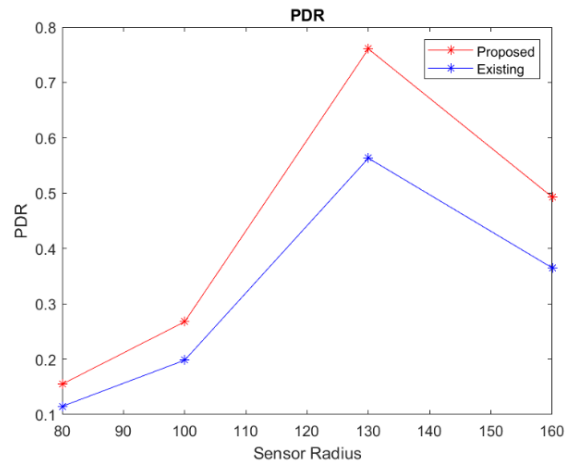


Fig. 3. Comparison of Existing with Proposed Approach in Terms of P.D.R.

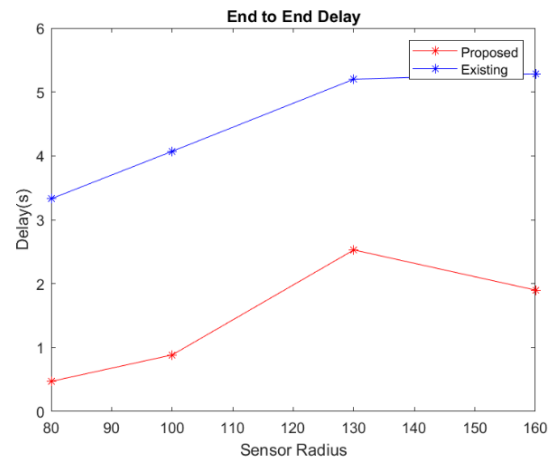


Fig. 4. Comparison of EESAA with m-EESAA in Terms of End-to-End Delay.

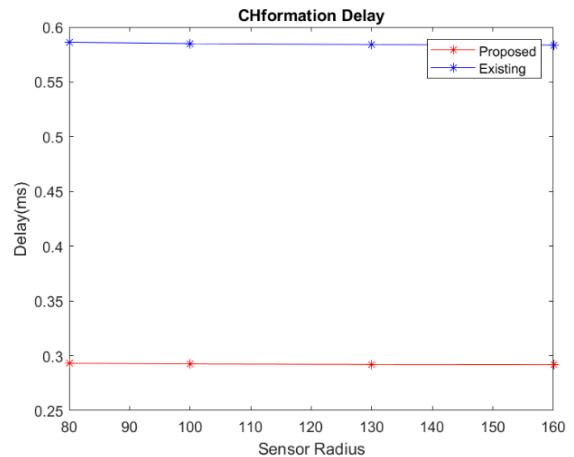


Fig. 5. Comparison of EESAA with m-EESAA in Terms of Cluster Head Formation Delay.

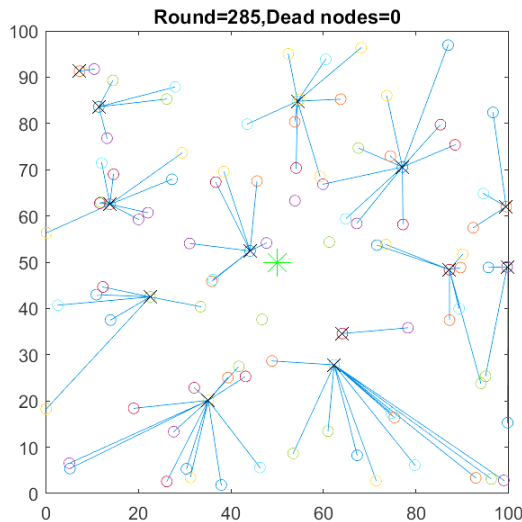


Fig. 6. Calculation of the Number of Rounds and Number of Dead Endpoints of WSN.

The simulation of several rounds and the number of dead endpoints of the wireless sensor network endpoint is captured during the run time during the code execution and is illustrated in Fig. 6. The same is further optimized for the modified protocol cluster networks for optimum clustering and routing protocol in wireless sensor networks (OCRSN). Fig. 7 illuminates the Cluster network formation for optimum clustering and routing protocol in wireless sensor networks (OCRSN). In simulations, our proposed protocol significantly enhanced network parameters illustrating that it could be a valuable option for WSNs. After performing additional optimization overhead to enhance the network lifetime of wireless sensors networks, the current algorithm can be compared to the LEACH protocol as illustrated in the following Fig. 8., Fig. 9. to Fig. 14. Fig. 8 depicts the comparison of routing and clustering protocol (OCRSN). LEACH clustering protocol in terms of the average energies of each endpoint of the wireless sensor network (WSN).

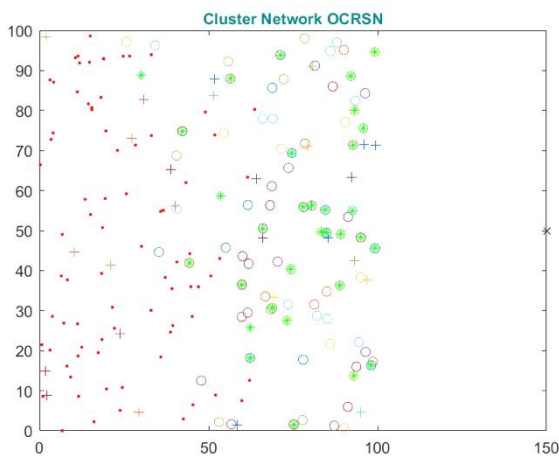


Fig. 7. Cluster Network Formation for Optimum Clustering and Routing Protocol in Wireless Sensor Networks (OCRSN).

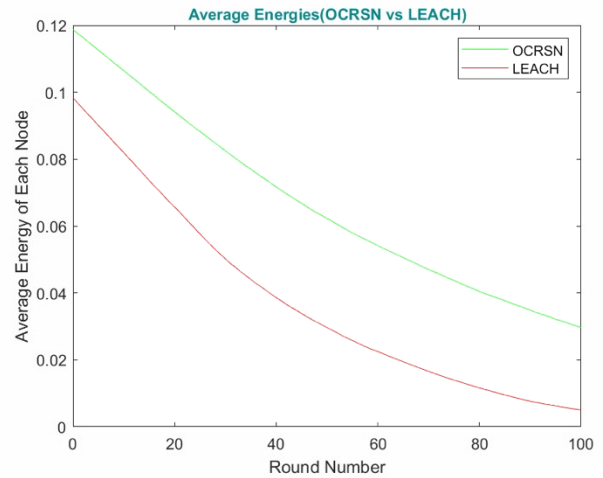


Fig. 8. Comparison of OCRSN vs. LEACH w.r.t to Average Energies.

Fig. 9 illustrates the formation of the LEACH clustering protocol cluster network and is obtained for comparisons with our work. Fig. 10 shows the calculation of several dead endpoints concerning the round number in OCRSN (Our Work) versus the LEACH protocols. It is observed that OCRSN has a smaller number of dead endpoints compared to the LEACH protocol. Fig. 11 illustrates the calculation of several alive endpoints concerning the round number in OCRSN (Our Work) versus the LEACH protocols. Again, it is observed that OCRSN has more alive endpoints compared to LEACH protocols.

Further, Fig. 12 presents the formation of head clusters versus the round number, and the number of cluster heads is compared with OCRSN (Our Work) versus LEACH protocol. It is observed that OCRSN (Our Work) has more cluster heads than LEACH protocol. Next, Fig. 13 depicts the number of packets to cluster heads to the round number, and the number of cluster heads is compared with OCRSN (Our Work) versus LEACH protocol. The Fig. 13. Illustrates the formation of several packets to the base station with respect to the round number.

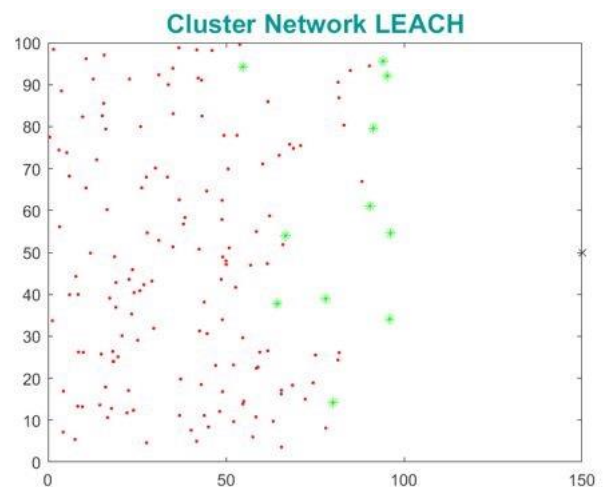


Fig. 9. Cluster Network of LEACH.

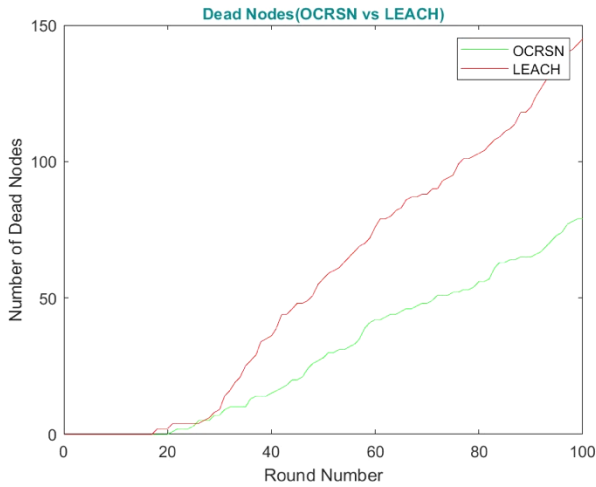


Fig. 10. Calculation of Number of Dead Endpoints (OCRSN vs. LEACH).

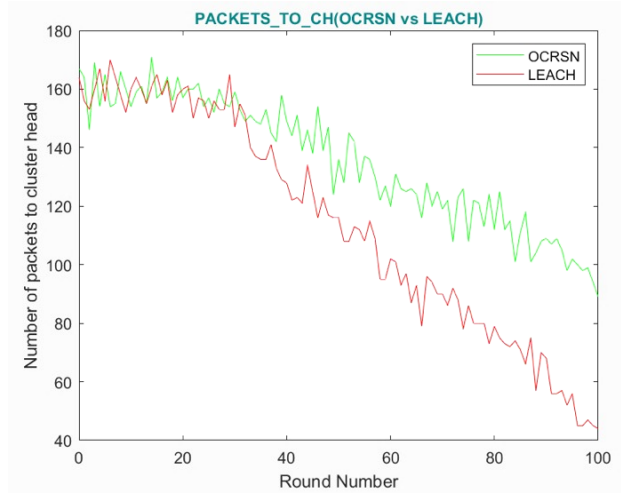


Fig. 13. Formation of Number of Packets to Cluster Head with respect to Round Number.

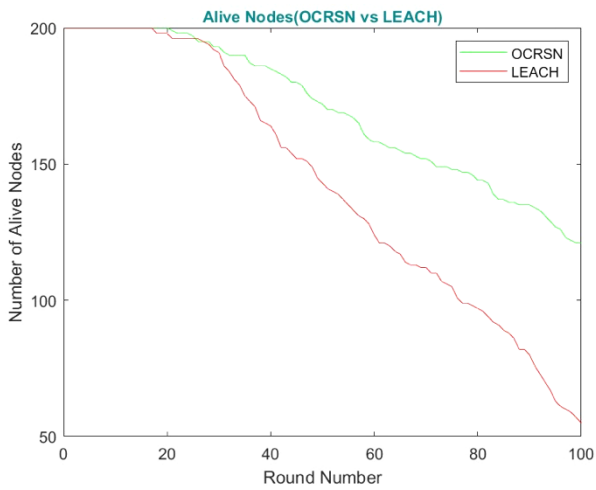


Fig. 11. Calculation of Number of Alive Endpoints (OCRSN vs. LEACH).

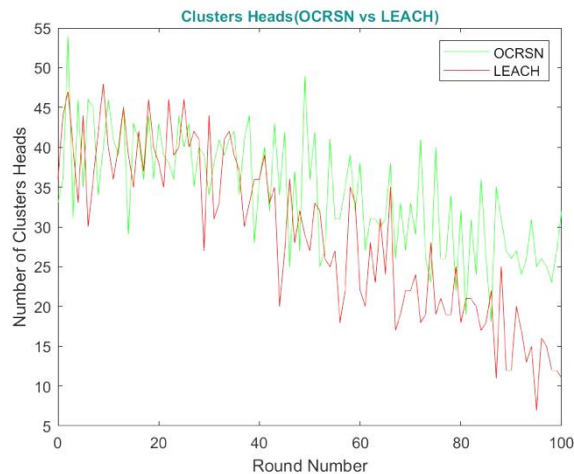


Fig. 12. Formation of a Head Cluster for Number of Rounds.

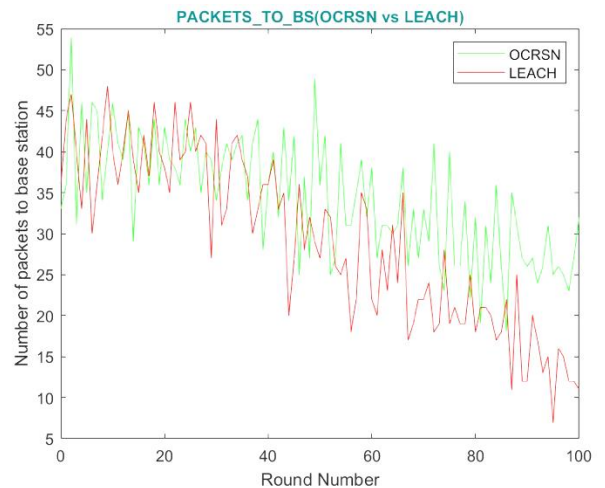


Fig. 14. Formation of Number of Packets to BS with respect to Round Number.

It is observed that OCRSN (Our Work) has more packets to the base station than the LEACH protocol. The enhanced network coupling node model is as illustrated in Fig. 14, it is observed that there are certain coupled node pairs aligned, and pipe connection is established between each of the aligned nodes. The isolated nodes are also observed at the bottom left and top right in Fig. 15. Table II illustrates the simulation parameters of measured simulation results obtained for the several network constraints with respect to the values obtained for each network constraint. Further from the overall simulations, it can be observed that:

- 1) LEACH can be chosen in reduced networks, where the sum of endpoints < 50 where achieves considerably enhanced performance than OCRSN.
- 2) OCRSN may be selected in more extensive topologies and once the experimental likelihood of cluster voting choice is more significant.

TABLE II. KEY SIMULATION PARAMETERS

Network Constraint	Value
a. Size of Network	100 x 100 m
b. Number of BS	2
c. Number of Nodes	100, 200, 300, 400
d. Packet Data Size	2K bits
e. Packet Control Size	20 bits
f. Node Initial Energy	3J
g. Calculated Rounds	52nJ/bit
h. Consumed Energy to drive transmit/receive signal	10pJ/bit/m ²
i. Free space parameter	0.0012 pJ/bit/m ³
j. Energy consumption by CH member	6nJ/bit/signal
k. Number of Rounds	1500

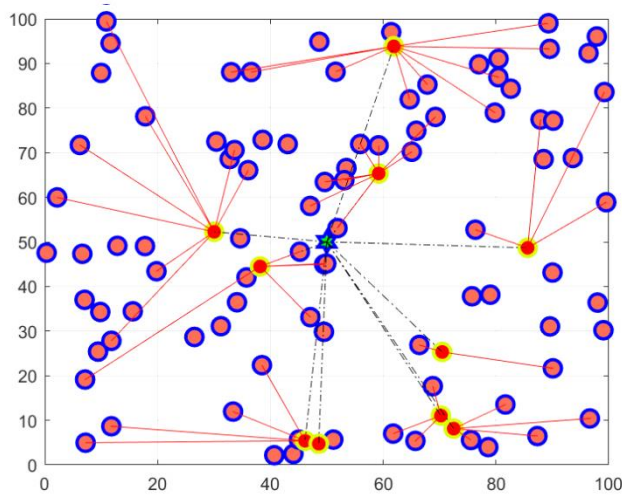


Fig. 15. Enhanced Network Coupling Node Model.

V. CONCLUSION

This paper presents the existing load balancing efficient-energy sleep awake, aware smart sensor network routing protocol. The modified protocol is developed for load-balancing efficient-energy sleep active alert smart routing system for wireless sensor networks, considering the network homogeneity. The modified protocol is the optimum routing and clustering protocol in wireless sensor networks (OCSRN). In the proposed modified approach, the study and enhancement of certain factors are proposed with memory considerations, and dependable transportation presents a hop-by-hop re-transmission strategy and congestion mitigation, a very consistent method based on a pipe flow model. The significance of characteristically pairing sensor endpoints is applied to maximize energy efficiency, and the simulations are obtained. The proposed protocol significantly improves network parameters, illuminating that it could be a valuable option for wireless sensor networks. After performing additional optimization overhead to enhance the network lifetime of wireless sensors networks, the current algorithm can be compared to the least energy adaptive clustering scheme protocol.

REFERENCES

- [1] Pantazis, N., & Vergados, D. (2007). A survey on power control issues in wireless sensor networks. *IEEE Communications Surveys & Tutorials*, 9(4), 86–107. doi:10.1109/comst.2007.4444752.
- [2] Sinde, R., Begum, F., Njau, K., & Kaijage, S. (2020). Refining Network Lifetime of Wireless Sensor Network Using Energy-Efficient Clustering and DRL-Based Sleep Scheduling. *Sensors*, 20(5), 1540. doi:10.3390/s20051540.
- [3] Sarkar, A., & Senthil Murugan, T. (2017). Cluster head selection for energy-efficient and delay-less routing in wireless sensor network. *Wireless Networks*, 25(1), 303–320. doi:10.1007/s11276-017-1558-2.
- [4] Gherbi, C., Aliouat, Z., & Benmohammed, M. (2018). A Novel Load Balancing Scheduling Algorithm for Wireless Sensor Networks. *Journal of Network and Systems Management*, 27(2), 430–462. doi:10.1007/s10922-018-9473-0.
- [5] Wang, J., Gao, Y., Liu, W., Sangaiah, A., & Kim, H.-J. (2019). An Improved Routing Schema with Special Clustering Using PSO Algorithm for Heterogeneous Wireless Sensor Network. *Sensors*, 19(3), 671. doi:10.3390/s19030671.
- [6] K.P, A. (2021). Comparison of Fuzzy-based Cluster Head Selection Algorithm with LEACH Algorithm in Wireless Sensor Networks to Maximize Network Lifetime. *Revista Gestão Inovação e Tecnologias*, 11(4), 1277–1288. doi:10.47059/revistageintec.v11i4.2186.
- [7] Jan, S. R. U., Jan, M. A., Khan, R., Ullah, H., Alam, M., & Usman, M. (2018). An Energy-Efficient and Congestion Control Data-Driven Approach for Cluster-Based Sensor Network. *Mobile Networks and Applications*, 24(4), 1295–1305. doi:10.1007/s11036-018-1169-x.
- [8] Punj, R., & Kumar, R. (2018). Technological aspects of W.B.A.N.'s for health monitoring: a comprehensive review. *Wireless Networks*, 25(3), 1125–1157. doi:10.1007/s11276-018-1694-3.
- [9] Khedr, A. M., Osamy, W., & Salim, A. (2018). Distributed coverage hole detection and recovery scheme for heterogeneous wireless sensor networks. *Computer Communications*, 124, 61–75. doi:10.1016/j.comcom.2018.04.002.
- [10] Farman, H., Javed, H., Jan, B., Ahmad, J., Ali, S., Khalil, F. N., & Khan, M. (2017). Analytical network process based optimum cluster head selection in wireless sensor network. *PLOS ONE*, 12(7), e0180848. doi:10.1371/journal.pone.0180848.
- [11] Qu, Y., Zheng, G., Ma, H., Wang, X., Ji, B., & Wu, H. (2019). A Survey of Routing Protocols in W.B.A.N. for Healthcare Applications. *Sensors*, 19(7), 1638. doi:10.3390/s19071638.
- [12] Chen, Z., & Shen, H. (2018). A grid-based reliable multihop routing protocol for energy-efficient wireless sensor networks. *International Journal of Distributed Sensor Networks*, 14(3), 155014771876596. doi:10.1177/1550147718765962.
- [13] Yong, Z., & Pei, Q. (2012). A Energy-Efficient Clustering Routing Algorithm Based on Distance and Residual Energy for Wireless Sensor Networks. *Procedia Engineering*, 29, 1882–1888. doi:10.1016/j.proeng.2012.01.231.
- [14] Mudathir, F.S.Y.; Rodrigues, J.J.P.C.; Khalifa, O.O.; Mohammed, A.B.; Korotaev, V. Service Redundancy and Cluster-based Routing Protocols for Wireless Sensor and Mobile Ad-Hoc Networks: A Survey. *Int. J. Commun. Syst.* 2020, 33, e4471.
- [15] Baranidharan, B. (2013). Energy Efficient Hierarchical Unequal Clustering in Wireless Sensor Networks. *Indian Journal of Science and Technology*, 7(3), 301–305. doi:10.17485/ijst/2014/v7i3.2.
- [16] Preeth, S. K. S. L., Dhanalakshmi, R., Kumar, R., & Shakeel, P. M. (2018). An adaptive fuzzy rule based energy efficient clustering and immune-inspired routing protocol for WSN-assisted IoT system. *Journal of Ambient Intelligence and Humanized Computing*. doi:10.1007/s12652-018-1154-z.
- [17] S. Raj, J., & Basar, A. (2019). QOS Optimization of Energy Efficient Routing in IoT Wireless Sensor Networks. *June 2019*, 01(01), 12–23. doi:10.36548/jismac.2019.1.002.
- [18] Guleria, K., & Verma, A. K. (2019). Meta-heuristic Ant Colony Optimization Based Unequal Clustering for Wireless Sensor Network. *Wireless Personal Communications*, 105(3), 891–911. doi:10.1007/s11277-019-06127-1.

- [19] Selvi, M., Santhosh Kumar, S. V. N., Ganapathy, S., Ayyanar, A., Khanna Nehemiah, H., & Kannan, A. (2020). An Energy Efficient Clustered Gravitational and Fuzzy Based Routing Algorithm in WSN's. *Wireless Personal Communications*, 116(1), 61–90. doi:10.1007/s11277-020-07705-4.
- [20] Elhoseny, M., Rajan, R. S., Hammoudeh, M., Shankar, K., & Aldabbas, O. (2020). Swarm intelligence-based energy efficient clustering with multihop routing protocol for sustainable wireless sensor networks. *International Journal of Distributed Sensor Networks*, 16(9), 155014772094913. doi:10.1177/1550147720949133.
- [21] D L, S. (2020). Energy Efficient Intelligent Routing in WSN using Dominant Genetic Algorithm. *International Journal of Electrical and Computer Engineering (I.J.E.C.E.)*, 10(1), 500. doi:10.11591/ijece.v10i1.pp500-511.
- [22] Ho, J.-W., Wright, M., & Das, S. K. (2012). ZoneTrust: Fast Zone-Based Node Compromise Detection and Revocation in Wireless Sensor Networks Using Sequential Hypothesis Testing. *IEEE Transactions on Dependable and Secure Computing*, 9(4), 494–511. doi:10.1109/tdsc.2011.65.
- [23] Praveen, J., & Nithya, V. (2016). Detection and Mitigation of Attacks in Cluster based Wireless Sensor Networks using Rule based I.D.S. *Indian Journal of Science and Technology*, 9(44). doi:10.17485/ijst/2016/v9i44/91477.
- [24] Hsueh, C.-T., Wen, C.-Y., & Ouyang, Y.-C. (2015). A Secure Scheme Against Power Exhausting Attacks in Hierarchical Wireless Sensor Networks. *IEEE Sensors Journal*, 15(6), 3590–3602. doi:10.1109/jsen.2015.2395442.
- [25] Thangaramya, K., Kulothungan, K., Logambigai, R., Selvi, M., Ganapathy, S., & Kannan, A. (2019). Energy aware cluster and neuro-fuzzy based routing algorithm for wireless sensor networks in IoT. *Computer Networks*, 151, 211–223. doi:10.1016/j.comnet.2019.01.024.
- [26] Nalband, A. H., Sarvagya, M., & Ahmed, M. R. (2021). Spectral Efficient Beamforming for mmWave MISO Systems using Deep Learning Techniques. *Arabian Journal for Science and Engineering*, 46(10), 9783–9795. doi:10.1007/s13369-021-05552-4.
- [27] Nalband, A. H., Sarvagya, M., & Ahmed, M. R. (2020). Power saving and optimal hybrid precoding in millimeter wave massive M.I.M.O. systems for 5G. *TELKOMNIKA (Telecommunication Computing Electronics and Control)*, 18(6), 2842. doi:10.12928/telkomnika.v18i6.15952.
- [28] Prashanth, B. U. V., & Ahmed, M. R. (2020). FPGA Implementation of Bio-inspired Computing Based Deep Learning Model. *Advances in Distributed Computing and Machine Learning*, 237–245. doi:10.1007/978-981-15-4218-3_24.
- [29] BENMAHDI, M. B., & LEHSAINI, M. (2020). A GA-based Multihop Routing Scheme using K-Means Clustering approach for Wireless Sensor Networks. *2020 Second International Conference on Embedded & Distributed Systems (EDiS)*. doi:10.1109/edis49545.2020.9296444.
- [30] Ramakrishnan, S., & Prayla Shyry, S. (2017). Distributed fuzzy logic based cluster head election scheme (D.F.L.C.H.E.S.) for prolonging the lifetime of the wireless sensor network. *International Journal of Engineering & Technology*, 7(1.5), 111. doi:10.14419/ijet.v7i1.5.9131.
- [31] K.P, A. (2021). Comparison of Fuzzy-based Cluster Head Selection Algorithm with LEACH Algorithm in Wireless Sensor Networks to Maximize Network Lifetime. *Revista Gestão Inovação e Tecnologias*, 11(4), 1277–1288. doi:10.47059/revistageintec.v11i4.2186.
- [32] Khan, B. M., & Bilal, R. (2020). Fuzzy-Topsis-Based Cluster Head Selection in Mobile Wireless Sensor Networks. *Sensor Technology*, 596–627. doi:10.4018/978-1-7998-2454-1.ch029.
- [33] Yahya, H., Al-Nidawi, Y., & Kemp, A. H. (2015). A dynamic cluster head election protocol for mobile wireless sensor networks. *2015 International Symposium on Wireless Communication Systems (IS.W.C.S.)*. doi:10.1109/iswcs.2015.7454362.
- [34] Zhang, H., Zhang, S., & Bu, W. (2014). A Clustering Routing Protocol for Energy Balance of Wireless Sensor Network based on Simulated Annealing and Genetic Algorithm. *International Journal of Hybrid Information Technology*, 7(2), 71–82. doi:10.14257/ijhit.2014.7.2.08.
- [35] Wicker, S. B. (2004). Self-Configuring Wireless Transmission and Decentralized Data Processing for Generic Sensor Networks. doi:10.21236/ada425425.

A Novel Approach for Small Object Detection in Medical Images through Deep Ensemble Convolution Neural Network

J. Maria Arockia Dass¹

Research Scholar, Department of Computer Science and Engineering, Saveetha School of Engineering, SIMATS
Saveetha Nagar, Thandalam, Chennai-602105

S. Magesh Kumar²

Associate Professor, Department of Computer Science and Engineering, Saveetha School of Engineering, SIMATS
Saveetha Nagar, Thandalam, Chennai-602105

Abstract—Small objects detection in medical image becomes an interesting field of research that helps the medical practitioners to focus on in-depth evaluation of diseases. The accurate localization and classification of objects face tremendous difficulty due to lower intensity of the images and distraction of pixel points that vary the decision on identifying the shape, structure etc. In many real-time cases, detection and classification of tiny objects in the medically treated images becomes mandatory. The proposed system is designed in the same criteria in which the semantic segmentation of tiny objects in the medical images is considered. The system design focused on implementing the model for different kinds of human organs such as lung and liver. The axial CT or PET images of Lung and Liver are considered as the prime input for the given system. Detection of tiny objects in the CT-PET images, segmenting it from the background and classification of segmented part as Tumor or Nodule is discussed. The preprocessed images are feature extracted after the morphology segmentation that determines the structural features of the tiny object being segmented. The feature vectors are nothing but the feature points from Kaze feature extraction and Morphology segmented image. These two inputs are fetched to the Deep ensemble Convolution neural network (DECNN) to obtain the dual classification results. Performing the quantitative measurements to evaluate the decision making system for nodule or tumor class is determined. The performance measure is done using accuracy, precision, recall and F1Score.

Keywords—Medical image processing; convolution neural network; lung tumor detection; early prediction; image enhancement

I. INTRODUCTION

Lung cancer becomes the most commonly occurring life threatening disease that needs to be detected and diagnosed in the early stages [1]. Most common lung cancers are detected using the Chest X-rays or CT images, rarely using the MRI images in the early stage itself because of the problems it causes in the normal activities of the body [2]. Since many lung cancers have higher chances of spreading it towards the liver, it is mandatory nowadays, the screening of lung and liver with high accuracy is focused. In recent days the test named Low Dose CT scan (LDCT) [3] has been used to detect lung cancer and liver cancer. Lung cancer is more frequent with people with smoking habits and unhealthy habitual changes. In

the case of early prediction the treatment of lung cancer is likely to be successful.

1) *Lung and liver tumor*: [4] Nearly 40% of patients with lung cancer have higher chances of metastasis to the neighborhood organs such as the liver. Metastasis is a kind of process held in the body, which migrates the cancer cells from one place to another. Cancer cells break away from the primary tumor and start to travel through the lymph channels or blood and affect the other organs. Hence early detection of tumor cells is highly important. Lung cancer cells migrate to other organs such as lymph nodes, the brain, the bones and the adrenal glands.

2) *Stages of tumor*: [5] Lung tumors are classified based on different stages as non-small cell, and small cell lung cancer. The early stage of non-small cell or NSCLC is also represented as carcinoma in Situ or CIS. Small cell tumor cancers are treated through radiation therapy or surgery.

3) *Role of medical imaging*: [6] There are almost six imaging modalities followed in screening the human organs. At each stage of the cancer it is required to screen, test and diagnose the cancer with accurate information. X-Rays, Computed Tomography(CT), Ultrasound(US), Magnetic resonance imaging (MRI) and Single photon emission Computed tomography(SPECT) and photon emission tomography(PET) [7] and optical imaging etc. The goal of the medical images is to produce a higher resolution to diagnose cancer cells properly. Determining the semantic objects present in the lungs are focused. Due to motion artifacts many noise factors interrupt the medical image being recorded accurately. Removal of noise from the images is an important task. Semantic segmentation of medical images are helpful in identifying the nature of abnormality occurring in the organs such as Lungs, liver etc. These lesions need to be treated in the early stage to stop the further transmissions. Considering Lung and Liver in the presented study, a comprehensive system model is created with Deep Ensemble Convolution neural network (DECNN).

The presented paper is organized as detailed background study in Section II, followed by methodology in Section III. Discussion on problem statement in the existing systems and

selection of software tool is discussed in Section IV. System design architecture is discussed in Section V. Followed by results and discussions in Section VI.

II. LITERATURE SURVEY

Systematic detection of lung cancer using Lung CT images is discussed with the presented system [8]. The model focused on image enhancement, segmentation process using binary lung mask etc. TCIA dataset images are considered for evaluation. The improved CT images are preprocessed and segmented with thresholding concept. The obtained mask is further fused with the ground truth to identify the tumor area alone. Further by using Support vector machines (SVM) algorithm the segmented area is classified. Image noise removal and its importance are clearly discussed in the paper.

The present paper [9] discuss the malignly detection of Lung CT images. Comparative study of one or more lung dataset is utilized such as LIDC, IDRI and LUNA16 are considered. Further the proposed approach uses two different architecture for evaluation such as U-Net architecture and VGG net is considered. The Multi-path 3D architecture used to classify the nodule and malignant part of the Lung images. The system achieved the accuracy of 95.6% and also the system suggested improving the further classification by improving the parameters considered.

Multi-resolution residual connected lung tumor detection system is discussed in [12]. The percentage system uses TCI open source lung tumor data set that consists of large count of lung patients and the CT images details helpful in analyzing the multi-resolution oil futures that impacts the prediction of lung tumor. Accessing system multistate convolutional neural network architecture is used to detect the lung tumor with multi resolution spectrum.

The present system discusses in detail about the clinical study and their impacts on lung tumor detection systems [13]. Epidemic growth receptor based decision tree model is discussed to detect the lung tumor without ignoring the residual factors that create similarity results. The author presented a system and discussed in detail on cell growth and its impact on lung tumor.

Knowledge based collaborative systems are required in many lung tumor detection systems in which each patient has unique problems and health records that impact the decision making process of tumor diagnosis [14]. The present system has developed a robust collaborative approach using ResNet-50 architecture. Most of their effects occurring because the present system is evaluated using a back propagation network. The presented knowledge based extraction method achieved the accuracy of 95.7% and the model training accuracy is achieved with 91.6% with ResNet-50 architecture.

Deep convolutional neural network architecture combined with artificial neural networks that create an impact on analyzing the lung tumor detection systems [15]. Most neural network architectures are less time consuming since the training and testing data will be formulated with the given configuration. The maximum of thousand approx. is allowed with the artificial intelligence networks in which the maximum accuracy will be achieved at any point of time with the given

iteration. The present system uses a light DC data set for the analysis of lung cancer prediction. Study is helpful in understanding the basic concepts that associated with the lung tumor detection systems. [16] Object tracking is discussed in the present paper. Small objects tracking using particle filter is focused with the present system. Based on energy accumulation, target trajectory process is done. The experimental results show the better signal to noise ratio with images of complex background.

III. METHODOLOGY

The proposed methodology is focused on incorporation of image processing techniques and deep learning algorithms to evaluate the lung tumor and liver tumor detection system. [1] The systematic approach uses the tuned layers of convolution neural networks to identify a tiny object present in the screening image as a tumor or nodule. In the aspect of image processing, the segmentation works on extracting the semantic object present in the test image through image processing techniques. To determine the class of the segmented objects, the features such as shape and size are required. Tumors larger than three centimeters are represented as masses. Pulmonary lung nodules are very common and they are identified clearly in many chest X-Rays. In case of lung or liver tumor, the early prediction is feasible if the system is able to detect the tiny nodes present in the medical images. The smaller nodule can also be developed into cancerous as it may appear in the early stage, detection of tiny objects that are less than nodule also focused.

1) *Data collection:* The lung images are collected from IQ-OTH/NCCD cancer patient's dataset and the Liver images are collected from TCIA publicly available dataset. The images are converted from DCM format to JPEG format. The images are labeled with respect to their age and patient name. The dataset modalities are completely differing from each other. The model created here utilize common Deep ensemble Convolution neural network (DECNN) only, whereas the primary processing steps varies separately for both Lung and Liver separately.

IV. SYSTEM DESIGN

The problem statement behind the small objects detection in medical images is lack of accuracy in low quality images like medical images [8], obtaining the accuracy, improving the precision in identifying the broken pixels of the objects. MATLAB is helpful in working out the detailed portions of the image through the image processing toolbox. The reason behind the selection of System tools is that MATLAB has numerous benefits over technical computing. Implement and test your algorithms easily. Develop the computational codes easily., Debug easily, Use a large database of built in algorithms, Process still images and create simulation videos easily, Symbolic computation can be easily done, Call external libraries and Perform extensive data analysis and visualization. Hence for image analysis, the system tool of MATLAB is more apt. using convolution neural network toolbox the improved DECNN structure is formulated.

V. DESIGN ARCHITECTURE

A. System Architecture

Fig. 1 shows the system architecture of proposed system using DECNN with BlobNet, in which the initial model creation is clearly depicted. The creations of model using training images are further tested with performance using the randomly selectable test images. The purpose of the Model created here is to provide fast and accurate segmentation of Semantic small object in the medical image as well as classify the object as tumor or nodule based on structural features.

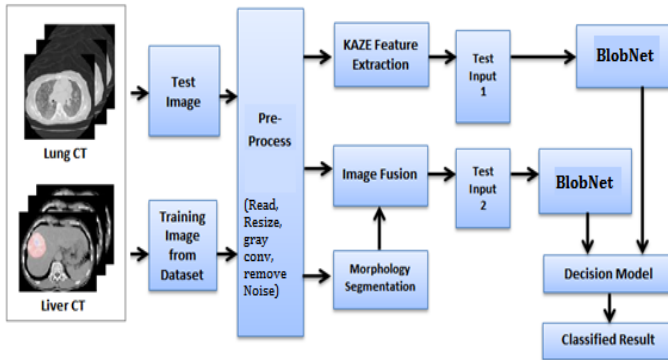


Fig. 1. System Architecture of the Proposed System DECNN with BlobNet.

B. Preprocessing

The input dataset is collected from TCIA and IQ-OTH/NCCD website, contains the [7] Lung CT images with detected Lung nodules and Lung tumor as well, also the IQ-OTH/NCCD dataset contains the Liver Tumor or Normal CT images of various patients. The input images are preprocessed before fetching it into the feature extraction stage. The input test image is read, resized into a common matrix for ease of handling. The processed image data is further applied to morphology image segmentation where the image is dilated, open and closed by the binary morphology operations.

C. KAZE Feature Extraction

The upgraded picture input is additionally prepared with KAZE highlight extraction method. Element descriptors are needed to be tuned in a manner the special pixel guides need toward be removed from the information test picture through non-straight space. For distinguishing central focuses, we figure the response of scale-normalized determinants of the Hessian at different scale levels. For multi-scale feature acknowledgment, the formula is given below.

$$L_{Hessain} = p^2 [LxLy-Lxy] \quad (1)$$

Differential heads ought to be normalized concerning scale, since by and large the assembly of spatial auxiliaries decay with scale. Where Lx , Ly go about as the flat subsidiary and vertical subordinate in the second request individually. The descriptor searches the exceptional focuses and applies to every one of the sifted pictures from the non-straight space. The finder reaction at different levels is being followed if there should be an occurrence of article following modules.

D. Image Fusion

The preprocessed image is further fused with the reference image through gradient mapping [10]. The fusion is required to highlight the tumor portion alone. The fused image with color mapped image is fetched to the DECNN model to make the pattern matching score with the trained dataset of lung and liver separately. MATLAB toolbox utilizes a composite image fusion process that blends the one image with another in case both images come under the same dimension. The formula to obtain the image composite process is given below.

$$f(x) = h[g(x)] \quad (2)$$

Where for every occurrence of x pixels the replacing the gradient color function of $g(x)$ is applied. The outcome of the image looks like the composite of two images.

E. Morphology Segmentation

The non-linear image processing technique handles the shape of the region or the features that determine the unique identification of the region that is segmented. The semantic object segmented after the binary conversion and fusion technique, further processed with few morphology steps includes, image dilation, opening the smaller area and closing the smaller holes etc. Once certain steps are applied, the sharpened image object is highlighted in the binary masked form.

F. Ensemble Model

1) *Feature based approach*: The proposed DECNN architecture is tuned to handle the given input images of different parameters. The lung images and Liver images are tested separately. The proposed Deep Net consists of 1×1000 samples of feature points to the input layer arranged with DECNN model 1. The ReLu layer and Classification layer follows. The fully connected layer extracts 384 samples. The database images are trained in the same way, extracting the features and forming $1 \times 1000 \times N$ training vectors.

Fig. 2 shows the feature based approach on small object detection in which the preprocessed images induced to feature extraction process, where the unique pixel intensity points systematically extracted by the KAZE feature detector. It acts as an extractor for Gaussian scale space with particular instance of linear diffusions of pixel intensity.

2) *Image based approach*: Another approach where the test image of dimension 100×100 is fetched to the input layer arranged with DECNN model 2. Certainly, the database images of both Lung and Liver are trained in the same way by applying morphology operation and cropped image of 100×100 is considered.

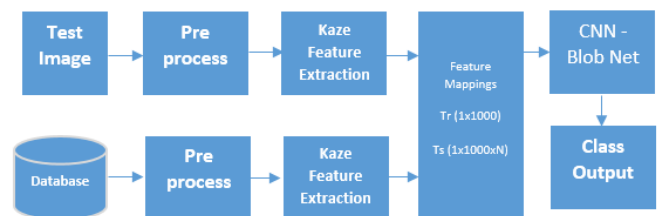


Fig. 2. Feature based Approach with DECNN – Blob Net.

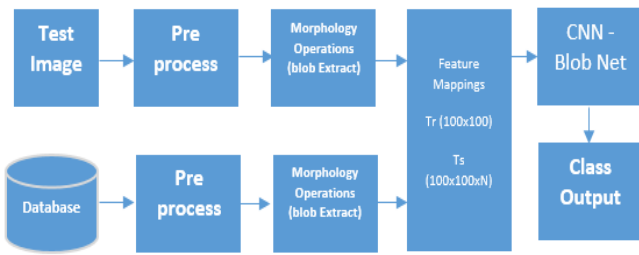


Fig. 3. Morphology based Approach with DECNN – Blob Net.

Fig. 3 shows the Morphology segmentation based image object extraction through Blob extraction process. The region oriented related boundary pixels are tuned to extract from the background image by selecting the initial similar pixels. Morphology segmentation is helpful in analysis of structural understanding of the semantic object. By tuning the structure the prediction quality will get improved.

3) *Decision model*: Based on the feature based result that runs up to 1000 epochs, to train and test the given input data, the decision is made using the quantitative measures such as accuracy and error tolerance. The system also focuses on reducing the false negative values. Hence in order to get the result with reduced false rate, the ROC curves are formed. The final decision classifies whether the given test image belongs to Class A = Tumor, Class B= Nodule or Class C= Normal. In few cases tested, Normal and nodule belong to the same class and regarding the similarity coincidences further the system is improved with tuned DECNN models.

ALGORITHM

```

Novel Deep BlobNet
Read x=Input Image
Y=preprocess(x);
[fea_1, ya]=kazeFea_1(Y);
[fea_2, ya]=MorpFea_2(Y);
Perform Fea Map;[fea_1,fea_2]
Store Fea Map -> fea.mat;
Train: DeepBlobNet (Train_images);
Pred_Y_1= DeepBlobNet (Train_Images, Test_images);
Pred_Y_2= DeepBlobNet (Train_fea, Test_fea);
Decision_model(Pred_Y_1, Pred_Y_2);
Plot Confusion (Pred_Y_1);
Plot Confusion(Pred_Y_2);
Perfrom Q_measure (Tp, Tn, Fp, Fn);
End
    
```

VI. RESULTS AND DISCUSSIONS

A. Preprocessing

Fig. 4 shows the complete pre-processing steps involved in the proposed system. The input image of the lung CT is read from the database. The image is preprocessed in which the

RGB image is converted into grayscale image. The grayscale image is converted into a binary image and colour space masking is done. After the masking process has completed morphological segmentation that enlarges the open pores and highlights the open area. The binary converter image is cropped and a binary mask with inverted images is applied.

B. Feature Extraction

Fig. 5 show the simulation result of case feature extraction of the one test image. The feature extracted area after the masking part is used to highlight the unique pixel points that vary with the intensity being verified. This feature information is mapped as a vector as training vector and testing vector before the DECNN classification is being applied.

C. Classification

Fig. 6 show the classification accuracy of proposed deep blob net which consists of pretrained images and the feature data as a vector map dinner randomly distributed scale. The training vector is framed and runs for 20 iterations. The higher the number of iterations is robust that the accuracy obtained will be noted. If maximum accuracy is obtained at the initial stage itself then the If maximum accuracy is obtained at the initial stage itself then the hydration would be stopped. Iterations would be stopped.

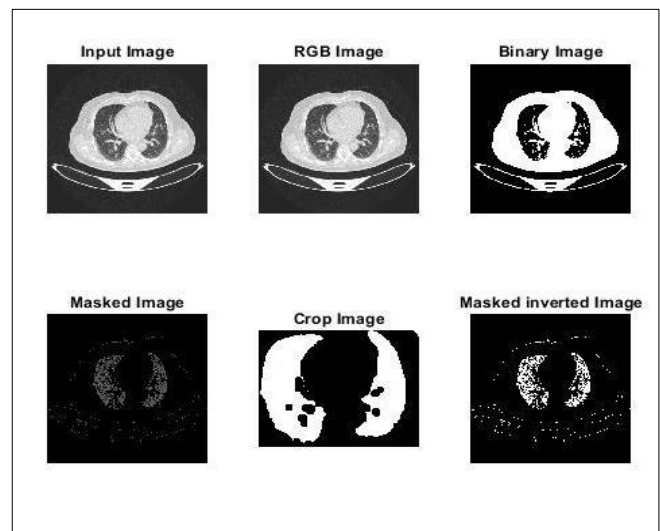


Fig. 4. Simulation Result showing Preprocessing Output, Masked and Morphology Extracted Outputs.

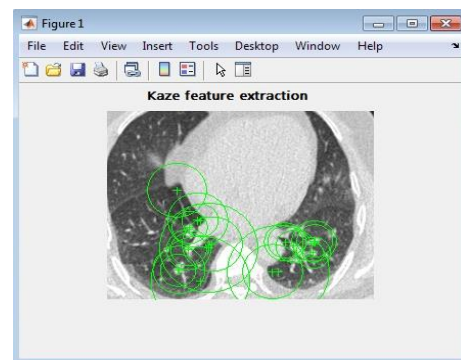


Fig. 5. Simulation Result showing Feature Extraction Output.

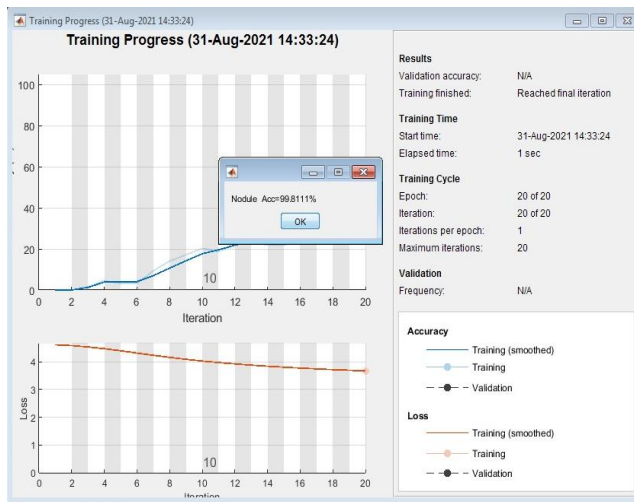


Fig. 6. Classification Notification and Internal Loss Function.

TABLE I. COMPARATIVE ANALYSIS OF ACCURACY WITH RESPECT TO EXISTING SYSTEM

Reference	Algorithm	Input Type	Accuracy
[10] M. Menikdiwela et al., (2017)	VGG16-RCNN	Spider Image dataset	84%
[11] Z. Yang et al., (2019)	YOLO V3-SlimNet	Traffic Image dataset	85%
Proposed System	Deep Blob-Net (pre-trained)	Medical images	99.8%

Table I shows the comparative study of existing lung tumor detection systems using VGG 16 architecture with recurrent convolutional neural network [10] and YoLo V3 model that detects the smaller objects in the given scene image. Comparatively the proposed architecture created using deep Blob-net utilizes the medical images for testing purposes and achieved the accuracy of 99.8% for the static data trained with the network.

D. Comparative Graphs on Accuracy

Fig. 7 shows the comparative performance of existing system and proposed system and its references. The proposed system uses the static data for developing the Novel structure. Further the system need to be improved with respect to real time data and dynamic analysis.

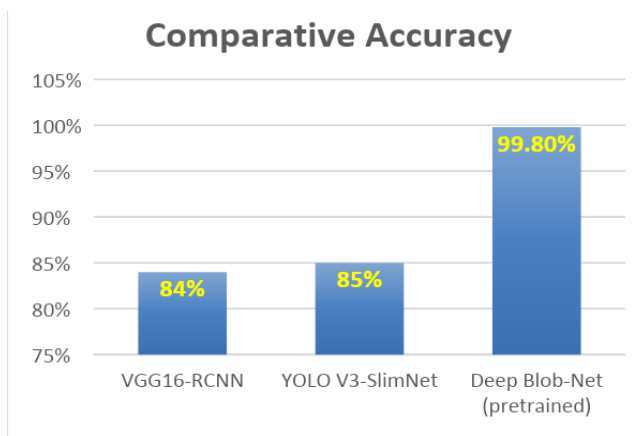


Fig. 7. Comparative Accuracy of Existing System and Proposed System.

VII. CHALLENGES

The development of blob-Net creates difficulty in tuning the layers since the parameters of the lung and liver vary. According to the static dataset the DECNN layers are tuned, whereas in case of application of dynamic dataset the accuracy and statistical performance is affected. Improving the number of images for training, obviously improve the performance of the convolution process.

VIII. CONCLUSION

Small objects' location in medical images turns into a fascinating field of research that assists the medical specialists to analyze diseases more accurately [2]. Due to intensity variations and motion artifacts, the images are in frequent sequence of motion; hence determining the tiny objects in the image is difficult. A Novel ensemble Deep learning network is developed using the convolution neural network. The system architecture is structured to ensemble two DECNN models with two variant input vectors. The first one utilizes feature based approach, and another method uses Image Morphology based approach. Based on the performance of both the results, a final decision model is developed to fetch the output class. Our proposed approach achieved 99.8% accuracy for static data and 75% accuracy approximately for dynamic data. Further the system is expanded to produce more dynamic results by training the real time input data. The performance is measured through loss function that lags during the increased epochs.

REFERENCES

- [1] W. Wei, "Small Object Detection Based on Deep Learning," 2020 IEEE International Conference on Power, Intelligent Computing and Systems (ICPICS), 2020, pp. 938-943, doi: 10.1109/ICPICS50287.2020.9202185.
- [2] P. Tresson, D. Carval, P. Tixier and W. Puech, "Hierarchical Classification of Very Small Objects: Application to the Detection of Arthropod Species," in IEEE Access, vol. 9, pp. 63925-63932, 2021, doi: 10.1109/ACCESS.2021.3075293.
- [3] X. Fu, L. Bi, A. Kumar, M. Fulham and J. Kim, "Multimodal Spatial Attention Module for Targeting Multimodal PET-CT Lung Tumor Segmentation," in IEEE Journal of Biomedical and Health Informatics, vol. 25, no. 9, pp. 3507- 3516, Sept. 2021, doi: 10.1109/JBHI.2021.3059453.
- [4] H. Ladjal, M. Beuve, P. Giraud and B. Shariat, "Towards Non-Invasive Lung Tumor Tracking Based on Patient Specific Model of Respiratory System," in IEEE Transactions on Biomedical Engineering, vol. 68, no. 9, pp. 2730-2740, Sept. 2021, doi: 10.1109/TBME.2021.3053321.
- [5] H. Hu, Q. Li, Y. Zhao and Y. Zhang, "Parallel Deep Learning Algorithms With Hybrid Attention Mechanism for Image Segmentation of Lung Tumors," in IEEE Transactions on Industrial Informatics, vol. 17, no. 4, pp. 2880-2889, April 2021, doi: 10.1109/TII.2020.3022912.
- [6] J. Deng, W. Zeng, W. Kong, Y. Shi, X. Mou and J. Guo, "Multi-Constrained Joint Non-Negative Matrix Factorization With Application to Imaging Genomic Study of Lung Metastasis in Soft Tissue Sarcomas," in IEEE Transactions on Biomedical Engineering, vol. 67, no. 7, pp. 2110- 2118, July 2020, doi: 10.1109/TBME.2019.2954989.
- [7] C. Lian, S. Ruan, T. Dencoux, H. Li and P. Vera, "Spatial Evidential Clustering With Adaptive Distance Metric for Tumor Segmentation in FDG-PET Images," in IEEE Transactions on Biomedical Engineering, vol. 65, no. 1, pp. 21-30, Jan. 2018, doi: 10.1109/TBME.2017.2688453.
- [8] N. S. Nadkarni and S. Borkar, "Detection of Lung Cancer in CT Images using Image Processing," 2019 3rd International Conference on Trends in Electronics and Informatics (ICOEI), 2019, pp. 863-866, doi: 10.1109/ICOEI.2019.8862577.

- [9] R. Tekade and K. Rajeswari, "Lung Cancer Detection and Classification Using Deep Learning," 2018 Fourth International Conference on Computing Communication Control and Automation (ICCUBEA), 2018, pp. 1-5, doi: 10.1109/ICCUBEA.2018.8697352.
- [10] M. Menikdiwela, C. Nguyen, H. Li and M. Shaw, "CNN-based small object detection and visualization with feature activation mapping," 2017 International Conference on Image and Vision Computing New Zealand (IVCNZ), 2017, pp. 1-5, doi: 10.1109/IVCNZ.2017.8402455.
- [11] Z. Yang, Y. Liu, L. Liu, X. Tang, J. Xie and X. Gao, "Detecting Small Objects in Urban Settings Using SlimNet Model," in IEEE Transactions on Geoscience and Remote Sensing, vol. 57, no. 11, pp. 8445-8457, Nov. 2019, doi: 10.1109/TGRS.2019.2921111.
- [12] J. Jiang et al., "Multiple Resolution Residually Connected Feature Streams for Automatic Lung Tumor Segmentation From CT Images," in IEEE Transactions on Medical Imaging, vol. 38, no. 1, pp. 134-144, Jan. 2019, doi: 10.1109/TMI.2018.2857800.
- [13] N. Kureshi, S. S. R. Abidi and C. Blouin, "A Predictive Model for Personalized Therapeutic Interventions in Non- small Cell Lung Cancer," in IEEE Journal of Biomedical and Health Informatics, vol. 20, no. 1, pp. 424-431, Jan. 2016, doi: 10.1109/JBHI.2014.2377517.
- [14] Y. Xie et al., "Knowledge-based Collaborative Deep Learning for Benign-Malignant Lung Nodule Classification on Chest CT," in IEEE Transactions on Medical Imaging, vol. 38, no. 4, pp. 991-1004, April 2019, doi: 10.1109/TMI.2018.2876510.
- [15] A. Amutha and R. S. D. Wahida Banu, "Lung tumor detection and diagnosis in CT scan images," 2013 International Conference on Communication and Signal Processing, 2013, pp. 1108-1112, doi: 10.1109/iccsp.2013.6577228.
- [16] Z. Wei and Y. Liu, "Research on Small Object Detection and Tracking Based on Particle Filter," 2009 Second International Conference on Intelligent Computation Technology and Automation, 2009, pp. 403-406, doi: 10.1109/ICICTA.2009.333.
- [17] W. Wei, "Small Object Detection Based on Deep Learning," 2020 IEEE International Conference on Power, Intelligent Computing and Systems (ICPICS), 2020, pp. 938-943, doi: 10.1109/ICPICS50287.2020.9202185.
- [18] H. Krishna and C. V. Jawahar, "Improving Small Object Detection," 2017 4th IAPR Asian Conference on Pattern Recognition (ACPR), 2017, pp. 340-345, doi: 10.1109/ACPR.2017.149.
- [19] Z. Wei and Y. Liu, "Research on Small Object Detection and Tracking Based on Particle Filter," 2009 Second International Conference on Intelligent Computation Technology and Automation, 2009, pp. 403-406, doi: 10.1109/ICICTA.2009.333.
- [20] J. Guo, W. Zeng, S. Yu and J. Xiao, "RAU-Net: U-Net Model Based on Residual and Attention for Kidney and Kidney Tumor Segmentation," 2021 IEEE International Conference on Consumer Electronics and Computer Engineering (ICCECE), 2021, pp. 353-356, doi: 10.1109/ICCECE51280.2021.9342530..

Software Reliability Prediction by using Deep Learning Technique

Shivani Yadav, Balkishan

Department of Computer Science & Applications
Maharshi Dayanand University, Rohtak-124001, Haryana, India

Abstract—The importance of software systems and their impact on all sectors of society is undeniable. Furthermore, it is increasing every day as more services get digitized. This necessitates the need for evolution of development and quality processes to deliver reliable software. For reliable software, one of the important criteria is that it should be fault-free. Reliability models are designed to evaluate software reliability and predict faults. Software reliability prediction is always an area of interest in the field of software engineering. Prediction of software reliability can be done using numerous available models but with the inception of computational intelligence techniques, researchers are exploring new techniques such as machine learning, genetic algorithm, deep learning, etc. to develop better prediction models. In the current study, a software reliability prediction model is developed using a deep learning technique over twelve real datasets from different repositories. The results of the proposed model are analyzed and found quite encouraging. The results are also compared with previous studies based on various performance metrics.

Keywords—Software reliability; deep learning; performance metrics; prediction; dense neural network; fault prediction

I. INTRODUCTION

Reliability is an essential and one of the most critical aspects of a software product and it is also one of the major attributes to determine software quality. Software reliability can be described as its ability to perform its intended functions accurately and successfully. Regular checks during software development ensure the prevention of faults which can further lead to failure and might incur huge efforts to correct or recover if detected later. Therefore, reliability prediction is an important aspect of any software development approach. For reliable software, it is important that it should be fault-free. Computational intelligence techniques like machine learning, genetic algorithm, deep learning, etc. are gaining the attention of researchers for reliability prediction. The current study uses a deep learning-based technique for software reliability prediction due to its potential to predict high accuracy on the huge amount of unstructured or unlabeled data [1]. Early fault prediction using deep learning models helps to improve the reliability of the software.

Deep learning is a subset of machine learning algorithms that are built on Artificial Neural Network (ANN). Neural networks are computational systems that respond to external inputs with dynamic state changes and try to determine underlying relationships within a dataset. ANN with two or three layers is a basic neural network and the neural network with more than three layers is considered as a deep learning

concept [38]. The label deep was inspired by the number of processing layers that data must pass through. Deep learning advances have resulted in the development of neural networks with more complexity to generate more powerful learning abilities. The deep learning model takes an input and performs a step-by-step nonlinear transformation and then uses the learnings to generate a statistical model as output. The model continues these iterations until the output is accurate enough. Due to the data-hungry nature of deep learning algorithms and increased dataset size, complex problems can be easily solved more accurately and efficiently.

Deep learning integration into Software Engineering (SE) tasks has become increasingly popular among software developers and researchers these days. Deep learning assists SE experts in extracting requirements from natural language text, generating source code, and predicting software faults for typical SE tasks. Deep learning in SE has increased the interest of both the SE and Artificial Intelligence (AI) experts.

This paper aims to develop a novel neural network-based deep learning reliability prediction model. The choice of the deep learning model has been determined because of its ability to automatically capture and learn the discriminative features from data, which results in an improved reliability prediction model. This research will open the road for other deep learning approaches to be used in fault prediction. So, that software engineers will be able to better predict the likelihood of faults which results in greater resource use, risk management and better quality control.

The remaining paper is organized into five sections. Section 2 conducts a literature review of related studies to explore the various models already used for predicting the software reliability and its accuracy so, that the scope of further improvement can be identified. Section 3 discusses the proposed model design for improving the accuracy of software reliability prediction. Step by step process is also discussed in this section. Section 4 implements the model and presents the results. Results are presented in tabular as well as graphical form and also discussed in detail. Section 5 compares the result of the current study with previous studies. In the final section of the paper, the work has been summarized with possible directions for future research.

II. LITERATURE REVIEW

The use of Computational Intelligence (CI) in the field of software engineering is expanding nowadays. It can be witnessed by the huge research work undergoing and still being

carried out by various researchers. Some important research work related to software reliability prediction is filtered and studied to conduct the current work.

The term CI can be traced back to 1983 when Nick Cercone and Gordon McCalla started the International Journal of Computational Intelligence (IJCI). Cercone and McCalla sought to differentiate their work from existing studies in the broad Artificial Intelligence domain [2]. Bezdek[2] was the first to propose a technical definition of CI and its relation to neural networks like computational networks. Marks [3] summarized that fuzzy systems, genetic algorithms, neural networks, and evolutionary programming is building blocks of CI. In the same year, Karunanithi et al. [4] explored the application of connectionist models based on a neural network for software reliability growth prediction and claim better results as compared to traditional parametric models. In the same field, Ho et al. [5] extended the research, the work compared traditional and connectionist models while extensively studying software reliability prediction using connectionist models. Therefore, neural networks give good results in predicting errors but do not provide appropriate results under different circumstances. In 2005, Tian and Noore[6] mentioned that neural networks are difficult to interpret physically the neurons in layer and proposed an alternative approach based on genetic algorithm predict software reliability and Costa et al. [7] proposed a hybrid approach which used both genetic algorithms and evolutionary neural networks for improving the reliability prediction. In this approach, a genetic algorithm is used to analyze the number of neurons in each layer of ANN. The use of hybridization became prominent since 2005 in the field of predicting software reliability. Another study by Pai and Hong [8] experimented combination of Simulated Annealing (SA) and Support Vector Machines (SVMs) for predicting software reliability. In this study, SA is used to choose the SVM parameters. However, the authors suggest exploring other searching techniques for improving the results. Hu et al. [9] used recurrent neural networks (RNNs) and genetic algorithms for designing generic software reliability models and showed better results with the larger datasets. In 2011, Lo [10] introduced techniques Support Vector Machine (SVM) and Autoregressive Integrated Moving Average (ARIMA), both the proposed models predict better results as compared to the results of the traditional model. Li et al. [11] used the Adaboost technique based on machine learning which combines weak predictors into a single predictor to improve prediction accuracy and the results are verified using two case studies. Similarly, Roy et al.[12]a proposed neuro-genetic algorithm in which ANN is trained using backpropagation and further the weights of the network are optimized using Genetic Algorithm (GA). Further the results are compared with traditional methods and good results are obtained by the model. Then, researchers focused more on machine learning and deep learning methods. Jin et al. [13] proposed a combination of Quantum Particle Swarm Optimization (QPSO) and hybrid Artificial Neural Network (ANN) for predicting fault-proneness of software modules. QPSO was used for dimensionality reduction whereas ANN classified modules into non-faulty and faulty categories. The approach is simple to implement, and results showed the correlation between a

module's software metrics and fault-proneness, which makes it possible to minimize cost and effort for software maintenance. Malhotra [14] reviewed various machine learning techniques for software fault prediction, performance is assessed and compared with statistical techniques. The study proved that machine learning technique models predict software fault better than traditional models, but these techniques are still limited. Wahono[15] proposed three influential frameworks i.e., Lessmann et al., Menzies et al., and Song et al. by combining Machine Learning (ML) classifiers for predicting software defects and improving the accuracy but these frameworks are not able to handle noisy data. Jaiswal and Malhotra [16] studied the application of various ML techniques including Instance-Based Learning (IBL), Cascading Forward Backpropagation Neural Network (CFBPNN), Multilayer Perceptron (MLP), General Regression Neural Network (GRNN), Feed Forward Backpropagation Neural Network (FFBPNN), Bagging, and Adaptive Neuro-Fuzzy Inference System (ANFIS) on industrial software. The results showed that ANFIS provides better reliability prediction compared to other methods. Several recent studies indicate the strength of the deep learning approach in software reliability prediction such as Clemente et al.[17] developed a predictive model using a deep learning technique that predicts security bugs with more accuracy (73.50%) as compared to machine learning techniques.[18][19][20][21][22] identified all the challenges, metrics required for finding faults and testing using different computational techniques.[23][24][25][26][27] fire reviewed, and assessed quality parameters for component-based software using different computational intelligence techniques. Qasem et. al. [28] predicted software faults using two deep learning algorithms i.e., the Multi-layer Perceptrons (MLP) and Convolutional Neural Network (CNN) using four NASA datasets and concluded CNN is a better model but implemented on limited datasets.

The literature review shows that there are a lot of techniques being used by various researchers in predicting software reliability, but more work needs to be done for predicting reliability for complex or large datasets. However, the neural network-based deep learning approach is gaining the attention of researchers due to its capability of providing better results. However, still, there is a scope on improving the accuracy of the reliability prediction by detecting faults in the software. To further improve prediction accuracy, a deep learning model is designed which is presented in subsequent sections.

III. DESIGN OF MODEL

Deep learning algorithms are based on ANN where hidden layers try to uncover relationships between data. An artificial neural network works by processing inputs through several dynamic state responses. The interconnected processing elements between different layers are called neurons and are responsible for facilitating the computational system. Artificial neural networks have evolved to provide increasingly complex structures with powerful learning abilities.

The framework used for building this model is shown in Fig. 1.

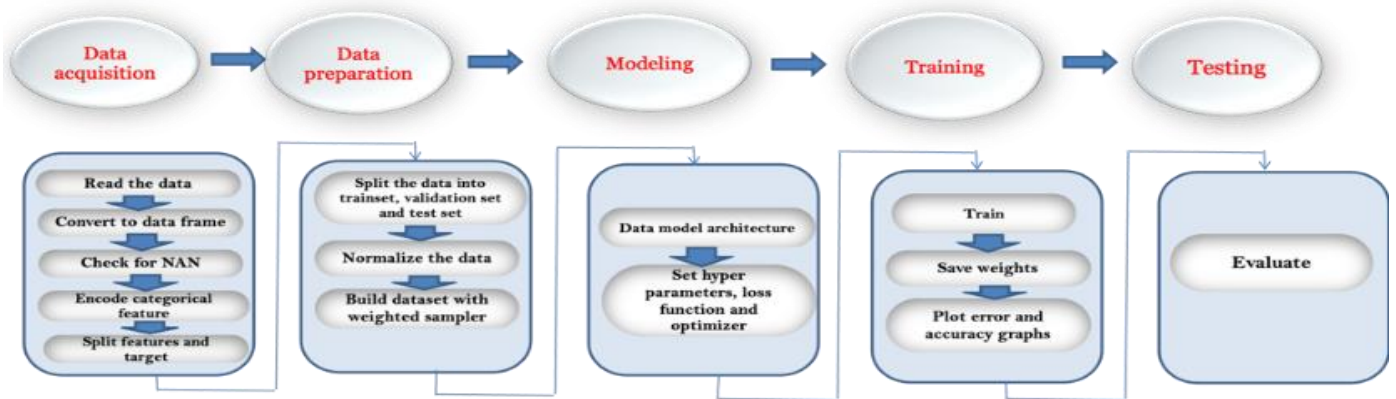


Fig. 1. Model Design Framework.

A. Data Acquisition

Data acquisition obtains meaningful data and transforms it into a digital form that can be processed by the model. The data used in the current study is obtained through various online sources and loaded into panda's data frames for further processing. A total of twelve datasets are used which consists of various features. Table VI presents the detail of all the datasets along with their sources. NAN (invalid or not a number) values check, and categorical features encoding are performed on the datasets. If the dataset contained NAN, it is ignored as they may create noise in further processing and lower the accuracy of the prediction. The attributes of the datasets are also divided into features and target attributes.

B. Data Preparation / Preprocessing

Collected data contains some impurities, therefore, not suitable for modeling in its raw form. It needs to be cleaned and pre-processed. For preprocessing the data transformation and normalization are carried out. This is accomplished by the application of natural logarithmic transformation and min-max normalization. Natural logarithmic transformation is used to reduce the skewness of the dataset distribution [38] and the min-max normalization technique provides high accuracy, learning speed and transforms the large value ranges into small range values. After normalization, a dataset is built using a weighted random sampler technique. The dataset is divided into sub-datasets for training, validation, and testing. This distribution is done randomly with 70% training data, 10% validation data, and 20% testing data. The purpose of training is to make the dataset applicable to train or fit for the model. Validation is used for unbiased evaluation at the time of hyperparameter tuning and the test set does unbiased evaluation of the final model.

The dataset contains many outliers which can affect the sample mean/variance and skew the results. To eliminate the noise due to outliers, considering the median and the interquartile range can yield better results. Therefore, Robust Scaling is applied to relevant features in the data set.

C. Modelling

The model is implemented using a dense neural network which consists of three types of layers: input, hidden, and output and shown in Fig. 2. In this type of network, all the

neurons at one layer are connected with all the neurons of the previous layer. Various configurations of the model are designed for each dataset and later the configuration with the best results is finalized. Activation functions along with the layers are decided to design a network. Also, the initial values of hyperparameters are decided.

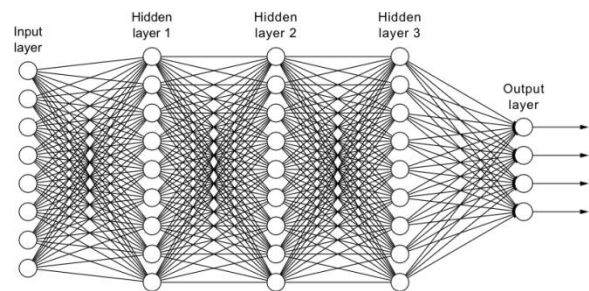


Fig. 2. Dense Neural Network Architecture.

For different configurations on each dataset different activation functions are used within the hidden layers in this study like ReLU (Rectified Linear Unit), GELU (Gaussian Error Linear Unit), Tanh (Hyperbolic Tangent), Softmax, and Sigmoid [29][30] and Table I represents all the activation functions with range.

- ReLU is a non-linear, differentiable, and computationally fast converge training phase of the network.
- A sigmoid activation function is non-linear, differentiable, and output ranges from 0 to 1 so that the output layer produces the result in probability for binary classification.
- Tanh is non-linear, differentiable, monotonic, and used for classification. The negative inputs are mapped strongly negative, and the zero inputs are mapped near zero.
- GELU is formed by combining properties of dropout, zoneout, and ReLU. It is a neuron activation function based on the Gaussian function.
- The softmax activation function normalizes the probability distribution of predicted target classes.

TABLE I. DIFFERENT ACTIVATION FUNCTION

Activation Function	Function f(x)	Range
ReLU	$\begin{cases} 0 & \text{if } x \leq 0 \\ x & \text{if } x > 0 \end{cases}$	[0,∞)
Sigmoid, $\sigma(y)$	$\frac{1}{(1 + e^{-y})}$	(0,1)
Tanh, $\tanh(y)$	$\frac{e^y - e^{-y}}{e^y + e^{-y}}$	(-1,1)
GELU	$x \cdot \frac{1}{2} \left[1 + \text{erf} \left(\frac{x}{\sqrt{2}} \right) \right]$ where erf(z) is the error function	(-0.17,∞)
Softmax	$\frac{e^{z_i}}{\sum_{i=1,2,3,\dots,j} e^{z_i}}$	(0,1)

D. Training

In the training section, cross-entropy is used as a loss function. Cross-entropy calculates the difference between two probability distributions. SGD (Stochastic Gradient Descent) and Adam (Adaptive Moment Estimation) are used for optimization. They are used to update the weights after each iteration. The updated weights are saved so that further, loss and accuracy can be calculated. SGD is used as the optimization technique because of its ability to learn faster by randomly selecting a subset of data, generally called batch, and performing gradient descent iteratively on that subset. Adam optimization is an enhancement over SGD. It brings the best of AdaGrad and RMSProp, which are extensions of SGD to provide an adaptive learning rate with little memory requirements and computational efficiency.

Cross entropy (L_{CE}) is a loss function that is used during training to adjust model weights and find optimal weights. The aim is to minimize the loss, where a perfect model has zero loss. While zero loss is often difficult to achieve practically, models are optimized to minimize the loss to the extent possible.

$$L_{CE} = - \sum_{j=1}^n t_j \log p_j \tag{1}$$

for n classes, where t_j is the truth label and p_j is the Softmax probability for the j^{th} class [31].

Further, the cost-sensitive learning method is used to tackle the class imbalance problem by assigning different weights to both classes (faulty and non-faulty). The difference in weights influences the classification of the classes during the training phase. The whole purpose is to penalize the misclassification.

E. Testing

In this phase, the evaluation of the model is done statistically using four standard performance metrics accuracy, precision, recall, and F1-score. The percentage of correct predictions for test data is referred to as accuracy. The confusion matrix along with all these four-performance metrics calculates support value. The support is the actual number of occurrences of a response class in a dataset. Further, the accuracy of the model is evaluated using formulas:

$$\text{Accuracy} = (TP + TN) / (TP + FP + FN + TN) \tag{2}$$

where, TP= True positive, TN= True negative, FP= False positive, FN= False negative.

Precision is the number of positive class predictions that are actually positive class predictions. It is calculated as number of correctly predicted positive observations divided by total predicted positive observations [32].

$$\text{Precision} = TP / (TP + FP) \tag{3}$$

A recall is defined as the number of correct positive predictions divided by all correct positive samples [32].

$$\text{Recall} = TP / (TP + FN) \tag{4}$$

F1-score measures the accuracy of a model on a dataset and is calculated as the harmonic mean of the model’s precision and recall [32],

$$F1 = 2 * (\text{precision} * \text{recall}) / (\text{precision} + \text{recall}) \tag{5}$$

IV. IMPLEMENTATION AND RESULTS

The deep learning model is implemented on various datasets as shown in 0and determines its software reliability prediction ability. The objective of the model is to classify modules as faulty or non-faulty, based on different features of the dataset and all the datasets are shown in Table II.

TABLE II. DATASET

Dataset	Data with defects	Data with no defects	Target Feature
MJ	14299	79849	Bugs
PC5	5176	16670	Defective
JM1	2106	8779	Defects
MC1	68	9398	C
PC2	23	5566	C
KC1	326	1783	Problem
PC4	178	1280	C
PC1	77	1032	Defects
PC3	77	1032	Defects
KC2	107	415	Problems
Datatrieve	11	119	Faulty
COCOMO NASA	26	34	Rely

The MadeyskiJureczko (MJ) dataset presents metrics that are used to build software defect prediction models for component-based software. Different metrics included are 6Chidamber and Kemerer (CK) metrics, 1 Henderson-Sellers (HS) metric, 5 Bansiy and Davis (BD) metrics, 3 Tang and 2 Martin metrics. Other metrics are based on McCabe’s complexity. The target attribute is named ‘bugs’.

Datasets MC1, PC1, PC2, PC3, PC4, and PC5 are used for software defect prediction with 40, 21, 36, 22, 37, 39attributes respectively. Each dataset has 1 target attribute for predicting faults. The target attribute for MC1, PC1, PC2, PC3, PC4, PC5 is named as ‘C’, ‘defects’, ‘C’, ‘defects’, ‘C’ and ‘defective’ respectively.

JM1, KC1, and KC2 datasets are used to encourage repeatable, verifiable, refutable, and improve predictive models of software engineering. All datasets have 22 attributes

consisting of 5 different lines of code measure, 3 McCabe metrics, 4 base Halstead measures, 8 derived Halstead measures, a branch count, and 1 target field. The JM1 target field is named as 'defects', KC1 target attribute is named as 'problem' and KC2 target attribute is classified as 'problems' which tells whether the module contains/does not contain reported defects in terms of 1 and 0.

Datatrieve dataset consists of a total of nine attributes including eight condition attributes and one target attribute. The target attribute is named 'faulty6_1' which has values of either 1 or 0. 0 indicates no faults are found and 1 indicates that faults are present. The purpose of the dataset is to study the correlation of code quality with the characteristics of the modules and the transition process between two versions of the software. The characteristics of the modules are recorded using attributes "LOC6_0", "LOC6_1", "AddedLOC", "DeletedLOC", "DifferentBlocks", "ModificationRate", "ModuleKnowledge", "ReusedLOC", "Faulty6_1".

The COCOMO NASA dataset attributes are used to find the required software reliability. The target feature is named 'Attribute Rely'. Values of various attributes are represented in the form of nominal, very high, high, low which are further converted into 0 and 1 during preprocessing. The seventeen attributes and its characteristics used are RELY (Required software reliability), DATA (Database size), CPLX (Process complexity), TIME (Time constraint), STOR (Main memory), VIRT, TURN (Turnaround time), ACAP (analysts), AEXP(Application), PCAP(Programmers), VEXP (Virtual machine), LEXP(Language), MODP (Modern Programming), TOOL (use of software), SCED (Schedule information), LOC (Line of code), ACT_EFFORT (Actual effort).

On all the twelve datasets, the same modeling approach is used with different configurations. In modeling, different layouts of neurons, and the values of hyperparameters (epoch, batch size, learning rate) have experimented and all the values are hyper tuned to achieve better results, the optimal combination of hyperparameters minimizes the loss function. Different dataset results in different values of parameters and different configurations for optimal results are shown in 0.

The loss and accuracy graph over the number of epochs for every dataset is shown in TABLE V Fig. 4 to 27. A good prediction model should have low loss and high accuracy. As observed from the loss and accuracy graphs from all the datasets, the accuracy of the model over the iterations is higher than the loss respectively.

An accuracy metric is used to measure how accurate the developed model's prediction is as compared to actual data. The loss values are calculated on training data and verified using validation data. Loss values are observed after each iteration of optimization to find the optimal model parameters. The model's loss and accuracy data for each epoch are saved in the history which is used by the model's developer to make more informed decisions about the architectural choices that must be made. Optimal Configuration for the datasets is represented in Table III.

TABLE III. OPTIMAL CONFIGURATION

Dataset	Layers in Model	Learning Rate	Activation Function
MJ	[24,1024,112,1]	0.04	ReLu
PC5	[39,1024,812,512,2]	0.0094	Tanh
JM1	[21,1024,512,256,1]	0.0004	Softmax, GELU, ReLu
MC1	[40,1024,2]	0.009	Softmax
PC2	[35,1024,256,2]	0.001	ReLu
KC1	[21,1024,512,256,128,64,2]	0.0099	Tanh
PC4	[37,1024,812,512,2]	0.0094	Tanh
PC1	[21,1024,2048,2]	0.0099	Tanh
PC3	[37,1024,512,2]	0.01	GELU
KC2	[21,1024,256,1]	0.005	Sigmoid, Tanh
Datatrieve	[9,256,512,64,1]	0.00001	Tanh, ReLu
COCOMO NASA	[17,512,128,1]	0.2	Tanh

The design model is tested using various performance metrics i.e., accuracy, precision, recall, and F1-score. These are the most commonly used reliable metrics for assessing the performance of a prediction model. The performance evaluation is done using a confusion matrix. The confusion matrix provides a summary of the individual class predictions for class-specific evaluations and provides information in terms of TP, TN, FP, and FN.

The results of the prediction model are shown in Table IV TABLE IV and Fig. 3.

TABLE IV. PERFORMANCE METRICS

Dataset	Accuracy	Precision	Recall	F1-score	Support
MJ	89%	0.90	0.96	0.93	55894
PC5	91%	0.99	0.90	0.95	11669
JM1	89%	0.92	0.95	0.93	5266
MC1	95%	0.99	0.95	0.97	7518
PC2	86%	0.99	0.86	0.93	3896
KC1	84%	0.90	0.91	0.91	1248
PC4	89%	0.99	0.87	0.93	895
PC1	85%	0.99	0.84	0.91	722
PC3	83%	0.99	0.81	0.89	1052
KC2	86%	0.89	0.94	0.92	311
Datatrieve	86%	0.97	0.87	0.92	83
COCOMO NASA	96%	0.99	0.91	0.95	23

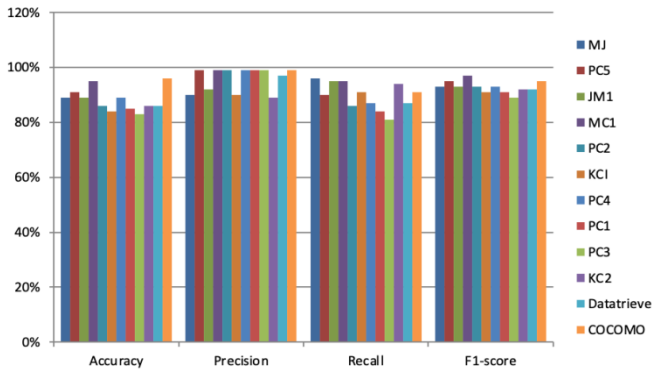


Fig. 3. Performance Metrics Graph.

From the results following are the observations that are made:

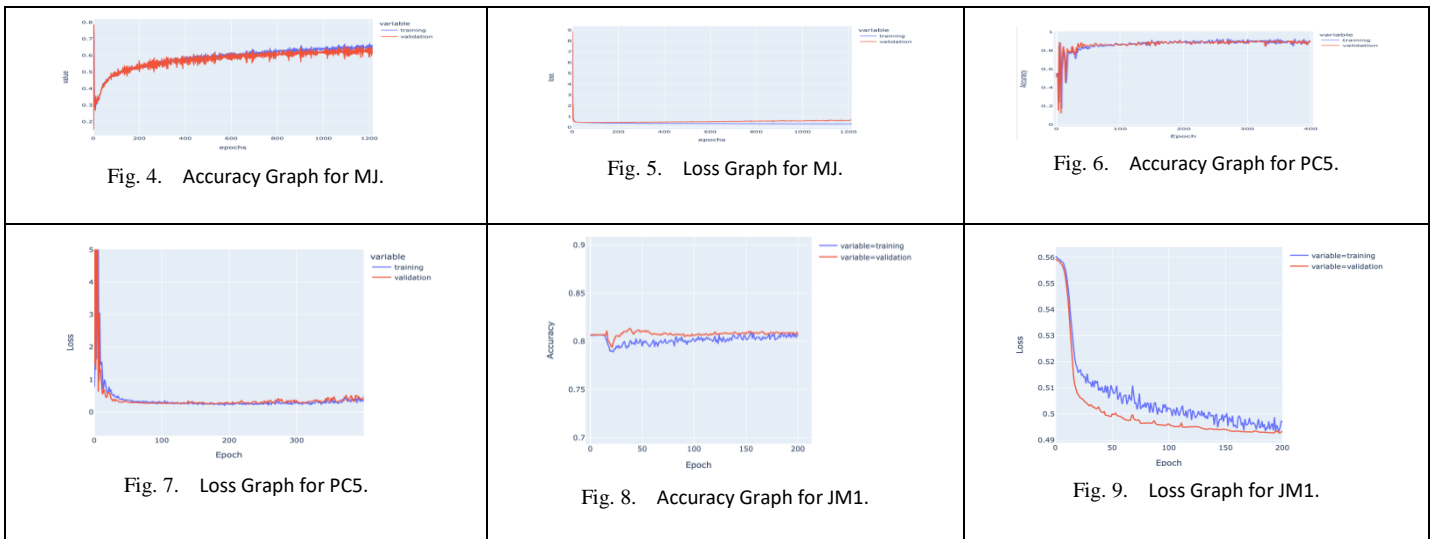
- Among all the datasets, the model showed the highest accuracy for the COCOMO NASA dataset i.e., 96% accuracy with precision 99%, recall 91% and f1-score 95% but it has the least instances among all the datasets. Datatrieve dataset also contains fewer instances and the model’s accuracy on Datatrieve is 86% with good precision 97%, recall 87%, and f1-score 92%.
- MJ dataset has the highest number of instances among all the datasets and prediction accuracy on this dataset is 89% which is validating the model as a good model. The model showed a precision of 90%, recall of 96%, and f1-score of 93%. This shows that this model is working well on a large dataset.
- The prediction accuracy on MC1 and JM1 datasets is 95%, 89% respectively, though its instances are less than MJ. Results of precision 99%; 92%, recall 95%; 95% and f1-score 97%; 93% respectively are also very promising.

- The prediction accuracy on PC1, PC2, PC3, PC4, and PC5 datasets is more than 80%. The results are average as compared to previous work on these datasets. It concludes that this model is giving optimum results on these datasets.

V. COMPARISON WITH EXISTING MODELS

Our proposed deep learning-based reliability prediction model shows better results in terms of accuracy, precision, recall, and f1-measure as compared to other techniques like decision tree, linear regression, backpropagation neural network, SVM, random tree, random forest, naïve bayes, hybrid machine learning techniques, etc. For the dataset KC1 accuracy is second highest after VOTE [34] proposed by the author Wang et.al achieved the highest precision but better as compared to other models like Under Sampling Strategy (USS), Random Forest (RF), and Naïve Bayes (NB), whereas KC2 dataset achieved the highest accuracy, precision, recall and f1-measure when compared with other machine learning techniques. Datatrieve dataset achieved the highest accuracy and precision when compared with the previous model (USS) result given by author Rao et al. [35]. COCOMO NASA dataset is evaluated with the highest score among all the datasets, but the result cannot be reliable because the dataset is small. Except for accuracy, where it is second after Random Forest by Wang et.al[34], the MJ dataset, which is the largest component-based dataset, outperforms all other approaches like Linear Regression (LR), Decision Trees (DT), Naïve Bayes (NB), SVM, Stochastic Gradient Boosting, KNN in all performance metrics[33]. While JM1 dataset results top in all the metrics as compared to models USS [35], VOTE, RT, NB [33]. Dataset MC1, PC1, PC2, PC3, PC4, and PC5 achieve the highest results in precision, recall, and f1-score. Performance metrics of various models for different datasets are listed in Table VII.

TABLE V. LOSS AND ACCURACY GRAPH FOR VARIOUS DATASETS



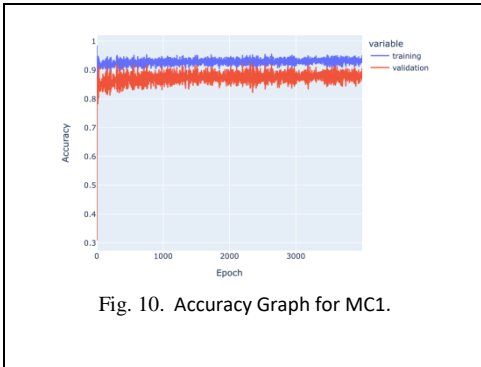


Fig. 10. Accuracy Graph for MC1.

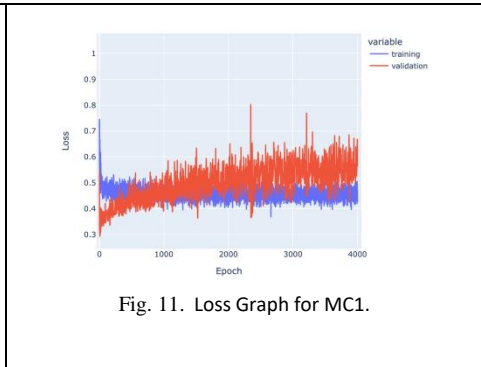


Fig. 11. Loss Graph for MC1.

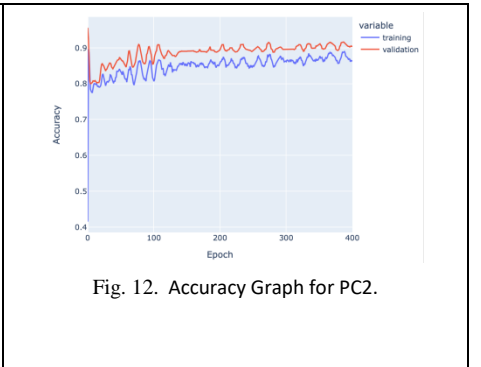


Fig. 12. Accuracy Graph for PC2.

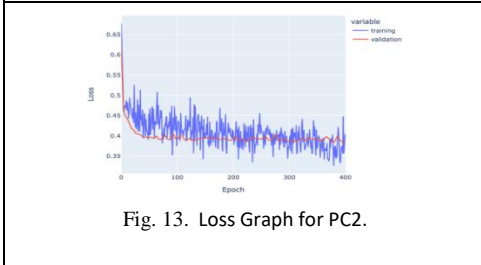


Fig. 13. Loss Graph for PC2.

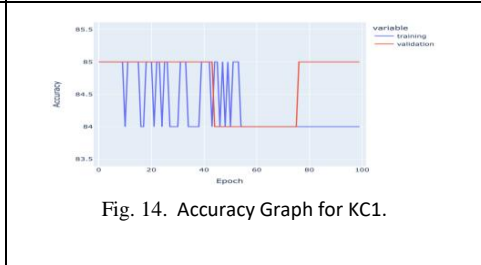


Fig. 14. Accuracy Graph for KC1.

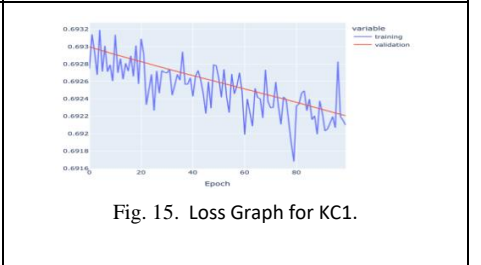


Fig. 15. Loss Graph for KC1.

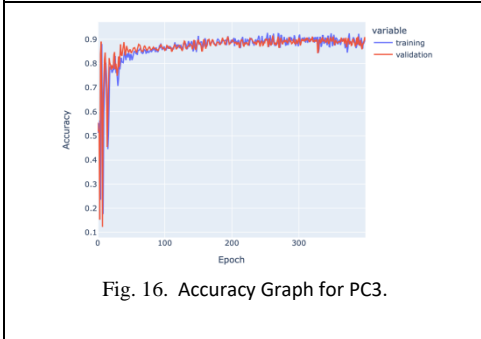


Fig. 16. Accuracy Graph for PC3.

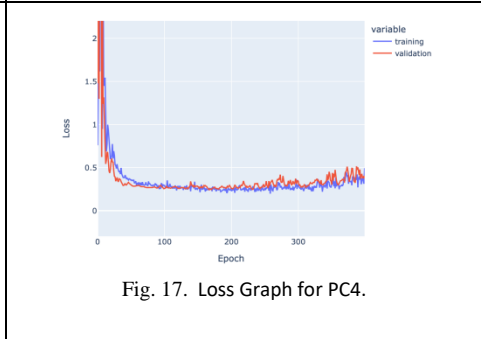


Fig. 17. Loss Graph for PC4.

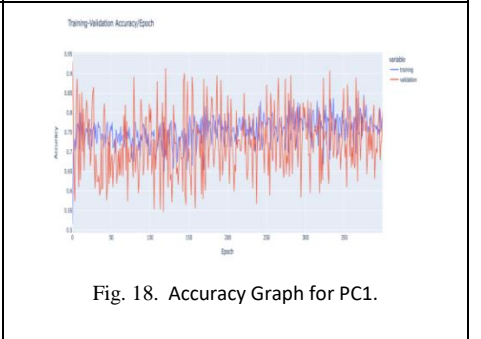


Fig. 18. Accuracy Graph for PC1.

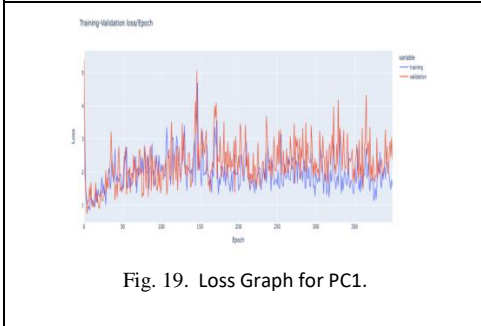


Fig. 19. Loss Graph for PC1.

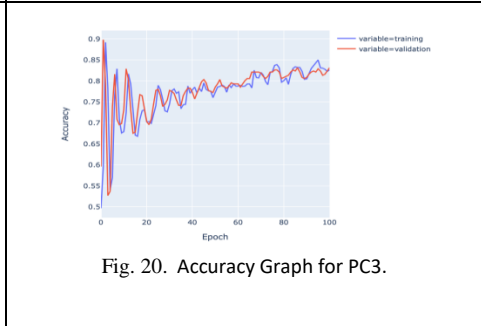


Fig. 20. Accuracy Graph for PC3.

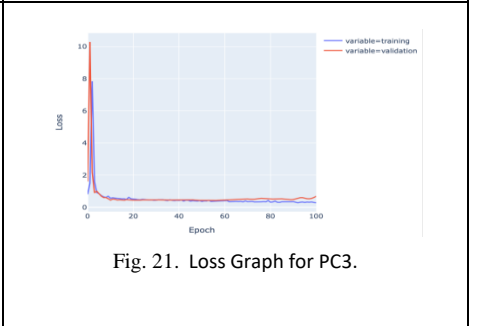


Fig. 21. Loss Graph for PC3.

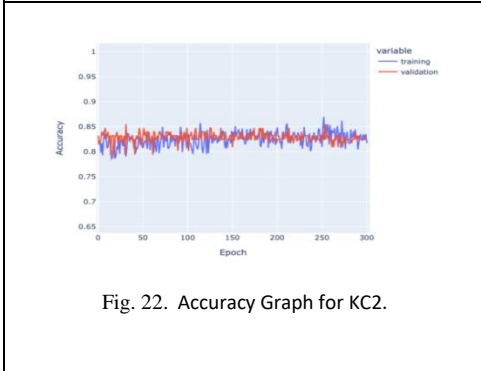


Fig. 22. Accuracy Graph for KC2.

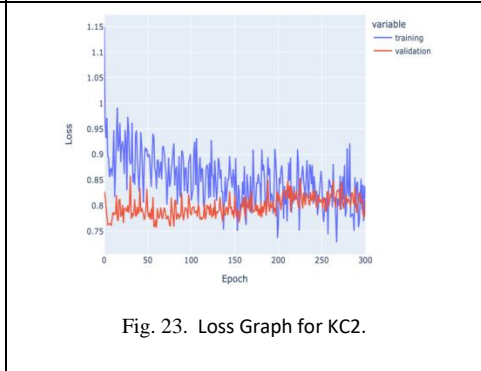


Fig. 23. Loss Graph for KC2.

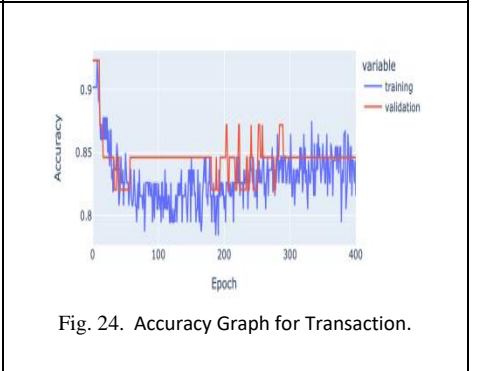


Fig. 24. Accuracy Graph for Transaction.

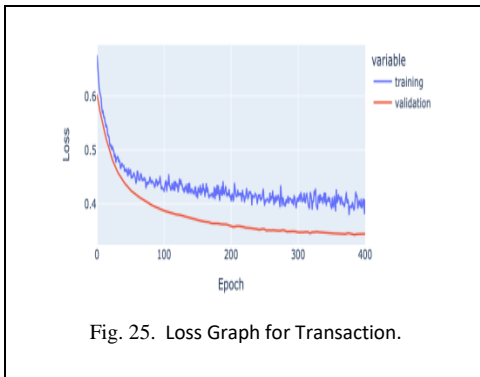


Fig. 25. Loss Graph for Transaction.

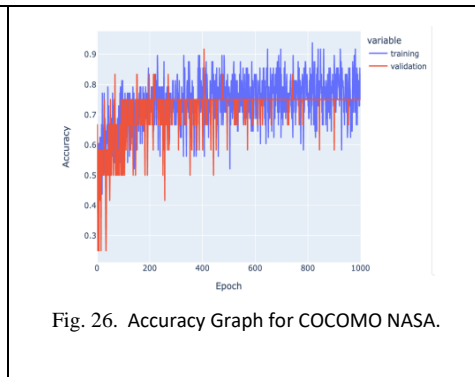


Fig. 26. Accuracy Graph for COCOMO NASA.

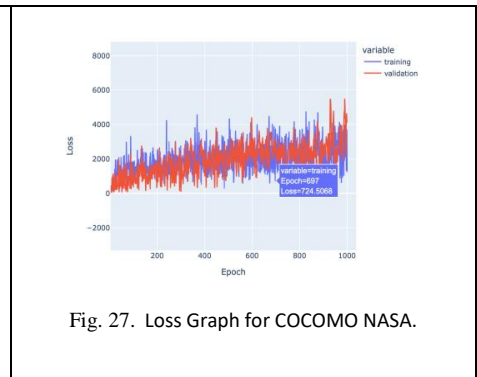


Fig. 27. Loss Graph for COCOMO NASA.

TABLE VI. DATASET DESCRIPTION

Dataset	Criterion	No. of Attributes	No. of instances	Source of Dataset
MJ	Software defect prediction	24	94148	https://madeyski.e-informatyka.pl/tools/software-defect-prediction/
PC5	Software defect prediction	39	17186	https://github.com/klainfo/NASADefectDataset/raw/master/OriginalData/MDP/PC5.arff
JM1	Software defect prediction	22	10885	http://promise.site.uottawa.ca/SERepository/datasets/jm1.arff
MC1	Software defect prediction	40	9466	https://www.openml.org/data/download/53939/mc1.arff
PC2	Software defect prediction	36	5589	https://www.openml.org/data/download/53952/pc2.arff
KC1	Software defect prediction	21	2109	http://promise.site.uottawa.ca/SERepository/datasets/kc1.arff
PC4	Software defect prediction	37	1458	https://www.openml.org/data/download/53932/pc4.arff
PC1	Software defect prediction	22	1109	http://promise.site.uottawa.ca/SERepository/datasets/pc1.arff
PC3	Software defect prediction	22	1109	https://www.openml.org/data/download/53933/pc3.arff
KC2	Software defect prediction	22	522	http://promise.site.uottawa.ca/SERepository/datasets/kc2.arff
Datatrieve	Success/ failure in the transaction	9	130	http://promise.site.uottawa.ca/SERepository/datasets/datatrieve.arff
COCOMO NASA	Required software reliability	17	60	http://promise.site.uottawa.ca/SERepository/datasets/cocomonasa_v1.arff

TABLE VII. COMPARISON OF ACCURACY WITH THE EXISTING MODELS IN THE LITERATURE

Dataset	Model	Accuracy	Precision	Recall	F - measure
MJ	Proposed	89%	90.00%	96%	93%
	Linear Regression (LR) [33]	74.99%		18.22%	
	Decision Tree (DT) [33]	74.45%		10.79%	
	Naive Bayes (NB) [33]	73.76%		22.28%	
	Support Vector Machine (SVM) [33]	78.19%		26.58%	
	Stochastic Gradient Boosting (GBM) [33]	76.16%		22.03%	
	K-Nearest Neighbor (KNN) [33]	84.24%		56.83%	
PC5	Proposed	91%	99%	90.00%	95%
	VOTE [34]	97.46%			
	Random Tree [34]	97.08%			
	Naive Bayes [34]	96.44%			

Dataset	Model	Accuracy	Precision	Recall	F - measure
JM1	Proposed	89%	92%	95%	93%
	USS[35]	66.40%	82.50%	96.90%	89.10%
	VOTE [34]	81.44%			
	Random Tree [34]	75.30%			
	Naive Bayes [34]	80.45%			
MC1	Proposed	95%	99%	95%	97%
	USS[35]	85.50%	67%	43.30%	49.70%
	VOTE [34]	99.42%			
	Random Tree [34]	99.43%			
	Naive Bayes [34]	93.80%			
PC2	Proposed	86%	99%	86%	93%
	VOTE [34]	99.53%			
	Random Tree [34]	99.29%			
	Naive Bayes [34]	97.11%			
KC1	Proposed	84%	90.00%	91%	91%
	USS[35]	78.50%	87.80%	95.30%	91.40%
	VOTE [34]	85.62%			
	Random Tree [34]	82.85%			
	Naive Bayes [34]	82.50%			
PC4	Proposed	89%	99%	87%	93%
	ILLE-SVM (Improved Locally Linear Embedding and Support)[37]	90.00%	62.50%	83.33%	71.43%
	VOTE [34]	90.28%			
	Random Tree [34]	87.74%			
	Naive Bayes [34]	87.11%			
PC1	Proposed	85%	99%	84%	91%
	USS[35]	84.10%	52.60%	36.30%	40.90%
	ILLE-SVM (Improved Locally Linear Embedding and Support)[37]	84.78%	78.26%	90.00%	83.68%
	LASSO-SVM[36]	78.26%	79.40%	75.46%	79.85%
	SVM[36]	71.32%	69.29%	69.25%	70.64%
	Linear regression (LR)[36]	84.20%	61.50%	69.60%	65.30%
	Back propagation neural network(BPNN)[36]	79.30%	60.60%	72.40%	66.90%
	Cluster Analysis (CA)[36]	71.60%	63.50%	71.20%	67.10%
	VOTE [34]	93.73%			
	Random Tree [34]	91.64%			
Naive Bayes [34]	89.12%				
PC3	Proposed	83%	99%	81%	89%
	USS[35]	76.60%	37.60%	26.10%	30.10%
	ILLE-SVM (Improved Locally Linear Embedding and Support)[37]	89.66%	73.08%	86.36%	79.05%
	VOTE [34]	89.12%			
	Random Tree [34]	86.01%			
	Naive Bayes [34]	48.30%			
KC2	Proposed	86%	89%	94%	92%
	VOTE [34]	82.91%			
	Random Tree [34]	79.86%			
	Naive Bayes [34]	83.62%			
Datatrieve	Proposed	86%			
	USS[35]	50.00%	91.20%	99%	95.40%
COCOMO NASA	Proposed	96%	99%	91%	95%

VI. CONCLUSION

Predicting software reliability has become an essential activity in software development to develop better quality software. Recently, the researcher community has identified that computational intelligence techniques can outperform traditional prediction methods. This study predicts the software reliability using a dense neural network which is implemented using deep learning. The classification is performed on twelve datasets KC1, KC2, Datatrive, COCOMO NASA, MJ, JM1, MC1, PC1, PC2, PC3, PC4, and PC5. The optimal model is designed with different configurations for each dataset for classification. Results are evaluated using four standard performance metrics, i.e., accuracy, precision, recall, and f1-score. The results obtained by our model show better results as compared to previous models in terms of accuracy, especially dataset MJ, JM1, KC2, and COCOMO NASA.

Hybridization of deep learning techniques with other computational intelligence techniques can be explored for better results. The same study can be extended with large industrial datasets to achieve better results and can also be experimented with other algorithms.

REFERENCES

- [1] C. Chen et al., "Reliability analysis using deep learning," International Design Engineering Technical Conferences and Computers and Information in Engineering Conference, vol. 51739, pp. 1–10, Aug. 2018.
- [2] J. C. Bezdek, "On the relationship between neural networks, pattern recognition and intelligence", International journal of approximate reasoning, vol. 6, pp. 85–107, 1992.
- [3] Robert J. Marks II, "Intelligence: Computational versus artificial," IEEE Trans. Neural Networks, vol. 4, pp. 737–739, 1993.
- [4] N. Karunanithi, D. Whitley and Y. K. Malaiya, "Prediction of software reliability using connectionist models," IEEE Transactions on software engineering, vol. 18, p. 563, 1992.
- [5] S. L. Ho, M. Xie and T. N. Goh, "A study of the connectionist models for software reliability prediction," Computers & Mathematics with Applications, vol. 46, pp. 1037–1045, 2003.
- [6] L. Tian and A. Noore, "Evolutionary neural network modeling for software cumulative failure time prediction," Reliability Engineering & system safety, vol. 87, pp. 45–51, 2005.
- [7] E. O. Costa, G. A. de Souza, A. T. R. Pozo and S. R. Vergilio, "Exploring genetic programming and boosting techniques to model software reliability," IEEE Transactions on Reliability, vol. 56, pp. 422–434, 2007.
- [8] P.F. Pai and W.C. Hong,, "Software reliability forecasting by support vector machines with simulated annealing algorithms," Journal of Systems and Software, vol. 79, pp. 747–755, 2006.
- [9] Q. P. Hu, M. Xie, S. H. Ng and G. Levitin, "Robust recurrent neural network modeling for software fault detection and correction prediction," Reliability Engineering & System Safety, vol. 92, pp. 332–340, 2007.
- [10] J. H. Lo, "A study of applying ARIMA and SVM model to software reliability prediction," International Conference on Uncertainty Reasoning and Knowledge Engineering, vol. 1, pp. 141–144, 2011.
- [11] H. Li, M. Zeng, M. Lu, X. Hu and Z. Li, "Adaboosting-based dynamic weighted combination of software reliability growth models," Quality and Reliability Engineering International, vol. 28, pp. 67–84, 2012.
- [12] P. Roy, G. S. Mahapatra and K. N. Dey, "Neuro-genetic approach on logistic model based software reliability prediction," Expert systems with Applications, vol. 42, pp. 4709–4718, 2015.
- [13] C. Jin and S. W. Jin, "Prediction approach of software fault-proneness based on hybrid artificial neural network and quantum particle swarm optimization," Applied Soft Computing, vol. 35, pp. 717–725, 2015.
- [14] R. Malhotra, "A systematic review of machine learning techniques for software fault prediction," Applied Soft Computing, vol. 27, pp. 504–518, 2015.
- [15] R. S. Wahono, "A Systematic Literature Review of Software Defect Prediction," Journal of Software Engineering, vol. 1, pp. 1–16, 2015.
- [16] A. Jaiswal and R. Malhotra, "Software reliability prediction using machine learning techniques," International Journal of System Assurance Engineering and Management, vol. 9, pp. 230–244, 2018.
- [17] C. J. Clemente, F. Jaafar and Y. Malik, "Is predicting software security bugs using deep learning better than the traditional machine learning algorithms?," IEEE International Conference on Software Quality, Reliability and Security (QRS), pp. 95–102, 2018.
- [18] O. Dahiya and K. Solanki, "An Efficient APHT Technique for Requirement-Based Test Case Prioritization," International Journal of Engineering Trends and Technology, vol. 69, pp. 215–227, 2021.
- [19] O. Dahiya and K. Solanki, "Prevailing Standards in Requirement-Based Test Case Prioritization: An Overview," ICT Analysis and Applications, pp. 467–474, 2021.
- [20] O. Dahiya and K. Solanki, "A Study on Identification of Issues and Challenges Encountered in Software Testing," In Proceedings of International Conference on Communication and Artificial Intelligence , pp. 549–556, 2021.
- [21] O. Dahiya, K. Solanki, and A. Dhankhar, "Risk-based testing: identifying, assessing, mitigating & managing risks efficiently in software testing," International Journal of advanced research in engineering and technology, vol. 11, pp. 192–203, 2020.
- [22] O. Dahiya and K. Solanki, "A systematic literature study of regression test case prioritization approaches," International Journal of Engineering & Technology, vol. 7, pp. 2184–2191, 2018.
- [23] S. Yadav and B. Kishan, "Reliability of Component-Based Systems- A Review", International Journal of Advanced Trends in Computer Science and Engineering, vol.8, pp. 293–299, 2019.
- [24] S. Yadav and B. Kishan, "Assessment of software quality models to measure the effectiveness of software quality parameters for Component Based Software (CBS)," Journal of Applied Science and Computations, vol. 6, pp. 2751–2756, 2019.
- [25] S. Yadav and B. Kishan, "Analysis and Assessment of Existing Software Quality Models to Predict the Reliability of Component-Based Software," International Journal of Emerging Trends in Engineering Research, vol. 8, pp. 2824–2840, 2020.
- [26] S. Yadav and B. Kishan, "Component-Based Software System using Computational Intelligence Technique for Reliability Prediction," International Journal of Advanced Trends in Computer Science and Engineering, vol. 9, pp. 3708–3721, 2020.
- [27] S. Yadav and B. Kishan, "Assessments of Computational Intelligence Techniques for Predicting Reliability of Component Based Software Parameter and Design Issues," International Journal of Advanced Research in Engineering and Technology, vol. 11, pp. 565–584, 2020.
- [28] O. Al Qasem and M. Akour, "Software fault prediction using deep learning algorithms," International Journal of Open Source Software and Processes (IJOSSP), vol. 10, pp. 1–19, 2019.
- [29] Wikipedia contributors, "Activation function," [Online]. Available: https://en.wikipedia.org/w/index.php?title=Activation_function&oldid=1076034609. [Accessed 2022].
- [30] Dishashree26, "Activation Functions | Fundamentals Of Deep Learning," January 2020. [Online]. Available: <https://www.analyticsvidhya.com/blog/2020/01/fundamentals-deep-learning-activation-functions-when-to-use-them/>. [Accessed December 2021].
- [31] Wikipedia contributors, "Cross entropy," 2022. [Online]. Available: https://en.wikipedia.org/w/index.php?title=Cross_entropy&oldid=1071450106. [Accessed 2022].
- [32] M. Sunasra, "Performance Metrics for Classification problems in Machine Learning," March 2019. [Online]. Available: <https://medium.com/@MohammedS/performance-metrics-for-classification-problems-in-machine-learning-part-i-b085d432082b>. [Accessed January 2022].

- [33] B. S. Deshpande, B. Kumar and A. Kumar, "Assessment of Software Reliability by Object Oriented Metrics using Machine Learning Techniques," *International Journal of Grid and Distributed Computing*, vol. 14, pp. 01–10, 2021.
- [34] T. Wang, W. Li, H. Shi and Z. Liu, "Software defect prediction based on classifiers ensemble," *Journal of Information & Computational Science*, vol. 8, pp. 4241–4254, 2011.
- [35] K. N. Rao and C. S. Reddy, "A novel under sampling strategy for efficient software defect analysis of skewed distributed data," *Evolving Systems*, vol. 11, pp. 119–131, 2020.
- [36] K. Wang, L. Liu, C. Yuan and Z. Wang, "Software defect prediction model based on LASSO--SVM," *Neural Computing and Applications*, pp. 8249–8259, 2021.
- [37] C. Shan, H. Zhu, C. Hu, J. Cui and J. Xue, "Software defect prediction model based on improved LLE-SVM," in *2015 4th International Conference on Computer Science and Network Technology (ICCSNT)*, vol. 1, 2015, pp. 530–535.
- [38] L. Qiao, X. Li, Q. Umer and P. Guo, "Deep learning based software defect prediction," *Neurocomputing*, vol. 385, pp. 100–110, 2020.

Performance Evaluation of Temporal and Frequential Analysis Approaches of Electromyographic Signals for Gestures Recognition using Neural Networks

Edwar Jacinto Gómez, Fredy H. Martínez Sarmiento, Fernando Martínez Santa
Technology Faculty, Universidad Distrital Francisco José de Caldas, Bogotá, Colombia

Abstract—Now-a-days, human-machine interfaces are increasingly intuitive and straightforward to design, but there is difficulty capturing electromyographic signal data using the least amount of hardware. This work takes the signals of a human forearm as input parameters describing a series of five gestures, using a dataset of 8 channels of electromyographic signals, using as a capture device a Thalmic Labs Inc. handle called Myo armband. The aim is to compare the performance of the artificial neural network using data in the time domain as input to the learning system. The same data are pre-processed to the frequency domain, looking for an improvement in the neural network's performance since transforming the input signals of the system to the frequency domain minimizes the problems inherent to this type of signal. This transformation is achieved using the fast Fourier transform. Consequently, it seeks to reach a neural network architecture that recognizes the gestures captured with the Myo armband in a high percentage of performance to be used in stand-alone applications, using the TensorFlow libraries of Python for its design. As a result, a comparison of the neural network trained with data in time versus the same data expressed in the frequency domain is obtained, seen from the increase in performance and the percentage of gesture detection.

Keywords—Neural networks; electromyographic signals; Myo armband; tensorflow; fast fourier transform

I. INTRODUCTION

Currently, there are different types of human-machine interfaces [1] (HMI) developed for applications in areas like automation [2], robotics [3], biomedicine [4], biometrics [5], among others. That has led to users needing specialized studies, knowledge, or skills on information technology to implement and operate such applications properly. For this reason, it is becoming important to minimize the complexity of these types of controls, design more straightforward and more intuitive human-machine interfaces, which take advantage of the benefits of human biomechanics, and make it easy and safer handling of the applications. Therefore, the aim is to have control interfaces that do not require much prior training and are as natural as possible, reaching non-invasive devices which can be used as a clothing accessory without needing the help of external personnel for configuration or startup.

For years one of the techniques that have been used for the development of HMI is electromyographic (EMG) signals [6]. The EMG signals measure the electrical currents generated in the muscles during their contraction, representing

neuromuscular activities [7]. An example of this is interfaces that detect the gestures of a human forearm, which use the electrical impulses of the forearm to control machinery, robots [8], prosthesis [9], [10], home automation systems [11], [12], personal identification systems [13], [14], IoT systems [15], among others.

On the other hand, a series of transformations have been used in the preprocessing of EMG signals for a couple of decades, taking into account problems present in periodicity, frequency behavior, stationary behavior, and fast transient behavior. Consequently, EMG signals have been acquired in the time domain, and mathematical transformations have been used to bring them to the frequency domain [16]. For example, Wavelet transform (WT) and the fast Fourier transform (FFT) are primary tools for analyzing and subsequent use of these signals.

Additionally, in recent years the use of Artificial Neural Networks (ANN) has become extensive for the classification of EMG signals [17], [18]. Due to the complexity of analyzing the intrinsic characteristics of these signals in terms of variance identification, average, length, zero crossing, median, and frequency, as to propose an algorithm. Thus, some previous works have focused on acquiring a database of signals in the time domain to use them as a knowledge base to train an ANN-based machine learning system [19], [20]. The amount of information to be analyzed becomes significant due to pure or "raw" EMG signals in the time domain.

Therefore, the objective of this research is to develop an algorithm in Python language that detects the gestures of a human forearm, using the EMG signals of this part of the body, to make a direct comparison between the use of these pure signals in time and the same signals transformed to the frequency domain through an FFT. These last to training and subsequent verification of an ANN and validate the algorithm's performance.

The paper is organized as follows: Section 2 presents the methodology proposed to detect EMG signals, create a dataset, preprocess the data in the time domain and get through FFT the data in the frequency domain, and design ANN to training and classification arm gestures. Section 3 presents the results of implementing the ANN algorithm in Python language, testing, and evaluating its performance. Section 4 presents the conclusions about this research's main ideas, including possible future jobs.

II. METHODOLOGY

A. Data Acquisition System

Technological advances in miniaturization and high performance of electronic devices have allowed advances in biomedicine, applied to human-machine interfaces, in this case, the use of wearable devices, particularly the Myo armband handle designed by the company Thalmic labs inc [21]. This armband is equipped with eight EMG electrodes, a 3-axis gyroscope, a 3-axis accelerometer, and a 3-axis magnetometer to perform IMU metrics. The EMG electrodes on the handle detect signals related to the muscular activities of the user's forearm, and the IMU detects forearm movements in three-dimensional space. This data acquired by the handle is sent via Bluetooth Low Energy (BLE), which allows a 3D reconstruction of human forearm movements, making it a good choice for this type of human-machine interface [22].

The Myo armband was chosen for this work as the EMG data acquisition system, running on Windows operating system using Myo Connect drivers as a base. Moreover, TensorFlow 'TFF' machine learning libraries were used to design the ANN in the software part.

As a first step to create a dataset, data from a human forearm was acquired as a control interface using the Myo™ Gesture Control armband tool. The signals were captured using Python scripts to read the data and store them in flat format.

Then, those EMG signals were analyzed to be used as a knowledge base for the training and verification of the ANN-based learning system. For this purpose, it was chosen five basic gestures made with the forearm, as shown in Fig. 1. Each gesture is captured by the Myo armband device for a time of one second, with a sampling frequency of 200Hz. These signals are considered a significant sample of gesture behavior. The data capture was performed through a Python script, which was in charge of measuring the time, completing the capture, and finally writing a flat file.

B. Characteristics of Artificial Neural Network

In recent years, ANNs have been used as a basis for recognition and classification tasks [23], [24]. Like in this case, it is required to associate patterns from a previously generated dataset, identifying from each muscular gesture performed by the arm those relevant characteristics that make it different from another gesture. It has been decided to use an ANN for this task because:

- it has the natural ability to acquire knowledge through experience,
- it can be easily adapted dynamically depending on the learning environment, and
- it has a high level of fault tolerance, supporting missing input data or significant damage to its structure and continuing with a good performance.

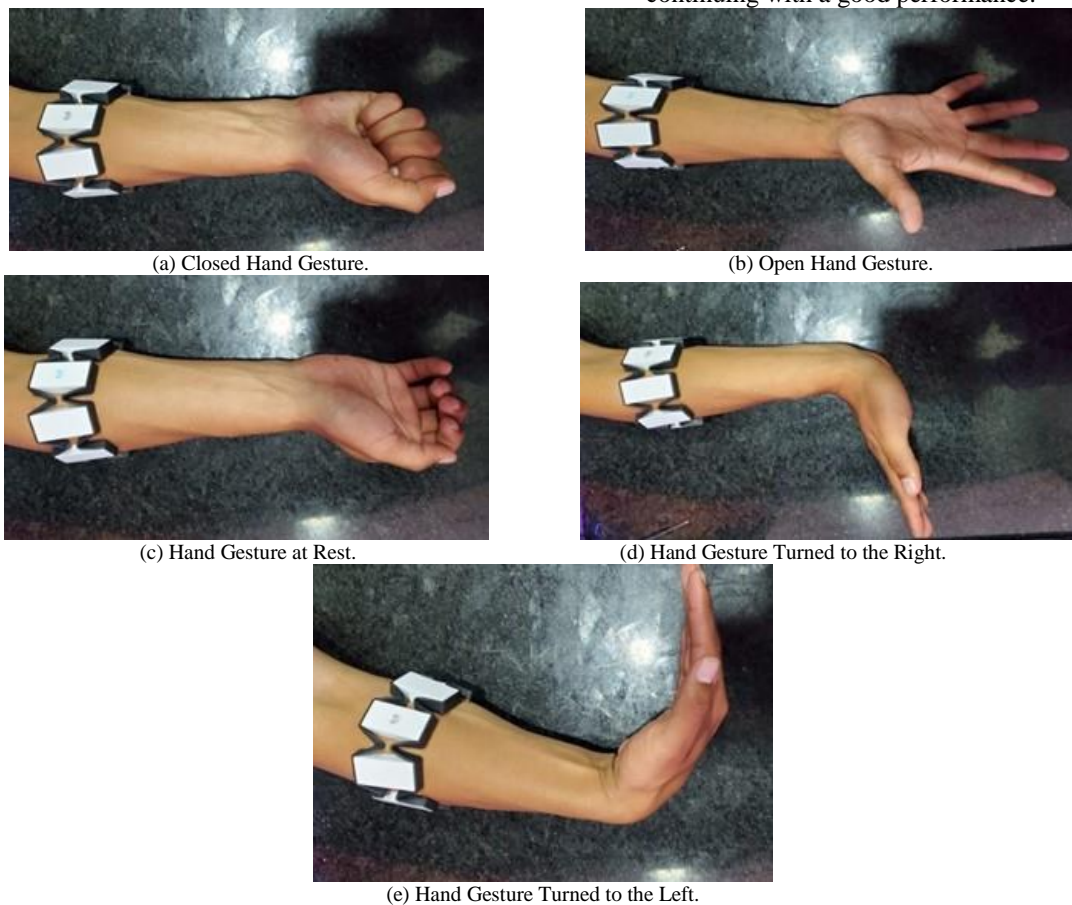


Fig. 1. Basic Gestures Captured with the Myo Armband.

So, the first methodological step was to collect the data, with specific characteristics, with a minimum amount of data, and in different individuals to have an adequate knowledge base. After that, it is necessary to decide which libraries must implement the learning system. Given its characteristics and ease of implementation, it chose to develop ANN using a library called TensorFlow Federated "TFF" developed by Google. It is an open-source framework for programming code for machine learning with decentralized data.

This library allows different architectures to be proposed in terms of the type of training, the platform on which they run and the different programming languages used, and the devices on which the final application will run. The architecture of TFF makes it possible to run on different platforms, i.e., CPUs, GPUs, and on a PC or a mobile device, in addition to being compatible with different programming languages such as Java, JavaScript, C, Go, Python, among others. However, it has been evidenced that the language most used to implement TFF is Python, so it is the one that will be used for the development of the algorithm to model the ANN.

After choosing the architecture, the device, and the programming language, it is necessary to define the size and characteristics of the dataset in terms of:

- the type of file to work with,
- the amount of data to be used for training, and
- the amount of data to be used to verify the learning performed.

Once it is clear if the dataset is local, built from its own data captures, the next step is to define the architecture of the ANN in terms of the number of neurons in the input and output layers, the number of hidden layers, and therefore the number of neurons used for the process. In addition to which activation function is indicated for the type of data being used.

Depending on the hardware characteristics, which in this case are local, using a CPU in a desktop PC, the performance of the neural network training software must be taken into account as a limiting parameter for the construction of the ANN model. In other words, the designed architecture and the processing time required must be considered to perform the training process. For this case, being local processing using a CPU requires a certain number of hours and does not allow significant changes to the neural network architecture in an agile way.

Finally, having the internal architecture of the ANN, it is necessary to perform learning tests, error quantity and verify if the system learned, for which TFF offers reports and graphs for error verification ROC curves, as well as verification of system learning through confusion matrices.

C. Block Diagram - Proposed Overall Solution

After defining the work methodology with which the solution will be designed and considering that such a scheme applies to different work scenarios, a general flow diagram is proposed in Fig. 2 to reach a system that detects gestures in a usable knowledge base for different applications. On the other hand, it is essential to emphasize that it seeks to compare the

data input, firstly the data as captured with the bracelet, in the time domain, simply with a normalization process, all this compared with a preprocessing of the input signals brought into a frequency domain.

D. Pre-process Time or FFT

Sixty-six thousand four hundred seventy-nine (66479) signals with a duration of one second were captured, corresponding to five different gestures using the Myo armband performed by three different individuals, as shown in Fig. 1. Subsequently, EMG signals of this dataset are preprocessed before being stored as local files, modeled, and classified to be usable for ANN training.

Fig. 3 shows a signals capture of the 8 EMG channels for a gesture, with a duration of one second and a sampling frequency of 200 Hz; it is possible to observe the characteristics of the signals captured in the time domain by the Myo armband. For this particular case, the signal is between a range of -50 and 50 units; it is evident that the most significant part of the signal is in its first 64 samples, in which the most substantial part of the gesture is found. For this reason, the ANN has an input layer of 64 neurons.

Fig. 4 shows the samples transformed to the frequency domain. A preprocessing of the EMG signals is performed, transforming those to the frequency domain, using the fast Fourier transform specifically. As base parameters for the Fourier transform, it used the criteria of twice the sampling frequency of the signal, i. e., the base frequency of the transform was performed at 400Hz. Also, the data of the magnitude and bilateral angle of the signal centered at zero were taken.

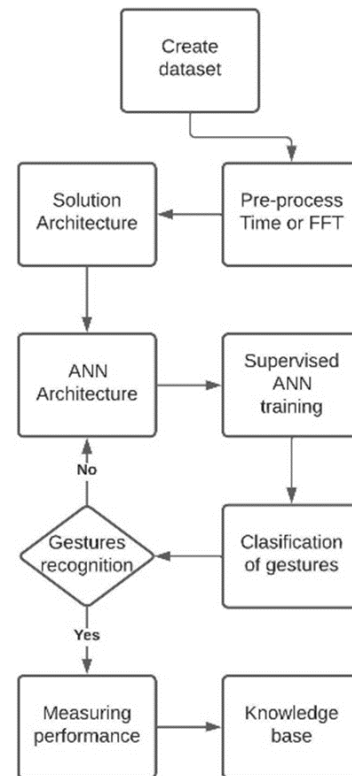


Fig. 2. Flow Chart of the Proposed Overall Solution.

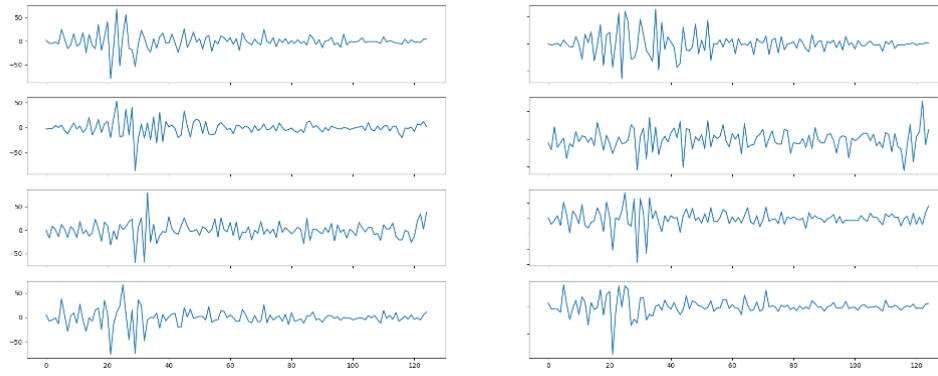


Fig. 3. EMG Signals Captured with the Myo Armband of the Left-hand Gesture in the Time Domain

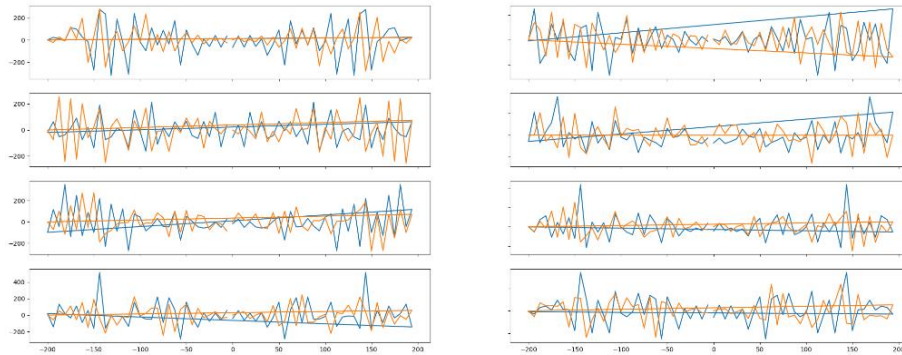


Fig. 4. EMG Signals Captured with the Myo Armband of the Left-hand Gesture in the Frequency Domain.

E. Architecture of Artificial Neural Network

Regarding the architecture of the solution, it was chosen to perform the data capture and network training process in a supervised manner using a local PC with the following hardware configuration: 5800x processor, RTX2070 GPU, 32Gb RAM at 3600Mhz, and the following software versions were used: Python version 3.9 and TensorFlow version 2.7.0.

Regarding the ANN creation and testing process, the first step is to characterize the data set that will be entered. Then, tests are performed with different numbers of training epochs or iterations to different configurations of the layers in the designed multilayer network. Subsequently, the architecture of the ANN must be defined, as shown in Fig. 5. The input layer has sixty-four neurons, that number of neurons taking into account the size of the dataset samples. The hidden layers have a number of neurons variable depending on the minimum performance required for this application; in Fig. 5. the change in the number of neurons is represented as N. The output layer has five neurons, that number of neurons considering the different gestures to be identified.

When talking about ANNs, it is necessary to have a minimum model to recalculate the weights that will model the behavior of the network. In this case, a simple backpropagation model is chosen that complies with the following equations,

$$\text{Input layer: } \quad (i) \quad (1)$$

$$\text{Hidden layer: } \quad a_1^{(i)} = \sigma(W_1 x^{(i)} + b_1) \quad (2)$$

$$\text{Output layer: } \quad \hat{y}^{(i)} = \sigma(W_2 a_1^{(i)} + b_2) \quad (3)$$

Where (i) is the input, the captures that were made of the three individuals performing the five gestures, W_1, b_1, W_2, b_2 are the matrices of weights and vectors of independent values used in the layers of (1) and (2), which are initialized randomly. The nonlinear activation function is σ . The result in (3) is represented by $\hat{y}^{(i)}$ where i is the desired output estimate [25].

Once it has a tentative ANN architecture, it is performed a series of tests with different network models until it achieves accuracy percentages greater than 80% and an amount of lost data less than 20%. Table I shows the different models of the ANN, taking as a knowledge base the data in the time domain.

The third ANN model uses an architecture with 66479 neurons in the first hidden layer and 300 neurons in the second hidden layer due to an activation method called RELU. RELU is a function that allows data to pass through or not to the next layer, depending on the result of the neuron weighting with equation (2). If the result of the neuron weighting is negative or zero, it does not pass to the next layer; otherwise, any positive number passes to the next layer. (Tf.Nn.Relu | TensorFlow Core v2.7.0, n.d.). Moreover, the first layer of the ANN has a dropout of 20%, which consists of randomly establishing in each iteration of training which neuron should be deactivated. The number of deactivated neurons in the layer will depend on the percentage entered into the dropout method. That is done not to overtrain the ANN. (Tf.Keras.Layers.Dropout | TensorFlow Core v2.7.0, n.d.).

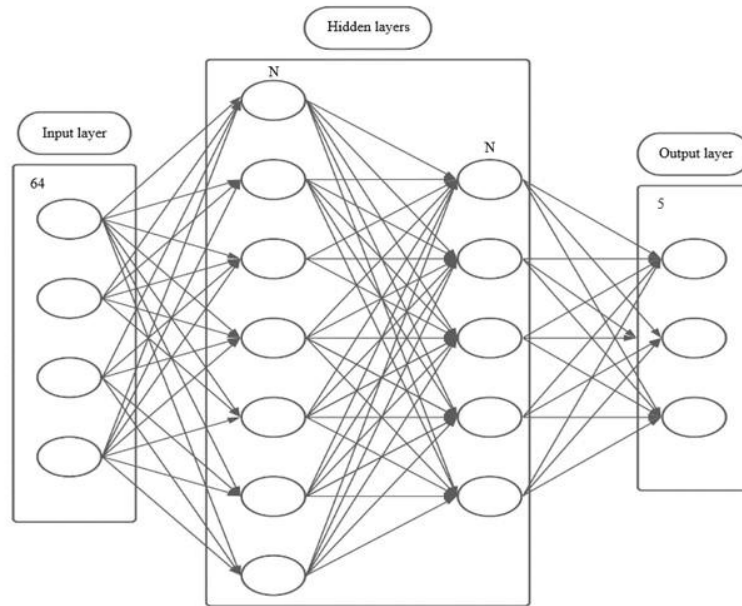


Fig. 5. Graphical Model of an ANN

TABLE I. DIFFERENT MODELS OF THE INTERNAL ARCHITECTURE OF THE ANN, USING THE DATA IN TIME

Model	Epochs	Neurons hidden layer 1	Neurons hidden layer 2	Neurons hidden layer 3	Accuracy	Lost
1	50	15000	100	N/A	20%	30%
2	2000	15000	100	20	25%	40%
3	1000	66479	300	100	90%	0,80%

TABLE II. MODEL OF THE INTERNAL ARCHITECTURE OF THE ANN, USING THE DATA AT FREQUENCY

Model	Epochs	Neurons hidden layer 1	Neurons hidden layer 2	Neurons hidden layer 3	Accuracy	Lost
Unique	1000	66479	300	100	95%	0,87%

When transforming the data to the frequency domain using FFT, it decreases the number of samples needed and minimizes some problems that the signals present in the time domain; in this case, it has the following ANN model, as shown in Table II.

F. Measuring Performance of Artificial Neural Network

Once the ANN model has been found, the parameters considered to verify the correct operation of the system are its performance and margin of error, in addition to analyzing possible training errors. This process has been done two previous times, modifying the data set and remodeling the ANN architecture, either by changing the weight of the neurons proportionally to the error or by reducing or increasing the layers of neurons to reduce overtraining or underfitting. When this architecture is already defined, the behavior of the error and performance of the network is analyzed. The results

for the third model are shown in Fig. 6; such data analysis is performed for the ANN with the input data in the time domain.

It can be seen that the probability of getting the gesture right is approximately 92%, and there is a loss of less than 0.4%; these results were obtained with the data set of 66479 captures or samples of the input signal in the time domain.

In the same way, tests were performed for the case of the chosen model, using the data in the frequency domain, such validation measurement of accuracy parameters and data loss, are shown in Fig. 7.

It can be seen that the probability of getting the gesture right is approximately 93%, and there is a loss of less than 0.21%; these results were obtained with the data set of 66479 captures or samples of the input signal in the time domain transform to the frequency domain.

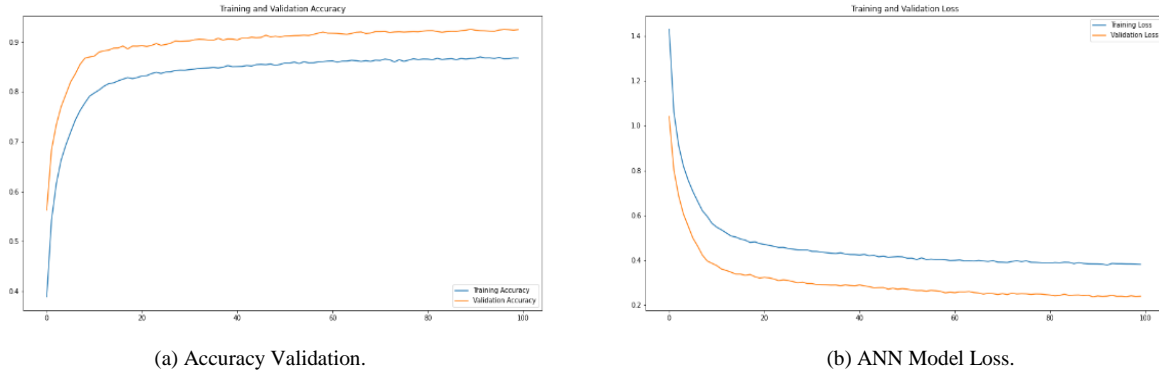


Fig. 6. Measurement of Training Parameters for Third Model with Time Domain Input Data.

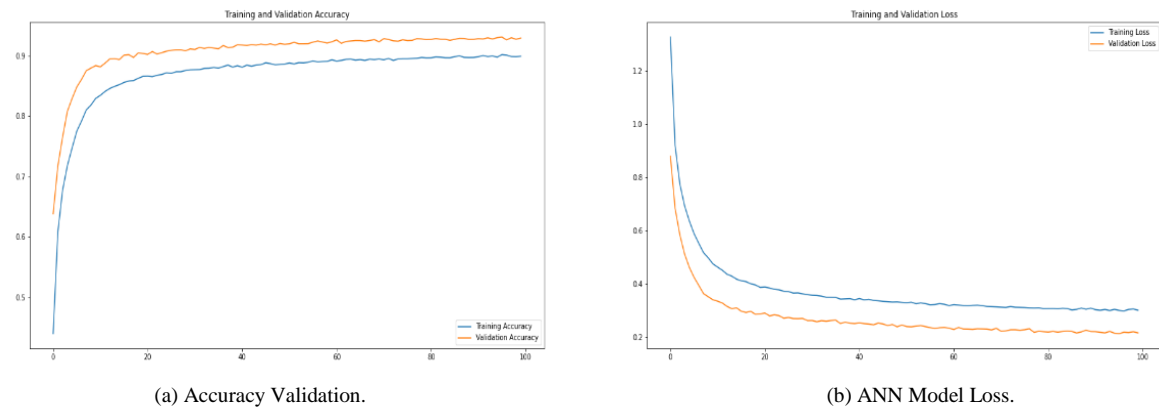


Fig. 7. Measurement of Training Parameters with Frequency Domain Input Data.

III. RESULTS

The ANN training yielded a data loss of 24.76% and an accuracy rate of 91.98%, with a thousand epochs in the training of the ANN data, data shown in Fig. 8, all this for the time domain data.

The ANN training yielded a 21.66% data loss and a 92.95% accuracy percentage, with a thousand epochs in the training of the ANN data, data shown in Fig. 9, all this for the data in the frequency domain.

One of the most used tools to validate the efficiency of the selected neural network model is the confusion matrix of the model, which is represented in a graph. This graph shows a matrix that shows the percentage of accuracy of the ANN when predicting a gesture, and it can also see the percentage of error when predicting another gesture that does not correspond to the one entered.

In order to appreciate the accuracy of the model, it is necessary to consider the diagonal of the matrix that begins in the upper left corner and ends in the lower right corner. The numbers that make up the diagonal indicate the percentage of accuracy in predicting the gesture correctly; the other fields of the matrix are the percentage of error in predicting the gesture. Fig. 10 shows the graphs of the confusion matrix for the time domain and frequency domain of the ANN model developed.

It can observe in confusion matrices that despite the pre-processing of the information, using the fast Fourier transform, the performance only improves by 1% for some gestures. These matrices clearly show that the system successfully classified the gestures, both in the time and frequency domains, consistently achieving prediction percentages higher than 88%.

```
831/831 - 3s - loss: 0.3864 - accuracy: 0.8656 - val_loss: 0.2430 - val_accuracy: 0.9220 - 3s/epoch - 4ms/step  
Epoch 99/100  
831/831 - 3s - loss: 0.3903 - accuracy: 0.8650 - val_loss: 0.2427 - val_accuracy: 0.9220 - 3s/epoch - 3ms/step  
Epoch 100/100  
831/831 - 3s - loss: 0.3881 - accuracy: 0.8653 - val_loss: 0.2476 - val_accuracy: 0.9198 - 3s/epoch - 3ms/step
```

Fig. 8. Test Values Obtained in ANN Training in the Time Domain.

```
831/831 - 3s - loss: 0.3044 - accuracy: 0.8989 - val_loss: 0.2178 - val_accuracy: 0.9301 - 3s/epoch - 3ms/step  
Epoch 99/100  
831/831 - 3s - loss: 0.3060 - accuracy: 0.8986 - val_loss: 0.2207 - val_accuracy: 0.9276 - 3s/epoch - 4ms/step  
Epoch 100/100  
831/831 - 3s - loss: 0.3015 - accuracy: 0.8994 - val_loss: 0.2166 - val_accuracy: 0.9295 - 3s/epoch - 4ms/step
```

Fig. 9. Test Values Obtained in the ANN Training in the Frequency Domain.

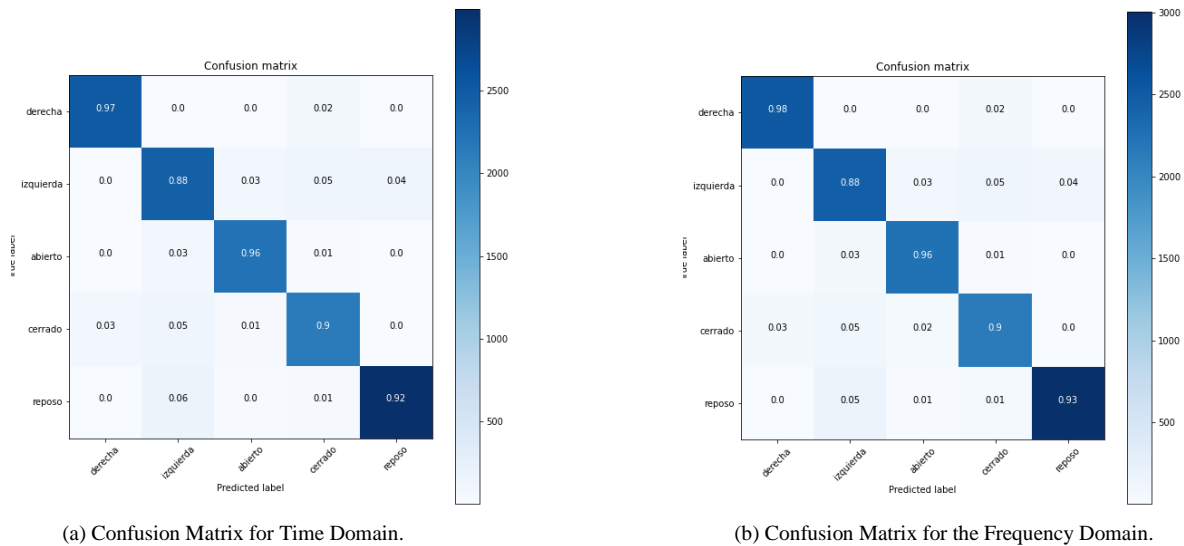


Fig. 10. Confusion Matrices of the ANN Model.

IV. CONCLUSION

This paper documents the training process of an ANN to detect five gestures captured from a human forearm of 3 different individuals, focusing on the differences between capturing the "raw" data in the time domain versus pre-processing them by transforming them to the frequency domain. It was verified that transforming dataset samples to the frequency domain removes some time-domain dataset issues such as delays, level offsets, and signal offsets. Also, it was possible to reduce the number of samples necessary to generate the minimal identification information of the gestures.

In some previous literature, a significant improvement was observed in working the systems in the frequency domain, avoiding problems inherent to the EMG signals. For this reason, it was expected that there would be an improvement in the detection process of the gestures. However, the increase in the measurement parameters and verification of the ANN has only reflected improvements close to 1%.

As future work, it is proposed to improve the data capture process, increasing the signal's sampling period over time to have more detectable harmonics in the frequency domain and have more elements to perform the training process of the ANN. Having a new sampling rate would increase the number of neurons in the input layer, and therefore the rest of the hidden capabilities would have to be modified. Finally, it would have to alter the epochs in the training process, having more samples of different individuals to have a complete dataset, looking for an improvement that exceeds the threshold of 90% detection of gestures.

ACKNOWLEDGMENT

The Universidad Distrital Francisco José de Caldas supports this work, with the research group belonging to the Technological Faculty; specifically, the research group SIE (Embedded Informatics Security). Currently, the work is focused on the digital processing of signals, images, and intelligent algorithms that seek to be applied in stand-alone solutions.

REFERENCES

- [1] M. A. Razzaq, M. A. Qureshi, K. H. Memon, S. Ullah, and R. Y. Khan, "A survey on user interfaces for interaction with human and machines," 2017. [Online]. Available: <https://blog.mozilla.org/labs/2007/07/the-graphical-keyboard-user>.
- [2] H. Oliff, Y. Liu, M. Kumar, and M. Williams, "A framework of integrating knowledge of human factors to facilitate hmi and collaboration in intelligent manufacturing," in *Procedia CIRP*, 2018, vol. 72, pp. 135–140. doi: 10.1016/j.procir.2018.03.047.
- [3] A. Grabowski, J. Jankowski, and M. Wodzyński, "Teleoperated mobile robot with two arms: the influence of a human-machine interface, VR training and operator age," *International Journal of Human Computer Studies*, vol. 156, Dec. 2021, doi: 10.1016/j.ijhcs.2021.102707.
- [4] S. P. Zavala, S. G. Yoo, and D. E. Valdivieso Tituana, "Controlling a wheelchair using a brain computer interface based on user controlled eye blinks." [Online]. Available: www.ijacsa.thesai.org.
- [5] N. Belgacem, R. Fournier, A. Nait-Ali, and F. Bereksi-Reguig, "A novel biometric authentication approach using ECG and EMG signals," *Journal of Medical Engineering and Technology*, vol. 39, no. 4, pp. 226–238, May 2015, doi: 10.3109/03091902.2015.1021429.
- [6] A. Patel, J. Ramsay, M. Imtiaz and Y. Lu, "EMG-based human machine interface control," 2019 12th International Conference on Human System Interaction (HSI), 2019, pp. 127–131, doi: 10.1109/HSI4729.8.2019.8942598.

- [7] M. B. I. Reaz, M. S. Hussain, and F. Mohd-Yasin, "Techniques of EMG signal analysis: detection, processing, classification and applications," *Biological Procedures Online*, vol. 8, no. 1, pp. 11–35, Mar. 2006, doi: 10.1251/bpo115.
- [8] S. Gowtham, K. M. A. Krishna, T. Srinivas, R. G. P. Raj and A. Joshua, "EMG-based control of a 5 DOF robotic manipulator," 2020 International Conference on Wireless Communications Signal Processing and Networking (WiSPNET), 2020, pp. 52-57, doi: 10.1109/WiSPNET48689.2020.9198439.
- [9] A. F. Ruiz-Olaya, C. A. Quinayas Burgos and L. T. Londoño, "A low-cost arm robotic platform based on myoelectric control for rehabilitation engineering," 2019 IEEE 10th Annual Ubiquitous Computing, Electronics & Mobile Communication Conference (UEMCON), 2019, pp. 0929-0933, doi: 10.1109/UEMCON47517.2019.8993080.
- [10] J. Vogel et al., "EDAN: An EMG-controlled daily assistant to help people with physical disabilities," in IEEE International Conference on Intelligent Robots and Systems, Oct. 2020, pp. 4183–4190. doi: 10.1109/IROS45743.2020.9341156.
- [11] P. J. Gonzalo and A. Holgado-Terriza Juan, "Control of home devices based on hand gestures," in 5th IEEE International Conference on Consumer Electronics - Berlin, ICCE-Berlin 2015, Jan. 2016, pp. 510–514. doi: 10.1109/ICCE-Berlin.2015.7391325.
- [12] Y. Muranaka, M. Al-Sada, and T. Nakajima, "A home appliance control system with hand gesture based on pose estimation," in 2020 IEEE 9th Global Conference on Consumer Electronics, GCCE 2020, Oct. 2020, pp. 752–755. doi: 10.1109/GCCE50665.2020.9291877.
- [13] L. Lu, J. Mao, W. Wang, G. Ding, and Z. Zhang, "A study of personal recognition method based on EMG signal," *IEEE Transactions on Biomedical Circuits and Systems*, vol. 14, no. 4, pp. 681–691, Aug. 2020, doi: 10.1109/TBCAS.2020.3005148.
- [14] J. S. Kim and S. B. Pan, "A Study on EMG-based Biometrics."
- [15] M. Nguyen, T. N. Gia, and T. Westerlund, "EMG-based IoT system using hand gestures for remote control applications," in 7th IEEE World Forum on Internet of Things, WF-IoT 2021, Jun. 2021, pp. 911–912. doi: 10.1109/WF-IoT51360.2021.9595957.
- [16] L. Lu, J. Mao, W. Wang, G. Ding and Z. Zhang, "An EMG-based personal identification method using continuous wavelet transform and convolutional neural networks," 2019 IEEE Biomedical Circuits and Systems Conference (BioCAS), 2019, pp. 1-4, doi: 10.1109/BIOCAS.2019.8919230.
- [17] R. Shioji, S. Ito, M. Ito and M. Fukumi, "Personal authentication and hand motion recognition based on wrist EMG analysis by a convolutional neural network," 2018 Joint 10th International Conference on Soft Computing and Intelligent Systems (SCIS) and 19th International Symposium on Advanced Intelligent Systems (ISIS), 2018, pp. 1172-1176, doi: 10.1109/SCIS-ISIS.2018.00184.
- [18] S. Shin, J. Jung and Y. T. Kim, "A study of an EMG-based authentication algorithm using an artificial neural network," 2017 IEEE SENSORS, 2017, pp. 1-3, doi: 10.1109/ICSENS.2017.8234158.
- [19] T. Wilaiprasitporn, A. Dittthaporn, K. Matchapam, T. Tongbuasirilai, N. Banluesombatkul, and E. Chuangsuwanich, "Affective EEG-based person identification using the deep learning approach," *IEEE Transactions on Cognitive and Developmental Systems*, vol. 12, no. 3, pp. 486–496, Sep. 2020, doi: 10.1109/TCDS.2019.2924648.
- [20] U. Côté-Allard et al., "Deep learning for electromyographic hand gesture signal classification using transfer learning," *IEEE Transactions on Neural Systems and Rehabilitation Engineering*, vol. 27, no. 4, pp. 760–771, Apr. 2019, doi: 10.1109/TNSRE.2019.2896269.
- [21] P. Visconti, F. Gaetani, G. A. Zappatore, and P. Primiceri, "Technical features and functionalities of Myo armband: an overview on related literature and advanced applications of myoelectric armbands mainly focused on arm prostheses," *International Journal on Smart Sensing and Intelligent Systems*, vol. 11, no. 1, pp. 1–25, 2018, doi: 10.21307/ijssis-2018-005.
- [22] T. Phienthrakul, "Armband gesture recognition on electromyography signal for virtual control," in 2018 10th International Conference on Knowledge and Smart Technology: Cybernetics in the Next Decades, KST 2018, Aug. 2018, pp. 149–153. doi: 10.1109/KST.2018.8426118.
- [23] J. Xu, T. Li, Y. Chen and W. Chen, "Personal identification by convolutional neural network with ECG signal," 2018 International Conference on Information and Communication Technology Convergence (ICTC), 2018, pp. 559-563, doi: 10.1109/ICTC.2018.8539632.
- [24] M. F. Guo, X. D. Zeng, D. Y. Chen, and N. C. Yang, "Deep-learning-based earth fault detection using continuous wavelet transform and convolutional neural network in resonant grounding distribution systems," *IEEE Sensors Journal*, vol. 18, no. 3, pp. 1291–1300, Feb. 2018, doi: 10.1109/JSEN.2017.2776238.
- [25] E. H. Galvis-Serrano, I. Sánchez-Galvis, N. Flórez, and S. Zabala-Vargas, "Classification of gestures of the colombian sign language from the analysis of electromyographic signals using artificial neural networks," *Informacion Tecnologica*, vol. 30, no. 2, pp. 171–179, Mar. 2019, doi: 10.4067/S0718-07642019000200171.